

Journal of

# Coastal Research

VOL. SI.70 • CERF • April 2014



Published by

*Proceedings of the 13th International Coastal Symposium*

Andrew Green  
Andrew Cooper  
Editors



**PROCEEDINGS OF THE INTERNATIONAL COASTAL  
SYMPOSIUM**

**DURBAN, KWAZULU-NATAL, SOUTH AFRICA**

**THE OYSTERBOX UMHLANGA ROCKS**

**13th TO 18<sup>th</sup> APRIL 2014**

Edited by Andrew Green and J. Andrew G. Cooper

Coastal Education and Research Foundation (CERF)

Geological Sciences, School of Agriculture, Earth and Environmental Sciences, University of  
KwaZulu-Natal

Journal of Coastal Research Special Issue 70

### **Organising committee**

Andrew Green (Chair), University of KwaZulu-Natal

Andrew Cooper (Chair), University of Ulster, University of KwaZulu-Natal

Bronwyn Goble, Oceanographic Research Institute, SAAMBR

Charles Finkl, CERF

Chris Makowski, CERF

Carlos Loureiro, Universidade do Algarve, University of KwaZulu-Natal

Lauren Hoyer, University of KwaZulu-Natal

Alan Smith, University of KwaZulu-Natal

### **Scientific committee**

Andrew Green (RSA)

Andrew Cooper (UK)

Bronwyn Goble (RSA)

Alan Smith (RSA)

Gonzalo Malvarez (ES)

Ana Vila-Concejo (AUS)

Oscar Ferreira (PT)

Javier Gracia (ES)

Paolo Ciavola (IT)

Samuel Etienne (Fr)

Helene Burningham (UK)

Rob Duck (UK)

Derek Jackson (UK)

Mike Phillips (UK)

ISSN 0749-0208

Front cover photo: Andrew Cooper

Published By

Marine Geology Research Unit, Geological Sciences

School of Agriculture, Earth and Environmental Sciences,

University of KwaZulu-Natal

Westville,

Durban 4000

South Africa

All the authors are responsible for the contents of their papers. The University of KwaZulu-Natal and CERF cannot be held responsible for any opinions and statements made by them.

## TABLE OF CONTENTS

### **Volume I Runup variability due to time dependence and stochasticity in the beach profiles: two extreme cases of the Spanish coast**

R. Díaz-Sánchez, J.S. López-Gutiérrez, A. Lechuga, V. Negro	1-6
<b>Analysis of wave attenuation and shore protection of a bulk carrier ship performing as a detached floating breakwater</b>	
A. Fernández Lázaro, R.M. Gutiérrez Serret, V. Negro, J.S. López-Gutiérrez	7-11
<b>The effect of scour protections in offshore wind farms</b>	
C. Matutano, V. Negro, J. López-Gutiérrez, M. D. Esteban, A. Hernández	12-17
<b>Using Combined Modelling Approaches to Improve Coastal Defence Design: a case study at Hopton, UK</b>	
J.J. Williams, L.S. Esteves, T. Conduche, P. Barber, A. Tindle	18-22
<b>On the use of the Radon transform to estimate longshore currents from video imagery</b>	
S. Larnier, R. Almar, R. Cienfuegos, A. Lejay	23-28
<b>Quantifying dispersion in an estuary: A Lagrangian drifter approach</b>	
D. Spencer, C.J. Lemckert, Y. Yu, J. Gustafson, S.Y. Lee, H. Zhang	29-34
<b>Monitoring of High Waves and Tsunami using HF Ocean Radar in the East Coast of Korea</b>	
J. Seo, B. Shin, K. Kim	35-40
<b>Impact of detached breakwaters on shoreline evolution: a case study on the Portuguese West Coast</b>	
M.A.V.C. Araújo, S.D. Bona, A. Trigo-Teixeira	41-46
<b>Growth of cusped spits</b>	
F. Bouchette, M. Manna, P. Montalvo, A. Nutz, M. Schuster, J. Ghienne	47-52
<b>Investigating the role of complex sandbar morphology on nearshore hydrodynamics</b>	
N. Cohn, P. Ruggiero, J. Ortiz, D.J. Walstra	53-58
<b>Volumetric changes of a soft cliff coast 2008-2012 based on DTM from airborne laser scanning (Wolin Island, southern Baltic Sea)</b>	
J. Dudzińska-Nowak, P. Wężyk	59-64
<b>Headland structural impacts on surf zone current circulations</b>	
M.S.A. Razak, A. Dastgheib, F. X. Suryadi, D. Roelvink	65-71

<b>Relationships between sand spit evolution, environmental forcing and inland inundation</b>	
T.Thomas, S.K. Lynch, M. R. Phillips, A.T. Williams , R.W. Duck	72-79
<b>Longshore drift cell development on the human-impacted Bight of Benin sand barrier coast, West Africa</b>	
R.A. Laïbi, E.J. Anthony, R. Almar, B. Castelle, N. Senechal, E. Kestenare	78-83
<b>Wave-driven circulation over a double nearshore bar system during storm conditions</b>	
N. Robin, R. Certain, F. Bouchette, E.J. Anthony, S. Meulé, N. Aleman	84-89
<b>Geomorphology of coastal formations on present and ancient sandy coasts</b>	
A. Anderson, K. Vilumaa, H. Tõnisson, A. Kont, U. Ratas, S. Suuroja	90-95
<b>Evolution of Corsican pocket beaches</b>	
B. Yann, B. Rémi, A. Merour, C. Riotte	96-101
<b>Travelling forelands: complexities in drift and migration patterns</b>	
H. Burningham, J.R. French	102-108
<b>Control of wave climate and meander dynamics on spit breaching and inlet migration</b>	
E. Chaumillon, F. Ozenne, X. Bertin, N. Long, F. Ganthuy	109-114
<b>Spur and groove distribution, morphology and relationship to relative wave exposure, Southern Great Barrier Reef, Australia</b>	
S. Duce, A. Concejo, S. Hamylton, E. Bruce, J.M. Webster	115-120
<b>A paraglacial coastal gravel structure: Connell’s Bank, NW Ireland</b>	
J. Knight, H. Burningham	121-126
<b>Time and spatial variability of sediment gradings in the surfzone of a large scale nourishment</b>	
B.J.A.Huisman, E.E. Sirks, L. van der Valk, D.J.R. Walstra	127-132
<b>Monitoring changes in suspended sediment concentration on the southwestern coast of Korea</b>	
J. Min, J. Choi, H. Yang, S. Lee, J. Ryu	133-138
<b>Regional variation in the dynamics of Estonia’s coastal landscapes</b>	
U. Ratas, R. Ravis, A. Kont, H. Tõnisson, K. Vilumaa, A. Anderson, R. Szava-Kovats	139-144
<b>Submarine hard-bottom substrates in the western Baltic Sea – human impact versus natural development</b>	
K. Schwarzer, B. Bohling, C. Heinrich	145-150

<b>Forecasting lagoon outlet erosion: KwaZulu-Natal, southeast Africa</b>	
A.M. Smith, L.A. Guastella, B.J. Goble	151-156
<b>Seasonal sedimentary processes of the macrotidal flat in Gomso Bay, Korea</b>	
J. Kang, H.J. Woo, Y. Lee, Y.B. Son	157-163
<b>Sea level fluctuation and shoreline evolution on decadal time scale. , Lithuanian Baltic Sea coast</b>	
D. Jarmalavičius, D. Pupienis, G. Žilinskas	164-169
<b>The role of beachrocks on the evolution of the Holocene barrier systems in Rio de Janeiro, southeastern Brazil</b>	
A.L.C. da Silva, M.A.M. da Silva, R.S. de Souza, M.L.V. Pinto	170-175
<b>Morphodynamic characterization of beaches on a Pacific atoll island: Tetiaroa, French Polynesia</b>	
M. Jeanson, E.J. Anthony, S. Etienne, F. Dolique	176-181
<b>Middle shoreface sand transport under the influence of a river plume</b>	
S. Meirelles, A. R. Horner-Devine, M. Henriquez, M. Stive, J. Pietrzak, A.J. Souza	182-186
<b>Megaripple dynamics on a dissipative sandy beach</b>	
J. Miles, A. Thorpe, P. Russell, G. Masselink	187-192
<b>Influence of storms on coastal retreat in SW Spain</b>	
M. Puig, L. del Río, T.A. Plomaritis, J. Benavente	193-198
<b>The natural causes of shoreline evolution of Capo Peloro, the northernmost point of Sicily (Italy)</b>	
G. Randazzo, C. Cigala, A. Crupi, S. Lanza	199-204
<b>Meandering fluvial system influencing the evolution of a Holocene regressive barrier in southern Brazil</b>	
A. Biancini da Silva, E.G. Barboza, M. L.C.C. Rosa, S.R. Dillenburg	205-210
<b>Dune coast changes caused by weak storm events in Miedzywodzie, Poland</b>	
N. Bugajny, K. Furmańczyk	211-216
<b>Morphological changes of a Mediterranean beach over one year (San Giovanni Sinis, western Mediterranean)</b>	
S. Simeone, G. De Falco, G. Quattrocchi, A. Cucco	217-222
<b>Multi-scale analysis of wave conditions and coastal changes in the north-eastern Baltic Sea</b>	
Ü. Suursaar, V. Alari, H. Tõnisson	223-228

<b>Field experiments with different fractions of painted sediments to study material transport in three coastal sites in Estonia</b>	
H. Tõnisson, Ü. Suursaar, A. Kont, K. Orviku, R. Ravis, R. Szava-Kovats, K. Vilumaa, T. Aarna, M. Eelsalu, K. Pindsoo, V. Palginõmm, U. Ratas	229-234
<b>Incorporating dynamic factors to the Environmental Sensitivity Index (ESI) shoreline classification – Estonian and Spanish examples</b>	
R. Aps, H. Tõnisson, G. Anfuso, J. A. Perales, K. Orviku, Ü. Suursaar	235-240
<b>The influence of interannual variability of mean sea level in the Adriatic Sea on extreme values</b>	
M.F. Bruno, M.G. Molfetta, A.F. Petrillo	241-246
<b>Overtopping hazard on a rubble mound breakwater</b>	
A.R. Carrasco, M.T. Reis, M.G. Neves, Ó. Ferreira, A. Matias, S. Almeida	247-252
<b>A contribution to climate change assessment of storm surges along the coast of Mozambique</b>	
A.C.F. Aramuge, A. Rocha, P. A. Silva	253-258
<b>Spatial distribution of storm wave energy dissipation for the assessment of beach morphodynamics</b>	
E. Guisado-Pintado, G. Malvárez, F. Navas, R. Carrero	259-265
<b>Hurricane Isaac storm surge deposition in a coastal wetland along Lake Pontchartrain, southern Louisiana</b>	
K. Liu, T.A. McCloskey, T.A. Bianchette, G. Keller, N.S.N. Lam, J.E. Cable, J. Arriola	266-271
<b>A preliminary study of the distribution, sizes and orientations of large reef-top coral boulders deposited by extreme waves at Makemo Atoll, French Polynesia</b>	
A.Y. Lau, S. Etienne, J. P. Terry, A.D. Switzer, Y. Sin Lee	272-277
<b>Responses of coastal waters in the Yellow Sea to Typhoon Bolaven</b>	
C S. Kim, H. Lim, J. Yong Jeong, J. Shim, I. Moon, Y. Jung Oh, H. Yoel You	278-283
<b>Transformation of small-scale meteorological tsunami due to terrain complexity on the western coast of Korea</b>	
T. Ha, J. Choi, J. Yoo, I. Chun, J. Shim	284-289
<b>Applicability of video-derived bathymetry estimates to nearshore current model predictions</b>	
M. Radermacher, M. Wengrove, J. van Thiel de Vries, R. Holman	290-295
<b>Extensive monitoring and intensive analysis of extreme winter-season wave events on the Korean east coast</b>	
S. Oh, W. Jeong	296-301



<b>Breach process simulation of coastal levees broken by the 2011 Tsunami</b>	
T. Iida, S. Kure, K. Udo, A. Mano, H. Tanaka	302-307
<b>Storm deposition induced by hurricanes in a rapidly subsiding coastal zone</b>	
J.D. Naquin, K. Liu, T.A. McCloskey, T.A. Bianchette	308-313
<b>Characterization of wave climate and extreme events into the SW Spanish and Wales coasts as a first step to define their wave energy potential</b>	
N. Rangel-Buitrago, G. Anfuso, M. Phillips, T. Thomas, O. Alvarez, M. Forero	314-319
<b>Influence of climate change on the Ria de Aveiro littoral: adaptation strategies for flooding events and shoreline retreat</b>	
J.M. Dias, C.L. Lopes, C. Coelho, C. Pereira, F.L. Alves, L.P. Sousa, I.C. Antunes, M. da Luz Fernandes, M.R. Phillips	320-325
<b>Non-uniformity of storm impacts on three high-energy embayed beaches</b>	
C. Loureiro, Ó. Ferreira, J. A.G. Cooper	326-331
<b>Effects of bathymetry on the propagation of tsunamis towards the east coast of Korea</b>	
S.B. Yoon, S.C. Kim, U. Baek, J.S. Bae	332-337
<b>Recording of selected effects and hazards caused by current and expected storm events in the Baltic Sea coastal zone</b>	
K. Furmańczyk, P. Andrzejewski, R. Benedyczak, N. Bugajny, Ł. Cieszyński, J. Dudzińska-Nowak, A. Giza, D. Paprotny, P. Terefenko, T. Zawisłak	338-342
<b>Global changes in mean tidal high water, low water and range</b>	
R.J. Mawdsley, I.D. Haigh, N.C. Wells	343-348
<b>Cliff-top storm deposits (55-63m amsl) from Morgan Bay, South Africa</b>	
Smith, A.M., Green, A.N., Cooper, J.A.G., Dixon, S., Pretorius, L., Wiles, E., Guastella, L.A.	349-353
<b>Nearshore bathymetry from video and the application to rip current predictions for the Dutch Coast</b>	
L. Sembiring, A. van Dongeren, G. Winter, M. van Ormondt, C. Briere, D. Roelvink	354-359
<b>Massive cooling water dispersion behavior in a shallow macro-tidal coastal zone in Korea</b>	
S. Suh	360-365
<b>RISC-KIT: Resilience-Increasing Strategies for Coasts – toolkit</b>	
A. Van Dongeren, P. Ciavola, C. Viavattene, S. de Kleermaeker, G. Martinez, O. Ferreira, C. Costa, R. McCall	366-371

<b>Incorporating dynamics factor to the Environmental Sensitivity Index (ESI) shoreline classification – Estonian and Spanish example</b>	
R. Aps, H. Tõnisson, G. Anfuso, J.A. Perales, K. Orviku, Ü. Suursaar	372-377
<b>Assessment of the Sensitivity of Salamina (Saronic Gulf) and Elafonissos (Lakonic Gulf) islands to Sea-level Rise</b>	
E. Karymbalis, C. Chalkias, M. Ferentinou, G. Chalkias, M. Magklara	378-384
<b>Preliminary coastal vulnerability assessment for Pico Island (Azores)</b>	
P. Borges, M.R. Phillips, K. Ng, A. Medeiros, H. Calado	385-388
<b>Coastal impacts of marine renewables: perception of breaker characteristics by beach water users</b>	
C. Stokes, E. Beaumont, P. Russell, D. Greaves	389-394
<b>Sandy beaches characterization and management of coastal erosion on western Sardinia island (Mediterranean Sea)</b>	
G. De Falco, F. Budillon, A. Conforti, S. De Muro, G. Di Martino, S. Innangi, A. Perilli, R. Tonielli, S. Simeone	395-400
<b>Guidelines for coastal zone management in the Amazon estuary (Amapá, Brazil)</b>	
R.K.S. Gomes, F.B.B. de Sousa, V.V. Amanajás, G.C. Santos, L.C.C. Pereira	401-406
<b>Managed realignment in practice in the UK: results from two independent surveys</b>	
L.S. Esteves, K. Thomas	407-413
<b>Artificial intelligence-based models to simulate land-use change around an estuary</b>	
R. Carrero, F. Navas, G. Malvárez, E. Guisado-Pintado	414-419
<b>Regional differences in recreational preferences of Estonian coastal landscapes</b>	
M. Reimann, Ü. Ehrlich, H. Tõnisson	420-425
<b>Beach user perceptions at the eastern Yucatan peninsula, Mexico</b>	
A.T. Williams, A. Barugh	426-430
<b>Are natural beaches facing extinction?</b>	
O.H. Pilkey and J.A.G. Cooper	431-436

**Trend Change(s) in Coastal Management Plans: the integration of short and medium term perspectives in the spatial planning process**

F.L. Alves, L.P. Sousa, T.C. Esteves, E.R. Oliveira, I.C. Antunes, M. da Luz Fernandes,  
L.Carvalho, S. Barroso, M. Pereira 437-442

**Productive Chain of the Mangrove Crab (*Ucides cordatus*) in the Town of Bragança, in the Northern Brazilian State of Pará (Amazon Region)**

M.A.B. Monteiro, F. P. Oliveira, J.N. Araújo, M.E.B. Fernandes 443-447

**An analysis of recent changes in Spanish Coastal Law**

V. Negro, J. López-Gutiérrez, M.D. Esteban, C. Matutano 448-453

**Creation of an alternative season based on sustainable tourism as an opportunity for Baltic Sea Region**

P. Łonyszyn, O. Terefenko 454-460

**Coastal and marine protected areas as key elements for tourism in small islands**

C. Fonseca, C. Pereira da Silva, H. Calado, F. Moniz, C. Bragagnolo, A. Gil,  
M. Phillips, M. Pereira, M. Moreira 461-466

**Framework for proper beach nourishment as an adaptation to beach erosion due to sea level rise**

J. Yoshida, K. Udo, Y. Takeda, A. Mano 467-472

**Assessment of vulnerability and adaptive capacity to coastal hazards in the Caribbean Region**

N.S.N. Lam, H. Arenas, P.L. Brito, K. Liu 473-478

**Methodology for the development of 3D GIS models in the Coastal Zone**

M.G. Magarotto, M.F. Costa, J.A. Tenedório, C.P. Silva, T.L. Martins Pontes 479-484

**A multi-scale analysis to support the implementation of a regional conservation policy in a small-island archipelago – the Azores, Portugal**

H. Calado, C. Bragagnolo, S.F. Silva, M. Pereira 485-489

**Beach nourishment experiment in Palanga, Lithuania**

D. Pupienis, D. Jarmalavičius, G. Žilinskas, J. Fedorovič 490-495

**How can Portugal effectively integrate ICM and MSP?**

M.A. Ferreira, D. Johnson, C. Pereira da Silva 496-501

**West African EBSAs: Building capacity for future protection**

D. Johnson, J. Lee, A. Bamba, C. Karibuhoye 502-506

**An interactive WebGIS observatory platform for enhanced support of integrated coastal management**

A. Oliveira, G. Jesus, J.L. Gomes, J. Rogeiro, A. Azevedo, M. Rodrigues, A.B. Fortunato, J.M. Dias, L.M. Tomas,  
L. Vaz, E.R. Oliveira, F.L. Alves, S. den Boer 507-512

**Coastal management and mis-management: comparing successes and failures at two lagoon outlets in KwaZulu-Natal, South Africa**

L. Guastella, A.M. Smith, T. Breetzke 513-520

**Beach users' profile, perceptions and willingness to pay for beach management in Cadiz (SW Spain)**

B. Alves, J. Benavente, Ó. Ferreira 521-526

**Evaluation of recreational quality, carrying capacity and ecosystem services supplied by sandy beaches of the municipality of Camaçari, northern coast of Bahia, Brazil**

J.R. de Souza Filho, R.C. Santos, I.R. Silva, C.I. Elliff 527-532

**Cross-shore variation of water surface elevation and velocity during bore propagation**

K. Lee, S. Shin, D. Kim 533-538

**Development of an oil spill hazard scenarios database for risk assessment**

S. den Boer, A. Azevedo, L. Vaz, R. Costa, A.B. Fortunato, A. Oliveira,  
L.M. Tomás, J.M. Dias, M. Rodrigues 539-544

**Tourism carrying capacity on estuarine beaches in the Brazilian Amazon region**

R.C. de Sousa, L.C.C. Pereira, R.M. da Costa, J.A. Jiménez 545-550

**The impact of processes associated with risk assessment and categorization of bathing waters on the water safety system development on the Polish Baltic coast**

T. Zalewski, T. Czapiewski 551-555

**Recreational parameters as an assessment tool for beach quality**

C. Botero, C. Pereira, G. Anfuso, O. Cervantes, A.T. Williams, E. Pranzini, C.P. Silva 556-562

**Sedimentation and erosion patterns in a low shoot-density *Zostera noltii* meadow in the fetch-limited Berre lagoon, Mediterranean France**

A. Paquier, S. Meulé, E.J. Anthony, G. Bernard 563-567

<b>Effects of mud flows from the LUSI mud volcano on the Porong River estuary, Indonesia</b>	
S. Kure, B. Winarta, Y. Takeda, K. Udo, M. Umeda, A. Mano, H. Tanaka	568-573
<b>Influence of mean sea level rise on tidal dynamics of the Ria de Aveiro lagoon, Portugal</b>	
C.L. Lopes, J.M. Dias	574-579
<b>The influence of the Maputo and Incomati rivers on the mixing and outflow of freshwater from Maputo Bay (Mozambique)</b>	
K. Markull, J.D. Lencart e Silva, J.H. Simpson, J. M. Dias	580-585
<b>Salinity modelling accuracy of a coastal lagoon: a comparative river flow analysis of basin model vs. traditional approaches</b>	
L.M. Tomas, M. Rodrigues, A.B. Fortunato, A. Azevedo, P.C. Leitão, A. Oliveira, A. Rocha, J.F. Lopes, J.M. Dias	586-591
<b>Hydrodynamics of a river-associated tidal inlet and maintenance of dynamic equilibrium: preliminary findings</b>	
M. Villagran, D. Caamaño, R. Cienfuegos	592-597
<b>Tidal dispersion and flushing times in a multiple inlet lagoon</b>	
J.D. Lencart e Silva, C.L. Lopes, A. Picado, M.C. Sousa, J.M. Dias	598-603
<b>Study of suspended sediment dynamics in a temperate coastal lagoon: Ria de Aveiro (Portugal)</b>	
S. Plecha, A. Picado, P. Chambel-Leitão, J.M. Dias, N. Vaz	604-609
<b>Residual currents and transport pathways in the Tagus estuary, Portugal: the role of freshwater discharge and wind</b>	
N. Vaz , J.M. Dias	610-615
<b>Analysis of the recent evolution of the sand spit at the Solís Chico river mouth</b>	
S. Solari, C. Chreties, G. López, L. Teixeira	616-620
<b>Differential short- and medium-term behavior of two sections of an urban beach</b>	
J. Benavente, T.A. Plomaritis, L. del Río, M. Puig, C. Valenzuela, B. Minuzzi	621-626
<b>Estimating the impact threshold for wind-blown sand</b>	
B. Li, J.T. Ellis, D.J. Sherman	627-632

**Rip currents and circulation on a high-energy low-tide-terraced beach (Grand Popo, Benin, West Africa)**

B. Castelle, R. Almar, M. Dorel, J. Lefebvre, N. Sénéchal, E.J. Anthony, R. Laibi,  
R. Chuchla, Y. du Penhoat 633-638

**Video monitoring and field measurements of a rapidly evolving coastal system: the river mouth and sand spit of the Mataquito River in Chile**

R. Cienfuegos, M. Villagran, J.C. Aguilera, P. Catalán, B. Castelle, R. Almar 639-644

**Storm-driven cusp behaviour on a high energy gravel beach**

T.G. Poate, G. Masselink, R.M. McCall, P.E. Russell, M.A. Davidson 645-650

**The Grand Popo beach 2013 experiment, Benin, West Africa: from short timescale processes to their integrated impact over long-term coastal evolution**

R. Almar and other authors. 651-656

**Intertidal beach classification in infrared images**

B. Hoonhout, F. Baart, J. van Thiel de Vries 657-662

**Contribution of swash processes generated by low energy wind waves in the recovery of a beach impacted by extreme events: Nha Trang, Vietnam**

J. Lefebvre, R. Almar, N.T. Viet, D.V. Uu, D.H. Thuan, L.T. Binh, R. Ibaceta, N.V. Duc 663-668

**Observed destruction of a beach cusp system in presence of a double-coupled cusp system: the example of Grand Popo, Benin**

N. Senechal, R.A. Laibi, R. Almar, B. Castelle, M. Biauxque, J.-P. Lefebvre, E. J. Anthony,  
M. Dorel, R. Chuchla, M.H. Hounkonnou, Y. Du Penhoat 669-674

**Nearshore and foreshore influence on overwash of a barrier island**

A. Matias, A.R. Carrasco, C. Loureiro, S. Almeida, Ó. Ferreira 675-680

**Morphodynamic variations of a macrotidal beach (Atalaia) on the Brazilian Amazon Coast**

L.C.C. Pereira, K.S.T. Pinto, A. Vila-Concejo 681-686

**Stratigraphic analysis applied on the recognition of the interface between marine and fluvial depositional systems**

E.G. Barboza, M.L.C.C. Rosa, S.R. Dillenburg, A.B. da Silva, L.J. Tomazelli 687-692

**Alongshore variations in beach-dune system response to major storm events on the Danube Delta coast**

F. Tătu, A. Vespremeanu-Stroe, L. Preoteasa 693-699

**Bedform Dynamics in a Rip Current**

A. Thorpe, J. Miles, G. Masselink, P. Russell 700-705

**Determining the role of exposure, wave force, and rock chemical resistance in marine notch development**

P. Terefenko, O. Terefenko 706-711

**Beach oscillation and rotation: local and regional response at three beaches in southeast Australia**

A.D. Short, M.A. Bracs, I.L. Turner 712-717

**A preliminary classification of coastal sand dunes of KwaZulu-Natal**

D.W.T. Jackson, J.A.G. Cooper, A.N. Green 718-722

**Integrating different records to assess coastal hazards at multi-century timescales**

A.D. Switzer, F. Yu, C. Gouramanis, J.L.A. Soria, D.T. Pham 723-728

**Wind-driven waves in a shallow estuarine lake with muddy substrates: St Lucia, South Africa**

V. Zikhali, K. Tirok, D. Stretch 729-735

**Beachrock facies variability and sea level implications: a preliminary study**

C.S. Kelly, A.N. Green, J.A.G. Cooper, E.A. Wiles 736-742

## PREFACE

As chairs of the 13th International Coastal Symposium, we would like to warmly welcome our delegates to the sunny east coast of South Africa. It was with great honour that we accepted the invitation, in 2012, from the Board of the Coastal Education and Research Foundation (CERF) to play host to this prestigious event, especially since it is the 30th Anniversary of the Journal of Coastal Research. We are very pleased to use this occasion to introduce to you some of the local research in coastal and marine sciences here in Durban.

This event is hosted by the University of KwaZulu-Natal's (UKZN) School of Agriculture, Earth and Environmental Sciences' Discipline of Geological Science. Geological Sciences at UKZN is a small unit concerned primarily with mineral exploration and the mining sectors. It has, however, maintained a strong focus on sedimentology and geomorphology since the pioneering work of the late Prof. Lester C. King. In the last four years, the emergence of a vibrant and productive Marine Geology Research unit at UKZN has led to a resurgence in the study of the coastal and marine areas of southern Africa. It was within this small unit that this conference was organised.

Out of the initial 820 abstracts submitted, 220 abstracts were accepted for presentation. Based on these abstracts, 136 full length, peer-reviewed papers now appear in Special Issue 70 of the Journal of Coastal Research. The production of this special issue could not have taken place without the assistance of the ICS2014's scientific committee, the anonymous reviewers and the small team of willing postgraduate students who went above and beyond to copy edit and proof every paper therein.

Of course, no event could take place without logistical and financial backing. In this light, we wish to thank the University of KwaZulu-Natal for providing the financial manpower, together with a large donation from the College of Agriculture, Engineering and Science, in order to ensure the ultimate success of ICS2014. We also wish to thank the Oysterbox, our host venue, for providing the sumptuous fare and surroundings within which the conference will take place. We are extremely grateful to Charlie Finkl, CERF President, for sponsorship of the conference dinner. He and Senior Vice President, Chris Makowski, provided constant support for the organisation of this conference since its inception.



Last but not least, we wish to thank you the delegates. Many have made a very long trip to be here in Durban. Without you, there would be little point to the conference. We hope that you will take this opportunity to renew old friendships, forge new ones, and establish new connections. Enjoy your stay.

Welcome, Welkom, Siyaalemukela, Amogela, Amohela, Amogela, Sondzela, Mi amukeriwile,  
Vho tangedzwa, Amkela, Emukela

Dr. Andrew Green and Prof. Andrew Cooper

Conference co-chairs ICS2014

# Runup variability due to time dependence and stochasticity in the beach profiles: two extreme cases of the Spanish coast

R. Díaz-Sánchez†, J.S. López-Gutiérrez‡, A. Lechuga∞, V. Negro§

† Centre for Harbours and Coastal Studies, CEDEX, Antonio López 81, Madrid, 28026, Spain  
roberto.diaz@cedex.es

‡ Research Group on Marine, Coastal and Port Environment and other Sensitive Areas.  
Universidad Politécnica de Madrid, Profesor Aranguren s/n, Madrid 28040, Spain  
josesantos.lopez@upm.es

∞ Centre for Harbours and Coastal Studies, CEDEX, Antonio López 81, Madrid, 28026, Spain  
antonio.lechuga@cedex.es



[www.cerf-jcr.org](http://www.cerf-jcr.org)

§ Research Group on Marine, Coastal and Port Environment and other Sensitive Areas.  
Universidad Politécnica de Madrid, Profesor Aranguren s/n, Madrid 28040, Spain  
Vicente.negro@upm.es



[www.JCRonline.org](http://www.JCRonline.org)

## ABSTRACT

Díaz-Sánchez, R., López-Gutiérrez, J.S., Lechuga, A., Negro, V., 2013. Runup variability due to time dependency and stochasticity in beach profiles. In: Conley, D.C., Masselink, G., Russell, P.E. and O'Hare, T.J. (eds.), 12<sup>th</sup> International Coastal Symposium Proceedings (Plymouth, England), *Journal of Coastal Research*, Special Issue No. 70, pp. 001-006, ISSN 0749-0208.

Equations for extreme runup worked out from several experimental studies are compared. Infragravitatory oscillations dominate the swash in a dissipative state but not in intermediate – reflective states. Therefore two kinds of equation depending on either significant wave height,  $H_0$ , or the Iribarren number,  $\xi_0$ , should be used. Through a sand bed physical model with a uniform sand bed slope, equations are proposed for both beach states, and results are compared with precedent field and physical model experiments. Once the equations are chosen, the time-longshore variability in a medium – long term time scale of the foreshore slope is evaluated in two extreme cases relating to the Spanish coast. The Salinas beach on the North coast ( Bay of Biscay) displayed a permanent dissipative beach state with small variations in the beach foreshore slope both along the shore and in time, so foreshore slope deviations in a medium-long term period were irrelevant and extreme runup is predicted with the wave height worked out from the design return period. Peñíscola beach on the East coast (Mediterranean sea) displayed an intermediate state. If only time variations are analysed, variations in determining extreme runup are irrelevant. In contrast, significant differences were found when the longshore variations were studied in this Mediterranean beach.

**ADDITIONAL INDEX WORDS:** *setup, runup, extreme runup, swash, beach processes.*

## INTRODUCTION

Extreme runup has been widely studied using the statistical approach. Several studies, whether field experiments or physical models, have proved the effectiveness of Iribarren number as an indicator of the surf and swash processes determining runup. The greater influence of infragravitatory frequencies on dissipative beaches leads to runup independence on the beach slope,  $\beta$ , (Guza and Thornton 1982; Stockdon *et al.* 2006). In contrast, for reflective states, energy in the swash spectra is distributed between both frequency ranges so beach slope becomes significant in runup estimation, (Holman 1986; Nielsen and Hanslow 1991).

Several equations have been developed from empirical studies to predict runup. Grouped into two general states on a beach, dissipative or reflective, these equations are separated so that different estimators are used as a function of the beach state. Basically for dissipative beaches, the commonly accepted

estimator is the significant wave height in deep water,  $H_0$ . The deep-water Iribarren number,  $\xi_0$ , Eq.(1) is used for the other kind, where  $L_0$  is the wave length estimated through the linear dispersion relationship, although scattering in the results remains high, mainly due to second order processes such as edge waves, or beach slope variations in time and space, both long-shore and cross-shore.

$$\xi_0 = \frac{\beta}{\sqrt{\frac{H_0}{L_0}}} \quad (1)$$

Since the beach's morphology influences runup dynamics, the variability of the beach profile, especially the beach slope at the foreshore,  $\beta_f$ , can yield high variance as a function of the longshore position or the time scale considered. In a risk analysis approach, the worst morphological state in a medium-long term period should be considered to evaluate the extreme runup on a

beach during a storm. Extreme runup may significantly vary due to longshore and time variability in the beach profiles.

In this study an equation worked out from a physical model is proposed. Data are also contrasted with prior field and physical model experiments. The physical model configuration with an initial uniform slope allows for an assessment of extreme runup on an unbalanced beach far from its theoretical equilibrium which involves ensuring a value less likely to be reached. Two extreme cases on the Spanish coast are analysed where the foreshore slope variance is measured longshore and in time on a medium-long term time scale.

## EXTREME RUNUP EQUATION

### Literature review

From prior studies, extreme runup,  $R_2$ , formulae can be grouped in those using the Iribarren number as an estimator and those others that remove the use of the beach slope. Some of the studies have provided both kinds of equation, with a limit to distinguish between dissipative and reflective states.

Among the prior results involving the Iribarren number, we might mention: Holman and Sallenger (1985); Mase (1989); Nielsen and Hanslow (1991); Ruggiero *et al.* (2001); Hedges and Mase (2004) and Stockdon *et al.* (2006). Generally speaking, these equations should be limited to non-dissipative conditions. Also, each author has usually provided an application range. When a range is not provided, it was worked out from the experiment's limits. The equations and relevant limits are presented in Table 1, where:  $SWL$  is an averaged water level defined by Nielsen and Hanslow (1991); and  $\Omega$  is the Dean parameter, (Dean 1977).

Table 1- Nondimensional extreme runup  $R_2/H_0$  – Iribarren number  $\xi_0$  prior equations

Reference	Proposed equation	Application range
Holman & Sallenger (1985)	$\frac{R_2}{H_0} = 0.2 + 0.83 \cdot \xi_0$	$\xi_0 > 0.5$
Mase (1989)	$\frac{R_2}{H_0} = 1.86 \cdot \xi_0^{0.71}$	$\frac{1}{30} < \beta < \frac{1}{5}$ $0.007 \leq \frac{H_0}{L_0}$
Nielsen & Hanslow (1991)	$\frac{R_2}{H_0} = SWL + 1.19 \cdot \xi_0$	$\beta_f > 0.10$ or $\Omega < 6$
Ruggiero <i>et al.</i> (2001)	$\frac{R_2}{H_0} = 0.27 \cdot \frac{\xi_0}{\sqrt{\beta}}$	$\xi_0 > 0.5$
Hedges & Mase (2004)	$\frac{R_2}{H_0} = 0.34 + 1.15 \cdot \xi_0$	$\xi_0 < 2.4$
Stockdon <i>et al.</i> (2006)	$\frac{R_2}{H_0} = 0.10 + 0.73 \cdot \xi_0$	$\xi_0 > 1.25$

Some relevant equations that removed the beach slope in the runup parameterization are: Guza and Thornton (1982); Nielsen and Hanslow (1991); Ruggiero *et al.* (2001); Stockdon *et al.* (2006) and; Roberts *et al.* (2010). In this kind of equation, the application is restricted to dissipative beaches although the authors provided an application range. Even if limits are not provided, it could be worked out from the experiment's limits. These prior studies are summarised in Table 2, where  $H_b$  is the breaking wave height.

Table 2- Extreme runup  $R_2$  – wave parameters  $H_0 - H_0L_0$

Reference	Proposed equation	Application range
Guza & Thornton (1982)	$R_2 = 0.55 \cdot H_0$	---
Nielsen & Hanslow (1991)	$R_2 = SWL + 0.1 \cdot (H_0 \cdot L_0)^{0.5}$	$\beta_f < 0.10$ or $\Omega > 6$
Ruggiero <i>et al.</i> (2001)	$R_2 = 0.5 \cdot H_0 - 0.22$	$\xi_0 < 0.5$
Stockdon <i>et al.</i> (2006)	$R_2 = 0.043 \cdot (H_0 \cdot L_0)^{0.5}$ $R_2 = 0.052 \cdot (H_0 \cdot L_0)^{0.5}$ $R_2 = 0.060 \cdot (H_0 \cdot L_0)^{0.5}$	$\xi_0 < 0.3$ or $\beta_f =$ 1/50 $\beta_f = 1/30$ $\beta_f = 1/20$
Roberts <i>et al.</i> (2010)	$R_2 = 1.00 \cdot H_b$	$\xi_0 > 0.3$

All these equations were compared with the physical model (described below) and field experiment data which have been obtained from previous studies that are described in the next section. Finally, equations for both dissipative and non-dissipative beaches are proposed.

### Physical model

This study analyses the extreme runup produced by the action of the random wave propagated vertically in a two dimensional flume - 2DV - on a sand seabed with an initial uniform slope. The purpose is to test the swash zone on a beach in an unbalanced state, so the results can be assumed as an envelope of the extreme runup  $R_2$  and, indeed, suitable for risk analysis.

The physical model was carried out in one of the wave flumes at the CEDEX Laboratory for Maritime Experimentation, Figure 1. The chosen wave flume is 36 metres long, 6.5 metres wide and 1.3 metres high. The water depth for wave generation was 0.55 metres. The physical model was designed to cover a reasonable range of parameters, three different slopes (1/50, 1/30 and 1/20), and it was filled up with two sand grain sizes (medium grain size,  $D_{50} = 0.12$  mm and 0.70 mm) and a range for the Iribarren number in deep water  $\xi_0$  from 0.1 to 0.6.



Figure 1. View of the physical model at the Laboratory for Harbours and Coastal Studies – CEDEX

The chosen range for the Iribarren number corresponds to the range that might occur on the Spanish coast in a storm, taking into account the extreme regime for maritime climate, (ROM 0.3-91 1991). Wave steepness in a storm for the Spanish coast varies between 0.01 and 0.06. The maximum limit for wave steepness relates to the maximum limit for the beach foreshore slope. For  $\zeta_0 = 0.6$  and  $H_0/L_0 = 0.06$  the beach slope is approximately 1/7. This is a very steep ratio for a sand beach. Hence the referred range is considered appropriate.

Swash measurements were made by means of two wave gauges set parallel to the beach profile on both sides minimizing law scale effects, under the assumption of Froude wave similitude. Due to the scale similitude, the flow is assumed to be in a rough turbulent flow in the swash. All cases were tested and the rough turbulent flow was the predominant flow, with velocities higher than 0.1 m/s. The sand bed provided more reliable swash oscillations due to permeability and friction factor.

Capacitive gauges were used for measuring surf characteristics and oscillations in the swash zone. Irregular waves were generated by software “ad hoc” whose principal inputs are: type of wave spectra, significant height, peak period, number of waves and acquisition time. Oscillations in the swash zone were measured by a hanging wire of 6 m in length parallel to the beach slope 1 cm high. Studies of the sea with 200 waves were performed, varying the time of the studies as a function of the averaged wave period.

From the data obtained in the 85 studies carried out, 79 were deemed as acceptable and statistical parameters of waves were calculated by spectra analysis. Time series of oscillations in the swash were also recorded. With the discrete distributions of runups, using the peak methodology, the extreme runup  $R_2$  was obtained in every test.

The significant wave height at 12 metres depth was calculated as the zeroth-moment of the wave spectrum and was assumed as the deep-water significant wave height and denoted as  $H_0$ . The wavelength  $L_0$  in deep water, was calculated by dispersion linear approximation with the peak period  $T_p$ . The Iribarren number is calculated using Eq.(1).

The time averaged setup  $\langle \eta \rangle$  is calculated for the extreme runup equations. Likewise, the significant spectra  $S_s$  is obtained as four times the root of the zeroth-moment of the swash spectra. Those parameters through the least-squared method are linear regressed and then  $R_2$  is calculated using Eq.(2). For more details see Díaz-Sánchez *et al.* (2013).

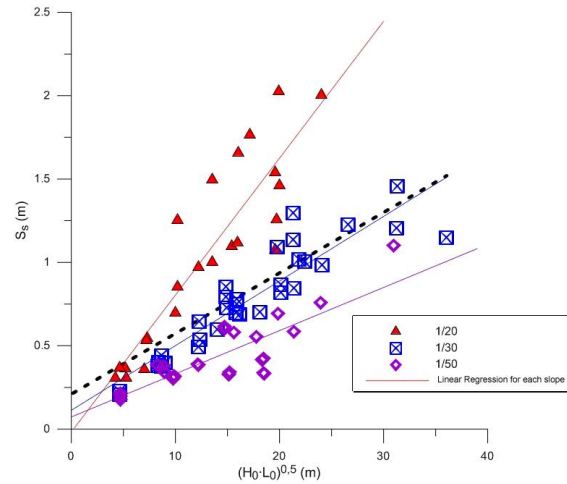


Figure 2: Significant swash,  $S_s$ , versus deep-water wave parameters  $H_0 L_0$ . Dashed line: Linear regression forced through origin

$$R_2 = 1.1 \cdot \left( \langle \eta \rangle + \frac{S_s}{2} \right) \quad (2)$$

## Results

The results of the experiment are grouped with data obtained from other experiments: Holman and Guza (1984); Mase (1989) and; Ruggiero *et al.* (2001). Finally a comparison between different equations was made so as to choose an equation for application to either dissipative or non-dissipative beaches.

Following Stockdon *et al.* (2006) who analysed data from several beaches in different states, the limit considered between dissipative and non-dissipative, also named intermediate – reflective, beaches was  $\zeta_0 = 0.3$ . The regression analysis through least squares, was made with the usual parameters, Iribarren number,  $\zeta_0$ , wave height,  $H_0$ , and pair wave height – wave length,  $H_0 L_0$ .

The pair wave height and wave length,  $H_0 L_0$ , showed bias, due to dependence on the beach slope, Figure 2. As the beach slope was significant, the use of these parameters is the same as the use of the Iribarren number.

For the Iribarren number,  $\zeta_0$ , the linear regression through the origin for  $\langle \eta \rangle$  and  $S_s$ , using Eq.(2) led to the Eq(3). This equation is similar to Nielsen and Hanslow (1991), but the definition of a SWL it is not required and the limit for application is the Iribarren number,  $\zeta_0$ , instead of the beach foreshore slope,  $\beta_f$ , or Dean parameter,  $\Omega$ .

$$\frac{R_2}{H_0} = 1.20 \cdot \zeta_0 \quad \text{for } \zeta_0 > 0.3 \quad (3)$$

With the significant wave height,  $H_0$ , the equation worked out following the same procedure mentioned above is expressed in Eq.(4). The application of this equation is restricted to dissipative cases.

$$R_2 = 0.32 \cdot H_0 \quad \text{for } \zeta_0 < 0.3 \quad (4)$$

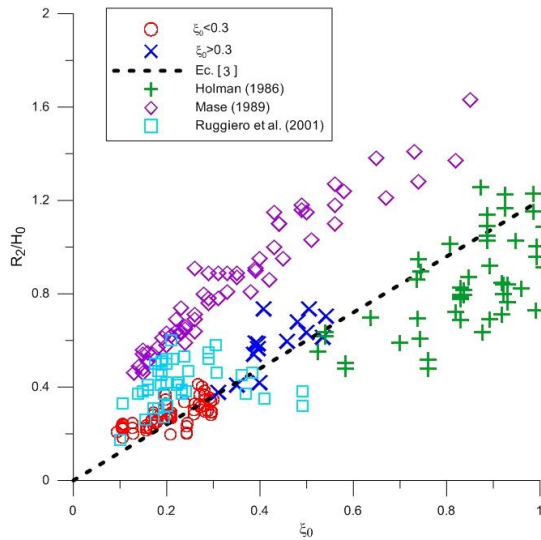


Figure 3. Non dimensional extreme runup  $R_2/H_0$  versus Iribarren number,  $\xi_0$ .

The comparison with other results is plotted in Figures 3 and 4. In both cases, Mase's data were underestimated by the equations and these data also disagree with the other results. The main reason is related with the impermeable slope used in Mase's model, that increases oscillations due to the absence of permeability which increases velocity in the uprush phase and decreases velocity in the backwash phase, and so yields less bore destruction at swash (Elfrink and Baldock 2002). The different friction factor might also affect the results (Puleo and Holland 2001). Then data from Mase (1989) are removed in the analysis of the equations' performance.

For the non-dissipative cases,  $\xi_0 > 0.3$ , is a good approximation for the data considered, with a root mean square error, RMSE, of

0.041 (non-dimensional), between 10 % and 3 % error of the non-dimensional extreme runup values. In the case of dissipative data, the RMSE is 0.046 m, which represents around 3 % error of the averaged extreme runup value.

## METHODOLOGY

### Field Data

Two extreme Spanish coast cases are studied with the aim to analyse the sensitivity of extreme runup due to beach morphology profile changes. From 2005 to 2012 several profiles are recorded in Salinas and Peñíscola beaches. Salinas beach is on the Bay of Biscay on the North coast of Spain and displays a dissipative beach state and is characterized for its strong three-dimensional, 3D, structure. In the case of the Peñíscola beach, the profile is more reflective like most of the beaches on the Mediterranean coast, and the morphodynamics can be assumed as two-dimensional, 2D.

This allows us to test the variability of the equation on two entirely different areas of the Spanish coast, where beach morphology and also incoming waves change. Generally speaking, one of the main differences between these areas is that wave steepness in the Bay of Biscay is gentler than in the case of the Mediterranean coast. Also, the storms on the Spanish North coast are stronger than in the East.

Topo-bathymetric surveys were made in a medium and long term period. For the Salinas beach, biannual bathymetric surveys were recorded over an 8-year period (2005-2012). For the other beach, surveys were conducted over a 4-year period (2006-2009). The longshore variation was also studied through several cross-shore transects on each beach, 5 for Salinas and 8 for Peñíscola. The profiles are plotted in Figure 5. The dry-beach profiles were collected by topographic methods at low tide. For the bathymetric survey, echo sounding equipment was used.

The foreshore slope was measured for every profile. To obtain this parameter, an averaged water level was estimated through the averaged tide high level as the tide level exceeded only 5 % of the

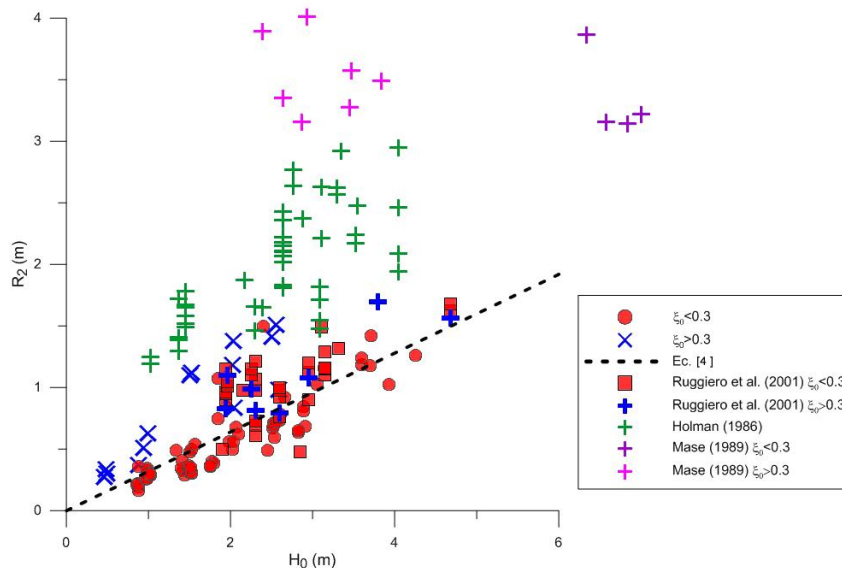


Figure 4: Extreme runup  $R_2$  scaled with significant wave height,  $H_0$ . Dashed line: Linear regression through origin.

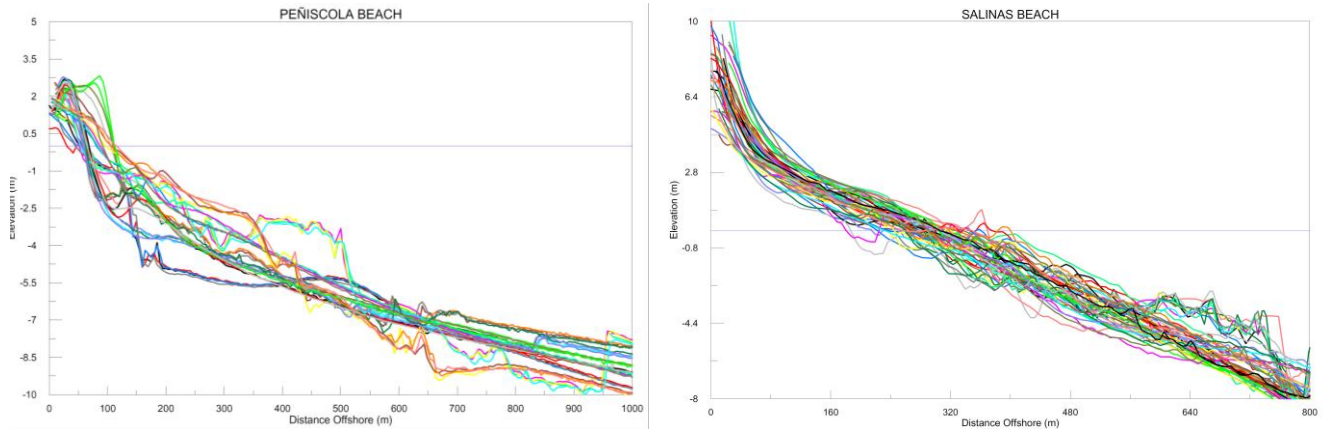


Figure 5: Recorded beach profiles

time in an annual period. Then the limits of the foreshore were estimated with the runup that would be obtained under a storm with a return period of 50 years. One of the main features is uniformity for the foreshore slope, the value does not vary significantly if return periods of the same order are selected for the limits of the foreshore estimation. Having obtained the foreshore slopes, foreshore variability in time and longshore was analysed.

**Climate wave parameters**

Wave parameters have to be selected for assessing runup. In the case of an extreme runup, a return period based on a socio-economical index should be determined. For this study, a return period of 50 years is selected which represents a “remote” event probability in a 30-year lifetime, Rock Manual (CIRIA et al. 2007)

The Spanish manual for maritime constructions (ROM 0.3-91 1991) was used to determine wave conditions. The storm was characterised through the significant deep-water wave height,  $H_0$  and the peak period,  $T_p$ . The data were obtained from the closest buoy. The details are presented in Table 3, where:  $K_\infty$  is the directional spread coefficient.

Table 3- Climate wave parameters

Beach	Buoy	Return Period (yrs)	$H_0$ (m)	$T_p$ (s)	$K_\infty$	$\frac{H_0}{L_0}$
Salinas	Gijón	50	9.5	12	1	0.04
Peñíscola	Valencia I	50	5.5	11	~ 1	0.03

**RESULTS AND DISCUSSION**

**Longshore variation**

For assessing longshore variation, profiles are time-averaged in each transect, and then the time-averaged beach foreshore slope for each transect within the recorded period is considered.

For the Salinas beach, the time-averaged foreshore slopes varied between 0.0160 and 0.0172 which implies a negligible variation in the Iribarren number (under storm conditions) which took a value around 0.08, so the longshore variation affecting the extreme runup for this parameter is negligible due to the dissipative state being expected in each transect. If the foreshore slopes had only been recorded in September-October, the averaged slope would have been steeper, but also within the dissipative range and a negligible 5% deviation in the maximum value.

In the Peñíscola beach the variation between longshore positions was more significant for the extreme runup estimation. The maximum foreshore slopes varied between transects from 0.019 to 0.108. With these values the Iribarren number took values between 0.11 and 0.62. In this case the variation is significant because it implies a change in the beach modal state. Alongshore the beach could be considered dissipative or intermediate involving different equations

The longshore variations of the foreshore slope are not relevant in Salinas but are in Peñíscola. Salinas beach presents a dissipative beach state in every transect time-averaged, due to the Iribarren number being under the value of 0.3 for all of the transects. Then the value of the beach foreshore becomes irrelevant since the extreme runup,  $R_2$ , was independent of the Iribarren number, Figure 6. In the case of the Mediterranean 2D beach, the values of the extreme runup can increase around 200 % if the intermediate beach state is reached, so the variations longshore are relevant, and should be analysed before applying an extreme runup equation.

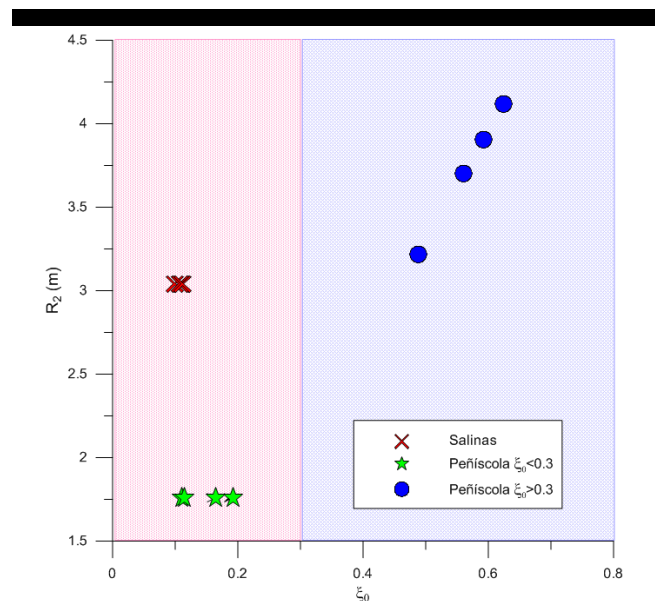


Figure 6. Extreme runup with time-averaged foreshore slope. Longshore variation.

### Medium-Long Term Time variation

Results are yearly longshore averaged for the foreshore slope's time variation and, therefore, a representative foreshore slope of the beach recorded for each year was obtained

As happened with the longshore variation in Salinas beach, the different values of the longshore averaged foreshore slope, are negligible and irrelevant. The foreshore slope varied between 0.0162 and 0.0176, which gave an Iribarren number between 0.08 and 0.09. Hence the dissipative state remained in time, and the extreme runup was independent from the foreshore slope over the years, so the value does not vary for the same return period.

For the Peñíscola beach, deviations were reduced in comparison with the longshore variation, which suggests that longshore changes are higher than time variations. The Iribarren number varied between 0.34 and 0.38 since the longshore averaged foreshore slope varied between 0.059 and 0.066. The extreme runup error is within 5% between extremes, i.e., 0.10 m, so can be assumed as negligible. Also in contrast with longshore variations, the dissipative state is never accomplished for the evaluated time period, Figure 7.

### CONCLUSIONS

A limit between dissipative and intermediate-reflective beaches has to be addressed for estimating extreme runup on a beach. This limit is estimated as a 0.3 Iribarren number value. Dissipative beaches independence on the beach foreshore slope implies that time and longshore deviations can be considered irrelevant for the extreme runup assessment.

The sand bed physical model provides more reliable oscillations in comparison with the results of field experiments and the physical model. The physical model with impermeable beds increases the runup values due to the friction factor and absence of subpressures.

In the case of a North Spanish beach with a strong wave climate, the dissipative state of the beach remains longshore and in time in a medium-long term evaluation. So, although the significant changes in the profile that could occur due to 3D

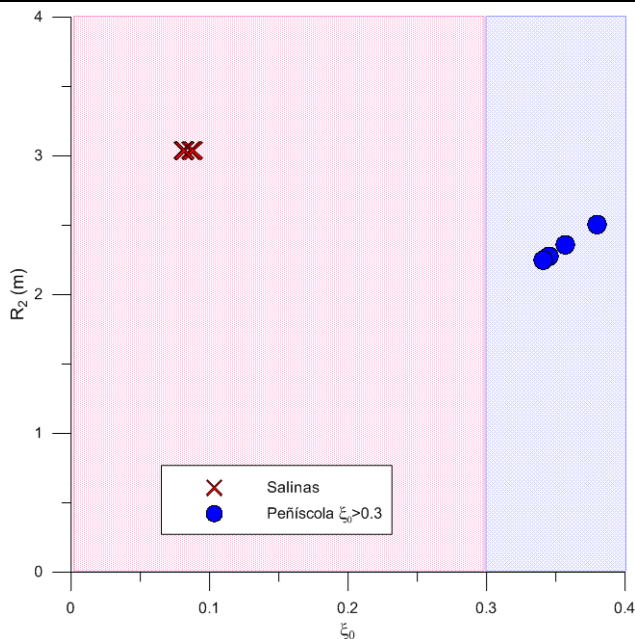


Figure 7: Extreme runup with longshore-averaged foreshore slope. Time variation.

morphology, at least, the foreshore slope changes do not influence the extreme runup estimation. Variations in extreme runup are determined by the wave height related to the return period considered.

For a Mediterranean Spanish beach, the time variations in the medium-long term were negligible. In contrast, significant deviations were found in the longshore analysis. This implies that this beach is characterized by strong longshore changes that should be carefully analysed to prevent major errors in the extreme runup assessment.

### ACKNOWLEDGEMENT

The experiment has been funded by the Spanish General Directorate for Sustainability of the Coast and Sea. The financial support of researcher training in CEDEX (Spanish Ministry for Civil Works), and also the collaboration of the Polytechnic University of Madrid to allow the PhD Thesis in its Institution have enabled this research to be carried out.

### LITERATURE CITED

- Bowen, A. J., 1967. "Rip currents". San Diego, USA: University of California, Ph.D. thesis, 115p.
- CIRIA; CUR; CETMEF, 2007. The Rock Manual. The use of rock in hydraulic engineering. 2nd edition. C683, CIRIA, London, UK.
- Dean, R. G., 1977. "Equilibrium beach profile." *Rep. No. 12*, University of Delaware.
- Díaz-Sánchez, R., López-Gutiérrez, J. S., Lechuga, A., Negro, V., and Esteban, M. D., 2013. "Direct estimation wave setup as a medium level in swash." *Journal of Coastal Research*, SI 65, 201-206.
- Elfrink, B., and Baldock, T. E., 2002. "Hydrodynamics and sediment transport in the swash zone: a review and perspectives." *Coastal Engineering*, 45(3-4), 149-167.
- Guza, R. T., and Thornton, E. B., 1982. "Swash Oscillations on a Natural Beach." *Journal of Geophysical Research-Oceans and Atmospheres*, 87(NC1), 483-491.
- Hedges, T. S., and Mase, H., 2004. "Modified Hunt's equation incorporating wave setup." *Journal of Waterway Port Coastal and Ocean Engineering-Asce*, 130(3), 109-113.
- Holman, R. A., 1986. "Extreme Value Statistics for Wave Runup on a Natural Beach." *Coastal Engineering*, 9(6), 527-544.
- Holman, R. A., and Guza, R. T., 1984. "Measuring Runup on a Natural Beach." *Coastal Engineering*, 8(2), 129-140.
- Holman, R. A., and Sallenger, A. H., 1985. "Setup and Swash on a Natural Beach." *Journal of Geophysical Research-Oceans*, 90(NC1), 945-953.
- Mase, H., 1989. "Random Wave Runup Height on Gentle Slope." *Journal of Waterway, Port, Coastal, and Ocean Engineering*, 115(5), 649-661.
- Nielsen, P., and Hanslow, D. J., 1991. "Wave Runup Distributions on Natural Beaches." *Journal of Coastal Research*, 7(4), 1139-1152.
- Puleo, J. A., and Holland, K. T., 2001. "Estimating swash zone friction coefficients on a sandy beach." *Coastal Engineering*, 43(1), 25-40.
- Roberts, T. M., Wang, P., and Kraus, N. C., 2010. "Limits of Wave Runup and Corresponding Beach-Profile Change from Large-Scale Laboratory Data." *Journal of Coastal Research*, 26(1), 184-198.
- ROM 0.3-91., 1991. Recomendación para Oleaje y Atlas de Clima Marítimo en Litoral español. *Gobierno de España, España*.
- Ruggiero, P., Komar, P. D., McDougal, W. G., Marra, J. J., and Beach, R. A., 2001. "Wave runup, extreme water levels and the erosion of properties backing beaches." *Journal of Coastal Research*, 17(2), 407-419.
- Senechal, N., Coco, G., Bryan, K. R., and Holman, R. A., 2011. "Wave runup during extreme storm conditions." *Journal of Geophysical Research-Oceans*, 116, C07032.
- Stockdon, H. F., Holman, R. A., Howd, P. A., and Sallenger, A. H., 2006. "Empirical parameterization of setup, swash, and runup." *Coastal Engineering*, 53(7), 573-588.

# Analysis of wave attenuation and shore protection of a bulk carrier ship performing as a detached floating breakwater

A. Fernández Lázaro†, R.M. Gutiérrez Serret‡, V. Negro∞, J.S. López-Gutiérrez§

† Laboratorio de Experimentación Marítima  
Centro de Estudios de Puertos y Costas CEDEX  
Antonio López, 81. Madrid, 28026, Spain  
angel.fernandezlazaro@cedex.es

‡ Laboratorio de Experimentación Marítima  
Centro de Estudios de Puertos y Costas CEDEX  
Antonio López, 81. Madrid, 28026, Spain  
ramon.m.gutierrez@cedex.es

∞ Research Group on Marine, Coastal and Port Environment and other Sensitive Areas  
Universidad Politécnica de Madrid, Profesor Aranguren, s/n. 28040, Spain  
vicente.negro@upm.es



[www.cerf-jcr.org](http://www.cerf-jcr.org)

§ Research Group on Marine, Coastal and Port Environment and other Sensitive Areas  
Universidad Politécnica de Madrid, Profesor Aranguren, s/n. 28040, Spain  
josesantos.lopez@upm.es



## ABSTRACT

Fernández Lázaro, A., Gutiérrez Serret R.M., Negro, V., López-Gutiérrez, J.S., 2014. Analysis of wave attenuation and shore protection of a bulk carrier ship performing as a detached floating breakwater. *Proceedings of the 13<sup>th</sup> International Coastal Symposium* (Durban, South Africa), *Journal of Coastal Research*, Special Issue No. 70, pp. 007-012, ISSN 0749-0208.

[www.JCRonline.org](http://www.JCRonline.org)

The effectiveness of a bulk carrier working as a detached floating breakwater to protect a stretch of coast and form salients or tombolos is assessed in this paper. Experiments were conducted in the Madrid CEDEX facilities in a 30 m long, 3 m wide, 1/150 scale flume. The bulk carrier ship is 205 m long, 29 m wide and 18 m in height with a draught of 13 m, and has been subjected to irregular waves with significant heights from 2 m to 4 m and peak periods from 6 s to 12 s at a depth of 15 m, all prototype dimensions. Three probes were placed between the wave paddle and the ship to record incident and reflected waves and four probes were placed between the ship and the coastline to measure the transmitted waves. Transmission, reflection and dissipation coefficients ( $C_t$ ,  $C_r$ ,  $C_d$ ) were calculated to determine wave attenuation. Results show good shelter in the lee of the ship with values of  $C_t$  under 0.5 for peak periods from 6 s to 11 s. In addition, forces on the mooring chains were measured showing maximum values of about 2000 tons at a 10 s peak period. Finally, two analytical models were used to determine the shoreline's response to the ship's protection and to assess the possible forming of salients or tombolos. According to the results, salients - but not tombolos - are formed in all tests.

**ADDITIONAL INDEX WORDS:** *Physical model tests, irregular waves, transmission coefficient, reflection coefficient, dissipation, shore's response, salient, tombolo, chain forces.*

## INTRODUCTION

The use of a ship as a detached floating breakwater to protect an area on the coastline from wave action may provide protection over a broader range than usual floating breakwaters, as well as advantages in terms of mobility, versatility, installation and dismantling. The subject was proposed and previously studied in preliminary research. More specifically, the use of a container ship at depths of 20 m and 35 m was tested with regular waves in a first investigation (Fernández Lázaro *et al.*, 2013a), and the use of an oil tanker subjected to irregular waves at a depth of 10 m was analyzed in a subsequent one (Fernández Lázaro *et al.*, 2013b). Among other findings, the former showed the need to bring the ship closer to the coastline into shallower water, while the latter recommended the use of a wider ship to improve its performance.

The aim of this study is to assess the effectiveness of a bulk carrier working as a detached floating breakwater to protect a

stretch of the coast and form salients or tombolos. Experiments were conducted in the Madrid CEDEX facilities in order to determine transmission, reflection and dissipation coefficients ( $C_t$ ,  $C_r$ ,  $C_d$ ). In addition, forces on the mooring chains were measured to check the feasibility of the mooring configuration.

Finally, two analytical models based on transmission coefficients were used to determine the shoreline's response to the ship's protection and to assess the possible forming of salients or tombolos. According to the results, salients - but not tombolos - are formed in all tests.

## EFFECTIVENESS OF A FLOATING BREAKWATER

The main purpose of a floating breakwater is to protect elements or facilities – such as a part of the coast, a structure, a marina or a set of mooring boats – from wave energy.

The processes by which a floating breakwater reduces wave energy to cause an area of calm water are mainly reflection, dissipation or turbulence and transformation of wave energy into

DOI: 10.2112/SI70-002.1 received 21 November 2013; accepted 21 February 2014. © Coastal Education & Research Foundation 2014



non-oscillatory movement. Finally, part of the incident waves, and, therefore, the associated energy, is transmitted through the breakwater. Accordingly, the incident wave energy ( $E_i$ ) is equal to the sum of the energy transmitted through the breakwater ( $E_t$ ), the energy reflected by the breakwater ( $E_r$ ) and the energy dissipated in turbulence ( $E_d$ ), giving rise to the following equation:

$$E_i = E_t + E_r + E_d$$

Since wave energy is proportional to the square of the wave height, the expression can be written in terms of wave heights:

$$H_i^2 = H_t^2 + H_r^2 + H_d^2$$

By dividing the terms of the equation by  $H_i^2$ , the equation can be expressed in dimensionless form:

$$1 = C_t^2 + C_r^2 + C_d^2$$

Where  $C_t$  is the transmission coefficient, which expresses the ratio between the transmitted wave height and the incident wave height ( $C_t = H_t/H_i$ );  $C_r$  is the reflection coefficient, which expresses the ratio between the reflected wave height and the incident wave height ( $C_r = H_r/H_i$ );  $C_d$  is the dissipation coefficient and expresses the ratio of the wave energy attenuated in turbulence ( $C_d = H_d/H_i$ ).  $C_t$  and  $C_r$  are usually calculated from data obtained from tests on a reduced scale physical model, while  $C_d$  is calculated from the previous two.

Most studies in floating breakwaters generally focus on determining the structure's transmission coefficient. A criterion normally used to determine whether the operation of the floating breakwater is successful is to set a maximum threshold of 0.5 for the transmission coefficient, following Koutandos *et al.* (2005), Heng (2006), Dong *et al.* (2008), Wang *et al.* (2010), Peña *et al.* (2012) and He *et al.* (2012). Thus, the floating breakwater would effectively attenuate those waves for which the transmission coefficient is equal to or less than 0.5 ( $C_t \leq 0.5$ ).

The main types of floating breakwater have been summarized and analyzed by authors such as Hales (1981), McCartney (1985) and Mani (1991). In general, floating breakwaters listed by these authors are effective in small waves, up to 2 m significant wave height and peak periods up to 5 s. More recently, the Monaco floating breakwater became an exception since it was designed for 5 m significant wave height and 11 s peak period (Peset *et al.*, 2002).

In previous research, a container ship of 275 m overall length and 32 m beam proved to be effective, according to the same

criterion ( $C_t \leq 0.5$ ), for waves up to 4 m significant height and 8 s period at a depth of 20 m (Fernández Lázaro *et al.*, 2013a), while an oil tanker of 139 m overall length and 17 m beam proved to be effective in a similar wave range at a depth of 10 m (Fernández Lázaro *et al.*, 2013b).

## TEST ON A PHYSICAL MODEL

### Description of the test

The test was carried out in the facilities of the Centro de Estudios de Puertos y Costas (CEPYC) – Centre for Ports and Coasts Studies - of the CEDEX in Madrid, Spain, in a wave flume 30 m long and 3 m wide, on a 1/150 scale. Froude's laws of similarity were used to establish the equivalence between model and prototype. Figure 1 shows a diagram of the test set up.

At one of its ends, the flume has a hydraulically driven translational motion wave generating paddle. At the other end, a gravel beach was built as a wave anti-reflection device inside the flume. The flume's bottom is flat over the first 10.5 m. As from this point, it slightly slopes to take the gradual closeness of the coast into account.

Eight probes were positioned to measure the waves. Probes 1, 2 and 3 provide an absorption system that separates the incident and reflected waves and real time calculates the corrected movement of the wave paddle by subtracting the reflected waves, according to Mansard and Funke's method (1980). Probes 1 to 4 assess incident waves while probes 5 to 8 measure transmitted waves. Probes 5 and 6 are 0.20 m from each other and the same applies for probes 7 and 8.

Previous research in ships working as floating breakwaters showed that the ship had to be brought closer to the coastline, to depths below 20 m (Fernández Lázaro *et al.*, 2013a), as well as the heavy influence the ship's beam had over the transmission coefficients (Fernández Lázaro *et al.*, 2013b). These reasons led to choosing a bulk carrier ship of 205 m overall length, 29 m beam, 18 m depth and 13 m draught under a full load condition, all prototype dimensions. The depth chosen was 15 m and the distance from the coast was about 400 m, prototype dimensions. The tidal range considered was 0, as in Mediterranean sea.

An anchoring system was reproduced by means of a chain and anchor with four chains, two on the exposed side of the ship, 3 m long in the model, and two on the land side, 1.5 m long in the model. Chains are initially subjected to their own weight, as a catenary, and they tense progressively as the waves act on the vessel.

The resulting tensile stress in the chains is measured by means

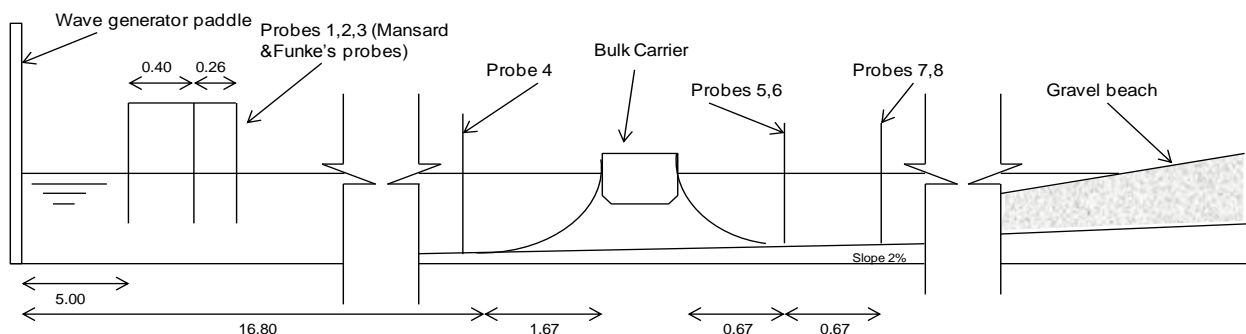


Figure 1. Diagram of the physical model test set up for assessing the ship's behaviour as a floating breakwater

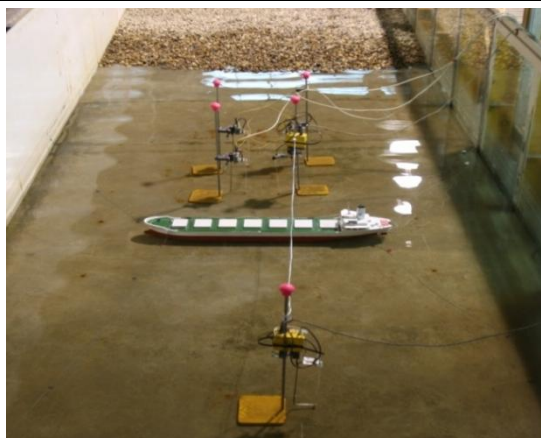


Figure 2. Photograph during the test run

of two previously calibrated strain gauges located on the ship's sea side. The ship was subjected to waves of 2 m to 4 m significant wave heights and peak periods from 6 s to 12 s. The number of waves was set to a minimum of 300 waves for the longest periods (12 s) up to 462 waves for the shortest period tested. Figure 2 shows a photograph taken whilst the test was running.

### Results obtained

Figure 3 shows how the transmission, reflection and dissipation coefficients vary with the peak period for the different significant wave heights studied at a depth of 15 m.

Graphs at the top of figure 3 show the transmission coefficients calculated from the transmitted waves measured at probes 5 to 8. According to the resulting values and taking into account the afore-mentioned criterion  $C_t \leq 0.5$ , the ship proves effective for attenuating waves up to 4 m significant wave height and up to an 11 s peak period. The variation of  $C_t$  with the peak period shows quite a horizontal tendency around 0.4 and 0.5 and only for the 12 s period does the transmission coefficient tend to increase up to 0.6. It can also be observed that results are not significantly sensitive to the variation in wave height, since  $C_t$  values corresponding to the different wave heights appear quite concentrated. Finally, probes in the second row (probes 7 and 8) show better results than those in the first row (probes 5 and 6) with transmission coefficients around 0.2 and 0.4 for peak periods from 6 s to 10 s.

Graphs in the middle of figure 3 show how reflection and dissipation coefficients vary with peak period. Reflection coefficients are below 0.5 in all cases and decline as the period increases. In particular, between 6 s and 9 s peak periods,  $C_r$  varies from nearly 0.5 to 0.4 and between 10 s and 12 s its value decreases below 0.4 to reach a minimum around 0.3. Dissipation coefficients show good, almost constant results for all periods tested, between 0.7 and 0.8.

Graphs at the bottom of figure 3 show the results of tensile stresses in the mooring chains. Forces show values under 1200 tonnes for peak periods up to 9 s, while for periods between 10 s and 12 s they considerably increase, reaching a maximum of about 2200 tonnes at 10 s peak period. Considering the variation of tensile stresses with the wave height, it can be observed that they do not exceed 600 tonnes for wave heights up to 3 m, while the highest values are obtained for 4 m wave heights in all cases. Differences between bow and stern mooring line forces are not significant.

### Conclusions from the test on a physical model

In view of the transmission coefficients, the conclusion may be drawn that the bulk carrier ship is effective for waves up to 4 m significant height and 11 s peak period. However, the values of transmission coefficient are slightly higher than those obtained in previous investigations (Fernández Lázaro *et al.*, 2013a, Fernández Lázaro *et al.*, 2013b). It can be inferred that the bulk carrier ship provides good protection for the coastline, slightly less effective than the container ship or the oil tanker, but in a wider range in terms of wave period. Besides, wave transmission is lower in the second row probes, which means that waves tend to soften in the lee of the ship as they approach the coast and the depth decreases.

Considering reflection and dissipation coefficients, the conclusion may be drawn that, although a great amount of wave energy is attenuated by reflection, dissipation is the main attenuation mode. Reflection is higher for short periods, while dissipation remains almost constant at values around 0.8. Dissipation occurs in the turbulence generated when waves hit the ship, from ship movements (mainly roll and heave) and from overtopping waves that reach the deck.

Finally, results of forces in the mooring lines show quite reasonable values - under 600 tonnes - for wave heights up to 3 m, for all the periods tested. Forces increase with the period and mainly with the wave height. The highest values are reached for 4 m wave heights. Several chains for each mooring line might be provided in order to restrain these maximum forces.

### RESPONSE OF THE COAST

A detached breakwater is a structure built some distance from the shore and generally parallel thereto in order to protect it from wave action by reducing the latter's energy in the sheltered area. This reduction in wave energy causes an alteration in sediment transport and sediment accumulates and deposits behind the breakwater. If sufficient material is deposited, a sand salient may form and develop until reaching the detached breakwater itself giving rise to a formation which is called a tombolo.

Numerous analytical models related to detached breakwater design are in existence and are used to either predict and define the response induced on the coast by a breakwater or system of detached breakwaters, or to calculate the geometrical characteristics of the works to be designed starting from the effect it is desired to achieve on the shoreline. In the case in question, two analytical models which, amongst other parameters, use the detached structure's transmission coefficient ( $C_t$ ) were chosen.

#### Hanson and Kraus (1990)

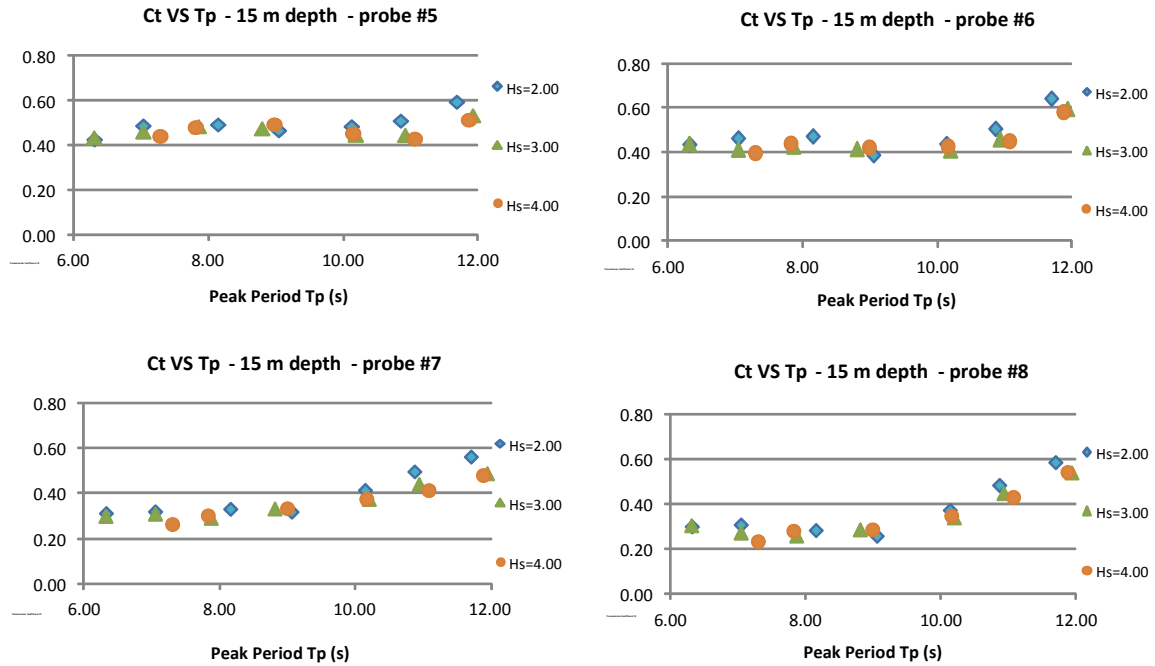
Based on results of simulations of the shoreline's evolution with a numerical model and on data from some detached breakwaters, Hanson and Kraus proposed the following model in 1990 to classify the shore's response behind a detached breakwater:

$$\frac{X}{L} \leq 48 \cdot (1 - C_t) \cdot \frac{H_0}{D} \rightarrow \text{salient}$$

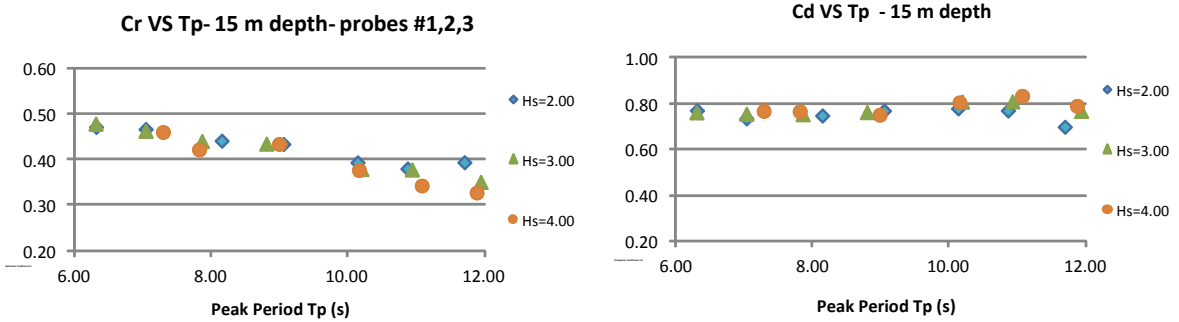
$$\frac{X}{L} \leq 11 \cdot (1 - C_t) \cdot \frac{H_0}{D} \rightarrow \text{tombolo}$$

where  $C_t$  is the transmission coefficient,  $X$  the structure's length,  $L$  the incident wave length,  $H_0$  the significant wave height in deep water and  $D$  the depth at which the breakwater is located. Table 1 gives the results obtained in the tests at a depth of 15 m.

**Transmission coefficients at probes 5 to 8**



**Reflection and dissipation coefficients**



**Maximum tensile stress in mooring chains**

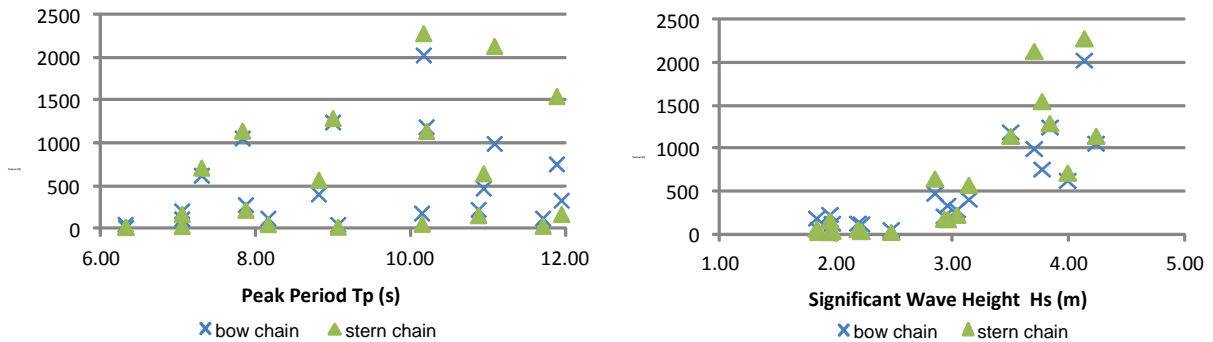


Figure 3. Top: transmission coefficients ( $C_t$ ) versus peak period ( $T_p$ ) at probes 5 to 8. Middle: reflection and dissipation coefficients ( $C_r$ ,  $C_d$ ) versus peak period ( $T_p$ ). Bottom: maximum tensile stresses ( $T$ ) versus peak period ( $T_p$ ) and significant wave height ( $H_s$ ) in mooring chains for the bulk carrier ship.

In order to take the effect of wave transmission into account, in 2003, Pilarzyk proposed that the factor  $(1-C_t)$  be considered in the elemental geometric formulas proposed by other authors to

classify the type of shoreline response in terms of the length of the structure and distance from the shore:

$$\frac{L_s}{X} > \frac{1.0 \text{ to } 1.5}{(1 - C_t)} \rightarrow \text{tombolo}$$

$$\frac{L_s}{X} < \frac{1.0}{(1 - C_t)} \rightarrow \text{salient}$$

where  $L_s$  is the length of the detached breakwater,  $X$  the distance to the shore and  $C_t$  the transmission coefficient.

Pilarzyk's proposed expressions allow the distance to the shore to be left as an unknown whilst setting all the other values so that the maximum distance at which the ship can be situated for a tombolo to be formed or the minimum distance to be kept for a salient to form can be calculated. The results obtained in tests at a depth of 15 m are shown in table 1.

### Discussion of results

Table 1 shows the results obtained from the tests carried out at a depth of 15 m. The conclusion may be drawn from the shoreline's response resulting from applying the Hanson and Kraus model, that protection as provided by a bulk carrier ship acting as a detached floating breakwater will give as a result the forming of salients for incident waves from 6 s to 12 s peak period and significant wave heights up to 4 m. The most determining parameters for the breakwater's effectiveness are the period, which appears to be more influential than the wave height, and the depth, which will, in most cases, be related to the distance from the coast.

The forming of tombolos is not foreseen in any of the cases tested. The results obtained from applying the Pilarzyk model to

determine the critical distance to the shoreline for tombolos or salients to form show a range of distances from approximately 55 m to 117 m. Specifically, for 11.69 s peak period and 1.97 m significant height, the distances between ship and shore for which a tombolo would form range from 55.17 m to 82.76 m, as from which distance a salient would form up to a maximum distance yet to be determined and as from which the ship would have no effect on the shore. Moreover, the distance as from which a salient would form for a 6.31 s peak period and significant wave height of 1.94 m is 117.33 m.

The transmission coefficients show good protection of the coast since less than 50% of the wave height is transmitted between 6 s and 11 s peak periods and less than 60% of the wave height is transmitted for a 12 s peak period.

### PROPOSALS FOR FUTURE LINES OF WORK

With respect to the ship, several research lines open related to different aspects. Since different types of ships have been tested in previous research, a first future line of work may be to test the effect of several ships, lined up in front of the coast, to assess their performance as shore protection as well as their mutual influence. However, this type of experiment cannot be carried out in a flume like the one described here, but in a three-dimensional facility. An alternative mooring system can also be tried, testing different configurations and materials. In particular, a short, pre-stressed chain mooring system might reduce ship movements as well as the occupied bottom surface. As far as mooring chains are concerned, some other topics to be taken into account are long term security,

Table 1. Response of a shore protected by a bulk carrier ship acting as a detached breakwater at a depth of 15 m, according to Hanson and Kraus (col. 6) and a breakwater's maximum and minimum distance to the shore for forming tombolos or salients according to Pilarzyk (col. 7 and 8)

Peak period $T_p$ [s]	Significant wave height $H_s$ [m]	Height transmitted $H_t$ [m]	Wave length $L$ [m]	Transmission Coefficient $K_t$ [-]	Hanson and Kraus shore response	Pilarzyk X max. for tombolo [m]	Pilarzyk X min. for salient [m]
6.31	1.94	0.83	57.60	0.428	salient	117.33	78.22
6.30	2.47	1.08	57.50	0.436	salient	115.59	77.06
7.03	2.22	1.09	68.10	0.490	salient	104.59	69.73
7.03	2.93	1.36	68.10	0.463	salient	110.15	73.43
7.29	3.99	1.77	71.71	0.443	salient	114.14	76.09
8.14	2.19	1.08	83.79	0.494	salient	103.69	69.12
7.85	3.04	1.48	79.75	0.487	salient	105.23	70.16
7.81	4.24	2.04	79.16	0.482	salient	106.09	70.73
9.05	1.85	0.86	96.19	0.468	salient	109.07	72.71
8.80	3.14	1.50	92.79	0.477	salient	107.17	71.45
8.98	3.84	1.90	95.30	0.496	salient	103.38	68.92
10.13	1.83	0.89	110.76	0.486	salient	105.28	70.19
10.19	3.50	1.57	111.53	0.448	salient	113.08	75.39
10.15	4.13	1.88	111.03	0.456	salient	111.61	74.41
10.86	1.95	0.99	120.42	0.511	salient	100.21	66.81
10.92	2.85	1.27	121.28	0.447	salient	113.31	75.54
11.06	3.70	1.60	123.14	0.431	salient	116.57	77.71
11.69	1.97	1.17	131.32	0.596	salient	82.76	55.17
11.93	2.96	1.58	134.42	0.535	salient	95.29	63.52
11.87	3.77	1.95	133.63	0.516	salient	99.21	66.14

maintenance and deterioration. Besides, some other interesting aspects beyond the scope of this paper such as the visual impact produced by the ship on the coastline, additional uses like berthage for small vessels or shelter for maritime works, or cost-benefit analysis of this alternative, may also be considered in related research.

The method employed enables the coast's response to the protection provided by the ship and the critical distance for creating one or the other formation to be determined. However, it does not indicate anything as regards the volume of accretion or about the stability or instability of the salient formed. Another possible line of investigation would therefore be to turn to other formulations or models (whether physical or analytical) in order to predict the shore's response to this effect. The use of mobile sediment models may be also considered. There is a limitation in the use of the Hanson & Kraus and Pilarzyk formulas - which are typical for wave transmission in a porous environment such as rubble mound breakwaters - for studying transmission in a floating element. In this respect, the test constitutes a first approach for determining the structural and functional response and certain test conditions will have to be modified enabling coastal models to be used.

Finally, mention must be made of the difficulties which arise, both in this test and those proposed, from considering the different scale factors and the geometrical similarities coming into play in work of this type. For example, the flume's width is a limitation to be borne in mind when choosing the ship's overall length. Another example is that the scale with which it is advisable to work with the ship (1/150 in this case) may not be the best for processing other factors such as wave action, sea bed or volume of sand. On the other hand, working with scales with a lower denominator makes it impossible to use the model of ship chosen.

## CONCLUSIONS

This article gives the results of the investigation carried out on the effectiveness of a bulk carrier ship acting as a detached breakwater for shore protection and the forming of salients or tombolos. Physical tests have proved that the ship provides good shelter for significant wave heights up to 4 m and peak periods up to 11 s. This result extends the range for using the most usual floating breakwaters to laminate the effects of incident waves.

Two analytical models based on the transmission coefficient have been used to assess the shore's response to the protection provided by the ship. In the light of the results obtained, the conclusion may be drawn that under test conditions, the coast is protected by the ship, giving rise to salients forming for peak periods between 6 s and 12 s. It is assumed that by bringing the ship closer to the shore, it will work better although the ship's draught should be borne in mind as an important conditioning factor.

Finally, results were discussed and new lines of work identified, amongst which the reproduction of physical model tests with several ships, alternative mooring configurations, a study of the stability of salients formed and estimation of the volume of accretion and use of more accurate analytical models for floating breakwaters may be highlighted. Mention should be made of the difficulties in factors of scale relating to the various elements present in the test such as the ship, the sea bottom and the waves. The main limiting factor in the physical model was the ship, which determines the test scale rather than the system hydrodynamics in generation conditions, wave-structure and wave-seabed interactions. Another limitation was given by the diffracted waves at the ends of the ship which, reflected on the walls of the flume, produce wave crossing that may alter the measurement of the

transmitted waves. This effect has been reduced by placing the leeward wave probes before the area where wave crossing occurs.

## ACKNOWLEDGEMENTS

The authors acknowledge the financial support of the Spanish Ministry of Public Works through the Researcher Staff Training Program developed by the CEDEX. They would also like to thank all the technical staff of CEPYC-CEDEX for their assistance during the experiments.

## LITERATURE CITED

- Dong, G., Zheng, Y.N., Li, Y.C., Teng, B. Guan, C.T., Lin, D.F., 2008. Experiments on wave transmission coefficients of floating breakwaters. *Ocean Engineering*, n° 35, pp.931-938.
- Fernández Lázaro, A., Gutiérrez Serret, R.M., Negro, V., López-Gutiérrez, J.S., 2013. Use of a scrapped ship as a floating breakwater for shore protection. *Proceedings 12th International Coastal Symposium* (Plymouth, England), Journal of Coastal Research, Special Issue No. 65, pp.225-230.
- Fernández Lázaro, A., Gutiérrez Serret, R.M., Negro, V., López-Gutiérrez, J.S., 2013. Use of a scrapped ship as a floating breakwater for shore protection in shallow water. *Proceedings 10th Institution of Civil Engineers Coasts, Marine Structures and Breakwaters conference* (Edinburgh, UK).
- Hales, Z., 1981. Floating breakwaters: state of the art literature review. USACE, Coastal Eng. Research Center (CERC).
- Hanson H., and Kraus, N.C., 1990. Shoreline response to a single transmissive detached breakwater. *Proceedings of the 22<sup>nd</sup> International Conference on Coastal Engineering, July 1990*, Delft (the Netherlands), ASCE, pp. 2034-2046.
- He, F., Huan, Z., Wing-Keung Law, A., 2012. Hydrodynamic performance of a rectangular floating breakwater with and without pneumatic chambers: An experimental study. *Ocean Engineering*, n° 51, pp.16-27.
- Heng, L., 2006. System performance of a composite stepped-slope floating breakwater. Doctoral Thesis, Uni. Tech. Malaysia.
- Koutandos, E., Prinos, P., Gironella, X., 2005. Floating breakwaters under regular and irregular wave forcing: reflection and transmission characteristics. *Journal of Hydraulic Research (IAHR)*, Vol 43, n° 2, pp. 174-188.
- Mani, J. SEC., 1991. Design of Y-frame floating breakwater. *Journal of Waterway Port Coastal and Ocean Engineering - ASCE*, n° 117(2), pp. 105-119.
- Mansard, E.P.D., and Funke, E.R., 1980. The measurement of incident and reflected spectra using a least squares method. *17th International Coastal Engineering Conference* (Sydney, Australia), pp. 154-172.
- McCartney, B. L., 1985. Floating breakwater design. *Journal of Waterway Port Coastal and Ocean Engineering - ASCE*, n° 111(2), pp. 304-318.
- Peña, E., Ferreras, J., Sánchez-Tembleque F., 2011. Experimental study on wave transmission coefficient, mooring lines and module connector forces with different designs of floating breakwaters. *Ocean Engineering* n° 38, 1150 – 1160.
- Peset L., Barceló J., & Troya L., 2002. El dique flotante de Mónaco. *Hormigón y Acero*, n° 223 a 226.
- Pilarzyk, K.W., 2003. Design of low-crested (submerged) structures – an overview-. *Proceedings of the 6<sup>th</sup> International Conference on Coastal and Port Engineering in Developing Countries*. September 2003, Colombo (Sri Lanka).
- Wang, H., & Sun, Z., 2010. Experimental study of a porous floating breakwater. *Ocean Engineering*, n° 37(5-6), pp. 520-527.

# The effect of scour protections in offshore wind farms

Clara Matutano†, Vicente Negro‡, José-Santos López-Gutiérrez∞, M. Dolores Esteban§, Andrés Hernández\*

† Research Group on Marine, Coastal and Port Environment and other Sensitive Areas  
Universidad Politécnica de Madrid, E28040, Madrid  
clara.mmolina@alumnos.upm.es

‡ Research Group on Marine, Coastal and Port Environment and other Sensitive Areas  
Universidad Politécnica de Madrid, E28040, Madrid  
vicente.negro@upm.es

∞ Research Group on Marine, Coastal and Port Environment and other Sensitive Areas  
Universidad Politécnica de Madrid, E28040, Madrid  
josesantos.lopez@upm.es

+ Research Group on Marine, Coastal and Port Environment and other Sensitive Areas  
Universidad Politécnica de Madrid, E28040, Madrid  
mariadolores.esteban@upm.es

\*Research Group on Marine, Coastal and Port Environment and other Sensitive Areas  
Universidad Politécnica Madrid, E28040, Madrid  
andres.hernandez@alumnos.upm.es



[www.cerf-jcr.org](http://www.cerf-jcr.org)



[www.JCRonline.org](http://www.JCRonline.org)

## ABSTRACT

Matutano, C., Negro, V., López-Gutiérrez, J. S., Esteban, M.D., Hernández, A., 2014. The effect of scour protections in offshore wind farms. In: Green, A.N. and Cooper, J.A.G. (eds.), *Proceedings 13<sup>th</sup> International Coastal Symposium* (Durban, South Africa), *Journal of Coastal Research*, Special Issue No. 70, pp. 012-017 ISSN 0749-0208.

The installation of offshore scour protection systems in offshore wind farms allows avoid the effect of scour phenomenon around these structures. Up to date, numerous research projects have been carried out to justify the necessity of the scour protection systems and also to optimize their design. Protection systems based on riprap is frequently used due to its low cost and easy availability compared to other solutions such as geotextile bags or prefabricated concrete blocks. The sizing of these structures can be performed according to a series of recommendations that can optimize the costs associated with them, but there have been only few studies with real data up to now which have allowed identify the need for such protections.

This investigation aims to assess the functionality of the scour protections adopted through the available data about their characteristics and the scour depth developed around the foundations. In this sense, this paper presents the results of a study that analyzes the functionality of scour protections in different European offshore wind farms.

**ADDITIONAL INDEX WORDS:** *scour protection, scour phenomenon, offshore wind farms, riprap.*

## INTRODUCTION

Scouring is a phenomenon that affects the overall stability of offshore structures. To avoid the consequences of this phenomenon, one solution that has been adopted in some offshore wind farms is the installation of an adequate scour protection system based on riprap (Matutano et al., 2013a; Matutano et al., 2013b). The design and sizing of these protection systems has been studied both in fluvial and marine environments by different authors such as Bounasoundas et al. (1973), Carstens (1976), or Den Boon et al. (2004) in particular.

The need for scour protection systems in offshore wind facilities has been investigated by Zaijjer et al. (2004). In spite of this, no author has come to analyze its utility using real data about scour protection systems installed in different offshore wind farms. Due to the absence of such research, and through the information collected in a series of offshore wind farms, this investigation aims to assess the functionality of the scour protections adopted through the available data about their characteristics and the edge scour developed around the foundations.

This paper presents firstly a summary of the current situation and the latest developments in the offshore wind market. Secondly, a representative selection of operating offshore wind farms from different countries in Europe is carried out. The publicly available information of different operating offshore wind farms in Europe are analyzed, especially the data regarding scour protection systems. The foundation present in all of the selected offshore wind farms is the monopole type (the most common foundation type used up to now in these facilities in 75% of European offshore wind farms (EWEA, 2013)). At the end of this paper, the results and conclusions obtained during the investigation are exposed.

## EUROPEAN OFFSHORE WIND ENERGY

Europe's commitment to developing marine renewable energy has been reflected in recent years through different European projects belonging to numerous calls of the Framework Programs of the European Commission. This support has led to an exponential growth in the offshore wind market since the installation of the first offshore wind farm in 1991 (Esteban et al., 2011a). Actually, according to EWEA (2013) around 5,000 MW had been installed in different countries in 2012 (see Figure 1). This important growth is also causing a rapid rise of

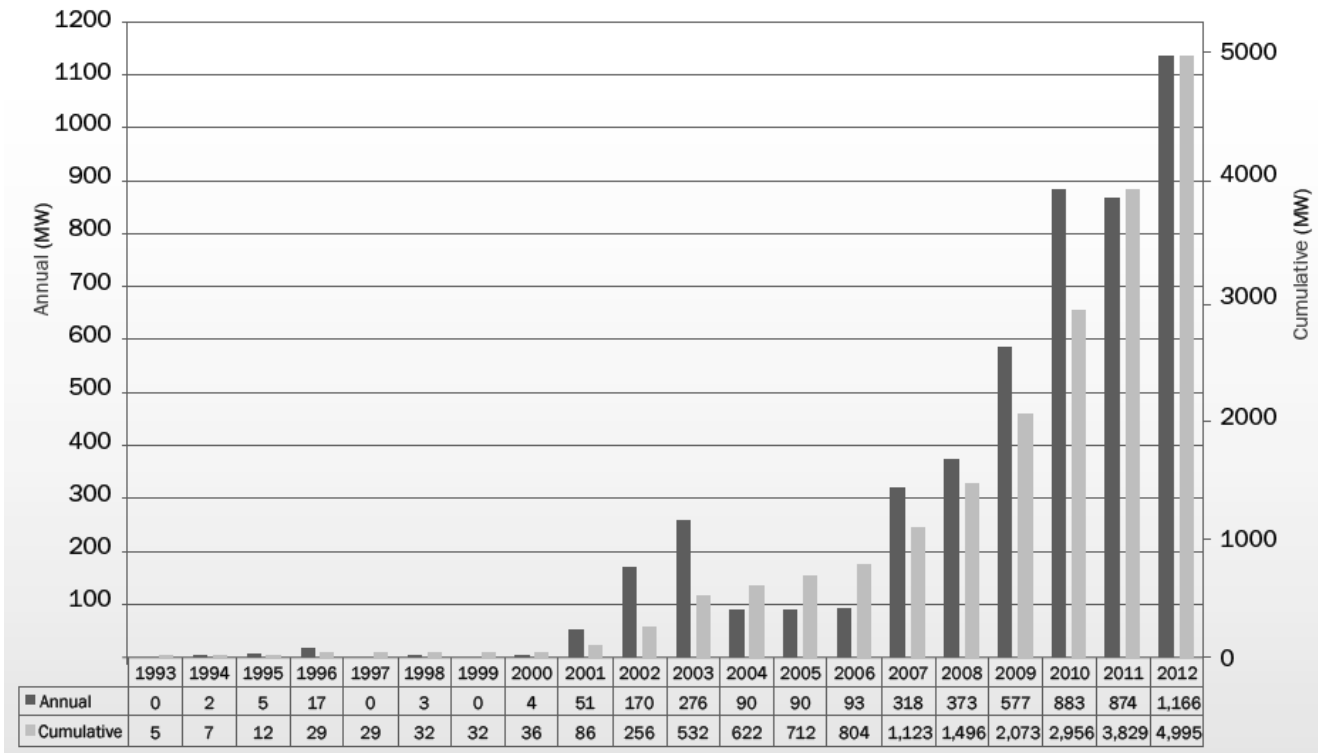


Figure 1. Cumulative and annual Offshore Wind installations (MW) from EWEA (2013)

engineering experience in design, construction and operation of offshore wind facilities. Thus, yearly new challenges arise in order to generate a greater number of MWs; these include greater depths of installations or the reduction in the costs associated with support structures (Negro et al., 2014).

To achieve some of these goals, prototypes of wind turbines with capacities up to 10 MW are being developed. Today, peak power installed is 5 MW; examples of this are Beatrice and Ormonde in UK and Thornton Bank in Belgium ([www.4coffshore.com](http://www.4coffshore.com)). This development associated with turbine design has caused an increase in the installed capacity in different European countries.

The installation of wind facilities at greater depths can be achieved through the proper selection of the foundation type (monopile, gravity based structures, jacket, tripod, tripile, suction bucket, etc.). Furthermore it can be achieved with improvements in foundation sizing, new innovation in their designs, or using new materials. Examples of this are the new designs of support structures such as the Space Frame Tower ([www.viciventus.com](http://www.viciventus.com)), or lightweight materials that are being used for the design of floating supports for wind turbines generators.

The major costs associated with foundation structures present in offshore wind farms are related to different variables such as the depth of the foundation, technical characteristics of the wind turbine to be installed and their design loads, the configuration and composition of the seabed, the actions (or loads) due to external agents (wind, waves, current, ice) etc.

The flow-structure interaction thus plays an important role in the design of the foundation and the support structure (Matutano et al., 2013b), and needs to be taken into account from the conceptual design phase. In fact, scour is a phenomenon that occurs as a result of this interaction, whose appearance around the

foundations can jeopardize the overall stability of the turbine, causing their failure (Matutano et al., 2013a).

The scour phenomenon and the design of the scour protections present in offshore wind farms have been studied by many authors, who have presented different publications (Den Boon et al., 2004; Zaaier et al., 2004; De Vos, 2008; Nielsen et al., 2010; Raaijmakers et al., 2010; or Simoons, 2012). Some of these are based on field data collected about the scouring occurring in offshore wind farms such as Egmond Aan Zee, or about the design of scour protections installed as in the case of Q7. In all cases the installation of a scour protection system was recommended to ensure the lifetime of any offshore wind farm.

Short term experience in the field of offshore wind technology has led to methodologies being established in order to recommend all necessary steps in the design of these facilities Esteban et al. (2009). On the other hand, it is important to know how the presence of offshore wind farms may affect littoral processes to prevent or avoid this impact Esteban et al. (2011b).

## METHODS

### Data Selection and Analysis

Facilities selection has been conditioned due to the limited available information about the main technical characteristics of different offshore wind farms in Europe. The lack of available data may be partly due to the confidentiality agreements related to the documentation associated with this type of projects. Despite the lack of available information, this study has been carried out successfully using gathered data about three offshore wind farms located in three different European countries (Denmark, UK and The Netherlands) (see Figure 2). The varied location of wind

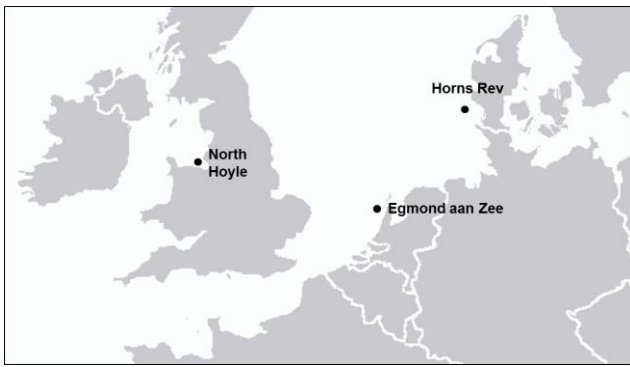


Figure 2. Location of offshore wind farms studied. Own research.

farms allowed us to research the same problem under different boundary and external conditions.

Table 1 shows the main features of offshore wind farms with scour protections that have been studied during this research. A brief description about the main characteristics of each offshore wind farm researched is then provided, in order to offer a better understanding of each particular case.

North Hoyle Wind Farm is located about 7.5 km from the north coast of Wales (UK), in Liverpool Bay. Sediments present in seabed are composed mainly by sandy gravel or gravely sand. The bathymetry of the area where the wind farm is located is essentially flat, although there are also rocky islands near the mouth of the Dee Estuary (Hilbre). The wind farm occupies a total area of 10 km<sup>2</sup>. Wind turbines are arranged over 5 columns and 6 rows, with a distance between their positions of 800 m and 350 m respectively. The foundation costs represent a high value of the total costs, comprising up to 34%.

During April and July of 2003, 30 wind turbines with a nominal capacity of 2 MW were installed through monopile foundations of 4 m of diameter. These piles were driven at depths of around 7 m and 11 m. As it can be seen in Figure 4, the piling procedure was carried out using a hydraulic hammer attached to a jack-up vessel, as typical of industry standards. The wind turbine generator model installed is a Vestas V80 2MW. The height of the nacelle above mean sea level is 70 m, and the rotor diameter is 80 m.

In Figure 3 (Carter et al., 2007), a foundation section can be observed. The transitional piece, cable connection, and scour protection installed is detailed. A scour protection system for “J-tube” cables and for the own monopile foundation was installed around the turbine foundation using rock pieces (riprap) with an average diameter of 0.3 m, in an extension up to 12 m around each turbine (COWRIE, 2010).

The main characteristics of marine climate were obtained through a report included in COWRIE (2010). In the Bay of Liverpool there are strong tidal currents along an east-west edge. Additionally, the propagation of waves inside this bay is usually caused by wind action, although there is also a swell waves that

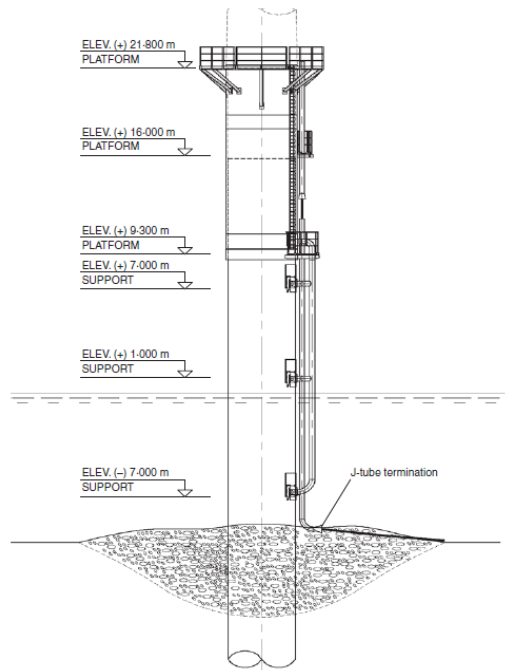


Figure 3. Detailed section of a foundation installed in North Hoyle. Carter et al. (2007)

come from the Atlantic Ocean.

The design parameters for a return period of 50 years in the location of the offshore wind farm are:

- Significant wave height ( $H_s = 4.66\text{m}$ )
- Wave period ( $T_{\text{medium}} = 6.8\text{s}$ )
- Maximum current velocity ( $U_{\text{cmax}} = 0.8\text{ m/s}$ )

As it is written in COWRIE (2010), a series of monitoring surveys to evaluate scour around the North Hoyle foundations were conducted during August and October of 2004, April and May of 2005, and during the springs of 2006 and 2007.

The scour depth registered during the field surveys of 2004 was less than 0.5 m, and occurred only in some wind turbines. Through field surveys made during 2006, sediment movement in the vicinity of many wind turbines was observed as part of the natural processes of sediment transport. During the scour monitoring carried out in 2007, it was observed that there was not registered erosion around wind turbines, and in the edge of scour protections (Whitehouse et al., 2011).

Horns Rev Wind Farm is located in an area known by the same name. This area is approximately 15 km from the west coast of Blavands Huk, a city of Denmark. The main problems for the wind farm installation were the great distance to the waterfront and the severe environmental conditions.

Horns Rev was the first wind farm built far away from the coast in the North Sea. This wind farm was constructed under the

Table 1. European offshore wind farms studied.

Name	Country	Year	Foundation	Turbines	Pile Diameter [m]	Capacity [MW]
Horns Rev	Denmark	2002	Monopile	80	4.25	2
North Hoyle	UK	2004	Monopile	30	4	2
Egmond Aan Zee	The Netherlands	2006	Monopile	36	4.6	3



Table 2. Characteristics of scour protections in different offshore wind farms.

Name	Year	D <sub>n50</sub> [m]	W <sub>n50</sub> [Kg]	Thickness [m]	Extension [m]
Horns Rev	2002	0.2 (filter), 0.4 (armor)	20 (filter), 170 (armor)	0.5 (filter), 1 (armor)	9.5 (filter)
Scroby Sands	2004	0.15	10	Unknown	Unknown
North Hoyle	2004	0.3	70	Unknown	Unknown
Arklow Bank	2004	0.425	200	Unknown	Unknown
Egmond Aan Zee	2006	0.05 (filter), 0.4 (armor)	0.3 (filter), 170 (armor)	1.4 (armor)	24 (filter), 18 (armor)
Thornton Bank	2009	0.35	120	0.7	50 (armor)

auspices of the Offshore Wind Turbine Action Plan developed by the Danish Energy Authority in 1997. That plan identified five areas close to the Danish coast for the implementation of offshore wind farms. The total cost of Horns Rev project, whose annual production is estimated at 600 GWh/yr, amounted to 278 million of Euros (Deutsche WindGuard, 2007).

Horns Rev Wind Farm consists of 80 wind turbines of 2 MW (Vestas V80) that were installed using monopile foundations of 4.25 m of diameter piled up to 25 m from the seabed (between 6 m and 13 m). The seabed is constituted by fine and coarse sand in a size range of 0.15-1 mm (Whitehouse et al., 2011). Wind turbines are distributed through a matrix of 10 rows and 8 columns, the distance between the turbines ~560 m, and occupying a total area of 27.5 km<sup>2</sup>.

The marine climate is very severe in this area of the North Sea, especially during the fall and winter seasons. The design wave height was calculated through directional registrations obtained during the last 15 years in a near location in the North Sea (COWRIE, 2010). The design parameter for a return period of 50 years in the location of the offshore wind farm is a maximum wave height ( $H_{max}$ ) of 8.1m. Wave period and current velocity data were not found during the research due to the limited available information.

Monopile foundations were protected against scour phenomenon using a protection system composed by two layers of rocks (filter and armor layers). The filter and armor layers were designed with a thickness of 0.5 m and 1 m respectively, with a total extension of 9.5 m from the axis of the pile. The scour protection system was installed by dumping the rock elements from a barge that was situated in the vicinity of wind turbines during scour protection positioning phase.

Field surveys undertaken between 2002 and 2005 in the wind farm confirm the appearance of a scour around the scour protections up to 0.5 m in depth. This represents a value of 0.12 times the pile diameter (Whitehouse et al., 2011).

Egmond Aan Zee was the first wind farm installed in the Dutch North Sea. The pilot project was located in an area known by the same name (Egmond Aan Zee). The offshore wind farm is located about 15 km from the coast, and occupies a total area of 30 km<sup>2</sup>. The wind turbine foundations are installed between 15 m and 20 m depth (Deutsche WindGuard, 2007).

In this wind farm 36 wind turbines of 3 MW (Vestas V90) were installed. 4.6 m diameter monopiles were driven 30 m into the seabed (www.noordzeewind.nl). The distribution of the wind turbines was performed by four separate columns of 6 wind turbines at a distance of about 1 km. The distance between each turbine was 600 m. These turbines have a total height of 115 m, a hub height of 70 m above mean sea level, and a rotor diameter of 90 m.

As it was stated in Lowersheimer (2007), the main characteristics of the marine climate considered for a return period of 50 years in the design of the Egmond Aan Zee Offshore Wind Farm were:

- Significant wave height ( $H_s = 3.6m$ )
- Wave peak period ( $T_p = 8s$ )
- Maximum current velocity ( $U_c = 0.7 m/s$ )

According to Raaijmakers (2009), a research about the scour protection systems installed in 2006 was conducted during the summer of 2007. The results obtained during the field studies confirm the appearance of scour around the edge of the scour protections. The maximum scour depth observed was between 0.7 m and 1.6 m, which approximately represent depth of scour values between 0.15 and 0.35 times the diameter of the piles. As it is shown in Figure 8, this erosion occurred at a distance of 17.5 m and 23 m from the center of the pile (4 or 5 times the pile diameter).

The wind turbine foundations were protected after their installation using a scour protection system of two layers of rocks (filter and armor layers). The filter layer of 0.4 m of thickness and 24 m of extension, is composed by rock elements of  $D_{n50} = 0.05$  m. The armor layer of 1.4 m thickness and 18 m of extension, is composed by rock elements of  $D_{n50} = 0.4$  m. Figures 9 and 10 indicate the scour protection installation.

## RESULTS

According to the information analysed regarding the offshore wind farms described above, a study to evaluate the functionality of scour protections installed through real cases is proposed here. This research thus aims to analyze the characteristics of scour protections jointly with scour phenomenon registered in each wind farm after the installation of such protections.

Protection systems designed to avoid the effects of the scour, based on riprap or rock elements, can be sized according to various recommendations proposed by different authors. Riprap is frequently used due to its low cost and easy availability compared to other solutions such as geotextile bags or prefabricated concrete blocks.

Table 3. Scour protection design recommendations.

Author	Protection extension [m]
Bonassoudas (1973)	2.5D-4.5D
Hjorth (1975)	2.5D
Hoffmans and Verheij (1997)	2.5D-4D
Melville and Coleman (2000)	3D-4D
May (2002)	2D

Table 4. Scour protection design recommendations.

Name	Max. scour depth [m]	Scour Estimated [m]	% Scour	% Scour Reduction
Horns Rev	0.12D	1.5D	8	92
North Hoyle	0.125D	1.5D	8.33	91.67
Egmond Aan Zee	0.34D	1.5D	22.67	77.33

## DISCUSSION

To characterize the scour protections, it is important to determine the average size of rocks ( $D_{n50}$ ), the extension, and the thickness of the different layers. In most cases, and as it has been described in two of the three wind farms selected, scour protection systems are composed by two different layers (filter and armor layers). The bottom layer is designed to act as a filter, while the top layer is designed to act as a protective layer.

The average size of the armor units ( $D_{n50}$ ) used for the design of the layers of the scour protection system (filter and armor layer) is different. According to the functionality of each layer, rock elements used in the filter layers has to have a smaller diameter than those used for armor layers.

A design recommendation included in Hoffmans and Verheij (1997) considers that armor layers should have a thickness of at least twice the average size of rock elements ( $D_{n50}$ ).

Table 2 shows the size of the elements ( $D_{n50}$ ), the thickness and the extension of the scour protection system present in different European offshore wind farms installed in the last decade, where information is available.

During the investigation, only Horns Rev, Egmond Aan Zee and North Hoyle Offshore Wind Farms were taken into account due to the limited availability of information. In order to carry out the design of the extension of the scour protections, as it is shown in Table 3, there are different recommendations that have been proposed by various authors. Note that these formulations were proposed under current conditions only in river environments. As such, their application in the design of offshore structures should be developed with caution.

As it can be seen, all recommendations summarized in Table 3, about the extension of rock protection systems are expressed in terms of the pile diameter ( $D$ [m]). Thus, these recommendations omitted wave climate variables such as wave height, wave period or wavelength, which are decisive in the design of these structures.

Authors like Den Boon et al. (2004) and Carstens (1976), have also developed formulations for the calculation of the optimum extension of the scour protection considering the maximum scour depth ( $S_{max}$  [m]), the angle of internal friction ( $\emptyset$  [rad]), and a safety factor ( $F_s$ ). Thus, the extension of scour protections can be defined as:

$$L_{ext} = F_s \cdot S \cdot \cot \emptyset \quad (1)$$

According to the international standard for the design of offshore wind farms, DNV (2011), the maximum extension of scour can be calculated according to the following formula:

$$L_{ext} = \frac{D}{2} + S_{max} \cdot \cot \emptyset \quad (2)$$

Where  $D$  [m] is the pile diameter,  $S_{max}$  [m] is the maximum scour depth, and  $\emptyset$  [rad] is the angle of internal friction of seabed. According to this formulation, it can be assessed that the extension of the scour protection should take a value greater than that obtained by this expression. The analysis of the validity of the formulations (1) and (2) is not within the objective of this research because this study rather focused on the adequacy of scour protections used in light of recent scouring data that were available.

In order to assess the adequacy of protection systems installed in offshore wind farms selected and described above, a summary of the main characteristics of scour protections and scour estimation of each wind farm was developed.

As it is described in Zaaier et al. (2004), during the installation of an offshore wind farm it is necessary to decide if a scour protection system will be used. In the absence of a scour protection, as a rule of thumb, and according to the experience gained, the scour depth around cylindrical structures drilled in the seabed can adopt a value of 1.5 times the diameter of the pile (Breusers et al., 1977).

In this sense, the scour data registered in offshore wind farms studied indicate that the use of an adequate scour protection system can reduce the effects of scour phenomenon up to 92% (see Table 4).

## CONCLUSIONS

According to the results obtained during the research, the following conclusions are presented:

- Currently, there are criteria for optimizing the design and sizing of protection systems that could reduce the overall costs that are associated with these foundations in offshore wind farms.
- In offshore wind farms, the protection system that is placed around the turbine allows only the scour development around the edge of scour protection. Then, the depth of drilled pile is not reduced.
- An adequate protection system reduces the effects of the scour phenomenon around wind turbines by up to 92%.
- Protection systems based on rock elements are a good option to prevent scour around monopile foundations present in offshore wind farms.
- It is necessary to carry out further research in order to optimize the dimensioning of scour protection systems and to study the use of new materials.

## ACKNOWLEDGEMENT

This study was supported by the ACCIONA Technological Centre of Madrid through the agreement for the promotion of PhD Thesis development with Technical University of Madrid.

## LITERATURE CITED

- Bonasoundas, M., 1973. *Strömungsvorgang und Kolkproblem am Pfeiler*, Versuchsanstalt für Wasserbau, Bericht 28, Technischen Universität München, Oskar v. Miller Institut, Germany.
- Breusers, H.N.C., Nicollet, G., Shen, H.W., 1977. Local scour around cylindrical piers, *J. Hydraulic Res. IAHR* 15 (3), 211-252.
- Carstens, T., 1976. Seabed scour by currents near platforms, *3th Conference on port and ocean engineering under arctic conditions*, University of Alaska, 1976, pp. 991-1006.
- Carter, J.M.F., 2007. North Hoyle Offshore Wind Farm: design and build, *Proceedings of the Institution of Civil Engineers, Energy* 160(EN1): 21-29.

- CIRIA/CUR, Manual on the use of rock in coastal and shoreline engineering. CUR 154, 1991.
- COWRIE Ltd., 2010. A further review of sediment monitoring data, Cowrie ScourSed-09 eBook, 106p, UK.
- Den Boon, J.H., Sutherland, J., Whitehouse, R., Soulsby, R., Stam, C.J.M., Verhoeven, K., Høgedal, M., Hald, T., 2004. Scour behavior and scour protection for monopile foundations of Offshore Wind Turbines, EWEC, London, UK.
- Deutsche WindGuard GmbH, Deutsche Energie-Agentur GmbH, University of Groningen, 2007. Case study: European Offshore Wind Farms- a survey for the Analysis of the Experiences and Lessons Learnt by Developers of Offshore Wind Farms, Final Report 2007.
- De Vos, L., 2008. *Optimisation of scour protection design for monopiles and quantification of wave run-up*, Ph. D. Thesis, Universiteit Gent, Belgium.
- Det Norske Veritas, Design of Offshore Wind Turbine Structures, Offshore Standard DNV-OS-J101, 2011 Edition.
- Esteban, M.D., Diez, J.J., López-Gutiérrez, J.S., Negro, V., 2009. Integral Management applied to Offshore Wind Farms, *J. Coastal Res.* SI 56 (2009), pp.1204-1208, Lisbon, Portugal.
- Esteban, M.D., Diez, J.J., López-Gutiérrez, J.S., Negro, 2011a. Why offshore wind energy? *Renewable Energy J., Elsevier*, N°36: 444-450.
- Esteban, M.D., Diez, J.J., López-Gutiérrez, J.S., Negro, 2011b. Methodology for the design of offshore wind farms, *Journal of Coastal Research*, Special Issue No. 64, pp. 496-500, Szczecin, Poland.
- European Wind Energy Association, 2013. The European offshore wind industry key trends and statistics, 2012, Technical Report of European Wind Energy Association.
- Hansen, E.A., Simonsen, H.J., Nielsen, A.W., Pedersen, J., Høgedal, M., 2007. Scour protection around offshore wind turbine foundations, full-scale measurements. *Presentation and Proceeding of European Offshore Wind Conference*, Milan (Italy), December 4–6, 2007, Paper 159, 13 pp.
- Hoffmans, G.J.C.M. and Verheij, H.J., 1997. *Scour Manual*, Rotterdam, The Netherlands: A.A.Balkema, 205 p.
- Hjorth, P., 1975. Studies on the nature of local scour. Institute of Technology, Dept. of Water Resources Engineering.
- Louwersheimer, W.F., 2007. *Scour around an offshore wind turbine*, MSc Thesis Delft University of Technology.
- May, R.W.P., Ackers, J.C., Kirby, A.M., 2002. *Manual on scour at bridges and other hydraulic structures*, CIRIA.
- Matutano, C., Negro, V., López-Gutiérrez, J.S., Esteban, M.D., 2013a. Scour prediction and scour protections in offshore wind farms. *Renewable Energy*, Volume 57, Elsevier, September, 2013.
- Matutano, C., Negro, V., López-Gutiérrez, J.S., Esteban, M.D., 2013b. Dimensionless wave height parameter for preliminary design of scour protection in offshore wind farms. *Journal of Coastal Research*, Special Issue No. 65, 2013.
- Melville, B.W., Coleman, S.E., 2000. *Bridge scour*, Water Resources Publications Highlands USA, 550p.
- Negro, V., López-Gutiérrez, J.S., Esteban, M.D., Matutano, C., 2014. Uncertainties in the design of support structures and foundations for offshore wind turbines. *Renewable Energy J.*, N°63: 125-132.
- Nielsen, A.W., Sumer, B.M., Fredsoe, J., and Christensen, E.D., 2010. Scour protection around offshore wind turbines, 5<sup>th</sup> *International Conference on Scour and Erosion*.
- Raaijmakers, T.C., 2009. Evaluation of performance of scour protection and edge scour development – Offshore Windpark Egmond aan Zee. Technical Report of Deltares.
- Raaijmakers, T. C., Oeveren, M. C. V., Rudolph, D., Leenders, V., and Sinjou, W. C. P., 2010. Field performance of scour protection around offshore monopiles. 5<sup>th</sup> *International Conference on Scour and Erosion*, San Francisco, USA.
- Simoons, E., 2012. *Edge scour around an offshore wind turbine*, MSc Thesis at TU Delft.
- Whitehouse, R. J.S., Harris, J.M., Sutherland, J., Rees, J., 2011. The nature of scour development and scour protection at offshore windfarm foundations, *Marine Pollution Bulletin* 62 (2011) 73-88.
- www.4coffshore.com  
 www.viciventus.no  
 www.noordzeewind.nl  
 www.ballast-nedam.nl/
- Zaaijer, MB., Van der Tempel, J., 2004. Scour protection: a necessity or a waste of money?, *Proceedings of the 43 IEA Topical Expert Meeting* (pp. 43-51), 2004, Stockholm: FOI.

# Using Combined Modelling Approaches to Improve Coastal Defence Design: a case study at Hopton, UK

J.J. Williams<sup>†</sup>, L.S. Esteves<sup>‡</sup>, T. Conduche<sup>†</sup>, P. Barber<sup>∞</sup>, A. Tindle<sup>+</sup>

<sup>†</sup> ABPmer, Quayside Suite,  
Medina Chambers, Town Quay,  
Southampton, SO14 2AQ, UK.  
jwilliams@abpmer.co.uk

<sup>‡</sup> School of Applied Sciences,  
Bournemouth University, Poole,  
BH12 5BB, UK  
lesteves@bournemouth.ac.uk

<sup>∞</sup> Shoreline Management Partnership,  
Talwryn Green, Townsditch, Wrexham,  
Clwyd, LL12 0AN, UK  
dr\_barber@btconnect.com

<sup>+</sup> Rosebay Services, 85 Moor  
Road North, Gosforth, Newcastle  
Upon Tyne, NE3 1RJ, UK.  
a.tindle@btinternet.com



[www.cerf-jcr.org](http://www.cerf-jcr.org)



## ABSTRACT

Williams, J.J., Esteves, L.S., Conduche, T., Barber, P., Tindle, A., 2014. Using Combined Modelling Approaches to Improve Coastal Defence Design: a case study at Hopton, UK. In: Green, A.N. and Cooper, J.A.G. (eds.), *Proceedings 13<sup>th</sup> International Coastal Symposium* (Durban, South Africa), *Journal of Coastal Research*, Special Issue No. 70, pp. 018-022, ISSN 0749-0208.

[www.JCRonline.org](http://www.JCRonline.org)

A storm that occurred close to the spring tidal maxima in March 2013 resulted in beach lowering and cliff recession of c. 5 m along a 110 m frontage at Hopton-on-Sea, UK and threatened the static caravan park of Bourne Leisure Ltd. This paper reports a study using XBeach and MIKE21 models to assist with the design of new coastal defences to reduce cliff and beach erosion. Two schemes are examined here: three fishtail rock groynes (Scheme 1); and ten 'double-head' curved rock groynes (Scheme 2). The selected design must provide acceptable level of protection and, to be granted consent, no adverse environmental impact must be demonstrated. Current practice using a single numerical model can provide a cost-effective tool for coastal defence assessments. However, the work presented here show that when good agreement between complementary models can be demonstrated, greater confidence can be given to model results. Specifically, refinements to the present scheme design were made possible by the use of the XBeach model, which allowed identification of the cross-shore limits of sediment transport in storm conditions, and by the MIKE21 model which allowed quantification of alongshore scheme impacts. Together, the model results have assisted the development of an improved final scheme design which minimizes potential environmental impacts.

**ADDITIONAL INDEX WORDS:** MIKE21 FM, XBeach, cliff erosion, fishtail breakwater, Hopton-on-Sea.

## INTRODUCTION

Hopton Holiday Park, owned by Bourne Leisure Ltd. (BLL), is located on an eroding cliff frontage at Hopton-on-Sea, between Great Yarmouth and Lowestoft on the east coast of the UK (Figure 1a). In March 2013, a storm closely coinciding with the spring tidal maxima resulted in beach lowering and cliff retreat (c. 5 m) threatening 110 m of the Park's frontage (Figure 2a). Temporary emergency works to protect the cliffs from further erosion were carried out by BLL with support from Great Yarmouth Borough Council (GYBC). For business reasons, relocation of the static caravan site is not an option being considered and Shoreline Management Partnership has been appointed to provide specialist advice to assist the design of a coastal defence scheme to prevent further lowering of the beach and to protect the existing defences (Figures 1 and 2). This paper reports results from a study using two complementary models undertaken to inform the design of coastal defences and to assess potential impacts on the adjacent beaches.

Local hydrodynamics and sediment transport processes are complex due to the presence of discontinuous offshore sand banks,

the Great Yarmouth Outer Harbour (GYOH) and the tidal/fluvial exchanges of water and sediments with the River Yare. Inshore of the banks tidal flows are parallel to the coast with net tidal residuals directed southwards. At Hopton-on-Sea, peak depth-averaged tidal flow speeds increase from 0.5 m/s at 250 m from the shoreline to 1.0 m/s at 2 km offshore.

It is widely reported that alongshore sediment transport is predominantly southwards along this stretch of the coast, with annual average drifts from 10,000 to 40,000 m<sup>3</sup>a<sup>-1</sup> (HR Wallingford, 2002). However, the beach width from Gorleston to Corton gradually declines in a southerly direction (Figure 1). At Hopton-on-Sea variations in alongshore sediment supply and differences in the exposure of the shoreline to waves and tides are complicated by the presence of the offshore sand bank system and coastal defences (SMP, 2013). Numerical modelling (HR Wallingford, 2011a) has indicated that the largest offshore waves originating from the north-east are refracted by the offshore banks to arrive with a low obliquity to the coast. The arrangement of sand banks and channels induce wave energy from the south and south-east sectors to concentrate along the Hopton-on-Sea frontage. Waves from the south-east sector also have greater obliquity providing greater potential for net northerly drift, as is evidenced by the accumulation of sediment south of coastal structures (Figure 1b, c).

DOI: 10.2112/SI70-004.1 received 8 December 2013; accepted 21 February 2014. © Coastal Education & Research Foundation 2014

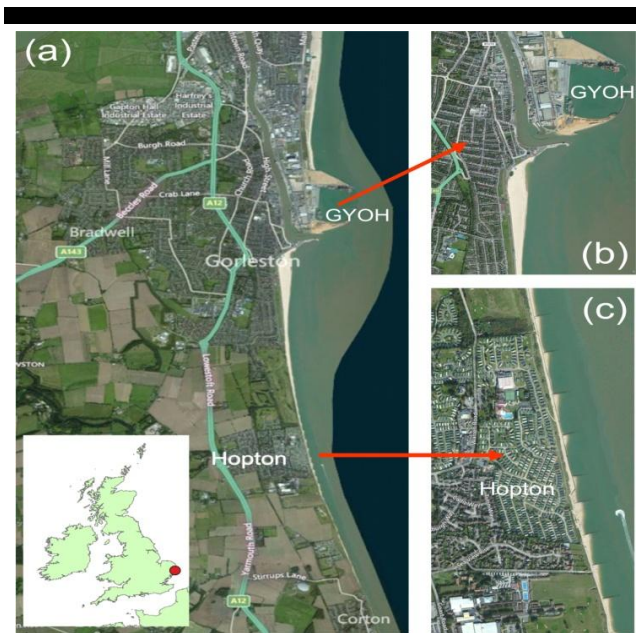


Figure 1. (a) Location of study site; (b) detail of GYOH and Gorleston beach; and (c) detail of Hopton-on-Sea.

HR Wallingford (2011b) and SMP (2013) show that Hopton beach exhibits a trend for beach erosion at its southern end and a trend of overall stability at its northern end derived from analysis of six-monthly beach profiles extending over the period 1991 to 2013. GYOH structures deflect the tidal streams and associated sediments offshore, likely reducing the southward sediment delivery feeding the sand banks system contributing to increased erosion along the Hopton-on-Sea frontage post GYOH construction (SMP, 2013).

### COASTAL DEFENCE STRUCTURES

The development of larger hydraulic machines over the last 30 years has provided the means to handle, place and profile large rock armour with individual boulder weights of up to 10 tonnes. Increasingly this shore-based construction approach is replacing the traditional steel piling and timber planking. This new construction method has led to the use of larger structures that are more akin to headlands than to traditional groynes. The evolution of more sophisticated models of nearshore coastal processes alongside the new alternative construction has produced a more refined design approach to such works.

There are two generic types of coastal defence classified as 'shore-parallel' and 'shore-normal'. A combination of these two types leads by logical progression to the 'fishtail' shape of breakwater employed in this study. Shore-normal construction essentially holds longshore currents away from the shoreline whilst allowing waves to advance into the calmer waters between structures where they can generate currents and move sediments during the breaking process. Shore-parallel construction essentially intercepts waves approaching the shoreline and when located offshore can use wave diffraction and refraction around structure extremities to stretch the length of wave crest and thereby reduce the wave energy incident at the shoreline per unit longshore length.

Key issues in the design of fishtail breakwaters / groynes are: (a) alongshore spacing of structures to restrict recovery of diverted longshore flows and avoid the generation of strong eddy-fields

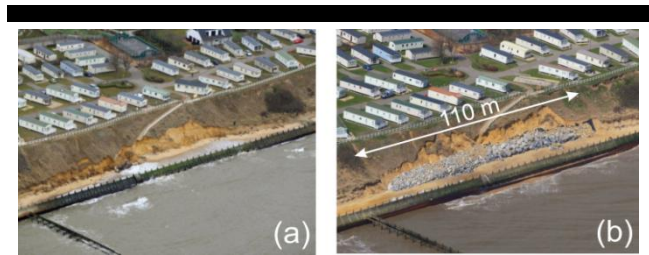


Figure 2. (a) March 2013 storm impact; and (b) emergency works at Hopton-on-Sea.

between structures; (b) on-offshore length of structures to provide sufficient depth of embayment to allow waves to respond to the changed conditions; (c) extent of shore-parallel wave interception to avoid adverse wave interaction along the on-offshore length of the structure and to achieve adequate wave dissipation between structures. Beyond these basic design parameters there are many more detailed considerations of structural form, roughness, stability and hydraulic performance across the structure. While these detailed considerations did not receive direct assistance from the modelling study reported here, the model results have provided specific inputs to the key design parameters set out above.

### MODELLING APPROACH

The modelling study has examined two coastal defence design options for Hopton-on-Sea: (Scheme 1) three *fishtail* rock groynes that are partly submerged at high water with alongshore spacing of 300 m and cross-shore extend of 150 m; and (Scheme 2) a linear scheme featuring ten curved rock groynes with a 'double head' at the offshore limit, an alongshore spacing of 100 m and a cross-shore extent of 55 m. The two schemes selected for test to provide coastal defence at Hopton represent two designs comprising firstly a multiplicity of shorter, closer-spaced structures and secondly fewer, larger structures. These are defined from experience for a specific site from consideration of: (a) inshore wave length, height and direction; (b) nearshore sea bed levels and tide range (including additions due to surge); and (c) the strength of longshore currents and their time of occurrence within the tidal cycle.

Information to support the design of the proposed schemes was obtained by coupling the Danish Hydraulic Institute's (DHI) MIKE21 Flexible Mesh (FM) models: hydrodynamics (HD); spectral wave (SW); and sediment transport (ST). In addition, a 2D XBeach model (Roelvink *et al.* 2009a,b) was used to provide an improved representation of complex nearshore hydrodynamics and sediment transport of relevance to the design of the proposed schemes. From a scientific point of view the approach would be to run a long series of computer model runs to assess the efficiency of the three key parameters at varied settings against other parameters calculated in the model. In practice the number of model runs is limited due to cost and specific runs are selected from experience once the shoreline exposure settings are known.

### MIKE21 FM

The MIKE21 FM model domain includes the sand banks systems and the Norfolk and Suffolk coast (from Horsey to Southwold) covering an area of approximately 60 km X 30 km (Figure 3). Fluvial inputs from the River Yare are negligible and are excluded. The north and south domain limits were configured to be perpendicular to the tidal streamlines and the offshore limits were designed to minimise wave obliquity at the open boundary.

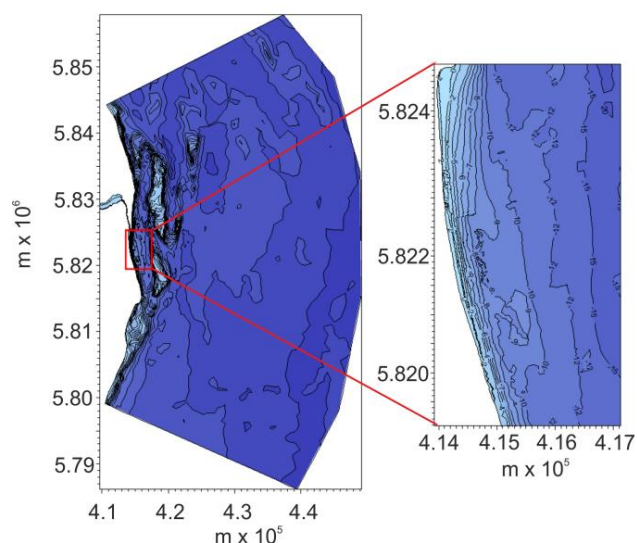


Figure 3. MIKE21 FM bathymetry for the whole domain (left) and detail of bathymetry at Hopton-on-Sea (right)

The bathymetry for the model (Figure 3) was derived from three data sources: (1) UKHO survey data; (2) Environment Agency beach profiles; and (3) BLL Hopton-on-Sea frontage survey data. In the offshore area the model resolution was 2 km, gradually reducing to 50 m in the coastal area and to 5 m along the Hopton-on-Sea frontage. Tidal forcing was applied at the northern and southern limits of the domain, and the offshore boundary tidal condition was set as a zero normal velocity. Water levels at the north and south boundaries were derived from harmonic analysis using DHI's global tidal harmonic database and Lowestoft tidal data from BODC. Wind forcing all over the domain was applied using 3 hourly wind data from the UKMO for the period of study (20-22 April 2008). Overall, the MIKE21 FM model performance agreed well with a Telemac model of the area reported by HR Wallingford (2012a, b; 2013).

### XBeach

Bathymetry for the 2D XBeach model was extracted from the MIKE21 FM model and used to create a non-linear grid with a variable spatial resolution across the model domain. For each scheme the grid mesh over the structures was 1 m and extended approximately three groyne lengths alongshore to the north and south of the schemes and offshore a distance of *c.* 500 m. The interpolated bathymetry for both schemes is presented in Figure 4. The scheme groynes were defined as 'hard structures' in the model (i.e. non-erodible). The model was run assuming that the representative median grain size ( $D_{50}$ ) for the beach sediments was 0.25 mm and  $D_{90} = 0.3$  mm (HR Wallingford 2012a). The depth of available sediment at all locations was assumed to be 2 m. Water levels, extracted from the MIKE21 FM-HD model, were applied at the northern and southern boundaries of the XBeach model to generate a shore-parallel tidal flow field with current speed and direction characteristics that agreed closely with the independently verified MIKE21 FM-HD model.

### Verification of the XBeach model

Beach profile GY28 is located approximately mid-way along the Hopton-on-Sea frontage surveyed by the Great Yarmouth Port

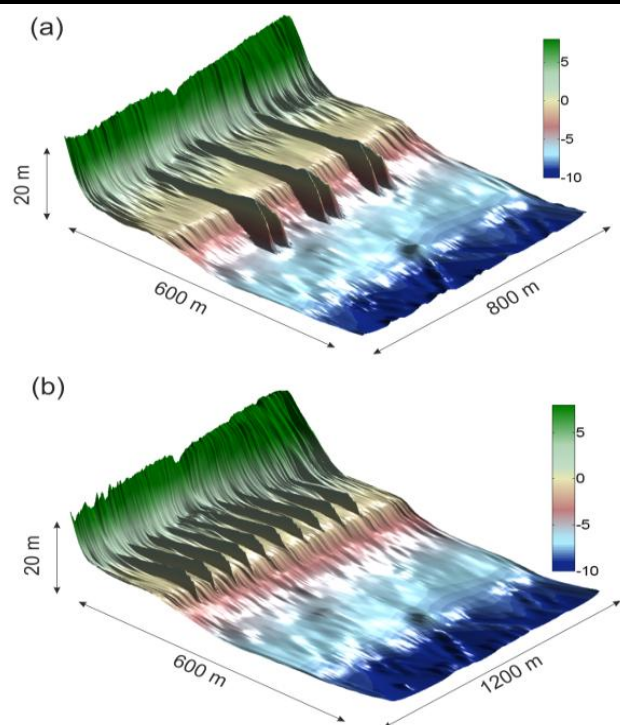


Figure 4. XBeach bathymetry: (a) Scheme 1; (b) Scheme 2.

Company as part of the monitoring of effects required under the enabling legislation. Figure 5 shows offshore time-series of tidal elevation ( $h$ ), wind speed ( $S_w$ ), wind direction ( $\theta_w$ ), significant wave height ( $H_s$ ) and peak wave period ( $T_p$ ) for an interval between successive GY28 profile measurements obtained on 5 October 2010 to 3 December 2010. Using XBeach in 1D mode, GY28 was extended offshore to -10 m ODN and the model was forced using the data shown in Figure 5.

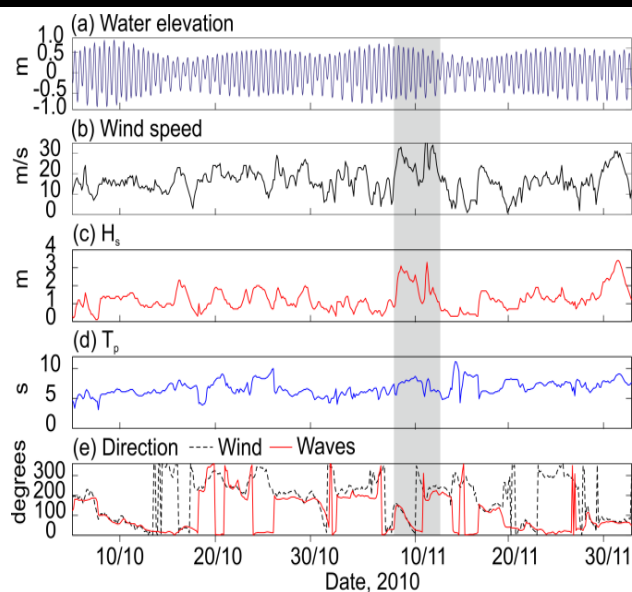


Figure 5. Time-series data used in XBeach model validation.

The measured and predicted GY28 beach profiles at the start (5 October 2010) and end (3 December 2010) of the model run are shown in Figure 6. The model predicts erosion in a cross-shore region spanning approximately 45 m between 2 m and -1 m ODN and accretion in a cross-shore region spanning approximately 25 m between -1 and -5 ODN (Figure 6). A Brier Skill Score (BSS) of 0.89 indicates excellent agreement between the observations and the model predictions (Van Rijn *et al.*, 2003). More than 90% of the changes to GY28 during the simulation period occurred during a storm beginning around 8 November 2010 when  $H_s > 2.5$  m (shown by the shaded region in Figure 5). Changes to GY28 during this storm are illustrated in Figure 6 (insert) which shows a surface fitted to a chronological time-stack of predicted beach erosion and accretion spanning a 12 hour period from the start of the storm. XBeach was also verified as being fit-for-purpose at 8 other locations between Hopton-on-Sea and Gorleston. Here it is assumed that the model performs equally well in 2D mode.

### Storm scenarios

Selecting wave sectors with the highest percentage of occurrence 1:35 year storm wave scenarios from approximately northeast by north (NEbN) and southeast by south (SEbS) directions were obtained from HR Wallingford (2011a) and used to define waves at the northern, southern and offshore boundaries of the MIKE21 FM-SW model (Table 1). Due to the limited fetch in the North Sea, wave directional spreading was set to  $30^\circ$ . The 2D XBeach model runs used wave data extracted from the MIKE21 FM-SW model at the offshore location coincident with the XBeach offshore boundary (i.e. -10m ODN, Table 1). Waves were introduced along the offshore boundary of the XBeach model as JONSWAP spectra and the directional spreading coefficient was set as time invariant.

## RESULTS

As numerical models have a potential to generate extensive data sets, it is important to select the information most relevant to a given study. The primary aim of this numerical modelling study

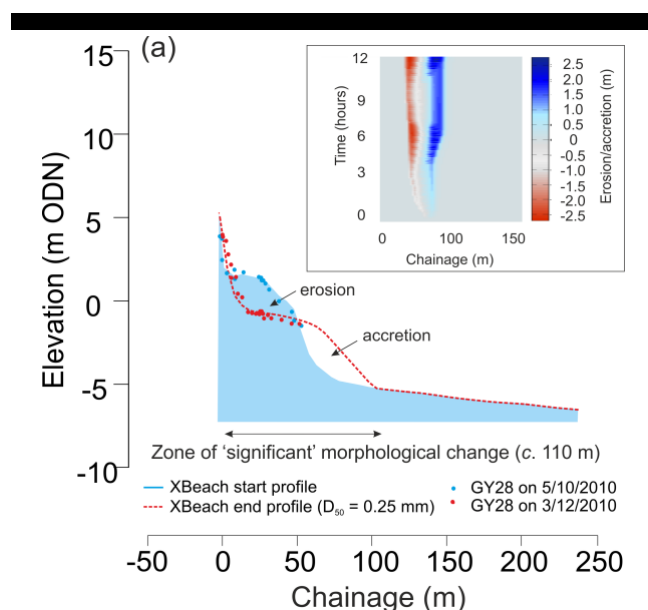


Figure 6. Beach profiles at the start and end of XBeach model run. Insert shows comparison between measured and predicted storm impacts at GY28.

Table 1. Offshore and inshore 1:35 year return period waves scenarios applied at the offshore boundaries of the MIKE21 FM-SW and 2D XBeach models.

Wave Scenario	MIKE21 FM-SW			2D XBeach		
	Hs (m)	Tp (s)	$\theta$ ( $^\circ$ N)	Hs (m)	Tp (s)	$\theta$ ( $^\circ$ N)
NEbN	4.53	10.3	30	1.71	7.0	72
SEbS	4.15	9.4	150	1.75	7.0	90

has been to assist scheme design and to assess near and far-field impacts. Therefore results presented here focus on the following model outputs over a tidal cycle: (a) average combined wave and tidal current (w-c) flows; (b) critical bed shear stress expressed as the percentage of time w-c flows exceed the critical bed shear stress for sediment entrainment ( $\tau_{crit}$ ), hereafter termed %T; (c) percentage change in total load sediment transport magnitude between the baseline condition and the scheme; and (d) changes in beach and nearshore morphology. It is assumed that  $\tau_{crit}$  for  $D_{50} = 0.25$  mm and  $\rho_s = 2650$  kg/m<sup>3</sup> is  $0.19$  N/m<sup>2</sup> (Soulsby, 1997).

Focussing on the nearshore flows for the NEbN baseline case, Figure 7a shows: w-c flow speed in the nearshore region is around 0.3 m/s and tidal currents in excess of 0.4 m/s are located offshore. For Scheme 1, a reduction in w-c flow speed occurs over the length of the scheme, especially between the structures (Figure 7b). Similar flow speed attenuation occurs in Scheme 2 (Figure 7c). Nearshore w-c flows for the SEbS scenario (c. 0.4 m/s) are higher than the NEbN scenario due to differences in the wave incidence angle. Flow attenuation by both schemes is shown in Figure 7e and 7f.

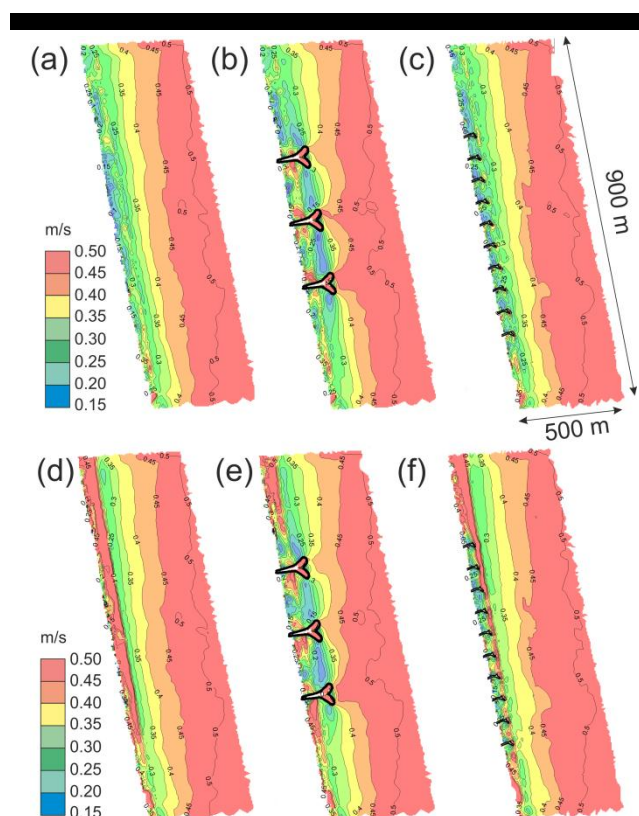


Figure 7. Tidally averaged w-c flow speeds: (a) baseline NEbN; (b) Scheme 1 NEbN; (c) Scheme 2 NEbN; (d) baseline SEbS; (e) Scheme 1 SEbS; (f) Scheme 2 SEbS.

If it is accepted that scheme impact alongshore is reflected by the distance over which the  $w$ - $c$  flow again attains a value above  $U_{crit}$  (i.e. the value competent to mobilise and transport sediments = 0.41 m/s, Soulsby, 1997), Figure 7 indicates that the scheme impact extends northwards less than one groyne length and two groyne lengths southwards in the NeBN scenario. The reverse is true for the SEbS scenario with impacts extending less than one groyne length southwards and two groyne lengths northwards. In both schemes the attenuation of  $w$ - $c$  flows to values  $< 0.3$  m/s in groyne embayments indicates sediment mobility will be reduced compared to the baseline case, thus providing beach protection and possibly accretion by the trapping of some proportion of the sediment moving alongshore. Deflection of flow streamlines around the groyne heads and wave action may also contribute to sedimentation processes within the groyne embayments.

The MIKE models showed that in the nearshore region,  $w$ - $c$  flows exceed  $\tau_{crit}$  for more than 90% of the time. This is primarily attributable to wave-induced flows (radiation stress-driven), as the tidal currents in this region are relatively weak (see Figure 7). Closer inshore, as a result of wave breaking and tidal flow attenuation by bed friction, the %T decreases from a maximum value in the breaker zone to zero at the shoreface. Similarly, the increase in water depth offshore reduces both  $w$ - $c$  bed shear stress and %T. The impacts of Scheme 1 are highly localised and principally confined to regions close to the structures. The local reductions in %T reflect wave sheltering and attenuation effects. There is no more than an approximate 10% reduction compared to the baseline to the north and south of Scheme 1. Seaward from the groyne heads, %T values are slightly enhanced compared with the baseline, probably due to the deflection of flow streamlines around the structures. Other than a very slight reduction in %T to the south of Scheme 2, no other impacts are evident. These results imply that waves are able to penetrate into the groyne embayments and generate approximately the same  $w$ - $c$  bed shear stress as the baseline case.

Percentage changes in total load sediment transport magnitude,  $Q_{tot}$ , between the baseline condition and the two schemes are shown in Figure 8 for ebb (tidal flow from south to north) and flood (tidal flow from north to south) flows and for each wave scenario (MIKE21 FM model). It should be noted, that although useful to illustrate **differences** between baseline and scheme cases, the percentage change can be misleading (e.g. a false impression of large changes when absolute values are small). There are several features common to each sub-plot in Figure 8: (a) a decrease in  $Q_{tot}$  of the order of 30% to 40% in inter-groyne embayments; (b) localised increases in  $Q_{tot}$  near the base and head of the scheme structures; (c) significant differences between ebb and flood flows especially for Scheme 2 as it is emerged around the time of peak ebb flow. The redistribution of wave energy, combined with a reduction in tidal current speed is shown to be responsible for the decrease in sediment transport at mid-distance between groynes.

Changes in bed elevation over a single spring tidal cycle (*c.* 12.5 hours) predicted by the 2D XBeach model for Schemes 1 and 2 are illustrated in Figure 9 for the NeBN and SEbS wave scenarios. Given limitations imposed by the surficial sediment depth defined in the model, the absolute changes in bed elevation may be either: (a) under-estimated due to depth-limited sediment cover; or (b) over-estimated because the depth of available sediment is less than 2 m and thus the patterns of erosion and accretion shown in Figure 9 indicate likely sedimentation patterns and must be interpreted with caution. Further, the 1:35 year wave return period wave events in the model represent an extreme event and thus the predicted beach impacts are correspondingly 'extreme'.

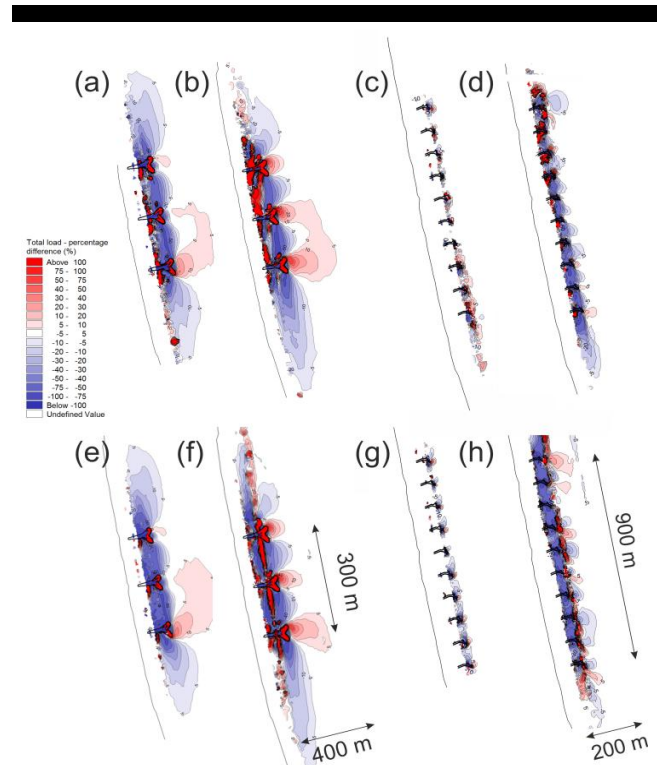


Figure 8. Percentage change in total load sediment transport magnitude between the baseline condition and schemes: (a) NEbN ebb tide Scheme 1; (b) NEbN flood tide Scheme 1; (c) NEbN ebb tide Scheme 2; (d) NEbN flood tide Scheme 2; (e) SEbS ebb tide Scheme 1; (f) SEbS flood tide Scheme 1; (g) SEbS ebb tide Scheme 2; and (h) SEbS flood tide Scheme 2.

Additionally, the initial beach morphology used in the 2D XBeach model is defined by the most recent beach survey data. This may reflect previous unknown and unrecorded erosive and/or accretionary phases and thus may not be representative of the 'typical' beach form. The erosion and accretion predicted by the 2D XBeach model is therefore predicated to some degree by the initial beach 'state' and should be taken into consideration when interpreting the model results.

Irrespective of the scheme or wave scenario Figure 9 exhibits two primary features: (a) a linear, approximately shore parallel, accumulation of sediments (hereafter termed a 'bar') that extends across the whole model domain; and (b) a zone of erosion that increases in depth shoreward from -0.5 m to -1.5 m. There is also evidence of erosion in the vicinity of the groyne heads and variable individual patterns of erosion and accretion in the inter-groyne embayments. Although exhibiting some spatial variability in accretion depth, the bar is homogeneous and, other than localised interactions with the structures, show no morphological signature that can be easily associated with the scheme. Similarly, the greatest predicted erosion depths are confined to the most shoreward regions and are similar alongshore across the model domain. In this respect the optimised linear scheme appears to have little or no impact on beach erosion compared with locations two or more groyne lengths to the north or south of the scheme.

## CONCLUDING REMARKS

Coastal defence funded privately (e.g. BLL scheme described here and Bunn Leisure, 2013) or in partnership with local and/or



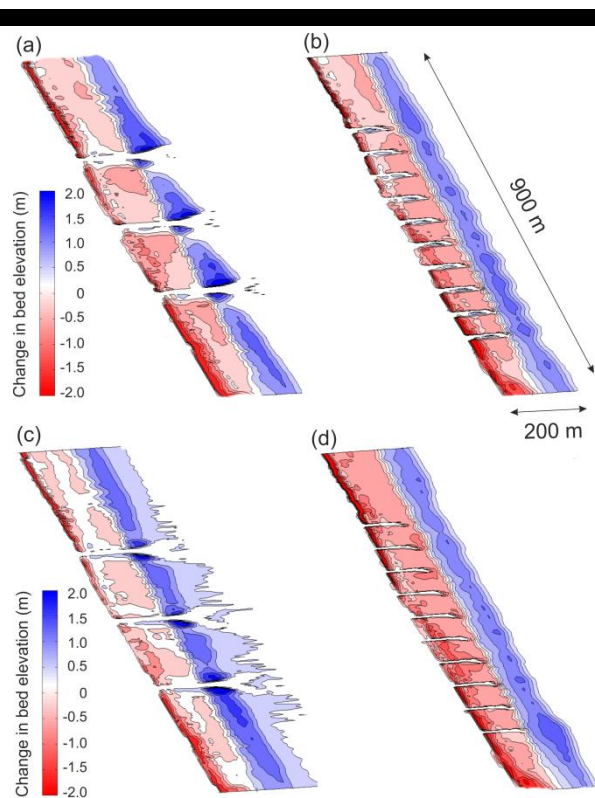


Figure 9. Changes in bed elevation predicted by the 2D XBeach model: (a) NEbN Scheme 1; (b) NEbN Scheme 2; (c) SEbS ebb tide Scheme 1; and (d) SEbS ebb tide Scheme 2.

national authorities is often undertaken when the value of an asset over a business cycle or the strategic importance of a site makes economic sense. The selected defence design must provide an acceptable level of protection and no adverse environmental impacts must be demonstrated. The work presented here has demonstrated that the use of complementary models that are designed to simulate specific processes and scenarios provide greater confidence in model results when good agreement between models predictions can be demonstrated. Specifically, refinements to the present scheme design were made possible by the use of the XBeach model which provided key information on the cross-shore limits of sediment transport in storm conditions and by the MIKE21 model which provided information on alongshore scheme impacts.

MIKE21 FM-HD/SW/ST and XBeach model results have assisted in the design of defence scheme structures (height, profile, length and spacing) and have provided guidance on how the scheme is likely to perform and the impacts it may have on the adjacent shorelines. They have also allowed preliminary material quantities and cost estimates to be confirmed.

The XBeach modelling has shown that storm waves with a 1:35 year return period from NebN and SebS directions will result in: (a) a linear alongshore, approximately shore parallel bar 2 m in height; and (b) a zone of erosion that increases in depth shoreward from c. -0.5 m to -1.5 m. Both models show that during a typical spring tidal cycle the maximum potential impacts of the optimised linear schemes extend no more than 150 m and 100 m to the north and south of the groyne field for Scheme 1 and 2, respectively. The exact distance to which these potential impacts extend is determined by the angle of incidence and the energy of the

incoming waves. However, the alongshore distance of potential impacts tends to be longest lee-ward of the groynes relative to the incoming wave direction. Together, the model results have therefore assisted the development of a cost-effective final scheme design which minimizes potential environmental impacts with respect to coastal and sediment processes.

It is acknowledged that the models used here can only look realistically at the two proposed schemes over short periods and thus cannot provide reliable information on the medium- or long-term scheme performance and impacts, where only experience and expert judgment can provide guidance. So that greater confidence can be given to results from similar modelling studies in the future, it is important that the medium- and long-term impacts of the final scheme to be built at Hopton-on-Sea are monitored and disseminated.

Finally, looking at the proposed scheme from an ecological perspective, rock structures will change the natural habitat and in turn may lead to unpredictable decreases or enhancements in local biodiversity. Further, depending on a personal viewpoint, the structures might be viewed as being visually intrusive and thus detrimental to environment aesthetics. These aspects of the scheme in the construction and operation phases, and those concerning water quality, fish and fisheries, noise and vibration, recreation, tourism and economics etc. are currently the subject of an independent environmental impact assessment process with key stakeholders. This will be prepared in accordance with the requirements of the EIA Directive (85/337/EEC as amended), the Town and Country (EIA) Regulations 2011 and the Marine Works (EIA) (Amendment) Regulations 2011.

## ACKNOWLEDGEMENT

Thanks are extended to Bourne Leisure Ltd. who funded the work described in this paper and granted permission for its publication.

## LITERATURE CITED

- Bunn Leisure, 2013. <http://beautifulbeach.bunn-leisure.co.uk/about-our-beautiful-beach.aspx>
- HR Wallingford, 2002. Southern North Sea Sediment Transport Study, Phase 2: Sediment Transport Report. Report EX4526.
- HR Wallingford, 2011a. Hopton Coastal Studies: Wave Modelling. Report EX 6680, Release 1.0, 80pp.
- HR Wallingford, 2011b. Great Yarmouth. Beach and nearshore monitoring report. EX 6469, Release 1.0, 76pp.
- HR Wallingford, 2012a. Hopton Coastal Studies: Numerical Hydrodynamic and Sediment Transport Modelling. Report EX 6595, 270pp.
- HR Wallingford, 2012b. Hopton Coastal Studies: Numerical Hydrodynamic and Sediment Dispersion Modelling. Report EX 6595-Addendum 2, 50pp.
- HR Wallingford, 2013. Hopton Coastal Studies: Numerical Hydrodynamic and Sediment Dispersion Modelling. Report EX 6595-Addendum 3, 96pp
- Roelvink, J.A., Reniers A., van Dongeren, A., de Vries, J., McCall, R., Lescinski, J., 2009a. Modelling storm impacts on beaches, dunes and barrier islands. *Coastal Engineering*, 56(11-12), 1133-1152.
- Roelvink, J. A., Reniers A., van Dongeren, A., de Vries, J., Lescinski, J., & McCall, R., 2009b. XBeach model description and manual, Deltares/TU Delft, The Netherlands, 96pp.
- SMP (Shoreline Management Partnership), 2013. An Investigation into the causes of beach erosion and effects of the Outer Harbour development at Hopton-on-Sea. Volumes I - IV.
- Van Rijn, L. C., Walstra, D. J. R., Grasmeyer, B., Sutherland, J., Pan, S. & Sierra, J. P., 2003. The predictability of cross-shore bed evolution of sandy beaches at the time scale of storms and seasons using process-based profile models. *Coastal Engineering*, 47, 295-327.

# On the use of the Radon transform to estimate longshore currents from video imagery



[www.cerf-jcr.org](http://www.cerf-jcr.org)

Stanislas Larnier†, Rafael Almar+, Rodrigo Cienfuegos∞, Antoine Lejay#

†LAAS-CNRS  
Université Paul Sabatier  
Toulouse, France  
[stanislas.larnier@laas.fr](mailto:stanislas.larnier@laas.fr)

+ IRD-LEGOS  
Université Paul Sabatier  
Toulouse, France  
[rafael.almar@ird.fr](mailto:rafael.almar@ird.fr)

∞ CIGIDEN  
Pontificia Universidad Católica  
Santiago, Chile  
[racienfu@ing.puc.cl](mailto:racienfu@ing.puc.cl)

# Inria-IECL  
Université de Lorraine  
Nancy, France  
[antoine.lejay@inria.fr](mailto:antoine.lejay@inria.fr)



[www.JCRonline.org](http://www.JCRonline.org)

## ABSTRACT

Larnier, S., Almar, R., Cienfuegos, R., Lejay, A., 2014. On the use of the Radon transform to estimate longshore currents from video imagery. In: Green, A.N. and Cooper, J.A.G. (eds.), *Proceedings 13<sup>th</sup> International Coastal Symposium* (Durban, South Africa), *Journal of Coastal Research*, Special Issue No. 70, pp. 023-028, ISSN 0749-0208.

In nearshore applications, the estimation of longshore currents is of primary importance since it controls the alongshore sediment transport and coastal evolution. Direct estimation of longshore currents using in-situ instruments is difficult and costly, especially under highly energetic wave climates. Low cost remote sensing systems based on video observations constitute a promising alternative when the drifting sea foam left after the passage of breaking waves is visible. In this paper we describe a method based on longshore timestacks that necessitates less data than approaches using the full video frames. Our approach uses the Radon transform applied on the time series derived from timestacks to produce an estimate of the longshore component of nearshore surface currents detected from the foam signature in video images. The Radon transform can be used to separate the wave crests from the drifting foam part. The identification of the longshore drift is enhanced with both a temporal and a spatial filters. The corresponding sinogram from the Radon transform is computed in order to find the angle of the alongshore drifting that is further converted into the longshore component of the surface currents. For the estimation of longshore currents, our approach is first tested using synthetic timestack examples created using anisotropic Gaussian random current fields. Comparisons between estimates derived by our algorithm and manual operator detection from videos are performed showing good agreement. These videos come from a field campaign conducted in the Mataquito River mouth area in the Maule region (Chile). Field test comparisons were also made against in situ current meter from the 2008 Truc Vert experiment in Aquitaine (France). It was taking place during an energetic event.

**ADDITIONAL INDEX WORDS:** *Longshore current, remote sensing, image processing, Radon transform, anisotropic Gaussian random fields.*

## INTRODUCTION

Wave energy is generated by converting the energy of ocean waves, swells, into other forms of electricity energy. Wave energy provides 15 to 20 times more available energy per square meter than either wind or solar and is also more regular (Muetze and Vining, 2006). With a long coastline where the Pacific Ocean is highly energetic, Chile, country partner of the project, plans to invest in this renewable energy.

The multi-disciplinary Franco-Chilean project behind this study intends to use low cost remote sensing systems based on video observations to determine the energy potential of a site. For this, we need to estimate the average period, average speed, and average wave height, average speed of coastal currents, the angle between incoming wave front and the coast, and bathymetry.

Remote sensing systems have been developed for over twenty years. They were used to detect morphology of submerged sandbars (Lippmann and Holman, 1990), period and direction of breaking waves (Lippmann and Holman, 1991), the time-varying location of the shore line (Plant and Holman, 1997) and nearshore bathymetry (Stockdon and Holman, 2000). Compared to the use of radar or sensors, this technique has the advantage of having a low cost of installation and use (Almar, 2009). In order to determine correctly geophysical variables, it is necessary to be able to transform the coordinates of the image in actual coordinates. Such a transformation is determined from a set of visible ground control points with known geophysical locations (Holman and al., 1993).

In this article, we are interested only in estimating the average velocity  $V$  of coastal currents using the moving mass of foam created when a wave breaks. The trajectories of the foam are dependent of current and waves.

DOI: 10.2112/S170-005.1 received 1 December 2013; accepted 21 February 2014. © Coastal Education & Research Foundation 2014

Methods consider only the current component parallel to the coast (Chickadel, 2003). Others use the whole video as Particle Image Velocimetry (PIV) (Holland *et al.*, 2001).

The videos used in this study come from two field campaigns. The ones from Chile were conducted in the Mataquito River mouth area in Maule region. These videos are part of a study on the post-tsunami coastal recovery of the Mataquito area after 2010 Chilean Tsunami (Villagran *et al.*, 2013). Unlike conventional installation of other campaigns, where the cameras are on a mast near the beach, the system is at the top of a hill in the coastal mountain range. Figure 1 presents two snapshots.

Field test comparisons were also made against in situ current meter from the 2008 Truc Vert experiment in Aquitaine (France). Figure 2 presents two snapshots. In the second one, a red dot marks the current meter location. This study was part of the ECORS program. It took place during an energetic event where rapid sandbar evolution was observed (Senechal *et al.*, 2011).

In section Timestacks, the definition of timestack is recalled then we present a simple approach to obtain synthetic data based on anisotropic Gaussian random fields. The section Radon transform and algorithm presents shortly the Radon transform, main tool of our approach, and the algorithm steps are given and illustrated with a real timestack from Truc Vert experiment. In section Numerical results, our approach is first tested using synthetic timestack examples, then comparisons between estimates derived by our algorithm and a manual operator detection from videos are performed showing good agreement and to conclude a field test comparisons is made against in situ current meter from the Truc Vert experiment.

## TIMESTACKS

### True timestacks

Timestacks are images created from a temporal sequence of selected pixels. Every horizontal line represents a line through the field of the camera to capture a given instant, as the red line, parallel to the coast, in Figure 3. Each vertical line shows the time evolution a fixed point on the line.

Figure 4 shows the resulting corresponding timestack about four periods of the wave front from the red line shown in Figure 3. Wave fronts give the white horizontal lines. The drift of persistent sea foam form oblique lines. The celerity of the surface currents



Figure 1. Snapshots from Mataquito cameras, Chile.

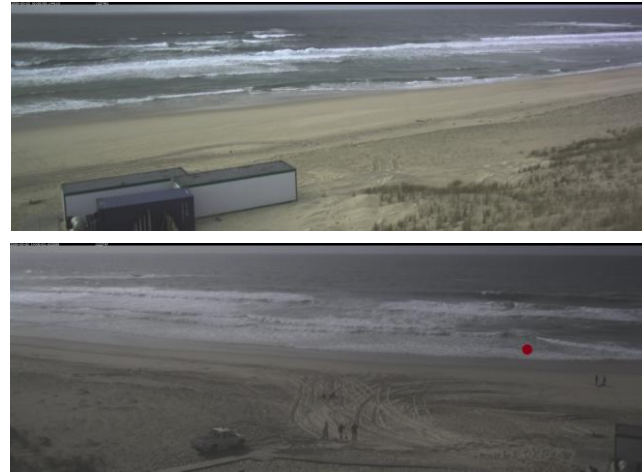


Figure 2. Snapshots from Truc Vert cameras, France.

can be estimated from the orientations of these lines. On this picture, the timestack was enlarged from temporal point of view to get a better understanding of the phenomena.

### Synthetic timestacks

It is possible to simulate synthetic longshore timestacks (Chickadel *et al.*, 2003). The approach proposed in this article is based on anisotropic Gaussian random fields.

The generation algorithm is:



Figure 3. View from Truc Vert site. The red line is the timestack position. The timestack is parallel to the wave front.



Figure 4. Associated timestack. The horizontal lines are wave crests. The orientation of the other lines created by the foam give the currents celerity along the shore.

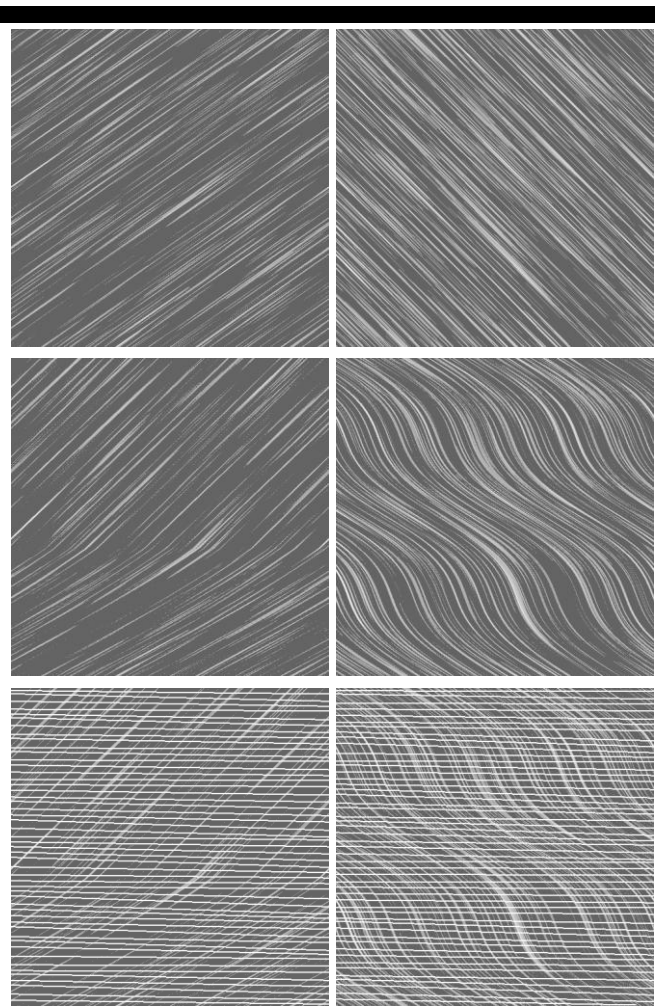


Figure 5. Creation of synthetic longshore timestacks. From up to down, anisotropic random Gaussian fields, deformations of the fields, same images where random wave crests have been added.

1. Creation of an anisotropic Gaussian random field with an orientation  $\theta$ ;
2. Deformation of the field;
3. Creation of random wave front with a mean period of  $T$ ;
4. Assemblage of the two.

Figure 5 presents two results from this algorithm. At the top,

there are two anisotropic random Gaussian fields with an orientation  $\theta=55^\circ$  at left and  $\theta=135^\circ$  at right. At the middle, there are modified in order to obtain a sudden acceleration for the left one and a sinusoidal behavior for the right one. At the bottom, the waves crests are added with a mean period of waves  $T=10$  pixels.

## RADON TRANSFORM AND ALGORITHM

### Radon transform

The Radon transform (Ramm and Katsevich, 1996; Mallat, 2009; Feeman, 2010)  $R(\rho, \theta)$  over a bidimensional field  $\eta(x,y)$  can be defined as:

$$R(\rho, \theta) = \iint \eta(x, y) \delta(x \cos \theta + y \sin \theta - \rho) dx dy$$

where  $\delta$  is the Dirac delta function,  $\theta$  and  $\rho$  are respectively the angle and distance from origin of the integration line defined as  $\rho = \cos(\theta)x + \sin(\theta)y$ . The origin is the center of the two-dimension field. The Radon transform is defined for all possible values of  $\theta$  from  $[0 \text{ to } 180^\circ]$  and  $\rho$  from 0 to the diagonal length.

From an image  $\eta$ , a sinogram, Radon transform data  $R$  depending of  $\rho$  and  $\theta$ , can be obtained, see Figure 7 for an example. It is possible to filter  $\eta$  by modifying the values of  $R$  then using the inverse Radon transform.

The Radon transform is especially used in medical image processing, notably in tomography. Recently, the Radon transform has been successfully applied to study nearshore wave dynamics where it allows the separation of incoming waves from reflected ones (Almar et al, 2013).

### Orientation detection algorithm

The algorithm is the following:

1. Use of Radon Transform to delete the horizontal lines (waves) and vertical ones (camera artefacts) with a range of more or less  $\mu$ ,
2. Temporal filter with a high pass filter;
3. Spatial filter in order to keep the high frequency information;
4. Study of Radon coefficients to determine the local maxima;
5. Deletion of extreme values outside of boundary values;
6. Mean of the best ones to obtain the best orientation.

In the majority of tests,  $\mu$  is equals to  $8^\circ$ . Figures 6 and 7 illustrate the algorithm steps on the 10th of March 2008 from 7h45 to 8h for Truc Vert campaign. From left to right. Figure 6 presents the timestack and the successive filters applied to the image.

The left image in Figure 6 presents the filtered image in which

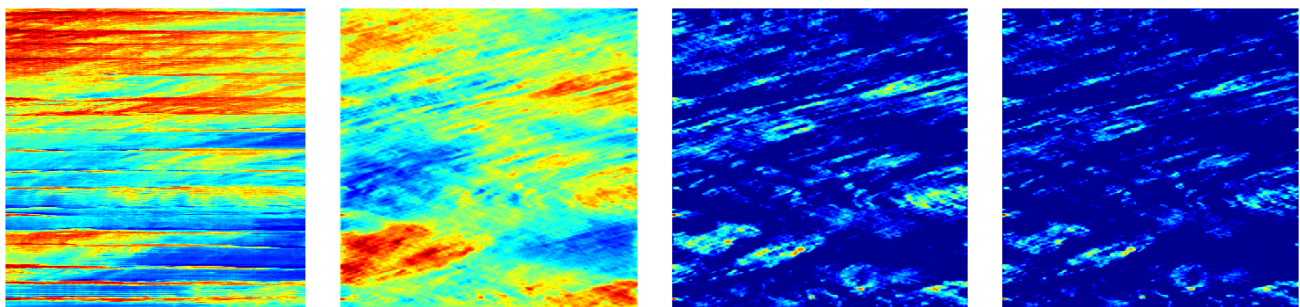


Figure 6. From left to right, original image, image filtered with Radon transform, then with a temporal filter, then with a spatial filter.

the orientation of the current will be determined. Even if some zones are not in the correct orientation, the obtained image is usually correct. Radon values for the filtered image are given in the right image of Figure 7 (the original image has been turned a quarter turn) with local maxima above a certain threshold surrounded by a red circle. The sensor has measured an average speed of -0.64 m/s and our algorithm returns -0.66 m/s.

## NUMERICAL RESULTS

### Tests on synthetic data

Synthetic stacks were created with an orientation  $\theta$  from  $5^\circ$  to  $175^\circ$  with a step size of  $10^\circ$  and with a mean period of waves  $T=10$  pixels. The synthetic image is a square of side 500 pixels and takes its gray values between  $[0,255]$ . Examples of synthetic stacks are shown in Figure 5.

In these tests, an additive Gaussian noise of standard deviation 50 is added. The correlation between true and detected angles is equals to 0.997. Figure 8 presents the plot of the true angles versus the detected ones. The blue crosses are the left type of synthetic data in Figure 5; the green crosses are the second one. The red thick line is the linear least square regression and follows the equation  $y=1.041x-3.626$ . The black dashed line is a perfect fit.

Note that for angles near a horizontal or a vertical orientation, the angle of deletion is lowered in step 1 of the orientation detection algorithm compared to real images.

### Comparison with human operator

Figure 9 shows two timestacks taken along the coast on Mataquito site in identical positions but in different light conditions. Manual operator found respectively  $13.8^\circ$  and  $12.6^\circ$  for the first and second timestack, against  $12.5^\circ$  and  $13.6^\circ$  for the algorithm. The detection algorithm gives results similar to those of a human operator.

Figure 10 presents the plot of manual operator current means versus the algorithm estimations at the Truc Vert during the 10<sup>th</sup> March 2008, from 12 a.m. to 4 p.m.. The linear least square regression is shown as the red thick line and follows the equation  $y=0.961x-0.084$ . The correlation is equals to 0.81. The black dashed line is a perfect fit. The worst results are for low velocity, it could come from the climate conditions which make it more difficult for manual operator to estimate the current mean on the studied windows.

### Comparison with current meter

Mean velocity was calculated from the data collected during three days of Truc Vert experiment. This acquisition was made from the 10<sup>th</sup> to the 12<sup>th</sup> of March 2008, from 7 a.m. to 6 p.m.. The position of the current meter is represented in Figure 2. It registers at 0.1 Hz, a mean of length 70 s is performed, and then an interpolation is used to obtain data at the same time than the detection. The detection algorithm gives information at each 240 s and a mean of length 720 s is performed.

Figure 12 presents three times series comparisons of mean longshore current estimates from the algorithm (red circles) with the ground thrust data returned from the current meter (blue crosses). Some data are not displayed because they have been taken at low tide and there is not enough water above the current meter to have correct measurements. The worst results are for the positive currents which are near the low tide so they are not completely accurate. The correlation is equals to 0.812.

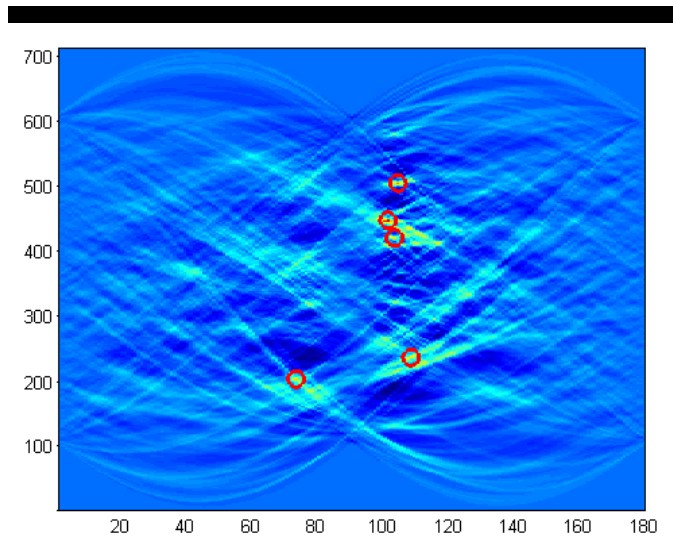


Figure 7. Sinogram (or Radon transform data) of the right image of Fig. 6. Local maxima are in a red circles.

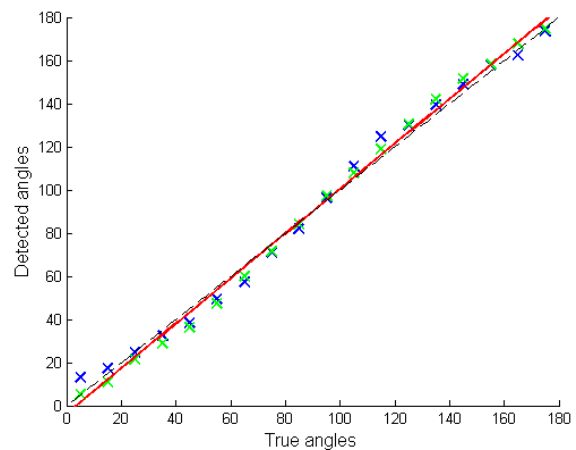


Figure 8. True angles versus detected ones for synthetic data. The blue crosses represent the first type and green crosses the second one, see Figure 5. The linear least squares regression is shown as the thick red line and the dash line is the line  $y=x$ .



Figure 9. Two timestacks from Mataquito with different illumination conditions.

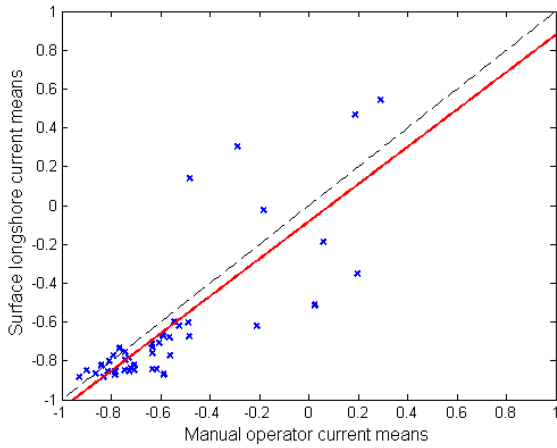


Figure 10. Manual operator current means versus detected ones at the Truc Vert during the 10<sup>th</sup> March 2008 from 12 p.m. to 4 p.m.. The linear least squares regression is shown as the thick red line and the dash line is the line  $y=x$ .

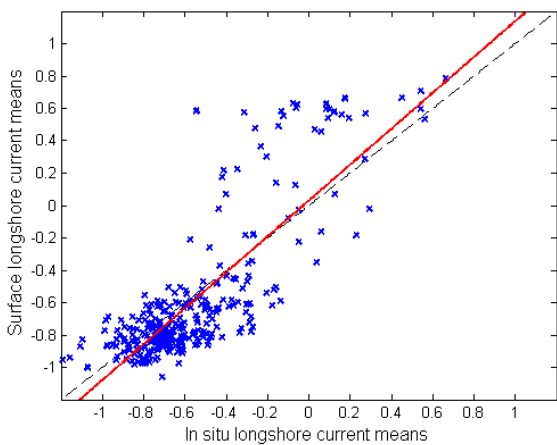


Figure 11. In situ longshore current means versus surface longshore current means. The linear least squares regression is shown as the thick red line and the dash line is the line  $y=x$ .

Figure 11 shows a more direct comparison between the two estimates. The linear least squares regression follows the equation  $y=1.109x+0.028$  and is the red thick line. The black dashed line is a perfect fit.

### CONCLUSION

This article presents a new approach to estimate longshore currents from video imagery timestacks using the Radon transform. The results on synthetic data, on normal condition or even in the case of an energetic event are promising. It is an alternative to other approaches (Chickadel et al., 2003; Holland et al., 2001). Extensive comparative study between these different approaches is under consideration, with also investigation to determine the optimal size windows and some indicators to avoid poor timestacks due to low contrast or undesirable marks due to for examples birds, boats or humans.

Future research under consideration is a comparison with the investigation of nearshore currents from parameters estimated in open sea in Benin (Laibi, R., et al., 2014).

Even if the longshore currents are often the most important part, it could be interesting to have the global current evolution from video imagery. During our study, we note that Radon transform, can be also used to separate wave crests and foam from a full camera snapshot. Two examples are given in Figure 12. Waves crests orientation is obtained from the sinogram of Radon transform. The separation part is performed like the first step of our estimation algorithm. Particle Image Velocimetry improvement exists (Larnier et al., 2013), and it will be interesting to dig also in this research perspective.

### ACKNOWLEDGEMENT

We acknowledge the Lorraine region, the associated franco-chilean team Anestoc-Inria, and the Centre Inria CIRIC for their financial support. R. Cienfuegos acknowledge partial support from the Fondap program 15110017. The ECORS experiment and Truc Vert video system were supported by the French “Service Hydrographique et Oceanographique de la Marine” (SHOM) and the “Délégation Générale de l’Armement” (DGA). R. Almar funded by the French programs INSU LEFE and EC2CO. R. Cienfuegos and Mataquito video system funded by Chilean project FONDECYT N°1120878.

### LITERATURE CITED

Almar, R., 2009. *Morphodynamique littorale haute fréquence par imagerie video*. PhD thesis, Université Bordeaux I, France.  
 Almar, R., Bonneton, P., Michallet, H. Cienfuegos, R. Ruessink, B.G., and Tissier, M., 2013. On the use of Radon transform in studying nearshore

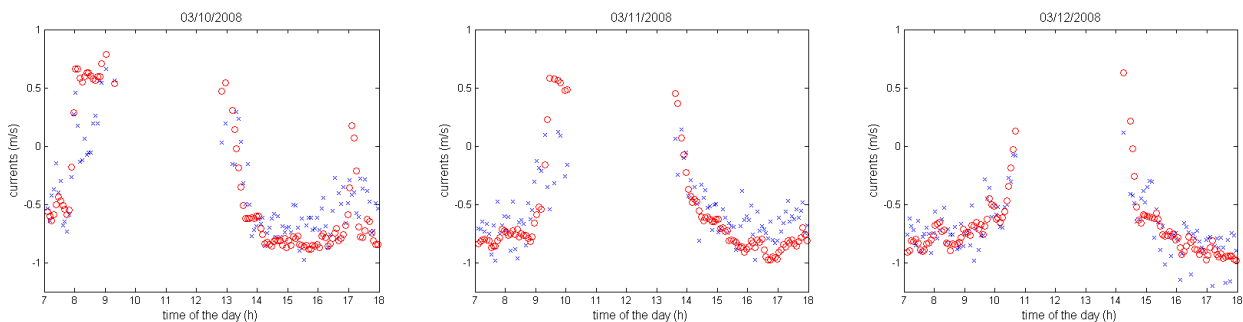


Figure 12. From left to right, optically measured man surface currents (circles) and in situ currents (crosses) for the 10<sup>th</sup> to the 12<sup>th</sup> March 2008 at Truc Vert experiment.

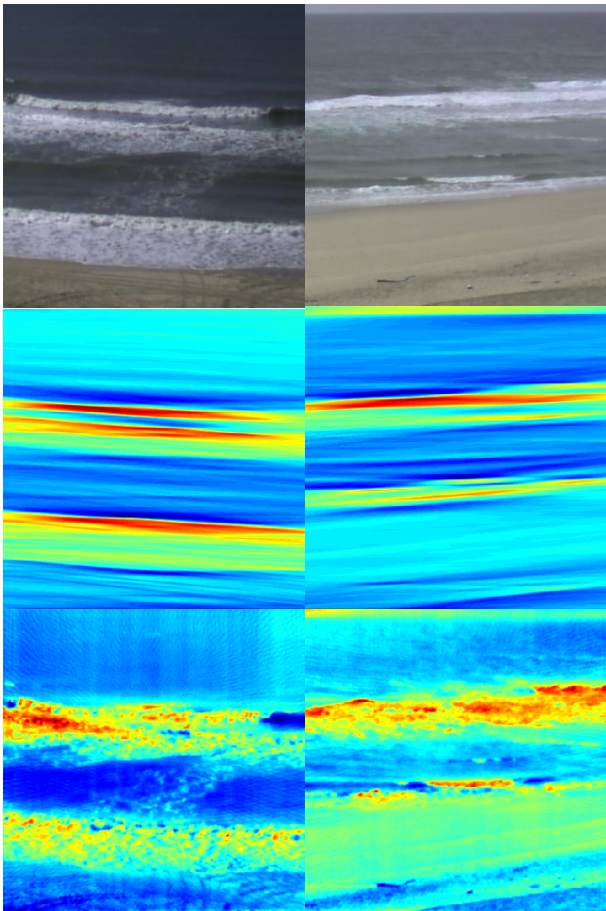


Figure 13. From up to down, original images, filtered to obtain the waves, filtered to obtain the foam.

- Mallat, S., 2009. *A wavelet tour of signal processing: The sparse way*. Elsevier/Academic Press, Amsterdam, 3 edition. With contributions from Gabriel Peyré.
- Muetze, A. and Vining, J.G., 2006. Ocean wave energy conversion — a survey. In *41st IAS Annual Meeting. Conference Record of the 2006 IEEE Industry Applications Conference*, vol. 3, 1410–1417.
- Plant, N.G. and Holman, R.A., 1997. Intertidal beach profile estimation using video images. *Maine. Geology*, 140, 1–24.
- Senechal, N., Abadie, S., Gallagher, E., MacMahan, J., Masselink, G., Michallet, H., et al., 2011. The ECORS-Truc Vert'08 nearshore field experiment: presentation of a three-dimensional morphologic system in a macro-tidal environment during consecutive extreme storm conditions. *Ocean Dynamics*, 61(12), 2073–2098.
- Stockdon, H.F. and Holman, R. A., 2000. Estimation of wave phase speed and nearshore bathymetry from video imagery. *J. Geophys. Research: Oceans*, 105(C9), 22015–22033.
- Ramm, A.G. and Katsevich, A.I., 1996. *The Radon transform and local tomography*. CRC Press, Boca Raton, FL.
- Villagran, M., Cienfuegos, R., Catalan, P. and Almar, R., 2013. Morphological response of central Chile sandy beaches to the 8:8 Mw 2010 earthquake and tsunami. In *Proceeding of Coastal Dynamics, 24-28 June 2013, Arcachon, France*, 1823–1834.

wave dynamics. In *Proceedings of Coastal Dynamics, 24-28 June, Arcachon, France*, 73–82.

- Chickadel, C.C., R.A. Holman, and Freilich, M.H., 2003. An optical technique for the measurement of longshore currents. *Journal of Geophysical Research: Oceans*, 108(C11).
- Feeman, T. G., 2010. *The mathematics of medical imaging, A beginner's guide*. Springer Undergraduate Texts in Mathematics and Technology. Springer, New York.
- Haralick, R.M. and Shapiro, L.G., 1993. *Computer and robot vision*. Computer and Robot Vision. Addison-Wesley Pub. Co..
- Holland, K.T., Puleo, J.A., and Kooney, T.N., 2001. Quantification of swash flows using video-based particle image velocimetry. *Coastal Engineering*, 44(2), 65–77.
- Holman, R.A., Sallenger, A.H. Jr., Lippman, T.C., and Haines, J.W., 1993. The application of video image processing to the study of nearshore processes. *Oceanography*, 6(3), 78–85.
- Laibi, R., Anthony, E., Almar, R., Castelle, B., Senechal, N., Kestenare, E., 2014. Longshore drift cell development on the human-impacted Bight of Benin sand barrier coast, West Africa. In *Proceedings 13th International Coastal Symposium (Durban, South Africa)*, Journal of Coastal Research, Special Issue No. 70, ISSN 0749-0208
- Larnier, S., Almar, R., Cienfuegos, R., and Lejay, A., 2013. *Détection de courants marins côtiers à partir de sequences video*. (submitted)
- Lippmann, T.C. and Holman, R.A., 1990. The spatial and temporal variability of sand bar morphology. *Journal of Geophysical Research: Oceans*, 95(C7), 11575–11590.
- Lippmann, T.C. and Holman, R.A., 1991. Phase speed and angle of breaking waves measured with video techniques. In N.C. Kraus, K.J. Gingerich, and D.L. Kriebel, editors, *Coastal Sediments*, 542–556.

# Quantifying dispersion in an estuary: A Lagrangian drifter approach

D. Spencer<sup>†</sup>, C.J. Lemckert<sup>‡</sup>, Y. Yu<sup>‡</sup>, J. Gustafson<sup>‡</sup>, S.Y. Lee<sup>†</sup>, H. Zhang<sup>‡</sup>

<sup>†</sup> Australian Rivers Institute  
Griffith University  
Gold Coast, 4222, Australia  
d.spencer@griffith.edu.au

<sup>‡</sup> School of Engineering  
Griffith University  
Gold Coast, 4222, Australia  
c.lemckert@griffith.edu.au



[www.cerf-jcr.org](http://www.cerf-jcr.org)



[www.JCRonline.org](http://www.JCRonline.org)

## ABSTRACT

Spencer, D., Lemckert, C.J., Yu, Y., Gustafson, J., Lee, S.Y., Zhang, H., 2014. Quantifying Dispersion in an Estuary: A Lagrangian Drifter Approach. In: Green, A.N. and Cooper, J.A.G. (eds.), *Proceedings 13<sup>th</sup> International Coastal Symposium* (Durban, South Africa), *Journal of Coastal Research*, Special Issue No. 70, pp. 029-034, ISSN 0749-0208.

Describing the physical drivers of water bodies plays an integral role in the marine environment. Lagrangian drifters are used to describe hydrodynamics, where tracking groups (clusters) of drifting floats is performed to determine the dispersion behaviour in the water. Using two types of Lagrangian drifters released in Moreton Bay, Australia, the dispersion behaviour is determined over the duration of a semi-diurnal spring tide cycle. A Self-Locating Datum Marker Buoy (SLDMB) was designed as the first drifter type. The second drifter (Small Drifter) was designed to be approximately half the size of the SLDMB. SLDMB and Small Drifter clusters were deployed for approximately 16hrs and 9-12hrs, respectively. Their trajectories and dispersion were influenced by the oscillating tidal current during the course of the drifter deployment, as well as fluctuating wind speed and direction. The Small Drifters exhibited a higher degree of dispersion than the SLDMBs; illustrating that the different drifter design had a significant impact on their susceptibility to wind induced shear dispersion – a consideration that all drogue based studies need to consider when interpreting results. A MIKE 3 model was used to assist with the investigation at hand using a dispersion coefficient of  $0.2\text{m}^2/\text{s}$ . The model required further adjustments with respect to tidal forcing and bathymetry resolution in order to enhance dispersion simulation.

**ADDITIONAL INDEX WORDS:** *Lagrangian drifter, dispersion, SLDMB, estuary.*

## INTRODUCTION

Coastal regions host unique environments that range from soft-shores to rocky shores, hilly or flat coastal plains, narrow or wide coastal shelves and a wide variety of wetlands. Among the wide variety of wetlands are shallow water environments known as estuaries. Estuaries act as the transition zone between rivers, land, and coastal oceans; providing habitats for a large diversity of marine life. These environments are commonly subject to processes such as planktonic larval distribution, discharged contaminants, and potentially harmful suspended sediment plumes. Analysing surface water dispersion provides very useful information; as it drives not only the flow field but also a lot of biological, chemical, and sedimentological constituents (Manley, 2010).

The analysis of Lagrangian dispersion in coastal environments has been extensively performed through many studies in order to investigate the trajectories of such various constituents. It has been proven that Lagrangian trajectory analysis is a very valuable tool when predicting the fate and origin of specific water masses (Jönsson et al., 2011). The data provided by trajectory analysis can be used to compute Lagrangian dispersion, delivering insight into the flow dynamics which is unforeseen when analysing Eulerian data (Sabet & Barani, 2011). In order to obtain such useful information from Lagrangian trajectories, methods have been implemented that practices the act of deploying surface tracers and

tracking their trajectory path.

Surface tracers need to be deployed in a manner that allows them to be carried by the surface current all the while tracking their geographic location. In theory, it is possible to compute the trajectories of drifting objects, with known shape and buoyancy, given the net result of the balance of forces acting on them from wind, surface currents, and waves (Zhang and Chan, 2003; Breivik & Allen, 2008). There are two main tracers commonly used in Lagrangian dispersion studies, surface drifters and fluorescent dye. Although tracking dye-patch growth is a valid method used for assessing water dispersion, solid floating objects are a lot easier to track both visually and with the aid of GPS units. With this in mind, the use of cleverly designed drifting floats deployed in the water has become a realistic option for measuring dispersion, commonly referred to as Lagrangian drifters.

Lagrangian drifters used in the water are floating instruments installed with different types of GPS devices, allowing the positions of the drifters to be retrieved after deployment or in real time. Since the early 1990's, evolutions of Lagrangian drifters have been made with the instrument float design and the equipment used to build them (Charria et al., 2012). For consideration during the design stage, drifters must be built with sufficient current following properties and therefore must be equipped with an effective drogue (Huhn et al., 2012). Tracking is performed using GPS satellite links for different types of drifters including Self-locating Datum Marker Buoys (SLDMB) (Marin & Delgado, 2007); or even small drifters made with basic materials such as PVC (Sabet & Barani, 2011). SLDMBs and small drifters



collect geographic displacement data over a specified time interval. In theory, windage and inertial forces should have a negligible effect on the drifters over time; as only a small portion of the drifters (casing where GPS units are contained) are exposed above the water surface (Sabet & Barani, 2011), and the portion of the drifter sitting above the water surface is highly aerodynamic. The data recorded from the drifters is then used to derive the dispersion behaviour of the water body. In order to calculate the dispersion characteristics of the drifters, the following equation can be used:

$$K = \frac{1}{4} \frac{\partial(\sigma_x \sigma_y)}{\partial t} \quad (1)$$

Where  $K$  is defined as the dispersion coefficient computed using the longitudinal ( $x$ ) and latitudinal ( $y$ ) cluster displacement variance,  $\sigma_x \sigma_y$ , of the drifters with respect to time,  $t$  (Tseng, 2002).

To assist with the dispersion study using Lagrangian drifters, a hydrodynamic model was used. Hydrodynamic models provide an administrative tool for decision making stakeholders to apply the right measures to restore endangered coastal environments (Zacharias & Gianni, 2008). Valuable information is produced from not only accurate results but also from the visual illustrations generated by the model output. The model used to assist with this study was MIKE 3; a 3D hydrodynamic model designed by the DHI Group. MIKE 3 is a generalised mathematical modelling system and is regularly applied to studies such as coastal circulation; water pollution; and environmental impact assessments (DHI Water & Environment, 2001). The system is based on the numerical solution of the 3D incompressible Reynolds-averaged Navier-Stokes (RANS) equations that are invoked with the hydrostatic pressure and Boussinesq assumptions. Many models are capable of reproducing state variables to within an order of magnitude, but most still need to be evaluated more intensively before their integrity can be verified (Lewis & Allen, 2009). The assessment of a hydrodynamic model begins with measuring physical factors that affect the hydrodynamics in the region of interest. For the study at hand, two types of Lagrangian drifters were used to spot check the dispersion modelling capability of a MIKE 3 model.

## METHODS

Quantifying dispersion in Moreton Bay estuary involved the use of two (2) types of Lagrangian drifters. A total of eight (8) drifters were deployed, four (4) for each type of drifter, at three (3) chosen locations with relatively unique spatial surroundings. The two types of drifters were deployed as two separate clusters from a research vessel during a semi-diurnal spring tide and their trajectory routes were tracked using GPS units. MIKE 3 was set up with a detailed domain map which included shoreline and bathymetric data as well as the wind and tide information. Results obtained from the drifters were to be spot checked against MIKE 3 to assess its capability when it comes to simulating dispersion.

## Study Site

Moreton Bay estuary is situated in southeast Queensland, Australia, just beyond the coastline of Queensland's capital city,

Brisbane. Brisbane has been the fastest growing city in Australia, with the highest population density occurring along the Brisbane River and major industrial ports occurring near the mouth of the river (Narayan & Pandolfi, 2010). This sub-tropical estuary is a large shallow embayment, ranging from depths of <1-50m, flanked by four large sand islands and contains several small islands (Chilvers *et al.*, 2005).

## Drifter Design

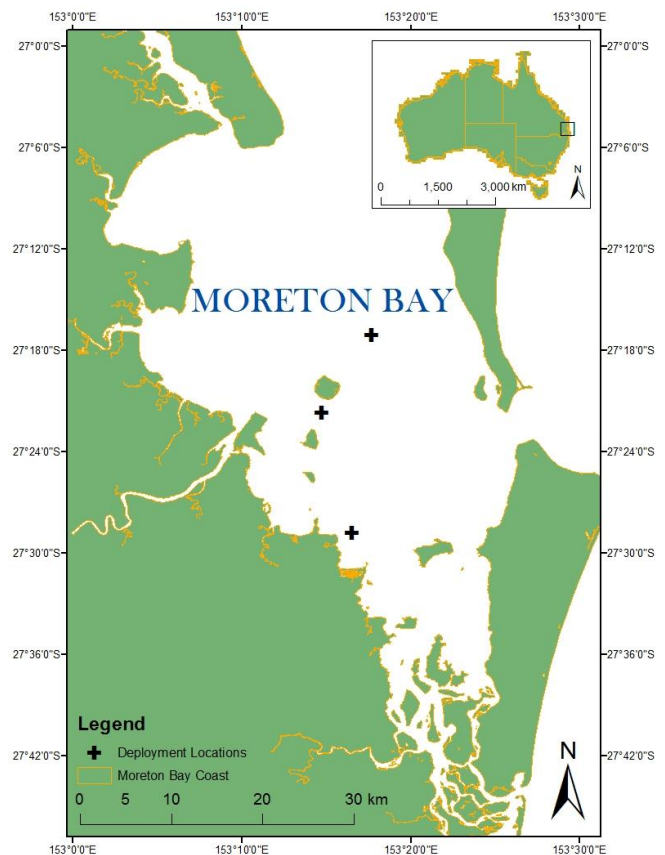


Figure 1. Map of Moreton Bay illustrating the three chosen locations for the drifters to be deployed.

Two different Lagrangian surface drifters were designed, constructed and used in this study: the SLDMB and Small Drifter. There were four (4) SLDMB drifters in total and these were large Self-Locating Datum Marker Buoys (SLDMB) built using strong aluminium materials for the frame (Figure 2a). The SLDMB was designed following a similar approach used by Poulain (1999), who designed drifters based on the Coastal Dynamics Experiment (CODE) study conducted in the early 1980's. A total of eight arms held four drag-producing vanes in place which acted together as a drogue for stability and control. A PVC container bolted to the top of the frame was used as water proof storage for the GPS unit. The GPS unit used for the SLDMB was the SPOT 2 Satellite GPS Messenger unit (Figure 2b) activated with the "Track Progress" feature, allowing the positions of the SLDMBs to be tracked in near real-time using Google Maps with a position fixing error of

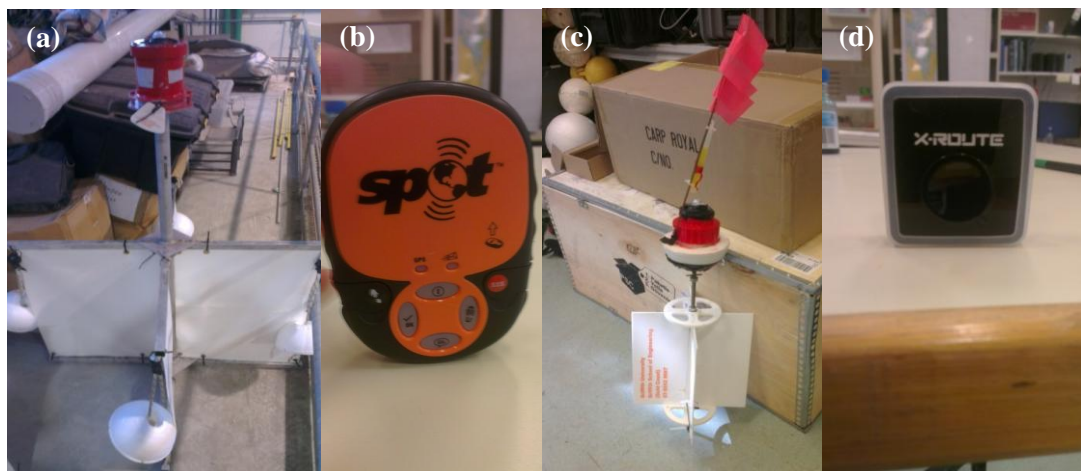


Figure 2. Self-Locating Datum Marker Buoy (a) tracked in near real-time using the Spot 2 Satellite Messenger (b). The Small Drifter (c) was tracked using the X-Route GPS (d) data logger.

~5m. For the Small Drifters, four (4) drifters were constructed and designed based on the SLDMB; however, the drifter was greatly reduced in size and more cost-effective materials were used (Figure 2c). For the GPS container, a small PVC union was capped at one end using high density plastic material and a pipe end cap sealed the other end. A threaded piece of rod was used to act as the spine of the drifter, allowing the rod to be screwed into the high density plastic end of the union. Two circular discs were used to hold in place four vanes at the top and bottom. The discs and vanes were laser cut and made entirely out of Perspex white acrylic. This smaller drifter was tracked using a simpler X-Route GPS data logger (Figure 2d), which logged the drifter's position throughout the duration of the deployment. Once each deployment was finished and the Small Drifters were retrieved the X-Route Manager software mapped their trajectory path using Google Maps with a position fixing error of ~25m.

### MIKE 3

The MIKE 3 domain map of Moreton Bay was generated using coastline data provided by the National Oceanic and Atmospheric Administration (NOAA) and bathymetry by Maritime Safety Queensland (Yu et al., 2013 a, 2013b). Predicted tidal heights provided by the DHI global tide model were used at the open boundaries in the domain (Figure 3). Wind conditions were accounted for using 1 minute datasets from the inner reciprocal marker wind station supplied by the Australian Bureau of Meteorology (BOM). Initial sea temperature and salinity data was described using satellite remote sensing observations provided by NASA and the Queensland Ecosystem Health Monitoring Program (EHMP). The "spin-up" period (time required for model to reach stable status) allocated for the model was one month and the trajectory started from rest with surface elevation and velocity set to zero. The dispersion was simulated using the MIKE 3 HD (Hydrodynamic) and PT (Particle Tracking) modules with a constant dispersion coefficient value of  $0.2\text{m}^2/\text{s}$ .

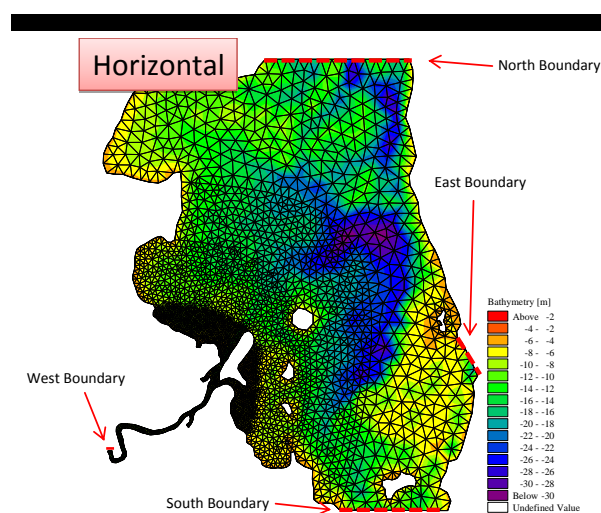


Figure 3. MIKE 3 horizontal spatial domain of Moreton Bay

### RESULTS

Field data obtained was used to quantify the dispersion behaviour of the two types of drifters. The physical drivers of their dispersion in Moreton Bay were evident. The tidal forcing had a significant effect on the fate of all the drifter trajectories as well as the dispersion behaviour. Evidence is illustrated using ArcMAP and a convex hull approach was implemented to exhibit both drifter types dispersion behaviour (Figure 4). Data was graphically presented using MATLAB for both the SLDMBs and Small Drifters. The dispersion coefficient ( $K$ ) was computed using linear regression of the displacement variance ( $\sigma_x\sigma_y$ ) shift after each recorded time step – 10min for the SLDMBs and 30min for the Small Drifters.

The trajectories of all the drifters from both the SLDMB cluster and Small Drifter cluster followed a very similar route as they all headed south-west in an anti-clockwise direction. The SLDMBs experienced very little dispersion until they were approaching peak high tide, where the drifters started to spread out; however, the largest amount of dispersion started to occur during the ebb tide. The Small Drifters experienced more dispersion than the SLDMBs before peak high tide and they also experienced more dispersion during the ebb tide.

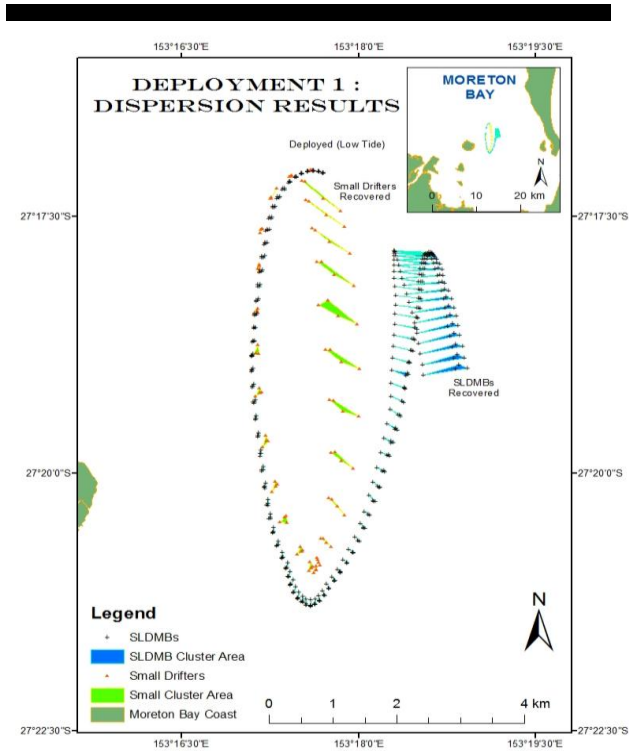


Figure 4. Trajectory paths and dispersion behaviour of the SLDMBs and Small Drifters at the first deployment location.

<b>Small Drifter deployment</b>	12hrs
<b>SLDMB deployment</b>	16hrs
<b>Tidal elevation</b>	0.2-2.5m
<b>Wind</b>	4-8m/s
<b>Surface current</b>	0-0.5m/s

Table 1. Deployment duration for each drifter type and physical driving conditions during deployment

The dispersion graphs reflect the behaviour illustrated in Figure 4, as the dispersion coefficient describes the dispersion “events” observed as the tide was approaching peak high and low (Figure 5a). A smaller spike is also observed just before the largest spreading starts to occur around the 9<sup>th</sup> hour. The gradual spreading is consistent with the maximum drifter distance and displacement variance, exhibiting a linear growth trend at the 9<sup>th</sup> hour before plateauing at ~14<sup>th</sup> hour (Figure 5b). On average, the Small Drifters revealed a greater value for the dispersion coefficient as well as a greater degree of fluctuation in comparison with the SLDMBs (Figure 5c). The dispersion coefficient shows a gradual increasing trend with the first peak related to the much quicker initial spread of the drifters before 2 hours. The second

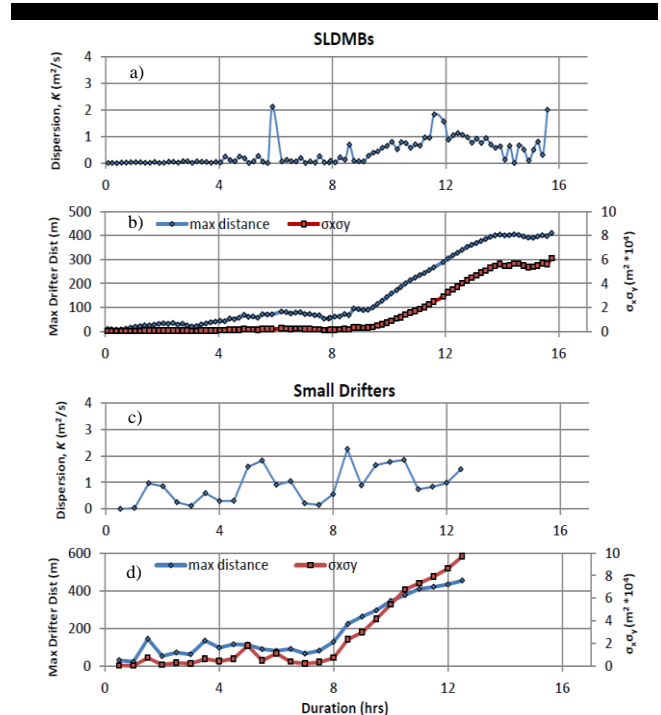


Figure 5. Dispersion and displacement variance of the SLDMBs and Small Drifters throughout the duration of the deployment

(larger) peak appears to be related to the drifters approaching high tide, and the greatest peak occurs just before the greatest spreading starts. The greatest spreading of the Small Drifters happened around the 8<sup>th</sup> hour (Figure 5d); ~1 hour earlier than the SLDMBs. Overall dispersion was greater than what was seen by the SLDMBs.

### SLDMBs vs. Small Drifters

Additional graphs were generated to help gain a better understanding of any relationships between the two different drifters. The drifters were different from one another with respect to their size, weight, materials, and GPS units used; however, both were designed based on the style used by Poulain (1999). Considering the SLDMBs and Small Drifters experienced very different dispersion behaviour, and consequently different values for their displacement variance and dispersion coefficient; they have been plotted together on the same graph in an attempt to identify similarities.

Figure 6 illustrates the dispersion and displacement variance for both the SLDMBs and Small Drifters over the deployment duration at the first location. The displacement variance of both drifters (Figure 6a) shows an obvious trend that they both share as the drifters spread out over time; however, the Small Drifters start spreading earlier. The Small Drifters clearly encounter a larger amount of dispersion and at a faster rate (Figure 6b). The dispersion coefficient for the Small Drifters is consistently higher than the SLDMBs until the last 1.5 hours where both clusters are closely correlating.

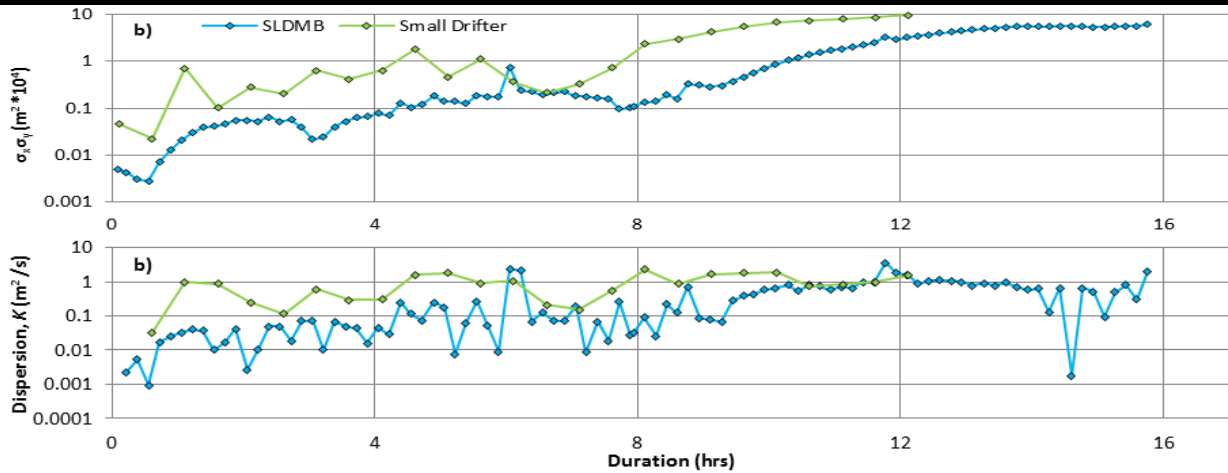


Figure 6. Dispersion behaviour comparison between SLDMBs and Small Drifters.

These analogies show that the Small Drifters were subject to greater dispersion than the SLDMBs the entire time. Both wind speed and direction were fluctuating during this trip, possibly causing chaotic Langmuir circulation (Li, 2000), which appears to be the cause for the larger amount of dispersion for the Small Drifters. Given their similar displacement variance trend, both drifters seem to be tidally dominated.

**MIKE 3 vs. Drifters**

The model results were compared by superimposing the dispersion results onto the map that illustrated the dispersion of the drifters at each location (Figure 7). The output results from the model produced point data for four particles (in this case hypothetical drifters) which were simulated for the duration the

drifters were in the water. Convex hulls were also used to represent the dispersion behaviour for the model results. The dispersion was overestimated for the first location during the first flood tide and, due to the steady nature of the dispersion simulated by the model, the dispersion did not increase during the ebb tide (as seen by the drifters). The difference in dispersion behaviour between the drifters and the model suggests that the dispersion coefficient of 0.2m<sup>2</sup>/s was insufficient. The model did not satisfy the amount of dispersion exhibited by both drifters, and therefore the dispersion coefficient value should be increased. The trajectory route simulation appears to be a flaw with the model, which may be caused by using tide information provided by the DHI global tide model.

Figure 8 reinforces the assumption that MIKE 3 better correlates with dispersion behaviour exhibited by the SLDMBs. Leading up to the 9<sup>th</sup> hour, both MIKE 3 and the SLDMBs experience *K* values around 0.1m<sup>2</sup>/s; whereas the Small Drifters experience values closer to 1m<sup>2</sup>/s. The mean and maximum dispersion values (Table 2) are larger than 0.1m<sup>2</sup>/s for the SLDMBs due to the increase after the 9<sup>th</sup> hour, reaching an average around 1m<sup>2</sup>/s.

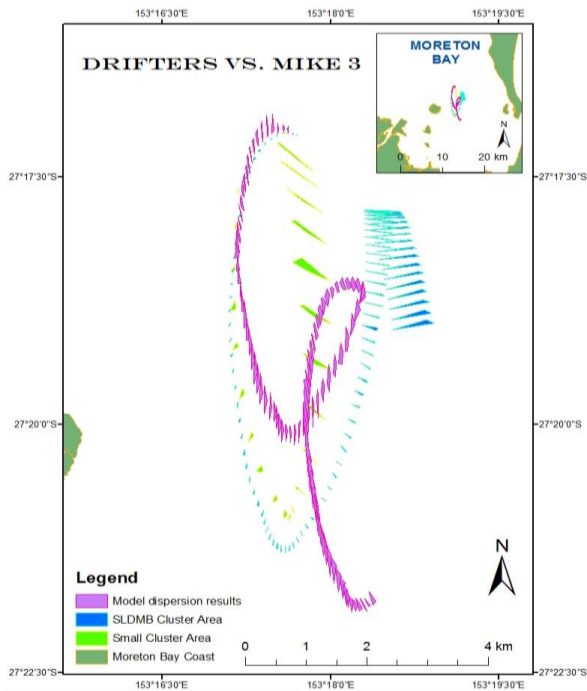


Figure 7. MIKE 3 dispersion and trajectory route compared to SLDMBs and Small Drifters

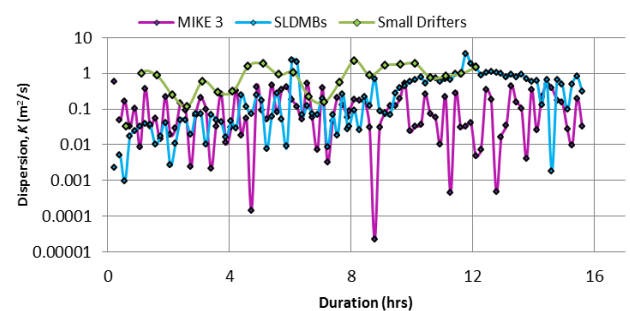


Figure 8. Dispersion showing a closer correlation with the SLDMBs

Table 2. Mean and maximum dispersion coefficient for MIKE 3, SLDMBs, and Small Drifters

Test	<i>K</i> mean	<i>K</i> max
MIKE 3	0.137	0.596
SLDMBs	0.414	3.54
Small Drifters	0.924	2.26

## CONCLUDING REMARKS

Two types of drifters were designed using a similar approach employed by Poulain (1999). In retrospect, it would have been ideal for the drifter designs to have been much more similar with respect to both the weight ratio and materials used. It would have been beneficial for the Small Drifters to have been made using the same cloth material for the vanes. Overall, the SLDMBs and Small Drifters clearly exhibited different dispersion behaviour. Results from this work highlights that drifters should be designed using well documented design regimes and any results need to be treated with great care. Further investigations should be performed to establish consistency with the dispersion and trajectory behaviour, including the impact of windage.

Adjustments to be made to MIKE 3 should certainly begin with developing a finer resolution spatial domain around the deployment locations. The model may benefit from using tidal predictions that are more accurate, which could potentially resolve issues associated with poor trajectory simulations.

## ACKNOWLEDGEMENT

David Spencer would like to thank the Griffith School of Engineering for funding the project and the staff for great support. The research presented in this paper was conducted through the Griffith School of Environment Honours Program which also assisted with funding and support.

## LITERATURE CITED

- Breivik, Ø. and Allen, A.A., 2008. An operational search and rescue model for the Norwegian Sea and the North Sea. *Journal of Marine Systems*, 69(1–2), 99–113.
- Charria, G., Lazure, P., Le Cann, B., Serpette, A., Reverdin, G., Louazel, S., Batifoulier, F., Dumas, F., Pichon, A. and Morel, Y., 2013. Surface layer circulation derived from Lagrangian drifters in the Bay of Biscay. *Journal of Marine Systems*, 109–110, S60–S76.
- Chilvers, B.L., Lawler, I.R., Macknight, F., Marsh, H., Noad, M. and Paterson, R., 2005. Moreton Bay, Queensland, Australia: an example of the co-existence of significant marine mammal populations and large-scale coastal development. *Biological Conservation*, 122, 559–571.
- DHI Water & Environment., 2001. MIKE 3 Estuarine and Coastal Hydraulics and Oceanography. *MIKE 3 Short Description Manual*
- Huhn, F., von Kameke, A., Allen-Perkins, S., Montero, P., Venancio, A. and Pérez-Muñuzuri, V., 2012. Horizontal Lagrangian transport in a tidal-driven estuary—Transport barriers attached to prominent coastal boundaries. *Continental Shelf Research*, 39–40, 1–13.
- Jönsson, B.F., Döös, K., Myrberg, K. and Lundberg, P.A., 2011. A Lagrangian-trajectory study of a gradually mixed estuary. *Continental Shelf Research*, 31, 1811–1817.
- Lewis, K. and J.I. Allen., 2009. Validation of a hydrodynamic-ecosystem model simulation with time-series data collected in the western English Channel. *Journal of Marine Systems*, 77, 296–311.
- Li, M., 2000. Estimating Horizontal Dispersion of Floating Particles in Wind-driven Upper Ocean. *Spill Science & Technology Bulletin*, 6, 255–261.
- Manley, T.O., 2010. Hands-on oceanography: Drifters, drogues, and circulation. *Oceanography*, 23, 165–171.
- Marín, V.H. and Delgado, L.E., 2007. Lagrangian observations of surface coastal flows North of the Humboldt Current system. *Continental Shelf Research*, 27, 731–743.
- Narayan, Y.R. and Pandolfi, J.M., 2010. Benthic foraminiferal assemblages from Moreton Bay, South-East Queensland, Australia: Applications in monitoring water and substrate quality in subtropical estuarine environments. *Marine Pollution Bulletin*, 60, 2062–2078.
- Poulain, P.M., 1999. Drifter observations of surface circulation in the Adriatic Sea between December 1994 and March 1996. *Journal of Marine Systems*, 20, 231–253.
- Sabet, B.S. and Barani, G.A., 2011. Design of small GPS drifters for current measurements in the coastal zone. *Ocean & Coastal Management*, 54, 158–163.
- Tseng, R.S., 2002. On the Dispersion and Diffusion Near Estuaries and Around Islands. *Estuarine, Coastal and Shelf Science*, 54, 89–100.
- Yu, Y., Zhang, H. and Lemckert, C., 2013a. Seasonal variations of the salinity and turbidity in the Brisbane River estuary, Queensland, Australia. *Journal of Coastal Research*, Special Issue No. 65, pp. 1253–1258, ISSN 0749-0208.
- Yu, Y., Zhang, H. and Lemckert, C., 2013b. Numerical analysis on the Brisbane River plume in Moreton Bay due to Queensland floods 2010–2011. *Environmental Fluid Mechanics*, 1–24.
- Zacharias, I. and Gianni, A., 2008. Hydrodynamic and dispersion modeling as a tool for restoration of coastal ecosystems. Application to a re-flooded lagoon. *Environmental Modelling & Software*, 23, 751–767.
- Zhang, H. and Chan, E., 2003. Modeling of the turbulence in the water column under breaking wind waves. *Journal of oceanography*, 59, 331–341.

# Monitoring of High Waves and Tsunami using HF Ocean Radar in the East Coast of Korea

Jinsung Seo<sup>†</sup>, Bumshick Shin<sup>††</sup>, Kyuhan Kim<sup>†††</sup>

<sup>†</sup> Department of Civil Engineering,  
Kwandong University, Gangneung,  
Korea  
popodong83@nate.com

<sup>††</sup> Waterfront and Coastal Research  
Center, Kwandong University,  
Gangneung, Korea  
sbs114@kd.ac.kr

<sup>†††</sup> Department of Civil Engineering,  
Kwandong University, Gangneung,  
Korea  
kkhkim@kd.ac.kr



[www.cerf-jcr.org](http://www.cerf-jcr.org)



[www.JCRonline.org](http://www.JCRonline.org)

## ABSTRACT

Jinsung Seo, Bumshick Shin, Kyuhan Kim, 2014. Monitoring System of High Waves and Tsunami using HF Ocean Radar in the East Coast of Korea, *Proceedings 13<sup>th</sup> International Coastal Symposium* (Durban, South Africa), *Journal of Coastal Research*, Special Issue No. 70, pp. 035-040, ISSN 0749-0208.

The east coast of Korea is exposed to the danger of tsunamis because it is contiguous to Japan. Damages took place in the region when tsunami occurred in the west of Japan in 1986 and 1993. Fear of the destruction caused by has increased following the 2011 Great Tsunami of Japan. The west coast of Japan embodies many high tsunami risk areas where tsunami may be triggered by earthquakes. As no earthquake has ever occurred there, these high risk areas contain high amount of potential energy. Furthermore, frequent high waves due to climate change have become one of the major factors with respect to coastal structure damage, beach erosion and various coastal disasters along the shoreline. In order to make a counterplan for coastal disaster, precise analysis of the high wave characteristics, through continuous monitoring, is essential. In this study, continuous long-term observation is implemented with an Ocean Radar. Ocean Radar conducts remote observation equipped with ground-based radars which enable series of simultaneous observations of extensive range of the coast with high frequency. Ocean Radar for continuous long-term observation is operated at Samcheok on the east coast of Korea. Samcheok has experienced tsunami damage in previous years and is where a nuclear power plant is located. In order to examine the reliability of the Ocean Radar, a pressure-type wave gauge, ultrasonic wave gauge, and ocean buoy are installed for data comparison and verification. The Ocean Radar used in this study is an array-type HF-RADAR named WERA (Wave RADAR). Data analysis of the continuous long-term observation verifies more than 90% of the wave data collected within 25km range from the center of two sites. Only less than 1% of the entire observation is unmeasured by time series analysis, but data from other wave gauges show similar features. Moreover, a comprehensive monitoring system supported by such observations is developed for the public for internet based real-time reports on waves and currents.

**ADDITIONAL INDEX WORDS:** *Ocean Radar, WERA, High Waves, Tsunami*

## INTRODUCTION

Korea has been confronting coastal structure damages by typhoon, storm surges, and high waves. And the east coast of Korea has experienced direct damages from Japanese tsunamis in 1986 and 1993 occurred in the west coast of Japan. The concern of massive destruction in the east coast of Korea has been arising after the 2011 Great Tsunami of Japan.

In order to hedge against coastal disasters, clear understanding of the external forces which trigger the natural disaster is necessary. Precise analysis is particularly essential for the east coast of Korea for its high waves and contiguous location to Japan.

Previous wave height measurement at coastal area has been using ocean buoys for deep ocean and ultrasonic or pressure-type wave gauges for shallow ocean. However, such observation is considered as a point measurement limited to target area, a comprehensive analysis of area measurement is unfeasible.

Therefore, an array-type HF-RADAR named WERA is

implemented for area measurement and consecutive wave observation. This study is the first to introduce and implement the WERA system in Korea.

The HF-RADAR used in this study was developed by Gurgel et al. in 1995 and it has been actively utilized at many sites for wave and current observations after 2000. In recent years, five HF-RADARs located in Hokkaido monitored the 2011 Great Tsunami by detecting a 9.0 scale earthquake in Sendai, Japan (Belinda Lipa et al, 2011).

The HF-RADAR ocean wave monitoring system utilizes the principle of the refraction and reflection of the electromagnetic waves against the conductive ocean surface. The system analyzes the electromagnetic signals transmitted via antenna (Figure 1). The

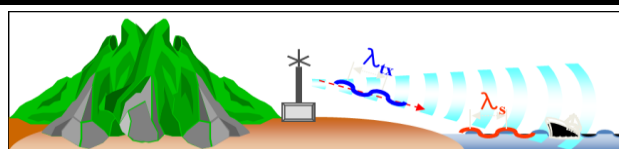


Figure 1. Performance property of Ocean Radar

electromagnetic signals are classified according to spectrum: First Order Peak and Second Order Return (Figure 2).

WERA enables high-resolution monitoring over extensive range. The high resolution system determines cell sizes from 300 m to 3km in distance and its data collection runs from 0.5sec to 10 min intervals with a time integration analysis for every 10 min.

WERA is a remote monitoring system based on internet making real-time adjustments for prevailing conditions possible. Also, the ground-based installation of WERA enables long-term observations without the risk of high wave damage.

In this study, the applicability of HF-RADAR is reviewed through the data collected from actual sites. The optimal installation sites are determined with the consideration of radio wave transmitting environment for 23~25 MHz. Ultrasonic wave gauges are also installed at the sites for the reliability verification of the HF-RADAR data.

## STUDY AREA AND FACILITY

### Study Area

The Samcheok City, Gangwondo is selected as the study area. Samcheok, located in the east coast of Korea, is famous for high waves and a nuclear power plant. The city experienced few natural disasters in the past, but is growing quickly with major development plans and constructions. Therefore, a monitoring system in the study area is unconditional.

The installation sites of WERA are determined with the optimal radio-wave transmitting environment, for data reliability, in mind. For proper HF-RADAR installation and use, the study environment must be examined with various factors such as accessibility and future development plan.

Four potential sites are selected based on geological conditions (Figure 3) and radio-wave transmitting environment examination is executed. SDR (Software Defined Radio)-IQ scanner is utilized for the examination for its convenient use.

In the examination, simulations of each installation sites are conducted in regards of 120° observation range of the RX antenna.

The devices are installed at the potential sites for radio-wave transmission verification. The HF-RADAR frequency of 24 MHz is tested twice, with maximum bandwidth of  $\pm 1$  MHz in 0.19 MHz intervals. The results of two frequency tests show no radio-wave interference at all potential sites.

Two sites, Imwon Harbor and Hujung Beach, are finalized as the installation sites by reviewing the feasibility, adaptability, and maintenance of radars.

The Ocean Radars operated in the subject area use 24.525 MHz frequency band. The azimuths of center beam at Imwon Harbor (Site A) and Hujung Beach (Site B) are 95.8° and 37.3° respectively with range of  $\pm 60^\circ$  from the central angle.

Each site has 30-minute cycle of wave and current data: wave data of max 27 km and current data of max 48 km. The bandwidth of 150 kHz is applied for 1 km lattice spacing resolution.

Figure 4 shows the range of Ocean Radar observation. Figure 5 indicates the azimuths of radars and the positions of RX & TX antennas.

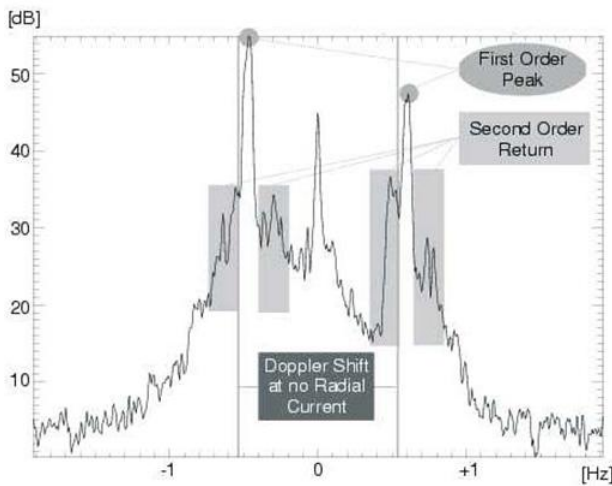


Figure 2. Doppler spectra in a Ocean Radar(Gurgel et al., 2006)

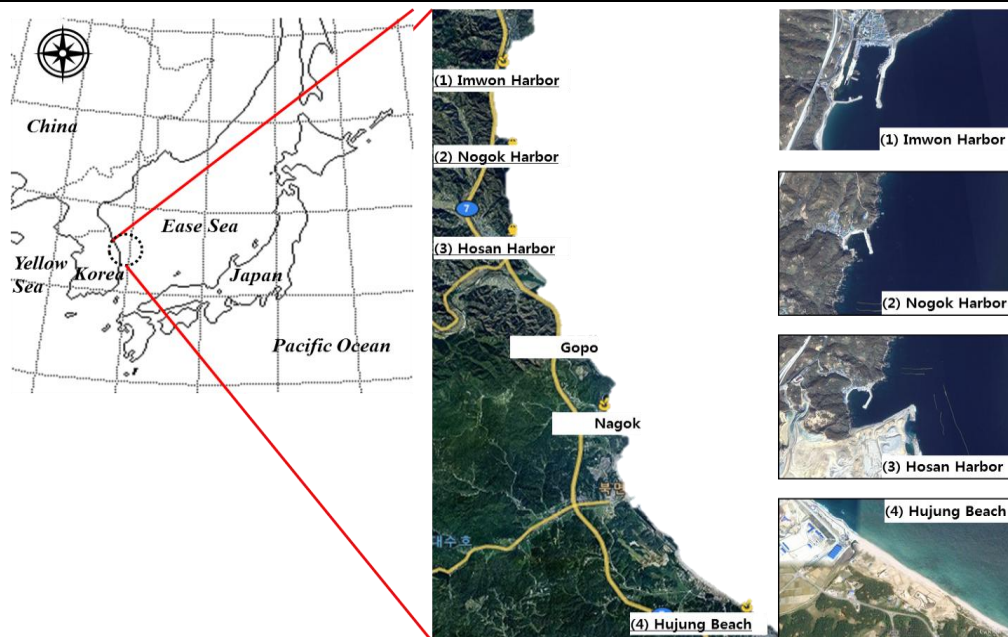


Figure 3. Study Area for Ocean Radar installation

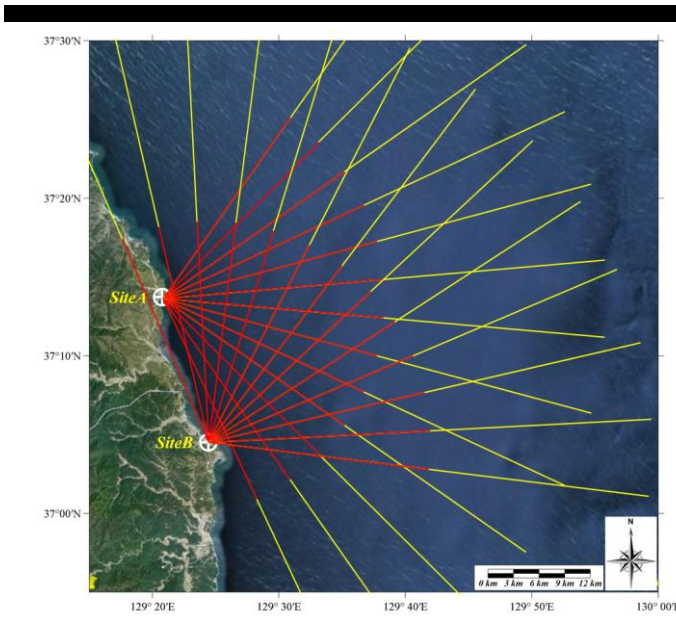


Figure 4. Monitoring Points and Range

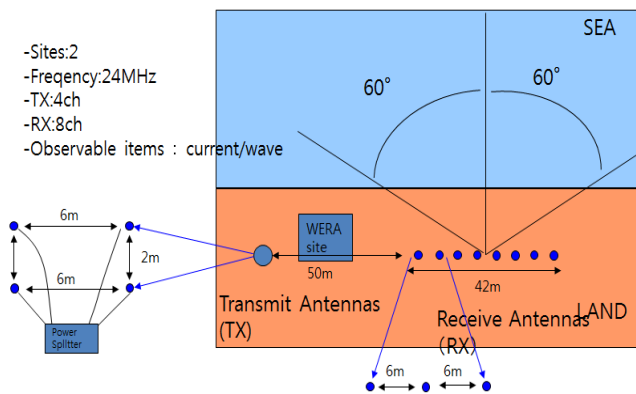


Figure 5. Installation of Ocean Radar



Figure 6. Facility of Ocean Radar

**Facility: Ocean RADAR (HF-Radar)**

Currently, HF-RADAR is manufactured in Germany, Japan and America. An array-type WERA (WavE RADar) is selected for this

study after thorough review with other devices. It was developed by a German company, Helzel, in 2000 and uses a frequency band of 24.525 MHz. WERA, used in this study, employs an 8-channel system composed of 4 transmitters and 8 receivers.

The devices needed for Ocean Radar installation (Figure 6) include: antennas, control server, GPS Receiver, and accessories. In particular, TX-SAT is a long-distance wireless antenna which has not been used previously anywhere in the world. The real time data of wave height and ocean circulation acquired by HF-RADAR can be browsed via web. The observed data (current, wave, wind) can be searched by time basis (UTC-base) that efficiency of the data is anticipated to increase in the future.

**WAVE MONITORING**

**Field Data Verification**

Figure 7 shows WERA data at the study areas: Site A (Imwon Harbor in Samcheok City, Gangwondo) and Site B (Hujeong Beach in Jukbyounmyoun, Uljngun). For quantitative analysis of WERA performance, the data acquisition rate for 15 days from July 30 to August 13, 2012 is calculated (Figure 8). The acquisition rate shows 95% of data are collected within 24km range and 90% within approximately 27km range from the centre of each site.

HF-RADAR observation requires data combination of at least two sites because RADIAL from a single site lacks the directions of currents and waves. RADIAL data overlapped in a straight-line is considered the least reliable, however RADIAL in perpendicular the most reliable.

Moreover, validity verification of the data by Ocean Radar is conducted by correlation coefficient analysis with AWAC (Acoustic Wave and Current Profiler), an ultrasonic wave gauge, data. The AWAC is installed at high GDOP (Geometric Dilution Of Precision) area because the extreme ocean depth in the east coast of Korea limits to 5km range from shoreline. The significant wave heights from WERA and AWAC are collected from Dec 2012 to Jan 2013 for correlation coefficient analysis. The principal component analysis of WERA and AWAC are indicated in Figure 10. Figure 10(a) indicates the significant wave-height observed by AWAC, 33% higher than that of HF-RADAR with tropic slope of 1.33. With 0 intercept and 18cm RMS deviation, the correlation coefficient is 0.87, a high correlation. Figure 10(b) indicates the significant wave-height observed by AWAC, 40% higher than that of HF-RADAR with tropic slope of 1.4. With 0 intercept and 19cm RMS deviation, the correlation coefficient is 0.84, again a high correlation.

**Long-term and Continuous Wave Monitoring**

The validity of WERA data is confirmed through reliability verification of HF-RADAR data to ultrasonic wave gauge data. The continuous wave monitoring data by WERA is shown in Figure 11.

During the consecutive observation period of 15 months, the significant wave-heights are in 1m~6m range with 10~15sec frequency when monitored in the high accuracy observation area of 24km range. Table 1 is a summary of the significant wave-heights observed during the period.

The analysis also reveals high swell waves of 5.95 meters with 14.7 sec wave period measured at around 13 hours on April 3, 2012. It suggests a new notion of spring high waves in which previous studies are confined to those in summer or winter.



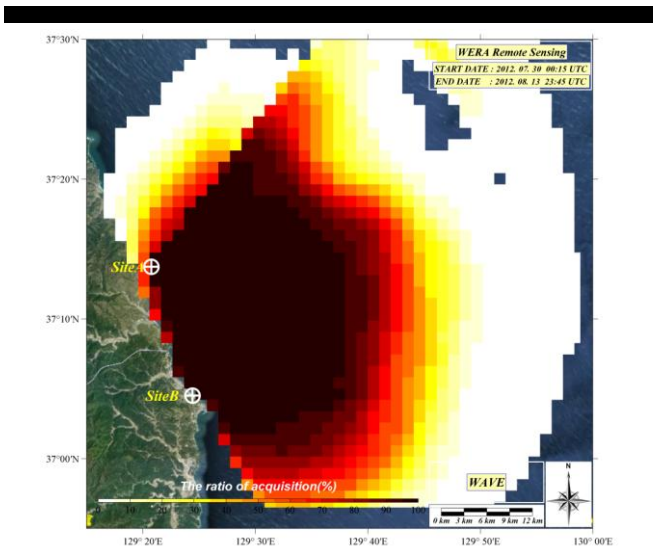


Figure 7. Acquisition of Ocean Radar Data

is calculated (Figure 8). The obtaining rate shows 95% of data acquisition within 24km range and 90% within approximately 27km range from the center of each site.

HF-RADAR observation requires data combination of at least two sites because RADIAL from a single site lacks the directions of currents and waves. RADIAL data overlapped in a straight-line is considered the least reliable but RADIAL in perpendicular the most reliable.

### CONCLUSION

This study is the first to introduce, implement, and utilize an array-type HF-RADAR in Korea for consecutive wave observation over extensive range of area.

The two installation sites of Ocean Radar are determined regarding the optimal radio-wave environment for 23~25MHz, installation and maintenance conditions, and surrounding factors.

The HF-RADAR data is compared to that of ultrasonic wave gauge for reliability and validation.

The data obtaining rate in winter shows 95% in 24km range and 90% in 27km range. Moreover, the correlation coefficient between Ocean Radar and ultrasonic wave gauge is 0.84~0.87 that the data has relatively high correlation and considered reliable.

### ACKNOWLEDGMENT

This research was partly supported by Manpower Development Program for Marine Energy and by MOF(Ministry of Oceans and Fisheries) and the RIC program of MOTIE (Ministry of Trade, Industry and Energy Republic of Korea).

### REFERENCES

- Barrick, D.E., 1972. Remote sensing of sea state by radar, In: Derr V.E., (ed.) *Remote Sensing of the Troposphere*, U.S. Govt. Printing Office, Washington, DC.
- Barrick, D.E., 1977. Extraction of wave parameters from measured HF sea echo Doppler spectra, *Radio Science*, 12, 415-424.
- Barrick, D.E., 1979. A coastal radar system for tsunami warning, *Remote Sensing of the Environment*, 8, 353-358.
- Crombie, D.D., 1955. Doppler spectrum of sea echo at 13.56 Mc/s, *Nature*, 175, 681-682.
- Graber, H.C. and Heron, M.L., 1997. Wave height measurements from HF radar, *Oceanography*, 10, 90-92.
- Gurgel, K.W., Antonischki, G., Essen, H.H., and Schlick, T., 1999. Wellen Radar (WERA), a new ground-wave based HF radar for ocean remote sensing, *Coastal Engineering*, 37 (3-4), 219-234.
- Gurgel, K.W., Essen, H.H., and Schlick, T., 2006. An Empirical Method to Derive Ocean Waves from Second-Order Bragg Scattering - Prospects and Limitations, *Journal of Oceanic Engineering*, 31 (4), 804-811.
- Heron, S.F. and Heron, M.L., 1998. A comparison of algorithms for extracting significant wave height from HF radar ocean backscatter spectra. *J Atmospheric and Oceanic Technology*, 15, 1157-1163.
- Heron, M.L. and Prytz, A., 2002. Wave height and wind direction from the HF Coastal Ocean Surface Radar.
- Helzel, T., Hansen, B., Kniephoff, M., Petersen, L., and Valentin, M., 2013. "Ocean Radar for Monitoring of Coastal Zones – new aspects after getting a worldwide frequency allocation for these instruments", *Journal of Coastal Research*, Special Issue No. 65
- Helzel, T., Kniephoff, M., Petersen, L., Mariette, V., and Thomas, N., 2011. Accuracy and reliability of ocean radar WERA in beam forming

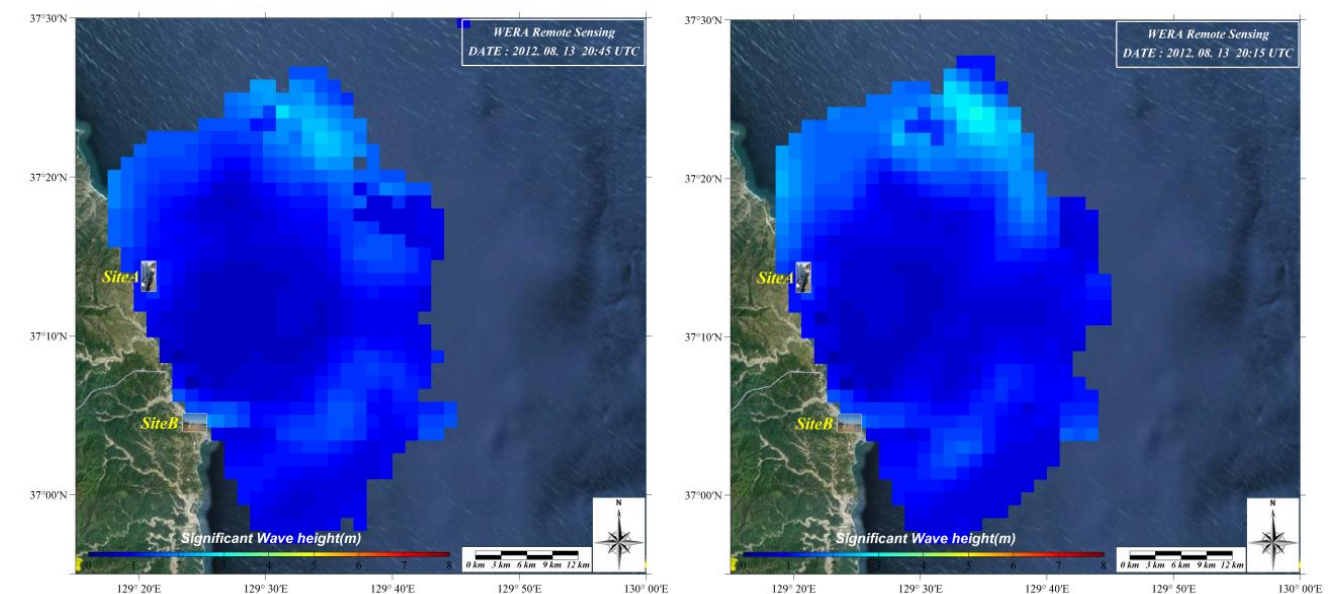


Figure 8. Wave Monitoring Results from Ocean Radar

or direction finding mode, pp.21 – 24, Current, Waves and Turbulence Measurements (CWTM).

Lipa, B., 2013. Japan Tsunami Current Flows Observed by HF Radars on Two Continents, *Remote Sensing*, 3 (8), 1663-1679

Wyatt, L.R. and Holden, G.J., 1994. HF radar measurement of multimodal directional wave spectra. *Global Atmosphere and Ocean System*, 2, 265-290.

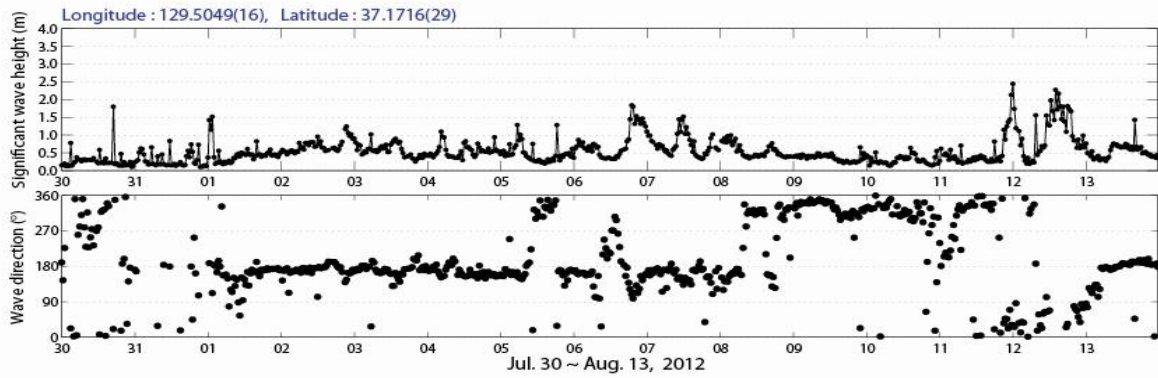


Figure 9. Time Series of Wave Monitoring (2012.7.30. ~ 2012. 8. 13)

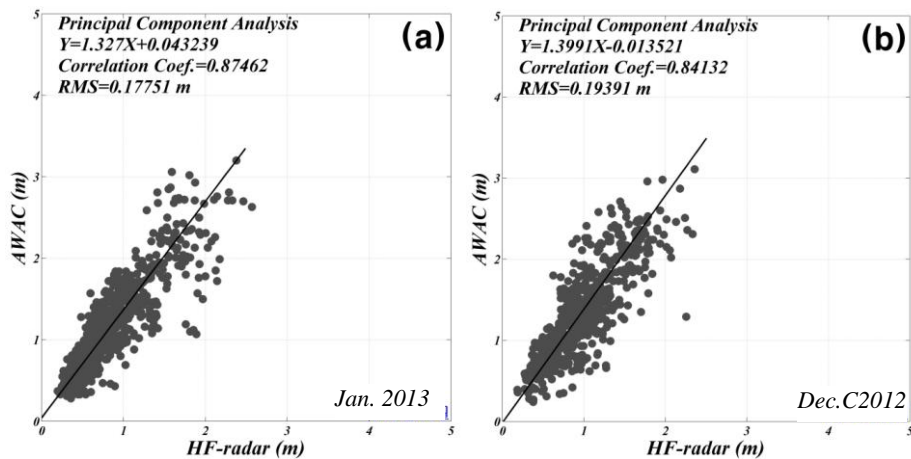


Figure 10. Correlation coefficient analysis results between Ocean Radar and AWAC

Table 1 Results of Wave Data(Range)

Duration(2012)	Significant Wave Height(m)	Significant Wave Period(sec)	Duration(2013)	Significant Wave Height(m)	Significant Wave Period(sec)
2012. 3. 12-13	2 ~ 5	10 ~ 13	2013. 1. 15-16	1 ~ 3	10 ~ 14
2012. 4. 03-04	2 ~ 6	12 ~ 15	2013. 1. 17-18	1 ~ 2	10 ~ 11
2012. 4. 19-20	2 ~ 4	10 ~ 15	2013. 1. 27-28	1 ~ 2	10 ~ 13
2012. 7. 14-15	1 ~ 3	11 ~ 13	2013. 2. 08-09	1 ~ 2	10 ~ 14
2012. 10. 11-13	1 ~ 2	10 ~ 12	2013. 3. 02-03	1 ~ 2	10 ~ 14
2012. 11. 01-03	1 ~ 3	10 ~ 12	2013. 3. 13-14	1 ~ 2	10 ~ 11
2012. 12. 06-07	1 ~ 3	10 ~ 11	2013. 4. 07-08	1 ~ 4	10 ~ 13
2012. 12. 11-12	1 ~ 2	10 ~ 12	2013. 5. 01-02	1 ~ 2	10 ~ 11

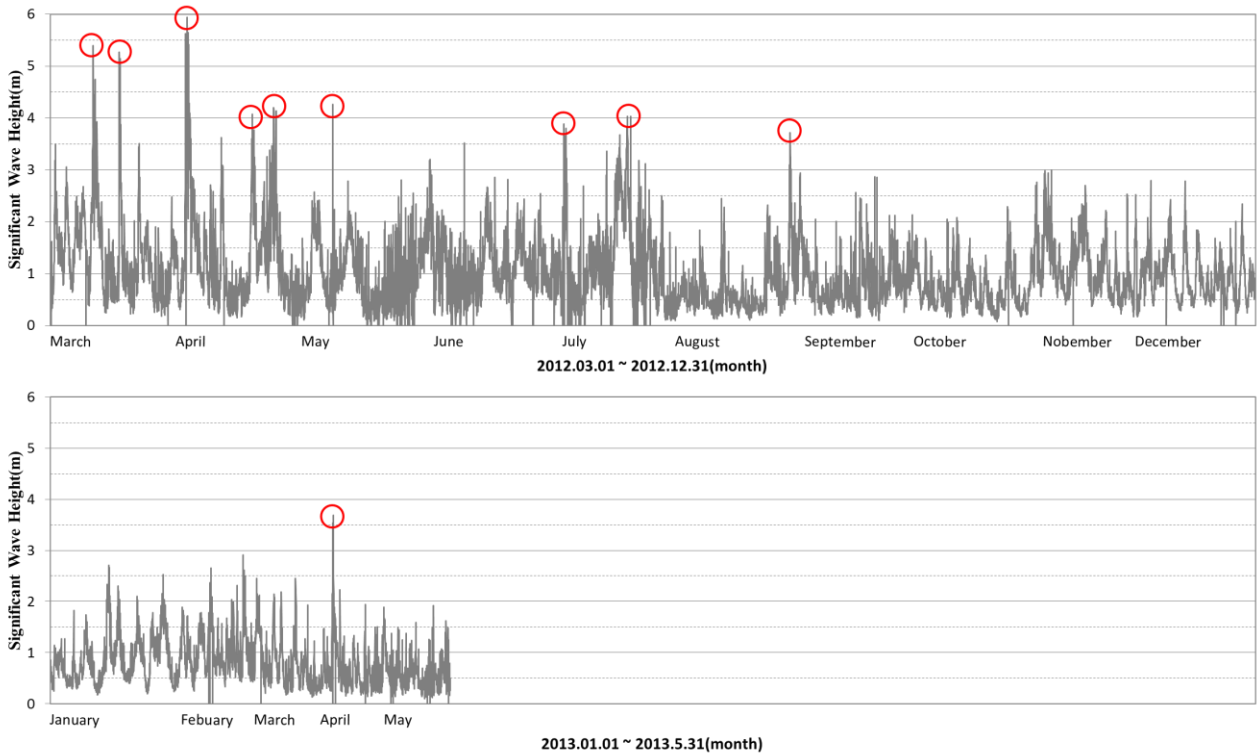


Figure 11. Time Series of WAVE Monitoring (2012.7.30. ~ 2012. 8. 13)

# Impact of detached breakwaters on shoreline evolution: a case study on the Portuguese West Coast

Maria A.V.C. Araújo†, Silvia D. Bona‡, António Trigo-Teixeira†

†CEHIDRO, Instituto Superior Técnico,  
Universidade de Lisboa, Av. Rovisco Pais 1,  
1049-001 Lisbon,  
Portugal  
amelia.araujo@tecnico.ulisboa.pt  
trigo.teixeira@tecnico.ulisboa.pt

‡ICEA Department  
University of Padova  
Via Ognissanti, 39  
35129 Padova  
Italy  
silviadibona8@gmail.com



[www.cerf-jcr.org](http://www.cerf-jcr.org)



[www.JCRonline.org](http://www.JCRonline.org)

## ABSTRACT

Araújo, M.A.V.C., Di Bona, S., Trigo-Teixeira, A., 2014. Impact of detached breakwaters on shoreline evolution: a case study on the Portuguese west coast. In: Green, A.N. and Cooper, J.A.G. (eds.), *Proceedings 13<sup>th</sup> International Coastal Symposium* (Durban, South Africa), *Journal of Coastal Research*, Special Issue No. 70, pp. 041-046, ISSN 0749-0208.

The Portuguese West Coast is facing severe erosion problems that threaten both the population and the immediate seaside properties. Some locations, such as the Vagueira region, are especially vulnerable. In an attempt to reverse the present erosional trend, a coastal defense scheme involving two detached breakwaters was introduced in a phased manner. In this work, the impact of those two detached breakwaters on the down-drift coast is investigated. The study area extends from south of the Costa Nova village southwards to Mira. The shoreline evolution is predicted, for various decades, using the GENESIS model. The present time shoreline position, from which future situations are predicted, was obtained using LIDAR data acquired in 2011. Two different future scenarios are investigated: the 'do-nothing' scenario, which assumes that no further engineering interventions will be performed on the coast; and the 'detached breakwaters protected' scenario, with the first breakwater introduced in 2011 and the second in 2026. Depending on sediment supply, two types of simulations are carried out: calibrated simulations, which assume that the amount of sediments in the future will be equal to those in the present situation; and extreme simulations, which assume an acute shortage in sediment supply. Results show that if no further interventions are executed at the Vagueira region, the entire coastal stretch will continue to erode, which could lead to extreme consequences in some locations, depending on sediment supply. If two detached breakwaters are introduced at different intervals, a new accreting trend is predicted at the Vagueira region, reversing the present erosional phase. However, the erosional trend will continue southwards, unless a 3<sup>rd</sup> detached breakwater is introduced in Mira.

**ADDITIONAL INDEX WORDS:** *coastal erosion, shoreline prediction, shoreline retreat, sediment shortage, GENESIS model, LIDAR data.*

## INTRODUCTION

With climate change it is fundamental to understand and predict coastal geomorphological changes in order to assess erosion risks, loss of territory and flooding. This knowledge will be crucial in developing sustainable coastal management solutions. From the beginning of the 20<sup>th</sup> century, human interference regarding shoreline evolution has become increasingly important due to the construction of defense structures such as seawalls, breakwaters or groins. Those structures interfere with the natural sediment flux, and may lead to coastal erosion, especially on sandy coasts (Gomes *et al.*, 1981). The way in which shorelines develop is also dictated by waves and currents. It is crucial to understand how littoral material moves for effective future coastal management. Several factors should be taken into account when measuring the geomorphological evolution of a stretch of coastline, such as the forcing and controlling mechanisms, pre existing conditions and the nature and composition of the coast. However, given the great variability of coastal processes, assessing whether or not there will be erosion or accretion is still a difficult issue to predict confidently over time (Hanson and Kraus, 1989).

At present, there is a trend for shorelines to retreat in many places of the world, related to erosion problems (Matteucci *et al.*, 2010). The Portuguese West Coast is heavily affected by high wave energy from the Atlantic Ocean, and some regions are particularly vulnerable to erosion. Human intervention has attempted to limit shoreline retreat, however it has been verified that, by disrupting longshore sediment transport, the stretches located further down-drift of the constructions became depleted in sediment and landward retreat rates increase locally. Longshore sediment transport takes place essentially within the surf zone, parallel to the coast, controlling beach morphology (Cooper and Pilkey, 2004) and can be interrupted by the construction of jetties or breakwaters; otherwise sediments can be trapped by inlets and submarine canyons (USACE, 2002). This emphasizes the idea that shore protection works, which are usually very expensive, do not always lead to satisfactory results (Gomes *et al.*, 1981).

In this work, the impact of the introduction of two detached breakwaters on the shoreline evolution of the Portuguese West Coast is assessed. A conceptual model to predict the long-term shoreline evolution is developed and an analysis of the coastal geomorphological change is performed, for a stretch of coast in the Vagos and Mira Municipalities (Figure 1). In addition, the

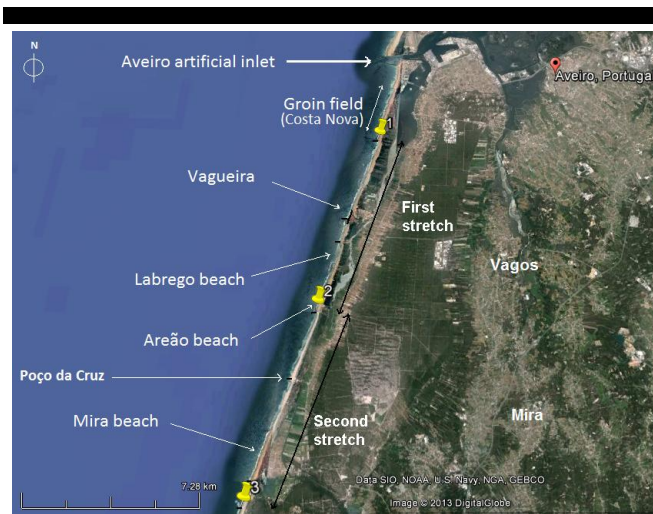


Figure 1. Study domain (adapted from Google Earth (2012)).

impact of past coastal management interventions on coastal geomorphological behavior is evaluated. This stretch of the coast is characterized by a rough wave climate, a strong potential littoral transport of sediments and a heavy erosional process.

The net littoral sediment transport is directed from north to south due to the prevailing northwesterly wave climate (Gomes *et al.*, 1981; Talbi *et al.*, 2008; Di Bona, 2013). The modeling of the shoreline evolution is performed using the GENESIS model (Hanson and Kraus, 1989) which, despite its shortcomings (Young *et al.*, 1995), is widely used by the coastal engineering community to simulate long-term shoreline evolution in places with spatial and temporal differences in longshore sediment transport (Hanson, 1989).

This work is a follow-up to a previous study carried out by Di Bona (2013). In that study, modeling of coastal evolution at Vagueira region was performed for the “First stretch” represented in Figure 1. This is one of the most vulnerable regions on the Portuguese coast, located south of the Aveiro lagoon, from south of Costa Nova village up to Areão beach. The main goal of that work was to investigate a coastal defense scheme to reverse the present erosional trend at the Vagueira region, without causing adverse effects on the down-drift area. The idea of introducing two detached breakwaters parallel to the present shoreline, as a solution for shore protection, was thus studied. However, further studies extending the domain southwards were recommended. Questions were raised regarding their impact on the down-drift coast, thus, the present work investigates that impact, extending the study domain southwards to Mira (“Second stretch” in Figure 1).

## METHODS

As previously mentioned, this work builds on a prior study, following the same methodology, using the same input data (except bathymetric/topographic data near the coastline) and investigating the same possible future scenarios. More detailed information is found in Di Bona (2013).

### Study Domain

The study area extends from south of Costa Nova village to Mira, and includes both stretches shown in Figure 1. The first is 9.2 km long and the second 9.8 km long. In this figure, defense structures present along the 19 km stretch of coast are represented

as small black lines corresponding to 7 groins and a seawall. From north to south: the first groin is located south of Costa Nova village (called the Vagueira north groin); followed by the seawall and a groin at Vagueira region (Vagueira groin); the other groin is located at Vagueira south, close to Labrego beach, and is called the Vagueira south groin; the next one is at Areão beach (curved groin 1); then the curved groin 2 at Poço da Cruz beach; and finally 2 groins located in Mira beach (Mira 1 groin and Mira 2 groin). These structures are also represented in Figure 2. The curved groins were built in an L shape with the purpose of, on the one hand, allowing sediment to accumulate up-drift and, on the other hand, allowing a certain degree of bypassing.

This stretch of the coast is especially vulnerable due to its sandy nature and low-lying lands (Coelho *et al.*, 2011), thereby endangering the urban waterfronts. At present Vagueira village is suffering with marked coastal erosion. Moreover, Vagueira region is located on the very narrow sand spit of the Aveiro lagoon and with shoreline retreat the prospect of barrier breaching is increasing. A recent occurrence of breaching took place on the 3<sup>rd</sup> of November 2011 during a storm event at Labrego beach during which the waters flooded the agricultural fields and breached the lagoon. This is a huge concern for the local authorities due to the economic and environmental impacts.

Since the beginning of the Aveiro artificial inlet opening, in 1808, adverse effects were immediately noted to the south of the inlet (Gomes *et al.*, 1981). The mean recession of the beach for the period between 1958 and 1978 was around 150 m, as shown in Figure 3. This figure also shows how the erosion process extended southwards. The construction of two long jetties, in the fifties, had also a strong negative impact on the littoral sediment transport southwards. Beach buildup on the up-drift side was accompanied by erosion down-drift of the jetties, (USACE, 2002). In 1973 a groin field was built in Costa Nova to protect this village, solving the problem locally, but worsening the situation on the down-drift area, with a beach recession occurring at a rate of 20 m/year between 1976 and 1978 (Gomes *et al.*, 1981). New structures of coastal defense have been built since then to face the strong erosion experienced at Vagueira region, which has been increasing to the present day.

Even though several protection works have been carried out in the last few years, such as the construction of several groins and an emergency seawall, this region of study continues to possess serious problems related to coastal erosion and shoreline retreat, as stressed in recent studies (Pais-Barbosa *et al.*, 2006; Coelho *et al.*, 2007).

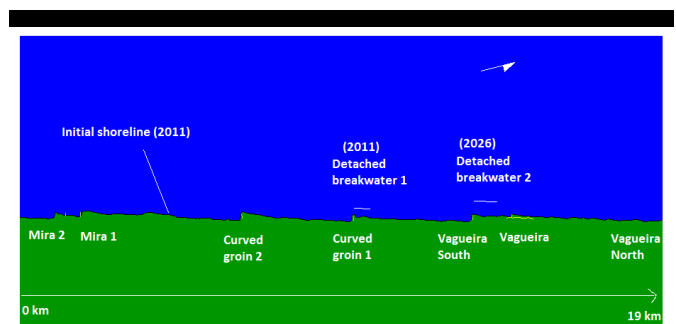


Figure 2. Existing structures along the study domain (coastal stretch of 19 km), with the curved groins introduced so as to be inclined slightly down-drift, together with a representation of the initial position for the shoreline (2011). The arrow indicates the northerly direction.

## Numerical Models and Data

The GENESIS (GENeralized model for SIMulating Shoreline change) model (Hanson, 1987; Hanson and Kraus, 1989) is used in this work to predict the shoreline evolution which results from spatial and temporal fluctuation in the rate of longshore sediment transport. This model is interfaced within NEMOS (Nearshore Evolution MODELing System), which includes a set of other models that operate as a cascade system. NEMOS belongs to a collection of Coastal Engineering Design and Analysis System (CEDAS) from the US Army Corps of Engineers. GENESIS model requires a large amount of data, including wave characteristics, shoreline position, boundary conditions, historical and recent shoreline position data for model calibration as well as data related to the coastal defense structures. Wave data were recorded at the buoy of Leixões, located to the north of Portugal at a depth of 83 m. The recording period was from July 1996 up to December 2011, every 3 hours, however, many gaps exist in the data. Great effort was put in obtaining a reliable wave climate, which constitutes the most important variable before running the GENESIS model (Young *et al.*, 1995). A detailed description on the methodology used in filling those gaps in order to obtain a continuous wave series is presented in Di Bona (2013). As expected, the main wave direction is northwest.

In the present work, the external wave transformation model STWAVE (Steady state spectral WAVE) (Smith *et al.*, 2001) is applied for near shore wind-wave growth and propagation. This model transforms waves over a specific bathymetry up to regions just outside the breaking point. The breaking wave characteristics are then determined and used by GENESIS to calculate the longshore sediment transport.

Bathymetric data were obtained from different data sources: for water depths from 13 m down to the 83 m depth contour

(corresponding to the depth of the recording buoy), nautical Portuguese charts at scale 1:150 000 were used. The remaining bathymetric and topographic data were obtained from a LIDAR survey which was performed in 2011. This yielded a high-resolution data 2 m square grid. This remote sensing allowed the positioning of a real-time and accurate shoreline from which simulations for the future evolution could be made.

No model calibration was carried out in this work since the calibration parameters obtained by Di Bona (2013) were applied. The depth of closure and berm height used in GENESIS were 14 m and 4 m, respectively. The characteristic sediment diameter,  $D_{50}$ , was set to 0.5 mm. The calibration parameters that control the sediment transport rate calculation ( $k_1$  and  $k_2$ ) were set to 0.8 and 0.64, respectively. All the existing engineering structures along the stretch were introduced in the model and adjusted in order to meet the model requirements in terms of position, shape and orientation. Non-diffracting groins were considered to have null permeability factors, and the breakwaters to have a null transmission coefficient. Regarding the lateral boundary conditions (BC), during the calibration process the “moving” type BC was considered from both left and right sides, assuming that the shoreline moved at a constant rate (-112 m and -84 m for left and right boundaries, respectively) over the calibration period (1996-2001) (for more details see Di Bona (2013)).

## Shoreline Evolution under Different Scenarios

Starting from 2011, which is considered to be the present time reference year, since LIDAR data was acquired in this year, two different future scenarios are investigated and the shoreline change evaluated following the methodology adopted by Di Bona (2013): the ‘do-nothing’ scenario and the ‘detached breakwaters protected’ scenario. While the first scenario assumes that no intervention will be made along the coastal stretch, i.e., that the coastal defense scheme will not change; the second one involves the introduction of two detached breakwaters parallel to the present shoreline (2011), at specific distances from the shore, to investigate their impact on the down-drift coast. As the simulation periods are longer than the input wave data (15 years), GENESIS runs by looping the wave data. Simulations are performed for various decades, with output every five years.

The lateral boundary conditions (BC) are one of the most important parameters in the model set-up because they restrict the longshore transport of sand at the boundaries. “Gated groin” BC are considered for both right and left sides corresponding to groins at Vagueira north and Mira 2, respectively. This condition can partially or completely prevent the sediments from entering/exiting the model, depending on the distance between the most northern groin tip and the shoreline position at the external right side of the model ( $YG_{north}$ ), and the distance between the shoreline and the most southern groin tip outside the left model boundary ( $YG_{south}$ ). If  $YG_{north}$  and  $YG_{south}$  are small compared with the groin length, sediments are able to bypass that groin (i.e., the shoreline is very close to the groin tip). Several tests were performed by Di Bona (2013) in determining the most realistic  $YG_{north}$  and  $YG_{south}$  values, since the simulation results depend mostly on those parameters. After a deep sensitivity analysis regarding both parameters on the model behavior, it was found that  $YG_{south}$  has no influence on the model results and  $YG_{north}$  is a key parameter in controlling the entrance of sediments into the domain. Those results were expected, given the dominant northwesterly direction of waves.

At present there are signs of a sediment shortage entering the northern boundary, by the breaching at Labrego beach (immediately south of the Vagueira south groin) in 2011. That

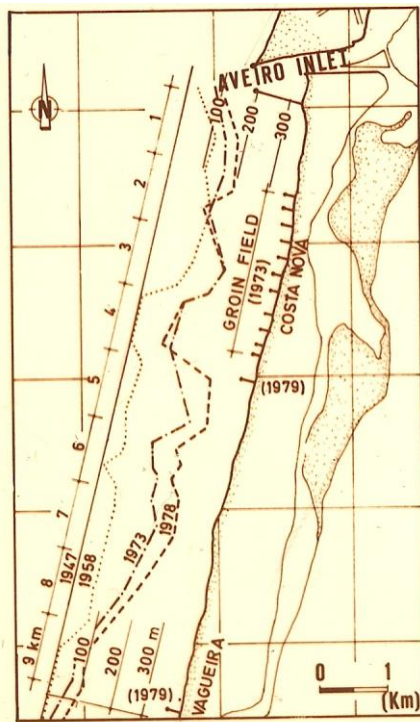


Figure 3. Shoreline evolution south of the Aveiro inlet (Gomes *et al.*, 1981).

shortage of sediment in this coastal stretch has further been stressed by Oliveira *et al.* (2001) and Veloso-Gomes *et al.* (2004). For that reason, and because the sediment supply in the future is unknown, two types of simulations are performed: calibrated simulations and extreme simulations. In calibrated simulations it is assumed that the amount of sediments entering the domain will remain constant and equal to those at the present time ( $YG_{north}=100$  m). Extreme simulations consider a complete absence of sediments entering the northern boundary, which is achieved by using a very high value for  $YG_{north}$  ( $YG_{north}=200$  m which is close to the Vagueira north groin length (285 m)).  $YG_{south}$  was considered to be 150 m for both cases, which is not critical since this parameter has very little effect. These YG values are the same as the ones used by Di Bona (2013).

With respect to the ‘detached breakwaters protected’ scenario, it is presented as a feasible alternative solution of coastal defense in trying to reverse the present erosional trend. Two detached breakwaters are introduced in the model at different instants in time: detached breakwater 1 in 2011 at Areão in front of curved groin 1 and detached breakwater 2 in 2026 at Vagueira south, as represented in Figure 2. Their placement, orientation and length were designed taking into account several criteria such as: the existing structures; an orientation parallel to the incoming wave crest direction; and a length of the same order of magnitude as the distance to the shoreline so as to promote tombolo formation (USACE, 2008). The tombolo formation is a requirement to induce an accretional trend, especially in the most vulnerable stretches of the domain. Different positions and orientations of breakwaters were tested by Di Bona (2013) and the most effective selected. Besides the formation of a tombolo, the absence of erosion is another prerequisite—especially at the Labrego beach, which is the most exposed area of the stretch. In the present study, a similar configuration for the detached breakwaters design is considered. Their length is set to 450 and 700 m for breakwaters 1 and 2, respectively, and their southern tip position is on the 3 m water depth contour.

## RESULTS

Results for shoreline position in the future, for both ‘do-nothing’ scenario and ‘detached breakwaters protected’ scenario, are presented considering both the case of present rate of sediment supply (calibrated simulations) and the absence of sediment supply (extreme simulations).

### ‘Do-Nothing’ Scenario

Figure 4 shows the results obtained from calibrated simulations with output every five years starting from the present time (2011) up to 2041. Shoreline evolution moves seaward (in the north) or shoreward (in the south) without changing its profile shape. Some fluctuations between the various shorelines can be verified in the order of 10-20 m, which are related to the fluctuations in the wave climate. The wave climate period is fairly long (15 years) when compared with the outputs presented in Figure 4, otherwise those fluctuations would be less evident. Yet, the beach presents a stable averaged configuration in the various stretches between groins.

The results of the coastal stretch evolution for the extreme simulations are represented in Figure 5, for the same outputs. Because in this case no sediments are entering at the northern boundary, erosion problems are evident everywhere. The averaged configuration almost coincides with the present time shoreline, which means that the stretch might be in sediment deficit, further suggested by the breaching at Labrego beach on 2011.

Results for 2026 are depicted in Figure 6, for both calibrated and extreme simulations. The future behavior of this stretch

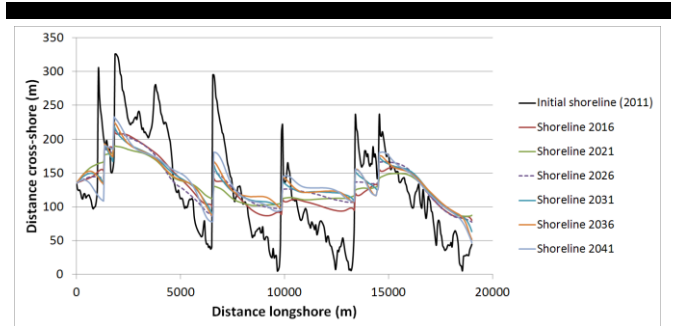


Figure 4. ‘Do-nothing’ scenario: predicted shoreline profiles for the calibrated simulations.

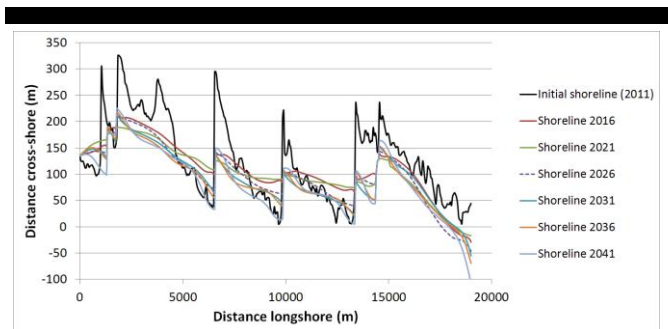


Figure 5. ‘Do-nothing’ scenario: predicted shoreline profiles for the extreme simulations.

Table 1. Averaged values of the distance between the calculated and the present shoreline positions. Negative distances mean erosion while positive mean accretion.

Year	$d_1$ (m)	$d_2$ (m)	$d_3$ (m)
<b>2026</b>			
<b>‘Do-nothing’ scenario</b>			
<i>Calibrated</i>			
	75.4	52.0	-31.4
<i>Extreme</i>			
	24.6	-65.5	-35.4
<b>‘Detached breakwaters protected’ scenario</b>			
1 breakwater			
<i>Calibrated</i>			
	172.0	55.1	-59.5
<i>Extreme</i>			
	123.0	-70.6	-60.2
<b>2056</b>			
2 breakwaters			
<i>Calibrated</i>			
	84.8	66.2	-125
<i>Extreme</i>			
	21.4	-50.1	-126.6

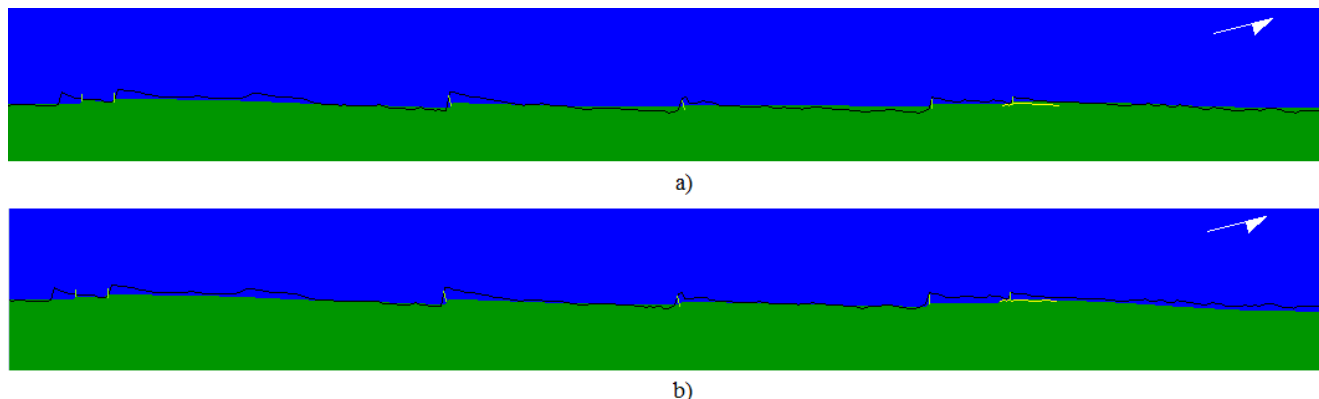


Figure 6. 'Do-nothing' scenario (in 2026): a) predicted shoreline position for the calibrated simulations; b) predicted shoreline position for the extreme simulations.

depends directly on the sediment supply. Assuming that the amount of sediment entering the domain will remain the same as at present (Figure 6a), the coastline will not face severe problems, especially north of the curved groin 1. Southwards the erosion process is more visible. However, in the event of a sediment shortage, the consequences on the northern stretch will be serious (Figure 6b). New breaching episodes of the sand spit barrier are expected to occur at Labrego beach.

#### 'Detached Breakwaters Protected' Scenario

Figure 7 presents the results for calibrated and extreme simulations, when detached breakwater 1 was introduced to the domain. Results are referred to 2026. In both cases the formation of the tombolo is verified. If sediments are available at the northern boundary (Figure 7a), the north stretch will not erode. In the case of a sediment shortage (Figure 7b), erosion takes place. The marked erosion south of curved groin 1 is related to the formation of a tombolo.

After including detached breakwater 2 in 2026, the stretch northwards of curved groin 1 was greatly accreted (Figure 8a), although some erosion still persists for the extreme situation where the sediment supply is not enough to form tombolos (Figure 8b). These results are referred to 2056. It is predicted that the shoreline will suffer landward translation. At the up-drift side of

the detached structures the shoreline tends to rotate, to be oriented parallel to the local direction of the incoming wave crests.

The introduction of two detached breakwaters, in different instants in time, improves the situation northwards of curved groin 1 as a new accretional trend is verified, namely at Labrego beach and Vagueira regions, which are more sensitive. However, ideally a 3<sup>rd</sup> detached breakwater should be introduced in Mira to sustain the severe erosion experienced southwards. This is a good example of the domino effect in shifting erosion down-drift (Cooper *et al.*, 2009). Areas south of Areão beach are not developed, thus their erosion is of less concern. Table 1 presents, for each scenario/simulation type, the averaged values of the distance between the calculated shoreline position and the present shoreline (2011) position, which are determined for three locations: immediately south of Vagueira south groin ( $d_1$ ), corresponding to the Labrego beach breaching location; close to Vagueira north groin ( $d_2$ ), where sediments are entering the domain; and in front of Mira village ( $d_3$ ). The distances predicted at Labrego beach are within the minimum required for safety.

#### CONCLUSION

This paper presents a study on the impact of two detached breakwaters on the Vagueira down-drift coast up to Mira, using the numerical model GENESIS. Two scenarios were investigated,

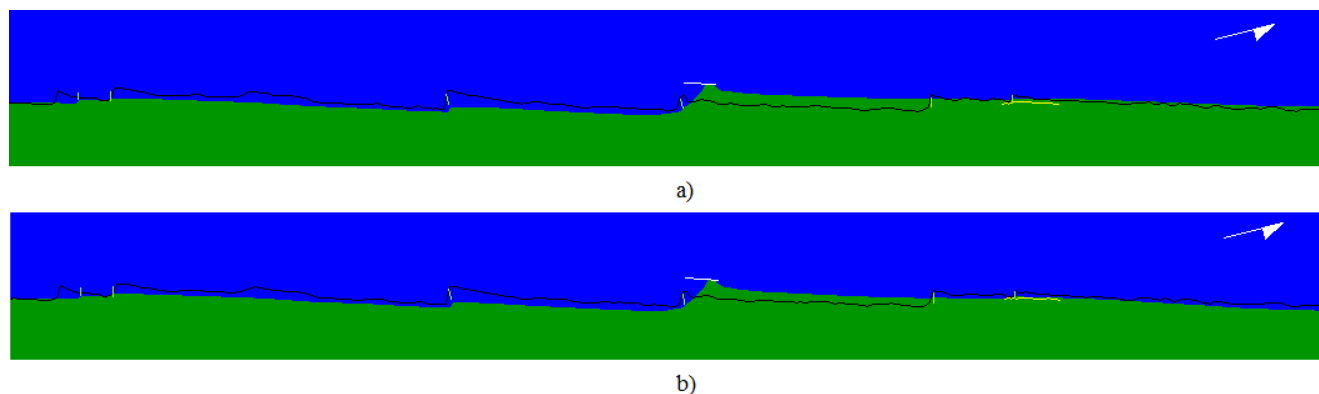


Figure 7. 'Detached breakwaters protected' scenario with 1 breakwater (in 2026): a) predicted shoreline position for the calibrated simulations; b) predicted shoreline position for the extreme simulations.



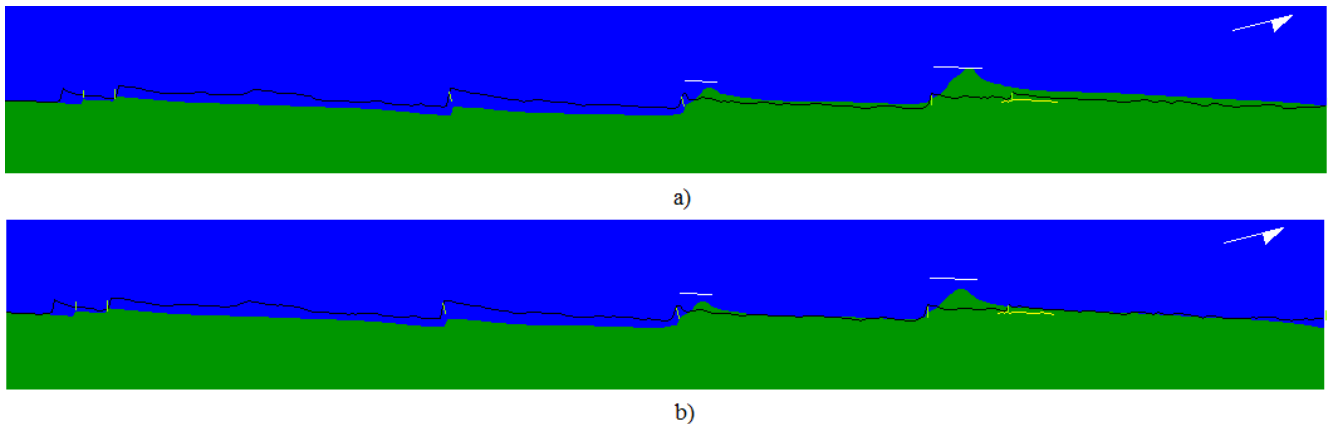


Figure 8. 'Detached breakwaters protected' scenario with 2 breakwaters (in 2056): a) predicted shoreline position for the calibrated simulations; b) predicted shoreline position for the extreme simulations.

considering the presence or absence of coastal defense structures at Vagueira and Areão beaches. Moreover, simulation tests were carried out for continued sediment supply and sediment shortage. The phased introduction of detached breakwaters promotes accretion on the northern stretch but an additional detached breakwater would then be needed at Mira to promote neither sedimentation nor widening of the beaches. There are no perfect or easy solutions to chronic erosion problems. In the long-term, the results from this work will enable better planning of coastal works and better understanding of the consequences of doing-nothing. Thus, this study will help coastal managers and local authorities in risk evaluation and decision-making.

### ACKNOWLEDGEMENT

The authors acknowledge the Portuguese Hydrographic Institute (IH) for providing the wave climate data and the National Institute of Cartography (IGP) for making available the LIDAR data.

### LITERATURE CITED

- Coelho, C., Silva, R., Veloso-Gomes, F. and Rodrigues, L., 2011. Artificial Nourishment and Sand By-Passing in the Aveiro Inlet, Portugal, *Proceedings of the International Conference on Coastal Engineering* (Shanghai, China), Paper No. 32 (2010).
- Coelho, C., Veloso-Gomes, F. and Silva, R., 2007. Shoreline coastal evolution model: two Portuguese case studies. *Proceedings of the 30th International Conference of Coastal Engineering* (San Diego, USA), 3430-3771.
- Cooper, J.A.G. and Pilkey, O.H., 2004. Longshore drift: trapped in an Expected Universe. *Journal of Sedimentary Research*, 74, 599-606.
- Cooper, J.A.G., Anfuso, G. and del Rio, L., 2009. Bad beach management: European perspectives. In: Kelley, J.T., Pilkey, O.H., and Cooper, J.A.G. (eds.) *America's Most Vulnerable Coastal Communities*. Geological Society of America Special Paper 460, pp 167-179.
- Di Bona, S., 2013. Modeling of coastal evolution: Long term simulation in the Vagueira region (Portugal). MSc thesis, University of Padova, Padova, Italy, 138 p.
- Gomes, N.A., Mota Oliveira, I., Pinto Simoes, J. and Pires Castanho, J., 1981. Coastal erosion caused by harbour works on the Portuguese coast and corrective measures. *25th PIANC Congress*. Edimburgh, 877-898.
- Hanson, H., 1987. GENESIS - A generalized shoreline change numerical model for engineering use. *Doctoral thesis*, Lund Institute of Technology, Report No. 1007, Department of Water Resources Engineering, Lund, Sweden.
- Hanson, H. and Kraus, N.C., 1989. GENESIS- Generalized model for simulating shoreline change. Technical report CERC-89-19. U.S. Army Corps of Engineers Waterways Experiment Station, Coastal Engineering Research Center, Vicksburg, Mississippi, 185 p.
- Hanson, H., 1989. GENESIS - A Generalized Shoreline Change Numerical Model. *Journal of Coastal Research*, 5, 1-27.
- Matteucci, G., Riccio, S., Rossini, P., Sisti, E., Bernucci, M.E., Pari, P. and Benedettini, M., 2010. Shoreline evolution trend connected to progressive construction of segmented defense structures (Rimini, North Adriatic Sea, Italy). *GeoActa*, Special Publication, 3, 135-141.
- Oliveira, I., Teixeira, A. and Valle, A., 2001. West Coast of Portugal (Espinho): A Comparison Between Project Predictions and Reality. *Coastal Engineering 2000*, 3552-3565.
- Pais-Barbosa, J., Veloso-Gomes, F. and Taveira-Pinto, F., 2006. Application of geographical information systems on Portuguese coastal projects. *Journal of Coastal Research*, SI 39, 1494-1501.
- Smith, J., Sherlock, A.R. and Resio, D.T., 2001. User's Manual for STWAVE, Version 3.0. *User's manual*. Coastal and Hydraulics Laboratory, Vicksburg, Mississippi, USA.
- Talbi, O., Moussa, M. and Trigo-Teixeira, A., 2008. Coastline change. Simulation in the Maceda-Torreira region. *1st Seminar on Coastal Research*, Porto.
- US Army Corps of Engineers (USACE), 2002. Longshore sediment transport. *Coastal Engineering Manual Part III, Chapter III-2*. Washington DC, USA: Army Corps of Engineers, *Engineer Manual 1110-2-1100*.
- US Army Corps of Engineers (USACE), 2008. Shore protection projects. *Coastal Engineering Manual, Part V, Chapter V-3*. Washington DC, USA: US Army Corps of Engineers, *Engineer Manual 1110-2-1100*.
- Veloso-Gomes, F., Taveira-Pinto, F., das Neves, L., Pais Barbosa, J. and Coelho, C., 2004. Erosion risk levels at the NW Portuguese coast: The Douro mouth - Cape Mondego stretch. *Journal of Coastal Conservation*, 10, 43-52.
- Young, R.S., Pilkey, O.H., Bush, D.M. and Thieler, E.R., 1995. A discussion of the generalized model for simulating shoreline change (GENESIS). *Journal of Coastal Research*, 11 (3), 875-886.

## Growth of cusped spits

Frédéric Bouchette<sup>†</sup>, Miguel Manna<sup>‡</sup>, Pablo Montalvo<sup>‡</sup>, Alexis Nutz<sup>∞</sup>, Mathieu Schuster<sup>∞</sup>, Jean-François Ghienne<sup>∞</sup>

<sup>†</sup>Geosciences-M / I3M  
Université Montpellier 2 / CNRS  
Montpellier, France  
bouchette@gm.univ-montp2.fr

<sup>‡</sup> Lab. Charles Coulomb  
Université Montpellier 2 / CNRS  
Montpellier, France  
manna@l2c.univ-montp2.fr

<sup>∞</sup>Institut de Physique du Globe  
Université Strasbourg / CNRS  
Strasbourg, France  
ghienne@unistra.fr, schuster@unistra.fr



[www.cerf-jcr.org](http://www.cerf-jcr.org)



[www.JCRonline.org](http://www.JCRonline.org)

### ABSTRACT

Bouchette, F., Manna, M., Montalvo, P., Nutz, A., Schuster, M., Ghienne, J.-F., 2014. Growth of cusped spits. In: Green, A.N. and Cooper, J.A.G. (eds.), *Proceedings 13<sup>th</sup> International Coastal Symposium* (Durban, South Africa), *Journal of Coastal Research*, Special Issue No. 70 pp. 047-052, ISSN 0749-0208.

The present work concerns cusped spits: slightly symmetrical geomorphic features growing along the shoreline in shallow waters. We develop a new formulation for the dynamics of cusped spits. Our approach relies on classical paradigms such as a conservation law to the shoreface scale and an explicit formula for alongshore sediment transport. We derive a non-linear diffusion equation and a fully explicit solution for the growth of cusped spits. From this general expression, we found interesting applications to quantify shoreline dynamics in the presence of cusped spits. In particular, we point out a simple method for the dating of a cusped spit given a limited number of input parameters. Furthermore, we develop a method to quantify the mean alongshore diffusivity along a shoreline perturbed by well-defined cusped spits of known sizes. Finally, we introduce a formal relationship between the geometric characteristics (amplitude, length) of cusped spits, which reproduce the self-similarity of these geomorphic features.

**ADDITIONAL INDEX WORDS:** *nearshore, sand spit, Pelnard-Considère, non-linear diffusion equation*

## INTRODUCTION

A wide range of large-scale long-standing geomorphic features occur in shallow water environments, from tens of metres of water depth to the shoreline, either in the open sea or on continental settings. Ripples, megaripples, dunes and sandwaves develop in rhythmic or isolated patterns at metre to kilometre scale (Bruun, 1954; Bakker, 1968; Lonsdale and Malfait, 1974; McBride and Moslow, 1991; Reynaud *et al.*, 1999; Lykousis, 2001; Todd, 2005; Raynal *et al.*, 2009; Bouchette *et al.*, 2010; Raynal *et al.*, 2010). Sandbanks are a part of this family of bedforms and include features such as mega-dunes, bars and ridges (Dyer and Huntley, 1999). Some sandbanks, termed shoreface-connected ridges and headland-associated banks, correspond to features that develop seaward from high points connected to the coast (McBride and Moslow, 1991; Dronkers, 2005). They are prograding down-drift and they usually extend down to deep waters. Obviously these local shoreline perturbations are associated with an accumulation of sand.

Zenkovitch (1959) first described cusped spits (Figure 1) as a limited category of shore-connected features that result from symmetrical wind/wave forcings and/or peculiar initial shore configuration (Bird, 1994; Coco and Murray, 2007). Asthon *et al.* (2001) and Asthon and Murray (2006) proposed that cusped spits, flying spits and other shoreline features are derived from instabilities inherent in the relationship between alongshore sediment transport and local shoreline orientation. They presented a comprehensive weakly non-linear theory for cusped and spit dynamics, and gave a striking numerical solution to the problem.

The present work focuses on cusped spits, also termed foreland spits, cusped foreland or v-notches (Gilbert, 1885; Gulliver, 1896;

Fisher, 1955; Zenkovitch, 1959), which are slightly symmetrical shoreline-connected features that grow along the shoreline of shallow water environments. Cusped spits belong to the class of self-similar pattern. That is to say, as the time proceeds, the shoreline varies whilst remaining geometrically similar. From this point, we develop a new formulation for the dynamics of cusped forelands. We derive a non-linear diffusion equation and an explicit solution for the dynamics of foreland spits. The final objective of this paper is to use the model developed to quantify mean growth velocity of cusped spits, to contribute to the determination of their age or to the mean longshore diffusivity at their origin. The paper also aims to provide additional ideas on the underlying physics of cusped spits.

First, we recall the mechanical context driving the edification of cusped spits, specifying what has been discussed in the literature and what we propose here. Then we present the main steps for the development and the proof of our mathematical model. Finally, we adapt our cusped model to various simple applied circumstances and initiate a discussion on the physics and origin of cusped spits.

### The Non-Linear Pelnard-Considère Equation

In this work, we make the assumption that seabed and shoreline changes driven by strict cross-shore dynamics smooth and counterbalance over time. We consider that the consequence for the net change in the shoreline position over years is weak (Ruessink and Terwindt, 2000; Marino-Tapia *et al.*, 2007). Indeed, at a long time scale, mean cross-shore profile is assumed to be at equilibrium (Hanson and Kraus, 1989; Dean, 1991), i.e. net cross-shore transport equals zero. The significant contribution to the long term shoreline change is thus from longshore dynamics



Figure 1. Examples of cusped spits along shorelines. (A) Cusped along the eastern basin of the Caspian Sea, the Garabogazköl Aylagy (Lat: 41.7813301; Lon: 54.3315601), (B) Cusped in the north-eastern part of the Langandensbyggö peninsula in Island (Lat: 66.3351803; Lon: -14.7930432), (C) String of cusped along the Lebanon shoreline (Lat: 32.8597276; Lon: 35.0629139), (D) Cusped morphology combining with the Belmonte river mouth, Brazil (Lat: -15.8595914; Lon: -38.8902677).

(Allen, 1981; Aagaard and Greenwood, 1995). This assumption is at the origin of the formulation proposed here for the development of cusped spits.

Having this in mind, a basic mass balance equation states that the volume of sand required to move a profile cross shore is the shift of shoreline times the height of the active profile. Let be  $y = S(x, t)$  in the equation of shoreline position in a fixed  $(x, y)$  coordinate system with the  $x$ -axis oriented alongshore, the  $y$ -axis oriented offshore and  $t$  the time (Figure 2A).  $S(x, t)$  satisfies:

$$\frac{dS}{dt} + \frac{1}{h_0 + B} \frac{dQ_L}{dx} = 0 \quad (1)$$

where  $h_0$  is the closure water depth (seaward of which no significant transport occurs),  $B$  is the active berm height,  $h_0 + B$  is the height of the active profile (Figure 2B). The total amount of sediment transported alongshore  $Q_L$  is related to the alongshore flux of energy available for the nearshore per unit length along the shoreline (Inman and Bagnold, 1963):

$$Q_L(x) = \frac{KF_L(x)}{(\rho_s - \rho)g(1-p)} \quad (2)$$

where  $\rho_s$  and  $\rho$  are densities of sediment and water respectively,  $p$  is the porosity,  $g$  is the acceleration of gravity. The dimensionless parameter  $K$  is an empiric constant. The energy flux to the beach  $F_L$  is defined by :

$$F_L = C_g \cdot \varepsilon_0 \cos(\delta_0 - \theta) \sin(\delta_0 - \theta) \quad (3)$$

where  $\cos(\delta_0 - \theta)$  is the ratio of incoming energy that flows from the closure water depth through the nearshore to the

shoreline. In other words, it is the ratio of energy between two infinitely ( $dL$ ) close wave rays that acts on an infinitely small  $dx$  shoreline segment (Figure 2A). Hence,  $\sin(\delta_0 - \theta)$  is the longshore contribution of the total incoming energy. At the closure water depth  $h_0$ , the incoming energy is classically defined with the expression derived from linear wave theory:

$$\varepsilon_0 = \frac{1}{8} \rho g H_0^3$$

with  $H_0$  representing the wave height. This energy propagates at the group velocity  $C_g$ . This velocity must be calculated at the point where the energy flows into the active domain, that is at the closure water depth  $h_0$ . In this case, the linear wave theory provides the simple formulation:

$$C_g = C_{g0} = \frac{g}{4\pi} T_0$$

The longshore transport rate  $Q_L$  is thus:

$$Q_L = 2C_L \cos(\delta_0 - \theta) \sin(\delta_0 - \theta) \quad (4)$$

with:

$$C_L = \frac{K\rho\rho_s g^2 T_0^2}{64\pi(\rho_s - \rho)(1-p)} \quad (5)$$

Several formulations for the alongshore transport rate were successively derived from Eq. (3) (e.g. Komar and Inman, 1970; Komar, 1971; Bailard, 1984). Reviews and compared analyses of alongshore transport formulae were also performed (Bayram *et al.*, 2001). Here the sediment transport is strictly controlled by  $F_L$ , the

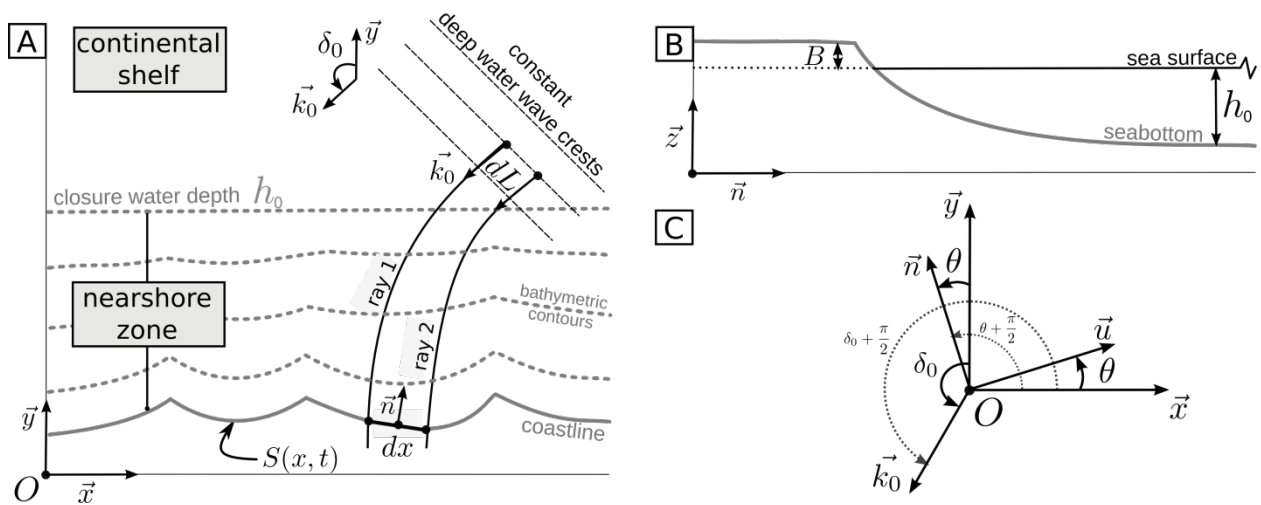


Figure 2. Sketches for the design of the mathematical model (A) a plan view of the nearshore and shoreline wherein the  $x$ -axis is oriented longshore and the  $y$ -axis is oriented seaward. From deep water, waves (example of Ray 1 and Ray 2) propagate from the top to the bottom of the figure and refract depending upon bathymetric contours (B) Definition of the normal  $n$  to the shoreline, the berm height  $B$ , and of the closure water depth  $h_0$ . (C) Relative orientation of vectors and angles used in the paper.

longshore portion of flux of energy  $\epsilon_0$  per shoreline unit length. No matter what type of wave transformation occurs in the nearshore, the only significant information is the fact that  $\delta_0 - \theta$  varies along the shoreline and that the energy that flows in the nearshore up dip of the shoreline depends upon this. This point of view is quite different from that chosen by other authors (for more explanations, see Ashton *et al.*, 2001).

The combination of Eqs (4) and (1) is a model of long-term shoreline changes  $S(x, t)$  under mean wave forcings and mean sediment texture conditions. To date, several strategies have been tested to find solutions for this kind of problem. First, Pelnard-Considère (1956) (and a significant amount of subsequent literature) linearized the problem so that a single linear diffusion equation describes the planform evolution of  $S(x, y)$ . More recently, Ashton *et al.* (2001) and Ashton and Murray (2006) solved the problem numerically with an expression of  $Q$  similar (but not equal) to that of Dean and Dalrymple (2002) and introduced a diffusion coefficient that depends on  $\theta$  (and may be thus negative). Ashton *et al.* (2001) focussed on rhythmic foreland spits. Another striking idea was to introduce some non-linearity with an “expansion of the flow and the bottom perturbations in a truncated series of eigenfunctions of the linear problem” (Calvete *et al.*, 2002; Falguères *et al.*, 2008) which is not discussed here. The latter works concerned more specifically rhythmic shoreline patterns like beach cusps. These works argued that shoreline-connected features including foreland spits originate in instabilities. We provide a new solution to the problem.

The angle  $\theta$  between the local normal to the shoreline and the  $y$ -axis (Figure 2C) satisfies:

$$\sin \theta = \frac{dS/dx}{\sqrt{1+(dS/dx)^2}} \tag{6} \text{ and } \tag{7}$$

$$\cos \theta = \frac{1}{\sqrt{1+(dS/dx)^2}}$$

Eq. (4) can be rewritten in the following Eq (8):

$$Q_L = C_L [\sin 2\delta_0 (\cos^2 \theta - \sin^2 \theta) - 2\cos 2\delta_0 \sin \theta \cos \theta]$$

Developing Eqs (6), (7) in Taylor series until order two in  $\partial S/\partial x$ , and combining Eqs (1) and (8) results in

$$\frac{dS}{dt} = G_0 \cos 2\delta_0 \frac{d^2 S}{dx^2} + 2G_0 \sin 2\delta_0 \frac{dS}{dx} \frac{d^2 S}{dx^2} \tag{9}$$

This is a nonlinear diffusion equation. When waves are directed along the  $x$ -axis (alongshore wind/wave forcings)  $\sin 2\delta_0$  is zero and Eq. (9) reduces to a classical diffusion equation (Pelnard-Considère, 1956) with  $G_0$  the longshore diffusivity. Another way to obtain Pelnard-Considère is to linearize Eq. (9). For this reason, we could name Eq. (9) the “non-linear Pelnard-Considère equation”. In such a formulation,  $G_0$  is given by:

$$G_0 = \frac{C_L}{h_0 + B} \tag{10}$$

and one will notice that

$$G_0 = G(H_0, T_0, \delta_0, \rho, \rho_s, p, h_0 + B) \tag{11}$$

which means that  $G_0$  is a function of wave properties, sediment properties and basic geometrical informations.

### Derivation of the Cusped Equation

From Eq. (11) we know that  $G_0$  depends upon most of the ‘environmental’ variables of the problem, i.e., those relative to the geometrical context and the forcings. As long term dynamics are mostly driven by mean values averaged to the historical/geological time scale, we can consider that  $H_0, T_0, \rho, \rho_s, p$  are constant through time or that they vary very slowly. In the same manner,  $h_0 + B$  may not change as sea bottom is always in equilibrium (Short, 1999, p. 45, Fig 3).

Let us consider the following particular scenario in the frame (0,  $x, y$ ) (Figure 2A). At  $t = 0$ , we have a non perturbed shoreline for  $x$  in  $[-\infty, +\infty]$ . At time  $t_0$ , an  $x$ -symmetric and positively defined perturbation appears that develops on both sides of the origin  $O$  and extends in  $[-x_f, +x_f]$ , being zero beyond. The building of such a cusped spit supposes that the alongshore sediment transport results from two main dominant forcings varying close enough to  $\delta_0 = \pm\pi/4$ . Under these conditions Eq. (11) splits in two equations with solutions  $S_R$  (for  $\delta_0 = +\pi/4$ ) and  $S_L$  (for  $\delta_0 = -\pi/4$ ) satisfying :

$$\frac{dS_{R/L}}{dt} = 2G_0 \sin(\pm \pi / 2) \frac{dS_{R/L}}{dx} \frac{d^2 S_{R/L}}{dx^2} \quad (12)$$

As one can consider that the two forcings compete through time, we can substitute the real system represented by the two Eqs. (12) by a model based on a distributed solution satisfying :

$$\frac{dS}{dt} = \begin{cases} 0 & \text{for } x \leq -x_f \\ 2G_0 \frac{dS_R}{dx} \frac{d^2 S_R}{dx^2} & \text{for } -x_f < x \leq 0 \\ -2G_0 \frac{dS_L}{dx} \frac{d^2 S_L}{dx^2} & \text{for } 0 \leq x \leq x_f \\ 0 & \text{for } x \geq x_f \end{cases} \quad (13)$$

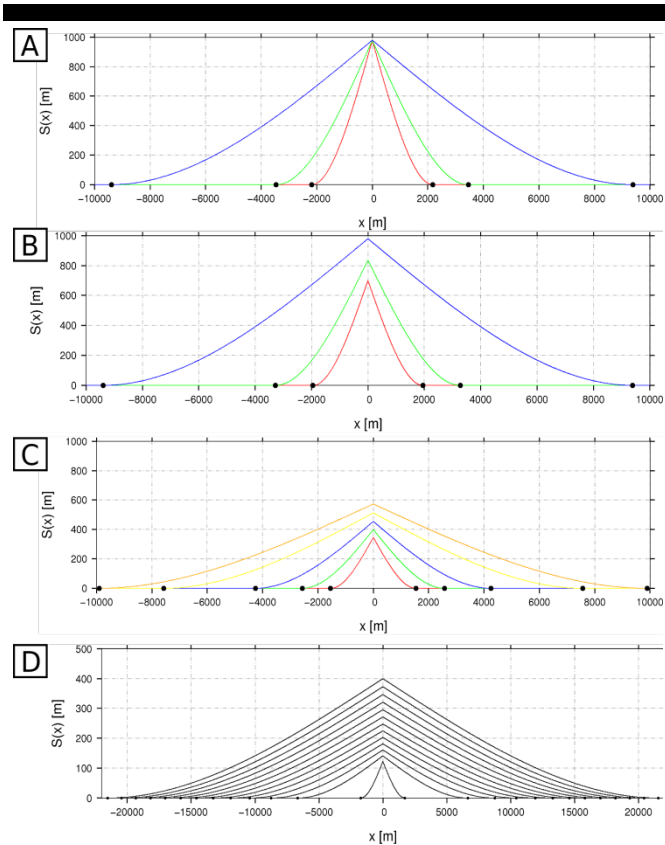


Figure 3. Various cusped spits calculated from the mathematical model proposed in Equation (16). The different plots correspond to the configurations given below. Parameters to be set are  $G_0$  and  $a$ .  $G_0$  is given by  $K = 0.77$ ,  $\rho = 1025 \text{ kg.m}^{-3}$ ,  $\rho_s = 2400 \text{ kg.m}^{-3}$ ,  $H_0=1.5 \text{ m}$ ,  $T_0 = 10 \text{ s}$ ,  $\kappa = 0.55$ ,  $h_0 = 10\text{m}$ . The definition of the parameter  $a$  (arising from the integration) changes in the various plots: (A) parameter  $a$  is a constant set to 20; (B) parameter  $a$  ranges from 16 to 20; (C) parameter  $a$  ranges from 10 to 14; (D) parameter  $a$  ranges from 5 to 11; the various curves represent cusped geometry from 1 year to 450 years.

We already recalled that cusped spits possess self-similar patterns. Thus it is obvious to take into account the  $(x,t)$  dependence of  $S$  through a self-similar variable  $\zeta$  so that:

$$S(x,t) \Leftrightarrow S(\zeta, \tau) \text{ with } \zeta = \frac{x}{t^{1/3}} \quad (14)$$

Applying this variable substitution to the operators  $d/dx$  and  $d/dt$ , we derive a new writing of Eq. (13):

$$\begin{cases} 2G_0 S_{R,\zeta\zeta} + \frac{1}{3}\zeta = 0, \zeta \in [-\zeta_0, 0] \\ 2G_0 S_{L,\zeta\zeta} - \frac{1}{3}\zeta = 0, \zeta \in [0, \zeta_0] \end{cases} \quad (15)$$

Integrating twice, we obtain another expression with 4 distinct constants to be determined by the geometrical behavior of the cusped spit. We impose to  $S$  to be continuous and positively defined at  $\zeta=0$ . In addition, we impose discontinuity of the derivative of  $S$  at  $\zeta=0$ . And we impose to  $S$  to be zero at the points  $\zeta_0$  where  $S_\zeta=0$ . We obtain a set of equations with a single unknown parameter  $a$ . Going back to the original coordinates  $(x,y)$ , we get a new equation.

This equation is an exact solution to the problem developed in Eq. (9) adapted to the growth of any cusped spit. Figure 3 displays some examples of plots of the expression  $S(x,y)$  derived here at various arbitrary times and for various values of the control parameters. Each curve could be cusped spits like those in Figure 1. The expression of the solution in the original coordinates is given by equation (16) given below.

$$\frac{dS}{dt} = \begin{cases} 0 & x \leq -\sqrt{6at}^{1/3} \\ \frac{1}{2G_0} \left\{ \frac{2}{3} a \sqrt{6a} + \frac{ax}{t^{1/3}} - \frac{x^3}{18t} \right\} & -\sqrt{6at}^{1/3} \leq x \leq 0 \\ \frac{1}{2G_0} \left\{ \frac{2}{3} a \sqrt{6a} - \frac{ax}{t^{1/3}} + \frac{x^3}{18t} \right\} & 0 \leq x \leq \sqrt{6at}^{1/3} \\ 0 & x \geq \sqrt{6at}^{1/3} \end{cases}$$

At this stage the model must be developed further. Indeed, unlike the longshore diffusivity  $G_0$  which affects the ability of the system to transport sediment alongshore, the parameter  $a$  has no clear physical meaning as it simply results from an integration process. The plots in the Figure 3 are consistent with highly symmetric geomorphic features; but, at this stage, we have no way to use the model for applications.

### Using the Cusped Model

From Eq. (27), the length  $\lambda(t)$  of the foreland spit is :

$$\lambda(t) = 2\sqrt{(6at)^{1/3}} \quad (17)$$

For  $x=0$ , Eq. (16) results in:

$$S(0) = \sqrt{(6)a^{3/2} / (3G_0)} \quad (18)$$

Making power three Eq. (28), and deleting  $a$  to the power of  $3/2$  from equations, we get the expression:

$$S(0) = \frac{\lambda^3}{2G_0 \cdot 72t} \quad (19)$$

If  $t_p$  is the present time, one may say that

$$\Delta t = t_p - t_0 \quad (20)$$

is the time required to nucleate and to develop the cusped spit from an initial moment  $t_0$ . For convenience, let us rename  $S(0)$  as  $A_p$ . With this formalism, Eq. (19) can be rewritten as:

$$\Delta T = \frac{1}{2G_0} \cdot \frac{\lambda_p^3}{72A_p} \quad (21)$$

where  $A_p$  and  $\lambda_p$  are the amplitude and the alongshore length of the cusped spit at the present day, respectively. These parameters can be easily measured on an aerial photograph or by satellite imagery (Figure 4) following the simple protocol described below.

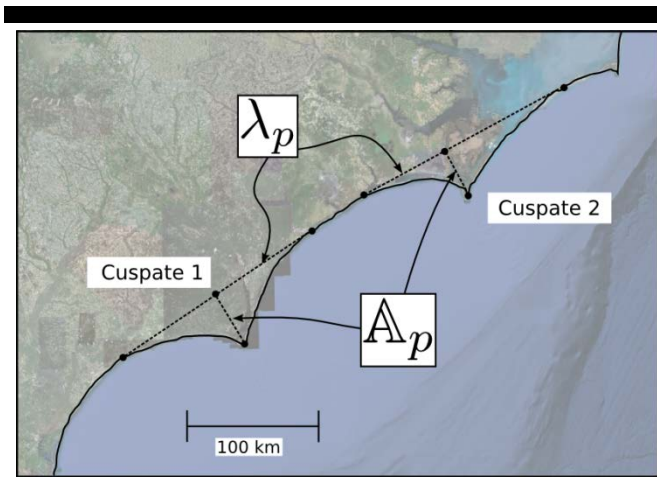


Figure 4. Sketch of two cusped spits along the Carolina Coast, from Ashton *et al.* (2001). The two cusped spits (1 and 2) display well defined wave lengths  $\lambda_p$  and wave amplitudes  $A_p$ . Those parameters can be estimated with the methodology described in the text.

To quantify  $A_p$  and  $\lambda_p$  for a given cusped spit, the following method is applied: a) draw a line at the tangent to the shoreline; it intersects the shoreline in two points. This defines a segment which is the cusped length  $\lambda_p$ ; (b) from the head of the cusped spit, draw the perpendicular line to the segment defined in (a); the point at their intersection and the point at the head of the cusped spit form a new segment whose length is the amplitude  $A_p$  of the cusped spit.

Eq. (21) can be considered as a method for the dating of a cusped spit knowing the mean alongshore diffusivity and the geometrical features of the cusped spit in the present day. Alternatively, the cusped spit model can be thought as a tool to quantify the mean alongshore diffusivity  $G_0$  having information on the geometry of the cusped spit and its age. Indeed, considering that the present day geometry of a cusped spit is known, as well as its age  $\Delta t$  (e.g. dated by its occurrence in an artificial continental water body dammed at a given period; or directly dated by any well-adapted dating method). This information can be robustly retrieved through field work by geologists. From Eq. (21) it reads directly:

$$2G_0 = \lambda_p^3 / (72 \cdot A_p \cdot \Delta T) \quad (22)$$

The calculation of such a mean alongshore diffusivity from parameters expressed on a geological/historical time scale is

interesting for the classification of the paleo-system concerned with respect to well-known existing littoral systems (such as described in Dean & Dalrymple (2002)).

Another obvious application is to calculate the mean active profile (or the mean wave height or period) for the system at a given time knowing the present day geometry and all the other long-term mean forcings. Combining Eqs (5), (10) and (21), we have:

$$h_0 + B = \frac{9K\rho g H_0^2 T_0 A_p \Delta T}{2\pi(\rho_s - \rho)(1-p)\lambda_p^3} \quad (23)$$

The benefit of this last application could be debated for recent cusped spits. Indeed, one will claim that there exist other ways of calculating an active profile directly from data in the field (e.g. considering the analysis of wave data at a buoy, and the subsequent extraction of a closure depth). Nevertheless, for ancient cusped spits it seems obvious that the calculation of

$H_0^2 T_0$  directly from Eq. (23) would provide significant semi-quantitative restraints for the reconstruction of paleo-wave regimes. Indeed, the parameters  $\rho_s$ ,  $\rho$  and  $p$  could be determined by analysis of sand properties within the cusped deposits.  $\lambda_p$  and  $A_p$  could be determined by direct surface observation (or seismic investigation if the cusped spit is buried).  $h_0$  could be determined by the identification of the location where wave ripples vanish and  $B$  by the identification of the position of the shoreline and the highest location concerned by wave impact.

## DISCUSSION

The cusped spit model offers the opportunity to calculate useful parameters for coastal engineering and geosciences. But applications under real conditions are beyond the objective of this paper, although they could be presented in future works.

Nevertheless, the cusped spit model highlights a more fundamental result. In their numerical analysis of the growth of cusped spits, Ashton & Murray (2006) suggested that there exists an approximate relationship between the age and the length of a cusped spit feature. They wrote (Eq. (10) in their paper):

$$\Delta t \approx \left( \frac{K_1}{D_{sf}} H_0^{12/5} T^{1/5} \right) \Delta x^2 \quad (24)$$

where  $\Delta t$  is our  $\Delta T$  (the age of the cusped spit),  $\Delta x^2$  is  $\lambda_p^2$  the cusped length squared, and  $D_{sf}$ ,  $K_1$  and other variables can be considered as constant and are ignored in the following. The authors derived this approximate relationship from the equation at the origin of their numerical model and from an analysis of numerical simulations.

In this paper we demonstrate with Eq. (21) that a formal relationship between the age and the length of the cusped spit is mathematically correct, and that this relationship is definitively controlled by a power law as Ashton & Murray (2006) suggested. Although the term to the power is different (3 in our case; 2 in the case of Ashton & Murray), these two totally independent proofs give more confidence in the reality of such a relationship. The occurrence of a power law suggests also that more underlying physics remain to be analyzed.

Finally, Ashton & Murray (2006) sustained the idea that, contrary to a traditional point of view, the wave angle in deep water strongly controls shoreline perturbations through their so-called anti-diffusional high wave angle instability. In this paper we demonstrate that deep water wave features  $H_0$  and  $T_0$  drive non-linear shoreline instabilities in a simple way with absolutely no dependence on what occurs to waves in the nearshore. This is also

a formal confirmation of what was suggested by Ashton & Murray (2006). Fourth, we demonstrate that there is no need to transform – by quite complex and obscure operations – shallow water variables into deep water ones (Equations (1), (4) and (5) of Ashton & Murray, 2006) to get this result.

## CONCLUSION

From what can be called the non-linear Pelnard-Considère equation, we develop an explicit formulation of the growth of a symmetrical cusped spit through time. This formulation can be applied (a) to the calculation of the age of a cusped spit, (b) to the determination of a mean alongshore diffusivity in the vicinity of a cusped spit, or (c) to the calculation of a paleo-active profile or information on paleo-wave regimes after some simple geological field data has been acquired. More substantially, the paper confirms the works of Ashton & Murray (2006) in the sense that it provides an alternative formal proof of what was suggested. In a near future the cusped spit model will be more deeply explored, tentatively extended to other geomorphic features and engineering/ geological applications will be engaged to confirm its relevancy.

## ACKNOWLEDGEMENT

This work was funded by NUCLEASPIT (CNRS Mathematics and Physics) and by KUNSHEN (ANR international program). The authors thank GLADYS (www.gladys-littoral.org) and SO LTC (www.soltc.org) for the comments on the original work as well as the reviewer of the previous version of the document.

## LITERATURE CITED

- Aagaard, T. and Greenwood, B., 1995. Longshore and cross-shore suspended sediment transport at far infragravity frequencies in a barred environment. *Continental Shelf Research*, 15, 1235-1249.
- Allen, J., 1981. Beach erosion as a function of variations in the sediment budget, Sandy Hook, New-Jersey, U.S.A. *Earth Surface Processes and Landforms*, 6, 139–150.
- Asthen, A. and Murray, B., 2006. High-angle wave instability and emergent shoreline shapes: 1) modeling of sand waves, flying spits and capes. *Journal of Geophysical Research*, 111, F04011.
- Asthen, A., Murray, B. and Arnault, O., 2001. Formation of coastline features by large-scale instabilities induced by high-angle waves. *Nature*, 414, 296-299.
- Bailard, J., 1984. A simplified model for longshore transport. *Proc. 19th Intl. Conf. Coastal Eng., ASCE, Houston*, 1454-1470.
- Bakker, W., 1968. Mathematical theory about sand waves and its applications on the Dutch Wadden Isle of Vlieland. *Shore and Beach*, 5-14.
- Bayram, A., Larson, M., Miller, H. C. and Kraus, N. C., 2001. Cross-shore distribution of longshore sediment transport: comparison between predictive formulas and field measurements. *Coastal Engineering*, 44 (2), 79-99.
- Bird, E. C., 1994. Chapter 2 physical setting and geomorphology of coastal lagoons. In: Kjerfve, B. (ed.), *Coastal Lagoon Processes. Vol. 60*, Elsevier Oceanography Series, 9-39.
- Bouchette, F., Schuster, M., Ghienne, J.-F., Denamiel, C., Roquin, C., Abderamane, M., Marsaleix, P. and Düringer, P., 2010. Hydrodynamics in the Holocene lake MegaChad. *Quaternary Research*, 73 (2), 226-236.
- Bruun, P., 1954. Migrating sand waves or sand humps, with special reference to investigations carried out on the Danish North Sea coast. *Proc. 5th international conference coastal engineering, ASCP*, 269-295.
- Calvete, D., de Swart and H. E., Falquès, A., 2002. Effect of depth-dependent wave stirring on the final amplitude of shoreface-connected sand ridges. *Continental Shelf Research*, 22 (18-19), 2763-2776.
- Coco, G. and Murray, A. B., 2007. Patterns in the sand: From forcing templates to self-organization. *Geomorphology*, 91 (3-4), 271-290.
- Dean, R., 1991. Equilibrium beach profiles: characteristics and applications. *Journal of Coastal Research*, 7, 53-84.
- Dean, R. and Dalrymple, R., 2002. Coastal processes with engineering applications, Cambridge University Press, 488p.
- Dronkers, J., 2005. *Dynamics of coastal systems. Vol. 25*. World Scientific, 255p.
- Dyer, K. and Huntley, D., 1999. The origin, classification and modelling of sand banks and ridges. *Continental Shelf Research*, 19, 1285-1330.
- Falquès, A., Dodd, N., Garnier, R., Ribas, F., MacHardy, L., Larroude, P., Calvete, D. and Sancho, F., 2008. Rhythmic surf zone bars and morphodynamic self-organization. *Coastal Engineering*, 55 (7-8), 622-641.
- Fisher, R. L., 1955. Cusped spits of saint lawrence island, alaska. *Journal of Geology*, 63, 133-142.
- Gilbert, G. K., 1885. The topographic features of lake shores. *US Geological Surv. Ann. Rep.*, 5, 69-123.
- Gulliver, E., 1896. Cusped forelands. *Geol. Soc. Am. Bull.*, 7, 399-422.
- Hanson, H. and Kraus, N., 1989. *Genesis: Generalized model for simulating shoreline change. report 1: Technical references*. US Army Eng. Waterways Experimentation station.
- Inman, D. and Bagnold, R., 1963. New York Interscience, *Littoral processes*, 529-533.
- Komar, P., 1971. The mechanics of sand transport on beaches. *Journal of Geophysical Research*, 76, 713-721.
- Komar, P., Inman, D., 1970. Longshore sand transport on beaches. *Journal of Geophysical Research*, 75, 5914-5927.
- Lonsdale, P. and Malfait, B., 1974. Abyssal dunes of foraminiferal sand on the canergie ridge. *Geol. Soc. Amer. Bull.*, 85, 1697-1712.
- Lykousis, V., 2001. Subaqueous bedforms on the Cyclades plateau (NE Mediterranean). Evidence of cretan deep water formation. *Continental Shelf Research*, 21, 495-507.
- Marino-Tapia, I., Russell, P., O'Hare, T., Davidson, M. and Huntley, D., 2007. Cross-shore sediment transport on natural beaches and its relation to sandbar migration patterns: 1. field observations and derivation of a transport parameterization. *Journal of Geophysical Research-Océans*, 112, C03002. doi: 10.1029/2005JC002894.
- McBride, R. A. and Moslow, T. F., 1991. Origin, evolution, and distribution of shoreface sand ridges, atlantic inner shelf, U.S.A. *Marine Geology*, 97 (1-2), 57-85.
- Pelnard-Considère, R., 1956. Essai de théorie de l'évolution des formes de rivages en plages de sable et de galets. *La Houille Blanche*.
- Raynal, O., Bouchette, F., Certain, R., Sabatier, P., Séranne, M., Lofi, J., Dezileau, L., Briquieu, L., Ferrer, P. and Courp, T., 2010. Holocene evolution of languedocien lagoonal environment controlled by inherited coastal morphology (Northern Gulf of Lions, France). *Bulletin Société Géologique Française*, 181 (2), 211-224.
- Raynal, O., Bouchette, F., Certain, R., Séranne, M., Dezileau, L., Sabatier, P., Lofi, J., Bui Xuan Hy, A., Briquieu, L., Pezard, P. and Tessier, B., 2009. Control of alongshore-oriented sand spits on the dynamics of a wave-dominated coastal system, Holocene deposits, northern Gulf of Lions, France. *Marine Geology*, 264 (3-4), 242–257.

# Investigating the role of complex sandbar morphology on nearshore hydrodynamics

N. Cohn<sup>†</sup>, P. Ruggiero<sup>†</sup>, J. Ortiz<sup>‡</sup>, D.J. Walstra<sup>∞</sup>

<sup>†</sup>College of Earth, Ocean, and Atmospheric Sciences  
Oregon State University  
Corvallis, OR, USA  
cohn@geo.oregonstate.edu  
pruggier@coas.oregonstate.edu

<sup>‡</sup> Department of Earth Sciences  
Dartmouth College  
Hanover, NH, USA  
john.p.ortiz.14@dartmouth.edu

<sup>∞</sup> Department of Hydraulic Engineering  
Deltares/TU Delft  
Delft, The Netherlands  
dirkjan.walstra@deltares.nl



[www.cerf-jcr.org](http://www.cerf-jcr.org)



## ABSTRACT

Cohn, N., Ruggiero, P., Ortiz, J., D.J. Walstra, 2014. Investigating the role of complex sandbar morphology on nearshore hydrodynamics. In: Green, A.N. and Cooper, J.A.G. (eds.), *Proceedings 13<sup>th</sup> International Coastal Symposium* (Durban, South Africa), *Journal of Coastal Research*, Special Issue No. 70, pp. 053-058, ISSN 0749-0208.

[www.JCRonline.org](http://www.JCRonline.org)

Coastal environments are characterized by complex feedbacks between flow, sediment transport, and morphology, often resulting in the formation of nearshore sandbars. In many locations, such as Hasaki (Japan), the Netherlands, and the Columbia River Littoral Cell (CRLC, USA), these sandbars exhibit a net offshore migration (NOM) cycle whereby these features form in the inner surf zone, migrate seaward and decay offshore on interannual cycles. Depending on the stage of the cycle, the number and configuration of the bars may differ widely. It has long been recognized that sandbars act as natural barriers during storm events by dissipating wave energy through breaking far from the beach face. Thus, dependent on the stage of the NOM cycle, one might expect significant variability in nearshore hydrodynamics. Using a non-linear wave model we demonstrate that inter-annual variability in sandbar configuration can significantly alter inner surf zone and swash zone processes. The model indicates that under different end-member NOM stages the same wave conditions can result in up to a 36% variance in the vertical extent of infragravity runup and can alter both the rate and direction of net cross shore sediment transport.

**ADDITIONAL INDEX WORDS:** *runup, setup, infragravity swash, coastal geomorphology, sandbar migration, cross shore sediment transport*

## INTRODUCTION

Sandy coastal systems are highly dynamic and under the combined forces of waves, winds, currents, and water levels are prone to many hazards that threaten valuable ecological, recreational, and commercial resources. Coastal erosion and backshore flooding, two primary hazards to these regions, are both largely governed by local extreme total water levels (TWL) which are defined as the combination of mean sea level, tides, non-tidal residuals including storm surge, and wave runup. The magnitudes of the various components of the TWL are influenced by atmospheric conditions (e.g., pressure, wind), oceanic parameters (e.g., wave height), and coastal morphology (e.g., beach slope). In some settings, such as the US West Coast, the wave-induced components of TWL typically dominate the overall TWL signal, particularly during extreme high water events. The wave induced portion of the TWL, runup, consists of two distinct components. Wave setup is the increase in mean water level due to gradients in radiation stresses whereas swash is the time-varying variance around the setup.

Traditionally, empirical metrics have been widely adopted by scientists and management agencies to predict the wave induced components of TWL. However, recent studies have recognized limitations in applying these empirically based formulae where complex morphologies, such as sandbars, are prevalent (e.g., Cox

*et al.*, 2013; Stephens *et al.*, 2011). In many locations throughout the world, including Japan, the Netherlands, and the US, a systematic trend of interannual net offshore sandbar migration (NOM) has been observed whereby bars form in the inner nearshore, migrate seaward across the surf zone, and eventually decay offshore in cyclic patterns (Walstra *et al.*, 2012). The presence of a sandbar that has migrated offshore could result in breaking occurring far from the shoreline during storm conditions and significantly different surf zone and intertidal hydrodynamics relative to a case with no offshore bar. Therefore the stage of the NOM has implications for the risk of coastal flooding and erosion.

Here we explore how nearshore hydrodynamics vary in response to different complex, multi-bar configurations. Specifically we apply a non-linear wave and current model (XBeach) to investigate how wave runup and cross-shore sediment transport vary during differing stages of NOM in the Columbia River Littoral Cell (CRLC, USA).

## BACKGROUND

### Columbia River Littoral Cell

The CRLC is a high energy, meso-tidal, progradational coastal system that extends approximately 165 km between Tillamook Head, OR and Point Grenville, WA on the Pacific coast of the US (Figure 1). The system consists of four prograded barrier plain sub-cells separated by the estuary entrances of the Columbia River, Willapa Bay, and Grays Harbor. Each barrier is generally characterized by wide, dissipative, gently sloping beaches with



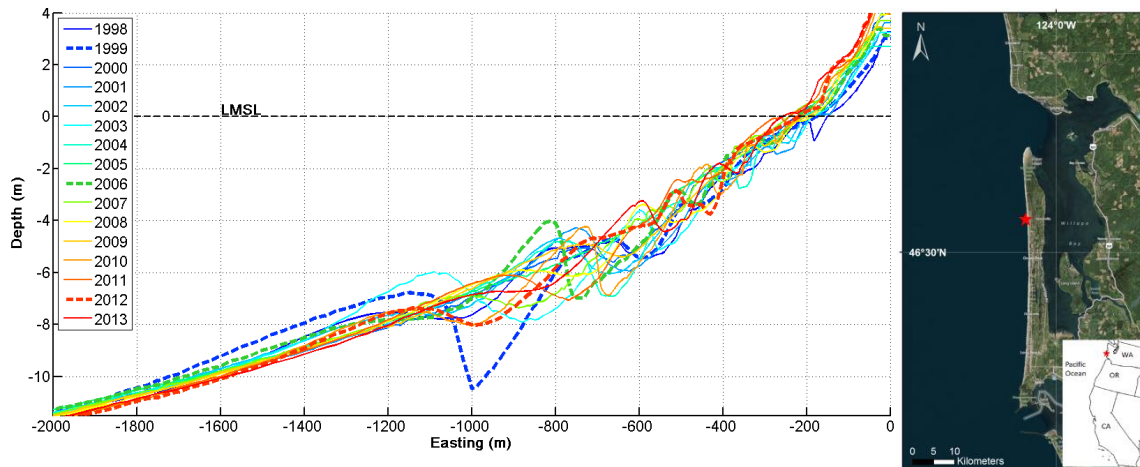


Figure 1. Annual bathymetric profiles from CRLC transect 66 from 1998 to 2013 and map with transect location (red star).

broad surf zones and multiple sandbars with fine sand derived from the Columbia River (Ruggiero *et al.*, 2005).

The Pacific Northwest experiences one of the most extreme wave climates in the world with annual deep-water significant wave heights (SWH) of about 3 m and peak wave periods of about 12 s. Large storms in the winter months regularly produce waves in excess of 8 m, with the approximately one storm per year generating SWHs greater than 10 m (Ruggiero *et al.*, 2010).

### Net Offshore Sandbar Migration

It has long been recognized that nearshore sandbars act as natural barriers to coastal erosion during storm events by dissipating wave energy through breaking far from the beach face. Changes in breaking wave patterns alter surf zone and intertidal wave and current characteristics, which consequently influence sediment transport and morphologic change. The number and configuration of these sandbars can therefore have a major influence on inner surf zone and intertidal processes.

Sandbars are common nearshore features on sandy coastlines throughout the world and are constantly evolving in response to hydrodynamic forces and gradients in sediment transport. Large waves result in a strong offshore directed current in the lower water column (undertow) that results in the seaward migration of sandbar systems (Hoefel and Elgar, 2003). However, during low wave conditions undertow is relatively weak and non-linear properties of the flow can drive net onshore sediment transport. Among the important factors in onshore directed transport are velocity skewness, acceleration skewness, and boundary layer streaming (Thornton *et al.*, 1996; Hoefel and Elgar, 2003; Aagard *et al.*, 2012). Resulting from the cumulative effects of these competing processes, an interannual trend of net offshore subtidal bar migration (NOM) is observed at many locations throughout the globe. Depending on the stage of the offshore migration cycle, the number of bars, their location, and their size can vary considerably (Ruessink *et al.*, 2003). Similarly, there is significant intersite variability in bar behavior. For example in Hasaki (Japan) bars typically are generated nearshore, migrate across the surf zone, and dissipate offshore all within a single year, while this cycle averages 15 years in Noord-Holland (the Netherlands).

A long term morphologic dataset from the CRLC (Ruggiero *et al.*, 2005) spanning 1998 to 2013 shows a clear trend of NOM (Figure 1). The data also demonstrates that there is large temporal variability in bar configuration. For example, in 2006 the outer bar

crest was located in a water depth of 4 m relative to local mean sea level with a crest to trough height of 3m while in 2012 it was 7.4 m deep with a height of 0.6 m. These conditions represent the shallowest (2006) and deepest (2012) outer bar configurations observed within the CRLC dataset. Further, the relatively shallow depth and proximity to the shoreline of the outer bar in 2006 suggests a much earlier stage of the NOM relative to the 2012 profile. The bar depth in the 1999 profile is between that of the 2006 and 2012 cases at 6.8 m, however exhibits an anomalously large bar height of 3.7 m. Bar height is a function of a number of morphodynamic processes and in the case of the 1999 profile represents an extreme end-member case likely the result of the storm event of record for the CRLC that occurred in March of that year (Allan and Komar, 2002).

The data indicates that the average life cycle of a bar in the Oysterville region of the Long Beach subcell of the CRLC is about 2.4 years. As bars progress through the cycle and migrate further offshore there is a clear trend of increasing mean bar depth as demonstrated in Figure 2. Therefore, depending on the stage of the NOM wave breaking patterns will vary considerably, especially during large storm events. For this reason it is expected that the stage of NOM will have a large control on inner nearshore and intertidal hydrodynamics within multi-barred systems.

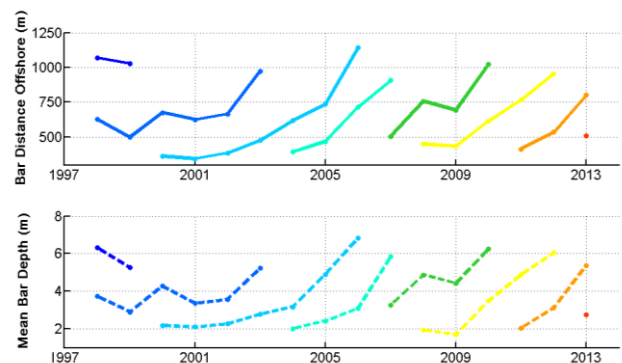


Figure 2. Average bar distance offshore (left panel) and mean bar depth (right panel) from 1998 to 2013 in the Oysterville region of the CRLC. Colors represent individual sandbars.

## Wave Runup

The TWL determines the horizontal and vertical extent of the interface between water and land and serves as an important metric for backshore flooding and beach erosion (e.g., Sallenger, 2000). In some physical settings extreme TWLs are primarily driven by storm surge, such as on the East and Gulf coasts of the US during major tropical cyclones. However, along the US West Coast, where the continental shelf width is relatively narrow, the wave induced component of extreme TWLs can dominate.

A number of field experiments using in-situ and remote sensing measurements have been completed in an attempt to correlate the instantaneous wet/dry beach interface to local wave conditions. Derived from Argus video monitoring data, the most commonly used formulation of runup is that of Stockdon *et al.* (2006). Data from 10 experiments on 6 different beaches was used to develop empirical relations of setup ( $\eta$ ), incident swash ( $S_{inc}$ ), and infragravity swash ( $S_{IG}$ ), which were parameterized as:

$$\eta = 0.35 B_f H_o L_o^{1/2} \quad (1)$$

$$S_{inc} = 0.75 B_f H_o L_o^{1/2} \quad (2)$$

$$S_{IG} = 0.06 H_o L_o^{1/2} \quad (3)$$

where  $H_o$  is the deepwater wave height and  $L_o$  is the deepwater wave period. They give the  $R_{2\%}$ , which is the runup that is exceeded only 2% of the time, as:

$$R_{2\%} = 1.1 \eta + \frac{S_{inc}^2 + S_{IG}^2}{2} \quad (4)$$

Though some of the beaches that were analyzed for these experiments had nearshore sandbars, the only explicit incorporation of the coastal morphology within this formulation is the foreshore slope. The authors did recognize that other metrics such as the surf zone slope could similarly be important for runup, although they did not find statistically significant correlations to justify incorporating those factors into their model.

In reality, however, it seems intuitive that nearshore morphologic features, such as sandbars, might have a considerable influence on runup. Recognizing this, researchers have sought to explicitly correlate swash and setup to properties of simple single bar geometries. Stephens *et al.* (2011) found that overall foreshore slope was a poor descriptor of the beach profile and that wave setup was strongly dependent on the presence and configuration of sandbars in the surf zone. Cox *et al.* (2013) used XBeach to correlate the presence of nearshore bars to infragravity (IG) swash. They found that in cases where waves broke seaward of the bar system that IG swash was reduced at the shoreline relative to cases without a bar. They propose a new model-derived empirical formulation for IG swash accounting for basic geometric considerations of the single bar system as an improvement on the Stockdon *et al.* (2006) model.

## Surf Zone Sediment Transport

Sediment transport within the inner surf zone remains poorly understood in part because of flow nonlinearities and the difficulty in obtaining in-situ measurements. However, many factors, including mean currents, incident waves, and IG waves, are known to influence the cross-shore fluxes of sediment in this environment (e.g. Roelvink and Stive, 1989).

A number of approaches exist that attempt to characterize cross-shore sediment transport fluxes often taking a form similar to:

$$q_x(x, y, t) = \frac{\partial h C u^E}{\partial x} + \frac{\partial}{\partial x} D_h h \frac{\partial C}{\partial x} \quad (5)$$

where  $C$  is the depth averaged sediment concentration,  $D_h$  is a sediment diffusion coefficient,  $h$  is the local water depth, and  $u^E$

is the cross-shore directed Eulerian velocity (Roelvink *et al.*, 2010). Equilibrium sediment concentrations are commonly predicted using the Soulsby-van Rijn formulation (Soulsby, 1997) to solve for advective and diffusive sediment transport along sandy coasts.

Just as sandbars have some influence on runup, morphology likewise alters inner nearshore hydrodynamics and sediment transport. For example wave breaking patterns will alter the asymmetric nature of the waves which will in turn influence advective transport. These morphodynamic feedbacks are important for whether a coastal system will be erosive or accretional. Therefore, in addition to investigating how nearshore morphology influences runup, we explore how bar configuration alters cross-shore sediment fluxes according to the sediment transport formulas available in XBeach.

## METHODS

In order to assess how complex morphology affects nearshore hydrodynamics and sediment transport, the eXtreme Beach (XBeach) model is applied for the CRLC under different stages of NOM. XBeach is a state of the art model that simulates spatially varying, depth averaged (2DH) flow characteristics and sediment transport in shallow water coastal environments (Roelvink *et al.*, 2010). The model is short-wave averaged, but resolves wave groups and infragravity wave motions as waves refract, shoal, break, and dissipate in the nearshore. Long period (infragravity) wave motions can dominate the hydrodynamics in the swash zone and are particularly important in the U.S. Pacific Northwest (Ruggiero *et al.*, 2004). As a non- short-wave resolving model, formulations do not directly take into account intra-wave properties. Wave shape induced velocity and acceleration skewness, are therefore parameterized using the Ursell number (Roelvink, 2010). Low frequency and mean flows are predicted using the nonlinear shallow water equations (NSWE). The Soulsby-van Rijn sediment transport formula is used to predict cross-shore and alongshore fluxes of sediment.

The XBeach model was applied to beach profiles from 1999, 2006, and 2012 from the CRLC dataset, which exhibit distinct phases of the NOM cycle (Figure 1). The model domain has variable spacing in the cross-shore direction with sub-meter resolution at the shoreline and up to 25 m resolution in intermediate water depths. The model domain extends 2,000 m offshore, which corresponds approximately to the 12m depth contour. The bathymetry was assumed to be uniform alongshore, however to generate bound long waves the model was run in 2DH mode and was extended 1 km in the alongshore direction with grid spacing of 25 m. For each nearshore bathymetric configuration the model is forced with combinations of offshore waves with SWHs of 1 to 10 m and periods of 6 to 18 s representing a realistic range of wave conditions for the CRLC. Offshore wave spectra using these heights and periods were modelled by the JONSWAP formulation and were linearly shoaled to the local XBeach model domain using the Simulating WAVes Nearshore (SWAN) model (Booij *et al.*, 1999). For simplicity all offshore waves input into SWAN were assumed to be propagating normally to shore. All other inputs to SWAN and XBeach were assumed to be the model default although morphologic updating is turned off such that our focus is on nearshore hydrodynamics and sediment transport.

For all 70 simulations that made up the run matrix for each bathymetric profile, XBeach was run for 1 hr and a time series of total water levels was extracted from the model output. Additional outputs such as current velocities and sediment fluxes were also obtained for select runs.

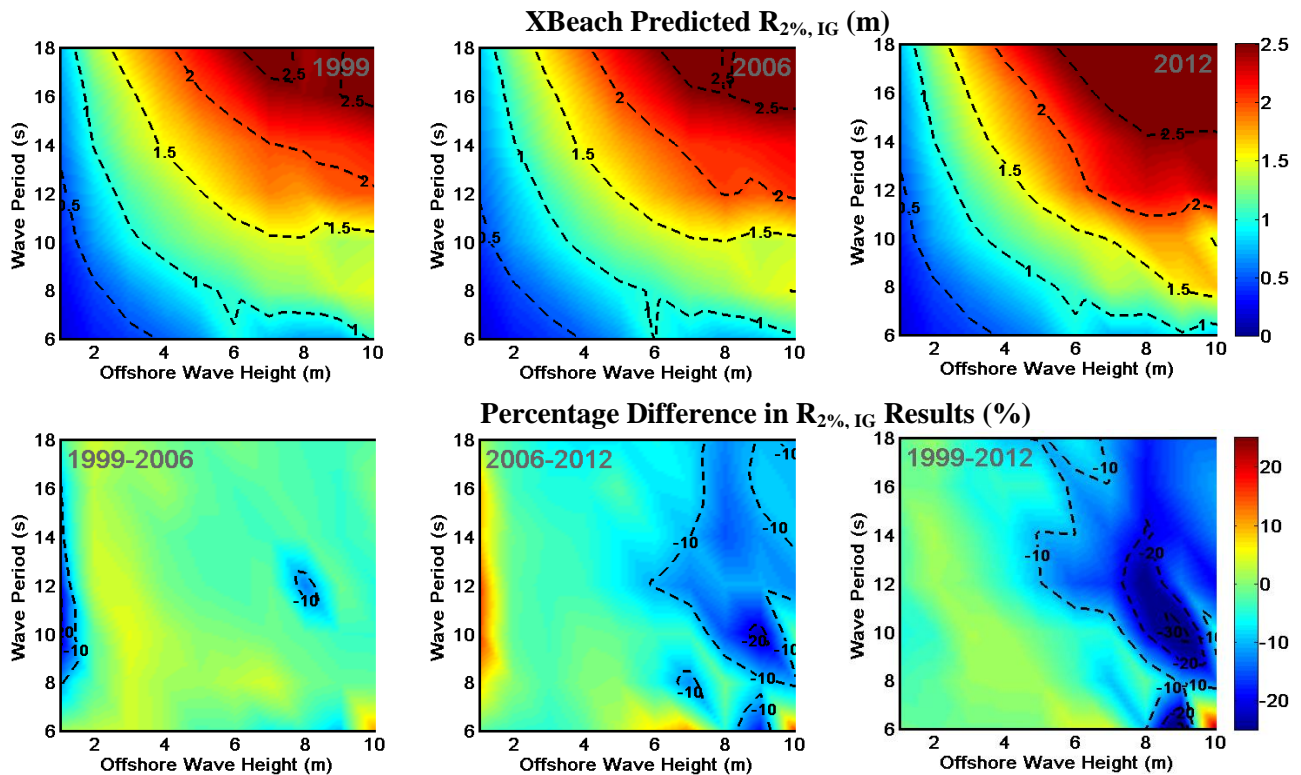


Figure 3. Model predicted  $R_{2\%, IG}$  for the 1999, 2006, and 2012 CRLC profiles from transect 66 under different combinations of offshore significant wave heights and peak wave periods (upper panels). Difference in results between 1999 and 2006, 2006 and 2012, and 1999 and 2012 (lower panels).

## RESULTS

### Wave Runup

XBeach simulated wave runup estimates are presented in Figure 3. The  $R_{2\%, IG}$  metric represents the water level that is only exceeded 2% of the time resulting from setup and infragravity swash (incident swash is not accounted for in XBeach) and is given by:

$$R_{2\%, IG} = 1.1 \eta + \frac{4\sigma_{IG}}{2} \quad (6)$$

where  $\sigma_{IG}$  is the standard deviation of the swash maxima. This approach is consistent with that used by Stockdon *et al.* (2006). As expected the results show that runup increases with increasing offshore wave height and increasing peak period. For a 2 m, 8 s wave (characteristic of average wave conditions in the CRLC), the  $R_{2\%, IG}$  is 0.45 m, 0.46 m, and 0.46 m, for the 1999, 2006, and 2012 cases, respectively. Under these moderate wave conditions, model results indicate that the influence of varying bathymetry is negligible – in part because wave breaking does not occur until relatively close to shore. However in the Pacific Northwest, waves reaching 10 m are not uncommon during winter storm events (Allan and Komar, 2002). An 8 m, 14 s wave (characteristic of a winter storm) results in predicted  $R_{2\%, IG}$  of 2.04 m, 2.08 m, and 2.45 m, for the 1999, 2006, and 2012 cases, respectively, demonstrating more variability in the predicted runup during high energy conditions. As shown in Figure 3, the differences between the three years can reach up to 36% for the same offshore conditions but differing nearshore morphology.

Numerical model results were also compared against the empirical model of Stockdon *et al.* (2006) for the setup and IG component of swash in Figure 4. The two approaches for computing  $R_{2\%, IG}$  show similar trends with some notable exceptions. XBeach underpredicts Stockdon for low energy conditions (small wave height and/or wave period), while XBeach typically predicts higher  $R_{2\%, IG}$  when wave height and period are larger such as is typical during storms. The mean difference between Stockdon and XBeach is -0.12 m, -0.12 m, and -0.21 m for the three bathymetries, with negative results representing an overprediction of the empirical model by XBeach. Overall the two approaches yield a difference of up to -0.7 m in magnitude (Table 1). The maximum percentage difference between the two approaches was 42%.

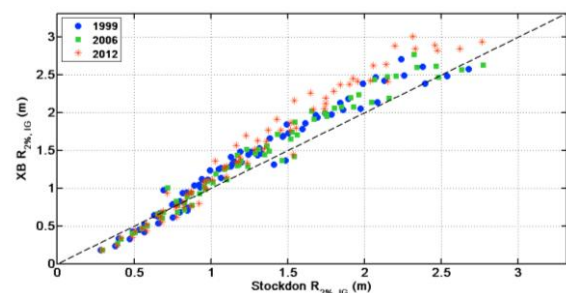


Figure 4. Comparison of  $R_{2\%, IG}$  between XBeach and Stockdon formulation for 1999, 2009, and 2012.

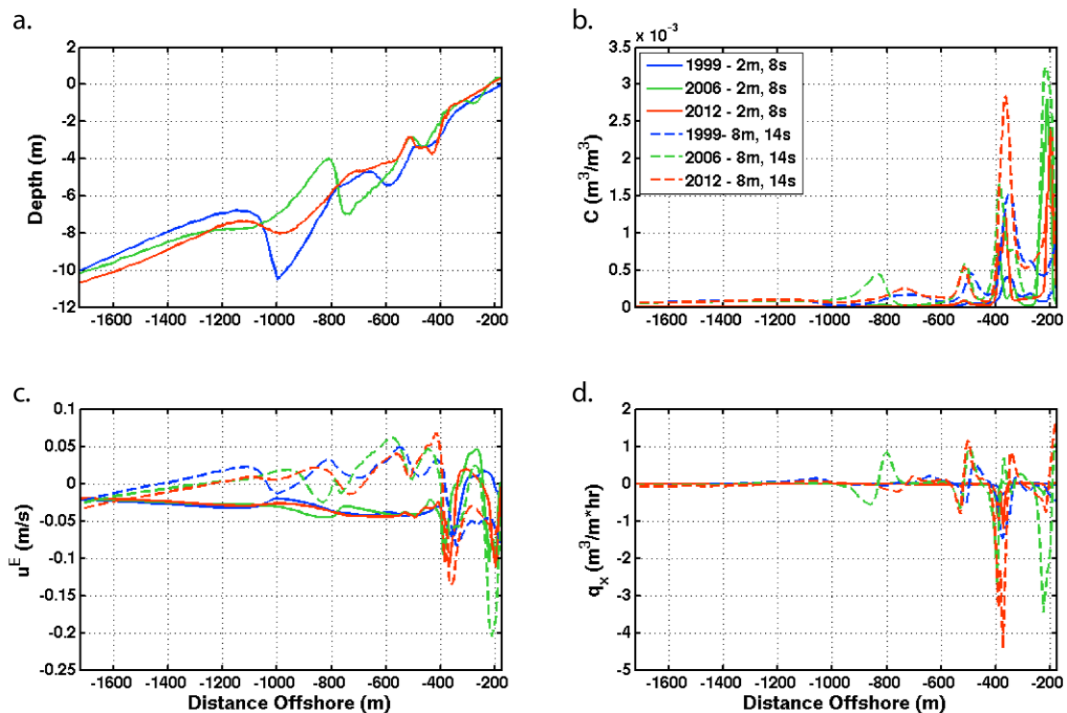


Figure 5. Average (b) total sediment concentration, (c) Eulerian transport velocity, and (d) cross shore sediment transport with distance offshore for the 1999, 2006, and 2012 simulations for **Scenario 1** –  $H_s = 2$  m,  $T = 8$  s (solid lines), **Scenario 2** –  $H_s = 8$  m,  $T = 14$  s (dotted lines). Bathymetry for the three years is shown in (a).

Table 1. Magnitude and percentage (in parentheses) differences between Stockdon and XBeach  $R_{2\%, 1G}$ . Negative values represent an overprediction of Stockdon by XBeach.

Metric	1999	2006	2012
Mean	-0.12 m (-6.5 %)	-0.12 m (-6.3%)	-0.21 m (-10.7%)
Minimum	-0.47 m (-41.7%)	-0.49 m (-42.4%)	-0.70 m (-40.0 %)
Maximum	0.14 m (37.5%)	0.12 m (37.2%)	0.16 m (37.4%)

### Surf Zone Sediment Transport

While a host of factors affect cross-shore sediment transport, our goal here is to assess the relative role that the net offshore bar migration cycle plays on nearshore hydrodynamics and sediment transport. Two specific scenarios were investigated to look at spatial trends in cross-shore transport: a 2 m, 8 s wave and an 8 m, 14 s wave. These are characteristic of U.S. Pacific Northwest average wave conditions and storm wave conditions as previously described. XBeach was used to calculate sediment transport fluxes for these two scenarios for each of the three bathymetries. Figure 5 shows alongshore and time averaged cross-shore sediment transport properties for the six cases.

In the outer sandbar zone, defined here as the region from the -10 m contour to the outer bar trough, the average total cross shore transport over the one hour simulation is  $-1.8 \times 10^{-3} m^3 m^{-1}$ ,  $-3.5 \times 10^{-3} m^3 m^{-1}$ , and  $-1.4 \times 10^{-3} m^3 m^{-1}$  for 1999, 2006, and 2012, respectively, for the average wave case, where negative values represent net offshore transport. For the storm event, the transport

is predicted to have transport rates of  $0.091 m^3 m^{-1}$ ,  $-0.022 m^3 m^{-1}$ , and  $-0.019 m^3 m^{-1}$  respectively for the three bathymetries.

The inner sandbar zone is defined here as the region from the outer sandbar trough to the mean water level. In this zone the average cross shore transport rate is  $-0.024 m^3 m^{-1}$ ,  $-0.042 m^3 m^{-1}$ , and  $-0.047 m^3 m^{-1}$  for the average wave case and  $-0.082 m^3 m^{-1}$ ,  $-0.15 m^3 m^{-1}$ , and  $-0.17 m^3 m^{-1}$  for the storm waves.

The sediment concentrations in the inner bar zone are quite different between the three bathymetries, which ultimately has a major influence on the net cross-shore transport. Unsurprisingly, the total sediment concentration (which here includes both bedload and suspended load transport) is higher for the storm wave cases relative to the average wave condition.

### DISCUSSION AND CONCLUSIONS

Many sandy coastal systems are characterized by a trend of net offshore sandbar migration. Dependent on stage of the NOM, the shoreline has different exposure to hazards such as flooding and erosion. The XBeach model results for three unique coastal profiles representing different stages of the NOM cycle in the CRLC show that  $R_{2\%, 1G}$  (runup minus incident band swash) varies by up to 36% for a given set of wave conditions (offshore significant wave height and peak period). The largest differences occur during high energy conditions when wave breaking occurs on the outer bar. The largest computed runup in our model tests generally occurred with the 2012 nearshore bathymetry when the outer bar was the deepest, especially under high wave conditions. This can in part be attributed to the role of the outer bar in dissipating wave energy far from the beach face, altering both the setup and infragravity swash components of runup. Interestingly, the results between 1999 and 2006 showed many similarities

despite having about a 3m difference in the depth of the outer bar. There are, however, other morphologic features of these profiles that could similarly alter the impact on nearshore hydrodynamics and offset the variance induced by the outer bar. More work must be completed to understand how the individual swash and setup components are altered by complex morphologic features such as these outer and middle bars. However, despite the profiles having different bar configuration all have generally the same foreshore slope. Therefore, this demonstrates that morphology exerts a strong control on runup and confirms that the foreshore slope alone is a poor descriptor of the nearshore morphology (Stephens *et al.*, 2012).

The Stockdon model predicted  $R_{2\%,IG}$  within 20 cm of the XBeach results on average. However, there were some conditions that resulted in over a 40% difference between numerical model and empirical estimates of  $R_{2\%,IG}$ . The largest differences occurred under moderate to high energy conditions where XBeach typically estimated larger  $R_{2\%,IG}$ . This is perhaps unsurprising given that the Stockdon formulation was developed using only limited high wave measurements. Since this formula is used by a wide range of practitioners for a range of applications, our work indicating possible limitations under high wave conditions with complex bathymetries suggests that further research is warranted.

To investigate the relation of NOM to surf zone sediment transport, two distinct wave scenarios were simulated. Under 2 m, 8 s waves XBeach predicted a net offshore transport of sediment for all three cross shore profiles. In the outer sandbar zone, the lowest rate of transport occurs in 2012 and the largest rate of transport occurs in 2006. This was expected based on the relative depths of the outer bars (2012 being the deepest and 2006 being the shallowest). In the inner bar zone the highest rate of transport occurs with the 2012 bathymetry, which could in part be a result of the deep water depth of the outer bar which results in waves breaking closer to shore, stirring up of sediment, and generating larger undertow.

Under the storm wave condition (8 m, 14 s) there is a net onshore sediment transport in the outer bar zone for the 1999 case and offshore predicted transport for 2006 and 2012. This demonstrates that even under the same wave conditions the morphology can alter both the rate and direction of net sediment transport. In the inner bar zone under storm waves all three profiles are expected to be erosional. However, Figure 5 demonstrates that there are highly complex spatial patterns in transport, with localized areas of onshore directed transport. The lowest net offshore sediment transport occurs with the 1999 bathymetry (intermediate offshore bar depth) and the highest transport occurs with the 2012 profile (deepest offshore bar depth). This suggests that there are other important factors in addition to the outer bar depth that influence inner surf zone sediment transport under very large wave conditions.

From these model simulations we have demonstrated that inter-annual variability in sandbar shape and position can significantly alter inner surf zone/swash zone processes. For this study, we have held the bathymetry constant and thus neglected some morphodynamic processes that would serve to alter the bar geometry in response to large wave events. These feedbacks can be highly complex as the coastal profile is constantly in flux. Thus while our findings may be limited due to the inherently dynamic nature of the system, we can conclude that sandbar configuration has a non-negligible influence on runup and surf zone sediment transport and it is apparent that significant work remains to further resolve the relationships between morphology, hydrodynamics, and ultimately coastal hazards.

## ACKNOWLEDGEMENT

This study was funded by Deltares, the Northwest Association of Networked Ocean Observing Systems (NANOOS), and the National Science Foundation Research Experience for Undergraduates (REU) program.

## LITERATURE CITED

- Aagard, T., Hughes, M., Baldock, T., Greenwood, B., Kroon, A., and Power, H., 2012. Sediment transport processes and morphodynamics on a reflective beach under storm and non-storm conditions. *Marine Geology*, 326-328, 154-165.
- Allan, J., and Komar, P., 2002. Extreme storms on the Pacific Northwest coast during the 1997-98 El Niño and 1998-99 La Niña. *Journal of Coastal Research*, 18, 175-193.
- Booij, N., Ris, R., and Holthuijsen, L., 1999. A third-generation wave model for coastal regions. *Journal of Geophysical Research*, 104, 7649-7666.
- Cox, N., Dunkin, L., and Irish, J., 2013. An empirical model for infragravity swash on barred beaches. *Coastal Engineering*, 81, 44-50.
- Hoefel, F. and Elgar, S., 2003. Wave-induced sediment transport and sandbar migration. *Science*, 299, 1885.
- Roelvink, D., Reniers, A., van Dongeren, A., van Thiel de Vries, J., Lescinski, J., and McCall, R., 2010. XBeach Model Description and Manual. Version 6.
- Roelvink, J. and Stive, J., 1989. Bar-generating cross-shore flow mechanisms on a beach. *Journal of Geophysical Research*. 94, 4785-4800.
- Ruessink, B., Wijnberg, K., Holman, R., and Kuriyama, Y., 2003. Intersite comparison of interannual nearshore bar behavior. *Journal of Geophysical Research*. 108, C8.
- Ruggiero, P., Holman, R., and Beach, R., 2004. Wave runup on a high-energy dissipative beach. *Journal of Geophysical Research*, 109: C6.
- Ruggiero, P., Kaminsky, G., Gelfenbaum, G., and Voigt, B., 2005. Seasonal to interannual morphodynamics along a high-energy dissipative littoral cell. *Journal of Coastal Research*, 21, 553-578.
- Ruggiero, P., Komar, P., and Allan, J., 2010. Increasing wave heights and extreme value projections: the wave climate of the U.S. Pacific Northwest. *Coastal Engineering*, 57, 539-552.
- Sallenger, A. 2000. Storm impact scale for barrier islands. *Journal of Coastal Research*, 16, 890-895.
- Soulsby, R., 1997. *Dynamics of Marine Sands*. Thomas Telford Publications, London.
- Stephens, S., Coco, G., and Bryan, K., 2011. Numerical simulations of wave setup over barred beach profiles: implications for predictability. *Journal of Waterway, Port, Coastal, and Ocean Engineering*. 137, 175-181.
- Stockdon, H., Holman, R., Howd, P., and Sallenger, A., 2006. Empirical parameterization of setup, swash, and runup. *Coastal Engineering*. 53, 573-588.
- Thornton, E., Humiston, R., Birkemeier, W. (1996). Bar-trough generation on a natural beach. *Journal of Geophysical Research*, 101, 12097-12110.
- Walstra, D., Reniers, A., Ranasinghe, R., Roelvink, J., and Ruessink, B., 2012. On bar growth and decay during interannual net offshore migration. *Coastal Engineering*. 60: 190-200.

# Volumetric changes of a soft cliff coast 2008-2012 based on DTM from airborne laser scanning (Wolin Island, southern Baltic Sea)

Joanna Dudzińska-Nowak†, Piotr Wężyk‡

†University of Szczecin  
Institute of Marine and Coastal Sciences  
Szczecin, Poland  
jotde@univ.szczecin.pl

‡ University of Agriculture in Krakow  
Laboratory of Geomatics  
Krakow, Poland  
rlwezyk@cyf-kr.edu.pl



[www.cerf-jcr.org](http://www.cerf-jcr.org)



[www.JCRonline.org](http://www.JCRonline.org)

## ABSTRACT

Dudzińska-Nowak, J., Wężyk, P., 2014. Volumetric changes of a soft cliff coast 2008-2012 based on DTM from airborne laser scanning (Wolin Island, southern Baltic Sea). In: Green, A.N. and Cooper, J.A.G. (eds.), *Proceedings 13<sup>th</sup> International Coastal Symposium* (Durban, South Africa), *Journal of Coastal Research*, Special Issue No. 70, pp. 59-64, ISSN 0749-0208.

A comparison of DTMs off a 2 km-long section of the southern Baltic Sea cliff coast at Wolin Island, composed of unconsolidated Pleistocene sediments with NW exposure and maximum height of 93 m, prepared on the basis of airborne laser scanning (ALS) data collected in 2008, 2009, 2011 and 2012 allowed the magnitude and spatial distribution of changes to be determined. Morphodynamic processes were spatially and temporally diverse. The time period 2008-2012 is dominated by erosion expressed by a negative sediment balance of  $-33,000 \text{ m}^3$ . The volume of eroded material was  $49,080 \text{ m}^3$ , while the volume of accumulated material –  $15,678 \text{ m}^3$ . The largest changes were observed in the upper parts of active cliff as a result of mass wasting triggered by loss of the slope stability due to erosion of the lower part of the slope. Significant erosion also occurred on the lower part of the cliff and on the beach. The accumulation is a consequence of material deposition on the beach and at the cliff base. Erosion could be correlated with the number of storm events and with water levels. The results confirm previous studies on the role of factors that regulate the magnitude of coastal erosion, the first being water level rise during the storm events as well as the influence of a series of storms.

**ADDITIONAL INDEX WORDS:** *volumetric cliff changes, airborne laser scanning, storm surges, coastal erosion.*

## INTRODUCTION

Sea coasts are sensitive to global climatic and environmental changes. These changes include accelerated sea level rise and increased intensity of extreme storm events (Sztobryn et al., 2005; Furmańczyk, Dudzińska-Nowak, 2009; Stanisławczyk, 2012). On the Southern Baltic Sea coasts these changes are accompanied by glacio-isostatic lowering of the land causing a relative sea level rise of up to 2 mm/y (Harff et al., 2007) as well strong storm events that cause progressive coast retreat (Zawadzka-Kahlau, 1999; Dudzińska-Nowak, 2006).

Access to the area, because of the narrow beach and cliff height, can be difficult and traditional survey and photogrammetric methods are not feasible. Implementation of airborne laser scanning technology (ALS; LiDAR- Light Detection and Ranging) to monitor coastal changes in 3D space opens new opportunities to identify precisely the magnitudes, structures and spatial distribution of changes occurring within the coastal zone. Use of digital terrain models (DTM), generated on the basis of ALS point clouds, is now a widely deployed method in many environmental management applications (Szostak et al., 2013) including morphometric analyses, landslide monitoring (Wójcik et al., 2013), geomorphological modelling and hydrological modelling.

In this study we assembled measurements using a diverse range of techniques over a five year interval with the aims of: (1) obtaining a coherent image of the changes taking place in

both the nearshore and the backshore environment as well as (2) collecting information on the main driving factor involved.

Bathymetric laser scanning, applied successfully in oceanic waters and even in the Northern Baltic Sea is inefficient within the study area due to a high degree of turbidity. The alternative is to merge bathymetric profiles with ALS data.

Combining information on the size and spatial behaviour of coastal and nearshore changes with the main drivers (storm events in the non-tidal Baltic Sea) of geomorphological evolution provides opportunities to analyse the morphodynamics of the cliffed coastline.

Analyses of the cliff coast in the area of Gosań hill (93,4 m A.S.L.; 53°57'12" N; 14°29'9" E) on Wolin island (408.7 – 410.7 Maritime Office km (km MO)) on the Southern Baltic Sea coast, using four sets of ALS data (2008, 2009, 2011 and 2012), are presented and discussed in this article. Pleistocene glacial sediments (mainly glacial till and sands) are exposed at the base of the analysed cliff. These are overlain by fluvio-glacial sand and sand with gravel mixtures as well as limno-glacial sandy and silty sediments. Within the nearshore, to a depth of 5 m (approx. 250 m off the coast), fine sands overlie glacial tills, whereas in the deeper nearshore (approx. 250-800 m off the coast), up to the 10-m isobath, fine sands are replaced by medium sands (Dobracki, Zachowicz, 2005). Despite the cliff comprising soft deposits, its slope is over 15° (Fig. 1), which places it in the “steep” category (Klimaszewski, 1994, ITB guidelines no. 424/2006). The inclination increases to “very steep” and even to “precipitous” at places where till deposits are exposed on the

lower parts of the cliff. Most of the cliff remains active. Only one part of the investigated section, between 409.5 – 410.5 km MO, is represented by inactive cliff covered by dense vegetation.

The aim of this study is to determine the magnitude and spatial distribution of changes to the active surface of the cliff and to the beach based on digital terrain models (DTM) generated from ALS point clouds. The obtained results are discussed in terms of hydrodynamic factors driving the changes as well as in view of geological and geomorphological settings.

**MATERIALS AND METHODS**

Water level changes and wave action trigger diverse effects depending on the geological and geomorphological settings. Various measuring techniques are needed to capture change on subaerial and underwater sections of the cliffed coast.

We utilized four series of airborne laser scanning data derived consecutively using the following scanners: LMS-Q560i Riegl (31.08.2008), TopEye SN 741 (30.11.2009), LMS-Q680i Riegl (21.03.2011) and LMS-Q680i Riegl (28.09.2012).

In case of analysis of ALS data derived by means of various scanners, attention must be paid to proper pre-preparation of the geodata. In order to make a credible comparison between individual years available, pre-processing should concern both the horizontal (X, Y) and the elevation (Z) adjustments of point

clouds as well as the selection of points which represent the ground (Weżyk 2008). The registered ALS point clouds from 2008, 2009 and 2011 were referenced to the ALS data from 2012. A comparison of georeference deviations (X, Y) was made for 12 points on roof ridges of buildings within the study area. The discrepancies between particular years and the reference year of 2012 are displayed as a root mean square (RMS) in Table 1. The differences in elevation (Z) were determined each time by means of a reference grid composed of 36 points, which were generated on the basis of the DTM of 2012 which was superimposed consecutively onto the other 3 digital terrain models.

Before generating DTMs, a transformation of ALS point clouds of 2008, 2009 and 2011 with a spatial vector was carried out in order to adjust the DTM models (Table 2). For this purpose, a macro command containing predefined spatial vector values was applied using TerraScan (Terrasolid Ltd.) software.

The analysis commenced with the filtering and classification of the ground. A macro command based on the active triangulation algorithm (adaptive TIN), which looks for the nearest neighbours in the “ground” class at a predefined distance and angular range (Axelsson, 2000), was used. Once a points classification and manual inspection combined with imposition discontinuity lines and structural lines were done (application of aerial photographs in TerraPhoto module), a DTMs (GSD 1.0m) was generated and saved in ASCII GRID format. The PL-1992 (EPSG2180) coordinate system was accepted as valid for this study (Journal of Laws of 2012, item 1247).

Further calculations and morphometric analyses were run in the ArcMap ArcGis 10.1 ESRI software applying the Spatial Analysis and 3D Analyst extensions. The calculations of accumulation and

Table 1. Georeference deviations of ALS point clouds of particular years in relation to the data of 2012 (reference data).

ALS data	RMS X (m)	RMS Y (m)	RMS XY (m)	RMS Z (m)
2008	0.17	0.35	0.39	0.16
2009	0.14	0.23	0.27	0.10
2011	0.15	0.52	0.54	0.01

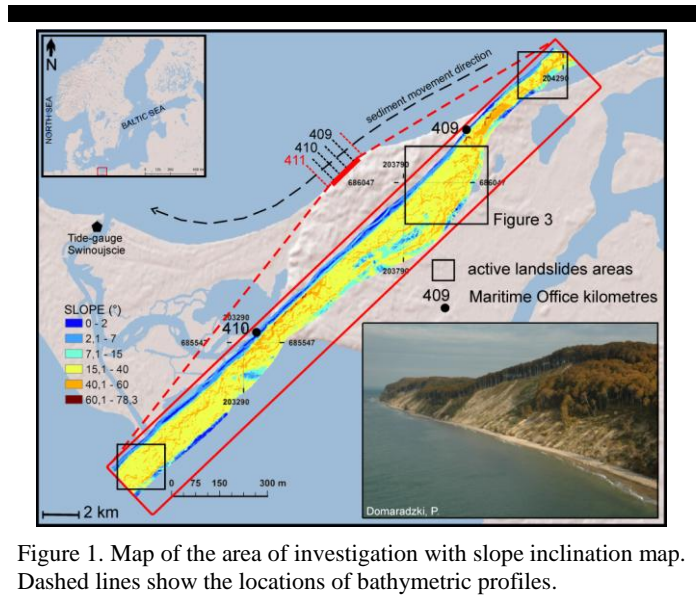


Figure 1. Map of the area of investigation with slope inclination map. Dashed lines show the locations of bathymetric profiles.

erosion volumes of the coastal changes were performed by means of the Cut/Fill command. This algorithm calculates the change of volume between two DTM surfaces, e.g., DTM 2008 and DTM 2012. This is typically used for cutting (removal/erosion – positive values in the attribute table) and filling (deposition/sedimentation – negative values in the attribute table) – GIS spatial operation. The coastal volume changes were analysed in relation to water level oscillations during storm events which occurred between LiDAR surveys. Tide gauge data from Świnoujście, located 14 km west of study area (Fig. 1), were provided by the Maritime Office in Szczecin (Fig. 2).

Bathymetric profiles carried out by means of echo sounder as a part of yearly coastal monitoring performed by the Maritime Office in Szczecin (Fig. 1) in 2008, 2009, 2010, 2011 and 2012 were used to analyse the changeability of the nearshore. These profiles are spaced at 500 m intervals along the coast and cover the nearshore zone out to 2 km seawards on average, within the depth range of -1.5 to -11 m. Four profiles are located within the area of investigation (409 km MO, 409.5 km MO, 410 km MO

Table 2. Vector values of applied corrections for sets of ALS point clouds from 2008, 2009 and 2011.

ALS data	dX (m)	dY (m)	dZ (m)
2008	0.17	0.35	0.16
2009	0.14	0.23	0.10
2011	0.15	0.52	0.01

and 410.5 km MO). Two neighbouring profiles: 408.5 km MO on the Eastern side and 411 km MO on the Western side were also analysed. The dates of bathymetric profiling do not correspond exactly to the dates of ALS data registrations (Fig. 2), however, accepting the assumption that considerable modifications of dynamic layer occur, mainly during strong storm events, an attempt was made to connect them with the backshore changes.

**RESULTS AND DISCUSSION**

The changes observed within the cliff active surface and presented on Figure 3 are the results of the impact of both storm events and slope processes determined by structure and geological setting as well as hydrodynamic conditions. A considerable dominance of erosion processes over accumulation is evident for

Table 3. Magnitude of volume changes of the cliff active surface and the beach in the analysed time periods (m<sup>3</sup>).

	2008-2009	2009-2011	2011-2012	2008-2012
<b>total volume changes</b>				
balance	2 600	-37 906	22 651	-33 402
active volume	41924	48 908	72 351	64 758
erosion	19 662	43 407	24 850	49 080
accumulation	22 262	5 501	47 501	15 678
<b>volume changes of the cliff</b>				
balance	-4 780	-20 921	-7 193	-32 895
active volume	32 274	32 895	38 705	58 068
erosion	18 528	26 908	22 949	45 482
accumulation	13 748	5 987	15 756	12 586
<b>volume changes of the beach</b>				
balance	7 380	-16 013	29 844	-506
active volume	9 648	16 985	33 646	6 690
erosion	1 134	16 499	1 901	3 598
accumulation	8 514	486	31 745	3 092

the entire analysed period of 2008-2012 and is expressed by a negative sediment balance of -33,402 m<sup>3</sup> (Table 3).

A total of 64,758 m<sup>3</sup> of material was displaced within the beach and cliff active surface. A significant spatial variability in change is evident. Three areas of active landslides are clearly visible: on the eastern and western edges of the area, near 408.8 km MO and 410.5 km MO, as well as at the greatest landslide, located in the eastern part within the coast section of 409.1-409.3 (Fig. 1). The sizes spanned from -7 m to 6.3 m. The changes occurred mainly in the eastern part of the area of investigation as well as on the western edge in the active cliff area. The greatest erosion was recorded in the upper parts of the cliff as a result of slope processes in the area of active landslides (Fig. 3) as well as in the lower parts of the cliff as a result of storm events. The volume of eroded material amounted to 49,080 m<sup>3</sup>, while the volume of accumulated material was 15,678 m<sup>3</sup>.

Between 2008 and 2009 a total amount of 41,924 m<sup>3</sup> of material was being displaced within the beach and cliff active surface. The volumes of accumulated and eroded material were similar (22,262 m<sup>3</sup> and 19,662 m<sup>3</sup>, respectively). The changes occurred mainly in the lower parts of the active cliff and on the beach, most probably as the result of storm events (Fig. 3) and resulting small landslides

which did not include the upper parts of the cliff. The magnitude of changes oscillated between -4.2 and 6.1 m. A positive sediment balance (2,600 m<sup>3</sup>) was the result of accumulation on the beach and colluvium at the cliff base. 48,908 m<sup>3</sup> of material was displaced during the subsequent period from 2009-2011. A considerable dominance of erosion over accumulation was visible. The volume of eroded material amounted to 43,407 m<sup>3</sup>, whereas the volume of accumulated material was only 5,501 m<sup>3</sup>. This resulted in a negative sediment balance of -37,906 m<sup>3</sup> in 2009-2011. The magnitude of change spanned from -8.2 to 13 m. The largest changes, which were caused indirectly via the influence of storm events, were observed in the upper parts of active cliff as a result of mass wasting triggered by loss of slope stability (Fig. 3). As in the previous period, significant erosion also occurred in the lower part of the cliff and on the beach. The reported accumulation is a consequence of material deposition at the cliff base. The period from 2011-2012 was characterised by the greatest amount of displaced material within the beach and cliff active surface - 72,351 m<sup>3</sup>. The accumulated volume almost doubled the eroded volume and amounted to 47,501 m<sup>3</sup> and 24,850 m<sup>3</sup>, respectively. This resulted in a positive sediment balance amounting to 22,651 m<sup>3</sup>. The magnitude of changes ranged from -6.7 to 5.5 m. Erosion was mainly visible in places of active landslides at the cliff slope and base. The accumulation of material occurred mainly on the beach and only to a slight extent on the lower part of the cliff.

A considerable diversification of erosion and accumulation volumes within the cliff active surface and beach was observed (Table 3). A comparable amount of material was displaced within the cliff active surface in all three time periods and amounted to: 32,274 m<sup>3</sup>, 32,895 m<sup>3</sup> and 38,705 m<sup>3</sup>, respectively. Accumulations in the form of colluvium accrued generally at the base, but also on the slope, and derived from the material that slid off the cliff slope amounted to 12,000 m<sup>3</sup> per year on average. All the analysed time periods reveal dominant erosion changes expressed by a negative sediment balance amounting to -4,780 m<sup>3</sup>, -20,921 m<sup>3</sup> and -7,193 m<sup>3</sup>, respectively. The lowest volume of eroded material was modeled for the interval spanning 2008-2009 (18,528 m<sup>3</sup>), when of the accumulation volume was 13,748 m<sup>3</sup>.

From 2009-2011, extremely significant sediment losses were expressed by a combination of negative sediment balance as well as the greatest volume of eroded material (26,908 m<sup>3</sup>) of the all investigated time periods. Also, the lowest volume of deposited material was observed (5,987 m<sup>3</sup>). The last investigated time period was characterised by a slightly smaller dominance of erosion over deposition when compared to the 2009-2011 interval. 22,949 m<sup>3</sup> of material was eroded, whereas a much greater volume of sediment was deposited (15,756 m<sup>3</sup>).

Within the beach setting, both the balance and the volume of displaced material within particular time periods are characterised by great diversity. 9,648 m<sup>3</sup> of material were displaced in the period from 2008-2009, while the sediment balance was positive and amounted to 7,380 m<sup>3</sup>. The volume of material deposited on the beach was 8,514 m<sup>3</sup>, whereas the volume of eroded material was 1,134 m<sup>3</sup>. Between 2009 and 2011 erosion predominated and was expressed by a negative sediment balance of -16,013 m<sup>3</sup>. The volume of material eroded from the beach was 16,499 m<sup>3</sup> (97% of the entire material displaced). The third time period (2011-2012) encountered strongly opposing conditions to that of the second (2009-2011). High degrees of accumulation were expressed by a positive sediment balance (29,844 m<sup>3</sup>) and almost double the volume of material was displaced (33,646 m<sup>3</sup>). The volume of material that accumulated on the beach accounted for 94% of the

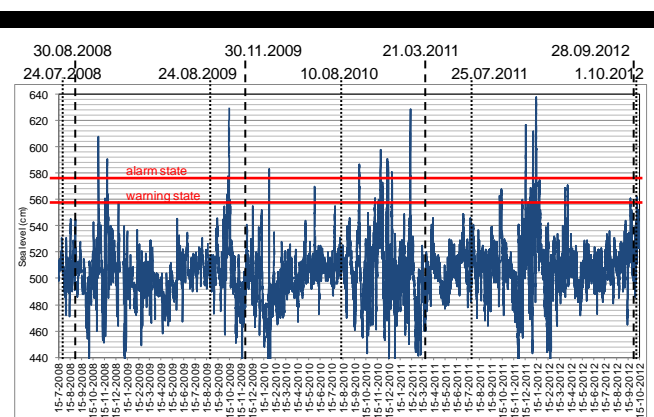


Figure 2. Water level at tide gauge in Świnoujście during the analysed time period (data source: Maritime Office in Szczecin), date of airborne laser scanning (dashed line) and bathymetric data surveys (dotted line).



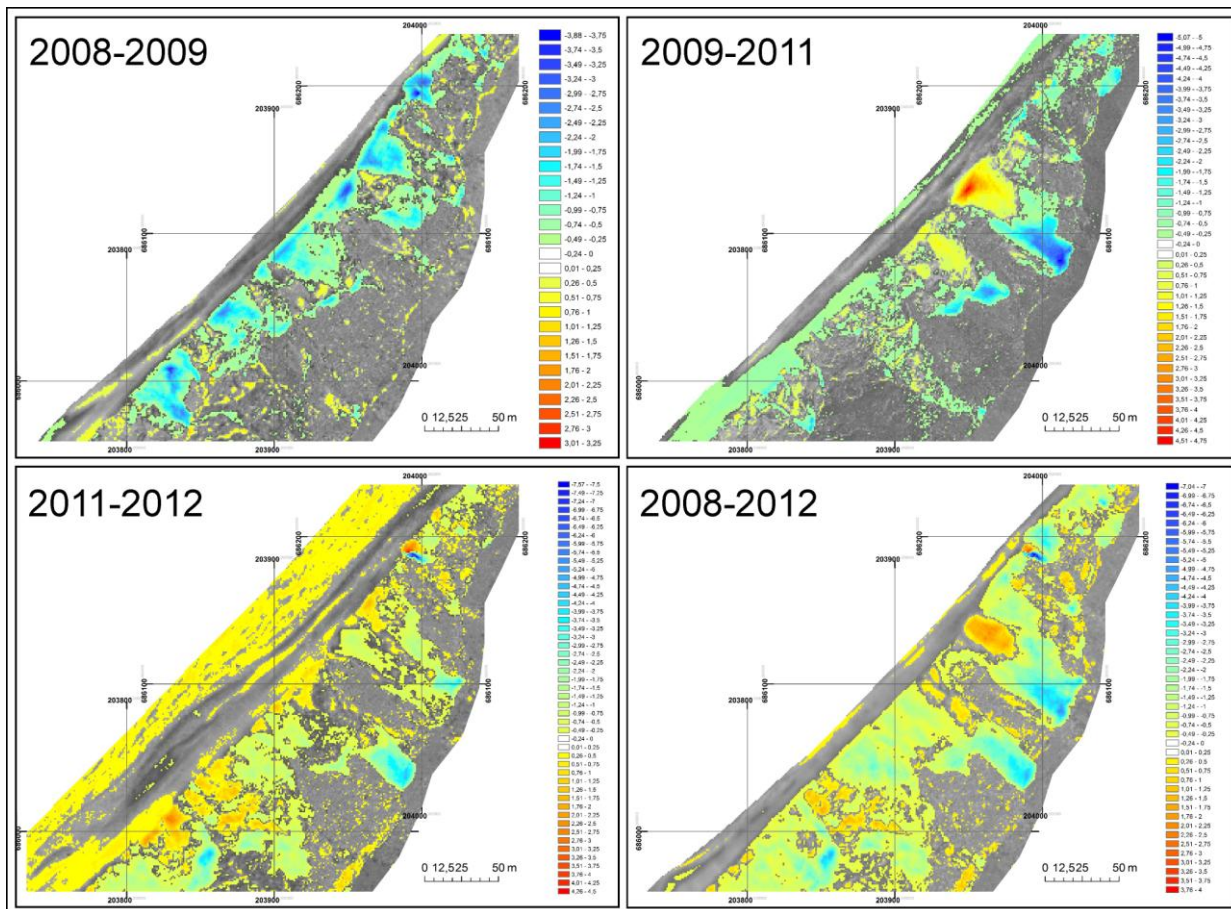


Figure 3. Spatial distribution of erosion and accumulation changes of the greatest active landslide located in the eastern part within the coast section of 409.1-409.3 in 2008-2009, 2009-2011, 2011-2012 and 2008-2012.

entire displaced material and the contribution of erosion was slight and amounted to only  $1,901 \text{ m}^3$ .

The greatest changes do not coincide with the steepest inclination of the slope, since these are associated with grey tills, which are significantly more resistant to erosion (Fig. 1).

On the basis of bathymetric profiles, nearshore changeability was analysed between consecutive measurements, moving from the East to the West in accordance with longshore sediment transport direction (Fig. 4). The main changes from 2008-2009 were mainly up to a depth of 2-2.5 m (100-120 m offshore). Accumulation was observed on the eastern edge of the study area, whereas the area of the active cliff erosion increased toward the west with a peak at the 409.5 km MO. In the area of inactive cliff, west of the 410 km MO, deposition of eroded material to a depth of 2 m was noted. No profile changes were observed at greater depths. Along the westernmost profile, a coastal berm moved towards the beach and a submerged bar was developing. In 2009-2010 the easternmost profile suffered changes over a considerably greater area out to a depth of 5 m. 0.5 m vertical accretion of the nearshore occurred down to that depth. Farther eastwards (409 km MO) a dominance of accumulation was also observed but it concerned only the submerged bar area 100 m offshore; while areas to a depth of 4 m suffered minor erosion of approximately 20 cm. The magnitude of changes along the profile decreased in the area of the greatest active landslide. Accumulation at the

coastal-front slope of the bar became negligible. Only a slight accretion of the seafront slope was noticed to a depth of 3.2 m. A significant degree of erosion between depths of 1.5 m to 2.5 m, that reached 80 cm locally, was noticed in the foreland of the inactive cliff. However, in the deeper parts, a slight accumulation of approximately 25 cm occurred. Further westwards, in the area of active landslide, continuous erosion of the seaward face of the bar (reaching 120 cm at the profile 410.5 km MO) as well as slight deposition at the seafront slope, were observed. Additionally, significant erosion of the nearshore between depths of 3-4 m was noted. In the 2010-2011 interval, erosion of the nearshore was dominant along the entire analysed section. The strongest erosion, however, occurred in the eastern sector. Erosion on the easternmost profile of 60-80 cm occurred down to a depth of 5 m. A distinct accumulation form with a height of 40 cm above the seabed was noticed in 2010 at a depth of 2 m. Profile 409.5 km MO suffered a complete washout of the second submerged bar of 1.2 m thickness, whilst deeper portions experienced 20 cm of erosion. Farther eastwards changes took place only to a depth of 2 m. Along the profile 409.5 km MO, a significant deposition of sediments caused accretion of the submerged bar to almost twice its original height as well as its slight landward movement. Significantly smaller changes occurred in the area of the inactive cliff and involved the reformation of the bar. Profile 410 km MO revealed mainly accumulation changes with the vertical accretion

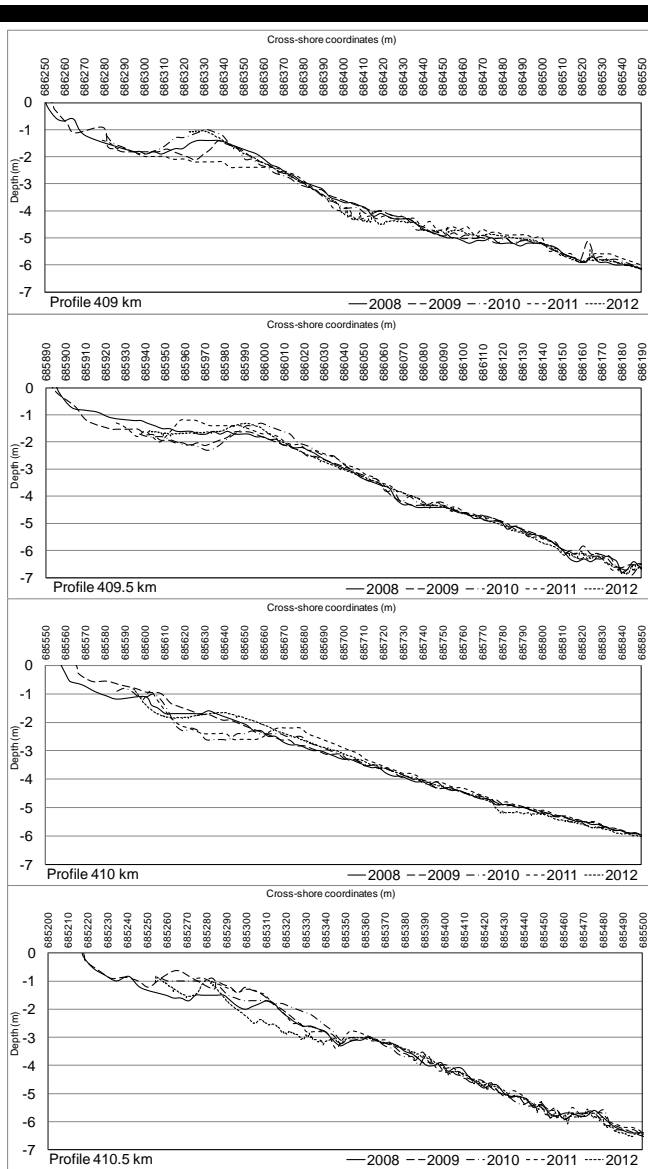


Figure 4. Nearshore changes on a base of bathymetric profiles for the analysed time period 2008-2012 (data source: Maritime Office in Szczecin).

of the seafront slope of the bar with a 40 cm thick layer. Farther westwards erosion predominated over accumulation and lowering of the nearshore by 40-60 cm was observed. The last analysed time period saw the smoothing of profile 408.5 km MO out to a depth of 6 m. The accumulation of a 40 cm – and locally a 60 cm – thick layer was observed to a depth of 2 m, whereas in the deeper parts washout of the submerged bar and erosion of a dynamic layer of 20 cm thickness were observed up to the end of the profile. In the area of the active landslide (409 km MO), significant deposition in the shallow nearshore to a depth of 2.4 m was observed, which led to restoration of a submerged bar of 1.2 m thickness. Slight erosional changes were also reported to a depth of 6 m. Further west changes occurred to a depth of 4 m. The lowering of the seaward face of the bar (40 cm) together with small accumulation of the seafront slope of the bar (25 cm) up to a depth of 1.8 m occurred. Further offshore, up to a depth of 3.6 m, erosion reaching 25 cm locally was noted. The area of the inactive

cliff suffered profile changes down to a depth of 6 m. A significant degree of accretion of the submerged bar (70 cm) occurred as well as its migration towards the coast. Consequently minor erosion of the seafront slope of approximately 30 cm occurred. Farther westwards, a significant 1 m of erosion was evident from 1 m to 3 m depths. Significant changes to the profile occurred to a depth of 3 m. A similar situation was observed on the westernmost profile. Considerable erosion to a depth of 2 m and slight accretion of the seaward face of the bar from a depth of 1.6 m to 2.4 m was observed.

Studies on the significance of particular storm parameters on the magnitude of coastal erosion show that the strongest correlation is associated first with water level, then with significant wave height and lastly, with significant wave direction (Furmańczyk et al., 2011); whilst the greatest coastal changes occur as a result of storm influence, during which a considerable surge –above warning and alarm levels– is observed (Furmańczyk and Dudzińska-Nowak, 2009). Catastrophic effects on the coast are observed in the case of a storm sequence, when storm events follow one after another in short intervals. In such cases, even a slight water level rise can cause significant damage to the coast (Ferreira, 2005; Furmańczyk and Dudzińska-Nowak, 2009).

The analysed period (31.08.2008 to 28.09.2012) contained 30 storm events recorded by means of a tide gauge in Świnoujście. 13 storm events exceeded the alarm level (580 cm), 6 of which exceeded 600 cm (Fig. 2). Therefore, the considerably greater coastal changes that were observed in the 2009-2011 interval compared to the 2008-2009 interval are the result of strong storm events registered in the autumn-winter storm season of 2010-2011. Eight storm events occurred within a three month period. The series began with a strong storm event from 27-29.09.2010, when water levels reached 587 cm and two smaller events came soon afterwards. The strongest storms occurred two months later. Within a month, between 23.11.2010 and 25.12.2010, four storm events were recorded during which the surge exceeded alarm level (580 cm). The strongest storm completed the series from 11-12.2.2011, when the sea level reached 629 cm. In the period 2011-2012, twelve storm events occurred, including three very strong ones, when water level exceeded 600 cm. They occurred just in a one month period (Fig. 2). From mid-January 2012 until the end of registration on 28.09.2012 no storm events were recorded that exceeded 580 cm. Most of the erosion changes reported within the study period are attributed to this series of very strong storm events, whilst the significant accumulation of the beach and shallow nearshore sediments are considered a result of natural processes of profile restoration under fairweather conditions.

Erosion changes in the nearshore profiles observed from 2008-2010 occurred mainly as a result of the strong storm of October 2009 (Fig. 4). The recorded accumulation changes in the eastern part of the investigated area are the result of the deposition of sediments that were eroded from the eastern side of the study area and moved via longshore transport. Most likely, a deficit of this material caused the erosion of the nearshore in the area of the inactive cliff. The observed accumulation on the seaward slope of the submerged bar is most probably a result of sediment deposition in the fairweather period from February to August 2010. Material that had been eroded as a result of storm events from the cliff, beach and nearshore was not deposited in the nearshore of the analysed section but partly deposited on the beach (hence a positive balance of nearshore changes for this period) and partly moved westwards or offshore. From 2010-2011 the dominance of erosion is a result of the series of strong storm events that also caused significant changes in the backshore. Nearshore changes covered a zone of 150 m width out to a depth

of 5 m. Only a small portion of the eroded material was deposited on the beach and in the nearshore. Most material was transported westwards and deposited on the seaward slope of the bar. Only in the area of 409.5 km MO was reconstruction and accretion of the submerged bar facilitated by the deposition of material. Erosion predominated in the nearshore sector between 2011 and 2012.

Accumulation occurred mainly in the eastern part of the area, in the foreland of the active cliff, whilst farther eastwards erosion was dominant. The material that was eroded from the cliff, beach and nearshore during strong storm events in the winter of 2011-2012 was re-deposited on the beach (Table 3) between April and October 2012.

## CONCLUSION

This study demonstrates the advantage of ALS technology over traditional survey methods. Application of this technology permitted precise assessment of the magnitude and spatial patterns of coastal volume changes over selected time intervals to be made.

A comparison of DTMs, prepared on the basis of airborne laser scanning data between 2008-2012, allowed the magnitude of coastal volume changes and their spatial distribution to be assessed. High spatial and temporal diversity in morphodynamic processes was evident. Three areas of intense changes were distinguished: two located in the place of active landslides, including the largest one in the eastern part of the investigated area and one on the western edge.

The entire analysed time period of 2008-2012 was characterised by the domination of erosion over accumulation, which is expressed by negative sediment balance amounting to  $-33,000 \text{ m}^3$ .  $64,000 \text{ m}^3$  of the material was displaced within the area of the beach and active cliff surface. The volume of eroded material was  $49,080 \text{ m}^3$ , while the volume of accumulated material was  $15,678 \text{ m}^3$ . Changes occurred mainly on the beach, on the lower parts of the cliff and within active landslides (Fig. 3).

These results confirm previous studies on the role of factors that regulate the magnitude of coastal erosion on the southern Baltic. First is the significance of sea-level rise during the storm events as well as the influence of a series of storms that increase the magnitude of changes and that occur one after another at very short intervals whereby the coast is unable to restore the balanced profile through the accumulation of material as occurred from 2009-2011. In the case of cliff coasts, hydrogeological factors provided damaging activity which was focused on the upper part of the cliff and was of great significance. Most slopes of the forested inactive cliff displayed stability. Soil creep was observed locally.

Bigger storm events cause changes in deeper parts of the bathymetric profile. From 2008-2009 and 2009-2010 profile changes reached a depth of 2-3 m, whereas for 2010-2011 and 2011-2012 the changes reached 5-6 m depths (Fig. 4). Long calm periods, without strong storm events, contribute to restoration of the nearshore profile.

In terms of presently occurring climate changes –an increase of number and intensity of storm events observed within the southern Baltic Sea and a general deficiency of sediments in the coastal zone– the determination of the accurate volumes and spatial distributions of change occurring on the coast through the application of state-of-the-art techniques (such as ALS) will allow more precise determination of the volume of sediment taking part in sediment balance. This is of particular importance for broadly defined coastal safety. The study presented here reveals that due to the wide variety of morphodynamic changes to neighbouring coastal sections within only a brief time span (a period of 5 years), a regular, long-term monitoring (through the application of remote

sensing surveying methods and GIS) is essential for effective coastal management.

## ACKNOWLEDGEMENTS

The authors would like to thank the Maritime Office in Szczecin and Mr Piotr Domaradzki in particular for providing the data sets of airborne laser scanning measurement data and bathymetrical profiles without which the execution of presented studies would have been impossible.

## LITERATURE CITED

- Axelsson, P., 2000. DEM generation from laser scanner data using adaptive TIN models, *International Archives of Photogrammetry and Remote Sensing*, Vol. XXXIII/4B, 110-117.
- Dobrcki, R. and Zachowicz, J., 2005. Objaśnienia do Mapy Geodynamicznej Polskiej Strefy Brzegowej Bałtyku, scale 1:10,000, 1 sheet. PIG OP.
- Dudzińska-Nowak, J., 2006. *Changes of the morphology as an indicator of the coastal tendency development (in polish)*. Szczecin, Poland: Institute of Marine and Coastal Sciences, University of Szczecin, Ph.D. thesis, 226p.
- Ferreira, O., 2005. Storm groups versus extreme single stores: predicted erosion and management consequences, *Journal of Coastal Research*, 42, 221-227.
- Furmańczyk, K. and Dudzińska-Nowak, J., 2009. Effect of extreme storms on coastline changes: a southern Baltic example, In: Pereira da Silva C., Vaz, B., Abrantes, P., Estanqueiro, R. (eds.), *Proceedings of the 10<sup>th</sup> International Coastal Symposium* (Lisbon, Portugal), *Journal of Coastal Research*, Special Issue No. 56, pp. 1637-1640.
- Furmańczyk K.K., Dudzińska-Nowak J., Furmańczyk K.A., Papińska-Swerpel B. and Brzezowska N., 2011. Dune erosion as a result of the significant storms at the western Polish coast (Dziwnow Spit example), In: Furmańczyk, K., Giza, A., Terefenko, P. (eds.), *Proceedings of the 11<sup>th</sup> International Coastal Symposium* (Szczecin, Poland), *Journal of Coastal Research*, Special Issue No. 64, pp. 756-759.
- Harff, J., Lemke, W., Lampe, R., Luth, F., Lubke, R., Meyer, M., Tauber, F. and Schmolcke, U., 2007. The Baltic Sea Coast – a Model of Interrelations between Geosphere, Climate and Anthroposphere. In: Harff, J., Hay, W.W. and Tetzlaff, D. (eds.), *Coastline Change - Interrelations of Climate and Geological Processes. The Geological Society of America Special Publications*, 426, pp 133-142.
- Instrukcja ITB nr 424/2006. Warszawa Instrukcja sporządzania mapy warunków geologiczno-inżynierskich w skali 1 : 10 000 i większej dla potrzeb planowania przestrzennego w gminach, 1999 (Państwowy Instytut Geologiczny, Warszawa s.). pp. 52-54.
- Journal of Laws, 2012. *The Council of Ministers of 15 October 2012 on National spatial reference system*, item 1247.
- Klimaszewski, M., 1994. *Geomorfologia (Geomorphology)*. Warszawa. Wydawnictwo Naukowe PWN, 280p.
- Stanisławczyk, I., 2012. Storm-surges Indicator for the Polish Baltic Coast. *International Journal on Marine Navigation and Safety of Sea Transportation*, 6 (1), 123-129.
- Sztobryn, M., Stigge, H.-J., Wielbińska, D., Weidig, B., Stanisławczyk, I., Kańska, A., Krzysztofik, K., Kowalska, B., Letkiewicz, B. and Mykita, M., 2005. *Storm Surges in the Southern Baltic Sea (western and central parts)*. Rostock Berichte des Bundesamtes für Seeschifffahrt und Hydrographie, 39, 74p.
- Szostak M., Węzyk P. and Tompalski P., 2013. Aerial Orthophoto and Airborne Laser Scanning as Monitoring Tools for Land Cover Dynamics: A Case Study from the Milicz Forest District (Poland). *Pure and Applied Geophysics*, 170, 4, DOI: 10.1007/s00024-013-0668-8.
- Węzyk P., Borowiec N., Szombara S. and Wańczyk R., 2008. Generation of digital surface and terrain models of the Tatra Mountains based on Airbone Laser Scanning (ALS) point cloud (in polish). *Archiwum Fotogrametrii, Kartografii i Teledetekcji*, 18 b, 651-661.
- Wójcik A., Węzyk P., Wojciechowski T., Perski Z. and Maczuga S., 2013. Geological and geomorphological interpretation of Airborne Laser Scanning (ALS) data of the Kasprowy Wierch area (Tatra Mts.) (in polish). *Przegląd Geologiczny*, 61 (4), 234-242.
- Zawadzka-Kahlau, E., 1999. *Tendencje rozwojowe polskich brzegów Bałtyku południowego*. Gdańsk. GTN. IBW, 220p.

# Headland structural impacts on surf zone current circulations

Mohd S.A. Razak<sup>†‡</sup>, Ali Dastgheib<sup>†</sup>, Fransiscus X. Suryadi<sup>†</sup>, Dano Roelvink<sup>†∞§</sup>

<sup>†</sup>Water Engineering & Science  
Department, UNESCO-IHE Institute for  
Water Education, 2601DA Delft, The  
Netherlands

[s.abrazak@unesco-ihe.org](mailto:s.abrazak@unesco-ihe.org)  
[a.dastgheib@unesco-ihe.org](mailto:a.dastgheib@unesco-ihe.org)  
[f.suryadi@unesco-ihe.org](mailto:f.suryadi@unesco-ihe.org)  
[d.roelvink@unesco-ihe.org](mailto:d.roelvink@unesco-ihe.org)

<sup>§</sup>Faculty of Civil Engineering &  
Geosciences, TU Delft, The Netherlands

<sup>‡</sup> Faculty of Engineering, Universiti Putra  
Malaysia, 43400 Serdang, Malaysia

<sup>∞</sup> Deltares, Rotterdamseweg 185, Delft,  
2629 HD Delft, The Netherlands



[www.cerf-jcr.org](http://www.cerf-jcr.org)



[www.JCRonline.org](http://www.JCRonline.org)

## ABSTRACT

Ab Razak, M.S., Dastgheib, A., Suryadi, F.X., Roelvink, D. 2014. Headland structural impacts on surf zone current circulation, *Proceedings 13<sup>th</sup> International Coastal Symposium* (Durban, South Africa), *Journal of Coastal Research*, Special Issue No. 70, pp. 065-071, ISSN 0749-0208.

The paper presents the morphodynamic investigation of embayed beaches through the impact of structural headlands. An XBeach model was successfully applied to predict the surf zone current pattern and to predict morphological features of three different embayment scales for low-moderate-high wave energy events. The formation of central rip currents in embayed beaches is linked to the presence of a sand bar, while topographical headland rips developed adjacent to the headland boundary are caused by the geological control of the headland structure itself. The effect of moderate and high waves has resulted to a decreased number of central rips in a longer embayment thus limiting the beach circulation to the cellular type. This type of rips could provide an initial insight into the offshore transport of sand from the coast. Whether wave breaking occurs outside or inside the embayment determines the initiation of large scale rip currents, megarips. Several factors that lead to the generation of megarip currents in literature should be taken into account as a guideline for morphodynamic studies in a high energy embayed coast. Nevertheless, the characteristics of surf zone current circulation in all cases presented in this study complies with the description of the theoretical embayment scaling parameter ( $\delta'$ ) (Short and Masselink, 1999 and Castelle and Coco, 2012). Further establishment of this parameter is needed to properly describe the surf zone current circulation in embayed beach systems.

**ADDITIONAL INDEX WORDS:** rips, headland, current circulation, XBeach, offshore transport

## INTRODUCTION

Embayed beaches comprise 50 % of the world's beach. Commonly bounded by two natural headlands or shore connected breakwaters, these curvilinear-shape bays are exposed to wave refraction/diffraction processes that may create a sheltering zone at the leeside of the headland, depending on the direction of the incoming waves. A complex pattern of current circulations leads to a dynamic behaviour of embayed beach morphology. This may be one of the reasons for the scarce research development for embayed beach systems. An obvious characteristic of embayed beaches compared to open straight beaches is its surf zone circulation. Headlands and engineering structures like groynes will impact the beach and surf zone through their influence on wave refraction and attenuation, thus limiting the development of longshore currents, rips, and rip feeder currents (Short and Masselink, 1999). Surf zone rip currents (e.g topographically controlled headland rips, normal beach rips and megarips) in embayed beach systems are responsible for the mechanism of cross-shore sediment exchange (Loureiro *et al.*, 2012; Short, 1985; Coutts-Smith, 2004). Rip currents are generated as a result of alongshore variations in wave height of the incoming waves (Bowen, 1969). The generation of rip currents in embayed beaches

is linked to the embayment size and variation of wave heights. Short and Masselink (1999) were the first to investigate the structural impact on surf zone current circulation. The novelty of embayment scaling parameter ( $\delta$ ) that was firstly developed by Short and Masselink (1999) and later was improved by Castelle and Coco (2012) is applicable to characterize the current circulation in different embayment scales under low wave energy conditions.

During storms, high wave energy may modify current patterns in embayed beaches. Beach rips which are normally developed in the middle of an embayment may increase in space to initially develop strong seaward rip currents. The variation of rip current strength was found to be directly related to incident wave height variations over periods of a few minutes. Strong rip currents developed in the middle embayment are associated with higher waves and waves of longer period (Mckenzie, 1958; Huntley *et al.*, 1988). However, Shepard and Inman (1950) opposed this opinion in which the minimum rip current strength is associated with high waves. This is not absolutely clear, but a possible explanation may be associated with the fact that Shepard and Inman (1950) were observing large scale rip currents on an open coast while observations of Mckenzie (1958) and Huntley *et al.*, (1988) were made in relatively enclosed bays. The generation of a central rip current may be through wave refraction around the bay. Long crested waves will refract to approach the shoreline in the bay at an oblique angle everywhere, except at the centre of the bay. This obliquity will drive feeder currents, inside the surf zone,

DOI: 10.2112/SI70-12.1 received 30 November 2013; accepted 21 February 2014. © Coastal Education & Research Foundation 2013

towards the centre of the bay, where the convergence might be expected to create seaward-flowing rip currents. Wright *et al.*, (1978) explained the formation of central rip currents in a highly compartmented beach driven by storm waves. The large rips exhibit a very low frequency and are very destructive in their effects. One or two rips may extend up to several kilometers seaward in highly compartmented beaches, like the one observed in Palm beach (Cowell, 1975) and Cronulla Beach (Lees, 1977).

Despite the fact that the number of studies on morphodynamics in embayed beaches have been increasing recently (e.g Gallop *et al.*, 2011; Ojeda *et al.*, 2011; Loureiro *et al.*, 2012), less attention is given to embayed beach morphodynamic modelling, with the exception of Reniers *et al.*, (2004), who found a relationship between rip current spacing and directional spreading. Furthermore, studies on surf zone morphodynamics in embayed beaches are restricted to a limited number of numerical studies, specifically for low wave energy conditions only. While surf zone retention is well documented on open beaches (e.g. Spydell *et al.*, 2007; Reniers *et al.*, 2009), it has never been addressed in detail on embayed beaches.

In this study a 2DH process based XBeach model (Roelvink *et al.*, 2009; 2010) was applied as a numerical tool to assess the confidence of the model in examining relevant morphodynamic processes that exist in embayed beach systems. Although the XBeach model is principally designed to predict dune erosion due to storm impact (e.g Roelvink *et al.*, 2010; Callaghana *et al.*, 2013; Splinter *et al.*, 2013 ), it can also be applied for small scale coastal problems (e.g Ab Razak *et al.*, 2013). The main objective of this study is to understand the morphodynamic behaviour of rip channel systems at different embayment scales based on the embayment scaling parameter ( $\delta$ ) for a range of wave heights. A research gap between this study and other researchers (e.g Castelle and Coco 2012) is the inclusion of higher wave energy events on the morphodynamic modelling of embayed beach systems.

### Embayment scaling parameter ( $\delta$ )

The embayment scaling parameter ( $\delta$ ) was used as a base guideline to predict the degree of headland impact on surf zone current circulation. This parameter relates the embayment configuration to the incident breaking wave conditions according to Eq.(1) (Short and Masselink, 1999):

$$\delta = \frac{S^2}{100C_l H_b} \quad (1)$$

where  $S$  is the embayment shoreline length,  $C_l$  is the embayment width and  $H_b$  is the breaking wave height. Based on  $\delta$ , three main beach circulations have been identified. On beaches with no headlands or obstacle structures, normal surf zone circulation prevails ( $\delta > 19$ ). When the embayment size and shape begins to increasingly influence surf zone circulation, by causing longshore currents to turn and flow seaward against each headland, while still maintaining some normal beach circulations away from the headlands, a transitional circulation exists ( $8 < \delta < 19$ ). If the headlands are closer together or if wave height increases, the entire beach circulation may be impacted by the headlands. At this stage, a topographically controlled large rip current (Short, 1985), prevails ( $\delta < 8$ ). This type of current generally promotes the cross-shore exchange of sediment transport. (e.g Loureiro *et al.*, 2012; Short, 1985; Coutts-Smith, 2004).

However, the parameter proposed by Short and Masselink (1999) has several limitations as has been addressed by Castelle and Coco (2012). They assumed that wave energy is redistributed along the whole wet-dry contour of the embayment. If the

headland length is greater than the surf zone width, the headland impact will be overestimated. Also, the amount of energy dissipated against the headland in most cases is small compared to the one dissipated along the beach. For that reasons, Castelle and Coco (2012) have established a non-dimensional embayment scaling parameter ( $\delta'$ ) which considers the surf zone width ( $X_s$ ) that fits into embayment length ( $L$ ) as presented in Eq.(2):

$$\delta' = \frac{L\gamma\beta}{H_s} \quad (2)$$

where  $\gamma$  is the breaking parameter,  $\beta$  is the nearshore slope and  $H_s$  is significant wave height. The degree of headland impact and circulation type in embayed beaches can still be estimated following Short and Masselink (1999) but with an improved description on the number of developing rips between normal and transitional beach circulations. If the number of rips that exist in the middle of the embayment is greater than four ( $n_{rip} > 4$ ) the beach is considered normal, while if  $n_{rip} < 4$  transitional beach circulation prevails. On the other hand, the cellular beach circulation is said to take place when there is a presence of headland rips at both sides of the headland and only one or two rips in the middle of the embayment. This parameter indeed requires further improvements in terms of beach curvature, prevailing wave angle, geometry of the headlands and directional wave spreading. Nevertheless, the degree of embayment predicted by  $\delta'$  has proved to be consistent with several observations of embayed beaches (Castelle and Coco, 2012). Their embayment scaling parameter was used in this study to quantify the number of resulting rip currents and rip channels.

### Two dimensional (2DH) process based XBeach model

The XBeach model consists of formulations for short wave propagation, shallow water equations, sediment transport and bed update. In this study, only a stationary wave solver was used. The Van Rijn sediment transport formula was selected in combination with the the advection-diffusion equation to compute total sediment transport, which can be used to update bathymetry. The seabed changes are updated with the use of a (low) morphological scale factor (Morfac) to accelerate the computational time. The avalanching module is activated to account for the slumping of sandy material. For detailed descriptions of XBeach model formulation, readers are referred to Roelvink *et al.*, (2009, 2010).

### NUMERICAL MODEL SETUP

Two groynes were used to represent headland structures with a length of 300 m while the alongshore beach length was varied ( $L = 500, 1500$  and  $4000$  m). The groyne length is long enough to prevent any sand bypassing, functionally designed for deeply enclosed beaches. A single barred coast was used as an initial bathymetry with an average slope of 0.01. The rip channel is assumed to exist only between the shoreline and the bar line (Gallop *et al.*, 2011). A sand bar located 100 m from the shoreline was placed with an amplitude of 1 m following the approach of Roelvink (1993). Wave height of 1 m, 2 m and 4 m associated with a period of 10 sec were imposed at the offshore seaward boundary. Neumann boundary was used as a lateral boundary at both right and left sides of the computational domain. Models were forced to run for ten morphological days with a morphological acceleration factor (Morfac) of 5. The shorter time scale addressed in this study is necessary to describe the dynamic environments of embayed beaches characterized by a variety of

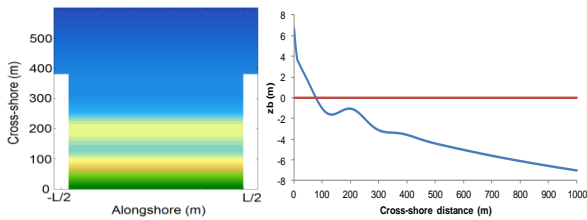


Figure 1. Model bathymetry and a nearshore barred bed profile. Red line indicates shoreline limit.

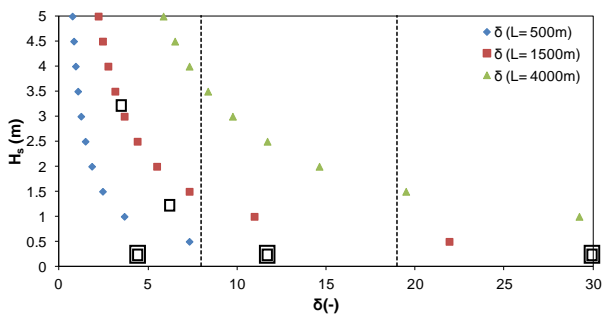


Figure 2. Embayment scaling parameter for different wave heights and embayment lengths. Vertical dotted lines delimit different beach circulation states. Double squares mean cases run with shore normal waves ( $\theta=0^\circ$ ) and an oblique wave ( $\theta=5^\circ$ ). Single square indicates cases run with only shore normal waves.

processes and a range of complex behaviour resulting in the presence of morphological patterns and the formation of rips (e.g. Holman *et al.*, 2006; Gallop *et al.*, 2011; Ojeda *et al.*, 2011, Castelle and Coco, 2012). Figure 1 shows the model embayment geometry and cross-shore bed profile. Figure 2 shows the beach circulation types and test cases. The  $\delta$  is calculated based on Equation 2. A typical current circulation for different

ranges of embayment sizes under low wave condition was first evaluated, followed by an investigation on the effect of increasing wave height. All tests performed in this study are graphically presented in Figure 2.

## RESULTS AND DISCUSSIONS

### Typical rip channel system on embayed beaches: Low wave energy condition

The morphodynamic rip channel of low wave energy was first investigated. For this analysis, a stationary wave of 1 m, period of 10 sec and wave angle perpendicular to the shore  $\theta = 0^\circ - 5^\circ$  was applied at the offshore boundary. The alongshore beach length was varied ( $L = 500, 1500$  and  $4000$  m) and corresponded to embayment scaling parameter of  $\delta = 3.7$  (cellular),  $10.9$  (transitional), and  $29.2$  (normal), respectively.

Figure 3 b,d,f shows the predicted morphodynamic pattern of embayed beaches for an oblique wave of  $5^\circ$ . These figures clearly show the influence of headland structure as well as embayment length on the development of surf zone rip currents and rip channels. Central rip currents appear in all ranges of embayment. For the  $L=1500$  m, three main rip channels are developed in the middle of the embayment with persistent topographical rips adjacent to each headland boundary. The presence of this central rip current is due to the accumulation of water in the shoreface, so that the water has to flow seaward to escape. Shore parallel wave propagating to the shore breaks over the bar, carrying extra water into the shoreface near the beach (wave setup). The bar and the waves block this accumulation of water from moving seaward over the bar. Instead, a rip current forms where a break (gap) opens up in the bar. Here, water that is piling up flows along between the bar and the beach and then turns and flows seaward through the gap in the bar. As the embayment length increases, the number of central rip channels also increases as shown in Figure 3(f) for  $L=4000$  m.

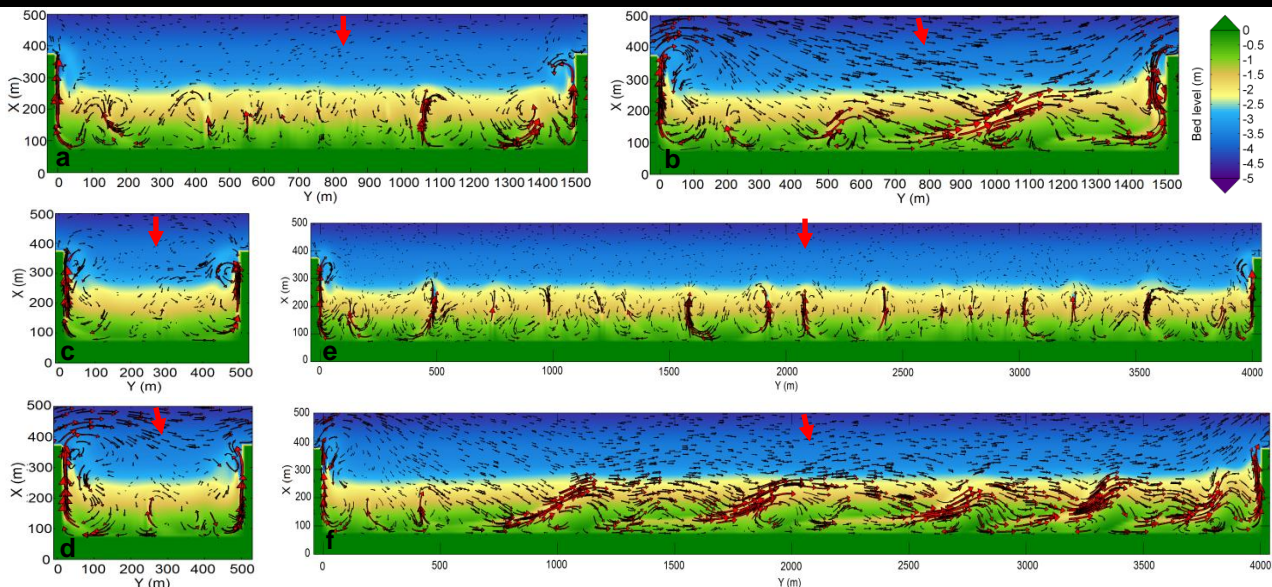


Figure 3. Morphodynamics of embayed beaches for different alongshore distances with  $H_{rms}=1$  m,  $T_p=10$  sec at the last time step. Red bold arrows indicate the incoming waves in two different directions.

This case is similar to the case of an unconstrained beach with no structure in between. The only difference is that headland rips occur at both sides of the structures. The shape of the rip seems to be dependent of the approaching wave angle. On the other hand, for the shorter embayment length ( $L=500$  m), the middle rip current hardly appears although there is evidence of a small developing rip at the centre of the embayment. Still, headland rips do occur.

The morphodynamic surfzone responses of the shore normal waves provide reasonable results, similar to the oblique wave. Figure 3 a,c,e shows the predicted morphodynamic pattern of three embayed beaches for the shore normal wave case. Rip currents and rip channels are observed in the middle of the larger embayment *i.e.*  $L=1500$  m and  $L=4000$  m. The perpendicular flow of the seaward currents provides a clear distinction between the shore normal wave and an oblique wave. In all cases, the development of rip channels complies with the description of theoretical embayed beach circulation.

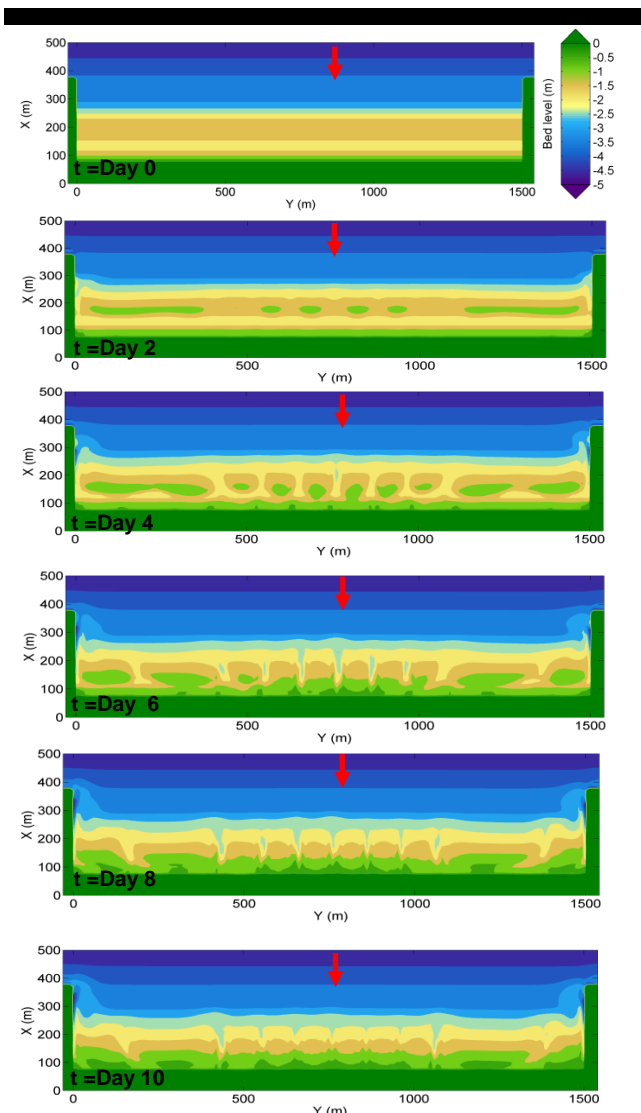


Figure 4. Morphological evolution of a rip channel system in a longer embayed beach ( $L = 1500$  m). Red arrows in each panel indicate shore normal wave direction with a  $H_{rms}$  of 1m.

The morphological development of a rip system can be inspected through the 2D numerical model. This may increase our understanding on the initial formation of a rip channel in embayed beaches. Figure 4 shows the example of the evolution of a rip channel for the case of longer embayment with shore normal waves. During the first two days, the sand bar starts to evolve but merely with small perturbations. A scouring channel develops at both headland extremities due to a strong rip flowing adjacent to the headland (headland rips). After day four, rip channels in the middle of the embayment continuously develop with seven rip currents draining the entire beach. More channels develop after day six, breaching the gap of the bar, carrying more water that is flowing back to the sea. While the rip channels progressively develop, the detached sandbars tend to move shoreward and finally merge with the beach. This happens as the shore normal wave pushes the sand consistently towards the coast. At the end of day 10, the rip channels are still present with four rips existing but their patterns are not as significant as those observed during day four. This model evolution also shows the transition between the longshore bar-trough state (day 4) and the transverse bar and rips state (day 6) which was observed in the field (see Figure 5). This was supported by Symonds *et al.* (1997), who described the slow onshore migration of sand bar to onshore during the period of low waves while developing the longshore variability and rip channels.



Figure 5. Rip channels and transverse bars with a rhythmic shoreline under low wave condition. Courtesy of Gallop *et al.* (2011).

### Effects of increasing wave height: The transition from a transitional to a cellular beach state

We further investigated the morphodynamic behaviour of a rip channel system when the wave height was increased to 2 m. In this case, an embayed beach with a length of 1500 m was only tested as this embayment indicates the transition between the transitional state to a cellular state based on embayment scaling parameter,  $\delta$ , as shown in Figure 2. The case of  $L=500$  m was tested also, but is not presented here as it does replicate the similar behavior pattern of 1 m wave height, with only headland rips occurring at both headland extremities. Additionally, the contribution of increasing wave height for the shorter embayment is not unique as it is already categorized in a cellular beach state as illustrated in Figure 2. The nearshore bed profile is kept constant similar to the previous analysis.

Figure 6 shows the evolution of bed level changes and current circulation pattern for the moderate wave height ( $H_{rms} = 2$  m). Based on  $\delta$ , it is categorized under cellular beach circulation as  $\delta = 5$ , less than the boundary limit of cellular beach state. This

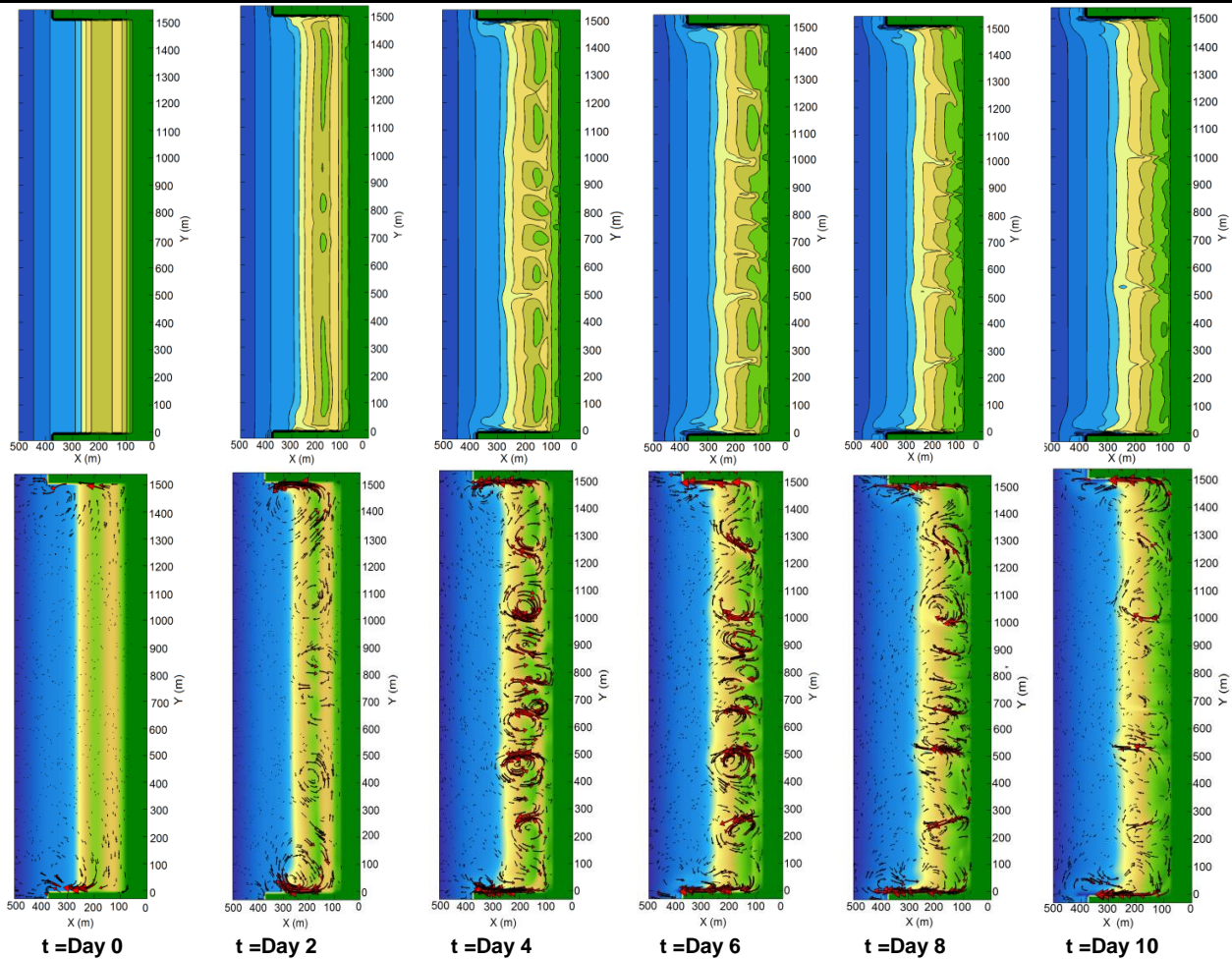


Figure 6. Evolution of bed level changes (upper panels) and current circulation pattern (lower panels) of  $H_{rms}$  2 m under shore normal waves. Bed level is represented as colorbar in Figure 3. In all upper panels iso-contours (0.5m intervals) are contoured in the background.

indicates that the number of central rip currents will be decreasing. At the beginning of simulation (day 4), there are seven rips developing in the middle of the embayment. These rips persistently remain at the same position until day 8. At the end of

To further investigate this we recorded the number of central rip currents that are developed during each day. The summary of mean rip spacing both for  $H_{rms}$  1 m and 2 m is presented in Table 1. Obviously, increasing wave height leads to a less number of rip currents developing in the middle of the larger embayment. This supports findings of Short (1985), who noted that under increasing waves, the alongshore rip spacing increases (decreasing number of rip currents) with the rips becoming more intense. Rips may configure by shifting, disappearing and more can re-appear (Short, 1985). The number of rip currents increases over the course of simulation inferring a decrease in alongshore mean rip spacing. As the channel starts to develop more channels appear (day 4) and slowly decrease as the bar slowly migrates inshore (day 10).

Table 1. Summary of resulting ranges of rip channel spacings for alongshore embayment,  $L=1500$  m.

Time evolution [days]	0	2	4	6	8	10
	Numbers of central rip currents [-]					
$H_{rms} = 1.0$ m	-	5	8	9	9	8
$H_{rms} = 2.0$ m	-	3	7	7	7	5
$H_{rms} = 4.0$ m	-	5	5	5	5	3

the simulation, the number of developing central rips decreases to only five rips thus increasing the mean alongshore rip spacing. The number of central rips for this case ( $H_{rms}=2$  m) is against the finding of low wave condition, *i.e.*  $H_{rms} = 1$  m.

The inclusion of extreme wave condition in investigating the morphodynamics of an embayed beach was incorporated. Referring to Figure 2, the beach circulation is categorized as cellular thus limiting the presence of rips in the middle of the embayment. For this particular case, an additional run for a wave height of 4 m was carried out to represent extreme wave conditions. The bed profile was extended offshore to a greater depth to prevent any disturbance at the seaward boundary. Figure 7 shows the morphodynamic behavior of an embayed beach for wave conditions of  $H_{rms}$  4 m and shore normal wave ( $\theta = 0^\circ$ ). The current circulation pattern and bed level changes are more or less similar to the case of  $H_{rms}$  2m with only a slight re-positioning of the rip channel. On the other hand, at the alongshore location of 800 m, an intense rip channel has developed, scouring the seabed up to -4 m, thus indicating the presence of a strong rip current in the middle of the embayment. In our simulation, the breaking wave height on the sand bar just before the bed is updated is rather low, merely 0.6 m for the wave height of 4 m, slightly above that for the moderate wave height of 2 m. This implies that the wave initially breaks further offshore, losing its energy and breaking again near the bar with less energy. The evolution of rip current



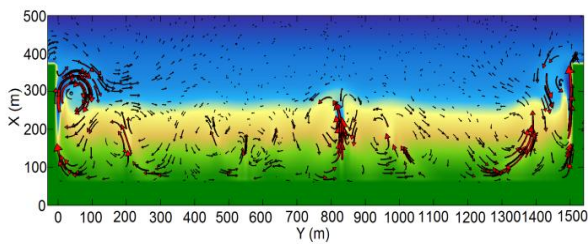


Figure 7. Surf zone current circulation and morphological bed changes of an embayed beach with  $H_{rms}$  of 4 m. Bed level is represented as colorbar in Figure 3.

rip channel for this particular extreme wave event shows a migration of the rip channel. This can be explained through the number of developing central rips as presented in Table 1. On day four, significant rip channels appear with five rips developed in the middle of the embayment. The number of central rips remains the same for the following days but is reduced to merely three rips when approaching day 10.

There are several studies that reported different surf zone current circulation behaviour in embayed coasts, which were not reproduced in our modelling study. For instance, Short (1985) reported the existence of large central rips in three Sydney beaches due to the influence of nearshore and adjacent embayment topography that prevented the development of a fully dissipative state by inducing wave refraction and persistent longshore gradients in surf zone dynamics. One or two megarips may drain the entire long embayed beach as the wave height increases, especially during extreme wave events (see Figure 8-left panel).

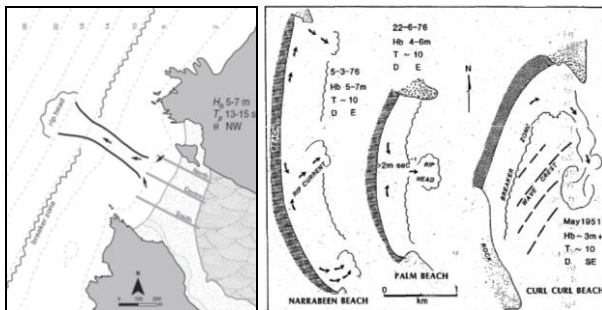


Figure 8. Schematic maps of megarip circulation. Left panel presents small Amoreira embayment (Portugal) during storm conditions (Loureiro *et al.*, 2012). Right panel shows large central rip circulations in the middle of three large embayments in Sydney region (Short, 1985).

In a different case, the storm oblique waves promote the formation of a meandering rip feeder current towards the east side of the headland. The rips sustain the same position, not experiencing significant alongshore movement as they remain topographically controlled. Likewise, Silva *et al.*, (2010) showed that the accumulation of water at the centre of the beach leads to the formation of a strong seaward rip. As the headland structures are close to each other and the shore-normal wave energy is evenly distributed along the beach, the rip current develops in the middle of embayment. Once the circulation is established, the increasing wave height would only strengthen and weaken the current velocities without modifying the circulation pattern (Silva *et al.*, 2010). On the other case study, Loureiro *et al.*, (2012)

described the formation of one large central rip developing roughly on the centre of the embayment during high energy events (see Figure 8-right panel) in Amoreira embayment, southwestern coast of Portugal. The beach is approximately 600 m long and generally exposed to energetic north-westerly waves. The formation of megarips is not related to the breaker gradients at this beach, but specifically due to the nearshore topographic control.

Nevertheless, it should be noted that in all examples described above, the condition of each study area is different from each other. Detailed investigation of the natural bottom topography at those particular study areas is highly recommended. In fact, small bathymetry irregularities can influence surf zone hydrodynamics, inducing wave gradient driven rip circulations (Calvette *et al.*, 2007; MacMahan *et al.*, 2008; Dalrymple *et al.*, 2011). On the other hand, wave breaking conditions either inside or outside the embayment also determine the generation of megarip currents. Short (1985, 2007, 2010) proposed a breaking wave height of 3 m as a threshold value for the generation of megarip currents. Further analysis on the formation of megarip currents should be investigated to understand the physical processes that govern their generation. The changes of nearshore bottom seabed, the effects of wave grouping and the variation of headland lengths are some of the "tasks to do" for future research. To date, none of the numerical studies were done to look into details of this particular process.

### Limitations of the embayment scaling parameter

In unconstrained coasts, intermediate beaches commonly with a single or multiple bar features are linked with the generation of beach rip currents. When the beach is fully dissipative or reflective, the normal beach rip (central rip) currents are likely to disappear. On the other hand, when natural or man-made structures like headlands, reefs or groynes are present, the surf zone currents are deflected seaward along the sides of the obstacles as topographically-controlled seaward flows of water known as topographic rips or headland rips (Short, 1985). These headland rips are the product of both embayment characteristics and wave height. An increase in wave height re-adjusts the morphological pattern of rip channels and limits the formation of rip currents.

The behaviour of current circulation in embayed beaches has been previously described by the embayment scaling parameter,  $\delta$ . However, both approaches still have limitations to predict the headland impact on the surf zone current circulation. Firstly, wave angle is one of the important factors that may contribute to the initiation of rip currents. Although rip currents are normally related to the shore normal waves, oblique waves may change the shape of the rip channel patterns thus limiting the generation of a rip current system. This study for instance, has shown the generation of rip channels both for shore normal ( $\theta = 0^\circ$ ) and oblique wave ( $\theta = 5^\circ$ ) under low wave energy conditions (see Figures 3c and d, respectively). In both cases, the number of rips present in longer embayments ( $L=1500$  m) for shore normal waves is greater than for oblique waves. Secondly, initial beach curvature may influence the dynamic circulation in embayed beaches. Although there are no cases tested in this study, Castelle and Coco (2012) have shown in their simulations that both beach curvature and directional spreading of waves influence the generation of central rip currents in a shorter embayed beach. Thirdly, rip current generation in embayed beaches is dynamic and unpredictable due to a variety of processes and a range of complex behaviour. Rip channels can be developed on a time scale of days to weeks (e.g. Gallop *et al.*, 2011; Ojeda *et al.*, 2011; Castelle and Coco, 2012; Ranasinghe *et al.*, 1999; Damgaard *et al.*, 2002) and

it is very difficult to reach an equilibrium state. A proper definition of time scale should be taken into account to properly explain the description of the beach circulation types.

### CONCLUDING REMARKS

The impact of headlands on surf zone current circulation under low to moderate to high wave energy was investigated. The surf zone current circulation behaviour showed different characteristics for different scales of embayment. The embayment scaling parameter that was used as a baseline to describe the characteristics of morphodynamics of embayed beaches proved to synchronize with the development of predicted current circulation patterns. Additionally, the transition between the transitional beach state to a cellular beach state has been proven under increasing wave energy for a longer scale embayment. The inclusion of extreme wave events in this modelling study showed a different behaviour of current circulation pattern which has not been seen in the field as reported in literature due to several factors *i.e.* nearshore and adjacent embayment topography and breaking wave conditions. Although a significant rip channel in the middle of embayment exists, this is only due to the increasing strength of the existing current. Wave breaking conditions play an important role in the generation of this large scale rip current. Further numerical investigation should be carried out to determine the related processes that drive the formation of this megarip current. Although results presented in this study are still purely hypothetical, they replicate the real phenomena observed in nature (*e.g.* Loureiro *et al.*, 2012 and Gallop *et al.*, 2011). Future study is recommended to include the storm wave grouping to observe the effects of real storm waves to the development of surf zone current circulation in small scale embayed beaches.

### ACKNOWLEDGEMENT

The work described in this publication was supported by the Ministry of Higher Education (MOHE) Malaysia and the Universiti Putra Malaysia (UPM).

### LITERATURE CITED

- Ab Razak, M.S., Dastgheib, A., Roelvink, D. (2013). Sand bypassing and shoreline evolution near coastal structure comparing analytical solution and XBeach numerical modelling, *Journal of Coastal Research*, Special Issue No. 65, 2038-2044.
- Bowen, A.J. (1969). Rip currents. 1. Theoretical investigation. *Journal of Geophysical Research*, 74, 5467-5478.
- Calvette, D., Coco, G., Falques, A., Dodd, N. (2007). (Un) predictability in rip channel systems, *Geophysical Research Letter*, 34, L05605
- Coutts-Smith (2004) The significant of megarrips along an embayed coastline. PhD thesis University of Sydney, Australia
- Castelle, B. Coco, G. (2012). The morphodynamics of rip channels on embayed beaches, *Continental Shelf Research*, 43, 10-23.
- Callaghana, D.P., Ranasinghe, R., Roelvink, D. (2013). Probabilistic estimation of storm erosion using analytical, semi-empirical, and process based storm erosion models. *Coastal Engineering*, 82, 64-75.
- Cowell, P.J. (1975). Morphodynamic aspects of the interactions between incoming waves and bed topography at Palm Beach, N.S.W. Unpublished Thesis, Department of Geography, University of Sydney, 179pp
- Dalrymple, R.A., Mac Mahan, J.H., Reniers, A.J.H.M., Nelko, V. (2011). Rip currents, *Annual Review of Fluid Mechanics*, 43, 551-581.
- Damgaard, J., Dodd, N., Hall, L., Chesher, T. (2002) Morphodynamic modelling of rip channel growth. *Coastal Engineering*, 45, 199-221
- Gallop, S.L., Bryan, K.R., Coco, G., Stephens, S.A. (2011). Storm-driven changes in rip channel patterns on an embayed beach, *Geomorphology*, 127, 179-188.
- Holman, R., Symonds, G., Thornton, E.B., Ranasinghe, R. (2006). Rip spacing and persistence on an embayed beach. *Journal of Geophysical Research*, 111, C01006
- Huntley, D.A., Hendry M.D., Haines, J., Greenidge, B. (1988). Waves and rip currents on a Caribbean Pocket Beach, Jamaica. *Journal of Coastal Research*, 4(1), 69-79.
- Lees, B.G. (1977). The effects of compartmentalization on beach processes and forms: Cronulia, N.S.W. Unpublished Thesis, Department of Geography, University of Sydney, 179pp
- Loureiro, C. Ferreira, O., Copper, J.G. (2012). Extreme erosion on high-energy embayed beaches; Influence of megarrips and storm grouping, *Geomorphology*, 139-140, 155-171.
- McKenzie, P (1958). Rip current systems. *Journal of Geology*, 66, 103-113.
- Mac Mahan, J.H., Thornton, E.B., Reniers, A.J.H.M., Stanton, T.P., Symonds, G. (2008). Low energy rip currents associated with small bathymetric variations, *Marine Geology*, 255, 156-164.
- Ojeda, E., Guillén, J., Ribas, F. (2011). Dynamics of single-barred embayed beaches, *Marine Geology*, 280, 76-90.
- Ranasinghe, R., Symonds, G., Holman, R. (1999). Quantitative characterisation of rip currents via video imaging, *Proceedings of Coastal Sediments '99*, New York, USA, pp. 987 - 1002.
- Reniers, A.J.H.M., J.A. Roelvink, and E.B. Thornton (2004). Morphodynamic modeling of an embayed beach under wave group forcing, *J. Geophys. Res.*, 109, doi:10.1029/2002JC001586.
- Reniers, A.J.H.M., Mac Mahan, J. H., Thornton, E.B., Stanton, T.P. Henriquez, M., Brown, J. W., Brown, J. A. Gallagher, E. (2009). Surf zone retention on a rip-channeled beach, *J. Geophys. Res.*, 114, doi:10.1029/2008JC005153.
- Roelvink, D., Reneir, Ad., van Dongeren, Ap., van Thiel de Vries, J., McCall, R., Lescinski, J. (2009). Modelling storm impacts on beaches, dunes and barrier islands. *Coastal Engineering*, 56 (11-12), 1133-52.
- Roelvink, J.A., Reniers, A., Dongeren, A., Vries, J.T., Lescinski, J., McCall, R. (2010). XBeach model description and manual. (UNESCO-IHE Institute for Water Education, Deltares, Delft University Technology).
- Roelvink, J.A. (1993). Surf beat and its effect on cross-shore profiles. PhD Thesis, Technical University of Delft, the Netherlands, 150pp
- Shepard, F.P., Inman, D.L. (1950). Nearshore water circulation related to bottom topography and wave refraction. *Transaction of the American Geophysical Union*, 31, 196-212.
- Short A.D. (1985) Rip current type, spacing and persistence, Narrabeen Beach, Australia, *Marine geology*, 65, 47-71.
- Short, A.D., Masselink, G. (1999). Embayed and structurally controlled beaches, In: Short, A.D. (ed.), *Handbooks of Beach and Shoreface Hydrodynamics*. Chichester, John Wiley & Sons.
- Short A.D. (2007). Australian rip systems: friend or foe? *Journal of Coastal Research* SI 50, 7-11.
- Short A.D. (2010). Role of geological inheritance in Australian beach morphodynamics. *Coastal Engineering*, 57, 92-97.
- Silva, R., Baquerizo, A., Loasada, M.A., Mendoza, E. (2010). Hydrodynamic of a headland-bay beach- Nearshore current circulation, *Coastal Engineering*, 57, 160-175.
- Splinter, K.D., Carley, J.T., Golshani, A., Tomlinson, R. (2013). A relationship to describe the cumulative impact of storm clusters on beach erosion. *Coastal Engineering*, 83, 49-55.
- Spydell, M., Feddersen, F., Guza, R.T. (2007). Observing surf-zone dispersion with drifters, *J. Phys. Oceanogr.*, 37, 2920-2939
- Symonds, G., Holman, R.A., Bruno, B. (1997). Rip currents. In: Coastal Dynamics '97, Thornton, E.B. (ed.), *American Society of Civil Engineering*, Reston, VA, pp:584-593.
- Wright, L.D., Thom, B.G., Chappell, J. (1978). Morphodynamics variability of high-energy beaches *Coastal Engineering*(1978), 1180-1194.

# Relationships between sand spit evolution, environmental forcing and inland inundation

Tony Thomas<sup>†</sup>, Shaun K Lynch<sup>‡</sup>, Michael R Phillips<sup>∞</sup>, Allan T Williams<sup>∞</sup>, Robert W Duck<sup>+</sup>

<sup>†</sup>G D Harries and Sons, Rowlands View, Templeton, Narberth, Pembrokeshire SA67 8RG  
tony.thomas@gdharries.co.uk

<sup>‡</sup>Technical Services, Carmarthenshire County Council, Carmarthen, Carmarthenshire SA31 3QZ  
SkLynch@carmarthenshire.gov.uk

<sup>∞</sup>University of Wales: Trinity Saint David (Swansea), Mount Pleasant, Swansea, Wales, UK. SA1 6ED  
mike.phillips@sm.uwtsd.ac.uk

<sup>∞</sup>University of Wales: Trinity Saint David (Swansea), Mount Pleasant, Swansea, Wales, UK. SA1 6ED  
emailAllan.williams@sm.uwtsd.ac.uk

<sup>+</sup>University of Dundee, DUNDEE, Scotland, UK, DD1 4HN  
Email: r.w.duck@dundee.ac.uk



[www.cerf-jcr.org](http://www.cerf-jcr.org)



[www.tl.konink.org](http://www.tl.konink.org)

## ABSTRACT

Thomas, T., Lynch, S.K., Phillips, M.R., Williams, A.T., Duck, R.W. 2014. Relationships between sand spit evolution, environmental forcing and inland inundation. In: Green, A.N. and Cooper, J.A.G. (eds.), *Proceedings 13<sup>th</sup> International Coastal Symposium* (Durban, South Africa), *Journal of Coastal Research*, Special Issue No. 70, pp. 072-077, ISSN 0749-0208.

Topographic field data and environmental forcing agents were used to assess morphological changes (1995-2010) at Ginst Spit, Pendine Sands, West Wales and flood potential at Laugharne, a town in the lee of the spit. Areal change between annual surveys showed variable distal end migration eastward extending into the channel of the Towy, Taf and Gwendreath estuaries. Dominant waves emanate from south toward southwest and suggest that the longshore sediment drift is from west toward east. However, sub-dominant waves from southeast are limited by fetch but engender a counter drift back toward the west at the distal end forming the customary northward hook. Wave model results showed significant modifications occurred between the inshore model boundary and the nearshore zone and overall results suggest that spit evolution is dependent on sediment movement that occurs during high spring tidal conditions within this macrotidal environment. Precipitation and flood events were correlated to spit evolution, which suggested that a combination of fluvial and coastal processes in combination contribute to the flooding of Laugharne town.

**ADDITIONAL INDEX WORDS:** *Sand spit evolution, wave models, precipitation, inland flooding.*

## INTRODUCTION

A spit ridge is an embankment of sediments attached to land at one end, whilst the other extends from low water to a depth of several metres (Davis and Fitzgerald, 2005; Teodoro *et al.*, 2011). Morales *et al.* (2001) found that a spit-platform downdrift of a barrier spit followed a cyclic pattern of downdrift migration and breaching. According to Vinther *et al.* (2005), spit-platforms draw little attention in the literature, despite their expected importance for understanding sediment transport mechanisms leading to siltation of tidal channels. The topographic boundary of a sand spit is not well-defined, because the boundary is not static in time, unlike the majority of water bodies (Teodoro *et al.*, 2011). The use of image classification tools reduces time consumption and makes for easier and more accurate identification of morphological and hydrodynamic features or patterns, and consequently, sand spit boundary extraction (Teodoro *et al.*, 2009).

Shoreline morphological changes are often estimated using various forms of topographic surveying techniques (Zhang *et al.*, 2002; Sorensen, 2006). Uncertainty in shoreline position depends on the accuracy and precision of survey measurements and stability of shoreline position indicators (Douglas and Crowell, 2000), and choice of a suitable shoreline change indicator is fundamental. In this environment, an ideal position indicator

would be easily identified both in the field and on all aerial photographs (Zhang *et al.*, 2002; Leatherman, 2003) and mean high water level (Zhang *et al.*, 2002) or alternatively, the vegetation line can be used (Morton, 1991).

Thomas *et al.* (2010; 2011) used the vegetation line with a combination of maps and aerial photographs when mapping shoreline changes at Tenby, South West Wales, as they found that the MHWL was difficult to obtain in a macrotidal environment. Nevertheless, they were able to map historic beach rotation that was subsequently linked to nearshore changes and to sand spit destruction. Ashton *et al.* (2001) showed that when the incident angle of deep water waves to the main shoreline exceeds 45°, shoreline instability occurs, which can result in development of a sand spit from a small shoreline perturbation. Thomas *et al.* (2011), using a 262 yr record of bathymetric maps, showed that certain spit formations can grow in the general direction of predominant longshore sediment transport, but can also erode commensurately with either a diminution of updrift sediment supply or changes in seabed and sandbank orientation. The spit may then become wave aligned and continue to grow in a different direction.

Laugharne township, Carmarthenshire, South West Wales, is located in the lee of Ginst Spit and has a history of flooding. Therefore, this research paper assesses sand spit evolution using meteorological data, topographic field studies and wave models and explores links to flooding events.

## Physical and geological background

The Bristol Channel/Severn Estuary is an inlet from the Atlantic Ocean on the west coast of Great Britain, partially enclosed and separating Wales from England (Phillips and Crisp, 2010; Uncles, 2010; Figure 1a). Carmarthen Bay on the northwest Bristol Channel is a shallow embayment which is bounded by the Worms Head to the east and by Caldey Island to the west (Halcrow, 2010; Figure 1b). The coastal strip is approximately 70 km long, with environments that vary from extensive sand beaches to muddy tidal flats or rocky cliffs, and human use varies from industrial to recreational and from agricultural to residential (Barber and Thomas, 1989). The foreshore of Pendine Sands forms the seaward part of an extensive, sandy coastal barrier within this shallow bay (Jago and Hardisty, 1984). The underlying intertidal zone and dune geology of Pendine Sands and Ginst spit (Figure 1c) comprises Old Red Sandstone laid down during the Devonian period while there is a small headland of Carboniferous Limestone on the western fringe, deposited down during the Carboniferous period (Halcrow, 2010). Centrally placed within the bay is the Taf, Towi and Gwendreath estuary complex. The geological characteristics extend below the present-day seabed, where the overlying morphology includes elements directly related to erosion and deposition associated with submarine valley formation, e.g., rock platforms and glacial deposits such as tills.

However, the seabed also includes morphological features

related to submergence by rising sea level following the last glaciation and sediment deposition and re-working, some of which may have fluvial and glacial origins (Mackie *et al.*, 2002). Strong winds and tides generated in the Bristol Channel, together with north Atlantic swells contribute to a high energy wave environment (Allan *et al.*, 2009). Dominant and prevailing south-westerly winds that expose the Bristol Channel to un-refracted North Atlantic waves ensure abundant wave action within these macrotidal, 7.5 m spring tidal range waters (Phillips and Crisp, 2010; Thomas *et al.*, 2011). Offshore recorded south to westerly waves of *circa* 1.2 m height and 5.2 s period predominate, although storm waves of >5.5 m with periods that range between 8 and 15 s are not uncommon (Thomas *et al.*, 2010).

## METHODS

Both total station and RTK network facilities were used to survey topographical changes annually between 1995 and 2010 and a total of 15 surveys were available for analysis. Each survey was directly referenced to the British Coordinate System. The output data was imported into Surfer 9<sup>®</sup>, a full-function 3D visualization, contouring and surface modelling programme. Using its sophisticated interpolation engine the XYZ data was digitised along the MHWL contour because this was clearly visible on all surveys. These data were subsequently imported into a Geographic Information System (GIS; MapInfo<sup>®</sup>) and areal changes between a shoreward baseline and both proximal (transect TR01 to transect TR02) and distal (area east of TR02) ends computed. Waves were modelled using the Nearshore Evolution Modelling system (NEMOS), a software package which consists of several modules coupled together to provide a complete picture of beach response to imposed wave conditions. A rectangular computational grid was developed within gridgen that encompassed the nearshore fronting Ginst Spit, with a square mesh size of 10 m × 10 m. To model inshore wave conditions a 23 yr time series (1987-2010) of offshore wave data supplied by the Meteorological Office, and the Weibull distribution was used to compute extreme waves and respective periods based upon a 1:10 year event (in line with annual data). Considered in the present study, were dominant south-westerly and sub-dominant south-easterly conditions. These offshore data were subsequently transformed using WISPHS3 and WWL to represent the inshore model boundary wave conditions. The Regional Coastal Processes WAVE propagation model (RCPWAVE), originally developed by Ebersole (1985) and documented by Ebersole *et al.* (1986), was used to model inshore waves fronting Ginst Spit.

## RESULTS

Table 1, produced from the data computed within GIS, shows the annual inter-survey and cumulative areal changes (m<sup>2</sup>). Figure 2, produced from Table 1, highlights a rising trend between 1995 and 2002 when areal changes were directly compared with time at the distal end and consistency was confirmed by a coefficient of determination that explains almost all data variation ( $R^2 = 0.86$ ). This was followed by a reversal in trend to the end of the assessment period (2002-2010;  $R^2 = 0.96$ ). Proximal areal changes showed a consistent rising trend throughout the assessed period (1995-2010;  $R^2 = 0.96$ ; Figure 3). Overall, the area of Ginst Spit increased with time ( $R^2 = 0.88$ ; Figure 4).

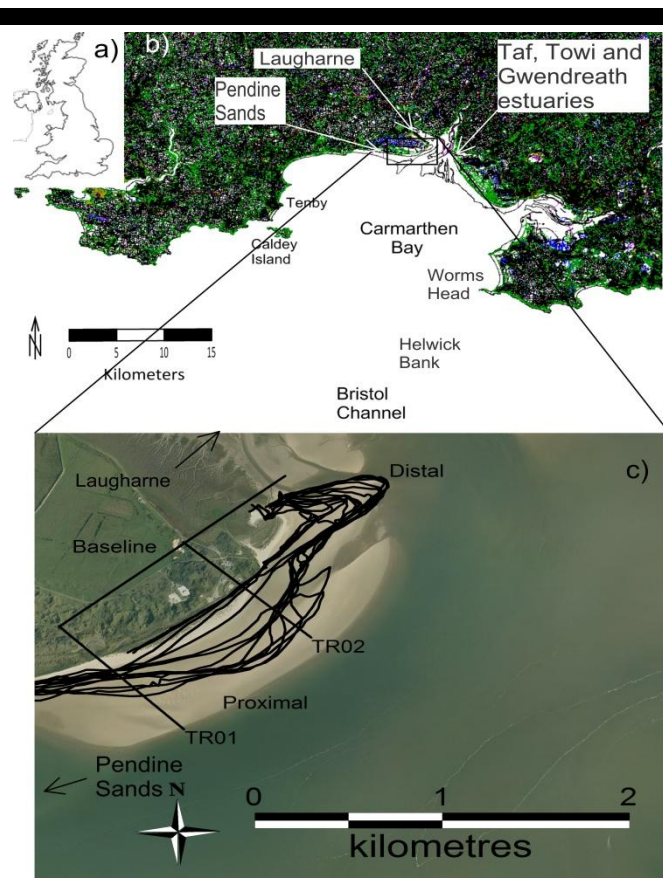


Figure 1. Study area Locality, a) UK, b) Carmarthen Bay and C) Ginst Spit location complete with baseline and transect locations form which areal changes were computed.

Table 1. Inter-survey and cumulative changes at Ginst Spit.

Date	Date	Inter-survey Areal Change (m <sup>2</sup> )			Cumulative areal Change (m <sup>2</sup> )		
		Distal	Proximal	Gross	Distal	Proximal	Gross
1999	2000	91500	39800	131300	91500	39800	131300
2000	2001	13900	57400	71300	105400	97200	202600
2001	2002	6100	102600	108700	20000	160000	180000
2002	2003	-2300	21600	19300	3800	124200	128000
2003	2004	-19100	52200	33100	-21400	73800	52400
2004	2005	-9800	15200	5400	-28900	67400	38500
2005	2006	-14000	24300	10300	-23800	39500	15700
2006	2007	-9100	26700	17600	-23100	51000	27900
2007	2008	-7000	33400	26400	-16100	60100	44000
2008	2009	-14140	10000	-4140	-21140	43400	22260
2009	2010	-33320	1900	-31420	-47460	11900	-35560

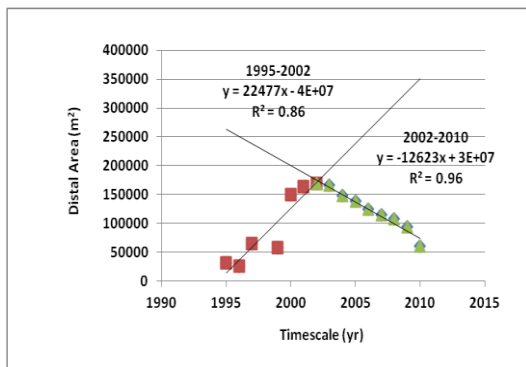


Figure 2. Temporal areal change at the distal end of Ginst Spit.

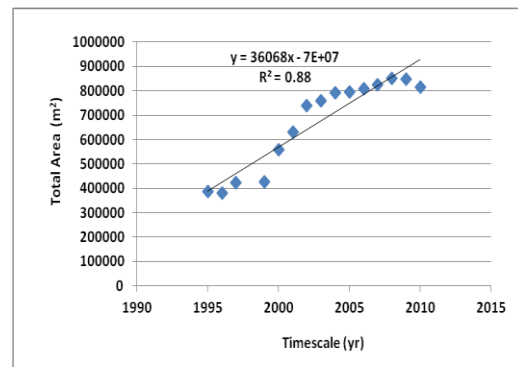


Figure 4. Combined (Proximal + Distal) Temporal areal changes at Ginst Spit.

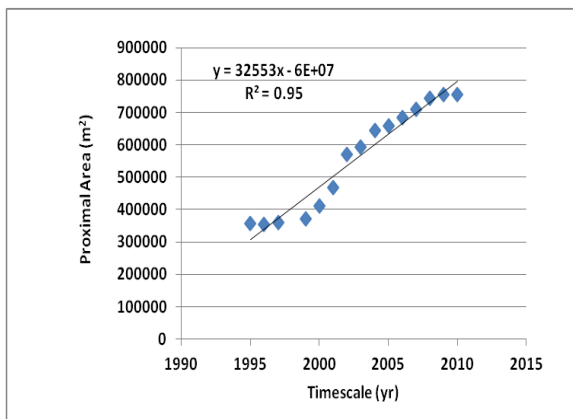


Figure 3. Temporal areal change at the proximal end of Ginst Spit.

Table 2 shows survey averaged precipitation and flooding events obtained from the Environment Agency, all averaged to correspond with the Inter-survey results given in Table 1. There was a temporal reducing trend of flooding at Laugharne given by the regression equation. The  $R^2$  value explains almost 60% of data variation (Figure 5). Precipitation also shows decreasing trends and an  $R^2$  value that explained 40% of data variation. These results agree with other Bristol Channel studies that have highlighted temporal reductions in storm occurrence and wind speed (Thomas *et al.*, 2010 and Phillips *et al.*, 2013, respectively). When flooding events are compared with annual averaged precipitation, a positive relationship existed between increasing floods and precipitation with  $R^2$  value that explained 50% of data variation given by regression equation (Figure 7).

Table 2. Survey averaged, wind, wave flood events and precipitation data from 1999-2010.

Date	Date	WSpd (ms-1)	RHs (m)	RTp (s)	RWadir (deg)	WWHs (m)	WWTp (s)	WWdir (deg)	SWHs (m)	SWTp (s)	SWdir (deg)	Flood Events (no)	Precipitation (mm)
1999	2000	12.7	2.9	6.6	232	2.8	6.6	232	0.9	10.8	204	16	566
2000	2001	12.9	2.6	6.3	196	2.5	6.2	194	0.8	10.3	206	44	667
2001	2002	12.7	2.7	6.4	225	2.7	6.5	228	0.6	9.0	168	61	722
2002	2003	12.5	2.6	6.3	210	2.5	6.3	210	0.8	10.8	208	47	608
2003	2004	12.3	2.5	6.1	225	2.4	6.1	226	0.7	9.3	187	42	568
2004	2005	12.4	2.7	6.4	226	2.7	6.5	225	0.6	9.2	176	32	615
2005	2006	12.3	2.7	6.4	226	2.6	6.4	226	0.8	10.6	202	18	606
2006	2007	12.6	3.0	6.8	228	2.9	6.7	227	0.9	11.8	212	19	474
2007	2008	12.6	3.0	6.8	235	2.9	6.7	237	0.9	11.8	224	26	444
2008	2009	12.5	2.4	6.5	221	2.3	6.5	215	0.7	9.7	199	31	602
2009	2010	13.4	2.5	7.2	224	2.3	7.6	216	0.9	10.6	225	25	569

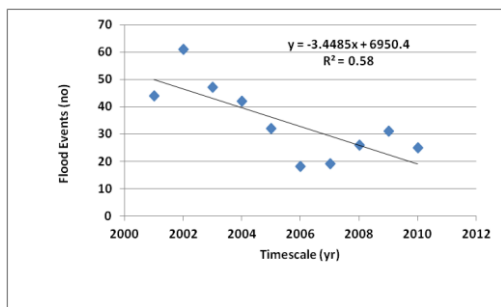


Figure 5. Temporal flood events.

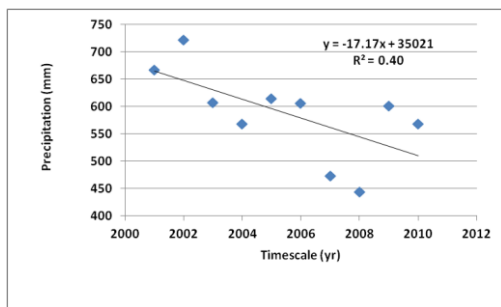


Figure 6. Temporal precipitation.

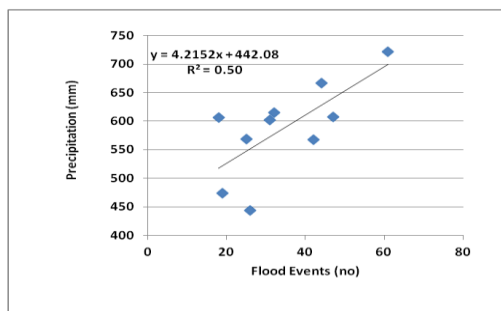


Figure 7. Comparison between floods and precipitation.

Table 2 also shows survey averaged environmental forcing, and comparison between the data of Table 1 and flood and precipitation data of Table 2 showed that both floods and precipitation were significantly correlated with almost all environmental variables with r values that ranged between -0.56 and -0.76 (p<0.05). The opposite was true when areal change was compared with environmental forcing where r values ranged between 0.09 and -0.33 (p>0.05). This was not surprising because of the temporal resolution data (i.e., annual average) that essentially filters out the storm events and also because of the macrotidal environment which makes MHWL to be only exposed to waves over a very limited timeframe.

Table 3, produced from Table 2, shows a Pearson correlation matrix set at zero lag, and highlights that flooding events are significantly correlated to both inter-survey and cumulative areal change with r values that ranged between 0.55 (p<0.05) and 0.90 (p<0.001). The positive value suggests that areal increase would result in a higher risk of floods at Laugharne Township. As the distal end of the spit migrates eastward there is a narrowing of the estuary mouth that diffracts waves refocusing their energy toward the foreshore area of Laugharne Township. Unsurprisingly, there was less correlation between precipitation and sand spit change with r values that ranged between 0.43 (p>0.05) and 0.61 (p<0.05) but the results still showed a linkage between increasing precipitation and areal increases suggesting that fluvial sediment contributes to the evolution of the spit.

Table 3. Pearson correlation matrix comparing sand spit changes with flood events and precipitation (Dist =distal end, Prox =proximal end, Precip = precipitation).

	Inter-survey Areal Change			Cumulative Areal Change		
	Dist	Prox	Gross	Dist	Prox	Gross
Floods	0.58	<b>0.75</b>	<b>0.76</b>	0.55	<b>0.90</b>	<b>0.82</b>
Precip	0.43	0.50	0.52	0.50	0.59	0.61

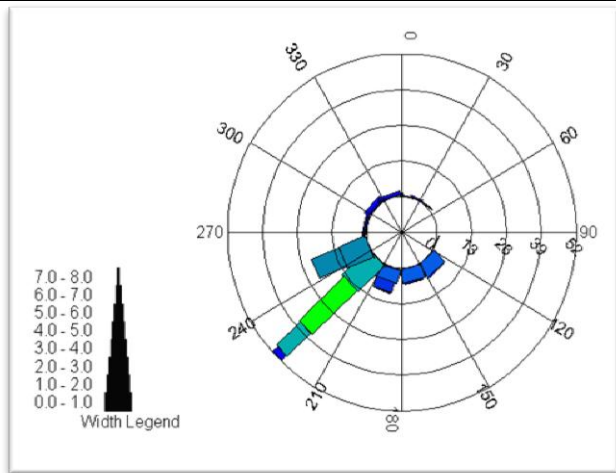


Figure 8. Wave Rose illustrating offshore waves prior to entering Carmarthen Bay.

Alongside the morphological change assessments, wave models were also used to predict beach behaviour based on extreme wave (1:10 year return period) conditions from the predominant (southwest; Figure 8) and sub-dominant (southeast) swell directions. Offshore south-westerly waves (c.f. Thomas *et al.*, 2013) approach Carmarthen Bay un-refracted and can reach as much as 9.7 m in height. On entering the bay they are heavily diffracted by Caldey Island before interacting with the bay's shallower waters. Refraction focuses their energy at an angle to the Ginst Spit shoreline. The inshore waves vary with differing extreme events, but can reach 4.59 m in the 1:10 yr condition (Figure 9).

Fetch limited south-easterly waves can reach 4.4 m offshore before entering Carmarthen Bay, but are heavily diffracted around Worms Head and refracted as they traverse the Helwick Bank before entering the bay. They approach the shoreline at Ginst Spit at an angle towards west and these extreme conditions produce inshore waves that rarely exceed 2.04 m.

According to Jago and Hardisty (1984) the sedimentological features of the macrotidal foreshore along the frontage of Pendine Sands and Ginst Spit reflect a tide-induced modification of nearshore wave characteristics. Ebb tide breaker heights decrease, as the surf zone widens and swash/backwash velocities diminish, causing a change from plunging to spilling breakers; increasingly symmetrical swash zone flows are associated with a decreasing beach gradient. This concurs with the work of Thomas *et al.* (2013) which highlighted a relatively stable intertidal zone and variable accretive/erosive subaerial zone. Therefore, it is reasonable to suggest that most alongshore sediment movement occurs during high tide and inshore propagating modelled southwest waves deviate by up to 30° (210° true), representing a 15° transposition toward south. Under these wave conditions sediments would be moved alongshore from west toward east (Figure 9). In contrast, southeast waves tend to deviate toward south (168° true) suggesting a sediment pathway from east toward west. Unlike the previous southeast breaking waves, which increase with offshore intensity but are relatively small (1 m) when compared to southwest waves, fetch limits the generation of energetic waves and therefore any counter drift would be relatively weak on the rare occasions on which easterly winds predominate (Figure 10).

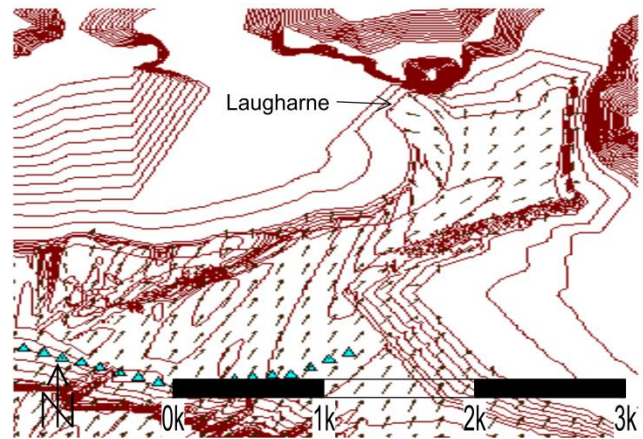


Figure 9. Plan showing wave direction vectors from southwest direction.

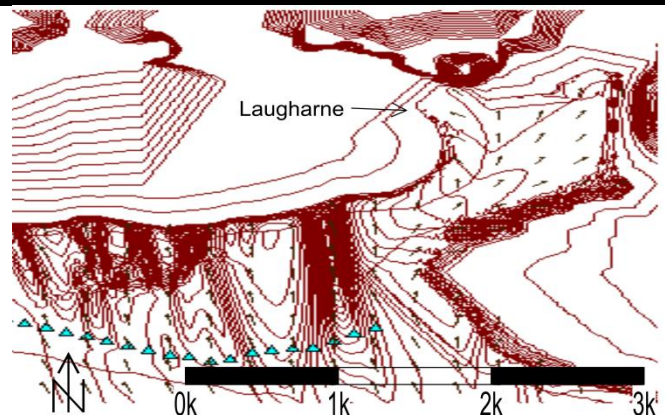


Figure 10. Plan showing wave direction vectors from southeast direction.

## DISCUSSION

Sand Spit changes based upon variations of the MHWL highlighted a cumulative increase in spit area through the 15 year period of assessment. This was confirmed by Regression analysis where the coefficient of determination ( $R^2$ ) values explained almost all data variation. This consistency, however, was not shown in the inter-survey results, caused by two distinct temporal trends; the first (between 1995 and 2002) highlighted a temporal areal increase and the second, an opposing trend to 2010. Interestingly, this variation approximately follows the nodal tide variation that causes a periodic change in mean tidal range and there was a decreasing trend between 1995 and 2004, followed by an increasing trend towards the end of the assessment period. The trend change also coincided somewhat with the highest recorded annual average precipitation which occurred in 2002.

There was a temporal reduction in rainfall and flooding events at Laugharne Township and correlation between them suggests that fluvial flows could also be a contributory factor. Correlation was also found between flooding, rainfall and spit evolution.

Numerical wave simulations and observations from inshore wave models provided insights into the sand spit responses, highlighting that wave heights at the shoreline are relatively consistent for all analysed wave events (not all shown in this paper), suggesting that wave energy attenuation across the extensive dissipative subaqueous and intertidal zones reduces coastal response to

changing wave conditions. The orientation of the beach and dune system west of Ginst Spit appears to be attuned to the modally high wave energy regime, suggesting that the system requires extreme storm conditions that coincide with high spring tidal range and at high water in order to produce any measurable significant morphological impact at Ginst Spit.

Overall the results would suggest that an increase in spit size may result in an increased risk of flooding which is quite the opposite of what would be expected. Spit migration across the estuary mouth probably causes additional diffraction of incumbent waves, refocusing their energy so as to impact the low lying foreshore area in front of Laugharne township, thereby increasing flood risk potential. However, in addition to the forcing agents analysed in this research, there is a likelihood that flooding can be caused by a combination of factors such as storm surges, fluvial flows and the impacts of sea level rise. These have not been considered here but form part of the continued regional research programme.

## CONCLUSIONS

Annual topographic field data provided a record of recent changes that took place at Ginst Spit, Pendine Sands, West Wales. Environmental forcing agents were used to understand both variations in sand spit morphology and inland flooding. Cumulative areal changes highlighted terminal end migration extending eastward into the estuary channel. Dominant waves emanate from southwest, and both offshore islands and bathymetry mean that they are significantly modified, resulting in longshore drift from west toward east. Sub-dominant waves from southeast engender a counter drift back toward the west albeit weakly. Wave model results found agreement with qualitative assessments. Annually averaged wave components demonstrated little correlation with the sand spit change but conversely, precipitation and spit growth were correlated to flood events, which suggested that a combination of fluvial and coastal processes in the flooding of Laugharne township. These assessments form part of a continued regional research programme. Similar behaviour should be exhibited at other coastal locations worldwide and should be replicated in order to establish specific responses, and underpin intervention or no active intervention strategies.

## LITERATURE CITED

- Allan, R., Tett, S.F.B. and Alexander, L.V., 2009. Fluctuations in autumn–winter severe storms over the British Isles: 1920 to present. *International Journal of Climatology*, 29, 357–371.
- Ashton, A., Murry, A. B. and Arnault, O., 2001. Formation coastline features by large scale instabilities induced by high angle waves. *Nature*, 414, 296–300.
- Barber, P. C. and Thomas, R. P. 1989. Case study of Carmarthen Bay. *Proceedings of the Maritime Engineering Board of the Institution of Civil Engineers* (London, England), pp. 243–260.
- Davis Jr, R. A. and Fitzgerald, D. M., 2005. *Beaches and Coasts*. Oxford, England: Blackwell Publishing, 385p.
- Douglas, B.C. and Crowell, M., 2000. Long-term Shoreline position Predictions and Error Propagation. *Journal of Coastal Research*, 16(1), 145–152.
- Ebersole, B.A., 1985. “Refraction, Diffraction Model for Linear Waves,”. *Journal of Water, Port, Coastal, and Ocean Engineering*, 3(6), 939–953.
- Ebersole, B.A., Cialone, M.A. and Prater, M.D., 1986. “Regional Coastal Processes Numerical Modelling System, Report 1, RCPWAVE- A linear Wave Propagation Model for Engineering Use,” *Technical Report CERC-86-4*, Coastal Engineering Research Centre, US Army Engineer Waterways Experiment Station, Vicksburg, MS.
- Halcrow, 2010. *Lavernock Point to St Ann’s Head SMP2*. <http://www.southwalescoast.org/contents.asp?id=55#SMP2MainDocument>. Accessed 06/09/2011.
- Jago, C.F. and Hardisty, J., 1984. Sedimentology and morphodynamics of a microtidal beach, Pendine Sands, SW Wales. *Marine Geology*, 60 (1–4), 123–154.
- Leatherman, S.P., 2003. Shoreline Change Mapping and Management along the U.S. East Coast. *Journal of Coastal Research*, S138, 5–13.
- Mackie, A.S.Y., James, J.W.C., Rees, E.I.S., Darbyshire, T., Philpot, S.L., Mortimer, K. and Jenkins, G.O., 2002. *BIOMOR 4. The Outer Bristol Channel Marine Habitat Study*. <http://www.marlin.ac.uk/obc/pdfs/report/chapter%202.pdf>. Accessed 10/10/2006
- Morales, J.A., Borrego, J., Jimenez, I., monterde, J. and Gil, N., 2001. Morphostratigraphy of an ebb-tidal delta system associated with a large spit in the Piedras estuary mouth (HuelvaCoast, Southwestern Spain). *Marine Geology*, 172, 225–241.
- Morton, R.A., 1991. Accurate shoreline mapping: past, present and future. *Proceedings of Coastal Sediments 91*, ASCE. 997–1010.
- Phillips, M.R. and Crisp, S., 2010. Sea Level Trends and NAO Influences: The Bristol Channel/Severn Estuary. *Global and Planetary Change*, 73, 211–218.
- Phillips, M.R., Rees, E.F. and Thomas, T., 2013. Winds, sea levels and North Atlantic Oscillation (NAO) influences: An evaluation. *Global and Planetary Change*, 100, 145–152.
- Sorensen, R.M., 2006. *Basic Coastal Engineering (3<sup>rd</sup> edition)*. New York: Springer, 319p.
- Teodoro, A.C., Pais-Barbosa, J., Gonçalves, H., Veloso-Gomes, F. and Taveira-Pinto, F., 2011. Extraction of Cabedelo sand spit area (Douro estuary) from satellite images through image processing techniques. *Journal of Coastal Research*, S1 64, 1740–1744.
- Teodoro, A.C., Pais-Barbosa, J., Veloso-Gomes, F. and Taveira-Pinto, F., 2009. Evolution of Beach Hydromorphological Behaviour and Classification Using Image Classification Techniques. *Journal of Coastal Research*, S1 56, 1607–1611.
- Thomas, T., Phillips, M. R., Williams, A. T and Jenkins, R. E., 2013. Rotation on two adjacent open coast macrotidal beaches. *Applied Geography*, 35, 363–376.
- Thomas, T., Phillips, M.R and Williams A.T., 2010. Mesoscale evolution of a headland bay: Beach rotation Process. *Geomorphology*, 123, 129–141.
- Thomas, T., Phillips, M.R., Williams and A.T. Jenkins, R.E., 2011. A Multi-century record of linked nearshore and coastal change. *Earth Surface Processes and Landforms*, 36, 995–1006.
- Uncles, R.J., 2010. Physical properties and processes in the Bristol Channel and Severn Estuary. *Marine Pollution Bulletin*, 61, 5–20.
- Vinther, N., Aagaard, T and Nielsen, J., 2005. Complex Sediment Transport Pattern on a Spit-Platform in the Danish Wadden Sea. *Journal of Coastal Research*, 21(4), 710–719.
- Zhang, K., Huang, W., Douglas, B.C. and Leatherman, S.P., 2002. Shoreline Position variability and Long Term Trend Analysis. *Shore and Beach*, 70, 31–35.



# Longshore drift cell development on the human-impacted Bight of Benin sand barrier coast, West Africa

Raoul A. Laïbi†, Edward J. Anthony‡, Rafael Almar∞, Bruno Castelle§, Nadia Senechal§, Elodie Kestenare∞

†Université Abomey Calavi  
Département des Sciences de la Terre,  
Faculté des Sciences et Techniques  
Cotonou, Republic of Benin  
raoulaibi@yahoo.fr

‡ Aix-Marseille Université,  
IUF, CEREGEUMR 34,  
Europôle de l'Arbois,  
13545 Aix en Provence cedex 04,  
France  
anthony@cerege.fr

∞ IRD-LEGOS  
Université Paul  
Sabatier/CNRS/CNES/IRD  
Toulouse, France  
rafael.almar@ird.fr  
elodie.kestenare@ird.fr



[www.cerf-jcr.org](http://www.cerf-jcr.org)

§EPOC  
Université de Bordeaux/CNRS  
Talence, France  
b.castelle@epoc.u-bordeaux1.fr  
n.senechal@epoc.u-bordeaux1.fr



[www.JCRonline.org](http://www.JCRonline.org)

## ABSTRACT

Laïbi, R. A., Anthony, E. J., Almar, N., Castelle, B., Senechal, E., 2014. Longshore drift cell development on the human-impacted Bight of Benin sand barrier coast, West Africa. In: Green, A.N. and Cooper, J.A.G. (eds.), *Proceedings 13<sup>th</sup> International Coastal Symposium* (Durban, South Africa), *Journal of Coastal Research*, Special Issue No. 70, pp. 078-083, ISSN 0749-0208.

The Bight of Benin is an open, microtidal, wave-dominated coast forming a 500 km-long mild embayment in the Gulf of Guinea, in West Africa, between the Volta River delta in Ghana, to the west, and the western confines of the Niger River delta in Nigeria to the east. The bight is exposed to energetic swells from the South Atlantic, and is characterised by Holocene sand barriers bounding lagoons. The barrier system has been sourced essentially by sand supplied through the Volta River delta, terminus of a large river catchment of 397,000 km<sup>2</sup>, although wave energy conditions and sand mineralogy also suggest inputs from the nearshore shelf. The long-term pattern of barrier progradation in the Bight of Benin culminated in a mildly embayed coast wherein incident wave behaviour, beachface gradient and the longshore sand transport system were intimately linked, generating what may be classified as an 'equilibrium drift-aligned' coast with a unique and homogeneous longshore drift cell stretching from the Volta River delta to the Niger River delta. This coast has, however, been significantly impacted over the last 50 years by the construction of three deepwater ports in Lomé (Togo), Cotonou (Benin) and Lagos (Nigeria) that have intercepted sand supply, as well as by a major dam on the Volta River, resulting in destabilization of the former single drift cell on this coast. The ensuing multi-cellular structure is characterised by long sectors of rampant coastal erosion that threatens parts of these cities, coastal villages and infrastructure.

**ADDITIONAL INDEX WORDS:** *wave-dominated coast, drift-alignment, deepwater ports, coastal erosion.*

## INTRODUCTION

One reason for the commonality of shoreline erosion induced by human activities on long open coasts is the lack of understanding of the spatial and temporal scales over which sediment redistribution processes that shape the coast occur. In many situations, small segments of coast, commonly of high value due to urbanisation, and with specific management preoccupations, are embedded in larger-scale aspects of coastal change that are not always well apprehended. From a coastal management point of view, a first step towards bridging the gap between these two scales of change has been the coastal cell concept. This is fundamentally hinged on open beaches (as opposed to short embayed or pocket beaches), alongshore wave gradients and longshore drift, which form the primary drivers of short-term coastal change on the scale of days to years (Carter, 1988). This concept has commonly been used in a purely sediment budgetary framework in which process gradients may be ignored, the emphasis being on the definition of each cell and on the net gains and losses of sediment within each coastal cell (van Rijn, 2011). This approach is valid and useful on coasts where cell

boundaries and their spatial and temporal changes are readily constrained, which is commonly the case of wave-dominated, microtidal coasts, such as in West Africa (Figure 1). The West African coast is characterised by two long stretches of wave-dominated coasts under the influence of long and regular swell and a minor component of shorter-fetch wind waves. A hallmark of this constant wave regime is strong sustained longshore drift that prevails along much of these two sectors of sandy coast. In conjunction with abundant fluvial sand supplies during the Late Pleistocene sea-level lowstand on the presently drowned inner shelf, this has resulted in the build-up of numerous barrier systems in the Gulf of Guinea and spit- and aeolian dune- systems on the Mauritania and Senegal coast.

Many of the barrier systems in the Gulf of Guinea are characterised by sequences of wave-formed beach ridges under dominantly 'drift-aligned' patterns (as defined by Davies, 1980), although locally, 'swash-aligned' patterns have developed in embayed settings bounded by bedrock headlands – notably in Liberia. Three sectors of sand barrier development with significant sequences of beach ridges bound by long, open beaches can be clearly distinguished: the coasts of southern Sierra Leone, Côte d'Ivoire, and the Bight of Benin (Figure 1). The long, open

DOI: 10.2112/SI70-014.1 received 29 November 2013; accepted 21 February 2014. © Coastal Education & Research Foundation 2013

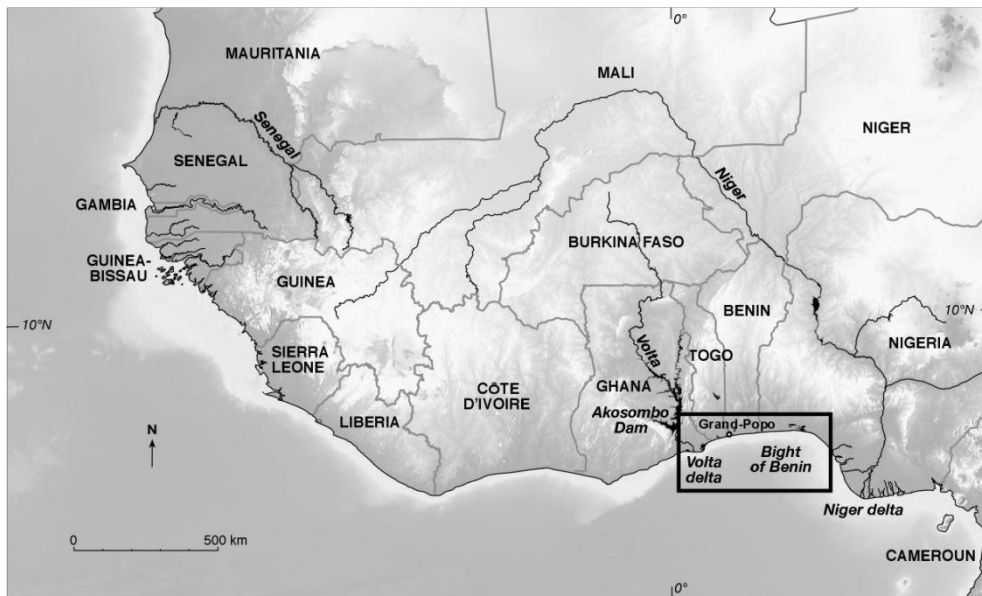


Figure 1. Wave-dominated sectors of the coast of West Africa characterized by moderate to strong longshore drift (Mauritania and Senegal, and from Sierra Leone to Cameroun), and the Bight of Benin coast between the deltas of the Volta and Niger Rivers

beaches of the last two sectors, subject to pronounced longshore drift, are also potentially highly susceptible to perturbations generated by anthropogenic activities.

This paper focuses on the drift cell structure of the barrier system off the Bight of Benin, which like that of the Côte d'Ivoire coast has been significantly impacted by human activities. Meanwhile, the coast of southern Sierra Leone, characterized by moderate drift by virtue of its overall orientation to Atlantic waves (Anthony, 1995), has remained totally exempt from direct human modifications. We show that following progradation towards an equilibrium shoreline characterized by a single major drift cell, the Bight of Benin coast has been undergoing rapid destabilization over the last 50 years, resulting in breakdown into a less well-defined multi-cell structure. We also contend that disentangling the impacts of human activities on this coast from natural trends requires a grasp of its long-term morphodynamics.

### STUDY AREA

The Bight of Benin is an open, microtidal, wave-dominated coast exposed to waves from the South Atlantic, and is characterised by Holocene sand barriers bounding lagoons. The bight is bounded by a narrow shelf 15 to 33 km wide, and is characterised by a fairly uniform, moderately steep shoreface with a gradient of between 1:120 and 1:150 up to a depth of -15 m – considered as the close-out depth for significant wave movements on this coast (Delft Hydraulics, 1990; Rossi, 1989). Beyond this depth, the inner shelf levels out to a low-gradient (1:350-1:400) plain covered by relict transgressive sands (Anthony and Blivi, 1999). The beaches bounding the sand barriers of the Bight of Benin coast are composed of relatively homogeneous medium to coarse (0.4–1 mm,  $D_{50}$ : 0.6 mm), iron-coated quartz sand, except at a pronounced shore break (step), where they also comprise rounded, fine gravel. Tides affecting this coast are semi-diurnal and have a mean spring tidal range of about 1.9 m. The wave setting is a 'cyclone- and storm-free West Coast swell environment' as defined by Davies (1980).

The Bight of Benin barrier system has been sourced essentially by sand supplied through the Volta River delta, which covers an area of about 5,000 km<sup>2</sup> at the outlet of a large river catchment of 397,000 km<sup>2</sup>. Minor additional inputs of sand come from the Mono River in Benin. Sand supply from the shoreface has been deemed to have been important in the early phases of barrier progradation as shoreface gradients in West Africa adjusted to sea level (Anthony, 1995). In the light of the cell dynamics discussed here, we surmise that this source may still be an important one. The Volta River discharge varied between a low of 1000 m<sup>3</sup>/s in the dry season and a high of over 6000 m<sup>3</sup>/s in the wet season before the commissioning of the Akosombo Dam in 1961, only 60 km upstream from the sea. Discharge downstream of the dam has been strongly reduced by the decrease in rainfall over the Sahel since 1975 (Oguntunde *et al.*, 2006). The sand load brought down annually by the river to its delta before dam construction has been estimated at about 1 million m<sup>3</sup> (Delft Hydraulics, 1990). Much of this sand was injected into the longshore drift system via a single delta river mouth (Figure 1). The only other river on this bight coast that supplies sand directly to the sea is the Mono (Anthony *et al.*, 1996). The estimated 100,000 m<sup>3</sup> of sand supplied by this river during the wet season months supplements the massive sand load transported by longshore drift from the Ghana and Togo coasts, however the commissioning of the Nangbéto dam on this river has also affected sand supply to the coast (Laïbi, 2011; Laïbi *et al.*, 2012).

The Bight of Benin barrier systems exhibit a relatively complex history, aspects of which have been documented by Anthony and Blivi (1999) and Anthony *et al.* (1996, 2002). Much of the bight coast exhibits a prograding single or double barrier. Once progradation of an inner barrier resulted in the regularisation of what was a hitherto indented shoreline; the succeeding phase of coastal development involved the emplacement of a more continuous outer barrier directly linked to the Volta river mouth. This suggests the establishment of a highly efficient drift alignment and transition to an economy of massive sediment sourcing by the Volta. Following the complex phases of barrier construction highlighted by the afore-mentioned studies, the

ensuing phase of net long-term longshore stability in Togo and Benin probably stemmed from some sort of equilibrium among shoreline orientation, the nearshore profile and the hydrodynamic regime (Anthony, 1995). This equilibrium alignment implied long-term shoreline stability, despite the massive drift potential. This long-term stability is now threatened by anthropogenic activities that affect longshore drift, especially deepwater ports.

## DATA AND METHODS

In order to estimate the longshore wave transport on the Bight of Benin coast, we had recourse to wave parameters (significant height, peak period and direction of both swell and wind waves) from hindcast data in the Atlantic Ocean between 1979 and 2012, generated by the ECMWF WAM wave model. The wave data are part of the ERA Interim dataset, which involves a reanalysis of global meteorological variables (Dee *et al.*, 2011, Sterl and Caires, 2005). Wave data were extracted from the ECMWF data server ([www.ecmwf.int/research/era](http://www.ecmwf.int/research/era)) on  $1^\circ \times 1^\circ$  grid and with a 6-hr temporal resolution. The ERA Interim reanalysis is the first in which an ocean wind-wave model is coupled to the atmosphere, and the quality of the wave data has been extensively validated against buoy and altimeter data. Sterl and Caires (2005) and Caires and Sterl (2005) demonstrated a very good correlation between the ERA Interim data and these sources, except for high waves (significant wave height,  $H_s > 5$  m) and low waves ( $H_s < 1$  m) which tend to be under- and over-estimated, respectively. These critical wave conditions are not typical of the relatively constant wave regime of the Gulf of Guinea. Sand drift volumes for this coast were determined using the formula of Kaczmarek *et al.* (2005)

$$Q = 0.023 H_b^2 V \quad \text{if } H^2 V < 0.15, \quad 1$$

$$Q = 0.00225 + 0.008(H_b^2 V) \quad \text{if } (H^2 V) > 0.15 \quad (2)$$

where  $H_b$  is the breaking wave height and  $V$  an estimation of the longshore current within the surf zone given by

$$V = 0.25k_v \overline{\gamma g H_b \sin 2\alpha} \quad (3)$$

where  $\alpha$  is the breaking wave angle;  $\gamma = H_b/h = 0.78$  is the constant breaker parameter according to Battjes and Janssen (1978);  $H_b$  the breaking wave height;  $h$  the local water depth and  $k_v$ , an empirical constant. Here we used  $k_v = 2.9$  according to the values in Bertin *et al.* (2008) for wave-dominated environments with similar grain size characteristics.

Field observations on wave breaking and beach morphology were further carried out in an experimental site at Grand-Popo in Benin (Fig. 1). Routine observations along much of the Bight of Benin coast show that the beach morphology and conditions at Grand-Popo are fairly representative of much of the bight coast, except in sectors undergoing massive accretion or erosion, which will be briefly evoked later.

Longshore drift cells were simply determined from morphological observations (especially using Google Earth images coupled with empirical knowledge of long-term barrier morphodynamics) as well as with more recent patterns of barrier development documented by Anthony *et al.* (1996, 2002) in Benin, Anthony and Blivi (1999) in Togo and more recently by Laïbi (2011) in Benin and Anthony (2013) in the Volta River delta sector in Ghana.

## RESULTS AND DISCUSSION

### Longshore transport potential

The Bight of Benin coast is exposed throughout the year to constant, moderate to high energy (ECMWF 1957-2012 Cotonou deep water closest node wave climatology:  $H_s = 1.36$  m,  $T_p = 9.4$  s) waves from the southwest ( $193.6^\circ$ ) (Fig. 2). The wave spectrum is strongly dominated by swell. Waves break on the coast after refraction, with angles of 4 to  $9^\circ$ . Wave breaking is dominantly in the plunging regime, and the grain-size conditions result in relatively steep-faced (slope  $\sim 12-17^\circ$ ) reflective beaches year-round with milder gradients in summer when swell waves are higher, as a result of northward migration, by a few degrees, of the wave-generating zone in the high latitudes of the South Atlantic ( $\sim 40^\circ$  to  $60^\circ$ S). Beach gradients are highly reflective in sectors subject to erosion and are more in the intermediate domain where sand is being sequestered by shore-normal structures.

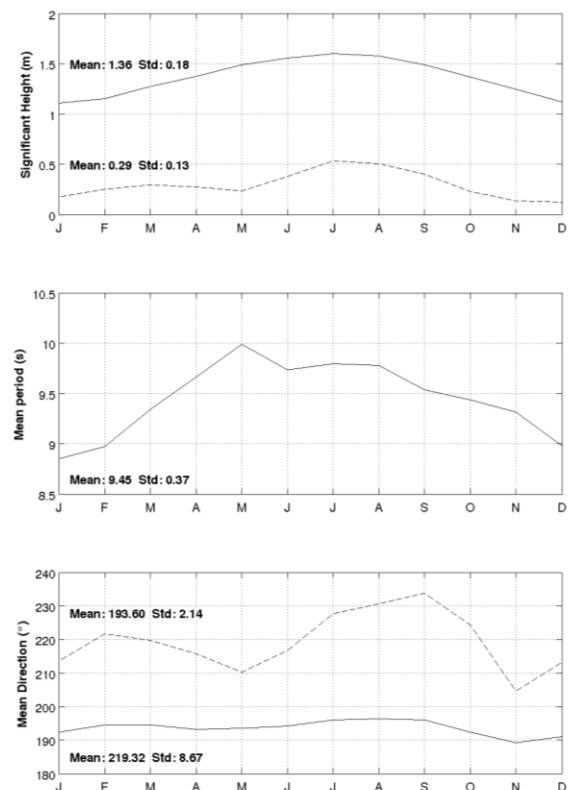


Figure 2. ERA Interim wave characteristics for the Bight of Benin near Cotonou, showing the largely dominant moderate-energy southwesterly swell. The solid line shows the swell and the dashed line is the wind wave. Note that mean periods of wind waves, not shown, are below 2.5 s.

The regularity of the southwesterly swell throughout the year, the small tidal range and the steep, dominantly reflective character of the beaches are three conditions that generate strong and persistent longshore drift from west to east. Past values estimated from intersection by harbour structures are 0.75-1.5 million  $\text{m}^3$  a year (Delft Hydraulics, 1990). The transport value computed from the ERA Interim reanalysed data using the formulation by Kaczmarek *et al.* (2005) is 0.6-0.8 million  $\text{m}^3$  a year (Fig. 3), which is not too different from the lower range identified from

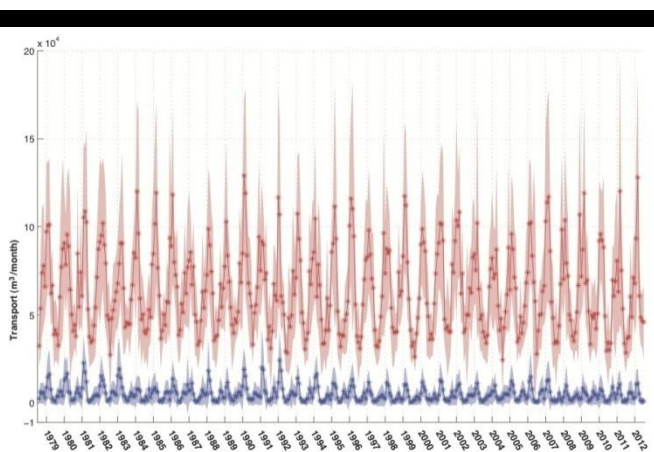


Figure 3. Potential monthly-integrated longshore drift on the Bight of Benin coast computed from ERA Interim wave statistics for the shoreface integrating refraction. Longshore drift, almost exclusively to the east (positive values) is very largely dominated by swell (red spikes), with a minor component associated with wind waves (blue spikes).

harbour interception. This transport is mostly driven by swell waves, rather than wind waves, and presents a large seasonal and interannual variability. Much of the sand is transported as bedload and in suspension in a narrow (30-50 m wide) zone between the wave breaker line and the swash-dominated beachface.

### Recent destabilization and drift cell structure

The present bight coast shows four identified erosional sectors, three of which are matched by downdrift- and one by updrift-accretion (Figure 4). The first of these erosional sectors corresponds to the sector of the coastal town of Keta, which constitutes a hinge point linking the Volta River sand supply to the rest of the Bight of Benin coast. Keta was once flourishing colonial port, probably located in a sector of stationary barrier in the transit zone for Volta delta sand to the Bight of Benin. Erosion has prevailed in this area since the mid-1880s (Kumapley, 1989), which largely predates the construction of the Akosombo dam (Ly, 1980), whereas the large Volta spit has accreted considerably over the last few decades. Anthony and Blivi (1999) estimated the amount of sand captured in this spit for the period 1968 to 1996 at about 750,000 m<sup>3</sup> a year, which accounts for nearly all the drift potential on the Bight of Benin coast (Fig. 3). As erosion around Keta has proceeded, this erosional sector became characterised by the 1990s by a narrow (<100 m wide) eroding transgressive barrier subject to overwash during the summer months of strong swell. A shoreline stabilisation project completed in 2002 and comprising several groynes and a seawall have reduced erosion in this sector, which is still nevertheless appreciable and estimated at about 5.5 m/yr in a recent study (Boateng, 2012). Downdrift of this sector erosion is even stronger (Addo *et al.*, 2011). Updrift of this sector, the Volta spit has continued growing, increasingly with a concave seaward plan-view shape due to accretion of successive beach ridges but with restricted longshore growth of the distal tip.

The other three erosional sectors are clearly associated with the construction of the three deepwater ports (Fig. 4) of Lagos (1957), Cotonou (1962) and Lomé (1967). These major offshore-protruding port breakwaters have significantly impacted the hitherto unidirectional drift, breaking down the equilibrium

shoreline alignment that prevailed prior to port construction, especially in the more updrift sectors of Togo and Benin. These structures have also generated sand accretion updrift, as well as several hundreds of metres of beach progradation over a shoreline distance of up to 5 km. The erosional sectors downdrift of the ports are longer (up to 20 km) and their erosion ensures continuity of the strong drift potential (Fig. 4). The highest degrees of accumulation and erosion have been observed at Lagos harbour. The erosional sector in Cotonou has been further complicated by a canal cut through the beach-ridge barrier in 1888 to alleviate river flooding of Lake Nokoué, the wide, circular lagoon in this sector.

The erosion downdrift of these ports is a threat to large areas of the cities of Cotonou, Lomé, and Lagos; to numerous villages, as well as to coastal infrastructure. Apart from the cell segmentation induced by the port breakwaters, highly localized drift reversal (counter-drift to the west) appears to operate in the immediate lee of these structures, as a result of strong wave refraction and diffraction.

The large accretion spit at the mouth of the Volta delta appears to be a relatively recent feature resulting from adjustments between sediment supply from the river, delta dynamics and the strong longshore drift along this coast (Anthony, 2013). The most likely reason for the dramatic erosion in the Keta sector is that sand supply from the Volta delta area has progressively become insufficient to compensate for strong drift supply to the rest of the Bight of Benin. This is probably because the distal delta barrier, between Anloga and Keta, had been increasingly sequestering a significant proportion of the river's sand supply to the coast, culminating in the inception of the Volta delta spit (Anthony, 2013). Under these conditions, the necessity to satisfy the strong longshore drift budget towards the rest of the bight coast has resulted in considerable reworking of the barrier, threatening coastal settlements such as Keta. In this sector, coastal erosion largely antedated dam construction. The situation has merely been aggravated since the 1960s by the construction of the Akosombo Dam.

## CONCLUSIONS

The morphology of the Bight of Benin coast is an outgrowth of beach-ridge progradation that generated a mildly embayed coast wherein incident wave behaviour, beachface gradient and the longshore sand transport system were intimately linked, generating what may be classified as an 'equilibrium drift-aligned' coast. The patterns of current beach shoreline orientation along much of this bight coast strongly reflect, however, the overarching impacts of human activities. The construction of three deepwater ports along a sector of coast exhibiting one of the world's highest rates of longshore sand drift has resulted in the destabilisation of such drift. A multiple drift cell system, characterised by short updrift sectors of important accretion but by longer downdrift sectors of erosion, has been generated. Such erosion has rendered large areas of the strongly growing cities of Lomé, Cotonou and Lagos increasingly vulnerable to the erosion that is set to continue within the coming decades. The general overview of longshore drift cell destabilization given here was initiated in February 2013 (see project overview in Almar *et al.*, this issue, as well as related studies by Castelle *et al.*, this issue, and Senechal *et al.*, this issue). This forms the prelude to an ongoing study of the morphodynamics and the longshore and cross-shore sediment dynamics of beaches bounding this bight coast.

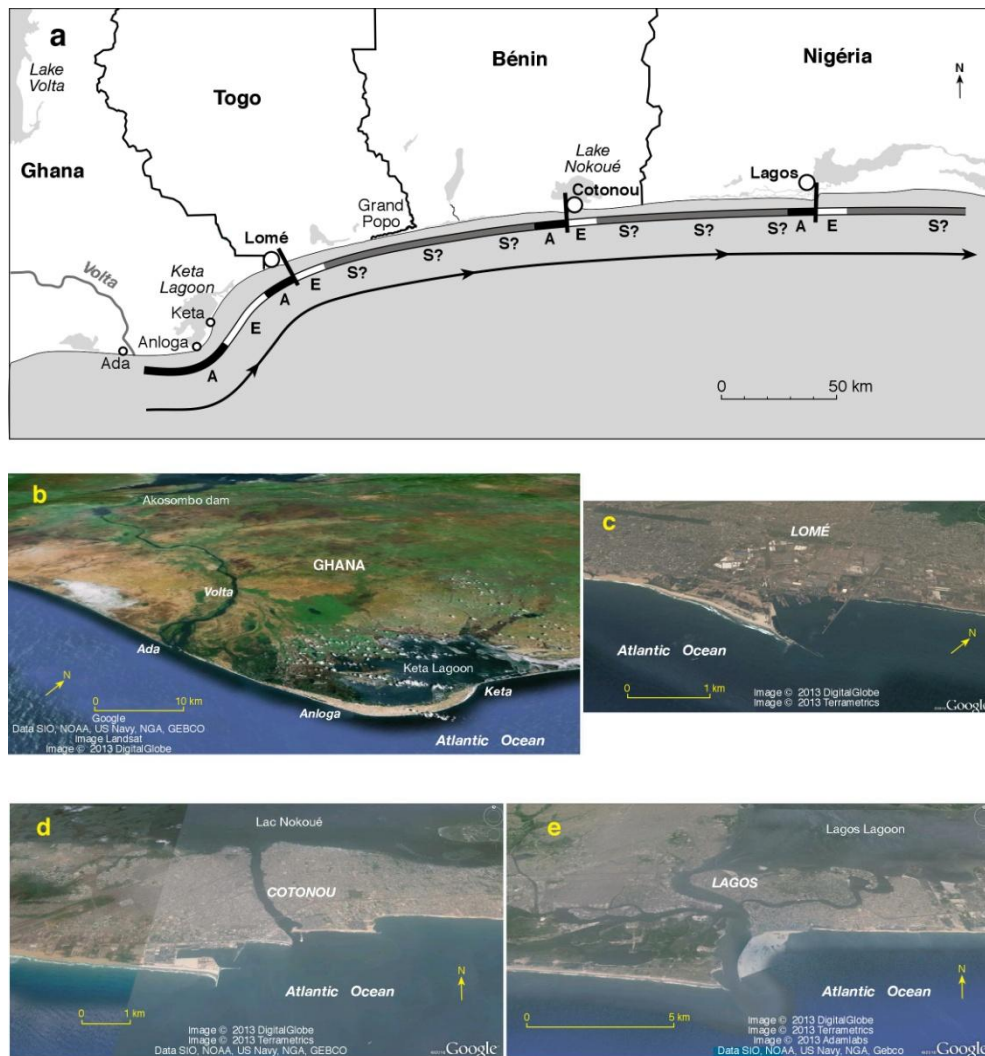


Figure 4. Current longshore drift cells and erosion and accretion associated with port breakwaters in the Bight of Benin. (a) Drift cell structure: a = accretion, e = erosion, s? = presumed stability; (b) the Volta delta; (c) port of Lomé; (d) port of Cotonou; (e) port of Lagos.

## ACKNOWLEDGEMENT

This study was funded by the French INSU LEFE and EC2CO programmes and the IRD (Action Incitative programme). We benefited the ECMWF ERA Interim dataset ([www.ecmwf.int/research/era](http://www.ecmwf.int/research/era)), made freely available.

## LITERATURE CITED

- Almar, R., Hounkonnou, N., Anthony, E., Castelle, B., Senechal, N., Laïbi, R., Mensah-Senoo, T., Degbe, G., Quenum, M., Dorel, M., Chuchla, R., Lefebvre, J-P, du Penhoat, Y., Laryea, W.S., Zodehougan, G., Sohoul, Z., Addo, K.A., and Kestenare, E., 2014. The Grand Popo beach 2013 experiment, Benin, West Africa: from short timescale processes to their integrated impact over long-term coastal evolution. In: Green, A.N. and Cooper, J.A.G. (eds.), *Proceedings 13th International Coastal Symposium* (Durban, South Africa), *Journal of Coastal Research*, Special Issue No. 66, ISSN 0749-0208
- Anthony, E.J., 1995. Beach-ridge progradation in response to sediment supply: examples from West Africa. *Marine Geology*, 129, 175-186.
- Anthony, E.J., 2013. Patterns of sand spit development and their management implications on deltaic, drift-aligned coasts: the cases of the Senegal and Volta River delta spits, West Africa. In: Randazzo, G. Cooper, J.A.G. (eds.), *Spits*, Springer, in review.
- Anthony, E.J. and Bliivi, A.B. 1999. Morphosedimentary evolution of a delta-sourced, drift-aligned sand barrier-lagoon complex, western Bight of Benin. *Marine Geology*, 158, 161-176.
- Anthony, E.J., Lang J. and Oyédé L-M., 1996. Sedimentation in a tropical, microtidal, wave-dominated coastal-plain estuary. *Sedimentology*, 43, 665-675.
- Anthony, E.J., Oyédé, L-M and Lang, J., 2002. Sedimentation in a fluvially infilling, barrier-bound, estuary on a wave-dominated, microtidal coast: The Ouémé River estuary, Benin, West Africa. *Sedimentology*, 49, 1095-1112.
- Addo, K.A., Jayson-Quashigah, P.N. and Kufogbe, K.S., 2011. Quantitative analysis of shoreline change using medium resolution satellite imagery in Keta, Ghana. *Marine Science*, 1, 1-9.
- Battjes, J.A. and Janssen, J.P.F.M., 1978. Energy loss and set-up due to breaking of random waves. *Proceedings 16th International Conference on Coastal Engineering*, ASCE, 569-587.
- Bertin, X., Castelle, B., Chaumillon, E., Butel, R and Quique, R., 2008. Longshore drift estimation and inter-annual variability at a high-energy dissipative beach: St. Trojan Beach, SW Oleron Island, France. *Cont. Shelf Res.*, 28, 1316-1332.
- Bliivi, A., Anthony, E.J. and Oyédé L-M., 2002. Sand barrier development in the Bight of Benin, West Africa. *Ocean and Coastal Management*, 45, 185-200.

- Boateng, I., 2012. An application of GIS and coastal geomorphology for large scale assessment of coastal erosion and management: a case study of Ghana. *Journal of Coastal Conservation*, 16, 383–397.
- Carter, R.W.G., 1988. *Coastal environments: An Introduction to the Physical, Ecological and Cultural Systems of Coastlines*. Academic Press: London, 617p.
- Castelle, B., Almar, R., Dorel, M., Lefebvre, J-P, Sénéchal, N., Anthony, E., Laïbi, R., Chuchla, R. and du Penhoat, Y., 2014. Flash rip dynamics on a high-energy low-tide-terraced beach (Grand Popo, Benin, West Africa). In: Green, A.N. and Cooper, J.A.G. (eds.), *Proceedings 13th International Coastal Symposium* (Durban, South Africa), *Journal of Coastal Research*, Special Issue No. 66, ISSN 0749-0208.
- Davies, J.L., 1980. *Geographical Variation in Coastal Development*. 2<sup>nd</sup> Ed. London, England: Longman, 212p.
- Dee, D.P., Uppala, S.M., Simmons, A.J., Berrisford, P., Poli, P., Kobayashi, S., Andrae, U., Balmaseda, M.A., Balsamo, G., Bauer, P., Bechtold, P., Beljaars, A.C.M., van de Berg, L., Bidlot, J., Bormann, N., Delsol, C., Dragani, R., Fuentes, M., Geer, A.J., Haimberger, L., Healy, S.B., Hersbach, H., Hólm, E.V., Isaksen, I., Kållberg, P., Köhler, M., Matricardi, M., McNally, A.P., Monge-Sanz, M., Morcrette, J.-J., Park, B.-K., Peubey, C., de Rosnay, P., Tavolato, C., Thépaut, J.-N. and Vitart, F., 2011. The ERA-Interim reanalysis: configuration and performance of the data assimilation system. *Q. J. R. Meteorol. Soc.*, 137, 553–597.
- Delft Hydraulics, 1990. National and regional aspects of coastal erosion in the Bight of Benin. Project 6607.43.94.155, European Development Fund, Brussels.
- Kaczmarek, L.M., Ostrowski, R., Pruszek, Z. and Rozynski, G., 2005. Selected problems of sediment transport and morphodynamics of a multi-bar nearshore zone. *Estuarine, Coastal and Shelf Science*, 62, 415–425.
- Kumapley, N.K., 1989. The geology and geotechnology of the Keta basin with particular reference to coastal protection. *Proceedings, KNGMG Symposium on Coastal Lowlands, Geology and Geotechnology*, pp. 311–320.
- Laïbi, R., 2011. Dynamique actuelle d'une embouchure fluviale estuarienne à flèche sableuse, la Bouche du Roi, Bénin, Golfe de Guinée : caractérisation hydrosédimentaire et géomorphologique. Dunkerque, France: Université d'Abomey-Calavi, Université du Littoral Côte d'Opale, Thèse de Doctorat Unique, 302p.
- Laïbi, R., Gardel, A., Anthony, E.J. and Oyédé, L-M., 2012. Apport des séries d'images LANDSAT dans l'étude de la dynamique spatio-temporelle de l'embouchure de l'estuaire des fleuves Mono et Couffo au Bénin, après la construction du barrage de Nangbéto sur le Mono. *Revue Télédétection*, 10, 179-198.
- Ly, C.K., 1980. The role of the Akosombo Dam on the Volta river in causing erosion in central and eastern Ghana (West Africa). *Marine Geology*, 35, 323–332.
- Oguntunde, P.G., Friesen, J., van de Giesen, N. and Savenije, H.H.G., 2006. Hydroclimatology of the Volta River Basin in West Africa: Trends and variability from 1901 to 2002. *Physics and Chemistry of the Earth*, 31, 1180-1188
- Rossi, G., 1989. L'érosion du littoral dans le Golfe du Bénin: un exemple de perturbation d'un équilibre morphodynamique. *Zeitschrift für Geomorphologie N.F., Supplement Band*, 73, 139–165.
- Senechal, N., Laïbi, R.A., Almar, R., Castelle, B., Biauxque, M., Lefebvre, J.-P., Anthony, E., Dorel, M., Chuchla, R., Houankonou, M.H. and Du Penhoat, Y., 2014. Observation of the destruction of a beach cusp system in presence of a double coupled cusp system: the example of Grand Popo–Benin. In: Green, A.N. and Cooper, J.A.G. (eds.), *Proceedings 13th International Coastal Symposium* (Durban, South Africa), *Journal of Coastal Research*, Special Issue No. 66, ISSN 0749-0208.
- Sterl, A. and Caires, S., 2005. Climatology, variability and extremes of ocean waves- the web-based KNMI/ERA-40 Wave Atlas. *Int. J. Climatol.*, 25, 963-977.
- Van Rijn, L.C., 2011. Coastal erosion and control. *Ocean & Coastal Management*, 54, 867-887.

# Wave-driven circulation over a double nearshore bar system during storm conditions

Nicolas Robin<sup>†</sup>, Raphael Certain<sup>†</sup>, Frederic Bouchette<sup>‡</sup>, Edward J. Anthony<sup>∞1</sup>, Samuel Meulé<sup>∞</sup>, Nicolas Aleman<sup>†</sup>

<sup>†</sup>CEFREM, UMR CNRS 5110  
Université de Perpignan Via-Domitia,  
52 Avenue Paul Alduy,  
66000 Perpignan,  
France  
[nicolas.robin@univ-perp.fr](mailto:nicolas.robin@univ-perp.fr)

<sup>‡</sup> Geosciences-Montpellier  
UMR 5243  
Cc 60, Université Montpellier II & CNRS,  
France

<sup>∞</sup> Aix-Marseille Université, IUF<sup>1</sup>,  
CEREGE UMR 34, Europole de l'Arbois,  
13545 Aix en Provence,  
France



[www.cerf-jcr.org](http://www.cerf-jcr.org)



[www.JCRonline.org](http://www.JCRonline.org)

## ABSTRACT

Robin, N., Certain, R., Bouchette, F., Anthony, E.J., Meulé, S., and Aleman, N., 2014. Wave-driven circulation over a double nearshore bar system during storm conditions. In: Green, A.N. and Cooper, J.A.G. (eds.), *Proceedings 13<sup>th</sup> International Coastal Symposium* (Durban, South Africa), *Journal of Coastal Research*, Special Issue No. 70, pp. 084-089, ISSN 0749-0208.

Current profiles and waves were recorded from a multi-instrumented transect over a double nearshore bar system in the Gulf of Lions, NW Mediterranean Sea (France) during storm conditions with shoreface significant wave heights of up to 3.2 m. The results constitute a preliminary analysis aimed at constraining the 3D nearshore circulation in a microtidal system. Significant time changes in the vertical distribution of nearshore velocities were observed, forced by the wind/wave conditions. Such vertical changes have been highlighted by theoretical velocity profiles in the literature, but our study demonstrates much larger variability than has hitherto been shown. Another result obtained was that the hydrodynamic pattern observed in the inner trough was distinct from that observed along the seaward flank of the inner bar. For a well-defined threshold in wave height, velocities in the trough increased abruptly and earlier, and remained strong over a longer time than those on the seaward flank. The trough thus behaves essentially as a drain for water piled against the shore. This behavior is altered by the width of the surf zone (and not only by the significant wave height), which modulates the mean current velocity. These results are a useful preliminary step in improving numerical modeling of the complex surf-zone circulation over bar-trough systems.

**ADDITIONAL INDEX WORDS:** *Current profile, longshore current, undertow, surf zone, ADCP, SHORECIRC*

## INTRODUCTION

Most sandy coasts display nearshore bars organized in single or multi-bar systems. Investigations of these nearshore bars are important in understanding wave breaking and hydrodynamic circulation on the shoreface because these features strongly influence the transformation and dissipation of waves that propagate to the shoreline, thus acting as a natural source of shoreline protection. Moreover, these features are important in terms of nearshore sand reservoirs (Certain *et al.*, 2005). Thus, in an integrated management approach of coastal hazards on shorelines subject to high socio-economic occupancy, enhanced understanding of hydrodynamic processes prevailing over bars, especially during storm conditions, is of significant interest.

Nearshore bars display various morphological features that have been identified by Wright and Short (1984) in their beach state classification model. The bars are dynamic at different timescales, notably changing in response to variations in wave energy. Depending on the intensity and characteristics of storm events, bars can undergo temporary offshore migration (Winjberg, 1995) when strong seawards currents (undertow) dominate the sediment transport. Onshore bar migration may occur between storm events

when wave energy is lower. At long timescales, this behaviour has been generally termed "Oscillation around a Position of Equilibrium" (OPE) (Certain and Barousseau, 2005). However, "Net Offshore Migration" (NOM), leading to long-term offshore bar migration and decay, has also been observed (Aleman *et al.*, 2013).

The hydrodynamics of the inner surf zone in which bars develop have long been studied in the literature as they strongly control changes in sandy shoreline morphology. In particular, the evolution of nearshore sand bars was early related to low-frequency changes in the mean current. However, the influence of vertical modulations of the water velocity in the water column has, to date, not been deeply explored in the field, despite the possible effect of such modulations on the morphodynamics. Furthermore, because of this scarce knowledge, numerical modelling often ignores, or largely underestimates, the variety of vertical distribution of velocities, thus resulting in unrealistic results.

In this context, this preliminary study aims at monitoring and analyzing the 3D circulation over a system of double nearshore sand bars forced by waves, especially during a storm event. The objectives of this paper are: (1) to estimate temporal profile variations of currents inside and outside the surf zone, (2) to compare differences in current characteristics on the inner trough

and the seaward flank of the inner bar, (3) to examine the importance of this type of in-situ data (2DV) in improving numerical models.

## STUDY AREA

The sand barrier bounding Thau lagoon is a 13 km long low-lying linear feature in the Gulf of Lions in the Mediterranean Sea (Figure 1). The study site is located in the northern part of the barrier, near Sète and has been affected by persistent erosion over the last few decades. The barrier is characterized by the presence of a double nearshore bar system (Certain and Barousseau, 2005) and a cusped shoreline usually in phase with the inner bar (seaward bulges in the shoreline being located in front of the bar shoals) with a cusp wavelength of 400 m (Balouin *et al.*, 2013). According to the Short and Aagaard (1993) classification, the field site is an intermediate beach ( $\Omega = 5.5$ ) and displays a Rhythmic Bar and Beach (RBB) inner bar and a Longshore Bar and Trough (LBT) outer bar (Aleman *et al.*, 2011).

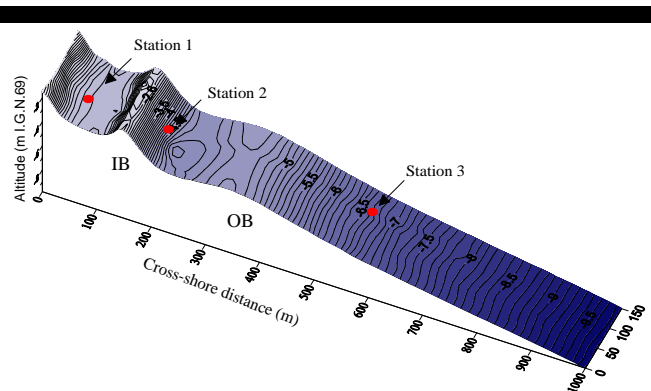


Figure 1. Cross-shore profile of the field site and location of the equipment deployed to measure vertical current profiles in the nearshore.

The field site is a typical example of a microtidal environment characterized by a very low tidal range ( $< 0.30$  m at mean spring tide). It is a wave-dominated system with very low mean energy, punctuated, especially during winter and autumn, by energetic storms. Just offshore of the study site, wave heights at the Datawell Sète buoy (water depth of 32 m) are less than 0.3 m for 75 % of the time. Wave heights larger than 2 m are observed only 10 % of the time for short periods less than 48 hours. The dominant wave regime is short-fetched with peak periods in the 3-4 second range, and waves are mainly from azimuths  $140$ - $220^\circ$ N generated by sea breezes.

## METHODS

Several instruments were deployed on a cross-shore transect over the sand bars for over 2 months, from 15 December 2008 to 25 February 2009. This study focuses only on a single storm event that lasted for few days in early February 2009 with significant offshore wave heights of up to 3 m.

Hydrodynamic measurements were obtained from three stations across the sand bar system. The first and second stations were located in the inner trough (3.3 m water depth) and in the seaward flank of the inner bar (4.6 m water depth). Each station contained one Acoustic Doppler Velocimeter (Sontek ADV) and one Acoustic Doppler Current Profiler (RDI ADCP, 600 kHz). This combination allowed measurements through the entire water

column. Indeed the ADV measure velocities at a point just above the seafloor (between 0.1 and 0.15 m) partly encompassing the blank space not covered by the ADCP. However, due to burial by sediment and corresponding bar morphological change, the ADV deployed on the seaward flank of the inner bar did not record starting from the peak of the storm. The data were collected at a frequency of 2 Hz during 1 minute with an interval of 3 or 6 minutes (inner trough and seaward flank of inner bar respectively) for the ADCP, and 20 minutes with an interval of 2h 40 mn for both ADVs. In this study, mean currents were averaged over every minute. Velocity measurements from both the ADVs and the ADCP tended to display noise in highly turbulent or aerated flows. Signal correlation values recorded by the instruments were used to identify such potentially incorrect data. Each instrument had a pressure sensor that measured wave characteristics with a burst duration of 20 minutes every 3 hours. The wave characteristics were processed by standard spectral analysis. In addition to the Doppler sensors, a self-recording electromagnetic current meter comprising a pressure sensor (Inter-Ocean S4DW) was deployed offshore of the outer bar at about 40 cm above the bed. Only the wave characteristics of this instrument are used in this study. Data were collected at a 2-Hz frequency with a burst duration of 20 minutes every 3 hours. In order to appreciate the current structure relative to the bar morphology, the mean currents were decomposed into cross-shore (onshore positive) and longshore (northward positive) components with respect to the crests of the bars ( $140^\circ$ N).

## RESULTS

The 2DV current characteristics in the trough and the seaward side of the inner bar that prevailed in the course of a storm from 31 January to 4 February 2009 are described and analyzed with reference to nine key periods selected following three phases: waxing storm (1, 2, 3), storm peak (4), and waning storm (5, 6, 7, 8, 9).

**Waxing storm:** At the beginning of the storm, mean currents in the inner trough were weak ( $< 0.15$  m.s<sup>-1</sup>), in relation to the moderate wave energy (Figure 3A, 3B). They intensified starting from  $H_s = 0.9$  m (in the trough) with strengthening of a pre-existent but weak longshore current (Figure 2D1). This first threshold corresponds to the inception of a surf zone over the inner bar-trough couplet (Figure 2A). Thereafter, mean currents became stronger, exceeding  $0.5$  m.s<sup>-1</sup> and up to  $0.8$  m.s<sup>-1</sup>. The longshore current was therefore the principal flow component (Figure 2D2, 2D3) compared to the cross-shore current (less than  $0.1$  m.s<sup>-1</sup>). As wave energy increased, the vertical distribution of the mean current direction became more uniform, and progressively tended to be parallel to the main axis of the bar-beach system (Figures 2F2, 2F3). On the seaward side of the inner bar, currents displayed characteristics influenced by the wind (mean velocity less than  $0.2$  m.s<sup>-1</sup> and relative heterogeneity of directions) (Figures 2E1, 2F1, 2E2, 2F2). Only the first metre of the water column was affected by stronger velocities of up to  $0.4$  m.s<sup>-1</sup> (Figure 2E1). This behavior was observed up to a significant wave height of 1.8 m on the inner bar. Starting from this second threshold corresponding to the inception of surf on the outer system, the current profile underwent a change with an increase in vertical homogeneity of the longshore current (up to  $0.4$  m.s<sup>-1</sup>), (except for the ADV near the bed which recorded lower velocities) (Figure 2C3). The cross-shore velocity was associated with an undertow that appeared as the threshold observed above (i.e.,  $H_s > 1.8$  m on the inner bar) was attained. However, this current was of very low velocity (less than  $0.1$  m.s<sup>-1</sup>) and was not constant over time.

This



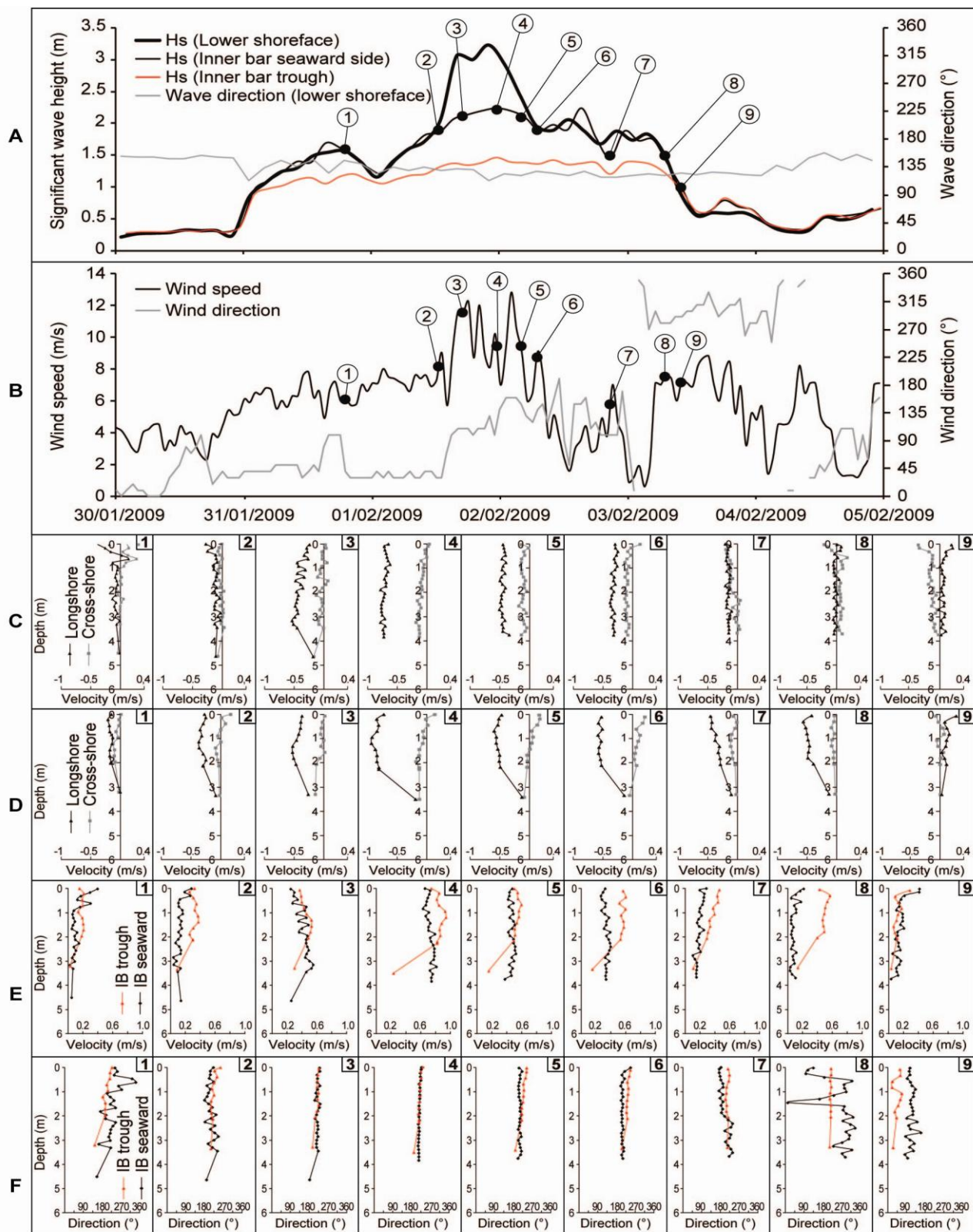


Figure 2. Meteorological forcing and hydrodynamic response during a storm in February 2009. (A) Significant wave height; (B) wind velocity and azimuth; (C) cross-shore/longshore components of the burst-averaged velocity profiles observed at different times on the flank of the inner bar; (D) same measured features in the trough itself; (E) burst-averaged velocities in the trough and the flank of the bar; (F) burst-averaged azimuth of the current in the trough and the flank.

behavior corresponded to an original profile of mean currents with relatively lower velocities at the surface and at the bottom ( $0.25 \text{ m.s}^{-1}$ ), and a maximum in the middle of the water column ( $0.55 \text{ m.s}^{-1}$ ) (Figure 2E3). During waxing of the storm, the current direction was relatively uniform throughout the water column in relation to the increase in significant wave height.

**Storm peak:** During the peak of the storm ( $H_s = 2.25 \text{ m}$  on the bar crest), the intensity and direction of the current were uniform throughout the water column ( $0.8 \text{ m.s}^{-1}$  on average) on the seaward side of the inner bar (Figure 2E4, 2F4). The longshore current was largely dominant and attained a maximum during this phase ( $0.7 \text{ m.s}^{-1}$ ). A weak return current ( $0.15 \text{ m.s}^{-1}$ ) was observed from 0.7 m depth to the bottom (Figure 2C4). In the inner trough, the current was also at its recorded maximum ( $0.93 \text{ m.s}^{-1}$ ) and almost totally longshore ( $0.9 \text{ m.s}^{-1}$ ) (Figure 2D4, 2E4). An undertow was also observed from a depth of 0.7 m, but with a weaker velocity ( $0.1 \text{ m.s}^{-1}$ ). The vertical velocity distribution in the water column was not as homogeneous as it was on the seaward side of the inner bar and reached a maximum at a depth of 1.2 m, whereas the current direction was uniform and parallel to the mean orientation of the bar-beach system.

**Waning storm:** The waning of the storm was characterized on the seaward side of inner bar by a high velocity which decreased down to the first threshold observed during the waxing stage. Velocities and directions were homogeneous throughout the water column up to about  $H_s = 1.5 \text{ m}$ , which corresponded to the disappearance of the undertow, throughout of lower intensity than the longshore current (Figure 2B6 and 2B7). Currents in the inner trough were always stronger than those on the seaward side of the inner bar, and they remained strong up to burst 8 ( $H_s = 1.2 \text{ m}$  in the trough,  $0.5 \text{ m.s}^{-1}$ ) (Figure 2E8). They then started getting weaker during burst 9 ( $H_s = 0.9 \text{ m}$  in the trough  $0.1 \text{ m.s}^{-1}$ ), corresponding to the second threshold previously observed.

## DICUSSION

### Vertical shearing of surf-zone currents

This study has examined the response of a current profile over a double nearshore sand bar system during a storm event. This type of in-situ data obtained inside or outside the surf zone is rare in the literature. It shows that the vertical distribution of nearshore velocities is strongly hinged on wind/wave conditions, as reported by Yamashita *et al.*, (1998) and Ferrer *et al.*, (2011), and the temporal variability of which can lead to significant changes in time distribution. During fair weather or moderate wave energy conditions, the velocity profile can exhibit numerous declinations, with, for instance, maximum velocities at the top, bottom, or middle of the water column, probably as a function of changing wind stress and wave conditions. Furthermore, the velocity distribution is of high heterogeneity, with values that can reach  $0.3\text{-}0.4 \text{ m.s}^{-1}$  (Figure 2). This quite complex representation can be erroneously interpreted when a depth-averaged velocity, a single point measurement, or lagrangian measurements are used to interpret the hydrodynamic circulation as well as the direction and intensity of sediment transport over bar systems. During the peak of the storm, velocities are higher and relatively uniform throughout the water column as reported in the literature (Yamashita *et al.*, 1998; Ferrer *et al.*, 2011). Only near the bottom are currents relatively weak, a kink observed by Aagaard *et al.*, (2012) on cross-shore velocities and which they attributed to bottom boundary layer streaming. In our study, this kink is essentially observed in the structure of the longshore current, which is much stronger than the cross-shore current, and is probably due to bed friction. Thus, however energetic the conditions are, there seems to be a difference between bottom

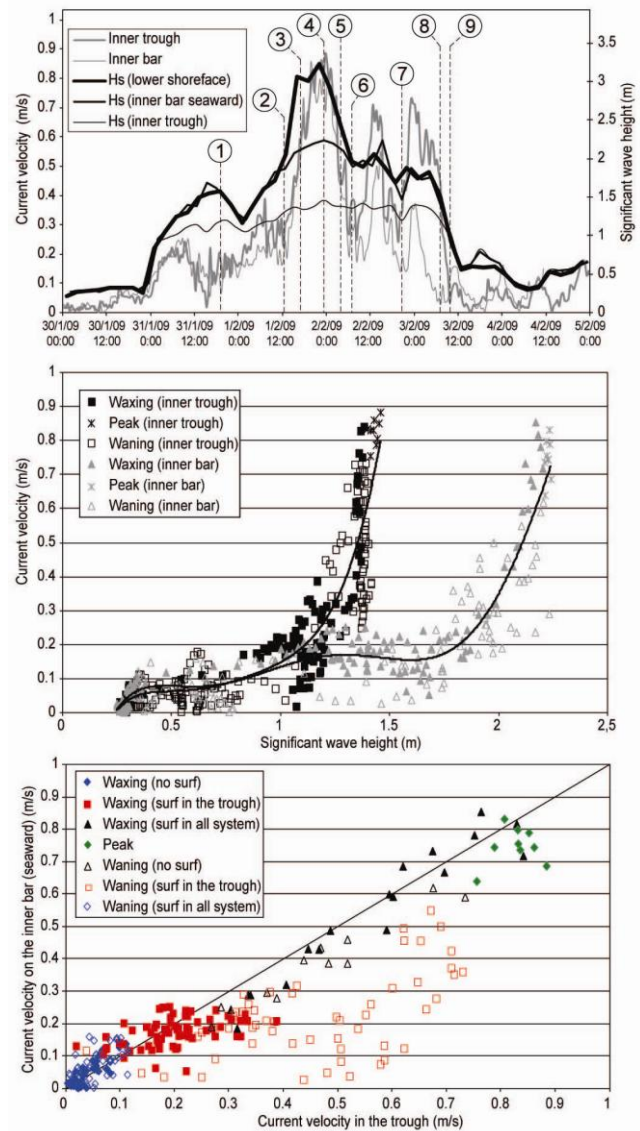


Figure 3. Top: Velocities measured at various locations in the course of the February 2009 storm. Bottom: correlation between velocities on the seaside flank of the inner bar and in the trough.

processes implied in sediment transport and the rest of the water column, and this has important implications regarding the interpretation of bar morphological response time to storms.

### Surf-zone control on current velocities

The system was mainly influenced by the longshore current as observed in other field sites (Greenwood and Sherman, 1986; Smith *et al.*, 1993). A distinctive hydrodynamic behavior is observed between the trough and the seaward flank of the inner bar involving the following characteristics. (1) The longshore velocities, which reach  $0.8 \text{ m.s}^{-1}$ , are slightly higher in the inner trough than over the bar during the waxing and peak phases of the storm. (2) The cross-shore velocities are weak and an undertow, fairly uniform over the water column, is observed mainly on the seaward flank of the inner bar. In the inner trough, the undertow is weaker and affects only the bottom of the column. The values of

the undertow ( $0.1$  to  $0.2 \text{ m}\cdot\text{s}^{-1}$ ) are similar to those described in the literature for similar wave energy conditions (Masselink and Van Heteren, in press). (3) A velocity increase is observed when the system is influenced by the surf zone (Figure 3A, 3B). The triggering of the longshore current is relatively synchronous in the different parts of the inner bar couplet. However, two thresholds in the increase of the velocities can be detected, with a first one when only the inner trough is affected by breaking waves ( $H_s = 0.9 \text{ m}$  in the trough) and a second one, even more intense, when the entire inner system is in the surf zone ( $H_s = 1.8 \text{ m}$  on the seaward flank of the bar). (4) Despite the difference in significant wave height over the inner system, mean velocities in the trough are relatively similar to those recorded on the seaward flank of the bar (Figure 3C). This behaviour is observed during the waxing and peaking of the storm but not during the waning period when breaking waves affect only the inner trough. During this period, mean velocities are higher in this part of this profile, notwithstanding the fact that this condition was not observed during the waxing period. This is probably due to the inner trough acting as a privileged drain for the water masses piled up on the shoreline.

### Input in terms of numerical modeling

The third objective of this preliminary study is to examine the utility of the type of in-situ data (2DV) we have reported here in enhancing the output of numerical modeling. The understanding of wave-driven nearshore hydrodynamics since the late 1960s, following the seminal work of Longuet-Higgins & Stewart (1962), has benefited from several major refinements regarding nearshore wave/current interactions. These include, in particular, the impact of a homogeneous current on wave dispersion (Burrows and Hedges, 1985), the combination of wave refraction and diffraction in the possible presence of a current (Kirby and Dalrymple, 1983; Holthuijsen *et al.*, 2003), and the calculation of quasi-3D current profiles forced by nearshore waves (Putrevu and Svendsen, 1999). Unfortunately, there is a significant lack of theoretical knowledge on wave transformation by vertically sheared currents (Booij, 1981; Liu, 1983). Thus, the dataset presented here and any other similar experiment in the field or in a wave flume, is of high importance to feed new theoretical insights regarding wave and sheared current interactions.

Over the last ten years, there have been a variety of numerical developments regarding the hydrodynamics of the nearshore zone that include the generalization of boundary conditions in coastal models (Haasa and Warner, 2009), the introduction of uncertainty in nearshore simulations (Mohammadi and Bouchette, 2013), and the elaboration of more robust numerical schemes (such as the so-called Green-Nagdi schemes; Marche, 2007). The present work demonstrates that these numerical refinements are of very limited use if a correct inclusion of wave-sheared current interactions is not achieved.

Another tendency in numerical modeling concerns simulations usually performed at the continental shelf-scale with models solving the primitive equations that tend to be downscaled to the nearshore zone. This enlargement of the use of these models requires robust 3D coupling with wave models such as WW3 (Bennis *et al.*, 2011). The practical suitability of this methodology is under debate in the literature. For example, Michaud *et al.* (2013) modeled 3D nearshore hydrodynamics based on a comprehensive coupling between SYMPHONIE (Marsaleix *et al.*, 2008) and WW3, and compared the results with a robust set of in-situ nearshore data. They obtained a correct agreement between simulations and measurements. However, although a lot of physics are embedded in the coupled model, waves and chiefly depth-dependent current patterns are altered by changes in the

bottom elevation through time, especially via sand bars. As a consequence, the next step for the improvement of these full 3D-coupled models is to fully consider the complex interactions between waves and bars, which, in particular, includes what has been brought to the fore in this paper.

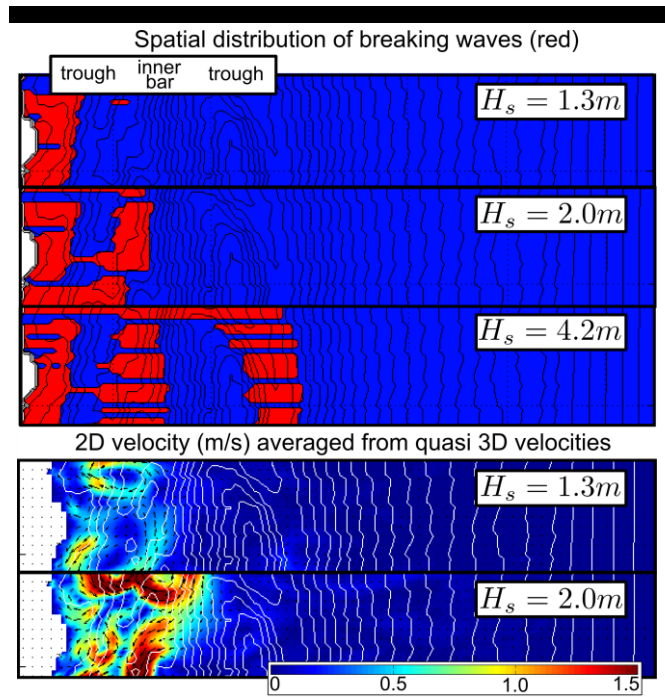


Figure 4. Cross-shore profiles with a limited longshore thickening-out extracted from SHORECIRC simulations. Top three: evolution of the spatial distribution of breaking waves with increasing wave height from  $1.3 \text{ m}$  to  $4.2 \text{ m}$ . Selected wave heights mark two thresholds where significant changes in the breaking wave distribution occur in the numerical results. Bottom: distribution of averaged velocities before ( $H_s=1.3\text{m}$ ) and after ( $H_s=2.0 \text{ m}$ ) the widening of the surf zone seaward of the inner trough.

Nonetheless, present models, either based on primitive equations or on strict nearshore physics, are already of help in enhancing results acquired in the field. To illustrate this, we computed with a modified version of SHORECIRC (Svendsen *et al.*, 2004), 3D velocity fields on a  $800 \times 600 \text{ m}^2$  domain with a sea bottom very similar to that observed in the field study site in Sète (Figure 1), and forced by similar waves ranging from  $H_s = 0.5 \text{ m}$  to  $5 \text{ m}$  and corresponding similar periods. A very basic analysis of the results gives numerical evidence for the occurrence of thresholds in the distribution of the wave height (linked to the extension of the surf zone) that controls the 3D velocity patterns (Figure 4). Although SHORECIRC does not allow the computation of strongly sheared profiles (the model presupposes the profiles partly), these numerical results are encouraging because they suggest that there exists a physical interpretation of what was observed in the course of the field experiment.

### CONCLUSION

The results presented in this study describe the complex configuration of current profiles over a double nearshore bar

system in a low microtidal setting, especially during fair weather and moderate wave energy. During storms, current profiles are vertically uniform, and the results further highlight the influence of breaking waves on the intensification of velocities and the establishment of undertow, which is confirmed by simple simulations dealing with 3D currents. However, the inner trough shows a peculiar behavior during storm waning probably due to its role as a privileged drain of the water masses accumulating over the bar-trough system during storm. These preliminary results will need to be confirmed by a fuller analysis of the extensive dataset obtained in the course of the > 2-month-long field experiment on the double bar system of the Gulf of Lions sand barrier coast, and which could lead to interesting insight into, and a better understanding of, the complex coupling between phases of waxing, peak and waning storm wave levels and sheared currents in the nearshore zone.

### ACKNOWLEDGEMENT

This work was supported by French National Research Agency (ANR) through projects VULSACO (ANR-06-VMC-009) and RELIEF MICROLIT. The authors are grateful to the GLADYS platform authorities (www.gladys-littoral.org and www.soltc.org) for loaning equipment.

### LITERATURE CITED

- Aagaard, T., Hughes, M., Baldock, T., Greenwood, B., Kroon, A. and Power, H., 2012. Sediment transport processes and morphodynamics on a reflective beach under storm and non-storm conditions. *Marine Geology*, 326-328, 154-165.
- Aleman, N., N. Robin, R. Certain, C. Vanroye, J. P. Barusseau and F. Bouchette (2011), Typology of nearshore bars in the Gulf of Lions (France) using LIDAR technology, *Journal of Coastal Research*, (SI.64), 721-725.
- Aleman, N., Robin, N., Certain, R., Barusseau, J.P. and Gervais, M., 2013. Net Offshore bar Migration variability at a regional scale : Inter-site comparaison (Languedoc-Roussillon, France). *Journal of Coastal Research*, (SI.65), 1715-1720.
- Balouin, Y., Tesson, J. and Gervais, M., 2013. Cuspate shoreline relationship with nearshore bar dynamics during storm events-field observations at Sete beach, France. *12<sup>th</sup> International Journal of Coastal Research*, (SI.65), 440-445.
- Bennis, A., F. Ardhuin, and F. Dumas, 2011. On the coupling of wave and three-dimensional circulation models: Choice of theoretical framework, practical implementation and adiabatic tests, *Ocean Modelling*, 40 (3-4), 260-272.
- Booij, N., 1981. Gravity waves on water with non uniform depth and currents. *Department of Civil Engineering, Delft University of technology. Tech. Rep.*, 81-1.
- Burrows, R. and Hedges, T.S., 1985. The influence of currents on ocean wave climates, *Coastal Engineering*, 9/3, 247-260.
- Certain, R. and Barusseau, J.-P., 2005. Conceptual modelling of sand bars morphodynamics for a microtidal beach (Sete, France). *Bulletin de la Societe Geologique de France*, 176 (4): 343-354.
- Certain, R., Tessier, B., Barusseau, J.P., Courp, T. and Pauc, H., 2005. Sedimentary balance and sand stock availability along a littoral system. The case of the western Gulf of Lions littoral prism (France) investigated by very high resolution seismic. *Mar. Petr. Geol.* 22, (6-7), 889-900.
- Ferrer, P., Certain, R., Aldoff, F., Bouchette, F., Barusseau, J.P., Meulé, S. and Robin, N., 2011. Hydrodynamics over a microtidal double crescentic barred under low energy conditions (Leucate Beach, France). *Journal of Coastal Research*, (SI.64), 2032-2036.
- Greenwood, B. and Sherman, D.J., 1986. Longshore current profiles and lateral mixing across the surf zone of a barred nearshore. *Coastal Engineering*, 10, 149-168.
- Haasa, K.A., and Warner, J.C., 2009. Comparing a quasi-3D to a full 3D nearshore circulation model : SHORECIRC and ROMS. *Ocean Modelling*, 26-(1-2), 91-103.
- Holthuijsen, L. H., Herman, A. and Booij, N., 2003. Phase-decoupled refraction-diffraction for spectral wave models. *Coastal Engineering*, 49, 291-305.
- Kirby, J.T. and Dalrymple, R.A., 1983. A parabolic equation for the combined refraction diffraction of Stokes waves by mildly varying topography. *J. Fluid. Mech.*, 136, 543-466.
- Liu, P. L.-F. 1983. Wave current interactions on a slowly varying topography., *J. Geophys. Res.*, 88 (C7), 4421-4426.
- Longuet-Higgins, M. S. and Stewart, R. W., 1962. Radiation stress and mass transport in gravity waves, with application to 'surf beats'. *Journal of Fluid Mechanics*, 13/4, 481-504.
- Marche F., 2007. Derivation of a new two-dimensional viscous shallow water model with varying topography, bottom friction and capillary effects. *European Journal of Mechanic /B : Fluid*, 2, 49-63.
- Masselink, G. and Van Heteren, S., in press. Response of wave-dominated and mixed-energy barriers to storms. *Marine Geology*.
- Marsaleix P., Auclair F., Floor J. W., Herrmann M. J., Estournel C., Pairaud I., Ulses C., 2008. Energy conservation issues in sigma-coordinate free-surface ocean models. *Ocean Modelling*, 20, 61-89.
- Michaud H., Robin N., Estournel C., Marsaleix P., Leredde Y., Certain R. and Bouchette F., 2013. 3D Hydrodynamic modeling of a microtidal barred beach (Sète, NW Mediterranean sea) during storm conditions. Proc. 7th Int. Conf. on Coastal Dynamics, Arcachon France, 139, 1183-1194.
- Miles, J. 2001. A note on surface wave generated by shear-flow instability. *J. Fluid Mech.*, 447, 173-177.
- Mohammadi, B. and Bouchette, F., 2013. Quantitative extreme scenarios for the evolution of a soft bed interacting with a fluid using the Value at Risk of the bed characteristics, *Computers & Fluids*, DOI: 10.1016/j.compfluid.2013.10.021.
- Putrevu, U. and Svendsen, I.A., 2001. Three-dimensional dispersion of momentum in wave-induced nearshore currents *European Journal of Mechanics - B/Fluids*, 18-3, 409-427.
- Smith, J.M., Larson, M. and Kraus, N.C., 1993. Longshore Current on a Barred Beach: Field Measurements and Calculation. *Journal of Geophysical Research*, 98 (C12): 22717-22731.
- Svendsen, I. A., Haas, K., and Zhao, Q., 2004. Quasi-3D Nearshore Circulation Model SHORECIRC: Version 2. *Research Report, Center for Applied Coastal Research, University of Delaware*.
- Wijnberg, K.M., 1995. *Morphologic behaviour of a barred coast over a period of decades*. PhD thesis Utrecht University, Netherlands Geographical Studies 195, KNAG, The Netherlands, 245 pp.
- Wright, L.D. and Short, A.D., 1984. Morphodynamic variability of surf zones and beaches: A synthesis. *Marine Geology*, 56 (1-4): 93-118.
- Yamashita, T., Yoshioka, H., Kato, S., Ming, L. And Shimoda, C., 1998. ADCP Observation of nearshore current structure in the surf zone. *Proceedings 26<sup>th</sup> International Conference on Coastal Engineering* (Copenhagen, Denmark), 787-800.

# Geomorphology of coastal formations on present and ancient sandy coasts

Agnes Anderson†, Kadri Vilumaa†, Hannes Tõnisson†, Are Kont†, Urve Ratas†, Sten Suuroja‡

† Institute of Ecology, Tallinn University,  
5 Uus-Sadama, 10120, Tallinn, Estonia  
agnes.anderson@tlu.ee  
kadri.vilumaa@tlu.ee  
hannes.tonisson@tlu.ee  
are.kont@tlu.ee  
urve.ratas@tlu.ee

‡ Geological Survey of Estonia  
82 Kadaka road, 12618, Tallinn, Estonia  
s.suuroja@egk.ee



[www.cerf-jcr.org](http://www.cerf-jcr.org)



[www.JCRonline.org](http://www.JCRonline.org)

## ABSTRACT

Anderson, A., Vilumaa, K., Tõnisson, H., Kont, A., Ratas, U., Suuroja, S., 2014. Geomorphology of coastal formations on present and ancient sandy coasts. In: Green, A.N. and Cooper, J.A.G. (eds.), *Proceedings 13<sup>th</sup> International Coastal Symposium* (Durban, South Africa), *Journal of Coastal Research*, Special Issue No. 70, pp. 090-095, ISSN 0749-0208.

Many coastal sites are experiencing land uplift, so coastal formations can be found many kilometres inland from the present day shoreline. However, due to the relatively rapid, site specific and complicated development, their evolution is not very thoroughly studied yet. In this study, we analyse sediments and subsurface stratigraphy to explain the evolution and geomorphology of coastal formations (from present to ancient coastlines) located in sediment supply-limited areas. Several study sites were chosen on Tahkuna Peninsula, Hiiumaa Island in Estonia, where the rate of land uplift is 2.8 mm yr<sup>-1</sup>. Due to deficiency of sediment, dunes and old beach ridges that developed during the last 3,500 years are low (dunes up to 6–7 m, the studied ridges mostly less than 2 m). The coastal formations studied are located at different distances (up to 1 km) from the shoreline and at different altitudes (up to 13.2 m above sea level).

In the current research, granulometric analysis was used for studying the coastal formations; grain size was determined by dry sieving of sediments. Additional studies were carried out with ground-penetrating radar (SIR-3000) to compare the present and former coastlines and to explain geomorphic differences. Drilling was also used and special pits were dug for the examination of mineral deposits. The preliminary results show that the sands on the present coastline are similar to those of former shorelines, which may be caused by the wind regime, time scale for coastal formation development, and underlying sediments.

**ADDITIONAL INDEX WORDS:** *Granulometry, beach ridges, foredunes, sand deposits, ground-penetrating radar.*

## INTRODUCTION

The evolution of coastal formations on sandy coasts is a complex system of movements of sand drift and dune stabilization. Natural dune stability and mobility are influenced by three major factors: climatic variables (wind, precipitation, moisture), sediment characteristics (availability, grain size) and vegetation cover (Mauz *et al.*, 2013). It is evident that enhanced storminess has often been invoked as a major causal factor for the initiation of dune activity (González-Villanueva *et al.*, 2013). Other well-known boundary conditions include wind directionality, grain size, watertable height and antecedent dune topography (Eastwood *et al.*, 2011).

However, explaining the geomorphology of coastal landforms on present coasts and ancient coastlines is poorly understood due to their relatively rapid, site specific and complicated development in Baltic region. Coastal formations as a record of climatic and geomorphic conditions are relatively unused in the Baltic region due to the difficulties to extract environmental information from geomorphic features.

(Fore)dune accretion depends on a sand supply to the beach; a

wide, dry beach across which the sand can be mobilized by aeolian activity and an accommodation space protected from wave erosion in which dunes can build up. It is evident that vegetation can subsequently affect the development of dunes, although, there is still a discussion going on about the factors that controlled sediment supply and coastal dune development in the past. It is not clear yet whether the formation of coastal dunes has occurred in response to sea level rise or sea level fall. As sea level (or lake level) falls, the former shoreface becomes exposed and wind may strip off the sediment to build foredunes. It is also suggested that (transgressive) dune formation may be due to sea level rise breaching pre-existing foredunes whereas regressive sea level tendencies result in dune stabilization by vegetation (Aasgard *et al.*, 2007).

Coastal waves and wind are the principal mechanisms involved in the transport of sand and the formation of beach ridges (Tamura, 2012). The lowermost parts of beach ridges on prograding coastlines are likely to have a high preservation potential and the internal architecture of the beach-ridge and swale deposits can be mapped using the ground-penetrating radar (GPR) method (Tamura, 2012; Clemmensen *et al.*, 2013; Hede *et al.*, 2013).

The aim of this article is to analyse the development of several coastal areas of Estonia using the information recorded in the coastal formations, including the grain size distribution, the



Figure 1. Location of study sites.

thickness of sand layers, the slope gradient of sand layers, the depth of water-resistant clay horizon and the location and dimensions of the beach ridges covered with peat.

### STUDY SITES

This work focuses on site specific and complicated development of the coastal formations from present to ancient coastlines. Our study sites are located on Tahkuna Peninsula, Hiiumaa Island, western Estonia (Figure 1). It is an active region in terms of both geomorphic and hydrodynamic conditions, and has experienced considerable human influences (intensive military activities associated with the Soviet period). The peninsula is bordered from three sides by the Baltic Sea. Prevailing winds in this part of the sea are from SW, W and NW. The winter ice-cover duration is usually between 40 and 60 days (Kont *et al.*, 2011). Tides are negligible (less than 10 cm) and the major hydrodynamic agents acting on seashores are waves and relatively infrequent storm surges reaching up to 2 m above mean sea level (Suursaar *et al.*, 2008; Tõnisson *et al.*, 2008; Orviku *et al.*, 2009).

As a result of sediment deficiency, the coastal formations are low (Raukas *et al.*, 1994). The study sites are experiencing land uplift with a current rate of about 2.5 to 2.8 mm yr<sup>-1</sup> (Vallner *et al.*, 1988). Beach ridges are situated at a distance from the contemporary shore and at different elevations above sea level.

Today, Tahkuna Peninsula is sparsely populated and densely covered by forests. It is characterized by different landforms. There is a glaciofluvial upland (SE–NW direction) in the western part of the peninsula (21 m above sea level), the seaward slope of which mainly consists of dunes. The eastern part of the peninsula is lower and complex. The nearshore waters are shallow (the 2-m isobath lies 150–300 m from the shoreline) (Anderson *et al.*, 2012).

The Quaternary cover is represented by till and varved clay, which are overlain by sand and peat. Due to the underlying varved clays, the groundwater level is one of the key factors in the development of the ridge-hollow landscape. Vegetation, soil, and

geomorphic factors are closely connected to each other across the whole area (Vilumaa *et al.*, 2013).

**Lõimastu study site** is located on the northern coast of Tahkuna Peninsula (Figure 1). Beach-dune system characterises the seaward side of the study site. The landforms here are up to 6 m a.s.l. The area of ancient beach ridges is located behind the beach-dune system, starting approximately 400 m inland from the sea. The area emerged from the sea in the middle of the Limnea Stage (2,500 cal yr BP). The coastal formations are situated between 6.0–7.8 m above sea level. The parallel long and narrow (10–50 m) sandy beach ridges are oriented from west to east. The peat layer is relatively thin (0.2–0.7 m).

**Röögu study site** is located on the eastern coast of the peninsula, approximately 1 km from the shoreline (Figure 1). This area emerged at the beginning of the Limnea Stage (3,500 cal yr BP). The coastal formations are situated between 10.2 and 13.2 m above sea level today. The long and narrow (usually 10–70 m) sandy beach ridges are oriented NW–SE. Adjacent depressions are 25–125 m wide. The thickness of peat layer is 0.5–1.0 m.

**Tõrvanina study site** is also located on the eastern coast of the peninsula, south of Lehtma harbour (Figure 1). The landward side of the beach is covered with forest and the beach is very narrow due to strong erosion (retreat rate 1–2.5 m yr<sup>-1</sup>) (Anderson *et al.*, 2012). Pine forests grow on the older coastal formations, which are up to 2–3 m a.s.l.

### METHODS

Different methods were used in studying the morphology and geological structure of the dunes and beach ridges. Fieldwork (from 2009–2013) consisted of landscape profiling, collecting sediment samples, GPR surveys and coring. Three transects were selected across Tahkuna Peninsula depending on the configuration of the present and ancient coastal landforms.

#### Granulometry

Sediment samples were collected for the examination of mineral deposits and soils on the basis of landscape profiles and the traces of radar facies. Landscape profiles were compiled and divided into zones: 90 sediment samples were collected along these transects. Samples from the present beach were collected much closer to the surface (depth 1–20 cm) as the parent material reaches almost up to the surface and is homogeneous. Samples from older coastal formations (landward part) were taken to a depth of 1 m. From each different layer, a sample was collected for granulometric analysis. Grain sizes were determined by dry sieving the sediments. Samples were dried in an oven at 105°C up to their constant weight. Dry samples were sieved for 15 minutes using an automatic shaker Vibratory Sieve-Shaker “Analysette 3” fitted with a standard set of sieves in an interval scale of > 63, 63, 100, 250, 500, 1000 and 2000 in µm. Weights of the sediment retained from each sieve were converted into the percentage of total sediment sample sieved.

#### Ground-Penetrating Radar (GPR)

Subsurface sedimentary architecture was investigated in Röögu and Lõimastu study sites using ground-penetrating radar. GPR reflection data was collected in March 2011, when average snow cover was ~ 60 cm and the studies were repeated in June 2013 (no snow).

Data from the GPR profiles was acquired almost perpendicular to the ridges using SIR-3000. A 100 MHz and 270 MHz frequency

antennae were used on two 1 km long landscape profiles. The processing of the GPR data was carried out using the *Road Doctor* software. Several markers were recorded along the GPR profiles and their locations were fixed using Garmin 60 CSx GPS. In order to verify the radar image interpretation, several approximately 4 m deep boreholes were drilled on the profiles. The coring data was used to calibrate the speed of electromagnetic waves in various layers in order to interpret the thickness of the layers. The EMW

(Electromagnetic wave) velocities were estimated using a depth-to-target method. In order to perform migration and time-depth conversion, radar wave velocities have to be known. GPR wave velocity is determined by factors such as grain size, porosity, and water saturation (Hede *et al.*, 2013). The average EMW speed value for peat was approximately  $0.035 \text{ m ns}^{-1}$ . For sand, the average EMW value was mostly between  $0.05\text{--}0.06 \text{ m ns}^{-1}$ . Low EMW values in sand are caused by high water content in the old

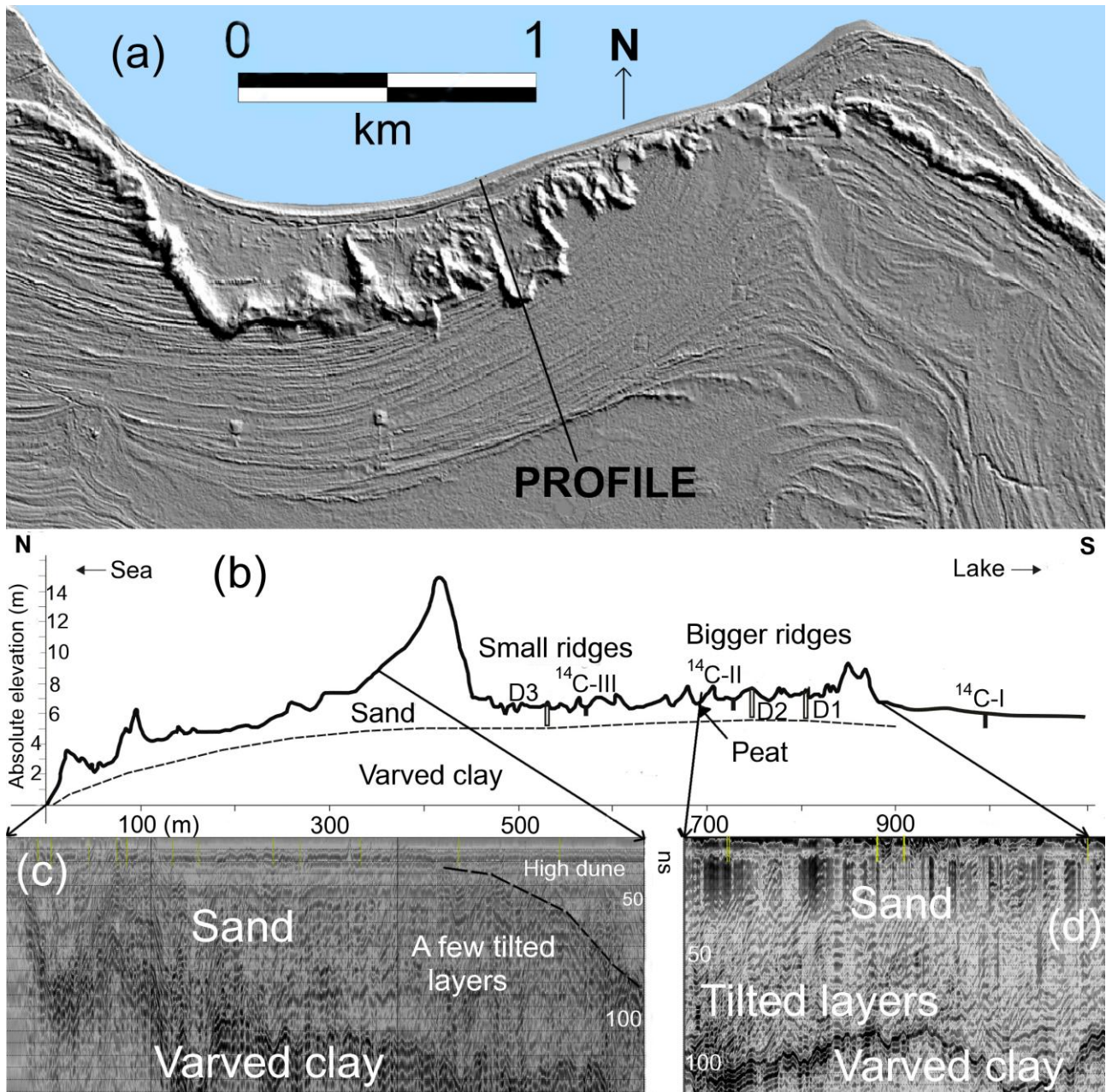


Figure 2. Lõimastu study site. (a) Relief map based on LIDAR. The map clearly shows how dunes are covering old beach ridges system. (b) Landscape profile (location on Fig. 2a), where D1-3 mark drill holes (cores) and  $^{14}\text{C-I-III}$  peat cores. (c) GPR profile (100 MHz) shows distinct sand and varved clay layer. (d) The beach ridges landward of the dune are characterised by many seaward tilted sand layers (GPR frequency 270 MHz).

beach formations. The vertical variation is likely caused by a change from saturated to unsaturated sediment controlled by the position of the groundwater table (Hede *et al.*, 2013).

### Radiocarbon Dating ( $^{14}\text{C}$ )

From Röögu and Lõimastu study sites, 7 peat cores in total were collected manually from swales using a Russian peat corer with a 50 cm sample chamber for radiocarbon dating. Bulk samples of ca. 5 cm in thickness were taken from the base of the basal peat unit (immediately above the substrate). The dating of the bulk samples was conducted in the radiocarbon dating laboratory of the Institute of Geology at Tallinn University of Technology using the standard liquid scintillation technique (Punning and Rajamäe, 1993). Calibration of the radiocarbon ages to calendar years BP was done using the age calibration online program of OxCal Version 4.2.

### In Addition to Previous

Landscape profiles were measured and topographic data were collected from three cross-shore profiles. Geological and soil maps were used for selecting the study areas and the routes for compiling landscape transects. Piezometric pipes were used to measure the water level in depressions. LIDAR survey based relief map compiled by Estonian Land Board was used as an additional information source to analyse the evolution of the study sites.

## RESULTS AND DISCUSSION

### Granulometry

For better understanding of the differences in sand along the horizontal profiles we collected sediment samples. Although we took sediment samples to a depth of 1 m, the results were not as different as expected. Comparing the Lõimastu study site with Röögu and Tõrvanina, we can see that in Lõimastu in the northern part of the peninsula fine sand (100–250  $\mu\text{m}$ ) is slightly dominant over medium sand (250–500  $\mu\text{m}$ ); the percentage ratio is 57/40. However, the present coast is dominated by medium to fine sand of 52/44. In the eastern part of the peninsula, the situation is more complicated. The Röögu profile is dominated by fine over medium sand, the percentage ratio is 75/25. It may refer to more aeolian activity in that region during the past. As said above, the study site at Tõrvanina is more complicated due to strong erosion. The percentage ratio is 10/80 on the beach. The older coastal formations show the ratio of fine to medium sand of 54/43 (Figure 3). The initial results did not show clear differences between aeolian and marine sand from this study based on grain size in the upper layers. Due to complexity of the over a size distribution additional data analyses is needed. Sediment granulometry and structures by themselves, however, may not always provide sufficient proof of foreshore and aeolian facies within a given beach ridge (Otvos, 2000). Therefore, we needed to collect sediment samples from deeper layers as well. We carried out drilling in Lõimastu and Röögu study sites. Preliminary results show that all the drilled boreholes reached the clay layer. The exact drilling locations were selected based on GPR data (visible tilted layers or other clear layers). Clear (visible by eye) cuts between marine and aeolian sand layers were found in several boreholes. The layers containing very coarse sand (also gravel particles) were assumed to be of marine (wave accumulated) origin. Sandy beach ridges also consist of coarse to fine sand on some modally low energy beaches (Hesp, 2006).

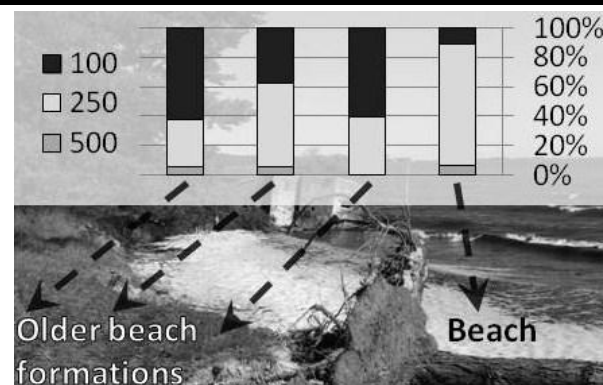


Figure 3. Grain size (in  $\mu\text{m}$ ) distribution at Tõrvanina site.

### Ground-Penetrating Radar (GPR)

The GPR survey in Lõimastu and Röögu study sites revealed two different textural patterns in the sands (Vilumaa *et al.*, 2013), which were confirmed by drilled boreholes. GPR studies in various settings suggest that the internal structure of the beach ridge is dominated by seaward dipping lamination (Clemmensen and Nielsen, 2010; Timmons *et al.*, 2010; Tamura, 2012), which stratification is formed in relation to beachface progradation, and is usually dissected in places by erosion surfaces resulting from episodic beach retreat (Tamura, 2012). These seaward tilted layers suggest that the accumulation of sediments took place in the result of wave activity during cross-shore transport (Vilumaa *et al.*, 2012; 2013).

**Lõimastu landscape profile** is ~ 1 km long and is divided into two parts by a high dune (Figure 2b).

The landward part of the profile is ~ 680 m long. The beach ridges landward of the dune are characterised by many seaward tilted sand layers (Figure 2d). The GPR profile showed that the last few ridges in the southern part lack tilted layers, which might refer to longshore drift. It is possible that part of the ridges is formed as a spit. Spit-like ridges can be also identified from the LIDAR based relief map (Figure 2a).

The seaward part of the profile is ~ 320 m long. As a contrast, the land surface in seaward (northern) side of the high dune is less undulating. The system of foredunes and dunes is presented at the seaside. Missing beach ridges could be related with the formation of the high dune. On relief map, it is visible how the high dune is covering the old ridges (probably this ridge system used to continue close to the shoreline). The GPR profile reveals only a few seaward tilted layers all of which are located in the close vicinity of that high dune (Figure 2c). Missing of tilted layers near the shore could be explained with the landscape changes during the formation of the high dune or with steeper surface elevation drop.

The high dune in the middle of the profile is up to 15 m a.s.l. (Figure 2a,b). The formation of it could be caused by local sea level changes (probably transgression) (Clemmensen *et al.*, 2013) or some extreme events in the past (ice attack, extreme storm, single extreme wave, etc.). There were probably small transgressions in the background of prevailing regression, but they were likely to have been of local origin (Hyvärinen *et al.*, 1988). Due to some reasons, there was enough available sediment (sand) during this period of time. The formation of the high dune changed the former landscape (beach ridges system) in the seaward part of the profile. The seaward border of the tilted layers



probably indicates the landward extent of the dune formation (according to GPR). The seaward border of these layers was probably the border of that past event. These layers were perhaps initially covered by a thick layer of sediments accumulated later in the dune. The dune gradually migrated landward and left those coarser (marine) layers at their original location.

Surface gradient has an important role in the formation of beach ridges as the analysis of landscape profiles shows. The highest and widest ridges seem to develop in an area with very small surface gradient. The area of well developed ridge system on landward side of Lõimastu study site, surface gradient elevation is only 0.5 m per ~ 220 m. The coastal landforms have the biggest parameters (up to 2 m) there. This area probably emerged from the sea during the regressive phase of Limnaea Sea (LimIII, 2500 yr BP) when the sea level was higher than during the formation of younger and smaller beach ridges (LimIV, 2000 yr BP). Due to the low surface gradient value, the sea level stays stable for a longer period of time, favouring the growth of ridges. Accumulation of aeolian sand on the beach ridges tends to heighten the formations while the shoreline progradation slows it down or ceases even without a change in wind climate. This means that slower progradation causes foredunes to receive sediments from the beach for a longer time (Tamura, 2012). The same can be seen on Juminda Peninsula, N Estonia where the sandy ridges have grown up to 4-5 m high in the area of low surface gradient value. In case of increase in the elevation gradient, the coastal formations' parameters decrease jointly (Vilumaa, *et al.* 2013). One important aspect is the availability of sediment supply, which depends on geological structure of a region.

The height of sandy beach ridges is often variable due to the unequal accumulation of aeolian sand. The interval varies both spatially and temporarily within a single beach-ridge system in relation to the different rate of shoreline progradation and ridge spacing, which are affected by lateral sediment supply and redistribution. The beach and aeolian facies are generally distinguishable: foreshore and backshore facies are mainly characterized by gentle seaward-dipping lamination, while aeolian dunes exhibit steeper cross lamination (Otvos, 2000; Tamura, 2012; Bendixen *et al.*, 2013). Foreshore lamination is possibly steeper on reflective beaches, and washover deposits may display high-angle cross lamination. On top of these deposits may lay aeolian dune facies with gentler cross lamination.

The drilled boreholes (3 in total) showed various sand layers. The first (4 m deep) borehole (D1) is located in the southern part of the profile (Figure 2b). There is a stronger layer at 3 m depth. In the second borehole (D2) (located in the middle of the area of higher beach ridges) in 2.5-3 m depth, the sand is coarser-grained (might be marine). In 3.5 m, the sand contains bigger dark quartz particles and is underlain (in 4-5 m) by varved clay. The third borehole (D3) is located almost in the middle of the smaller ridge system. In this drill hole, in 3 m depth the sand layer is also coarser and even some gravel particles are visible. This data confirms that the tilted layers in the lower section of the GPR profiles are most probably of marine origin. The upper 2-3 m deep layer of sand is probably of aeolian origin or was mixed during various coastal processes.

**Röögu landscape profile** is 1 km long. The internal structure of the Röögu beach ridge system according to the GPR data shows a number of beach ridges, which have been covered by peat and have eventually levelled. The top layers (1–1.5 m) are almost parallel to the surface of the initial beach ridges. Most of the lower layers are tilted north (probably seaward side during their formation) (Vilumaa *et al.*, 2013). The dipping reflectors are interpreted as representing beachface deposits formed under

swash- and backwash processes (Hede *et al.*, 2013). The uppermost reflections running mainly parallel with the ground surface may be interpreted as representing aeolian cap deposits (Lichter, 1995; Hede *et al.*, 2013) or a result of accumulated longshore drift or a combination of both processes.

The dimensions of the beach ridges at Röögu study site are comparable to those in the southern part of Lõimastu study site. The reason might be again in low surface gradient (~ 0.5 m per 1000 m). The ridge system has NW-SE orientation. We can assume that the area was more exposed to NE and E in the past and less to strong wave activity from W (Tõnisson *et al.*, 2011).

Three boreholes in total were drilled at the beginning, in the middle and at the end of the landscape profile. According to the GPR records and the data from the three drilling holes, the sand layer is approximately 3.5-4 m thick and is underlain by varved clay. Unexpectedly, the coring showed that the sand is fine grained even in deeper layers. This could be related to the exposure to the sea, past sediment transport and origin.

### Radiocarbon Dating

Due to the acidic environment (pHKCl 2.7–4.6), the beach ridges on Tahkuna Peninsula are non-calcareous and therefore lack of material available for radiocarbon dating. Radiocarbon dating of soil and peat in inter-ridge swales is problematic because these materials were not necessarily deposited synchronously with the adjacent beach ridges (Tamura, 2012), but it still gives us information about the development of the swales.

A total of seven radiocarbon ages were obtained from peat in swales resting directly on sandy substrate along a bathymetric gradient.

At **Lõimastu**, all the 3 peat samples were collected from landward side of the high dune (Figure 2b). The oldest peat (<sup>14</sup>C-I) 1,386 cal. yr BP (1501±45 BP Tln3501, 75 cm depth) was dated in the southernmost part of the profile in lake depression area. The peat (<sup>14</sup>C-II) between higher and clearly developed beach ridges is approximately 1,141 cal. yr BP (1213±50 BP Tln3502, 69 cm depth) old and the youngest (<sup>14</sup>C-III) 581 cal. yr BP (553±50 BP Tln3503, 45 cm depth) layer was recorded in the area of smaller ridge system near the high dune. The peat thickness and swales' location correlates well with the radiocarbon data.

At **Röögu** the peat layer between the oldest ridges, which are located the most inland of the profile is quite young 981 cal. yr BP (1066±50 BP Tln3506, 60 cm depth). The oldest 1,581 cal. yr BP (1673±50 BP Tln3507), 1,735 cal. yr BP (1801±45 BP Tln3508) and deepest (85-100 cm) peat layers have developed in the middle part of the landscape profile. The youngest peat layer 601 cal. yr BP (608±45 BP Tln3509, 55 cm depth) was found between the youngest ridges on seaward side.

The radiocarbon results and the topographic setting (age) of the ridge system do not always correlate. The dating results show that the development of peat layer between ridges is more dependent on the coastal formation parameters and water movement than on the altitude and age of the beach ridges. The same was recorded in Juminda Peninsula, where the deepest and oldest peat profile was found to be in seaward side swales. The thickness of the peat layer varies a lot along the profiles. There is no clear trend between the age (elevation) of the ridges-swale systems and the thickness of peat layer (Vilumaa *et al.*, 2013).

### CONCLUSIONS

The study of the coastal formations confirmed the following. Granulometric analysis showed that no final conclusion about the origin of the sand can be made due to the difficulty to differentiate lithofacies. The studied beach ridges have developed under retreat

of shorelines and probably in low-energy wave conditions. The initial height of the ridge depends on the exposure to wind erosion and vegetation, which may later cause an enlargement of the coastal formation. The sandy beach ridges are often variable due to the unequal accumulation of aeolian sand and sediment supply. Due to the difficulties in determining the original beach-ridges we used GPR and radiocarbon dating.

GPR reflections showed us the internal structures of the study areas where seaward tilted layers on radar facies could be interpreted as beachface deposits formed as a result of swash- and backwash processes. The uppermost reflections running mainly parallel with the ground surface may reflect aeolian cap deposits or refer to longshore drift. It is possible that part of the ridges is formed as a spit.

Radiocarbon datings from swales do not always correlate with the topographic settings. The development of peat layers between the ridges is more dependent on geomorphology and hydrological conditions. Therefore, the peat between younger beach formations might be older than the peat between older beach formations.

### ACKNOWLEDGEMENT

This paper was supported by the target-financed project No.SF0280009s07, funded by the Estonian Ministry of Education and Research and by the Estonian Science Foundation grants No. 7564, 8549, 9191, Tallinn University Centre of Excellence "Studies of Natural and Man-Made Environments" and the EstKliima project of the European Regional Fund programme No. 3.2.0802.11-0043.

### LITERATURE CITED

- Aagaard, T., Orford, J. and Murray, A., 2007. Environmental controls on coastal dune formation: Skallingen Spit, Denmark. *Geomorphology*, 83, 29-47.
- Anderson, A., Ratas, U., Rivis, R. and Palginõmm, V., 2012. Relationship between coastline changes and dynamics of coastal ecosystems of Tahkuna Peninsula, Estonia. *IEEE/OES Baltic 2012 International Symposium*, 1-6.
- Bendixen, M., Clemmensen, L.B. and Kroon, A., 2013. Sandy berm and beach-ridge formation in relation to extreme sea-levels: A Danish example in a micro-tidal environment. *Marine Geology*, 344, 53-64.
- Clemmensen, L.B. and Nielsen, L., 2010. Internal architecture of a raised beach ridge system (Anholt, Denmark) resolved by ground-penetrating radar investigations. *Sedimentary Geology*, 223, 281-290.
- Clemmensen, L.B., Bendixen, M., Hede, M.U., Kroon, A., Nielsen, L. and Murray, A.S., 2013. Morphological records of storm floods exemplified by the impact of the 1872 Baltic storm on a sandy spit system in south-eastern Denmark. *Earth Surf. Process. Landforms*. doi: 10.1002/esp.3466
- Eastwood, E.N., Joanna, M., Baas, A. and Kocurek, G., 2011. Modelling controls on aeolian dune-field pattern evolution. *Sedimentology*, 58, 1391-1406.
- González-Villanueva, R., Costas, S., Pérez-Arlucea, M., Jerez, S. and Trigo, R.M., 2013. Impact of atmospheric circulation patterns on coastal dune dynamics, NW Spain. *Geomorphology*, 185, 96-109.
- Hede, M.U., Bendixen, M., Clemmensen, L.B., Kroon, A. and Nielsen, L., 2013. Joint interpretation of beach-ridge architecture and coastal topography show the validity of sea-level markers observed in ground-penetrating radar data. *Holocene*, 23 (9), 1238-1246.
- Hesp, P.A., 2006. Sand beach ridges: Definition and re-definition. *J. Coastal Research*, SI 39, 72-75.
- Hyvärinen, H., Donner, J., Kessel, H. and Raukas, A., 1988. The Litorina Sea and Limnea Sea in the Northern and Central Baltic. *Ann. Acad. Sci. Fennicae, Series A. III. Geol.-Geogr.* 148, 25-35.
- Kont, A., Jaagus, J., Orviku, K., Palginõmm, V., Ratas, U., Rivis, R., Suursaar, Ü. and Tõnisson, H., 2011. Natural development and human activities on Saaremaa Island (Estonia) in the context of climate change and integrated coastal zone management. *In: Schernewski, G., Hofstede, J. and Neumann, T. (eds.), Global change and Baltic coastal zones.* Springer, pp. 117-134.
- Lichter, J., 1995. Lake Michigan beach-ridge and dune development, lake level, and variability in regional water balance. *Quaternary Research*, 44, 181-189.
- Mauz, B., Hijma, M.P., Amorosi, A., Porat, N., Galili, E. and Bloemendal, J., 2013. Aeolian beach ridges and their significance for climate and sea level: Concept and insight from the Levant coast (East Mediterranean). *Earth-Science Reviews*, 121, 31-54.
- Orviku, K., Suursaar, Ü., Tõnisson, H., Kullas, T., Rivis, R. and Kont, A., 2009. Coastal changes in Saaremaa Island, Estonia, caused by winter storms in 1999, 2001, 2005 and 2007. *Journal of Coastal Research*, SI 56, 1651-1655.
- Otvos, E.G., 2000. Beach ridges – definitions and significance. *Geomorphology*, 32, 83-108.
- Punning, J.M. and Rajamäe, R., 1993. Radiocarbon dating organic detritus: implications for studying ice sheet dynamics. *Radiocarbon*, 35, 449-455.
- Raukas, A., Bird, E. and Orviku, K., 1994. The Provenance of Beaches on the Estonian Islands of Saaremaa and Hiiumaa. *Proc. Estonian Acad. Of Sci. Geol.* 43, 2, 81-92.
- Suursaar, Ü., Jaagus, J., Kont, A., Rivis, R. and Tõnisson, H., 2008. Field observations on hydrodynamic and coastal geomorphic processes of Harilaid Peninsula (Baltic Sea) in winter and spring 2006-2007. *Estuarine Coastal and Shelf Science*, 80, 31-41.
- Tamura, T., 2012b. Beach ridges and prograded beach deposits as palaeoenvironment records. *Earth-Science Reviews*, 114, 279-297.
- Timmons, E.A., Rodriguez, A.B., Mattheus, C.R. and DeWitt, R., 2010. Transition of a regressive to a transgressive barrier island due to back-barrier erosion, increased storminess, and low sediment supply: Bogue Banks, North Carolina, USA. *Marine Geology*, 278, 100-114.
- Tõnisson, H., Orviku, K., Jaagus, J., Suursaar, Ü., Kont, A. and Rivis, R., 2008. Coastal damages on Saaremaa Island, Estonia, caused by the extreme storm and flooding on January 9, 2005. *Journal of Coastal Research*, 24 (3), 602-614.
- Tõnisson, H., Suursaar Ü., Orviku K., Jaagus, J., Kont A., Willis, D.A. and Rivis, R., 2011. Changes in coastal processes in relation to changes in large-scale atmospheric circulation, wave parameters and sea levels in Estonia. *Journal of Coastal Research*, SI64-1, 701-705.
- Vallner, L., Sildvee, H. and Torim, A., 1988. Recent crustal movements in Estonia. *J. Geodyn.* 9, 215-223.
- Vilumaa, K., Kont, A., Ratas, U. and Tõnisson, H., 2012. Ground-penetrating radar study of coastal landscape on Hiiumaa Island, Estonia. *IEEE/OES Baltic 2012 International Symposium*, 1-6.
- Vilumaa, K., Tõnisson, H., Kont, A. and Ratas, U., 2013. Ground-penetrating radar studies along the coast of Estonia. *Journal of Coastal Research*, SI65, 612-617.

# Evolution of Corsican pocket beaches

Balouin Yann†, Bélon Rémi‡, Anne Merour‡, Camille Riotte‡

†BRGM, French Geological Survey, Dir.  
Languedoc-Roussillon  
Montpellier, France  
y.balouin@brgm.fr

‡ BRGM, French Geological Survey, Dir.  
Corse  
Bastia, France  
r.belon@brgm.fr



[www.cerf-jcr.org](http://www.cerf-jcr.org)



[www.JCRonline.org](http://www.JCRonline.org)

## ABSTRACT

Balouin, Y., Belon, R., 2014. Evolution of Corsican pocket beaches. In: Green, A.N. and Cooper, J.A.G. (eds.), *Proceedings 13<sup>th</sup> International Coastal Symposium* (Durban, South Africa), *Journal of Coastal Research*, Special Issue No. 70, pp. 096-101, ISSN 0749-0208.

Pocket beaches are small beaches that are formed between headlands and within coves along rocky shorelines. They can be composed of a mix of boulders, pebbles, sand and mud and therefore have the attributes of a combination of shoreline types. Their evolution depends on wave forcing and morphological characteristics, and the most commonly observed dynamic is that of beach rotation due to prevailing wave direction. In this study, 44 pocket beaches off Corsica Island, in the Mediterranean were studied. The absence of significant tides and the generally weak coastal currents restrict significant beach morphology changes to the most important storm events though the variability of coastal evolution suggests that other factors played a role. To assess these evolution parameters, the morphological characteristics of the beaches as well as the historical evolution of the shoreline were studied. This analysis, based on aerial photos and DGPS surveys, allowed for the behavior of beaches over historical (1948-2012) period to be assessed. Over this period, 15 beaches are considered to be in erosion, 16 are stable and the others show shoreline progression. The historic analysis, through several increments of time, shows that beaches have been in perpetual movement. Moreover, some periods are particularly erosive (i.e., 1996 to 2002) for a number of beaches. Several parameters must be considered to explain the beach behavior changes such as: beach orientation, closure, geology, hydro-climatic regime, grain size and length. The wave backward modeling ANEMOC was used to analyze wave characteristics and the occurrence and direction of the most important storm events. The entire dataset was used to obtain a conceptual model describing the most important factors involved in the contrasting coastal evolutions observed, i.e., symmetric or asymmetric beach rotation, homogeneous retreat or progradation and rapid shoreline movements due to the presence of beach-cast *Posidonia Oceanica* seagrass litter.

**ADDITIONAL INDEX WORDS:** *shoreline, beach stability, sea grass litter.*

## INTRODUCTION

A large majority of the world's continental and island margins consist of rocky coastlines. Along these coasts, typical beach morphology is characterized by the presence of hard rock headlands (Short and Masselink, 1999). These embayed beaches, are usually small beaches known as curved, embayed, pocket and headland-bay beaches. Detailed studies of these pocket beaches have been made (Hsu and Evans, 1989, Klein *et al.*, 2002, Bowman *et al.*, 2009, Daly *et al.*, 2011, van de Lageweg *et al.*, 2013). It is widely accepted that the morphological behavior of these beaches is determined by beach planform and indentation ratio, beach type and slope, grain size and the presence or absence of nearshore bars. The morphological evolution of these systems is also driven by wave conditions which influence both the hydrodynamics at the coast (alongshore and rip-currents) (Short and Masselink, 1999) and beach rotation processes.

The planform geometry approach (Hsu *et al.*, 1989) has been widely used to obtain a first insight into the study of embayed coasts. This approach is based on an equilibrium form of the planview beach that fits either logarithmic, parabolic or power functions. This method thereby permits us to evaluate the equilibrium state of a given embayed beach, by evaluating the

relationship between indentation ratio ( $a/r_0$ ) of the beach and wave angle ( $\beta$ ).

Several studies have, however, shown that models using averaged environmental parameters were insufficient to clearly explain the morphological evolution of embayed beaches (Loureiro *et al.*, 2009, 2013), with reflective and lower intermediate beaches showing more agreement with parametric approaches than intermediate beaches. Beach state classification, using parameters such as dimensionless fall velocity (Wright and Short, 1984), therefore provides additional information on the applicability of planform approaches and also gives an information on the nearshore circulation that is to be expected (Short and Masselink, 1999).

The objective of this contribution is to evaluate the geometry, evolution and morphodynamics of a complete dataset obtained from 44 embayed beaches on Northern Corsica Island in the south of France.

## FIELD STUDY

The study site is the Haute-Corse division on Corsica Island; located in the Mediterranean Sea (Figure 1). There, the coast is divided into a sandy coastal plain along the eastern coast and a long rocky coast in the north where 44 pocket beaches with variable exposure, morphologies and evolution patterns are observed. Mean tidal range is around 0.2 m and can reach 0.3 m during spring tides. Modal wave conditions are weak ( $H_s$  mean = 0.8 m;  $T_s$  mean  $\approx$  4.5 s) but important wave events and winter

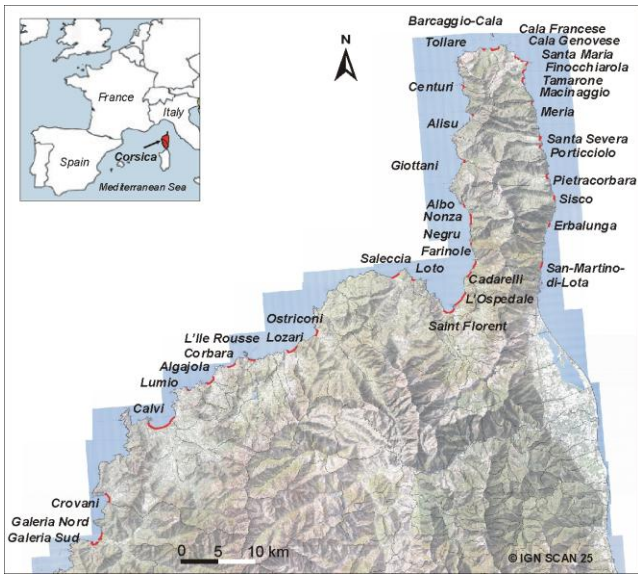


Figure 1. Localisation of the study area and the 44 pocket beaches of Haute-Corse.

storms are rather frequent. The 1 yr return period height for waves is around 4.7 m, but significant wave heights of more than 8 m were observed. Most of the field sites are reflective beaches composed of fine sand to large gravel. For most of the sites, the erosion rate of the nearby cliffs is low and the sediment supply is thus very limited. The cliffs along the Cape are composed of ophiolites and glossy schists, while the western coastline is formed by high-magnesium and -potassium, granitic rocks.

**METHODS**

**Beach morphology and shoreline evolution**

An analysis of shoreline evolution was performed using aerial photographs available since 1948 (1948, 1951, 1960, 1983, 1985, 1996, 2002, 2007). Photographs taken before 1990 are at the scale 1:25000, while more recent ones are at the scale 1:5000. Both the vegetation line and the wet/dry line were digitised, but as the upper beach limit is very often marked by a cliff or human infrastructures, the wet/dry line was used in this study to evaluate

the long-term shoreline change. Given the higher variability of this indicator, and the resolution of images, the extracted position of the shoreline has an accuracy of +/-10 m for the old photographs (before 1996) and +/- 5 m for the more recent ones. Some of the studied beaches have been monitored yearly since 2000 within the Coastal Monitoring Network of Corsica (ROL, Balouin *et al.*, 2013), to evaluate the short-term changes in shoreline position. A DGPS survey of the shoreline for all studied beaches was performed in 2012. Beach profiles, sediment samples, photographs and geomorphological observations (e.g., of vegetation, seagrass litter and the presence/absence of a developed berm, beach cusps or nearshore bars) were also collected.

All shorelines were digitized using ArcGIS® software. To measure the shoreline evolution with time and the evolution speeds, the DSAS module developed by USGS (Thieler *et al.*, 2009) was used. It allows for the comparison of shoreline position for a large number of points to be carried out automatically (see example on Fig. 2). Pocket beach characteristics were evaluated both by aerial photographs and by field data analysis. Characteristics assessed included: beach orientation, slope, length, sheltering, degree of embayment, closure, geology and the presence/absence of seagrass litter. This information permitted a morphodynamic indicator (Wright and Short, 1984) and a stability indicator (Hsu and Evans, 1989) to be calculated. Finally, a description of the main morphological behavior was defined for the 44 beaches distinguishing between beach stability, unidirectional beach rotation, bi-directional beach rotation, homogeneous retreat and accretionary behaviours.

**Hydrodynamics**

Wave measurements are scarce along Corsica shorelines, and most of the thus-far collected data has no directional information. In order to analyze the wave climate and storm characteristics, the ANEMOC database (© CETMEF / EDF R&D-LNHE 2010/2011) was used. ANEMOC (Digital Atlas of State Oceanic and Coastal Sea; <http://anemoc.cetmef.developpement-durable.gouv.fr>) was built from hindcasts over a period of 30 years from 01/01/1979 to 31/12/2008 for the Mediterranean coast. Five virtual buoys (MEDIT 4655, 6530, 6771, 7846, 8110) were used to analyze wave climate along the Haute-Corse shoreline (Fig. 3). The mean wave climate was obtained as well as storm characteristics: maximum wave height, cumulated energy, frequency, duration, maximum run-up and set-up using the formula of Stockdon *et al.* (2006). A storm event along this coastline is defined by a

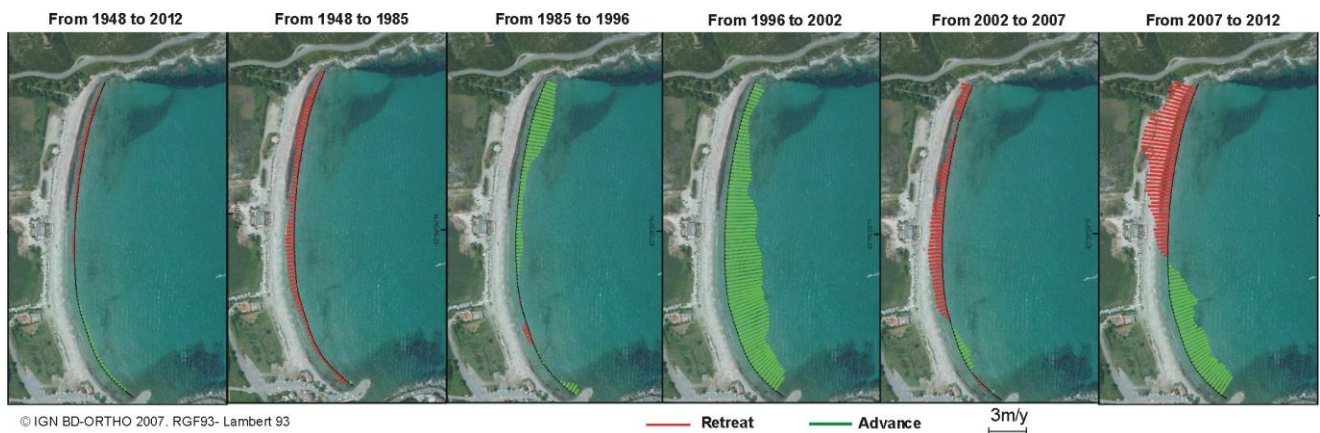


Figure 2. Example of shoreline evolution from 1948 to 2012 at Pietracorbara beach on the eastern coast of Corsica.

significant wave height above 2 m (more than two times the mean significant wave height).

## RESULTS

### Hydrodynamics

ANEMOC hindcast database was used to obtain the mean wave climate along the northern Corsican coastline, but also the characteristics of storm events during the period 1979-2008. Particular storm wave conditions were extracted for all beaches depending on their orientation, aperture. Figure 3 illustrates the prevailing wave direction. More than 750 events with  $H_s > 2$  m were analyzed. Most of the storms have significant wave heights around 3 m. However, at this site  $H_s$  can reach more than 6 m as observed in November 2004. Mean duration of these events is around 21 hours. However, the maximum duration was 113 hours in February 1990. At most of the beaches, there is a prevailing storm direction (see Figure 3). However, smaller events can occur with an opposite direction thus contributing to the alternation in the direction of sediment transport and beach rotation processes along the surveyed period. Moreover, even if the storm characteristics are comparable for all beaches with a slight higher energy on the west coast where the fetch is longer, the frequency of storm events is more important on the northern and the western coast than the eastern one. While less than 500 storm events ( $H_s > 2$  m) were recorded on the east coast, more than 1000 were recorded on the northeast coast during the period 1979-2008 (see Figure 4). To calculate the mean wave climate, the prevailing direction was used (see  $\Omega$  and incidence in Figure 4).

### Shoreline evolution

Evolution of shoreline position was calculated for the 44 beaches (see example on Figure 2). Over the long-term (from 1948 to 2012), very few beaches have been enlarged. The beaches of Galeria North and Cala Genovese (see location on Figure 1) show a respective advance of 20 and 15 m. Two beaches of the western Cap Corse, Albo and Nonza, present a very strong enlargement reaching more than 300 m between 1948 and 1960. This evolution is however anthropogenic and derive from the mining activities in the vicinity of these bays (Mine of Canari) and the human deposition of large quantities of material extracted from the mine. Sixteen beaches are stable, 11 in erosion and 4 in strong erosion: Tollare, Giottani and Negru where the retreat reaches 40 m and Saleccia where a 60 m retreat was observed in the southern part of the bay.

The recent evolution, from 2007 to 2012, gives the trend of the current evolution, onto all the studied beaches, 4 are stable, 16 are in accretion and 23 are in erosion. This evolution is much more contrasted than the historic evolution, 13 beaches have an important accretion and 16 have marked erosion.

The analysis of the historical shoreline evolution shows contrasted behaviors of beaches exposed to the same forcing parameters, evidencing the importance of local parameters. The short-term evolution (see Figure 4) shows the high temporal variability of the erosional process. This is particularly the case for the beaches where an important seagrass litter covers the beach (Figure 4). The quantity of seagrass litter is highly variable in time because the destruction of the meadow is linked to storm occurrence, and some of the beaches are "cleaned" before the summer touristic season.

Some periods show a very rapid shoreline retreat, as during 1996-2002 along the eastern coast of the cape. The wave conditions during this period were not more energetic, but

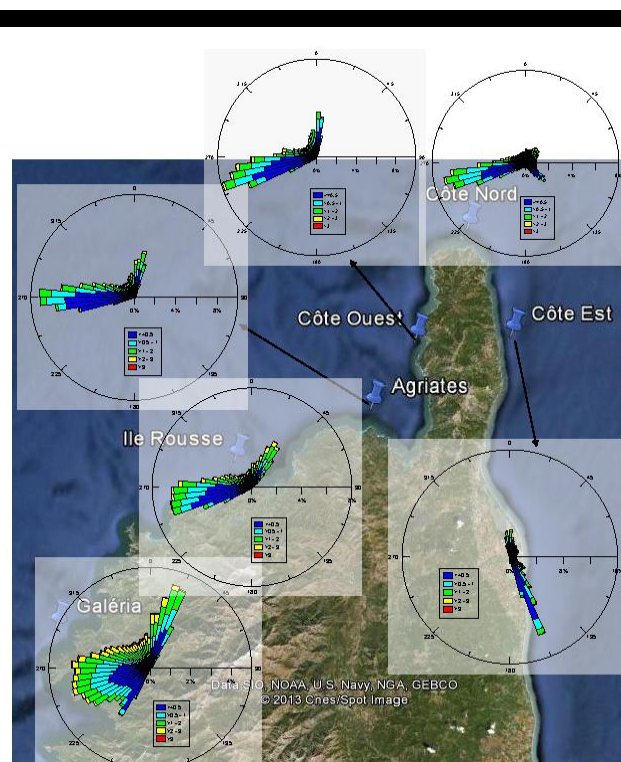


Figure 3. Wave characteristics along the coastline of northern Corsica. Vectors indicate the frequency of wave direction while colours indicate the associated significant wave high ( $H_s$ , m).

duration between two successive events was slightly shorter, preventing beach recovery, and could explain the observed strong retreat.

### Morphodynamics

To understand the differences in shoreline evolution of the Corsican pocket beaches, several parameters were analyzed (Figure 4). The first parameter was wave incidence at 10 m depth. Given the prevailing wave direction from north and south-east along the east coast and from east and north-east along the northern coastline, wave incidence is highly variable. Apart from their orientation, beaches on the east coast are much more exposed to highly oblique waves. In such cases, wave refraction is higher, and energy supposed to be lower at the coast.

The number of storm events during the last 30 years was also lower than on the northern coast. This wave climate is in agreement with the main morphological behavior of these beaches which was characterized by beach rotation that could be either unidirectional or bi-directional based on the orientation and closure of the beach. On the west coast of the Cape, the most significant storm events reach the coast with a very low incidence. The main morphological behavior observed was a homogeneous retreat of the shoreline, except for the anthropogenic-driven beaches of Nonza and Albo. Along the rest of the coast, wave direction is mostly shore-normal, but beach orientation is much more variable so a general trend cannot be defined.

In order to take into account the morphology of the bays, the stability state of the beaches using the indentation ratio ( $a/R_o$ ) and the wave crest angle ( $\beta$ ) (see Figs. 4 and 5) were examined. This concept was widely used in a first step to evaluate the equilibrium

state of the beaches. The results (Figure 5) indicated that most of the beaches of the eastern coast are unstable. The main reason for this is the high wave incidence, particularly during storms from

the south-east. These beaches, and some others along the coastline usually have reduced lengths, large indentations and are known to have a large amount of *Posidonia oceanica* beach casts. Despite

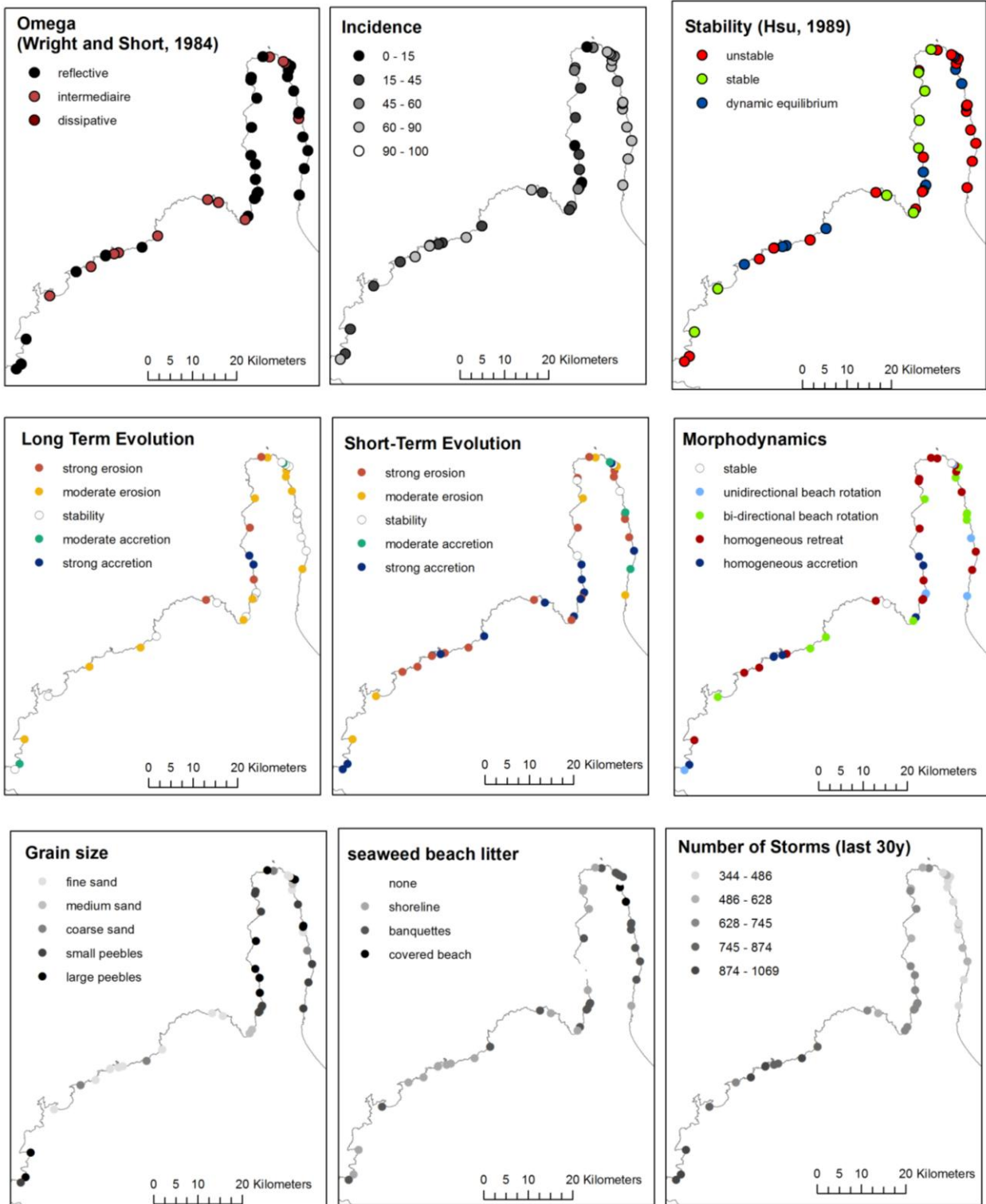


Figure 4. Morphological indicators obtained from the 44 pocket Beaches along Northern Corsica. Upper panel: dimensionless fall velocity  $\Omega$ ; wave incidence at 10 m depth and stability test results (Hsu and Evans, 1989); Middle panel: long-term (1948 to 2012) shoreline evolution, short-term (2002-2007) shoreline evolution and main morphological processes observed (both on the historical photographs and the yearly surveys undertaken on some of the beaches); Lower panel: grain size, presence and quantity of seagrass litter on the beach and number of storm events (with  $H_s > 2m$ ) during the period 1979-2009.

this apparent unstable state, they have shown a quite stable position of the shoreline during the last few decades.

## DISCUSSION

Results on the evolution and morphological changes of 44 embayed beaches located along northern Corsica Island reveal contrasting responses, even for beaches submitted to the same forcing conditions. Beach orientation drastically affects shoreline evolution, with higher erosion where wave incidence is the lowest. This is particularly true for the beaches of Tollare, Giottani, Saint-Florent, Lumio. However, several beaches, like Ostriconi, have a low incidence and are exposed to energetic storms yet they remain quite stable on the long term.

As was physically observed by Dai *et al.* (2010) and numerically simulated by Daly *et al.* (2011), beaches with a stable shape experience greater degrees of beach oscillation (onshore or offshore movement) than of beach rotation. This was observed at several beaches (Meria, L'Ile Rousse, Corbara, Lumio). The directional spreading was very large at all beaches, with a bimodal directional spectrum at all sites (Fig. 3). Nevertheless, only 13 beaches displayed a clear rotation tendency on the observed shoreline. Despite the occurrence of opposite storms, some of these beaches showed an alternation of beach rotation direction, while others presented a unidirectional evolution, with one part of the bay always providing sediment to the other. Of course, this observation was taken along several shorelines and short-term evolution in relationship with storm events was not taken into account. This could point towards a significantly different behavior between storm evolution and the mid- and long-term tendency.

Stability analysis has shown that only 9 of the 44 studied beaches possessed a stable planform. Most of these beaches were on the western coast of the Cape and are characterized by a low wave incidence; they are among the few intermediate beaches of northern Corsica. Beaches expected to be stable (in green on Figure 4) are supposed to keep a stable planform shape. In Corsica those beaches have shown an erosional trend during the last decade, but according to the available dataset, did not present an important modification of their planform shapes. At those sites, erosion concerned the entire bay and no rotation processes were visible. According to the classification of Hsu *et al.* (2008), eight of the 44 beaches were in a state of dynamic equilibrium. As expected, these displayed long-term erosional trends and the evolution of their shorelines could be either via homogeneous retreat or via beach rotation processes that also yielded a decrease in beach surface.

For beaches in stable and in dynamic equilibrium, the stability analysis gave expected results and comprehensively explained shoreline evolution, even if the rate of shoreline retreat was highly variable and dependent upon local morphological parameters (e.g., beach orientation, beach length).

Unstable beaches represent the main part of the Corsican pocket beaches (27 out of 44). Their dynamics and evolution are highly variable. On the east coast, where storms are less frequent and wave incidence higher, the long term shoreline evolution involves either stability or moderate erosion, whereas short-term evolution indicates a high temporal variability. Even if storm events are less frequent and more refracted, these beaches have quite significant morphological responses during storms; as in 2003, when the coastal road in Porticciolo was partly destroyed by breaking

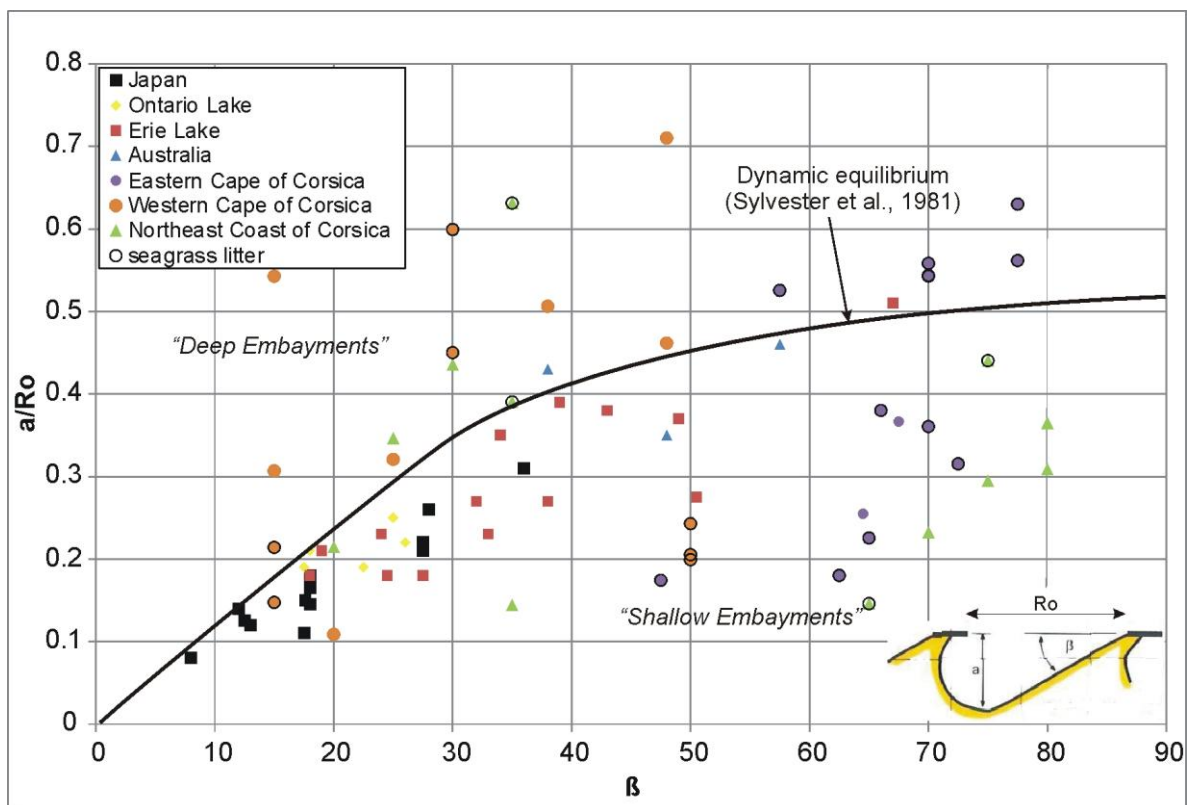


Figure 5. Relationship between indentation ratio ( $a/R_o$ ) and angle between the incident wave crest at the wave diffraction point and the control line joining the updrift diffraction point to the near straight downdrift beach (modified from Bishop (1983), in Simeoni *et al.* (2012)). Black circles on data points from Corsica (this study) indicate a significant amount of seagrass litter on the beach.

waves. Evolution of these beaches is poorly predicted by currently used classifications. However, the characteristics of these beaches and their exposures were quite comparable to the others; the only common characteristic being the presence of seagrass litter along the shoreline and, for some of the sites, upon the entire beach.

This biogenic beach litter has a very important role on the erosion trend: when a large quantity of leaves is present on the beach and in the nearshore zone, it protects the beach from storm waves. However, a storm can have a split impact on the quantity of leaves on the beach: large waves can induce the destruction of the seagrass meadows, favoring the deposition of leaves on the beaches; meanwhile, the most energetic storms can erode the beach cast, enhancing the vulnerability of beaches to subsequent storm events. For these beaches, the stability classification of course does not reflect the real beach state. The seagrass leaves have a very particular behavior. When only a few leaves grow at the shoreline, they tend to be moved easily by waves, but when they form a banquette, their structure is more solid and only more energetic events can move them. Moreover, when leaves are dispersed in water close to the shoreline, they give the water a more viscous behavior that attenuates wave energy at the coast. In this study, the available dataset was not sufficient to clearly understand the role of the seagrass litter and its dynamics (when it is deposited/eroded and why?). However, real-time monitoring using video systems could be useful to determinate the dynamics of these beaches which represent the main part of Corsican beaches.

## CONCLUSION

A dataset on 44 pocket beaches located along Corsica island in France was obtained, describing the mid- and long-term shoreline evolution, local beach characteristics and wave exposures. Hsu *et al.* (1989) stability analysis was applied to evaluate the pertinence of such a method in Corsica. The study indicates that this methodology gives quite interesting results for predicting the behavior of stable and dynamic equilibrium beaches. However, for most of the beaches, the method is not useful because of the presence of seagrass litter on the beach which fully modifies the morphodynamics. Further studies on the impact of seagrass litter on coastal evolution are needed to be able to anticipate the evolution of Corsican pocket beaches.

## ACKNOWLEDGEMENT

The work described in this publication was supported by the Direction Départementale du Territoire et de la Mer de Haute-Corse. For this study, backward modeling results from the ANEMOC database (EDF R&D and CETMEF) were used.

## LITERATURE CITED

- Balouin, Y., Stepanian, A. and Belon, R., 2013. The Corsican coastal monitoring network. In: Cipriani, L.E. (ed.), *Coastal erosion monitoring – a network of regional observatories*. Nuova grafica fiorentina.
- Bishop, C.T., 1983. A shore protection alternative: artificial headlands. *Proc. Candian Coastal Conf., NRCC*, 305-319.
- Bowman, D., Guillen, J., Lopez, L. and Pellegrino, V., 2009. Planview geometry and morphological characteristics of pocket beaches on the catalan coast (Spain). *Geomorphology*, 108, 191-199.
- Daly, C.J., Bryan, K.R., Roelvink, J.A., Klein, A.H.F., Hebbeln, D. and Winter, C., 2011. Morphodynamics of embayed beaches: the effect of wave conditions. *Journal of Coastal Research*, SI64, 1003-1007.
- Dai, Z., Liu, J.T., Lei, Y.P. and Zhang, X.L., 2010. Patterns of sediment transport pathways on a headland beach – Nawan Beach, South China: a case study. *Journal of Coastal Research*, 26(6), 1096-1103.
- Hsu, J.R.C. and Evans, C., 1989. Parabolic bay shapes and applications. *Proc. of the Institution of Civil Engrs.*, 87, 556-570.

- Hsu, J.R.C., Silvester, R. and Xia, Y.M., 1989. Generalities on static equilibrium bays. *Coastal Engineering*, 12, 353-369.
- Klein, A.H.F., Filho, L.B. and Schumacher, D.H., 2002. Short-term beach rotation processes in distinct headland bay beach systems. *Journal of Coastal Research*, 18, 442-458.
- Loureiro, C., Ferreira, O. and Cooper, J.A.G., 2009. Contrasting Morphologic behavior at embayed beaches in Southern Portugal. *Journal of Coastal Research*, SI56, 83-87.
- Loureiro, C., Ferreira, O. and Cooper, J.A.G., 2013. Applicability of parametric beach morphodynamic state classification on embayed beaches. *Marine Geology*, 346, 153-164.
- Short, A.D. and Masselink, G., 1999. Embayed and structurally controlled beaches. In: Short A.D. (ed.), *Handbook of beach and shoreface dynamics*. Chichester, England: John Wiley and Sons, 392p.
- Simeoni, U., Corbau, C., Pranzini, E., Ginesu, S., 2012. Pocket Beach. In: Angeli, F. (ed.), *Dinamica e gestione delle piccole spiagge*, 171 p.
- Van de Lageweg, W.I., Bryan, K.R., Coco, G. and Ruessink, B.G., 2013. Observation of shoreline-sandbar coupling on an embayed beach. *Marine Geology*, 344, 101-114.



# Travelling forelands: complexities in drift and migration patterns

H. Burningham†, J.R. French

Coastal and Estuarine Research Unit  
UCL Department of Geography  
University College London  
London, WC1E 6BT, UK  
†email: h.burningham@ucl.ac.uk



[www.cerf-jcr.org](http://www.cerf-jcr.org)



[www.JCRonline.org](http://www.JCRonline.org)

## ABSTRACT

Burningham, H., French, J.R., 2014. Travelling forelands: complexities in drift and migration patterns. In: Green, A.N. and Cooper, J.A.G. (eds.), *Proceedings 13<sup>th</sup> International Coastal Symposium* (Durban, South Africa), *Journal of Coastal Research*, Special Issue No. 70, pp. 102-108, ISSN 0749-0208.

Cusate forelands have been described from a range of shorelines around the world, but in the majority of cases, the foreland maintains a constant position relative to the neighbouring shoreline. Here, we describe the contemporary geomorphology and historical evolution of a small cusate foreland on the Suffolk coast, UK, which has been migrating northward for several centuries. Benacre Ness, a mixed sand and gravel sedimentary accumulation, is currently located at Kessingland, 5 km to the north of Benacre, from which it gained its name when adjacent to it in the 19th century. The foreland was previously called Covehithe Ness, having been adjacent to Covehithe (3 km south of Benacre) early in the 19th century. Previous sediment transport experiments and modelling studies have demonstrated a net southerly transport direction on this coastline, yet the foreland has continued to migrate northward over several centuries. Local reversals in sediment transport direction and rates are likely responsible for the northward migration of the foreland, but substantial changes in behaviour over the last 400 years suggest a close relationship between foreland dynamics and coastal configuration.

**ADDITIONAL INDEX WORDS:** *ness, beach ridges.*

## INTRODUCTION

Cusate forelands are low-lying sedimentary depositional landforms, comprising beach ridges and/or sand dunes, which are attached to and project from a mainland coast. Johnson (1919) described cusate forelands as ‘forms in which the shoreline is systematically prograded by wave and current action’ where ‘an appreciable area of more or less continuous dry land added to that previously existing’. By definition, they extend the shoreline seaward of what might be a previous erosional shoreline or a sedimentary coastal plain, and exist on scales of hundreds of metres to several kilometres in longshore and/or cross-shore extent. Gulliver (1899) recognised three stages in foreland development: the V-bar stage in which a lagoon separates the seaward barrier beaches from the mainland; the lagoon-marsh stage during which some infilling and encroaching has taken place; and the filled stage in which any enclosed lagoon or marsh has been entirely infilled, or within which no wetland exists. In all cases, dominance of depositional processes leads to the accumulation of beach ridge structures and the extension of a foreland environment. Examples of marsh and lagoon-enclosing forelands are plentiful on the east coast of the USA where they are locally referred to as ‘capes’. Where these forelands exist in a barrier island context, progradation can occur in combination with barrier overwash (Moslow and Heron, 1981). In the UK, cusate forelands such as Dungeness, Sussex are largely lacking in such lagoons or extensive marshes. They are considered to be mature forms (Gulliver, 1897) and their extensive beach ridge plains

provide evidence of multiple depositional phases representing several millennia of development (Long and Hughes, 1995). The cusate forelands found in the UK are colloquially referred to as ‘nesses’, a term that has been used for several centuries and which is embedded in a number of place names around the coast. The vast majority of these sites comprise extensive areas of sand-gravel beach ridges (e.g., Dungeness, Sussex and Orfordness, Suffolk).

The cusate (i.e., triangular and/or projecting) nature of these forelands and the mechanisms responsible for their development have been considered for decades by numerous authors (e.g. Gulliver, 1896; Johnson, 1919; Moslow and Heron, 1981; Semeniuk et al., 1988; McNinch et al., 2000) linking foreland development and behaviour to bathymetric, geological and headland controls; opposing wind and wave or sea versus swell directions and to spatial and temporal variability in tidal currents. Reshaping associated with changing patterns of erosion and deposition can result in significant changes to the foreland shoreline, but more often than not, the foreland itself does not move relative to the neighbouring hinterland. However, Escoffier (1954) described travelling forelands as truncated cusate forelands that move along a shoreline in response to differences in rates of sediment removal and supply.

This paper describes the geomorphology and historical behaviour of the Benacre Ness foreland on the east coast of England. We present an extended history of development, in addition to analysis of shoreline change over the last 130 years and explore the evidence for bimodal wave-driven sediment transport along this shoreline in order to establish the likely mechanisms for foreland migration.

## PHYSICAL SETTING

Benacre Ness is located on the north Suffolk coastline, between Lowestoft and Southwold. This shoreline is bounded to the north by Lake Lothing and to the south by the Blyth estuary, but importantly the hinterland alternates between cliff and lowland valleys. The former are less than 15m high, formed of Pleistocene deposits (comprising clays, sand and gravel) and glacial tills, whilst the latter contain permanently flooded lagoons and extensive marshes, where drainage is blocked by the continuous sand-gravel barrier beach stretching from Lowestoft to Southwold (Figure 1). Sedimentology of the beach is spatially and temporally variable, particularly in terms of the relative dominance of sand and gravel (McCave, 1978). This is also true of the depositional foreland of Benacre Ness, formed of multiple beach ridges that are aligned northwest to southeast (Figure 1) and which comprise a mixture of sand and gravel. It is currently backed by a 10 to 15 m scarped cliff face that defines a previous (~100 year old) erosional shoreline.

The upper shoreface changes substantially from north to south along this section of shoreline. Water depths of 10 m and more are found within ~1 km of the coast between Benacre Broad and Southwold, but are 2.6 to 3.6 km offshore between Kessingland and Lowestoft (Figure 1) due to the presence of shallow offshore banks (Newcome Sands and Barnard Sands) to the north. These banks play an important role in beach dynamics and sediment transport, but there is also some suggestion that Benacre Ness maintains an important control on the position and behaviour of the Newcome-Barnard Sands bank system (Coughlan et al., 2007; Dolphin et al., 2007; 2009).

The tidal regime between Lowestoft and Southwold is high microtidal, with a spring tidal range of 1.9 m. Waves recorded offshore from Southwold have a median significant height ( $H_s$ ) of 0.71 m and a median period ( $T_z$ ) of 3.7 s (2010-2012). But this wave climate is strongly bimodal: waves from the northeast (0-90°N) account for 49% of the record whilst those from the south (135-225°N) account for 40%. The differences in the wave climate associated with these opposing directions are relatively small. The median  $H_s$  and  $T_z$  are 0.72 m and 4 s from the northeast and 0.76m and 3.5 m from the south; the 99th percentile  $H_s$  is 2.69 m from the northeast and 2.36 m from the south. Significant wave heights greater than 2 m account for 1.8% of the northeasterly climate and 0.9% of the southerly climate. In summary, waves from the northeast are more frequent and marginally larger than those from the south. Sea-level rise recorded at the Lowestoft tide gauge is 2.66 mm yr<sup>-1</sup> (1956 to 2012), although the trend over the most recent 30 years (1972 to 2012) is 3.95 mm yr<sup>-1</sup> (PSMSL, 2013).

## METHODS

The long-term historical context for shoreline behaviour in north Suffolk was evaluated from a range of pre-1800 maps sourced from the British Library, National Maritime Museum and additional online archives. These include 1575-79 Christopher Saxton and 1695-1722 Robert Morden maps of Suffolk (Figure 2). Ordnance Survey maps, at 1:2500 and ~ 1:10000 scales, published since the late 1880s, were georectified and analysed within a GIS. The mean high water shoreline was digitised from each. LiDAR data from 1999, 2008 and 2012 (Environment Agency) were analysed relative to the local tidal frame and the position of mean high water was derived from each. Aerial photography from 1945 (Google) and 2011 (Bing) were georeferenced and the position of mean high water was estimated and digitised. Digitised shorelines were collated and analysed for change using the DSAS (Digital Shoreline Analysis System (Thieler et al., 2009)) in ArcGIS 10.

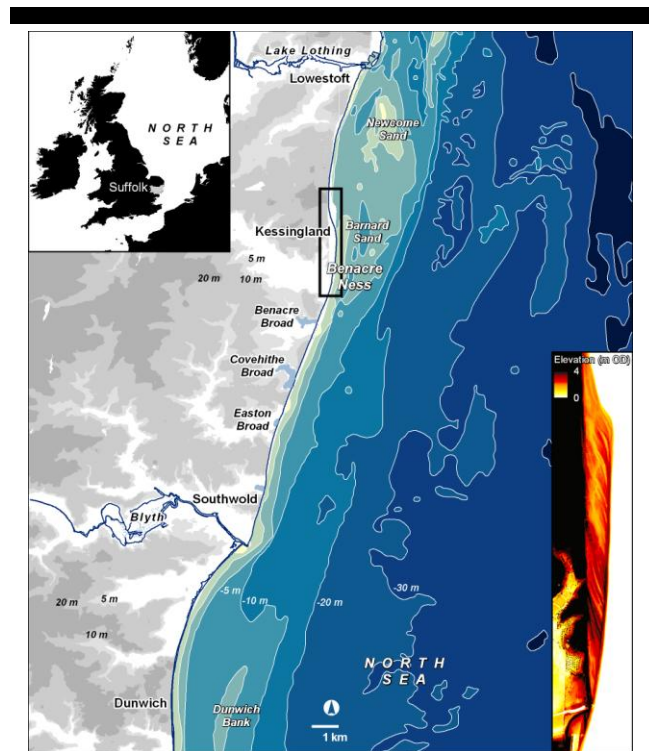


Figure 1. The north Suffolk coastline, from Lowestoft to Dunwich, showing the location and topography of Benacre Ness, a mixed sediment, travelling foreland.

Nearshore wave climate between Lowestoft and Southwold was evaluated using the SWAN model (Booij et al., 1999). Bathymetric data from 2003 were digitised from georeferenced charts and interpolated onto a 100 m grid. The model was run in GEN1 mode using median and extreme (99th percentile) scenarios from the northeasterly and southerly wave climates. Water level was set at mean high water. Wave parameters were derived from the Southwold wave records (Table 1). No attempt was made here to validate the wave model results given that the aim was to simply characterise and compare the nearshore wave climate to the north and south of the Benacre Ness foreland. Specifically, SWAN wave modelling was used here to evaluate the role of contrasting seabed morphology to the north (Newcome and Barnard Sands) and south (no offshore banks) on the nearshore wave climate around the foreland and to consider the relative importance of the two wave climate modes.

## RESULTS AND DISCUSSION

### Century-scale coastal evolution

The earliest map depicting the Suffolk coastline dates from the late 16th century (Saxton, 1575). Many maps were produced throughout the 17th and 18th centuries, although a large proportion of these were copies or were redrawn from earlier versions. Figure 2 presents a summary of these early maps. Lowestoft, Southwold and Dunwich are clearly depicted in most, which improve the potential to position other specific coastal features in the context of this geography. The 1575 map shows a large foreland just north of Southwold (Sowowilde), named Easton Ness. This is a well-documented eastward-extending promontory, where the settlement of Easton Bavent was once located.



Figure 2. Historical mapping of north Suffolk, showing 16th - 18th century evidence of a foreland at Easton, just north of Southwold: A) Saxton (1575), B) Van Keulen (1682), C) Morden (1703) and D) Bowen (1767).

Described as a city in some early publications (UKHO, 1869), it was an active parish with church and chapel in the Early Middle Ages (Cromwell, 1819), but is little more than a small hamlet now, testament to significant erosion here. Even by the early 1800s, it had been described as ‘of very little importance having suffered considerably from repeated encroachments of the sea’ (Bell, 1836).

The foreland of Easton Ness was considered for several centuries to be the easternmost point on the English coast (Camden, 1722; Cromwell, 1819; UKHO, 1869), and it is possible that its continued depiction as a key feature on maps of the region throughout the 17th and 18th centuries is a consequence of this notoriety. But the examples shown in Figure 2 do allude to a changing structure that might once have been formed of extensive beach deposits at the base of an eroding cliff (Figure 2B), that gradually receded (maps from 1703 (2C) and 1767 (2D) clearly show a reduction in easterly projection) and possibly started exhibiting a northward shift in position (Fig. 2D).

It is clear that by the very late 18th century, all that remained at the original location of Easton Ness were eroding cliffs and a handful of houses (Cromwell, 1819). Evidence for its northward migration during the late 1700s to early 1800s is relatively limited as independent maps at that time were increasingly derived from earlier versions, and the formal, country-wide mapping undertaken

by the Ordnance Survey (OS) was in its infancy. But by the early 1800s, a small foreland was evident at Covehithe Broad (~ 2.75 km north of Easton Bavents) and it was around this time that the name Covehithe Ness was first used. The earliest evidence of this feature is that of the Thomas 1824 chart (Lowestoft to Orford) and it is important to note that there is no reference to Covehithe Ness in any earlier maps or documents. In Wake’s (1839) description of Southwold and its vicinity, he notes of the walk back from Covehithe (before reaching Easton Bavent) ‘glistening and many coloured pebbles, which garnish the wide breadth of beach’. This could reflect a dispersed foreland, post-breakdown of Easton Ness.

The earliest OS map (1 inch to 1 mile, published in the 1830s) shows the foreland ~ 2.4 km north of Covehithe Broad, centred on Benacre Broad. The name Covehithe Ness was present on maps until the early 1900s: the first revision of the OS 1:2500 map (1904-7) bears this name, but by the second revision (1926-8), the foreland was labelled Benacre Ness. This name continues to present day, although the entire foreland had migrated north of Benacre Broad by the 1940s. The foreland is currently located over 3.5 km north of Benacre Broad, adjacent to Kessingland.

**Decadal shoreline change**

Shoreline change analysis (1880s to present) shows large-scale patterns of retreat and growth between Lowestoft and Southwold

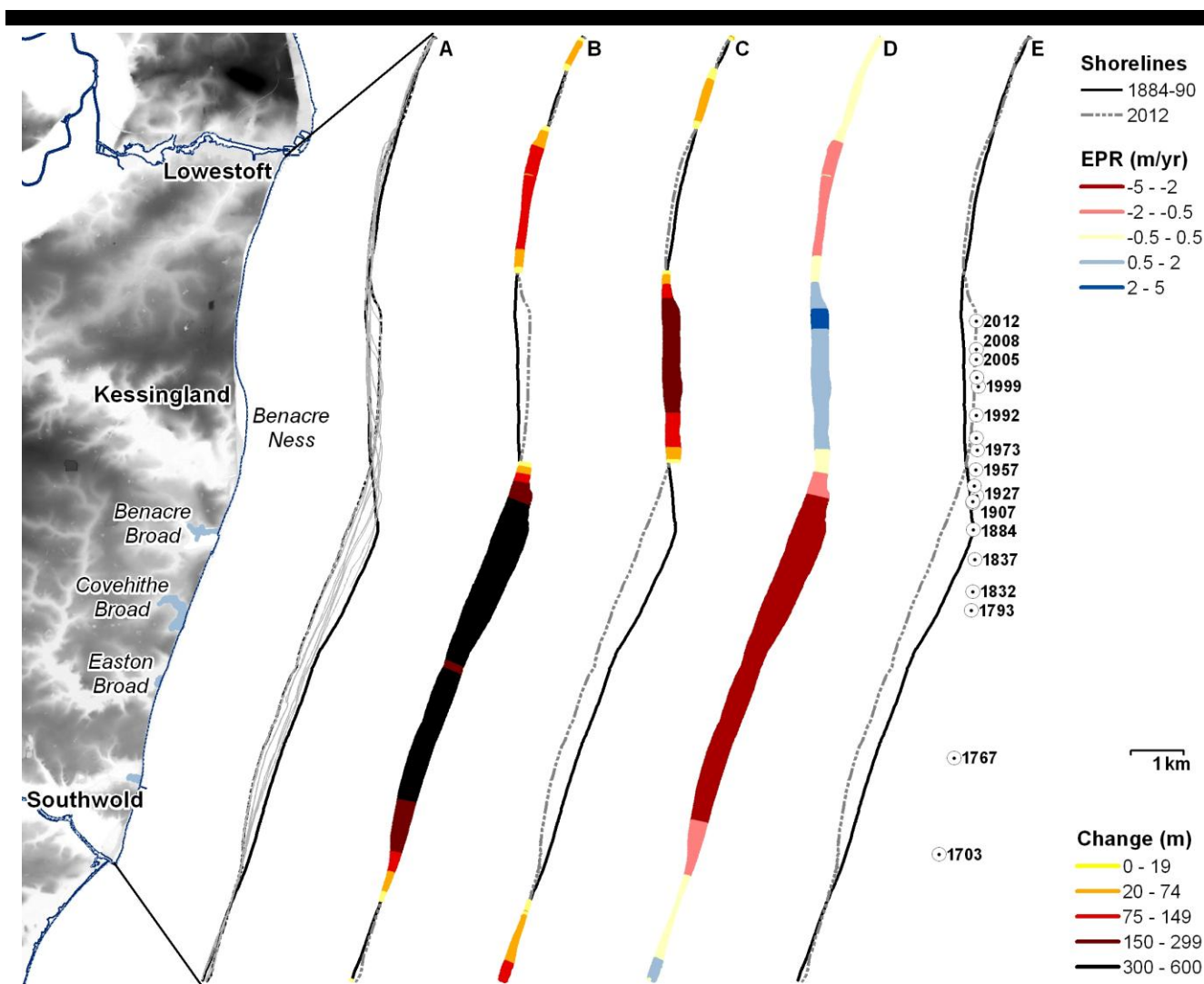


Figure 3. Shoreline change analysis of the Lowestoft to Southwold coastline, showing A) shoreline change envelope; net shoreline B) recession and C) advance; D) historical rate (end-point) of shoreline change and E) historical change in the position of Benacre foreland.

that are dominated by the alongshore movement of the foreland (Fig. 3). Most of this coastline (64%) has experienced recession over the last 130 years (Fig. 3B) and the average net shoreline movement across all DSAS transects is  $-130$  m. But this is not wholly a product of foreland migration: only around a third of this retreat can be explained by the shift in foreland position. Northward migration of the foreland has exposed cliffs to the north of Southwold, leading to retreat of the cliff-line by 250-350 m south of Easton Broad increasing to 500-800 m north of Covehithe Broad. The barriers fronting the coastal lagoons ('broads') have rolled-back a similar amount, significantly reducing the extent of these important habitats (Spencer and Brooks, 2013). The Lowestoft frontage is relatively stable by comparison, though this is largely due to the presence of sea defences. Just to the south of Lowestoft, cliffs are undefended and here some coastal recession (around 100 m) has occurred. Seaward advances in shoreline position (Fig. 3C) are dominated by the growth of the foreland seaward of Kessingland, where repeated construction of beach ridges has prograded the shoreline by 200-400 m. Foreland development here has protected what was previously a retreating cliff-line.

In terms of shoreline trends, this part of Suffolk could be described as a rapidly changing coastline where rates of erosion and deposition around the foreland are  $>2$   $\text{m yr}^{-1}$ . The Benacre Broad shoreline exhibits the maximum rates of change ( $4\text{--}5$   $\text{m yr}^{-1}$ ) due to the combined impact of a northward migration in foreland followed by continued cliff erosion and barrier rollover.

Although accurate mapping is not available prior to the late 1800s, positions of the foreland extracted from earlier maps (based on local geography) suggest the foreland migrated northward at around  $40$   $\text{m yr}^{-1}$  until the mid-1800s (Fig. 4). From the mid-1800s until the 1980s, the northward movement reduced to around  $15$   $\text{m yr}^{-1}$  but has since rapidly increased to an average northward movement of  $75$   $\text{m yr}^{-1}$  since the 1980s. Comparison of LiDAR surveys from 1999 to 2012 shows that the apex of the foreland has migrated northward by 1230 m, equivalent to a rate of  $95$   $\text{m yr}^{-1}$ . The period of significant change in the rate of northward migration is the 1980s to early 1990s, when the apex of the foreland was adjacent to the southern extent of the Kessingland cliff, and the entire foreland was north of the Benacre hinterland (Fig. 3E). This position on the coastline marks a significant shift in shoreline orientation from northeast-southwest (south of

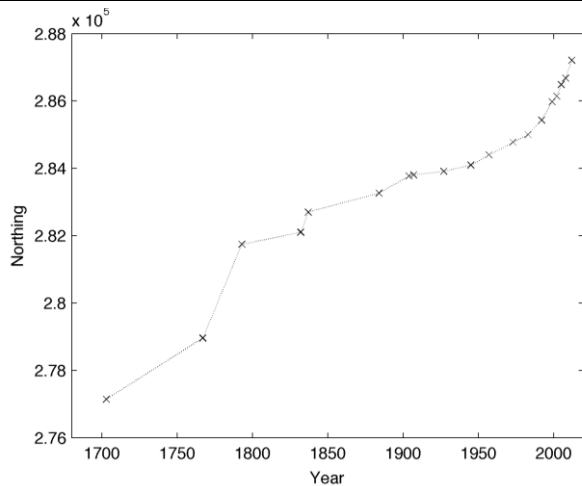


Figure 4. Changes in the alongshore position of Benacre foreland (apex). Positions prior to 1880 are locations estimated from very old maps.

Benacre) to north-south (north of Benacre). Foreland dynamics are therefore responding directly to the configuration of the hinterland shoreline along which the accumulation is positioned

Morphologically, the foreland has changed shape significantly over the last 130 years. Historical records of topography do not exist, but it is possible to establish that the foreland was ~343 m wide at its broadest (at the apex, where the maxima in shoreline protrusion occurs) in the 1880s and extended alongshore around 2.25 km. The 2012 foreland is 275 m wide at its apex, but ~3.4 km long. Despite these changes in shape, the total area covered by the foreland has changed marginally from 589397 m<sup>2</sup> in the 1880s to 593076 m<sup>2</sup> presently: this is an increase of 3679 m<sup>2</sup> or 0.6% of the 1880s area, so well within the error margin of historical mapping and analysis. It is not possible to establish whether the beach ridge structures have substantially changed in elevation but beach ridges elsewhere in Suffolk do not achieve heights of greater than 5 m above mean sea level (Burningham, 2014; Pontee et al., 2004), and recent LiDAR data from Benacre Ness is consistent with this. It is thus entirely possible that minimal change has occurred in the total volume of material contained within the foreland.

### Contemporary wave climate and sediment flux

Results from the analysis of historical shoreline changes imply that the orientation of the neighbouring shoreline exerts an important control on foreland dynamics and, specifically, that a north-south orientation presents less resistance to northward migration than a northeast-southwest orientation. This likely reflects the relative ability of waves from different directions to transport sediment north or south along this shoreline. Sediment transport directions and fluxes along the Suffolk coast have received some attention over the last few decades but are still poorly understood, primarily owing to the bimodal wave climate and the mixed (sand and gravel) sedimentology. Geomorphologically, the net direction of sediment transport is to the south, based on the southerly-oriented accumulations at the estuary mouths (Steers, 1964; McCave, 1978). Beach sediments from this shoreline have in the past exhibited coarsening to both the north and south of Covehithe cliffs, implying sediment transport to the north and south of Covehithe, which would explain the northward migration of Benacre Ness (McCave, 1978).

Dolphin et al. (2011) found that Pakefield beach, between Kessingland and Lowestoft, experiences annual rotation cycles where winter periods are dominated by northward sediment transport (clockwise shoreline rotation) whereas summer months see a shift to southward transport and anti-clockwise rotation. There is evidence for longer-term or larger-scale controls on this change in transport direction as the rotation cycles vary from year to year, most likely associated with changes in wave climate and complexities arising from interactions with the offshore banks Newcome Sands and Barnard Sands. Sand wave asymmetry and migration across these banks implies a net southward transport (UKHO, 2008; UKHO, 2010), which may lead to a supply of sand to the Kessingland - Lowestoft shoreline, but gravel is not present in these systems so there is unlikely to be a sediment supply connection associated with this coarser grade of material important to the development of the Benacre Ness foreland.

Previous analyses of bathymetric change and modelling of sediment transport have suggested that sand is predominately transported southward along this shoreline (Onyett and Simmonds, 1983; Halcrow, 2001), with local northward transport along the Kessingland shoreline. Sand is also readily lost from the shoreline to the offshore banks and Barnard Sand has shown significant growth in the short-term, but an extensive review concluded that Kessingland could be classed as a ‘drift null point’ (HR Wallingford, 2002). Application of the SWAN wave model to the Lowestoft-Southwold shoreline highlights the role of the Newcome/Barnard Sands in refraction and attenuation of nearshore waves north of Kessingland (Fig. 5). Waves from the northeast, which correspond to 49% of records, are reduced in height by 36% (median) and 64% (99th percentile) north of Kessingland, but only by 26% (median) and 44% (99th percentile) south of Kessingland. Waves from the south (40% of the record) are significantly attenuated north of Kessingland (49% and 66% respectively), but the lack of interaction with the offshore banks

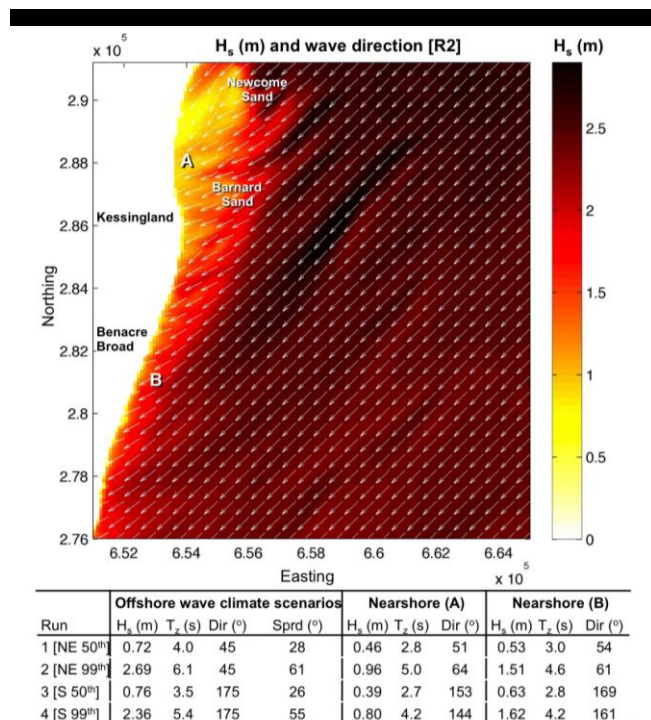


Figure 5. Example SWAN output (run 2), and summary nearshore results from selected offshore wave climate scenarios.

south of Kessingland sees only a reduction of 17% (median) and 31% (99th percentile). In summary, the Newcome and Barnard Sands influence all nearshore waves between Lowestoft and Kessingland, but only significantly impact northeasterly waves along the Benacre-Southwold nearshore. Southerly waves produce slightly larger waves at Benacre than northeasterly waves but northeasterly waves result in larger waves north of Kessingland. Overall, these wave analyses do not offer a simple answer to the question of sediment transport directions, but the dominance of a northeasterly wave climate over the southerly wave climate implies a likelihood of a net southward transport direction.

## CONCLUSION

The Benacre Ness foreland has experienced three stages of movement over the last 400 years. From the 16th century through to the mid-1800s, a previous foreland and possibly headland feature (Easton Ness) at Easton Bavent broke down and receded, leading to a northward reshaping and migration of a gravel-based shoreline accumulation. By the early 1800s, this structure was referred to as Covehithe Ness and its northward migration was well established. Northward movement was possibly discontinuous, although map evidence is limited. The second stage, from the mid-1800s through to the 1980s, saw the foreland migrate northward progressively at a rate of around 15 m yr<sup>-1</sup>, moving from a position adjacent to Covehithe to between Benacre and Kessingland. The 1980s marked the start of the third stage, notable for a significant acceleration in migration rate to an average of 75 m yr<sup>-1</sup>, but reaching 95 m yr<sup>-1</sup> in the last decade. This stage of development marks the shift in foreland position from a northeast-southwest to north-south oriented shoreline. The increased rate of movement might be facilitated by increased obliquity of southerly waves, but may also reflect more complex interactions with the Barnard and Newcome offshore banks, particularly in terms of sand sourcing/supply.

SWAN wave modelling supports conclusions from other studies and shows that the bidirectional wave climate is variously modified by the presence of significant offshore banks to the north of Kessingland and by the lack of similar features to the south. The slight temporal dominance of the northeasterly wave climate and the limited difference in energy regime (based on wave height and period) between the two modes, still implies a net transport to the south. However, it is more likely that sediment transport by oblique waves from the south is more effective in facilitating northward littoral drift in comparison to the closer to shore-normal nearshore waves produced by the northeasterly climate.

Foreland dynamics are a product of a bidirectional wave climate and a simple segmented linear coastline. The shift from northeast-southwest orientation to north-south is instrumental in the changing migratory behaviour of the foreland.

## ACKNOWLEDGEMENT

The authors are grateful to the Environment Agency for the provision of LiDAR data through the NERC iCOASST project.

## LITERATURE CITED

Bell, J., 1836. *A New and Comprehensive Gazetteer of England and Wales: Vol I*. Fullarton and Co: Glasgow, 472p.  
 Booij, N., Ris, R.C. and Holthuisen, L.H., 1999. A third generation wave model for coastal regions; Part I: model description and validation. *Journal of Geophysical Research*, 104, 7649–7666.  
 Burningham, H., 2014. Gravel spit-inlet dynamics: Orford Spit, UK. *In review*.

Camden, W., 1722. *Britannia or a chorographical description of Great Britain and Ireland, together with the adjacent islands: Vol I*. London, England: Gibson, 1248p.  
 Coughlan, C., Vincent, C.E., Dolphin, T.J., and Rees, J., 2007. Effects of tidal stage on the wave climate inshore of a sandbank. *Journal of Coastal Research*, SI 50, 751 – 756.  
 Cromwell, T.K., 1819. *Excursions in the county of Suffolk: Vol II*. London, England: Longman, 198p.  
 Dolphin, T.J., Vincent, C.E., Coughlan, C. and Rees, J.M., 2007. Variability in Sandbank Behaviour at Decadal and Annual Time-Scales and Implications for Adjacent Beaches. *Journal of Coastal Research*, SI50, 731 – 737.  
 Dolphin, T.J., Vincent, C.E., Wihsgott, J., Belhache, M. and Bryan, K.R., 2011. Seasonal rotation of a mixed sand-gravel beach. *Journal of Coastal Research*, SI 64, 65-69.  
 Goadby, R., 1776. *A New Display of the Beauties of England: or A description of the most elegant or magnificent public edifices, royal palaces, noblemen's and gentlemen's seats and other Curiosities, natural or artificial, in different Parts of the Kingdom*. London, 633p.  
 Gulliver, F.P., 1897. Dungeness Foreland. *The Geographical Journal*, 9 (5), 536-546.  
 Gulliver, F.P., 1899. Shoreline Topography. *Proceedings of the American Academy of Arts and Sciences*, 34 (8), 151-258.  
 Halcrow, 2001. *Lowestoft to Thorpe Ness Coastal Process and Strategy Study Volume 2: Coastal Processes*.  
 HR Wallingford, 2002. *Southern North Sea Sediment Transport Study, Phase 2*. Report EX4526, 146p.  
 Johnson, D.W., 1919. *Shore Processes and Shoreline Development*. New York, USA: Wiley, 604p.  
 Kirby, J., 1839. *A topographical and historical description of the county of Suffolk*. London, England: Munro, 522p.  
 Long, A.J. and Hughes, P.D.M., 1995. Mid- and late-Holocene evolution of the Dungeness foreland, UK. *Marine Geology*, 124 (1-4), 253-271.  
 McCave, I.N., 1978. Grain-size trends and transport along beaches: Example from Eastern England. *Marine Geology*, 28, M43-M51.  
 McNinch, J.E. and Luettich Jr, R.A., 2000. Physical processes around a cusped foreland: implications to the evolution and long-term maintenance of a cape-associated shoal. *Continental Shelf Research*, 20 (17), 2367-2389.  
 Moslow, T.F. and Heron, S.D., Jr., 1981. Holocene depositional history of a microtidal cusped foreland cape: Cape Lookout, North Carolina. *Marine Geology*, 41, 251-270.  
 Onyett, D. and Simmons, A., 1983. *East Anglian Coastal Research Project Final Report*. Norwich, England: Geobooks, 125p.  
 Pontee, N.I., Pye, K. and Blott, S.J., 2004. Morphodynamic behaviour and sedimentary variation of mixed sand and gravel beaches, Suffolk, U.K.. *Journal of Coastal Research*, 20 (1), 256–276.  
 PSM SL, 2013. Permanent Service for Mean Sea Level: Lowestoft tide gauge. <http://www.psm sl.org/data/obtaining/stations/754.php>: Nov 2013  
 Semeniuk, V., Searle, D.J. and Woods, P.J., 1988. The sedimentology and stratigraphy of a cusped foreland, southwestern Australia. *Journal of Coastal Research*, 4 (4), 551-564.  
 Spencer, T. and Brooks, S.M., 2012. Methodologies for measuring and modelling change in coastal saline lagoons under historic and accelerated sea-level rise, Suffolk coast, eastern England. *Hydrobiologia*, 693, 99-115.  
 Steers, J.A., 1964. *The Coastline of England and Wales: 2<sup>nd</sup> edition*. Cambridge, England: Cambridge University Press, 750p.  
 Thieler, E.R., Himmelstoss, E.A., Zichichi, J.L. and Ergul, A., 2009. *Digital Shoreline Analysis System (DSAS) version 4.0—An ArcGIS Extension for Calculating Shoreline Change*. U.S. Geological Survey, Open-File Report 2008-1278.  
 UKHO, 1869. *North Sea Pilot: Part III East Coast of England*. Admiralty, 270p.  
 UKHO, 2008. *East Anglia - Approaches to Lowestoft: Assessment on the analysis of routine resurvey area EA10 from the 2008 survey*, 23p.  
 UKHO, 2010. *East Anglia - Approaches to Lowestoft: Summary assessment on the analysis of routine resurvey area EA10 from the 2009 survey*. UKHO, 28p.  
 UKHO, 2012. *East Anglia - Approaches to Lowestoft: Summary assessment on the analysis of routine resurvey area EA10 from the 2011 survey*. UKHO, 5p.

UKHO, 2013. *East Anglia - Approaches to Lowestoft: Assessment on the analysis of routine resurvey area EA10 from the 2012 survey*, 2p.

Wake, R., 1839. *Southwold and its vicinity, ancient and modern*. Skill: Yarmouth, 420p.

# Control of wave climate and meander dynamics on spit breaching and inlet migration

Chaumillon Eric†, Ozenne Florian, Bertin Xavier, Long Nathalie, Ganthly Florian

University of La Rochelle  
UMR CNRS 7266 LIENSs  
2 Rue Olympe de Gouges  
17000 La Rochelle, France  
†eric.chaumillon@univ-lr.fr



[www.cerf-jcr.org](http://www.cerf-jcr.org)



[www.JCRonline.org](http://www.JCRonline.org)

## ABSTRACT

Chaumillon E., Ozenne F., Bertin X., Long N., Ganthly F., 2014. Wave climate and inlet channel meander bend control spit breaching and migration of a new inlet: La Coubre Sandspit, France. In: Green, A.N. and Cooper, J.A.G. (eds.), *Proceedings 13<sup>th</sup> International Coastal Symposium* (Durban, South Africa), *Journal of Coastal Research*, Special Issue No. 70, pp. 109-114, ISSN 0749-0208.

This study focuses on the mid-term (infra annual and pluri annual; over the period 1999-2013) morphological evolutions of a sandspit (La Coubre Sandspit, West coast of France), with a particular emphasis on spit breaching, new inlet opening and migration. Morphological evolutions are observed from a large number of aerial photographs and satellite images and are compared with wave parameters and extreme events (periods where significant wave height exceeds the 1% largest waves with water level exceeding the 90% highest water level) obtained from a high resolution hindcast wave modelling. It appears that extreme events are likely to be responsible for spit breaching and new inlet opening. Once opened, the new inlet migrates downdrift, but its migration rate is not correlated with the wave climate variations. Detailed geomorphological observations suggest that the main control on downdrift inlet migration is related to orientation of the meander bend of the tidal inlet main channel. When the meander bend is convex in an updrift direction, it counteracts the littoral drift and slows the inlet migration. Oppositely, when the meander bend is convex in a downdrift direction, the meander-induced transport is in the same direction as wave-induced longshore transport, which allows the inlet to migrate much faster.

**ADDITIONAL INDEX WORDS:** *Spit breaching, tidal inlet opening and migration, extreme storms, longshore drift, meander bend dynamic, autocyclic control versus climate control, satellite images, wave model.*

## INTRODUCTION

In the context of a growing population along the coast line and a changing climate, the capacity to provide reliable morphological and water quality predictions of coastal zones has become a priority. This capacity requires a great deal of improvement in the level of understanding of coastal system dynamics. Among them, tidal inlets are some of the most dynamic features around coastlines worldwide (Fitzgerald, 1996) and are of critical and growing socio-economical and environmental importance, due to their intense use for aquaculture and tourism. Tidal inlets are often exceptionally dynamic, due to the combination of strong tidal currents, shallow channels and an energetic wave climate. Among those morphological changes, breaching and new inlet development and migration can strongly impact the morphology of barrier islands and adjacent shorelines (Fitzgerald, 1996) as well as water circulation in backbarrier lagoons (Dias *et al.*, 2009). To study inlet opening and migration and adjacent coastline dynamics, we chose, as a field laboratory, La Coubre Sandspit, located on the northern margin of the Gironde Estuary Mouth (Figure 1), because this stretch of coastline was shown to be one of the most rapidly evolving coastlines in France (Bertin and Chaumillon, 2005). Tidal amplitude at the mouth of the Gironde Estuary ranges from 1.5 to 5 m. Offshore wave climate is

energetic with 15–27% of the annual wave climate being characterized by  $H_s = 2.5\text{--}9.4$  m,  $T_p = 11\text{--}15$  s; occurring mostly during winter months (November–March; Bertin *et al.*, 2008). La Coubre Sandspit was a 5.5 km long and about 250 m wide sandspit in 2012 (Figure 1). It is a hooked sandspit that bounds the Bonne Anse Bay (5.7 km<sup>2</sup>). La Coubre Sandspit and Bonne Anse Bay were absent in the 19<sup>th</sup> century, which illustrates the huge sediment dynamic and associated coastline evolutions in this area. The historical morphological evolutions of the La Coubre Sandspit have already been described in earlier studies (Jouanneau, 1974; Carbonel and Jouanneau, 1982). Since 1977, the termination of La Coubre Sandspit has almost reached the downdrift coast, located eastward and upstream in the estuary mouth and separated from it by a single tidal inlet. The aim of this study is to focus on the mid-term (infra annual and pluri annual) morphological evolutions at the end termination of the sandspit, with a particular emphasis on spit breaching, new inlet opening and migration during the last decades. The first objective of this study is to quantify the observed morphological evolutions, based on the most complete dataset available on this area and to analyze the interactions between the different morphological compartments at the end termination of the spit. Given that sandspit morphological evolutions are mostly driven by wave-related processes (Evans, 1942; King, 1970; Schwartz, 1982), themselves depending on the wave climate variations (Allard *et al.*, 2008), the second objective is to compare the observed morphological changes with the modeled local wave climate.

DOI: 10.2112/SI70-019.1 received 30 November 2013; accepted 21 February 2014. © Coastal Education & Research Foundation 2014



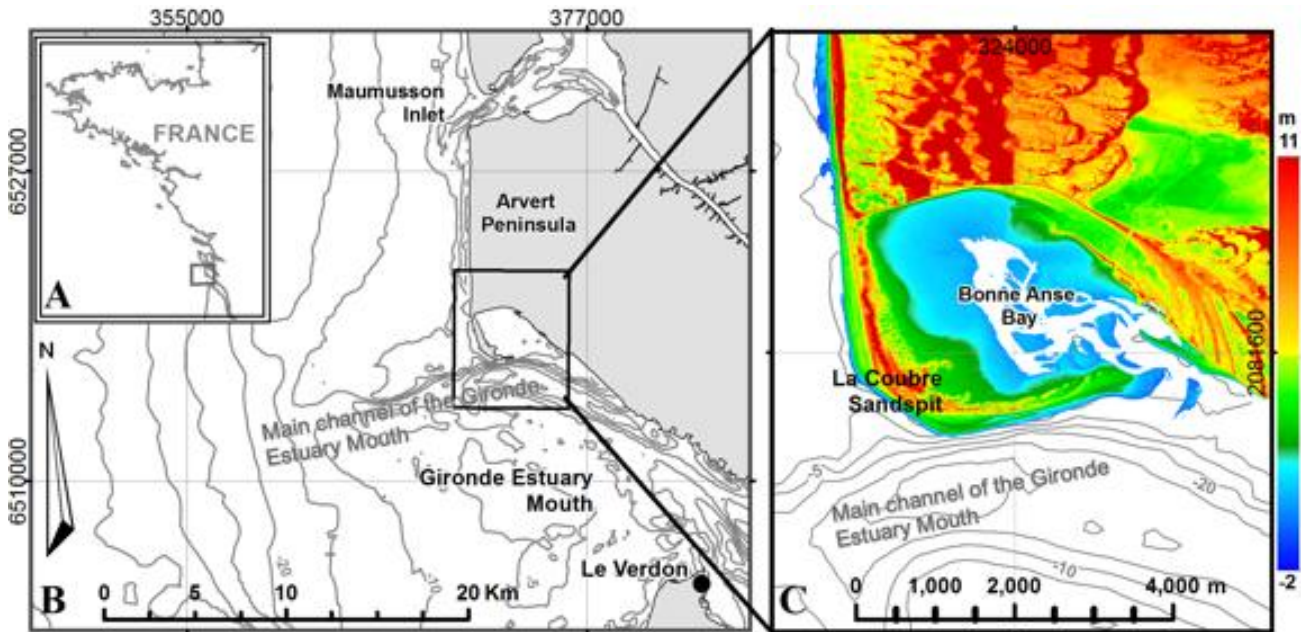


Figure 1. Locality map of the study area (Lambert 93 horizontal projected coordinate system in meters). (A) Map of France showing the location of the study area. (B) Simplified bathymetric map of the Gironde Estuary Mouth with bathymetric intervals of 5 m. (C) LiDAR derived Digital Terrain Model and bathymetric map (bathymetric intervals of 5 m) of the study area. Elevation is shown in meters NGF.

From this study, we propose working hypothesis that will be further verified through numerical experiments.

**METHODS**

**Satellite images and aerial photographs**

Morphological evolutions of La Coubre Sandspit over the period 1999–2013 are demonstrated from a set of satellite images (SPOT and Landsat) and aerial photographs. Aerial photographs were taken from a microlight at a low altitude with a frequency of 2 photos per year at low spring tide over the period 2002–2013.

These photos are very accurate with a resolution of less than 1 m, but as they cannot be georeferenced they are used only for qualitative observations and to help interpretations of satellite images. For quantitative observations, SPOT images obtained at low tide were mainly used. Available satellite SPOT images, recorded by the French National Centre of Space Studies (CNES) during low tide, include the following: 20 satellite SPOT images over the period 1987–2012 with a 20 m.pixel<sup>-1</sup> spatial resolution; 22 satellite SPOT images over the period 1988–2010 with a 10 m.pixel<sup>-1</sup>; and 5 satellite SPOT images over the period 2002–2011 with a 2.5 m.pixel<sup>-1</sup> spatial resolution. To complete this dataset, 110 Landsat images with a 30 m.pixel<sup>-1</sup> spatial resolution over the

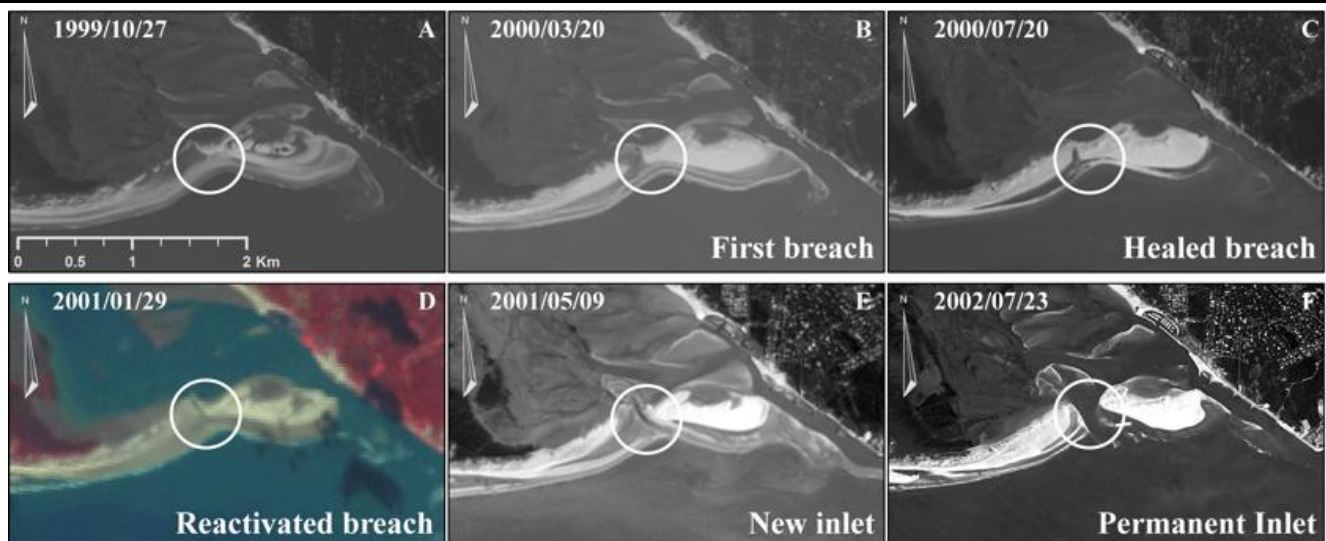


Figure 2. Breaching and new inlet opening in the La Coubre Sandspit from 1999 to 2002 evidenced by Landsat and SPOT satellite images.

period 1984–2013 and 5 vertical aerial photographs taken in 1999, 2000, 2003, 2006 and 2010 were used. Spatial resolution of vertical photographs ranges from 0.5 to 1 m.pixels<sup>-1</sup>. Vertical aerial photographs and satellite images have been georeferenced and processed using Arcview10.1 GIS. The georeferenced images and vertical photos have been used to quantify the migration rate of the new inlet, by calculating the distance between the axis of the main channel within the new inlet and a fixed point of the updrift coast (Figure 3).

### Modeled local wave climate

The wave climate in the Bay of Biscay was hindcast for the period 1998–2013 by means of a regional application of the Wave Watch III model (hereafter WWIII; Tolman, 2009) for the North Atlantic Ocean. The model was forced by wind fields originating from the ERA-INTERIM reanalysis (Dee *et al.*, 2011) and more details on this hindcast can be found in Dodet *et al.* (2010), with further improvements in Bertin *et al.* (2013). To investigate the local wave climate at the entrance of Bonne-Anse Bay, the spectral wave model SWAN (Boijj *et al.*, 1999) was employed. A Shell script was developed to perform a series of stationary runs, accounting for water-level variations and local wave generation. A first grid was implemented over the whole continental shelf with a 1000 m resolution and the model was forced along its open boundaries with time-series of spectra originating from WWIII. A second grid was nested over the Gironde Estuary mouth (Figure 1) with a 200 m resolution. A 1h-time step was selected to account properly for water level variations, which strongly affect wave propagation in the region. Water levels used to force the model correspond to observations at the nearby tide gauge of Le Verdon (Figure 1) and the gaps in the record were filled in using harmonic synthesis. Finally, model results were archived at a point located in front of the bay entrance with a water depth sufficient to avoid wave breaking. Extreme events likely to produce overwash were arbitrarily defined as periods where significant wave height ( $H_s$ ) exceeds the 1% largest waves over the period (hereafter  $H_{s99}$ ) with water level exceeding the 90% highest water levels ( $WL_{90}$ ).

## RESULTS

In 1977, La Coubre Sandspit stopped its lengthening and its termination was separated from the downdrift human-fixed coast by one single inlet. Since 1977, new inlets have opened twice, in 1978 and 2001, respectively. Those new inlets opened a few hundred meters updrift with respect to the preexisting inlet (Figure 2). We focus on the spit breaching and the new inlet opening and migration over the period 1999–2013 because, during this period of time, the morphological evolutions are well constrained by many available satellite images and aerial photographs every years.

### Breaching and new inlet opening

The breaching of La Coubre Sandspit and the opening of a new inlet in an updrift location over the period 1999–2013 followed 4 steps (Fig. 2). A first breach occurred between October 1999 and March 2000 and was filled by sand during the summer 2000. The reactivation of the first breach occurred during the winter 2000–2001 as shown by the Landsat image taken in March 2001. Following this reactivated breach, a narrow new inlet developed in May 2001 and widened to become a permanent inlet in July 2002.

### New Inlet Migration

Following the opening of the new inlet, the Bonne Anse Bay communicated with the Atlantic Ocean via two inlets from July 2002 to May 2005 (Figure 3). Between February and November 2004 the preexisting inlet, located along the downdrift coast was progressively filled by sediments, in response to both natural processes and artificial channel-fill, and the new inlet became the unique communication between the bay and the ocean. From 2001 to 2012, the new inlet migrated downdrift with an average migration rate of 120 m.yr<sup>-1</sup>. Beyond this average rate, important variations in the downdrift migration rate occurred and allow for the defining of four periods (Figure 3): from 2001 to 2004, the migration rate was 42 m.yr<sup>-1</sup>; from 2004 to 2007, the migration rate was 14 m.yr<sup>-1</sup>; from 2007 to 2010, the migration rate was 193 m.yr<sup>-1</sup>; and from 2010 to 2012, the migration rate was 115 m.yr<sup>-1</sup>.

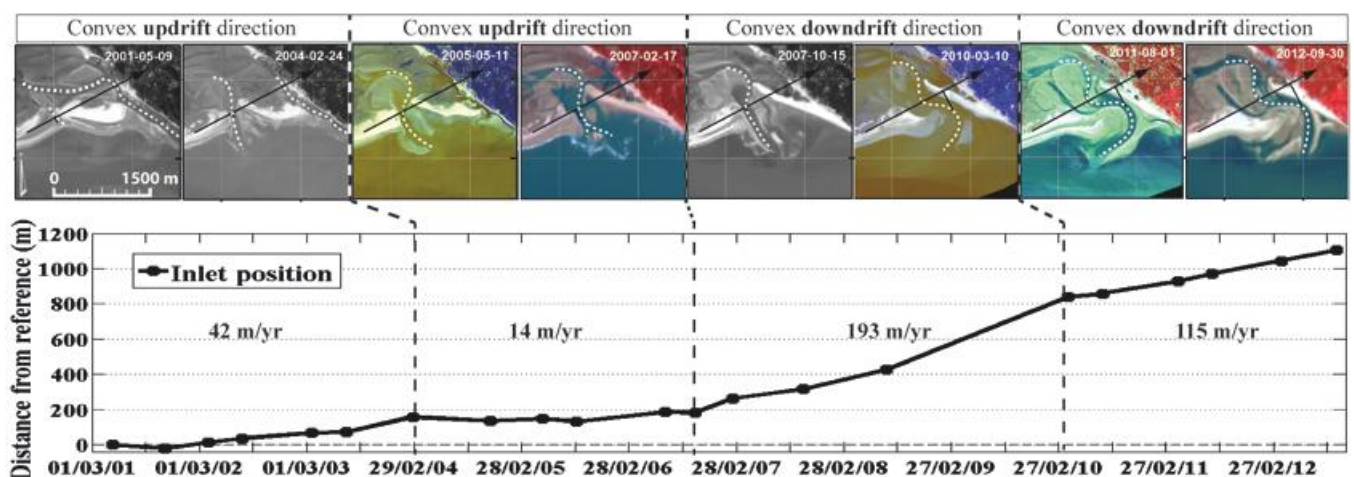


Figure 3. New inlet migration at La Coubre Sandpit from 2001 to 2012 deduced from SPOT satellite images. Upper panel: Selected SPOT images showing typical morphologies of the inlets for the four periods defined on the basis of the new inlet migration rate (the new inlet is located updrift with respect to the preexisting inlet in 2001, 2004 and 2005). “Convex” refers to the meander bend orientation of the main channel within the new inlet. White dotted lines show the axis of the main channel within the inlets and black arrows represent the vector of growth characterizing the main direction of the spit elongation and along which the new inlet migration rate was calculated. Lower panel: Distance between the new inlet channel axis and the reference point located updrift and migration rates of the new inlet from 2001 to 2012.

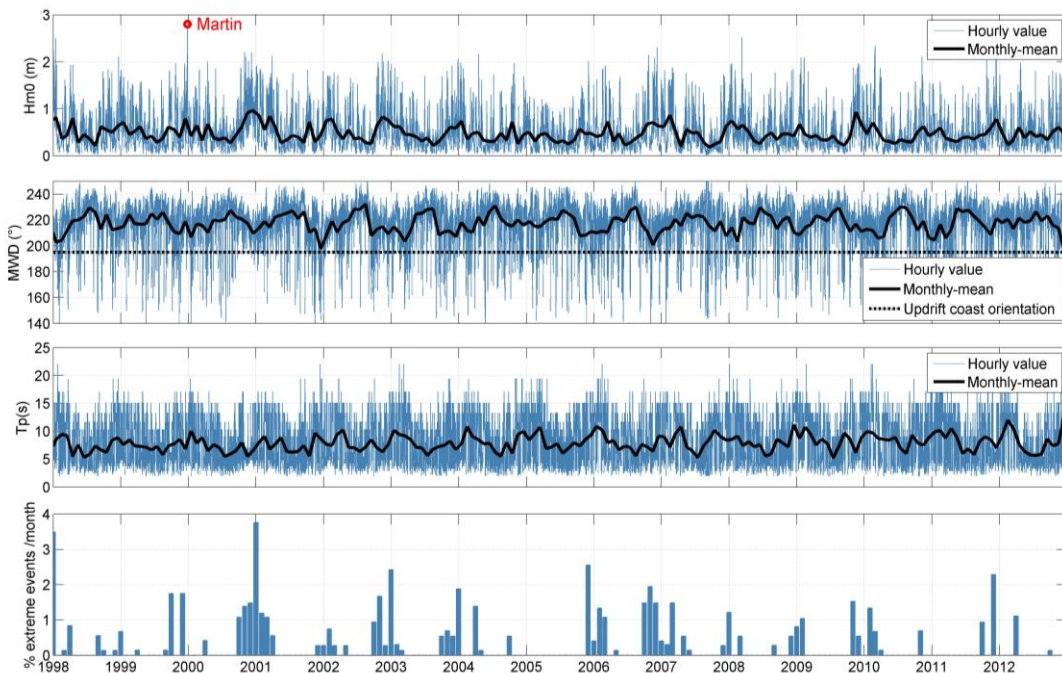


Figure 4. Three upper panels: Time series of modelled wave parameters between 1998 and 2013 at a point located in front of the Bonne Anse Bay entrance. From top to bottom: (a) significant wave height (m), (b) wave angle ( $^{\circ}$ N), (c) and peak period (s). Lower panel: time series of percentage of extreme events per month (periods where significant wave height exceeds the 1% largest waves with water level exceeding the 90% highest water level).

## Wave Climate

The nearshore wave climate was computed from 1998 to 2013 and shows both a seasonal and an interannual variability (Fig. 4). Overall, winter periods (November-March) are characterized by larger waves, longer wave periods and wave directions more frequently coming from the southwest. More interesting to our study is the inter-annual variability which is clearly evidenced by the percentage of extreme events ( $H_{s99}$ -TR70; Fig. 4). Winter 2000-2001 was a highly energetic winter, compared with other winters during the 1998-2013 period, as during this year extreme events occur more than 10% of the time. 2001 was also characterized by a succession of extreme events that took place during 7 consecutive months (Fig. 4).

## DISCUSSION

### Wave climate control on spit breaching and new inlet migration

Of particular note, during winter 1999 was the superstorm “Martin” that took place on December 27<sup>th</sup> (Figure 4) with extreme gusts over  $40 \text{ m}\cdot\text{s}^{-1}$  (Ulbrich *et al.*, 2001; Salomon, 2002), which caused a 1.3 to 2.2 m-high storm surge in the Gironde Estuary (Salomon, 2002), marine flooding and severe coastal erosion. Model results suggest that  $H_s$  exceed 12 m offshore and 2.8 m at the entrance of the lagoon. The sandspit topography revealed by the LiDAR (Figure 1) together with the waves and surge associated with this superstorm would suggest that a large part of the sandpit was flooded during this event. It is also likely that this storm was responsible for the breaching as observed on the SPOT image taken on March 20<sup>th</sup> 2000 (Figure 2). Overwash events are usually associated with storms (Sallenger, 2000; Matias

*et al.*, 2008). The fair weather during summer 2000 allowed this first breach to be filled by sand (Figure 2). The exceptional percentage of extreme events together with the high frequency of successive energetic events that occurred during winter 2000-2001 is probably responsible for the reactivation of this partly healed breach (Figure 2). Reactivation of partly healed breaches has previously been documented (Wright *et al.*, 1979; Morton, 2002) and this mechanism shows that beyond the key role of extreme storms, the high frequency of successive energetic events is critical for barrier breaching. Hits by successive storms occurring at spring high tide have created breaches that have not had the time to heal, with breach widening and new inlet opening as a result. The reactivated breach observed in January 2001 was widened and evolved rapidly to a new permanent inlet in May 2001 (Figure 2). Similar breach widening and inlet opening from an initially small breach was documented in similar settings (Houser *et al.*, 2008; Pries *et al.*, 2008; Buynevich and Donnelly, 2006; Gervais *et al.*, 2012). Following its opening, the new inlet migrated downdrift with important migration rate variations (Figure 3). Downdrift migration of tidal inlets is partly the result of the littoral drift itself related to wave parameters and beach slope and grain size (e.g., Kamphuis, 1991). It is noteworthy that the 4 periods defined from variations of downdrift migration rates are not correlated with the wave climate variations. Slow migration rates ( $<50 \text{ m}\cdot\text{yr}^{-1}$ ) occurred during both low-energy and highly energetic winters (2005 and 2001, respectively; Figs. 3 and 4) and the highest migration rate was observed during the 2007-2010 period, which was characterized neither by higher waves nor by longer period waves nor by more oblique waves relative to the coast (Fig. 4). This lack of correlation between the downdrift migration of the new inlet and the wave climate variations suggests that autocyclic processes produced within the La Coubre sedimentary systems could take place.



Figure 5. Oblique aerial photographs (obtained from a microlight) showing the two main orientations of the tidal inlet meander bend. Upper photo (Courtesy of Les Mattes Municipality): In 2005, the meander bend was convex in an updrift direction and counteracted the littoral drift leading to a slow downdrift migration of the tidal inlet. Lower photo (Courtesy of Les Mattes Municipality): In 2010, the meander bend was convex in a downdrift direction and the meander-induced transport was in the same direction as the longshore transport leading to a fast downdrift migration of the tidal inlet.

### Tidal channel morphology control on spit breaching and new inlet migration

An autocyclic geomorphological control of tidal channel morphology on inlet migration rates is suggested from La Coubre Sandspit example. From 2002 to 2007 (period of slow to moderate migration rate of the new inlet), the meander bend of the tidal inlet main channel was convex in an updrift direction, with the cutbank located updrift and the point bar located downdrift (Figs. 3 and 5). This channel curvature induced erosion of the updrift coast and progradation of the downdrift coast, which counteracted the shoreward littoral drift and resulted in a stable setting with slow migration rate. Conversely, from 2008 to 2012 (period of rapid migration rate of the new inlet), the meander bend of the tidal inlet main channel was convex in a downdrift direction with the cutbank located downdrift and the point bar located updrift. In this

setting, meander-induced transport was in the same direction as wave-induced longshore transport, which allowed the inlet to migrate much faster. A similar mechanism was already described by Abrey and Speer (1984), who even reported updrift inlet migration. It is likely that the change in meander convexity of the main channel within the new inlet (from 2007 to 2008) was driven by the littoral drift, but at a time-scale of few years, it appears that the meander convexity of the inlet channel has a control on the migration rate of inlet.

### CONCLUSION

A large number of aerial photographs and satellite images (a total of 184 photos and images over the period 1999-2013) have been used to accurately reconstruct the evolution of the end termination of a rapidly evolving sandspit (La Coubre Sandspit, France) during the last decades. The main geomorphological changes included: spit breaching, new inlet opening and new inlet migration. The comparison of those evolutions with wave model results has shown that extreme storms occurring during high water levels are likely to generate sandspit breaching and new inlet opening. This comparison has also suggested that beyond the key role of extreme storms, the high frequency of successive energetic events is critical for barrier breaching. Finally, this comparison has shown that, once opened, the new inlet migration rate was not correlated with wave climate variations. The main control on downdrift inlet migration may be related to the meander bend orientation of the tidal inlet channel. Slow migration of the tidal inlet occurred when the meander bend was convex in an updrift direction and counteracted the littoral drift. Oppositely, fast migration of the tidal inlet occurred when the meander bend was convex in a downdrift direction because the meander-induced transport was in the same direction as wave-induced longshore transport. Other coastal evolutions driven by self adjustment have been already reported in another tidal inlet-barrier system (Cooper *et al.*, 2007). Our findings show an interesting example of coastal system behavior driven by both allocyclic and autocyclic processes with important implications for the interpretation of coastal evolutions in a context of climate change.

### ACKNOWLEDGEMENT

This study was conducted in the scope of project DYNAMO, funded by the French Agency for Research (Grant agreement n°ANR-12-JS02-00008-01). The developing teams of WWIII and SWAN are greatly acknowledged as well as ECMWF for ERA-INTERIM reanalysis. Satellite SPOT images were supplied by the Centre National d'Etude Spatial (CNES). Developers of the USGS Earth Explorer tool are acknowledged for making the Landsat satellite images available.

### LITERATURE CITED

- Allard, J., Bertin, X., Chaumillon, E. and Pouget, F., 2008. Sand spit rhythmic development: A potential record of wave climate variations? *Arçay Spit, western coast of France. Marine Geology*, 253, 107-131.
- Audrey, D.G. and Speers, P.E., 1984. Updrift Migration of Tidal Inlets. *Journal of Geology*, 92, 531-545.
- Bertin, X. and Chaumillon, É., 2005. Apports de la modélisation sur bathymétries historiques dans la compréhension des évolutions des bancs de sable estuariens. *Comptes Rendus Geoscience*, 337, 1375-1383.
- Bertin, X., Prouteau, E. and Letetrel, C., 2013. A significant increase in wave height in the North Atlantic Ocean over the 20th century. *Global and Planetary Change*, 106, 77-83.
- Bertin, X., Castelle, B., Chaumillon, E., Butel, R. and Quique, R., 2008. Longshore transport estimation and inter-annual variability at a high

- energy dissipative beach: Saint Trojan beach, SW Oléron Island, France. *Continental Shelf Research*, 28, 1316-1332.
- Booij, N., Ris, R.C. and Holthuijsen, L.H., 1999. A third-generation wave model for coastal regions, Part I, Model description and validation, *Journal of Geophysical Research C4*, 104, 7649-7666.
- Buynevich, I.V. and Donnelly, J.P., 2006. Geological signatures of barrier breaching and overwash, southern Massachusetts, USA. *Journal of Coastal Research*, SI 39 (Proceedings 8th International Coastal Symposium), 112-116. Itajaí, SC, Brazil, ISSN 0749-0208.
- Carbonel, P. and Jouanneau, 1982. The evolution of a coastal lagoon system: hydrodynamics determined by ostracofauna and sediments, The Bonne-Anse Bay (Pointe de la Coubre, France). *Geo-Marine Letters*, 2, 065-070.
- Cooper, J.A.G., McKenna, J., Jackson, D.W.T. and O'Connor, M., 2007. Mesoscale coastal behavior related to morphological self adjustment. *Geology*, 35, 187-190.
- Dee, D.P., *et al* Uppala, S.M., Simmons, A.J., *et al.*, 2011. The ERA-interim reanalysis: configuration and performance of the data assimilation system. *Quarterly Journal of the Royal Meteorological Society*, 137 (656), 553-597.
- Dias, J.M., Sousa, M.C., Bertin, X., Fortunato, A.B. and Oliveira, A., 2009. Numerical modeling of the impact of the Ancão Inlet relocation (Ria Formosa, Portugal). *Environmental Modelling and Software*, 24 (6), 711-725.
- Dodet, G., Bertin, X., and Taborda, R., 2010. Wave climate variability in the North-East Atlantic Ocean over the last six decades. *Ocean Modelling*, 31, 120-131.
- Evans, O.F., 1942. The origin of spits, bars and related structures. *J. Geol.*, 50, 846-865.
- FitzGerald, D. M. (1996), Geomorphic variability and morphologic and sedimentologic control on tidal inlets. *Journal of Coastal Research*, SI23, 47-71.
- Gervais, M., Balouin, Y. and Belon, R., 2012. Morphological response and coastal dynamics associated with major storm events along the Gulf of Lions Coastline, France. *Geomorphology*, 143-144, 69-80. doi:10.1016/j.geomorph.2011.07.035.
- Houser, C., Hapke, C. and Hamilton, S., 2008. Controls on coastal dune morphology, shoreline erosion and barrier island response to extreme storms. *Geomorphology*, 100, 223-240. doi: 10.1016/j.geomorph.2007.12.007.
- Jouanneau, J. M., 1974. *Etude sédimentologique d'un système côtier évolutif: la Pointe de la Coubre (embouchure de la Gironde, France)*. France: University of Bordeaux, Ph.D. thesis, 161p.
- Kamphuis, J.W., 1991. Alongshore sediment transport rate. *Journal of Waterway, Port, Coastal and Ocean Engineering*, 117 (6), 624-640.
- King, C.A.M., 1970. Changes in the Spit at Gibraltar Point, Lincolnshire, 1951 to 1969. In: Schwartz, M.L. (eds), *Spits and Bars. East. Midl. Geol.*, 5, 19-30.
- Matias, A., Ferreira, O., Vila-Concejo, A., Garcia, T., Alveirinho Dias, J., 2008. Classification of washover dynamics in barrier islands, *Geomorphology*, 97, 3-4, 15, 655-674.
- Morton, R.A., 2002. Factors controlling storm impacts on coastal barriers and beaches – A preliminary basis for real-time forecasting. *Journal of Coastal Research*, 18, 486-501.
- Pries, A.J., Miller, D.L. and Branch, L.C., 2008. Identification of structural and spatial features that influence storm-related dune erosion along a barrier-island ecosystem in the Gulf of Mexico. *Journal of Coastal Research*, 24, 168-175. doi: 10.2112/06-0799.1.
- Sallenger, A.H., Jr., 2000. Storm impact scale for barrier islands. *Journal of Coastal Research* 16, 890-895. <http://www.jstor.org/stable/4300099>.
- Salomon, J.-N., 2002. Flooding in the Garonne valley and the Gironde estuary caused by the "storm of the century" (27-28 December 1999). *Géomorphologie: relief, processus, environnement*, 2, 127-134.
- Schwartz, M.L., 1982. *The encyclopedia of beaches and coastal environments*. Stroudsburg, Penn: Hutchinson Ross Pub. Co., 960p.
- Tolman, H.L., 2009. *User manual and system documentation of WAVEWATCH III version 3.14*. NOAA/NWS/NCEP/MMAB Technical Note 276, 194p.
- Ulbrich, U., Fink, A. H., Klawa, M. and Pinto, J. G., 2001. Three extreme storms over Europe in December 1999. *Weather*, 56, 70-80.
- Wright, L.D., Chappell, J., Thom, B.G., Bradshaw, M.P. and Cowell, P. 1979. Morphodynamics of reflective and dissipative beach and inshore systems: Southeastern Australia. *Marine Geology*, 32, 105-140.

# Spur and groove distribution, morphology and relationship to relative wave exposure, Southern Great Barrier Reef, Australia



[www.cerf-jcr.org](http://www.cerf-jcr.org)

Stephanie Duce†, Ana Vila-Concejo†, Sarah Hamylton‡, Eleanor Bruce†, Jody M. Webster†

†Geocoastal Research Group  
School of Geosciences  
University of Sydney  
Sydney, Australia  
stephanie.duce@sydney.edu.au

‡ School of Earth and Environmental  
Sciences  
University of Wollongong  
Wollongong, Australia



[www.JCRonline.org](http://www.JCRonline.org)

## ABSTRACT

Duce, S., Vila-Concejo, A., Hamylton, S., Bruce, E., Webster, J. M., 2014. Spur and groove distribution, morphology and relationship to relative wave exposure, Southern Great Barrier Reef, Australia. In: Green, A.N. and Cooper, J.A.G. (eds.), *Proceedings 13<sup>th</sup> International Coastal Symposium* (Durban, South Africa), *Journal of Coastal Research*, Special Issue No. 70, pp. 115-120, ISSN 0749-0208.

Spur and groove features occur on the seaward reef slope of coral reefs around the world. They are believed to act as important natural breakwaters, regulating the hydrodynamic energy and nutrients received by reef platforms. They also represent one of the most diverse and productive zones of modern reefs. However, the formation processes and morphodynamics of spur and groove systems are poorly understood, particularly in the Great Barrier Reef (GBR). This paper constitutes the first broad scale analysis of spur and groove systems in the Capricorn Bunker Group (CBG) in the southern GBR. It uses remotely sensed imagery coupled with ground-truthed data to measure groove length at four reefs (Wreck, Heron, One Tree and Lady Elliot). A total of 2621 grooves were digitised across the four study reefs. Groove length was found to vary both between and within the study reefs. The maximum groove length was 536 m. Average groove length ranged from 93 m at Wreck Reef to 32 m at Heron Reef. This data was compared to relative wave exposure estimates derived from the fetch scenario at each reef. Strong positive correlation was found with groove length increasing as wave exposure increased. Groove length was highly spatially dependant and varied around the reef platforms according to the degree of wave exposure. The longest grooves were found on the most exposed, eastern sides of all reefs. These results provide valuable insight into spur and groove function, formation and likely response to future environmental changes in the CBG and further afield.

**ADDITIONAL INDEX WORDS:** *Spur and Groove, Reef Zonation, Wave Energy, Reef Front; Geomorphology, Ecomorphology*

## INTRODUCTION

Spur and groove features (SaGs) are a distinctive characteristic of reef edges worldwide and are formed by a series of parallel, linear ridges (spurs) separated by channels (grooves) creating finger-like shapes extending down the reef slope into deeper water at the margins of reef platforms (Guilcher, 1988). Spur and groove systems are commonly reported on the windward sides of exposed coral reefs and are believed to act as natural breakwaters playing an important role in the dissipation of wave energy at the reef crest (Munk and Sargent, 1954). They are critical to the reef's ability to resist erosion (Sheppard, 1981). Their regulation of the energy, sediments and nutrients received by the reef platform makes them extremely important to reef health and the geomorphic and biologic zonation of the reef platform (Odum and Odum, 1955). Corals forming the SaGs are thought to be faster growing than the rest of the reef and may represent the front line of seaward reef growth allowing lateral reef expansion to occur (Kan *et al.*, 1997; Shinn, 1963). Despite underpinning many reef flat processes SaG systems remain poorly understood (Gischler, 2010). To our knowledge no literature explicitly examining SaGs in the Great Barrier Reef (GBR) exists. This paper constitutes the first broad

scale analysis of SaG systems in the southern GBR. It aims to quantify the distribution and geomorphic metrics of SaGs at four reefs: Wreck, Heron, One Tree and Lady Elliot. It also aims to determine if a relationship exists between relative wave exposure and groove length. This will provide insights into how, where and why spur and groove systems form both in the southern GBR and globally.

## STUDY SITE

The Capricorn and Bunker Groups (CBG) of reefs and Lady Elliot Reef are the southern-most reefs in the Great Barrier Reef Marine Protected Area (GBRMPA). The CBG extends from North Reef A (-23.18° Lat; 151.9° Lon) approximately 135 km south to Lady Elliot Island (-24.11° Lat; 152.7° Lon) and comprises numerous reefs and 14 reef islands (Figure 1). The reefs occur in depths of between 35 and 60 m on the mid to outer continental shelf, approximately 80 km offshore of Gladstone, Queensland (Jell and Webb, 2012). The region is dominated by south-easterly trade winds, with average speeds of 20 to 40 km/hr from approximately April to August. North westerlies prevail from August to December and cyclones can occur between December and April (Shannon *et al.*, 2013).

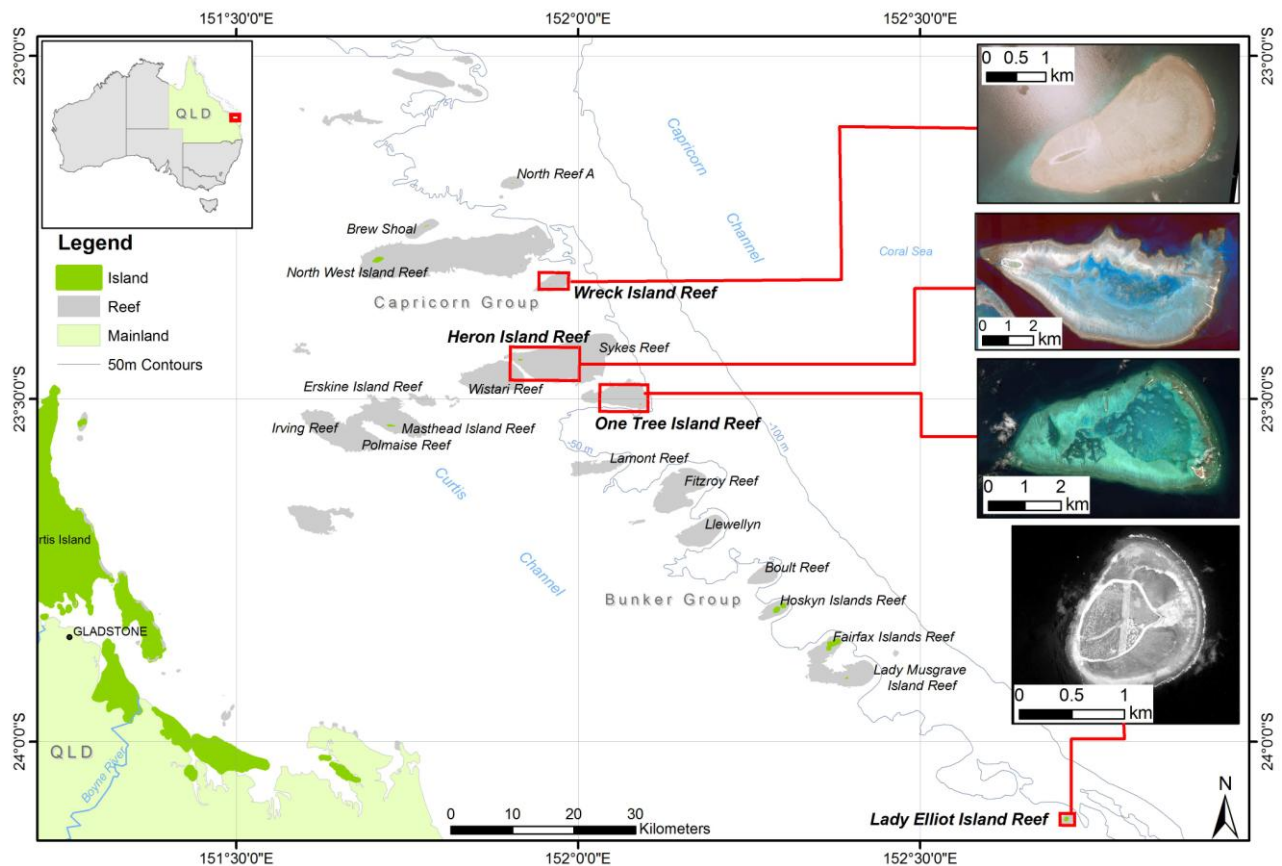


Figure 1. Locality map of the Capricorn and Bunker Groups in the southern GBR showing the four reefs studied in this paper. The 100 m contour denotes the seaward edge of the Continental Shelf. The reefs studied in this project are (a) Wreck Reef; (b) Heron Reef, which is located behind Sykes Reef and One Tree Reef and therefore is less exposed to ocean swell; (c) One Tree Reef; and (d) Lady Elliot Reef

Tides are semi-diurnal with spring tidal heights of approximately 3 m. Tidal currents can reach considerable velocities as they flow between reefs, for example reaching 7.5 km/hr between Heron and Wistari Reefs (Jell and Webb, 2012). Waves are mostly swell, generated from the predominating south-easterly trade winds (Harris and Vila-Concejo, 2013). However, no broad scale assessment of the wave climate of the region has been conducted.

This study focuses on the SaG systems of Wreck, Heron, One Tree and Lady Elliot reefs (Figure 1). Wreck, Heron and Lady Elliot reefs are classified as Planar (Senile) reefs having reached the most advanced state of reef flat evolution recognised by Hopley *et al.* (2007). One Tree is classified as a Lagoonal (Mature) system and has a prominent infilling southern sand apron (Harris *et al.*, 2011, Vila-Concejo *et al.*, 2013). All four reefs are approximately 20 km east of the continental shelf margin (100 m depth contour in Figure 1). Heron is sheltered to the east and south-east while the other study reefs are exposed to ocean swell on their eastern sides (Figure 1).

Wreck and Heron house vegetated solitary sand cays on their leeward sides while One Tree and Lady Elliot have vegetated solitary shingle cays (Hopley *et al.*, 2007). Wreck, Heron and One Tree are within the Capricornia Cays National Park with Wreck and One Tree having additional management protection as “Scientific Zones” which are not accessible to the public. Their high level of protection and distance from the populated coastline mean all four reefs are relatively pristine and free from direct

anthropogenic impacts. Thus, they provide ideal sites to assess SaG systems and their relationship to natural processes without human influence.

## METHODS

The location of SaG systems on the exposed reef front makes them difficult to access and map *in situ* (Guilcher, 1988). This study employed high resolution remotely sensed imagery to determine the distribution and groove length of SaG systems at the four study reefs. Statistical analysis of SaG metrics and modelled relative wave energy were then used to determine if SaGs were spatially auto correlated and if their length could be related to wave exposure.

### Image Analysis

Remotely sensed images of the study reefs were examined and SaGs were identified around the periphery of each reef platform. Table 1 lists the remotely sensed imagery used at each reef. Attempts to automatically classify SaGs using supervised and unsupervised image classification were unsuccessful due to the variable nature of the features and their often small spatial scale. Thus, it was necessary to manually interpret and digitise the features at a 1:1000 scale using *ArcGIS 10.1*. Grooves were found to be the most prominent feature and most easily identifiable in the imagery. Grooves were defined broadly as a linear break in the

surface of the substrate and were digitised by tracing a line down their centre from the reef-ward end (i.e., the head of the groove) as far seaward as the feature was visible (Figure 2).

While this manual digitisation method provided a detailed data set of groove location and length, there were limitations associated with the spatial resolution of the imagery and depth penetration. The sub-meter resolution of imagery at all sites increased the likelihood that all grooves were captured to their full extent, although very narrow grooves (<1 m in width) may have been missed. Multiple factors, including water clarity, light, atmospheric conditions and sensor spectral and spatial resolution, inhibit the depth to which sub-aqueous features can be captured in remotely sensed imagery (Green *et al.*, 2000). Lee *et al.* (2011) found that, under ideal conditions on coral reefs, WorldView-2 imagery can be used to map features to depths of 20 m. In this study grooves were digitised to a maximum depth of ~19 m at Wreck (Table 1).

Interpretation of groove features was sometimes difficult. Grooves may bifurcate (Figure 2) and it can be complicated to define where one groove ends and another begins. Each groove was only ever digitised once. Where bifurcation points were encountered the dominant groove would be continued and a new groove would be created from the point of divergence. This results in some relatively short grooves amongst longer grooves, although they are connected. This should be kept in mind when considering the average and standard deviation groove length statistics presented below. If grooves are not covered by spectrally distinct material (e.g., sand or smoothed rubble) it may not be possible to distinguish them in the imagery. Broken waves and sun glint on the water can also obscure subsurface features. Where two images, from different dates were available at a site (Table 1), both were used to inform the interpretation of grooves addressing the identified limitations in some places. Ground truthing was conducted by snorkel and SCUBA diving at four sites on One

Table 1. Sensor, spatial and spectral resolution and date of acquisition for the imagery used in this study and the max. depth to which grooves were digitised

Reef	Image Sensor	Spatial Res.	Spectral Res.	Date	Max. Depth
Wreck	WV-2	2.0 m	8 band	Oct. 2006	19 m
	Aerial Photo	0.35 m	RGB	Jun. 1980	
Heron	WV-2	0.6 m	4 band	Aug. 2006	13 m
One Tree	Aerial Photo	0.15 m	RGB	Mar. 1978	17 m
	WV-2	0.6 m	4 band	Dec. 2009	
Lady Elliot	Quickbird	0.6 m	Pan.	Aug. 2008	No data

Tree (Figure 2) in October 2013 and confirmed that the features digitised were grooves and the manual digitisation method defined their length well.

### Relative Wave Exposure

To determine if wave exposure and by extension, wave energy, could be related to groove length at the study sites, relative wave exposure data was employed based on the fetch scenario and typical wind conditions of each reef platform (Hamilton and Puotinen, 2012). This dataset gave relative wave exposure at 1 km intervals around each reef flat as a dimensionless value ranging from 0 to 1, with 1 being completely exposed and 0 entirely sheltered. A continuous relative wave exposure surface was created using kriging interpolation and the relative wave exposure value was extracted at each groove. It must be noted that, while

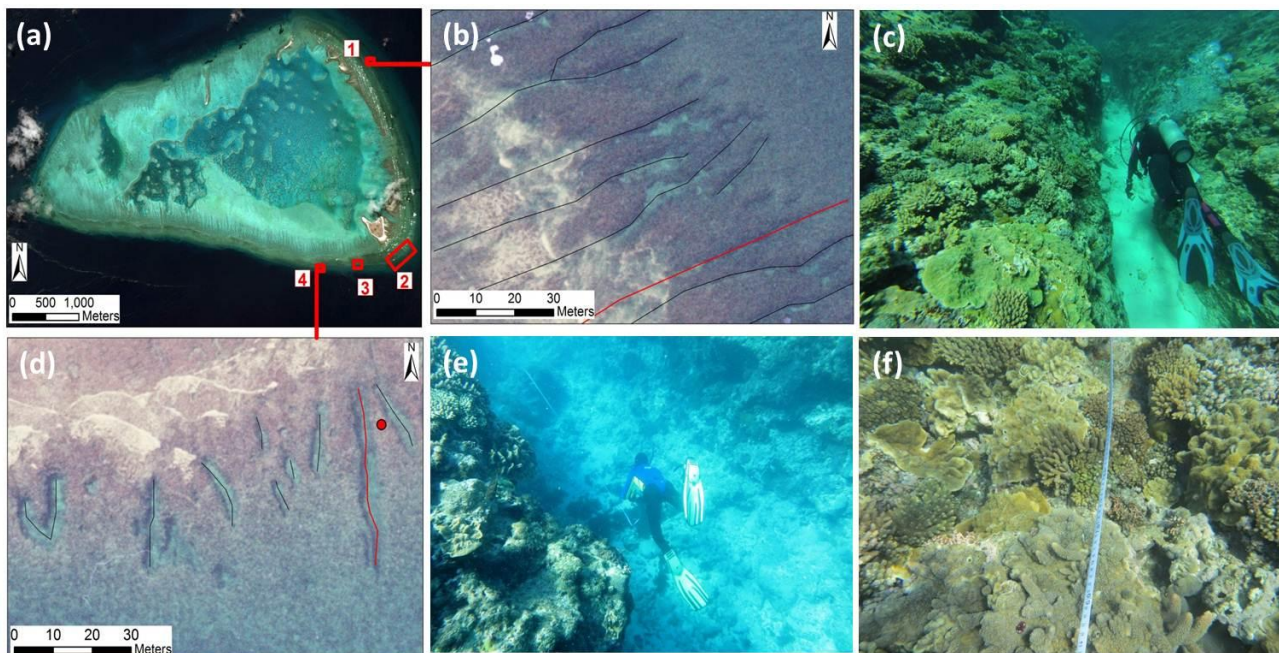


Figure 2. Ground truthing of the SaG zones at One Tree. (a) Sites at which ground truthing was conducted are labeled 1 to 4. (b) Aerial image of site 1 showing digitized grooves. Image (c) was taken in the red groove. (c) Diver swimming towards the head of the red groove shown in (b). Coral covered spurs can be seen either side of the sandy bottomed groove. (d) Aerial image of site 4. Image (e) was taken in the red groove. The red point shows the approximate location of photo (f). (e) Diver swimming towards the head of a wide groove show in figure (d). Mixed boulders, gravel and sand can be seen on the bed. (f) Coral cover on the spur at the site denoted by a red dot in figure (d).



these values are a good proxy for wave energy, they do not take into account wave refraction and other smaller scale hydrodynamic processes and are not a direct measure of local wave power. Rather, they present a useful basis for internal comparison of the relative wave regime for localised subsets of SaGs.

### Statistical Analysis

The *GeoDa 1.4.1* spatial statistics package (Anselin *et al.*, 2006) was used to perform exploratory spatial data analysis on the groove data for each site. Ordinary least squares regressions were used to assess the correlation between groove length and wave exposure at each reef. Univariate Local Moran's I tests were performed to determine if the groove length variable was spatially auto correlated. A spatially lagged regression, maximum likelihood estimation was run with groove length as the dependent variable and wave exposure as the independent variable. A quartile map of the lag predicted groove length was created and used to group the grooves into spatially relevant sectors. One-way ANOVA tests were performed in *IBM SPSS Statistics Software Version 22* to determine if measured groove length was statistically significantly different between the sectors defined.

### PRELIMINARY RESULTS

This study found that SaG systems were present at all four of the reefs examined and occurred on all sides of the reef platforms. A total of 2621 grooves were digitised across the four study reefs. One Tree Reef had the highest number of grooves (1214) and the highest average groove density with one groove every 12.5 m when averaged around the reef perimeter (Table 2). Lady Elliot had the second highest average density of grooves (one every 15.55 m), followed by Wreck (one every 20.95 m). The lowest average groove density occurred at Heron with an average distance of 40 m between grooves (Table 2). These results correspond reasonably well with the maximum relative wave exposure values at each reef. Heron has the lowest maximum exposure (0.03) due to wind shadow from Sykes reef while Wreck, One Tree and Lady Elliot had similar maximum wave exposure values. Wreck was the highest (0.044) followed by One Tree (0.043) and Lady Elliot (0.039) (Table 2).

Groove length was found to vary between reefs, but also varied significantly within reefs (Figs. 3 and 4). The maximum groove length at any reef was 536 m at Wreck. Wreck had the overall longest average groove length (93 m), followed by One Tree (66 m) and Lady Elliot (34 m). Heron had the shortest average grooves (32 m). It should be remembered that bifurcation of grooves can decrease the average lengths calculated. Figure 3 shows the measured length of each groove plotted against the relative wave exposure value at that location. All reefs exhibited positive correlations between the two variables with groove length increasing as wave exposure increased (Figure 3). The strongest correlation was at Lady Elliot ( $R^2 = 0.504$ ). The weakest correlation was at Heron ( $R^2 = 0.119$ ) (Figure 3). Heron Reef also had the lowest relative wave exposure, being protected to the south and east (Figure 1). It is possible that some of these relationships may be stronger if the bifurcated grooves were treated differently.

Calculated Moran's I values were positive for all reefs showing that the groove length data was spatially dependant (Table 2). Given the spatial dependence of the data a spatially lagged, maximum likelihood estimation regression was run. This model improved the  $R^2$  value for all sites (Table 2). The model predicted groove length based on relative wave exposure well at Wreck,

Table 2. Sensor, spatial and spectral resolution and date of acquisition for the imagery used in this study and the max. depth to which grooves were digitised

	Wreck	Heron	One Tree	Lady Elliot
<b>No. Grooves</b>	408	719	1214	280
<b>Groove Density</b> (Perimeter/No. Grooves)	20.29	40.06	12.5	15.55
<b>Max. Relative Wave Expos.</b>	0.044	0.03	0.043	0.039
<b>Moran's I</b>	0.752	0.327	0.57	0.63
<b>R<sup>2</sup> Spatial Lag</b>	0.719	0.287	0.461	0.519
<b>Z-Value</b>	27.405	15.54	7.529	10.128
<b>Lag coeff. (Rho)</b>	0.759	0.71	0.441	0.52

Lady Elliot and One Tree but not so well at Heron Reef (refer to  $R^2$  Spatial Lag values in Table 2). The high z-values at all sites indicate a highly significant (>99% confidence) degree of positive spatial auto correlation.

The groove lengths predicted by the spatial lag model were divided into quartiles and plotted on the imagery (Figure 4). These quartiles delineate different sectors of the reef based on groove length and exposure. Six SaG sectors were identified at Wreck, One Tree and Lady Elliot and ten sectors were identified at Heron (Figure 4). One-way ANOVA tests confirmed that differences in measured groove length between these sectors were statistically significantly. Figure 4 shows the average groove length and standard deviation (in parenthesis) for each sector in boxes. It can be seen that the longest grooves are always found on the eastern side of the reef flats. These grooves also tend to be the most regularly aligned, spaced, and linear. The shortest average grooves are always found on the western side of the reef platforms and tend to be less linear and regular in terms of length, spacing and alignment (Figure 4). The sectors at Heron are not as uniformly distributed around the reef platform and ten sectors were distinguished. The mean groove lengths between sectors were significantly different but not to the same extent as the other reefs, as indicated by the lower F score in the one-way ANOVA (Figure 4).

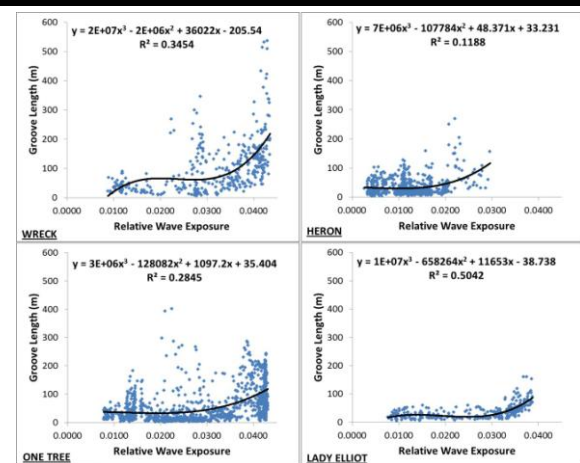


Figure 3. Measured groove length (m) plotted against the relative wave exposure value at each groove for the four study reefs. Polynomial trend lines are shown along with the equation of the line and the associated  $R^2$  value.

DISCUSSION

Hydrodynamic conditions modify the morphology of reef features, simultaneously these features interact with and alter their hydrodynamic environment. This creates a complex and inextricably linked morphodynamic feedback loop (Kench and Brander, 2006). SaG systems may provide an excellent example of this feedback loop. This study found that groove length varies significantly around all the reef platforms studied. This variation is highly spatially dependant, with the longest grooves occurring on the eastern sides of the studied reefs. A relationship between exposure to wave energy and groove length was revealed, with greater exposure corresponding with longer grooves. To our knowledge, no other studies have explicitly examined groove length with respect to wave energy.

Munk and Sargent (1954) reported a correlation between wave power and groove distribution at Bikini Atoll in the Pacific, with grooves only found on reef fronts exposed to the direction of wave action. They also noted that reef slope plays a role in groove length, with steeper slopes at their study site housing shorter grooves though wave energy was equal. The inclusion of reef slope was beyond the scope of this study but could explain the shorter average length of grooves in the eastern sector of Lady Elliot, which has similar wave exposure values to One Tree and Wreck. Roberts *et al.* (1977) found that, at Grand Cayman Island in the Caribbean, areas with higher average annual wave power were characterised by narrower, more closely spaced SaGs. Storlazzi *et al.* (2003) measured SaGs in detail at Hawaii's Molokai Reef. They found that spur height and distance between adjacent spurs both increased with depth. Mean SaG height and spacing were found to be inversely proportional to wave energy i.e. greater wave energy, lower spur height and closer spacing. Increasing the length and frequency of grooves increases the surface area of the reef front available to dissipate wave energy and is likely to be a geomorphic response of reefs exposed to higher energy.

In general, the grooves were parallel to one another but were not always perpendicular to the reef rim (Figure 4) and most likely reflect the direction of the dominant refracted wave orthogonal as reported by Sneh and Friedman (1980). Quartile groupings of the lag predicted groove lengths (Figure 4) defined statistically distinct sectors around the reef platforms. These sectors correspond well to variation in SaG characteristics beyond that of groove length, including spacing, orientation, linearity, regularity and connection to the reef rim. It is likely that these characteristics are also controlled primarily by exposure to wave energy which varies around the reef platform. These radial sectors provide an alternative approach to the geomorphic zoning of reef platforms which typically follow concentric bands parallel to the reef rim in accordance with the assumption that distance from the reef rim is the primary factor controlling energy and geomorphic zonation of the reef flat (Geister, 1977). The identification of these energy-driven differences in reef front morphology suggest that the reef flat may also exhibit radial zonation. Indeed, Shannon *et al.* (2013) divided the eastern rubble flat at One Tree into northern and southern zones based on the geomorphology, rate of change in rubble features and infill to the lagoon. The sites defined by Shannon *et al.* (2013) align almost perfectly with the different SaG zones delineated independently in this study. Hamylton (2011) found that deeper grooves were associated with a higher degree of linearity in adjacent sand and seagrass patches on the reef flat of Alphonse Atoll, Indian Ocean. This shows the potential merit of defining radial geomorphic zones based on energy exposure gradients around the reef flat. It also suggests that

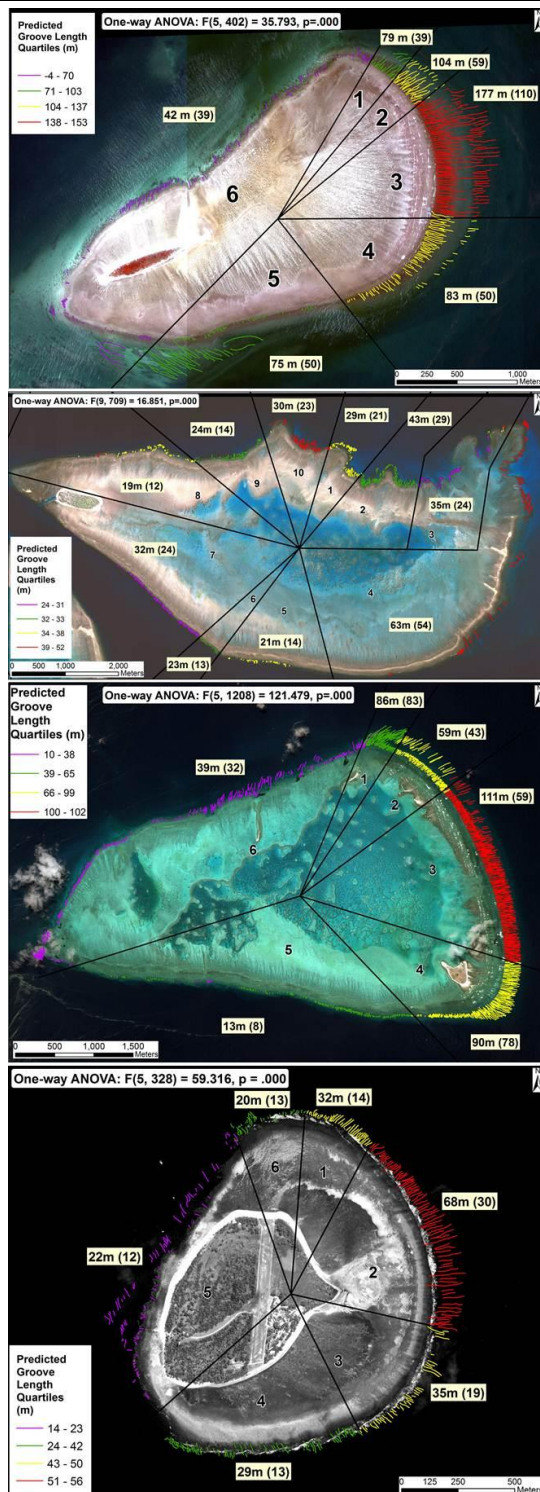


Figure 4. Digitised grooves displayed in coloured quartiles based on groove length predicted by the spatially lagged regression. Numbered sectors were defined based on these quartiles. The boxes in each sector show the average, measured groove length (m) and the standard deviation (in parenthesis). Results of the one-way ANOVA of groove length by sector are also presented (top left)

differences in spur and groove character could translate into differences in the morphodynamics of the adjacent reef flat.

### CONCLUDING REMARKS

This study found that spur and groove systems occur at all sides of reef margins at three exposed reefs and one semi-protected reef in the Southern GBR. Average groove length varied between reefs and around the reef platform. SaG systems were found to be less defined and regular in less exposed environments. Groove length varied significantly around each reef platform with the longest average grooves occurring on the most exposed, eastern sides of the reefs. A strong positive correlation was found between relative exposure to wave energy and groove length. This supports the belief that SaG systems act as effective natural breakwaters for reef environments by increasing the surface area of the reef front available to dissipate wave energy.

These results provide insight into spur and groove function and formation and provide a basis for understanding their likely response to future environmental changes. The application of the methodology, used on a reef by reef basis here, to more reefs could assist to establish a model that can be broadly applied to SaG systems beyond the CBG. The influence of other factors including depth, slope, antecedent topography, substrate, tides and currents should also be assessed. Such assessments fall beyond the scope of this paper but are being conducted as part of ongoing research to improve our understanding of SaG systems, both regionally in the southern GBR and globally.

### ACKNOWLEDGEMENT

Duce is funded by an Australian Postgraduate Award and USYD Merit Award. Vila-Concejo is funded by an Australian Research Council Future Fellowship. The fieldwork conducted was funded by Vila-Concejo's Future Fellowship and Women in Science Return to Work Fellowship, USYD. Fieldwork was carried out at USYD's One Tree Island Research Station. The authors would like to thank the Station Managers Glen and Wendy Shaw and Matthew Kosnic and Andrew Irvine for their assistance in the field. The imagery of Wreck, Lady Elliot and Heron were provided by Hamylton and GeoScience Australia. The One Tree imagery was purchased using a USYD Start-up Program Grant to Webster.

### LITERATURE CITED

- Anselin, L., Syabri, I. and Youngih, K., 2006. Geoda: An introduction to spatial data analysis. *Geographical Analysis*, 38, 5-22.
- Geister, J., 1977. The influence of wave exposure on the ecological zonation of caribbean coral reefs. *Proceedings int Coral Reef Symp*, 3.
- Gischler, E., 2010. Indo-pacific and atlantic spurs and grooves revisited: The possible effects of different holocene sea-level history, exposure, and reef accretion rate in the shallow fore reef. *Facies*, 56, 173-177.
- Green, E.P., Edwards, A.J. and Mumby, P.J., 2000. Mapping bathymetry. In: Green, E. P., Mumby, P. J., Edwards, A. J. and Clark, C. D. (eds.), *Remote sensing handbook for tropical coastal management* (Paris, France), UNESCO.
- Guilcher, A., 1988. *Coral reef geomorphology*. New York, USA: John Wiley and Sons, 228p.
- Hamylton, S., 2011. Estimating the coverage of coral reef benthic communities from airborne hyperspectral remote sensing data: Multiple discriminant function analysis and linear spectral unmixing. *International Journal of Remote Sensing*, 32, 9673-9690.
- Hamylton, S. and Puotinen, M., 2012. Assessing reef island response to environmental conditions on the GBR. *12th International Coral Reef Symposium*, 2012 (Cairns, Australia).
- Harris, D.L. and Vila-Concejo, A., 2013. Wave transformation on a coral reef rubble platform. In: Conley, D.C., Masselink, G., Russell, P.E. and O'hare, T.J. (eds.) *12th International Coastal Symposium* (Plymouth, England), *Journal of Coastal Research*, Special Issue No. 65, 506-510.
- Harris, D.L., Webster, J.M., De Carli, E.V. and Vila-Concejo, A., 2011. Geomorphology and morphodynamics of a sand apron, one tree reef, southern great barrier reef. *Journal of Coastal Research*, 760-764.
- Hopley, D., Smithers, S.G. and Parnell, K.E., 2007. *The geomorphology of the great barrier reef: development, diversity and change*, Cambridge University Press.
- Jell, J.S. and Webb, G.E., 2012. Geology of heron island and adjacent reefs, great barrier reef, australia. *Episodes*, 35, 110-119.
- Kan, H., Hori, N. and Ichikawa, K. 1997. Formation of a coral reef-front spur. *Coral Reefs*, 16, 3-4.
- Kench, P.S. and Brander, R.W., 2006. Wave processes on coral reef flats: Implications for reef geomorphology using australian case studies. *Journal of Coastal Research*, 22, 209-223.
- Lee, K.R., Kim, A.M., Olsen, R. and Kruse, F.A., 2011. Using worldview-2 to determine bottom-type and bathymetry. *SPIE Defense, Security, and Sensing*. International Society for Optics and Photonics.
- Munk, W.H. and Sargent, M.C., 1954. Adjustment of bikini atoll to ocean waves. *U.S. Geological Survey Professional Paper*, 260 C, 275-280.
- Odum, H.T. and Odum, E.P., 1955. Trophic structure and productivity of a windward coral reef community on eniwetok atoll. *Ecological Monographs*, 25, 291-320.
- Roberts, H.H., Murray, S.P. and Suhayda, J.N., 1977. Physical processes in a fore-reef shelf environment. *Third International Coral Reef Symposium* (Miami, USA).
- Shannon, A.M., Power, H.E., Webster, J.M. and Vila-Concejo, A., 2013. Evolution of coral rubble deposits on a reef platform as detected by remote sensing. *Remote Sensing*, 5, 1-18.
- Sheppard, C.R.C., 1981. The groove and spur structures of chagos atolls and their coral zonation. *Estuarine Coastal and Shelf Science*, 12, 549-560.
- Shinn, E.A., 1963. Spur and groove formation on the florida reef tract. *Journal of Sedimentary Petrology*, 33, 291-303.
- Sneh, A. and Friedman, G.M., 1980. Spur and groove patterns on the reefs of the northern gulfs of the red-sea. *Journal of Sedimentary Petrology*, 50, 981-986.
- Storlazzi, C.D., Logan, J.B. and Field, M.E., 2003. Quantitative morphology of a fringing reef tract from high-resolution laser bathymetry: Southern molokai, hawaii. *Geological Society of America Bulletin*, 115, 1344-1355.
- Vila-Concejo, A., Harris, D.L., Power, H.E., Shannon, A.M. and Webster, J.M., 2013. Sediment transport and mixing depth on a coral reef sand apron. *Geomorphology*.

# A paraglacial coastal gravel structure: Connell's Bank, NW Ireland

Jasper Knight†, Helene Burningham‡

† School of Geography, Archaeology & Environmental Studies, University of the Witwatersrand, Private Bag 3, Wits 2050, Johannesburg, South Africa  
jasper.knight@wits.ac.za

‡ Department of Geography, University College London, Gower Street, London, WC1E 6BT, UK  
h.burningham@ucl.ac.uk



[www.cerf-jcr.org](http://www.cerf-jcr.org)



[www.JCRonline.org](http://www.JCRonline.org)

## ABSTRACT

Knight, J., Burningham, H., 2014. A paraglacial coastal gravel structure: Connell's Bank, NW Ireland. In: Green, A.N. and Cooper, J.A.G. (eds.), *Proceedings 13<sup>th</sup> International Coastal Symposium* (Durban, South Africa), *Journal of Coastal Research*, Special Issue No. 70, pp. 121-126, ISSN 0749-0208.

Coastal gravel structures have been well documented worldwide and are formed dominantly by onshore wave transport of gravel, mainly during storm events. They are commonly observed along paraglacial coastlines where their origins are more ambiguous because of the effects of antecedent patterns of sediment supply, glacioisostatic sea-level change, and contemporary coastal processes. This paper describes the properties and polygenic origin of Connell's Bank, a small paraglacial gravel structure on the Atlantic-facing coast of NW Ireland. This feature has been shown on historical maps, air photos and satellite imagery since ca. 1850 but its outline has varied depending on seasonal migration, expansion and contraction of a sand veneer. It has also acted as a major control on tidal channel position within the estuary, and thus on sensitivity of the estuary system to ocean forcing. In detail, the bank surface is composed of cobbles sourced from outside of the immediate catchment. These surface cobbles are strongly winnowed, forming a lag deposit, whereas below the surface, cobbles exist within a granule and shell matrix. A significant proportion of surface cobbles show evidence for recent ventifaction by blown sand at low tide. The paraglacial evolution of Connell's Bank since the last glaciation comprises the following stages: (1) deposition of coarse glacial sediment as a moraine or proximal outwash fan during the late Pleistocene lowstand; (2) reworking of sediments onshore during early Holocene sea-level rise; (3) surface winnowing during mid to late Holocene tides and storms; and (4) surface cobble modification by contemporary wind abrasion.

**ADDITIONAL INDEX WORDS:** *Paraglacial, glacial sediment, ventifacts, erosional lag, gravel barrier, landscape palimpsest.*

## INTRODUCTION

A range of coastal gravel structures including barriers, bars, banks and spits has been well documented worldwide. Most gravel structures are found where coastline orientation changes abruptly. They are usually elongate structures with a steep shoreface, attain a height of several metres above sea level, and are often characterised by systematic changes in clast size along the length of the structure (Carter, 1983; Orford *et al.*, 2002). Most of the documented examples of gravel structures are formed by onshore transport of clasts during storm events and associated with strong storm wave setup and in response to long-term changes in sea level (Forbes *et al.*, 1991; Carter and Orford, 1993; Orford and Anthony, 2011). As such, most gravel structures are assumed to form episodically under contemporary conditions, and to attain a maximum threshold height with respect to incoming storm waves and/or sea-level position (Orford *et al.*, 1995). However, coarse clastic (gravel) structures that are documented from glaciated coasts are more ambiguous and probably polygenic in origin (Carter and Orford, 1988). This is because glacier retreat often leaves gravel-rich moraines and drumlins in coastal lowland settings where eustatic and glacioisostatic sea-level rise can

rework these sediments, leaving a winnowed lag of glacial clasts from which the finer matrix has been washed away (Carter *et al.*, 1990; Forbes and Syvitski, 1994; Greenwood and Orford, 2007; Hayes *et al.*, 2010; Hoffmann *et al.*, 2010). It is notable that many coastal dune fields across northwest Europe are anchored on gravel ridges (e.g. Orford *et al.*, 2003) which are likely to have a similar history. Such gravel landforms are commonly overstepped by postglacial sea-level rise, forming a drowned or welded barrier, and winnowing may result in formation of sandy beaches, saltmarsh or lagoonal sediments adjacent to a residual moraine core (Carter and Orford, 1988). The term paraglacial has been applied to such coastal landforms (Forbes and Syvitski, 1994) because their morphology and post-depositional evolution have been strongly influenced by glaciation (cf. Church and Ryder, 1972). Although examples of coarse clastic paraglacial structures, in particular barriers, have been described from eastern Canada and USA (Forbes *et al.*, 1995a; FitzGerald and van Heteren, 1999), few have been described from other glaciated coastal lowlands or drowned continental shelves (Ruz, 1989; Johnston, 2001). Here, we describe one element of a paraglacial coastal landscape in northwest Ireland – a cobble-mantled bank – where a combination of high glacial sediment supply and postglacial sea-level rise has resulted in a complex history of sediment reworking, morphological evolution, and polygenic physical attributes of these elements in today's landscape.

DOI: 10.2112/SI65-021.1 received 2 December 2013; accepted 21 February 2014. © Coastal Education & Research Foundation 2013

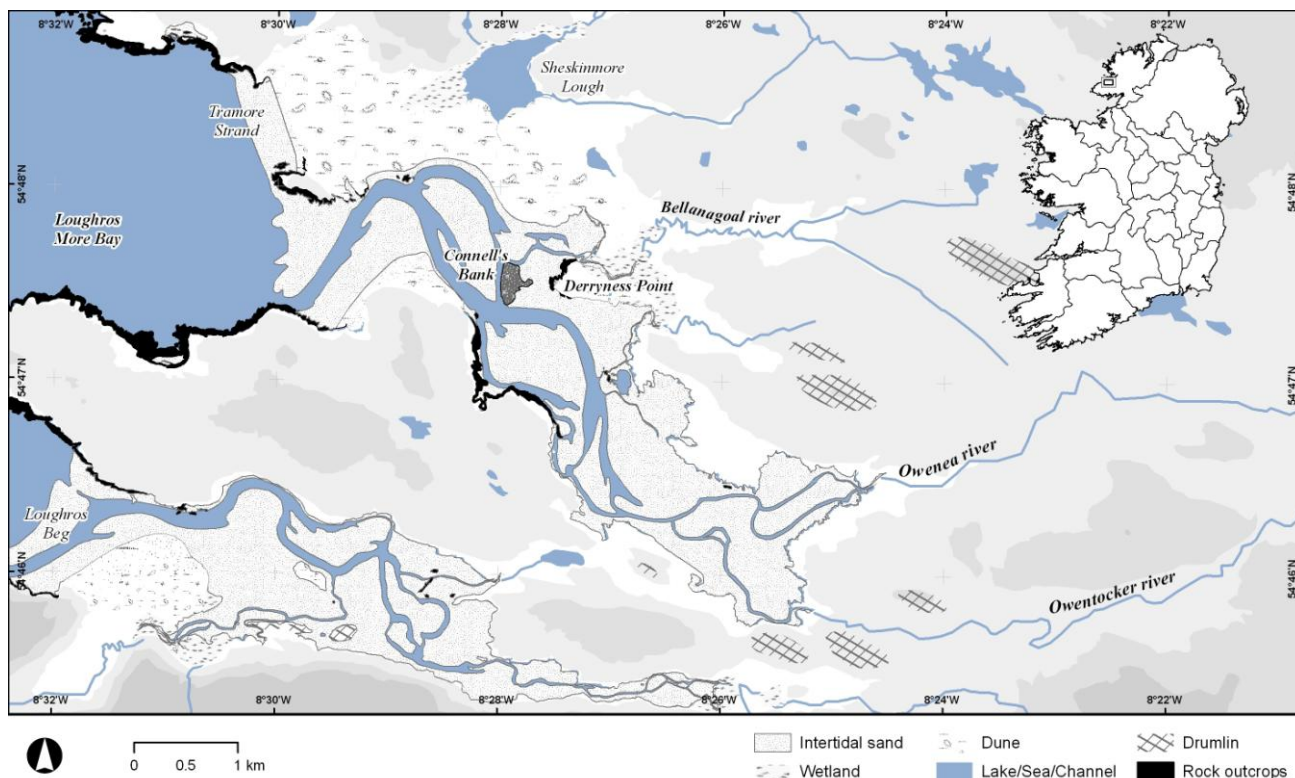


Figure 1. Location of Connell's Bank in the Loughros More estuary, northwest Ireland.

## LOCATION AND GEOLOGIC SETTING

The west coast of County Donegal, northwest Ireland, is dominated by a headland-embayment system which reflects a combination of relatively hard granite and metasediment rock types, and fault zones which have acted as lines of weakness for fluvial and glacial erosion. The coastline is macrotidal and with high wave energy and onshore winds from the adjacent Atlantic. Typical sedimentary landforms include sand dunes, saltmarsh, tidal sand flats and ebb deltas primarily associated with estuarine settings that lie within glacially eroded valleys or larger coastal embayments (Figure 1). Although sand dune, sandy beach and ebb-channel dynamics have been described in detail from some of these west coast estuaries (Burningham, 2002, 2008), there has been little consideration of the glaciogenic controls on postglacial estuary evolution (Shaw and Carter, 1994). Here, we describe the properties and origins of Connell's Bank, a gravel structure located within Loughros More Bay, the estuary of the underfit Owenea and Owentocker rivers (Figure 1). The gravel bank exerts an important control on ebb channel dynamics in Loughros More estuary, particularly in terms of preventing the northward migration of the mid-estuary ebb channel (Burningham, 2008). This feature (450 x 300 m dimensions) has a relative relief of < 1.5 m and is fully exposed within the lower intertidal zone (Figures 2, 3). During spring tides, the uppermost part of the bank is not covered by water. The area of Connell's Bank is underlain by quartz monzodiorite that corresponds to one part of the zonal differentiation within the Ardara granite pluton (Stevenson *et al.*, 2008). The quartz monzodiorite outcrops on the adjacent Derryness headland. Coarse crystalline tonalite from the same pluton outcrops on low-lying areas adjacent to this headland. The

core of the pluton, located 1.5 km to the east, is composed of granodiorite.

During the late Pleistocene glaciation in west Donegal, ice flowed generally westwards through embayments and on to the Atlantic continental shelf. Evidence for this comes from the presence of glacial erosional and depositional landforms, including moraines, found onshore and offshore (Knight, 2009, 2011, 2012; Ó Cofaigh *et al.*, 2012). Glacial abrasion helped break down the coarse-grained granite and quartzite bedrock of west Donegal into sand-sized particles. This sand was then largely reworked onshore from the continental shelf and into adjacent estuaries and embayments, particularly during postglacial sea-level rise. Most of the present coastal landforms appear to have been built as a consequence of a stable sea-level position attained around 7 kyr BP (Carter and Wilson, 1993). There is very little preserved evidence for coastal events prior to this period.

## METHODS

Historic map, air photo and satellite data from different dates between c. 1850 and 2012 were imported into and georeferenced within a GIS in order to examine centennial and shorter time-scale changes in the area and position of Connell's Bank, and the boundary between sand and exposed cobble substrates, which can be clearly identified from these data sources. Episodic field surveys between 2007 and 2013 mapped the sand-cobble boundary in more detail using a handheld GPS, and differential GPS surveys in 2005 and 2008 captured the topographic context, in particular with reference to the vertical tidal frame (Figure 4). These spatial data were compared quantitatively within the GIS. Field surveys also examined the surface and immediate subsurface lithology and structure of the bank itself. The lithology and

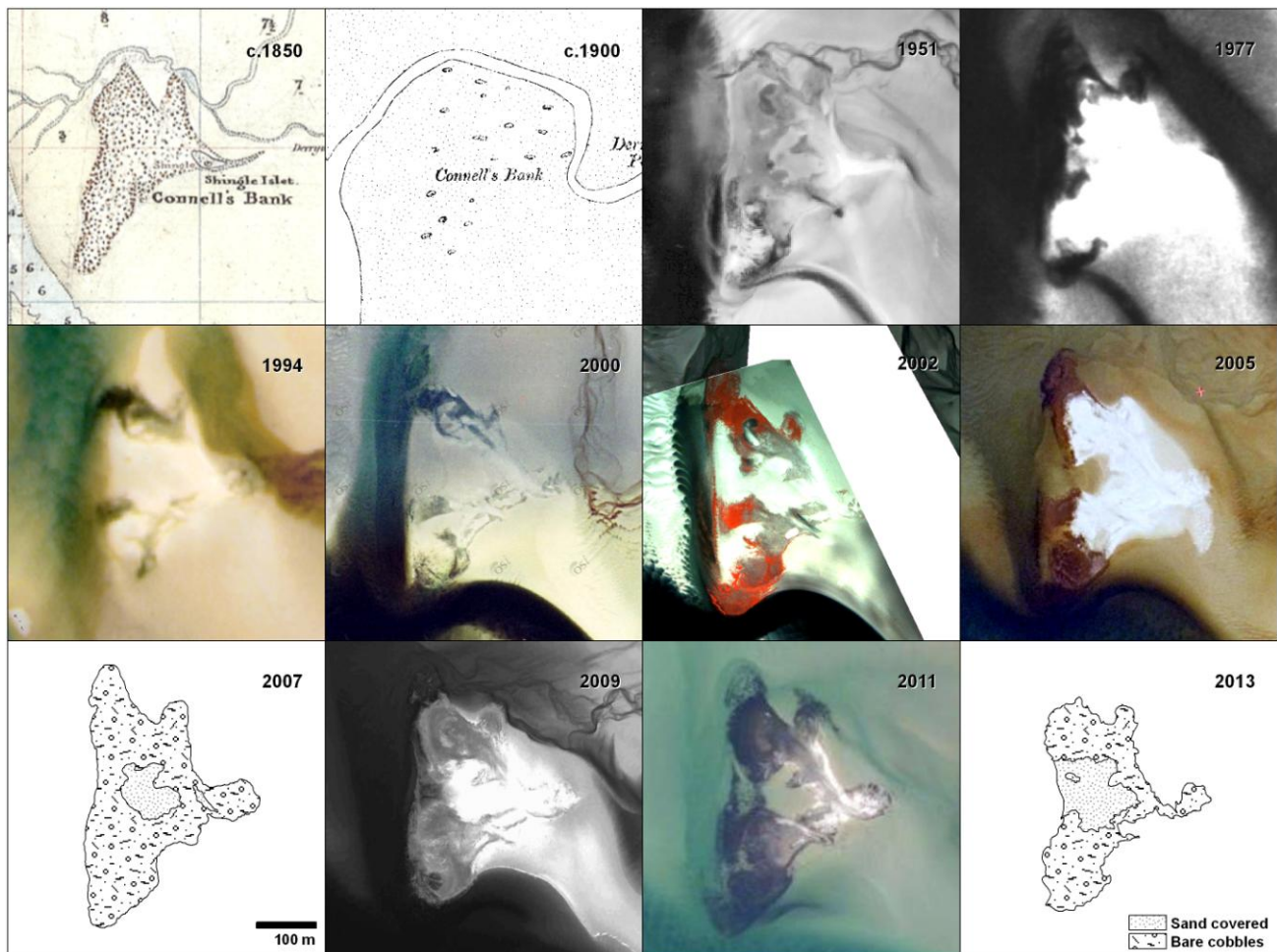


Figure 2. Change in the surface character and planform of Connell's Bank from map, aerial photograph and field surveys, 1850–2013.

properties of representative surface cobbles were examined in twenty 1 x 1 m quadrats. These quadrats were identified using a stratified sampling method in which a north-south and east-west grid was marked across the bank, with a line spacing of approximately 20 m, and quadrats were placed at grid intersections. Thirty randomly selected clasts were sampled from the bank surface within each quadrat (600 clasts in total). Clast lithology; clast shape based on the scheme of Zingg (1935) using a, b, c axial measurements; relative degree of weathering (qualitative scale from 0 [not weathered] to 5 [highly weathered]); and angularity/roundness using the Powers (1953) scheme (quantified where rounded has a value of 1 and angular a value of 4) were noted and averaged for the quadrat as a whole. As each quadrat was located with the GPS, this yielded consideration of spatial patterns of clast features. Summary (averaged) data are presented here. Test pits (< 60 cm deep) were excavated in the bank top in order to examine its subsurface structure.

## RESULTS AND INTERPRETATION

### Spatial Analysis

From spatial mapping of the sand-cobble boundary around Connell's Bank over the last 160 years, it is evident that the

landform has not changed significantly in size and shape over this time period (Figure 2). However, over the shorter timescales of field mapping, it is notable that the landward (easterly) side of the bank remains relatively fixed but that the seaward boundary migrates over tens of metres, which reflects seasonal to interannual variations in wave intensity and to a lesser extent variations in ebb tide velocity. Sand accumulates as an overlapping wedge against both the seaward and landward sides of Connell's Bank during flood and ebb tides respectively, or in response to small movements of the ebb channel (Figure 3). As such, the bank acts as a sediment capture point. This outermost part of the estuary is ebb-dominant, shown by the orientation of asymmetric ripples and the onlap of a low-density, therefore quickly-deposited, sand wedge against the landward side of the bank. The relative permanence of Connell's Bank, irrespective of northwest Ireland's exposure to Atlantic storms and large waves (Dawson *et al.*, 2004), suggests that it is a relict feature that is largely insensitive to today's coastal climate. A further point is that, although the broader Loughros More estuary contains extensive sands at a range of elevations, the high mobility of the sand cover around Connell's Bank suggests that this location is the focus of a specific set of processes that are conducive to sand mobilisation and transport.



Figure 3. Photographs showing (i) view south over Connell's Bank into the estuary; (ii) view north showing the raised cobble bank (foreground); (iii) view south showing the cobble/sand boundary; and (iv) ventifacted cobble on the bank surface.

### Clast Analysis

When data from all 20 quadrats are aggregated together, clasts ( $n=600$ ) are dominantly quartzite (64.5%), with subordinate appinite (10.8%), tonalite (6.2%), granodiorite (4.3%) and

Falcarragh Limestone (3.1%). It is notable that the majority of clasts are not derived from the immediate catchment but from sources outside of the watershed, in particular to the south and southeast (quartzite, appinite). Aggregated data on clast shape ( $n=600$ ) show that 44.2% are tabular, 34% are equant, 12.6% are prolate and 9.1% are bladed. There are no significant differences between these percentage splits between different quadrats. The index of relative weathering shows that 14.3% of all clasts show little or no weathering and 5.8% of all clasts are highly weathered, but there is some spatial variability in this pattern whereby both these weathering end-members are more common at slightly lower elevation sites on the bank, and in more proximal positions. This may suggest that clasts may be turning over as a consequence of undercutting wave action. With respect to clast angularity, angular clasts only make up 1% of all clasts observed, and are only observed in those quadrats where clasts are also variably weathered. Most clasts (53%) are subrounded. In total, 18% of all clasts observed show evidence for ventifaction, with 106 clasts showing a surface polish caused by the rubbing of wind-blown sand grains, and two clasts showing pits caused by saltating sand grains. The quadrats in which over 30% of clasts are polished are located at lowest elevations closest to the low tide channel. It is notable that no clasts show clear evidence for glacial transport, such as faceting and striations, which may reflect overprinting by more recent marine and aeolian processes (Figure 3).

Excavation into the cobble surface to around 60 cm depth shows vague planar stratification of openwork well-rounded cobbles with a poorly sorted coarse sand to granule matrix. The cobbles are a similar size, shape and lithology to those forming the surface lag. Intact marine shells are present within the matrix, in particular cockles (*Cerastoderma edule*) and periwinkles (*Littorina littorea*), indicating that the surface layer of the bank has been reworked and redeposited in a full marine setting. As the present lagged surface is, according to the spatial data presented in Figure 2, relatively geomorphically stable, we suggest that sediment reworking and development of this lagged surface layer took place during the mid-Holocene sea-level transgression, and that this is marked by a basal erosional unconformity (transgressive surface). The timing of this sea-level rise is uncertain as a consequence of uncertainty in the rate of glacioisostatic adjustment (Brooks *et al.*, 2008) but took place between around 6.5–5 kyr BP (Shaw and Carter, 1994). Since this time period, sea level has been relatively stable and the estuary has evolved through sediment infilling and development of fringing sand dunes and saltmarsh (Burningham, 2002). This is very similar to the gravel barrier-overstepping model presented by Forbes *et al.* (1991).

## DISCUSSION

### Connell's Bank as a Glacigenic Feature

Although no diagnostic evidence for glacial abrasion is seen on Connell's Bank cobbles, the embayment geomorphic setting, positive relief morphology, erratic lithologies and wider glacial context suggest that Connell's Bank formed as a glacigenic feature, most probably as a moraine during late Pleistocene ice retreat, and formed by a valley glacier extending northwards from the Glengesh peninsula (e.g. Dury, 1957; Knight, 2012). It is also likely that during deglaciation and in the early Holocene, rivers were more vigorous than they are at present, and transported glacigenic materials into the present-day estuary valley. This may be considered as a paraglacial response to deglaciation (Knight and Harrison, 2009).

## Paraglacial context of Connell's Bank

Paraglacial coasts are generally characterised by high sediment supply and significant changes in sea level that affect coastal evolution over millennial timescales following ice retreat (Forbes and Syvitski, 1994; Forbes *et al.*, 1995b). As such, paraglacial coasts evolve in response to antecedent factors that in turn give rise to a palimpsest of relict, reactivated and contemporary landforms. Within Loughros More Bay are located examples of all these landform types, including bedrock shore platforms, sand and boulder (storm) beaches, coastal sand dunes, saltmarsh and ventifacts (Burningham, 2002, 2008; Knight, 2008), as well as Connell's Bank itself. This suite of landforms results from a range of processes operating on different spatial and temporal scales, and are also set against a typical postglacial history of estuary infilling and thus long-term reduction of tidal prism and sediment accommodation space. This fits with similar themes in recent literature. For example, Hein *et al.* (2012) described the paraglacial and 'post-paraglacial' evolution of barrier islands in Maine, USA, in which recent morphodynamic behaviour is both much reduced in magnitude and is spatially constrained by landforms and structures of the paraglacial past. The coastline of western Ireland also shows this general behaviour (Shaw and Carter, 1994; Delaney and Devoy, 1995).

## Recent morphodynamics of Connell's Bank

The physical properties and range of morphological features found in association with Connell's Bank confirm that it has a polygenic origin, formed as a glacial moraine which is lithologically sourced from outside of the catchment, and subsequently modified by postglacial marine reworking by tides and waves, and with aeolian ornamentation of surficial clasts. The presence of Connell's Bank as a positive-relief obstruction within the estuary has helped control the position of the flanking ebb channel, at least over the time scale of available map data, because it has acted as an obstruction to channel migration (Burningham, 2008) (Figure 4). Furthermore, as a consequence of this channel control, it allowed for the coeval eastward migration of sand dunes located on the northerly estuary margin, which closed off Sheskinmore Lough (Barrett-Mold and Burningham, 2010). Thus, it could be argued that this paraglacial control on ebb channel configuration has subsequently influenced Holocene morphodynamic behaviour of the whole estuary and surrounding coastal landscapes and ecosystems.

It is notable that at low tide, when the landward part of the estuary is exposed, wind processes are dominant with streamers driven by strong offshore winds transporting saltating sand grains across the bank from east to west. This is a geomorphically-significant process, as seen by the presence of well-developed ventification of surface cobbles. These clasts commonly show small (mm-scale) pits and larger smooth and abraded surfaces typical of *dreikanter*-type ventifacts. This fits with regional evidence for geomorphically-significant wind-driven sand transport, forming ventifacts of different types and scales under the contemporary wind regime (Knight and Burningham, 2001; Knight, 2005, 2008). There is no particular clustering of ventifacted clasts, although some have been abraded on several sides, suggesting that clasts may have moved position, probably by wind-wave undercutting.

## CONCLUSIONS

Despite Ireland having a strong glacial imprint, paraglacial landscape responses in the coastal zone are poorly documented. Connell's Bank is a glacial structure that has exerted a

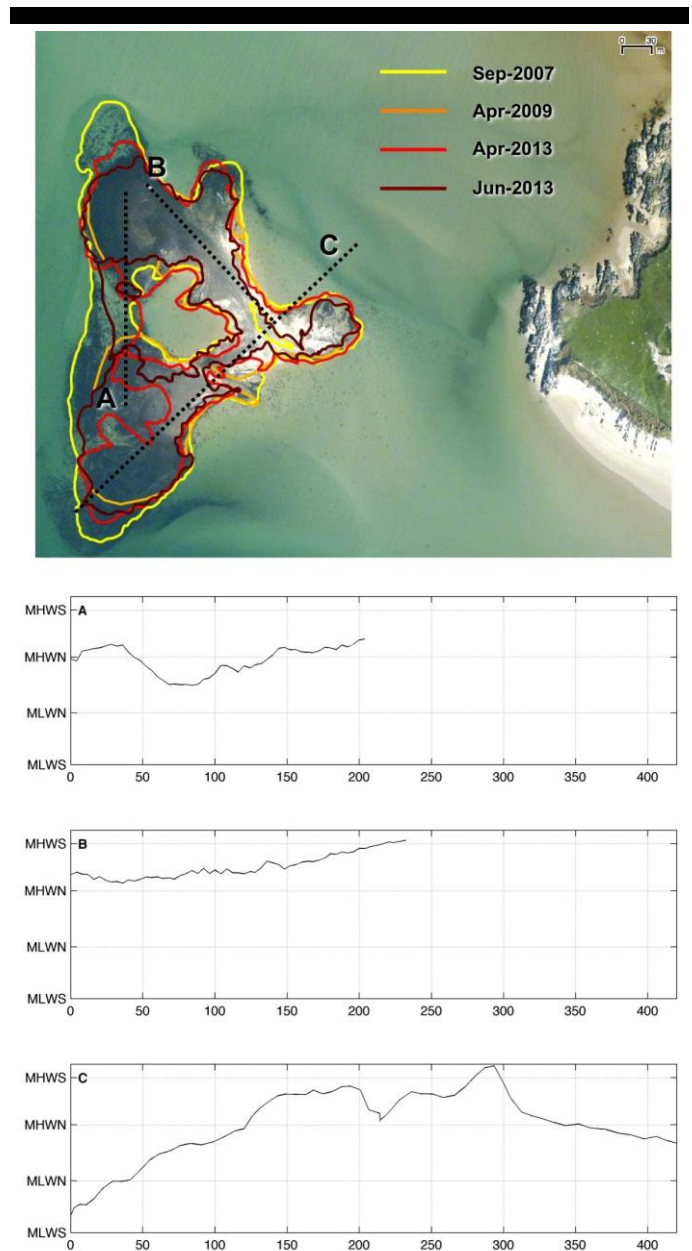


Figure 4. Detailed field surveys of sand/cobble boundary at Connell's Bank, and representative topographic transects A-C.

significant impact on subsequent paraglacial coastal evolution. The permanence of this structure over mapping timescales shows that it is largely relict with a surface cobble lag that has protected underlying sediments from contemporary wave disturbance. Such features are common throughout the western Ireland coast, suggesting that the present-day coastal landscapes are a palimpsest of past and contemporary geologic and climate-driven processes, and of recent human activity. Identifying the relative age and origins of different coastal landforms within a single region, such as an estuarine basin, can yield a better understanding of the nature of coastal palimpsests and thus the sensitivity of coastal landscapes to forcing.



## LITERATURE CITED

- Barrett-Mold, C. and Burningham, H., 2010. Contrasting ecology of prograding coastal dunes on the northwest coast of Ireland. *Journal of Coastal Conservation*, 14, 81–90.
- Brooks, A.J., Bradley, S.L., Edwards, R.J., Milne, G.A., Horton, B. and Shennan, I., 2008. Postglacial relative sea-level observations from Ireland and their role in glacial rebound modelling. *Journal of Quaternary Science*, 23, 175–192.
- Burningham, H., 2002. Meso-scale morphological changes in the Loughros More estuary. *Littoral 2002: The Changing Coast*, 3, 265–270.
- Burningham, H., 2008. Contrasting geomorphic response to structural control: the Loughros estuaries, northwest Ireland. *Geomorphology*, 97, 300–320.
- Carter, R.W.G., 1983. Raised coastal landforms as products of modern process variations and their relevance in eustatic sea-level studies: examples from eastern Ireland. *Boreas*, 12, 167–182.
- Carter, R.W.G. and Orford, J.D., 1988. Conceptual model of coarse clastic barrier formation from multiple sediment sources. *Geographical Review*, 78, 221–239.
- Carter, R.W.G. and Orford, J.D., 1993. The morphodynamics of coarse clastic beaches and barriers: A short- and long-term perspective. *Journal of Coastal Research*, Special Issue No. 15, 158–179.
- Carter, R.W.G., Orford, J.D., Forbes, D.L. and Taylor, R.B., 1990. Morphosedimentary development of drumlin-flank barriers with rapidly rising sea level, Story Head, Nova Scotia. *Sedimentary Geology*, 69, 117–138.
- Carter, R.W.G. and Wilson, P., 1993. Aeolian processes and deposits in northwest Ireland. In: Pye, K. (ed.), *The Dynamics and Environmental Context of Aeolian Sedimentary Systems*. Geological Society Special Publication, 72, pp. 173–190.
- Church, M. and Ryder, J.M., 1972. Paraglacial sedimentation: a consideration of fluvial processes conditioned by glaciation. *Bulletin of the Geological Society of America*, 83, 3059–3071.
- Dawson, A., Elliott, L., Noone, S., Hickey, K., Holt, T., Wadhams, P. and Foster, I., 2004. Historical storminess and climate ‘see-saws’ in the North Atlantic region. *Marine Geology*, 210, 247–259.
- Delaney, C. and Devoy, R., 1995. Evidence from sites in Western Ireland of late Holocene changes in coastal environments. *Marine Geology*, 124, 273–287.
- Dury, G.H., 1957. A glacially breached watershed in Donegal. *Irish Geography*, 3, 171–180.
- FitzGerald, D.M. and Van Heteren, S., 1999. Classification of paraglacial barrier systems: coastal New England, USA. *Sedimentology*, 46, 1083–1108.
- Forbes, D.L., Shaw, J. and Taylor, R.B., 1995a. Differential preservation of coastal structures on paraglacial shelves: Holocene deposits of southeastern Canada. *Marine Geology*, 124, 187–201.
- Forbes, D.L., Orford, J.D., Carter, R.W.G., Shaw, J. and Jennings, S.C., 1995b. Morphodynamic evolution, self-organisation, and instability of coarse-elastic barriers on paraglacial coasts. *Marine Geology*, 126, 63–85.
- Forbes, D.L. and Syvitski, J.P.M., 1994. Paraglacial coasts. In: Carter, R.W.G. and Woodroffe, C.D. (eds.), *Coastal Evolution – Late Quaternary shoreline morphodynamics*. Cambridge University Press, pp. 373–424.
- Forbes, D.L., Taylor, R.B., Orford, J.D., Carter, R.W.G. and Shaw, J., 1991. Gravel-barrier migration and overstepping. *Marine Geology*, 97, 305–313.
- Greenwood, R.O. and Orford, J.D., 2007. Factors controlling to the retreat of drumlin coastal cliffs in a low energy marine environment – Strangford Lough, Northern Ireland. *Journal of Coastal Research*, 23, 285–297.
- Hayes, M.O., Michel, J. and Betenbaugh, D.V., 2010. The intermittently exposed, coarse-grained gravel beaches of Prince William Sound, Alaska: comparison with open-ocean gravel beaches. *Journal of Coastal Research*, 26, 4–30.
- Hein, C.J., FitzGerald, D.M., Carruthers, E.A., Stone, B.D., Barnhardt, W.A. and Gontz, A.M., 2012. Refining the model of barrier island formation along a paraglacial coast in the Gulf of Maine. *Marine Geology*, 307, 40–57.
- Hoffmann, G., Lampe, R. and Barnasch, J., 2005. Postglacial evolution of coastal barriers along the West Pomeranian coast, NE Germany. *Quaternary International*, 133, 47–59.
- Johnston, M.R., 2001. Nelson Boulder Bank, New Zealand. *New Zealand Journal of Geology & Geophysics*, 44, 79–88.
- Knight, J., 2005. Controls on the formation of coastal ventifacts. *Geomorphology*, 64, 243–254.
- Knight, J., 2008. The environmental significance of ventifacts: A critical review. *Earth-Science Reviews*, 86, 89–105.
- Knight, J., 2009. Subglacial erosion forms in northwest Ireland. *Boreas*, 38, 545–554.
- Knight, J., 2011. Drumlin formation in a confined bedrock valley, northwest Ireland. *Boreas*, 40, 289–302.
- Knight, J., 2012. The last glaciation of Aran Island and Cruit Island, County Donegal, north-west Ireland. *Irish Journal of Earth Sciences*, 30, 49–58.
- Knight, J. and Burningham, H., 2011. Boulder dynamics on an Atlantic-facing coastline, northwest Ireland. *Marine Geology*, 283, 56–65.
- Knight, J. and Harrison, S., 2009. Periglacial and paraglacial environments: a view from the past into the future. In: Knight, J. and Harrison, S. (eds.), *Periglacial and paraglacial processes and environments*. Geological Society Special Publication 320, pp. 1–4.
- Ó Cofaigh, C., Dunlop, P. and Benetti, S., 2012. Marine geophysical evidence for Late Pleistocene ice sheet extent and recession off northwest Ireland. *Quaternary Science Reviews* 44, 147–159.
- Orford, J.D. and Anthony, E.J., 2011. Extreme events and the morphodynamics of gravel-dominated coastal barriers: Strengthening uncertain ground. *Marine Geology*, 290, 41–45.
- Orford, J.D., Carter, R.W.G., Jennings, S.C. and Hinton, A.C., 1995. Processes and timescales by which a coastal gravel-dominated barrier responds geomorphologically to sea-level rise: Story Head Barrier, Nova Scotia. *Earth Surface Processes and Landforms*, 20, 21–37.
- Orford, J.D., Forbes, D.L. and Jennings, S.C., 2002. Organisational controls, typologies and time scales of paraglacial gravel-dominated coastal systems. *Geomorphology*, 48, 51–85.
- Orford, J.D., Murdy, J.M. and Wintle, A.G., 2003. Prograded Holocene beach ridges with superimposed dunes in north-east Ireland: mechanisms and timescales of fine and coarse beach sediment decoupling and deposition. *Marine Geology*, 194, 47–64.
- Powers, M.C., 1953. A new roundness scale for sedimentary particles. *Journal of Sedimentary Petrology*, 23, 117–119.
- Ruz, M.-H., 1989. Recent evolution of the southeast barrier coast of Ireland. *Journal of Coastal Research*, 5, 523–539.
- Shaw, J. and Carter, R.W.G., 1994. Coastal peats from northwest Ireland: implications for late-Holocene relative sea-level change and shoreline evolution. *Boreas*, 23, 74–91.
- Stevenson, C.T.E., Hutton, D.H.W. and Price, A.R., 2008. The Trawenagh Bay Granite and a new model for the emplacement of the Donegal Batholith. *Transactions of the Royal Society of Edinburgh: Earth Sciences*, 97, 455–477.
- Zingg, T., 1935. Beitrag zur Schotteranalyse. *Schweizerische Mineralogische und Petrographische Mitteilungen*, 15, 38–140.

## Time and spatial variability of sediment grading in the surfzone of a large scale nourishment

B.J.A. Huisman<sup>†‡</sup>, E.E. Sirks<sup>†</sup>, L. van der Valk<sup>∞</sup>, D.J.R. Walstra<sup>†‡</sup>

<sup>†</sup> Civil Engineering & Geosciences  
Technical University of Delft  
P.O. Box 5048  
2628 CN Delft, The Netherlands  
Bas.huisman@deltares.nl

<sup>‡</sup> Harbour, Coastal and Offshore  
Engineering  
Deltares, P.O. Box 177  
2600 MH Delft, The Netherlands

<sup>∞</sup> Morphology and Sedimentary Systems  
Deltares, P.O. Box 177  
2600 MH Delft, The Netherlands



[www.cerf-jcr.org](http://www.cerf-jcr.org)



[www.JCRonline.org](http://www.JCRonline.org)

### ABSTRACT

Huisman, B.J.A., Sirks, E.E., van der Valk, L., Walstra, D.J.R., 2014. Time and spatial variability of sediment grading in the surfzone of a large scale nourishment. In: Green, A.N. and Cooper, J.A.G. (eds.), *Proceedings 13<sup>th</sup> International Coastal Symposium* (Durban, South Africa), *Journal of Coastal Research*, Special Issue No. 70, pp. 127-132-134, ISSN 0749-0208.

Temporal and spatial variations in sediment gradation in the surfzone were investigated for a large scale nourishment (Sand Motor) at the Dutch coast (~ 21.5 million m<sup>3</sup> sand). This nourishment provides an excellent opportunity to investigate the effect of hydrodynamic conditions on the spatial and temporal development of sediment grading. A strong point of the Sand Motor is that it has a well-known initial sediment composition. Measurements of the sediment grading at the Sand Motor were carried out during and after its construction to investigate the sorting process. Samples were taken for six cross-shore rays at ten depth contours (from MSL -1m to MSL -10m). A weighted average of the grain size distribution was determined for each cross-shore transect to investigate the alongshore sorting process. Similarly, cross-shore averaged sediment properties were determined for the samples above and below MSL -4m to assess the cross-shore sorting process. The sieved samples showed that: (1) significant sediment sorting takes place across the surfzone of the Sand Motor. Typically, the sediment in the surfzone of the exposed part of the Sand Motor is 20 to 30% coarser than the average for the survey; (2) a large depositional area with relatively fine material (150 to 200 μm) from the Sand Motor has developed on the Northern side of the Sand Motor; and (3) an alongshore band with finer sediment was found at water depths of 4 to 6 meter below MSL as a result of selection processes at the waterline.

**ADDITIONAL INDEX WORDS:** *Coastline perturbation, Nourishment, Sediment characteristics, Morphology.*

### INTRODUCTION

The relevance of heterogeneous bed sediment composition for bed forms, sediment transport and coastal evolution has been pointed out by many authors (e.g., Komar, 1987; Moutzouris *et al.*, 1991; Hoekstra *et al.*, 1997; Anthony, 1998). Field investigations have shown trends for the spatial variation in sediment properties at sand and gravel coasts. Sediment grading at the shoreface is represented by a fining of sediment grain size in offshore direction (Richmond & Sallenger, 1984) with coarsest sediment being found in the swash zone (e.g., Pruszek, 1993). Moutzouris *et al.* (1991) explains that coarse sediments are found in the troughs of barred beaches and fine sediments at the bar crests. For the Dutch coast, however, coarser material was found at the bar crests (Guillén and Hoekstra, 1996). Temporal variations in sediment gradation in the surfzone were studied by Medina *et al.* (1994) showing the largest seasonal variability in the swash zone.

Local sediment gradation is affected by a combination of hydrodynamic conditions and sediment availability. This implies that the antecedent morphology and geological history play an important role (Eisma, 1968; Van Straaten, 1965). In practice, however, it is often difficult to establish whether temporal and spatial variability in sediment gradation should be attributed to the substrate heterogeneity (i.e., sedimentary history) or to hydrodynamic sorting processes as such analyses are often

hampered by relatively low spatial and temporal sampling resolutions. To overcome this difficulty, more controlled



Figure 1. Aerial Photograph of the Sand Motor after completion (September 2011) looking southward showing clouds of fine-grained material. Picture courtesy of Rijkswaterstaat/Joop van Houdt.

situations in laboratory wave tunnels have been investigated to assess small scale sorting, transport processes and bedform evolution (e.g., Sonu, 1972; Táncoz, 1996). The complex hydrodynamics and larger scale sorting processes in the surfzone of sandy coasts can, however, not be captured sufficiently in laboratory scale experiments.

### Sand Motor

The recent construction of the Sand Motor along the Dutch coast (i.e., a nourishment of 21.5 million m<sup>3</sup> sand; see Fig. 1) provides an excellent opportunity to observe large scale sediment sorting at a natural beach (Mulder & Tonnon, 2010; Stive *et al.*, 2013). The size of the intervention makes it possible to better distinguish the impact of hydrodynamic processes on sediment sorting than for other nourishments (Guillén & Hoekstra, 1996). Furthermore, the influence of antecedent morphology and geological history will be reduced since the Sand Motor has a well-known sediment composition.

The Sand Motor is located between Monster and Kijkduin on the southern part of the Holland coast (i.e., Delfland coast). The local coastline prior to the nourishment was almost straight and had an average orientation of 312°N. Original beach and dune sediment generally consisted of fine sands (~100 to 200 µm), with mostly medium sized sand in the swash and surf (~200 to 400 µm) and finer sands in an offshore direction (~100 to 300 µm) up until 8-10 meter depths (Van Straaten, 1965). However, patches with coarse material (i.e., >500 µm) can occasionally be found.

### Aims

It is hypothesized that sorting processes at the Sand Motor shoreface will have a large scale impact on the sediment grading in the area. Significant coarsening is expected at the Sand Motor shoreface due to the exposure to waves and tide, while fine sediment patches are expected to develop at the coast directly north and south of the Sand Motor. Magnitude and time scale of the sorting process are, however, not known. The aim of this research is to characterize the spatial and temporal development of the sediment grading in the first one and a half years after the construction of the Sand Motor. This will provide a basis for further research regarding the impact of sediment sorting on the redistribution of large scale nourishments.

## APPROACH

### Field sampling

Field surveys (Fig. 2) were carried out pre-construction of the Sand Motor from 12-14<sup>th</sup> October 2010 (T<sub>0</sub>), during construction in April to June 2011 (T<sub>1</sub>) and post-construction from 20-29<sup>th</sup> August 2012 (T<sub>2</sub>) and from 21 to 22 February 2013 (T<sub>3</sub>). It is noted that the T<sub>1</sub> samples were collected by the dredgers at the dry beach during construction. The T<sub>0</sub> and T<sub>2</sub> surveys were carried out by IMARES and the T<sub>3</sub> survey by the TU-Delft. The surfzone sediment samples were collected with a Van Veen grab sampler at depth contours spanning MSL -1m to MSL -10m. All surveys used the same sampling and sieving methodology.

The wave conditions during the surveys were similar. Average wave heights ranged from 1 to 1.2 m with average wave periods of about 4 seconds. Wave directions varied from North (T<sub>0</sub>) to West (T<sub>2</sub>) and North-North-East (T<sub>3</sub>). The variation of the wave height over the period of the measurements and the month preceding the measurements was similar for all surveys, with a wave height ranging from 0.2 to 4 m and wave periods from 2.5 to 7 s.

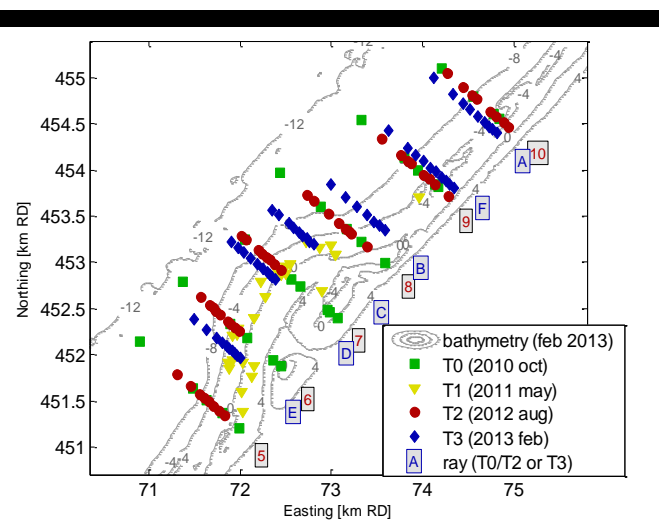


Figure 2. Overview of sample locations for the three field measurement surveys and the labelling of transects. T<sub>0</sub> and T<sub>2</sub> transects are labelled 5 to 10 and T<sub>3</sub> is labelled A to F.

The number of samples per transect was 5 points for the T<sub>0</sub> survey and 7 to 10 points for the T<sub>2</sub> and T<sub>3</sub> survey. The T<sub>1</sub> survey consisted of scattered samples over the Sand Motor area.

The difference in alongshore spacing of the samples resulted in a selection of five transects (A, B, D, E and F in Fig. 2) which were used for the analysis. Representative sediment compositions at transects A, D and F were obtained for the surveys T<sub>0</sub> and T<sub>2</sub> by using data of the nearest transects. Data from transect 5 and 6 were combined (with a ratio of 27% and 73%) to obtain a bed composition for transect E for surveys T<sub>0</sub> and T<sub>2</sub>. Similarly, transect B data is a combination of data of transect 8 and 9 (74% and 26% respectively).

### Sieving and Analyses

The dry or wet sieve method was applied (British Standards 812, 1975) for the 2013 survey and the Malvern for the other surveys. The proportion of shells was determined by pre-treatment with acid for a selection of the samples.

The analysis of the samples consisted of an investigation of the measured sediment properties. For this purpose the weight percentiles of the grain size and median grain size were determined. This information was then used to assess the uniformity coefficient ( $D_{60}/D_{10}$ ), graphical sample standard deviation and skewness (Folk & Ward, 1957; McLaren, 1981). These characteristics of the sediment distributions were then used in the evaluation of the origins of the sediment as McLaren and Bowles (1985) indicated that the mean, standard deviation and skewness change in the direction of the sediment path.

Variability in the alongshore sediment characteristics was investigated on the basis of alongshore averaged sediment properties per transect. A weighted average of the grain size distribution was determined per cross-shore transect (Medina *et al.*, 1996), which weighs the contribution of each sample depending on the cross-shore extent for which it is representative. This extent is determined by attributing half of the distance to the neighboring samples. Samples of each transect are used only up till the most seaward sample of the 2013 survey. Similarly, aggregated sample properties were computed for samples above and below MSL -4m to assess the cross-shore sorting process.

## RESULTS AND ANALYSIS

The overall changes in the sediment properties in the study area (Table 1) show that the average median grain size for the considered surveys ranged from 230 to 300  $\mu\text{m}$  with a moderate width of the distribution (standard deviation  $\sim 0.6$  to  $0.7$ ). The median grain size after construction of the Sand Motor was 30 to 70  $\mu\text{m}$  higher than in the  $T_0$  situation, which indicates a small shift towards coarser sediment as a result of the construction of the Sand Motor. The average width of the distributions (i.e., standard deviation) was similar for the different surveys. Average skewness was found to be small for all the surveys. Although construction of the Sand Motor may have affected the average sediment composition of the area to some extent, it is considered a small change in overall sediment properties when compared to the expected natural variability in sediment properties.

Table 1. Overview of average sediment properties for the considered measurement surveys

	D10 [ $\mu\text{m}$ ]	D30 [ $\mu\text{m}$ ]	D50 [ $\mu\text{m}$ ]	D60 [ $\mu\text{m}$ ]	D90 [ $\mu\text{m}$ ]	Std* [-]	Skew* [-]
$T_0$ (oct 2010)	125	185	232	275	469	0.73	-0.07
$T_1$ (jun 2011)	151	204	278	309	482	0.64	0.06
$T_2$ (aug 2012)	166	240	301	360	591	0.70	0.01
$T_3$ (feb 2013)	157	218	268	295	459	0.61	-0.03

\* graphical standard deviation and skewness were computed from the Phi values of the sediment (i.e.  $-\log_2(D \text{ percentile})$ )

## Spatial and temporal patterns

Spatial plots of observed median grain diameter for the  $T_0$ ,  $T_2$  and  $T_3$  surveys (Fig. 3) show considerable variability in the sediment composition in time and space within the observed area. A transition from coarse sediment in shallow water to finer sediment offshore is observed for the reference situation  $T_0$ , which is in line with observations in literature (e.g., Richmond and Sallenger, 1984). The construction of the Sand Motor affected the median grain diameter considerably. Samples with coarser sediment are noticeable in deeper water at the Sand Motor in the August 2012 survey ( $T_2$ ). This survey also shows a band of finer sediment along the Sand Motor at depths ranging from MSL -4m to MSL -8m. The  $T_3$  survey (February 2013) shows a more pronounced distinction between coarser sediment at the Sand Motor and finer sediment in the area North of it. The width of the grain size distribution within each survey differs considerably over space and time (Fig. 4). The uniformity coefficient for all surveys ranges between 1.5 and 3, but it is much narrower in the Sand Motor area in the  $T_3$  survey. This is expected to be related to the coarsening of the sediment at the Sand Motor over time. A relatively wide uniformity coefficient is found North of the Sand Motor area. This is expected to be due to the accumulation of much finer material than was naturally present in the bed.

Aggregated sediment parameters per transect will be used to quantify the alongshore and cross-shore development of the bed sediment composition over time.

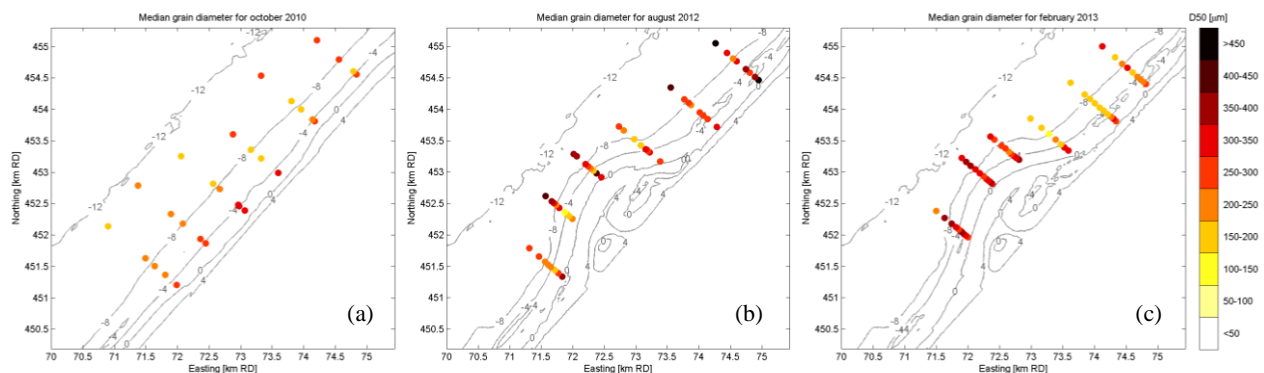


Figure 3. Median grain diameter of sediment samples for  $T_0$ ,  $T_2$  and  $T_3$  measurement surveys ( $T_1$  surveys are located on land)

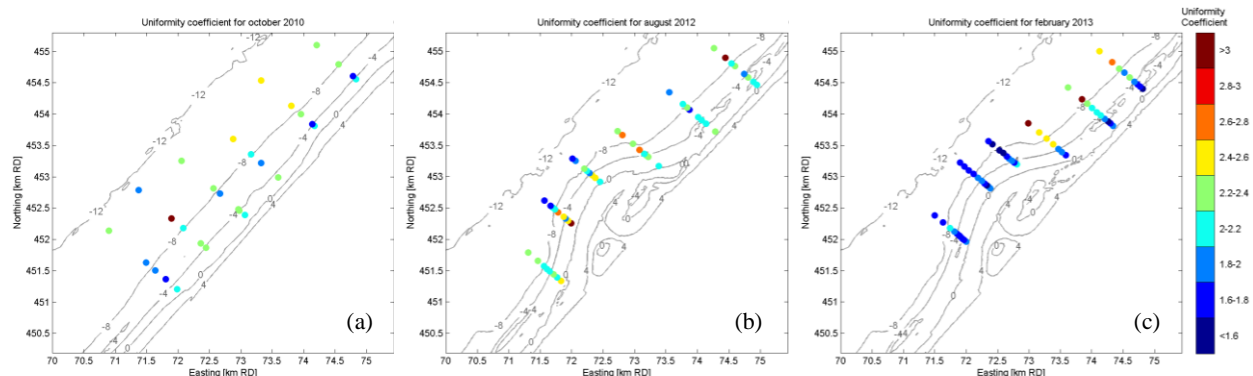


Figure 4. Uniformity coefficient of sediment samples for  $T_0$ ,  $T_2$  and  $T_3$  measurement surveys ( $T_1$  surveys are located on land)

**Alongshore**

The alongshore variation of the sediment parameters in time and space is quantified by using a cross-shore weighted average of the median grain diameter along the considered transects (i.e., A, B, D, E and F of the 2013 survey; also see Section ‘Approach’).

An overview of the bed sediment composition in space and time is provided in Table 2. This table shows the weighted median grain diameters per transect (referred to as ‘Master Samples’) and the weighted average for the whole measurement survey. The Master Samples per transect are then compared relatively to the weighted average grain diameter for the whole survey. Such a relative measure will reduce the influence of study specific aspects (e.g. the monitored area, sampling and sieving methodology). The first three rows of the table are located North of the Sand motor and the last two rows at the Sand Motor.

Table 2. Master samples of the median grain diameter per transect for the three measurement surveys (i.e., as an absolute value and relative to ‘weighed average’ of all transects).

transect	T <sub>0</sub> (Oct 2010)		T <sub>2</sub> (Aug 2012)		T <sub>3</sub> (Feb 2013)	
	D50 [µm]	relative impact*	D50 [µm]	relative impact	D50 [µm]	relative impact
A	241	4%	381	26%	251	-6%
B	207	-11%	302	0%	197	-27%
F	242	4%	260	-14%	189	-30%
D	227	-2%	324	8%	343	28%
E	240	3%	286	-5%	320	19%
<i>weighted avg.</i>	232		301		268	

\* Relative deviation from the weighted average for the whole survey

The transect-averaged median grain diameters in Table 2 show that the reference survey (T<sub>0</sub>) has a relatively smaller variation in the alongshore averaged median grain size (i.e., -11% to +4%) than the other surveys. Small scale changes less than 10%, however, are considered insignificant. The changes in August 2012 survey (T<sub>2</sub>) are considerable but still patchy, whereas the 2013 survey (T<sub>3</sub>) shows very significant alongshore variation in bed sediment composition.

The 2013 survey (T<sub>3</sub>) shows considerable coarsening of the sediment in transects D and E and fining of the sediment in transects B and F. This alongshore variation is attributed to a large scale sorting process at the Sand Motor. It is expected that predominant erosion of the finer sediment fractions at the Sand Motor results in a relative coarsening of the sediment composition at transects D and E. The average median grain size at these transects changed from 305 µm to 332 µm between measurement surveys T<sub>2</sub> and T<sub>3</sub>. This sediment is then transported along the coast towards deeper and less energetic areas, which creates the patch with finer sediment in transects B and F. The decrease of the uniformity coefficient in the area of the Sand Motor (T<sub>3</sub> survey in Fig. 4) also provides evidence for larger scale sorting processes since the difference between the D<sub>10</sub> and D<sub>60</sub> decreased as a result of washing out of the finer sediment fractions. This is also confirmed by 10<sup>th</sup> weight percentiles of the grain size at these transects (Fig. 5), which is significantly coarser at the Sand Motor.

It is noted that the coarser sediment in Transect A of the 2012 survey T<sub>2</sub> (see Fig. 3b) is not considered to be related to the processes at the Sand Motor as it is influenced strongly by a single very coarse sample in deep water (MSL -10m). It is hypothesized that a patch with coarser sediment was present just below the surface of the bed at this location.

The width of the grainsize distribution in the 2013 survey T<sub>3</sub> (see Fig. 7b) was smaller at the Sand Motor and the transect north

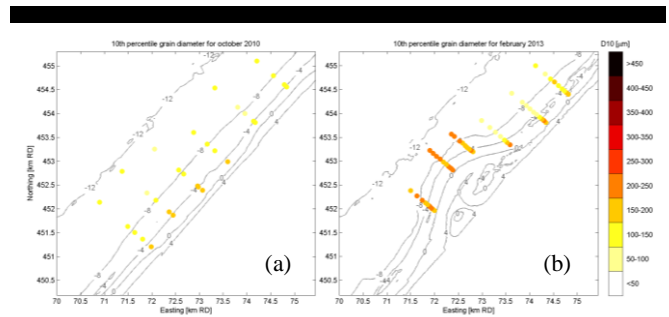


Figure 5. 10<sup>th</sup> weight percentiles of the grain size distribution for the October 2010 and February 2013 surveys (T<sub>0</sub> and T<sub>3</sub>).

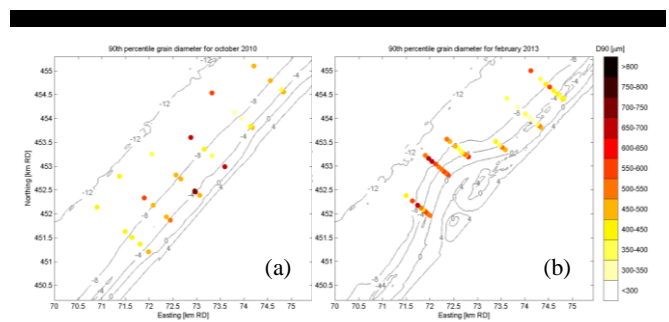


Figure 6. 90<sup>th</sup> weight percentiles of the grain size distribution for the October 2010 and February 2013 surveys (T<sub>0</sub> and T<sub>3</sub>).

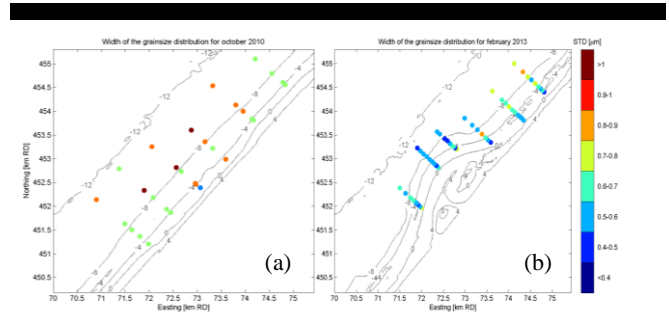


Figure 7. Graphical standard deviation of the grain size distribution for the October 2010 and February 2013 surveys

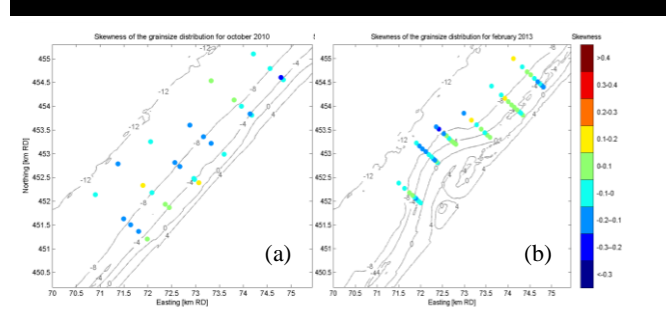


Figure 8. Graphical skewness of the grain size distribution for the October 2010 and February 2013 surveys (T<sub>0</sub> and T<sub>3</sub>)

of it (standard deviation  $\sim 0.5 \mu\text{m}$ ) than for the surrounding transects (standard deviation  $\sim 0.6$  to  $0.8 \mu\text{m}$ ). This indicates that sediment is better sorted at the Sand Motor. The sediment distributions had quite symmetrical shapes near the shore, with increasing negative skewness for the more offshore points (Fig. 8), which provides an indication for a net offshore directed path of the sediment (McLaren & Bowles, 1985).

### Cross-shore

The impact of the Sand Motor on the cross-shore distribution of the sediment gradings is investigated by comparing the Master Samples of the nearshore and offshore transect data (Table 3). A threshold at MSL -4m was chosen since this depth approximately demarcates the location of the bars. It is noted that differences in sediment composition of similar magnitude are found for the offshore and nearshore part of the profile if depth thresholds at MSL -3m or MSL -5m are applied.

The median grain diameter of the offshore part of the transects was smaller than the nearshore sediment for the reference survey  $T_0$  (i.e.,  $D_{50 \text{ offshore}}$  was 22% finer than the  $D_{50}$

Table 3. Master samples of the median grain diameter of the samples below MSL -4 m for each transect for the three measurement surveys (i.e., absolute and relative value).

Transect	T0 (oct 2010)			T2 (aug 2012)			T3 (feb 2013)		
	Off* <sup>1</sup>	Nsh* <sup>2</sup>	Dev* <sup>3</sup>	Offs.	Nsh.	Dev.	Offs.	Nsh.	Dev.
A	240	257	-7%	383	377	2%	255	232	10%
F	204	238	-15%	311	288	8%	183	255	-28%
B	218	306	-29%	242	282	-14%	162	288	-44%
D	210	327	-36%	329	318	3%	347	333	4%
E	233	282	-17%	314	217	45%	320	320	0%
W.Avg* <sup>4</sup>	221	282	-22%	316	297	+6%	253	286	-11%

\*1 Master sample of  $D_{50}$  for offshore samples ('Off')

\*2 Master sample of  $D_{50}$  for nearshore samples ('Nsh')

\*3  $D_{50}$  deviation of offshore sample from nearshore sample ('Dev')

\*4 Weighted average for each survey ('W.Avg')

nearshore), while the other surveys show a smaller difference of the median grain diameter of the offshore and nearshore sediment (+6% and -11%). This is expected to be related to the construction of the Sand Motor after which the sediment composition became much more homogeneous.

When specific transects are investigated it is found that the transects North of the Sand Motor (i.e., B and F) have experienced a considerable fining of the offshore sediment composition over time from the  $T_2$  to the  $T_3$  survey (e.g., a change of the  $D_{50}$  of the

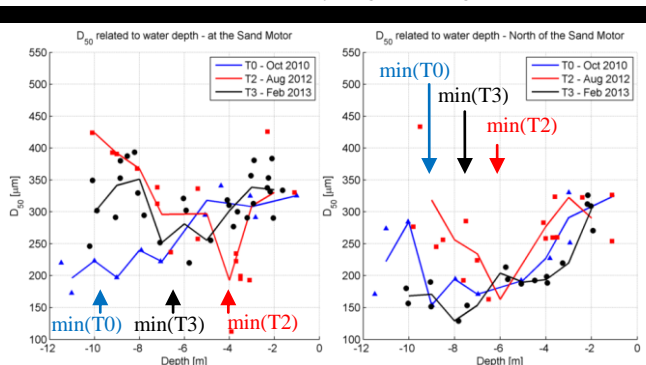


Figure 9. Average cross-shore sediment composition ( $D_{50}$ ) for transects at the Sand Motor (C, D and E) and for transects North of the Sand Motor (A, B and F). The lines represent the moving average of the cross-shore sediment composition.

offshore sediment from +8% to -28% of the  $D_{50}$  of the nearshore sediment). No clear differences between offshore and nearshore sediment composition can be found for the other transects in survey  $T_3$ . The observed overall fining of the transects B and F (Table 2) is therefore expected to take place predominantly in the offshore part of transects B and F, which is the deeper, less energetic portion of these transects.

The average cross-shore sediment composition for the transects at the Sand Motor and for the transects North of it (Fig. 9) shows that a minimum in the median grain diameter can be found in each of the surveys. This minimum is located most seaward for the reference survey ( $T_0$ ), it is located at about 4 m water depth in the 2012 survey after construction of the Sand Motor ( $T_2$ ) and has shifted to about 6 m water depth in the 2013 survey ( $T_3$ ). It is hypothesised that the area with the minimum median grain diameters demarcates the offshore extent of the sorting process at the Sand Motor, as the most extreme wave conditions after construction of the Sand Motor have transported fine sediment from the shoreline to deep water during erosive events.

### DISCUSSION

The current surveys show large scale sorting of sediment at the Sand Motor over a period of 1.5 years. Despite the limited number of available surveys, the large signal in the final survey (-30% and +30% in median grain diameter) provides strong evidence for the observed coarsening of the sediment at the Sand Motor and subsequent fining of sediment North of the Sand Motor. Specific aspects of the sampling and sieving methodology may, however, have some impact on the results. Sections below elaborate on:

- 1) Van Veen grab sampling method
- 2) Method of sieving and analysis
- 3) Shells, organic matter and fines
- 4) Nourishments preceding the Sand Motor
- 5) Intra-survey changes in bed sediment composition.

Sediment sampling with a Van Veen mini grabber inherently means that only the first five to ten centimeters of the bed sediment are sampled. For the specific situation at the Sand Motor it is, however, expected that the differences in the vertical composition of the sediment deposits are small since the study area shows quite persistent and steady patterns of erosion and sedimentation.

Impact from the methodology for determining the grain size distribution (e.g., Murray & Van Holtum, 1996) is expected to be small for the current study since the study focuses mainly on the median grain diameters, which are shown to be better correlated for the different analysis techniques (e.g., Malvern or sieving) than derived properties of the distribution like Skewness and Kurtosis (Rodríguez & Uriarte, 2009).

The applied dry sieving method (and wet sieving method for a selection of samples) can be influenced by the content of shells and organic matter since the samples were not pre-treated with acid. For this reason, a total of 14 samples at 7 representative locations were pre-treated with acid and sieved again. This resulted in an estimate of the influence of shells and organic matter on the median grain diameter. On average the median grain size of the pretreated samples was  $14 \mu\text{m}$  smaller than the original result, while the 10<sup>th</sup> and 90<sup>th</sup> weight percentiles were  $5 \mu\text{m}$  and  $50 \mu\text{m}$  smaller, respectively. Some samples of transects North of the Sand Motor can therefore be slightly finer than determined in the current analysis, which would strengthen the conclusion of alongshore sorting.

It is noted that the coast adjacent to the Sand Motor is expected to be influenced by regular nourishments with medium size sand (i.e., 200 to 300  $\mu\text{m}$ ). The last nourishment was constructed in 2009 as part of the 'Zwakke Schakels' project and affected the whole Delfland coast. The actual changes in bed composition as a result of this nourishment, however, are expected to have already taken place before the survey in 2010, since most of the redistribution in the cross-shore has taken place and the resulting impact is expected to be smaller than the seasonal variability in sediment composition (Medina *et al.*, 1994).

The details of the intra-survey developments are difficult to quantify since this requires a higher frequency of the surveys or more insight in the time scales at which the processes act. For now, it is hypothesized that alongshore sorting is a steady process over time, since it is expected to be driven by the ongoing large scale erosion at the Sand Motor. The cross-shore time scale is expected to be much shorter and is likely to depend on temporary wave conditions that move finer sediment offshore, which is likely the cause of the band with finer sediment between 4 and 6 m water depths. These issues should, however, be verified by additional research.

It is envisaged that additional research should focus on: (1) the causes for the observed sediment sorting process; (2) the effects of sediment sorting on the morphological evolution of nourishments; and (3) observation of specific aspects of the sediment sorting. For example, it can be investigated whether the time scale of cross-shore changes is predominantly influenced by specific conditions (e.g., storms) or by the entire climate. Numerical models can be used to assess the potential impact of sediment sorting on sediment transport paths and morphological development of nourishments. From an observational point of view, it is relevant to see whether the impact of wave conditions differs for specific areas of the Sand Motor and how sharp the transitions in sediment grading along the coast can be. It is envisaged that data will be needed on longer term development as well as on specific events.

## CONCLUSIONS

The analysis of sediment sampling data from four field surveys at the Sand Motor showed the following:

- Significant coarsening of the sediment took place along the exposed part of the Sand Motor. On average a 20 to 30 % larger median grain diameter (300 to 350  $\mu\text{m}$ ) was found for transects at the Sand Motor in the February 2013 survey compared to the average for the area.
- A large depositional area with relatively fine material (150 to 200  $\mu\text{m}$ ) has developed on the Northern side of the Sand Motor. This sediment is expected to originate from the Sand Motor. Most of the accumulation took place in the deeper part of these transects below MSL -4m.
- An alongshore band with finer sediment was found at water depths of about 4 to 6 m below MSL for the surveys after construction of the Sand Motor (i.e., T<sub>2</sub> and T<sub>3</sub>). This is expected to be the result of cross-shore sediment transport of fine material from the shoreline.

## ACKNOWLEDGEMENT

The European Research Council of the European Union is acknowledged for the funding provided for this research by the ERC-advanced Grant 291206-NEMO. Sampling data for the years

2010 and 2012 were collected with support of the European Fund for Regional Development. Joep Storms of the Delft University of Technology is thanked for strengthening this paper by providing comments, while Matthieu de Schipper and Saulo Meirelles are thanked for their support during the sediment collection.

## LITERATURE

- Anthony, E.J., 1998. Sediment-wave parametric characterization of beaches. *Journal of Coastal Research*, 14, 347-352.
- British Standards (BS) 812, 1975. *Sampling, Shape, Size and Classification, part 1*.
- Eisma, D., 1968. Composition, origin and distribution of Dutch coastal sands between Hoek van Holland and the Island of Vlieland. *Netherlands Journal of Sea Research*, 4, 123-267.
- Folk, R.L. and Ward, W.C., 1957. Brazos River bar: a study in the significance of grain size parameters. *Journal of Sedimentary Petrology*, 27, 3-26
- Guillén, J. and Hoekstra, P., 1996. The 'equilibrium' distribution of grain size fractions and its implications for cross-shore sediment transport: a conceptual model. *Marine Geology*, 135, 15-33.
- Hoekstra, P., Houwman, K., Kroon, A., Ruessink, B., Roelvink, J. and Spanhoff, R., 1997. Morphological development of the Terschelling shoreface nourishment in response to hydrodynamic and sediment transport processes. In: Edge, B. (ed.), *Proceedings of the 25th International Conference on Coastal Engineering*, ASCE, 2897-2910.
- Komar, P.D., 1987. Selective grain entrainment by a current from a bed of mixed sizes: a reanalysis. *Journal of Sedimentary Petrology*, 57 (2), 203-211.
- McLaren, P.A., 1981. Interpretation of trends in grain-size measurements. *Journal of Sedimentary Petrology*, 51, 611-624.
- McLaren, P.A. and Bowles, D., 1985. The effects of sediment transport on grain-size distributions. *Journal of Sedimentary Petrology*, 55, 457-470.
- Medina, R., Losada, M.A., Losada, I.J. and Vidal, C., 1994. Temporal and spatial relationship between sediment grain size and beach profile. *Marine Geology*, 118, 195-206.
- Moutzouris, C.I., Kraus, N.C., Gingerich, K.J., Kriebel, D.L., 1991. Beach profiles vs. crossshore distributions of sediment grain sizes. In: Laxhan, V. (ed.), *Advances in Coastal Modeling*. New York, USA: American Society of Civil Engineers, 860-874.
- Mulder, J.P.M. and Tonnon, P.K., 2010. "Sand Engine " : Background and Design of a Mega-Nourishment Pilot in the Netherlands. *Proceedings of the 32nd International Conference on Coastal Engineering*.
- Murray, D.M. and Holtum, D.A., 1996. Technical Note: Inter-conversion of Malvern and Sieve Size Distributions. *Minerals Engineering*, 9 (12), 1263-1268.
- Pruszk, Z., 1993. The analysis of beach profile changes using Dean's method and empirical orthogonal functions. *Coastal Engineering*, 19, 245-261.
- Richmond, B.M. and Sallenger, A.H., 1984. Cross-shore transport of bimodal sands. *Proceedings of the 19th International Conference on Coastal Engineering*, ASCE, 1997-2008.
- Rodríguez, J. G. and Uriarte, A., 2009. Laser Diffraction and Dry-Sieving Grain Size Analyses Undertaken on Fine- and Medium-Grained Sandy Marine Sediments: A Note. *Journal of Coastal Research*, 251, 257-264.
- Sonu, C., 1972. Bimodal composition and cyclic characteristics of beach sediment in continuously changing profiles. *Journal of Sedimentary Petrology*, 42, 852-857.
- Stive, M.J.F., De Schipper, M.A., Luijendijk, A.P., Aarninkhof, S.G.J., Van Gelder-Maas, C., Van Thiel de Vries, J.S.M., De Vries, S., Henriquez, M., Marx, S. and Ranasinghe, R., 2013. A New Alternative to Saving Our Beaches from Sea-Level Rise: The Sand Engine, *Journal of Coastal Research*, 29 (5), 1001-1008.
- Tanczos, L.C., 1996. *Selective Transport Phenomena in Coastal Sands*. Groningen, The Netherlands: University of Groningen, Ph.D. thesis.
- Van Straaten, L.M.J.U., 1965. Coastal barrier deposits in South- and North Holland in particular in the area around Scheveningen and IJmuiden. *Mededelingen van de Geologische Stichting*, 17, 41-75.

## Monitoring changes in suspended sediment concentration on the southwestern coast of Korea

Jee-Eun Min<sup>†</sup>, Jong-Kuk Choi<sup>†</sup>, Hyun Yang<sup>†</sup>, Seok Lee<sup>‡</sup>, Joo-Hyung Ryu<sup>†</sup>

<sup>†</sup> Korea Ocean Satellite Center  
Korea Institute of Ocean Science and Technology  
Ansan 426-744, Korea  
[jemin@kiost.ac](mailto:jemin@kiost.ac)  
[jkchoi@kiost.ac](mailto:jkchoi@kiost.ac)  
[yanghyun@kiost.ac](mailto:yanghyun@kiost.ac)  
[jhyru@kiost.ac](mailto:jhyru@kiost.ac)

<sup>‡</sup> Marine Environments & Conservation Research Division  
Korea Institute of Ocean Science and Technology  
Ansan 426-744, Korea  
[lees@kiost.ac](mailto:lees@kiost.ac)



[www.cerf-jcr.org](http://www.cerf-jcr.org)



[www.JCRonline.org](http://www.JCRonline.org)

### ABSTRACT

Min, J. E., Choi, J. K., Yang, H., Lee, S., Ryu, J. H. 2014. Monitoring changes in suspended sediment concentration on the southwestern coast of Korea. In: Green, A.N. and Cooper, J.A.G. (eds.), *Proceedings 13<sup>th</sup> International Coastal Symposium* (Durban, South Africa), *Journal of Coastal Research*, Special Issue No. 70, pp. 133-138, ISSN 0749-0208.

Concentrations and distribution patterns of suspended sediment (SS) are key indicators of marine environmental change, particularly in coastal areas, which gives good information on the deposition and migration of sediments from land. In this study we analyzed 632 scenes (79 days × 8 scenes) of Geostationary Ocean Color Imager (GOCI) data in order to investigate SS variations relating to tides, tidal currents, bottom morphology, river discharge, and so on. We also compared them to the numerical model of tidal currents for the Yellow Sea. The study area, the coastline of Mokpo, is characterized by shallow water depths (<50 m), a relatively large tidal range (8 m) and by strong tidal currents (1 to 2 m/s). The coastal area of Mokpo shows extremely high SS concentrations (SSC) caused by a resuspension of bottom sediments. GOCI, the world's first geostationary ocean color observation satellite, can obtain data hourly during daylight. Therefore, GOCI is well equipped for the detailed analysis of time-series variations in SSC with regard to tides and tidal currents along Mokpo. The concentrations and distribution patterns of SS in the study area were mainly affected by tidal currents. During flood tide, SSC showed higher values than during ebb tide, and the SS distribution pattern flowed in a northerly direction. On the other hand, during ebb tide, the SS distribution pattern flowed towards the south. Bottom morphology also displayed a similar pattern to the SS distribution.

**ADDITIONAL INDEX WORDS:** GOCI (Geostationary Ocean Color Imager), suspended sediment, coastal waters, monitoring

### INTRODUCTION

The concentrations and distribution patterns of suspended sediment (SS) play an important role when monitoring marine environmental change, especially in coastal areas (May *et al.*, 2003; Torres and Morelock, 2002; Zhang *et al.*, 2010). High SS concentrations (SSC) reduce underwater vertical transmittance and phytoplankton productivity, which affect whole ecosystems (Cloern, 1987; Cole and Cloern, 1987; May *et al.*, 2003). Suspended sediment may also affect nutrient dynamics (Mayer *et al.*, 1998) and pollutant movement (Olsen *et al.*, 1982). In particular, short-term SS variations, due to civil construction in coastal regions, can lead to large changes in marine environments (Jung and Kim, 2005; Min *et al.*, 2012).

SS variations are generally related to environmental characteristics, such as tidal conditions, seasons, bottom morphology, discharge flow from rivers, and so on. In the study area, SSC variations may have been affected by these variables. Therefore, we endeavoured to find out which environmental factors highly affect to the SSC variations within this area of the Yellow Sea. A long-term time series analysis was required for the analysis of seasonal, and a short-term time series analysis was needed for the analysis of tidal direction variations. Existing

ocean color remote sensing satellite data, like as SeaWiFS (Sea-viewing Wide Field-of-view Sensor) and MODIS (Moderate Resolution Imaging Spectroradiometer), do not possess a sufficiently short 'revisit' cycle, so new satellite data with a shorter 'revisit' cycle needed to be acquired.

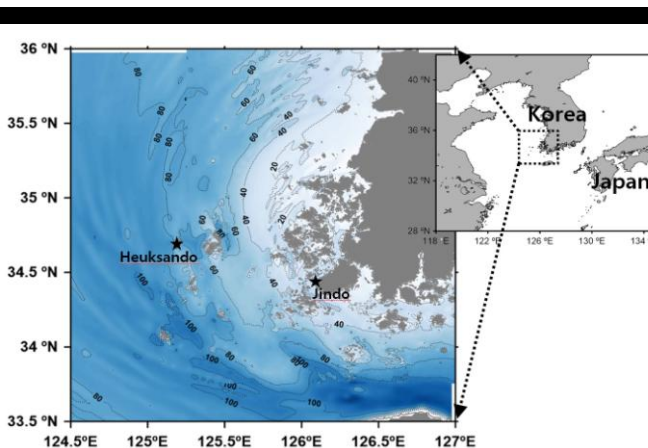


Figure 1. Study area with corresponding bathymetric map.

DOI: 10.2112/SI70-023.1 received 1 December 2013; accepted 21 February 2013. © Coastal Education & Research Foundation 2014



The Geostationary Ocean Color Imager (GOCI) is the world's first geostationary ocean color satellite and is now continuously observing our study area in its geostationary orbit. Because GOCI provided data every hour from 09h00 to 16h00 local time, we were able to analyze the short-term time series variations in SS distribution (Ryu *et al.*, 2011).

The study area, (i.e., the Mokpo coast), is located on a southwestern coastal part of the Yellow Sea (hereafter referred to as CM) (Figure 1). The area is characterized by shallow water depths (<50 m), relatively strong tidal currents (1 to 2 m/s) and complicated coastlines with numerous islands and extensive tidal flats (Kang *et al.*, 2009). There are semi-diurnal tides with an ebb-dominant tidal flow characterized by long flood and short ebb tides (Byun *et al.*, 2004). Freshwater is supplied to open sea by the Youngsan River. The SSC of this coastal area yielded relatively high values (>20 g/m<sup>3</sup>). During the winter season extremely high SSC values (>200 g/m<sup>3</sup>) occurred in shallow areas because of the strong northwest monsoon. In this study, we extracted front lines and current vectors using GOCI SS data, with the aim of observing spatial and seasonal variations as well as tide direction changes.

## DATA

A total of 632 scenes of GOCI data were used for SS analysis from January 2012 to March 2013. To retrieve the SS concentration from GOCI TOA (top-of-atmosphere) data, atmospheric correction was initially performed for all GOCI images. The modified MUMM approach was used (Ruddick *et al.*, 2000; Choi *et al.*, 2012; Choi *et al.*, 2013; Lee *et al.*, 2013), in which contributions by aerosol and water to satellite reflectance are estimated on a per-pixel basis, with the assumption of spatially constant band-7:band-8 ratios for aerosol reflectance ( $\epsilon$ ) and water reflectance ( $\alpha$ ). Each GOCI image was converted to radiance on the sea surface ( $L_w$ ), and  $L_w$  was converted to remote sensing reflectance ( $R_{rs}$ ) using the extraterrestrial solar irradiance ( $F_o$ ) values for each GOCI band. For the verification of atmospheric correction, we selected data matched within  $\pm 10$  minutes to the GOCI observation time. So obtained 25 matching data sets and these GOCI data showed a good correlation with matching in-situ  $R_{rs}$  values ( $R(490) = 0.89$ ,  $R(555) = 0.95$  and  $R(660) = 0.95$ ), as illustrated in Figure 2.

Tidal-, wind- and water depth-data were used for the comparison of SS variations with environmental factors. Data concerning tidal conditions (Jindo & Heuksando tidal station) and wind variations (Heuksando ocean observation station) were obtained from the Korea Hydrographic and Oceanographic Administration website (KHOA, <http://www.khoa.co.kr>). Current speed and direction data were obtained using a recording current meter (RCM) instrument between 23<sup>rd</sup> and 28<sup>th</sup> October 2013 off Mokpo. This data was used for the analysis of SS movement with respect to semi-diurnal tides along with the tidal model.

## METHODS

### SS Algorithm for GOCI

We developed a new empirical SS algorithm in a band combination format using 3 bands, as proposed by Siswanto *et al.* (2011). For the algorithm development, an in-situ dataset of SS concentrations and  $R_{rs}$  data were acquired within our study area. SS concentration (g/m<sup>3</sup>) was determined by gravimetric means and

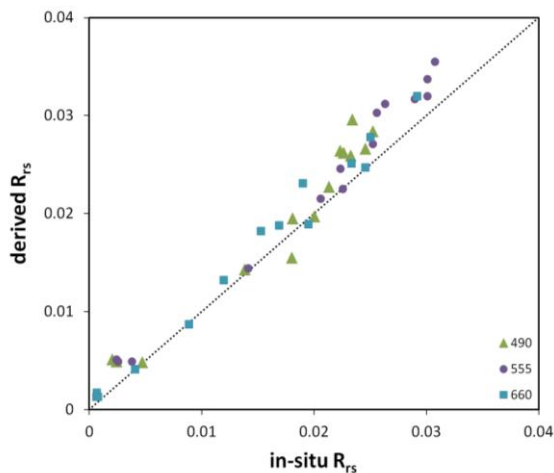


Figure 2. Verification of the atmospheric correction for GOCI (modified MUMM) using matching datasets on flyover time (within  $\pm 10$  minutes).

surface  $R_{rs}$  data were measured by the hyperspectral radiometer of ASD FieldSpec® portable spectroradiometer (Analytical Spectral Devices, Inc.). The equation below shows a newly developed SS algorithm for GOCI data. This algorithm showed best squared correlation coefficients ( $R^2$ ) of 0.97.

$$SS \text{ (g / m}^3\text{)} = 10^{(c_0+c_1(555+660)+c_2(\frac{490}{555}))} \quad (1)$$

$$c_0 = 0.6567, \quad c_1 = 28.83, \quad c_2 = -0.6917$$

### SS front and current vector analysis

For SS variation analysis, front lines of SS distribution were extracted and water current vectors were analyzed using time-series GOCI SS data. Front lines were extracted based on the boundary value of a 10 g/m<sup>3</sup> TSS concentration. The study area possesses highly turbid coastal waters with shallow water depths, so SS concentration was dynamically decreased offshore. Owing to this characteristic of the area, a SS front was easily extracted and a SS concentration of 10 g/m<sup>3</sup> was the best boundary value for extraction. Figure 4 shows extracted front lines for each SS image.

The water current vectors were analyzed using Ocean Surface Current Estimation (OSCE) algorithm developed by Choi *et al.* (2012). The OSCE is a method for current vector extraction using maximum cross correlation (MCC). GOCI has the advantage of a high temporal resolutions at 1 hour intervals. This unique feature enables the monitoring of dynamic changes in coastal water properties, especially for tidal currents in the CM area. We verified the OSCE results using in-situ RCM measurements obtained on the 23<sup>rd</sup> October 2013. A numerical model for tidal currents was used for comparison with the current vector analysis, which was developed by Lee *et al.* (2008) for the Yellow Sea. *In situ* tidal current data from RCM instrument were also used for comparison with the current vector results.

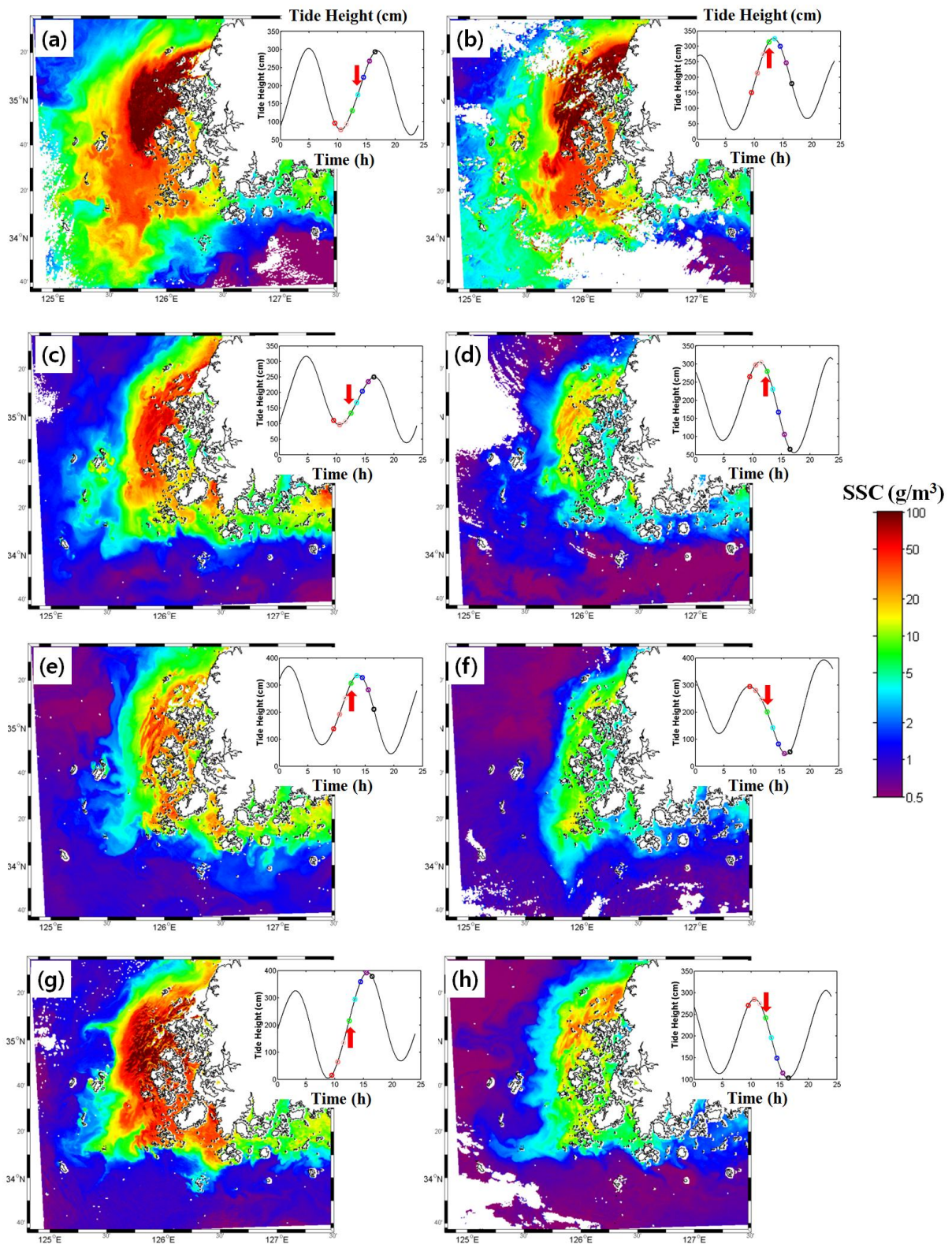


Figure 3. Comparison of SS distribution according to different tidal conditions of flood (a, c, e, and g) and ebb (b, d, f, and h) tide within same season (a and b for winter; c and d for spring; e and f for summer; and g and h for autumn). Images represent the SS distribution on the 27<sup>th</sup> Feb., 20<sup>th</sup> Feb., 26<sup>th</sup> Apr., 3<sup>rd</sup> May, 31<sup>st</sup> Aug., 31<sup>st</sup> Jul., 18<sup>th</sup> Oct., and 25<sup>th</sup> Oct., respectively.

## RESULTS AND DISCUSSION

### Spatial and seasonal variations

SS distribution off the coast of Mokpo was widely spread out towards the southwest, having higher SS concentrations during spring and winter seasons. Figure 3 showed seasonal SS images processed using GOCI. Figures 3a, c, e, g showed SS distribution maps acquired during flood tide in winter, spring, summer and autumn seasons, respectively. Conversely, Figures 3b, d, f and h showed SS distribution maps acquired during ebb tide in winter, spring, summer and autumn seasons, respectively. SS showed higher values during flood tide than during ebb tide conditions. It is assumed that the resuspension of bottom sediment is stronger during flood tide. This may be owing to a longer flood tide than ebb tide (Byun *et al.*, 2004).

Seasonal variation of SS distribution represented maximum extent during the winter season and minimum extent during the summer season. Maximum SS extent decreased toward the end of winter, whilst the minimum SS extent in summer expanded as winter approached. High SS concentrations and extents during the winter season were owing to strong north-westerly monsoon winds and the resulting resuspension of sediment. To confirm the influence of strong wind for high concentrations and wide areas of expansion, we processed front analysis, extracted from GOCI SS data using boundary value of 10 g/m<sup>3</sup>, and compared this with wind speed and direction data measured at the Heuksando Ocean Observation Station (Fig. 4). Wind speed during the winter season, during which SS values and areal coverage were greater, was

observed to be stronger than for summer months.

### Directional variations

Figure 5 displays the results of current vectors extracted from the GOCI SS data –tidal currents calculated from the numerical model and in-situ current data measured by RCM instruments on 26<sup>th</sup> October 2012. Figure 5a represents current vector results obtained from the GOCI SS data captured at 9 and 10 a.m.; Figure 5b represents the model result at 9:30 a.m.; and Figure 5c represents current direction and speed measured at 9:30 a.m. using RCM. Figures 5d, e, and f represent data obtained at 10:30 a.m., and Figures 5g, h and i represent data obtained at 11:30 a.m. in a same way. The results of current vectors (Figs. 5a, d, g) and tidal currents (Figs. 5b, e, h) showed similar patterns in direction toward southwestern area and reduction of vector size. In the case of *in situ* current data from RCM, its result at 10:30 a.m. shows very similar patterns to the current vectors and tidal currents at 10:30 a.m. Unfortunately the other data were not matched to the GOCI and model data and may be caused by the instantaneous flow of *in situ* measurements.

Figure 6 shows time-series variations for fronts (10 g/m<sup>3</sup>) extracted by the GOCI SS data as well as time-series current vector distributions processed by GOCI on 26<sup>th</sup> March 2012. During flood tide, currents moved in a clock-wise direction close to shore. During flood conditions, a strong northwesterly-flowing tide appeared along the southern part of Jindo. And along the coastline of Heuksando, currents moved slightly towards a southwesterly direction and changed to northerly a direction. The movement along the Youngkwang coast was toward the northeast.

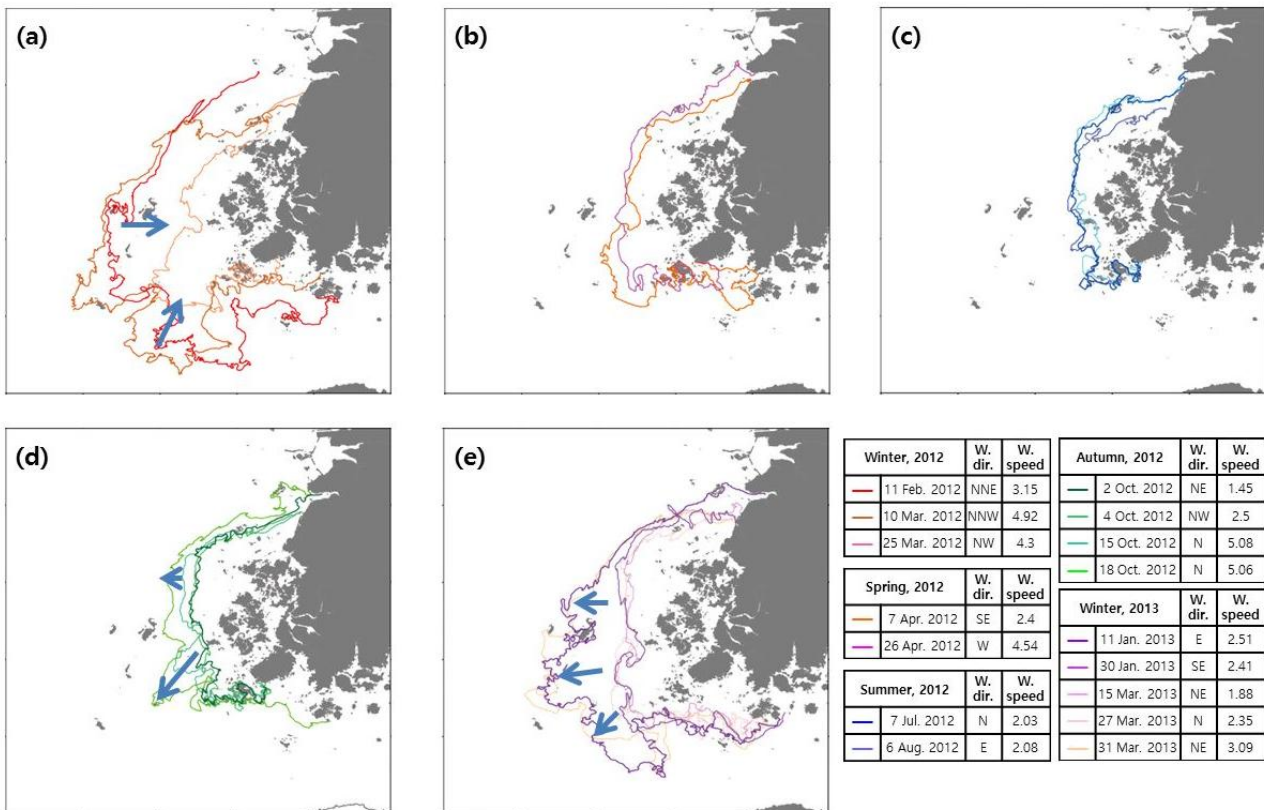


Figure 4. Seasonal variations for the distribution front of suspended sediment (10 g/m<sup>3</sup> boundary) together with wind data (Heuksando ocean observation station).

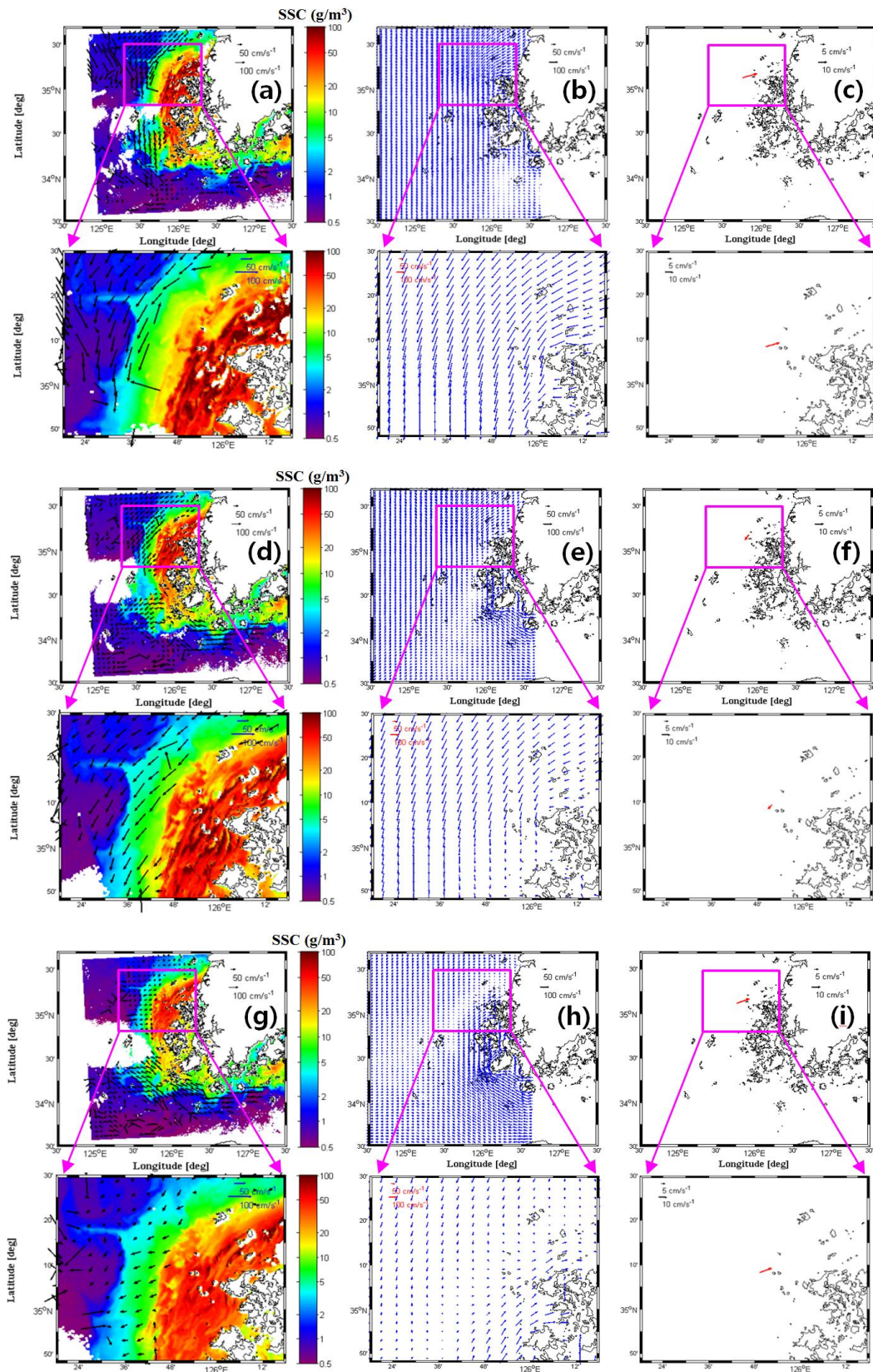


Figure 5. Comparison of results for tidal current extraction using: (a, d, and g) the current vector method of GOCI TSS data; (b, e, and h) a numerical model for tidal currents; and (c, f, and i) *in-situ* RCM data.

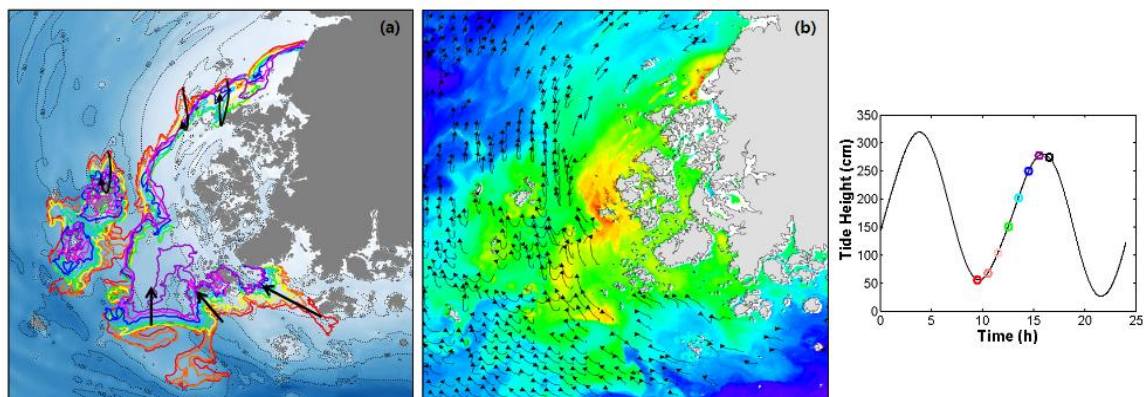


Figure 6. (a) Time-series for the movement of a SS front between 09h30 and 16h30; (b) continuous current vector movement on 26<sup>th</sup> March 2012 (line colors denote each capture time used for vector extraction) and tidal height variation at the Heuksando tidal station.

## CONCLUSION

In this study, we analyzed the time-series variation of SS movement and distribution along the coastal area of Mokpo using GOCI data. The Mokpo coastline is mainly affected by tidal currents and bathymetric expression. The flood tide is highly influential on SS distribution in this area. The current vector analysis, using time-series GOCI SS data, provide invaluable information regarding current directions and sediment movement within this area. GOCI current vector results were very well matched to the numerical tide models. If the accuracy of SS algorithms and atmospheric corrections for use on coastlines with extremely high SS concentrations were to be improved, time-series variations (using GOCI data) would be very helpful in coastal environmental monitoring in the northwest Pacific.

## ACKNOWLEDGEMENT

This research was supported by projects titled “Research for Applications of Geostationary Ocean Color Imager” and “Development of satellite based ocean carbon flux model for seas around Korea”; funded by the Ministry of Oceans and Fisheries, Korea. This research was part of a project titled “Satellite Application Techniques for Coastal Ocean Environmental Monitoring (SATCOM)” funded by the Korea Institute of Ocean Science and Technology (KIOST).

## LITERATURE CITED

- Byun, D.S., Wang, X.H. and Holloway, P.E., 2004. Tidal characteristic adjustment due to dyke and seawall construction in the Mokpo Coastal Zone, Korea. *Estuarine, Coastal Shelf Science*, 59(2), 185-196. doi:10.1016/j.ecss.2003.08.007.
- Choi, J.K., Park, Y.J., Ahn, J.H., Lim, H.S., Eom, J. and Ryu, J.H., 2012. GOCI, the world's first geostationary ocean color observation satellite, for the monitoring of temporal variability in coastal water turbidity. *Journal of Geophysical Research*, 117, C09004.
- Choi, J.K., Yang, H., Han, H.J., Ryu, J.H. and Park, Y.J., 2013. Quantitative estimation of suspended sediments in coastal region using GOCI. *Journal of Coastal Research*, Special Issue No. 65, 1367-1372.
- Choi, J.K., Park, Y.J., Lee, B.R., Eom, J. Moon, J.E. and Ryu, J.H., 2013. Application of the Geostationary Ocean Color Imager (GOCI) to mapping the temporal dynamics of coastal water turbidity. *Remote Sensing of Environment*. http://dx.doi.org/10.1016/j.rse.2013.05.032
- Cloern, J.E., 1987. Turbidity as a control on phytoplankton biomass and productivity in estuaries. *Continental Shelf Research*, 7, 1,367-1,381.
- Cole, B.E. and Cloern, J.E., 1987. An empirical model for estimating phytoplankton productivity in estuaries. *Marine Ecology Progress Series*, 36, 299-305.
- Jung, T.S. and Kim, S.G., 2005. Monitoring system of coastal environment changes due to the construction on the sea. *Journal of the Korean Society for Marine Environmental Engineering*, 8, 53-59.
- Kang, J.W., Moon, S.R., Park, S.J. and Lee, K.H., 2009. Analyzing sea level rise and tide characteristics change driven by coastal construction at Mokpo Coastal Zone in Korea. *Ocean Engineering*, 36 (6-7), 415-425. doi:10.1016/j.oceaneng.2008.12.009.
- Lee, B., Ahn, J.H., Park, Y.J. and Kim, S.W., 2013. Turbid water atmospheric correction for GOCI: Modification of MUMM algorithm. *Korean Journal of Remote Sensing*, 29 (2), 173-182.
- Lee, S., Lie, H.J., Song, K.M., Cho, C.H., and Lim E.P., 2008. Tidal modification and its effect on sluice-gate outflow after completion of the Saemangeum Dike, South Korea. *Journal of Oceanography*, 64, 763-776.
- Min, J.E., Ryu, J.H., Lee, S. and Son, S.H., 2012. Monitoring of suspended sediment variation using Landsat and MODIS in the Saemangeum coastal area of Korea. *Marine Pollution Bulletin*, 64, 382-390.
- Olsen, C.R., Cutshall, N.H. and Larsen, I.L., 1982. Pollutant-particle associations and dynamics in coastal marine environments: a review. *Marine Chemistry*, 11, 501-533.
- Ryu, J.H., Choi, J.K., Eom, J. and Ahn, J.H., 2011. Temporal variation in Korean coastal waters using Geostationary Ocean Color Imager. *Journal of Coastal Research*, Special Issue No. 64, 1731-1735
- Torres, J.L. and Morelock, J., 2002. Effect of terrigenous sediment Influx on coral cover and linear extension rates of three Caribbean massive coral species. *Caribbean Journal of Science*, 38, 222-229.
- Zhang, M., Tang, J., Dong, Q., Song, Q. T. and Ding, J., 2010. Retrieval of total suspended matter concentration in the Yellow and East China Seas from MODIS imagery. *Remote Sensing of Environment*, 114, 392-403.

## Regional variation in the dynamics of Estonia's coastal landscapes

Urve Ratas†, Reimo Rivas†‡, Are Kont†, Hannes Tõnisson†, Kadri Vilumaa†, Agnes Anderson†, Robert Szava-Kovats∞

† Institute of Ecology at Tallinn University, Uus-Sadama 5-537 Tallinn, 10145, Estonia, Europe  
Urve.Ratas@tlu.ee  
Reimo.Rivas@tlu.ee,  
Are.Kont@tlu.ee  
Hannes.Tonisson@tlu.ee  
Kadri.Vilumaa@tlu.ee  
Agnes.Anderson@tlu.ee

‡ Institute of Mathematics and Natural Sciences, Tallinn University, Narva road 29, 10120 Tallinn

∞ Institute of Ecology and Earth Sciences, Tartu University, Lai St. 40, 51005 Tartu  
robszav@ut.ee



[www.cerf-jcr.org](http://www.cerf-jcr.org)



[www.JCRonline.org](http://www.JCRonline.org)

### ABSTRACT

Ratas, U., Rivas, R., Kont, A., Tõnisson, H., Vilumaa, K., Anderson, A., Szava-Kovats, R., 2014. Regional variation in the dynamics of Estonia's coastal landscapes. In: Green, A.N. and Cooper, J.A.G. (eds.), *Proceedings 13th International Coastal Symposium* (Durban, South Africa), *Journal of Coastal Research*, Special Issue No. 70, pp. 139-144, ISSN 0749-0208.

The coastal landscapes of Estonia are young (less than 10,000 years old). Their development is affected by the Baltic Sea, by pre-existing geomorphology and by regional tectonic uplift. Since emerging from the sea ~5,000 years ago, the coastal landscapes have been evolving under regressive sea conditions. The landscape diversity is greatest on coasts with variable topographies and those exposed to wind and waves. Low and flat parts of the coast, which are seasonally inundated, exhibit less variable landscapes. Landscape changes in coastal areas no longer affected directly by the sea have been caused largely by human activity. Abrupt socio-political and economic changes over the last century led to a cessation of traditional land use during the Soviet era with urban sprawl and expansion of recreation areas after re-independence in the beginning of the 1990s. The aim of this paper is to analyze the structure, formation conditions, and the velocity and extent of change in coastal landscapes (for both natural and human-induced impacts) along different coastal regions of Estonia. The Estonian coast can be divided into four distinct regions: 1) Gulf of Finland; 2) Baltic Proper; 3) Gulf of Livonia and 4) Coast of Väinameri, making it possible to compare the influence of sea exposure, geological structure, vegetation, soil productivity, age of human settlements and character of land use on the development of coastal landscapes. The results of the current study are applicable to coastal conservation, to the development of sustainable coastal land use and to the facilitation of transnational tourism.

**ADDITIONAL INDEX WORDS:** *Land cover change, coastal landscape, human impacts, Baltic Sea, Estonia.*

### INTRODUCTION

A general pattern of landscape variability results from the character of landforms and parent materials, and is expressed by the existence of various ecosystems (Forman and Gordon, 1981). The properties of a landscape depend upon both local and regional variations of the environment (Urban *et al.*, 1987). The coastal zone is special because its natural processes occur at the interface between the land and the sea. Crustal tectonics and sea-level fluctuations in a region play an important role in the development of coastal landscapes, leading to changes in shoreline contour and position (Woodroffe, 2003).

The coastal landscapes of Estonia are young (less than 10,000 years old) and are rapidly developing in an area of tectonic uplift. Due to the geomorphic variability of the coast, coastal landscapes in Estonia vary greatly from site to site. The ancient topography, lithological composition of the bedrock, accumulation or erosion pattern, distribution of glacial deposits and landforms, and human impacts have all played an important role in contemporary landscape development. Abrupt changes in water levels in the Baltic Sea basin during the Holocene epoch have also had a major impact on the formation and dynamics of coastal landscapes. For instance, during the earlier stages of development of the Baltic Sea sea levels were transgressive; whereas during the last ~5,000 years—since the middle of Litorina stage—the sea has been

regressive (Hyvärinen *et al.*, 1988).

The contemporary coast of Estonia is washed by the waters of different parts of the Baltic Sea (Figure 1) – the Gulf of Finland, the Baltic Proper, the Gulf of Livonia and Väinameri (an inland sea between the west Estonian archipelago and the mainland). These parts differ in their configurations, seabed topographies and in the hydrodynamics of their coastal waters. Till- and silt-dominated shores comprise much of the Estonian coast. Sand and gravel-pebble shores are less common (Orviku *et al.*, 2009; Tõnisson *et al.*, 2011). There are scarp shores (1/3 of the total length of all shore types) and cliff shores, i.e., eroded in the bedrock (~ 5%), in areas with variable topography and active shore processes (Orviku *et al.*, 2013). Artificial shores comprise less than 2% of the total length of the Estonian coastline and are concentrated along the northern coast (Orviku *et al.*, 2010). Most changes near the current shoreline are caused by natural processes. The most exceptional changes in shoreline position and shape in many coastal areas of Estonia are attributable to a combination of strong storms, high sea level and mild (ice-free) winters. Depositional coasts, particularly beaches, are most vulnerable to this combination. As a result, the balance between erosion and deposition is fragile and an initial coastal shape cannot be restored during the intermediate period between storms (Orviku *et al.*, 2013).

As a rule, landscapes become older with more stable natural processes and greater human impact as we travel farther inland to

locations where seawater has no direct impact (Puurmann *et al.*, 2004; Antso *et al.*, 2013). The establishment of coastal settlements and the beginning of anthropogenic land use began at higher elevations and subsequently expanded to lower areas towards the sea. Most of the contemporary coast of Estonia emerged from the sea during the period of anthropogenic influence. For centuries, the coastal regions have been used in different ways depending both on the natural conditions and on the economic development level and intensity of foreign trade (Palginõmm *et al.*, 2007). The greatest changes in the coastal landscapes during the last century have been caused by abrupt socio-political and economic changes, for example, the cessation of traditional land use during the Soviet era, urban sprawl and the expansion of recreation areas after re-independence in the beginning of the 1990s. Most of the coastal areas used as crop fields or pastures half a century ago are now overgrown by shrubs and forest. Reconstruction of abandoned harbours and construction of new harbours as well as the expansion of coastal cities and urban sprawl around Tallinn, have also had a strong influence on coastal landscapes (Orviku *et al.*, 2008; Tammaru *et al.*, 2009).

### STUDY SITES

In this study, the Estonian coast is divided into four distinct regions in order to compare the influence of sea exposure, geological structure, vegetation, soil productivity, age of human settlements and character of land use on the development of coastal landscapes. These four coastal regions exemplify different landscape regions of Estonia each with a distinctive palaeogeographical history and character (Figure 1).

1) The western and central parts of the Gulf of Finland coastline are characterized by a strongly dissected shorelines consisting of a number of peninsulas, bays and small islands. The eastern part is a fairly straight cliff shore formed by the ( $\leq 56$  m high) limestone

Baltic Klint adjacent to a narrow strip of coastal plain. The western shores of the peninsulas, which are well exposed to storm waves, consist of eroded till, gravel and pebbles. The eastern (leeward) shores are silt-dominated. Sand usually accumulates at the end of the bays, forming sandy beaches with adjacent dune ridges. These sites are high in recreation value.

2) The coast of the Baltic Proper is associated with geologically active shores where shore processes are the most active and coastal changes are most rapid. Sandy beaches with foredunes and dune systems are the most vulnerable, whereas till, cliff and rocky shores are more resistant to erosion. Cliff and rocky shores are often adjacent to unique coastal landscapes called *alvars*: dry, species-rich calcareous grasslands.

3) The coast of the Gulf of Livonia is a semi-enclosed part of the Baltic Sea with the greatest sea-level fluctuations on the coast of Estonia. The area between Pärnu and Ikla is well-known for its sandy beaches with the highest dunes in Estonia alternating with species-rich seashore grasslands on silt-dominated shores.

4) The coast of Väänameri (a very shallow, semi-enclosed basin) is characterized by extensive reedbeds on silty shores adjacent to crop fields and pastures. This area concentrates a number of small islands with unique and diverse landscapes. The flat and low-lying silty shores are subject to temporary inundation, are geologically passive and are often overgrown by reeds and bushes.

The landscape structure of these coastal regions is rather diverse. The study sites were selected from the most representative parts of these regions (Figure 1). The results from the study sites show the differences in formation, structure, land use and trends of development in various parts of the coastal zone of Estonia.

Two study sites were selected from the region of the Gulf of Finland: the Kolga Bay islands and Ontika. These sites differ from each other in age, topography, natural processes as well as in land use. The islands of Kolga Bay are the highest parts of drumlin-like



Figure 1. Location of coastal landscape regions and study sites (coast types after Orviku (2010)).

NW-SE orientated glacial landforms which emerged from the sea less than 4,000 years ago (Karukäpp and Malkov, 1993). The landscapes of the islands have been shaped by the water bodies preceding the contemporary Baltic Sea. The Ontika study site represents the highest part of the Baltic Klint. This is a cliff shore, the upper part of which changed to a terrestrial development over 10,000 years ago. Harilaid Peninsula in NW Saaremaa Island is the study site from the region of the Baltic Proper. This area is characterised by the most active shore processes and the most rapid changes in shoreline displacement and beach profiles. The Rannametsa study site, in the region of the Gulf of Livonia, is an area of sandy shores and the highest dune ridges in Estonia, and is of a high recreational value. The landscapes of this area have been formed as the result of transgressions and regressions of the Baltic Sea. The Salinõmme study site in the Väinameri region represents a typical flat and low-lying seashore grassland with saline plant communities and has been used intensely for grazing in the past, but less so today.

## METHODS

This study is based on fieldwork in the study sites as well as on analysis of existing maps and datasets. Most of the landscape field studies were carried out between 1995 and 2012. Different methodologies were used to investigate the study sites. A variety of maps were examined in order to identify changes in landscapes, shoreline contours and shoreline position (e.g., geological, soil, topographic etc.).

Landscape analysis and historical-geographical interpretation were the main research methodologies used to assess changes in land cover pattern and their relationships with human impact. We applied several methods to analyze important geographical, cultural and socio-economic factors contributing to the development of coastal landscapes and to estimate the rate and nature of these changes. Changes in land cover patterns and shoreline position were analyzed by comparing maps from different periods. The land cover units were distinguished and the trends of changes were analysed using *MapInfo* or *ArcGIS*. The maps used were of 1:10,000 scale, except for the oldest map from 1900 which was of a 1:42,000 scale.

We analyzed the data obtained from landscape profiles compiled at each study site in order to distinguish trends in landscape change. These used data collected along transects with time intervals of 5-10 years. The landscape profile method is one of the best ways to analyze the complete spatial structure of a landscape or an ecosystem, and to reveal mutual relationships between natural components of the system. The method is also well suited to an assessment of the rate of human impact on landscape changes.

## RESULTS AND DISCUSSION

The marine and terrestrial effects on the coastal areas have resulted in unique landscape types, ensuring high and concurrently fragile biological diversity and productivity in these regions (Turner *et al.*, 1996). The formation and development of coastal landscapes in Estonia has been in progress since the last deglaciation ~10,000 years ago. The development of the preceding stages of the contemporary Baltic Sea and concurrent shore processes have played an important role in shaping coastal landscapes. Environmental factors (e.g., velocity of land uplift, sea level fluctuations, climatic changes, etc.) have drastically changed over this period. As the general trend of development of the Estonian coast since the beginning of Holocene has been generally the same (at least in regressive sea conditions), we assume that the

main processes that shaped the coastal landscapes in the past still occur today.

The oldest coastal landscape in Estonia is located along the eastern part of the Gulf of Finland and is densely connected with the greatest bedrock landform – the Baltic Klint. The klint – up to 56 m high at Ontika – is eroded into the northern slope of the Viru limestone plateau. The Ontika study site is located along the eastern part of the cliff. Here the cliff is compact and straight and is exposed to northerly winds. Due to erosion over the entire Holocene epoch, the cliff has steadily receded inland and a narrow (~100 m wide) coastal plain has formed at its foot (Suuroja, 2006). The lower part of the cliff is buried under colluvial deposits, which form an expansive talus. The cliff is made up of Ordovician limestone underlain by Cambrian clays. The water-bearing surface of the clays often causes landslides in the talus. Storm waves during high sea-level enhance erosion of the down-slid or collapsed sediment. The talus of the cliff is covered with broad-leaved forest where nutrient-rich soil is present. This is a unique vegetation type in Estonia due to its species-rich composition containing many rare species (Paal *et al.*, 2001; Rooma and Paal, 2001). Its natural elements along with its high relief make the site one of the most attractive landscapes in Estonia (Figure 2).

Most of the coastal zone emerged from the sea during the Limnea Sea stage (~4,000 years ago). Uplift of the land together with the variable topography of the seabed (comprising landforms of both Quaternary deposits and bedrock) led to the transition of a considerable portion of current coast into a terrestrial development

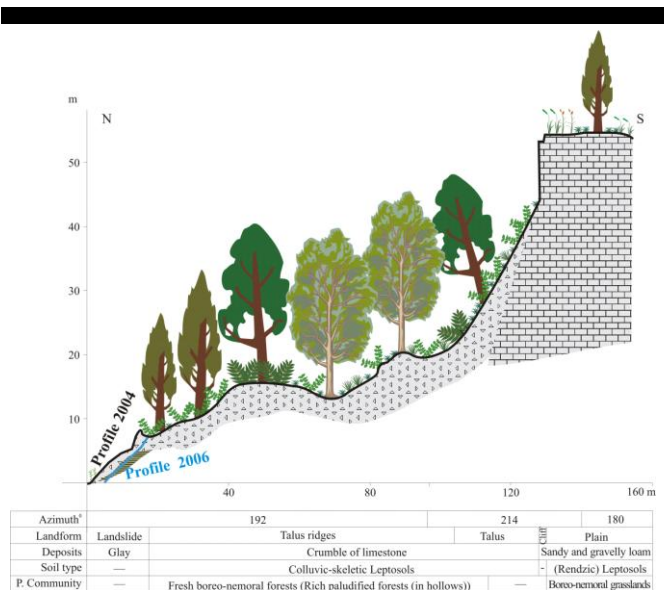


Figure 2. Landscape transect of Ontika study site.

in the form of islands. The general trend of development has been an enlargement of the area of these islands as they merged with one another or with the mainland. The character of formation of certain coastal areas is a natural basis for the development and diversity of coastal landscapes. In addition to the geomorphic characteristics of a site, location in relation to coastal waters and exposure to prevailing winds and waves are also important in landscape formation.

The group of islands in Kolga Bay in the Gulf of Finland is closely related to the coastal plain of the mainland. The archipelago consists of 10 small islands in different stages of development and of different size (the biggest island is > 1 km<sup>2</sup>)



and elevation ( $\leq 13$  m a.s.l.). The sea surrounding the islands is  $\sim 90$  m deep. The islands are the tops of drumlin-like glacial landforms in the bay with relative altitudes of  $> 100$  m, which have been reshaped by the waters of the Limnea stage of the Baltic Sea. The islands have been subject to active shore processes, as indicated by the presence of beach formations with dunes in the highest and oldest central parts. Some paludified depressions and overgrowing lakes among them diversify the landscape. Active shore processes are characteristic also of the contemporary shores. Erosion is predominant on windward shores; sediments are transported and accumulated to the leeward sides of the islands.

The character of shore processes has remained unchanged for decades (Lepland, 1995), while the intensity has increased due to an increase in the frequency of strong storms and higher storm surges over the last few decades (Orviku *et al.*, 2003, 2013). The most susceptible to erosion are sandy beaches and scarps, which are well-exposed to storm winds and waves. For instance, a sandy scarp on the western coast of Rammu Island has receded by 0.2–0.5 m per year during the last decades, as measured by repetitive GPS survey. The development of soil-vegetation complexes is presumably rather slow due to the active shore processes. Diverse plant communities from open grasslands to forests are present on the sandy sediments in the central part of the island (Ratas *et al.*, 1995). Crowberry heaths, which are usually characteristic of tundra zones, provide a unique plant community here at the southernmost boundary of their extent. The forests on larger islands were planted at the end of the 20<sup>th</sup> century. The landscapes on the islands were most influenced by humans between the 18<sup>th</sup> and mid-20<sup>th</sup> centuries on permanently inhabited islands such as Rammu (102.6 ha; 4 m a.s.l.) and Koipse (34.3 ha; 7 m a.s.l.). Even some small, uninhabited islands display evidence of human impact in their landscapes (Figure 3). For example, there was an inn on Suur-Malusi which was a centre of contraband trade between Estonia and Finland centuries ago. The Soviet occupation dramatically changed the face these islands: traditional land use was interrupted and the population deported. Since the liberation of Estonia from Soviet occupation at the end of the 20<sup>th</sup> century, the islands of Kolga Bay have been under nature conservation with only limited tourism.

Dramatic changes in the coastal landscapes of Estonia can be detected even over a few years. Harilaid Peninsula ( $> 4$  km<sup>2</sup>; 4.3 m a.s.l.) in NW Saaremaa Island in the region of Baltic Proper is an area where shoreline changes are the most rapid in the country.

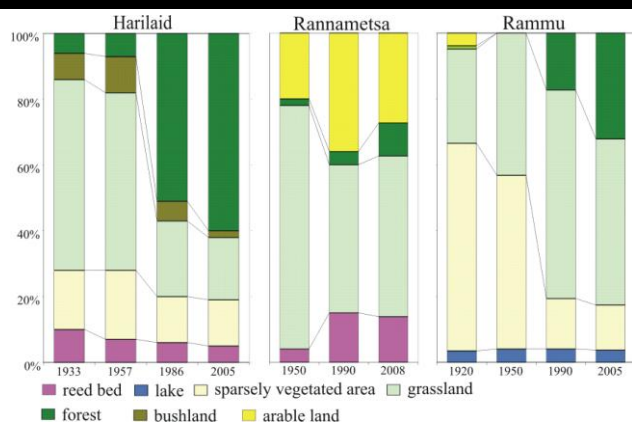


Figure 3. Changes in land cover on Harilaid Peninsula, in the western part of Rannametsa and on Rammu Island.



Figure 4. Shoreline changes in Harilaid over the last decades.

years ago. Harilaid is geologically young; its highest points started emerging as a result of uplift much later than Saaremaa  $\sim 2,000$  years ago. It is joined to Saaremaa by a narrow tombolo in the east. The axis of the peninsula is oriented NW-SE and the entire coastal zone is well-exposed to storm waves. A wave cut bench formed in a submarine glacial ridge extends from the north-westernmost tip of Harilaid to the NW. This is the main source of fine-grained sediments in the accumulation areas. Sandy beaches prevail in the northern part of the peninsula, whereas the southern part is characterised by alternating beach ridges comprising well-rounded pebbles and by backing lagoons (Orviku *et al.*, 2003).

The continuous accumulation of new beach ridges elongates the spit. The mean annual increment of spit elongation during the last 25 years has been 45 m, while the mean areal expansion has reached 2270 m<sup>2</sup>/yr (Tõnisson *et al.*, 2011). The seabed around the northern part of Harilaid is shallow (2 m isobaths lie  $\sim 1$  km from the shoreline). The existence of a relatively thick (4–8 m) layer of sand and openness to prevailing strong winds have favoured the formation of sandy beaches with foredunes and dunes. The earlier accumulative shoreline positions at Cape Kiipsaare are evidenced by a series of parallel beach ridges that cross the current shoreline at an angle of 30–35°. Shore processes during the last century have caused the north-westernmost point of the peninsula to migrate to the north-east. The western shore of Cape Kiipsaare is subject to strong erosion. The eroded sand is transported around the cape and accumulated on the eastern shore. A sandy scarp on the western shore has receded by 3–8 m/yr during the last 25 years (Figure 4). This has led to the loss of some characteristic dune habitats. The zone of active shore processes has no permanent plant cover. The formation of vegetation along the inner part of the peninsula has been strongly influenced by human activity. The study site is characterised by dry, species-poor grasslands and pine stands on sandy soils. Formerly an open area with moving sands, the area was planted with willows in the middle of the 19<sup>th</sup> century. At the beginning of the 20<sup>th</sup> century, the peninsula was used as a pasture. The willows partly disappeared as a result of grazing and the sand subsequently started to move again. We have a precise description of the species composition of vegetation at Harilaid from the

The peninsula existed as a group of small isles as recently as 300

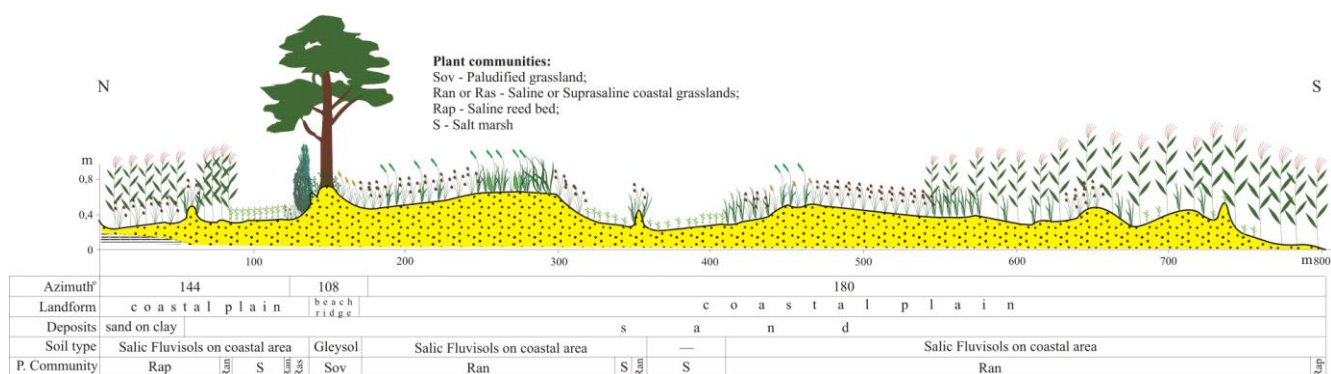


Figure 5. Landscape transect of the Salinõmme study site.

1930s (Pastak, 1935). Comparison of the results of that time with the data from the 1950s reveals some minor changes during the 20 year interval. Later, the peninsula was planted with pine, which once again changed the landscape of Harilaid (Figure 3).

Active shore processes are inoperative when a shoreline is isolated from the open sea. The characteristic features of shore dynamics in such areas are a slow displacement of the shoreline due to uplift along with the formation of grasslands and reedbeds. Changes in the structure of coastal landscapes in geologically passive areas are caused mainly by human impact. Mowing and grazing have been the major traditional economic activities which have kept the landscape open and enhanced biodiversity (Puurmann *et al.*, 2002). Their cessation has resulted in the overgrowth of grasslands by shrubbery and the expansion of reedbeds along the shore. An example of such an area is the Salinõmme study site on SE Hiiumaa Island, in the region of Väinameri. This site is subject to regular inundation. The coast consists of marine sand and silt, which are underlain by varved clay. The sediments and micro-topography determine the character of the water regime. The extent and duration of inundation by salty seawater plays a crucial role in the formation of saline soil-vegetation complexes in this area. The landscape transects show a strong dependence of vegetation pattern on the micro-topography (20-30 cm) of the site (Figure 5). Cessation of human activity in Salinõmme over the last 50 years has led to a decline in the area of typical saline plant communities and an expansion in reedbeds. The rise of the adjacent causeway some decades ago has excluded inundation and enhanced overgrowth of the grasslands.

The transgressions of the Baltic Sea during the transition from the Ancyclus Lake stage to the Litorina Sea (Hyvärinen *et al.*, 1988) led to the formation of notable coastal landforms in the region of the Gulf of Livonia. Two roughly parallel ridges of coastal formations possessing the tallest dunes in Estonia are located at the Rannametsa study site (Figure 6). These ridges are separated from the sea by a low and flat coastal plain, which originated as a coastal terrace during the Limnea stage age. The landward ridge (8-14 m a.s.l.) formed during the Ancyclus Lake stage, whereas the seaward ridge (4-9 m a.s.l.) is the product of the Litorina Sea transgression (Kessel and Raukas, 1967). Due to a much slower uplift rate (< 1 mm/yr) (Vallner *et al.*, 1988), the coastal formations in SW Estonia are lower-lying than the formations of the same age in northern Estonia. The dune ridges at Rannametsa are covered by dry pine forest on nutrient-poor sandy soils (Aringo *et al.*, 2003). A raised bog is located in the depression between the ridges. The formerly active shore processes have ceased and the coastal plain is now covered by

vegetation. The lower parts of the plain suffered from occasional inundation. In the 1960s a dam was erected to protect the land against floods. Nowadays, seashore grasslands overgrown with reeds dominate between the dam and the shoreline. The landward

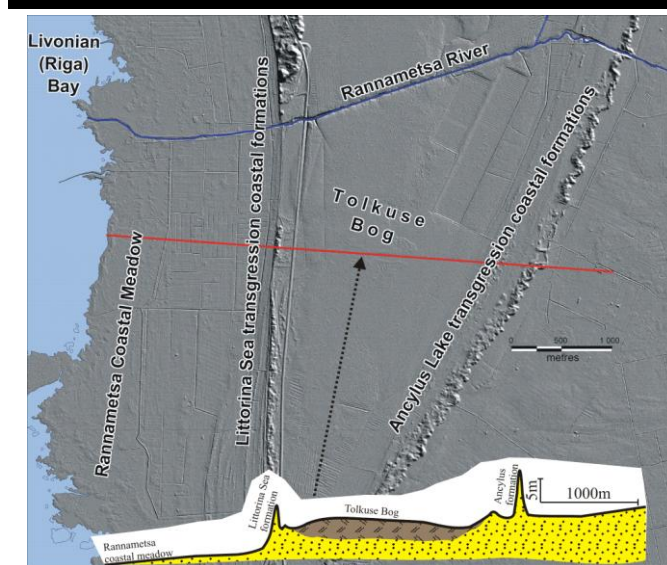


Figure 6. Shoreline changes and schematic profile along the Rannametsa study site.

area behind the dam is currently largely neglected while mowing and grazing on the grasslands between the dam and the shore are becoming more and more frequent and are financially supported by the Life Project and the European Regional Development Foundation.

## CONCLUSIONS

The coastal landscapes of Estonia are variable and exhibit considerable differences from site to site. These depend largely on geomorphology, exposure to the open sea, and the character and duration of land use. Although the structure and dynamics of coastal landscapes have been formed by natural processes, the effect of human impact is continuously increasing. The most drastic changes in the coastal landscapes of Estonia during the last century are human-induced. Coastal landscapes are a part of the

national landscapes of Estonia, and are seen as expressing the unique, but also the most typical features of the country.

### ACKNOWLEDGEMENTS

This work was supported by ESF Grants No. 8549 and 9191, target financed theme No SF0280009s07 and the Est Kliima project of the European Regional Fund program No. 3.2.0802.11-0043.

### LITERATURE CITED

- Antso, K., Kont, A., Palginõmm, V., Ratas, U., Rivis, R. and Tõnisson, H., 2013. Changing natural and human impacts on the development of coastal land cover in Estonia. *Journal of Coastal Research*, Special Issue No. 56, 862-867.
- Aringo, M., Rivis, R. and Ratas, U., 2003. Landscape changes in the Rannametsa River catchment area. In: Järvet, A., Lode, E. (eds.), *Ecological processes in northern wetlands. Selected papers of International Conference & Educational Workshop*. Tallinn, Estonia: Tartu University Press. Tallinn-Tartu, pp. 293-303.
- Forman, R.T.T. and M. Gordon, M., 1981. Patches and structural components for a landscape ecology. *BioScience*, 31(10), 733-740.
- Hyvärinen, H., Donner, J., Kessel, H. and Raukas, A., 1988. The Littorina Sea and Limnea Sea in the Northern and Central Baltic. *Ann. Acad. Sci. Fennicae, Series A. III. Geol.-Geogr.*, 148, 25-35.
- Karukäpp, R. and Malkov, B., 1993. Pinnamood. In: Lutt, J. Raukas, A. (eds.), *Geology of the Estonian shelf*. Tallinn, Estonia: Academy of Sciences of Estonia, pp. 22-29.
- Kessel, H. and Raukas, A. 1967. *The deposits of the Ancylus Lake and Littorina Sea in Estonia*. Tallinn, Estonia: Valgus (in Russian).
- Lepland, A., 1995. Kolga lahe saarte randade geoloogia. In: *Year-book of the Estonian Naturalists' Society*, 76. Tallinn, Estonia: Estonian Academy Publishers, pp. 109-136.
- Orviku, K., Jaagus, J., Kont, A., Ratas, U. and Rivis, R., 2003. Increasing Activity of Coastal Processes Associated with Climate Change in Estonia. *Journal of Coastal Research*, 19, 364-375.
- Orviku, K., Tõnisson, H., Aps, R., Kotta, J., Kotta, I., Martin, G., Suursaar, Ü., Tamsalu, R. and Zalesny, V., 2008. Environmental impact of port construction: Port of Sillamäe case study (Gulf of Finland, Baltic Sea). In: *2008 IEEE/OES US/EU-Baltic International Symposium: US/EU-Baltic International Symposium "Ocean Observations, Ecosystem-Based Management & Forecasting"*. Tallinn, Estonia: IEEE-Inst Electrical Electronics Engineers Inc, pp. 350-359.
- Orviku, K., Suursaar, Ü., Tõnisson, H., Kullas, T., Rivis, R. and Kont, A., 2009. Coastal changes in Saaremaa Island, Estonia, caused by winter storms in 1999, 2001, 2005 and 2007. *Journal of Coastal Research*, Special Issue No. 56, 1651-1655
- Orviku, K., Kont, A. and Tõnisson, H., 2010. Estonia. In: Bird, E. (ed.), *Encyclopedia of World's Coastal Landforms*. Dordrecht, Heidelberg, London, New York: Springer, pp. 605-611.
- Orviku, K., Tõnisson, H., Kont, A., Suuroja, S. and Anderson, A., 2013. Retreat rate of cliffs and scarps with different geological properties in various locations along the Estonian coast. *Journal of Coastal Research*, Special Issue No. 65, 552-557.
- Paal, J., Vellak, K. and Ingerpuu, N., 2001. Eesti pangametsade liigiline koosseis, klassifikatsioonistruktuur ja seos peamiste mullaparametritega. *Metsanduslikud uurimused XXXV*, 104-132.
- Palginõmm, V., Ratas, U. and Kont, A., 2007. Increasing human impact on coastal areas of Estonia in recent decades. *Journal of Coastal Research*, Special Issue No. 50, 114-119.
- Pastak, E., 1935. Harilau taimkate. *Acta Instituti et Horti Botanici Universitatis Tartuensis*, 5, 1-2, 1-44.
- Puurmann, E., Ratas, U. and Rivis, R., 2002. The change in plant diversity of seashore meadows on Estonian uplifting lowshores. In: Fock, T., Hergarden, K., Repasi, D. (eds.), *Salt grasslands and coastal meadows in the Baltic region* (Neubrandenburg, Germany), *Proceedings of the 11th conference*, 18, 292-296.
- Puurmann, E., Ratas, U. and Rivis, R., 2004. Diversity of Estonian Coastal Landscapes: Past And Future. In: Palang, H., Sooväli, H., Antrop, M., Setten, G. (eds.), *European rural landscapes: persistence and change in a globalising environment* (Tartu, Estonia), *20th Permanent European Conference for the Study of the Rural Landscape*, 411-424.
- Ratas, U., Nilson, E., Truus, L. and Kannukene, L., 1995. Development of landscapes on the islands of the Kolga Bay. In: *Year-book of the Estonian Naturalists' Society*, 76. Tallinn, Estonia: Estonian Academy Publishers, 137-163.
- Rooma, I., Paal, J., 2001. Eesti pangametsade mullad. In: *Eesti Loodusuurijate Seltsi aastaraamat 80* (Tallinn, Estonia), pp. 178-209.
- Suuroja, K., 2006. *Baltic Klint in North Estonia as a Symbol of Estonian Nature*. Tallinn, Estonia: Ministry of Environment, 224p.
- Tammaru, T., Leetmaa, K., Silm, S. and Ahas, R., 2009. Temporal and Spatial Dynamics of the New Residential Areas around Tallinn. *European Planning Studies*, 17 (3), 423-439.
- Turner, R.K., Subak, S. and Adger W.N., 1996. Pressures, Trends, and Impacts in Coastal Zones: Interactions Between Socioeconomic and Natural Systems. *Environmental Management*, 20, 2, 159-173.
- Tõnisson H., Suursaar Ü., Orviku K., Jaagus J., Kont A., Willis D.A. and Rivis, R., 2011. Changes in coastal processes in relation to changes in large-scale atmospheric circulation, wave parameters and sea levels in Estonia. *Journal of Coastal Research*, Special Issue No. 64, 701-705.
- Urban, D.L., O'Neill, R.V. and Shugart, H.H., 1987. Landscape ecology. *BioScience*, 37, 119-127.
- Vallner, L., Sildvee, H. and Torim, A., 1988. Recent crustal movements in Estonia. *Journal of Geodynamics*, 9, 215-223.
- Woodroffe, C.D., 2003. *Coasts, form, process and evolution*. Cambridge University Press, 623p.

## Submarine hard-bottom substrates in the western Baltic Sea – human impact versus natural development

Klaus Schwarzer<sup>†</sup>, Björn Bohling<sup>‡</sup>, Christoph Heinrich<sup>∞</sup>

<sup>†</sup>Institute of Geosciences, Sedimentology, Coastal- and Continental Shelf Research, Kiel University, 24118 Kiel, Germany  
Email: [kls@gpi.uni-kiel.de](mailto:kls@gpi.uni-kiel.de)

<sup>∞</sup> Institute of Geosciences, Sedimentology, Coastal- and Continental Shelf Research, Kiel University, 24118 Kiel, Germany  
Email: [ch@gpi.uni-kiel.de](mailto:ch@gpi.uni-kiel.de)

<sup>‡</sup>Fugro Survey AS, Hoffsvæien 1 C, 0275 Oslo, Norway  
Email: [b.bohling@fugro.no](mailto:b.bohling@fugro.no)



[www.cerf-jcr.org](http://www.cerf-jcr.org)



[www.JCRonline.org](http://www.JCRonline.org)

### ABSTRACT

Schwarzer, K., Bohling, B., Heinrich, C., 2014. Submarine hard-bottom substrates in the western Baltic Sea – human impact versus natural development. In: Green, A.N. and Cooper, J.A.G. (eds.), *Proceedings 13<sup>th</sup> International Coastal Symposium* (Durban, South Africa), *Journal of Coastal Research*, Special Issue No. 70, pp. 145-150, ISSN 0749-0208.

Large areas of the seafloor in the western Baltic Sea are covered by lag deposits of Pleistocene origin, consisting of gravel, stones and boulders. From about 1800–1974, commercial extraction of stones and boulders from these shallow submarine areas was carried out. These activities have fundamentally changed the sediment distribution patterns and ecological conditions of the seafloor. Based on comparisons between old analogue and modern digital sidescan sonar images and direct abrasion measurements on the seafloor by scuba divers, the development of this hard-bottom substrate was studied on a decadal to seasonal scale. We show that due to abrasion processes the amount of boulders has been increased over a 22 year period. Thus, natural regeneration of hard-bottom substrate and improvement of the ecological status of the shallow marine environment is possible. This needs to be considered in order to reestablish a “good ecological status” as demanded by administrative guidelines like the EU Water Framework Directive and the Marine Strategy Framework Directive.

**ADDITIONAL INDEX WORDS:** *Seafloor abrasion, marine resources, lag deposits, habitat mapping, EU Water-Framework Directive, Marine Strategy Framework Directive.*

### INTRODUCTION

Wide areas of the seafloor of the western Baltic Sea (Figure 1) are built up of Pleistocene deposits –mainly glacial till– composed of a grain size spectrum ranging from clay to boulders (Kolp, 1966; Harff *et al.*, 2011; Niedermeyer *et al.*, 2011). Abrasion of submarine platforms results in the erosion and export of fine fractions and the formation of lag deposits ranging from gravel to boulders. From about 1800 to 1974 commercial exploitation of stones and boulders from the seafloor down to -20 m NN (German reference level) –called “stone fishing” (Figure 2)– was undertaken in shallow marine areas (Healy and Wefer, 1980; Bock *et al.*, 2003). According to Kolp (1966), big stones range from 20–63 cm in diameter, boulders are >63 cm. Lacking hard rock resources on land, these stones were used for constructions: mainly harbor moles, jetties and shore protection. About  $3.5 \times 10^6$  tons of boulders ranging from 60 to 160 cm in diameter were taken from the seafloor (Bock *et al.*, 2003), of which  $3.0 \times 10^6$  tons were “fished” from 1930 to 1976. Due to local requirements, exploitation was not carried out everywhere with the same

intensity. Since 1930 “stone fishing” was prohibited in water depths shallower than -6 m NN and in less than 200 m distance from the shore. The total number of exploited boulders corresponds to about  $2.5 \times 10^6$ , equivalent to a loss of 5.6 km<sup>2</sup> of hard-bottom substrate. Zander (1991) estimated a loss of even  $100 \times 10^6$  tons of stones and boulders for the entire Baltic Sea, which equals a loss of about 100 km<sup>2</sup> of hard-bottom substrate. This “stone fishing” has fundamentally changed the sediment distribution pattern and ecological condition of the seafloor, as hard-bottom substrates form the most important living resource for macrophytobenthos (Karez and Schories, 2005). Additionally, stones and boulders act as a protection shield against abrasion (Healy and Wefer, 1980). Due to environmental requirements, the protection of areas with hard-bottom substrate has become a key issue as the EU Water Framework Directive (DIRECTIVE 2000/60/EC, 2000), the Marine Strategy Framework Directive (DIRECTIVE 2008/56/EC, 2008) and HELCOM (Baltic Marine Environment Protection Commission) claim efforts to reach a “good ecological status” in the Baltic Sea (Silva *et al.*, 2006). Also, the design of protected habitat types according to NATURA 2000 requirements desires knowledge of the recovery-potential of areas which have been affected by “stone fishing”.

As stones and boulders are exposed naturally by abrasion, a potential “natural regeneration” of hard-bottom habitats might be an alternative to the deployment of artificial reefs as compensation measure. In the western Baltic Sea rates of seafloor abrasion down to -7 m NN range from 1 to 5 cm/yr, depending on water depth and exposure (Wefer *et al.*, 1976; Schwarzer *et al.*, 2000). Besides hydrodynamic forcing, the abrasion process is strongly influenced by the spatially highly variable composition and structure of the till, determining the resistance against erosion (Schrottke, 2001; Kasten, 2012). Submarine sediment distribution offshore bluff coasts is additionally characterized by a highly dynamic variability due to long- and cross-shore sand transport and the mobility of gravel and small-sized stones (Schrottke *et al.*, 2006).

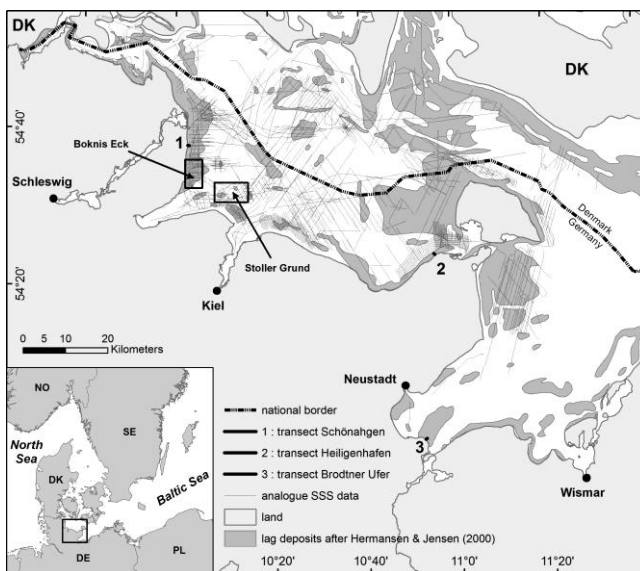


Figure 1. Study areas StollerGrund, Boknis Eck (squares) and the profiles in front of the bluffs Brodtener Ufer, Heiligenhafen and Schönhagen.



Figure 2. Historical picture showing the vessel A.M.4 by hauling up a big boulder (Karez *et al.*, 2003).

We present results from research projects which have been carried out in Kiel- and Mecklenburg Bight (western Baltic Sea), focusing on the resistance against abrasion and the temporal development

of hard-bottom substrates. Study areas are StollerGrund (an abrasion platform reaching up to -7 m NN), Boknis Eck (a nearshore abrasion platform in front of a bluff) and 3 shore-normal profiles (extending up to 500 m offshore in front of the bluffs Schönhagen, Heiligenhafen and Brodten) (Figure 1). As Kiel Bight was the study area for several previous research projects, old data about sediment distribution and geological built up are in existence (Flemming and Wefer, 1973; Wefer *et al.*, 1976; Werner *et al.*, 1976; Bohling *et al.*, 2009). Close to Boknis Eck, a platform for oil extraction was built in 1984 and was active until 2000. Two pipelines extending from the platforms to the mainland (Figure 4) were placed in approximately 0.5 m deep channels on the seafloor. They crossed the study area and were monitored in the frame of an EIAS-study. These data are used to assess long term seafloor changes.

Questions arising in the context of the potential of natural regeneration of hard-bottom substrates in the Baltic Sea are:

- Are areas of “stone fishing” still characterized by a lack of stones and boulders?
- How effective is the natural regeneration of hard-bottom substrate by natural abrasion processes?
- Do the sediment properties of the seafloor and activities of macrobenthic organisms influence abrasion rates?

## METHODS

### Data Acquisition

To study temporal variations of seafloor conditions, time series data are required. Maps of sediment distribution usually show grain-size data based on sediment sampling, sediment-analyses and interpolation between sampling stations (Harff *et al.*, 1995; Tauber *et al.*, 1999). This approach is suitable for mapping large areas in deep waters. For areas under wave influence, these maps often show inaccuracies regarding borders between different sediment facies. Additionally an estimation of the amount of stones and boulders is not possible due to inappropriate sampling devices for residual sediments. Sidescan sonar and multibeam echosounder technology offer the possibility to create high resolution maps on sediment distribution patterns, seafloor morphology and the distribution of boulders (Blondel, 2009; Katsnelson *et al.*, 2012).

Since the early 1970s, sidescan sonar surveys have been carried out by the Institute of Geosciences of Kiel University (IfG). Data recording from 1972 to 1992 was done using analogue storing techniques (printouts on paper) with a limited accuracy in positioning due to DECCA navigation. Nevertheless, the existence of old analogue data provides a unique possibility to assess the evolution of the seafloor by comparing old data with recent digital records. Kubicki and Diesing (2006) have shown that this combination of old analogue data with new digital data from the same area is a useful tool to study sediment dynamics and the sedimentological development of the seafloor on a decadal time scale. Processing and georeferencing of our analogue data was done following this methodology excluding slant range and altitude corrections, as this information is missing in some old data sets. The equipment used in our studies from 2007/08 was a dual frequency (100 & 500 kHz), high-resolution sidescan sonar system (Klein Assoc. Inc., Model 595) with digital data acquisition and processing (ISIS Sonar Software, Triton Int.). Navigational data was obtained by GPS. To get high resolution sonographs, the 500 kHz mode with a tilt angle of 20° was chosen. The sonar-fish was towed behind the vessel with a survey speed of 4 knots. A range of 52 m on each side was applied. Track spacing was designed with an overlap of 40%. Mosaicing was done using Delph Map (Triton Int.). For ground-truthing, ROV-surveys,

observations by scuba-divers and sediment sampling with a Van Veen grab at selected stations were conducted during the cruises. Additionally, bathymetric data were acquired with the hull-mounted multibeam echosounder system SeaBeam 1185 (L3-Communications, ELAC Nautik GmbH), operating with a frequency of 180 kHz. Data are recorded with the software Hydrostar (L3-Communications, ELAC Nautik GmbH) and processed with HDP-post and Fledermaus IVS. The surveys were limited to areas deeper than -5 m NN.

The sidescan sonar records are presented as images using a grayscale color map where high backscatter corresponds with dark-gray values (Figure 5); boulders appear as dark spots (Figure 3). On the far side of the acoustic pulse, the area behind a boulder remains white as it represents the acoustic shadow. The height of boulders was calculated by applying the theorem on intersecting lines.

Boulders were counted in the Boknis Eck (May, 2008) and StollerGrund (Mosch, 2008) study areas to evaluate the development of hard-bottom substrate. For this purpose, areas overlapping with old analogue sonographs and recent records were selected from different water depth. For Boknis Eck the selected areas are indicated in figure 6. To get a spatial reference, the areas were subdivided into cells of 10 m x 10 m. In total, 750 cells were investigated for boulders with a diameter >60 cm, as this was the minimum size of 95% of all boulders which were exploited by stone fishing (Bock, 2003). For the detection of objects, a size >60 cm in diameter is a good value to obtain reliable data from old analogue and modern sidescan sonar records. The counting of boulders, especially based on old analogue records, requires that some limiting issues are taken into account:

- The quality of old analogue sidescan sonar records is sometimes poor, impeding the detection of boulders.
- The georeferencing process can cause some distortion resulting in further lowering the accuracy of the analogue record, as digital post-processing, like beam angle or beam pattern corrections or destripping are difficult to apply.

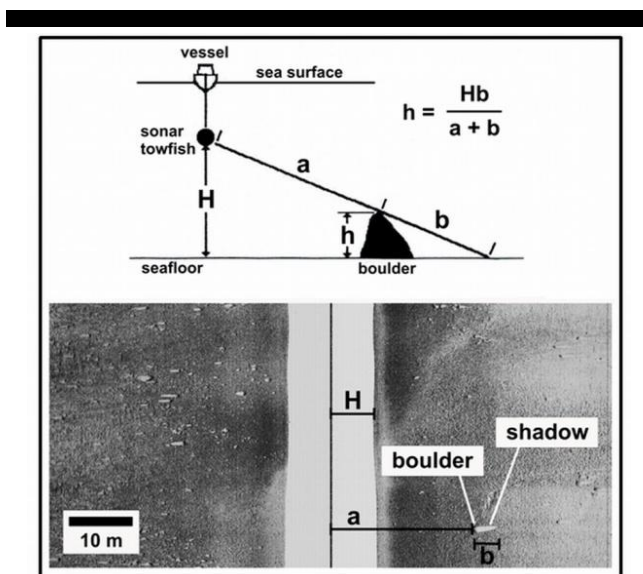


Figure 3. Sidescan sonar record showing boulders on the seafloor and a sketch how to calculate the height of boulders (adapted from Mazel, 1985). H = height of towfish above seafloor, h = height of boulder, a = distance from towfish to boulder, b = length of shadow

- From scuba-divers and ROV observations it is known that boulders are often covered by macrophytobenthos (Figure 7), which may lead to a falsified estimation of their size.
- Where sand appears adjacent to lag sediments, boulders may be occasionally covered partly by sand, influencing their measurable size in sidescan sonar records.

Besides sidescan sonar data acquisition, abrasion was measured directly at the seafloor by scuba divers. An abrasion measurement table was first used by Wefer *et al.* (1976). A so called Micro Erosion Meter (MEM) was developed and used efficiently by Askin and Davidson-Arnott (1981) in coastal environments of the Great Lakes (Davidson-Arnott and Ollerhead, 1995; Davidson-Arnott and Langham, 2000). We used a modified device to measure the distance between a plate made of acrylic-glass, in which 36 measuring sticks were implemented, arranged on a 10 x 10 cm grid (Figure 4). The plate itself is placed on fixed piles, which were driven into the seafloor to mark the measuring positions. The fixed piles remain in the seafloor as the stations were revisited several times each year since 1997. The divers are able to measure in mm-accuracy the distance between the 36 distinct positions on the plate (Figure 4) and the seafloor. As the acrylic-glass is diaphanous, divers can control easily every measurement, especially the contact between the base of the scale and the seafloor (Schwarzer *et al.*, 2000). Abrasion measurements have been carried out on platforms along three transects perpendicular in front of the bluffs “Brodter Ufer”, “Heiligenhafen” and “Schönhagen” (Schrottke, 2001; Kasten, 2012; see Figure 1). In total, 15 offshore stations have been established, starting from 25 m offshore (1,7 m water depth) up to 500 m offshore (6.5 m water depth). The period from 1997 to 2012 could be covered with up to 4 abrasion measurements per year, with a short break from 2001 to 2003.

The investigation site Boknis Eck comprises an area of 21 km<sup>2</sup> where boulders occur over an area of about 14.6 km<sup>2</sup>. StollerGrund, being one of the most exploited sites, comprises an area of about 38 km<sup>2</sup>, of which boulders are present on 21 km<sup>2</sup>. The amount of boulders at both sites correlates with water depth, with a decrease in numbers towards deeper waters. In the StollerGrund area there were no boulders below 15 m NN. In both sites boulders occurred together with lag deposits in shallow areas

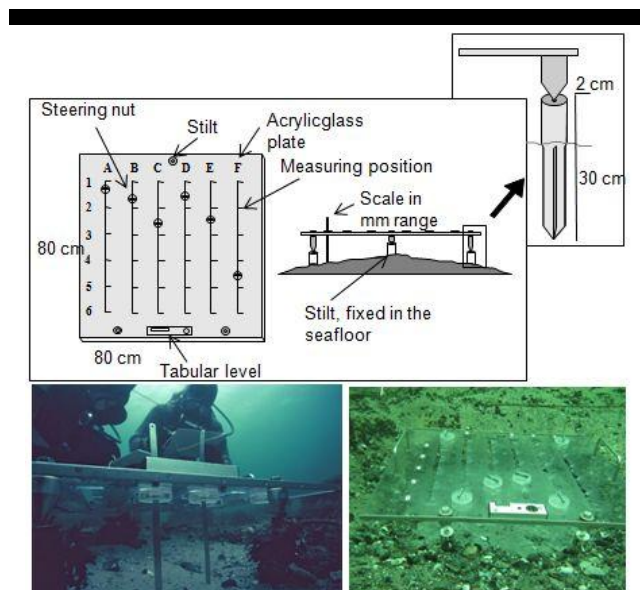


Figure 4. Schematic view (top) and scuba divers using the abrasion measuring table (bottom).

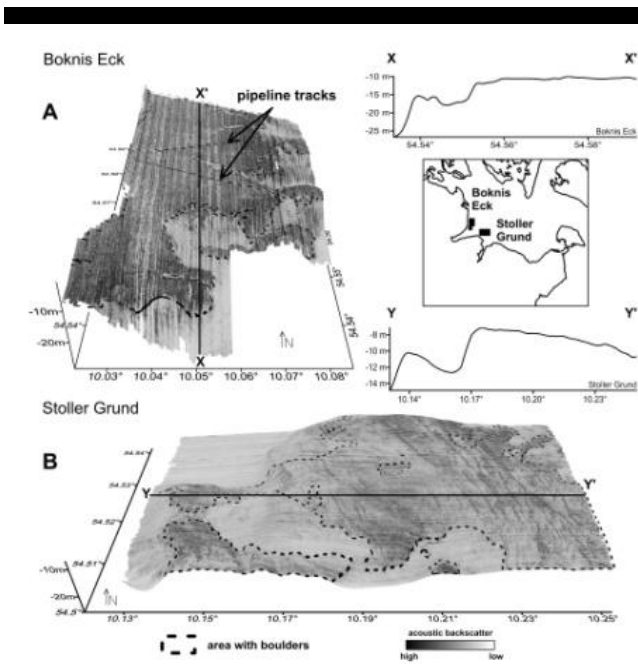


Figure 5. Sidescan sonar mosaics from the study areas Boknis Eck and StollerGrund, combined with bathymetric data. Dashed lines are surrounding the areas where boulders occur.

(<20 m water depth at Boknis Eck, <15 m water depth at StollerGrund), represented by a high backscatter (Figure 5). The difference between Boknis Eck and StollerGrund may be explained by their geographical position, as Boknis Eck is exposed to a longer fetch and higher waves offshore ( $H_{max}$  up to 3.9 m; Dette and Stephan, 1979). Wave activities are strong enough to abrade the seafloor causing newly exposed boulders in areas below 15 m NN (Wefer et al., 1976).

An overview of georeferenced old analogue sonographs from Boknis Eck area and an example of a high resolution image from the same area is shown in Figure 6. In both images, single boulders on the sea floor are visible as black spots with white shadows. The pipeline track, refilled with sand, can be observed in image A. It is still preserved even with detailed structures after 21 years (1986 to 2007). These structures are useful benchmarks for the georeferencing of analogue sidescan sonar records.

For both time-slices (1985/6 and 2007) we observe a decreasing number of boulders with increasing water depth (Table 1). Compared to 1985/86, there is an increase in the amount of boulders for all water depths at Boknis Eck in 2007. This increase is lesser for deeper waters than for shallower areas closer to the coast. From 1985/86 to 2007 the total amount of boulders increased by approximately 125% (from 823 to 1855). Thus, 1032 boulders were newly exposed during this period. In the StollerGrund area, which is amongst the most exploited sites, only 501 boulders could be counted. A comparison to old data failed due to the insufficient quality of old records and poor spatial and temporal coverage. Table 1 presents the boulder density for the 100 m<sup>2</sup> cells for different water depth and periods for Boknis Eck. During the observation period, the amount of cells with none or only one boulder decreased. The number of cells with a density of three or four boulders per 100 m<sup>2</sup> represents the class with the highest increase. The mean boulder density increased from 1 boulder per 100 m<sup>2</sup> to 2.5 boulders from 1985/86 to 2007. The maximum density of boulders per 100 m<sup>2</sup> amounted to 7 in

1985/86 and 9 in 2007. In both cases, this occurred in the shallowest water depths (6 to 8 m).

Table 1. The amount of 10 x 10 m<sup>2</sup> cells with different boulder densities in the study area Boknis Eck.

Year	1985/86			2007			Change
	Water depth [m]			Water depth [m]			
Boulders / 100 m <sup>2</sup>	6-8	10-13	15-16	6-8	10-13	15-16	
0	71	103	97	18	46	55	-152
1	122	85	45	57	56	43	-96
2	73	45	28	58	59	36	+7
3	19	16	23	60	51	25	+78
4	10	1	3	48	24	22	+80
5	3	0	3	33	10	14	+51
6	1	0	1	19	2	4	+23
7	1	0	0	10	1	2	+12
8	0	0	0	10	3	0	+13
9	0	0	0	1	0	0	+1

### Regeneration of hard-bottom substrate

Fishermen reported that a single fished boulder had a weighted mean diameter of about 1 m with a mean surface area of 3.14 m<sup>2</sup>. Bock (2003) assumes that 75% of a boulder is exposed above the seafloor and can potentially be colonized by macrozoobenthos and macrophytobenthos (Figure 7). Bock (2003) and Karez and Schories (2005) estimated the surface area which was lost due to “stone fishing” in the territorial waters of the state of Schleswig-Holstein to about 5.6 km<sup>2</sup>. The area of lag sediments in the study area Boknis Eck (14.6 km<sup>2</sup>) and the amount of exposed boulders (1032) are used to estimate the increase of hard-bottom substrate (Figure 8B). An exposure of 0.47 km<sup>2</sup> is calculated for Boknis Eck within the 22-year period, corresponding to 0.2 x 10<sup>6</sup> individual boulders.

Boulders are common in areas composed of lag deposits covering boulder clay of Pleistocene origin. Only these areas have the potential for hard-bottom regeneration by natural abrasion. According to the sediment distribution map for the western Baltic

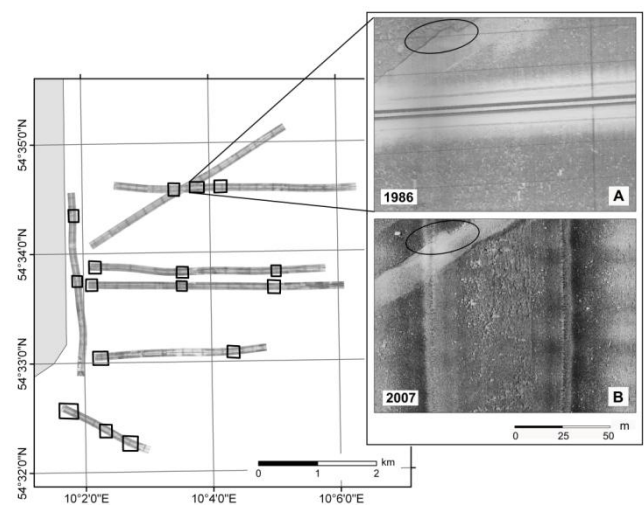


Figure 6. Analogue sidescan sonar records from Boknis Eck recorded in 1985 and 1986. Selected areas for counting boulders are marked with squares. A and B show the comparison with a high resolution image from 1986 and 2007, respectively. The track of a pipeline and boulders can be observed.

Sea (Hermansen and Jensen, 2000), about 250 km<sup>2</sup> of the seafloor belonging to territorial waters of Schleswig-Holstein is covered by lag deposits (Figure 1). Transferring the results obtained from Boknis Eck to this area, hard-bottom substrate of 8.12 km<sup>2</sup>, equivalent to  $3.44 \times 10^6$  single boulders (assumed diameter is 1 m), can be exposed during this period (Figure 8B). This estimation shows an impressive regeneration potential within 22 years, exceeding the loss of 5.6 km<sup>2</sup>. However, it has to be considered that these calculations are based on measurements in the study area in Boknis Eck where high abrasion rates occur. Furthermore, abrasion is a process with a high spatial variability. Also local scour processes can influence erosion and may locally enhance the exposure of boulders (Shamloo *et al.* 2001). Thus hard-bottom regeneration is characterized by a high degree of inhomogeneity and an extrapolation to other areas of the Baltic Sea –as done in Figure 8B– requires more site specific information.

Counting boulders on analogue sidescan sonar records inherit inaccuracies, which may result in underestimated numbers of detected boulders and thus in regeneration-rate estimates for hard-bottom substrates that are too high. In a first estimation of the influence of corrected values on the amount of regenerated hard-bottom substrate, two corrections have been done: In contradiction to Bock (2003), we assume that only 50% of a boulder is exposed above the sea floor. Additionally we reduce the amount of newly exposed boulders based in the results from StollerGrund by 50% to account for the above mentioned problems with counting boulders on analogue records. Previous calculations are repeated

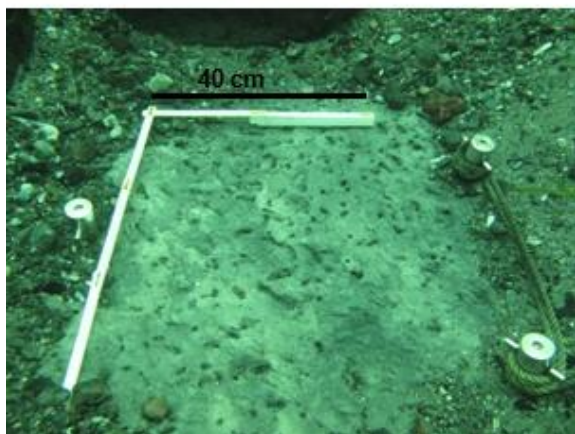


Figure 7. Top: A boulder covered with macrozoo- and macrophyto-benthos. Bottom: Seafloor with holes of boring organisms.

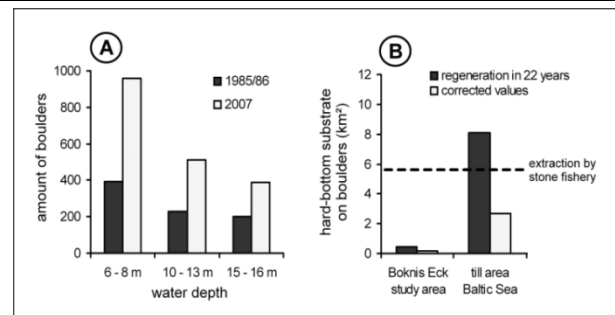


Figure 8. (A) The amount of boulders at Boknis Eck for different water depths in 1985/86 and 2007 (May, 2008). (B) Estimated potential for the spatial regeneration of hard-bottom substrate for the Baltic Sea.

with corrected values (Figure 8B). The results reveal that with a boulder surface area of 0.16 km<sup>2</sup> for Boknis Eck and 2.70 km<sup>2</sup> for the entire Baltic Sea area of Schleswig-Holstein, the growth of hard-bottom substrate is still a significant process for the recovery of this habitat.

Data of abrasion measurements carried out in front of 3 active cliffs support the values obtained above. The measured values of abrasion vary depending on water depth, composition of the boulder clay, activities by boring organisms (Figure 7) and partial coverage with mobile sand. Monthly abrasion rates vary from 0.06–0.3 cm, or an abrasion rate of 0,72–3,6 cm/year. According to Schrottke (2001), there is no strong gradient of decreasing abrasion rates from onshore towards offshore in the 3-year observation period. Apart from wave energy, the shear strength of the boulder clay and its saturation with water –thereby weakening of the upper layer even when covered with sand (Davidson-Arnott *et al.*, 1999)– as well as the activities of boring organisms (Kasten, 2012) all play a dominant role in the abrasion processes. Lowering of the seafloor within the measured 22-year period reached between 16 cm and 80 cm. For the long term period, reduced abrasion rates towards deeper waters were observed due to a decrease in wave influence. These data support the results obtained from the analyses of sidescan sonar records.

## CONCLUSION

Comparisons of old analogue with modern digital sidescan sonar records are a suitable tool to evaluate the development of hard-bottom substrates. Our results show that boulders are still present as lag sediments in the western Baltic Sea, in spite of the removal of boulders by previous “stone fishing” activities until 1974. Furthermore, the amount of boulders increased during an observation period of 22 years because of abrasion processes exposing additional boulders. Thus, new hard-bottom substrate is provided by newly exposed boulders. A natural regeneration is possible on a time scale of decades. Actual abrasion rate data support these results, obtained through the comparison of side scan sonar data over various years. The natural process of exposure of new boulders has to be considered when the regeneration of marine habitats in the Baltic Sea is intended, for example, in combination with the construction of artificial reefs.

## ACKNOWLEDGMENT

Data was acquired from the projects “Hard bottom substrates” and “Regeneration of subaquatic stone-fields in the western Baltic



Sea”, supported by the State Agency for Nature and Environment Schleswig-Holstein (LLUR). Fieldwork was assisted by captain and crew of the research vessel “Littorina” from Kiel University and GEOMAR, and by the scientific scuba diving group of Kiel University.

### LITERATURE CITED

- Askin, R.W. and Davidson-Arnott, R.G.D., 1981. Micro-erosion meter modified for the use underwater. *Marine Geology*, 40, 45-48.
- Blondel, P., 2009. *The handbook of sidescan sonar*. Chichester, England: Springer and Praxis Publishing, 316p.
- Bock, G., 2003. Quantifizierung und Lokation der entnommenen Hartsubstrate vor der Ostseeküste Schleswig-Holsteins. Eine historische Aufarbeitung der Steinfischerei, Rep. *Landesamt für Natur und Umwelt des Landes S.-H (LANU)*, 52p.
- Bock, G. F., Thiermann, H., Rumohr, H. and Karez, R., 2003. Ausmaß der Steinfischerei an der schleswig-holsteinischen Ostseeküste. *Jahresbericht Landesamt für Natur und Umwelt des Landes S.-H. (LANU)*, 111-116.
- Bohling, B., May, H., Mosch, T. and Schwarzer, K., 2009. Regeneration of submarine hard-bottom sunstare by natural abrasion in the western Baltic Sea. *Marburger Geographische Schriften*, 145, 66-79.
- Davidson-Arnott, R.G.D. and Ollerhead, J., 1995. Nearshore erosion on a cohesive shoreline. *Marine Geology*, 122, 349-365.
- Davidson-Arnott, R.G.D., van Proosdij, D., Ollerhead, J. and Langham, D., 1999. *Canadian Coastal Conference 1999*, pp. 627-636.
- Davidson-Arnott, R.G.D. and Langham, D.R.J., 2000. The effects of softening on nearshore erosion of a cohesive shoreline. *Marine Geology*, 166, 145-162.
- Directive 2000/60/ec of the European Parliament and of the Council of 23 October 2000, 2000. *Establishing a framework for Community action in the field of water policy*.
- Directive 2008/56/ec of the European Parliament and of the Council of 17 June 2008, 2008. *Establishing a framework for community action in the field of marine environmental policy (Marine Strategy Framework Directive)*.
- Detle, H.H. and Stephan, H.J., 1979. Über den Seegang und Seegangswirkung im Küstenvorfeld der Ostsee. *Mitteilungen des Leichweiß Instituts für Wasserbau*, 65, 89-136.
- Diesing, M. and Schwarzer, K., 2006. Identification of submarine hard-bottom substrates in the German North Sea and Baltic Sea EEZ with high-resolution acoustic seafloor imaging. In: Nordheim, H. v., Boedecker, D. and Krause, J.L. (eds.), *Progress in marine conservation in Europe. Natura 2000 sites in German offshore waters*. Berlin, Heidelberg, New York: Springer, pp. 111-125.
- Fish, J.P. and Carr, H.A., 1990. *Sound underwater images. A guide to the generation and interpretation of side scan sonar data*. Orleans, MA: Lower Cape Publishing, 188p.
- Flemming, B. and Wefer, G., 1973. Tauchbeobachtungen an Wellenrippeln und Abrasionserscheinungen in der Westlichen Ostsee südöstlich Bokniseck. *Meyniana*, 23, 9-18.
- Harff, J., W., Lemke, W., Tauber, F. and Emelyanov, E.M., 1995. Geologische Kartierung der Ostsee. *Geowissenschaften*, 13 (11), 442-447.
- Harff, J., Björck, S. and Hoth, P., 2011. *The Baltic Sea Basin*. Heidelberg, Dordrecht, London, New York: Springer, 449p.
- Healy, T. and Wefer, G., 1980. The efficiency of submarine abrasion vs. cliff retreat as a supplier of marine sediment in Kiel Bight, Western Baltic. *Meyniana*, 32, 89-96.
- Hermansen, B. and Jensen, J.B., 2000. *Digital seabottom sediment map around Denmark 1:500,000*, Danmarks Og Groenlands Geologiske Undersøegelse, Copenhagen.
- Karez, R. and Schories, D., 2005. Die Steinfischerei und ihre Bedeutung für die Wiederansiedlung von *Fucus vesiculosus* in der Tiefe. *Rostocker Meeresbiologische Beiträge*, 14, 95-107.
- Kasten, S., 2012. *Der erosive Einfluss von Sedimentbedeckung, Morphologie und Bioturbation auf verschiedene Abrasionsplattformen in der Kieler und Lübecker Bucht*. Kiel, Germany: University, Inst. of Geosciences, Diplom thesis, 127p.
- Katsnelson, B., Petnikov, V. and Lynch, J., 2012. *Fundamentals of Shallow Water Acoustics*. New York, Dordrecht, Heidelberg, London: Springer, 540p.
- Kolp, O., (1966): Die Sedimente der westlichen und südlichen Ostsee und ihre Darstellung (Berlin, Germany). Akademie-Verlag, *Beiträge zur Meereskunde*, 17-18, 9-60.
- Kubicki, A. and Diesing, M., 2006. Can analogue sidescan sonar data still be useful? An example of a sonograph mosaic geo-coded in Decca Navigation System. *Continental Shelf Research*, 26, 1858-1867.
- May, H., 2008. *Seegrundkartierung und Analyse der Entwicklung subaquatischer Steinfelder mittels hydroakustischer Methoden bei Boknis Eck (Eckernförder Bucht)*. Keil, Christian-Albrechts-University, Diplom thesis, 108p.
- Mosch, T., 2008. *Veränderungen der Sedimentverteilungen auf dem StollerGrund seit den siebziger Jahren*. Kiel, Germany: Christian-Albrechts-University Kiel, Diplom thesis, 91p.
- Mazel, C., 1985. *Sidescan sonar record interpretation*. Klein Associates Inc., New Hampshire, 144p.
- Niedermeyer, R.-O., Lampe, R., Janke, W., Schwarzer, K., Duphorn, K., Kliewe, H. and Werner, F., 2011. *Die deutsche Ostseeküste. Sammlunggeologischer Führer*, 105, 370 p.
- Schrottke, K., 2001. Retreat dynamics of Schleswig-Holsteins' scifl-coasts with special regard to submarine abrasion and residual sediment mobility. *Ber.-Rep., Inst. of Geosciences*, 16, 186p. (in German).
- Schrottke, K., Schwarzer, K. and Fröhle, P., 2006. Mobility and transport directions of residual sediments on abrasion platforms in front of active cliffs (southwestern Baltic Sea). *Journal of Coastal Research*, Special Issue No. 39, 459-464.
- Schwarzer, K., Schrottke, K., Stoffers, P., Kohlhasse, S., Fröhle, P., Fittschen, T., Mohr, K., Riemer, J. and Weinhold, H., 2000. *Einfluss von Steiluferabbrüchen an der Ostsee auf die Prozessdynamik angrenzender Flachwasserbereiche*. Final Report, Inst. of Geosciences, 182p.
- Shamloo, H., Rajaratnam, N. and Katopodis, C., 2001. Hydraulics of simple habitat structures. *Journal of Hydraulic Research*, 39 (4), 351-366.
- Silva, J. P., Jones, W., Eldridge, J. and Sarvan, E., 2006. *Life and the marine environment. Promoting sustainable management of Europe's seas*. European Commission Environment Directorate-General, Brussels, 53p.
- Tauber, F., Lemke, W. and Endler, R., 1999. Map of sediment distribution in the western Baltic Sea (1:100,000), Sheet Falster-Møn. *Deutsche Hydrographische Zeitschrift*, 51(1), 5-32.
- Wefer, G., Flemming, B. and Tauchgruppe Kiel, 1976. Submarine Abrasion des Geschiebemergels vor Bokniseck (Westl. Ostsee). *Meyniana*, 28, 87-94.
- Werner, F., Altenkirch, J., Newton, R.S. and Seibold, E., 1976. Sediment patterns and their temporal variation on abrasion ridges in a moderate flow regime (StollerGrund, Western Baltic). *Meyniana*, 28, 95-103.
- Zander, C.D., 1991. Die biologische Bedeutung der Lebensgemeinschaft “Miesmuschelgürtel” in der Ostsee. *Seevögel*, 12 (1), 127-131.

# Forecasting lagoon outlet erosion: KwaZulu-Natal, southeast Africa

A.M. Smith<sup>†</sup>, L.A. Guastella<sup>‡</sup>, B.J. Goble<sup>+</sup>

<sup>†</sup>School of Geological Sciences,  
University of KwaZulu-Natal, Durban  
4001, South Africa,  
asconsulting@telkomsa.net

<sup>+</sup>Oceanographic  
Research Institute,  
Durban, 4056, South  
Africa.  
bgoble@ori.org.za

<sup>‡</sup> Oceanography Department, University  
of Cape Town, Private Bag X3,  
Rondebosch, South Africa,  
lisagus@telkomsa.net

<sup>∞</sup>Bayworld Centre for Research and  
Education (BCRE), Riesling Rd,  
Constantia, South Africa



[www.cerf-jcr.org](http://www.cerf-jcr.org)



[www.JCRonline.org](http://www.JCRonline.org)

## ABSTRACT

Smith, A.M., Guastella, L.A., Goble, B.J., 2014. Forecasting lagoon outlet erosion: KwaZulu-Natal, southeast Africa. In: Green, A.N. and Cooper, J.A.G. (eds.), *Proceedings 13<sup>th</sup> International Coastal Symposium* (Durban, South Africa), *Journal of Coastal Research*, Special Issue No. 70, pp. 151-156, ISSN 0749-0208.

The Amanzimtoti Lagoon is at the mouth of the Amanzimtoti River. The lagoon outlet changes systematically in response to the 18 year long Dyer-Tyson summer rainfall cycle (DTC). During the dry part of the DTC the lagoon is generally closed, opening only during heavy rainstorms. When closed the lagoon is separated from the sea by a baymouth bar, varying from 30 to 60 m wide. The open-days per year have increased dramatically as the DTC has entered the wet phase. Early in the DTC the lagoon rarely opened, and when this occurred it breached near the centre of the headland bound bay, but as the DTC-driven runoff cycle has progressed the outlet has remained open. However, during this open phase the outlet has been forced southward along the back beach until it deflected seaward by the southern headland outcrop. This appears to be brought about by longshore drift and an increased beach width. We suggest that this is due to the shoreward reworking of sediment by waves. This sediment has been brought down by the river in increasing amounts as the wet part of the DTC waxes, strengthening the seasonal rainfall and the river flow cycle. Wave reworking has forced the outlet along the back beach causing erosion of the coastal dune behind the back beach. Thus, the lagoon mouth enters a predictable erosion phase as the DTC progresses. This cyclicity can be used to forecast this type of lagoon outlet erosion. The Amanzimtoti Lagoon has strong similarities to the Hapua Lagoon-type recognized from New Zealand.

**ADDITIONAL INDEX WORDS:** *Hapua Lagoon, Longshore drift, Dyer-tyson cycle*

## INTRODUCTION

KwaZulu-Natal (KZN) is located on the east coast of South Africa in the subtropical zone and, as such, experiences summer rainfall. Rainfall varies year-on-year, controlled by an 18-year cycle (Dyer and Tyson, 1977; Tyson, 1986), likely as a result of the lunar nodal cycle (LNC). Recent research (Smith et al., 2010; 2013; Corbella and Stretch, 2012a) shows that the KZN coast is prone to coastal (beach) erosion during the LNC peak.

Two types of Erosion Hot Spots (EHS) have been recognized on the coast of KwaZulu-Natal (KZN) and correlated with the lunar nodal cycle (LNC) peak (Smith et al., 2010; 2013) (Figure 1). EHS<sub>1</sub> is triggered by highswells, whereas EHS<sub>2</sub> is caused by seasonal megarip activity produced headlands perturbing the longshore drift (Smith et al., 2013). This paper reports on a new EHS type [EHS<sub>3</sub>], associated with lagoon mouth dynamics which is correlatable with the eighteen year summer rainfall cycle or Dyer-Tyson Cycle (DTC) (Dyer and Tyson, 1977; Tyson, 1986; Malherbe et al., 2012), which, although 80<sup>0</sup> out of phase, also correlates with the LNC. The South African mean annual precipitation controls the coastal sediment input, its severity is controlled by the multi-annual DTC. The relationship between the DTC and LNC, although not understood, allows for the forecasting of long-term coastal erosion and EHS.

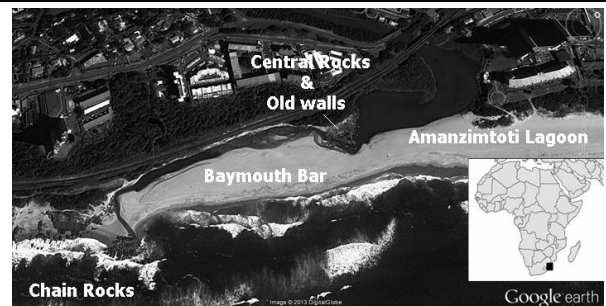


Figure 1. Location map and context of the Amanzimtoti River and Lagoon.

The Amanzimtoti is a small coastal river (Figure 1; Table 1) which enters the sea within a headland-bound bay. This paper discusses an example of lagoon mouth dynamics on the KZN coast and comments on the time and place of erosion. This erosion can at times be catastrophic, for example, on 11 December 2012 it led to the collapse and failure of an urban railway line adjacent to the Amanzimtoti Lagoon outlet (Guastella et al., *this volume*). In this paper we concentrate on the Amanzimtoti Lagoon (Figure 1) which has been the subject of ongoing video assessment (Guastella and Smith, 2014) and frequent field observation since

April 2010. We relate lagoon outlet erosion to the intensity of the DTC. From this cyclicity we have established a baseline by which lagoon outlet erosion can be forecast. This adds to the existing Coastal Erosion Model presented by Smith *et al.* (*in press*).

The KZN tidal range varies from a maximum (highest astronomical) tide of 2.3 m and mean neap high of 1.36 m (Durban) and a highest astronomical tide of 2.47 m and mean neap high tide of 1.48 m (Richards Bay); thereby making it a microtidal to low mesotidal system (Hayes, 1979). The coast is exposed to the Indian Ocean with the nearest offshore landmass being Antarctica, hence it is exposed to the full brunt of swell generated in the Southern Ocean. The continental shelf is narrow, varying from 2 km to a maximum of 47 km (Bosman *et al.*, 2007; Cawthra *et al.*, 2012). The 1:1 year significant wave height ( $H_s$ ) is estimated at 5.5 m (Corbella and Stretch, 2012b). The highest recorded  $H_s$  is 9 m (Guastella and Rossouw, 2012), being produced by Tropical Storm Imboa (1984). A Cut-off Low system (COL) produced waves ( $H_s$ ) of 8.5m in 1966 and 2007 (Smith *et al.*, 2007; 2010). A maximum  $H_s$  of 11.36 has been estimated from Mission Rocks in northern KZN by Salzmann and Green (2012) using megalith dimensions (Figure 1.). The wave climate drives a generally northerly flowing longshore drift (Cooper, 1991a, 1991b, 1994; Guastella and Smith, 2014), although this can reverse on synoptic- and seasonal- scales (Smith *et al.*, 2013).

## METHODS

Using a CCTV camera of opportunity (set up for tourism purposes by a cellphone company), daily images have been collected for the period spanning March (2010) to the present. Images have been captured at low tide (and at other times of interest). This imagery has been augmented by images collected from frequent ground truthing and any other available imagery. Over this time period we have documented changes in the bay mouth bar, outlet behavior and breaching events.

This imagery was manually analysed to identify any patterns. Smith *et al.* (2010; 2013; *in press*; 2014) and Guastella and Smith (2014) established that seasonal and multi-annual trends are present on the KZN coast. This work continues that line of research but analyses, specifically, changing sub-seasonal, synoptic and daily trends throughout the DTC multi-annual cycle.

## RESULTS

When closed the lagoon outlet is separated from the sea by a baymouth bar (Figure 2). There is a systematic seasonal change of lagoon mouth morphodynamics driven by river run-off, itself driven by the mean annual precipitation. Between 2010 and 2013 the dominant lagoon outlet morphology changed significantly. During the latter half of 2010 and 2011 the lagoon outlet was generally closed, breaching only rarely. When breaching occurred it took place at the river mouth (Figure 2a) or when closed water ponded behind the baymouth bar (Table 2). During this period river freshes and freshettes (driven by summer rainfall) opened the lagoon.

As the multi-annual seasonal rainfall cycle progressed, the Amanzimtoti lagoon mouth opened more frequently until in 2013 where it has been permanently open. With this change the beach has widened and the lagoon outlet was forced to flow southward along the back beach. Towards the end of 2012, the pattern changed to a southward, shore-parallel inlet migration along the backbeach in response to a widening of the beach spit (from 100 to 200 m and an increase in elevation) (Figure 2).

The Amanzimtoti Lagoon outlet is deflected seaward in its coast-parallel course by a dolerite outcrop (Figure 2). Much of the time this outcrop is partly buried under sand, especially when the

lagoon outlet is closed. The outlet gradually extended southward until it was blocked and deflected seaward by the Chain Rocks rocky promontory that marks the southern boundary of the headland-bound bay, some 600 m to the south (Figure 1). During this migration, the outlet channel caused erosion and undercutting of the coastal dune behind the back beach. Importantly, the coastal dune has been heavily modified by the construction of a railway, dating back to the late 19<sup>th</sup> century. Outlet erosion resulted in instability and ultimately failure of the coastal railway line at Amanzimtoti. The behavior of this lagoon is summarized in Table 1.

Breaching events (between March 2010 and September 2013) are plotted in Figure 3. From this it can clearly be seen that the number of breaching events has varied markedly (logarithmically) over this period. This has not been a smooth process but an episodic one.

Lagoons similar to the one described here are elsewhere referred to as ICOLLs (Roy *et al.*, 2001; Figueiredo, 2002; Figueiredo *et al.*, 2007; Serpa *et al.*, 2011), however the specific genera that the Amanzimtoti Lagoon best fits is the 'Hapua Lagoon morphotype' (Hart, 2007; 2009). These are characterised by dynamic outlet systems that often extend along the coast, separated from the sea by a coast-parallel bar, driven by longshore drift. Hapua lagoons are an extreme form of wave-dominated delta. As in the Amanzimtoti case, the Hapua Lagoon is in a dynamic equilibrium between fluvial input and wave reworking (Hart, 2009). The Amanzimtoti lagoon seems to be an extreme version of the Hapua lagoon, enclosed within a headland-bound bay.

## DISCUSSION

Previous lagoon research has relied on serendipitous coastal air imagery (Cooper, 2002; Garden and Garland, 2005; Green *et al.*, 2013). These image points are often several years apart and cannot account for hourly, daily, synoptic or seasonal changes (Guastella and Smith, *in press*) or long-term tidal cycles (Smith *et al.*, 2010; 2013, *in press*; Corbella and Stretch, 2012a). All previous southeast African coastal geomorphological research has neglected these shorter-term changes with the exception of Smith *et al.* (2010; 2013) who highlighted seasonal- and synoptic- driven geomorphological changes on KZN beaches. Elsewhere Hart (2009) analysed some New Zealand Hapua lagoons, utilizing a year of images.

The Amanzimtoti lagoon catchment was characterized by high and sudden coastal-rainfall events during late 2011 and most of 2012. This increased water flow to the sea resulted in increased sediment deposition at the inlet mouth. This sediment was reworked back onto the beaches which widened and inflated the beach, preventing the outlet from breaching the spit bar. The lagoon outlet was forced to flow southward along the backbeach. This movement is controlled by an eddy in the longshore drift which produces a localized, topographically controlled, reversal of the longshore drift (Guastella and Smith, 2014), and consequently the baymouth bar is built from north-south. This forces the lagoon outlet to cut a path along the backbeach to the Chain Rocks headland (southern boundary of the headland bay, where breaching occurs as a result of hydraulic head build up. This process results from wave activity dominating fluvial processes and inflating the beach. The mouth will stay open as long as the hydraulic head can dominate wave processes. In mid-late 2012 the Amanzimtoti lagoon outlet was squeezed against the railway berm (modified coastal dune) due to the widening and inflation of the Amanzimtoti lagoon beach bar from 2011 to 2012. This was brought about by reworking of fluvial sediment brought down during the stronger rainy season. Squeezing of the outlet against



Figure 2. Amanzimtoti River and Lagoon morphodynamics. A. Baymouth bar breached after thunderstorm; B. Baymouth bar breached after thunderstorm, note that the southern outlet channel has been abandoned; C. Lagoon outlet moving to the south; D: Lagoon outlet flowing southward.

the dune, led to undercutting and subsequent slope failure and, ultimately, a train derailment.

Danger to the railway line was first noticed in late August, when the lagoon outlet had been pushed landward and squeezed against the berm flowing until blocked by the rocky point, that

MONTH	2010	2011	2012	2013
Jan	n/a	C/S to Chain Rocks	Central Rocks	Chain Rocks
Feb	n/a	C/S	Central Rocks	Chain Rocks
Mar	n/a	C/S	Central Rocks	Chain Rocks
Apr	Chain Rocks	C/S	Central Rocks	Chain Rocks
May	Chain Rocks to C/S to Chain Rocks	C/S	Central Rocks	Chain Rocks
June	Chain Rocks to C/S	C/S	Central Rocks	Chain Rocks
July	C/S	Central Rocks	Central Rocks	Chain Rocks
Aug	C/S	Central Rocks	Central Rocks	
Sep	C/S	Central Rocks	Central Rocks to C/S	
Oct	C/S	?	C/S to Chain Rocks	
Nov	C/S	?	F/S to C/S	
Dec	C/S	Central Rocks	F/S	

Table 1: Position of the Amanzimtoti lagoon outlet 2010-2013 from a CCTV source (C/S is 400m south of the river mouth; F/S is 600m south of the river and Central Rocks is where the old walls were constructed (see Figure 1).

marks the southern end of Chain Rocks Bay, it entered the sea. A rainstorm overnight (10-11<sup>th</sup> December) triggered the final conditions that caused the railway failure. The likelihood of such an event was obvious and had been communicated to the authorities, however no action was taken. During this time it was also noted that other lagoon outlets along the coast behaved in a similar way.

Coastal erosion, which correlates with the dry climatic cycle of river runoff (Smith *et al.*, *in press*) dominated from 2005-2011 (Smith *et al.*, 2010; 2013) (Figure 2). Towards the end of the dry climatic phase (2009) and especially during 2012 it was noted that the Amanzimtoti lagoon outlet showed a strong tendency to migrate southwards. No northwards migration has been observed. During ground-thruthing exercises the existence of failed walls were noted. These structures had apparently been built to prevent the lagoon outlet's southward movement and to maintain a full lagoon for paddling canoes and holidaymakers. As far as we were able to determine these had been built during the previous DTC peak indicating that this type of lagoon outlet behaviour is cyclic and consequently predictable.

Cooper (2002) summarized the role of extreme floods in lagoon dynamics, stating that erosion of river banks, barrier and tidal deltas produced an ephemeral sand delta to seaward. Post-flood wave-reworking of these sediments provides a source of sediment for rebuilding the pre-flood morphology. Cooper (2002) highlights that this process takes place on a scale of months, years and possibly decades. In contrast Smith *et al.* (2010) identified that the Natal Flood (1987), one of the largest on record (occurred during a major coastal erosion phase) did not prevent dramatic coastal erosion during the 1987 to 1989 period. There appears to be a significant difference between floods produced by the major rivers and those produced by limited fetch rivers.

There is a clear correlation between the DTC, which drives runoff and consequently river flow, and the 18.61 year LNC (Dyer and Tyson, 1977; Visagie, 1985; Malherbe *et al.*, 2012). Further the  $\pm 4.4$  year Lunar Perigean subharmonic (LPS) cycle is evident in the coastal erosion record (Corbella and Stretch, 2012a; Smith *et al.*, 2013) with the LNC apparently dominating. The latter effect is due to the masking effect of the DTC driven sediment runoff, consequently erosion is only noticed during the dry part of the DTC cycle (Smith *et al.*, *in press*).

Extreme flood events do not seem to affect coastal erosion episodes, however, the clear link between the DTC and LNC sparks a conundrum. We suggest that during extreme flood events most sediment bypasses the nearshore zone to be deposited on the inner shelf. This was clearly demonstrated by the extreme seaward

position of the surf zone in images of the Natal Flood (Perry, 1989). It is also becoming increasingly well known that a significant offshore facies break occurs at depths of  $\pm 13$ -16m depth, a location characterized by the presence of shoreface-connected ridges (Cawthra *et al.*, 2011; Bosman, 2013), built by sediment that has bypassed the surf zone (nearshore zone) and which cannot be returned to the shore (Smith *et al.*, 2010) during the process of marine transgression (Swift *et al.*, 1978). Sediment transported by flooding in the smaller rivers does not bypass the nearshore surf zone and consequently is available to be reworked back onto the coast by fair-weather processes and build or rebuild beaches and dunes as suggested by Cooper (2002).

During flooding the Amanzimtoti lagoon outlet generally opens at the river mouth when the beach is deflated and thin, but when the beach is wide and inflated the mouth is forced southward. The southward migration pattern shows that the river has been progressively unable to breach the containing baymouth bar and hence is forced southwards. Other researchers (Garden and Garland, 2005; Green *et al.*, 2013) have noted that lagoon outlet movement is in response to littoral drift flow. The fact that some outlets flow in opposition to the littoral drift direction is recorded (Garden and Garland, 2005) but is not discussed. In the Amanzimtoti lagoon case the southward reversal in direction is in response to a coastal topographic-driven eddy in the longshore drift (Guastella and Smith, 2014).

## CONCLUSION

The Amanzimtoti Lagoon outlet changes systematically in response to the 18 year long Dyer-Tyson summer rainfall cycle (DTC). During the dry part of the DTC the lagoon was generally closed, opening only during rainstorms. When closed off from the sea the lagoon is separated from it by a baymouth bar, varying from 30 to 60 m wide.

The lagoon outlet open-days per year have increased dramatically as the DTC has entered the wet phase. Early in the DTC the lagoon opened rarely, and when this occurred it breached near the centre of the headland bound bay, but as the DTC-driven runoff cycle has progressed the outlet has remained open. However during this open phase the outlet has been forced southward along the back beach till it is deflected seaward by the southern headland outcrop. This appears to be brought about by increased baymouth bar/beach width. We suggest that this is due to the shoreward reworking of sediment by waves. This sediment has been brought down by the river in increasing amounts as the wet part of the DTC waxes and strengthens the seasonal rainfall and river flow cycle.

As the behavior of the Amanzimtoti Lagoon outlet is related to regular cycles, such as the mean annual precipitation, and the eighteen year DTC, its behavior is predictable. This knowledge will allow forecasting of lagoon outlet erosion events and allow beach managers to become better informed about coastal dynamics and plan ahead. This information could have been used to prevent disasters such as the Amanzimtoti train smash on 12 December (2012) which was directly related to lagoon outlet erosion (Guastella *et al.*, 2014).

We suggest that the dominance of wave-sediment reworking has forced the lagoon outlet along the back beach. This shoreward forcing causes erosion of the coastal dune behind the back beach.

Thus the lagoon mouth enters a predictable erosion phase as the DTC progresses. This cyclicity can be used to forecast this type of lagoon outlet erosion. The Amanzimtoti lagoon has similarities to the Hapua lagoon type recognized from New Zealand.

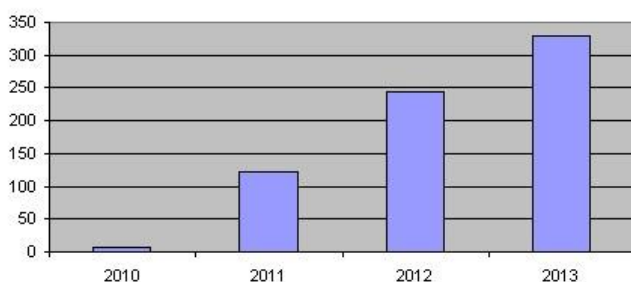


Figure 3: Increase in frequency of lagoon outlet days in an open condition. As well as this increase in open-ness, the outlet has been continually routed south.

## ACKNOWLEDGEMENT

We would like to acknowledge Vodacam SA for allowing the authors to make use of CCTV footage and Google Earth for further coastal imagery. This project was self-funded by the authors.

## LITERATURE CITED

- Bosman, C., 2013. *The marine geology of the Aliwal Shoal, Scottburgh, South Africa*. Durban, South Africa: University of KwaZulu-Natal, Ph.D. thesis, 550p.
- Cooper, J.A.G., 1991a. *Shoreline changes on the Natal coast: Mkomanzi River mouth to Tugela River mouth*. Natal Town and Regional Planning Commission Report 77. The Town and Regional Planning Commission, P/B 9038, Pietermaritzburg, 3200, pp. 53.
- Cooper, J.A.G., 1991b. *Shoreline changes on the Natal coast: Tugela River mouth to Cape St Lucia*. Natal Town and Regional Planning Commission Report 76. The Town and Regional Planning Commission, P/B 9038 (Pietermaritzburg, South Africa), 3200, pp. 57.
- Cooper, J.A.G. 1991c. *Sedimentary models and geomorphological classification of river-mouths on a subtropical, wave-dominated coast, Natal, South Africa*. Durban, South Africa: University of Natal, Ph.D. thesis, 330p.
- Cooper, J.A.G., 1994. *Shoreline changes on the Natal coast: Mtamvuna River mouth to the Mkomazi River mouth*. Natal Town and Regional Planning Commission Report 79, The Town and Regional Planning Commission, P/B 9038, Pietermaritzburg, 3200, pp. 53.
- Cooper, J. A. G., 2002. The role of extreme floods in estuary-coastal behaviour: contrasts between river- and tide-dominated microtidal estuaries. *Sedimentary Geology*, 150, 123–137.
- Corbella, S. and Stretch, D.D., 2012a. Decadal trends in beach morphology on the east coast of South Africa and likely causative factors Natural Hazards Earth Systems Science 12, 2515–2527. [www.nat-hazards-earth-syst-sci.net/12/2515/2012/](http://www.nat-hazards-earth-syst-sci.net/12/2515/2012/). doi:10.5194/nhess-12-2515-2012.
- Corbella, S and Stretch, D.D, 2012b. The wave climate on the KwaZulu-Natal coast of South Africa. *J. S. Afr. Inst. Civ. Eng.*, 54. [http://www.scielo.org.za/scielo.php?pid=S1021-20192012000200005&script=sci\\_arttext](http://www.scielo.org.za/scielo.php?pid=S1021-20192012000200005&script=sci_arttext).
- H.C. Cawthra, H.C Neumann, F.C Uken R, Smith, AM, Guastella, LA and Yates, A., 2012). Sedimentation on the narrow (8 km wide), oceanic current-influenced continental shelf off Durban, Kwazulu-Natal, South Africa. *Marine Geology*, 323–325, 107–122.
- Dyer, T.G.J. and Tyson, P.D., 1977. Estimating above and below normal rainfall periods over South Africa, 1972–2000. *Journal of Applied Meteorology*, 16, 145–147. DOI: 10.1175/1520-0450(1977)016<0145:EAABNR>2.0.CO.
- Figueiredo, S.A., 2002. *Distribuição espaço-temporal dos sangradouros na costa gaúcha no trecho São José do Norte – Farol de Mostardas*. Rio Grande, Rio Grande do Sul: Universidade Federal do Rio Grande. Graduation Thesis, 43p.
- Figueiredo, S.A., Cowell, P. and Short, A., 2007. Intermittent backbeach discharge to the surfzone: modes and geomorphologic implications. *Journal of Coastal Research*, Special Issue No. 50, 610–614.
- Garden, S.E. and Garland, G.G., 2005. Spit development in the Mdloti River estuary, KwaZulu-Natal. *South African Journal of Geology*, 108, 257–270.
- Green, A., Cooper, J.A.G., and LeVieux, A., 2013. Unusual barrier/inlet behaviour associated with active coastal progradation and river-dominated estuaries. In: Kana, T.; Michel, J., and Voulgaris, G. (eds.), *Proceedings, Symposium in Applied Coastal Geomorphology to Honor Miles O. Hayes* (Coconut Creek, Florida), *Journal of Coastal Research*, Special Issue No. 69, 35–45. ISSN 0749-0208.
- Guastella, L.A. and Rossouw, M., 2012. What will be the impact of increasing frequency and intensity of coastal storms along the South African coast? *Reef Journal*, 2, 129–139.
- Guastella, L.A. and Smith, A.M., 2014. Coastal dynamics on a soft coastline from serendipitous webcams: KwaZulu-Natal, South Africa. *Estuarine, Coastal and Shelf Science* (2014), <http://dx.doi.org/10.1016/j.ecss.2013.12.009>.
- Guastella, L.A., Smith and A.M., Breetzke, T., 2014. Coastal management and mis-management: comparing successes and failures at two lagoon outlets in KwaZulu-Natal, South Africa. In: Green, A.N. and Cooper, J.A.G. (eds.), *Proceedings 13<sup>th</sup> International Coastal Symposium* (Durban, South Africa), *Journal of Coastal Research*, Special Issue No. 66, pp. ISSN 0749-0208.
- Hart, D. E., 2007. River-mouth lagoon dynamics on mixed sand and gravel barrier coasts. *Journal of Coastal Research*, SI50, 927–931.
- Hart, D., 2009. Morphodynamics of Non-estuarine River mouth Lagoons on High-Energy Coasts. *Journal of Coastal Research*, 56 (2), 1355–1359.
- Hayes, M. O., 1979, Barrier island morphology as a function of wave and tide regime. In: Leatherman, S. P. (ed.), *Barrier islands from the Gulf of St. Lawrence to the Gulf of Mexico*. New York, Academic Press, pp. 1–29.
- Malherbe, J., Engelbrecht, T., Landman, F.A. and Engelbrecht, C.J., 2012. *Tropical systems from the southwest Indian Ocean making landfall over the Limpopo River Basin, southern Africa: a historical perspective*. Water Research Commission, South Africa WRC Project No. K5/1847.
- Perry, J.E., 1989. The impact of the September 1987 floods on the estuaries of Natal/ Kwazulu.: A hydro-photographic perspective. *Earth, Marine and Atmospheric Science and Technology* (Stellenbosch, South Africa), *CSIR Research Report*, 640, 29p.
- Roy, P. S., Williams, R. J., Jones, A. R., Yassini, R., Gibbs, P. J., Coates, B., West, R. J., Scanes, P. R., Hudson, J. P. and Nichol, S., 2001. Structure and Function of South-East Australian Estuaries. *Estuarine, Coastal and Shelf Science*, 53, 351–384.
- Salzmann, L. and Green, A., 2012. Boulder emplacement on a tectonically stable, wave-dominated coastline, Mission Rocks, northern KwaZulu-Natal, South Africa. *Marine Geology*, 323–325, 95–106.
- Serpa, C.G., Romeu, M.A.R., Fontoura, J.A.S., Calliari, L.J., Melo, E. and Albuquerque, M.G., 2011. Study of the responsible factors for the closure of an intermittent washout during a storm surge, Rio Grande do Sul, Brazil. *Journal of Coastal Research*, SI 64, 2068 – 2073.
- Smith, A.M., Guastella, L.A., Bundy and S.C., Mather, A.A., 2007. Combined marine storm and Saros spring–high tide erosion event, March 19–20, 2007: A preliminary assessment. *South African Journal of Science*, 103, 274–276.
- Smith, A.M., Mather, A.A., Bundy, S.C., et al., 2010. Contrasting styles of swell-driven coastal erosion: examples from KwaZulu-Natal, South Africa. *Geological Magazine*, 147, 940–953.
- Smith, A. M., Guastella, L.A., Mather, A.A., LA, Bundy and S.C. Haigh, I., 2013. KwaZulu-Natal coastal erosion in time and space: a predictive tool? Comparisons between the 2011 and 2007 erosion event. *South African Journal of Science*, 109, 1–4.
- Smith, A.M., Guastella, L.A., Botes, Z.A. Bundy S.C., and Mather A.A., 2014. Forecasting cyclic coastal erosion on a multi-annual to multi-decadal scale: southeast African coast. *Estuarine and Continental Shelf Science*. <http://dx.doi.org/10.1016/j.ecss.2013.12.009>
- Swift, D.J.P., Parker, G., Lanfredi, N.W., Perillo, G. and Figge, K., 1978. Shoreface-connected sand ridges on American and European shelves: a comparison. *Estuarine Coastal Mar. Sci.*, 7, 257–273.
- Tyson, P.D., 1986. *Climate Change and Variability in Southern Africa*. Cape Town: Oxford, 220p.
- Visagie, P.J., 1985. An investigation into wet and dry cycles of rain fall in South Africa. Report to Hydrology Engineering Division, Electricity Supply commission, Sandton. In: Tyson, P.D., *Climate Change and Variability in Southern Africa*. Cape Town, South Africa: Oxford, 220p.

# Seasonal sedimentary processes of the macrotidal flat in Gomso Bay, Korea

Jeongwon Kang<sup>†</sup>, Han J. Woo<sup>‡</sup>, Yoon-Kyung Lee<sup>∞</sup>, Young B. Son<sup>§</sup>

<sup>†</sup> Korean Seas Geosystem Research Unit  
Korea Institute of Ocean Science and  
Technology (KIOST), 787 Haeanro,  
Ansan 426-744, Korea  
jwkhang7@kiost.ac

<sup>‡</sup> Korean Seas Geosystem Research Unit  
Korea Institute of Ocean Science and  
Technology (KIOST), 787 Haeanro,  
Ansan 426-744, Korea  
hjwoo@kiost.ac

<sup>∞</sup> Korea Ocean Satellite Center  
Korea Institute of Ocean Science and  
Technology (KIOST), 787 Haeanro,  
Ansan 426-744, Korea  
eunicelee@kiost.ac

<sup>§</sup> Marine Ecosystem Research Division  
Korea Institute of Ocean Science and  
Technology (KIOST), 787 Haeanro,  
Ansan 426-744, Korea  
sonyb@kiost.ac



[www.cerf-jcr.org](http://www.cerf-jcr.org)



[www.JCRonline.org](http://www.JCRonline.org)

## ABSTRACT

Kang, J., Woo, H.J., Lee, Y.-K., Son, Y.B., 2014. Seasonal sedimentary processes of the macrotidal flat in Gomso Bay, Korea. In: Green, A.N. and Cooper, J.A.G. (eds.), *Proceedings 13<sup>th</sup> International Coastal Symposium* (Durban, South Africa), *Journal of Coastal Research*, Special Issue No. 70, pp. 157-163, ISSN 0749-0208.

To understand seasonal sedimentary processes, we analyzed sediment grain size, short-term sedimentation rates, and chemical tracers to determine sediment provenance in the Gomso tidal flat, which is located on the western coast of Korea. It is a funnel-shaped embayment with a mean tidal range of 4.3 m. Calculating the elevation from a digital elevation model (DEM), the landward inner bay was relatively higher than that of the outer bay. Sandy sediments generally dominated the outer bay, whereas sandy mud sediments were distributed in the inner bay. The middle bay consisted of muddy sand sediments. From February 2011 to February 2012, the net deposition rate in the inner tidal flat of the bay was 41 mm/year. Erosion dominated the middle and outer tidal flats of the bay, with net erosion rates of -30 and -10 mm/year, respectively. Seasonal variations in sedimentation in the Gomso tidal flats occurred with deposition via the inflow of fine-grained sediments during spring and summer and winnowing from the bay during autumn and winter. The rare earth element (REE) analysis proved that the fine-grained sediments were transported from Jujin Stream in the southern bay and deposited on the middle bay tidal flats, especially during the rainy season. The source of the outer bay sediments was related to the inflow of fine sediments of alluvial origin. Therefore, the major forcing factors affecting the seasonal variation in sedimentation involve a combination of tidal currents and waves, together with heavy rainfall.

**ADDITIONAL INDEX WORDS:** *Sedimentation rate, Rare earth elements, Rainfall, Monsoon.*

## INTRODUCTION

The tidal flats located on the western coast of Korea are broad, with gentle slopes and macrotidal ranges of 4 to 10 m. The dispersal and transport of suspended fine-grained sediments along this Yellow Sea sect of the coast is associated with tidal flat sedimentation within coastal bays (Lee *et al.*, 1999; Ryu, 2003). Generally, the western coast of Korea is classified by either semi-closed or open type tidal flats, each with characteristic sedimentological processes (Ryu, 2003 and references therein); the geographic north and south zones are embayed tide-dominated coasts, while the central west coast is relatively straight and wave-dominated (Yang *et al.*, 2006; Figure 1).

The sedimentary process of the open-type tidal flat involves a monsoon climate with strong storms during winter. These generate high hydrodynamic stress which affects the surficial fine

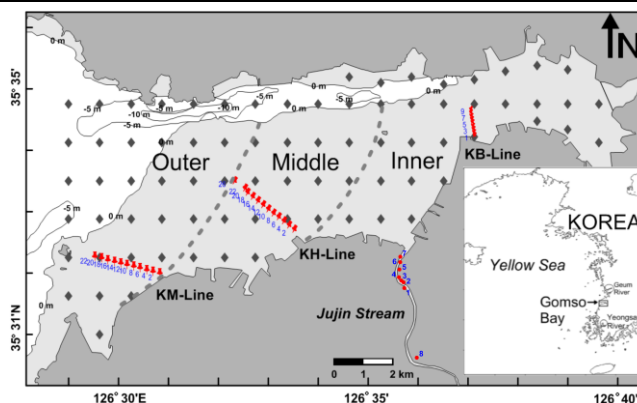


Figure 1. Map of the study area, including the transect lines, 79 surface sediment sampling locations (◆), three zones along the southern tidal flat flank and sampling stations for Jujin Stream.

DOI: 10.2112/SI70-027.1 received 27 November 2013; accepted 21 February 2014. © Coastal Education & Research Foundation 2014

sediments deposited during summer. In winter, these are winnowed offshore to form a suspended plume (Lee *et al.*, 2004). However, the sedimentary cycles of tidal flats characterized by semi-closed bays appear to be complicated. The most important factor causing different seasonal sedimentary processes is thought to be the inner coastline geometry of a bay relative to the wind direction and hence the degree of the effect of wind-generated waves on different sites within the bay (Ryu *et al.*, 2004). In addition, heavy rainfall during the flooding season (and possibly typhoons) can significantly alter the sediment flux within a bay (Ryu *et al.*, 2004; Lee *et al.*, 2013a).

Gomso Bay is a piedmont-type estuary due to its mountainous catchment area (~300 km<sup>2</sup>, Figure 2) (Yang *et al.*, 2007). Since the early 1990s, the bay has been the focus of intense research regarding its sedimentological characteristics—including its Holocene stratigraphy (Chang *et al.*, 1996; Yang *et al.*, 2006)—, spatial and temporal changes in sedimentary facies (Chang *et al.*, 2007; Yang *et al.*, 2007), tidal sedimentation (Lee, 2010a; Choi, 2011) and long-term changes in sedimentary bedforms from satellite data (Ryu *et al.*, 2008). These have shown that the Gomso tidal flats consist of a basement (Precambrian gneiss and Jurassic granite), a pre-Holocene oxidized unit (subglacial stage before 12,000 years BP), and Holocene sequences with surface sands that reflect a Holocene sea-level rise and have accumulated since ~1,800 years BP (Chang *et al.*, 1996; Lee, 2010a). In addition, bedform (including chenier) migration indicates that Gomso Bay is affected by a high-energy environment, especially during winter, with strong winds and waves combined with the macrotidal current. During summer, only the macrotidal current develops. As a result, sedimentation within the bay is influenced by the combination of tides and waves (Yang *et al.*, 2007; Lee, 2010a).

There is no direct sediment supply from river runoff, and the bay is distant from Korean rivers (i.e., the Geum River to the north and Yeongsan River to the south; Figure 1). The main tidal channel, with water depths up to 20 m, runs west-east in the northern part of the bay and connects directly with the Kangsun Stream at the bay head, while a southern branch links to the Jujin Stream (Figs. 1 and 2). In previous studies (e.g., Yang *et al.*, 2007; Ryu *et al.*, 2008), sedimentologists have ignored the supply of terrigenous sediments via both streams, due to the presence of dams upstream. However, the Jujin Stream channel (Figure 2)

appears to be ebb-dominated during the summer rainy season, when over 60% of the annual precipitation (1,100–1,300 mm; Yang *et al.*, 2007) occurs (Kim, 2010; Lee, 2010a; Choi, 2011); hence, the bay might receive terrigenous sediments with fresh runoff.

Therefore, this paper:

- Investigated the seasonal variation in sedimentation to understand sedimentary processes in the Gomso tidal flats, and
- Characterized the rare earth element (REE) geochemistry of the tidal flat and compared it with possible end members, such as Korean rivers (e.g., the Geum and Yeongsan Rivers) and the local Jujin Stream.

## METHODS

### Sedimentary data processing

Surface sediments for observing sediment facies were collected from 79 stations in Gomso Bay in March 2011. In addition, three transect lines (KM, KH, and KB) along the tidal flat were used to monitor the variation in morphology and sedimentary process by burying a plate from February 2011 to February 2012. Bottom sediments along Jujin Stream were sampled in September 2011 (Figure 1). In the laboratory, grain size was analyzed using an automatic particle size analyzer (SediGraph 5100, Micromeritics) for the mud fraction (>4 Ø) and the standard sieving method for the sand fraction (<4 Ø), after removing carbonate with 0.1 N HCl and organic matter with 10% H<sub>2</sub>O<sub>2</sub>. The inclusive graphic method was used to determine the sediment characteristics (Folk and Ward, 1957).

Landsat TM/ETM+ satellites were used to construct an intertidal digital elevation model (DEM) with the waterline method combined with a survey using an echo-sounder (Figure 2). The waterline method is a useful practical application of satellite remote sensing when topographically mapping a tidal flat. Levelling data obtained from the echo-sounder survey were used as a reference elevation for the extracted waterline (Choi *et al.*, 2010 and references therein).

For the REE analysis, the bulk sediments were dried overnight at 60°C in an oven and then powdered and homogenized using an agate mortar. The powdered samples (~0.2 g) were digested with

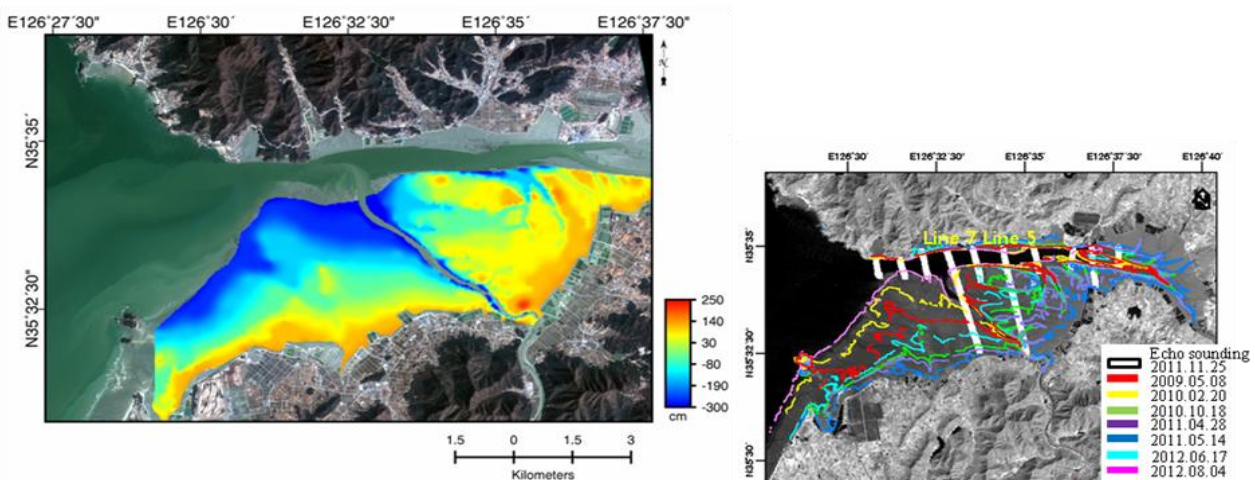


Figure 2. Morphological image of the Gomso tidal flats (left) based on a digital elevation model (DEM) and echo-sounding track lines (right). Echo-sounding survey data were converted into benchmark standards equivalent to the tide gauge data and then assigned to the waterlines.



mixed acids ( $\text{HNO}_3 + \text{HClO}_4 + \text{HF}$ ) in a tightly sealed Teflon vessel on a hot plate at 120–150°C for 24 h. Then, the acid solution was evaporated to dryness on a hot plate after removing the screw lid, and the resultant white cake was extracted with 1%  $\text{HNO}_3$ . REEs were measured using inductively coupled plasma mass spectrometry (ICP-MS; model X-7; Thermo Elemental, UK) at the Korea Basic Science Institute. Analytical quality was evaluated using the reference material MAG-1 (United States Geological Survey) together with the batch of sediment samples. The relative deviations between the measured and certified values were generally < 20%, indicating satisfactory recovery.

## RESULTS

The DEM showed that landward inner bay had a higher elevation and that the seaward outer bay had relatively lower elevation (Figure 2). There was a considerable gradient in the outer bay from the high water line to the low water line. Line KB was approximately 1.0–1.5 m above the mean sea level (MSL), while most of lines KM and KH were below the MSL (Figure 3).

The surface sedimentary facies of the Gomso tidal flats were mainly classified into sand (S), silty sand (sS), and sandy silt (sZ) from the grain size characteristics (Figure 4). In spring (March 2011), the average mean grain sizes (Mz) of those facies were 2.3, 3.7, and 5.1  $\phi$ , respectively. In the tidal flats of the bay, the sand fraction was predominant in the outer bay area, indicating that fine sediments were winnowed offshore by storm events in winter.

Figure 5 shows the sedimentation rates from transects KM, KH, and KB over 1 year; these appeared to be different. In the tidal flat at the inner bay (line KB), surface sediments accumulated during spring, autumn and winter, and they were eroded during summer, which concurred with the sediment movement vectors (not shown here) and with a net sedimentation rate of 41 mm yr<sup>-1</sup>. Therefore, Mz became somewhat coarser during summer (average 4.4  $\phi$ ) compared with the other seasons (average 4.8–5.3  $\phi$ ). By contrast, transects KM and KH faced the bay opening and showed erosion during autumn and winter with net sedimentation rates of –10 and –30 mm yr<sup>-1</sup>, respectively. The average Mz during autumn and winter ranged from 2.3 to 4.0  $\phi$ , while it was 2.7 to 4.7  $\phi$  during spring and summer. In general, the tidal flats of the outer bay were undergoing considerable erosion.

In the Jujin Stream, the Mz in samples from eight stations was 4.2–7.0  $\phi$ . Mz was somewhat coarser (4.2–4.8  $\phi$ ) at the stream mouth (stations 6 and 7) and upstream site (station 8). The sand,

silt, and clay contents in the bottom sediments were 5.4–29.8%, 40.6–79.7%, and 7.9–47.0%, respectively, indicating that silt-sized grains were dominant.

In August, the upper continental crust (UCC)-normalized light REEs (LREEs: La, Ce, Pr, and Nd) were more enriched than the middle (MREEs: Sm, Eu, Gd, Tb, and Dy) and heavy (HREEs: Ho, Er, Tm, Yb, Lu) REEs, resulting in  $(\text{La}/\text{Yb})_{\text{UCC}} > 1$  (KM, 1.7±0.2; KH, 2.3±0.3) and  $(\text{Gd}/\text{La})_{\text{UCC}} < 1$  (KM, 0.8±0.1; KH, 0.7±0.1). In the Jujin Stream, their ratios (1.5±0.2 and 0.8±0.1, respectively) from stations 1–7 were similar to those for line KM, while station 8 had values close to line KH.

## DISCUSSION and CONCLUSIONS

The sediment transport paths of surface sediments during spring (March), calculated using the grain-size parameters mean, sorting, and skewness (Gao and Collins, 1992), showed two different paths (Figure 6). In the main channel in the north, the sediment transport vectors were directed toward the northeastern side of the bay, while the majority of the transport vectors were directed southeastward from the sub-tidal zone in the tidal flat.

Woo *et al.* (2013, *in press*) conducted time-series (12.5 h) measurements of the current, tide level, and suspended sediment concentration at the bay mouth, revealing that a large amount of suspended sediment was transported into the bay at the rate of 82,700 kg/m during a tidal cycle in the spring (May). The springtime currents were generally flood-dominant with easterly (landward direction of 90°) residual currents varying between 10 and 13 cm/s in the water column. The net sediment fluxes were significantly higher in bottom water ( $110 \times 10^{-3}$  kg/m<sup>2</sup>/sec) compared with the surface ( $20 \times 10^{-3}$  kg/m<sup>2</sup>/sec), suggesting the resuspension of bottom sediments. In addition, Lee (2010a) made hydrodynamic measurements using a benthic tripod in Gomso Bay during the summer (August). Suspended sediments were transported landward over the tidal flats and in the middle to upper reaches of the main tidal channel. Therefore, the results of this study and Lee (2010a) indicate that tidal currents supply fine-grained sediments to the bay during the spring and summer, hence the tidal flat becoming muddier.

The change in sedimentary facies from sand to silty sand toward the inner bay (Figure 4) is associated with wave-dominated conditions in the outer and middle bays where erosion occurs. Thereafter, the fine sediments are transported landward by flood tides (Yang *et al.*, 2007).

For the fine sediments, however, the characteristics of the REE

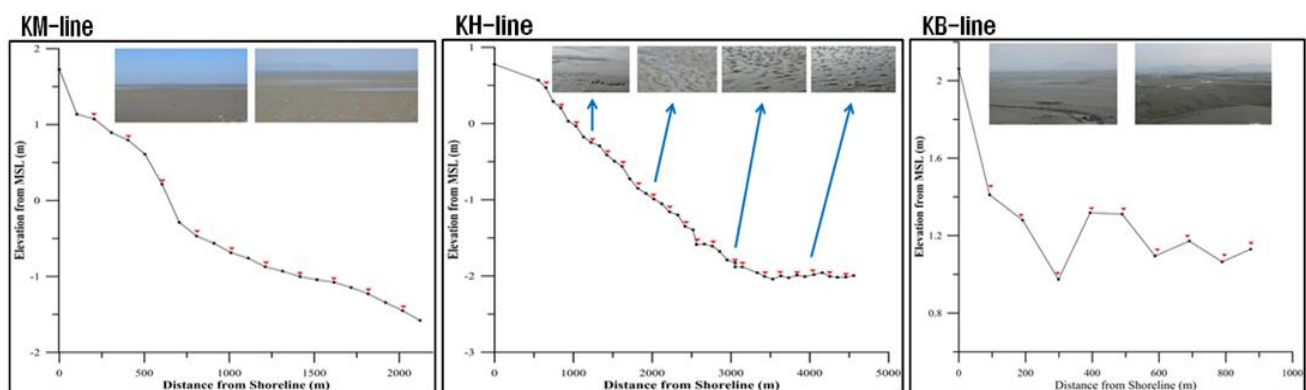


Figure 3. Variation in the elevation from the MSL along transects KM, KH, and KB. The elevation was measured using a leveling instrument (Pentax Pal 2S Level) and a differential global positioning system (DGPS).

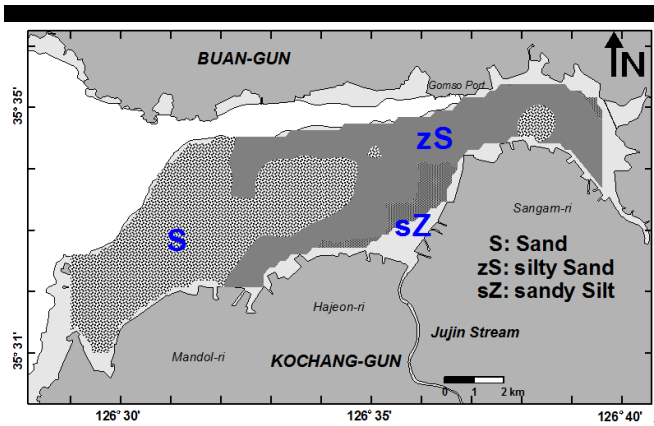


Figure 4. The sedimentary facies of Gomso tidal flats in spring (March 2011). Fine-grained sediments (sandy silt) were distributed in the upper tidal flats of the inner bay, while coarse sediments (sand and silty sand) were dominant in the outer bay and lower tidal flats.

geochemistry in summer (August) and spring (May) differed along line KH (Figure 1); during summer, relatively more sediments that were enriched in light LREEs (La-Nd) but depleted in Eu were distributed there (Kang *et al.*, *in press*). This might be influenced by REE-rich minerals, such as zircon, monazite and allanite, with grain sizes <63 μm (Li *et al.*, 2009). Based on these REE characteristics, we discuss the provenance of fine sediments transported into the bay using Eqs. (1) and (2) (Jung *et al.*, 2006).

$$M_{(MREEs/LREEs)} = \frac{(\sum_{j=Sm}^{Dy} \frac{C_j(sample)}{C_j(UCC)})/5}{(\sum_{i=La}^{Nd} \frac{C_i(sample)}{C_i(UCC)})/4} \quad (1)$$

$$L_{(LREEs/HREEs)} = \frac{(\sum_{j=La}^{Nd} \frac{C_j(sample)}{C_j(UCC)})/4}{(\sum_{i=Ho}^{Eu} \frac{C_i(sample)}{C_i(UCC)})/5} \quad (2)$$

The values of  $M_{(MREEs/LREEs)}$  and  $L_{(LREEs/HREEs)}$  for sediments collected along the two lines in August are well distributed on the regression line ( $r^2=0.83$ ) for the rivers and Jujin Stream (Figure 7). These distributions indicate that there are two sources of fine-sediments: Korean rivers and the Jujin Stream (located on the

southern coast of the inner bay) (Figure 1). Satellite Landsat TM/ETM+ images showed that the suspended sediment concentrations increased (more turbid water) along the southern coast of the study area during high tide, indicating that the riverine sediments distributed in coastal regions are resuspended and transported into the bay by southwest to northeast tidal currents (Min *et al.*, 2012; Lee *et al.*, 2013b).

In Figure 7, the  $M_{(MREEs/LREEs)}$  and  $L_{(LREEs/HREEs)}$  values of samples collected at stations 1-7 along the Jujin Stream (JS) indicated a riverine origin, suggesting the transport of muddy riverine sediments via tides. The sedimentary facies downstream showed that rhythmically laminated silt facies (i.e., tidal rhythmites) developed, with the exception of the upstream part around station 8 where tidal deposits decrease as fewer tides approach this station. This indicates that tidal currents are a major factor generating tidal rhythmites (Choi, 2011). During summer floods, however, obvious morphological changes were observed in the Jujin tidal channel (Figure 2), including a terrigenous yellow-brown mud layer in core sediments, as a result of enhanced ebb currents due to increased runoff discharge from the Jujin Stream (Kim, 2010). Therefore, the REE fingerprints from line KH in August suggest that the stream sediments could be transported and remain in surface sediments of the bay after heavy rainfall (Kang *et al.*, *in press*).

Over the long-term, from 1991 to 2000 (Ryu *et al.*, 2008) and from 2000 to 2010 (Lee *et al.*, 2013b), the morphological changes in the tidal flats showed a maximum deposition of about 60 cm, which occurred mainly in the inner bay (to the east of the Jujin Stream). The maximum erosion, approximately -90 cm, determined using the DEM approach, was seen in the outer bay (to the west of the Jujin Stream). However, the changes in the annual mean budgets for sand (-58,800 m<sup>3</sup>/yr), silty sand (-197,900 m<sup>3</sup>/yr), and finer sandy silt (-52,600 m<sup>3</sup>/yr) from 1991 to 2000 showed that erosion dominated the tidal flat (Ryu *et al.*, 2008), although fine sediments were periodically deposited in spring and summer (lines KM and KH, Figure 5).

The long-term erosion processes seem to be associated with changes in hydrodynamic conditions resulting from human activities, such as sea-wall construction, land reclamation and the position of farms near the low water line within Gomso Bay, which have led to change of the sedimentary facies (Chang *et al.*, 2007). In addition, correlation of a large dyke, Saemangeum, in the northern part of the bay with the changes in physical and biological conditions including abrupt mass extinction of benthic animals, particularly shellfish, in Gomso Bay is little known (Lee, 2010a). But, tidal current velocity from hydrodynamic modeling

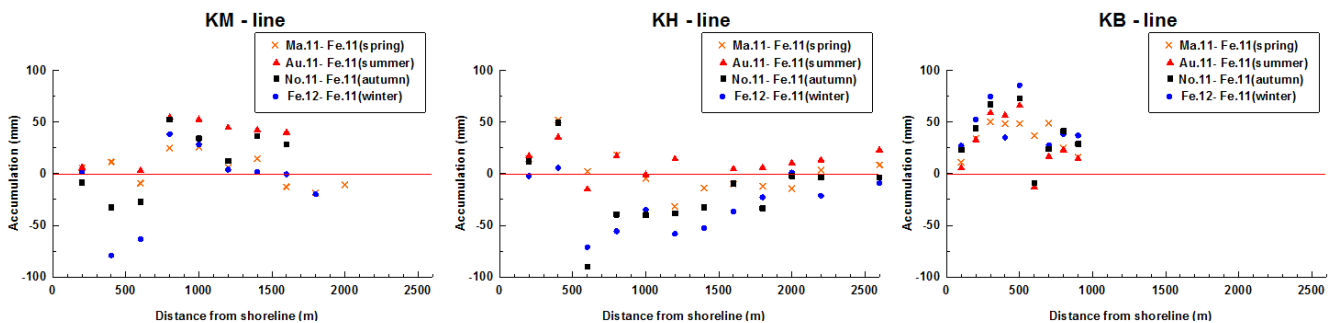


Figure 5. Seasonal variation in the surface accumulation rates along transects KM, KH, and KB in the Gomso tidal flats from February 2011 to February 2012. Each seasonal accumulation rate was calculated by subtracting the initial value for February 2011 (e.g., March 2011–February 2011).

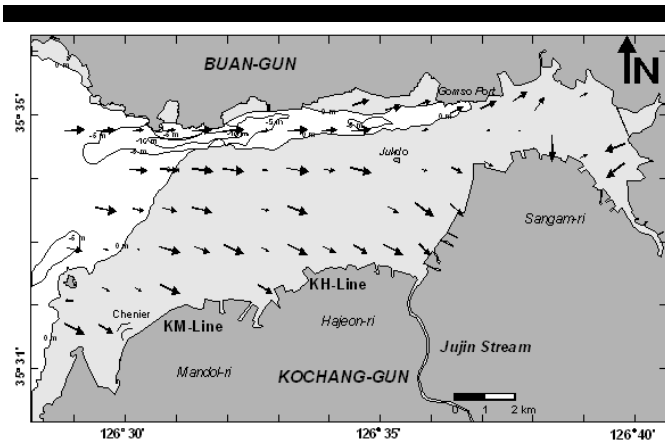


Figure 6. Residual patterns of grain-size trends from surface sediments investigated in spring, March 2011.

in coastal regions has been increased after the dyke construction (Lee *et al.*, 2013b).

Seasonal erosion processes in Gomso Bay, especially along transects KM and KH during autumn and winter, were likely associated with the fact that the bay opened directly westward into the Yellow Sea (Figure 1). In the southeastern Yellow Sea, the storm frequency tends to increase in autumn and winter (Lee and Chu, 2001). During winter, strong northerly winds are sufficient to generate wave heights of up to 4 m in the vicinity of Gomso Bay, while the wave height during summer is less than 1 m (Yang *et al.*, 2007). The northerly winds can cause wind-generated currents that increase the hydrodynamic energy, moving sands as a bedload during tidal current movements (Lee, 2010b). Therefore, the combination of tide and waves is the major factor controlling the sedimentation in Gomso Bay, where waves reach the outer and middle bay, while tides dominate conditions in the inner bay (Yang *et al.*, 2007).

The sedimentary processes during summer in the inner bay were different from those of the outer and middle bays. Along line KB in the inner bay, channel-related erosion occurred during

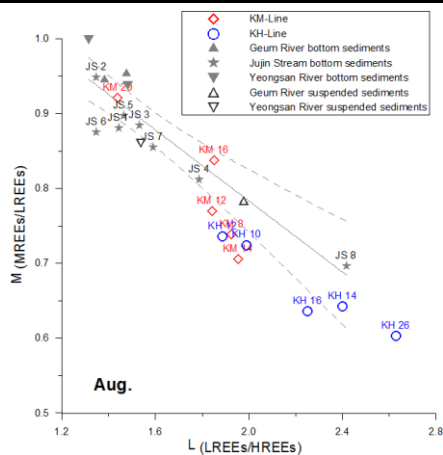


Figure 7. Relationships between  $M_{(MREEs/LREEs)}$  and  $L_{(LREEs/HREEs)}$  for Geum and Yeongsan River bottom sediments  $< 20 \mu m$  (Song and Choi, 2009), together with their suspended sediments (Yang *et al.*, 2003) and sediments from the Jujin Stream and lines KM and KH in summer (August 2011) (Kang *et al.*, in press).

summer. This erosion is likely due to the heavy rainfall that enhances softening (reducing shear strength) of the fine surface sediments; hence, they are flushed by local runoff (Ryu *et al.*, 2004; Yang *et al.*, 2007). On the other hand, the supply of fine sediments from local runoff (Jujin Stream; Figure 1) due to heavy rainfall might be considerable in the middle bay near line KH. This implies that heavy rainfall alters the sediment budget within Gomso tidal flats (e.g., Lee *et al.*, 2013a).

### ACKNOWLEDGMENTS

This study was a part of the ‘‘Satellite Application Techniques for Coastal Ocean Environmental Monitoring (SATCOM)’’ programme and was funded by the Korea Institute of Ocean Science and Technology (KIOST).

### LITERATURE CITED

Chang, J.H., Park, Y.A. and Han, S.-J., 1996. Late Quaternary stratigraphy and sea-level change in the tidal flat of Gomso Bay, west coast of Korea. *Journal of the Korean Society of Oceanography*, 1, 59-72.

Chang, J.H., Ryu, S.-O. and Jo, Y.-J., 2007. Long-term variation of tidal-flat sediments in Gomso Bay, west coast of Korea. *Journal of the Korean Earth Science Society*, 28, 357-366.

Choi, J.-K., Ryu, J.-H., Lee, Y.-K., Yoo, H.-R., Woo, H.J. and Kim, C.H., 2010. Quantitative estimation of intertidal sediment characteristics using remote sensing and GIS. *Estuarine Coastal and Shelf Science*, 88, 125-134.

Choi, K., 2011. Tidal rhythmites in a mixed-energy, macrotidal estuarine channel, Gomso Bay, west coast of Korea. *Marine Geology*, 280, 105-115.

Fork, R.L. and Ward, W.C., 1957. Brazos river bar: a study in the significance of grain size parameters. *Journal of Sedimentary Petrology*, 27, 3-26.

Gao, S. and Collins, M., 1992. Net sediment transport patterns inferred from grain-size trends, based upon definition of transport vectors. *Sedimentary Geology*, 81, 47-60.

Jung, H.-S., Lim, D.-I., Yang, S.Y. and Yoo, H.-S., 2006. Constraints of REE distribution patterns in core sediments and their provenance, northern East China Sea. *The Korean Society of Economic and Environmental Geology*, 39, 39-51.

Kang, J., Woo, H.J., Jeong, K.-S., Jang, S. and Lee, J.H., 2014. Rare earth element fingerprints in Korean coastal bay sediments: association with provenance discrimination. *Estuarine Coastal and Shelf Science*, in press.

Kim, M., 2010. *Seasonal variation of morphology and spatial distribution of sedimentary facies in estuarine intertidal channel, Gomso Bay, west coast of Korea*. Gwangju, South Korea: Chonnam National University, Master's thesis, 100p.

Lee, H.J. and Chu, Y.S., 2001. Origin of inner-shelf mud deposit in the southeastern Yellow Sea: Huksan Mud Belt. *Journal of Sedimentary Research*, 71, 144-154.

Lee, H.J., 2010a. Preliminary results on suspended sediment transport by tidal currents in Gomso Bay, Korea. *Ocean Science Journal*, 45, 187-195.

Lee, H.J., 2010b. Enhanced movements of sands off the Saemangeum Dyke by an interplay of dyke construction and winter monsoon. In: Lie, H.-J. and Ishimatsu, A. (eds.), *Coastal Environmental and Ecosystem Issues of the East China Sea*, pp. 49-70.

Lee, H.J., Chu, Y.S. and Park, Y.A., 1999. Sedimentary processes of fine-grained material and the effect of seawall construction in the Daeho macrotidal flat-nearshore area, northern west coast of Korea. *Marine Geology*, 157, 171-184.

Lee, H.J., Jo, H.R., Chu, Y.S. and Bahk, K.S., 2004. Sediment transport on macrotidal flats in Garolim Bay, west coast of Korea: significance of wind waves and asymmetry of tidal currents. *Continental Shelf Research*, 24, 821-832.

- Lee, Y.G., Kim, S., Jeong, E.U., Kim, J.K. and Woo, H.J., 2013a. Effects of heavy rainfall on sedimentation in the tidal salt marsh of Suncheon Bay, South Korea. *Journal of Coastal Research*, 29, 566-578.
- Lee, Y.-K., Kim, K.-L., Woo, H.-J., Ryu, J.-H. and Choi, J.-K., 2013b. Preliminary results on the analysis of geomorphologic change of the tidal flat in Gomso Bay by the construction of Saemangeum Dyke. *International Symposium on Remote Sensing* (Tokyo, Japan).
- Min, J.-E., Ryu, J.-H., Lee, S. and Son, S.-H., 2012. Monitoring of suspended sediment variation using Landsat and MODIS in the Saemangeum coastal area of Korea. *Marine Pollution Bulletin*, 64, 382-390.
- Ryu, J.-H., Kim, C.-H., Lee, Y.-K., Won, J.-S., Chun, S.-S. and Lee, S., 2008. Detecting the intertidal morphologic change using satellite data. *Estuarine Coastal and Shelf Science*, 78, 623-632.
- Ryu, S.O., 2003. Seasonal variation of sedimentary processes in a semi-enclosed bay: Hampyong bay, Korea. *Estuarine Coastal and Shelf Science*, 56, 481-492.
- Ryu, S.O., Lee, H.J. and Chang, J.H., 2004. Seasonal cycle of sedimentary process on mesotidal flats in the semi-enclosed Muan Bay, southern west coast of Korea: culminating summertime erosion. *Continental Shelf Research*, 24, 137-147.
- Song, Y.-H. and Choi, M.S., 2009. REE geochemistry of fine-grained sediments from major rivers around the Yellow Sea. *Chemical Geology*, 266, 328-342.
- Woo, H.J., Kang, J., Lee, J.H. and Jeong, K.-S., 2013. *Seasonal changes of sedimentary environment at the macrotidal flat in Gomso Bay, west coast of Korea* (San Diego, California). CERF 2013.
- Yang, B., Dalrymple, R.W., Gingras, M.K., Chun, S. and Lee, H., 2007. Up-estuary variation of sedimentary facies and ichnocoenoses in an open-mouthed, macrotidal, mixed-energy estuary, Gomso Bay, Korea. *Journal of Sedimentary Research*, 77, 757-771.
- Yang, B.C., Dalrymple, R.W., Chun, S.S. and Lee, H.J., 2006. Transgressive sedimentation and stratigraphic evolution of a wave-dominated macrotidal coast, western Korea. *Marine Geology*, 235, 35-48.
- Yang, S., Li, C., Lee, C.B. and Na, T.K., 2003. REE geochemistry of suspended sediments from the rivers around the Yellow Sea and provenance indicators. *Chinese Science Bulletin*, 48, 1135-1139.

# Sea level fluctuation and shoreline evolution on decadal time scale, Lithuanian Baltic Sea coast

Darius Jarmalavičius, Donatas Pupienis, Gintautas Žilinskas

Institute of Geology and Geography  
Nature research centre  
Vilnius, Lithuania  
donatas.pupienis@gf.vu.lt  
jarmalavicius@geo.lt  
zilinskas@geo.lt



[www.cerf-jcr.org](http://www.cerf-jcr.org)



## ABSTRACT

Jarmalavičius, D., Pupienis, D., Žilinskas, G., 2014. Sea level fluctuation and shoreline evolution on decadal time scale, Lithuanian Baltic Sea coast. In: Green, A.N. and Cooper, J.A.G. (eds.), *Proceedings 13<sup>th</sup> International Coastal Symposium* (Durban, South Africa), *Journal of Coastal Research*, Special Issue No. 70, pp. 164-169, ISSN 0749-0208.

[www.JCRonline.org](http://www.JCRonline.org)

Fluctuations in sea level are reflected in shoreline dynamics. Depending on the nature of the change, the coast is dominated by either erosion or accumulation processes. However, despite considerable attention to this subject, few works have been dedicated to the direct research of coastal development dependence on these determining factors. The objective of this paper was to assess the impact of sea level fluctuations on shoreline dynamics based on coastal monitoring data. The monitoring of coastal dynamics has been carried out since 2002. Annual shoreline displacement was determined based on the obtained data. In addition to morphometric data, sea level data from the Klaipėda gauge station from 2002–2012 were used. The results showed that the long-term tendency of shoreline displacement was not uniform. From 2002–2012, a shoreline recession of the mainland coast was observed, whereas accumulation processes prevailed in the Curonian Spit. Also, a trend of rising sea level was observed from 2002–2012. No significant correlation between shoreline displacement and sea level on a decadal time scale was found. This may be due to the fact that the long-term trend in sea level was negligible and had no distinct impact on coastal dynamics. Short-term changes in sea level, on the other hand, have had a greater impact on coastal dynamics. A good correlation between the short-term change in yearly sea-level and shoreline displacement was observed.

**ADDITIONAL INDEX WORDS:** Coastal erosion, sandy beach, coastal monitoring, Baltic Sea.

## INTRODUCTION

Sea-level fluctuation is reflected in the dynamics of shoreline position. Depending on the nature of the change, the coast may be dominated either by erosion or accumulation processes. Many authors hold the opinion that coastal erosion is directly controlled by sea-level rise (Bruun, 1962; Barth and Titus, 1984; Nicholls *et al.*, 1995; Rotnicki *et al.*, 1995; Zeidler, 1992, 1995; Pruszk and Zawadzka, 2005; Corbella and Stretch, 2012). According to IPCC projections (Meehl *et al.*, 2007), sea level in the 21st century might rise by 59 cm. Consequently, the extent of coastal erosion in the future may increase. However, other factors are also crucial for coastal dynamics besides sea-level fluctuations: e.g., sand availability (Selivanov, 1996; Carter *et al.*, 1987; Storms *et al.*, 2002; Thom, 1983), wave climate (Guillén *et al.*, 1999; Cooper and Navas, 2004), storminess (de Ruig and Louise, 1991; Corbella and Stretch, 2012), coastal morphology (Roy *et al.*, 1994; Cowell *et al.*, 2003; Aagaard and Sørensen, 2012), and human impact (Žilinskas *et al.*, 2010; Jarmalavičius *et al.*, 2012; Pupienis *et al.*, 2013a; Kriaučiūnienė *et al.*, 2013). Furthermore, particular factors have different effects at different time scales (Stive *et al.*, 2002). Therefore, for the assessment of the impact of sea level rise on shoreline dynamics it is important to consider wave and wind climate, coastal morphology, sand supply and human impact. Since 2002, monitoring along the Lithuanian Baltic sea coast has

been carried out regarding shoreline position. Based on this data, the analysis of coastal dynamics from 2002–2012 was performed. The main objective of this paper is to assess the impact of sea-level fluctuations on shoreline dynamics on the decadal time scale.

## STUDY AREA AND METHODS

The Lithuanian coast consists of two segments of different genesis: the mainland shore (38 km) and the Curonian Spit (51 km) which are separated by the Klaipėda Strait (1.6 km) (Fig. 1). The nearshore of the Curonian Spit includes a well-developed bar system consisting of 2 to 5 bars reaching 400–670 m in width. The 30–80 m wide beaches are composed of fine and medium sand (Jarmalavičius and Žilinskas, 2006). The volume of beach sediment is 42–115 m<sup>3</sup>/m and the altitude of the foredune reaches up to 16 m (Jarmalavičius and Žilinskas, 2006; Bitinas *et al.*, 2004). The abundance of sand in this section determines the northward longitudinal sand migration. It enables a large amount of sand to reach the Lithuanian territory from the Russian (Kaliningrad Oblast) southward part of the spit (Gudelis, 1998). Due to the Klaipėda port jetties, which block alongshore sediment migration flow, a large proportion of sand does not reach the mainland coast. For this reason mainland coastal deposits are scarcer and the bar system is not well developed. One to three bars are present, although not always persistent along strike (Bitinas *et al.*, 2004). Locally at a depth of 1.5–3.0 m, moraine is exposed. 20–85 m wide beaches are mostly composed of fine and medium sand.

DOI: 10.2112/SI70-028.1 received 1 December 2013; accepted 21 February 2014. © Coastal Education & Research Foundation 2014

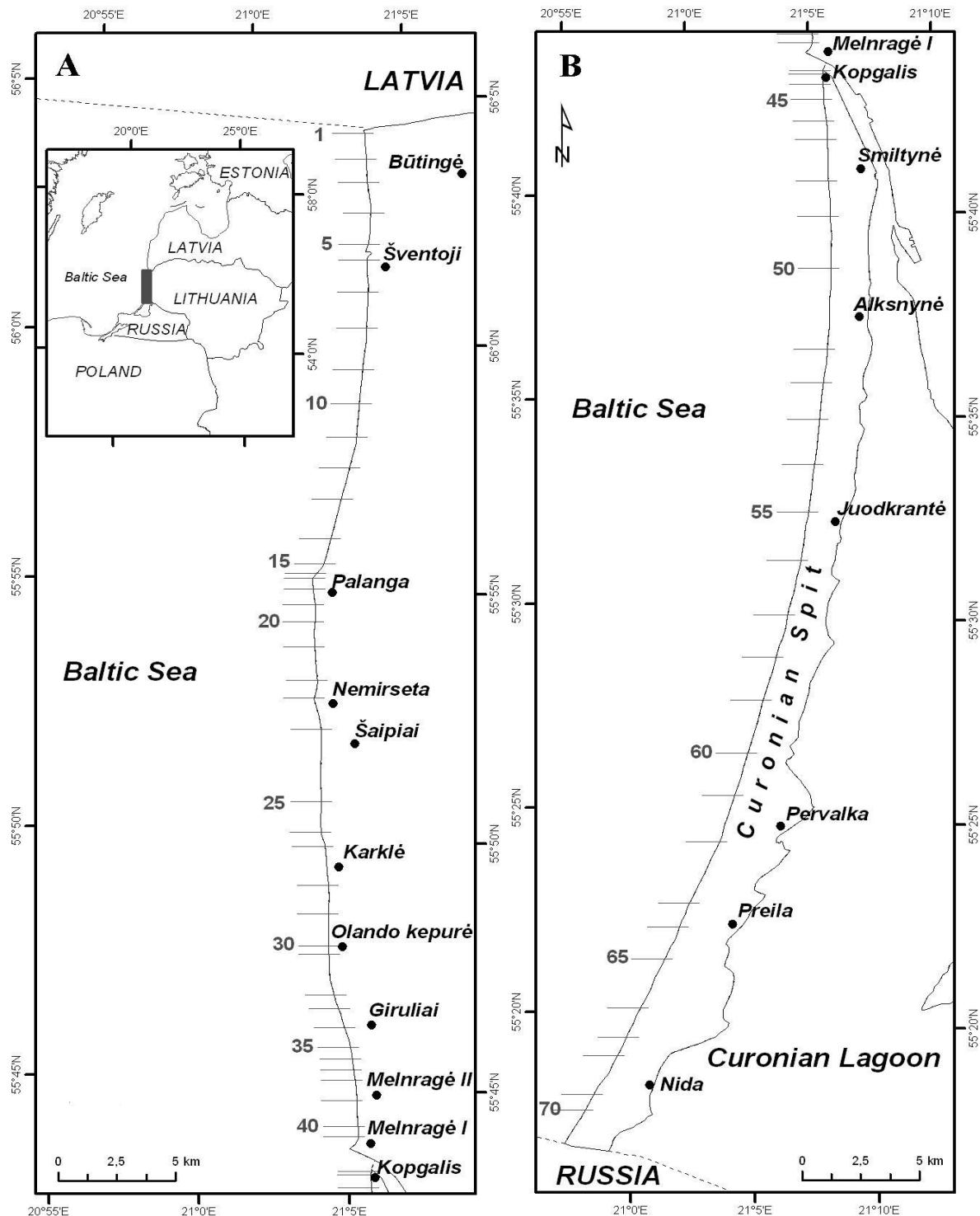


Figure 1. Location map. A – Mainland coast; B – Curonian Spit coast. Lines with numbers show sites of cross-shore profiles.

The average volume of beach sediments was estimated at  $65.5 \text{ m}^3/\text{m}$ . The highest dune ridge at Šventoji reaches 12 m in height, whereas in Būtingė and Melnragė II dunes are only 4 m high. It should be noted that the shore between Šaipiai and Karklė is dominated by moraine cliffs.

The assessment of changes in shoreline position was based on coastal monitoring data from 2002–2012. During the monitoring process, the cross-shore profile was measured by levelling (41 profiles in the mainland coast and 29 profiles in the Curonian Spit) (Fig. 1) once a year, in May, when relatively calm weather predominates. Therefore, accidental storm surges have no visible

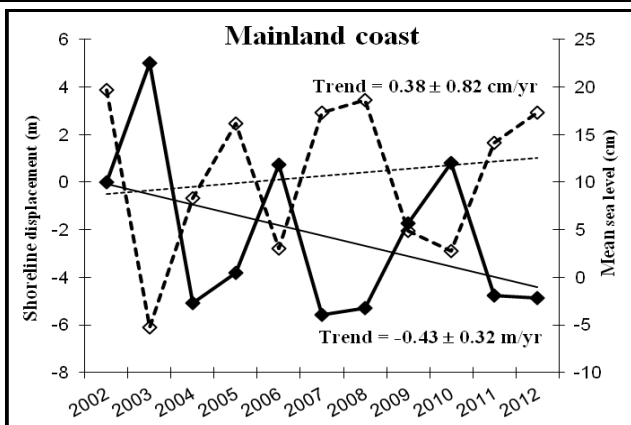


Figure 2. Shoreline displacement (solid line) calculated from reference year (2002) and sea level (dashed line) in mainland coast and their linear trends.

influence on shoreline position in spring. Also, tidal range is inconsequential as the Baltic Sea is tideless. For an evaluation of the decadal trend, shoreline dynamics were calculated taking shoreline position in 2002 as a starting point. The annual shoreline change rate (m/yr) was calculated from linear regression. The yearly variations were calculated between the shoreline positions for two consecutive years. To avoid random local fluctuations due to rhythmic topography in shoreline position, data were averaged separately for the mainland coast and the Curonian Spit coast over a longer coastal stretch (Thom and Hall, 1991; Farris and List, 2007).

The mean monthly sea level-, wind speed- and wave height- data from the Klaipėda gauge and meteorological station were collected between 2002 and 2012 by the Department of Marine Research of the Environmental Protection Agency. Since coastal monitoring was carried out in May, the shoreline fluctuations reflected variations taking place over one-year periods, from May to the subsequent April. Therefore, the annual mean of sea level similarly was calculated for the same period based on the average monthly values.

## RESULTS

An assessment of shoreline trends for the time frame spanning

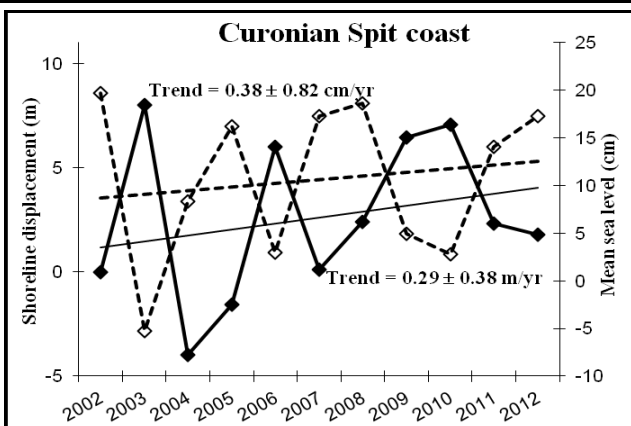


Figure 3. Shoreline displacement (solid line) calculated from reference year (2002) and sea level (dashed line) in Curonian Spit coast and their linear trends.

2002-2012 showed that shorelines did not develop uniformly along the coast. The shoreline in the mainland coast migrated from 2.8 m/yr landward (near Melnragė II) to 1.9 m/yr seaward (near Giruliai). The Curonian Spit shoreline, similarly, did not experienced uniform change over this period. The shoreline in Curonian Spit coast migrated from 1.4 m/yr landward (near Nida), to 3.4 m/yr seaward (between Preila and Nida). It can be seen that both the mainland and the Curonian Spit shorelines did not have the same development tendencies, but rather their development was of cyclical nature related to changes in shoreline configuration (Pupienis *et al.*, 2012). Due to the displacement of embayments along the coast, the shoreline position may change by up to 52 m within 2 km alongshore (on the mainland coast) and up to 53 m within 8 km alongshore (on the Curonian Spit coast). The high variability of shoreline position may be related to coastal morphology and human intervention through jetty installations at Klaipėda and Šventoji Ports and artificial nourishment on Palanga beach (Žilinskas *et al.*, 2010; Jarmalavičius *et al.*, 2012; Pupienis *et al.*, 2013b).

Between 2002 and 2012, weak erosion took place on the mainland coast (mean shoreline migration landward was 0.43

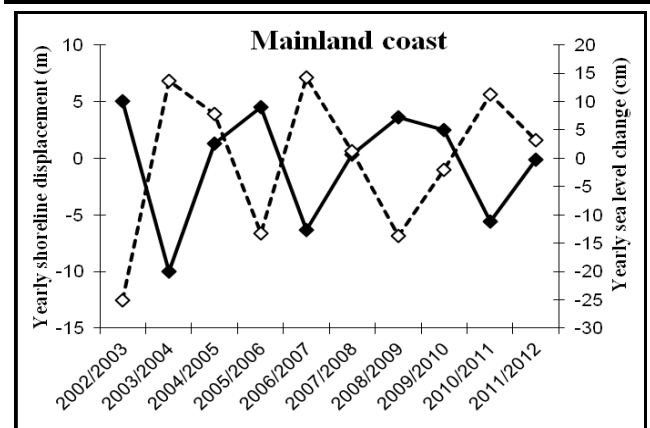


Figure 4. Yearly shoreline displacement (solid line), and yearly sea level change (dashed line) on the mainland coast.

m/yr), whilst on the Curonian Spit coast accumulation was recorded (mean shoreline migration seaward was 0.29 m/yr). It should be noted that there are no confident trends for such short time scales ( $p = 0.207$  for mainland coast shoreline displacement,  $p = 0.463$  for Curonian Spit shoreline displacement and  $p = 0.654$  for sea level trend) due to large inter-annual fluctuations. Nevertheless, common tendencies are obvious.

Figures 2 and 3 show that sea level rose by  $0.38 \pm 0.82$  cm/yr from 2002–2012. Although this tendency is not confident ( $p = 0.654$ ), it can be stated (based on the history of long-term sea level fluctuation) that the rising tendency has been observed from the beginning of the 20th century (Jarmalavičius and Žilinskas, 1996). For example, over the period of 1898–2012, sea level has been rising at a rate of  $0.15 \pm 0.02$  cm/yr ( $p = 0.000$ ) and from 1975 to 2012 sea level has risen at a rate of  $0.37 \pm 0.1$  cm/yr ( $p = 0.001$ ). Meanwhile, observing the mean trends of shoreline displacement along a longer coastal stretch, it can be noticed that, despite sea level rise, the mainland coastline is characterised by a retreating trend whilst the Curonian Spit coastline is characterised by an accumulation trend (Fig. 2 and 3).

Figures 2 and 3 show that the trends of sea level and shoreline change are not identical but that sea level fluctuation and shoreline

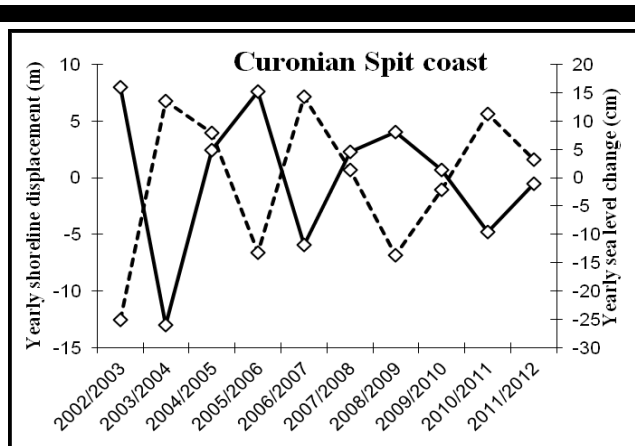


Figure 5. Yearly shoreline displacement (solid line) and yearly sea level change (dashed line) for the Curonian Spit coast.

position for individual years were in opposite phase. These differences are apparent for yearly relative shoreline and sea level changes. Figures 4 and 5 show that the yearly sea level fluctuations are in good agreement with the yearly shoreline displacements, yet in an opposite phase.

This dependence is clearly visible in relationship graphics presented in Figures 6 and 7. It should be pointed out that this dependence is similar, both on the mainland and on the Curonian Spit coasts.

## DISCUSSION

The research results demonstrated that from in 2002–2012, despite sea level rise, the shoreline position displacement trends on the mainland and the Curonian Spit coasts differed. The mainland shoreline retreated landward, while the Curonian Spit shoreline migrated seaward.

This disagreement between shoreline evolution and sea level fluctuation has been indicated by other authors (e.g., Clarke and Eliot, 1983; Lacey and Peck, 1998; Le Cozannet et al., 2013), who have noticed that shoreline erosion and accumulation processes on a decadal time scale do not coincide with the sea level rise. It was found that the slight trend in sea level rise (1.8 mm/yr) will not have a significant impact on the shoreline for at least 30–50 years (Pye and Blott, 2006), yet would produce an impact if sea level rise exceeded a certain threshold (Hoffmann and Lampe, 2007). Our studies, however, have shown that even in the case of more rapid sea level rise (> 3 mm/yr), the shoreline erosion processes will not necessarily intensify. These disparities can be explained by the influence of other factors such as morphology and sand supply. It has been shown that accumulation processes may take place on gently sloping coasts (gradients of <math>< 0.8^\circ</math>) even whilst sea level is rising (Roy et al., 1994; Aagaard and Sørensen, 2012). The average nearshore slope of the Lithuanian mainland coast is

(Žilinskas et al., 2001). Large amounts of sand on the Curonian Spit coast indicate the prevalence of an accumulation processes. In contrast, a sparse volume of sand on the mainland coast shows the trend of erosion. The importance of sediment supply was demonstrated by other authors who investigated coastal changes on a geological time scale (Carter et al., 1987; Thom, 1983; Hoffmann and Lampe, 2007). The rise of sea level results in an increase in coastal erosion, which enhances sediment supply, leading to the emergence of accumulation forms (particularly sand barriers systems). The same processes of intensive shore erosion were observed during the period of rapid transgression of the Littorina Sea, ~7000 years ago, which caused intensive erosion to the Sambia moraine's headland (situated to the southwest of the Curonian Spit in Kaliningrad Oblast). At the same time large amounts of sand were carried northward predetermining the formation of the Curonian Spit (Gudelis, 1998). Thus, on a long-term time scale, slow rise in sea level may initiate coastal erosion in areas of sediment starvation. In areas of excess sand supply, small increments of sea-level rise may induce accumulation.

A more noticeable impact of sea level on shoreline change occurs on a short-term time scale. An inverse relationship was established between yearly shoreline position change and yearly

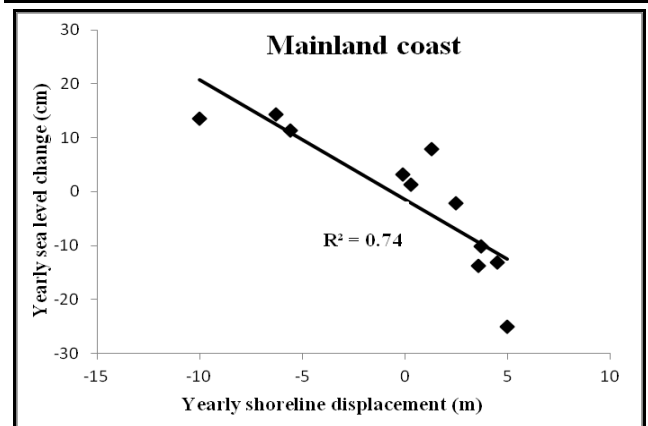


Figure 6. Relationship between yearly shoreline displacement and yearly sea level change for the mainland coast.

sea level change (Figs. 6 and 7), regardless of sand supply (e.g., the mainland coast ( $r = -0.85$ ) with a sediment supply deficit or

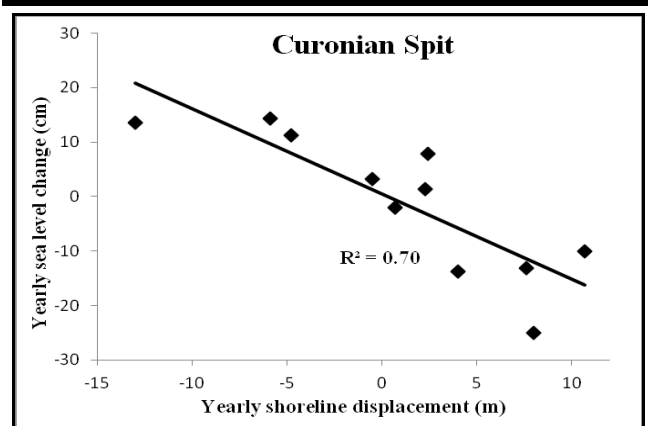


Figure 7. Relationship between yearly shoreline displacement and yearly sea level change on the Curonian Spit coast.



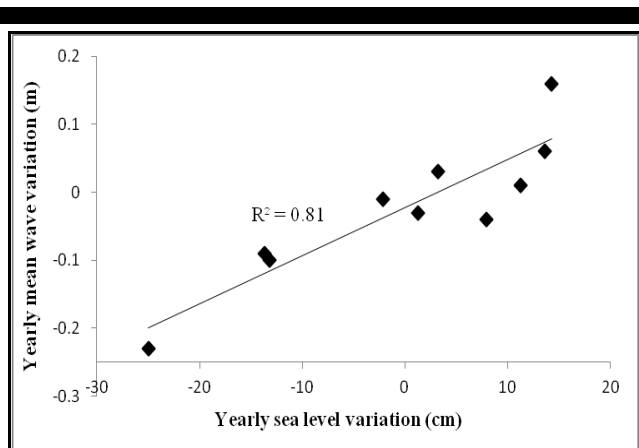


Figure 8. Relationship between yearly sea level change and yearly mean wave change.

the Curonian Spit coast ( $r = -0.84$ ) with a sediment excess). The relationship between beach-width variation and sea-level fluctuations over a short-time cycle (1 and 3.5 years) was also noted by Clarke and Eliot (1983).

Mean yearly sea level amplitude at the Klaipėda gauge station is 1.36 cm/yr (i.e., 150 cm total rise in RSL) between 1902 and 2012, whilst in the 2002–2012 interval sea-level rise only amounted to 0.38 cm/yr. This difference shows that sea-level rise over the course of several years may not have as much of a substantial effect on shoreline position as yearly sea-level changes. On the other hand, yearly sea-level changes are predetermined by hydrometeorological characteristics – particularly by wind-wave climate. A good correlation was established between changes in the yearly sea-level variation and yearly mean wave variation (i.e., the difference between yearly mean wave heights for two consecutive years) ( $r^2 = 0.90$ ) (Fig. 8). Due to the close relationship between these factors, it is difficult to evaluate the direct effects of sea level fluctuation isolated from the effects of other processes. It can additionally be stated that yearly shoreline position was influenced by the frequency and intensity of storms. According to the data collected by the Department of Marine Research in Klaipėda, the period from 2003–2012 was characterized by a low frequency of storms (i.e., extreme winds of  $>25$  m/s), with a frequency of, on average, one storm per year (Navašinskienė, 2013). The interval between 1997 and 2002, however, was characterised by four storms per year. This decrease in storminess could result in intensification of coastal accumulation processes, thus the increase in extreme storm frequency has a crucial impact on shoreline displacement on a short-term scale. However, over a period of recovery, the coast profile is restored. Corbella and Stretch (2012) found out that the shoreline recovery takes two years on average. Thus, extreme storms may not affect the long-term shoreline trend if recurrence of storms is less frequent than once every two years.

## CONCLUSION

The investigation showed that there is no evident agreement between sea level rise and shoreline displacement on a decadal time scale. The magnitude of shoreline displacement depends on other factors, particularly sediment supply, nearshore morphology and storm activity.

Rising sea levels may inhibit coastal erosion and lead to an increase in sediment volume at the nearshore. Thus, conditions are created for development of coastal accumulation forms (e.g., sand

barrier systems). Together with prevailing accumulation processes in the coastal zone, sand volumes may decrease, which in turn results in the initiation of erosion. In this way the feedback mechanism between sand volume and shoreline displacement is created. Trends of low sea-level rise may not have an appreciable effect on coastal dynamics.

Over a shorter period of time (i.e., within a year or between consecutive years) sea-level fluctuations of higher amplitude may produce a greater impact on shoreline displacement. Nevertheless, it is difficult to assess the sole influence of sea level fluctuation without taking into consideration other factors such as yearly variations of sea level, mean wave height and extreme events, all of which showed high levels of agreement with shoreline displacement.

## ACKNOWLEDGEMENT

The authors wish to thank the Department of Marine Research of the Environmental Protection Agency for access to sea-level data from Klaipėda gauge station.

## LITERATURE CITED

- Aagaard, T. and Sørensen P., 2012. Coastal profile response to sea-level rise: a process-based approach. *Earth Surface Processes and Landforms*, 37, 354-362.
- Barth, M.C. and Titus, J.G., 1984. *Greenhouse effect and sea level rise. A challenge for this generation*. New York, USA: VNR company, 368 p.
- Bitinas, A., Aleksa, P., Damušytė, A., Gulbinskas, S., Jarmalavičius, D., Kuzavinis, M., Minkevičius, V., Pupienis, D., Trimonis, E., Šečkus, R., Žaromskis, R. and Žilinskas, G., 2004. *Geological Atlas of Lithuanian coast of the Baltic Sea*. Vilnius, Lithuania: Lietuvos Geologijos Taryba.
- Bruun, P., 1962. Sea-level rise as a cause of shore erosion. *Journal of Waterways and Harbours Division*, 88(ww1), 117-130.
- Carter, R.W.G., Johnston, T.W., McKenna, J. and Orford, J.D., 1987. Sea level, sediment supply and coastal changes: examples from the coast of Ireland. *Progress in Oceanography*, 18(1-4), 79-101.
- Clarke, D.J. and Eliot, I.G., 1983. Mean sea-level and beach-width variation at Scarborough, Western Australia. *Marine Geology*, 51, 251-267.
- Cooper, J.A.G. and Navas, F. 2004. Natural bathymetric change as a control on century-scale shoreline behavior. *Geology*, 32(6), 513-516.
- Corbella, S. and Stretch, D. D., 2012. Predicting coastal erosion trends using non-stationary statistics and process-based models. *Coastal engineering*, 70, 40-49.
- Cowell, P.J., Stive, M.J.F., Niedoroda, A.W., Swift, D.J.P., de Vriend, H.J., Buijsman, M.C., Nicholls, R.J., Roy, P.S., Kaminsky, G.M., Cleveringa, J., Reed, C.W. and de Boer, P.L., 2003. The coast-tract (Part 2): applications of aggregated modeling of lower-order coastal change. *Journal of Coastal Research*, 19(4), 828-848.
- de Ruig, J.H. M. and Louise, C.J., 1991. Sand budget trends and changes along the Holland coast. *Journal of Coastal Research*, 7(4), 1013-1026.
- Farris, A.S. and List, J.H., 2007. Shoreline change as a proxy for subaerial beach volume change. *Journal of Coastal Research*, 23(3), 740-748.
- Gudelis, V., 1998. *The Lithuanian offshore and coast of the Baltic Sea*, Vilnius, Lithuania: Lietuvos mokslas, 442 p. (in Lithuanian).
- Guillén, J., Stive, M.J.F. and Capobianco, M., 1999. Shoreline evolution of the Holland coast on a decadal scale. *Earth Surface Processes and Landforms*, 24, 517-536.
- Hoffmann, G. and Lampe, R., 2007. Sediment budget calculation to estimate Holocene coastal changes on the southwest Baltic Sea (Germany). *Marine Geology*, 243, 143-156.
- Jarmalavičius, D. and Žilinskas, G., 1996. Peculiarities of long-term oscillations of sea water level near the Lithuanian coasts on the dynamical background of S and SE Baltic Sea level. In: Žaromskis, R., Eitmanavičienė, N., Žilinskas, G. (eds.). *Geography in Lithuania*. Vilnius: Lithuania: Institute of geography, pp. 100-109.
- Jarmalavičius, D. and Žilinskas, G., 2006. Peculiarities of sand sorting on the Lithuanian coast of the Baltic Sea. *Geologija*, 56, 36-42.

- Jarmalavičius, D., Žilinskas, G. and Pupienis, D., 2012. Impact of Klaipėda port jetties reconstruction on adjacent sea coast dynamics. *Journal of Environmental and Landscape Management*, 20(3), 240-247.
- Kriauciūnienė, J., Žilinskas, G., Pupienis, D., Jarmalavičius, D. and Gailiusis, B., 2013. Impact of Šventoji port jetties on coastal dynamics of the Baltic Sea. *Journal of Environmental Engineering and Landscape Management*, 21(2), 114-122.
- Lacey, E.M. and Peck, J.A., 1998. Long-term beach profile variations along the South shore of Rhode Island, U.S.A. *Journal of Coastal Research*, 14(4), 1255-1264.
- Le Cozannet, G., Garcin, M., Petitjean, L., Cazenave, A., Becker, M., Meyssignac, B., Walker, P., Devilliers, C., Le Brun, O., Lecacheux, S., Baills, A., Bulteau, T., Yates, M. and Wöppelmann, G., 2013. Exploring the relation between sea level rise and shoreline erosion using sea level reconstructions: an example in French Polynesia. *Journal of Coastal Research*, SI 65: 2137-2142.
- Meehl, G.A., Stocker, T.F., Collins, W.D., Friedlingstein, P., Gaye, A.T., Gregory, J.M., Kitoh, A., Knutti, R., Murphy, J.M., Noda, A., Raper, S. C.B., Watterson, I.G., Weaver, A.J. and Zhao Z.C., 2007. Global climate predictions. In: Solomon, S., Qin, D., Manning M., Chen, Z., Marquis M., Averyt, K. B., Tignor, M. and Miller, H. L. (eds.). *Climate Change 2007: The Physical Science Basis. Contribution of Working Group I to the Fourth Assessment Report of the Intergovernmental Panel on Climate Change*. Cambridge, UK: Cambridge University Press, pp. 747-846.
- Navašinskiėnė, J., 2013. Extreme events on the seacoast. In: Milerienė, R., Minevičiūtė, I. (eds.) *Jūros ir krantų tyrimai*. Klaipėda, Lithuania: Klaipėda University, pp. 172-174. (in Lithuanian).
- Nicholls, R.J., Leatherman, S.P., Dennis, K.C. and Volonte, C.R., 1995. Impact and responses to sea-level rise: qualitative and quantitative assessments. *Journal of Coastal Research*, SI 14, 26-43.
- Pruszk, Z. and Zawadzka, E., 2005. Vulnerability of Poland's coast to sea-level rise. *Coastal engineering journal*, 47(2-3), 131-155.
- Pupienis, D., Jarmalavičius, D. and Žilinskas, G., 2012. Coastline dynamics tendencies of the Baltic Sea in 1910-2010. In: Rukšėnas, O., Turčimavičienė, J., Slapšytė, G., Bukelskis, E., Valiuškevičius, G., Gadeikytė, S. (eds.) *Mokslas Gamtos mokslų fakultete 7*. Vilnius, Lithuania: Vilnius university, pp. 141-152. (in Lithuanian).
- Pupienis, D., Jonuškaitė, S., Jarmalavičius, D. and Žilinskas, G., 2013a. Klaipėda port jetties impact on the Baltic Sea shoreline dynamics, Lithuania. *Journal of Coastal Research*, SI65, 2167-2172.
- Pupienis, D., Buynevich, I.V., Jarmalavičius, D., Žilinskas, G. and Fedorovič, J., 2013b. Regional distribution of Heavy-mineral concentrations along the Curonian Spit coast of Lithuania. *Journal of Coastal Research*, SI65, 1844-1849.
- Pye, K. and Blott, S. J., 2006. Coastal processes and morphological change in the Dunwich-Sizewell area, Suffolk, UK. *Journal of Coastal Conservation*, 22(3), 453-473.
- Rotnicki, K., Borowka, R.K. and Devine, N., 1995. Accelerated sea level rise as a threat to the Polish coastal zone – quantification of risk. *Journal of Coastal Research*, SI 22, 111-135.
- Roy, P.S., Cowell, P.J., Ferland, M.A. and Thom, B.G., 1994. Wave-dominated coasts. In: Carter, R. W. G., Woodroffe, C. D. (eds.). *Coastal evolution. Late Quaternary Shoreline Morphodynamics*. Cambridge, UK: Cambridge University Press, pp. 121-186.
- Selivanov, A.O., 1996. Morphological changes on Russian coasts under rapid sea-level changes: examples from the Holocene history and implications for the future. *Journal of Coastal Research*, 12(4), 824-830.
- Stive, M.J.F., Aarninkhof, S.G.J., Hamm, L., Hanson, H., Larson, M., Wijnberg, K.M., Nicholls, R.J. and Capobianco, M., 2002. Variability of shore and shoreline evolution. *Coastal Engineering*, 47, 211-235.
- Storms, J.E.A., Weltje, G.J., van Dijke, J.J., Geel, C.R. and Kroonenberg, S.B., 2002. Process-response modelling of wave-dominated coastal systems: simulating evolution and stratigraphy on geological timescales. *Journal of Sedimentary Research*, 72(2), 226-239.
- Thom, B.G., 1983. Transgressive and regressive stratigraphies of coastal sand barriers in Southern Australia. *Marine Geology*, 56, 137-158.
- Thom, B.G. and Hall, W., 1991. Behavior of beach profiles during accretion and erosion dominated periods. *Earth Surface Processes and Landforms*, 16, 113-127.
- Zeidler, R.B., 1992. *Assessment of the Vulnerability of Poland's Coastal Areas to Sea Level Rise*, Gdansk, Poland: HTC, 165 p.
- Zeidler, R.B., 1995. Vulnerability of Poland's coastal areas to sea level rise. *Journal of Coastal Research*, SI 22, 99-109.
- Žilinskas, G., Jarmalavičius, D. and Minkevičius, V., 2001. *Aeolian processes on sea coast*. Vilnius, Lithuania: 283 p.
- Žilinskas, G., Pupienis, D. and Jarmalavičius, D., 2010. Possibilities of regeneration of Palanga coastal zone. *Journal of Environmental and Landscape Management*, 18(2), 92-101.

## The role of beachrocks on the evolution of the Holocene barrier systems in Rio de Janeiro, southeastern Brazil

André L.C. da Silva<sup>†</sup>, Maria A.M. da Silva<sup>‡</sup>, Rogério S. de Souza<sup>#</sup>, Márcio L.V. Pinto<sup>∞</sup>

<sup>†</sup> Department of Geography  
Universidade do Estado do Rio de Janeiro  
São Gonçalo, RJ, Brazil  
[andreclsilva@ig.com.br](mailto:andreclsilva@ig.com.br)

<sup>‡</sup> Department of Geology/LAGEMAR  
Universidade Federal Fluminense  
Niterói, RJ, Brazil  
[mamsgeo@gmail.com](mailto:mamsgeo@gmail.com)

<sup>#</sup> PETROBRAS/CENPES  
Cidade Universitária - Ilha do Fundão  
Rio de Janeiro, RJ, Brasil  
[schiffer@petrobras.com.br](mailto:schiffer@petrobras.com.br)



[www.cerf-jcr.org](http://www.cerf-jcr.org)

<sup>∞</sup> Department of Geography  
Universidade Federal Fluminense  
Niterói, RJ, Brazil  
[marciogeouff@yahoo.com.br](mailto:marciogeouff@yahoo.com.br)



[www.JCRonline.org](http://www.JCRonline.org)

### ABSTRACT

Silva, A.L.C., Silva, M.A.M., Souza, R.S., Pinto, M.L.V., 2014. The role of beachrocks on the evolution of the Holocene barrier systems in Rio de Janeiro, southeastern Brazil. In: Green, A.N. and Cooper, J.A.G. (eds.), *Proceedings 13<sup>th</sup> International Coastal Symposium* (Durban, South Africa), *Journal of Coastal Research*, Special Issue No. 70, pp. 170-175, ISSN 0749-0208.

Beachrocks at different locations along Rio de Janeiro coast (southeastern Brazil) play an important role in the understanding of coastal evolution and sea-level fluctuations in the Holocene. The studied area presents a long and wide stretch of coastal plain characterized by two sandy barriers, which confine a series of small isolated chain-like lagoons in addition to large lagoons on the reverse side of the inner barrier. The beachrocks occur at different positions in relation to present-day mean sea level. These can be observed as submarine outcrops and along the beaches. The 8.100 years old B.P. beachrocks reveal a phase of retrogradation of the barrier system, and the drowning and partial preservation of this barrier during the sea transgression through the Holocene. The beachrocks are composed of medium-to coarse sand grained bioclastic quartz-rich sandstones which are strongly cemented by calcite. Three successive events of calcite cementation have drastically reduced the porosity of the rock. Calcite cement occurs as three basic forms: isophacous fringe of very fine crystalline calcite, aphanocrystalline calcite and coarsely crystalline calcite. Each textural type indicates different geochemical composition of the pore waters during the very early diagenetic evolution within the intertidal zone of the coastal barrier system.

**ADDITIONAL INDEX WORDS:** *Beachrock; Holocene evolution; coastal barrier system; calcite cementation; southeastern Brazil.*

### INTRODUCTION

The coastal geology of the Rio de Janeiro state (SE, Brazil) (Figure 1) is mainly characterized by Pre-Cambrian granites, migmatites and gneisses, forming impressive mountain ranges. The coastal plain geomorphology of Maricá and Rio de Janeiro cities (Figure 1) presents two barriers, an inner Pleistocene barrier and an outer Holocene barrier (Ireland, 1987; Turcq *et al.*, 1999; Pereira, 2001; Pereira *et al.*, 2003; Silva, 2011). These two barriers confine a series of nearly dry, small, and isolated chain-like lagoons. A large lagoon usually occurs on the reverse side of the Pleistocene barrier (Figure 1).

Beachrocks appear parallel to the present-day coastline and are visible at the intertidal zone of the beaches or as submarine outcrops (Figure 2A, B and C). Mansur *et al.* (2011) presented the history of the first observations and descriptions of the Brazilian beachrocks, highlighting the important visit of Charles Darwin, who in 1842 presented a first description of the Jaconé beachrock in Rio de Janeiro. Beachrocks are more common in places where

temperatures are high enough to promote seawater evaporation (mainly from 35° N to 35° S latitudes), which, in turn, raises the concentration levels of calcium carbonate in the water and interstitial waters favoring the precipitation of calcium carbonate (Friedman and Sanders, 1978; Cooper, 1991; Friedman *et al.*, 1992). The increase of CaCO<sub>3</sub> saturation levels is further enhanced as CO<sub>2</sub> evaporates during exposure of the beaches at low tides (Bathurst, 1976). CaCO<sub>3</sub> precipitation is likely to occur at the beach vadose zone, where waters of different compositions mix (Bathurst, 1976). Bathurst (1976) also points out the importance of the metabolism of microorganisms, which can play an important role on the overall complex diagenetic process. As a consequence of their nature, beachrocks can be very significant in the understanding of the evolution of barrier systems.

The evolution of Rio de Janeiro state coastal plain has been under investigation since the works of Lamago (1940, 1945) when based on the surface geomorphology, he proposed that the closing of large embayments through spit growth gave rise to the barrier-lagoon systems. That hypothesis was reinforced by surveys carried on the Jacarepaguá coastal plain (Figure 1) (Roncarati and Neves, 1976). Sea-level fluctuations began to be considered as an

important factor for the Rio de Janeiro coastal plain evolution much latter, implying the submergence of the low-lying areas and barrier formation (Perrin, 1984; Coe Neto *et al.*, 1986; Ireland, 1987; Muehe and Correa, 1989; Turcq *et al.*, 1999; Pereira *et al.*, 2003). In addition to sea-level fluctuations, longshore currents have also been proposed as a controlling mechanism for the formation of the barrier-lagoon systems in the area (Perrin, 1984; Pereira, 2001; Pereira *et al.*, 2003; Silva, 2011). The study area is a wave-dominated coast with predominant and more intense S-SW stormy waves during winter months (Muehe, 1979; Silva *et al.*, 2008a). Maximum spring tidal fluctuation is 1.5 m (DHN, 1974).

Holocene sea-level history along RJ coast is marked by an important transgressive event at around 5100 years B.P., which achieved about 5 meters above present-day sea level. This was

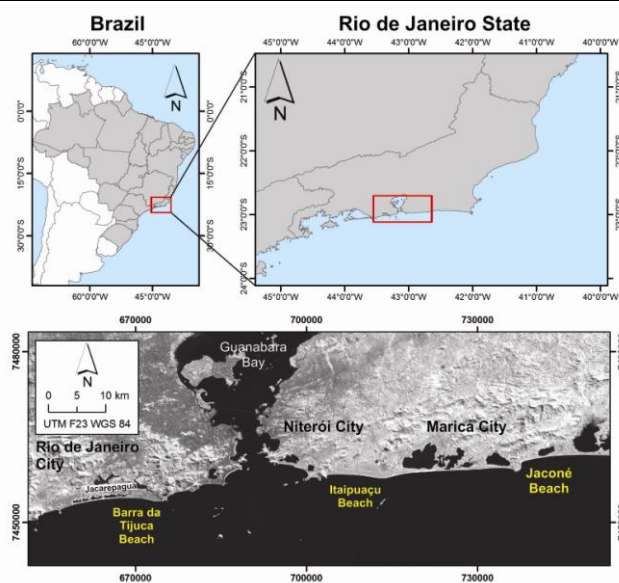


Figure 1. Location map of the studied area and the beachrocks in Rio de Janeiro coast, southeast Brazil.

then followed by a regression at about 2.800 years B.P., which caused progradation of the coastline (Martin *et al.*, 1993; Martin *et al.*, 2003). Today, a new phase of transgression is causing the retrogradation of the barrier at a rate of 15 m over the past 30 years (Lins-de-Barros, 2005; Silva, 2006; Silva *et al.*, 2008b). As a consequence of this, the beachrocks can be seen as outcrops at the Jacomé and Barra da Tijuca beaches or as a submarine outcrop in Itaipuaçu beach (Figure 1; 2A, B and C). This has served as good evidence for the present-day retrogradation of the barriers in Rio de Janeiro (Muehe, 1984). However, the beachrocks have not been dated. Muehe (1984) hypothesises that the beachrock could have been formed during the regression of 2800 B.P. This paper provides new insights on the beachrock aiding in the understanding of the timing of the beachrock formation and its role on the evolution of the Rio de Janeiro coastal plain.

## METHODS

Fragments of beachrocks were collected at the beaches after storms. Out of 30 samples, 20 were chosen from Itaipuaçu beach and 10 from Barra da Tijuca beach. These were photographed and described. Thin sections of the most representative samples for each place were made: 4 from Itaipuaçu and 3 from Barra da Tijuca. The thin sections were saturated with Blue Oracet for



Figure 2. Beachrocks at different locations in relation to present-day mean sea level along Rio de Janeiro coast: a submarine outcrop at Itaipuaçu beach (a) Barra da Tijuca beach (b) and Jacomé beach (c). Photos by Novaes, F., 2007 (a); Luís and Sidnei, 2011 (b); Silva, A. L. C., (2013).

porosity analysis and examined under transmitted as well as polarized light using a petrographic microscope. A sample containing whole well preserved shells from the Itaipuaçu beachrock was sent to the Center for Applied Isotope Studies (CAIS) at the University of Georgia (USA) for radiocarbon dating using the Accelerator Mass Spectrometry (AMS 14C) method.

The Jaconé beachrock ages presented in this study are from Mansur *et al.* (2011).

## RESULTS AND DISCUSSION

### The Itaipuaçu and Barra da Tijuca beachrocks

The Itaipuaçu beachrocks (Figure 2A) occur at 5 to 7 m water depth range and roughly 100 m in distance from the present-day beach water-line mark (Muehe, 1984; Muehe and Ignarra, 1987). These beachrocks extend for about 2 500 m along the coast, ranging from 20 to 100 m in width, with stratification dipping 5° seaward (Souza, 1988). Large fragments of the beachrock are easily found along the western part of the beaches after storms (Figure 3A and B). Itaipuaçu beach is famous for its rounded, poorly sorted, very coarse sand and gravel grained particles.

The beachrock is a quartz-rich sandstone akin to the present-day beach sediments (quartz grains content ranges from 65 to 70% of the bulk rock volume), with a minor amount microcline and

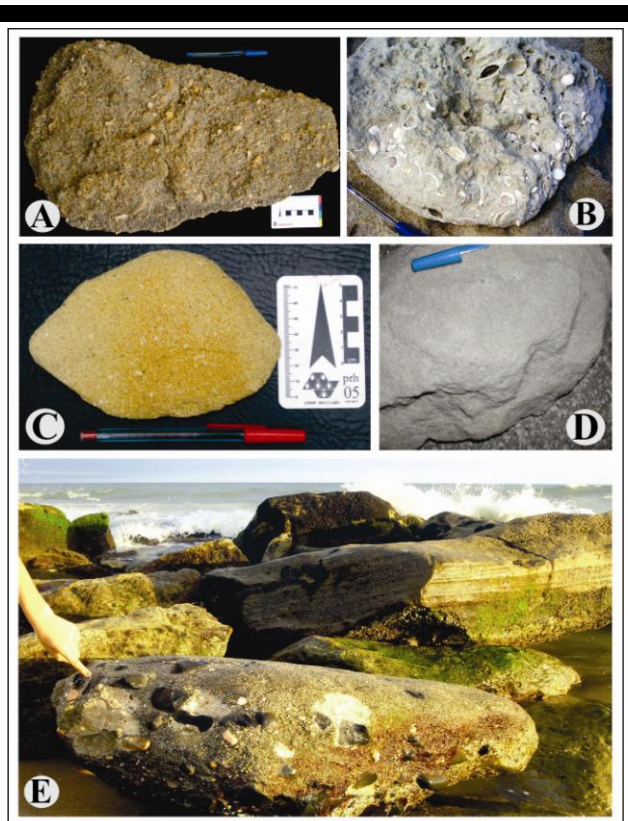


Figure 3. Beachrock fragments found at the beaches after storms: Itaipuaçu (a,b) and Barra da Tijuca (c,d). Beachrock blocks in the intertidal zone at Jaconé (e). Photos by Silva, A. L. C. (a, c, e); Silva, M. A. M. (b); Pinto, M. L. V. (d).

plagioclase feldspar (up to 3 to 5% of the bulk rock volume), bioclasts mostly composed of bivalve shells (5 to 7% of the bulk rock volume) and trace amounts of heavy minerals (epidote, tourmaline, garnet, magnetite, ilmenite and zircon). Whole and fragmented shells appear in different sizes and degrees of dissolution. Some of these are well preserved and, in the case of bivalves, with both shells closed (Figure 3B). Very well preserved shells provided the age of  $8110 \pm 30$  years B.P. for the beachrock. (Figure 4A). Sedimentary structures are abundant predominating

plane-parallel laminations, low angle cross bed stratification, cut-and-fill and heavy mineral laminations (sparse).

The Barra da Tijuca beachrock (Figure 2B) occurs: (1) at about 80 to 130 m from the beach, at water depths of about 5 meters and (2) a second outcrop, discussed in this work, can be seen at low tides at the beach (Figure 2B) (Muehe and Ignarra, 1984). As in Itaipuaçu, fragments of the beachrock are found at the beach after

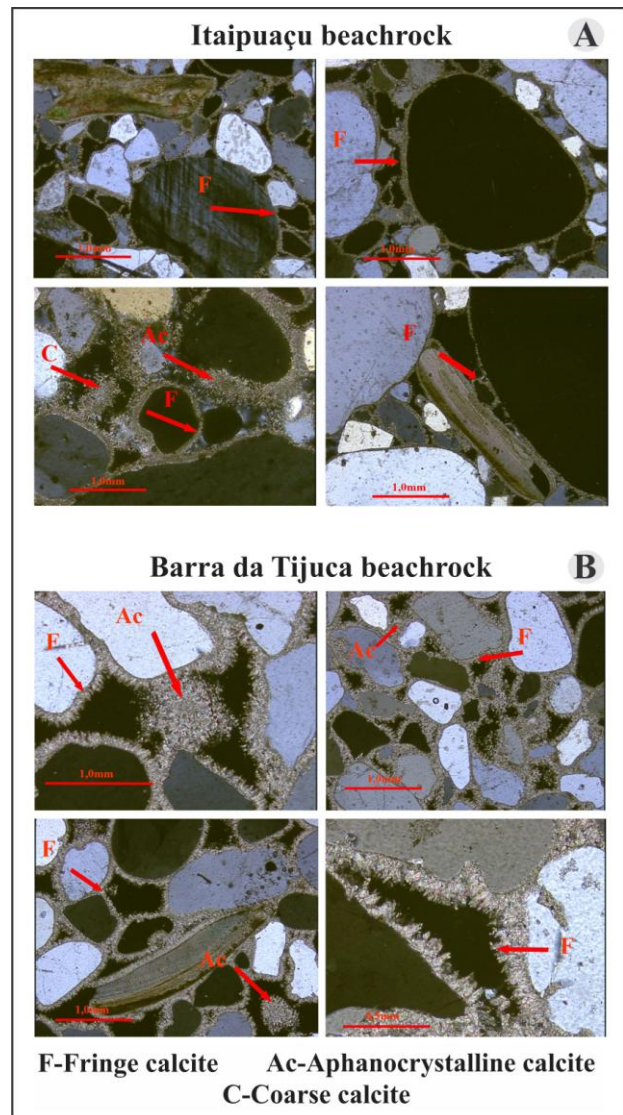


Figure 4. Photomicrographs of beachrock fragments from Itaipuaçu (a) and Barra da Tijuca (b).

storms (Figure 3C and D). The beachrock is siliciclastic, quartz being the dominant component, with a subordinate amount of microcline feldspar (Figure 4B). It is made up of rounded and well sorted medium to coarse sand (Figure 4B). Common sedimentary structures observed in the samples are plane-parallel beds, laminations and planar-cross stratification. Shells are mostly fragmented; therefore no means of dating is available for the Barra da Tijuca beachrock.

Cements, in both cases, are composed of calcite (Figure 4A and B). The cementation process appears to have been very pervasive and has drastically reduced the porosity of the beachrock. Three

types of calcite are predominant: isopachous fringe of prismatic “dog-tooth” very fine crystalline (.0000319 - .00015369 mm) calcite (according Folk, 1974, classification scheme based upon crystal size), aphanocrystalline (0.0000319 - 0.00015369 mm) and coarsely crystalline (.25 - 1.00 mm) calcite. The isopachous fringe calcite is observed around particles, and the well formed crystals are oriented perpendicularly to the grain surface (Figure 4A and B). This type of cement is considered to form in the marine phreatic zone, where porous in the sediments are completely filled by seawater (Bathurst, 1976; Souza, 1988). Aphanocrystalline calcite occurs as anhedral to subhedral crystals (Figure 4A and B) and is the result of precipitation of  $\text{CaCO}_3$  in the vadose or phreatic zone of the beach under the influence of the mixing of marine and meteoric waters (Souza, 1988). Coarse crystals of calcite (Figure 4A and B) are developed when the ideal conditions for  $\text{CaCO}_3$  precipitation are stable for a low period of time allowing the growth of calcite crystals. Souza (1988) proposed three consecutive stages for the beachrock cementation: (1) cementation by isopachous fringe of prismatic “dog-tooth” fine crystalline calcite precipitated under phreatic marine conditions where porous were entirely filled by seawater; (2) precipitation of aphanocrystalline calcite at the vadose zone or phreatic zone when pores were filled by mixed marine and meteoric waters; (3) second phase of isopachous fringe of prismatic “dog-tooth” fine crystalline calcite that continues up to the present day, in the marine phreatic zone of the submarine outcrops entirely saturated with marine water.

### The Jaconé beachrock

The beachrock at Jaconé beach (Figure 1, 2C) has been studied by Mansur *et al.* (2011). It extends for approximately 1100 m and is most visible at low tide. According to Mansur *et al.* (2011); the beachrock is a siliciclastic sandstone, conglomeratic in places, and has the distinct presence of diabase pebbles as a result of the local geology (Figure 3E). The cement is also carbonate in nature and is considered to be the result of  $\text{CaCO}_3$  precipitation in the marine phreatic environment. The age of the beachrock is 8198-7827 cal B.P.; the cement has also been dated as 6008-5786 cal B.P.

### Evolution of the Holocene barrier and beachrock system

The Itaipuaçu and Jaconé beachrocks indicate the existence of a barrier system at around 8000 years B.P. on the study coast of Rio de Janeiro (Figure 5). Another example of beachrock which is similarly located has been dated as  $7870 \pm 60$  and  $8050 \pm 80$  years B.P. and comes from São Paulo state (about 400-500 km south of Rio de Janeiro city) (Furtado *et al.*, 1998, in Klein and Mahiques, 2003). These examples, together with Barra da Tijuca beachrock, are good indicators of a stable and lower than today sea level.

A 6000 years B.P. layer of peat under the present day barrier suggests the existence of a lagoon associated with the former barrier (Pereira, 2001; Pereira *et al.*, 2003) (Figure 5). The beachrock, thus a remnant of this former barrier (Figure 5A and B), was subsequently drowned as the Holocene transgression proceeded forcing the retrogradation of the coast. This is seen in the case of Itaipuaçu (Figure 5D). The barrier, where the beachrock was formed, constitutes the first record of Holocene sedimentation in the area, as shown by GPR images and borehole

data (Silva, 2011). The beachrock overlies an erosional surface which marks the limit between the Pleistocene and Holocene Sequences (Silva, 2011). Therefore, the beachrock is at the base of the Holocene Coastal Sequence as defined by Silva (2011) and helps to recognise the first Holocene coastal sediments after an interval of erosion and subsequent subaerial exposure of a Pleistocene barrier system. Towards the top, the sequence is represented by sediments deposited during the Holocene transgression and retrogradation of the coast. During the Holocene, sea level reached its maximum of 3 to 5 m above present-day sea level around 5000 years ago (Angulo and Lessa, 1997; Martin *et al.*, 1993; Martin *et al.*, 2003). The retrograding coast reached roughly 200 m distance inland. Following this event, GPR images show a phase of progradation of the barrier (Silva, 2011; Silvestre, 2013). For the past 30 years, the barrier has continued to retreat by approximately 15 m (Lins-de-Barros, 2005; Silva, 2006; Silva *et al.*, 2008b). The locations of the beachrocks reinforce the notion of a retreating coast, as proposed by Muehe (1984).

The beachrock plays an important role helping to establish the timing of Holocene sedimentation in the area as well as the retrogradation of the barrier that followed as sea level rose throughout the Holocene. The different locations where the beachrocks are found, in relation to present-day sea level, may be a consequence of the different wave dynamics of each particular area. Itaipuaçu, where the beachrock is completely immersed, is well known in Rio de Janeiro for its very high-energy waves (Muehe, 1979; Silva, 2006; Silva *et al.*, 2008a; Pardal, 2009). Such behavior of a coast has also been observed in Rio Grande do Sul (southernmost state of Brazil) where wave energy seems to control the tendency of the coast to prograde or recede (Dillemburg *et al.*, 2003).

### CONCLUSION

Along the Rio de Janeiro coast, several occurrences of beachrocks allow the understanding of sedimentation during the Holocene. The beachrocks in this study provide an age of about 8100 years B.P. They are siliciclastic, quartz-rich mostly coarse well rounded sand with gravel. Calcite occurs as very fine crystalline fringes around the grains, aphanocrystalline and coarsely crystalline cements drastically reducing the porosity of the rock. Based upon the paragenetic sequence at least three events of calcite cementation are recognized that suggest variation of the composition of the pore filling waters from marine to mixed marine and meteoric waters. They represent an early Holocene barrier-lagoon system that migrated as sea level fluctuated through time. Today, they are found at different locations in relation to sea level, as a submarine outcrop (Itaipuaçu) or along the beaches observed at low tides (Barra da Tijuca and Jaconé), and that may be the result of the transgression which is moving the barrier inland, but also the consequence of different gradients in the wave intensity (Itaipuaçu presents the most intense wave conditions along the year). The beachrock is at the base of the Holocene Coastal Sequence, resting on top of an erosional surface, which represents the limit Peistocene/Holocene. The beachrock is, thus, a good evidence for the first record of sedimentation in the Holocene in this area.

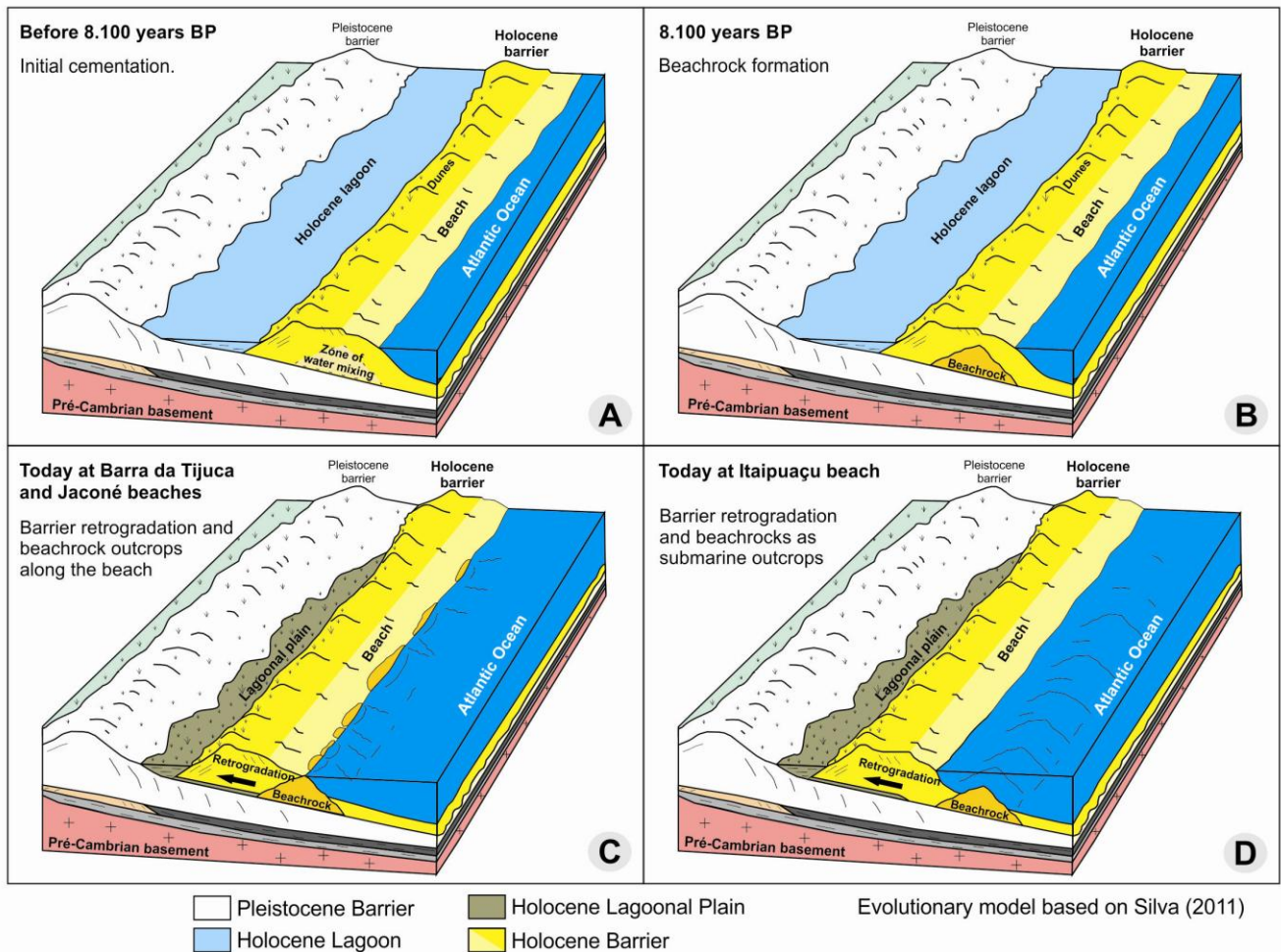


Figure 5- Evolutionary model for the Holocene barrier systems in Rio de Janeiro, southeastern Brazil.

## ACKNOWLEDGEMENT

This project was funded by FAPERJ (E-26/170 452/07). André Silva acknowledges the award of doctoral scholarship from CAPES. The authors would like to thank the responsible for the Maricá APA for permitting access to the study area. We are very grateful to friends and students who helped during field works.

## LITERATURE CITED

- Angulo, R. J. and Lessa, G. C. 1997. The Brazilian sea-level curves: a critical review with emphasis on the curves from Paranaguá and Cananéia regions. *Marine Geology*, 140, 141-166.
- Bathurst, R. 1976. Carbonate Sediments and Their Diagenesis. Developments In: *Sedimentology*. Elsevier, 12, 658p.
- Coe Neto, R., Froidefond, J. M. and Turcq, B. 1986. Géomorphologie et chronologie relative des dépôts sédimentaires récents du littoral brésilien à l'est de Rio de Janeiro. *Bull. Inst. Géol. Bassin d'Aquitaine*, Bourdeaux, 40, 67-83.
- Cooper J.A.G. 1991. Beachrock formation in low latitudes: implications for coastal evolutionary models. *Marine Geology*, 98, 145-154.
- DHN - Departamento de Hidrografia e Navegação. 1974. Correntes de Maré - Baía de Guanabara, RJ.
- Dillenburg, S. R., Tomazelli, L. J. and Clerot, L. C. P. 2003. Gradientes de energia de onda: o principal fator controlador da evolução costeira no Rio Grande do Sul durante o Holoceno Superior. *IX Congresso da Associação Brasileira de Estudos do Quaternário*, 1-3.
- Folk, R.L., 1974. *Petrology of Sedimentary Rocks*. Hemphill Publishing Company, Austin, Texas, 184p.
- Friedman, G. M. and Sanders, J. E. 1978. *Principles of Sedimentology*. New York, John Wiley and Sons. 792p.
- Friedman, G. M.; Sanders, J. E. and Kopaska-Merkel, D. C. 1992. *Principles of Sedimentary Deposits: Stratigraphy and Sedimentology*. New York, Oxford, Singapore, Sydney: Maxwell Macmillan International, 403 - 441.
- Furtado, V.V., Bonetti Filho, J., Rodrigues, M. and Barcellos, R.L. 1998. Aspectos da sedimentação no Canal de São Sebastião. Relatório do Projeto de Oceanografia da Plataforma Interna de São Sebastião (OPISS). *Relat. Téc. Inst. Oceanografia*, São Paulo, 43, 15-31.
- Ireland, S., 1987. The Holocene sedimentary history of the coastal lagoons of Rio de Janeiro State, Brazil. In: Tooley, M. and Shennan, I. (ed.) *Sea Level Changes*. Oxford: Brazil Blackwell Ltd, pp. 25-66.
- Klein, D. A. and Mahiques, M. M. 2003. Evidências de variações do nível relativo do mar durante o último ciclo glacial, na porção norte do canal de São Sebastião, litoral norte do estado de São Paulo. *II Congresso sobre Planejamento e Gestão das Zonas Costeiras dos Países de Expressão Portuguesa*. Florianópolis, 1-5.
- Lamego, A. R. 1940. *Restingas na Costa do Brasil*. Divisão de Geologia e Mineralogia. Boletim 96, DNPM, 63p.

- Lamego, A. R. 1945. *Ciclo Evolutivo das Lagunas Fluminenses*. Divisão de Geologia e Mineralogia. Boletim 118, DNPM, 47p.
- Lins-de-Barros, F. M., 2005. Risco, Vulnerabilidade Física à Erosão Costeira e Impactos Sócio-econômicos na Orla Urbanizada do Município de Maricá, Rio de Janeiro. *Revista Brasileira de Geomorfologia*, Ano 6, 2, 83-90.
- Mansur, K. L., Ramos, R. R. C., Godoy, J. M. O., and Nascimento, V. M. R. 2011. Beachrock de Jacané, Maricá e Saquarema - RJ: importância para a história da ciência e para o conhecimento geológico. *Revista Brasileira de Geociências*, 41 (2), 290-303.
- Martin, L., Suguio, K. and Flexor, J. M. 1993. As flutuações de nível do mar durante o Quaternário Superior e a evolução geológica de “deltas” brasileiros. *Boletim IG-USP*, 15, 186p.
- Martin, L., Dominguez, J. M. L. and Bittencourt, A. C. S. P. 2003. Fluctuating Holocene Sea Levels in Eastern and Southeastern Brazil: Evidence from Multiple Fossil and Geometric Indicators. *Journal of Coastal Research*. West Palm Beach, Florida, 19, 1, 101-124.
- Muehe, D. C. E. H. 1979. Sedimentology and Topography of a High Energy Coastal Environment between Rio de Janeiro and Cabo Frio – Brazil. *Anais da Academia Brasileira de Ciências*, 51 (3), 473-481.
- Muehe, D. C. E. H. 1984. Evidências de recuo dos cordões litorâneos em direção ao continente no litoral do Rio de Janeiro. In: Lacerda, L. D., Araújo, D. S. D., Cerqueira, R. and Turcq, B. (ed.), *Restingas: origem, estruturas e processos*. CEUFF – Universidade Federal Fluminense, 75-80.
- Muehe, D. C. E. H and Corrêa, C. H. T. 1989. The Coastline between Rio de Janeiro and Cabo Frio. Coastlines of Brazil. *American Society of Civil Engineers*. New York, 110-123.
- Muehe, D. C. E. H. and Ignarra, S. 1987. O Arenito de Praia de Itaipuaçu e sua influência no fluxo de sedimentos. In: Lamego, A. R. (ed.), *Anais do I Simpósio de Geologia Regional RJ-ES*. Sociedade Brasileira de Geologia. Rio de Janeiro, 57-62.
- Pardal, M. T. C. 2009. *Mudanças morfológicas e suas implicações para a estabilidade da praia na Região do Recanto de Itaipuaçu, Maricá, RJ*. Niterói, Brasil: Programa de Pós Graduação em Geologia e Geofísica Marinha da Universidade Federal Fluminense, Dissertação de Mestrado, 148p.
- Pereira, A. J. 2001. *Investigação da Estratigrafia da Região Costeira de Maricá – Praia de Itaipuaçu (RJ) – Através do Ground Penetration Radar (GPR)*. Niterói, Brasil: Programa de Pós Graduação em Geologia e Geofísica Marinha da Universidade Federal Fluminense, Dissertação de Mestrado, 93p.
- Pereira, A. J., Gamboa, L. A. P., Silva, M. A. M., Rodrigues, A. R. and Costa, A. A. 2003. Utilização do Ground Penetrating Radar (GPR) em Estudos de Estratigrafia na Praia de Itaipuaçu - Maricá (RJ). *Revista Brasileira de Geofísica*, EDUFF, Niterói, 21 (2), 163-171.
- Perrin, P. 1984. Evolução da Costa Fluminense entre as Pontas de Itacoatiara e Negra, preenchimentos e restingas. In: Lacerda, L. D., Araújo, D. S. D., Cerqueira, R. and Turcq, B. (ed.), *Restingas, origens, processos*. CEUFF, 65-74.
- Roncarati, H. and Neves, L. E. 1976. *Estudo geológico preliminar dos sedimentos recentes superficiais da Baixada de Jacarepaguá, Município do Rio de Janeiro* - RI. PETROBRAS, CENPES. DEXPRO, 89p.
- Silva, A. L. C. 2006. *Comportamento Morfológico e Sedimentológico do Litoral de Itaipuaçu (Maricá) e Piratininga (Niterói), RJ, nas últimas três décadas*. Niterói, Brasil: Programa de Pós Graduação em Geologia e Geofísica Marinha da Universidade Federal Fluminense, Dissertação de Mestrado, 153p.
- Silva, A. L. C. 2011. *Arquitetura sedimentar e evolução geológica da planície costeira central de maricá (RJ) ao longo do Quaternário*. Niterói, Brasil: Programa de Pós Graduação em Geologia e Geofísica Marinha da Universidade Federal Fluminense, Tese de Doutorado, 185p.
- Silva, A. L. C., Silva, M. A. M. and Santos, C. L. 2008a. Comportamento Morfológico e Sedimentar da Praia de Itaipuaçu (Maricá, RJ) nas Últimas Três Décadas. *Revista Brasileira de Geociências*, Sociedade Brasileira de Geologia, 38 (1), 89-99.
- Silva, A. L. C., Silva, M. A. M., Santos, C. L. Ribeiro, G. B., Santos, R. A. and Vasconcelos, S. C. 2008b. Retrogradação da Barreira Arenosa e Formação de Leques de Arrombamento na Praia de Itaipuaçu (Oeste de Maricá, RJ). *Revista Brasileira de Geomorfologia*, Ano 9, 2, 75-82.
- Silvestre, C. P. 2013. *Estrutura interna da barreira holocênica e seus condicionantes geológicos (Maricá – RJ)*. Niterói, Brasil: Programa de Pós Graduação em Geologia e Geofísica Marinha da Universidade Federal Fluminense, Dissertação de Mestrado, 128p.
- Souza, R. S. 1988. Cimentação carbonática do beachrock de Itaipuaçu, Maricá, Rio de Janeiro, RJ. XXXV Congresso Brasileiro de Geologia, Belém, Pará, Vol.2, 975-987.
- Turcq, B., Martin, L., Flexor, J. M., Suguio, K., Pierre, C. and Tasayaco-Ortega, L. 1999. Origin and Evolution of the Quaternary Coastal Plain between Guaratiba and Cabo Frio, State of Rio de Janeiro, Brazil. *Environmental Geochemistry of Coastal Lagoon Systems*, Rio de Janeiro, Brazil, Série Geoquímica Ambiental, 6, 25-46.



# Morphodynamic characterization of beaches on a Pacific atoll island: Tetiaroa, French Polynesia

Matthieu Jeanson<sup>†</sup>, Edward J. Anthony<sup>‡</sup>, Samuel Etienne<sup>†§</sup>, Franck Dolique<sup>∞</sup>

<sup>†</sup>Laboratoire de Géomorphologie et Environnement Littoral, Ecole Pratique des Hautes Etudes, CNRS UMR 8586 Prodig, 15 Boulevard de la Mer, 35800 Dinard, France  
matthieu.jeanson@ephe.sorbonne.fr

<sup>‡</sup> Aix Marseille Université, Institut Universitaire de France, CEREGE UMR 34, Europôle Méditerranéen de l'Arbois, B.P. 80, 13545 Aix en Provence Cedex, France  
anthony@cerege.fr

<sup>∞</sup> Université Antilles-Guyane, Campus de Martinique, BP 7207, 97275 Schoelcher Cedex, France.  
fdolique@martinique.univ-ag.fr



[www.cerf-jcr.org](http://www.cerf-jcr.org)

<sup>§</sup> Laboratoire d'excellence "CORAIL", France



[www.JCRonline.org](http://www.JCRonline.org)

## ABSTRACT

Jeanson, M., Anthony, E.J., Etienne, S., Dolique, F., 2014. Morphodynamic characterization of beaches on a Pacific atoll island: Tetiaroa, French Polynesia. In: Green, A.N. and Cooper, J.A.G. (eds.), *Proceedings 13<sup>th</sup> International Coastal Symposium* (Durban, South Africa), *Journal of Coastal Research*, Special Issue No. 70, pp. 176-181, ISSN 0749-0208.

Beach profile types and wave characteristics were monitored in April 2013 on the small islet of Onetahi in the south Pacific coral reef atoll of Tetiaroa, French Polynesia, with the aim of characterizing atoll islet beach morphodynamics. Twelve beach profiles were each surveyed using a theodolite, and water levels and wave characteristics measured over four semi-diurnal tidal cycles using four miniature pressure sensors deployed in the subtidal zone. Water levels corresponded to a very narrow microtidal range (~0.2 m). Wave heights were extremely low throughout (<0.15 m), and spectral decomposition showed a mix between gravity and infragravity energy. The latter dominant at high water, whereas energy was virtually nil at low tide. The wave characteristics, which reflect significant filtering of large Pacific waves by the atoll reef, were not in phase with the intertidal beach morphology. These were interpreted as largely inherited from differential exposure to higher-energy events that occasionally impacted the atoll, notably Cyclone Oli in February 2010. Sand aprons in the lagoon, moving from the eastern to the southern and ultimately the western shores of the island in response to wave pumping, locally enhance build-up of the lower beach where shoreline orientation changes. Confrontation of these observations with long-term islet shoreline trends identified by Le Cozannet et al. (2013) suggests that high-energy event-scale changes and daily background beach cosmetic changes associated with subtidal sand apron mobility, and intertidal swash reworking during the narrow tidal excursion are embedded in long-term morphological stability likely hinged on sand circulation around the islet.

**ADDITIONAL INDEX WORDS:** coral reef, atoll, beach profiles, wave spectrum, infragravity energy, Cyclone Oli, Tetiaroa, French Polynesia.

## INTRODUCTION

The importance of physical processes in driving geological and ecological processes in reef environments has been abundantly recognized. To date, however, the majority of process studies have been conducted, on fringing and barrier reefs, with an initial clear focus on two themes: the mechanisms forcing lagoon circulation and water exchanges between ocean and lagoon, and transformation of wave energy across reef flats (e.g., Brander et al., 2004; Ogston et al., 2004; Storlazzi et al., 2005; Tamura et al., 2007; Jeanson et al., 2013). Less attention has been paid to atoll environments where a few studies have highlighted the importance of wave energy modulation and wave gradients in space and time (e.g., Kench, 1998; Kench et al., 2006, 2009; Samorson and Woodroffe, 2008). Unlike fringing and barrier reef systems, which may be sheltered by landmasses, isolated atolls are commonly equally exposed to ocean waves and high-energy events from all sectors and their oceanography is not influenced by inter-reef

hydrodynamic complexities associated with shallow barrier reef systems (Kench, 1998). Atolls and their associated islands or cays are thus essentially shaped by waves. Waves are responsible for transporting sediments, commonly generating focal points of wave convergence, for instance, that contribute to reshaping the islands and cays over time (Flood, 1986; Gourlay, 1988; Samorson and Woodroffe, 2008). Wave transformation patterns across the more commonly studied fringing reefs and barriers are important in elucidating reef and barrier stability. Similarly, wave transformations across atoll systems are important in determining sand distribution patterns, local variations in atoll island erosion and accretion, and long-term atoll stability. The low elevation of atolls is considered to be a source of vulnerability to the impacts of extreme wave events (Etienne, 2012; Collin et al., 2013), and to sea-level rise associated with climate change (Hopley et al., 2007; Le Cozannet et al., 2013). In this study, beach profile types and incident wave characteristics were monitored on an atoll island in Tetiaroa, French Polynesia (Figure 1a,b), with the aim of

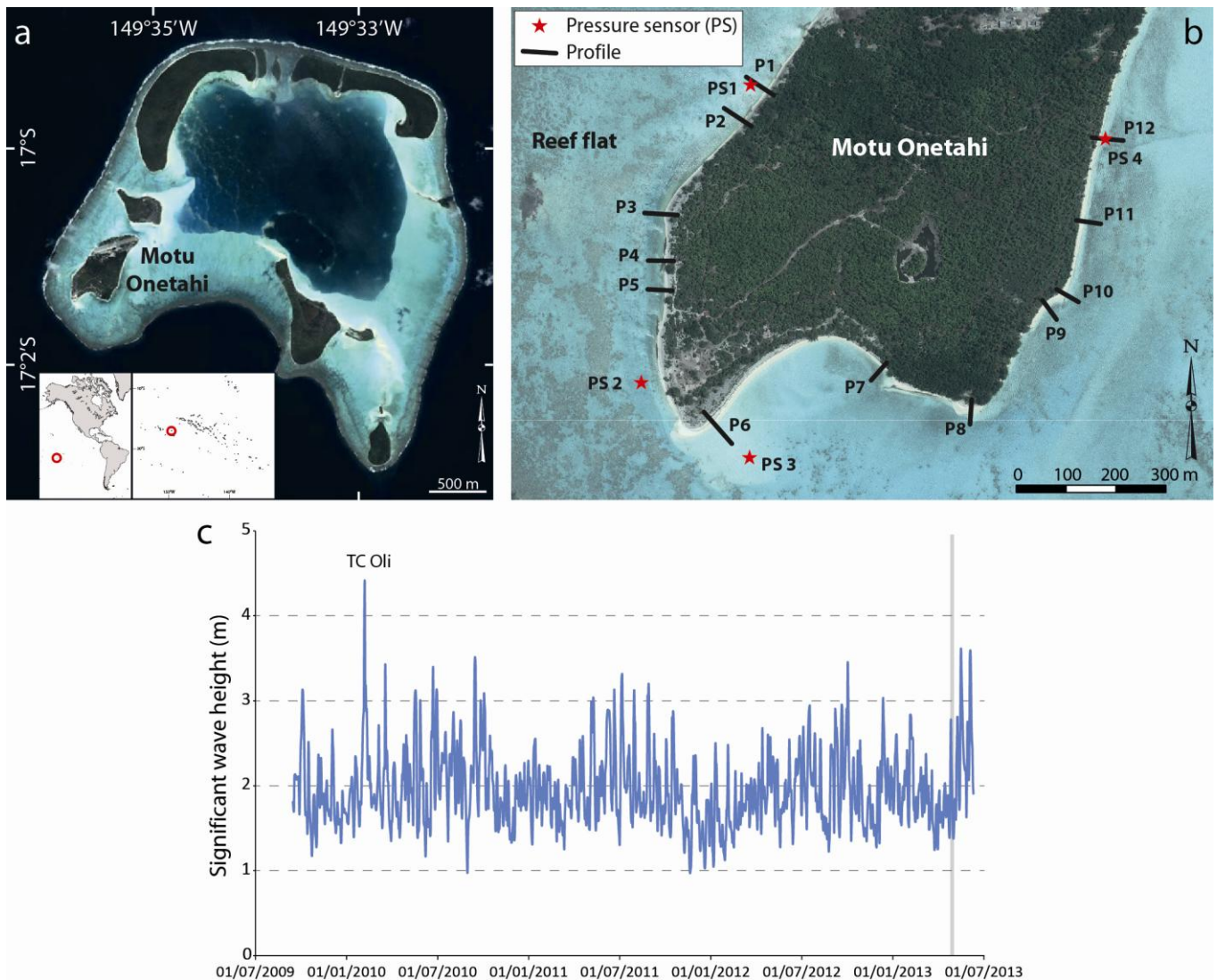


Figure 1. (a) Tetiaroa atoll in the South Pacific, and Motu (islet) Onetahi; (b) Locations of field measurement sites on Onetahi; (c) AVISO data from spatial altimetry showing deepwater significant wave heights from July 2009 to July 2013. Grey line on the right corresponds to the April 2013 survey period of beaches on Onetahi, TC = Tropical Cyclone.

identifying spatial variability in atoll island beach morphology and the characteristics of the incident wave spectrum. The results are then analysed with reference to the ambient wave exposure conditions of this cyclone-exposed Pacific atoll, and confronted with longer-term (multi-decadal) results on patterns of evolution recently documented for Tetiaroa by Le Cozannet *et al.* (2013).

## METHODS

Tetiaroa is a south Pacific atoll in the Society Islands of French Polynesia (Figure 1a), about 55 km from Tahiti. The atoll comprises 12 islets, covering a total surface area of 520 ha (5.2 km<sup>2</sup>), and occupies 22% of the reef flat (Le Cozannet *et al.*, 2013). The atoll has an outer reef perimeter of 28 km. The highest points of the islets are situated up to 3 m above the low tide level and are associated with wide coalescent sand aprons at less than 0.5 to 1.5 m depth at high tide. The mean tidal range is extremely narrow (> 0.5 m). The outer reef platform exhibits remnants of one or two peripheral ridges 1 to 2 m high. These are composed of rubble.

Parts of this reef platform comprise large boulders associated with high-energy events (Etienne, 2012; Collin *et al.*, 2013).

Tetiaroa experiences a tropical climate with a rainy season from November to April and a relatively dry season from May to October. East-southeasterly trade winds are dominant throughout the year (70-80%) and are strongest during the southern hemisphere winter months. During the rainy season, organized depressions can generate winds from north to northwest. The maximum wind speeds occur during the passage of tropical storms or cyclones between November and April. AVISO spatial altimetry data show that the South Pacific wave climate around Tetiaroa is characterized by moderate to high waves (1-3.5 m, Figure 1c). The wave climate is closely related to the ESE trade-wind regime. Wave heights and periods measured during breaking over the reefs surrounding Tetiaroa during the course of the fieldwork for this study, in April 2013, were in the order of 1-1.5 m and 7 to 12 s, respectively.

The experiment was conducted on Motu Onetahi (area: 0.745 km<sup>2</sup>; perimeter: 3.98 km), which lies in the southwest corner of the atoll (Figure 1a). Onetahi comprises beaches of fine carbonate sand. In order to monitor spatial variations in beach profile characteristics and wave energy gradients, 12 profiles were established in April 2013 on the west, south, and east shores of Onetahi using a theodolite, and four portable pressure sensors deployed in the subtidal zone in order to measure water level fluctuations and non-directional wave characteristics (Figure 1b). In the absence of benchmarks on the atoll, the beach surveys were referenced relative to the low water level at the time of the surveys (LWL), which coincided with average tide-range conditions. Given the very narrow tidal range, LWL is considered as an adequate reference. Self-recording miniature pressure sensors (length: 10 cm; diameter: 2 cm) were fixed on an iron rod driven into the subtidal sand apron fronting the beaches with the measuring gauge membrane located about 10 cm above the sandy surface. The gauges continuously measured tide and wave-induced pressure with the frequency of acquisition set at 2 Hz. The water level and wave characteristics were obtained from the measured

time series by spectral analysis using Fast Fourier Transforms. The Fourier coefficients of the free surface elevation fluctuations were obtained from corresponding coefficients computed which were from the pressure time series. To achieve this, the frequency dependent transfer function inferred from linear theory was used. Field observations were carried out on wave shoaling, breaking and swash, as well as on bedform mobility in the intertidal and subtidal zones.

## RESULTS

Onetahi is characterized by relatively narrow beaches ranging in width from 10 to 40 m between an upper beach platform or berm, that may be eroded, and LWL. The lower beach commonly grades into a subtidal sand apron (Figure 2). Beach rock is locally present near LWL on the southwestern shores of the islet. The beach profiles show significant differences in morphology (Figure 3) imprinted in alongshore variations. Profiles 1, 2, and 3 on the west shore of the islet exhibit a relatively well-developed linear morphology. The beach grades further southwest into a more or less pronounced concave morphology represented by profiles 4



Figure 2. Grounds photographs of Onetahi beaches: (a) low intertidal beach near profile P6 showing successive wrack lines associated with the swash excursion; (b) scarped upper beach near profile P12; (c, d) subtidal sand apron characterized by migrating low-amplitude (order of a few cm) sand waves. Sand apron is wider (as in d) where shoreline orientation changes, creating a shadow zone of accumulation.

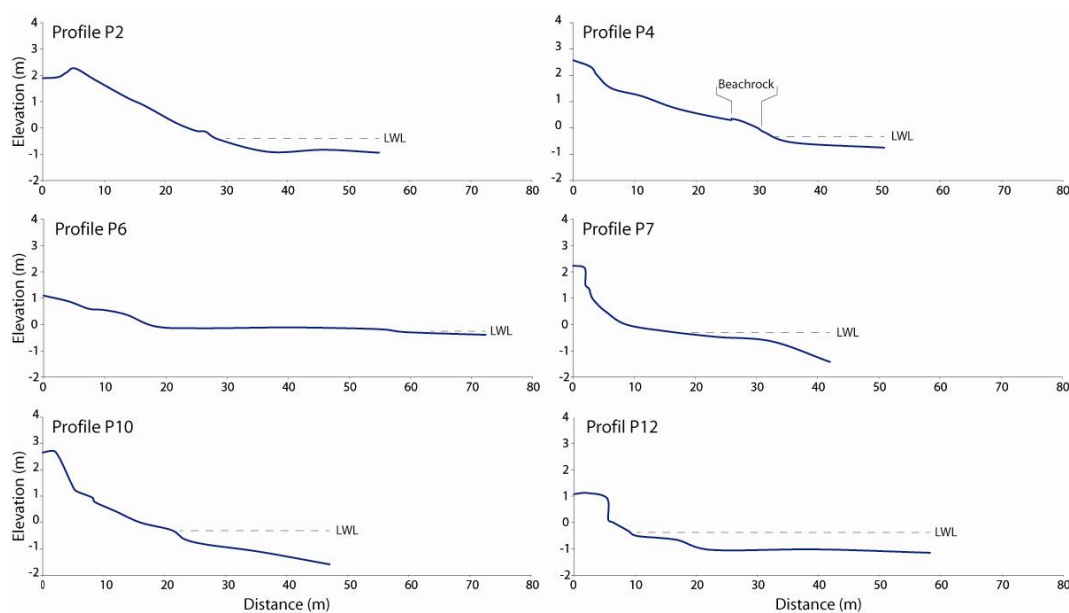


Figure 3. Representative profiles of beaches of Onetahi islet.

and 5. The upper beach elevation drops significantly along profile 6 at the southern apex of the islet, which exhibits a much lower gradient, the low beach grading into a well-developed sand-rich subtidal apron. Profiles 7 to 10 have similar elevation to those of profiles 1 to 5, and exhibit a concave morphology with a well-defined beach scarp on profiles 7, 9 and 10. The lower beach and subtidal sand apron are substantially lower in these sections. A further nuance is exhibited by profiles 11 and 12, which is characterized by a much lower upper beach elevation (1-1.2 m above LWL), and by scarping on profile 11.

Water level fluctuations occurred within a very narrow window that hardly exceeded 0.2 m over four tides (Figure 4a), confirming the very low tidal range hinged on that of the oceanic tide. The relatively good coherence of the water levels of the four pressure sensors suggests the quality of the measured data. PS 3 and 4 had a tendency to record slightly higher water levels ( $\sim 0.02$  m) than the others. Significant wave heights ( $H_s$ ) were low ( $< 0.15$  m) throughout the four sites (Figure 4b), but showed clear differences between PS 3 and 4, which recorded values 30-40% higher than those of PS 1 and 2.  $H_s$  decreased by half (max: 0.06 m) during tide 4. Mean zero up-crossing wave periods ( $T_z$ ) ranged from 5 s at low tide to 30 s at high tide (Figure 4c). The  $T_z$  patterns were similar for all four sensors during tide 1 but PS 1 and PS 2 showed overall lower  $T_z$  values during the next three tides. The  $T_z$  variation also tended to be narrower (5-15 s) during the last two tides. Spectral decomposition shows that wave energy was largely dominated by the infragravity band (Figure 4d). At high tide, peak energy for the four pressure sensors ranged between 0.006 and 0.015 Hz (i.e., periods between 160 and 60 s), with PS 3 and PS 4 having a higher energy density. A secondary peak between 0.035 and 0.05 Hz (30 to 25 s) was recorded by PS 1 and PS 2. This peak is much weaker in PS 3 and is absent in PS 4. At low tide, energy is virtually zero. Field observations show that swash wave periods were much lower (2-3 s) than the mean zero up-crossing wave periods shown in Figure 4c. Swash run-up on the beaches was weak (order of 0.1-0.2 m for each swash event) and was controlled by the narrow tidal excursion. Minor sand drift patterns associated with the narrow swash zone were observed. The

subtidal sand apron was commonly characterized by low-amplitude (order of a few cm) migrating dunes (Figure 2c,d).

## DISCUSSION

The AVISO wave climate offshore during the April 2013 experiment was characterized by significant wave heights of 1 to 3 m, which are the modal conditions in this part of the South Pacific. When compared with the data recorded by the pressure sensors show that Pacific waves (Figure 1c), field observations of wave characteristics beyond the reef platform (prior to and during breaking) are largely dissipated by the atoll reef, resulting in a highly attenuated regime in the lagoon (Figure 4). Variations in wave height, mean zero up-crossing periods, and infragravity energy were further strongly controlled by the semi-diurnal tidal variation.

At high tide, strong filtering of gravity waves occurred, resulting in the dominance of infragravity energy (Figure 4d). At low tide, almost complete dissipation resulted in a nearly nil energy spectrum. These aspects are similar to those described from other atoll reef settings (e.g., Kench *et al.*, 2006; Samosorn and Woodroffe, 2008), and highlight the importance of atoll morphology in modulating wave characteristics. This modulation feeds back, in turn, on beach morphology by reducing the amount of work done by the highly attenuated low-energy waves recorded on the atoll islet beaches. The measured wave characteristics and observed swash behaviour on the beaches are not in phase with the beach morphology, which is, undoubtedly, a heritage of the differential spatial impacts, on Onetahi, of higher-energy events associated with the ambient Pacific wave climate. The linear to convex beach profiles (Figure 3) such as profiles 1 to 3 (west shore), and 6 (south), represent stable to accretionary conditions which differ quite markedly from adjacent concave profiles such as 4, 5 (southwest), and 7 to 12 (southeast to east). The persistent eroded southeast and east shoreline beach morphology highlighted by these latter profiles may be the result of the impact of directional exposure of these islet shores to Tropical Cyclone (TC) Oli in February 2010. TC Oli was the most severe storm to hit French Polynesia since TC Zita and Arthur (both category 2 at their peak intensity), which affected the western part of French

Polynesia in January 2007 (Collin *et al.*, 2013). Etienne (2012) showed that the geomorphic impacts of TC Oli included submarine reef erosion (coral colony breakage and massive colony displacement), fine and coarse sediment transport and beach erosion, and the displacement of large coral blocks as seen at Tetiaroa atoll on the exposed northern outer reef fringes. Field observations in May 2010, July 2011 and November 2011 on the beaches of Tetiaroa show that the alongshore-alternating spatial pattern of beach morphology has been persistent. The alternations of accretion-type profiles (1-3) and concave profiles (4-5) on the usually less wave-exposed western flanks of the islet may reflect the effect of beachrock outcrops on the latter that act as obstacles to sand transfers between the subtidal sand apron and intertidal beach. Alongshore outcrops of beachrock may also create a channel-effect on the lower beach on backwash flows. Local variations in islet beach exposure may also be due to the effect of perforations in the reef rim during wave propagation towards the islet beaches.

The morphology of the beaches of Onetahi is also affected by sand mobility over the subtidal apron. This is associated with currents in Tetiaroa lagoon which were probably generated by a small degree of tidal pumping, but more likely, to a greater degree, by wave pumping. Wave pumping has been described from other reef settings, and is considered an extremely efficient mechanism in the hydrodynamic circulation of certain coral reef systems, especially where the tidal range is very narrow (Callaghan *et al.*, 2006; Nielsen *et al.*, 2008). The currents generated by this pumping process, in conjunction with the dominant Pacific wave directional window from the east-southeast, lead to significant mobility of sand in the lagoon. This is generally observed from the

eastern to the southern as well as southwestern shores of the island, as attested by the abundance of migrating subtidal bedforms (Figure 2c,d). According to this mechanism, the waves on the exposed side (east to southeast) are deemed to push water into the lagoon, while water leaves the lagoon on the less exposed side (west) for most of the tidal cycle duration. This may explain the slightly higher water levels, wave heights and larger energy recorded by pressure sensors PS 3 and 4 (Figure 4). This sand migration may slow down the recovery of the eroded eastern beaches as sand is slowly transported alongshore, and ultimately westward. Where shoreline re-entrants occur, sand drift leads, locally, to significant buildup of the subtidal beach, reducing the beach gradient and enhancing wave dissipation throughout the tide. Such local build-up in areas of shoreline orientation change also generates spits (as in the accreting section of profile 6 between adjacent eroding profiles), or small headland shoals (as in the case of profile 8).

The limited field data acquired in the course of this study and their confrontation with observations of longer-term patterns of evolution of Tetiaroa Atoll recently published by Le Cozannet *et al.* (2013) lead us to suggest that the long-term morphological evolution of Onetahi islet beaches, and probably other mid-oceanic atoll islet beaches, is determined mainly by high-energy events that leave lasting (order of years) morphological testimony. Cosmetic changes generated by modal swash zone processes and sand transport patterns generated by currents over the sand apron are progressively overprinted on such inherited antecedent morphology, which may, however, survive over long periods of modal wave energy. Le Cozannet *et al.* (2013) identified five cyclones between 1977 and 2001 with deepwater wave heights of

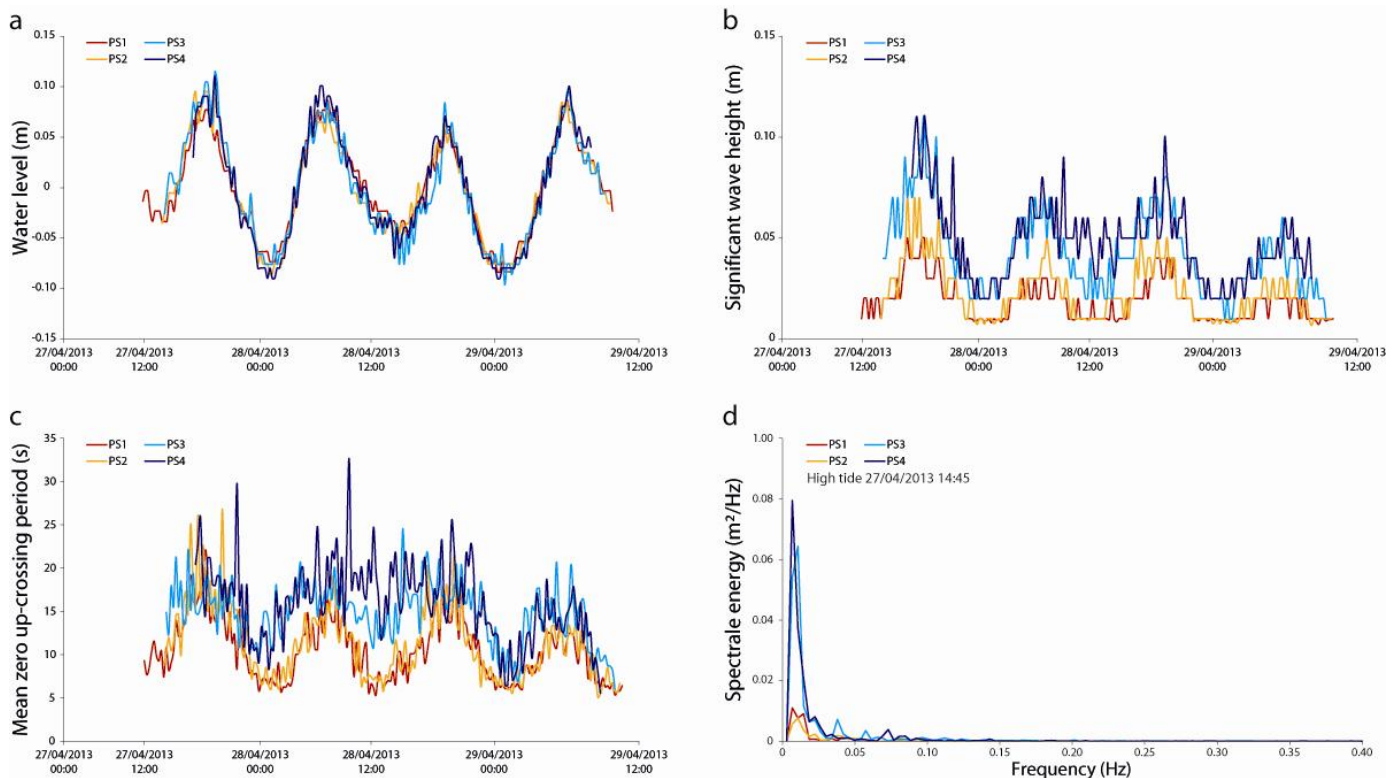


Figure 4. Water levels (a), significant wave heights (b), mean zero up-crossing wave periods (c) and energy spectrum (d) of the four experimental sites shown in Figure 1b.

ca. 3 to 8 m that were deemed to have impacted Tetiaroa. From an analysis of aerial photographs of Tetiaroa atoll islands over a 47-year period (1955-2002), these authors also found relatively insignificant changes in the overall size of the atoll (-0.01%), and showed that overall atoll island shoreline accretion and erosion were relatively balanced over this period, although individual islands exhibited significant differences. They also concluded that human influences and sea-level change have not been significant actors in recent atoll evolution. Onetahi islet exhibited the overall atoll trend with relatively minor changes over the 47-year period, thus showing a high degree of resilience. Since cyclone wave directional incidence on the atoll has been variable (Le Cozannet *et al.*, 2013), erosion and accretion may have been relatively balanced over time, although, locally, one or the other process has been dominant. Tying up our summary, observations with these long-term islet shoreline trends suggests that high-energy event-scale changes and continuous background beach cosmetic changes under highly dissipated wave conditions, associated with subtidal sand apron mobility and intertidal swash reworking during the narrow tidal excursion are embedded in long-term morphological stability. This stability is likely to be hinged on sand circulation around the islet, which is probably associated with long-term rotation dominated by a net sand flux from the eastern to the western shores. This constitutes a theme for future work.

## CONCLUSION

Beach profiles and wave characteristics were monitored in April 2013 on the small islet of Onetahi in the south Pacific coral reef atoll of Tetiaroa, French Polynesia, in order to characterize atoll islet beach morphodynamics. The recorded wave characteristics reflect significant filtering of large Pacific waves by the atoll reef, and also show that the eastern and southern shores of the islet are more exposed to waves. The highly attenuated waves recorded near the islet beaches in the course of four tides during which Pacific modal wave heights at breaking were about 1-1.5 m were not in phase with the intertidal beach morphology, which has been interpreted as largely inherited from differential exposure to higher-energy events that occasionally impact the atoll, notably Cyclone Oli in February 2010. Sand aprons in the lagoon, migrating in response to wave pumping, locally enhance build-up of the lower beach where shoreline orientation changes. When confronted with long-term islet shoreline trends identified by Le Cozannet *et al.* (2013), these observations suggest that high-energy event-scale changes and daily background beach cosmetic changes are embedded in long-term morphological stability that is likely associated with sand circulation around the islet. Future work on these beaches will seek to elucidate more clearly the link between beach profile changes, high-energy events, and wave-generated mechanisms such as wave pumping.

## ACKNOWLEDGEMENT

We wish to thank Hinano Bagnis and the NGO *Tetiaroa Society* for access to Tetiaroa Atoll and for their logistic support during fieldwork on Motu Onetahi. EA received support from an Institut Universitaire de France research grant for the field mission; SE and MJ from CPER Rinalpof (University of French Polynesia) allocated by the French Government and the Territory of French Polynesia.

## LITERATURE CITED

Brander, R.W., Kench, P.S., Hart, D., 2004. Spatial and temporal variations in wave characteristics across a reef platform, Warraber Island, Torres Strait, Australia. *Marine Geology* 207, 169-184.

- Callaghan, D.P., Nielsen, P., Cartwright, N., Gourlay, M.R., Baldock, T.E., 2006. Atoll lagoon flushing by waves. *Coastal Engineering*, 53, 691-704.
- Collin, A., Etienne, S., Planes, S., 2013. High-energy events, boulder deposits and the use of very high resolution remote sensing in coral reef environments. *Journal of Coastal Research*, SI 65, 690-695.
- Etienne, S., 2012. Marine inundation hazards in French Polynesia: geomorphic impacts of Tropical Cyclone Oli in February 2010. *The Geological Society of London, Special Publications*, 361, 21-39.
- Flood, P.G., 1986. Sensitivity of coral cays to climatic variations, southern Great Barrier Reef, Australia. *Coral Reefs*, 5, 13-18.
- Gourlay, M.R., 1988. Coral cays: products of wave action and geological processes in a biogenic environment. In: *Proceedings of the 6th International Coral Reef Symposium*, Townsville, Australia, pp. 491-496.
- Hopley, D., Smithers, S.G., Parnell, K.E., 2007. *The geomorphology of the Great Barrier Reef: development, diversity and change*. Cambridge University Press, Cambridge, 532p.
- Jeanson, M., Anthony, E.J., Dolique, F., Aubry, A., 2013. Wave characteristics and the morphology of pocket beaches fronted by a coral reef-lagoon system, Mayotte Island, Indian Ocean. *Geomorphology*, 182, 190-209.
- Kench, P.S., 1998. Physical processes in an Indian Ocean atoll. *Coral Reefs*, 17, 155-168.
- Kench, P.S., Brander, R.W., Parnell, K.E., McLean, R.F., 2006. Wave energy gradients across a Maldivian atoll: Implications for island geomorphology. *Geomorphology*, 81, 1-17.
- Kench, P.S., Brander, R.W., Parnell, K.E., O'Callaghan, J.M., 2009. Seasonal variations in wave characteristics around a coral reef island, South Maalhosmadulu atoll, Maldives. *Marine Geology*, 262, 116-129.
- Le Cozannet, G., Garcin, M., Petitjean, L., Cazenave, A., Becker, M., Meyssignac, B., Walker, P., Devilliers, C., Lebrun, O., Lecacheux, S., Baills, A., Bulteau, T., Yates, M., Wöppelmann, G., 2013. Exploring the relation between sea level rise and shoreline erosion using sea level reconstructions: an example in French Polynesia. *Journal of Coastal Research*, SI 65, 2137-2142.
- Nielsen, P., Guard, P.A., Callaghan, D.P., Baldock, 2008. Observations of wave pump efficiency. *Coastal Engineering*, 55, 69-72.
- Ogston, A.S., Storlazzi, C.D., Field, M.E., Presto, M.K., 2004. Sediment resuspension and transport patterns on a fringing reef flat, Molokai, Hawaii. *Coral Reefs*, 23, 559-569.
- Samosorn, B., Woodroffe, C.D., 2008. Nearshore wave environments around a sandy cay on a platform reef, Torres Strait, Australia. *Continental Shelf Research*, 28, 16, 2257-2274.
- Storlazzi, C.D., Brown, E.K., Field, M.E., Rodgers, K., Jokiel, P.L., 2005. A model for wave control on coral reef breakage and species distribution in the Hawaiian Islands. *Coral Reefs*, 24, 43-55.
- Tamura, H., Nadaoka, K., Pringit, E.C., 2007. Hydrodynamic characteristics of a fringing coral reef on the east coast of Ishigaki Island, southwest Japan. *Coral Reefs*, 26, 17-34.

# Middle shoreface sand transport under the influence of a river plume

Saulo Meirelles†, Alexander R. Horner-Devine‡, Martijn Henriquez†, Marcel Stive†, Julie Pietrzak†, Alejandro J. Souza∞

†Civil Engineering & Geosciences  
Technical University of Delft  
Delft, The Netherlands  
s.meirellesnunesdarocha@tudelft.nl

‡ Civil & Environmental Engineering  
University of Washington  
Seattle, Washington, USA  
arhd@u.washington.edu

∞ National Oceanography Center  
Joseph Proudman Building  
6 Brownlow Street  
Liverpool, UK  
ajso@noc.ac.uk



[www.cerf-jcr.org](http://www.cerf-jcr.org)



[www.JCRonline.org](http://www.JCRonline.org)

## ABSTRACT

Meirelles, S., Horner-Devine, A.R., Henriquez, M., Stive, M., Pietrzak, J., Souza, A.J., 2014. Middle shoreface sand transport under stratified regimes. In: Green, A.N. and Cooper, J.A.G. (eds.), *Proceedings 13<sup>th</sup> International Coastal Symposium* (Durban, South Africa), *Journal of Coastal Research*, Special Issue No. 70, pp. 182-186, ISSN 0749-0208.

Observations from a field experiment along the south-Holland coast, the Netherlands, were carried out in order to obtain new insights about the impacts of the Rhine ROFI (Region of Freshwater Influence) on the sand transport patterns. The net alongshore sand transport is generally governed by tides. The sediment concentration in the middle shoreface increased significantly with approaching waves of higher than ~1 m and  $T_{m0} > 5$  s. The southward net transport of the alongshore component does not agree with the literature. Modulations of the net cross-shore transport direction were observed. The net transport is more relevant during the neap tides where the velocity magnitudes are smaller.

**ADDITIONAL INDEX WORDS:** *NEMO project, Sand Engine, STRAINS Experiment, sediment concentration.*

## INTRODUCTION

This paper presents observations of the middle shoreface at the south-Holland coast. This middle shoreface is the transition zone between the surfzone and the lower shoreface and ranges from -8 to -20 m NAP (Normaal Amsterdams Peil which is the Dutch datum equal to approximately mean sea level) (Walstra, *et al.*, 1998). The above observations are part of the STRAINS experiment (STRAtification Impacts on Nearshore Sediment transport) (see Horner-Devine, *in prep*). The STRAINS experiment combines several projects: two of these are science projects, known as the NEMO project (Nearshore Monitoring and Modelling, see Stive *et al.*, 2013), looking at inter-scale coastal behaviour of this coastal stretch; and the STW project (Sustainable ROFIs) which investigates the effect of Regions Of Freshwater Influence (ROFIs) on sediment transport. The other project is the MOS2 project between the Port of Rotterdam and Deltares that studies the impacts of the expansion of the Rotterdam harbour.

The experiment was located ~10 km North of the mouth of the Rotterdam Waterway and was influenced by the Rhine ROFI (de Boer *et al.*, 2006), a tidally dominated river plume that extends along the Dutch coast. The Rhine ROFI plays a key role in the hydrodynamic circulation patterns along much of the coast and over the entire water column (Souza & Simpson, 1996, Simpson *et al.*, 1997).

The periodic stratification of the Rhine ROFI has been observed to affect the transport of the fine material (Simpson *et al.*, 1993,

Joordens *et al.*, 2001) and may also influence the coarser fraction. Work by Souza & Lane (2013) has shown how baroclinic effects in the Liverpool Bay ROFIs can dramatically change sediment pathways. Many researchers have focused on the sediment transport along the south-Holland coast (e.g., Stive & de Vriend, 1995; van Rijn, 1997; Walstra, *et al.*, 1998; van de Meene & van Rijn, 2000), however none have investigated how the Rhine ROFI impacts the sand transport in this region. The sediment transport on the middle shoreface is important since it is believed to be highly relevant to the sediment supply to the surfzone and the adjacent nourished coast. The response of the middle shoreface to changes such as sea-level rise and the Sand Engine (see Stive *et al.*, 2013) remains unclear.

This study aims to elucidate the qualitative contribution of the net sand transport during the field observations. The sampling strategy was planned such that a full spring-neap cycle was measured in the area under the Rhine ROFI influence.

## METHODS

### Study Area

The STRAINS experiment was located in the southern part of the Holland coast which is considered to be an uninterrupted straight sandy part of the Dutch littoral zone. The experiment site is in the middle of the domain NEMO project domain (see Figure 1), with its southern border approximately 10 km away from the Rotterdam Waterway. Scheveningen harbour is located at the northern limit, ~7.3 km from the deployment location. The offshore boundary of the experimental domain is near the depth contour of -20 m.

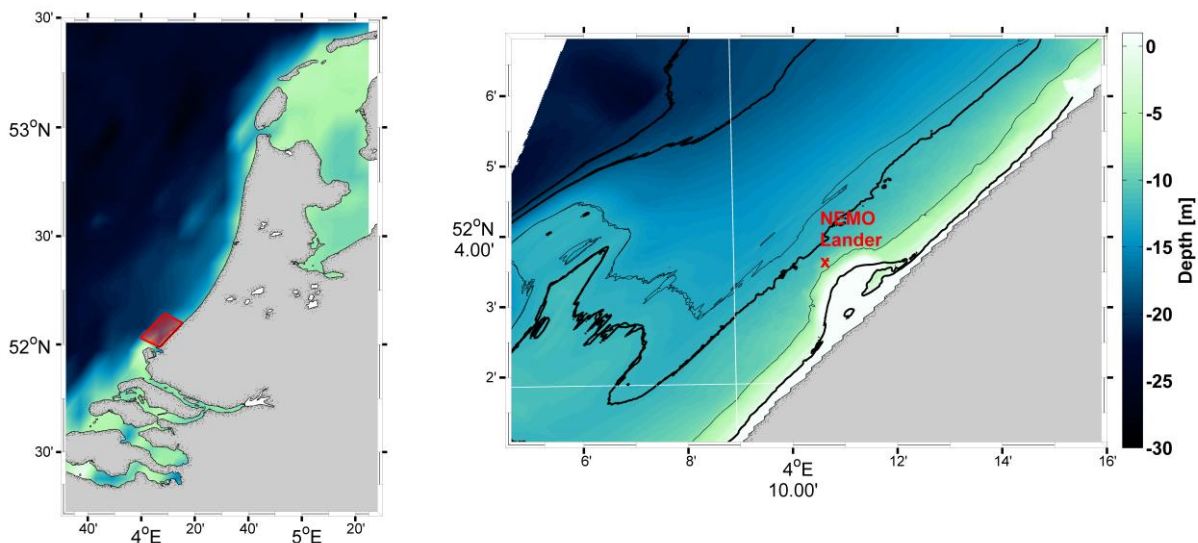


Figure 1: Left panel – The coast of the Netherlands with the experimental domain of the NEMO project delineated by the red rectangle. Right panel – detail of the NEMO domain depicting the site where the NEMO Lander was deployed. The hook-shaped mega-nourishment is the Sand Engine.

There is a large coastal perturbation within the experimental domain as a result of the Sand Engine (Stive *et al.*, 2013). This prominent feature is an artificial hook-shaped peninsula which was created to nourish the Dutch beaches (21.5 Mm<sup>3</sup> of sand) following the “building with nature” concept (de Vriend & van Koningsveld, 2012).

The Rhine ROFI influences the entire domain extending over 100 km along the coast (northward) and coincides with the NEMO domain which covers 30 km immediately northward. The stratified and mixed regimes vary according to the neap-spring cycles (Simpson *et al.*, 1993) and due to wind and waves (Souza *et al.*, 1997). Souza & James (1996) and De Boer *et al.* (2008) showed that advection and tidal straining modulate the stratification on the intra-tidal time scale, and Pietrzak & De Boer (*in prep.*) also showed that the wind plays an important role. Under normal conditions, fronts associated with the release of freshwater on the ebb tide are present.

### Experimental Set-Up

An instrumented bed-frame (coined the ‘NEMO Lander’) was deployed in February 2013 (see Figure 2). The Lander was at a nominal depth of -12 m NAP.

In the framework of the STRAINS experiment, other instruments were deployed besides the Lander. Among these were two bottom frames and two moorings that focussed on the ROFI hydrodynamics and suspended sediment concentrations. Due to the presence of the Sand Engine, Rijkswaterstaat (Dutch agency for water management) monitors the area intensively. Continuous observations are made with Radar, Wave Rider Buoy and ARGUS imaging system. Bathymetry data are collected periodically.

The NEMO Lander measured currents and waves for a duration of 21 days. Current profiles were measured with a downward-facing Aquadopp-HR which was mounted ~50 cm above the bed and recorded 1320 samples at 2 Hz every hour and averaged over

1 s. Current profiles throughout the water column were recorded from an upward-facing Aquadopp, which sampled at 1 Hz alternately with waves that were recorded at 2 Hz in burst of ~17 minutes. Near-bottom flow was also continuously measured using an ADV (Vectors) at 8 Hz. Density was estimated using Conductivity-Temperature-Depth (CTDs) sensors mounted in a mooring deployed in the vicinity of the NEMO Lander location. Bottom sediment samples were collected with a van Veen grab sampler.

### Intensity of acoustic backscatter

The acoustic backscatter signal from the downward-facing Aquadopp-HR was used to provide qualitative information of the coarse suspended material. The signal intensity in dB was corrected for acoustic spreading and sound attenuation in dB/m due to seawater, as follows:

$$I = 20 \log(R) + 2\alpha_w R \quad (1)$$

where  $I$  is the corrected echo intensity,  $R$  is the range along the acoustic beam given by  $r/\cos(25)$ . Here  $r$  is the distance from the transducer. The seawater absorption,  $\alpha_w$ , was equal to 1.262 dB/m (Lohrmann, 2001).

The correction for particle attenuation was not taken into account in this study, however, details on this methodology can be found in Thorne & Campbell (1992), Thorne *et al.* (1995), Merkelbach (2006) and Russo & Boss (2012). This is because the backscatter signal was not calibrated for the typical grain size found in the measurement site. Consequently, the conversion from acoustic signal in dB to concentration units (e.g., g/l) was not possible.



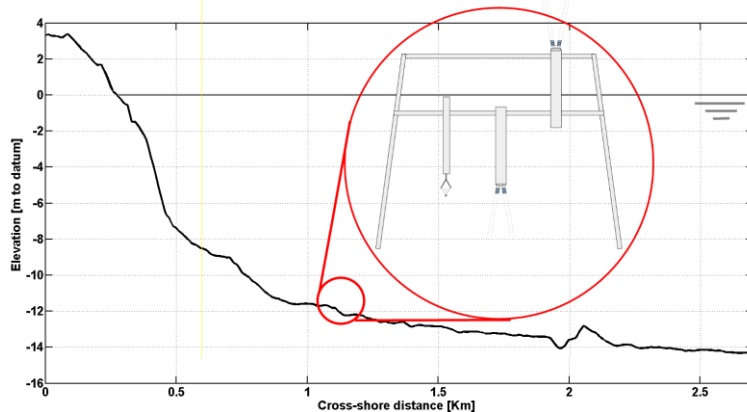


Figure 2: Left panel – Cross-shore profile where the NEMO Lander was deployed detaching a sketch of the instrumentation mounted on it. Right panel – picture of the NEMO Lander during its lowering. The bed-frame was deployed -12 m NAP (Normal Amsterdam Water Level) for about 21 days.

However, the aim of this work is to indicate the sediment concentration and net sediment transport direction. Therefore, the intensity of the corrected acoustic backscatter was summed along the vertical profile and used as an indicator for sediment concentration. To get an estimate for the transport direction, the velocity profile was multiplied by the intensity profile, and thereafter, summed over depth.

### Velocities

In order to extract the tidal signal from the ADV measurement, a running average of 10 minutes was applied in order to filter out, for example, orbital velocities due to waves and random fluctuations due to turbulence. The down-facing Aquadopp velocities were also averaged over 10 minutes.

### Conditions

Figure 3 shows the oceanographic conditions during the experiment. The measurement duration included the spring-neap-spring tidal cycles. During the spring tides, the vertical tide was approximately 2 m. The high water amplitudes ranged between 1.5 m and about -0.5 m during low water. Shortly before day 46, the higher low water reached -1.5 m, which was the minimum observed. During the neap tide, the vertical range varied between 1 m and 1.5 m. Water amplitudes ranged from around -0.5 to 0.7 m during low and high water, respectively. Those values are typical for the tidal range of the Netherlands.

The prevailing meteorological conditions were characterized by winds blowing from NNE-ESE. A moderate gale with winds up to 15 m/s was observed between day 55 and 57.

Waves were generally low, with wave heights  $H_{m0} < 1$  m. In the period between day 55 and 57, the waves reached  $H_{m0} \approx 1.5$  m. The variations of the significant wave height corresponded to the changes in wind speed. There were no significant differences between the peak period ( $T_p \approx 5$  s) and the mean wave period ( $T_{m0} \approx 5$  s) throughout the measurements. This suggests that the wave regime was driven by the local winds. The greatest wave frequency was from a Northerly direction.

### PRELIMINARY ANALYSIS

The results are shown in Figure 4. The alongshore-tidal velocities were in phase with the tidal surface elevations. The cross-shore tidal velocities were onshore prior to the peak of flood velocities. Thereafter, the cross-shore velocity was directed offshore until prior to the peak of the ebb velocities essentially keeping this modulation constant at every tidal period.

The daily average of the acoustic backscatter intensity followed the trend of the wave height (see Figure 4, second panel from top). The period of day 48 to 54, along with relatively low wave energy, produced relatively low acoustic backscatter intensities. On the contrary, the period of day 54 to 58, during the passage of the moderate gale, produced relatively high acoustic backscatter intensities.

On the time scale of hours, large peaks marked the acoustic backscatter intensities in the period of day 43 to 46 and day 58 to 61. The larger peaks occurred during the peak high tide velocities and the lower secondary peaks occurred during the peak low tide velocities.

The alongshore transport varied along with the tidal cycle and was dependent on the magnitude of tidal velocities (see Figure 4, third panel from top). The gradient of the curve in the graph is near to zero at the beginning of the experiment (year day  $< 47$ ). Therefore, the net alongshore transport is likely to be insignificant at that point. During the neap tide (after year day 49), a negative gradient is observed suggesting a net alongshore transport in the south direction. In the next spring tide (starting at approximately year day 57) the net alongshore transport was near to zero once again, as shown by the decreasing gradients in the graph.

According to Figure 4 (lower panel), the cross-shore transport within a tidal cycle was lower than the alongshore transport. The results indicate that before year day 46, the net cross-shore transport was negligible. Thereafter, a positive gradient is observed until year day 58. It can be inferred that a net transport in the shore direction took place during this period. This situation reverses between year days 58 and 61 when an offshore net transport is seen in the graph.

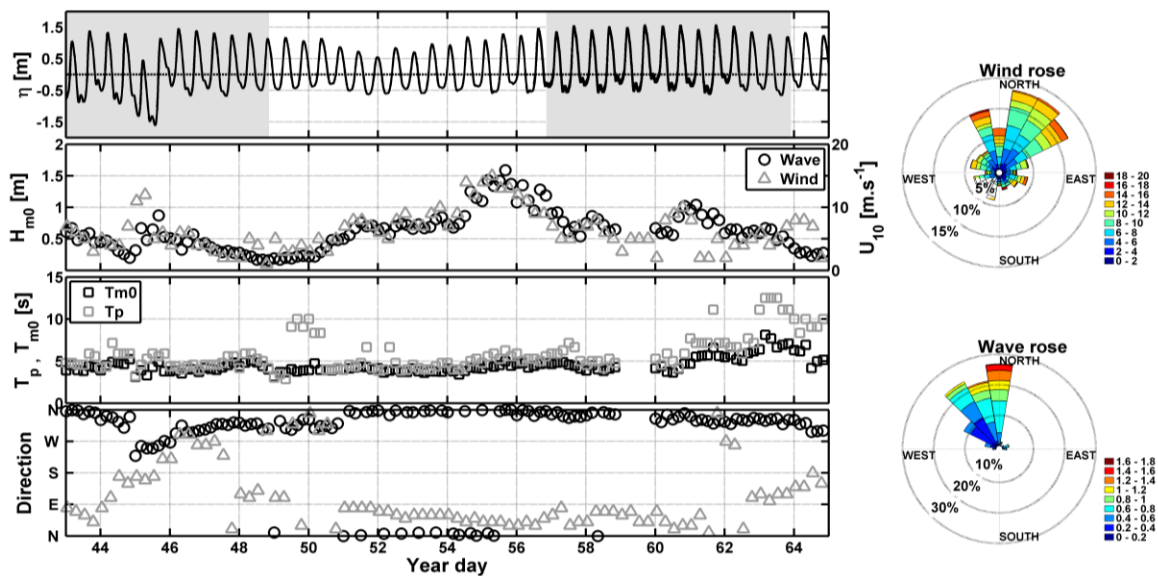


Figure 3: Oceanographic conditions during the STRAINS experiment. From top to bottom: [1] water elevation (the shaded area indicates spring tides); [2] significant wave height (left axis; black circles) and wind speed (right axis; grey triangles); [3] peak period,  $T_p$  (grey squares) and mean wave period,  $T_{m0}$  (black squares); [4] wind (grey triangles) and wave direction (black circles). The wind rose [m/s] and the wave rose [m] are shown on the right side.

### CONCLUSION AND DISCUSSION

It is possible to speculate that during the STRAINS experiment, the magnitude of the sediment transport on the middle shoreface (-12 NAP) followed the magnitude of the tidal velocities. Waves of  $H_{m0} > 1$  m increased the time-average sediment concentration. Over the 21 days of the experiment the net alongshore sediment transport was in the southwest direction presenting higher magnitudes during neap tide. Over the measurement period the net

cross-shore transport reversed to offshore for a period of 3 days.

The downward-facing Aquadopp measured the current profiles in the first 0.5 m above the bed. Transport estimated from these profiles included only the coarse suspended material and hence excludes the bed-load transport. Fine sediments were not incorporated in the present analysis mainly because acoustic signals reflect better on coarser sediment (in contrast to optical instruments).

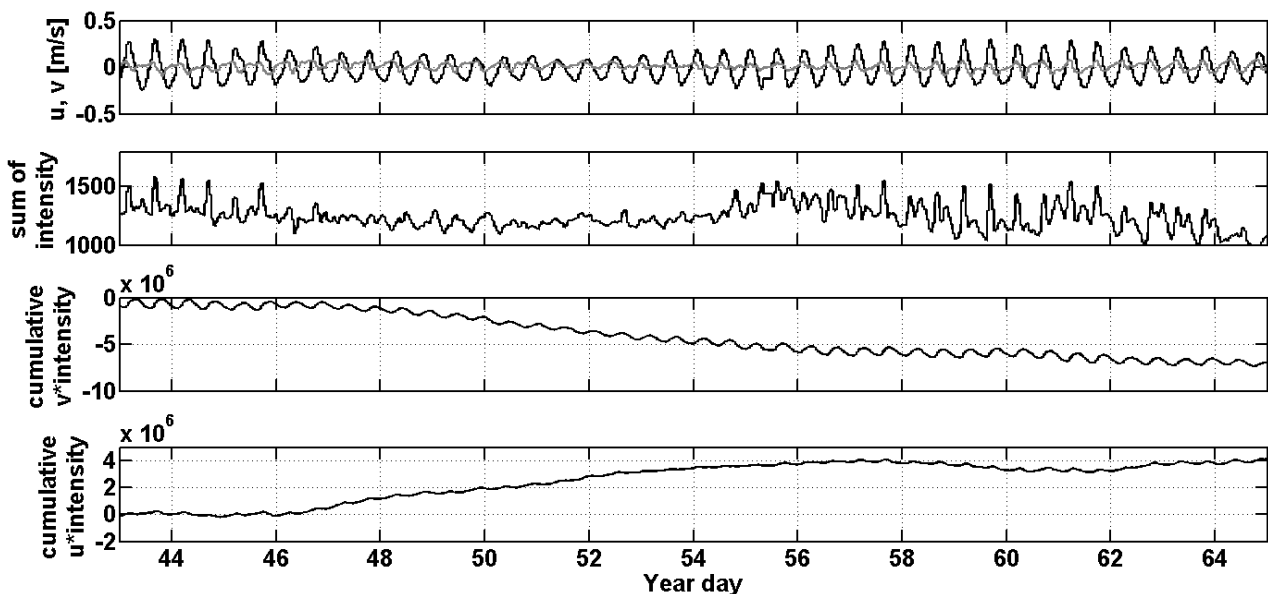


Figure 4: From top to bottom: [1] the tidal velocity, the black line represents the alongshore ( $v$ ) component and the light grey line the cross-shore ( $u$ ) one; [2] Sum of the acoustic backscatter intensity along the vertical profile; [3] cumulative alongshore transport; [4] cumulative cross-shore transport.

The southwest direction of the net alongshore transport is unlikely. Instead, a northeast direction is expected as is indicated in e.g., van Rijn (1997).

In conclusion the results show that a substantial amount of sand is locally re-mobilized during spring tides (note well-pronounced peaks of acoustic backscatter signal), however, that does not affect the net transport in general. On the other hand, the net transport is more relevant during the neap tide where the velocities are slower, but when tidal straining is likely to play a more dominant role. Waves also play an important role, especially in the volume of sand being transported.

The change in direction of the net cross-shore sediment transport between year day 58 and 61 is not directly attributed to either tides or waves and it is therefore the focus of future research. Connection to the dynamics of the Rhine ROFI will be investigated using field observations and model results.

### ACKNOWLEDGEMENT

The authors would like to thank the EU Research Council for funding this research, though the NEMO project. The authors are indebted to Rijkswaterstaat (in particular Ad Stolk) for providing the M/V Arca and its crew for carrying out the STRAINS Experiment. We also wish to thank The Port of Rotterdam, Wil Borst and Onno van Tongeren for their support. Alejandro Souza contribution was supported by NERC-NC through direct funding to NOC.

### LITERATURE CITED

- De Boer, G. J.; Pietrzak, J. D. and Winterwerp, J. C., 2006. On the vertical structure of the Rhine region of freshwater influence, 198-216. In *Ocean Dynamics*, 56, 3-4.
- De Boer, G. J., Pietrzak, J. D., & Winterwerp, J. C. 2008. Using the potential energy anomaly equation for tidal straining and advection of stratification in a ROFI. *Ocean Modelling*, 22, 1-2.
- De Vriend, H. J.; van Koningsveld, M., 2012. *Building with Nature: thinking, acting and interacting differently*, EcoShape: Dordrecht, The Netherlands, 39 pp.
- Joordens, J.C.A., Souza A.J. and Visser, A. W., 2001. The Influence of tidal straining and wind on suspended matter and phytoplankton dynamics in the Rhine outflow region, *Continental Shelf Research*, 21, 3, 301-325.
- Lohrmann, A., 2001. Monitoring sediment concentration with acoustic backscattering instruments. Technical Note 003, Nortek AS, Rud, Norway.
- Merckelbach, L. M., 2006. A model for high-frequency acoustic Doppler current profiler backscatter from suspended sediment in strong currents. *Cont. Shelf Res.*, 26, 1316-1335.
- Russo, C. R., Boss, E. S. 2012: An Evaluation of Acoustic Doppler Velocimeters as Sensors to Obtain the Concentration of Suspended Mass in Water. *J. Atmos. Oceanic Technol.*, 29, 755-761.
- Simpson J. H., Bos W. G, Schirmer F, Souza A. J., Rippeth T.P., Jones S.E., Hydes D., 1993. Periodic stratification in the Rhine ROFI in the north-sea. *Oceanologica Acta*, 16(1), 23-32.
- Souza, A. J., & Simpson, J. H. 1996. The modification of tidal ellipses by stratification in the Rhine ROFI. *Continental Shelf Research*, 16(8), 997-1007.
- Souza, A. J. and J. H. Simpson; 1997. Controls on stratification in the Rhine ROFI system, *Journal of Marine Systems*, 12, 311-323.
- Souza, A. J., Simpson, J. H. and Schirmer F.; 1997. Circulation in the Rhine ROFI. *Journal of Marine Research* 55, 2, 277-292.
- Souza, A. J., and Lane, A., 2013 Effects of freshwater inflow on sediment, *J. Operational. Oceanogr.*, 6, 1, 27-31.
- Stive, M. J. F. and De Vriend, H. J., 1995. Modelling shoreface profile evolution. *Marine Geology*, 126, 235-248.
- Stive, M. J. F., de Schipper, M. A., Luijendijk, A. P., Aarninkhof, S.G.J., van Gelder-Maas, C., van Thiel de Vries, J.S.M., de Vries, S., Henriquez, M., Marx, S., and Ranasinghe, R., 2013. A new alternative to saving our beaches from local sea-level rise: the sand engine. *Journal of Coastal Research*, 29(5), 1001-1008.
- Thorne, P. D. and Campbell, S. C., 1992. Backscattering by a suspension of spheres. *J. Acoust. Soc. Am.*, 92 (2), 978-986.
- Thorne, P. D., Holdaway, G. P., Hardcastle, P. J., 1995. Constraining acoustic backscatter estimates of suspended sediment concentration profiles using the bed echo. *J. Acoust. Soc. Am.*, 98 (4), 2280-2288.
- van de Meene, J. W. H., van Rijn, L. C., 2000b. The shoreface-connected ridges along the Dutch coast—part 2: morphological modelling. *Continental Shelf Research*, 20:2325-2345.
- van Rijn, L. C., 1997. Sediment transport and budget of the central coastal zone of Holland. *Coastal Engineering*, 32, 61-90.
- Visser, A., Souza, A. J., Hessner, K., and Simpson, J. H., 1994. The effect of stratification on tidal current profiles in a region of freshwater influence. *Oceanologica Acta*, 17, 369-381
- Walstra, D. J. R., van Rijn, L. C and Aarninkhof, S., 1998. *Sand transport of the middle and lower shoreface of the Dutch coast: simulation of SUNTRENCH-model and proposal for large scale laboratory test*, Report Z2378, Delft Hydraulics, Delft, The Netherlands.

# Megaripple dynamics on a dissipative sandy beach

Jon Miles<sup>†</sup>, Antony Thorpe<sup>†</sup>, Paul Russell<sup>†</sup>, Gerd Masselink<sup>†</sup>

<sup>†</sup>School of Marine Science and Engineering  
Plymouth University  
Plymouth, United Kingdom  
J.R.Miles@plymouth.ac.uk  
antony.thorpe1@plymouth.ac.uk  
P.Russell@plymouth.ac.uk  
gerd.masselink@plymouth.ac.uk



www.cerf-jcr.org



[www.JCRonline.org](http://www.JCRonline.org)

## ABSTRACT

Miles, J., Thorpe, A., Russell, P., Masselink, G., 2014. Megaripple dynamics on a dissipative sandy beach. In: Green, A.N. and Cooper, J.A.G. (eds.), *Proceedings 13<sup>th</sup> International Coastal Symposium* (Durban, South Africa), *Journal of Coastal Research*, Special Issue No. 70, pp. 187-192, ISSN 0749-0208.

Conventional force models of bedform dimensions link bedform wavelength and height to wave orbital excursion and wave orbital velocity. Self-organization models, however, suggest that bedform wavelengths either: grow, remain stable, or are wiped flat, but are unable to reduce in length. This paper presents measurements of megaripple evolution on a macrotidal sandy dissipative beach at Perranporth, England, using measurements from a Sand Ripple Profiler. Measurements were made as the tide flooded and ebbed over the instruments, producing a cross-section of the moving surf zone for 12 separate tides. Water depths varied from 1 to 6 m, and wave heights were up to 2.2 m. The data allowed megaripple dimensions to be observed with heights up to 30 cm and wavelengths up to 1.8 m. Megaripples were observed to grow *and* decay in both length and height. Megaripple spacing did not increase consistently with age of ripple. Megaripple lengths changed at rates of up to 5 cm/minute, and height changed at rates of up to 0.5 cm/minute. Maximum changes took place in large orbital velocity conditions. At orbital velocities > 0.5 m/s, ripples attempted to stabilize at a wavelength related to the orbital excursion, suggesting a forced mode. The most stable ripples had the greatest height and steepness. At orbital velocities < 0.5 m/s the spacing was greater than the orbital excursion, suggesting self-organized growth may be a more appropriate model for small orbital velocities.

**ADDITIONAL INDEX WORDS:** megaripples, self-organization, surf zone, bedforms, dissipative beach.

## INTRODUCTION

Bedforms develop on the seabed in sandy nearshore environments, and make an important contribution to bottom boundary layer hydrodynamics and sediment transport (Fredsoe and Deigaard, 1992). Bedforms take on a variety of length scales, including wave ripples, megaripples and sandbars. Megaripples are particularly important in the surf zone, as they are reasonably ubiquitous features (Clarke and Werner, 2004) and make an important contribution to the overall bed roughness (Gallagher *et al.*, 2003). Megaripples typically have heights of ~0.5 m and wavelengths of 1 to 5 m (Gallagher *et al.*, 1998).

Nielsen (1992) identified that wavelength and height of ripples increase as a function of orbital excursion and mobility number through empirical modeling of laboratory tests. However, field measurements of megaripple spacing in a saturated surf zone suggest that bedform spacings (i.e. wavelengths) are not solely dependent on forcing and are not well represented by these empirical models (Gallagher, 2003). Video observations of megaripples on a natural beach suggest that megaripple spacing increases with time (Clarke and Werner, 2004). Their results suggest that spacing growth is approximately linear for low age (0.01 days to 0.5 days) and is logarithmic beyond this. The scatter in the age/spacing relationship was large, but the bed state was uncorrelated with offshore wave height, period or direction.

Self-organization based models have provided a mechanism for

wavelength growth, and are able to predict both stable wavelengths and replicate growth characteristics (Coco and Murray, 2007; Gallagher, 2011). Gallagher (2011) modelled self-organized megaripples in the nearshore and found that the self-organization model of bedform spacing leads to the prediction that the megaripples will grow continually. The predictive curve takes a similar form to that of Clarke and Werner (2004). Werner and Kocurek (1999) modelled the evolution of bedform patterns for linear and oscillatory flows using defect dynamics and identified that for dunes in a linear flow their spacing increased with time. For oscillating flows in constrained channels, the ripple spacing was a function of the near-bed orbital excursion, with wavelength  $\lambda = 0.65 D$ , where  $D$  is the orbital excursion.

When hydrodynamic conditions change, it has been shown that there is potential for ripples to no longer be in equilibrium with forcing hydrodynamic conditions (Austin *et al.*, 2007) and that it takes a certain amount of time for the ripples to respond. This is also the case for megaripples and is a particular problem for macro-tidal beaches, which may experience relatively rapid changes of conditions as the tide floods or ebbs, and the wave height and position in the surf zone change. If the self-organization model is appropriate, the megaripples should grow when conditions are favorable, remain stable if the hydrodynamic conditions (mobility number) are too weak, or become washed flat if conditions become too energetic. In this paper, therefore, we look at observations of the growth rates of megaripples, in order to

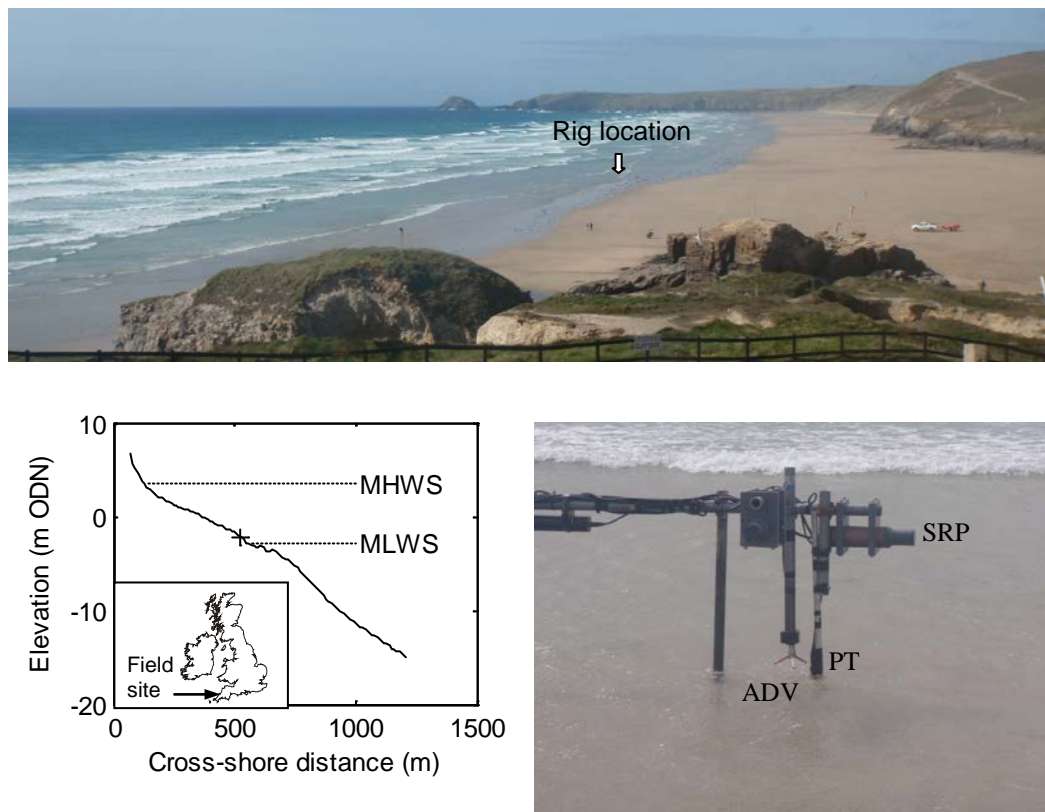


Figure 1. The field site at Perranporth (top), with approximate rig position indicated. The beach profile for the experiment period (bottom left) indicates the deployment location (+) relative to the position of Mean High Water Springs and Mean Low Water Springs (ODN refers to Ordnance Datum Newlyn, which is the approximate UK mean sea level datum). Instrumentation (bottom right) comprised a Sand Ripple Profiler (SRP), an Acoustic Doppler Velocimeter (ADV) and a Pressure Transducer (PT).

ascertain if they do indeed grow in length until flattened, or if they are capable of reducing in size.

### FIELD MEASUREMENTS

Field measurements were made at a high energy, macrotidal dissipative sandy beach at Perranporth (North Cornwall, UK) (Figure 1). Two separate field deployments were carried out in May and October, 2011, each for six separate high tides. The tides described in this paper are identified as tides 11 - 16 and 21 - 26, representing the May and October deployments, respectively.

Perranporth has a mean tidal range of 6.1 m, and a mean offshore wave height of 1.6 m (Davidson *et al.*, 1997). Sediments at the site are medium sand sized ( $D_{50} = 0.28$  mm). The beach profile was reasonably linear, with an average slope of 1/80.

Measurements were made by deploying an instrumented rig near the low water mark, roughly between the spring and neap low tide level. The instruments logged data as the tide flooded and ebbed over the rig, and this allowed measurements to be made in a variety of water depths from 1 to 6 m, and in a variety of wave/current conditions in the surf and shoaling zones.

A Sand Ripple Profiler (SRP) measured a line scan of seafloor elevation. The SRP was positioned 90 cm above the bed, and measured a 2-m on-offshore line, once per minute. Data was post-processed to give regular horizontal (on-offshore) spacing between points of  $\sim 1$  cm over the 2-m footprint of the scanner. Flow velocities were measured using an Acoustic Doppler Velocity meter (ADV) with a sensing volume 25 cm above the bed. Mean water depths and wave heights were measured using a Pressure Transducer (PT) deployed at bed level. Hydrodynamic data were recorded at 16 Hz for tides 11 - 16 and 8 Hz for tides 21 - 26. Data from the SRP, ADV and PT were divided into 10-minute runs for processing. Only hydrodynamic data were considered for runs when bedform data from the SRP was available. This limited the data set to water depths greater than 1 m, because only then was the SRP covered by water sufficiently to yield continuous information on the seabed topography.

### HYDRODYNAMICS

Hydrodynamic conditions for each of the tides recorded at the rig are shown in Figure 2. Each 'run' represents a 10-minute

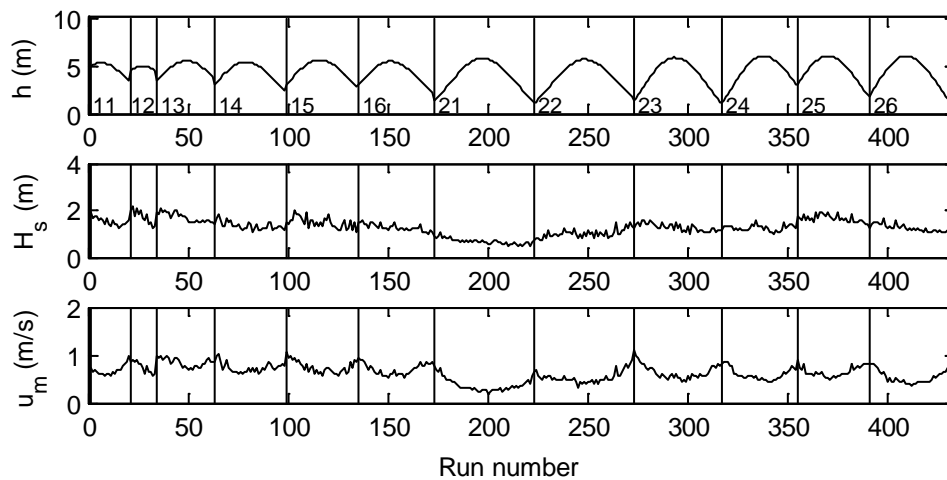


Figure 2. Hydrodynamic data: water depth  $h$ , wave height  $H_s$  and orbital velocity  $u_m$ . Each 'Run' represents a 10-minute section of data. Vertical lines indicate when instruments were dry at low tide or between deployments.

section of data. The run numbers start when data collection started on the first tide. The instruments were dry at low water and between experiments, and these time periods with no data have been removed. Average water depths ( $h$ ) were calculated for each run, allowing for offsets of instrument heights and atmospheric pressure. Significant wave heights ( $H_s$ ) were calculated with a correction for depth attenuation, and were in the range  $H_s = 0.48 - 2.19$  m. Wave periods ( $T_{1/3}$ ) indicate mostly swell waves for the measured tides, with  $T_{1/3} = 10 - 11$  s, although data were also collected for  $T_{1/3} = 7 - 8$  s (tides 25 and 26). The wave orbital velocity was calculated as  $u_m = 2\sqrt{\sigma_u^2}$  (where  $\sigma_u^2$  is the cross-shore velocity variance) following Masselink *et al.* (2007).

### BEDFORMS

Sequential profiles from the SRP were time-stacked and are displayed as an image plot to illustrate different features of interest (Figure 3). Megaripples migrated shoreward for the majority of the time (Miles *et al.*, 2013), i.e., crests move down the image as

time passes. In terms of ripple wavelength, the plots show that there are instances where (a) megaripples increase in wavelength (e.g., latter part of tide 25) and (b) reduce in wavelength (e.g., tide 11).

Crawford and Hay (2001) identified that the heights of wave ripples and megaripples could be determined directly from the variance of the bed-level trace as  $\eta = \sqrt{8(\sigma^2(z))}$ . To separate out the megaripple component, each bedform scan was first low-pass filtered below a cut-off of 35 cm to remove wave ripples and reduce noise. The Crawford and Hay (2001) calculation was carried out on the filtered elevation data, to give megaripple heights.

Megaripple wavelengths were calculated from an autocorrelation of the scan, to identify the distance from crest to trough (Masselink *et al.*, 2007). The wavelength was quantified as twice the spatial lag corresponding to the strongest negative autocorrelation peak. The maximum value was limited by the requirement for at least half a wavelength to be visible in the scan.

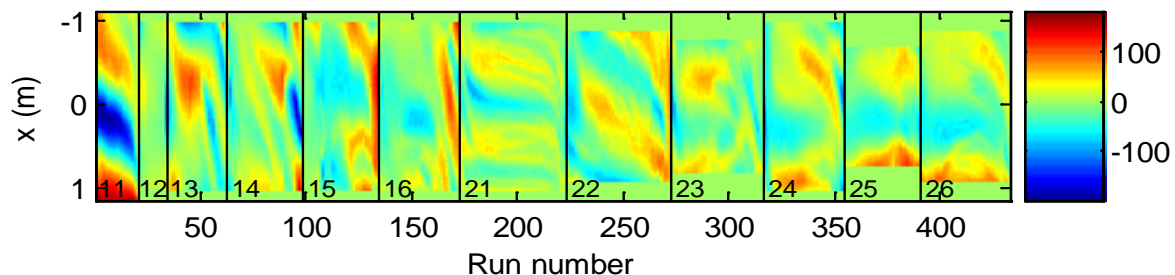


Figure 3. Timestacks of bedforms measured by the SRP. Colourscale indicates vertical relief with +ve (-ve) values in red (blue) and a vertical scale of mm. The SRP is fixed at ' $x = 0$ ', and the shore is towards the base of the plot. Data are shown for one scan per minute. Run numbers shown are synchronous with hydrodynamic data and 1 run = 10 minutes. On-offshore data resolution is 1 point per cm. Vertical lines indicate the gaps when the instruments were dry after/before each tide or between deployments.

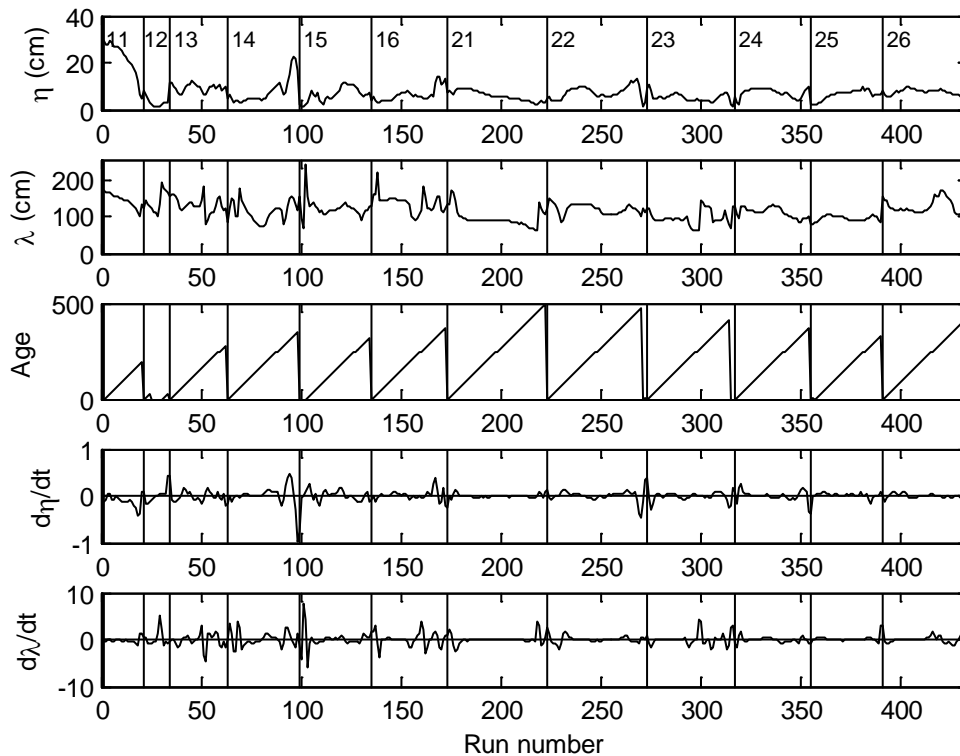


Figure 4. Bedform parameters: height  $\eta$  and wavelength  $\lambda$  of megaripples. The age of the megaripples is the time since the bed was last flat (minutes). Rates of change of height ( $d\eta/dt$ ) and wavelength ( $d\lambda/dt$ ) have units of cm/minute.

Megaripple age was quantified for each run as the length of time since either (a) the bed was last flat, or (b) since the bed had last been dry at low tide or between experiments. A 'flat' bed was determined as when the bedform height was  $< 2$  cm. In reality, a flat bed was rare, so the general 'age' statistic for this position in

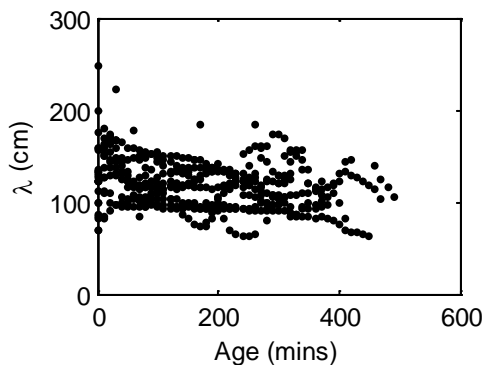


Figure 5. Wavelength of bedforms ( $\lambda$ ) as a function of age, timed from either the previous flattening or from the first measurement after the previous low tide.

the intertidal is most dependent on the time since the last dry period at low tide. Megaripple ages therefore reach a maximum of  $\sim 500$  minutes at this location due to the semi-diurnal tide.

Megaripples ranged in height from flat bed to 30 cm (Figure 4). They were  $> 10$  cm for 13.4% of the time, and were greater than 6.6 cm high for 50% of the time. Megaripple wavelengths were typically in the range 1 to 2 m. When megaripple heights were  $> 6.6$  cm (i.e. the highest 50% of megaripples), the average megaripple wavelength was 1.25 m. Both growth and decay of elevation and wavelength are evident. The changes, in general, appear to happen towards the start and end of the tides, when water is most shallow and orbital velocities are largest.

Megaripple wavelength is plotted against megaripple age in Figure 5. Examining the sequences of data points in the plot, it is possible to identify sets of data where the spacing is both increasing and decreasing. Despite large scatter in the data, there is some evidence that the megaripples reduce in size over the time of a tide. The average reduction in spacing is 3.5 cm/hr, but the r-squared is low (0.075).

The rate of change of megaripple morphology (height and wavelength) is related to the orbital velocity (Figure 6). The most rapid changes appear to occur when the orbital velocity is largest. Changes of both wavelength and height can be positive (up to 5 cm/min) or negative (5 cm/min), suggesting that the rates of growth and decay are broadly similar. However, a large orbital velocity does not necessarily mean that wavelength change will take place, and in many instances no change takes place when the

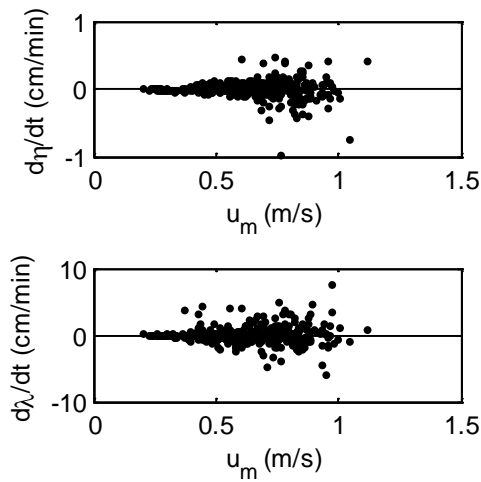


Figure 6. Rate of change of megaripple height ( $d\eta/dt$ ) and megaripple wavelength ( $d\lambda/dt$ ) (from SRP data) plotted against orbital velocity ( $u_m$ ) (from ADV data). Positive (negative) values indicate growth (decay) of the megaripples.

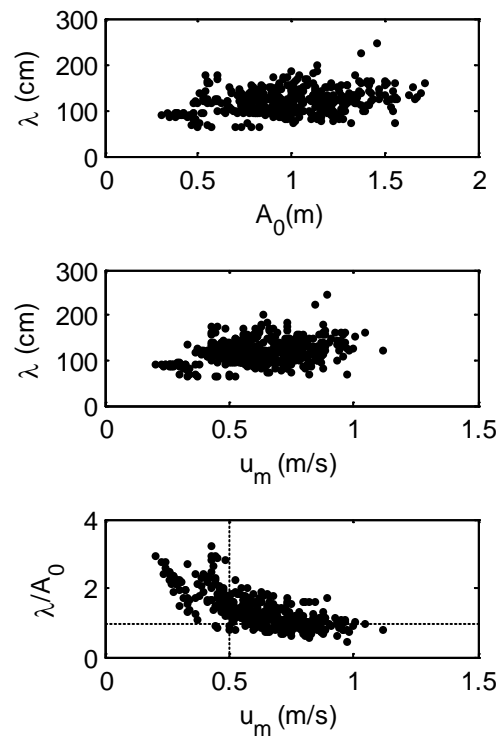


Figure 8. Megaripple wavelength ( $\lambda$ ) as a function of orbital semi-excursion ( $A_0$ ) and orbital velocity ( $u_m$ ).  $\lambda/A_0$  is a normalised excursion, frequently used in predictive models of bedform wavelength. As  $u_m$  increases,  $\lambda/A_0$  stabilises at  $\sim 0.95$ .

orbital velocity is large. This may occur because the ripples are in equilibrium with the hydrodynamic forcing.

The rates of wavelength change, may be considered in terms of the megaripple height and steepness (Figure 7). The fastest changes in wavelength (positive and negative) happen when the megaripple height is smallest ( $< 10$  cm). Rates are least when the ripple height and steepness is largest. This suggests that as the megaripples grow in height and become steeper, a stable condition is gradually reached.

There is evidence that the megaripple wavelengths are attempting to match the conditions dictated by forcing hydrodynamics (Figure 8). Wavelength broadly increases with both wave semi-orbital excursion (calculated as  $A_0 = u_m T/2\pi$

following Soulsby (1997)) and with orbital velocity, but the scatter is large. At low values of  $u_m$  ( $< 0.5$  m/s), the normalised wavelength  $\lambda/A_0$  increases with reducing  $u_m$ . As  $u_m$  increases,  $\lambda/A_0$  appears to stabilise at a value of roughly 0.95. The implication of this is that as the orbital velocity increases, the bedform spacing becomes more constrained by the orbital velocity. An approximate cut off value between the two regimes appears to exist at  $u_m = 0.5$  m/s.

### DISCUSSION

The data presented here are limited to a relatively narrow on-offshore scan length ( $\sim 2$  m), and only one on-offshore line was possible (spatially). Measured and quantified information on the orientation of the ripples and on the three-dimensional patterns is therefore not available. Low tide wading observations suggest that the ripple crests were reasonably shore parallel and were approximately constant in the alongshore direction for distances of several meters. The adjacent crests and troughs evident in the SRP data are therefore taken as a reasonable indication of megaripple wavelength.

It is possible that the bedforms are responding to mean flows as well as orbital velocities. The orientation of the megaripples indicates that these are responding to on-offshore flows, rather than longshore flows. The magnitude of the oscillatory on-offshore flows is large (up to 1 m/s) compared to the mean flow (up to 0.3 m/s). The influence of these different parameters is difficult to separate in the surf zone, because the strongest offshore flows (e.g., undertow) occur at the same time as the

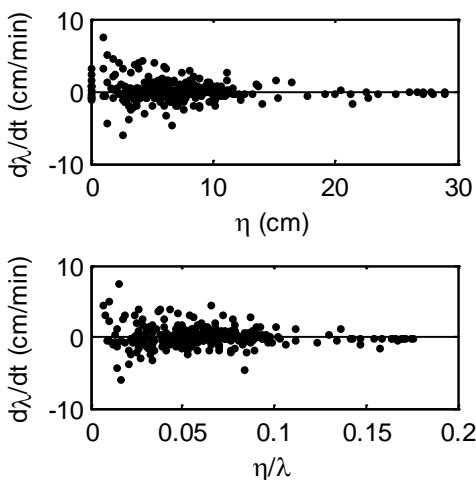


Figure 7. Rate of change of megaripple wavelength ( $d\lambda/dt$ ) plotted against megaripple height ( $\eta$ ) and steepness ( $\eta/\lambda$ ).



largest orbital velocity. In this investigation, the magnitude of the mean cross-shore flow was small compared to the orbital velocity, and the orbital flow was assumed to be the most important hydrodynamic variable driving wavelength change.

Austin *et al.* (2007) identified that a lag can occur between the forcing hydrodynamics and the bed response. The large tidal range at this site means that putting the ripple age concept into context is complex, because the water depth and flow velocity conditions vary as the tide floods and ebbs over the sensors. However, the results do indicate that there is a reduction in the rate that bedforms change shape as they become more developed (i.e., rates of wavelength change reduce as the ripples become higher and steeper). Any lags between flow conditions and bedform will therefore be short lived during the early developmental phases, but exacerbated when bed features are well developed.

Self-organisation models (e.g., Gallagher *et al.*, 2011) suggest that megaripple spacing grows in time under oscillatory flow conditions, but that the bed will either not change if a threshold shear stress is not passed, or be flattened if the flow strengths are too strong. The self-organisation approach offers an interesting solution to the observations of Clarke and Werner (2004), which identified megaripple spacing increasing with ripple age. The rates of growth and decay of megaripple spacing identified here are ~5 cm per minute. These growth rates are similar to those reported by Clarke and Werner (2004) for newly developing ripples. Their predictive curve suggests growth rates of 5 cm/minute for ripple age of 21 minutes, 0.28 cm / minute for ripple age of 0.5 days (720 minutes). The main difference identified here is that the ripples appear to decay as well as grow.

Werner and Kocurek (1999) indicate that the wavelength of dunes in unidirectional flows increase with age, but that for reversing flows the wavelength is related to the orbital excursion (D), and may be approximated by  $\lambda = 0.65 D$  (equivalent to  $\lambda/A_0 = 1.3$  in this data) for small  $\lambda$ . In the present contribution, when orbital velocities are large, the value of  $\lambda/A_0$  appears to reach a minimum of ~0.5 (i.e.  $\lambda = 0.25 D$ ), and stabilises at approximately 0.95 (i.e.  $\lambda = 0.475 D$ ), suggesting that the forced model may be appropriate at high orbital velocities. For smaller orbital velocities, the value of  $\lambda/A_0$  is larger, and increases as the orbital velocity reduces. The wavelengths are over-sized for a given orbital excursion, possibly indicating self-organised growth is dominating over the forced relationship with  $A_0$ . It is possible that an evolved self-organization model, or a combined forced / self-organized model may cope with the differences and offer a more consistent predictor for ripple behavior than the existing individual approaches.

## CONCLUSION

Megaripples were observed to grow and decay in both length and height. Megaripple spacing did not increase consistently with age of ripple. Megaripple lengths changed at rates of up to 5 cm/minute, and height changed at rates of up to 0.5 cm/minute. The greatest changes took place in larger orbital velocity conditions. In high orbital velocity conditions ( $u_m > 0.5$  m/s), the ripples attempted to stabilize at a wavelength related to the orbital excursion, suggesting a traditional empirical forced model may be appropriate. In lower orbital velocities ( $u_m < 0.5$  m/s), the relative spacing of wavelength to orbital excursion increased, suggesting self-organized growth may be prevalent. The most stable ripples had the greatest height and steepness.

## ACKNOWLEDGEMENTS

The fieldwork for this project was funded by a partnership grant

from the UK Natural Environment Research Council (NERC) and the UK Royal National Lifeboat Institution (RNLI), 'Dynamics of Rip Currents and Implications for Beach Safety (DRIBS)', (NERC ref: NE/H004262/1).

## LITERATURE CITED

- Austin, M.J., Masselink, G., O'Hare, T.J., Russell, P.E., 2007. Relaxation time effects of wave ripples on tidal beaches. *Geophysical Research Letters*, Vol 34, L16606, doi:10.1029/2007GL030696.
- Clarke, L.B., and Werner, B.T., 2004. Tidally modulated occurrence of megaripples in a saturated surf zone. *Journal of Geophysical Research*, 109. C01012, doi: 10.1029/2003JC001934
- Coco, G. and Murray, A.B., 2007. Patterns in the sand: From forcing templates to self-organisation. *Geomorphology*, 91. 271-290.
- Crawford, A.M., and Hay, A.E., 2001. Linear transition ripple migration and wave orbital velocity skewness: Observations, *Journal of Geophysical Research*, 106, 14,113-14,128.
- Davidson, M., Huntley, D., Holman, R., George, K., 1997. The evaluation of Large Scale (km) Intertidal Beach Morphology on a Macrotidal Beach Using Video Images. *Proceedings Coastal Dynamics 97*. 385-394.
- Fredsoe, J. and Deigaard, R., 1992. *Mechanics of coastal sediment transport*. Advanced series on ocean engineering, vol. 3. World Scientific. London.
- Gallagher, E.L., 2003. A note on megaripples in the surfzone: evidence for their relation to steady flow dunes. *Marine Geology*, 193. 171-176.
- Gallagher, E.L., 2011. Computer simulations of self-organised megaripples in the nearshore. *Journal of Geophysical Research* 116 F01004. Doi:10.1029/2009JF001473.
- Gallagher, E.L., Elgar, S., Thornton, E.B., 1998. Megaripple migration in a natural surfzone. *Nature*, 394. 165-168.
- Gallagher, E.L., Thornton, E.B., and Stanton, T.P. 2003. Sand bed roughness in the nearshore. *Journal of Geophysical Research* 108 C2 3039 doi:10.1029/2001JC001081.
- Masselink, G., Austin, M., O'Hare, T. and Russell, P., 2007. Geometry and dynamics of wave ripples in the nearshore of a coarse sandy beach. *Journal of Geophysical Research* 112, C10022, doi:10.1029/2006JC003839.
- Miles, J., Thorpe, A., Russell, P., and Masselink, G., 2013. Observations of bedforms on a macrotidal dissipative beach, *Proceedings of Coastal Dynamics 2013*, Bordeaux.
- Nielsen, P., 1992. *Coastal bottom boundary layers and sediment transport*. Advanced series on ocean engineering. World Scientific. London.
- Soulsby, R.L. 1997. *Dynamics of Marine Sands*, Thomas Telford Publications.
- Thorpe, A., Miles, J., Masselink, G., Russell, P., Scott, T., and Austin, M., 2013. Suspended sediment transport in rip currents on a macrotidal beach. *Proceedings 12<sup>th</sup> International Coastal Symposium* (Plymouth, England), *Journal of Coastal Research*. Special Issue No 65. 1880-1885. doi: 10.2112/SI65-318.1.
- Werner, B. T., and Kocurek, G. 1999. Bedform spacing from defect dynamics. *Geology* 27 (8), 727-730.

# Influence of storms on coastal retreat in SW Spain

María Puig†, Laura del Río†, Theocharis A. Plomaritis†, Javier Benavente†

†Dpt. Earth Sciences, CASEM  
University of Cadiz  
11510 Puerto Real, Cádiz, Spain  
[maria.puig@uca.es](mailto:maria.puig@uca.es)



[www.cerf-jcr.org](http://www.cerf-jcr.org)



[www.JCRonline.org](http://www.JCRonline.org)

## ABSTRACT

Puig, M., Del Río, L., Plomaritis, T.A., Benavente, J., 2014. Influence of storms on coastal retreat in SW Spain. *Proceedings 13<sup>th</sup> International Coastal Symposium* (Durban, South Africa), *Journal of Coastal Research*, Special Issue No. 70, pp. 193-198, ISSN 0749-0208.

Natural and anthropogenic controls contribute to coastal change at diverse temporal and spatial scales. This study presents an analysis of storminess and a correlation with the medium-term shoreline erosion rates in two sand spits of the Gulf of Cadiz (SW Spain). Recession rates were assessed by means of aerial photographs and orthophotographs considering the dune foot as an appropriate proxy. Storm events were obtained from a combination of coastal wave buoy data and the hindcast database of the HIPOCAS project. The characteristics of the storms were compared with shoreline changes determined using the aerial photographs, and the correlation between them was estimated and discussed. The best agreement between storms and shoreline change was observed in section 1 of Sancti Petri sand spit, while Valdelagrana sand spit showed a lower dependence between shoreline erosion and storminess. This is related to the contrasting exposure of both sites, with Sancti Petri being more exposed and thus more sensitive to storm impact. It is suggested that the main causes of retreat in Valdelagrana are human interventions performed on the coast and in the nearby rivers (breakwaters, jetties and dams). Nevertheless, storminess contributes to modulate recession rate, so that erosion rates increase when the number of storms is higher.

**ADDITIONAL INDEX WORDS:** *Coastal evolution, coastal storms, coastal erosion, aerial photographs, Gulf of Cadiz.*

## INTRODUCTION

Over past decades, the interest in knowledge of shoreline behavior has increased due to climate change predictions and population growth in coastal areas. Medium-term shoreline recession is the result of a large number of mechanisms and processes (Komar, 2000). Numerous authors have studied the contribution of natural and anthropogenic factors in shoreline change. Within natural controls, geological framework (e.g. Riggs *et al.*, 1995; Jackson *et al.*, 2005; Rossi *et al.*, 2011), sediment supply (e.g. Aagaard *et al.*, 2010; Lima *et al.*, 2013) and wave climate (e.g. Houser *et al.*, 2008; Anderson *et al.*, 2010; Jiménez *et al.*, 2012) are the main contributing agents. Based on these controls, numerous models have been developed in order to predict future shoreline changes (e.g. Cowell *et al.*, 1995; Frazer *et al.*, 2009; Davidson *et al.*, 2010).

In the Gulf of Cadiz (SW Spain), coastal evolution and storm characterization have been well studied (e.g. Reyes *et al.*, 1999; Benavente *et al.*, 2002a; Plomaritis *et al.*, 2010; Rangel-Buitrago and Anfuso, 2011; Del Río *et al.*, 2013). However, there are no detailed studies on the main factors that contribute to beach behavior and how storms control coastal evolution.

In this context, in the present study a comparison between medium term shoreline changes and wave climate data is undertaken and the influence of storminess in coastal evolution is analysed and discussed.

## STUDY AREA

The study area constitutes two sites located in the eastern part of the Gulf of Cadiz (SW Spain) (Figure 1). Tides in this area are mesotidal and semidiurnal. Swell waves are dominant approaching from the W and SW, with an average significant wave height of about 1 m and associated periods of 5-6 seconds (Benavente *et al.*, 2002b).

Both test sites comprise well-developed sand spits with contrasting exposure and development characteristics. The Valdelagrana sand spit is protected as dominant waves coming from W and SW are refracted around Cadiz tombolo (Figure 1). It has a total length of 7 km and it is considered to be a single unit because it is limited by hard structures (Guadalete river jetties at the northernmost end and Matagorda shipyard dykes at the southern one). The northern part is heavily urbanized, while the central and southern sectors belong to the Cadiz Bay Natural Park. On the other hand, the Sancti Petri sand spit is a natural exposed area situated in the southern part of the Bay of Cadiz. It extends from Punta Poniente to Punta del Boqueron for 7.7km, also being part of Cadiz Bay Natural Park (Figure 1). Both areas are occupied by a sandy beach and dune ridges, backed by extensive salt marshes.

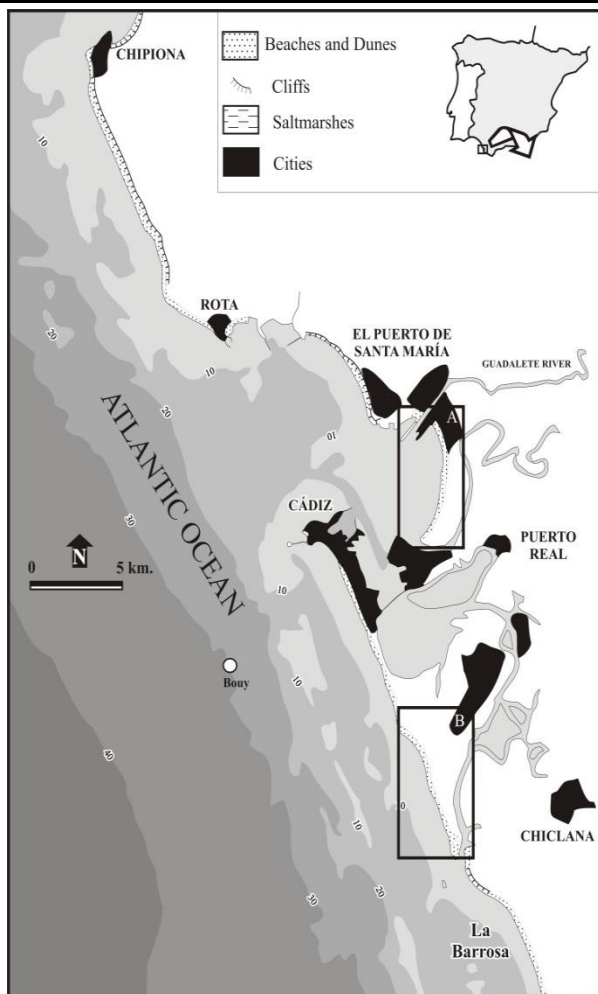


Figure 1. Location of the study area and the analysed geomorphological units A (Valdelagrana sand spit) and B (Sancti Petri sand spit).

## METHODS

### Aerial photographs

Changes in shoreline position were measured on several sets of aerial photographs and orthophotographs dating between 1956 and 2010, at scales ranging from 1:15,000 to 1:33,000. For each test site an average of 15 photographs were used. Georeferencing, digitization of shoreline proxies and calculation of shoreline changes and associated uncertainty were performed in GIS environment following the methodology described in Del Río *et al.* (2013). According to this, the dune foot (considered as the contact line between the backshore and the foredune) was chosen as the preferred proxy to reflect storm impacts in the study area. Its limitation was that the significant time lag for showing accretion was not considered relevant, as the periods between photographs were longer than a year (Boak *et al.*, 2005).

Rates of shoreline change were obtained calculating the mean slope of the regression line between consecutive sets of photographs. Here, the Digital Shoreline Analysis System (DSAS) extension for ArcGIS™ (Thieler *et al.*, 2009) was used for measuring the distance between shorelines along shore-normal

transects spaced at 20 m intervals. Although these transects were created along the entire coast, the surroundings of tidal creeks were not included.

### Storm record

The storm record was obtained by combining the coastal wave buoy of Cadiz (Puertos del Estado, Figure 1) and the hindcast database of the HIPOCAS project (Guedes-Soares *et al.*, 2002). These two datasets were inter-calibrated for the overlapping period, using the peak over threshold (POT) analysis, with emphasis on agreement during storms (Del Río *et al.*, 2012).

Storm waves in the study area approach mainly from WSW, with a typical wave height over 2 m. Based on the above characteristics, the storm events were identified for the periods from sets of aerial photographs. A restriction on storm duration of at least 72 hours was used. Furthermore, consecutive storm events with calm periods of less than 72 hours between them were considered as a single storm-group event.

In order to characterize storm-induced impacts in shoreline change, different parameters were determined, namely the total, peak and average wave energy, wave energy at high tide, wave power and wave erosivity, as well as storm duration and the number of storms for each time interval between consecutive sets of photographs. Wave erosivity factor is considered as an indication of the erosive potential of incident waves and details of its formula are described in Benavente *et al.* (2000).

Finally, the above parameters were normalized for the corresponding period between photographs and a Pearson correlation analysis was performed between the results and the calculated shoreline changes along both study areas.

## RESULTS AND DISCUSSION

### Shoreline change

Figure 2 and Table 1 show the mean shoreline trends of both study areas during the period 1956-2010. Since this analysis follows the results of Benavente *et al.* (2006) and Del Río *et al.* (2013), this work summarized the results of previous studies in order to compare them with the storm record.

Both areas were divided into three sections based on different evolutionary behavior. Overall, the northern part of Valdelagrana sand spit (section 1) showed an accretionary trend with stabilization in the past two decades. Section 2 experienced a similar accretion between 1956 and 1977, and then defined erosion was measured reaching up to  $-10.1$  m/y in 1984. The southern part (section 3) was characterized by extreme erosion that appeared between 1976 and 1977 ( $-10.6$  m/y) after the construction of the above mentioned jetties (Martinez-del-Pozo *et al.*, 2001). This erosion was intensified between 1984 and 1985 with an average retreat rate of  $-22.6$  m/y. From 1998 onwards, erosion slowed down and in the recent years it increased again, reaching values of  $-7.6$  m/y.

On the other hand, Sancti Petri sand spit was characterized by alternating behavioral styles along its coast. The frequency of spatial changes in shoreline trend increased in the southern part of the spit due to the presence of washover fans which modified dune morphology, thus creating advances and retreats in the dune foot. The first section, which extended from the northern end to the southern one and had the longest stretch located in the middle portion of the area (Figure 2), indicated an erosional nature with a mean retreat rate of  $-0.96$  m/y. Section 2, situated in the northern part of the spit, recorded accretion between 1956 and 1986,

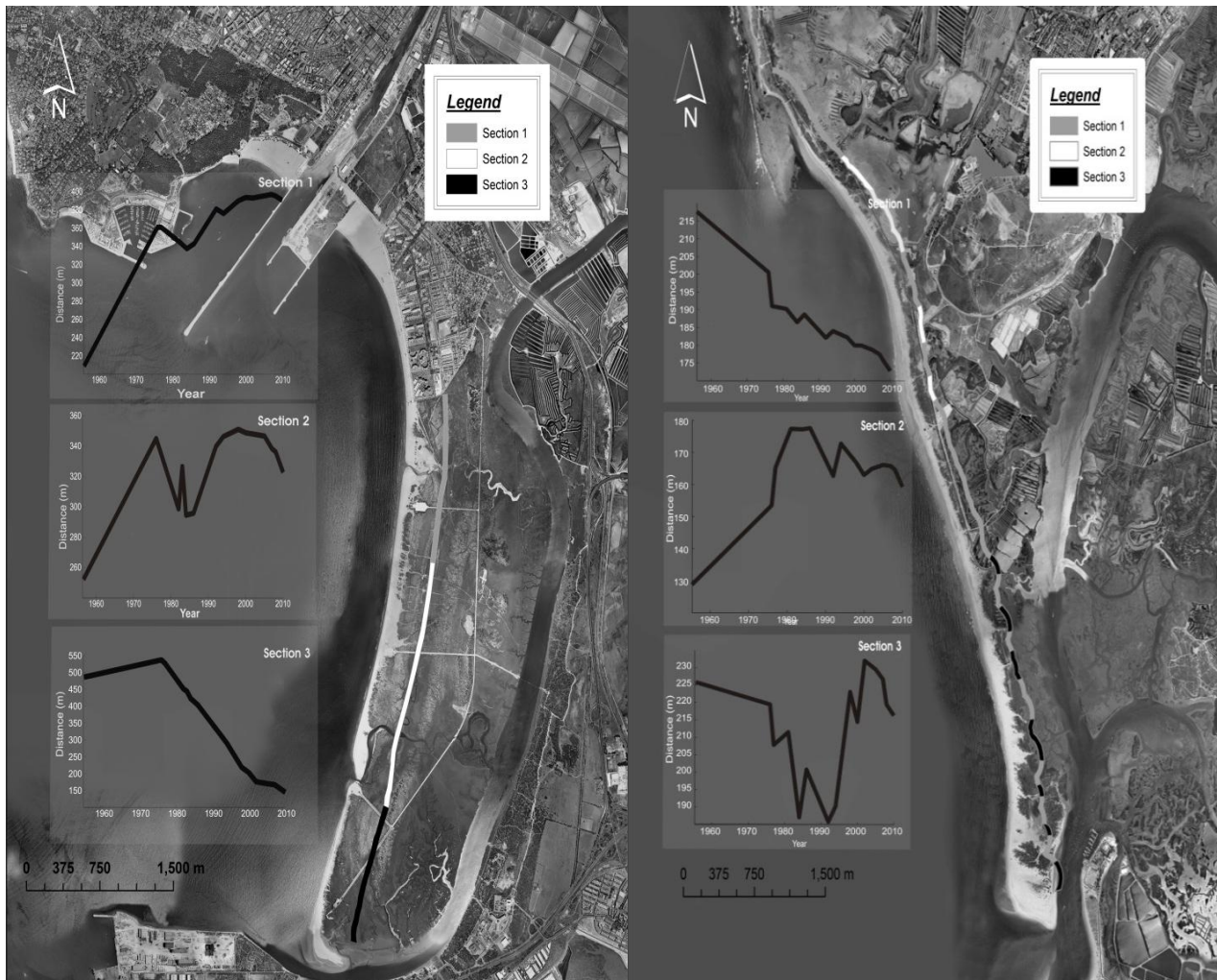


Figure 2. Shoreline trend of the study sites (left: Valdelagrana; right: Sancti Petri).

Table 1: Shoreline changes in the study area (\*Recession rate for the period 1982-1984, as the 1983 aerial photographs were not available for this area). For details on the assessment of uncertainty, see Del Río *et al.*, (2013).

Valdelagrana change rate (m/yr)				Sancti Petri change rate (m/yr)				
Period	Uncertainty	Sect. 1	Sect. 2	Period	Uncertainty	Sect. 1	Sect. 2	Sect. 3
1956-1976	0.11	7.75	4.87	1956-1976	0.11	-1.07	1.21	-0.29
1976-1977	1.94	0.01	-7.60	1976-1977	1.97	-6.53	11.76	11.46
1977-1982	0.34	-3.21	-7.78	1977-1981	0.46	-0.25	3.05	0.94
1982-1983	2.05	-	5.38	1981-1984	0.65	-1.10	-0.05	-7.48
1983-1984	1.78	-3.30*	-10.09	1984-1986	1.23	1.40	0.25	8.74
1984-1985	2.12	6.32	1.55	1986-1992	0.24	-1.05	-2.38	-2.31
1985-1992	0.22	5.48	6.32	1992-1994	0.70	0.97	5.14	1.88
1992-1994	0.75	-2.60	3.35	1994-1998	0.33	-0.45	-1.49	7.81
1994-1998	0.34	3.46	1.18	1998-2000	0.95	-1.18	-2.03	-5.62
1998-2000	0.93	1.95	-1.21	2000-2002	0.72	-0.03	0.87	7.98
2000-2002	0.70	-0.24	-0.37	2002-2005	0.29	-0.41	0.42	-0.81
2002-2005	0.29	0.79	-0.45	2005-2007	0.61	-0.62	-0.19	-1.38
2005-2007	0.61	0.74	-4.14	2007-2008	1.11	-1.70	-1.04	-7.12
2007-2008	1.11	-1.28	-2.14	2008-2010	0.35	-1.49	-2.72	-1.54
2008-2010	0.25	-2.47	-6.79					

followed by gradual erosion with an average recession rate of -0.4 m/y. Finally, the third section corresponded to washovers situated in the southern part of the spit. Here shoreline trends were highly variable, with recession rates ranging from -0.3 to -7.5 m/y and accretion rates between 0.9 and 11.5 m/yr.

### Storm analysis

The temporal evolution of the energetic parameters (energy, wave power and erosivity) of the investigated database shows a slightly negative trend with similar patterns during the period of study (Figure 3). Overall, energy and wave power decreased gradually from 1956 to 1990 reaching the lowest values in the 1980s-90s. From then on, they increased gently with peaks of high energy and wave power between 1994-1998 and 2008-2010. On the other hand, the wave erosivity factor is characterized by a clearly negative trend with the same peaks along the study period. These peaks correspond with the negative NAO (North Atlantic Oscillation) phases reported in Ribera *et al.* (2011) and Rangel-Buitrago and Anfuso (2012).

Figure 4 shows 11 of the 14 parameters that were calculated on the storm dataset. It presents the peak, mean and total energy at high tide, number of storms and storm duration for the Valdelagrana sand spit, and the peak, mean and total energy and erosivity for the Sancti Petri sand spit during the periods between photographs. The main differences between the patterns of the two study areas were observed from 1977 to 1992 (periods 3 to 7 in Valdelagrana and 3 to 6 in Sancti Petri) due to photo availability.

A total of 111 storms were recorded within the studied time span, with a total duration of 756 days. The distribution of storminess along the periods is variable (Figure 4). Periods with more than three storms per year and 18 days of duration correspond to the following time spans: 1984-1985 (Valdelagrana), 1984-1986 (Sancti Petri), 2002-2005 and 2008-2010. These results match the years of high Storm Power Index obtained by Rangel-Buitrago and Anfuso (2012) and the study of Almeida *et al.* (2011) that analyse the storminess in Faro, located in the western Gulf of Cadiz. Nevertheless, other years with high storm record according to these studies (1987, 1989, 1995, 1996 and 1997), which correspond to the periods 1985-1992 (Valdelagrana), 1986-1992 (Sancti Petri) and 1994-1998, are not reflected in the present work.

Concerning the rest of parameters showed in Figure 4, overall, energy at high tide presents more variable pattern than energy and erosivity. Although they differ from the general storm pattern, the

peaks of total parameters, i.e. 1984-1985 (Valdelagrana), 1984-1986 (Sancti Petri), 2002-2005 and 2008-2010, coincide with stormy periods as expected. On the other hand, mean and peak energy at high tide show the same distribution, although differences are found between both study areas during 1983-1984. Consequently, a stable distribution with lower variations is observed in Sancti Petri sand spit. Finally, mean energy and erosivity show a stable pattern, while peak energy and erosivity present important variations in the past decades.

### Correlation analysis

Through use of a Pearson correlation analysis between the above mentioned parameters and shoreline changes, it was found that the mean energy at high tide showed the best correlation values, which are presented in Table 2. Within the Valdelagrana geomorphological unit, the central part (section 2) exhibited the best correlation, with a lower Pearson value ( $r=-0.52$  and  $P$ -value=0.04), followed by the southern part (section 3) ( $r=-0.41$  and  $P$ -value=0.12) and the northern part (section 1) ( $r=-0.20$  and  $P$ -value=0.48). The low correlation value in section 1 reveals the influence of other factors in shoreline changes, such as the construction of jetties in the mouth of the Guadalete River, that affects shoreline behavior by protecting the coast from wave incidence, and the urban construction on a tidal creek that led to dune development. The moderate degree of correlation observed in the rest of the area reflected certain dependence between variables. This was expected in section 2 as it is the most exposed sector of the sand spit to wave attack. Nevertheless, other factors not included in the analysis could affect the central and southern parts, namely the lack of sediment supply due to dam construction in the Guadalete river basin and the jetties at its mouth (Martinez-del-Pozo *et al.*, 2001; Benavente *et al.* 2006).

In Sancti Petri sand spit the correlation analysis reveals that the

Table 2: Pearson correlation values between shoreline change and mean energy at high tide for the study areas

		Correlation	P-value
Valdelagrana	Section 1	-0.20	0.48
	Section 2	-0.52	0.04
	Section 3	-0.41	0.12
Sancti Petri	Section 1	-0.60	0.02
	Section 2	0.46	0.09
	Section 3	-0.46	0.09

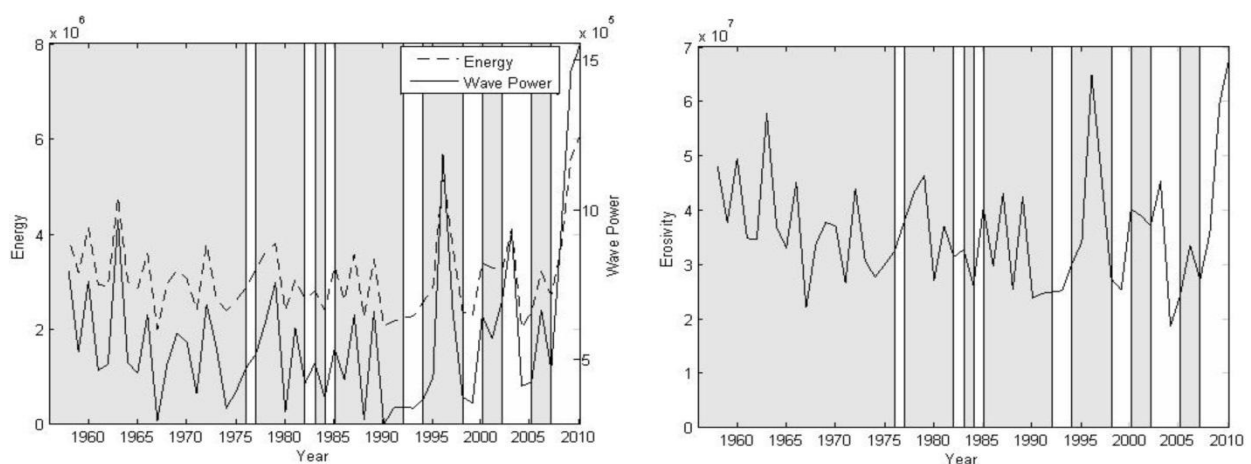


Figure 3. Temporal evolution of the energetic parameters indicating the sets of photographs available for the geomorphological area of Valdelagrana sand spit.

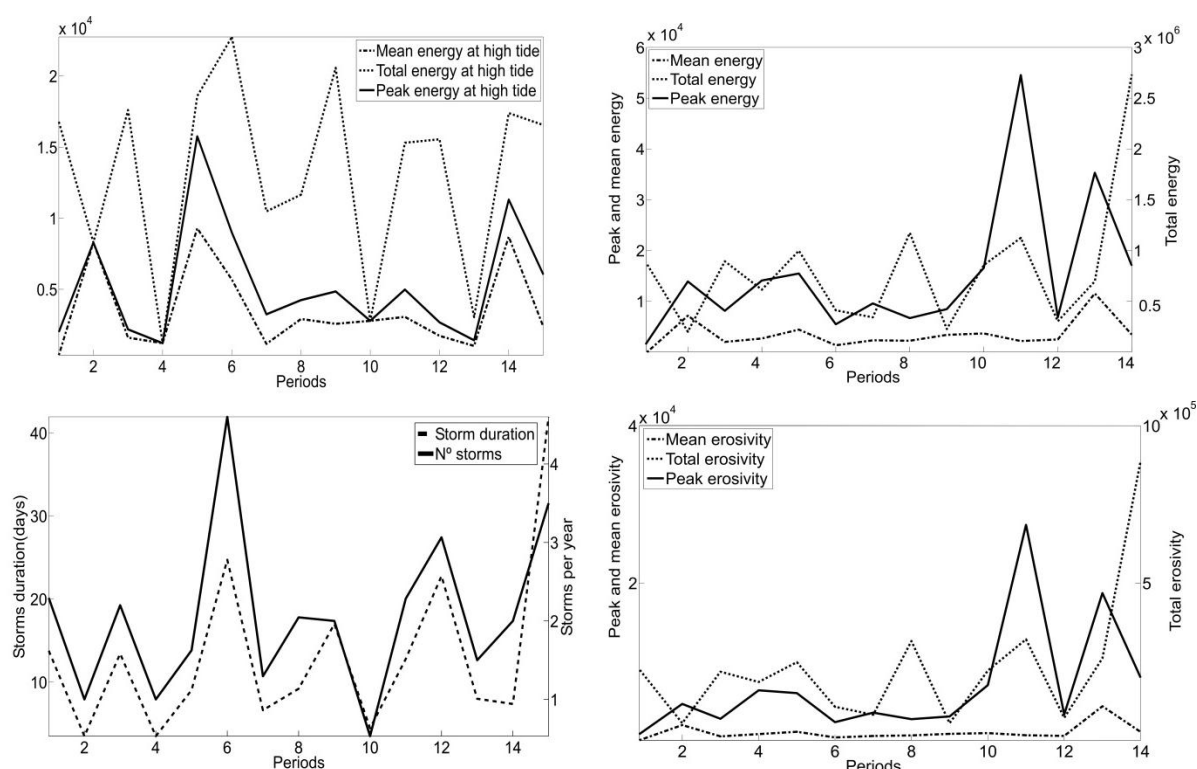


Figure 4. Temporal evolution of the high-tide energy parameters, number of storms and storm duration for the central and southern parts of Valdelagrana (left) and the energy and erosivity parameters for Sancti Petri (right).

stretch most sensitive to storms is section 1, with a negative correlation of  $-0.60$  and P-value of  $0.02$ . This is supported by the recent study of Benavente *et al.* (2013), where vulnerability to storm impacts in this area is reflected by the low storm intensity needed to produce washover reactivation. Section 2 with a lower coefficient was moderately correlated ( $r=0.46$  and P-value= $0.09$ ), with this positive correlation suggesting that sand eroded from adjacent zones could accumulate in this section. Finally, the highly variable shoreline trend in washovers at the southern section (section 3) was negatively correlated with storm energy ( $r=-0.46$  and P-value= $0.09$ ), thus reflecting the presence of other factors that influence its behavior.

## CONCLUSION

This work provides insights into the influence of storminess on shoreline change recorded from two study sites of the Gulf of Cadiz with contrasting exposure and development characteristics.

From the results obtained suggest that medium-term shoreline change shows different behavior depending on the characteristics of the area. Overall, erosion rates are observed along both study sites with variable storminess contribution. Storm-related rates of erosion are greater in exposed areas, such as section 2 of the Valdelagrana sand spit and section 1 of the Sancti Petri sand spit. However, erosion rates are also influenced by the dependence on river sediment supply and human interventions, namely urban construction and coastal engineering structures. On the other hand, sections of the study areas showing low correlation coefficients between storm parameters and shoreline change (i.e. section 1 of Valdelagrana sand spit) are mainly influenced by the aforementioned factors. Nevertheless, it is suggested that in these areas storms contribute to modulate erosion rates, increasing the amount of years with higher storm frequency.

Coastal management plans should be designed according to the main factors that affect shoreline change. Thus, the analysis presented in this work constitutes a useful tool for coastal managers to gain insight into the impacts associated with storms and coastal erosion.

## ACKNOWLEDGEMENT

The work is a contribution to the research group RNM-328 of the Andalusian Research Plan (PAI), the project RNM-6547 funded by the Regional Government of Andalusia and the project GERICO (CGL 2011-25438) funded by the Spanish Ministry of Economy and Competitiveness. M. Puig was supported by the FPI grant (BES-2012-053175) associated to the above project.

## LITERATURE CITED

- Aagaard, T., Kroon, A., Greenwood, B. and Hughes, K.G., 2010. Observations of offshore bar decay: Sediment budgets and the role of lower shoreface processes. *Continental Shelf Research*, 30, 1497-1510.
- Almeida L.P., Ferreira, O., Voudouskas, M.I. and Dodet, G., 2011. Historical variation and trends in storminess along the Portuguese Southcoast. *Natural Hazards Earth Systems Science*, 11, 2407-2417.
- Anderson, T.R., Frazer, L.N. and Fletcher, C.H., 2010. Transient and persistent shoreline change from a storm. *Geophysical Research Letters*, 37, L08401.
- Benavente, J., Gracia, F.J. and López-Aguayo, F., 2000. Empirical model of morphodynamic beachface behaviour for low-energy mesotidal environments. *Marine Geology*, 167, 375-390.
- Benavente, J., Martínez, J.A., Gracia, F.J., Reyes, J.L., Del Río, L., 2002a. Procesos de desbordamiento en la flecha litoral de Sancti-Petri (Bahía de Cadiz): riesgos asociados. In: Serrano, E., García de Celis, A. (eds.), *Estudios Recientes en Geomorfología*. Valladolid, Spain: University of Valladolid, pp. 23-32.

- Benavente, J., Del Río, L., Anfuso, G., Gracia, F.J. and Reyes, J., 2002b. Utility of morphodynamic characterisation in the prediction of beach damage by storms. *Journal of Coastal Research*, 36, 56-64.
- Benavente, J., Del Río, L., Gracia, F.J. and Martínez-del-Pozo, J.A., 2006. Coastal flooding hazard related to storms and coastal evolution in Valdelagrana spit (Cadiz Bay Natural Park, SW Spain). *Continental Shelf Research*, 26, 1061-1076.
- Benavente, J., Del Río, L., Plomaritis, T.A. and Menapace, W., 2013. Impact of coastal storms in a sandy barrier (Sancti Petri, Spain). In: Conley, D.C., Masselink, G., Russell, P.E. and O'Hare, T.J. (eds.), *Proceedings 12th International Coastal Symposium* (Plymouth, England), *Journal of Coastal Research*, Special Issue No. 65, pp. 666-671.
- Boak, E.H. and Turner, I.L., 2005. Shoreline definition and detection: a review. *Journal of Coastal Research*, 21, 688-703.
- Cowell, P.J., Roy, P.S. and Jones, R.A., 1995. Simulation of large-scale coastal change using a morphological behaviour model. *Marine Geology*, 126, 45-61.
- Davidson, M.A., Lewis, R.P. and Turner, I.L., 2010. Forecasting seasonal to multi-year shoreline change. *Coastal Engineering*, 57, 620-629.
- Del Río, L., Plomaritis, T.A., Benavente, J., Valladares, M. and Ribera, P., 2012. Establishing storm thresholds for the Spanish Gulf of Cádiz coast. *Geomorphology*, 143, 13-23.
- Del Río, L., Gracia, F.J. and Benavente, J., 2013. Shoreline change patterns in sandy coasts. A case study in SW Spain. *Geomorphology*, 196, 252-266.
- Guedes-Soares, C., Weisse, R., Carretero, J.C., Alvarez, E., 2002. A 40 years hindcast of wind, sea level and waves in European waters. *Proceedings. 21st International Conference on Offshore Mechanics and Arctic Engineering* (Oslo, Norway), ASME, pp.28604
- Frazer, L.N., Anderson, T.R. and Fletcher, C.H., 2009. Modeling storms improves estimates of long term shoreline change. *Geophysical Research Letters*, 36, L20404.
- Houser, C., Hapke, C. and Hamilton, S., 2008. Controls on coastal dune morphology, shoreline erosion and barrier island response to extreme storms. *Geomorphology*, 100, 223-240.
- Jackson, D.W.T., Cooper, J.A.G. and Del Río, L., 2005. Geological control of beach morphodynamic state. *Marine Geology*, 216, 297-314.
- Jimenez, J.A., Sancho-García, A., Bosom, E., Valdemoro, H.I. and Guillén, J., 2012. Storm-induced damages along the Catalan coast (NW Mediterranean) during the period 1958–2008. *Geomorphology*, 143–144, 24-33.
- Komar, P.D., 2000. Coastal erosion-underlying factors and human impacts. *Shore & Beach*, 68, 3-16
- Lima, L.G., Dillenburg, S.R., Medeanic, S., Barboza, E.G., Rosa, M.L.C.C., Tomazelli, L.J., Dehnhardt, B.A. and Caron, F., 2013. Sea-level rise and sediment budget controlling the evolution of a transgressive barrier in southern Brazil. *Journal of South American Earth Sciences*, 42, 27-38.
- Martínez del Pozo, J.A., Anfuso, G. and Gracia, F.J., 2001. Recent evolution of a tidal delta in Cádiz Bay (SW Spain) due to human interventions. In: Özhan, E. (Ed), *Proceedings of the Fifth International Conference on the Mediterranean Coastal Environment* (Hammamet, Tunisia). MEDCOAST, 1, pp. 1425-1433.
- Plomaritis, T.A., Del Río, L., Benavente, J. and Valladares, M., 2010. Storm thresholds for the Spanish Gulf of Cadiz coast. *Geophysical Research Abstracts*, 12, EGU2010-10781.
- Rangel-Buitrago, N. and Anfuso, G., 2011. Coastal storm characterization and morphological impacts on sandy coasts. *Earth Surface Processes and Landforms*, 36, 1997-2010.
- Rangel-Buitrago, N. and Anfuso, G., 2012. Winter wave climate, storms and regional cycles: The SW Spanish Atlantic coast. *International Journal of Climatology*, 33, 2142-2156.
- Reyes, J., Martins, J., Benavente, J., Ferreira, O., Gracia, F., Alveirinho-Dias, J. and López-Aguayo, F., 1999. Gulf of Cadiz beaches: a comparative response to storm events. *Boletín-Instituto Español de Oceanografía*, 15, 221-228.
- Ribera, P., Gallego, D., Pena-Ortiz, C., Del Río, L., Plomaritis, T. and Benavente, J., 2011. Reconstruction of Atlantic historical winter coastal storms in the Spanish coasts of the Gulf of Cadiz, 1929–2005. *Natural Hazards and Earth System Sciences*, 11, 1715-1722.
- Riggs, S.R., Cleary, W.J. and Snyder, S.W., 1995. Influence of inherited geologic framework on barrier shoreface morphology and dynamics. *Marine Geology*, 126, 213-234.
- Rossi, V., Amorosi, A., Sarti, G. and Potenza, M., 2011. Influence of inherited topography on the Holocene sedimentary evolution of coastal systems: An example from Arno coastal plain (Tuscany, Italy). *Geomorphology*, 135, 117-128.
- Thieler, E., Himmelstoss, E.A., Zichichi, J.L. and Ergul, A., 2009. The Digital Shoreline Analysis System (DSAS) Version 4.0- An ArcGIS Extension for Calculating Shoreline Change. *U.S. Geological Survey open-file report*, 2008-1278.

## The natural causes of shoreline evolution of Capo Peloro, the northernmost point of Sicily (Italy)



Giovanni Randazzo†, Claudia Cigala‡, Antonio Crupi‡, Stefania Lanza †

† Department of Physics and Earth Sciences  
University of Messina  
Via F. Stagno D'alcontres, 31 - 98166 –  
Messina, Italy  
grandazzo@unime.it

‡ CERISI (Centro di Eccellenza Ricerca e Innovazione Strutture e Infrastrutture di grandi dimensioni)  
University of Messina  
Via Consolato del Mare, 41 is 317 -  
98100 – Messina, Italy  
claudia.cigala@hotmail.it

‡ CERISI (Centro di Eccellenza Ricerca e Innovazione Strutture e Infrastrutture di grandi dimensioni)  
University of Messina  
Via Consolato del Mare, 41 is 317 -  
98100 – Messina, Italy  
antoniocrupi5@hotmail.it

[www.cerf-jcr.org](http://www.cerf-jcr.org)

† Department of Physics and Earth Sciences  
University of Messina  
Via F. Stagno D'alcontres, 31 - 98166 –  
Messina, Italy  
lanzas@unime.it



[www.JCRonline.org](http://www.JCRonline.org)

### ABSTRACT

Randazzo, G., Cigala, C., Crupi, A., Lanza, S., 2014. The natural causes of shoreline evolution of Capo Peloro, the northernmost point of Sicily (Italy). In: Green, A.N. and Cooper, J.A.G. (eds.), *Proceedings 13<sup>th</sup> International Coastal Symposium* (Durban, South Africa), *Journal of Coastal Research*, Special Issue No. 70, pp. 199-204, ISSN 0749-0208.

During recent times, the world's coastline has been constantly changing, and factors such as: the absence of sediment transport from rivers, urbanization of the coastal zone, construction of protective structures and ports, contribute to such change. An increase in frequency and intensity of storm events may also play a role. In the area of Capo Peloro (eastern Sicily) in the last 180 years, the changing coastline has been assessed using maps, aerial photographs, urban plans, historical notes, and surveys from 1824 to 2013 with the support of a long winded dataset series (1951 to 2012).

The area of Capo Peloro is the northernmost headland of Sicily, dividing the Tyrrhenian from the Ionian Sea and stretching into the Strait of Messina. The four beaches which constitute the continuous coastal system of the cape show rapid evolution. Analysis of the wind records shows a decreasing trend for winds coming from the orientation range of 290°-330°, while there is an increasing trend for those coming from the range of 331°-20° and, in general, wind intensity has increased in the last 9 years. Comparison of the coastal evolution pattern and the wind data set, a direct relationship has been recognized, while urbanization has not affected this trend.

The beach of Tiro a Volo lost its capability to regenerate and protect itself naturally in 2012, which was the windiest year of the series considered. Erosion in 2012 uncovered old anthropic structures, eliminating the morphological connection between the beach and the alluvial plain. The hardening of the landward limit of the beach caused a loss of beach resilience. Due to the exposed structures, an artificial redistribution of the sedimentary material in the area is now necessary.

**ADDITIONAL INDEX WORDS:** *Strait of Messina, coastal erosion, resilience, wind analysis*

### INTRODUCTION

Coastal erosion is a natural process which occurs along the world's coastlines through the action of currents and waves, and is also most frequently a result of human action. In both cases the result is sediment loss in some areas and accretion in others.

There are areas where humans have encroached on the dynamic beach environment only to suffer the consequences of the erosion, and others where anthropic pressure has interfered with coastal processes leading to accelerated coastal erosion (Short, 2009).

Along many of the world's coastlines, coastal erosion has dramatically increased over the last three decades, and this is expected to continue as sea levels rise, storm frequency, and severity increase (Brown and McLachlan, 2002). However, natural and anthropogenically induced erosion does not occur as a continuous process but, much rather, in strong bursts during storm

events as a result of increased wave height and storm intensity (Smith *et al.*, 2010; Cooper *et al.*, 2004). Therefore, it is impossible to distinguish a trend in how time constrains these processes as they are often confined to very time-concentrated events. Changing shoreline position on two successive charts, aerial photographs or satellite images of the coastline can enable an impression of historical scale evolution.

In this paper, we analyse the coastal evolution of Capo Peloro, the northernmost point of Sicily, since Smith's survey in 1824 and using a 60-year wind series to interpret the evolution of the coastline due to natural and anthropogenic factors. Analysis of the oldest historical data, that lacks corresponding wind data, shows an evolutionary trend which is free of human interference. Using more recent maps, it is possible to attribute coastal evolution to both natural and human causes. It is possible to examine any relationship between wind and erosion using the wind data set.



## GEOGRAPHICAL SETTING

The area of Capo Peloro (eastern Sicily) divides the Tyrrhenian from the Ionian Sea (Figure 1a). Along the coastline, four beaches are present: Massone, Tiro a Volo, Pylon and Nose. These beaches are situated within the English Channel, connecting Lake Faro and the Tyrrhenian Sea as well as the last of series of breakwaters, in front of Torre Faro village along the Ionian Sea. The four beaches represent a continuous 2.7km long system which in the past was much wider and energetic, with a multi-berm structure and several dune ridges.

The headland, according to Barrier (1995), originated from tectonic movement along the Strait of Messina during the Pliocene and Pleistocene. The erosion of the emerging structure has created the present day coastal plan which characterizes the area from Messina to Capo Peloro. The hills bordering the alluvial plan show a diffuse presence of a conglomerate sequence (Sands and Gravels of Messina). This Formation overlaps the metamorphic rock outcrops of the Peloritani Mountains (Bonfiglio, 1999; Bonfiglio *et al.*, 1993). The steep slope of the hills, shaped by terraces and smoothed by colluvium sedimentation, is a result of the presence of NE-SW faults (Atzori *et al.*, 1978; Montenat *et al.*, 1991). These faults have contributed to the formation of the marine sedimentary basins, which at a later stage began to form the headland of Capo Peloro.

The study area contains the coastal lagoon, Ganzirri, and the lake, Faro. Also included, is the ancient Margi swamp which is currently dry with remnants of the Margi Channel. The two bodies of water are connected to the sea by two artificial channels which require continuous maintenance (Ferrarin *et al.*, 2013). The evolution of these bodies of water is not clear: the 1,700m long lagoon of Ganzirri (maximum depth 7 m), as suggested by Chillemi (1995), represents the classic evolution of a bay closed by the westward moving sand bar. Margi swamp probably followed the same path of evolution and was previously part of the lagoon of Ganzirri. Lake Faro, according (Bonfiglio, 1999), is a small coastal lake that has formed due to tectonic processes. It is nearly circular in shape, measuring about 500 m in diameter and about 30 m deep in the central part and it has meromictic circulation (Manganaro *et al.*, 2011).

The headland of Capo Peloro extends into the Strait of Messina.

The strait connects the Tyrrhenian and the Ionian Sea and along the direction of Capo Peloro to Punta Pezzo (in southern Italy). There is a morphological structure, locally called a “sella” (saddle), which has a depth of 80 to 120 m below sea level, which sinks gradually westwards to reach 1,000 m in depth between the Milazzo Peninsula and the Aeolian Islands. Eastwards, its depth descends sharply to hundred meters (Selli, 1979).

Climatically, the area of the Strait of Messina is protected by its shape. In the south, the “reverse funnel” formed by the two sides of the coast protects it against waves from the first and second quadrants. On the eastern and northern sides, the Sicilian coastline is shielded from winds blowing from the third and fourth quadrants, by the peninsula of Milazzo and the archipelago of Aeolian Islands, and the southern part of the Italian peninsula. From NW-WNW, in Messina the wind often comes from those quadrants but does not create waves (Figure 1b).

Along the coastline, the presence of the two seas, differing in terms of density and shape of the sea floor, develop a strong reversing coastal current (Berdar *et al.*, 1986). However, this current does not register significant tidal amplitudes (Arena and Barbaro, 2013).

The area of Capo Peloro also attracts attention for various economic reasons, such as: aquaculture (mainly mussels), vacation homes, and intense beach use (sunbathing, swimming, and water sports) during summer.

## COASTAL EVOLUTION

A great variety of graphic works (e.g. engravings, watercolours) portraying the area of Capo Peloro have survived from the 14th to the 17th century. However, the map drawn by Smith (1824) is the first document which could be considered modern cartography. This was used as the starting point of this study. This map clearly depicts the entire coastal area, with the two lakes and a largely undeveloped coastal zone. The channels of the lake of Faro are well depicted, while the two of lagoons of Ganzirri are not visible, occupied by salt works, indicating the economic interest of the area. The nose of the cape is curved and the beach (called “nose” in this paper) appears large and well defined. The lighthouse is situated in the north, which has lasted to the present, while the English barracks disappeared in later documents.

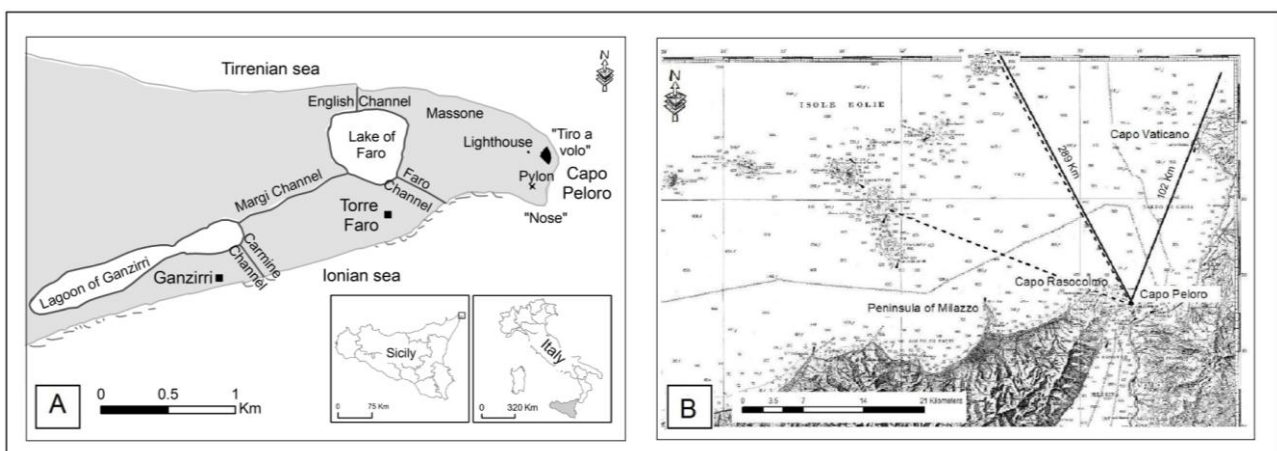


Figure 1 – a) Location of the study area of Capo Peloro on the northernmost point of Sicily, south Italy; in this figure the beaches considered in the study and the other toponymis are shown (“Massone”, “Tiro a Volo”, Pylon and “nose”). b) Wind sectors: dashed line indicates the section between 290° and 330, sheltered by the Aeolian Islands and the solid one the sector between 331° and 20° with the longest fetch.

In 1889 the first Italian map was drawn (edited by Royal Geographic Military Institute) on the basis of the survey of 1865-66, at the scale 1:50,000. The shape of the coastline is similar to that of the previous map, with some change in the road network, indicating village growth and new names of localities such as “Massone” on the Tyrrhenian side (Figure 2).

Ten years later (1899), at the same scale, a new version of this map was published, clearly defining the progress of hydraulic works on the landward side of the lagoon which was evidently connected to the sea by a channel. The most important change occurred on the nose of the cape, with a severe loss of about 1 sq. km, with no explanatory information available.

The new edition of the map of the area (1:25,000 scale), was edited in 1906. The area maintained the same placenames and the constructions still occupied a very limited surface area, whereas almost the entire territory, both at sea level and on the hills, was covered by vineyards. In the few years between the two maps, the beach had grown and the isobaths showed a gentler slope along the northern side while the southern coast had a steeper slope.

After 1906, three cartographic documents become available (1947, 1952, and 1956) from a study for the construction of an electrical pylon which connected Sicily to Italy. These maps were compared with respect to the 1889 shoreline (Figure 3).

A composite map, made by the manual overlapping of several coastlines, shows a major coastline progression advance between 1889 and 1947 (the study does not consider 1906 map). In this time period, Messina was completely destroyed by the December

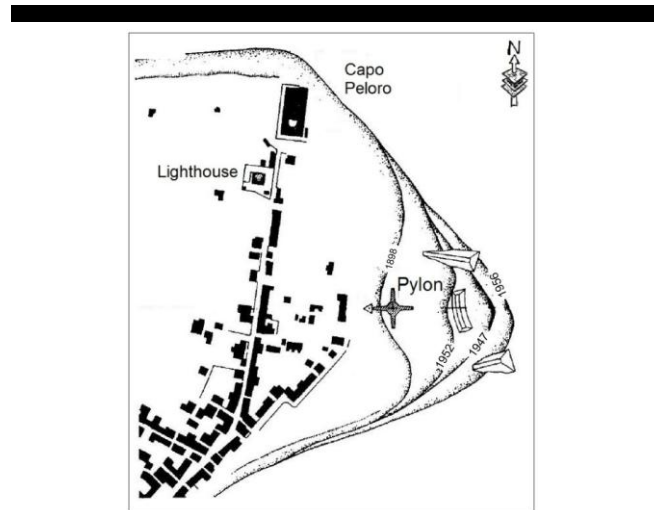


Figure 3 - Position of the shoreline before and after 1908 earthquake; 1956 shoreline shows hard structures engineered to protect the base of the Pylon.

1908 earthquake and was rapidly reconstructed. The enormous volumes of ruins were in part left in the same area where they fell (the actual city of Messina is 3-5 m higher than the previous one) but a significant proportion was dumped into the sea, facilitating the expansion of the beaches.

In the next map, dated 1952, a major shoreline retreat is evident, while in 1956 the map shows a clear seaward movement. The nautical map based on the 1889 coastline, with the improved information of the 1957 map clearly depicts the geomorphology of the area. A modest coastal chain crossed by several water courses produced an alluvial plain which, together with the southern side, shows sedimentary evolution in the form of expansion of the plain and the closure of the lagoon. Meanwhile, along the northern side, tectonic evolution predominates as illustrated in a wider framework by Doglioni *et al.* (2012).

In 1962, a Military Geographic Institute (I.G.M.) map derived from the 1956 aerial photograph, which was used in the previous study, shows the area was still sparsely populated and the vineyards were still dominant. However, in subsequent years the panorama changed. In the 1967 aerial photograph, growth of the constructed area is evident with some of the channels being protected by jetties as well as the first breakwaters were built along the southern coastline. The northern coastline appears to be stable and the beach remains large; a better picture is not possible because the area of Capo Peloro has been blanked out in maps for military purposes.

From this map we can start to analyse the coastal evolution with a georeferenced overlapping which considers dated documents (Figure 4): 1967 (I.G.M., aerial photograph, scale about 1:33,000), 1985 (Regional Map, scale 1:10,000), 1997 (Technical Regional Map, scale 1:10,000), 2007 (Technical Regional Map, scale 1:10,000) and 2012 (surveying by GPS). In general, it is possible to see where the coastline has moved seaward or landward, with erosion of some parts and accretion in others. The northern coastal area (Massone beach) has maintained a certain equilibrium, while along the southern beaches (Tiro a Volo, Pylon and “nose”) it is evident that continuous disequilibrium has involved only the beach section. It is important to note that the coastline evolution has involved only the beach section and it has at no time damaged the morphologic step (vegetated on the aerial

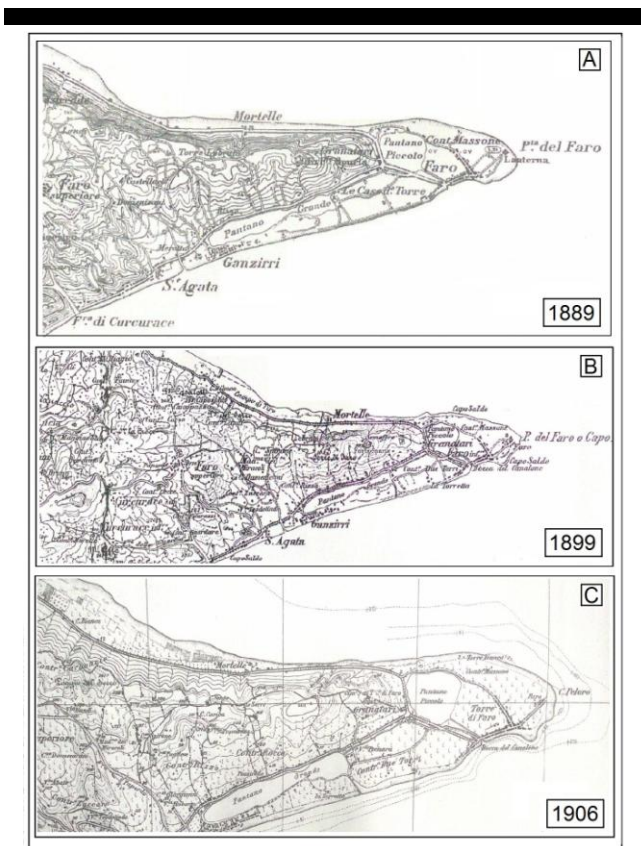


Figure 2 -The first three maps edited by the Royal Geographic Military Institute after its constitution at the time of Italian unification (1861): A and B were originally at 1:50,000 scale, while C was at 1:25,000 scale.

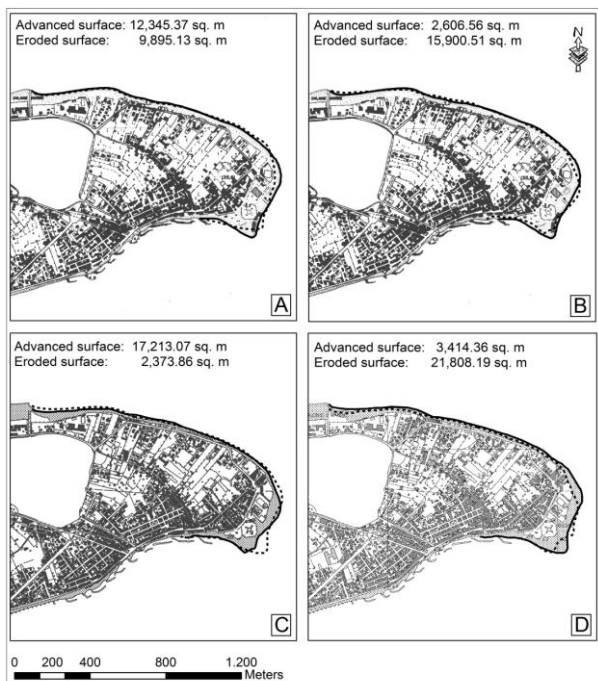


Figure 4 - Recent evolution of the coastline: the solid line represents the topographic base (1985 in A and B, 1997 in C and 2007 in D). The dotted lines represent, respectively, the 1967 contour in A, 1997 in B, 2007 in C and 2012 surveyed contour in D.

photograph) which separates the beach from the coastal plain or the brittle structure protecting the Pylon.

During fall 2011 and winter 2012, the beach of Tiro a Volo was strongly eroded and retreated landwards more than previously recorded and attacked the base of the alluvial plain behind the beach. Furthermore the erosion uncovered the hard structures placed to protect the boundary of Tiro a Volo. In March 2012, at the end of winter, a topographic survey of the area was performed and the drawing of coastline was reconstructed in comparison to the 2007 Technical Regional Map. The erosion of the shoreline was evident in several parts of the coastal area. The deepest erosional process was shown where the foundation of old constructions were exposed by the energy of the waves. This trend has been confirmed by the surveys performed in November 2013 (Figure 5).

### WIND ANALYSIS

The Strait of Messina with its particular morphology is somewhat protected from marine weather and, despite being affected by strong winds often coming from the second quadrant, the waves that form are relatively small. From the whole eastern sector (the first and second quadrants) waves are gentle, and when the wind affects the strait between Italy and Sicily, it generates low, foaming waves which are generally absorbed six hours of alternate flux. From both the third and the fourth quadrants the fetch is limited between  $290^\circ$  by the Capo Rasocolmo and  $20^\circ$  (partially in the first quadrant) by the Capo Vaticano in the Italian peninsula.

Between  $290^\circ$  and  $330^\circ$ , the area is screened by the presence of the Milazzo Peninsula and the Aeolian Archipelagos. Therefore, the waves do not have the space to generate strong energy,

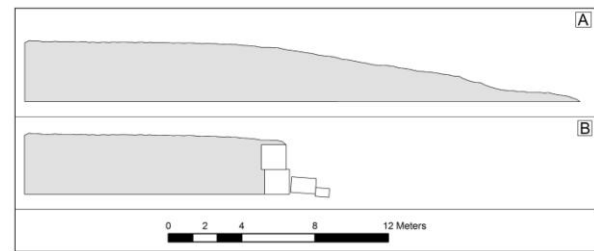


Figure 5 - Section of "Tiro a Volo" beach: A in 2007 and B in 2013.

whereas from  $331^\circ$  to  $20^\circ$  is the longest fetch reaching Italy's coast (between 289 and 102 km). Because of this configuration, we divide our observations into two sets: between  $290^\circ$  and  $330^\circ$ , the sheltered Aeolian area; and between  $331^\circ$  and  $20^\circ$ , the free fetch. The study was further concentrated on winds blowing at speeds exceeding 30 km/h, which have the energy to generate more erosive waves. The entire wind dataset is composed of three different sources:

- January 1951 to December 1999 data from Military Aviation Station of Messina with a three-hour cadence (131,631 inputs) measured in km/h.
- January 2000 to December 2011 data pre-analysed from Superior Institute for Environmental Research (ISPRA), coming from the same observatory of the Station of Messina with an hourly cadence (103,347 inputs) measured in km/h and normalized to a three-hour cadence, for 12,922 inputs measured in km/h.
- January 2012 to December 2012 data from a private station, recording hourly (7,593 inputs) in km/h, normalized to the three-hour cadence with 949 observations.

The dataset was used as a comparison between events occurring over a period of several years. Winds blow more intensely on the coast in autumn and winter, with peaks generally concentrated between December and March.

For the 60 years comprehensively analysed (1951-2011), the winds from  $290^\circ$ - $330^\circ$  (Figure 6a), which occur at an annual average of 10 events, tend to slightly decline in the number of events when above 30 km/h in speed. There were 2 peaks in occurrence, for a total of 7 years around the years 1951 and 1966, which were triple the annual average, while it was doubled in 1954, 1965, 1969-70, and 1979. From this direction, in the whole period, only 6 events exceeded 60 km/h.

Winds from the sector  $331^\circ$ - $20^\circ$  (Figure 6b) follow the opposite trend, with an average of 10 events, but with peaks that double or triple the average only in the coincidence of two periods identified for the previous sector (1951 and 1965-66). These winds remain close to the average until 1999, when there was a peak of 27 occurrences (78% above 60 km/h), followed by a series of occurrences which were always above average (with several peaks above the two and three times the average). Between 1987 and 1990 the highest frequency of wind over 60 km/h was recorded.

The year 2012 was the windiest of the entire time series for the sector  $290^\circ$ - $330^\circ$  and was the third peak of the entire observation period for those coming from the sector  $331^\circ$ - $20^\circ$ .

Regarding the number given by the sum of the appearance of winds from both directions over the entire observation period (Figure 6c), and with reference to the average value of 20 occurrences per year, we find that for the first 20 years of observation (51-70), there is a regular alternation of pairs or triads of the windiest years (more than average) with couples or single

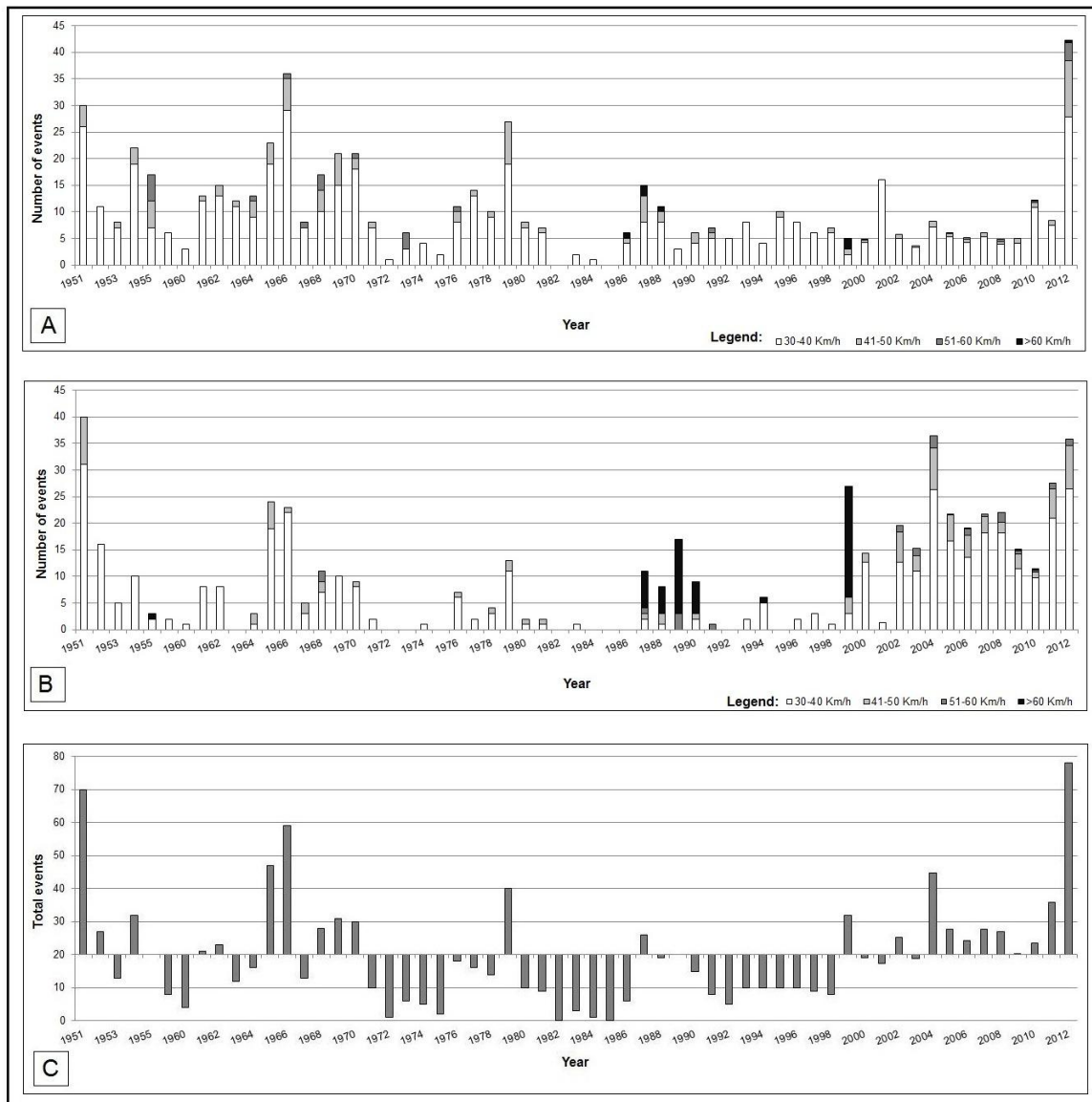


Figure 6 - Wind time series divided by sectors: a) 290°-330° and b) 331°-20° (white bar indicates wind speed 30-40 km/h, light grey 41-50, dark grey 51-60 and black >60 km/h. c) shows the sum of the two series respect to the average of the annual events.

years that are less windy. Between 1972 and 2004 we generally have below-average events, with the exception of four years. Finally, the time interval from 2005 to the present has been characterized by a succession of years, culminating in the windy peak of 2012, which is the windiest year in the dataset.

## DISCUSSION

The coastline is a dynamic environment subject to erosion and accretion processes as a result of both natural and human causes. These are particularly evident in the area of Capo Peloro and are documented by past and more recent cartography using aerial photography as well as direct evidence.

In this study, the coastal evolution has been analysed taking into consideration all of the above wind data sets. Considering that we find a direct correlation between wind cycles and coastal change,

the increase in urbanization looks less influential. In particular, the analysis of shoreline evolution of Capo Peloro, between 1824 and 1957, shows that without the presence of urbanization, the response of the beach towards the force of the waves is vigorously dynamic, with several metres of variation over the years. A determining role was played by the 1908 earthquake in the evolution, after which thousands of tons of material of different origin and size was deposited on the beach from the destroyed buildings.

Baratta (1910) states that the central part of the town of Faro was completely destroyed, the church had collapsed and the houses next to it were ruined. This author also affirmed that the buildings were normally constructed either with pebbles and mud or using hydrated lime, composed of unwashed marine sand or unwashed ground sand. The accretion caused by deposition of this material is even more evident on the 1947 shoreline, whereas in

1952 a portion of this material was removed, probably due to sea storms approaching from the fourth quadrant. In 1951 extreme weather conditions and winds with a velocity of more than 30 km/h were recorded and were only exceeded in 2012. After 1952, the materials that were not completely dispersed offshore were re-deposited at their former sites, during calm periods. In the absence of urbanization, the area maintained a balance between periodic erosion and accretion.

Between 1967 and 1985 the eroded material from the Massone and Pylon beaches enlarged the beaches of Tiro a Volo and the “nose”.

During these 20 years, two windy peaks from sector 290°-330° were recorded, while winds from sector 331°-20° were practically absent. Between 1985 and 1997 the trend reversed, with erosion of the Tiro a Volo beach and an accretion of Pylon. Between 1987 and 1991, strong winds from sector 331°-20° were registered, with a greater number of winds exceeding 60 km/h. Between 1997 and 2007 the remodelling of the beaches concerned only the sector of Pylon, with erosion of the northern part of the beach and a lengthening of the “nose” towards the north. In this period the dominant winds came from sector 331°-20°, but the beach of Tiro a Volo was not subjected to any particularly erosive event.

This trend confirms that, as long as the beaches maintain the space for their physiological resilience (EUROSION, 2007), they tend to be naturally stable within the same sector, resulting in a change in shape without any loss in volume. However, in 2012 this balance was broken by an extraordinary succession of winds between autumn 2011 and winter 2012. These events completely eliminated the beach up to the morphological step that separated it from the Holocene terrace and uncovered ancient foundations of a probable ancient port. This provoked the hardening of the coastal area and the formation of an artificial “step” which cannot be covered by sediments that circulate in the area.

The last survey performed in November 2013 still confirms the equilibrium of the coastal system of Capo Peloro. Tiro a Volo beach, with the exposed foundation, is still in the same condition as the previous year, and has broken the continuous contour.

On Tiro a Volo beach, 12,000 m<sup>2</sup> was lost, whereas the northern area of Pylon beach recorded accretion of about 5,000 m<sup>2</sup>. The southern beach, Pylon, lost about 4,000 m<sup>2</sup> in surface area, with a further accretion of the “nose” beach of about 1,000 m<sup>2</sup>. During the same period Massone beach remained more or less stable. Considering the medium slope of the beach, the area recorded a loss of about 16,000 m<sup>3</sup> of material and an accretion of about 5,000 m<sup>3</sup>, with a total deficit of about 11,000 m<sup>3</sup>. The material available is unable to cover the eroded beach of Tiro a Volo because of the rigid wall that deflects waves, preventing any type of sedimentation.

The restoration of resilience will require an artificial redistribution of the material present in the area either made up of dredged spoil from the English Channel or from adjacent accreting beaches. In this way the sea will redistribute the sediments following a natural process according to the physiological variation of the shoreline in relation to weather and marine events. Unfortunately, the area is subject to strict limitations that prevent any intervention.

## LITERATURE CITED

- Arena, F. and Barbaro, G., 2013. The Natural Ocean Engineering Laboratory, NOEL, in Reggio Calabria, Italy: A commentary and announcement. *Journal of Coastal Research*, 29 (5), 7–10.
- Atzori, P., Ghisetti, F., Pezzino, A. and Vezzani, L., 1978. Strutture ed evoluzione geodinamica recente dell'area peloritana (Sicilia nord-orientale). *Boll. Soc. Geol. It.*, 97 (4), 31-56.
- Baratta, M., 1910. *La Catastrofe Sismica Calabro – Messinese*. Società Geografica Italiana, 425 p.
- Barrier, P., 1995. The Straits of Messina during Pliocene and Pleistocene times (Italy). In: Guglielmo, L., Manganaro, A. and De Domenico E. (eds), *Proceedings of the Symposium held (Messina, Italy) 4-6 April 1991*, pp 71-81.
- Berdar, A., Riccobono, F. and Bonfiglio, L., 1986. *Le meraviglie dello stretto di Messina*. EDAS, Messina 672 p.
- Bonfiglio, L., 1999. La distribuzione dei siti archeologici, il contesto stratigrafico e la ricostruzione paleoambientale. In: Bacci, G.M. and Tigano, G. (eds.), *Da Zancle a Messina, un percorso archeologico attraverso gli scavi*, pp. 9-17.
- Bonfiglio, L., Bacci, M. G., Barra, D., Bonaduce, G., Di Geronimo, D., Manfra, L., Proposito, A. and Violanti, D., 1993. Paleoeological, radiometric and archeological core analysis of Holocene deposits in the Messina harbour area (North-Eastern Sicily). In Matteucci et al. (eds.), *Studies on Ecology and Palaeoecology of Benthic Communities*. Boll. Soc. Paleontol. Ital., Spec. Mucchi, Modena, Vol. 2, pp. 47-60.
- Brown, A.C. and McLachlan, A., 2002. Sandy shore ecosystems and the threats facing them: some predictions for the year 2025. *Environmental Conservation*, 29 (1), 62-77.
- Chillemi, F., 1995. Capo Peloro e la spiaggia di Tono. In Edas (ed.), *I Casali di Messina*.
- Cooper, J.A.G., Jackson, D.W.T., Navas, F., McKenna, J. & Malvarez, G., 2004. Identifying storm impacts on an embayed, high energy coastline: western Ireland. *Marine Geology*, 210, 261-280.
- Doglion, C., Ligi, M., Scrocca, D., Bigi, S., Bortoluzzi, G., Carminati, E., Cuffaro, M., D’Orlando, F., Forleo, V., Muccini, F., and Riguzzi, F., 2012. The tectonic puzzle of the Messina area (southern Italy): insights from new seismic reflection data. *Scientific Report* 2, 970; DOI:10.1038/srep00970.
- EUROSION, 2007. Living with coastal erosion in Europe; sediment and space for sustainability. Luxembourg: Office for Official publications of the European Communities 40p.
- Ferrarin C., Bergamasco, A., Umgiesser, G. and Cucco, A., 2013. Hydrodynamics and spatial zonation of the Capo Peloro coastal system (Sicily) through 3-D numerical modelling. *Journal of Marine Systems*. 117-118, 96-107.
- Manganaro, A., Pulicanò, G. and Sanfilippo, M., 2011. Temporal evolution of area of Capo Peloro (Sicily, Italy) from pristine site into urbanized area. *Transitional waters bulletin*, 5 (1), 23-31.
- Montenat, C., Barrier, P. and Ott d’Estevou, P., 1991. Some aspects of the recent tectonics in the Straits of Messina, Italy. *Tectonophysics*, 194, 203-215.
- Selli, R., 1979. Geologia e sismotettonica dello stretto di Messina. *Acc. Naz. Lincei, Att. Cov.* 43, pp. 1-17.
- Short 2009. Impact of coastal erosion in Australia. <http://www.coastalwatch.com/news/article.aspx?articleId=4524>
- Smith, A., Mather, A., Guastella, L., Cooper, J.A.G., Ramsay, P.J. and Theron, A., 2010. Contrasting styles of swell-driven coastal erosion: examples from KwaZulu-Natal, South Africa. *Geological Magazine*, 147, 940-953.
- Smith, W. H., 1824. *Memoir descriptive of the resources, inhabitants, and hydrography of Sicily and its islands, interspersed with antiquarian and other notices*. John Murray Editor. In the translation by Catinella G.D. and De Franchis G. (1987), Giada.

## Meandering fluvial system influencing the evolution of a Holocene regressive barrier in southern Brazil

Anderson Biancini da Silva†, Eduardo G. Barboza‡, Maria Luiza C.C. Rosa†, Sérgio R. Dillenburg‡

† Programa de Pós Graduação em Geociências, Universidade Federado Rio Grande do Sul, Porto Alegre – RS – Brasil  
anderson.biancini@ufrgs.br

‡ Centro de Estudos de Geologia Costeira e Oceânica, Instituto de Geociências, Universidade Federal do Rio Grande do Sul  
Caixa Postal 15.001 – Porto Alegre – RS – Brasil  
eduardo.barboza@ufrgs.br  
sergio.dillenburg@ufrgs.br  
luiza.camara@ufrgs.br



[www.cerf-jcr.org](http://www.cerf-jcr.org)



[www.JCRonline.org](http://www.JCRonline.org)

### ABSTRACT

Biancini da Silva, A., Barboza, E.G., Rosa, M.L.C.C., Dillenburg, S.R., 2014. Meandering Fluvial System Influencing the Evolution of a Holocene Regressive Barrier in Southern Brazil. In: Green, A.N. and Cooper, J.A.G. (eds.), *Proceedings 13<sup>th</sup> International Coastal Symposium* (Durban, South Africa), *Journal of Coastal Research*, Special Issue No. 70, pp. 205-210, ISSN 0749-0208.

A meandering fluvial system changes its course according to geological time, eroding rocks and pre-existing deposits and transporting large volumes of sediment to the coastal plains. Understanding the evolution of channels and paleochannels in regions showing coastal barriers and relating them to changes in sea level becomes extremely important to comprehend the factors that contribute to the behavior of coastal barriers. During the Holocene the barrier at Passo de Torres located northeast of the Mampituba River, along the southern coast of Santa Catarina state, prograded approximately 5.5 km. The barrier comprises both foredune ridges, which occur in the landward portion, and transgressive dune ridges, which occur seawards. One feature that stands out in the region is that the regressive barrier morphologies are truncated (eroded) by paleochannels and channels of a meandering fluvial system, which can be related to the dynamics of the Mampituba River. These paleochannels have elongated morphologies with SW – NE orientation and are up to 25 km long. With the purpose of characterizing the longer paleochannels, the geophysical method of ground penetrating radar (GPR) was used, associated with drill hole and radiocarbon dating. The GPR profile reveals continuous reflectors ( $\pm 5$  m depth) with great contrast and lateral continuity for over 450 m. These represent an erosive surface, interpreted as the base of the fluvial channel. The granulometric results indicate that around 5 m, an increase in grain size (fine sand grading to medium sand) and the presence of several shells. These are very fragmented, characterizing a probable bedload transport. However, shells of the genus *Donax* sp. were collected intact with no signs of abrasion. This genus inhabits beach environments (specifically foreshore) and cannot survive in freshwater environments. These shells were incorporated to the bedload of the fluvial channel through an inlet, probably during storm surge events. These events carried beach sands, associated with shells (mainly *Donax* sp.), towards the continent, which were incorporated into the fluvial sediments. The dating of these species revealed an age between 5.6 – 5.4 cal ka. The ages obtained are consistent with the maximum sea level of the Postglacial Marine Transgression (PMT) in southern Brazil. Because these shells are exclusive to beach environments, dating allowed us to infer that this channel was active and had connection with the ocean at about 5.5 ka, concomitant with the maximum sea level of PMT.

**ADDITIONAL INDEX WORDS:** *Paleochannels, GPR, Coastal barriers, Maximum sea level Holocene.*

### INTRODUCTION

The development of Holocene barriers and the paleogeographic evolution of coastal plains are intimately related to the morphodynamics of estuarine-fluvial systems (Boucher *et al.*, 2006; T. van der Schriek *et al.*, 2007; Angulo *et al.*, 2009; Costas and Fitzgerald, 2011; Hein *et al.*, 2013). The channels of the meandering fluvial systems shift laterally and migrate longitudinally according to geological time. Understanding the evolution of coastal channels and paleochannels, and relating them to changes in sea level becomes extremely important to comprehend the factors that contribute to the behavior of coastal barriers. During the Holocene, the barrier at Passo de Torres situated northeast of the Mampituba River, along the southern

coast of Santa Catarina state, prograded approximately 5.5 km. The regressive barrier is composed of foredune ridges that occur in the landward portion and transgressive dune fields, which occur seawards (Silva, 2009) (Figure 1). One feature that stands out is that barrier morphology is truncated (eroded) by paleochannels and channels of a meandering fluvial system, which can be related to the dynamics of the Mampituba River. These paleochannels have elongated morphology with SW – NE orientation, associated with the littoral drift of the region. In this paper we intend to characterize of the longer paleochannel ( $\pm 25$  km) and link its development with sea level changes which have occurred during the Holocene. Subsurface data was acquired using the geophysical method of ground penetrating radar (GPR), associating sedimentological data obtained through one drill hole and radiocarbon dating.

DOI: 10.2112/SI70-035.1 received 1 December 2013; accepted 21 February 2014. © Coastal Education & Research Foundation 2013

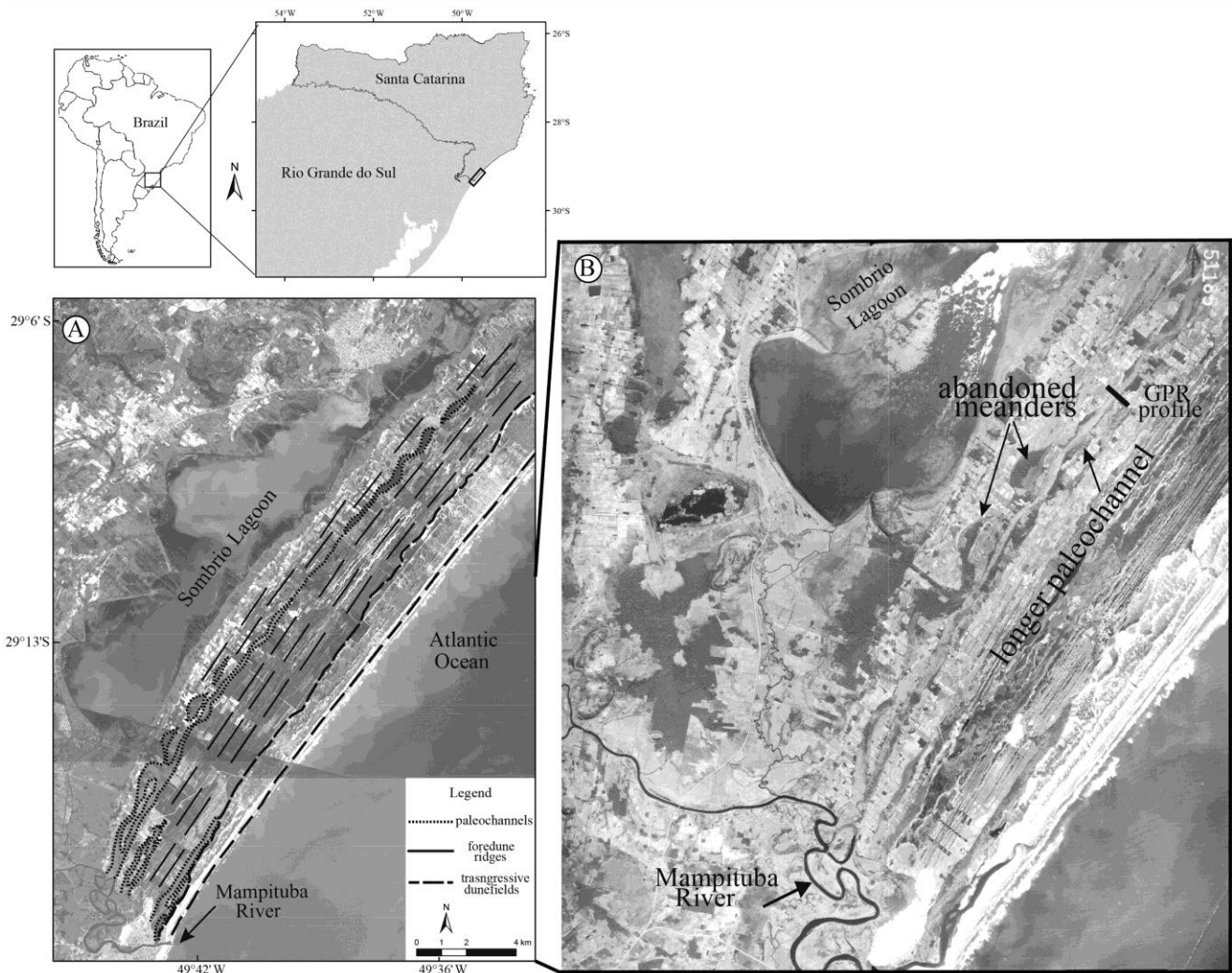


Figure 1. A) Spot panchromatic satellite image (date 2005) showing the Holocene regressive barrier at Passo de Torres. The foredune ridges and transgressive dunefields are truncated (eroded) by paleochannels. B) Historical aerial photography (scale of 1:60.000 from 1965) where it is possible to observe the coastal region without anthropogenic influence. This photo shows the longer paleochannel, abandoned meanders and GPR profile location. The paleochannels have elongated form, 2 up to 25 km long with SW – NE orientation, parallel to the coast.

## REGIONAL SETTING

The study area is situated at the emerged portion of the Pelotas Basin, southern Brazil. This basin's genesis was related to the South Atlantic opening, which began in the Lower Cretaceous. The coastal plain of Pelotas Basin has evolved mainly in response to 400 ka glacioeustatic cycles, being recognized as four barrier-lagoon depositional systems (Villwock *et al.*, 1986; Villwock and Tomazelli, 1995). Each system corresponds to high-frequency depositional sequences (Rosa *et al.*, 2011) that have developed during the Pleistocene and Holocene.

The Holocene coastal system, related to the younger depositional sequence, evolved in response to the last glacial cycle. The maximum sea level of the Postglacial Marine Transgression (PMT) reached  $2.1 \pm 1$  m higher than present at around 5.6 cal ka, subsequently followed by a slow sea level fall (Angulo *et al.*, 2006) (Figure 2). The regressive barrier at Passo de Torres is located in a coastal embayment, northeast of the

Mampituba River (bordering the Rio Grande do Sul state – RS) in southernmost coast of Santa Catarina state. This river is characterized by a low energy meandering fluvial system, which is connected to the ocean at the city of Torres (RS).

The climate is subtropical, with mean temperatures of 23°C in summer and 14°C in winter. The humidity is around 80%, and average precipitation rate is 1,500 mm per year (SEMA, 2000). Winds from E and NE directions predominate during the warmer months of spring-summer, while cyclonic winds from S and SW produced by cold fronts predominate during autumn-winter (Machado, 2005). The most frequent wave period is 8 s for easterly waves and 12 s for southerly waves, and their significant heights are 1.15 and 2 m, respectively (Araújo *et al.*, 2003). According to Siegle and Asp (2007), the swell is approaching from southern and eastern quadrants, and although less frequent, have high energy and long periods. These control the alongshore transport of sediments (littoral drift) in a northeast direction.

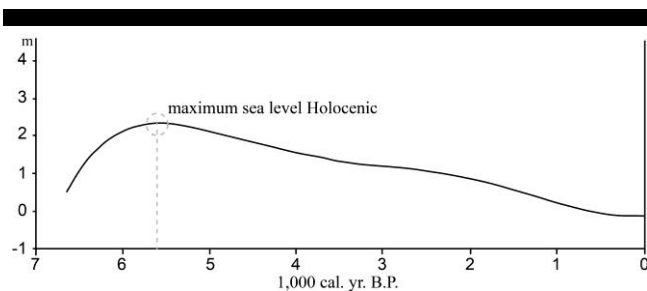


Figure 2. Holocene sea level curve for the southern coast of Brazil (Modified from Angulo *et al.*, 2006). Sea level reached  $2.1 \pm 1$  m higher than present at approximately 5.6 cal ka. In this period the longer paleochannel was active and connected with the ocean. Posteriorly sea level fall slowly, and the channel began its filling process.

This coast is microtidal with semidiurnal tides having a mean range of 0.5 m. If the mean variation related to meteorological effects is added to this value, the total tidal range, estimated with regards to field observations, is slightly larger than 1 m (Giannini, 1993). According to Gruber *et al.* (2006) the external morphologic limit of the dynamics of the shoreface is between -16 and -25 m depth.

## METHODS

This study is based on the analysis of ancient aerial photographs (scale of 1:40.000 from 1953, and a scale of 1:60.000 from 1965) with the purpose of eliminating the anthropic effect on the coastal region, profile elevation obtained through a Differential Global Positioning System (DGPS), Ground Penetration Radar (GPR) records, one drill hole survey and radiocarbon dating. A SIR-3000 data acquisition system of GSSI™ (Geophysical Survey Systems, Inc.) with 200 MHz antenna was used. The GPR system was connected to DGPS, achieving a real time topographic survey. A dielectric constant for sand (10) was used, representing a velocity of 0.1 m/ns (Davis and Annan, 1989). This constant was validated by lithological data obtained from the drill hole. The Common Off-set array was used. The field records of GPR were processed and interpreted through the software RADAN™ 6.6 and Reflex-Win®. The interpretation was based in the method of seismostratigraphy (Payton, 1977) adapted to the GPR (Neal, 2004). This method is based on termination (onlap, downlap, toplap and truncations), geometry and pattern of reflectors (Abreu *et al.*, 2010; Catuneanu *et al.*, 2009; Mitchum Jr. *et al.*, 1977; Vail, 1987).

The granulometric results refer to the mean diameter and standard deviation calculated by the analytical technique (sieve and settling tube). The mean diameter is expressed in the nominal scale of Wentworth (1922) and the standard deviation values are converted to the nominal sorting classes of Folk and Ward (1957). The morphoscopic analysis was based on comparative table of the Krumbein (1941) for roundness, and classification proposed by Bigarella (1955) for surface texture. These aspects in conjunction define the grain maturity, which is related to their properties (original shape, hardness, durability, i.e. resistance), and the sedimentary environment (agent of transportation, time or distance and the reworking in the accumulation basin).

Radiocarbon dating of a shell sample (shell *Donax* sp.) was performed by Beta Analytic Inc. The age of the shell sample was corrected considering a reservoir effect of  $8 \pm 17$  years, as defined

by Angulo *et al.* (2005) for the southern and southeastern Brazilian coast.

## RESULTS

Through the analysis of aerial photographs several features that truncate (erode) the adjacent foredune ridges and transgressive dunefields deposits were observed. These have elongate forms, 2 up to 25 km long, with SW – NE orientation, parallel to the coast. They exhibit a width between 150 and 350 m, and a thinning pattern toward the northeast. These features are interpreted as paleochannels. The direction showed by the inflection to the north of the paleochannels is in accordance with the littoral drift. Also observed, are semi-circular forms that represent abandoned meanders. Swales (shoals) between successive foredune ridges show narrow width (20 – 100 m) when compared to the paleochannels.

The DGPS and GPR profiles were acquired across the axis of the longer paleochannels. In the DGPS profile an observed concave form, revealed a broad floodplain, around 650 m wide. Using integrated interpretation of GPR and drill hole data, three radar facies (RFA, RFB and RFC) and one erosive surface were identified (Figure 3).

At the base of the GPR section, contorted and wavy reflectors with large wavelengths represent deposits generated in the shallow marine environment (upper shoreface – RFA). Similar sets of reflectors are described by Silva *et al.* (2010); Dillenburg *et al.* (2011) and Barboza *et al.* (2009, 2010, 2011, 2013). Due to limitations of the drill hole survey the lithology of this deposit was not defined.

Between approximately -5 and -5.5 m depth, reflectors with great contrast and lateral continuity for over 450 m were observed. These represent an erosive surface, interpreted as the base of the paleochannel. The erosive surface truncates reflectors that constitute the RFA. The sample obtained from drill hole indicates very well-sorted, quartzose medium sand (~85%) with large amounts of shell fragments (15%). Shells of the genus *Donax* sp. were collected intact with no signs of abrasion. This genus inhabits beach environments (specifically the intertidal zone – foreshore), not surviving in freshwater environments. The dating of these species revealed an age between 5,590 and 5,448 cal years BP (Beta Analytic – 337817). The morphoscopy reveals high irregularity with predominance of sub-angular grains and a sacaroidal superficial texture. These characteristics suggest a highly selective agent of transportation with a moderate degree of maturity.

The channel filling is initially represented by a set of non-continuous and undulated reflectors (RFB) with a downlap termination over the base of the paleochannel. The granulometry indicates well-sorted, quartzose fine sand with minor amount of shell fragments (2%). Medium sand is present in around 10%. The morphoscopy reveals high irregularity, with predominance of sub-angular to sub-rounded grains and a sacaroidal to mamelonada superficial texture. These characteristics suggest an agent of transportation moderately selective and an environment with a moderate degree of maturity. The initial filling is represented by fluvial sands.

Posteriorly the channel filling is represented by a set of reflectors parallel and continuous (RFC). In this radar facies the reflectors do not present a sharp contrast, evidencing homogeneous deposits, which is suggested by the granulometry (very well – sorted, quartzose fine sand, without medium sand). The morphoscopy reveals high regularity, with predominance of sub-rounded to rounded grains and a mamelonada superficial texture. These characteristics suggest an agent of transportation



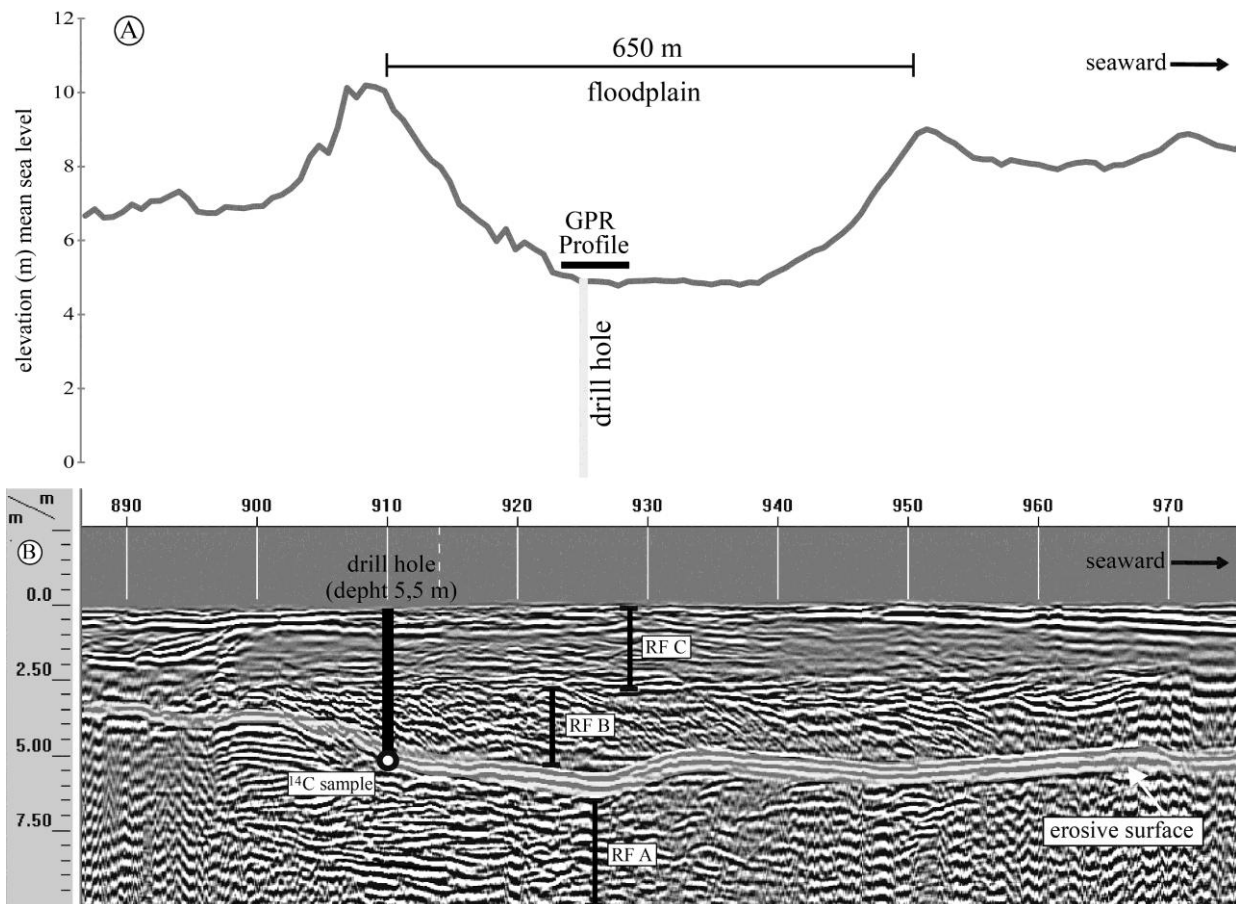


Figure 3. A) DGPS profile acquired across the axis of the longer paleochannels, evidencing the broad floodplain. B) GPR profile acquired with a frequency of 200 MHz, showing drill hole and dating location. Radar facies A (RFA) is characterized by deposits generated in shallow marine environment. This deposit is truncated by an erosive surface, interpreted as the base of the paleochannel. This surface is composed by medium sand and shell fragments (mainly *Donax* sp.). The dating radiocarbon of *Donax* sp. revealed an age between 5,590 and 5,448 cal years BP. RFB represents the initial phase of filling by fluvial sands and RFC represents the final filling by aeolian sands.

highly selective and an environment with moderate to high degree of maturity. The end of the filling is interpreted as aeolian sand.

## DISCUSSION AND CONCLUSION

The presence of several features of paleochannels indicates that these were active at some time during the Holocene. The GPR profile across the axis of the longer paleochannels showed an erosive surface that represents the base of paleochannel. This surface truncates reflectors of the RFA, suggesting that this paleochannel eroded deposits of the upper shoreface of the barrier. The granulometric results indicate that around 5 m depth an increase in grain size (fine sand grading to medium sand) and the presence of several shell fragments are characterizing a probable bedload transport. Shells of the genus *Donax* sp. collected intact provides evidence that this paleochannel once in the past had some connection with the sea (by an inlet), because this genus inhabits beach environments (foreshore) and does not survive in freshwater environments (Figure 4).

This paleochannel was developed in the form of a shore-parallel fluvial channel, with a SW – NE orientation, staying active even after progradation of the barrier. Simultaneously, or slightly after

the continuation of progradation, the fluvial action through the migration of the inlet results in the erosion of the backshore/foreshore deposits. The channel erosion may have resulted from a combination of high precipitation and high energy waves. Similar coast-parallel channel meanders was described in Green *et al.* (2013) for the east coast of South Africa.

The *Donax* sp. shells were incorporated in to bedload of the fluvial channel (medium sand) through an inlet, probably during storm surge events. These events carried beach sands by rolling and saltation, associated with the shells, towards the continent, which were incorporated into the fluvial sediments. The dating of these species revealed an age between 5.6 – 5.4 cal ka. The ages obtained are consistent with the maximum sea level of the PMT in southern Brazil. According to Angulo *et al.* (2006) sea level reached  $2.1 \pm 1$  m higher than present approximately 5.6 cal ka, subsequently followed by a slow fall.

Due to the fact that these shells inhabit exclusively beach environments, the dating allowed it to be inferred that this channel was active and had connection with the ocean at about 5.5 ka, concomitant with the maximum sea level of PMT. In this period the barrier in front of the channel was very narrow, no more than 300 m, probably analogous with the modern Araranguá River (60

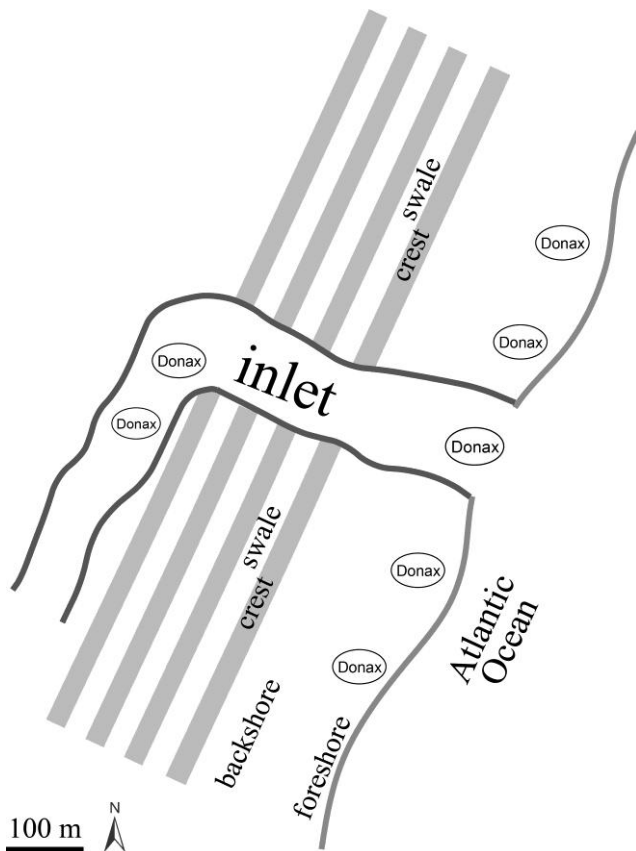


Figure 4. Illustrative figure showing the shore-parallel fluvial channel, with a SW – NE orientation. During the period between 5.6 – 5.4 cal ka, the barrier in front of the Mampituba River was narrow, no more than 300 m. The shells of *Donax* sp. that inhabits foreshore environment, was carried along the inlet, probably during storm surge, and deposited in the base of the channel.

km to the northeast of the study area – Figure 5). As the barrier in front of the channel was narrow, shells *Donax* sp. may have been carried to the river course through overwash process. The recognition of the interface between systems of marine and fluvial deposition of the Araranguá River is discussed in Barboza *et al.* (2014).

With the sea level fall associated with a high sediment budget, the barrier was influenced by a regime of forced regression. A decrease in the intensity of the water flow through the inlet conditioned the initiation of its filling. Sands load of the own channel (quartzose fine sand, well selected, irregular morphoscopy – RFB) initiated this process. Afterwards aeolian sands (quartzose fine sand, very well selected, regular morphoscopy – RFC) filled the channel. Therefore, the presence of a meandering fluvial system (actual Mampituba River) is an important factor, influencing the processes associated with the development of the regressive barrier at Passo de Torres.

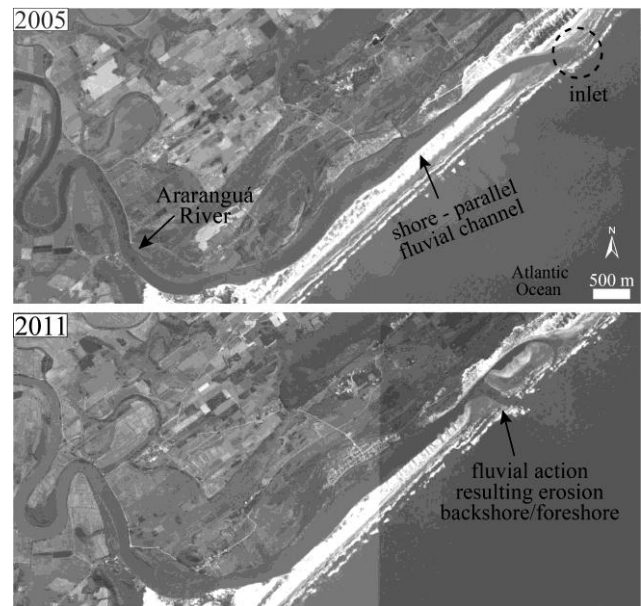


Figure 5. Satellite image (Google Earth) of the modern Araranguá River (60 km to the northeast of the study area). Image 2005 shows shore-parallel fluvial channel. The barrier in front of the channel is narrow, no more than 300 m. Image 2011 observed fluvial action through the migration of the inlet, which resulted in the erosion of the backshore/foreshore deposits. This coastal fluvial system is a modern example of the past behavior of the river Mampituba.

#### ACKNOWLEDGEMENT

This study was funded by Conselho Nacional de Desenvolvimento Científico e Tecnológico (CNPq – Brazil) via project n° 473227/2010-0. The authors Biancini da Silva, Barboza, Rosa and Dillenburg thank CNPq for their research grants.

#### LITERATURE CITED

- Abreu, V.S., Neal, J. and Vail, P.R., 2010. Integration of Sequence Stratigraphy concepts. In: Abreu, V.S., Neal, J., Bohacs, K.M. and Kalbas, J.L. (eds.), *Sequence Stratigraphy of siliciclastic systems – The ExxonMobil Methodology: atlas of exercises*, 209-224.
- Angulo, R.J., Souza, M.C., Reimer, P. and Sasaoka, S.K., 2005. Reservoir effect of the southern and southeastern Brazilian coast. *Radiocarbon*, 47, 67-73.
- Angulo, R.J., Lessa, G.C. and Souza, M.C., 2006. A critical review of Mid- to Late-Holocene sea-level fluctuations on the eastern Brazilian Coastline. *Quaternary Science Reviews*, 25, 486-506.
- Angulo, R.J., Lessa, G.C. and Souza, M.C., 2009. The Holocene Systems of Paranaguá and Northern Santa Catarina Coasts, Southern Brazil. In: Dillenburg, S.R. and Hesp, P.A. (eds.), *Geology and Geomorphology of Holocene Coastal Barriers of Brazil*. Springer, Lecture Notes in Earth Sciences, 107, 135-176.
- Araújo, C.E.S., Franco, D., Melo, E. and Pimenta, F., 2003. Wave regime characteristics of the southern Brazilian coast. *International Conference on Coastal and Port Engineering in Developing Countries*, COPEDEC VI, Colombo, Sri Lanka. Proceedings. Paper 97. CD-ROM.
- Barboza, E.G., Dillenburg, S.R., Rosa, M.L.C.C., Tomazelli, L.J. and Hesp, P.A., 2009. Ground-penetrating radar profiles of two Holocene regressive barriers in southern Brazil. *Journal of Coastal Research*, SI 56, 579-583.
- Barboza, E.G., Rosa, M.L.C.C., Dillenburg, S.R. and Tomazelli, L.J., 2010. The Holocene Coastal Barrier of Rio Grande do Sul (Southern Brazil): an Evaluation Based on GPR Data. In: 2010 Meeting of the Americas. Eos Trans. AGU, *Meet. Am. Suppl.*, v. 91. p. NS11A-03.

- Barboza, E.G., Rosa, M.L.C.C., Hesp, P.A., Dillenburg, S.R., Tomazelli, L.J. and Ayup-Zouain, R.N., 2011. Evolution of the Holocene Coastal Barrier of Pelotas Basin (Southern Brazil) - a new approach with GPR data. *Journal of Coastal Research*, SI 64, 646-650.
- Barboza, E.G., Rosa, M.L.C.C., Dillenburg, S.R. and Tomazelli, L.J., 2013. Preservation potential of foredunes in the stratigraphic record. *Journal of Coastal Research*, SI 65, 1265-1270.
- Barboza, E.G., Rosa, M.L.C.C., Dillenburg, S.R., Biancini da Silva, A. and Tomazelli, L.J., 2014. Stratigraphic analysis applied on the recognition of the interface between marine and fluvial depositional systems. *Journal of Coastal Research*, SI 66, 221-227.
- Bigarella, J.J., Hartkopf, C.C., Sobanski, A. and Trevisan, N., 1955. Textura superficial dos grãos de areias e arenitos (Contribuição à metodologia). Curitiba, *Arq. Biol. Tecn.*, X(11): 253-275.
- Boucher, E., Arseneault, D. and Héту, B., 2006. Holocene development of a floodplain along a small meandering stream, northern Québec, Canada. *Geomorphology*, 80, 267-281.
- Catuneanu O., Abreu, V.S., Bhattacharya, J.P., Blum, M.D., Dalrymple, R.W., Eriksson, P.G., Fielding, C.R., Fisher, W.L., Galloway, W.E., Gibling, M.R., Giles, K.A., Holbrook, J.M., Jordan, R., Kendall, C.G.S.T.C., Macurda, B., Martinsen, O.J., Miall, A.D., Neal, J.E., Nummedal, D., Pomar, L., Posamentier, H.W., Pratt, B.R., Sarg, J.F., Shanley, K.W., Steel, R.J., Strasser, A., Tucker, M.E. and Winker, C., 2009. Towards the standardization of sequence stratigraphy. *Earth-Science Reviews*, 92, 1-33.
- Costas, S. and FitzGerald, D., 2011. Sedimentary architecture of a spit-end (Salisbury Beach, Massachusetts). *Marine Geology*, 284, 203-216.
- Davis, J.L. and Annan, A.P., 1989. Ground-penetrating radar for high resolution mapping of soil and rock stratigraphy. *Geophysical Prospecting*, 37, 531-551.
- Dillenburg, S.R., Barboza, E.G., Hesp, P.A. and Rosa, M.L.C.C., 2011. Ground Penetration Radar (GPR) and Standart Penetration Test (SPT) records of a regressive barrier in southern Brazil. *Journal of Coastal Research*, SI 64, 651-655.
- Folk, R.L. & Ward, W.C., 1957. Brazos River Bar: Study and significance of grain size parameters. *Journal Sedimentary Petrology*, 27(1):03-26.
- Giannini, P.C.F., 1993. *Sistemas Depositionais no Quaternário Costeiro entre Jaguaruna e Imbituba, SC*. Universidade de São Paulo - SP, Tese, 439p.
- Green, A., Cooper, J.A.G. and LeVieux, A., 2013. Unusual barrier/inlet behavior associated with active coastal progradation and river-dominated estuaries. *Journal of Coastal Research*, SI 69, 35-45.
- Gruber, N.L.S., Corrêa, I.C.S., Nicolodi, J.L. and Barboza, E.G., 2006. Morphodynamic limits of shoreface and inner shelf at the northern coast of Rio Grande do Sul, Brazil. *Journal of Coastal Research*, SI 39, 664-668.
- Hein, C.J., Fitzgerald, D.M., Cleary, W.J., Albernaz, M.B., Menezes, J.T. and Klein, A.H.F., 2013. Evidence for a transgressive barrier within a regressive strandplain system: Implications for complex coastal response to environmental change. *Sedimentology*, 60 (2), 469-502.
- Krumbein, W.C., 1941. Measurements and geologic significance of shape and roundness of sedimentary particles. *Journal of Sedimentary Petrology*, 11, 64-72.
- Machado, C., 2005. *Morfodinâmica do trecho praiado entre Morro dos Conventos - Balneário Gaivota, SC*. (Dissertação de Mestrado). Programa de Pós-Graduação em Geografia, Universidade Federal de Santa Catarina, Florianópolis. 87p.
- Mitchum Jr., R.M., Vail, P.R. and Sangree, J.B., 1977. Seismic Stratigraphy and Global Changes of Sea Level, Part 6: Stratigraphy interpretation of seismic reflection patterns in depositional sequences. In: Payton, C.E. (ed.), *Seismic Stratigraphy — Applications to Hydrocarbon Exploration*. Tulsa, AAPG, 26, 117-133.
- Neal, A., 2004. Ground-penetrating radar and its use in sedimentology: principles, problems and progress. *Earth Science Reviews*, 66, 261-330.
- Payton, C.E., 1977. *Seismic Stratigraphy — Applications to Hydrocarbon Exploration*. Tulsa, AAPG, (Memoir # 26), 516 p.
- Rosa, M.L.C.C., Barboza, E.G., Dillenburg, S.R., Tomazelli, L.J. and Ayup-Zouain, R.N., 2011. The Rio Grande do Sul (southern Brazil) shoreline behavior during the Quaternary: a cyclostratigraphic analysis. *Journal of Coastal Research*, 64, 686-690.
- Sema - Secretaria do Meio Ambiente do Estado do Rio Grande do Sul. 2002. Relatório Anual sobre a situação dos Recursos Hídricos do Rio Grande do Sul. Região Hidrográfica das Bacias Litorâneas. Disponível em [www.sema.rs.gov.br/sema/html/pdf/modulo3.pdf](http://www.sema.rs.gov.br/sema/html/pdf/modulo3.pdf).
- Siegle, E. and Asp, N.E., 2007. Wave Refraction and Longshore Transport Patterns along the Southern Santa Catarina Coast. *Brazilian Journal of Oceanography*, 55, 109-120.
- Silva, A.B., 2009. *Mapeamento e Caracterização dos Depósitos em Subsuperfície do Setor Meridional da Planície Costeira de Santa Catarina*. Porto Alegre. Trabalho de Conclusão de Curso de Graduação em Geologia, Instituto de Geociências, Universidade Federal do Rio Grande do Sul. Porto Alegre - RS. 66p.
- Silva, A.B., Barboza, E.G., Rosa, M.L.C.C. and Fracalossi, F.G., 2010. Caracterização dos Depósitos Sedimentares em Subsuperfície no Setor Meridional da Planície Costeira Sul de Santa Catarina. *Gravel* 8, 1-7.
- T. van der Schriek., Passmore, D.G., Rolão, J. and Stevenson, A.C., 2007. Estuarine-fluvial floodplain formation in the Holocene Lower Tagus valley (Central Portugal) and implications for Quaternary fluvial system evolution. *Quaternary Science Reviews*, 26, 2937-2957.
- Vail, P.R., 1987. Seismic Stratigraphy Interpretation Using Sequence Stratigraphy. Part 1: Seismic Stratigraphy Interpretation Procedure. In: Bally, A.W. (ed.), *Atlas of Seismic Stratigraphy*. Tulsa, AAPG, 27 (1), 1-9.
- Villwock, J.A. and Tomazelli, L.J., 1995. Geologia Costeira do Rio Grande do Sul. Centro de Estudos de Geologia Costeira e Oceânica, Instituto de Geociências, Universidade Federal do Rio Grande do Sul, Porto Alegre - RS, *Notas Técnicas*, 8, 45p.
- Villwock, J.A., Tomazelli, L.J., Loss, E.L., Dehnhardt, E.A., Horn, N.O., Bachi, F.A. and Dehnhardt, B.A., 1986. Geology of the Rio Grande do Sul Coastal Province. In: Rabassa, J. (Ed.), *Quaternary of the South America and Antarctic Peninsula*, vol. 4. A.A. Balkema, Rotterdam. 79-97.
- Wentworth, C.K., 1922. A scale of grade and class terms for clastic sediments. *Journal of Geology*, 30, 377-392.

# Dune coast changes caused by weak storm events in Miedzywodzie, Poland

Natalia Bugajny† and Kazimierz Furmańczyk

Institute of Marine and Coastal Sciences  
University of Szczecin  
Szczecin, Poland  
†natalia.bugajny@univ.szczecin.pl



[www.cerf-jcr.org](http://www.cerf-jcr.org)



[www.JCRonline.org](http://www.JCRonline.org)

## ABSTRACT

Bugajny, N. and Furmańczyk, K., 2014. Dune coast changes caused by weak storm events in Miedzywodzie, Poland In: Green, A.N. and Cooper, J.A.G. (eds.), *Proceedings 13<sup>th</sup> International Coastal Symposium* (Durban, South Africa), *Journal of Coastal Research*, Special Issue No. 70, pp. 211-216, ISSN 0749-0208.

This paper describes the impact of weak storm events on morphological changes of the sandy, non-tidal Southern Baltic coast. It was initially assumed that weak storms do not cause any significant changes on the coast, i.e. dune erosion. For this purpose, 14 RTK-GPS surveys were carried out during June to December 2012, consisting of a cross-shore profile every 100 m along a 2 km stretch of coast. Offshore wave data (WAM model) and water level data (tide gauge) were also collected. The hydrodynamic conditions were grouped into 3 groups by Ward's hierarchical cluster analysis to investigate relationships with morphological changes on the coast. Correlation between volume changes and shoreline displacement for profiles and each group of hydrodynamic conditions were obtained. The correlation coefficient value for profiles ranged from  $R=0.41-0.91$ ; and for groups  $R=0.79-0.82$ . It was found that for the first group ( $H_s < 1$  m), accumulation was observed almost in the whole area. For the second hydrodynamic group, some profiles accumulated while others experienced erosion. For the last group, erosion processes were dominant. The study reveals the oscillating nature of the coast within the study area. Volumetric changes between the first and last survey ranged from  $+0.8$  m<sup>3</sup>/m to approximately  $-1.2$  m<sup>3</sup>/m and the shoreline changed from rough to smooth.

**ADDITIONAL INDEX WORDS:** RTK-GPS, shoreline displacement, beach volume changes, dune coast, storm events, Southern Baltic coast

## INTRODUCTION

Sandy coasts are dynamic environments which are continuously changing. Morphological changes can be considered at different time and spatial scales. In the short-term, coastal changes are primarily due to variability in wave energy, whereas in the long-term scale (centuries, millennia), coastal variability is mostly related to relative oscillations of sea level and river sediment supply, caused mainly by climatic changes (Cowell and Thom, 1994). Beach topographical profiling by RTK-GPS survey, which is being successfully deployed to sandy coasts (Harley *et al.*, 2011; Hansen and Bernard, 2009, Ortega-Sanchez, *et al.*, 2008) and for some aspects to cliffs as well (Wziątek *et al.*, 2011), is the most common technique allowing monitoring of morphological changes in a short-term scale. These measurements are usually repeated at regular intervals, in order to measure daily as well as monthly to annual variations of specific parameters to understand physical aspects of coastal environments (Komar, 1998; Short, 1999).

The aim of this study is to assess the influence of weak storms on the morphological changes of the coastal zone. This paper presents the results of the examination of short-term (2 weeks interval, on average) profile variability using beach and shallow water (1 m depth) profile data combined with wave data and water level data collected at the study area. The investigated area is a 2 km-long section of dune coast of the non-tidal Baltic Sea. The section is located in the central part of the Pomeranian Bay, in the western part of the Dziwnow Spit. The entire Dziwnow Spit is

approximately 14 km long and is divided into western and eastern parts by an inlet. The western part is 2 km wide and has a well-developed dune system. Some dunes are 12 m high and act as natural protection for the hinterland, where the town of Miedzywodzie is located. The dunes are fronted by a 30-50 m wide beach. The nearshore slopes dip gently northwestwards. A system of 2-3 nearshore bars (2 m high) is present. The beach and bottom sediments consist of fine and medium sand. Due to the erosive tendency of the coast (Zawadzka-Kahlau, 1999; Dudzińska-Nowak, 2006a), the entire eastern part and a portion of the western part of the spit are protected by various hydro-engineering structures (Figure 1), which significantly modify the natural morphodynamic processes and cause local intensification of coastal erosion (Dudzińska-Nowak, 2006b).

Long-term research on coastline changes along the Dziwnow Spit was carried out using cartographic methods for the period 1875-1979 on the basis of historical topographic maps (Zawadzka-Kahlau, 1999) and for the period 1938-1996 on the basis of aerial images (Dudzińska-Nowak, 2006a). The research revealed strong erosive tendencies of over 0.7 m/yr for this section of the coast. Another study on evolution of the coastline of Pomeranian Bay, at different time scales, was also carried out by Schwarzer *et al.*, (2003). From their observations, short-term changes (storm events, which were the shortest in this study), superimpose seasonal variations and seem to strongly influence processes occurring at the decadal scale. Thus, processes on different time scales appear to interact.

Comprehensive knowledge on forcing and related processes affecting shoreline changes is essential, in order to improve to the

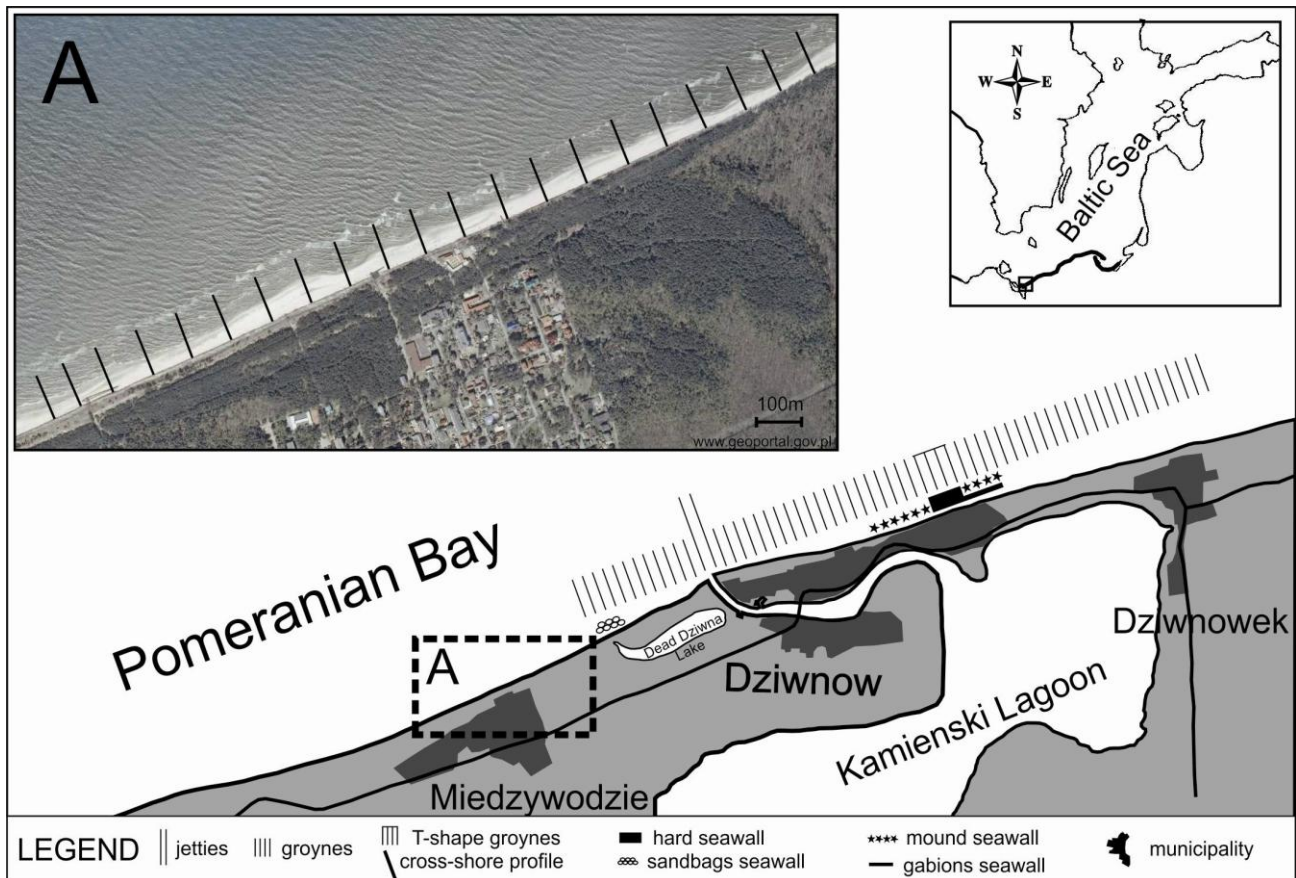


Figure 1. Investigated area with location of the twenty one cross-shore profiles of RTK-GPS surveys.

efficiency of coastal zone management and to improve future projections of coastal behaviour, for the Pomeranian Bay (Deng *et al.*, 2013).

The wave climate in the Pomeranian Bay was based on the wave measurements (Paplińska, 2001) and on a 44-year hind cast (1958-2001) of wave field over the Baltic Sea performed within the HIPOCAS project (Cieślakiewicz and Paplińska-Swerpel, 2008). The mean value of the significant wave height over the period of measurements was 0.75 m and the mean significant period - 4.0 s. The greatest measured height of an individual wave was 6.5 m and the maximum value of a measured wave period was 9.5 s. The highest significant wave height was 3.3 m. Significant wave height over 1.0 m occurred 28% of the time. 25% of waves moved in an easterly direction, 21% and 20%, respectively SW and SE. Only 16% of the waves moved southwards.

Analysis of wave modelling results shows that wave fields are not homogeneous in the Pomeranian Bay. A gradual increase (up to 50%) of yearly mean values of selected wave parameters can be observed from the south-west to north-east. Wind climate and shape of the basin determine directional distribution of significant wave height which prevails in easterly, south-easterly, south-westerly directions.

## METHODS

Wave parameters were obtained from the WAM model (Wave Model) Cycle 4 (WAMDI Group, 1988) provided by the

Interdisciplinary Centre for Mathematical and Computational Modelling of Warsaw University (ICM). The WAM model for the Baltic Sea was validated as described by Cieślakiewicz and Paplińska-Swerpel (2008). Hourly data including offshore significant wave height, peak period and mean wave direction were collected for a point located approximately 6 km north of the town of Miedzywodzie (54.0579°N, 14.664°E). The data refer to the period from June to December 2012.

Water level data were derived from the tide gauge of Institute of Meteorology and Water Management (IMGW), which is installed in the Dziwna mouth. The data are available on the IMGW's website [www.pogodynka.pl](http://www.pogodynka.pl) exclusively. These are hourly data on water level value referred to Kronstadt zero-level.

The time series of wave parameters and water level for the period of research is presented on figure 2. Additionally, trends of water level variations were calculated for the particular time intervals. The collected data were analysed and grouped by means of Ward's hierarchical cluster analysis (Ward, 1963), in order to find group hydrodynamic conditions in time intervals and effects in form of morphological changes occurring on the coast.

Coastal monitoring was carried out on the 2 km-long section of the dune coast of the southern Baltic Sea in the area of Miedzywodzie. 14 surveys were carried out from June to December 2012, where RTK-GPS of horizontal ( $\pm 1.5$  cm) and vertical ( $\pm 2$  cm) accuracy was deployed. Cross-shore profiles were measured from the dune base to a depth of approximately -1 m every 100 m along the coast (Figure 1).

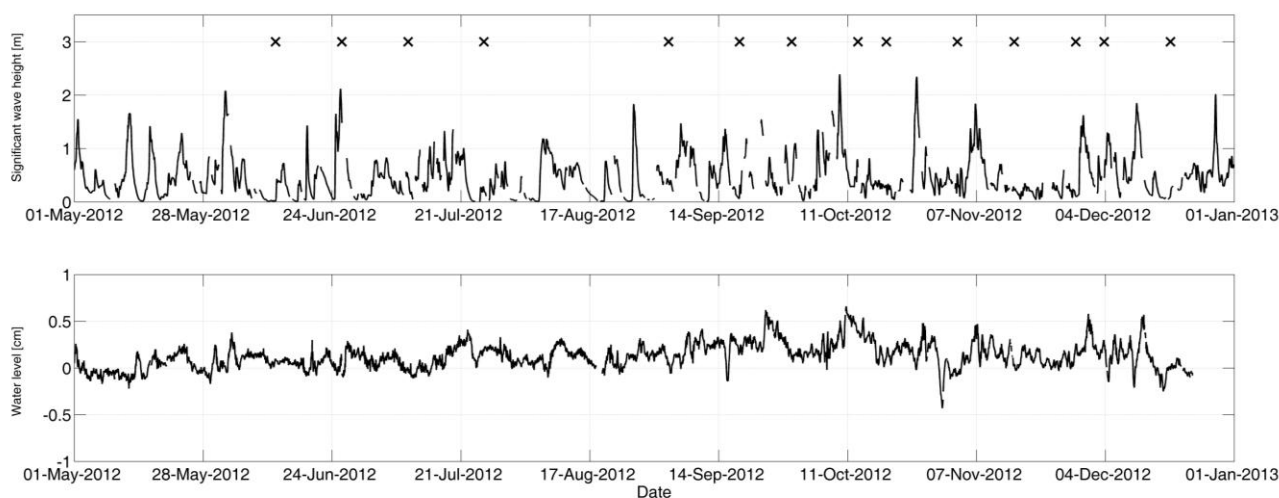


Figure 2. Time series of significant wave height (upper) and water level (lower) from May to December 2012. RTK-GPS survey times are marked by x-es.

Height of profiles was referred to the Konstadt zero-level. The dates of particular surveys depended on hydrological and meteorological conditions. Time interval between subsequent surveys was not constant and averaged every 2 weeks roughly. This study defined a storm event if significant wave height exceeds 1 meter ( $H_s > 1$  m). No significant storm events, i.e. events that cause dune erosion (Furmańczyk *et al.*, 2012), were recorded within the period of the study. However, weak storm events occurred that did not cause dune erosion. Due to difficult meteorological conditions during the last two surveys measurements were taken only on the every second profile, i.e. every 200 m.

Each profile was interpolated every 1 m, which allowed comparison of particular measurement series at the same elementary points. Widely applied statistics were deployed for each created elementary point. The statistics were: mean value, standard deviation, difference between particular measurements, difference between maximal and minimal height. Additionally, an average of the shoreline position along the investigated area and its deviations as well as minimum and maximum location values were defined. The shoreline in the studies was a datum-based shoreline, which is defined as the intersection of a specific elevation datum equal mean sea level (zero Kronstadt). Moreover, the sand volume in each profile was calculated between mean sea level (zero Kornstadt) point and dune base point, in order to calculate the correlation coefficient, similar to Farris and List (2007).

## RESULTS AND DISCUSSION

### Hydrodynamic characteristics

The period from June to December 2012 was characterized by predominance of waves of significant wave height less than 0.5 m (63%). Waves of 0.5-1.0 m height accounted for 23% of the wave height, whereas waves of over 1.0 m occurred only in 10% of the study period. Easterly, south-easterly, south-westerly directions

were dominant wave directions over that time. These directions accounted for 20%, 30% and 20%, respectively.

Water level changes recorded during the studies oscillated between -0.43 and +0.56 m relative to mean sea level (zero Kronstadt).

### Hydrodynamic classification

Classification of the hydrodynamic conditions was carried out by means of Ward's hierarchical cluster analysis (Figure 3). Five parameters that specify each time interval were considered. They included: maximum significant wave height for the time interval, coefficient of trend of water level variations for the time interval, time spans from the last storm event within the time interval to the end of the period (days), duration time of the last storm event for the time interval (hours) and number of storms for the time interval (when  $H_s > 1$  m).

Three classes of hydrodynamic conditions were identified. The first class (3 occurrences) is characterised by lack of storm events, so that the significant wave height did not exceed 1 m. The second class (4 occurrences) is characterised by the occurrence of 2-3 weak storm events of significant wave height from 1.4 m to 1.9 m. The third class (6 occurrences) includes 1 to 5 storms of significant wave height from 1.5 to 2.4 m.

### Morphological changes

Beach volume changes between the first and last survey are shown on figure 4a. Maximal changes that occurred there amounted to 1.6 m<sup>3</sup>/m. Fig 4a shows the situation, where beach accumulation appeared among the middle beach, while erosion focused on the lower beach and shallow water. Volumetric changes ranged from +0.8 m<sup>3</sup>/m to approximately -1.2 m<sup>3</sup>/m. The shoreline position changed from the very rough in the beginning of the measuring season to very smooth at the end of it, while the western part was receding, the eastern part accreted. Mean width of the beach over the entire study period oscillated between 29 and 53 m, with the lowest mean values at the edges of the study site, during the investigated period.

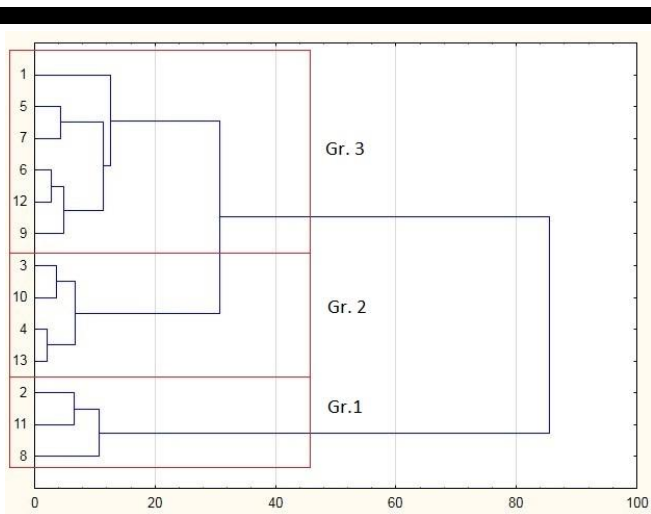


Figure 3. Cluster dendrogram presenting the separation of the three groups of hydrodynamic conditions using hierarchical Ward cluster analysis. Hydrodynamic intervals are listed on vertical axis.

Analysis of the standard deviation values of volumetric changes for each elementary point shows that the greatest changes occur in shoreline displacement (Figure 4b). Three types of profile with distinctive dynamics were distinguished on the basis of maximal standard deviation values of volumetric changes and maximal changes of shoreline displacement for the entire investigated period of time. Limit values between particular groups were: mean value of maximal standard deviation value,  $0.36\text{m}^3/\text{m}$  and mean value of maximal change of shoreline displacement in the profile,

10 m. The first group is consists of very dynamic profiles. These profiles are characterized by above mean value of shoreline displacement oscillation and above mean standard deviation values of volumetric changes. The second group contains profiles that are characterized by below mean values of the aforementioned parameters, which means that they are of low dynamics. The third group is composed of profiles that are diverse in terms of dynamics, so that they received values over or below the mean values of the parameters.

The spatial analysis of the results proves that the most dynamic profiles are located in the western and central-eastern parts of the investigated area, while the stable ones are in the central part. The location of dynamic profiles in the western part can be related to dominance of storm waves that arrive from the western sector during storm events (see wave characteristics), whereas the eastern part of the investigated area is protected by a group of groynes (Figure 1).

Furthermore, correlation coefficients between shoreline displacement and beach volume changes were calculated for all surveys with division into particular profiles. Their spatial distribution is presented on figure 5. The value of correlation coefficient along the investigated area oscillates between  $R=0.41-0.91$  and its mean value is  $R=0.79$ . Most of the profiles reveal good correlation between shoreline displacement and volume changes. Only 2 profiles stand out and they have  $R$  values less than 0.6

Correlations between shoreline displacement and volume changes of the beach for all measurements and with the division into 3 profile groups of hydrodynamic conditions are demonstrated on figure 5. The correlation coefficient for all measurements amounts to  $R=0.79$  (Figure 5a), which means a good correlation.

The group which contains no storm events, i.e.  $H_s < 1$  m

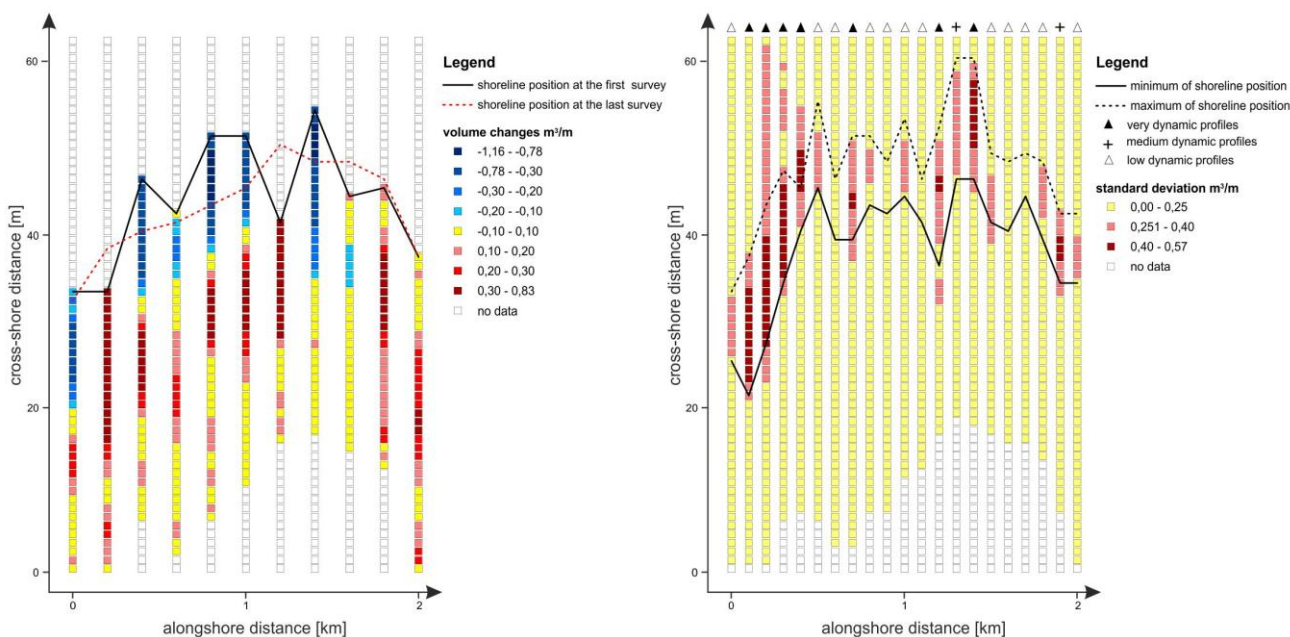


Figure 4. Morphological changes between first and last RTK-GPS survey with shoreline position at these particular surveys (left), standard deviations of volume changes with maximum and minimum positions of shoreline (right). Types of dynamic profiles are marked by triangles and crosses.

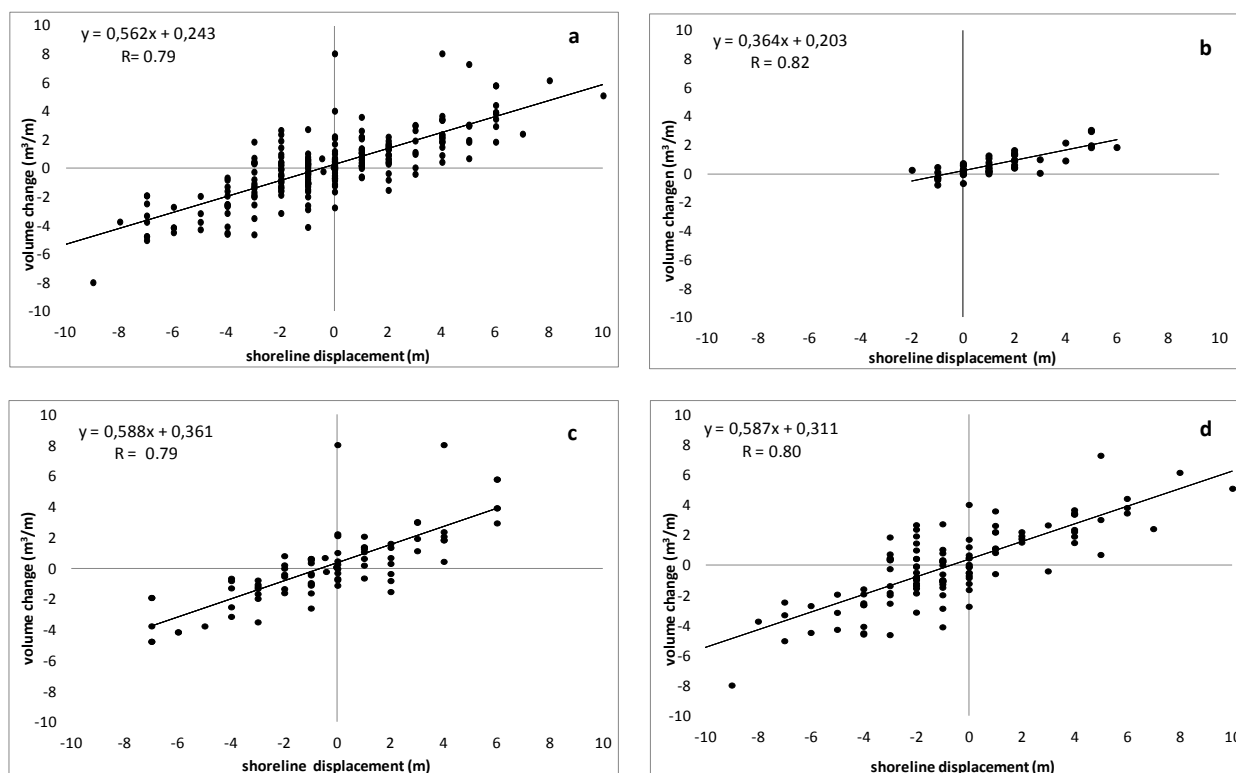


Figure 5. Beach volume changes vs. shoreline displacement. a) all observations, b) the first group of hydrodynamic conditions, c) the second group of hydrodynamic conditions, d) the third group of hydrodynamic conditions.

(Figure 5b), experiences accumulation, both in terms of shoreline displacement (30/7) and beach volume changes (46/7). The values in brackets refer to the number of profiles with registered accumulation/erosion in time interval qualified to particular groups. The correlation coefficient for this group is  $R=0.82$ . Maximal differences in shoreline accumulation values amounts to 6 m, while beach volume changes are approx.  $4 \text{ m}^3/\text{m}$ . The second group (Figure 5c), where time intervals contain 2-3 weak storm events of significant wave height smaller than 1.9 m, reveals similar accumulation and erosion changes, both for shoreline displacement (30/41) and beach volume changes (41/41), so the processes are in equilibrium. The correlation coefficient for this group is  $R=0.79$ . Maximal differences of shoreline accumulation values amount to 6-7 m, while beach volume changes are up to  $8 \text{ m}^3/\text{m}$ . The third group (Figure 5d), where time intervals can contain up to 5 weak storm events and significant wave height oscillates between 1.5 and 2.4 m, also shows accumulation and erosion changes. The changes of beach volume are similar (57/59), whereas the changes of shoreline are dominated by erosion (31/69). The correlation coefficient for this group is  $R=0.80$ . Maximal differences of shoreline accumulation values amounts to 10 m, while beach volume changes are up to  $8 \text{ m}^3/\text{m}$ .

Therefore, waves with heights  $<1 \text{ m}$  cause beach volume increase in most of the investigated areas with a simultaneous advance of the shoreline. This is related to onshore sediment transport and beach accretion during calm wave conditions. The wave increase to the range of 1.4-1.9 m causes activation of erosion processes, however, they remain temporally in equilibrium with accumulation processes. Further increase to the values 1.5-2.4 m however, causes dominance of erosion processes.

The correlation coefficients between the shoreline displacement and beach volume changes for all measurements in the investigated area ( $R=0.79$ ) as well as for particular profiles ( $R=0.41-0.91$ ) which are similar to those reported by Farris and List (2007). They obtained a correlation coefficient of  $R=0.73-0.96$  for 4 investigated areas. The spatial diversification of correlation coefficient values was also visible and it oscillated between  $R=0.43$  and  $R=0.98$  for particular profiles. Likewise, a high correlation between the shoreline displacement and beach volume changes that amounted to  $R=0.90$  was also obtained by Lee *et al.* (1995), whereas Dail *et al.*, (2000) correlated average values of shoreline displacement and beach volume changes in their studies with a correlation coefficient of  $R=0.98$ . This confirms the assumption that there is a positive relationship between shoreline displacement and beach volume changes.

Additionally, Farris and List (2007) investigated the dependency of shoreline displacement and volume changes in two characteristic profiles, with accumulation and erosional nature. On the other hand, the 100 m-spaced profiles in the in the 2 km-long study area, show that the same storm event has caused diverse effects on the coast.

## CONCLUSION

On the basis of 14 RTK-GPS surveys carried out from June to December 2012, shoreline changes and beach volume changes short-term periods (every 2 weeks at average) for 21 cross-shore profiles located on dune coast were analysed.

The most dynamic volume changes took place within the area of maximum shoreline displacement. Correlation coefficients of shoreline displacement and beach volume changes for all



observations ( $R=0.79$ ) and for all profiles of the investigated period of time ( $R=0.41-0.91$ ) were good. Furthermore, 3 profile groups of diversified dynamics were distinguished.

Hydrodynamic conditions in the study period were classified by means of Ward's method into 3 time temporal groups. The first group is associated with waves below 1 m, i.e. no storm events; the second group contains 2-3 storm events of significant wave height oscillating between 1.4 and 1.9 m; the last group includes 1-5 storm events with significant wave height oscillating between 1.5 and 2.4 m.

Furthermore, a correlation coefficient between shoreline displacement and beach volume changes divided into 3 time interval groups of specific hydrodynamic conditions was high for all groups.

Individual time intervals associated with particular hydrodynamics caused diverse effects on the shore. The group containing no storms caused accumulation in most of the investigated area, both in terms of shoreline displacement and beach volume changes. The second dynamic group yielded both erosion and accumulation, although these processes are equilibrating each other. The third group was characterised by both erosion and accumulation, but erosion was dominant.

Weak storms (which do not cause dune erosion) cause diverse effects within the study area (of the non-tidal sea). These include both accumulation and erosion, the magnitude of which depends on hydrological conditions and proves of oscillating nature of the coast.

#### ACKNOWLEDGEMENT

The authors would like to thank ICM (Interdisciplinary Centre for Mathematical and Computational Modeling) for providing wave data from the WAM model.

#### LITERATURE CITED

- Cieślakiewicz, W. and Paplińska-Swerpel, B., 2008. A 44-year hindcast of wind wave fields over the Baltic Sea. *Coastal Engineering*, 55 (11), 894-905.
- Cowell, P.J. and Thom, B.G., 1994. Morphodynamics of coastal evolution. In: Carter, R.W.G and Woodroffe, C.D. (eds.), *Coastal evolution, Late Quaternary shoreline morphodynamics*, Cambridge University Press, 33-86.
- Dail, H.J., Merrifield, M.A. and Bevis, M., 2000. Steep beach morphology changes due to energetic wave forcing. *Marine Geology*, 162, 443-458.
- Deng, J., Zhang, W., Harff, J., Schneider, R., Dudzińska-Nowaka, J., Terefenko, P., Giza, A. and Furmańczyk, K., 2013. A numerical approach for approximating the historical morphology of wave-dominated coasts – A case study of the Pomeranian Bight, southern Baltic Sea. *Geomorphology*, 204, 425-443.
- Dudzińska-Nowak, J., 2006a. Coastline long-term changes of the selected area of the Pomeranian Bay. In: Tubielewicz, A. (ed.), *Proceedings 8<sup>th</sup> International Conference LITTORAL* (Gdańsk, Poland), *Coastal Dynamic, Geomorphology and Protection*, pp. 163-170.
- Dudzińska-Nowak, J., 2006b. Wpływ metod ochrony brzegu morskiego na zmiany położenia linii podstawy wydmy na wybranym przykładzie. In: Koźmiński, Cz., Dutkowski, M. i Radziejewska, T. (ed.), *Człowiek i środowisko przyrodnicze Pomorza Zachodniego: III. Środiwsko przyrodnicze i problemy społeczno-ekonomiczne*. Szczecin, pp. 91-98.
- Farris, A.S and List, J.H., 2007. Shoreline changes as a proxy for subaerial beach volume change. *Journal of Coastal Research*, 23, 740-748.
- Furmańczyk, K. K., Dudzińska-Nowak, J., Furmańczyk, K. A., Paplińska-Swerpel, B. and Brzezowska, N. 2012. Critical storm thresholds for the generation of significant dune erosion at Dziwnów Spit, Poland. *Geomorphology*, 143-144, 62-68.
- Komar, P.D., 1998. *Beach Processes and Sedimentation*. 2nd ed. Prentice-Hall, Englewood Cliffs, NJ, 544pp.
- Lee, G., Nichols, R.J., Birkemeier, W.A. and Latherman, S., 1995. A conceptual fair-weather-model of beach nearshore profile evolution at Duck, North California, USA. *Journal of Coastal Research*, 11, 1157-1166.
- Ortega-Sanchez, M., Fachin, S., Sancho, F. and Losada, M.A., 2000. Relation between beachface morphology and wave climate at Trafalgar beach (Cadiz, Spain). *Geomorphology*, 99, 171-185.
- Paplińska, B., 2001. Specific features of sea waves in the Pomeranian Bay. *Archives of Hydro-Engineering and Environmental Mechanics*, 48 (2), 55-72.
- Short, A.D., 1999. *Beach and Shoreface Morphodynamics*. John Wiley and Sons, Chichester, 379 pp.
- Schwarzer, K., Diesing, M., Larson, M., Niedermeyer, R.O, Schumacher, W. and Furmańczyk, K., 2003. Coastline evolution at different time scales: examples from the Pomeranian Bight, southern Baltic Sea. *Marine Geology*, 194, 79-101.
- Ward, J.H., 1963. Hierarchical grouping to optimize an objective function. *Journal of the American Statistical Association*, 58, 236-244.
- WAMDI Group, 1988. The WAM model-a third generation ocean wave prediction model. *Journal of Physical Oceanography*, 18, 1775-1810.
- Wziętek, D., Vousdoukas, M.V. and Terefenko, P., 2011. Wave-cut notches along the Algarve coast, S. Portugal: Characteristics and formation mechanisms, In: Furmańczyk, K. (ed.), *Proceedings 11<sup>th</sup> International Coastal Symposium* (Szczecin, Poland), *Journal of Coastal Research*, Special Issue No. 64, pp. 855-859.

## Morphological changes of a Mediterranean beach over one year (San Giovanni Sinis, western Mediterranean)

Simone Simeone†, Giovanni De Falco†, Giovanni Quattrocchi†, Andrea Cucco†

†Istituto per l'Ambiente Marino Costiero.  
IAMC – CNR. U. O. Oristano, loc Sa  
Mardini 09072  
Torregrande, Or.  
[simone.simeone@iamc.cnr.it](mailto:simone.simeone@iamc.cnr.it)  
[giovanni.defalco@iamc.cnr.it](mailto:giovanni.defalco@iamc.cnr.it)  
[giovanni.quattrocchi@iamc.cnr.it](mailto:giovanni.quattrocchi@iamc.cnr.it)  
[andrea.cucco@iamc.cnr.it](mailto:andrea.cucco@iamc.cnr.it)



[www.cerf-jcr.org](http://www.cerf-jcr.org)



[www.JCRonline.org](http://www.JCRonline.org)

### ABSTRACT

Simeone, S., De Falco, G., Quattrocchi, G., Cucco, A. 2014. Morphological changes of an Mediterranean beach over one year (San Giovanni Sinis, western Mediterranean). In: Green, A.N. and Cooper, J.A.G. (eds.), *Proceedings 13<sup>th</sup> International Coastal Symposium* (Durban, South Africa), *Journal of Coastal Research*, Special Issue No. 70, pp. 217-222, ISSN 0749-0208.

Mediterranean beaches experience major modifications in their morphology and grain size features mainly during intense storms and extreme meteo-marine events. The assessment of beach response to storms can be useful in the evaluation of coastal hazards, and in relation to the efficiency of management projects such as artificial nourishment. This paper aims to establish the subaerial morphological response of a beach located in western Sardinia (western Mediterranean) during the period of a year. Both experimental and numerical approaches were adopted to investigate the beach system. In particular, beach profiles, acquired by means of Differential Positioning System were used to analyze the morphological changes of the beach and wave parameters and current velocity data were collected by means of an Acoustic wave and current meter (ADCP). Numerical techniques were also applied to investigate the hydrodynamics in the area of study. Coupled wind wave - 3D hydrodynamic finite element model were used to reproduce the wave propagation and the wind, tide and wave induced 3D water circulation along the coastal areas, and it displayed a good accuracy. During the year, the beach experienced intense morphological changes in the area where submerged beach is not occupied by rocky outcrops and the model was also able to reproduce the related observed periods of strong wind wave events. The interdisciplinary approach allowed an evaluation to be made about the response of the beach morphology in respect to meteo-marine forcings.

**ADDITIONAL INDEX WORDS:** *beach morphology, storms, beach profile, numerical model.*

### INTRODUCTION

The morphology of beaches can be influenced by different factors such as wave climate, geological inheritance and sediment grain size. These can combine to influence beach shape and dynamics (Short, 1996). The interactions between these factors, or alternatively acting alone, can influence the characteristics of the beach system.

Storm events can cause coastal erosion, coastal flooding and damage to the infrastructure. The impact of such events can be influenced by large, medium-range and local scale processes (Del Rio *et al.*, 2011). Main large and meso-scale processes are represented by tide and onshore winds which can locally have an effect only on the change of the sea surface elevation. On the other hand, at local scale, near the shore, the main forces are the waves breaking and swash processes (Benavente *et al.*, 2006), which play an important role on both changing the SSE (wave set-up) and on changing the beach sediment budget. The combination of the

aforementioned processes is the main force affecting the evolution of a beach profile at seasonal and yearly time scales.

In the Mediterranean Sea the tide can be neglected as a factor influencing the morphological evolution of the littoral zones. Only the wind and the waves can be considered as the main forcing acting at both meso and local scale (Basterretxea *et al.*, 2004). Thus, the beaches experience profound modifications in morphology and grain size composition only during intense storms and extreme meteo-marine events. The response of beaches to storms can also be influenced by the geomorphic context of the coastline, such as coastal orientation, presence of reef closer to the shoreline and the topography of the nearshore, as well as storm parameters (Gallop *et al.*, 2012; Gallop *et al.*, 2011; Almeida *et al.*, 2010; Backstrom *et al.*, 2008).

The assessment of beach response to storms can be useful in the evaluation of coastal hazards in particular on artificial nourishment projects, and in general, to improve the effectiveness of coastal management plans.

DOI: 10.2112/SI70-037.1 received 29 November 2013; accepted 21 February 2014. © Coastal Education & Research Foundation 2014

The aim of this study was to establish the sub-aerial morphological response of a beach located in western Sardinia (western Mediterranean Sea) during a whole meteorological year.

An interdisciplinary approach, encompassing both numerical and experimental methods, was followed to investigate the morphological changes as well as the natural recovery of the beach of interest after intense storm events.

In particular, the morphological variability of the beach profiles on its sub-aerial part was analyzed by using a Differential Global Positioning System. At the same time, and for the whole investigated period, bottom mounted ADCP probe were used to collect wave data. Finally, a high resolution coupled waves-currents numerical model SHYFEM3D-WWM (Cucco *et al.*, 2012; Umgiesser *et al.*, 2004;) was applied to reproduce the temporal and spatial variability of the main wave features along the whole investigated period and for the domain of interest. The influence of both large and local scale forcings were simulated and the obtained data have been used to investigate the relationship between the morphological changes and the wind waves features in the study area.

## STUDY AREA

San Giovanni beach is located on the Sinis Peninsula (SGS hereafter) in the western side of Sardinia, western Mediterranean (Figure 1). It is included in the Marine Protected Area of the “Penisola del Sinis, Isola di Maldiventre”, established in 1997 by the Italian Minister of the Environment. The geological setting of the Sinis peninsula includes a sequence of volcanic and sedimentary rocks (marls, sandstone and limestone) dating from the Neogene to the present (Marini and Murru, 1977). The coastline is characterized by several rocky outcrops built up by well cemented Late Pleistocene aeolian sandstones (Lecca and Carboni, 2007; Davaud *et al.*, 1991).

The sediment grain size of the San Giovanni beach ranges between fine-medium sand and coarse sand. The sediments have a bimodal distribution due to the presence of both siliciclastic and biogenic carbonate grains the latter prevalent (80% of the total sediments) in the submerged beach from the depth of 1m (De Falco *et al.*, 2003).

The prevailing winds are mainly from the north-west (Mystral), often in the form of severe storms, especially during winter. In autumn and winter, southwestern winds (Libeccio) are also important (Corsini *et al.*, 2006). The tides are negligible with a maximum water displacement of < 0.2 m (Cucco *et al.*, 2006). Climatology spanning an observation period of ten years is provided by a buoy located in Alghero where wave heights and related directions were collected. Recorded wave heights, of more than 3 m high, are found along the prevalent incoming direction, located in the north-west sector between 280 and 330 degrees. Beside, twenty percent of the observations display relevant wave heights (up to 3 m/s) coming from the south-west sector, between 220 and 270 degrees (Corsini *et al.*, 2006).

## METHODS

An interdisciplinary approach was followed to investigate the relationship between the sea state and the morphological changes of the SGS coastline. In the following sections, field activities including the GPS and wave data measurements and the adopted numerical methods are described.

### Beach Morphology

In order to evaluate the beach morphology and the variability of the different areas of the sub-aerial beach, a total of 8 beach

profiles were analyzed (Figure 1, right panel). The beach profiles were carried out by using a DGPS system, collecting a point every 2.5 m along each profile (Morton *et al.*, 1993). DGPS profile collections were analyzed from the shoreline (beach step) up to the end of the dune system landward or man-made structures.

To establish the trend of the shoreline during the last years the measured beach profiles were compared to the Digital Terrain Model data obtained from LIDAR survey (about 1 m and 14 cm in horizontal and vertical accuracy) of the studied beach, available from the website [www.sardegnaoportale.it](http://www.sardegnaoportale.it) and acquired by the Regione Autonoma della Sardegna during the 2008.

The Northern section of the beach, where the profiles 1\_1 and 1\_2 were recorded, was characterized by a wide submerged sandy beach with the presence of bars and by a vertical sandstone cliff,

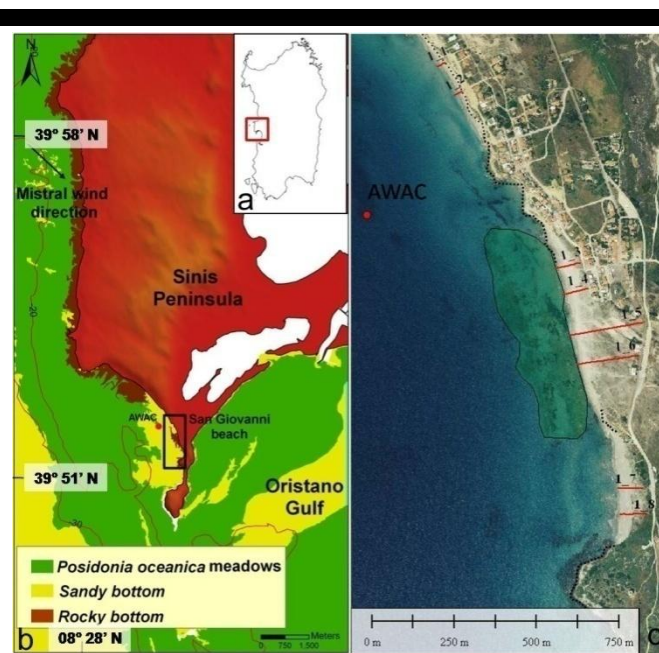


Figure 1. Study area; a) location of Sinis Peninsula; b) location of San Giovanni Beach; c) position of beach profiles, the green transparent area represents the submerged beach in which rocky outcrop occurs, the dotted lines represent the cliff edges.

of 10 m high, limiting the beach landward (Figure 1c). The central area of the beach, where profiles 1\_3, 1\_4, 1\_5, and 1\_6 were recorded, was characterized by an extended dune field and by several rocky outcrops in the submerged beach domain (Figure 1c). The southern section of the beach was characterized by dunes and a submerged sandy beach with one or more bars (Figure 1c). In this section, two beach profiles were recorded: 1\_7 and 1\_8.

Acoustic wave and current profiler (AWAC) was used to measure the wave parameters. The wave gauge was located at a depth of about 12 m (Figure 1b,c), with the recording interval of the wave parameters being three hours with a frequency of 1 Hz. The data recorded by AWAC were also used to calibrate the numerical model and validate the simulation results

### Numerical model

The SHYFEM3D-WWM is a coupled 3D hydrodynamic and wave model based on the finite element method (Ferrarin *et al.*, 2013; Cucco *et al.*, 2012; Umgiesser *et al.*, 2004). These two-module systems were adopted in order to reproduce the wind wave propagation in the study area, as directly influenced by the wind

action, and the wave interactions with surface water currents and the sea floor features.

The hydrodynamic module solves the primitive shallow water equations (Umgiesser *et al.*, 2004) integrated over each vertical layer in their formulations with water level and transport. The system of equations is implemented on a finite element unstructured mesh for spatial discretization, z-layers for vertical discretization and a semi-implicit algorithm is used for integration in time. A detailed description of numerical treatments can be found in Umgiesser *et al.*, (2004).

The wave module is a phase averaging numerical model, which solves the wave action equations (WAE) by means of the finite element integration method. They describe the net source terms defined by the energy input due to wind, the nonlinear interaction in deep and shallow water, the energy dissipation due to white capping and depth induced wave breaking as well as the energy dissipation due to bottom friction. A further comprehensive description of this numeric approach is found in Roland *et al.* 2009.

The wave-current interaction processes were simulated using the wave induced surface stresses computed according to the radiation stress theory of Longuet-Higgins and Stewart (1964). A two-way coupling procedure between the hydrodynamic and the wave module, based on the FIFO (First In First Out) file generation, allowed the calculation of the wave effects on the momentum and continuity equations and the current effects on the WAE.

The model integration domain includes the whole Western Mediterranean Sea, between the longitude of 5° W and 6° E, from the Gibraltar Strait to the western Sardinian island. An unstructured mesh based on triangular elements were implemented covering the whole area of interest with a spatial resolution varying between 10 km for the open ocean and 50 to 10 m for the San Giovanni bay shallow water area. The vertically discretization of the hydrodynamic module was defined by 14 logarithmically spaced z-levels with depths ranging between 2 and 100 m and a further bottom layer up to 4000 m.

The spectral space domain in the WWM was reproduced by a discrete distribution of 32 regularly spaced frequency intervals ranging between 1 and 0.04 Hz, with a relative frequency distribution of approximately 1.2 Hz, whereas the directional space domain was discretized using 24 regular intervals of 15°. An integration time step of 100 sec was adopted for both modules.

All the model domain boundaries were considered as closed. The numerical simulation was conducted using, as top boundary forcing, hourly data of wind speed and direction obtained by a high-resolution atmospheric model covering the whole Mediterranean Sea with a spatial resolution of 5 km (SKIRON, <http://forecast.uoa.gr>; Kallos and Pytharoulis, 2005). Either tide or other oceanographic forcing, such as open ocean thermohaline gradients, were not considered.

The model set-up described allowed for the reproduction of the effects of wind on the water level set-up (medium-range forcings), the wind wave generation and the water current interaction (local forcings) in the shallow water areas of interest, without taking into account any open boundary conditions. In fact, the extension of both the meteorological dataset and model domain permits to simulate all the wind wave generation processes occurring along the main wave fetch lengths characterizing the area.

## RESULTS

The beach profile analysis showed that the main variability of the sub-aerial beach was located in the southern part of the beach (see profiles 1\_7 and 1\_8 in Figure 4).

The northern profiles (profiles 1\_1 and 1\_2) showed a uniform variation along the whole sub-aerial beach, also highlighted by an absolute standard deviation value of about 0.2-0.4m (Figure 2 and Figure 5). In particular, these profiles showed a lowering of the beach surface among the first survey and subsequent ones. An exception is the last survey, carried out in October, which showed that the beach surface was rising toward the initial conditions (Figure 2 and Figure 5).

The central profiles were located in the area of beach where wide dune fields and rocky outcrops along submerged beaches exist. These profiles showed lower variation in foreshore. Variability along the profiles was found in the berm area and in both, the top and the toe of the most elevated and not vegetated dunes (Figure 2).

Along the southern beach profiles, the variability in elevation along beach accounts for about 2 m among the third, fourth and fifth survey. The changes occurred from the toe of the dune up to the shoreline causing a retreat of the dune of about 12 m landward and a lowering of the level of the beach surface of about 2m. This process occurred on profiles 1\_7 and 1\_8 between February and May when the major north western storms occurred (Figure 2 and Figure 3).

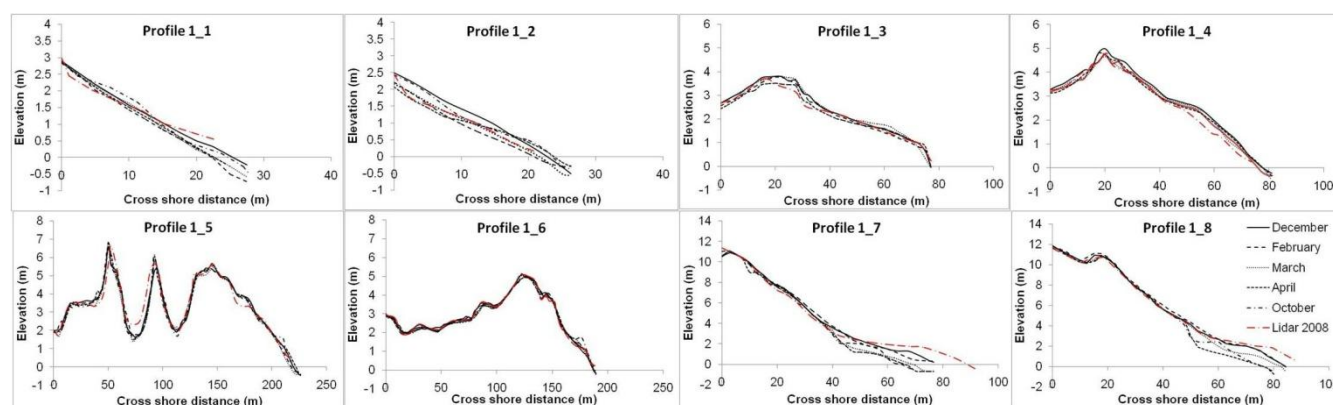


Figure 2: Morphological changes in the San Giovanni Beach along the beach profiles from December 2012 to October 2013. A further survey carried out by Lidar in 2008 was added to represent the general trend of the beach morphology.

During the last survey, carried out in late October 2013, the beach recovery was not complete and as a result the shoreline retreated about 10m with respect to the first survey.

With respect to the DTM data collected by the Regional

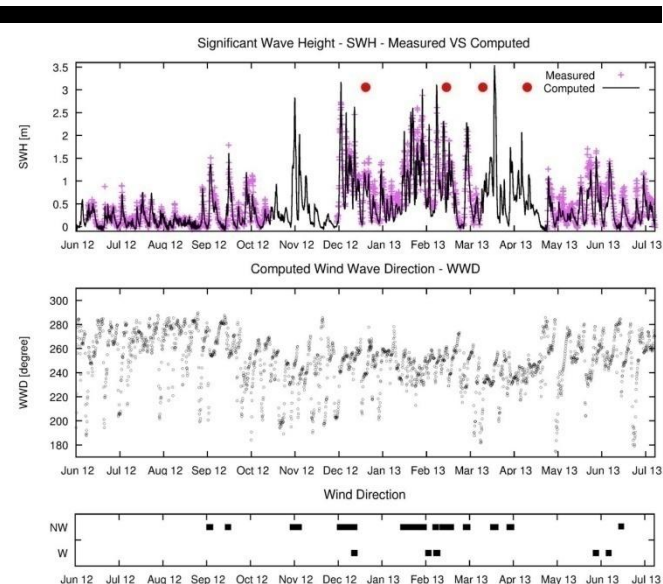


Figure 3. Wave parameters. Upper panel: significant wave height measured (magenta crosses) versus computed (continuous black line), the red dots represent the data of the beach profile acquisition. The last acquisition was carried out at the end of October and is not shown in the figure. Central panel: wind wave direction. Lower panel: direction of provenance of storms.

Authority of Environment in the 2008, the beach showed a considerable retreat in the southern sector (Profiles 1\_7 and 1\_8) of about 10~20 m (Figure 2), while in the other sections the shoreline did not show any retreat. Along the profile 1\_5, which crosses the dune field, a lowering of the trough by about 1m was found between the highest dunes by comparing the DGPS beach surveys and the LIDAR data (Figure 2).

The AWAC provided in situ data of wave heights, propagation direction, and energy. The observed year has displayed a maximum wave height (SWH) of 3.2 m and a prevailing propagation direction coming from the south-west sector, between 220 and 270 degrees. The wave propagation direction did not pass through relevant changes during both Mistral and Libeccio events; indeed, the local orientation of the isobaths and the submerged beach promoted the diffraction of the incoming waves. The higher wave heights and the greater part of the recorded wave events were found during Mistral wind events, whereas modest wave heights (below 1.1 m) were found during Libeccio wind events. The highest observed wave energy was localized between 220 and 270 degrees; the maximum energy amount, accounted for wind waves with a frequency ranging between 0.12 and 0.49 Hz, was of 0.8 m<sup>2</sup>/Hz, whereas swell waves (0.06 – 0.11 Hz) accounted for 6.3 m<sup>2</sup>/Hz of energy during all the observed, recorded year.

A 375 day long simulation run was conducted. A preliminary set of calibration runs aimed to determine the most suitable wave and current bottom friction coefficient to use were carried out. A trial and error approach based on the sequential comparison between simulation results and ADCP wave data was conducted, and the proper value for the model parameter defined.

The 3-hourly SWH measured dataset was selected for comparison with hindcast results to provide a model validation. In Figure 4 the scatter diagram is reported. The Pearson correlation coefficient, R, computed for the whole dataset, indicated an overall high accuracy of the model results along the whole simulated period (R = 0.958). In particular, good model performances were found for computed SWH comprised between the 0 and 2 m (green crosses and green stars in Figure 4) whereas lower model accuracy was found for SWH computed higher than 2 m (green dots).

The very low mean bias between the measured and computed SWH time series (see Figure 3) was about 0.07 m, with highest discrepancy of about 0.78 m found in correspondence of a single event, characterized by measured SWH values of more than 1.5 m. The bias analysis reflects a slight underestimation of the measured dataset that was also evidenced by the position of the best fit line in the scatter plot diagram (see Figure 4). Concerning the simulated wave propagation direction (see middle panel of Figure 3), the model accuracy was generally high. The computed directions varied between 170° and 290° with an average deviation between the measured and the computed ones spanning 5 to 10 degrees, which is less than the selected discretization interval of the WWM directional space. Confirming the results obtained by the ADCP data analysis, majority of the computed events high energetic events were generated by Mistral wind (see Figure 3).

**DISCUSSION AND CONCLUSION**

The high model accuracy, as illustrated in the previous paragraph, allowed the use of this numerical tool to reproduce, with a good degree of certainty, the propagation and evolution of the wind waves in the study domain. Both the lack of temporal continuity in the ADCP measurements (see Figure 3) and the lack of synopticity of the punctual measurements, with reference to the spatial scale of the investigated phenomena, were highly offset by the numerical applications.

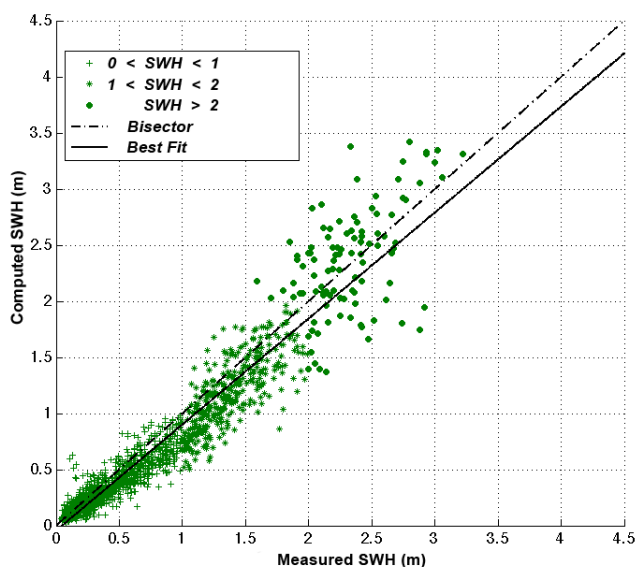


Figure 4. Model performance: correlation between measured wave height and computed wave height (R=0.958).

In particular, the highest and most energetic event simulated by the model occurred in a period during which the ADCP probe was not collecting data (see Figure 3). The event was generated by a Mistral wind blowing for about 38 hours between the 2013/03/13 and 2013/03/14 with peak speed of more than 20 m/s. The SWH reached the 3.5 m in the ADCP location (see Figure 5) and the computed peak and average periods were more than 8 and 7 seconds respectively.

During the period of study, the most intense storms involving this section of western Sardinia occurred from December 2012 to April 2013 in form of singles or groups of consecutive storms (Figure 3). Particularly from late January to middle February, a series of storms affected the beach (Figure 3), whilst in the middle of March the most intense storm occurred. The models results, reproducing the significant wave height during the most intense storm (2013/03/13), showed that the significant wave height mainly affected the southern sector of beach and the cliff located between the northern and southern sectors of beach (see Figure 5).

Also the profile analyses showed that the beach, particularly in the southern sector, experienced changes in subaerial morphology among the surveys of December, February and March. These changes became drastic (see Profile 1\_7 and 1\_8 in Figure 2, acquired on March and on late April, respectively) during the period of the monitored year in which the main storm occurred (2013/03/13). The numerical simulation for San Giovanni beach confirms the persistence of energetic events in the same period (see SWH in Figure 3), and the presence of higher wave height in the area where the beach profiles showed the main changes in morphology (Figure 5). In this area the modification of beach morphology consists of a retreat of the shoreline of about 10m, a pronounced erosion scarp in the foredune and a lowering in the

beach level of about 2 m (Figure 2 and Figure 5). In particular the shoreline retreat is confirmed by a comparison between the DGPS beach profiles data and the DTM LIDAR data acquired in 2008 (Figure 2).

The other profiles, in the northern and central sections of the beach, were less variable in the foreshore area.

The northern sector of the beach (Profiles 1\_1 and 1\_2) showed that morphological changes involved the whole subaerial beach profile. During the monitoring period, the beach profiles do not present relevant morphological features (e.g. storm berm) and the variability consists in an increasing or decreasing of the beach level. This behavior may be related to the presence of a sandstone cliff (10 m high) in the backshore, close to the shoreline.

The central profile is characterized by an extended dune field in the backshore area, with changes up to about 0.4 m in the top of the unvegetated dunes. Thus, the wind transport and the anthropogenic structures (i.e. beach access for beachgoers) may represent the main forcing affected the morphology of the dunes. The submerged area of this sector is characterized by extended rocky outcrops from the shoreline up to 4 m depth (Figure 1); their presence can influence the beach storm response, increasing the stability of the beach (Gallop *et al.*, 2012, Eversole and Fletcher, 2003). In fact the morphology of the foreshore of the central sector of San Giovanni results more stability with respect to other sections (see profiles 1\_3, 1\_4, 1\_5 and 1\_6 in Figure 2).

As highlighted before by using the numerical model, the highest waves directly affect the foreshore of the southern sector of beach. The observed morphological changes are related to this phenomenon which may affect beach recovery and lead to a new morphological shape of this section of beach. In fact, beach profile analyses (see profiles 1\_7 and 1\_8 in Figure 2) confirmed that in

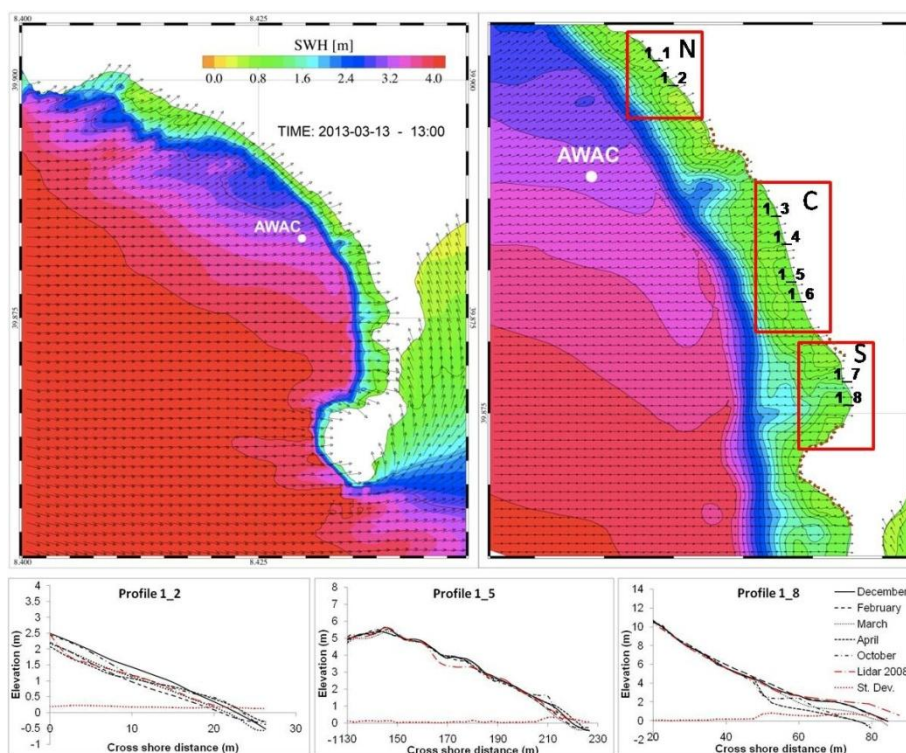


Figure 5. Wave height obtained by model run during the most intense storm. The wave height resulted higher in the southern sector of beach in which were found a significant retreat of shoreline and a erosive scarp morphology. Dotted lines represent the cliffs. Standard deviation has been computed for the profiles acquired from December 2012 to October 2013.

the southern section the morphology of the beach and foredune is deeply modified as a result, whereas beach recovery only occurred in the northern and central sections (see profile 1\_2 and 1\_5 in Figure 5).

In conclusion the interdisciplinary approach provided the evaluation of storms intensity and related morphological beach responses, defining the vulnerable areas where relevant erosion and low recovery capabilities were revealed using the in-situ measurements.

### ACKNOWLEDGMENT

This work was funded by RESMAR project (funded by P. O. Marittimo, European Union) and RITMARE project (flag project funded by Italian Ministry of University and Scientific Research).

### LITERATURE CITED

- Almeida, L. P., Ferreira, O., Pacheco, A., 2011. Threshold for morphological changes on an exposed sandy beach as a function of wave height. *Earth Surface Processes and Landforms*, 36, 523-532
- Backstrom J. T., Jackson D. W. T., Cooper J. A.G., Malvarez, G. C. 2008. Storm-driven shoreface morphodynamics on a low wave energy delta: the role of the nearshore topography and shoreline orientation. *Journal of Coastal Research*, 24 (6), 1379-1387.
- Basterretxea, G.; Orfica, A.; Jordi, A.; Casas, B.; Lynett, P.; Liu, P.L.F.; Duarte, C. M., and Tintoré, J., 2004. Seasonal Dynamics of a Microtidal Pocket Beach with *Posidonia oceanica* Seabed (Mallorca, Spain). *Journal of Coastal Research*, 20 (4), 1155-1164.
- Benavente, J., Del Rio, L., Gracia, F. J., Martinez del Pozo, J. A. 2006. Coastal flooding hazard related to storms and coastal evolution in Valdelagrana spit (Cadiz Bay Natural Park, SW Spain). *Continental Shelf Research*, 26, 1061-1076.
- Cucco, A., Sinerchia, M., Ribotti, A., Olita, A., Fazioli, L., Sorgente, B., Perilli, A., Borghini, M., Schroeder, K., Sorgente, R., 2012. A high resolution real time forecasting system for predicting the fate of oil-spills in the Strait of Bonifacio (western Mediterranean). *Marine Pollution Bulletin*, 64, 6, 1186-1200
- Davaud, E.; Kindler, P.; Martini, R., and Strasser, A., 1991. Enregistrement des variations eustatiques dans des dépôts littoraux du Pleistocène supérieur de San Giovanni di Sinis (Sardaigne occidentale). *Société Géologique de France*, 162, 523-533.
- De Falco, G., Molinaroli, E., Baroli, M., Bellacicco, S., 2003. Grain size and compositional trends of sediment from *Posidonia oceanica* meadows to beach shore, Sardinia, Western Mediterranean. *Estuarine Coastal and Shelf Science*, 58: 299-309.
- Del Rio, L., Plomaritis, T. A., Benavente, J., Valladares, M., Ribera, P. 2012. Establishing storm threshold for the Spanish Gulf of Cadiz coast. *Geomorphology*, 143-144, 13-23.
- Eversole D., Fletcher, C. H. 2003. Longshore sediment transport rates on a reef-fronted beach: field data and empirical models Kaanapali beach, Hawaii. *Journal of Coastal Research*, 19 (3), 649-664.
- Ferrarin, C., Roland, A., Bajo, M., Umgiesser, G., Cucco, A., Davolio, S., Buzzi, A., Malguzzi, P., Drofa, O., 2013. Tide-surge-wave modelling and forecasting in the Mediterranean Sea with focus on the Italian coast. *Ocean Modelling*, 61, 38-48.
- Gallop S. L., Bosserelle, C., Eliot, I., Pattiaratchi, C. B. 2012. The influence of limestone reefs on storm erosion and recovery of a perched beach. *Continental Shelf Research*, 47, 16-27.
- Gallop, S. L., Bosserelle, C., Pattiaratchi, C. B., Eliot, I. 2011. Hydrodynamic and morphological response of a perched beach during sea breeze activity. *Journal of Coastal Research*, 64 (S.I.), 75-79.
- Kallos G., and Pytharoulis, I. 2005. Short-term predictions (weather forecasting purposes). In Anderson, M.G. (Ed.), *Encyclopedia of Hydrological Sciences*, Wiley, London, pp. 2791-2811.
- Lecca, L.; and Carboni, S., 2007. The Tyrrhenian section of San Giovanni di Sinis (Sardinia): Stratigraphic record of an irregular single high stand. *Rivista Italiana di Paleontologia e Stratigrafia*, 113 (3), 509-523.
- Longuet-Higgins and Stewart, 1964. Radiation stress in water waves: a physical discussion with applications. *Deep Sea Research*, 11 (1964), pp. 529-562
- Morton, R. A., Leach, M. P., Paine, J. G, and Cardoza, M. A., 1993. Monitoring Beach Changes Using GPS Surveying Techniques. *Journal of Coastal Research*, 9 (3); 702-720.
- Marini, A. and Murru, M., 1977. Rilevamento geologico della penisola del Sinis (Sardegna centro meridionale). *Rendiconti Seminario Facoltà di Scienze Università di Cagliari*, 24, 95-108.
- Roland, A.,Cucco, A., Ferrarin, C., Hsu, TW, Liau, JM, Ou, SH.,Umgiesser, G., Zanke.U., 2009. On the development and verification of a 2-D coupled wave-current model on unstructured meshes. *Journal of Marine Systems*, 78, S244-S254.
- Umgiesser, G, Canu, DM, Cucco, A, Solidoro C., 2004. A finite element model for the Venice Lagoon.Development, set up, calibration and validation. *Journal of Marine Systems*, 51 (1), 123-145
- Short, A.D., 1996. The role of wave height, period, slope, tidal range and embaymentisation in beach classifications: a review. *Revista Chilena de Historia Natural*, 69, 589-604.

# Multi-scale analysis of wave conditions and coastal changes in the north-eastern Baltic Sea

Ülo Suursaar<sup>†</sup>, Victor Alari<sup>‡</sup>, Hannes Tõnisson<sup>∞</sup>

<sup>†</sup> Estonian Marine Institute,  
University of Tartu,  
Mäealuse St. 14, Tallinn 12618,  
Estonia  
ulo.suursaar@ut.ee

<sup>‡</sup> Marine Systems Institute at Tallinn  
University of Technology,  
Akadeemia St. 15a, Tallinn 12618,  
Estonia  
victor.alari@msi.ttu.ee

<sup>∞</sup> Institute of Ecology at Tallinn  
University,  
Uus-Sadama 5-537, Tallinn 10120,  
Estonia  
hannes.tonisson@tlu.ee



[www.cerf-jcr.org](http://www.cerf-jcr.org)



[www.JCRonline.org](http://www.JCRonline.org)

## ABSTRACT

Suursaar, Ü., Alari, V., Tõnisson, H., 2014. Multi-scale analysis of wave conditions and coastal changes in the north-eastern Baltic Sea. In: Green, A.N. and Cooper, J.A.G. (eds.), *Proceedings 13<sup>th</sup> International Coastal Symposium* (Durban, South Africa), *Journal of Coastal Research*, Special Issue No. 70, pp. 223-228, ISSN 0749-0208.

Temporal variations of shoreline changes have been analyzed and interpreted in three differently exposed Estonian coastal sections. Using coastline contours that have been recorded frequently over the last twelve years, as well as recently digitized aerial photographs, orthophotos and old topographic maps (some of them dating back to 1900), all overlaid in the Mapinfo software, areal changes over different sub-periods were calculated. To explain the shoreline changes, two different wave modelling approaches were used and mutually compared. Both the BaltAn65+ reanalysis (an ERA-40 refinement) forced SWAN model hindcast (1965–2005) and the point model runs (1966–2012), locally and independently calibrated against extensive wave measurements in these coastal study sites, confirmed specifically higher (and increasing) intensity of coastal processes in the westerly exposed study sites, and a decrease in northerly exposed sites. Some common quasi-periodic cycles with high stage approximately in 1985–1995, and probably also from 2007 can be found. However, the role of a few randomly occurring extreme winter storms (such as in 1967, 2005, 2007 and 2012) was often decisive within the sub-periods.

**ADDITIONAL INDEX WORDS:** *Waves, shorelines, coastal erosion, modelling, storms, wind climate.*

## INTRODUCTION

Wind waves gain energy, propagate, undergo transformation and dissipate over a wide range of spatial and temporal scales. As a result, wave fields in near-coastal areas have large variability which can be analyzed by means of multi-scale modelling or using altogether different experimental datasets and individual models that are suited for capturing processes in specific scales. Usually, multi-scale modelling of an oceanographic variable can be achieved by increasing the density of computational points, either by using nesting techniques or unstructured meshes (Anselmi-Molina *et al.*, 2012; Rusu and Soares, 2012; Chubarenko *et al.*, 2013). For relatively small model domains, outputs of high-resolution and long-term modelling runs can reproduce, to a certain extent, variations in different time scales. However, owing to the specific properties of existing input data, the practical usability of various scales may be quite different, and validation in different temporal spans is therefore advisable.

In the Estonian coastal sea, starting from the 2000s, a few process-oriented wave measurement series were obtained for certain locations where adjoining coastal studies were also carried out. For these specific locations, independently calibrated long-term (1966–2012) high resolution (1h time step) wave hindcasts exist (Suursaar, 2013), which can be used for comparison of gridded modelling results obtained e.g. by WAM (e.g. Soomere and Räämet, 2011) or SWAN (Alari and Raudsepp, 2010) for the same areas and in several time scales.

Also, in coastal geomorphic studies, accumulation of observational datasets over different periods of time has made a

multi-scale approach possible. A number of Estonian coastal study sites have been regularly examined by coastal scientists since the 1960s (Orviku, 1974). Some of them have exhibited rather spectacular developments. Three sites have been chosen for this study: the westerly exposed Harilaid Peninsula in the western part of Saaremaa Island, the northerly exposed Letipea – Sillamäe site, and the north-westerly exposed Osmussaar Island (Figure 1).

Since the 2000s, use of gradually improving GPS instruments and GIS software has enabled year-to-year changes in the shoreline to be tracked and the calculation of the corresponding areas or volumes due to accumulation and erosion (Rivis, 2004; Tõnisson *et al.*, 2008; 2013). On the other hand, studies of recent coastal geomorphic changes can benefit greatly from the availability of old maps and aerial photographs (Tõnisson *et al.*, 2013; Suursaar *et al.*, 2013). The recently digitized aerial photographs of the study sites, as well as orthophotos and old topographic maps (some of them dating back to 1900), all overlaid in the Mapinfo software, enable the calculation of areal changes over different, relatively long sub-periods.

Hence, we have observed both long-term shoreline changes, as well as eye-witnessed and in-situ recorded rapid impacts of severe storm events, such as winter storms in 2005 and 2007 (Tõnisson *et al.*, 2008; Suursaar *et al.*, 2008), storm Berit in 2011 and Ulli in 2012; (Tõnisson *et al.*, 2013) and more recently the St. Jude storm in late 2013. The aim of the paper is: (1) to compare and validate the two wave hindcasts obtained by different modelling methods using different time scales; (2) to analyze the observed coastal changes in three differently exposed Estonian coastal sections (covered by the wave hindcasts) and (3) to explain these changes



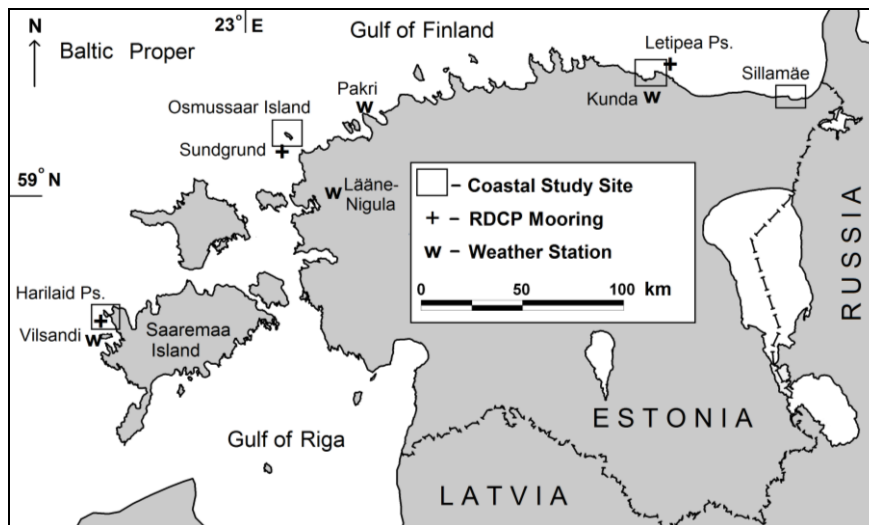


Figure 1. Map of the study area together with case study sites, RDCP mooring and weather stations.

using experimental datasets and wave hindcasts with different temporal spans and spatial resolutions.

## STUDY AREA

All three study sites are located in the eastern section of the practically tideless and semi-enclosed Baltic Sea. Cape Kelba in the southern part of Harilaid Peninsula (Figure 1) comprises a series of beach ridges forming an approximately 2 km long spit with a maximum crest height of 3.8 m a.s.l. in its proximal part. The predominantly accumulative distal part consists of well-rounded crystalline gravel, pebbles, cobbles and boulders (Tõnisson *et al.*, 2013). The spit emerged from the sea in the early 1900s, and it has grown gradually since then. The westerly exposed marine region has the roughest wave climate along the Estonian coastal sea (Soomere and Räämet, 2011).

The study site on the southern part of the Osmussaar Island (Figure 1) is composed of 2–3 m high accumulative gravel-pebble beach ridges. The up to 7 m high Ordovician limestone cliff in the northern part of the island is gradually eroded by storm waves and storm surges, feeding the southward longshore transport of sediment (Suursaar *et al.*, 2013). Increments of the spits occasionally rejoin the main island and several brackish-water coastal lagoons can be found behind the spits. The Kunda–Letipea–Sillamäe study sites in north-eastern Estonia are exposed to northerly winds and have relatively straight coastlines. The Baltic Glint (limestone cliff), which attains a maximum height of up to 56 m a.s.l., lies behind a narrow coastal plain landward from the contemporary shoreline. Gravel-pebble and sandy shores alternate depending on the curves in the shoreline, whereas east of Sillamäe a 10 km long sandy beach is present.

## MATERIALS AND METHODS

### Coastal Studies

Topographic and geomorphic assessment of coastal changes was based on a combination of field and GIS-based study methods. Since 2000, shoreline positions were determined *in situ* 1–3 times a year at irregular time intervals, including at least one annual complex survey and additional surveys after major storm events. From 2000 until 2004, a handheld Garmin 12 GPS

navigator with a maximum horizontal accuracy of 3 m was used. The accuracy attainable in the field was 3–5 m. From 2004 until 2010, shoreline positions and the contours of beach ridges were measured using Garmin 60CSx and 60CS devices (accurate to within 3 m), and after 2010, shoreline positions were measured using a Leica RTK-GPS GS09, accurate to within 1–2 cm. Precise leveling studies were performed annually since 2004 using a Leica Sprinter Digital Level 180M. The RTK-GPS GS09 has been used to increase the quality and speed of measuring profiles since September 2011; the number of profiles has also increased.

The shoreline contours obtained both from the GPS surveys, as well as from the digitized maps and photographic sources were overlaid and analyzed using the Mapinfo software. The map sources varied somewhat between the study sites. For instance, at Osmussaar, topographic maps from the years 1900, 1935, 1939, 1947, 1961 and 1981 were used. In addition, aerial photographs from 1987 and orthophotographs (pixel sizes between 25 and 100 cm) from 1998, 2005, 2008 and 2010 were compared. Areal changes over different sub-periods were calculated. The rate of coastal change was calculated as a ratio of the sum of volume to the duration of the measured period for both erosion and accumulation (as an average per shoreline metre).

### SWAN Model and BaltAn65+ Wind Input

To explain the shoreline changes, two different wave modelling approaches were used. They were supposed to be methodologically independent from each other and to provide the possibility for mutual validation of their results. Firstly, the Simulating Waves Nearshore (SWAN) model was used for the 1965–2005 Baltic Sea wave hindcast.

SWAN is a third generation phase averaged spectral wave model developed at Delft University of Technology (Booij *et al.*, 1999). The model (SWAN cycle III, version 40.91) was run in a non-stationary mode with a 15 minute integration timestep. Structured grid with spherical coordinates and resolution of 1' along latitudes and 2' along longitudes included 629 meshes along longitudes and 734 along latitudes. Digital topography covering the entire Baltic Sea with a resolution of 1 nautical mile (Seifert *et al.*, 1995) was used in this study. Physical processes, such as third-generation formulations with respect to wave-wave interactions (triad and quadruplet), whitecapping (Westhuysen *et al.*, 2007),

wind input, bottom friction and depth-induced breaking were included. Linear growth term for wind growth was activated.

The depth-induced breaking was due to Battjes and Janssen (1978) with the breaker parameter set to 0.73. JONSWAP form of bottom friction with the bottom friction coefficient of  $0.067 \text{ m}^2 \text{ s}^{-3}$  was used (Alari and Raudsepp, 2010). The ice concentrations used in this wave study were calculated at the Swedish Meteorological and Hydrological Institute by using a coupled Rossby Centre Ocean ice-ocean model and Helsinki Multicategory Sea Ice Model HELMI. As SWAN has no special treatment of ice, the seasonal ice was introduced to the wave model with the water level switch.

The wave model was forced by the gridded winds from the Baltic Sea reanalysis database BaltAn65+ (Luhamaa *et al.*, 2011). It is a regional refinement of the ERA-40 dataset (see e.g. Sterl and Caires, 2005) with a horizontal grid resolution of 0.1 degrees (approximately 11 km). The period of reanalysis (1965–2005) determines the span of the wave hindcast. High Resolution Limited Area Model (HIRLAM) was used for the reanalysis (Rööm *et al.*, 2007). Wind velocity components were saved every 6 hours. Velocity components were interpolated to model integration time-steps internally in SWAN and the interpolation was strictly energy conservative. The output parameters (with time interval of 3 hours) included significant wave height, average wave direction, peak wave period and wave period corresponding to the first moment of spectrum.

### Locally Calibrated Point Model (LCPM)

Long-term wave hindcasts were performed for the selected coastal study locations (Harilaid, Letipea, Osmussaar) using a simple point model which was independently calibrated against the wave measurements made in those locations earlier. The SMB-type model, also known as the significant wave method, further modified in the Shore Protection Manuals of the U.S. Army Corps of Engineers (USACE, 1984), calculates the significant wave height, period and wavelength as a function of wind speed, effective fetch length and water depth. In fact, the manuals and handbooks include a wide choice of such equations with slightly different empirical coefficients and terms, which should take into account different wind conditions and shallow-water effects. Our central idea was to calibrate the wave model using high-quality wave measurements, so that afterwards the model can act as a virtual extension of the fixed-point applications both for hindcasts and forecast. The role of remotely generated waves (swell) is small and the memory time of the wave fields in the Baltic Sea is relatively short (Soomere and Räämet, 2011).

For supplying the wave model with wind speed and direction, we acquired data from the meteorological stations operated by the Estonian Environment Agency (previously known as the EMHI). For each of the three wave modelling sites, we used wind data from the closest station (digitized records available since 1966). The Vilsandi station is merely 7 km from the Harilaid Peninsula and the Kunda station is just 10 km west of the Letipea site (Figure 1). As the long-term wind input data from the closest coastal meteorological station to the Osmussaar (i.e. Pakri station) could not be considered homogeneous (Keevallik *et al.*, 2007), data from the more distant (37 km) Lääne-Nigula station were used. Calibration of the model was based on wave measurements at Letipea ( $59^{\circ}34'N$ ,  $26^{\circ}40'E$ , 16 October – 25 November 2006), Harilaid ( $58^{\circ}28'N$ ,  $21^{\circ}49'E$ , 20 December 2006 – 23 May 2007), and Sundgrund ( $59^{\circ}15'N$ ,  $23^{\circ}24'E$ , 18 September – 10 November 2011) using a RDCP-600 oceanographic measuring complex. The upward facing instrument manufactured by AADI was deployed at the seabed at a depth between 10 and 14 m. The chosen locations were all 1–3 km off the nearest coast. The 1 hour measuring

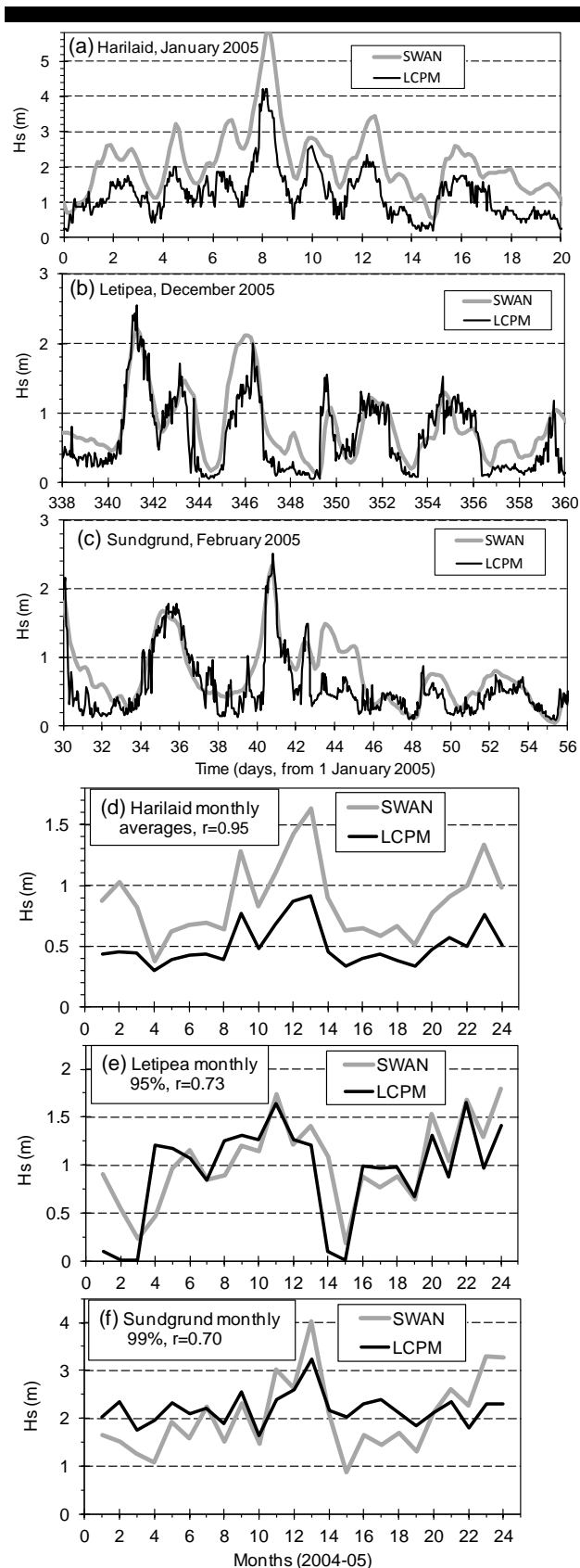


Figure 2. Comparison of wave hindcast results in three study locations in hours-days time scale (a,b,c; excerpts) and in monthly statistics (averages, percentiles) in 2004–2005 (d,e,f).

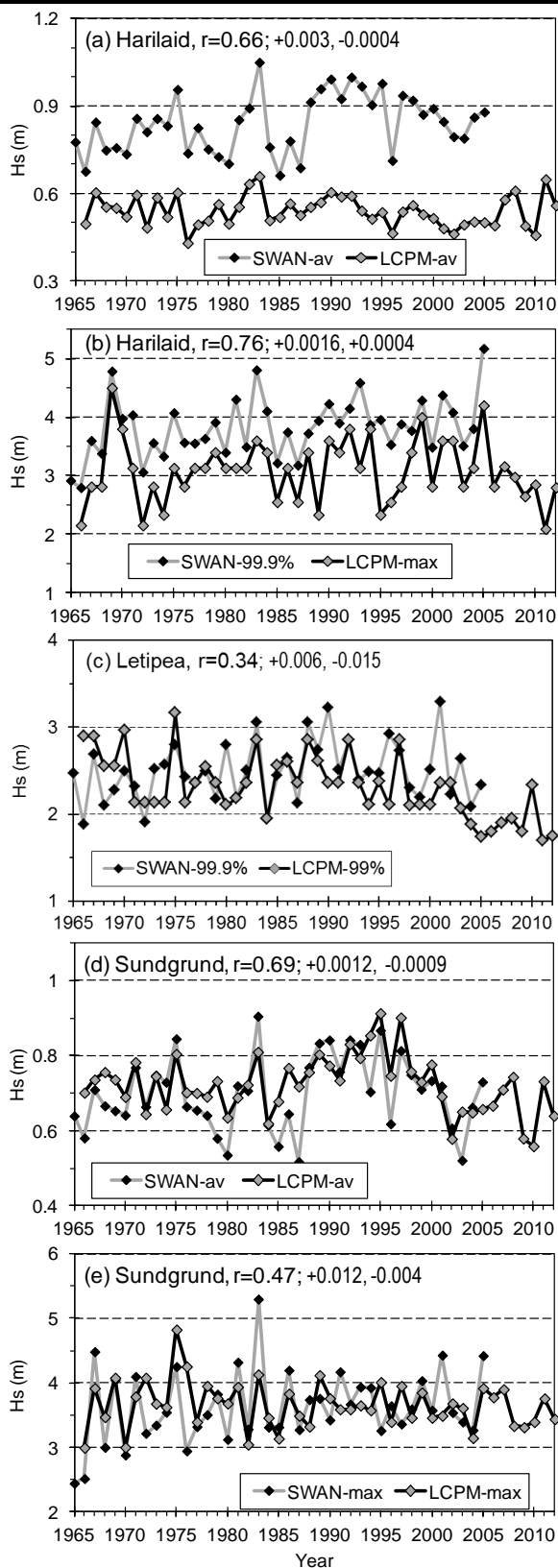


Figure 3. Comparison of annual statistics (averages, percentiles) of wave hindcasts. Additional information in the legend includes correlation coefficients and trend slopes (SWAN, LCPM).

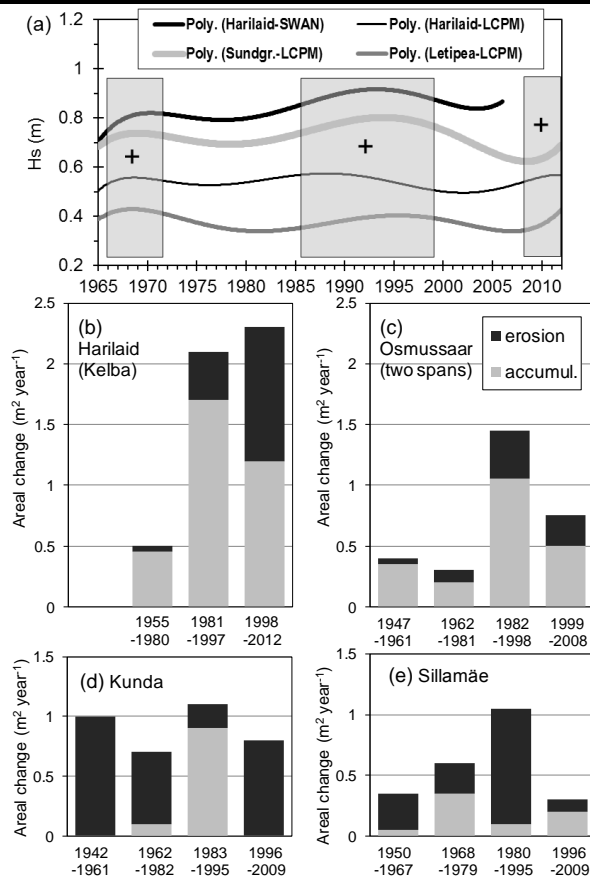


Figure 4. Smoothed (generalized) decadal variations in average wave conditions (a), average areal changes (accumulation and erosion per one shoreline meter and year) in the study sites (b-e).

interval was the same as for the routinely measured meteorological data used in the calibration and hindcast. Although the model calibration also includes a search for the appropriate depth, the most important item was prescribing the fetch for different wind directions. After measuring the fetches from nautical charts, a series of new distributions of fetches was created by maximizing the correlation coefficient and minimizing the root square error by means of consecutively adjusting the fetch in all  $20^\circ$  wide sectors. By trying to keep the maximum and average wave heights equal in the modelled and reference series, the iterative calibration procedure found the best set of fetches and, somewhat, compensated for local wind impediments around the specific weather station. The calibration results at Harilaid and Letipea were highly successful (Suursaar, 2013). The somewhat lower calibration quality for Sundgrund appeared to be a result of the larger distance between the wind data source and the actual wave modelling site (Suursaar *et al.*, 2013). Eventually, using the specific calibration settings and wind input sources, the long-term hindcasts were obtained independently at the three locations for 1966–2012. The hindcast had an interval of 3 hours from January 1966 to August 2003, and 1 hour thereafter.

## RESULTS AND DISCUSSION

### Comparison of SWAN and LCPM Outputs in Different Time-Scales

**Days:** In addition to some good calibration results (Suursaar, 2013), a few independent validation examples between the pre-calibrated LCPM runs and field measurements can be found (e.g. Fig. 3b in Suursaar, 2010). LCPM output retained a very similar visual appearance and statistical structure to the RDCP measurements, both having a 1 hour time step. Obviously, the LCPM can successfully be used for fast hind- or forecasts on a short-term scale. Owing to the 3 hour time step and inherited temporal properties from the BaltAn65+ reanalysis wind data, the SWAN output was more smooth (Figure 2abc). The systematic difference (bias) between the Harilaid series appeared as a result of a mismatch between the calculation locations in a rather complex, rugged coastline of the Harilaid region. While the LCPM was calibrated to exactly mimic the RDCP measurements at the specific 14 m deep location, 1.5 km off the Kelba coast, the 2 km SWAN mesh-cell was obviously misplaced along the near-coastal depth gradient. Being somewhat more offshore and thus allowing higher waves to evolve, the time series still displays remarkable similarity to the LCPM. The model outputs at Letipea-Kunda and Sundgrund were both spatially well-positioned and behaved similarly with time (Figure 2).

**Months:** Analysis on a monthly or annual basis can be made as a comparison between the series composed from summary statistics (e.g. averages, maxima, quantiles) of monthly or annual data samples, respectively. The two-year excerpts display normal seasonal variations for the Baltic Sea with higher values from November to January (Figure 2def). Despite the systematic bias in the case of Harilaid, the series correlated well with each other.

**Years:** Although the correlations between the two model outputs vary (0.3–0.8) depending on the statistics and locations, the models yielded similar results, which captured both inter-annual variability as well as basic long-term trends (Figure 3). While certain quasiperiodic (i.e. NAO-based) cycles or “regimes” can be found in time series of annual mean wave properties (e.g. Figure 3ad), the maximum or high-end values show more randomly-behaving temporal variations (Figure 3bce). Strong storms may occur equally during the high or low NAO phase (Jaagus and Suursaar, 2013). The length of the long-term series composed from annual statistics is somewhat different (1965–2005 for SWAN and 1966–2012 for LCPM) and the full-series trends are not exactly comparable. Also, in many cases the SWAN series begin with relatively low values and end with higher values than the LCPM series, thus yielding more upward trends. However, even if considering the common time span, the SWAN series tends to display more increasing trends. Most likely, long-term wind input for the LCPM has a small decreasing, artificial trend component. Although the influence of most obvious instrument change in 1976 was eliminated in the older data, there may be other smaller inhomogeneity sources left. The BaltAn65+ reanalysis series are less sensitive in that sense, although the amount and consistency of the assimilated source data have also changed over time (Luhamaa *et al.*, 2011).

### Coastal Changes and Their Relationships With Wave Climate

Based on consensus between the two wave modelling outcomes, the long-term wave conditions exhibited some quasi-periodic cycles with a high stage in 1985–1995, and probably also starting from 2007 (Figure 4a); a near stable trend in mean wave heights

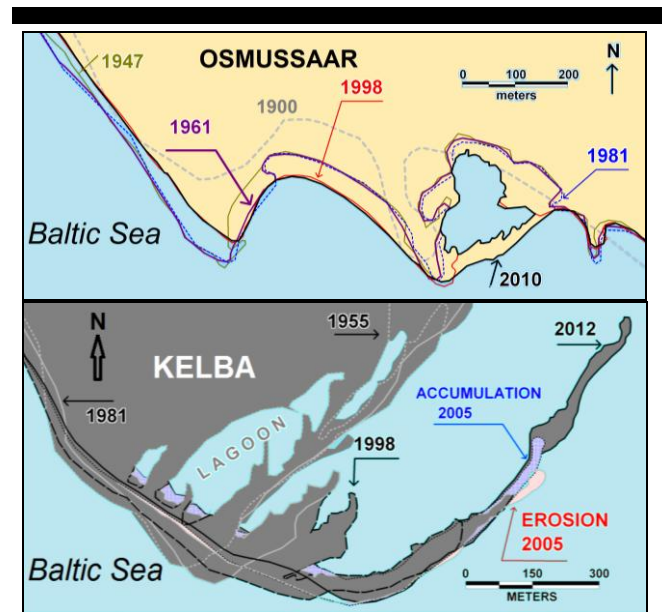


Figure 5. Selected shoreline positions at Osmussaar and Kelba in some sub-periods and after the storms in 2005 and 2012.

and an increase in high wave events at the windward coasts of West Estonia, but decrease at the northerly and easterly exposed coasts (Figure 3; Suursaar, 2013). The spatially contrasting results for differently exposed coasts reflect the corresponding changes in wind climate, and, on the other hand, evoke spatially different developments on the coasts.

Over all the coastal study sub-periods, the shore processes (erosion and accumulation) were the most intense at the westerly exposed Harilaid, where the wave climate is the roughest; the intensity of shore processes was the smallest at the northerly exposed Kunda–Sillamäe region, leaving Osmussaar Island in the middle (Figure 4). We have found that the current rate of coastal change in western Estonia is approximately 10 times higher than it was in the 1950s. The changes also include an increase of erosion areas. Slightly increasing rate of shore processes can be observed also on the north-westerly located Osmussaar. However, a slight decrease has been observed in the northernmost Letipea–Kunda site, which confirms the quasi-cycles in wave climate (Figures 3,4a). As a whole, such changes in the shore processes are most probably caused by changes in the large-scale atmospheric circulation patterns above North Europe and a poleward shift of cyclones trajectories (e.g. Pinto *et al.*, 2007), resulting in an increase of regional storminess (Jaagus and Suursaar, 2013). Over the last decades there have been more cyclones, which bypass Estonia from the north, creating strong westerly winds. On the other hand, there are fewer such cyclones that cross over Estonia, thus leading to a decrease in northerly winds.

### Long-term Changes vs. Changes During Storms

In general, the sub-periods (Figure 4) included a different number of storms. There is a crucial need to understand and better quantify the impact of extreme storms on the coastal zone. The energy of strong storms and their impact on shore dynamics is exponentially larger than that of moderate storms and they may even alter the evolution paths of the existing shore formations. Just within a few days of a violent storm, the magnitude of coastal changes may exceed the total changes that occur over a period of many years without such strong storms. Although it is difficult to

determine exactly the impact of a single violent storm during 1940–1990 (Figure 5), we have eye-witnessed and instrumentally measured the impacts of several strong storms in recent years (Tõnisson *et al.*, 2008; 2013; Suursaar *et al.*, 2008). While the prominent storms in the past include the events in 1967 and 1969, the storms that left a lasting impression on the coast of Estonia in recent twelve years include the winter storms in 2005 (Gudrun/Erwin), 2007 (Hanno/Per), 2011–12 (Berit and Ulli), and 2013 (St.Jude). The 9–10 January 2005 hurricane-force Gudrun was probably the most influential storm in recorded Estonian history. The distal part of Cape Kelba became elongated by about 75 m and the area of the spit increased by about 4300 m<sup>2</sup> (Figure 5). During the storm on 14–15 January 2007, the distal tip of the spit advanced a further 60–70 m, while in the proximal part the shoreline has receded by up to 15 m along a 400 m stretch, accounting for approximately 3500 m<sup>2</sup> of land loss. Including the changes in beach face, the estimated volume of erosion within the study site was up to 5000 m<sup>3</sup> (gravel, cobbles, boulders) and the accumulation in the distal part was 13000 m<sup>3</sup>. The magnitudes of changes during the storms in 2005, 2007 and 2012 were comparable with those of the overall changes during the longer periods (Figures 4 and 5).

## CONCLUSION

The overlapping time period of two independent wave hindcasts (1966–2005) enabled the models to be cross-validated and their scopes and scales for coastal applications to be defined. The models showed a good agreement both in short-term and decadal scales. In explaining the coastal changes during the recent violent storms, the locally calibrated point model can be used. BaltAn65+ reanalysis forced SWAN model gave the spatial results for long term changes, while the LCPM confirmed the most important inter- and intra-annual variability features. The results showed specifically higher (and increasing) intensity of coastal processes in westerly exposed study sites, and a decrease in northerly exposed sites. Some common quasi-periodic cycles with a high stage, approximately in 1985–1995, and probably also from 2007 can be found. However, the role of a few randomly occurring extreme winter storms (such as in 2005, 2007 and 2012) was often decisive within the sub-periods.

## ACKNOWLEDGEMENT

The study was supported by the Estonian target financed project 0104s08, the Estonian Science Foundation grants No 8549, 8980 and 9191 and by the EstKliima project of the European Regional Fund programme No 3.2.0802.11-0043.

## LITERATURE CITED

- Alari, V. and Raudsepp, U., 2010. Depth induced breaking of wind generated surface gravity waves in Estonian coastal waters. *Boreal Environment Research*, 15, 295–300.
- Anselmi-Molina, C.M., Canals, M., Morell, J., Gonzalez, J., Capella, J. and Mercado, A., 2012. Development of an operational nearshore wave forecast system for Puerto Rico and the U.S. Virgin Islands. *Journal of Coastal Research*, 28, 1049–1056.
- Battjes, J.A. and Janssen, J.P.F.M., 1978. Energy loss and set-up due to breaking of random waves. *Proceedings of the Coastal Engineering Conference*, 1, 569–587.
- Booij, N., Ris, R.C. and Holthuijsen, L.H., 1999. A third-generation wave model for coastal regions 1. Model description and validation. *Journal of Geophysical Research C: Oceans*, 104 (C4), 7649–7666.
- Chubarenko, B.V., Leitsina, L.V., Esiukova, E.E. and Kurennoy, D.N., 2012. Model analysis of the currents and wind waves in the Vistula Lagoon of the Baltic Sea. *Oceanology*, 52, 748–753.
- Jaagus, J. and Suursaar, Ü., 2013. Long-term storminess and sea level variations on the Estonian coast of the Baltic Sea in relation to large-scale atmospheric circulation. *Estonian Journal of Earth Sciences*, 62, 73–92.
- Keevallik, S., Soomere, T., Pärj, R. and Žukova, V., 2007. Outlook for wind measurement at Estonian automatic weather stations. *Proceedings of the Estonian Academy of Sciences, Engineering*, 13, 234–251.
- Luhamaa, A., Kimmel, K., Männik, A. and Rõõm, R., 2011. High resolution re-analysis for the Baltic Sea region during 1965–2005 period. *Climate Dynamics*, 36, 727–738.
- Orviku, K., 1974. *Estonian Seacoasts*. Tallinn: Valgus, 112 p. (in Russian).
- Pinto, J.G., Ulbrich, U., Leckebusch, G.C., Spanghel, T., Reyers, M. and Zacharias, S., 2007. Changes in storm track and cyclone activity in three SRES ensemble experiments with the ECHAM5/MPI-OM1 GCM. *Climate Dynamics*, 29, 195–210.
- Rivis, R., 2004. Changes in shoreline positions on the Harilaid Peninsula, West Estonia, during the 20th century. *Proceedings of the Estonian Academy of Sciences. Biology, Ecology*, 53, 179–193.
- Rõõm, R., Männik, A., Luhamaa, A. and Zirk, M., 2007. Nonhydrostatic semi-elastic hybrid-coordinate SISL extension of HIRLAM. Part II: Numerical testing. *Tellus Series A-Dynamic Meteorology and Oceanography*, 59, 661–673.
- Rusu, L. and Soares, C.G., 2013. Evaluation of a high-resolution wave forecasting system for the approaches to ports. *Ocean Engineering*, 58, 224–238.
- Seifert, T., Kayser, B. and Tauber, F., 1995. *Bathymetry data of the Baltic Sea*. Baltic Sea Research Institute, Warnemünde.
- Sterl, A. and Caires, S., 2005. Climatology, variability and extreme of ocean waves – the web-based KNMI/ERA-40 wave atlas. *International Journal of Climatology*, 25, 963–977.
- Soomere, T. and Räämet, A., 2011. Spatial patterns of the wave climate in the Baltic Proper and the Gulf of Finland. *Oceanologia*, 53(1-T1), 141–150.
- Suursaar, Ü., 2010. Waves, currents and sea level variations along the Letipea – Sillamäe coastal section of the southern Gulf of Finland. *Oceanologia*, 52, 391–416.
- Suursaar, Ü., 2013. Locally calibrated wave hindcasts in the Estonian coastal sea in 1966–2011. *Estonian Journal of Earth Sciences*, 62, 42–56.
- Suursaar, Ü., Jaagus, J., Kont, A., Rivis, R. and Tõnisson, H., 2008. Field observations on hydrodynamic and coastal geomorphic processes off Harilaid Peninsula (Baltic Sea) in winter and spring 2006–2007. *Estuarine Coastal and Shelf Science*, 80, 31–41.
- Suursaar, Ü., Tõnisson, H., Kont, A. and Orviku, K., 2013. Analysis of relationships between near-shore hydrodynamics and sediment movement on Osmussaar Island, western Estonia. *Bulletin of the Geological Society of Finland*, 85, 35–52.
- Tõnisson, H., Orviku, K., Jaagus, J., Suursaar, Ü., Kont, A. and Rivis, R., 2008. Coastal Damages on Saaremaa Island, Estonia, Caused by the Extreme Storm and Flooding on January, 9 2005. *Journal of Coastal Research*, 24, 602–614.
- Tõnisson, H., Suursaar, Ü., Rivis, R., Kont, A. and Orviku, K., 2013. Observation and analysis of coastal changes in the West Estonian Archipelago caused by storm Ulli (Emil) in January 2012. *Journal of Coastal Research*, SI 65, 832–837.
- USACE, 1984. *U.S. Army Coastal Engineering Research Center, Shore Protection Manual*, Vol.1, Third Ed., U.S. Govt. Printing Office, Washington D.C., 719 p.
- Westhuysen, A.J., Zijlema, M. and Battjes, J.A., 2007. Nonlinear saturation-based whitecapping dissipation in SWAN for deep and shallow water. *Coastal Engineering*, 54, 151–170.

## Field experiments with different fractions of painted sediments to study material transport in three coastal sites in Estonia

Hannes Tõnisson†, Ülo Suursaar‡, Are Kont†, Kaarel Orviku†, Reimo Rivis†, Robert Szava-Kovats+, Kadri Vilumaa†, Triin Aarna†, Maris Eelsalu#, Katri Pindsoo#, Valdeko Palginõmm†, Urve Ratas†

† Institute of Ecology at Tallinn University,  
Uus-Sadama 5-537, Tallinn 10120, Estonia  
hannes.tonisson@tlu.ee

‡ Estonian Marine Institute, University of Tartu,  
Mäealuse St. 14, Tallinn 12618, Estonia  
ulo.suursaar@ut.ee

# Institute of Cybernetics at Tallinn University of Technology,  
Akadeemia tee 15a, Tallinn 12618, Estonia  
maris.eelsalu@ioc.ee

+Institute of Ecology and Earth Sciences,  
Tartu University, Lai 40, Tartu, 51014, Estonia  
robszav@ut.ee



[www.cerf-jcr.org](http://www.cerf-jcr.org)



[www.JCRonline.org](http://www.JCRonline.org)

### ABSTRACT

Tõnisson, H., Suursaar, Ü., Kont, A., Orviku, K., Rivis, R., Szava-Kovats, R., Vilumaa, K., Aarna, T., Eelsalu, M., Pindsoo, K., Palginõmm, V., Ratas, U. 2014. Field experiments with different fractions of painted sediments for studying material transport in three coastal study sites in Estonia. *In: Green, A.N. and Cooper, J.A.G. (eds.), Proceedings 13<sup>th</sup> International Coastal Symposium* (Durban, South Africa), *Journal of Coastal Research*, Special Issue No. 70, pp. 229-234, ISSN 0749-0208.

Our current understanding of the morphodynamics in swash and surf zones is limited due to their turbulent and irregular nature. The importance of this zone to sediment transport led us to perform a sophisticated field experiment using painted sediments. Sediments collected locally from beach ridges were sorted into the following diameters: 1–2.5 cm, 2.5–5 cm and 5–10 cm. The sediments were painted, amassed in piles and placed at 0.5–10 m depths in three sites near the Estonian coast. The locations were recorded with GPS devices and photographed. The sediment piles placed in the sea were monitored at least once after an intense storm or once before and after the storm season. Some sediments were placed on the shoreline and monitored daily for a shorter period. Hydrodynamic parameters were also measured or hindcasted during the experiment. We found that wave breaking during storms can take place even at 6 m depth, but mostly between 2–4 m depth. Sediment fractions between 1–10 cm diameters can be transported over 20 m towards the shore. Even sediment piles at 10 m depth were moved 2–4 m, but towards the open sea. Sediments accumulated on the shoreline moved up to 3 m/hour along the shore and approximately 350 m during three months. We also found that calm periods can be more influential in places where regular vessel-generated waves wash the shores. As vessel-generated waves often approach from a different angle than natural waves, they can cause notable erosion during the periods when natural waves are weak or absent.

**ADDITIONAL INDEX WORDS:** *Coastal evolution, sediment transport, wave measurements, Baltic Sea.*

### INTRODUCTION

Estonia is a small country, but has a relatively long coastline (about 4,000 km in length) and has an abundance of islands (over 1,500). Recent years have seen coastal geomorphic research conducted at several sites along the Estonian coast. Coastal geomorphic surveys have been carried out routinely since the beginning of the 2000s, and aerial photographs and old charts dating back to 1900 have been analysed. Moreover, several “in situ” measurements and field experiments’ data from the 1960s and 1970s have been digitized. These data have given us the opportunity to analyse long term trends in coastal evolution, discern fluctuations in these trends and find the relationships between coastal processes, hydrodynamic conditions and meteorological parameters in decadal scale (Rivis, 2004; Tõnisson *et al.*, 2011; Suursaar *et al.*, 2008; 2013).

Surf and the swash zones comprise regions of the coastal zone where waves dissipate or reflect their remaining energy after

propagation from the open sea towards the coast (Brocchini and Baldock, 2008). Indeed, it has been acknowledged that within this region most of the sediment transport occurs giving rise to the generation of rapid coastal changes (e.g. Masselink and Russell, 2006). However, our current understanding of the morphodynamics in this region is limited. This is partly ascribed to the strong, unsteady flows and high turbulence, which hinder reliable measurement of wave kinematics and sediment fluxes in the transient aerated flow. Therefore, swash/surf zone hydrodynamics and sediment transport have been active topics of research over the past decade. Laboratory experiments aiming at analysing and quantifying the role of wave-form asymmetries (around a vertical and a horizontal axis) and wave-current interaction have been conducted to provide a better description of the near-bed sediment dynamics (e.g., Watanabe and Sato, 2004; Silva *et al.*, 2011; Dong *et al.*, 2013). However, few experiments have been carried out in the natural environment.



Figure 1. Location of the study sites.

Our recent “in situ” studies on single extreme storm events (Tõnisson *et al.*, 2008; 2012; 2013) led us to conduct field experiments using painted sediments. In fact, fieldwork was carried out by K. Orviku and his colleagues in the 1970s to determine the origin of accumulative material in beach ridges and the sediment flow directions in both the Black Sea and the Baltic Sea (Orviku, 1974). Great amounts of painted sediments were placed at several depths. However, at that time it was not possible to relate these studies to hydrodynamic parameters and exact changes on the shores, and irregular access to the shores lessened the scientific significance of their studies.

Such studies done in a more sophisticated and regular manner enable us to determine the extent of feeding areas, directions of sediment transport and to gain information on accumulation patterns. The main aim of this study is to develop and test methodology for “in situ” sediment tracing, which enables us to locate sediment transport zones and directions in the coastal zone. Moreover, simultaneous wave measurements help us to estimate the extent of changes caused by a single storm.

### STUDY AREA

Three study areas were chosen representing different geological characteristics and wave conditions. All three study sites are located in the eastern section of the nearly tideless and semi-enclosed Baltic Sea. Cape Kelba in the southern part of Harilaid Peninsula (Figure 1) consists of a series of beach ridges forming an approximately 2 km long spit with the maximum crest height of 3.8 m a.s.l. in its proximal part (Tõnisson *et al.*, 2007). The predominantly accumulative distal part consists of well-rounded crystalline gravel, pebbles, cobbles and boulders (Tõnisson *et al.*, 2013). The coastal slope of the spit is rather steep; 5 m isobath is approximately 100 m from the shoreline, while 10 m depth is approximately 300 m from the shoreline. Kelba Spit is exposed to waves from the SW, W and NW. The westerly exposed marine region has the roughest wave climate along the Estonian coastal sea (Soomere and Räämet, 2011). Maximum waves near the site attain 5 m while Hs often reach over 3 m during storm events.

The study site on the south-western part of the Osmussaar Island (Figure 1) consists of 2–3 m high accumulative gravel-pebble beach ridges. The up to 7 m high Ordovician limestone cliff in the northern part of the island is gradually being eroded by storm waves and storm surges, feeding the southward long-shore transport of sediment (Suursaar *et al.*, 2013). Increments of the

spits occasionally rejoin the main island and several brackish-water coastal lagoons are located behind the spits. The coastal sea is less than 2 m deep beyond the 200–300 m wide limestone bench on the western side of the island. Depth increases rapidly further offshore. As in Kelba, maximum waves near the site attain 5 m while Hs often reaches over 3 m during storm events.

Aegna study site (Figure 1) is somewhat different than the others. Gravel, pebble and boulders are the most characteristic features on the shore while the coastal slope is typically covered by sand and single boulders. Sand covers the back-shore as well. The coastal slope is less steep; 5 m depth is over 200 m from the shoreline while 10 m depth lies more than 500 m from the shoreline. This site is situated in a semi-closed basin and exposed to waves mainly from the W and NW. The highest waves are expected to be over 2 m high (Kelpšaitė *et al.*, 2009). This site is also heavily affected by vessel wakes approaching the coast from directions different than wind waves (Soomere *et al.*, 2009). Experimental data suggest typical wave height in completely calm weather is about 1.2 m, the largest ship wave heights in calm conditions are 1.5 m. Wave heights resulting from the combination of wind and ship can attain 1.7 m (Parnell *et al.*, 2008). Wind waves up to 0.5 m high produced runup events up to 20–30 cm above the still water level. The runup events of ship waves frequently exceeded 1 m above the still water level and a few attained more than 1.5 m above the still water level (Torsvik *et al.*, 2009; more information in Parnell *et al.*, 2008).

## MATERIAL AND METHODS

### Coastal Studies

A sophisticated analysis of painted sediments was carried out for the current study. Collected locally from beach ridges, sorted particles with the following diameters were used: 1–2.5 cm (yellow), 2.5–5 cm (red) and 5–10 cm (blue). The sediments were painted with non-fluorescent, water and wear resistant, asphalt paints, stacked in piles (approximately 10 liters of sediment in each pile) and placed at depths of 0.5–10 m (intervals of 0.5 m in Osmussaar study site and 1.0 m intervals at the other sites) at three different study sites near the islands of Saaremaa, Osmussaar and Aegna – all located along the Estonian coast and representing different geological and hydrodynamic conditions.

The locations were positioned with RTK-GPS (on the shore and shallow sea) or Garmin 60 CSx GPS (in the deeper sea) and were photographed. A Leica RTK-GPS GS09, accurate within 1–2 cm, enabled us to record exact locations and elevations of the painted sediments and a Garmin 60 CSx (accurate within 3 m), was precise enough to record the locations of sediment piles in deeper sea. The sediment piles placed in the sea were monitored at least once after an intense storm or once before and after the storm season.

Additional tests were carried out on the swash zone in Aegna and Kelba site, where the sediments were accumulated in a continuous line from -0.5...+1.3 m. Sediments placed on the swash zone on Aegna study site were monitored daily for 10 days and once three months after the start of the experiment. Kelba site was also monitored twice on the following day and once 3 months later. GPS data were overlaid and analyzed using *ArcGIS* and *MapInfo* software. Maximum and average distance from the initial source of the sediments as well as the elevation of the painted sediment particles was calculated and analyzed. Direction of the sediment transport can be tracked on specially designed thematic maps.

## Wave Data

Information on wave conditions was obtained from real time measurements and calibrated hindcasts. Wave measurements were carried out at Harilaid (58°28'N, 21°49'E, 20 December 2006 – 23 May 2007 and 29 July – 3 November 2013) and at Sundgrund (59°15'N, 23°24'E, 18 September – 10 November 2011) using a RDCP-600 oceanographic measuring complex. In addition, wave hindcasts were performed for Osmussaar and Kelba study locations for periods when real time measurements were not taken. A simple point model was used which was previously calibrated against the wave measurements made at these locations. The SMB-type model, also known as the significant wave method, further modified in the Shore Protection Manuals of the U.S. Army Corps of Engineers (USACE, 1984) was used to calculate the significant wave height, period and wavelength as a function of wind speed, effective fetch length and water depth (For further information see: Suursaar, 2013; Suursaar *et al.*, 2013). Data from the meteorological stations operated by the Estonian Environment Agency were obtained to supply the wave model with wind speed and direction. The Vilsandi station is 7 km from the Harilaid Peninsula and the Lääne-Nigula station (37 km) was used for Osmussaar site.

Wave data for Aegna study site came from previous studies (e.g. Soomere, 2005; Kelpšaitė *et al.*, 2009). Unlike the other two sites, fast-ferry vessel-wakes may influence shore processes at Aegna. However, the vessel wakes are more influential in summer; therefore measurements taken for previous studies were used (Soomere *et al.*, 2009; Torsvik *et al.*, 2009).

## RESULTS AND DISCUSSION

### Fate of Sediment Piles: Osmussaar Island

The initial results of the field experiments, carried out on gently sloping limestone bench, indicate that, during the first two months, fresh wind conditions (wind speed 13 m/s, Hs up to 2 m, sea-level around zero) were able to move 1–10 cm diameter sediments in depths between 2.5–4 m, i.e. in the zone where most storm waves break (Suursaar *et al.*, 2013). The sediment piles at those depths were completely dispersed.

Therefore, we can assume that erosion takes place over the steeper section of the underwater limestone bench, i.e., from 2.5 m to 5 m isobaths – the zone where storm waves typically break and dissipate. There was no observed movement at shallower depths. Above the shallow (0–2.5 m) and gently sloping limestone bench waves lose energy and local wave heights are constrained by shallow conditions.

The next period, from autumn 2011 to autumn 2012, saw several strong storms during winter. We recorded that a storm with winds up to 21 m/s, sea level up to 1.2 m and waves up to 4.3 m (strongest event during the study period) was able to move sediments at depths between 0.5–1.5 m (the smallest particles was transported as much as 28 m shoreward). This storm accompanied by a higher sea level probably allowed higher energy waves to reach closer to the shore and transport these sediments. The sediments at depths between 1.5 and 2.5 m remained unaffected. This area remains vegetated by bladderwrack (*Fucus vesiculosus*), which shows that the sediments eroded from greater depths were accumulated on the vegetation border and were not moved shoreward even during strong storm conditions.

Most waves break at depths of greater than 2.5 m and the sediments eroded from the deeper sea are deposited here as small submerged ridges that protect bottom vegetation. On the other hand, vegetation prevents shoreward movement of the sediments.

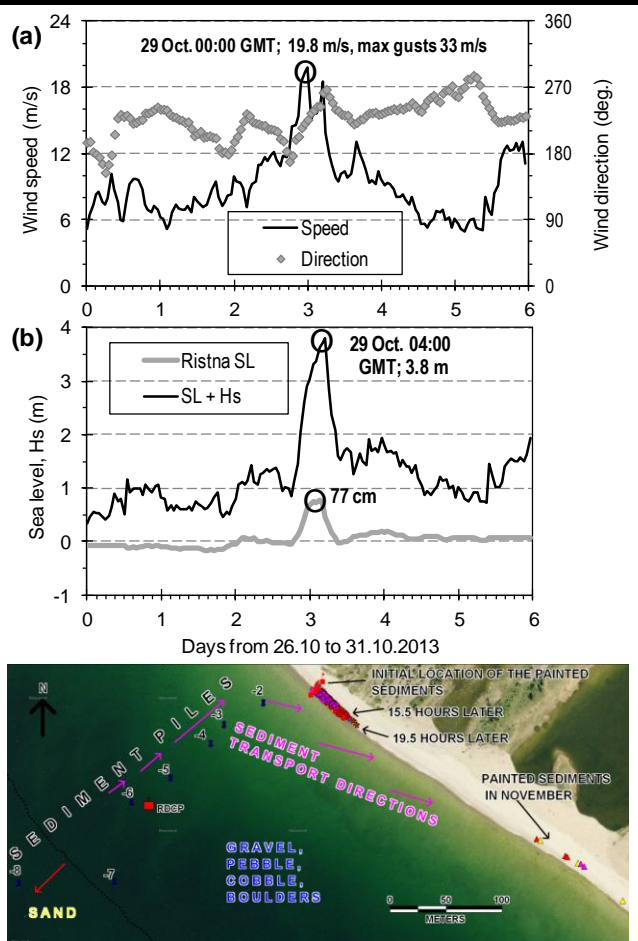


Figure 2. Measurements at Kelba on October-November 2013. Winds at Vilsandi station (a); measured sea level (SL) at Ristna tide gauge station and combined sea level - significant wave height (Hs) at Kelba during the St. Jude storm (b); movement of painted sediment at Kelba coast (c).

Under extreme-high sea-level conditions, a secondary wave breaking zone may form, in which sediments are transported shoreward from a depth of 1 m (landward border of vegetation).

### Kelba Peninsula

The sediments were placed on the sea bottom in August 2012 and the site was first revisited in August 2013. The sediments were placed at 1 m depth intervals due to the steeper coastal slope. Bottom sediments are mostly gravel, pebbles, cobbles and a few boulders until 7 m depth (Figure 2c). Medium sand is most commonly at deeper depths.

The first hours of the experiment showed that at a site waves induced by wind speeds of 5–6 m/s can distort sediment piles at 0.5 m depth (breaker zone) already due to the steep and narrow beach slope. Thus, the narrower breaking zone allowed small waves to move sediments in this shallow depth.

The 2012 – 2013 winter was relatively calm. There were two rather modest storms: on 26 October 2012 and on 3 March. The average wind speed attained 18 m/s and the sea-level was close to zero during the both events. During the second storm, negative storm surge occurred as the sea-level dropped to -40 cm (due to the wind blowing from the north).



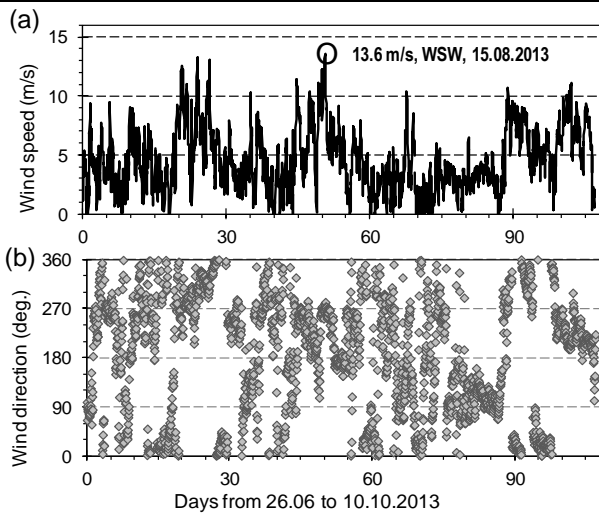


Figure 3. Sustained wind speed (a) and direction (b) at Rohuneeme meteorological station (5 km south of Aegna) in summer 2013.

Significant wave heights for these storms attained 2.3 and 1.8 m, respectively, far less than the maximum  $H_s$  wave heights in the previous winter (2.8 m, storm Ulli; Tõnisson *et al.*, 2013) and after (3.3 m, St. Jude).

Despite moderate storm conditions, noteworthy changes in sediment piles were observed. The piles at depths from 7–10 m moved 2–4 m seaward, forming an approximately 0.5 m wide line covered by painted sediments of all sizes. Sediments were partly buried under freshly accumulated sand. We assume that seaward moving sand moved the painted sediments to greater depths as well (there is a gentle seaward tilted slope). Piles from 6–4 m depth were distributed over similar 0.5 m wide lines with the sediments being moved shoreward by 4–12 m (4 m at 6 m depth and 12 m at 4 m depth). All the sediments were completely dispersed and moved across- and along the shore at the depths of 2 and 3 m. Not a single sediment particle was found at lower depths.

As at Osmussaar site, wave braking during the storm took place at depths of 2–4 m where sediments have been completely dispersed or transported shoreward. Piles at lower depths were probably located in the swash zone and therefore transported on or along the shore.

New piles were placed in August 2013 at the same depths. The site was revisited at the beginning of November. The period witnessed one of the strongest storms in recent years (St. Jude). Average wind speed was nearly 20 m/s with gusts attaining 33 m/s (Vilsandi station, 7 km from the site; Figure 2a). Sea-level reached nearly 80 cm above the long-term average (or zero) while the combined sea level – wave height was up to 3.8 m (Figure 2b). In addition to the wave hindcast (representative for the 14 m deep location 1.5 km off the Kelba), the RDCP measured significant wave heights close to 3.2 m and maximum wave heights up to 5.2 m at a 5.5 m depth site 0.25 km off the Cape Kelba during the storm.

We failed to find any sediment piles from the line at the start of the sandy bottom (7.5 m isobath). The entire area was covered by a thick layer of freshly accumulated sand. We assume that massive amounts of sand leveled and covered the sediment piles. The pile at 7 m depth was somewhat distorted and the pile at 6 m depth was dispersed over a 0.5 wide and 8 m long shoreward directed band. No sediments were found at 5 m depth; the sea bottom showed signs of extensive erosion. There were several freshly formed

holes and depressions around larger boulders (owing to the higher surrounding turbulence). RDCP, which was initially deployed at 5.5 m depth, was found more than 20 m landward from its initial location. The sediments placed at 4 m depth were dispersed along a 20 m long and approximately 1 m wide shoreward directed band. The pile at 3 m depth was completely dispersed. We failed to find painted sediments at 1 and 2 m depths.

During fieldwork between 31 July and 1 August 2013, the sediments accumulated as a continuous line from -0.5 m to 1.3 m and started to move along the shore towards the nearby spit. In the first 15.5 hours, yellow, red and blue sediments moved up to 37 (2.4 m/h), 38 (2.4 m/h) and 24 m (1.5 m/h), respectively. Four hours later, the same sediments were moved a further 12, 11 and 2 m. Therefore, the maximum speed for these sediments was 3 m/h during the last 4 hours of the experiment, which was characterized by relatively windy conditions. Wind speed attained 7.1 m/s (initially from S and later from W). Waves ( $H_s$  up to 1.1 m) approached the shore at a sharp angle, which is favorable for long-shore transport.

We were able to find a few painted sediments as far as 350 m towards the tip (red-particles) of the spit after the storm in November. The furthest yellow and blue particles were found 330 and 285 m from their initial location. Therefore, the average daily travelling speed was between 3.0 and 3.7 m (0.13–0.16 m/h). The fact that we were able to find so many sediment particles in such a mobile environment indicates that the mobile layer of the sediment is relatively thin. All the particles were found at elevations between 0.95 and 1.18 m above sea-level. This is confirmed by the profiles measured in summer and just after the storm. The mixed layer at around 1 m elevation was mostly between 20 and 40 cm; in a few locations it reached 0.5 m.

We can conclude that waves typically break at depths between 2 and 4 m. However, this zone might extend to at least 5.5 m in very strong storms. Gravel, pebble and cobble particles are initially transported towards the shore at such depths. Longshore transport of sediments usually begins in the swash zone, typically located at the depths of less than 2 m. However, it can extend to 3 m in extreme events. Theoretically, the wave generated flow speed outside the breaking zone must be between 80 and 160 cm/s (Bagnold, 1963) to move the painted sediments (size 1–5 cm) and even faster for the biggest particles (5–10 cm), which were transported together with smaller particles. The sediments reaching the foreshore can be considered the most mobile. Their travelling speed has been determined to be as high as 3 m/h, depending mostly on wave direction, sea-level and wave height.

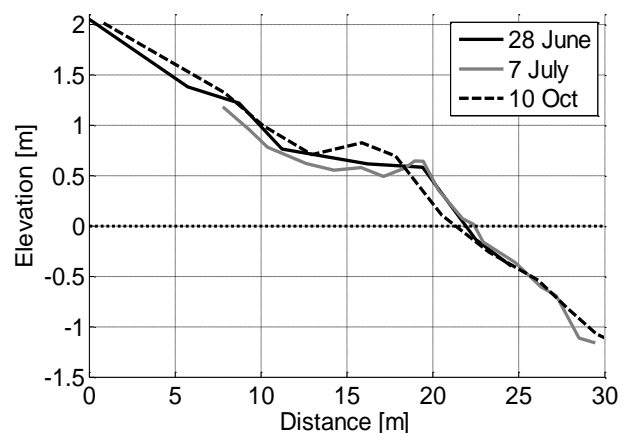


Figure 4. Changes in the beach profile during Aegna experiment.

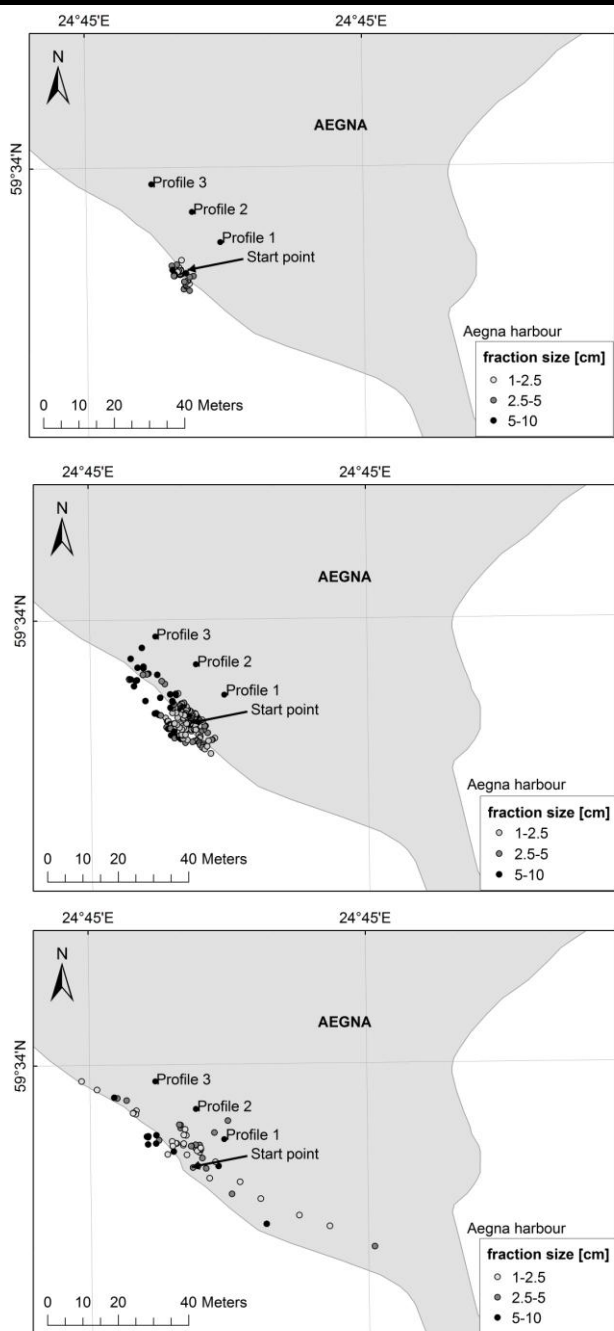


Figure 5. Locations of painted sediments: a) one day, b) 10 days and three months after their placement to the start point.

It is also worth noting that painted sediments lost most of their paint in three months in such a highly dynamic environment. However, the smallest (yellow) particles and particles with rough surfaces remained easily recognizable.

### Aegna Island

Aegna Island is located in a zone with some of the highest vessel wakes in Estonia. Fieldwork was carried out between 26 June and 10 October 2013, during which the winds conditions were often fresh wind (up to 13–14 m/s, Figure 3a,b). Sea level fluctuated slowly between -30 and +30 cm from the long-term

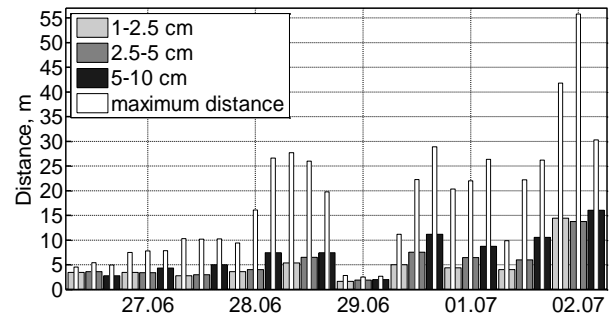


Figure 6. Movement of painted sediments from their initial location, Aegna Island.

mean, being maximal during the strong wind event on August 15 and minimal during persistent northerly or easterly winds on days 25–35 and 80–95 (Figure 3b).

In addition to the sediment piles at 1 m depth intervals, we placed a few hundred litres of painted sediments in the swash zone. There was no movement observed deeper than 1 m during the first 10 days. Three months later, in October, there were still no change at 1.5 m depth. Therefore, deeper sediment piles were not monitored. We observed that these ship-produced waves were able to move painted sediments at depths up to 1 m. The furthest sediment particle (in size category from 5–10 cm) was found about 29 m long-shore from its original position only 10 days later (Figure 5). The highest located sediment particle was also from the same size category and located 0.8 m above sea level. These 10 days were generally calm and therefore, sediment transport was dominated by ship waves. Most of the sediments moved north during the first 10 days (Figure 5).

Most of the painted sediments had been buried by the second visit three months later. The burial might be related to natural waves caused by small storm events and resulting profile change on the beach (Figure 4). However, we managed to find over 50 painted sediment particles. This indicates that the mixed layer of sediments at this location is relatively thin as well. Profiles (Figure 4) also show that the mixed layer is usually less than 25 cm deep.

Natural waves typically approach from the N and NW and therefore we found more sediments south of their initial location by the end of the experiment (Figure 5). The travelled distance from the initial location was greater for medium particles from 26 to 56 m (Figure 6) while the furthest large particles were found about 31 m from their initial location. It is also worth noting that the furthest found particle was found south of the original pile. Notably, the highest sediment particle was recovered at 1.6 m elevation. No particles at deeper depths (up to 1.5 m) were recovered; 0.4 m was the deepest registered depth.

The sediments were typically transported between elevations of -0.5 m to 1.0 m. Vessel wakes transported the sediments mostly to the north, while natural waves re-transported them to the south. There are abundant sediments available to the north while the site is bordered by the harbor jetty to the south. Therefore, long quiet periods might influence the beach profile more than stormy periods, which are largely return ship-wave transported sediments to their initial location.

### CONCLUSION

We can conclude that most storm waves break at depths of 2–4 m. However, this zone might extend seaward during extreme storm events and wave braking may occur even at 6 m depth. There is very active sediment transport in this zone and particles

with a 1–10 cm diameter are usually transported towards the shore.

The mobile layer of sediments on the gravel shores on the Baltic Sea seems to be smaller than initially expected. This study was able to confirm only that typically a 20–40 cm thick layer is mixed even during strong storms and in the most mobile and energetic environments for gravel shores.

It is controversial that calm periods can be more influential in locations where regular vessel-generated waves wash the shores. As vessel-generated waves often approach from the different angle than natural waves, they can cause notable erosion during periods when natural waves are weak or absent. However, these events can take place in specific locations with a relatively steep coastal slope and during calm periods.

### ACKNOWLEDGEMENT

The study was supported by Estonian target financed projects 0104s08 and SF0140007s11, Estonian Science Foundation grants No 8549, 8980, 9125 and 9191, by the EstKliima project of the European Regional Fund programme No 3.2.0802.11-0043 and through support of the ERDF to the Centre of Excellence in Non-linear Studies CENS and the Mobilitas project MTT63.

### LITERATURE CITED

- Bagnold, R.A., 1963. Mechanics of marine sedimentation. In: M.N.Hill, ed., *The Sea*, Vol. 3. New York: Wiley and Sons, 507-528.
- Brocchini, M. and Baldock, T.E., 2008. Recent advances in modelling swash zone dynamics: Influence of Surf–Swash interaction on nearshore hydrodynamics and morphodynamics. *Reviews of Geophysics* 46, RG3003.
- Dong, L.P., Sato, S. and Liu, J., 2013. A sheetflow sediment transport model for skewed-asymmetric waves combined with strong opposite currents. *Coastal Engineering*, 71, pp. 87-101.
- Kelpšaitė, L., Parnell, K.E. and Soomere, T., 2009. Energy pollution: the relative influence of wind-wave and vessel-wake energy in Tallinn Bay, the Baltic Sea. *Journal of Coastal Research*, SI 56(1), 812-816.
- Masselink, G. and Russell P., 2006. Flow velocities, sediment transport and morphological change in the swash zone of two contrasting beaches. *Marine Geology*, 227, 227-240.
- Orviku, K., 1974. *Estonian Seacoasts*. Tallinn: Valgus, 112 p. (in Russian).
- Parnell, K., Delpeche, N., Didenkulova, I., Dolphin, T., Erm, A., Kask, A., Kelpšaitė, L., Kurennoy, D., Quak, E., Räämet, A., Soomere, T., Terentjeva, A., Torsvik, T. and Zaitseva-Pärmaste, I., 2008. Far-field vessel wakes in Tallinn Bay. *Estonian Journal of Engineering*, 14(4), 273-302.
- Rivis, R., 2004. Changes in shoreline positions on the Harilaid Peninsula, West Estonia, during the 20th century. *Proceedings of the Estonian Academy of Sciences. Biology, Ecology*, 53, 179-193.
- Silva, P. A., Abreu, T., van der A, D.A., Sancho, F., Ruessink, B.G., Van der Werf, J.J. and Ribberink, J.S., 2011. Sediment transport in non-linear skewed oscillatory flows: the Transkew experiments. *Journal of Hydraulic Research*, 49 (1), 72-80.
- Soomere, T., 2005. Wind wave statistics in Tallinn Bay. *Boreal Environment Research*, 10 (2), 103-118.
- Soomere, T., Parnell, K.E. and Didenkulova, I., 2009. Implications of fast-ferry wakes for semi-sheltered beaches: a case study at Aegna Island, Baltic Sea. *Journal of Coastal Research*, SI 56(1), 128-132.
- Soomere, T. and Räämet, A., 2011. Spatial patterns of the wave climate in the Baltic Proper and the Gulf of Finland. *Oceanologia*, 53(1-T1), 141-150.
- Suursaar, Ü., 2013. Locally calibrated wave hindcasts in the Estonian coastal sea in 1966–2011. *Estonian Journal of Earth Sciences*, 62, 42-56.
- Suursaar, Ü., Jaagus, J., Kont, A., Rivis, R. and Tõnisson, H., 2008. Field observations on hydrodynamic and coastal geomorphic processes off Harilaid Peninsula (Baltic Sea) in winter and spring 2006–2007. *Estuarine Coastal and Shelf Science*, 80, 31-41.
- Suursaar, Ü., Tõnisson, H., Kont, A. and Orviku, K., 2013. Analysis of relationships between near-shore hydrodynamics and sediment movement on Osmussaar Island, western Estonia. *Bulletin of the Geological Society of Finland*, 85, 35-52.
- Torsvik, T., Didenkulova, I., Soomere, T. and Parnell, K.E., 2009. Variability in spatial patterns of long nonlinear waves from fast ferries in Tallinn Bay. *Nonlinear Processes in Geophysics*, 16(2), 351-363.
- Tõnisson, H., Orviku, K., Kont, A., Suursaar, Ü., Jaagus, J. and Rivis, R., 2007. Gravel-pebble shores on Saaremaa Island, Estonia, and their relationships to formation conditions. *Journal of Coastal Research*, SI 50, 810-815.
- Tõnisson, H., Orviku, K., Jaagus, J., Suursaar, Ü., Kont, A. and Rivis, R., 2008. Coastal Damages on Saaremaa Island, Estonia, Caused by the Extreme Storm and Flooding on January, 9 2005. *Journal of Coastal Research*, 24, 602-614.
- Tõnisson, H., Suursaar, Ü., Orviku, K., Jaagus, J., Kont, A., Willis, D.A. and Rivis, R., 2011. Changes in coastal processes in relation to changes in large-scale atmospheric circulation, wave parameters and sea levels in Estonia. *Journal of Coastal Research*, SI64-1, 701-705.
- Tõnisson, H., Suursaar, Ü., Suuroja, S., Ryabchuk, D., Orviku, K., Kont, A., Sergeev, Y. and Rivis, R., 2012. Changes on coasts of western Estonia and Russian Gulf of Finland, caused by extreme storm Berit in November 2011. In: IEEE/OES Baltic 2012 International Symposium: May 8-11, 2012, Klaipeda, Lithuania, *Proceedings: IEEE*, 2012, 1-7.
- Tõnisson, H., Suursaar, Ü., Rivis, R., Kont, A. and Orviku, K., 2013. Observation and analysis of coastal changes in the West Estonian Archipelago caused by storm Ulli (Emil) in January 2012. *Journal of Coastal Research*, SI 65, 832–837.
- USACE, 1984. *U.S. Army Coastal Engineering Research Center, Shore Protection Manual*, Vol.1, Third Ed., U.S. Govt. Printing Office, Washington D.C., 719 p.
- Watanabe, A. and Sato, S., 2004. A sheet-flow transport rate formula for asymmetric, forward-leaning waves and currents. *Proceedings of the 29th International Conference on Coastal Engineering, ASCE*, Lisbon, Portugal, pp. 1703-1714.

## Incorporating dynamic factors to the Environmental Sensitivity Index (ESI) shoreline classification – Estonian and Spanish examples

Robert Aps†, Hannes Tõnisson‡, Giorgio Anfuso+, José Antonio Perales#, Kaarel Orviku‡, Ülo Suursaar†

† Estonian Marine Institute, University of Tartu, Mäealuse St. 14, Tallinn, 12618, Estonia, robert.aps@ut.ee

‡ Institute of Ecology at Tallinn University Uus-Sadama 5, Tallinn, 10120, Estonia, hannes.tonisson@gmail.com

+ Departamento de Ciencias de la Tierra, Facultad de Ciencias del Mar y Ambientales, Universidad de Cádiz, Puerto Real, Spain, giorgio.anfuso@uca.es

# Departamento de Tecnologías del Medio Ambiente, Centro Andaluz de Ciencia y Tecnologías Marinas (CACYTMAR) Universidad de Cádiz, Puerto Real, Spain, joseantonio.perales@uca.es



[www.cerf-jcr.org](http://www.cerf-jcr.org)



[www.JCRonline.org](http://www.JCRonline.org)

### ABSTRACT

Aps, R., Tõnisson, H., Anfuso, G., Perales, J.A., Orviku, K., Suursaar, Ü. 2014. Incorporating dynamic factors to the Environmental Sensitivity Index (ESI) shoreline classification – Estonian and Spanish examples. In: Green, A.N. and Cooper, J.A.G. (eds.), *Proceedings 13<sup>th</sup> International Coastal Symposium* (Durban, South Africa), *Journal of Coastal Research*, Special Issue No. 70, pp. 235-240, ISSN 0749-0208.

Oil transportation is growing in the Baltic Sea area and especially in the Gulf of Finland where it will reach approximately 180–200 million tons a year by 2020. Growing oil transportation is considerably contributing to the risk of accidental spill-related shoreline oiling. This paper focuses on amending the Environmental Sensitivity Index (ESI) related shoreline classification to local conditions by dynamically changing the categorization of the shoreline in terms of its susceptibility to spilled oil caused by extreme meteorological events. This takes into consideration a number of natural physical factors. The paper presents the results of two European case studies: the Estonian shoreline of the Gulf of Finland (Baltic Sea), and the Spanish coast of the Gibraltar Strait. Susceptibility to spilled oil of some categories of the Estonian shoreline (sandy shores, till shores and gravel shores) occasionally changes over time from low to high sensitivity and back; especially conditioned to the influence of heavy storms. The studies carried out in Spain revealed a well recognizable indirect proportionality between foreshore slope and the tidal range. At many locations, the dynamic morphological characteristics of the beach appeared to be largely determined by contouring and specific conditions that are modifying the initial ESI related categorization of the sandy beaches concerned. The novelty of this work is in attempt to move from the standard ESI related, and locally adapted, static shoreline classification towards more dynamic shoreline monitoring based on characterization of the elements sensitive to oil pollution on shorelines.

**ADDITIONAL INDEX WORDS:** *Dynamic shoreline classification, oil pollution, risk, Baltic Sea, Gibraltar Strait.*

### INTRODUCTION

Oil transportation has been growing significantly all around the world: it increased from 100 millions of tons in 1935 to approximately 3 billion tons today. Oil transportation is growing also in the Baltic Sea area and especially in the Gulf of Finland where it is reaching approximately 180–200 million tons a year by 2020 (Brunila and Storgård, 2012). Growing oil transportation is considerably contributing to the risk of accidental spill-related shoreline oiling and, nowadays, advice on sensitive shorelines likely to be impacted by oil is of critical importance in order to support decision-makers, whether or not a response is necessary or what kind and extent of response is appropriate.

According to NOAA (National Oceanic and Atmospheric Administration 2002), the Environmental Sensitivity Index (ESI) maps have been an integral component of oil-spill contingency planning and response since 1979, serving as quick references for oil spill responders. These comprise three general types of information: 1) shoreline classification, 2) biological resources and 3) human-use resources. The more than three decades of

development of ESI applications have resulted in a considerable body of research into the sensitivity mapping of the different coastal zones in relation to the potential incidental oil pollution. According to NOAA (2002) classification, there are 10 main types of shores, based on an understanding of the physical and biological character of the shore environment. 1 is the least and 10 is the most sensitive. Within these 10 types there may be several sub-types (A, B, etc.) according to more location-specific environmental conditions.

A growing number of studies in this direction proceeded from the pioneering research by Gundlach and Hayes (1978), Michel *et al.* (1978) and Dicks and Wright (1989). Further development of an ESI mapping was based on an extensive application of GIS (Krishnan, 1995) and remote sensing techniques with the aim to reduce the environmental consequences of the spill and cleanup efforts (Jensen *et al.*, 1990; 1998). ESI atlases have been generated from digital databases using GIS techniques for the Svalbard intertidal zone (Moe *et al.*, 2000), Cardoso Island State Park and surrounding areas, São Paulo, Brazil (Wieczorek *et al.*, 2007), the Mediterranean coast of Israel (Adler and Inbar, 2007), the Portuguese coast (Santos and Andrade, 2009), the northern coast of the Gibraltar Strait (Bello Smith *et al.*, 2011).

The aim of the paper is to present the ESI-related results of two European case studies: 1) the Estonian shoreline of the Gulf of

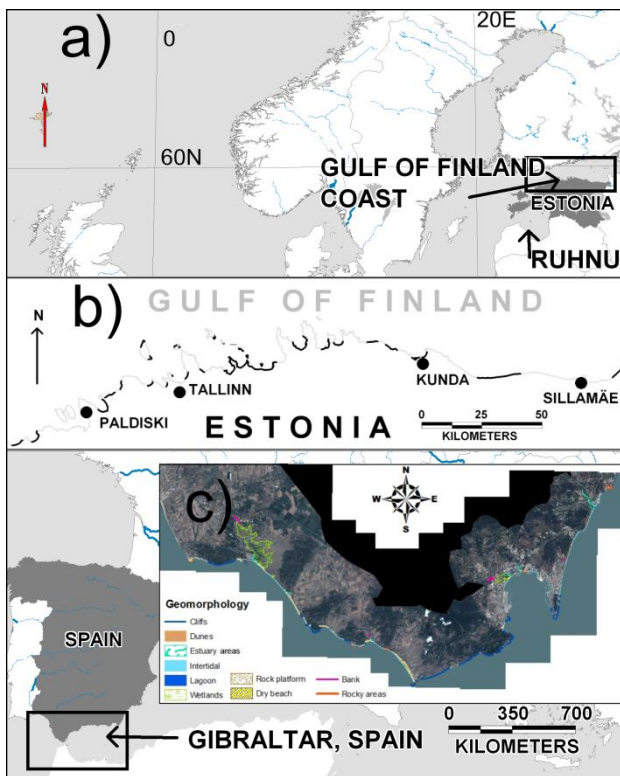


Figure 1. Location of the studied sites in Europe (a); Gulf of Finland coast (b), black-colored shoreline marks the classified sandy shores; geomorphic map of Gibraltar coast, Spain (c).

Finland (Baltic Sea), and 2) the Spanish coast of the Gibraltar Strait. Both are among the most endangered (by tanker accidents) sites in Europe due to their very intense, rapidly growing oil transport and relatively short distances from shipway to the shore makes the reaction time short. Therefore, the current study introduces new level of ESI mapping by including the most considerable dynamical components. Finally, such results increase the preparedness to disaster and help to reduce clean-up costs and impact to nature.

### STUDY AREA

The Estonian and Spanish study sites represent particularly endangered areas because they show intense ship traffic in naturally sensitive shallow continental seas and narrow straits (Figure 1). In such environments, the risk associated with ship grounding or collision is rather high and, if the oil spill occurs, it is almost impossible to prevent the oil from washing ashore due to the limited extent of the sea area concerned and often narrow “window of opportunity” determined by the possibly unfavorable weather conditions.

Estonia has a comparatively long shoreline (approximately 4,000 km) due to a number of peninsulas, bays and islands (over 1,500 islands). The shores are geologically diverse and serve a variety of societal functions. The Estonian seashores in general are characterized by embayments with a variety of beach types experiencing land uplift ranging from 0.5 to 2.8 mm/year (Vallner *et al.*, 1988). The Estonian coast of the Gulf of Finland is a nontidal bay (tidal range is less than 5 cm) exposed to the waves from the west, north-west and north. Despite virtually nonexistent tides, the Gulf of Finland frequently experiences rapid meteorologically

forced sea-level fluctuations, including up to 4 m high storm surges in the area of St. Petersburg (Russia) and up to 2–3 m high surges on the Estonian coast (Suursaar, 2010). Based on long-term studies in coastal geology, the Estonian shoreline of the Gulf of Finland has probably one of the most detailed geological classifications of the shore types in Europe. In the previous studies this classification has been taken as a basis for adapting the standard ESI shoreline classification to the local conditions of the Estonian shoreline of the Gulf of Finland. The standard ESI shoreline classification adapted to the Estonian shoreline revealed that over 2/3 of the shoreline concerned has very high environmental sensitivity in relation to potential oil pollution. Moreover, this is the most densely populated coastal area in Estonia including the capital (over 400,000 inhabitants) and a number of towns. Another example from the western coast of Estonia is also considered to demonstrate and explain the mechanisms of the findings (Ruhnu).

The studied area in Spain includes the Gibraltar Strait, a microtidal environment (tidal range is 1.3 m) exposed to winds and waves from the east and, secondarily, from the west. The shoreline is composed of high cliffs, bluffs, rocky shore platforms and sand beaches. Within this zone, several small quartz-rich beaches are observed at Algeciras Bay, which is the most populated area (around 250,000 inhabitants) with coastal towns, port activities, a petrochemical industry and fisheries.

### METHODS

The data on shore dynamics are collected in the frames of several monitoring programs and scientific research projects of the Estonian coast. Repetitive photographs are taken and profiles are measured from the studied locations.

The collected profiles and photographs in the database are analyzed. Regular orthophotos have been taken along the Estonian coast since 1995 and for the studied sections in 1995–1998 (grayscale, pixel size 75 cm), 2002–2005 (color, pixel size 50 cm) and 2008–2012 (color, pixel size 25 cm). The orthophotos are analyzed using *Mapinfo Professional*. We were not able to fit all the orthophotos in the article, but each orthophoto can be freely accessed via the Estonian Land Board portal (<http://geoportaal.maaamet.ee/eng/>) The classification of the shoreline geology of Estonia is elaborated by Dr K. Orviku (Orviku *et al.*, 2010), which is later converted into ESI classification by the authors.

The Internet GIS technologies are increasingly used worldwide in conjunction with oil spill modeling tools as a means of integration and visualization of the oil spill response decision support related information. The methodology used in the example from Estonia is based on a coupled Seatrack Web – SmartResponse Web (SW-SRW) simulation framework developed by the EU Central Baltic INTERREG IVA Project “Minimizing risks of maritime oil transport by holistic safety strategies (MIMIC)”. The Estonian shoreline ESI map layers are imported as the Web Map Services into the coupled SW-SRW simulation framework and used for building situation awareness in oil spill response operations.

Relative exposure to wave and tidal energy, shoreline slope, and substrate type have been investigated in SW Spain in the framework of different studies and monitoring programs, especially focused on the design of Environmental Sensitivity Maps for the Gibraltar Strait area (Bello Smith *et al.*, 2011) or the characterization of beach morphodynamics and wave climate along the SW Andalusia littoral (Anfuso *et al.*, 2002; Anfuso, 2005; Rangel and Anfuso, 2011). These studies serve as a

discussion source for the current paper. Moreover, several monitoring results are taken into account.

## RESULTS AND DISCUSSION

The recent studies in Estonia and Spain have clearly revealed that shore dynamics might be an important factor to be taken into account in regional ESI classifications. Mixing layer, seasonality, changing shore types due to the deficit of the sediment and abundance of strong storms are the biggest concerns considered in the following chapter.

### Dynamics Factor: Estonian Example

Estonian coast is experiencing a sediment deficit. Thin layers of soft, mobile sediments combined with very variable shore types make the use of ESI sensitivity classes rather difficult. The datasets originating from the monitoring programs and various scientific research projects indicate rapid changes in beach morphology and shore types in several locations along the Estonian coast (Orviku *et al.*, 2003; 2009; Tõnisson *et al.*, 2007; 2013). Changes in beach type will automatically and rapidly change the sensitivity class and the sensitivity to pollution as well.

Storm surges have an important role in the shore processes on the coasts of the nearly tideless Gulf of Finland leading to changes in beach morphology and (ESI) type. It is worth noting that storm surges in Estonia are caused by westerly storms. Very strong easterlies result in low sea level events, also known as “negative surges”, which have no significant geomorphic effect. The highest sea levels recorded in Estonia have always occurred during westerly storms. The highest sea-level (in the history of instrumental measurements) reached 275 cm above mean sea level; recorded during the storm Gudrun in 2005 (Tõnisson *et al.*, 2008).

According to the analyzed field data recorded after the storms and available cartographic data, we found out that a few extreme or unusual events have caused the most drastic changes on the shores, including changes in their type (Orviku *et al.*, 2009). The best recorded example originates from the western coast of Estonia on Ruhnu Island (Figure 1a). Changes were first discovered on the repetitive photographs (Figure 2) and were later also detected on the orthophotos (Figure 3). In 1990, the whole western coast of the island was fringed by at least 20–30 m wide sandy beach while by 1996, most of the western coast was turned into a till shore (Figure 2). The length of the sandy beaches decreased more than 2.5 km in 5 years (monitoring data). The southeastern part of Ruhnu Island is characterized by wide sandy beaches and dunes whereas most of the eastern and north-eastern part is till shore bordered by a small scarp. There is usually a slow sediment transport from north to south and accumulation in the southern part of the island (Orviku *et al.*, 2003). However, in January and February 1990 two very strong storms occurred when average wind speeds reached 19 m/s, sea level +171 cm in January and 25 m/s, +166 cm in February. In both cases the wind blew from the S or SSW elongating the sandy beaches nearly 2.5 km northward. There were no major storms in the next five years and the initial situation was restored – sand was transported back to the south (Figure 2). Later on, we have spotted similar shifts after major winter storms in 2005, 2007 and 2011/2012 (based on several orthophotos). However, most of the sand stayed in the northern part of the island due to frequent storms.

Another example can be taken from the northern coast of Estonia (Gulf of Finland) in the vicinity of Aa village. However, the geomorphic system here is different. There is a constant sediment transport from west to east on the southern coast of the gulf. Negative storm surges during the eastern storms make the



Figure 2. Winter storms from unusual direction accompanied with high sea level (over 150 cm) created over 2 km long and 20 m wide sandy beach on Ruhnu Island in 1990. In 1996, the same sandy beach changed to a till shore.

westward transport almost impossible. Similarly to the previous study area, we can witness wide sandy beaches after strong storm periods here. This section of the coast is experiencing sediment deficit like most of the Estonian coast. The sand layer on the shore is usually very thin (less than 0.5 m). The sand is eroded from the scarps and is taken onto the shore or into the shallow sea during strong storms (like in 2005, 2007 and 2011/2012) associated with high sea levels. The orthophotos and the photos taken from the shores the following summer indicate a rapid expansion of sandy beaches. However, this sand continues a slow but constant eastward movement during ordinary storm events and accumulates in the bays or in the deeper sea leaving the shores, which are well exposed to waves, without sand in a few years. These sandy beaches are temporarily restored during the next strong storm accompanied by high sea-level.

These sandy beaches can be considered ESI 3B beaches (fine-to medium-grained sandy beaches – based on geological databases and visual observations) and after the loss of sand they change for 6A or 6B (gravel beaches and rip-rap gravel beaches). Their sensitivity to oil pollution increases rapidly (due to much deeper penetration of oil difficult cleanup). Lack of sand may create a situation when the upper layers cannot stop the penetration of possible oil pollution and oil reaches the deeper 6A or 6B type layers, which makes the cleanup process more complicated.

Nearly 25% (approximately 150 km) of the Gulf of Finland shores are mapped as sandy shores of ESI class 3B shores. However, these shores have mostly been mapped only once (field visits over past 30 years) and we cannot be sure if they persist or change their type from time to time. There are approximately 30

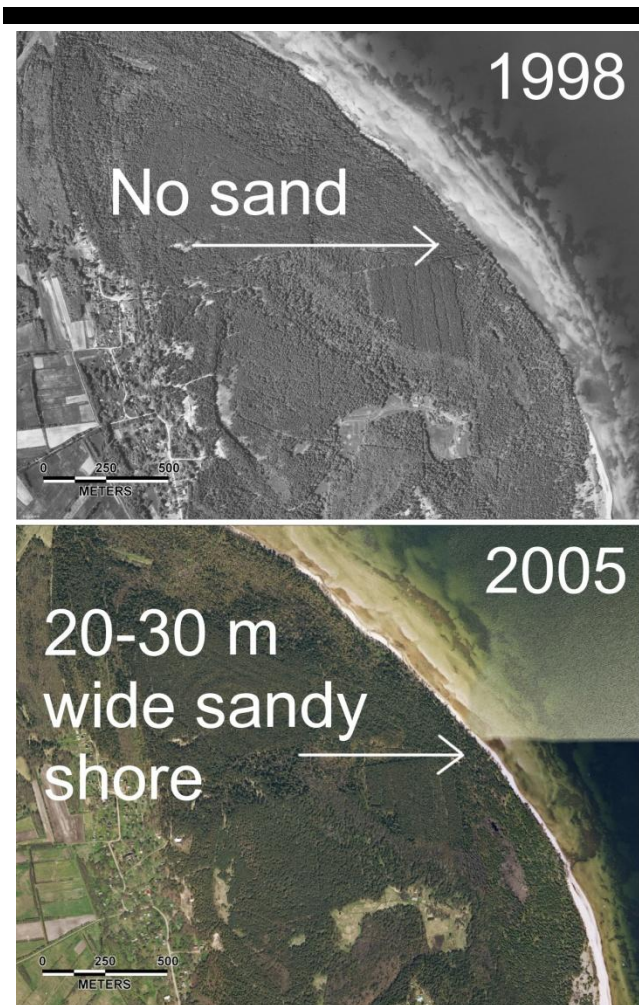


Figure 3. Winterstorms from unusual direction accompanied with high sea level (over 150 cm) created more than 2 km long and 20 m wide sandy beach (white color on the orthophoto) in Ruhnu Island. In 1995, no more sand was left (orthophotos by Estonian Land Board).

separate units of sandy beaches on the coast of the Gulf of Finland and even if we assume that their length may change by approximately 2 km it still means approximately 60 km (30 units  $\times$  2km), which is 10% of the total length of the shores here. These 10 % can be classified as ESI 6A or 6B making the southern coast of the Gulf of Finland more sensitive than it was expected.

There is a certain relationship between the shoreline substrate type (shoreline substrate sensitivity) and the associated seafloor habitat's sensitivity (sensitivity of macrophytes and benthic invertebrates) to oil pollution (Leiger *et al.*, 2012). Therefore, the dynamic changes in shoreline substrate type are dynamically changing also the relationship with the associated seafloor habitat's sensitivity.

The ESI maps of the Estonian Baltic Sea shoreline are used by the oil spill response authorities for contingency planning, personnel training and in real emergency situations. Therefore, having the up-to-date and reliable information as an input to the coupled SW-SRW simulation framework used by the authorities is essential. However, the solution for making our ESI classification more reliable is rather time-consuming. We see that all the shores classified as ESI 3B (sandy beaches) must be re-mapped on the

existing orthophotos (at least 6 different datasets depending on the location). We assume that the changes take place mostly between classes 6A, 6B and 3B, and luckily, these types can be easily identified and delimited from the orthophotos and no further fieldwork is needed. This enables us to identify the shores with very dynamic behavior. Furthermore, comparison of different datasets makes it possible to identify the directions of changes and find out the relationships with the forcing conditions (threshold values for storm parameters like direction, sea-level, wave height etc.) and the recorded changes on the shores. We suggest that the comparison of maps and analyses of forcing conditions, together with the monitoring program enables the elaboration of the methodology to predict the extent and direction of changes in the beach morphology and ESI type. Such a methodology helps us to make ESI classification dynamic and match more closely the real situations that we might face on the shores. This all contributes to the better state of our shores and coastal waters. However, solutions to this problem require extensive fieldwork (regular monitoring) for the verification (including thickness of sand layer) of the cartographic data and it must be handled in a separate study.

### Dynamics Factor: Spanish Example

The current study on the Spanish coast is focusing on geomorphic characteristics and especially on sandy littoral sectors in order to consider the importance of beach behavior, morphological changes and beach grain size in determining the sensitivity of the shores.

Concerning the relative exposure and according to Rangel and Anfuso (2011), storm characterization and distribution can be easily carried out by means of the Storm Power Index (Dolan and Davis, 1992) used to divide storms into five classes, from Class 1 (Weak) to Class 5 (Extreme). Following Rangel and Anfuso (2011), the analysis of different wave data sets allowed identifying storm wave height threshold and storm energy and characteristics such as temporal and spatial distribution along the SW Atlantic littoral of Andalusia. Obtained information constituted a key issue in the determination and prediction of beach erosion and accretion processes and associated risk for oil burial or re-appearance. Potential burial of oil in beaches is an important issue that must be taken into account in ESI and Emergency Plans (NOAA, 2002).

Shoreline slope is an important aspect that affects oil persistence in the littoral and beach dynamics. It is related to grain size characteristics. In fact, there is a well-known direct relationship between these parameters. Anyway, it is important to observe as, at places, beach slope values can be altered because of contouring conditions (Anfuso *et al.*, 2002). In this sense, an "artificial" slope, e.g. a slope value not well related to grain size characteristics can be linked to a rock shore platform extended in the nearshore area (the rock platform affects wave propagation), or to other kinds of natural or human structures. Examples are beaches laterally limited by groins or backed by cliffs and/or seawalls or rip-rap revetments (Anfuso *et al.*, 2002; Bello Smith *et al.*, 2011). In such cases, slope values must be treated carefully because they are usually overestimated. Beach slope is also affected by tidal range and this point is not taken into account in NOAA (2002). In the framework of the beach monitoring carried out by Bello Smith *et al.* (2011), the micro-tidal beaches recorded extremely high slope values when compared with the ones recorded in the tidal areas. This is because of a well-known inverse relationship between tidal range and beach slope. Hence, it could be probably interesting to differentiate between beach slopes of micro and tidal beaches because they show similar numeric values but different width and behavior.

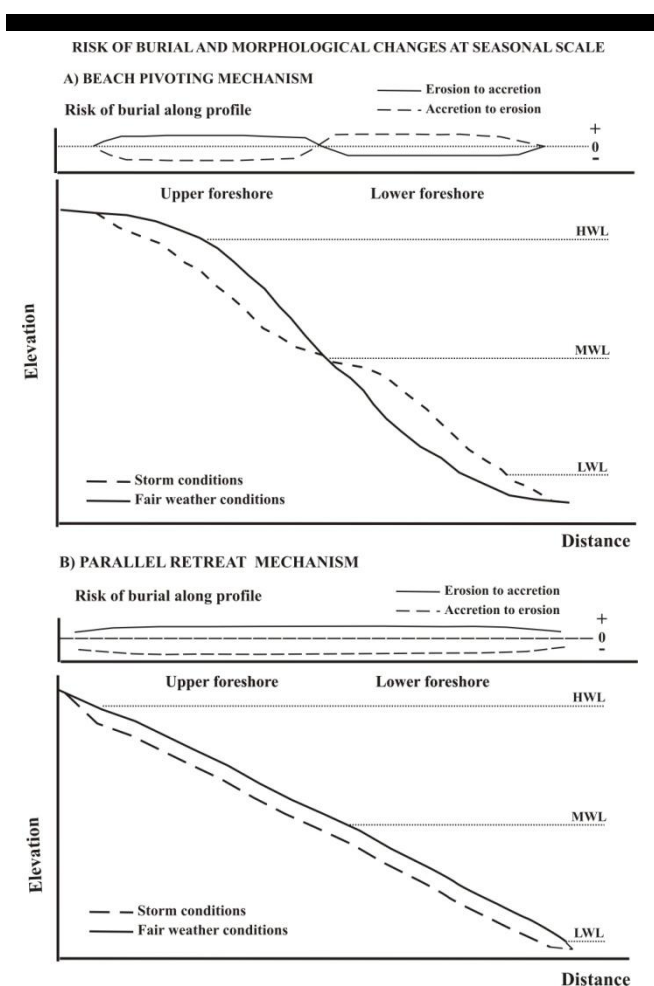


Figure 4. Pivoting and parallel retreat risk of burial at seasonal scale.

Additionally, it must be underlined that beach slope is a useful indicator of beach characteristics and morphodynamic state, but it records great seasonal and short term variations. It is consequently of great interest to achieve as much data as possible on beach morphological characteristics and changes. In this sense, Bello Smith *et al.* (2011) carried out a monitoring program with a monthly periodicity, for the reconstruction of characteristics, behavior and seasonal variability of sandy beaches. Specifically, they investigated the Gibraltar Strait area during the spring-summer period when, after winter storm season, natural beach recovery and berm formation take place.

Different beach types were identified and classified according to the NOAA (2002) and the Wright and Short (1984) and Masselink and Short (1993) classifications. The use of the latter two classifications is of great importance because it allows useful, additional information concerning the morphodynamic beach state (relevant for natural beach cleaning processes, the determination of cleaning techniques and beach mobility) and presence of bar/berm and beach cusps, relevant for oil burial. In addition, the monitoring program allowed the investigation of seasonal changes. In this sense it was possible to observe: i) beach morphodynamic changes over the year, this being an important point which controls practical aspects such as beach mobility, and ii) vertical variations along the cross-shore profile, an important point for oil burial potential. Such changes can be categorized as

“beach pivoting” and “parallel retreat” mechanisms (Nordstrom and Jackson, 1992). The knowledge of such types of beach response to erosion process is important for oil burial and estimation of beach trafficability (Figure 4). Following the “beach pivoting mechanism”, a fair weather profile, usually characterized by a well developed berm and associated high foreshore slope, is affected by processes that create erosion in the upper foreshore and give rise to accretion in the lower foreshore, with a beach pivoting at mean sea level position (Figure 4). In this sense, maximum probabilities of oil burial and re-appearance are respectively expected in the lower and upper foreshore. During fair weather conditions the berm will be formed with sediments coming from the lower foreshore and burial potential will be maximum in the upper foreshore with high probability of oil re-appearance at the lower foreshore.

According to the “parallel retreat mechanism” erosion and accretion are generally of minor importance with respect to the previous case, and are homogeneously distributed along the foreshore. Oil burial and re-appearance probability show a homogeneous trend along the foreshore too (Figure 4).

As an example, in Galicia (Spain), after the Prestige accident (13<sup>th</sup> November 2002), the cleaning activities continued during several years because of the sporadic appearance of reduced quantities of fuel (Gonzalez *et al.*, 2009). In the period between winter 2002 and summer 2006, along beaches investigated by previous authors, more than 10,000 tons of residual materials were removed from the berm and intertidal zone. This was because the intermediate-reflective beach state and great morphological variability favored the oil to become partly buried. Lorenzo *et al.* (2009) observed similar processes in nearby beaches and used ground-based radar to investigate the depth of oil burial that ranged from a few centimeters to 1–2 m.

Furthermore, in order to assess an important issue such as oil burial at the hourly scale (e.g. linked to tidal related morphological variations) specific field assessments on the determination of disturbance depth can be carried out. Anfuso (2005) used both rods with loose-fitting washers and marked sand to determine the disturbance depths, which were related to beach slope, breaking wave height and type; and morphodynamic beach state to propose different equations that have a broad validity. Specifically, the author found a good linear relationship between disturbance depth (y) and beach slope (x, expressed as  $\tan \beta$ ):

$$y = 0.22 + 115 x \quad r = 0.90 \quad (1)$$

The obtained expression is valid for a great range of beach gradients, from gentle beach faces ( $\tan \beta = 0.02$ ,  $\sim 1.3^\circ$ ) to steep foreshores ( $\tan \beta = 0.14$ ,  $\sim 8.8^\circ$ ). Aforementioned values belong to the first two classes of the NOAA classification, e.g.  $< 5^\circ$  and  $5 - 30^\circ$ . No cases have been reported for sand beaches with foreshore slopes  $> 10^\circ$  nor for the NOAA third class ( $> 30^\circ$ ); these large values probably related to gravel, cobbles and blocks. Considering the great range in disturbance values presented by Anfuso's (2005) equation (1): 2.52 cm for a slope of  $1.3^\circ$ , 8.27 cm for  $5^\circ$  and 16.32 cm for  $8.8^\circ$ , it could be helpful to further subdivide the first two NOAA classes into subclasses. Regarding the substrate type, the monitoring program carried out by Anfuso *et al.* (2002) evidenced the importance of studying seasonal changes in beach sediments, with coarser sediments observed in winter and vice versa. These granulometric differences in SW Spain being of 0.06 mm.



## CONCLUSION

The study reminds us that shores cannot be handled as static systems and all kind of classifications for the shores, including ESI classification, must take into account the shore dynamics. The shoreline ESI maps that are used by the oil spill response authorities for contingency planning, personnel training and in real emergency situations need to contain up-to-date and reliable information. Therefore, it is essential to move from the standard ESI related and locally adapted static shoreline classification towards more dynamic shoreline monitoring based on the characterization of the shore's sensitivity to oil pollution shoreline elements.

## ACKNOWLEDGEMENT

This work was supported by ESF grants No. 8549, 9191 and 8980, target financed themes SF0280009s07 and SF0180104s08, and by the EstKliima project of the European Regional Fund program No. 3.2.0802.11-0043. The study was also supported by the Estonian Environmental Investment Centre and by Central Baltic INTERREG IVA Program Project MIMIC "Minimizing risks of maritime oil transport by holistic safety strategies". This research was partially developed in the frame of the ALBORAN Project (Project Ref. 0066\_ALBORAN\_2\_E), co-funded by the FEDER-POCTEFEX Program and with matched funding provided by the Regional Ministry of Environment of Andalusia and Andalusia (Spain) Research PAI Group RNM-328. Special thanks to Dr. Are Kont for his assistance in providing English language editorial comments and suggestions.

## LITERATURE CITED

- Adler, E. and Inbar, M., 2007. Shoreline sensitivity to oil spills, the Mediterranean coast of Israel: assessment and analysis. *Ocean & Coastal Management*, 50, 24-34.
- Anfuso, G., 2005. Sediment-activation depth values for gentle and steep beaches. *Marine Geology*, 220, 101-112.
- Anfuso, G., Martínez del Pozo, J.A., Gracia, F.J. and López-Aguayo, F., 2003. Long-shore distribution of morphodynamic beach states along an apparently homogeneous coast in SW Spain. *Journal of Coastal Conservation*, 9, 49-56.
- Bello Smith, A., Cerasuolo, G., Perales, J.A. and Anfuso, G., 2011. Environmental Sensitivity Maps: the north coast of Gibraltar Strait example. *Journal of Coastal Research*, SI 64 875-879.
- Brunila, O. and Storgård, J., 2012. Oil transportation in the Gulf of Finland in 2020 and 2030. *Publications from the Centre for Maritime Studies University of Turku*, A 61, 72 p.
- Dicks, B. and Wright, B., 1989. Coastal sensitivity mapping for oil spills. In: Dicks, B. (Ed.) *Ecological impacts of the oil industry*. New York: J. Wiley & Sons: 235-259.
- González, M., Medina, R., Bernabeu, A.M. and Novoa, X., 2009. Influence of beach morphodynamics in the deep burial of fuel in beaches. *Journal of Coastal Research*, 25, 799-818.
- Gundlach, E.R. and Hayes, M.O., 1978. Vulnerability of coastal environments to oil spill impacts. *Marine Technology Society Journal*, 12, 18-27.
- Jensen, J.R., Halls, J.N. and Michel, J., 1998. A Systems Approach to Environmental Sensitivity Index (ESI) Mapping for Oil Spill Contingency Planning and Response. *Photogrammetric Engineering & Remote Sensing*, 64, 1003-1014.
- Jensen, J.R., Ramsey, E.W., Holmes, J.M., Michel, J.E., Savitsky, B. and Davis, B.A., 1990. Environmental Sensitivity Index (ESI) Mapping for Oil Spills Using Remote Sensing and Geographic Information System Technology. *International Journal of Geographical Information Systems*, 4, 181-201.
- Krishnan, P., 1995. Research report – a geographical information-system for oil-spills sensitivity mapping in the Shetland-islands (United Kingdom). *Ocean & Coastal Management*, 26, 247-255.
- Leiger, R., Aps, R., Kotta, J., Orviku, K., Pärnoja, M. and Tõnisson, H., 2012. Relationship between shoreline substrate type and sensitivity of seafloor habitats at risk to oil pollution. *Ocean & Coastal Management*, 66, 12-18.
- Lorenzo, H., Rial, F.I., Aris, P. and Armesto, J., 2009. Fighting against coastal oil spill pollution by means of ground-based radar. *Journal of Coastal Research*, SI 56, 846-850.
- Masselink, G. and Short, A.D., 1993. The effect of tide range on beach morphodynamics and morphology: a conceptual beach model. *Journal of Coastal Research*, 9, 785-800.
- Michel, J., Hayes, M.O. and Brown, P.J., 1978. Application of an oil spill vulnerability index to the shoreline of lower Cook Inlet, Alaska. *Environmental Geology*, 2, 107-117.
- Moe, K.A., Skeie, G.M., Brude, O.W., Løvås, S.M., Nedrebø, M. and Weslawski, J.M., 2000. The Svalbard intertidal zone: a concept for the use of GIS in applied oil sensitivity, vulnerability and impact analyses. *Spill Science & Technology Bulletin*, 6, 187-206.
- NOAA, 2002. Environmental Sensitivity Index Guidelines, Version 3. NOAA Technical Memorandum Nos OR and R11. Hazardous Materials Response Division, National Ocean Service, Seattle, WA, 192 p.
- Nordstrom, K.F. and Jackson, N.L., 1992. Two-dimensional change on sandy beaches in meso-tidal estuaries. *Zeit. für Geomorph.*, 36, 465-478.
- Orviku, K., Jaagus, J., Kont, A., Ratas, U. and Rivis, R., 2003. Increasing activity of coastal processes associated with climate change in Estonia. *Journal of Coastal Research*, 19, 364-375.
- Orviku, K., Suursaar, Ü., Tõnisson, H., Kullas, T., Rivis, R. and Kont, A., 2009. Coastal changes in Saaremaa Island, Estonia, caused by winter storms in 1999, 2001, 2005 and 2007. *Journal of Coastal Research*, SI 56, 1651-1655.
- Orviku, K., Kont, A. and Tõnisson, H., 2010. Estonia. Bird, E. (Eds.). *Encyclopedia of the World's Coastal Landforms* (605-611). Dordrecht, Heidelberg, London, New York: Springer.
- Rangel, N. and Anfuso, G., 2011. Coastal storm characterization and morphological impacts on sandy coasts. *Earth Surfaces Processes and Landforms*, 36, 1997-2010.
- Santos, C.F. and Andrade, F., 2009. Environmental sensitivity of the Portuguese coast in the scope of oil spill events - Comparing different assessment approaches. *Journal of Coastal Research*, SI 56, 885-889.
- Suursaar, Ü., 2010. Waves, currents and sea level variations along the Letipea – Sillamäe coastal section of the southern Gulf of Finland. *Oceanologia*, 52, 391-416.
- Tõnisson, H., Orviku, K., Kont, A., Suursaar, Ü., Jaagus, J. and Rivis, R., 2007. Gravel-pebble shores on Saaremaa Island, Estonia, and their relationships to formation conditions. *Journal of Coastal Research*, SI 50, 810-815.
- Tõnisson, H., Orviku, K., Jaagus, J., Suursaar, Ü., Kont, A. and Rivis, R., 2008. Coastal damages on Saaremaa Island, Estonia, caused by the extreme storm and flooding on January 9, 2005. *Journal of Coastal Research*, 24, 602-614.
- Tõnisson, H., Suursaar, Ü., Rivis, R., Kont, A. and Orviku, K., 2013. Observation and analysis of coastal changes in the West Estonian Archipelago caused by storm Ulli (Emil) in January 2012. *Journal of Coastal Research*, SI 65, 832-837.
- Vallner, L., Sildvee, H. and Torim, A., 1988. Recent crustal movements in Estonia. *Journal of Geodynamics*, 9, 215-223.
- Wieczorek, A., Dias-Brito, D. and Milanelli J.C.C., 2007. Mapping oil spill environmental sensitivity in Cardoso Island State Park and surrounding areas, São Paulo, Brazil. *Ocean & Coastal Management*, 50, 872-886.
- Wright, L.D. and Short, A.D., 1984. Morphodynamic variability of surf zones and beaches: a synthesis. *Marine Geology*, 56, 93-118

## The influence of interannual variability of mean sea level in the Adriatic Sea on extreme values

M.F. Bruno†, M.G. Molfetta†, A.F. Petrillo†

†DICATECh  
Technical University of Bari,  
Bari, Italy  
f.bruno@poliba.it,  
m.molfetta@poliba.it,  
a.petrillo@poliba.it



[www.cerf-jcr.org](http://www.cerf-jcr.org)



[www.JCRonline.org](http://www.JCRonline.org)

### ABSTRACT

Bruno, M.F., Molfetta, M.G., Petrillo, A.F., 2014. The influence of interannual variability of mean sea level in the Adriatic Sea on extreme values. In: Green, A.N. and Cooper, J.A.G. (eds.), *Proceedings 13<sup>th</sup> International Coastal Symposium* (Durban, South Africa), *Journal of Coastal Research*, Special Issue No. 70, pp. 241-246, ISSN 0749-0208.

The analysis of sea level data, in the low and middle Adriatic (south of Italy), collected by 6 stations belonging to the National Tide Gauge Network and to Apulia Region Meteorological Network, shows a generalized increase in the mean sea level from 2008. The change between 2007 and 2009 is in the order of about 10 cm. A GPD distribution has been fitted to extreme series (5 extremes per year from 1999 to 2012) of sea level observed values, observed levels corrected with current annual mean sea level and tidal residuals. The analysis shows a significant increase in extremes of sea level values, while the extremes of corrected observed values and tidal residuals are quite similar respect to those found using observed data updated to 2006. Due to the sea level increase, the extremes, in observed sea level, rise drastically when updating time series to 2012, but, removing the effect of Mean Sea Level (MSL), these differences significantly decrease in the return levels.

**ADDITIONAL INDEX WORDS:** *Sea level extremes, Mean sea level, Coastal flooding.*

### INTRODUCTION

The risk assessment and the coastal management have, in recent years, become of paramount importance in environmental policies and civil protection. The high attention is, primarily, attributable to intensive exploitation of coastal areas subjected to a progressive increase in the resident population and to a growing concentration of activities becoming more and more important from a socio-economic perspective (Eurosion, 2004).

In the planning and management of the coastal zone, sea level variation (IPCC, 2007; IPCC, 2013) must be taken into account; for the specific case of sandy coasts this may lead to an increase in the present trend of eroding shorelines.

The change in sea level is a phenomenon linked to various environmental and physical factors, global and local, with a strong temporal frequency. The question is of great importance since the rise in average sea level leads to a natural retreat of sandy beaches and an increased risk of flooding of low-lying coastal areas (Sanchez-Arcilla *et al.*, 2011).

The Integrated Coastal Zone Management (ICZM) underlines the necessity to define a coastal setback zone (Sano *et al.*, 2011) as an area, with a minimum width of 100m from the highest winter waterline, where construction is not allowed. The ICZM Protocol (UNEP, 2008) sets that the zone must be delimited as "taking into account, inter alia, the areas directly and negatively affected by climate change and natural risks".

In Italy, in the last few years, several studies have been conducted to evaluate coastal flooding due to sea level increase

(Antonioli and Leoni, 2007), and marine inundation assessment along the coastline due to storm surge and run up (Armaroli *et al.*,



Figure 1. Geographic localization of examined National Tide Gauge Network stations (green squares) and Apulia Region tidal gauges (red circles) along the Apulian Coast, Southern Italy, Adriatic Sea.

Table 1. Overview of the examined tide stations with the maxima of observed levels, observed levels corrected with the current year mean sea level and tidal residual. The starred values are affected by the presence of an outlier in the time series.

Station	Period	Geographical Coordinates (WGS84)	Observed Level (m)	Observed Level -MSL (m)	Tidal Residual (m)
<i>National Tidegauge Network</i>					
Ortona	1/09/1999-31/08/2013	42°21'21.24"N 14°24'53.50"E	0.84*	0.80*	0.68
Vieste	1/09/1999-31/08/2013	41°53'17.10"N 16°10'37.24"E	0.61	0.65	0.54
Bari	1/09/1999-31/08/2013	41°08'24.74"N 16°51'57.72"E	0.56	0.63	0.49
Otranto	1/09/1999-31/08/2013	40°08'49.74"N 18°29'49.52"E	0.32	0.49	0.48
<i>Apulia Region Tide Gauges</i>					
Manfredonia	1/09/2006-31/08/2013	41°37'28.39"N 15°54'51.27"E	--	0.59	0.46
Brindisi	1/09/2006-31/08/2013	40°39'21.14"N 17°58'2.71"E	0.48	0.58	0.46

2009; Martinelli *et al.*, 2010).

All these studies focuses on low-lying coastal areas along the Adriatic Sea, that are characterized by the occurrence of severe rises in sea level induced by the combination of high astronomical tide and high levels of meteorological tide, caused by low pressures and strong south winds that push water to the northern part of the basin. The storm surge, defined as the sum of the effects of the barometric pressure, wind stress, Coriolis force, and wave breaking have on sea level, reaches its maximum in the area of the Venice lagoon, giving rise to the well known "acqua alta" phenomena.

Similar studies are ongoing in the Apulia Region where, due to its low-lying areas associated with the progressive disappearance of coastal dune belts and coastal erosion, the regional coastline is at risk of coastal flooding (Antonoli and Leoni, 2007).

The coastal flooding risk along the Apulian coast has been analyzed, within the IPA-SHAPE project (deliverables published at <http://www.shape-ipaproject.eu/>), using a GIS-based approach (Lichter and Feslsteiner, 2012) and a two-dimensional hydraulic modeling software model to simulate a storm surge approaching a low sandy beach (O'Brien, 2005).

These studies, together with the Regional Coastal Plan (PRC) and the Coastal Defense Plan (PDC) (Bruno *et al.*, 2012), can be seen as a first decisive step towards ICZM, which entered into force in the EC in March 2011, but in many countries, among them Italy, not yet been fully implemented.

The hydraulic and GIS-based models, for coastal flooding evaluation, require the water levels at the shoreline. This is a

function of time, calculated as the sum of storm surge, astronomical tide, and wave run-up.

The sea level in the Adriatic Sea shows large interannual and multiannual fluctuations, due to meteorological conditions (Raicich, 2003). Hence, for this purpose, sea levels along the Adriatic coast have been analyzed, and in particular, an in depth analysis has been conducted on extreme events that occurred in recent years. Furthermore, over the last century since seamless and reliable tide data are available, the long term Relative Sea Level Ratio (RSLR) of the Adriatic Sea has risen between  $0.5 \pm 0.2$  and  $1.2 \pm 0.1$  mm/year (Marcos and Tsimplis, 2008; Raicich, 2007). In comparison, the tide gauges of Venice (in the northern Adriatic) have registered  $2.5 \pm 0.1$  mm/year due to anthropogenic subsidence.

In the period from 2007 to 2009, the tide gauges located in the northern Adriatic Sea, reported an increase of about 150 mm and a similar rise has been observed along all the Adriatic Sea with an escalation in extreme events with several flooding events. The sudden increase in MSL in the Mediterranean Sea, as reported by Tsimplis *et al.* (2013) and Landerer and Volkov (2013), has suggested an update of the extreme levels, in order to consider the latest significant events recorded in the Adriatic Sea.

## ANALYSIS AND DISCUSSION

The sea surface elevation recorded by tide gauges is the sum of mean sea level ( $Z_0$ ), astronomical tide ( $x$ ) and meteorological tide ( $y$ ) induced by wind, storms, atmospheric pressure disturbances (Pugh and Vassie, 1979):

$$\xi(t) = x(t) + y(t) + Z_0 \quad (1)$$

The analysis of sea level data has been extended to 6 stations in the low and middle Adriatic belonging to the National Tide Gauge Network (located at Ortona, Vieste, Bari and Otranto) and to Apulia Region tidal gauges (located at Manfredonia and Brindisi). Figure 1 shows the geographical location of the tide gauges and in Table 1 the main characteristics of the time series are reported.

The Apulia Region Meteorological Network, since 2006, has integrated the national network, allowing a total covering of the regional coastline. This local network has been realized in the framework of a monitoring program of coastal areas and protection structures, that has been carried out in the last ten years

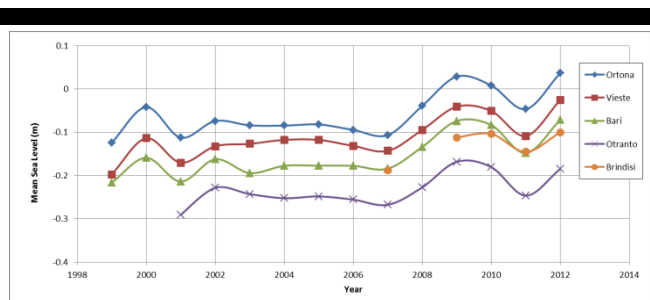


Figure 2. Annual MSL at examined stations from 1999 to 2012

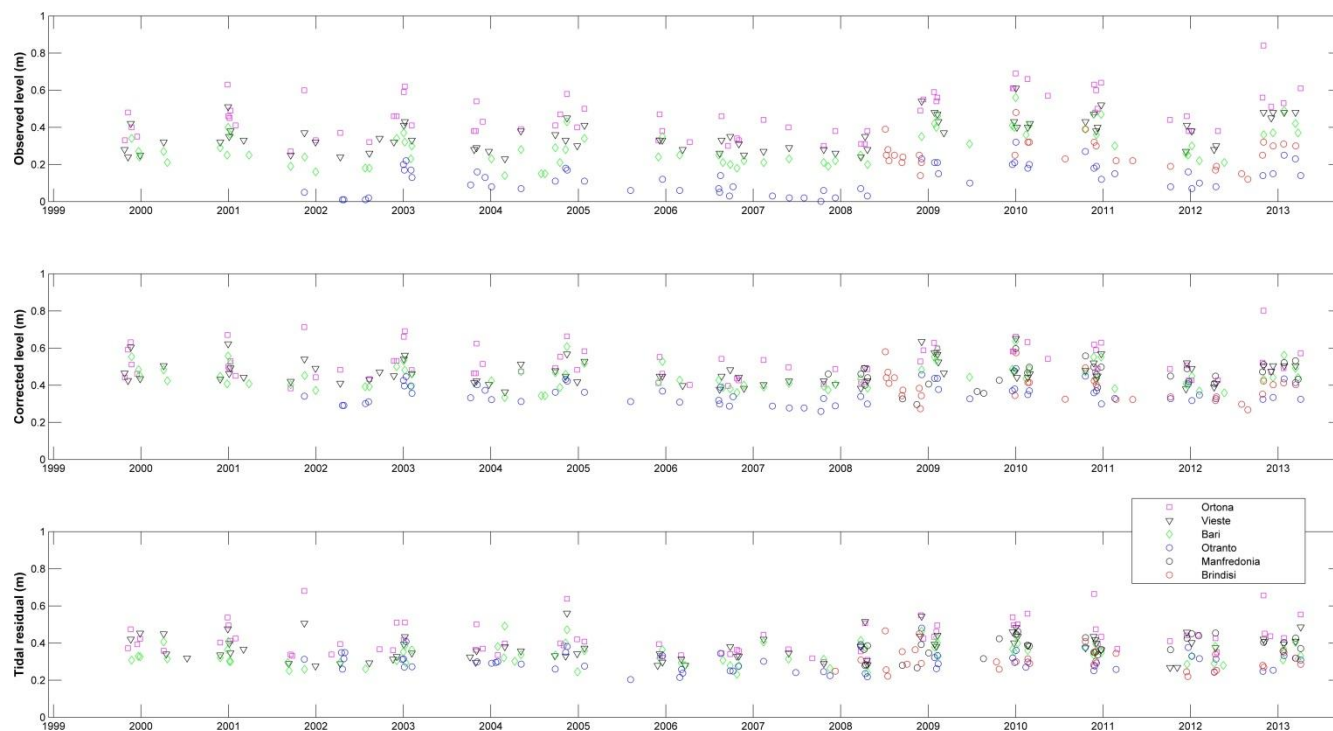


Figure 3. Extreme series (5-largest values per year) of observed levels (upper panel), corrected observed values (central panel), tidal residuals (lower panel).

(Damiani *et al.*, 2007) and it includes two wave buoys, four tide stations and six anemometric stations.

The Manfredonia site, in particular, was chosen because there was a lack of data in the Gulf of Manfredonia. Additionally, due to the low quotes and sea bottom topography, that area is at high risk of coastal flooding (Krestenitis *et al.*, 2011).

The hourly sea level records, before proceeding to the analysis, have been subjected to a quality control for the identification of anomalous data, spikes and timing errors. Data were visually inspected before and after the time for continuity and consistency; this was implemented following the recommendations reported in the (NDBC, 2009). All dubious records have subsequently been removed from the time series.

The maximum deviation  $\sigma_T$  between two successive records has been estimated:

$$\sigma_T = 0.58 \times \sigma \sqrt{T} \quad (2)$$

where  $\sigma$  is the standard deviation calculated for each station and  $T$  is the time lag (in hours).

The application of harmonic analysis to the time series using the software T-TIDE (Pawlowicz *et al.*, 2002), has allowed an additional quality control on the data: records related to years of observation with harmonic constant values not consistent for the site have been discarded.

In a preliminary phase, the yearly mean sea level has been calculated from the observed data with the application of Doodson filters (Doodson, 1954). This is based on years that run from September 1 to August 31 in order to avoid winter splitting.

All the examined stations (Figure 2) show a sudden increase in mean sea level from the winter 2008-2009, with a variation between 2007 and 2009 on the order of about 10 cm. This was followed by a decrease in 2011. The mean sea level in 2012 increases again slightly beyond the level of 2009.

The observed level data have also been subjected to a statistical analysis to get the annual frequency of high tides greater than a fixed threshold. This remained fairly steady up to 2008 with a net increase of events in winter 2009-2010.

The time series check revealed a vertical shift in Manfredonia data in the very first years of observation; hence, in the following, only the corrected levels and tidal residuals will be examined, since, removing MSL, the shift datum disappears. The tidal residual time series have been reconstructed by subtracting the astronomical tide calculated using the harmonic constants with the ratio signal to noise greater than 2 (Pawlowicz *et al.*, 2002). The classical approach to provide an estimation of the probability distribution of extreme levels are based on the generalized extreme value (GEV) distribution (Tsimplis and Blackman, 1997; Lionello *et al.*, 2003) and the generalized Pareto distribution (GPD).

The meteorological tide can be predicted implementing extremal analysis to tidal residuals in order to obtain events with a given return period. Marcos *et al.* (2009) analyzed sea level extremes, updated to 2006, estimating 50-year return levels for sea level observations, tidal residuals and tide-surge probability for 73 tide gauge records located along the coast of Southern Europe.

Haigh *et al.* (2010) investigated the probability distribution of extreme still water levels in the English Channel; they found that the revised joint probability method (Tawn and Vassie, 1989; 1991; Tawn, 1992) is more appropriate than the annual maxima method (Gumbel, 1958), the  $r$ -largest annual events (Tawn, 1988) and the joint probability method (Pugh and Vassie, 1978, 1980) for describing the probability distribution of extreme sea level data in that area.

The study presented in this paper provides an estimation of the probability distribution of extreme sea level using a GPD distribution fitted to the  $r$ -largest values per year, with  $r = 5$  (Marcos *et al.*, 2009)

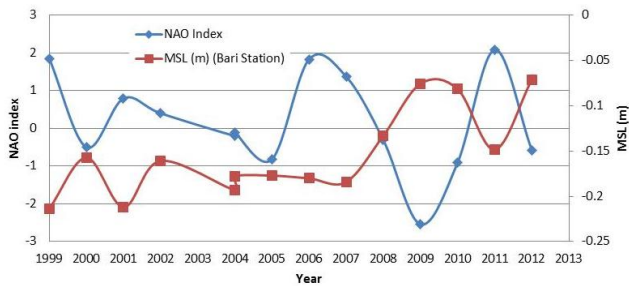


Figure 4. NAO Index versus Annual MSL recorded at Bari station in the period 1999-2012

Additionally, the 5-largest per year observed levels moved sharply higher from the winter 2008-2009, after 2 years characterized by mild weather conditions (Figure 3, upper panel). After removing the mean sea level, the observed levels (Figure 3, central panel) show only a slight increase and also the tidal residual shows the same (Figure 3, lower panel). Particular attention has been paid to the outlier event recorded at Ortona station in the late 2012, because, even after the SML subtraction, the value remains exceptionally high. This exceptional event has been recorded during a severe storm that caused coastal flooding along the Ortona coastline. Although the check control was positive, the value remains ambiguous.

The distribution of exceedances  $Y_i$  over large threshold  $u$  has been asymptotically distributed following a Generalized Pareto Distribution (GPD):

$$F(y) = 1 - \left(1 + \xi \frac{y}{\sigma}\right)^{-\frac{1}{\xi}} \quad (3)$$

where  $y_i = X_i - u \mid X_i > u$ ,

$\sigma$  is a scale parameter and  $\xi$  is a shape parameter that can be estimated using simple likelihood model.

The N-year return level  $Z_N$  can be calculated as

$$Z_N = u + \frac{\sigma}{\xi} \left( N^\xi - 1 \right) \quad (4)$$

The GPD distribution has been fitted to the series of extreme sea level values observed, to observed levels corrected with current annual mean sea level and to tidal residuals. The 5 extremes per year are lagged by at least 78 hours as suggested by Masina and Ciavola (2011), in order to consider the seiche decay time after surge events (Raichich, 1999) and to select only independent events.

The analysis (Table 2) shows a significant increase in extremes of observed sea level values, while the extremes of corrected values and tidal residuals are quite similar respect to those found by Marcos *et al.* (2009) using observed data updated to 2006. The increase in return levels estimated from observed sea levels, updated to 2012, is mainly imputable to MSL raise. In fact, considering only levels depurated of MSL, the estimated return levels do not rise significantly. Only Ortona station behaves differently and the return levels are considerably higher. Return levels are consistent with other stations if the outlier value is discarded, and the event requires further analysis for reliability assessment.

This is in agreement with Tsimplis *et al.* (2013) and Landerer and Volkov (2013); in both studies, authors report a sudden increase in mean sea level that has been related to large scale

forcing over the North Atlantic (North Atlantic Oscillation-NAO) that forces water to enter into the Mediterranean Sea. The NAO index, calculated as the difference between normalized sea level pressure over Gibraltar and Southwest Iceland, has a significant yearly variability (Jones *et al.*, 1997) and in the winter 2009/10 had the most negative value measured during the almost 190-year record (Osborn, 2011). Figure 4 shows the variability of the NAO index (calculated by Osborn and published at <http://www.cru.uea.ac.uk/~timo/datapages/naoi.htm>) together with the MSL recorded at the station of Bari.

Local changes in meteorological conditions, such as barometric pressure values and winds, have also been investigated where the National Tide Gauge Network stations are equipped with pressure sensors and anemometers. The hourly data of pressure have been examined and significant changes have been found (Figure 5, upper panel). After a relative minimum recorded in 2000, the values of mean atmospheric pressure held quite steady from 2001 to 2008 but dropped in 2009 to the lowest value in the last 10 years. Furthermore wind frequency analysis shows, from 2008, a slight increase in southern wind events (Figure 5, lower panel). In the Adriatic Sea, these are responsible for wind set-up. These peculiar local meteorological conditions in the latest years could be responsible for slightly higher tidal residuals than the values of the previous period.

### CONCLUSION

The study presented in this paper provides an analysis of sea level data collected by 6 stations in the low and middle Adriatic Sea belonging to the National Tide Gauge Network and to Apulia Region Meteomarine Network.

All the examined stations show a sudden increase in mean sea level from the winter 2008-2009, with a variation between 2007 and 2009 of the order of about 10 cm. This was followed by a decrease in 2011. The mean sea level in 2012 increases again slightly beyond the level of 2009.

The increase in return levels estimated from observed sea levels, updated to 2012, is mainly imputable to MSL rise. In fact, considering only levels depurated of MSL, the estimated return levels do not rise significantly.

Furthermore the local meteorological conditions have been

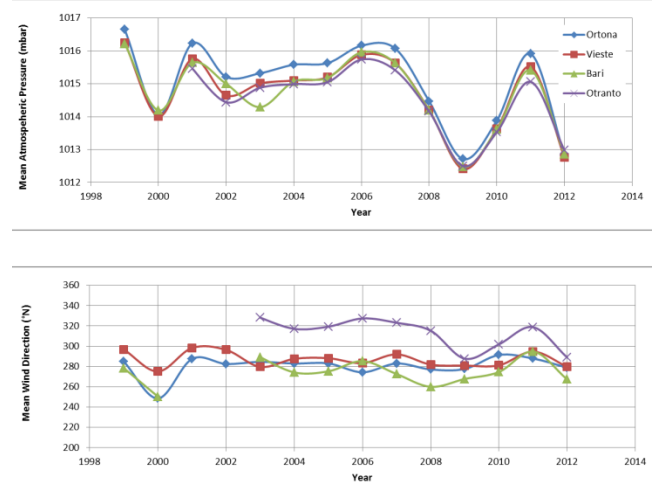


Figure 5. Annual mean atmospheric pressure (upper panel) and annual mean wind direction (lower panel) at examined stations from 1999 to 2012

Table 2. Estimated return level. RL observed= observed level, RL corrected= observed level corrected with the current year mean sea level and RL residual= tidal residual. The return level have been estimated with N=5, 10 and 50 years. The starred results are affected by the presence of an outlier in the time series.

		N-year Return (years)		
		5	10	50
Ortona	RL observed(m)	0.65*	0.74*	0.81*
	RL corrected(m)	0.66*	0.74*	0.79*
	RL residual(m)	0.57	0.63	0.67
Vieste	RL observed(m)	0.49	0.55	0.59
	RL corrected(m)	0.56	0.61	0.64
	RL residual(m)	0.49	0.53	0.55
Bari	RL observed(m)	0.42	0.48	0.54
	RL corrected(m)	0.56	0.60	0.63
	RL residual(m)	0.42	0.46	0.48
Otranto	RL observed(m)	0.19	0.23	0.29
	RL corrected(m)	0.43	0.46	0.48
	RL residual(m)	0.39	0.44	0.47
Manfredonia	RL observed(m)	--	--	--
	RL corrected(m)	0.52	0.56	0.59
	RL residual(m)	0.44	0.45	0.46
Brindisi	RL observed(m)	0.39	0.44	0.47
	RL corrected(m)	0.51	0.55	0.58
	RL residual(m)	0.40	0.44	0.46

investigated. It was found that in 2009 and 2012, mean atmospheric pressure values dropped. In the same period a slight increase in southern winds has been observed. These peculiar local meteorological conditions in the latest years could be responsible for slightly higher tidal residuals than the values of the previous period. This research has provided updated extreme values of sea level and meteorological residual that could be useful for coastal risk management and design of nearshore structures.

### ACKNOWLEDGEMENT

The authors wish to thank Dr. Marta Marcos for the useful discussion.

### LITERATURE CITED

- Antonoli, F. and Leoni, G., 2007. Mappa Nazionale delle aree a rischio di allagamento da parte del mare. *Dossier ENEA per lo studio dei cambiamenti climatici e loro effetti*. RT ENEA, pp 83.
- Bruno, M.F.; Francioso, R.; Nobile, B. and Petrillo, A.F., 2012. Integrated studies for coastal erosion and littoral planning: the apulian experience. *Proceedings of the 4th international conference on the application of physical modelling to port and coastal protection - Coastlab12*, Ghent, Belgium, pp. 1-8.
- Damiani, L., Bruno, M.F., Molfetta, M.G. and Nobile, B., 2007. "Coastal zone monitoring in Apulia region: first analysis on meteomarine climate". *Proceedings of 5th International Symposium on Environmental Hydraulics (ISEH 2007)* Arizona (USA).
- Doodson, A.T., 1954. Appendix to circular-letter 4-H. The harmonic development of the tide-generating potential. *International Hydrographic Review* 31, 37-61.

- EuroSION 2004 Living with coastal erosion in Europe: sediment and space for sustainability. *Major findings and policy recommendations of the EUROSION project*. European Commission, Directorate General Environment, Service contract B4-3301/2001/329175/MAR/B3.
- Gumbel, E. J. (1958). Statistics of extremes. *Dover Publications. com*.
- Haigh, I. D., Nicholls, R. and Wells, N., 2010. A comparison of the main methods for estimating probabilities of extreme still water levels. *Coastal Engineering*, 57(9), 838-849.
- Krestenitis, Y.N., Androulidakis, Y.S., Kontos, Y.N. and Georgakopoulos, G., 2011. Coastal inundation in the north-eastern mediterranean coastal zone due to storm surge events. *Journal of Coastal Conservation*, 15(3), 353-368.
- IPCC 2007, Fourth Assessment Report of the Intergovernmental Panel on Climate Change, *Cambridge University Press*.
- IPCC 2013, Fifth Assessment Report of the Intergovernmental Panel on Climate Change, *Cambridge University Press*.
- Jones, P.D., Jonsson, T. and Wheeler, D., 1997. Extension to the North Atlantic Oscillation using early instrumental pressure observations from Gibraltar and South-West Iceland. *International Journal of Climatology* 17, 1433-1450.
- Landerer, F. W. and Volkov, D. L., 2013. The anatomy of recent large sea level fluctuations in the Mediterranean Sea. *Geophys. Res. Lett.*, 40, doi:10.1002/grl.50140.
- Lichter, M. and Felsenstein, D., 2012. Assessing the costs of sea-level rise and extreme flooding at the local level: A GIS-based approach. *Ocean & Coastal Management*, 59, 47-62.
- Lionello, P., Nizzero, A. and Elvini, E., 2003. A procedure for estimating wind waves and storm-surge climate scenarios in a regional basin: the Adriatic Sea case. *Climate Research*, 23(3), 217-231
- Marcos, M. and Tsimplis, M. N., 2008. Coastal sea level trends in Southern Europe. *Geophysical Journal International*, 175(1), 70-82.
- Marcos, M., Tsimplis, M.N. and Shaw, A.G.P., 2009. Sea level extremes in southern Europe. *Journal of Geophysical Research*, 114, C01007, doi:10.1029/2008JC004912.
- Martinelli, L., Zanuttigh, B. and Corbau C., 2010. Assessment of coastal flooding hazard along the Emilia Romagna Littoral, IT. *Coastal Engineering*, 57(11-12), Nov-December 2010, 1042-1158. (doi:10.1016/j.coastaleng.2010.06.007)
- Masina, M. and Ciavola, P., 2011. Analisi dei livelli marini estremi e delle acque alte lungo il litorale ravennate. *Studi Costieri*, 18, 87-101.
- NDBC, 2009: NDBC Technical Document 09-02, *Handbook of Automated Data Quality Control Checks and Procedures*
- Osborn, T.J., 2011. Winter 2009/2010 temperatures and a record-breaking North Atlantic Oscillation index. *Weather* 66, 19-21.
- Pawlowicz, R., Beardsley, B. and Lentz, S., "Classical tidal harmonic analysis including error estimates in MATLAB using T\_TIDE", *Computers and Geosciences* 28 (2002), 929-937
- Pugh, D.T. and Vassie, J.M., 1978. Extreme sea levels from tide and surge probability. *Coastal Engineering Proceedings*, 1(16).
- Pugh, D.T. and Vassie, J.M., 1980. Applications of the joint probability method for extreme sea level computations. *ICE Proceedings* (Vol. 69, No. 4, pp. 959-975). Thomas Telford.
- Raicich, F., Orlic, M., Vilibic, I. and Malacic, V., 1999. A case study of the Adriatic seiches (December 1997). *Nuovo Cimento - Società Italiana di Fisica Sezione C*, 22, 715-726.
- Raicich, F., 2003. Recent evolution of sea-level extremes at Trieste (Northern Adriatic). *Continental Shelf Research*, 23(3), 225-235.
- Sánchez-Arcilla, A., Mösso, C., Sierra, J. P., Mestres, M., Harzallah, A., Senouci, M. and El Raey, M., 2011. Climatic drivers of potential hazards. *Mediterranean coasts Regional Environmental Change September* 2011, Volume 11, Issue 3, pp 617-636
- Sano, M., Jiménez, J.A., Medina, R., Stanica, A., Sanchez-Arcilla, A. and Trumbic, I., 2011. The role of coastal setbacks in the context of coastal erosion and climate change. *Ocean & Coastal Management*, 54(12), 943-950.
- Tawn, J.A., 1988. An extreme-value theory model for dependent observations. *Journal of Hydrology*, 101(1), 227-250.
- Tawn, J.A. and Vassie, J.M., 1989. Extreme sea levels; the joint probabilities method revisited and revised. *ICE Proceedings* (Vol. 87, No. 3, pp. 429-442). Thomas Telford.
- Tawn, J.A. and Vassie, J.M., 1991. Recent improvements in the joint probability method for estimating extreme sea levels. *Tidal Hydrodynamics* (Parker, PB, ed.).

- Tawn, J.A., 1992. Estimating probabilities of extreme sea-levels. *Applied Statistics*, 77-93.
- Tsimplis, M.N. and Blackman, D., 1997. Extreme sea-level distribution and return periods in the Aegean and Ionian Seas. *Estuarine, coastal and shelf science*, 44(1), 79-89.
- Tsimplis, M.N., Calafat, F. M, Marcos, M., Jordà, G., Gomis, D., Fenoglio-Marc, L., Struglia, M.V., Josey, S.A. and Chambers D. P., 2013. The effect of the NAO on sea level and on mass changes in the Mediterranean Sea. *Journal of Geophysical Research Oceans*, 118, 944-952, doi:10.1002/jgrc.20078.
- UNEP, 2008 Protocol on Integrated Coastal Zone Management in the Mediterranean

## Overtopping hazard on a rubble mound breakwater

Ana R. Carrasco†, Maria T. Reis††, Maria G. Neves††, Óscar Ferreira†, Ana Matias†, Sílvia Almeida†

†CIMA, Universidade do Algarve,  
Campus de Gambelas  
8005-139, Faro, Portugal  
azarcos@ualg.pt  
oferreir@ualg.pt  
ammatias@ualg.pt  
smalmeida@ualg.pt

††LNEC – National Laboratory for Civil  
Engineering  
Av. do Brasil, 101  
1700-066 Lisboa, Portugal  
treis@lnec.pt  
gneves@lnec.pt



[www.cerf-jcr.org](http://www.cerf-jcr.org)



[www.JCRonline.org](http://www.JCRonline.org)

### ABSTRACT

Carrasco, A.R., Reis, M.T., Neves, M.G., Ferreira, Ó., Matias, A., Almeida, S., 2014. Overtopping hazard on a rubble mound breakwater. In: Green, A.N. and Cooper, J.A.G. (eds.), *Proceedings 13<sup>th</sup> International Coastal Symposium* (Durban, South Africa), *Journal of Coastal Research*, Special Issue No. 70, pp. 247-252, ISSN 0749-0208.

A major concern of coastal engineering is not only to assess the damage to coastal structures by severe wave overtopping, but also the hazard imposed to users. Local hazard is often associated to the volume of overtopping water per unit of time (called overtopping discharge). Despite two decades of intensive research, it is yet not fully clear to practitioners what is the best method to compute the discharge parameter and its application on the assessment of local hazard. This work provides insight into the overtopping characterization in rubble mound breakwaters, by distinguishing different methods to assess hazardous overtopping. Fieldwork was conducted over a tidal cycle in a breakwater located at Albufeira Harbour (South coast of Portugal) under storm conditions ( $H_{so} \sim 3$  m;  $T_p \sim 9$  s). Mean overtopping discharges were calculated from field measurements of flow depths and velocities at the breakwater slope armour and at the impermeable crest. Two different velocities were calculated: overtopping leading-edge velocity and overtopping peak velocity. The two methods provided similar results, with higher velocities occurring during high-tide (between 2 and 10 m/s). Mean overtopping discharges at the beginning of the impermeable crest ranged between 0.2 and 0.8 l/s/m. Under the measured hydrodynamic conditions, the breakwater offers risk to all types of pedestrians. Additionally it is shown that field measurements compare relatively well with empirical prediction methods (for the overall analysed overtopping events), namely the corrected NN\_OVERTOPPING2 neural network tool. Besides contributing to the overall database on wave overtopping in coastal structures, the presented results can also be used for calibration and validation of overtopping evaluation methods (empirical formulae, artificial neural networks and numerical and physical models).

**ADDITIONAL INDEX WORDS:** *wave, discharge, velocities, hazard, empirical prediction.*

### INTRODUCTION

Most sea defence structures are constructed primarily to limit overtopping volumes that might cause flooding (Shankar and Jayaratne, 2003). Flooding potential is determined from the quantity of overtopping water per unit of time (overtopping discharge) and storm duration (Chini and Stansby, 2012; Hughes *et al.*, 2012; Tonelli and Petti, 2013). Over a storm or tide, the overtopping volumes that can be tolerated will be site specific, as the volume of water that can be permitted will depend on the size and use of the receiving area, extent and magnitude of drainage ditches, damage versus inundation curves, and return period (Pullen *et al.*, 2007). Ideally, return periods at which overtopping hazards are analysed, and against which a defence might be designed, should be constantly set by national regulation or guidelines, yet that is not common practice (Geeraerts *et al.*, 2007).

The main hazards on or close to sea defence structures are of death, injury, property damage or disruption from direct wave impact or by drowning (Geeraerts *et al.*, 2007). Some guidance has been given on the basis of the tolerable discharges and overtopping volumes for a range of circumstances or uses (Pullen

*et al.*, 2007; Geeraerts *et al.*, 2007), which have been widely used in several locations. The EurOtop Manual gives guidance on allowable overtopping when people are present or vehicles are moving behind the structure.

Hazard-driven flow parameters are essentially the mean overtopping discharge and the maximum overtopping volume, as well as overtopping flow depths and velocities. The mean overtopping discharge is the most widely used to judge allowable overtopping. An extensive database on mean overtopping discharge has been gathered in the scope of the CLASH project (<http://www.clash-eu.org>). However, the mean discharge does not always describe the real behaviour of wave overtopping, where only the larger incoming waves will reach the top of the structure and promote overtopping. There remain also two difficulties in specifying safety levels with reference to maximum volumes rather than to mean discharges. Firstly, methods to predict maximum volumes are available for limited structure types, and are not well-validated. Secondly, data relating individual maximum overtopping volumes to hazard levels are still very rare (Pullen *et al.*, 2007).

The ideal situation is to instrumentally collect data at each required location and locally define the hazard thresholds. That is however a very remote possibility for the vast majority of the existing structures. Even if it is possible to collect data, often there is no constant discharge over the crest of a structure. That is the



case when accessing very thin water layers of run-up tongues, which are common in rubble mound revetments, because they are porous and have sloping layers, dissipating a large proportion of the incident wave energy (Pullen *et al.*, 2007). In fact, few investigations have been conducted on rough slopes of different sizes of armour (Shankar and Jayaratne, 2003). Hazard driving flow parameters are nowadays recurrently predicted based on engineering models and formulae resulting from recent experiments. Indeed, in the past two decades, wave overtopping was investigated in a large number of studies and projects, mostly of experimental nature (e.g. De Rouck *et al.*, 2005; Van der Meer *et al.*, 2006), which led to the development of several empirical prediction formulae and artificial neural networks (Verhaeghe, 2005; Pullen *et al.*, 2007). Notwithstanding, the overtopping results obtained from the derived models still have a large degree of uncertainty, as the models themselves demand a continued calibration. The present work uses a dataset of collected overtopping flow depths and velocities in a rubble mound breakwater in Portugal with two aims: (a) full characterization of overtopping conditions based on fieldwork data, and (b) their comparison with mean discharges predicted by empirical tools.

## METHODS

### Experimental setting

Overtopping experiments were conducted at the west breakwater of Albufeira Harbour (South coast of Portugal, Figure 1) on the 19th January 2013 from 4 am till 12 pm. The chosen breakwater is a relatively low-crested structure (4.3 m above mean sea level, MSL) with about 42 % porosity (Eric Didier, personal communication). It is of easy access and it is often overtopped by waves higher than 3 m during spring tides. In the fishing harbour protected by the breakwater, small fishing boats are anchored more than 20 m from the rear slope of the structure. Details about the structure can be found in Didier *et al.* (2011). The collected and analysed data included tidal levels, wave characteristics

(offshore and at the structure), and overtopping parameters (flow depth, velocity and associated discharge). For the analysis of the overtopping variability, the monitored tidal cycle was divided in several blocks of 30 minutes.

### Nearshore and offshore measurements

Tidal data were obtained from Huelva tide gauge (Spain), located at about 100 km to the East of the study area. The recorded levels (referred to the local harbour level) were corrected for the Portuguese datum and mean sea level (MSL). A time correction (~30 minutes tide delay in Albufeira) was also performed. Offshore wave height (significant,  $H_{so}$ , and maximum,  $H_{maxo}$ ) and peak period ( $T_p$ ) were obtained from Faro wave buoy (belonging to Instituto Hidrográfico), located 30 km to the East of the study area (Figure 1a) in a water depth of 93 m MSL. Overtopping parameters (flow depth and velocity) were measured along a profile in the middle section of the western breakwater (Figure 1b and c). Flow depth was measured with a series of pressure transducers along the breakwater crest. Video images from crest overtopping at the profile of instrumentation were recorded from a higher position at a nearby cliff (100 m in horizontal distance, Figure 1b). Ground Control Points (GCPs) were placed and georeferenced to support overtopping flow analysis using video image.

### Nearshore wave propagation

Offshore wave conditions were propagated to the breakwater toe (3.5 m below MSL) using SWAN (Simulating Waves Near-shore; Booij *et al.*, 1999). Grid resolutions of 45 m and 5 m were chosen for the large and small grids, respectively (Figure 2).

Model predictions were initialized on the two open boundaries of the larger grid with the parametric input from the wave buoy time series, using a JONSWAP spectral shape to represent the wave field. Input boundary conditions for the small grid were determined from the computations over the large grid. SWAN simulations accounted for non-linear triad wave-wave interactions,

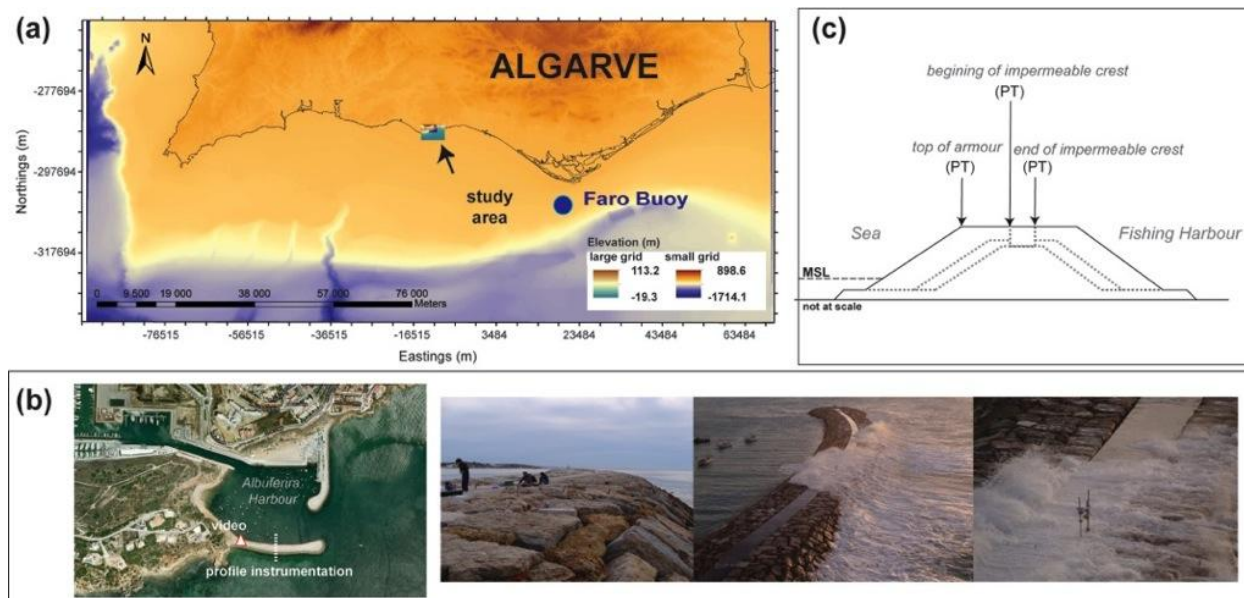


Figure 1. (a) Study area; (b) Albufeira Harbour and photos from fieldwork profile instrumentation and overtopping occurrence; and (c) Pressure transducers (PT) location across the breakwater profile.

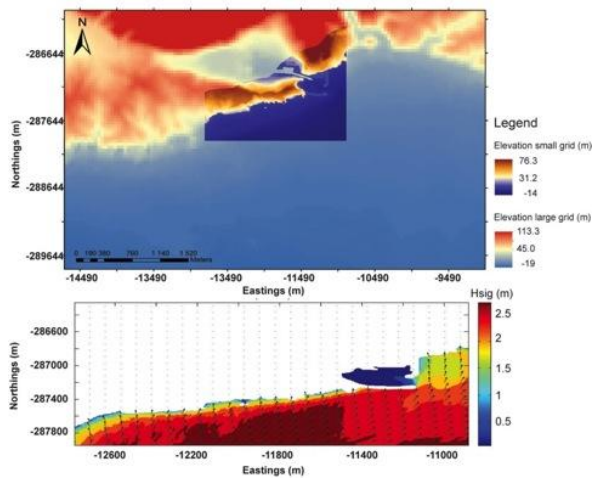


Figure 2. Nested grids used in SWAN runs (depths referred to MSL, upper panel). Significant wave height ( $H_s$ ), and wave direction (arrows), during high tide (lower panel).

as they are rather important in shallow coastal areas (Booij *et al.*, 1999; Holthuijsen, 2007), for bottom friction dissipation using the default variable JONSWAP expression according to Hasselmann *et al.* (1973), and for breaking dissipation according to the default bore-based model of Battjes and Janssen (1978).

### Overtopping velocities and discharge computations

Each overtopping event was defined as a single passage of water above the structure crest. Data were collected at the top of the armour slope and at the beginning of the impermeable crest of the breakwater (distant 5.2 m). These data were used to identify overtopping frequency, and to calculate flow depth and flow velocity.

The leading-edge flow velocity ( $v_f$ ) represents the water velocity between the sensors located at the top of the armour slope and at the beginning of the impermeable crest, and is obtained using the time delay between sensors:

$$v_f = \frac{d}{t_f - t_i} \quad (1)$$

where  $d$  is the horizontal distance between the sensors,  $t_i$  and  $t_f$  correspond to the arrival time at the top of the slope armour and the arrival time at the beginning of the impermeable crest, respectively. The leading-edge velocity,  $v_f$ , represents the mean velocity of each event. Besides, peak overtopping flow velocity ( $v_p$ ) was also computed by considering the difference between arrival times of maximum overtopping flow depths (peak):

$$v_p = \frac{d}{t_{pf} - t_{pi}} \quad (2)$$

where  $t_{pi}$  and  $t_{pf}$  correspond to the arrival times at the top of the armour and at the beginning of the impermeable crest, respectively. Overtopping leading-edge volumes ( $V_f$ ) and overtopping peak volumes ( $V_{max}$ ), were also calculated for all overtopping events, using the flow depths, flow velocities (leading-edge velocity and peak velocity) and the duration of each event.

### Empirical tools prediction

Calculated mean overtopping discharges based on field measurements at the top of the armour (Qarmour) and at the beginning of the impermeable crest (Qcrest) were compared with mean discharges predicted by the EurOtop empirical formulae

available online ([http://www.overtopping-manual.com/calculation\\_tool.html](http://www.overtopping-manual.com/calculation_tool.html)) and by the NN\_OVERTOPPING2 tool (Coeveld *et al.*, 2005) also available online. For comparison, the calculated mean overtopping discharges for each block of 30 minutes (Qarmour and Qcrest), were obtained by adding all event volumes and dividing by 1800 s.

The geometrical characteristics of the structure adopted for the discharge prediction were defined according to six cross-sections measured around the instrumented profile. For the EurOtop formulae the structure geometry was assumed as “armoured composite slope with crest berm”. The input wave parameters at the toe of the structure and the structure parameters are described in Ferreira *et al.* (2013). Input wave parameters for the NN\_OVERTOPPING2 tool included the wave data at the toe of the structure and the angle between the wave direction and the normal to the structure. Details about the NN\_OVERTOPPING2 input parameters are presented in Coeveld *et al.* (2005). For both methods, EurOtop formulae and NN\_OVERTOPPING2, the predicted mean overtopping discharges are provided per meter run of seawall.

### Hazard assessment

Hazard assessment was conducted by comparing calculated mean overtopping discharges and maximum volumes, both based on field measurements, with the values indicated in the EurOtop Manual (2007) and Geeraerts *et al.* (2007). The overtopping limits suggested in Table 1 derive from a general precautionary principle based on observations and measurements undertaken by the CLASH project (Allsop *et al.*, 2008). Above the presented limits, both humans and goods are at risk; risk to structure integrity is not evaluated here.

## RESULTS AND DISCUSSION

Overtopping parameters (flow depths and flow velocities) were measured during neap tides and storm conditions ( $H_{so} \sim 3-4$  m and  $T_p \sim 8-10$  s, Figure 3), with dominant wave direction from SW, frequent during winter. Maximum wind intensities were close to 7 m/s, occurring during high tide. For the analysis of the overtopping variability along the monitored tidal cycle, four blocks of 30 minutes, beginning at 05h, 07h, 08h and 10h, were chosen; each time block represents different tide stages. The time block of 05h represents the beginning of overtopping occurrence, whereas the time blocks of 07h and 08h are representative of high tide, and the time block of 10h is representative of mid tide (Figure 3a).

### Overtopping frequency and associated discharges

Overtopping flow was generally turbulent across the armour and the end of the impermeable crest of the breakwater, similar to ‘white water’ flow defined by Pullen *et al.* (2007). Indeed, most recorded flows are classified with mean Froude number of 9 (supercritical). The maximum overtopping duration was 5 s, and mean overtopping flow depths were on average below 3 cm (Figure 4). There is no significant correlation between the flow depths and related velocities, which means that the higher velocities were not always related with deeper water flows. Mean  $v_f$  and  $v_p$  values are of the same order of magnitude, less than 6 m/s; maximum values obtained for  $v_f$  are slightly higher than for  $v_p$ , due to differences in the methodology (Figure 4). Results for  $v_f$  were corroborated with velocities obtained with video analysis (using wave arrival at each GCPs). The velocities obtained with

Table 1. Indicated limits for overtopping mean discharges and peak volumes (adapted from Geeraerts *et al.*, 2007).

Hazard type/reason	Mean discharge	Peak volume
<i>Pedestrians</i>	Q (l/s/m)	V <sub>max</sub> (l/m)
Unaware pedestrian, no clear view of the sea, narrow walkway or close proximity to edge	Q > 0.03	2 – 5 at high level or velocity
Aware pedestrian, clear view of the sea, wider walkway	Q > 0.1	20 – 50 at high level or velocity
Trained staff, well shod and protected, overtopping flows at lower levels only, no falling jet, low danger of fall from walkway	Q [1 – 10]	500 at low level
<i>Marinas</i>		
Sinking of small boats set 5-10 m from wall, damage to larger yachts	Q > 10	1000-10000
Significant damage or sinking of larger yachts	Q > 50	5000-50000

video image were, on average 5 m/s, with maximum values of 12 m/s.

Larger overtopping volumes were recorded during high tide (07h and 08h, Table 2), as well as higher flow depths and higher velocities (Figure 4). The increased velocities might be partially ascribed to an increase in overtopping depth and also to an increase of wind velocity over that period. Wind affected incoming waves by blowing up-rushing water over the crest of the structure, resulting in a possible modification of the physical form of the overtopping volume or jet (Pullen *et al.*, 2007), and ultimately, contributing to the total volume of overtopping. Wind also affects the way that hazard might be assessed (Shankar and Jayaratne, 2003; Allsop *et al.*, 2008). Obtained records are, however, scarce to yield conclusions.

Except for 05h time block, mean  $V_{max}$  values are of higher magnitude than  $V_f$ , indicating that this last method is more useful when describing individual maximum overtopping events, whereas  $V_f$  is mostly representative of average conditions. Mean  $V_f$  volumes are of the same order of magnitude as the individual discharges recorded in Pullen *et al.* (2003), at the Samphire Hoe (about 300 l/s to 500 l/s) and the individual maximum discharges estimated by Hughes *et al.* (2012), in laboratory. However, Qarmour exceeds the mean overtopping discharges obtained at Zeebrugge by Geeraerts and Boone (2004),  $Q < 0.86$  l/s/m for  $H_{mo} = 3.9$  m and  $T_p = 8.6$  s, and Qarmour and Qcrest exceed the mean overtopping discharges obtained at Ostia,  $Q < 0.36$  l/s/m for  $H_{mo} = 2.0$  m and  $T_p = 9$  s by De Rouck *et al.* (2005), as can be seen in Table 3. The differences are due to the intrinsic differences between the structures, the wave conditions and, of course, also the type of data acquisition and methodology adopted for discharge computation.

### Calculated vs. predicted overtopping

Maximum mean overtopping discharges predicted with the EurOtop formulae were 1.2 l/s/m and  $1.5 \times 10^{-1}$  l/s/m at the top of the armour slope and at the beginning of the impermeable crest, respectively (Table 3). For the NN\_OVERTOPPING2 tool, maximum mean overtopping discharges corrected to account for

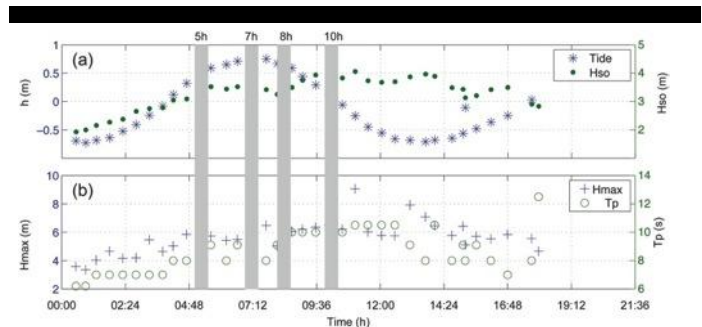


Figure 3. (a) Tide (h) and significant wave height (Hso) during fieldwork; (b) Maximum wave height (Hmax) and wave peak period (Tp) during fieldwork. Vertical grey bars mark 05h, 07h, 08h and 10h time blocks chosen for analysis of overtopping.

model, scale and wind effects in prototype situations,  $Q'_{NN}$ , were 1.8 l/s/m at the top of the armour slope and  $5.5 \times 10^{-1}$  l/s/m at the beginning of the impermeable crest.  $Q'_{NN}$  and  $Q_{NN}$  exhibit a similar pattern (Figure 5).

NN\_OVERTOPPING2 mean discharges presented relatively small variations along the studied period, while the calculated mean discharges based on field measurements revealed higher variability (Figure 5, left panel). At both locations (armour and crest), the  $Q'_{NN}$  predicted discharges present a good agreement with the calculated discharges (Qarmour and Qcrest), when considering the entire period of analysis, and are generally included in the 95% confidence intervals obtained from the NN\_OVERTOPPING2 tool. Differences can be found when comparing each time block individually. At the top of the armour slope, the mean relative error between Qarmour and  $Q'_{NN}$  is less than 1%, whereas the maximum relative error is of 60%. At the beginning of the impermeable crest, the mean relative error between Qcrest and  $Q'_{NN}$  is higher, about 20%, whereas the maximum relative error is similar, 60%. The correction applied by this tool improves significantly the agreement between predicted and calculated

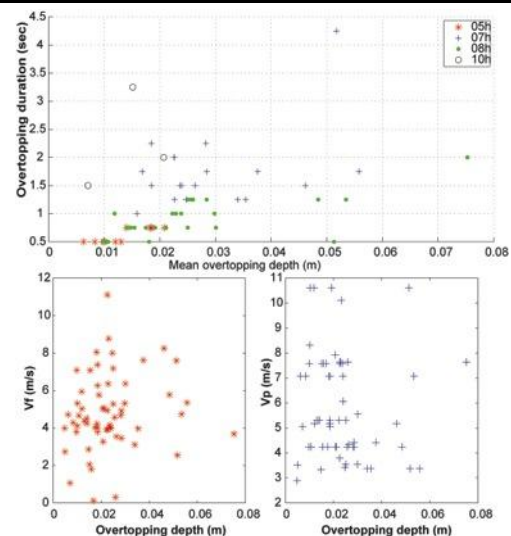


Figure 4. Overtopping duration vs. mean overtopping depth (upper panel);  $v_f$  and  $v_p$  vs. mean overtopping depth at the top of the breakwater armour slope (lower panel).

Table 2.  $V_f$  and  $V_{max}$  (l/m) at the beginning of the impermeable crest of the breakwater.

Parameters	$V_f$			
	05h	07h	08h	10h
Mean	166	170	185	181
Max	166	209	231	205
Parameters	$V_{max}$			
	05h	07h	08h	10h
Mean	166	188	308	204
Max	166	297	508	261

discharges (Figure 5).

There is a fair agreement between  $Q'_{NN}$  and  $Q_{armour}$ , with three of the four data points included in-between  $1/2 < Q'_{NN}/Q_{armour} < 2$  (Figure 5, right panel). At the beginning of the impermeable crest, calculated mean overtopping discharges are also fairly predicted by NN\_OVERTOPPING2 tool. In contrast, the probabilistic EurOtop formulae clearly underpredict the discharges at both locations, but especially at the impermeable crest, by one order of magnitude (Figure 5, right panel). Similar situation occurs for the uncorrected NN\_OVERTOPPING2 results (Figure 5, left panel).

Deviations between fieldwork data and tools predictions can be partially explained by the natural wave variability, namely wave-wave interaction near the structure (specifically due to reflected waves) and also by the important 3D processes that occur at the field including the longshore variability of the overwash progression through structure, induced by alongshore differences between wave crest and structure. Furthermore, the calculation of overtopping discharges from field measurements use tide levels and wave conditions at the structure predicted from measurements elsewhere, which might introduce some uncertainty. Moreover, most data used for developing the tools were obtained from physical model tests, where some scale effects affect the results and where 3D effects are often neglected. The 95% confidence interval obtained from the NN\_OVERTOPPING2 tool already accounts for differences on wave characteristics at the toe of the structure (before or after breaking, for example) and differences

Table 3. Results of mean overtopping discharges based on field measurements ( $Q_{armour}$  and  $Q_{crest}$ ) and on predictions from NN\_OVERTOPPING2 and EurOtop formulae (l/s/m).

	$Q_{armour}$	$Q_{NN}$	$Q_{NN}$ (2.5%)	$Q_{NN}$ (97.5%)	$Q'_{NN}$
Min	$3.5 \times 10^{-01}$	$2.1 \times 10^{-01}$	$3.5 \times 10^{-02}$	1.3	$5.5 \times 10^{-01}$
Max	2.1	1.5	$2.7 \times 10^{-01}$	6.6	1.8
	$Q_{crest}$	$Q_{NN}$	$Q_{NN}$ (2.5%)	$Q_{NN}$ (97.5%)	$Q'_{NN}$
Min	$1.8 \times 10^{-01}$	$3.0 \times 10^{-02}$	$5.4 \times 10^{-03}$	$1.5 \times 10^{-01}$	$1.9 \times 10^{-01}$
Max	$7.5 \times 10^{-01}$	$2.2 \times 10^{-01}$	$6.6 \times 10^{-02}$	$7.9 \times 10^{-01}$	$5.5 \times 10^{-01}$
EurOtop formulae					
	$Q_{armour}$	$Q_{crest}$			
Min	$1.9 \times 10^{-01}$	$1.7 \times 10^{-02}$			
Max	1.2	$1.5 \times 10^{-01}$			

on the measurements due to scale effects. Other deviations between fieldwork data and tools predictions can also be explained by difficulties inherent to the field measurements.

Summing up, results from the corrected NN\_OVERTOPPING2 ( $Q'_{NN}$ ) are the best predictions for mean overtopping discharges calculated based on field measurements of flow depths and velocities (Figure 5).

### Hazard assessment

Because in almost all instances, the use of empirical methods involves some degree of simplification of the actual situation, the hazard analysis of the monitored conditions is discussed based on the recorded field data only.

For the calculated mean overtopping discharges ( $0.2 < Q_{crest} < 0.8$  l/s/m), the breakwater offers risk mostly to unaware and aware pedestrians ( $Q > 0.1$  l/s/m, Table 1). However, for the calculated overtopping peak volumes ( $166 < V_{max} < 508$  l/m), the breakwater offers risk to all types of pedestrians ( $V_{max} > 500$  l/m, Table 1), confirming visual observations during fieldwork and video monitoring. There was no related risk to small boat in the fishing harbour, since they were more than 20 m

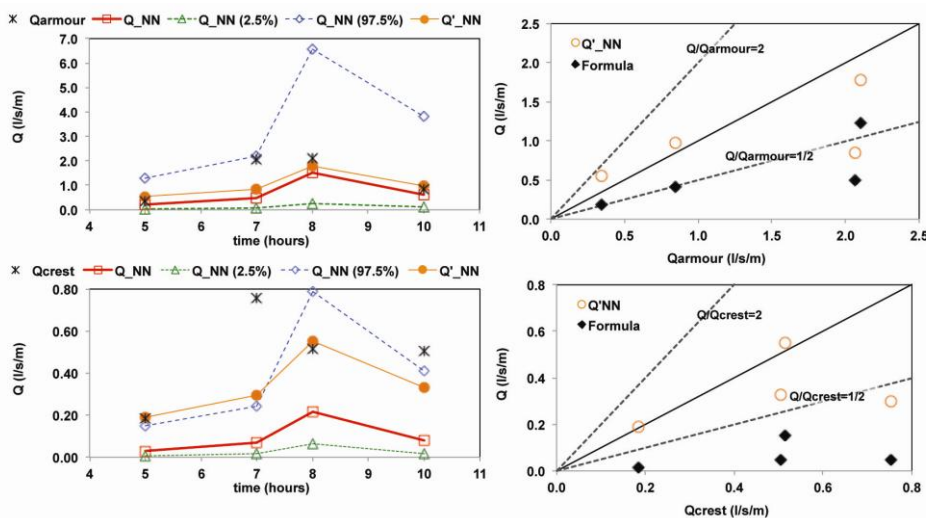


Figure 5. Comparison between calculated mean overtopping discharges based on field measurements at the top of the armour slope ( $Q_{armour}$ , upper panel) and at the beginning of the impermeable crest ( $Q_{crest}$ , lower panel), and NN\_OVERTOPPING2 tool parameters ( $Q_{NN}$ , 95% confidence intervals,  $Q_{NN}(2.5\%)$ ,  $Q_{NN}(97.5\%)$ ) (left panel); and comparison between calculated mean overtopping discharges and results from both EurOtop formulae and the NN\_OVERTOPPING2 tool  $Q'_{NN}$  (right panel).

apart from the structure. There is a limitation when comparing the recorded hydrodynamic conditions with the classification from Table 1 since discharge intervals presented in Table 1 concern hazard assessment behind the breakwater, and the discharges presented here are related to measurements at the beginning of the impermeable crest, which seems more adequate to pedestrians at the walkway. Moreover, limits presented in Table 1 concern to overtopping velocities below 10 m/s (Allsop *et al.*, 2008). Individual maximum velocities recorded here were above 10 m/s (Figure 4), therefore, lower volume intervals should be preferably used as guideline.

Differences between the calculated mean and maximum overtopping volumes ( $V_f$  and  $V_{max}$  in l/m, Table 2), confirm the randomness of the overtopping spectrum (as suggested by Allsop *et al.* (2008)). In fact, in a precautionary management approach, individual maximums would be more adequate to characterise local overtopping hazard. Tests on the effects of overtopping flows on people suggest that values on mean discharges alone may not give reliable information (Allsop *et al.*, 2008). Thus, an increased effort to develop methods to predict maximum volumes for the overall structure types, and their validation, should be performed. The methodology applied here allows the computation of both mean and maximum volume intervals. Although it was only validated for this breakwater, it is likely suitable to be adopted in other locations. Simultaneously, besides flow depths and overtopping discharges, research should also explore in more detail the overtopping hazard estimates based on overtopping velocities.

## CONCLUSIONS

This paper presents a comparison of mean overtopping discharges calculated from flow field measurements of depths and velocities at a breakwater armour and crest, with mean discharges predicted by empirical tools. The corrected NN\_OVERTOPPING2 is the method that better predicted the mean discharges calculated based on field data, for the overall analysed overtopping events, but presents significant errors when predicting individual mean discharges. EurOtop formula underpredicts calculated mean discharges, and is unsuitable to predict local overtopping volumes. Towards an increase of validation of the empirical/numerical tools (*e.g.*, discharge predictions for short-term intervals) efforts should be concentrated on fieldwork data acquisition.

The recorded hydrodynamic conditions offer risk to all types of pedestrians at the walkway and to small boats, if located at less than 20 m of the breakwater. Hazard assessment has different results when using calculated mean overtopping discharges or overtopping peak volumes, thus it is recommended that peak volumes should be more often used as a parameter to infer local hazard. Future work should aim at the understanding and quantification of overtopping effects, in an attempted to solve structure design problems before construction.

## ACKNOWLEDGEMENTS

This work is a contribution to the project SPACE (PTDC/ECM/114109/2009), funded by FCT. A. R. Carrasco was supported by SFRH/BPD/88485/2012. Ana Matias was supported by Programme Investigator FCT. This is also a contribution for the RUSH project (PTDC/CTE-GIX/116814/2010). Tidal data were kindly supplied by Puertos del Estado and offshore wave data by Instituto Hidrográfico.

## LITERATURE CITED

- Allsop, W., Bruce, T., Pullen, T. and van Der Meer, J., 2008. Direct Hazard from wave overtopping – the forgotten aspect of coastal flood risk assessment? DEFRA. *Proceedings of Flood and Coastal Management Conference*, Manchester, UK, 11 p.
- Battjes, J.A. and Janssen, P.A.E.M., 1978. Energy loss and set-up due to breaking of random waves, *Proceedings of 16th International Conference on Coastal Engineering*, ASCE, 569-587.
- Booij, N., Ris, R.C. and Holthuijsen, L.H., 1999. A third-generation wave model for coastal regions, Part I, Model description and validation, *Journal of Geophysical Research*, C4, 104, 7649-7666.
- Chini, N. and Stansby, P.K., 2012. Extreme values of coastal wave overtopping accounting for climate change and sea level rise, *Coastal Engineering*, 65, 27-37.
- Coeveld, E.M., Van Gent, M.R.A. and Pozueta, B., 2005. Neural Network. Manual NN\_OVERTOPPING 2. CLASH WP8, WL Delft Hydraulics Report, Delft, The Netherlands.
- De Rouck, J., Geeraerts, J., Troch, P., Kortenhaus, A., Pullen, T. and Franco, L., 2005. New results on scale effects for wave overtopping at coastal structures. *Proceedings of ICE Coastlines, Structures & Breakwaters '05*, Thomas Telford, London, 29-43.
- Didier E., Ferreira O., Matias A., Neves M.G., Reis M.T. and Pacheco A., 2011. Desenvolvimento e validação de um modelo Smoothed Particle Hydrodynamics para aplicação a estruturas costeiras. *Proceedings of 7as Jornadas Portuguesas de Engenharia Costeira e Portuária*, eds. Delegação Portuguesa da PIANC, pp 30 (15 p. CD Rom), Porto, Portugal.
- Ferreira, Ó., Reis, M.T., Carrasco, A.R., Neves, M.G., and Didier, E., 2013. Small Overtopping discharges at Albufeira Harbour: field measurements and modelling. *Proceedings of 6th SCACR – International Short Course/Conference on Applied Coastal Research*, LNEC, Lisboa.
- Geeraerts, J. and Boone, C., 2004. CLASH: Full Scale Measurements on the Zeebrugge breakwater - Second Winter Season, Ghent University, Belgium.
- Geeraerts, J., Troch, P., Rouck, J.D., Verhaeghe, H. and Bouma, J.J., 2007. Wave overtopping at coastal structures: prediction tools and related hazard analysis. *Journal of Clear Production*, 15, 1514-1521.
- Hasselmann, K., Barnett, T.P., Bouws, E., Carlson, H., Cartwright, H., Cartwright, D.E., Enke, K., Ewing, J.A., Gienapp, H., Hasselmann, D.E., Kruseman, P., Meerburg, A., Muller, P., Olbers, D.J., Richter, K., Sell, W. and Walden, H., 1973. Measurements of wind-wave growth and swell decay during the Joint North Sea Wave Project (JONSWAP). *Dtsch. Hydrogr. Z. Suppl.* 12 (A8), 1-95.
- Holthuijsen, L.H., 2007. *Waves in Oceanic and Coastal Waters*, Cambridge University Press.
- Hughes, S., Thornton, C., van der Meer, J. and Scholl, B., 2012. Improvements in describing wave overtopping processes. *Proceedings of 3rd International Conference Coastal Engineering (ICCE)*, ASCE, Santander, Spain, 1-6.
- Pullen, T., Allsop, N.W.H., Bruce, T. and Geeraerts, J., 2003. Violent wave overtopping: CLASH field measurements at Samphire Hoe. *Proceeding of Coastal Structures*, 12 p.
- Pullen, T., Allsop, N.W.H., Bruce, T., Kortenhaus, A., Schürtrumpf, H. and Van der Meer, J.W., 2007. EurOtop: Wave Overtopping of Sea Defences and Related Structures: Assessment Manual. Environment Agency, UK, Expertise Netwerk Waterkoren, NL, and Kuratorium für Forschung im Küsteningenieurwesen, DE.
- Shankar, N.J. and Jayaratne, M.P.R., 2003. Wave run-up and overtopping on smooth and rough slopes of coastal structures. *Ocean Engineering*, 30, 221-238.
- Tonelli, M. and Petti, M., 2013. Numerical simulation of wave overtopping at coastal dikes and low crested structures by means of a shock-capturing Boussinesq model. *Coastal Engineering*, 79, 75-88.
- Van der Meer, J.W., Snijders, W., and Regeling, H.J. 2006. The wave overtopping simulator. *Proceedings of 30th International Conference Coastal Engineering*, ASCE, San Diego, 4654-4679.
- Verhaeghe, H., 2005. Neural Network Prediction of Wave Overtopping at Coastal Structures. PhD Thesis, Ghent University, Belgium.

# A contribution to climate change assessment of storm surges along the coast of Mozambique

Adérito C.F. Aramuge, Alfredo Rocha, Paulo A. Silva.

CESAM and Department of Physics,  
University of Aveiro,  
3810-193 Aveiro, Portugal  
aderito@ua.pt  
alfredo.rocha@ua.pt  
Psilva@ua.pt



[www.cerf-jcr.org](http://www.cerf-jcr.org)



## ABSTRACT

Aramuge, A., Rocha, A., Silva, P.A., 2014. A contribution to climate change assessment of storm surge along the coast of Mozambique. In: Green, A.N. and Cooper, J.A.G. (eds.), *Proceedings 13<sup>th</sup> International Coastal Symposium* (Durban, South Africa), *Journal of Coastal Research*, Special Issue No. 70, pp. 253-258, ISSN 0749-0208.

[www.JCRonline.org](http://www.JCRonline.org)

About two-third of total population of Mozambique lives along the coast which is 2700 km long. Mozambique is affected by tropical cyclones which are formed in the Indian Ocean, most of them inducing storm surges along the coast. This study presents an analytical model to estimate sea level changes, particularly extreme events (storm surges) from atmospheric pressure and wind data. The meteorological tides, for Maputo tide gauge station, were obtained by applying a low pass filter, with a cut off frequency of 33 hours. The analytical model was validated by comparing the generated meteorological residuals, trough inverted barometer and wind forcing, against the meteorological residual obtained from the tidal gauge. The analysis of the distribution curves of relative and cumulative frequencies, allowed the definition of three classes of storm surges namely: significant, very significant and highly significant for the percentile of 95, 99 and 99.9 respectively. There is a good agreement with a high correlation between the results obtained from the two methods. The alongshore wind, mainly from south or southeast, represents the main contribution for storm surge generation. The analytical model will be used to evaluate changes in the statistical properties of storm surges for future climate change scenarios along the Mozambican coast.

**ADDITIONAL INDEX WORDS:** Mozambique coast, climate change, storm surge, time series.

## INTRODUCTION

Mozambique has the third largest coastline in Africa, spanning approximately 2700 km. Due to its geographical location, Mozambique lies in the favored path of potentially deadly tropical cyclones, which are formed in the Indian Ocean basin and proceed towards land (Figure 1). These tropical cyclones cause frequent storm surge along the Mozambican coast. According to Emanuel (2008), model results suggest that for the Indian Ocean, there is an overall tendency toward decreasing frequency of tropical cyclones but increasing cyclone intensity. It is known that the atmosphere influences the oceans, mainly by wind stress exerted on the interface of both (Peixoto and Oort, 1992). Therefore, cyclones represent potential disaster conditions for the population and infrastructures along the coast, taking into consideration that the more intense the wind, the greater the amount of water displaced coastwards. The low-lying nature of the coastal zone and its dense human occupation (nearly two-thirds of the Mozambique total) has made this country one of the most vulnerable to natural disasters (INGC 2009).

In a total of 80 developing countries studied, one of the top 10 countries at risk from intensification of storm surges is Mozambique, occupying the 10<sup>th</sup> place with 51.7% due to coastal population, 5<sup>th</sup> place with 55% due to coastal gross domestic



Figure 1. Southern Indian Ocean tropical cyclone tracks, 2004-2007. (Source: NOAA - Adapted)

product (GDP) and 8<sup>th</sup> place with 55.1% due to coastal urban areas (Dasgupta et al. 2009).

According to Santos and Miranda (2006), for a given site and time, the sea level is determined by the combination of two effects: the astronomical and meteorological tide. By neglecting resonances and second-order effects, the storm surge can be

determined by wind and atmospheric pressures alone. While the astronomical tide is deterministic, the meteorological effects have a stochastic nature. The sea level oscillation responds continuously to astronomical, oceanographic and atmospheric (pressure and near-surface winds) interactions over a wide range of periods (Pugh 1987). The combined effects of atmospheric pressure and wind forcing on sea level produce oscillations known as meteorological tides or low frequency sea level oscillations (storm surge), relative to that due of the tides alone. The height of surge is given by the difference between the recorded level and the predicted tidal level. A surge can be either positive or negative, i.e. the actual sea level can be either higher or lower than expected from tidal predictions (Bowden 1983). According to Faggioni *et al.* (2006), when a high-pressure area moves on a free water surface it produces an additional weight on it causing a water out-flow (low meteorological tide). On the contrary, when a perturbed front produces a drop in atmosphere weight, the isostatic compensation adjustment will be realized in a bump produced by a flow of incoming tide (high meteorological tide). The increased pressure of 1 hPa results in a decrease in sea level of approximately 1 cm. This response, called inverted barometer effect, is explained through a theoretical model derived from hydrodynamic equations considering an ocean with constant depth (Proudman, 1953). When a low atmospheric pressure system coincides with a high water spring tide, extreme sea level can be expected.

According to Dasgupta, *et al.* (2009) and Rahmstorf (2007), the scientific evidence indicates that climate change will intensify storm surges and there are evidences which suggest that sea-level rise could reach 1 meter or more during this century. There are no such studies carried out on the meteorological tides along the Mozambican coast. The few that exist are discussed by Mavume and Brundrit (2009) and Dasgupta *et al.* (2009).

This study is mainly concerned with the validation of an analytical model which will help in understanding the future behavior of storm surge on the coast of Mozambique. This work regards the risks inherent in coastal occupation and provides a useful tool for weather forecasting during the cyclone season. This will aid decision makers in their planning activities in Mozambique with respect to cyclone hazards.

## Study Area

The study area lies along the coastal zone of Mozambique between the latitudes  $-10^{\circ} 20'$  (Rovuma) and  $-26^{\circ} 50'$  (Maputo); a length of about 2700 km. The continental shelf extends to the 200 meter isobath and has an area of 104 km<sup>2</sup> (Figure 2). It is narrow in the south and in the north, with two banks of ecological importance (Hoguane and Pereira, 2003). The coastal zone is characterized economically by the main cities, services and industries such as tourism, trade and ports. The population gains their livelihood at the expense of the resources existing there. The ports are strategically associated with roads, providing services with intense movement of loads from national clients as well as for neighboring countries.

## Climatological Description of the Region

Due to its location on the eastern coast of Africa, the Mozambican coastline is subject to the influence of the warm current of the Mozambique/Agulhas Current and the corresponding maritime prevailing East quadrant winds (Muchangos, 1999). The tides are semi-diurnal with fairly significant diurnal inequality (Hoguane, 1999). The pattern of movement of ocean water along the coast of Mozambique, according to Saetre and Silva (1982), is characterized by three

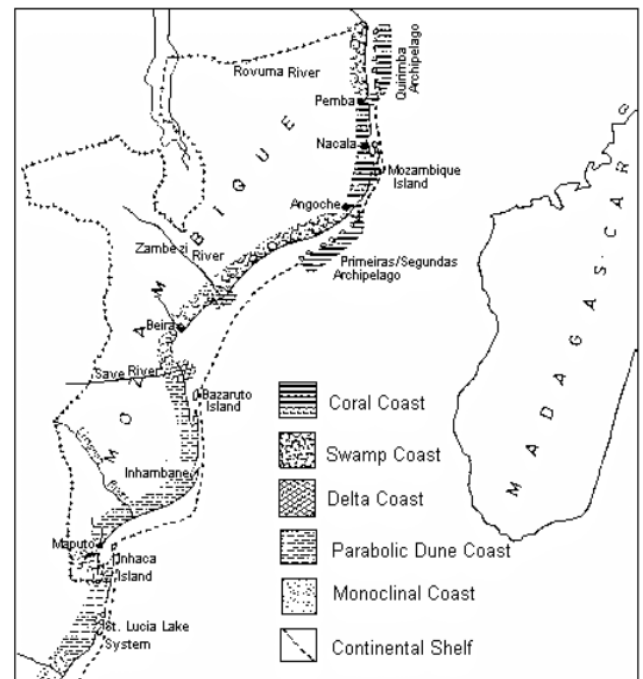


Figure 2. The study area. The dashed line represents the 200 m isobaths. Source: Hoguane and Pereira (2003).

anti-cyclonic cells, which vary in position throughout the year, and by small wind vortices between the large anti-cyclonic eddies.

The weather in Mozambique is determined by the location of the equatorial low pressure zone, tropical anticyclone cells and Antarctic polar fronts. Anticyclonic cells are located on both sides of the southern Africa over the Atlantic and Indian oceans, determining, under the influence of equatorial and polar low pressure centers, the regime of monsoon winds that blow consistently (Muchangos, 1999). The climate is generally tropical humid with two distinct seasons: dry or winter and wet or summer. The annual average atmospheric temperature is about 23°C to 26°C for the coastal zones of southern and northern Mozambique. The average annual precipitation is about 1200 mm, and occurs mainly during the summer (November to April). The climate in the region north of the Zambezi River is under the influence of the equatorial low-pressure zone, with the NE monsoon occurring in the warm season. The climate south of the Zambezi River is influenced by a subtropical anti-cyclonic zone. North of Sofala, along the Zambezi River, a transitional zone occurs. This is termed the Intertropical Convergence Zone (ITCZ) which experiences high rainfall (Saetre and Silva, 1979). According to Tinley (1971) northern Mozambique is affected by the extension of the East African monsoon system with winds blowing North to Northeast during the austral summer and South to Southwest during the austral winter. Central and southern Mozambique is affected by the Southeast Trade Wind System and receives easterly prevailing winds throughout the year. In the North of the Zambezi River, the atmospheric circulation is characterized by influence of equatorial low pressure area, with winds of NE monsoon during the summer, while in the South of the Zambezi River, it is characterized by the anti-cyclonic subtropical circulation. The winds in the South and central zone are predominantly trades, and in the North are influenced by a

monsoon regime with NE winds during the summer and SW during the winter.

According to INGC (2009), in the period 1980-2007, 56 tropical cyclones and tropical storms entered the Mozambique Channel. Fifteen (25%) of them made landfall on the coast of Mozambique. Four cyclones hit the North, eight hit the Centre and three hit the South. Only four occurred in the period 1980-1993, whilst the other eleven occurred in the later period from 1994-2007. Two cyclones in the period 1980-1993 were classified as category 3-5 compared to seven in the period 1994-2007. Observations also suggest a recent southward shift in their trajectories and landfall locations. The tropical cyclones are more frequent between January and February and cause rains accompanied by thunderstorms and strong winds, sometimes reaching over 100 km/h.

## METHODS

### Data Source and Collection

The sea level records database of Mozambique is not continuous since it has many missing data and a limited number of tide gauges (Table 1). The station of Maputo is the only one with a near complete data set (~13 years). The scarcity of tide gauge data has led to the use of proxy data sets of sea level pressure, wind speed and direction to proceed with this study. The atmospheric pressure and observed wind data from 7 meteorological stations, namely Maputo, Xai-Xai, Inhambane, Beira, Quelimane, Angoche and Pemba were used as input for running the analytical model along the coast of Mozambique to generate storm surge. The data period is from 1973 to 2011 and was downloaded from the Climate Data Online (CDO) site, at National Climate Data Center (NCDC) of the National Oceanic and Atmospheric Administration (NOAA). The wind was measured at a height of 10 meters. The hourly sea level records data used to validate the analytical model are from Maputo tide gauge station for 1974, since this the only year with a complete time series of data.

### Data Processing and Analysis

Tides and inertial motions usually cause a high-frequency noise in sea level records used to analyze low-frequency motion in the ocean (Thompson 1983). Hourly tide gauge series were statistically analyzed by calculating averages, standard deviations, percentile and variances. For the identification of the meteorological component in combined sea level records, the low-pass filter PL33 was used to remove the astronomical high frequency components. The digital filter, which operates on hourly data values, replaces each point with a weighted average of the 33 points on either side of the central point. The filtering reduces the total length of the time series by 66 hours (33 hours on each end). The filter transfers signals at unreduced amplitude that have periods longer than about 50 hours. The half-amplitude period of the filter is at 33 hours and the half power period is at 38 hours (Rosenfeld, 1983).

Storm surge is usually considered to be driven by two processes namely the atmospheric pressure and extreme wind stress. An analytical model was used, which considered the atmospheric pressure and wind components. The inverted barometric effect, which is the response of sea level to changes in atmospheric pressure, was used with sea level pressure data to estimate the perturbations of the sea level by using equation 1. This equation can be obtained from the fundamental equations for sea level rise and the result was added to the one obtained from the wind setup effects. This was decomposed into an onshore and alongshore

component, described in equations 2 and 3 respectively (Santos and Miranda, 2006). Those equations represent the three storm surge types of forcing used in the study. Equation 2 is used for the wind setups due to cross-shore winds.

When the wind blows perpendicular to a coastline, a steady-state balance is quickly established between the surface wind stress and a pressure force due to the slope of the sea surface (Csanada, 1982). Equation 3 is used for the wind setup due to alongshore wind. According to Garrett (1983), there is considerable evidence to suggest that the alongshore wind component is much more important than the cross-shelf wind component in producing coastal sea level changes at low frequency. The wind forcing produces an Ekman current to the left of the wind in the Southern Hemisphere, which causes the surface to rise at a constant rate within a distance on the order of the barotropic Rossby radius of deformation from the coast.

$$\eta_{sh} = \frac{\Delta P_a}{\rho g} \tag{1}$$

$$\eta_{sn} = \frac{\tau_{sx}}{\rho_w g h} L \tag{2}$$

$$\eta_{st} = \frac{f}{g} \left( \frac{\tau_{sy}}{\rho_w \kappa} \right)^{1/2} L \tag{3}$$

In the above equations,  $\Delta P_a$  is the atmospheric pressure disturbance,  $\eta_{sh}$  the displacement of water level from the mean due to pressure disturbance,  $\rho$  the air density,  $\eta_{sn}$  the displacement of water level from the mean due to onshore wind,  $\tau_{sx}$  the zonal surface wind stress,  $L$  the platform width,  $\rho_w$  the sea water density,  $g$  the gravitational acceleration,  $h$  the depth of the water column,  $\eta_{st}$  is the displacement of water level from the mean due to alongshore wind,  $f$  Coriolis parameter,  $\tau_{sy}$  the meridional surface wind stress and  $\kappa$  bottom drag coefficient.

A cross correlation among the filtered sea level, atmospheric pressure and wind stresses was calculated. The zonal and meridional wind stresses were calculated by using equations 4 and 5, where  $C_D$  is a drag coefficient,  $w$  wind speed at height of ten (10) meters,  $u$  and  $v$  are zonal and meridional wind components, respectively.

$$\tau_{sx} = C_D \rho |w| u \tag{4}$$

$$\tau_{sy} = C_D \rho |w| v \tag{5}$$

The drag coefficient links the easily measured wind velocity with the more difficult direct measurement of wind stress and is the key parameter for the determination of the momentum transfer between atmosphere and ocean. The drag coefficient for the ocean surface is found to increase with wind speed (Smith, 1980). For the present study this coefficient was estimated by using equations 6, 7 and 8 for the ranges of different wind speed. According to Large and Pond (1981), Smith (1980) and Powell, et al. (2003)

Table 1. Observed tide gauge data available and missing, from the network stations along the coast of Mozambique, by 2012.

Tide Gauge Station	Data Period Range	Total Missing Data (%)
Maputo	1974, 1980-1986, 1995-2002	33
Xai-Xai	No data	100
Inhambane	1994-1995	71
Beira	1996-2000, 2002	29
Quelimane	1995	25
Angoche	No data	100
Nacala	1995-2007	45
Pemba	1984, 1996-2004, 2007-2010	39



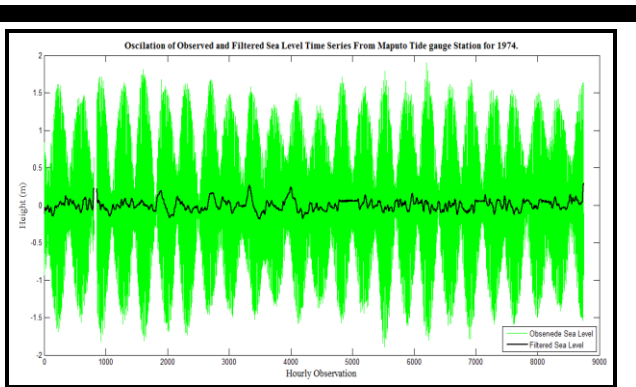


Figure 3. Oscillation of observed (green) and filtered (black) sea level time series from Maputo tide gauge Station, for 1974.

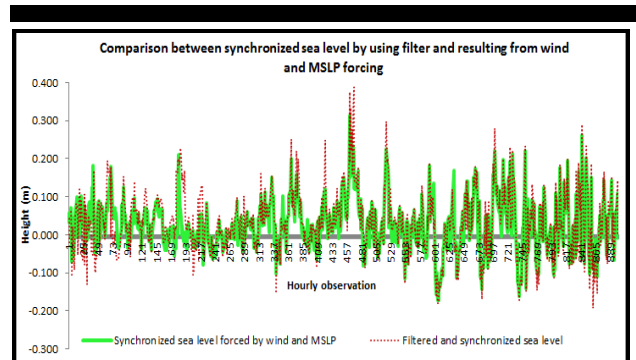


Figure 4. Graphical comparison between synchronized sea level by using filter (red dashed line) and resulting from wind and mean sea level pressure (green line).

respectively; these are:

$$C_D = 1.1 \cdot 10^{-3} \quad \text{If } w < 6 \text{ m s}^{-1} \quad (6)$$

$$C_D = (0.61 + 0.063W) \cdot 10^{-3} \quad \text{If } 6 \text{ m s}^{-1} \leq w < 22 \text{ m s}^{-1} \quad (7)$$

$$C_D = 2.5 \cdot 10^{-3} \quad \text{If } w \geq 22 \text{ m s}^{-1} \quad (8)$$

The following are the constants used:  $\rho = 1.25 \text{ kg.m}^{-3}$ ,  $k = 0.002$  (Feddersen et al. 2003),  $\rho_w = 1027 \text{ kg.m}^{-3}$ ,  $g = 9.8 \text{ m.s}^{-2}$ ,  $f = 8.5 \times 10^{-5} \text{ s}^{-1}$ ,  $h = 200 \text{ m}$ . The value of  $L$  was considered as being the distance from the coast to the 200 m depth zone, taking in consideration that the continental shelf is narrow in the South and in the North. We force the model with recorded pressure and wind data to generate meteorological tide time series which are later compared against the meteorological tide time series obtained by filtering observed sea level time series.

### RESULTS

The meteorological tides, from the observed sea level time series at Maputo tide gauge station, were obtained by applying a low pass filter, with a cut off frequency of 33 hours (Figure 3). The filtered records generated the time series of the sea level responsible for the meteorological system affected at the respective point. All the values of meteorological tides in this study are in meters (m). The analytical model was validated by comparing the generated meteorological residuals, trough inverted barometer and wind forcing, against the meteorological residual

obtained by using the low pass filter. Both data were synchronized in order to eliminate the gaps due to the time discrepancy in both time series. The analysis of the distribution curves of relative and cumulative frequencies allowed the definition of three classes of storm surges namely: significant, very significant and highly significant for the percentile that appears above 95, 99 and 99.9 respectively. This analysis was done as a tool for the validation of the analytical model, by making a comparison in the end between the meteorological tides from filtered sea level and from the analytical model. It is noticed that the analytical model underestimate the intensity of the storm surge, however the differences are very small which does not reduce the model quality (Table 2).

In order to verify the linear correlation, the peaks of the meteorological tides, obtained from both methods, were analyzed through the coherence between them. In figure 4, there is an agreement between the two meteorological residuals despite some difference in amplitude which can be neglected. The correlation between both meteorological tides calculated by using the two different methods (Figure 5a) is 0.8.

The meteorological tide and the atmospheric pressure are strongly correlated (Figure 5b). The contribution of the parameters in the storm surge was of 62% for the wind and 38% for the sea level pressure. The alongshore wind setup has more contribution than onshore wind setup.

After the analytical model validation, the pressure and wind data for the seven points along the coast of Mozambique was

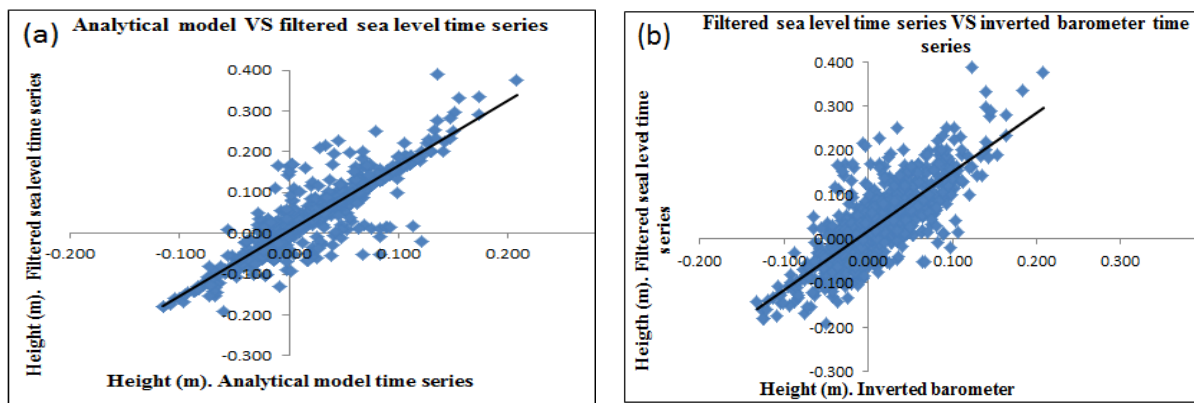


Figure 5. Comparison: (a) Between the meteorological tides from filtered time series and analytical model. (b) Between the meteorological tides from filtered time series and from inverted barometer for Maputo, 1974.

Table 2. The three significant storm surge levels for the filtered sea levels and from analytical model, for Maputo, 1974.

	Filtered sea level time series	Analytical model time series
<b>Significant Storm Surge</b>	0.17	0.15
<b>Very significant Storm Surge</b>	0.25	0.21
<b>Highly significant Storm Surge</b>	0.38	0.36
<b>Maximum Storm Surge</b>	0.39	0.38

applied in the model to estimate storm surges. The results were grouped, also, in 3 storm surge significance levels (Table 3), as mentioned above. For all seven stations, the contribution of alongshore wind setup is predominant if compared against onshore wind. The highest storm surge value occurred in Angoche followed by Maputo and Inhambane.

### CONCLUSIONS

For some simplified conditions of balance, analytical solutions exist that allow one to understand the main mechanisms involved in storm surge or even calculates it, in simplified form, from meteorological data. A simple analytical model which generates storm surge by using wind and sea level pressure time series was validated against the tide gauge records. Statistical analysis defined three significant levels of storm surge, which helps in understanding the characteristics of this natural phenomenon. Despite its great simplicity, the method of calculating storm surge from meteorological data allows useful results to be obtained with a minimum effort in the calculation. This is a purely static method and enables a simple interpretation of the fundamental processes that generate storm surge. It also highlights the importance of the effect of tangential (alongshore) wind to the shoreline. The results show that the amplitude of generated storm surge, when using the analytical model, is slightly different, although there is a good agreement with meteorological residuals obtained from both methods. The analytical method can be useful to study storm surge for the areas where there is no tide gauge data, by using sea level pressure and wind forcing. From the theoretical arguments and numerical results obtained, it was established that the alongshore wind, mainly from south or southeast, represents the main contribution for the storm surge generation along the coast.

The heights for the storm surge along the coast of Mozambique, according to this study seem to be small. However when taking into account that some cities are located below the mean sea level, we cannot neglect these results. The analytical model simulates the storm surge events in the considered location well, despite the model only consider the atmospheric pressure and wind for its calculation and neglecting other factors. This model does not consider the cyclonic system dynamics itself: everything else being equal, storm surge values at the coast are very different with fast-moving and slow-moving systems. Further, this analytical model will be used with atmospheric data generated by climate change simulations to evaluate changes in the statistical properties of storm surges for future climate change scenarios along the Mozambican coast.

Table 3. The three significant storm surge levels for the below studied stations for the period 1973-2011.

	Significant Storm Surge	Very significant Storm Surge	Highly significant Storm Surge	Maximum Storm Surge
<b>Maputo</b>	0.09	0.14	0.22	0.96
<b>Xai-Xai</b>	0.10	0.16	0.23	0.56
<b>Inhambane</b>	0.14	0.19	0.25	0.81
<b>Beira</b>	0.12	0.17	0.24	0.67
<b>Quelimane</b>	0.12	0.15	0.20	0.77
<b>Angoche</b>	0.09	0.14	0.28	1.10
<b>Pemba</b>	0.08	0.13	0.13	0.68

### ACKNOWLEDGEMENT

Appreciation is expressed to the National Institute of Hydrography and Navigation of Mozambique for providing the tide gauge data, the National Institute of Meteorology of Mozambique (INAM) for the samples of meteorological data, the National Climate Data Center (NCDC-NOAA) for the sea level pressure and wind data, the government of Portugal, through the Science and Technology Foundation (FCT), for sponsoring the PhD scholarship.

### LITERATURE CITED

- Bowden, K. F., 1983. Physical oceanography of coastal waters. *Ellis Horwood series in marine science*.
- Dasgupta, S., Laplante, B., Murray, S., and Wheeler, D., 2009. Climate Change and the Future Impacts of Storm-Surge Disasters in Developing Countries. *CGD Working Paper 182. Washington, D.C.: Center for Global Development*.
- Csanady, G. T., 1982. *Circulation in the Coastal Ocean*. Reidel, 279 pp.
- Emanuel, K., Sundararajan, R., and William, J., 2008. Hurricanes and global warming: Results from downscaling IPCC AR4 simulations. *Journal of Climate*, 89, 347-367.
- Oswaldo Faggioni, O., Arena, G., Bencivenga, M., Bianco, G., Bozzano, R., Canepa, G., Lusiani, P., Nardone, G., Piangiamore, G., Soldani, M., Surace, L., and Venzano, G., 2006. The Newtonian approach in meteorological tide waves forecasting: Preliminary observations in the East Ligurian harbours. *Annals of geophysics*, vol. 49, n.6, December 2006.
- Fedderson, F., Gallagher, E. L., Guza, R. T., and Elgar, S., 2003. The drag coefficient, bottom roughness, and wave-breaking in the nearshore. *Coastal Eng.*, 48, 189 – 195.
- Garrett, C., 1983. Variable sea level and strait flows in the mediterranean: A theoretical study of the response to meteorological forcing. *Oceanol. Acta*, 6, 79–87.
- Hoguane, A., 1999. Sea level measurements and analysis in the western Indian Ocean. *National Report, Mozambique. IOC, UNESCO, 6-7 21*.
- Hoguane, A.M. and Pereira, M.A.M., 2003. National Report: Marine Biodiversity in Mozambique the known and the unknown. pp 138-155. In: C. Decker, C. Griffiths, K. Prochazka, C. Ras and A. Whitefield Marine Biodiversity in Sub-Saharan Africa: the known and the unknown. Proceedings of the marine biodiversity in Sub-Saharan Africa: the known and the unknown Cape Town, South Africa 23-26 September 2003.
- INGC (National Institute for Disaster Management), 2009a. Main Report: INGC Climate Change Report: Study on the impact of climate change on disaster risk in Mozambique. (K. Asante, G. Brundrit, P. Epstein, A. Fernandes, M.R. Marques, A. Mavume, M. Metzger, A. Patt, A. Queface, R. Sanchez del Valle, M. Tadross, and R. Brito, eds.). Maputo, Mozambique:INGC.

- Large, W.G. and Pond, S., 1981. Open ocean momentum fluxes in moderate to strong winds. *Journal of Physical Oceanography* 11: 324-336.
- Mavume, A and Brundrit, G., 2009. Main Report: INGC Climate Change Report. *INGC, Mozambique 2009*.
- Muchangos, A., 1999. Moçambique paisagens e regiões naturais. Tipografia Globo,Lda. República de Moçambique, 01048/FBM/93, 163p.
- Peixoto, J. P.; Oort, A., 1992. *Physics of Climate. 1. ed. New York: American Institute of Physics, 1992, 520 p.*
- Powell, M.D., Vickery, P.J., and Reinhold, T. A., 2003. Reduced drag coefficient for high wind speeds in tropical cyclones. *Nature* 422: 278-283.
- Proudman, J., 1953. *Dynamical Oceanography. 1. ed. London, Methuen and Co., 1953.*
- Pugh, D. T., 1987. *Tides, Surges and Mean Sea Level. Great Britain: John Wiley and Sons, 1987, 472 pp.*
- Rahmstorf, S., 2007. A Semi-Empirical Approach to Projecting Future Sea-Level Rise. *Science Vol. 315 no. 5810 pp. 368-370.*
- Rosenfeld, S., 1983. WHO I Technical Report 85-35. p. 21.
- Saetre, R. and Silva, R. P., 1979. The Marine Fish Resources of Mozambique. Reports on Surveys with the R/V "Dr. Fridtjof Nansen", Serviço de Investigação Pesqueira. Maputo. Institute of Marine Research, Bergen.
- Saetre, R. and Silva, R. P., 1982. Water masses and circulation on the Mozambique channel. *Rev. Inv. Pesq:* 3-38.
- Santos, F.D., Miranda, P., (eds), 2006. Alterações climáticas em Portugal, cenários, impactos e medidas de adaptação. *Projecto SIAM II, Gradiva, Lisboa 2006.*
- Smith, S. D., 1980. Wind stress and heat flux over the ocean in gale force winds, *J. Phys. Oceanogr.*, 10, 709-726.
- Thompson, R. O. R. Y., 1983. Low-pass filters to suppress inertial and tidal frequencies. *J. Phys. Oceanogr.*, 13, 1077-1083.
- Tinley, K., 1971. Determinants of coastal conservation: dynamics and diversity of the environment as exemplified by the Mozambique coast. *Proc. Symp: Nature Conservation as a form of land use Gorongosa National Parks – 13-17 September 1971. Sarcus 125-153.*
- Web site: The National Oceanic and Atmospheric Administration (NOAA). Retrieved in January 12<sup>th</sup>, 2014. <http://www.csc.noaa.gov/hurricanes/#>

# Spatial distribution of storm wave energy dissipation for the assessment of beach morphodynamics

E. Guisado-Pintado†, G. Malvárez‡, F. Navas‡, R. Carrero†

† Coastal Environments Research Group  
University Pablo de Olavide  
Seville, Spain  
esguipin@upo.es

‡ Area of Physical Geography,  
University Pablo de Olavide,  
Seville, Spain



[www.cerf-jcr.org](http://www.cerf-jcr.org)



[www.JCRonline.org](http://www.JCRonline.org)

## ABSTRACT

Guisado-Pintado, E., Malvárez, G., Navas, F., Carrero, R., 2014. Storms based morphodynamics from wave energy dissipation for beach characterisation. In: Green, A.N. and Cooper, J.A.G. (eds.), *Proceedings 13<sup>th</sup> International Coastal Symposium* (Durban, South Africa), *Journal of Coastal Research*, Special Issue No. 70, pp. 259-265, ISSN 0749-0208.

High energy events are responsible for most significant and visible changes in beach morphology and sediment disposal in a short temporal scale. Storms are associated with damage to the coastal ecosystem and societal services such as severe shoreline erosion, collapse of coastal infrastructures and properties (ports, seawalls). These also affect the effectiveness of coastal defence works such as beach nourishment. In a scenario of climate change, with predictions of sea level rise and an increase in storminess being the most important threats affecting the coastal environments, the understanding of wave climate and the role of high energy events are of key importance. In this paper an index for the characterisation of modal regimes and extreme wave events, based on a 10-year wave hindcast on a 1-hour basis, is developed to characterize wave storms regime of the Andalusia region of southern Spain. Results of the implementation of this method are presented through two case studies; one concerning a low-energy environment located on the Mediterranean coast and other for the higher energy Atlantic coast. Analysis and characterisation of the wave parameters during modal and storm conditions and the study of the spatial distribution of wave energy dissipation patterns, among other hydrodynamic parameter such as wave orbital velocity, are carried out and implemented through a morphodynamic index for nearshore environments. Results show the variability of wave energy dissipation patterns among both study sites, the role of the nearshore topography and the adaptation of the surf zone in wave hydrodynamic processes. Further, the morphodynamic resilience helps in identifying the potential for changing behaviour in energy dissipation and morphological effects derived from high energy events when compared with low-energy modal conditions.

**ADDITIONAL INDEX WORDS:** *wave energy dissipation, SWAN, surf zone, morphodynamic resilience, storms.*

## INTRODUCTION

The characterisation of storms and extreme wave and wind events affecting the coast has been widely studied by researchers during past decades (Zhang *et al.*, 2002; Rodriguez *et al.*, 2003; Ferreira, 2004; Rangel-Buitrago and Anfuso, 2013). The knowledge and understanding of storm patterns is one of the main issues in coastal and marine studies, and a valuable basis for coastal management, as it provides worthy information, not only for planning and regulation of coastal uses in the short term, but also for the forecasting of coastal risks and associated coastal vulnerability. In a scenario of climate change, coastal systems would have to adapt to new energy conditions derived from variations not only in storm frequency and wave climate, but also those caused by sea-level rise (Komar and Allan, 2008; Phillips and Crisp, 2010). Thus, understanding variations in the dynamic equilibrium achieved during the current (interglacial) period by sedimentary coastal systems is of paramount relevance to the comprehension of future scenarios of change. Research on storm identification and their effects on coastal morphodynamics frequently characterize and isolate events based on either wave conditions (height, period and direction) (CMA, 2003) or wind

data -speed and duration- (Cook and Prior, 1988; MacClenahan *et al.* 2001), or through the combination of both (Carter and Stone, 1989). Nevertheless, there is no common criterion in the identification of storm events, mainly due to the variability of conditions associated with coastal areas and marine environments. Further, storm characterisation should include criteria to indicate the independence of events, a minimum period of time to be considered between storms to avoid overlapping. For instance, whereas for Morton *et al.* (1997) and Dorsch *et al.* (2008) this independency factor has a value of 30 hours, Rangel-Buitrago and Anfuso (2013) set the threshold at 24 hours. Additionally, analyses of storm patterns for beach morphodynamic studies need to address storm duration, since in nearshore dynamics the accumulation of wave-related work (energy dissipation density) may be a significant parameter. However, duration is a parameter that differs among authors. For MacClenahan *et al.* (2001) the storm duration threshold is set from the biggest storm registered in the dataset, while Carter and Stone (1989) established that a minimum duration of 5 hours is needed to produce erosion on the foredune. For the Regional Government of Andalusia (CMA, 2003), the duration threshold value is set at 5 hours for an event to be considered a storm.

Frequently in the literature, storms have been used to characterise morphodynamic beach state in comparison with fair wave conditions (e.g. Benavente *et al.*, 2002; Gomez-Pujol *et al.*,

2007; Backstrom *et al.*, 2008) as they are considered the primary driver responsible for long term beach erosion (Fenster and Dolan, 1994). In contrast, other authors (Zhang *et al.*, 2002) proved that the short-term erosion induced by storms is only a temporary deviation from the long-term morphosedimentary trend for beaches, because no matter the intensity of storm event, the system seems to recover after storms at varying paces.

When the context moves purely to beach morphodynamics, the key element to understand the effect of storms must carefully consider wave propagation and attenuation in nearshore environments. Waves represent the dominant source of energy in the nearshore, and most waves acting on coasts hit by storms include an element related to waves generated or greatly enhanced by local winds. In the nearshore waves are substantially transformed and their energy is dissipated due to shoaling, turbulence and friction in the surf zone where key wave-driven processes such as refraction and breaking induce sediment transport. Furthermore, given certain deep water storm wave conditions (at depths <2–3 m) the surf zone behaves in a very dynamic way and processes become highly nonlinear (Pruszek *et al.* 2008). It is thus in this critical region that storm wave energy affects beach morphodynamics and where it makes sense to study spatial patterns of energy dissipation. Within this context the *morphodynamic resilience* of a coastal system is understood by the authors as the ability of a system to absorb changes and disturbances. Thus, the *resilience envelope* indicates the capacity of the system to shift from a narrow to a wide area for energy dissipation (i.e. the breadth of the range over which a system can adapt the surf zone at varying wave energy inputs). In this paper no intentions to detect thresholds for collapse of the system are included.

The morphodynamic approach needs to focus on changes in nearshore features, surf zone adjustments, shoreline evolution, and processes dependant of wave-seabed interaction such as wave dissipation patterns, orbital velocities distribution, wave induced currents, etc. Understanding processes driven by waves under both modal and storm conditions, acquires special relevancy since there are a number of assumptions made on potential behaviour of low energy coasts that may need further investigation. This is the case of storm level energy behaviour in low energy modal environments which, in theory, should present stronger reactions (for instance erosion processes) to higher energy levels than those of coastal settings developed under high energy regimes.

Previous studies have assessed how wave energy dissipation patterns differ from dissipative to reflective beaches and further, how the wave frequencies in the nearshore are distributed (Anthony, 2009). Given that the wave breaker zone is particularly relevant in characterising beach states into either dissipative, reflective or intermediate, the spatial analyses on how the energy is distributed across the shoaling and surf zones under different wave conditions and along different submerged beach topographies is of great relevance. However, most of the research has been devoted in the development and application of beach morphodynamic state models (e.g. Surf Scaling, Dean Parameter), which are insufficient to understand beach behaviour when conditions are controlled by a complex scenario such as geological control, wide ranges of energy dissipation and or heavily fluctuating sediment sourcing (Loureiro *et al.* 2013).

This paper aims to investigate morphodynamic changes derived from storm events in high and low energy environments based on the analysis of wave energy dissipation profiles, and further to provide a preliminary assessment on the amplitude of the envelope for balance in coastal systems based on the concept of coastal morphodynamic resilience.

## STUDY AREA

Wave climate and coastal morphologies change significantly between nearby locations along the coast of Andalusia where Atlantic and Mediterranean beaches are exposed to different wave typologies and energies, wind climate and storms events. Thus, local dynamics and mechanisms of wave energy dissipation depend on many factors: the wave climate, the physical features of the cross-shore profile and the beach morphological profile (e.g. surf zone) among others, all of them influencing the patterns of wave energy dissipation and, potentially, beach morphology.

The coast of Andalusia, in southern Spain, is a complex system with two basins facing the Atlantic Ocean in the west and the Mediterranean Sea in the east. Coastal and marine morphologies vary from the Atlantic where a relatively flat and gentle sloping continental platform extends to the 100 m isobath (30–50 km width); whereas in the Mediterranean a steep continental shelf dominates the first 10 km seaward reaching 200 m in depth. Although the Andalusian coast is not influenced by big storms over a large area, it registers an intense storm activity (Guisado *et al.* 2013). Storm events are slightly different among the two coastal exposures of Andalusia: along the Atlantic coast the wide continental platform allows swells to approach from distant low pressure centres with a southwesterly direction bringing storms that have a normal (orthogonal) approach to the SW exposed coastline.

In the Mediterranean coast the fetch is limited and thus sea waves are mostly common. In general, wind climate is characterised by the alternation, almost 50% in the southern part of the Andalusian coast, of westerly and easterly winds. Westerly winds, called *Poniente*, originate in the Atlantic Sea due to low

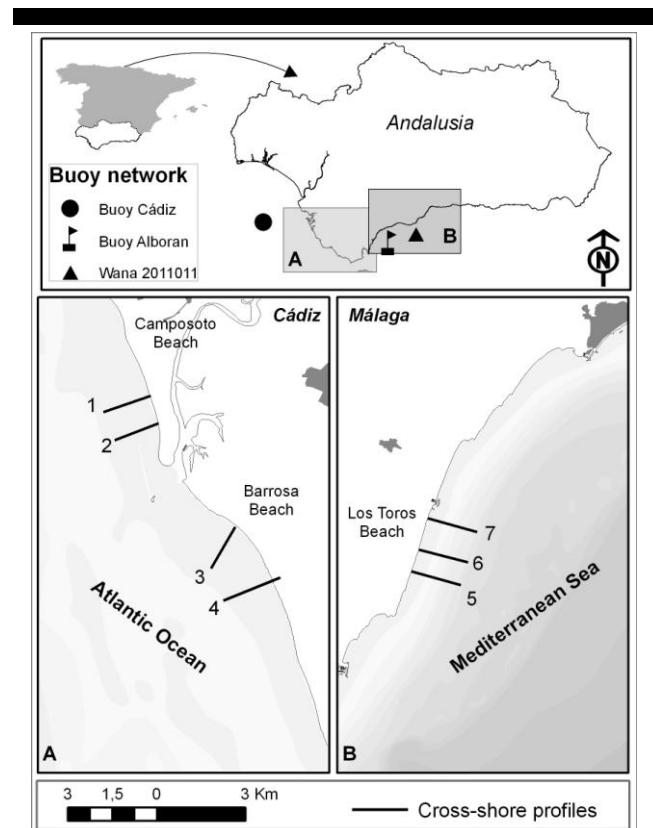


Figure 1. Coastal study sites, offshore buoy network used for climate analysis and cross-shore profiles.

pressure systems and reach the Atlantic coast with WNW and WSW orientations. On the contrary, easterly and south-easterly winds, known as *Levante*, are originally from the Mediterranean Sea. Given these conditions and the wide range of driving energy comprised in a relatively small geographic setting (< 200 km) the duality of coastal environments in Andalusia allowed the direct comparison of two study sites: the Atlantic Coast stretch of Camposoto and Barrosa Beach (Cádiz) with a high-energy dominated setting, and Los Toros beach (Málaga) in a typically low-energy environment of the Mediterranean coast of Andalusia (Figure 1).

### Atlantic coast

The Atlantic coast is characterised by a gentle topography where coastal features such as estuaries, salt-marshes and extensive sand beaches are dominant. Defined as mesotidal and semidiurnal, the tidal range varies from 1 m during neap tides to 4.15 m in the Guadiana river mouth (to the west of the study site). Winds are persistent and intense, with two main components, westerly and easterly, with mean wind speeds of around 5 to 7 m/s. Waves normally have a bi-directional approach, from either the south-east or west, with mean significant wave height (Hs) in winter of 1.90 m and a 7 s period. In contrast, during summer waves rarely exceed 1.07 m and their period is around 5 s. Beaches are composed of fine sediments that range from fine to medium-coarse sand. The beach profiles have mild slopes adjusted to low frequency waves and the surf zone is flat and wide where breakers associated with swell waves are dominant. Thus, beaches are mostly of a dissipative morphodynamic type, sometimes turning into intermediate, with waves breaking in spilling modes that allows sediment transport in a landward direction. This is the case of Camposoto and Barrosa, two Atlantic dissipative beaches exposed to swell waves and occasionally to significant storms.

### Mediterranean coast

The proximity of Sierras to the Mediterranean coastline influences the presence of a narrow continental platform and thus the predominance of coastal cliffs, pocket beaches and delta systems. Tidal range is microtidal (rarely > 1 m) and semidiurnal. Therefore the main hydrodynamic influence on the coast is wave action, characterised by long periods of calm (over 77% per year) in which the wave heights are less than 1 m and periods are short (e.g. 4 s) corresponding with short crested waves originated by local winds and limited fetch (Guisado *et al.* 2013). The wave and wind approach is characterised by the alternation, almost 50%, of westerly and easterly winds. The beach profiles have steep slopes, adjusted to high frequency waves and the surf zone is steep and narrow, with significant depths (e.g. >200 m) reached within 10 km from the coast. The effective fetch is limited to an average 500 km and only rarely do swell waves filter from the Atlantic Ocean. This results in a concentration of wave action on a narrow fringe of steep coastal shelf (Malvárez, 2012). Intermediate to reflective beaches are commonly found in the area, associated with plunging breakers. Los Toros beach, western Málaga, with a NNE-SSE orientation is a typical beach within this Mediterranean setting.

## METHODS

### Storm identification

Wave climate characterization for storm identification consisted in the analysis of a 10 year long wave buoy dataset recorded at Cádiz (offshore buoy) and Málaga (Alborán offshore buoy and WANA 2011011) (SNPA, 2010). Data were logged at 1 h

intervals and included a time series of 85365 wave height and period records acquired between 2000 and 2010 from the offshore buoy network operated by Puertos del Estado (Spanish Ministry of Public Works). The method used to identify storm events throughout the two study cases is based on criteria from previous research (Cook and Prior, 1988; MacClenahan *et al.* 2001). Storms are defined as a climatic event during which Hs exceeds a threshold for a specific period of time. The following criteria were set:  $H_s \geq 2.5$  m for the Atlantic and  $H_s \geq 2$  m for the Mediterranean Sea (following CMA, 2003). The minimum storm duration was set to 12 hours. To separate events, an “independence” criterion of 24 hours was used, in line with the proposal of Rangel-Buitrago and Anfuso (2013). Finally, to characterise the storm record in terms of energy density the Storm Power Index (Dolan and Davis, 1992) was calculated. This is a valuable indicator of storm strength (Li *et al.* 2011). The Index categorises storms in five classes from *Weak* to *Extreme* based on the maximum significant wave height (Hs) and the event duration in hours (td).

### Wave propagation analysis

The SWAN (Simulating WAVes Nearshore) numerical model (Booij *et al.* 1999) was used to simulate the development of wave spectra propagating from deep to shallow water for modal and storm conditions. The input data was the bathymetry, wind speed/direction and wave direction, period and significant wave height. Simulations were carried out along two grids: a 250 x 250 m grid nested into a 40 x 40 m grid for each study site. Computational grids were defined according to offshore buoy location: Alborán buoy and 2011011 WANA for Los Toros Beach and Cádiz offshore buoy for Camposoto / Barrosa beach in the Atlantic coast. In addition, previous calibration analyses were carried out to assess the representativeness of the chosen buoy for the given coastal area. From the model, wave propagation results were obtained for a 40 x 40 m grid including wave energy dissipation and bottom orbital velocities among other wave related parameters.

### Wave energy dissipation analysis

To study the spatial distributions of the wave energy dissipation on both study areas, the output obtained from wave model was placed into a spatial framework using a Geographical Information System (GIS). Based on the wave energy dissipation distribution, from closure depth to shoreline, wave dissipation patterns (peak of energy, distance to the shoreline, surf zone width) along 7 cross-shore profiles were analysed (see Figure 1). At each profile, wave parameters were extracted from the SWAN grid results at 10 m resolution and plotted in bi-dimensional graphs. Statistical analyses were undertaken to interpret the resulting graphs of wave energy dissipation by studying the shape of the curve and the dissipation pattern along the entire cross-shore profile for each location. This took into account the shape of the curve, the location of peaks of energy dissipation, the distance of these peaks to the shoreline and the overall and peak energy related to waves across the shoaling and surf zones.

## RESULTS

### Storm identification analyses

Through the wave climate analysis a characterisation of the modal and extreme wave regime was carried out for both Atlantic and Mediterranean beaches. As expected, modal conditions are more energetic in the Atlantic coast with waves of 1.9 m height

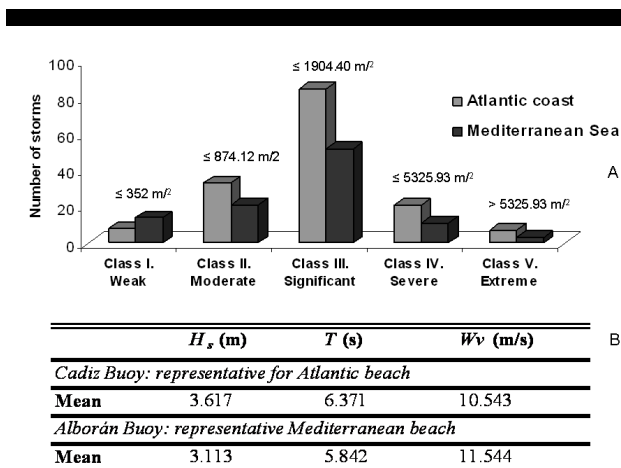


Figure 2. A) Storm Power Index values for Atlantic and Mediterranean coast. B) Mean wave parameters for last decade (2000-2010) storm record.  $H_s$  = significant wave height;  $T$  = wave period and  $Wv$  = wind velocity.

and 7 s periods than in the Mediterranean beach of Los Toros where shorter waves of 1 m height and 5 s are dominant. However, the wave analysis showed that both systems received similar amounts of energy during storm events, though the occurrence in the Mediterranean Sea was more infrequent. In this sense, out of the 20 most energetic storm events that occurred during the past decade in Andalusia, 8 are localised in the Mediterranean Sea and 10 in the Atlantic (Guisado *et al.*, 2013). Once isolated, storms were classified into 5 classes following the parameterisation proposed for the Storm Power Index (Dolan and Davis, 1992). Storms from class I defined as *Weak*, with an estimated storm power of  $\leq 353.22 \text{ m}^2/\text{h}$ , are mainly found in the Mediterranean Sea whereas storms from class II *Moderate* ( $353.22 < \text{storm power} \leq 874.12$ ), class III *Significant* ( $874.12 < \text{storm power} \leq 1904.40$ ), class IV *Severe* ( $1904.4 < \text{storm power} \leq 5325.93$ ) and class V *Extreme* (storm power  $> 5325.93$ ) are more frequent in the Atlantic. These are also likely to occur in the Mediterranean (Figure 2A). Given the direct relationship between the wave height and the designation of a class, *Severe* and *Extreme* events are characterised by waves of around  $H_s$  4.5 m and waves of  $H_s$  2.3 m to 3.3 m are typical of classes I, II and III. Furthermore, analysing the mean wave parameters for each storm record it was found that both coastal environments are exposed to similar energy conditions (Figure 2B), in terms of mean  $H_s$  and wave period reached during storms, though the duration of storms (hours) in the Atlantic are slightly greater. In this sense, offshore storms were found to have similar conditions but different wave/wind directions in both settings. In particular two storms from the records were used to analyse wave energy patterns. For the Atlantic coast the offshore buoy of Cadiz registered waves of 4.7 m height and 9 s period, SW direction, and wind speed of 12.8 m/s during the storm of 24/12/2009; similarly during the storm of the 11/10/2008, waves of 4.7 m and 10 s period, 14.0 m/s wind speed and SE orientation were recorded offshore in the Mediterranean coast.

### Wave energy dissipation patterns

Nearshore wave propagation results showed that under modal conditions in the Mediterranean energy dissipation takes place on the steep foreshore, almost over the shoreline, with a breaking zone that extends no wider than 170 m. The peak of energy

dissipation is  $0.003 \text{ W/m}^2$  and is found around 2 m seaward (50 cm depth), and thus energy dissipation takes place rapidly along a short shallow-water section. On the contrary, Atlantic surf zones are wider under modal conditions (390 m) with a peak of dissipation of  $0.006 \text{ W/m}^2$  occurring at around 1 m depth at 40 m away from the shoreline (Table 1, Figure 3A). This dissipation shows a progressive tendency and very low energy values reach the shore.

Results from storms displayed very different patterns to those observed under modal conditions. In both settings a wider surf zone is identified, with a 780 m width at Barrosa and a 600 m width at Los Toros. In terms of wave energy dissipation, the peak occurs at depths of around 2.1 m with  $0.016 \text{ W/m}^2$  for the Atlantic case studied (150 m seaward), whereas a peak of  $0.051 \text{ W/m}^2$  correspond to the Mediterranean beach (at depths of about 3.5 m); and thus differing significantly from what was found under modal conditions (Table 1). Significant shoaling (in terms of wave energy dissipation) seems to occur in Atlantic beaches from 9.5 m and around 10 m in the Mediterranean. These results, induced by wave geometry, imply that the spatial pattern of the Mediterranean beach dissipation is very steep (Figure 3B) reaching the peak at depths of around 3.5 m, whilst the most significant peak is found in the Atlantic profile at 2.1 m. Regarding the morphology of the dissipation, wave energy dissipates in Atlantic beaches following a soft pattern in which gradually small peaks of dissipation are detected. On the contrary, patterns of wave energy dissipation in the Mediterranean are characterised by the existence of a significant peak where most of the energy is dissipated, both in modal and storm conditions.

## DISCUSSION AND CONCLUSIONS

The common assumption that intermediate systems are adjusted to medium-low energy settings suggests that the energy envelope introduced by presence of storms may induce greater stress in the morphodynamic stability of the nearshore. The concept of resilience refers to the ability of a natural system to maintain its structure and function in the event of a hazard or disturbance; (Walker *et al.*, 2004). Moreover, resilience is a measure of the ability of a dynamic system to absorb changes and thus the adaptive capacity it shows (Holling, 1973). This adaptability, inherent to coastal systems, refers to the capacity of being resistant but vulnerable when stress is exceeded. *Morphodynamic resilience* is here measured as a function of wave energy dissipation pattern and surf zone adaptability to varying energy conditions in two coastal systems. Measuring the *resilience envelope* (shifting capacity) of semi-reflective systems, such as the Mediterranean beach of Los Toros, could help to establish when these systems become unstable and may potentially enter into a new phase beyond dynamic equilibrium. In this sense, it could be questioned whether low energy settings are more or less susceptible to storm

Table 1. Overview of the preliminary results of wave energy dissipation patterns. Sw=surf zone width; Peak= peak of wave energy dissipation; Sd=Shoreline distance of maximum dissipation and Depth= depth of maximum dissipation.

Parameter	Sw (m)	Peak ( $\text{W}^2/\text{s}$ )	Sd (m)	Depth (m)
<i>Atlantic beach</i>				
<b>Modal</b>	390	0.0062	40	0.8
<b>Storm</b>	780	0.0016	150	2.1
<i>Mediterranean beach</i>				
<b>Modal</b>	170	0.0030	2-5	0.5
<b>Storm</b>	600	0.0500	220	3.5

morphodynamic instability (i.e. severe erosion or accretion) than high energy coasts. Which degree of dynamic adaptation could have a coastal system in terms of wave energy input? How much disturbance can a system absorb before switching to an alternate state?

Beaches experience a wide range of morphodynamic states providing widely varying conditions. Furthermore, single average values for storm related beach morphodynamics scarcely represent the environmental conditions of a beach system (Loureiro *et al.* 2013), especially when wave conditions vary abruptly between modal and high energy events as is common on the Mediterranean coasts. Along these lines, the preliminary results presented in this article, based on wave energy dissipation distribution over the surf zone, provide insights on how beaches in high and low-energy environments (typically ranging from dissipative to an intermediate-reflective state) develop the capacity to adapt and adjust their equilibrium at variable wave energy conditions. This demonstrates that their morphodynamic *resilience envelope* is not only wider than expected for the “low energy” setting, but also somehow as effective as the adaptation typical of dissipative coastal systems. Beaches in Mediterranean shores presented in this

study depict curves for wave energy dissipation under severe storm simulations that are surprisingly efficient. The surf zone during storms seems to cope with higher energy levels through the translation towards deeper water of the most active dissipation area (potentially breaker). This would suggest that intense instability promotes collapsing breaking types, thus enhancing off-shore sediment transport. In comparison, Atlantic beaches seem to modulate wave energy dissipation, spreading various minor peaks all over the shoaling and surf zones. This, although predictable, implies that the higher energy setting provides a permanent buffer to cope with peaks in energy surges (i.e. storms) and very consistent spilling breaker types make storms a mechanism for potential progradation, if the water levels are not influenced by coincidence with high tides and surges.

In the context of resilience, where the key element is the ability to absorb changes, it could be established that the spatial distribution of wave energy dissipation over the extended Mediterranean surf zone shows a significant adaptation capacity. The variability of surf zone extension from modal to storm conditions demonstrates that the system is not immediately collapsing against conditions that may have surpassed all

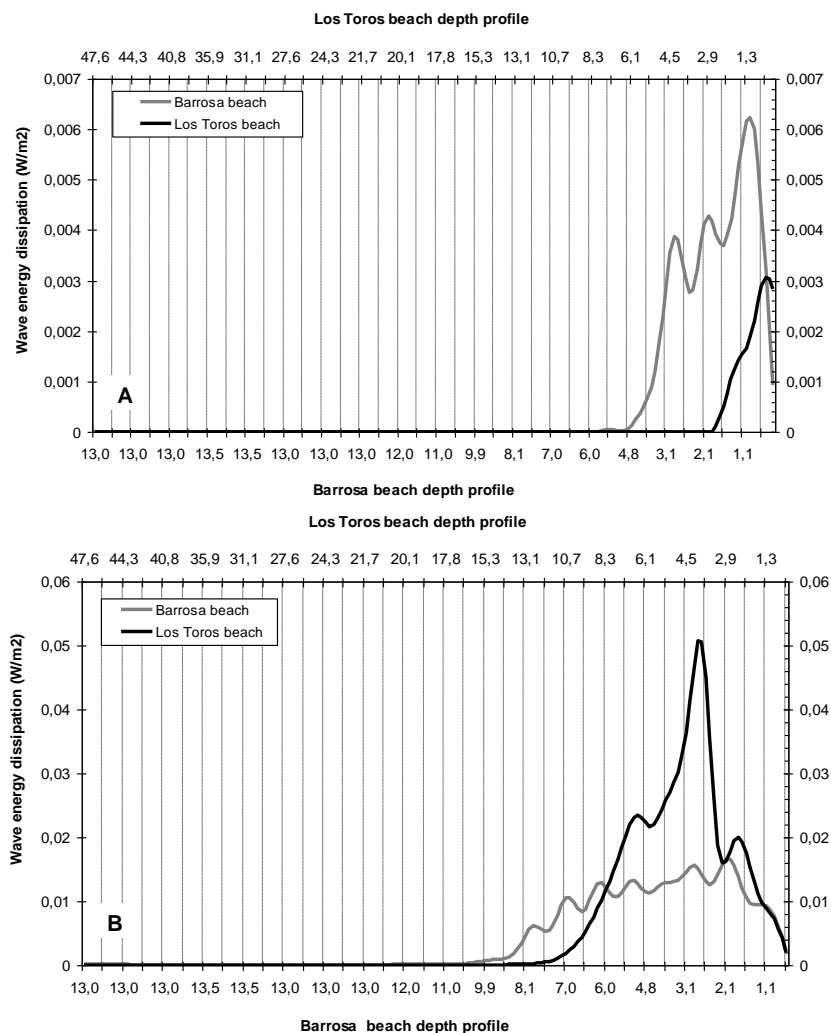


Figure 3. Wave energy dissipation results at cross-shore profiles during modal conditions (A), and storm conditions (B). Results correspond to profile 4 in Barrosa beach and profiles 6 in Los Toros beach.



thresholds given the infrequent occurrence and the extremely low modal energy conditions. The surf zone changes from some 170 m long across modal conditions to over 600 m in the severe storm conditions, yet the maximum peak of dissipation is well away from the shoreline. Wave base moves significantly beyond predicted values of depths potentially inducing currents in deeper zones that are commonly predicted for coastal engineering design. Atlantic beaches also show an expansion of the surf zone, but the dissipation morphology remains similar to that found under modal conditions. This is due to wave energy conditions not being as different as those of the Mediterranean. However, resilience implies that beyond a threshold of disturbance, that varies from place to place, the system may collapse. Mediterranean beaches seem to have a high capacity of adjustment independent of the shoreline effects that this adjustment might have (i.e. erosion, sediment remobilisation, flooding). In contrast, the Atlantic showed a narrower range of energy adaptation. Nevertheless, the effect of storm groups for beach recovery is paramount to assess morphodynamic effects on beaches associated with erosion (Ferreira, 2004). In addition the analysis of recovery pace and collapse thresholds is important; results on energy dissipation patterns suggest despite the fact that Mediterranean beaches show more adaptability, the cumulative impact of storms could produce a significant effect on the morphodynamics, greater than for the Atlantic.

The following conclusions can be drawn:

- **A new approach** to understand beach morphodynamics is proposed and applied to Atlantic (high-energy) and Mediterranean (low-energy) beaches in Southern Spain. Preliminary results showed that the analysis of wave dissipation patterns provides insights about the width of the beaches' active morphodynamic zones.
- **Results show differences** in the *morphodynamic envelope* between low and high energy settings through the variation of wave energy dissipation patterns across the studied profiles. Furthermore, detailed analysis on the surf zones helps in identifying the adaptation of the two, apparently opposite, beach environments. This is the case of storm level energy behaviour in low energy environments which, contrary to what was expected, adapt their surf zones similarly to the way coastal settings developed under high energy regimes do.
- **Given that beach state models** are proven insufficient for characterising beaches under wave energy fluctuations, intermediate states and geologically controlled coastal systems (Loureiro *et al.* 2013), new considerations based on the characterisation of wave energy dissipation patterns and *morphodynamic resilience* could be used in combination with classical methods.
- **Further studies** should assess the effect of storm groups and extreme events in *morphodynamic resilience* in low and high energy settings, beach recovery analysis and the medium-term effects in shoreline and beach evolution.

## LITERATURE CITED

- Anthony, E.J., 2009. Shore processes and their palaeoenvironmental applications. Oxford: Elsevier, 519 p.
- Backstrom, J.T., Jackson, D.W.T., Cooper, J.A.G. and Malvárez, G.C., 2008. Storm-Driven Shoreface Morphodynamics on a Low-Wave Energy Delta: The Role of Nearshore Topography and Shoreline Orientation. *Journal of Coastal Research*, 24 (6), 1379-1387.
- Benavente, J., Del Río, L., Anfuso, G., Gracia, F.J. and Reyes, J.L., 2002. Utility of morphodynamic characterization in the prediction of beach damage by storms. In: Cooper, J.A.G. y Jackson, D.W.T. (eds), *Proceedings of the 7th International Coastal Symposium (ICS)*, (Northern Ireland, United Kingdom), *Journal of Coastal Research*, Special Issue No. 36, pp. 56-64.
- Booij, N., Ris, R.C. and Holthuijsen, L.H., 1999. A third generation wave model for coastal regions, Part I, Model description and validation. *Journal of Geophysical Research*, 104 (C4), 7649-7666.
- Carter, R.G.W. and Stone, W.G., 1989. Mechanisms associated with the erosion of sand dune cliffs, Magilligan, Northern Ireland. *Earth surface and Landforms*, 14, 1-10.
- CMA (Consejería de Medio Ambiente), 2003. *Informe de Medio Ambiente de Andalucía (IMA)*. Junta de Andalucía, 495 pp.
- Cook, N.J. and Prior, M.J., 1988. Extreme wind climate of the United Kingdom. *Journal of Wind Engineering and Industrial Aerodynamics*, 28, 11-20.
- Dolan, R., and Davis, R.E., 1992. An intensity scale for Atlantic coast northeast storms. *Journal of Coastal Research*, 8, 352-364.
- Dorsch, W., Newland, T., Tassone, D., Tymons, S., and Walker, D., 2008. A statistical approach to modeling the temporal patterns of ocean storms. *Journal of Coastal Research*, 24 (6), 1430-1438.
- Fenster, M. and Dolan, R., 1994. Large-scale reversals in shoreline trends along the U.S. mid-Atlantic coast. *Geology*, 22, 543-546.
- Ferreira, O., 2004. Storm groups versus Extreme Single Storms: Predicted Erosion and Management Consequences. *Journal of Coastal Research*, 42, 221-227
- Gómez-Pujol, L., Orfila, A., Cañellas, B., Álvarez-Ellacuría, A., Méndez, F.J., Medina, R. and Tintoré, J., 2007. Morphodynamic classification of sandy beaches in low energetic marine environment. *Journal of Marine Geology*, 242, 235-246.
- Guisado, E., Malvárez, G. and Navas, F., 2013. Morphodynamic environments of the Costa del Sol, Spain. In: Conley, D.C., Masselink, G., Russell, P.E. and O'Hare, T.J. (eds.), *Proceedings 12th International Coastal Symposium* (Plymouth, England), *Journal of Coastal Research*, Special Issue No. 65, pp. 500-505.
- Holling, C. S., 1973 Resilience and stability of ecological systems. *Annual Review of Ecology and Systematics* 4, 1-23.
- Komar, P. and Allan, J.C., 2008. Increasing hurricane-generated wave heights along the U.S. East Coast and their climate controls. *Journal of Coastal Research*, 24 (2), 479-488.
- Li, F., Roncevic, L., Bicknell, C., Lowry, R. and Ilich, K. 2011. Interannual variability and trends of storminess Perth, 1994-2008. *Journal of Coastal Research*, 27 (4), 738-745.
- Loureiro, C., Ferreira, O. and Cooper, J.A.G., 2013. Applicability of parametric beach morphodynamic state classification on embayed beaches. *Marine Geology*, 346, 153-164.
- MacClenahan, P., Mackenna, J., Cooper, J.A.G. and O'Kane, B., 2001. Identification of highest magnitude coastal storm events over Western Ireland on the basis of wind speed and duration Thresholds. *International Journal of Climatology*, 21, 829-842.
- Malvárez, G.C., 2012. The history of Shoreline Stabilisation on the Spanish Costa del Sol. In: Cooper A. and Pilkey J. (ed.), *Pitfalls of Shoreline Stabilization: Selected Case Studies*. Springer Netherlands, pp 235-249
- Morton, I., Bowers, J., and Mould, G., 1997. Estimating return period wave heights and wind speeds using a seasonal point process model. *Coastal Engineering*, 26, 251-270.
- Phillips, M. and Crisp, S., 2010. Sea level trends and NAO influences: the Bristol Channel/Seven Estuary. *Global and Planetary Change*, 73,211-218.
- Pruszek, Z., Szymkiewicz, P., Ostrowski, R., Skaja, M. and Szymkiewicz, M., 2008. Shallow-water wave energy in a multi-bar coastal zone, *Oceanologia*, Vol. 50 (1), 43-58.
- Rangel-Buitrago, N. and Anfuso, G., 2013. Winter wave climate, storms and regional cycles: the SW Spanish Atlantic coast. *International Journal of Climatology*, 33 (9), 2142-2156.
- Rodríguez, A., Ruiz, F., Caceres, L.M., Rodriguez, J., Pino, R. and Muñoz, J.M., 2003. Analysis of the recent storm record in the south western Spanish coast: implications for littoral management. *The Science of Total Environment*, 303, 189-201.
- SNPA, Spanish National Port Authority, 2010. Wave and wind data records. Oceanographic Database. Eds Public Works Ministry.
- Walker, B. H., Holling, C. S., Carpenter, S. and Kinzig, A., 2004. Resilience, adaptability, and transformability in social-ecological systems. *Ecology and Society*, 9(2), art.5.

Zhang, K., Douglas, B. C. and Leatherman, S. P., 2002. Do storms cause long-term beach erosion along the U.S. East Barrier Coast?. *Journal of Geology*, 110, 493-502.

## Hurricane Isaac storm surge deposition in a coastal wetland along Lake Pontchartrain, southern Louisiana

Kam-biu Liu<sup>†</sup>, Terrence A. McCloskey<sup>‡</sup>, Thomas A. Bianchette<sup>+</sup>, Gregory Keller<sup>∞</sup>, Nina S.N. Lam<sup>#</sup>, Jaye E. Cable<sup>@</sup>, Jill Arriola<sup>§</sup>

<sup>†</sup>Dept of Oceanography and Coastal Sciences  
Louisiana State University  
Baton Rouge, LA, USA, 70803  
kliu1@lsu.edu

<sup>‡</sup> Dept of Oceanography and Coastal Sciences  
Louisiana State University  
Baton Rouge, LA, USA, 70803  
tmcclo1@tigers.lsu.edu

<sup>+</sup> Dept of Oceanography and Coastal Sciences  
Louisiana State University  
Baton Rouge, LA, USA, 70803  
tbianc1@tigers.lsu.edu

<sup>∞</sup>Dept of Geology and Geophysics  
Louisiana State University  
Baton Rouge, LA, USA, 70803  
gkelle6@lsu.edu

<sup>#</sup> Dept of Environmental Sciences  
Louisiana State University  
Baton Rouge, LA, 70803  
nlam@lsu.edu

<sup>@</sup>Dept of Marine Sciences  
University of North Carolina  
Chapel Hill, NC, USA, 27599  
jecable@email.unc.edu

<sup>§</sup>Dept of Marine Sciences  
University of North Carolina  
Chapel Hill, NC, USA, 27599  
arriola@email.unc.edu



[www.cerf-jcr.org](http://www.cerf-jcr.org)



[www.JCRonline.org](http://www.JCRonline.org)

### ABSTRACT

Liu, K., McCloskey, T.A., Bianchette, T.A., Keller, G., Lam, N.S.N., Cable, J.E., Arriola, J. 2014. Hurricane Isaac Storm Surge Deposition in a Coastal Wetland along Lake Pontchartrain, Southern Louisiana. In: Green, A.N. and Cooper, J.A.G. (eds.), *Proceedings 13<sup>th</sup> International Coastal Symposium* (Durban, South Africa), *Journal of Coastal Research*, Special Issue No. 70, pp. 266-271, ISSN 0749-0208.

Hurricanes play an important role in shaping the coast of Louisiana. Although the sedimentary signatures of hurricane deposits have been documented in several different coastal environments along the northern Gulf coast, no studies have as yet documented the signatures in wetlands adjacent to large, inland brackish water bodies. In this paper we present results of a case study documenting the distribution and characteristics of storm surge deposits related to Hurricane Isaac (2012) in a wetland on the western shore of Lake Pontchartrain, Louisiana. Hurricane Isaac, a category 1 storm, made landfall near the mouth of the Mississippi River on August 28, 2012. Due to its large size and slow movement, Isaac generated strong easterly winds across Lake Pontchartrain, producing a large storm surge along the west shore of the lake and unprecedented flooding in the surrounding lowlands. Loss-on-ignition, XRF, radioisotopic, and grain-size analyses conducted on sediment cores and surface samples from the area identify two distinct sedimentary signatures for the Hurricane Isaac deposits. Near the lake shore the signature is characterized by a laminated silty sand with a geochemical profile closely resembling that of lake bed material. Storm deposits located in a brackish swamp ~ 1km inland consist of a dark, low-organic mud with low concentrations of terrestrial metals and elevated concentrations of Br, S, and Cl. Differences in the storm signal are explained by the differing effect of topographical features on the depositional and transportation processes occurring at the two sites. Utilizing the geochemical/compositional signatures as a hurricane-generated storm surge proxy indicates the possible occurrence of a similar event predating the historical record.

**ADDITIONAL INDEX WORDS:** *Paleotempestology, Hurricane Isaac, storm surge, storm deposit, wetland sedimentation, Lake Pontchartrain, Louisiana.*

### INTRODUCTION

Coastal erosion has been a very serious problem in Louisiana for decades (Barras et al., 2008). Although many of the proximate causes such as subsidence, sea level rise, and landward transgression of salinity are gradual processes, erosion often occurs in pulses, driven by the passage of tropical cyclones (TCs), particularly hurricanes (<http://coastal.er.usgs.gov/hurricanes/isaac/coastal-change/>). Because of the importance of these TC-generated geomorphic changes, including a debate over the relative importance of hurricane-delivered sediments and their effect on marsh elevation (Turner et al., 2006; Törnqvist et al., 2007), several studies have investigated the depositional signatures of TCs along the northern Gulf coast. Studied

environments include coastal wetlands (Turner et al., 2006), a deltaic marsh (Reese et al., 2008), a backbarrier lagoon (Liu et al., 2011), and beach-ridge plains (Williams, 2009, 2011). However, as the severely indented coastline of Louisiana is immensely varied, consisting of a large number of bays, lakes, marshes and swamps that vary greatly in terms of size, salinity, vegetational communities and degree of fluvial influence, it can be expected that geomorphic response to TCs will also vary by location and environment type. Therefore, expanding the spectrum of environments for which depositional signatures of TCs are known is an important objective, in order not only to improve our ability to accurately assess the geomorphologic impact of TCs, but also increase our understanding of the sedimentary processes involved. In this study we advance this objective by examining the geochemical and stratigraphic characteristics of material deposited

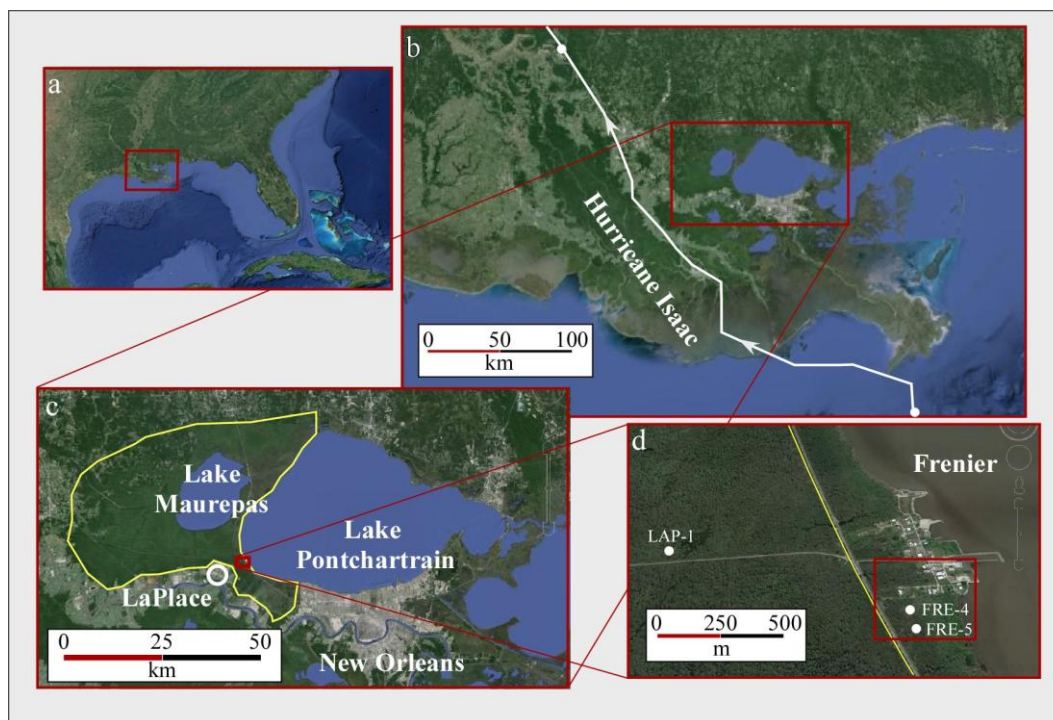


Figure 1. Location of study site. Google Earth imagery displays a), the northern Gulf of Mexico, b), southeastern Louisiana, c), the western margin of Lake Pontchartrain, d) the community of Frenier, showing the locations of cores LAP-1, FRE-4 and FRE-5, and the elevated rail line (marked in yellow). The white line in b) represents the track of Isaac during the 36 hour period from 5 PM, August 28 (lower white dot) through 5 AM, August 30 (upper white dot). The red box in d) is the area displayed in Figure 2.

by Hurricane Isaac (2012) in a wetland on the margins of Lake Pontchartrain in southern Louisiana.

### STUDY SITE

Lake Pontchartrain is a large (1,600 km<sup>2</sup>), shallow (~4 m) oval-shaped brackish lagoon lying east of the Mississippi River just north of New Orleans (Li et al., 2008). As the lake receives freshwater input along the northern and western edges and is connected to the Gulf of Mexico by a few small openings along the eastern edge, salinity decreases from east to west. Immediately to the west of Lake Pontchartrain and connected to it by two narrow passes lies Lake Maurepas, a smaller (240 km<sup>2</sup>), shallower (~3 m), and fresher lake (Keddy et al., 2007). An extensive wetland, occupied by cypress swamps and bottomland hardwood forests, surrounds Lake Maurepas, extending from the western edge of Lake Pontchartrain to the city of LaPlace, located on the eastern bank of the Mississippi River (Figure 1c). During Hurricane Isaac the entire area suffered unprecedented flooding, forcing the closure of the interstate highway in LaPlace, and requiring the evacuation of trapped residents in several neighborhoods (Boquet, 2012; Thibodeaux, 2012). Frenier is a small community located in a bottomland hardwood forest along the western edge of Lake Pontchartrain. A raised (~2 m) railroad line runs parallel to the lake's shoreline ~250-400 m inland behind the community (Figures 1, 2). Although Frenier regularly floods during tropical cyclones, local residents relate that the inundation associated with Isaac was significantly deeper and longer-lasting than for other recent events (Hurricanes Katrina, 2005; Rita, 2005; Gustav, 2008) (L. Lipps, personal communication).

We extracted cores from two sites in the area. Core LAP1 was extracted ~1 km west of Lake Pontchartrain in a low area consisting of a mix of cypress swamp, innumerable black-water ponds, and hardwood forest, with a water table generally at or above ground level (Figure 1d). Cores FRE4 and FRE5 were extracted from the area immediately around the community of Frenier, which is much dryer, with no open water. Our coring sites in this area were selected to capture the area of maximum storm surge and wave energy as determined by the spatial distribution of the storm debris, with cores FRE4 and FRE5 taken from the area most heavily covered by hurricane debris (Figures 1d, 2).

### HURRICANE ISAAC

Hurricane Isaac made landfall near the mouth of the Mississippi River on August 28, 2012 as a category 1 hurricane, with maximum sustained wind speed of 70 kts (Berg, 2013) (Figure 1b). However, due to an unusual combination of features, both the societal and biophysical effects of this storm greatly exceeded the norm for hurricanes of this magnitude along the northern Gulf coast. Isaac was a very large storm; tropical-storm-force winds extended >320 nautical miles at landfall. It was also a very slow moving storm, at times remaining either stationary and drifting backwards on its path. This resulted in an extremely long duration for sustained tropical force winds (up to 45 hours) in coastal areas, heavy rainfall (>50 cm in New Orleans), and a vast amount of water pushed westward against the southeastern shoreline of Louisiana (Berg, 2013, US Army Corps of Engineers, 2013).

These conditions were powerful enough to force the Mississippi River to flow backwards for 24 hours, with the storm surge



Figure 2. Frenier coring site. Red lines mark the approximate boundaries of a fairly narrow debris field resulting from Hurricane Isaac. As the debris originated in the lakeside buildings, the location and orientation of the field indicate the primary direction (from the northeast) of wind and waves at the time of maximum impact. Cores FRE4 and FRE5 were sited within the debris field.

advancing >300 river miles upstream (US Army Corps of Engineers, 2013). In Lake Pontchartrain the sustained easterly wind piled water against the western shore, and storm surge occurred during a period of already elevated water levels (Berg, 2013, US Army Corps of Engineers, 2013), resulting in unprecedented inundations for the area. In the area immediately surrounding Frenier the elevated rail line acted as a barrier to the free movement of water, resulting in differing depths and durations of inundation for the areas east and west of the line. Although both areas were connected hydrologically during the time of maximum water level, drainage was very different for the two areas. Flood waters in the area east of the rail line were able to drain directly back into Lake Pontchartrain, while the area to the west remained flooded much longer as drainage in that area required a slow traverse across the large wetlands and Lake Maurepas.

## METHODS

Cores FRE4 and FRE5 were extracted by means of a 7.62 cm diameter aluminum push tube. FRE4 reached a depth of 46 cm, the 36 cm of sediments contained in the core indicates that 10 cm of compaction occurred. FRE5 captured the top 30 cm of sediments without compaction. LAP1, extracted with a Russian peat borer, consists of three overlapping sections pulled from within a small (~25 cm diameter) area with a total core length of 119 cm. A sample of surface material, ~5 cm in depth, was obtained at the same location by means of a putty knife.

Peat borer sections and surface samples were photographed in the field. All coring and sampling locations were determined by a handheld GPS unit. Cores were sealed in the field and transported to The Global Change and Coastal Paleoecology Laboratory at Louisiana State University, where they were kept in a cold room (4°C) until opened, at which time the cores were photographed and the composition, structure, color and stratigraphy described. Loss-on-ignition (LOI) analysis was conducted continuously at 1 cm resolution (Liu and Fearn, 2000) to determine water, organic, carbonate, and residual percentages. Grain size analysis was

performed on 38 clastic samples for FRE4 with a Beckman Coulter ls 13 320 laser diffraction particle size analyzer. Sampling resolution was 0.5 cm until a depth of 3 cm, after which material was sampled every cm, except for cm 33. Both the top of LAP1 and the surface material collected from the immediate area were analyzed for the short-lived radioisotopes,  $^7\text{Be}$  ( $t_{1/2} = 53$  days; 477 keV gamma emission) and  $^{234}\text{Th}$  ( $t_{1/2} = 24$  days; 63 keV gamma emission) by gamma spectrometry using an intrinsic germanium well detector (Canberra®) at the University of North Carolina. All sediment material was collected on 9/26/2012, 29 days after Hurricane Isaac made landfall. Sediment samples were shipped to UNC where they were homogenized and packed into 10-mm diameter gamma vials. Samples were counted within 1 to 3 months of collection for 1 to 2 days each. Total  $^{234}\text{Th}$  and  $^7\text{Be}$  activities were determined on all samples and corrected using the detector efficiency for each gamma peak as determined from counting standard reference material calibrated by the International Atomic Energy Agency (IAEA-300 marine sediment). Supported  $^{234}\text{Th}$  was determined after greater than six half-lives of  $^{234}\text{Th}$  had passed and the excess  $^{234}\text{Th}$  activity had decayed to less than 1%. Sediments were recounted and the remaining  $^{234}\text{Th}$  was taken as the supported activity. Supported  $^{234}\text{Th}$  was deducted from the total  $^{234}\text{Th}$  (first count), and the excess  $^{234}\text{Th}$  and  $^7\text{Be}$  activities are reported as decay-corrected to the time of collection ( $\pm 1\sigma$  analytical error). We evaluate the new or event deposition based on the presence and magnitude of these decay-corrected activities. Elemental concentrations were determined for four sediment samples taken from the bed of Lake Pontchartrain in front of the study site and for all three cores at 2 cm resolution by a Delta Premium DP-4000 X-ray fluorescence (XRF) analyzer. A small quantity of gray clay from a depth of 101 cm in LAP1 was sent to Beta Analytic, Inc. in Miami, FL, USA for bulk sediment radiocarbon dating. Dates were calibrated to calendar years with the Calib 6.0 program (<http://calib.qub.ac.uk/calib/calib.html>), using the Reimer *et al.* (2009) dataset.

## RESULTS

### LAP1 and surface samples

LAP1 is dominated by a very uniform grayish-brown, low-organic clay. Except for a minor peak in organics at 90 cm, from 13-101 cm there is no significant stratigraphic change, with very little variation in either the wet weight percentages of water (30-40%), or the dry weight percentages of organics (seldom above 7%), carbonate (always <3%), or residual (generally >90%). However, both the top 12 cm and the bottom 17 cm do display clear stratigraphic changes. The top 4 cm are a slightly organic (13-22%) mud, with water content from 64-75%. The next four cm (5-8) are much wetter (water percentages >80%) and more organic (32-65%). From 8-12 cm, water and organic values decrease to levels only slightly above that associated with the clay, which begins at 13 cm (Figure 3). A similar pattern occurs at the bottom of the core, as below 101 cm organic and water percentages first rise, reaching values of 28% and 65% respectively at 107 cm, and then drop, until by 111 cm water and organic levels are only slightly higher than the clay. Another very small organic rise occurs at 118-119 cm at the very bottom of the core.

Shifts in elemental concentrations mirror these compositional changes, as the core top and bottom share an elemental signature, which is distinctly different from the clay signature. The clay interval occupying the middle of the core is characterized by high

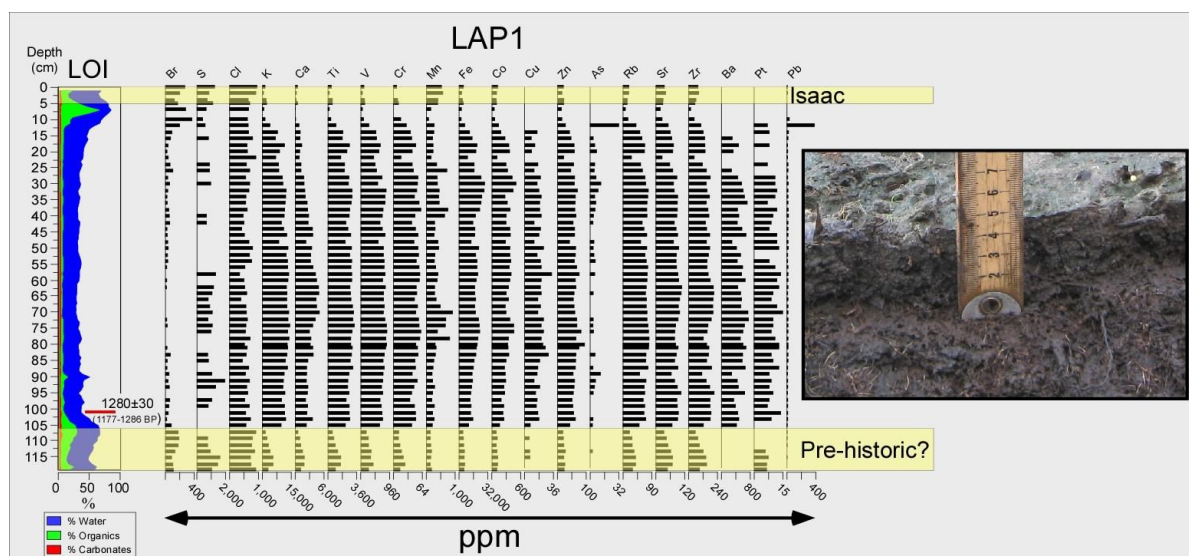


Figure 3. Core LAP1. LOI curves (left) display water, organic and carbonate contents of the core at 1-cm resolution, resolution of concentrations of selected elements (center) is 2 cm. Photo (right) shows the sharp contact between the ubiquitous mud layer found around LAP1 and the underlying organic material.  $^7\text{Be}$  analysis shows the mud layer to have been deposited shortly before the time of collection, which occurred 29 days after the passage of Hurricane Isaac. The  $^{14}\text{C}$  age and the  $2\sigma$  calibrated date range are listed next to a red bar indicating the depth of the sample (101 cm) on the LOI curves (left).

concentrations of such terrestrial metals as Ti, V, Cr, Fe, and Zn, and low concentrations of Br, Sr, and Ca, while the more organic sections at the top and bottom of the core display the reverse pattern (Figure 3).

The bulk sediment sample from 101 cm in LAP was dated at  $1280 \pm 30$   $^{14}\text{C}$  yr BP, which calibrates to a single calendar date range of 1177-1286 BP (Table 1). Significant amounts of both  $^7\text{Be}$  and  $^{234}\text{Th}$  were found to be present in all four samples that were analyzed, with  $^7\text{Be}$  values ranging from 2.47 to 8.37 dpm/g and  $^{234}\text{Th}$  values ranging from 1.30 to 34.1 dpm/g (Table 2).

### FRE4, FRE5

FRE4 and FRE5 have very similar chemical elemental profiles (Figure 4). A thin section of laminated brown sandy material at the top of each core (3 cm thick in FRE4, 2 cm in FRE5) is characterized by extremely low water and organic percentages, (in fact, in both cores both water and organics values reach core minima in this interval). These sediments occur immediately above rooty silt intervals (from 4-12 cm in FRE4, from 3-6 cm in FRE5) with either the highest water and organic values (FRE4) or

four cm is the largest in the core (Figure 4). Elemental concentrations in the uppermost unit in both FRE4, and FRE5 are markedly different from downcore material, although achieving a good match with sediment samples taken from the lake bed immediately off shore, having much higher concentrations of Ca,

Table 2. Shortlived radioisotopic results for samples from the LAP1 site.

Sample	Depth (cm)	$^7\text{Be}$ (dpm/g)	$^{234}\text{Th}$ excess (dpm/g)
Surface sample	0-1	$3.55 \pm 0.17$	$1.30 \pm 0.19$
	1-2	$8.37 \pm 0.17$	$3.56 \pm 0.19$
LAP1	0-4	$6.96 \pm 0.42$	$11.57 \pm 0.85$
	4-7	$2.47 \pm 0.44$	$34.05 \pm 0.77$

Sr, Zr, and Mn and lower concentrations of Fe, Co, and Br than other core material (Figure 5).

## DISCUSSION

### Sedimentary signatures

$^{234}\text{Th}$  and  $^7\text{Be}$  are short-lived, particle reactive radionuclides.  $^7\text{Be}$  is derived from cosmic ray spallation in the upper atmosphere and is deposited on the earth's surface during precipitation events.  $^{234}\text{Th}$  is a daughter of the ubiquitous primordial earth element,  $^{238}\text{U}$ , and occurs in excess of its  $^{238}\text{U}$  parent when sediment is washed into an area from another location. Because both radionuclides appear in sediments from an external source, we can use them to evaluate the initiation of an event and/or ascertain how rapidly sediments were deposited. The presence of these isotopes within the mud layer at the top of LAP1 constrains the

Table 1. Radiocarbon results for the bulk sediment sample from core LAP1.

Lab #	Core	Depth (cm)	Age $^{14}\text{C}$ yr BP	Age (2 $\sigma$ ) Cal yr BP	%
360464	LAP1	101	$1280 \pm 30$	1177-1286	1

the highest water and second highest organic values (FRE5) in their respective cores. Farther downcore the material is gray silt that transitions into clay near the core bottoms. Occasional intervals with slightly elevated organic values occur. Grain size analyses conducted on FRE4 indicate that the material in the top

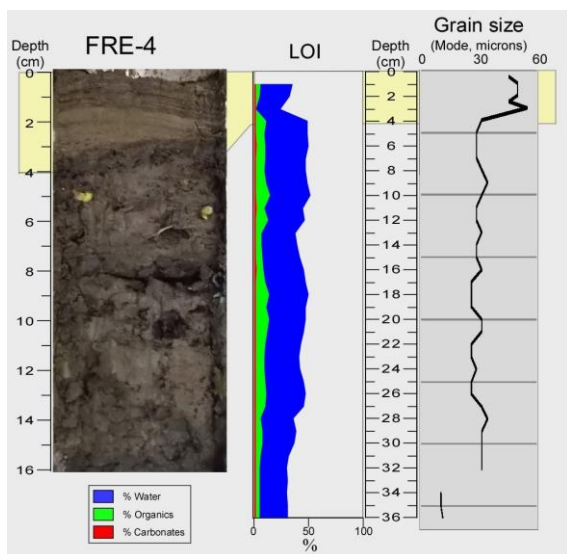


Figure 4. Core FRE4. LOI curves for FRE4 (middle) show a distinctive dip in the top four cm (shaded box), which presents as a laminated clastic material (top left), with appreciably larger grain size.

date of the initiation of deposition of this layer to a point in time shortly before our collection, which occurred 29 days after Hurricane Isaac made landfall. Additionally, the high activities of both excess  $^{234}\text{Th}$  and  $^7\text{Be}$  indicate that the sediments were deposited over an extremely short time span. The contact between this material and the underlying higher-organic sediments is both visually striking and ubiquitous among samples; random sampling in the area surrounding LAP1 produced nearly identical results at multiple sites. Often a layer of well-preserved intact leaves and forest debris could be observed immediately below the mud. The dramatic stratigraphic mismatch between the mud cap and the underlying material is paralleled by equally clear differences in elemental concentrations, which are marked by a downcore increase in terrestrial metals and a decrease in Br, S, and Cl (Figure 3). The most likely interpretation of this sequence is that the surficial mud was deposited by Hurricane Isaac and that the more organic underlying layer represents the forest floor at the time of the storm. The sedimentary signature at LAP1 seems clear; namely a dark, low-organic mud, with low concentrations of terrestrial metals and high concentrations of Br, S, and Cl.

As at the LAP1 site, the surface units in the Frenier cores display major differences with the underlying material in terms of grain size, color, texture, and structure, as seen in FRE4 (Figure 4). FRE5 exhibits a nearly identical stratigraphy, capped by the same unique top unit. It seems reasonable to identify these anomalous surface units as Hurricane Isaac storm deposits. Their elemental profiles suggest that a significant portion of this material was derived from lake bed material. The signature of this deposit is characterized by a light-colored, low-organic, laminated silty sand with high concentrations of Ca, Sr, Zr, and Mn, and low concentrations of Fe, Co, and Br. This does not match the signature from LAP1.

## Topographic/geographic controls

The fact that we have clear, but differing, sedimentological/geochemical storm signals for the two locations raises some interesting avenues of investigation. Because both signatures originated with the same event, the differences must be due to variations in the effects of the transportation and/or depositional processes. Investigating these differences should therefore help us better understand the working of these processes during tropical cyclones.

Geographical and topographic features can exert important control over the hydrodynamics of storm waves and the movement of water during periods of sustained flooding (Bianchette *et al.*, 2009). Of particular importance in this case is the elevated rail line just to the west of Frenier. Roughly ~2 m in height, the road bed acted as an effective barrier to water movement and the transport of materials during Isaac, as evidenced by the stranding of a small fishing boat and large cargo container on the lake side of the embankment by the storm. This suggests that large-grained traction load material would not have been transported inland of the rail line. The presence of this barrier also likely complicated wave and sedimentation patterns east of the rail line, with sediment-laden bottom flow rebounding lakeward after colliding with the embankment. Conceivably, the resulting temporal variability in wave energy and direction and velocity of flow could have contributed to the laminated nature of the storm deposit by affecting the parameters determining the settling of large-grained sediments. Therefore, very different patterns of storm activity may have occurred at the two coring sites. Lakeward of the embankment (FRE4, FRE5), we can hypothesize a turbulent storm surge-driven mixture of nearshore/beach lake bed sediments (light-colored, larger-grained) and loose/dislodged surface material from the bottomland forest, with the energy reflected from the constraining embankment causing erratic movement of both bottom sediments and surface water. After passage of the storm, the relatively quick drainage of the flood water would have carried much of the suspended load back to the lake. However, a very different flood event could have occurred at LAP1, west of the embankment. Due both to distance and the presence of the rail line, only small-grained lake material, carried as suspended load in the upper part of the water column, would have reached the site.

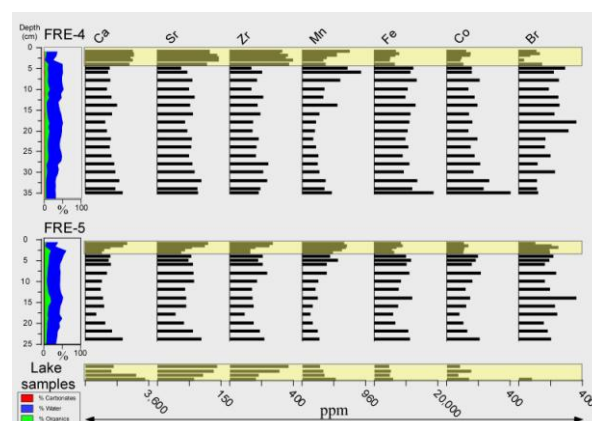


Figure 5. Core FRE4, FRE5 and lake material. The surface units are distinctly different from downcore material, both compositionally and in elemental concentration for both FRE4 (top) and FRE5 (bottom). The elemental concentrations of this material is very similar to that from lake bed samples (bottom).

This lake material would have formed a smaller portion of the total sediment load than at FRE4, FRE5, as the flood waters, though less turbulent, entrained large amounts of the loose, fine-grained dark swamp material forming the forest floor or floating in or resting on the bottom of the small pothole ponds. Much of this material would have subsequently been deposited at the site, after settling out of the water column during the long, slow drainage process.

This variability in the sedimentary response to tropical cyclones highlight the difficulty in creating viable proxies for correctly identifying hurricane events in the sedimentary record. The field of paleotempestology uses such signatures derived from historical storms as sedimentary proxies for establishing multi-millennial landfall records for coastal locations. The ultimate purpose is to correlate these records with known paleoclimatic conditions in order to identify the climatic/atmospheric mechanisms forcing changes in tropical cyclone activity (Liu and Fearn 2000; Donnelly and Woodruff, 2007; McCloskey and Liu, 2012). As nearly all previously described modern analogs have been derived from sea-edge locations, the identification of sedimentary signatures from this inland site may prove useful. The FRE4, FRE5 signature is similar to the common coastal proxy, which uses large-grained, light-colored clastics as a proxy for hurricane-generated overwash lobes. The LAP1 proxy is a bit more subtle. Because the storm deposit consists mainly of autochthonous material (resuspended pond/forest sediments) with a very small marine/lake component, the event layer itself may not be recognizable in the sedimentary record. However, in this case the mud deposit may have created a recognizable, though indirect, proxy by covering, and thereby preserving, the underlying forest surface. This higher-organic sediment, which by a combination of weathering and bioturbation would normally degrade into the featureless, low-organic silty clay found lower in the core, will perhaps, by its burial, be preserved as a distinct layer. Recognizing a buried forest surface layer as marking a hurricane provides another tool for researchers looking to extend the landfall record, particularly, given the necessity of thick draping mud layer at large distances inland, for the identification of extremely large events. A potential candidate layer occurs near the bottom of LAP1, dated to ~1200 yr BP (years before present) (Figure 3), although further investigation is needed.

## CONCLUSIONS

Anomalous surface layers, 2–4 cm in thickness occur over a wide area of forested wetlands on the western edge of Lake Pontchartrain, Louisiana, USA. Short-lived radioisotopic analysis strongly suggests that this material was deposited rapidly, as a unit, at the approximate time of the passage of Hurricane Isaac, a category 1 hurricane which caused unprecedented flooding in the area in August, 2012. The surface layer covering a swamp forest ~1 km inland consists of a dark, low-organic mud, with low concentrations of terrestrial metals and high concentrations of Br, S, and Cl. However, the distinguishing characteristics of the posited storm deposit in a bottomland hardwood forest <300 m inland from Lake Pontchartrain are very different, consisting of a light-colored, low-organic, laminated silty sand with high concentrations of Ca, Sr, Zr, and Mn, and low concentrations of Fe, Co, and Br. The disparity of the storm signals is attributed to differing hydrodynamic conditions that occurred during the storm at the two locations as a result of differences in shore-to-site distance and the presence of a topographic barrier located between the two sites. The lakeside storm signal resembles the signature commonly identified from coastal areas, generated by storm-surge driven overwash lobes. The inland signal, less distinctive due to

the large contribution of autochthonous material, is possibly of little value in itself as a sedimentary proxy. However, the possible ability of the storm deposit to preserve the forest surface creates the potential for the development of a new, indirect proxy.

## ACKNOWLEDGEMENTS

This material is based upon work supported by the National Science Foundation under Grant Number CNH-1212112. Any opinions, findings, and conclusions or recommendations expressed in this material are those of the authors and do not necessarily reflect the views of the National Science Foundation. A special thanks to Nicholas Janzen for help in the field.

## LITERATURE CITED

- Barras, J.A., Bernier, J.C. and Morton, R.A., 2008. Land area change in coastal Louisiana—A multidecadal perspective (from 1956 to 2006). *U.S. Geological Survey Scientific Investigations Map 3019*, scale 1:250,000, 14 p. pamphlet.
- Berg, R. 2013. Hurricane Isaac tropical cyclone report. *National Hurricane Center*, 1-78.
- Bianchette, T. A., Liu, K.B., Lam, N. and Kiage, L. M., 2009. Ecological impacts of Hurricane Ivan on the Gulf Coast of Alabama: A remote sensing study. *Journal of Coastal Research*, SI56, 1622-1626.
- Boquet, J., 2012. Isaac's waters result in 3,500 residents evacuated from St. John Parish. *The New Orleans Times-Picayune*, 8-30-12.
- Donnelly, J. P. and Woodruff, J. D., 2007. Intense hurricane activity over the past 5,000 years controlled by El Niño and the West African monsoon. *Nature*, 447, 465-468.
- Keddy, P.A., Campbell, D., McFalls, T., Shaffer, G.P., Moreau, R., Dranguet, C. and Heleniak, R., 2007. The wetlands of lakes Pontchartrain and Maurepas: past, present and future. *Environmental Reviews*, 15, 43-77.
- Li, C., Walker, N., Hou, A., Georgiou, I., Roberts, H., Laws, E., McCorquodale, J.A., Weeks, E., Li, X. and Crochet, J., 2008. Circular plumes in Lake Pontchartrain estuary under wind straining. *Estuarine, Coastal and Shelf Science*, 80, 161-172.
- Liu, K.B. and Fearn, M.L., 2000. Reconstruction of prehistoric landfall frequencies of catastrophic hurricanes in northwestern Florida from lake sediment records. *Quaternary Research*, 54, 238-245.
- Liu, K.B., Li, C., Bianchette, T. A., McCloskey, T. A., Yao, Q. and Weeks, E., 2011. Storm deposition in a coastal backbarrier lake in Louisiana caused by Hurricanes Gustav and Ike. *Journal of Coastal Research*, SI64, 1866-1870.
- McCloskey, T. A. and Liu, K.B., 2012. A sedimentary-based history of hurricane strikes on the southern Caribbean coast of Nicaragua. *Quaternary Research*, 78, 454-464.
- Reese, C.A., Strange, T.P., Lynch, W. D. and Liu, K.B., 2008. Geologic evidence of hurricane Katrina recovered from the Pearl River Marsh, MS/LA. *Journal of Coastal Research*, 24, 1601-1607.
- Reimer, P.J., Baillie, M.G.L., Bard, E., Bayliss, A., Beck, J.W., Blackwell, P.G., Bronk Ramsey, C., Buck, C.E., Burr, G.S., Edwards, R.L., Friedrich, M., Grootes, P.M., Guilderson, T.P., Hajdas, I., Heaton, T.J., Hogg, A.G., Hughen, K.A., Kaiser, K.F., Kromer, B., McCormac, F.G., Manning, S.W., Reimer, R.W., Richards, D.A., Southon, J.R., Talamo, S., Turney, C.S.M., van der Plicht, J. and Weyhenmeyer, C.E., 2009. IntCal09 and Marine09 radiocarbon age calibration curves, 0–50,000 years cal BP. *Radiocarbon*, 51, 1111–1150.
- Thibodeaux, R. 2012. Hurricane Isaac floodwaters take LaPlace and Slidell by surprise. *The New Orleans Times-Picayune*, 8/30/2012.
- Törnqvist, T.B., Paola, C., Parker, G., Liu, K.B., Mohrig, D., Holbrook, J.M. and Twilley, R.R., 2007. Comment on "Wetland sedimentation from hurricanes Katrina and Rita." *Science*, 316, 201.
- Turner, R.E., Baustian, J.J., Swenson, E.M. and Spicer, J.S., 2006. Wetland sedimentation from hurricanes Katrina and Rita. *Science*, 314, 449-452.
- Williams, H.F.L., 2009. Stratigraphy, sedimentology, and microfossil content of Hurricane Rita storm surge deposits in southwest Louisiana. *Journal of Coastal Research*, 25, 1041-1051.
- Williams, H.F.L., 2011. Shell bed tempestites in the Chenier Plain of Louisiana: late Holocene example and modern analogue. *Journal of Quaternary Science*, 26, 199-206.
- US Army Corps of Engineers, 2013. Hurricane Isaac with and without 2012 100-year HSDRRS evaluation, Final Report. 230 pp.



# A preliminary study of the distribution, sizes and orientations of large reef-top coral boulders deposited by extreme waves at Makemo Atoll, French Polynesia



[www.cerf-jcr.org](http://www.cerf-jcr.org)

A. Y. Annie Lau<sup>†</sup>, Samuel Etienne<sup>‡\*</sup>, James P. Terry<sup>∞</sup>, Adam D. Switzer<sup>§</sup>, Ying Sin Lee<sup>+</sup>

<sup>†</sup> Department of Geography,  
National University of Singapore,  
AS2, 1 Arts Link,  
Kent Ridge 117570, Singapore  
lauaya@nus.edu.sg

<sup>‡</sup> Ecole Pratique des Hautes Etudes,  
CNRS UMR 8586 Prodig,  
Laboratory of Coastal Geomorphology  
and Environment,  
15, boulevard de la mer  
35800 Dinard, France  
samuel.etienne@ephe.sorbonne.fr

<sup>∞</sup> Department of Geography,  
National University of Singapore,  
AS2, 1 Arts Link,  
Kent Ridge 117570, Singapore  
geojpt@nus.edu.sg

<sup>§</sup> Earth Observatory of Singapore and  
Division of Earth Sciences,  
Nanyang Technological University,  
50 Nanyang Avenue,  
Singapore 639798, Singapore  
aswitzer@ntu.edu.sg

<sup>+</sup> Earth Observatory of Singapore,  
Nanyang Technological University,  
50 Nanyang Avenue,  
Singapore 639798, Singapore

<sup>\*</sup> Laboratoire d'excellence CORAIL,  
"Les récifs coralliens face au changement  
global", CRILOBE, BP 1013, 98729,  
Papetoai, Moorea, Polynésie française



[www.JCRonline.org](http://www.JCRonline.org)

## ABSTRACT

Lau, A.Y.A., Etienne, S., Terry, J.P., Switzer, A.D., Lee, Y.S., 2014. A preliminary study of the distribution, sizes and orientations of large reef-top coral boulders deposited by extreme waves at Makemo Atoll, French Polynesia. In: Green, A.N. and Cooper, J.A.G. (eds.), *Proceedings 13<sup>th</sup> International Coastal Symposium* (Durban, South Africa), *Journal of Coastal Research*, Special Issue No. 70, pp. 272-277, ISSN 0749-0208.

The history of extreme wave events on the Tuamotu Archipelago of French Polynesia in the central South Pacific remains poorly understood, even though huge wave deposited coastal boulders were identified in the area decades ago. Numerous large coral boulders deposited on the reef flats of Makemo Atoll (16.56°S, 143.73°W) were investigated in this study in an attempt to understand the characteristics of extreme wave events in the region. The positions, dimensions and orientations of 286 boulders were measured along over 15 km of the northern coastline of the atoll. The biggest clast measures over 130 m<sup>3</sup> in size and it weighs more than 310 tonnes. The size-distribution of the Makemo boulders suggests that these huge clasts were transported by extreme storm waves. The long-axes of boulders are mostly aligned parallel to sub-parallel to the shoreline. However, a relationship between the boulder size and orientation was not found, suggesting the orientation of boulders is not representative of boulder transport mode.

**ADDITIONAL INDEX WORDS:** *Storms, Tropical cyclones, South Pacific islands, Boulder transport, Extreme waves*

## INTRODUCTION

Reef-derived boulders deposited on reef flats are valuable geomorphological features indicating the occurrence of extreme wave events in the past (e.g. Noormets *et al.*, 2002, 2004; Scheffers *et al.*, 2002; Goto *et al.*, 2009; Etienne *et al.*, 2011; Richmond *et al.*, 2011; Terry and Etienne, 2011; Engel and May, 2012). The characteristics of individual coastal boulders and boulder fields can be studied to elucidate the behaviour of extreme waves at the coast (Terry *et al.*, 2013). On Makemo, an atoll in the Tuamotu Archipelago of French Polynesia, numerous large coral boulders are present on the reef flat of the northern windward island. This is another boulder field identified in the Tuamotus group, in addition to the huge boulder deposits described on Rangiroa Atoll by Stoddart (1969) and Bourrouilh-Le Jan and Talandier (1985) where a large block measuring 15 x 10 x 5 m which Bourrouilh-Le Jan and Talandier suggested weighed around 1500 tonnes. Recent work by Etienne suggests that the boulder

actually has dimensions of 14 x 8 x 4.5 m and the weight is ~1000 tonnes. Boulders studied on Nukutipipi Atoll were up to 30 m<sup>3</sup> in size and were transported by one of the tropical cyclones during the 1982-83 El Niño Southern Oscillation (ENSO) period (Salvat and Salvat, 1992).

The aim of this research is to assess the risk of extreme marine inundation hazards of the Makemo Atoll and the larger area of the Tuamotu Archipelago, where exceptionally large boulders have been dislodged and emplaced onto the reef platforms. At the Tuamotu Archipelago, the historical record of tsunami is limited (Etienne, 2012). The impact of historical tsunami waves on these atolls seems minimal, as exemplified by small effects of recent trans-Pacific tsunamis, the 2010 Chile and the 2011 Tohoku tsunamis (Reymond *et al.*, 2012). It has been suggested that the steep submarine slope of atolls does not amplify the long period tsunami waves effectively; therefore tsunamis have relatively little effect on the atolls (Vitousek, 1963; Stoddart and Walsh, 1992). However, the atolls of Maldives have received waves up to 1.8 m above mean sea level in the 2004 Indian Ocean tsunami, with geomorphic changes of the atoll islands widely observed, flooding

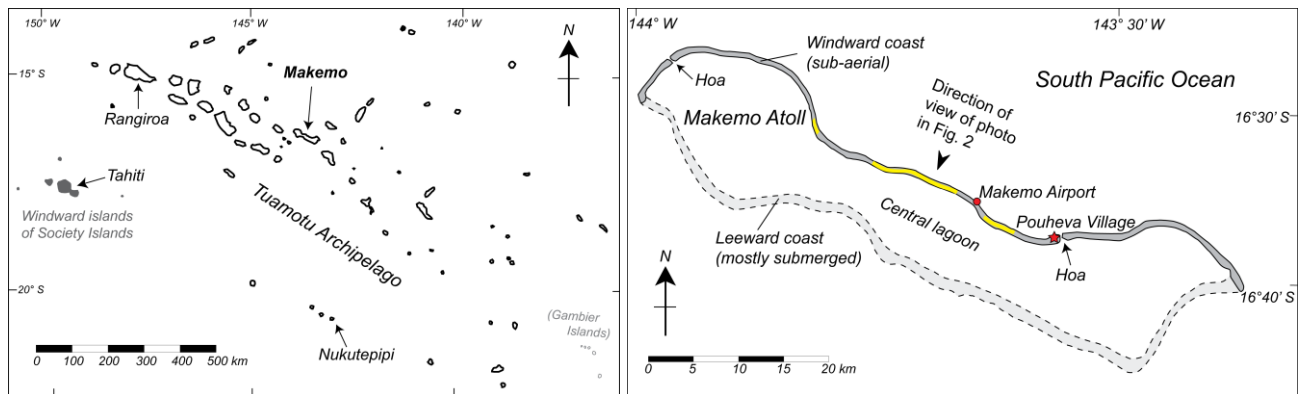


Figure 1. (Left) Location map of Makemo in the Tuamotu Archipelago. Rangiroa and Nukutepipi are the other two atolls with large coastal boulder deposits reported. (Right) Makemo Atoll of Tuamotu Archipelago, French Polynesia in the Central South Pacific. It consists of the windward low islands at the NE coast, a central lagoon and the mostly absent leeward shore at the SW. There are only 2 hoia (passages) connecting the lagoon to the open sea. Parts of the reef flat at the NE shore (indicated by 3 sections with yellow shades) were visited for boulder data collection.

and destruction of Male city and its infrastructure, and the loss of more than 80 lives in the island nation (Kench *et al.*, 2006, 2008). On the other hand, waves from storms including tropical cyclones and cyclonic swells are more common causes of high-energy marine inundation events in the area. Severe damage and high death tolls from the Tuamotu atolls have been reported in the 1982-1983 tropical cyclone season (Reymond *et al.*, 2012), and swells with amplitude up to 10-15 m have been reported from the same period (Laboute, 1985).

This paper presents the preliminary results from field research on Makemo Atoll, with a focus on the size and distribution of large boulders. We examine whether these are products of storm waves, or could they alternatively be the result of a tsunami event? A discussion of how this type of extreme-wave event moves the boulders, and how it is reflected on boulder orientation and other physical features is also included.

### STUDY AREA

Makemo (16°37'S, 143°40'W) is the fourth largest atoll in the Tuamotu Archipelago. The atoll is NW-SE orientated with an axis length of more than 65 km (Figure 1). Its morphology is asymmetrical with the windward NE coast consisted of low isles with vegetation cover and human habitation, while across the central lagoon the SW leeward coast is almost absent, so that the atoll consists of an arc facing north-east. On the windward coast, wave deposited coral boulders are present on parts of the reef flat of 70-100 m in width, where the reef is expanding by accretion to the open Pacific Ocean to the north (Fig. 2). Makemo is a low-lying atoll, with elevation of the windward islands not exceeding 5 m above sea level. No raised reef or other outcrop is present on the atoll, so the boulders on the reef flat could not be products of mass wasting and are not likely the remnants of the weathered raised reef, but were definitely sourced from the modern reef itself.

The windward shore of Makemo is approximately 65 km in length. Due to limited accessibility and time on the atoll, only a 15 km stretch of the island has been investigated for this research. The visited areas include the coastlines with road access, plus a small area in the west, to which a day trip was taken on a boat to collect data from the large boulders at the site.

### METHODS

#### Field and laboratory methods

Boulders investigated at the visited coasts were chosen mainly based on their size. At the western area (approx. 0.7 km of shoreline) where there is no road access, only the largest clasts were measured due to time constraints. At the other area where more time was available, large and medium-sized boulders were chosen, but clasts with b-axes less than 1 m were generally excluded from the dataset. Nevertheless, 7 smaller boulders of b-axes < 1 m were included because they were deposited significantly far inland, and their presence can reflect the inundation limit of waves.

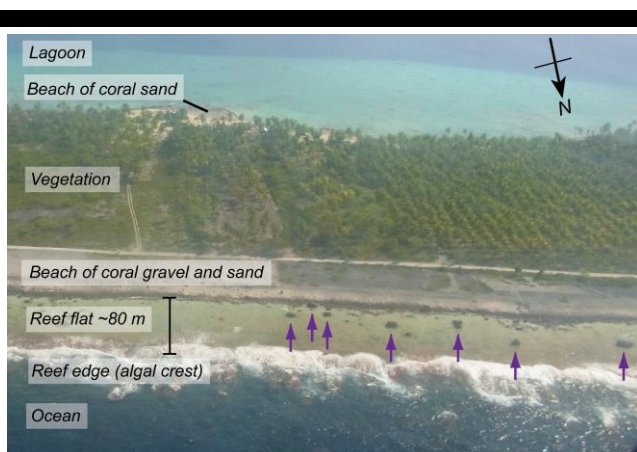


Figure 2. Zonation of geomorphic features on the windward island. Arrows are pointing at coral boulders measured on the reef flat. The largest boulder in this photo (at the right end) measures 7.4 m in length and is oriented almost parallel to the shore / algal crest reef edge.



Figure 3. (Upper) The 2 boulders in the upper picture were evidently transported as one but later broken into 2 pieces at time of emplacement or post-depositional. They are regarded as a whole boulder and were measured and recorded as one for analysis. The sizes of the separated boulders were also recorded, so they could be traced if they are remobilised and repositioned by the next wave event. (Lower) Although these boulders appear to come from an adjacent source from the proximal reef edge, they could be entrained in the flow separately. In such case they are considered as 2 individual boulders for analyses.

For each selected boulder, information was recorded on its (1) dimension in 3 axes measured by tape, (2) orientation of the long (a-) axis, (3) shape, (4) GPS location (*Mobile Mapper 10*; x,y accuracy 0.5 m) and (5) the distance from the algal crest reef edge by a laser range finder. In a case where the distance to the reef edge cannot be measured when an obstruction was present, the distance was estimated from satellite images. In addition to the basic boulder information, the primary coral type, presence of bioerosion, weathering stage of the clast, and the direction of coral growth were recorded where observable. Samples were taken from more than 20 boulders for dating of coral mortality age at a later stage, and also for density measurement. The volume and weight of each sample were measured in the laboratory, hence an average density of these coral samples was applied to calculate the weight of every measured boulder on Makemo based on their volume estimated based on their shapes.

### Data treatment

Some pairs of boulders were observed in the field as being once connected. They were likely broken into separate pieces (1) at their source at the time of boulder dislodgement and being emplaced adjacently after transportation; (2) during transportation or emplacement, or (3) due to post-depositional erosion processes.

Considering the difficulty in accurately identifying the time of fracture, and in order not to overestimate the power of waves, only pairs of boulders that are evidently broken at time of emplacement or by post-depositional processes were regarded as one piece during initial transportation and used for boulder size and orientation analyses (Figure 3).

For orientation analyses, only the boulders with a-axis 20% longer than the b-axis were included as square boulders would not be representative if the clast does not present a significant longer edge. As the shore orientation varies across the 15-km long field site, the shore is divided into 5 zones, named A to E from west to east, according to the shore orientation (see Figure 5 on following page). The direction of the shore was determined from satellite photos. The number of boulders present in each zone varies from 24 to 151 because the division of zones was based purely on the shore orientations. The boulder orientations were plotted on rose diagrams for each zone, the dominant orientation at each zone was then identified as the major boulder orientation.

## RESULTS AND DISCUSSIONS

### Boulder size and distribution

A total of 291 boulders were recorded in the first trip to Makemo (number decreased to 286 for analysis after considering 5 cases in which the boulders were originally one piece during initial transportation but later split into two pieces). Some of the largest clasts reached the 'block' category (scale following Blair and McPherson, 1999), with the largest sized 7.5 x 5.5 x 3.35 m and smallest measured 0.77 x 0.68 x 0.66 m. Average density of the Makemo boulders is 2.3 t/m<sup>3</sup> as determined from 24 rock samples collected. With a size of 138 m<sup>3</sup>, the largest block weighs 318 tonnes. The average size and weight of coral boulders measured are 16.04 m<sup>3</sup> and 36.90 t respectively.

Regarding the transport distance of boulders, the minimum distance between a measured clast to the reef edge is 11 m. The maximum distance is 162 m, where one of the small spherical boulders (1.17 x 1.16 x 1.14 m) was emplaced behind the beach on the vegetation. This boulder was likely transported by the flow and rolled to the present position before it finally stopped due to

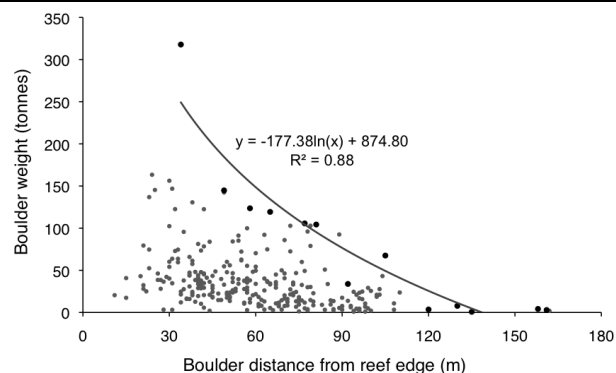


Figure 4. Size-distribution of boulders on the Makemo shore. A landward fining trend is exhibited by the arrangement of 286 measured boulders. A strong exponential correlation ( $R^2 = 0.88$ ) is present among the largest boulders in 10 m grid cell (bigger black dots). Boulders situated within 30 m from the reef crest are excluded in the correlation plotting considering that clasts close to the reef edge are remobilized by waves more frequently.

increased friction with the land surface.

The distribution of boulders on the coast follows a clear landward fining trend (Figure 4), except for < 10 m from the algal crest reef edge where there are no boulders, possibly because this section is consistently exposed to breaking waves. Any clast originally deposited within this short distance from the reef edge is likely to have been remobilized further inland. Following the approach taken by Goto *et al.* (2009), the largest boulder in every 10-m grid was selected for plotting; a strong exponential correlation of landward fining trend can be established for boulders situated in excess of 30 m from the reef crest. We compare the boulder distribution on Makemo to the storm and tsunami boulder fields on Ishigaki and Kudaka Islands of Japan as presented in Goto *et al.* (2010a) who found a similar landward fining trend in the reef flat boulder distribution in 2 sets of storm deposited boulders. Goto *et al.* (2010a) proposed that in contrast to storm-deposited boulders tsunami-deposited boulders do not follow such fining trend but are scattered randomly further inland than storm boulders due to the longer wave period of tsunami (Goto *et al.*, 2010a, 2010b). Following this rationale, these large boulders on Makemo are likely deposited by storm waves based on their size and distribution.

### Boulder orientation and transport mode

The majority of the boulders in all zones except zone B are orientated parallel to slightly sub-parallel to shore (Figure 5). Zone B shows a different result from the other zones as no preferred orientation could be observed. From the statistics of the boulder sizes in each zone (Table 1), the small sizes of boulders present in zone B could be the reason for this lack of preferred boulder orientation. This result appears similar to the study from the boulder field in Bonaire carried out by Watt *et al.* (2010), who concluded that the biggest clasts would orientate parallel to the shore as they were transported by rolling or sliding; whereas smaller clasts deposited normal to shore imply they were carried in turbulent suspension and saltated during transportation (Inman, 1949; Collinson and Thompson, 1982; Williams and Hall, 2004, Watt *et al.*, 2010). However, this hypothesis on the relationship between boulder orientation and boulder size cannot be further

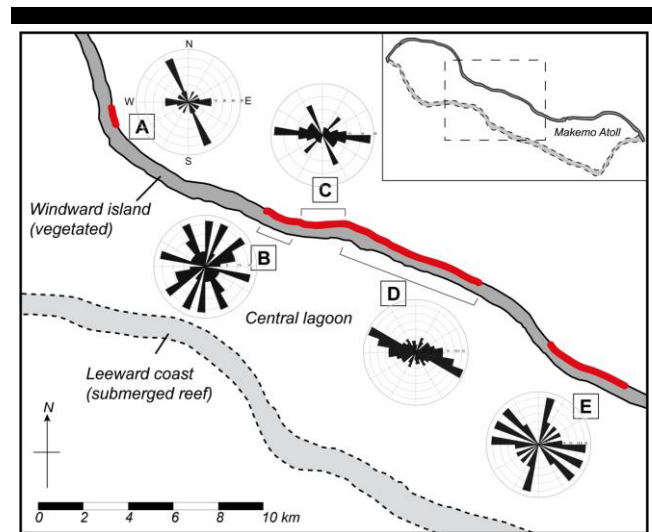


Figure 5. Rose diagrams of boulder orientation at zone A to E. The boulder orientations were group into  $10^\circ$  grid for calculation. At all zones except B, the majority of boulders are aligned with long axes parallel to the shore.

verified by the size and orientation of individual boulders, as the larger boulders in each zone may also have orientated normal to shore (Figure 6). The lengths of b-axes of boulders do not show a correlation with its alignment relative to shore. To date we have no explanation for the different orientations of boulders on Makemo.

Regarding the boulder transport mode, it should be highlighted that all boulders on Makemo were likely initially lifted and entrained in the flow, as this is the only possible transport mechanism that can bring these reef-derived boulders from the submerged reef framework onto the reef flat as sub-aerial features. As presented in the work of Nandasena *et al.* (2011), initiating boulder transport by lifting or saltating the boulder requires the highest wave velocity, as compared to transportation by sliding

Table 1. Information on the divided zones A to E, with the shore and preferred boulder orientation present at each zone. The category for boulder orientation relative to shore is divided in the same way as in Watt *et al.* (2010). Orientation within  $\pm 10^\circ$  to shoreline orientation is considered 'shore parallel',  $\pm 50^\circ$  to shoreline is 'sub-parallel'; similarly, boulder orientation within  $\pm 10^\circ$  of shoreline normal is 'shore normal', and  $\pm 50^\circ$  to shoreline normal is 'sub-normal'. (# Due to the presence of the largest coral block in zone E, the standard deviation of boulder weight is very high. If this extreme sample is removed from the statistics, the mean boulder weight and the standard deviation of zone E would be 42.88 tonnes and 29.92 respectively.)

Zone	A	B	C	D	E
No. of boulders plotted (n) / Total no. of boulders (t)	n=15 t=24	n=28 t=44	n=32 t=43	n=79 t=151	n=13 t=24
Length of shore (km)	0.7	1.2	2.2	5.9	3.8
Mean boulder weight (tonnes)	49.33	17.67	29.66	39.82	54.34 <sup>#</sup>
Standard deviation of boulder weight	37.02	18.72	27.80	33.59	63.29 <sup>#</sup>
Shore orientation	160°	100°	90°	110°	120°
Major boulder orientation relative to shore	150°-160° (Parallel)	No obvious preferred orientation	90°-100° (Parallel)	100°-120° (Parallel)	90°-140° (Parallel to Sub-parallel)

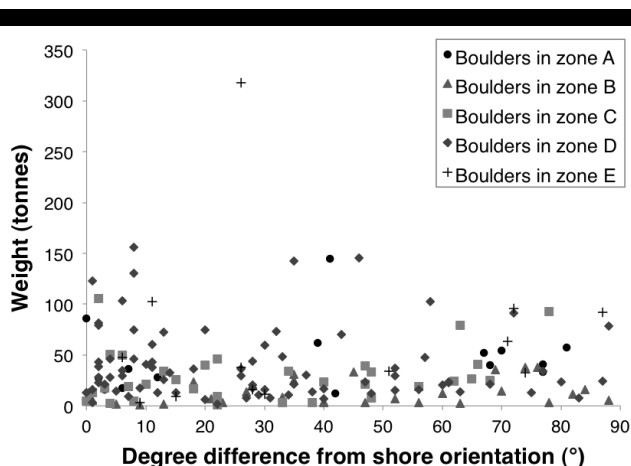


Figure 6. The relationship between individual boulder orientation and boulder size (as weight). The horizontal axis is the degree difference between the orientation of a boulder from the shore orientation ( $0^\circ$  difference between boulder and shore orientation indicates the boulder is aligned parallel to shore,  $90^\circ$  suggests the boulder is normal to shore). No correlation can be established, as the  $R^2$  value for the overall trend is  $2.20 \times 10^{-6}$ , whereas the value for each separate zone varies from 0.009 to 0.097.

and rolling. This implies that the waves of the unknown storm(s) that emplaced the Makemo boulders were exceptionally fast flowing. Once the boulder is lifted onto the reef flat, it could be dropped from the entrainment if the wave velocity lowered. It has been proposed that this sudden drop of boulder to the reef surface may be the cause of boulders splitting/breaking into two parts along the mechanically weak middle section (Goto et al., 2010b). While this splitting/breaking of a boulder was not observed in the storm boulders in Japan but only found among tsunami boulders, this feature is exhibited by some boulders on Makemo. This splitting of boulders again confirmed that these boulders were once lifted and dropped by turbulent waves, which are likely of storm origin, an interpretation supported by the landward fining distribution of boulders on the reef flat. If this is the case, it implies that storm waves can also be as turbulent as tsunami waves, and the splitting of boulders is not a signature of tsunami clasts. Sliding and rolling of boulders may be the secondary transport mechanisms, as the boulders may continue to move inland in these modes in the slower flow before stopping completely. This is when the long axis of boulder rotates and finally aligns perpendicular to the flow (Nandasena and Tanaka, 2013), which is parallel to the shoreline if the flow comes normal to shore as in most cases.

## CONCLUSION

- 1) From the size-distribution of boulders deposited on the reef flat and the beach of the Makemo windward island, it is believed that the boulders were emplaced by storm waves as an exponential landward fining trend in boulder size is present.
- 2) The majority of these boulders are orientated with long-axes parallel to the shoreline, with the exception of a zone with smaller measured clasts where a more random boulder orientation was observed.
- 3) There seems no relationship between the boulder size and the orientation of boulders relative to shore, hence we cannot

conclude that the boulder orientation is a reflection of transport mode, which is relative to size of clasts. All boulders on Makemo would have been lifted in the flow at least once, when they were emplaced onto the reef flat from the submarine reef structure.

- 4) More analyses and results on the Makemo boulder field, including the modelling of wave propagation on the reef flat and the timing of the ancient storm event(s) will be presented in future publications.

## ACKNOWLEDGEMENTS

Fieldwork by S Etienne and AYA Lau was supported by CPER-Rinalpof grant (French Government and Territory of French Polynesia). This is Earth Observatory of Singapore contribution 57. AYA Lau is supported by the National University of Singapore Research Scholarship. The contribution of AS and YSL is supported by National Research Foundation Singapore under its Singapore NRF Fellowship scheme (National Research Fellow Award No. NRF-RF2010-04) and administered by Earth Observatory of Singapore. This paper is a contribution to the IGCP project "IGCP-588 Preparing for Coastal Change".

## LITERATURE CITED

- Blair, T.C. and McPherson, J.G., 1999. Grain-size and textural classification of coarse sedimentary particles. *Journal of Sedimentary Research*, 69, 6-19.
- Bourrouilh-Le Jan, F.G. and Talandier, J., 1985. Sédimentation et fracturation de haute énergie en milieu récifal: Tsunamis, ouragans et cyclones et leurs effets sur la sédimentologie et la géomorphologie d'un atoll: motu et hoa, à Rangiroa, Tuamotu, Pacifique SE (Major high-energy events in a reef environment: Tsunamis, hurricanes and tropical cyclones and their effects on the sedimentology and geomorphology of an atoll: Rangiroa, Tuamotu, SE Pacific). *Marine Geology*, 67, 263-333.
- Collinson, J.D. and Thompson, D.B., 1982. *Sedimentary structures*. London: George Allen & Unwin, 194p.
- Engel, M. and May, S.M., 2012. Bonaire's boulder fields revisited: Evidence for Holocene tsunami impact on the Leeward Antilles. *Quaternary Science Reviews*, 54, 126-141.
- Etienne S., Buckley M., Paris R., Nandasena A.K., Clark K., Strotz L., Chagué-Goff C., Goff J., Richmond B., 2011. The use of boulders for characterising past tsunamis: lessons from the 2004 Indian Ocean and 2009 South Pacific tsunamis. *Earth-Science Reviews*, 107, p. 76-90.
- Etienne, S., 2012. Marine inundation hazards in French Polynesia: geomorphic impacts of Tropical Cyclone Oli in February 2010. *Geological Society, London, Special Publications*, 361, 21-39.
- Goto, K., Okada, K. and Imamura, F., 2009. Characteristics and hydrodynamics of boulders transported by storm waves at Kudaka Island, Japan. *Marine Geology*, 262, 14-24.
- Goto, K., Miyagi, K., Kawamata, H. and Imamura, F., 2010a. Discrimination of boulders deposited by tsunamis and storm waves at Ishigaki Island, Japan. *Marine Geology*, 269, 34-45.
- Goto, K., Kawana, T. and Imamura, F., 2010b. Historical and geological evidence of boulders deposited by tsunamis, southern Ryukyu Islands, Japan. *Earth-Science Reviews*, 102 (1-2), 77-99.
- Inman, D.L., 1949. Sorting of sediments in the light of fluid mechanics. *Journal of Sedimentary Petrology*, 19, 51-70.
- Kench, P.S., McLean, R.F., Brander, R.W., Nichol, S.L., Smithers, S.G., Ford, M.R., Parnell, K.E. and Aslam, M., 2006. Geological effects of tsunami on mid-ocean atoll islands: The Maldives before and after the Sumatran tsunami. *Geology*, 34, 177-180.
- Kench, P.S., Nichol, S.L., Smithers, S.G., McLean, R.F. and Brander, R.W., 2008. Tsunami as agents of geomorphic change in mid-ocean reef islands. *Geomorphology*, 95, 361-383.
- Laboute, P., 1985. Evaluation of damage done by the cyclones of 1982-1983 to the outer slopes of the Tikehau and Takapoto atolls (Tuamotu Archipelago). *Proceedings of the Fifth International Coral Reefs Congress (Tahiti)*, Volume 3, pp. 320-328.

- Nandasena, N.A.K. and Tanaka, N., 2013. Boulder transport by high energy: Numerical model-fitting experimental observations. *Ocean Engineering*, 57, 163-179.
- Noormets, R., Felton, E.A. and Crook, K.A.W., 2002. Sedimentology of rocky shorelines: 2 Shoreline megaclasts on the north shore of Oahu, Hawaii—origins and history. *Sedimentary Geology*, 150, 31-45.
- Noormets, R., Crook, K.A.W. and Felton, E.A., 2004. Sedimentology of rocky shorelines : 3. Hydrodynamics of megaclast emplacement and transport on a shore platform, Oahu, Hawaii. *Sedimentary Geology*, 172, 41-65.
- Reymond, D., Hyvernaud, O. and Okal, E.A., 2012. The 2010 and 2011 Tsunamis in French Polynesia: Operational Aspects and Field Surveys. *Pure and Applied Geophysics*, 170, 1169-1187.
- Richmond, B.M., Watt, S., Buckley, M., Jaffe, B.E., Gelfenbaum, G. and Morton, R.A., 2011. Recent storm and tsunami coarse-clast deposit characteristics, southeast Hawai' i. *Marine Geology*, 283, 79-89.
- Salvat, F. and Salvat, B., 1992. Nukutipipi Atoll, Tuamotu Archipelago; geomorphology, land and marine flora and fauna and interrelationships. *Atoll Research Bulletin*, 357, 1-43.
- Scheffers, A.M., 2002. Paleotsunami evidences from boulder deposits on Aruba, Curaçao and Bonaire. *Science of Tsunami Hazards*, 20, 26-37.
- Stoddart, D.R., 1969. Reconnaissance geomorphology of Rangiroa Atoll, Tuamotu Archipelago. *Atoll Research Bulletin*, 125, 1-32.
- Stoddart, D.R. and Walsh, R.P.D., 1992. Environmental variability and environmental extremes as factors in the island ecosystem. *Atoll Research Bulletin*, 356, 1-71.
- Terry, J.P. and Etienne, S., 2011. "Stones from the dangerous winds" – reef platform mega-clasts in the tropical Pacific Islands. *Natural Hazards*, 56, 567-569.
- Terry, J.P., Lau, A.Y.A. and Etienne, S., 2013. Reef-Platform Coral Boulders. Evidence for high-energy marine inundation events on tropical coastlines. Springer Briefs in Earth Sciences, Springer, 105 p.
- Vitousek, M.J., 1963. The Tsunami of 22 May 1960 in French Polynesia. *Bulletin of the Seismological Society of America*, 53, 1229-1236.
- Watt, S.G., Jaffe, B.E., Morton, R.A., Richmond, B.M. and Gelfenbaum, G., 2010. *Description of extreme-wave deposits on the northern coast of Bonaire, Netherlands Antilles*. USGS Open-File Report 2010-1180, 64p.
- Williams, D. and Hall, A.M., 2004. Cliff-top megaclast deposits of Ireland, a record of extreme waves in the North Atlantic--storms or tsunamis? *Marine Geology*, 206 (1-4), 101-117.

## Responses of coastal waters in the Yellow Sea to Typhoon Bolaven

Chang S. Kim<sup>†</sup>, Hak-Soo Lim<sup>†</sup>, Jin Yong Jeong<sup>†</sup>, Jae-Seol Shim<sup>†</sup>, Il-Ju Moon<sup>‡∞</sup>, You Jung Oh<sup>‡</sup>, Hak Yoel You<sup>□</sup>

<sup>†</sup>Coastal Disaster Research Center, Korea Institute of Ocean Science & Technology, 787 Haeanro, Ansan 426-744, Korea  
surfkim@kiost.ac, hslim@kiost.ac  
jyjeong@kiost.ac, jsshim@kiost.ac

<sup>‡</sup>College of Ocean Science, Jeju National University, 102 Jeju-Univ. St., Jeju, Korea, ijmoon@jeju.ac.kr, ou90@daum.net  
<sup>∞</sup> Corresponding author

<sup>□</sup>Oceanographic Division, Korea Hydrographic and Oceanographic Administration, 351 Haeyang-ro, Yeongdo-gu, Busan, Korea  
peterhak@korea.kr



[www.cerf-jcr.org](http://www.cerf-jcr.org)



[www.JCRonline.org](http://www.JCRonline.org)

### ABSTRACT

Kim, C.S., Lim, H.S., Jeong, J.Y., Shim, J.S., Moon, I.J., Oh, Y.J., You, H.Y., 2014. Response of Coastal Waters in Yellow Sea to Typhoon Bolaven. In: Green, A.N. and Cooper, J.A.G. (eds.), *Proceedings 13<sup>th</sup> International Coastal Symposium* (Durban, South Africa), *Journal of Coastal Research*, Special Issue No. 70, pp. 278-283, ISSN 0749-0208.

In August 2012, Typhoon Bolaven (1215) passed through the East China Sea (ECS) and the Yellow Sea (YS), leading to severe coastal damages in Korea. This study investigated the responses of the coastal waters along the meridional direction of the YS and the ECS to Typhoon Bolaven. This included the causes of record-breaking high waves in the ECS, the possible danger of coincident peak surges and high tides, resonant coupling between the typhoon, tides and topography, and the impact of Bolaven-induced sea surface cooling on the intensity of Typhoon Tembin (1214). Analyses were conducted using observations from an ocean platform, buoys, and tidal stations, as well as a numerical model during the passage of Bolaven. Results revealed that the western coast of the Korean Peninsula fortunately avoided severe storm surge damages due to weak tidal action during the passage of Bolaven, although pure surge components were significantly high. However, we found that there was the possibility of resonant coupling between surges, tides and topography in the YS, which would contribute to further enhancement of the storm surge. Based on the wave simulations, it was revealed that a straight track and fast translation of Bolaven maximized the production of record-breaking high waves in the ECS.

**ADDITIONAL INDEX WORDS:** Typhoon Bolaven, sea surface cooling, coastal water responses, storm surge, tide, resonance, waves

### INTRODUCTION

On average, about three tropical cyclones (hereafter referred to as typhoons) per year influence the Korean peninsula (KP) and about one typhoon per year makes landfall on the KP. These typhoons sometimes lead to extensive damages from strong winds, high waves, storm surges, and flooding, which has long been one of the most serious natural hazards to people living in Korea.

In 2012, four typhoons made landfall on the KP, which was the largest number recorded since 1960. Among them, Typhoon Bolaven (1215), which hit the Jeju Island (JI) and passed through the Yellow Sea (YS), caused serious property damages, particularly for aquaculture and breakwaters along the southwest coast of the KP due to high waves. At 00 UTC 28 August, the maximum wind speed (MWS) of Bolaven was 33 m/s (10 min average value) around the JI, but ocean waves that were higher than expected destroyed many breakwaters along the coast. This study investigated the possible causes for the unusually high waves based on wave simulations and measurements. In addition, we examined the potential danger of storm surges along the coast of the YS due to coincidence of peak surges and high tides as well as resonant coupling between the typhoon, tides, and topography.

Two days after the passage of Bolaven, Typhoon Tembin (1214) also made landfall on the KP, but the intensity of the typhoon was not so strong. It was assumed that Bolaven changed

the oceanic conditions ahead of Tembin, resulting in the weakened intensity of Tembin. This assumption was also verified in this study.

### DATA AND METHODS

To investigate the responses of waters along the coast of the KP to Bolaven, we collected all available data observed during the passage of the typhoon. The observations came from the Ieodo Ocean Research Station (IORS), two Korea Ocean Gate Arrays (KOGA), four Korean Meteorological Administration (KMA) buoys, and 14 tidal stations (see Figure 1 and Table 1). In particular, IORS, the KOGA buoys, and the Marado buoy were very close to Bolaven's track (Figure 1). We also used satellite images (Kim *et al.*, 2013; Ryu *et al.*, 2012) and numerical model results (Lim *et al.*, 2013; Moon *et al.*, 2003b) for the analysis. The surge heights were calculated by subtracting the predicted tidal elevation from the observed sea level at the 14 tidal stations. The predicted tidal elevation was estimated using a harmonic analysis.

Wave simulations were conducted using the WAVEWATCH III (WW3) model. The WW3 is an ocean surface wave model developed at NOAA/NCEP in the spirit of the WAM model. The WW3 has been used in many research programs to study surface wave dynamics, and as the operational wave model of NCEP for global and regional wave forecasts (Tolman 2002; Tolman *et al.*, 2002).

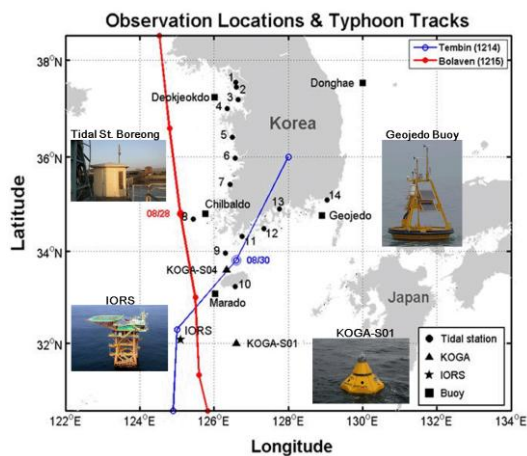


Figure 1. Observation locations and tracks of Typhoons Bolaven and Tembin. Names of tidal station are listed in Table 1.

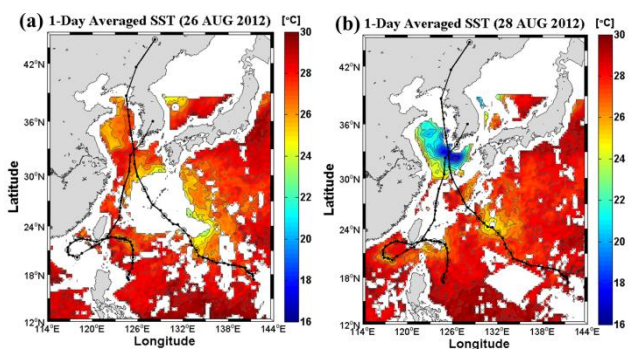


Figure 2. Change in sea surface temperature (SST) after the passage of Bolaven: (a) before arrival of Bolaven (26 August), (b) after the passage (28 August). Tembin passed through the cooled areas before landfall on the KP.

## RESULTS

### Bolaven-induced Sea Surface Cooling and its Impacts

In summer, the surface waters in the YS are moderately warm, approximately 27°C–28°C, while the bottom waters are relatively cool at approximately 10°C (Kim *et al.*, 2004) due to the year-round presence of Yellow Sea Bottom Cold Water (YSBCW). Considering that the average water depth in the YS is about 60 m, this area is distinguished by a large vertical temperature gradient of up to 18°C. This unique environment, rarely found in other regions, produces a strong sea surface cooling when typhoons pass over the area (Moon and Kwon, 2012).

Figure 2 shows the sea surface cooling after the passage of Typhoon Bolaven. Warm surface waters of 27°C–28°C were suppressed to 16°C–20°C, particularly in the southern and western coastal waters of the KP. Typhoon Tembin passed over the cooled areas two days after the passage of Bolaven. Considering that

2.5°C cooling in the inner core is sufficient to shut down the entire energy production of a storm (Emanuel *et al.*, 2004), the large SST drop seemed to have a significant weakening effect on Typhoon Tembin when it passed over the area on 28–29 August 2012 (Figure 3).

### Potential Danger of Coincident Peak Surges and High Tides

The west coast of Korea is one of the strongest tidal areas in the world. The tidal range is about 4 m in the south and increases to about 10 m in the north. During the high spring tides, the tidal elevation is significantly increased. If the astronomically enhanced tide levels coincide with the passage of a typhoon, it might be very threatening to the low land of coastal regions in Korea (Moon *et al.*, 2003a).

Figure 4 shows the temporal variations of minimum central pressures, wind speeds, and surge heights during the passages of Typhoons Bolaven and Tembin. Here, the surge heights were calculated by subtracting the predicted tidal level from observed sea level. For the 14 tidal stations, we also calculated peak surge height (A) and time ( $t_A$ ), predicted tide level (B) at  $t_A$ , nearest high tide level (C) and time ( $t_C$ ), nearest spring high tide level (D) and time ( $t_D$ ), observed sea level (A+B) at  $t_A$ , extreme sea level scenario 1 (A+C) at  $t_C$ , extreme sea level scenario 2 (A+D) at  $t_D$ , and time differences ( $|t_C - t_A|$ ,  $|t_D - t_A|$ ) during the passage of Typhoon Bolaven (see Table 1). The peak surge heights ranged from 50.2 cm (Busan) to 167.3 cm (Goheung). The surge heights above 140 cm were among the highest records in this region. However, it was fortunate that the peak surges occurred near low tide ( $04\text{h } 45\text{m} < |t_C - t_A| < 06\text{h } 57\text{m}$ ) at most stations on the western coast along Bolaven's track (1–10, including JI). Furthermore, Bolaven's arrival avoided the spring tide ( $|t_D - t_A| > 67\text{h}$ ).

We estimated extreme sea levels at the tidal stations assuming the worst case scenarios that Bolaven landfall at high tide (scenario 1, A+C) and at spring high tide (scenario 2, A+D). For example, the observed sea level of 458 cm at YB reached 985 cm in scenario 1 and 1094 cm in scenario 2. At the other stations, potential extreme sea levels were estimated based on these scenarios (Table 1). These results suggested that the coincidence of peak surge and high tides present tremendous danger along the coast of the KP and proper preparedness is necessary for the worst case scenarios.

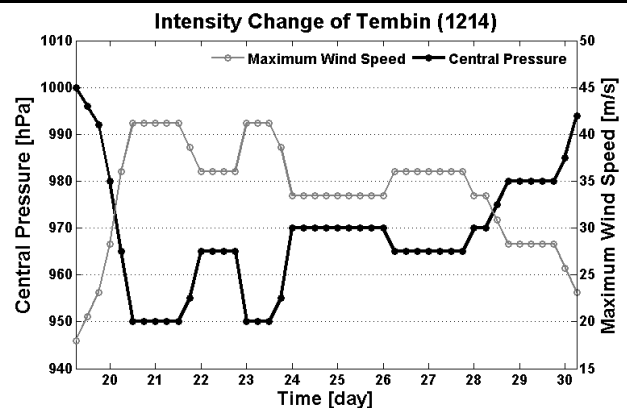


Figure 3. Change in intensity of typhoon Tembin (1214) in terms of minimum central pressure and maximum wind speed.



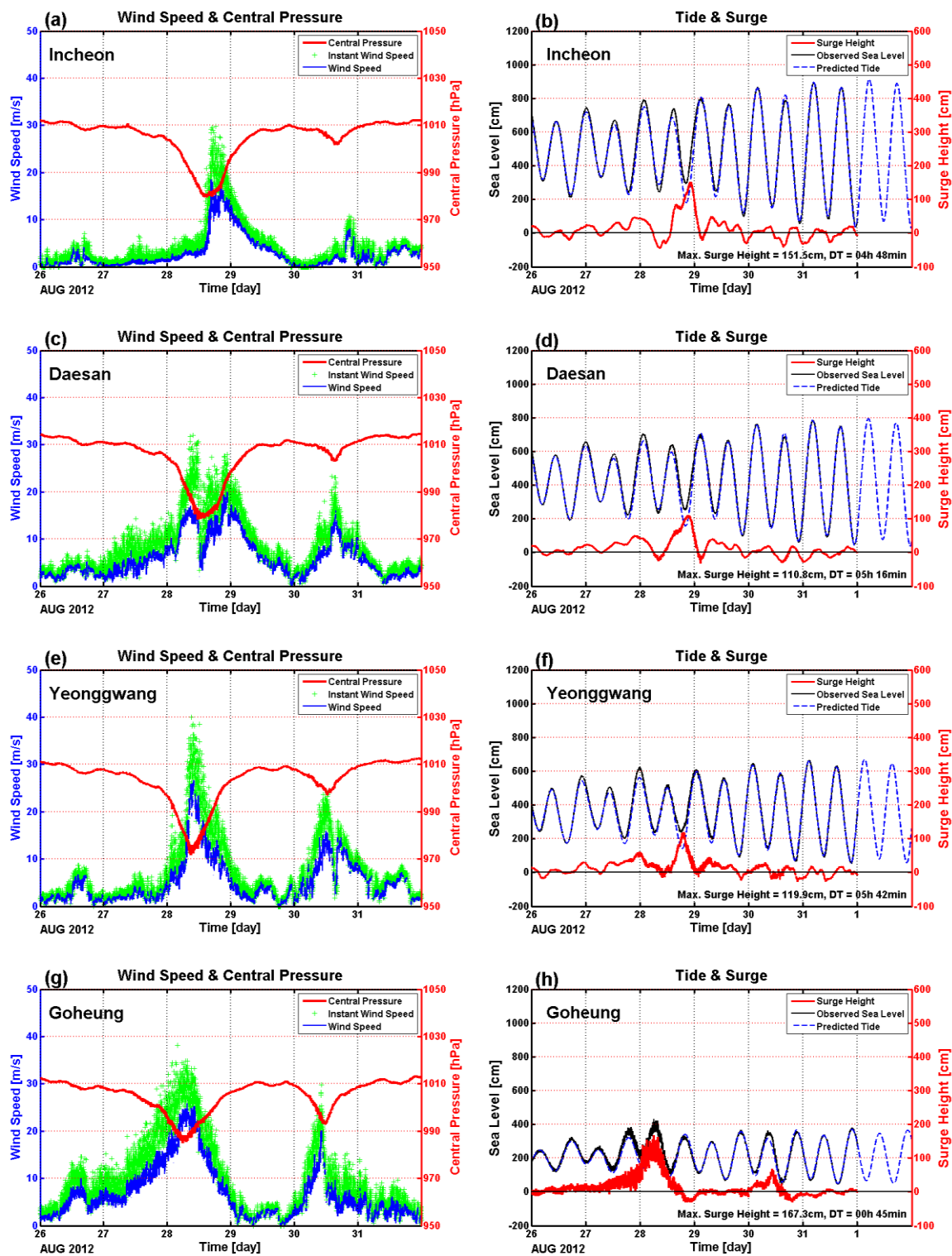


Figure 4. Time series of minimum central pressure, instant wind speed, 10 min average wind speed (a, c, e, g) and predicted tidal elevation, observed sea level, surge height (b, d, f, h) with the time difference (DT) between high tide and surge peak occurrence at various coastal stations in Korea: (a, b) Incheon, (c, d) Daesan, (e, f) Yeonggwang, and (g, h) Goheung during the passages of Typhoons Bolaven and Tembin.

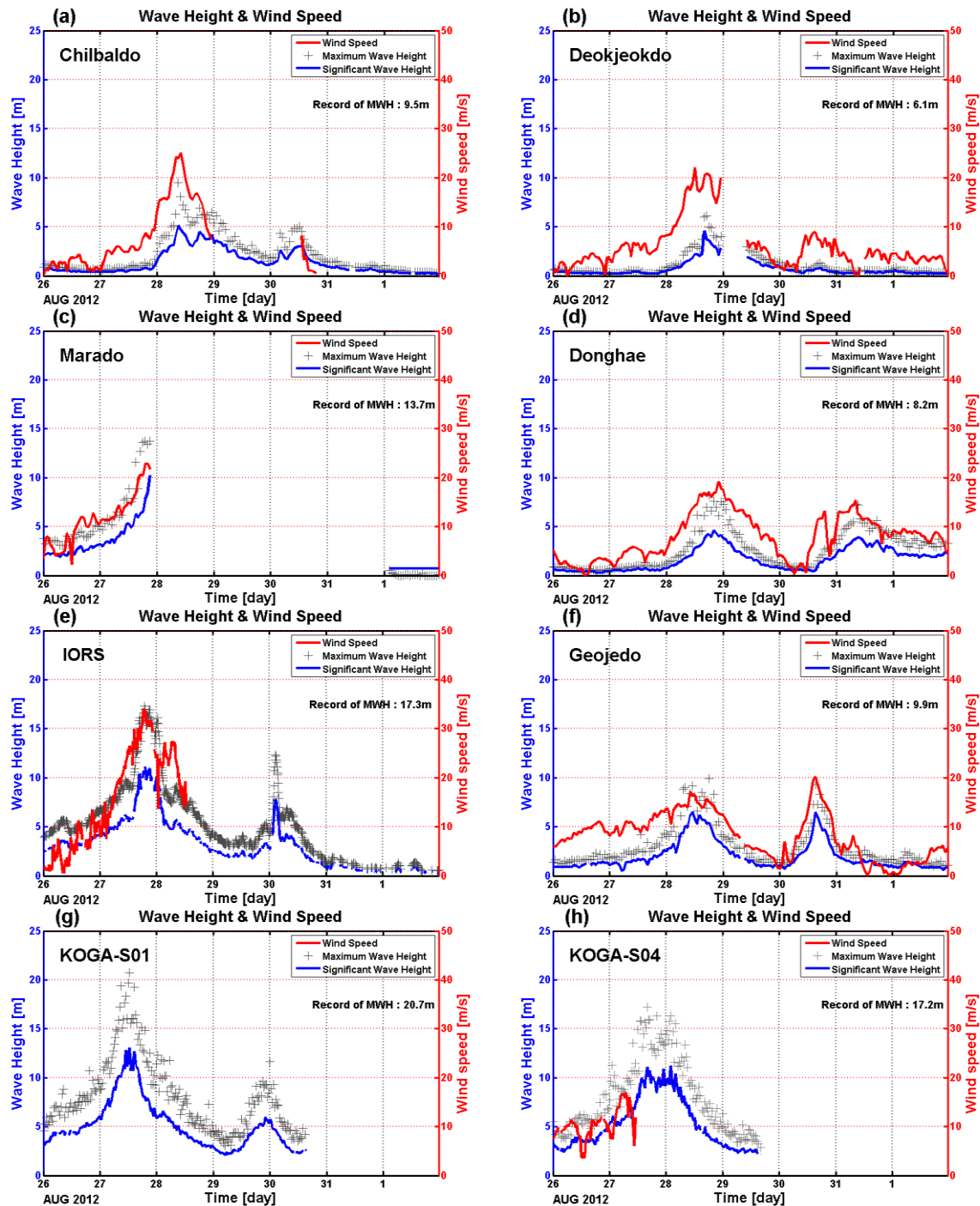


Figure 5. Temporal variation of wind speed, significant wave height, and maximum wave height observed at oceanographic buoys and platforms during the passing of Typhoon Bolaven.

### Resonant Coupling Between Typhoon, Tides, and Topography

In this region, another critical situation can occur due to resonant coupling of typhoon and tide when the storm translation speed (STS) is comparable to that of the tide. According to the tidal chart (Fang *et al.*, 2004) and observed tidal data (Lee *et al.*,

2013), the tidal wave propagates from south to north along the western coast of Korea and there is a six hour difference in high tide between Jeju Harbour in the south and Incheon Harbour in mid-western Korea. The distance between the two tidal stations is approximately 438 km, yielding a phase speed of about 70 km/h

Table 1. Peak surge height (A) and time ( $t_A$ ), predicted tide level (B) at  $t_A$ , nearest high tide level (C) and time ( $t_C$ ), nearest spring high tide level (D) and time ( $t_D$ ), observed sea level (A+B) at  $t_A$ , extreme sea level scenario 1 (A+C) at  $t_C$ , extreme sea level scenario 2 (A+D) at  $t_D$ , and time differences ( $|t_C-t_A|$ ,  $|t_D-t_A|$ ) at 14 tidal stations during the passage of Typhoon Bolaven. The unit of sea level is [cm]. Here,  $|t_C-t_A| = 0$  hour and  $|t_C-t_A| = 6$  hours represent that the peak surges occur at high and low tides, respectively.

	Station	A	B	C	D	A+B	A+C	A+D	$ t_C-t_A $	$ t_D-t_A $
1	Yeongjong Bridge (YB)	159.6	298.4	825.4	934.6	458	984.9	1094.1	04h 50m	79h 06m
2	Incheon	151.5	289.5	807.3	911.7	441	958.8	1063.2	04h 49m	79h 01m
3	Ansan	142.3	270.7	763.1	862.9	413	905.4	1005.2	04h 45m	78h 55m
4	Daesan	110.8	211.2	712.2	797.5	322	823	908.3	05h 16m	79h 26m
5	Boreong	143.2	178.9	676.1	757	322	819.2	900.1	06h 46m	80h 54m
6	Gunsan(out)	124.5	164.5	645.4	721.4	289	769.9	845.9	05h 58m	80h 07m
7	Yeonggwang	119.9	151.1	599.2	670.8	271	719.2	790.7	05h 43m	79h 55m
8	Daehuksando	84.4	145.7	324.4	362.2	230	408.7	446.6	06h 57m	92h 21m
9	Chujado	98.4	139.6	297.6	317.2	238	396	415.6	06h 24m	67h 37m
10	Seogwipo	111.8	145.2	262	295.3	257	373.8	407.1	06h 06m	92h 24m
11	Wando	136.6	258.4	285.3	384.9	395	421.9	521.5	01h 41m	88h 27m
12	Goheung	167.3	262.7	268.6	369.2	430	436	536.5	00h 47m	87h 37m
13	Gwangyang	101.3	258.7	287.8	385	360	389.1	486.3	01h 35m	85h 14m
14	Busan	50.2	111.8	113.8	145.9	162	164	196.1	00h 40m	86h 07m

for the co-tidal line. If the STS is similar to the phase speed, the storm surge can ride on the high tide.

Based on the best track data of the typhoon, the STS of Bolaven was about 40 km/h when it passed over the YS, which is much slower than the propagation of the co-tidal line in this region. However, the STS of some historical storms such as Kompasu in 2010 reached up to 70 km/h, suggesting that in the worst case scenario, the storm surge peaks could be amplified by a resonant coupling of tides and typhoon along the west coast.

On the other hand, the YS is a semi-enclosed marginal sea of the northwestern Pacific Ocean, surrounded by the KP, the Chinese coast, and the Ryukyu Islands. If we assume that the YS is an open channel closed at one end with a length of 820 km and depth of 60 m, the natural period of the channel,  $T_n$ , can be given by:

$$T_n = \frac{4L}{n\sqrt{gh}} \quad (1)$$

where  $n$  is the number of nodes ( $n = 1, 3, \dots$ ),  $L$  is the length of the channel,  $g$  is the gravity acceleration, and  $h$  is the water depth. For  $n = 1$  and  $n = 3$ , the natural periods,  $T_1$  and  $T_3$ , are 37.8 hours and 12.6 hours, respectively. The period  $T_3$ , with three nodes, is known to reinforce tides by resonance with the semi-tidal period, resulting in strong tides in this area (Choi, 1980). If the natural periods ( $T_1$  and  $T_3$ ) are similar to the predominant period ( $T_{surge}$ ) of the surge generated from typhoons passing over this region, the storm surge can be significantly enhanced by the resonant coupling (Moon *et al.*, 2003a). The  $T_{surge}$  can be expressed by:

$$T_{surge} = \frac{L_{surge}}{V_{storm}} \quad (2)$$

where  $L_{surge}$  is the length scale of the typhoon and  $V_{storm}$  is the STS. In the case of Typhoon Bolaven, if we consider that  $L_{surge}$  was 600 km (based on mean distributions of wind and air pressure) and  $V_{storm}$  was 40 km/h, the predominant period of the surge was about 15 hours, resulting in no significant resonant coupling. However, depending on the combination of STS and storm size, a potential

enhancement of the storm surge always exists in this region due to the coupling.

### Occurrence of Record-Breaking High Waves

One of the most interesting responses of coastal waters during the passage of Typhoon Bolaven was the observation of high maximum wave heights (MWH). The MWHs observed at KOGA-S01, KOGA-S04, IORS, and Mardo buoys were 20.7m, 17.2m,

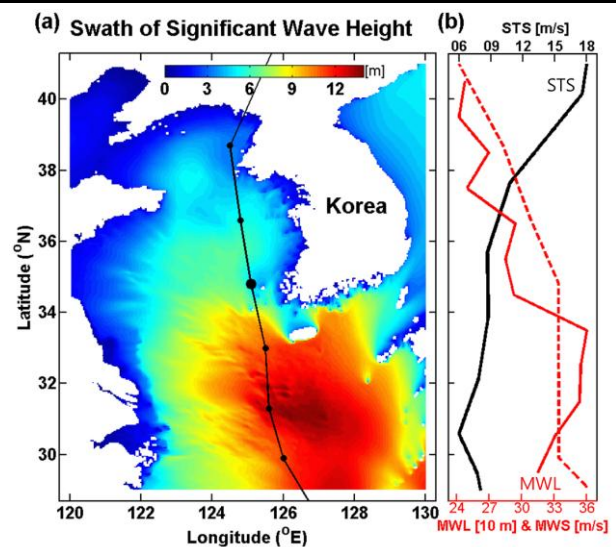


Figure 6. (a) Swath of SWH during the passage of Typhoon Bolaven. Line is the storm track. (b) Dominant MWL ( $\times 10$ , red solid line), MWS (red dotted line), and STS (black solid line) along the typhoon track.

17.3 m, and 13.7 m respectively (Figure 5). The extraordinarily high values broke observational records in these regions although Bolaven was not the strongest typhoon based on the historical best-track archives of the Regional Specialized Meteorological Center (RSMC).

It is known that as the STS increases and becomes comparable to the group speed of dominant waves, waves to the right of the typhoon track are exposed to prolonged forcing from wind; that is, they become “trapped” within the typhoon (resonance effect or dynamic fetch) and grow continuously (Moon *et al.*, 2003b). The straight translation of the typhoon can maximize the increase of the dynamic fetch.

Typhoon Bolaven was moving quickly along a straight track with a high STS of about 9–18 m/s in the ECS and YS (Figure 6), which may have provided favorable conditions for wave growth. To support this hypothesis, we simulated the significant wave height (SWH) for Typhoon Bolaven using the WW3 model (Tolman, 2002) and calculated the maximum SWH at all grid points (swath in Figure 6) as well as the dominant mean wave length (MWL) along the typhoon track (red solid line in Figure 6). This indicated that asymmetric distribution of the SWH was evident due to the resonance effect, resulting in high waves to the right of the typhoon track.

## CONCLUSIONS

In 2012, five typhoons affected the Korean coastal waters, and among them, three typhoons made landfall on the KP from late August to early September. This investigation focused on the response of coastal waters to the passage of Typhoon Bolaven (1215) which was the strongest to hit the KP in 2012, and passed through the ECS and YS, leading to severe damages in Korea. We analyzed observations from an ocean platform, buoys, and tidal stations as well as numerical modeling results during the passage of Bolaven.

Analysis revealed that the western coast of the KP avoided severe storm surge damages due to weak tidal action during the passage of Bolaven, although pure surge components were significantly high. In fact, sea level at the coastal stations along the track of Bolaven reached peak surges ranging from 50 to 150 cm over the tidal elevation. However, the peak surges fortunately occurred with a time difference of approximately 4–5 hours from high tide.

We examined the possible dangers due to coincident peak surges and high tides as well as resonant coupling between the typhoon, tides, and topography. Results suggested that if the STS is similar to the co-tidal amplitude propagation (70 km/h) or the predominant period of the surge is similar to the natural period of the YS (12.6 or 37.8 hours), the coasts along the YS would be very vulnerable to coastal inundation during high and spring tides, requiring a systematic warning system for the worst situation.

Wave observations and modeling results showed that the straight and fast translation of Typhoon Bolaven caused unusually high waves in this region. The SST measurements also indicated that when Typhoon Bolaven passed through the YS, the surface water was vertically mixed, lowering the SST from 27°C–28°C to 16°C–20°C. Due to the cooler SST, Typhoon Tembin, which followed closely after Bolaven, lost energy and ended up a moderate typhoon.

## ACKNOWLEDGEMENTS

This research was supported by the project entitled, “Functional improvement of the Korea Ocean Satellite Center”, funded by the Korea Institute of Ocean Science & Technology as well as the project entitled, “Advanced Research on Applied Meteorology”,

funded by the National Institute of Meteorological Research. Partial support was provided by the projects entitled, “Construction of Ocean Research Station and their Application Studies”, “Development of Coastal Erosion Control Technology”, and “KOOS II”, funded by the Ministry of Oceans and Fisheries, Korea, and this support was greatly appreciated.

## LITERATURE CITED

- Choi, B.H., 1980. *A tidal model of the Yellow Sea and the East China Sea*. Korean Ocean Research and Development Institute (KORDI) Report 80-02, 72p.
- Emanuel, K.A., DesAutels, C., Holloey, C. and Korty, R., 2004. Environmental control of tropical cyclone intensity. *Journal of the Atmospheric Sciences*, 61, 843-857.
- Fang, G.H., Wang, Y.G., Wei, Z., Choi, B.H., Wang, X. and Wang, J., 2004. Empirical Cotidal Charts of the Bohai, Yellow, and East China Seas from 10 years of TOPEX/Poseidon altimetry. *Journal of Geophysical Research*, 109, c11006.
- Kim, C.S., Lim, H.S., Yoon, J.J., Oh, J.H. and Fangli, Q., 2004. Numerical simulation of hydrodynamics and water properties in the Yellow Sea. *Journal of Korean Society of Oceanography*, 39(10), 72-95.
- Kim, C.S., Park, Y.J., Park, K.S., Shim, J.S. and Lim, H.S., 2013. Application of GOCI Satellite Data to Ocean Modeling. *Journal of Coastal Research*, SI65, pp. 1409-1414.
- Lee, S.H., Kang, C.Y., Choi, B.J. and Kim, C.S., 2013. Surface Current Response to Wind and Plumes in a Bay-shape Estuary of the eastern Yellow Sea. *Ocean Science Journal*, 48, 117-139.
- Lim, H.S. Chun, I.S. Kim, C.S. Park, K.S. Shim, J.S. and Yoon, J.J., 2013. High-resolution operational coastal modeling system for the prediction of hydrodynamics in Korea using a wave-current coupled model. *Journal of Coastal Research*, SI65, pp. 314-319.
- Moon, I.-J. and Kwon, S.J., 2012. Impact of upper-ocean thermal structure on the intensity of Korean peninsular landfall typhoons. *Progress in Oceanography*, 105, 61-66.
- Moon, I.-J., Oh, I.S., Murty, T. and Yoon, Y.H., 2003a. A study on the cause of the unusual coastal flooding generated by typhoon Winnie along the western coast of Korea. *Natural Hazards*, 29(3), 485-500.
- Moon, I.-J., Ginis, I., Hara, T., Tolman, H., Wright, C.W. and Walsh, E.J., 2003b. Numerical simulation of sea-surface directional wave spectra under hurricane wind forcing. *Journal of Physical Oceanography*, 33, 1680-1706.
- Ryu, J.H., Han, H.J., Cho, S., Park, Y.J. and Ahn, Y.H., 2012. Overview of Geostationary Ocean Color Imager (GOCI) and GOCI Data Processing System (GDPS). *Ocean Science Journal*, 47(3), 223-233.
- Tolman, H.L., 2002. Validation of WAVEWATCH III version 1.15 for a global domain. NOAA/NWS/NCEP/OMB Tech. Note 213, 33 pp. [Available online at <http://polar.ncep.noaa.gov/waves/references.html>]
- Tolman, H.L., Balasubramanian, B., Burroughs, L.D., Chalikov, D., Chao, Y.Y., Chen, H.S. and Gerald, V.M., 2002. Development and implementation of wind-generated ocean surface wave models at NCEP. *Weather and Forecasting*, 17, 311-333.

## Transformation of small-scale meteorological tsunami due to terrain complexity on the western coast of Korea

Taemin Ha†, Jin-Yong Choi†, Jeseon Yoo†, Insik Chun‡, Jaeseol Shim∞

† Coastal Disaster Research Center,  
Korea Institute of Ocean Science and  
Technology, Ansan 426-744, Korea  
tmha@kiost.ac  
dol76@kiost.ac  
jyoo@kiost.ac

‡ Department of Civil Engineering,  
Konkuk University, 120 Neungdong-ro,  
Gwangjin-gu, Seoul 143-701, Korea  
ischun@konkuk.ac.kr

∞ Corresponding Author, Operational  
Ocean Science and Technology  
Department, Korea Institute of Ocean  
Science and Technology, Ansan 426-744,  
Korea  
jsshim@kiost.ac



[www.cerf-jcr.org](http://www.cerf-jcr.org)



[www.JCRonline.org](http://www.JCRonline.org)

### ABSTRACT

Ha, T., Choi, J.-Y., Yoo, J., Chun, I., Shim, J., 2014. Transformation of small-scale meteorological tsunami due to terrain complexity on western coast of Korea. In: Green, A.N. and Cooper, J.A.G. (eds.), *Proceedings 13<sup>th</sup> International Coastal Symposium* (Durban, South Africa), *Journal of Coastal Research*, Special Issue No. 70, pp. 284-289, ISSN 0749-0208.

On the 4th of May, 2008, a meteorological tsunami occurred in the Yellow Sea and abnormal waves were observed at Jukdo Island, located on the western coast of Boryeong, Korea. The event attracted the attention of many engineers and scientists because it caused extreme waves only at Jukdo Island, unlike the meteorological tsunami event in 2007, which caused abnormal extreme waves along the western coast of Korea. In general, a meteorological tsunami can be forecasted using large-scale meteorological observation data and climate modeling systems. However, a small-scale meteorological tsunami like the event that occurred in 2008, which can cause abnormal extreme waves only in specific coastal areas, should be analyzed using a high-resolution modeling system because water motions can be affected by local terrain. In this study, numerical experiments were conducted to identify the generation and amplification mechanisms of the meteorological tsunami that hit Jukdo Island in 2008. To achieve this objective, we generated virtual meteorological tsunamis using atmospheric pressure disturbances observed in 2008 and simulated the propagation and run-up of the meteorological tsunamis over real topographies by varying specific characteristics of the local terrain. A three-dimensional hydrodynamic model, MOHID, and a Boussinesq-type wave model, FUNWAVE-TVD Version 2.0, were employed to simulate the generation and transformation of the meteorological tsunamis, respectively. The numerical models were first validated by comparing the numerical results with the available tidal records observed during the event, and then used to identify the generation and amplification mechanism of the meteorological tsunami that hit Jukdo Island. Finally, the transformation of a small-scale meteorological tsunami due to terrain complexity is discussed in detail.

**ADDITIONAL INDEX WORDS:** *Meteotsunami, Numerical modeling, Yellow Sea.*

### INTRODUCTION

Meteorological tsunamis or meteotsunamis are destructive tsunami-like long-period oceanic waves associated not with seismic activity but with atmospheric pressure disturbances. They have occurred regularly in oceans around the world (cf. Monserrat *et al.*, 2006; Rabinovich, 2008; Vilibic *et al.*, 2008), and have been recorded under local names such as “bravezas” in Chile (Paskoff, 1970); “Rissaga” in the Balearic Islands (Ramis and Jansa, 1983, Gomis *et al.*, 1993; Monserrat *et al.*, 2006); “Marubbio” in Sicily (Candela *et al.*, 1999), “Milghuba” in Malta (Drago, 2008), and “Abiki” in western Japan (Kakinuma *et al.*, 2009; Tanaka, 2010). They have also been documented in the Yellow Sea (Wang *et al.*, 1987), the Adriatic Sea (Vilibic and Sepic, 2009), the English Channel (Haslett and Bryant, 2009), Florida (Churchill *et al.*, 1995), the north-western Atlantic coast (Mercer *et al.*, 2002), the Argentine coast (Dragani *et al.*, 2002), the New Zealand coast (Goring, 2005), and in other regions (Vilibic *et al.*, 2010). According to Shiga *et al.* (2007), meteorological tsunamis are

recorded approximately five times per year on average, with certain tidal stations recording them more than ten times per year.

The generation mechanism of meteorological tsunamis can be described as follows (Monserat *et al.*, 2006; Sepic *et al.*, 2012): (i) an air pressure disturbance in the atmosphere, which is characterized by a relatively long duration and an abrupt initial change of at least 2-4 hPa over 5-10 min; (ii) transference of this energy to long-period sea waves that can increase the wave height by up to 5 times when compared to the air pressure change; (iii) harbor seiche resonance of long-period sea waves in coastal areas. The first step of the generation mechanism is related to an atmospheric condition, whereas the second and third steps are strongly dependent on topographic properties: the former is more dependent on the sea bathymetry, whereas the latter is more dependent on the characteristics of the coastline (Sepic *et al.*, 2012). The amplification mechanism of the second step is well established (Liu *et al.*, 2003; Vilibic *et al.*, 2008): in essence, when the speed of propagation of the atmospheric disturbance equals the oceanic local gravity wave speed, the Froude number equals 1 and a Proudman resonance (Proudman, 1929) amplifies the open

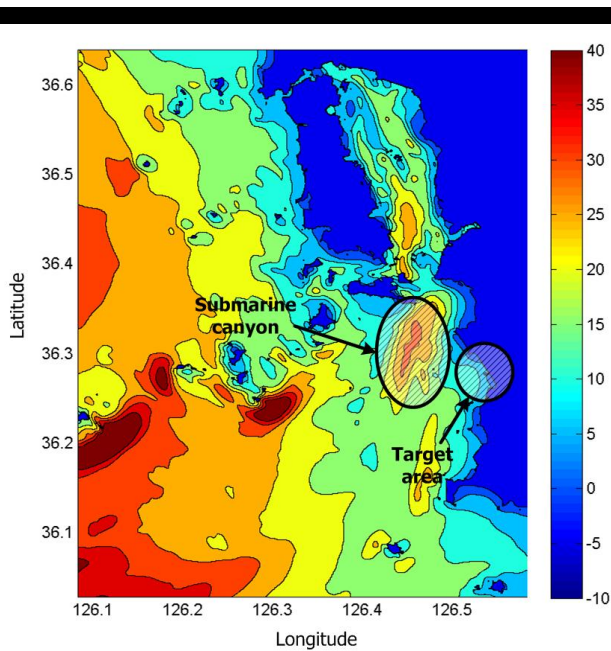


Figure 1. Local characteristics of coastal bathymetry data around Boryeong, Korea.

ocean inverse barometer response (Renault *et al.*, 2011). As for the

third step, it occurs when atmospherically generated open sea waves hit bays that are prone to strong seiche activity (Rabinovich, 2009; Sepic *et al.*, 2012).

On 4 May 2008, a meteorological tsunami occurred in the Yellow Sea, and abnormal extreme waves were observed at Jukdo Island, located on the western coast of Boryeong, Korea (Yoo *et al.*, 2010). The event attracted the attention of many engineers and scientists because it caused extreme waves only at Jukdo Island, unlike the previous meteorological tsunami that occurred in 2007, which caused abnormal extreme waves along the western coast of Korea. There have been some studies to identify the generation mechanism of the 2008 tsunami (Choi *et al.*, 2008; Choi and Lee, 2009; Cho *et al.*, 2013), but many unknown processes, including

propagation over irregular bathymetry and the generation of a large run-up at the coast, remain unidentified. In general, a meteorological tsunami can be forecasted using large-scale meteorological observation data and climate modeling systems. A small-scale meteorological tsunami like the event that occurred in 2008, however, should be analyzed using a high-resolution modeling system because water motions can be affected by local terrain which can cause abnormal extreme waves only in the specific coastal area. For example, a small submarine canyon is located on the western coast of Boryeong (Figure 1) and it could transform the amplification mechanism of meteorological tsunamis in coastal areas. Variable topographies can affect the transformation of sea waves causing features such as depth-induced refraction and shoaling, and these should be considered in order to identify the amplification mechanism.

In this study, numerical experiments were performed to identify the generation and amplification mechanism of the meteorological tsunami that hit Jukdo Island. In order to achieve this objective, we generated virtual meteorological tsunamis using atmospheric pressure disturbances observed in 2008, and simulated the propagation and run-up of the meteorological tsunamis over real topographies by varying specific characteristics of the local terrain. A three-dimensional hydrodynamic model, MOHID, and a Boussinesq-type wave model, FUNWAVE-TVD Version 2.0, were employed to simulate the generation and transformation of the meteorological tsunamis, respectively. The numerical models were first validated by comparing the numerical results with the available tidal records observed during the event, and then used to identify the generation and amplification mechanism of the meteorological tsunami that hit Jukdo Island in 2008. Finally, the transformation of the small-scale meteorological tsunami due to terrain complexity is discussed in detail.

## METHODS

### Data Analysis of the 2008 Event

According to interviews with eyewitnesses (Yoo *et al.*, 2010), during the 4 May 2008 event, a large abnormal oscillation of the sea level lasted for tens of minutes and tsunami-like waves washed away 36 people who were near the breakwater, into the ocean. From analyses of CCTV video data, Yoo *et al.* (2010) observed that the maximum trough-to-crest height of the abnormal waves reached 1.3 m and that the dominant period was approximately 185 s (3.1 min). However, this large oscillation was not recorded

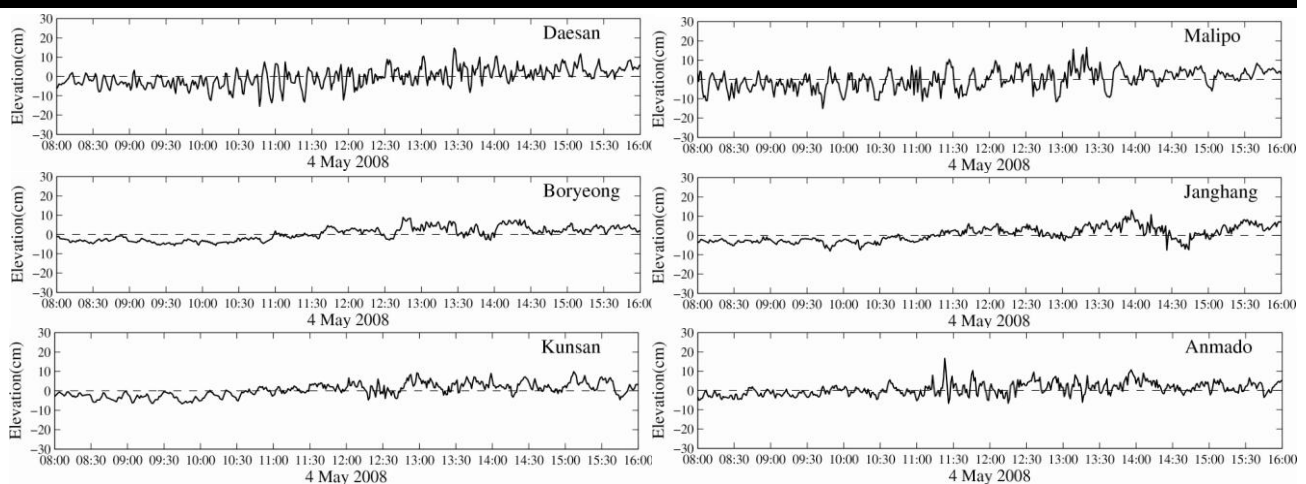


Figure 2. Observational data recorded in the national tidal stations (KHOA) and the temporary wave observation stations (KIOST) during the meteorological tsunami that occurred on 4 May 2008.

by the national tidal stations of the Korea Hydrographic and Oceanographic Administration (KHOA) and the temporary wave observation stations established by the Korea Institute of Ocean Science and Technology (KIOST) along the western coast of the Korean Peninsula (Figure 2). This is quite uncommon because tsunami-like long-period oceanic waves can travel long distances without significant energy dissipation and should have thus been observed by most observation stations. In fact, a similar large oscillation was observed by most national tidal stations when a meteorological tsunami occurred in 2007. Therefore, it was inferred that the abnormal oscillation observed during the 2008 event might have originated from certain other factors.

Choi and Lee (2009) analyzed observed wave data for the 2008 tsunami and obtained a time series of the significant wave height and period to identify the influence of wind waves, but the wind waves were observed to only increase the wave heights a day after the event (Figure 3). They also analyzed the automatic weather system data and weather radar images and observed that the pressure jump moved from the southwest to the northeast at a speed of approximately  $23.0 \text{ m}\cdot\text{s}^{-1}$  on average and that the mean magnitude of the pressure jumps was 1–3 hPa. Figure 4 shows the variation in precipitation concentration in radar data from 10:40 am to 12:40 pm on 4 May 2008. The moving atmospheric pressure disturbance, indicated by red lines, is clearly detected in Figure 4 (Choi and Lee, 2009; Cho *et al.*, 2013). In general, the mean water depth is approximately 44.0 m in the Yellow Sea and long period waves can move at a speed of  $c = \sqrt{gh} \approx 20.98 \text{ m}\cdot\text{s}^{-1}$  with the pressure jump. Thus, a long period sea wave generated by local-scale pressure jumps might be amplified during propagation owing to a Proudman resonance. In this case, the wave heights would be 5.0–10.0 cm since the amplification is generally multiplied by up to five times when compared to the air pressure change. The predicted wave heights agree well with observational data collected from national tidal stations and temporary wave stations. However, the abnormal oscillation observed at Jukdo Island is exceptional, and it might have originated from certain local conditions, such as rapid variations in topography.

### Computational Set-Up

The fully nonlinear and weakly dispersive Boussinesq model, FUNWAVE (Wei *et al.*, 1995), was initially developed and validated for coastal wave dynamics problems, including many successful tsunami case studies (cf. Chen *et al.*, 2003; Ioualalen *et al.*, 2007). Recently, the model has been improved and upgraded to FUNWAVE-TVD (Shi *et al.*, 2012) using a total variation diminishing (TVD) shock-capturing algorithm to simulate wave breaking and inundation more accurately, and is fully parallelized through a message passing interface protocol. This model was employed to simulate the run-up and inundation of the 2011 Tohoku-Oki tsunami (Grilli *et al.*, 2013) and has been validated for simulations of tsunami-like sea level oscillations on real topography.

MOHID, the three-dimensional baroclinic model developed by Marine and Environmental Technology Research Center at the Instituto Superior Tecnico at the Technical University of Lisbon, has been successfully applied to various studies in coastal and estuarine areas, as well as to oceanic processes and reservoirs, and it has shown reasonably good results in simulating complex features of the flows (cf. Vaz *et al.*, 2009). The model is capable of treating atmospheric forcing as a boundary condition for simulating hydrodynamics processes in oceans and can thus be applied to generate atmospheric disturbances in the Yellow Sea.

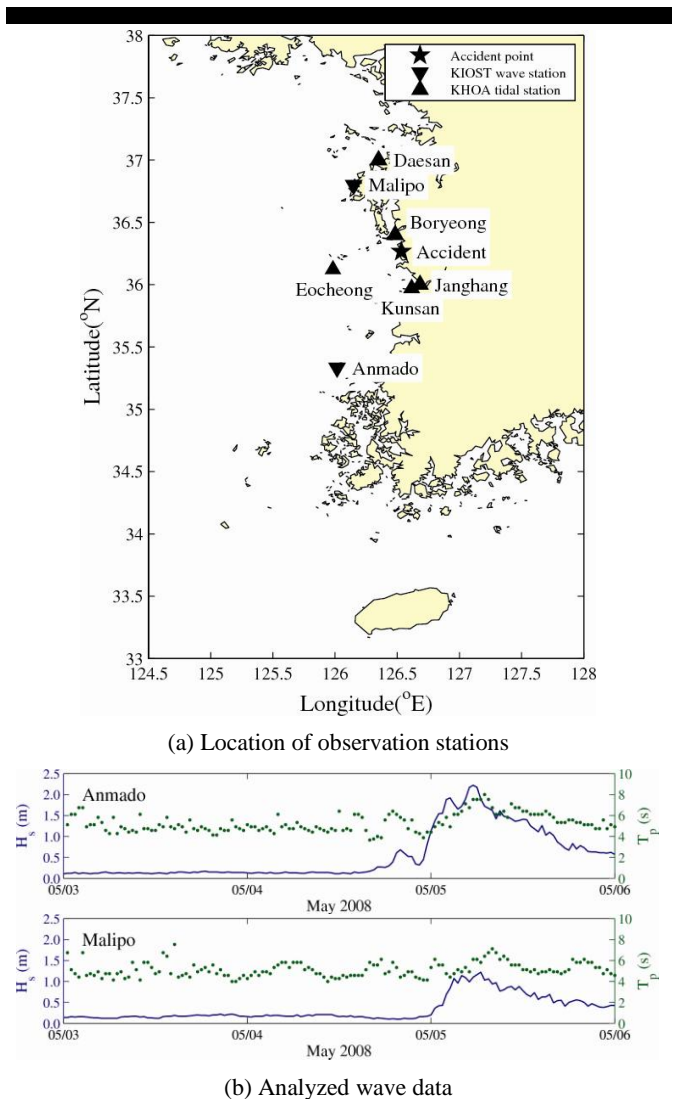


Figure 3. Time series of the significant wave height and period analyzed from observed wave data (Choi and Lee, 2009).

An atmospheric pressure disturbance moving over the Yellow Sea was generated using the MOHID model, according to the previous analysis performed by Choi and Lee (2009). Then, the model simulated hydrodynamic processes in the Yellow Sea from the source of the atmospheric forcing on the target area and provided a corresponding boundary condition for the FUNWAVE-TVD model. In the target area, the FUNWAVE-TVD model was employed to simulate complex transformations of the meteorological tsunami to account for depth-induced refraction, diffraction, and shoaling effects. The computational grid was constructed by utilizing 30 arc-second KorBathy30s bathymetry data (Seo, 2008), 1 arc-minute global relief model ETOPO1 bathymetry data, and the electronic navigational charts produced by KHOA (Figure 5). Resolution of the grid system ranged from 300.0 m to 1.5 km for the coarse grid used in the MOHID model and a uniform fine grid of 20.0 m was used in the FUNWAVE-TVD model.

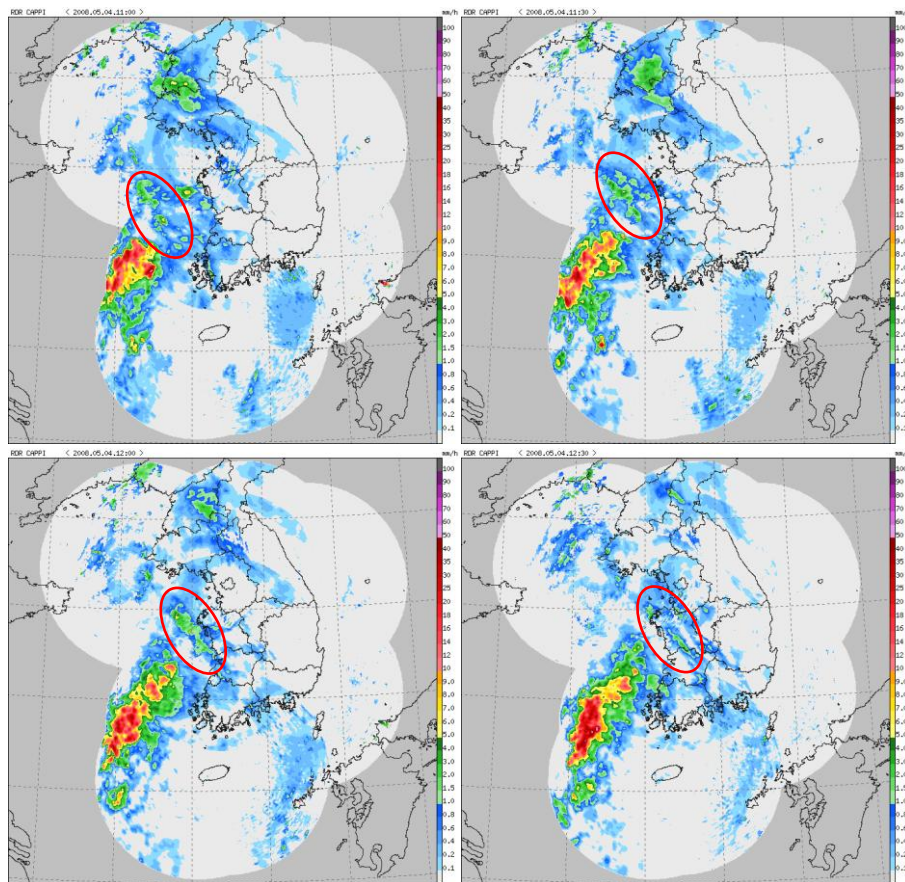


Figure 4. Moving atmospheric pressure disturbance observed in weather radar images from 10:30 am to 12:30 pm on 4 may 2008.

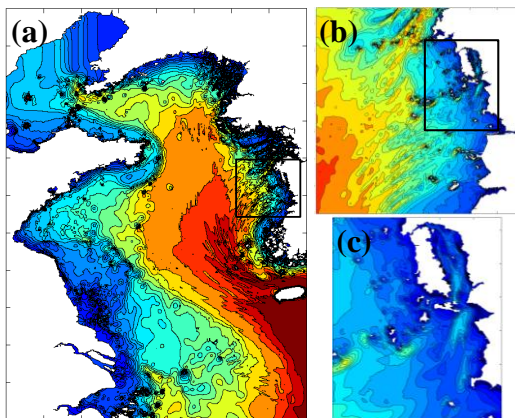


Figure 5. Detailed bathymetry in Yellow Sea and corresponding computational grid system [(a), (b): MOHID, (c): FUNWAVE-TVD].

## RESULTS AND DISCUSSION

As a preliminary test, a solitary wave was generated at the left boundary and its propagation was simulated to identify the amplification process in the target area using the FUNWAVE model. A solitary wave with an Ursell number of 0.1 was

generated, as the nonlinearity of a meteorological tsunami is usually small in the ocean. In Figure 6, the numerical results are represented and the time-dependent transformation of a solitary wave is shown around Boryeong. The numerical results show that while the incident solitary wave propagated through the Yellow Sea, it experienced variation in water depth and topography, and subsequently underwent depth-induced wave transformation. Thus, the incident wave was scattered into several wave trains of various wave heights and periods. These wave trains were focused in front of the target area (Figure 6), and the wave heights were increased owing to the effect of the combined wave trains. Furthermore, in the target area, both the first wave and the following wave trains were amplified simultaneously, and thus the whole amplification process clearly distinguished this area from the neighboring areas. The numerical results suggest the possibility of wave focusing in the target area during the 2008 event. As a result, an abnormally high run-up height might have originated only at the target area.

In general, the FUNWAVE-TVD model predicted the complex wave transformations in the surf zone better than the MOHID model since the former is a primitive equation model solving fully nonlinear Boussinesq equations and can consider physical dispersion effects as well as nonlinear effects in the shallow water region, whereas the latter focusses on simulating middle-scale ocean motions. Therefore, the MOHID model can be used in a straightforward manner to provide a corresponding boundary condition to the FUNWAVE-TVD model. In Figure 7, free surface profiles obtained on the basis of the numerical results



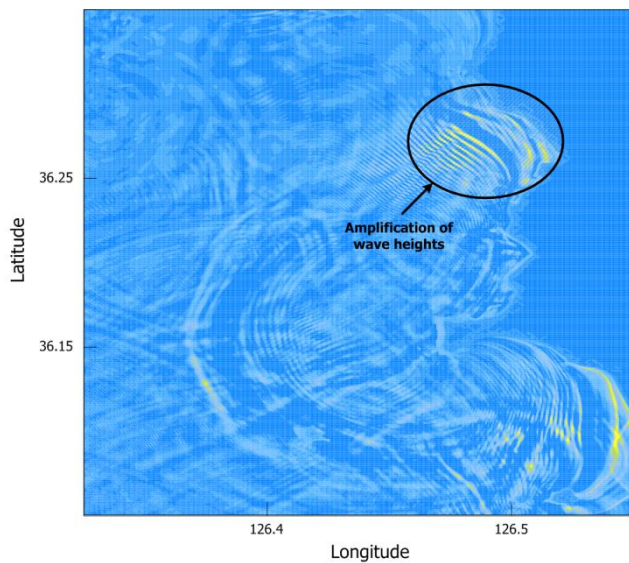


Figure 6. Propagation of solitary wave and amplification process by FUNWAVE-TVD around Boryeong, Korea.

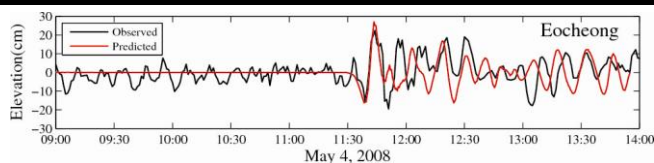


Figure 7. Comparison of free surface profiles between MOHID model and observational data at Eocheong Island.

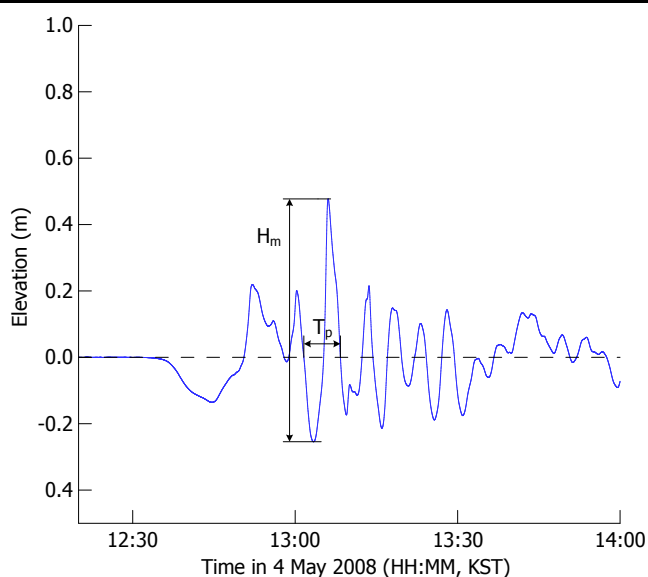


Figure 8. Computed free surface profile at Jukdo Island using FUNWAVE model.

computed by the MOHID model are compared with those based on observational data from a tidal station in Echeong Island.

According to a post-tsunami field survey, the meteorological tsunami hit Eocheong Island at 11:40 am, and the numerical results agree with the observational data with respect to the arrival time. The leading wave height and phase are also predicted well by the model.

Yoo *et al.* (2010) analyzed CCTV video data and calculated the wave height observed near the breakwater at Jukdo island. Figure 8 displays the maximum wave height and period computed by the FUNWAVE model. The maximum wave height and dominant wave period were calculated to be approximately 0.7 m and 400 s, respectively. However, Yoo *et al.* (2010) calculated the maximum trough-to-crest height and the dominant period was approximately 1.3 m and 185 s, respectively. In the numerical simulations, the amplification process for an incident wave was quite reasonable and an abnormal high wave was qualitatively well predicted, but the model slightly underestimated the wave height as compared to observational data. Although the model is capable of simulating complex wave transformation in the surf zone, including wave shoaling, breaking and breaking-induced current, a detailed run-up process on a coastal structure can only be roughly predicted because the process contains many uncertainties such as turbulent energy dissipation, wave interaction with porous media, bottom friction, and amplification of wave energy according to the dimension of structures. The results can be enhanced by employing additional analysis, such as experimental run-up formulas and high-resolution numerical simulations.

## CONCLUSION

In this study, the transformation of a small-scale meteorological tsunami on the western coast of Korea due to terrain complexity was investigated using numerical experiments. During the 2008 meteorological tsunami, an abnormally high wave oscillation was recorded only at Jukdo Island. We simulated the transformation of an incident wave at Jukdo Island using a coastal engineering model and briefly investigated the amplification process at this area. From the numerical simulations, it was identified that local topographic characteristics caused waves to be focused in front of Jukdo Island, following which combined waves arrived at Jukdo Island with high wave heights. However, the numerical model underestimates the wave heights, and additional analysis is required to improve this numerical modeling. Furthermore, the cause of the atmospheric pressure disturbance above the Yellow Sea is still unknown and needs to be identified to understand the whole amplification process in detail.

## ACKNOWLEDGEMENT

This research was a part of the project titled 'Development of Coastal Erosion Control Technology', funded by the Ministry of Oceans and Fisheries, Korea. This work was also supported by the Korea Institute of Ocean Science & Technology (Grant: PE99183).

## LITERATURE CITED

- Candela, J., Mazzola, S., Sammari, C., Limeburner, R., Lozano, C. J., Patti, B. and Bonnano, A., 1999. The "Mad Sea" phenomenon in the Strait of Sicily. *Journal of Physical Oceanography*, 29, 2210-2231.
- Chen, Q., Kirby, J.T., Dalrymple, R.A., Shi, F. and Thornton, E.B., 2003. Boussinesq modeling of longshore currents. *Journal of Geophysical Research*, 108(C11), 3362, doi:10.1029/2002JC001308.
- Cho, K.-H., Choi, J.-Y., Park, K.-S., Hyun, S.-K., Oh, Y. and Park, J.-Y., 2013. A synoptic study on tsunami-like sea level oscillations along the west coast of Korea using an unstructured-grid ocean model. In: Conley, D.C., Masselink, G., Russell, P.E. and O'Hare, T.J. (eds.), *Proceedings*

- 12th International Coastal Symposium (Plymouth, England), *Journal of Coastal Research*, Special Issue No. 65, pp. 678-683.
- Choi, B.-J., Park, Y. and Kwon, K., 2008. Generation and growth of long ocean waves along the west coast of Korea in March 2007. *Ocean and Polar Research*, 30, 453-466 (in Korean).
- Choi, J.-Y. and Lee, D.-Y., 2009. Analysis of small-scale atmospheric pressure jumps related to the generation of abnormal extreme waves at Boryeong. *Ocean and Polar Research*, 31, 379-388 (in Korean).
- Churchill, D.D., Houston, S.H. and Bond, N.A., 1995. The Daytona Beach wave of 3-4 July 1992: A shallow water gravity wave forced by a propagating squall line. *Bulletin of the American Meteorological Society*, 76, 21-32.
- Dragani, W.C., Mazio, C.A. and Nuñez, M.N., 2002. Sea level oscillations in coastal waters of the Buenos Aires province, Argentina. *Continental Shelf Research*, 22, 779-790.
- Drago, A.F., 1999. A study on the sea level variations and the 'Milghuba' phenomenon in the coastal waters of the Maltese Islands. University of Southampton, *Ph.D. thesis*.
- Gomis, D., Monserrat, S. and Tintore, J., 1993. Pressure-forced seiches of large amplitude in inlets of the Balearic Islands. *Journal of Geophysical Research*, 98(14), 437-445.
- Goring, D.G., 2005. Rissaga (long-wave events) on New Zealand's eastern seaboard: A hazard for navigation. In: Townsend, M.R. and Walker, D. (eds.), *Coasts and Ports: Coastal Living Coast; Australian Conference 2005*, Institution of Engineers, Barton, Australia, pp. 137-141.
- Grilli, S.T., Harris, J.C., Tajalli Bakhsh, T.S., Masterlark, T.L., Kyriakopoulos, C., Kirby, J.T. and Shi, F., 2013. Numerical simulation of the 2011 Tohoku tsunami based on a new transient FEM co-seismic source: Comparison to far- and near-field observations. *Pure and Applied Geophysics*, 170, 1333-1359.
- Haslett, S.K. and Bryant, E.A., 2009. Meteorological tsunamis in Southern Britain: An historical review. *Geographical Review*, 99(2), 146-163.
- Ioualalen, M., Asavanant, J., Kaewbanjak, N., Grilli, S., Kirby, J. and Watts, P., 2007. Modeling the 26th December 2004 Indian Ocean tsunami: Case study of impact in Thailand. *Journal of Geophysical Research*, 112, C07024, doi:10.1029/2006JC003850.
- Kakinuma, T., Asano, T., Inoue, T., Yamashiro, T. and Yasuda, K., 2009. Survey of February 2009 abiki disaster in Urauchi bay, Kamikoshiki Island. *Annual Journal of Coastal Engineering, JSCE*, B2-65, 1391-1395 (in Japanese).
- Liu, P. L.-F., Monserrat, S., Marcos, M. and Rabinovich, A.B., 2003. Coupling between two inlets: Observation and modeling. *Journal of Geophysical Research*, 108(C3), 3069, doi:10.1029/2002JC001478.
- Mercer, D., Sheng, J., Greatbatch, R. and Bobanovic, J., 2002. Barotropic waves generated by storms moving rapidly over shallow water. *Journal of Geophysical Research*, 107(C10), 3152, doi:10.1029/2001JC001140.
- Monserrat, S., Vilibić, I. and Rabinovich, A.B., 2006. Meteotsunamis: atmospherically induced destructive ocean waves in the tsunami frequency band. *Natural Hazards and Earth System Sciences*, 6, 1035-1051.
- Paskoff, R., 1970. *Le Chili semi-aride. Recherches géomorphologiques*. Bordeaux: Biscaye Frères, 420p.
- Proudman, J., 1929. The effects on the sea of changes in atmospheric pressure. *Monthly Notices of the Royal Astronomical Society. Geophysical Supplement*, 2(4), 197-209.
- Rabinovich, A.B., 2009. Seiches and harbour oscillations. In: *Handbook of Coastal and Ocean Engineering*, Singapore: World Scientific, 193-236.
- Ramis, C. and Jansa, A., 1983. Condiciones meteorológicas simultáneas a la aparición de oscilaciones del nivel del mar de amplitud extraordinaria en el Mediterráneo occidental, *Revista de Geofísica*, 39, 35-42 (in Spanish).
- Renault, L., Vizoso, G., Jansa, A., Wilkin, J. and Tintore, J., 2011. Toward the predictability of meteotsunamis in the Balearic Sea using regional nested atmosphere and ocean models, *Geophysical Research Letters*, 38, L10601, doi:10.1029/2011GL047361.
- Seo, S.-N., 2008. Digital 30sec gridded bathymetric data of Korea marginal seas - KorBathy30s. *Journal of Korean Society of Coastal and Ocean Engineers*, 20, 110-120 (in Korean).
- Sepic, J., Vilibić, I. and Strelec Mahovic, N., 2012. Northern Adriatic meteorological tsunamis: observations, link to the atmosphere, and predictability. *Journal of Geophysical Research*, 117, C02002, doi:10.1029/2011JC007608.
- Shi, F., Kirby, J.T., Harris, J.C., Geiman, J.D. and Grilli, S.T., 2012. A high-order adaptive time-stepping TVD solver for Boussinesq modeling of breaking waves and coastal inundation. *Ocean Modelling*, 43-44, 36-51.
- Shiga, T., Ichikawa, M., Kusumoto, K. and Suzuki, H., 2007. A statistical study on seiche around Kyushu and Satsunan Islands, *Papers in Meteorological Geophysics*, 74, S139-S162 (in Japanese).
- Tanaka, K., 2010. Atmospheric pressure-wave bands around a cold front resulted in a meteotsunami in the East China Sea in February 2009. *Natural Hazards and Earth System Sciences*, 10, 2599-2610.
- Vaz, N., Dias, J.M. and Leitao, P.C., 2009. Three-dimensional modelling of a tidal channel: The Espinheiro Channel (Portugal). *Continental Shelf Research*, 29(1), 29-41.
- Vilibić, I., Monserrat, S., Rabinovich, A. and Mihanovic, H., 2009. Numerical Modelling of the Destructive Meteotsunami of 15 June 2006 on the Coast of the Balearic Islands, *Pure and Applied Geophysics*. 165, 2169-2195.
- Vilibić, I. and Sepic, J., 2009. Destructive meteotsunamis along the eastern Adriatic coast: overview, *Physics and Chemistry of the Earth*, 34, 904-917.
- Vilibić, I., Šepić, J., Rangelov, B., Strelec Mahovic, N. and Tinti, S., 2010. Possible atmospheric origin of the 7 May 2007 western Black Sea shelf tsunami event. *Journal of Geophysical Research*, 115, C07006, doi:10.1029/2009JC005904.
- Wang, X., Li, K., Yu, Z. and Wu, J., 1987. Statistical characteristics of seiches in Longkou Harbour, *Journal of Physical Oceanography*, 17, 1963-1966.
- Wei, G., Kirby, J.T., Grilli, S.T. and Subramanya, R., 1995. A fully nonlinear Boussinesq model for surface waves. I. Highly nonlinear, unsteady waves. *Journal of Fluid Mechanics*, 294, 71-92.
- Yoo, J., Lee, D.-Y., Ha, T., Cho, Y.-S. and Woo, S.-B., 2010. Characteristics of abnormal large waves measured from coastal videos. *Natural Hazards and Earth System Sciences*, 10, 947-956.

# Applicability of video-derived bathymetry estimates to nearshore current model predictions



Max Radermacher<sup>†</sup>, Meagan Wengrove<sup>‡</sup>, Jaap van Thiel de Vries<sup>†</sup>, Rob Holman<sup>∞</sup>

<sup>†</sup> Delft University of Technology  
Faculty of Civil Engineering  
Stevinweg 1  
2628CN Delft, The Netherlands  
m.radermacher@tudelft.nl  
j.s.m.vanthieldevries@tudelft.nl

<sup>‡</sup> University of New Hampshire  
Durham, NH, U.S.A.  
med36@wildcats.unh.edu

<sup>∞</sup> Oregon State University  
Corvallis, OR, U.S.A.  
holman@coas.oregonstate.edu



[www.JCRonline.org](http://www.JCRonline.org)

## ABSTRACT

Radermacher, M., Wengrove, M.E., Van Thiel de Vries, J.S.M., Holman, R.A., 2014. Applicability of video-derived bathymetry estimates to nearshore current model predictions. In: Green, A.N. and Cooper, J.A.G. (eds.), *Proceedings 13<sup>th</sup> International Coastal Symposium* (Durban, South Africa), *Journal of Coastal Research*, Special Issue No. 70, pp. 290-295, ISSN 0749-0208.

In the framework of swimmer safety, coastal managers desire accurate nearshore current predictions obtained from numerical models. To this end, detailed and up-to-date bathymetry is a necessity. Remote sensing techniques for bathymetry estimation are a promising solution. The focus of this paper is to assess the performance of wavenumber-based bathymetric inversion using Argus imagery (also known as the cBathy algorithm) as a feasible input bathymetry for numerical models to make reasonable nearshore current predictions. Numerical flow simulations on a cBathy bed are compared to simulations on an in-situ surveyed bathymetry. Results demonstrate that simulated nearshore currents on a cBathy bathymetry have a root-mean-square error in the order of 10 cm/s (magnitude) and 40 degrees (direction) when compared to simulated currents on a surveyed bathymetry. In the intertidal zone cBathy should be combined with a different method for bathymetry estimation in order to decrease these errors.

**ADDITIONAL INDEX WORDS:** *Remote sensing, Argus, Numerical modeling, Sand Motor, Swimmer safety.*

## INTRODUCTION

In the nearshore, many processes are strongly influenced by the bed topography. Surfzone currents, which are studied here in relation to swimmer safety, are a clear example. The beach profile has its influence on the cross-shore distribution of currents (Ruessink *et al.*, 2001), whereas alongshore variable bar patterns may induce rip cell circulations (Dalrymple *et al.*, 2011). As a result of wave and current action, the bed is highly dynamic and bathymetry will change continuously. Such that there is a great need for frequent bathymetric data of the nearshore.

In-situ survey methods, such as echo sounders attached to floating equipment, are accurate and can be used for any desired spatial resolution. However, their maintenance and costs inhibit the implementation of high-frequency operational survey schedules. In contrast, remote sensing (RS) survey methods have a lower accuracy and limited spatial resolution, but are much less time-consuming and have low operational costs. The survey purpose determines if the accuracy and resolution achieved by a specific RS method are sufficient.

The relation between surfzone currents and bathymetry is not trivial, in that significant bathymetric errors do not necessarily lead to low accuracy in calculated currents on top of the bed. A bathymetry can be thought to consist of various features of different length scales, superimposed on each other. Through the

use of smoothing, Plant *et al.* (2009) assessed the influence of these bathymetric length scales on numerically simulated flow fields. They concluded that alongshore variability of intermediate scale features, associated with sand bar patterns, has a particularly strong influence. In this paper, the applicability of the cBathy algorithm (Holman *et al.*, 2013), based on the Argus system for coastal imagery (Holman and Stanley, 2007), to nearshore current simulations is explored. The capability of this method to resolve sand bar patterns is hypothesized to be crucial for accurate model predictions of nearshore currents.

## METHODS

cBathy results are obtained from the Sand Motor Argus station in the Netherlands. The Sand Motor (also known as Sand Engine or Zandmotor) is a vast beach nourishment of approximately 20 Mm<sup>3</sup> near the town of Ter Heijde, which primarily serves as a means of coastal protection against flooding (Stive *et al.*, 2013). In this study, one bathymetric survey conducted between 1 and 4 July 2013 is used for groundtruth comparison. In-situ bathymetry is measured using RTK-DGPS and a single-beam echo sounder (SBES) mounted on a personal water craft (PWC) for the wet section of the beach profile and an RTK-DGPS mounted on an all-terrain vehicle (ATV) for the dry section. With a comparable PWC-mounted system, MacMahan (2001) found that the root-mean-squared (RMS) deviation with respect to measurements by a traditional coastal survey vessel remain below 6 cm. The error

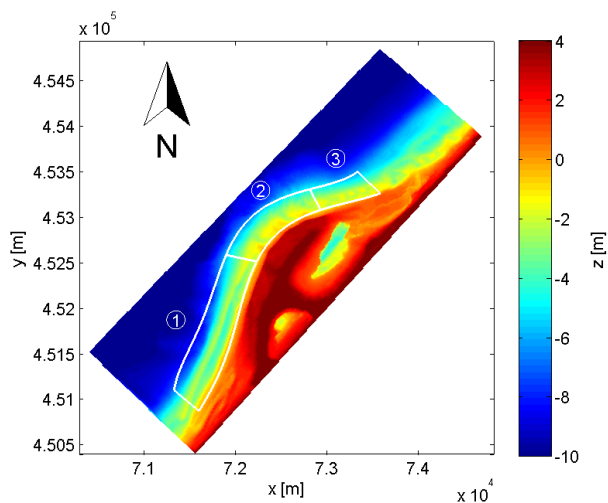


Figure 1. Bathymetry of the Sand Motor as captured during the July 2013 in-situ survey. Horizontal coordinates are according to the Dutch RD system; elevations with respect to the Dutch datum NAP. Numbers indicate nearshore subdomains used in this paper.

margin for the ATV is even smaller, as it is not susceptible to wave response or deviations due to the SBES.

The cBathy algorithm subjects wave-induced modulations of camera pixel intensity to cross-spectral analysis and complex EOF analysis in order to derive frequency and wavenumber pairs over a spatial analysis array. Inversion of the linear dispersion relation subsequently yields estimates of the water depth. Robustness of the algorithm is promoted by Kalman filtering in time (Kalman, 1960).

cBathy estimates are collected every 4 hours, so here both the highest and the lowest skill bathymetry (when comparing cBathy results to the in-situ measurements) during this 4-day period are assessed. Recent studies have reported average cBathy RMS errors (with respect to in-situ surveys) of 0.51 m for Duck, NC, 0.56 m for Agate Beach, OR (Holman *et al.*, 2013) and 1.14 m for

Kijkduin in the Netherlands (Wengrove *et al.*, 2013), the latter based on individual estimates before application of the Kalman filter.

A rectified and merged plan view image created from the 8 installed Argus cameras is presented as Figure 2. cBathy provides depth estimates at an analysis grid with a spacing of 10 m in the cross-shore and 20 m in the alongshore direction, contained within the white shape in the figure. As a result of noise, new estimates cannot be given every 4 hours for the full analysis domain. Over the first four days of July 2013 an average return rate of 42% of all analysis points was achieved, with a maximum of 85% and a minimum of 9%. Because of the relatively large cBathy analysis domain at the Sand Motor, combined with a low graze angle, average return rates reported by Holman *et al.* (2013) are much higher: 84% at Duck (small analysis domain) and approximately 85% at Agate Beach (high graze angle). Using the Kalman filtering procedure, effectively a running average of depth estimates is computed in time, bridging the gaps created by return rates less than 100%.

The bathymetries obtained from this analysis procedure are not directly applicable in numerical flow simulations. Especially in the off-shore regions, approximately outside the 6 m depth contour, moving objects in the camera images like small craft vessels and drifting navigation buoys are a very coherent source of errors. They are erroneously interpreted as wave-like signals by the cBathy algorithm, typically resulting in very shallow depth estimates with a high confidence. This problem is partly mitigated by rejecting depth estimates resulting from the lowest frequencies used in the analysis, as these tend to contain most of the energy associated with the errors. Furthermore, analysis tiles including pixels on the dry beach create deep troughs near the shoreline. Finally, only cBathy estimates that fall inside the three nearshore regions of Figure 1 (approximately the first 500 meters from the shoreline) are incorporated in the input bathymetry. The rest of the domain is filled with data from the in-situ survey, as cBathy results are too contaminated in these regions.

Numerical flow simulations on top of a cBathy bed are compared to simulations using a groundtruth bathymetry. The latter is assumed here to be the 'target': cBathy is judged suitable for nearshore current simulations if flow simulation results on both bathymetries compare well. The Delft3D suite (Lesser *et al.*,

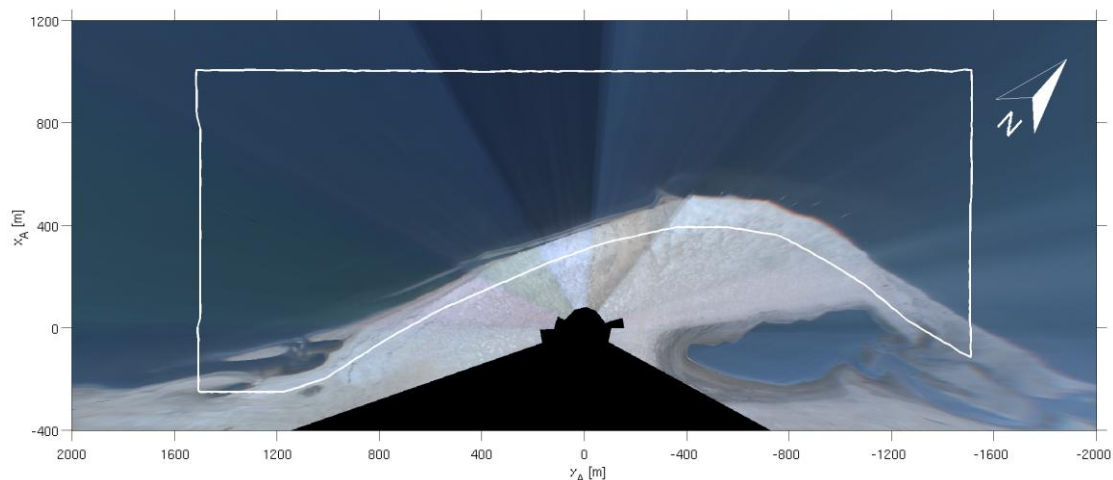


Figure 2. Merged and rectified (i.e. plan view) image of the Sand Motor collected by the Argus station at the Sand Motor on 8 July 2013. The initially hook-shaped peninsula shows clear signs of gross sediment fluxes in both northward and southward direction since construction was completed in fall 2011. The white polygon indicates the extent of the cBathy pixel grid. Horizontal coordinates are in the local Argus coordinate system.

2004) is used to conduct the flow calculations. This model has been used before to study nearshore currents over complex bathymetries, *e.g.* by Smit *et al.* (2008), Garcia *et al.* (2013) and Van Dongeren *et al.* (2013). The Sand Motor is embedded in a rectangular computational grid covering roughly 9.6 x 3.8 km in the alongshore and cross-shore directions respectively. The grid cell resolution varies from 50 m x 50 m in the offshore corners towards 17 m x 17 m in the region of interest.

Both bathymetric data sources are interpolated to the numerical grid, but first a limited amount of smoothing is added to the cBathy data on a uniform 17 m x 17 m grid using a Hanning filter with a length of 17 m in all directions to reduce potential aliasing of sub-grid scale features (Plant *et al.*, 2009), to average out noise in the cBathy bed and to provide a smooth transition at the edge of the nearshore subdomains. Although the cBathy algorithm already introduces a similar amount of smoothing (Holman *et al.*, 2013), RMS error statistics showed a significant improvement after applying this additional, limited amount of smoothing.

Boundary conditions are obtained from the operational Coastal Storm Modelling System (CoSMoS; Van Ormondt *et al.* 2012). This train of numerical wave and flow models is driven at the highest level by wave predictions for the Atlantic Ocean from NOAA's WaveWatch III model, meteorological predictions from the High Resolution Limited Area Model (HIRLAM) and astronomic water level predictions from the TPXO 6.2 model. More detailed models are nested down to the desired grid cell size at the Dutch coast. Finally, CoSMoS provides directional wave spectra, water levels and water level gradients to the Sand Motor model's boundaries and initial conditions.

Boundary conditions from the four days of the groundtruth survey have not been used, because accurate measurements with the single-beam echo sounder require mild hydrodynamic conditions ( $H_s < 0.5$  m) in order to limit dynamic response of the PWC. This inhibits analysis of rip current formation on the cBathy bed, which would be an interesting process to study given the swimmer safety background of this research, as these currents only develop with sufficient wave-forcing. Hence boundary conditions have been taken from the last three days of June, when hydrodynamics were slightly more energetic (waves with  $H_s \approx 1$  and directions between NW and N). The westerly wind is

moderate, with an average speed of 6.1 m/s and a maximum of 9.4 m/s computed by HIRLAM.

## RESULTS

In this section, first the cBathy depth estimates are compared to the groundtruth target bathymetries in order to select the best and worst matching 4-hourly cBathy results during the 4-day groundtruth survey campaign. Secondly, the results of the flow simulations are presented.

### Bathymetry

Figure 1 shows the bathymetry of the Sand Motor as captured during the groundtruth survey campaign of 1 to 4 July 2013. In the alongshore direction, three distinct regions can be indicated based on the prevailing bathymetric features. The southernmost region is characterized by a single, alongshore uniform bar (subdomain 1 in Figure 1). At the most seaward part of the Sand Motor, the bar welds to the shoreline and forms wide transverse bars incised by pronounced channels (subdomain 2). Along the spit towards the inlet of the lagoon, more rhythmic bar patterns can be distinguished (subdomain 3). Due to all these different regions, simulated flow patterns are also expected to show interesting spatial variability.

Because the in-situ bathymetric survey was conducted over a 4 day period, the RMS error over time is assessed to choose which cBathy estimate during this period best matches the PWC bathymetry. In the development of the RMS error over time a slight trend is present, with a minimum error around 3 July. This trend is very likely to be the result of noise rather than natural morphological evolution, as environmental conditions were very mild during the first four days of July and longer term development of RMSE shows a more scattered behavior rather than a smooth development. Errors in the nearshore domain (Figure 1) range from 48-66 cm. The collective RMS error over the three nearshore regions was used to rank the 4-hourly cBathy estimates. Both the highest (0.48 m at 2 July 18:40 UTC) and the

lowest ranked (0.66 m at 4 July 10:40 UTC) estimates were applied in the numerical modeling phase, as to represent the full range of results. The presented RMS errors in the nearshore are

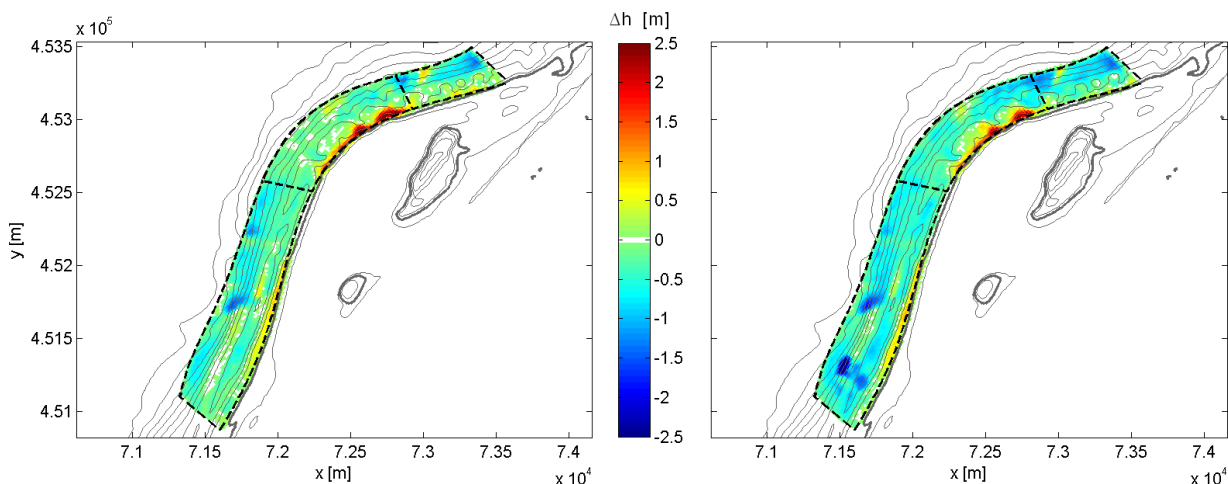


Figure 3. Highest (left) and lowest (right) ranked cBathy results. Both panels show deviations of cBathy bed levels with respect to groundtruth (red indicating cBathy estimate is too deep) together with depth contours of the groundtruth bathymetry. Outside the nearshore domains differences are absent, since cBathy estimates are omitted there.

comparable to those found by Holman *et al.* (2013), as mentioned in the previous section.

The spatial distribution of deviations of the highest ranked cBathy estimate are shown in the left panel of Figure 3. The calculated differences between the cBathy estimate and the in-situ survey demonstrate that cBathy resolves the seaward side to be too shallow and the shoreward side to be too deep (maximum deviations up to  $\pm 2.5$  m), in accordance with results from Holman *et al.* (2013) and Wengrove *et al.* (2013). This is highly noticeable in the upper part of the shore-connected bars in subdomain 2, where a trough separates the bar from the shoreline. Also, the southernmost rip channel in subdomain 2 is estimated to be too shallow by 50 cm, which could be the result of strong wave-current interaction when rips are active. The right panel of Figure 3 represents the lowest ranked (or worst) cBathy estimate. The error patterns are comparable, but the absolute deviations are larger. In subdomain 1 an erroneous shore-connected bar appears, whereas alongshore variability in subdomain 3 almost vanishes.

### Nearshore currents

The simulation results are summarized in Figure 4. It shows the temporal development of the RMSE in both magnitude (middle panel) and direction (lower panel) of currents on a cBathy bed with respect to currents on a groundtruth bathymetry. Modeled timeseries of environmental conditions, depicted in the upper panel, were obtained from a location offshore of subdomain 2. Altogether the velocity RMS errors remain below 15 cm/s in all subdomains for both the best and the worst cBathy result. The figure shows a clear tidal modulation, which peaks during low water.

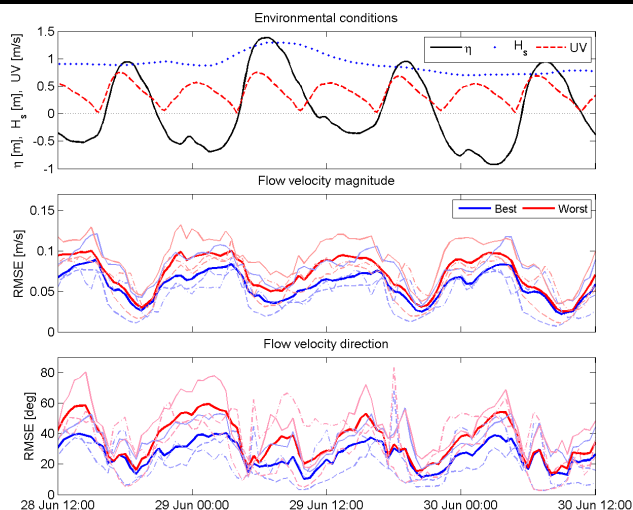


Figure 4. Environmental conditions as observed offshore of subdomain 2: tidal elevation  $\eta$ , significant wave height  $H_s$  and flow velocity magnitude  $UV$  (upper panel). Root-mean-square errors of flow velocity magnitude (middle panel) and direction (lower panel), using the best (blue) and worst (red) cBathy results. Individual subdomains are shown in thin, shaded lines: subdomain 1 (dashed), subdomain 2 (solid) and subdomain 3 (dash-dotted).

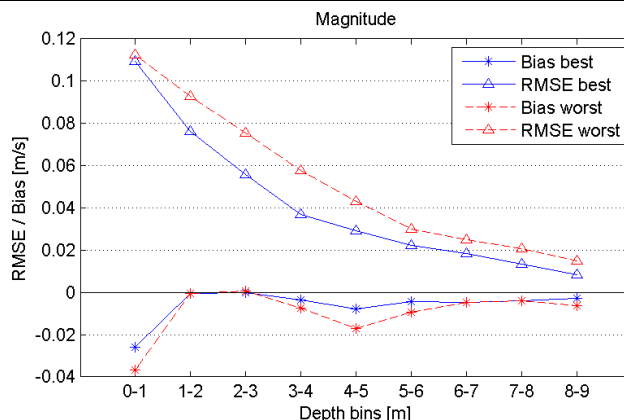


Figure 5. Time-averaged bias (stars) and RMS errors (triangles) of current magnitude deviations per (PWC) depth bin. Values based on the best cBathy estimate are shown in solid blue lines, those based on the worst estimate are shown in dashed red lines.

Figure 4 showed domain-averaged error statistics over time. In order to assess the spatial distribution of these errors, they can also be presented in a time-averaged plot. In Figure 5, bias and RMSE are shown per depth bin and averaged over time. It becomes apparent that the biggest error sources reside near the shoreline, as the shallowest depth bins have the highest bias and RMSE. To take the tidal modulation (Figure 4) into account, separate time-averaged statistics were calculated for the high water (HW,  $\eta > 0$ ) and low water (LW,  $\eta < 0$ ) phase. The HW-averaged statistics are rather straightforward (not shown here): subdomain 1 and 2 are dominated by an alongshore tidal current, which shows only very small deviations between both bathymetries. In subdomain 3, errors between currents on the cBathy and PWC bed are somewhat larger, due to the separation of tidal flow and the associated formation of a gyre. The LW-averaged statistics for the best bathymetry are shown in the left column of Figure 6. In subdomain 1, there is a small offset in the shore-parallel current through the longshore trough, which clearly shows from the adjacent red and blue bands in the middle panel. Shifting the focus to subdomain 2, good agreement between both simulations in the two distinct rip channels can be observed. Only the feeder currents near the shoreline show relatively large deviations, obviously resulting from the coarse overestimation of water depth by cBathy in the intertidal zone (recall Figure 3). This mainly goes for the northernmost part of subdomain 2, where the trough estimated by cBathy is particularly deep and flow directions deviate accordingly. In subdomain 3 there is again good agreement between both simulations, judging from the small differences in magnitude and direction. The rhythmic bar patterns do not seem to evoke strong rip currents, but the slightly off-shore directed flow in the eastern part of the subdomain is well represented.

The flow field obtained with the worst bathymetry is less capable of reproducing the flow field on a groundtruth bed. HW-averaged statistics do not show a large additional error, as this tidal phase is dominated by a strong shore-parallel tidal current, which is less influenced by bar patterns. Deviations in magnitude during HW are slightly higher compared to those of the highest ranked bathymetry, due to the more pronounced underestimation of water depth on the outer bar face by cBathy (Figure 3). LW-averaged statistics are shown in the right column of Figure 6. Observed deviations in subdomain 1 computed with the worst cBathy estimate (offset of current through longshore trough) are

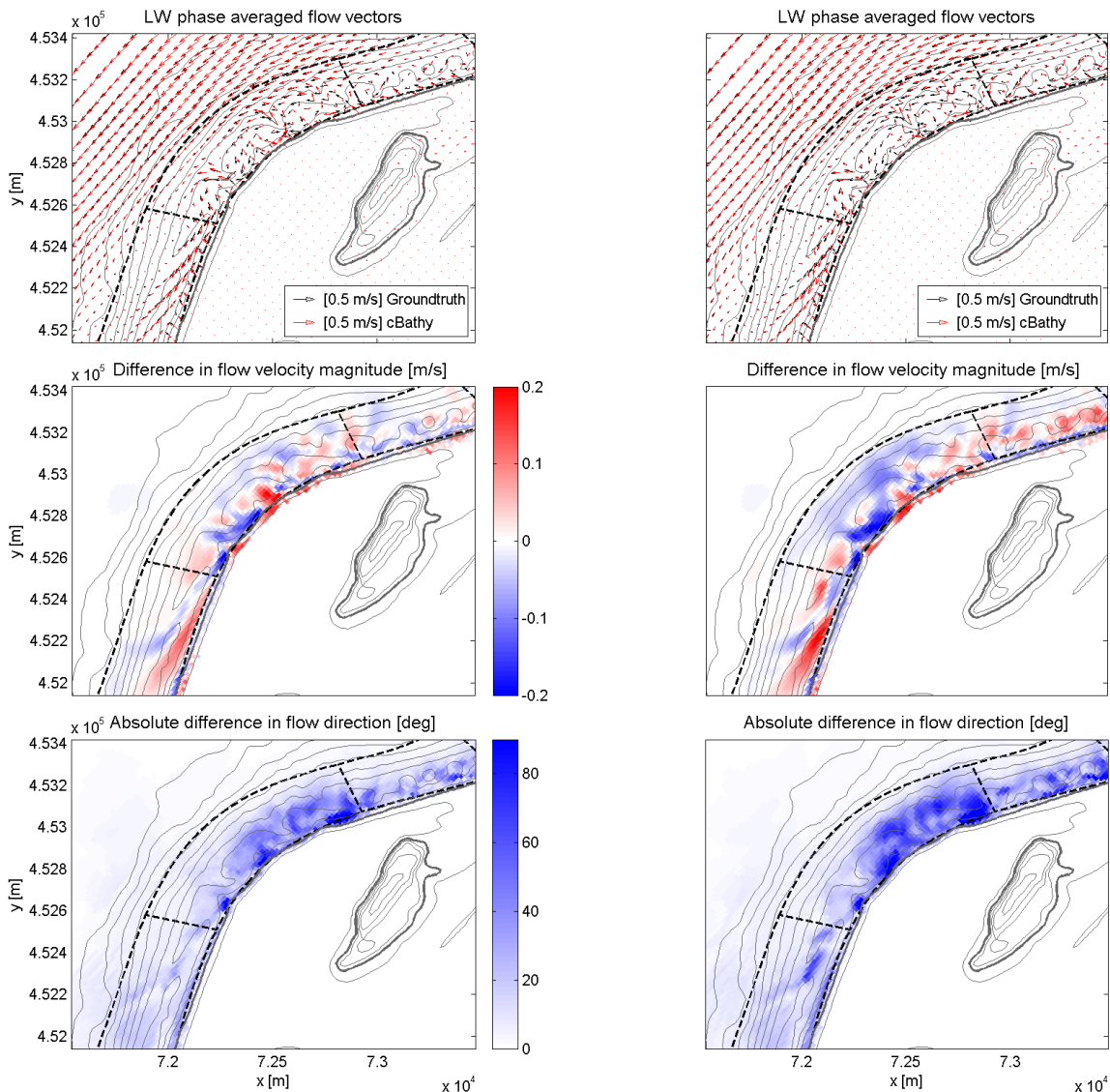


Figure 6. Comparison of low water phase-averaged currents over a cBathy bed (left column for best estimate, right column for worst estimate) and groundtruth bathymetry. The upper panels show velocity vectors (red for cBathy, black for groundtruth; only 1 in every 3 arrows is shown), the middle panels show the difference in magnitude (red indicating overestimation of velocities using a cBathy bed) and the lower panels show the absolute difference in direction. Grey contour lines represent the groundtruth bathymetry.

similar to those computed with the best cBathy estimate, but stronger. In subdomain 2, the rip current in the lower left channel is still well predicted using the worst estimate. This does not hold for the upper right part of this subdomain, where the trough near the shoreline is deeper than in the best estimate and completely disturbs the flow field. This influences currents in the left part of subdomain 3 as well, resulting in larger deviations.

## DISCUSSION

Results show velocity deviations simulated on the best cBathy bed averaged over HW and LW tidal phases remain below 10 cm/s, except for several locations close to the shoreline, where deviations reach up to 20 cm/s during LW. When compared to maximum flood currents of 70 cm/s and maximum ebb currents of 55 cm/s at 13 m water depth (see upper panel of Figure 4) and about 50 cm/s in the nearshore (which also happens to be the order of magnitude of human swimming speed), these deviations seem

reasonably small. Using the worst cBathy bed, flow fields compare less well and deviations increase over the full nearshore domain. Generally, the tidal modulation of the error can potentially be explained by the increasing relative importance of absolute errors in the cBathy bed as the water level decreases, or could be related to specific features in the flow field during the subsequent tidal phases. When the flood phase is initiated, a uniform current develops along the shoreline, directed to the North-East. At the lee-side of the Sand Motor, this causes flow separation and the creation of a large-scale gyre near subdomain 3. Before the gyre gets advected northward, the ebb phase commences and the gyre dies out. During the ebb phase, lowering of the water level causes waves to break over the prominent transverse bars in subdomain 2. In line with rip current theory and observations, this drives strong seaward currents in the rip channels (Dalrymple *et al.*, 2011). Although the rips are resolved well in both magnitude and direction on the cBathy bed, directional RMSE peaks up to 80 degrees in subdomain 2 for the

worst bathymetry (lower panel of Figure 4). This is mainly caused by differences in nearshore circulations on the cBathy and PWC bed, locally leading to directional deviations around 180 degrees. The ebb flow again creates a gyre, which is now located south-west of the Sand Motor and partly passes through subdomain 1. Subsequently the flood phase sets in and the cycle starts over.

Similar flow simulations for the first four days of July, when environmental conditions were very mild, yielded smaller deviations. In an operational current forecasting scheme, e.g. for swimmer safety purposes, even the worst cBathy estimate combined with highly energetic environmental conditions should yield flow errors that remain within acceptable limits. More extreme environmental conditions and bathymetric deviations will be explored in more detail in follow-up research.

Improving remotely sensed bathymetric estimates near the shoreline is expected to reduce errors in flow predictions. cBathy estimates several troughs in the intertidal zone that do not only disturb the calculated flow at those locations, but also influence a wider region (in the order of 10's to 100's of meters). An example of this relates to erroneous predictions of a feeder current effecting the strength and timing of the associated rip current. An Argus-based tool for the estimation of intertidal bathymetry using shoreline tracking has been described by Aarninkhof *et al.* (2003) and Uunk *et al.* (2010). Future research will focus on incorporating this source of up-to-date RS bathymetry in the numerical model simulations. Another possible solution strategy would be to reduce anomalies in the cBathy bed through the use of smoothing, thereby partly removing the troughs. Additional simulations have been conducted with a smoothed bathymetry, using a Hanning window which spans 4 surrounding grid cells in both horizontal dimensions (Plant *et al.*, 2009). Although error statistics of this smoother bathymetry show a slight decrease of RMSE in flow magnitude and direction, important flow features to hydrodynamic predictions for swimmer safety purposes like rip currents are damped through the removal of rip channels.

This research has only focused on model-model comparison of bathymetries and flow fields so far, because an extensive set of hydrodynamic field data around the Sand Motor is currently lacking. During the MegaPEX field campaign in fall 2014 a robust dataset of hydrodynamic conditions will be collected, that can be used to validate hydrodynamic model simulations.

## CONCLUSIONS

In this paper, a comparison has been presented between remotely sensed bathymetric data obtained with the cBathy algorithm and groundtruth bathymetric data of the Sand Motor, as well as a comparison of flow fields simulated on these bathymetries using a 2DH hydrodynamic model. Despite considerable root-mean-squared errors in the depth estimates, cBathy bathymetries generally induced fairly small deviations in the flow field. The main source of errors resides around the shoreline, where the water depth is heavily overestimated by cBathy.

In conclusion, cBathy seems to be a suitable tool for application in operational nearshore current predictions. However, please note that depth estimates for deeper parts of the analysis domain (all data from the area indicated in Figure 2 that fall outside the nearshore domains indicated in Figure 1) have been rejected in the final bathymetry.

## ACKNOWLEDGEMENTS

Max Radermacher is supported by STW Perspectief program Nature-driven nourishments of coastal systems (NatureCoast), project 12686: S1 Coastal Safety. The authors would like to

acknowledge Roderik Hoekstra and Cilia Swinkels from Deltares for providing the basis of the Delft3D model used in this research, along with the associated CoSMoS boundary conditions.

## LITERATURE CITED

- Aarninkhof, S.G.J., Turner, I.L., Dronkers, T.D.T., Caljouw, M. and Nipius, L., 2003. A video-based technique for mapping intertidal beach bathymetry. *Coastal Engineering*, 49, 275-289.
- Dalrymple, R.A., MacMahan, J.H., Reniers, A.J.H.M. and Nelko, V., 2011. Rip currents. *Annual Review of Fluid Mechanics*, 43, 551-581.
- Garcia, I.D., El Serafy, G., Heemink, A. and Schuttelaars, H., 2013. Towards a data assimilation system for morphodynamic modeling: bathymetric data assimilation for wave property estimation. *Ocean Dynamics*, 63, 489-505.
- Holman, R.A. and Stanley, J., 2007. The history and technical capabilities of Argus. *Coastal Engineering*, 54, 477-491.
- Holman, R.A., Plant, N.G. and Holland, K.T., 2013. cBathy: A robust algorithm for estimating nearshore bathymetry. *Journal of Geophysical Research: Oceans*, 118, 2595-2609.
- Kalman, R., 1960. A new approach to linear filtering and prediction problems. *Journal of Basic Engineering*, 82, 35-45.
- Lesser, G.R., Roelvink, J.A., Van Kester, J.A.T.M. and Stelling, G.S., 2004. Development and validation of a three-dimensional morphological model. *Coastal Engineering*, 51, 883-915.
- MacMahan, J.H., 2001. Hydrographic surveying from personal watercraft. *Journal of Surveying Engineering*, 127, 12-24.
- Plant, N.G., Edwards, K.L., Kaihatu, J.M., Veeramony, J., Hsu, L. and Holland, K.T., 2009. The effect of bathymetric filtering on nearshore process model results. *Coastal Engineering*, 56, 484-493.
- Ruessink, B.G., Miles, J.R., Feddersen, F., Guza, R.T. and Elgar, S., 2001. Modeling the alongshore current on barred beaches. *Journal of Geophysical Research*, 106, 22,451-22,463.
- Smit, M.W.J., Reniers, A.J.H.M., Ruessink, B.G. and Roelvink, J.A., 2008. The morphological response of a nearshore double sandbar system to constant wave forcing. *Coastal Engineering*, 55, 761-770.
- Stive, M.J.F., De Schipper, M.A., Luijendijk, A.P., Aarninkhof, S.G.J., Van Gelder-Maas, C., Van Thiel de Vries, J.S.M., De Vries, S., Henriquez, M., Marx, S. and Ranasinghe, R., 2013. A new alternative to saving our beaches from sea-level rise: the Sand Engine. *Journal of Coastal Research*, 29, 1,001-1,008.
- Uunk, L., Wijnberg, K.M. and Morelissen, R., 2010. Automated mapping of the intertidal beach bathymetry from video images. *Coastal Engineering*, 57, 461-469.
- Van Dongeren, A., Van Ormondt, M., Sembiring, L., Sasso, R., Austin, M., Briere, C., Swinkels, C., Roelvink, D. and Van Thiel de Vries, J., 2013. Rip current predictions through model-data assimilation on two distinct beaches. In: Proceedings of the Coastal Dynamics 2013 conference (Arcachon, France).
- Van Ormondt, M., Van Dongeren, A., Briere, C., Sembiring, L., Winter, G., Lescinski, J. and Swinkels, C., 2012. Simulating storm impacts and coastal flooding along the Netherlands coast. In: Klijn, F. and Schwenkendiek, T. (eds.), *Comprehensive Flood Risk Management*. Proceedings of the Flood Risk 2012 conference (Rotterdam, Netherlands).
- Wengrove, M.E., Henriquez, M., De Schipper, M.A., Holman, R.A. and Stive, M.J.F., 2013. Monitoring morphology of the Sand Engine leeside using Argus' cBathy. In: Proceedings of Coastal Dynamics 2013 (Arcachon, France), 1893-1904.



## Extensive monitoring and intensive analysis of extreme winter-season wave events on the Korean east coast

Sang-Ho Oh<sup>†,‡</sup>, Weon-Mu Jeong<sup>†</sup>

<sup>†</sup>Coastal Engineering and Ocean Energy Research Division  
Korea Institute of Ocean Science and Technology  
Ansan, Republic of Korea  
ohsangho@kiost.ac  
wmjeong@kiost.ac

<sup>‡</sup> Department of Convergence Study on the Ocean Science and Technology  
Ocean Science and Technology School  
Korea Maritime and Ocean University  
Busan, Republic of Korea



[www.cerf-jcr.org](http://www.cerf-jcr.org)



[www.JCRonline.org](http://www.JCRonline.org)

### ABSTRACT

Oh, S.-H., Jeong, W.-M., 2014. Extensive monitoring and intensive analysis of extreme winter-season wave events on the Korean east coast. In: Green, A.N. and Cooper, J.A.G. (eds.), *Proceedings 13<sup>th</sup> International Coastal Symposium* (Durban, South Africa), *Journal of Coastal Research*, Special Issue No. 70, pp. 296-301, ISSN 0749-0208.

Extensive wave monitoring was carried out over nine consecutive years at nine different locations along the east coast of Korea in order to examine the overall wave statistics and to investigate the generation and propagation mechanism of occasional high waves in this region. This type of long-term wave observation at multiple stations has never been performed on the Korean east coast. Appearances of high waves, defined by criteria of  $H_s \geq 3$  m and  $T_p \geq 9$  s at any of the nine stations within a single day accounted for approximately 5% of the total data. These high waves mostly occurred in winter under the influence of strongly developed winter storms over the East Sea. Among these high wave events, three representative cases were subjected to a further intensive analysis by using the corresponding wave data together with meteorological data at that time. Based on such a synthetic analysis, it was possible to understand details regarding the general patterns in the development of low pressures and subsequent formation of strong wind fields around the coastal zone, which eventually affected the characteristics of the high waves that were observed.

**ADDITIONAL INDEX WORDS:** *Winter storm, High waves, extra-tropical cyclone, wave observation, East Sea.*

### INTRODUCTION

During winter seasons in the recent few years, extremely high storm waves greater than 3 m occasionally appeared on the Korean east coast at a frequency of several times per year. These high waves caused many casualties and the damage of infrastructures along the coastline. Several researchers recently examined the reason why such high waves are occurring during the winter season around the east coast of Korea or the west coast of Japan (Jeong *et al.*, 2009; Lee *et al.*, 2010; Kim *et al.*, 2011; Lee, 2013; Oh and Jeong, 2013). According to them, high waves tend to be generated when strong northeasters continuously blow over the water surface of the East Sea. These are as a result of excessive development of extra-tropical low pressure system or cyclones over the sea.

In the winter season, the wind and wave climate around Korea is predominantly influenced by steady northwesterers governed by the winter monsoon. However, in the case of the east coast of Korea, intermittently blowing strong northeasters, rather than the ordinary northwesterers, can bring about more severe weather conditions in winter. This is because it faces the East Sea in an easterly direction. While it is not clear at the present whether such stormy weather is occurring more often than previously, as a result of possible impacts of climate change around this region (e.g., Vanem *et al.*, 2012), the scale of human casualties, beach erosion,

and damage of coastal structures is obviously increasing in the last decade. Basically, the strong development of extra-tropical cyclones and subsequent stormy weather several times during the winter season is a prevailing phenomenon in the mid-latitudes of the Northern Hemisphere (Hoskins and Hodges, 2002; Chang and Fu, 2002). In the sea waters of the North Atlantic Ocean and the North Sea, harmful winter storms have caused many casualties and huge economic losses over the European countries repeatedly. In this light, a number of studies have been carried out to understand the nature, dynamics, and variability of the European winter storms (e.g. Ulbrich *et al.*, 2001; Wernli *et al.*, 2002; Liberato *et al.*, 2013). Meanwhile, storms that are generated in the East Sea, or the western boundary of the North Pacific Ocean, have received relatively less attention so far; partly because there have been little notable disasters due to the storms until recently. The appearance of high storm waves on the Korean east coast has become more common in the recent decades, and the loss of human lives and property damage accompanied by such high waves is now receiving more attention from the local populace.

Hence, it is required to understand, in detail, the characteristics of the generation and propagation of these winter storms that are occurring in the East Sea. These are prerequisites for the accurate prediction of the storm tracks and consequent establishment of countermeasures. As a means to accomplish such a goal, extensive nearshore wave monitoring has been continued for the past decade at nine different stations covering the Korean east coast. Such an extensive wave observation program has never been carried out in



Figure 1. Location map of the wave measurement stations.

the past in Korea; the acquired wave observation data are thus considered a valuable database for studying the wave climate on the Korean east coast. In this paper, major findings related to the extreme winter storm events are presented based on the intensive analysis of the long-term wave monitoring data.

## DATA

### Wave Data from Nine Measurement Stations

The coastal waves were measured at the nine measurement stations along the east coast of Korea by using pressure gauges deployed on the sea bottom as shown in Figure 1. Information about the geographical coordinate and water depth of each wave station is presented in Table 1. The wave observation period and number of data were different depending on the stations as the number of measurement stations has increased until 2008. The pressure gauges recorded the raw data at a sampling rate of 2 Hz. By using the first 2048 data points during every 30 minutes, the wave spectrum was calculated from the spectrum of water pressure by using the transfer function between the wave pressure and the water surface elevation.

### Supplementary Meteorological Data

The weather chart and wind observation data provided by the Korean Meteorological Agency (KMA) were also used in this study to assist in the understanding of the generation and propagation mechanism of the high wave event. The weather chart is officially released every three hours by KMA. Meanwhile, the wind data were obtained at the weather station nearest to each of the wave measurement locations shown in Figure 1. Mean wind speed and direction at every one hour for each weather station were used in the analysis. Since the elevation from the mean sea level at each of the weather stations is different, the wind speed was converted to the value at 10 m above the land by assuming the logarithmic profile of the mean wind speed.

## BASIC WAVE STATISTICS

Table 1. Information on the nine wave measurement stations.

Station	Observation period	Geographical coordinate	Water depth (m)	Number of data
Daejin	2007.11.09~ 2012.06.19	38.521°N 128.427°E	17.5	75,691
Sokcho	2005.11.24~ 2012.11.29	38.208°N 128.617°E	18.5	122,944
Gangneung	2005.02.27~ 2012.10.27	37.798°N 128.929°E	15.0	133,202
Mukho	2004.03.07~ 2012.06.18	37.548°N 129.125°E	15.5	138,708
Jukbyeon	2006.03.15~ 2012.11.30	37.060°N 129.433°E	18.5	104,275
Hupo	2006.05.04~ 2012.09.20	36.700°N 129.484°E	18.5	102,311
Weolpo	2008.01.29~ 2012.05.16	36.212°N 129.398°E	17.0	75,294
Yangpo	2007.10.31~ 2012.10.30	35.886°N 129.539°E	18.5	87,360
Jinha	2005.10.20~ 2012.10.30	35.387°N 129.361°E	19.0	112,952

### Distributions of wave height and period

While our main interest is placed on extreme wave events that have occurred on the Korean east coast, it is also meaningful to know the general wave climate over the region where wave measurements were carried out. Figure 2 shows the cumulative distributions of the significant wave heights and periods at the nine measurement stations. These were calculated by using all the available data during the observation period as shown in Table 1.

Although the general pattern in the distributions of wave heights and periods is similar among the measurement locations, there exists a difference among the stations with respect to the portion of samples exceeding a certain wave height or period. Taking some examples, 15.4% of the measured significant wave heights were greater than 1 m at Jinha, while the ratio became almost double at Jukbyeon (28.5%). Meanwhile, the exceedance probability of a significant wave period of 10 s was 6.8% at Jinha and 2.04% at Sokcho. One noteworthy thing in Figure 2 is that the probability of exceeding a certain significant wave height is generally much higher in the mid-latitude locations such as Jukbyeon and Mukho than in the low-latitude locations of Jinha or Wolpo. In contrast, the trend for the significant wave period is different, showing an obviously greater exceedance probability in the low-latitude locations than in the high-latitude locations (such as Sokcho or Gangneung). This may be due to the differences in relative fetch from the wave source region between the different wave measurement stations. Since the overall wave direction is northeast on the Korean east coast, waves tend to first arrive at the relatively high or mid-latitude wave stations.

### Probabilities of high wave occurrence

By utilizing all the available wave observation data from March 2004 to November 2012, some extremely high wave events were detected, with a criterion of  $H_s \geq 3$  m and  $T_s \geq 9$  s, which was suggested by Oh *et al.* (2010) as threshold values for discriminating large-height swell-like waves. The term *swell-like waves* was used in their study because the high waves appearing on the Korean east coast are typically a mixture of relatively longer period swell and ordinary wind waves. Table 2 shows the occurrences of such high wave events, where the numbers of days

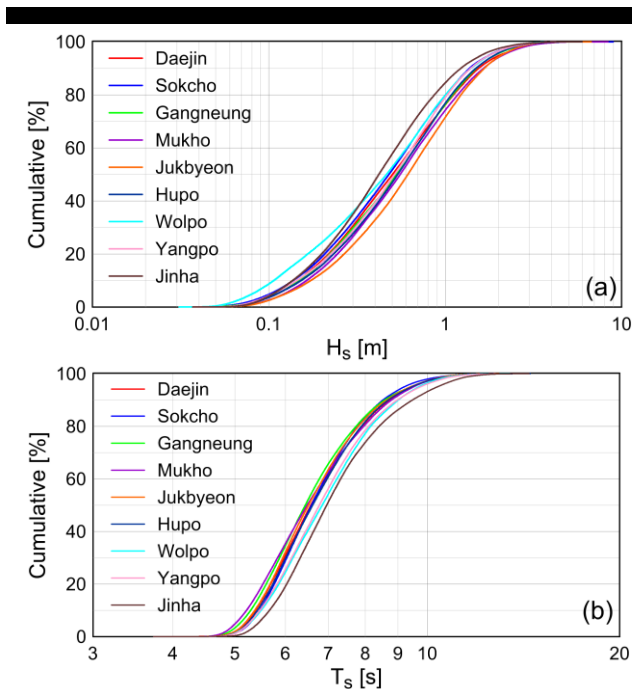


Figure 2. Cumulative distributions of the significant wave heights and periods at the nine measurement stations.

in each month satisfying the above criteria at any of the nine wave stations are listed.

In Table 2, it is clearly seen that high waves tend to appear more often in winter than in summer. It shows that 91.3% of the high wave days occurred during the eight months starting from September to April. Among them, in particular, 38.8% belonged to December or January. Within these two months, the probability of days experiencing high waves was 11.5% during the total observation period, which implies high waves of  $H_s \geq 3$  m and  $T_s \geq 9$  s may appear 7.1 days during the two months on average. With respect to the annual variation, a slight increase in this tendency is found in the table, although there exists large scattering in the numbers of days with high waves in each year. Overall, high waves associated with the above criterion took place 161 days during the total consecutive observation period of 105 months, which corresponds to a probability of occurrence of 5.0%.

In Korea, a high wave alert or advisory is issued by KMA when high winds greater than 14 m/s are probable for more than three hours or when the significant wave height within the specified coastal area is expected to surpass 3 m. Hence, the aforementioned criteria of  $H_s \geq 3$  m and  $T_s \geq 9$  s by Oh *et al.* (2010) corresponds to the high wave alert criteria of KMA. In order to investigate the occurrence probability of further extreme wave events, however, a stricter set of criteria of  $H_s \geq 4$  m and  $T_s \geq 12$  s were applied to recognize more unusually high wave case among the observation data. The results are also shown in Table 2, where the numbers in the parentheses denote the numbers of days fulfilling the stricter criterion. In total, 10 days were detected as listed in the table, on which day waves of  $H_s \geq 4$  m and  $T_s \geq 12$  s visited at least one of the nine measurement stations on the Korean east coast. This corresponds to a probability of occurrence of 0.3% during the whole observation period.

Table 2. Numbers of days when high waves  $H_s \geq 3$  m and  $T_s \geq 9$  s appeared on any of the nine measurement stations during the whole wave observation period. The numbers in the parentheses indicate the days of  $H_s \geq 4$  m and  $T_s \geq 12$  s.

Month	'04	'05	'06	'07	'08	'09	'10	'11	'12	Total
Jan.	-	2	0	3	3	6	6	5(1)	3	28
Feb.	-	0	4	0	3(2)	1	2	6	3	19
Mar.	0	0	0	0	1	1	3	0	2	7
Apr.	1	0	0	2	0	4	1	2	2(1)	12
May	0	0	0	0	0	0	5	0	0	5
Jun.	0	0	0	0	0	0	0	0	0	0
Jul.	0	0	0	0	0	0	0	2	0	2
Aug.	0	1	2	0	4	0	0	0	0	7
Sep.	0	1	4	2	0	0	0	7	1	15
Oct.	1	2(2)	5(2)	1	0	3	1	2	0	15
Nov.	2	0	2	4	0	9	0	4	1	22
Dec.	5(1)	4(1)	4	0	3	3	6	4	-	29
All	9	10	21	12	14	27	24	32	12	161

## ANALYSIS OF HIGH WAVE EVENTS

### Three extremely high wave events

Among the wave records related to the stricter criteria of  $H_s \geq 4$  m and  $T_s \geq 12$  s, three wave events that occurred in October 2006, February 2008, and January 2011 were selected for examining the general characteristics of the growth and decay patterns of the high waves. These three events showed clear dissimilarity as well as similarity with respect to the wave development patterns, the spatio-temporal variations of wave height and period among the wave measurement stations, and the dynamics of the associated low pressure systems. Figures 3 to 5 show the time series of the significant wave heights and periods observed at all the available measurement stations during the three wave events, respectively.

In the case of October 2006, the wave records were only acquired at the five locations as shown in Figure 3. The wave height started to rapidly increase and reached its maximum within less than 20 hours for all the measurement stations. In particular, the maximum significant wave height at Sokcho reached 9.69 m on 23rd October, which was the record-high wave height on the Korean east coast. Another feature found in Figure 3 is the considerable distinction in the time of sudden increase of wave heights and periods among the five locations. This indicates a temporal difference in terms of the first arrival of high waves depending on the measurement stations. In general, the first appearance of high waves tended to be delayed with progressively lower latitude. This indirectly implies that the waves may approach the coast from the northern direction. Indeed, supplementary wave measurement carried out by using a directional buoy showed that the principal wave direction on the Korean east coast is mostly northeast in winter time (Oh *et al.*, 2013).

The time histories of  $H_s$  and  $T_s$  are shown in Figure 4. For the high wave events in February 2008, these also displayed a tendency of earlier arrival of high waves at the measurement stations located more northward. In this case, however, the variation patterns of wave heights and periods showed marked discrepancy from those in October 2006 (Figure 3). Although the maximum wave height was significantly smaller than the previous case, the high waves continued about 2 days after the peak, rather than gradually decaying as in October 2006. In fact, the wave heights and periods doubled on the 23rd and 24th February respectively, as shown in Figure 4. The reason for this type of

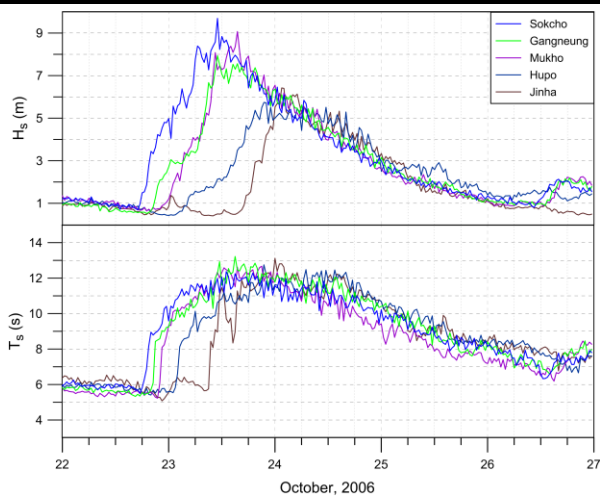


Figure 3. Time series of  $H_s$  and  $T_s$  for the high waves during 22nd to 26th October 2006.

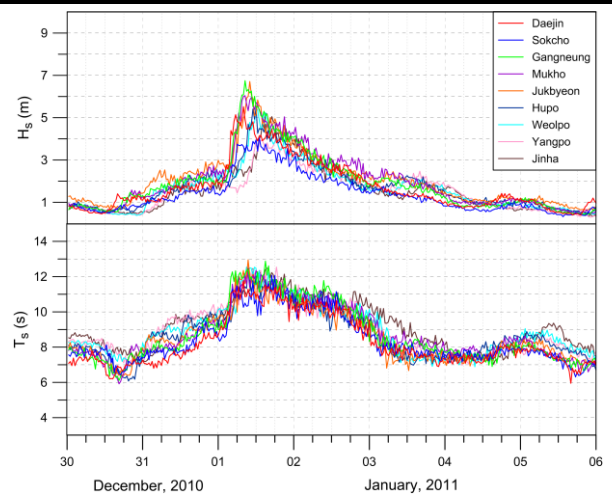


Figure 5. Time series of  $H_s$  and  $T_s$  for the high waves during 30th December 2010 to 5th January 2011.

two-stage increase in  $H_s$  and  $T_s$  is ascribed to the development and movement of two discriminated low pressure systems over the East Sea at that time (See Figure 6 presented in the below).

A final high wave event occurred in January 2011; shown in Figure 5. Similarly as with the two previous cases, the high waves arrived first at the northern stations on the Korean east coast than the southern stations. However, the gap between the arrival times was relatively shorter when compared with the two cases. As mentioned in the above, the high waves appearing on the Korean east coast are a mixture of swell and wind waves. The gap in arrival times among the measurement stations seems to be longer or shorter, influenced by whether the wave field is dominantly composed of either swell or wind waves, depending on each high wave event. Meanwhile, the overall trends of  $H_s$  and  $T_s$  shown in Figure 5 were almost similar as that of the high wave case in October 2006, with a sudden rise to the peak and subsequent gradual decrease of wave heights and periods at all the measurement stations.

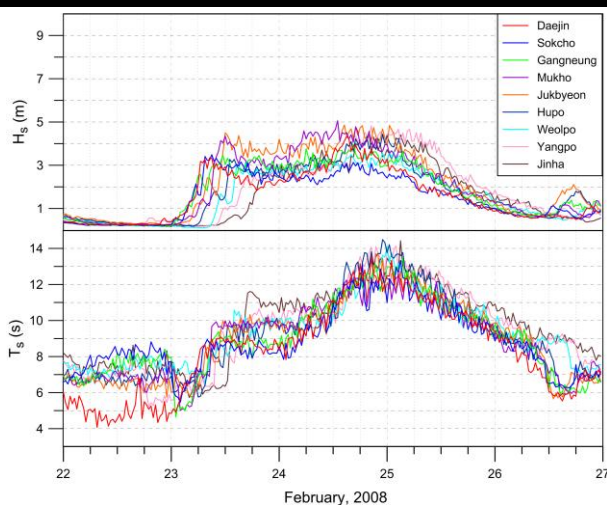


Figure 4. Time series of  $H_s$  and  $T_s$  for the high waves during 22nd to 26th February 2008.

### Low pressures during the high waves

During the time period corresponding to the appearance of the extremely high waves on the east coast of Korea, there existed one or multiple strong low pressure systems over the East Sea. The low pressures were originally generated inland of China and then moved eastward into the East Sea, while developing in strength by absorbing water vapors provided by the ocean surface. In some atmospheric situations favorable to rapid development of the low pressures, they are excessively developed comparable to a small- or medium-size typhoon. In such a case, a strong baroclinic gradient is formed around the East Sea which eventually makes strong wind fields and results in high wave phenomenon over the sea.

One of such examples that show the low pressures developed during the high wave event in February 2008 is shown in Figure 6. There are four weather charts from 12KST (Korea Standard Time) 22nd to 15KST 23rd February, showing the atmospheric pressures at the earth surface. At that period, two different low pressures, or extra-tropical cyclones, were separately developed over the East Sea. With time elapsed, the two low pressures moved eastward by lowering their central pressures. As a result, the very narrow isobaric contour lines were formed around each low pressure, implying steep gradients in atmospheric pressure across the isobaric lines. As seen in the last weather chart (lower right panel in Figure 6), the isobaric contours were mostly shaped in a north to south direction over the sea; very favourable to the formation of a strong wind field heading to the south. Indeed, abnormal waves as high as 10 m hit the west coast of Japan, centered at Toyama bay (Lee *et al.*, 2010). At that time, high waves also approached the Korean east coast as shown in Figure 4. However, their magnitudes were significantly smaller than those on the Japanese west coast.

This type of strong development of low pressures was always observed in the weather charts corresponding to the time period of high wave occurrence on either the Korean east coast or the Japanese west coast. However, the detailed pattern related to the moving tracks of the low pressures was very unique for each wave event, while a broad classification of the moving path was suggested by Lee *et al.* (2010). It seems that the overall atmospheric conditional structure over the entire sea region,

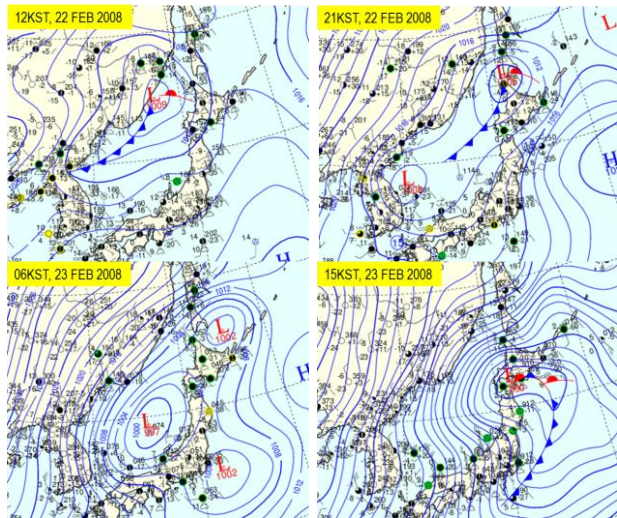


Figure 6. Four weather charts starting from 12KST (Korea Standard Time) 22th February 2008 at an interval of nine hours.

incorporated with the rapidly developing single or multiple low pressure systems, also plays an important role in determining the specific wind field favorable to generation of extremely high waves.

### Synthetic analysis of the data

In order to comprehensively understand the generation and development of the three extremely high waves, along with the contemporary variation of the meteorological conditions, all the available data used in the analysis were put together into a single picture as in Figures 7 to 9, similarly as to Lee (2013). The moving paths of the two low pressures formed during the high waves in October 2006 were graphically displayed in the upper panel of Figure 7. The numbers inside the arrow tag attached to the moving paths indicate the central pressures (in hPa) of the low pressures. As seen in the figure, two low pressures were generated individually but merged into one later. The central locations of the united low pressure were distributed very near to the measurement stations on the Korean east coast so that wind waves were likely to suddenly develop around the region.

The temporal variations of central pressures are also presented in the lower panel of Figure 7, where the time series of  $U$  as well as  $H_s$  and  $T_s$  at Sokcho are also plotted. As the maximum wave height at Sokcho was the largest among the measurement stations, the physical quantities there are presented in Figure 7. For the high waves of February 2008 and January 2011, the data obtained at Mukho and Jukbyeon were respectively selected for the same reason. Note that the right axis of the time series plot corresponds to the magnitude of the significant wave height and period, but just half of the mean wind speed. It is very clear that the central pressure declined in advance of the augmentation of wave height and period. In addition, the growth and subsequent decay trend of the mean wind speed coincided fairly well with those of the significant wave height. This implies that the locally formed strong wind field might be a dominant factor for the high wave occurrence in October 2006.

A similar picture for the high wave event in February 2008 is presented in Figure 8. In this case too, two different low pressures were generated, but they moved independently across the middle

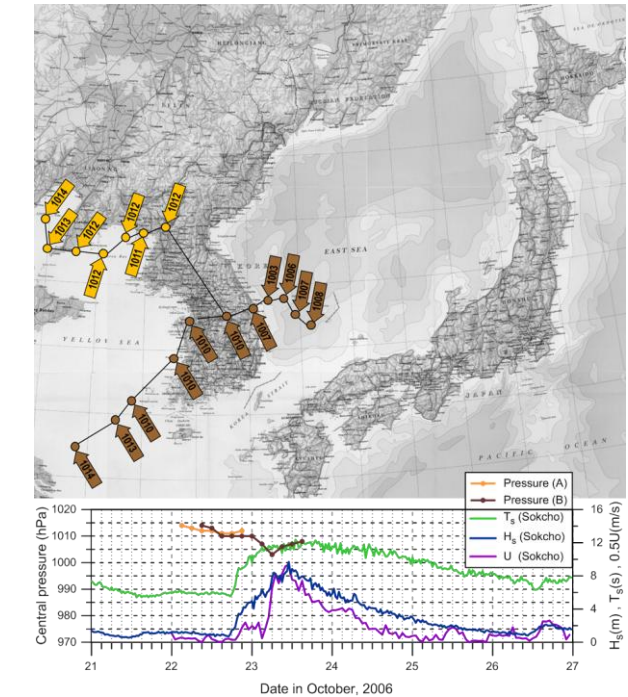


Figure 7. Tracks of the two extra-tropical cyclones and the variation of central pressures during their movement (upper panel). Time series of central pressures of the two cyclones together with those of  $T_s$ ,  $H_s$  and  $U$  measured at Sokcho during 21st to 26th October 2006 (lower panel).

and northern regions of the East Sea, respectively. While there existed considerable fluctuation, the local wind speed at Mukho started to increase with the drop of central pressures of the two low pressures. This in turn resulted in the rise of the significant wave height and period at Mukho on 23rd February. Meanwhile, the second increment of wave height and period the next day seems to have little relation with the local wind field as it occurred when the local wind speed was gradually decreasing. This implies that the second-stage increase in  $H_s$  and  $T_s$  was likely to not be associated with the local wind waves but rather with the swell that might be propagated from far offshore. According to Oh *et al.* (2013), indeed, the waves that contributed to the second increase of wave height and period were predominantly swell, which was presumed to be generated under the influence of the low pressure that existed over the northern end of the East Sea, between the Russia and Hokkaido island of Japan (the upper low pressure in Figure 8).

In the case of the high waves that appeared in January 2011, the general patterns in the time series of low pressure, significant wave height and period, and mean wind speed were almost the same as those of October 2006. In particular, the agreement in growing/decaying trend between  $H_s$  and  $U$  was remarkably good (Figure 9). It is noteworthy the extraordinary drop in central pressure down to 976 hPa ahead of the high wave appearance. Compared to the previous case shown in Figure 7, the amount of pressure drop was more than 2.5 times in this case, but the local mean wind speed and the significant wave height was not much greater than October 2006. The reason for may be ascribed to the difference in the central locations of the low pressures. The locations were very close to the Korean east coast in October 2006 so that the very strong wind field seemed to be generated around

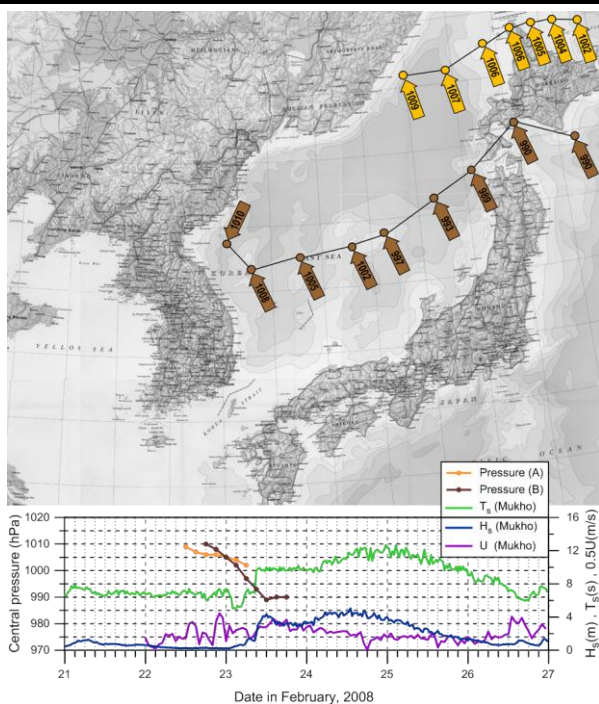


Figure 8. Same as Figure 7, but  $H_s$ ,  $T_s$  and  $U$  measured at Mukho during 21st to 26th February 2008.

the coastal zone. In contrast, the development of the low pressure itself was more powerful in January 2011, but its central location was far away from the Korean east coast. This might result in comparatively less impressive local wind fields around the coastal area.

### CONCLUDING REMARKS

This paper presented a detailed analysis of the high waves that have been repeatedly observed on the east coast of Korea. Extensive wave monitoring at nine measurement stations over approximately a decade revealed that the occurrence probability of  $H_s \geq 3$  m and  $T_s \geq 9$  s at any of the measurement stations within a certain day was 5.0% on average. With a stricter criterion of  $H_s \geq 4$  m and  $T_s \geq 12$  s, the probability was 0.3%. Such high waves mostly appeared during winter when extra-tropical low pressures were strongly developed around the East Sea prior to the wave appearance. The strong wind field formed by the low pressures incurred the development of the extremely high waves, while their detailed characteristics significantly varied depending on the overall atmospheric conditions over the East Sea at that time.

### ACKNOWLEDGEMENT

This research was supported by a grant (12-RTIP-B01) from Regional Technology Innovation Program by Ministry of Land, Infrastructure and Transport of Korean government and the research project (PE99223) of Korea Institute of Ocean Science and Technology.

### LITERATURE CITED

Chang, E.K.M. and Fu, Y., 2002. Interdecadal variations in northern hemisphere winter storm track intensity. *Journal of Climate*, 15, 642-658.

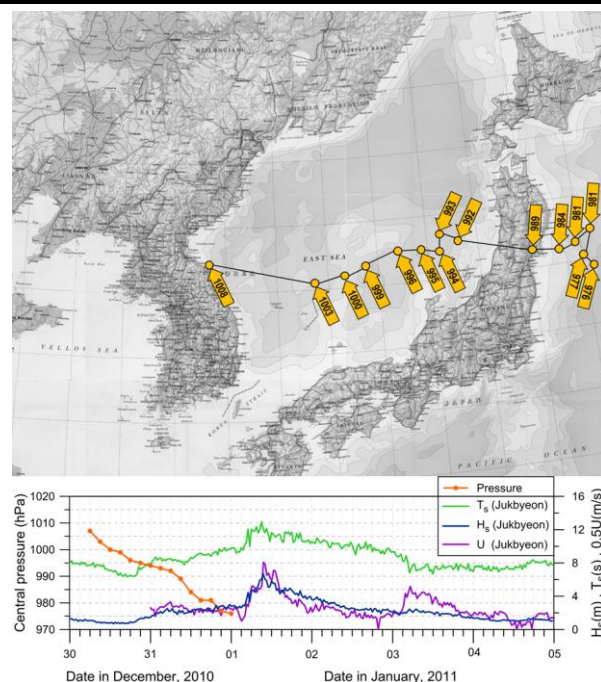


Figure 9. Same as Figure 7, but  $H_s$ ,  $T_s$  and  $U$  measured at Jukbyeon during 30th December 2010 to 4th January 2011.

- Hoskins, B.J. and Hodges, K.I., 2002. New perspectives on the northern hemisphere winter storm tracks. *Journal of the Atmospheric Sciences*, 59, 1041-1061.
- Jeong, W.-M., Oh, S.-H., Ryu, K.-H., Lee, D.Y. and Chae, J.W., 2009. Multi-station observation of the high swell along the east coast of Korea. *Proceedings of the 5th International Conference on Asian and Pacific Coasts* (Singapore).
- Kim, K.O., Lee, H.S., Min, B.I. and Choi, B.H., 2011. Hindcasting of high swell waves off the eastern Korean coast on 24 February 2008 using structured and unstructured wave models. *Proceedings of 11th International Coastal Symposium* (Szczecin, Poland), *Journal of Coastal Research*, Special Issue No. 64, pp. 1073-1077.
- Lee, H.S., 2013. Abnormal storm waves in the East Sea (Japan Sea) in April 2012. *Proceedings of 12th International Coastal Symposium* (Plymouth, England) *Journal of Coastal Research*, Special Issue No. 65, pp. 748-753.
- Lee, H.S., Kim, K.O., Yamashita, T., Komaguchi, T. and Mishima, T., 2010. Abnormal storm waves in the winter East/Japan Sea: generation process and hindcasting using an atmosphere-wind wave modelling system. *Natural Hazards and Earth System Sciences*, 10, 773-792.
- Liberato, M.L.R., Pinto, J.G., Trigo, R.M., Ludwig, P., Ordóñez, P., Yuen, D. and Trigo, I.F., 2013. Explosive development of winter storm Xynthia over the subtropical North Atlantic Ocean. *Natural Hazards and Earth System Sciences*, 13, 2239-2251.
- Oh, S.-H., Jeong, W.-M., Lee, D. Y. and Kim, S.I., 2010. Analysis of the reason for occurrence of large-height swell-like waves in the east coast of Korea. *Journal of Korean Society of Coastal and Ocean Engineers*, 22, 101-111 (written in Korean with English abstract).
- Oh, S.-H. and Jeong, W.-M., 2013. Characteristics of high waves observed at multiple stations along the east coast of Korea. *Natural Hazards and Earth System Sciences*, accepted.
- Ulbrich, U., Fink, A.H., Klawns, M. and Pinto, J.G., 2001. Three extreme storms over Europe in December 1999. *Weather*, 56, 70-80.
- Vanem, E., Natvig, B. and Huseby, A.B., 2012. Modelling the effect of climate change on the wave climate of the World's oceans. *Ocean Science Journal*, 47(2), 123-145.
- Wernli, H., Dirren, S., Liniger, M.A. and Zillig, M.S., 2002. Dynamical aspects of the life cycle of the winter storm 'Lothar'. *Quarterly Journal of the Royal Meteorological Society*, 128, 405-429.

# Breach process simulation of coastal levees broken by the 2011 Tsunami



Tatsuki Iida†, Shuichi Kure‡, Keiko Udo∞, Akira Mano+, Hitoshi Tanaka#

†Department of Civil and Environmental Engineering, Tohoku University, Sendai, Tohoku University, Sendai, 9808579, Japan

t-iida@potential1.civil.tohoku.ac.jp

+ International Research Institute of Disaster Science, Tohoku University, Sendai, 9808579, Japan

mano@civil.tohoku.ac.jp

‡International Research Institute of Disaster Science, Tohoku University, Sendai, 9808579, Japan

kure@irides.tohoku.ac.jp

#School of Engineering, Tohoku University, Sendai, 9808579, Japan

tanaka@tsunami1.tohoku.ac.jp

∞ International Research Institute of Disaster Science, Tohoku University, Sendai, 9808579, Japan

udo@potential1.civil.tohoku.ac.jp

[www.cerf-jcr.org](http://www.cerf-jcr.org)



[www.JCRonline.org](http://www.JCRonline.org)

## ABSTRACT

Iida, T., Kure, S., Udo, K., Mano, A., Tanaka, H., 2014. *Breach process simulation of coastal levees broken by 2011 tsunami*. In: Green, A.N. and Cooper, J.A.G. (eds.), *Proceedings 13<sup>th</sup> International Coastal Symposium* (Durban, South Africa), *Journal of Coastal Research*, Special Issue No. 70, pp. 302-307, ISSN 0749-0208.

On March 11, 2011, a tsunami hit the Sendai Bay Coast and broke 80% of the coastal levees. The areas around the breached levees were scoured deeply, causing serious adverse effects on post-disaster reconstruction efforts. This motivated us to analyze the mechanism of the local scour in the areas around breached levees. We collected and investigated various data such as aerial photographs and tsunami videos. As the results of the investigation, we found the breach points progressing in two steps. Firstly, the brittle structure was destroyed by the first leading wave. Secondly, the concentration of the return flow eroded and breached levees with the broken points from the first step. In order to understand the details of the second step, a numerical simulation was conducted using a finite volume method. From the result of the simulation, the scouring mechanism around breached levees was analyzed and discussed.

**ADDITIONAL INDEX WORDS:** tsunami, coastal levee, breach, return flow, two-dimensional finite volume method

## INTRODUCTION

A tsunami caused by the 2011 Tohoku Earthquake on March 11, 2011 hit and broke about 80% of the coastal levees on the Sendai Bay Coast (Figure 1). The national and local governments defined the following two kinds of hazard concerning future tsunamis, deciding the targets to be protected and the responsive measures against each kind of hazard. For “Level 1 Tsunami” which has a higher frequency, lower tsunami height and causes severe damages, the construction of shore protection facilities is advocated with the object of protecting human lives and residents’ property, stabilizing local economic activities and protecting production bases. For “Level 2 Tsunami” which has a much lower frequency, a substantially greater tsunami height and causes extremely significant damages, integrated provisions carrying all possible measures are to be established with the evacuation of residents and saving their lives given the highest priority. Regarding coastal levees, a levee height is decided by choosing the higher height between Level 1 Tsunami and the assumed storm surge. The government’s aim is to reconstruct levees which are robust enough to extend the time to collapse or reduce the possibility of total collapse, even though the levees are completely washed away by a tsunami higher than Level 1 Tsunami flowing over the coastal levees.

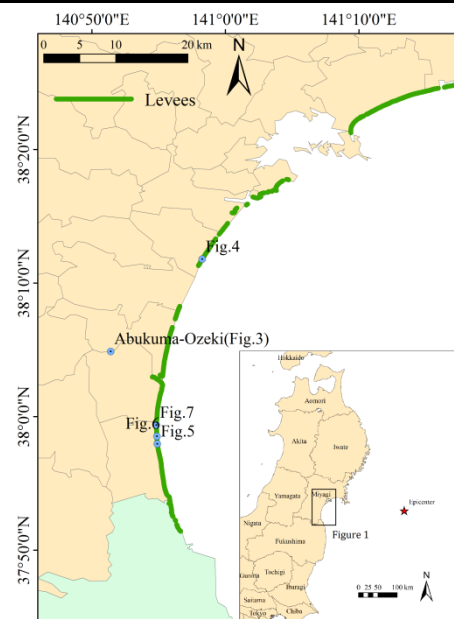


Figure 1. The map of the Sendai Bay Coast and the location taken in respective following figures.



Figure 2. The Yamamoto Coast before (left) and after (right) the tsunami, taken by MLIT on March 2010 and by Kyodo News on March 19, 2011 respectively.

There are various breaking patterns of coastal levees by the 2011 tsunami. Among them, levee breaching is most significant. Figure 2 shows the Yamamoto Coast, located in the southern part of Sendai Bay Coast, before and after the tsunami. Before the tsunami the beaches disappeared, while after the tsunami the back land of the coastal levees was widely eroded and the coastal levees were breached in many places. The areas around the breached levees were deeply eroded, allowing the succeeding wave groups to invade the present inland area, as well as causing serious adverse effects on post-disaster reconstruction efforts. In this light, it is urgent to analyze the breaching mechanism to consider adaptation measures for future tsunamis.

The coastal disaster by the 2011 Tsunami has been investigated by various research institutes. By analyzing aerial photographs or topography data observed by a laser profiler before and after the tsunami, the bed elevation change of the Sendai Bay Coast is clarified (Tanaka et al, 2011; Udo et al, 2012).

Regarding the damage of coastal levees by the 2011 Tsunami, it is confirmed, by hydraulic experiments and numerical simulations (Hatogai et al, 2012; Kato et al; 2012), that the collapse of levees is due to the scour on the back of levees as a result of the tsunami flowing over the levees. The scouring mechanism is further outlined by Kato et al. (2012) who used a cone penetration test applied at the back of levees: Firstly, the tsunami flowing over levees scoured the area in the back of levees. Secondly, backwash accelerated the scour around the breached levees. The study suggests that we should consider not only the leading wave but also backwash. Furthermore, a numerical simulation of the 2011 Tsunami around shore protection facilities indicated that very strong flows occurred around the breached shore protection facilities. (Nagasawa et al, 2012). Before the 2011 Tsunami, external forces damaging the shore protection facilities was studied in terms of tsunami height or inundation depth. As mentioned above, however, the 2011 Tsunami had massive waves that overtopped the coastal levees and with repeated force, making the damaging conditions complex and thus detailed analysis of the causes extremely difficult. Regarding the 2004 Indian Ocean Earthquake Tsunami considered as a mega tsunami, it is concluded that excess pore water pressure begot liquefaction, causing the scour (Yeah et al, 2006). Also, through the experimentation and simulation of scouring by soliton; it was identified that scouring, other than bottom friction, is attributable

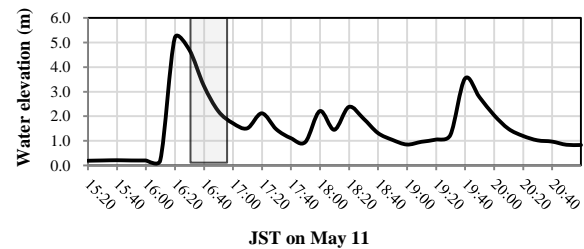


Figure 3. Observed tsunami records: Abukuma-Ozeki 10km upstream of the Abukuma River mouth measured by MLIT.

to liquefaction by excess pore water pressure (Tonkin et al, 2003; Pan et al, 2012). We thus considered that it is necessary to analyze whether this mechanism worked in the 2011 tsunami. This study thus aims to analyze local scouring around the breached points of levees hit by the 2011 tsunami so as to prevent scouring by future mega tsunamis.

## METHODS

### Breaching Factor Analysis

We collected aerial photos before and after the tsunami from the Geospatial Information Authority of Japan (GSI), together with the tsunami record and video from Tohoku Regional Development Bureau (TRDB) of the Ministry of Land, Infrastructure, Transport and Tourism (MLIT). "Michinokugo" the TRDB's helicopter took off from the Sendai Airport at 15:23 JST, 37 minutes after the main shock and about 20 minutes before the inundation of the airport by the tsunami. It flew south along the Sendai Bay Coast and videoed the tsunami. The time stamp of the video is compared with the tsunami record to reconcile the video to the tsunami phase. Spatial information of aerial and onsite photos and topographical map is matched by GIS, in addition to a field survey that was undertaken.

### Scouring Analysis

We simulated conditions to analyze the scouring mechanism in a quantitative way after a calculation model and conditions were decided using the results obtained by breaching factor analysis. The details of the calculation model and conditions are described in the section SCOURING SIMULATION.

## BREACHING PROCESS ANALYSIS

### Feature of 2011 Tsunami

Observed tsunami records in Figure 3 indicate that the first wave appears as the maximum wave with an amplitude 5.2 m and sharp rise. The following waves are smaller at Abukuma-Ozeki 10km upstream of the Abukuma River mouth. The many residents witnessed the tsunami's first wave running up the river like a turbid wall, which agrees with the sharp rise of the leading wave in the river. The higher inundation height could be interpreted as the local amplification by reflection, run-up, wave concentration, etc. The incident tsunami height of the leading wave is comparable to the coastal levee height, but the tsunami height of the following waves is less than that.





Figure 4. Return flow issued from broken levees at the junction of Fujitsuka, 2.5km north from the Natori River mouth at 16:15 JST.

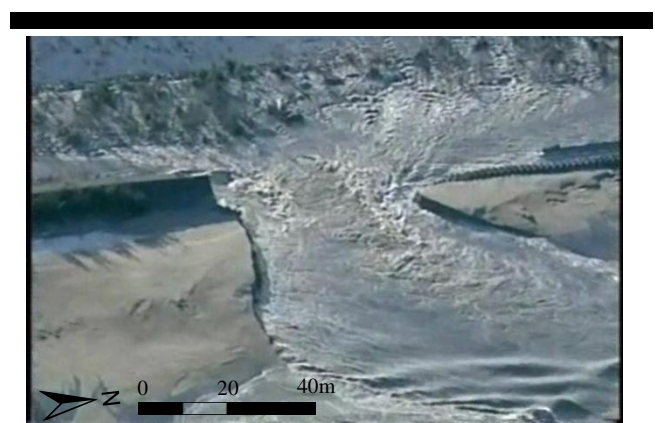


Figure 6. Tsunami video at 16:35 JST in northern part of the Yamamoto Coast.

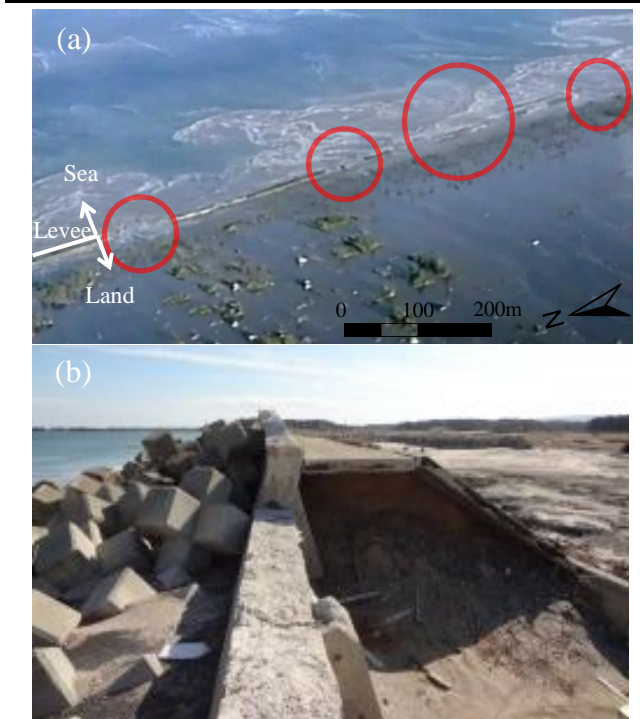


Figure 5. Levee broken on the Yamamoto Coast. (a) The tsunami video at 16:39 JST on the Yamamoto Coast. (b) The broken parapets on the Yamamoto Coast.

### Estimating Breaching Factor

Figure 4 shows a capture of the video taken by Michinokugo at 16:15 JST in Fujitsuka Area, located 2.5 km northward from the Natori River. There was a structural junction of a mild slope levee and an upright levee in this area. The return flow on the sea issued from this structural junction. This suggests that the return flow had already started inland, although the tsunami was in the leading wave phase at that time. It should be noted that the structural junction is weaker than the other part of levees. Therefore, it is considered that the junction was broken by the first, highest leading wave.

Figure 5 shows a capture of the video by Michinokugo at 16:39 JST on the Yamamoto Coast. In this figure, it is also identified that the muddy return flows on the sea issued from sections where some parts of levees were broken. In this area on the Yamamoto Coast, upright levees with parapets had been built. The parapets were weak against pressure from the one side. This allowed the hard hydraulic pressure of the first leading wave to break the parapets, and the return flow to be issued from the broken point.

Figure 6 shows a capture of the video by Michinokugo at 16:35 JST in the northern part of the Yamamoto Coast. It is identified from this figure that the return flow was concentrated at the breached point. This concentrated strong return flow grew stronger in the breached section, and scoured, at a large scale, the area around the breached levees.

Figure 7 shows the aerial photos after the tsunami, together with the topographical map at the same scale and the same area on the Yamamoto Coast. Each tsunami bay corresponds to an old or active channel. This indicates that the tsunami bay was formed with the active or old channel having extended coastward. This kind of erosion is possible only by the return flow. The concentration of return flow at the active or old channel intensifies the erosion. That was attributable to influx going into the lower height of alive or old channel.

In summary, the following two-step process is considered regarding the breach of coastal levees hit by the 2011 tsunami:

- (1) The leading wave broke the weak points of the levees.
- (2) The concentrated return flow led to levee breaching and large scale scouring at the points broken by the first high leading wave.

### SCOURING SIMULATION

In this section, we describe a numerical simulation of the local scour around the levees breached by the return flow of the first wave. This is based on the consideration that the local scour around the breached levees was severely affected by the return flow, deformed by tsunami run-up to landwards as mentioned in the previous section.

Previously, local scouring problems have been studied using numerical simulations by many research institutes. The development of computing technology has made possible the numerical simulation of various kinds of three-dimensional models (e.g. Onda *et al.*, 2007; Round *et al.*, 2005). However, enormous calculation time is needed for the simulation of return-flows, in spite of the recent computing technology because

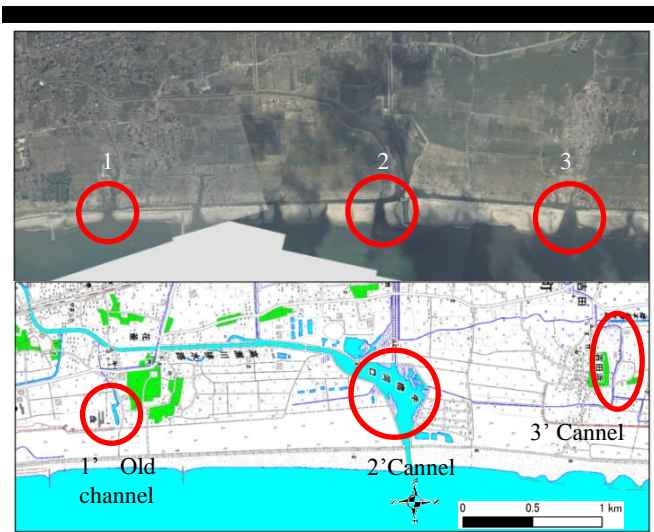


Figure 7. Aerial photos taken on March 12, 2011 by GSI (upper) and topographical map measured in 2009 by GSI (lower).

of the need of an expansive calculation area. Therefore, this study chooses a two-dimensional model which allows the calculation to be completed in a short period of time.

**Two-dimensional Model Used**

This numerical model is constructed from the combination of a flow model and a sediment model. The flow model uses non-linear shallow water equations integrated vertically.

$$\frac{\partial}{\partial t} \eta + \frac{\partial}{\partial x} q_x + \frac{\partial}{\partial y} q_y = 0 \tag{1}$$

$$\begin{aligned} \frac{\partial}{\partial t} q_x + \frac{\partial}{\partial x} u q_x + \frac{\partial}{\partial y} u q_y \\ = -gD \frac{\partial \eta}{\partial x} + \frac{\tau_{bx}}{\rho} + \nu_t \left( \frac{\partial^2 q_x}{\partial x^2} + \frac{\partial^2 q_x}{\partial y^2} \right) \end{aligned} \tag{2}$$

$$\begin{aligned} \frac{\partial}{\partial t} q_y + \frac{\partial}{\partial x} v q_x + \frac{\partial}{\partial y} v q_y \\ = -gD \frac{\partial \eta}{\partial y} + \frac{\tau_{by}}{\rho} + \nu_t \left( \frac{\partial^2 q_y}{\partial x^2} + \frac{\partial^2 q_y}{\partial y^2} \right) \end{aligned} \tag{3}$$

in which

$$\tau_{bx} = -\frac{\rho n^2 g}{D^{7/3}} q_x \sqrt{q_x^2 + q_y^2} \tag{4}$$

$$\tau_{by} = -\frac{\rho n^2 g}{D^{7/3}} q_y \sqrt{q_x^2 + q_y^2} \tag{5}$$

$$\nu_t = 0.11 \frac{ng^{1/2}}{D^{1/6}} \sqrt{q_x^2 + q_y^2} \tag{6}$$

where  $t$  = time;  $x, y$  = Cartesian coordinates;  $\eta$  = water surface elevation;  $q_x, q_y$  = quantity of flow per unit width;  $u, v$  = depth-averaged velocity;  $D$  = depth of water;  $g$  = gravitational acceleration;  $\tau_{bx}, \tau_{by}$  = stress of bottom friction;  $\nu_t$  = viscosity coefficient;  $\rho$  = water density (= 1000kg/m<sup>3</sup>);  $n$  = Manning's roughness.

Bed elevation change is calculated by the following equation:

$$\frac{\partial Z_b}{\partial t} = \frac{1}{1-\lambda} (C_{bottom} - C_a) \bar{w}_0 \tag{7}$$

where  $Z_b$  = bed level;  $\lambda$  = porosity;  $C_{bottom}$  = reference deposition concentration;  $C_a$  = reference pick-up concentration;  $w_0$  = settling velocity. The reference deposition concentration depends on the Rouse's vertical suspended concentration distribution (Rouse, 1937) based on a depth-averaged suspended concentration:

$$\frac{C}{C_{bottom}} = \frac{1}{1-z_a^*} \int_{z_a^*}^t \left[ \left( \frac{1-z^*}{z^*} \right) \left( \frac{z_a^*}{1-z_a^*} \right) \right]^{R_o} dz^* \tag{8}$$

in which

$$R_o \equiv \frac{w_0}{\kappa u_*} \tag{9}$$

where  $C$  = depth-averaged suspended concentration;  $z_a^*$  = dimensionless reference height;  $R_o$  = Rouse number;  $\kappa$  = Karman constant (= 0.4);  $u_*$  = bottom friction velocity. The depth-averaged suspended concentration is derived from solving a sediment transport equation integrated vertically.

$$\begin{aligned} \frac{\partial C}{\partial t} + \frac{1}{D} \frac{\partial q_{sx}}{\partial x} + \frac{1}{D} \frac{\partial q_{sy}}{\partial y} = \frac{C}{D} \left( \frac{\partial q_x}{\partial x} + \frac{\partial q_y}{\partial y} \right) \\ + \frac{\partial}{\partial x} \left( \varepsilon_s \frac{\partial C}{\partial x} \right) + \frac{\partial}{\partial y} \left( \varepsilon_s \frac{\partial C}{\partial y} \right) + \frac{w_0}{D} (C_a - C_{bottom}) \end{aligned} \tag{10}$$

where  $q_{sx}, q_{sy}$  = sediment quantity per unit width;  $\varepsilon_s$  = depth-averaged diffusion coefficient. Additionally, the reference pick-up concentration depends on the Van Rijn's equations (1993).

$$C_a = 0.015 \frac{d}{a} D_*^{-0.3} \left( \frac{\theta - \theta_c}{\theta_c} \right)^{1.5} \tag{11}$$

where  $d$  = grain diameter;  $D_*$  = non-dimensional diameter;  $\theta$  = shields number (=  $\rho u_*^2 / (\rho_s - \rho) g d$ );  $\theta_c$  = critical shields number;  $\rho_s$  = density of sand;  $a$  = constant number (=  $\Delta / 2 = 50d$ );  $\Delta$  = height of sand waves.

**Discretization Methods**

We adopt an unstructured grid finite volume method (FVM) as a discretization method. The FVM is capable of dividing meshes finely around the breached levees where the flow variation is considered to be large. Also, the FVM can accurately calculate variables of focusing areas around the breached levees by creating the boundary of calculating area along the levee.

**Data Set**

For calculation, we prepare a calculation area (Figure 8b) equal to the breached point where the strong return flow was concentrated at the breached point in Fujitsuka Area (Figure 8a), and run the simulation of return flow from the land to the sea. The calculation area has 7,684 cells, and the minimum size of meshes is 3.0 m in the area where the flow moves severely, and the maximum size of meshes is 30 m (Figure 8 c). The topographical condition is configured by setting the x-way gradient to be 0 and the y-way gradient 0.002 to meet the average gradient of the entire Sendai Bay Coast. Regarding approach flow, we need to simulate some conditions, because it is difficult to apply the condition of the 2011 Tsunami. In this paper, a typical case is shown to qualitatively analyze the mechanism. Namely, water discharge is 5600 m<sup>3</sup>/s, and the corresponding Reynolds number is 2.0\*10<sup>6</sup>.

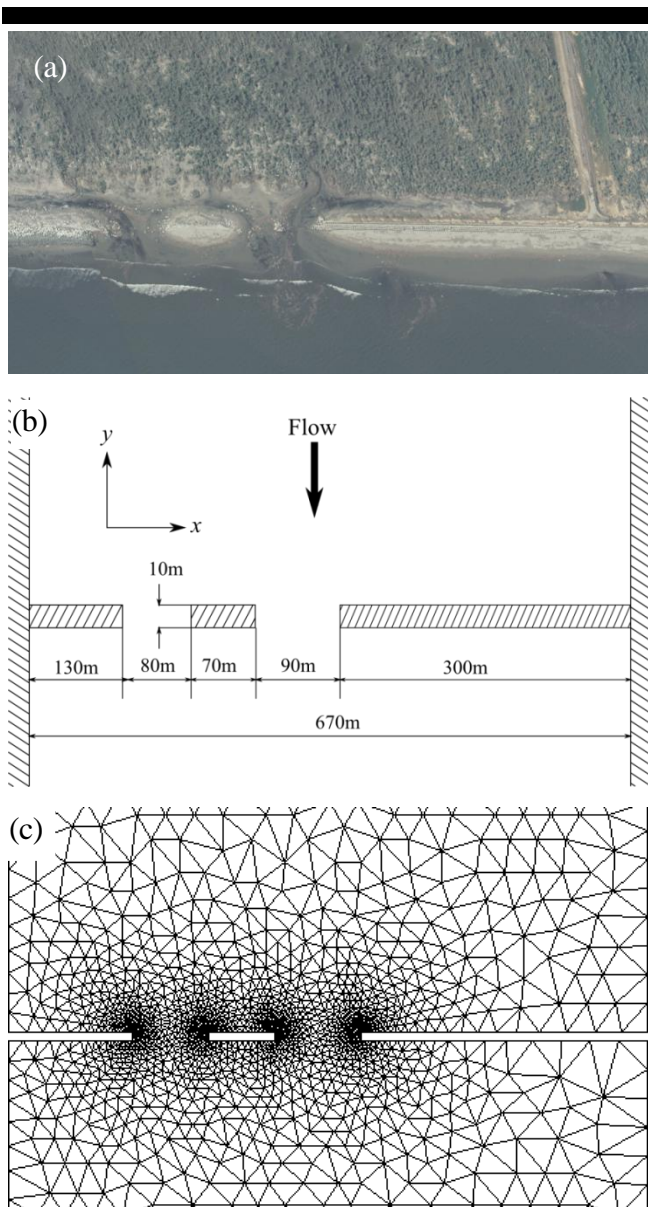


Figure 8. Calculation area. (a) Aerial photo in the Fujitsuka Area by GIS. (b) Calculation area prepared. (c) Meshes divided in the calculation area

This is based on the configuration of an approach flow depth equal to nearly 3.0 m in the uniform flow condition. The approach flow depth is decided by the height of vegetation snapped toward the landward side due to the leading wave shown in the video when the return flow moved. Manning's roughness and grain size are uniformly defined as 0.035 and 0.2 mm in all areas. For the downstream flow on the seaward side, a complete overflow condition is adopted, and the weir height is adjusted to meet the beach width of 50 m in the Fujitsuka Area. Also, the wall surface was set as the boundary of the levees, and a non-slip condition is adopted for the boundary. The time step size is set as 0.025s. Note that the breaking process is not considered in this study because it is difficult to simulate the process.

The proposed simulation enables the calculation of flow conditions from inland sub-critical flows to high-velocity critical flows accompanying deep soil scour around the levees.

## Results and Discussion

Figure 9a shows a water elevation counter map around the breached point 30 minutes after the start of return flow ( $t = 30$  min). In the figure, it is identified that water elevation on the upstream side is higher than the downstream side with water dammed up by the unbreached levees on the upstream side. A hydraulic jump does occur because of the rise of the water elevation on the downstream side in the breached section.

Figure 9b shows a map of streamlines and velocity contours around the breached point at  $t = 30$  min. The return flow coming from the land side moves toward the breached section, and is concentrated at the section, forming a strong flow in the breached section, especially at the center of the section. The velocity at the right side of the breached section is higher than at the left side because the unbreached levees of the right side continue to extend longwise.

Figure 9c shows a bed elevation change contour map around the breached levees, and Figure 9d is an aerial photo after the 2011 Tsunami which shows the same area of (c). The calculated result of bed elevation change compared to the aerial photo indicates that it is similar to the actual bed elevation, proving the validity of this simulation. Especially, the scouring trace arc with a focus on the toe of the unbreached levees is identified in the aerial photo, and this scouring trace is portrayed in the simulation. The calculated result of the maximum scouring depth exceeding 10 m, however, may be an overestimation, because the maximum bed elevation change of 5.7 m was observed at the breached point at Ninokura, located 12 km southward from the Fujitsuka Area where the return flow concentrated. The characteristics of scouring from the calculation are: Significant local scour at the toe of unbreached levees; and a scouring trace behind the levees continuing along levees from the breached section. Severe local scouring at the edge of levees mostly corresponds to the strong flow area, indicating that the strong flow is the main cause of scouring. Also, the scouring trace behind the levees continuing along the levees from the breached section is found to result from the concentrated return flows toward the breached section moving toward the deeply scoured site behind the breached levees.

## CONCLUSIONS

In this study, we estimated the breaching factor of defense levees by analyzing the tsunami video and the aerial photos of the 2011 Tohoku Earthquake Tsunami. We further simulated the phenomenon based on the estimation, and discussed the results. From the present study, we can conclude as follows:

- (1) The return flows are channeled into the breached coastal levees, and the strong flow was formed around the breached levees by the concentrated flow. Therefore, it is estimated that the return flow was concentrated at the point having been broken by the first high leading wave and scoured significantly around the breached point.
- (2) We made a simulation using a two-dimensional model to analyze the scouring phenomenon around the breached levees by the return flow of the first wave. The calculated bed elevation change was similar to the actual bed elevation, proving that the calculation is qualitatively accurate: The flow was concentrated and the strong flow was formed in the breached section. The area at the toe of unbreached levees was scoured significantly, and the scouring trace

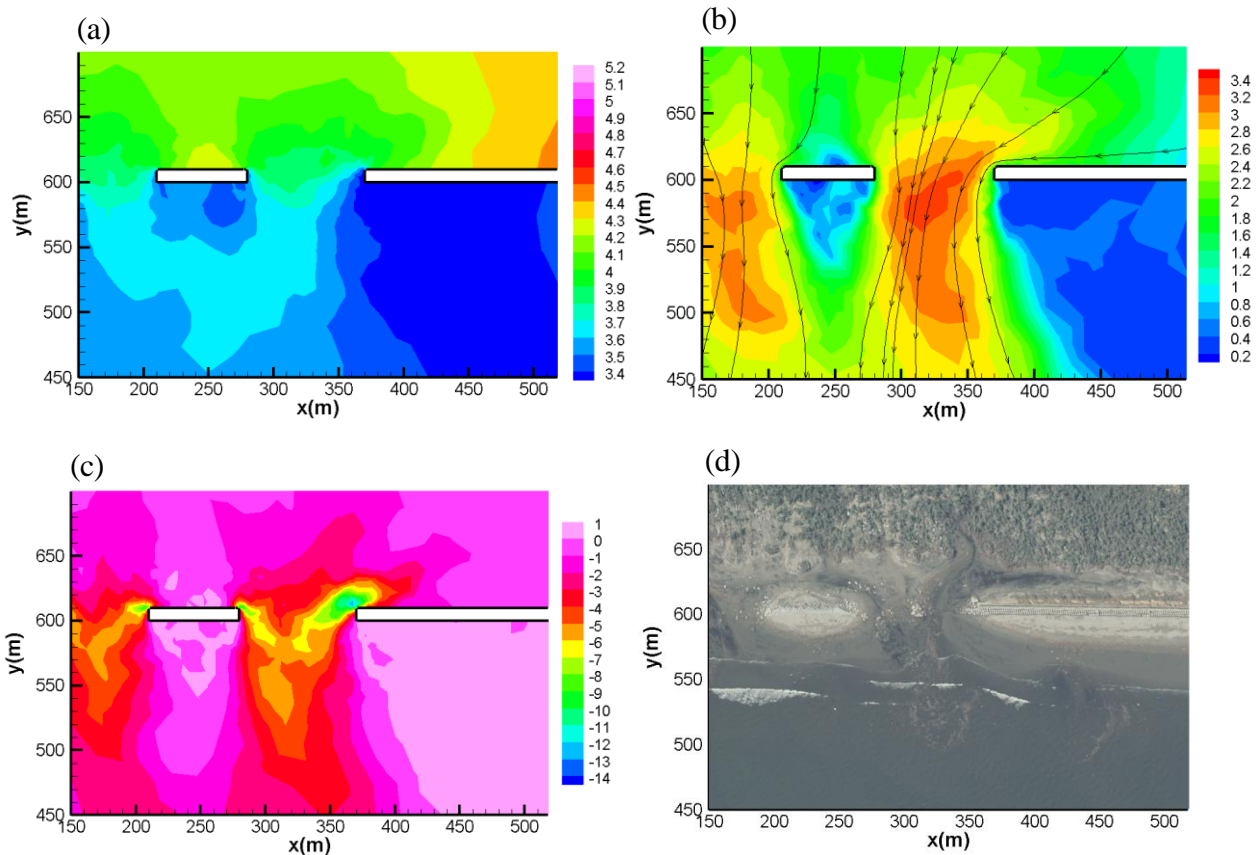


Figure 9. Calculation result 30 minute after the start of return flow vs. calculation situation. (a) Water elevation contour. (b) Streamline and velocity contour. (c) Bed elevation change contour. (d) Aerial photo after tsunami in same area of (c) by GSI

behind the unbreached levees was formed by the flow moving toward the area and damming up by the levees.

### LITERATURE CITED

- Hatogai, S., Suwa Y. and Kato, F., 2012. Hydraulic model experiments on scour landward of the coastal dike induced by tsunami overflow. *Journal of Japan Society Civil Engineers Ser. B2 (Coastal Engineering)*, 68, 406-410.
- Kato, F., Noguchi, K., Suwa, Y., Kimura, A., Kawai, M., Takagi, T. and Omata, M., 2012. Field survey on coastal dike damage and scouring in the southern part of the Sendai Plain induced by the Great East Japan Earthquake Tsunami. *Journal of Japan Society Civil Engineers Ser. B2 (Coastal Engineering)*, 68, 1396-1400.
- Kato, H., Hayashi, K., Nakamura, T., Nakayama, A., Yagi, H., Mori, K., Igarashi, Y. and Suzuki, A. 2012. Research on damage factors of coastal conservation facilities due Tohoku Earthquake Tsunami. *Journal of Japan Society Civil Engineers Ser. B2 (Coastal Engineering)*, 68, 1386-1390.
- Morales, R. and Ettema, R. M. ASCE, 2013. Insights from depth-averaged numerical simulation of flow at bridge abutments in compound channels. *Journal of Hydraulic Engineering*, 139(5), 470-481.
- Nagasawa, T. and Tanaka, H., 2012. Analysis of Structural Damages with massive Geomorphic Change due to Tsunami. *Journal of Japan Society Civil Engineers Ser. B2 (Coastal Engineering)*, 68, 1361-1365.
- Onda, S., Hosoda, T., Kimura, I. and Iwata, M., 2007. Numerical simulation on local scouring around a spur dike using equilibrium and non-equilibrium sediment transport models. *Annual Journal of Hydraulic Engineering*, 51, 943-948.
- Rijn, L., C., V., 1993. Principles of sediment transport in rivers, estuaries and coastal seas. *Aqua Publications*.
- Roulund, A., Sumer, B. M., Fredsoe, J. and Michelsen, J., 2005. Numerical and experimental investigation of flow and scour around a circular pile. *Journal of Fluid Mechanics*, 534, 351-401.
- Rouse H., 1937. Modern conceptions of the mechanics of fluid turbulence. *American Society of Civil Engineers*, 102, 461-543.
- Tanaka, H., Mano, A. and Udo, K., 2011. Beach morphology change induced by the 2011 Great East Japan Earthquake Tsunami. *Journal of Japan Society Civil Engineers Ser. B2 (Coastal Engineering)*, 67, 571-575.
- Udo, K., Sunagawa, D., Tanaka, H., Imai, K. and Mano, A., 2012. Impact of 2011 Tohoku Earthquake and Tsunami on beach morphology along the Northern Sendai Coast. *Coastal Engineering Journal*, 54, 1250009.

## Storm deposition induced by hurricanes in a rapidly subsiding coastal zone

James D. Naquin, Kam-biu Liu, Terrence A. McCloskey, Thomas A. Bianchette

Department of Oceanography and Coastal Sciences  
School of the Coast and Environment  
Louisiana State University  
Baton Rouge, LA 70803, USA  
jnaqui6@lsu.edu  
kliu1@lsu.edu  
tmcclo1@lsu.edu  
tbianc1@lsu.edu



[www.cerf-jcr.org](http://www.cerf-jcr.org)



[www.JCRonline.org](http://www.JCRonline.org)

### ABSTRACT

Naquin, J.D., Liu, K.B., McCloskey, T.A., Bianchette, T.A., 2014. Storm Deposition Induced by Hurricanes in a Subsiding Coastal Zone. In: Green, A.N. and Cooper, J.A.G. (eds.), *Proceedings 13<sup>th</sup> International Coastal Symposium* (Durban, South Africa), *Journal of Coastal Research*, Special Issue No. 70, pp. 308-313, ISSN 0749-0208.

To understand the geological processes induced by tropical cyclones, geochemical and sedimentological analyses were performed on a 3 m sediment core (basal  $^{14}\text{C}$  date of 940  $\pm$  50 years BP) extracted from a marsh adjacent to a backbarrier lake along Louisiana's Gulf of Mexico coast (USA). This study was conducted in order to identify the geologic changes within a subsiding coastal region in the light of coastal recession and past hurricane activity. Previous studies show that Bay Champagne, a semi-circular lake near Port Fourchon, Louisiana, is subjected to subsidence rates between 1.0 and 1.2 cm year<sup>-1</sup>, the highest rate of retreat within the entire northern Gulf of Mexico. Loss-on-ignition (LOI) and X-ray fluorescence (XRF) analyses, employed to generate lithological and geochemical core profiles, identified three distinct sand layers measuring up to 50 cm in thickness deposited by recent hurricanes. LOI shows large decreases in water, organic, and carbonate contents, indicating the occurrence of marine inundation. Within each marine incursion layer terrestrial elemental concentrations as determined by XRF display large depletions. Grain size analysis of a portion of the core (30-86 cm) indicates the presence of two series of sequential high-energy storm deposits followed by intense fluvial flooding within Bay Champagne. These events are attributed to Hurricanes Katrina/Rita in 2005 and Gustav/Ike in 2008.

**ADDITIONAL INDEX WORDS:** *paleotempestology, hurricanes, subsidence, marine geochemistry, storm surge*

### INTRODUCTION

Paleotempestology, the study of ancient hurricanes, has emerged to the forefront of science in recent decades due to its ability to extend tropical cyclone record beyond the historical period. Commonly used proxies include oxygen isotopic ratios in cave deposits and tree rings, beach ridge formation, microfossil assemblages, and storm deposits in coastal backbarrier lakes and marshes (Liu, 2013). The detection of ancient storm deposits by means of stratigraphical analyses in coastal sediments serves as an effective tool for reconstructing past hurricane activities. Because the instrumental tropical cyclone record is constrained to the past 150 years, the long-term perspective provided by sedimentary paleotempestology can be used to improve the estimate of return periods of intense hurricanes.

Since coastal backbarrier lakes and deltaic lowlands are frequently impacted by tropical cyclones and the related sedimentary processes, they function as key repositories for storm-driven morphological changes, with overwash sand layers

commonly being used as a proxy for large storm events. The thickness and texture of these deposits have often been used to assess the relative intensity of prehistoric events, with the intensity levels calibrated by comparison with the sedimentary signatures of known historic or modern events (Liu, 2004). Such studies have indicated that repeated hurricane strikes will be marked in coastal sediments by interspersed organic and clastic layers, and that these layers can often be identified by visible inspection, LOI, and grain size analyses.

Paleoenvironmental changes stimulated by hurricanes strikes have been well recorded along the Northern Gulf of Mexico coast (Liu, 2004; Liu and Fearn, 2000; Liu et al., 2008). However, data from regions subjected to rapid subsidence that also serve as a major contributor to regional economies have remained fairly elusive. This study serves as a companion study to Liu et al. (2011), which measured the hydrodynamic and sedimentological changes caused by Hurricanes Gustav and Ike in Bay Champagne near Port Fourchon, southern Louisiana (LA).

Coastal wetlands are multi-functional systems that not only serve as a vital sink for the global carbon budget, but also provide a natural buffer zone for inland areas against destructive forces

associated with tropical cyclones (Long, 2011). However, the current eustatic sea-level rise combined with anthropogenic modifications of wetland structures have yielded rapid rates of subsidence in many coastal zones such as the Mississippi River deltaic plain of Louisiana (USA) (Blum and Roberts, 2009). This area is unique in comparison to other coastal zones along the northern Gulf of Mexico and is characterized by inundated or saturated soils that contain vegetation adapted to these conditions. The formation of the first Mississippi River delta emerged approximately 6000-7000 BP and throughout its existence, the Mississippi River has avulsed a new deltaic lobe every 1000-1500 years (Day *et al.*, 2007). This study is focused on the Lafourche deltaic lobe which actively received freshwater and sediment derived from the Mississippi River from 2500-600 BP (Blum and Roberts, 2009). Situated on the coastal front of this deltaic plain is Port Fourchon, LA, Louisiana's southernmost and largest port, and an important player in regional, national, and global economies. Port Fourchon annually accounts for \$1.5 billion and \$350 million in business sales and household earnings, respectively. A 30-year projection shows that Port Fourchon is expected to cater to 60% of all natural gas and petroleum drilling services off the coasts of Louisiana, Mississippi, and Alabama (Brewton *et al.*, 2009). Port Fourchon (Figure 1) originally encompassed 700 acres of naturally deposited marsh while a 400-acre area was artificially expanded in 2008 to compensate for the rising industrial economy (Brewton *et al.*, 2009). This region is subjected to rapid subsidence rates of approximately 1.0-1.2 cm per year, the greatest rate within the entire northern Gulf of Mexico coast (Day *et al.*, 2007). Factors contributing to this high rate of coastal retreat include lack of incoming sediments and nutrients, local sea-level rise, and hurricane-induced erosion (Blum and Roberts, 2009). This study presents a recent geologic record of hurricane activity in the context of a rapidly subsiding coast.



Figure 1. Aerial photograph of Port Fourchon (outlined in white) and Bay Champagne (white arrow). Image supplied by Google Earth (2008).

### STUDY SITE

The study site, Bay Champagne (Figure 2), is a semi-circular backbarrier lagoon along the Caminada-Moreau headland, located immediately to the southeast of Port Fourchon. It receives water

input from fresh and salt-water sources, is aligned along a WSW to ENE axis, and separated by the Gulf of Mexico by a narrow sandy barrier ~1 m in height. This barrier prevents marine waters from entering the bay during normal tidal processes, although it cannot prevent marine inundation during storm surge events generated by coastal or landfalling hurricanes.

Bay Champagne existed as a fully-circular body of water during the early 1950s. Since then, the coastline has rapidly retreated inland (Henry and Twilley, 2013). Consequently, Bay Champagne is currently much reduced in area, and has become semi-circular in shape (Figure 3). In the past decade, Bay Champagne and surrounding areas have been repeatedly impacted by hurricanes (Figure 4). Hurricane Lili, a category 2 storm on the Saffir-Simpson scale, produced a 3-m storm surge in Port Fourchon and deposited an extensive sediment overwash fan on the east side of the bay (Liu *et al.*, 2011). In 2005, two intense hurricanes—Katrina and Rita—inundated coastal Louisiana approximately one month apart from each other. These two hurricanes caused extensive scouring and erosion (~527 km<sup>2</sup>) to low-salinity wetlands along the western Chenier Plain as well as marsh flats southeast of New Orleans (Howes *et al.*, 2010). The most recent hurricanes to affect this area were Hurricanes Gustav (1 September 2008) and Ike (13 September 2008); these storms produced 3-m and 1.2-m storm surges in Port Fourchon, respectively. (Berg, 2009)

### METHODS

A 3-m sediment core (BCM) was extracted from the seaward margin of a marsh located along the far southwestern edge of Bay Champagne (29°07'N, 90°10'W) in October 2009 by means of a Vibra-corer (10 cm inside diameter), and transported to Louisiana State University where it was stored in a cold room at 4° C. After opening, the core was photographed and subjected to Loss-on-ignition (LOI) analysis at 1-cm resolution, as described by Liu and Fearn (2000). Elemental profiles of 26 chemical species were determined by a handheld Innov-X Delta X-ray fluorescence (XRF) device at 2-cm intervals. Charcoal and wood fragments were extracted from the base of the core (308 cm) and sent to the National Ocean Sciences AMS lab at Woods Hole Oceanographic Institution in Massachusetts, USA for radiocarbon dating. This date was converted to calendar years by the Calib 7.0 program. Grain-size analysis was conducted by using a Beckman Coulter LS 13 320 SW laser diffraction particle size analyzer.

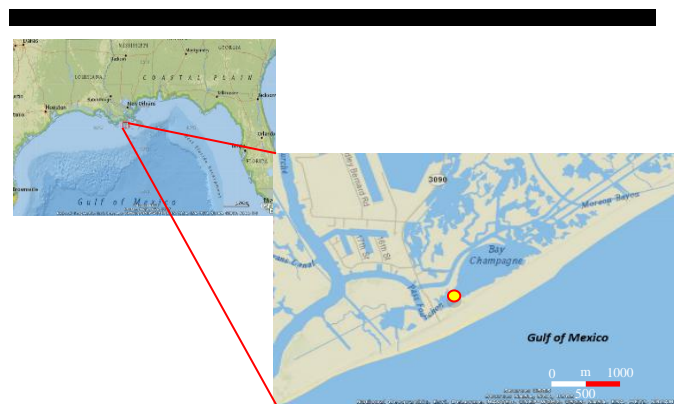


Figure 2. GIS map created by ArcGIS Explorer (2012) of Bay Champagne in relation to the Gulf of Mexico. Yellow dot denotes the BCM coring site.

## RESULTS

Core BCM shows four distinct sedimentological zones according to its lithology (Figure 5). Zone I (318-294 cm) mainly consists of silt with a dark 5 cm sandy layer present from 299-294 cm. Zone II (293-296 cm) is predominantly composed of dark brown mud while containing large *in situ* roots at multiple depths. In Zone III (275-108 cm), the sediment is generally a homogenous light grey clay with black laminations on the order of 0.5-1.0 mm in thickness occurring throughout the entire zone. Zone IV (107-0 cm) is dominated by three distinct medium-grained sand layers present at 105-55 (A), 40-45 (B), and 18-3 (C) cm (orange bands, Figure 5).

Zone I is characterized by ~30% water and ~10% organic content, with a 5% increase in carbonate concentration occurring in the middle of the zone. Elemental analysis shows moderate values of Co, Cl, Fe, S, and Zn in relation to other zones (II and III) within the stratigraphy. Zone II is distinguished by relatively high water and organic contents (~60% and 20%, respectively). This zone also displays a secular increase in S concentration throughout the entire depth of the zone, followed by a large depletion upon entering Zone III. Zone III spans nearly half of core BCM. The sediment within this zone shows overall high concentrations of terrestrial elements (Co, Fe, S, Ti, V, and Zn), and a maximum of ~65-70% water content from 230-220 cm. This interval also displays ~30% organic content with a maximum peak of ~40% occurring from 207-202 cm (green shading, Figure 5). Following this spike, water and organic contents decrease steadily towards the upper part of Zone III and drop sharply across the boundary with Zone IV.

The sand layers found in Zone IV differ in elemental composition compared to the layer found near the bottom of the core (299-294 cm). Overall, the sand units found in Zone IV are coarser in texture, possess lower water contents (~30% difference), and have lower concentrations of Co, Cl, Fe, S, and Zn. The sand layers C, B, and A are easily distinguishable due to their abrupt contacts with muddy sediments found in Zone IV (Figure 6). The alternating muddy sediment found within this portion of core BCM shows similar elemental and lithological signatures to the mud found within Zones I, II, and III.

Grain size analysis of layer B and a section of C determined kurtosis (degree of sorting or "peakedness"), standard deviation, mean grain size, and skewness (degree of asymmetry). This data is presented in the Phi scale found in Figure 7 for sediments ranging from 30-86 cm in depth. Kurtosis displays a secular increase from 86-65 cm and a large increase at 36-35 cm. Mean grain size of BCM ranges from 2.5 and 5 phi and shows an overall fining upward trend with deviations at 79, 53, 40, and 33 cm, indicating the presence of fine grained material. These textural variations are also present in standard deviation and skewness profiles and correspond to the thin (~1-3 mm in thickness) dark brown and black laminations. Sediments found in this portion of the core contain medium-sized sand to silty grained material.

Table 1. Radiocarbon date for BCM

Lab No.	Core	Depth (cm)	Age <sup>14</sup> C yr BP	Age 2σ cal yr
OS-95830	BCM	308	940±50	742-933

## DISCUSSION

We interpret Zone I as the transition period between deltaic lobes due to its high abundance of silt, the presence of a fine-textured sand layer at 299-294, and the location of a radiocarbon date (940 +/- 50 BP, Table 1) taken from 308 cm, which corresponds to the approximate time of the Lafourche deltaic lobe switch. Sediment deposition in coastal Louisiana wetlands is typically composed of silt and clay (Blum and Roberts, 2009; Day et al., 2013), however, delta lobe avulsion causes crevasse overbank and fluvial flooding of fine-textured sand derived from inland sources. As accommodation space within a deltaic lobe diminishes, fine sand is often scoured from river channels and deposited laterally into seaward wetlands (Kemp et al., 2013). This explains the presence of this material within the lower depths of BCM. Within the past half century, Bay Champagne has transgressed approximately 1 km inland (Figure 3). It is highly likely that coastal retreat in this area has been occurring since the termination of the Lafourche deltaic lobe (Day et al., 2007). Therefore, the sandy layer found at the bottom of the core is not attributable to hurricane-induced overwash processes due to its postulated distance from the sea during that time. The uppermost portion of Zone II likely marks the post-termination period of the

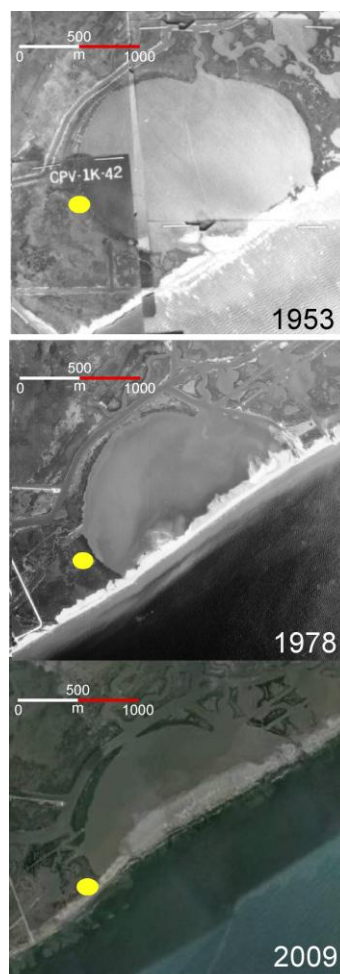


Figure 3. Satellite images showing coastal transgression occurring in the Bay Champagne area between 1953 and 2009. Coring site of BCM is denoted by the yellow dot. Image courtesy of the Louisiana State University Map Library.

deltaic lobe. It is understood that during this time, the BCM coring site existed as a subaerial vegetated river bank, as supported by the large *in situ* roots and high organic content found within this zone. The contact between Zones II and III signifies a period in which the site was inundated by freshwater. This is likely due to the submergence of the inactive Lafourche delta. Zone III, the thickest zone within the core (167 cm), represents the coastal regression that followed submergence of the area, as noticed by the steady decrease in water content following the high organic level found at 207-202 cm and the secular increase in Ba, S, V following this layer (Figure 5). Bay Champagne has become increasingly susceptible to coastal retreat and hurricane-induced overwash sand deposition (Zone IV). The deposition of sand in backbarrier coastal systems usually only occurs during high-energy events (Liu et al., 2008; Liu et al., 2011). The formation of cm-thick sand layers as a result of aeolian transport can be eliminated, given the generally moist beach systems resulting from the narrow beaches. Possible events of sufficient magnitude include tsunamis, winter storms, and tropical cyclones. Given the lack of historical tsunamis for this region (Chaytor, 2010) and the relatively low wave height produced by frontal winter storms (Pepper and Stone, 2004), hurricane-driven storm surges are by far the most likely producers of the large-grain clastic layers occurring in BCM. The repeated passage of hurricanes can result in alternating layers of terrestrial material and marine-derived overwash sand layers.

We attribute the three sand layers occupying Zone I of BCM to recent hurricanes. Due to its surface position, the upper 3-cm of the core, consisting of silty clay, is posited as having been deposited during the 15-month period between the passage of Hurricanes Gustav and Ike (September 2008) and the extraction of the core (December 2009). Beneath this topmost layer lies an abrupt transition to the 15-cm thick sand layer C, apparently a storm deposit attributable to the storm surges and overwash processes produced by Gustav/Ike (Figure 6). This is supported by large decreases in water content and elements indicative of terrestrial origin (Co, Fe, Ti, V, Zn) (Sabatier, 2012). The two

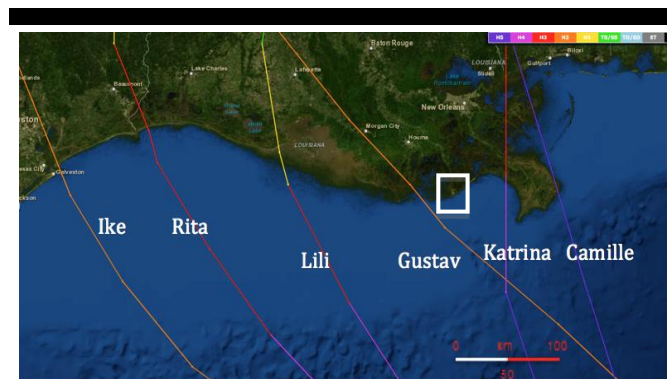


Figure 4. Aerial image of south Louisiana and east Texas showing 6 hurricanes that affected Bay Champagne (white box) from 1969-2008. Figure modified from <http://www.nhc.noaa.gov/> National Oceanic and Atmospheric Administration (2013).

sand layers B and A were probably deposited by Hurricanes Rita and Katrina, respectively, in 2005, as inferred from their stratigraphic positions in the sequence. The alternating mud and sand layers, suggested by the LOI and grain size data (Figures 5 and 7), possibly indicate the occurrence of differing energy levels both between and within the storms.

The occurrence of pure sand at the bottom of layer A (105-85 cm) can possibly be correlated with the initial wave runup and intense storm surge effects of Katrina, while the oscillations in water content and skewness of grain size occurring at the top of the unit (~35, 40, 65 cm) may reflect energy pulses relating to heavy precipitation intervals. As the intense rain bands passed over the study site it caused fluvial flooding of the system, thus giving rise to bimodal deposition originating from both riverine and marine sources (Liu et al., 2011). The rise in water content, suggesting an increase in clay and silt contents in the sediment, towards the top of sand layer A (see LOI curve, Figure 5)

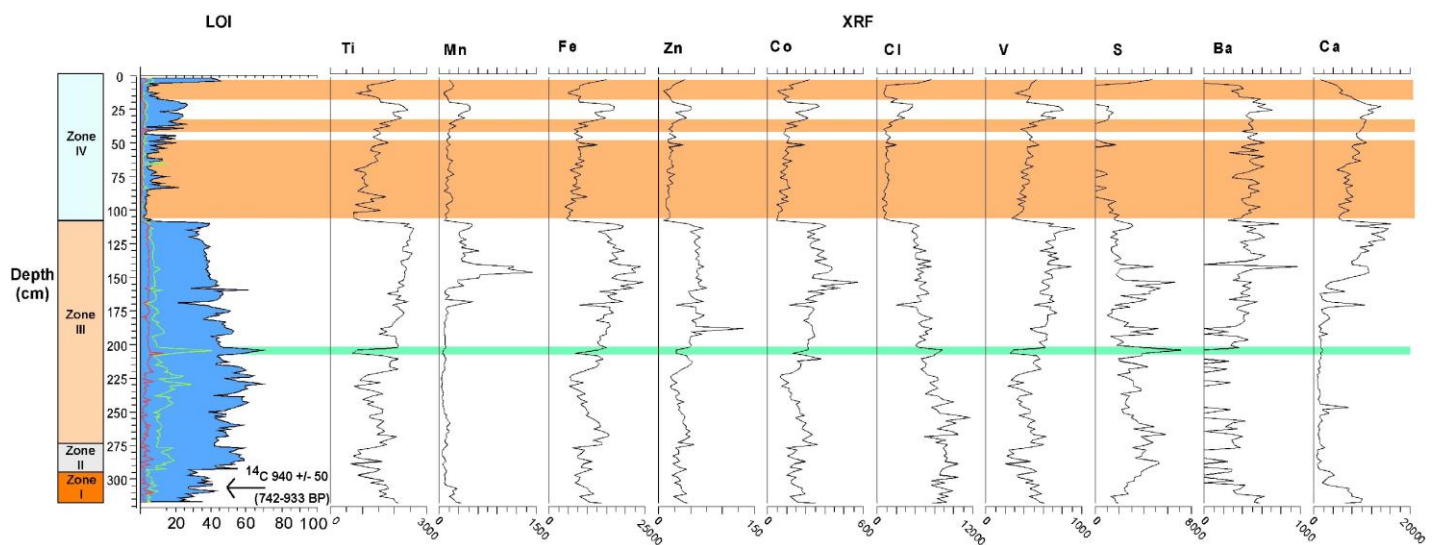


Figure 5. LOI curve (left) and elemental composition as determined by XRF (right). Blue, green, and red curves are representative of water, organic, and carbonate content, respectively. Overwash sand layers (orange bands) are distinguished from muddy sediments (white, background) and peat material (green band).





Figure 6. Photograph of the upper 26 cm of core BCM. Red arrows denote abrupt changes found between facies caused by Hurricanes Gustav/Ike.

probably resulted from the extensive riverine flooding that occurred in the aftermath of Hurricane Katrina (Day et al., 2013; Howes et al., 2010; Liu et al., 2011). The 5-cm thick sand layer B was likely deposited by the storm surge that accompanied Hurricane Rita ~30 days later. While obtaining precise radiometric dating is difficult for sandy sediments due to their low adhesive ability to radioisotope tracers (i.e.,  $^{137}\text{Cs}$ ,  $^{210}\text{Pb}$ ,  $^{234}\text{Th}$ ) (Madsen et al., 2005), the sediment stratigraphy occurring in BCM achieves a close match with the meteorological features of these known storms, and is in keeping with storm intensity and distance from the site. The strength of the geologic signature is related to the proximity of the storm to the sampling site and also the strength of the storm. In this instance, the higher intensities of Hurricanes Katrina/Rita in comparison to the Gustav/Ike series are reflected by the thicknesses of overwash sand in the sediment column.

The fact that overwash sand layers dominate the upper meter of the core does not indicate higher frequency of landfalling hurricanes during the recent past, but is an artifact of relative sea level rise and coastal recession. This suggests that a threshold exists in which a site can be paleotempeologically sensitive to

recording overwash deposition. Hurricane Camille (Category 5, 1969) is not found within the stratigraphy due to the large distance between the coring site and the Gulf of Mexico at that time (Figure 3). In a rapidly subsiding coastal area, as the distance between coring site and the rising sea decreases over timescales of decades and centuries, this coring site has become increasingly susceptible to storm surges and overwash processes generated by coastal or landfalling hurricanes. Consequently, this leads to a corresponding increase in “paleotempestological sensitivity” (*sensu* Liu, 2004) for the coring site over time. Thus the occurrence of multiple thick overwash sand layers in the top meter of the BCM core cannot be interpreted as suggesting an increase in the frequency or intensity of landfalling hurricanes in the recent decade, but is attributable simply to an increase in the paleotempestological sensitivity of the coring site so that these recent hurricane events are more likely to be recorded in the coastal sedimentary record.

## CONCLUSIONS

A core extracted from a marsh bordering Bay Champagne on

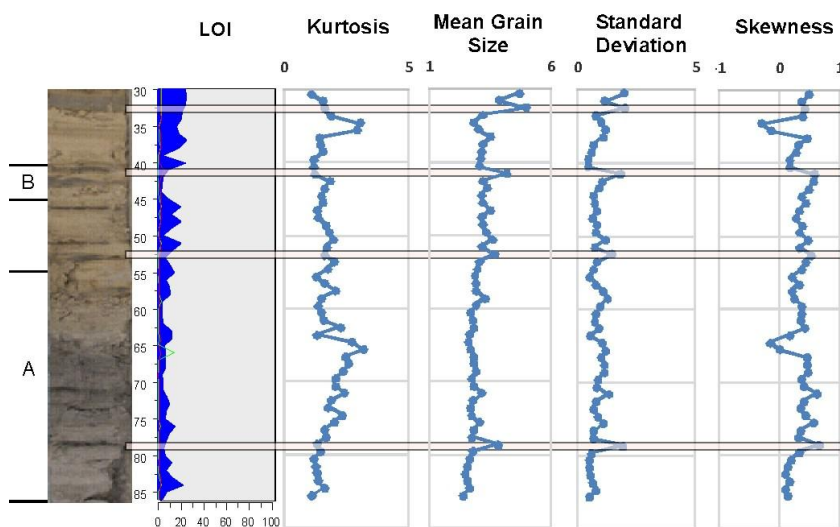


Figure 7. Grain size data of overwash layer (30-86 cm) deposited by Hurricanes Katrina/Rita. Grain size and corresponding statistical analyses are calculated from mean grain size (Phi scale). Spikes in mean grain size and standard deviation are outlined by the shaded lines.

the southeastern coast of Louisiana has allowed a geologic reconstruction of recent hurricanes within the area, namely, Gustav and Ike of 2008, and Katrina and Rita of 2005. Sediment-stratigraphic analyses reveal four periods that reflect different paleoenvironmental regimes. The stratigraphy has recorded the avulsion of the Lafouche deltaic lobe (approximately 0.7 ka), the post-deltaic lobe termination period, the resulting submergence of the area, and a period in which the coastline is rapidly subsiding. Due to rapid coastal subsidence within this area, Bay Champagne has transgressed from a circular body of water to a semi-circular backbarrier bay that is geologically sensitive to hurricane-generated overwash processes. Storm surge from Hurricane Katrina deposited nearly 50 cm of coarse grained sand, while heavy precipitation and fluvial flooding produced intercalated bands of silty material at the uppermost levels of the overwash layer. About a month later, Hurricane Rita inundated the area again, giving rise to a 5 cm sand layer similar to the material deposited by Katrina. The effects of Hurricanes Gustav/Ike only deposited a 15 cm coarse grained sand layer with no distinctive boundaries between the two storms due to the short time span between storms.

This study adds new insight to the paleotempestology of a rapidly subsiding, yet economically important, coastal zone in an oil-producing state. It reinforces the concept that a coastal backbarrier site can serve as a sensitive repository for hurricane overwash deposition only when it is situated not too far from the sea (Liu, 2004). In a rapidly retreating coastal zone like Port Fourchon, this time window of "paleotempestological sensitivity" could be quite narrow. This poses a challenge for locating sensitive sites for paleotempestological investigations in Louisiana, where the rate of coastal subsidence is high compared with more stable coastal zones like Alabama and Florida from which multi-millennial proxy records of hurricane activities have been produced (Liu and Fearn, 1993, 2000).

### ACKNOWLEDGMENTS

This research was funded in parts by grants from the Inter-American Institute for Global Change Research (IAI grant CRN2050) and the National Science Foundation. (NSF Grant No. CNH-1212112). Any opinions, findings, and conclusions or recommendations expressed in this material are those of the authors and do not necessarily reflect the views of the National Science Foundation. The authors would like to acknowledge Dr. Kevin Xu for his help in grain size analysis and Qiang Yao for his assistance in field sampling.

### LITERATURE CITED

- Berg, R., 2009, Tropical cyclone report: Hurricanes Gustav and Ike, *National Hurricane Center*, AL092008, 1-55.
- Blum, M.D. and Roberts, H.H., 2009, Drowning of the Mississippi Delta due to insufficient sediment supply and global sea-level rise, *Nature Geoscience*, 2, 10, 488-491.
- Brewton, A., Baud, R., Yam, F., Almasy, L., DeCort, T., Uli, M., Riches Jr, T., Kazanis, E., Josey, A., and Bongiovanni, R., 2009, Gulf of Mexico Oil and Gas Production Forecast: 2009-2018, *U.S. Department of the Interior-Minerals Management Service*, 1-19.
- Chaytor, J.D., 2010, Distribution and tsunamigenic potential of submarine landslides in the Gulf of Mexico, *Advances in Natural and Technological Hazards Research*, 28, 745-754.
- Day, J., Boesch, D., Clairain, E., Kemp, P., Laska, S., Mitsch, W., Orth, K., Mashriqui, H., Reed, D., Shabman, L., Simenstad, C., Streever, B., Twilley, R., Watson, C., Wells, J., and Whigham, D., 2007, Restoration of the Mississippi Delta: Lessons from hurricanes Katrina and Rita, *Science*, 315, 1679-1684.
- Day, J., Lane, R., Moerschbaeche, M., DeLaune, R., Mendelsohn, I., Baustian, J., and Twilley, R.R., 2013, Vegetation and soil dynamics of a Louisiana estuary receiving pulsed Mississippi River water following Hurricane Katrina, *Estuaries and Coasts*, 36, 665-682.
- Henry, K.M. and Twilley, R.R., 2013, Soil development in a coastal Louisiana wetland during a climate-induced vegetation shift from salt marsh to mangrove, *Journal of Coastal Research*, 29(6), 1273-1283.
- Howes, N.C., FitzGerald, D.M., Hughes, Z.J., Georgiou, I.Y., Kulp, M.A., Miner, M.D., Smith, J.M., and Barras, J.A., 2010, Hurricane-induced failure of low salinity wetlands, *Proceedings of the National Academy of Sciences*, 107, 32, 14014-14019.
- Kemp, G.P., Day, J.W., and Freeman, A.M., 2013, Restoring the sustainability of the Mississippi River Delta, *Ecological Engineering*, 10, 1-16.
- Liu, K.B., 2004, Paleotempestology: Principles, methods, and examples from Gulf coast lake sediments. In: Murnane, R.J. and Liu, K.B. (eds.) *Hurricanes and Typhoons: Past, Present, and Future*, pp. 13-57. New York: Columbia University Press.
- Liu, K.B., 2013, Paleotempestology. *Encyclopedia of Quaternary Science*, 3, 209-221, Amsterdam: Elsevier.
- Liu, K.B. and Fearn, M.L., 1993, Lake sediment record of late Holocene hurricane activities from coastal Alabama. *Geology*, 21, 793-796.
- Liu, K.B. and Fearn, M.L., 2000, Reconstruction of prehistoric landfall frequencies of catastrophic hurricanes in northwestern Florida from lake sediment records. *Quaternary Research*, 54, 238-245.
- Liu, K.B., Houyuan, L., and Caiming, S., 2008, A 1200-year proxy record of hurricanes and fires from the Gulf of Mexico coast: Testing the hypothesis of hurricane-fire interactions, *Quaternary Research*, 69, 29-41.
- Liu, K.B., Li, C., Bianchette, T.A., McCloskey, T.A., Yao, Q., and Weeks, E., 2011, Storm deposition in a coastal backbarrier lake in Louisiana caused by Hurricanes Gustav and Ike, *Proceedings 12<sup>th</sup> International Coastal Symposium (Poland)*, *Journal of Coastal Research*, Special Issue No 64, 1866-1870.
- Long, S.P., 2011, Comparing carbon sequestration in temperate freshwater wetland communities, *Global Change Biology*, 5, 1636-1647.
- Madsen, A.T., Murray, A.S., Anderson, T.J., Pejrup, M., and Beruning-Madsen, H., 2005, Optically stimulated luminescence dating of young estuarine sediments: a comparison with <sup>210</sup>Pb and <sup>137</sup>Cs dating, *Marine Geology*, 214, 251-268.
- Pepper, D.A. and Stone, G.W., 2004, Hydrodynamic and sedimentary responses to two contrasting winter storms on the inner shelf of the northern Gulf of Mexico, *Marine Geology*, 210, 43-62.
- Sabatier, P., Dezileau, L., Colin, C., Briqueu, L., Bouchette, F., Martinez, P., Siani, G., Raynal, O., and Grafenstein, U., 2012, 7000 years of paleostorm activity in the NW Mediterranean Sea in response to Holocene climate events, *Quaternary Research*, 77, 1-1

# Characterization of wave climate and extreme events into the SW Spanish and Wales coasts as a first step to define their wave energy potential

Nelson Rangel-Buitrago<sup>†</sup>, Giorgio Anfuso<sup>†</sup>, Mike Phillips<sup>∞</sup>, Tony Thomas<sup>+</sup> Oscar Alvarez<sup>‡</sup>, Manuel Forero<sup>‡</sup>



[www.cerf-jcr.org](http://www.cerf-jcr.org)

<sup>†</sup>Faculty of Marine Science  
University of Cadiz,  
Cadiz

11510 Puerto Real, Spain  
nelson.rangel@mail.uca.es  
giorgio.anfuso@uca.es

+ G D Harries and Sons, Rowlands  
View, Templeton, Narberth,  
Pembrokeshire SA67 8RG  
tony.thomas@gdharries.co.uk

<sup>‡</sup> Applied Physics Department  
University of Cadiz,  
Cadiz

11510 Puerto Real, Spain  
oscar.alvarez@mail.uca.es  
manolo.forerofernandez@alum.uca.es

<sup>∞</sup> University of Wales Trinity Saint  
David (Swansea),  
Mount Pleasant, Swansea, Wales  
m.phillips@sm.uwtsd.ac.uk



[www.JCRonline.org](http://www.JCRonline.org)

## ABSTRACT

Rangel- Buitrago, N., Anfuso, G., Alvarez, O., Phillips, M., Thomas, T., M. Forero. 2013. Characterization of wave climate and extreme events into the SW Spanish and Wales coasts as a first step to define their wave energy potential. *Proceedings 13<sup>th</sup> International Coastal Symposium* (Durban, South Africa), *Journal of Coastal Research*, Special Issue No. 70, pp. 314-319, ISSN 0749-0208.

The characterization of wave climate and extreme events is a key issue for planning coastal and offshore activities. The energy sector is obliged to use alternative sources directed towards environment friendly renewable energy. Ocean waves constitute a potential source of this kind of energy and detailed knowledge of site specific wave climates constitutes the first step in developing a wave energy system. Consequently, this work deals with the analysis of wave climate at Cadiz (SW Spanish Atlantic coast) and Tenby (S Wales, UK). At the former site, wave records include 22 years of data covering the period between 1987 and 2008. Offshore wave climate showed clear cyclic variations in average monthly significant wave height ( $H_s$ ). Waves were usually low ( $H_s < 0.8$  m, Cadiz -  $H_s < 1.0$  m, Tenby) from May to August (late spring to summer), reaching minimum values in August ( $H_s = 0.6$  m Cadiz -  $H_s = 1.0$  m Tenby). Winter waves rapidly increased in height, reaching peak values ( $H_s = 1.2$  m, Cadiz,  $H_s = 2.1$  m, Tenby) between December and January. Energy patterns calculated using the equation of wave energy flux, showed monthly averages at Cadiz and Tenby of circa 5 kW/m and 15 kW/m respectively that reached average values of 37 kW/m and 155 kW/m respectively, during winter. Despite this, Atlantic coastal locations receive less attention when compared with other coastlines around the world since they are considered to be relatively calm areas. Wave power values recorded in this research suggest that the SW Spanish Atlantic and South Wales coastal areas are potential sources of renewable energy.

**ADDITIONAL INDEX WORDS:** *Wave climate, wave energy, renewable energy, Spain, Wales*

## INTRODUCTION

The energy sector is obliged to use a renovating process directed towards environment friendly renewable energy (Vanucchi and Cappiotti, 2011). In this sense waves can potentially contribute large amounts of renewable energy to different world societies (Duckers, 1994). New large scale technologies have been tested in real sea conditions and are near a commercial stage but in order for the Wave Energy Converters (WECs) to be efficient, they have to be adapted to the local wave climate. A detailed knowledge of the wave climate of a specific area is essential for developers of wave energy systems to optimize the technology and make it much more viable and competitive.

In order to assess the viability of development energy plants based on WECs in Cadiz (Spain) and Tenby (Wales), a proper characterization of the local wave climate and an estimate of the available wave energy potential are crucial. In this sense, the

Atlantic Ocean has received less attention since it is considered "calm" in comparison to other coastlines around the world (Vanucchi and Cappiotti, 2011). Therefore, the Atlantic Ocean wave energy would be of interest, particularly when WECs are embodied into new designs or retro fitted to oil platforms or harbor breakwaters. In these cases, they become multifunctional and the required costs for both functionalities are combined (structure and energy production) thus enhancing the value of the use of the WECs.

This research analyses the specific wave climate and energy potential of two Atlantic Ocean coastlines, Cadiz (SW Spanish Atlantic coast) and Tenby (SW Wales), utilizing 22 years of wave data captured between 1987 and 2008. Both wave climates are presented in terms of significant wave height, energy flux and annual energy distribution. Results are then discussed from a wave power perspective and the questions arise around WECs; ultimately the driving force behind this work.

DOI: 10.2112/SI70-053.1 received 1 December 2013; accepted 21 February 2014. © Coastal Education & Research Foundation 2014

Although recent studies have been conducted detailing Atlantic Ocean wave climate, documentation associated with the wave fields and wave energy resources of the investigated areas is extremely sparse and these results fill important gaps in the research.

**STUDY AREA**

This study investigates the wave climate and energy potential of two Atlantic Ocean coastal areas facing the city of Cadiz (SW Spain) and seaside town of Tenby (SW Wales, UK - Figure 1). The Cadiz area corresponds with a northwest-southeast oriented coastline which is characterized by a diversity of coastal landforms and environments including sand spits, beaches, dunes, saltmarshes, cliffs and rocky shore platforms. Tides have a semidiurnal periodicity and mesotidal range, with mean values for neaps and springs of 1.0 and 3.50 m respectively. The littoral zone is affected by western and eastern winds. Westerly winds are related to Atlantic low pressure systems that can continue for several days and affect large portions of the Iberian Peninsula. They blow from the WNW to WSW with a mean annual velocity of 16 km/h and a frequency of 13%. Easterly winds, blowing from the E to SE, with an annual frequency of 20% and a mean velocity of 28 km/h, are originally formed in the Mediterranean Sea and greatly increase their velocity due to the canalization of the Gibraltar Strait. Due to the coastline orientation, westerly winds give rise to both sea and swell waves and easterly winds have no important fetch principally giving rise to sea waves; the main longshore drift thus flows south-eastward.

Tenby, located in Carmarthen Bay, is a relatively wide (30 km), shallow (10 km) embayment bounded by Gower Peninsula in the east and Giltar point, Caldey and St Margaret’s Islands in the west. The area is mainly characterized by rocky cliffs and

sediment movement within South Beach moves from south to north (Thomas *et al.*, 2010), influenced by heavily refracted Atlantic swell waves before undergoing diffraction as they encounter the south coast of Pembrokeshire, and offshore Caldey and St Margaret’s Islands. Winds predominate from south and southwest (alongshore and offshore), where Giltar promontory and the offshore islands give shelter. Caldey Sound, the stretch of water between the mainland and offshore islands, is approximately 1 km wide; its depth below the lowest astronomical tide is 16 m.

**METHODS**

**Wave Data**

Real-time wave measurements along the Spanish littoral were available from the coastal buoy network operated by *Puertos del Estado* (Spanish Ministry of Public Works). Specifically, this work was based on the analysis of data obtained from the scalar buoy n° 1316 (36.50°N; 6.33°W), a waverider-datowell instrument which is located at a water deep of 21 m, in front of Cadiz city (Figure 1). The Tenby wave climate was characterized using data captured at a point located 9 kilometers to the southeast (51.6°N; 4.58°W) within Carmarthen Bay, derived from hind-casts produced by the MetOffice (Figure 1). This point is located at a depth of 28 m, and records significant wave conditions at three hourly intervals.

All data contained a time series acquired during the 1987-2008 period. In the present work, average annual and monthly winter values of significant wave height ( $H_s$ ) were used for the characterization of wave climate and the definition of wave energy flux.

**Wave Power Calculations**

It is well known that, in case of regular waves, the specific wave power is equal to:

$$P = \frac{1}{8} \gamma H^2 C_g \tag{1}$$

Where  $\gamma$  being specific weight ( $N/m^3$ ),  $H$  is wave height (m) and  $C_g$  is the group celerity (m/s). Irregular waves can be considered a superposition of an infinity number of regular components and the total power is calculated as the sum of the power associated to any component, according to the equation 2:

$$P = \sum_{i=1}^{\infty} \frac{1}{8} \gamma H^2(f_i) C_g(f_i) \tag{2}$$

In terms of frequency spectrum,  $S(f_i)$ , the wave height squared is expressed as in equation 3:

$$H^2(f_i) = 8S(f_i)\Delta f \tag{3}$$

The group celerity is computed as in equation 4:

$$C_g(f_i) = \frac{1}{4} \frac{g}{\pi f} \tag{4}$$

Being  $g$  the gravity acceleration ( $m/s^2$ ),  $\pi$  is Pi Constant and  $f$  frequency (1/s). Substituting equations 3 and 4 into equation 2, the equation 5 is obtained:

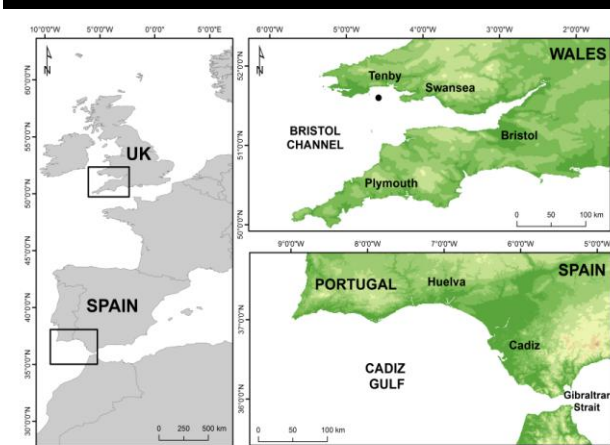


Figure 1. Study areas with location of used wave buoys.

small bays which contain pocket beaches, formed as a result of differential erosion of the softer mudstone-rich Carboniferous Coal Measures and Millstone Grit. In this area tides are semi-diurnal and macro, with a mean spring tidal range of 7.5 m. The shape of the modern coast is dominated by a high-energy south-westerly wave regime (Barber and Thomas, 1989). Incident waves usually approach from south to westerly directions with an average wave height recorded from an offshore position of circa 1.2 m, with associated mean periods centered around 5.2 s; however, storm waves of 5.5 m, and periods of 8.2 s are common (UK Met Office, 2008). Longer-term longshore

$$P = \frac{g\gamma}{4\pi} m_{-1} \frac{m_0}{m_0} \quad (5)$$

Where

$$m_k = \sum_{i=1}^{\infty} S(f_i) f_i^k \Delta f \quad (6)$$

Finally, wave power per unit length of wave front is calculated as in equation 7:

$$P = \frac{1}{64} \frac{g^2}{\pi} \rho H_s^2 T \quad (7)$$

With  $\rho$  water density and providing that  $H_s$  is the significant wave height and  $T$  is the mean wave period.

## RESULTS

### Wave Climate

The monthly average significant wave height ( $H_s$ ) during the investigated period (1987-2008) and associated linear regression analysis are shown graphically in figure 2. Wave Height ( $H_s$ ) results showed a clear cyclic pattern, with waves usually low ( $H_s < 0.8$  m, Cadiz -  $H_s < 1.0$  m, Tenby) from May to August (late spring to summer), reaching their minimum values in August ( $H_s = 0.6$  m, Cadiz -  $H_s = 1$  m, Tenby).

During the winter season, waves rapidly increased in height, reaching peak values ( $H_s = 1.2$  m, Cadiz,  $H_s = 2.1$  m, Tenby) between December and January. When consideration was given to the entire investigated period, there was a significant variation in average monthly wave height. Low winter season  $H_s$  values ( $< 1$  m) were recorded within the 1990/1-1994/5, 1998/9-2001/2 and 2004/5-2007/8 periods and high values ( $H_s \geq 1.3$  m) recorded during the 1989/0, 1995/6, 1996/7, 1997/8, 2002/3 and

2003/4 winter seasons. When extreme wave conditions were considered, the highest monthly value was December 1989, with an average value of extreme wave height of 4.6 m in Tenby and 2.5 m in Cadiz.

Data trends showed small decreases in monthly  $H_s$  values (-0.007 in Cadiz and -0.008 in Tenby). However, Pearson Correlation analyses highlighted that these trends were statistically insignificant for both study cases. Similar results were obtained using Mann-Kendall trend and Wilcoxon rank-sum tests that are commonly used in such studies (Carter and Draper, 1988; Bacon and Carter, 1991; Allan and Komar, 2000). Finally, figure 2 highlighted quasi-periodic 2 to 4 year cyclical behavior in significantly high wave. Similarly, spectral analysis of the time series of extreme waves, based on the Fourier transformation (Boashash, 2003), indicated a cyclic trend of 3 years.

### Wave Energy

Maximum values of monthly mean power for the two areas are shown in Figure 3. Results show that the monthly average wave energy flux was 4.7 kW/m in Cadiz and 14.7 kW/m in Tenby, and reached values of 36.6 kW/m and 155.5 kW/m respectively during the winter season.

When consideration was given to monthly energy power in Cadiz and Tenby areas, the most energetic years were 1987/88, 1989/90, 1994/96, 2000/01 and 2002/03. No clear trend was observed using the 5 step moving average in energy power occurrence and variations indicated a yearly cyclical behavioral pattern and energy peaks observed in 1987/88, 1989/90, 1995/96 and 2000/01 winter seasons.

Linear regressions analysis, Mann-Kendall trend and Wilcoxon rank-sum tests did not show any clear trends throughout the study period. However, the most energetic years showed similarity in the wave energy power in both studied areas. Higher wave energy powers are concentrated during winter seasons (months of October, November, December and January). It is worth noting that during these periods the mean power in the studied domains was always greater than 5Kw/m and during the summer months this energy value ranged from 2 to 6 kW/m.

## DISCUSSION

The obtained results confirmed the seasonal nature of wave height and energy power variations in both Cadiz and Tenby areas.

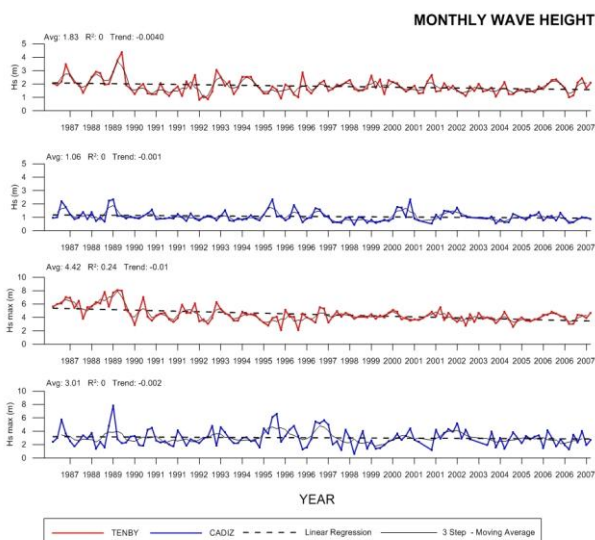


Figure 2. Monthly  $H_s$  and  $H_{s \max}$  for the 1987 – 2008 period.

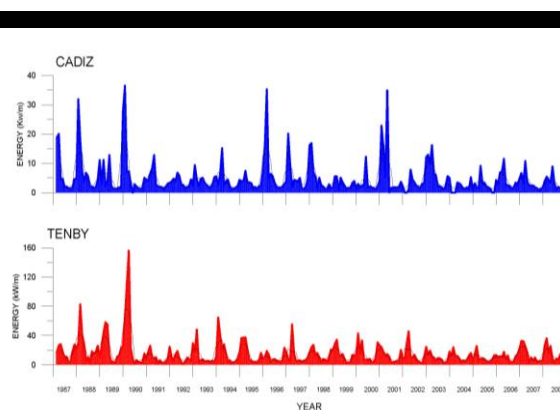


Figure 3. Monthly energy power for the 1987 – 2008 period.

The average monthly time series showed a lack of any clear trends within both features and importantly disagreed with observations carried out by several authors (Carter and Draper, 1988; Bacon and Carter, 1991) suggesting increasing mean significant wave heights in many Oceans around the World that includes the Northern part of the North Atlantic Ocean. Nevertheless, results confirmed observations carried out at the mid and southern latitudes of the North Atlantic Ocean by, for example, Dolan *et al.* (1989) and WASA (1998), and at regional scale, e.g. Cadiz Gulf, by Menéndez *et al.* (2004), Ferreira *et al.* (2009) and Almeida *et al.* (2011).

Almeida *et al.* (2011) used offshore wave buoy data recorded in Southern Portugal and affirmed that the energetic years were the 1987, 1989, 1995, 1996, 1997, 2002 and 2003. All mentioned energetic years (but one, e.g. 2003) confirmed observations carried out in this study. Similarities among previously mentioned studies point to a general homogeneity of wave climate in the Cadiz Gulf, broadly exposed to storms approaching from the third and fourth quadrants. This was observed by Rangel and Anfuso (2011) who analyzed HIPOCAS data sets at 5 locations along the Atlantic littoral of Andalusia Region.

Previous Bristol Channel studies highlighted a predominance of high energy third quadrant Atlantic waves and subdominant first quadrant waves that caused beach rotation at Tenby (Thomas *et al.* 2011a) and to a lesser extent at Penarth 120 km to the east (Phillips and Williams, 2007). Other studies also highlighted a general reduction in swell wave heights for this region (Thomas *et al.*, 2010, 2011b).

Storm generation and high energy fluxes across Central and Southern Europe are related to the Arctic Oscillation (AO) and North Atlantic Oscillation (NAO). Specifically, the NAO is defined as the difference in normalized sea level pressure computed between a station in The Azores (Ponta Delgada) or Southern Europe (e.g., Gibraltar) and another station in Iceland (Stykkisholmur). Negative NAO values give rise to changes in the surface westerly winds across the North Atlantic that eventually affects The Azores and the western European coasts (Andrade *et al.*, 2008). In this respect, severity of winters in northern and western Europe (WMO, 1995; Esteves *et al.*, 2011), temperature anomalies (Hurrell, 1995; Trigo *et al.*, 2002), intensity and frequency of winter daily precipitation and storms over the Iberian Peninsula (Muñoz-Díaz and Rodrigo, 2003; Gallego *et al.*, 2005; Almeida *et al.*, 2011) are partially influenced by this teleconnection pattern.

The AO is an atmospheric circulation pattern reflecting the non-seasonal sea-level pressure variations north of 20° N latitude and varies over time with no particular periodicity; it is characterized by pressure anomalies of opposite sign, one located in the Arctic and the other centered at 37–45° N latitude (Thompson and Wallace, 1998). The AO is believed to be causally related to, and thus partially predictive of, weather patterns in locations many thousands of miles away, including many of the major population centers of Europe and North America. In the same way, negative AO values play an important role in determining extreme conditions such as frozen

precipitations, strong winds and extreme weather events in general over the Northern Hemisphere and in particular over the North East USA, the Mediterranean area and China (Thompson and Wallace, 2000; Higgins *et al.*, 2002; Wettstein and Mearns, 2002; Xoplaki, 2002; Türkeş and Erlat, 2008; Mao *et al.*, 2011).

Within this study, high energy conditions prevailed during negative values of AO and NAO as previously observed by Hurrell (1995) in Southern Europe, Rodríguez *et al.* (2003) in the Gulf of Cadiz and Thomas *et al.* (2011) and Phillips and Crisp (2010) in Wales (Figure 4). During NAO positive values, low cyclonic activity is recorded and winters are dryer (and less energetic) than normal (Rodwell *et al.*, 1999). It is interesting to remark that high energy values were observed when neutral to strong negative NAO and AO phases occurred and also when there were abrupt changes moving between positive and negative phases without passing through a neutral phase. Thompson and Wallace (1998) observed behavioral patterns of both NAO and AO indices and concluded that the AO resembles the NAO in many respects. However, the AO's primary center of action covers more of the Arctic, giving it a more zonal symmetric appearance. Hence, even though the AO and the NAO patterns resemble each other, there is a clear distinction that could play a guiding role in determining the physical mechanisms that control Northern Hemisphere climate variability (Wallace, 2000).

Climatic anomalies were associated with an extreme persistence of negative phases of AO and NAO indices and an exceptional Northern Hemisphere mean atmospheric circulation episode (Wang *et al.*, 2010) reflected by the distribution of the geo-potential height anomalies at 500 mb. This parameter exhibited a strong zonal hemispheric pattern, with anomalously high pressures over the pole during 1995/1996 (Figure 5). Such a distribution favored the development of negative phases for the AO and NAO at the same time (Thompson and Wallace, 1998; L'Heureux *et al.*, 2010). Similar results were recorded by Cohen *et al.* (2010) and L'Heureux *et al.* (2010) which highlighted that the negative AO phase of December 1995 was a record result of an unusual occurrence of two troposphere–stratosphere coupling events (NAO–AO) that occurred more rapidly than usual and in quick succession.

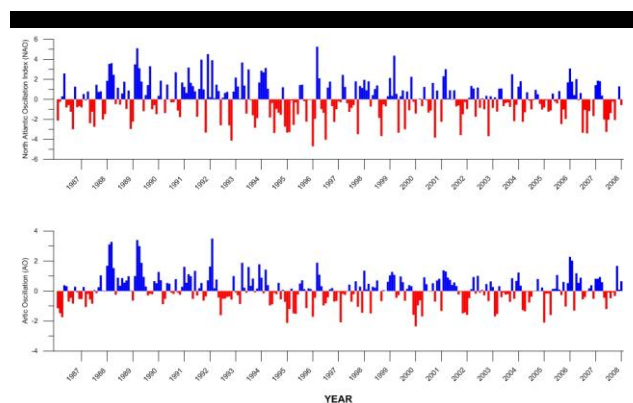


Figure 4. Monthly NAO and AO for the 1987 – 2008 period.

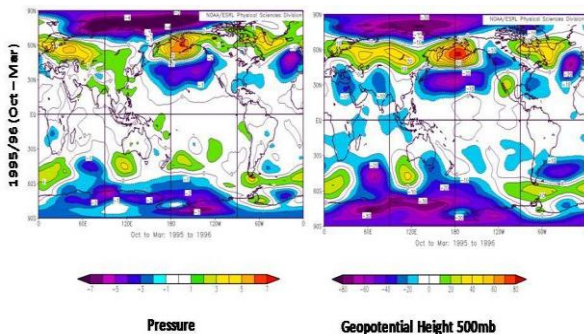


Figure 5. Pressure and Geo-potential height anomalies at 500 mb over the 1995/96 (from NCEP-NCAR reanalysis). Wave energy and extremely coldest conditions were recorded during the aforementioned winter seasons.

Finally, in the realm of the WECs, the irregular nature of the waves is a problematic area for the ocean wave energy capture. Principally, the extreme energy differences experienced in extreme events (such storms) when compared to average power levels can have a harmful consequence on the possible development and survivability of these schemes.

Authors such as Walters *et al.* (2009) clarify that when designing a wave energy converter for a certain site, for example Cadiz or Tenby, there are many parameters to consider, one of them being the average energy power. The plan choices may vary a great deal depending on where one chooses to focus, and any decision will be a compromise.

The average levels of energy flux are a reality in the oceans that all designers of wave energy converters must consider. Although most likely published only in regular media rather than in scientific journals, the harsh conditions of the oceans and the extreme power of ocean waves have wrecked many attempts to make use of wave energy conversion.

The WECs must be designed to survive in these conditions. However, since a wave energy converter cannot be designed to have an installed power corresponding to the 100-year wave some compromise is needed in order for the WEC to be of realistic proportions from an economical perspective.

## CONCLUDING REMARKS

In a global scenario of climate change, renewable energies are achieving a rising importance. Waves are powerful energetic agents but their characteristics and spatial and temporal distributions are still deeply unknown in many coastal sectors. In this study, this substantial energy resource was investigated using wave buoy data and hindcast data respectively for the Cadiz (SW Spanish Atlantic coast) and Tenby (Wales, UK) areas over a period of 22 years between 1987 and 2008.

It was found that wave climates present a clear seasonal behavior at both sites and most of the energy is provided by waves during winter months. Essentially December and January are most energetic, with significant wave height average values of  $H_s = 1.2$  m in Cadiz and  $H_s = 2.1$  m, in Tenby. The average monthly wave energy flux is 5 kW/m in both Cadiz and Tenby. During winter, it may reach an average value of 37 kW/m and 155 kW/m in Cadiz and Tenby, respectively.

## ACKNOWLEDGEMENT

This work is a contribution to the RESISTE Research Project (CGL2008-00458/BTE, supported by the Spanish Ministry of Science and Technology and by European Funds for Regional

Development – F.E.D.E.R.), the Research Project GERICO (CGL 2011–25438) and to the Andalusia P.A.I. Research Group no. RNM-328. Thanks to Puerto del Estado (Spanish Ministry of Public Works) and MetOffice in Wales for offshore wave data records. This work has been partially developed at the Centro Andaluz de Ciencia y Tecnología Marinas (CACYTMAR), Puerto Real (Cadiz, Spain).

## LITERATURE CITED

- Allan, J.C. and Komar, P.D., 2000. Are ocean wave heights increasing in the eastern North Pacific?. *EOS, Transactions of the American Geophysical Union*, 47, 561-567.
- Almeida, L.P., Ferreira, O., Voudoukas, M.I. and Dodet, G., 2011. Historical variation and trends in storminess along the Portuguese Southcoast. *Natural Hazards Earth Systems Sciences*, 11, 2407-2417.
- Andrade C., Trigo R.M, Freitas M.C., Gallego, M.C., Borges, P. and Ramos A.M., 2008. Comparing historic records of storm frequency and the North Atlantic Oscillation (NAO) chronology for the Azores region, *The Holocene*, 15 (5), 745-754.
- Bacon, S. and Carter, D.J.T., 1991. Wave climate changes in the North Atlantic and North Sea. *International Journal of Climatology*, 11, 545-558.
- Barber, P.C., and Thomas, R. R. P., 1989. Case study of Carmarthen bay. *Coastal Management*, 25, 243-262.
- Boashash, B., 2003. Time-Frequency signal analysis and processing: A comprehensive reference, Oxford: Elsevier Science: 135p.
- Carter, D.J.T. and Draper, L., 1988. Has the north-east Atlantic become rougher?. *Nature*, 332: 494.
- Cohen, J., Foster, J., Barlow, M., Saito, K., Jones, J., 2010. Winter 2009–2010: a case study of an extreme Arctic Oscillation event. *Geophysical Research Letters*, 3, L17707, DOI: 10.1029/2010GL044256.
- Dolan, R., Lins, H. and Hayden, B., 1989. Mid-Atlantic coastal storms. *Journal of Coastal Research*, 4, 417-433.
- Esteves, L.S, Williams, J.J. and Brown, J.M., 2011. Looking for evidence of climate change impacts in the eastern Irish Sea, *Natural Hazards and Earth System Sciences*, 11, 1641-1656.
- Ferreira, O., Voudoukas, M.V. and Ciavola, P., 2009. MICORE review of climate change impacts on storm occurrence, Florence:MICORE, 120p.
- Gallego, M.C., Garcia, J.A and Vaquero, J.M, 2005. The NAO signal in daily rainfall series over the Iberian Peninsula, *Climate Research*, 29(2), 103-109.
- Higgins, R.W., Leetman, A. and Kousky, V.E., 2002. Relationships between climate variability and winter temperature extremes in the Unites States, *Journal of Climate*, 15, 1555-1572.
- Hurrell, J.W., 1995. Decadal trends in the North Atlantic Oscillation: Regional temperatures and precipitation. *Science*, 269, 676-679.
- L'Heureux, M., Butler, A., Jha, A., Kumar, A., Wang, W., 2010. Unusual extremes in the negative phase of the Arctic Oscillation during 2009. *Geophysical Research Letters*, 37, L10704, DOI: 10.1029/2010GL043338.
- Mao, R., Gong, D., Bao, J. and Fan, Y., 2011. Possible influence of Arctic Oscillation on dist storm frequency in North China. *Journal of Geographical Sciences*, 21(2), 207-218.
- Menéndez, M., Méndez, F., Losada, I., Medina, R. and Abascal, A., 2004. Variaciones del régimen extremal del clima marítimo en el litoral español en el periodo 1958–2001. In *El Clima entre el Mar y la Montaña*. Concha D, Garcia J, Alvarez D. (eds) Universidad de Cantabria: Santander, Spain.
- Muñoz-Díaz, D. and Rodrigo, F.S., 2003. Effects of the North Atlantic oscillation on the probability for climatic categories of local monthly rainfall in southern Spain. *International Journal of climatology*, 23(4), 381-397.
- Phillips, M. and Crisp, S., 2010. Sea level trends and NAO influences: the Bristol Chanel/Seven Estuary, *Global and Planetary Change*, 73, 211-218.
- Rangel-Buitrago, N. and Anfuso, G., 2011. An application of Dolan and Davis (1992) classification to coastal storms in SW Spanish littoral. *Journal of Coastal Research*, SI64, 1891 - 1895.
- Rodríguez, A., Ruiz, F., Caceres, L.M., Rodríguez, J., Pino, R. and Muñoz, J.M., 2003. Analysis of the recent storm record in the south western

- Spanish coast: implications for littoral management. *The Science of the Total Environment*, 303, 189-201.
- Rodwell, M.J., Rowell, D.P. and Folland, C.K., 1999. Ocean forcing of the wintertime North Atlantic Oscillation and European climate, *Nature*, 358, 320-323.
- Thomas, T., Phillips, M. R. and Williams, A. T., 2010. Mesoscale evolution of a headland bay: beach rotation process. *Geomorphology*, 123, 29-41.
- Thomas, T., Phillips, M.R., Williams, and A.T., Jenkins, R.E., 2011a. A Multi-century record of linked nearshore and coastal change. *Earth Surface Processes and Landforms*, 36, 995-1006.
- Thomas, T., Phillips, M.R., Williams, A.T. and Jenkins, R.E. (2011b), “Short-term beach rotation, wave climate and the North Atlantic Oscillation (NAO)”, *Progress in Physical Geography*, 35(3), 333-352.
- Thompson, D.W.J. and Wallace, J.M., 1998. The Arctic Oscillation signature in the wintertime geopotential height and temperature fields, *Geophysical Research Letters*, 25, 1297-1300.
- Trigo, R.M., Osborn, T.J. and Corte-Real, J., 2002. The North Atlantic Oscillation influence on Europe: climate impacts and associated physical mechanism, *Climate Research*, 20, 9- 17.
- Türkeş, M. and Erlat, E., 2008. Influence of the Arctic Oscillation on the variability of winter mean temperatures in Turkey, *Theoretical and Applied Climatology*, 92, 75- 85.
- Wallace, J.M. and Gutzler, D.S., 1981. Teleconnections in the geopotential height field during the Northern Hemisphere winter, *Monthly Weather Review*, 109, 784-812.
- Wallace, J.M., 2000. North Atlantic Oscillation /annular mode: Two paradigms – one phenomenon. *Quarterly Journal of the Royal Meteorological Society*, 126, 791-805.
- Walters, R., Engstrom, J.I., Isberg, J. and Leijon, M., 2009. Wave climate off Swedish west coast, *Renewable Energy*, 1600-1606.
- Wang, C., Liu, H., Lee, S., 2010. The record-breaking cold temperatures during the winter of 2009/2010 in the Northern Hemisphere, *Atmospheric Science Letters*, 11, 161-168.
- WASA, 1998. Changing waves and storms in the northeast Atlantic, *Bulletin of the American Meteorological Society*, 79, 741-760.
- Wettstein, J.J. and Mearns, L.O., 2002. The influence of the North Atlantic-Arctic Oscillation on mean, variance and extremes of temperature in the northeastern United States and Canada, *Journal of Climate*, 15, 3586-3600.
- WMO (World Meteorological Organization), 1995. The global climate system review. Climate system Monitoring 1991-1993. WMO: Switzerland.
- Xoplaki, E., 2002. *Climate Variability over the Mediterranean*. Bern, Switzerland: University of Bern, PhD. Thesis, 230 p.



## Influence of climate change on the Ria de Aveiro littoral: adaptation strategies for flooding events and shoreline retreat



João M. Dias<sup>†</sup>, Carina L. Lopes<sup>†</sup>, Carlos Coelho<sup>‡</sup>, Carla Pereira<sup>‡</sup>, Fátima L. Alves<sup>∞</sup>, Lisa P. Sousa<sup>∞</sup>, Inês C. Antunes<sup>∞</sup>, Maria da Luz Fernandes<sup>∞</sup>, Mike R. Phillips<sup>+</sup>

<sup>†</sup> NMEC, CESAM  
Physics Department  
University of Aveiro  
3810-193, Aveiro, Portugal  
joao.dias@ua.pt  
carinalopes@ua.pt

<sup>‡</sup> CESAM,  
Civil Engineering Department  
University of Aveiro  
3810-193, Aveiro, Portugal  
ccoelho@ua.pt  
alexandrapereira@ua.pt

<sup>∞</sup> CESAM,  
Environment and Planning Department  
University of Aveiro  
3810-193, Aveiro, Portugal  
malves@ua.pt  
lisa@ua.pt  
ines.antunes@ua.pt  
maria.luz@ua.pt

<sup>+</sup> University of Wales:  
Trinity Saint David  
(Swansea),  
Mount Pleasant,  
Swansea,  
SA1 6ED, Wales, UK  
m.phillips@smu.ac.uk

[www.cerf-jcr.org](http://www.cerf-jcr.org)



[www.JCRonline.org](http://www.JCRonline.org)

### ABSTRACT

Dias, J.M., Lopes, C.L., Coelho, C., Pereira, C., Alves, F.L., Sousa, L.P., Antunes, I.C., Fernandes, M. da L., Phillips, M.R., 2014. Influence of mean sea level rise on Ria de Aveiro littoral: adaptation strategies for flooding events and shoreline retreat. In: Green, A.N. and Cooper, J.A.G. (eds.), *Proceedings 13<sup>th</sup> International Coastal Symposium* (Durban, South Africa), *Journal of Coastal Research*, Special Issue No. 70, pp. 320-325, ISSN 0749-0208.

Floods and shoreline retreat in coastal areas threaten many millions of people across Europe. Moreover, it is agreed that climate change can amplify the magnitude and frequency of flooding events and accelerate the shoreline retreat. The main goal of this work is to assess flood and shoreline retreat risk, and define adaptation strategies under present conditions and future climate change scenarios on the Ria de Aveiro and its littoral. The hydrodynamic model ELCIRC was implemented for the Ria de Aveiro lagoon and GENESIS (U.S. Army Corps of Engineers) and LTC (Long-Term Configuration) shoreline evolution models for the littoral stretch between Esmoriz and Mira. Numerical results in present and future scenarios were used to map the flooded lagoon extension and the shoreline evolution of this coastal stretch. Analysis showed an increase of the lagoon's flooded area, relative to the present, with regions more exposed to sea level rise being lowland areas located at the margins of the lagoon's deeper channels. Examination of the littoral stretch showed a slight increasing trend of shoreline retreat under predicted future climate change scenarios, thereby increasing the probability of sand spit rupture. Data from numerical predictions were integrated into Geographical Information Systems covering the coastal and lagoon study areas, and produced hazard and risk maps including the identification of regional use and activities. Structural and non-structural measures were subsequently developed in order to mitigate flood and shoreline retreat effects.

**ADDITIONAL INDEX WORDS:** Numerical modeling, flood risk, coastal vulnerability, sea level rise, mitigation

### INTRODUCTION

Flood events are part of nature and one of the most common hazards all over the world. The shoreline retreat also endangers coastal areas worldwide. Together they threaten millions of people, goods and ecosystems. Management of flood and coastal erosion risk involves many different public and private entities worldwide, each accountable for different aspects of risk management. Ensuring the emergency services and public knowledge of where and when the flood or coastal erosion will occur and how serious these hazards will be is a very complex task. The minimization of damages caused by floods or coastal retreat involves reducing the likelihood of these hazards and their impacts when they occur. At the same time, there are underlying pressures that are increasing the risk, such as climate change, urban development or changes in land use.

In 2007, the European Union recognized the threats of floods and approved an European Directive (2007/60/EC) on the assessment and management of flood risk. This directive states that all member states must prepare flood hazard maps and flood risk maps for all water courses and coastlines and establish flood risk management plans to reduce the risk, taking into account

climate change effects. In response, the scientific project ADAPTAR<sup>ia</sup> (<http://climetua.fis.ua.pt/legacy/adaptaria/en/index.html>) was developed to study the impact of climate change on flooding events and shoreline retreat in the Ria de Aveiro lagoon and its littoral (Figure 1). The lagoon is a shallow coastal system located in central Portugal exposed to fluvial and coastal flooding. The adjacent coastal stretch of Esmoriz to Mira has several coastal erosion problems with a high probability of sand spit rupture. The main goal of this work is to perform flood and shoreline retreat risk assessment and define adaptation strategies under present and future climate change scenarios. To achieve this target, the flood extension in the lagoon and the shoreline position under present (P) and future (F) climate conditions were estimated through numerical modelling. Then, the numerical results were incorporated into a Geographical Information Systems and vulnerability and risk maps were built. Finally, mitigation and adaptation strategies were designed for the region in order to minimise flood and shoreline retreat effects, aiming to reduce risk and mitigate the damages caused by these hazards.

### STUDY AREA

The Ria de Aveiro is a shallow coastal lagoon located on the northwest Portuguese coast (40°38'N, 8°45'W). A sand spit separates the lagoon from the ocean in most of its extension,

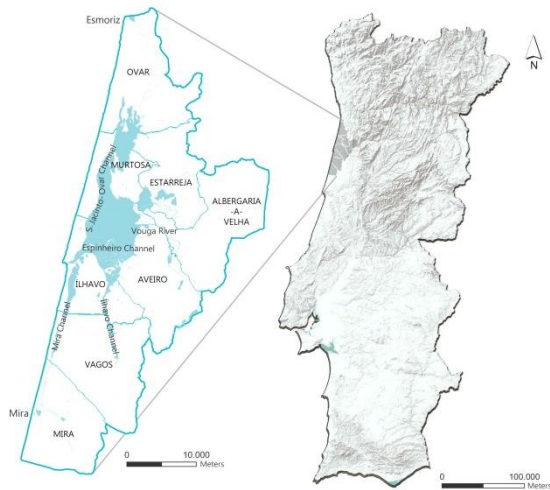


Figure 1. Location of Ria de Aveiro region, indicating the lagoon main channels and its municipalities.

except at the middle where the lagoon connects with the Atlantic Ocean through a single artificial inlet built in 1808. It is 45 km long and 10 km wide and covers an area of 89.2 km<sup>2</sup> in spring tide which is reduced to 64.9 km<sup>2</sup> in neap tide conditions (Lopes *et al.*, 2013). The astronomical tidal range varies between a maximum of 3.2 m in spring tide and a minimum of 0.6 m in neap tide (Dias *et al.*, 2000). The meteorological tide, although infrequent, can reach a maximum height of ~ 1 m (Picado *et al.*, 2013). When high tides and/or significant meteorological tide occur, certain areas adjacent to the lagoon are flooded, endangering agricultural productivity as well as the local biodiversity. In the Espinho channel, the Vouga River enters and represents approximately 2/3 of the overall lagoon fluvial input. The Antuã River enters into the Laranjo bay the, while at the heads of S.Jacinto, Ílhavo and Mira channels, the Cáster, Boco and Ribeira dos Moinhos Rivers enter respectively. The adjacent regions of the Vouga river mouth are flooded when its discharge is high. This area is called *Bloco do Baixo Vouga Lagunar* (BBVL), and presents unique biophysical characteristics that confer to this region high nature conservation and biodiversity values. For these reasons, Ria de Aveiro and its littoral are included in the Natura 2000 network as a Special Protection Zone.

The Esmoriz-Mira stretch is mainly a sandy coastal system, under a very energetic maritime wave climate. The wave climate presents a significant wave height of about 2 or 3 meters, with wave periods between 8 and 12 seconds. The significant wave height during storm events exceeds 8 meters, with wave periods from 16 to 18 seconds (Coelho *et al.*, 2009). Major storms reaching the Northwest Portuguese coast are from the Northwest quadrant. As a consequence of the wave climate, littoral drift currents act mainly in a North-South direction. This can easily be demonstrated by areas of accretion located north of groins and areas of erosion at the south (Coelho and Veloso-Gomes, 2006).

## METHODOLOGY

The first step of this study was the application of the 2D hydrodynamic model ELCIRC (Zhang *et al.*, 2004) to the Ria de Aveiro lagoon in order to determine the lagoon's flooded area and

of the GENESIS (U.S. Army Corps of Engineers) and LTC (Long-Term Configuration) models to the Esmoriz-Mira stretch in order to predict the evolution of the shoreline.

Concerning the lagoon hydrodynamic simulations, the model configuration used was previously calibrated for tidal propagation by Lopes *et al.* (2013). Six runs were defined (Table 1), corresponding to combinations of different tidal ranges (TR), storm surge (SS), mean sea level (MSL) and fluvial flow (FF) conditions. Additionally, the model was run for mean tide conditions, without any other forcing, to define the reference conditions. Mean, spring and equinoctial tide conditions were determined from statistical analysis of tidal gauge data recorded at the lagoon entrance between 1976 and 2005. Storm surge amplitudes of 0.58, 0.84 and 1.17 m determined by Picado *et al.* (2013) for 2, 10 and 100 years return periods, respectively, are used. The fluvial flow for 2, 10 and 100 years return periods was determined at the five most important lagoon tributaries for both climates (Table 2), from daily discharges predicted by the watershed model SWAT. This model was forced with observed precipitation (1932-2010) for the present climate and with forecasted precipitation from ECHAM5 model for the future (2071-2100), considering the SRES A2 scenario from IPCC. A mean sea level rise of 0.42 m was adopted, corresponding to Lopes *et al.* (2011) local estimation for the end of the 21<sup>st</sup> century considering the SRES A2 scenario from IPCC.

The shoreline evolution simulations include coastal defense works at the studied stretches after all the necessary considerations related to their position, together with wave propagation effects and permeability, thus establishing the most appropriate calibration results. The initial shoreline position, defined as elevation +2.0 m (Cartographic Datum) required some adjustments in bathymetry and topography, being coincident with the position obtained by the satellite image of 2010 (Pereira *et al.*, 2013). Two runs were defined, one considering the current mean sea level and wave climate and other considering the future mean sea level (0.42 m) and wave climate. The wave regimes used are presented in Pereira *et al.* (2013) and were determined based on the application of the WW3 wave model to the North Atlantic (Ribeiro *et al.*, 2012). The two runs were forced by wind fields generated by the climatic model ECHAM5 for the reference (1971-2000) and future (2071-2100 – IPCC SRES A2 scenario) situations (Ribeiro *et al.*, 2012). Following the guidelines of the Decree 115/2010 of October 22 – which transposes the EU Floods Directive (2007/60/EC) to the national law – the data from numerical predictions were introduced into a Geographical Information Systems along with thematic data (such as Census data, land cover, infrastructures, buildings, etc.). The results of the runs of flood extent for the lagoon (Figure 2) and shoreline evolution for the littoral stretch (Figure 3) were analysed and combined, resulting in a present (A) and a future scenario (B). These results were used to map the probability of occurrence, the vulnerability of the territory, and the risk of flooding and shoreline retreat for both scenarios. Finally, based on the risk analysis were proposed interventions to adapt, control, and manage the risk of floods in the lagoon and the risk of shoreline retreat.

Table 1. Summary of boundary conditions used in the hydrodynamic simulations.

	Run1	Run2	Run3	Run4	Run5	Run6
<b>Tide</b>	Mean	Spring	Equino.	Mean	Spring	Equino.
<b>SS</b>	2	10	100	2	10	100
<b>MSL</b>	P	P	P	F	F	F
<b>FF</b>	P-2	P-10	P-100	F-2	F-10	F-100

**RESULTS AND DISCUSSION**

**Lagoon marginal flooding**

The flood extent maps (Figure 2) result from the identification, in model grid, of cells that were flooded along each tidal cycle. These maps show that changes to the lagoon flooding drivers resulted in different marginal flooded regions. Globally, the margins of the lagoon main channels are flooded under extreme events, mainly at the S.Jacinto and Espinheiro channels given their low altitude and reduced topography. It should be highlighted that under high fluvial discharges the flood extension increases at BBVL, as well as in other lowlands located close to the mouth of the lagoon tributaries. For the future climate, the marginal inundation tends to increase at the lagoon central area and around the lagoon main channels. Close to the mouth of the tributaries, the marginal inundation decreases as a consequence of the predicted reduction in fluvial discharge for the future climate.

**Shoreline retreat**

The shoreline retreat, the lost territory areas and the alongshore sediment transport volumes in several cross sections were determined from model predictions. An erosion trend was observed for both climates, with few exceptions in very short lengths (Figure 3). Strong erosion downdrift of the groins along this stretch is found for both runs. The maximum retreat after 90 years was recorded in the Labrego-Areão stretch, corresponding to about 400 meters, for the climate change scenario. The lowest retreat rates are located in the confined stretches of smaller extension, being therefore less susceptible to coastal erosion. Comparing the results for present and future runs, a slight clockwise rotation of the shoreline was predicted, increasing the average shoreline retreat rate by about 6% (Figure 3). Regardless of the considered runs, it was found that the areas south of Costa Nova and Labrego (located south of Vagueira) have the higher probability of sand spit rupture and therefore represent the most likely location for opening a new inlet between the lagoon and the ocean.

**Vulnerability and flood risk**

The first step was to integrate the results of the flood extent for the lagoon and of the shoreline evolution for the littoral stretch. In

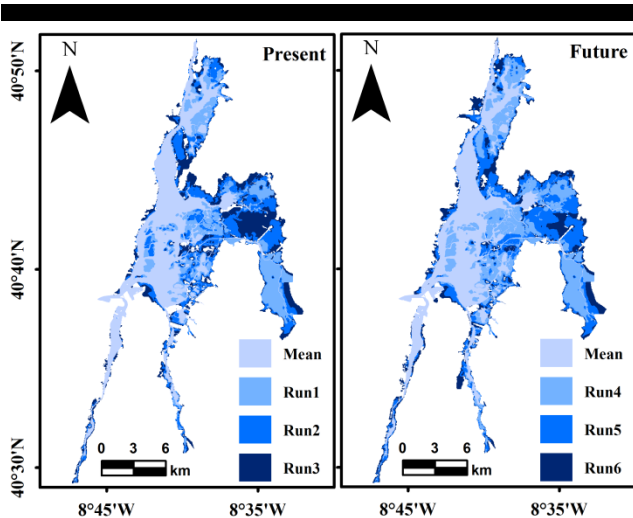


Figure 2. Lagoon flooded extent maps for each model run.

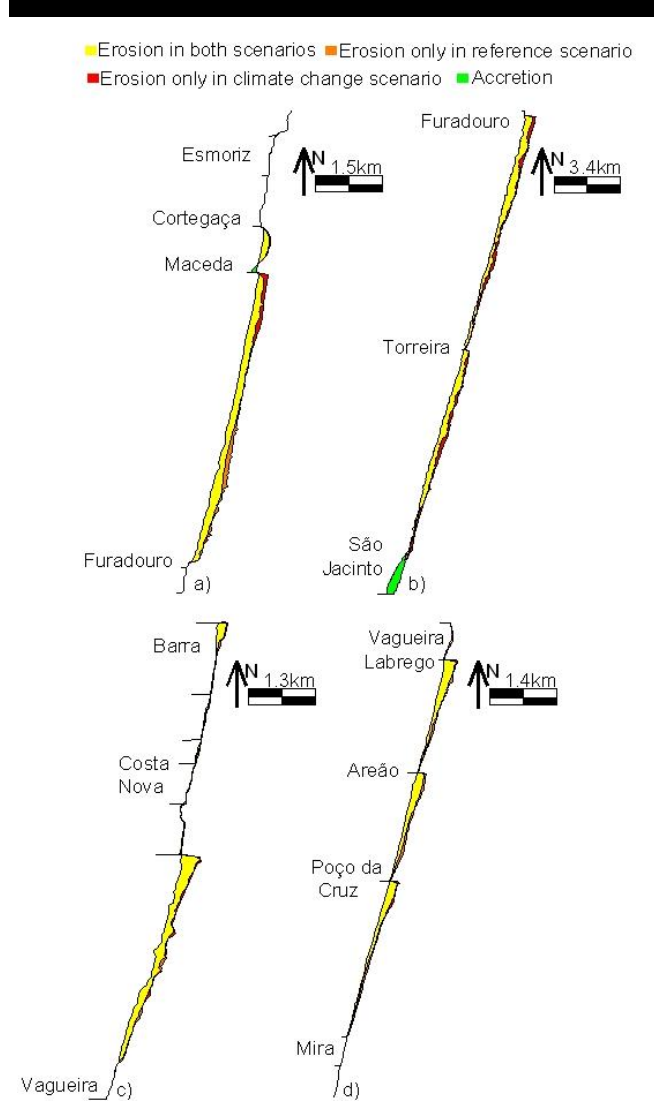


Figure 3. Territory lost until 2100, for both runs: a) Esmoriz-Furadouro; b) Furadouro-São Jacinto; c) Barra-Vagueira; d) Vagueira-Mira.

order to simplify the analysis, the model runs were reduced to a present (A) and a future scenario (B). The scenario A takes into account the current conditions of mean sea level, wave climate, fluvial discharge, storm surge and tidal range. The scenario B considers future climate change scenarios, taking into account the mean sea level rise combined with wave climate and fluvial discharge forecasts for 2100.

The probability of occurrence (Figure 4) of flooding in the lagoon was determined based on the return period of fluvial discharge and storm surge. For the coastal area, it was assumed that the largest retreats are less likely to be achieved (shoreline position in 2100 has a lower probability of being reached than the shoreline position in 2070, that has lower probability of being reached than shoreline position in 2040). Probability maps were built for each scenario, combining lagoon and coastal area results.

Vulnerability (Figure 5) is understood as the characteristics of a territory, which make it susceptible to degradation or damage (Barroca *et al.*, 2006; UNISDR, 2009) caused by flooding and/or

shoreline retreat. Given the geographic scale of analysis, a correspondence between the degree of vulnerability and the 2006 CORINE Land Cover classes (Caetano *et al.*, 2009) was made. It was assumed that the vulnerability was:

- high in artificial surfaces;
- medium in agricultural, forest and semi natural areas, when they are subject to flooding by salt water, and whenever the shoreline reaches the lagoon;
- low in agricultural, forest and semi natural areas, when they are subject to flooding by freshwater;
- residual in wetlands and water bodies.

The risk map (Figure 5) results from the combination of the probability of occurrence with the vulnerability of the territory. This means that the risk is higher in areas identified with high probability and high vulnerability. This approach integrates both socioeconomic and ecological aspects of the territory.

**Mitigation and adaptation strategies**

The analysis of present and future flood risk in the lagoon and shoreline retreat risk in the littoral shows:

- increase of the lagoon flooded area – particularly in the alluvial plains – as result of the mean sea level rise, which is not nullified by the predicted decrease in fluvial discharge;
- increase in the average shoreline retreat rate (~6%), also increasing the threatening to the sand spit stability close to Vagueira settlement, as result of mean sea level rise and new wave climate.

Flood risk and shoreline retreat risk can be reduced by managing hazard characteristics, such as flood probability or extent, and/or by reducing the vulnerability of people and territory at risk. There are several measures that can contribute to control, adapt and manage the risk (Klijn *et al.*, 2009):

- structural measures – intervene directly in biophysical environment. These can be hard (e.g. dikes, dams, groins), soft (e.g. recovery of water courses, beach nourishment) or mix (where direct physical adaptation interventions into

nature structures are done through the application of specialized treatment techniques);

- non-structural measures - comprises the definition of policies and strategies (including the management of water resource), financial instruments (e.g. incentives and penalties) and communication strategies (e.g. public awareness, warning systems).

Table 3 summarizes the proposed interventions to adapt, control, and manage the risk of flooding in the lagoon and the risk of shoreline retreat.

**CONCLUSIONS**

This multidisciplinary work reports the influence of climate changes on the flooding of the Ria de Aveiro and on shoreline retreat of the adjacent littoral. This also incorporates proposals to reduce their adverse impacts. Globally, the lagoon’s flooded area increases under predicted future climate conditions relative to the present; essentially driven by the mean sea level rise predicted for the region. Nevertheless, a reduction of the flooded extension was forecast close to the mouth of the lagoon tributaries, motivated by the reduction of fluvial discharges expected for the future. Regarding shoreline evolution, an increase of about 6% in the average retreat rate for the future, with a slight clockwise rotation of the shoreline is predicted. Erosion problems will induce a high risk of sand spit rupturing in the coastal stretch between Costa Nova and Mira, and consequently the opening of a new inlet in this stretch is predicted.

From the combined analysis of risk of flooding and shoreline retreat, the most critical situations and ensuing strategies to adapt to climate change were identified. These are within the framework of the Portuguese government international responsibilities, and developed in the frame of the national strategy for climate change adaptation. In this context the formulated proposals intend to anticipate the consequences of planned interventions, and incorporate the 'uncertainties' inherent to hazard and risk. This is particularly relevant for areas of significant socioeconomic and

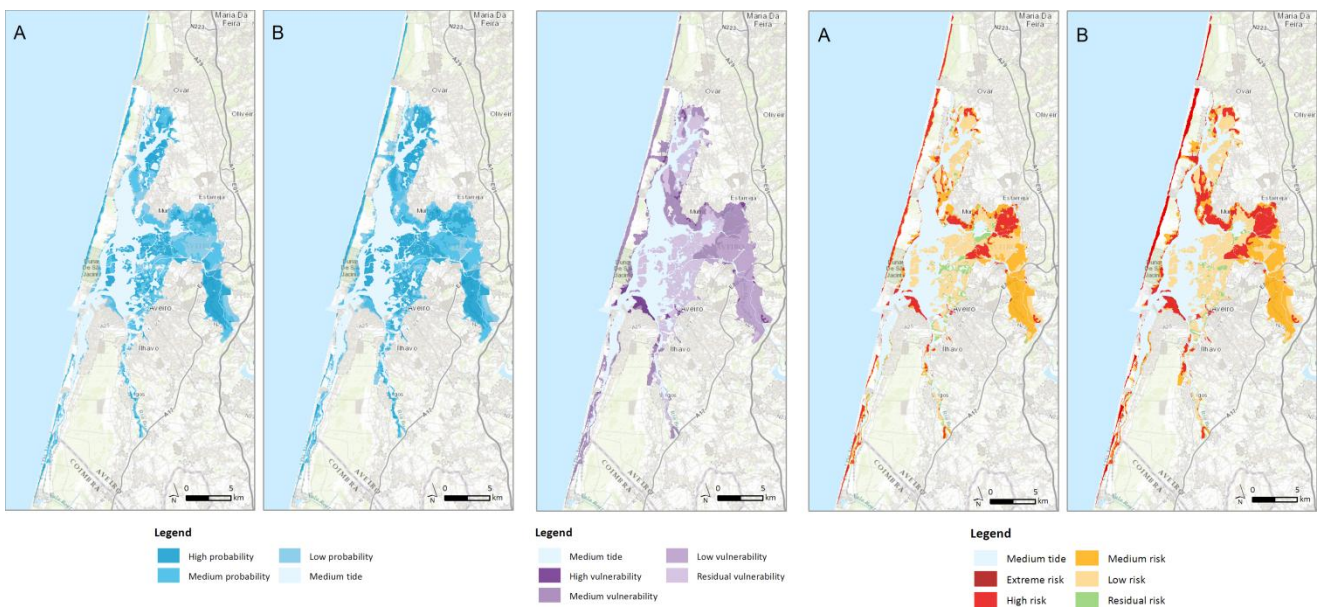


Figure 4. Probability of occurrence in scenarios A and B, global vulnerability of the territory, and flood and shoreline retreat risk maps in scenarios A and B (Source: adapted from Alves and Sousa, 2013).

Table 3. Proposed interventions (Source: adapted from Alves *et al.*, 2013a).

			Type	
Structural Measures of Adaptation	<b>Tide Protection System</b>			
	'Esteiros' (watercourses)	Recovery and stabilization of watercourses banks through biophysical engineering techniques and establishment of riparian shrub borders in order to avoid uncontrolled overtopping.	<u>Event:</u> Floods, overtopping and bank rupture. <u>Damage:</u> Salinization of agricultural fields and flooding in urban areas.	Mix
	<b>Flood Adaptation System</b>			
	Vouga river	Land surface recovery and biophysical stabilization in and along Vouga river channel through biophysical engineering techniques and establishment of riparian shrub borders in order to avoid uncontrolled overtopping and bank ruptures, characteristic at flood season.	<u>Event:</u> Overtopping, bank rupture and waterlogging. <u>Damage:</u> Flooding of BBVL fields, bank rupture, deposition of unwanted sediments, destruction of agricultural roads and waterlogging (when the drainage is not done on time).	Mix
	Other rivers	Land surface recovery and biophysical stabilization in and along rivers channels through biophysical engineering techniques and establishment of riparian shrub borders in order to avoid uncontrolled overtopping.	<u>Event:</u> Floods, overtopping, bank rupture and waterlogging. <u>Damage:</u> Flooding of agricultural fields and urban areas, bank rupture, deposition of unwanted sediments, destruction of agricultural roads and waterlogging (when the drainage is not done on time).	Soft
	Structural Measures of Control	<b>Tide Protection System</b>		
Dikes		Protection of BBVL fields through the extension of a physical main existing structure (dike) against salt water intrusion.	<u>Event:</u> Overtopping and bank rupture. <u>Damage:</u> Salinization of BBVL fields and consequently destruction of cultures and banks.	Hard
Hydraulic structures		Construction of hydraulic structures constituted by tidal gates, which allow the drainage of excess water to Ria de Aveiro in flood season and constitute a barrier to the entrance of salt water.	<u>Event:</u> Flooding, waterlogging and salinization. <u>Damage:</u> Waterlogging and salinization of BBVL fields and consequently destruction of cultures.	Hard
<b>Coastal Erosion Protection System</b>				
Artificial sand nourishment of beaches and reinforcement of dune system		Sand nourishment in Barra, Costa Nova and Vagueira beaches, and in the south dune system of Costa Nova, Vagueira and Areão beaches in order to maintain the environmental and recreational values and to preserve the natural coastal defence systems (beaches and dunes).	<u>Event:</u> Beach area reduction. <u>Damage:</u> Decrease of beach area, losing the recreational and bathing use values.	Soft
Groins		Construction or extension of a groin in Barra beach, in order to fix the shoreline position and allow filling the eroded beaches by the intersection of longshore sediments transport, with accumulation updrift.	<u>Event:</u> Shoreline retreat and beach area reduction. <u>Damage:</u> Losing of territory, recreational and bathing uses values, damages in infrastructures and properties.	Hard
Longitudinal revetment works	Construction or extension of longitudinal revetments works in Costa Nova, Vagueira, Areão and Poço da Cruz beaches in order to fix the shoreline position and reduce the wave action by absorption the energy in the structure slope.	<u>Event:</u> Shoreline retreat and waves overtopping. <u>Damage:</u> Territory loss, sandbank rupture, overtopping and floods, damages in infrastructures and properties.	Hard	
Non-Structural Measures	<b>Primary and Secondary Drainage System</b>			
	Ditches	Ditches cleaning	<u>Event:</u> Clogged ditches and waterlogging. <u>Damage:</u> Poor drainage of excess water in flood season.	Management
	<b>Main Green Structure</b>			
Hedges	Pruning	<u>Event:</u> Clogged roads. <u>Damage:</u> Difficulties in circulation.	Management	
Hedges	Riparian borders and hedges reinforcement.	<u>Event:</u> Unprotected areas against the advance of water due to the lack of protection shrubs or trees. <u>Damage:</u> Bank ruptures, faster intrusion of salt or fresh water into the fields.		

ecological value at risk, such as Ria de Aveiro lagoon and its coastal zone.

### ACKNOWLEDGEMENTS

This work has been supported by FCT and by European Union (COMPETE, QREN, FEDER) in the frame of the research project ADAPTARia (PTDC/AAC-CLI/100953/2008). The second and

sixth authors benefits from PhD grants (SFRH/BD/78345/2011 and SFRH/BD/79170/2011, respectively) given by the Portuguese FCT (Fundação para a Ciência e Tecnologia). The seven author was financed by Homme-Milieu International Network (BI/DAO/OHMI2013\_FA). The eighth author was financed by DG Maritime Affairs through the TPEA project (EU MARE/2012/08; BI/UI88/6389/2013).

## LITERATURE CITED

- Alves, T., 2012. *Análise económico-ambiental espacial de esporões no centro de Portugal*. MSc thesis, University of Aveiro, 119 pp. <http://hdl.handle.net/10773/9584>
- Alves, F.L., Sousa, L.P., 2013. Cartas Globais de Vulnerabilidade e Risco. In: Dias, J.M. and Alves, F.L. (Eds.), *Risco de Cheia e Estratégias de Adaptação para a Zona Costeira e Lagunar da Ria de Aveiro*. Aveiro: Universidade de Aveiro, CESAM - Centro de Estudos do Ambiente e do Mar, p. 27-35, ISBN: 978-989-98755-0-0.
- Alves, F.L., Coelho, C.D., Antunes, I.C., Sousa, L.P., Pereira, C., Fernandes M.L., Roebeling, P.C., 2013a. Estratégias de Adaptação. In: Dias, J.M. and Alves, F.L. (Eds.), *Risco de Cheia e Estratégias de Adaptação para a Zona Costeira e Lagunar da Ria de Aveiro*. Aveiro: Universidade de Aveiro, CESAM - Centro de Estudos do Ambiente e do Mar, p. 36-49, ISBN: 978-989-98755-0-0.
- Alves, F.L., Sousa, L.P., Almodovar, M., Phillips, M.R., 2013b. Integrated coastal zone management (ICZM): a review of progress in Portuguese implementation. *Regional Environmental Change*, 13:1031-1042.
- Alves F., Roebeling P.C., Pinto P., Batista P., 2009. Valuing ecosystem service losses from coastal erosion along the central Portuguese coast: a benefits transfer approach. *Journal of Coastal Research*, SI 56, 1169–1173.
- Barroca, B., Bernardara, P., Mouchel, J.M., Hubert, G., 2006. Indicators for identification of urban flooding vulnerability. *Natural Hazards and Earth System Sciences*, 6, 553-561.
- Caetano, M., Nunes, V., Nunes, A., 2009. CORINE Land Cover 2006 for continental Portugal, Relatório Técnico, Instituto Geográfico Português.
- Coelho, C., Silva, R., Veloso-Gomes, F. and Taveira-Pinto, F., 2009. Potential effects of climate change on northwest Portuguese coastal zones. *ICES Journal of Marine Science*, 66: 1497-1507.
- Coelho, C., Veloso-Gomes, F. 2006. Crossshore Beach Profile Models – Application to Aveiro Coast. *Journal of Coastal Research*, SI 39, 345-350.
- Dias, J.M., Lopes, J.F., Dekeyser, I., 2000. Tidal propagation in Ria de Aveiro lagoon, Portugal. *Physics and Chemistry of the Earth Part B-Hydrology Oceans and Atmosphere*, 25, 369-374.
- Klijn, F., Bruijn, K., Ölfert, A., Penning-Rowsell, E., Simm, J., Wallis, M., 2009. Flood risk assessment and flood risk management - an introduction and guidance based on experiences and findings of FLOODsite (an EU-funded Integrated project). Report Number T29-09-01, 127 pp.
- Lopes, C.L., Azevedo, A. and Dias, J.M., 2013. Flooding assessment under sea level rise scenarios: Ria de Aveiro case study. *Journal of Coastal Research*, SI 65, 766-771.
- Lopes, C.L., Silva, P.A., Dias, J.M., Rocha, A., Picado, A., Plecha, S., Fortunato, A.B., 2011. Local sea level change scenarios for the end of the 21st century and potential physical impacts in the lower Ria de Aveiro (Portugal). *Continental Shelf Research*, 31, 1515-1526.
- Pereira, C., Coelho, C., Ribeiro, N., Fortunato, A., Lopes, C.L., Dias, J.M., 2013. Numerical modelling of shoreline evolution in the Aveiro coast, Portugal – climate change scenarios. *Journal of Coastal Research*, SI 65, 2161-2166.
- Picado, A., Lopes, C.L., Mendes, R., Vaz, N. and Dias, J. M., 2013. Storm surge impact in the hydrodynamics of a tidal lagoon: the case of Ria de Aveiro. *Journal of Coastal Research*, SI 65, 796-801.
- Ribeiro, N.A., Fortunato, A.B., Rocha, A.C., 2012. Efeito das alterações climáticas no regime de agitação marítima no Atlântico Norte e costa portuguesa, *2as Jornadas de Engenharia Hidrográfica*, 163-166.
- Roebeling, P.C., Coelho, C.D., Reis, E.M., 2011. Coastal erosion and defense interventions: a cost-benefit analysis. *Journal of Coastal Research*, SI 64, 1415-1419.
- UNISDR, 2009. UNISDR Terminology on Disaster Risk Reduction. United Nations International Strategy for Disaster Reduction, 13 pp.
- Zhang, Y.L., Baptista, A.M., Myers, E.P., 2004. A cross-scale model for 3D baroclinic circulation in estuary-plume-shelf systems: I. Formulation and skill assessment. *Continental Shelf Research*, 24, 2187-2214.

# Non-uniformity of storm impacts on three high-energy embayed beaches

Carlos Loureiro†‡∞, Óscar Ferreira†, J. Andrew G. Cooper‡∞

† CIMA - Centre for Marine and Environmental Research  
Universidade do Algarve  
Faro, Portugal  
[cloureiro@ualg.pt](mailto:cloureiro@ualg.pt)  
[oferreir@ualg.pt](mailto:oferreir@ualg.pt)

‡ Centre for Coastal and Marine Research  
School of Environmental Sciences  
University of Ulster  
Coleraine, Northern Ireland, UK  
[jag.cooper@ulster.ac.uk](mailto:jag.cooper@ulster.ac.uk)

∞ Geological Sciences  
School of Agriculture, Earth and Environmental Sciences  
University of KwaZulu-Natal  
Westville, Durban, South Africa



[www.cerf-jcr.org](http://www.cerf-jcr.org)



[www.JCRonline.org](http://www.JCRonline.org)

## ABSTRACT

Loureiro, C., Ferreira, Ó., Cooper, J.A.G., 2014. Non-uniformity of storm impacts on three high-energy embayed beaches. In: Green, A.N. and Cooper, J.A.G. (eds.), *Proceedings 13<sup>th</sup> International Coastal Symposium* (Durban, South Africa), *Journal of Coastal Research*, Special Issue No. 70, pp. 326-331, ISSN 0749-0208.

Coastal storms are highly significant and destructive events and important natural hazards that have major impacts upon the physical and human-cultural coastline environments. Exceptional coastal storms in the last decades have emphasized the urgent need to reinforce scientific knowledge regarding the frequency, impact and role of these extreme events. This is particularly relevant for embayed beaches, where geomorphological control promotes characteristic morphodynamic responses that are distinct from the better studied long-linear beaches. This paper analyses storm response from datasets of morphological change obtained from three embayments located in three distinct wave environments. Analysis of the morphological response to extreme storm events, particularly the 2007 March Equinox storm in eastern South Africa, the January-February 2009 storm group in southwestern Portugal and the December 2011-January 2012 storm group in northwestern Ireland, demonstrate that storm-induced morphological change in the Durban Bight, Arrifana beach and Portstewart Strand is highly variable alongshore. Retreat values for the mean high water spring shoreline are shown to differ significantly within each embayment. This alongshore non-uniform response to storm-events is attributed to boundary effects triggered by the presence of natural headlands or outcrops and/or artificial engineering structures. Megarip development drives variability in storm response in Arrifana, while wave shadowing and interruption of longshore sediment movement under south-easterly/west-northwesterly storm waves promotes the northward/westward increase in shoreline retreat in the Durban Bight and Portstewart Strand, respectively. Boundary effects significantly influence short-term morphodynamic behaviour during storms and, consequently, determine alongshore non-uniform morphologic response to storm events, irrespective of embayment dimensions and event magnitude.

**ADDITIONAL INDEX WORDS:** *beach surveys, erosion, alongshore variability, geological control.*

## INTRODUCTION

Storms have a major impact upon the physical and human-cultural environments of coastlines (Lozano *et al.*, 2004), and a significant body of storm-dedicated coastal research exists nowadays. Nevertheless, exceptional coastal storms in the last decade have caused intense human suffering and extensive economic losses (Ciavola *et al.*, 2011; Coumou and Rahmstorf, 2012), emphasizing an urgent need to reinforce scientific knowledge regarding the frequency, impact and role of coastal storms (Ciavola *et al.*, 2011). Major efforts have, however, been focussed on coastal barriers of the North American coastline, prone to the impacts of hurricanes and tropical storms (Anthony, 2013). In such low-lying and geologically unconstrained environments, the relations between extreme water levels (produced by storm surge and wave setup) and beach morphology are quite well understood (*c.f.* Sallenger, 2000), as is the coastal response to event frequency (Houser and Hamilton, 2009). Still, the devastating impacts of recent extreme coastal storms (*e.g.* hurricanes Katrina and Sandy) highlight that the improved

knowledge of storm-driven beach morphodynamics on low-lying unconstrained shorelines has not been successfully translated into an effective reduction of coastal risks (Ciavola and Jiménez, 2013).

Along the western coasts of Europe, and many other locations worldwide, progress in developing a comprehensive framework for the impacts of mid-latitude extra-tropical cyclones has been hindered by marked geomorphological variability (Ciavola *et al.*, 2011; Anthony, 2013). Recent extreme events, such as the Xynthia storm that affected the western coast of France in early 2010, the 2007 March equinox storm in eastern South Africa, or the Pasha Bulker storm that hit the eastern Australian coastline in June 2007, have underlined the potential devastating effects of extra-tropical coastal storms, further demonstrating that the knowledge of storm-induced coastal change remains incomplete (Ciavola *et al.*, 2011). This is due to the complexity of coastal response to storms, which depends on nonlinear interactions between multiple parameters related to incident storm characteristics (including waves, water level, atmospheric pressure, wind speed and direction) and coastal setting (Anthony, 2013; Masselink and van Heteren, 2013). These interactions are further complicated along embayed coastlines, where geological control significantly influences morphological

behaviour (Jackson *et al.*, 2005) and storm impacts are highly site-specific (Cooper *et al.*, 2004). Significant efforts have been made in improving the knowledge of storm response along sandy coastlines, with a wealth of literature addressing the impacts of storms on unconstrained beaches (Anthony, 2013). Embayed sandy beaches, however, are ubiquitous and arguably dominant around the world's coastlines (Short and Masselink, 1999), and the literature suggests that the overall morphodynamic behaviour and, particularly, storm response is different from unconstrained beaches (Loureiro *et al.*, 2012a). Because of the influence of headlands and rocky outcrops in compartmentalising coastal sediment budgets, restraining longshore sediment transport and altering nearshore circulation, distinctive storm dynamics occur on embayed beaches. Recent work on energetic embayments demonstrated that embayment rotation is more complex than previously assumed, and this is partly due to distinctive sheltering effects by headlands during storms (Harley *et al.*, 2011). Unlike unconstrained beaches, storm response within embayed beaches was also found to be highly variable, with distinctly alongshore variability driven by 3-dimensional circulation patterns (Loureiro *et al.*, 2012a). Such new insights into embayment response to storms were built on the availability of a few datasets of embayed beach morphological change and, whereas availability of representative datasets is a general limitation to all studies of coastal storm impact (Ciavola *et al.*, 2011), scarcity of observational data for embayed beaches has been particularly stressed (e.g. Cooper *et al.*, 2004; Harley *et al.*, 2011; Castle and Coco, 2012). Owing to such incomplete knowledge of 3-dimensional coastal processes and morphological responses to storms in embayed settings, research based on extensive datasets of embayed beach morphology is particularly required.

The overall aim of this work is to present an integration and analysis of datasets of morphological change obtained from three embayed beaches located in three distinct energetic global wave environments. The specific objective of the paper is to explore the spatial variation in morphological response to storms between different sites as mediated by distinct geomorphologic settings.

## STUDY SITES

Aiming to obtain a comprehensive analysis of embayed beach morphological response to storms, three embayments were regularly monitored. To maintain consistency in the analysis, only wave-dominated settings exposed to energetic conditions were considered and, to provide wide representation, sites on the three major global wave environments were included. These are, according to Davies (1972), storm waves, here represented by Portstewart Strand in the northwestern coast of Ireland; west coast swell, which dominates the wave conditions along Arrifana beach in the southwestern coast of Portugal; and the east coast swell that reaches the Durban Bight in the eastern coast of South Africa (Figure 1). Selection of study locations was data-driven, as availability of high-resolution survey programs was identified as a major constraint. The sites are integrated in a framework that encompasses a wide array of embayment dimensions and types, from small double headland-bound embayment a few hundred meters long in southwestern Portugal, to the 7 km-long, single headland-bound and crenulated-shaped embayment of the Durban Bight (Figure 2; Table 1). A brief description of the major geomorphological and oceanographic characteristics of the study areas is provided in the next sections.

### Northwestern Ireland (Portstewart Strand)

The coast of northwest Ireland is bedrock-framed, irregularly shaped and highly indented, with glacially-derived sandy to

Table 1. Overview of major hydrodynamic and morphologic characteristics of study sites.  $H_s$  – mean annual offshore significant wave height (m);  $T_m$  – mean wave period (s);  $MSR$  – mean spring tidal range (m);  $d_{50}$  – median grain diameter (mm);  $Tan\beta$  – mean intertidal slope;  $B_l$  – beach length (km).

Site	$H_s$	$T_m$	$MSR$	$d_{50}$	$Tan\beta$	$B_l$
Portstewart <sup>1</sup>	2.3	7.1	1.5	0.16	0.025	2.75
Arrifana <sup>2</sup>	1.8	6.5	2.9	0.27	0.039	0.75
Durban <sup>3,4,5</sup>	1.7	6.4	1.8	0.39	0.053	7.00

<sup>1</sup>Jackson *et al.* (2005); <sup>2</sup>Loureiro *et al.* (2012b); <sup>3</sup>Smith *et al.* (2010);

<sup>4</sup>Corbella and Stretch (2012a); <sup>5</sup>CSIR (2009).

gravely deposits accumulating usually as headland-embayment beaches or as barriers at estuary mouths (Cooper *et al.*, 2004; Jackson *et al.*, 2005). Strong indentation and a steep shoreface (Backstrom *et al.*, 2009) preclude alongshore sediment exchange between embayments, and contemporary sediment supply is negligible (Cooper *et al.*, 2004). This implies that sediment available for beach construction comes from reworking of shelf sands and also from erosion of dunes and bluffs (Carter, 1991), and is highly contained within each embayment (Jackson and Cooper, 2010).

Location within the major northeast Atlantic storm tracks renders this coastline exposed to high-energy wave and wind events, particularly during the boreal winter. Average deepwater significant wave height is around 3.6m (O'Connor *et al.*, 2011), yet large-scale refraction along northwestern Ireland attenuates wave heights to about 2 to 2.5 m offshore the study area (Jackson and Cooper, 2010). Tidal range is highly variable along the Irish coastline, but for the coastal section that includes Portstewart strand, mean spring tidal range is 1.5 m (Jackson *et al.*, 2005). Details of Portstewart embayment (Figure 2a) are given in Table 1 and further description is provided by Carter (1991) and Jackson *et al.* (2005).

### Southwestern Portugal (Arrifana)

Headland-bound embayed beaches are also characteristic of the southwestern coast of Portugal, occurring in re-entrants along the

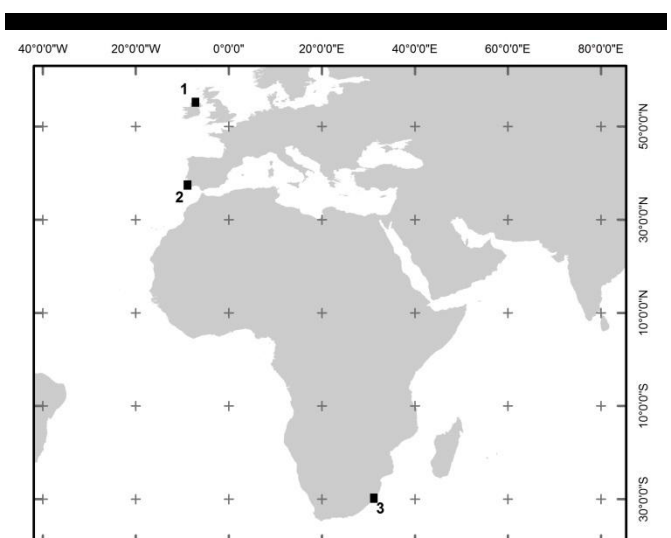


Figure 1. Geographical location of the study sites: 1) Portstewart Strand - northwest Ireland; 2) Arrifana - southwest Portugal; 3) Durban Bight - eastern South Africa.





Figure 2. Aerial and oblique photography of the study sites showing the varied geomorphological settings analysed: a) Portstewart Strand; b) Arrifana; c) Durban Bight. Aerial photographs from Bing Maps ArcGIS Web Mapping Service.

rocky cliffs or in association with small coastal streams. Despite evidences of sediment reworking across the Portuguese continental shelf during the Holocene transgression (Dias *et al.*, 2002) and, particularly, evidences of abundant aeolian deposits along the southwestern Portuguese margin (Pereira, 1987), the present day coastline is sediment starved, presenting negligible sediment supply. Contemporary beach dynamics are, therefore, mostly restricted to the limited amounts of sediment contained within embayments and reworking of adjacent nearshore sands.

Western facing embayments along this coastline are fully exposed to the North Atlantic swell and storms, experiencing a high-energy wave climate with a marked oceanographic seasonality (Loureiro *et al.*, 2011). Average deepwater significant wave heights range from 1 to 1.5 m in summer to values in excess of 2 m during the northern hemisphere winter (Costa and Esteves, 2010). Tides are characterized by a mesotidal, semi-diurnal regime with maximum spring tidal range around 3.5 m. Detailed description of morphologic features of Arrifana (Figure 2b) embayment is given by Loureiro *et al.* (2012a) and a synthesis of general characteristics is provided in Table 1.

### Eastern South Africa (Durban Bight)

The coastline of southern and central KwaZulu-Natal (KZN), located in the eastern seaboard of South Africa (Figure 1), is characterized by an almost continuous succession of variable-sized headland-bound embayments, along which sandy embayed beaches of variable lengths have developed (Cooper, 1991). A very steep hinterland, associated with a sub-tropical humid climate, promotes active terrigenous sediment supply to the coast by the large number of rivers that reach the KZN coastal zone

(Cooper, 1991, 2001). Such availability of sediment delivery led to the development of the long sandy embayment known as the Durban Bight (Figure 2c). Extensive coastal development and engineering since the early 1900's has significantly modified natural dynamics in the area (Cooper, 1991). However, despite the fact that the Durban Bight is within the most intervened beaches worldwide, with sediment nourishment activities initiated as soon as 1926 and the emplacement of a sand pumping scheme in 1935 (Barnett, 1982), chronic beach erosion is still a major concern along the Durban shoreline (Corbella and Stretch, 2012b).

High-energy wave conditions characterize the KZN coastline (Table 1), with average significant wave height around 1.7m and peak storm activity during the austral autumn (Corbella and Stretch, 2012a). However, given a wide variety of storm origins (Smith *et al.*, 2010) energetic events can be experienced year-round. Tides are semidiurnal with an average spring tidal range of 1.8 m. Further details of the Durban Bight coastal geomorphology and provided by Cooper (1991).

### MONITORING PROGRAMS

Different motivations for undertaking the beach monitoring programs determined the use of variable survey methods, survey frequencies and monitoring periods between the various embayments. This has implications in terms of dataset suitability for analysing the morphological response to storms, as well as in the investigation of the morphodynamic mechanisms driving such responses. Details of each monitoring program are provided for each site.

### Northwestern Ireland (Portstewart)

Topographic surveys were initiated in 2005 with the objective of investigating beach morphology and morphodynamics. Surveys were conducted using an RTK-GPS system, composed by a base station and a mobile unit mounted on an all-terrain quad bike. Predefined cross-shore beach profiles were surveyed during low-tide, and extended from the dune base down to the low water level. Survey frequency is variable, most of the years sampling is approximately monthly, but occasionally intervals of a few months have occurred between surveys. Due to the gentle slopes and fine compacted sand that characterizes the Portstewart Strand, measurement errors due to sinking of the quad-bike and tilting of the GPS antenna are considered to be within a sub-decimetres range, typical of RTK-GPS surveys.

### Southwestern Portugal (Arrifana)

RTK-GPS was also the survey method used for monitoring in southwestern Portugal. Cross-shore topographic profiles were monitored regularly every two months from September 2007 to September 2009. Event-driven surveys complemented the monitoring, with the site being surveyed after each storm event and afterwards to record beach recovery. Surveys were always performed on foot using a telescopic pole and during low tide conditions, extending from the cliff base to waning depths. Measurements errors are also considered to be within sub-decimetres range, given RTK-GPS errors of up to 5 cm and operation errors related to tilting and ground offset within an interval of 5 cm. Further details regarding the monitoring program for southwestern Portugal are presented in Loureiro *et al.* (2012a).

### Eastern South Africa (Durban Bight)

Due to severe and continued erosion problems in the Durban Bight since the early decades of the XX century, the Council for Scientific and Industrial Research (CSIR) in South Africa was commissioned in 1973 to implement the Durban Beach Monitoring Programme. Practical management concerns were at the basis of this programme, given the need to maintain a functional beach requiring continuous bypassing or frequent sand nourishment as a measure to mitigate the northwards littoral drift cut-off by Durban harbour jetties (Barnett, 1982; Laubscher *et al.*, 1990; CSIR, 2009). This program consists of topographic beach surveys along a series of 28 cross-shore beach profiles from the Durban Harbour north jetty up to the Umgeni river mouth (Figure 2c). The surveys, conducted every month for most of the period since 1973, but with intervals that can span half a year, were performed using theodolite measurements taken at variable intervals, and extend from a fixed benchmark landward up to waning depths (Corbella and Stretch, 2012b). Theodolite measurements are potentially affected by sequential steeping, with additional inaccuracy introduced by linear interpolation between surveyed points that, in the Durban case, can be cross-shore spaced up to 15 m. Errors for this dataset are estimated to be higher, but lower than 20 cm, which is within the 0.1 to 0.4 m range of accuracy for widely-used image-derived shorelines (Plant *et al.*, 2007; Harley *et al.*, 2011b).

## MORPHOLOGICAL STORM IMPACTS

Mining the embayment datasets for storms allowed to identify a few events that, given the magnitude of the oceanographic forcing and widespread erosion observed, are here presented to provide an overview of morphological impacts of extreme storms in high-energy settings.

Between the 18<sup>th</sup> and 20<sup>th</sup> of March of 2007, the combined occurrence of unusually high spring tides and extreme wave conditions, with offshore significant wave heights in excess of 8 m, generated by an intense cuff-off low pressure system off the eastern coast of South Africa, prompted widespread erosion along the KZN coastline (Smith *et al.*, 2010). Within the Durban Bight, retreat of the mean high water spring (MHWS) shoreline averaged 22 m, reaching values of 63 m in the northernmost section of the embayment. Despite significant variation in shoreline retreat for the 28 beach profiles analysed, a clear trend is observed for higher retreat in the northern sector, with decreasing shoreline retreat for the southern section (Figure 3). Considering the south-easterly direction of more energetic waves for this event and the shadowing effect of the harbour jetties, such southward decrease in shoreline retreat was expected. The northward increase in shoreline retreat, although also expected, revealed to be of much higher magnitude. Average retreat for the 10 northern profiles more than tripled the average retreat for the 10 southern ones (-35 m versus -9 m, respectively). It is noteworthy to consider that the presence of the underwater mound (Figure 3), emplaced using dredged sediment as an attempt to protect the central to northern beach sectors by reducing incoming wave energy (Barnett, 1982), does not appear to have been effective during the 2007 March Equinox storm, despite indications that it should offer some protection to the northern Bight section under extreme conditions (Laubscher *et al.*, 1990). Located downdrift of a series of piers and engineering structures (Figure 3) that have been shown to trap the long-term sediment movement (Corbella and Stretch, 2012b), the northern section of the Durban Bight is more susceptible to sediment depletion, and consequently larger shoreline retreat, given that the sediment entrained under south-easterly waves storm waves is impeded by the coastal engineering structures to move naturally to the northern section of the Bight.

At Portstewart Strand, following a group of four storms reaching the coast of Northern Ireland between the 13<sup>th</sup> of December 2011 and 5<sup>th</sup> of January 2012, with deepwater significant wave heights peaking at 14.7 m, 11.6 m, 10.3 m and 10 m, widespread beach erosion was observed (Figure 3). Also here, significant differences can be observed within the embayment, with higher shoreline retreat values, in excess of 17 m, measured in the westernmost profile, closer to the Bann river jetties, while in the easternmost profiles retreat averages to 5.5 m. Considering the west-northwest direction of storm waves during the storm-group (Figure 3), the westward increase in shoreline retreat is consistent with the progressive sediment depletion from west to east, given the downdrift interruption of sediment movement by the Bann river jetties. The approximately 200 m offset in dune base line position between the sides of the river mouth (Figure 3) further highlights the long-term adjustment of the shoreline to such littoral drift cut-off, triggered in the late XIX century with the inlet stabilization works (Carter, 1991). Increased storm erosion in the westernmost section is indicative that despite coastal stabilization has been emplaced in Portstewart for over a century, by interrupting the longshore sediment transport the Bann river jetties still determine the present patterns of shoreline response to storms. However, even though widespread intertidal beach erosion revealed by MHWS shoreline retreat, no significant foredune trimming was observed for the event analysed. This is consistent with previous reports of the impacts of extreme storms along the Irish coastline, which have found these high-energy dissipative embayments to be attuned to energetic conditions, which means that despite significant intertidal beach changes, longer-term shoreline retreat in the form of dune scarping and erosion is often precluded during storm events (Cooper *et al.*, 2004).

The impacts of the January-February 2009 storm group along the southwestern coast of Portugal, presented in detail in Loureiro *et al.*, (2011, 2012b), further highlight the within-embayment variability in the morphological response to storms (Figure 3). Despite the reduced dimensions of Arrifana, with a beach length of roughly 750 m (Table 1), MHWs shoreline retreat in the northern section (20.8 m) more than doubles the retreat in the centre (7.9 m) of the embayment (Figure 3). Considering the north-westerly direction of high-energy waves from the 5 storms that composed the January-February storm group, it would be expected that the northern section of the embayment was protected by the prominent northern headland. However, given suitable conditions for cellular nearshore circulation, megarips develop in the extremities of the embayment (Loureiro *et al.*, 2012a), enhancing beach erosion in such locations, while the centre of the beach presents only moderate shoreline retreat (Figure 3).

Boundary effects of coastal engineering structures or natural headlands and outcrops have been shown to significantly influence the seasonal to yearly morphological behaviour of coastal embayments (Miller and Dean, 2007; Loureiro *et al.*, 2012b), driving the development of cellular circulation mechanisms, beach rotation phenomena and limiting profile fluctuation. Examples from only three embayments, and considering exclusively one storm event at each site, further demonstrate that short-term morphological response to storms is also significantly affected by boundary effects. When cellular circulation mechanisms dominate the storm response of an embayment, particularly in the form of megarip development as in the case of Arrifana, the direction of the storm waves appears to be less relevant. On the other hand, when variability in storm response is determined by wave shadowing and longshore sediment transport, evidenced in the cases of the Durban Bight and Portstewart Strand, the direction of storm waves and their interaction with coastal engineering structures becomes fundamental for understating the nature and patterns of storm impacts within embayments. The results presented here for three embayed beaches and three extreme events suggest that irrespective of embayment dimensions and magnitude of storms, morphological responses are unlikely to be homogenous within any embayment. Similar findings of alongshore variability in storm response (e.g. Harley *et al.*, 2011b; Loureiro *et al.*, 2012a; Coco *et al.*, 2014) suggest that non-uniformity in storm impacts may be the norm, not the exception.

## CONCLUSIONS

This paper presents an overview of the morphological response to extreme storm events, particularly the 2007 March Equinox storm in eastern South Africa, the January-February 2009 storm group in southwestern Portugal and the December 2001-January 2012 storm group in northwestern Ireland. Morphological response to storms in each of the three embayments analysed is highly variable alongshore, and this is attributed to the presence of natural headlands or outcrops and/or artificial engineering structures. Cellular circulation mechanisms in the form of megarips drive the alongshore variable response in Arrifana, with increased erosion in embayment extremities. Wave shadowing and interruption of longshore sediment by coastal engineering structures drives a northward increase in shoreline retreat in the Durban Bight, while sand depletion driven by sediment supply cut-off in Portstewart Strand explains the westward increase in shoreline erosion under west-northwest storm waves. Boundary effects are, therefore, considered to significantly influence short-term morphodynamic behaviour during storms and, consequently, determine alongshore non-uniform morphologic response to storm events, irrespective of embayment dimensions.

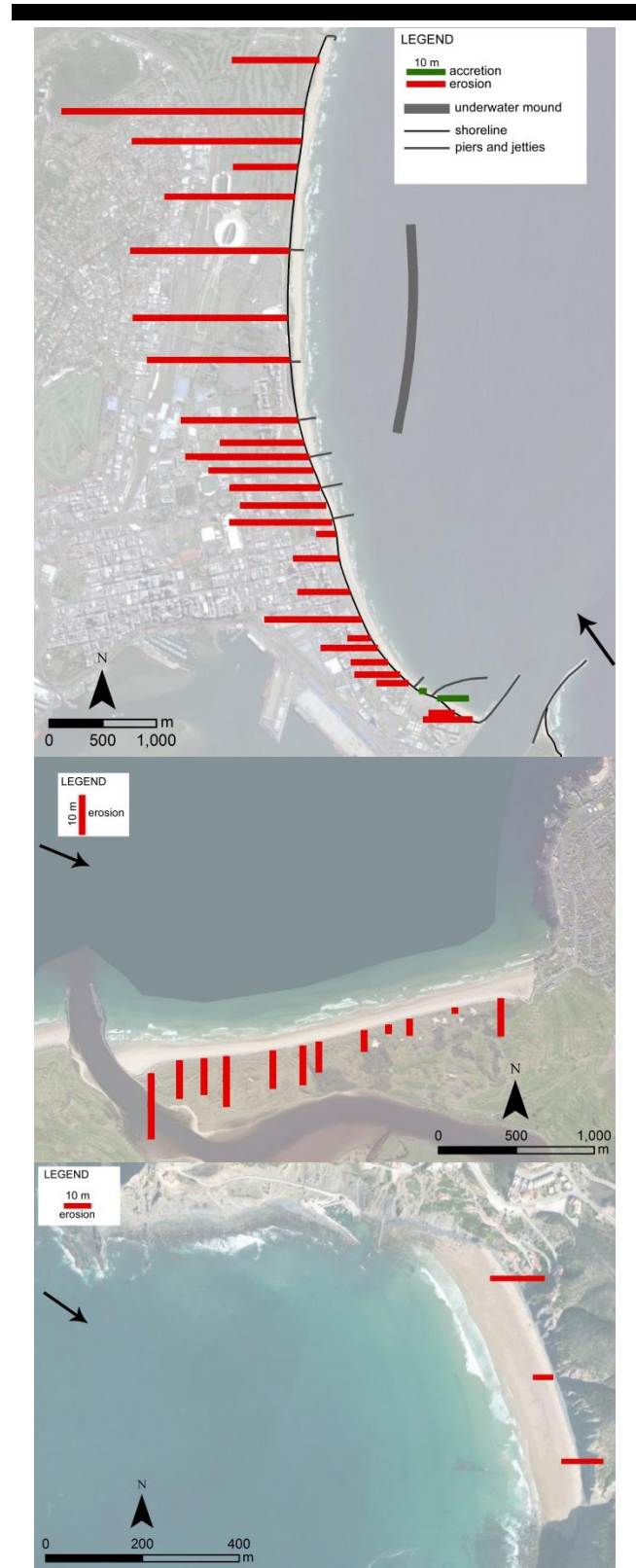


Figure 3. Storm-driven mean high water shoreline variation for: Durban bight during the 2007 March Equinox storm (upper image); Portstewart Strand during December 2011-January 2012 storm group (middle image); and Arrifana during the January-February 2009 storm group (lower image). Black arrows indicate offshore wave direction during storm events analysed.

Ongoing research considering datasets from an extended number of embayments, aimed at building a multi-embayment catalogue of storm events, evaluate their morphological impacts and explore the morphodynamic mechanisms that drive the observed behaviour, is expected to provide comprehensive insights into the wide variability of embayment response to storms, further extending our understating of storm impacts in high-energy embayed beaches.

### ACKNOWLEDGEMENTS

The datasets used for this work have been collected over the years by several institutions and people. To all of them we wish to thank, particularly eThekweni Municipality for providing the Durban Bight dataset; Robert Stewart, Sam Smith and especially David Rogers for collecting and processing the datasets for northwestern Ireland; the Coastal Research team at CIMA/UALG for assistance in fieldwork for southwestern Portugal, which was financially supported by FCT within the scope of project BAYBEACH (PTDC/CTE-GEX/66893/2006). The development of this collaborative project is financially supported by an FCT postdoctoral fellowship awarded to Carlos Loureiro (grant SFRH/BPD/85335/2012). Óscar Ferreira's participation was funded by FCT project SPACE (PTDC/ECM/114109/2009).

### LITERATURE CITED

- Anthony, E.J., 2013. Storms, shoreface morphodynamics, sand supply and the accretion and erosion of coastal dune barriers in the southern North Sea. *Geomorphology*, 199, 8-21.
- Backstrom, J.T., Jackson, D.W.T., Cooper, J.A.G., 2009. Shoreface morphodynamics of a high-energy, steep and geologically constrained shoreline segment in Northern Ireland. *Marine Geology*, 257, 94-106.
- Barnett, K.A., 1982. Durban beaches reclamation: practical aspects. *Proceedings of the 18th Conference of Coastal Engineering* (Cape Town, South Africa), ASCE, pp. 1970-1991.
- Carter, R.W.G., 1991. *Shifting Sands: a study of the coast of Northern Ireland from Magilligan to Larne*. HMSO, Belfast, 49p.
- Castelle, B., Coco, G., 2012. The morphodynamics of rip channels on embayed beaches. *Continental Shelf Research*, 43, 10-23.
- Ciavola, P., Ferreira, Ó., Haerens, P., van Koningsveld, M., Armaroli, C. and Lequeux, Q., 2011. Storm impacts along European coastlines. Part 1: the joint effort of the MICORE and ConHaz Projects. *Environmental Science and Policy*, 14, 912-923.
- Ciavola, P. and Jiménez, J.A., 2013. The record of marine storminess along European Coastlines. *Natural Hazards and Earth System Sciences*, 13, 1999-2002.
- Coco, G., Senechal, N., Rejas, A., Bryan, K.R., Capo, S., Parisot, J.P., Brown, J.A., MachMahan, J.H.M., 2014. Beach response to a sequence of extreme storms. *Geomorphology*, 204, 493-501.
- Cooper, J.A.G., 1991. *Shoreline Changes on the Natal coast: Mkomanzi River mouth to Tugela River mouth*. Natal Town & Regional Planning Commission Reports, vol. 77. Pietermaritzburg, 57p.
- Cooper, J.A.G., 2001. Geomorphological variability among microtidal estuaries from the wave-dominated South African coast. *Geomorphology*, 40, 99-122.
- Cooper, J.A.G., Jackson, D.W.T., Navas, F., McKenna, J., Malvarez, G., 2004. Identifying storm impacts on an embayed, high-energy coastline, examples from western Ireland. *Marine Geology*, 210, 261-280.
- Corbella, S. and Stretch, D., 2012a. The wave climate on the KwaZulu-Natal coast of South Africa. *Journal of the South African Institution of Civil Engineering*, 54, 45-54.
- Corbella, S. and Stretch, D., 2012b. Decadal trends in beach morphology on the east coast of South Africa and likely causative factors. *Natural Hazards and Earth System Sciences*, 12, 2515-2527.
- Costa, M. and Esteves, R., 2010. Clima de agitação marítima na costa oeste de Portugal Continental. Proceedings of XI Jornadas Técnicas de Engenharia Naval - O Sector Marítimo Português. Edições Salamandra, Lisboa, Portugal, pp. 413-426.
- Coumou, D. and Rahmstorf, S., 2012. A decade of weather extremes. *Nature Climate Change*, 2, 491-496.
- CSIR, 2009. *Durban beach monitoring progress report: July 2007 to June 2008*. Report No. CSIR/NRE/CO/ER/2009/0105/C, Vol. 2, Council for Scientific and Industrial Research, Stellenbosch, South Africa, 233p.
- Davies, J.L., 1972. *Geographical Variation in Coastal Development*. Edinburgh: Oliver & Boyd, 204p.
- Dias, J.M.A., Boski, T., Rodrigues, A. and Magalhães, F., 2002. Coastline evolution in Portugal since the Last Glacial Maximum until present - a synthesis. *Marine Geology* 170, 177-186.
- Harley, M.D., Turner, I.L., Short, A.D. and Ranasinghe, R., 2011a. A reevaluation of coastal embayment rotation: the dominance of cross-shore versus alongshore sediment transport processes, Collaroy-Narrabeen Beach, southeast Australia. *Journal of Geophysical Research*, 116, F04033.
- Harley, M.D., Turner, I.L., Short, A.D. and Ranasinghe, R., 2011b. Assessment and integration of conventional, RTK-GPS and image-derived beach survey methods for daily to decadal coastal monitoring. *Coastal Engineering*, 58, 194-205.
- Houser, C. and Hamilton, S., 2009. Sensitivity of post-hurricane beach and dune recovery to event frequency. *Earth Surface Processes and Landforms*, 34, 613-628.
- Jackson, D.W.T., Cooper, J.A.G. and del Rio, L., 2005. Geological control of beach morphodynamic state. *Marine Geology*, 216, 197-314.
- Laubscher, W.I., Swart, D.H., Schoonees, J.S., Pfaff, W.M. and Davis, A.B., 1990. The Durban beach restoration scheme after 30 years. *Proceedings of the 22nd Conference of Coastal Engineering* (Delft, The Netherlands), ASCE, pp. 3227-3238.
- Loureiro, C., Ferreira, Ó. and Cooper, J.A.G., 2011. Morphologic change and morphodynamics at high-energy embayed beaches in southwestern Portugal. *Proceedings of Coastal Sediments 2011*, vol. 2. World Scientific Publishing, Singapore, 1375-1389.
- Loureiro, C. Ferreira, Ó. and Cooper, J.A.G., 2012a. Extreme erosion on high-energy embayed beaches: influence of megarips and storm grouping. *Geomorphology*, 139-140, 155-171.
- Loureiro, C. Ferreira, Ó. and Cooper, J.A.G., 2012b. Geologically constrained morphological variability and boundary effects on embayed beaches. *Marine Geology*, 329-331, 1-15.
- Lozano, I., Devoy, R.J.N., May, W. and Andersen, U., 2004. Storminess and vulnerability along the Atlantic coastlines of Europe: analysis of storm records and of a greenhouse gases induced climate scenario. *Marine Geology*, 210, 205-225.
- Masselink, G. and van Heteren, S., 2013. Response of wave-dominated and mixed-energy barriers to storms. *Marine Geology (in press)*.
- Miller, J.K. and Dean, R.G., 2007. Shoreline variability via empirical orthogonal function analysis: Part 1 temporal and spatial characteristics. *Coastal Engineering*, 54, 111-131.
- O'Connor, M.C., Cooper, J.A.G. and Jackson, D.W.T., 2011. Decadal behaviour of tidal inlet-associated beach systems, Northwest Ireland, in relation to climate forcing. *Journal of Sedimentary Research*, 81, 38-51.
- Pereira, A.R., 1987. Acumulações arenosas eólicas consolidadas do litoral do Alentejo e Algarve ocidental. *Linha de Acção de Geografia Física, Centro de Estudos Geográficos*, 27, 113p.
- Plant, N.G., Aarninkhof, S.G.J., Turner, I.L., Kingston, K.S., 2007. The performance of shoreline detection models applied to video imagery. *Journal of Coastal Research*, 23, 658-670.
- Sallenger, A.H., 2000. Storm impact scale for barrier islands. *Journal of Coastal Research*, 16, 890-895.
- Short, A.D. and Masselink, G., 1999. Embayed and structurally controlled beaches. In: Short, A.D. (Ed.), *Handbook of Beach and Shoreface Morphodynamics*. John Wiley and Sons, Chichester, pp. 230-250.
- Smith, A.M., Mather, A.A., Bundy, S.C., Cooper, J.A.G., Guastella, L.A., Ramsay, P.J. and Theron, A., 2010. Contrasting styles of swell-driven coastal erosion: examples from KwaZulu-Natal, South Africa. *Geological Magazine*, 147, 940-95.

## Effects of bathymetry on the propagation of tsunamis towards the east coast of Korea

Sung B. Yoon†, Seok C. Kim‡, Unil Baek∞, Jae S. Bae§

†Hanyang University, ERICA Campus  
Ansan, Korea  
sbyoon@hanyang.ac.kr

‡ Hanyang University  
Seoul, Korea  
schk37@nate.com

∞ Hanyang University  
Seoul, Korea  
builhjoo@dic.co.kr

§ Hanyang University, ERICA Campus  
Ansan, Korea  
bjjae194@hanyang.ac.kr



[www.cerf-jcr.org](http://www.cerf-jcr.org)



### ABSTRACT

Yoon, S.B., Kim, S.C., Baek, U., Bae, J.S., 2014. Effect of Bathymetry on Propagation of Tsunamis towards the East Coast of Korea. In: Green, A.N. and Cooper, J.A.G. (eds.), *Proceedings 13<sup>th</sup> International Coastal Symposium* (Durban, South Africa), *Journal of Coastal Research*, Special Issue No. 70, pp. 332-337, ISSN 0749-0208.

[www.JCRonline.org](http://www.JCRonline.org)

In this study the effect of underwater topography of the East Sea on the propagation of tsunamis towards the Korean Peninsula is investigated using the dispersion-correction finite difference numerical model. A series of numerical simulations are conducted for three tsunami events including the 1964 Niigata Tsunami, the 1983 Central East Sea Tsunami and the 1993 Hokkaido South-West Sea Tsunami for the cases of examining the individual or combined influence of underwater topographic features. These include the Yamato Rise, a submerged ridge connecting Yamato Rise and the Shimane Peninsula of Japan, and K-shaped submerged ridges emerging from the east coast of Korea towards the East Sea. In particular, in order to evaluate quantitatively the effects of underwater topography on the propagation of tsunamis, a new concept of energy discharge per unit width is introduced. Using this concept, the quantitative analyses of energy propagation during tsunami events are performed. The analyses show that the underwater topographies including the submerged rises and ridges capture the tsunami energy and transport it to coastal areas connected to those topographies.

**ADDITIONAL INDEX WORDS:** *Tsunami, Energy flux, Submarine topography, East Sea*

### INTRODUCTION

On May 26, 1983, the Central East Sea Tsunami was generated by an undersea earthquake of magnitude  $M_w$  7.9 off the Akita coast of Honshu in Japan. The tsunami caused 104 casualties in Japan. This tsunami propagated towards the east coast of Korea, and destroyed many ships and houses and caused 3 deaths. The damages to the east coast of Korea were not significant in comparison with those of Japan. Two more tsunamis occurred in this sea in 1964 and 1993. The damages along the east coast of Korea were not serious, while severe damages were reported along the Okushiri coast of Japan including 197 casualties such as in the case of the 1993 tsunami event. The major reason for this reduction of tsunami damages along the east coast of Korea is the long distance from the tsunami source. However, the damages at two different areas were totally different, even though the two areas are located with the same distance from the tsunami source. For example, the damage due to the 1983 Tsunami event along the Shimane coast of Japan was much more severe than that on the east coast of Korea, even though the distance and the orientation from the source are nearly the same.

In the present study, the effects of the underwater topography including submarine rises and ridges on the propagation of tsunamis are quantitatively investigated based on the concept of energy flux. The effect of the location of the tsunami source is first investigated using a simplified topography and eliminating the submerged rises and ranges. Three tsunami sources including

the 1964, 1983 and 1993 events are simulated, and the energy flow patterns for each case are compared. To understand the effect of particular topography, the Yamato Rise and the submarine range connecting Yamato Rise to the Shimane coast of Japan is added to the simplified topography. Finally, the numerical simulation is conducted using the real topography by including the K-shaped submarine ridges. By comparing the energy flow patterns for the various bathymetries, the role of the particular underwater topography can be easily understood.

### GOVERNING EQUATIONS

#### Far Field Propagation Model

The wave length of tsunamis is long, and the amplitude is small when the tsunamis are propagating over a deep ocean. Thus, the following linear shallow water equations are frequently used.

$$\frac{\partial \zeta}{\partial t} + \frac{\partial P}{\partial x} + \frac{\partial Q}{\partial y} = 0 \quad (1)$$

$$\frac{\partial P}{\partial t} + \frac{\partial \zeta}{\partial x} = 0 \quad (2)$$

$$\frac{\partial Q}{\partial t} + gh \frac{\partial \zeta}{\partial y} = 0 \quad (3)$$

where,  $\zeta$  is the free surface displacement from the still water level (m),  $P$  and  $Q$  are the flow rates per unit width in  $x$ - and  $y$ -directions, respectively.  $g$  is the gravity acceleration ( $m/s^2$ ), and  $h$  is the water depth from the still water level to the bottom (m).

Imamura et al. (1988) developed a finite difference model using the staggered leap-frog scheme. However, when the source region of tsunamis is narrow, the dispersion effect of tsunami waves should be considered. Thus, Cho et al. (2007) developed a modified technique to include the dispersion effect while the linear shallow water equation is still used. The modified numerical scheme of Cho et al. (2007) is further extended by Cho (2012) to include the Coriolis effect as in the following:

$$\frac{\zeta_{i,j}^{n+1} - \zeta_{i,j}^n}{\Delta t} + \frac{P_{i+1/2,j}^{n+1/2} - P_{i-1/2,j}^{n+1/2}}{\Delta x} + \frac{Q_{i,j+1/2}^{n+1/2} - Q_{i,j-1/2}^{n+1/2}}{\Delta y} = 0 \quad (4)$$

$$\begin{aligned} & \frac{P_{i+1/2,j}^{n+1/2} - P_{i+1/2,j}^{n-1/2}}{\Delta t} + gh_{i+1/2,j} \frac{\zeta_{i+1,j}^n - \zeta_{i,j}^n}{\Delta x} - fQ_{i+1/2,j}^n \\ & + \frac{\alpha}{12\Delta x} gh_{i+1/2,j} [\zeta_{i+2,j}^n - 3\zeta_{i+1,j}^n + 3\zeta_{i,j}^n - \zeta_{i-1,j}^n] \\ & + \frac{\gamma}{12\Delta x} gh_{i+1/2,j} \begin{matrix} \zeta_{i+1,j+1}^n - 2\zeta_{i+1,j}^n + \zeta_{i+1,j-1}^n \\ -(\zeta_{i,j+1}^n - 2\zeta_{i,j}^n + \zeta_{i,j-1}^n) \end{matrix} = 0 \end{aligned} \quad (5)$$

$$\begin{aligned} & \frac{Q_{i,j+1/2}^{n+1/2} - Q_{i,j+1/2}^{n-1/2}}{\Delta t} + gh_{i+1/2,j} \frac{\zeta_{i,j+1}^n - \zeta_{i,j}^n}{\Delta y} + fP_{i,j+1/2}^n \\ & + \frac{\alpha}{12\Delta y} gh_{i,j+1/2} [\zeta_{i,j+2}^n - 3\zeta_{i,j+1}^n + 3\zeta_{i,j}^n - \zeta_{i,j-1}^n] \\ & + \frac{\gamma}{12\Delta y} gh_{i,j+1/2} \begin{matrix} \zeta_{i+1,j+1}^n - 2\zeta_{i,j+1}^n + \zeta_{i-1,j+1}^n \\ -(\zeta_{i+1,j}^n - 2\zeta_{i,j}^n + \zeta_{i-1,j}^n) \end{matrix} = 0 \end{aligned} \quad (6)$$

where,  $f (= 2\omega\sin\Phi)$  is the Coriolis coefficient,  $\omega (= 7.27 \times 10^{-5}\text{rad/s})$  is the angular velocity of earth rotation, and  $\Phi$  is the latitude.  $\alpha$  and  $\gamma$  are the correction factors introduced by Cho et al. (2007) to consider the dispersion effect of tsunami waves as in the following.

$$\alpha = \frac{4h^2 + gh\Delta t^2 - \Delta x^2}{\Delta x^2} \quad (7)$$

$$\gamma = \alpha + 1 \quad (8)$$

**Near Field Inundation Model**

In the near field along the coast, the bottom friction and the nonlinearity of waves are also important. Thus, the two dimensional nonlinear shallow water equations, (9) ~ (11), are employed. Additionally, a dry-wet scheme developed by Yoon and Cho (2001) is applied along the moving land boundary.

$$\frac{\partial \zeta}{\partial t} + \frac{\partial P}{\partial x} + \frac{\partial Q}{\partial y} = 0 \quad (9)$$

$$\begin{aligned} & \frac{\partial P}{\partial t} + \frac{\partial P^2}{\partial x} + \frac{\partial P Q}{\partial y} \\ & + gD \frac{\partial \zeta}{\partial x} + \frac{gn^2}{D^{7/3}} P \sqrt{P^2 + Q^2} = 0 \end{aligned} \quad (10)$$

$$\begin{aligned} & \frac{\partial Q}{\partial t} + \frac{\partial P Q}{\partial x} + \frac{\partial Q^2}{\partial y} \\ & + gD \frac{\partial \zeta}{\partial y} + \frac{gn^2}{D^{7/3}} Q \sqrt{P^2 + Q^2} = 0 \end{aligned} \quad (11)$$

where,  $n$  is the Manning's roughness coefficient ( $\text{s/m}^{1/3}$ ), and  $D (= h + \zeta)$  is the total water depth (m). The nonlinear shallow

water equations are solved using the conventional staggered leap-frog finite difference scheme.

**ENERGY FLUX**

Energy flux of tsunami waves provides useful information for analyzing the effect of submarine topography. Based on the long wave theory, Kowalic et al. (2006) proposed the energy flux vector  $E$  as

$$E = \int_{-h}^{\zeta} P_d u \, dz \quad (12)$$

where  $P_d$  is the dynamic pressure of waves, and  $u = (u, v)$  is the horizontal velocity vector. Because the tsunamis are long waves, the dynamic pressure can be represented by

$$P_d = \rho g \zeta \quad (13)$$

where  $\rho$  is the density of water ( $\text{kg/m}^3$ ). Thus, Eq. (12) can be rewritten as

$$E = \rho g D u \zeta \quad (14)$$

Each component of the energy flux vector  $E$  is given as

$$E_x = \rho g D u \zeta, \quad E_y = \rho g D v \zeta \quad (15)$$

Net energy flow per unit width during the time interval,  $t_1 < t < t_2$ , can be evaluated by integrating the energy flux over the time interval (Baek, 2013) as

$$E_{tx} = \int_{t_1}^{t_2} E_x \, dt = \int_{t_1}^{t_2} \rho g D u \zeta \, dt \quad (16)$$

$$E_{ty} = \int_{t_1}^{t_2} E_y \, dt = \int_{t_1}^{t_2} \rho g D v \zeta \, dt \quad (17)$$

When the time interval is sufficiently long to include the whole period of tsunami duration, the net energy flow,  $E_{tx}$  and  $E_{ty}$ , represents the total energy flow which passes the given location.

The integrated energy flux,  $E_{sx}$  and  $E_{sy}$ , normal to the segments  $y_1 < y < y_2$  and  $x_1 < x < x_2$ , respectively, can be obtained by

$$E_{sx} = \int_{y_1}^{y_2} E_x \, dy = \int_{y_1}^{y_2} \rho g D u \zeta \, dy \quad (18)$$

$$E_{sy} = \int_{x_1}^{x_2} E_y \, dx = \int_{x_1}^{x_2} \rho g D v \zeta \, dx \quad (19)$$

In the previous study (Yoon, 2002; Lim et al., 2008) the energy flow pattern was represented by the distribution of maximum tsunami heights. However, as pointed out by Kowalic et al. (2006), the sense of energy flow direction can be misleading when the tsunamis propagate normal to a submerged ridge. In Figure 1 a submarine ridge is aligned parallel to the  $y$ -direction. Two tsunamis are generated internally along  $x=0$  by releasing a 20m-high Gaussian hump of water. One tsunami propagates along the positive  $x$ -axis, and the other in the opposite direction. The tsunami energy should propagate in the same direction, i.e., normal to the ridge. As shown in Figure 2 the distribution of the net energy flow,  $E_{tx}$ , shows correctly the direction of energy flow, i.e., normal to the ridge, while the distribution of maximum tsunami height does not give any sense of energy flow direction. On the other hand, as shown in Figure 3, the energy flux,  $E_x$ , proposed by Kowalic et al. (2006) shows the distribution of instantaneous energy flux. Thus, it is hard to understand the overall picture of energy flow pattern. In this study the effect of each submerged topography on the propagation of tsunamis

generated in the East Sea is quantitatively investigated using the newly introduced energy flux concept.

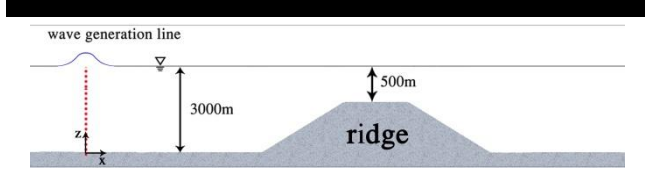


Figure 1. Schematic wave tank with a submerged ridge.

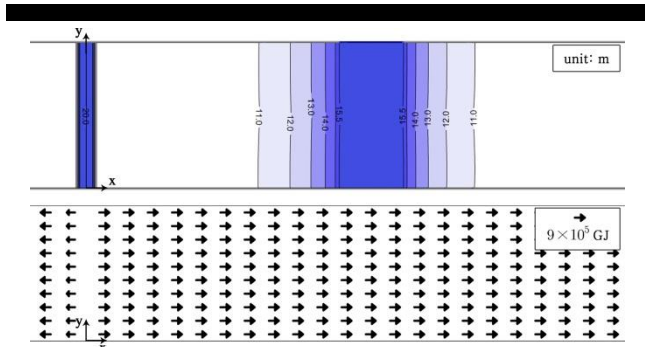


Figure 2. Distribution of maximum tsunami height (upper) and net energy flow (lower).

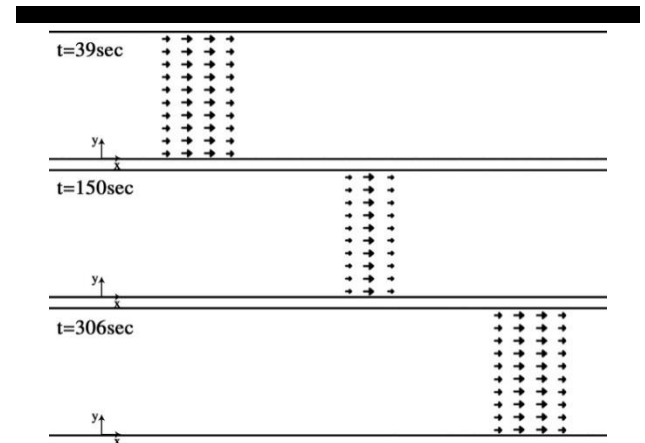


Figure 3. Distribution of instantaneous energy flux.

**VERIFICATION OF NUMERICAL MODEL**

The finite difference model developed by Cho (2012) was verified for the case of 1983 Central East Sea Tsunami. The fault parameters proposed by Aida (1984) was used to determine the initial free surface distribution at the source region. The simulated results were compared with the free surface displacements observed at Sokcho, Mukho, Pohang and Ulsan harbours located along the east coast of Korea. Good agreements between calculated and observed data were obtained (Baek, 2013).

**EFFECTS OF SUBMARINE TOPOGRAPHY**

Submarine topography of the East Sea is very complex as shown in Figure 4. In the figure the topography including the Yamato Rise and the submerged ridge connecting the Yamato Rise and Shimane coast of Japan is denoted by Region A. The topography including the K-shaped ridges emerging from the east coast of Korea towards the East Sea is denoted by Region B.

Figure 5 shows the simplified bathymetry of the East Sea by eliminating the submerged topographies inside the two regions of

Region A and Region B. When the submerged topographies are eliminated, the background bathymetry of the East Sea can be characterized by the so-called shallow-south-deep-north (SSDN) topography. In Figure 5 the tsunami sources of the historical tsunamis occurred in the East Sea are also presented along with the fault line between the Eurasian Plate and the North American Plate. Two straight lines in Figure 5 represent the lines where the energy flux is evaluated. To understand the basic energy flow pattern of the tsunamis generated in the eastern rim of the East Sea, numerical simulations are performed using the simplified geometry shown in Figure 5 for the cases of 1964 Niigata Tsunami, 1983 Central East Sea Tsunami, and 1993 Hokkaido South-West Sea Tsunami.

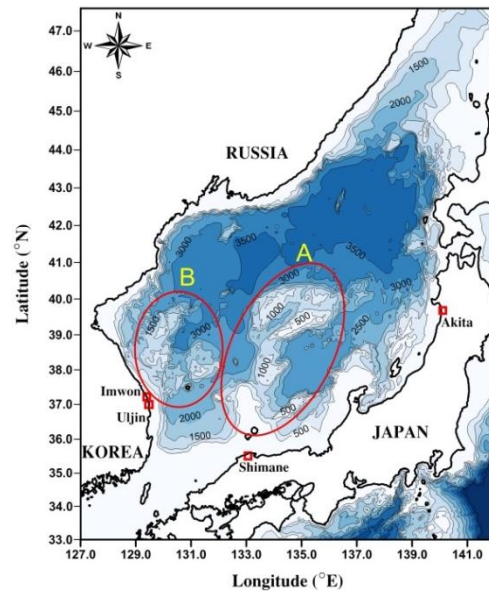


Figure 4. Submarine topography of the East Sea. A indicates the Yamato Rise and the submerged ridge. B indicates the K-shaped submerged ridges.

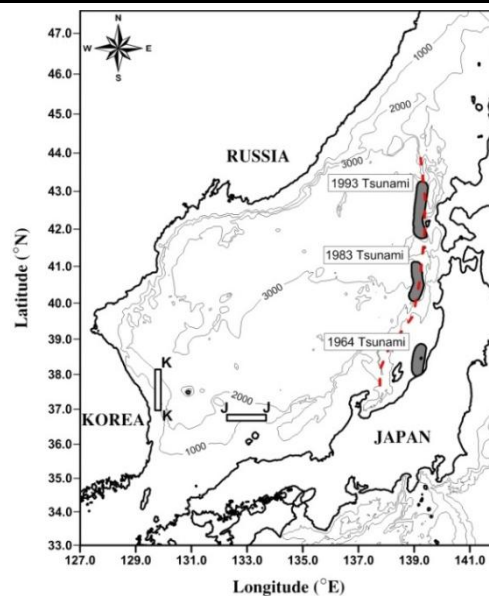


Figure 5. Simplified background bathymetry of the East Sea and source areas of historical tsunamis (shaded regions).

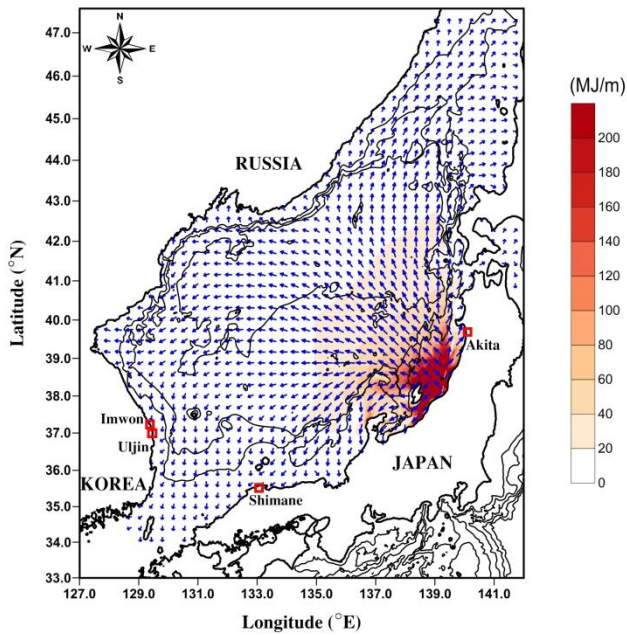


Figure 6. Energy flow pattern for the case of background bathymetry (1964 Niigata Tsunami).

Figure 6 shows the energy flow pattern due to 1964 Niigata Tsunami. Because the tsunami source is located in the shallow area of the south corner of the East Sea, even though the orientation of the source is towards the Russian coast, the major part of tsunami energy is refracted back to the Japanese coast. As a result the east coast of Korea is well protected.

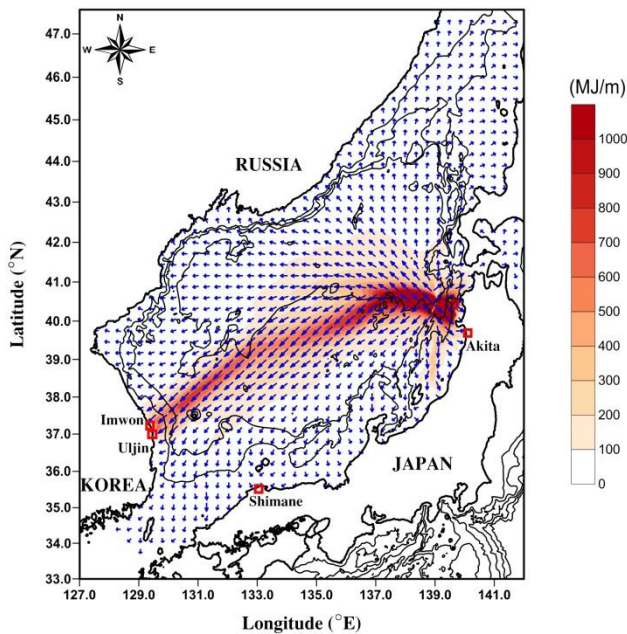


Figure 7. Energy flow pattern for the case of background bathymetry (1983 Central East Sea Tsunami).

Figure 7 shows the energy flow pattern due to the 1983 Central East Sea Tsunami. One branch of energy stream towards the north coast of Korea turns slowly towards the east coast of Korea due to refraction over the shallow-south-deep-north (SSDN) topography.

As a result the major energy of tsunami is concentrated on the east coast of Korea, while the tsunami intensity along the Shimane coast is weak. However, in reality, the damage due to 1983 Tsunami was much more severe along the Shimane coast than the east coast of Korea. Thus, it can be realized that the previously neglected submerged topography does play an important role in the propagation of tsunamis generated in the central part of the east rim of this sea. Figure 8 shows the time history of the integrated energy flux which passes perpendicular to the segments K-K and J-J. The energy flow across the line K-K is much stronger than that of line J-J. The main energy starts to pass the segment K-K at 83min after the tsunami generated, while 70min for the case of segment J-J. These arrival times are much shorter than those observed. The elimination of Yamato Rise and the submerged ridge should be responsible for the shortening of arrival time.

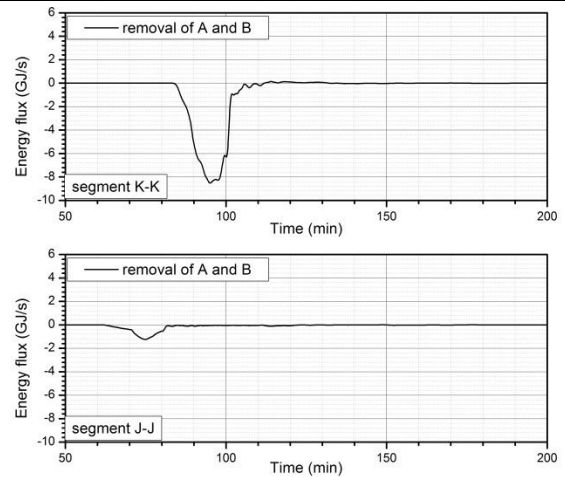


Figure 8. Time history of the energy flux integrated along the segments K-K and J-J when the background bathymetry is used (1983 Central East Sea Tsunami).

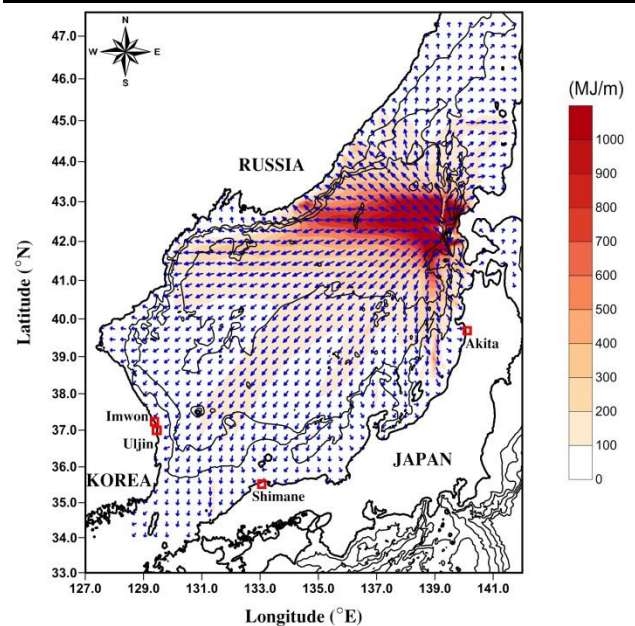


Figure 9. Energy flow pattern for the case of background bathymetry (1993 Hokkaido South-West Sea Tsunami).



Figure 9 shows the energy flow pattern due to the 1993 Hokkaido South-West Sea Tsunami. Because the tsunami source is located in the northern corner of the East Sea where the refraction due to shallow-south-deep-north topography is weak, the major energy flows towards the Russian coast.

From the analyses of simulation results with the simplified background topography the location of the tsunami source is very important. When the source is located in the north or south corner of the fault line, the tsunami intensity along the east coast of Korea is weak due to the so-called shallow-south-deep-north topography of the East Sea. If the source is located in the middle of the fault line, the tsunami action can be strong along the east coast of Korea.

To check the role of the Yamato Rise and the submerged ridge connecting the Yamato Rise and the Shimane coast of Japan the Region A is added to the background bathymetry and the numerical simulation is conducted for the case of 1983 Central East Sea Tsunami. Figure 10 shows the energy flow pattern for 1983 Tsunami. The main stream of energy is trapped by the southern peak of the Yamato Rise and the submerged ridge connected to the Shimane coast of Japan. Thus, the tsunami energy is concentrated on the Shimane coast of Japan instead of the east coast of Korea. Figure 11 shows the time history of the integrated energy flux through the lines K-K and J-J. The energy flow across the line J-J is much stronger than that of the line K-K. This confirms quantitatively that the Yamato Rise and the ridge act as a wave guide which captures and transfers the main energy of tsunami to the Shimane coast of Japan. Comparison between Figure 7 and 10 clearly shows why the damage from the 1983 Tsunami was much more severe on the Shimane coast than the east coast of Korea. It is noteworthy that the main energy starts to pass the segment K-K at 117min after the tsunami was generated, while it is 110min for the case of segment J-J. The arrival time of the tsunami is approximately 40 min longer than that for the case of eliminating the topography included in Region A. This indicates that the main energy of the tsunami flows along the Yamato Rise and the submerged ridge where the water depth is shallow.

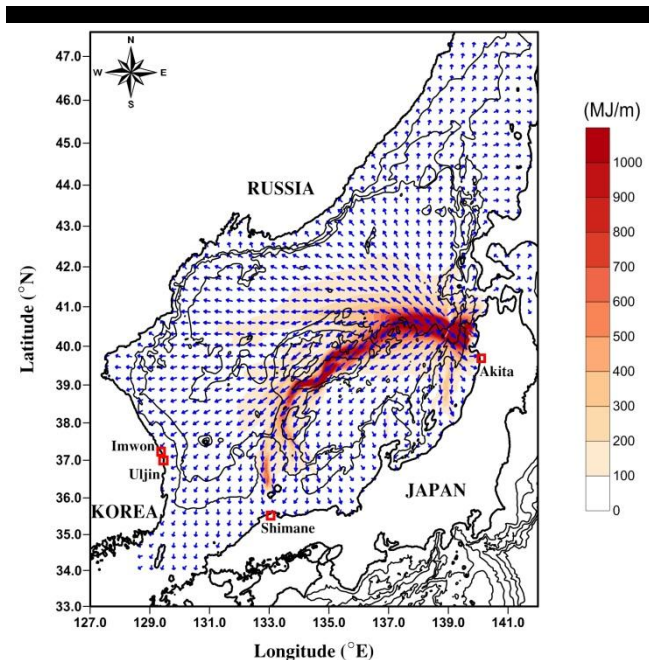


Figure 10. Energy flow pattern for the case of Region A added to background bathymetry (1983 Central East Sea Tsunami).

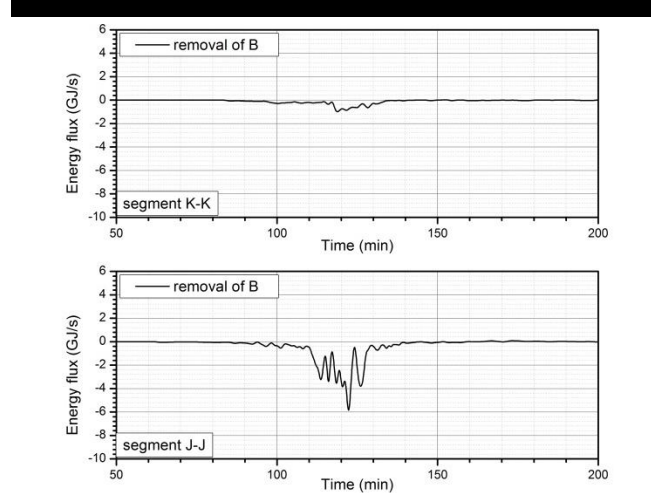


Figure 11. Time history of the energy flux integrated along the segments K-K and J-J when the Region A is added to the background bathymetry (1983 Central East Sea Tsunami).

Finally, the role of the K-shaped submerged ridge denoted by Region B in Figure 4 is investigated for the case of the 1983 Central East Sea Tsunami. The K-shaped ridge is added to the bathymetry used in the previous simulation. Thus, all the real topography is included. As shown in Figure 12 the energy flow pattern is similar to the previous case. However, a small difference due to the presence of K-shaped ridges can be noticed along the east coast of Korea. Some energy which escaped from the Yamato Rise due to diffraction is captured by the K-shaped ridge and is transferred to the Imwon coast of Korea where the K-shaped ridge meets the land. As a result the tsunami intensity has a local maximum at the Imwon area. The numbers of casualties, 100 at the Akita Coast of Japan, 4 at the Shimane Coast of Japan, and 3 at the Imwon Coast of Korea, support the results obtained in this study.

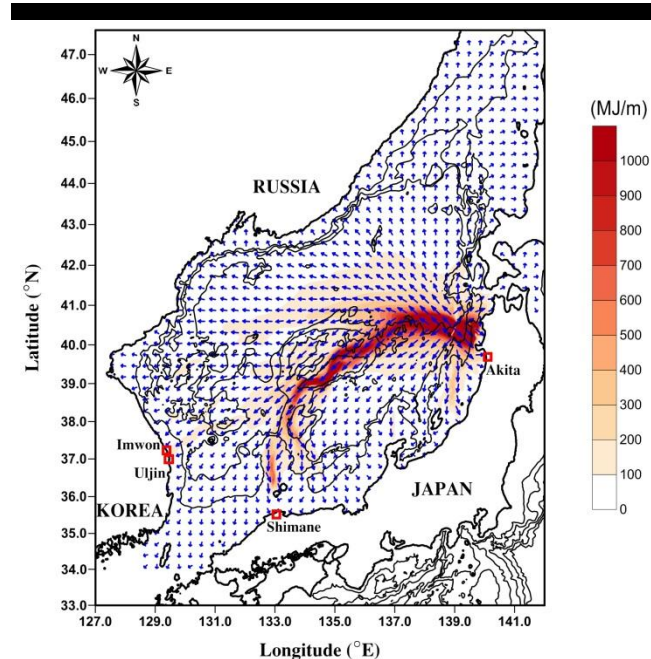


Figure 12. Energy flow pattern for the case of original bathymetry (1983 Central East Sea Tsunami).

Figure 13 shows the time history of the integrated energy flux across segments K-K and J-J. In comparison with Figure 11 for the case of neglecting the K-shaped ridge the energy flow across the line J-J remains unchanged, while the energy flow across the segment K-K is stronger than the case of neglecting the K-shaped ridge. This confirms that the K-shaped ridge captures and transfers the tsunami energy diffracted from the Yamato Rise to the Imwan coast of Korea.

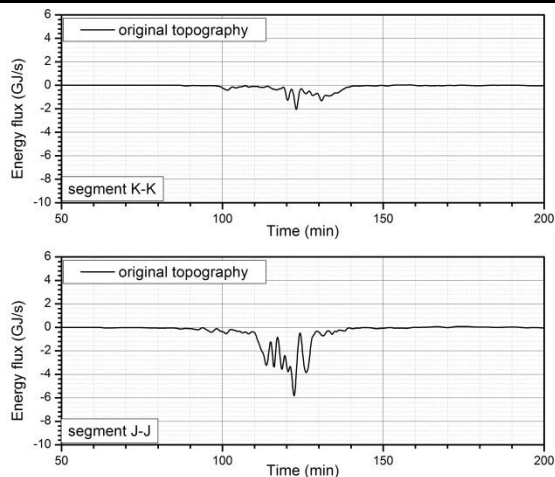


Figure 13. Time history of the integrated energy flux integrated along the segments K-K and J-J for the case of original bathymetry (1983 Central East Sea Tsunami).

Figure 14 compares the time histories of the water surface displacement due to 1983 Tsunami event at the Imwon harbour located in the east coast of Korea for the cases of various bathymetry. When the topographies included in the Regions A and B are eliminated, the tsunami arrives much faster and the intensity is much stronger than observed ones at the Imwon area of Korea. On the other hand, when only the topography included in the Region B is eliminated, the overall pattern of tsunami action is similar to that of the original bathymetry except for the smaller maximum tsunami height than the observed. Thus, it can be concluded that the topographies included in Region A, i.e., the Yamato Rise and the submerged ridges connected to Shimane coast of Japan, are the most important in the propagation of tsunamis generated in the eastern rim of the East Sea.

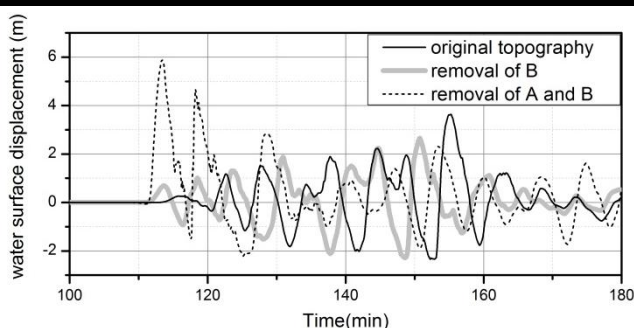


Figure 14. Comparison of the water surface displacement at Imwon harbour (1983 Central East Sea Tsunami).

## CONCLUSION

The underwater topography of the East Sea is very complex. Thus, the underwater topography plays an important role in the

propagation of tsunami occurred in this sea. The major findings of the present study are summarized as follows:

First, the refraction of tsunamis due to the so-called shallow-south-deep-north topography of the East Sea plays an important role to determine the path of main energy flow. When the tsunami source area is located to the northern or southern part of the East Sea, the paths of main energy flow digress from the path towards the east coast of Korea. As a result, the effect of tsunamis along the east coast of Korea is relatively weak. On the other hand, if the tsunami source area is located in the central part of the East Sea, the paths of main energy flow direct towards the east coast of Korea. As a result the effect of tsunamis along the east coast of Korea is intensified.

Second, the Yamato Rise and the submerged ridge connecting the Yamato Rise and the Shimane coast of Japan capture the tsunami energy radiated from the tsunami source located in the central part of the East Sea, and transport it to the Shimane coast of Japan. Thus, the tsunami intensity along the east coast of Korea becomes weaker.

Finally, the K-shaped submerged ridges emerging from the Imwon of the east coast of Korea capture the tsunami energy and transport it towards the Imwon area located at the end of the K-shaped submerged ranges. As a result, the K-shaped submerged ridges play an important role of an energy concentrator for the tsunamis generated in the East Sea regardless of the location of tsunami source.

## ACKNOWLEDGEMENT

This research was a part of the project titled 'Countermeasure System against Hazards of Typhoons and Tsunamis in Harbor Zones (South Coast) – Stage2', funded by the Ministry of Oceans and Fisheries, Korea.

## LITERATURE CITED

- Aida, I., 1984. A source models of the 1983 Nihonkai-earthquake tsunami. *Proceedings of Symposium on Nihonkai Chubu Earthquake Tsunami*, JSCE, 9-21.
- Baek, U., 2013. *Effects of Underwater Topography of East Sea on Propagation of Tsunamis towards Korean Peninsula*. Seoul, Korea: Hanyang University, Ph.D. Thesis, 127p.
- Cho, Y.J., 2012. *Development of Far-Field Tsunami Numerical Model*. Seoul, Korea: Hanyang University, Master's Thesis, 50p.
- Cho, Y.S., Sohn, D.H. and Lee, S.O., 2007. Practical modified scheme of linear shallow-water equations for distant propagation of tsunamis. *Ocean Engineering*, 34, 1769-1777.
- Imamura, F., Shuto, N., and Goto, C., 1988. Numerical simulation of the transoceanic propagation of tsunamis. *Proc. of 6th Congress Asian and Pacific Regional Division(Japan)*, IAHR, 265-271.
- Kowalik, Z., Knight, W., Logan, T. and Whitmore, P., 2006. The tsunami of 26 December, 2004: Numerical modeling and energy considerations. *Pure and Applied Geophysics*, 164, 1-15.
- Lim, C.H., Bae, J.S., Lee, J.I., and Yoon, S.B., 2008. Propagation characteristics of historical tsunamis that attacked the east coast of Korea. *Natural Hazards*, 47, No. 1, 95-118.
- Yoon, S.B., 2002. Propagation of distant tsunamis over slowly varying topography. *J. Geophys. Res.*, AGU, 107, No. C10, 4-1-4-11.
- Yoon, S.B. and Cho, J.H., 2001. Numerical simulation of coastal inundation over discontinuous topography, *Water Engineering Research*, Korea Water Resources Association, 2, No. 2, 75-87.

## Recording of selected effects and hazards caused by current and expected storm events in the Baltic Sea coastal zone

Kazimierz Furmańczyk, Paweł Andrzejewski, Rafał Benedyczak, Natalia Bugajny, Łukasz Cieszyński, Joanna Dudzińska-Nowak, Andrzej Giza, Dominik Paprotny, Paweł Terefenko, Tomasz Zawisłak

Institute of Marine and Coastal Sciences  
University of Szczecin  
Szczecin, Poland  
kaz@univ.szczecin.pl



[www.cerf-jcr.org](http://www.cerf-jcr.org)



[www.JCRonline.org](http://www.JCRonline.org)

### ABSTRACT

Furmańczyk, K., Andrzejewski, P., Benedyczak, R., Bugajny, N., Cieszyński, Ł., Dudzińska-Nowak, J., Giza, A., Paprotny, D., Terefenko, P., Zawisłak, T., 2014. Recording of selected effects and hazards caused by current and expected storm events in the Baltic Sea coastal zone. In: Green, A.N. and Cooper, J.A.G. (eds.), *Proceedings 13<sup>th</sup> International Coastal Symposium* (Durban, South Africa), *Journal of Coastal Research*, Special Issue No. 70, pp. 338-342, ISSN 0749-0208.

Routine monitoring has already become a legal obligation and apparent necessity for EU members, especially of such dynamic and important habitat as the Baltic Sea and its shores. One of the subsystems of *SatBaltyk*, a Polish research project for maritime observation, is dedicated to coastal monitoring. It focuses on recording and forecasting the consequences of storm events along the Baltic's Polish shoreline. Three sites (7–12 km-long sections of dune coast) were selected for detailed research: the Dziwnów Spit, Jamno and Bukowo lakes' spits and part of the Hel Peninsula. Work started in 2010 and will continue until 2015. A numerical model, XBeach, was implemented in order to provide forecasts of several parameters, i.e. beach flooding, dune erosion, suspension of matter in the water after storm and rip current occurrence. It combines external data with in situ measurements by the researchers. Many pieces of equipment were installed for this research: a satellite receiving station, underwater probe ADCP (Acoustic Doppler Current Profiler), a tide gauge, a hyperspectral radiometer and two video cameras for constant shoreline observation. The system is currently being calibrated and verified; an online visualisation available to the public is due to be launched as a long-lasting outcome of the project.

**ADDITIONAL INDEX WORDS:** numerical modelling, visualisation, remote sensing, coastal management, coastal monitoring, coastal hazard.

### INTRODUCTION

The Baltic is a semi-enclosed sea in north-eastern Europe. It constitutes a small (415,000 km<sup>2</sup>) and relatively shallow (52 m deep on average) basin of brackish water (Ziedler *et al.*, 1995). It is considered a non-tidal sea, since the amplitude of tides rarely exceeds a few centimetres (Medvedev, Rabinovich, Kulikov, 2013). The Baltic's catchment area contains 85m people in 14 countries (Omstedt *et al.*, 2004).

Partially enclosed seas such as the Baltic play an important role in the world ocean's ecosystem. Their biological productivity is far greater than that of deep ocean waters, but is at the same time particularly endangered by the consequences of economic activities inland. Such a complex environment as the Baltic is shaped by numerous events and processes, therefore managing it requires substantial knowledge about its condition and variability. Continuous monitoring of key indicators is regarded as essential in its management. Moreover, efficient control measures and forecasting the Baltic's reaction to divert factors are needed in order to use its resources and economic potential in a sustainable way.

The desire to acquire accurate and up-to-date information on the Baltic Sea's environment had been the main motivation behind activities undertaken in the *SatBaltyk* project ('Satellite Monitoring of the Baltic Sea Environment'), launched in 2010 and due to finish in 2015. The project's main objective is to create the

technical infrastructure and implement practical procedures, so that the Baltic's environment can be represented on maps. A remote sensing-based system is planned, which, when operational, will publish selected parameters of the ecosystem online, as a form of routine monitoring of the entire basin (Woźniak *et al.*, 2011a). Therefore, the project's outcome will be the *SatBaltyk Operating System*, generating a set of maps on daily basis, including maps of organic material production, oxygen dispersed by photosynthesis, short- and longwave radiation balance in the sea and atmosphere, concentrations of chlorophyll and other phytoplankton pigments, dynamic state of the sea surface, temperature, upwelling and many others.

An important feature of the system will be its ability to generate those maps even when input data – satellite images from Tiroso N/NOAA, MSG (currently Meteosat 9), EOS, AQUA, DMSP, ENVISAT or other spacecraft – are temporarily unavailable. If a situation like this occurs, e.g. when a particular area is overcast by clouds, the missing data will be replaced by the results from automatic algorithms based on ecohydrodynamic models. Data obtained by this procedure fit well with present measurements.

The work performed in the *SatBaltyk* project is well-positioned within the contemporary legal framework, which established mandatory monitoring and protection of the Baltic's natural environment and climate, such as the Convention on the Protection of the Marine Environment of the Baltic Sea Area (1992), the EU Water Framework Directive (2000), the Integrated Maritime Policy for the European Union (2007). One of the EU's

flagship projects is the European Earth Observation Programme *Copernicus*, while a report of the Marine Research Infrastructures Experts Group (also an EU-governed body) identified a combination of satellite imaging, mathematical modelling and *in situ* measurements as the most effective method of ocean observation.

*SatBaltyk Operating System-Shores* is an integral subsystem of *SatBaltyk* concerned with forecasting and recording the effects and threats associated with current and expected storm surges, as well as calculating important hazard parameters in selected coastal sectors of the Baltic. In accordance to global standards, like those implemented by U.S. Geological Survey's Coastal and Marine Geology Program (Brock and Sallenger, 2001; Morton and Sallenger, 2003; Sallenger *et al.*, 2003; Stockdon *et al.*, 2010), several technologies were included in the operating system, including lidar, video recording, aerial photography, field surveying with GPS devices and, in future, hyperspectral satellite imaging. Thanks to *SatBaltyk's* unique, holistic approach to maritime observation the Baltic's environmental conditions and dynamics can be presented in their entirety, with the inclusion of coastal zone monitoring which is often omitted in other systems or established as a separate system, mainly due to different scale of processes.

## DESCRIPTION OF RESEARCH AREAS

The Baltic coastline amounts to over 15,000 km and is very diverse in character. Three general types of shores are identified, namely (1) coasts made of narrow, fjord-like valleys, (2) hilly and rocky archipelagos (skerries) and (3) coasts made of moraine and fluvioglacial deposits and associated modern deposits. The Polish coast is located in the southern Baltic and has a total length of 500 km. It belongs to the third type, with 80% of the shore covered by beaches and dunes, while the rest forms a cliff coast. Most of the coastline is natural, though artificial coastal protection measures can be found on 25% of its length (Musielak and Furmańczyk, 1999). Low-lying shores are exposed to flooding caused by storm surges, which are a result of high wind velocity, deep low pressure systems and increased amount of water in the sea. The most extreme surges occur during strong westerly winds, when the Baltic fills up with water from the North Sea via the Danish Straits (Ekman, 2009). The research carried out in *SatBaltyk* focuses on, but is not limited to, three research areas of dune coast located in the western, central and eastern parts of the Polish coast, as shown in Figure 1.

The first research area, Dziwnów Spit, is the one where applied research is most currently in its most advanced stages. It includes 10 km of shore between the settlements of Międzywodzie and Dziwnówek, with the Dziwna Strait and the town of Dziwnów located in the middle. The western part is about 2 km wide and includes a dune barrier that is up to 12 m high. The eastern part is much narrower, measuring 300–500 m at its narrowest point and the dunes are lower: 3–4 m in some locations. The spit is made of fine-grained deposits. The shore includes a sandy beach of 30–50 m in width and a flat profile. The shoreline in this area is oscillating, though erosion is stronger than accumulation and consequently it has been protected by seawalls, groins and beach nourishments. The permanent population of the spit is around 4,000, while the number of tourists exceeds 80,000 per year (Central Statistical Office). In effect, it is densely built up with housing and summer resorts.

The area in the central coast, where research is still in its early stages, covers the spits of two coastal lakes, Jamno and Bukowo, between their connection with the sea, Jamieński and Szczuczy inlets (12 km in total). Jamno Lake's spit is about 400 m wide

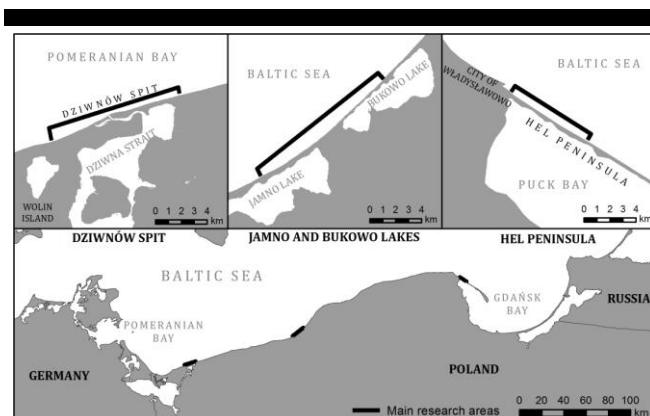


Figure 1. Polish Baltic coast and main research areas.

with a 5–10 m high dune bar. The second spit is far less developed: its width is only 150–200 m and the dune bar is only 50 m wide and 5–7 m wide. The spits are made of fine and medium sands. The shore in this area is eroding; the dunes at Bukowo Lake were overtopped several times in recorded history. This part of the coast is protected with timber groynes. The spits are sparsely populated: only two small settlements of less than 100 persons are located there.

The final research area, where fieldwork is yet to start, is a 7 km long fragment of the Hel Peninsula from the connection with mainland to Chałupy village. This section of peninsula is only 180–430 m wide and made of medium and coarse sands. Its dune elevation is highly variable; at some locations it is only 2 m above mean sea level. When extreme storm surges occur, seawater can overflow it, turning the peninsula into an island (Furmańczyk, 1995). To mitigate this hazard, several protection measures are being used, including timber groynes, a kilometer-long seawall (partially concrete) and gabions installed inside the dunes. Still, in order to compensate an estimated yearly loss of 100,000 m<sup>3</sup> of sediment (Basiński, 1995) the beach is continuously being replenished. The whole research area officially belongs to an urban area of Władysławowo city, but in fact its population does not exceed 500.

## STORM IMPACT INDICATORS

*SatBaltyk-Shores* system was created to supplement environmental data on the Baltic with information about the coastal zone. Unfortunately, precise observations of the shore from the satellites being used in *SatBaltyk* are not yet possible, as the images' resolution is inadequate. A 1 km pixel excludes them from any kind of analysis of the coastal zone, since the beach, dunes and underwater bars are all less than the resolution. In consequence an alternate concept was developed: to use numerical models, land surveying, aerial photography and video cameras. Combining the methods allows the researchers to assess the current and predicted state of the coastal environment using a set of indicators.

State of the coastal environment is defined here as the degree of shore transformation and impacts of the sea on the coast in the aspect of potential hazards to the shore itself, the population or the infrastructure located on it. The system operationally assesses potential threats in the shoreface, beach and dune bars due to water level changes and waves through a parameterization of selected coastal processes and classifying their consequences. Storm impact indicators (*SatBaltyk* indicators) were defined for this purpose. They form two groups: present storm impacts and

predicted storm impacts. The first group includes the following indicators:

- Magnitude of dune erosion;
- Volume of sand eroded from the coastal zone;
- Amount of suspended matter in the water immediately after the storm.

For these the simulation is started only after the storm has ended, so that actual data from the event can be used, instead of predicted ones. The second group has two indicators:

- Possibility of rip current occurrence;
- Extent of beach inundation.

This time the simulation is run using data from numerical models of the sea environment. The entire output is recorded in a database and presented online. To make the results easily understandable for ordinary users, a four-grade hazard scale originally created by Sallenger (2000) and commonly used by various meteorological websites (e.g. Meteolarm) was applied.

### SATBAŁTYK-SHORES SYSTEM STRUCTURE

The system is based on the experience gained during the preparation of an early warning system (EWS) under MICORE project (2008-2011), which was financed by the EU's 7<sup>th</sup> Framework Programme (Furmańczyk *et al.*, 2012). SatBałtyk-Shores is a modification and expansion of that EWS.

The core of the system is a numerical model developed by a Dutch and American consortium for the U.S. Army Corps of Engineers – XBeach (eXtreme Beach behaviour model). Three types of data are required for the model in order to deliver forecasts: sea levels, wave parameters and coastal morphology measured during fieldwork. Simulation results in the form of physical parameters generated by the model are compared with threshold values of indicators, so that the consequences of the storm impact are recorded in the database and presented online. The system's structure is depicted in Figure 2.

SatBałtyk-Shores uses three prognostic models: WAM for wave parameters, M3D for water levels and the aforementioned XBeach. WAM (Wave Model) Cycle IV model (WAMDI Group, 1988) was validated by Cieślíkiewicz and Papińska-Swercel (2008) for the Baltic Sea. Data are supplied by the Interdisciplinary Centre for Mathematical and Computational Modelling, an advanced research unit of the University of Warsaw in the form of a 84-hour forecast including significant wave height, wave direction, mean wave period and other, all of one-hour resolution. M3D is part of a ecohydrodynamic model, developed by the University of Gdańsk's Institute of Oceanography (Kowalewski, 1997). It was validated for the Pomeranian Bay by Kowalewski and Kowalewska-Kalkowska (2011) based on several storm events. Data are available online as a 48-hour forecast of numerous parameters, including water levels used for XBeach simulations.

XBeach was designed for modelling the behaviour of a dune coast in various hydrological and meteorological conditions (Roelvink, 2009). Notwithstanding the shortcomings of coastal morphodynamic models (Thieler *et al.*, 2000), the 1D version of the model was applied on the southern Baltic coast for the first

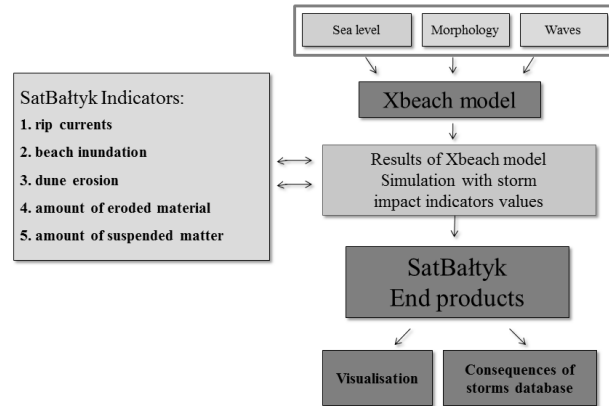


Figure 2. *SatBałtyk-Shores* system structure.

time in MICORE. It was calibrated using 8 profiles of Dziwnów Spit's shore and a single storm surge by Bugajny *et al.* (2013). For the purpose of forecasting and recording the effects and hazards in the coastal zone, caused by current and expected storm events (Woźniak *et al.*, 2012), build in the *SatBałtyk* project, XBeach was preliminarily calibrated in 1D using more up-to-date profiles (Furmańczyk *et al.*, 2013).

The validation process of the model for the Dziwnów Spit has ended for two storm impact indicators mentioned above, i.e. the possibility of rip current occurrence and the extent of beach inundation. The first indicator is based on an assumption that rip currents appear when waves break over submerged longshore bars near the shoreline (Short and Aagaard, 1993). Using XBeach modelling the threshold value of a certain parameter depicting wave breaking was obtained. When it exceeds 0.6 in a 0–1 scale rip currents may occur (Figure 3) (Furmańczyk *et al.*, 2013).

Calibration of the indicator dealing with beach inundation was based upon a few storm events for which a complete set of data was acquired, including morphology, hydro-meteorology and images from a video camera. The modelled extent of wave run-up on the beach was juxtaposed with real data measured on the images (Table 1). The difference between the model and measurements was on average 4.4 m, proving the method accurate enough for use in *SatBałtyk-Shores* (Furmańczyk *et al.*, 2013).

The remaining three other indicators are currently undergoing the calibration process. To do that, land surveying with GPS RTK devices is conducted, along with continuous recording of images from video cameras and cyclic measurements of suspended matter.

### VISUALISATION AND DATABASES

An XBeach simulation is run every morning with a 6-hour output time step giving a 48-hour forecast. For every time step both rip current and flood inundation are calculated. The results are transferred to *SatBałtyk Operating System's* home website (Figure

Table 1. Difference between modelled and measured wave run-up on the beach for three storm events.

Event	Elapsed time of events (hours)																						Event average (m)	Average (m)
	1	2	3	4	5	6	7	8	9	10	11	12	13	14	15	16	17	18	19	20	21	22		
1	6	-3	12	-3	9	0	-3	12	0	6	6	3	12	0	12	0	6	9	0	6	-6	3	3.95	4.38
2	9	15	15	6	12	6	12	9	6	12	3	9	6	12	3								9.00	
3	-3	12	-3	-3	3	-9	9	0	-3	-3	-9	0											-0.75	



Figure 3. Output from XBeach modelling indicating breaking waves and the possibility of rip current occurrence.

4) and *SatBaltyk-Shores*'s subsite (Figure 5), with the latter giving more detailed information. Additionally, all data are stored in databases.

The model's output is transformed with appropriate automatic algorithms. They save the information in databases and generate results in graphic form. Moreover, for on-line presentation, graphics are created as well as KML files with coloured circles for every 1 km sector. The circles use a 4-colour legend mentioned earlier. On the map of the entire Baltic Sea the results are presented as points (Figure 4). When one is clicked, the map zooms into the proper area and shows a detailed legend. From this point, the user can go to the *SatBaltyk-Shores* subsite.

When visualised, the simulation results are shown over a basemap from Google, in order to ensure clarity and accuracy. The website's functionality allows the user to choose a forecast date and indicator he or she is looking upon. The requested information is then loaded from an KML file. A indicator-specific legend is always presented. Additional layers can be put on the map, like the location of bathymetric profiles or Maritime Office's kilometer points. The graphs are displayed below the map with information about the indicators and the model's input data, i.e. significant wave height, wave mean period, wave direction and sea level.

In summary, the system consists of a numerical model, input data, database structures, server solutions and automated scripts for the results of storm events in the coastal zone. At the same time it presents the results in a simple and easily understandable form for a casual user of the website.

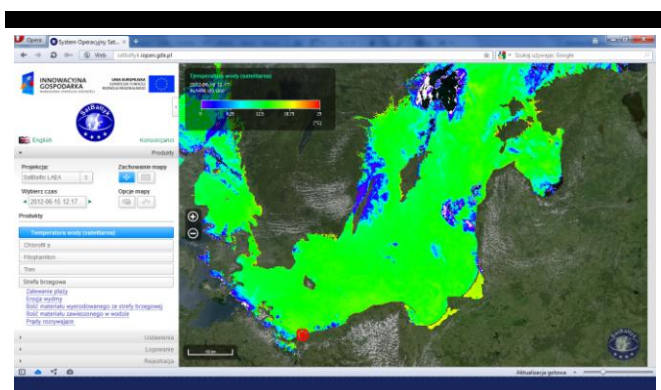


Figure 4. *SatBaltyk Operating System* website's visualisation page ([satbaltyk.iopan.gda.pl](http://satbaltyk.iopan.gda.pl)).

## SUPPORTING ACTIVITIES

*SatBaltyk-Shores* system required many data for calibration and validation, which were obtained through the use of several pieces of scientific equipment.

Continuous monitoring of the shore at two sites is accomplished by two digital cameras which record visual information about the beach and shoreface. The cameras are operated through algorithms prepared by the researchers and run in Matlab software. Images are recorded with a 3 Mpix resolution during the day and 1 Mpix during the night.

A local server in the Remote Sensing and Marine Cartography Unit, which operates *SatBaltyk-Shores* system, stores and calculates the data for the system. The output is transferred in the form of ready-to-use KML files to the *SatBaltyk*'s main server for visualisation.

Data on coastal morphology are acquired using GPS RTK devices – Topcon HiPer Pro II. Measurements are made in profiles perpendicular to the shoreline, located in the research areas. They are located 1 km one from another, what gives a total of 10 profiles for the Dziwnów Spit and 12 for the spits of Jamno and Bukowo lakes. Additionally, a single profile was chosen at the western side of a 400-meter pier in Międzyzdroje in order to conduct research on matter suspended in the water. The profiles include the dune, beach and shoreface. Because underwater measurements could be made only up to 1 m in depth, the profiles are located in such a manner so that data from Maritime Office's bathymetric surveys could be used.

Moreover, the researchers are experimenting with an innovative method to calculate bathymetry in the surf zone. Upon completion, an algorithm will compute it directly from colour aerial images, substantially enhancing the quality of underwater morphology, which is an important input information for XBeach.

Furthermore, the spectral characteristics of the water and seafloor are investigated, as they have an impact on aerial and satellite imagery. A hyperspectral radiometer is used for this research. It also provides additional information about the matter suspended in the water.

In November 2012 an underwater probe, ADCP (Acoustic Doppler Current Profiler) was placed in the Pomeranian Bay north

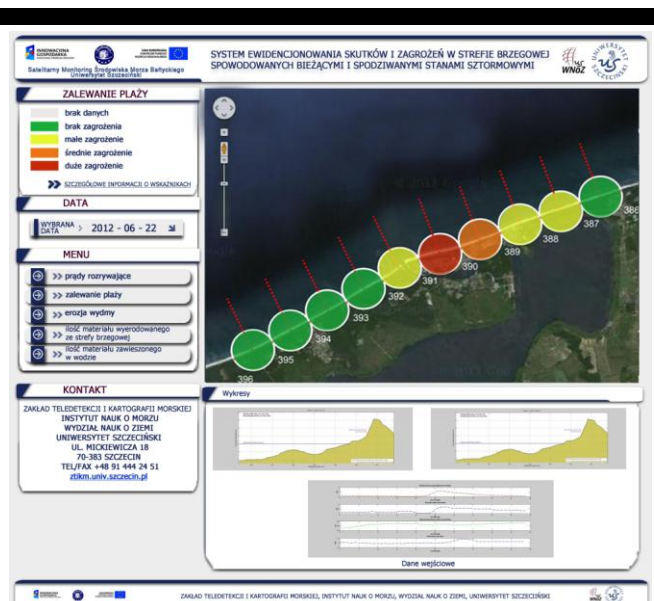


Figure 5. *SatBaltyk-Shores* pilot website.

of Dziwnówek (54°5'19.8" N 14°33'59.24" E). It records the height and direction of waves, the velocity and direction of sea currents, so that the WAM model could be locally calibrated. It could also help to analyse suspended matter transport in the water.

Finally a satellite scene-receiving station (SeaSpace) was established. It downloads continuously images from AVHRR radiometers installed on NOAA spacecraft. The data are converted into sea surface temperature and chlorophyll concentration in the water.

## CONCLUDING REMARKS

In the framework of *SatBałtyk* project a system has been built that automatically processes data from prognostic models and presents them on the internet using a set of specially designed indicators. In a simple and easily accessible way a typical non-professional user can obtain information about current and expected storm impacts.

Assessing the hazards in the coastal zone in an operational manner is important for the system's end-users (governmental authorities responsible for coastal protection, the local administration which manages the coasts and, the local population and tourist directly at risk from storm impacts).

Data stored in the system that pertains to the consequences of storms will allow in the future a temporal analysis of coastal zone variability. Such information could lead to a more effective and sustainable coastal management along the Baltic Sea.

## ACKNOWLEDGEMENT

This work was done within the *SatBałtyk* project, which is funded by the European Union through the European Regional Development Fund – contract No. POIG.01.01.02-22-011/09, project entitled 'Satellite Monitoring of the Baltic Sea Environment'.

## LITERATURE CITED

- Basiński, T., 1995. Protection of the Hel Spit. In: Rotnicki, K. (ed.), *Polish Coast: Past, Present and Future*, Journal of Coastal Research, Special Issue No. 22, pp. 197-202.
- Brock, J.C. and Sallenger, A.H. Jr., 2001. *Airborne topographic lidar mapping for coastal science and resource management*. U.S. Geological Survey Open-File Report 01-0046.
- Bugajny, N., Furmańczyk, K., Dudzińska-Nowak, J. and Paplińska-Swerpel, B., 2013. Modelling morphological changes of beach and dune induced by storm on the Southern Baltic coast using XBeach (case study: Dziwnów Spit). In: Conley, D.C., Masselink, G., Russell, P.E. and O'Hare, T.J. (eds.), *Proceedings 12<sup>th</sup> International Coastal Symposium* (Plymouth, England), *Journal of Coastal Research*, Special Issue No. 65, pp. 672-677.
- Central Statistical Office. Local Data Bank. <http://www.stat.gov.pl/bdlen/>
- Cieślakiewicz, W. and Paplińska-Swerpel, B., 2008. A 44-year hindcast of wind wave fields over the Baltic Sea. *Journal of Coastal Engineering*, 55, 894-905.
- Dudzińska-Nowak, J., 2006. Coastline long-term changes of the selected area of the Pomeranian Bay. In: Tubielewicz, A. (ed.), *Proceedings 8th International Conference LITTORAL* (Gdańsk, Poland), *Coastal Dynamic, Geomorphology and Protection*, pp. 163-170.
- Ekman, M., 2009. *The changing level of the Baltic Sea during 300 years: a clue to understanding the Earth*. Åland Islands, Finland: Summer Institute for Historical Geophysics, 168p.
- Furmańczyk, K., 1995. Coast changes of the Hel Spit over the last 40 years. In: Rotnicki, K. (ed.), *Polish Coast: Past, Present and Future*, *Journal of Coastal Research*, Special Issue No. 22, pp. 193-196.
- Furmańczyk, K., Bugajny, N., Dudzińska-Nowak, J., Andrzejewski, P., Terefenko, P., Giza, A., Benedyczak, R. and Cieszyński, Ł., 2012. Projekt MICORE – podsumowanie zrealizowanych zadań. In: Furmańczyk, K. (ed.), *Zintegrowane Zarządzenie Obszarami Przybrzeżnymi – stan obecny i perspektywy 4. Zagrożenia i systemy ostrzegania*. Szczecin, Poland, Institute of Marine and Coastal Sciences.
- Furmańczyk, K., Bugajny, N., Dudzińska-Nowak, J., Andrzejewski, P., Cieszyński, Ł. and Paprotny D., 2013. *Raport z realizacji zadania S4.1 w roku 2013*. Szczecin: Internal scientific report of the *SatBałtyk* project.
- Kowalewski M., 1997. A three-dimensional, hydrodynamic model of the Gulf of Gdańsk. *Oceanological Studies*, 26 (4), 77-98.
- Kowalewski M. and Kowalewska-Kalkowska H., 2011. Performance of operationally calculated hydrodynamic forecasts during storm surges in the Pomeranian Bay and Szczecin Lagoon, *Boreal Environment Research*, 16 (Suppl. A), p. 27-41.
- Medvedev, I.P., Rabinovich, A.B. and Kulikov, E.A., 2013. Tidal oscillations in the Baltic Sea. *Oceanology*, 53(5), 526-538.
- Meteoalarm. Alerting Europe for extreme weather. [www.meteoalarm.eu](http://www.meteoalarm.eu)
- Morton, R.A. and Sallenger, A.H., Jr., 2003. Morphological impacts of extreme storms on sandy beaches and barriers. *Journal of Coastal Research*, 19, 560-573.
- Musieliak, S. and Furmańczyk, K., 1999. Baltic coast types. In: Lundin, L. C., (ed.), *Water in nature. Sustainable water management in the Baltic Sea basin*. Uppsala, Sweden: Baltic University Publication, p. 30-33.
- Omstedt, A., Elken, J., Lehmann, A. and Piechura, J., 2004. Knowledge of the Baltic Seaphysics gained during the BALTEX and related programmes. *Progress in Oceanography*, 63 (1-2), 1-28.
- Projekt MICORE, [www.micore.ztikm.szczecin.pl](http://www.micore.ztikm.szczecin.pl)
- Projekt SATBAŁTYK, [www.satbaaltyk.iopan.gda.pl](http://www.satbaaltyk.iopan.gda.pl)
- Roelvink, D., Reniers, A., van Dongeren, A., van Thiel de Vries, J., McCall, R. and Lescinski, J., 2009. Modelling storm impacts on beaches dunes and barrier islands. *Coastal Engineering*, 56 (11-12), 1133-1152.
- Sallenger A.H. Jr., 2000. Storm impact scale for barrier islands, *Journal of Coastal Research*, 16, 890-895.
- Sallenger, A.H., Jr., Krabill, W.B., Swift, R.N., Brock, J.C., List, J., Hansen, M.E., Holman, R.A., Manizade, S., Sontag, J., Meredith, A., Morgan, K.L.M., Yunkel, J.K., Frederick, E.B. and Stockdon, H.F., 2003. Evaluation of airborne scanning lidar for coastal change applications: 1. beach topography & changes. *Journal of Coastal Research*, 19, 125-133.
- Short, A.D. and Aagaard T., 1993. Single and Multi-Bar Beach Change Models. In: Short, A.D. (ed.), *Beach and Surf Zone Morphodynamics*, *Journal of Coastal Research*, Special Issue No. 15, pp. 141-157.
- Stockdon, H.F., Doran, K.S. and Serafin, K.A., 2010. *Coastal change on Gulf Islands National Seashore during Hurricane Gustav: West Ship, East Ship, Horn, and Petit Bois Islands*. U.S. Geological Survey Open-File Report 2010-1090.
- Thieler, E.R., Pilkey, O.H., Young, R.S., Bush, D.M., Chai Fei. 2000. The use of mathematical models to predict beach behavior for US Coastal Engineering: a critical review. *Journal of Coastal Research*, 16, 48-70.
- WAMDI Group, 1988. The WAM model—a third generation ocean wave prediction model. *Journal of Physical Oceanography*, 18, 1775-1810.
- Woźniak B., Bradtke K., Darecki M., Dera J., Dudzińska-Nowak J., Dzierzbicka-Głowacka L., Ficek D., Furmańczyk K., Kowalewski M., Krężel A., Majchrowski R., Ostrowska M., Paszkuta M., Stoń-Egiert J., Stramska M. and Zapadka T., 2011a. *SatBaltic – a Baltic environmental satellite remote sensing system- an ongoing project in Poland*. Part 1: Assumptions, scope and operating range, *Oceanologia*, 53(4), 897-924.
- Woźniak B., Bradtke K., Darecki M., Dera J., Dudzińska-Nowak J., Dzierzbicka-Głowacka L., Ficek D., Furmańczyk K., Kowalewski M., Krężel A., Majchrowski R., Ostrowska M., Paszkuta M., Stoń-Egiert J., Stramska M. and Zapadka T., 2011b. *SatBaltic – a Baltic environmental satellite remote sensing system- an ongoing project in Poland*. Part 2: Practical applicability and preliminary results, *Oceanologia*, 53(4), 925-958.
- Zeidler, R.B., Wróblewski, A., Miętus, M., Dziadziuszko, Z., Cyberski, J., 1995. Wind, Wave, and storm surge regime at the Polish Baltic coast. In: Rotnicki, K. (ed.), *Polish Coast: Past, Present and Future*, *Journal of Coastal Research*, Special Issue No. 22, pp. 33-55.

# Global changes in mean tidal high water, low water and range

R.J. Mawdsley†, I.D. Haigh, N.C. Wells

National Oceanography Centre,  
Southampton,  
University of Southampton  
Southampton, UK  
†robert.mawdsley@noc.soton.ac.uk



[www.cerf-jcr.org](http://www.cerf-jcr.org)



[www.JCRonline.org](http://www.JCRonline.org)

## ABSTRACT

Mawdsley, R.J., Haigh, I.D., Wells, N.C., 2014. Global changes in tidal high water, low water and range. *In: Green, A.N. and Cooper, J.A.G. (eds.), Proceedings 13<sup>th</sup> International Coastal Symposium* (Durban, South Africa), *Journal of Coastal Research*, Special Issue No. 70, pp. 343-348, ISSN 0749-0208.

Impacts of extreme sea levels are increasing as the population and infrastructure in coastal zones increases. Extreme high sea levels generally increased at a similar rate to mean sea level through the twentieth century at most sites around the world, suggesting that the same mechanisms are driving both increases. However, the simplicity of this conclusion belies the fact that many mechanisms known to act on the different components of sea level, have been observed to change in local and regional studies. Using a 'quasi-global' dataset of sea level records, this paper investigates changes in the tidal component of sea level and shows that changes in mean high and low waters, and hence tidal range, are occurring over long-time scales at many sites around the world. Over half of the selected sites show significant trends in tidal range datums, but no clear spatial patterns of change exist, suggesting that mechanisms are affecting the tide on local scales. Trends are dependent on the tidal datum selected which has wide-ranging practical applications given the variety of uses of tidal datums.

**ADDITIONAL INDEX WORDS:** *Sea level, tide, extremes.*

## INTRODUCTION

Extreme sea levels (ESL) can have devastating effects on life and infrastructure in the coastal zone and the impact of these events may increase due to continued population growth and development in this zone. Therefore, long-term predictions of changes in ESL are of vital importance to aid coastal engineering, management, planning and policy.

In a quasi-global assessment, Menendez and Woodworth (2010) showed that ESL have increased over the 20<sup>th</sup> century at most locations around the world. They also showed that this increase was primarily a direct result of increases in mean sea level (MSL) over this period. However, the simplicity of this conclusion belies the fact that many mechanisms act on the three main components of sea level (MSL, tide and the non-tidal residual). In addition, the findings of a number of local and regional scale studies that have observed significant changes in both tides and storm surges, which appears to contradict these findings. For example, changes in storm surge, the predominant cause of non-tidal residual, have been shown to significantly change in the Mediterranean (Lionello et al., 2005; Raicich, 2004; Ullmann et al., 2007), the North Sea (Mudersbach et al., 2013) and the north-east Pacific (Cayan et al., 2008; Abeyirigunawardena and Walker, 2008).

In this paper however, the focus is on long term changes in the tidal component. The tide propagates as a shallow water wave with speed  $c = \sqrt{gh}$ , where  $h$  is the water depth and  $g$  is the acceleration due to gravity. Therefore changes in the tidal component can occur with changes in water depth, even though the astronomical forces driving tides remain constant. Modelling studies have suggested that a 1 m change in MSL could lead to a 1-2% increase in tidal range due to changes in the propagation

speed of the tidal wave (Muller et al., 2011). However modelling studies in the North Sea have shown that large changes in water depth are required to change tidal characteristics significantly (Flather et al., 2001; Pickering et al., 2012). Eustatic or isostatic sea level change can indirectly change tides by changing the resonance of a basin to particular tidal frequencies. Changes in resonant periods have been the suggested cause of observed increases in the amplitude of the  $M_2$  tide in the Gulf of Maine and along the north-east American coast, as well as a larger decrease, of up to 10% per century, in the  $S_2$  tide (Ray, 2006; Ray 2009). However, along the Pacific coast of North and South America increases in amplitude of both the  $M_2$  and  $K_1$  tides north of 18°N increased by 2.2% per century. The spatial extent of consistent trends suggests the influence of large scale processes, while consistent spatial patterns of the  $M_2$  and  $K_1$  tides excludes mechanisms with a strong frequency dependence (Jay, 2009). Large regional changes have not been observed in Europe or the Far East, although there is evidence of smaller regionally consistent changes in the  $M_2$  and  $S_2$  constituents in the German bight (Woodworth, 2010). The smaller regional patterns have been attributed to the movement of the local amphidromic point, due to changes in wave propagation and energy dissipation due to friction changes (Pickering et al., 2012).

Changes in mean tidal range (MTR), calculated from high waters (HW) and low waters (LW), have been observed at many sites around the United Kingdom (Woodworth et al., 1991), in the German Bight (Führböter et al., 1990), and at many sites around the United States (Flick et al., 2003). However, the regional trends seen in individual constituents are not always present in these studies which assess the whole tidal signal. A number of local scale mechanisms appear to be causing these changes,



Table 1. Summary of selected tidal datums and the description of their calculation.

Tidal Range Datum	HW/LW Datums	Description
Great Diurnal Tidal Range (GDTR)	Mean Higher High Water (MHHW) Mean Lower Low Water (MLLW)	Annual average of highest high water minus the lowest low water of each day.
Mean Tidal Range (MTR)	Mean High Water (MHW) Mean Low Water (MLW)	Annual average of all high waters minus the average of all low waters.
Lesser Diurnal Tidal Range (LDTR)	Mean Lower High Water (MLHW) Mean Higher Low Water (MHLW)	Annual average of lowest high water minus the highest low water of each day.
Spring Tidal Range (STR)	Mean High Water Spring (MHWS) Mean Low Water Spring (MLWS)	Annual average of all high waters minus all low waters during spring periods.
Neap Tidal Range (NTR)	Mean High Water Neap (MHWN) Mean Low Water Neap (MLWN)	Annual average of all high waters minus all low waters during neap periods.

including bathymetric changes. These changes occurring in coastal waters, harbours or estuaries include: natural changes such as vertical land movements, natural accretion and erosion in river deltas (Araújo *et al.*, 2008); or anthropogenic causes caused by dredging of a navigation channel or creation of a sea wall, which are usually easier to assign if accurate port histories are kept (Woodworth *et al.*, 1991). Other processes that can cause tidal variations are: sea ice cover (St. Laurent *et al.*, 2008); and water column stratification, which modifies vertical viscosity and bottom friction (Muller, 2012) and has been shown to cause changes of up to 10% between seasons, in the  $M_2$  tide in the East China Sea (Kang *et al.*, 2002). Both of these are likely to change with global warming and influence tides on local to regional scales. These studies demonstrate that changes in the tides are widespread and large enough to be considered an important factor during investigation of sea level rise (Woodworth *et al.*, 1991) and in the calculation of ESL.

This study will address to key questions: First, do changes in the tide occur globally? Second, are trends and spatial patterns in observed tidal data significantly different from those of the major tidal constituents?

## DATA & METHODS

The 'quasi-global' Global Extreme Sea Level Analysis (GESLA) dataset was used here. This dataset was compiled by staff from the Permanent Service for Mean Sea Level (PSMSL) in the UK, the Antarctic Climate & Ecosystems Cooperative Research Centre (ACE CRC) in Australia and the University of Hawaii Sea Level Center (UHSLC). It contained 675 individual sea level records from 450 unique locations around the world.

The initial task of the study was to extend the datasets, from 2004, to the end of 2012, where possible. Data were downloaded from the websites of the UHSLC for global sites, the British Oceanographic Data Centre (BODC) for UK sites, the National Oceanic and Atmospheric Administration (NOAA) for US sites, Marine Environmental Data Service (MEDS) for Canadian sites and Bureau of Meteorology (BOM) for Australian sites. Since the quality control (QC) procedures of the different governmental bodies varied, further data checks were conducted on all sites and at all stages of analysis, to standardised the QC and ensure data quality. Comparisons were conducted where different datasets were to be concatenated or consolidated, such as where duplicate datasets existed in the inherited GESLA dataset or with the extension of datasets. QC was conducted after harmonic analysis with a particular focus on: datum shifts, phase shifts and outliers. Further checks were carried out throughout the analysis and where data were deemed invalid they were removed.

A preliminary set of sites were selected, giving a near-global coverage, to assess global patterns, while also generating a region of high data density around the United Kingdom to assess regional patterns.. The data requirements for tidal analysis are strict, since events ranging from hours (e.g. tropical storm surges, tidal high water), to decades (e.g. the lunar nodal cycle) must be captured and accurately resolved. The following requirements were imposed on the selected sites:

1. Data must be of research quality. Data downloaded from various websites have been through quality control (QC) procedures, but further checks were conducted to remove any remaining erroneous data;
2. Data must be hourly to capture the variations in tide;
3. Each year of data must contain at least 75% of potential hourly values. Seasonal cycles influence the tide so a high percentage of data is required for each year to be accurately represented;
4. The dataset must span at least 28 years and contain 15 years of data that conform to requirement 3 within that period (Woodworth *et al.*, 1991). This allows representation of inter-decadal variations in tide, such as the lunar nodal cycle.

In total 38 sites passed the selection criteria and are used for analysis in this paper.

## Tidal Analysis

The measured data was separated into the three main component parts. MSL was calculated using a 30-day running mean. With this removed, the remaining data (tide and residual) were separated into calendar years and run through the harmonic analysis software T\_Tide (Pawlowicz *et al.*, 2002). Annual analysis means important long constituents, such as the nodal cycle, are not removed and hence are accounted for later in the analysis.

From the tide component, every HW and LW was extracted by locating the turning points of the tide. An initial automated extraction was checked manually to ensure they were correctly located and assigned. The tidal datums used to classify the tide were calculated from a number of different subsets of HW and LW (Table 1; Figure 1). The spring/neap periods were calculated using the highest HW of successive 14 day periods, and then splitting the time into quarters between each set of consecutive highest HW. Spring period is therefore the quartile before (Q4) and the quartile after (Q1) a highest HW, while the neap period is Q2 and Q3. (Figure 1). Each tidal datum was calculated per annum to give a time series of heights to which a linear regression model with a nodal term added. Equation 1 gives the example for MTR.

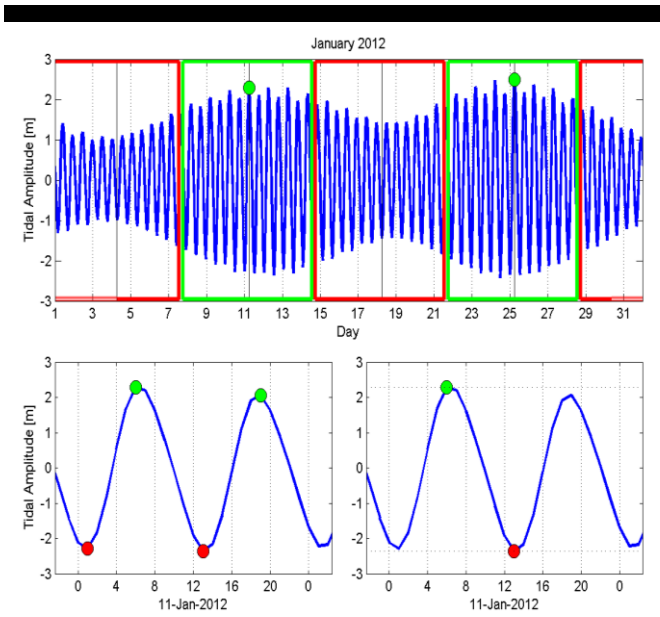


Figure 1. Different subsets of HW and LW illustrated using data from Newlyn, UK: top panel, shows relationship of spring (green boxes) and neap (red boxes) to the highest HW of consecutive 14-day periods. Bottom left: all HW and LW selected, as per MTR calculation; bottom right, highest HW and lowest LW of each day selected, as per calculation for GDTR.

$$MTR t = a + bt + c \cos \omega t - d \quad (1)$$

MTR(t) is a function of a linear trend ( $a + bt$ ) and a nodal term, where  $\omega = 2\pi/18.61$  radians per year, and  $c$  and  $d$  are constants. The nodal term is included to ensure that trends are not biased by inter-decadal nodal modulations.

### RESULTS

The magnitude of the trend in tidal datums varies from  $1.7 \text{ mmyr}^{-1}$  in STR at North Shields, UK to  $-1.5 \text{ mmyr}^{-1}$  in MTR at Fishguard, UK (Figure 2). The greatest contribution to tidal range from a HW tidal datum is the  $1.2 \text{ mmyr}^{-1}$  in MHWS at Heysham, UK, while the greatest increase from a LW tidal datum is the  $-1.0 \text{ mmyr}^{-1}$  change in MLWS at Stornoway, UK. Large trends in range, HW and LW are not limited to the UK however, with large significant increases in tidal range datums at Cananea, Brazil, and significant decreases in tidal range datums at Fort Denison, Australia amongst others. Large changes occur at sites with small tidal ranges, such as Fremantle, as well as large tidal range, such as Fishguard.

Variation between the different tidal datums is evident at all selected sites (Figure 2), with significant differences observed at 5 sites: Fremantle in Australia, Atlantic City in the USA, Cananea in Brazil, Kungsholmsfort in Sweden and North Shields in the UK. Strong consistency between trends in different tidal datums is observed at Balboa in Panama, Brest in France, Fishguard & Newlyn in the UK, Fort Denison in Australia, Pago Pago in American Samoa, Simon's Town in South Africa, Tumaco in Colombia, and Wellington in New Zealand.

The spatial analysis focuses on the tidal datum GDTR, and its

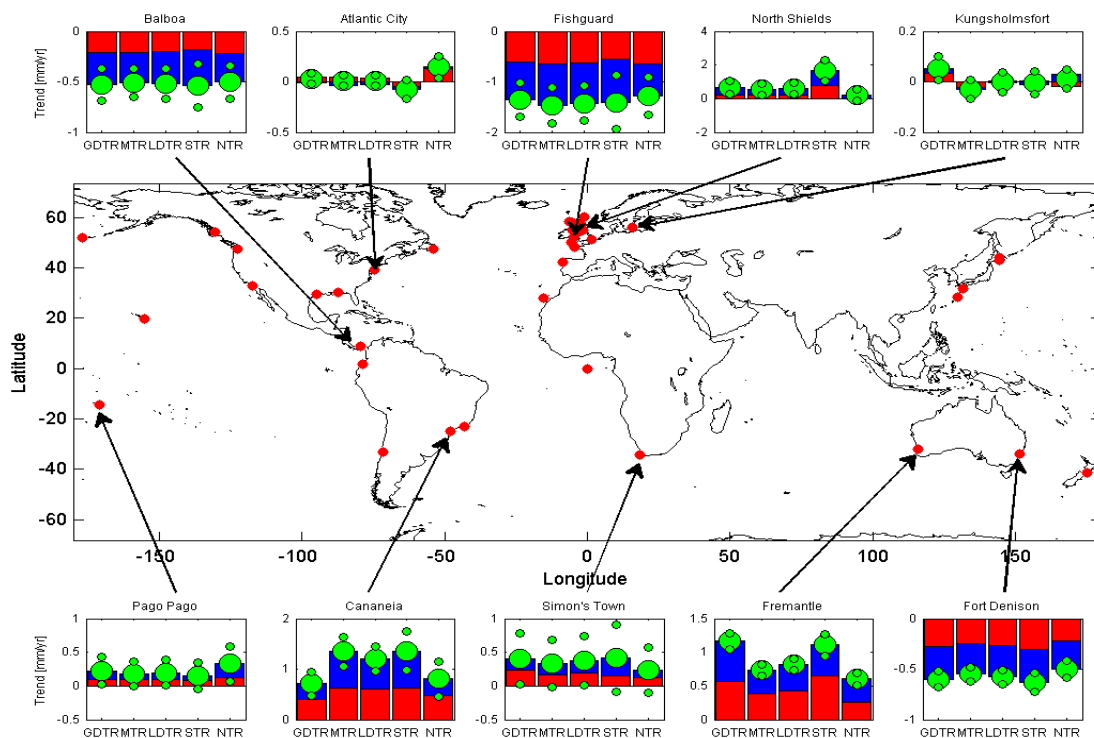


Figure 2. Map showing position of selected sites (red dots). Plots surrounding the map show the linear trends in tidal datums at 10 sites referenced in the text. The trend in tidal range datum (large green dots) is plotted with 95% confidence limits (small green dots) for five tidal range datums (see Table 1). Stacked bar charts show the contribution towards the tidal range datum trend of changes in the respective HW subsets (blue) and LW subsets (red). For example, at Fishguard the contribution toward STR from HW is negative (i.e. trend in MHWS is negative) while the contribution from LW is negative (i.e. positive trend in MLWS).

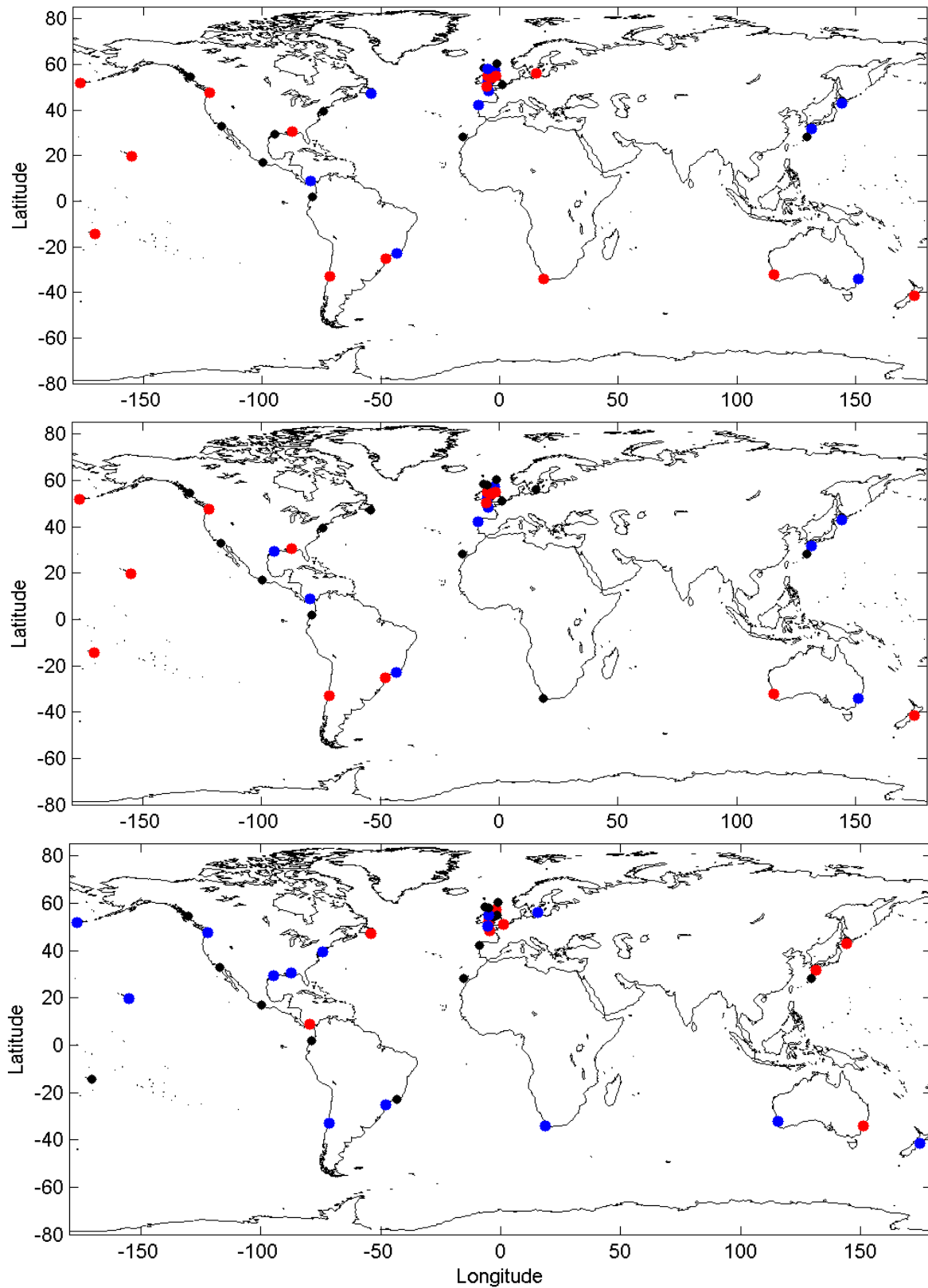


Figure 3: Global map showing where trends in GDTR (top), MHHW (middle) and MLLW (bottom) are: significant positive (red), significant negative (blue) or not significant (black) trends are shown for each location.

corresponding HW and LW tidal datums, MHHW and MLLW (defined in Table 1). GDTR provides spatial and temporal continuity in its sampling of HW and LW between semi-diurnal or diurnal tidal regimes. However, the trends in GDTR vary from other datums and therefore values presented in Figure 3 and 4 should not be applied to other tidal datums.. Global patterns are not clear in the data, with roughly equal numbers of positive, negative and non-significant trends (Table 2; Figure 3). Regional patterns are also unclear. Some regions display some consistency, such as negative trends in GDTR around the US, or negative trends in MLLW around Japan (Figure 3), but data density is not sufficient to resolve this accurately.

Globally, trends in GDTR and MHHW are almost identical, because of the direct relationship of a change in MHHW on GDTR, while most sites also had a corresponding trend with the opposite sign in MLLW.

Trends in GDTR, MHHW and MLLW around the UK show considerable spatial variability (Figure 4), but with no regional spatial pattern. GDTR trends around the UK are significantly positive at 4 sites, significantly negative at three sites non-significant at 2. While the significance of trends in GDTR and MHHW follow the global pattern and are virtually identical, the corresponding trends in MLLW around the UK were not all reversed as with most sites around the world (Figure 4). These deviations at Dover, Heysham and North Shields imply a more complex solution than just an increased in the amplitude of the tide.

## DISCUSSION

Large changes in tide occur around the world, with variations in observed tidal datums seen at sites not previously reported, such as Cananea, Brazil and Simon's Town, South Africa. The magnitude of trends exceeded  $1 \text{ mmyr}^{-1}$  at a number of sites, which is of similar magnitude to the rate of MSL rise observed over the 20th century. This coupled with the fact that over half of the selected sites had significant trends in 9 out of 15 tidal datums including GDTR, MTR and STR, shows that studying changes in the observed tide is vitally important for ESL calculations. However, no spatially coherent pattern was observed globally (Figure 3) or even regionally around the UK (Figure 4). Previous

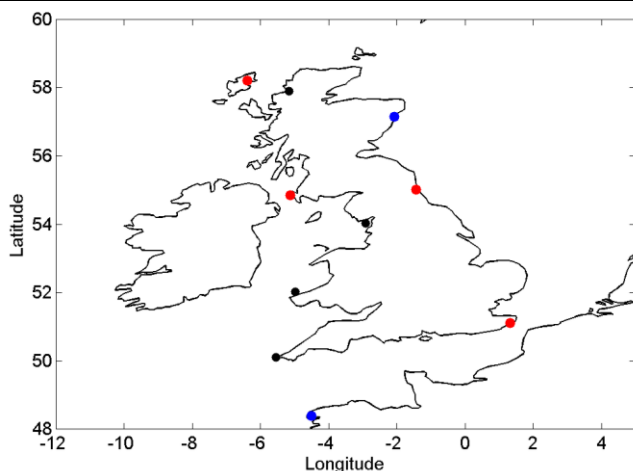


Figure 4. UK map showing where trends in GDTR are significant positive, significant negative or not significant. Significant positive (red), significant negative (blue) and not significant (black) trends are shown for each location.

Table 2: Number of selected sites with either significant positive, non-significant or significant negative trends for each datum.

Datum	Positive	Non sig.	Negative
GDTR	15	12	11
MHHW	13	15	10
MLLW	9	15	14
MTR	13	14	11
MHW	12	15	11
MLW	10	18	10
LDTR	8	21	9
MLHW	11	15	12
MHLW	11	18	9
STR	10	18	10
MHWS	11	21	6
MLWS	9	20	9
NTR	8	21	9
MHWN	3	29	6
MLWN	7	23	8

studies that used individual tidal constituents observed regional patterns around the eastern North Sea (Woodworth, 2010), the Atlantic coast of North America (Ray, 2009) and the Pacific coast of North and South America north of  $18^{\circ}\text{N}$  (Jay, 2009). While these previous studies show that there are mechanisms acting on regional scales this research indicates that the observed tide, composed of many tidal constituents, has additional influences effecting it. It is not possible to determine the active mechanisms in this preliminary set of selected sites, but the global coverage and increased data density provided by the 250-300 sites that will be included in the final study will allow better examination of the mechanisms.

These mechanisms may be indirect effects of changing MSL such as: the changing resonance of ocean basins, suggested previously Ray, 2006), which would cause a change in specific near resonant constituents; or a shift in amphidromic points due to a change in the propagation of the tidal wave, which would vary observed tidal range parameters. Alternatively, morphological change may be the cause creating very localised impacts (Araújo et al., 2008). Comparing different sites and different representations of the tide (i.e. constituents, tidal datums), combined with the construction of simple numerical models of the response of a basin to MSL change may help to determine the mechanism(s) causing the observed changes.

Their many practical applications mean that all tidal datums are of interest and not just GDTR and MTR, along with their respective HW datums previously used. This study shows that at a small number of sites significant differences exist between different tidal datums, and that the magnitude of significant trends in tidal range, HW or LW depend on the choice of tidal datum. The differences occur due to the different subsets of HW and LW used in their calculations, which has important consequences in the calculation of ESL. There is a greater probability of ESL during spring tides because the increased tide component reduces the magnitude of storm surge needed to exceed a given threshold. Increases in MHWS therefore lead to an increase in likelihood of exceedence at the times of high water. Conversely, large increases in MHWN, will generally have little impact on the magnitude

ESL, because HW levels are still likely to be below a given threshold. An increase in neap tide parameters in a region of small spring/neap variation may increase the frequency of exceedence. Further research is required to quantify the relative importance of changes in different tidal datums in this case, but it is clear that different tidal datums cannot be used interchangeably. MHWS and MHHW, and the corresponding parameters for low and neap tides, are sometimes documented as representing the same level (PCTMSL, 2013), but this research shows that this cannot be universally assumed. Many sources state that certain tidal datums should only be used to characterise the tide in a particular tidal regime (Parker, 2007; PCTMSL, 2013). This report has however shown that using these different subsets of HW or LW provide a different interpretation of how the tide is changing and therefore, all tidal datums should be included in the analysis at all sites.

While HW tidal datums are of most interest to this study, since high ESL have the most devastating impact on the coastal zone, the results demonstrate that understanding changes in the LW tidal datums important as well. The large changes observed at many sites will be of particular interest in legal matters, since many international, national and jurisdictional boundaries are determined by MLLW or LAT.

## CONCLUSION

Using observed tidal data this paper showed that significant changes in tidal datums occur at sites around the world including regions, such as Brazil and South Africa that have not been reported in previous studies. In 9 out of 15 tidal datums assessed, over 50% of the selected sites had significant trends, and the magnitude of some trends was similar to global trends observed in MSL, up to  $1.7 \text{ mmyr}^{-1}$ . Global or regional scale patterns are not evident, in contrast to previous studies that have analysed individual tidal constituents. The mechanisms driving changes appears therefore not to be a global response to MSL increase, but more likely a dominant local affect in response to increases in MSL or changes in local morphology.

It has been shown that the selection of tidal datum is important. This study shows for the first time that at a small number of sites significant differences exist between different tidal datums, and that at many more the magnitude of significant trends in range, HW or LW depend on the choice of tidal datum. All the tidal datums present values for average tidal range, HW or LW, but the considerable variations between them is due to the different subsets of HW and LW for each use in their calculations. These differences show the tidal datums should not be used interchangeably and that given the number tidal datums that are used for practical applications, one tidal datum cannot be assumed relative to another without site-specific study.

Understanding changes in this component is clearly important in investigating ESL. This is only a preliminary analysis and further assessment is underway on a more extensive dataset. This is crucial to determination of spatial patterns of long-term change in tidal datums because only with a global coverage coupled with data dense regions will it be possible to determine the mechanisms changing the tide.

## ACKNOWLEDGEMENT

This study was funded by the University of Southampton, School of Ocean and Earth Science and the National Environmental Research Council (NERC).

## LITERATURE CITED

- Abeyirigunawardena, D.S. and Walker, I.J., 2008. Sea level responses to climatic variability and change in northern British Columbia. *Atmosphere & Ocean*, 46(3): 277-296.
- Araújo, I., Dias, J. and Pugh, D., 2008. Model simulations of tidal changes in a coastal lagoon, the Ria de Aveiro (Portugal). *Continental Shelf Research*, 28(8): 1010-1025.
- Cayan, D.R. et al., 2008. Climate change projections of sea level extremes along the California coast. *Climatic Change*, 87: S57-S73.
- Flather, R.A., Baker, T.F., Woodworth, P.L., Vassie, I.M. and Blackman, D.L., 2001. Integrated effects of climate change on coastal extreme sea levels. Proudman Oceanographic Laboratory Internal Document No.140: 20pp.
- Flick, R.E., Murray, J.F. and Ewing, L.C., 2003. Trends in United States tidal datum statistics and tide range. *Journal of Waterway, Port, Coastal, and Ocean Engineering*, 129(4): 155-164.
- Führböter, A., Dette, H. and Töppe, A., 1990. Recent changes in sea level rise. *Proceedings of the Skagen Symposium*, p.^pp. 2-5.
- Gill, S.K. and Schultz, J.R., 2001. Tidal datums and their applications. National Oceanic and Atmospheric Administration.
- Jay, D.A., 2009. Evolution of tidal amplitudes in the eastern Pacific ocean. *Geophysical Research Letters*, 36(4): L04603.
- Kang, S.K. et al., 2002. Two-layer tidal modeling of the yellow and east china seas with application to seasonal variability of the M2 tide. *Journal of Geophysical Research*, 107(C3): 3020.
- Lionello, P., Mufato, R. and Tomasin, A., 2005. Sensitivity of free and forced oscillations of the Adriatic Sea to sea level rise. *Climate Research*, 29(1): 23-39.
- Menendez, M. and Woodworth, P.L., 2010. Changes in extreme high water levels based on a quasi-global tide-gauge data set. *Journal of Geophysical Research-Oceans*, 115.
- Mudersbach, C., Wahl, T., Haigh, I.D. and Jensen, J., 2013. Trends in high sea levels of german north sea gauges compared to regional mean sea level changes. *Cont Shelf Res*, 65: 111-120.
- Muller, M., 2012. The influence of changing stratification conditions on barotropic tidal transport and its implications for seasonal and secular changes of tides. *Continental Shelf Research*, 47: 107-118.
- Muller, M., Arbic, B.K. and Mitrovica, J.X., 2011. Secular trends in ocean tides: Observations and model results. *Journal of Geophysical Research - Oceans*, 116.
- Parker, B.B., 2007. Tidal analysis and prediction. US Department of Commerce, National Oceanic and Atmospheric Administration, National Ocean Service, Center for Operational Oceanographic Products and Services.
- Pawlowicz, R., Beardsley, B. and Lentz, S., 2002. Classical tidal harmonic analysis including error estimates in MATLAB using `t_tide`. *Computers & Geosciences*, 28(8): 929-937.
- PCTMSL, 2013. Australian tides manual: Special publication no. 9.
- Pickering, M.D., Wells, N.C., Horsburgh, K.J. and Green, J.A.M., 2012. The impact of future sea-level rise on the European shelf tides. *Continental Shelf Research*, 35: 1-15.
- Raicich, F., 2003. Recent evolution of sea-level extremes at Trieste (Northern Adriatic). *Continental Shelf Research*, 23(3-4): 225-235.
- Ray, R.D., 2006. Secular changes of the M2 tide in the Gulf of Maine. *Continental Shelf Research*, 26(3): 422-427.
- Ray, R.D., 2009. Secular changes in the solar semidiurnal tide of the western North Atlantic ocean. *Geophysical Research Letters*, 36(19).
- St-Laurent, P., Saucier, F.J. and Dumais, J.F., 2008. On the modification of tides in a seasonally ice-covered sea. *Journal of Geophysical Research -Oceans*, 113(C11).
- Ullmann, A., Pirazzoli, P.A. and Tomasin, A., 2007. Sea surges in Camargue: Trends over the 20th century. *Continental Shelf Research*, 27(7): 922-934.
- Woodworth, P.L., 2010. A survey of recent changes in the main components of the ocean tide. *Continental Shelf Research*, 30(15): 1680-1691.
- Woodworth, P., Shaw, S. and Blackman, D., 1991. Secular trends in mean tidal range around the British Isles and along the adjacent European coastline. *Geophysical Journal International*, 104(3): 593-609.

# Cliff-top storm deposits (55-63m amsl) from Morgan Bay, South Africa

Smith, A.M.,<sup>†</sup> Green, A.N.,<sup>†</sup> Cooper, J.A.G.,<sup>\*\*</sup> Dixon, S.,<sup>†</sup> Pretorius, L.,<sup>†</sup> Wiles, E.,<sup>†</sup> Guastella, L.A.<sup>‡</sup>

<sup>†</sup> Geological Sciences, School of Agricultural, Earth and Environmental Sciences, University of KwaZulu-Natal, South Africa  
[asconsulting@telkomsa.net](mailto:asconsulting@telkomsa.net)

<sup>\*\*</sup> School of Environmental Science, University of Ulster, Coleraine BT52 1SA, UK

<sup>‡</sup> Department of Oceanography, University of Cape Town, Private Bag X3, Rondebosch, Cape Town, 7701, South Africa.



[www.cerf-jcr.org](http://www.cerf-jcr.org)



[www.JCRonline.org](http://www.JCRonline.org)

## ABSTRACT

Smith, A.M., Green, A.N., Cooper, J.A.G. *et al.*, 2014. Cliff-top storm deposits (55-63m amsl) from Morgan Bay, South Africa. In: Green, A.N. and Cooper, J.A.G. (eds.), *Proceedings 13<sup>th</sup> International Coastal Symposium* (Durban, South Africa), *Journal of Coastal Research*, Special Issue No. 70, pp. 349-353, ISSN 0749-0208.

Cliff-top storm deposits (CTSDs) occur south of Morgan Bay, South Africa at elevations varying from ±55- to 63m. These occur as a ±10m-wide horizontal fringe of shell breccia mixed into a very thin (>15cm) sandy soil on the cliff top platform. Visually it is evident that the shell breccia is of various ages. Comparisons with proven wave breccia from this area indicate the same source. We suggest that this breccia was deposited as fall-out from wave and wind-borne plumes produced by wave bores striking the cliff base. These bores would likely have been produced by waves at least ~40m in height. Alternative interpretations, such as a perched marine deposit or tsunamite are rejected in favour of CTSDs produced by multiple large wave events.

**ADDITIONAL INDEX WORDS:** *Shell breccia, storm deposits, storm waves, tsunami.*

## INTRODUCTION

Cliff-top storm deposits (CTSDs) range from shelly material to boulders located on marine cliff-tops. CTSDs at heights of up to 50m have been described from Shetland, Orkney, Caithness and the Outer Hebrides in Scotland and from the Aran Islands in Galway Bay, Ireland (Hall *et al.*, 2006). In this paper we describe CTSDs from marine cliff-tops up to 60m high from the Eastern Cape coastline, South Africa.

## ENVIRONMENTAL SETTING

Morgan Bay, on the Eastern Cape Coast of South Africa, faces the Indian Ocean (Fig. 1). The location climate is warm temperate (Cooper *et al.*, 2013) and the sea temperatures vary from 22°C in summer to 14°C in winter. Average daily air temperatures vary from 14°C to 23°C. The driest months are June, July and August and are followed by the spring rains. Coastal winds are bimodal: southwesterly and northeasterly in roughly equal proportions (Cooper *et al.*, 2013). Marine storms are common in September, although less common, tropical cyclone swells are also experienced (South African Weather Service).

The regional geology comprises gently dipping Beaufort sandstones that have been intruded by thick dolerite sills (Fig. 3A). A well-developed shore platform coated by boulders is present on the adjacent coast, but not at the foot of the sea cliffs where the CTSDs are found. Morgan Bay is a small tourist village within a headland-bound bay. It is fronted by a narrow rocky beach, which grades from a boulder beach in the south to a sandy beach in the north. The southern headland is flanked to the south by plunging cliffs up to 65 m high, whereas the northern headland is subdued and capped by a high coastal dune (Smith *et al.*, 2011). CTSDs (Hall *et al.*, 2006) were found on the tops of exposed bluffs which collectively form the southern headland. These headlands are aligned south-south easterly and project into the Indian Ocean. They have elevations varying from ~16 to ~63m amsl (Fig. 2). In some instances a well-defined step is present on

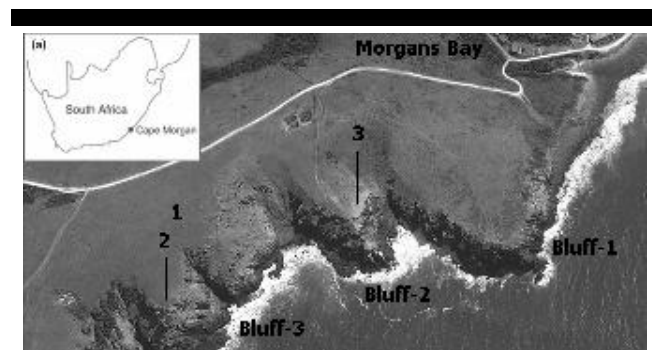


Figure 1A: Location of field area (32°42'14"S 28°20'10"E; 34 °S); B: The sample sites.

these cliffs where the dolerite-sandstone contact coincides with sea level (Fig. 2B). The immediate cliff top area is relatively flat but slopes gradually landward. The cliffs are relatively undisturbed by human activity and contemporary cliff-top land use is restricted to cattle grazing and hunter gathering.

## OCEANIC ENVIRONMENT

### Bathymetry

The shelf is very narrow (±10km wide) and consequently swell attenuation due to bottom friction is minimal. The coast is microtidal, with a mean high tide of 1.25 m and a high astronomical tide (HAT) of 2.08 m (<http://www.satides.co.za/>).

### Meteorology

Swells and seas are generally produced by cold fronts and cut-off-low pressure systems, although tropical storms and cyclones can also contribute. The wave record extends from 1992 (for the port of East London 40km south) to the present (van der Borch and van Werolde, 2004; CSIR wave rider buoy). The prevailing

swell systems move in association with the west-to-east synoptic weather patterns and produce a net south-to-north littoral drift although this can reverse through topographic forcing and during easterly swells.

### Wave climate

Wave heights of 8 m and periods of 11–17 s are common during winter storms (Smith *et al.*, 2011). The average significant wave height is 4.45 m, with a period of 14 s. The mean peak period is 13.7 secs (vdbvW, 2004). The longest period measured was 18.3s, associated with a comparatively low 5.24  $H_{mo}$  swell in 1993 (the swell propagation direction is not available)(Rousouw and Rousouw, 1999). Most swells approach from 170 to 190° with a measured range varying from 62 to 224° (vdBvW, 2004). Extreme events (>4m  $H_{mo}$ ) occur between March and September, (van der Borch and van Werolde, 2004).

Between 31<sup>st</sup> August and the 1<sup>st</sup> September 2008, 9 to 10.7 m waves were generated by an extremely deep cold front that passed south-west of the country during equinox tides (Table 1) (Guastella and Rossouw (2013). This high swell caused considerable coastal flooding at Morgan Bay and elsewhere in the Eastern Cape. A high swell which struck on the March (2007) equinox had higher swells (Table 1) but passed without much notice, whereas the 2008 September equinox event had an unusually high (7-8m) runup and caused significant flooding and damage to coastal infrastructure. This was probably due to the fact that the 2008 September equinox swell came from an unusually easterly direction (Table 1). It is also possible that the nearshore and inner shelf had not fully recovered from the high swells of 2007, as was the case during the austral winter (2007) erosion in KwaZulu-Natal to the north (Smith *et al.*, 2010). It appears that 10 m ( $H_{max}$ ) swells are not uncommon on a decadal scale (Table 1). However, storm damage was extreme during the 09/2008 event which had a comparatively low swell height. The 1997 event appears anomalous, however it is likely that its propagation direction (Table 1) was too far west and that most of the energy would have been lost to friction as the swells wrapped in across the shelf.

## METHODS

The cliffs below the CTSDs show several important morphological characteristics. There is a small 1 m-wide step at



Figure 2: An oblique view (from the south) of the lower sampled site (#3) showing stack (A) development two thirds of the way up the cliff. B) A closer oblique view of the Morgan Bay cliff showing the stepped edge (arrowed) due to rock removal.



Figure 3: Shell debris in situ on cliff-top platform at an elevation of 60 m.

the upper sill-sandstone junction (Fig. 2A). In addition there are rock projections reminiscent of marine stacks at this boundary. Table 1. The largest swells on record for East London, 40km south of Morgan Bay.

Date	$H_s$ (m)	$H_{max}$ (m)	T (s)	Bearing	Source
06/1997	9.3	13.79	15.5	?SW	CSIR
02/2007	4.59	7.98	12.5	173	CSIR
03/2007	6.25	10.13	13.3	155	CSIR
05/2007	4.97	10.3	10.3	148	CSIR
09/2008	4.73	8.76	11.1	145	CSIR

The cliff-top edge can also show a distinct step (Fig.2B). No marine platform is present below the highest cliffs. Both Bluffs 2 and 3 (Fig. 1) are capped by a flat cliff-top platform, whereas Bluff 1 slopes steeply northeast. The cliff-top platform is a grassland, with occasional stunted bushes, although the inter-Bluff areas can be more densely vegetated. Rock outcrop is present. The soil is sandy and very thin, varying from zero to about 15cm. Field mapping was employed to describe the extent of the CTSDs on the cliff-top platform. Four sites were investigated of which three were sampled.

## RESULTS

The cliff top sampled deposit locations were recorded and samples were taken for microscopy (both optical and SEM) analysis (Table 2). These samples were compared with unequivocal wave deposits from the storm swash terrace (e.g. McKenna *et al.*, 2012) at the cliff base. The results of this are described below.

### Shell Breccia

Scattered marine shell breccia debris was noted within the thin soil horizon (zero to 20 cm thick) on the flat surface above the cliff edge, at elevations of up to ~63 msl (Fig.2). No bedding is preserved, most likely having been destroyed by terrestrial bioturbation. The sample characteristics are described in Table 2.

### 3<sup>rd</sup> Bluff-South

Samples were taken from the highest ( $\pm 63$ m) locality investigated. Two samples were collected (Fig.4) (Table 2). At this locality the shell breccia occurs within the soil, commonly exposed in mole hills and as a lag deposit concentrated in the base of sandstone tarn pools. Material has been washed in from the

surrounding soil to concentrate in the tarn pools. Shell breccia deposition is patchy, but only found within 10m of the cliff edge. Occasional rounded shale and quartzite pebbles (0.5 to 1 cm diameter) are present in the CTSDs. Careful inspection of this locality showed that the shell fragments become more numerous and larger towards the cliff edge (Table 2). The CTSDs form a 10m-wide shell breccia fringe adjacent to the cliff edge, the clasts of which fine rapidly inland. No shell breccia was seen more than 10m inland from the cliff edge.

## 2<sup>nd</sup> Bluff-South

On the cliff-top platform ( $\pm 49$ m), shell fragments are exposed in mole hills within 10m of the cliff edge (Table 2). The cliff top soil is composed of very fine sand. A single sample (3) was taken.

## 1<sup>st</sup> Bluff-South and Inter- Bluff areas

This site is steeply inclined ( $\pm 16$ m highest point) and no shell breccia was found here, or in the intervening area, consequently it was not sampled (Fig.1).

## General observations

Comparison with unequivocal wave deposits show a strong similarity with wave shell breccia. They too comprise granules, very coarse sand and shell hash of variegated composition (Fig. 4A and B). The CTSDs are only found on cliff-top platforms where they form a 10m-wide detrital shell breccia fringe adjacent to the cliff edge, the clasts of which fine rapidly inland showing that the shell breccia is related to the marine environment. shell breccia was only found on horizontal surfaces. The absence of CTSDs on Bluff 1 may be related to the geomorphology, as there is no cliff-top platform. Instead it slopes steeply to the northeast and would make it less likely that material would settle, but rather flow back down the back slope.

## Binocular microscope and SEM analysis

No detailed statistics was attempted as the sample is small. A detailed textural examination revealed a combination of older and younger shell clasts (Fig. 5A and B). SEM analysis of surface weathering features on the shell fragments showed variable degrees of weathering, implying that the breccia clasts are of variable age. The breccia in sample 3 was less weathered and younger than that of sample 1 (Table 2). The shell fragments from sample 2 were more etched than those of sample 3, suggesting them to be older. Further, sample 2 fragments showed evidence of a patchy biological layer, such as might be expected to cover a younger shell fragment (Fig. 5A and B).

## DISCUSSION

There is no evidence that the Morgan Bay cliffs have been overtopped by "green water" but the presence of shell breccia in the soil indicates relatively recent introduction of marine debris to the cliff top. The cliff edge often shows a prominent step, associated with stacks at the top of the dolerite. The cliff top is also associated with a prominent step, reminiscent of marine quarrying, however, no loose boulders were noted landward of the cliff edge. In contrast the cliff step is littered with fallen boulders. The cliff-top socket may be the result of extreme wave quarrying but the lack of a boulder fringe argues against this. Optical and SEM inspection of the CTSD breccia shows various degrees of weathering and indicates that the breccia is of variable ages, but absolute dating is beyond the scope of this study, however the more weathered fragments were found at higher levels.

Table 2. Summary of sample properties and locations.

Sample	Dimensions	From cliff edge	Elevation (amsl)	Location
1	1<5 mm most 1-2 mm	5 m	$\pm 63$ m	Bluff 3
2	<20mm most 4-5 mm	10 m	$\pm 62$ m	Bluff 3
3	<30m most 5-10 mm	5 m	$\pm 49$ m	Bluff 2
No sample taken	Not present	Not present	$\pm 16$ m	Bluff 1
Cliff Base	variable	n/a	8 m	Storm surge terrace

This coastline faces the Indian Ocean and is very exposed to high swell and storm waves. The cliff-top shell breccia is clearly ocean-derived as proved by their similarity to unequivocal wave deposits and the proximity to the cliff edge. Waves are known to spray sand (Cooper *et al.*, 1999) and further CTSDs have been described from cliff tops in Scotland and Ireland (Hanson and Hall, 2006). In Shetland, at the Villians of Hamnavoe and Eshaness Lighthouse, CTSDs are present at an elevation of 50 m (Hall *et al.*, 2006). They interpreted this as air throw debris produced by very large waves striking the cliff and the ensuing debris being transported onshore by strong winds. within the spray. In the Morgan Bay case wave scour is recognized at an elevation of 40 m, well below the CTSDs. In the Morgan Bay case, the position of the CTSDs on Bluff 2 and Bluff 3 would suggest that the source is a giant southeasterly swell and associated onshore wind (Fig. 2). Hanson *et al.* (2008) state that 10m high waves can form vertical jets capable of transporting large blocks. In the Morgan Bay case no unequivocal large blocks were observed on the cliff tops but the runoff from such might be capable of eroding the cliff edge. In Morgan Bay the cliffs have clearly been eroded at the dolerite sandstone contact and this must be due to wave action. This is at a level of  $\sim 40$ m. If the wave spray height in figure 6 is used, then simply scaling up the 2008 September Equinoctial event statistics indicates that air throw deposits could easily have been flung 60m upward. For the observed CTSDs to exist on the Morgan Bay cliffs, we theorise that waves in the 40m ( $H_{max}$ ) category must have occurred from time to time. We propose that these CTSDs are the result of spray thrown up by bores from very large broken waves striking the cliff (Fig. 6).

The relationship between  $H_s$  and  $H_{max}$  is probably dependent on wave period and swell order (Table1). Long-range swells are better ordered than storm seas. For this research the proxy used in

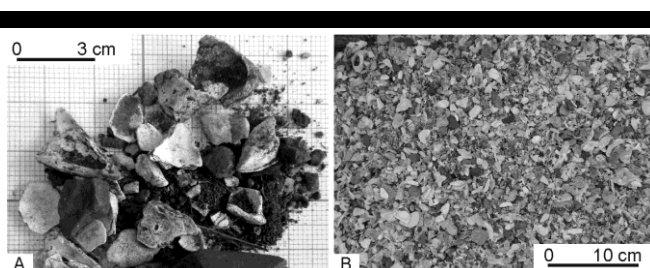


Figure 4. Comparison between (A) CTSD shell hash and pebble deposit of sample 1 and (B) storm wave-deposited sheet of variegated shell hash and pebble material. Note the similarity.



this study is wave height, as period and direction are unknown for ancient swells and we can only surmise direction (a probable southeasterly or coast-normal wave propagation direction).

On a global scale, satellite altimetry has indicated that 100 foot waves (33 m) occur several times per year, one such wave was recently surfed at Nazare, Portugal.

The Agulhas Current flows southwestward, off Morgan Bay, and is famous for 'rogue waves', with a 30 m example having been recorded in 1977 (Faulkner, 2006). Rogue waves are defined

variously as  $H_{max}/H_s > 2$  (Wolfram *et al.*, 2000) or  $2 \times H_s$  (O'Brien *et al.* 2013) or  $> 2.4 \times H_s$  (Faulkner, 2006). Using the maximum  $H_{mo}$  (9 m), waves  $> 20$  m are quite possible at Morgan Bay. The largest wave surfed in SA (2008) was in Cape Town (1000km south) and estimated to be 22 m. The open ocean tug Wolraad Woltemade sailed over a 21 m swell in 2001 off Cape Town (Candy, pers. com.). On breaking, this swell could conceivably have had a +30 m face. Clearly 20 m waves are not uncommon on the South African coast. The age of the proposed Morgan Bay CTSDs is not known, consequently we have no idea what the prevailing climatic regime was, but the preservation does point to a Holocene age of deposition.

### Alternate Formative mechanisms

Probable wave deposits at a high elevation automatically attract a tsunamiite hypothesis for their genesis. No tsunamiite deposits are on record for the South African coastline and although such an origin cannot be ruled out, it seems unlikely as the CTSDs are clearly the product of multiple events.

An alternative hypothesis is that the shelly debris were deposited at a raised shoreline during a period of higher sea level. A Tertiary age boulder horizon ('Boulder Bed'), dated at 4 Ma (Erlanger *et al.*, 2012) is well known at about 70m amsl from the South African coast (Davies, 1970; Erlinger, 2012). The "Boulder Bed" is located 10m above and several hundred metres landward of the highest proposed CSTDs (site 1). No shell material has ever been found to be associated with the 'Boulder Bed'. The "Boulder Bed" is a very distinctive unit (0.5-1 m thick) comprising very-well rounded cobbles and small boulders. These boulders can be recognized within colluvium below the outcrop. No such clasts have been found to be associated with the CTSDs. Finally the shell debris is from existing marine species that occur around the base of the cliffs, thus precluding an ancient raised shoreline origin.

### CONCLUSIONS

CTSDs are found at levels of up to  $\pm 63$  m amsl at Morgan Bay. This deposit comprises a shelly breccia fringe adjacent to the marine cliff top. Comparisons with wave breccia from the lower supratidal (6m amsl) show them to be similar but older based on micro-textural characteristics of the shell debris. The CTSD fragments are variable in age. We suggest that this breccia was emplaced as air throw from wave and wind-borne plumes produced by the bores of broken waves struck the base of the cliffs. These bores would likely have been produced by waves ~40 m in height. Both a tsunamiite and perched beach origin were considered as alternative means of emplacement, however these origins seem unlikely.

### LITERATURE CITED

- Candy, R., pers. com. CSIR wave rider buoy. <http://wavenet.csir.co.za/OnlineData/EastLondon/eastlondonwaveD.htm>
- Cooper, J.A.G. and Jackson, D.W.T., 1999. Wave spray-induced sand transport and deposition during a coastal storm, Magilligan Point, Northern Ireland. *Marine Geology*, 161, 377-383.
- Cooper, JAG, Smith, A.M. and Green, A.N., 2013. Backbeach deflation aprons: morphology and sedimentology. *Journal of Sedimentary Research*, 83, 395-405.
- Davies, O (1970). Pleistocene beaches of Natal. *Annals of the Natal Museum*, 20, 403-442.
- Erlanger, E.D., Granger, D.E., Gibbon, R.J., 2012. Rock uplift rates in South Africa from isochron burial dating of fluvial and marine terraces. *Geology*, 40, 1019-1022.
- Draper, L., 1964. "Freak" Ocean Waves, *Oceanus*, X:4. Reprinted in *Rogue Waves 2004: Proceedings of a Workshop*.
- Faulkner, D., 2000. *Rogue Waves – Defining Their Characteristics for*

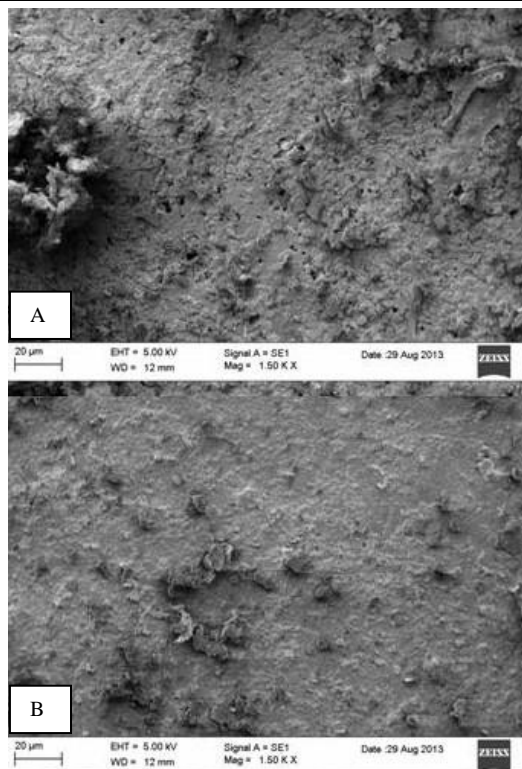


Figure 5. Photomicrographs of shell surface textures. A and B are fragments from sample 1, showing older weathered and younger less weathered material, respectively.



Figure 6. September (2008). Spray from a wave bore ( $H_s=4.73$ ;  $H_{max} \sim 8$  m), reaching a height of ~12m against a  $\pm 16$  m cliff at Morgan Bay. Photo R. Smith.

- Marine Design. Rogue Waves 2000: Proceedings of a Workshop.
- Guastella, L.A., Rossouw, M., 2012. What will be the impact of increasing frequency and intensity of coastal storms along the South African coast? *Reef Journal*, 2, 129-139.
- Hall, A.M., Hansom, J.D., Williams, D.M., Jarvis, J., 2006. Distribution, geomorphology and lithofacies of cliff-top storm deposits: examples from the high-energy coasts of Scotland and Ireland. *Marine Geology*, 232, 131-155.
- Hansom, J.D., Barltrop, N.D.P. and Hall, A.M., 2008. Modelling the processes of cliff-top erosion and deposition under extreme storm waves. *Marine Geology*, 253, 36-50.
- O'Brien, L., Dudley, J.M., and Dias, F., 2012. Extreme wave events in Ireland: 14 680 BP. *Natural Hazards and Earth Systems Science*, 13, 625-648, 2013.
- McKenna, J., Cooper, J.A.G., Jackson, W.T., 2012. Storm Swash Terraces: A Previously Overlooked Element of the Cliff-Shore Platform System. *Journal of Sedimentary Research*, 82, 260-269.
- Rossouw, J., Rossouw, M., 1999. Re-evaluation of recommended design wave methods. Proceedings of the 5th International Conference on Coastal and Port Engineering in Developing Countries (COPEDEC), Cape Town, South Africa, April 1999.

# Nearshore bathymetry from video and the application to rip current predictions for the Dutch Coast

Leo Sembiring<sup>†</sup>, Ap van Dongeren<sup>‡</sup>, Gundula Winter<sup>∞</sup>, Maarten van Ormondt<sup>‡</sup>, Christophe Briere<sup>‡</sup>, Dan Roelvink<sup>†‡</sup>,

<sup>†</sup> Department of Water Engineering  
UNESCO-IHE  
Delft, The Netherlands  
[l.sembiring@unesco-ihe.org](mailto:l.sembiring@unesco-ihe.org)

<sup>‡</sup> Marine and Coastal System  
Deltares, Delft The Netherlands

<sup>∞</sup> Civil Engineering and Geosciences  
Delft University of Technology  
Now at The University of Western  
Australia



[www.cerf-jcr.org](http://www.cerf-jcr.org)



[www.JCRonline.org](http://www.JCRonline.org)

## ABSTRACT

Sembiring, L., Van Dongeren, A., Winter, G., Van Ormondt, M., Briere, C., Roelvink, D., 2014. Nearshore bathymetry from video and the application on rip current predictions for The Dutch Coast. In: Green, A.N. and Cooper, J.A.G. (eds.), *Proceedings 13<sup>th</sup> International Coastal Symposium* (Durban, South Africa), *Journal of Coastal Research*, Special Issue No. 70, pp. 354-359, ISSN 0749-0208.

This paper demonstrates the potential use of nearshore bathymetry estimated from video data in a coastal operational model for the Dutch Coast, which provides daily forecast of waves, water levels and (rip) currents. Two video techniques to obtain beach bathymetry from video data- Beach Wizard and CBathy are validated against jet ski surveyed bathymetry. Both methods show good agreement with surveyed data, and bathymetric features of the beach are adequately produced. To assess the applicability of video-derived bathymetry for the purpose of rip current predictions, a model is built for Egmond aan Zee in The Netherlands, in which rip current predictions based on video-derived bathymetry are compared with those based on the jetski survey. Results show that predicted maximum mean offshore-directed (rip) velocities are in good agreement when using surveyed bathymetry (reference model) and video-derived bathymetry. Finally, to address the rip current forecasting skill, this local model is forced by wave boundary conditions obtained from a larger-scale wave prediction model, in addition to the bathymetry from video. Results show that useful information can still be obtained regarding the rip currents' flow where maximum offshore-directed velocities obtained from the predictive model resemble adequately rip currents pattern in the reference model. This paper will discuss each component of the model system and the validation result on hindcasting and forecasting rip currents.

**ADDITIONAL INDEX WORDS:** *operational model, beach hazard, Argus video technique, nearshore modeling.*

## INTRODUCTION

Rip currents are some of the most dangerous hazards at beaches for swimmers. In Australia and United States, they are responsible for 100s of fatalities every year (Lushine, 1991; Short, 2007). Moreover, in the southwest of England coasts, 71 percent of beach accidents are due to rip currents (Scott et al., 2007). In the Netherlands, which is adjacent to a shelf sea, these numbers are not so high. However, lifeguards at Egmond aan Zee in The Netherlands (*personal communication*), reported that the number of rescues due to rip currents increases every year. In order to plan the deployment of lifeguards, they need a predictive tool to have an advanced warning of rip current timing, location and strength.

Several approaches have already been taken to provide a risk assessment of rip current events for public safety. Using empirical correlations of drowning statistics and meteorological conditions, a rip current risk has been implemented on the U.S. coast (Lushine, 1991; Lascody, 1998; Engle et al., 2002). A slightly different approach in providing alert to swimmers is by using an operational wave forecasting system and then transforms the condition towards the nearshore as was done on the Balearic Islands, Spain (Alvarez-Ellacuria, et al., 2009). The hazard level is determined based on nearshore wave conditions derived from a

database, and alerts are sent through short message system via mobile phone and published on the local authority's website. This approach makes use of a 2DH Navier-Stokes model for the nearshore to predict surfzone waves and currents, and they suggest an improvement by utilizing video technique to have an up-to-date bathymetry for the 2DH model (Alvarez-Ellacuria, et al., 2010). Similarly, Kim et al., 2011 introduced a prediction system for rip currents for Haeundae Beach in Korea, which integrates a nearshore circulation model with a morphological model to obtain the current state of the bathymetry. The prediction results show good agreement with measurements in terms of wave induced currents and set up. They propose further research on the morphological model to improve the overall prediction skill. Austin et al., (2012) presented a validation of an operational rip risk prediction model for the southwest England coast, where field data and beach incidents statistics are analyzed. They show the potential use of a nearshore hydrodynamic model to provide rip current forecasts and provide hazard ratings. They also address an integration of the hydrodynamical model with a data assimilation method in order to obtain nearshore sub tidal bathymetry to be used in the model system.

Efforts which try to locate rips based on remote sensed technology have also been in place, for instance through video (Ranasinghe et al., 1999; Bogle et al., 2000; Gallop et al., 2009),

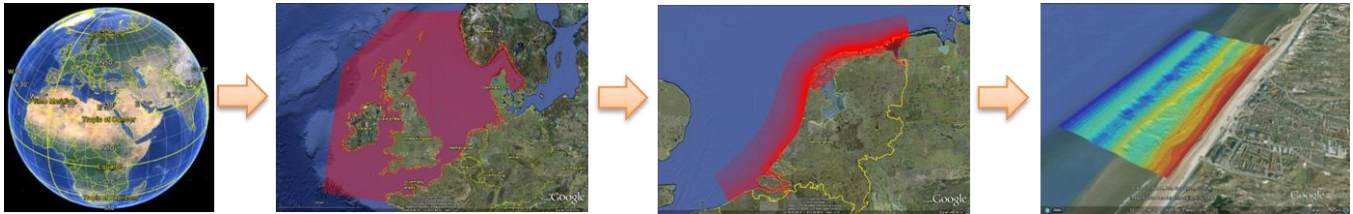


Figure 1. Model chain within COSMOS, showing model domains starting from entire globe, the Dutch Continental Shelf, the Dutch Coast, and finally Egmond aan Zee .

and high frequency radar (Kohut et al., 2008). Detection of rip locations using video techniques was reported to be successful. However, the detection of rips is not done in operational mode at the moment. Also, high frequency radar systems can now predict surface current patterns on a regional spatial scale at a resolution too coarse for application on the detailed bar-trough scale.

In this paper we present an approach to simulate and predict the occurrence of topographically-controlled rip currents by making use of process based models in combination with video-derived bathymetries. For the Dutch Coast, a model system named COSMOS has been built (Van Ormondt et al., 2012), where predictions of waves and water levels are provided on the surf zone scale model domain. To this end, having an accurate and up to date bathymetry is necessary for the COSMOS to provide accurate predictions in the nearshore zone because the rip currents are bathymetrically-controlled (Dalrymple, 1978; Van Dongeren et al., 2013). Here, the nearshore bathymetry will be obtained using video techniques. Each component of the system will be discussed in the following sections.

## METHODS

### COSMOS prediction system

The COSMOS system can accommodate and manage several models which are nested in each other. For the Dutch Coast, the operational model system consists of two main models and one (or more) local models in the surfzone area, which is the area of interest. Models are increasing in spatial resolution going from regional to beach scale domain. The Dutch Continental Shelf Model (DCSM, Gerritsen et al., 1995) is used as regional model which covers The North Sea and provides boundary conditions to the Dutch Coast Strip model nested within it. Finally a local surfzone model will obtain boundary conditions from the Dutch Coast model (Fig. 1).

The model system simulates waves, surge, and currents. The wave model SWAN is used (Booij et al., 1999) where meteorological forcing is obtained from HIRLAM (High resolution limited area model, Unden et al., 2002). In addition, swell boundary conditions are obtained from the Global Wave Watch 3 model (NOAA, Tolman, 2009) and imposed on the open boundaries of the DCSM wave model. For the flow model, Delft3D is used where tidal constituents are obtained from tide model TPX062 (Egbert and Erofeeva, 2002) and assigned on the open boundary which is divided into 23 segments. Moreover, HIRLAM wind is used for the flow model as meteorological forcing to simulate surge. The model structure within the system appears in Fig. 2.

The system is designed on the MATLAB platform, where the initiation of operational run is performed every 12 hours, and managed by a so called timer loop. There are two timer loops in the system that dictate the operational run. First, the main loop,

which will define the starting time and end time of a model run and trigger the overall initiation of the system. Within this timer loop, necessary wind and air pressure data to be used by the wave WW3 and SWAN model are also downloaded. The second time loop is the model loop, in which a model run will be executed in good sequence after starting and end time of simulation has been defined. Downloaded forcing data and simulation results from models are stored on the OpenDAP server (Van Ormondt et al., 2012).

### Bathymetry from video technique

We use Beach Wizard (Van Dongeren et al., 2008) and CBathy (Holman et al., 2013) to obtain nearshore bathymetric estimates. Beach Wizard is a technique where 10 minutes time exposure images from the Argus video (Holman and Stanley, 2000) are used and considers the pixel intensities as a proxy of wave roller dissipation. Based on the difference between simulated and observed intensities, the bathymetry is adjusted using a Kalman filter (after Kalman, 1960). The implementation of the algorithm is carried out within the XBeach model (Roelvink et al., 2009) where wave roller dissipation is computed by the model in stationary mode.

CBathy (Holman et al., 2013) is an algorithm which uses time stacks of Argus video images to obtain the bathymetry. The algorithm consists of three steps. First, the four most coherent frequencies  $f$  are determined from the video signal time series at each pixel point in the video image. Then, the first EOF is extracted from the cross spectral matrix and the associated eigenvalue is determined. The wave number  $k$  then is computed by a nonlinear fit of the first EOF from video towards a forward model. For every  $f$ - $k$  pair, a unique depth ( $h$ ) then is obtained. In the second step, one single best value of depth is obtained by performing a weighted best fit between the frequency-wave

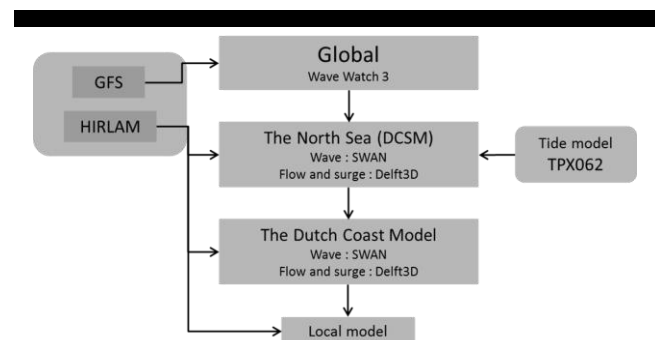


Figure 2. Model structure used in the COSMOS.

number (f-k pair) obtained from step 1 and the linear dispersion relationship. Finally, in the third step a running average of the depth estimate from step 2 is smoothed using the previous result (in time) by applying a Kalman filter. Applying the algorithm for semi- enclosed beaches like the Dutch Coast requires some adjustments of the parameters used as described in Holman *et al.*, 2013. Here, we apply some changes relative to the default settings such that the method will work in wind sea-dominated environments with shorter wave lengths.

### Nearshore model

A process-based numerical model XBeach (Roelvink *et al.*, 2009) is used to simulate nearshore hydrodynamics. The model solves the wave action balance and shallow water equations simultaneously, allowing us to take into account interaction between wave, wave-driven currents and tidal currents. Wave groups are imposed on the offshore boundary and are propagated through the domain in wave group mode. In addition, a tidal current is generated by imposing water level signal at two boundary points offshore with a certain spatial lag. The model is executed using different bathymetry sources (from survey and from video) to assess applicability. The model is validated using measurement of Lagrangian mean flow data, obtained using floating drifter deployment mounted by GPS device (Winter *et al.*, 2012). Fig. 3 presents drifter trajectory from the field survey (left) and the model result (right) as an example. The model results are in good agreement with the field data where the drifters move offshore due to the rip and later on drifted parallel to the shore line due to alongshore currents. This model scenario will be referred as reference model for the rest of this paper.

## RESULTS AND DISCUSSION

### Nearshore bathymetry estimation

A validation is performed for the Beach Wizard model using a data set of jetski surveys obtained during field work conducted in August 2011 (Winter *et al.*, 2012). Using an alongshore uniform topography as the initial bathymetry input, Beach Wizard evolves the bathymetry towards the ground truth. Fig. 4 shows the bathymetry using Beach Wizard (a) and bathymetry from the jetski survey (b). In general, the bathymetry features are produced very well by Beach Wizard. The outer sand bar, which is located around  $x = 400$  m is reproduced well. In addition, features near the shoreline, where the inner sand bar typically disrupted by channels is also very well predicted. Two channels and three berm features appear clearly in the bathymetry estimate as they appear in the jet ski bathymetry. However, outer bar-crest is shifted too much onshore, and the trough depth is underestimated (Fig. 4c). In contrast, alongshore bar-crest profiles along the inner sand bar show that the bathymetry from Beach Wizard can accurately produce the features in the surveyed bathymetry where the rip channels are clearly observed at  $y = -400$  m and  $y = -50$  m (Fig. 4d). The root mean square error of the Beach Wizard estimate is 0.8 m with a bias of 0.13 m.

For CBathy, a validation is performed using jetski data obtained during field work conducted on June 2013. In contrast with bathymetry situation on August 2011, during this period the actual morphology does not exhibit distinct regular rip channels as observed in 2011 bathymetry data. In Fig. 4, bathymetry from CBathy (e) and the jetski survey (f) are presented. The sand bar at approximately  $x = 400$  m is produced very well by CBathy. Moreover, features near the shoreline produced by the CBathy resemble the jet ski bathymetry adequately. Bar crests and troughs from CBathy are in very good agreement with jetski survey (Fig.4g). Moreover, the alongshore bar crest transect shows that

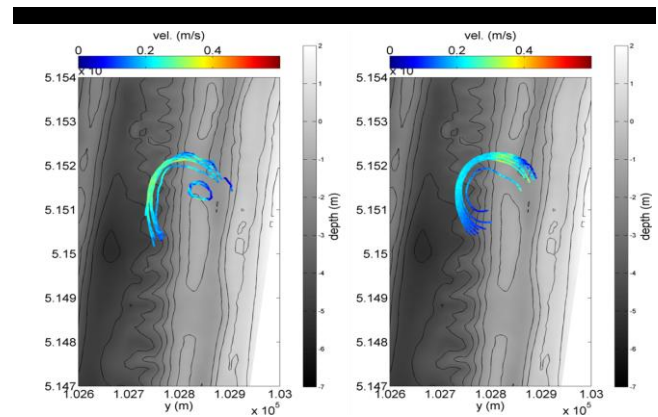


Figure 3. Drifters' trajectory during a deployment on 22 August 2011, left: obtained from field measurement, right: hindcast result using reference model. Color shading indicates drifter speed; grey color map in the background is jet ski bathymetry in local Dutch coordinate system (shore line is on the right).

CBathy result can adequately produce bathymetric features as in jetski bathymetry (Fig. 4h). The root mean square error of the CBathy estimate is 0.45 m with bias of -0.16 m.

### Rip current hindcast and forecast

An XBeach model is constructed where the jetski bathymetry from August 2011 is used. Tidal currents are simulated by assigning water level signal interpolated from two tidal stations, IJmuiden and Petten. The model domain location is centered between the two stations. For the waves, wave group forcing is used, where wave condition is changed every 20 minutes when the sea state changes. Wave current interaction is taken into account for grid cell with water depth less than 3 meters and greater than 0.1 meter. Wave data is obtained from a nearby wave buoy which is located 10 km to the North of the location.

Besides this model, another model is set up where the bathymetry from video -Beach Wizard- is used. Boundary conditions and forcing are similar to the reference model previously mentioned. Having these two models, an evaluation can be performed on how well the model results using video bathymetry will agree with model results using surveyed bathymetry. Moreover, to assess forecasting skill, another model will also be set up where wave forcing for the model is obtained from 2 days forecast of COSMOS.

In Fig. 5, maximum cross shore component of mean velocity for different model set up is shown. Offshore-directed flow pattern (reddish colour shading), present clearly in the results and the locations are associated with the location of two regular channels. For the reference model (Fig. 5a), the peak of the maximum offshore-ward velocities is in order of 0.5 m/s at both rip channels. When the bathymetry from Beach Wizard is used, results also show offshore-directed flows (Fig. 5b). Visually, the cross shore velocity map of (b) does not completely resemble the ones in (a). However, when we focus mainly on offshore-directed velocities, model results clearly exhibit the flows. Finally, when wave forcing for the model is obtained from COSMOS forecast- in addition to bathymetry data from video-, results show that presence of offshore-directed flows associated with rip channels are still apparent (Fig. 5c). However, there is a tendency of underestimation by the model result of the magnitude of the velocity. This is due to the less pronounced bathymetric features in the Beach Wizard bathymetry.

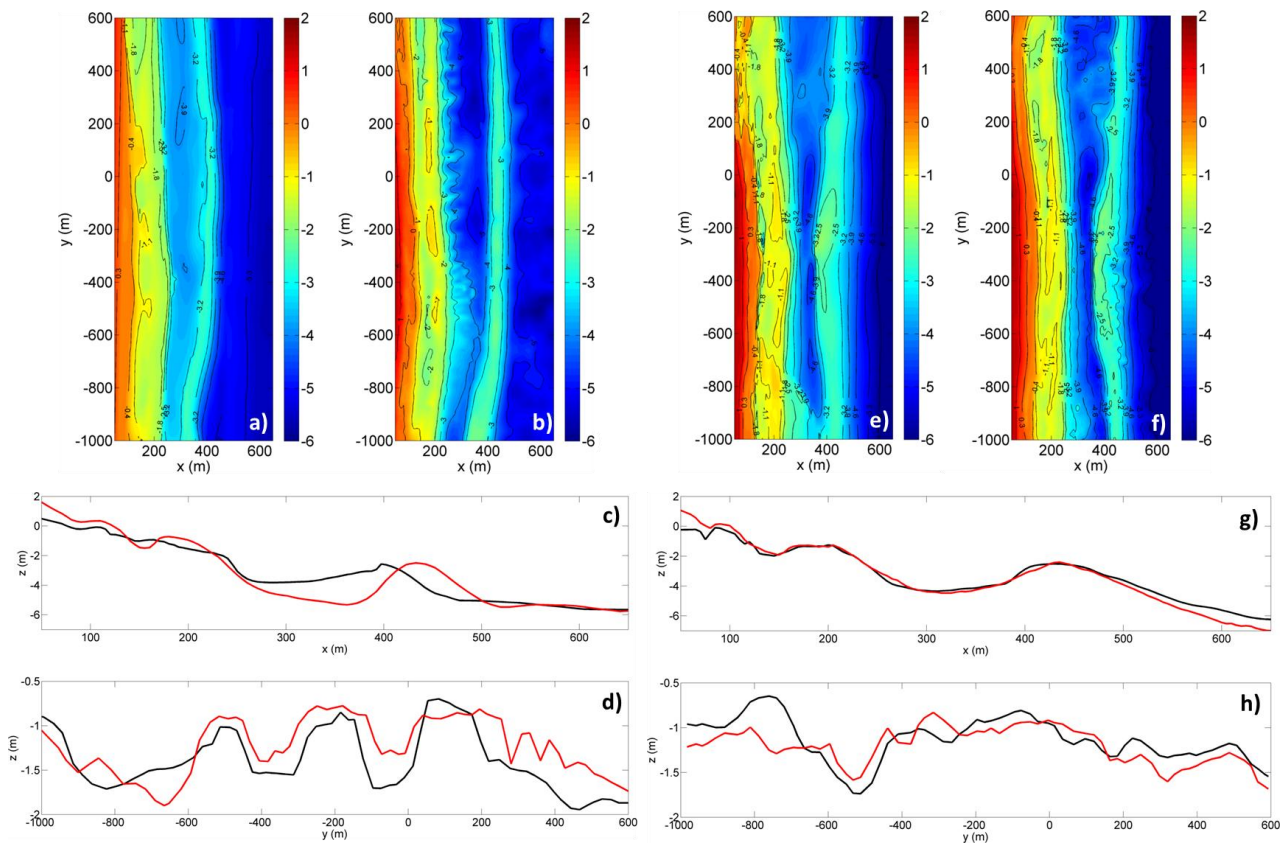


Figure 4. Bathymetry estimate from video compared with jet ski survey in Argus grid coordinate system, color shading represents bed level. a) Beach Wizard estimate for August 2011, b) jet ski bathymetry of August 2011; e) CBathy result for June 2013, f) jet ski bathymetry of June 2013; c) and g): cross shore transect of bathymetry at  $y = -200$  m, red line is jet ski bathy and black line is Beach Wizard bathymetry estimate (c) and CBathy (g); d) and h) alongshore inner bar-crest transect of bathymetry ( $\sim x = 180$  m), red line is jet ski and black line is bathymetry estimate from Beach Wizard (d) and CBathy (h).

In Fig. 6, alongshore transects of the maximum cross shore component of velocity (from Fig. 5), are presented. The black line, which represents the results of the reference model, clearly shows the rip currents around  $y \sim -400$  m and  $y \sim -50$  m, with peak velocity magnitude of  $\sim 0.5$  m/s. When the bathymetry from Beach Wizard is used (red line), both the location and the magnitude of the maximum offshore-directed velocities show good agreement with reference model. The peak location of the maximum velocities is shifted 59 m and 27 m for the first and the second channel respectively, and the magnitude is underestimated. Finally, when the COSMOS forecast is used as wave boundary, offshore-ward flows obtained from the model still resembles adequately the presence of rip currents. The peak locations are shifted 38 m and 48 m for the first and second channel respectively. Moreover, the magnitude is under predicted for both channels' location. Overall, it is clearly seen that model results using bathymetry from video and wave forcing from COSMOS forecast still resemble adequately the presence of rip currents as in reference model.

## CONCLUSIONS AND RECOMMENDATIONS

An operational model for nearshore zone has been built with which waves, water levels, and rip currents are predicted. Up to date beach bathymetry is essential to provide good prediction of

the location, strength and timing of rip currents. To that end, a video-derived nearshore bathymetries using Beach Wizard and CBathy are applied. A validation of the two methods shows a good agreement using either method with bathymetry obtained from jetski surveys. Typical double sand bar features are reproduced well by the methods. Using the August 2011 jetski bathymetry data as ground truth, Beach Wizard is able to produce fairly accurate rip channel features around the inner bar where the bar is occasionally interrupted by channels. However, outer bar-crest location is too much onshore and the trough depth is underestimated. For CBathy, the method produces a nearshore bathymetry with very good agreement with jetski data. Features near the shoreline are reproduced very well and outer bar crest and the trough are very well predicted by CBathy.

An XBeach model for Egmond beach is constructed to simulate rip currents. When the bathymetry from Beach Wizard is used in the model, results show the high potential use of such bathymetry when forecasting rip currents, as the results show fairly good agreement with results from reference model (using surveyed bathymetry). Locations of maximum offshore-directed velocities are matched with associated rip channels. Moreover, in forecast mode, the maximum offshore-directed flows obtained from the model still resemble adequately the presence of rip currents as they are in hindcast results using reference model. This shows that

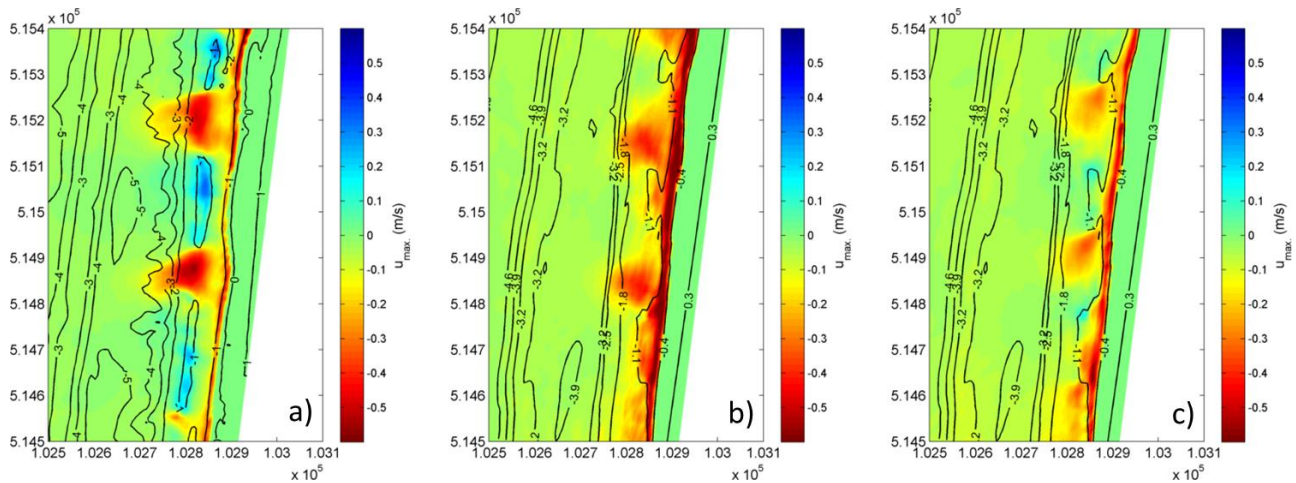


Figure 5. Maximum cross shore component velocity for three different model set up, a): reference model, b): using Beach Wizard bathymetry, c): using Beach Wizard bathymetry and wave boundary from COSMOS forecast. Presence of rip currents clearly observed visually which associated with underlying rip channels.

the model and video-derived bathymetries from video are potential tools to be used for rip current predictions for the Dutch Coast.

Each of the prediction system components contributes to the error in the prediction results that lead to rooms for improvement. First of all, the COSMOS prediction system provides boundary conditions for the nearshore model is a system that involves many inputs and models. Further investigation is recommended where improvement in the wave prediction can be made and uncertainties of the model results are addressed. Second, the nearshore bathymetry update model CBathy shows great potential, since it shows higher skill on providing beach bathymetry compared with Beach Wizard method which is used in the model in the present paper. Moreover, further investigations on applying bathymetries obtained from video on nearshore modeling is suggested to address the potential and limitation of such an approach. Finally, further research on rip currents characteristics in wind sea environment like the Dutch Coast is recommended which will add to our current knowledge on rip current behavior.

## ACKNOWLEDGEMENT

This research has been carried out in the framework of project: Real-Time Safety on Sandy Coasts funded by the Flood Control 2015 research program (project code 2010.05), and the Deltares' strategic research program on Event-driven Hydro- and Morphodynamics (project code 1202362).

The authors thank the many volunteers involved in the field campaign in August 2011: Andrew Pomeroy, Antoon Hendriks, Arnold van Rooijen, Brice Blossier, Claire Bouchigny, Cilia Swinkels, Dirk Knipping, Erwin Bergsma, Giorgio Santinelli, Greta van Velzen, Hesseltje Hoogeveen, Ivan Garcia, Jamie Lescinski, Jeroen Stark, Lisa de Graaf, Roland Vlijm, Timon Pekkeriet; and volunteers during June 2013 field campaign: Amr Elgamel, Andrianto Rahmadha, Elena Zervou, Gisha Prathita, Hendiek Setiantoro, Huda Bachtiar, Juma Haineni, Li Shouqian, Nawisworo, Renny Ratmaningsih, Seyedabdolhossein Mehvar, Shiranee Mahaarachchi, Sifat Sarwar, Sihan Yang, Thais da Costa Borba, Yu Rong. We thank Willem Verbeek for sharing knowledge about rip currents at Egmond aan Zee. The help and support provided by Shore Monitoring (Roeland de Zeeuw, Sierd

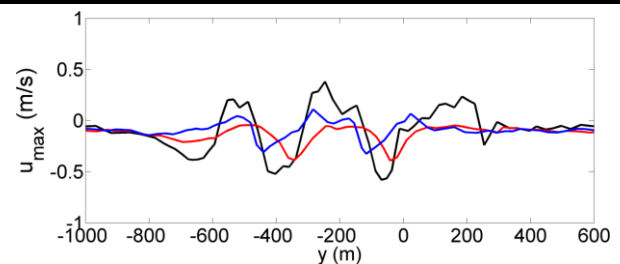


Figure 6. Alongshore transect of maximum cross shore velocity. Black: reference model, red: using Beach Wizard bathymetry, blue: using Beach Wizard bathymetry and wave boundary from COSMOS prediction.

de Vries, and Matthieu de Schipper) are highly appreciated. Rijkswaterstaat is greatly appreciated for providing wave buoy data used in this study.

## LITERATURE CITED

- Alvarez-Ellacuria, A., Orfila, A., Olabarrieta, M., Gómez-pujol, L., Medina, R., & Tintoré, J., 2009. An Alert System for Beach Hazard Management in the Balearic Islands. *Coastal Management*, 37(6), 569-584.
- Alvarez-Ellacuria, A., Orfila, A., Olabarrieta, M., Medina, R., Vizoso, G., & Tintoré, J., 2010. A Nearshore Wave and Current Operational Forecasting System. *Journal of Coastal Research*, 503-509.
- Austin, M. J., Scott, T. M., Russell, P. E., & Masselink, G., 2012. Rip Current Prediction: Development, Validation, and Evaluation of an Operational Tool. *Journal of Coastal Research*, 283-300.
- Bogle, J. A., Bryan, K. R., Black, K. P., Hume, T. M., & Healy, T. R., 2000. Video observations of rip formation and evolution. *Journal of Coastal Research*, SI 34, 117-127.
- Booij, N., Ris, R. C., & Holthuijsen, L. H., 1999. A third-generation wave model for coastal regions 1. Model description and validation. *J. Geophys. Res.*, 104(C4), 7649-7666.
- Dalrymple, R., 1978. Rip currents and their causes. *Proceedings International Conference on Coastal Engineering* (Hamburg), pp. 1414-1427.
- Engle, J., MacMahan, J. H., Thieke, R. J., Hanes, D. M., & Dean, R. G., 2002. Formulation of a Rip Current Predictive Index Using Rescue

- Data. *National Conference on Beach Preservation Technology* (Biloxi, MS).
- Gallop, S. K., Bryan, K. R., & Coco, G., 2009. Video Observations of Rip Currents on an Embayed Beach. *Journal of Coastal Research*, SI 56.
- Gerritsen, H., de Vries, J. W., & Philippart, M. E., 1995. The Dutch Continental Shelf Model. In: D. Lynch & A. Davies (Eds.), *Quantitative Skill Assessment for Coastal Ocean* (Washington DC), pp. 425-467
- Holman, R., Plant, N., & Holland, T., 2013. cBathy: A robust algorithm for estimating nearshore bathymetry. *Journal of Geophysical Research: Oceans*, 118(5), 2595-2609.
- Kalman, R. E., 1960. A New Approach to Linear Filtering and Prediction Problems. *Transactions of the ASME – Journal of Basic Engineering* (82 (Series D)), 35-45.
- Kim, I. H., Kim, I. C., & Lee, J. L., 2011. Rip Current Prediction System Combined with a Morphological Change Model. *Journal of Coastal Research* SI 64.
- Kohut, J., Roarty, H., Lichenwalner, S., Glenn, S., Barrick, D., Lipa, B., & Allen, A., 2008. Surface current and wave validation of a nested regional HF radar Network in the Mid-Atlantic Bight. *Proceeding of the IEEE - Conference on Current Measurement Technology* (Charlston, SC), pp. 203 – 207.
- Lascody, R. L., 1998. East Central Florida Rip Current Program. *National Weather Digest*, 22:2, 25-30.
- Lushine, J. B., 1991. A study of rip currents drownings and related weather factors. *National Weather Digest*, 16:3, 13-19.
- Ranasinghe, R., Symonds, G., & Holman, R. A., 1999. Quantitative characterization of rip dynamics via video imaging. *Coastal Sediments* (Virginia), pp. 987-1002.
- Roelvink, D., Reniers, A., van Dongeren, A., van Thiel de Vries, J., McCall, R., & Lescinski, J., 2009. Modelling storm impacts on beaches, dunes and barrier islands. *Coastal Engineering*, 56(11-12).
- Scott, T., Russel, P., Masselink, G., Wooler, A., & Short, A., 2007. Beach Rescue Statistics and their relation to Nearshore Morphology and Hazard: A case study for Southwest England. *Journal of Coastal Research*, SI 50.
- Short, A. D., 2007. Australian Rip System-Friend or Foe. *Journal of Coastal Research*, SI 50.
- Tolman, H. L., 2009. User manual and system documentation of WAVEWATCH-III version 3.14. NOAA / NWS / NCEP / MMAB Technical Note 276.
- Uden, P., Rontu, L., Heikki, Jarvinen, P. L., Javier Calvo, G. C., Joan Cuxart, Kalle Eerola, Carl Fortelius, J. A. G.-M., Colin Jones, Geert Lenderlink, A. M., Ray McGrath, Beatriz Navascues, Tjmm., 2002. HIRLAM-5 Scientific Documentation.
- Van Dongeren, A., Plant, N., Cohen, A., Roelvink, D., Haller, M. C., & Catalán, P. (2008). Beach Wizard: Nearshore bathymetry estimation through assimilation of model computations and remote observations. *Coastal Engineering*, 55(12).
- Van Dongeren, A., Van Ormondt, M., Sembiring, L., Sasso, R., Austin, M., Briere, C., Van Thiel de Vries, J. (2013). Rip current predictions through model data assimilation on two distinct beaches. *Coastal Dynamics* (Bordeaux, France).
- Van Ormondt, M., Van Dongeren, A., Briere, C., Sembiring, L., Winter, G., Lescinski, J., & Swinkels, C. (2012). Simulating storm impacts and coastal flooding along the Netherlands Coast. *Flood Risk 2012*, (Rotterdam, The Netherlands).
- Winter, G., Van Dongeren, A., de Schipper, M., & Van Thiel de Vries, J. (2012). A field and numerical study into rip currents in wind-sea dominated environments. *International Conference on Coastal Engineering* (Santander).



# Massive cooling water dispersion behavior in a shallow macro-tidal coastal zone in Korea

SeungWon Suh

Department of Ocean Science and  
Engineering  
Kunsan National University  
Kunsan, Korea  
suh@kunsan.ac.kr



[www.cerf-jcr.org](http://www.cerf-jcr.org)



[www.JCRonline.org](http://www.JCRonline.org)

## ABSTRACT

Suh, S.W., 2014. Massive Cooling Water Dispersion in a Shallow Macro-tidal Coastal Zone in Korea. In: Green, A.N. and Cooper, J.A.G. (eds.), *Proceedings 13<sup>th</sup> International Coastal Symposium* (Durban, South Africa), *Journal of Coastal Research*, Special Issue No. 70, pp. 360-365, ISSN 0749-0208.

The Hanbit Nuclear Power Plant is located on a macro-tidal coastline in mid-western Korea; it generates 5900 MW of electricity through 6 units. It discharges  $354.6 \text{ m}^3 \text{ s}^{-1}$  of cooling water, with excess temperature of  $\Delta T = 7.6 \text{ }^\circ\text{C}$ , into the shallow coastal water. The mean depth around the Hanbit NPP is  $\sim 10 \text{ m}$ , in which strong tidal currents of  $>1.0 \text{ m s}^{-1}$  occur during spring tides. This study examines the complex thermal dispersion in a shallow sea environment. To accurately delineate the dispersion characteristics, 15 sets of seasonal field observations for wave, tide, tidal currents, and water temperature were conducted over 3 years from 2002 to 2004. Water temperature at 30 stations around the power plant was measured simultaneously over a 15-day period to investigate seasonal changes in the tidal hydrodynamics. Spectral analysis was employed to understand the dominant semidiurnal forcing upon thermal plume movement. The results revealed that wide thermal plumes were spreading beyond the regional tidal excursion. Numerical models based on two-dimensional hydrodynamic advanced circulation (ADCIRC) and fine-grid Eulerian-Lagrangian transport models were also developed, which reproduced the results of the field observations with satisfaction.

**ADDITIONAL INDEX WORDS:** nuclear power plant, thermal pollution, plume, surface heat loss

## INTRODUCTION

There are 23 Nuclear Power Plant (NPP) units operating in Korea, providing almost 30% of the national electricity generation. On the east coast, adjacent to the East Sea (Sea of Japan), there are 3 NPPs incorporating 17 units. The YongGwang NPP, renamed the Hanbit NPP (HNPP), is the only power plant located on the west coast and it generates 5900 MW through 6 units. This power plant is situated on the Yellow Sea coast in an area with well-developed tidal flats, as shown in Figure 1. The region adjacent to the HNPP is a shallow coastal sea, which has a sea bed with a very mild slope of the order of 0.0006 in the offshore direction. This area experiences a large tidal range with a mean spring tide of 6 m. At low tide, the area to the north of the power plant is predominantly exposed as tidal flats. The region around the HNPP is characterized by tidal currents with a strong recursive pattern exceeding  $1.1 \text{ m s}^{-1}$  in the northeast direction during the flood tide and in the southwest direction during the ebb. A 1136-m-long flow-guiding dike has been constructed near to the discharge channel of the HNPP to lessen the impact of heat dispersion on the neighboring sea and to prevent recirculation of heated water. Cooling water (CW) is discharged at a rate of  $354.6 \text{ m}^3 \text{ s}^{-1}$  with a temperature of  $7.6 \text{ }^\circ\text{C}$ . Thus,  $1.305 \times 10^{10} \text{ J s}^{-1}$  of heat is discharged continuously, assuming the density of sea water is  $1023 \text{ kg m}^{-3}$  and its specific heat is  $4182 \text{ J kg}^{-1} \text{ }^\circ\text{C}^{-1}$ .

Heated water discharged into coastal regions from power plants is regarded as thermal pollution. It raises the temperature of the

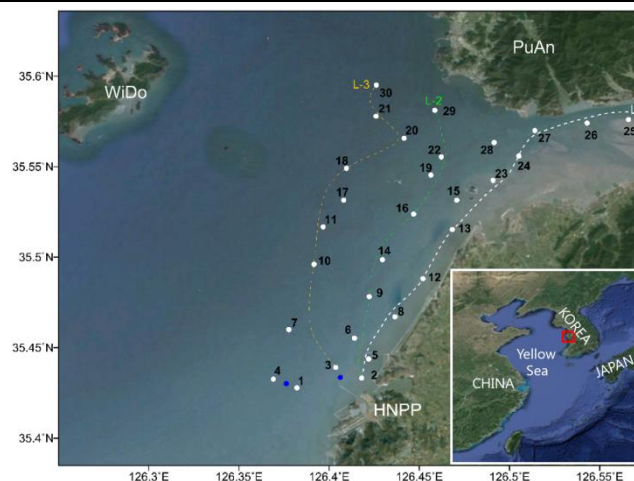


Figure 1. Map showing study area around HNPP on the west coast of Korea. In which temperature observation station numbers are shown along reference lines L-1, L-2 and L-3.

environment and could affect aquatic life in the ecosystem (Jan *et al.*, 2004; Abbaspour *et al.*, 2005). To understand and solve this problem, precise assessment of the heat pollution is required by

taking into account both the thermal dispersion pattern and the hydrodynamic and meteorological variations in the vicinity of the power plant. Moreover, it is necessary to define a region of interest (ROI), for example, the impact of thermal pollution on the germination of seaweed, regardless of governmental regulations.

Field observations and modeling are two approaches to performing an analysis of CW discharge (Wu *et al.*, 2001). For the analysis of the thermal plume (TP) at the HNPP, Ahn *et al.* (2006) used the indirect method of analyzing satellite infrared data. According to their results, the occurrence of both strong coastal currents and winds during the winter and summer monsoons often results in a high rate of thermal dispersion. Yanagi *et al.* (2005) took field observations for one month in spring 2003, under conditions of spring tides and fine weather, and performed 3d numerical modeling on the HNPP. Because of the limited data sampling, they found that the computed isotherm contours ran parallel to the coastline. To overcome this, in the present study, we intensively measured the water temperatures in the region around the HNPP over a longer timeframe. Specifically, we obtained temperature data at 30 locations around the HNPP over a 3-year period, recording data for at least 15 days per season.

Many approaches using numerical models have been applied to understanding CW behavior. Wu *et al.* (2001) studied not only the air-water heat exchange for power plants, but also the water-sediment heat exchange. Jiang *et al.* (2003) used embedded grids incorporating near and far fields simultaneously. German *et al.* (2007) proposed a simple characteristic Galerkin finite element method, using an unstructured grid system, to address the stabilization technique. However, they addressed it using grids that were almost the same size as those used in resolving the problem, and they were unable to perform any calibration exercises to verify the accuracy of some of the parameters used. Abbaspour *et al.* (2005) considered several scenarios when determining the optimal separation distance. Even though several numerical models (KOPEC, 1997; KOPEC, 1999; KHNP, 2001) have been applied in assessing the environmental impact of the HNPP, actual verification has not been undertaken. Because the study area has shallow depth, an integrated 2d approach is sufficient to explain thermal dispersion (Martin and McCutcheon, 1999). Thus, in this study, both a 2d model ADCIRC (Luettich *et al.*, 1992) and an Eulerian-Lagrangian model (Adams and Cosler, 1987) were applied to find the ROI of 1 °C.

## METHODS

### Direct temperature observation

To obtain continuous direct measurements of the temperature distribution, we recorded 15 distinct datasets for at least 15 days from March 2002 to April 2005. Much effort was expended on obtaining simultaneous measurements of temperature from the 30 stations located to the north of the HNPP. In addition, to develop an understanding of the coastal hydrodynamics, tide and wave characteristics and tidal currents were also measured 8 times simultaneously at selected stations. Effluent discharging conditions of HNPP and the measurements of ambient environments for tide, tidal currents and waves are listed in Table 1 for selected observations. The locations of the stations are shown in Figure 1 as numbers. In designing the distribution of stations, we set three separate lines: L-1 (stations 2-12-13-24) along the coastline; L-2 (stations 3-9-16-29), a middle line representing the principal movement of the TP; and L-3 (stations 3-10-18-30), furthest from the HNPP, to capture the impact of the TP on the surrounding environment. Each temperature station was equipped with a Minilog-12 measuring device with a resolution

and accuracy of 0.01 °C and 0.1 °C, respectively. For recording hydrodynamic data, the stations were equipped with RCM-9 and UCM60 current meters, and a WTR-9 wave tide recorder. The depth mean temperature was measured at 10-minute intervals over 15-day periods, selected to encompass the spring and neap tidal impact on thermal dispersion.

Table 1. Selected summary of field observations

Sequence	Period	Tide and Current Obs. Devices	Water Temp. Sensors Installed Total(lost)	Status of Operating NPP Units
2 <sup>nd</sup>	2002.5.20~6.3	R,U,W	31(2)	1,2,3,4,5
4 <sup>th</sup>	2002.9.13~9.24	R,U,W	30(4)	1,2,5
5 <sup>th</sup>	2003.1.7~1.22	-	30(5)	1,2,3,4,5,6
7 <sup>th</sup>	2003.7.30~8.13	-	27(4)	1,2,3,4,5,6
11 <sup>th</sup>	2004.4.30~5.15	R,W	30(1)	1,2,3,5,6
12 <sup>th</sup>	2004.7.26~8.9	R	29(1)	1,2,3,4,5,6

Devices R:RCM-9, U:UCM-60, W:WTR-9

### Numerical modeling

One of the purposes of this study is to delineate an ROI that has a consistent excess temperature of 1 °C. The simulation of thermal pollution, which encompasses the prediction of the 1 °C excess temperature induced by CW discharge, is particularly important in evaluating seaweed germination during the winter. We applied the 2d ADCIRC model for the hydrodynamic simulations with consideration of the dry-rewet treatment, and we applied the Eulerian-Lagrangian model for the simulation of heat dispersion, as in a previous analysis (Suh, 2001), where the near field is treated as Gaussian puff and is patched into a far field model. At the beginning of the simulation, turbulent flow due to tidal excursion enhances dispersion in the offshore direction; however, the TP cannot last because heat loss at the surface behaves as a balancing term, maintaining quasi-steady dispersion. In this regard, it is important to note the role of the heat loss coefficient in modeling, which is often represented as a linear decaying term in water quality modeling. A previous modeling approach (KOPEC, 1999) for the NPP used a constant heat loss coefficient value of 32 W m<sup>-2</sup> °C<sup>-1</sup> throughout the entire simulation period, which is equivalent to a linear decay coefficient of 7 × 10<sup>-6</sup> s<sup>-1</sup> (Jirka *et al.*, 1996). This value was not justified clearly in that study, but was regarded simply as a typical surface heat loss coefficient. It is equivalent to a wind speed of 4 m s<sup>-1</sup> when the ambient water temperature is 15 °C and the excess temperature is within the range of 0–3 °C (Jirka *et al.*, 1996). However, for a wind speed of 1 m s<sup>-1</sup>, the coefficient would be 12 W m<sup>-2</sup> °C<sup>-1</sup>, and under calm conditions it would decrease to 5 W m<sup>-2</sup> °C<sup>-1</sup>. Thus, great care must be taken in choosing proper coefficients in modeling. In model calibration, this starts with a low wind speed and increases until the modeling results match appropriate verification values.

## RESULTS

### Spatial behavior of CW

To analyze the dispersion of CW, we first analyzed its spatial distribution. Of the 15 datasets over the 3-year period, 3 sets were chosen arbitrarily to determine the spatial behavior: the 5th dataset (January, 2003), representing winter; and the 7th and 12th datasets (August of 2003 and 2004, respectively) showing summer seasonal variations. Figure 2 illustrates the excess temperature versus distance from the discharge point along analysis lines L-1

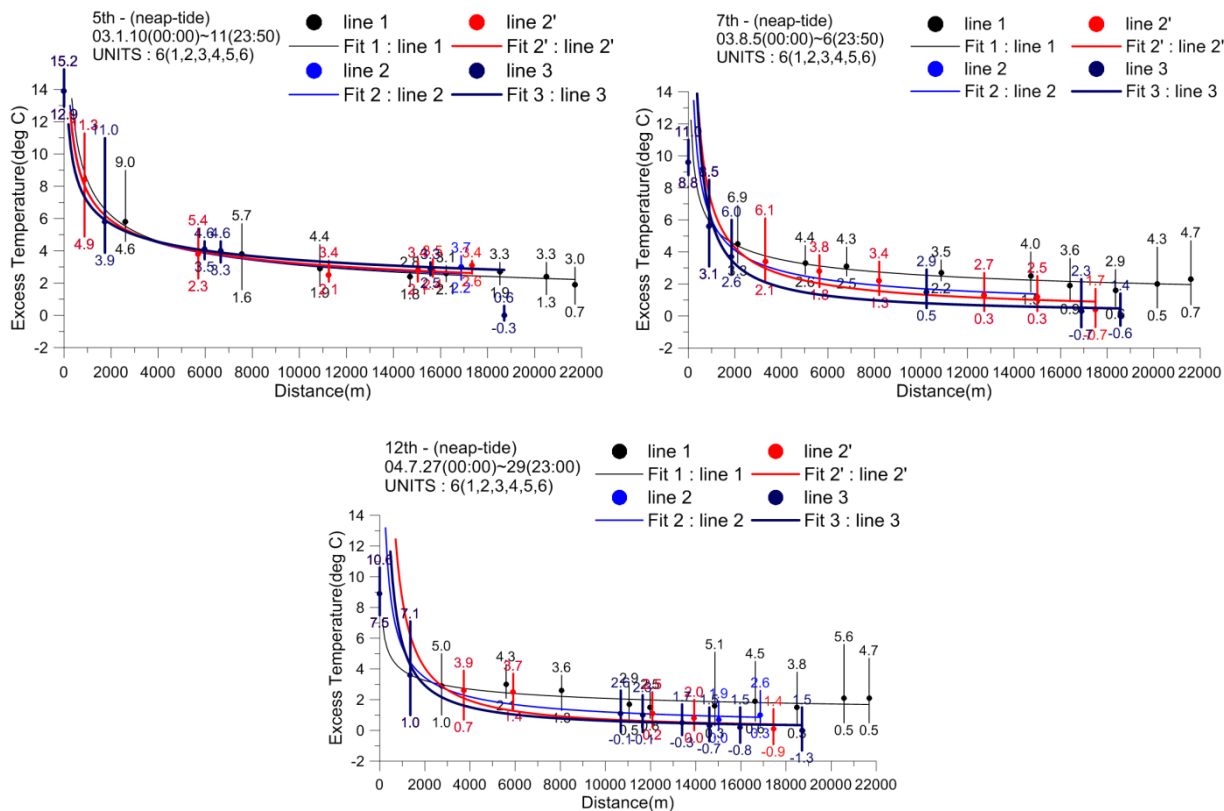


Figure 2. Spatial variation of excess temperature along reference lines L-1, L-2 and L-3 on the 5th (winter of 2003), 7th (summer of 2003) and 12th (summer of 2004).

to L-3. In preparing these diagrams, the mean temperature at the station furthest from the HNPP (T30, station #30) was regarded as the background temperature, and the excess temperature at the other stations was determined by subtracting the background temperature from that recorded at each station. The trends of excess temperature in summer are almost the same in 2003 and 2004, despite the one-year time lag. In this plot, the diurnal mean temperature is marked at each station along each analysis line, and a bar is used to illustrate the diurnal minimum and maximum temperatures. The advantage of this analysis scheme is that we can compare variation between same seasons, regardless of the ambient conditions when we are using excess values. Specifically, in both summers, the excess temperature decreased suddenly in front of the discharge point and then diminished gradually before plateauing to a constant value.

For the 5th dataset representing winter, the exponential decay curves for lines L-1 to L-3 fall approximately on a single line. An explanation for the similarity of these curves could be that the major and minor flow directional variations happened to be equal in the winter season because of the effect of the relatively strong wind compared with the magnitude of the flow.

The curve fitting shows that the time-averaged heat dispersion around the HNPP decreases according to an exponential law. In contrast to the trend in the mean temperature with distance from the discharge point, the maximum temperature values along L-1 do not decrease exponentially. This finding can be attributed to the fact that L-1 runs adjacent to the coastline in close proximity to the well-developed tidal flats. It behaves as a heating source due to solar radiation or cooling when it loses heat at night or during

the winter season and hence, may be subject to geo-environmental heating effects (Yanagi *et al.*, 2005). The spatial distributions of excess temperature recorded in summer and winter are similar, except for some high temperatures recorded around the tidal flats during summer. According to this spatial distribution, neglecting the temporal component, we can use one of the empirical or numerically proven relationships provided by CORMIX3 (Jirka *et al.*, 1996) in the analysis of intertidal temperature behaviors, but it

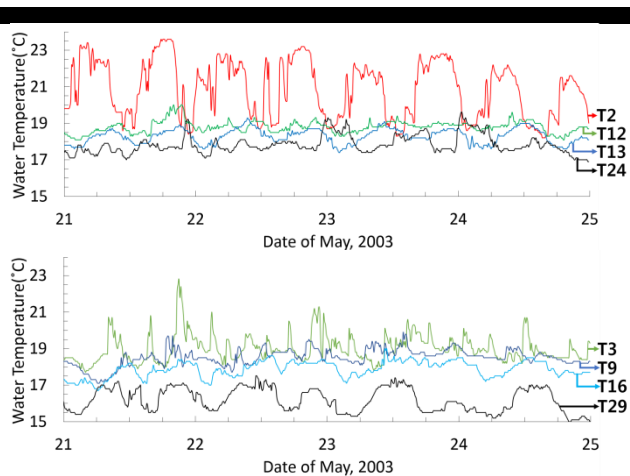


Figure 3. Temporal variation of temperatures along L-1 and L-2 measured in May 2003.

is inadequate to define an ROI.

### Temporal tendency of TP

In addition, we analyzed the temporal variation of temperature along the three analysis lines. As can be seen in Figure 3, thermal peaks move northwards from the discharge point according to the flooding tidal flow. The lag time between the peak temperatures at successive stations is almost the same as that of the tide, indicating that tidal motion drives the movement of the temperature peaks from station to station. Thus, tidal forcing plays a major role in water temperature variability associated with the TP, as it does in natural cases along a channel (Sousa *et al.*, 2011) and in an estuary (García-Lafuente *et al.*, 2012). In particular, the semi-diurnal tidal constituents  $M_2$  and  $S_2$  act as primary forces in the form of advection in a shallow coastal region.

According to the temporal plot for L-1, the thermal peak exhibits a relatively flat shape near the discharge point at station T2, but it becomes sharper at T12 and T13. It is also clear that thermal peaks occur twice daily, in accordance with the dominant semi-diurnal coastal hydrodynamics. Moreover it should be noticed that high temperatures were recorded around midnight at T24 which is 16.6 km apart from the discharging point. Because the TP extends to a tidal excursion distance of 8–9 km, even for a spring tide, the temporal variation of temperature beyond this region must be affected by the dispersion of the TP. The temporal variation along L-2, which runs through stations T3, T9, T16, and T29, shows some interesting features (lower panel of Figure 3). Temperature peaks occur twice daily, as they do with L-1, but the time lag between the peaks at successive stations does not match exactly the tidal velocity. Temperature variations along L-2 reveal that the peaks can occur four times a day. Specifically, this is more common in cases of calm or low wind fields because of reduced dissipation. The reason for this is that the moving TP affects the stations along L-2 twice during the flooding tide, and an additional two times during the ebb tide. That is, off L-2, the TP spreads out in front of the HNPP and moves with the tidal current. As can be seen in the figure, if we take the background water temperature as the mean value at the most distant point, which is 16 °C for the 2nd observation, then the maximum temperature difference at each station  $\Delta T_{\max}$  would be 23.6 °C at station T2 and 22.8 °C at T3, which gives  $\Delta T_{T2} = 7.6$  °C and  $\Delta T_{T3} = 6.8$  °C. Even though station T2 is far from the discharge point, the excess temperature at that station approaches the design value of excess temperature, indicating that a recirculation effect is occurring.

It is also clear from the spectral analysis with tide and temperatures of T6, F9, T16 and T30 stations for the 12th datasets,

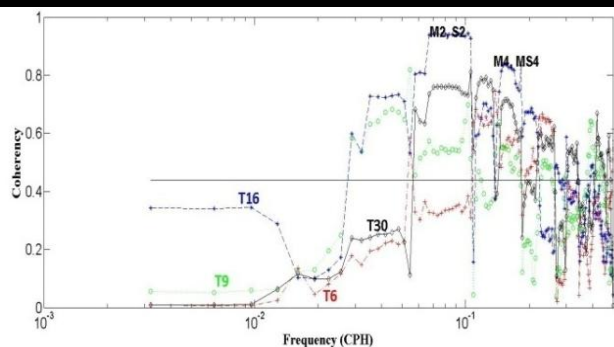


Figure 4. Coherent analysis with tide and temperatures along L-2 line measured in August 2004.

shown in Figure 4, that the major forcing of peak temperature is by the semi-diurnal tidal component  $M_2$ ,  $S_2$  and the others are over and compound tides,  $M_4$ , and  $MS_4$ , due to nonlinear interactions because of the shallow depth.

To understand the behavior of the TP more precisely, we examined animations of the time evolution of the distribution of excess temperature. These animations showed the time evolution of the tidal elevation, air temperature, and wind speed and direction. According to the animation, the TP moves almost the entire tidal excursion distance within each tidal cycle. The animation analysis also revealed that the TP spreads further in response to the tidal current rather than the wind effect, indicating that tidal currents play a major role in the dispersion mechanism, and that wind speed and direction might have a minor effect.

### Dispersion patterns by numerical modeling

The dispersion mechanism is dependent on diverse effects, for example, ambient flow conditions, effluent discharges, discharge shape, designed excess temperature, discharge type (surface or submerged), ambient geomorphologic distribution. In addition, meteorological variations affect the dispersion indirectly, because heat loss or gain at the air-sea interface is a major sink or source. Thus, we must investigate carefully the ambient physics in order to enhance the model's reliability. In our numerical modeling, the designed excess temperature is set as 7.6 °C. One limitation of numerical modeling is that it only represents a typical situation, such as the mean spring or neap tide, regardless of other physical phenomena.

The simulated result of the quasi-steady state reveals that the TP has a relatively broad width in the offshore direction. As seen in Figure 5, the results show the well-developed spread of the TP, not only along the main axis of the tidal current direction (i.e.,

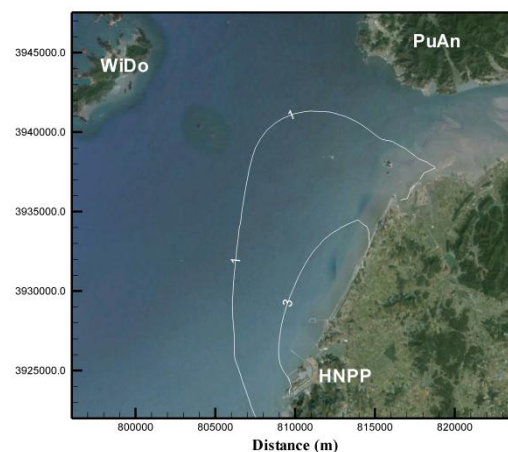


Figure 5. Distribution of excess isotherms in °C around HNPP by numerical modeling.

northeast to southwest, parallel to the coastline), but also along the minor axis (i.e., offshore direction). This numerical tendency has never been reported in previous modeling studies (KHNP, 2001; Yanagi *et al.*, 2005). The inability of previous models to simulate this may come from the application of a relatively high surface heat loss coefficient,  $32 \text{ W m}^{-2} \text{ °C}^{-1}$ . Our simulations show that the application of a proper heat loss coefficient is very important. Initially, the TP develops and then moves along the coast, broadening until it reaches an equilibrium state. One of the reasons for this might be due to the horizontal additive dispersion

effect (Suh, 2006) induced by the massive buoyancy of the CW. Numerical results also show that the thermal distribution around the HNPP is not only a result of newly discharged water, but is also affected by the movement of the existing TP.

## DISCUSSION

To understand the behavior of the massive TP, continuous direct measurements were obtained. Because of the significant quantity of data comprising water temperature, and tide, wave, and wind velocities at each station, it is difficult to determine typical movements of the TP. Even though we performed spatial, temporal, and statistical analyses, we are unable to depict precisely the instantaneous occurrence and duration of peak water temperature. Covariance results show that the movement of the TP coincides with the major tidal forcing of the  $M_2$  constituent, as has been found for the natural water temperature in other shallow coastal zones (Sousa *et al.*, 2011; García-Lafuente *et al.*, 2012). However, the duration of peak temperature shows significant differences with distance from the point for discharge as seen in Figure 3. Directly in front of the NPP, the peak temperature persists for several hours, which is shown by the flat shape in the time series graph, whereas a shape that is sharper arises as the distance of the ambient tidal movement increases. Furthermore, the duration time decreases rapidly and exhibits a sharp shape along the minor tidal axis, i.e., it decreases more rapidly offshore than it does in the major direction along the coast. According to Yanagi *et al.* (2005) sometimes tidal flats might act as a heat source, but this may be possible only during daytime. The method of direct observation conducted in this study is very efficient in catching the real movement of the TP with the tidal current, not just during daytime but also at night. Therefore, we could distinguish the effects of solar radiation on thermal movement. From the analysis, radiation may act only on the exposed tidal flats during daytime, but its magnitude is not significant compared with the total heat released from the HNPP.

It is meaningful to examine the behavior of the TP both spatially and temporally. To understand the effect of tidal flat

heating and other meteorological side effects, we analyzed the spatial and temporal variations for a selected group of stations for the summer season only. Specifically, we compared spring tide data from one day of the 2003 summer season (the 7th dataset) with those of a corresponding day to cover low to high tide from the 2004 summer season (the 12th dataset). In the analysis, the time scales for all stations in the two datasets were shifted to synchronize the tidal elevation and current. The results of the comparison are plotted in Figure 6. As expected, directly in front of the discharge point, the fluctuations in excess temperature over the 24-hour period are almost the same despite the 1-year gap between the measurements. Similarly, the temporal fluctuations in the region furthest from the discharge point are almost the same in both years, which can be interpreted as the water far from the discharge point showing normal daily variations. The temporal fluctuations along the outer stations, such as those along L-3, of the 2003 and 2004 datasets almost coincide, indicating that the plume-affected region is almost unchanged. By contrast, the variations in excess temperature at stations close to the coast, such as those along L-1, show deviations of within 1 °C. These deviations can be attributed to geological and meteorological effects rather than variations in effluent. However, at most stations, the overall variation in excess temperature shows similar tendencies. Therefore, we can conclude that the behavior of the TP has a unique periodic tendency affected by ambient tidal conditions.

We could not find any distinct variation of thermal behavior, even with a gap of one year and furthermore, there was no seasonal behavior apparent, except for some shrinkage of the TP due to surface heat loss and an attachment to the shoreline caused by winter surface wind stress. Peak temperature in front of the HNPP occurs four times daily, even in the environment of a dominating semi-diurnal tidal constituent. This is because it is not just the newly discharged CW that has an effect during the flood tide, but also the existing plume that follows the ebb tide.

It is difficult to depict the instantaneous occurrence of high temperature, which is rather more harmful to marine ecosystems than a constant high temperature, in the prevailing analysis

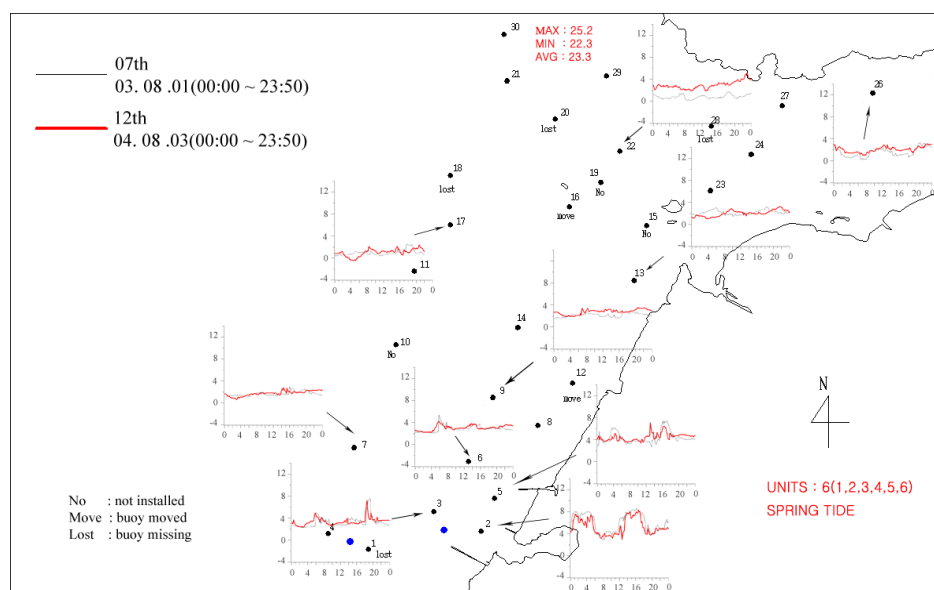


Figure 6. Comparison of 2 days excess temperature variations for the 2003 and 2004 summer data on selected stations.

scheme, because the peak value is almost always filtered or ignored in the data analysis. However, we can easily understand the behavior of the TP through the animation analysis, which includes all the effects in one sense.

The numerical modeling analysis produces almost the same results as those obtained from the three-year period of field observations. However, we could not account for all phenomena or extraordinary cases in the modeling because of the lack of information. Thus, we could expect that a somewhat greater spread of the TP exists than that suggested by the numerical modeling. The results of the numerical modeling can be understood as complementary to the direct field observations, but the selection of the heat loss coefficient is most important in understanding the behavior of the TP. In modeling tests, we obtained a heat loss coefficient of  $20 \text{ W m}^{-2} \text{ }^{\circ}\text{C}^{-1}$  after several calibrations.

## CONCLUSION

In this work, we sought to clarify the pattern of thermal dispersion in shallow coastal waters, associated with the discharge of CW from a nuclear power plant, by both intensive field measurements over a three-year period and numerical simulations using ADCIRC and an Eulerian-Lagrangian scheme. The field observations revealed very clear movements of the TP, even during the night. Through the analysis of the temperature variations over time, we found that the time lag between thermal peaks at successive measurement stations was almost the same as that of the tidal motion, indicating that the thermal peaks move in association with tidal motion. The covariance analysis showed almost the same result. The temporal variation of temperature beyond the tidal excursion distance of 8–9 km arises clearly from the combined effects of the upward existing TP and the downward ebb tidal currents. It is due to the massive discharge of CW as a thermal source of  $1.305 \times 10^{10} \text{ J s}^{-1}$  being continuously injected into the shallow coastal zone. Even though macro tidal fluctuations can cause rapid vertical and horizontal mixing, the continuous release of heat from the HNPP causes a huge TP, which is unable to decay in an acceptable manner because of the low surface wind stress. Thus, we can conclude that a single massive discharge of cooling effluent would not dissipate within one tidal cycle, but would persist for several cycles and thus, it causes an effect stretching at least twice the tidal excursion length. Analysis of the tidal mean variation of temperature along three lines revealed that the water temperature decays exponentially with distance from the discharge point.

In the numerical modeling, we found that careful attention should be given to selecting an appropriate value for the heat loss coefficient, in order to simulate properly the dispersal behavior of the massive TP. Following several calibration simulations, using wind speeds obtained from meteorological data, we determined that a heat loss coefficient of  $20 \text{ W m}^{-2} \text{ }^{\circ}\text{C}^{-1}$  is reasonable in almost all cases. Our simulation results revealed an expansion in the offshore direction that almost coincided with the observed data. It should also be noted that the well-developed plume directly in front of the HNPP persists for two or three days in connection with tidal flow movements along the coast. That is, the plume develops initially due to the thermal discharges and then moves along the coast, increasing in width until it reaches an equilibrium state. These findings indicate that thermal distribution in the waters near the HNPP is not affected only by newly discharged water, but also by the movement of the existing TP discharged earlier. This is a unique phenomenon discovered during this study, which has not been detected at other thermal

power plants in Korea owing to their relatively low thermal discharges.

## ACKNOWLEDGEMENT

This research was a part of the projects “Countermeasure system against typhoons and tsunamis in harbor zones” of frontier harbor project and “Development of coastal erosion control technology” funded by the Ministry of Oceans and Fisheries, Korea. The comments of anonymous reviewers were much appreciated.

## LITERATURE CITED

- Abbaspour, M. Javid, A.H., Moghimi, P. and Kayhan, K., 2005. Modeling of thermal pollution in coastal area and its economical and environmental assessment. *Int. J. Environ. Sci. Tech.*, 2, 1, 13-26.
- Adams, E.E. and Cosler, D.J., 1987. *Predicting circulation and dispersion near coastal power plants: Applications using models TEA and ELA*. Report No. MIT-EL 87-008, MIT.
- Ahn, Y.H., Shanmugam, P., Lee, J.H. and Kang, Y.Q., 2006. Application of satellite infrared data for mapping of thermal plume contamination in coastal ecosystem of Korea. *Marine Environmental Research*, 61, 186-201.
- García-Lafuente, J., Delgado, J., Navarro, G., Calero, C., Díez-Minguito, M., Ruiz, J. and Sánchez-Garrido, J.C., 2012. About the tidal oscillations of temperature in a tidally driven estuary: The case of Guadalquivir estuary, southwest Spain. *Estuarine, Coastal and Shelf Science*, 111, 60-66.
- German, A., Espino, M., Blasco, J. and Maidana, M., 2007. Finite element modeling of the thermal outflow of three power plants in Huelva Estuary. *Advances in Engineering Software*, 38, 379-385.
- Jan, S. Chen, C.A., Tu, Y.Y. and Tsai, H.S., 2004. Physical properties of thermal plumes from a nuclear power plant in the southernmost Taiwan. *Journal of Marine Science and Technology*, 12, 5, 433-441.
- Jiang, J., Fissel, D.B. and Topham, D., 2003. 3D numerical modeling of circulations associated with a submerged buoyant jet in a shallow coastal environment. *Estuarine Coastal and Shelf Science*, 58, 475-486.
- Jirka, G.H., Doneker, R.L. and Hinton, S.W., 1996. *User's manual for CORMIX: A hydrodynamic mixing zone model and decision support system for pollutant discharges into surface water*. US EPA.
- KHNP, 2001. *A review report on reduction scheme of thermal effect of YGNPP due to delaying of Kusipo project (in Korean)*.
- KOPEC, 1997. *A review report on reduction scheme of thermal effect of YGNPP (in Korean)*.
- KOPEC, 1999. *A re-review report on reduction scheme of thermal effect of YGNPP (in Korean)*.
- Luettich RA, Westerink JJ, Scheffner NW (1992) *ADCIRC : an advanced three-dimensional circulation model for shelves, coasts and estuaries. report 1 : Theory and methodology of ADCIRC-2DDI and ADCIRC-3DL*, Dredging Research Program Technical Report DRP-92-6, US Army Corps of Engineers WES, Vicksburg, MS.
- Martin, J.L. and McCutcheon, S.C., 1999. *Hydrodynamics and transport fort water quality modeling*, Lewis publishers.
- Sousa, M.C., Vaz, N. and Dias, J.M., 2011. Physical forcing of the water temperature variability along the Espinheiro Channel (Ria de Aveiro, Portugal). *J. of Coastal Research*, SI 64, 1594-1598.
- Suh, S.W., 2001. A hybrid near-field/far-field thermal discharge model for coastal areas. *Marine Pollution Bulletin*, 43, 7-12, 225-233.
- Suh, S.W., 2006. A hybrid approach to particle tracking and Eulerian-Lagrangian models in the simulation of coastal dispersion. *Environmental Modelling & Software*, 21, 234-242.
- Wu, J., Buchak, E.M., Edinger, J.E. and Kolluru, V.S., 2001. Simulation of cooling-water discharges for power plants. *J. of Environmental Management*, 61, 77-92.
- Yanagi, T., Sugimatsu, K., Shibaki, H., Shin, H.R. and Kim, H.S., 2005. Effect of tidal flat on the thermal effluent dispersion from a power plant. *J. of Geophysical Research*, 110, C03025.

## RISC-KIT: Resilience-Increasing Strategies for Coasts - toolKIT

Ap Van Dongeren<sup>†</sup>, Paolo Ciavola<sup>‡</sup>, Christophe Viavattene<sup>∞</sup>, Simone de Kleermaeker<sup>§</sup>, Grit Martinez<sup>+</sup>, Oscar Ferreira<sup>#</sup>, Cristina Costa<sup>@</sup>, Robert McCall<sup>¶</sup>

<sup>†</sup> Deltares,  
Dept. ZKS,  
Delft, The Netherlands  
ap.vandongeren@deltares.nl

<sup>‡</sup> Dip. Fisica e Sc. Terra,  
U. Ferrara,  
Ferrara, Italy  
cvp@unife.it

<sup>∞</sup> Flood Hazard Research Center  
Middlesex University,  
London, United Kingdom  
C.Viavattene@mdx.ac.uk

<sup>§</sup> Deltares,  
Dept. ZKS,  
Delft, The Netherlands  
simone.dekleermaeker@deltares.nl

<sup>+</sup> Ecologic Institute,  
Berlin, Germany  
grit.martinez@ecologic.eu

<sup>#</sup> CIMA,  
Universidade do Algarve,  
Faro Portugal  
oferreira@ualg.pt

<sup>@</sup> EurOcean  
Lisbon, Portugal  
costa.cristina@fct.pt

<sup>¶</sup> Deltares,  
Dept. ZKS,  
Delft, The Netherlands  
Robert.mccall@deltares.nl



[www.cerf-jcr.org](http://www.cerf-jcr.org)



[www.JCRonline.org](http://www.JCRonline.org)

### ABSTRACT

Van Dongeren, A., Ciavola, P., Viavattene, C., De Kleermaeker, S., Martinez, G., Ferreira, O., Costa C., R. McCall, 2014. RISC-KIT: Resilience-Increasing Strategies for Coasts – toolkit. In: Green, A.N. and Cooper, J.A.G. (eds.), *Proceedings 13<sup>th</sup> International Coastal Symposium* (Durban, South Africa), *Journal of Coastal Research*, Special Issue No. 70, pp. 366-371, ISSN 0749-0208.

Recent and historic high-impact events have demonstrated the flood risks faced by exposed coastal areas. These risks will increase due to climate change and economic development. This requires a re-evaluation of coastal disaster risk reduction DRR strategies and prevention, mitigation and preparedness PMP measures. To this end, the UN Office for Disaster Risk Reduction formulated the Hyogo Framework for Action, and the EU has issued the Floods Directive. By their nature, neither is specific about the methods to be used to assess coastal risks, particularly those risks resulting from dune and structure overtopping, the non-stationarity of surge and flash flood events, and coastal morphodynamic response. This paper describes a set of open-source and open-access methods, tools and management approaches to fill this gap. A Coastal Risk Assessment Framework will assess coastal risk at a regional scale. Thus critical *hotspots* can be identified for which an impact-oriented Early Warning System/Decision Support System is developed. This can be applied in dual mode: as a forecast and warning system and as an ex-ante planning tool to evaluate the vulnerability. The tools are demonstrated on case study sites on a range of EU coasts with diverse geomorphic settings, land use, forcing, hazard types and socio-economic, cultural and environmental characteristics. Specific DRR plans will be developed for all sites. A management guide of PMP measures and management approaches is to be developed. The toolkit will benefit forecasting and civil protection agencies, coastal managers, local government, community members, NGOs, the general public and scientists.

**ADDITIONAL INDEX WORDS:** *Coastal risk, impacts, hazards, early-warning systems, Bayesian modeling, numerical modeling, eco-systembased approaches, socio-cultural aspects, impact-oriented data base.*

### INTRODUCTION

Recent and historic low-frequency, high-impact events such as Xynthia which inundated the French Atlantic Vendee coast in February 2010 (Garnier and Surville, 2010; Bertin, et al. 2012), the Ligurian Flash Floods which occurred in October 2011 (Silvestro et al 2012), 1953 North Sea storm surge which inundated parts of the Netherlands, Belgium and the UK have demonstrated the flood risks faced by exposed coastal areas in Europe. Typhoons in Asia (such as Typhoon Haiyan in the Phillipines in November 2013), hurricanes in the Caribbean and Gulf of Mexico, and Superstorm Sandy, impacting the northeastern U.S.A. in October 2012, have demonstrated how even larger flooding events pose a significant risk and can

devastate and immobilise large cities and countries.

Risk can be defined as the product of the probability of a hazard and its consequences (Helm, 1996). Both are likely to increase in the future. The hazard probability may go up due to a changing climate (Emmanuel, 2007) with more frequent and violent hazards of surge-driven floods, wind damage, erosion, overtopping and rain-driven flash floods. Also, the consequences will increase. These consequences (or impacts) are composed of two factors: the direct exposure (the density of receptors, e.g. number of people and buildings in an affected area) and vulnerability (receptor value and their sensitivity to experience harm; Samuels et al., 2009). The number and value of receptors in the coastal area increases due to continued economic development and population growth. The sensitivity is also increasing e.g. due to unsuitable building

types. Moreover, due to ripple effects of disasters, indirect impacts will affect the hinterland of coastal areas.

This projected increase in risk along coasts requires a re-evaluation of coastal disaster risk reduction (DRR) strategies and a new mix of prevention (e.g. dike protection), mitigation (e.g. limiting construction in flood-prone areas; eco-system based solutions) and preparedness (e.g. Early Warning Systems, EWS) (PMP) measures. Even without a change in risk due to climate or socio-economic changes, a re-evaluation is necessary in the light of i) shrinking public works budgets which drives cost-efficiency, and ii) a growing appreciation of ecological and natural values which drive ecosystem-based approaches. One step further is the “Building with Nature” (De Vriend and Van Koningsveld, 2012) approach, which in effect uses natural processes and environments to help protect the hinterland. In addition, as free space is becoming sparse, coastal DRR plans need to be spatially efficient, allowing for multi-functionality (eg., use of ecosystem services as flood defence; combining coastal protection with benefits for tourism).

DRR planning should be viewed as an integrated chain of actions. This chain starts with understanding the present and historic situation and context in an area, assessing coastal risk for present and future hazard probabilities, identifying critical (hot spot) areas of higher risk, designing DRR plans including suitable prevention, mitigation and preparedness measures (such as EWS) to reduce coastal risk, and building trust and societal acceptance of these measures. In this way effective DRR solutions can achieve a strong societal basis and become part of the culture. Developing methods and tools to decrease risk and increase resilience requires an interdisciplinary approach and a supranational effort.

In one such supranational effort to drive the agenda on DRR, the United Nations Office for Disaster Risk Reduction (UNISDR) formulated the disaster reduction goals in the Hyogo Framework for Action (HFA). Concurrently, the EU has issued the Floods Directive, focused on the hazard of flooding, which requires Member States to implement flood risk management plans by 2015.

By their nature, neither the HFA nor the EU Floods Directive are specific about the methods to be used to assess coastal risks, particularly those resulting from multiple, synergistic hazards such as overtopping, breaching, and erosion. On coasts, river flood risk assessment methods (GIS-based flood mapping) will misrepresent the risk because the non-stationarity of surge and flash flood events. Also, the morphodynamic response of the coast has a strong effect on the flooding of the hinterland. Finally, effective preparedness measures, specifically coastal EWS, do not as yet play an integral role in the European approach, even though they are encouraged in the EU Floods Directive and have been identified as the most effective method for reducing the risks of loss of life and economic value (UNISDR, 2002).

## OBJECTIVES

The main objective of the EU-funded RISC-KIT project is to develop methods, tools and management approaches to reduce risk and increase resilience to low-frequency, high-impact hydro-meteorological events in the coastal zone. These products will enhance forecasting, prediction and early warning capabilities, improve the assessment of long-term coastal risk and optimise the mix of prevention, mitigation and preparedness measures. Specific objectives are:

1. Review and analysis of current-practice coastal risk management plans and lessons-learned of historical large-scale events;

2. Collection of local socio-cultural-economic and physical data at case study sites through end-user and stakeholder consultation to be stored in an impact-oriented coastal risk database;
3. Development of a regional-scale coastal risk assessment framework (CRAF) to assess present and future risk due to multi-hazards;
4. Development of an impact-oriented Early Warning and Decision Support System (EWS/DSS) for hot spot areas consisting of: i) a free-ware system to predict hazard intensities using coupled hydro-meteo and morphological models and ii) a Bayesian-based Decision Support System which integrates hazards and socio-economic, cultural and environmental consequences;
5. Development of potential DRR measures and the design of ecosystem-based and cost-effective, (non-)technological DRR plans in close cooperation with end-users for a diverse set of case study sites on all European regional seas and on one tropical coast;
6. Application of CRAF and EWS/DSS tools at the case study sites to test the DRR plans for a combination of scenarios of climate-related hazard and socio-economic vulnerability change and demonstration of the operational mode;
7. Development of a web-based management guide for developing integrated DRR plans along Europe’s coasts and beyond and provide a synthesis of lessons learned in RISC-KIT in the form of policy guidance and recommendations at the national and EU level.

## THE RISC-KIT PROJECT

The Resilience-Increasing Strategies for Coasts - toolKIT (RISC-KIT) project will consist of a set of innovative open-source and open-access methods, tools and management approaches (the RISC-KIT) in support of coastal managers, (emergency) decision-makers and policy makers. In detail they are

### Coastal Risk Assessment Framework

As a *first tool*, a quick-scan Coastal Risk Assessment Framework (CRAF) will be able to assess coastal areas at a regional scale of about 100 km of coastal length, a typical “administrative” or “jurisdictional” scale (visualised in the top panel of Figure 1). The CRAF evaluates coastal risk along transects (the grey lines in the figure) with a resolution of about 1 km. With this tool, coastal managers can identify critical coastal areas (*hotspots* of about 10 km in alongshore length, indicated by the red crosses in the figure) so that resources can be directed to the areas that need it most under present but also under future (climate-change induced) conditions.

The first innovation of this tool will be to derive the hazard itself (e.g. breaching, erosion, wave run-up and overtopping) from the external boundary conditions using physics-based models which properly consider the nonlinear dynamics of the processes involved. In particular, an efficient 1D (transect) version of the XBeach model (Roelvink et al., 2009) will be applied. Thus, this methodology will allow associating probabilities of occurrence not just to the forcing elements (waves, surges) but also to the hazards (erosion, inundation). This is especially relevant as most of the considered hazards depend upon more than one variables.

The second advancement is to consider various forcing terms and their associated probabilities and to include all these in the probability of the hazard itself. To do this for all potential coastal hazards, the methodology developed Jimenez et al. (2009) and Bosom and Jimenez (2011) will be extended.



The third advancement is in the assessment of the vulnerability of exposed entities, where RISC-KIT will better recognize the variation in the sensitivity value of groups in response to external factors, such as the characteristics of the hazard, the nature of the surrounding environment, and the existence of PMP measures. This will be done by developing a consistent and exhaustive library which will enhance the vulnerability assessment of the exposed entities and will make vulnerability comparable on a pan-European scale.

Fourthly, we will evaluate the long-term risk based on the resilience of the system, i.e. the ability of a system or a sub-system to return to the prior state after a disturbance (Birkman, 2006), and thus stimulate sustainable coastal development. A key challenge is to incorporate additional non-monetary social indicators such as the Human Development Index and the Wellbeing index (Stiglitz *et al.*, 2009). Finally, rather than focussing on directly-exposed elements, RISC-KIT will advance knowledge by considering potential ripple effects within and between the socio-economic, cultural and environmental systems inside and outside the immediate disaster area, and develop specific indicators to reveal the vulnerability of the system as a whole.

### Early Warning System/Decision Support System

The CRAF will identify hotspots of high risk. For these hotspots, a more detailed *second tool*, the impact-oriented Early Warning System/Decision Support System (EWS/DSS) is developed to provide real-time (short-term) forecasts and early warnings based on generic tools so that a common functionality across Europe can be achieved. The EWS (Figure 1; middle panel) component is a 2D model train of hydro-meteo and morphological models which computes hazard intensities, in the example in the figure a hazard of marine-origin. From the hazard intensity for every hazard type and the attributes (density, sensitivity and value) of every receptor type, the total expected impact can be obtained using the Decision Support System (DSS).

The first advancement will be to expand the functionality of Delft-FEWS (Werner *et al.*, 2013), now used in riverine environments, to coastal environments, including models of wave transformation, tides and wind-induced surge. The second advancement is to include morphodynamical and flash flood models. To the first aspect, the storm-response model XBeach (Roelvink *et al.*, 2009; Van Dongeren *et al.*, 2009) will be incorporated in a 2D efficient mode and expanded in functionality. In order to compute rain-driven flash floods, the modules developed in EU projects such as DRIHM and IMPRINTS (Alfieri *et al.*, 2011; Berenguer *et al.*, 2011) will be incorporated. The third advancement is the distribution of EWS information to the field. The goal is to develop a means to supply decision-makers with a stand-alone EWS/DSS which uses information from ex-ante scenario computations and which can be updated with the latest available information. We will develop a Bayesian-based Decision Support System which will connect hazard intensity and socio-economic, environmental and cultural distributions and thus allow the transition from hazards to impacts. An important innovation of the EWS/DSS lies in its application in dual mode: as a forecast and warning system and as a consistent ex-ante planning tool to evaluate the long-term vulnerability due to multiple (low-frequency) coastal hazards, under various climate-related scenarios. This innovative dual function application will thus integrate long-term planning and short-term forecasts and warnings to their mutual benefit. RISC-KIT will demonstrate the robustness and applicability of the CRAF and EWS/DSS tools on case study sites on the coasts of all EU regional seas with diverse

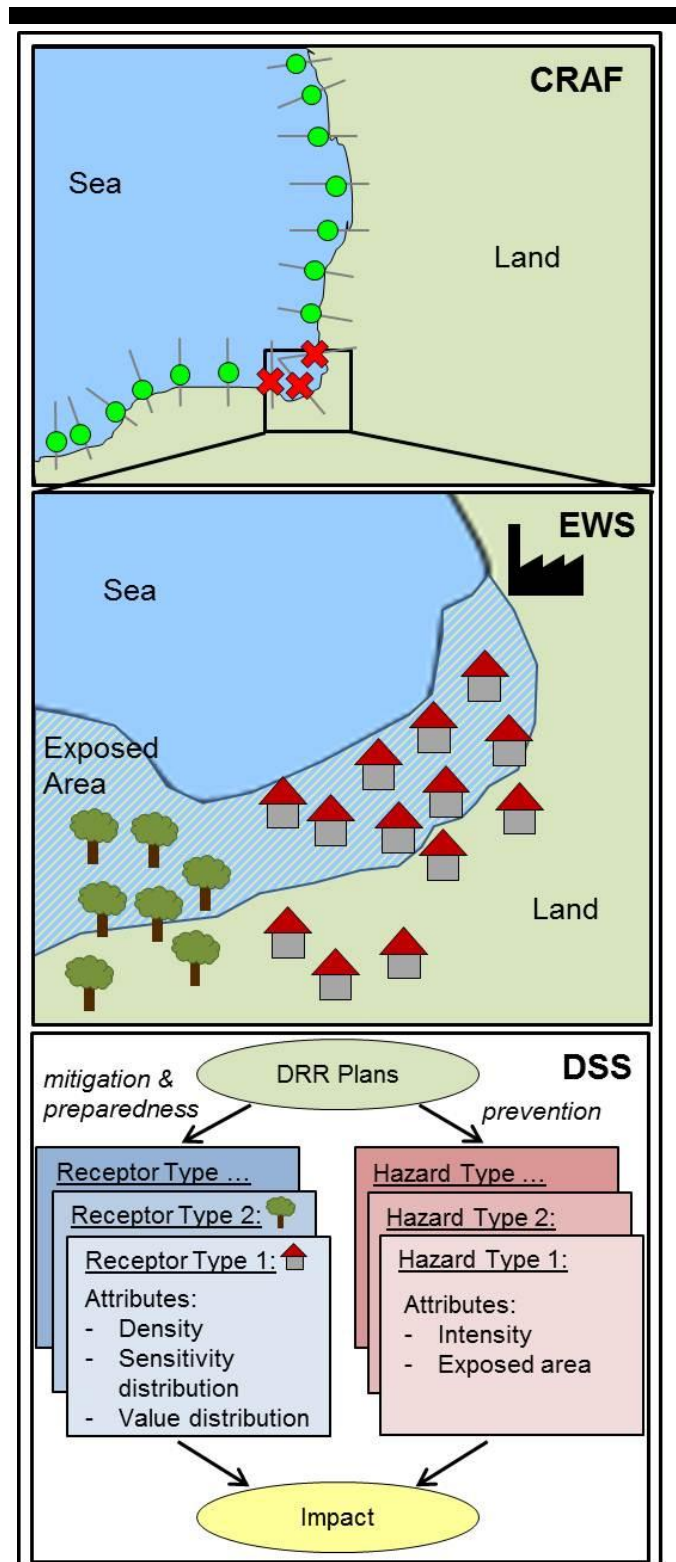


Figure 1. Conceptual drawing of the CRAF (top panel), the EWS (middle panel) and the DSS (bottom panel).

geomorphic settings (open coasts, lagoons, salt marshes, deltas and estuaries), land use (industrial infrastructures, coastal towns, marinas, tourist areas, natural parks and cultural heritage), forcing

(tides, surges, waves), hazard types (erosion, overtopping, coastal rain-driven flash floods) and socio-economic, cultural and environmental characteristics, see Figure 2. The list also includes one site in Bangladesh characterised by a high population density in a delta plain affected by typhoons. Several of the study sites will be affected by consequences of climate change such as sea level rise or wave height increase. Sea level rise will be relevant for the majority of the studied sites, potentially inducing increased coastal erosion and shoreline retreat on sandy shores (e.g. ocean shores of Ria Formosa, North Norfolk, Bocca di Magra, La Faute sur Mer and Tordera Delta), problems related to safety and protection at harbors (e.g., Zeebrugge), but mainly contributing to an increase on the flood potential to the low-lying areas (e.g. Kristianstad, Ria Formosa lagoon, Tordera Delta, Garibaldi-Bellocchio, La Faute sur Mer estuary, North Norfolk saltmarshes and Sandwip Island at the GBM Delta). Wave height increase on the North Atlantic will account for an increase in coastal erosion on the Atlantic exposed coastal areas (e.g. La Faute sur Mer) as it can also be damaging for harbor infrastructures (e.g. Zeebrugge). The consequences mentioned above will have a direct impact on the economy with tourism and housing being the most threatened economic values but also resulting in increased difficulties to execute certain harbor activities. In low lying areas economic threats also include loss of agricultural land (e.g. North Norfolk, Kristianstad) and clam farming areas (e.g., Ria Formosa), and inundation of urban areas (e.g. Kristianstad, Ria Formosa).

### Management guide of PMP measures and approaches

Specific DRR plans and alternatives will be developed for all sites. The DRR plans will be tested using the EWS/DSS in ex-ante planning tool mode in order to optimise the effect that such plans have on hazard intensities (through e.g. prevention) and receptor attributes (through mitigation and preparedness), see Figure 1 bottom panel. This optimisation will provide valuable information to develop a management guide of adequate ex-ante prevention, mitigation and preparedness measures and management approaches (the *third tool* in the RISC-toolkit) which will help to minimise socio-economic loss and environmental impacts.

RISC-KIT will demonstrate practical ways in which the multi-hazards from the sea and the land can be integrated into DRR approaches. Thus, we will show how Integrated Coastal Zone Management (ICZM) and Integrated Water Resources Management (IWRM) can be linked with DRR strategies which go over and beyond the scope of the Flood Directive. Through this integration, RISC-KIT aims to encourage greater policy effectiveness and to increase coherence with existing systems, policies approaches and goals to ensure their sustainability and cost-effectiveness. In a second advancement, risk reduction and resilience plans developed in RISC-KIT will constitute a tailor-made mix of DRR plans, which will explicitly include adaptive management measures that move away from a worldview of preventing or avoiding risk, towards accepting risks. Therefore, apart from traditional hard-infrastructure technological solutions, the project will consider ecosystem-based solutions (Johannessen and Hahn, 2013) and ways of 'living with hazards' (Nienhuis and Leuven, 2001). In a third advancement, as resilience to natural events is deeply rooted in social systems, local and community-level understandings of risk are acknowledged as legitimate descriptions of system dynamics. Thus, for effective DRR at an EU and international level, it is essential that lessons learned and user knowledge of local socio-economic, historic and cultural factors are shared between actors. To account for this, RISC-KIT will make use of participatory methods (live-polling, moderated

discussion groups or round table discussions). This approach will also help build ownership amongst coastal end-users and stakeholders and contribute to improved multi-level governance and institutional accountability (Wachinger et al., 2012). Fourthly, acceptability of the plans will be improved by evaluating them against a range of climate scenarios at the case study sites, using an integrated assessment that as a progress-beyond-the-state-of-the-art combines a multi-criteria analysis and a soft systems methodology (Checkland, 2000). The first will assess the technical and economic feasibility and the capacity to reduce disaster risk. The soft systems methodology takes different viewpoints of end-users and stakeholders into consideration.

### Impact-oriented coastal risk database

Finally, as a *fourth tool*, a more complete and impact-oriented database will be created. This type of database is not publicly-available as of now, despite efforts at the European and global (UNISDR) level. Currently, Europe lacks a comprehensive database of marine storm occurrence *and* their impact on all European coastlines. In some cases national databases combining hazards and impacts exist, but often only contain recent data. The first advancement will be the expansion of the data set with historical sources. The reconstruction of the human and financial costs in the current coastal setting caused by events comparable to those in the historical analysis, will lead to better understanding of the stakes and vulnerabilities of the case study sites in a long-term perspective (>200 years) and will strengthen prevention and the preparation strategies for extreme events. In addition, the knowledge gained will supply examples regarding memory of risks, which will constitute useful tools for mediation with elected representatives and local communities. The second advancement is the inclusion of socio-economic, cultural and environmental information (where possible from interviews of contemporary witnesses) to characterise the *impact* of the events. The social and economic aspects of post disaster appraisal will also be examined, as well as cultural and health related aspects such as the number and type of casualties experienced both during and after an event. The third advancement is that the database will integrate data from different hazards, ie. will be multi-hazard (storms, surges, winds, flash floods) in a systematic way.

### Target audience and users

The above toolkit will directly benefit end-users (primary users of the project's deliverables such as forecasting agencies, civil protection agencies, coastal managers) and stakeholders (those affected by project outcomes, such as mayors, community members, NGOs, the general public and scientists), because it will enable them to identify hot spot areas, to produce timely forecasts and early warnings for these critical hotspots, to evaluate climate-related, socio-economic and cultural changes and to design DRR plans with the optimal mix of prevention, mitigation and preparedness measures for their specific situation. The Bangladesh site will serve to test the applicability of the toolkit in the developing world in the context of the UNISDR policy.

To ensure uptake and acceptance of these tools, RISC-KIT has assembled an End-User Board which includes representatives from disaster management agencies (National Civil Protection in Italy), coastal managers (Environment Agency in UK; Schleswig-Holstein Coastal Defence Agency, Germany; Catalunya Water Agency, Spain), local government (La Faute sur mer mayor, Kristianstad Chief Executive and Varna Governor), regional government (Water Agency, Spain; Regione Emilia-Romagna, Italy; Flanders Government) and interest groups (Kiel Marina) who have a vested interest in the case study sites.

## METHODOLOGY

The project is structured into seven Work Packages (WP) as follows (Figure 3). WP1 will firstly review current DRR management policy and will analyse representative disastrous hydro-meteorological events to derive lessons learned from the past (to be used in WP4). Secondly, WP1 will collect physical, socio-economic, cultural and environmental data at the case study sites on the basis of stakeholder consultations and compile them in an easily accessible database (to be used in WP5).

WP2 will develop the CRAF at regional scale (~100 km) to identify hot spots of risk (first component of the RISC-toolKIT). The CRAF will be a combination of the Coastal Hazard Assessment module and the Coastal Vulnerability Indicator Library. This enables the evaluation of risk as the product of hazard, derived from the underlying physical processes, and vulnerability, based on socio-economic, cultural, environmental and system-related indicators. The multi-criteria analysis to be developed will weigh these criteria according to user preferences and to map risk levels spatially.

WP3 will develop a detailed EWS/DSS (second component of the RISC-toolKIT) for hot spots of risk (~10 km). The EWS will predict hazard intensities (e.g. flood levels and erosion) at a high resolution and can be used for real time and ex-ante scenario simulations. The Bayesian DSS will link the predicted hazard intensities to socio-economic, cultural and environmental impacts. Thus, the EWS/DSS will provide early-warnings for decision making not based on hazard intensities, but on expected impacts.

WP4 will develop new management and policy approaches to reduce coastal risk and increase resilience. It will develop a potential PMP measures, and compile them into site-specific DRR plans. Based on the evaluation of these plans after extensive scenario testing at the case study sites (WP5) and feedback consultations with end-users and stakeholders, WP4 will make recommendations on the use of PMP measures and will publish these in the form of a web-based management guide.

In WP5 the RISC-toolkit will be applied to a set of diverse field sites. At a priori selected hot spots the EWS/DSS (WP3) will be set up to test a range of climate-change and socio-economic scenarios against the DRR plans proposed in WP4. The results of these tests will be fed back to WP4 to evaluate the effectiveness and acceptance of the DRR plans.

All dissemination activities will be centrally streamlined through WP6 and will run alongside the entire project as will do WP7 in which the project will be managed and coordinated. Figure 3 displays the organisation and inter-linkages of the Work Packages.

## PARTNER INSTITUTES

The RISC-KIT consortium consists of the following partners. Case study partners are indicated with a \*:

1. Deltares, Delft, NL (Coordinator and WP3 leader)
2. Consorzio Ferrara di Ricerche, Ferrara, IT (WP1 leader, \*)
3. Middlesex University, London, UK (WP2 leader)
4. Ecologic Institute, Berlin, DE (WP4 leader)
5. U. Algarve, Faro, PT (WP5 leader, \*)
6. EurOcean Foundation, Lisbon, PT (WP6 leader)
7. Stockholm Environmental Institute (\*)
8. Bundesanstalt für Wasserbau, Hamburg, DE (\*)
9. University of Cambridge, Cambridge, UK (\*)
10. International Marine and Dredging Contractors, Antwerp, BE (\*)
11. Centre National de la Recherche Scientifique, La Rochelle, FR (\*)
12. Universitat Politècnica de Catalunya, ES (\*)



Figure 2. Case study sites (stars), RISC-KIT case study site partners (blue solid dots) and non-case study site partners (red open circles).

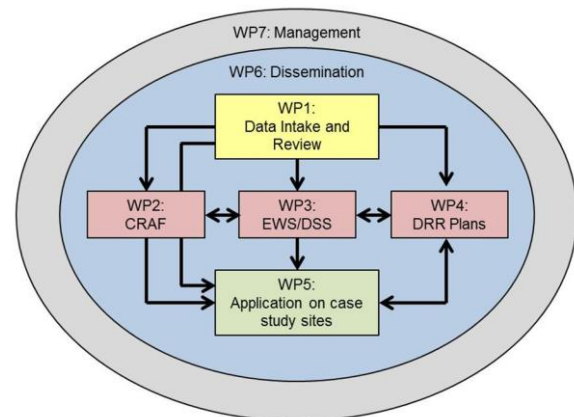


Figure 3. Diagram showing the interaction (in terms of exchange of results) between different Work Packages (WP).

13. Centro Internazionale in Monitoraggio Ambientale, Savona, IT (\*)
14. Institute of Oceanology – Bulgarian Academy of Sciences, Varna, BG (\*)
15. World Meteorological Organization, Geneva, CH (\*)
16. Université de Caen Basse Normandie, Caen, FR
17. UNESCO-IHE, Delft, NL (\*)
18. Delft University of Technology, Delft, NL.

## IMPACTS

### Faster attainment of the DRR goals of UNISDR

RISC-KIT contributes directly to the DRR goals of the UNISDR, summarised in five Priorities for Action (Pfa's).

*Pfa1: Ensure that disaster risk reduction is a national and local priority with a strong institutional basis for implementation;* RISC-KIT provides DRR methods, tools and approaches that are applicable across the EU and beyond. When used by local

governments, RISC-KIT helps to decentralise resources and responsibilities.

*PfA 2 Identify, assess and monitor disaster risks – and enhance early warning;* The collection of local socio-economic and physical data into an impact-oriented coastal risk database allows for data sharing. The CRAF and EWS/DSS enables regional authorities to identify and assess multi-hazards and their impacts.

*PfA3 Use knowledge, innovation, and education to build a culture of safety and resilience at all levels;* The CRAF and the impact-oriented coastal risk database will integrate hazard data and vulnerability information and facilitate information sharing and cooperation across industries. To build a culture of safety and improve public awareness, RISC-KIT will target and involve regional end-users through information exchange and summer schools

*PfA4 Reduce the underlying risk factors;* RISC-KIT recognizes that sustainable ecosystems and environmental management are a key ingredient in designing cost-effective DRR plans.

*PfA5 Strengthen disaster preparedness for effective response at all levels;* Through dissemination to end users and stakeholders, RISC-KIT increases capacity building on coastal risk management and contribute to risk reduction at policy, technical and institutional levels.

### Design of cost-effective risk-reduction plans, based on the proposed tools and solutions.

Coastal managers will be able to assess coastal risk at the regional (administrative) scale and identify hot spot (priority) areas for which detailed EWS can be implemented and innovative, cost-effective and ecosystem-based DRR plans can be designed. These plans will be ‘environmentally sustainable, economically equitable, socially responsible and culturally sensitive’, combining all relevant aspects of Integrated Coastal Zone Management. Evaluation criteria will ensure that these options will strive for policy coherence and cost-effectiveness.

### Improve risk governance and preparedness through the provision of timely information and warnings to decision-makers.

The EWS/DSS will improve risk governance and preparedness through the provision of timely information and warnings to decision-makers. In the event of an impending disaster, the EWS/DSS will allow managers to take rapid decisions based on the latest information on impacts. The CRAF and the scenario evaluation tool will help decrease the ex-ante coastal risk by providing policy makers with information on vulnerable hot spots. Through on-going end-user interaction, RISC-KIT will foster information exchange between disaster managers and technical developers.

### ACKNOWLEDGEMENTS

The work described in this publication was supported by the European Community's 7th Framework Programme through the grant to the budget of RISC-KIT, contract no. 603458, and by contributions by the partner institutes.

### LITERATURE CITED

Alfieri, L., Velasco, D., and Thielen, J., 2011. Flash flood detection through a multi-stage probabilistic warning system for heavy precipitation events, *Adv. Geosci.*, 29, 69-75, doi:10.5194/adgeo-29-69-2011.

- Berenguer, M., D. Sempere-Torres, G.S. Pegram, 2011. SBMcast – An ensemble nowcasting technique to assess the uncertainty in rainfall forecasts by Lagrangian extrapolation, *Journal of Hydrology*, Volume 404, Issues 3–4, 11 Pages 226-240, ISSN 0022-1694, <http://dx.doi.org/10.1016/j.jhydrol.2011.04.033>.
- Birkmann, J. (ed.), 2006. *Measuring vulnerability to natural hazards: towards disaster resilient societies*. United Nations University Press. 523 p. ISBN 92-808-1135-5
- Bertin, X., Bruneau, N., Breilh, J. F., Fortunato, A. B., & Karpytchev, M. (2012). Importance of wave age and resonance in storm surges: The case Xynthia, Bay of Biscay. *Ocean Modelling*, 42, 16-30.
- Bosom, E. and Jiménez, J.A., 2011. Probabilistic Coastal vulnerability assessment to storms at regional scale - application to Catalan beaches (NW Mediterranean). *Natural Hazards and Earth System Sciences*, 11, 475-484.
- De Vriend, H. J., & Van Koningsveld, M., 2012. *Building with Nature: Thinking, acting and interacting differently*. Dordrecht, the Netherlands: EcoShape, Building with Nature, 39
- Checkland, P., 2000. Soft systems methodology: a thirty year retrospective. *Systems Research and Behavioral Science*, 17, 11-58.
- Emanuel, K., 2007. Environmental factors affecting tropical cyclone power dissipation. *Journal of Climate*, 20(22), 5497-5509.
- Garnier, E., Surville, S.F., 2010. *Le Croît Vif, Saintes*, p. 176, ISBN 978-2-36199-009-1.
- Samuels, P., Gouldby, B., Klijn, F., Messner, F., van Os, A., Sayers, P. and Udale-Clarke, H. (2009). Language of risk—project definitions. *Floodsite project report T32-04-01*.
- Helm, P. 1996. Integrated Risk Management for Natural and Technological Disasters. *Tephra*, vol. 15, no. 1, June 1996, pp. 4-13.
- Jiménez, J.A., Ciavola, P., Balouin, Y., Armaroli, C., Bosom, E. & Gervais, M., 2009. Geomorphic coastal vulnerability to storms in microtidal fetch-limited environments: Application to NW Mediterranean & N Adriatic Seas. *Journal of Coastal Research*, SI 56, 1641-1645.
- Johannessen, Å., and T. Hahn. (2013). Social learning towards a more adaptive paradigm? Reducing flood risk in Kristianstad municipality, Sweden. *Global Environmental Change* 23:372–381, <http://dx.doi.org/10.1016/j.gloenvcha.2012.07.009>
- Nienhuis, P. and R. Leuven, 2001. River restoration and flood protection: controversy or synergism. *Hydrobiologia* 444: 85–99
- Roelvink, J.A., A. Reniers, A. Van Dongeren, J. Van Thiel de Vries, R. McCall, J. Lescinski. 2009. Modeling storm impacts on beaches, dunes and barrier islands. *Coastal Engineering*, doi: DOI: 10.1016/j.coastaleng.2009.08.006.
- Silvestro, F., Gabellani, S., Giannoni, F., Parodi, A., Rebora, N., Rudari, R., and Siccardi, F., 2012. A hydrological analysis of the 4 November 2011 event in Genoa, *Nat. Hazards Earth Syst. Sci.*, 12, 2743-2752, doi:10.5194/nhess-12-2743-2012.
- Stiglitz, J.E. A. Sen, & J.-P. Fitoussi (Eds.), 2009. *Report by the commission on the measurement of economic performance and social progress*. Paris: Commission.
- UNISDR, 2002. *Guidelines for reducing flood losses*. United Nations. Retrieved from [http://www.unisdr.org/files/558\\_7639.pdf](http://www.unisdr.org/files/558_7639.pdf).
- Van Dongeren, A. Bolle, M. Voudoukas, T. Plomaritis, P. Eftimova, J. Williams, C. Armaroli, D. Idier, P. Van Geer, J. Van Thiel de Vries, P. Haerens, R. Taborda, J. Benavente, E. Trifonova, P. Ciavola, Y. Balouin and J.A. Roelvink, 2009. MICORE: Dune erosion and overwash model validation with data from nine European field sites, *Proceedings of Coastal Dynamics* 2009, pp. 1–15, doi:10.1142/9789814282475\_0084
- Wachinger, G., Renn, O., Begg, C., & Kuhlicke, C. (2012). The risk perception paradox—implications for governance and communication of natural hazards. *Risk Analysis*.
- Werner, M., J. Schellekens, P. Gijsbers, M. van Dijk, O. van den Akker and K. Heynert, 2013. The Delft-FEWS flow forecasting system. *Environmental Modelling & Software* 40, pp. 65-77.

## Incorporating dynamics factor to the Environmental Sensitivity Index (ESI) shoreline classification – Estonian and Spanish example

Robert Aps<sup>†</sup>, Hannes Tõnisson<sup>‡</sup>, Giorgio Anfuso<sup>+</sup>, José A. Perales<sup>#</sup>, Kaarel Orviku<sup>‡</sup>, Ülo Suursaar<sup>†</sup>

<sup>†</sup> Estonian Marine Institute, University of Tartu, Mäealuse St. 14, Tallinn, 12618, Estonia, robert.aps@ut.ee

<sup>‡</sup> Institute of Ecology at Tallinn University Uus-Sadama 5, Tallinn, 10120, Estonia, hannes.tonisson@gmail.com

<sup>+</sup> Departamento de Ciencias de la Tierra, Facultad de Ciencias del Mar y Ambientales, Universidad de Cádiz, Puerto Real, Spain, giorgio.anfuso@uca.es

<sup>#</sup> Departamento de Tecnologías del Medio Ambiente, Centro Andaluz de Ciencia y Tecnologías Marinas (CACYTMAR) Universidad de Cádiz, Puerto Real, Spain, joseantonio.perales@uca.es



[www.cerf-jcr.org](http://www.cerf-jcr.org)



[www.JCRonline.org](http://www.JCRonline.org)

### ABSTRACT

Aps, R., Tõnisson, H., Anfuso, G., Perales, J.A., Orviku, K., Suursaar, Ü. 2014. Incorporating dynamics factor to the Environmental Sensitivity Index (ESI) shoreline classification – Estonian and Spanish example. In: Green, A.N. and Cooper, J.A.G. (eds.), *Proceedings 13<sup>th</sup> International Coastal Symposium* (Durban, South Africa), *Journal of Coastal Research*, Special Issue No. 70, pp. 372-377, ISSN 0749-0208.

Oil transportation is growing in the Baltic Sea area and especially in the Gulf of Finland where it is reaching approximately 180–200 million tons a year by 2020. Growing oil transportation is considerably contributing to the risk of accidental spill related shoreline oiling. This paper focuses on amending the Environmental Sensitivity Index (ESI) related shoreline classification to local conditions by dynamically changing the categorization of shoreline in terms of its susceptibility to spilled oil caused by extreme meteorological events and taking into consideration a number of natural physical factors. The paper presents the results of two European case studies: the Estonian shoreline of the Gulf of Finland (Baltic Sea), and the Spanish coast of the Gibraltar Strait. Susceptibility to spilled oil of some categories of the Estonian shoreline (sandy shores, till shores and gravel shores) is occasionally changing over time from low to high sensitivity and back, and that especially conditioned to the influence of heavy storms. The studies carried out in Spain revealed a well recognizable indirect proportionality between foreshore slope and the tidal range. At many locations, the dynamic morphological characteristics of the beach appeared to be largely determined by contouring and specific conditions that are modifying the initial ESI related categorization of the sandy beaches concerned. The novelty of this work is in attempt to move from the standard ESI related and locally adapted static shoreline classification towards more dynamic shoreline monitoring based on characterization of the sensitive to oil pollution shoreline elements.

**ADDITIONAL INDEX WORDS:** *Dynamic shoreline classification, oil pollution, risk, Baltic Sea, Gibraltar Strait.*

### INTRODUCTION

Oil transportation has been growing significantly worldwide: it increased from 100 million tons in 1935 to approximately 3 billion tons presently. Oil transportation is also growing in the Baltic Sea area and especially in the Gulf of Finland where it will be reaching approximately 180–200 million tons a year by 2020 (Brunila and Storgård, 2012). Expanding oil transportation is contributing considerably to the risk of accidental spill related shoreline oiling. Nowadays, advice on sensitive shorelines is likely to be impacted by oil as it is of critical importance in order to support decision-makers, whether or not a response is necessary, and what kind and extent of response is appropriate.

According to NOAA (National Oceanic and Atmospheric Administration, 2002), the Environmental Sensitivity Index (ESI) maps have been an integral component of oil-spill contingency planning and response since 1979, serving as quick reference for oil spill responders, providing three general types of information: 1) shoreline classification, 2) biological resources and 3) human-use resources. The more than three decades of development of ESI

applications have resulted in a considerable body of research relating to sensitivity mapping of the different coastal zones in relation to the potential incidental oil pollution. According to NOAA (2002) classification, there are 10 main types of shores, these are based on an understanding of the physical and biological character of the shore environment. 1 being the least and 10 is the most sensitive. Within these 10 types there may be several sub-types (A, B, etc.) according to more location-specific environmental conditions.

A growing number of studies in this direction proceeded from the pioneering research done by Gundlach and Hayes (1978), Michel *et al.* (1978) and Dicks and Wright (1989). Further development of an ESI mapping was based on the extensive application of GIS (Krishnan, 1995) and remote sensing techniques with the aim to reduce the environmental consequences of the spill and cleanup efforts (Jensen *et al.*, 1990; 1998). ESI atlases have been generated from digital databases using GIS techniques for the Svalbard intertidal zone (Moe *et al.*, 2000), Cardoso Island State Park and surrounding areas: São Paulo, Brazil (Wieczorek *et al.*, 2007), Mediterranean coast of Israel (Adler and Inbar, 2007), Portuguese coast (Santos and Andrade, 2009), the northern coast of the Gibraltar Strait (Bello Smith *et al.*, 2011).

DOI: 10.2112/SI70-063.1 received 30 November 2013; accepted 21 February 2014. © Coastal Education & Research Foundation 2014

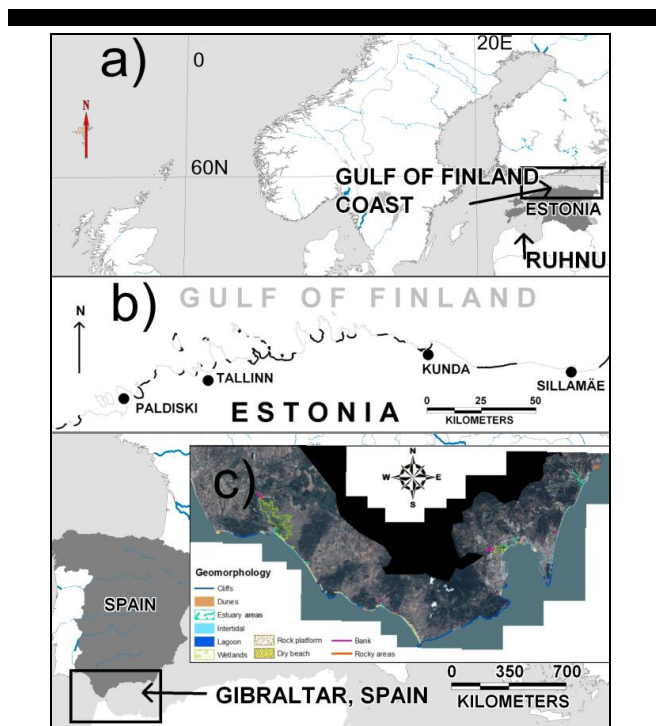


Figure 1. Location of the studied sites in Europe (a); Gulf of Finland coast (b), black-colored shoreline marks the classified sandy shores; geomorphic map of Gibraltar coast, Spain (c).

The aim of the paper is to present the ESI-related results of two European case studies: 1) the Estonian shoreline of the Gulf of Finland (Baltic Sea), and 2) the Spanish coast of the Gibraltar Strait. Both are among the most endangered (as a result of tanker accidents) sites in Europe due to their very intense, rapidly growing oil transport and relatively short distances from shipway to shore which makes the reaction time short. Therefore, the current study introduces a new level of ESI mapping by including the most considerable dynamic components. Finally, such results increase the preparedness to disaster and help to reduce clean-up costs and impact to the nature.

### STUDY AREA

The Estonian and Spanish study sites represent particularly endangered areas because they show intense ship traffic in naturally sensitive shallow continental seas and narrow straits (Figure 1). In such environments, the risk associated with ship grounding or collision is rather high, and if the oil spill occurs it is almost impossible to prevent the oil from washing ashore due to the limited extent of the sea area concerned and often narrow “window of opportunity” determined by the possibly unfavorable weather conditions.

Estonia has a comparatively long shoreline (approximately 4,000 km) due to a number of peninsulas, bays and islands (over 1,500 islands). The shores are geologically diverse and serve a variety of societal functions. The Estonian seashores in general are characterized by embayed nature with a variety of beach types experiencing land uplift ranging from 0.5 to 2.8 mm/year (Vallner *et al.*, 1988). The Estonian coast of the Gulf of Finland is a non-tidal bay (tidal range is less than 5 cm) exposed to the waves from the west, north-west and north. Despite virtually nonexistent tides, the Gulf of Finland frequently experiences rapid meteorologically

forced sea-level fluctuations, including up to 4 m high storm surges in the area of St. Petersburg (Russia) and up to 2–3 m high surges on the Estonian coast (Suursaar, 2010). Based on long-term studies in coastal geology, the Estonian shoreline of the Gulf of Finland has probably one of the most detailed geological classifications of shore types in Europe. In previous studies this classification has been taken as a basis for adapting the standard ESI shoreline classification to the local conditions of the Estonian shoreline of the Gulf of Finland. The standard ESI shoreline classification, adapted to the Estonian shoreline, revealed that over 2/3 of the shoreline concerned has very high environmental sensitivity with respect to potential oil pollution. Moreover, this is the most densely populated coastal area in Estonia including the capital (over 400,000 inhabitants) and a number of towns. Another example from the western coast of Estonia is also considered to demonstrate and explain the mechanisms of the findings (Ruhnu).

The studied area in Spain includes the Gibraltar Strait, a micro-tidal environment (tidal range is 1.3 m) exposed to winds and waves from the east and, secondarily, from the west. The shoreline is composed of high cliffs, bluffs, rocky shore platforms and sand beaches. Within this zone, several small quartz-rich beaches are observed at Algeciras Bay, which is the most populated area (around 250,000 inhabitants) with coastal towns, port activities, petrochemical industry and fisheries.

### METHODS

The on shore dynamic data are collected in the frames of several monitoring programs and scientific research projects of the Estonian coast. Repetitive photographs are taken and profiles are measured from the studied locations.

The collected profiles and photographs in the database are analyzed. Regular orthophotos have been taken along the Estonian coast since 1995 and for the studied sections in 1995–1998 (gray-scale, pixel size 75 cm), 2002–2005 (color, pixel size 50 cm) and 2008–2012 (color, pixel size 25 cm). The orthophotos are analyzed using *Mapinfo Professional*. We were not able to fit all the orthophotos in this article, but each orthophoto can be freely accessed via Estonian Land Board portal (<http://geoportaal.maaamet.ee/eng/>). The classification of the shoreline geology of Estonia was elaborated by Dr K. Orviku (Orviku *et al.*, 2010), which was later converted into ESI classification by the authors.

The Internet GIS technologies are increasingly used worldwide in conjunction with oil spill modeling tools as a means of integration and visualization of the oil spill response decision support related information. The methodology used in the example from Estonia is based on a coupled Seatrack Web – SmartResponse Web (SW–SRW) simulation framework developed by the EU Central Baltic INTERREG IVA Project “Minimizing risks of maritime oil transport by holistic safety strategies (MIMIC)”. The Estonian shoreline ESI map layers are imported as the Web Map Services into the coupled SW–SRW simulation framework and used for building situation awareness in oil spill response operations.

Relative exposure to wave and tidal energy, shoreline slope, and substrate type have been investigated in SW Spain using the framework of different studies and monitoring programs, especially focusing on the design of Environmental Sensitivity Maps for the Gibraltar Strait area (Bello Smith *et al.*, 2011) or the characterization of beach morphodynamics and wave climate along the SW Andalusia littoral (Anfuso *et al.*, 2002; Anfuso, 2005; Rangel and Anfuso, 2011). These studies serve as a discussion source for the current paper. Moreover, several monitoring results are taken into account.

## RESULTS AND DISCUSSION

The recent studies in Estonia and Spain have clearly revealed that shore dynamics might be an important factor to be taken into account in regional ESI classifications. Mixing layer, seasonality, and changing shore types due to the deficit of the sediment and abundance of strong storms, are the biggest concerns considered in the following chapter.

### Dynamics Factor: Estonian Example

The Estonian coast is experiencing a sediment deficit. Thin layers of soft, mobile sediment combined with largely variable shore types make the use of ESI sensitivity classes rather difficult. The datasets originating from the monitoring programs and various scientific research projects are indicating rapid changes in beach morphology and shore types in several locations along the Estonian coast (Orviku *et al.*, 2003; 2009; Tõnisson *et al.*, 2007; 2013). Changes in beach type automatically and rapidly change the sensitivity class as well as the sensitivity to pollution.

Storm surges have an important role in the shore processes on the coasts of the nearly tideless Gulf of Finland, leading to changes in beach morphology and (ESI) type. It is worth noting that storm surges in Estonia are caused by storms with westward approach directions. Very strong easterlies result in low sea level events, also known as “negative surges”, which have no significant geomorphic effect. The highest sea levels recorded in Estonia have always occurred during westerly storms. The highest sea-level (in the history of instrumental measurements) reaching 275 cm above mean sea level was recorded during the storm Gudrun in 2005 (Tõnisson *et al.*, 2008).

According to the analyzed field data, which was recorded after the storms and available cartographic data, we found that a few extreme or unusual events have caused the most drastic changes on the shores, including changes in their type (Orviku *et al.*, 2009). The best recorded example originates from the western coast of Estonia on Ruhnu Island (Figure 1a). Changes were first discovered on the repetitive photographs (Figure 2) and were later also detected on the orthophotos (Figure 3). In 1990, the whole western coast of the island was fringed by at least 20–30 m wide sandy beach while by 1996, most of the western coast was transformed into a till shore (Figure 2). The length of sandy beaches decreased more than 2.5 km in a space of 5 years (monitoring data). The southeastern part of Ruhnu Island is characterized by wide sandy beaches and dunes whereas most of the eastern and north-eastern parts are till shore bordered by a small scarp. Sediment transport is usually slow from north to south and accumulation occurs in the southern part of the island (Orviku *et al.*, 2003). However, in January and February of 1990, two very strong storms occurred with average wind speeds reaching 19 m/s, sea level +171 cm in January, and 25 m/s, +166 cm in February. In both cases the wind blew from S or SSW, elongating the sandy beaches nearly 2.5 km northward. No major storms occurred in the next five years and the initial situation was restored – sand was transported back to the south (Figure 2). Later on, similar shifts after major winter storms in 2005, 2007 and 2011/2012 (based on several orthophotos) were identified. However, most of the sand remained in the northern part of the island due to frequent storm activity.

Another example can be taken from the northern coast of Estonia (Gulf of Finland) in the vicinity of Aa village. However, the geomorphic system here is different. There is a constant sediment transport from west to east on the southern coast of the gulf. Negative storm surges during the eastern storms make westward transport almost impossible. Similar to the previous study area, wide sandy beaches after strong storm periods have



Figure 2. Winter storms from unusual direction accompanied with high sea level (over 150 cm) created over 2 km long and 20 m wide sandy beach on Ruhnu Island in 1990. In 1996, the same sandy beach changed to a till shore.

been observed here. This section of the coast is experiencing sediment deficit like most of the Estonian coast. The sand layer on the shore is usually very thin (less than 0.5 m). The sand is eroded from the scarps and is transported onto the shore or into the shallow sea during intense storms (like in 2005, 2007 and 2011/2012) and associated high sea levels. The orthophotos and photos taken from the shores the following summer indicate a rapid expansion of sandy beaches. However, this sand continues slow but constant eastward movement during ordinary storm events and accumulates in the bays or in the deeper sea leaving the shores, which become well exposed to waves without sand in a couple of years. These sandy beaches are temporarily restored during the next intense storm accompanied by high sea-levels.

These sandy beaches can be considered ESI 3B beaches (fine- to medium-grained sandy beaches – based on geological databases and visual observations) and after the loss of sand they change to 6A or 6B (gravel beaches and rip-rap gravel beaches). Their sensitivity to oil pollution increases rapidly (due to much deeper penetration of oil difficult cleanup). Lack of sand may create a situation when the upper layers cannot stop the penetration of possible oil pollution and oil reaches the deeper 6A or 6B type layers, which makes the cleanup process more complicated.

Nearly 25% (approximately 150 km) of the Gulf of Finland shores are mapped as sandy shores of ESI class 3B shores. However, these shores have mostly been mapped only once (field visits over past 30 years) and we cannot be sure if they persist or change their type from time to time. There are approximately 30 separate units of sandy beaches on the coast of the Gulf of Finland and even if we assume that their length may change approximately 2 km it still amounts to approximately 60 km (30 units x 2km), which is 10% of the total length of the shores here. This 10 % can



Figure 3. Winterstorms from unusual direction accompanied with high sea level (over 150 cm) created more than 2 km long and 20 m wide sandy beach (white color on the orthophoto) in Ruhnu Island. In 1995, no more sand was left (orthophotos by Estonian Land Board).

be classified as ESI 6A or 6B making the southern coast of the Gulf of Finland more sensitive than it was expected.

There is a certain relationship between the shoreline substrate type (shoreline substrate sensitivity) and the associated seafloor habitat's sensitivity (sensitivity of macrophytes and benthic invertebrates) to oil pollution (Leiger *et al.*, 2012). Therefore, the dynamic changes in shoreline substrate type are also dynamically changing the relationship of the associated seafloor habitat's sensitivity.

The ESI maps of the Estonian Baltic Sea shoreline are used by the oil spill response authorities for contingency planning, personnel training as well as in real emergency situations. Therefore, having the up-to-date and reliable information as an input to the coupled SW-SRW simulation framework, used by the authorities, is essential. However, the solution for making our ESI classification more reliable is rather time-consuming. We see that all the shores classified as ESI 3B (sandy beaches) must be re-mapped on the existing orthophotos (at least 6 different datasets depending on the location). We assume that the changes take place mostly between classes 6A, 6B and 3B, and luckily, these types can be easily identified and delimited from the orthophotos and no further fieldwork is needed. This enables us to identify the shores with very dynamic behavior. Furthermore, comparison of different datasets makes it possible to identify the directions of changes and find out the relationships with the forcing conditions (threshold

values for storm parameters like direction, sea-level, wave height etc.) and the recorded changes on the shores. We suggest that the comparison of maps and analyses of forcing conditions together with a monitoring program enables elaboration on the methodology to predict the extent and direction of changes in the beach morphology and ESI type. Such a methodology helps us to make ESI classification dynamic and match more closely the real situations that we might face on the shores. This all contributes to the better state of our shores and coastal waters. However, a solution to this problem requires extensive fieldwork (regular monitoring) for the verification (including thickness of sand layer) of the cartographic data and it must be handled in a separate study.

### Dynamics Factor: Spanish Example

The current study on the Spanish coast is focusing on geomorphic characteristics and especially on sandy littoral sectors in order to consider the importance of beach behavior, morphological changes, and beach grain size in determining the sensitivity of the shores.

Concerning the relative exposure, according to Rangel and Anfuso (2011), storm characterization and distribution can be easily carried out by means of the Storm Power Index (Dolan and Davis, 1992) used to divide storms into five classes, from Class 1 (Weak) to Class 5 (Extreme). Following Rangel and Anfuso (2011), the analysis of different wave data sets allowed the identification of storm wave height threshold and storm energy as well as characteristics such as temporal and spatial distribution along the SW Atlantic littoral of Andalusia. Information obtained constituted a key issue in the determination and prediction of beach erosion and accretion processes and associated risk for oil burial or re-appearance. Potential burial of oil in beaches is an important issue that must be taken into account in ESI and Emergency Plans (NOAA, 2002).

Shoreline slope is an important aspect that affects oil persistence in littoral and beach dynamics. It is related to grain size characteristics. In fact, there is a well-established direct relationship between mentioned parameters. Anyway, it is important to observe that, at places, beach slope values can be altered because of contouring conditions (Anfuso *et al.*, 2002). In this sense, an "artificial" slope, e.g. a slope value not well related to grain size characteristics, can be linked to a rock shore platform extended in the nearshore area (the rock platform affects wave propagation), or to other kinds of natural or human structures. Examples are beaches which are laterally limited by groins or backed by cliffs and/or seawalls or rip-rap revetments (Anfuso *et al.*, 2002; Bello Smith *et al.*, 2011). In such cases slope values must be treated carefully because they are usually overestimated. Beach slope is also affected by tidal range and this aspect is not taken into account in NOAA (2002). In the framework of beach monitoring carried out by Bello Smith *et al.* (2011), the micro-tidal beaches recorded extremely high slope values when compared with the ones recorded in the tidal areas. This is because of a well known inverse relationship between tidal range and beach slope. Hence, it would probably be interesting to differentiate between beach slopes of micro and tidal beaches as they show similar numeric values but different width and behavior.

Additionally, it must be underlined that a beach slope is a useful indicator of beach characteristics and morphodynamic state but it records exceptional seasonal and short term variations. Consequently, it is of great interest to achieve as much data as possible with regards to beach morphological characteristics and changes. In this sense, Bello Smith *et al.* (2011) carried out a monitoring program with a monthly periodicity, for the



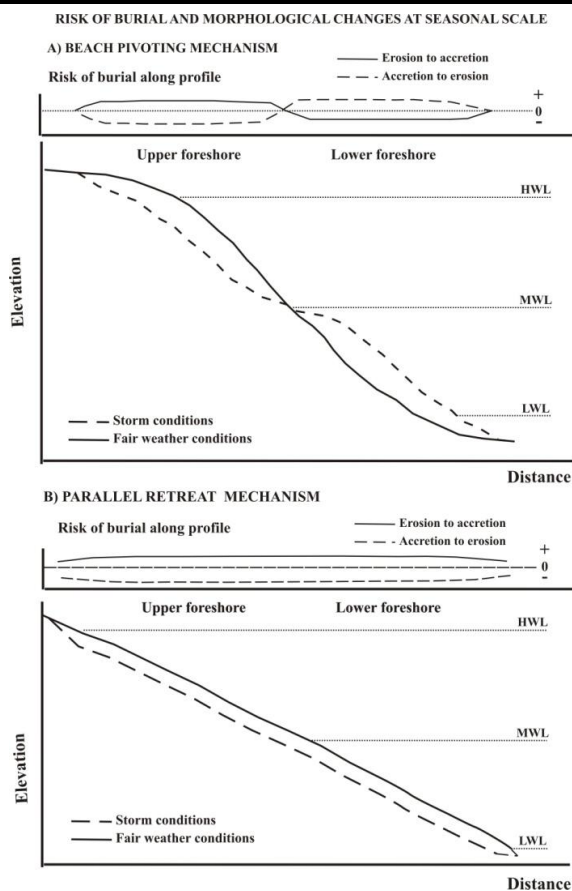


Figure 4. Pivoting and parallel retreat risk of burial at seasonal scale.

reconstruction of characteristics, behavior and seasonal variability of sandy beaches. Specifically, they investigated the Gibraltar Strait area during the spring-autumn period when, after the winter storm season, natural beach recovery and berm formation took place.

Different beach types were identified and classified according to the NOAA (2002) and the Wright and Short (1984) and Masselink and Short (1993) classifications. The use of the latter two classifications is of great importance because it allows useful additional information concerning the morphodynamic beach state (relevant for natural beach cleaning processes, the determination of cleaning techniques and beach mobility) and presence of bar/berm and beach cusps, relevant for oil burial. In addition, the monitoring program allowed investigation of seasonal changes. In this sense, it is possible to observe: i) beach morphodynamic changes over the year, this being an important point which controls practical aspects as beach mobility, and ii) vertical variations along the cross-shore profile, an important point for oil burial potential. Such changes can be categorized as “beach pivoting” and “parallel retreat” mechanisms (Nordstrom and Jackson, 1992). The knowledge of such types of beach response to erosion process is important for oil burial and estimation of beach congestion potential (Figure 4). Following the “beach pivoting mechanism”, a fair weather profile, usually characterized by a well developed berm and associated high foreshore slope, is affected by processes that create erosion in the upper foreshore and give rise to accretion in the lower foreshore, with a beach

pivoting at mean sea level position (Figure 4). In this sense, maximum probabilities of oil burial and re-appearance are respectively expected at lower and upper foreshore. During fair weather conditions the berm will be formed with sediments coming from the lower foreshore and burial potential will be at its maximum in the upper foreshore with high probability of oil re-appearance at the lower foreshore.

According to the “parallel retreat mechanism”, erosion and accretion are generally of minor importance with respect to the previous case, and are homogeneously distributed along the foreshore. Oil burial and re-appearance probability also show a homogeneous trend along the foreshore (Figure 4).

As an example, in Galicia (Spain), after the Prestige accident (13<sup>th</sup> November 2002), cleaning activities continued for several years because of the sporadic appearance of reduced quantities of fuel (Gonzalez *et al.*, 2009). In the period between the winter 2002 and the summer of 2006, along beaches investigated by previous authors, more than 10,000 tons of residual materials were removed from the berm and intertidal zone because the intermediate-reflective beach state and great morphological variability, which favored the oil to become partly buried. Lorenzo *et al.* (2009) observed similar processes in near beaches and used ground-based radar to investigate the depth of oil burial that ranged from few centimeters to 1–2 m. Furthermore, in order to assess an important issue such as oil burial at hourly scales, e.g. linked to tidal related morphological variations, specific field assessments on disturbance depth determination can be carried out. Anfuso (2005) used both rods with loose-fitting washers and marked sand to determine the disturbance depths, which were related to beach slope, breaking wave height and type, and morphodynamic beach state; different equations that have a broad validity were proposed. Specifically, the author found a good linear relationship between disturbance depth ( $y$ ) and beach slope ( $x$ , expressed as  $\tan \beta$ ):

$$y = 0.22 + 115x \quad r = 0.90 \quad (1)$$

The obtained expression is valid for a great range of beach gradients, from gentle beach faces ( $\tan \beta = 0.02$ ,  $\sim 1.3^\circ$ ) to steep foreshores ( $\tan \beta = 0.14$ ,  $\sim 8.8^\circ$ ). The aforementioned values belong to the first two classes of the NOAA classification, e.g.  $< 5^\circ$  and  $5 - 30^\circ$ , no cases have been reported neither for sand beaches with foreshore slopes  $> 10^\circ$  nor for the NOAA third class ( $> 30^\circ$ ), being such great values probably related to gravel, cobbles and blocks. Considering the great range in disturbance values presented by Anfuso (2005), e.g. equation (1): 2.52 cm for a slope of  $1.3^\circ$ , 8.27 cm for  $5^\circ$  and 16.32 cm for  $8.8^\circ$ , it could be probably helpful to further subdivide the first two NOAA classes in subclasses. Regarding the substrate type, the monitoring program carried out by Anfuso *et al.* (2002) evidenced the importance of studying seasonal changes in beach sediments, with coarser sediments observed in winter and vice versa, the granulometric differences in SW Spain being of 0.06 mm.

## CONCLUSION

Shores cannot be handled as static systems and all kind of classifications for the shores, including ESI classification, must take into account the shore dynamics. The shoreline ESI maps that are used by the oil spill response authorities for contingency planning, personnel training and in real emergency situations need to contain the up-to-date and reliable information. Therefore, it is essential to move from the standard ESI related and locally adapted static shoreline classification towards more dynamic shoreline monitoring based on characterization of the sensitivity to oil pollution shoreline elements.

## ACKNOWLEDGEMENT

This work was supported by ESF grants No. 8549, 9191 and 8980, target financed themes SF0280009s07 and SF0180104s08, and by the EstKliima project of the European Regional Fund program No. 3.2.0802.11-0043. The study was also supported by the Estonian Environmental Investment Centre and by Central Baltic INTERREG IVA Program Project MIMIC "Minimizing risks of maritime oil transport by holistic safety strategies". This research was partially developed in the frame of the ALBORAN Project (Project Ref. 0066\_ALBORAN\_2\_E), co-funded by the FEDER-POCTEFEX Program and with matched funding provided by the Regional Ministry of Environment of Andalusia and Andalusia (Spain) Research PAI Group RNM-328. Special thanks to Dr. Are Kont for his assistance in providing English language editorial comments and suggestions.

## LITERATURE CITED

- Adler, E. and Inbar, M., 2007. Shoreline sensitivity to oil spills, the Mediterranean coast of Israel: assessment and analysis. *Ocean & Coastal Management*, 50, 24–34.
- Anfuso, G., 2005. Sediment-activation depth values for gentle and steep beaches. *Marine Geology*, 220, 101–112.
- Anfuso, G., Martínez del Pozo, J.A., Gracia, F.J. and López-Aguayo, F., 2003. Long-shore distribution of morphodynamic beach states along an apparently homogeneous coast in SW Spain. *Journal of Coastal Conservation*, 9, 49–56.
- Bello Smith, A., Cerasuolo, G., Perales, J.A. and Anfuso, G., 2011. Environmental Sensitivity Maps: the north coast of Gibraltar Strait example. *Journal of Coastal Research*, SI 64 875–879.
- Brunila, O. and Storgård, J., 2012. Oil transportation in the Gulf of Finland in 2020 and 2030. *Publications from the Centre for Maritime Studies University of Turku*, A 61, 72 p.
- Dicks, B. and Wright, B., 1989. Coastal sensitivity mapping for oil spills. In: Dicks, B. (Ed.) *Ecological impacts of the oil industry*. New York: J. Wiley & Sons: 235–259.
- González, M., Medina, R., Bernabeu, A.M. and Novoa, X., 2009. Influence of beach morphodynamics in the deep burial of fuel in beaches. *Journal of Coastal Research*, 25, 799–818.
- Gundlach, E.R. and Hayes, M.O., 1978. Vulnerability of coastal environments to oil spill impacts. *Marine Technology Society Journal*, 12, 18–27.
- Jensen, J.R., Halls, J.N. and Michel, J., 1998. A Systems Approach to Environmental Sensitivity Index (ESI) Mapping for Oil Spill Contingency Planning and Response. *Photogrammetric Engineering & Remote Sensing*, 64, 1003–1014.
- Jensen, J.R., Ramsey, E.W., Holmes, J.M., Michel, J.E., Savitsky, B. and Davis, B.A., 1990. Environmental Sensitivity Index (ESI) Mapping for Oil Spills Using Remote Sensing and Geographic Information System Technology. *International Journal of Geographical Information Systems*, 4, 181–201.
- Krishnan, P., 1995. Research report – a geographical information-system for oil-spills sensitivity mapping in the Shetland-islands (United Kingdom). *Ocean & Coastal Management*, 26, 247–255.
- Leiger, R., Aps, R., Kotta, J., Orviku, K., Pärnoja, M. and Tõnisson, H., 2012. Relationship between shoreline substrate type and sensitivity of seafloor habitats at risk to oil pollution. *Ocean & Coastal Management*, 66, 12–18.
- Lorenzo, H., Rial, F.I., Aris, P. and Armesto, J., 2009. Fighting against coastal oil spill pollution by means of ground-based radar. *Journal of Coastal Research*, SI 56, 846–850.
- Masselink, G. and Short, A.D., 1993. The effect of tide range on beach morphodynamics and morphology: a conceptual beach model. *Journal of Coastal Research*, 9, 785–800.
- Michel, J., Hayes, M.O. and Brown, P.J., 1978. Application of an oil spill vulnerability index to the shoreline of lower Cook Inlet, Alaska. *Environmental Geology*, 2, 107–117.
- Moe, K.A., Skeie, G.M., Brude, O.W., Løvås, S.M., Nedrebø, M. and Weslawski, J.M., 2000. The Svalbard intertidal zone: a concept for the use of GIS in applied oil sensitivity, vulnerability and impact analyses. *Spill Science & Technology Bulletin*, 6, 187–206.
- NOAA, 2002. *Environmental Sensitivity Index Guidelines, Version 3*. NOAA Technical Memorandum Nos OR and R11. Hazardous Materials Response Division, National Ocean Service, Seattle, WA, 192 p.
- Nordstrom, K.F. and Jackson, N.L., 1992. Two-dimensional change on sandy beaches in meso-tidal estuaries. *Zeitschrift für Geomorphologie*, 36, 465–478.
- Orviku, K., Jaagus, J., Kont, A., Ratas, U. and Rivas, R., 2003. Increasing activity of coastal processes associated with climate change in Estonia. *Journal of Coastal Research*, 19, 364–375.
- Orviku, K., Suursaar, Ü., Tõnisson, H., Kullas, T., Rivas, R. and Kont, A., 2009. Coastal changes in Saaremaa Island, Estonia, caused by winter storms in 1999, 2001, 2005 and 2007. *Journal of Coastal Research*, SI 56, 1651–1655.
- Orviku, K., Kont, A. and Tõnisson, H., 2010. Estonia. Bird, E. (Eds.). *Encyclopedia of the World's Coastal Landforms* (605-611). Dordrecht, Heidelberg, London, New York: Springer.
- Rangel, N. and Anfuso, G., 2011. Coastal storm characterization and morphological impacts on sandy coasts. *Earth Surfaces Processes and Landforms*, 36, 1997–2010.
- Santos, C.F. and Andrade, F., 2009. Environmental sensitivity of the Portuguese coast in the scope of oil spill events - Comparing different assessment approaches. *Journal of Coastal Research*, SI 56, 885–889.
- Suursaar, Ü., 2010. Waves, currents and sea level variations along the Letipea – Sillamäe coastal section of the southern Gulf of Finland. *Oceanologia*, 52, 391–416.
- Tõnisson, H., Orviku, K., Kont, A., Suursaar, Ü., Jaagus, J. and Rivas, R., 2007. Gravel-pebble shores on Saaremaa Island, Estonia, and their relationships to formation conditions. *Journal of Coastal Research*, SI 50, 810–815.
- Tõnisson, H., Orviku, K., Jaagus, J., Suursaar, Ü., Kont, A. and Rivas, R., 2008. Coastal damages on Saaremaa Island, Estonia, caused by the extreme storm and flooding on January 9, 2005. *Journal of Coastal Research*, 24, 602–614.
- Tõnisson, H., Suursaar, Ü., Rivas, R., Kont, A. and Orviku, K., 2013. Observation and analysis of coastal changes in the West Estonian Archipelago caused by storm Ulli (Emil) in January 2012. *Journal of Coastal Research*, SI 65, 832–837.
- Vallner, L., Sildvee, H. and Torim, A., 1988. Recent crustal movements in Estonia. *Journal of Geodynamics*, 9, 215–223.
- Wieczorek, A., Dias-Brito, D. and Milanelli J.C.C., 2007. Mapping oil spill environmental sensitivity in Cardoso Island State Park and surrounding areas, São Paulo, Brazil. *Ocean & Coastal Management*, 50, 872–886.
- Wright, L.D. and Short, A.D., 1984. Morphodynamic variability of surf zones and beaches: a synthesis. *Marine Geology*, 56, 93–118.

## Assessment of the Sensitivity of Salamina (Saronic Gulf) and Elafonissos (Lakonic Gulf) islands to Sea-level Rise

Efthimios Karymbalis†, Christos Chalkias†, Maria Ferentinou‡, George Chalkias†, Maria Magklara†

† Department of Geography  
Harokopio University  
Athens, Greece  
Karymbalis@hua.gr

‡ Geological Sciences  
University of KwaZulu Natal,  
Durban, South Africa  
Ferentinou@ukzn.ac.za



[www.JCRonline.org](http://www.JCRonline.org)

### ABSTRACT

Karymbalis, E., Chalkias, C., Ferentinou, M., Chalkias, G., Magklara, M. 2014. Assessment of the Sensitivity of Salamina (Saronic Gulf) and Elafonissos (Lakonic Gulf) islands to Sea-level Rise. In: Green, A.N. and Cooper, J.A.G. (eds.), *Proceedings 13<sup>th</sup> International Coastal Symposium* (Durban, South Africa), *Journal of Coastal Research*, Special Issue No. 70, pp. 378-384, ISSN 0749-0208.

This paper deals with the classification of the coasts of two Greek islands (Salamina and Elafonissos), according to the sensitivity to long-term sea-level rise by applying the Coastal Sensitivity Index (CSI). Salamina lies in the Saronic Gulf about 2 km off-coast from Piraeus (the port of Athens). The island has an area of 93.5 km<sup>2</sup> while the total length of the coastline is 131.3 km. Elafonissos has an area of 19 km<sup>2</sup> (coastline length: 30.4 km) and lies west of cape Maleas in the Lakonic Gulf (South-east Peloponnese). CSI calculation involves the physical variables of geomorphology, coastal slope, relative sea-level rise rate, shoreline change rate, mean tidal range and mean wave height, in a quantifiable manner. Every section of the coastline is assigned a risk ranking based on each variable, and the CSI is calculated as the square root of the product of the ranked variables divided by the total number of variables. CSI maps which were produced for the studied islands showed that Elafonissos is more susceptible to a future sea-level rise since an extensive length of its coast (16.7 km, corresponding to 54.5% of the entire coastline) is characterized as highly and very highly sensitive primarily due to the low topography and the presence of extensive sandy beaches. On the other hand only 2 km of Salamina's shoreline, corresponding to 1.5% of the entire coast of the island, is of high sensitivity. Areas of high and very high CSI values host socio-economically important land uses (urban areas and recreational activities).

**ADDITIONAL INDEX WORDS:** *Sea-level rise, coastal geomorphology, sensitivity, Greece.*

### INTRODUCTION

Human-induced climate change is expected to cause a profound series of changes, including rising sea-level (Nicholls, 2011). From 1990 to the last decade of the twenty-first century, the Intergovernmental Panel on Climate Change (IPCC) Fourth Assessment Report (AR4) has forecast a total sea-level rise in the range of 18-59 cm (Meehl *et al.*, 2007). The assessment of coastlines' response to sea-level rise has become an important issue in recent years. Various approaches have been proposed to predict the evolution of the coastal zone under the influence of long-term sea-level rise. The relative susceptibility of different coastal environments to sea-level rise may be quantified by considering information regarding the important variables that contribute to coastal evolution in a given area such as coastal geomorphology and slope, shoreline shifting, rate of sea-level rise and other related factors. An index that is based on the physical variables of coastal landforms, geology, relief, shoreline displacement, relative sea-level change, tide range and wave height, has been used to assess the sensitivity of coasts in the USA, Europe, Brazil, India, and Greece (Gornitz, 1991; Thieler

and Hammar-Klose, 1999; Pendleton *et al.*, 2004; Nageswara Rao *et al.*, 2008; Gaki-Papanastassiou *et al.*, 2011; Karymbalis *et al.*, 2012).

A similar formula, referred to as a sensitivity index, was applied by Shaw *et al.* (1998) along the Canadian coast. Abuodha and Woodroffe (2010) in an attempt to assess the susceptibility of southern Australia to sea-level rise introduced an index with two more physical variables concerning the type of the barrier and the exposure of the shoreline. In this approach the authors used two - instead of one- parameters to express the geomorphology variable: coastal landforms and rock types. Boruff *et al.* (2005) used physical risk indicators along with a quantitatively derived social vulnerability index (SoVI; incorporating population and demographic data, variables relevant to economic activities, etc.) for the comparative spatial assessment of human-induced vulnerability to coastal hazards in US coastal counties.

The aim of this paper is to classify the coasts of the Greek islands of Salamina and Elafonissos, with respect to their sensitivity to long-term sea-level rise through the calculation of the Coastal Sensitivity Index (CSI). CSI is similar to the formula proposed by Thieler and Hammar-Klose (1999) that modified the initial Coastal Vulnerability Index (CVI) produced by Gornitz *et al.* (1994). In this approach the ranges, which were used for



Figure 1. Location of Salamina and Elafonissos islands.

sensitivity ranking of the involved variables, are those proposed by Karymbalis *et al.* (2012) for the coastal environment of Greece.

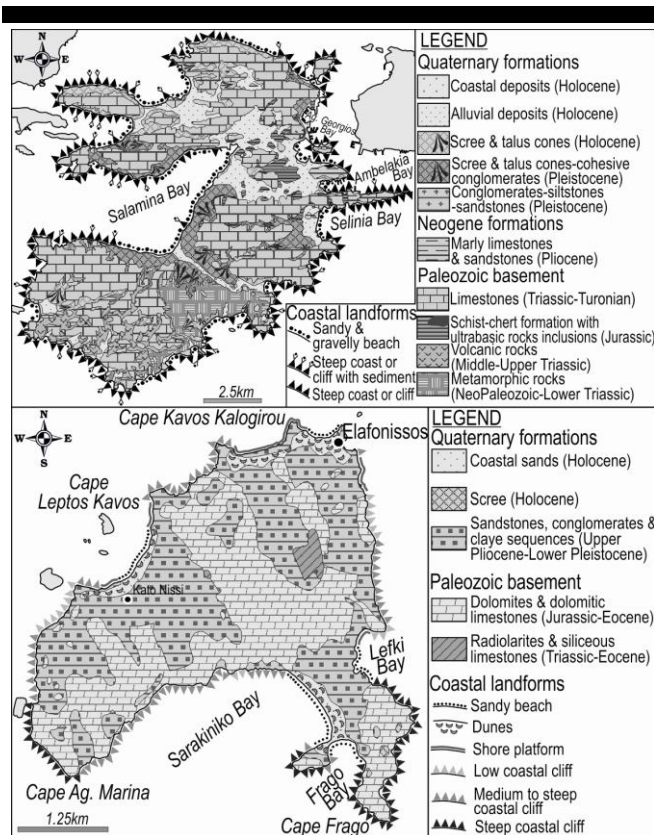


Figure 2. Simplified lithological maps of Salamina and Elafonissos. The map also depicts the coastal geomorphology of the island. Geological formations mapping is based on geological maps of the Institute of Geology and Mineral Exploration of Greece (IGME, 1982; 1984, 2002) while coastal landforms were mapped through fieldwork.

### STUDY AREAS

Salamina is the largest of the Saronic Gulf islands. It has an area of 93.5 km<sup>2</sup> while the total coastline length of the island is 131.3 km. It lies about 2 km off-coast from Piraeus (the port of Athens) (Figure 1).

The Paleozoic basement of the island is made up of limestones of Triassic-Turonian age, metamorphic rocks of Neopaleozoic-Lower Triassic age, middle Upper Triassic volcanic rocks and the schist-cert formation (shales alternating with red radiolarites and limestones with cherts and tectonic inclusions of serpentinized ultra-basic rocks) of Jurassic age (IGME, 1982;1984). Pliocene formations are composed of marly limestones and sandstones while Pleistocene formations consist of consolidated talus cones and scree and small outcrops of fluvialite deposits such as conglomerates alternating with breccias, siltstones, sandstones and marly sands (IGME, 1982;1984). Recent unconsolidated scree and talus cones cover the slopes of the island whereas Holocene alluvial deposits occur along the main channels of the drainage networks.

A part of the island’s coast consists of steep and medium marine cliffs composed of relatively difficult-to-erode rocks (mainly limestones of Paleozoic age). Cliffs of various gradients are also developed where talus cones of Pleistocene age, which have the form of cohesive conglomerates, meet the sea(Figure 2). Several shingle to sandy pocket beaches occur between rocky headlands. The pocket beaches of the south island are relatively short in length, as compared to those of the north shore of Salamina.

The island of Elafonissos is located along the southeastern coast of the Lakonic Gulf, northwest of Cape Maleas (Figure 1). It is separated from the Peloponnese by a narrow channel of 1250m width. The depth of the channel is very low and does not exceed 2.5 m. The island has an area of 19 km<sup>2</sup> while its total coastline length is 30.4 km (Figure 1). The Paleozoic basement of the island is composed of dolomites and dolomitic limestones of Jurassic-Eocene age while there is a small outcrop of radiolarites and siliceous limestones at the central part of the island (IGME, 2002). An extensive area of the island consists of marine and lacustrine clastic and biogenic sediments of Upper Pliocene-Lower Pleistocene age (Figure 2). This formation includes sandstones, conglomerates and arenaceous-clayey sequences (IGME, 2002).

Steep coastal cliffs occur there where the dolomites, dolomitic limestones and conglomerates reach the sea (Figure 2). The steepest marine cliffs of the island are found at the south-west (cape Ag. Marina) and south-east (Frago Peninsula) parts of the island and along the west shore of Sarakiniko Bay. The geomorphology of the north coast, (west of Cape Kavos Kalogirou) is characterized by the presence of a rocky shore platform partially covered by sand dunes. Sandy beaches occur along the north (between the settlement of Elafonissos and Kavos Kalogirou cape) and north-west (between Leptos Kavos cape and Kato Nissi) coasts of the island. Low cliffs are the dominant geomorphic characteristic of the eastern coast interrupted by the sandy pocket beach of Lefki. Extensive sandy beaches backed by well developed sandy dunes stabilized with vegetation are found along the eastern shore of Sarakiniko bay, at Frago bay, south of cape Leptos Kavos and west of the Elafonissos settlement.

Both islands can be characterized as microtidal environments with an average mean tidal range lower than 0.15 m (Tsimplis, 1994). Wave climate is primarily wind driven with offshore mean significant wave heights averaging <0.6 m for Elafonissos and <0.4 m for Salamina (Soukisian *et al.*, 2007).

The islands of Salamina and Elafonissos have been selected as case study areas for the application of the CSI predominantly due to the variability of their coastal landforms and the prevailing

Table 1. Ranges for sensitivity ranking of the six variables.

VARIABLES	Sensitivity Categories				
	1	2	3	4	5
Geomorphology	Rocky, cliffed coasts, artificially armored coasts	Medium cliffs, indented coasts	Low cliffs, alluvial plains	Cobble Beaches, Lagoon	Barrier beaches, beaches, deltas
Shoreline Erosion (-) /Accretion (+) rate (m/yr)	>(1.5)	(1.5)-(0.5)	(0.5)-(0.5)	(-0.5)-(-1.5)	<(-1.5)
Coastal Slope (%)	>12	12 - 9	9 - 6	6 - 3	<3
Relative Sea-Level rise (mm/yr)	<1.8	1.8 - 2.5	2.5 - 3.0	3.0 - 3.4	> 3.4
Mean Wave Height (m)	<0.3	0.3 - 0.6	0.6 - 0.9	0.9 - 1.2	>1.2
Mean Tide Range (m)	<0.2	0.2 - 0.4	0.4 - 0.6	0.6 - 0.8	>0.8
CSI	Very Low	Low	Moderate	High	Very High

socioeconomic conditions. Salamina is a densely populated, urbanized island while tourism and recreational activities is an essential part of the economy of the Elafonissos island.

## METHODOLOGY AND DATA ACQUISITION

The CSI is calculated as the square root of the product of six variables divided by their total number.

$$CSI = \sqrt{\frac{a \cdot b \cdot c \cdot d \cdot e \cdot f}{6}} \quad (1)$$

where a: geomorphology, b: coastal slope, c: shoreline erosion/accretion rate, d: relative sea-level rise rate, e: mean tide range and f: mean significant wave height.

The variables are ranked from 1 to 5 according to Table 1, with rank 1 indicating very low sensitivity and rank 5 indicating very high sensitivity. The ranges of sensitivity ranking, used in this study, are those proposed by Karymbalis *et al.* (2012) for the coastal environment of Greece.

Categorization of geomorphology classes in this study was undertaken using recent orthorectified aerial photographs (taken in 2009) and detailed (at the scale of 1:5,000) field coastal geomorphological mapping of the islands. Because this variable also represents the bedrock outcropping along the shoreline, data for the rock types were interpreted from the geological maps of the islands at a scale of 1:50,000 published by the Greek Institute of Geology and Mineral Exploration (IGME, 1982; 1984; 2002).

To estimate the coastal slope values, slope maps of the coastal zone of the islands were created with the use of the detailed, 1:5,000 scale, topographic maps. With these maps as the main elevation source, the Digital Elevation Model (DEM) of the coastal belt with an elevation from 0 to 50 m were created for each island. Next, for this zone, the slope maps were implemented within the ArcGIS spatial analysis extension environment, and maps of slope zones (according to Table 1) were constructed. Finally, for the assignment of the proper slope categorization to each coastline segment, the intersection of slope zones with the coastline was performed.

Shoreline change rates were derived from orthorectified aerial photographs taken in 1945 and 2009, obtained from the Hellenic Military Geographical Service and the Hellenic Cadastre (Ktimatologio S.A.) respectively. The photomosaics of these photographs were manipulated within the GIS environment to digitize the shorelines of 1945 and 2009. The thematic layers of the 1945 and 2009 shorelines (in vector format) were overlaid, and

with the use of GIS-based distance analysis functions, the final shoreline change map for the 64-year time period was obtained with estimated accretion and erosion rates.

For the islands of this study relative sea-level change is the sum of the eustatism component and the local long-term tectonic vertical land movements. Published information concerning the Late Holocene relative sea-level trends at the broader area of the islands was considered.

The tidal range was deduced from published information (Tsimplis, 1994) whereas the mean annual values of significant wave height were abstracted from the Wave and Wind Atlas of the Hellenic Seas (Soukiasian *et al.*, 2007), which is based on offshore measurements for the period between 1999 and 2007 (POSEIDON program).

To obtain a preliminary assessment of the impacts of anticipated sea-level rise on the socio-economic activities, land cover of the islands' coastal zone was identified utilizing the relevant map of the Corine 2000 Land Cover Program. Ten land cover categories were recognized and compared with the highly and very highly sensitive segments of the shoreline.

GIS software ArcGIS (ver. 9.3), provided the platform for the coastal mapping and the calculation of the CSI. For each variable, the entire coastline of the study area is segmented into five sensitivity classes, and a sensitivity rank number is assigned to each segment of the coast. The method of computing the CSI in the present study is similar to that applied by Pendleton *et al.* (2005), Thieller and Hammar-Klose (1999) and Abuodha and Woodroffe (2010). The difference is that instead of the "raster" approach, input parameters and final CSI values were estimated in coastline segments. This modified approach seems appropriate for medium scale. To display the results of the index derived from integration of the variables, a template of segments was derived for the coast. The segment-based template was used to store and present data for each of the variables in an attribute table (in vector format using shape-files in ArcGIS) for adjacent segments along the coast. As mentioned above, for each of the six variables, a ranking on a scale of 1-5 was assigned to each segment. The final CSI maps were generated by combining all of the variables. These maps contain 7959 segments of the coastline, each of which has a unique identity in its corresponding attribute table. Another column was added to this attribute table for the CSI formula so that the system generated the CSI values for all of the coastline segments of the islands. The combined CSI value was added as an attribute value for each coastline segment. Subsequently, the "equal interval" classification method was used to categorize coastline segments according to their CSI magnitude for the

construction of the final CSI zonation maps. The minimum and maximum CSI values of both islands' coastline segments were implemented in this classification.

## RESULTS

### Coastal Geomorphology

The predominant coastal landforms identified in the study areas (ranging from very high to very low sensitivity) were marine cliffs (moderate to steep) composed of various rock types, such as limestones, dolomites, metamorphic rocks, old talus cones and scree (in the form of cohesive conglomerates), and Plio-Pleistocene formations, small pebbly to sandy pocket beaches, and extensive sandy beaches with stabilized dunes. (Figure 2). The different landforms recognized and mapped were classified as shown in Figure 3 - 1a, 2a.

The coastline of Salamina has a series of small sandy to pebbly pocket beaches occupying a total length of 4.2 km, which corresponds to 3.2 % of the total coastline of the island (Figure 3-1a). The predominant coastal landform of the island is marine cliffs made up of limestones or metamorphic rocks and artificially armored coasts (55.9 km – 42.5%) followed by low limestone cliffs (36.8 km, which is 28.0 % of the coastline), steep marine cliffs composed of volcanic rocks, cohesive conglomerates, marly limestones and sandstones (19.7 km – 15.0 %), cobble pocket beaches (14.8 km – 11.3%) and sandy beaches located along coastal alluvial plains (4.2 km – 3.16%). Steep cliffs made of hard rocks (limestones and metamorphic rocks) offer maximum resistance and were classed with a rank of 1 whereas cliffs of weaker lithologies (volcanic rocks, conglomerates, marly limestones and sandstones) or medium elevations were assigned sensitivity ranks of 2 and 3, respectively. Notably, the artificially protected shoreline segments have a length of 21.5 km, which corresponds to 16.4% of the coastline length of Salamina, and were considered as composed of a particularly resistant to erosion rock type (rank 1). Shingle pocket beaches are sensitive to the effects of both natural marine processes and relative sea-level rise and are given a rank of 4 (high sensitivity). The predominant coastal landforms of Elafonissos are low cliffs composed of dolomites and dolomitic limestones, conglomerates and sandstones (12.0 km, which is 39.4 % of the island's coastline), followed by steep rocky cliffs (7.1 km – 23.4 %), shore rocky platforms and sandy beaches with stabilized dunes (7.0 km – 20 %), rocky cliffs of moderate slope (2.9 km – 9.4 %) and sandy beaches without dunes (6.1 km – 7.6%) (Figure 3 -2a). Sandy beaches were assigned a sensitivity rank of 5, while stabilized dune formations are considered that provide a kind of protection to the land behind them and were assigned a sensitivity rank of 4.

### Coastal Slope

The low-lying coasts of Salamina Island are occupied by beaches developed along the fronts of coastal alluvial plains. The 23.6% of the island's coastal zone, corresponding to 31.0 km, located along the west coast (Salamina Bay) as well as along the densely urbanized east coast of the island is characterized as very highly susceptible to inundation (Figure 3-1b). Most of the island's coastal zone (nearly 51.5% of the coast - 67.6 km) is of very low susceptibility to inundation as its slope is higher than 12%.

Most of the Elafonissos coastal zone (63.9 % which corresponds to 11.8 km) that lies mainly along the northwest as well as along the east coast of Sarakiniko Bay is low-lying and is characterized as very highly susceptible to inundation (Figure 3-2b). A

significant section of the east as well as the south coast of the island (6.3 km - 20.7%) is classified as having high sensitivity due to the presence of relatively low slopes (between 3% and 6%).

### Shoreline Change

The island of Salamina experienced mean shoreline change rates from -1 m/yr of erosion (moderate sensitivity) to +1.6 m/yr of accretion (low sensitivity) between 1945 and 2009. A shoreline length of 121.1 km, which corresponds to 92.2% of the coastline, is relatively stable (mean shoreline shifting rate within  $\pm 0.5$  m/yr), whereas 0.4 km (0.3 %) of the coastline is retreating with a mean rate between -0.5 and -1.5 m/yr (Figure 3-1c). 8.8 km (6.7 %) of the shoreline has been prograded with a mean accretion rate between +0.5 and +1.5 for the period between 1945 and 2009, while a very small percentage of the coastline (0.8% - 1.0 km) is prograding faster with a mean accretion rate higher than 1.5 m/yr. Accretion occurs at the mouth of the torrents due to increased sediment supply, especially during the rainy period of the year but mainly along artificially protected parts of the island.

Mean shoreline change along the coastline of Elafonissos range between +1.5 m/yr and -1 m/yr. A shoreline length of 23.6 km, which corresponds to 77.7% of the coastline, is relatively stable (mean shoreline shifting rate within  $\pm 0.5$  m/yr), whereas 4.2 km (13.7 %) of the coastline is retreating with a mean rate between -0.5 and -1.5 m/yr (Figure 3-2c). Retreat is the main process along the low-lying extensive sandy beaches of the island.

### Relative Sea-level Change

Due to the lack of recent accurate sea-level measurements, the values for the variable of relative sea-level rise were estimated coupling the effects of eustatism and local land level movements caused by tectonics. The relative sea-level rise is considered to have the same value along the coastline of both islands and took the value of 1.0 mm/yr based on estimations from studies relevant to eustatic sea-level rise in Greece (Lambeck, 1996). Additionally, publications about the relative sea-level trend during the Late Holocene for the broader area of the studied islands were taken into account.

At least six submerged harbors and port installations of Classical and Roman antiquity are found along the Saronic Gulf coast (Mourtzas and Kolaiti, 2013). Among them the submerged Classical harbor of Salamina (1400  $\leq$  100 years B.P.) is the main past sea-level indicator of known age of the island. It lies at -1.5 m below the present sea-level and indicates a time averaged rate of relative sea-level rise of 1.0 mm/yr (Lolos, 1995). This rate is similar to the estimations from studies of eustatic sea-level rise in Greece (Lambeck, 1996).

Signs of submerged Holocene coastlines, which reveal sea-level rise trend, are highly presented in the island of Elafonissos. At the western part of Cape Frago, old shoreline can be observed up to a depth of -1.6 m. These lines are created from shells of organisms which live near the sea level. Remains of a settlement from Helladic times (about 5000-3000 BP) near the small rocky island of Pavlopetri, which is located between Elafonissos and Cape Punda, are at -1.0 m below sea-level. There are also found remnants of the associated necropolis, as well partly submerged. This archaeological setting indicates that since the mid-Holocene, the relative sea-level has obviously never been higher than the modern one (Scheffers *et al.*, 2008).

### Tidal Range

For the sensitivity ranking of the tidal range variable for the islands of Salamina and Elafonissos the ranges proposed for

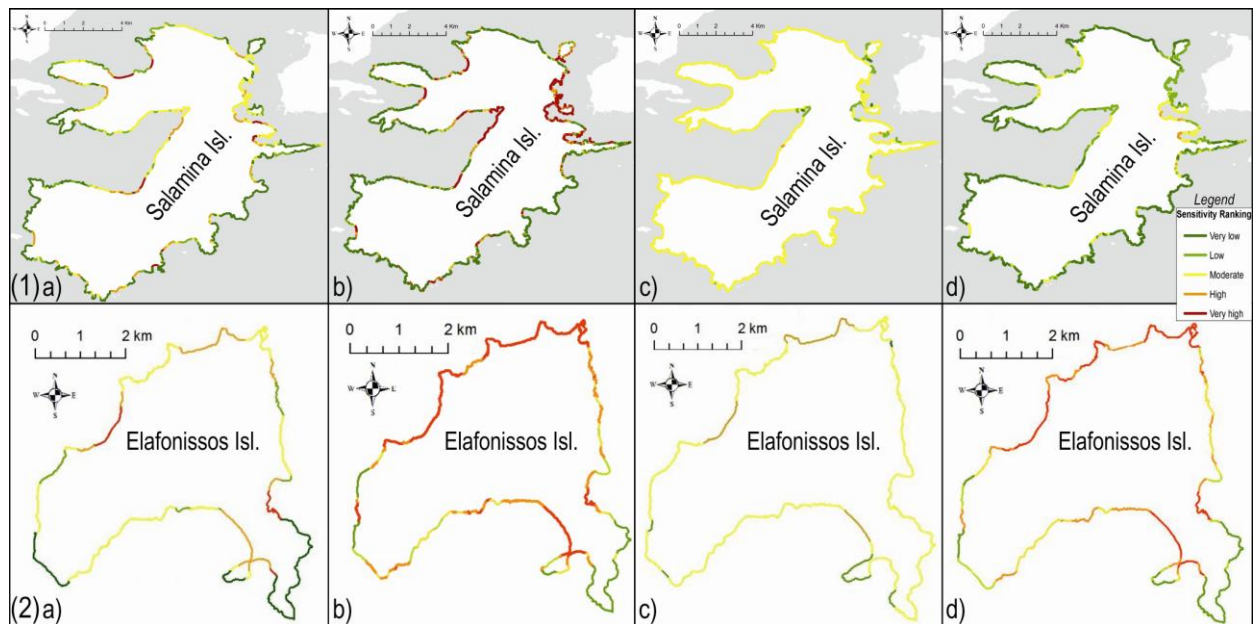


Figure 7. Maps of classification of (1) Salamina and (2) Elafonissos island coasts according to the variables of a) geomorphology, b) coastal slope, c) shoreline change and d) Coastal Sensitivity Index (CSI) values. The maps indicate the sensitivity ranking of various segments of the coast based on the categorization of the values into five classes.

Greece were considered (Table 1). These ranges were proposed taking into account the tide range variations for the Greek seas which are generally less than 0.87 m (Tsimplis, 1994) (Table 1).

In this study, tidal range is ranked such that extremely microtidal (tidal range < 0.2 m) coasts are at low risk and less microtidal (tidal range > 0.8 m) coasts are at high risk. The reasoning is that although a large tidal range dissipates wave energy limiting beach or cliff erosion to a brief period of high tide it also delineates a broad zone of intertidal area which will be most susceptible to inundation following long-term sea-level rise (Gornitz, 1991). Furthermore, the velocity of tidal currents depends partially on the tidal range. High tidal range is associated with stronger tidal currents, capable of eroding and transporting sediment (Gornitz, 1991). Salamina and Elafonissos are microtidal islands with tidal (astronomical) range < 0.15 m. As such, the tidal range variable is ranked according to Table 1 with the value 1 (very low sensitivity).

### Mean Significant Wave Height

The wave climate of the west coastline of Salamina is dominated by offshore significant wave heights < 0.3 m, whereas mean annual significant wave heights off the east coast of the island range between 0.3 and 0.4 m according to the output of the wave model (POSEIDON program), which has been calibrated with the use of offshore field measurements (Soukisian *et al.*, 2007). Hence, the west coastline of the island is considered to have very low sensitivity (rank 1) while the east coastline is of low sensitivity (rank 2). According to wind and wave atlas of the Hellenic seas the wave climate of the Elafonissos Island is characterized by offshore significant wave heights between 0.5 and 0.6 m (Soukisian *et al.*, 2007). The mean significant wave height variable for the entire coast of the island is ranked according to Table 1 with the value 2 (low sensitivity).

### The CSI Values

CSI values for both islands were classified into five groups. The CSI values along the coastline of Salamina islands range between 0.6 and 5.0. The median value of the index for the island is 1.6, and the standard deviation is 1.0. The geographical distribution of the sensitivity of Salamina Island coast to potential sea-level rise is presented schematically in Figure 3-1d. Nearly 1.5% of the coastline (2.0 km) is classified as having high sensitivity (CSI values between 4.2 and 5.6), 14.1% (18.5 km) as moderately sensitive (CSI values between 2.8 and 4.2) and 31.6% (41.4 km) with low sensitivity (CSI values between 1.4 and 2.8). Finally, values below 1.4 are assigned to the very low sensitivity category. A significant part of the island's shoreline (69.2 km - 52.8%) belongs to this very low sensitivity class. The moderate and high sensitivity categories are primarily located along pocket beachfronts in most of the bays around the island. The high sensitivity segments of the shoreline are located along the east coast of the island (Ambelakia Bay, Agios Georgios Bay and Selinia Bay). These areas are of high sensitivity primarily due to the low regional coastal slope and the high sensitivity of the coastal landforms (unconsolidated shingle to sandy sediments). The low and very low sensitivity categories correspond to steep, relatively stable, cliffed coasts composed of hard rocks (limestones, metamorphic rocks and cohesive conglomerates).

In terms of the socio-economic impacts of the anticipated sea-level rise, the highly sensitive coastal segments and a large part of the moderately sensitive coast is occupied by urban activities (cities and settlements as well as tourism activities and facilities). Many settlements, constructions and facilities are already artificially armored and belong to the low and very low sensitivity coast of the island.

The CSI values along the coastline of Elafonissos islands range between 1.2 and 7.1. The median value of the index for the island is 2.8, and the standard deviation is 2.4. Figure 3-2d depicts the

geographical distribution of the sensitivity of the coast of Elafonissos to potential sea-level rise. Nearly 9.7 km, corresponding to 31.4% of the total coastline length, was assigned to the very high sensitivity category. The extensive sandy beaches of the north, northwest and south part of the island are characterized by very high levels of sensitivity, primarily due to the low regional coastal slope, the high erodibility of the fine grained unconsolidated sediments, and the relatively higher (compared with Salamina) mean significant wave high that affects the coast. Nearly 23.1% of the coastline (7.0 km) is classified as having high sensitivity (CSI values between 4.2 and 5.6), 17.2% (5.2 km) as moderately sensitive (CSI values between 2.8 and 4.2) and 8.7% (2.64 km) with low sensitivity (CSI values between 1.4 and 2.8). Finally, 21.4 km; 14.6% of the shoreline has values below 1.40 and belongs to the very low sensitivity class. The low and very low sensitivity categories are primarily located at the southwestern and southeastern parts of the island and correspond to coastal cliffs of various gradients developed where dolomites, dolomitic limestones and consolidated talus cones and scree, which have the form of cohesive conglomerates, meet the sea.

Most of the coastal settlements, tourism facilities and recreational activities of Elafonissos are located along the very highly sensitive segments of the coast. Some 2.0 km along the shoreline (26.0% of the very highly sensitive coast) is characterized by the presence of continuous and discontinuous urban fabric and tourism facilities. Additionally, a length of the highly and very highly sensitive coastal zone is occupied by agricultural land. Some 1.3 km, corresponding to 16.7% of the very highly sensitive coastal plains' shoreline, host agricultural activities. Similarly, these agricultural uses extend for 2.8 km, representing 30.4% of the highly sensitive coast. These findings are of high importance because tourism sector, and agricultural activity, plays a significant role for the socioeconomic development of the island.

## CONCLUSIONS

In this study, the relative sensitivity of the islands of Salamina and Elafonissos to environmental changes due to the anticipated long-term rise in sea-level is assessed with the calculation of the CSI. Calculated CSI values along the shoreline of the islands vary between 0.6 and 7.1. Of the six variables, geomorphology and regional coastal slope introduce the greatest variability to the CSI values. Among the other four parameters, shoreline change rate and mean significant wave high shows a small variation, while tidal range, and relative sea-level rise rate have the same values along the entire coastline of both islands. According to the criteria of coastal sensitivity, as defined in this study, Elafonissos is more sensitive to a potential rise of sea-level than Salamina. An extensive segment of the coast is of high (7.0 km) and very high (9.7 km) sensitivity. The sections of coast with high and very high CSI ratings include low gradient coasts of the island, underlain by unconsolidated fine grained sediments. These areas are most susceptible to both inundation and erosion and host economically important tourism facilities and recreational activities. The settlement of Elafonissos is very highly susceptible to sea-level rise. Highly sensitive areas are numerous low-lying shingle to sandy pocket beaches of Salamina located mainly along the east coast of the island, occupied by densely populated settlements. In this study, the entire coastline is analyzed as a line feature with the use of GIS-based vector analysis procedures, which gives a more precise assessment of the sensitivity-vulnerability level of any point along the shoreline. Additionally, a segment-based template provides a visual representation, which may enable coastal planners and managers to appreciate the contrast between the most

susceptible / vulnerable areas and the less susceptible / vulnerable areas along the islands. This approach can assist in prioritizing efforts to enhance the natural resilience of the coast or assist in the formation of adaptation policies.

## LITERATURE CITED

- Abuodha, P.A.O. and Woodroffe, C.D., 2010. Assessing vulnerability to sea-level rise using a coastal sensitivity index: a case study from southeast Australia. *Journal of Coastal Conservation*, 14, 189-205.
- Boruff, B., Emrich, C. and Cutter, S.L., 2005. Erosion hazard vulnerability of US coastal countries. *Journal of Coastal Research*, 21(5), 932-942.
- Gaki-Papanastassiou, K., Karymbalis, E., Poulos, S., Seni, A. and Zouva, C., 2011. Coastal vulnerability assessment to sea-level rise based on geomorphological and oceanographical parameters: the case of Argolikos Gulf, Peloponnese, Greece. *Hellenic Journal of Geosciences*, 45, 109-121.
- Gornitz, V., Daniels, R.C., White, T.W. and Birdwell, K.R., 1994. The development of a coastal vulnerability assessment database: vulnerability to sea-level rise in the U.S. southeast. *Journal of Coastal Research*, Special Issue 12, 327-338.
- Gornitz, V., 1991. Global coastal hazards from future sea-level rise. *Palaeogeography, Palaeoclimatology, Palaeoecology (Global and Planetary Change Section)*, 89, 379-398.
- IGME, 1982. *Geological Map of Greece - Athinaï-Piraeïvs sheet*. Institute of Geology and Mineral Exploration, scale 1:50,000.
- IGME, 1984. *Geological Map of Greece - Megara sheet*. Institute of Geology and Mineral Exploration, scale 1:50,000.
- IGME, 2002. *Geological Map of Greece - Pappadhianika-Potamos sheet*. Institute of Geology and Mineral Exploration, scale 1:50,000.
- Karymbalis, E., Chalkias, Ch., Chalkias, G., Grigoropoulou, E., Manthos, G. and Ferentinou, M., 2012. Assessment of the sensitivity of the Southern Coast of the Gulf of Corinth (Peloponnese, Greece) to sea-level rise. *Central European Journal of Geosciences*, 4(4), 561-577.
- Lambeck, K., 1996. Sea-level change and shore-line evolution in Aegean Greece since Upper Palaeolithic time. *Antiquity*, 70(269), 588-611.
- Lolos, Y., 1995. Notes of Salaminian harbours. In: H., Tzalas (ed.) *TROPIS III, 3rd International Symposium on Ship Construction in Antiquity*, (Athens, Greece) Hellenic Institute for the Preservation of Nautical Tradition, pp. 291-308.
- Meehl, G.A., Stocker, T.F., Collins, W., Friedlingstein, P., Gaye, A., Gregory, J., Kitoh, A., Knutti, R., Murphy, J. and Noda, A., 2007. Global climate protections. In: Solomon, S., Qin, D. and Manning, M. (eds.) *Climate Change 2007: The physical science basis. Contribution of Working Group I to the Fourth Assessment Report of the Intergovernmental Panel on Climate Change*. Cambridge, UK: Cambridge University Press.
- Mourtzas, N.D. and Kolaiti, E., 2013. Historical coastal evolution of the ancient harbour of Aegina in relation to the Upper Holocene relative sea-level changes in the Saronic Gulf, Greece. *Palaeogeography, Palaeoclimatology, Palaeoecology*, 392, 411-425.
- Nageswara Rao, H., Subrauelu, P., Venkateswara Rao, T., Hema Malini, B., Ratheesh, R., Bhattacharya, S., Rajawat, A.S. and Ajai, 2008. Sea-level rise and coastal vulnerability: an assessment of Andhra Pradesh coast, India through remote sensing and GIS. *Journal of Coastal Conservation*, 12, 195-207.
- Nicholls, R.J., 2011. Planning for the impacts of sea-level rise. *Oceanography*, 24(2), 144-157.
- Pendleton, E.A., Thieler, E.R. and Jeffress, S.W., 2005. *Coastal vulnerability assessment of Goldan Gate National Recreation Area to sea-level rise*. USGS Open\_file Report, 2005-1058.
- Pendleton, E.A., Thieler, E.R. and Williams, S.J., 2004. Coastal vulnerability assessment of Cape Hattaras National Seashore (CAHA) to sea-level rise. USGS Open File Report 2004-1064. Available from <http://pubs.usgs.gov/of/2004/1064/images/pdf/caha.pdf> accessed on 15 Dec 2011.
- Scheffers, A., Kelletat, D., Vott, A., May, S.M. and Scheffers S., 2008. Late Holocene tsunami traces on the western and southern coastlines of the Peloponnese (Greece). *Earth and Planetary Science Letters*, 269, 271-279.
- Shaw, J., Taylor, R.B., Forbes, D.L., Ruz, M.H. and Solomon, S., 1998. Sensitivity of the Canadian Coast to Sea-Level Rise. *Geological Survey of Canada Bulletin*, 505, 114p.



- Soukisian, T., Hatzinaki, M., Korres G., Papadopoulos, A., Kallos, G. and Anadranistakis, E., 2007. *Wave and wind Atlas of the Hellenic Seas*. Anavyssos: Hellenic Centre for Marine Research Publication, 270p.
- Thieler, E.R. and Hammar-Klose, E.S., 1999. National Assessment of Coastal Vulnerability to Sea-Level Rise, U.S. Atlantic Coast. U.S. Geological Survey. Open-File Report, 99-593.
- Tsimplis, M.N., 1994. Tidal oscillations in the Aegean and Ionian Seas. *Estuarine, Coastal and Shelf Science*, 39, 201-208.

# Preliminary coastal vulnerability assessment for Pico Island (Azores)

P. Borges†, M.R. Phillips‡, K. Ng§, A. Medeiros§, H. Calado§

† Department of Geosciences  
University of the Azores  
Ponta Delgada, Portugal  
pb@uac.pt

‡ University of Wales: Trinity Saint  
David (Swansea)  
Wales, UK  
mike.phillips@sm.uwtsd.ac.uk

§ Department of Biology  
CIBIO-University of the Azores  
Ponta Delgada, Portugal  
kiat@uac.pt; calado@uac.pt



[www.cerf-jcr.org](http://www.cerf-jcr.org)



[www.JCRonline.org](http://www.JCRonline.org)

## ABSTRACT

Borges, P., Phillips, M.R., Ng, K., Medeiros, A., Calado, H., 2014. Preliminary coastal vulnerability assessment for Pico Island (Azores). In: Green, A.N. and Cooper, J.A.G. (eds.), *Proceedings 13<sup>th</sup> International Coastal Symposium* (Durban, South Africa), *Journal of Coastal Research*, Special Issue No. 70, pp. 385-388, ISSN 0749-0208.

The SMARTPARKS project (PTDC/AAC-AMB/098786/2008), funded by the Portuguese Foundation for Science and Technology (FCT), aims at establishing a planning and management system for small island (SI) protected areas (PA). Diverging from traditional no-take zone protected areas this project strives to integrate human activities, economic and cultural development, and conservation objectives. Pico Island in the Azores archipelago was selected as a suitable case study site. Pico is a Natural Park with 35% of its area being classified as PAs. This paper presents the assessment of relative coastal vulnerability of Pico to erosion and coastal flooding in order to determine how best to manage the PAs with respects to coastal hazards. A Coastal Vulnerability Index (CVI) was developed based on remote sensing and fieldwork data whereby a set of physical coastal parameters, which serve as indicators of vulnerability, were obtained: type of cliff; exposure to swell/storm waves; outcrop flooded; and coastal defences. The CVI values were used to rate coastal segments into five classes ranging from extremely low to very high based on its relative degree of vulnerability. CVI will provide input into a decision support tool to facilitate effective planning and management on Pico Island Natural Park with the potential of adapting and extending this approach to the other SIs.

**ADDITIONAL INDEX WORDS:** *small islands, coastal erosion, coastal flooding, protected area, coastal vulnerability index.*

## INTRODUCTION

Small islands (SIs) are vulnerable to the effects of climate change, sea-level rise and extreme events (Mimura et al., 2007). In light of global sea level rise and storm trends (i.e. frequency, intensity and track), there is a need to understand coastal vulnerability to these potential impacts based on available, accessible and best known information. Global sea level has been suggested to rise by possibly 1 m or more by 2100 due to accelerated decline of polar ice sheet mass (Pfeffer et al., 2008). Keim et al. (2004) suggested an increase in frequency of very intense storms, particularly at high latitudes, in agreement with other global and North Atlantic Ocean studies (Young et al., 2011; Bertin et al., 2013).

The SMARTPARKS project (PTDC/AAC-AMB/098786/2008) funded by the Portuguese Foundation for Science and Technology (FCT) was undertaken to establish a planning and management system for protected areas (PAs) in SIs that can be integrated into territorial management. Diverging from the traditional no-take zone PAs scheme, this project aims to provide a sustainable plan that integrates human activities, cultural, economic and conservation objectives. Pico Island was subsequently selected as a suitable case study site. For an effective planning and management, coastal vulnerability to the main identified coastal hazards (e.g. erosion and coastal flooding) needs to be understood (Calado et al., 2011). A coastal vulnerability index (CVI) based on four key physical parameters was established to provide a relative ranking of the erosion and flooding vulnerability of Pico coasts.

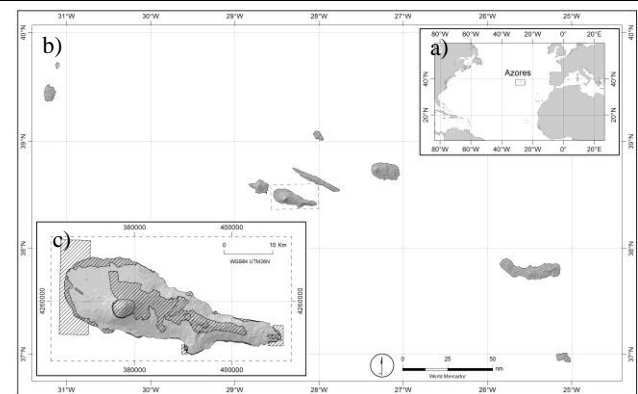


Figure 1. Map of the study area: a) Azorean islands (bordered) in relation to North Atlantic Ocean; b) Azores archipelago; c) Pico island and its protected areas (dark shade).

The CVI will assist in the planning and management of coastal PAs in Pico Island.

## STUDY AREA

Located in the middle of the North Atlantic Ocean, Pico Island is one of the nine volcanic SIs forming the Azores archipelago in Portugal (Fig. 1). It is an Island Natural Park with 35% of its area being classified as protected areas (PAs). The coastal zone where most of the social and economic activities concentrate is vital to Pico residents. Over the past few decades, tourism has become an

important economic sector, while human occupation has increased along the coast.

Pico's shoreline is approximately 167 km long and represents 15% of the total Azorean coastline. According to Borges (2003), circa 50% of Pico's sea cliffs are less than 10 m high. There are some areas with very gentle slopes where the edges of cliffs are less than 1 m above mean sea level (msl), while areas with cliffs higher than 100 m are rare and confined only to the eastern part of the island. Borges (2003) classified the coast into four main geomorphic compartments based on the composition of the material and the pattern of their deposition layers (Fig. 2). The dominant type of coastal cliff for Pico island is Type IV.

According to Borges et al. (2002), the long fetch that characterizes the Azores results in a high-energy wave climate where both sea and swell waves are relevant. The north-facing shores of each island are generally more exposed than the south-facing shores. However, a significant part of Pico's northern shore is sheltered by São Jorge island. Borges (2003) suggested that the Azorean storms have slightly increased in frequency between 1835 and 1998, characterized by an elevated inter-annual and inter-decadal variation, while Andrade et al. (2008) indicated that the average storm lasts for two days with an average frequency of three storms yr<sup>-1</sup>. Furthermore, medium intensity storms occur four times every five years, while an extreme storm occurs on average once every seven years. Storms are usually short, frequent and intense, and an extreme storm usually coincides with southwesterly waves (Borges, 2003). Tides and tidal currents are minor contributors to coastal morphology and sediment dynamics; they are semi-diurnal with a yearly average and maximum spring tidal range of 0.75 – 1 m and 1.3 m, respectively (Andrade et al., 2006). In general, impacts from storm surges are negligible (0.3 m) because wind build-up is limited due to the exposed nature of the coast and steep submarine slopes (Roger et al., 1982; Carter, 1999). However, field data at Lajes (Pico Island) indicate that surge heights reaching at least 0.6 m to 0.8 m were observed in 1963 and 2005, respectively.

**METHODS**

This study is a preliminary coastal vulnerability assessment that employs a modified CVI that has been successfully undertaken in other locations (e.g. Palmer et al. 2011; Davies, 2012). This preliminary approach assesses Pico coastline according to geomorphic compartments following similar concepts as Gutierrez et al., 2007, instead of uniform coastal cells (e.g. Pendleton et al., 2010; Palmer et al., 2011). Four accessible and representative physical parameters were employed as indicators for this vulnerability assessment: a) type of coastal cliffs; b) coastal exposure to swell and storm waves; c) outcrop flooded; and d) coastal defenses.

The application of this CVI aims to provide a simple approach that could easily be utilized to evaluate the general coastal vulnerability of a SI. Therefore, only four physical parameters were used to assess the vulnerability to natural and anthropogenic-modified coastal and physical processes. The rationale behind the

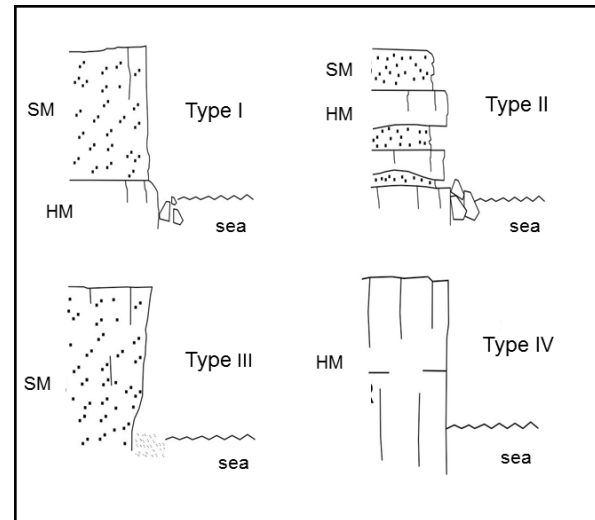


Figure 2 Types of coasts. SM - soft material; HA – hard material (modified from Borges, 2003).

selection of these parameters was emphasizing the most representative for SIs that are easily accessed and assessed. The type of coastal cliffs, as defined by Borges (2003) for the coasts of the Azores (Fig. 2), provides an indication of erosion rates (stability) of the cliff. While the type of cliff represents the vulnerability to coastal erosion hazard, the exposure to swell/storm addresses the vulnerability to the extreme events. In this study, only swell and storm waves coming from SW (225°) through W to NW (315°) were considered as they correspond to the dominant and worst case scenarios (Borges, 2003; Andrade et al., 2008; Ng, 2013). The percentage of area of flooded outcrop to 7 m was determined as an indicator to represent the coastal vulnerability to coastal flooding hazard, as 7 m has been indicated as the modal run-up for extreme events (Borges and Andrade, 1999; Borges, 2003). To calculate the percentage of this area, a buffer zone of 100 m inland from shore for the entire island was considered as the flooding zone as this value corresponds to the maximum modal inland penetration of coastal flooding during an extreme event (Borges and Andrade, 1999).

Coastal defences are constructed to protect shorelines from natural processes. These modified coasts reduce vulnerability to coastal hazards, and consequently, coastal defense was included as an indicator. These indicators were rated according to five grades ranging from (1) extremely low to (5) very high (Table 1) and were assessed and validated based on pre- and post-storm field surveys, along with the utilization of orthophotographs, nautical charts, coastal typological maps, topographic maps and ArcGIS geoprocessing tools. Taking into consideration these indicators, each coastal segment was rated in terms of its degree of relative vulnerability using the following total relative vulnerability score. To emphasize highly vulnerable sites, i.e. cases where Type III coast coincide with > 80% exposure to swell/storm waves and

Table 1. Rating of physical parameters.

	Physical parameter	Extremely low (1)	Low (2)	Moderated (3)	High (4)	Very high (5)
a	Type of cliff	IV	II	I	III	
b	Exposure to swell/storm waves (%)	<20	20-40	40-60	60-80	>80
c	Outcrop flooded (%)	<20	20-40	40-60	60-80	>80
d	Coastal defences (%)	>80	80-60	60-40	40-20	<20

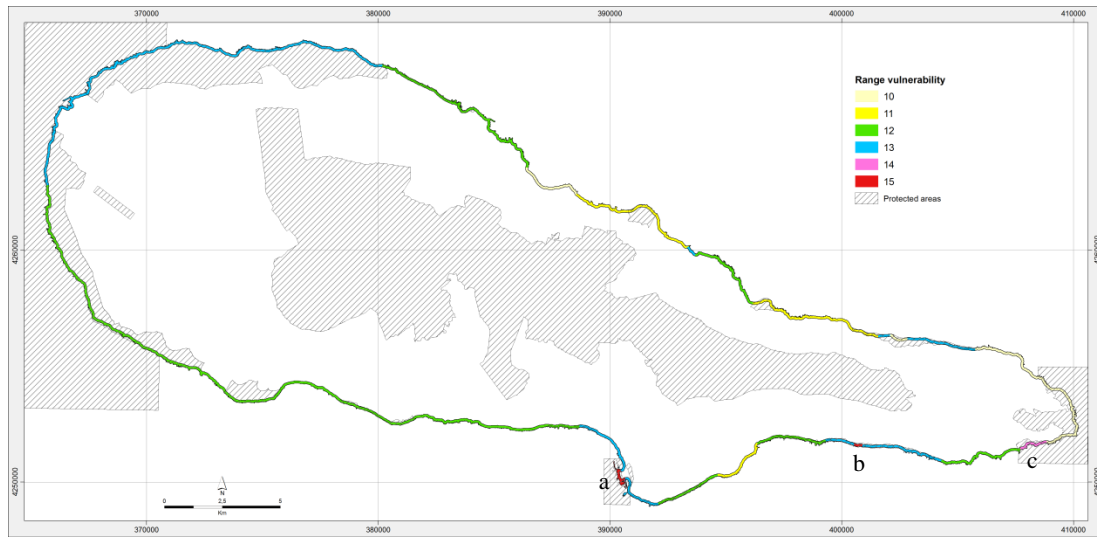


Figure 3. Relative coastal vulnerability for Pico island and an overlay of its protected areas: a) Lajes; b) Fajã de Ribeira Grande; and c) Baía Domingos Pereira.

outcrop flooded, and < 20% of the coastal segment with coastal defenses, an additional factor “e” was included in the total score to provide additional weighting to the rCVI of these sites. Therefore, the total relative CVI (rCVI) score ranges from (4) minimum to (20) maximum.

$$relative\ CVI = a + b + c + d + e$$

Where a = type of cliff vulnerability score, b = exposure to swell and storm waves vulnerability score, c = outcrop flooded vulnerability score, d = coastal defences vulnerability score, e = additional weighting of highly vulnerable sites (if b, c, d = 5).

### RESULTS AND DISCUSSION

A total of 35 coastal segments were identified with rCVI ranging from 10 to 15 (Fig. 3) and 46% of the coastal segments has rCVI score of 10. This result finds agreement with field survey observation. The additional factor “e” was not needed in this case as the potential scenario of extremely high vulnerability does not exist in Pico coast after analysis, however it is likely needed for the other Azorean islands. Overlaying the PAs with this result shows that the highest rated relative vulnerability Baía Domingos Pereira (rCVI = 14) and Lajes (rCVI = 15) lie within PAs. Baía Domingos Pereira is located in two protected areas (i.e. for natural resources and management, and for vineyards cultural heritage), while Lajes is located in the protected area for natural resources and management and is a Natura 2000 site. Lajes is one of the three most important Pico villages in terms of economic, social, cultural and conservation significance. Fajã de Ribeira Grande also received the highest score (rCVI = 15). However being a talus debris platform which does not lie within or near any PAs, it is not considered an area that requires nature conservation or cultural heritage preservation, and therefore no specific action is needed.

To inform planning and management, a simple representation of coastal vulnerability for Pico was presented where rCVI scores were transposed into a CVI ranking (CVI = rCVI/4) using a scale of (1) lowest to (5) highest (Fig. 4). This exercise suggests that coastal vulnerability in Pico is relatively uniform with the entire coast being ranked either 3 or 4, corresponding to 161.9 km and

5.4 km of Pico’s shoreline, respectively. Future management needs to ensure the maintenance of important natural areas, evaluate the safety of existing near-shore developments and prevent any future near-shore developments in the vulnerable sites. Palmer et al. (2011) highlighted the importance of including social, economic and ecological components into the vulnerability study to understand how to manage risks, e.g. the degree of vulnerability of structures and features of social, economic and ecological importance located inland depends on their proximity to the high water mark. For that reason, the next phase of work will include these components to help identify areas of risk for Pico Island.

### CONCLUSIONS

Coastal vulnerability in Pico Island is relatively uniform, with some coastal segments showing relatively high vulnerabilities. Physical parameters that consider the existing natural geomorphology conditions, wave exposure to extreme events, coastal flooding and erosion, and coastal defenses were used to evaluate the relative coastal vulnerability for Pico Island. Overlaying PAs and the rCVI scores helps to identify PAs that are relatively more vulnerable, thereby requiring a different planning

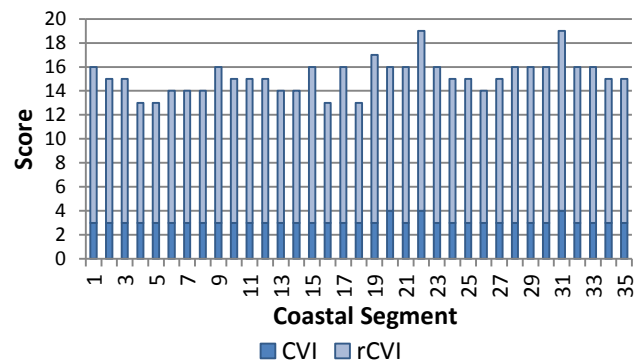


Figure 4. rCVI and transposed CVI along Pico coast.

and management approach than the relatively less vulnerable PAs. This preliminary approach provides a simple and useful tool to decision-makers for the PAs in Pico Island and could be adapted to other PAs in SIs. However, future work could include human vulnerability and risk to coastal hazards by assessing social and economic indicators, and data such as sea level rise and storm trends and patterns, regional wave statistics need to be updated as they become available and accessible.

### ACKNOWLEDGEMENTS

Authors would like to thank Fabiana Moniz (Department of Biology, University of the Azores) for her help and support. This work received support from the Portuguese national funds through the Portuguese Foundation for Science and Technology (Fundação para a Ciência e Tecnologia, FCT) under SMARTPARKS Project (PTDC/AAC-AMB/098786/2008).

### LITERATURE CITED

- Andrade, C., Borges, P. and Freitas, M.C., 2006. Historical tsunami in the Azores Archipelago (Portugal). *Journal of Volcanology and Geothermal Research*, 156, 172-185.
- Andrade, C.; Trigo, R.M.; Freitas, M.C.; Gallego, M.C.; Borges, P. and Ramos, A.M., 2008. Comparing historic records of storm frequency and the North Atlantic Oscillation (NAO) chronology for the Azores region. *The Holocene*, 18(5), 745-754.
- Bertin, X., Prouteau, E., and Letetrel, C., 2013. A significant increase in wave height in the North Atlantic Ocean over the 20th century. *Global and Planetary Change*, 106, 77-83.
- Borges, P. and Andrade, C., 1999. *Storm characterization in the Azores archipelago on the XIX and XX centuries*. Unpublished Technical Report/Project STORMS - Storminess and Environmentally Sensitive Atlantic Coastal Areas of the European Union.
- Borges, P., Andrade, C. and Freitas, C., 2002. Dune, bluff and beach erosion due to exhaustive sand mining – the case of Santa Bárbara, S. Miguel (Azores, Portugal). *Journal of Coastal Research*, SI 36, 89-95.
- Borges, P., 2003. *Ambientes litorais nos grupos Central e Oriental do arquipélago dos Açores, conteúdos e dinâmica de microescala*. Ponta Delgada, Portugal: University of the Azores, Ph.D. thesis, 413p.
- Calado, H., Borges, P., Phillips, M., Ng, K., Alves, F., 2011. The Azores archipelago, Portugal: improved understanding of small island coastal hazards and mitigation measures. *Natural Hazards* 58(1), 427-444.
- Carter, R.W.G., 1999. *Coastal environments: an introduction to the physical, ecological and cultural systems of coastlines*, 7a ed. Academic Press, London.
- Davies, W.T.R., 2012. *Applying a Coastal Vulnerability Index (CVI) to the Westfjords, Iceland: a preliminary assessment*. Ísafjörður, Iceland: University of Akureyri, Master's thesis, 109p.
- Gutierrez, B.T., Williams, S.J., and Thieler, E.R., 2007. Potential for shoreline changes due to sea-level rise along the U.S. Mid-Atlantic region: *U.S. Geological Survey Open-File Report* 2007-1278. Web only, available at <http://pubs.usgs.gov/of/2007/1278>.
- Keim, B.D., Muller, R.A., and Stone, G.W., 2004. Spatial and temporal variability of coastal storms in the North Atlantic Basin. *Marine Geology*, 210, 7-15.
- Mimura, N., Nurse, L., McLean, R.F., Agard, J., Briguglio, L., Lefale, P., Payet, R., and Sem, R., 2007. *Small islands - Climate Change 2007: Impacts, Adaptation and Vulnerability*. Contribution of Working Group II to the Fourth Assessment Report of the Intergovernmental Panel on Climate Change, M.L. Parry, O.F. Canziani, J.P. Palutikof, P.J. van der Linden and C.E. Hanson, Eds., Cambridge University Press, Cambridge, UK, 687-716.
- Ng, K., 2013. *Feasibility study on multifunctional artificial reefs for the Azores*. Ponta Delgada, Portugal: University of the Azores, Ph.D. thesis, 125p.
- Palmer, B J., Van der Elst, R., Mackay, F., Mather, A A., Smith, A M., Bundy, S C., Thackeray, Z., Leuci, R. and Parak, O., 2011. Preliminary coastal vulnerability assessment for KwaZulu-Natal, South Africa, *Journal for Coastal Research*, 64, 1390-1395.
- Pendleton, E.A., Barras, J.A., Williams, S.J., and Twichell, D.C., 2010. Coastal Vulnerability Assessment of the Northern Gulf of Mexico to Sea-Level Rise and Coastal Change: *U.S. Geological Survey Open-File Report* 2010-1146.
- Pfeffer, W.T., Harper, J.T., and O'Neel, S., 2008. Kinematic constraints on glacier contributions to 21st-century sea-level rise. *Science*, 321 (5894), 1340-1343.
- Roger, J.B., Turpin, R.N. and Brand, S., 1982. *Hurricane havens handbook for the North Atlantic Ocean*. AVENVPREDRSCH-FAC Technical Report TR 82-03.
- Young, I.R., Zieger, S., and Babanin, A.V., 2011. Global trends in wind speed and wave height. *Science*, 332, 451-455.

## Coastal impacts of marine renewables: perception of breaker characteristics by beach water users

Christopher Stokes, Emily Beaumont, Paul Russell, Deborah Greaves

School of Marine Science and  
Engineering,  
University of Plymouth,  
Plymouth, UK  
PL4 8AA

christopher.stokes@plymouth.ac.uk  
emily.beaumont@plymouth.ac.uk  
p.russell@plymouth.ac.uk  
deborah.greaves@plymouth.ac.uk



[www.cerf-jcr.org](http://www.cerf-jcr.org)



[www.JCRonline.org](http://www.JCRonline.org)

### ABSTRACT

Stokes, C., Beaumont, E., Russell, P., Greaves, D., 2014. Coastal Impacts of Marine Renewables: Perception of Breaker Characteristics by Beach Water Users. In: Green, A.N. and Cooper, J.A.G. (eds.), Proceedings 13th International Coastal Symposium (Durban, South Africa), Journal of Coastal Research, Special Issue No. 70, pp. 389-394, ISSN 0749-0208.

Beach water users such as bathers and surfers are of economic importance to tourism in Cornwall, UK. Wave energy converters soon to be trialed at the 'Wave Hub' marine renewables test site in Cornwall, may reduce inshore wave heights and have an unknown effect on wave period, therefore potentially affecting water recreation and tourism on the beaches in its lee. There is little existing research to indicate what surf conditions are 'preferred' by various beach water user groups, and how they perceive different wave conditions has never been investigated. Without an understanding of how waves are observed and described by water users, little can be said about how likely they are to be affected by, or if they will correctly perceive, any changes to inshore waves caused by Wave Hub or future renewables projects. To investigate how waves are perceived, nearshore wave buoy measurements collected in 10 m water depth and transformed to breaking height, were compared to concurrent visual observations of mean breaker height and period made by 354 participants. Ratios of observed over measured height and period were used to quantify the perceptions. The vast majority of water users underestimated significant wave height and period at breaking, and their average perceptions can be approximated by  $H_{vis} \approx 0.70H_b$  and  $T_{vis} \approx 0.83T_{1/3}$  (for waves  $0.5 \leq H_b \leq 3.5$  m and  $3 \leq T_{1/3} \leq 15$  s). Although perceptions were highly varied, average perceptions did not change significantly under different wave conditions. Perception of wave period did not change significantly between the different water user groups considered. Expert water users and surfers generally under predicted wave height the most, especially for small and/or short period waves, while novices and non-surfing water users made height observations closer to measurements.

**ADDITIONAL INDEX WORDS:** Perception, wave observation, water users, wave energy, coastal recreation

### INTRODUCTION

#### Wave Hub controversy

Recreational water-users such as surfers and bathers bring ~£300 million of tourism a year to Cornwall, UK (Environment Agency, 2007). There was initially some concern that wave energy converters soon to be trialed at the 'Wave Hub' marine renewables test site (10 km off the coast of St Ives, Cornwall, [www.wavehub.co.uk](http://www.wavehub.co.uk)) would reduce inshore wave heights, and have an unknown effect on wave period, potentially affecting water recreation and tourism on beaches in its lee. During the initial Wave Hub consultation, a collective of surfers argued that the facility would be better sited elsewhere (see figure 1), as the potential value of the electricity that would be harvested was considered to be less than the value of the surfing industry in Cornwall considered to be threatened by the project (Baxendale, 2007). Most modelling studies have indicated that the impact to surfing waves will be quite minor. One study predicted an average reduction in inshore wave height of <2% at Perranporth beach in a

scenario of 30% energy extraction (Millar *et al.*, 2007). Another study indicated < 0.5% reduction in inshore height under a scenario of 30% energy extraction (Smith *et al.*, 2012)). Nevertheless, surfing and water sports industries are crucial to Cornwall's economy, and impacts to inshore waves from future renewables deployments may exceed these initial predictions as device efficiency increases, or if arrays of devices increase in size.

To manage waves as a shared commodity, and avoid clashes of interest between renewables and tourism stakeholders, it is necessary to understand what wave conditions are of most value to each group. Globally, there has been little research to indicate what surf conditions are 'preferred' by recreational beach water users, and more fundamentally, how such individuals perceive different wave conditions has never been investigated. Without an understanding of how waves are observed and described by water users, their wave preferences cannot be interpreted correctly. It is therefore unknown how likely they are to be affected by, or if they will correctly perceive, any changes to inshore waves caused by Wave Hub or future renewables projects. As part of the E.U. funded project 'Streamlining of Offshore Wave Farm Impacts Assessment' (SOWFIA, [www.sowfia.eu](http://www.sowfia.eu)), a questionnaire survey has been conducted at two beaches on the north Cornish coast in the lee of Wave Hub to investigate water user perceptions of

breaking waves. Nearshore wave buoy measurements (collected in 10 m water depth and transformed to breaking height) were compared to concurrent visual observations of mean breaker height and period made by participants. This study aims to investigate how different groups of beach water users perceived those wave conditions.

### Wave perceptions

A number of studies have investigated the relationship between concurrently recorded visual and measured wave heights and periods, usually for the purpose of validating a long running visual record. These include observations of the height and period of unbroken waves in deep water (amongst others, Nordenstrom, 1969; Jardine, 1980; Guedes Soares, 1986), and breaking waves at the coast (Perlin, 1984; Plant and Griggs, 1992; Caldwell, 2005; Caldwell and Aucan, 2007), typically using observations made by scientists or mariners. For brevity, measurements made visually with the human eye will herein be referred to as ‘observations’ and measurements made with instrumentation such as wave gauges or buoys will be called ‘measurements’. Wave characteristics are difficult to observe consistently and accurately with the naked eye due to the dynamic and complex nature of waves. Observations are therefore variable and subjective, and often include bias (Battjes, 1984; Caldwell, 2005); what one person might consider to be a 2 m high wave might be considered a 1.5 m high wave from another viewpoint, or by another person.

Another factor influencing a person’s perception of wave height and period is the form of averaging they use in order to report a single height or period from a sea of mixed (non-monochromatic) waves, which are ubiquitous in ocean and inshore waters. Comparing observed and measured data from weather ships in the Atlantic ocean, Nordenstrom (1969) found that the average of the largest 1/3 of measured wave heights,  $H_{1/3}$ , most closely corresponded to concurrent human observations. Significant wave height ( $H_{1/3}$  or  $H_s$ ) is widely used for this reason, and the World Meteorological Organisation now recommends that observers average ~20 of the larger waves in several wave groups to determine wave height or period. Although many studies have found good correlation between measured and observed wave heights, poor correlation and a large degree of scatter tends to occur in comparisons of observed and measured wave period (Battjes, 1984; Perlin, 1984).

Systematic bias in observations has been found in visual wave height records made since the 1960’s by Hawaiian lifeguards. Although the reason for its use is disputed, the ‘Hawaiian scale’ of observation appears to consistently underestimate wave height by approximately half of the measured trough to crest height (Caldwell, 2005; Caldwell and Aucan, 2007). Scarfe *et al.* (2009) propose that surfers may therefore perceive wave heights quite differently to measurements, although there is no evidence to suggest whether or not the Hawaiian scale is used elsewhere, or by other water user groups. There is also no report of a similar systematic bias being used when describing wave period.

## METHODS

### Sampling

Questionnaire data, collected on 30 different survey dates between May and November 2013, are presented here. Perranporth and Porthtowan beach on the North Coast of Cornwall, UK, were chosen as the study sites as they lie in the middle of the area predicted to experience the greatest reduction in wave heights from Wave Hub (see figure 1). To determine

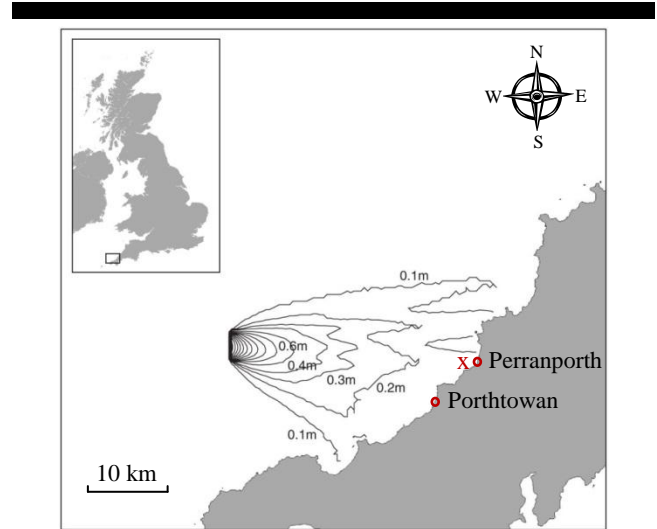


Figure 1. Location of study sites, Waverider buoy (x), and a ‘worst-case’ model prediction of wave shadowing from the Wave Hub, adapted from Millar *et al.* (2007). Contours show predicted change in  $H_s$ , for unidirectional, monochromatic swell and 0% energy transmission. (Reference state:  $H_s$  3.3 m,  $T_m$  11 s,  $269^\circ$  from North).

characteristics of the entire population of water-users at the two sites, a random (probability) sample was sought. This was achieved by predetermining the survey dates and start times using a random number generator on a computer. The two beaches were visited alternately, and questionnaires were collected for 2 hours on each visit. On average, 12 questionnaires were completed on each visit, with a total sample of  $n = 354$ . During each survey, participants were randomly sampled from either the water’s edge, or at an adjacent car park or area that overlooked the water. The researcher(s) would walk in circuits around the water’s edge or car park, and the closest available person was approached and asked if they used the water at that beach, and if they would take part in the survey. After completing a questionnaire the researcher would continue the lap and approach the next closest person.

In addition to answering demographic questions relating to their use of the sea (see figure 2), participants were asked to report a visual estimate of the average wave height,  $H_{vis}$ , and period,  $T_{vis}$ , over the 30 minutes prior to the questionnaire, or as long as they had been within view of the sea if less than 30 minutes. Wave height was defined as ‘the face height of the waves as they break’, and period as ‘the time in seconds between each wave passing a fixed point’. These definitions were intended to provide a guideline for the participants, while remaining relatively vague so that the perception of the individual would be apparent. Only participants over 18 years old were asked to partake, and ethical permission was granted by Plymouth University to conduct the surveys.

To investigate how much perceptions vary between different water user groups, observations were binned by each participant’s ‘experience factor’,  $E_f$ , and by their preferred water activity.  $E_f$  is the product of: the number of years they have been participating in their preferred water activity and the percentage of days in a year they typically participate (see figure 2b).  $E_f$  therefore approximates the total number of days the individual has participated in their lifetime (units are years). ‘Novice’ water users were classed as those with  $0 < E_f < 0.3$ , ‘experienced’ water users as  $0.3 \leq E_f < 4$ , and ‘expert’ water users as  $4 \leq E_f$ . These

thresholds are approximately the 25th and 75th percentile, respectively, of the experience levels within the sample. Two activity bins were created, those from participants who put surfing as their preferred activity, and those who stated any other preferred activity (approximately 55% and 45% of the sample respectively, see figure 2a). Experience level and activity will be considered separately to maximize the size of each subsample.

### Wave data

Wave data was collected by a directional wave-rider buoy just offshore of Perranporth beach located in approximately 10 m depth (see figure 1). In order to compare breaking wave observations to measurements, wave heights from the nearshore buoy were transformed to breaking heights. The rms wave height at breaking was estimated using linear wave theory that takes into account shoaling and refraction (Plant *et al.*, 1999) –

$$H_{b(rms)} = \left(\frac{\gamma}{g}\right)^{1/5} [H_o^2 C_{go} \cos(\theta_o)]^{2/5} \quad (1)$$

where  $g$  is gravitational acceleration and  $\gamma$  is the empirically determined ratio of wave height to water depth at breaking. At Perranporth beach, a conservative value for  $\gamma$  is 0.4, and is used here (Miles *et al.*, 2013 (in press)).  $H_o$  and  $\theta_o$  are the rms wave height and peak wave direction relative to shore normal (in radians), respectively, taken at the wave buoy.  $C_{go}$  is the offshore group velocity calculated using linear wave theory, which considers peak period,  $T_p$ , and water depth, both at the location of the buoy.  $H_{b(rms)}$  was adjusted to estimate significant wave height at breaking,  $H_b$ , by  $H_s \approx H_{rms}/0.7$  (Komar, 1998). Wave period was not transformed from the buoy and was taken as the significant period,  $T_{1/3}$ , calculated as either  $T_{1/3} \approx 0.95T_p$  for windsea spectra (Goda, 1978), or  $T_{1/3} \approx T_p$  for swell (Goda, 1988a). Plant and Griggs (1992) argue that when bimodal spectra occur an observer is likely to report a significantly reduced wave period, due to the interaction of the swell and windsea components. Despite this, for bimodal cases, the  $T_{1/3}$  value associated with the dominant component (swell or wind sea) was used, as this resulted in the best agreement with the visual observations. Swell and windsea were identified in the 1D spectra, and bimodal spectra partitioned, using the methods of Portilla *et al.*, (2009).

As there is no other source of wave data more local to

Porthtowan, it has to be assumed that there are no significant differences in the nearshore conditions between Porthtowan and Perranporth, despite their 10 km separation and slight difference in orientation ( $292^\circ$  and  $283^\circ$  from North, respectively; See figure 1). Scott (2009) and Poate (2011) used data output by a Mike21 wave model at the 15 m depth contour to assess differences in the wave climate along the North coast of Cornwall. They found that differences in the annual wave statistics were negligible under non-extreme conditions, with 0.8% difference in  $H_{s50\%}$  between Perranporth and Porthtowan (1.24 and 1.23 m respectively) and 2% difference in  $T_p$  between Perranporth and Porthtowan (9.7 and 9.5 s respectively). Under larger wave conditions the disparity between the sites increases however, with 13.6% difference in  $H_{s10\%}$  between Perranporth and Porthtowan (2.95 and 2.55 m respectively). Given that the waves considered in this study are generally under  $H_s$  2 m, the Perranporth wave buoy should provide a reasonable surrogate source of data for Porthtowan.

### Statistical analysis

Outliers in the wave height and period observations were objectively removed, as they are unlikely to represent typical water-user perceptions and will reduce the quality of the regression analysis to be performed on the data. Firstly the ratios of observed over measured wave height ( $H_{vis}/H_b$ ) and period ( $T_{vis}/T_{1/3}$ ) were calculated for each participant. The ‘boxplot’ approach was then used to identify unusually large or small ratios, whereby outliers lie outside the range:  $IQR \pm (1.5 * IQR)$ , where IQR is the interquartile range. This method doesn’t rely on the assumption of normally distributed data, as the IQR depends on the median of the data and not the mean (McGill *et al.*, 1978). In total, 3.4% of wave height observations and 7.9% of wave period observations were excluded from the data set.

To provide an estimate of how well the statistics derived from this sample represent the entire population of water users at the two sites, and to identify when statistics are significantly different to one another, 95% confidence intervals are reported. These indicate the bounds within which the true population parameter is likely to lie. Bootstrapping has been used to calculate this, as it provides accurate confidence bounds for relatively small samples and also performs well for non-normally distributed data (DiCiccio and Efron, 1996), which will be beneficial for the small

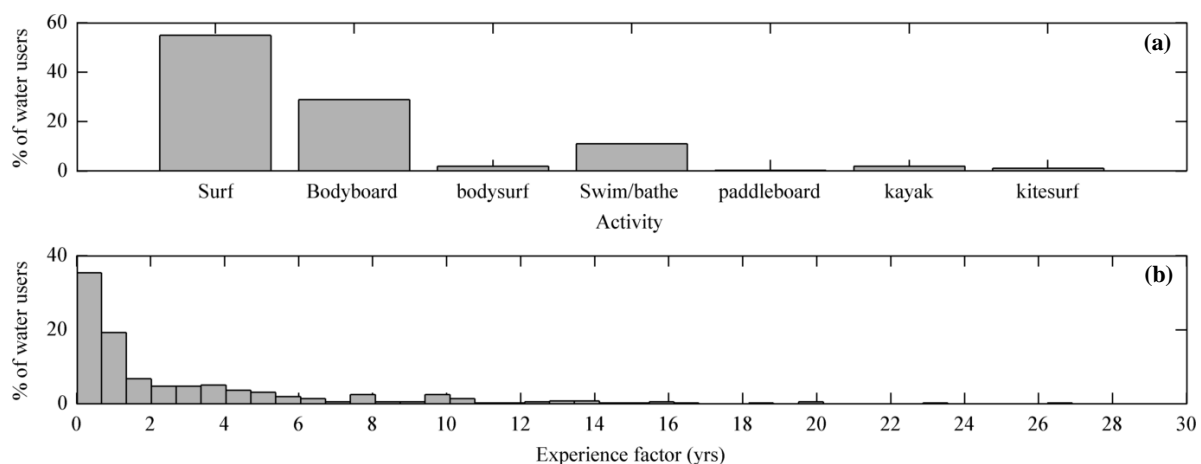


Figure 2. Water use statistics for the sample. (a) ‘Preferred’ water activity (activity they most often do) (b) Experience level of the participants, calculated as the product of the number of years of experience of each individual and the typical percentage of days in a year they participate (herein referred to as their ‘experience factor’,  $E_f$ ).



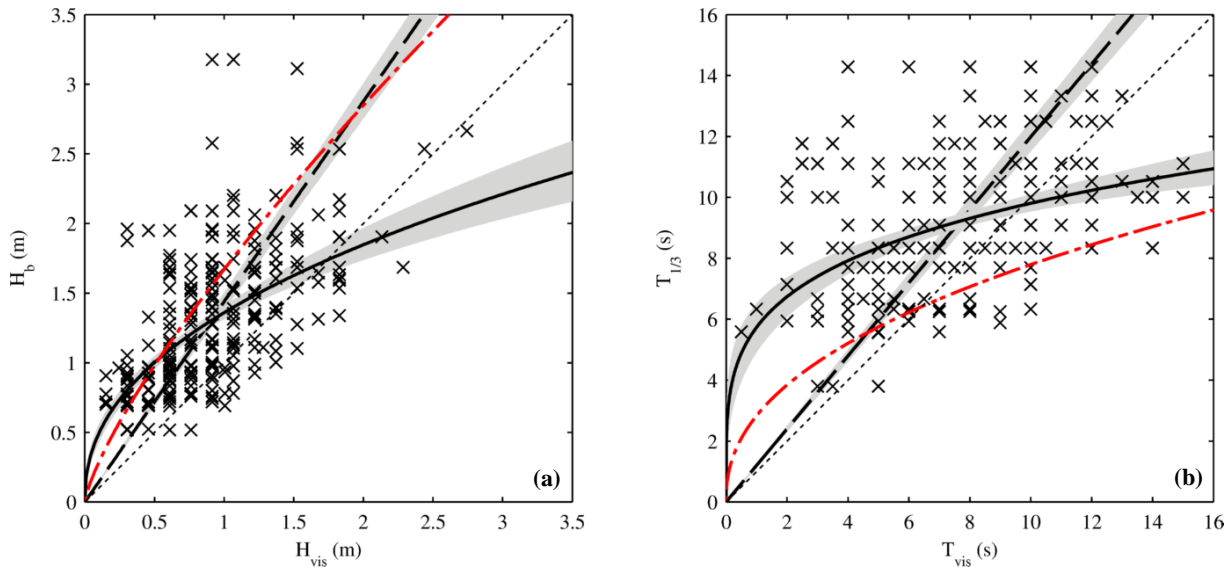


Figure 3. (a)  $H_{vis}$  plotted against significant wave height at breaking,  $H_b$ , for all water users (outliers removed). (b)  $T_{vis}$  plotted against  $T_{1/3}$  for all water users (outliers removed). The solid black curve in each plot is a power law, least squares fitted to the data. The dashed black lines are the mean perception ratios. The dot-dashed curves are the power law curves determined by Nordenstrom (1969). The shaded areas are 95% confidence intervals. The thin dotted line is a line of perfect correlation for reference only.

subsamples examined later (minimum size  $n = 10$ ). Bootstrapping simulates the task of resampling from the population, making many ‘artificial’ samples by randomly resampling from the available data. 5000 bootstrap samples were used to calculate each confidence interval, and stabilization of the statistic usually occurred well before this number was reached. For the regression confidence intervals described later, the percentile bootstrapping method was used, and for the mean ratios the accelerated and bias corrected method was used. DiCiccio and Efron (1996) provide an assessment and summary of each method.

### RESULTS

Figure 3 shows visual observations of wave height and period plotted against concurrent measurements. At all measured heights (periods) the majority of participants under-predicted the breaking wave height (period). There is a fair degree of scatter in the relationships, particularly between observed and measured wave period, which indicates that participant’s perceptions varied widely. To model these relationships, power law curves were least-squares fitted to the data and are plotted in figure 3 (solid curves; RMS error is 0.41 in (a) and 2.03 in (b)) alongside the power law curves derived by Nordenstrom (1969) in a similar study (dot-dashed curves; RMS error is 0.51 in (a) and 5.65 in (b)). Our power law curves fit the data reasonably well up to  $H_b$  1.5 m, and  $T_{1/3}$  10 s, and suggest that a water user’s observations can be estimated from  $H_b$  and  $T_{1/3}$  by the following relationships –

$$H_{vis} = \frac{0.44}{\sqrt{1.36}} H_b^{0.44} \quad (\text{for } 0.5 \leq H_b \leq 1.5 \text{ m}) \quad (2)$$

$$T_{vis} = \frac{0.23}{\sqrt{5.73}} T_{1/3}^{0.23} \quad (\text{for } 6 \leq T_{1/3} \leq 10 \text{ s}) \quad (3)$$

A simpler relationship is the mean ratio of observation over measurement; the ‘perception ratio’,  $P$  (figure 3, thick dashed lines; RMS error is 0.52 in (a) and 3.22 in (b)). These do not fit the bulk of the data as well as our power law curves, but do fit better at larger heights ( $2 < H_b < 3.5$  m) and periods ( $12 < T_{1/3} < 15$

s) and, like the data, suggest that these heights and periods will be under predicted by water users. From figure 3 the mean wave height perception ratio,  $P_H$ , for all participants was 0.70 (std. dev. 0.28), while the mean wave period perception ratio,  $P_T$ , was 0.83 (std. dev. 0.29). Therefore on average –

$$H_{vis} \approx 0.70 H_b \quad (\text{for } 0.5 \leq H_b \leq 3.5 \text{ m}) \quad (4)$$

$$T_{vis} \approx 0.83 T_{1/3} \quad (\text{for } 3 \leq T_{1/3} \leq 15 \text{ s}) \quad (5)$$

### Effect of varying conditions on perceptions:

To investigate how much perceptions change under different incident wave conditions, observations were binned by measured wave height (0.5-1, 1-1.5, and 1.5-2 m) and measured wave period (6-8, 8-10, 10-12, and 12-14 s). Mean  $P_H$  and  $P_T$  values were then calculated for each bin with 10 or more observations in, along with 95% confidence bounds. Significant variations in perception due to the incident conditions are seen where there is no overlap between the confidence bounds of different height or period bins in figure 4 (grey bars with diamonds). Although some significant differences in height (period) perception occurred at different wave heights (periods), there were no significant differences between the binned perceptions and the overall mean perceptions described by equation (4) (shown as a grey dashed line in figure 4) and equation (5). This suggests that equations (4) and (5) are sufficient in describing the average water user perception within any of the height and period bands considered.

### Effect of differing experience level and preferred activity on perception:

Significantly different wave height perceptions by the different experience level (activity) groups can be identified in figures 4a and 4b (4c and 4d) where there is no overlap between the confidence bars for novice, experienced, and expert water users (surfers and non-surfers). Additionally, a group’s perception is adequately described by equations (4) or (5) if the confidence bounds of that group’s perception overlap the bounds of (4) or (5).

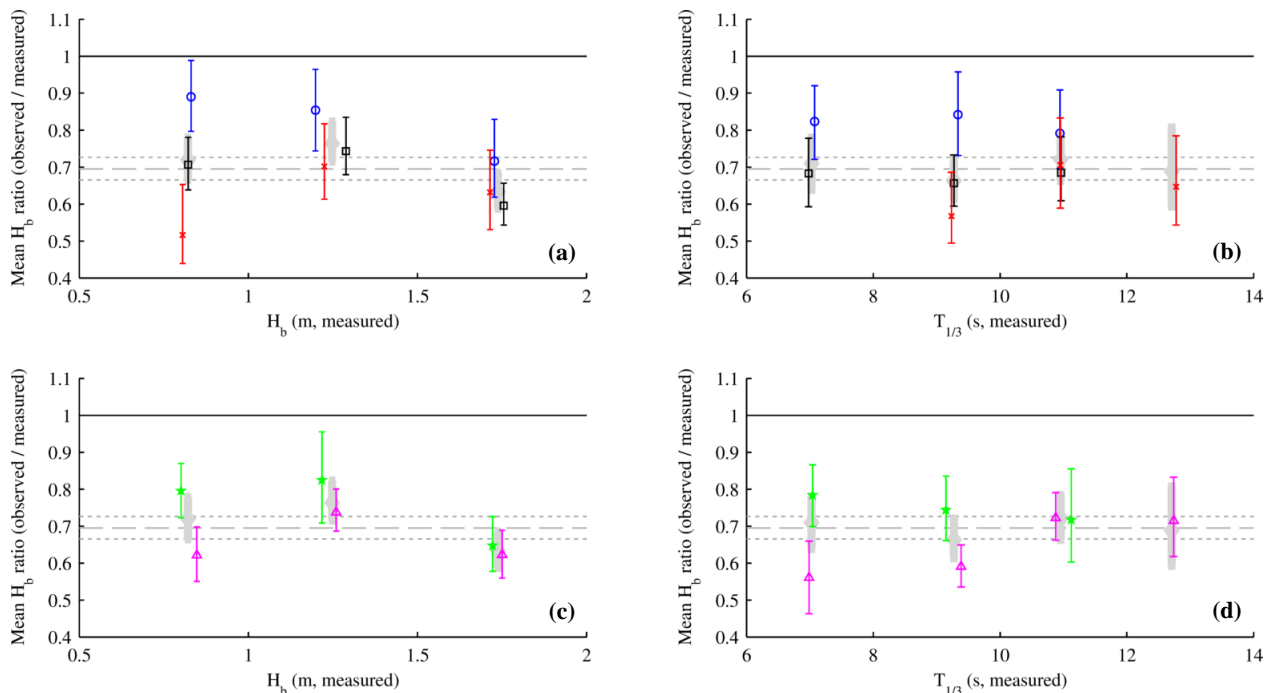


Figure 4. Mean ratios of observed/measured wave height ( $P_H$ ) plotted against mean measured wave height in each band (a and c) and mean measured wave period in each band (b and d). In (a) and (b) blue circles = novice water users, black squares = experienced water users, red crosses = expert water users. In (c) and (d) Magenta triangles = surfers, green stars = non-surfers. In each panel grey diamonds = all water users. The grey dashed and dotted lines are the mean perception and confidence intervals, respectively, for all water users at all heights and periods. As there were few significant differences between mean period perceptions, they are not shown.

There were no significant differences in  $P_T$  for participants of differing experience level or activity, (hence  $P_T$  not being plotted), and Equation (5) adequately describes the average wave period perception of all water user groups. There were however significant differences in the perception of wave height. At small wave heights (0.5-1 m) and medium periods (8-10 s) there is disparity between the height perception of novices and experts. At these bands wave height was underestimated more by the more experienced water users, and the perception ratio in equation (4) does not sufficiently describe the various perceptions. Unsurprisingly, as they are the majority group, experienced water user's perceptions were much better accounted for by equation (4), although at larger wave heights (1.5-2 m) the  $P_H$  of experienced water users was slightly lower than that given by equation (4).

A similar result was seen for the activity groups, where at small wave heights (0.5-1 m) and short periods (6-10 s) surfers under predicted height significantly more than non-surfers. The wave height and period perception of non-surfers is sufficiently described by equation (4), whereas surfer's perceptions were significantly different to equation (4) during short period waves (6-10 s). At measured heights of 1-1.5 m and periods of 10-12 s the perceptions of all water users were most similar to one another, and wave heights and periods were under predicted the least by surfers and more experienced water users.

## DISCUSSION

The scatter in figure 3 (a) and (b) demonstrates the large degree of variability in people's perception of wave heights and periods. Perception could vary due to the presence or absence of a comparison object (e.g. a person or a rock) to provide scale to the waves or a benchmark for timing wave period (Caldwell and

Aucan, 2007). It might also be affected by the position and elevation of the observer or their level of observational experience (Perlin, 1984; Guedes Soares, 1986; Caldwell and Aucan, 2007). In addition the observer may have made an observation based on very few waves, whereas the wave buoy averages over 30 minutes. Further to these potential sources of observational 'error', bias also undoubtedly contributes to the variation in perception. Bias may be caused by differences in what each observer considers to be the trough and crest of each wave; expert water users may only consider the steeper part of the wave face, while novices the entire face from trough to crest. It has not been possible in this study to differentiate between inaccuracy and bias in each observation, but small observational errors (noise) should average out over a large number of observations, while systematic bias should remain apparent (signal).

The pronounced scatter in the wave period observations is not unusual (Battjes, 1984; Perlin, 1984; Plant and Griggs, 1992), and the relationship between  $T_{vis}$  and  $T_{1/3}$  must be considered cautiously. In other studies variability has been attributed to difficulties in counting wave period, or even identifying one wave from another during mixed seas (Perlin, 1984; Plant and Griggs, 1992). It was noted that the untrained participants in this study rarely counted wave period properly, and their observations were therefore often based on a wave forecast (53% had recently seen a forecast), or were merely a quick estimate. Despite this, the mean  $P_T$  found here (0.83) was not significantly different to any of the water user group's mean perception ratios, and is similar to the  $P_T$  found in other studies (0.89-0.95 (Battjes, 1984)). The power law curves in figure 3 suggest that wave heights (periods) under 1.5 m (10 s) will be under predicted and larger heights (periods) will be over predicted, despite the fact that there is predominantly under

prediction occurring in the data. This results from the curves fitting to the bulk of the data at heights (periods) <1.5 m (10 s); at greater heights (periods) they fit the data poorly. The divergence of our wave height curve from that of Nordenstrom (1969) at heights >1 m could be a result of the difference between observing/measuring wave height in deep water (e.g. Nordenstrom, 1969) and observing/estimating breaking height with linear theory, as has been done here. However Nordenstrom's curve is fitted over a greater range of heights, considering waves of up to 10 m. It is therefore likely that with data from larger waves, our curve would be closer to theirs, and may not show over prediction of larger waves.

The ratios in equations (4) and (5) seem to adequately describe the average perception of most water user groups. Because they indicate that water users will, on average, under predict height and period (as is apparent in the data in figure 3), and because they fit the data better at larger wave heights and periods, the ratios are deemed to be better models of wave perception than the power law curves. It should be noted however that the ratios relate to  $H_s$  and  $T_{1/3}$  as calculated above. Linear shoaling is not infallible, and on shallow coasts usually overestimates  $H_b$  because bottom friction is not considered, although this has possibly been mediated by using a conservative value for  $\gamma$ . There are also other methods for calculating  $T_{1/3}$ .

For waves of 1-1.5 m or 10-12 s all water user groups had approximately the same perception of wave height, and height was under predicted the least. Interestingly, the annual mean  $H_s$  and  $T_{1/3}$  at Perranporth fall exactly within these ranges, indicating that during average wave conditions, height and period are more accurately and consistently described by water users than during non-average conditions. Novice water users and/or non-surfers often had wave height perceptions closest to measurements, while experts and/or surfers often significantly under predicted height, especially for small waves (0.5-1 m), or short period waves (6-10 s). The perceived height of small, short period waves therefore changes through increased water use, which may be a result of these waves seeming less threatening as experience and water ability increases. There may also be a culturally bred bias in the surfing world that has not yet permeated into other water sports, which would explain the lower height perception of surfers. This may have originated from the Hawaiian scale of height observation, where  $P_H \approx 0.5$ , as Hawaiian surf culture has had a widespread influence on global surf culture. Machismo may be a cause of such wave height underestimation, as an observer may seek to play down the size of surf to inflate their apparent confidence. Comparison of perceptions by gender may be used to explore this further.

## CONCLUSIONS

Overall, participants generally underestimated measured wave height and period at breaking, and the average perception can be approximated by  $H_{vis} \approx 0.70H_b$  and  $T_{vis} \approx 0.83T_{1/3}$  (for waves  $0.5 \leq H_b \leq 3.5$  m and  $3 \leq T_{1/3} \leq 15$  s). Although perceptions were highly varied, average perceptions did not change significantly under the different (aforementioned) wave conditions analyzed in the study. Perception of wave period did not change significantly between the different water user groups, but expert water users and surfers generally under predicted wave height the most, while novices and non-surfing water users made observations closer to measurements. Using specific height perception ratios for expert water users and surfers may therefore better describe their perceptions. Observations at greater wave heights and periods are needed to further explore the perception of breaking waves.

## ACKNOWLEDGEMENTS

We would like to thank all the participants that gave their time to take part in this study. Additional thanks go to Eleanor Woodward, Claire Earlie, and Emma Rendle for their hard work collecting data on a number of the survey dates.

## LITERATURE CITED

- Battjes, J. 1984. A review of methods to establish the wave climate for breakwater design. *Coastal Engineering*, 8, (2), 141-160.
- Baxendale, J. 2007. Are we waving goodbye to surfing? Martin, A. The Telegraph Newspaper. Available online at: [www.telegraph.co.uk/news/uknews](http://www.telegraph.co.uk/news/uknews).
- Caldwell, P. C. 2005. Validity of north shore, Oahu, Hawaiian Islands surf observations. *Journal of Coastal Research*, 1127-1138.
- Caldwell, P. C. and Aucan, J. P. 2007. An empirical method for estimating surf heights from deepwater significant wave heights and peak periods in coastal zones with narrow shelves, steep bottom slopes, and high refraction. *Journal of Coastal Research*, 1237-1244.
- DiCiccio, T. J. and Efron, B. 1996. Bootstrap confidence intervals. *Statistical Science*, 189-212.
- Environment Agency 2007. *Enjoying water. A strategy for water-based recreation in the South-West 2009 - 2014*.
- Goda, Y. 1978. The observed joint distribution of periods and heights of sea waves. *Coastal Engineering Proceedings*, 1, (16),
- Goda, Y. 1988a. Statistical variability of sea state parameters as a function of wave spectrum. *Coastal Eng. Japan*, 31, (1), 39-52.
- Guedes Soares, C. 1986. Assessment of the uncertainty in visual observations of wave height. *Ocean engineering*, 13, (1), 37-56.
- Jardine, T. 1980. The reliability of visually observed wave heights. *Coastal Engineering*, 3, 33-38.
- Komar, P. 1998. *Beach processes and sedimentation*. (Second ed), Prentice Hall, New Jersey.
- McGill, R., Tukey, J. W. and Larsen, W. A. 1978. Variations of box plots. *The American Statistician*, 32, (1), 12-16.
- Miles, J., Thorpe, A., Russell, P. and Masselink, G. 2013 (in press). Observations of bedforms on a dissipative macrotidal beach. *Ocean Dynamics CD13 Topical Collection*,
- Millar, D., Smith, H. and Reeve, D. 2007. Modelling analysis of the sensitivity of shoreline change to a wave farm. *Ocean engineering*, 34, (5-6), 884-901.
- Nordenstrom, N. 1969. *Methods for Predicting Long Term Distributions of Wave Loads and Probability of Failure for Ships*. Report No. 69-22-S. Det Norske Veritas, Research Department, Oslo.
- Perlin, M. 1984. Statistical analysis of visual wave observations and gage/radar measurements. *Final Report Coastal Engineering Research Center, Vicksburg, MS.*, 1,
- Plant, N. G. and Griggs, G. B. 1992. Comparison of visual observations of wave height and period to measurements made by an offshore slope array. *Journal of Coastal Research*, 957-965.
- Plant, N. G., Holman, R. A., Freilich, M. H. and Birkemeier, W. 1999. A simple model for interannual sandbar behavior. *Journal of Geophysical Research. C. Oceans*, 104, 15.
- Poate, T. G. 2011. *Morphological Response of High Energy Macrotidal Beaches*. Plymouth: Plymouth University, Ph.D. thesis, 255p.
- Portilla, J., Ocampo-Torres, F. J. and Monbaliu, J. 2009. Spectral partitioning and identification of wind sea and swell. *Journal of atmospheric and oceanic technology*, 26, (1), 107-122.
- Scarfe, B. E., Healy, T. R. and Rennie, H. G. 2009. Research-based surfing literature for coastal management and the science of surfing-a review. *Journal of Coastal Research*, 539-557.
- Scott, T. M. 2009. *Beach morphodynamics and associated hazards in the UK*. University of Plymouth,
- Smith, H. C. M., Pearce, C. and Millar, D. L. 2012. Further analysis of change in nearshore wave climate due to an offshore wave farm: An enhanced case study for the Wave Hub site. *Renewable Energy*, 40, (1), 51-64.

## Sandy beaches characterization and management of coastal erosion on western Sardinia island (Mediterranean Sea).



[www.cerf-jcr.org](http://www.cerf-jcr.org)

Giovanni De Falco†, Francesca Budillon‡, Alessandro Conforti†, Sandro De Muro∞, Gabriella Di Martino‡, Sara Innangi‡, Angelo Perilli†, Renato Tonielli‡, Simone Simeone†

† Istituto per l'Ambiente Marino Costiero  
CNR, Località Sa Mardini Torregrande  
Oristano, Italy  
[giovanni.defalco@cnr.it](mailto:giovanni.defalco@cnr.it)

‡ Istituto per l'Ambiente Marino Costiero  
CNR, Calata Porta di Massa Napoli, Italy

∞ Dipartimento di Scienze Chimiche e  
Geologiche, Università di Cagliari, Italy



[www.JCRonline.org](http://www.JCRonline.org)

### ABSTRACT

De Falco, G., Budillon, F., Conforti A., De Muro, S., Di Martino G., Innangi, S., Perilli, A., Tonielli, R., Simeone, S. 2014. Sandy beaches characterization and management of coastal erosion on western Sardinia island (Mediterranean sea). In: Green, A.N. and Cooper, J.A.G. (eds.), *Proceedings 13<sup>th</sup> International Coastal Symposium* (Durban, South Africa), *Journal of Coastal Research*, Special Issue No. 70, pp. 395-400, ISSN 0749-0208.

Coastal erosion is a global problem which affects sandy and rocky shores worldwide. Coastal erosion can be triggered by several causes. Local processes can generate erosion hot spots, whereas at the global scale, the main forces are sea level rise, changes in storm climate and human interference. Beaches along the Mediterranean sea are strongly affected by coastal erosion. Recently, the Protocol on Integrated Coastal Zone Management in the Mediterranean (PAP/RAC 2007) recommended the prevention of erosion processes by restoring the natural adaptive capacity of the coast and by improving the knowledge on the state, development and impact of coastal erosion. In order to achieve the objective of the PAP/RAC protocol, we characterized 24 sandy beaches along ~270 km of the western coastline of the Sardinia island (western Mediterranean). Grain size and mineralogy of the foreshore sediments were analyzed and the intertidal elevation/bathymetric profile were measured using the Differential Global Positioning System. Aerial photos were used to identify the shoreline configuration, the number of bars and morphodynamic features. A digital elevation model (DEM) of the adjacent shelf was produced and acoustic backscatter, grab and box-corer sediment samples were collected in order to characterize the seafloor and to identify the substrate lithology, particularly the distribution of sandy sediments. The investigated coastline is characterized by linear, multibarred beaches and wide transgressive dune fields formed by terrigenous and coarse sand. These linear beaches are alternated with embayed beaches which locally show a mixed terrigenous/bioclastic carbonate composition. Large sandy bodies were found in the inner shelf, often forming dune fields which were uncovered by mud drapes. A database was created to facilitate the characterization of the beach systems along the studied coastline and adjacent inner shelf. It is anticipated that the database will be used by policy makers in support of the implementation of coastal erosion management strategies.

**ADDITIONAL INDEX WORDS:** *sand reservoir, beach, management.*

### INTRODUCTION

The management of coastal erosion has received increasing attention during the past decade (Jimenez et al., 2011). Several projects funded by the European Commission (Eurosion, Conscience, Micore) were launched to achieve the strategic objective of developing guidelines of sustainable management of coastal erosion in Europe (Marchand et al., 2011; Ciavola et al., 2011).

The management of coastal erosion is recognized as a main topic in the "Protocol on Integrated Coastal zone Management in the Mediterranean" (PAP/RAC, 2007). The protocol recommends "to adopt the necessary measures to maintain or restore the natural capacity of the coast to adapt to changes, including those caused by the rise in sea levels. The Parties will anticipate the impacts of coastal erosion through the integrated management of activities, including adoption of special measures for coastal sediments and

coastal works. The Parties undertake to share scientific data that may improve knowledge on the state, development and impacts of coastal erosion".

A basic concept of coastal erosion management is the 'favorable sediment status', defined by Eurosion project as the situation where the availability of coastal sediments supports the objective of promoting coastal resilience in general and of preserving dynamic coastlines in particular (Merchand et al., 2011, Gault et al, 2011, Sánchez-Arcilla et al., 2011). Within this framework, the strategic sediment reservoirs are an essential component and they can be used as sediment supply for nourishment as an intervention measure.

The project RITMARE represents the main research effort of Italian scientific community in marine science, with a specific work package dedicated to the beach sedimentary budget along several test areas of the Italian coast.

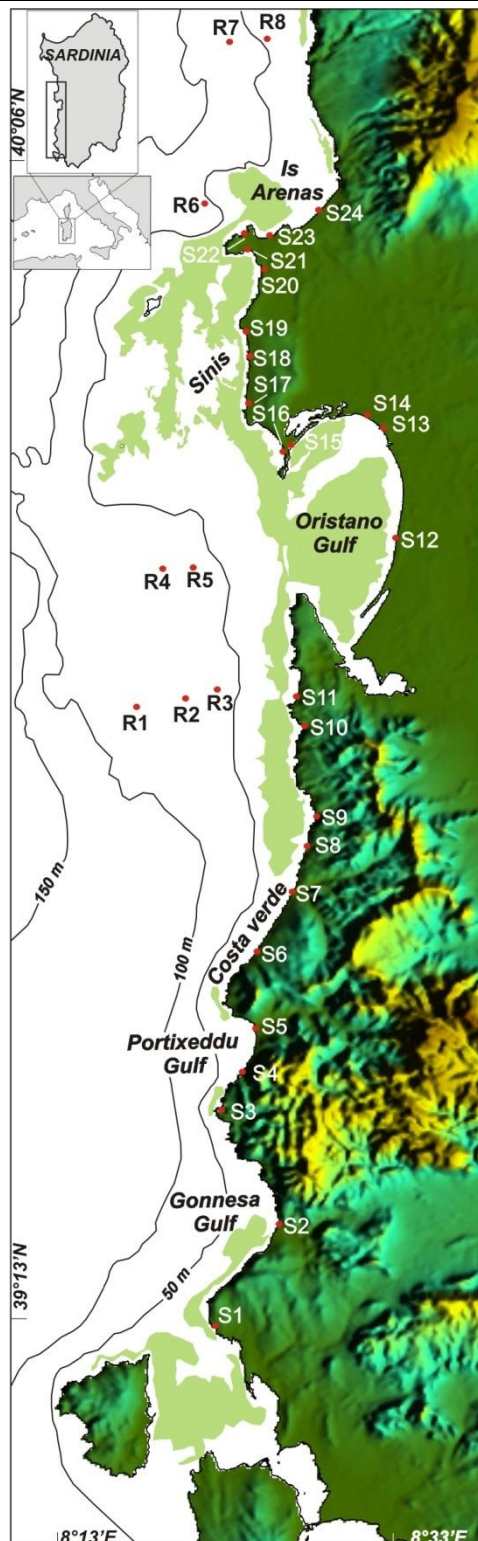


Figure 1. Location of beaches and sampling point of offshore sediments along the western Sardinian shelf. The distribution of the seagrass *Posidonia oceanica* is reported (green area).

One of these test areas is the western coast of Sardinia (Western Mediterranean), is characterized by a low degree of urbanization

and extended pristine coastal sectors. The sandy shores of this sector are extremely varied, including: long linear beaches, wide large transgressive dune fields, embayed beaches and barrier-lagoon systems (Simeone and De Falco, 2012; Simeone *et al.*, in press). Beach sediments are heterogeneous in composition (terrigenous vs. biogenic carbonate) and grain size (De Falco *et al.*, 2003).

The aim of this paper is to analyze the relationships between the sediment characteristics of beach systems and the adjacent offshore sediment deposits in terms of grain size and composition. Several data sets (e.g. geophysical data, sediment sampling and morphological measures) obtained by different projects were used, in order to assess the level of coastal resilience in terms of sediment availability along a ~270 km stretch of the western Sardinian coastline.

## METHODS

### Beach morphology

A total of 24 beaches were considered (Figure 1). The foreshore slope was measured along one cross-shore transect located on the central area of each beach. Differential Global Positioning System (DGPS) technology was used to collect positioning data (X, Y, Z), with one point every 2.5 m, by using Stop and Go modality (Coelho *et al.*, 2009; Morton *et al.*, 1993). In order to obtain the foreshore slope the measured beach profiles were acquired from the top of the storm berm up to the beach step. Foreshore slope was considered as a synthetic indicator of the morphological aspect of the foreshore of the beaches (Hegge *et al.* 1996). The main morphological features of the beaches (e.g. dune field morphology, number of bars, etc.) were described by using aerial images of the coastline of Sardinia Island available from the Informative System of the Regione Autonoma della Sardegna. The Embayment Index was computed as the ratio between the beach length and distance between the capes, according to Spagnolo *et al.* (2008).

### Offshore geophysical data

Multibeam echosound (MBS) data were collected throughout the western margin of Sardinia providing a comprehensive morphostructural definition of the mid-outer continental shelf/upper slope sectors, down to 600 m depth. Data were collected in five oceanographic cruises from 2009 and 2011 using the R/V Maria Grazia and Urania of Italian National Research Council (CNR) equipped with different instruments.

In the 50 and 150 meters depth range, data were acquired using the Kongsberg EM 3002D (293-307 kHz) with a depth resolution of 1cm. The system was equipped with two heads angled at approximately 33° which provided a wide swath up to 150 meters deep. For deeper sectors (from 150 to 700-800 meters) the Kongsberg EM 710 and SeaBat Reson 7111 were used, both devices operate at a sonar frequency of 100 kHz.

All MBS devices also provided the seabed backscatter which was used for interpreting the characteristics of the seabed. All data were processed using Caris Hips and Sips software. Finally, Digital Terrain Models (DTM) at 2.5 meters (shelf) and 5 meters (slope) resolution were produced.

Very high resolution seismic data were collected along the same routes of the multibeam survey by using different devices. In this paper we show seismic data collected on bedform fields using a Datasonic Chirp II operating at 3.5 kHz.

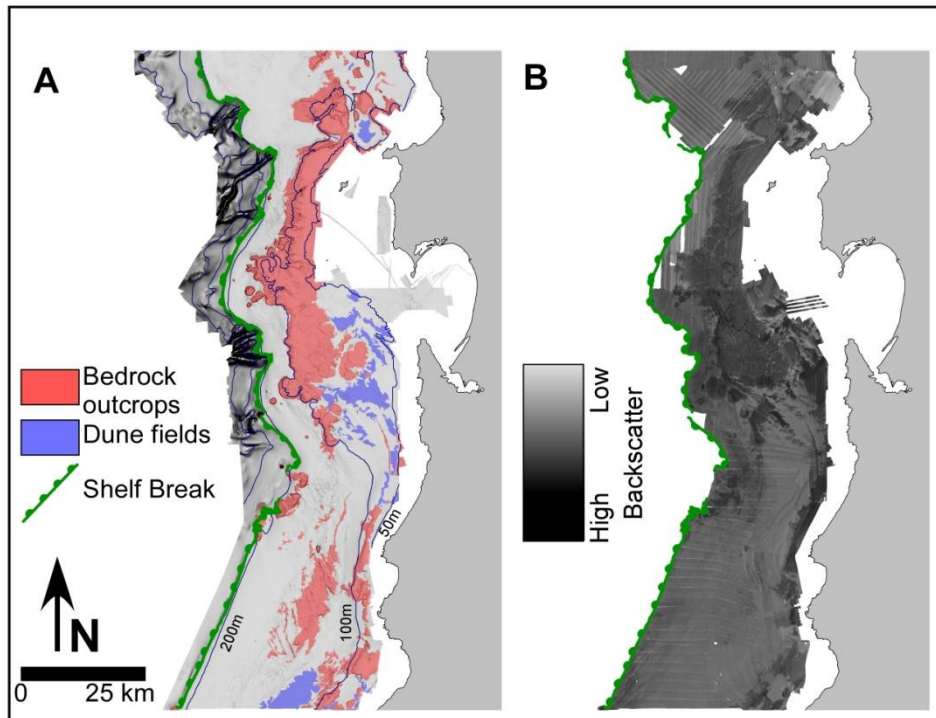


Figure 2. A) Digital Terrain Model of the shelf-upper slope of central western margin of Sardinia obtained from multibeam echosounder data and B) backscatter intensity. The sectors with large dune fields represent potential sand reservoirs: those areas are characterized by lower backscatter values.

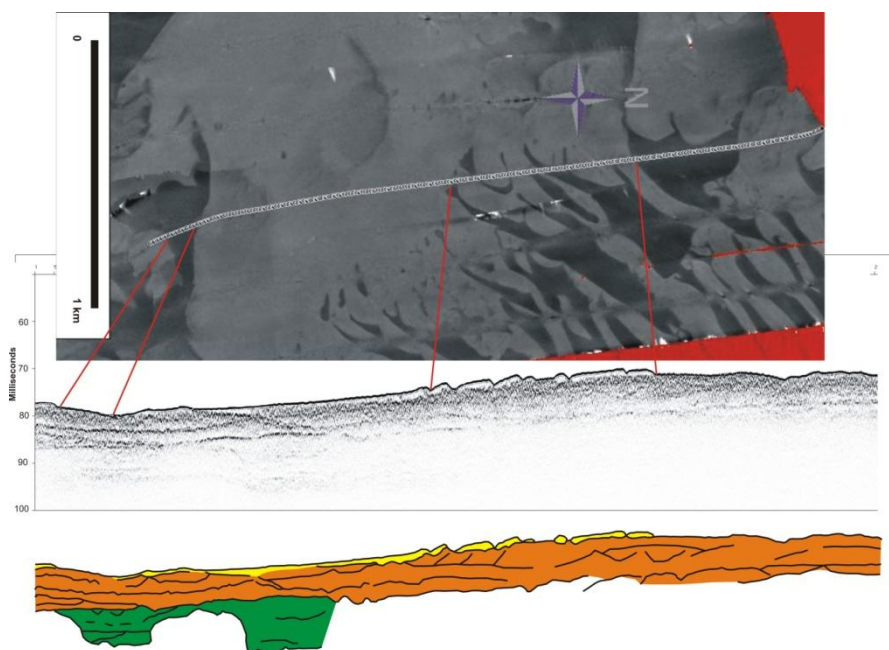


Figure 3. Very high resolution seismic profile of the offshore sand deposits: the superficial seismic unit (yellow unit) is characterised by lower backscatter values, and is composed of medium to fine sands, with a thickness < 3m, which overlie a thicker seismic unit with internal reflectors denoting cross stratification, and characterised by high backscatter values associated to coarse sediments.

## Sediment analysis and data processing

Two sediment samples were collected in the foreshore of the central section of each beach. A total of 26 short cores were collected in 8 sites along the offshore region (Figure 1) by using a box-corer which penetrated 20-30 cm into the sand deposits. Two/three sub-samples were further retrieved along the vertical profile of each core.

Grain size and carbonate content of beach and offshore sediments were determined by dry sieving (1/2 phi interval) and using the Dietrich-Fruhling calcimeter.

The sediment samples were preliminarily classified into three groups based on biogenic carbonate contents: terrigenous (carbonate <20%), mixed (20-60%) and biogenic carbonate (>60%). The similarity and differences between sediment texture of beach and offshore sediments within each compositional group were determined by multivariate statistics of grain size data. Factor analysis was applied to grain size data and expressed at half phi interval considering samples as cases and grain size intervals as variables. Data were previously transformed, by using the ranking method, in order to avoid artifacts due to the closure to 100 of grain size data (De Falco et al., 2008).

## RESULTS AND DISCUSSION

### Beach characterization

Wide linear multibarred beaches, with large parabolic dunes, characterize the open coastline from the Gulf of Gonnesa to Costa Verde (S1-S11, Table 1 and Figure 1), with a few embayed beaches. Foreshore sediments are mainly terrigenous and are characterized by coarse grain size, ranging from slight gravelly to gravelly sands.

In the Gulf of Oristano (S12-S15), the morphology is characterized by the presence of a foredune and the absence of bars in the shoreface. The sediment composition is terrigenous, with the exception of the northern sector of the gulf where sediments are mixed.

In the Sinis Peninsula (S16-S24), the morphology is more variable depending on the configuration of the coast. The main feature of this sector is the mixed or mainly biogenic sediment composition, with grain size being coarse.

The foreshore slope does not show a clear trend along the investigated coastline, and is driven by the sediment grain size.

### Offshore sediment reservoir

The shallower shelf sector (<50m) is largely colonised by the seagrass *Posidonia oceanica* (Figure 1), a protected marine species. Consequently, the analysis of sediment reservoirs was focussed in the deeper shelf areas (>50 m), outside the deep limit of the seagrass meadows.

The digital elevation model of the study area is reported in Figure 2. Large sections of the shelf, down to 130-140 m depth, were characterized by the presence of an irregular seabed surface which can be attributed to the outcropping bedrock. The rocky outcrop encompasses small basins in the inner shelf which display wide dune fields in the bathymetric range of 50-110 m, with a surface of up to 90km<sup>2</sup>.

The backscatter data further support and better define the identification of the bedrock outcrops and provide an outline of the type of sediment which is present on the shelf. As largely reported in literature and tested in the area, a high backscatter can be related to the outcropping bedrock and to coarse sediments, whereas low backscatter can be associated with finer sediments

(De Falco et al, 2010). Lower backscatter values are found between 50 and 100 m and are often associated with dune fields.

Table 1. Morphological characteristics and sediment composition and grain size of the studied beaches (see Figure 1 for location). The description of beach morphology includes the Embayment Index, the morphology of the shoreface (Rk=rocky; NB=no bars; SB = single bar; MB = multiple bars), the dune (ND= no dune; FD = foredune; LPD = large parabolic dunes) and the foreshore slope. The sediment characteristics include the composition (T=terrigenous; BC= biogenic carbonate; Mx= mixed, and the median diameter.

Beach ID.	Morphology			Sediments		
	Emb. Ind.	Shoreface	Dune	For. Sl. (°)	Comp.	D50 (µm)
S1	1.53	NB	ND	n.a	Mx	236
S2	1.22	MB	LPD	4.9	Mx	838
S3	3.65	SB	LPD	n.a	T	1503
S4	1.58	SB	FD	7.9	T	506
S5	1.12	MB	LPD	6.7	T	441
S6	1.02	MB	LPD	4.5	T	473
S7	1.04	MB	LPD	6.3	T	1044
S8	1.18	NB	FD	11.1	T	1217
S9	1.07	MB	ND	5.6	T	420
S10	1.75	NB	ND	n.a	T	4326
S11	1.15	MB	LPD	7.3	T	1293
S12	1.05	NB	FD	6	T	125
S13	1.40	NB	FD	6.1	T	1421
S14	1.40	NB	ND	7.1	T	1554
S15	1.28	NB	FD	3.7	Mx	186
S16	1.14	MB	LPD	8.9	Mx	810
S17	1.26	SB	LPD	5.1	Mx	1641
S18	1.97	Rk	ND	6.9	T	1672
S19	1.21	NB	ND	7.3	Mx	1961
S20	1.29	SB	ND	4.4	T	817
S21	1.54	SB	FD	2.4	Mx	165
S22	*	*	LPD	4.1	BC	1155
S23a	1.22	Rk	FD	n.a	BC	573
S23b	1.22	Rk	FD	3.3	BC	603
S24	1.19	MB	LPD	5.9	Mx	1004

Those patches were particularly extended in the central sector of the shelf, off the Gulf of Oristano, where lobed and slightly raised, striated patches with low backscatter values (Figure 3) alternated with a flat, high backscatter seabed. The analysis of very high resolution seismic data shows that the low backscatter values are associated with bedforms developed within a shallow and

acoustically transparent unit only a few meters thick. This unit overlies a stratified unit that, when outcropping, shows high backscatter (Figure 3). Those are sedimentary deposits which represent the potential offshore reservoirs. The analysis of superficial sediment samples collected on these deposits revealed that they were mainly composed of medium-fine sands with carbonate or mixed carbonate terrigenous composition, whereas only two samples were mainly terrigenous.

### Beach systems vs. offshore sediment deposits

Factor analysis showed that the grain size of beach and offshore sediments with mainly biogenic carbonate composition was very different (Figure 4, upper plot: explained variance 81% - factor 1 43%, factor 2 38%): offshore sediments are finer, in the range of fine medium sand, whereas beach sediments are coarse sand. Those differences are due to the mechanism of sediment selection: the grain size of offshore sediments result from sediment transport and deposition along the shelf driven by hydrodynamics (e.g. bottom currents), while the size of beach sediments depends on local conditions (i.e. closeness to sediment source, coastal morphology). Beach and offshore deposits with mixed carbonate/siliciclastic composition are more scattered in the plot of the factor score (Figure 4, mid plot: explained variance 75% - factor 1 41%, factor 2 34%). Offshore, mixed sediments are generally finer with the exception of two coarse samples (from R1 sampling station, Figure 1) which show a grain size comparable to the grain size of S16 beach.

The beach with terrigenous sediments are clearly divided into three groups (Figure 4, lower plot: explained variance 63% - factor 1 39%, factor 2 24%) with prevailing very coarse sands, medium sands and fine sands respectively. Only two offshore samples (collected at R5 station) showed a terrigenous composition with a grain size comparable to the sediments of S1 and S20 beaches.

### CONCLUSIONS

The preliminary results reported in this work show that along the western Sardinian shelf a large amount of offshore sand deposits are present, and their volume can be tentatively estimated as  $> 100 \cdot 10^6 \text{ m}^3$ , considering the seafloor surface where they occur and the thickness revealed by seismic profiles. In general terms the presence of offshore deposits is considered strategic for the evaluation of coastal resilience (Merchand et al., 2011), and an evaluation of stratigraphic and sedimentary feature is needed to assess the resource availability and the potential environmental effects of relict sand dredging (Paganelli et al., 2013). The evaluation of compatibility of sediment from potential dredging areas with beach sediment is required according to specific protocols established by national agencies (Nicoletti et al., 2006). In the case of Italy the sediment compatibility is mainly considered in term of grain size and sediment geochemistry (e.g. pollutant concentration).

In our case, the first evaluation of sediment similarity, which was roughly made using grain size and terrigenous vs. biogenic carbonate content, revealed that only three beaches (out of 24) have a comparable offshore sediment reservoir, and beach sediments are generally coarser than respective offshore deposits.

This low degree of similarity can be attributed to the different processes which sorted beach and offshore sediments, the former characterized by an extremely variable composition and grain size (De Falco et al., 2003), due to specific local conditions (coastal morphology and geology, nearshore carbonate factories) which enhance a strong coastal compartmentalization (Sanderson and

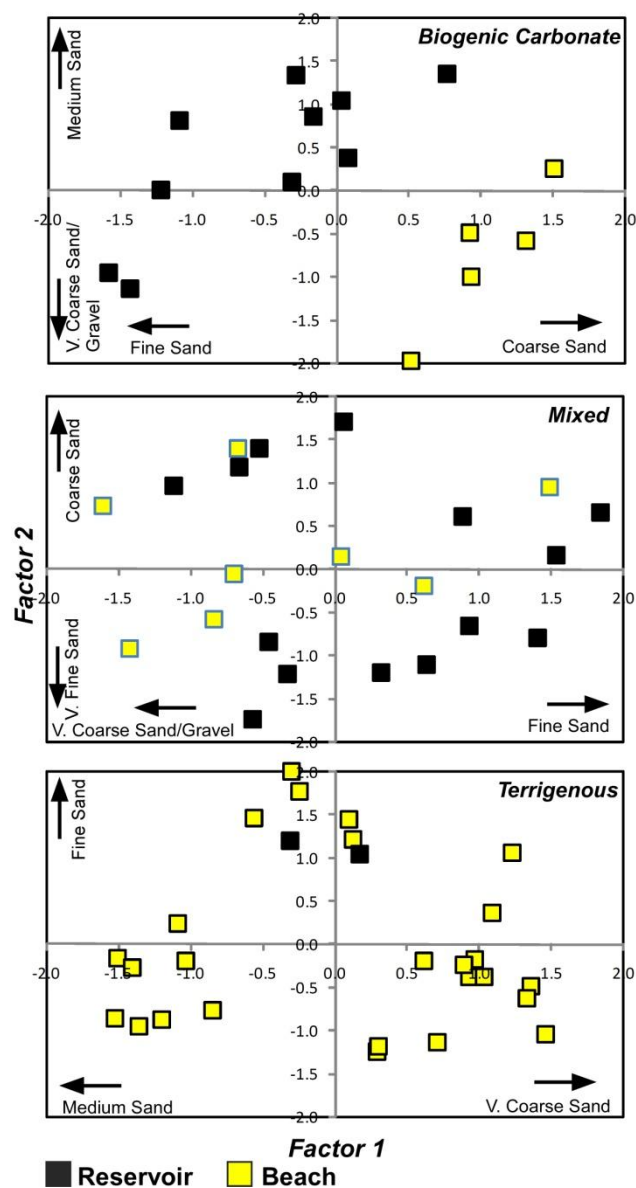


Figure 4. Results of Factor Analysis applied to beach and offshore sediments divided for their composition (see Table 1). The variables which correlate with Factor scores are indicated along the axes.

Eliot 1999), the latter were probably selected under similar conditions driven by shelf hydrodynamics.

Furthermore the evaluation of similarity must take into account other parameters (e.g. sediment color, grain roundness, mineralogy, Nicoletti et al., 2006) which are important for the coastal landscape. Those sediment features are particularly important for pristine coastal sectors, such as the western Sardinia coast, where the specific beach sediment typology is a fundamental component of the coastal landscape. Considering this broader definition of sediment features, few beaches of western Sardinia have a corresponding sediment reservoir and consequently a loss of natural sediments due to erosion will be irreversible.



In summary this case study highlights that large volumes of offshore deposits occur along the western Sardinian shelf. However the beaches of this coastal sector cannot be considered to be in a 'favorable sediment status' regarding the availability of offshore deposits for beach nourishment, due to the low degree of similarity between beach and offshore sediments.

Coastal management policies must address their effort toward natural beach conservation avoiding to consider beach sediment renewable with nourishment as an intervention measure.

### ACKNOWLEDGEMENT

Data were collected in the framework of the following projects: RITMARE - the Italian research for marine science, funded by MIUR; BEACH - Beach Environment, Management and Coastal Hazard, funded by Sardinian Region - L7; MAGIC - Marine Geohazard along the Italian Coasts, funded by Italian Civil Protection Department.

### LITERATURE CITED

- Ciavola, P., Ferreira, O., Haerens, P., Van Koningsveld, M., Armaroli, C. and Lequeux, Q., 2011. Storm impacts along European coastlines. Part 1: The joint effort of the MICORE and ConHaz Projects. *Environmental Science & Policy*, 14, 912-923.
- Coelho, C.; Lopes, D., and Freitas, P., 2009. Morphodynamics classification of Areao Beach, Portugal. In: da Silva, C.P. (ed.), Proceedings of the ICS (Portugal, 2009), *Journal of Coastal Research*, Special Issue No. 56, pp. 34-38.
- De Falco, G., Tonielli, R., Di Martino, G., Innangi, S., Simeone, S., Parnum, I.M., 2010. Relationships between multibeam backscatter, sediment grain size, and *Posidonia oceanica* seagrass distribution. *Continental Shelf Research* 30, 1941-1950.
- De Falco, G., Molinaroli, E., Baroli, M., Bellacicco, S., 2003. Grain size and compositional trends of sediments from *Posidonia oceanica* meadows to beach shore, Sardinia, Western Mediterranean. *Estuarine Coastal and Shelf Science* 58 (2), 299-309.
- De Falco, G., Baroli, M., Cucco, A., Simeone, S., 2008. Intrasbasinal conditions promoting the development of a biogenic carbonate sedimentary facies associated with the seagrass *Posidonia oceanica*. *Continental Shelf Research*, 28/6, 797-812.
- Gault, J., O'Hagan, A.M., Cummins, V., Murphy, J., Vial, T. 2011. Erosion management in Inch beach, South West Ireland. *Ocean and Coastal Management*, 54 (12), 930-942.
- Hegge, B., Eliot, I., Hsu, J., 1996. Sheltered sandy beaches of south western Australia. *J. Coast. Res.* 123., 748-760.
- Jiménez, J.A., Gracia, V., Valdemoro, H.L., Mendoza T., Sánchez-Arcilla A., 2011. Managing erosion-induced problems in NW Mediterranean urban beaches. *Ocean & Coastal Management*, 54, 907-918
- Marchand, M., Sánchez-Arcilla, A., Ferreira, M., Gault, J., Jiménez, J.A., Markovic, M., 2011. Concepts and science for coastal erosion management - An introduction to the CONSCIENCE framework. *Ocean & Coastal Management*, 54, 859-866.
- Morton, R.A.; Leach, M.P.; Paine, J.G., and Cardoza, M.A., 1993. Monitoring beach changes using GPS surveying techniques. *Journal of Coastal Research*, 9(3), 702-720.
- Nicoletti, L., Paganelli, D., Gabellini, M., 2006. Aspetti ambientali del dragaggio di sabbie relitte a fini di ripascimento: proposta di un protocollo di monitoraggio. *Quaderno ICRAM n. 5*: 159 pp.
- Paganelli, D., Nonnis, O., Finoia, M.G. and Gabellini M., 2013. The role of sediment characterization in environmental studies to assess the effect of relict sand dredging for beach nourishment: the example of offshore sand deposits in Lazio (Tyrrhenian Sea) In: Conley, D.C., Masselink, G., Russell, P.E. and O'Hare, T.J. (eds.), Proceedings 12th International Coastal Symposium (Plymouth, England), *Journal of Coastal Research*, SI 65, 1015-1020.
- PAP/RAC, 2007. ICZM Protocol in the Mediterranean (as signed in Madrid on 21 January 2008).
- Sánchez-Arcilla, A., Jiménez, J.A., Marchand, M., 2011. Managing coastal evolution in a more sustainable manner. The Conscience approach. *Ocean & Coastal Management*, 54, 951-955.
- Sanderson, P.G., and Eliot, I., 1999. Compartmentalisation of beachface sediments along the southwestern coast of Australia. *Marine Geology*, 162, 145-164
- Simeone, S., De Falco G., 2012. Morphology and composition of beachcast *Posidonia oceanica* litter on beaches with different exposures. *Geomorphology*, 151-152, p.224-233.
- Simeone, S., Palombo, L., and De Falco, G., 2012. Morphodynamics of a Nontidal Embayed Beach: The Case Study of Is Arutas (Western Mediterranean). *Journal of Coastal Research*, In-Press.
- Spagnolo, M., Llopis, I.A., Pappalardo, M., Federici, P.R., 2008. A new approach for the study of the coast indentation index. *Journal of Coastal Research* 24, 1459-1468.

## Guidelines for coastal zone management in the Amazon estuary (Amapá, Brazil)



[www.cerf-jcr.org](http://www.cerf-jcr.org)

Raimunda K.S. Gomes†, Francelle B.B. de Sousa†, Viviane V. Amanajás‡, Gilvane C. Santos†, Luci C.C. Pereira∞

† Universidade do Estado do Amapá, Humanismo, 2449, Renascer II, 68907-407, Macapá-AP, Brazil. rkellysgomes@yahoo.com.br francelesousa@bol.com.br cordeirosantos@yahoo.com.br

‡ Instituto de Ordenamento Territorial e Meio Ambiente, Av. Coaracy Nunes, 68900-010, Macapá-AP, Brazil. vivi\_amanajas@yahoo.br

∞ Universidade Federal do Pará, Alameda Leandro Ribeiro, sn, Aldeia, 68600-000, Bragança-PA, Brazil. cajueiro@ufpa.br



[www.JCRonline.org](http://www.JCRonline.org)

### ABSTRACT

Gomes, R.K.S., Sousa, F.B.B., Amanajás, V.V., Santos, G.C., Pereira, L.C.C., 2014. Guidelines for the management of the coastal zone of the Amazon estuary in the Brazilian state of Amapá. In: Green, A.N. and Cooper, J.A.G. (eds.), *Proceedings 13<sup>th</sup> International Coastal Symposium* (Durban, South Africa), *Journal of Coastal Research*, Special Issue No. 70, pp. 401-406, ISSN 0749-0208.

The study area is located in the district of Anauerapucu, at the watershed of the hydrographic basins of the Matapi and Vila Nova rivers. The objective of this study was to contribute to the social diagnosis of this estuarine community. Guidelines for the effective management of this coastal area were proposed. Data were collected using structured and semi-structured questionnaires in interviews with 63.3% of the local families, and all the association leaders, as well as a survey of the available services and infrastructure, and direct observations. Following this phase, a participative approach was employed in the local community. A socio-economic profile dominated by relatively young individuals (51.1% of population under 20 years of age), with agriculture and the extraction of natural resources as the primary occupations. However, the primary source of monetary income (73%) is government benefits. The community was also characterized by low levels of schooling. The principal health problems are diarrhea and hepatitis, reflecting the poor quality of the local drinking water. Due to the lack of a public sanitation system, most households (62.3%) have cesspits, which drain into the estuary. The community has five associations, although they do not participate in the social movements that campaign for the improvement of the quality of life of the population. The principal environmental problems of the community are the poor quality of the water supply and the inadequate disposal of domestic refuse. Overall, the results of this study indicate clearly that the socio-environmental problems of the local community are derived from the lack of effective public policies or management of the estuarine coastal zone of the state of Amapá. We provided some suggestions for the improvement of the current situation found within the study area.

**ADDITIONAL INDEX WORDS:** *Human activities, environmental degradation, Amazon coast.*

### INTRODUCTION

Coastal zones contain some of the world's most productive, diverse and valuable ecosystems. Coastal areas comprise 20% of the Earth's land area (Burke et al., 2001) and host almost half the planet's population (Small and Nicholls, 2003). Worldwide, population growth in coastal areas has resulted in a range of economic, social, and environmental impacts (Christie, 2005). Anthropogenic impacts on coastal regions thus present a significant challenge for ecosystem management, including the resolution of land use conflicts and the maintenance of the quality of life.

With a land area of 8.5 million square kilometers, Brazil is the fifth largest country in the world, and the fifth most populous, but also presents extreme of economic inequality. The Brazilian coastline is 8500 km long, of which around 35% of the northern limit is located in the Amazon region. The occupation of the Amazon coast varies from medium- to densely-populated urban

centers to isolated areas that are sparsely inhabited by native populations (Pereira et al., 2007; Pereira et al., 2010; Szlafsztein, 2012).

Coastal processes operating in this coastal zone are a consequence of several dominant features, such as: macrotides, moderate wave energy, strong currents, and the enormous discharge of freshwater from dozens of rivers, including the Amazon (Geyer et al., 1996). Located within one of the largest and best preserved tropical rainforests of the planet, the Amazon coast demands special attention for the planning of land use, environmental conservation and the sustainability of its natural resources. However, local authorities tend to show reduced interest in the improvement of local service and infrastructure.

Part of the Amazon coast, the Brazilian state of Amapá, has a land area of 142,828.521 km<sup>2</sup> and 734,996 inhabitants (IBGE, 2013). Overall, 72% of the state is located within environmental protection areas (ZEE, 2011). The state's 698 km-long coastline

encompasses estuarine (236 km) and Atlantic (462 km) sectors (Takyama and Silva, 2009).

This study focuses on the estuarine sector, where more than 80% of the state's population lives. According to Gomes et al. (2011), local problems are related primarily to: (i) inadequate economic development, (ii) unplanned land occupation and use, (iii) lack of infrastructure and services, and (iv) natural impacts (such as flooding).

Given this, the aim of this study was to contribute to the social diagnosis of an estuarine community located in the region of the Amazon estuary. For this, the social characteristics of the community (i.e., sex, age, marital status, occupation, and education and income levels) were evaluated and the perceptions of its inhabitants on local infrastructure and services, as well as the region's principal environmental problems were recorded. Based on this analysis, a number of guidelines for the effective management of this coastal area were proposed, with the primary aim of improving the quality of life of the local inhabitants.

### STUDY AREA

The estuarine sector of Amapá is located between the coordinates 1°30'N, 49°30'W and 1°30'S, 52°30'W, and includes fluvial-marine environments, dry grasslands, forests, secondary habitats, rivers, streams, lakes, and seasonally-flooded grasslands.

The local climate is characterized by two distinct seasons (rainy and dry). Around 88% of the annual precipitation falls during the rainy season, mainly in March and April when intense fluvial flooding occurs. Minimum and maximum temperatures are normally around 26°C and 29°C, respectively, with an annual mean of 27°C (Cohen et al., 1989, Silva and Portela, 2002).

The majority of the communities found along the margins of the Amazon River have low income, limited education and poor living conditions (Takiama and Silva, 2009). Inadequate services and infrastructure include a lack of public sanitation and water supplies, refuse collection, schools, and medical assistance (Gomes et al., 2011). The local economy is supported by family-based fishing, farming and extractive activities. The study area (Figure 1) is located in the district of Anauerapucu, located at the watershed of the hydrographic basins of the Matapi and Vila Nova rivers. This community contains 235 houses and 998 inhabitants (IBGE, 2010).

The community can be reached by road or riverboat. Logistics (public transport, commerce, access to schools and medical assistance) depend on the tide, season, and climatic conditions, especially for the villages located along tidal creeks (Silva, 2010).

### METHODS

A total of 159 questionnaires were applied during the present study, including all the local association leaders (five) and 63.3%

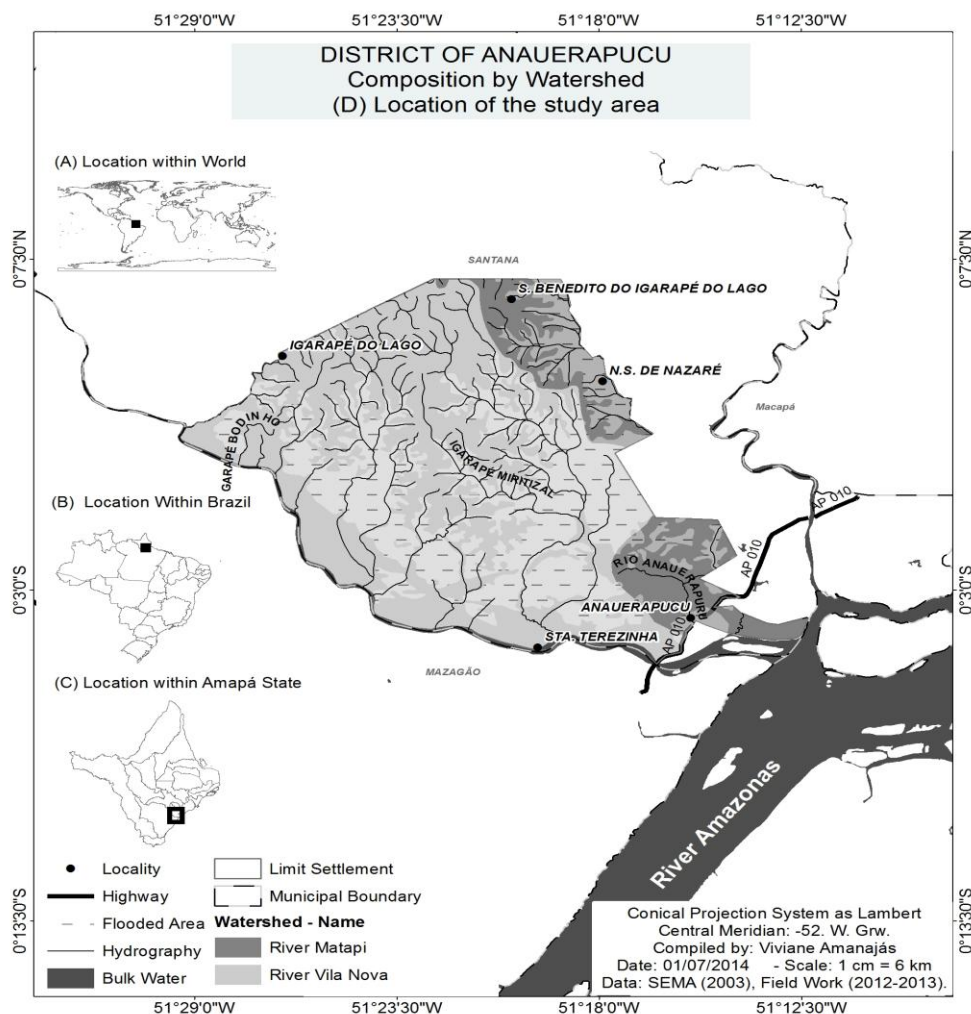


Figure 1. Location of the study area (C) within Brazil (A), and Amapá state (B). Source: IMAP (2013).

of the families. According to Gunther (2006), the questionnaires covered two principal areas: (i) inhabitant profiles, and (ii) perceptions of the main social and environmental problems. A

check-list was used to collect qualitative and quantitative data on access, services, infrastructure, and the types of land use. Data were collected between August 2012 and May 2013.

The participative approach was based on the establishment of an integrated, open and effective channel of communication on a broad level, including continuous, interactive, and adaptive procedures that provide ongoing support in the decision-making process (Takyama and Silva, 2009). Guidelines for coastal management were proposed in the context of local conflicts of interest, and the lack of any prospects of investments on the part of local or regional authorities.

## RESULTS

### Socioeconomic profile

More than half of the families in Anauerapucu contain 4 to 6 members (Table 1). Just over half (52.53%) of the local inhabitants are male, young (51.1% less than 20 years old) and single (62.0%). Almost 40% of the inhabitants are students, and 14.2% are farmers or depend on the extraction of natural resources. The main source of income (73.0%) is federal and state government benefits, such as pensions, family and farming grants, and fishery benefits. About 75.6% of the interviewees have an income of less than one minimum wage (US\$312.80<sup>1</sup>). Only 1.2% of the interviewees have a college degree, while 12.6% are illiterate.

### Housing conditions and services/infrastructure

The majority of the residences are built on the margins of the Anauerapucu estuary (Figure 2a). Most (91.8%) are stilt houses due to the effects of tides and seasonal flooding (Figure 2b).

There is no public sanitation system and in most cases (80.5%), waste disposal is based on the use of cesspits located under bathrooms (Figure 2c). Unfortunately, the sewage is discharged directly into the Anauerapucu (also known as Vila Nova) estuary, causing health problems such as diarrhea and hepatitis reported in 58.5% of households.

Public refuse collection is irregular and a large quantity of household trash can be observed (Figure 2d) on the river margins or in the water (82.4% of households). Many families (44.6%) depend on wells for their water supply, whereas about 40.9% use the turbid estuarine water (Figure 2e), and 14.5% are supplied by other sources. Each five liter container of well water is sold for US\$1.38. The water is consumed untreated.

### Perception of the main social and environmental problems

According to the interviewees, the principal environmental problems are derived from deforestation, the destruction of riverside forests, soil degradation, wildfires, logging, effluent disposal, and uncollected refuse (Table 1). The majority of the residences (92.5%) are linked to the public power grid. Riverboats, known locally as *catraias* (Figure 2f), are the only means of public transport for access to outlying villages.

Public health facilities consist only of community clinics, where 11.3% of residents are treated. Most people are cared for in urban centers, such as Santana (54.7%) and Macapá (18.8%). Two percent of residents are cared for at home.

Table 1. Socioeconomic profile (%) of the population of the study area and perceptions of environmental problems by local residents.

Socioeconomic profile and environmental perception		(%)
<b>Number of family members</b>	1 to 3	22.8
	4 to 6	55.2
	7 to 9	17.2
	> 9	4.80
<b>Sex</b>	Male	52.53
	Female	47.40
<b>Age</b>	0 to 20	51.1
	21 to 40	28.3
	41 to 60	13.5
	61 to 80	7.10
<b>Marital status</b>	Married	30.6
	Single	62.0
	Widower	1.50
	Other	5.90
<b>Occupation</b>	Student	39.9
	Farming or harvesting of natural resources	14.2
	Administrative employee	2.90
	Housewife	12.9
	Fishing	3.90
	Retired	4.90
	Freelance	1.60
	Other	19.7
	<b>Source of income</b>	Government benefits
Public employees		11.9
Other		15.1
<b>Income (in minimum salaries)</b>	< 1	75.6
	1 to 2	17.5
	3 to 4	3.3
	> 5	3.6
<b>Schooling</b>	Unfinished primary school	30.9
	Primary school graduate	25.0
	High school graduate	18.6
	University graduate	1.20
	Illiterate	12.6
	Below school age (< 3 years old)	11.7
<b>Environmental problem</b>	Deforestation	20.8
	Destruction of riverside forests	1.8
	Degradation of the soil	1.8
	Wildfires	18.8
	Logging	9.5
	Hunting	20.2
	Pollution of water sources	17.6
	No problems	9.5

The community has three schools, two of which are municipal primary schools attending to pupils of up to the fifth grade, although the school located at the mouth of the Vila Nova River employs the multi-series system, an approach which mixes pupils of different ages. The state school located in the main community is the only one that provides both primary and high-school teaching, although during the present study, the interviewees were informed that, due to truancy levels and the lack of teachers, high school classes would no longer be offered in subsequent years.

There are no banks, post office or telephone services in the community, and there is only one grocery shop. In other words, access to most goods and services requires a trip (around 1 hour) to

<sup>1</sup> US\$ 1 = R\$ 2.33 in December 13, 2013 (www.uol.com.br).

the local town or the state capital, Macapá. The cost of each trip is approximately US\$ 3.43.



Figure 2. Housing and service conditions. Typical residence (a). Occupation of the river margin (b). Cess-pit (c). Waste (d). Water supply (e). School transport (f).

Within the study area, deforestation has resulted from four main processes: (i) occupation of the margins of the Anauerapucu estuary, which has resulted in the erosion of the banks and the silting of the estuary (Figure 3a-b), (ii) extraction of firewood for the local brickworks (Figure 3c), (iii) logging to supply the local furniture factory (Figure 3d), and (iv) clay quarrying (Figure 3e-f). These activities have led to an increase in the number of cases of malaria (58.5% of households), and they are completely unmonitored by the relevant environmental organizations, which should provide guidelines and assistance for the minimization of impacts and the improvement of public health standards.

### Participative activities

When community members were asked what needs to be done to improve the exploitation of the coastal environment, they responded unanimously with regard to the need for a collective consciousness in relation to the importance of the local coastal ecosystems for the improvement of the quality of life of the population. Suggestions provided by local residents for participative coastal management included: (i) training programs, (ii) landowner registration, (iii) the establishment of alternative sources of income, and (iv) the installation of basic health, education, and sanitation services.

The participative meetings also indicated that, while the local residents demand improvements to reduce the exploitation of the ecosystems, they are unaware that socio-environmental problems are part of their daily lives, given that they refer only to the public authorities as the source of a solution. In other words, they fail to comprehend that the community itself could contribute to the improvement of the socio-environmental conditions within the study area.

It is important to emphasize that the intervention of the public authorities will be essential to ensure the installation of basic public services available to the community and the conservation of the local coastal ecosystems. However, it is also essential that local residents participate in the planning of land occupation and use, considering that one of the principal obstacles encountered in this part of the study was the difficulty of bringing community members together to discuss their problems as a group.

In addition, while the community has a number of social associations, these organizations are not effectively active in any way on local environmental problems. This reflects in part the political conflicts within the associations, which hamper the struggle for the improvement of basic services, or the conservation of local coastal ecosystems.

### DISCUSSION

The economically-active population of Amapá has a mean income that is not only below the national average, but is also lower than that of the Legal Amazon macroregion (Pedroso, 2010). This situation is derived from a number of historic and cultural factors, in particular the fact that the subsistence of many families depends on the exploitation of natural resources (Diegues, 2004). A number of studies of other rural communities of the Amazon coast have also shown that the majority of families subsist on fishing and agricultural activities (Glaser, 2003; Krause and Glaser, 2003; Guimarães *et al.*, 2011; Gorayeb *et al.*, 2011; and others). Resende and Oliveira (2008) have reported that the governments of many developing countries increasingly use social and economic programs to combat poverty. In Brazil, federal benefits obtained through social security programs are the principal source of income for many families, especially in the country's northern and northeastern regions. The lack of employment opportunities, logistic problems, economic instability, and the harsh socio-economic reality that is typical of the riverside communities of the Amazon region all contribute to the reduced levels of income recorded in the study area (Gomes *et al.*, 2011).

Despite the social programs adopted by the federal government, the high illiteracy rates and low levels of schooling found throughout, most of the Amazon region contributes to the lack of progress in the improvement of the quality of life of local populations. In particular, the formal education system provided in rural areas, including those within conservation units, has little or no relevance to the culture of the region's inhabitants, historically linked to the extraction of forest products and subsistence agriculture (Diegues, 2004; Silva, 2010; Simonian *et al.*, 2010; Gomes *et al.*, 2011; Silva *et al.*, 2013). The poor quality of the education system has also contributed to the rural exodus of coastal communities in Amapá. Clearly, the system needs to be reformulated urgently in order to better attend to the socio-cultural and environmental diversity of the region, primarily by recognizing the value of traditional local knowledge and community organizations as a means of guaranteeing the formation of a sustainable and integrative society (Sachs, 2004).

Fearnside (1999) has emphasized the fact that deforestation in the Amazon region is not considered relevant at a political level, which impedes the effective monitoring and control of this activity by the public authorities. Worse still, the National Institute for Colonization and Agrarian Reform (INCRA), while enforcing the legal settlement of many regions within the Brazilian Amazon basin, has not implemented any alternative strategies for the use and regulation of the land (Fearnside, 1999, 2000; Loureiro, 2009). The present study area provides a good example of this problem – while approximately 200 families were found living in the area, INCRA has assigned plots of local land to 400 families. These

landowners have not settled their plots, but use them as weekend homes, without any obligation as far as the regulation of the use of the land or local environmental problems are concerned.



Figure 3. Environmental problems. Erosion (a-b). Local furniture factory (c). Logging (d). Clay quarrying (e-f).

Amapá presents widely conflicting scenarios (Ceí, 2010). While its natural ecosystems are the best protected of any Brazilian state, piles of refuse are a common sight in many areas, including the margins of its rivers, and the general lack of public sanitation has grave implications for the health of its population. The lack of adequate public policies necessary for the social inclusion of the traditional populations of the Amazon region and the conservation of its environment have resulted in a total lack of socio-environmental sustainability (Simonian et al., 2010).

During the period of this study, many of the families surveyed were suffering from a lack of drinking water, despite living at the margin of the world's largest river by volume (Szlafsztein and Sterr, 2007) and on the watershed between two of the largest of the state's thirty-three hydrographic basins (SEMA, 2003). Ceí (2010) reported that the incidence of diseases in coastal communities caused by environmental problems has exhausted the productive capacity of the ecosystems. Similar problems have been found in many other riverside communities in the Amazon region (Gorayeb, 2009; Guimarães et al., 2009a, 2009b; Simonian et al. 2010; Pereira et al., 2007, 2010; Silva et al., 2011, 2013), as well as in other countries with similar socio-economic conditions, such as China, Mexico and Chile. In most cases, efforts have been made to guarantee both the development of rural/urban areas and the adequate use of local natural resources (Xue et al., 2004; Sánchez-Gil et al., 2004; Alviaal and Recule, 1999). However, the majority of these communities have been affected by rapid population growth associated with unregulated urban/rural expansion and the ongoing expansion of anthropogenic impacts.

Overall, the implementation of participative management plans that emphasize the most urgent socio-environmental problems will be essential to the development of coastal communities. This will not only allow for improvement in the quality of life of the population, but also in the occupation and land use of coastal

ecosystems (Krelling et al., 2008; Szlafsztein, 2012), as well as involving coastal populations in the debate necessary for the construction of a truly participative coastal management program.

## FINAL CONSIDERATIONS

The social-environmental problems of the study community are clearly derived from the lack of effective public policies, and the absence of services, such as a supply of drinking water, basic sanitation, regular refuse collection, drainage system, medical assistance, and adequate schools. It is also important to understand the ways in which the land is occupied and used by the coastal communities of the Amazon region, and their way of life, in order to develop alternatives that will guarantee improvements in the quality of life of the local populations, together with a more adequate exploitation of the environment. Given this, a number of strategies can be recommended for the improvement of the current situation found within the study area, including (i) regulation of land use and monitoring of settlements by INCRA, (ii) introduction of a program of participative environmental management designed to minimize the degradation of habitats and guarantee the adequate exploitation of natural resources, (iii) the effective prohibition of unplanned settlement, (iv) investment in local services and infrastructure, in order to improve the quality of life of the local population, and (v) the development of programs of environmental awareness appropriate to the reality of the local population. Considering that these issues are typical of the whole Amazon coast, as well as in other parts of the globe, these proposals could be applied to other locations that suffer similar social and environmental problems anywhere in the world.

## ACKNOWLEDGEMENT

We are grateful to the Amapá State Science and Technology Ministry (SETEC/AP) and the Brazilian National Research Council (CNPq).

## LITERATURE CITED

- Amapá. Instituto de pesquisa científica e tecnológica do Amapá, 2011. Zoneamento ecológico econômico das áreas ressaca. <http://www.iepa.ap.gov.br> (accessed September 20, 2013).
- Amapá. Secretaria estadual de meio ambiente (2003). Definição de bacias hidrográficas do estado do Amapá. <http://www.sema.ap.gov.br> (accessed June 10, 2013).
- Alviaal, A. and Reculé, D., 1999. Fundacion Chile and the integrated management of the coastal zones. *Ocean & Coastal Management*, 42, 143-154.
- Burke, L., Kura, Y., Kassem, K., Revenga, C., Spalding, M. and McAllister, D., 2001. *Coastal ecosystems*. Washington, DC. World Resource Institute, 75 p.
- Ceí, I.L.F., 2010. Condições sanitárias dos resíduos sólidos no Amapá e política adotada pelo ministério público do estado. In: Simonian, L.T.L. (org.). Políticas públicas, desenvolvimento, unidades de conservação e outras questões socioambientais no Amapá, Belém-PA, Brasil: NAEA-UFPA/MPEAP, pp. 443-483.
- Christie, P., 2005. Is Integrated Coastal Management Sustainable?. *Ocean & Coastal Management*, 48, 208-232.
- Cohen, J.C.P., Dias, M.A.S. and Nobre, C.A., 1989. Aspectos climatológicos das linhas de instabilidade na Amazônia. *Climadnise*. Campos do Jordão - SP, 4 (11), 34-40.
- Diegues, A.C., 2004. Comunidades Tradicionais e Manejo dos Recursos Naturais da Mata Atlântica, São Paulo: Hucitec Nupaub, Brasil. 2. Edição, 395 p.
- Fearnside, P.M., 1999. Biodiversity as an environmental service in Brazil's Amazonian forests: risks, value and conservation. *Environmental Conservation*, 26, 305-321.
- Fearnside, P.M., 2000. Global warming and tropical land-use change: greenhouse gas emissions from biomass burning, decomposition and

- soils in forest conversion, shifting cultivation and secondary vegetation. *Climatic Change*, 46, 115-158.
- Geyer, W.R., Beardsley, R.C.; Lentz, S.J., Candela, J.; Limeburner, R., Johns, W.E.; Castro, B.M., and Soares, I.D., 1996. Physical oceanography of the Amazon shelf. *Continental Shelf Research*, 16, 575-616.
- Glaser, M., 2003. Interrelations between mangrove ecosystem, local economy and social sustainability in Caeté Estuary, North Brazil. *Ecological Economics*, 11, 361-373.
- Gomes, R.K.S., Takiyama, L.R., Pereira, L.C.C. and Ferreira, R.C.M., 2011. Social Diagnosis and Guidelines for Coastal Management in Environmental Protection Areas of the Amazon Littoral (Amapá, Brazil). *Journal of Coastal Research*, SI 64, pp. 1331 – 1335.
- Gorayeb, A., Lombardo, A.M. and Pereira, L.C.C., 2011. Natural Conditions and Environmental Impacts in a Coastal Hydrographic Basin in the Brazilian Amazon. *Journal of Coastal Research*. SI 64, pp.1340 - 1344
- Gorayeb, A., Lombardo, M.A. and Pereira, L.C.C., 2009. Aspectos Sociais e Condições Ambientais da Bacia Hidrográfica do Rio Caeté Amazônia Oriental-Brasil. *Revista de Gestão Costeira Integrada*, 9 (2), 59-70.
- Guimarães, D.O., Pereira, L.C.C., Gorayeb, A. and Costa, R.M., 2011. Exploitation and management of natural resources by rural communities in the Caeté River Basin in northern Brazil. *Journal of Coastal Research*. SI 64, pp.1228 – 1232.
- Guimarães, D.O., Pereira, L.C.C. and Costa, R.M., 2009a. Aspectos Socioeconômicos e Ambientais das Comunidades Rurais da Bacia Hidrográfica do Rio Caeté (Pará-Brasil). *Revista de Gestão Costeira Integrada*, 9, 71-84.
- Guimarães, D.O., Pereira, L.C.C., Monteiro, M., Gorayeb, A. and Costa, R.M., 2009b. Effects of the urban influence on the Cereja River and Caeté Estuary (Amazon littoral, Brazil). *Journal of Coastal Research*, SI59 (2), pp. 1219-1223.
- Gunther, H, 2006. Pesquisa qualitativa versus Pesquisa quantitativa: esta é a questão. *Revista psicologia: teoria e pesquisa*, 22 (2), 201-210.
- IBGE, 2010. Censo Demográfico. Brazil. <http://www.ibge.gov.br> (accessed October 15, 2013).
- IBGE, 2013. Divisão de Territórios. Brazil. available in: <<http://www.ibge.gov.br> (accessed October 15, 2013).
- Krause, G. and Glaser, M., 2003. Co-evolving geomorphological and socio-economic dynamics in a coastal fishing village of the Bragança region (Pará, North Brazil). *Ocean and Coastal Management*, 46, 859-874.
- Krelling, A.P., Polette, M., and Delvalls, A.C., 2008. Coast Learn: Lessons learnt from a web-based capacity building in Integrated Coastal Zone Management (ICZM). *Ocean and Coastal Management*, 51, 789- 796.
- Loureiro, V.R., 2009. *A Amazônia no século XXI: novas formas de desenvolvimento*. 1ª Ed. São Paulo: Empório do Livro, 279 p.
- Pedroso, J.S., 2010. Reserva de desenvolvimento sustentável do rio Iratapuru: um estudo sobre sustentabilidade e atividades humanas. In: Simonian, L.T.L. (org). Políticas públicas, desenvolvimento, unidade de conservação e outras questões socioambientais no Amapá. NAEA-UFPA/MPEAP, p. 267-286
- Pereira, L.C.C., Guimarães, D.O., Costa, R.M. and Souza Filho, P.W.M., 2007. Use and Occupation in Bragança Littoral, Brazilian Amazon. *Journal of Coastal Research*, SI 50, pp. 1116-1120.
- Pereira, L.C.C., Monteiro, M.C., Guimarães, D.O., Matos, J.B. and Costa, R.M., 2010. Seasonal effects of wastewater on the water quality of the Caeté river estuary, Brazilian Amazon. *Anais da Academia Brasileira de Ciências* (Impresso), 82, 467-478.
- Resende, A.C.C., Oliveira, A.M.H.C. , 2008. Avaliando Resultados de um Programa de Transferência de Renda: o Impacto do Bolsa Escola sobre os Gastos das Famílias Brasileiras. *Est. econ.*, São Paulo, 38 (2), p. 235-265.
- Sachs, I., 2004. *Desenvolvimento: incluídos, sustentável, sustentado*. Rio de Janeiro: Garamond.
- Silva, I.R., Pereira, L.C.C., Trindade, W.N., Magalhães, A. and Costa, R. M., 2013. Natural and anthropogenic processes on the recreational activities in urban Amazon beaches. *Ocean and Coastal Management*, 76, 75-84.
- Silva, J.B., 2010. Populações tradicionais sul-amapaenses de unidade de conservação: valores, condutas e o papel da pedagogia da alternância In: Simonian, L. T. L. (org). Políticas públicas, desenvolvimento, unidade de conservação e outras questões socioambientais no Amapá. NAEA-UFPA/MPEAP, p. 287-324.
- Silva, L.M., Portela, B.T.T., 2002. Um estudo da precipitação, temperatura e umidade relativa do ar na costa norte-nordeste do Brasil. [www.cbmet.com/cbm](http://www.cbmet.com/cbm) (accessed November 10, 2013).
- Silva, N.I.S., Pereira, L.C.C., Gorayeb, A., Vila-Concejo, A., Sousa, R.C., Asp, N.E. and Costa, R.M., 2011. Natural and social conditions of Princesa, a macrotidal sandy beach on the Amazon Coast of Brazil. *Journal of Coastal Research*, SI 64, pp. 1979 - 1983.
- Simonian, L.T.L., Silva, J.B., Andrade, R.F. and Almeida, A.C.P.C., 2010. Floresta nacional do Amapá: um histórico breve, políticas públicas e (in) sustentabilidade. In: Simonian, L.T.L. (org.). Políticas públicas, desenvolvimento, unidades de conservação e outras questões socioambientais no Amapá, Belém-PA, Brasil: NAEA-UFPA/MPEAP, p. 115-180.
- Small, C. and Nicholls, R.J., 2003. A global analysis of human settlement in coastal zones. *Journal of Coastal Research*, 19 (3), 584-599.
- Szlafsztein, C. and Sterr, H., 2007. A GIS-based vulnerability assessment of coastal natural hazards, state of Pará, Brazil. *Journal of Coastal Conservation*, 11, 53-66.
- Szlafsztein, C.F., 2012. The Brazilian Amazon coastal zone management: implementation and development obstacles. *Coastal Conservation*, 16, 335-343.
- Sánchez-Gil, P. Yáñez-Arancibia, A. Ramírez-Gordillo, Day, J. W. Templet, P. H. (2004). Some socio-economic indicators in the Mexican states of the Gulf of Mexico. *Ocean & Coastal Management*, 47, 581-596.
- Takiyama, L.R. and Silva, U.R.L., 2009. Experiences on Utilization of Participative Methodology for the Construction of Coastal Management Instruments in the Amapá State, Brazil. *Revista de Gestão Costeira Integrada*, 9 (2), 33-45.
- Xue, X. Hong, H. Charles, A. T. (2004). Cumulative Environmental Impacts and Integrated Coastal Management: The Case of Xiamen, China. *Journal of Environmental Management*, 71, 271-28.

# Managed realignment in practice in the UK: results from two independent surveys

Luciana S. Esteves<sup>†</sup> and Karen Thomas<sup>‡</sup>

<sup>†</sup> School of Applied Sciences  
Bournemouth University  
Poole, UK  
lesteves@bournemouth.ac.uk

<sup>‡</sup> Environment Agency  
Flood and Coastal Risk Management  
Ipswich, UK  
karen.thomas@environment-agency.gov.uk



[www.cerf-jcr.org](http://www.cerf-jcr.org)



[www.JCRonline.org](http://www.JCRonline.org)

## ABSTRACT

Esteves, L.S., Thomas, K., 2014. Managed realignment in practice in the UK: results from two independent surveys. In: Green, A.N. and Cooper, J.A.G. (eds.), *Proceedings 13<sup>th</sup> International Coastal Symposium* (Durban, South Africa), *Journal of Coastal Research*, Special Issue No. 70, pp. 407-413, ISSN 0749-0208.

Shoreline Management Plans in England envisage implementation of managed realignment along 550 km or 10% of the coastline length by 2030. About 66 km of the coastline has been realigned between 1991 and the end of 2013. Therefore, an eight-fold increase in the length of realigned shorelines is expected in the next 20 years. It is now timely to gather and evaluate experiences and lessons learned from existing experience to inform future projects. This article presents results from two surveys concerning experiences and perceptions of managed realignment in the UK. The UK is often recognised as leading the implementation of managed realignment worldwide and it is anticipated that the national experience attracts great interest of international researchers and practitioners. Findings from a qualitative survey focusing on practitioners experience are contrasted by the results from a quantitative survey allowing comparison of practitioners', consultants', researchers' and stakeholders' views. Three key issues identified through the analysis of the responses are discussed in this article: (1) the multiple functions of realignment sites should be emphasised to increase buy-in from stakeholders; (2) working in partnership with relevant organisations and landowners from the inception of project planning is highly beneficial; and (3) knowledge has greatly advanced in many aspects, but improved understanding about the long-term evolution of sites is needed. Stakeholders' views are considerably more negative about the outcomes of managed realignment, especially concerning flood risk management, when compared with other groups assessed here. Consultants' and practitioners' views are more positive, although many indicate results vary depending on the site and aspects being assessed. More than 60% of all groups agree that better understanding about long-term evolution of realigned sites is needed, especially sedimentation and biogeochemical processes. This study identifies aspects about which stakeholders' views most differ from the practical knowledge gathered from consultants, practitioners and researchers. It is suggested here that improved practice and stakeholders engagement can be achieved by obtaining and disseminating quantifiable and reliable evidence of the multiple benefits offered by realigned sites. Although these findings reflect the UK experience, they are likely to be useful to inform future initiatives elsewhere.

**ADDITIONAL INDEX WORDS:** *flood risk, habitat creation, stakeholder, Environment Agency United Kingdom.*

## INTRODUCTION

The *Making Space for Water* policy (Defra, 2005) has set out a 20-year vision for managing flood and erosion risk in England. The policy challenges the traditional hold-the-line approach and promotes soft engineering options to create space for coastlines to evolve more naturally. Managed realignment (MR) involves breaching existing defences to create wetland areas and has been promoted as an option to deliver sustainable flood risk management with added environmental benefits. MR projects usually have multiple objectives, including: creation of intertidal habitats, improvement of flood defences, reduction of costs to maintain defences and compensation for habitat loss. Creation of intertidal habitats offers aggregated benefits through the provision of ecosystem services, such as: storm protection, recreation, nutrient cycling, carbon storage and water quality (e.g. Luisetti et al., 2011; Spencer and Harvey, 2012; Burden et al., 2013).

Land use and land cover changes resulting from MR, and the

associated potential for climate regulation (e.g. carbon sinks) and flood control, are part of the UK's National Adaptation Programme (Defra, 2013). Although the primary objective of MR originally concerned flood risk management, the main focus of most MR projects in the UK has been the creation of habitats to address the legal requirement "to take appropriate conservation measures to maintain and restore the habitats and species" protected under the EU Habitats Directive<sup>1</sup>. About 80% of MR projects are within or adjacent to designated protected areas (Esteves, 2013).

The *Online Managed Realignment Guide* (ABPmer, 2013) describes and maps 51 MR projects implemented in the UK since 1991, the majority through breaching or removal of flood defences. About 66 km of England's coastline have been realigned (as in November 2013) and Shoreline Management Plans suggest an eight-fold increase in the length of realigned shorelines by 2030, a total of 550 km or 10% of the coastline (Committee on

DOI: 10.2112/SI70-069.1 received 29 November 2013; accepted 21 February 2014. © Coastal Education & Research Foundation 2014

<sup>1</sup> <http://ec.europa.eu/environment/nature/legislation/habitatsdirective/>



Climate Change, 2013). Implementation of MR at this scale and rate requires identifying sites that have both suitable physical characteristics (e.g. subjected to tidal levels favourable to the development of the habitat to be created) and the willingness of landowners (i.e. to embrace the project or sell the land). Challenges known to delay or hinder MR projects (e.g. stakeholders acceptance) will need to be addressed timely and efficiently.

Considering that *Making Space for Water* is reaching its mid-life and the important role MR plays on government's plans for climate change adaptation and environmental obligations, it is timely to establish the current understanding about MR performance in the UK. This article summarises the main results obtained from two surveys designed and conducted independently by the authors to collate current views and experiences on MR projects in the UK. By contrasting practitioners, consultants, researchers and stakeholders responses, this study identifies three key issues that need to be addressed to improve current practice. It is anticipated that these key findings are applicable to inform future policy developments in the UK and elsewhere.

## METHODS

Two surveys were designed independently from each other and conducted concomitantly by the authors in 2013 with the objective of understanding the current experiences and perceptions concerning managed realignment in England. The scope and methods of the two surveys (identified by the initials of the author's affiliation) were different and are described below. Table 1 summarises the composition of participants in each survey per sector and geographical distribution.

### Bournemouth University Survey (BUS)

BUS was a quick quantitative survey designed to obtain a general view about managed realignment across sectors and countries (EU and non-EU). To reach a wider range of participants, BUS was distributed to targeted groups and individuals through email, twitter and LinkedIn. Results presented here focus on responses from UK participants. Participants represented the expected range of public and private sectors (Table 1), most directly or indirectly involved in planning, design, delivery and researching MR projects across the UK. About 15% of BUS respondents have not been involved in MR projects but have an interest on the subject. Stakeholders include farmers, private businesses and members of the public. Non-governmental organisations (NGOs) include large national charities and smaller local groups. Respondents were distributed across all UK regions (except Northern Ireland) with dominance of respondents from East and South England.

### Environment Agency Survey (EAS)

EAS was a qualitative extensive questionnaire distributed to key practitioners with experience in planning or delivery of MR projects, including: Environment Agency staff, the Environment Agency Coastal Business User Group and relevant external partners or consultants. The EAS aimed to compile knowledge and experience to benchmark current thinking and provide evidence to inform future projects and policy developments. Responses cover 15 specific MR sites led by a range of organisations and four strategies that include MR policy options. Most of EAS respondents have also taken part in BUS.

Table 1. Composition of the participants in each survey.

BUS	EAS
<b>Number of respondents (n)</b>	
139	16
<b>Represented Sectors</b>	
29% consultants	31% EA practitioners
22% stakeholders	25% private consultants
21% researchers/academics	25% independent consultants
14% government	19% NGO (Royal Society for the Protection of Birds)
14% NGO	
<b>Geographical Distribution</b>	
35% East England	63% East England
26% South England	19% South England
17% Southwest England	12% Northeast England
8% Northeast England	6% Wales
6% Scotland	*responses cover projects in the Southwest, despite the lack of participants from the region
4% Wales	
4% Northwest England	
<b>Direct involvement in managed realignment</b>	
85% of respondents	100% of respondents

## RESULTS AND DISCUSSION

Analysis of responses obtained from EAS allowed identification of lessons learned from practical experiences that relate to a range of aspects, including: strategic issues (policy), statutory process (regulations, licensing etc.), technical knowledge, funding and communications (to/from wider stakeholders and the public). Many cross-cutting issues were identified, which relate to more than one of the listed aspects. A non-comprehensive summary of the main issues of wider applicability (site-specific issues are not included) is provided here.

At the strategic level, it is necessary to improve dissemination and communication about the multiple (socio-economic and environmental) benefits of planned climate change adaptation compared with unmanaged breach of defences. Organisations involved in managed realignment vary in scope and may expect different outcomes. In order to attract interest from a range of stakeholders and the public, projects must offer outcomes that benefit society and the environment more widely. Multi-functional sites are more likely to attract greater public support and funding than single-purpose sites.

Working in partnership with landowners and relevant organisations reduce the overall costs of projects (e.g. eliminating the need for land purchase) and expedite implementation (e.g. delays due to local opposition are minimised). Partnerships are facilitated when different parties 'buy-in' the potential benefits of the project. Buy-in depends on perceptions landowners might have about MR and the benefits on offer (e.g. diversification of land use; lower costs to maintain flood defences; grants from the Environmental Stewardship scheme). There is a lack of clarity and confidence in relation to the legal obligations associated with MR projects that can lead to over-prescriptive demands from stakeholders during the licensing process. Partnerships with stakeholder organisations can facilitate progress of the statutory licensing process, especially in sites where features of public interest are affected (e.g. archaeological and historic sites; footpaths and public right of way).

In England, compulsory purchase mechanisms to secure land for strategic plans exist, but the Government chooses not to use them for MR projects. Land purchase is negotiated case-by-case and subjected to high price variability. Many projects were implemented in areas of high grade agricultural land, which have a

current average value in the UK of £18,400/ha (RICS, 2013). MR projects are often implemented in areas behind flood defences in poor state of conservation, where land usually have a discounted value (e.g. £5,000/ha in Wallasea Island) and landowners are more willing to sell or work in partnership. Unmanaged breaches of defences create intertidal land that immediately revert to Crown Estate; resulting in loss of ownership unless previous arrangements are made. Demand for land is high near ports and areas planned for future development. In locations such as along the Thames and Humber estuaries prices can be twice the average agricultural value.

Technical knowledge has advanced and now there is a better understanding about how sites will respond to seawall breaches in the short-term. There is a need to advance knowledge about the long-term evolution of sites. Key issues identified by respondents relate to the selection of sites with favourable characteristics and the need to better understand macro-hydrodynamics at the early stages of project planning. Land elevation in relation to tidal levels determines duration and frequency of inundation and must be suitable to the type of habitat that is intended to be created. Sediment availability and hydrodynamics influence sediment dynamics and how sites will respond in the long-term (e.g. vertical accretion, lateral erosion etc.). The use of adequate modelling tools to improve the understanding of macro-hydrodynamics influencing the sites is of paramount importance to inform project design. Therefore, the tender process needs to be modified so contractors can be selected based on technical quality and modelling suitability (instead of solely on the lowest cost).

Effective communication and public engagement are key elements for the success of MR as a national and regional strategy and for the implementation of individual projects. Public and stakeholders perceptions affect all issues mentioned previously. Societies tend to resist and oppose to change and changing public perception usually requires time and effort. The process requires clear and transparent communication of plans and targets and a justifiable rationale, so communities can understand common questions (e.g. why here; why now). Communication of uncertainty related to evolution of sites is important and requires a sound understanding of coastal processes and a knowledge transfer strategy able to reach the wider public (e.g. clear language, accessible formats, local public meetings etc.).

Continuous public engagement from early planning stages will help understanding the benefits that are of interest to local communities and stakeholders and allow customising project design to meet local expectations. A participatory process that offers opportunities for shared decision-making creates a sense of

ownership and is more likely to agree common targets and accept compromises. However, there is a need to substantiate the ‘promise’ of benefits with unquestionable evidence from existing projects. The risk otherwise is to rely that communities will indefinitely be willing to exchange the certain loss for the uncertain gains at unknown time-frames.

Not all the aspects described above were directly addressed in BUS. However, responses and open comments provide insights about the difference in perceptions about MR across the sectors. Understanding these differences will help address some of the issues identified by practitioners in the EAS. In particular, three cross-cutting issues are discussed here taking into consideration results from BUS.

**All MR functions need to be equally emphasised**

EAS participants indicate that to increase public acceptance and attract funding from a wider range of stakeholders, it is necessary to promote the multiple benefits of MR both at the strategic level and locally. Practitioners are becoming increasingly aware that the current strong focus on habitat creation is hindering wider acceptance of MR. Comments provided by different stakeholders corroborate with this view and also indicate concern with dry land assets and environment that are being lost:

“A useful tool has become a plaything for environmentalists.” (stakeholder from South England)

“this realignment for the birds, is barmy...” (member of the public from East England)

“...We have lovely habitats in the UK, and we live on dry land... If we want to increase intertidal habitats, (which we should do), then stop the water companies from over-drawing water... as they have with the Blackwater in Essex. STOP REALIGNMENT NOW.” (landowner from East England)

“...One of my personal biggest issues has always been 'why do various so called environmentalists think that they can 'play God' in deciding that land that is home to a huge variety of land animals, plants and crops, insects and birds is all of a sudden flooded for some wading birds!’” (stakeholder from East England)

Results from BUS show clear differences in the views of stakeholders concerning the suitability of MR to achieve different objectives in comparison with other groups of respondents. Stakeholders are considerably more negative about the potential contribution of managed realignment to flood risk management. Less than 5% of stakeholders agree and 76% disagree that MR is a promising strategy to reduce flood risk and the costs to maintain

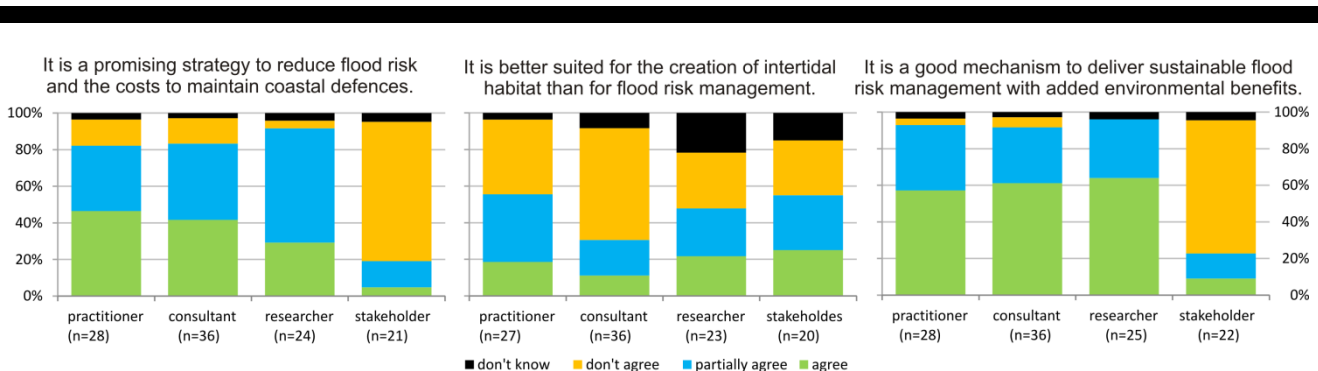


Figure 1. Results from BUS showing difference between groups of respondents concerning their views about the suitability of managed realignment to achieve different objectives. Stakeholders are considerably more negative about the potential contribution of managed realignment to flood risk management.

coastal defences; contrasting with over 40% of practitioners and consultants agreeing with the statement and about 14% disagreeing (Figure 1 left).

Greater contrast is observed concerning the statement that MR is a good mechanism to deliver sustainable flood risk management with added environmental benefits. While around 60% of practitioners, consultants and researchers agree with the statement, 73% of stakeholders disagree and only 9% agree (Figure 1 right, note that none of the researchers have disagreed).

Negative comments from stakeholders often express concern with loss of land without a clear benefit and mistrust in the parties involved in policy, planning and implementation of MR. A clear and transparent participatory process is necessary to establish confidence amongst parties. The statement below reflects the lack of trust in the engagement and communication process:

*“Authorities claimed MR was for flood defence. Would not admit that it was... for compensatory habitat, until nearly 5 years into the engagement process. Pretty clear to stakeholders that the driving force was compensatory habitat early on... so-called independent consultants (paid for by the [funders]) were never going to ascribe a decent [benefit:cost] ratio to any flood protection scheme on this part of the coastline that did not involve major managed realignment.”* (stakeholder from South England)

Stakeholders and researchers responded similarly (roughly showing equally divided opinions) to the statement that MR is better suited for the creation of intertidal habitats than for flood risk management (Figure 1 centre). On the other hand, 61% of consultants and 41% of practitioners disagree with the statement. Most consultants responding to BUS are involved in the design of MR projects aiming to deliver both habitat creation and flood risk management. Therefore, it is expected that consultants will have a more positive view about the suitability of MR to deliver both functions. Based on comments provided by practitioners in both surveys, it is possible to infer that the partial agreement on this

issue reflect differences across sites, including time since completion (i.e. many believe it is too early to evaluate performance, see Figure 2).

### Working partnerships are essential to the implementation of MR

Working in partnership with relevant organisations and landowners is the best way to maximise efforts and resources. This was a clear message from the EAS as all but one respondent acknowledged that projects would be unviable without partnerships. Partnerships usually involve landowners, businesses, government and NGOs concerned with wildlife conservation).

MR implementation costs considerably more to the taxpayer in cases where the Environment Agency has to purchase land. Figure 2 (top centre) shows that over 60% of stakeholders perceive MR to be too expensive for the benefits it may create; contrasting with 72% of consultants and 58% of practitioners and researchers who think otherwise. Funding might be a bigger issue in the future as suitable land becomes scarcer. The government plans to realign a total of 111 km by 2016 and 550 km by 2030 resulting in the creation of 6,200 ha of intertidal habitat at a cost of £10-15 million per year (Committee on Climate Change, 2013). The estimated cost would not suffice to maintain current rate of MR; therefore it is likely that government is relying on external funding sources.

If partners with different interests are involved, there are better opportunities for the delivery of multiple benefits; which in turn may enhance local acceptance of MR. EAS respondents stated that public acceptance requires a much longer and persistent engagement than usually foreseen. More than 60% of stakeholders believe MR results are not very convincing so far (Figure 2 top right). Working in partnership also offers opportunity for knowledge transfer and exchange amongst partners, facilitating changes in perception, especially when supported by evidence and/or practical experience. Resolution of complex issues (e.g.

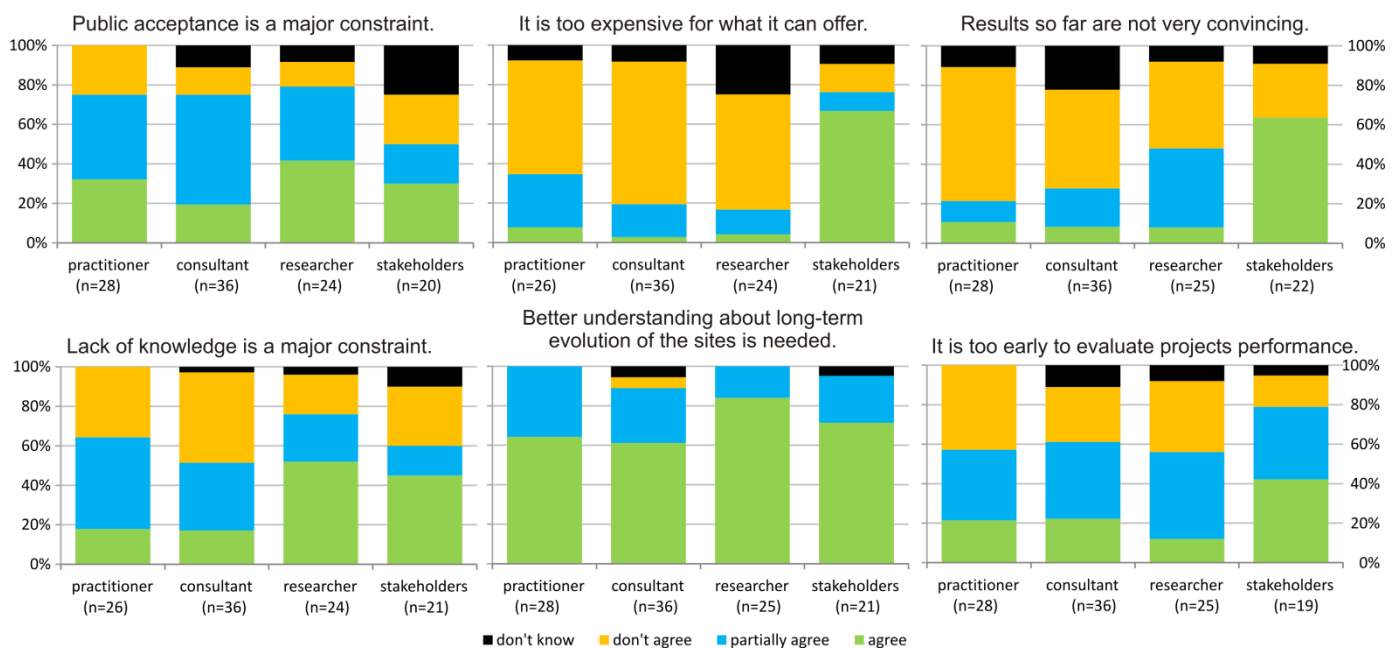


Figure 2. Results from BUS showing difference between groups of respondents concerning their views about managed realignment. Stakeholders are considerably more negative about the outcomes from managed realignment and the associated costs. Generally, stakeholders are less likely to agree/partially that public acceptance is a major constraint.

relocation of footpaths, public access to sites etc.) is also more easily and quickly resolved if affected parties are included in the partnership.

Analysis of BUS responses to the statement “public acceptance is a major constrain” was inconclusive as opinions were generally divided (Figure 2 top left). Although, more respondents agree than disagree with the statement in all groups, partial agreement is high, especially amongst practitioners and consultants. Opinions seem to reflect individual experiences and further investigation is required to clarify the reasons underlying partial agreement. About 42% of researchers agree that public acceptance is a major constraint (Figure 2) and this might reflect findings from the literature (e.g. Myatt-Bell et al., 2002; Milligan et al., 2009; Roca and Villares, 2012) rather than practical experience.

Considering that some stakeholders offered strong views against MR, it is surprising that agreement and disagreement is expressed by similar proportion of respondents in this group. It is possible that some respondents have disagreed with the statement as they might believe that public opposition may delay but will not stop implementation of MR projects; therefore public acceptance is not considered a major constraint.

Working with landowners at opportunistic sites means that costs can be greatly reduced. However, if coastal processes at these sites are not favourable, the project will be poorly justified and delivery of objectives will be challenging.

**Better understanding of long-term evolution of realigned sites is needed**

Over 60% of BUS respondents in all groups agree that better understanding about long-term evolution of the realigned sites is needed (Figure 2). EAS respondents indicate great confidence in the tools available to assist project design and engineering but improvement of hydrodynamic modelling capabilities and/or uptake of model results concerning sediment processes is required. Lack of knowledge is considered a major constraint by less than 20% of practitioners and consultants, but by more than 40% of stakeholders and 50% of researchers (Figure 2 bottom left).

BUS responses indicate that not all MR sites have benefited from systematic monitoring and they think all sites should be monitored and for longer than current general practice. Notably, the majority of researchers and stakeholders indicate that vegetation, sedimentation and biogeochemical processes should be monitored for at least 10 years or longer (Figure 3). Consultants and practitioners more often think the minimum monitoring could be 5 years or less.

Sedimentation processes greatly influence the type of habitat

that might develop within the realigned site and together with biogeochemical processes affect the ecosystem functioning and the delivery of wider ecosystem services. Long-term monitoring of these processes is fundamental to quantify environmental changes and assess whether site evolution is occurring towards the desired objectives. High sediment input (decreasing physical accommodation space) will favour saltmarsh development while mudflats will develop in sites of low sediment input (increasing physical accommodation). Therefore, creation of specific habitats may require more prescriptive engineering solutions (e.g. larger breaches to reduce sedimentation would favour mudflats).

Understanding the type of habitat that is likely to develop is important for quantifying the effects of the realigned site on flood risk and other ecosystem services (e.g. carbon storage, nutrient cycling, enhanced conditions for fisheries, etc. Impact on shell-fisheries is another aspect noted by EAS respondents that needs to be better considered in early stages of planning, including both the engagement with fishery owners and lessons learned from other sites from the inception project planning. More detailed modelling studies might be necessary in sites close to shell-fisheries to assess potential for increase sedimentation or erosion impact and early engagement with fishery owners is recommended. More generally, MR can have a positive impact on local commercial and recreational fishing.

**General perception of MR performance**

Figure 4 shows that opinions are divided about the performance of MR projects against the planned objectives. Only 22% of all respondents think projects are performing well but even less (7%) think they are not performing well. Practitioners show the most positive views with 36% of respondents indicating projects are performing well in all objectives (none indicated projects are not performing well so far). This result is not surprising as practitioners are usually directly involved in implementation and management of projects. Considering that consultants are usually involved in designing and delivering MR projects, it is surprising that only 19% of consultants think projects are performing well towards all objectives.

Once again stakeholders show the most negative views, with 23% of respondents thinking projects are not performing well. A good proportion of respondents from all groups think projects are performing well in some aspects and not so well in others (23% to 53%) or that it is too early to judge (24% to 38%). Projects are at different stages of development (some still in planning others have just being implemented) and therefore these perceptions may change through time depending how sites evolve and whether projects have clear set targets (so performance can be assessed).

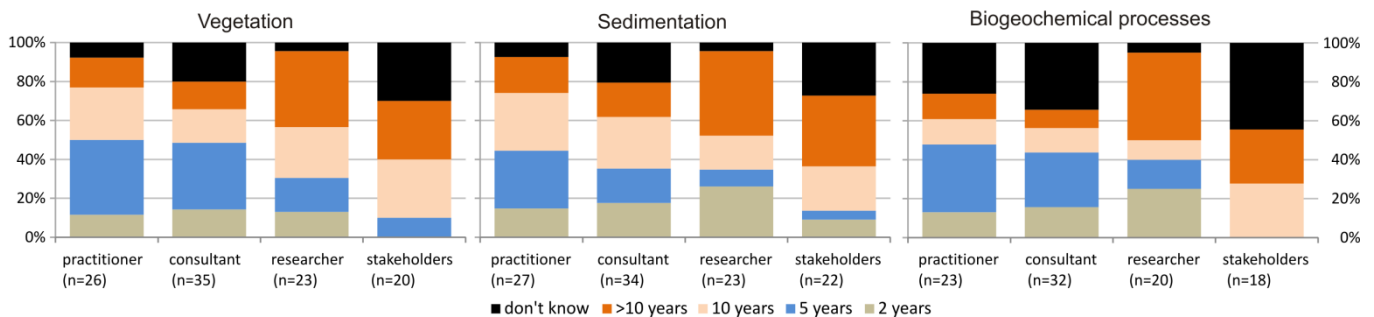


Figure 3. BUS participants’ response to the question: What do you think should be the minimum required systematic monitoring? Note that the question also included birds, fisheries and benthic fauna (not shown here)

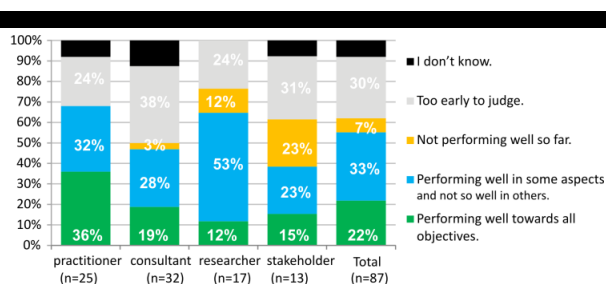


Figure 4. BUS participants' response to the question: Based on your understanding, how are the managed realignment projects you have been involved with performing against the intended objectives?

It is understandable that sites are performing differently due to a number of reasons (e.g. geographical location; mechanism of implementation; stage of development etc.). However, it might be difficult to engage stakeholders and the public with MR projects, if the majority of the practitioners and consultants are not themselves certain about projects' performance. The proportion of consultants thinking it is too early to judge might suggest to stakeholders that this is a slow process and perhaps too risky to invest as benefits might not realise.

Effective communication might help increase the proportion of stakeholders with favourable views. It is important that organisations and practitioners involved in MR send out clear and consistent messages about projects targets, time-frames for attaining benefits and associated uncertainties. Providing convincing evidence about quantifiable benefits is critical and independent academic research is more likely to be trusted by stakeholders and the public than results from consultants involved in project design and implementation (see comment from South England stakeholder provide above).

## CONCLUSIONS

This study provides evidence on current perceptions and experiences concerning the implementation of MR in the UK through the analysis of two independent surveys. By contrasting practitioners, consultants, researchers and stakeholders views, this study identifies key issues that need to be considered to improve current practice. It is anticipated that the key findings and suggestions presented here are applicable to inform future policy and practice in the UK and elsewhere.

Practitioners, consultants and researchers perceive MR as a promising coastal management approach with potential for delivering benefits associated with flood risk management and habitat creation. Stakeholders have more negative views about the potential to deliver multiple benefits, the performance of existing projects and the associated costs. Practitioners are increasingly aware that the current focus on habitat creation is hindering a wider uptake of MR. To increase public acceptance and attract funding from a wider range of stakeholders, it is necessary to promote equally the multiple benefits of MR at the strategic level and locally.

It is suggested here that uptake by stakeholders and the public can be enhanced through a more consolidated message from practitioners (views are still greatly divided in some aspects) and provision of tangible evidence of benefits. Communication of potential benefits resulting from future projects must be supported by undisputed evidence of benefits accruing through time from existing realigned areas. More than 60% of respondents across all groups (practitioners, consultants, researchers and stakeholders)

agree that better understanding of the long-term evolution of realigned sites is required. Knowledge about how sites evolve through time cannot be realised without long-term monitoring of sedimentation and biogeochemical processes (ten years or longer is suggested by more than 50% of researchers and stakeholders). Evidence of performance can only be credible if measured against set targets and their associated time-frames. Similarly, policy objectives must be clearly defined and widely communicated to guide implementation of projects and allow systematic review of achievements at the local, regional and national levels.

Working partnerships formed by landowners and a range of national and local organisations with various interests are essential for the viability of MR implementation at the scale planned by the government in the next 20 years. Partnerships can be developed through continuous engagement with stakeholders and local communities from early planning stages to ensure projects are designed to deliver agreed targets. Continuous engagement also offers opportunity to raise awareness about uncertainties related to natural variability, coastal processes and long-term site evolution.

## ACKNOWLEDGEMENTS

The authors are very grateful for the contribution provided by all survey respondents. Dr Esteves would like to thank the support received from Bournemouth University's Fusion Investment Funds and Grants Academy Networking funds.

## LITERATURE CITED

- ABPmer, 2013. *Online Managed Realignment Guide (OMRG)*. Available from: [www.abpmer.net/omreg/](http://www.abpmer.net/omreg/), last accessed on 30 Nov 2013.
- Burden, A.; Garbutt, R.A.; Evans, C.D.; Jones, D.L. and Cooper, D.M., 2013. Carbon sequestration and biogeochemical cycling in a saltmarsh subject to coastal managed realignment. *Estuarine, Coastal and Shelf Science*, 120, 12–20.
- Committee on Climate Change, 2013. *Managing the land in a changing climate*. Chapter 5: Regulating services – coastal habitats. Last accessed on 1st Dec 2013. <http://www.theccc.org.uk/publication/managing-the-land-in-a-changing-climate/>, pp. 92–107.
- Defra (Department for Environment, Food and Rural Affairs), 2005. *Making space for water - Taking forward a new Government strategy for flood and coastal erosion risk management in England*. First Government response to the autumn 2004 consultation exercise. London.
- Defra (Department for Environment, Food and Rural Affairs), 2013. *National Adaptation Programme: Making the country resilient to a changing climate*. London: The Stationery Office, 182p.
- Esteves, L.S., 2013. Is managed realignment a sustainable long-term coastal management approach? *Journal of Coastal Research*, Special Issue 65, 933–938.
- Ledoux, L.; Cornell, S.; O'Riordan, T.; Harvey, R. and Banyard, L. 2005. Towards sustainable flood and coastal management: identifying drivers of, and obstacles to, managed realignment. *Land Use Policy*, 22(2), 129–144.
- Luisetti, T., Turner, R. K., Bateman, I. J., Morse-Jones, S., Adams, C. and Fonseca, L. 2011. Coastal and marine ecosystem services valuation for policy and management: Managed realignment case studies in England. *Ocean & Coastal Management*, 54(3), 212–224.
- Milligan, J.; O'Riordan, T.; Nicholson-Cole, S.A.; Watkinson, A.R., 2009. Nature conservation for future sustainable shorelines: Lessons from seeking to involve the public. *Land Use Policy*, 26(2), 203–213.
- Myatt-Bell, L.B.; Scrimshaw, M.D.; Lester, J.N. and Potts, J.S., 2002. Public perception of managed realignment: Brancaster West Marsh, North Norfolk, UK. *Marine Policy*, 26(1), 45–57.
- Roca, E. and Villares, M., 2012. Public perceptions of managed realignment strategies: The case study of the Ebro Delta in the Mediterranean basin. *Ocean & Coastal Management*, 60, 38–47.
- Spencer, K.L. and Harvey, G.L., 2012. Understanding system disturbance and ecosystem services in restored saltmarshes: Integrating physical and

biogeochemical processes. *Estuarine, Coastal and Shelf Science*, 106, 23-32.

RICS (Royal Institution of Chartered Surveyors), 2013. *Rural Land Market Survey H1*. Available from <http://www.rics.org/uk/knowledge/market-analysis/ricsrac-rural-market-survey/ricsrau-rural-land-market-survey-h1-2013/>.

## Artificial intelligence-based models to simulate land-use change around an estuary

Carrero, R.†, Navas, F.‡, Malvárez, G.‡, and Guisado-Pintado, E.†.

† Coastal Environments Research Group  
University Pablo de Olavide  
Seville, Spain  
rcargom1@upo.es

‡ Physical Geography Area  
University Pablo de Olavide  
Seville, Spain



[www.cerf-jcr.org](http://www.cerf-jcr.org)



[www.JCRonline.org](http://www.JCRonline.org)

### ABSTRACT

Carrero, R., Navas, F., Malvárez, G., Guisado-Pintado, E. 2014. Artificial intelligence-based models to simulate land-use changes around an estuary. In: Green, A.N. and Cooper, J.A.G. (eds.), *Proceedings 13<sup>th</sup> International Coastal Symposium* (Durban, South Africa), *Journal of Coastal Research*, Special Issue No. 70, pp. 414-419, ISSN 0749-0208.

Understanding human-driven land-use changes is a key element for successful coastal management and planning. Land-use change modelling helps to increase our comprehension of the patterns of these changes and the interacting factors affecting them. In previous years, a wide variety of land-use modelling approaches have arisen, however not all of them fit with the complex and especially dynamic behaviour of land use changes in coastal areas. In this sense, the so called ‘fifth generation’ of models represent an opportunity, as they integrate computer modelling with artificial intelligence technology allowing a more flexible and non-linear approaches that better emulate the real and complex behaviour of land use changes in rapidly evolving environments such as coastal areas. In this paper the applicability of artificial intelligence-based models to simulate land-use changes is explored and applied to a specific case in a coastal stretch. First the potential of a Cellular Automata (CA) is compared with other modelling approaches. In the study CA proved to be a powerful approach due to its capacity of performing dynamic and complex spatial modelling, its affinity to work with geographic and remote sensing data, and its compatibility with other models. Second, a specific CA-Stochastic model is tested in an estuary located in southwestern Spain. The model is applied to simulate land-use changes from 1999-2007, using a spatial resolution of 10x10 m-cell, considering eight representative land-use classes, 30 different land-use transitions and fifteen variables affecting each transition. Validation based on a fuzzy similarity method is performed to compare the real and simulated maps. Results show high analytic capacity and good performance of the model. Four major strengths are identified: i) the integration of physical variables with human-controlled variables; ii) the successful simulation of multiple, simultaneous land-use changes; iii) the management of high-resolution spatial data; and iv) the flexibility of the model. In terms of its application to coastal management and planning, CA-based models not only help to understand past land use changes and the natural and human factors behind them, but also represent a great potential to forecast land use changes and create future spatial-explicit scenarios to assist decision-making in the mid-long term.

**ADDITIONAL INDEX WORDS:** *Land-use change modelling, artificial-intelligence, cellular-automata, coastal management.*

### INTRODUCTION

Land-use change is one of the major factors affecting global environmental change (Meyer and Turner, 1994) and it is associated to global environmental problems such as biodiversity loss, habitat fragmentation, soil degradation or climate change. Natural land which covers forests or wetlands are rapidly being transformed to human-dominated ecosystems. This is due to economic growth and human expansion both in developed and developing regions at rates that reach 1.3 million/ha/year worldwide (FAO, 2010). Land-use change is of special concern in coastal areas, where urbanisation, infrastructure demand or agriculture intensification are taking place at faster rates than in any other region. With about 40 percent of the world’s population living within 100 km of the sea (Tundi and Alder, 2005), land use change is taking place at rates that threaten the sustainability of these sensitive areas. In this context, understanding the factors influencing land-use change has been the focus of scientific study across multiple disciplines (Parker *et al.*, 2003) and it is a key

element for a successful coastal management and planning. Land-use change models help to increase our comprehension of the spatial patterns of these changes and the interacting factors affecting them. During the last decades land-use models have emerged to assist the analysis of the causes and consequences of land-use change, in order to better understand the functioning of land-use systems and to support land-use planning and policy (Verburg *et al.*, 2004). Although originally developed in the field of urban and transportation modelling in the United States during the 1950’s, the acknowledgement that land-use change is behind many environmental problems spread land-use change models in environmental sciences from the nineties onwards. At first most environmental land-use models were mainly focused on deforestation (Lambin, 1997) but more recent efforts also address other land-use conversions such as urbanization or agricultural intensification (Verburg *et al.*, 2002). In parallel to their thematic expansion, land-use models have progressively evolved during the last six decades from static, deterministic approaches to more dynamic and non-linear approaches that better emulate the real and complex behaviour of land-use changes. Abbott (1989)

DOI: 10.2112/SI70-070.1 received 1 December 2013; accepted 21 February 2014. © Coastal Education & Research Foundation 2014

introduced the notion of “generations” to explain the progression of land-use models and Silva and Wu (2012) applied this notion to explain the evolution of land-use models. This evolution goes from a first generation –which developed large scale urban models based on static and deterministic principles on the 1950s- to the current fifth generation of models, which is acknowledged to integrate computer dynamics with ‘Artificial Intelligence’ (AI) technology, such as artificial life, intelligent stochastic simulation models, evolutionary computing, spatial DNA, and knowledge-based intelligent systems (Wu and Silva, 2010). The fifth generation of models represents an opportunity for coastal management, as it allows for a more flexible and non-linear approach which better reproduces the true behaviour of land-use changes in rapidly evolving environments such as coastal areas. In this paper the applicability of AI-based models to simulate land-use changes in coastal areas is explored. First, the potential of Cellular Automata (CA) is presented in comparison with other modelling approaches; and second, a specific Stochastic-CA model is tested in an estuary located in southwestern Spain.

### STUDY SITE

The study site is the municipality of Ayamonte, located in the Region of Andalusia, southwestern Spain (Figure 1). Ayamonte lies on the western margin of the Guadiana river estuary, the border between Spain and Portugal, having the Atlantic Ocean as its southern boundary. The municipality covers a surface of 142.78 km<sup>2</sup> with gentle topography which reaches a maximum high of 160 m above sea level. The littoral physiography of the study is strongly influenced by the presence of the Guadiana estuary, one of the most important mesotidal-fluvio-marine systems of the Iberian Peninsula. The river mouth was formed as a narrow channel excavated by fluvial incision during the Pleistocene lowstand and flooded 6.500 years ago. Coastal morphology is controlled by wave activity, fluvial sediment supply and exposure/submersion levels related to tidal activity, highly influenced by the wave-dominated regime of the estuary. Tidal range is mesotidal with a mean tidal range of 2 m, and a maximum spring tide of 3.4 m (Morales, 1997). The coastal environment is characterized by low to medium energy waves, including Atlantic swell waves and local sea waves, with an average offshore significant wave height is about 0.9 m, with an average period of 4.6 s (SNPA, 2013). Dominant wave approach (about 50% of occurrences) is from the southwest and west directions (Lobo *et al.*, 2003) producing a strong longshore littoral drift from west to east that generates an estimated sediment transport rate of 18x10<sup>3</sup> m<sup>3</sup> yr<sup>-1</sup> (Garel *et al.*, 2009). In socio-economic terms, the site is a medium-size municipality for regional standards, with a current population of 20 000 inhabitants, mostly concentrated in Ayamonte town. The municipality has faced significant socio-economic transformations in past decades; from being an important regional port in the 1950s, to becoming heavily reliant on the tourism industry. Ayamonte’s coastal settlement (Isla Canela) was the focus of a tourism plan in 1963, which intended to create a large international resort. Since then, different strategies have been put in place to develop the tourism industry in the area, driving an increase in housing, facilities and infrastructure mainly concentrated on the closest areas to the beach and the river margins. Since the beginning of the 2000s important transformations occurred in the area due to the development of a macro-tourist centre in Costa Esuri, north of town Ayamonte (Figure 1). Aquaculture was also introduced during the 1970s causing important transformations on the wetlands. Agriculture has expanded and intensified during the early 2000s with an

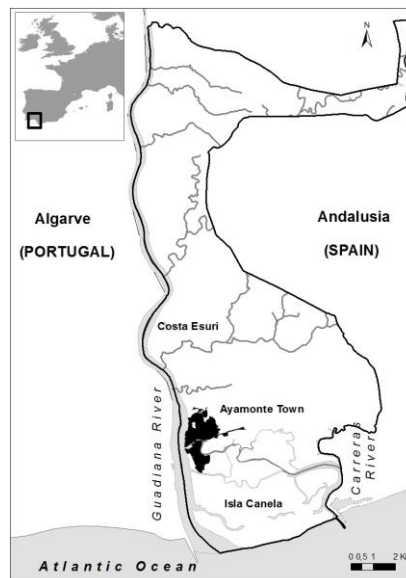


Figure 1. Study site: Ayamonte municipality, SW Spain.

associated deforestation process. Urban migration to the coast has caused coastal urbanisation to reach a 15-29% of the land cover on the first 250m-400m of the coastline (Tejada, 2005) and has led to an increase in commercial and urban areas as well as infrastructure in Isla Canela. As an effort to relieve part of the physical distress caused by anthropogenic activities and to protect the ecological values of the site, a natural protected area was created in 1989, covering 1 385 hectares of the marshes. In 2003 the protected area was included in the Natura 2000 network, confirming the high ecological values of the wetlands. Due to the many land-use changes occurred during the last decades, the area perfectly represents the great dynamism of coastal areas and the heavy and intense influence of land-use change on coastal estuarine environments.

### METHODS

#### Land-use change model selection

A literature review was performed to compare five different land-use change modelling approaches (four AI-based approaches and one non-AI based). The approaches based on AI techniques included: i) *Cellular Automata* (CA), ii) *Agent-Based Models* (ABM) both from the field of ‘artificial life’; iii) *Genetic Algorithm* belonging to the intelligent stochastic optimization processes; and iv) *Artificial Neural Networks*, from the field of evolutionary computing. The non-AI based modelling approach included in the comparative analysis was *Empirical-Statistical modelling*, which was included given its wide application and importance in current land-use change modelling research. All modelling approaches were compared in terms of models’ strengths for land-use change analysis, spatial nature capacity to work with geo-data and models examples. After surveying the different land-use change modelling approaches, and identifying the most suitable approach for this research, a second literature review was performed to evaluate four specific land-use change models: one Empirical-Statistical based model and three Cellular Automata-based models. The four land-use change models were compared by: the spatial allocation of change procedure, land-use maps needed for the calibration, spatial resolution, factors included to explain land-use change, types of land-use changes



Table 1. Comparison of various land-use change modelling approaches.

Modelling approach	Strengths for land use change analysis	Spatial nature	Capacity to work with geo-data	Examples
<i>Non-Artificial Intelligence Approaches</i>				
<b>Empirical-Statistical Modelling</b>	Can provide information on the behaviour of key drivers of change. Data can be managed at multiple scales.	No	If coupled with other model	Verburg <i>et al.</i> , 2004
<i>Artificial- Intelligence based Approaches</i>				
<b>Cellular Automata (CA)</b>	Show a strong potential to represent spatial processes at the local scale. Can replicate real-world spatial patterns, particularly fractal structures.	Yes (cells/grid)	Yes, natural affinity to work with spatial data	Jantz <i>et al.</i> , 2004
<b>Agent-Based models (ABM)</b>	Can incorporate individual decision-making and the interactions with the environment. It is possible to include cross-scale feedbacks.	No	If coupled with other model	Polhill <i>et al.</i> , 2001
<b>Genetic Algorithm</b>	Can deal with nonlinear optimization problems (optimal spatial configuration of land-uses). Can help to define land allocation rules.	No	If coupled with other model	Seixas <i>et al.</i> , 2007
<b>Artificial Neural Networks</b>	Useful for land use classification/cluster and land pattern learning. Can help to select suitable input parameters for land-use change models.	No	If coupled with other model	Pijanowskia <i>et al.</i> , 2002

taken into account, and inclusion of a validation procedure in the model. After analysing the four land-use change models, the CA-based model Dinamica EGO (Soares-Filho *et al.*, 2002) was finally selected for this study. This is a spatially explicit CA model that simulates land-use change dynamics and where the *rate of change* is calculated by a coupled Markovian model and the *location of changes* can be inferred by calculating transition probability maps that quantify and integrate the influence of specific determinants on the spatial prediction of land-use changes (Soares-Filho *et al.*, 2001).

### Input data preparation

The application of the model needed a pre-processing of the input data in a GIS environment. Input spatial data for the model included: *land-use maps* and *explanatory variables maps*, which covered both physical variables (e.g. slope, elevation) and socio economic variables (e.g. urban spots, infrastructures). For the *land-use maps* an initial 1999 map of Ayamonte municipality and a final 2007 land use map were considered (CMA, 2013). The time span selected, included the years in which Costa Esuri began its construction. Original maps were reclassified into 8 classes in order to maximize the explanatory power of the model. Reclassification was based on the analysis of the behaviour and the net change of the original classes (i.e. classes behaving similarly-as different types of crops- were unified into one category). The 8 land-use classes finally considered were: urban, industrial, crops, shrubs, wetlands, beach, water and non-vegetated areas. For the *explanatory variables maps*, fifteen variables were taken into account to explain land-use change in the study site, including *physical variables* -elevation, slope, lithology, presence of wetlands, presence of aquifers, distance to rivers- and *human-related variables*- distance to roads, distance to trails, planned industrial areas, planned touristic areas, distance to industrial areas, distance to golf courses, distance to ports, distance to commerce and the existence of protected areas. The human-related variables were selected based on a participatory identification of driving forces in the study area (Navas *et al.*, 2012; Carrero *et al.*, 2013). All the spatial data used as input was transformed and homogenized before being exported to the model. A spatial resolution of 10x10 m cell was selected taking into account the local-scale application of the model.

### Model Calibration

The rate of land-use changes was quantified by a Markov matrix obtained from the comparison of the initial and final land-use maps, as suggested by Soares-Filho (2001). The matrix indicates the number of changing cells for each transition and can be transformed into a Markov chain probability matrix for the entire period. From the probability matrix, yearly transition rates were obtained, that is, the percentage of land-use that will change to another state each year (Soares-Filho *et al.*, 2002). Afterwards, relationships between the explanatory variables and land-use were quantified with the *Weights of Evidence Method* (Goodacre *et al.*, 1993; Bonham-Carter, 1994) applied in Dinamica EGO model as described by Soares-Filho *et al.* (2002, 2004). Weights of Evidence method (WoE) is based on a Bayesian approach where the weight of *each variable* for *each land-use transition* is performed through a conditional probability analysis. In order to calibrate the WoE, the data structure of each variable was transformed as described by Soares-Filho *et al.* (2002). Each variable was divided into representative categories (for categorical variables) or intervals (for continuous variables), and the specific logarithmic value of each weight for each category/range for each transition was calculated in order to quantify their positive or negative correlation with the analysed land-use transitions. To ensure the spatial independence assumption among the considered variables (i.e. avoiding double-counting effect of factors), two correlation analyses were performed in the model: Cramer's Coefficient and the Joint Information Uncertainty (Bonham-Carter, 1994). These tests showed the degree of association or dependence between the explanatory variables, both of them being based on the ratio of overlapping areas among the different categories belonging to two maps of explaining variables. For the correlation analyses, according to Ximenes *et al.* (2011), the threshold value used to exclude a variable was >0.50 for both indexes. In order to increase the model fitness, all the 15 weights were individually analysed and modified for all transitions. Four types of modifications were performed according to (Quiroz, 2009): no modification, when the variable behaviour followed a logical trend; slight modification, in order to soften the trend; strong modification when there was a strange uncorrelated system behaviour; and elimination, when values were close to 0 or when there was a high degree of noise for a specific land-use transition.

**Simulation and validation**

After the calibration procedure, the WoE method was further applied to the Dinamica EGO model to calculate a *probability map*, which depicted the favourable areas for change according to the explanatory variables influence (Soares-Filho *et al.*, 2002, 2004). The spatial transition probability determines the likelihood that a specific cell has to change from one state to other over a period of time (Soares-Filho *et al.*, 2001), e.g. a change from non-vegetated areas to industrial surface in relation to potential evidences as the roads proximity. To perform the *spatial allocation of changes* (i.e. selection of the pixels that actually change from one category to another) two cellular automata transition functions based on stochastic selection algorithms were used within the model. The first function simulates expansion and contraction of previous patches of a certain class, whereas the second function is designed to generate new patches through a seeding mechanism (Soares Filho *et al.*, 2002). Increasing the patch size leads to a model with a less fragmented landscape, and

increasing the patch size variance leads to a more diverse landscape. In this research an external landscape analysis package was used (PatchAnalyst) to support the selection of the input parameters for the two CA functions. Simulation was run from the initial year (1999) to the final year (2007). A validation of the spatial accuracy of the simulation was performed through a modification of the *K fuzzy similarity* based on the concept of fuzziness of location, in which coincidence is not restricted to a cell-by-cell overlay but also includes the cells in a neighbourhood (Hagen, 2003). Through this method the real and simulated 2007 land-use maps were compared, and the spatial fitness of the model was measured.

**RESULTS**

Results from the literature review on the different land-use change modelling approaches are summarized in Table 1. Both Empirical-Statistical models and CA-based models show a high potential. However, CA presents a natural affinity to work with

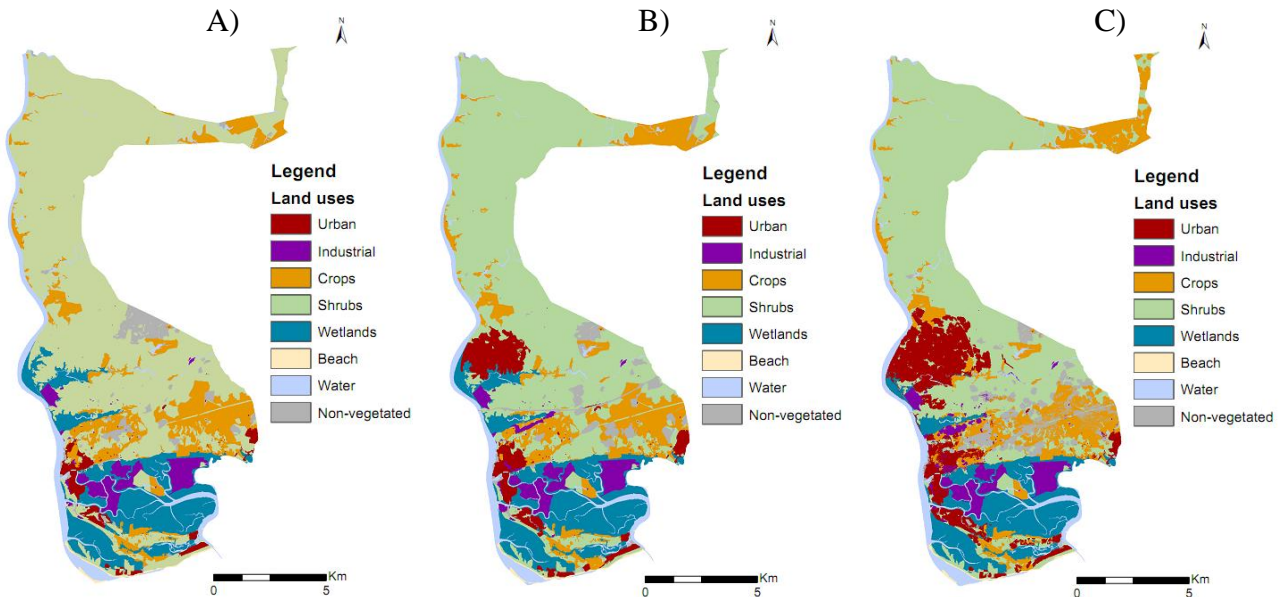


Figure 2. From left to right: A) Real land-use map 1999; B) Real land-use map 2007; and C) Simulated land-use map for 2007.

Table 2. Comparison of specific land-use change models (Empirical-Statistical vs. Cellular Automata).

Model	Spatial allocation of changes	Land-use maps for calibration	Spatial resolution	Factors included to explain land-use change	Land-use changes	Validation included in the model
CLUE (Empirical-Statistical)	Logistic regression analysis and decision-rules	At least 2	Changeable (Designed for <1x1 km)	Biophysical (e.g. precipitation) and Socio-economic (e.g. economic conditions)	Multiple	No
SLEUTH (CA)	Self-modifying cellular automata	5 for urban uses	1 km to 30 m	Six: slope, land use, urban, exclusion, transportation, and hill shading	Urbanisation	No
Metronamica (CA)	CA transition rules	At least 2	Changeable (max. 25 x 25 m)	Biophysical and Socioeconomic	Multiple	No
Dinamica EGO (CA)	Marcov chains and CA	At least 2	Changeable	Biophysical and Socioeconomic. Unlimited number.	Multiple	Yes

spatial data and also to represent real, complex and dynamic land-use change processes as the ones that usually take place on estuarine/coastal areas. Considering this, four different models—three CA and one logistic regression based model—were compared as shown in Table 2. Among all the analysed models, Dinamica EGO presents the highest potential for the analysing land-use change in coastal areas at the local scale, given the flexibility of the model in terms of spatial resolution, a number of factors and land-use change included in the analysis, and inclusion of a results' validation procedure.

After applying Dinamica EGO in the study site the following results were obtained. Regarding the quantification of changes, thirty land-use change transitions were detected by the Markov matrix between 1999 and 2007. Significant transitions ( $>1\%$  change per year) in this period were: non-vegetated areas to shrubs ( $11\% \cdot y^{-1}$ ), non-vegetated areas to crops ( $5.2\% \cdot y^{-1}$ ), shrubs to urban ( $1.6\% \cdot y^{-1}$ ), crops to non-vegetated areas ( $1.4\% \cdot y^{-1}$ ) and wetland to urban ( $1.3\% \cdot y^{-1}$ ). In terms of the effects of the explanatory variables over land-use changes, all fifteen explanatory variables were found to have an effect on the 30 analysed land-use change processes. Correlation analysis through *Crammers* and *Joint Uncertainty indexes* showed pairs of variables were dependent for land-use transitions in 41 cases. In all the cases where both indexes were above the threshold value, the weight of one of the explanatory variable was excluded, i.e. for the transition from urban to industrial land, the pair of variables 'protected areas' and 'wetlands surface' had a *Crammers* and *Joint Uncertainty index* above 0.55 and consequently, the weight of wetlands was eliminated for that transition. To increase the model fitness, 168 weights were modified and 96 were eliminated following the criteria explained in the methodology. To perform the simulation, first the WoE method was applied to obtain 30 probabilities maps (one for each land-use transition) depicting the most favourable areas for a change according to the explanatory variables influence. Second, the two cellular automata transition functions included in Dinamica EGO were calibrated for each transition with the support of the landscape metrics analysis of PatchAnalyst software. The resulting simulated 2007 land-use map reproduced the most important land-use change over the study site as shown in Figure 2. The fuzzy validation test showed a 40% land-use change prediction at a resolution of 30x30 m.

## DISCUSSION AND CONCLUSIONS

During past decades empirical-statistical land-use change models -such as the CLUE model (Veldkamp and Fresco, 1996)- have been widely used in the scientific community and successfully applied from transnational to sub-regional scales all over the globe. Nevertheless, an important drawback of these models is that the linear approaches of statistics do not accurately represent the complexity of land-use changes and can constrain simulation (Koomen and Stiwel, 2007). In this sense, the application of Artificial Intelligence (AI) methods to land-use change modelling is a promising line of research as it opens new possibilities in the simulation of non-linear, complex and dynamic land-use change patterns. Approaches such as Genetic Algorithm and Artificial Neural Networks present a great potential for specific phases of land-use change modelling -e.g. selecting the input variables or optimising land-uses spatial configurations- although these models cannot be used by themselves for a comprehensive spatial modelling analysis and need to be integrated with other modelling approaches. In this regard, Agents-Based Modelling (ABM) and Cellular Automata (CA) - both belonging to the *artificial life techniques* (Wu and Silva, 2010)- are rapidly gaining ground and being increasingly

implemented in land-use change studies. Whereas ABM is focused on the human influence over land-use change and it is a recommendable approach to represent the non-spatial dynamics of land-use change by incorporating the social processes on decision making (Matthews *et al.*, 2007), CA is a powerful tool to simulate the spatial dynamics of land-use change given their natural affinity to represent complex spatial forms through relatively simple rules (White and Engelen, 1997). Moreover CA models show a high capacity of performing dynamic spatial modelling, they can easily incorporate geographic and remote sensing data and they can integrate a diversity of other models, including ABM. With regards to limitations of CA, Verburg *et al.* (2002) point out that these models are not capable of explicitly addressing the competition between different land-use types, thus they can only simulate the conversion of only one land-use type. Verburg *et al.* (2004) also consider CA simplicity and the rudimentary quantification of the neighbourhood functions as important restrictions to take into account. However, some authors state CA can overcome such limitations when combined with other methods such as ABM, Fuzzy logics, Artificial Neural Networks (Wu and Silva, 2010) or Stochastic methods (Almeida *et al.*, 2003). In this paper, agreeing with Almeida *et al.* (2003), the CA-model Dinamica EGO has been successfully applied in an estuary to simulate multiple processes (urban sprawl, industrialisation, agriculture intensification, etc.), model 8 representative land-use classes and 30 different land-use transitions, as well as analyse the individual effect of 15 variables for each transition. These results demonstrate that it is possible to address the competition between different land-use types, to reproduce multiple land-use changes at the same time and to quantify the neighbourhood functions through complex and flexible mechanisms. Moreover the simulation spatial accuracy (40% land-use changes were predicted within a 30x30 m window) is more than acceptable in comparison with other works in the field (e.g. Pereira *et al.*, 2010). Regarding the application of Dinamica EGO to coastal areas and considering that the transformation of the coastal system responds to a combination of natural and anthropogenic forces, one of the greatest advantages of this model is its capacity of integrating both physical variables (e.g. slope) with human-controlled variables (e.g. existence of protected areas). Moreover the model is able to include different anthropogenic-related spatial determinants of changes such as: proximate causes (e.g. building a road), preferable sites (e.g. more fertile soil), or restrictive conditions (e.g. protected areas) (Soares-Filho *et al.*, 2010). Coastal managers and decision-makers could take advantage of this, as it allows to analyse the influence of certain spatial decisions over specific land-use changes (e.g. building new infrastructure can trigger urbanisation over a certain ratio). In this way the model can help to elucidate or even measure the factors that lead to coastal artificialisation. For instance in the pilot site, results show that the presence of golf courses or commercial surfaces facilitate the creation of coastal resorts in the surroundings. In addition, the result of past planned decisions (as creating an urban reserve) in terms of land-use changes, can be analysed and even discussed within the community. Analogously, and as an exciting possibility to coastal planning, the model could be used to simulate future changes, including multiple spatial decisions and comparing how different spatial planning options can influence future changes in land-use. In other words, CA-models not only aid in the understanding of the complex processes underneath past land-use changes, but also represents a great potential to forecast future land-use changes in coastal areas. Considering the current population growth trend in coastal areas and the associated urbanisation processes, land-use change may occur at faster rates

and wider scales in the next decades, leading to environmental impacts at unprecedented levels. The use of artificial intelligence techniques such as CA-model represents an exceptional opportunity to explore the consequences of future decisions on the coasts. The results obtained in this paper indicate that further research could be focused on testing the applicability of Dinamica EGO to simulate alternative spatially-explicit future scenarios in coastal areas to assist decision making and coastal planning in the mid and long term.

### LITERATURE CITED

- Abbott, M. B., 1989. Review of Recent Developments in Coastal Modelling. In *Hydraulic and Environmental Modelling of Coastal, Estuarine and River Waters*, Eds. R. A. Falconer, P. Goodwin, and R. G. S. Mathew, 3–39. Avelbury Technical.
- Almeida, C. M., Batty, M., Vieira, A. M., Câmara, G., Silveira, B., Coutinho, G. and Lopes, C., 2003. Stochastic cellular automata modeling of urban land use dynamics: empirical development and estimation. *Computers, Environment and Urban Systems*, 27, 481–509.
- Bonham-Carter, G.F., 1994. Geographic Information Systems for Geoscientists: Modelling with GIS. In: *Computer Methods in the Geosciences*, vol. 13, p. 398. New York, Pergamon.
- Carrero, R., Navas, F., Malvárez, G. and F. Cáceres., 2013. Participative Future Scenarios for Integrated Coastal Zone Management. *Journal of Coastal Research*, SI 65, 898–903.
- CMA, 2013. *Mapas de Usos y Coberturas Vegetales de Andalucía, 1999, 2007*. Sevilla, España: Consejería de Medio Ambiente, Scale 1:25.000.
- FAO, 2010. *Global Forest Resources Assessment 2010*. FAO Forestry Paper, 163. Rome, Italy: FAO Forestry Department. ISBN 978-92-5-106654-6. 340 p.
- Garel, E., Pinto, L., Santos, A., and Ferreira, Ó., 2009. Tidal and river discharge forcing upon water and sediment circulation at a rock-bound estuary (Guadiana estuary, Portugal). *Estuarine, Coastal and Shelf Science*, 84, 269–281.
- Goodacre, C. M., Bonham-Carter, G. F., Asterberg, F. P. and Wright, D. F., 1993. A statistical analysis of spatial association of seismicity with drainage patterns and magnetic anomalies in western Quebec. *Tectonophysics*, 217, 285–305.
- Hagen, A., 2003. Fuzzy set approach to assessing similarity of categorical maps. *International Journal of Geographical Information Science*. 17 (3), 235–249.
- Jantz, C. A., Goetz, S. J., Shelley, M., 2004. Using the SLEUTH urban growth model to simulate the impacts of future policy scenarios on urban land use in the Baltimore Washington metropolitan area. *Environment and Planning B: Planning and Design*, 31, 251–271.
- Koomen, E. and Stillwell, J., 2007. Modelling land-use change. Chapter 1. In: Koomen E, Stillwell J, Bakema A, Scholten HJ (eds) *Modelling land-use change; progress and applications*. Springer, Dordrecht, p 1–21.
- Lambin, E.F., 1997. Modelling and monitoring land-cover change processes in tropical regions. *Progress in Physical Geography*, 21 (3), 375–393.
- Lobo, F.J., Dias, J.M.A., González, R., Hernández-Molina, F.J., Morales, J.A. and Díaz Del Río, V., 2003. High-resolution seismic stratigraphy of a narrow, bedrock-controlled estuary: The Guadiana estuarine system, SW Iberia. *Journal of Sedimentary Research*, 73, 973–986.
- Matthews, R.B., Gilbert, N., Roach, A., Polhill, J.G. and Gotts, N.M., 2007. Agent-based land use models: a review of applications. *Landscape Ecology*, 22, 1447–1459.
- Meyer W.B. and Turner B.L. 1994. Changes in land use and land cover: a global perspective. University Press, Cambridge, UK.
- Morales, J.A., 1997. Evolution and facies architecture of the mesotidal Guadiana River Delta (S.W. Spain-Portugal). *Marine Geology*, 138, 127–148.
- Navas, F., Carrero, R. and Cáceres, F., 2012. *A new approach to Future Scenarios for the EU COASTANCE Project: A coastal governance experience in Andalusia*. A report to the Ministry of the Environment of the Regional Government of Andalusia-128 pp.
- Parker, D. C., Manson, S. M., Janssen M., Hoffmann, M. J. and Deadman, P. J., 2003. Multi-agent systems for the simulation of land use and land cover change: a review. *Annals of the Association of American Geographers* 93(2), 314–337.
- Pereira, R.S., Ferrari, R., Dal Santo, M.A., 2010. Dynamic Modeling of Land Use and Coverage at Quarta Colônia, RS, Brazil. FIG Congress 2010, Facing the Challenges – Building the Capacity, Sydney, Australia, 11–16 April 2010. 11 p
- Pijanowskia, B. C., Brown, D. G., Shellitoc, B. A., and Manikd, G. A., 2002. Using neural networks and GIS to forecast land use changes: a land transformation model. *Computers, Environment and Urban Systems*, 26(6), 553–575.
- Polhill, J.G., Gotts, N.M. and Law, A.N.R., 2001. Imitative Versus Non-Imitative Strategies in a Land Use Simulation. *Cybernetics and Systems*, 32 (1–2), 285–307.
- Quiroz, Y., 2009. Modelo dinámico de cambio de cobertura y uso de suelo en una zona de transición urbano-rural entre la ciudad de Morelia y el ejido Jesús del Monte. Mexic: Universidad Nacional Autónoma de México, PhD Thesis, 215 p.
- Seixas J., Nunes J.P., Lourenço P. and Corte-Real J., 2007. GENETICLAND: modeling land-use change using evolutionary algorithms. In *Modelling land-use change*. Eds. Eric Koomen, Aldrik Bakema, John Stillwell and Henk Scholten. Springer Verlag, ISBN: 978-1-4020-5647-5.
- Silva, E. and Wu, N., 2012. Surveying Models in Urban Land Studies. *Journal of Planning Literature*, 27, 139–152.
- Soares-Filho, B., Assunção, R., Pantuzzo, A., 2001. Modeling the spatial transition probabilities of landscape dynamics in an Amazonian colonization frontier. *BioScience* 51, 1039–1046
- Soares-Filho, B.S., Pennachin, C.L. and Cerqueira, G., 2002. DINAMICA a stochastic cellular automata model designed to simulate the landscape dynamics in an Amazonian colonization frontier. *Ecological Modeling*, 154 (3), 217–235.
- Soares-Filho, B., Alencar, A., Nepstad, D., Cerqueira, G., Vera Diaz, M., Rivero, S., Solorzano, L. and Voll, E., 2004. Simulating the response of land-cover changes to road paving and governance along a major Amazon highway: the Santarém-Cuiabá corridor. *Global Change Biology*, 10, 745–764.
- Soares-Filho, B., Moutinho, P., Nepstad, D., Anderson, A., Rodrigues, H., Garcia, R., Dietzsch, L., Merry, F., Bowman, M., Hissa, L., Silvestrini, R. and Maretti, C., 2010. Role of Brazilian Amazon protected areas in climate change mitigation. *Proceedings of the National Academy of Sciences*, 107, 10821–10826.
- SNPA, Spanish National Port Authority, 2013. *Clima medio oleaje. Nodo SIMAR 1050048*. Oceanographic Database. Eds Public Works Ministry. 47 pp.
- Tejada, M., 2005. Evaluación de la resiliencia en el marco de la Gestión de Áreas Costeras. Seville, Spain: Pablo de Olavide University, PhD Thesis, 378 p.
- Tundi, A. and Alder, J. 2005. Coastal Systems. In Hassan, R., Scholes, R., and Ash, N. (eds), *Ecosystems and Human Well-Being: Current State and Trends*, Volume 1. Washington, DC: Island Press. 513–549.
- Veldkamp A. and Fresco, L.O., 1996. CLUE: a conceptual model to study the conversion of land use and its effects. *Ecological Modelling*, 85, 253–270.
- Verburg, P.H., Soepboer, W., Limpiada, R., Espaldon, M.V.O., Sharifa, M.A. and Veldkamp, A., 2002 Modelling the spatial dynamics of regional land use: The CLUE-S model. *Environmental Management*, 30, 391–405.
- Verburg P.H., de Nijs T.C.M., van Eck J.R., Visser H. and K. de Jong, 2004. A method to analyse neighbourhood characteristics of land use patterns. *Computers, Environment and Urban Systems*, 28, 667–690.
- White, R. and Engelen, G., 1997. Cellular automata as the basis of integrated dynamic regional modeling. *Environment and Planning B*, 24, 235–246.
- Wu, N. and Silva, E., 2010. Artificial Intelligence Solutions for Urban Land Dynamics: A Review. *Journal of Planning Literature*, 24, 246–265.
- Ximenes, A.C., Almeida, C.M., Amaral, S., Escada, M.I.S., and Aguiar, A.P.D., 2011. Spatial Dynamic Modelling of Deforestation in the Amazon, *Cellular Automata - Simplicity Behind Complexity*, (Ed.) Dr. Alejandro Salcido ISBN: 978-953-307-230-2.

# Regional differences in recreational preferences of Estonian coastal landscapes

Mart Reimann†, Üllas Ehrlich‡, Hannes Tõnisson∞

† Department of Leisure Sciences, Tallinn University; Institute of Ecology and Earth Sciences, Tartu University  
mart.reimann@tlu.ee

‡ Tallinn School of Economics and Business Administration at Tallinn University of Technology  
Ullas.Ehrlich@ttu.ee

∞ Institute of Ecology, Tallinn University, Uus-Sadama 5, Tallinn 10120, Estonia  
hannes.tonisson@tlu.ee



[www.cerf-jcr.org](http://www.cerf-jcr.org)



[www.JCRonline.org](http://www.JCRonline.org)

## ABSTRACT

Reimann, M., Ehrlich, Ü., Tõnisson, H., 2014. Regional differences in recreational preferences of Estonian coastal landscapes. In: Green, A.N. and Cooper, J.A.G. (eds.), *Proceedings 13<sup>th</sup> International Coastal Symposium* (Durban, South Africa), *Journal of Coastal Research*, Special Issue No. 70, pp. 420–425, ISSN 0749-0208.

Estonia has rich and valuable coastal landscapes. Estonian natural coastline is classified into five shore types: cliffs, till, gravel, sandy and silty. Those shore types are well distinguishable and recognised by scientists and the general public. Shoreline types are not distributed equally, some shore types occur in all counties, other shore types are found only in certain parts of Estonia. The main aim of the current study is to assess whether people's preferences for shore types are related to the types occurring in their home county. A survey (N=1,519) was carried out on an Estonian working age population in all 15 counties, of which 7 counties have a coastline. The questionnaire contained information on Estonian shores, which were presented in coloured photos. Respondents were asked to rank the photos according to the question: "Which shore type do you prefer to visit in your leisure time?" Differences were found among preferences in various regions; however, sandy shores were highly preferred among all respondents. In other types, differences appeared. Respondents are less likely to prefer shore types which are dominant in their region than shore types which are absent or less common in their county.

**ADDITIONAL INDEX WORDS:** *Shore types, landscape preferences, human-landscape relationship, landscape values, recreational use of landscape.*

## INTRODUCTION

Landscape preferences are widely studied worldwide. The preference approach is an integrative approach used to study human-landscape relationships. It combines psychophysical methods, visual landscape stimuli and statistical analysis in the assessment of landscape visual quality (Lothian, 1999; Daniel, 2001; Tveit, 2009; Sevenant and Antrop, 2010). Majority of landscape preference researches have dealt with general aesthetical preferences. But people could prefer different landscapes for different purposes (Pinto-Correia and Carvalho-Ribeiro, 2012). For example, Kellomäki and Savonlainen (1984) found preferences for natural beauty and recreation to be different. Ribe (2002) found that a livestock grazer may see a dense and contiguous forest aesthetically pleasing, while acknowledging that his/her own livestock will not be able to thrive in such a habitat. Tahvanainen *et al.* (2001) suggest that a forest, clear cut, might be appreciated by someone picking berries even though the scenic beauty is likely to be compromised.

Landscape preferences are dependent on many factors, including: respondents' profession, education, age, gender and regional origin (Kaplan and Kaplan, 1989; Herzog *et al.*, 2000; Tveit, 2009). Another important factor is familiarity, which is dependent on regional origin. Familiarity is a product of experience, and experience comes in many forms. One gains such familiarity from many circumstances, such as where one lives,

where one has visited, what one has studied and the cultural norms of one's group (Kaplan and Kaplan, 1989).

Some studies indicate that the respondents from very different geographic regions prove that their landscape preferences are similar and regional familiarity does not play an important role in landscape preferences (Wellmann and Buhyoff, 1980; Larsen and Harlan, 2006). On the other hand, several studies show that regional familiarity plays an important role in landscape preferences (Lyons, 1983; Kaplan and Herbert, 1987; Herzog *et al.*, 2000; Tveit, 2009). Kaplan and Herbert (1987) found that familiarity with a landscape does not necessarily contribute to preference, while preference is affected by familiarity, people do not necessarily prefer what they are familiar with. Purcell (1992) suggests that preferences are higher for landscapes outside one's home environment because the unfamiliar is found more interesting. Some preference studies have proved that the further one lives from certain landscape the less negative aspects one sees in it (Tyrvänen, 2001).

Objectives of this study are to determine recreational preferences for coastal landscapes and regional differences between them. The aim is to assess whether peoples' preferences for shore types are related to the types occurring in their home county. The first chapter contains a description of Estonian coastal landscapes. Then the method of the preference survey is explained. The results of the questionnaires are presented. The paper concludes with the suggestions for coastal recreation management.

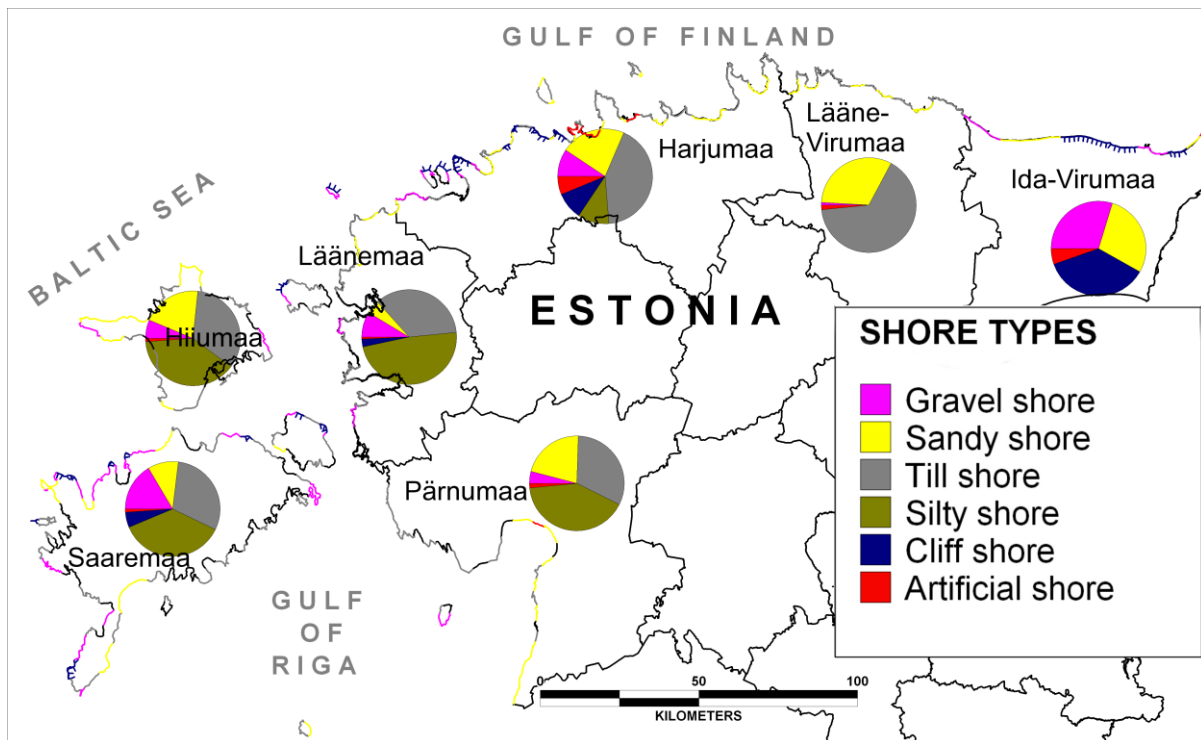


Figure 1. Estonian shore types distribution by counties (based on Orviku *et al.*, 2010).

## ESTONIAN COAST

Estonia is located in a transition zone between regions with maritime climate in the west and continental climate in the east. It is a relatively small country (45,227 km<sup>2</sup>), but due to its geographical location between major geological structures (Fennoscandian Shield and East European Platform) and comparatively long coastline (over 4,000 km), numerous peninsulas, bays and islands (over 1,500 island), it is rich in different shore types and valuable coastal ecosystems (Tõnisson *et al.*, 2013).

The western coast is exposed to waves generated by prevailing westerly winds, with NW waves dominant along the north-facing segment beside the Gulf of Finland, contrasting with southern relatively sheltered sectors located on the inner coasts of islands (Väinameri Sea) and along the Gulf of Livonia (Riga).

The coastline classification is based on the concept of wave processes straightening the initially irregular outlines, via erosion of capes, deposition in bays, or a combination of the two (Orviku, 1974; Orviku and Granö, 1992; Gudelis, 1967). Much of the coast (77%) has an irregular configuration showing capes and bays formed by hard bedrock or unconsolidated Quaternary deposits. The north-eastern cliff coast in Ida-Virumaa has been straightened by erosion, whereas the beach-fringed Narva Bay has an outline smoothed by deposition (Orviku and Romm, 1992). Coasts straightened by a combination of erosion and deposition can be found on the northern shore of Hiiumaa, and around the Gulf of Livonia (Saaremaa and Pärnumaa).

Based on the initial relief slope, geological character of the substrate and dominant coastal processes, the following shore types are distinguished (Orviku, 1974; Orviku *et al.*, 2010): cliff shore, scarp shore, till shore, gravel shore, sand shore, silty shore

and artificial shore. The distribution of the shore types along the Estonian coast is not equal (Figure 1 and Table 1). Geological settings, exposure to the sea as well as human influence are the most significant factors controlling their distribution. We can see that the distribution of the shore types in Saaremaa is very close to the average in Estonia; this island is a small-scale model of the shore types distribution in Estonia.

Table 1. How much shore types in counties differ from Estonian average (%). Art=artificial.

	Art. shore	Till shore	Sandy shore	Cliff shore	Gravel shore	Silty shore
<b>Ida-Virumaa</b>	3.1	-34.4	12.3	31.1	18.9	-31.0
<b>Lääne-Virumaa</b>	0.7	31.1	15.8	-5.2	-10.0	-31.0
<b>Harjumaa</b>	4.0	7.7	6.2	4.1	-1.6	-20.4
<b>Läänemaa</b>	-1.6	0.7	-11.4	-2.6	-2.3	17.1
<b>Pärnumaa</b>	-0.7	-2.6	5.4	-5.3	-6.8	9.9
<b>Saaremaa</b>	-1.1	-4.2	-5.7	0.0	5.6	5.4
<b>Hiiumaa</b>	-1.1	-1.0	4.3	-5.3	-4.6	7.6

The most notable difference can be seen on the northern coast of Estonia. Silty shores are not represented between the Estonian border and Harjumaa county, where silty shores are considerably less represented than the national average. These three counties form the whole northern coastline of Estonia. The national average is inflated due to the silty shores occurring along nearly half of Pärnumaa and Läänemaa shores. Silty shores can be described as: beautiful, high biodiversity, gentle coastal slope resulting in low

wave energy and often sensitive to human impact. Another notable fact is the abundance of cliff shore in northern Estonia (called also a North-Estonian cliff). It borders over 1/3 of the Ida-Virumaa coast and nearly 10% of the Harjumaa coast. Cliff shores do not occur in Lääne-Virumaa (but the cliff is still visible a few kilometres inland from the shore), or in Hiiumaa, Pärnumaa, but can be found in a very short section in Läänemaa.

Northern Estonia has the highest percentage of sandy shores. Much lower percentage of sandy shores can be seen in Läänemaa – the county with one of the lowest population density. Moreover, most of Läänemaa's sandy beaches are close to the Harjumaan border and are located on the northern tip of the county – far away from major settlements in Läänemaa. Till shore is the most characteristic shore in Estonia. We can also see that most of Estonian counties have plenty of till shores and the deviation from the average is minimal. However, there is one exception. Till shores are not present in Ida-Virumaa, while its neighbouring county – Lääne-Virumaa – has the highest percentage of till shores (Table 1).

## METHODS

The preference survey was conducted according to commonly used procedures in landscape research (Kaplan and Herbert, 1987; Kaplan and Kaplan, 1989; Herzog *et al.*, 2000; Larsen and Harlan, 2006; Tveit, 2009). The questionnaire contained photos of five shore types (Figure 2) and descriptions of all shore types. The preference question in the questionnaire was formulated as follows: "Please rank the shore types according to your preference to visit them for your leisure time (5 - most preferred, 1 - least preferred)". All the respondents were also asked to comment on their preferences. The sample included respondents from all counties proportionally to the number of inhabitants. A total of 1,519 questionnaires were included in the study, which is sufficient for drawing conclusions on Estonia (approx. 1.3 million inhabitants).

## RESULTS

Sandy shores received, by far, the highest average score of 4.6. The comments on sandy shore are quite stereotyped, especially underlining the most typical shore-related recreational activities like swimming and sunbathing. The high preference rating is quite logical considering that for most Estonians associates the sandy shore with the most typical place to spend one's vacation. Gravel shore had the lowest average preference score (2.5). The low rating of this shore type is related to the following: it is not comfortable to walk barefoot on gravel; it lacks visually striking landforms (e.g. steep cliff shore, eye-catching large rocks and boulders of the moraine shore and the cosiness of the silty shore). Silty shore and cliff shore received equally 2.6 points. Comments indicate that the latter is the preferred shore type for hiking and bird watching. Owing to the fact that cliff shore in Estonia ascends from the sea (depending on the region) to 10–50 metres, it offers a better view of the sea compared to other types of shore.

Preferences of different respondent groups classified on the basis of the sociometric indicators used in the survey are not significantly different from average preferences of all respondents. However, some differences can be detected when taking a closer

look. The ratings on the basis of gender differ for all shore types with the exception of the silty shore. Average preferences of men are similar (2.6) for all shore types except for the sandy shore. Till shore is valued by men lower (2.6) and women higher (2.8) than average (2.7). Till shores are the second highest preferred type by female respondents. Many female respondents prefer till shores, but they do not like to sunbathe there, however simply enjoy the presence of the sea. Many males, on the other hand, have pointed to the protective nature of the till shore from erosion of numerous rocks. A slightly lower than average rating (2.6) is given by women to the cliff shore (2.5), which according to voluntary comments written in the questionnaire may be caused by the unsuitable nature of the steep cliff shore for walking with children. Some women believe the cliff shores give a threatening impression. The sandy shore is rated by men on average slightly lower (4.5). In comments both men and women are concerned about the large anthropogenic impact on the sandy shore, considering just this type of shore more threatened than others. The concern is well justified, because a large part of organized recreational activities and tourism are related to sandy shores, which received the highest preference. The sandy shore is also specifically picked out as a very suitable place for a family vacation, for swimming and sunbathing. It is the only shore type in Estonia where you can walk barefoot stress-free, without focusing attention to what is underfoot.

The effect of the educational level on differences in preferences is revealed first of all in the case of the silty shore. The average preference score by people with primary education is 3.0, which is the highest average rating for a non-sandy shore in all the survey on the basis of any sociometric indicator. At the same time, people with technical secondary education rate the silty shore relatively very low (2.4). The respondents with higher education value the till shore and cliff shore (2.8) higher than other educational groups, at the same time rating the sandy shore (4.4) lower than others. The comments allow concluding that in comparison with other educational groups people with higher education prefer cliff shore and till shore related active recreational forms (e.g. hiking, bird watching), preferring those activities to classical sunbathing and swimming. Respondents with higher education value also gravel shore lower (2.4) than average (2.5).

To some extent, the preferences are affected also by the respondents' age. For example, the highest rated coastal type on average, the sandy shore has been rated relatively low among older than 70 year old people. The average rating for this age group is 4.1, which is the lowest score for the sandy shore with all indicators considered. This can be explained by the fact that older than 70 year old people are no longer as active with respect to sunbathing. At the same time, this age group has rated all other shore types either at least on average level or above average. The youngest age group (18–23 year old) surprisingly gave the lowest rating (2.4) to cliff shore (average for all respondents 2.6). Also conspicuous is four middle age groups' (30–69 year old) lower than average rating for the silty shore. The age group of 60–69 year olds rates this type of shore the lowest (2.3; all respondents' average 2.6) in comparison with the ratings by groups on the basis of all indicators.



Figure 2. Estonian shore types. a – silty shore, b – till shore, c – cliff shore, d – gravel shore, e – sandy shore.

The effect of income on preferences is relatively smaller than other sociometric indicators, remaining relatively similar to the all respondents' average notwithstanding the income group. The fact that relatively better material opportunities to visit shores do not influence the preferences is somewhat surprising. It can be pointed out also that lower income respondent groups rate the cliff shore relatively lower, the lowest income group (monthly income smaller than 128 euro) has rated the cliff shore even as low as 2.4, which is clearly different from the average (2.6). The highest

income group (more than 1278 euro per month) rates after the sandy shore, which is the most preferred by all groups, the till shore the highest (2.9); the income as a determinant of preferring other types of shore is relatively insignificant.

The regression analysis results of the dependence of shore type preferences on sociometric indicators and the place of residence are provided in Table 2. Preferences of most numerous shore types are influenced by gender and age. Women's preference of the moraine shore and sandy shore and men's preference of the gravel



Table 2. Shore type preference (5 – most preferred, 1 – least preferred) dependence on sociometric indicators and respondent's place of residence (inland 1, coast 2), OLS

Independent variables	Dependent variable				
	Silty shore	Till shore	Cliff shore	Gravel shore	Sandy shore
<b>C</b>	3.048	2.186	2.776	2.721	4.263
<b>SITE</b>	-0.029	-0.020	-0.107	0.110	0.056
<b>SEX</b>	0.021	0.149***	-0.152**	-0.171***	0.155***
<b>AGE</b>	-0.057***	0.052***	0.008	0.026	-0.026
<b>EDUCATION</b>	-0.111***	0.067*	0.029	-0.019	0.023
<b>INCOME</b>	0.014	0.001	0.027	-0.029	-0.009
<b>Adjusted R-squared</b>	0.011	0.016	0.005	0.006	0.006
<b>F-statistic</b>	4.186	5.879	2.594	2.750	2.774
<b>Durbin-Watson</b>	1.787	1.931	1.760	1.703	1.812

\*, \*\* and \*\*\* indicate significance at the 10%, 5% and 1% levels, respectively

Table 3. Preferences by counties

	Preferences' average (5 – most preferred)				
	Silty shore	Till shore	Cliff shore	Gravel shore	Sandy shore
<b>Läänemaa</b>	2,3	2,7	2,7	2,6	4,7
<b>Harjumaa</b>	2,7	2,7	2,6	2,5	4,5
<b>Hiiumaa</b>	2,5	2,3	2,4	2,9	4,8
<b>Ida-Virumaa</b>	2,9	2,6	2,2	2,5	4,8
<b>Lääne-Virumaa</b>	2,4	2,8	2,2	2,9	4,7
<b>Pärnumaa</b>	2,6	3,0	2,6	2,3	4,5
<b>Saaremaa</b>	2,4	2,5	2,5	2,7	4,9
<b>Total seaside counties</b>	2,6	2,7	2,5	2,5	4,6
<b>Inland</b>	2,7	2,7	2,6	2,5	4,5
<b>Total, average</b>	2,6	2,7	2,6	2,5	4,6

shore are statistically significant at the level of 1%. Men's preference of the cliff shore is significant at 5% level. Silty shore preferences are not statistically dependent on gender. Possible causes of the preferences have been discussed above. Another statistically significant indicator that determines the rating is age. The silty shore is in strong negative correlation with age (at 1% level) (i.e. preference decreases with age) and the moraine shore is in strong positive correlation with age (preference increases with age). The result that the silty shore preference by young people is greater in comparison with older age groups is based on the respondents' comments caused by the quality of the silty shore to offer privacy. Not many tourists go to the silty shore and often the silty shore has grown into reeds and the reeds offer good hiding places, if necessary. Older people prefer the moraine shore. One comment by an older age group respondent, for example, points to the moraine shore as a good place to sit on a rock and watch the sunset. Preferences of the cliff, gravel and sandy shore are not statistically dependent on age. Education has less influence than expected. Only silty shore preferences are in strong negative

correlation with education. The comments do not indicate why people with lower education value the silty shore more than higher educated people, but one explanation could be that age and education are not completely independent sociometric indicators. Young people who prefer the silty shore more than older people in general have lower education already because of the age. Also the moraine shore is in weak positive correlation (at 10% level) with education. Dependence of preferring the cliff, gravel and sandy shore on education is not statistically proven. Surprisingly, preferences are correlated to neither respondents' income nor place of residence in none of the shore types. The factors that determine the preferences definitely need to be investigated further, and in addition to quantitative methods also qualitative methods (e.g. in-depth interview) should be used.

### Regional differences

Dependence of preferences on residents' geographic-regional identity is presented in Table 3. In separate rows are the seaside counties, data on inland counties (without sea border) are summed up (see Figure 1). For the sake of comprehensiveness, preferences of people living in seaside counties are also summed up in Table 3. As the statistical analysis in Table 3 indicates, preferences do not depend on whether the county of the respondent's residence is by the sea or inland. Preferences on the basis of this indicator do not differ more than 0.1 points for not even one shore type. Inland people attach slightly higher value to the silty shore and cliff shore, residents of seashore counties, on the other hand, sandy shores. For the moraine and gravel shore the preference average is equal. However, some differences in the ratings at the level of individual counties can be detected. Residents of seaside counties value their typical shore type lower than average and the shore type which is either rare or does not exist in their home county is valued higher. For example, people living in Ida-Virumaa have a relatively high preference (2.9) of the silty shore, which is scarce in that county. At the same time, the most typical shore type in that county, cliff shore, receives only 2.2 points on average. In Läänemaa, where the silty shore is one of the most typical shore types, it receives only 2.3 points on average. At the same time, the cliff shore, which is nearly absent in Läänemaa, got the highest

rating, 2.7 in comparison with other shore types from the residents of Läänemaa.

## DISCUSSION AND CONCLUSIONS

Most popular shores among the respondents were sandy shores. The highest density of population in Estonia can be seen in northern Estonia as well as the highest percentage of sandy shores. Thus, we can say that people live quite close to their favourite shores. Regional differences within counties were obvious and the most preferred shores are the ones less represented in the respondents' country of residence. These results are similar to previous studies indicating that unfamiliar landscapes are found more interesting (Purcell, 1992) and the further one lives from certain landscape, the less negative aspects one sees in it (Tyrvänen, 2001).

In Ida-Virumaa, where cliff shore is dominant, respondents prefer it the least. In Läänemaa, where cliffs are almost non-existent, cliff shores were the second most preferred after sandy shores. Läänemaa respondents see cliff shores attractive and symbolic for Estonia. Ida-Virumaa residents, living close to cliffs, see several negative aspects (e.g. dangerous to walk etc.). Cliff shores have been pointed out as the Estonian identity landscape in previous studies (Palang *et al.*, 2003), but people who are more familiar with those landscapes see also negative aspects in addition to the romantic bias. Similar findings were found concerning silty shores. Respondents living in counties without silty shores pointed out that reeds offer privacy, while respondents living close to silty shores pointed out that reeds disturbed their view to the sea. The coastal landscape preferences require more qualitative research in the future to find out more about the public recreational preferences. This study offers a basic overview to assist management of Estonian shores. Residents of different regions may prefer different shore types. Taking this understanding into consideration, better efforts can be made to offer adequate level of protection to sensitive coasts to minimize human-induced impacts (e.g. people in regions where only a few silty shores exist might overuse these fragile shores and therefore adequate management must be implemented there like wooden tracks to the shores, marked tracks etc).

## ACKNOWLEDGEMENT

The study was partly supported by Estonian Science Foundation grants No 8549 and 9191 and by the EstKliima project of the European Regional Fund programme No 3.2.0802.11-0043.

## LITERATURE CITED

- Daniel, T.C., 2001. Whither scenic beauty? Visual landscape quality assessment in the 21st century. *Landscape and Urban Planning*, 54, 267–281.
- Gudelis, V.K. 1967 Morphogenetic types of coasts and shores of Baltic Sea. (in Russian, English summary) *Baltica*, 3, 123–145.
- Herzog, T.R., Herbert, E.J., Kaplan, R. and Crooks, C. L., 2000. Cultural and Developmental comparison of landscape perceptions and preferences. *Environment and Behavior*, 32, 3, 323–346.
- Kaplan, R. and Kaplan, S., 1989. *The Experience of Nature: A Psychological Perspective*, CUP, Cambridge, 340 p.
- Kaplan, R. and Herbert, E.J., 1987. Cultural and sub-cultural comparisons in preferences for natural settings. *Landscape and Urban Planning*, 14, 281–293.
- Kellomäki, S. and Savolainen, R., 1984. The scenic value of forest landscape as assessed in the field and the laboratory. *Landscape planning*, 11, 97–108.
- Larsen, L. and Harlan S.L., 2006. Desert dreamscapes: Residential landscape preference and behavior. *Landscape and Urban Planning*, 78, 85–100.
- Lothian, A., 1999. Landscape and the philosophy of aesthetics: is landscape quality inherent in the landscape or in the eye of the beholder? *Landscape and Urban Planning* 44 (4), 177–199.
- Lyons, E., 1983. Demographic correlates of landscape preference. *Environment and Behaviour*, 15, 487–511.
- Orviku, K. 1974. *Estonian Seacoasts*. (in Russian with English summary) Academy of Sciences of Estonia, Tallinn. 112 pp.
- Orviku, K., Kont, A. and Tõnisson, H., 2010. Estonia. Bird, E. (Toim.). *Encyclopedia of the World's Coastal Landforms* (605–611). Dordrecht, Heidelberg, London, New York: Springer.
- Orviku, K. and Granö, O., 1992. Contemporary coasts. (In Russian, English summary) (In), Raukas, A. and Hyvarinen, H. (eds.) *Geology of the Gulf of Finland*, Tallinn: 219–238.
- Orviku, K. and Romm, G., 1992. Litho-morphodynamical processes of Narva Bay. (In Russian, English summary). *Proceedings of the Estonian Academy of Sciences*. Geology. 41/3: 139–147.
- Palang, H., Printsman, A., Alumäe, H., Kaur, E., Oja, T., Prede, M., Pungas, P., Reimann, M. and Sooväli, H., 2003. Local people as shapers of sustainability of rural landscapes. In: Tiezzi, E., Brebbia, C.A., Usó, J.L. (Eds.), *Ecosystems and Sustainable Development*, Vol. 2 (Advances in Ecological Sciences, 19). Wessex Institute of Technology Press, Southampton, pp. 873–882.
- Pinto-Correia, T. and Carvalho-Ribeiro, S., 2012. The Index of Function Suitability (IFS): A new tool for assessing the capacity of landscapes to provide amenity functions. *Land Use Policy*, 29, 23–34.
- Purcell, A.T., 1992. Abstract and specific physical attributes and experience of landscape. *Journal of Environmental Management*, 34, 159–177.
- Ribe, R.G., 2002. Is scenic beauty a proxy for acceptable management? The influence of environmental attitudes on landscape perceptions. *Environment and Behavior*, 34, 757–780.
- Sevenant, M. and Antrop, M., 2010. The use of latent classes to identify individual differences in the importance of landscape dimensions for aesthetic preference. *Land Use Policy*, 27, 827–842.
- Tahvanainen, L., Tyrvaäinen, L., Ihalainen, M., Vuorela, N. and Kolehmainen, O., 2001. Forest management and public perceptions – visual versus verbal information. *Landscape and Urban Planning*, 53, 53–70.
- Tyrvänen, L., 2001. Economic valuation of urban forest benefits in finland. *Journal of Environmental Management*, 62, 75–92.
- Tveit, M.S., 2009. Indicators of visual scale as predictors of landscape preference; a comparison between groups: environmental and landscape change: addressing an interdisciplinary agenda. *Journal of Environmental Management*, 90, 9, 2882–2888.
- Tõnisson, H., Orviku, K., Lapinskis, J., Gulbinskas, S. and Zaromskis, R., (2013). The Baltic States - Estonia, Latvia and Lithuania. Panzini, E. and Williams, A. (Toim.). *Coastal erosion and protection in Europe* (47 – 80). UK, US and Canada: Routledge.
- Wellman, J.D and Buhoff, G.J., 1980. Effects of regional familiarity on landscape preferences. *Journal of Environmental Management*, 11, 105–110.

## Beach user perceptions at the eastern Yucatan peninsula, Mexico

A.T. Williams, A. Barugh

Built Environment, Swansea,  
University of Wales Trinity St. David,  
Mount Pleasant, Swansea, Wales, SA1  
6ED, UK  
allan.williams@smu.ac.uk.

e-geo Group  
Geography Dept.  
Nova Universidade de Lisboa  
Lisboa, Portugal  
angela.barugh@hotmail.com



[www.cerf-jcr.org](http://www.cerf-jcr.org)



[www.JCRonline.org](http://www.JCRonline.org)

### ABSTRACT

Williams, A. T., Barugh, A., 2014. Beach user perceptions at the eastern Yucatan peninsula, Mexico. In: Green, A.N. and Cooper, J.A.G. (eds.), *Proceedings 13<sup>th</sup> International Coastal Symposium* (Durban, South Africa), *Journal of Coastal Research*, Special Issue No. 70, pp. 426-430, ISSN 0749-0208.

Socio-demographic parameters and beach user preferences and priorities were analysed from 160 questionnaire interviews at Playa Linda and Playa Choc-Mool in Cancun - a mega resort; Playa del Carmen (lower level resort) and Tulum, which was located in a protected area, all located along the Yucatan peninsula, Mexico. Prioritisation of 50 beach qualities were undertaken and a strong relationship ( $p < 0.05$ ) was found at all four beaches between perceived water quality and the presence of visual litter pollution. Litter free white sand and water quality was the highest preference and scenery was considered more important than safety at Tulum. Fifty per cent of users expressed a preference for visiting an undeveloped beach with just a few facilities (bar/toilet), with only 9.6% expressing a preference for a highly developed resort. A significant difference ( $p < 0.05$ ) occurred between females and males, the former preferring a beach with few facilities, the latter an undeveloped one. Similar differences were found for the presence of harmful sea creatures, the importance of toilets, presence of oil on the beach, cooking smells; sun bed hire had a much higher significant difference ( $p = 0.02$ ). American visitors preferred a large range of restaurants, car parks, tarmac roads; Europeans seemingly the opposite. Beach users who had travelled the furthest seemed to prefer a more natural beach, but facilities and access at commercial resorts were appreciated. Fifty percent wanted a dog ban on all beaches.

**ADDITIONAL INDEX WORDS:** *Findings and comparisons, Europe, Columbia.*

### INTRODUCTION

Coastal environments are now viewed as increasingly important for providing open space and leisure opportunities as a balm to and increasingly urbanised and pressurised world. A world, where long stretches of coast line have been urbanised to the  $n^{\text{th}}$  degree, e.g. Spain, which has inevitably lead to a decline in the local cultural heritage, natural resource destruction and exclusion of local residents. The past 40 years has seen the rise of coastal management, but apart from a few exceptions, e.g. the Great Barrier Reef and preferences of beach users have rarely been taken into management consideration. User perception research has been carried out in several other fields, e.g. forest management in Denmark and the Netherlands, but it was Cutter *et al.*, (1979) who pioneered beach user studies. Their conclusions were that water and beach cleanliness were the main priorities of beach users followed by the quality of the natural attributes of beaches. Their studies showed that users in New Jersey, USA were selecting a less than optimal beach environment with respect to their priorities, other factors, such as, access, social interaction and facilities playing a major role in selection. A 'trade off' was involved purely for convenience.

Questionnaire surveys carried out on tourist beach user preferences in Wales ( $n = 2,360$ ), UK; Hollywood beach, Florida ( $n = 83$ ); the Costa Dorada ( $n = 157$ ), Spain; Malta ( $n = 154$ ), and

Turkey's Aegean coast ( $n = 245$ ), showed that five parameters were of the greatest importance on beach choice, These were safety, facilities, water quality, litter and scenery (Ergin, *et al.*, 2004; Williams and Micallef, 2009). In contrast, in Columbia, proximity and a friendly atmosphere were deemed to be important to the detriment of scenery (Botero *et al.*, 2013). Personality factors, such as extroversion, anxiety and neuroticism also have an effect on leisure, as shown by many early works, e.g. Williams *et al.*, (1992). Additionally, age, stay length, sex, socio-economic status, etc. all contributes to this point.

Coastal occupation has been increasing in the past few decades especially due to coastal tourism-related activities. Travel and tourism is probably the world's largest growth industry (Klein *et al.*, 2004) and it is expected to grow at 4.0% per year reaching 1.6 billion international tourists (WTB). Within this industry, beaches are a pivotal parameter (Houston, 2008) being worth billions of tourist dollars (Clark, 1996). Europe is currently still the world's largest source region (UNWTO, 2011), generating just over half of international arrivals worldwide, followed by Asia and the Pacific (22%), the Americas (16%), the Middle East (4%) and Africa (3%). The UNWTO (2011) showed that international tourist arrivals grew by 4% in 2012 to reach 1.035 billion. Growth is expected to continue in 2013 only slightly below the 2012 level (+3% to +4%) and in line with UNWTO long term forecast. In the

Caribbean, international tourist arrivals have increased from 11.4 million in 1990 to 20.9 millions in 2012.

Tourism, employing some 7 million people is one of the most important Mexican economic sectors providing 13% of the Mexican GDP (Pelaez, 2011). In 2012, Mexico received 23 million international tourists - the majority from the U.S.A and Canada with others coming from the UK, Spain and South America, and 178 million domestic tourists, generating US\$12.7 billion in foreign exchange. This represented a 10.5% increase from 2011, trailing manufacturing, oil remittances and foreign direct investment, as the nation's biggest source of revenue. Yucatan has followed this trend and in past years, the regional economy has moved from traditional agriculture towards manufacturing/service industries, with tourism, producing 90% of the state GDP (Pelaez, 2011). This paper is a *pilot* study for some Yucatan beaches.

### STUDY AREA

The Yucatan peninsula, occupies *circa* 113,000 km<sup>2</sup> with a shoreline of >1,600 km (Figure 1a). The peninsula includes the Mexican states of Yucatan on the north coast, Campeche on the west along the Gulf of Mexico, and Quintana Roo on the east coast adjacent to the Caribbean. The peninsula comprises a vast (some 350,000 km<sup>2</sup>) limestone platform extending northwards into the Gulf of Mexico, hence all surficial rocks are carbonates displaying a plethora of karst features. The submerged portion varies in width from some 225 km on the west coast to <10 km on the east coast (Ward *et al.*, 1985). The climate is constant with a minimum average of 23°C in January to a maximum of 30°C in May and two rainfall periods (June/July and September/October), can be found of 100cm/year at Cancun to 150 cm/year at Tulum. The area sits on one of the main hurricane paths, which usually arrive in September/October, e.g. Gilbert, 8-19<sup>th</sup> Sept, 1988-a category 5 on the Saffir-Simpson scale, which caused great sand loss and serious infrastructure damage; Ivan, Emily and Wilma in 2004, 2005. These had huge negative economic effects Felix-Delgado *et al.*, (2008).

Four beaches were visited (Figure 1b). On the northern windward side of the mega resort of Cancun, facing the sea at Bahía de Mujeres, lies Playa Linda. It has a flat white sand beach of *circa* 1 km lined with a number of four/five star hotels. At the eastern end is a pier giving boat access to Isla Mujeres beach. The water is very calm and admirably suited to water sports. Just south of the above is Playa Choc-Mool extending 5 km facing the Caribbean Sea, which has a tidal range of 0.3-0.6 m (Thieler and Bush, 1991). The water depth is shallow (1-2 m) for *circa* 15 m from the beach and then deepens considerably. Four/five star hotels, restaurants/bars/changing-rooms etc. front the beach. Playa Del Carmen lies 68 km south of Cancun and has been converted from a picturesque village to a mega resort, with beaches extending many km north and south of the pier. Accommodation runs from ultra deluxe hotels, e.g. Continental Plaza Playacar), to camping. Tulum ('wall' in Maya) lies 130 km south of Cancun, in a protected area and encompasses the largest coastal fortified Mayan fort. The coastline is rock cliffs and beaches and the area, dominated by an ancient castle, 'el Castillo', is a famous tourist destination for Cancun tourists. Two miles south of the Mayan ruins is Tulum beach where accommodation is relatively basic.

### METHODS

Since no similar data has been collected in the Yucatan area, this paper represents a pilot investigation. Few workers, e.g. Botero *et al.*, (2011, 2012, 2013), Daza (2012), have studied beach users' needs in the Latin American Caribbean area. Essentially, a questionnaire was devised encompassing a multi faceted approach



Figure 1a. Location. 1. Cancun; 2. P del Carmen; 3. Tulum



Figure 1b. Location views. Clock-wise from top left: Questionnaire surveys at P. Linda; Choc-Mool; Cancun; Effects of Hurricane Gilbert; Tulum castle; P Del Carmen entrance.

involving physical, biological and social parameters that reflected users' priorities and preferences. The questionnaire was drafted in English and Spanish and took some 15 minutes to complete. Forty were distributed at each of the four investigated beaches *via* a stratified sampling policy. Questions were coded and visitors socio-economic class derived (Office of Population and Censuses and Surveys, 1991), as well as journey origin, sex, age and preferences, and priorities analysed *via* SPSS. Differences between groupings, e.g. male/female were carried out by Mann-

Whitney tests and one way Kruskal-Wallis ANOVA tests were performed at all beaches to obtain ranking values for priorities, together with Principal Component analysis. Spearman Rank correlations were conducted between overall parameters (160) and for individual beaches (40).

## DISCUSSION

Fifty four percent of users were from the USA (Great Lakes 26, Frontier West 23 and Far West 19; (Crompton, 1979 sub divisions) and 41% were based at Cancun, 23% were European, 14% Canadian; 8% Mexican and the rest were from Latin America. Findings agreed with those of Crompton (1979) who assessed 617 USA students who had picked Mexico as a tourist destination. Interestingly, he found that the number of American visitors increased as distance from the country increased. This could reflect experiences of border towns, or a reflection that the lowest number of USA tourists came from the south/south east areas where hurricane knowledge is a very real entity. Over 40 years ago, Rowntree (1974) showed that hurricane knowledge exhibited a direct economic relationship with enlightened hazard perception.

Table 1. Correlation between socio demographic factors.

**Bold** = negative.

Environment					
Parameter	Age	Sex	SES	Area	Length
No cooking smells	0.212	0.526	0.812	0.104	0.991
No traffic fumes	0.337	0.019	0.785	0.018	0.198
No commerce noise	0.944	0.045	0.635	0.006	0.172
No traffic noise	0.545	0.078	0.554	0.149	0.197
No seaweed/fish smell	<b>0.034</b>	0.607	0.081	0.01	0.256

Beach Safety					
Parameter	Age	Sex	SES	Area	Length
No dangerous cliffs	0.901	0.964	0.74	0.029	0.046
No rock pits in beach	0.529	0/193	0.430	0.808	0.668
No harmful animals	0.609	0.028	0.686	0.279	0.741
Lifeguards present	<b>0.049</b>	0.113	0.162	0.329	0.604
No large waves	0.217	0.566	0.27	0.063	0.506
No large currents	0.409	0.630	0.300	0.010	0.801
No rips	0.196	0.893	0.415	0.030	0.573

P. Linda had the greatest age range and the largest number of respondents aged 20 or younger with an average age of 33.1 years. P. Choc-Mool displayed the narrowest age range with 85% of respondents aged < 25 years, with the average age being 22.2. At P. Del Carmen, the modal age group was 21-25 years with an average age of 31.6. At Tulum, 19 respondents were aged from 24-30 (85% being <30 years of age), with an average of 27.2. Table 1 gives some examples of the demographics associated with the beaches. Figure 2 gives the replies to length of time spent at the various beaches. Modal arrival time was between 11.30 and 13.30, in accord with the findings of Silva *et al.*, (2008) in Brazil. It is interesting to note that 20.7% and 37.7% of respondents from P. Linda and P. Choc-Mool respectively expressed a preference for an undeveloped/few facilities beach, compared with 73.3% and 87.5% respectively from P. Del Carmen and Tulum (Table 2). Morgan and Williams (1995) found similar results in Wales, but there, only 9% expressed a preference for an undeveloped beach (as against 19% in Mexico) and for a large resort, only 1% expressed a preference as opposed to circa 10% there, only 9% expressed a preference for an undeveloped beach (as against 19%

in Mexico) and for a large resort, only 1% expressed a preference as opposed to circa 10% in Mexico.

The largest priorities selected via Principal Component analyses were as follows.

**Factor 1**, Water Quality: No litter on beach/sea; no sea pollution.

**Factor 2**, Environment: No traffic/commerce noise; no smells.

**Factor 3**, Safety: No rip/strong longshore currents.

**Factor 4**, Climate: Good temperatures, long sunshine hours.

European and American respondents at the investigated beaches had some interesting differences with regard to the preference question

**American:** Cafes with wide food/drink selections, Tarmac beach path and signposted roads, car park <200m from beach, very exposed beach.

**European:** Emphasis was on basic refreshments, narrow/rough beach access path, no beach car park, a sheltered beach but with a breeze, no alcohol.

Tourism is a business and the product sold is an experience e.g. enjoyment, memories, pleasure (Butler, 1991). In the seventies, Harris (1972) was amongst the first to attribute safety and sanitation as the two main parameters in determining a beach vacation in Mexico. Coastal landscapes can be the resultant of natural forces or the effects of economic activity and certain landscape points could make a landscape appealing. A flat plain is of less interest than rocky hill, e.g. Tulum, which represents a natural area, in contrast to Cancun, with its plethora of water sports and facilities. The latter exists due to political vacuum, international private sector finance and organised funding. In the '60s, it was an undeveloped, snake-infested; 30km, L shaped coastal area that in 2000 received its first two million tourists. However, the extremely rapid growth has resulted in several problems, the most notable being beach erosion and sand dune destruction.

Beach perception studies have been researched several times in Europe (Morgan *et al.*, 1993, 1996; Micallef *et al.*, 1999; Tudor and Williams, 2006; Roca, and Villares, 2008; Vaz, 2008, Marin *et al.*, 2009); but research details are sparse, for example, in Brazil (Polette, 2009) and Columbia, (Borero *et al.*, 2011, 2012, 2013). Questionnaire surveys carried out on many diverse European and USA beaches regarding user preferences and priorities, showed that five parameters were of the greatest importance on beach choice: safety (swimming), facilities (sun beds, shades, toilets, etc), water quality, litter and scenery. In the Botero *et al.*, (2013) study, safety was linked with security from crime, but this aspect was not mentioned in the case studies presented. The pre-eminent beach aspect at ALL Yucatan investigated beaches confirmed that sand and water quality was the number 1 priority and preference, the last being access and parking (Table 3).

Significant differences were found between males and females

Table 2 Beach type preferences

Beach type	1	2	3	4	5
Undeveloped	2.6	7.5	22	42.5	19.1
Few facilities - toilet/bar	35.1	12.5	51.2	45.0	36.5
Small resort	27.0	30	12.2	12.5	20.5
Medium resort	18.9	27.5	9.8	0.	14.1
Large resort	16.2	22.5	4.8	0.	9.6

1 P.Linda, 2 P.Choc-Mool, 3 P.Del Carmen, 4 Tulum, 5 Overall  
(the lower the value, the greater the preference),

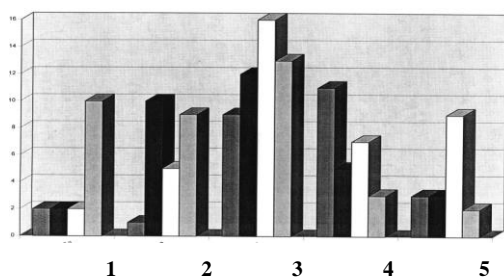


Figure 2. Time spent (*hours*) on the beach. 1-<2; 2- 3; 3- 4; 4- 5; 5->5. Bar graph order, left to right: P. Linda, P. Choc-Mool, P. Del Carmen, Tulum.

regarding the presence of harmful animals ( $p=0.5$ ); presence of oil on the beach ( $p=0.05$ ), cooking smells ( $p=0.05$ ) and sun bed hire ( $p=0.02$ ), with females being more conscious of all of the above. Males seemingly preferred more remote beaches ( $p=0.01$ ), as females were very concerned with the safety of children, as well as facilities such as toilets. The question of dogs on beaches resulted in a 50:50 split.

Water quality, safety for swimming and sand cleanliness (sewage/litter), were the most important aspects for beach management. Studies in Turkey and the UK have shown that water colour and clarity, noise absence, historic buildings, quality of built environment and landscape features are among the other top parameters reflecting beach preferences (Ergin *et al.*, 2004). Visual factors influence users' perception, associating an absence of litter with clean water, or the evidence of a drain or discharge with questionable water quality. Similar preferences have been identified by Cervantes *et al.*, (2008), in Brazil, Mexico and USA, where users at all places wanted no beach litter and an unpolluted sea.

At Tulum (especially for the castle; Figure 1b), a protected site since 1981 together with P. Del Carmen, relatively unspoiled beach scenery was rated highly, in fact at the latter beach, it ranked higher than safety. Tulum attracted a higher proportion of visitors than any other investigated beach and 11 out of 40 had travelled there on that day. In contrast, only one had travelled to P. Del Carmen and none to the Cancun beaches.

A high ranking for scenery is common for many European and USA beaches, although recent work has indicated that it is not the case in Columbia. Botero *et al.*, (2013), showed that results differed in that the main aspect in beach selection was "proximity" for both local and national visitors. Aspects such as "a relaxed friendly" atmosphere and "party atmosphere" were mentioned, by Botero *et al.*, (2013) although 'peddlers' and loud music

frequently prevailed. However, in Brasil, Silva *et al.*, (2008) found that scenery was highly rated as an attribute for tourist choice. Several authors, e.g. Cutter *et al.*, (1979), have found this and it is a crucial factor for beach managers and ICM decision making especially for urban areas. With regard to these aspects, similar viewpoints of preferences were reported by McKenna *et al.*, (2011) in Ireland, but with less relevant scores.

## CONCLUSIONS

Global estimates by 2020 are at 1.6 billion international tourists (UNWTO, 2008). In Latin America 55% of jobs are in the service industry (Weller, 2004). Along the Caribbean, tourist arrivals have increased five-fold, from 166 million in 1970 to 935 million in 2010 and cruise arrivals grew even more rapidly over the same period increasing from 1.3 in 1970 to >20 millions in 2012 (Caribbean Tourism Organization, 2012). In past years, coastal tourism has acquired a great importance in Yucatan and in Quintana Roo state alone has been responsible for 90% of the state GDP (Pelaez, 2011).

Questionnaires of beach user priorities and preferences have not been carried out previously in the region and this pilot study has shown that similar traits hold well to those found in Europe and the USA, i.e. safety, facilities, water quality and scenery were the main parameters for people's preferences. This is not surprising in that tourists interviewed mainly come from these countries. The contrast from findings in nearby Columbia was that scenery was not as important as a 'friendly atmosphere.' The priority for a beach however was one of distance - the closer the better!

A difference in outlook between USA and European visitors was found in that the former desired more of a 'resort' location. Male and female differences were also marked *viz.* the chances of meeting harmful animals, cooking smells, facilities and pollution.

## ACKNOWLEDGEMENT

This work is a contribution to the E-Geo research group, Nova Universidade, Lisbon, Portugal.

## LITERATURE CITED

- Botero, C., Pereira., C. and Escudero E. M. 2011. *Informe del programa de investigación en calidad ambiental de playas turísticas (CAPT) en el Caribe Norte Colombiano 2010 – 2013. Periodo AGO-DIC 2010*. Documento de trabajo, Grupo de Investigación en Sistemas Costeros, Universidad del Magdalena, Santa Marta, Colombia, 50pp
- Botero, C., Zielinski, S., Pereira., C. and Escudero E. M. 2012. *Informe del programa de investigación en calidad ambiental de playas turísticas (CAPT) en el Caribe Norte Colombiano 2010 – 2014. Periodo ENE – DIC 2011*. Informe Técnico, Grupo de Investigación en Sistemas Costeros, Universidad del Magdalena, Santa Marta, Colombia, 60 pp.
- Botero, C., Anfuso, G., Zielinski, S., Silva, C, Cervantes, O., Silva, L., Cabrera, A., and A. T., Williams, 2013. Reasons for beach choice: European and Caribbean perspectives. *Journal of Coastal Research*, SI65, 850-885.
- Butler, R.W., 1991. Tourism, environment and sustainable development, *Environmental Conservation*, 18, 3, 201-208
- Caribbean Tourism Organization. 2012. *Caribbean tourism - State of the industry*, 2012 edition.
- Cervantes, O., Espejel, I., Arellano, E. and Delhumeau, S. 2008. Users' Perception as a Tool to Improve Urban Beach Planning and Management. *Environmental Management*, 42 (2), 249-264.
- Clark, J. R. 1996. *Coastal zone management handbook*. Boca Raton, Florida, USA: CRC Press/Lewis Publishers.
- Crompton, J.L., 1979. An assessment of the image of Mexico as a vacation destination and influence of geographical location upon image. *Jn, Travel Research*, 17, 4, 18-23.
- Cutter, S.L., Nordstrom, K.F., and Kuema, G.A. 1979. Social and environmental factors influencing beach site selection. *In Proc. 5th Ann.*

Table 3. Overall ranking of beach aspects

Parameter/Place	1	2	3	4	5
Sand/water quality	1.22	1.2	1.16	1.32	1.27
Safe bathing	2.67	2.6	2.66	2.68	2.64
Facilities	2.72	2.85	3.71	4.18	3.37
Scenery	3.39	3.15	2.61	2.14	2.63
Access/parking	4.44	4.9	4.68	4.68	4.68

1 P.Linda, 2 P.Choc-Mool, 3 P.Del Carmen, 4 Tulum, 5 Overall.  
(the lower the value, the greater the preference),

- Conf. Resource allocation issues in the coastal environment*, (ed.), N. West, 183-194, The Coastal Society, USA.
- Daza, A. 2012. *Propuesta de un instrumento de evaluación para la playa turística de la zona urbana de Riohacha mediante el uso de variables ambientales, socioculturales y de infraestructura*. Master's thesis on, 'Integrated Coastal Management'. University of Magdalena. Santa Marta, Colombia, 113 pp.
- Ergin, A., Karaesmen, E., Micallef, A., and Williams, A. T. 2004. A new methodology for evaluating coastal scenery: fuzzy logic systems. *Area*, 36: 367-386.
- Felix-Delgado, A., Mendoza, E., Silva, R., Riviera-Arriaga, E., and Palacio, A. 2008. Analysis of the natural and anthropogenic evolution of Cancun beach, Mexico, as a contribution to its sustainable development. First ProCoast seminar on Coastal Research, (Porto, Portugal), May 26-28.
- Harris, L., 1972, The challenge of research in the coming era of travel. *Proc. Travel Research Assoc. Third Annual Conf.* (Salt Lake City) 13 pp, cited in Crompton, 1979.
- Houston, J. R. 2008. The economic value of beaches: a 2008 update. *Shore and Beach*, 76(3), 22-26.
- Klein, Y. L., Osleeb, J. P., and Viola, M. R. 2004. Tourism generated earnings in the coastal zone: a regional analysis. *Journal of Coastal Research*, 20(4), 1080-1088.
- Marin, V., Palmisani, F., Ivaldi, R., Dursi, R., and Fabiano, M. 2009. Users' perception analysis for sustainable beach management in Italy. *Ocean & Coastal Management* 52, 268-277.
- McKenna, J., MacLeod, M., Power, J., and Cooper, A., 2000. *Rural Beach Management: A Good Practice Guide*. Donegal County Council, Lifford Co. Donegal, Ireland
- Micallef, A., Morgan, R., and Williams, A. T. 1999. User preferences and priorities on Maltese beaches: Findings and potential importance for tourism, in Randazzo, G. (ed.), *Coastal Environmental Management*, EUCC-Italy/EUCC. (electronic disc)
- Morgan, R., Jones T.C., and Williams A.T. 1993. Opinions and perceptions of England and Wales Heritage Coast beach users: Some management implications for the Glamorgan Heritage Coast Wales. *Journal of Coastal Research*, 9, 1083-1093.
- Morgan, R., and Williams, A. T. 1995. Socio-demographic parameters and user priorities at Gower Beaches, UK. In: Healy, M. G., and Doody, J. P., (eds.), *Directions in European Coastal Management*, 83-90, Cardigan, EUCC and Samara Publishing.
- Morgan, R., Gatell, E., Junyant, R., Micallef, A., Ozhan, E. and Williams, A. T., 1996. Pilot studies of Mediterranean beach user perceptions, (In), Pilot studies of Mediterranean beach user perceptions, (In), Ozhan, E. (ed.), *ICZM in the Mediterranean and Black Sea: Immediate Needs for Research*, 99-110, Ankara, Turkey, METU, Turkey.
- Office of Population and Censuses and Surveys, 1991, *Classification of occupations*
- Pelas, H.R. 2011. *Tourism development in Cancun, Mexico: an analysis of state developed tourism initiatives in a developing nation*. unpub. Master's thesis. Georgetown University, Washington, DC, USA, 81 pp.
- Polette, M. 2009. Analysis of Users' Perceptions at Praia Central, Balneário Camboriú (Santa Catarina, Brazil), 317-324. (In), Williams, A. T., & Micallef, A. *Beach Management: Principles and practices*. London, UK: Earthscan.
- Roca, E., and Villares, M. 2008. Public perceptions for evaluating beach quality in urban and semi-natural environments. *Ocean & Coastal Management*, 51:314-329.
- Rowntree, R. A., 1974, Coastal erosion: the meaning of a natural hazard in Britain and the USA. *Applied Geography*, July, 197 pp.
- Silva, J.S., Leal, M.M.V., Araújo, M.C.B., Barbosa S. C. T, and M. F., Costa (2008) Spatial and Temporal Patterns of Use of Boa Viagem Beach, Northeast Brazil. *Journal of Coastal Research*, 24, Issue 1A: 79 - 86.
- Thieler, E.R., and Bush, D.M., 1991. Hurricane Gilbert and Hugo send powerful messages for coastal development. *Jn. Geol. Educ.* 39, 291-296.
- Tudor, D. T. and Williams, A. T., 2006. A rationale for beach selection by the public on the coast of Wales, UK, *Area*, 38, 2, 153-164.
- UNWTO 2011 (United Nations World Tourism Organization). *Tourism Highlights*, 2011 Edition.
- Vaz, B. 2008. *Contributos para a avaliação e gestão de traíais: a importância da percepção dos seus utilizadores.*, Human ecology and contemporary social problems. Unpub. Master's thesis, Nova Universidade of Lisbon, Lisbon, 115 pp.
- Ward, W. C., Weidie, A. E., and W. Back, 1985. *Geology and hydrogeology of the Yucatan and Quaternary geology of the North-east Yucatan peninsula*. New Orleans Geol. Soc, 1-14.
- Weller, J. 2004. Tertiary sector employment in Latin America. Between modernity and survival. *CEPAL Review* 84, 157-174.
- Williams, A.T., Jones, T.C., Davies, P., and R C H., Curr. 1992. Psychological Profile of the beach/dune user in South Wales, UK. *Shore and Beach*, 60 (2), 26 - 30.
- Williams, A.T., and Micallef, A. 2009. *Beach Management: Principles and Practices*, 454 pp, Earthscan, London, UK.
- WTB. World Tourism Barometer (<http://media.unwto.org/en/press-release/2013-01-28/international-tourism-continue-robust-growth-2013>, (accessed 19 February 2013)

## Are natural beaches facing extinction?

Orrin H. Pilkey<sup>†</sup> and J. Andrew G. Cooper<sup>‡†</sup>

<sup>†</sup> Earth and Ocean Sciences  
Duke University, Durham,  
NC 27708, USA  
opilkey@duke.edu

<sup>‡</sup> School of Environmental Science  
University of Ulster  
United Kingdom  
jag.cooper@ulster.ac.uk

<sup>†</sup> Geological Sciences  
School of Agriculture, Earth and  
Environmental Sciences  
University of KwaZulu-Natal, Westville,  
South Africa



[www.cerf-jcr.org](http://www.cerf-jcr.org)



[www.JCRonline.org](http://www.JCRonline.org)

### ABSTRACT

Pilkey, O.H. and Cooper, J.A.G. 2014. Are natural beaches facing extinction? *In: Green, A.N. and Cooper, J.A.G. (eds.), Proceedings 13th International Coastal Symposium (Durban, South Africa) Journal of Coastal Research, Special Issue, No. 70 pp. 431-436. ISSN 0749-0208.*

On a generational scale, on developed shorelines, the world's recreational beaches are doomed. This is largely because of the widespread assumption that preservation of buildings is a higher priority than preservation of beaches in response to sea level rise. Continuing beach degradation will be inevitable through active or passive processes. Active degradation means the actual removal of the beach, mostly as a result of shoreline engineering or mining. By far, the most important cause of beach loss in this category will be hard structures, especially seawalls. The incorrectly but widely perceived panacea of each replenishment will become economically impossible because of raised sea levels. Replenishment leads to intensified beachfront development and this ironically and inevitably will increase the future construction of seawalls. Passive degradation refers to reduction of the quality of the beach to the point that human usage drops, along with political support for costly beach preservation by nourishment. Passive degradation includes trash accumulation, oil spills, beach driving and most importantly, pollution, which is increasing rapidly apace with population growth and remains largely unrecognized by the beach-using public.

**ADDITIONAL INDEX WORDS:** *sea level rise, pollution, litter, beach management.*

### INTRODUCTION

The rush to the shore continues unabated in spite of the incontrovertible evidence of global sea level rise (Pilkey and Young, 2009; Gornitz, 2013). The world's coasts are being developed at rapid rates, and the lessons of the economic downturn of 2007/8 (Cooper and McKenna, 2009a) appear not to have been learned. There is a clear disconnect between land-use planning systems that regulate shoreline development and scientific knowledge of how shorelines respond to rising sea level and storms. This we attribute to a misplaced reliance on engineering to solve the problems that poorly planned development creates. The situation is sustained and exploited by current beachfront development practice.

A consequence of this situation is that worldwide there are thousands of miles of densely developed beachfront communities, including the many miles of high-rise-lined beaches in Florida and Spain. Almost universally, to date in these communities, buildings and infrastructure are considered to be more valuable than beaches when it comes to responding to sea level rise. Consequently many beaches are now backed by seawalls and unable to migrate landwards or absorb the impacts of storms. In this diminished state, beaches provide a small recreational platform and impaired ecosystem function (Figure 1). The longer this prioritization persists, the denser the

development becomes, and the more difficult it is to respond to sea level rise using anything other than hard defences.

It is clear (to scientists and planners but not necessarily to the general public) that the next generation will face major disruptions of shorefront development and its infrastructure, and widespread loss of beaches. The most visible disruption will be in the coastal cities, especially those at low elevations, such as Miami, New York, Philadelphia, Dhaka, Rotterdam, Alexandria, Belem, Durban, and Hong Kong, to name a few. Funding the protection of cities from flooding and shoreline recession is likely to be higher priority than funding protection of the thousands of miles of shorelines with relatively small beachfront tourist communities. We believe that there is a significant chance that beaches along these developed shorelines will be utterly destroyed within 40 to 50 years if sea level rise projections are close to reality. The same scenario applies to scattered coastal developments whether privately or corporately owned. At present, many of these developments are buffered from the costs of defence by government intervention. This will diminish and disappear as a result of more pressing demands on public funds.

In this paper we review and categorize the ways in which beach degradation is likely to occur. All are already happening but will increase in scale and distribution in the near future in response to increasing development and sea-level rise. We recognise two general modes of beach destruction: active and passive. Active destruction of beaches occurs as a result of emplacement of hard stabilization structures and/or removal of sand by mining. Such activities damage the physical integrity of the beach. Passive destruction refers to loss of beach function

DOI: 10.2112/SI70-073.1 received 30 November 2013; accepted 21<sup>st</sup> February 2014. © Coastal Education & Research Foundation 2014



because of pollution, trash, driving and oil spills. Passive degradation results in beaches becoming difficult or unpleasant to use, which removes their utility and ultimately results in loss of political support for beach preservation. Both types of beach destruction are discussed in the following sections.

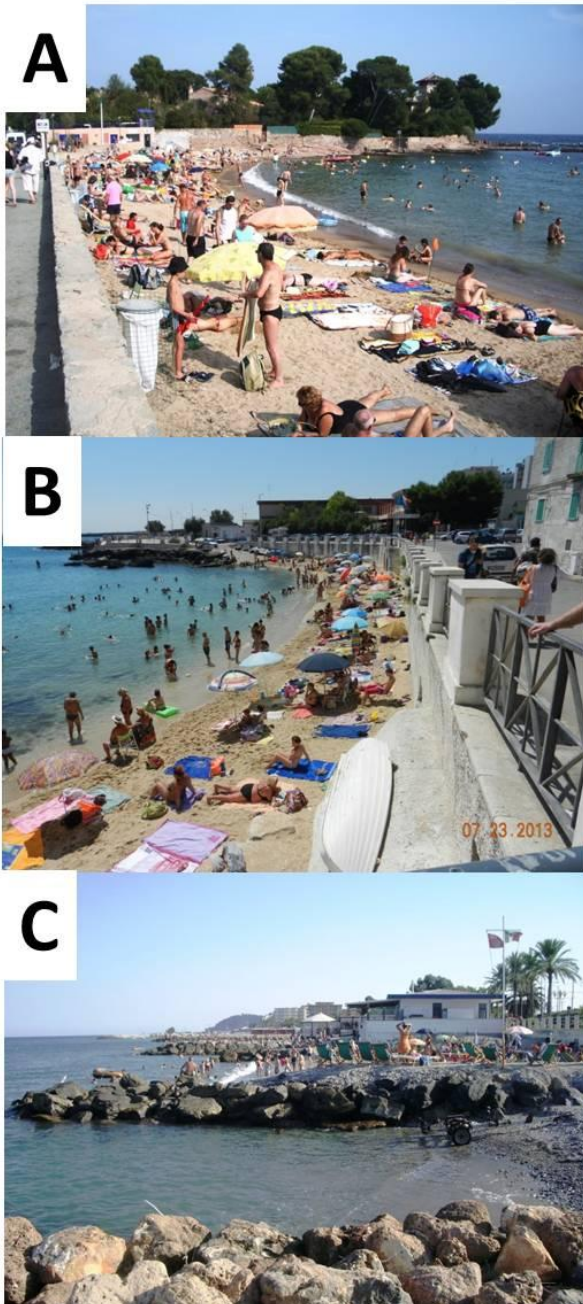


Figure 1. Small recreational beaches backed by seawalls. A) Esterel, France; B) Monopoli, Italy (photo: Norma Longo); C) Albenga, Italy.

## ACTIVE BEACH LOSS

Two main groups of human activity contribute to active beach loss: mining and coastal engineering. They diminish the physical extent of the beach and cause loss of ecosystem functioning.

### Mining

Beach sand is ideal for concrete aggregate and other construction uses. It tends to be relatively uniform in size with no silt and clay, and it is easily mineable. Such mining is carried out on several scales on many of the world's beaches (Figure 2). In Morocco and Singapore, mining is conducted on a very large scale. In Morocco, as in all of North Africa, wood is hard to come by and concrete provides the basis for most construction. The massive dunes that characterize the shorelines of the northern parts of Morocco are being removed on a large scale for use as construction sand. As in most countries, sand mining is illegal, but in Morocco and many other countries the law is largely ignored. In Singapore, sand is being used on a very large scale for the purpose of increasing the area of the country by 20% within the next decade (Levitt, 2010). Some of this sand is mined from the sea floor, but most of Singapore's new sand is obtained from the beaches of other countries including Malaysia, Indonesia, Viet Nam, and Laos. Such mining is illegal in these countries, but nonetheless, officials can be convinced (or bribed) to allow mining. The mining going on for Singapore is in some cases damaging the future of the tourist industry in those source countries (Sand Wars, 2013).

Mining on the beaches of Sierra Leone (IRIN, 2013) is carried out on a smaller scale to obtain construction sand (partly to rebuild the many buildings destroyed in the country's recent civil war). Unfortunately, the Sierra Leone beaches tend to be small and without extensive dunes like those in Morocco. They are thus easily removed entirely. On the island of Barbuda in the Caribbean the beaches are being virtually stripped of sand to be sold to other Caribbean islands (and further afield) for construction purposes. Such mining of beaches is actively damaging a very important tourist industry as well as removing the beaches' ecosystem function, including its attributes as a natural storm defence.

### Coastal Structures: The Seawall Family

Hard stabilization was carried out by the Romans, Greeks and Phoenicians in the early times, mostly for formation and protection of harbours. In the last few centuries, helped along by modern machines capable of moving large volumes of sand and large rocks, stabilization of shorelines to preserve buildings has become a common practice (Figure 3). Widespread recognition of the price paid for seawall construction (i.e. loss of the beach) seems not to have arrived until a few decades ago. The loss of beaches caused by seawalls and groins has led in recent decades to a preference for widespread beach replenishment using dredged sand from adjacent lagoons or the seafloor in front of the beaches (Coburn, 2012). Tourist communities that have been the recipient of beach nourishment

have not had to face the problems caused by seawalls because replenishment has been available.

However, as sea level rises, beaches on shorelines that are being held in place by repeated replenishment will be lost at increased rates because the man-made beaches will be out of equilibrium with the level of the sea. The costs of replenishment and the volumes of sand required to hold the shoreline in place increase greatly with rising sea level (e.g. Cooper and Lemckert, 2012). Meanwhile, as beaches are re-replenished numerous times, development on the shoreline intensifies (Coburn, 2012). Inevitably, as replenishment becomes too costly, seawalls will be considered an absolute necessity to preserve costly buildings (Cooper and Pilkey, 2012). Thus, in Florida, for example, where there are hundreds of miles of high-rise-lined shorelines, future loss of the beach due to seawall construction is inevitable (Kelley et al., 2010).



Figure 2. Beach sand mining takes place at various scales. These examples are in A) Morocco and B) Sierra Leone.

As beaches become narrower in front of seawalls, the extent of the dry beach diminishes and with it the capacity to accumulate beach litter. Natural beach litter (seagrass and seaweeds) is the base of many beach ecosystems. In a study of beaches in southern California, for example, Dugan et al. (2008) found preferential loss of dry beach and with it, a loss in wrack accumulation and associated invertebrate fauna on seawalled beaches.

## PASSIVE BEACH LOSS

In this category we include actions that degrade the beach and diminish its natural ecosystem functions and/or amenity values to humans. They are usually unintended impacts of activities carried out on beaches themselves or in the surrounding waters or catchment areas (Finkl and Krupa, 2003). While they do not necessarily impact on the physical integrity of the beach, they nonetheless degrade it and render it less useable.

### Pollution

Pollution has long been an issue in beach management and beach utilization. Indeed many studies have shown that cleanliness is a key element in selection of a particular beach for recreation (McKenna et al., 2010). Pollution has diverse origins and comes in various forms on beaches. As coastal populations increase along with the amount of impermeable surfaces in the landscape, pollution of nearshore waters and beaches will increase. The presence of faecal bacteria, which is easily analyzed, is widely used as a measure of beach pollution. Recent studies have shown that faecal bacteria are typically more abundant in beach sands than in the water (Bonilla et al., 2007) but testing of beach suitability for recreation is almost always based solely on testing of the water (Haliday and Gast, 2012).

Besides sewage outfalls and septic tanks, sources of faecal bacteria are often assumed to be dogs, but in some cases other creatures are responsible. In Hawaii for example, pigeons and mongooses were found to be the source (Oshiro & Fujioka, 1995). Runoff from fields with dispersed livestock and the direct effect of livestock droppings on the beach can also contribute to faecal contamination. In many parts of the developing world, however, including India and Pakistan and in the atoll nations, human faecal matter on beaches is common and must be a major source of health problems for swimmers or beach-goers. Other pollution problems include accumulations of green algae caused by nutrients from nearby over-fertilized farmlands.

There is a large technical literature concerned with beach sand pollution but it has largely escaped public recognition. The literature recommends wearing shoes on the beach, not lying directly on beach sand, and never, ever being buried in the sand. Other suggestions include not swimming after heavy rainfall runoff to beaches and avoiding beaches with direct urban storm water runoff and treated sewage effluent discharge systems nearby.

It is widely recognized by various health agencies that swimmers are affected by gastrointestinal and pulmonary illnesses. According to the US Environmental Protection Agency, 3.5 million American beach-goers are sickened each year (NRDC, 2013). Most of these illnesses are minor and are often difficult to distinguish from other non-beach sources (e.g. food poisoning or gastroenteritis). But increasingly there are serious illnesses related to beach activities. For example, co-author Pilkey's grandson contracted MRSA while surfing on a remote Washington State beach with a cut on his foot. Elsewhere, notably in Louisiana and Florida, 'flesh-eating bacteria' have caused serious illnesses and sometimes death. In each case the infected persons had cuts or scrapes and even insect bites.

### Oil spills

As recent high profile events have shown, oil spills are an important source of beach pollution (Gundlach and Hayes, 1978) and they can lead to a reduction the availability of beaches for recreation (Deacon and Kolstad, 2000) as well as causing ecological impacts (Schlacher et al., 2007). Large spills such as the BP Deep Horizon spill in the Gulf of Mexico, the Exxon Valdez spill in Alaska, and the First Gulf War oil spill in the Persian Gulf have dramatic immediate consequences but may also pollute beaches for long periods of time. Such large-scale pollution makes beaches unusable for a period of time and costs a great deal to clean up. Oil spills from shipping are difficult to control and despite improvements in maritime law, enforcement remains a problem in some areas.

### Trash

Trash also pollutes beaches and reduces their utility (Figure 4). Single events plus the effects of continuous low-level inputs create a litter problem on beaches. The Japanese tsunami of 2011 produced large amounts of floating trash, some of which is still coming ashore on North America. In addition, tons of plastic trash are concentrated in the large garbage patch in the central portion of all the world's oceans (ocean gyres), some of which spins off to nearshore waters. The arrival of trash on beaches produces a plastisphere that supports an entirely foreign flora and fauna. As the plastic trash degrades, it creates small particles that are sometimes consumed by birds and fish, killing them, and also results in changes in the ocean ecosystem. Styrofoam is a particularly deadly type of trash on beaches.

### Beach Driving

The use of vehicles on beaches has impacts on both the beach ecosystem (Schlacher and Thompson, 2007) and on recreational use of the beach (Cooper and McKenna, 2009b). Numbers of



Figure 3. Various types of seawalls destroy beaches and cause loss of recreational potential as well as ecosystem functioning. A) The former beach at Pondicherry, India replaced by a seawall. B) The former beach at Recife, Brazil, replaced by a seawall. Note the beach volleyball pitch constructed in a sandpit on top of the wall. C) Gabion baskets at the rear of a beach in Tubuai, French Polynesia. D) The tourist resort of Nusa Dua, Bali, Indonesia where beaches have been replaced by concrete structures.

infauna are reduced by driving and there are direct impacts on beach-dwelling or beach-using organisms, including turtles, seals, and birds, from driving on beaches. On recreational beaches driving causes a hazard to other users. In South Africa a countrywide ban on beach driving was introduced in 2002.

Claimed ecological benefits include recovery of some surf-zone fishes now outside the range of anglers who must now walk rather than drive (Dunlop and Mann, 2010) and improved integrity of foredune systems.

## CONCLUSIONS

Active degradation of beaches by mining and by shoreline engineering, as sea level rises, will result in the extensive loss of recreational beaches. Beach replenishment can be viewed as a process leading to seawalls and to the destruction of beaches in the next generation. This is because beach replenishment encourages development intensification, making the eventual retreat from the shoreline more and more difficult and intensifying the need for seawalls.

The problem of beach pollution in all of its forms will not directly destroy beaches, but it will undermine the ecosystem services provided by beaches. It will also cause recreational use of the beaches to decrease and, perhaps in some places, to be discontinued altogether. If no one is using the beaches, the critical element of political support to preserve beaches is absent and the priority of buildings over beaches will become even more entrenched. Under such a scenario, we envision that promenading on the top of seawalls will be the principal activity of tourists such as has happened in many former resorts. Beaches will of course remain in less developed and less populated countries (Namibia and Siberia come to mind) and beaches will remain in protected areas (e.g. National Seashores in the United States), but hard stabilization of adjacent shorelines will likely lead eventually to shoreline stabilization in parks and national seashores as well.

Preservation of beaches on developed shorelines will require demolition of buildings or moving buildings back, although these options can be expensive and have the potential to cause additional pollution. Along Florida and other intensely developed coasts, suitable sites for relocating buildings behind the beachfront or barrier islands may not be available. Other alternatives include building bigger and better seawalls, accepting beachfront development as a future artificial reef, or strengthening the base of buildings and exchanging cars for boats. All of these structural approaches will destroy the beach.

It is likely that implementing any of these alternatives will be extremely difficult because when the beachfront tourist communities are in trouble from sea level rise, the coastal cities will be in greater trouble (Pilkey and Young, 2009). The coastal cities will certainly trump the smaller communities for funding when it comes to sea level rise response, leaving a potentially chaotic scramble for resources as communities attempt to preserve their property.

## LITERATURE CITED

- Bonilla, T.D., Nowosielski, K. Cuvelier, M., Hartz, A., Green, M., Esiobu, N., McCorquodale, D.S., Fleisher, J.M. and Rogerson, A. 2007. Prevalence and distribution of faecal indicator organisms in South Florida beach sand and preliminary assessment of health

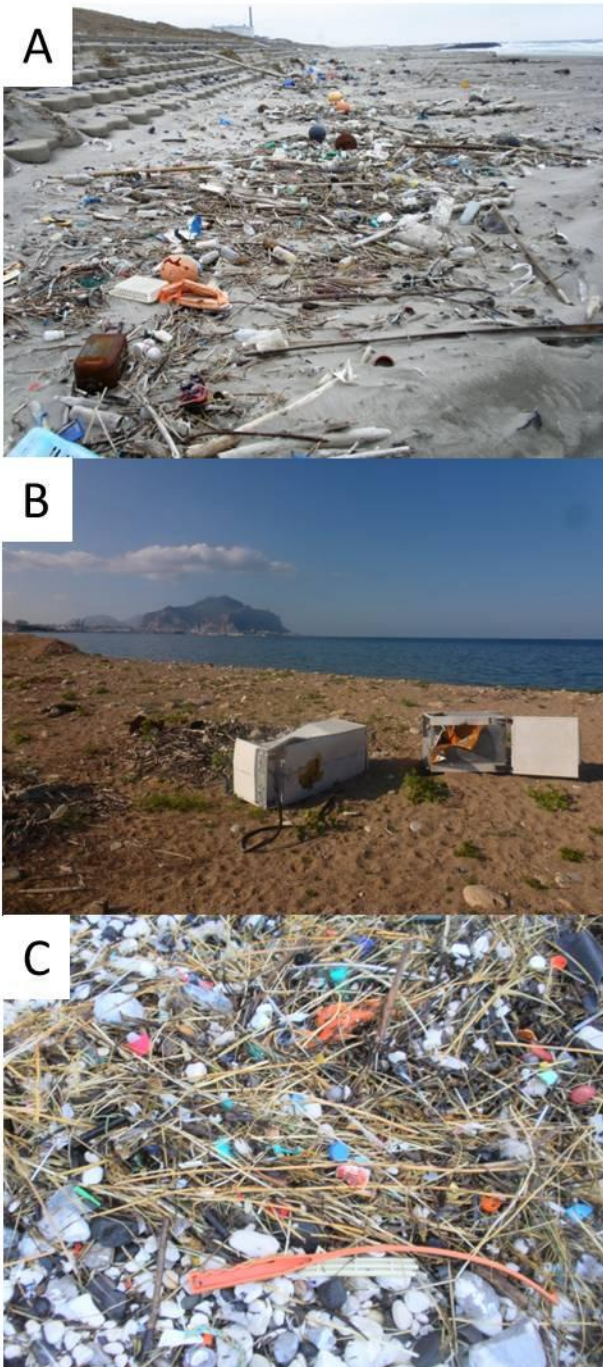


Figure 4. Trash accumulates on beaches from many sources and has many forms. A) Marine debris, Kashima, Japan; B) Domestic appliances dumped on beach, Palermo, Italy; C) Fine plastic debris, Portrush, Northern Ireland.

- effects associated with beach sand exposure. *Marine Pollution Bulletin*, 54, 1472-1482.
- Coburn, A.S. 2012. Beach Nourishment in the United States. In: Cooper, J.A.G. and Pilkey O.H. (eds.): *Pitfalls of Shoreline Stabilization: Selected Case Studies*, Coastal Research Library 3. Springer, Heidelberg, pp. 105-119.
- Cooper, J.A.G. and Lemckert, C. 2012. Extreme sea level rise and adaptation options for coastal resort cities: a qualitative assessment from the Gold Coast, Australia. *Ocean and Coastal Management*, 64, 1-14.
- Cooper, J.A.G. and McKenna, J., 2009a. Boom and Bust: the influence of macroscale economics on the world's coast. *Journal of Coastal Research*, 25, 533-538.
- Cooper, J.A.G. and McKenna, J. 2009b. Managing cars on beaches: A case study from Ireland. In: Williams, A. & Micallef, A., *Beach Management. Principles and Practice*. Earthscan Publishers, London.
- Cooper, J.A.G. and Pilkey O.H. (eds.) 2012. *Pitfalls of Shoreline Stabilization: Selected Case Studies*. Coastal Research Library 3. Springer, Heidelberg, 235-245.
- Deacon, R. and Kolstad, C. 2000. Valuing Beach Recreation Lost in Environmental Accidents. *J. Water Resour. Plann. Manage.* 126, 374-381.
- Demirbilek, Z. Lin, L. and Seabergh, W.C. 2009. Laboratory and numerical studies of hydrodynamics near jetties. *Coastal Engineering Journal* 51, 143-175.
- Dugan, J.E., Hubbard, D.M., Rodil, I.F., Revell, D.L., and Shroeter, S., 2008, Ecological effects of coastal armoring on sandy beaches: *Marine Ecology*, v. 29, suppl. 1, p. 60-170.
- Dunlop, S.W., Mann, B.Q., 2012. An assessment of participation, catch and effort in the KwaZulu-Natal shore-based marine linefishery, with comments on management effectiveness. *African Journal of Marine Science*, 34, 479-496.
- Finkl, C.H. and Krupa, S.L. 2003. Environmental impacts of coastal-plain activities on sandy beach systems: hazards, perception and mitigation. *Journal of Coastal Research*, 35, 132-150.
- Gornitz, V., 2013. *Rising Seas: Past, Present and Future*. Columbia University Press, 360 pp.
- Gundlach, E.R. and Hayes, M.O. 1978. Vulnerability of coastal environments to oil spill impacts. *Marine Technology Society Journal*, 12, 18-27.
- Halliday, E. and Gast, R.J. 2011. Bacteria in beach sands: An emerging challenge in protecting coastal water quality and bather health. *Environ. Sci. Technol.* 45, 370-379.
- IRIN, 2013. Sierra Leone: Sand-mining threatens homes and livelihoods in Sierra Leone. Nairobi, Kenya: IRIN News (Integrated Regional Information Networks), UN Office for the Coordination of Humanitarian Affairs, 4 Feb. 2013. <http://reliefweb.int/report/sierra-leone/sand-mining-threatens-homes-and-livelihoods-sierra-leone>
- Kelley, J.T., O.H. Pilkey and J.A.G. Cooper (eds.), 2009. *America's Most Vulnerable Coastal Communities*. Geological Society of America, Special Paper 460, 179 pp.
- Levitt, T., 2010. The damage caused by Singapore's insatiable thirst for land. *The Ecologist*. May 11th, 2010. [http://www.theecologist.org/News/news\\_analysis/481729/the\\_damage\\_caused\\_by\\_singapores\\_insatiable\\_thirst\\_for\\_land.html](http://www.theecologist.org/News/news_analysis/481729/the_damage_caused_by_singapores_insatiable_thirst_for_land.html)
- NRDC (Natural Resource Defense Council) 2013. Annual Report: Testing the Waters. [www.nrdc.org/water/oceans/ttw/](http://www.nrdc.org/water/oceans/ttw/)
- Oshiro, R. and Fujioka, R., 1995. Sand, soil and pigeon droppings: sources of indicator bacteria in the waters of Hanauma Bay, Oahu, Hawaii. *Water Science and Technology*, 31, 251-254.
- Phillips, M.C., Solo-Gabriele, H.M., Piggot, A.M., Klaus, J.S. and Zhang, Y., 2011. Relationships between sand and water quality at recreational beaches. *Water Research*, 45, 6763-6769.
- Pilkey, O.H., Neal, W.J. Kelley J.T. and Cooper, J.A.G. 2011. *The World's Beaches: A Global Guide to the Science of the Shoreline*. University of California Press, 355 pp.
- Pilkey, O.H. and Young, R. 2009. *The Rising Sea*. Island Press, 203 pp.
- "Sand Wars" (documentary film), 2013. [coastalcare.org/](http://coastalcare.org/)
- Schlacher, T.A. and Thompson, L.M.C. 2007. Exposure of fauna to off-road vehicle (ORV) traffic on sandy beaches. *Coastal Management*, 35, 567-583.
- Schlacher T.A., Dugan J., Schoeman D.S., Lastra M., Jones A., Scapini F., McLachlan A., Defeo O. 2007. Sandy beaches at the brink. *Diversity & Distributions*, 13, 556-560.

## Trend Change(s) in Coastal Management Plans: the integration of short and medium term perspectives in the spatial planning process



[www.cerf-jcr.org](http://www.cerf-jcr.org)

Fátima L. Alves †, Lisa P. Sousa †, Tanya C. Esteves †, Eduardo R. Oliveira †, Inês C. Antunes †, Maria da Luz Fernandes †, Luís Carvalho ‡, Sérgio Barroso ‡, Margarida Pereira §

† CESAM (Centre for Environmental and Marine Studies), Departamento de Ambiente e Ordenamento Universidade de Aveiro Campus de Santiago, 3810-193 Aveiro, Portugal  
malves@ua.pt, lisa@ua.pt, tanyae@ua.pt, eduardo.oliveira@ua.pt, inesantunes14@gmail.com, maria.luz@ua.pt

‡ CEDRU (Centro de Estudos e Desenvolvimento Regional e Urbano) Rua Fernando Namora, 46 A 1600-454 Lisboa, Portugal  
luis.carvalho@cedru.com, sergio.barroso@cedru.com

§ e-GEO, Faculdade de Ciências Sociais e Humanas da Universidade Nova de Lisboa, 1069-061 Lisboa, Portugal  
ma.pereira@fcsh.unl.pt



[www.JCRonline.org](http://www.JCRonline.org)

### ABSTRACT

Alves, F.L., Sousa, L.P., Esteves, T.C., Oliveira, E.R., Antunes, I.C., Fernandes, M.L., Carvalho, L., Barroso, S., Pereira, M., 2014. Trend Change(s) in Coastal Management Plans: the integration of short and medium term perspectives in the spatial planning process. In: Green, A.N. and Cooper, J.A.G. (eds.), *Proceedings 13<sup>th</sup> International Coastal Symposium* (Durban, South Africa), *Journal of Coastal Research*, Special Issue No. 70, pp. 437-442, ISSN 0749-0208.

Spatial planning can be seen as an interdisciplinary science that ensures sustainable development and land use, since it integrates policy, social, cultural, economic and environmental management issues. Marine and coastal spatial planning is particularly challenging due to their vulnerable, dynamic and complex nature and to the problems associated with sea level rise, erosion processes and land-use pressures in the coastal zone. Coastal erosion, flooding and shoreline retreat are serious problems along the coast of mainland Portugal. By using an innovative approach of coastal zone spatial planning, this study developed an Integrated Coastal Zone Management Plan for the Portuguese central region (stretch Ovar - Marinha Grande), where alternative planning policies to the previous ones were suggested. The study revealed that socio-economic analysis and the identification and valuation of ecosystems services and land use need to be incorporated in spatial planning to support decision-making favouring sustainable development. According to these approaches the Coastal Plan was developed considering three environmental scenarios to respond to the coastal erosion trends, based on a development model for the coastal region. In addition, the scenarios consider the public investments constraints (national budget) expected in the next decade and the short and medium term of the Plan. This Plan is differentiated from the previous by attempting to lessen further coastal erosion through the integration of different jurisdictions, legislations and directive measures and applying them to the terrain. This strategy shows itself as relevant to promote further forward-thinking Plans for other Portuguese coastal areas.

**ADDITIONAL INDEX WORDS:** *Coastal erosion. Shoreline evolution. Coastal management. Scenarios.*

### INTRODUCTION

Coastal areas are highly dynamic natural systems being densely inhabited throughout major European cities, where Portugal is no exception. The Portuguese mainland coast is over 900 km long, with a high environmental value (35% of protected area, which is included in the National Network of Protected Areas). It is also subject to extreme amounts of stress, with 75% of Portugal's population located along the coast and 85% of the national GNP is generated by these coastal metropolitan areas (urban, industry and tourism). These activities have led to overwhelming coastal inland asymmetries as well as to the so-called "coastal compression", a phenomenon that relates the dissemination of constructed areas and infrastructures over more area and closer to the shoreline (Alves *et al.*, 2011; Alves *et al.*, 2007). This doesn't comply with the sustainable principles present in the European Commission's proposal for establishing a framework for maritime spatial

planning and integrated coastal management (Commission Proposal COM (2013) 133 final).

If the influence of climate change was added to these factors along coastal regions (e.g. sea-level rise, extreme storm events, shoreline recession, low-land flooding), threats to coastal areas are enhanced, not only in terms of natural patrimony, but also economically (Carrero *et al.*, 2013; Esteves, 2013). This is due to coastal zone being major metropolitan centres and impacts may potentially affect a large part of the population, thus affecting coastal zone access and occupation (Alves *et al.*, 2013).

### Coastal Management Plans

It is now becoming clear that we need to review the norms and practices that have guided human development over the past decades, especially in the field of territorial planning. Spatial planners have to adopt new integrated and adaptive models for

governance, facilitating inclusive debate between stakeholders, with focus orientated on delivery rather than on regulation (Kidd and Shaw, 2013; Schmidt *et al.*, 2013).

Several European countries have used leadership to adopt this new paradigm for maritime planning: an integrated coastal zone management (ICZM) approach is, in general, a process where a scope of harmonized policies and decision-making structures concert action towards achieving sustainable goals. The potential of this strategy is patent in the increasing amount of European level initiatives that refer to it specifically (Reis, *et al.*, 2014). European countries now focus more on identifying and resolving conflicts among different sea users and attempt to include all waters under their jurisdiction, ensuring that conservation objectives are not impaired by human activity (Douvere and Ehler, 2009).

Study results of Reis, *et al.* (2014) show that current coastal management practices in Europe are based on “principals” of good management, which encourage approaches that are more holistic, participatory, long term and adaptive. Although the author’s studied areas aren’t themselves ICZM projects, the applied science and methodologies could certainly support such an approach. There are a wide range of European-level instruments set to guide this process, however practical implementation throughout some countries have still found several levels of success.

## New Generation Coastal Management Plans in Portugal

The legal framework of the Portuguese Coastal Zone Management Plans (CZMP) was originally created in 1993 (Decree no. 390/93, of September 2), which formed the basis of spatial and land use coastal zone planning, beach management, sustainable tourism and nature conservation. In 2012, the legal regime for the coastal zone was revised (Decree no. 159/2012 of July 24) in order to promote a new more flexible, integrated and adaptive approach. This new generation of CZMP reinforces the need for mechanisms of risk prevention, environment safeguarding and user safety.

New national CZMP should base their strategic principals on:

- **Sustainability:** to promote the compatibility between the socio-economic development and nature, biodiversity and geodiversity conservation, to preserve life quality of existing and future populations;
- **Precaution:** to foresee and anticipate consequences, adopting a cautious attitude, minimizing risk and negative impacts;
- **Cohesion:** to assure social and territorial balance, as well as a balanced distribution of resources and opportunities.

As for the intervention area of the CZMP, it is now divided into two fundamental subspaces: Maritime Protection Zone (MPZ) and Terrestrial Protection Zone (TPZ). This new Decree introduced significant changes in the territorial configuration of CZMP, such as the integration of the areas under port jurisdiction and the possibility of extending the planned intervention area up to 1.000 m (rather than the previous 500 m) (Figure 1).

## Objectives for the study

This study aims at delineating an innovative revision process for the first of the new generation CZMP for the Ovar-Marinha Grande stretch, creating a plan that encompasses the whole of the shoreline, including the maritime and terrestrial areas. Besides their normal regulatory and normative character, this more flexible, adaptive and integrated logic will give the CZMP the means to identify and program management, protection, conservation and valorisation strategies for water resources and

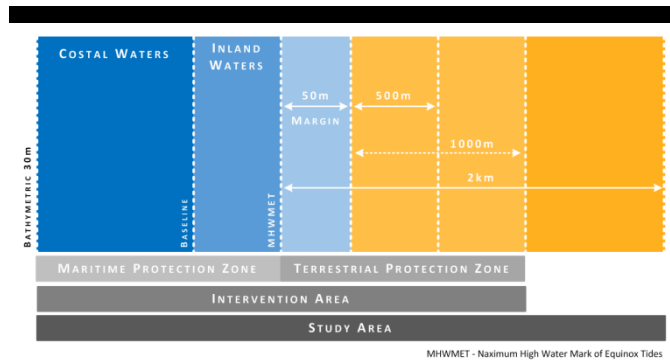


Figure 1. Incidence area of CZMP-OMG (Source: adapted from APA, 2012)

natural systems associated to them. Thus, this plan positions itself to be one of the first for the Portuguese coastal areas, serving as a beacon to future coastal management plans.

## STUDY AREA

Located in the central region of mainland Portugal, the study area includes a coastline of 140 km (with around 905 km<sup>2</sup>), eleven coastal municipalities, distributed throughout three NUTS III: Baixo Vouga (Ovar, Murto, Aveiro, Ílhavo, Vagos); Baixo Mondego (Mira, Cantanhede, Figueira da Foz); and Pinhal Litoral (Pombal, Leiria e Marinha Grande) (Figure 2). In its whole, these municipalities correspond to one of the highest population concentrations of the Centre Region of Portugal, with 538.442 inhabitants (2011) (Alves, *et al.*, 2007; APA, 2012). Due to its extensive coverage of the mainland coastline, the Ovar - Marinha Grande (OMG) stretch has a privileged geographical location and a set of singularities that urge valorisation and preservation. The diversity and biophysical abundance are marking characteristics of the territory which include marine and lagoon ecosystems, dunes, cliffs, etc. (APA, 2012). Prime examples are the Ria de Aveiro and the Mondego river ecosystems. In the Ria de Aveiro case, this shallow coastal lagoon covers almost 120 km<sup>2</sup>, including 158 740 inhabitants in the adjoining parishes, a large multifunctional port and it is considered an area of ecological significance, including a nature reserve and a wide range of habitats used as nursery areas by several species that include bivalves, crustaceans, fish and birds (Oliveira *et al.*, 2013; Sousa *et al.*, 2013).

With two of the six major Portuguese ports in the OMG region (Aveiro and Figueira da Foz), this is a highly dynamic economic area, having registered an economic growth higher than the national mean, partly due to its prime conditions in terms of infrastructures and support services to business activities. Tourism is also presented as one of the sectors with high strategic value for the intervention area, given the great diversity and attractiveness of the available resources and the excellent conditions for the development of this activity, e.g., nationally referenced quality beaches such as Furadouro; Torreira; Barra; Costa Nova; Praia da Tocha; Figueira da Foz; Praia da Vieira and São Pedro de Moel (APA, 2012).

The OMG coastline is one of the greatest national littoral challenges in terms of integrated management of resources and activities, and minimization of risk upon people and assets. This territory is distinguished by its fragile geology that when allied with wave climate energy and sediment availability, it results in one of the most intense erosive processes along the Portuguese coast. This stress can lead to many issues, which include coastal

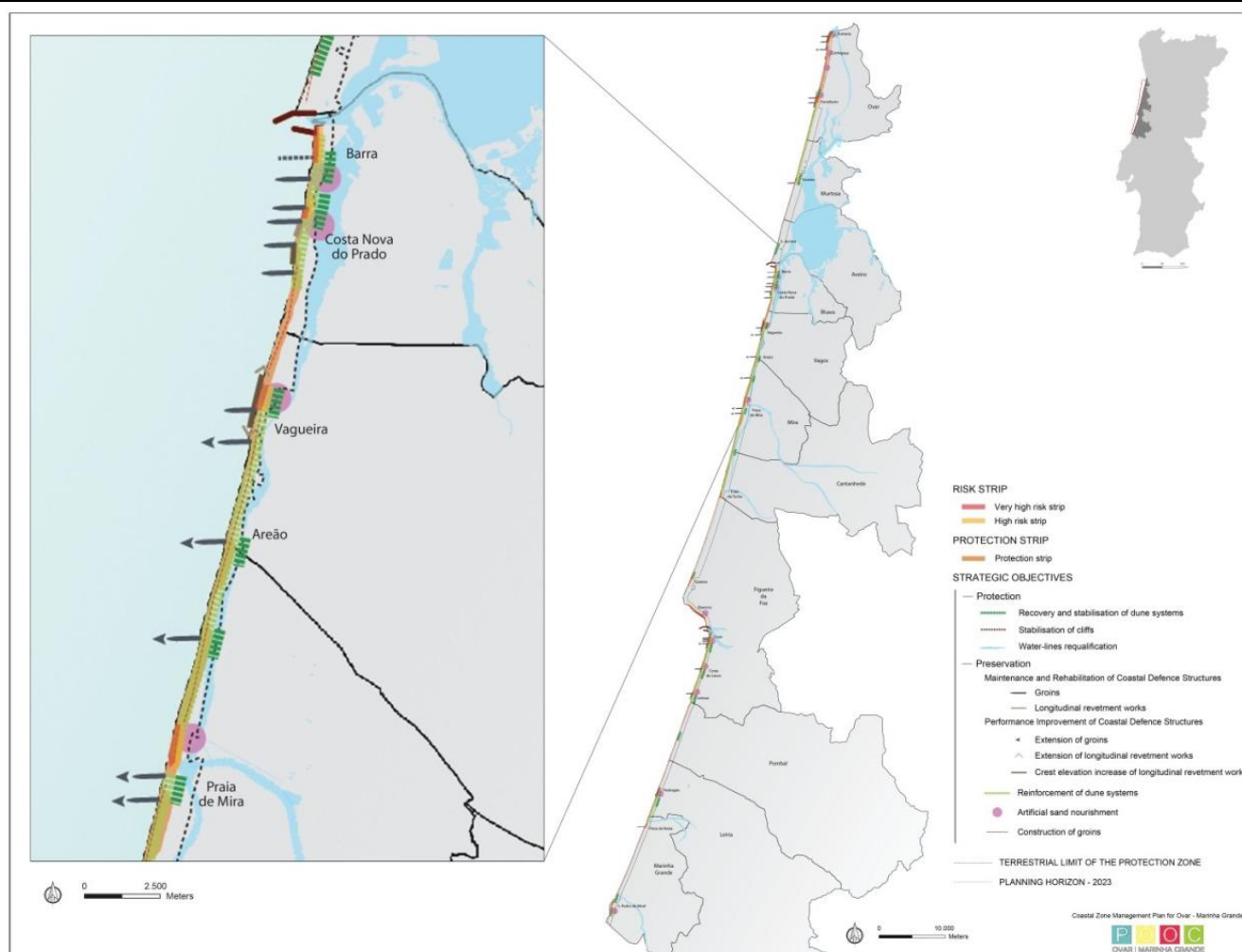


Figure 2. Strategic Map for the CZMP-OMG. Detail for the actions defined for the Barra – Mira stretch.

planning and management problems (chaotic and casuistic construction); coastal erosion (use of prone-hazard areas, coastline and sediment supply interference); and coastal and estuarine pollution (lack of adequate waste treatments) (Alves *et al.*, 2011). Allying the preservation of ecological values, public and economic use of resource demands an integrated approach of the limitations and potentials of the OMG stretch (APA, 2012).

The intensity of coastal erosion in this coastal stretch, which largely exceeds the prediction of the shoreline's evolution made in the first Coastal Zone Management Plan for Ovar - Marinha Grande (CZMP-OMG), was enough to justify the Plan's revision (Alves *et al.*, 2013). It is also important to review the final results of the original Plan, once they fell short of expectations (Alves *et al.*, 2011; Alves *et al.*, 2013).

## METHODOLOGY

Due to resulting pressures existing along the coastline area, the prodigious natural and landscape value, and because of its great sensitivity, the territory should be safeguarded by an adequate strategy for spatial planning of the land use and soil occupation.

For this second generation CZMP, 5 phases are considered to enable an improved implementation of this Plan (Figure 3) (APA, 2012) and allow the short and medium term perspective of its application.

Phase 1, *Evaluation, Characterization and Prospective Diagnosis*, generally consists on evaluating the results for the implementation of the first generation CZMP-OMG (Council of Ministers Resolution no. 142/2000, of October 20), leading to the establishment of expectations for the second generation CZMP-OMG. It also identifies the territories' main characteristics to assess its current state.

Phase 2, *Plan Proposal*, involves producing different scenarios (Figure 4) to evaluate the territory's short and medium term conditions, and to create preliminary versions for strategic frameworks and models.

Phase 3, *Plan Project for an Intervention Proposal*, seeks to generate proposals and technical specifications for the protection, conservation and valorisation regimes of the coastline, and to create the Execution and Financing programmes.

Phase 4, *Public Consultation and Discussion*, aims to prepare elements, participate in, analyse results and write the final report of the public consultation and discussion stage.

Phase 5, *Final Elements*, aim to produce the final CZMP-OMG, which include products such as; several reports, models (strategic and planning models), plans (execution, intervention, financing plans), Plan regulation and maps (summary, conditioning, framing, current situation maps).

The scenario creation exercise of Phase 2 aims to (APA, 2013a): (i) foresee and clarify the study area's main threats; (ii)



establish a coastal defence approach adjusted to the problems that the CZMP-OMG will face until 2023; (iii) promote a precautionary principle by framing medium-term planning solutions (50 years) envisaging a sustainable management for the coastline; (iv) allow the establishment of anticipated coastal defence responses for emerging problems that compromise the territory's inhabitants; (v) and beacon the variability problems to define flexibility/adaptability mechanisms that guarantee response capacity and efficiency.

Accordingly, scenario creation results in a chained process of five tasks, which view the concretization of each one of the components that integrate the scenario model for the CZMP-OMG (Figure 4) (APA, 2013b). Task 1 (T1) defines the environmental scenarios for two reference years for the planning process – 2023 and 2063 –, coincident with the Plan's term and the Execution Programme (10 years) and for the medium-term adaptive and precautionary response framework (50 years). Using these scenarios as reference, and taking into account the high hazard level that affects the OMG coastline, T2 takes place. This task delimits the risk strips for 50 years accounting for variables for short and medium-term periods. In T3, a baseline situation is created by using the short-term environmental scenario for 2023 (from T1), by mapping an eventual shoreline evolution for the next 10 years in case no coastline defence intervention is made in the study area. Next, the definition of the response scenarios for coastal defence is made in T4, where these are a central task of the model (Scenario 1 – Emergency reactive; Scenario 2 – Volunteer maintenance; Scenario 3 – Volunteer anticipation). Finally, T5 analyses the implications resulting from the conjugation of the environmental scenario (2023) with each response scenario, seeking to identify the resulting costs for the concretion of each scenario and to understand the gains in terms of the minimization of the territorial impacts resulting from the evolution of the related phenomena to coastline dynamics, namely shoreline retreat and overtopping's.

## RESULTS

The definition of the CZMP-OMG **Strategic Model** takes into account the general and specific goals of the CZMP and the particular features of the territory, previously analysed in the characterization and prospective diagnosis studies. Despite its strategic nature, this model is designed in a way that meets its operational framework. The Strategic Model is structured with four strategic goals and 12 strategic lines, consistent with the territory it regulates, which must be implemented by the Spatial Planning and Intervention models:

- **Protect the territory:** ensure the protection of the biophysical integrity of the area and preservation of the environmental and landscape values. This may be done by safeguarding the dune

and cliff ecosystems by preserving the natural patrimony and geodiversity of the coastline; protecting the water resources to ensure the bathing water quality; protecting and valuing the marine habitats and the coastal lagoon systems; and protecting and valuing the agricultural and forest patrimony.

- **Value the space:** promote the value and the safe public fruition of the maritime public domain, as a social, cultural and economic resource. For that, it is necessary to value and qualify the beaches, reinforcing their importance as a natural, social and economic resource; promote an adaptive management of the beaches, guaranteeing safety settings for their use and viability of the associated economic activities; and by qualifying and planning the maritime front, conjugating the urban fruition with the mitigation of the effects of sea overtops and water advances.
- **Preserve the territory:** guarantee the territorial preservation and risk mitigation by promoting the sustainable use and occupation of the coastline. This may be achieved by maintaining the integrity of the coastline by anticipating the response to emerging problems; and defining a coastline use and occupation model that is adequate for a culture that is precautionary, has sustainable management and is inter-generationally solidary with the territory.
- **Guarantee its development:** create appropriate conditions for the development of activities that contribute towards the local development and the sea economy. It may be done by creating conditions for dynamism and planning of a sustainable use of the marine resources; create means to promote the development of the coastal fishing activities; and qualify and value the coastline's multiple tourism resources.

The **Spatial Planning Model** is the central element of the CZMP and is supplemented by the Intervention Model. This Model combines a strategic vision of the territorial development with the zoning of uses, activities and functions and land-use regulations. As previously mentioned, coastal erosion is considered the main threat to this territory. In order to adequately respond to this threat and protect the coastal resources, the Plan should anticipate the medium-term (50 years) threats and implement actions, such as adaptation measures, within its timeframe (10 year). Therefore, this Model is designed based upon the principles of Sustainability and Intergenerational Solidarity, Prevention and Precaution, and Operation and Adaptability. In this context it is based on the scenario exercise, where two risk strips (for a period of 50 and 100 years) were defined for each urban area along the intervention area. Thus enabling the fundamental spatial elements of the Plan Proposal to finally be constructed:

- Constraints Map – identify the legal constraints arising from administrative measurements and public utility restrictions;
- Land-use Map – represents the management system translated

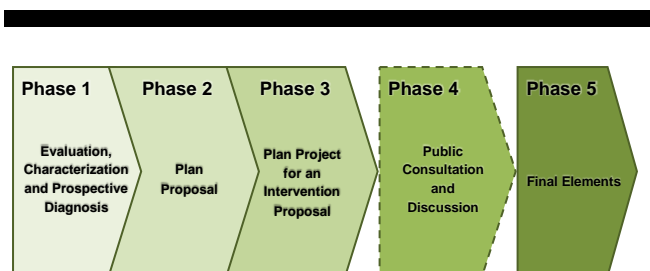


Figure 3. Methodological diagram of the CZMP-OMG (Source: adapted from APA, 2013b).

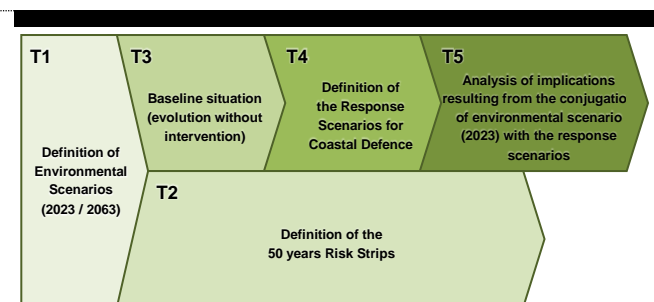


Figure 4. Tasks for the Scenario creation process (Source: adapted from APA, 2013b).

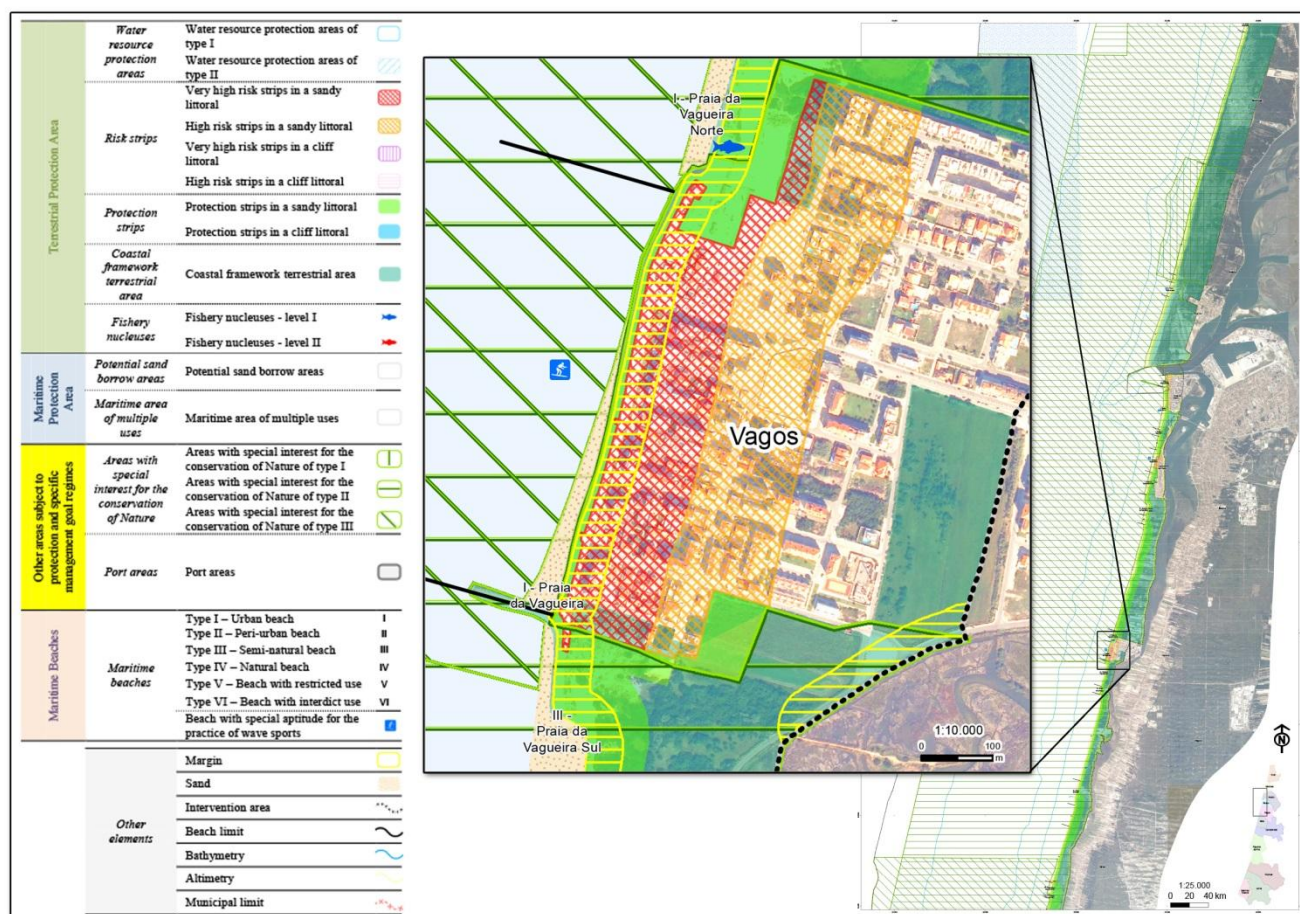


Figure 5. Structure of the Spatial Planning Model and detail of the Land-Use Map.

in the spatial distribution of the uses and activities (and their intensity) compatible with the sustainable use of the territory.

Figure 5 shows the structure of the Spatial Planning Model and illustrates an example of the detail required for the Land-Use Map.

The **Intervention Model** follows the strategic goals and lines defined in the Strategic Model, encompassing an execution and financial program. In other words, the four goals underpinning the Strategic Model (Protection, Recovery, Preservation and Development) are also those that structure the execution program, and each strategic line, intervention typologies (25) and actions (207) are set in order to meet the proposed Strategy. Some of these actions are spatially represented in the Strategic Map. Figure 2 shows in detail the actions defined for the Barra – Mira stretch. Under the Protection goal, there are actions such as recovery and stabilisation of dune systems, stabilisation of cliffs or water-lines requalification. The maintenance, rehabilitation and performance improvement of coastal defence structures is addressed to preserve goals as well as artificially nourishment and construct new groins.

Several local, sub-regional and national entities responsible for the implementation of each programmed actions were identified. The timeframe set for the CZMP-OMG implementation extends from 2014 to 2023. So, the temporal distribution of the proposed actions is planned regarding the urgency of the action, the ongoing projects and the next period of programmed EU funds (2014-2020). Although some of the actions have a preventive and adaptive nature, and are designed to address future problems/challenges, they must be achieved within the Plan's horizon (10 years). Finally the financial plan for the execution

program is designed as a result of the estimated costs of each action.

## FINAL REMARKS

As previously referred to the Portuguese spatial planners now face a challenge of reviewing their first generation spatial plans in order to implement a new innovative strategic tool that should not only be adapted to the territory in its present state, but should look ahead to try to prevent/mitigate future coastline impacts. This second generation Plan for OMG aims to do exactly that. It currently includes features that were not initially considered when the first CZMP was created in 2000 and is using GIS (Geographic Information Systems) and other modelling systems to foresee what may happen to the territory in order to adequately adapt the Plans' aims and goals. The ever changing territorial reality combined with the issues that are now relevant (but possibly won't be in the future, where new issues will arise) creates a strong management tool to help oversee present and future activities and effects.

Although the plan is being built for a time span of 10 years, the issues considered when constructing it went beyond this 10 year horizon. Risk parameters for the next 50 years were taken into consideration to avert or moderate more serious impacts for a medium-term future.

Challenges arise when creating a Management Plan for delicate coastal areas, once these are both influenced by and incur influences on several sectors: social, politics, economy, regulatory, natural and cultural. It is quite difficult to balance out

these different points of view nowadays. When trying to export these concerns in a 10 or 50 year span, this planning exercise has to deal with not only foreseeable influences of the territory (e.g., change in legislation, political changes, etc.), but also the factors that are currently unknown (e.g., climate change, coastline erosion, etc.). The review process of the second generation CZMP-OMG is now arriving to the end of its third phase. Even in this stage, it is safe to say that this process is not an easy task and great challenges are imposed when revising the CZMP-OMG. Several factors influence the intermediate decisions along the process as well as the end result. Some factors give unforeseeable outcomes, such as the accentuated increase of coastal erosion, the increase of oceanic overtopping situations and the future implications of coastal erosion and climate change. Practical issues are hard to assess and apply, such as the level of qualification of maritime beaches and relevant changes in their appeal. New regulatory issues further influence the review of the CZMP-OMG, such as the new regulatory context of the CZMPs (Decree no. 159/2012, of July 24) and the increasing strategic importance of the Sea (National Sea Strategies, Maritime Space Management Plan and the Basic Law on Maritime Space Planning and Management). Another factor which is a greater participatory in the planning process includes culture (6 thematic technical work meetings, several rounds of meetings with local authorities, 11 municipal technical work meetings).

To aid in the evaluation of the future coastal shoreline location, modelling is of extreme importance. Although modelling results don't tell us exactly what will happen, they may give us a very good idea because important information that may not have been visible initially can now be contemplated. Based on these results, the CZMP may be considerably improved, greatly aiding the decision-making process.

Currently there are multiple models which are available and applied, some more accurate than others, risk regulation has several real-world technical challenges. When an unused area is located in the risk strip, what should be done? Should we leave the area abandoned, creating an undesirable waste of space or an eyesore? The straight answer is no. But it is not easy achieving an optimum solution. If to prevent these situations certain exceptions should be done in order to maximize the territories' utilization, then the Plan should regulate these exceptions to minimize the risk level for inhabitants in that area.

As for a more practical analysis of the results, with Figure 2 one can verify that with the Strategic and Intervention Models two important areas to intervene can be identified, in order to protect the coastal zone from erosion, floods, shoreline retreat and the possibility of climate changes. These areas are located immediately south of the ports of Aveiro and Figueira da Foz and combine a higher number of priority actions to protect the coastal ecosystem dynamics and urban areas.

## ACKNOWLEDGEMENT

This work has been financed by Agência Portuguesa do Ambiente (APA; I.P.), QREN, Programa Operacional Regional do Centro and FEDER and has been developed under the Consórcio CEDRU/UA – Revisão do Plano de Ordenamento da Orla Costeira Ovar - Marinha Grande Protocol (cc. 2.10.400.67). Lisa P. Sousa benefits from a PhD grant (SFRH/BD/79170/2011) given by the Portuguese FCT (Fundação para a Ciência e Tecnologia). Tanya Esteves is financed by the Consórcio CEDRU/UA (BI/DAO/TanyaEsteves /2013). Eduardo R. Oliveira is financed by the European Regional Development Fund and INTERREG IV B: Atlantic Area Transnational Programme (SPRES-2011-1/168) (BI-FIS-31/SPRES-OUT2012). Inês C.

Antunes is financed by Homme-Milieu International Network (BI/DAO/OHMI2013\_FA). Maria da Luz Fernandes is financed by DG Maritime Affairs through the TPEA project (EU MARE/2012/08; BI/UI88/6389/2013).

## LITERATURE CITED

- Alves, F.L., Silva, C.P. and PINTO, P., 2007. The Assessment of Coastal Zone Development at a Regional Level – the case study of the Portuguese Central Area. In: *Proceedings of the 9th International Coastal Symposium* (Gold Coast, Australia), *Journal of Coastal Research*, Special Issue No. 50, 72 – 76. ISSN 0749-0208.
- Alves, F.L., Coelho, C., Coelho, C.D., Pinto, P., 2011. Modelling coastal vulnerabilities - Tool for decision support system at inter-municipality level. *Journal of Coastal Research*, Special Issue 64, 966-970.
- Alves, F. L., Sousa, L. P., Almodovar, M., Phillips, M. R., 2013. Integrated Coastal Zone Management (ICZM): a review of progress in Portuguese implementation. *Regional Environmental Change*, 13:5, 1031-1042. DOI: 10.1007/s10113-012-0398-y.
- APA. 2012. Relatório de Caracterização e Diagnóstico Prospectivo (Fase I – Relatório 2, Volume I). Lisbon: Agência Portuguesa do Ambiente, I.P.. Report developed by CEDRU and University of Aveiro.
- APA. 2013a. Relatório de Fase 2 – Proposta de Plano. (Fase II – Volume I). Lisbon: Agência Portuguesa do Ambiente, I.P.. Report developed by CEDRU and University of Aveiro.
- APA. 2013b. Relatório de Fase 3 – Projecto de POOC e Plano de Intervencões. (Fase III – Volume I). Lisbon: Agência Portuguesa do Ambiente, I.P.. Report developed by CEDRU and University of Aveiro.
- Carrero, R., Navas, F., Malvárez, G., and Cáceres, F., 2013. Participative Future Scenarios for Integrated Coastal Zone Management. In: Conley, D.C., Masselink, G., Russell, P.E. and O'Hare, T.J. (eds.), *Proceedings 12th International Coastal Symposium* (Plymouth, England), *Journal of Coastal Research*, Special Issue No. 65, pp. 898-903, ISSN 0749-0208.
- Commission Proposal COM., 2013. 133 final. Proposal for a Directive of the European Parliament and of the Council on establishing a framework for maritime spatial planning and integrated coastal management.
- Douvere, F., Ehler, C.N., 2009. New perspectives on sea use management: Initial findings from European experience with marine spatial planning. *Journal of Environmental Management*, 90, 77–88. DOI: 10.1016/j.jenvman.2008.07.004.
- Esteves, L.S., 2013. Is managed realignment a sustainable long-term coastal management approach? In: Conley, D.C., Masselink, G., Russell, P.E. and O'Hare, T.J. (eds.), *Proceedings 12th International Coastal Symposium* (Plymouth, England), *Journal of Coastal Research*, Special Issue No. 65, pp. 933-938, ISSN 0749-0208.
- Kidd, S. and Shaw, D., 2013. Reconceptualising territoriality and spatial planning: insights from the sea. *Planning Theory & Practice*, 14:2, 180-197. DOI: 10.1080/14649357.2013.784348.
- Oliveira, E.R., Silveira, B., Alves, F.L., *in press*. Support mechanisms for oil spill accident response in coastal lagoon areas (Ria de Aveiro, Portugal), *Journal of Sea Research*, Available online 14 November 2013. <http://dx.doi.org/10.1016/j.seares.2013.11.002>.
- Reis, J., Stojanovic, T., Smith, H., 2014. Relevance of systems approaches for implementing Integrated Coastal Zone Management principles in Europe. *Marine Policy*, 43, 3-12. DOI: 10.1016/j.marpol.2013.03.013.
- Schmidt, L., Delicado, A., Gomes, C., Granjo P., Guerreiro, S., Horta, A., Mourato, J., Prista, P., Saraiva, T., Truninger, M., O'Riordan, T., Santos, F.D., and Penha-Lopes, G., 2013. Change in the way we live and plan the coast: stakeholders discussions on future scenarios and adaptation strategies In: Conley, D.C., Masselink, G., Russell, P.E. and O'Hare, T.J. (eds.), *Proceedings 12th International Coastal Symposium* (Plymouth, England), *Journal of Coastal Research*, Special Issue No. 65, 1033-1038, ISSN 0749-0208.
- Sousa, L.P., Lillebø A.I., Gooch G.D., Soares J.A., Alves F.L., 2013. Incorporation of Local Knowledge in the Identification of Ria de Aveiro Lagoon Ecosystem Services (Portugal). In: Conley, D.C., Masselink, G., Russell, P.E. and O'Hare, T.J. (eds.), *Proceedings 12th International Coastal Symposium* (Plymouth, England), *Journal of Coastal Research*, Special Issue No. 65, pp. 1051-1056, ISSN 0749-0208.

## Productive Chain of the Mangrove Crab (*Ucides cordatus*) in the Town of Bragança, in the Northern Brazilian State of Pará (Amazon Region)



[www.cerf-jcr.org](http://www.cerf-jcr.org)

Marcos A.B. Monteiro†, Francisco P. Oliveira‡, José N. Araújo‡, Marcus E.B. Fernandes†

† Instituto de Estudos Costeiros,  
Universidade Federal do Pará, Campus de  
Bragança. Alameda Leandro Ribeiro, s/n,  
Bragança, Pará, Brasil, CEP: 68.600-000.  
Corresponding author: Phone/Fax: ++55  
91 34251209 / E-mail address:  
marcosborgesmonteiro@gmail.com;  
foliveiranono@yahoo.com.br;  
mebf@ufpa.br

‡ Instituto de Ciências Sociais Aplicadas,  
Universidade Federal do Pará, Faculdade  
de Ciências Econômicas - FACECON  
Rua Augusto Corrêa, nº 01, Setor  
Profissional, Guamá, Belém-PA, Brasil,  
CEP 66073-044, E-mail address:  
jonaz@ufpa.br



[www.JCRonline.org](http://www.JCRonline.org)

### ABSTRACT

Monteiro, M.A.B., Oliveira, F.P., Araújo, J.N., Fernandes, M.E.B. 2014. Productive Chain of the Mangrove Crab (*Ucides cordatus*) in the Town of Bragança, in the Northern Brazilian State of Pará (Amazon Region). In: Green, A.N. and Cooper, J.A.G. (eds.), *Proceedings 13<sup>th</sup> International Coastal Symposium* (Durban, South Africa), *Journal of Coastal Research*, Special Issue No. 70, pp. 443-447, ISSN 0749-0208.

The present study focuses on the production chain of the mangrove crab (*Ucides cordatus*), one of the key animal species in the mangrove forests of the Brazilian Amazon coast. The study began in the principal restaurants of the town of Bragança, in the northeastern extreme of the state of Pará, from which the principal components of the productive chain were identified, working back along this process until the primary producers, the crabbers, were detected. Questionnaires were applied each month throughout an annual cycle. The present study also identified the marketing processes (formal and informal) adopted by these social actors and analyzed the profit margins generated by the sale of the crabs at different stages in the process. All the social actors that compose this productive chain were monitored over an annual cycle. The Kruskal-Wallis nonparametric analysis of variance was used to evaluate the level of variation in the parameters analyzed. The results indicated that the *U. cordatus* productive chain in Bragança is composed of six social actors – crabbers, crabmeat pickers, primary and secondary traders, restaurants, and final consumers. While this chain is ramified, it is not complex, being formed by primary producers, wholesale and retail markets, and final consumers. All these levels are linked by the flow of capital, material, and information.

**ADDITIONAL INDEX WORDS:** *Social actors, mangrove land crab trade, wholesale and retail markets, Brazilian Amazon coast.*

### INTRODUCTION

The coastline of Brazil extends over a total length of 7408 km, and encompasses approximately 70% of the country's population, and 75% of its principal urban centers (CNIO, 1998). Around 40% of this littoral is located on the Amazon coast, formed by the seaboard of the states of Amapá, Pará, and Maranhão, which together stretch over a total distance of 2500 km (Isaac & Barthem 1995; Lara & Cohen 2003). Biologically, this region is extremely diverse and highly productive, with a highly characteristic fauna and flora, which are found in a heterogeneous landscape of estuaries, rivers, and tropical forests, interlinking terrestrial and aquatic ecosystems (Carvalho & Rizzo, 1994, Souza-Filho *et al.*, 2005).

One of the most important crustaceans that inhabit the mangrove forests of the Brazilian coast is the mangrove crab, *Ucides cordatus* Linnaeus, 1763. This species is characterized by its coloration pattern of blue, purple, and reddish tones. Its carapace has a diameter of approximately 10 cm, and the distance

between the tips of its outstretched limbs may reach 30 cm. The internal surfaces of the legs are covered with large, stiff bristles. Reproduction occurs between January and March, when the adults come out of their dens (Nordi, 1994). The crabs dig complex galleries or individual burrows of approximately one meter in depth under the mangrove forest in which they remain hidden during the rest of the year, when they are especially difficult to capture, given that they stock their dens with the food necessary to last through the period of ecdysis (Pinheiro, 2001).

The mangrove crab is a valued economic resource, and for this reason, it is important to better understand its productive chain, that is, the set of interactive components, including productive systems, the suppliers of goods and services, processing facilities, and distribution and marketing agents, as well as the role of the final consumers (Marques & Aguiar, 1993; Batalha, 1995). The marketing of the product involves the exchange of goods and services for monetary gain. Exchange condition or rates and product prices are generally determined by market forces, that is, the equilibrium of supply and demand, which permit the transfer of goods and services in exchange for money. In this context, the

product reaches the consumer through a series of different market levels (Rezende & Aguiar, 1996).

In the Brazilian state of Pará, the harvesting of crabs is one of the mangrove forest's oldest productive occupations (Fiscarelli, 2001; Pinheiro, 2001). In the present day, it is one of the most important socio-economic activities of traditional local populations, such as those found in the municipality of Bragança, where the local economy is heavily dependent on the artisanal harvesting of these crustaceans and other fishery resources.

In Bragança, *U. cordatus* is the most important fishery resource found in the local mangroves, in terms of both subsistence foraging and the generation of monetary income. More than half of the households in rural areas and those adjacent to mangrove forests depend on the harvesting, processing, transportation or marketing of crabs for the bulk of their income. However, crabbers are considered to represent one of the poorest social groups in rural coastal areas, where *U. cordatus* constitutes a fundamentally important source of income (Glaser & Grasso, 1998; Grasso, 2000).

The mangrove crab is the main source of income for both coastal communities and for those of large cities. Its marketing has been taken from living individuals and portions, i.e. crabmeat, both for household consumption and for sale in bars and restaurants. Moreover, in recent years, restrictions on labor supply and employment in cities of the Amazon region have provided an additional quota of skilled manpower for activities related to the extraction of mangrove crab. As a consequence, local stocks have been the subject of exhaustive collections by capturing, with the increasing number of local crab fishermen, as well as the post-capture, with the involvement of communities in processing the meat, generating socio-economic situation in the region (Manesch, 2003).

In this context, the present study focuses on the productive chain, analyzing its structure and processes, and identifying the bottlenecks and levels of competition among the participants of this system. In order to better understand the marketing process, the social agents that make up the chain in the town of Bragança were identified and the formal and informal strategies adopted by these actors for the sale of mangrove crabs were investigated.

## Study area

The Bragança coastal plain, in the northeastern extreme of the Brazilian state of Pará, extends from Maiaú Point to the mouth of the Caeté River, covering a total area of approximately 1570 km<sup>2</sup> (Souza-Filho, 1995). The Ajuruteua Peninsula is bisected by the PA-458 highway, which links Bragança to the village of

Ajuruteua. The highway is 36 km long, of which the northernmost 20 km cross the local mangrove forest (Carvalho, 2002).

The town of Bragança (01°03'48"S, 46°46'24"W) is located on the left margin of the Caeté River (Figure 1), 220 km east of the state capital, Belém (Costa, 2001). The municipality is limited to the North by the Atlantic Ocean, to the south by the municipalities of Santa Luzia do Pará and Viseu, to the east by Augusto Corrêa, and to the west by Tracuateua. It has a total population of 113,165 inhabitants (approximately 51% male and 49% female), of which, 64.15% live in the urban zone, while the remaining 35.85% are distributed among the 173 rural and fishing communities that make up the municipality, which are organized into seven administrative districts – Almoço, Bacuriteua, Bejamim, Bragança, Caratateua, Nova Mocajuba, and Treme (IBGE, 2010).

## METHODS

### Procedures

The dynamics of the productive chain of the mangrove crab in Bragança was investigated by interviewing the different agents that make up the chain (i.e., restaurateurs, traders, crabmeat pickers, and crabbers) using questionnaires. These social actors participate directly in the crab marketing system in Bragança. Complementary documentary input was collected through the systematic analysis of secondary data obtained from research institutions and government agencies, as well as searches of the specialist literature.

The data were stored and organized in Excel spreadsheets. This approach permitted the use of descriptive elements based on statistical methods. The quantitative data from the spreadsheets were condensed and analyzed using descriptive statistics run in Statistica 8.0.

The data were examined for normality using the Lilliefors test. Since assumptions for normality were not satisfied, even after the transformation of the data, the Kruskal-Wallis nonparametric analysis of variance was used to evaluate the levels of variation in the different parameters analyzed (Zar, 1996).

### Interviews

Questionnaire-based interviews were used to characterize the *U. cordatus* marketing system in the town of Bragança. The questions were structured or semi-structured and emphasized both qualitative and quantitative approaches (Chizzotti, 2000). The interviews (based on specific questionnaires) were conducted each month over an annual cycle, focusing on (i) Bars and restaurants, (ii) Traders, (iii) Crabmeat pickers, and (iv) Crabbers.

## RESULTS

### The productive chain of the mangrove crab in Bragança (Pará, Brazil)

The productive chain of the mangrove crab in the Brazilian town of Bragança is shown in the flow chart in Figure 2. This scheme shows that the first segment of the chain, represented by the crabbers, involves the supply of the input necessary to initiate the process. This segment includes the transportation costs, rations, fuel, insect repellent, and medical supplies used during the harvesting of the crabs. The traders represent another segment of the productive chain. The primary traders buy live crabs directly from the crabbers, and sell them to the final consumer or other types of buyers. The secondary traders are responsible for marketing processed crabmeat in bulk to local restaurants and

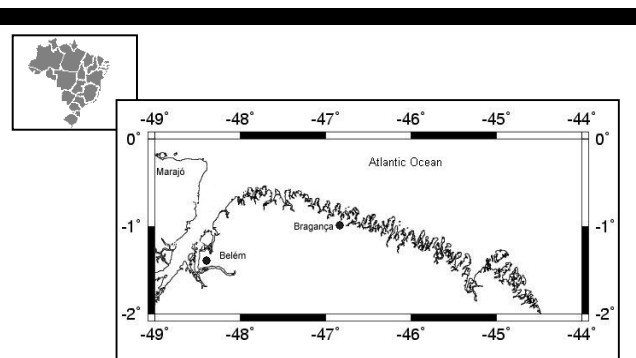


Figure 1. Map showing the town of Bragança in the northeastern extreme of the Brazilian state of Pará. Modified from Monteiro (2007).

other buyers in Bragança, as well as other towns in the region, with little or no onus or investment.

As an integral component of the productive chain, local restaurants purchase the majority of the processed crabmeat sold by the traders and crabbers. The restaurants pass on all the inputs of the process – including the harvesting, processing, and distribution – through the dishes served to the final consumer, the last link in the chain. These social actors, in turn, stimulate the local market in *U. cordatus*.

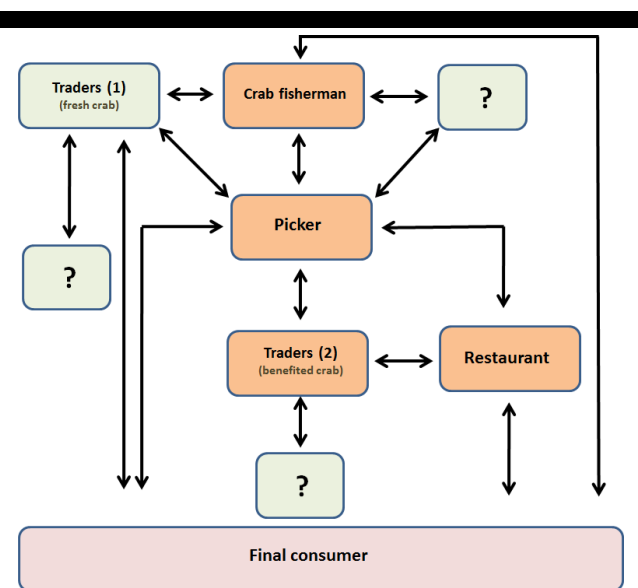


Figure 2. Flow chart of the *U. cordatus* productive chain in Bragança (Pará, Brazil).

### Crabbers

The crabbers collect “cords” of crabs, each of which contains 14 crabs (Pinheiro & Fiscarelli, 2001). The mean numbers of cords harvested each month by the local crabbers are shown in Figure 3. The mean number of cords collected by different crabbers varied significantly ( $H = 11.02$ ;  $df = 4$ ;  $p < 0.05$ ), as did the mean number of cords produced each month ( $H = 28.41$ ;  $df = 11$ ;  $p < 0.01$ ). Significant variation was also found in the income of different crabbers ( $H = 29.88$ ;  $df = 4$ ;  $p < 0.0001$ ). Figure 5 shows crabbers and traders in different stages of the process.

### Crabmeat pickers

An average minimum of 11 cords (154 crabs) and a maximum of 21 cords (294 crabs) are picked (meat extracted) per day of work. According to the crabmeat pickers, 40 crabs are required for the extraction of 1 kg of crabmeat and 200 g of claws. The pickers work eight hours a day on average, three to six days a week. The crabmeat and claws are normally sold by the pickers to traders, who distribute the products to restaurants and other consumers in Bragança. Significant variation was found in the income of different crabmeat pickers (Kruskal-Wallis:  $H = 20.52$ ;  $df = 4$ ;  $p < 0.001$ ).

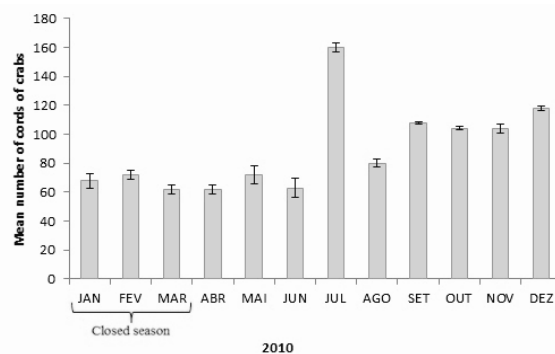


Figure 3. Mean number of cords of crabs (1 cord = 14 crabs) harvested by the crabbers each month over an annual cycle in the mangroves of the Ajuruteua Peninsula, Bragança (Pará, Brazil). Standard error bars.

### Traders

The traders buy the crabmeat and claws in Apeú, Augusto Corrêa, Cajueiro, Caratateua, Furo da Salina, and Treme. However, the pickers obtain the live crabs in the open-air markets of Bragança and process the animals in their homes in this municipality. The traders sell 500–700 kg of crabmeat per month to the local restaurants, and 80–140 kg of claws, presenting the same range of standard error (Figure 4). Crabmeat is also marketed to other cities in Pará, and other Brazilian states, such as Amazonas (Manaus). No significant variation was found in the income of different traders ( $H = 0.22$ ;  $df = 1$ ;  $p = 0.64$ ).

### Restaurants

During the study period, the Bragança restaurants purchased most crabmeat in July and December. Overall, a mean of 28 kg of crabmeat was obtained each month per restaurant. Prices in these

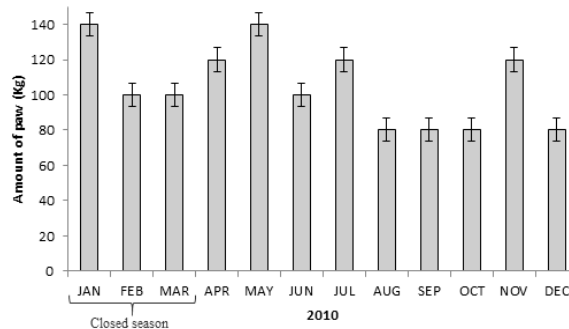


Figure 4. Monthly variation in the purchase of crab meat (kg) by the restaurants of the town of Bragança over an annual cycle. Standard error bars.



Figure 5. Images of crabbers and traders from Bragança (Pará, Brazil), showing the complete process from the capture of the mangrove crabs to their sale: (a) crabbers preparing to enter the mangrove forest, (b) crabbers accessing the mangrove by boat, (c) crabber capturing *U. cordatus* in the mangrove, (d) crabber with a full cord, (e) stallholder selling crabs in the open-air market in Bragança, (f) cords of crabs ready to be sold to traders, and (g) trader selling crabs on a stall in another part of Bragança.

months, when large numbers of tourists visit the town (due to the school holidays and local festivities) ranged from R\$14 to R\$16 (US\$5–6), the kilogram. Significant variation was found among months in the income of the restaurants ( $H = 28.51$ ;  $df = 3$ ;  $p < 0.001$ ).

## DISCUSSION

### The productive chain of the mangrove crab in Bragança (Pará, Brazil)

In Bragança, the primary producers (crabbers and crabmeat pickers) depend on traders for the marketing of their product, that is, the mangrove crab. The local productive chain is made up of four components – the primary producers, wholesale market, retail market, and final consumers. All these components are linked by a flow of capital, materials, and information. However, Besanko *et al.*, (2006) considered the chain to be simple, that is, made up of isolated transactions without formal or contractual relationships between the different components.

#### Crabbers

*Ucides cordatus* is harvested from the mangrove forest by crabbers. The sustainable exploitation of this resource will require a better understanding of this environment (Schaeffer-Novelli, 1996). In this context, the harvesting of *U. cordatus* in the state of Pará is considered to be primarily a subsistence activity and a source of income for the local communities that exploit this natural resource (Martins, 2010).

#### Crabmeat pickers

The present study showed that the crabmeat pickers buy crabs directly from the crabbers or, in the urban setting, from traders. In some cases, the crabbers' family members extract the meat, which is then sold to traders. A similar situation was found in the studies of Mendes (2003) and Reis (2007), which described the relationships among crabbers, pickers, and traders. In this case, the crabbers sold their catch directly to the pickers, who wait for the crabs at the landing point, although some crabbers also took their catches home for processing.

#### Traders

In the study area, the traders are the intermediary between the crabbers and local or regional markets, supplying crabmeat and claws to local restaurants. Sarmento (1998) reports that live mangrove crabs are generally sold by the crabbers themselves, or by traders who sell the crabs on to other suppliers. The traders may also sell other products on the local market. It is important to note, however, that these traders usually cultivate a close working relationship with the local restaurant owners to whom they may work on credit, sometimes receiving payment for the crabmeat only once a week, for example. This emphasizes the trust between these two actors in the productive chain, despite the informal relationship between them.

#### Restaurants

Based on the data collected in the questionnaires and the calculation of profit margins, it was possible to confirm that the restaurants of the town of Bragança are the component of the

productive chain that most profit from the process. While no comparable studies of the *U. cordatus* productive chain are available for comparison with the results of the present study, Takahashi (2008) has studied the productive chain of the blue land crab (*Cardisoma guanhumi*) in Paraíba, northeastern Brazil, where a closely similar system was observed, in which the local bars were the most important components of the chain. This study did not report on profit margins, however.

### CONCLUDING REMARKS

The results of the present study indicate that the social actors who make up the productive chain of the mangrove crab in the Brazilian town of Bragança are the crabbers, crabmeat pickers, traders, restaurants, and final consumers. The trade of the mangrove crab in Bragança is more profitable for the wholesale and retail market, maintaining the low level of income of the primary producers, i.e., the fisherman and collector. This sale is part of a productive chain whose flow is much branched, but it does not culminate in a complex productive chain, by lacking formalities between their social agents. According to the flow of the productive chain of the mangrove crab in Bragança, the biggest beneficiaries of this are the social marketing agents downstream of this flow, i.e. the traders and restaurants. It was noticed throughout the present study that the period of the closure of the mangrove crab (January, February, and March/2010) there was a significant reduction in fishery, processing, transportation, and marketing of this resource. Such behavior, explicit in the different actors of the productive chain, may reflect several factors, which are linked to various sectors of society.

### ACKNOWLEDGEMENTS

We are grateful to the Federal University of Pará, the Graduate Program in Environmental Biology (Masters and Doctorate in the Biological Resources of the Amazon Coastal Zone), the Coastal Ecosystems Institute for graduate training, and the Mangrove Ecology Laboratory on the Campus of Bragança for the opportunity to develop this research.

### LITERATURE CITED

- Ayres, M., Ayres-Junior, M., Ayres, D. L., Santos, A., S., 2007. Aplicações Estatísticas nas Áreas das Ciências Biológicas e Médicas. Instituto de Desenvolvimento Sustentável Mamirauá. BioEstat 5.0, 364p.
- Batalha, M. O., 1995. As cadeias de produção agro industriais: uma perspectiva para o estudo das inovações tecnológicas. Revista de Administração, São Paulo, v30, n42, 43-50.
- Besanko, D; Dranove, D; Shanley, M; Schaefer, S., 2006. A Economia da Estratégia. 3ª edição. Artmed Editora. Porto Alegre – RS, 608p.
- Carvalho, M. L., 2002. Aspectos da produtividade primária Aspectos da produtividade primária dos bosques de mangue do Furo Grande, Furo Grande, Bragança-Pará. Dissertação (Mestrado) – Universidade Federal do Pará, Belém-Pará, 68p.
- Carvalho, V. C. & Rizzo, H. G., 1994. A Zona Costeira Brasileira: subsídios para uma avaliação ambiental. Ministério do Meio Ambiente e Amazônia Legal. Secretaria de Coordenação de Assuntos de Meio Ambiente. Brasília-DF, 40p.
- Chizzoti, A., 2000. Pesquisa em Ciências Humanas e Sociais. 4ª Ed. – São Paulo: Cortez, 164 p.
- Costa, N. dos S., 2001. Estrutura da Comunidade de Peixes capturados nos currais pesqueiros do rio Caeté, Bragança-PA. Trabalho de Conclusão de Curso apresentado ao Colegiado do Curso de Biologia – Campus de Bragança – UFPA, 29p.
- CNIO – Comissão Nacional Independente Para os Oceanos. 1998. O Brasil e o mar no século XXI: relatório aos tomadores de decisão do país. Rio de Janeiro – Comissão Nacional Independente para os Oceanos, 248p.
- Glaser, M., Grasso, M., 1998. Fisheries of a mangrove estuary: dynamics and inter-relationships between economy and ecosystem in Caeté bay, northeastern Pará, Brazil. Boletim do Museu Paraense Emílio Goeldi, Belém-PA, 95-125.
- Grasso, M., 2000. Understanding, modeling and valuing the linkages between local communities and the mangroves of the Caeté river Bay, PA, Brazil. Phd, Dissertation – Faculty of the graduate School of the University of Maryland, US, 554p.
- IBGE. 2010. Instituto Brasileiro de Geografia e Estatística. Bragança-PA. <http://www.ibge.br/cidadesat/default2.php>.
- Lara, R.J.; Cohen, M.C.L., 2003. Sensoriamento remoto, p. 11-28. In: Fernandes. M.E.B. Os manguezais da costa norte brasileira. São Luís, Fundação Rio Bacanga, 142p.
- Isaac, V.J.; Barthem, R. B., 1995. Os Recursos Pesqueiros da Amazônia Brasileira. Museu Paraense Emílio Goeldi. Universidade Federal do Pará. Série, 11(2), 151-194.
- Manesch, M.C., 2003. Sócio-Economia: Trabalhadores e Trabalhadoras nos Manguezais. In: M.E.B. Fernandes (org.), Os manguezais da costa norte brasileira. Vol 2. Fundação Rio Bacanga, São Luís, 135–165.
- Marques, P.V.; Aguiar, D. R. D., 1993. Comercialização de produtos agrícolas. São Paulo. Edusp. V.13, 291p.
- Martins, L.F., 2010. Caracterização socioambiental da extração e comercialização do caranguejo-uçá realizado na RESEX “Mãe Grande de Curuçá”, Pará. Monografia (Especialização). Núcleo de Altos Estudos Amazônicos – NAEA e Universidade Federal do Pará – UFPA, 96p.
- Mendes, P.M., 2003. Quatipuru: Sobrevivendo do Mangue: Alimentação e Trabalho na Produção de Caranguejo. Monografia de Especialização. Núcleo de Altos Estudos Amazônicos (NAEA-UFPA), Belém-PA, 46p.
- Monteiro, M.A.B., 2007. O Livro Didático e os Atores Educacionais da Comunidade de Tamatateua - Bragança: uma experiência no litoral nordeste do Pará. Trabalho de Conclusão de Curso (TCC), Universidade Federal do Pará, Campus de Bragança-Pará, 60p.
- Nordi, N., 1994. A captura do caranguejo-uçá (*Ucides cordatus*) durante o evento reprodutivo da espécie: o ponto de vista dos caranguejeiros. Revista Nordestina de Biologia 9, 41-47.
- Pinheiro, M.A., 2001. A Biologia do caranguejo-uçá (*Ucides cordatus*, Linnaeus, 1763) no litoral sul do Estado de São Paulo. Relatório Científico Final do Projeto Uçá. FAPESP. Jaboticabal, SP, 211p.
- Fiscarelli, A.G., 2001. Manual de Apoio à Fiscalização do Caranguejo-uçá (*Ucides cordatus*). CEPISUL. Itajaí (Santa Catarina), 43p.
- Reis, M.R.R., 2007. Na Friadagem do Mangal: organizar e tirar caranguejos nos fins de semana em Bragança (Vila do Acarajó). Dissertação de Mestrado em Ciências Sociais. Universidade Federal do Pará. Belém/Pará, 115 p.
- Rezende, A.M.; Aguiar, D.R.D., 1996. Comercialização, Complexo, Agroindustrial e Marketing Rural. Brasília-DF. ABEAS, 43p.
- Sarmiento, I. L. F., 1998. O caranguejo é mina? Dimensões socioeconômicas e ambientais de uma atividade extrativista no litoral do Pará. Monografia (Especialização) – Núcleo de Altos Estudos Amazônicos/Universidade Federal do Pará (NAEA/UFPA), Belém-PA, 51p.
- Schaeffer-Novelli, Y., 1996. Ecosistema manguezal: conhecer para conservar. Anais do VI Encontro Nacional de Educação Ambiental em áreas de manguezais, 39p.
- Souza-Filho, P.W.M., 1995. A planície costeira bragantina (NE do PA): influência das variações do nível do mar na morfoestratigrafia costeira durante o Holoceno. Dissertação (Mestrado) – Universidade Federal do Pará, 123p.
- Souza-Filho, P.W.M., Sales, M.E.C.; Prost, M.T.R.C., Costa, F.R., Sousa, L.F.M.O., 2005. Zona Costeira Amazônica: O cenário regional e os indicadores bibliométricos em C&T. In: Souza Filho, P.W.M. Cunha, E.R.S.P., Sales, M.E.C., Souza, L.F.M.O., Costa, F.R. (org) Bibliografia da Zona Costeira Amazônica – Brasil. Museu Paraense Emílio Goeldi. Universidade Federal do Pará, Belém, 9-20.
- Takahashi, M.A., 2008. Conhecimentos locais e a cadeia produtiva do goiamium (*Cardisoma guanhumi*, Latreille, 1825) no litoral paraibano. Universidade Federal da Paraíba / Universidade Estadual da Paraíba. Dissertação de Mestrado. Programa regional de Pós-graduação em desenvolvimento e Meio Ambiente, 88p.
- Zar, J.H., 1996. Biostatistical Analysis. 3ª. ed. Prentice-Hall International Editions, New Jersey, 662p.



## An analysis of recent changes in Spanish Coastal Law

Vicente Negro†, José-Santos López-Gutiérrez‡, M. Dolores Esteban∞, Clara Matutano§

†Research Group on Marine, Coastal and Port Environment and other Sensitive Areas  
Universidad Politécnica de Madrid,  
E28040, Madrid  
vicente.negro@upm.es

‡ Research Group on Marine, Coastal and Port Environment and other Sensitive Areas  
Universidad Politécnica de Madrid,  
E28040, Madrid  
josesantos.lopez@upm.es

∞ Research Group on Marine, Coastal and Port Environment and other Sensitive Areas  
Universidad Politécnica de Madrid,  
E28040, Madrid  
mariadolores.esteban@upm.es



[www.cerf-jcr.org](http://www.cerf-jcr.org)

§ Research Group on Marine, Coastal and Port Environment and other Sensitive Areas  
Universidad Politécnica de Madrid,  
E28040, Madrid  
matumol@gmail.com



[www.JCRonline.org](http://www.JCRonline.org)

### ABSTRACT

Negro, V., López-Gutiérrez, J.S., Esteban, M.D., Matutano, C., 2014. An analysis of recent changes in Spanish Coastal Law. In: Green, A.N. and Cooper, J.A.G. (eds.), *Proceedings 13<sup>th</sup> International Coastal Symposium* (Durban, South Africa), *Journal of Coastal Research*, Special Issue No. 70, pp. 448-453, ISSN 0749-0208.

Spanish coastal legislation has changed in response to changing circumstances. The objective of the 1969 Spanish Coastal Law was to assign responsibilities in the Public Domain to the authorities. The 1980 Spanish Coastal Law addressed infractions and sanctions issues. The 1988 Spanish Coastal Law completed the responsibilities and sanctions aspects and included others related to the delimitation of the Public Domain, the private properties close to the Public Domain, and limitations on land use in this area.

The 1988 Spanish Coastal Law has been controversial since its publication. The “European Parliament Report on the impact of extensive urbanization in Spain on individual rights of European citizen, on the environment and on the application of EU law, based upon petitions received”, published in 2009 recommended that the Spanish Authorities make an urgent revision of the Coastal Law with the main objective of protecting property owners whose buildings do not have negative effects on the coastal environment.

The revision recommended has been carried out, in the new Spanish Coastal Law “Ley 2/2013, de 29 de mayo, de protección y uso sostenible del litoral y de modificación de la Ley 22/1988, de 28 de Julio, de Costas”, published in May of 2013. This is the first major change in the 25 years since the previous 1988 Spanish Coastal Law. This paper compares the 1988 and 2013 Spanish Coastal Law documents, highlighting the most important issues like the Public Domain description, limitations in private properties close to the Public Domain limit, climate change influence, authorizations length, etc. The paper includes proposals for further improvements.

**ADDITIONAL INDEX WORDS:** *Public domain, Coastal law, Auker Report, Spanish coastal legislation.*

### INTRODUCTION

Over the period 1969-2013, various Spanish Coastal Law documents with different approaches have been approved. This paper tracks the changing legislation with particular attention to the most recent amendments. In April 1969 (B.O.E., 1969), the first Coastal Law was approved in Spain. Previously, the land-sea domain regulation depended on existing port laws that were developed. Port laws were focused solely on navigation and naval facilities, and ignored environmental management.

The 1969 Coastal Law was approved during a dictatorship. During this period, in order to strengthen the economy, the regime opted to promote the tourism industry on the Spanish coasts. Thus, property development experienced a spectacular growth within the

coastal environments (Figure 1 and Figure 2). One of the main problems faced by the subsequent democracy was the existence of property rights acquired through the 1969 Coastal Law. Most of these properties were within the maritime-terrestrial public domain.

The new Spanish Constitution, approved in 1978, stated the intention of limiting private property rights by the Central Administration. In order to do this, it was necessary to develop a specific law to regulate the maritime-terrestrial areas. Ten years later, the 1988 Coastal Law (B.O.E., 1988) was implemented.

In the justification of the 1988 Coastal Law it was noted that the Spanish coast, comprising 24% beaches, represents a valuable asset for the great possibilities offered. In spite of this, little effort was made in understanding the extent of human modification of the coast (Cooper and Alonso, 2006) or how to recover its physical balance.

DOI: 10.2112/SI70-076.1 received 21 November 2013; accepted 21<sup>st</sup> February 2014. © Coastal Education & Research Foundation 2014



Figure 1. High rise buildings in the coastal environment (Benidorm, Spain) (M.A.R.M., 2013)

The 1988 Coastal Law was approved with the main objective of recovering coastal areas by restricting private property in the public domain. However, this law did not achieve this challenge and Spain continued to suffer a poorly planned development of the coastal zone. The great technical and legal complexity of the application of this law was due to numerous technical, social and economic problems related to expropriation, the limits of the public domain and the practicalities of carrying out demolitions (Torres, 2010).

Various property owners who were affected by the new law created a new association in an effort to protect their assets. The new organization “Asociación Europea de los Perjudicados por la Ley de Costas (AEPLC)” submitted a petition to the European Parliament. Margarete Auken, Danish Deputy from the Green/EFA group, wrote a complete report supporting the association’s claims, denouncing the impact of the extensive urbanization in Spain and defending the individual rights of European citizens. EU approved the Auken report. Based on the conclusions of the Auken report, the 2013 Coastal Law (B.O.E.,

2013) was written because of the ineffectiveness of the 1988 Coastal Law. The reasons leading to this reform were mainly the legal uncertainty for owners of private properties constructed in public domain, and the lack of legal surety for occupations and economic activity.

In the following sections the highlights of the two Spanish coastal laws of 1988 and 2013 will be described. Later, a comparative analysis of both indicating the improvements and shortcomings of both will be included.

### THE 1988 COASTAL LAW

The privatization of the public domain was excluded explicitly by the 1988 Coastal Law. This Law transformed the rights of private owners whose properties were within the public domain. They were given a right of occupancy of their properties for thirty years. This concession can be extended another thirty years. Obviously, this caused many political and social reactions, although the most vigorous reaction was carried out by the different Spanish coastal cities, which received information about

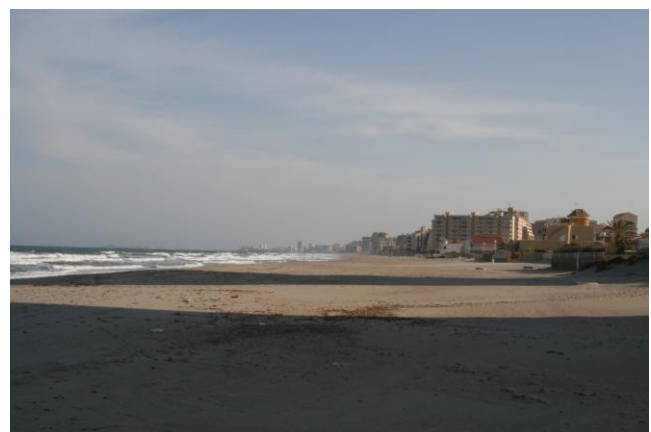


Figure 2. La Manga sand barrier: pictures before (www.marmenonline.com) and after the huge growth of private properties

the new Coastal Law reform a few months before final approval.

These coastal municipalities, aware of the impact of the future Coastal Law, rapidly developed numerous General Urban Plans in order to maintain the smallest distance of easement in their territories.

With the approval of 1988 Coastal Law, the following actions were developed:

- Change in the nomenclature and size of easements.
  - Protection easement, which occupies 20 or 100 meters depending on the classification of the territory: 20 meters in urban and building land with partial planning approved, and 100 meters in undeveloped land or land for building development without partial planning approved.
  - Transit easement of transit of 6 meters width.
  - Access to the sea easement. In urbanized areas free public access to the coast is guaranteed at a distance of every 200 meters for pedestrians, and every 500 meters for traffic.
- Numerous properties were considered as public domain.
- Owners of properties located in the public domain will become holders of a right of temporary occupation without the right of compensation. After the period of occupation, such properties will be demolished.

Analyzing all these actions is clear that the 1988 Coastal Law focused on regulation of the public domain limits and private property on the coast (B.O.E., 1989).

The approval of the 1988 Coastal Law and its General

Regulations required the complete definition of the public domain limits. Thus, it was intended to ensure the public use of the shoreline and consequently regulate the degree of coastal privatization (M.M.A., 2005).

The delimitation process of the public domain had important legal, economic, political, social and environmental implications. On one hand, the technical consequences were associated with the large number of technical studies needed to justify the extent of the public domain. On the other hand, the administrative impact was due to the large number of affected population. And finally, social impact was related with the consequences suffered by owners of its properties.

Throughout the years, the process of delimitation of public domain limits increased its complexity. A huge number of cases were brought before the Court of Justice, performing new technical studies to analyze the suitability of the approved limits.

With the intention that the entire public domain limits were completely defined in a maximum period of four years, the Spanish Ministry of Environment developed a specific Plan of delimitation of these territories between 2004 and 2008 (M.A.R.M., 2009).

According to the data provided by the Spanish Ministry of Environment, in 2005, 70% of the public domain of Spanish coast was defined. In 2009, this percentage reached 87.19% and in 2010, it was of 94%. Figure 3 shows the percentages obtained in the last month of 2011. Only 3 territories present figures of 100%.

As a result of the controversial actions associated with the implementation of the 1988 Coastal Law, the National Platform of

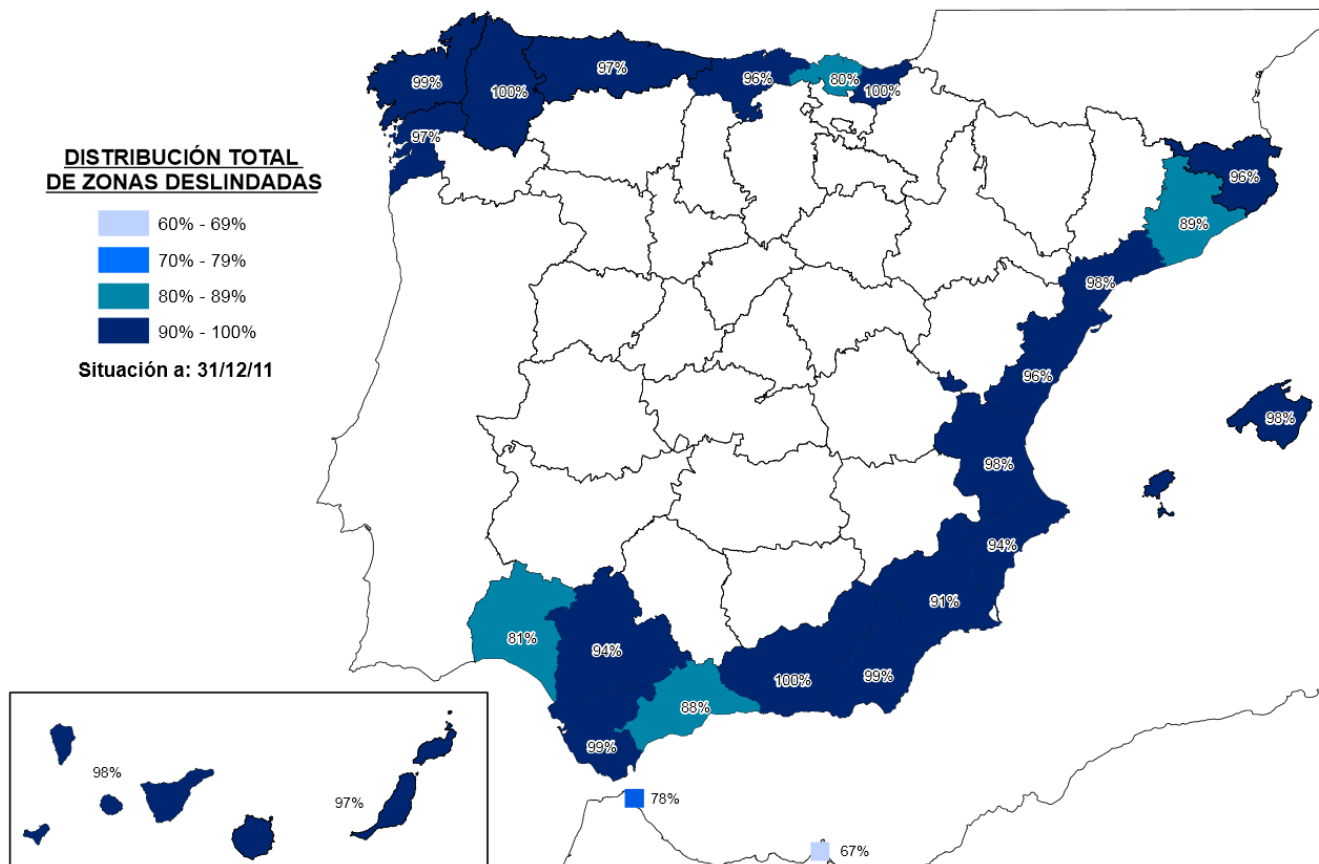


Figure 3. Percentages of public domain delimited (December, 2011) ([www.magrama.gob.es](http://www.magrama.gob.es))

people affected by the Coastal Law was founded in 2008. This platform filed a complaint with the European Parliament arguing an abusive and retroactive application of the Coastal Law. In this sense, The European Parliament decided to prepare a detailed study ended with the presentation of the Auken Report (Auken, 2009). This report analyzed the impact of extensive urbanization in Spain on individual rights of European citizens, on the environment and on the application of EU law, based upon petitions received.

The Auken report identified an unsustainable model which serious environmental, social and economic consequences. Although the impact of this report was limited (it was not a mandatory). It contained a number of recommendations to the Spanish government.

After 25 years of its existence, the 1988 Coastal Law had become disconnected from reality. Over the years it has come to be seen as ineffective in protecting the coast against the excesses of construction.

It is important to note that the economic crisis which began in 2008 reduced significantly the number of constructions on the Spanish coastline (Cooper and McKenna, 2009). Although, nowadays, the consequences of poorly regulated construction is still present in the landscape (García-Ayllón and Estrella, 2013). This, coupled with the following issues described in Table 1, culminated in the development of the 2013 Coastal Law, “Ley 2/2013, de 29 de mayo, de protección y uso sostenible del litoral y de modificación de la Ley 22/1988, de 28 de Julio, de Costas”.

### THE 2013 COASTAL LAW

The reform of 1988 Coastal Law was justified by the need for an effective tool for coastal protection and conservation, in order to ensure the legal security of private owners, and reconcile the protection of natural areas with economic activities that create jobs and generate wealth.

The 1988 Coastal Law promoted an erratic and sometimes arbitrary application at times, which caused legal uncertainty for owners and rights holders on the coast.

From 1988 to present, major degradation of the coast due to urban overcrowding and the expansion of private constructions has taken place. The 2013 Coastal Law distinguishes between “urban” zones on beaches, and “natural” zones located in protected areas away from urbanizations. Applying a different regimen in each case, with the objective of providing a high level of protection of beaches and that environmental values are maintained.

The 2013 Coastal Law emphasizes the desirability of the

Table 1. Weaknesses of 1988 Coastal Law.

Weaknesses of 1988 Coastal Law
Lack of clarity and consistency of the Public Domain boundary
Existence of more than 10.000 residential occupancies in the Public Domain
Absence of guarantees to purchasers. Urban abuses and loss of credibility of the Spanish property market in Europe
No protection for owners: massive demolitions in 2018 on certain uses and activities that create jobs and wealth
Degradation of buildings and facilities on the coast

existence of a mechanism for rapid and effective reaction by the Administration to avoid the occurrence of illegal situations (see Figure 4). According to the called “Anti-Algarrobrico” clause, The Administration could address each problem from the beginning with total autonomy.

In order to eliminate legal uncertainty contained in the 1988 Coastal Law, the new law introduces significant improvements, such as the clarification of the maritime-terrestrial public domain, and the clear definition of the beach and the elements it includes, especially the dunes, among others.

A second line of improvement, within the objective of increasing legal certainty was to ensure that citizens have all the information about properties constructed in public domain areas. It was made possible through an effective coordination process between the cadaster and the property registry.

A third pillar of the reform is based on reconciling protection of the coast with economic activities, on the premise that it is necessary to protect the integrity of the maritime-terrestrial public domain, and contribute to their conservation. In this sense, the right of occupancy of the private properties situated on public domain during thirty years renewable for another thirty was extended to seventy five years.

It should be noted that according to the 7<sup>th</sup> disposition of this law, a list of twelve different Spanish territories have been excluded from the public maritime domain. An example of this can be seen in Figure 5, corresponding to an important territory of the Malaga coast, and in Figure 6, corresponding to Ampuriabrava. In these figures, the territories excluded are shaded.



Figure 4. The Algarrobrico Hotel located in Almeria (Spain) (www.efe.com)



Figure 5. Malaga coast (B.O.E., 2013 and Google Earth capture)



Figure 6. Ampuriabra coast (B.O.E., 2013 and Google Earth capture)



Figure 7. Flooding episodes in Spanish coast (R.O.P.,2013a)

## CONCLUSIONS

The decision of placing a fixed line that divides the land in two types of property –public domain and privately owned land- in a changeable environment is the considerable potential source of conflict. This line has to move its position time to time in order to adapt to the movements of the shoreline.

The two Coastal Laws (1988 and 2013) attempt to reduce the problems that any change of demarcation line can cause in the urban areas.

The 2013 Coastal Law, as it is written now, is not a single document because it is necessary to read together both 1988 and 2013 Law documents to have a complete view of the current Spanish Coastal Law. It will be an advantage to write a single document in the next future, including the full complete final text.

The right of occupancy of private properties located on the Public Domain was increased from thirty to seventy five years. Furthermore, it is possible to transmit these private properties, and two new concepts have been included in the Law: energy efficiency and sustainable economic activities.

The 2013 Coastal Law do not include with issues related to marine renewable energies, maritime spatial planning indicating the uses and activities (aquaculture, offshore wind farms, wave energy converters facilities, etc.) to be implemented in the different zones, risk maps and physiographic units distribution. The inclusion of these all issues would be very interesting and recommended.

As is stated in different Spanish publications (R.O.P, 2013b) the 2013 Coastal Law was legally developed in order to avoid the devastation of the Spanish coastline. Although in reality its application defends private properties ahead of the protection of these areas. An example of this is the list of territories excluded from the public domain, a decision carried out without taking into account a study about the numerous episodes of flooding that these and many others territories suffered in the last decades (B.O.E., 2013a) as can be seen in Figure 7.

The new Coastal Law has been written with the main objective to guarantee legal security for European citizens with private properties in the Spanish coastal zone.

## LITERATURE CITED

- Auken, 2009. Resolución del Parlamento Europeo, de 26 de marzo de 2009, sobre el impacto de la urbanización extensiva en España en los derechos individuales de los ciudadanos europeos, el medio ambiente y la aplicación del Derecho comunitario, con fundamento en determinadas peticiones recibidas (2008/2248(INI)).
- B.O.E., 1969. Ley 28/1969, de 26 de abril, sobre Costas.
- B.O.E., 1988. Ley 22/1988, de 28 de julio, de Costas.
- B.O.E., 1989. Real Decreto 1471/1989, de 1 de diciembre, por el que se aprueba el Reglamento General para el desarrollo y ejecución de la Ley 22/1988, de 28 de julio, de Costas.
- B.O.E., 2013. Ley 2/2013, de 29 de mayo, de protección y uso sostenible del litoral y de modificación de la Ley 22/1988, de 28 de julio, de Costas.
- Cooper, J.A.G. and Alonso, I. 2006. Natural and anthropic coasts: challenges for coastal management in Spain. *Journal of Coastal Research Special Issue*, 48, 1-7.
- Cooper, J.A.G. and McKenna, J., 2009. Boom and Bust: the Influence of macroscale economics on the world's coast. *Journal of Coastal Research*, 25, 533-538.
- García-Ayllón, S. and Estrella, E., 2013. Causas y fundamentos de la asimetría territorial en el desarrollo litoral de la Región de Murcia. *Revista de Obras Públicas* nº 3547, pp. 49-63.
- M.M.A., 2005. El deslinde del dominio público marítimo-terrestre, *Ambienta* nº 47, septiembre 2005, pp. 16-20.
- M.A.R.M., 2009. Plan de deslindes. El deslinde del dominio público marítimo-terrestre.
- M.A.R.M., 2013. Proyecto de Ley de Protección y Uso Sostenible del Litoral y de modificación de la Ley 22/1988, de 28 de julio, de Costas.
- R.O.P., 2013a. La modificación de la Ley de Costas de 1988. El inicio de un nuevo ciclo devastador. *Revista de Obras Públicas* nº 3543, pp 51-58.
- R.O.P., 2013b. Mitos y verdades sobre la reforma de la Ley de Costas. *Revista de Obras Públicas* nº 3543, pp 47-50.
- Torres Alfosea, F.J., 2010. Cuarenta años de leyes de costas en España (1969-2009). *Investigaciones geográficas*, nº52, pp. 167-198 ISSN: 0213-4691.
- [www.efc.com](http://www.efc.com). EFE Web Page.
- [www.marmenoronline.com](http://www.marmenoronline.com). Mar Menor Web Page.

# Creation of an alternative season based on sustainable tourism as an opportunity for Baltic Sea Region

Przemysław Lonyszyn†, Olga Terefenko‡

†Faculty of Geosciences  
University of Szczecin  
70-383 Szczecin, Poland  
lonyszyn@onet.eu

‡ Faculty of Geosciences  
University of Szczecin  
70-383 Szczecin, Poland  
olga.terefenko@univ.szczecin.pl



[www.cerf-jcr.org](http://www.cerf-jcr.org)



[www.JCRonline.org](http://www.JCRonline.org)

## ABSTRACT

Lonyszyn, P., Terefenko, O., 2014. Creation of an alternative season based on sustainable tourism as an opportunity for Baltic Sea Region. In: Green, A.N. and Cooper, J.A.G. (eds.), Proceedings 13th International Coastal Symposium (Durban, South Africa), *Journal of Coastal Research*, Special Issue No. 70, pp. 454-460, ISSN 0749-0208.

For several years, the Baltic Sea was divided by the Iron Curtain. However, though this situation changed over 20 years ago and this body of water has since become an internal sea of the European Union, there are still visible differences in the welfare and mentality of the people from the Baltic Sea Region. It's the world's largest body of brackish water, its beaches are exceptionally picturesque, and due to the concentration of iodine it is an exuberant source of medical richness. However, people view the coastal regions of the Baltic Sea countries almost exclusively as a destination for summer vacations. This results in the existence of an expansive, harmful tourist industry for a short time and distinct stagnancy throughout the rest of the year. The majority of local resorts from autumn to spring become examples of "ghost towns" where the inhabitants don't have regular incomes. The problem is, according to scholars, that extending the summer season is impossible in the Coastal Baltic Sea Region due to the local climate and economic conditions of the areas around the sea. The solution could be the creation of an alternative season based on sustainable tourism, as the extension of a summer season could only reduce the problem of the area's degradation due to mass tourism instead of solving it. This paper presents how an alternative season could be a real chance for a gradual end of the problem. Moreover, it shows real examples of transnational cooperation that could become the base for sustainable tourism in the Coastal Baltic Sea Region.

**ADDITIONAL INDEX WORDS:** *Coastal BSR, ICZM, cultural heritage tourism, health tourism, Baltic Sea sustainable tourism.*

## INTRODUCTION

The sustainable tourism has been implemented from the term of the sustainable development and, as such, has been based on three pillars: environment, economy and society. Nevertheless, even earlier Hetzer created a definition of the responsible tourism where he selected her four pillars (Durydiwka *et. al.*, 2010). Throughout the years scientists have created many definitions of sustainable tourism. Coccossis (1996) has collected them in four groups:

- a sectoral point of view such as the economic sustainability of tourism,
- an ecological point of view emphasizing the need for ecologically sustainable tourism,
- a tourism viability point of view recognizing the competitiveness of destinations,
- a point of view accepting tourism as a part of strategy for sustainable development throughout the physical and human environments.

The literature with reference to this term is extensive but this

paper is largely based on a couple of key sources, which are particularly relevant to the main topic, especially the three-pillars-based definition proposed by the World Tourism Organization according to the sustainable tourism should:

- Make optimal use of environmental resources that constitute a key element in tourism development, maintaining essential ecological processes and helping to conserve natural heritage and biodiversity.
- Respect the socio-cultural authenticity of host communities, conserve their built and living cultural heritage and traditional values, and contribute to inter-cultural understanding and tolerance.
- Ensure viable, long-term economic operations, providing socio-economic benefits to all stakeholders that are fairly distributed, including stable employment and income-earning opportunities and social services to host communities, and contributing to poverty alleviation.

During the summer season at the sandy beaches of the southern part of Baltic Sea one will find thousands of tourists. This is normal, as beaches always were, are, and will be natural destinations for people wanting a place to relax during holidays,

and Baltic beaches are special as their sand is soft and has an attractive shiny gold colour. For the inhabitants along Baltic coastline it's obvious that their lands should be used for tourism and they focus their efforts on income from that source. The coastal areas have their own, unique development tendency that comes as a result of diversification and dynamics of natural phenomena and processes as well as through the focusing of the major part of local economies on coastal potential and access to the sea (Dutkowski, 2001).

The problem is that the climate conditions for tourism are acceptable for only 2 months of the year (Szwichtenberg, 2001). During the rest of the year these picturesque beaches are empty leaving the local people to think of ways to extend the summer season. Unfortunately, desolate villages could only deter potential visitors.

The Baltic Sea Region (BSR) consists of all countries around that body of water. The authors have used only regions classified by Eurostat (The Statistical Office of the European Community) as NUTS3 for analysis (Figure 1). Throughout the European Union there are 446 of them with access to coastline but only 71 of them are in the BSR. Regardless of the coastline access the NUTS3 regions sometimes reach deep inland. That is why the authors take into consideration only seaside regions that stretch up to 50 km in from the coastline.

A typical community in the Coastal Baltic Sea Region (Coastal BSR) has its own problems such as a dependency of external demand for recreational values and tourism services, or the degradation of coastal ecosystems due to the expansion of tourism and touristic spatial planning (Dutkowski, 2001). That creates only two possibilities – to benefit from tourism as much as possible during that 2 month period and accept those threats, or to create an alternative season based on sustainable tourism in forms adequate to the potential of the Coastal Baltic Sea Region.

The contemporary economy has a global dimension and metropolises, regions, and touristic areas compete in the global market. Matching the increasing global competition require paradoxically, an improvement in cross-border, regional, and local cooperation (Dutkowski, 2001). Regarding the BSR, it should be mentioned that for centuries the sea was a factor that united people rather than divided them. During the late Middle Ages the well-known Hanseatic League clustered market towns from all over the Baltic Sea – from Lübeck in Germany to Novogrod in Russia (Schulte Beerbühl, 2012). Later, thanks to the Deluge in the 50's of seventeenth century, almost the entire Baltic belonged to Kingdom of Sweden and was treated as their internal sea. The European Union (EU) achieved the same in a more peaceful manner. With the exception of a few parts belonging to the Russian Federation, the majority of the Baltic Sea coastline is situated within the borders of EU members and the Schengen Area which simplifies travels and cooperation.

The Iron Curtain, dividing Europe and its region in opposite political systems, made cross-border activities nearly impossible. However it was not only the political situation, but also the lack of awareness and understanding which prevented common efforts (Steingrube, 2010). Nowadays, the situation has changed as the fall of the Berlin Wall has opened new possibilities. Is the potential correctly utilized by local stakeholders or does the lack of awareness and understanding still hinder the growth of the BSR? In this paper, the authors try to answer that question by showing existing examples as well as niches yet to be explored.

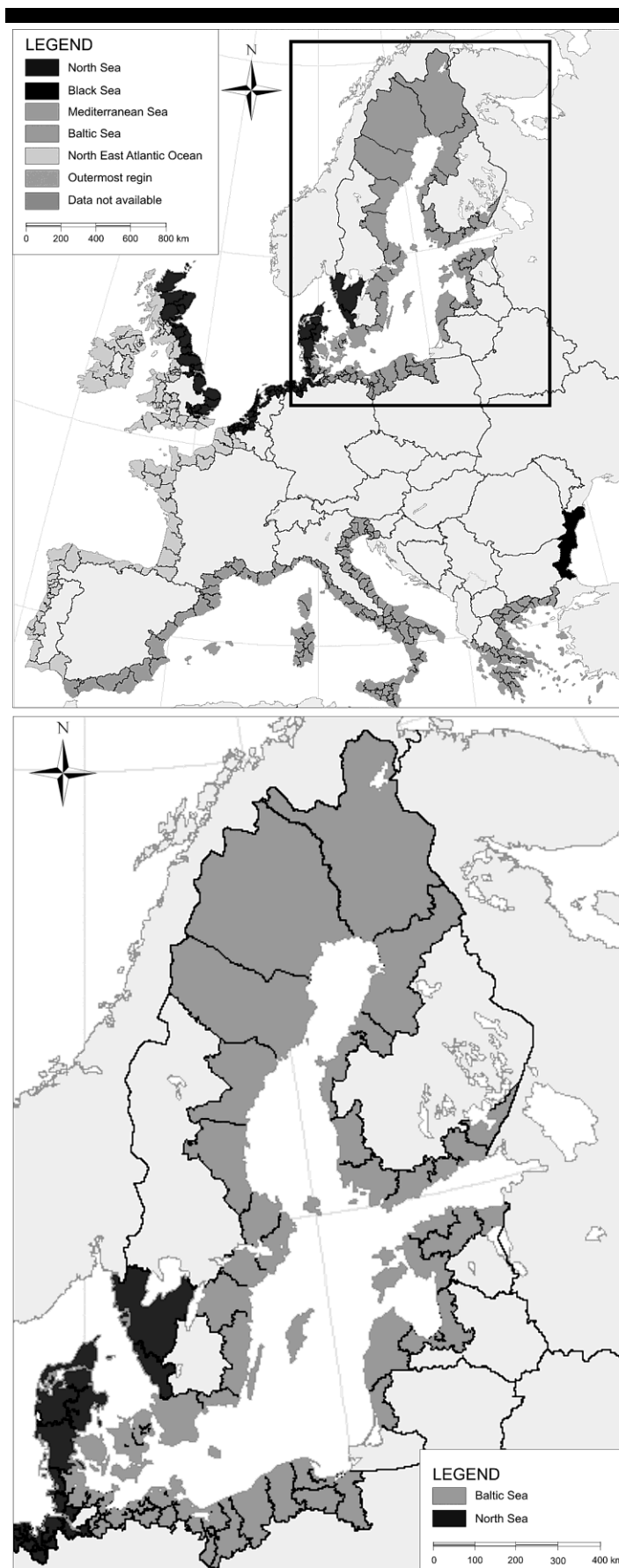


Figure 1: The coastal NUTS 3 regions of all Europe (above) and of the Baltic Sea Region (below) (source: Coastal region statistics, 2013)



## STUDY SITE

The Baltic Sea stretches from the Gulf of Finland to the Kattegat (over 1,200 km in the east-west direction) and from the Pomeranian Bay to the Gulf of Bothnia near the Arctic Circle (over 1,300 km in the north-south direction). It covers an area of 415,266 km<sup>2</sup> and has a water volume of approximately 21,000 km<sup>3</sup>. (Schiewer, 2010). It is the world's largest body of brackish water.

The Baltic Sea is bordered by the coasts of nine countries: Denmark, Germany, Poland, Lithuania, Latvia, Estonia, Finland, Sweden and Russia as the only non-EU country. The length of the coastline is 69,027 km and its shoreline is varied. You can find 12 types of major classes of shores (Schiewer, 2010).

The Baltic Sea Region belongs to moderate climate zone. The moderate warm zone is on the southern part, and the moderate cold zone on the northern part. It implicates that even during summer season the weather conditions are not pleasant enough for 3S tourism (Sea, Sand and Sun), as even in the warmest regions the temperature in June doesn't exceed 16 centigrade (according to the E-OBS).

## METHODS

As a part of the analysis, a review has been done of institutionalized examples of cross-border cooperation in the Coastal Baltic Sea Region, specifically those created as a consequences of "EU Strategy for the Baltic Sea Region" coordinated by European Commission as well as for those created by stakeholders. It is impossible to determine, due to the way the range of the study has been described, if one will be able to grasp all cases of cross-border cooperation regarding touristic growth. Regardless, there are a sufficient number of selected institutions to move on to next stage of the analysis. Specifically, searching for those cases that can, in the future, contribute to sustainable tourism in the Coastal Baltic Sea Region and create an alternative season.

The authors have selected elements that fulfills the criteria as listed below:

- health tourism,
- fishing tourism,
- bird-watching tourism,
- cultural heritage tourism,
- maritime heritage tourism,
- military tourism.

All types mentioned above are an alternative for 3S tourism, primarily because seasonal climate changes do not impede their realization. From the authors' point of view, maritime tourism, regarding the Coastal BSR is mostly based on cross-border cooperation, and is not an element that fulfills the assumed principles. Its growth does not cut into traveling to areas that empty out during the summer tourism season. Seaports are in big cities which already attract many tourists and give other sources of livelihood for the local inhabitants.

	Germany	Czech Republic	Poland	Israel	Lithuania
Brest augmentation	7500	4321	3712	4037	3224
Liposuction	4499	3054	2800	2500	1400
Cataract surgery	1973	921	1714	3500	1232
Knee joint arthroplasty	11375	---	8348	---	5691
Knee joint arthroscopy	2625	---	912	3200	1200
Hemorrhoids removal surgery	3400	2888	1026	2325	1200
Varicose veins surgery	3150	3588	751	---	720
Dental implantation	3000	1950	973	2000	860

Figure 2: Prices of the some medical services in selected European countries – all prices in USD (source: litcare.com).

As the aim of the paper is to bring attention to some tendencies that are already happening and should become examples to be followed by others. The authors focus mostly on samples of cross-border cooperation that could be a base for sustainable tourism in the Coastal BSR.

## RESULTS

### Medical tourism

Medical tourism is one of the fastest developing branches of tourism. For the European Union, possibilities for further growth have been created by the Directive 2011/24/EU of the European Parliament and of the Council of March 9, 2011 "on the application of patients' rights in cross-border healthcare" that should have been implemented by the legislation of all member states by October 25, 2013. This document gives patients an advantage in being European citizens. The access to medical care in any other Member State cannot be denied from now on. The only exclusions are long-term care services, organ transplants, and public vaccination.

As the BSR is composed of countries with different cost of living, there are different prices for medical services. Already Baltic States (Lithuania, Latvia and Estonia) promote their medical tourism industries. There are plenty of clusters that prepare a comprehensive offer for potential tourists so that they could also spend a nice time in that countries. The offer of medical care is very attractive when we compare the prices of some services (Figure 2).

On 13th of November 2013 the representatives of medical clusters from the Baltic States had signed a memorandum of understanding to lead them to tighter and more integrated collaboration and cross-border cooperation. This was a reaction to changes in EU legislative. It was a big step to help the Baltic States become one of the world leaders in medical tourism. Already Lithuania is the 10th best medical tourism destination on our planet.

The Coastal Baltic Sea Region has big potential regarding spa and wellness tourism. There are many of these kinds of resorts around this body of water as local climate – moderate temperatures and high iodine concentration – can augment the effects of treatments, especially among people with hypothyroidism or heart problems.

### Fishing tourism

Fishing tourism is an option that can make use Coastal BSR potential regarding fishing in the deep sea as well as on rivers and coastal inland bodies of water. The fishing is independent of the weather, but also depends on fishing season for various species. The fishers are not invaders - on the contrary, they integrate almost invisibly with nature and local heritage.

The most popular fishing destination is Sweden, but there are also some attempts to develop this branch of tourism in other regions. As an example of cooperation one can reference the cross-border project: "Fishing tourism in the South Baltic Region" that has been instituted by the Polish commune Stegna and Lithuanian - Nerynga. As the webpage of the project presents "the main purpose of the project it is promotion of finishing tourism that has the chance to influence the extending of the summer season and the creation of the new worksites". Between those two communes there is a wide coastline that belonged to the Kaliningrad Oblast, and maybe in the near future this type of project will be instituted in cooperation with a non-EU partner (Kropinova, 2011).

"The West Pomeranian Sailing Route" instituted by the West Pomeranian Tourism Organization within the EU Operational Programme 'Innovative Economy' for the years 2007-2013 - 6.4 "Investments in tourism products of supra-regional importance" is a natural extension of the "Cross-border Cluster - Water Route Berlin-Szczecin-Baltic" (ZROT, 2013). Thanks to this, even in small towns alongside the water route which are vibrant during the summer season and empty during the rest of the year, it is possible to sustain tourism through fishing for those who have their own boat and want to fish on rivers or other bodies of water connecting Berlin with the Baltic Sea. The Water Route Berlin-Szczecin-Baltic can also promote locks and other interesting structures along its route like the oldest German working boat lift in Niederfinow (1927-1934) (Poland Travel, 2013).

### Bird-watching tourism

The Coastal Baltic Sea Region is less urbanized and populated than, for example, the Mediterranean and North Sea regions (Figure 3). The same is true regarding tourism carrying capacity. In the year 2007 the density of tourism capacity in the Italian coastal region of Rimini was greater than 290 bed places per km<sup>2</sup>. In contrast, the density was less than 1 bed place per km<sup>2</sup> in the Finnish region of Lappi (Collet, 2010). Due to these circumstances, it is no surprise that plenty of places exist close to the Baltic coastline where you can find very suitable conditions for bird-watching. The access to Ramsar Sites and other restricted places is now easier to those who are interested in observing natural heritage. Because of this factor, together with wider ornithological education, there are more and more people interested in a bird-watching.

Sweden has much to offer bird lovers, but in other countries there are also interesting places like in Latvia with the famous Slitere Nature Reserve (Eco-tours, 2013b), or in Poland's Slowinski National Park and Odra River Valley (Eco-tours, 2013a). Nevertheless, the Baltic Sea Region is yet to start real cross-border cooperation within this branch of tourism. It would be worth a closer look at the examples of the cooperation regarding fishing tourism as these two branches could really go hand in hand.

### Cultural heritage tourism

Cultural heritage tourism could easily cooperate with historical festivals or walks through open-air museums. Countries of the BSR are competing with North Sea countries regarding the attraction of viking culture fans. Most festivals dedicated to the Vikings are in the western part of Europe, yet around the Baltic Sea there are a few. The most important ones take place during the heat of the summer season, such as the ones in Danish Trelleborg or Polish Wolin. Yet not all of them are during the summer season. There are some that you can visit in other months. For example there is one in Foteviken in Swedish Scania (Jelledragon, 2013). The promotion of the Viking culture is an example of the active preservation of cultural heritage connected with maritime traditions and ethnic history.

The Vikings are only the example of an enormous potential hidden in the Coastal Baltic Sea Region. Viking culture is extinct, but there are some indigenous minorities in almost all of the countries around the Baltic Sea (six in small Estonia) as well as some small and almost forgotten remnants of peoples also living in the Baltic rim, for example Kashubes in Poland and Karaims in Central Lithuania (Ryden *et al.*, 2003). Together, they comprise the local colour and ethnic diversity of the Coastal BSR (Figure 4). Festivals are the force that drives the cultural heritage business

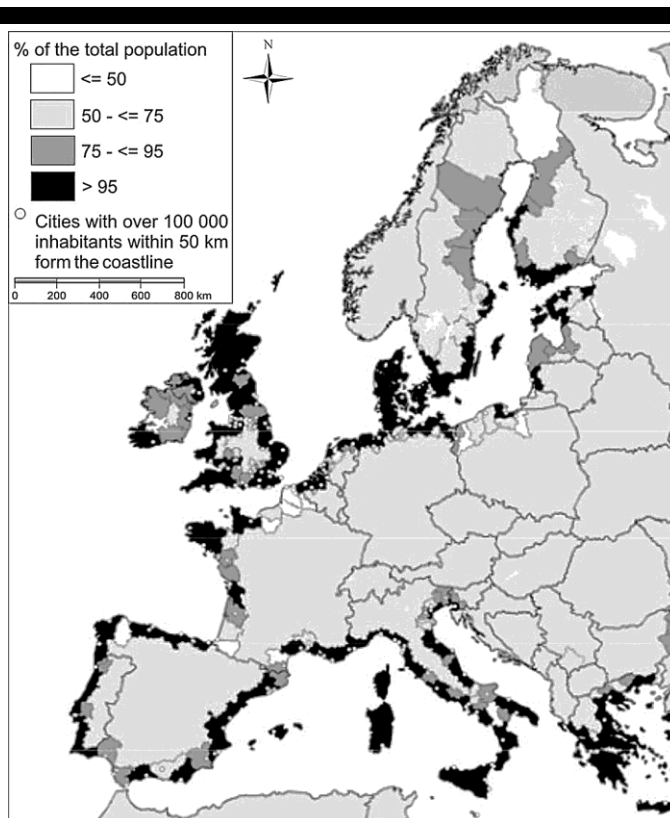


Figure 3: The density of population in the coastal NUTS3.

cycle, as they take place in the summer. Meanwhile, the Baltic climate is not an obstacle for contacts with local culture. One does not even need a museum for this. To spend time with ethnic minorities (to sample their food, habits or artisanal handicraft) can be done with those groups who are also local stakeholders of the alternative season. This would allow them to live following their traditions and survive.

Undoubtedly, everything depends on the preparation of adequate tourism opportunities offered by local authorities. "Is it not amazing to imagine out a future scenario where western developed countries preserve their own heritage because it becomes their main source of revenue through mass tourism, and where simultaneously less developed countries will preserve their own heritage because it becomes their main source of investment opportunities" (Ost, 2012).

### Maritime heritage tourism

Through the years the Baltic Sea was a very busy body of water, due to the turbulent history of its countries. Because of this, there are plenty of nautical devices and buildings around that greatly generate the interest of tourists. Mostly, they are interested in lighthouses and navigational signs. Lighthouses usually are available for visitors who will jump at the opportunity to see them, as is illustrated by wild crowds climbing to the top balconies of such buildings. The beauty of the lighthouses resides not only in their architecture, but also in the unforgettable view of the local surroundings. Such a view is often the reward for breathtaking efforts during the climb, as most of lighthouses are high towers.



Figure 4: The localization of ethnic minorities in the Coastal Baltic Sea Region (source: own work).

In the BSR countries there are numerous associations that gather enthusiasts of lighthouses, for example: Svenska Fyrsällskapet, Suomen Majakkaseura and Stowarzyszenie Miłośników Latarni Morskich, which cooperate in an informal and casual, but eager manner. The tourists can count on them for assistance while visiting the network of Baltic lighthouses spread around the very long shoreline.

There were some efforts on the governmental level. For example: Baltic Sea Heritage Co-operation founded in 1997 in Lübeck by Ministers of Culture of countries in the BSR. One of the areas of interest was the „Coastal Culture and Maritime Heritage”. Unfortunately, there were only some minor achievements regarding the promotion of the lighthouses' network spread around the Baltic Sea (Baltic Sea Heritage Co-operation, 2005).

It looks like the potential of the nautical heritage is not fully exploited. The number of websites about lighthouses and nautical devices is so large that there is no doubts that there is a significant demand to visit them. The truth is, there is no cross-border tourism offer prepared by the associations mentioned above or by the authorities managing these buildings and devices. After all, visiting them does not depend on the weather and provides a strengthened connection between a coastal region and a sea treated as a local heritage site. Moreover, lighthouses could be used as restaurants and cafes, conference centres, guest and pleasure boat harbours, nature centres and bird observation stations. The

adoption of new uses could also contribute revenue towards the ongoing maintenance costs of the buildings (Baltic Lights, 1997). Some of them are already transformed, and they works just fine.

### Military tourism

Military tourism is an another branch of tourism independent of the weather, and it does not require any artificial meddling into the cultural and natural landscape. Regarding the Baltic Sea Region this branch is one of the most important form of preservation of cultural heritage. As has been mentioned, during the Cold War the Iron Curtain divided this region into two fronts which are clearly visible in countless military constructions. Most of them, after geopolitical changes is closed which makes them perfect places for people who like that branch of tourism, or as an educational tool, or for fans of physical activity as places to walk, run, or play paintball. Moreover, there are a lot of military installations from the II World War, most of them well maintained, that are a multidimensional memorial of traumatic events in human history.

Within the project Baltic Green Belt which gathered more than twenty partners from Russia, Estonia, Latvia, Lithuania, Poland and Germany (non-governmental, governmental and scientific), a network was set up for the conservation and sustainable development of the Baltic Sea coast. One of its realized actions was a creation of military heritage management guidelines. The project had demonstrated the scale of the military heritage potential in the BSR. By themselves, the number of military installments currently working as tourism locations is very impressive – in Latvia along there were 63 such places. The guidelines instructed how to promote and use that legacy in sustainable tourism, and pointed out the need for cross-border cooperation (Military Heritage management guidelines, 2011).

There are many places that could not be classified within the range of such projects, but still determine the potential of the Coastal BSR. For example Prora's legacy – what is left from the longest beach resort in the world (the buildings extend over a length of 4,5 kilometers) that Adolf Hitler ordered built in Rügen for his followers.

### DISCUSSION

The main goal of tourism development in the Baltic countries is to ensure sustainable economic, social, cultural and spatial development based on preservation, maintenance and enhancement of cultural heritage sites as well as the welfare of host communities through increased supply and demand, diversity, quality, and sale of viable cultural tourism services (UNESCO and Baltic Countries National Commissions, 2004). In other words, sustainable tourism.

According to Aleksander Schwichtenberg it is impossible to extend the summer season beyond a July-August interval. He uses arguments like: mediocre bioclimatic conditions, a dominant model of spending holidays, and an inflexible system of summer break planning in schools and universities (Terefenko, Łonyszyn, 2012). The same situation exists in all regions of the BSR. The problem is that the majority of papers about the development of tourism (including papers about the development of sustainable tourism) speak about the extension of the summer season in the Coastal BSR, and that it appears to be a mistake. There are some relevant divergences between developmental goals based on sustainable tourism for the Baltic countries that are included in “Baltic Sea Region Strategy” and the principles presented in this paper. The rejection of goals like city tourism or cruise tourism seems to be obvious, as they favour groups of influences that do not include the stakeholders of seasonal coastal tourism. This does not mean a total rejection of such a strategy. It is merely an



Figure 5: A street sign in two languages: Polish (above), and Kashubian (below) in Ostrzyce village. (fot. Aotearoa).

observation that what could be good for deep inland areas would not be beneficial for the coastal areas.

The lack of serious treatment of the Coastal BSR can be seen in other areas of life. For example there is no comprehensive strategy for that region regarding Integrated Coastal Zone Management (ICZM) (Coastal Challenges, 2010). Thus, one would not expect a reliable tourism strategy?

An important element worthy of special emphasis regarding the Coastal BSR, is doubtless ethnic heritage diversity. There are still many places where one can walk down various streets and find signboards or street names in languages considered by many to be extinct or non-existent (for example in Kashubia in Poland - Figure 5). If connected with a dynamically developing culinary tourism that will allow visitors to taste local delicacies, a product will be created that responds to challenges of the modern and aware tourist. Unfortunately, the members of ethnic minorities are acting in an opposite manner. Usually they abandon their own culture and try to adjust to the popular model of 3S tourism. Thus, they forget that their own heritage builds the potential for creating a year-round, attractive image of their region.

There is another problem regarding locals. As the tourist season is only 2 months, they have to use it as much as possible to earn money for the rest of the year. Due to this, the non-metropolitan inhabitants of the Coastal BSR are deprived of summer joy. This season, that commonly is treated as period of joy and rest, only means a hard work for the locals. The lack of summer holidays increases exhaustion and consequently cause social stagnation. These unfavourable circumstances cause other alarming effects like an escape of youngsters. Tourism is an attractive industry that gives opportunities for self-development. Meanwhile there is a registered outflow of the young people, and the high prices of the building plots in the coastal zone are successfully threatening a potential inflow of youngsters from inland regions.

## CONCLUSION

The possibilities for growth in coastal communities are significant, but their utilization requires coordinated actions. The word "cooperation" is a leading catchphrase (Dutkowski, 2001). Because the position on the world tourism market of the Baltic Sea Region decreases, the countries of the BSR should cooperate with each other, and not compete. The examples presented in this

paper have shown that 20 years after the fall of the Berlin Wall it is very possible.

## LITERATURE CITED

- Baltic Lights. 1997. Cultural Heritage in the Baltic Sea States. <http://www.cmm.pl/balticlights/> [Accessed 29 Nov 2013].
- Baltic Sea Heritage Co-operation. 2005 <http://balticheritage.raa.se> [Accessed 29 Nov 2013].
- Coastal Challenges. 2010. The Baltic Sea in need of integrated management. Updated - 15 may 2010. <http://coastalchallenges.com/2010/05/15/456/> [Accessed 29 Nov 2013]
- Coastal region statistics. 2013. [http://epp.eurostat.ec.europa.eu/statisticsexplained/index.php/Coastal\\_regio](http://epp.eurostat.ec.europa.eu/statisticsexplained/index.php/Coastal_regio) [accessed 29 Nov 2013].
- Collet I., 2010. Portrait of EU coastal regions. In: Eurostat. Statistics in focus, No. 38/2010, 12p.
- Durydiwka M., Kowalczyk A. Kulczyk S., 2010. Definicja i zakres pojęcia 'turystyka zrównoważona', In: Kowalczyk A.(ed.), Turystyka zrównoważona, Warszawa: Wydawnictwo Naukowe PWN, pp. 21–43
- Dutkowski M., 2001. Szanse rozwoju społeczno-gospodarczego gmin nadmorskich. In: Szwichtenberg A. (ed.) Turystyka szansą rozwoju społeczno-gospodarczego regionu nadmorskiego, XVII Sejmik Morski. Gdańsk-Hel: Katolickie Stowarzyszenie "Civitas Christiana, pp. 50-59.
- Eco-tours. 2013a. Along the Lower Odra River valley [http://www.ecotours.pl/birdwatching\\_tour\\_lower\\_odra\\_valley.php](http://www.ecotours.pl/birdwatching_tour_lower_odra_valley.php) [Accessed 29 Nov 2013].
- Eco-tours. 2013b. Baltic States – with a particular focus on bird [http://www.eco-tours.pl/birdwatching\\_tour\\_baltic\\_countries.php](http://www.eco-tours.pl/birdwatching_tour_baltic_countries.php) [Accessed 29 Nov 2013].
- Jelledragon.,2013. <http://www.jelledragon.com/links.htm> [accessed 29 Nov 2013].
- Kropinova E., 2011. Факторы формирования трансграничного туристско-рекреационного региона "Юго-Восточная Балтика" In: Балтийский регион, No. 1 (7). Kaliningrad: Immanuel Kant Baltic Federal University, pp. 106-114.
- Military Heritage management guidelines. 2011. LCTA Lauku Celjotas. Latvija. Pp. 54.
- Cocossis H., 1996. Tourism and Sustainability: Perspectives and Implications. In: Priestley G.K., Edwards J.A., Cocossis H.(eds), Sustainable Tourism? European Experience. Wallingford: CAB International, pp.1-21.
- Ost C., 2012. Cultural Heritage, Local Resources and Sustainable Tourism: Towards an Operational Framework for Policy and Planning. In: Fusco Girard L., Nijkamp P., Cultural Tourism and Sustainable Local Development. Farnham: Ashgate Publishing, pp. 319.
- Poland Travel. 2013. The West Pomeranian Sailing Route <http://www.poland.travel/en/yachting/the-west-pomeranian-sailing-route/> [Accessed 29 Nov 2013].
- Ryden L., Mugula P., Andersson M., 2003. Environmental Science. Uppsala: The Baltic University Press, 824p.
- Schiewer U., 2010 Ecology of Baltic Coastal Waters. Berlin: Springer-Verlag 428 p.
- Schulte Beerbühl M., 2012. Networks of the Hanseatic League. In: European History Online. Leibniz Institute of European History. Mainz. <http://www.ieg-ego.eu/en/threads/european-networks/economic-networks/margrit-schulte-beerbuehl-networks-of-the-hanseatic-league> [accessed 29 Nov 2013].
- Steingrube W., 2010. Introduction In: EcoRegion Perspectives. Sustainable Tourism as a Part of the EU Strategy for the Baltic Sea Regio. First Issue. Berlin, Baltic 21. pp. 4
- Szwichtenberg A., 2001. Współczesne problemy funkcjonowania turystyki w polskiej nadmorskiej strefie turystycznej. In: Szwichtenberg A. (ed.) Turystyka szansą rozwoju społeczno-gospodarczego regionu nadmorskiego, XVII Sejmik Morski. Gdańsk-Hel: Katolickie Stowarzyszenie "Civitas Christiana, pp. 97-112.
- Terefenko O., Lonyszyn P., 2012. Ochrona dziedzictwa kulturowego i przyrodniczego podstawą zrównoważonego rozwoju nadmorskich gmin w Polsce na przykładzie gminy Rewal. In: Rydzewski T., Smutek J. (eds.), Współczesne aspekty badań przestrzeni geograficznej. Poznan: Boguski Wydawnictwo Naukowe, pp.123-136

UNESCO and Baltic Countries National Commissions. 2004. Baltic Cultural Tourism Policy Paper. Estonian, Latvian and Lithuanian National Commissions for UNESCO 2001-2003. 91p.

ZROT. 2013. Projekt. <http://zrot.pl/szlak/projekt.php> [Accessed 29 Nov 2013].

## Coastal and marine protected areas as key elements for tourism in small islands

Catarina Fonseca†, Carlos Pereira da Silva†, Helena Calado‡, Fabiana Moniz‡, Chiara Bragagnolo∞, Artur Gil§, Mike Phillips#, Margarida Pereira†, Miguel Moreira‡

† e-GEO, Research Centre for Geography and Regional Planning

FCSH Universidade Nova de Lisboa  
Lisboa, Portugal

[catarinafonseca7@gmail.com](mailto:catarinafonseca7@gmail.com)

[cpsilva@fcs.unl.pt](mailto:cpsilva@fcs.unl.pt)

[ma.pereira@fcs.unl.pt](mailto:ma.pereira@fcs.unl.pt)

§ Azorean Biodiversity Group, CITA-A  
Department of Biology, Universidade dos Açores

Ponta Delgada, Portugal

[arturgil@uac.pt](mailto:arturgil@uac.pt)

‡ CIBIO, Research Center in Biodiversity and Genetic Resources (Azores Unit)

Universidade dos Açores

Ponta Delgada, Portugal

[calado@uac.pt](mailto:calado@uac.pt)

[geografia@uac.pt](mailto:geografia@uac.pt)

[migueldmoreira@uac.pt](mailto:migueldmoreira@uac.pt)

# University of Wales Trinity Saint David (Swansea)

[mike.phillips@smu.ac.uk](mailto:mike.phillips@smu.ac.uk)

∞ Institute of Biological and Health Sciences, Federal University of Alagoas (UFAL)

Maceió, Brazil

[chiara.bragagnolo@yahoo.com.br](mailto:chiara.bragagnolo@yahoo.com.br)



[www.cerf-jcr.org](http://www.cerf-jcr.org)



[www.JCRonline.org](http://www.JCRonline.org)

### ABSTRACT

Fonseca, C., Pereira da Silva, C., Calado, H., Moniz, F., Bragagnolo, C., Gil, A., Phillips, M., Pereira, M., Moreira, M., 2014. Coastal and marine protected areas as key elements for tourism in small islands. *In: Green, A.N. and Cooper, J.A.G. (eds.), Proceedings 13<sup>th</sup> International Coastal Symposium* (Durban, South Africa), *Journal of Coastal Research*, Special Issue No. 70, pp. 461-466, ISSN 0749-0208.

The Azores Archipelago (Portugal) is composed of 9 small islands located in the North Atlantic. To overcome the common challenges of this type of territory (e.g. isolation, closed systems, limited physical space and natural resources, endemism, small economies, small populations) and taking advantage of the natural and cultural heritage, the Regional Government of the Azores has based its Tourism Strategy on the high value of nature, landscape, flag species and outdoor experiences with a strong environmental friendly label. Pico Island offers the perfect scenario to enjoy such nature-based tourism activities, welcoming around 15,000 tourists per year, equivalent to the number of residents on the island. The island's natural and cultural heritage is outstanding and Pico Island Natural Park represents 35% of the territory, including several coastal and marine areas. Tourists' awareness about Pico protected areas, their activities and preferences can be extremely important to the management of the Island Natural Park. Integrated in the research project SMARTPARKS, a survey was conducted with 134 tourists, revealing the importance assigned to Pico protected areas and coastal zone. Among coastal and maritime activities, bathing and whale watching are the most frequent activities (57% and 44% of respondents, respectively) and 20% of respondents think whale watching should be promoted. This exploratory study gathered important information for decision-making agencies with respect to solving problems and possible solutions through tourism, namely the application of a fee system to help manage and conserve protected areas.

**ADDITIONAL INDEX WORDS:** *Azores; Pico Island; island natural park; sustainable tourism*

### INTRODUCTION

Small islands' encounter particular challenges (their isolation, limited physical space and natural resources, closed systems, endemism, terrestrial/marine ecosystems linkages) which increase their vulnerability to threats such as climate variability, proliferation of invasive exotic species, natural catastrophes and overexploitation of natural resources (Rietbergen *et al.*, 2007). At the same time, economic and social development is a major concern in territories with small economies, seriously dependent on external markets, high transport costs and small populations (Millennium Ecosystem Assessment, 2005). Such characteristics make planning and management on small islands more demanding in scientific and technical terms (Calado *et al.*, 2007). Island systems represent the challenge of our time: how to balance ecological integrity with economic development and collective quality of life (Baldacchino and Niles, 2011).

Tourism can play an important role in small islands' economies, presenting some advantages over export of goods and traditional services, namely through job creation, tax revenues and increased

value of local products (Schubert *et al.*, 2011; Seetanah, 2011). Extraordinary natural and cultural assets found in small islands can be major attractions for tourists. In fact, nature-based tourism has a growing economic relevance and protected areas offer unique opportunities for visitor experiences (Tisdell & Wilson, 2012). Moreover, since protected areas restrict most primary sector activities, tourism is one of the few suitable tools for local development and also for financing protected areas management (Kafyri *et al.*, 2012; Emerton *et al.*, 2006).

### Azores Islands Natural Parks

The Azores Archipelago is a Portuguese autonomous region, located in the North Atlantic. It consists of nine islands of volcanic origin situated between 37 to 40 °N and 25 to 31 °W. Due to their geographical distribution, the islands are divided into three groups: the Western Group (Flores and Corvo), the Central Group (Pico, Faial, São Jorge, Graciosa and Terceira) and the Eastern Group (São Miguel and Santa Maria) (fig. 1).

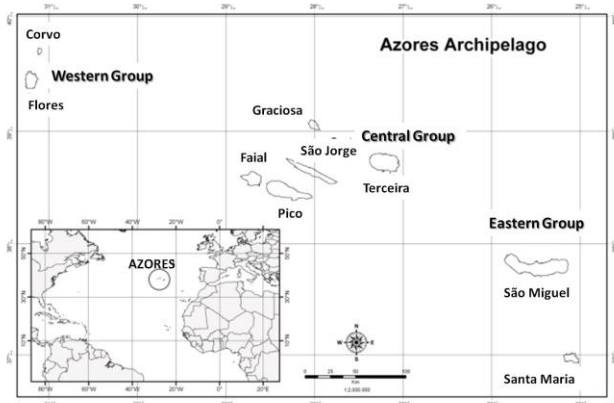


Figure 1. Azores Archipelago (Source: Centre of Geographic Information Systems, University of the Azores).

Considering UNESCO criteria for small islands' definition – an area equal to or less than 10.000 km<sup>2</sup> and 500.000 residents or less (Hess, 1990) – each of the Azorean islands is included in this classification (the archipelago itself occupies only 2.330 km<sup>2</sup> and has just over 246.000 inhabitants).

The environment is assumed to be a transverse pillar for all of the Region's social and economic activities and sectors (Azorean Regional Government, 2008a). This assumption is confirmed by the quantity (16) and diversity of current legal land-based instruments with environmental and spatial incidence in the Azores, regulating and acting at the archipelagic, island and municipal scale (Gil *et al.*, 2012). Azores natural characteristics, linked with its rich historical, architectural and cultural heritage, provide opportunities for the development of tourism as an economic activity of regional significance (DROTRH/IA, 2001; Moniz, 2009; Cruz *et al.*, 2011). In fact, tourism in the Azores has grown since the mid-1990s, and maritime and coastal recreational activities are major tourist attractions, namely whale watching and diving (Bentz *et al.*, 2013; Calado *et al.*, 2011). Therefore, the local authorities based its Tourism Strategy on the high value of nature, landscape, flag species (whales and dolphins) and outdoor experiences (hiking, bicycling), with a strong environmental friendly label (Azorean Regional Government, 2008b).

Although part of the Macaronesia Biogeographic Region, the Azores Archipelago presents distinctive characteristics in terms of climate and species composition, due to a stronger influence of northern European species (Sundseth, 2009). When compared to other archipelagos of Macaronesia, the diversity of terrestrial species is relatively poor but the occurrence of endemism makes it equally important for conservation (Cardoso *et al.*, 2008).

The regional network of protected areas includes 9 Island Natural Parks, one for each island of the archipelago. This scheme is the outcome of a reclassification process, undertaken in 2007, in which was applied the IUCN classification system. As a result, each island has a single park comprising several management units, each of which is assigned with one of the following categories: nature reserve, natural monument, protected area for habitat/species management, protected landscape and protected area for resources management. Such classification seeks to highlight the link between the statutory level of a protected area, its natural and cultural values and required management actions.

## SMARTPARKS Project

SMARTPARKS Project - *Planning and Management System for Small Islands Protected Areas* – is a research project coordinated by Azores University and funded by the Portuguese Foundation for Science and Technology. It attempts to facilitate the development of sustainable protected areas, based on an active involvement of stakeholders, economic and cultural activities compatible with nature conservation and an innovative planning and management scheme for protected areas at island scale. Pico Island Natural Park was selected as the case study due to its singularity, percentage of classified area, diversity and representativeness of protection categories. It comprises Pico Mountain (highest point in Portugal, 2.351 m), important coastal sections and the unique vineyard landscape, classified as UNESCO World Heritage Site.

Involving stakeholders in planning and management brings important benefits: increased sense of 'ownership'; greater support for the protection of the area; greater public involvement in decision-making; and closer links between conservation and development. This promotes communication potentially leading to the identification and resolution of problems (Gil *et al.*, 2011). Therefore, stakeholders' involvement in the management of Pico Natural Park was one of the ambitions of SMARTPARKS and the methodological approach included public presentations, interviews and thematic workshops and surveys to residents and tourists (Fonseca *et al.*, 2011). Stakeholders are individuals, groups or communities likely to affect or to be affected by the management of the protected area (Alexander, 2008), thus tourists were targeted by the project. To better understand tourism activities and tourists' expectation, an exploratory survey was developed and applied. The objectives of such a survey were to identify the reasons to choose Pico as a destination, understand how tourists perceive the island and the existing offered tourism, identify preferred areas and activities and their relation with protected areas.

This paper presents preliminary results of the tourists' survey, highlighting the relevance of coastal areas and maritime tourist activities as an attractiveness factor and discussing the relation between protected areas and tourism in Pico Island.

## METHODS

### Study area

Pico Island is the second largest in the archipelago, with a total surface of 445 km<sup>2</sup> and 152 km of coastline length. The main economic activities, relevant for the island's competitiveness and sustainability, are linked with traditional value chains: agriculture, livestock, fisheries and tourism. The island has 14.144 inhabitants (2011) and receives a similar number of tourists per year, mostly attracted by landscape, natural and cultural values. Pico Island offers 40 tourist accommodation establishments, from which 35 are classified as rural tourism and country houses. There are 16 enterprises providing maritime tourist activities such as whale watching, boat tours, boat rental, diving, recreational fishing and windsurfing. Despite the absence of sandy beaches, bathing is also a significant attraction with 57 classified bathing areas.

Pico Island Natural Park is composed by 22 areas: 4 classified as nature reserve, one as natural monument, 8 as protected area for habitat/species management, 6 as protected landscape and 3 as protected area for resource management (fig. 2). The total protected area represents 35% of the island territory.

Pico Mountain is a majestic landscape feature and major tourism attraction, especially for hiking enthusiasts. It is classified

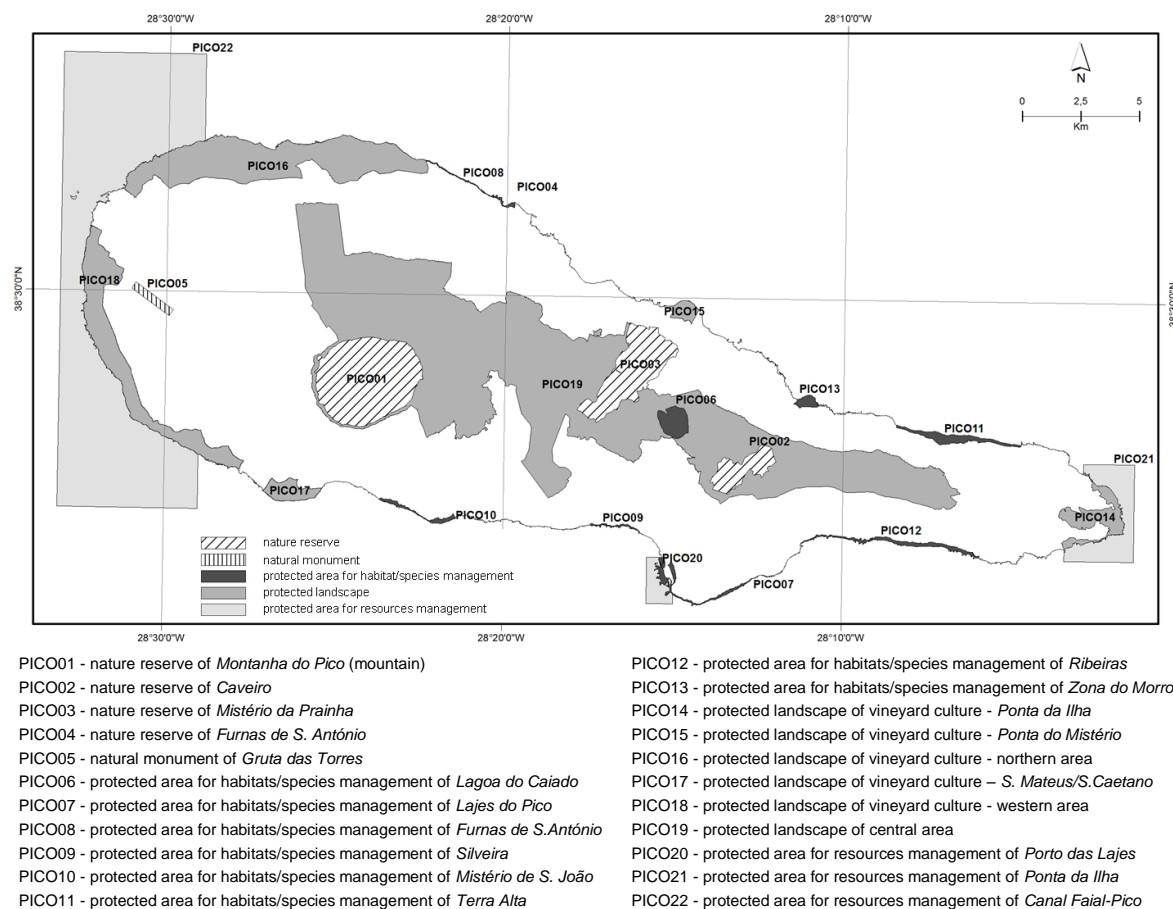


Figure 2. Pico Island Natural Park (Source: Centre of Geographic Information Systems, University of the Azores).

as a nature reserve (PICO 01 – fig. 2) and host protected habitats and species.

Protected areas in the coastal zone are divided in two categories: a) protected landscape of vineyard culture (PICO 14, 15, 16, 17 and 18 – fig. 2), and; b) protected areas for habitat/species management (PICO 07, 08, 09, 10, 11, 12 and 13 – fig. 2). The first group includes larger areas, mainly concentrated in the western part of the island, with well preserved structures of small walled vineyard fields (Portuguese: *currais*). Some are classified as UNESCO World Heritage Site. The second group comprises areas included in Natura 2000 network and some important bird areas, particularly relevant for protected seabirds such as *Sterna dougallii*, *Sterna hirundo* and *Calonectris deomedeae*.

The marine protected areas included in Pico Island Natural Park (PICO 20, 21 and 22 – fig. 2) are near shore and contiguous to terrestrial protected areas and coincide with areas closed to limpets harvesting.

## Survey

A total of 134 questionnaires were conducted during July 2011 with national and international tourists visiting Pico Island. The following information was collected on respondents: gender, age, occupation and nationality. The full questionnaire was composed of 22 questions taking around 20 minutes to complete. It was divided into three main sections: i) information about the respondent's visit to the island (motivation, duration, expenses,

visited sites and activities); ii) perceptions and preferences (knowledge about the island, positive and negative aspects), and; iii) position towards protected areas.

This paper focuses on two first sections, including the following questions:

Q1 - Why did you choose Pico as vacations' destination?

Q2 - Please indicate which activities have you done/plan to do during your vacations at Pico (it was possible to select more than one activity).

Q3 - Please indicate, on the map, the areas you have visited/plan to visit during your vacations at Pico.

Q4 - What do you associate to Pico landscape?

Q5 - Which are the 3 places you like the most at Pico?

Q6 - Which are the 3 places you dislike the most at Pico?

Q7 - Please indicate the 3 most positive aspects of Pico.

Q8 - Please indicate the 3 most negative aspects of Pico.

Q9 - Which are the activities developed at Pico that you consider positive and that you would like to see promoted/protected?

Q10 - Would you be willing to pay a fee to help to protect Pico protected areas? If yes, that fee should be directly applied for the protection of which areas or species?

Valid responses to Q5 and Q6 were classified as coastal or inland locations (considering the characteristics of Pico Island, inland landscape is associated to higher altitudes, usually more than 400 meters).



### Sample characterization

The sample was composed of 73 males and 50 females (11 persons have chosen not to answer), belonging mostly to the age group 45-54 years (27%) and 25-34 (24.6%).

As for occupation, the majority was: intellectual/scientific professionals (32 respondents), associate professionals (18 respondents), senior executives (16 respondents), administrative professionals (11 respondents) and students (11 respondents).

Regarding nationality, 35% were national tourists and international visitants were from different countries, mostly European, with France slightly standing out (11%) (Table. 1).

Table 1. Distribution of respondents by their nationality (frequency and percentage).

Nationality	Frequency	%
American	1	1%
Austrian	5	4%
Belgian	8	6%
Canadian	6	4%
Dutch	7	5%
English	10	7%
French	15	11%
German	6	4%
Italian	8	6%
Polish	3	2%
Portuguese	47	35%
Scottish	1	1%
Spanish	5	4%
Swiss	5	4%
Not responding	7	5%
<b>Total</b>	<b>134</b>	<b>100%</b>

### RESULTS

Tourists tend to choose Pico Island as vacations' destination (Q1) mainly because of its landscape and natural values (21.6%), maritime tourist activities (20.1%) and peculiarity (14.9%).

As for recreational activities during their stay (Q2), tourists indicated mainly: visits to museums, others cultural manifestations and events (63%), pedestrian trails (59%), bathing (57%), mountain climbing (45%) and whale watching (44%) (fig. 3).

Regarding the most visited areas (Q3), 34.3% of respondents indicated marine protected areas, 45.5% the Pico Mountain (PICO 01), 55.2% the central plateau area (PICO 19), 66.4% the Lajes village (where most of the whale watching companies are located), 67.2% vineyard areas (mainly PICO 16 and PICO 18) and 84.3% of respondents pointed protected areas other than those already mentioned.

The landscape of Pico Island (Q4) was inevitably associated to the mountain (40.3%) and to other landscape and natural values (34.3%).

Despite the relevance of the mountain, most of the preferred areas (Q5) are largely coastal (60%). The same applies to most disliked places (Q6), 85% of responses are placed on the coast.

When asked about Pico Island most positive aspects (Q7), 73.1% of respondents indicated landscape and natural values (other than the mountain and vineyard areas), 33.6% people's hospitality and 25.4% the sea. As for negative aspects (Q8), the most mentioned were: access and transports (other than aerial transport) (18.7%), spatial planning and urban development related issues (17.2%) and environmental quality problems (15.7%).

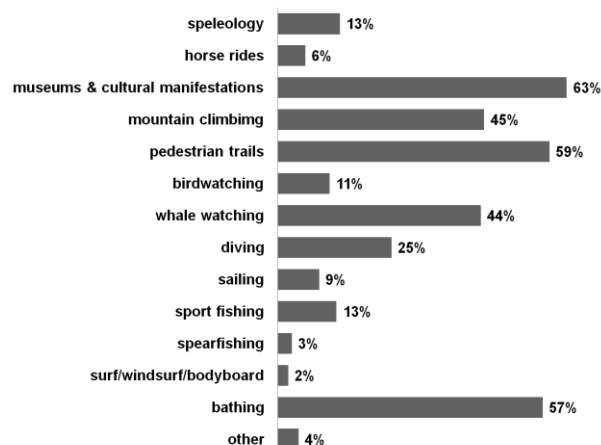


Figure 3. Recreational activities tourists enjoyed during their stay at Pico (Q2).

Activities considered positive and to be promoted (Q9) were mainly maritime tourist activities (20.1%), handicraft and culture (17.2%) and outdoor activities (13.4%).

Regarding willingness to pay a fee to help Pico's protected areas (Q10), 61.2% of the answers were positive. Of these, 27.6% think the fee should be directed to the conservation of the vineyard culture landscape, 20.9% to the mountain and 9% to the conservation of areas not yet classified as protected.

### DISCUSSION

Results show that Pico Island is much appreciated for its landscape and natural values, validating the Regional Government's strategy based on the promotion of natural heritage.

Maritime tourist activities play an important role in Pico attractiveness with a potential to increase since visitors think these activities are positive and should be promoted. Currently, whale watching is the most significant of those activities but diving and bathing are also relevant. Other popular activities, such as pedestrian trails and visits to museums (fig. 3), can be partially linked with coastal and marine features. A significant part of existing trails have coastal segments and the two most important museums on the island (alongside with the vineyard culture interpretation centre) are related to the old whaling industry.

The relevance of the coastal zone in Pico Island can be explained by the typical territorial organization of an island with volcanic origin and high altitude. The combination of biophysical structure, climate and dependence on sea as a privileged route of communication contributes to concentrating human settlements along the coast and population tends to decrease with an elevation of above 350 meters (Azorean Regional Government, 2008b). Therefore, it is natural that both preferred and problematic places are pinpointed in the coastal zone, this being the most used, enjoyed and impacted area on the island.

Although coastal areas are highly valued and the sea is indicated as one of the main positive aspects of the island, Pico Mountain is a unique and imposing scenic feature attracting tourists inland. This mountain/sea contrast can be explored as complementary tourism products, based on a high environmental quality label.

But, if the mountain “speaks for itself”, maritime tourism activities should be promoted and diversified. Birdwatching industry should also be fostered, mostly at coastal sites, in order to establish synergies with further coastal-based touristic activities.

The good state of conservation of the island’s natural environment seems to play a crucial role in Pico’s attractiveness and the existing protected areas are expected to contribute highly to its maintenance. However, with 35% of the island’s territory included in the Island Natural Park, management can be a challenge, both in terms of human and financial resources. On the other hand, tourism can have negative effects on protected areas and biodiversity. The implementation of a fee system can help finance protected areas and minimize environmental impacts of visitors. There are several examples worldwide where fee systems have been successfully implemented, providing revenues for protecting, monitoring and restoring protected areas (Steckenreuter & Wolf, 2013). However, tourism-related benefits can generate socio-economic inequalities if not properly shared among local communities, accruing human-conservation conflicts and increasing environmental impacts (e.g. exceeding carrying capacity, etc.) (Brockington *et al.*, 2008).

With 61.2% of respondents declaring their willingness to pay a fee to help maintain Pico’s protected areas, responsible agencies, namely the Island Natural Park management board, can explore suitable alternatives to implement such a fee, including voluntary tools.

## CONCLUSION

Tourism is expected to grow in the Azores in the next years, drawn by the high environmental quality of its territory. This is a key element for the development of these small islands, counterbalancing their natural disadvantages.

Our study at Pico Island explores the role of protected areas in tourism attractiveness and highlights the contribution of coastal and marine areas and activities. There is a clear potential for the growth of tourism on this island (as well as in others islands with similar characteristics) but such potential must be carefully exploited, ensuring the maintenance of the natural and cultural heritage and the environmental quality and crucial elements of Pico’s attractiveness as a tourism destination. To this end, tourist activities must be managed through an integrated approach promoting diversity and complementarity. Also, the adequate management of protected areas must be ensured in order to guarantee the preservation of natural values. Further studies should be conducted regarding carrying capacity and limits of acceptable change to determine the parameters which will allow the balance between conservation and enjoyment.

By facing visitors as stakeholders in the management of protected areas, SMARTPARKS Project gathered important information for decision-making agencies with respect to problems to be addressed and their possible solutions through tourism.

## ACKNOWLEDGEMENT

The authors want to express their gratitude to Andrea Zita Botelho, Cláudia Gomes, Inês Carapinha, Kiat Ng and José Benedicto Royuela for their assistance during surveys. Also, thank to Fernando Oliveira and Manuel Paulino da Costa, as Directors of Pico Island Natural Park, and Madalena, Lajes do Pico and S. Roque municipal councils for all their support to SMARTPARKS Project’s activities. At last, the authors wish to acknowledge “Fundação para a Ciência e Tecnologia” (FCT, Portugal) for funding Project PTDC/AAC-AMB/098786/2008.

## LITERATURE CITED

- Alexander, M., 2008. *Management planning for nature conservation: a theoretical basis and practical guide*. Dordrecht, The Netherlands: Springer, 426p.
- Azorean Regional Government., 2008a. An Assessment of “Strategy for the Outermost Regions: Achievements and Future Prospects” (Communication COM (2007) 507 Final). Ponta Delgada, Portugal: 35p.
- Azorean Regional Government., 2008b. Plano Regional de Ordenamento do Território para a Região Autónoma dos Açores. Região Autónoma dos Açores. Portugal (in Portuguese).
- Baldacchino, G. and Niles, D. (Eds.), 2011. *Island Futures: Conservation and Development Across the Asia-Pacific Region*. Tokyo, Japan: Springer, 182 pp.
- Bentz, J., Dearden, P. And Calado, H., 2013. Strategies for marine wildlife tourism in small islands – the case of the Azores In: Conley, D.C., Masselink, G., Russell, P.E. and O’Hare, T.J. (eds.), Proceedings 12th International Coastal Symposium (Plymouth, England), *Journal of Coastal Research*, Special Issue No. 65, pp. 874-879, ISSN 0749-0208.
- Brockington D., Duffy R. and Igoe J., 2008. *Nature Unbound. Conservation, capitalism and the future of Protected Areas*. London, UK: Earthscan, 249p.
- Calado, H., Ng, K., Borges, P., Alves, F., and Sousa, L., 2011. Climate Change and Coastal Tourism in Azores Archipelago. In: Jones, A.J. and Phillips, M. (eds.) *Disappearing Destinations: Climate Change and the Future Challenges for Coastal Tourism*. UK and USA: CAB Intl., 296p.
- Calado H., Quintela A. and Porteiro J., 2007. Integrated Coastal Zone Management Strategies on Small Islands. *Journal of Coastal Research*, SI 50 (Proceedings of the 9th International Coastal Symposium), 125 - 129. Gold Coast, Australia, ISSN 0749.0208
- Cardoso, P., Borges, P. A. V., Costa, A. C., Cunha, R. T., Gabriel, R., Frias Martins, A. M., Silva, L., Homem, N., Martins, M., Rodrigues, P., Martins, B. and Mendonça; E., 2008. A perspectiva arquipelágica: Açores. In: Martín, J.L., Arechavaleta, M., Borges, P.A.V. and Faria, B. *Top 100. Las 100 especies amenazadas prioritarias de gestión en la región europea biogeográfica de la Macaronesia*. Espanha: Consjería de Medio Ambiente y Ordenación Territorial, Gobierno de Canarias, pp 421-449 (in Portuguese).
- Cruz, A., Benedicto, J. and Gil, A., 2011. Socio-economic Benefits of Natura 2000 in Azores Islands – a case study approach on the ecosystem services provided by a Special Protected Area. *Journal of Coastal Research*, SI 64 (Proceedings of the 11th International Coastal Symposium), 1955 – 1959. Szczecin, Poland, ISSN 0749-0208
- DROTRH/IA. 2001. *Plano Regional da Água - Relatório Técnico - Versão para Consulta Pública*. Secretaria Regional do Ambiente, Direcção Regional do Ordenamento do Território e dos Recursos Hídricos, 414p (in Portuguese).
- Emerton, L., Bishop, J. and Thomas, L., 2006. *Sustainable Financing of Protected Areas: A global review of challenges and options*. Gland, Switzerland and Cambridge, UK: IUCN. x + 97p.
- Fonseca, C., Calado, H., Pereira da Silva C. and Gil, A., 2011. New approaches to environment conservation and sustainability in Small Islands: The Project SMARTPARKS. *Journal of Coastal Research*, SI 64 (Proceedings of the 11th International Coastal Symposium), 1970-1974. Szczecin, Poland, ISSN 0749-0208.
- Gil, A., Fonseca, C., Lobo, A. and Calado, H., 2012. Linking GMES Space Component to the development of land policies in Outermost Regions - the Azores (Portugal) case-study. *European Journal of Remote Sensing*, 45: 263-281. DOI: 10.5721/EuJRS20124524.
- Gil A., Calado H., Costa L.T., Bentz J., Fonseca C., Lobo A., Vergílio M. and Benedicto J., 2011. A Methodological Proposal for the Development of Natura 2000 Sites Management Plans. *Journal of Coastal Research*, SI 64 (Proceedings of the 11th International Coastal Symposium), 1326 – 1330. Szczecin, Poland, ISSN 0749-0208.
- Hess, A.L., 1990. Overview: Sustainable Development and Environmental Management of Small Islands. In: D’Ayala, W.B.P. and Hein, P. (eds.). *Sustainable Development and Environmental Management of Small Islands*. Paris, France: UNESCO, pp. 3–14.
- Kafyri, A., Hovardas, T. and Poirazidis, K., 2012. Determinants of Visitor Pro-Environmental Intentions on Two Small Greek Islands: Is Ecotourism Possible at Coastal Protected Areas?. *Environmental Management*, 50: 64-76,

- Millennium Ecosystem Assessment., 2005. *Ecosystems and human well-being: current state and trends*. Millennium Ecosystem Assessment Series, vol. 1. Washington, DC, USA: Island Press.
- Moniz, A., 2009. A sustentabilidade do turismo em ilhas de pequena dimensão: o caso dos Açores. Ponta Delgada, Centro de Estudos de Economia Aplicada do Atlântico (in Portuguese).
- Rietbergen, S. Hammond, T. Sayegh, C., Hesselink F. and Mooney, K., 2007. *Island voices – island choices: Developing strategies for living with rapid ecosystem change in small islands*. Gland, Switzerland: IUCN, 40 p.
- Schubert, S.F., Brida, J.G. and Risso, W.A., 2011. The impacts of international tourism demand on economic growth of small economies dependent on tourism. *Tourism Management*, 32, 377-385.
- Seetanah, B., 2011. Assessing the dynamic economic impact of tourism for island economies. *Annals of Tourism Research*, 38(1), 291-308.
- Steckenreuter, A. and Wolf, I.D., 2013. How to use persuasive communication to encourage visitors to pay park user fees. *Tourism Management*, 37, 58-70.
- Sundseth, K., 2009. *Natura 2000 in the Macaronesian Region*. European Commission, Environment Directorate General. Luxembourg: Office for Official Publications of the European Communities, 12p.
- Tisdell, C. and Wilson, C., 2012. *Nature-based Tourism and Conservation: New Economic Insights and Case Studies*. UK and USA: Edward Elgar Publishing Limited, 520p.

# Framework for proper beach nourishment as an adaptation to beach erosion due to sea level rise

Jun Yoshida†, Keiko Udo‡, Yuriko Takeda‡, Akira Mano‡

†Department of Civil and Environmental Engineering, Tohoku University, Sendai 980-8579, Japan  
j-yoshida@potential1.civil.tohoku.ac.jp

‡International Research Institute of Disaster Science, Tohoku University, Sendai 980-8579, Japan  
udo@irides.tohoku.ac.jp  
takeda@irides.tohoku.ac.jp  
mano@irides.tohoku.ac.jp



[www.cerf-jcr.org](http://www.cerf-jcr.org)



[www.JCRonline.org](http://www.JCRonline.org)

## ABSTRACT

Yoshida, J., Udo, K., Takeda, Y., Mano, A., 2014. Framework for proper beach nourishment as adaptation to beach erosion due to sea level rise. In: Green, A.N. and Cooper, J.A.G. (eds.), *Proceedings 13<sup>th</sup> International Coastal Symposium* (Durban, South Africa), *Journal of Coastal Research*, Special Issue No. 70, pp. 467-472, ISSN 0749-0208.

Beach erosion caused by sea level rise is a serious problem for people over the world. Beaches play important roles in disaster prevention, recreational use, and nurturing unique ecosystems. Beach nourishment is capable of maintaining the position of the shoreline and the natural environment. However, applying artificial nourishment to the whole beach area is not a practical method due to high costs and the large quantity sand required. There has been no framework for effective adaptation of beach nourishment to solving coastal erosion issues. In this study, we focus on the beach nourishment as an adaptation to beach erosion due to sea level rise and attempt to construct a framework for proper beach nourishment. The framework for the adaptation proposal is as follows: (i) Prediction of shoreline changes and future beach width due to sea level rise; (ii) Determination of beach width to be protected in terms of disaster prevention, ecosystem conservation and recreation respectively; (iii) Specifying vulnerable areas where the area of and width of the beach Step; (iv) Estimation of sand volume and its cost applied only to the vulnerable area. This framework was applied to Japanese beaches where the determine beach width indicated that when a beach width of more than 10 m is needed for prevention against disasters, more than 20 m for ecosystem conservation, and more than 30 m for recreation use. The volume of sand required to maintain the beach width along the whole Japanese beach varies from  $61 \times 10^6$  to  $2,300 \times 10^6 \text{ m}^3$ , and by the use of this framework, it is possible to estimate practical nourishment volume and its associated costs for disaster prevention, ecosystem conservation and recreation use.

**ADDITIONAL INDEX WORDS:** *sea level rise, beach erosion, adaptation, beach nourishment, framework.*

## INTRODUCTION

Coastal erosion caused by sea level rise and climate change is a serious problem for people over the world. The IPCC 5th Assessment Report (2013) estimated that global sea level for 2081-2100 will likely be in the range of 0.26 to 0.82 m under all RCP scenarios due to thermal expansion and melting glaciers and ice sheets. With the change in wave characteristics due to climate change presenting another concern, such as the growth of wave height due to extreme storms. The future shoreline would retreat due to sea level rise and the increase in wave heights during storms, which consequently, would cause harmful impacts on socio-economics in coastal regions as 10% of the world's population live in low-lying coastal regions within 10 m above the present sea level (McGranahan et al. 2007). Sandy beach play important roles in disaster prevention with existing unique ecosystems and recreational use, they have the ability to dissipate wave energy, preventing waves from overtopping coastal defenses therefore decreasing the force of incoming waves. Coastal areas with no beaches are affected by high energy waves during storm events. Beaches are important for tourism because people visit for various activities and during vacation and therefore the economic value of recreational beaches was estimated using the travel cost

method at 9.2 billion US dollars per year for the whole Japanese beach (Ohno et al., 2009). Unique ecosystems existing on these beaches which encompass as beach vegetations and nesting sea turtles. It is necessary to carefully consider adapting beaches for recreational use so as to maintain ecosystems, and prevent possible disasters.

In order to make an adaptation against beach erosion, evaluation of the possible impacts due to sea level rise and climate change and associated beach erosion should be carried out. The effects of sea level rise have previously been estimated using Bruun rule (Zhang et al., 2004). In Japan, Yoshida et al. (2013) estimated shoreline change in the five Japanese beaches with the causes of past long-term beach erosion taken into consideration which showed that the main cause of beach erosion is sea level rise.

Examples of recent proposed adaptations based on the impact assessments include periodic beach nourishment, associated with breakwaters and dune afforestation, which could protect tourist resorts from erosion and inundation risks (Snoussi et al., 2008). Stabilization and accretion of the beach requires artificial beach nourishments (Marcinkowski et al., 2013). The average cost per beach nourishment project was estimated in the USA at \$175,400 by Corporations of Engineers, with the average cost of \$12 million for hard structure, which is significantly more expensive than beach nourishment (Sudar et al., 1995). Beach nourishment is the method where sand is sourced from an outside region and used to

replace sediment lost through longshore drift, high wave energies or sea level rise; factors which progressively eroding beach areas. This method has previously been used for preventing the undermining of coastal defenses foundation, such as sea wall and levees, and exposing or making beach width wider in the coastal resort city where the existing beach conditions are indispensable (e.g. Miami beach from 1976 to 1981). According to the relationship between hurricane damage and prior beach width, it is evident that the damage incurred drastically decreases in wide beach (Dean *et al.*, 1988). In other words, beach nourishment that maintains a wide beach width can mitigate seacoasts hazards.

It is ideal to maintain beaches without hard structures considering beach benefits for disaster prevention, environment conservation and recreational use. Applying beach nourishment to the whole beach area is not a practical method because of its high cost and large sand quantities (Cooper *et al.*, 2012). This paper focuses on the beach nourishment as an adaptation however, as no new frameworks for proper beach nourishment have been identified. Therefore, this study aims to construct a framework for a proper beach nourishment regarding disaster prevention, preservation of ecosystems and recreation use, as an adaptation to beach erosion due to sea level rise.

## STUDY SITE AND PHYSICAL FEATURES

Figure 1 shows the location of Japan with twenty-five percent of Japan's entire coastline (35000 km) consisting of sandy beaches of which 50% are natural beaches without artificial coastal structures (Nature Conservation Bureau of the Environment Agency, 1994). The study sites consist of 77 coastal areas in Japan, categorized in terms of topographical and oceanographic similarities, and longshore sediment transport; continuity according to the Basic Policy for Coastal conservation in Japan. Seawalls and levees were installed from the 1950's in potential disaster coasts to prevent typhoon and storm surge inland. From the 1950s-1990s coastal structures and developed seaside structures after World War II decreased longshore drift, causing erosion along the Japanese beaches. However, from 1990 to 2008, the shoreline did not change significantly because the coastal law revised in 1999, to focus on beach conservations under the consideration of "use" and "environment" besides disaster prevention (Yoshida *et al.*, 2013).

The annual mean and maximum tide level tended to increase over the past few decades in Japan according to Sugawa *et al.* (2011). The Nationwide Ocean Wave Information Network for Port and Harbours (NOWPHAS) of the Ministry of Land, Infrastructure and Transport has been observing waves. The sea of Japan is characteristics by high waves in winter and low waves in summer, with a high frequency of swell throughout the year on the Pacific Ocean side, with a small seasonal change of wave height and the period (Sugimoto *et al.*, 2008).

## METHODS

### Framework for proper beach nourishment

Considering the important roles of beaches, it is desirable to preserve sandy beaches as much as possible. However, applying beach nourishment to the whole beach area is not a practical method. Therefore, beach nourishment need only be applied to vulnerable areas for disaster prevention, preservation of ecosystems, and recreation, using beach width as a vulnerable evaluation index. Thus a framework for estimating a proper beach nourishment volume based on this concept may be applied, using the following proposal (Figure. 2).

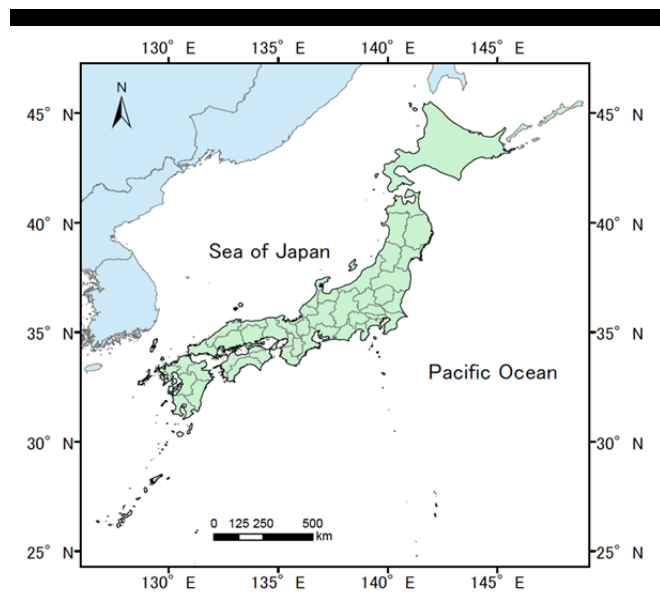


Figure 1. Location of Japan.

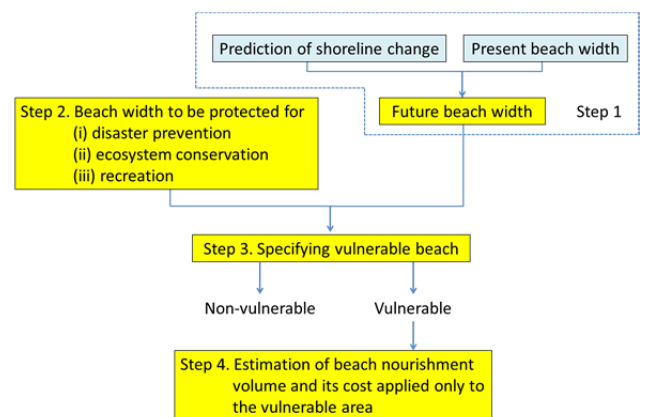


Figure 2. Framework for proper beach nourishment.

1. Prediction of shoreline changes and future beach width due to sea level rise.
2. Determination of beach width to be protected for disaster prevention, ecosystem conservation, and for recreation.
3. Specifying vulnerable areas where the area of beach width of Step 2 is narrower than the beach width of Step 1.
4. Estimation of sand volume and its cost to maintain the beach width to be protected in terms of disaster prevention, recreation and beach ecosystems respectively.

The step 1 is to estimate beach width for 2100 by obtaining differences between predicted shoreline change and present beach width. The predicted shoreline change we used in this paper is the results of the estimation using the Bruun rule (Bruun, 1962) as Udo *et al.*, (2013) estimated for 75 beaches over the whole Japan which is divided from geographical features, marine phenomenon and continuity of longshore drift. For the grain size of 0.2 mm,

shoreline would retreat between 26 and 56 m under RCP2.6, between 28 and 62 m under RCP4.5, between 26 and 57 m under RCP6.0, and between 37 and 84 m under RCP8.5 by the end of 21st century. For the grain size of 0.6 mm, shoreline would retreat between 11 and 24 m under RCP2.6, between 12 and 27 m under 4.5, between 11 and 25 m under 6.0, and between 16 and 36 m under RCP8.5 by the end of 21st century. The Bruun rule can easily estimate shoreline change in large-scale areas; however, the rule has been criticized due to its limitation and assumptions (Cooper and Pilky, 2004). On the other hand, the model tests have claimed to provide verification of Bruun rule (Zhang et al., 2004). The present dry beach width of 75 beaches was obtained by dividing each beach area by the corresponding shoreline length. The beach area and length were extracted from 1/25000 scale maps from 1990 by Kishida and Shimizu (2000).

The step 2 is to determine the beach width in order to protect the beach from disaster, preserve ecosystems, and recreation. We determine that the beach width of 10 m is required for disaster prevention, 20 m for ecosystem conservation, and 30 m for recreation. The focus was placed on the wave-dissipating property on the beach, as risk reduction. In Japan, the determination of beach width against wave-overtopping has been evaluated by using wave run-up height. Wave run-up is estimated by using the improved Saville's hypothetical slope concept (Nakamura et al., 1975). Many examples show that the beach width against wave-overtopping should be more than 10 m in beaches where a seawall exists (e.g. Sendai Bay Coast and Kujukurihama Beach Coast). For ecosystems, we consider the width in order to protect plant habitats. Analyses of aerial photographs of the Kashimanada Coast and the Kujukurihama Beach Coast showed that at least 20 m beach widths are required for plant to inhabit along coast fronting the Pacific Ocean (Kato et al., 2001). The necessary width for recreational use requires more than 30 to 50 m beach widths, with foreshore slope of 0.10 to 0.02 at high tide (Japan Travel and Tourism Association, 1987; Ministry of Land, Infrastructure, Transport and Tourism, 1992). The specification of 30 m was required to estimate the minimum sand volume required for recreation.

The step 3 specifies vulnerable areas where the future beach width of Step 1 is narrower than the beach width of Step 2 that is 10 m against wave-overtopping, 20 m for preserving ecosystem and 30 m for recreational use. Beach nourishment applies only to the vulnerable beaches of step 3.

The step 4 is to estimate beach nourishment volume and its cost for maintaining beach width to be protected in step 2.

### Beach nourishment model with sea level rise

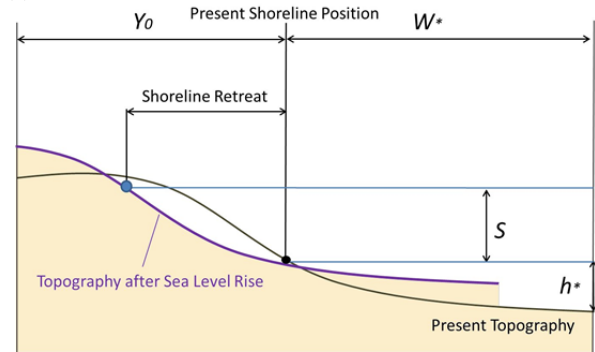
The current beach profile is assumed to be in equilibrium (Dean, 1977). The profile can be described by the equation (1):

$$h = Ay^{2/3} \tag{1}$$

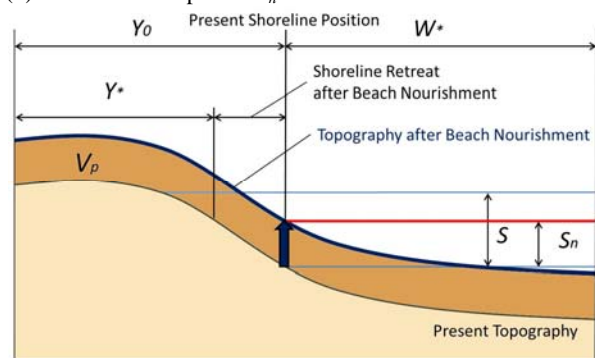
where  $h$  is the water depth,  $y$  is the distance offshore and  $A$  is the scaling parameter based on sediment characteristics. Dean (1977) found that the scaling parameter,  $A$ , depends on grain size alone.

Beachs maintain equilibrium profile when sea level does not rise. On the other hand, the beach profile spreads towards offshore and shoreline tends to retreat landward without additional sand input to the beach under rising sea level (Figure 3a). In order to maintain the beach equilibrium profile facing future sea level rise, the entire beach profile would have to increase vertically with the same amount of sea level rise (Astrid, 2010; Cooper et al., 2013). Based on this, the necessary additional sand volumes are calculated by the following equation (2):

(a) Shoreline retreat without beach nourishment



(b) Increase of the profile  $S_n$



(c) Shoreline retreat after beach nourishment

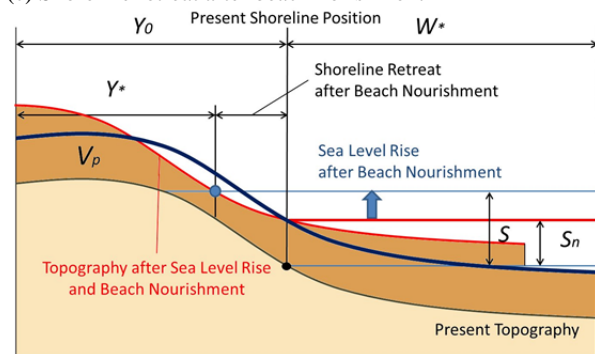
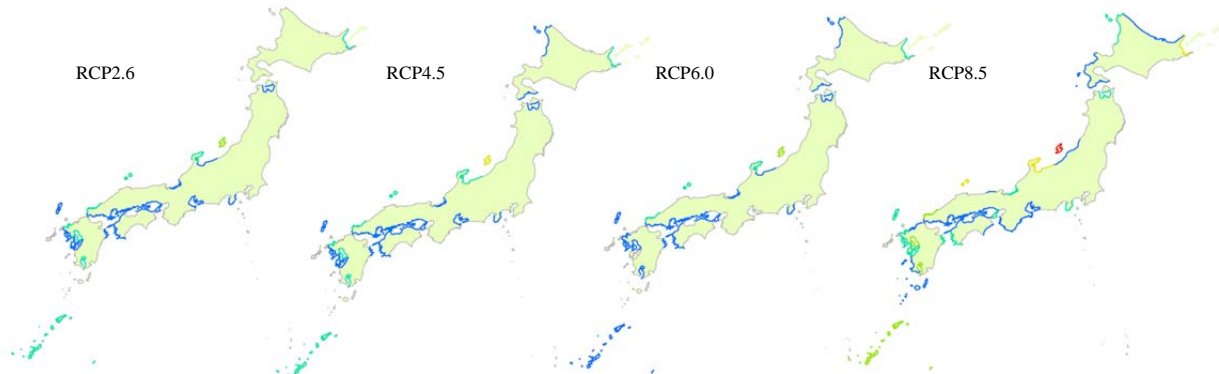


Figure 3. The concept of beach nourishment for keeping beach width to be protected. (b) The profile increases the amount of  $S_n$  by adding sand. (c) The shoreline would retreat due to sea level rise after beach nourishment. The blue point on the figure (c) is shoreline position after beach nourishment. This nourishment prevents future beach width from being narrower than  $Y_*$  while allowing shoreline to be retreated when the future beach width will be wider than the beach width of step 2 after rising sea level.

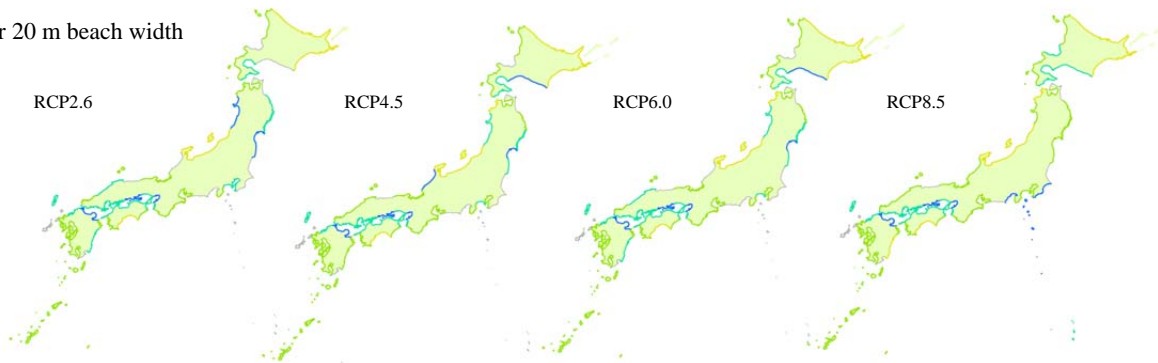
$$V_p = S_n Y_0 + \int_0^{W_*} (Ay^{2/3} + S_n) dy - \int_0^{W_*} Ay^{2/3} dy \tag{2}$$

where  $V_p$  is the profile change volume ( $m^3 m^{-1}$ ),  $Y_0$  is the dry beach width,  $S_n$  is the height of beach nourishment, i.e. the amount of vertical increase of equilibrium profile, to maintain the beach width to be protected,  $Y_*$ , and  $W_*$  is the cross-shore distance to closure the depth  $h_*$ . The amount of vertical increase of equilibrium profile  $S_n$  is given by the following equation (3) obtained from the Bruun equation:

(a) For 10 m beach width



(b) For 20 m beach width



(c) For 30 m beach width

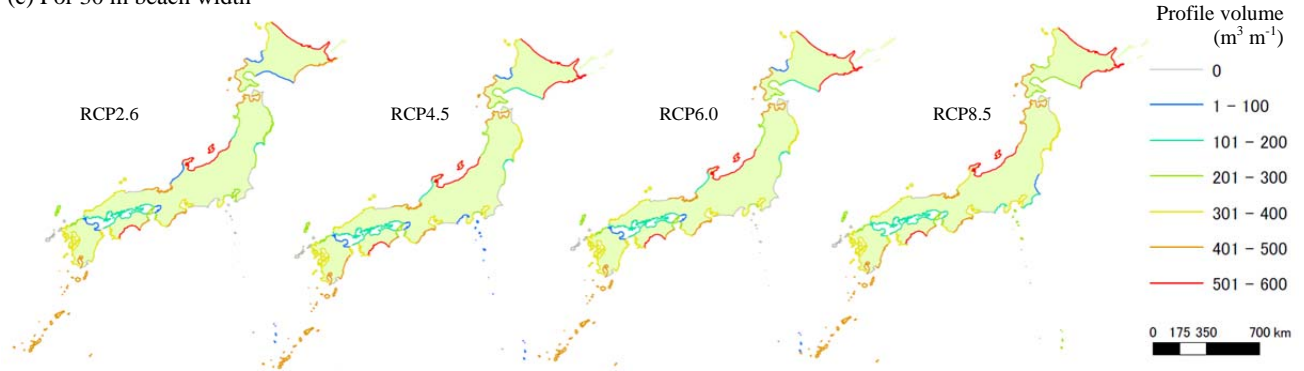


Figure 4. The profile volume (grain size of 0.2 mm) required for (a) beach width of 10 m for disaster prevention, (b) 20 m for ecosystem conservations, and (c) 30 m for recreational use under RCP2.6, RCP4.5, RCP6.0, and RCP8.5.

$$S_n = S - \left( \frac{h_* + B_h}{W_*} \right) (Y_0 - Y_*) \quad (3)$$

$S$  is the sea level rise,  $h_*$  is the closure depth and  $B_h$  is the berm height. The amount of sea level rise after beach nourishment causes a permissible retreat ( $Y_0 - Y_*$ ) after the profile increases the amount of  $S_n$  (Figure 3b).  $V_p$  is the additional profile volume for preventing future beach width from being narrower than  $Y_*$ , while this nourishment allows shoreline to be retreated when the future beach width becomes wider than the beach width of step 2 after sea level rises. The additional sand volume is estimated from multiplying profile change volume of equation (2) by beach length.

The closure depth,  $h_*$  is given by the following equation (Hallemeier, 1981):

$$h_* = 2.28H_m - 68.5 \left( \frac{H_m^3}{gT_m^3} \right) \quad (4)$$

where  $H_m$  is the maximum significant mean wave height,  $T_m$  is the maximum significant mean wave period,  $g$  is gravity acceleration. The cross-shore distance,  $L_*$ , was used for the distance offshore,  $y$ , calculated by substituting the scaling parameter,  $A$ , and the closure depth,  $h_*$ , into Eq. (1). The berm height,  $B_h$ , is given by the equation mentioned by Takeda and Sunamura (1983):

$$B_h = 0.125H_b^{5/8} (gT_s^2)^{3/8} \quad (5)$$

where  $H_b$  is the breaker wave height,  $H_s$  is the mean significant wave height,  $T_s$  is the mean significant wave period.  $H_b$  is given by the following equation (Sunamura, 1983):

$$\frac{H_b}{H_s} = (\tan \alpha)^{0.2} \left( \frac{H_s}{L_s} \right)^{-0.25} \tag{6}$$

where  $\tan \alpha$  is the beach gradient, and  $L_s$  is mean significant wave length. The shoreline change was thus estimated by using the data of sea-level rise, grain size, beach gradient and wave conditions.

The data used in this framework was sea level rise, waves, grain size and foreshore slope. The sea level rise used in this study was of sea level rise data of Udo et al. (2013) added with the contribution from ice sheet melt under RCP2.6, RCP4.5, RCP6.0, and RCP8.5 scenarios. The sea level rise ranges between 0.41 and 0.49 m under RCP2.6, between 0.46 and 0.51 m under RCP4.5, between 0.45 and 0.47 m under RCP6.0, and between 0.59 and 0.69 m under RCP8.5 by the end of 21st century. We obtained annual mean and maximum significant wave heights from NOWPHAS. Average annual mean and maximum significant wave heights and periods were assigned as the wave conditions required by estimating beach nourishment volumes. We uniformly used the grain sizes of 0.2 and 0.6 mm throughout Japanese beaches because it is difficult to examine each size over the whole beach in Japan. About 80 % of sand particle size of 35 prefectures in Japan was found to be between 0.125 and 1.0 mm according to 120 literatures surveyed (Udo et al., 2013). The sediment scale parameter,  $A$ , we used for equilibrium equation is 0.10 for 0.2 mm and 0.17 for 0.6 mm in grain sizes. The slope we used in this paper is 0.014 for 0.2 mm and 0.11 for 0.6 mm in grain sizes. The input data we use in this study such as grain sizes, beach slope and beach width are uniformly applied to the whole Japanese beaches because it is difficult to obtain detailed data of large scale areas.

### RESULTS

We applied the constructed framework to the 77 beaches in Japan to estimate necessary nourishment volume and its cost until

2100. Figure 4 shows the profile volumes (only 0.2 mm of grain size because of the limited pages) required for keeping the 10 m of the beach width against wave-overtopping, 20 m for inhabiting plants, and 30 m for recreational use under RCP2.6, RCP4.5, RCP6.0, and RCP8.5. For the grain size of 0.2 mm, the profile volume estimates between 120 and 1600 m<sup>3</sup>/m for maintaining the present position of the shoreline, 11 and 197 m<sup>3</sup>/m against wave-overtopping, 13 and 394 m<sup>3</sup>/m for inhabiting plants, and 1 and 591 m<sup>3</sup>/m for recreation. For the grain size of 0.6 mm, the profile volume estimates between 51 and 680 m<sup>3</sup>/m for keeping present shoreline position, 2 and 194 m<sup>3</sup>/m against wave-overtopping, 2 and 390 m<sup>3</sup>/m for inhabiting plants, and 1 and 580 m<sup>3</sup>/m for recreation.

Table 1 shows the total nourishment volume for keeping shoreline position and considering beach width. For the grain size of 0.2 mm, the additional volume to keep the present shoreline position ranges from  $3,700 \times 10^6$  to  $5,200 \times 10^6$  m<sup>3</sup>. As for protection against wave-overtopping, the additional volume ranges from  $600 \times 10^6$  to  $720 \times 10^6$  m<sup>3</sup>. As for inhabiting plants, the additional volume ranges from  $1300 \times 10^6$  to  $1,500 \times 10^6$  m<sup>3</sup>. As for recreational use, the additional volume ranges from  $2,000 \times 10^6$  to  $2,300 \times 10^6$  m<sup>3</sup>. For the grain size of 0.6 mm, the additional volume to keep the present shoreline position ranges from  $1,700 \times 10^6$  to  $2,300 \times 10^6$  m<sup>3</sup>. As against wave-overtopping, the additional volume ranges from 61 to  $240 \times 10^6$  m<sup>3</sup>. As for inhabiting plants, the additional volume ranges from  $350 \times 10^6$  to  $720 \times 10^6$  m<sup>3</sup>. As for recreational use, the additional sand volume ranges from  $870 \times 10^6$  to  $1400 \times 10^6$  m<sup>3</sup>. The necessary sand volume depends on the grain size. All beaches require additional volumes according to the increase of the beach width determined in the step 2. For the grain size of 0.6 mm, beach nourishment for keeping the 10 m beach width would not be needed under RCP2.6 and RCP6.0 because the future beach width would be maintained at least 10 m over entire Japanese beaches under these scenarios. Table 2 shows the maximum and minimum cost of beach nourishment. Beach nourishment cost in Japan mostly ranges from \$20/m<sup>3</sup> to \$60/m<sup>3</sup> (Nishi et al, 2005).

Table 1. Sand volume (10<sup>6</sup> m<sup>3</sup>) to keep present shoreline position: beach width of 10 m for disaster prevention, 20 m for ecosystem conservation, and 30 m for recreational use.

Grain size	0.2 mm				0.6 mm				
	Scenario	RCP2.6	RCP4.5	RCP6.0	RCP8.5	RCP2.6	RCP4.5	RCP6.0	RCP8.5
Keeping shoreline									
10m for protection	3,700	4,100	3,800	5,200	1,700	1,900	1,700	2,300	
20 m for ecosystem	600	640	630	720	66	93	61	240	
30 m for recreation	1,300	1300	1,300	1,500	350	420	370	720	
	2,000	2,100	2,100	2,300	870	980	910	1,400	

Table 2. Maximum and minimum cost of beach nourishment (million dollar, 1dollar = 100 Japanese yen). Maximum is estimated from nourishment cost of \$60/m<sup>3</sup> with 0.2 mm in grain size, and minimum from \$20/m<sup>3</sup> with 0.6 mm in grain size.

Case	Maximum cost				Minimum cost				
	Scenario	RCP2.6	RCP4.5	RCP6.0	RCP8.5	RCP2.6	RCP4.5	RCP6.0	RCP8.5
Keeping shoreline									
10m for protection	220,000	250,000	230,000	310,000	34,000	38,000	34,000	46,000	
20 m for ecosystem	36,000	38,000	38,000	43,000	1,300	1,900	1,200	4,800	
30 m for recreation	78,000	78,000	78,000	90,000	7,000	8,400	7,400	14,000	
	120,000	130,000	130,000	140,000	17,000	20,000	18,000	28,000	



We use \$20/m<sup>3</sup> as a cost for the case of 0.6 mm grain size to estimate minimum expenditure, and \$60/m<sup>3</sup> for the case of 0.2 mm grain size to estimate maximum expenditure for the next century. Minimum expenditure would be \$1.2 billion for beach nourishment assuming that the beach width has to be maintained at 10 m for the RCP6.0 scenario, \$140 billion would be required for beach nourishment assuming that the beach width be maintained as wide as 30 m for the worst (RCP8.5) scenario. From these results, the necessary sand volume and its cost would be smaller, than the volume and its cost required for maintaining the present shoreline position against sea level rise by the end of 21st century.

## CONCLUSION

In this study, we constructed the framework for proper beach nourishment for disaster prevention, ecosystem conservation and recreation, estimating the volume of sediment required for beach nourishment in Japan associated with maximum and minimum costs.

We uniformly applied the beach width to be protected for disaster prevention, ecosystem, and recreation, throughout Japanese beaches, by using data obtained from Japanese local governments. This framework only takes into consideration the impact of sea level rise on the coast without considering existing erosion. Determining beach width required for disaster prevention must therefore be integrated with evaluation of risks associated to other forms of coastal erosion in order to improve this framework. An appropriate beach width and more reliable input data according to beach characteristics are needed when applying this framework to smaller areas. However, it would be useful to deal with an adaptation in large scale areas such as the whole Japanese coastal because this framework can estimate overviews of beach nourishment against sea level rise. If a necessary beach width of each region can be obtained, it is possible to estimate realistic and practical nourishment volumes required for disaster prevention, ecosystem conservations and recreation by using this framework.

## ACKNOWLEDGEMENT

This study was supported in part by the Environment Research and Technology Development Fund (S-8) of the Ministry of the Environment, Japan. We express our deepest gratitude to Professor So Kazama of Tohoku University for valuable suggestions regarding how to treat the estimation data of climate change. We are also grateful to an anonymous reviewer for encouraging and constructive comments.

## LITERATURE CITED

- Astrid, F., 2010. Influence of climate change on beach nourishment and the seawall design at the Gold Coast, Australia, Bergische University, Diploma thesis. No. 42551.
- Bruun, P., 1962. Sea-level rise as a cause of shore erosion, *Journal. Waterways and Harbors Division*. ASCE, 88, 117-130.
- Chiba prefecture. 2003. Master plan for storm surge protection projects at the Kujukuri Beach coast, Japan. (in Japanese)
- Cooper, J.A.G. and Pilkey, O.H., 2004. Sea-level rise and shoreline retreat: time to abandon the Bruun Rule, *Global and Planetary Change*, 43, 157-171.
- Cooper, J.A.G. and Lemckert, C., 2012. Extreme sea-level rise and adaptation options for coastal resort cities: A qualitative assessment from the Gold Coast, Australia, *Ocean & Coastal Management*, 64, 1-14.
- Dean, R.G., 1977. Equilibrium beach profiles: U.S. Atlantic and Gulf coasts. Ocean Engineering Technical Report 12, Department of Civil Engineers., University of Delaware: Newark, DE; 45 pp.
- Dean, R.G., 1988. Realistic economic benefits from beach nourishment, *Proceedings of 21st Coastal Engineering Conference*, pp.1558-1572.
- Hallermeier, R. J., 1981. A profile zonation for seasonal sand beaches? from wave climate, *Coastal Engineering*, 4, 253-277
- Intergovernmental Panel on Climate Change (IPCC). 2013. Climate Change 2013. The Physical Science Basis. Working Group I Contribution to the IPCC 5th Assessment Report - Changes to the Underlying Scientific/Technical Assessment (IPCC-XXVI/Doc.4).
- JapanTravel and Tourism Association. 1987. Guide of marine tourist resort plan pp.33
- Kishida, H., and Shimizu, M., 2000. Extraction of coastal erosion and deposition through coastal information survey, *Proceeding of Coastal Engineering, JSCE*, 47, 681-685. (in Japanese)
- Marcinkowski, T. and M. Szmytkiewicz., 2013. Performance of submerged breakwaters as improvement of beach fill effectiveness in Gdynia, Poland. *Journal of Coastal Research*, Special Issue No. 65, pp.326-331.
- McGranahan, DA., Balk, D., and Anderson, B., 2007. The rising tide: assessing the risk of climate change and human settlements in low elevation coastal zones. *Environ. Urban*. 19:17-39
- Ministry of Land, Infrastructure and Transport Tohoku Regional Bureau. 2009. The report of project appraisal committee at the south Sendai Bay coast, Japan. (in Japanese).
- Ministry of Land, Infrastructure, Transport and Tourism, 1992. Manual of beach planning and design, pp.118. (in Japanese).
- Nature Conservation Bureau of the Environment Agency, 1994. The 4<sup>th</sup> National Survey on the Natural Environment, pp.48. (in Japanese)
- Nishi, R., Robert G. Dean., Tanaka, R., 2005. Beach nourishment projects in Japan in terms of its size and cost. *Proceedings of civil engineering in the ocean No. 21*, pp. 355-360. (in Japanese)
- Ohno, E., Hayashiyama, Y., Morisugi, H. and Nohara, K., 2009. Global warming damage cost of sandy beach loss: travel cost method approach. *Proceedings of the Symposium on Global Environment*, Volume 14, 291-297. (in Japanese)
- Port and Airport Research Institute, Marine Information Group, Marine Information Division Marine Environment and Engineering Department. Nationwide Ocean Wave Information Network for Ports and Harbours (NOWPHAS), Wave Data.
- Sudar, R. A., J. Pope., T. Hillyer, and J. Crumm., 1995. Shore protection projects of the U.S. Army Corps of Engineers, *Journal of Shore and Beach*, pp. 3-16.
- Sugawa, T., Udo, K., Mimura, N., and Mano, A., 2011. Projection of Shoreline Retreat due to Sea Level Rise along Japanese Coasts. *Journal of Japan Society of Civil Engineers*, Ser. B2 (Coastal Engineering), 67, 1196-1200. (in Japanese)
- Sugimoto, S., Chikasawa, M., 2008. A Study on Japanese Coastal Wave Characteristics Using Coastal Wave Observation by Japan Meteorological Agency. Weather service bulletin No. 75, pp. 77-95.
- Sunamura, T., 1983. Determination of Breaker Height and Depth in the Field, Annual Report No.8, Institute of Geoscience, University of Tsukuba, Japan, 53-54.
- Snoussi, M., Ouchani, T., and Niazi, S., 2008. Vulnerability assessment of the impact of sea-level rise and flooding on the Moroccan coast: The case of the Mediterranean eastern zone. *Estuarine, Coastal and Shelf Science*, 77, 206-213.
- Takeda, I., and Sunamura, T., 1983. Topographic evolution of sandy beaches in the accretion process, *Proceedings of Coastal Engineering, JSCE*, 30, 254-258 (in Japanese).
- Udo, K., Takeda, Y., Yoshida, J. and Mano, A., 2013. Future projection of beach erosion in Japan using sea level change data of MIROC5 model. *Journal of Japan Society of Civil Engineers*, Ser. G (Environmental Research), 69, 239-247. (in Japanese)
- Yoshida, J., Udo, K., Takeda, Y., and Mano, A., 2013. Potential impact of climate change at five Japanese beaches. *Journal of Coastal Research*, Special. Issue.No. 65, pp. 2185-2190.
- Zhang K., Douglas B.C., and Leatherman S.P., 2004. Global Warming and Coastal Erosion. *Climatic Change*. 64, 41-58.

# Assessment of vulnerability and adaptive capacity to coastal hazards in the Caribbean Region

Nina S.-N. Lam<sup>†</sup>, Helbert Arenas<sup>‡</sup>, Patricia L. Brito<sup>∞</sup>, Kam-Biu Liu<sup>§</sup>

<sup>†</sup> Department of Environmental Sciences,  
Louisiana State University  
Baton Rouge, USA.  
[nlam@lsu.edu](mailto:nlam@lsu.edu)

<sup>‡</sup> Department of Informatique  
University of Burgundy  
Dijon, France.  
[helberius@gmail.com](mailto:helberius@gmail.com)

<sup>∞</sup> Department of Transportation  
Engineering and Geodesy  
Federal University of Bahia  
Salvador, Brazil.  
[patricia.brito@ufba.br](mailto:patricia.brito@ufba.br)



[www.cerf-jcr.org](http://www.cerf-jcr.org)

<sup>§</sup> Department of Oceanography and  
Coastal Sciences  
Louisiana State University  
Baton Rouge, USA.  
[kliu1@lsu.edu](mailto:kliu1@lsu.edu)



[www.JCRonline.org](http://www.JCRonline.org)

## ABSTRACT

Lam, N.S.N., Arenas, H., Brito, P.L., Liu, K.B., 2014. Assessment of vulnerability and adaptive capacity to coastal hazards in the Caribbean region. In: Green, A.N. and Cooper, J.A.G. (eds.), *Proceedings 13<sup>th</sup> International Coastal Symposium* (Durban, South Africa), *Journal of Coastal Research*, Special Issue No. 70, pp. 473-478, ISSN 0749-0208.

It has been documented that given the same type of climate related hazard and degree of exposure, the vulnerability of a region to the hazard and its resultant damages could be very different, depending on a number of natural and socioeconomic factors. An understanding of the factors contributing to the vulnerability of a region requires a good assessment method. This paper reports the results of a vulnerability assessment to hurricane hazards for the countries in the Caribbean region. The resultant index is a weighted combination of variables. The paper demonstrates a methodology to validate the weights of the variables used to compute the index through regression analysis with the storm damage data. The refined vulnerability indices for the 25 countries studied were found to range from 0.31 to 0.77. Small island countries were generally more vulnerable than large countries, with the highest vulnerability indices (>0.6) found in The Bahamas, Montserrat, St. Kitts and Nevis, and Turks and Caicos Is. Although the hurricane exposure was originally considered a key variable contributing to high vulnerability, low adaptive capacity in the form of low socioeconomic status, high electricity consumption, and low infrastructure development were found to have a higher weight contributing to the overall vulnerability index.

**ADDITIONAL INDEX WORDS:** *Resilience, sustainability, climate change impacts.*

## INTRODUCTION

Climate change poses a serious threat to low-lying coastal areas throughout the world. Climate change impacts include both slow-moving threats such as accelerated sea-level rise, as well as increase in frequency of extreme events such as hurricanes and associated storm surges (Emanuel, 2005; Webster et al., 2005). Countries in the Caribbean region and Central America, as well as the Gulf Coast and East Coast of the United States, are especially prone to these coastal hazards, as these regions are under threats of hurricane strikes every year (Pielke et al., 2003; Pulwarty et al., 2010). These climate-related coastal hazards, when compounded with inadequate planning and poor social-economic conditions of the countries, could lead to very devastating effects with significant loss of lives, property damages, and economic losses (Lam et al., 2009a).

As examples of hurricane hazard, the 1998 Hurricane Mitch devastated several Central American nations and caused a combined death toll of over 18,000 people and economic losses in the billions of US dollars. In Honduras alone, although Mitch had already weakened to a category 1 hurricane at landfall, the damage

was over 14,000 deaths and \$3.8 billion economic losses (Pielke et al., 2003). In the United States, the deadliest and costliest hurricane in recent decades was Katrina, which hit the Gulf Coast in 2005. A category 3 hurricane at landfall near the City of New Orleans, Katrina devastated the region and resulted in over 1,800 deaths and \$108 billion in damages (Lam et al., 2009b; Lam et al., 2012a).

It is obvious that given the same type of hazard and exposure, the vulnerability of a region to the hazard and its resultant damages could be very different in different regions. The vulnerability would depend on the physical and socio-economic conditions of the region such as elevation, proximity to the coast or water bodies, degree of preparedness, and the level of poverty. Therefore, it is critical to understand what makes a region more vulnerable than the others. In order to answer this question, the first step would be the development of a comprehensive quantifiable measure, or an index, to assess the vulnerability of the region. Through the assessment process, the key factors that contribute to a decrease in vulnerability, and ultimately an increase in resilience, could be identified. This information would be extremely helpful to the planning and management of coastal regions in response to climate change. Moreover, the quantitative

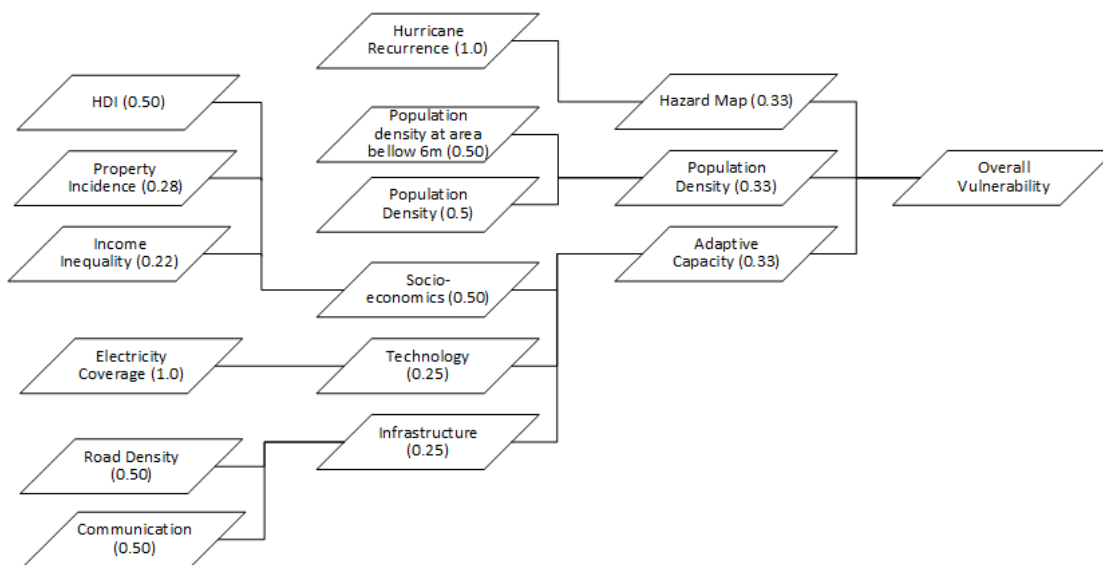


Figure 1. The original method used in deriving the hurricane vulnerability index; values within the parentheses are the weights (adapted from Yusuf and Francisco, 2009; Brito and Arenas, 2009).

measures, or indices, developed could serve as an effective planning tool for monitoring the progress of adaptive measures applied to reduce vulnerability (Reams et al., 2012; Lam et al., 2013).

However, developing a comprehensive measure of vulnerability and/or resilience to coastal hazards is not an easy task due to: (1) the many different definitions of vulnerability and its related concepts of resilience, adaptive capacity, and sustainability (Holling 1996; Folke et al., 2002; Adger et al., 2005); and (2) the arbitrariness of the method and the lack of empirical validation for the indices developed. In addition, high-quality, comparable data needed for the assessment across different countries are not easily available, especially for the countries in the Caribbean region.

This paper reports the results of, and the issues associated with, a commonly used approach to assess the vulnerability of the Caribbean and Central American countries to climate-related coastal hazards. The method is based on the definition described in the Third Assessment of the Intergovernmental Panel on Climate Change, which defines vulnerability as a function of exposure, sensitivity, and adaptive capacity (IPCC, 2001, p.995; Yusuf and Francisco, 2009). The vulnerability index is derived by combining the different variables representing the three dimensions using an arbitrary weighting scheme. To validate the derived vulnerability index, we used the actual storm damage data and conducted regression analysis between the actual damage and the variables used to construct the index. The weights were revised according to the resultant regression coefficients, and the vulnerability index was recalculated and compared. The goal of the study is to demonstrate the theoretical as well as technical issues related to the vulnerability assessment, and to suggest future research directions for a validation-based and inference-based approach to vulnerability and adaptive capacity assessment.

## METHODS

There is a long-standing extensive literature on climate-change vulnerability and its related concepts, including resilience, adaptive capacity, hazards and risks, and sustainability (Holling 1996; Adger et al., 2005). Definitions of the term “vulnerability”

vary greatly in the literature, depending on the field of study and its emphasis. In fact, the two terms, vulnerability and resilience, have been used interchangeably. While some researchers have expanded the definition of vulnerability to include resilience and its underlying concept of adaptive capacity (Folke et al., 2002; Turner et al., 2003), others have focused on vulnerability within a social system (Cutter et al., 2003; Cutter and Finch, 2008), and yet some others have considered vulnerability to include both social and ecological elements (Adger, 2006). Lately, the concept of sustainability, which emphasizes the tradeoffs between the natural and social systems, has been used to bridge the three concepts: vulnerability, resilience, and sustainability (Turner, 2010). Furthermore, recent literature shows that the coupled natural-human system dynamics approach can be viewed as the path to understand how vulnerability can be reduced, resilience can be increased, and sustainability can be maintained (Lam et al., 2012b).

This paper uses the IPCC definition of vulnerability and follows the methodology as described in Yusuf and Francisco (2009), which applied the IPCC definition to compute the vulnerability to climate change indices for the Southeast Asian countries. Brito and Arenas (2009) used a similar method to derive the vulnerability indices to hurricane hazards for the Caribbean countries. The IPCC defines vulnerability ( $V$ ) as a function of exposure ( $E$ ), sensitivity ( $S$ ), and adaptive capacity ( $C$ ):

$$V = f(E, S, C)$$

Exposure refers to “the nature and degree to which a system is exposed to significant climatic variations”; sensitivity refers to “the degree to which a system is affected”; and adaptive capacity is defined as “the ability of a system to adjust to climate change (including climate variability and extremes)”. Variables representing each dimension were selected, weighted (somewhat arbitrarily based on related research), and added to become a composite index of the vulnerability of each country or region. Hence, according to the IPCC definition, adaptive capacity is considered part of the overall vulnerability.



Figure 2. The original vulnerability index by country mapped using four equal intervals.

The above assessment method is straight-forward; however, the index is limited by the arbitrary nature of weight assignments and a lack of empirical verification. In this paper, we first computed a vulnerability index for all the Caribbean and Central American countries using similar variables and weight assignment as in Yusuf and Francisco (2009) and Brito and Arenas (2009). Figure 1 shows the model and the variables used in deriving the first set of vulnerability indices.

In the second step, we validated the meaning of the vulnerability index and the weight of each variable using the actual storm damage data. Regression analysis was conducted between the actual damage data (dependent variable) and the predictor variables representing the three dimensions of vulnerability (Figure 1). The results of the regression analyses, especially the beta regression coefficients, were used as an aid to revise the weighting scheme. The second set of vulnerability indices was then computed and compared with the first set of indices.

### STUDY AREA AND DATA

The countries selected for this study were limited by the availability of the data. In particular, fine-scale storm damage data at a subnational level are rarely available. Consequently, a sub-national study similar to the one conducted previously by members of this research group was not possible (Brilo and Arenas, 2009). After considering data quality and consistency, 25 countries were included in the analysis, and they are: Antigua & Barbuda, Bahamas, Barbados, Belize, Colombia, Costa Rica, Cuba, Dominica, Dominican Republic, Grenada, Guatemala, Haiti, Honduras, Jamaica, Mexico, Nicaragua, Panama, St. Kitts & Nevis, St. Lucia, St. Vincent, Trinidad & Tobago, Venezuela, Montserrat, Netherlands Antilles, and Turks & Caicos Is. (Figure 2).

The following documents the sources of the data and the methods used in deriving each variable. ArcGIS was the main software used for calculating:

- Hurricane Recurrence (kDensityHurricanes): it was calculated using NOAA (National Oceanographic and Atmospheric Administration) hurricane tracks vector data. All Caribbean hurricanes documented from 1842 to 2008 were included. A kernel density surface using a radius of 50 km and a cell size of 5 km was generated and weighted according to the hurricane intensity category (i.e., category  $x = \text{weight } x$ ). The cells were then aggregated and averaged for each national unit. This variable represents the long-term exposure: the higher the density value, the higher the exposure to hurricane hazards, and potentially better awareness and adaptation by the community to minimize damage.
- Percent population living below 6 meters (%Pop<6m): This variable was derived using three data sources: (i) elevation: the ASTER GDEM (Advanced Spaceborne Thermal Emission and Reflection Radiometer – Global Digital Elevation Model) elevation data obtained from the NASA EOSDIS (Earth Observing System and Data and Information System) website (<http://earthdata.nasa.gov>). (ii) Landscan population data in 2006 with a cell size of 1 km by 1 km, which were obtained from the Oak Ridge National Laboratory website (<http://www.ornl.gov/landscan/index.html>). (iii) Political boundary data for the Caribbean countries were obtained from the ESRI (Environmental System Research Institute). Using the GIS method as documented in Lam et al. (2009a), the percent of population living below 6 m for each country was retrieved.
- Population density in 2012 (PopDen2012): Population data in 2012 (and in 2000) were obtained from the United Nations (<http://hrstats.unep.org/en/tables/>). Country area data were obtained from the Latin America and the Caribbean (LAC)

Population Database from the International Center for Tropical Agriculture (<http://gisweb.ciat.cgiar.org/population/report.htm>).

- Human Development Index (HDI2012): Obtained from the same United Nations website, the HDI combines normalized measures of life expectancy, literacy, educational attainment, and GDP per capita. The higher the index, the better in human development.
- Percent of population below poverty line (Poverty): The variable was obtained from World Bank website (<http://data.worldbank.org/indicator/SI.POV.NAHC>). Dates for the data are not the same for all countries; for instance, Bahamas is 2004, while Costa Rica is 2011. There were 8 missing values and they were replaced with the average of the variable.
- Income inequality as represented by the Gini coefficient (Gini): The variable was obtained from the World Bank (<http://data.worldbank.org/indicator/SI.POV.GINI/>). Gini coefficient was computed based on the Lorenz curve between cumulative population and cumulative income, with a score of 0.0 indicating perfect equality and a score of 1.0 total inequality. The higher the Gini coefficient, the more unequal the income distribution. The dates of the values in this data set ranged from 1993 to 2007. There were 12 missing values in this variable.
- Electricity coverage (Electricity): It represents electricity consumption per capita in 2010. The variable was obtained from the World Bank website (<http://data.worldbank.org/indicator/EG.USE.ELEC.KH.PC>). There were 8 missing values.
- Road density (KDensityRoads): The road network data, except for Mexico, was obtained from the U.S. Geological Survey. The Mexico road network data was obtained from INEGI (Instituto Nacional de Estadística e Geografía de México, base map scale of 1:1,000,000; [http://mapserver.inegi.org.mx/data/inf\\_e1m/](http://mapserver.inegi.org.mx/data/inf_e1m/)). The road density value for each national unit is an average of a kernel density surface generated using a search radius of 50 km and a cell size of 5 km.
- Communication (telephones): The communication capacity was estimated from the variable of fixed and mobile telephone subscribers per 100 people. The variable was obtained from the United Nation website.
- Damage data: The storm damage data were obtained from the EM-DAT (Emergency Disasters Data Base, Centre for Research on the Epidemiology of Disasters, <http://www.em-dat.net/>). This is the only publicly available global database on human impacts from hazardous events (Peduzzi et al., 2009). Several damage data variables were derived and tested: the damage in dollars variable was from 1987-2012; damage dollars per capita was adjusted using population in 2012; damage dollars for coastal population was adjusted using the population living in areas below 6 m elevation. In addition, the following data variables were adjusted using the 2012 population, including percent population killed, percent population injured, percent population affected, percent population becoming homeless, and percent of total population affected (killed + injured + affected + homeless).

## RESULTS

The model as displayed in Figure 1 can be represented in equation form:

$$V = 0.33(HZ) + 0.33(PD) + 0.34(1-AC) \quad (1)$$

Table 1. The original (W1) and validated (W2) indices. The rankings were delineated using four equal intervals.

Country	W1-index	W1-rank	W2-rank	W2-index
Costa Rica	0.11	1	1	0.31
Venezuela	0.12	1	1	0.36
Panama	0.12	1	1	0.33
Colombia	0.15	1	1	0.41
Mexico	0.17	1	1	0.30
Nicaragua	0.20	1	1	0.31
Honduras	0.23	1	1	0.30
Guatemala	0.24	1	1	0.32
Trinidad and Tobago	0.26	2	2	0.43
Barbados	0.35	2	2	0.44
Netherlands Antilles	0.35	2	2	0.53
Dominican Republic	0.35	2	1	0.40
Jamaica	0.36	2	1	0.39
Cuba	0.36	2	2	0.42
Belize	0.44	3	2	0.53
Dominica	0.46	3	3	0.56
St. Vincent & The Grenadines	0.47	3	3	0.59
Montserrat	0.48	3	3	0.64
Antigua and Barbuda	0.49	3	3	0.58
The Bahamas	0.51	3	4	0.67
St. Lucia	0.51	3	3	0.58
Grenada	0.52	3	3	0.58
St. Kitts and Nevis	0.53	4	3	0.64
Haiti	0.61	4	2	0.47
Turks and Caicos Is	0.66	4	4	0.77

where  $PD = 0.5(PopD) + 0.5(Pop6m)$ ;

$AC = 0.5(SocEc) + 0.25(Tech) + 0.25(Infra)$ ;

$SocEc = 0.5(HDI) + 0.28(1-Pov) + 0.22(1-Gini)$ ;

$Infra = 0.5(Road) + 0.5(Comm)$

It was necessary to invert the adaptive capacity variable and the poverty and Gini coefficient variables so that the final vulnerability would mean that the higher the index, the more vulnerable the country to hurricane hazards. All variables were normalized before the computation.

Table 1 lists the results from applying the above model (W1\_index). The countries were sorted from the lowest vulnerability to the highest. Figure 2 maps the indices using four equal-class intervals. The results show that the vulnerability indices ranged from 0.11 to 0.66. The top three countries that had the lowest vulnerability were Costa Rica, Venezuela, and Panama, whereas Turks & Caicos Is. and Haiti were found to have the highest vulnerability to hurricane hazards.

To validate if the vulnerability index corresponds with meaningful outcome variables such as storm damage, we conducted a number of regression analyses between the damage variables and the variables used to compute the vulnerability index. The regression between damage per capita and the 9 predictor variables was found to be the best, with an R-square value of 0.63 and a significance level of  $p=0.03$ . Table 2 lists the beta regression coefficients of the model. These beta coefficients can be used to develop a new weighting scheme to calculate a new index (W2\_index). The regression results indicate two major differences from the original model. The variable "percent of population below poverty line" (Poverty) was found to be negatively associated with the damage per capita variable, whereas "electricity consumption" (Electricity) was found to be positively associated with the damage per capita. It is noted that both variables were not significant. The beta coefficients also show that hurricane recurrence and road density were the most influential variables; the former was positively associated with the damage per capita ( $\beta=0.568$ ), whereas road density was found to be negatively associated with the damage per capita ( $\beta=-0.539$ ).

Based on the beta coefficients, the weights in Equation 1 can be modified as follows:

Model	Unstandardized Coefficients		Standardized Coefficients
	B	Std. Error	Beta
(Constant)	21.781	36.768	
kDensityHurricanes	46.563	16.109	.568
%Pop<6m	-.313	.161	-.401
PopDen2012	-.016	.013	-.221
hdi2012	-47.273	39.964	-.364
poverty2	-.144	.208	-.195
gini3	.452	.434	.192
electricity	.142	.191	.220
kRoadDensity	-166.246	64.744	-.539
telephones	-.044	.038	-.229

Table 2. The regression coefficients between the damage per capita and the 9 predictor variables.

$$V = 0.2(HZ) + 0.2(PD) + 0.6(1-AC) \quad (2)$$

$$\begin{aligned} \text{where } PD &= 0.36(PopD) + 0.64(Pop6m); \\ AC &= 0.43(SocEc) + 0.13(1-Tech) + 0.44(Infra); \\ SocEc &= 0.5(HDI) + 0.25(Pov) + 0.25(1-Gini); \\ Infra &= 0.7(Road) + 0.3(Comm) \end{aligned}$$

The new index (W2\_index) for each country was computed and is listed in Table 1, along with the indices from the original model. The range of the new indices was from 0.31 to 0.77. The countries were classified into four groups using four equal intervals. The higher the rank is, the higher the vulnerability. The results show that the two rankings were very similar. Dominican Republic and Jamaica were upgraded slightly from rank 2 to rank 1, and Belize from rank 3 to rank 2. The Bahamas was downgraded from rank 3 to rank 4. An unexpected result was Haiti, which was upgraded from rank 4 to rank 2, implying that Haiti—the poorest nation in the study region—may have already been adapted to frequent hurricane strikes, and hence it is more resistant to hurricane hazards and resulted in smaller damage relative to the other countries in the region.

## DISCUSSION

There have been several attempts towards the development of a robust index for measuring vulnerability, adaptive capacity, and/or resilience. Some indices focus more on the physical aspects of a place such as the Coastal Vulnerability Index (Iglesias-Campos et al., 2010), whereas others rely on the socioeconomic characteristics such as the Social Vulnerability Index (Cutter et al., 2003). Very few studies have been successful in empirically validating the developed index with satisfactory results. Cutter and her research group attempted to validate the Social Vulnerability Index, which is derived through factor analysis of 42 socioeconomic variables, by correlating it with the number of presidential declarations after disaster for each county. They found no correlation between the two variables (Cutter et al., 2003). By contrast, the regression results from our study are encouraging, as it explained a reasonable amount of variance (R-square of 0.63).

Peduzzi and others (2009) developed a Disaster Risk Index using a regression approach similar to this study. They used the

number of persons killed by a certain type of hazard as the dependent variable and regressed with a set of socioeconomic and land cover variables. They then used the relative number of persons killed (divided by the country population) as dependent variable to derive another set of regressions. The two estimates were averaged into a combined Disaster Risk Index. They found that human vulnerability is mostly linked to human development and environmental quality. While their approach emphasizes validation, the developed index lacks an important dimension, which is the resiliency, or the adaptive capacity or recovery ability, of a region after disasters.

Lam et al. (2013) proposed the use of a new framework to measure community resilience to coastal hazards. The new framework, called the Resilience Inference Measurement (RIM) model, measures a region's resiliency using three dimensions—exposure, damage, and recovery—and two abilities—vulnerability and adaptability (Li, 2011). Future studies on vulnerability should include some aspects of recovery indicators so that they can be identified and used to help planning and mitigating impacts. This would be a useful future research direction towards better assessment of vulnerability and resilience in the region.

Data availability and data quality remain to be a very difficult challenge for the accurate assessment of vulnerability across countries. The damage dollar variable will need better adjustment across different countries. There were many missing values for the variables used in this study, and some of the data items were not of the same dates. Continuous effort will need to be made to develop a better-quality world database for disaster and climate-change impact research.

Furthermore, the index calculated in this study is relative and comparable only among the 25 countries used in the sample. Future research should focus on developing assessment models that can be used to apply to other study regions, such as the RIM model currently being developed by this research group (Lam et al., 2013).

## CONCLUSION

This paper demonstrated the use of a model to compute the vulnerability index to hurricane hazards for the countries in the Caribbean and Central America region, as well as the use of a validation technique to refine the model. The computation method is straightforward; it follows a conceptual framework and is easily understandable. It could be a useful planning tool for assessment and for monitoring the progress of a country in reducing vulnerability and increasing resilience. The same model can be applied to other types of hazard, such as drought, earthquakes, and tornados. Through the validation and recalculation, this study found that small island countries were generally more vulnerable than large countries in the context of hurricane hazards, with the highest vulnerability indices (a revised vulnerability index >0.6) found in The Bahamas, Montserrat, St. Kitts and Nevis, and Turks and Caicos Is. Although the hurricane exposure was a key variable contributing to high vulnerability, low adaptive capacity in the form of low socioeconomic status, high electricity consumption, and low infrastructure development were found to have a more important role (higher beta coefficients) in increasing vulnerability.

## ACKNOWLEDGEMENT

This research was funded in part by grants from the Inter-American Institute for Global Change Research (IAI) (award number: CRN-2050), the U.S. National Science Foundation (award number: 1212112), and the U.S. Department of

Agriculture (award number: USDA 2010-65401-21312). The statements, findings, and conclusions are those of the author and do not necessarily reflect the views of the funding agencies.

### LITERATURE CITED

- Adger, W.N., 2006. Vulnerability. *Global Environmental Change*, 16, 268-281.
- Adger, W. N., Hyghes, T.P., Folke C., Carpenter, S.R. , and Rockstrom, J., 2005. Social Ecological Resilience to Coastal Disasters. *Science*, 309, 1036-1039.
- Brito, P.L. and Arenas H., 2009. Vulnerability mapping for Caribbean countries. Baton Rouge, Louisiana, USA.: Technical Report, RSGIS Laboratory, Louisiana State University.
- Cutter, S.L. and Finch, C., 2008. Temporal and spatial changes in social vulnerability to natural hazards. *Proceedings of the National Academy of Sciences*, 105(7), 2301-2306.
- Cutter, S.L., Boruff, B.J., and Shirley, W.L., 2003. Social vulnerability to environmental hazards. *Social Science Quarterly*, 84, 242-261.
- Emanuel, K., 2005. Increasing destructiveness of tropical cyclones over the past 30 years. *Nature*, 436, 686-688.
- Folke, C., Carpenter, S., Elmqvist, T., Gunderson, L., Holling, C.S., and Walker, B., 2002 Resilience and Sustainable Development: Building Adaptive Capacity in a World of Transformations. *Ambio*, 31, 437-440.
- Holling C.S., 1996. Engineering resilience versus ecological resilience. In Schelze P, eds. *Engineering within Ecological Constraints*, pp. 31-44. Washington, DC: National Academy Press.
- Iglesias-Campos, A., Simon-Colina, A., Fraile-Jurado, P., and Hodgson, N., 2010. Methods for assessing current and future coastal vulnerability to climate change. ETC/ACC Technical Paper. Bilthoven, the Netherlands: European Topic Centre on Air and Climate Change.
- IPCC (Inter-governmental Panel on Climate Change 2001. MaCarthy J., Canziani O., Leary N., Dokken, D., and White, K., eds. *Climate Change 2001: Impacts, Adaptation, and Vulnerability*. Cambridge, UK: Cambridge University Press.
- Lam, N.S.-N., Arenas, H., Li, Z., and Liu, K.B., 2009a. An estimate of population impacted by climate change along the U.S. Coast. *Journal of Coastal Research*, SI 56, 1522-1526.
- Lam, N.S.N., Pace, K., Campanella, R., LeSage, J., and Arenas, H., 2009b. Business return in New Orleans: Decision making amid post-Katrina uncertainty. *Public Library of Science (PLoS ONE)* 4(8); e6765. doi:10.1371/Journal.pone.0006765.
- Lam, N.S.N., Arenas, H., Pace, R.K., LeSage, J.P., Campanella, R., 2012a. Predictors of Business Return in New Orleans after Hurricane Katrina. *PLoS One* 7(10), e47935: 1-8.
- Lam, N.S.N., Liu, K.B., Rivera-Monroy, V., Reams, M., Xu, J., Pace, K., and Dismukes, D., 2012b. CNH: Coupled Natural-Human Dynamics in a Vulnerable Coastal System. Washington, DC, USA: National Science Foundation website. Award Abstract.
- Lam, N.S.N., Reams, M.A., Li, K., Li, C., and Mata, L., 2013. A framework for community resilience measurement. Manuscript in Review, Department of Environmental Sciences, Louisiana State University.
- Li, K., 2011. *Temporal Changes of Coastal Community Resilience in the Gulf of Mexico Region*. Baton Rouge, Louisiana, USA: Louisiana State University, M.S. Thesis, 68p.
- Peduzzi, P., Dao, H., Herold, C., and Mouton, F., 2009. Assessing global exposure and vulnerability towards natural hazards: the Disaster Risk Index. *Natural Hazards and Earth Systems Science*, 9, 1149-1159.
- Pielke, R.A. Jr., Rubiera, J., Landsea, C., Fernandez, M.L., Klein, R., 2003. Hurricane vulnerability in Latin America and The Caribbean: Normalized damage and loss potentials. *Natural Hazards Review*, 4(3), 101-114.
- Pulwarty, R.S., Nurse, L.A., and Trotz, U.O., 2010. Caribbean islands in a changing climate. *Environment; Science and Policy for Sustainable Development*, 52(6), 16-27.
- Reams M.A., Lam, N.S.N., Baker, A., 2012. Measuring capacity for resilience among coastal counties of the U.S. Northern Gulf of Mexico Region. *American Journal of Climate Change*, 1, 194-204.
- Turner, B.L., 2010. Vulnerability and resilience: Coalescing or paralleling approaches for sustainability science? *Global Environmental Change* 20, 570-576.
- Turner, B.L., Kasperson, R.E., Matson , P.A., McCathy, J.J., Corell, R.W., Christensen, L., Eckley, N., Kasperson, J.X., Luers, A., Martello, M.L., Polsky C., Pulsipher, A., and Schiller, A., 2003. Science and technology for sustainable development special feature: A framework for vulnerability analysis in sustainability science. *Proceedings of the National Academy of Sciences*, 100(14), 8074-8079.
- Webster, P.J., Holland, G.J., Curry, J.A., and Chang, H.R., 2005. Changes in tropical cyclone number, duration, and intensity in a warming environment. *Science*, 309, 1844-1846.
- Yusuf A.A. and Francisco, H., 2009. Climate change vulnerability mapping for Southeast Asia. Singapore: Economy and Environmental Program for Southeast Asia (EEPSEA).

# Methodology for the development of 3D GIS models in the Coastal Zone

Mateus G. Magarotto<sup>†‡</sup>, Monica F. Costa<sup>‡</sup>, José A. Tenedório<sup>†</sup>, Carlos P. Silva<sup>†</sup>, Ted L. Martins Pontes<sup>‡</sup>

<sup>†</sup> e-GEO, Research Centre for Geography and Regional Planning, Faculdade de Ciências Sociais e Humanas, Universidade Nova de Lisboa, Lisboa, Portugal  
email: mateus\_magarotto@fch.unl.pt  
email: ja.tenedorio@fch.unl.pt  
email : cpsilva@fch.unl.pt

<sup>‡</sup>Laboratório de Ecologia e Gerenciamento de Ecossistemas Costeiros e Estuarinos. Departamento de Oceanografia. Universidade Federal de Pernambuco.  
email: mfc@ufpe.br  
email: tedlincoln@hotmail.com



[www.cerf-jcr.org](http://www.cerf-jcr.org)



[www.JCRonline.org](http://www.JCRonline.org)

## ABSTRACT

Magarotto, M., Costa, C., Tenedório, J.A., Silva, C.P., Pontes, T., 2014. Methodology for the development of 3D GIS models in the Coastal Zone. In: Green, A.N. and Cooper, J.A.G. (eds.), *Proceedings 13<sup>th</sup> International Coastal Symposium* (Durban, South Africa), *Journal of Coastal Research*, Special Issue No. 70, pp. 479-484, ISSN 0749-0208.

The present work involved a methodology which analyzes land use changes, from 1961 - 2011 using digital image processing and visual analysis of one satellite image and aerial photos. A simplified methodology using GIS 3D generates models of the coastal zone and its index of vertical growth. The GIS method uses SPRING - INPE (freeware) and ArcScene (ESRI). The data was obtained in the field (2011). The base area used was seventeen census sectors of the Brazilian Institute of Geography and Statistics (IBGE). To analyze vertical growth, a Volumetric Compactness Index (CVI) was created. It is able to track the tallest buildings over the years studied. The sectors were analyzed for spatial (N-S; E-W) and temporal (50 years) variations, where they were divided into North, Central and South zones of Boa Viagem. At all sectors occupation indexes are presently high, a strong trend of vertical growth exist that results in high volumetric compactness. Occupation and vertical growth are especially accentuated in the 1981 - 1996, reaching a maximum in 2011. Vertical growth increased from shore- inland being more prevalent towards the Central Zone, followed by the North and South. As a result of these processes, several problems arose with the most relevant including: impermeable coverings; large volumes of urban runoff; increasing temperatures; wind funneling; traffic jams; air pollution and; deficient water supply, wastewater collection and solid wastes collection. The results obtained using this methodology may be useful for the management of coastal areas and the potential for its development in relation to urban planning and development. The models obtained can prioritize mitigation actions in similarly developed neighborhoods.

**Keywords:** *Urban Density, Urban Models, Volumetric Index.*

## INTRODUCTION

Vertical growth in urban coastal zones occurred both abruptly and irregularly, from the middle of the twentieth century, mainly in South American countries. This vertical growth causes problems related to the natural environment in coastal zones which are home to approximately 60% of the population. However, the factors influencing coastal zone changes are more complex and interrelated, including both natural and anthropogenic causes (Del Rio *et al.*, 2013). Currently the coastal urban areas are considered symbols of human development. The reproduction of this urban space originates inequality through spatial and social segregation, supported by real estate speculation (Polidoro *et al.*, 2012). This integrated process in horizontal expansion, through decentralization, with the intensification of urban land use (Pereira, 2003), resulting in denser urban areas and buildings designed for the redevelopment of the urban environment (Yu *et al.*, 2010).

These factors aggravate fragile natural systems located in coastal areas (Lin *et al.*, 2013). Thus the appropriate environmental and territorial planning at local levels can help solve the problems and conflicts associated with urban development of coastal areas (Fresca, 2007).

DOI: 10.2112/SI70-081.1 received 1 December 2013; accepted 21 February 2014. © Coastal Education & Research Foundation 2014

Management of the coastal zones with the help of Remote Sensing (RS) and Geographic Information Systems (GIS) may provide solutions to the problems which occur during the development of coastal areas, home to fragile ecosystems (Silva *et al.*, 2007, Costa *et al.*, 2008 and Henriques and Tenedorio, 2009; Paula *et al.*, 2012). One of the possibilities, still not fully explored by coastal planning are the three-dimensional (3D) representations of the real world. Although these facilitate the visualization of objects for analysis, it is still difficult to realize their advantages, due to the poor exploitation of these models (Fosse *et al.*, 2006; Teka *et al.*, 2012). Thus it is necessary that users are aware of the range of possibilities that 3D GIS may offer (Sahin *et al.* 2012).

With the intention of creating a better understanding and management processes for the vertical growth in coastal zones, it is necessary to develop new method that can provide answers to current socio-urban problems. This paper introduces a methodology based on Geographic Information Systems (GIS) in three-dimensions (3D) and the use of census tracts as IBGE with Minimum Mapping Area (MMA). This procedure can analyses the vertical growth and create the Volumetric Compactness Index (CVI). This new method has the potential to assist in understanding the problems caused by rapid urban development,



population issues associated with the consequences of vertical urban growth; e.g. decrease in public spaces due to compaction of urban space, congestion, decreased carrying capacity, attended by transport, water supply, solid wastes collection, etc.

The objective of the methodology presented in this paper is not based on complex models for simulation of urban growth, but rather offers a new alternative to the study of urban land occupation. This allows for the identification of certain elements of the urban landscape at different scales using the SIG 3D. These models are based on the geo-referencing database and of easy access. This can monitor urban conflicts, through the information space and computational procedures, facilitating the analysis, management and representation of space (Câmara *et al.*, 1996). The SIG 3D, associated with Minimum Area Mapping (AMM), can monitor all the urban management and analyzes the buildings present within the spatial distribution (Ding, 2013). These procedures can generate models that help describe the main areas of conflict between different social classes and the decreased quality of life (Lin *et al.*, 2013). It acts as a platform to point out the existing problems and contributes to a more rational urban development while offering the public with crucial information.

The study area chosen, where this method was implemented, was a developed neighborhood of Boa Viagem, the capital of the state of Pernambuco—Brazil, located within a coastal environment south of Recife, (Fig 1). The study area selected has an area of 747.06 ha (IBGE, 2010) and average temperatures of 25°C; with a hot and humid climate. The dry seasons occur from September to February and a rainy season from March to August. The average rainfall is 1600mm/a and the Quaternary geomorphology of the area is flat and composed of quartz and sandstone, located in plain fluvial plains and marine topography, with an elevation not exceeding five meters (Costa and Araujo, 2008). To the north Pina and Piedade neighborhoods are located (Municipality of Jaboatão dos Guararapes), to the south Ipsep neighborhoods and Afogados neighborhoods to the west with the Atlantic Ocean to the east. The geographic coordinate: Y2:9105000 – Y1: 9098000 and X2: 292080 – X1: 290000 (Figure 1).

## METHODS

### Development of methodology for the model in three dimensions

The first step was to create the Geodatabase georeferenced in a GIS environment using the software SPRING 5.2 and ArcScene 10. The QuickBird satellite image 2002 was uploaded in the Geodatabase, as well as the administrative boundaries of the study area and census tracts of IBGE. The Second step was to conduct a field visit to the study area to obtain real estate data. The systematic data collection of properties always started at a point north and east of each block. Street intersections and / or avenues were identified through their names, from right to left and from the start to the finish in each block. Within the sector the blocks were numbered according to a proximity factor to the beach. Buildings identified were characterized as residential, commercial, ranch houses or buildings with the number of stories indicated. Others aspects were obtained including the distance to the sidewalk, use of real estate, condition and vegetated areas. All the data was collected digitally using a Mobile Mapping System (Mobile Mapper System), with the most relevant information for the 3D GIS model being the number of stories, the building area and the date of occupation of the real estate.

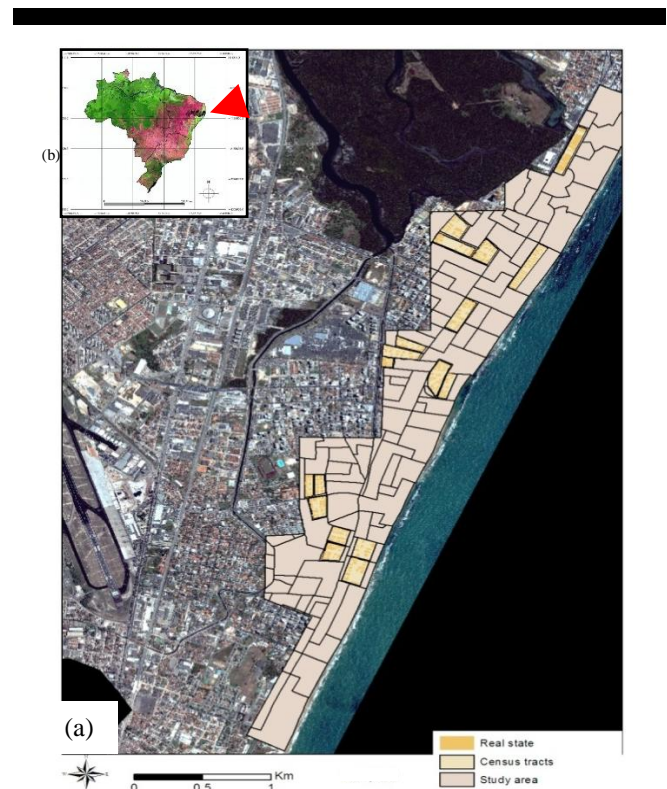


Figure 1. Study area (a). The light brown polygon represents the Study area, the lighter polygon represents the census tracts and the other the real state. Northings and eastings are in metres, UTM zone 25S. Localization (b) in the Brazil the area that is the Estate of Pernambuco in SE of Brazil.

### Volumetric index.

The volumetric index measures the vertical growth and is presented within this methodology, as the 3D model allows the development of a "Volumetric Index" which considers the volume built on the area of each census tract. The index is calculated as the sum of the area of real estate included in the census tracts, multiplied by the sum of the number of building stories, divided by the total area of the census tract, as follows:

$$VI = \frac{\sum ar \cdot (\sum nf \cdot 3)}{U} / ac \quad (\text{Equation 1})$$

Where: VI = Volumetric index; ar = constructed area of real estate; nf = number of floors of buildings; ac = area census tract.

## RESULTS

The results of this study show the effectiveness of using three dimensions (3D) models of the coastal urban zones using the described methodology. The vertical growth at different angles is shown and the locations which will have a visual impact in real estate are speculated. The vertical growth was divided into three zones within the study area, these included: North Zone (from the Pina neighborhood border to the Padre Carapuêiro street); Central Zone (from Padre Carapuêiro to Cel. Benedito Chaves street); South Zone (from Cel. Benedito Chaves street to the border of the Piedade neighborhood, in the municipality of Jaboatão dos Guararapes).

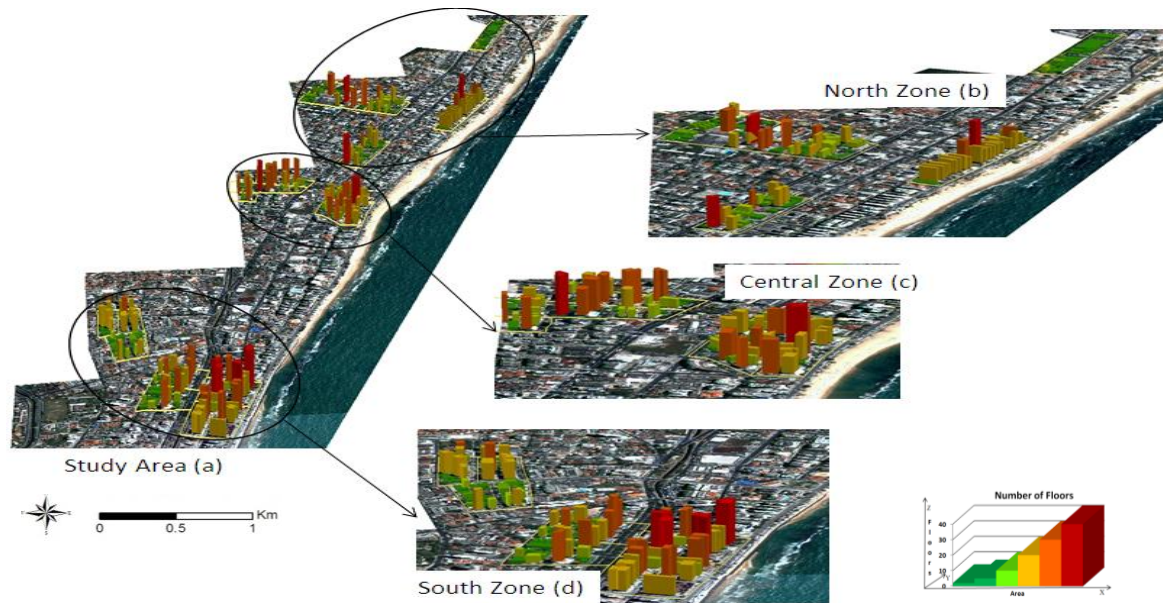


Figure - 2. Representation of the 3D model of the vertical growth Boa Viagem neighborhood. Visualization of the study area (a) and in detail the division of the three zones (North Zone (b), Central Zone (c) and South Zone (d)). The colors represent the different floors of buildings present.

The results of the method are of a higher precision, quantify and qualify the vertical growth in the neighborhood of Boa Viagem. (Figure 2).

The census tract samples show that the neighborhoods vertical growth is not limited to the beach, but occurs within the center of the neighborhood. Within the city center the avenues (Engenheiro Domingos Ferreira, Conselheiro Aguiar and Jequitinhonha) had a lower vertical growth rate and a higher concentration of two story buildings. North and south of the study area vacant lots / parcels and buildings with two floors were prevalent; these areas may be affected by vertical growth in the next few years.

**Analysis of vertical growth in the North Zone.**

The North Zone (ZN), located close to the Pina neighborhood has five census tracts: 181 (beach line), 401 and 186 (near the main avenues of connection with the city center), 182 and 468 (inland study area) (Table 1).

In the North Zone the vertical growth was more evident in the census tract 181 with 85%. In this sector there were three lots / parcels with building with two floors remaining. Two of the properties are intended for businesses (traditional Padaria e Pastelaria Boa Viagem located on Av Boa Viagem, and a hair salon at Rua dos Navegantes) with the third allotment currently under construction and will possibly be a new building (Figure 3).

The census tract 401 has not been included in this analysis; however real estate present have a maximum of two floors, within

Table - 1. Parcel by sector - North Zone.

Census Tracts	Quantity lots / parcels
181	27
401	25
186	31
182	25
468	30
<b>Total</b>	<b>138</b>

this sector there is no current vertical growth. This may be due to the real estate being intended for traditional shops as a commercial gallery within the neighborhood. However, further south on the same line, the census tract 186 has 60% vertical growth and within this sector, the real estate with two floors is intended for businesses and other buildings are assigned to private residences.

Inland of the North Zone the analyzed census tracts 182 and 468 have 65% and 50% vertical growth, respectively, and it was found that their rate of vertical growth was moderate with a high potential development of new buildings. This future development is associated with the construction of Via Mangue; a new roadwork that will connect the Boa Viagem neighborhood with the center of Recife; there is a possibility that vertical growth will continue in this direction due to the high number of empty lots and two story building in the area.

**Analysis of vertical growth in the Central Zone.**

This is the most central zone of the Boa Viagem beach near the “Shopping Center Recife”. This position is highly valued with the vertical growth in this area progressing faster over time due to its central position within the neighborhood.

The census tract 149 shows a vertical growth of 85%, this sector is central to the beach; a popular tourist attraction and meeting point for swimmers. Within this sector only two building on the beach remain with two floors which are intended for trade. It offers public utilities and various trades.

Table - 2. Parcel by sector - Central Zone.

Census tracts	Quantity lots / parcels
149	13
147	35
385	25
146	19
136	06
<b>Total</b>	<b>99</b>

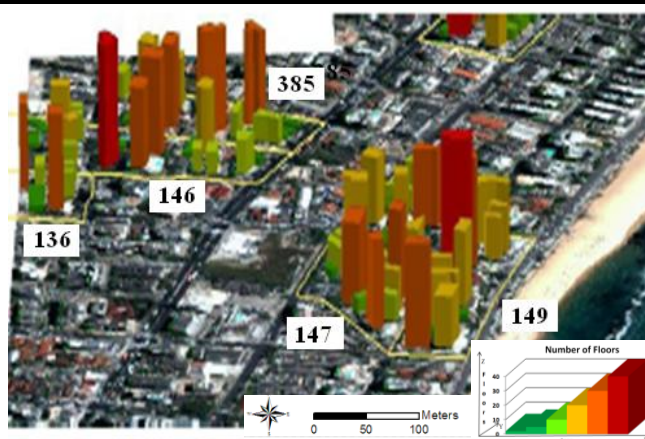


Figure – 3. Detail of sample sectors vertical growth North Zone. Figure – 4. Detail of sample sectors vertical growth Central Zone.

The census tract 147 shows a vertical growth of 71%, with the largest quantity of property with two floors either abandoned or intended for trade. This census tract is beside a deteriorating building called ‘Holiday’, which is ironic as this building was an icon of development in the latter half of the 20<sup>th</sup> century. It is apparent that development in this sector is stagnant.

The census tracts 385, 146 and 136 inland of the Central Zone, have vertical growths of 60%, 58% and 80%, respectively. Along census tracts 385 and 146 it was found that two new buildings were under construction in each sector. Residential houses designed for small trade which occurs due to the great demand by the middle class population to live in this neighborhood and makes one think that *“if business does not prosper they will be converted into residential buildings.”* The census tract 146 has a high index of vertical growth, with four tall buildings with more than 30 floors and only two houses with two floors; a sports gym and a supermarket with a petrol station.

This area is the most representative of the neighborhood and its vertical growth due to its proximity to the Boa Viagem beach and the “Shopping Center Recife”.

**Analysis of vertical growth in the South Zone.**

The South Zone is composed of seven census tracts; 330 and 197 in the first and second line from the beach, 193 and 412 in an intermediate position and 196, 195 and 413 inland from the study area (Figure 5).

The census tracts 330 and 197 have vertical growth rates of 75% and 92%, respectively, with no real estate with two floors. The census tracts 193 and 412 have vertical growth rates of 47%

and 44%, respectively with residential homes and small trade. An important observation is the presence of Madre Deus School which occupies several buildings with two floors.

The census tracts 196, 195 and 413, inland from the South Zone, have 85%, 38% and 20% vertical growth respectively. The census tracts 195 and 413 have houses, galleries, small trade, guesthouses, restaurants, and others buildings. Tract 413 has new buildings such as the Residential Barcelona that was completed in 2011. It is speculated that vertical growth is yet to occur in this neighborhood, due to the availability of residential houses and its close proximity to the beach.

**The Volumetric Index.**

The creation of 3D models provides the opportunity to study the creation of Volumetric Index able to measure the volume buildings. A representation of the sectors distributed over the study area shows the degree of vertical growth (Figure 6).

The data obtained through this confirms the observation shown visually within the census tracts. It also provides the possibility of creating a graph of the IV to show the vertical growth of the census tracts. Thus it can be verified with the IV, that the waterfront of Boa Viagem neighborhood has high rates of vertical growth (sector: 330, 136, 149, 147, 181). Along the avenues: Conselheiro Aguiar e Engenheiro Domingos Ferreira and the main street access we find the census tract with the lowest volumetric index (sectors: 401, 468, 412 and 413). In the inner district the volumetric index are low, but with potential for vertical growth in the coming years.

Table - 3. Parcel by sector - South Zone.

Census tracts	Quantity lots / parcels
330	12
197	17
193	30
412	25
196	13
195	16
413	43
<b>Total</b>	<b>156</b>

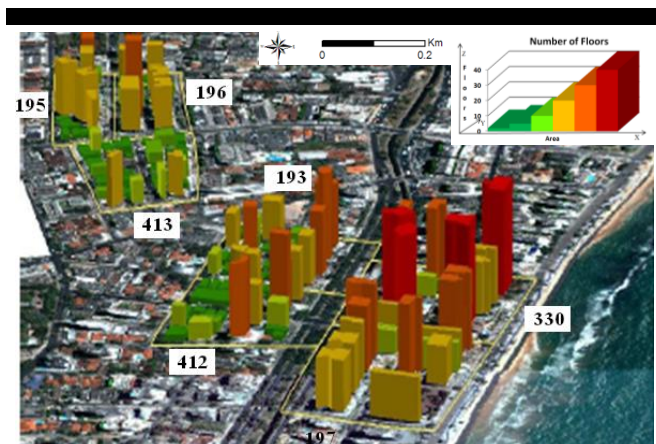


Figure – 5. Detail of sample sectors vertical growth South Zone.

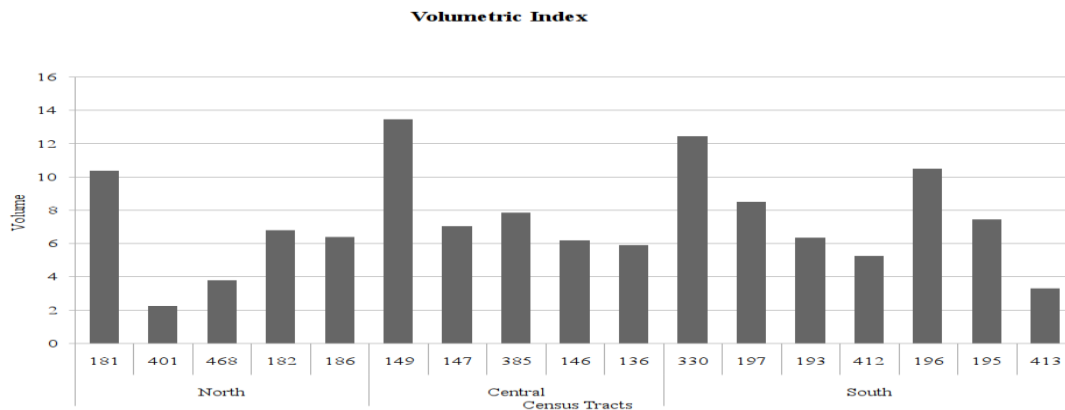


Figure – 6. Volumetric index sample of census tracts in the neighborhood of Boa Viagem. This table shows the vertical growth in the year 2011. The major indexes are relative of the census tracts near the beach. Adaptive of Magarotto, 2012.

However along the avenues low volumetric indices are maintained by small businesses that occupy Real Estate with two floors.

The census tract 149 has higher volumetric rates due to its central position in relation to the beach of Boa Viagem. In the South Zone we can identify high levels of volumetric rates mainly in the 330 and 197. These census tracts are representative because of the lots / parcels consisting of high buildings. The census tracts 193, 412 and 413, have a greater number of properties with two floors and low volumetric indexes, which may indicate that the vertical growth will continue in these parts of the district.

Thus, the data concerning the volume index confirm the vertical growth of the neighborhood of Boa Viagem. This vertical growth causes problems associated with the welfare of the population, conduit the sea wind, little ventilation inside the neighborhood, urban heating, heat islands and traffic congestion.

## DISCUSSION

The urban spatial expansion is a continuous process dependent on urban planning appropriate for urban development (Lin *et al.*, 2013). Urban planning is the most influential tool in guiding spatial development. In the initial phase of urbanization, the neighborhood of Boa Viagem had little planning, initially concentrated next to the beach mainly for holiday homes. Since the creation of Beira Mar Avenue the main functions of the area was recreation, tourism and national defense (Araújo, 2007; Pereira *et al.*, 2007) and the lack of urban planning associated with land can be observed. This caused problems within the neighborhood and transformed pleasant areas, such as coastal zones, into place of intense vertical growth. Since 1960, rapid urbanization of coastal lands resulted in high buildings.

In this work the vertical growth in the neighborhood of Boa Viagem was collected in census tracts. The parameter selected to observe the vertical growth of the census tracts was the amount of real estate with more than two floors. This parameter can be discussed and debated to measure the degree of vertical growth. Many authors use different heights or floors in the analysis, this was done within the neighborhood of Santa Cecilia in the city of São Paulo where building with more than six floors were considered as a vertical growth factor (Moura and Nucci, 2008). In Mossoró / Rio Grande do Norte vertical growth was rated from heights of four floors (Morais *et al.*, 2007). Other authors have developed analyses of vertical growth which used other criteria (Costa *et al.*, 2008; Scussel and Salter, 2010; Paula *et al.*, 2012).

A consensus standard does not exist to determine the index of vertical growth and as such, it was decided that real estate with more than two floors should be considered. This resulted in a quantitative analysis according to the degree of vertical growth in each census tract, allowing comparisons to be made between different sectors within the study area.

One of the aspects present in this option is the comprehension of the physical form of the real estate. A two story house may be a residence to single or multiple families and may also be a commercial enterprise. Within the structure the physical form the physical form may contribute to the understanding of vertical growth.

In this context the establishment of the 3D model enables visibility for others aspects of the vertical growth and assists in local management (Ding, 2013), besides giving the models a more realistic aspect. The 3D models have the ability to integrate different data sets to gain new insights of the built environment. (Zhu, 2010) thus enabling planners with sustainable long-term plans for the future development of the cities (Zhu, 2010; Lin *et al.*, 2012). The availability of data in the 3D model gave way to the development of the Volumetric Index enabling census tracts with a higher degree of vertical growth to be identified. The detailed results of the application can be found in Magarotto (2012).

An index to establish the volume in urban areas is not used frequently in literature, with authors preferring to work with percentage values of vertical growth. Creating an indicator that can help in monitoring work in areas with vertical growth is of great interest to coastal management. This indicator can graphically compare different areas and provide information on the extent of vertical growth in an area. The study by Santos *et al.*, (2013) and Magarotto, (2012) attempted to measure vertical growth through a volumetric index.

An important observation in this sample analysis with 3D GIS is the fact that the green area was not found on the analyzed census tracts. This indicates little concern in local urban planning for the environment and environmental protection of the marine shore at Recife. The absence of green spaces causes problems related to air pollution and sound/noise levels, urban heating, the recharge of aquifers, flooding caused by soil impermeability etc. (Freire *et al.*, 2009). Another negative aspect of the lack of green areas is that there are no spaces for recreation, sport and socialization.

Therefore, urban planning needs to seek alternatives in relation to the appropriation of urban space. This neighborhood is based on real estate speculation and infrastructure that degrades and

destroys the natural environment. Public authorities have to request that builders and real estate agents construction new projects taking into consideration social and environmental implications.

## CONCLUSION

The presented methodology enabled the generation of a database in three dimensions with results on the vertical neighborhood of Boa Viagem and its current and future development.

The methodology was aimed at complementing the analysis of this research study. It can validate the ability to obtain data on urban development with concrete percentage values of the vertical growth in the studied census tracts. The use of satellite image of high spatial resolution enabled the drawings of “real” polygons and opens the possibility of improvements using other 3D design software. Thus proving the analysis of data can create a Volumetric Index and can be an important step in the future evaluation of vertical growth in local areas. It also makes it possible to develop more economic methods.

The methodology can be used both for coastal projects and projects in larger urban centers. It may also be used in other urban planning projects in Brazil or elsewhere.

There is also the opportunity for this work to be used for improving the monitoring of coastal areas and improving methodology with the insertion of other variables. It is also enables the possibility of comparative studies between different locations inside or outside the country. Thus it can monitor developments and create future scenarios.

This project/investigation shows that 3D model analysis and integration with Volumetric Index are two powerful tools for coastal urban planning. Through landscape analysis the most vulnerable areas affected by spatial urbanization will be identified.

## ACKNOWLEDGEMENT

To the Recife City Municipal Administration and to the IBGE - Recife, and their staff, for access to the data banks. To the UFPE (Departments of Oceanography and Cartographic Engineering) and the CONDEPE/FIDEM for the aerial photographs and satellite images. MFC is a CNPq fellow.

## LITERATURE CITED

- Araújo, R. C. B., 2007. *As praias e os dias: história social das praias do Recife e de Olinda*. Ed.: Fundação da Cultura Cidade do Recife, Recife.
- Bertaud, A. and Brueckner J., K., 2005. Analyzing Building-height Restrictions: Predicted Impacts and Welfare Costs. *Regional Science and Urban Economics*, 35 (2), 109–125.
- Câmara, G., Souza, R.C.M., Freitas, U.M. and Garrido, J., 1996. SPRING: Integrating remote sensing and GIS by object-oriented data modeling. *Computers & Graphics*. 20 (3), 395-403.
- Costa, M.F., Araújo, M.C.B., Souza, S.T., and Silva-Cavalcanti, J.S., 2008. Verticalização Da Praia Da Boa Viagem (Recife, Pernambuco) e Suas Consequências Socioambientais. *Revista Da Gestão Costeira Integrada* 8 (2), 233–245.
- Del Río, L., Javier Gracia, F. and Benavente, J., 2013. Shoreline Change Patterns in Sandy Coasts. A Case Study in SW Spain. *Geomorphology*, 196: 252–266.
- Ding, C., 2013. Building height restrictions, land development and economic costs. *Land Use Policy*. 30(1), 485-495.
- Fresca, T.M., 2007 A Área Central de Londrina: Uma Análise Geográfica. *Revista Geografia (Londrina)*, 16, 2: 143-166.
- Fosse, J.M., Centeno, J.A.S. and Sluter, C.R., 2006. Avaliação De Variáveis Gráficas Para a Representação Cartográfica Tridimensional. *Revista Brasileira De Cartografia*. 58/01, 81–90.
- Henriques, C. and Tenedório, J.A., 2009. “Remote Sensing, GIS Application and Simulation of Coastal Land Use Changes Based on Cellular Automata: A Case Study of Maputo, Mozambique.” *Journal of Coastal Research*. 56, 1518–1521.
- Lin, T., Xue, X., Shi, L., and Gao, L., 2013. Urban Spatial Expansion and Its Impacts on Island Ecosystem Services and Landscape Pattern: A Case Study of the Island City of Xiamen, Southeast China. *Ocean & Coastal Management*. 81, 90–96.
- Morais, L.S., Silva, P., Moura M., and Medeiros, W.D.A., 2007. “Análise do processo de verticalização na área urbana do município de Mossoró-rn: aspectos jurídicos e ambientais.” *Revista Verde De Agroecologia e Desenvolvimento Sustentável* 2,2: 171–182.
- Moura, A.R. and Nucci, J.C., 2008. A Verticalização Como Parâmetro Na Avaliação Da Qualidade Ambiental Urbana. In: *XIII Simpósio Brasileiro de Geografia Física Aplicada*, 1–14.
- Paula, D.P., Dias, J.A., Ferreira, O. and Morais, J.O., 2013. High-rise Development of the Sea-front at Fortaleza (Brazil): Perspectives on Its Valuation and Consequences. *Ocean & Coastal Management*. 77,14–23.
- Pereira, M., 2003. Os próximos desafios do planejamento municipal. *GeoNova – Revista do Departamento de Geografia e Planejamento Regional*,7: 179 – 199.
- Pereira, L.C.C., Jimenez, J. A., Medeiros, C., and Costa, R.M., 2007. Use and occupation of Olinda littoral (NE, Brazil): guidelines for an integrated coastal management. *Environmental Management*, 40(2): 210–8.
- Polidoro, M., Lollo, J., and Barros, M., 2012. Urban Sprawl and the Challenges for Urban Planning. *Journal of Environmental Protection*, 03 (09): 1010–1019.
- Sahin, C., Alkis, A., Ergun, B., Kulur, S., Batuk, F. and Kilic, A., 2012. Producing 3D City Model with the Combined Photogrammetric and Laser Scanner Data in the Example of Taksim Cumhuriyet Square. *Optics and Lasers in Engineering*. 50 (12), 1844–1853.
- Scussel, M.C.B., and Sattler, M.A., 2010. Cidades Em (trans) Formação: Impacto Da Verticalização e Densificação Na Qualidade Do Espaço Residencial. *Ambiente Construído* 3, 10: 137–150.
- Silva, C., Alves, F., and Rocha, R., 2007. The management of beach carrying capacity: The case of northern Portugal. *Journal of Coastal Research*, 50, 135–139.
- Teka, O., Sturm-Hentschel, U., Vogt, J., Bähr, HP., Hinz, S., and Sinsin, B., 2012. “Process Analysis in the Coastal Zone of Bénin Through Remote Sensing and Socio-economic Surveys.” *Ocean & Coastal Management* 67: 87–100.
- Yu, B., Liu, H., Wu, J., Hu, Y., and Zhang, L., 2010. Automated Derivation of Urban Building Density Information Using Airborne LiDAR Data and Object-based Method. *Landscape and Urban Planning*, 98, 3–4.
- Zhu, S.T. Butler, R. Sander, J.M.A., and Lawrence, M.G., 2010. Impact of dust on tropospheric photochemistry over polluted regions: A case study of the Beijing megacity. *Atmospheric Chemistry and Physics* 10:3855–3873.

## A multi-scale analysis to support the implementation of a regional conservation policy in a small-island archipelago – the Azores, Portugal.



[www.cerf-jcr.org](http://www.cerf-jcr.org)

Helena Calado†, Chiara Bragagnolo‡, Susana F. Silva†, Margarida Pereira∞

† CIBIO – Research Centre in Biodiversity and Genetics Resources, Department of Biology/Geography Section, University of the Azores, Rua da Mãe de Deus, Apartado 1422, 9500-855 Ponta Delgada, Portugal  
[calado@uac.pt](mailto:calado@uac.pt), [susana.silva@uac.pt](mailto:susana.silva@uac.pt)

‡ Institute of Biological and Health Sciences, Federal University of Alagoas (UFAL)  
Av. Lourival Melo Mota, s/n, Tabuleiro do Martins, Maceió, AL 57072-900, Brazil  
[chiara.bragagnolo@yahoo.com.br](mailto:chiara.bragagnolo@yahoo.com.br)

∞ e-Geo – Centro de Estudos de Geografia e Planeamento Regional. Faculdade de Ciências Sociais e Humanas, Universidade NOVA de Lisboa, Avenida de Berma 26C, 1069-050 Portugal  
[ma.pereira@fch.unl.pt](mailto:ma.pereira@fch.unl.pt)



[www.JCRonline.org](http://www.JCRonline.org)

### ABSTRACT

Calado, H., Bragagnolo, C., Silva, S.F., Pereira, M. 2014. A multi-scale analysis to support the implementation of a regional conservation policy in a small-island archipelago – the Azores, Portugal. In: Green, A.N. and Cooper, J.A.G. (eds.), *Proceedings 13<sup>th</sup> International Coastal Symposium* (Durban, South Africa), *Journal of Coastal Research*, Special Issue No. 70, pp. 485-489, ISSN 0749-0208.

Small islands present both exceptional biodiversity and higher vulnerability. Their isolation has been identified as the main driver contributing to preserve the unique natural capital (10 of the 34 terrestrial biodiversity hotspots listed by Conservation International are wholly comprised of islands). However, small-island archipelagos may present a great variability among islands in terms of size and population, remoteness, incomes, natural and cultural landscapes, human pressures and vulnerabilities to global changes. This inexorably leads to different values, life-styles, and land use forms, which combine to shape cultural and socio-economic relationships of archipelagos, creating inter- and intra- island networks. Therefore, exploring inter- and intra-island relationships (based on historical, geographical, political and economic factors) can support a better understanding of networks and scale-dependent processes (ecological, economic, political, etc.), facilitating a more effective implementation of sustainable and biodiversity conservation policies at different levels. In this contribution, we present a multi-scale analysis to support the implementation of a regional conservation policy in a small-island archipelago (The Azores, Portugal). It represents a decision-making challenge for biodiversity conservation where a new management system of Protected Areas (PAs) was recently adopted. Three spatial units are considered: archipelago, island groups and island *per se*. The analysis integrates qualitative information, quantitative indicators and land use analyses in order to identify key areas of concern and relevant challenges for implementing the regional conservation policy at multiple levels. Findings underlined the importance to provide appropriate arrangements to better deal with scale mismatches arising from the divergence between spatial scale (where conservation challenges are identified) and administrative levels (where management interventions can be made).

**ADDITIONAL INDEX WORDS:** *Small islands, conservation, planning, archipelagos, the Azores, Pico island.*

### INTRODUCTION

Regional island studies previously indicated that islands occupy unfavourable position with respect to the mainland (Niles and Baldacchino, 2011). As a result, small-island archipelagos are generally considered vulnerable, threatened by sea-level rise, climate change, over-dependence on sea resources, changes in agriculture trends, changing markets for their limited commodities and scale economies (van Beukering *et al.*, 2007; Rietbergen *et al.*, 2007).

However, archipelagos are complex systems made up of different island groups characterised by widely spread spatial units, mosaic of values, different life-styles and land-use forms (Ankre, 2009; Stratford *et al.*, 2011), which combine to shape

cultural and socio-economic relationships of Archipelagos, creating inter- and intra- island networks.

Therefore, analysing different spatial units and multi-scale relationships of archipelagos (based on historical, geographical, political and economic factors) may support a better understanding of scale-dependent processes (Cumming *et al.*, 2006; Guerrero *et al.*, 2012), improving the implementation of policies at different levels (Bunce, 2008).

Exploring multi-scale processes (ecological, socioeconomic, cultural, and political) further represents a key issue for island ecosystem conservation. Island ecosystems have been considered some of the most threatened in the world (Mueller-Dombois and Loope, 1990) as well as those hosting about one third of the terrestrial biodiversity hotspots (Mittermeier *et al.*, 2005).

According to Poiani *et al.* (2000), biodiversity conservation operates at multiple scales. Planning for conservation is about

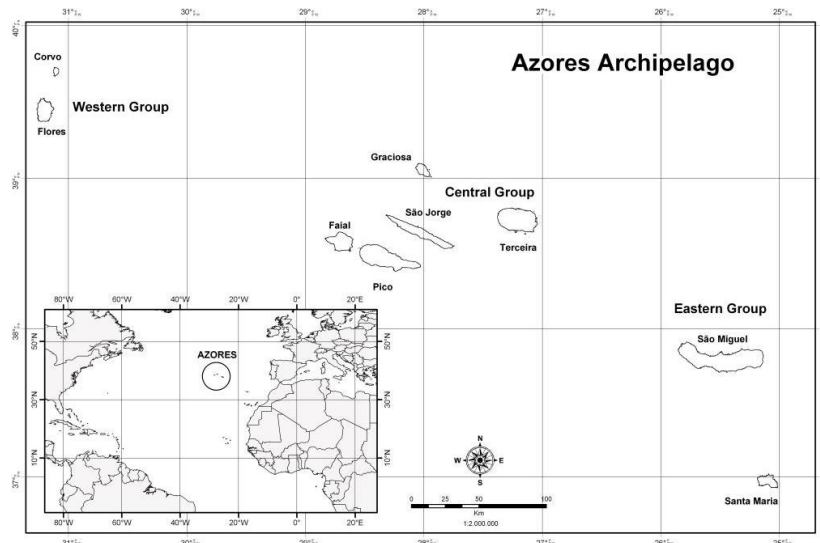


Figure 1. Azores geographic localization (Centre of Geographic Information Systems, University of the Azores).

translating conservation policies into actions at appropriate geographical scale and administrative level (Guerrero *et al.*, 2012). In this context, exploring the positioning of islands with respect to archipelago may contribute to a better understanding of the social-ecological systems in which conservation policies are to be implemented (Cumming *et al.*, 2006; Paloniemi *et al.*, 2012).

This paper presents a multi-scale analysis to support the implementation of a regional conservation policy in the Azores archipelago. Three spatial units are considered: Archipelago, groups of islands and the island *per se* (example of Pico Island). The study integrates qualitative information, quantitative indicators and land use analyses. Relevant challenges for achieving conservation objectives at each scale are identified and discussed.

### THE STUDY REGION

The Azores Archipelago is an Autonomous Region located in the centre of the North Atlantic Ocean (Figure 1), formed by nine volcanic islands, characterized by both exceptional endemism and high vulnerability (Cardoso *et al.*, 2008).

The archipelago presents a unique natural and cultural capital, which is vital for maintaining the health of ecosystems and supporting local livelihoods and regional economy (Petit and Prudent, 2010). However, during the last decades, human pressures on the archipelago's biodiversity have increased, leading to habitat loss and fragmentation, pollution, invasion of exotic species and unsustainable exploitation of resources (McGinley, 2007; Calado *et al.*, 2011a).

The current economy of the Archipelago is mainly based on small domestic markets, depending mostly on biodiversity and natural resources (the main economic sectors are: agriculture, cattle grazing, tourism and fisheries). Manufacturing mostly relies on primary products (mainly livestock, dairy and fish) and tourism which is currently increasing in terms of both supply (lodging capacity) and demand (number of tourists per year).

In this context, biodiversity and natural resource conservation has become a priority of the regional policy agenda, in a way that 20% of the Azorean coastal and terrestrial surface is under protection, including Natura 2000 European Network sites.

In 2007, nine Island Natural Parks (one for each island – territorial sea up to 12 nautical miles) and a Marine Park were created by the Regional Government through the introduction of a new regional conservation policy. This was achieved by implementing a new management system of Protected Areas (PAs) which aims at preserving biodiversity and cultural landscapes of the archipelago.

The criteria developed by the International Union for Conservation of Nature (IUCN) were applied and adapted to assign different categories of protection to existing (Natura 2000, Ramsar sites, regional woodland reserves, etc.) and potential natural sites, leading to a network of Parks made up by PAs under the same designation and management regime.

The policy further created a series of Park Authorities (one per each island) and in this way designed the Parks to become key features in conservation and sustainable management of island resources. Nevertheless, to be implemented, the model needs to be effectively down-scaled and carefully tailored to local circumstances

### METHODOLOGY

The method integrates qualitative information, socioeconomic indicators (i.e. GDP per island, number of international flights per island, etc.), expert opinions (this analysis is part of the Smartparks Project and informal opinions of the project team are used), and land use analyses.

Firstly, a scoping process was followed to analyse both the regional context (archipelago – *scale 1*) and three groups of islands (*scale 2*). Qualitative information, informal expert opinions and regional statistics were collected and applied to identify the most relevant socioeconomic drivers and the most important challenges with respect to key conservation issues (natural and cultural capital, Protected Areas management and governance, etc.).

Then, the island of Pico was analysed (*scale 3*). A simplified model of small volcanic islands was used to better explore land use patterns, conservation opportunities and conflicts at this scale. It distinguishes three spatial units of an island: coastal zone (0 m-150 m above the sea level), middle crown (between 150 m and

600 m above sea level) and core area (more than 600m above the sea level).

## MULTI-SCALE ANALYSIS

### Scale 1: The Azores Archipelago

The Archipelago is characterized by a "double" insularity, driven by the combination of its remoteness (about 1,500 km from the mainland and 4,000 km from the North American East-coast) and the large distance among the constituent islands (Table 1).

On one hand, these natural and physical barriers tend to increase the vulnerability of the archipelago, limiting the development of terrestrial and marine connections, increasing the dependence on distant external markets, and leading to an overspecialisation of the regional economy.

On the other hand, the Azores have started to achieve a significant importance in the management of the North Atlantic Ocean (the Economic Exclusive Zone surrounding the Azores represents the 55% of the national EEZ). Moreover, the strategic role of the Azores has recently increased, particularly concerning the protection of marine environments and the formulation of international transportation and maritime policies. The peculiar status of the Portuguese Autonomous Regions makes the Archipelago an active actor in ocean governance and environmental planning, giving it the right to define regional environmental policies and to participate in the negotiation of accords and international agreements concerning marine pollution, nature conservation, and the exploitation of living species (Calado *et al.*, 2011b).

The introduction of the new regional conservation policy (DLR, 2007) represents one of the greatest challenges for the future development of the region. The establishment of a network of nine Island Natural Parks and an offshore Marine Park has redesigned the governance system of the region, introducing new conservation authorities (each Park is represented by an authority), and redefining planning, management and administration issues.

However, there are many uncertainties threatening the effectiveness of this policy. Issues faced include the global economic crisis which could move the focus from conservation to prioritising human and financial resources for other purposes. There may be many institutional and non-institutional barriers, including: information gaps on biodiversity (mostly on marine ecosystems), scarce coordination among authorities, lack of coherent establishment or implementation of management plans, scarce involvement of public and poor attitude to participation and a restricted perception associated with PAs, etc.

These issues should be mainly addressed at this scale, by providing management guidelines and alternatives (e.g. financial options, development of tourism-related benefits, etc.) for a successful down-scaling of the regional conservation policy.

### Scale 2: Groups of Islands

The Azores are made up by three groups of islands geographically separated, namely: Oriental, Central and Occidental.

1. The Oriental Group (islands: São Miguel and Santa Maria) represents the main gate of the archipelago, connecting the region with the world (during the last three year 78% of total international flights connecting Azores to foreign countries have departed from or landed in these two islands). The group further concentrates the largest population (more than 50% of total inhabitants) and density (about 15%) which influences the economy of the entire Archipelago (i.e. final demand of goods and services). Haddad *et al.* (2012) estimated the multipliers effect of the economic base on Azores, showing that more than half of Azores economy was represented by São Miguel.

The group presents unique natural features (fossil deposits with great scientific interest, exclusive geological formations with volcanic activity such as volcanic craters and cones, lake-filled calderas, lava domes, hydrothermal vents, etc.) and host endemic habitats and species (Laurissilva natural forest and inland birds), representing important sites for geo- and biodiversity conservation.

They are host to multiple research centres and environmental institutions (university, environmental ONGs, governmental agencies) presenting a greater conservation capacity, which may facilitate the implementation of the regional conservation policy.

2. The Central group (Graciosa, Terceira, São Jorge, Pico, Faial) was characterised by little interaction with foreign countries and strong integration among the constituent islands (sharing infrastructure, services, and exchanging basic goods). Inter-island connections of this group were significant; with 60% of the total inter-island flights departing/landing and 90% of the total passengers transported by inter-island ferries, were between this island group within the last three year.

The group presents a heterogeneous pattern of natural and cultural sites, including: active volcanos, UNESCO agricultural landscapes and heritage sites, wetlands, endemic terrestrial and marine habitats and species, volcanic ridges and marine caves, presence of significant colonies of seabirds, lava caves, peculiar rural architecture and colonial urbanism, etc.

The strong connection of the constituent islands gives the opportunity to develop combined strategies and initiatives to preserve and manage this huge natural and cultural capital, as different ecotourism activities and education programmes can be developed and integrated based on common natural features of islands. This would improve environmental attitudes and conservation knowledge of tourists and residents (e.g. bird and whale watching, scientific diving, mountain climbing and trekking, speleological activities, etc.), contributing to biodiversity conservation.

3. The Occidental Group (Flores and Corvo) is the most isolated sector of the Azores (with no international transportation and limited connection with other groups). These islands are interlinked and mutually dependent with a small economy with a highly vulnerable declining population and social problems, demanding strong investment in halting the abandonment of human activities and maintaining local livelihoods (Table 2).

### Scale 3: The Island – the case of Pico

Pico is the second biggest island of the Azores and, with the largest area of protected land (35%) with various categories of protection represented by the island Park (five IUCN management categories were associated to this Island Park), it represents a challenge for regional conservation policies.

Table 1. Distance among Azores islands [km]

Islands	Santa Maria	São Miguel	Terceira	Graciosa	São Jorge	Pico	Faial	Flores	Corvo
Santa Maria	0	100	265	345	330	340	360	575	585
São Miguel	100	0	170	250	250	260	280	500	510
Terceira	265	170	0	95	120	125	145	360	370
Graciosa	345	250	95	0	75	80	85	270	280
São Jorge	330	250	120	75	0	20	40	250	260
Pico	340	260	125	80	20	0	25	240	250
Faial	360	280	145	85	40	25	0	235	245
Flores	575	500	360	270	250	240	235	0	15
Corvo	585	510	370	280	260	250	245	15	0



Table 2. Demographic and economic baseline

Island	Population		Population density [inhab./km <sup>2</sup> ]	Ageing ratio	GDP* [%]
	[inhab.]	%			
Corvo	507	0,21	29,65	204,2	0,1
Faial	15.784	6,42	91,18	91,3	6,6
Flores	4.168	1,70	29,56	138,6	1,2
Graciosa	4.950	2,01	81,55	146,0	1,1
Pico	14.923	6,07	33,55	149,2	4,8
Santa Maria	5.557	2,26	57,35	73,1	2,7
São Jorge	9.403	3,83	38,60	124,0	2,7
São Miguel	134.662	54,78	180,85	50,3	59,6
Terceira	55.857	22,72	139,54	82,0	21,2
<b>Azores Archipelago</b>	<b>245.811</b>	<b>100,00</b>	<b>105,86</b>	<b>68,8</b>	<b>100</b>

By applying a simplified model for small volcanic islands, three geographical rings can be recognised at island scale: a coastal zone, a middle crown and a core area (Figure 2).

According to this model, the coastal zone is where settlements, human activities and transportation infrastructures are mainly developed. The coastal zone of Pico is mainly covered by urban areas (approximately 8% of the coastal zone) and agricultural areas (approximately 30%), including a traditional viticulture area with a strong socio-cultural identity - *Landscape of the Pico Island Vineyard Culture* - designed as the UNESCO world heritage site.

The main conservation challenges include the protection of seabird habitats, the connection between fragmented PAs, the reduction of tourist pressures on designated sites and the improvement of environmental education activities and monitoring programs. Harmonising of human activities and biodiversity conservation in cultural vineyard landscapes is considered a priority, due to emerging conflicts between the preservation of the cultural landscapes and the conservation of protected endemic species and habitats which have recently occupied several abandoned vineyards.

The middle ring is mostly covered by pastures (approximately 40%) and semi-natural land with a significant presence of invasive non-indigenous species (more than 40%) with PAs covering only 7% of the ring. The creation of ecological corridors between coastal zone and core area should be considered. Appropriate actions for containing invasive species could be considered and assessed (e.g. habitat restoration, use of invasive woodland biomass for energy production, etc.).

Areas with large pastures and natural areas, with a significant presence of endemic species, predominantly occur in the core area (peatbogs, ancient volcanic lakes, etc.) where the majority of PAs are concentrated. The protected land includes Nature Reserves

(IUCN category I), areas for the protection of singular species or habitats (IUCN category IV), and a large natural landscape (IUCN category V), covering about 9,500 ha (70% of the core). The conversion of natural and semi-natural lands into pastures represents the main pressure for conservation with negative conservation behaviours frequently observed (e.g. animal grazing in habitats with natural high-level value) suggesting that human-conservation conflicts may increase without mobilizing the support of local communities.

## DISCUSSION

Assuming that archipelagos are systems made up of spatial units with different features and values, a multi-scale analysis could then be applied. This enabled a better understanding of the social-ecological system in which the regional conservation policy to be implemented, generating insights for down-scaling the strategy at multiple levels.

Archipelagos represent a suitable context for applying a multi-scale analysis since the selection of spatial units is facilitated by their physical limits.

The Azores Archipelago was considered an excellent case study for performing this multi-scale analysis due to the recent implementation of the regional conservation policy, aiming at translating conservation principles into local actions.

The study identified a “double insularity” symptom in the Azores, associated with a greater dependence on external inputs and a poorly diversified economy (Kerr, 2005). Another archipelagic effect relies on its strategic location contributing to the management of the Atlantic space and to adaptation strategies for global environmental change. The new conservation policy seems to be a powerful way for promoting the sustainable future of the Archipelago. However, for a successful down-scaling of this policy a strategic approach to conservation is required where the major challenges for its implementation are:

- defining the role of conservation actors including duties and responsibilities;
- building expertise and improving institutional, technical and financial capacity;
- promoting inter-agencies coordination and integrating conservation and sectorial policies and;
- identifying financial needs and suitable funding programmes.

In island groups, the analysis highlighted the importance of connections among them to support appropriate conservation strategies and measures. Collaborative approaches should be adopted to provide overarching directions and objectives for sustainable development and conservation. The three main objectives for the implementation of the regional conservation policy at this scale are:

- identification of inter-island networks and promoting inter- and intra-institutional collaborations;
- definition of conservation strategies and desirable objectives for each group and;
- Optimisation of human and financial resources to capitalize on economies

At the island scale, the key challenges identified were the need to find consensual solutions for avoiding conflicts between conservation and local livelihoods. It may require a participatory approach, where public participation is crucial to find consensual solutions for implementing conservation and management measures.

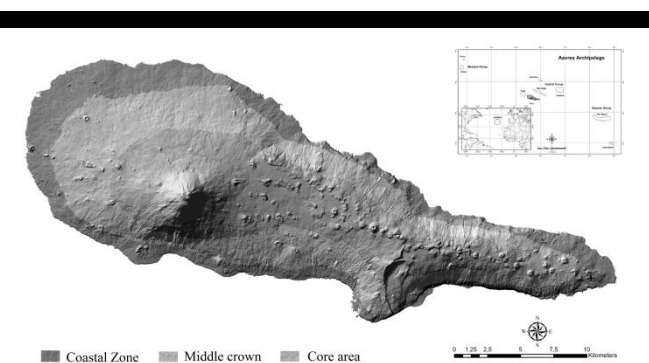


Figure 2. Simplified model of volcanic small islands in Pico island

## CONCLUSION

The selection of an appropriate scale of analysis is critical for conservation planning as many conservation problems may occur when the levels at which management interventions are made do not correspond to the scales at which ecological processes and problems occur (Cumming *et al.*, 2006; Guerrero *et al.*, 2012).

This study has presented a multi-scale analysis to support the implementation of a regional conservation policy in the Azores archipelago. Three scales were selected (Archipelago, groups of islands and island per se) based on bio-physical and socio-cultural aspects. Among them, only the archipelago clearly aligns with an administrative level (Autonomous Region) and, to some extent, the island (even though the Park Authority does not represent an elective body). In this context, it is vital to strengthen cross-scale communication, cooperation and participation, through mechanisms that could facilitate to downscale the regional policy such as: the creation of a forum of Island Park Authorities, the establishment of inter- and intra-island partnerships for conservation, etc.

Finally, although the nature of the analysis was mainly qualitative, it showed a potential way for analysing naturally nested geographic units such as archipelagos. We believe that this multi-scale approach could be applied in the future in other small-island archipelagos and extended to support the implementation of other policies (e.g. spatial planning or sectorial policies). Nevertheless, criteria for selecting scales will always need to be re-formulated based on specific features and objectives of the study.

## ACKNOWLEDGEMENT

The work described in this publication was developed under the Project SMARTPARKS – Planning and Management System for Small Islands Protected Areas (PTDC/AAC-AMB/098786/2008) funded by Fundação para a Ciência e a Tecnologia (FCT).

The authors wish to express their gratitude to Professor Richard James Ladle for providing important suggestions in this study.

## LITERATURE CITED

- Ankre, R., 2009. Zoning in a future coastal biosphere reserve - Planning for tourism and outdoor recreation in the Blekinge archipelago, Sweden. Working paper 2009:1. Östersund: ETOUR Mid Sweden University.
- Bunce, M., 2008. The 'leisuring' of rural landscapes in Barbados: New spatialities and the implications for sustainability in small island states. *Geoforum* 39:969–979
- Calado, H., Borges P., Phillips M., Ng K. and Alves F., 2011a. The Azores archipelago, Portugal: improved understanding of small island coastal hazards and mitigation measures. *Natural Hazards*. 58:427–444
- Calado, H., Ng, K., Lopes C. and Paramio L., 2011b. Introducing a legal management instrument for offshore marine protected areas in the Azores – The Azores Marine Park. *Environmental Science & Policy*. 14(8):1175–1187
- Cardoso, P, Borges, P.A.V., Costa, A.C., Tristão da Cunha, R., Gabriel, R., Martins, A.M.F., Silva, L., Homem, N., Martins, M., Rodrigues, P., Martins, B, and Mendonça, E., 2008. A perspectiva arquipelágica: Açores. In: Martin JL, Arechavaleta M, Borges PAV, & Faria B (eds.), Top 100. Las 100 espécies amenazadas prioritárias de gestión en la región europea biogeográfica de la Macaronesia, pp. 421-449.
- Cumming, G.S., Cumming, D.H.M., and Redman, C.L., 2006. Scale mismatches in social ecological systems: causes, consequences, and solutions. *Ecology and Society* 11(1): 14
- Decreto Legislativo Regional (DLR) n. 15/2007/A de 25 de Junho, Diário da República, 1ª série - Nº 120, que procede à revisão da Rede Regional de Áreas Protegidas da Região Autónoma dos Açores e determina a reclassificação das áreas protegidas existentes.
- Guerrero, A.M., McAllister, R.R.J., Corcoran, J. and Wilson, K.A., 2013. Scale Mismatches, Conservation Planning, and the Value of Social-Network Analyses. *Conservation Biology* 27: 35–44
- Kerr, S.A., 2005. What is small island sustainable development about? *Ocean & Coastal Management* 48:503–524
- McGinley. 2007. Azores temperate mixed forests. The Encyclopedia of Earth – available online: [http://www.eoearth.org/article/Azores\\_temperate\\_mixed\\_forests](http://www.eoearth.org/article/Azores_temperate_mixed_forests)
- Mendonça, L., 2000. História dos Açores: visão geral (sécs XV-XIX). Ponta Delgada, Açores. 208 p.
- Mittermeier, R.A., da Fonseca, G.A.B., Hoffman, M., Pilgrim, J., Brooks, T., Gill, P.R., et al., 2005. Hotspots revisited: Earth's biologically richest and most endangered terrestrial ecoregions. In: CEMEX, Conservation International, Washington DC, USA.
- Mueller-Dombois, D., Loope, L.L., 1990. Some unique ecological aspects of oceanic island ecosystems. *Monog. Syst. Botan.* 32, 21–28.
- Niles, D. and Baldacchino, G., 2011. Introduction: On Island Futures. In: Island Futures: Conservation and Development across the Asia-Pacific Region. Baldacchino G. and Niles D. (eds.). 2011. Tokyo, Springer, 2011.
- Paloniemi, R., Apostolopoulos, E., Primmer, E., Grodzinska-Jurczak, M., Henle, K., Ring, I., Kettunen, M., Tzanopoulos, J., Potts, S., van der Hove, S., Marty, P., McConville, A., and Similä, J., 2012. Biodiversity conservation across scales: lessons from a science-policy dialogue. *Nature Conservation* 2: 7–19
- Petit, J. and Prudent, G. (eds). Climate Change and Biodiversity in the European Union Overseas Entities. Gland, Switzerland and Brussels, Belgium: IUCN. Reprint, Gland, Switzerland and Brussels, Belgium: IUCN, 2010. 192 pp.
- Poiani, K.A., Richter, B.D., Anderson, M.G. and Richter, H.E., 2000. Biodiversity conservation at multiple scales: functional sites, landscapes, and networks. *BioScience* 50(2): 133-146
- Rietbergen, S. Hammond, T. Sayegh, C., Hesselink, F. and Mooney, K., 2007. Island voices – island choices: Developing strategies for living with rapid ecosystem change in small islands. Gland, Switzerland: IUCN, 40 pp.
- Serviço Regional de Estatística dos Açores (SREA). 2009. PIB por Ilha. Contas Regionais.
- Serviço Regional de Estatística dos Açores (SREA). 2010. Anuário estatístico. Região Autónoma dos Açores. Angra do Heroísmo, Portugal.
- Stratford, E., Baldacchino, G., McMahon, E., Farbotko, C., Harwood, A., 2011. Envisioning the Archipelago, *Island Studies Journal* 6(2):113-130
- van Beukering P., Brander, L., Tompkins, E. and McKenzie, E., 2007. Valuing the Environment in Small Islands - An Environmental Economics Toolkit. Available from: <http://www.jncc.gov.uk/page-4065>

## Beach nourishment experiment in Palanga, Lithuania

Donatas Pupienis†, Darius Jarmalavičius‡, Gintautas Žilinskas‡, Julija Fedorovič‡

Faculty of Natural Sciences, Vilnius  
University, Lithuania  
donatas.pupienis@gf.vu.lt

‡Institute of Geology and Geography  
Nature research centre  
Vilnius, Lithuania  
jarmalavicius@geo.lt  
zilinskas@geo.lt  
julijafed@inbox.lt



[www.cerf-jcr.org](http://www.cerf-jcr.org)



[www.JCRonline.org](http://www.JCRonline.org)

### ABSTRACT

Pupienis, D., Jarmalavičius, D., Žilinskas, G., Fedorovič, J., 2014. Beach nourishment experiment in Palanga, Lithuania. In: Green, A.N. and Cooper, J.A.G. (eds.), *Proceedings 13<sup>th</sup> International Coastal Symposium* (Durban, South Africa), *Journal of Coastal Research*, Special Issue No. 70, pp. 490-495, ISSN 0749-0208.

Palanga is one of the most popular Lithuanian seaside resorts, which has previously been valued for its wide beaches composed of light yellow fine-grained quartz sand. At the turn of the 20<sup>th</sup> and 21<sup>st</sup> centuries, intensified erosion processes in recreation zones led to shoreline retreat and the volume of beach sand reduced. Increased coastal erosion resulted in diminishing recreational space. In order to rebuild the eroded beaches, a decision to implement a beach nourishment project was made. From 2006 to 2012, through several stages along a 2.5 km stretch of shoreline, over half a million m<sup>3</sup> of sand was added to the beach, dredged from the onshore Kunigiškiai sand quarry or offshore from the Baltic Sea floor. From 2004 to 2013, along the nourished stretch, coastal monitoring was carried out once a year in the spring; the beach's condition was assessed based on 10 cross-shore profiles: cross-shore levelling was carried out and sand samples were collected. On the basis of repeated cross-shore levelling, changes in the morphometric characteristics of the beach and dune ridges and sand volume were undertaken. Sand samples allowed the identification of its granulometric composition. The results showed that the shoreline has partially stabilised after the beach reclamation; the beach has become wider and higher, thus recreational conditions have partially improved, i.e. beach recreational space has increased. However, beach nourishment has not changed the coastal dynamic patterns. The beach is relatively stable due to the additional nourished sand. It should be noted that the morphometric parameters of the beach profile depend on the nourished sand volume. Due to the increased beach width, aeolian processes have intensified, resulting in an increased sand volume carried towards the coastal backdune forest. These shore reclamation operations have changed in the prevailing sand's granulometric composition. Previously, predominantly light yellow fine sand was replaced by dark brown medium sand. The beach restoration was the reason for an increase in beach slope.

**ADDITIONAL INDEX WORDS:** *beach nourishment, morphometric characteristics, grain size, sand volume, Palanga, Lithuania.*

### INTRODUCTION

The sandy shoreline of Lithuania, according to prevailing dynamic processes, can be divided into regions: those which are eroded - 18.6 km, those which are stable or have negligible erosion rates - 32.0 km, and accreting shores - 38.0 km (Pupienis *et al.*, 2012). Only 20.5 % of all Lithuanian beaches are classified as eroding beaches, but the majority of them have the status of recreational space. At the turn of the 20<sup>th</sup> and 21<sup>st</sup> centuries, intensified erosion processes in recreational areas led to shoreline retreat, narrowing of wide beaches, coastal land loss and sand volume reduction. Consequently, increased coastal erosion resulted in diminishing recreational space.

Various shore protection methods are practised in effort to manage beach erosion and satisfy social and economic needs. In recreation zones, beach or coast sand replenishment is widely applicable for sandy beach reconstruction as a common 'soft' shore protection measure. Beach nourishment is a preferable measure for shore protection and beach restoration in today's world (Clayton, 1991; Dean, 2002; Finkl and Walker, 2002; Castelle *et al.*, 2009; Cai *et al.*, 2010; Cooke *et al.*, 2012), as well

as being a priority tool in coastal management applied in the UE countries (Dubrawski, 1995; Zawadzka, 1996; Hanson *et al.*, 2002; Žilinskas *et al.*, 2008; Weisner and Schernewski, 2013; van der Spek and Elias, 2013; Silva *et al.*, 2013).

In Lithuania a beach nourishment operation with imported sand was carried out for the first time in 1991, when 30 000 m<sup>3</sup> of sand was refilled along a 1 km-long stretch of shore near Kunigiškiai (Kirllys, 1993). In 2001, along a 2 km-long stretch between Melnragė and Giruliai, 537 282 m<sup>3</sup> of sand was pumped onto the beach at a depth of 6-7 m (Žilinskas *et al.*, 2002). Based on data provided by Klaipėda Seaport, beach re-nourishment operations (297 045 m<sup>3</sup> of sand) along this stretch were carried out in 2005, 2009 and 2012, but their effects have not been analysed in detail. Most of the researchers' attention was focused on the Palanga beach nourishment experiment initiated in 2006, and which was continued intermittently until 2012. Detailed results from the first three years of this experimental project, when the beach was nourished with sand imported from Kunigiškiai sand quarry, was summarised by Žilinskas *et al.* (2008).

The objective of this paper is to identify the beach sand granulometric composition, the beach morphometric characteristics and changes in sand volume from 2004-2013 before and after the beach nourishment.

## PHYSICAL SETTING

The study region (Palanga beach) is located along the Baltic Sea coast of Lithuania (Figures 1a and 1b). The study spans a 2.5 km long coastal strip from Birutė Hill to Ražė Stream (Figure 1c). Palanga is one of the most popular Lithuanian seaside resorts, which has previously been valued for its wide beaches composed of light-yellow fine-grained quartz sand. The investigated stretch of shoreline has a south-north orientation from Birutė Hill to Palanga pier and a southwest-northeast orientation from Palanga pier to the concrete embankment near Ražė Stream. Until 1997 the open sea beach sites ranged from 50 to 80 m in width and the elevation of the foredune toe ranged from 2 to 3 m above mean sea level, and was backed by 6-10 m-high foredunes. The beach consisted predominantly of well-sorted ( $S_p=1.34-1.35$ ) fine quartz sand with a mean grain size ( $d_{50}$ ) ranging from 0.17 to 0.22 mm. During the period 1995–1999 coastal erosion in the Palanga area reached a catastrophic scale: the shoreline retreated about 115 m (23 m per year) (Žilinskas *et al.*, 2004); during the period 1995–2003 the annual loss of sediment volume per one linear meter was 130 m<sup>3</sup> (Jarmalavičius, Žilinskas, 2003).

The mean annual wind speed is 4.7 m/s (Strolytė, Rimkus, 2012). During the period 2004-2013 the Lithuanian seaside experienced seven severe storms with wind speeds equaling or exceeding 25-29 m/s (Navašinskienė, 2013). Since the Baltic Sea near the Lithuanian coast is tideless, swell and wind waves are the only drivers of water motion in the nearshore zone. The mean annual significant offshore wave height ( $H_s$ ) at the 7 m isobath is about 0.7 m, and the mean annual significant offshore wave period ( $T_s$ ) is about 5.8 s. The prevailing wind and wave directions are SW, W and S (Kelpšaitė, Dailidienė 2011). This causes a predominant alongshore sediment transport along the southeast Baltic Sea coast from south to north (Gudelis, 1998). This alongshore sediment transport is blocked by an 80 m-long groyne situated south of Palanga pier (Figure 1c).

## METHODS

Since 2004, along the nourished 2.5 km long stretch, coastal monitoring has been carried out once a year in May when the weather is calm, and the sea level is close to the long term mean (Jarmalavičius *et al.*, 2012). The levelling of the cross-profiles of the beach was carried out (applying electronic tachymeter TOPCON GTS 229) at 10 observation stations installed along the coastal strip under investigation (from Birutė Hill to Ražė Stream). Four monitoring stations are situated north, and six south of Palanga pier. The locations of the beach profile benchmarks are shown in Figure 1c.

Along each transect, sediment samples were collected from the middle of the beach. The sand samples were taken from the 'active' layer (upper 5 mm). Based on the measurement data, the following parameters were calculated: shoreline position changes, positions of the crest and foot of the foredune, and sediment volume in the subaerial beach in the foredune and on the coast in general (beach + foredune) (Jarmalavičius *et al.*, 2012). The sediment volume was calculated with the ArcMap 10.1 computer programme. Sand samples were screened (using 'Fritsch Analysette 3 PRO' laboratory equipment) to determine the distribution of different sand fractions, the average diameter of grains and sorting. Statistical parameters of sand granulometric composition were calculated using 'Gradistat v4.0', and by applying the Geometric method after Folk and Ward (1957). This calculation method was chosen in order to compare the previous and current results of granulometric composition analysis (Jarmalavičius, Žilinskas, 2003; Žilinskas *et al.*, 2008).

## RESULTS

From 2006 to 2012, through four stages, 574 648 m<sup>3</sup> of sand was pumped onto the beach over a 2.25 km-long stretch of shoreline (Table 1). The places of sand nourishment on the beach

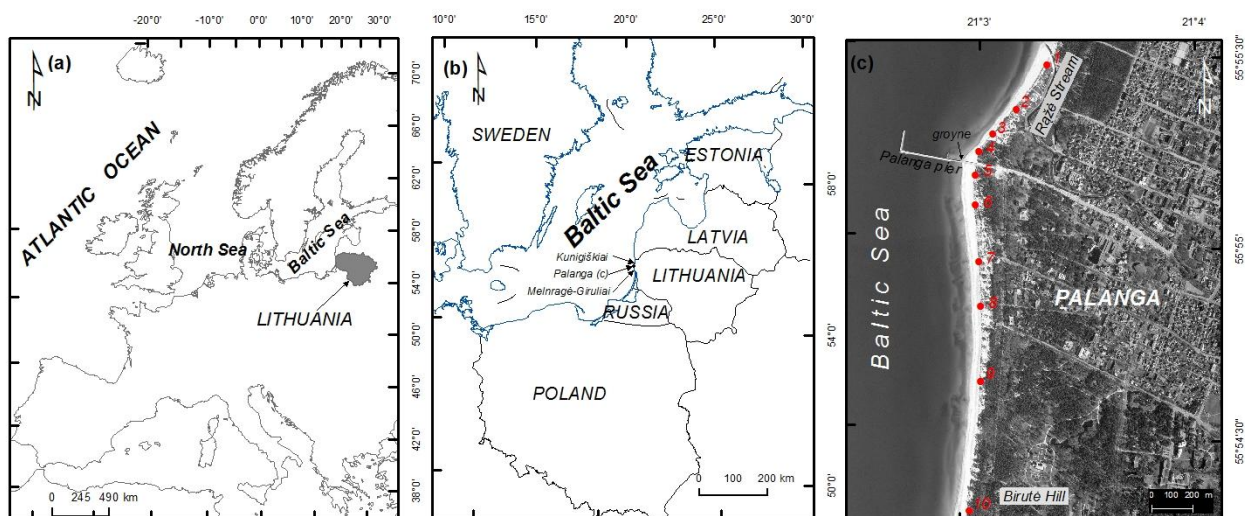


Figure 1. Location of study area. Red points - cross-shore profile benchmarks.

Table 1. Palanga beach nourishment project history based on data provided by Ministry of Environment of the Republic of Lithuania.

Date (Project)	Length (m)	Total volume placed (m <sup>3</sup> )	Sediment mean grain size (mm)	Cost, EUR
February-March 2006 (I)	800	40000	0.37	347544
April 2008 (II)	1680	111000	0.35	1757993
April-May 2011 (III)	1295	131631	0.38	1853000
April-May 2012 (IV)	2250	292017	0.33	4110792

are shown in Figure 2. Replenishment operations on Palanga beach cost over 27.8 mln Lt. in total (or 8.05 mln EUR).

In the spring of 2006, during the first nourishment project, sand dug out of Kunigiškiai sand quarry was pumped onto the beach along an 800 m-long coastal stretch located south of Palanga pier (Figure 2a). The sand was poorly sorted ( $S_o=2.17$ ) and of medium size ( $d_{50}=0.37$  mm), i.e., 1.7 times coarser than native sand with lesser sorting (Figure 3). Sand imported from Kunigiškiai sand quarry was made up of 26.34 % particles coarser than 0.40 mm, and sand finer than 0.063 mm constituted 0.37% (Figure 4). After the nourishment operation the beach widened by 10-20 m and rose in height by 1.0-1.5 m on average (Figure 5). The beach was nourished with about 50 m<sup>3</sup> of sand per one linear meter.

Despite the fact that over one year the average sand particle

size and sorting was restored to the granulometric composition parameters of those in 2005. Thus the decision was made to reject sand coming from Kunigiškiai quarry as it did not satisfy the beach replenishment requirements (Žilinskas *et al.*, 2008). In 2008, after a two-year break, it was decided to nourish the beach in Palanga with sand dredged from the Baltic Sea floor. During the second nourishment project 111 000 m<sup>3</sup> of sand was added to the beach along a 1680 m-long stretch located south of Palanga pier, in place of the emerging embayment (Figure 2b). The mean size of the sand particles ( $d_{50}=0.35$  mm) was similar to those nourished in 2006 (Figure 3); however, both the finest and coarsest fractions constituted a smaller percentage. The marine sand was moderately sorted ( $S_o=1.70$ ). An analysis of the sand's granulometric composition showed that particles larger than 0.40 mm constituted 34.19 %, but the amount of silt was reduced by 10 times - 0.04% (Figure 4). The beach nourishment resulted in the beach widening



Figure 2. Documented beach nourishment sites in Lithuania and comparison of satellite images of nourished beach at different times. Numbers in legend: 1 – shoreline position in 01-06-2003, 2 – beach nourishment place, project number and date.

by 10-15 m and a slowing down of erosion processes (Figure 5). During the third nourishment project in 2011, 131 631 m<sup>3</sup> of sand dredged from the Baltic Sea bottom was pumped onto the beach along a 1295 m-long stretch (Table 1). 43.4% of the sand volume was refilled along a 330m-long stretch north of Palanga pier, and 56.6% - south of Palanga pier along a 965 m-long stretch (Figure 2c). The decision to nourish the beach north of Palanga pier was made after the erosion processes caused by a groyne intensified. Erosion processes led to the beach narrowing by up to 30 m, substantial erosion of the dune ridge and a significant reduction in beach sand volume in 2006-2010 – the remaining sediment volume did not exceed 22 000 m<sup>3</sup> (Figure 6). The sand was medium ( $d_{50}=0.39$  mm) and moderately sorted ( $S_o=1.82$ ). In terms of granulometric composition the sand was characterised by particles coarser than 0.40 mm (43.30 %) and finer than 0.063 mm (0.01 %) (Figure 4). The beach after nourishment widened by 10–15 m on average in comparison with the previous years, and their height reached 1.5–2.0 m.

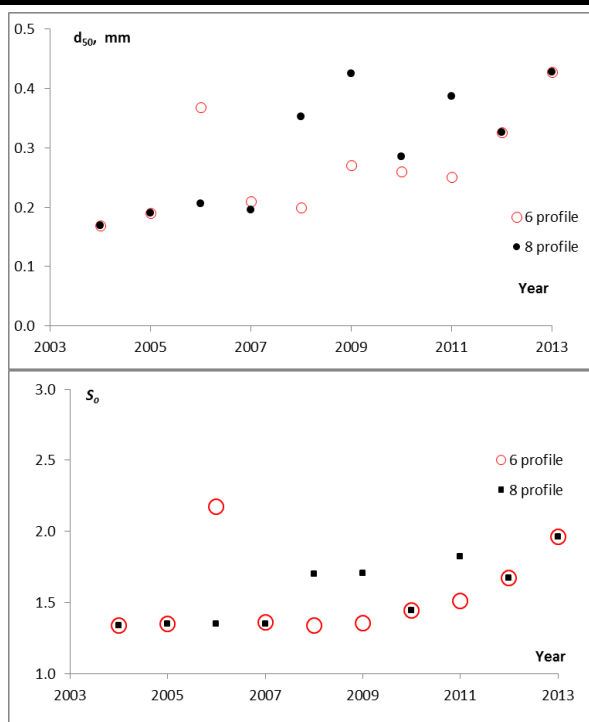


Figure 3. The changes of mean grain size and sorting in 2004–2013.

In April of 2012, during the fourth nourishment project, 292 017 m<sup>3</sup> of sand was placed on the beach along a 2250 m-long stretch, i.e. 78.1 % of the entire volume along the southern stretch (Birutė Hill – Palanga pier), and 21.9% - along the northern stretch (Palanga pier – Rąžė stream) (Figure 2d). In this case the sand was the finest ( $d_{50}=0.33$  mm) and best-sorted ( $S_o=1.67$ ) in comparison with the sand's granulometric parameters in the previous years (Figure 3). The sand's granulometric composition was characterised by a reduction in quantity of coarser particles (>0.40 mm) and an increase in quantity of finer particles (<0.063 mm), which constituted 28.67 % and 0.22 % respectively (Figure 4). The average height of the beach increased to 3 m and the width expanded by 80 m as a result of the beach replenishment (Figure 5).

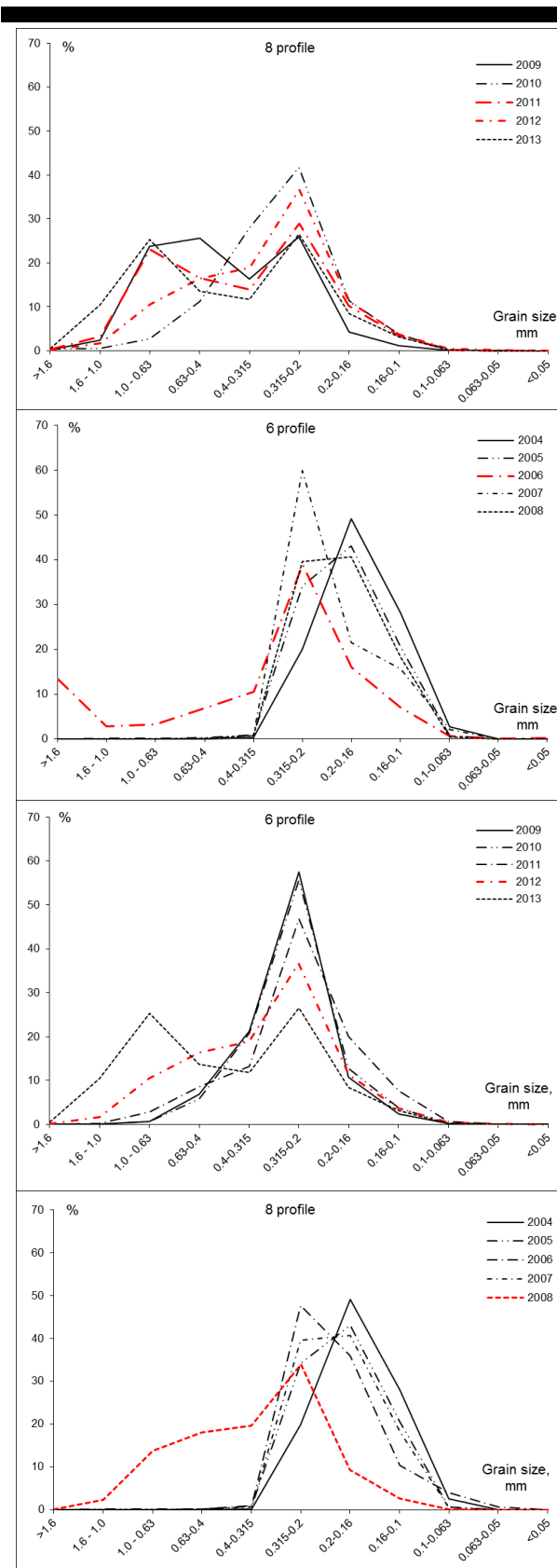


Figure 4. The changes in beach sand granulometric composition in 2004–2013. Red line – sand granulometric composition after beach nourishment.

Based on the levelling of cross-shore profile data, the dynamics of the subaerial beach volume from 2005–2013 were calculated. The sand volume dynamics showed that along the southern stretch from 2006 to 2007 the prevailing coastal erosion ( $-9.2 \text{ m}^3/\text{m}$  per year) was replaced by accumulation ( $10.1 \text{ m}^3/\text{m}$  per year). Along the northern stretch, from Palanga pier to Ražė stream, accumulation processes ( $13.6 \text{ m}^3/\text{m}$  per year) began in 2011, whereas up to 2011 this coastal section was reduced by  $-1.91 \text{ m}^3/\text{m}$  of sand per year.

The largest volume of sediment along the coastal sections discussed occurred in 2012, i.e.  $107.0 \text{ m}^3/\text{m}$  along the southern stretch and  $80.1 \text{ m}^3/\text{m}$  along the northern by one linear meter (Figure 6).

## DISCUSSION

The beaches in Palanga after nourishment have become relatively stable. It should be noted that beach nourishment besides changes in hydrometeorological conditions affected the coast's stability. During the first nourishment project about  $50 \text{ m}^3/\text{m}$  of sand was pumped onto the beach, and one year later only

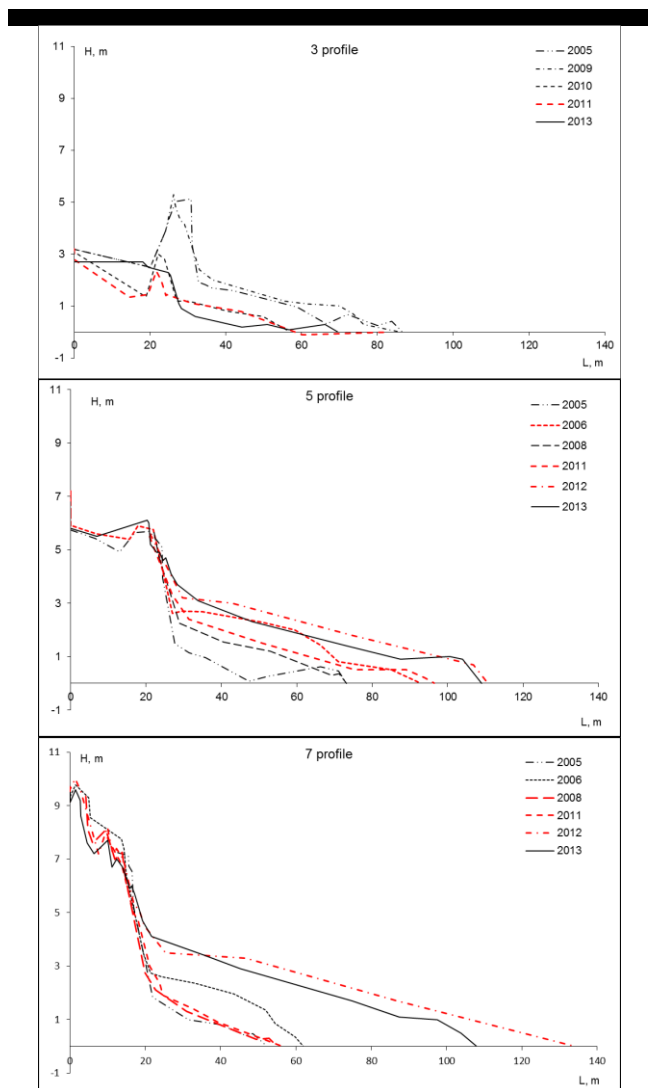


Figure 5. Cross-shore profiles change on the Palanga beach in 2005–2013. Red line – profiles measured after beach nourishment.

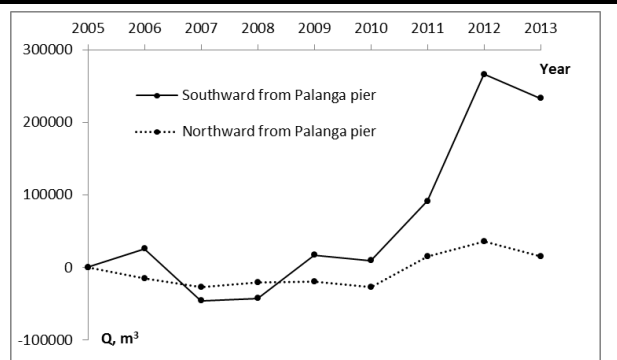


Figure 6. Sand volume dynamics in the Palanga beach in 2005–2013.

20% of this added sand volume remained; while the last project involved  $130 \text{ m}^3/\text{m}$  of sand on average, and the sand remaining one year later constituted around 95% of the added volume. A similar theoretical volume loss over a one-year period was indicated by other authors (Dean, 2002; Kirlyš, 1993; Zawadzka, 1995).

The amount of eroded sand from the beach partly depends on the nourished sand volume. A relatively larger amount of nourished sand means a more stable beach because sand is eroded at a slower pace. However, the eroded volume of nourished sand is largely conditioned by the hydrometeorological conditions. It was found that one year after the beach nourishment in 2006, the relative mean annual sea level reached 14 cm, i.e. in 2007 it was higher than in 2006. Meanwhile, one year after the last beach nourishment in 2012, the relative mean annual sea level was 10 cm, i.e. in 2013 it was lower than in 2012. Moreover, in 2006–2007 there were 37 days when the average westerly wind speed exceeded  $10 \text{ m/s}$ , and in 2012–2013 there were only 4 days.

There are other factors besides sediment volume that have influenced the sand dynamics: sand granulometric composition mismatch and groyne impact (Žilinskas *et al.*, 2008). A comparative analysis of the native material and ‘foreign’ material coming from outside sources (Kunigiškiai sand quarry and the Baltic Sea bottom), by applying the  $R_j$  and  $R_A$  indicators (James, 1975), showed that these two sand materials did not match satisfactorily. The sand from Kunigiškiai quarry was closer to the native nearshore sand in terms of composition, so its use was more accurate for nearshore nourishment in Palanga and the formation of the sandbar (Žilinskas *et al.*, 2010). During the second and third projects a large part of the sand composition constituted coarse sand. After storms it is possible to find packs of coarse sand on the beach along the shoreline and on the foredune, which is not typical for the coastal stretch under consideration. The beach's morphometric characteristics changed simultaneously with a larger amount of coarse sand. Before the beach replenishment the prevailing beach slope ( $tg\theta$ ) was 0.035, while artificially nourished beaches were formed with an average slope of 0.032. Over one year after the last nourishment the beach slope increased to 0.045, since the beach width was reduced and the height increased. Naturally coarser sand determined the increase in beach slope.

In order to protect the beach in Palanga from further erosion, an impermeable groyne was built in the summer of 2005 in the place of the old pier. It was not determined that the shoreline in the northern part of the Palanga groyne would develop in accordance with the parabolic bay equation. The diffraction of the

prevailing SW, W and S waves (Kelpšaitė, Dailidienė, 2011) resulted in the formation of an embayment in the northern stretch (Pupienis *et al.*, 2013).

The beach nourishment provided a more favourable recreational space by making the beach wider and higher. However, the emergence of large quantities of sand and the elongation of the fetch length (due to the widening beaches) created favourable conditions for the intensification of aeolian processes. Recently, sand blowing over Palanga pier and the recreational infrastructure has been observed. In addition, alongshore sediment transport in a south to north direction has blocked the Rąžė stream mouth. The beach nourishment led to a decrease in the relative height of the dune ridge as an effect of the increasing height of the foredune toe. As a result, large quantities of sand are more easily transported over the dune ridge towards the backdune forest, threatening to bury the trees. Similar effects of beach nourishment are listed by Dubrawski (1995), Zawadzka (1996). The above facts were the reasons for changes in coastal management strategy. The previous priority task was to stop beach erosion and the preservation of recreational space; currently, the main focus is on backdune forest protection against sand overblowing and constant Rąžė stream dredging, transferring the dredged sand to the adjacent coastal stretches.

It should also be noted that the main purpose of beach nourishment is to ensure the stability of the coast; therefore granulometric composition is most frequently highlighted and at the same time less emphasis is put on the aesthetic properties of sand, i.e. sand colour. Italian researchers point out that the colour of the beach is important in terms of both aesthetic value and ecology (Pranzini, Vitale, 2011). After the beach restoration in Palanga, the predominantly light yellow sand ('gold') was replaced by dark brown sand. However, any aesthetic change on the beach has not been investigated until now.

## CONCLUSION

The results showed that after the beach reclamation the shoreline partially stabilized; the beach became wider and higher and thus recreational conditions have partially improved, i.e. the beach recreational space has increased. However, beach nourishment has not changed the coastal dynamic patterns. The beach is relatively stable due to the addition of nourished sand. It should be noted that the morphometric parameters of the beach profile depend on the nourished sand volume. Due to the increased beach width, aeolian processes have intensified, which have resulted in increasing sand volume carried towards the coastal backdune forest. The shore reclamation works which were carried out have determined the change in the prevailing sand's granulometric composition and statistical parameters (mean grain size and sorting). Beach nourishment caused an increase in the beach slope and the previously light yellow fine sand was replaced by dark brown medium sand.

## ACKNOWLEDGEMENTS

The authors would like to thank Valerija Portapienė from the Klaipėda Seaport and Dalia Gudaitienė-Holiman from the Ministry of the Environment of the Republic of Lithuania for the precise data they provided on the nourished sand volume.

## LITERATURE CITED

Cai, F., Dean, R. G., and Liu, J., 2010. Beach nourishment in China: status and prospects. *Proceedings of 32<sup>nd</sup> Conference on Coastal Engineering*, Shanghai, China. 32.

- Castellea, B., Turner, I.L., Bertinc, X., and Tomlinson, P., 2009. Beach nourishments at Coolangatta Bay over the period 1987–2005. Impacts and lessons. *Coastal Engineering*, 56(9), 940-950.
- Clayton, T.D., 1991. Beach replenishment activities on U.S. Continental Pacific Coast. *Journal of Coastal Research*, 7 (4), 1195-1210.
- Cooke, B.C., Jones, A.R., Goodwin, I.D., and Bishop M.I., 2012. Nourishment practices on Australian sandy beaches: A review. *Journal of Environmental Management*. 113. 319-327.
- Dean, R.G., 2002. Beach Nourishment: Theory and Practice. World Scientific Publishing, New Jersey, pp. 420.
- Dubrawski, R., 1995. Analysis of shore and offshore of Hel Peninsula during beach nourishment in 1989-1995. Int. Rep. IM WW 4864, Gdansk. (in Polish).
- Finkl, C.W., and Walker, H.J., 2002. Beach nourishment. In: Chen, J.; Hotta, K.; Eisma, D., and Walker, J. (eds.), *Engineered Coasts*. Dordrecht: Kluwer, pp. 1–22.
- Folk, R.L., and Ward, W.C., 1957. Brazos River bar: a study in the significance of grain size parameters. *Journal of Sedimentary Petrology* 27, 3–26.
- Gudelis, V., 1998. Lithuanian coastal region. Vilnius, Lithuanian Acad. Sci. Monogr., 442. (In Lithuanian)
- Hanson, H., Brampton, A., Capobianco, M., Dette, H. H., Hamm, L., Lastrup, C., Lechuga, A., and Spanhoff, R., 2002. Beach nourishment projects, practices, and objectives – a European overview. *Coastal Engineering*, 47, 81–111.
- James, J.R., 1975. *Techniques in evaluating suitability of borrow material for beach nourishment*. Technical memorandum No. 60, Coastal Engineering Research Center, U.S. Vicksburg.
- Jarmalavičius, D., Satkūnas, J., Žilinskas, G., and Pupienis, D., 2012. Dynamics of beaches of Lithuanian coast (the Baltic Sea) for the period 1993-2008 based on morphometric indicators. *Environmental Earth Sciences*, 65(6), 1727-1736.
- Kelpšaitė, L., and Dailidienė, I., 2011. Influence of wind wave climate change to the coastal processes in the eastern part of the Baltic Proper. *Journal of Coastal Research*, SI 64, 220-224.
- Kirlyš, V., 1993. The shallow nearshore and beaches stabilisation methods and tools of natural analogues example. *Baltic Sea coast dynamics and Palaeogeography issues*, 2, 7-14. (In Lithuanian).
- Navasinskienė, J., 2013. Extreme events on the seacoast. In: Milerienė, R., Minevičiūtė, I. (eds.) *Jūros ir krantų tyrimai*. Klaipėda, Lithuania: Klaipėda University, pp. 172-174. (In Lithuanian).
- Pranzini, E., and Vitale, G., 2011. Beach Sand Colour: the Need for a Standardised Assessment Procedure. In: Micallef, A. (ed.), *MCRR3-2010 Conference Proceedings*, *Journal of Coastal Research*, SI61, 66-69.
- Pupienis, D., Jarmalavičius, D., and Žilinskas, G., 2012. Coastline dynamics tendencies of the Baltic Sea in 1910-2010 (In Lithuania). In: Rukšėnas, O., Turčinavičienė, J., Slapšytė, G., Bukelskis, E., Valiūškevičius G., Gadeikytė S. (eds.), *Proceedings 7th Science, Faculty of Natural Sciences*, Vilnius University, 141-152.
- Pupienis, D., Jonuškaitė, S., Jarmalavičius, D., and Žilinskas, G., 2013. Klaipėda port jetties impact on the Baltic Sea shoreline dynamics, Lithuania. In: Conley, D.C., Masselink, G., Russell, P.E. and O'Hare, T.J. (eds.), *Proceedings 12<sup>th</sup> International Coastal Symposium* (Plymouth, England), *Journal of Coastal Research*, SI 65, pp 2167-2172.
- Silva, R., Veloso-Gomes, F. and Pais-Barbosa, J., 2013. Morphological Behaviour of Costa da Caparica Beaches Monitored during Nourishment Operations. In: Conley, D.C., Masselink, G., Russell, P.E. and O'Hare, T.J. (eds.), *Proceedings 12<sup>th</sup> International Coastal Symposium* (Plymouth, England), *Journal of Coastal Research*, SI 65, 1862-1867.
- Stroltytė, S., and Rimkus, E., 2012. Changes of wind direction and speed in Lithuania in 1971-2010. *Geografija*, 48(2), 97-107. (In Lithuanian).
- van der Spek, A., and Elias, E., 2013. The effects of nourishments on autonomous coastal behaviour. Proceedings 7<sup>th</sup> International Conference on Coastal Dynamics. In: *Coastal Dynamics 2013*, 1753-1762.
- Zawadzka, E., 1996. Coastal zone Dynamics during artificial nourishment. *Coastal Engineering. Part IV: Coastal Processes and Sediment Transport*, 2955-2968.
- Žilinskas G., Pupienis, D., and Jarmalavičius, D., 2010. Possibilities of regeneration of palanga coastal zone. *Journal of Environmental Engineering and Landscape Management*, 18(2), 92-101.



## How can Portugal effectively integrate ICM and MSP?

Maria A. Ferreira<sup>†</sup>, David Johnson<sup>‡</sup>, Carlos Pereira da Silva<sup>†</sup>

<sup>†</sup>e-GEO, Research Centre for Geography and Regional Planning, FCSH Universidade Nova de Lisboa, 1069-061, Portugal  
[adelaide.ferreira@fcsh.unl.pt](mailto:adelaide.ferreira@fcsh.unl.pt)  
[cpsilva@fcsh.unl.pt](mailto:cpsilva@fcsh.unl.pt)

<sup>‡</sup> Seascope Consultants Ltd., Belbins Valley, Belbins, Romsey, SO51 0PE, UK  
[david.johnson@seascopeconsultants.co.uk](mailto:david.johnson@seascopeconsultants.co.uk)



[www.JCRonline.org](http://www.JCRonline.org)

### ABSTRACT

Ferreira, M.A., Johnson, D., Pereira da Silva, C., 2014. How can Portugal effectively integrate ICM and MSP? In: Green, A.N. and Cooper, J.A.G. (eds.), *Proceedings 13<sup>th</sup> International Coastal Symposium* (Durban, South Africa), *Journal of Coastal Research*, Special Issue No. 70, pp. 496-501, ISSN 0749-0208.

In 2013, the European Commission proposed a Directive to spur the integration of Maritime Spatial Planning (MSP) and Integrated Coastal Management (ICM) within and across Member States. To ascertain if key elements for integration exist, fundamental questions should be addressed: Are there (compatible) national policies/plans for the coast and ocean? Are ICM strategies in line with MSP policies? Are the agencies responsible for ICM and MSP coordinated? Are there common goals, indicators and integrated measures between both types of policies/plans?

Portugal is one of the world's largest maritime nations, and is actively engaged in preparing policies and planning/management legislation for the ocean. An analysis of the current Portuguese policy/legislative framework, in terms of the above mentioned questions, suggested that: coordination among coastal and maritime policies and strategies is unclear, as is the articulation between institutions and between spatial plans for coastal and maritime zones; objectives of relevant policies are mismatched; there are yet no indicators to evaluate coastal and ocean policies/plans, and the articulation between measures to integrate ICM and MSP is unclear. Despite language barriers and people/institutional resistance to change, effective integration of MSP/ICM requires: flexibility and novel approaches, public participation and stakeholder involvement, systemic approaches, and finding strategic level indicators to evaluate integrated policies. Portugal can play a lead role in setting an example for other coastal nations worldwide. If appropriately tackled, the mismatches highlighted in this analysis provide pointers that may contribute to a more effective integration of ICM and MSP in Portugal and in other coastal nations.

**ADDITIONAL INDEX WORDS:** *marine spatial planning, ICZM, ICOM, plan evaluation, indicators*

### INTRODUCTION

The coastal zone (including estuaries) is the gateway (entry and exit point) of all maritime activities: shipping, fisheries and aquaculture, marine (renewable) energies, mineral's/ore extraction, cables and pipelines, etc. All require dedicated space for the installation of related infrastructure. As such, integrated coastal planning and management must take into account maritime activities and, therefore, be integrated with Maritime Spatial Planning (MSP). Perhaps one of the most consensual definitions of MSP is "a public process of analyzing and allocating the spatial and temporal distribution of human activities in marine areas to achieve ecological, economic, and social objectives that are usually specified through a political process." (Ehler and Douvere, 2009, p.18). The recent proposal (March 2013) of a new European Directive establishing a framework for MSP and Integrated Coastal Management (ICM) (European Commission, 2013), is recognition of the need to achieve coherence between ICM and MSP within and across national borders. It is evident that despite the obvious importance of a concerted approach and of various calls for action, European Member States have yet to comprehensively apply the principles and practice of ICM or effectively link ICM with MSP. Worldwide, other coastal nations are faced with this same challenge. Why has it been so difficult to

coherently combine coastal and maritime policy, planning and management and how can this integration be achieved?

Various questions can be asked to try to approach this issue:

- Are there national policies and plans in place for both the coastal zone and the ocean?
- Are ICM strategies in line with MSP policies?
- Are planning instruments for coast and ocean compatible?
- Is there coordination between the agencies responsible for ICM and MSP?
- Are there common goals/overarching objectives between the two types of policies?
- Are there common indicators? In what areas/fields?
- Is there scope for integrated measures?

Portugal is one of the world's largest maritime nations: the Portuguese EEZ (mainland+Madeira+Azores) totals 1,700,000 km<sup>2</sup> (MAOT, 2011). It is also the 2<sup>nd</sup> biggest EEZ in the territory of the European Union (Sea Around Us Project, 2013). About ¾ of the Portuguese population lives on the coast, which contributes to 85% of the national GDP (APA, 2012). As such, the Portuguese case can be used to illustrate some of the challenges facing the effective integration of ICM with MSP.

Portuguese national policies and plans specifically addressing ICM and MSP were reviewed and compared to try to answer the

DOI: 10.2112/SI70-085.1 received 30 November 2013; accepted 21 February 2014. © Coastal Education & Research Foundation 2014

Table 1. Portugal’s main policy and planning framework for ICM and MSP. HWST: High water spring tide; nm: nautical miles.

	ICM	MSP
National Policy	2009 – National Strategy for Integrated Coastal Zone Management (ENGIZC)	2013 – National Ocean Strategy (ENM) (revision of 2006 version)
Geographic range	Landward: 2 km inland from max. equinoctial HWST Seaward: territorial waters (12 nm) incl. the seabed.	Coastal to 200 nm/Outer Continental Shelf
Planning	1993/2012 – Shoreline Spatial Plans (Planos de Ordenamento da Orla Costeira)	2013 – Draft Framework Law for Maritime Spatial Planning and Management
Geographic range	Coastal & interior maritime waters (excl. ports), their seabed & margins from the 30 m isobath to a line 500-1000 m inland from the sea margin (50m inland from max HW)	From the baseline (the low water line along the coast) to the outer limit of the continental shelf beyond 200 nautical miles.

questions highlighted above and to contribute to an assessment of how ICM and MSP connect in the current Portuguese framework.

Some of the legislation is still under discussion (reflecting in other words the fact that this is a relatively new policy and planning field). We present results of an in-depth analysis of the Portuguese situation with integrating ICM and MSP and discuss challenges facing all EU coastal Member States, having noted similar challenges and efforts in other parts of the world.

### THE PORTUGUESE SITUATION

#### Policy and planning framework for ICM and MSP

The main policy and planning framework for ICM and MSP in Portugal is summarized in Table 1 and their territorial expression is depicted in Figure 1.

The national policy for integrated coastal management in Portugal is the National Strategy for Integrated Coastal Zone Management (ENGIZC) adopted in 2009. Its stated vision is to

achieve, by 2029, “A coastal zone which is harmoniously developed and sustainable based on a systemic approach and on the valorization of its resources and identity values, sustained on scientific knowledge and managed according to a model which articulates institutions, coordinates policies and instruments, and ensures the participation of the different stakeholders involved.” (Resolution 82, 2009, p. 6067). Valorization is a term very frequently used in Portuguese policies and planning legislation. According to the Merriam-Webster dictionary it means “to enhance or try to enhance the price, value, or status (of something) by organized and usually governmental action” (Merriam-Webster, 2013).

The ENGIZC lists 4 thematic objectives and 4 transversal objectives (cf. Table 2): thematic objectives cover all the “sectors” traditionally considered as the pillars of sustainable development (environmental, social and economic objectives, together with objectives which are technical (prevent/manage risk situations)) (Defra, 2006) and relates to the promotion of the knowledge base required for action; transversal objectives are geared towards bettering the governance structure required for implementing the

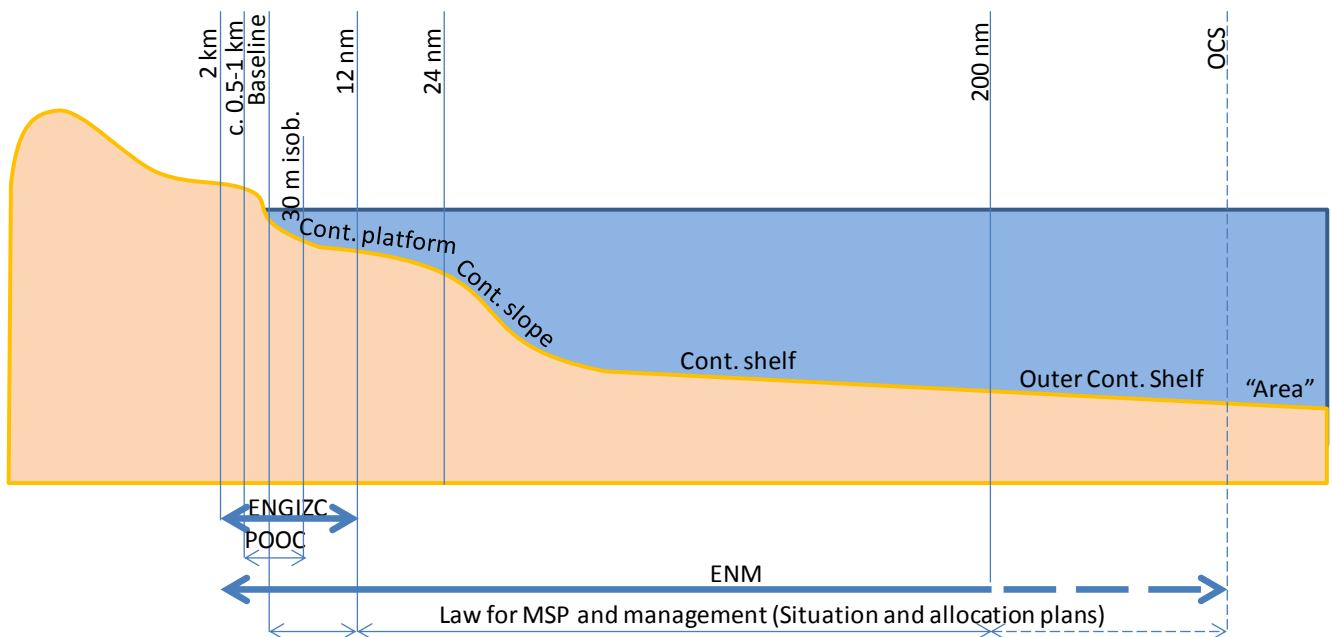


Figure 1. Schematic representation of the features and limits of the Portuguese coastal zone and maritime area, including the boundaries of relevant policies and plans. nm: nautical miles. ENGIZC: National Strategy for Integrated Coastal Zone management. POOC: Shoreline Spatial plans; ENM: National Ocean Strategy. OCS: Outer Continental shelf.

Table 2. Objectives of Portuguese policies and planning instruments for ICM and MSP. En: Environmental; Soc: social; Ec: Economic; Kn: Knowledge; G: Governance; F: Framework; T: Technical.

	ICM	MSP
Objectives	<p><b>ENGIZC (2009)</b>  <i>Thematic objectives</i></p> <p>a) Conserve and valorize resources and the natural, landscape and cultural heritage (En)</p> <p>b) Anticipate, prevent and manage risk situations and environmental, social and economic impacts (T)</p> <p>c) Promote the sustainable development of activities which generate wealth and contribute to the valorization of specific resources of the coastal zone. (Soc, Ec)</p> <p>d) Deepen the scientific knowledge on coastal systems, ecosystems and landscapes. (Kn)</p> <p><i>Transversal objectives</i></p> <p>a) Develop international cooperation (G)</p> <p>b) Strengthen and promote institutional articulation and the coordination of policies and instruments (G)</p> <p>c) Develop observation and monitoring mechanisms and networks (Kn);</p> <p>d) Promote public information and participation (G).</p>	<p><b>ENM (2013)</b></p> <ul style="list-style-type: none"> <li>• Reaffirm the national maritime identity in a modern, proactive and entrepreneurial framework. (F, Ec)</li> <li>• Achieve the economic, geostrategic and geopolitical potential of the national maritime territory, turning the Portuguese Sea into an active (asset) with permanent economic, social and environmental benefits. (F, Ec, En)</li> <li>• Create conditions to attract national and international investment in all sectors of the sea economy, promoting growth, employment, social cohesion and territorial integrity, and increasing by 2020, the direct contribution of the sea sector to the national GDP by 50% (Ec).</li> <li>• Strengthen the national scientific and technological capacity, stimulating the development of new areas of action which promote knowledge of the Ocean and enhance, in an effective, efficient and sustainable way, its resources, uses, activities, and ecosystem services (Kn, Soc, Ec, En).</li> <li>• Consecrate Portugal, at the global level, as a maritime nation and as an inescapable part of the IMP and of EU's maritime strategy, namely for the Atlantic area (F).</li> </ul>
Planning legislation objectives	<p><b>Shoreline Spatial Planning Law (Planos de Ordenamento da Orla Costeira) (1993/2012)</b></p> <p>a) Establish regimes to safeguard resources and natural values, and sustainable coastal zone management (En);</p> <p>b) Foster the sustainable development of the coastal zone (En, Ec)</p> <p>c) Make different coastal zone uses compatible (Ec)</p> <p>d) Promote the requalification of water resources (En)</p> <p>e) Value and qualify strategic beaches (En, Ec)</p> <p>f) Classify and discipline bathing beaches's use (En, Ec)</p> <p>g) Protect and valorize marine and terrestrial ecosystems (En)</p> <p>h) Identify and establish safeguard mechanisms of areas at risk (G)</p> <p>i) Ensure the articulation among territorial management instruments applicable in the area of the POOC (G)</p>	<p><b>Framework Law for Maritime Spatial Planning and Management (Draft Law 113/XII, 2013)</b></p> <p>“promotion of the economic, rational and efficient exploitation of marine resources and ecosystem services, ensuring the compatibility and sustainability of the diverse uses and of the activities developed within it, considering the intergenerational responsibility in the spatial use of the national maritime space and aiming at job creation. (Ec)</p>
Planning instruments	POOCs – shoreline spatial plans	Situation plans and Allocation plans (yet to be implemented)

strategy. The ENGIZC determined that a set of indicators to evaluate its efficiency and efficacy should be defined within 6 months of its entry into force. According to Alves *et al.* (2013), a national monitoring program (M18, Table 3) was initiated. It isn't clear if an evaluation of efficiency/efficacy has been performed.

The main planning instruments for the coast are the Shoreline Spatial Plans (*Planos de Ordenamento da Orla Costeira*, POOC), created in 1993. POOC implementation started in 1998 and presently the entire coast of the mainland, except ports/harbors, is covered by one of these plans (for a recent discussion of POOC implementation, see Ferreira *et al.*, 2013). The POOCs did not propose indicators for their evaluation. Their legal regime, including their territorial scope and objectives, was revised in 2012 (cf. Table 2). POOCs have a great stated focus on environmental objectives (Table 2) and cover coastal and interior maritime waters, their seabed and margins, including marine and terrestrial protection zones from the 30 m isobath to a line 500-1000 m inland from the sea margin (50 m inland from maximum high water) (Decree-Law 159, 2012).

The National Ocean Strategy (*Estratégia Nacional para o Mar – ENM*) is the national policy for the Ocean. The ENM was first published in 2006. A new strategy was put up for public consultation in March 2013, and was approved on November 16<sup>th</sup> 2013 (DGPM, 2013). The revised National Strategy clearly reflected the focus on Blue Growth of the European Integrated Maritime Policy (IMP) and of the new proposed Directive for MSP and ICM. The EC views “Blue growth” as “an initiative to harness the untapped potential of Europe's oceans, seas and coasts for jobs and growth.” (European Commission, 2012, p.2). The ENM's proposed vision for the period 2013-2020 is that “the Portuguese Sea is a national goal/ambition whose potential will be fulfilled through the economic, social and environmental valorization of the ocean and coastal zones for the benefit of all Portuguese” (Governo de Portugal, 2013a, p. 55). The new strategy's objectives are mainly framework (*sensu* Defra, 2006), economic, and, to a lesser extent, environmental. There is also an objective of development of the knowledge base (cf. Table 2).

In terms of MSP, there was a first planning exercise for the Exclusive Economic Zone (EEZ) of the mainland – the POEM –

Table 3. ENGIZC measures (M) potentially related to ENM. MPA: Marine Protected Area; R&amp;D: Research&amp;Development.

M01	Strengthen and promote a normative framework for coastal zone (CZ) management
M03	Clarify licensing procedures of main activities valorizing specific resources carried out in the CZ
M04	Complete the constitution of a coherent and integrated network of MPAs
M06	Promote integrated management of coastal mineral resources
M08	(Re)evaluate the need of “hard” coastal engineering
M09	Incorporate in contingency plans specific risks of CZ
M12	Create a strategic reference framework for the development of economic activities with high added value aimed at valorizing marine resources
M13	Promote favourable conditions to host and develop recreational boating and sustainable tourism
M14	Promote technical publications on good practices for sustainable uses and activities in the CZ
M15	Create a R&D knowledge platform for the CZ
M16	Ensure adequate technical training adapted to the demands of ICM
M17	Promote development of cooperation mechanisms between states/regions in terms of ICM
M18	Develop a national monitoring program for coastal systems, biotic communities and environmental quality
M19	Put in place a cooperation platform involving public and private institutions to be a mechanism for the integrated interpretation of the evolution of the CZ
M20	Develop a CZ information and awareness program

which started in 2008 and underwent public consultation in 2010-2011. In 2012, a governmental dispatch determined that the studies making up the POEM would be published online but made no determination regarding the validity/implementation of the plan (Dispatch 14449, 2012).

A draft Framework Law for Maritime Spatial Planning and Management is currently being discussed in the Portuguese Parliament (Draft Law no. 133/XII, 2013). Its stated objective is the “promotion of economic, rational and efficient exploitation of marine resources and ecosystem services, ensuring compatibility and sustainability of the diverse uses and activities developed within it, considering the intergenerational responsibility in the spatial use of the national maritime space, and aiming at job creation” (ibid., p.7). It creates two new figures of planning instruments in the Portuguese legal framework: situation plans (*planos de situação*) and allocation plans (*planos de afectação*): the former should identify protection and preservation sites of the marine environment and the spatial and temporal distribution of present and potential uses and activities; the latter should allocate areas and/or volumes to different uses and activities.

Tables 3 and 4 highlight measures contained in the ENGIZC and program areas proposed in the ENM (Governo de Portugal, 2013b) that may be relevant for the integration of ICM with MSP.

### Articulating ICM with MSP in Portugal

The analysis of the emerging Portuguese policy and planning framework for ICM and MSP highlighted aspects that may constitute challenges to their effective integration:

- **Coordination between coastal and maritime policies and strategies is unclear:** The ENGIZC highlighted the need to be closely integrated with the ENM. The new ENM refers the need to establish articulation mechanisms between

Table 4. ENM Program Areas (*Áreas Programáticas*, AP) potentially related with ENGIZC measures.

ENM	ENGIZC
<b>Governance</b>	
AP1 Administration	M01
AP2 Strategic thinking and action	M12
AP3 Education, Science and Technology	M20
AP4 Identity and culture	-
AP5 Protection and Safeguard	M18
<b>Natural resources – system</b>	
AP1 Ocean (environmental and anthropogenic pressures on fisheries; indicators; MPAs)	M4
AP2 Atmosphere (research)	M18
AP3 Integrated system (observation, risk evaluation, impact mitigation, preservation)	M18
<b>Natural resources – living resources</b>	
AP1 Fisheries and industry (fish. related products)	
AP2 Aquaculture (zoning)	M03
AP3 Marine biotechnology	
<b>Natural resources – non-living resources</b>	
AP1 Mineral and marine resources (exploitation)	M06,09, 12
AP2 Marine energy resources	
<b>Other uses and activities</b>	
AP1 Ports, transportation and logistics	M09
AP2 Recreation, sports and tourism (recreational boating)	M13
AP3 Ship building and repair	M09
AP4 Maritime works (coastal engineering): research, exploitation & preservation	M08

coastal and ocean management (and MSP) (Governo de Portugal, 2013b), but makes no reference to the ENGIZC. References to the articulation with ICM relate mainly to spatial planning and to the national action plan to protect and valorize the littoral (APA, 2012). Although, as in the previous version (Carneiro, 2007), the ENM “appears to attempt to establish a bridge between the ocean policy and the ICZM strategy (ibid., 431), an unclear coordination between them may lead either to duplicated efforts or to lack of implementation of certain program areas.

- **Unclear articulation between spatial plans for coastal and maritime zones:** Although there are still no plans in place for the maritime space, there will be territorial overlap between plans for the coastal zone (POOCs) and for the areas open for maritime spatial planning and management (cf. Figure 1). POOCs were created 20 years ago and they have at least 15 years of implementation. Situation and allocation plans for MSP are new planning figures, and it is still unclear what they will encompass, how they will work and how they will be articulated with plans for the coastal environment. Under existing national legislation, POOCs are spatial plans of national relevance whose articulation with all other spatial plans for the terrestrial territory is defined in a national framework law for spatial planning and urbanism. Such a law is currently also under revision. The proposed new law states that, when necessary, plans for the terrestrial and the maritime environment shall be articulated and be made compatible “in accordance with the law” (Draft Law no 183/XII, 2013, p.38). This wording is very vague and does not explain how this articulation will be achieved; including if there will be prevalence of one type of plans over the other (hierarchical relationship).

- **Institutional articulation is unclear:** Up until recently, there was one ministry responsible for coastal and ocean policy and planning in Portugal – the Ministry of Agriculture, Sea, Environment and Spatial Planning (*Ministério da Agricultura, Mar, Ambiente e Ordenamento do Território*, MAMAOT,). In 2013, a government reshuffle divided it in two: the Ministry of Agriculture and Sea (*Ministério da Agricultura e do Mar*, MAM) and the Ministry of Environment, Spatial Planning and Energy (*Ministério do Ambiente, do Ordenamento do Território e da Energia*, MAOTE). MAM, through the national Directorate-General For Maritime Policy (*Direção-Geral de Política do Mar*, DGPM) has responsibility over maritime spatial planning. The ministry of the Environment, through the National Environmental Agency (*Agência Portuguesa do Ambiente*, APA) has jurisdiction over coastal zone planning and management. Although such a split does not make it impossible for the two agencies to work together, additional effort will be required to coordinate and communicate at a technical level.
- **Mismatched objectives:** In order to promote effective articulation of ICM with MSP, relevant policies should have matching or shared objectives. Whereas the national strategy for ICZM and the national plans for spatial planning of the coastal zone prioritize environmental concerns, these seem to be secondary in the ENM and non-existent in the objective of the draft law for MSP and management, which is clearly oriented towards an economic objective. In this instance, how can both policies be matched?
- **Indicators to evaluate the environmental effects of policies and plans for the coast and ocean are not defined:** Indicators are the link between objectives and action in management (IOC, 2006; Day, 2008; Ehler and Douvère, 2009; Douvère and Ehler, 2011). To understand policy/plan performance, i.e., what is happening to the environment and/or natural resources as a result of the implementation of plans and policies, it is vital to evaluate their effects, namely, through the use of environmental indicators (Johnson, 2008). As mentioned above, it is unclear if an evaluation of the ENGIZC has been performed. The new ENM proposes to address this by developing a monitoring framework, and a corresponding set of appropriate indicators.
- **Unclear articulation between management measures relevant for integration of ICM and MSP:** As Alves et al. (2013) point out, Portuguese ICM and MSP “needs strict articulation and balancing of coastal and marine management tools” (p.1032). Although there is a parallel between measures proposed in the ENGIZC and in the ENM (cf. Tables 3 and 4), that does not ensure that their implementation will be articulated.

As mentioned above, this analysis is based on the Portuguese national policies and legislation available as of November 2013. While some were just finalized, others are undergoing discussion in the Portuguese Parliament. It will be interesting to analyze, in the coming years, if and how, despite these perceived mismatches, their implementation and articulation will take place.

## CHALLENGES IN MATCHING ICM AND MSP

In the previous section we highlighted the main aspects of the Portuguese political and planning framework for ICM and MSP, and how, if not carefully approached, they may impair the necessary articulation between coastal and maritime planning and

management. Tackling the abovementioned mismatches is a first step towards such integration.

Throughout the world, there are already some noteworthy examples. For instance, the USA has adopted a Federal (national) policy of Coastal and Marine Spatial Planning (CMSP). New marine spatial plans (recently developed or underway), usually encompassing the territorial seas of each State, are being merged with existing (sometimes decades old) statewide coastal zone management programs, and are being managed (or at least centralized) by the same agencies (e.g. OCMP, 2013; RICRMC, 2010). Such practice contributes to promote effective integration of data, maps, etc., and also to coherence between goals, objectives, indicators and management actions. It must be highlighted that States have only jurisdiction over their territorial sea, which in most cases, extends to 3 nautical miles. Consistency of planning options and management actions between State and Federal waters is ensured by a tool called ‘Federal consistency’.

Although approaches vary, coastal nations throughout the world face similar challenges in effectively integrating the planning and management of these two very different environments. Some main challenges include, in no particular order:

- **Integrating MSP and ICM requires flexibility and novel approaches** as it brings together different technical languages/expertise, including an adaptation of traditional planning practices (coastal planning being usually tilted towards its terrestrial component and being different from planning for a 3-D fluid/dynamic environment), merging of different work scales, etc.
- **People and institutions resist change.** Integrating coastal and maritime planning requires bringing together and articulating different governance structures/jurisdictions, sometimes restructuring existing institutions or creating new ones, and may bring about shifts (often perceived as losses) in traditional power balances. Because integration of ICM and MSP is also required across national borders, this challenge is expanded.
- **Public participation and stakeholder involvement**, which are key both for MSP and for integrated coastal planning and management processes, are often still considered as time-consuming and expendable parts of the planning process. However, they are unique venues to highlight issues or concerns that would not otherwise stand out, as they are often not organized in stakeholder groups, such as non-consumptive recreational uses (e.g. surfing, beachgoing or seascape aesthetics).
- **Different languages and terminologies:** the adoption of a systemic approach implies i.a., the breaking of a number of linguistic barriers within and among institutions and practitioners. Such barriers may be caused by different backgrounds, training, and experiences. These hurdles are twofold: not only established terms (e.g. “sustainability”) may have different meanings for different people in the same team, potentially undermining discussions, but the plethora of terms and acronyms related to the field (e.g. ICM, ICZM, CMSP, ICOM, MSP) may give an erroneous impression of distinct approaches and methodologies when, in fact, they may be different names for the same thing.
- **Adopting a systemic vs. a sectoral approach.** Although this should already be the focus of ICM and MSP, it is still difficult to implement in practice, because of the complexity of the issues at stake. This comprehends tackling the mismatches mentioned in this and previous sections and more. One critical aspect is considering human activities taking place on land and how they affect coastal and marine

environments (e.g. through drainage basins and atmospheric pathways), and integrating them in planning and management of coastal and maritime spaces.

- **Finding appropriate indicators.** Coming up with relevant indicator sets for the monitoring and evaluation of overlapping coastal and marine policies and plans poses specific challenges, such as finding common management objectives, establishing links between activities (pressures) and impacts, selecting common priority indicators to monitor, and defining comparable methodologies to allow results to be adequately compared. In this respect, the European Environment Agency list of indicators for coasts and seas (EEA, 2013), could be an interesting starting point for the definition of such a set of integrated indicators.

Effectively integrating ICM and MSP is a new challenge for most coastal nations and a paramount step towards achieving sustainable human development. From the rivers to the sea, policies, management plans, institutions, and society at large must work together to tackle the number and magnitude of the challenges involved. Understanding what they are and looking for appropriate ways to approach them should be every coastal nation's priority in the coming years.

As one of Europe's (and the world's) largest maritime nations, Portugal has a very important role to play in paving the way and setting an example for other coastal nations worldwide. The Portuguese experience in the last 20 years with integrating coastal and marine planning and management, has been rich in "enthusiastic" launches of new initiatives, which, despite "good intentions and commitment of many professionals", were then "undermined by the lack of continuing political support" (Carneiro, 2007, p. 431). Hopefully, this will no longer be the case. The mismatches highlighted in this analysis provide pointers to aspects that, if appropriately tackled, can contribute to a more effective integration of ICM and MSP in Portugal and in other coastal nations.

## ACKNOWLEDGEMENTS

All translations from Portuguese are from the first author. The first author has a Ph.D. grant from the Foundation for Science and Technology – FCT (*Fundação para a Ciência e a Tecnologia*: SFRH/BD/88549/2012). This paper presents research results of the Strategic Project of e-GEO (PEst-OE/SADG/UI0161/2011) Research Centre for Geography and Regional Planning funded by the Portuguese State Budget through FCT. The authors are grateful to the anonymous reviewer whose comments helped to improve the quality of this manuscript.

## LITERATURE CITED

- Alves, F.L., Sousa, L.P., Almodovar, M. and Phillips, M.R., 2013. Integrated Coastal Zone Management (ICZM): a review of progress in Portuguese implementation. *Reg. Environ. Change*, 13, 1031-1042.
- APA, 2012. Plano de Ação de Proteção e Valorização do Litoral 2012-2015. Agência Portuguesa do Ambiente. 86p.
- Carneiro, G., 2007. The parallel evolution of ocean and coastal management policies in Portugal. *Marine Policy*, 31, 421-433.
- Day, J., 2008. The need and practice of monitoring, evaluating and adapting marine planning and management – lessons from the Great Barrier Reef. *Marine Policy*, 31, 823-831.
- Decree-Law 159. 2012. Decreto-Lei n.º 159/2012, de 24 de Julho. Diário da República, 1ª série, 142, 3881-3889. Lisbon: INCM.
- DEFRA., 2006. Shoreline management plan guidance. Volume 1: Aims and requirements. Department for Environment, Food and Rural Affairs. 48p.
- DGPM, 2013. Estratégia Nacional para o Mar 2013-2020. Online at <http://www.dgpm.gov.pt/Pages/ENM.aspx>. Accessed 29 October 2013.
- Dispatch 14449. 2012. Despacho n.º 14449/2012, de 8 de Novembro. Diário da República, 2ª série, n.º 216, 36606. Lisbon: INCM.
- Douvere, F. and Ehler, C.N., 2011. The importance of monitoring and evaluation in adaptive maritime spatial planning. *Journal of Coastal Conservation*, 15, 305-311.
- Draft Law no. 133/XII. 2013. Proposta de Lei n.º133/XII. Online at: <http://www.parlamento.pt/ActividadeParlamentar/Paginas/DetalheIniciativa.aspx?BID=37600>. Accessed 29 October 2013.
- Draft Law no. 183/XII. 2013. Proposta de Lei n.º 183/XII. Online at: <http://www.parlamento.pt/ActividadeParlamentar/Paginas/DetalheIniciativa.aspx?BID=38024>. Accessed 20 November 2013.
- EEA. 2013. Indicators. Online at [http://www.eea.europa.eu/data-and-maps/indicators#c5=coast\\_sea&c7=all&c0=10&b\\_start=0](http://www.eea.europa.eu/data-and-maps/indicators#c5=coast_sea&c7=all&c0=10&b_start=0). Accessed, 20 November 2013.
- Ehler, C. and Douvere, F., 2009. Marine Spatial Planning: a step-by-step approach toward ecosystem-based management. *IOC Manual and Guides No. 53, ICAM Dossier No. 6*. Paris: UNESCO.
- European Commission. 2012. Blue Growth: opportunities for marine and maritime sustainable growth. COM(2012) 494 final. 12p.
- European Commission. 2013. Proposal for a Directive of the European Parliament and of the Council establishing a framework for MSP and ICM. COM(2013) 133 final. Brussels, 12.3.2013.
- Ferreira, M.A., Williams, A.T. and Silva C.P., 2013. Portuguese shoreline spatial plans: integrating lessons from the past into second generation plans. *Coastal Management*, 41:1, 1-18
- Governo de Portugal. 2013a. Estratégia Nacional para o Mar 2013-2020. 73 p. Online at <http://www.dgpm.gov.pt/Documentos/ENM.aspx>. Accessed 10 April 2013.
- Governo de Portugal. 2013b. Estratégia Nacional para o Mar 2013-2020: Anexo B – Apêndice 1 – Adenda A: Índice dos Programas de Ação. 427p. Online at <http://www.dgpm.gov.pt/Documents/ENM.aspx>. Accessed 10 April 2013.
- IOC. 2006. A Handbook for Measuring the Progress and Outcomes of Integrated Coastal and Ocean Management. *IOC Manuals and Guides, 46; ICAM Dossier, 2*. Paris, UNESCO.
- Johnson, D., 2008. Environmental indicators: their utility in meeting the OSPAR Convention's regulatory needs. *ICES Journal of Marine Science*, 65, 1387–1391.
- MAOT. 2011. POEM Volume 3: Relatório Ambiental. Online at [http://www.dgpm.gov.pt/Documents/POEM\\_Volume3\\_RelatorioAmbiental.pdf](http://www.dgpm.gov.pt/Documents/POEM_Volume3_RelatorioAmbiental.pdf); Accessed 20-11-2013.
- Merriam-Webster Dictionary, 2013. Online at <http://www.merriam-webster.com/dictionary/valorize>. Accessed 20 November 2013.
- OCMP. 2013. Oregon's Territorial Sea Plan TOC. Online at: [http://www.oregon.gov/LCD/OCMP/Pages/Ocean\\_TSP.aspx](http://www.oregon.gov/LCD/OCMP/Pages/Ocean_TSP.aspx). Accessed 20 November 2013.
- Resolution 82. 2009. Resolução do Conselho de Ministros no. 82/2009, de 8 de Setembro. Diário da República, I série, 6056–6088. Lisbon: Imprensa Nacional Casa da Moeda.
- RICRMC. 2010. Rhode Island Ocean SAMP. Online at [http://seagrant.gso.uri.edu/oceansamp/pdf/samp\\_crmc\\_revised/RI\\_Ocean\\_SAMP.pdf](http://seagrant.gso.uri.edu/oceansamp/pdf/samp_crmc_revised/RI_Ocean_SAMP.pdf). Accessed, 20 November 2013.
- Sea Around Us Project. 2013. EEZs. Sea Around Us Project: Fisheries, Ecosystems and Biodiversity. The Pew Charitable Trusts. Online at <http://www.seaaroundus.org/eez/>. Accessed September 30 2013.

## West African EBSAs: Building capacity for future protection

David Johnson<sup>†</sup>, Jihyun Lee<sup>‡</sup>, Abou Bamba<sup>∞</sup>, Charlotte Karibuhoye<sup>#</sup>

<sup>†</sup> Seascope Consultants Ltd  
Belbins Valley, Belbins  
Romsey, SO51 0PE, UK  
david.johnson@seascopeconsultants.co.uk

<sup>‡</sup> Secretariat of the Convention of  
Biological Diversity  
413 St Jacques Street, suite 800  
UNEP, Montreal, QC H2Y 1N9  
jihyun.lee@cbd.int

<sup>∞</sup> UNEP Abidjan Convention Secretariat  
01 PO Box 1747  
Abidjan, Cote d'Ivoire  
abou.bamba@unep.org



[www.cerf-jcr.org](http://www.cerf-jcr.org)

<sup>#</sup> WCPA Vice-Chair  
Central and Western Africa  
Foundation Internationale du Banc d'Arguin  
Mamelles, Rue 210km, Villa F46  
BP24939, Ouakam-Dakar, Senegal  
[karibuhoye@lafiba.org](mailto:karibuhoye@lafiba.org)



[www.JCRonline.org](http://www.JCRonline.org)

### ABSTRACT

Johnson, D., Lee, J., Bamba, A., Karibuhoye, C. 2014. West African EBSAs: Building capacity for future protection. In: Green, A.N. and Cooper, J.A.G. (eds.), *Proceedings 13<sup>th</sup> International Coastal Symposium* (Durban, South Africa), *Journal of Coastal Research*, Special Issue No. 70, pp. 502-506, ISSN 0749-0208.

The Convention on Biological Diversity (CBD)'s commitment to describe marine Ecologically or Biologically Significant Areas (EBSAs) through the organisation of a series of regional workshops has resulted in the collation and synthesis of relevant physical and biological datasets. Groups of typically 30-50 experts have pooled knowledge, with the support of technical facilitators, to undertake these intensive scientific and technical exercises in a growing number of marine regions around the world. The results, which are then subject to consideration by the Conference of the Parties to the CBD, describe areas meeting scientific criteria for EBSAs that may require enhanced conservation and management measures. For the South-East Atlantic (West Africa), such a regional workshop took place in Namibia 8-1 April 2013 and, subject to consideration by CBD scientific subsidiary body, the Conference of the Parties to the CBD should eventually be presented with a suite of descriptions of 45 areas meeting EBSA criteria in this region in October 2014 at its 12th meeting. This paper explains the processes that took place both before and after the West African Workshop. Firstly, the Sustainable Ocean Initiative (SOI) supported a first ever regional capacity building Workshop to facilitate the implementation of efforts towards Aichi Target 6 (sustainable fisheries) and 11 (marine protected areas), and to make connections between these targets and the EBSA process. This successful effort, held in Senegal in February 2013, prepared the ground for the subsequent EBSA Workshop. Experts became familiar with available data, with the challenges to be met and had an opportunity to exchange experiences. Sharing scientific information related to descriptions of areas meeting EBSA criteria toward achieving the Strategic Plan for Biodiversity 2011-2020 and Aichi Biodiversity Targets requires sustained effort and collaboration among various partners and experts. The Global Ocean Biodiversity Initiative (GOBI) brings together partners who can contribute skills and research results to inform this process. Areas meeting EBSA criteria in the South-East Atlantic region reflect transboundary connections – from river to sea, from inshore to offshore and deep-sea ecosystems. Ultimately their sustainable use should involve spatial area management tools including, where appropriate, an ecosystem-based approach to fisheries and networks of marine protected areas. The work of selected countries since the EBSA Workshop illustrates possibilities.

**ADDITIONAL INDEX WORDS:** *CBD, SOI, Aichi Biodiversity Targets, GOBI, marine spatial planning*

### INTRODUCTION

The Convention on Biological Diversity (CBD), at its tenth meeting (COP-10), adopted the Strategic Plan for Biodiversity 2011-2020, with its Aichi Biodiversity Targets. The mission of the Strategic Plan is to take effective and urgent action to halt the loss of biodiversity in order to ensure that by 2020 ecosystems are resilient and continue to provide essential services, thereby securing the planet's variety of life, and contributing to human wellbeing and poverty eradication.

CBD COP-10 (Decision X/29, para 36) also set place a series of regional workshops to facilitate the description of ecologically or biologically significant areas (EBSAs) through the application of scientific criteria in Annex 1 of Decision IX/20 (see Table 1). Dunn et al. (in press) review the origins, development

and current status of EBSAs. Outcomes of the first two CBD convened regional Workshops, in the South West Pacific hosted by Fiji in November 2011 and the Wider Caribbean and Western Mid-Atlantic hosted by Brazil in February 2012, were presented to the CBD Subsidiary Body on Scientific, Technical and Technological Advice (SBSTTA) at its 17th meeting and CBD COP-11. At both meetings African nations expressed a strong interest in Regional EBSA Workshops for Africa. A Regional EBSA Workshop for the Southern Indian Ocean was held in July 2012, hosted by Mauritius and another for the South-Eastern Atlantic, the focus of this paper, in April 2013.

West Africa hosts a diverse and extensive range of marine ecosystems spanning three of the world's 12 marine realms (Temperate North Atlantic, Tropical Atlantic, Temperate South Atlantic). At its heart is one of the world's most diverse and economically important fishing zones upon which large coastal

Table 1. CBD Ecologically or Biologically Significant Area (EBSA) Criteria

Criterion	Interpretation
1 Uniqueness or rarity	Areas contain either (i) unique ("the only one of its kind"), rare (occurs only in a few locations) or endemic species, populations or communities, and/or (ii) unique, rare or distinct, habitats or ecosystems; and/or (iii) unique or unusual geomorphological or oceanographic features
2 Special importance for life-history stages of species	Areas that are required for a population to survive and thrive
3 Importance for threatened, endangered or declining species and/or habitats	Area containing significant assemblages or is critical for the survival and recovery of endangered, threatened, declining species and/or habitats
4 Vulnerability, fragility, sensitivity, or slow recovery	Areas that contain a relatively high proportion of sensitive habitats, biotopes or species that are functionally fragile (highly susceptible to degradation or depletion by human activity or by natural events) or with slow recovery
5 Biological productivity	Area containing species, populations or communities with comparatively higher natural biological productivity
6 Biological diversity	Area contains comparatively higher diversity of ecosystems, habitats, communities, or species, or has higher genetic diversity
7 Naturalness	Area with a comparatively higher degree of naturalness as a result of the lack of or low level of human-induced disturbance or degradation

populations rely heavily for both food and foreign Exchange. Sustainable development is at the core of the African Union's '2050: Africa's Integrated Maritime Strategy' ([www.au.int/maritime](http://www.au.int/maritime)), and the continent is mindful of implications of climate change (Arusha Declaration on Africa's Post Rio+20 Strategy for Sustainable Development). Such commitments build upon large scale, long-term, multidisciplinary and cooperative scientific research and data gathering projects initiated to understand West African marine ecosystems. Both bilateral and multi-lateral subregional projects have a long track record from the Coastal Upwelling Ecosystems Analysis Project of the 1970s and 1980s, to the current FAO Fridtjoff Nansen Project and three large marine ecosystem programmes (the Canary Current, Guinea Current and Benguela Current LMEs).

This paper explains how a suite of EBSA descriptions for West Africa were derived and provides examples of how the information gathered is informing initiatives intending to secure better protection of biodiversity assets against the adverse effects of human activities.

### THE SOI SENEGAL WORKSHOP

The Sustainable Ocean Initiative (SOI) was conceived in the margins of CBD COP-10, through the leadership of Japan, COP-10 Presidency. SOI is being evolved as a global platform to build partnerships and enhance capacity to achieve Aichi Biodiversity Targets related to marine and coastal biodiversity in a holistic manner (in particular Targets 6 and 11; see Table 2). The SOI Capacity Building Workshop for West Africa, hosted by the Government of Senegal, took place in Dakar from 4-8 February 2013. The emphasis of the Workshop was on exchange of information and experiences, active learning of skills and tools, and building regional level partnership for continuous information sharing. There was an emphasis on technical tools, particularly the use of Geographic Information Systems (GIS) for compiling data and use of the Ocean Biodiversity Information System (OBIS) database, to compile, for example, Kernel Density estimations to identify important areas for specific species.

Achieving Aichi Target 6 (sustainable fisheries) requires integration of objectives and policies set by different sectors and the costs of inaction and correcting action, together with significant costs and benefits of available solutions.

Table 2. Summary of Aichi targets 6 and 11

**Aichi Target 6:** *By 2020, all fish and invertebrate stocks and aquatic plants are managed and harvested sustainably, legally and applying ecosystem based approaches, so that overfishing is avoided, recovery plans and measures are in place for all depleted species, fisheries have no significant adverse impacts on threatened species and vulnerable ecosystems and the impacts of fisheries on stocks, species and ecosystems are within safe ecological limits;*

**Aichi Target 11:** *By 2020, at least 17 per cent of terrestrial and inland water areas, and 10 per cent of coastal and marine areas, especially areas of particular importance for biodiversity and ecosystem services, are conserved through effectively and equitably managed, ecologically representative and well-connected systems of protected areas and other effective area-based conservation measures, and integrated into the wider landscapes and seascapes.*

The Ecosystem Approach to Fisheries is a sectoral application of the Ecosystem Approach, which demands societal responsibility, interdisciplinary considerations based on science and compatibility of measures. In fisheries this is made more difficult by complex feedback loops, complicating variables (such as genetics) and natural environmental variations.

Achieving Aichi Target 11 (marine protected areas) emphasizes the protection of areas of 'particular importance for biodiversity and ecosystem services'. Establishing that MPA stops the cycle of genetic truncation that other fisheries management measures cannot achieve, allowing normal genetic populations to flourish. The MPA creates a buffer or 'insurance' policy, albeit one that can also cause social and/or economic hardship. Therefore good planning is required to select the right places that balance ecological and economic values. Network design, drawing upon many criteria, aims to bring together complementary sites. A representative selection of presentations by Workshop participants illustrated region-specific challenges and opportunities. Even in South Africa, where the national MPA network is relatively advanced, the offshore area is significantly under-represented. Some West African nations have yet to establish any MPAs and



the existing network of MPAs (RAMPAO) covers mostly coastal sites. Protocols and legislation are at different stages of updating. A variety of scientific programmes and protection measures have been applied and stakeholders have been involved at different levels. Several countries were concerned about how resources can be mobilised for marine biodiversity conservation.

The Workshop also explored the data needed to describe EBSAs. This is best illustrated with reference to three key examples from the Indian Ocean which were used to demonstrate the approaches and data that a previous Workshop had used as follows:

- Coral Seamount: a large seamount in the southern central Indian Ocean that has benefitted from both scientific surveys and mapping by the Southern Indian Ocean Deep-sea Fishing Association. Fine-scale backscatter data was used, along with information from scientific surveys to delimit the area, which is also an area closed to fishing;
- Agulhas Front: a large highly productive feature extending from southern Africa across the Indian Ocean. This is an area of high primary productivity that provides important habitat for breeding colonies of seabirds, southern right whales and Bluefin tuna. It is the only productivity feature of its kind in the Indian Ocean;
- Protea Banks and sardine run: a unique deep reef feature that provides habitat for endemic species and four shelf incising submarine canyons. It is a key migration route for several species, notably the sardine *Sardinops sagax*. The sardines are followed by large numbers of sharks, cetaceans and seabirds.

The Workshop sought to identify synergies between the Aichi Biodiversity Targets and the EBSA process. This included expert opinion on the use of area-based planning tools such as Marxan and cost-benefit of fisheries closures. There was also a focus on integration – between shared goals and objectives, building in compliance, and achieving flexibility to adapt to new information or situations (e.g. climate change related factors). Ultimately

application of the EBSA criteria is a scientific and technical exercise and areas identified as such by CBD COP may require enhanced conservation and management measures selected by States and competent intergovernmental organisations.

### SOUTH-EAST ATLANTIC EBSA WORKSHOP

The South-East Atlantic Regional Workshop to Facilitate the Description of Ecologically or Biologically Significant Marine Areas, in collaboration with the Convention for Cooperation in the Protection, Management and Development of the Marine and Coastal Environment of the Atlantic Coast of the West, Central and Southern Africa Region (Abidjan Convention), the Food and Agriculture Organisation of the United Nations (FAO) and the South East Atlantic Fisheries Organisation (SEAFO) was hosted by the Government of Namibia and took place in Swakopmund from 8-12 April 2013. Experts participated from 17 States and 16 Inter-governmental and non-governmental organisations. It was acknowledged that the SOI Dakar Workshop had helped by providing a necessary training and facilitating compilation of scientific information through networking. The close collaboration between CBD's work on EBSAs and FAO's work on vulnerable marine ecosystems was also noted.

The biogeography of the South-East Atlantic is governed by three main current regimes (*viz.* Canary, Guinea and Benguela current systems) and gyre dynamics. Available descriptions of the biogeography covering the entire pelagic and benthic zones were therefore essential context for the EBSA description discussions. EBSAs must also be described on the basis of best available scientific knowledge and cannot be described on the basis of modeling results alone. Whilst all parts of the ocean support marine biodiversity, EBSA criteria are applied in a relative context in order to call attention to areas that are particularly rich in the properties associated with one or more criteria. Four types of areas were identified as possibly meeting one or more criteria (see Table 3).

In general, the physical data layers provided by the technical team for open ocean areas were much more comprehensive than the biological layers. The Workshop also considered other sources of information from published literature, but the amount and

Table 3. Guidance on types of area

<b>Spatially stable features, whose positions are known and individually resolved on the maps</b>
Examples include individual seamounts and feeding areas for sharks and seabirds. Such areas do not have to be used all year round, nor does all the area have to be used every year. However, all the area within the corresponding map polygon has the feature(s) that are described in the template as meeting the criterion being considered.
<b>Spatially stable features, whose individual positions are known but a number of individual cases are being grouped</b>
Examples include a group of coastal areas, seamounts or seabird breeding sites where the location of each is known but a single polygon on the map and corresponding template encompasses all the members of the group. The grouping may be done because there may be insufficient knowledge to evaluate each separately or the information is basically the same for all members of the group, so no message can be applied to all group members.
<b>Spatially stable features, whose individual positions are not known</b>
Examples include areas where coral or sponge concentrations are likely based on for example modelling of suitable habitats, but information is insufficient to specify locations of each individual concentration. Each such area may be represented by a single map polygon and template, but the entire area inside the polygon is not to be interpreted as filled with the feature(s) meeting the criteria. Narrative about these areas should stress the importance of getting better information on the spatial distribution of these features.
<b>Features that are inherently not spatially fixed</b>
An example is a frontal transition zone. The position of this front moves seasonally and among years. The map polygon for such a feature should include the full range occupied by the front (or other feature) during a typical year. The text for the description should also make very clear that at any given time, the ecological importance usually is highest wherever the feature is located at that time and often decreases as distance from the feature increases. It may even be the case that at any given time some parts of the total area contained in the polygon are ecologically little different from areas outside the polygon.

quality of information on biodiversity and ecology for this area is sparse. The data, combined with expert knowledge, were used to describe those areas meeting EBSA criteria, and groups used prominent geomorphological and hydrographical features (e.g. frontal zones) that were likely to support biota and create significant ecological processes. Relatively shallow areas comprising seamounts and seamount chains, and near-surface hydrographic features such as major convergence zones clearly met EBSA criteria. Deep-sea habitats (i.e. pelagic and benthic habitats deeper than the photic zone) were more difficult to describe based on current information. Ecosystem linkages between shallow and deep waters are however very significant and were recognized in the description of areas meeting EBSA criteria. The workshop noted that the Mid Atlantic Ridge was a prominent feature in the South East Atlantic but felt reluctant to describe the entire ridge as an area meeting EBSA criteria without more information. The workshop noted that there are also significant additional data holdings in both countries represented at the Workshop and those unable to attend, which would be useful in the future EBSA description. The official report of this Workshop has yet to be finalized and the 45 EBSA descriptions compiled by the South-East Atlantic experts will be subject to consideration by SBSTTA 18 and CBD COP-12. Prior to these CBD meetings the Abidjan Convention COP-11 to be held from 17 to 21 March 2014 in Cape Town, South Africa, will also consider a draft decision on EBSAs to be approved by the 22 African ministers in charge of marine and coastal issues of the South-East Atlantic.

### **ROLE OF THE GLOBAL OCEAN BIODIVERSITY INITIATIVE (GOBI)**

Supporting the EBSA process is an international partnership advancing the scientific basis for conserving biological diversity in the deep seas and open oceans. It aims to help countries, as well as regional and global organisations, to use and develop data, tools and methodologies to identify EBSAs with an initial focus on the high seas and areas beyond national jurisdiction.

GOBI began in 2008 and has been supported to date financially by the German Federal Agency for Nature Conservation (BfN). Since then Partner organisations have been involved with all the Regional EBSA Workshops and have actively promoted the CBD EBSA process in other international forums. The work under this initiative ultimately aims to help countries meet the goals adopted under the CBD, United Nations General Assembly resolutions, and the three Earth Summits (Rio 1992, Johannesburg 2002; Rio 2012). These global goals relate to reducing the rate of biodiversity loss, applying ecosystem approaches, determining EBSAs and VMEs as well as establishing representative marine protected area networks.

Of particular note has been the support provided to each of the Regional EBSA Workshops by technical teams from the Commonwealth Scientific and Industrial Research Organisation (CSIRO Australia) and Duke University (USA). Both organisations are GOBI Partners and they have facilitated data provision to southern and northern hemisphere Regional Workshops respectively. As set out earlier, the data to support EBSA descriptions is drawn from a wide range of data types, ranging from global data sets that are readily available to national and local scale data sets. Regional organisations such as Regional Fisheries Management Organisations, Large Marine Ecosystems Projects and Regional Seas Partnerships are also all important sources of data.

Several GOBI Partners are also data providers, either in terms of biological data or physical data. Examples of the former are survey data from individual researchers, dedicated organisations

such as BirdLife International or data repositories such as OBIS. Other initiatives associated with the Census of Marine Life, such as CenSeam, are also important. Physical data is generally publically available and derived from large-scale global and regional datasets, comprising either information on the seafloor (e.g. seamount, and vent locations, geology and canyons) or the upper pelagic biome (e.g. global climatologies, satellite observations and derived oceanic data layers). GOBI Partners have been instrumental in overcoming data sensitivities, which include data availability, ownership and sharing, and problems of combining datasets for trans-boundary features.

GOBI has also set out practical illustrations relating to species, habitats and oceanographic features for each of the seven CBD scientific criteria, as well as examples of various scientific methods and techniques relevant to each criterion ([www.gobi.org](http://www.gobi.org)).

### **OPPORTUNITIES TO APPLY EBSA DESCRIPTIONS**

Whilst describing and identifying EBSAs for all marine Regions remains a short-term priority, it is clear that EBSA descriptions make explicit marine physical and biological information previously often held by diverse scientific institutions and individual experts. In addition, whilst the EBSA process is not perfect, it stands as an extremely positive initiative that has gained considerable momentum in a short space of time. It is likely that EBSA descriptions will be strengthened and added to in future as a result of further scrutiny and as new data becomes available. Furthermore, several commentators have identified the potential of large scale marine spatial planning (for example, Ehler and Douvère, 2009; Agardy *et al.*, 2011) and some consider that EBSAs provide the context for such an exercise (Weaver and Johnson, 2012). Two examples serve to illustrate how the data compiled for the South-East Atlantic EBSA Workshop is helping to inform biodiversity protection actions.

Firstly, UNESCO's World Heritage Marine Programme has commissioned a study to consider the feasibility of a Particularly Sensitive Sea Area (PSSA) for the Banc d'Arguin and an adjacent sea area in Mauritania. The Banc d'Arguin National Park extends a maximum of 60km into the shallow sea and 35km inland into the Sahara. However, the ecological connections extend offshore into the Mauritanian Exclusive Economic Zone and beyond. Most specifically this includes the Cap Blanc upwelling system, an extensive area that straddles the 200nm limit. The Canary Current group at the South-East Atlantic EBSA Workshop recognised the ecological and biological significance of a larger area. For the upwelling area sea surface temperature measurements clearly show a divide between relatively cool, upwelled water across the continental shelf and upper slope region compared with deeper warmer Waters (Wynn and Kniefelkamp, 2004). The area is at the junction between Afrotropical and Palaearctic biogeographic realms and hosts the largest concentration of wintering waders in the world. PSSA qualification criteria, as promulgated by the International Maritime Organisation, include ecological criteria closely reflecting (although not matching directly) the EBSA selection criteria. Thus making use of the same justification data has distinct advantages and the EBSA Workshop provides a rich source of relevant information. This feasibility study is ongoing and results will be available in 2014. Furthermore, three additional EBSAs that were described during the Namibia workshop have been taken into consideration in the ongoing drafting process of the national MPA strategy in Mauritania.

The second example relates to the Benguela Current Large Marine Ecosystem (BCLME), which stretches along the coast of South Africa, Namibia and Angola and is considered a global

biodiversity hotspot. Although the countries concerned are to a large extent dependent on their natural marine resources, conservation and sustainable use of biodiversity and its sustainable management are arguably insufficiently well anchored in national policies. Regionally unbalanced management capacities as well as human resources at all levels have an additional adverse effect. From 2014-2019 the Benguela Current Commission (BCC) will therefore partner with the German Implementing Agency for Development Cooperation (GIZ) to strengthen the region's capacities for enhanced sustainable management of the BCLME's marine biodiversity and natural resources. This project, to be funded by the German Federal Ministry for the Environment, Nature Conservation and Nuclear Safety (BMU), seeks to support the BCC and its member states through refining the existing EBSA descriptions, potential descriptions of additional EBSAs and implementation of appropriate and effective management and governance measures for their conservation and sustainable use. In addition, the project aims at implementing and institutionalising marine spatial planning. As such, the project will take the EBSAs from maps to action (Gunnar Finke, pers com. 2013) and may provide a model for the other two West African LMEs.

### ACKNOWLEDGEMENTS

The authors wish to recognise colleagues who contributed to both the SOI Capacity Building Workshop and the South-East Atlantic EBSA Workshop whose views we have reflected in this paper by drawing upon draft reports of both meetings.

### LITERATURE CITED

- Agardy, T., Notarbartolo di Sciara, N. and Christie, P., 2011. Mind the gap: Addressing the shortcomings of marine protected areas through large scale marine spatial planning. *Marine Policy* 35 (2011): 226-232
- Dunn, D., Ardron, J., Bax, N., Bernal, P., Cleary, J., Cresswell, I., Donnell, B., Dunstan, P., Gjerde, K., Johnson, D., Kaschner, K., Lascelles, B., Rice, J., von Nordheim, H., Wood, L., and Halpin, P.N., In press. The Convention on Biological Diversity's Ecologically or Biologically Significant Areas: origins, development, and current status
- Ehler, C. and Douvère, F., 2009. *Marine Spatial Planning: a step-by-step approach toward ecosystem-based management*. Intergovernmental Oceanographic Commission and Man and the Biosphere Programme. IOC Manual and Guides No. 53, ICAM Dossier No. 6. Paris: UNESCO.
- Weaver, P. and Johnson, D., 2012 Think big for Marine Conservation. 22 March, Vol. 483, *Nature* 399.
- Wynn, R.B. and Knefelkamp, B., 2004 Seabird distribution and oceanic upwelling off northwest Africa. *British Birds* 97 (July): 323-325

## An interactive WebGIS observatory platform for enhanced support of integrated coastal management

A. Oliveira†, G. Jesus†, J.L. Gomes†, J. Rogeiro†, A. Azevedo, M. Rodrigues†, A.B. Fortunato†, J.M. Dias‡, L.M. Tomas‡, L. Vaz‡, E.R. Oliveira∞, F.L. Alves∞, S. den Boer†

†National Civil Engineering Laboratory  
Av. do Brasil, 101  
1700-066 Lisbon, Portugal  
aoliveira@lnc.pt

‡CESAM, Department of Physics  
University of Aveiro  
Campus Universitário de Santiago  
3810-193 Aveiro, Portugal

∞CESAM,  
Environment and Planning Department  
University of Aveiro  
Campus Universitário de Santiago  
3810-193, Aveiro, Portugal



[www.cerf-jcr.org](http://www.cerf-jcr.org)



[www.JCRonline.org](http://www.JCRonline.org)

### ABSTRACT

Oliveira, A., Jesus, G., Gomes, J.L., Rogeiro, J., Azevedo, A., Rodrigues, M., Fortunato, A.B., Dias, J.M., Tomas, L.M., Oliveira, E.R., Alves, F.L., den Boer, S., 2014. An interactive WebGIS observatory platform for enhanced support of coastal management. In: Green, A.N. and Cooper, J.A.G. (eds.), *Proceedings 13<sup>th</sup> International Coastal Symposium* (Durban, South Africa), *Journal of Coastal Research*, Special Issue No. 70, pp. 507-512, ISSN 0749-0208.

A new WebGIS observatory platform is presented, tailored for risk assessment and emergency preparation and response in coastal areas. The tool combines a sophisticated forecast modeling system for multi-scale analysis of water bodies, including waves, hydrodynamics and oil spills prediction, with real-time monitoring networks for forcing and continuous validation purposes. Tailor-made visualization and analysis products, conceptualized for multiple uses through a service-oriented framework, provide an easy and interactive access to both data and predictions. The system was customized for oil spills risk assessment and the rapid response to an oil spill emergency, and applied to the Aveiro lagoon. The tool addresses oil spill problems in two complementary ways: 1) a detailed risk assessment through georeferenced hazard and vulnerability maps and GIS layers of information to support the definition of contingency plans; and 2) the visualization of georeferenced oil spill predictions produced by a real-time oil spill forecasting system. Improvements relative to existing risk systems are 1) the possibility of selecting quick-access predictions for fast emergency response or high-quality, georeferenced GIS prediction products, 2) the flexibility in accessing products to evaluate local impacts of oil spills both in the water column and in the intertidal areas, and 3) the enhanced hazard and risk analysis through a combination of a multi-scenarios approach with the historical database of spill predictions, forced by daily hydrodynamic forecasts. Dependability of information, for both model results and monitoring data, is being implemented through innovative ways, targeting the robustness and quality control of the WebGIS platform.

**ADDITIONAL INDEX WORDS:** *WebGIS, risk management, oil spill, real-time monitoring, forecast systems.*

### INTRODUCTION

The timely prediction and monitoring of environmental conditions as well as the anticipation of hazardous events are essential parts of integrated coastal and harbor management, providing the necessary information for safe navigation and harbor operation, and the protection of valuable natural assets.

Coastal observatories have been under development for over a decade in the USA and in Europe (Baptista, 2006, Daniel et al., 2004), addressing many problems and spanning several disciplines, through the monitoring and prediction of several variables, such as wind, waves, sea surface elevation and some geochemical quantities (Gonzalez et al., 2008; Rodrigues et al., 2013). These observatories encapsulate our ability to characterize the behavior of water bodies, by integrating numerical models, monitoring networks and information technology systems, to provide real-time predictions of the main drivers in coastal zones. With the recent emergence of reliable and cost-effective automatic data acquisition systems and highly efficient and reliable numerical water quality models, the most important constraints for

the operational use of real-time forecasting and monitoring systems have been minimized (David et al., 2013; Rodrigues et al., 2013).

Herein, an interactive and flexible computational GIS-based platform is presented. Named RDFS-PT, this platform takes advantage of novel technologies to provide on-line, intuitive and geographically-referenced access to real-time data and model predictions, and to produce on-demand services in support of routine management of coastal resources and harbor operations. This platform is intended for the daily use of harbor authorities and coastal management entities and is available at each deployment site to the relevant end-users.

The enhanced interface is based on a previous deployment using Drupal, a PHP-based Content Management System (CMS) used to access model metadata, status and products. To allow for geospatial placement of monitoring and forecast products, as well as model output query capabilities, map server support (Geoserver) providing Web Map Services (WMS) have been added to the RDFS-PT. A WebGIS was developed in Flex, using the OpenScales library to handle geospatial information. This

WebGIS is being built in a modular and generic way, to allow future inclusions of new models, sensor networks and services required by coastal authorities and emergency agents. The requirements analysis of this platform was developed in close cooperation with several harbor and coastal management authorities, to promote its usefulness for management purposes.

The WebGIS platform is demonstrated in the recent deployment for the oil spill risk management in the Aveiro coastal lagoon, developed in the scope of the Portuguese Science and Technology Foundation (FCT) research project PAC: MAN and INTERREG project SPRES ([spres.ihcantabria.com](http://spres.ihcantabria.com)). Particular attention is given to the reliability of the real-time monitoring network and the automatic validation of model results, supported by dependable concepts applied to sensors and models.

The paper is organized in three sections, besides this introduction. The conceptualization of the generic nowcast forecast system, including technological choices presented in the next section. This is followed by the implementation of the generic technological system to the oil risk management in the Aveiro lagoon. The Aveiro lagoon is a large coastal system in Portugal, which is presented here to demonstrate the flexibility, service-provision and usefulness of the system. The paper closes with the major conclusions and the identification of the research directions ahead.

## RDFS-PT: A MULTI-PURPOSE NOWCAST-FORECAST INFORMATION SYSTEM

### Conceptual vision and building blocks

The ability to simulate and forecast the dynamics of estuarine and coastal zones is essential to assess the social, ecological and economic impacts of human interventions and climate variability and changes, and to support the sustainable management of these regions. A growing pressure on coastal management, fuelled in Europe by multiple legislation (Water Framework Directive - <http://ec.europa.eu/environment/water/water-framework/>, OSPAR Convention - <http://www.ospar.org/>, Marine Strategy Framework Directive - <http://ec.europa.eu/environment/marine/eu-coast-and-marine-policy/marine-strategy-framework-directive>), has fostered the development of computational nowcast-forecast systems (NFS) that provide predictions of several quantities at short time scales, by integrating numerical models and field data.

The reliability of the predictions of NFS depends on the accuracy of the models behind them and on the availability of real-time field data for the automatic validation of the predictions. However, the hydrodynamic and water quality simulation of water bodies poses a number of challenges: 1) on the adequate temporal and spatial scales for all relevant processes; 2) on the computational requirements for its use within a forecast system; and 3) on the methodology to quantify and reduce error propagation within the chain of cascade modelling. These difficulties, often combined with a lack of real-time data for the validation of model predictions, have prevented the development of nowcast-forecast systems that account for all relevant processes and interactions.

Integrated modelling approaches, combining both cross-scale, unstructured grids hydrodynamic and water quality models, are thus required to cover the full range of the relevant spatial and temporal scales of the processes in coastal systems. Usage of high-performance computational resources and optimized models also play major role in providing the necessary accuracy at computational times compatible with forecasting uses (Costa *et al.*, 2009).

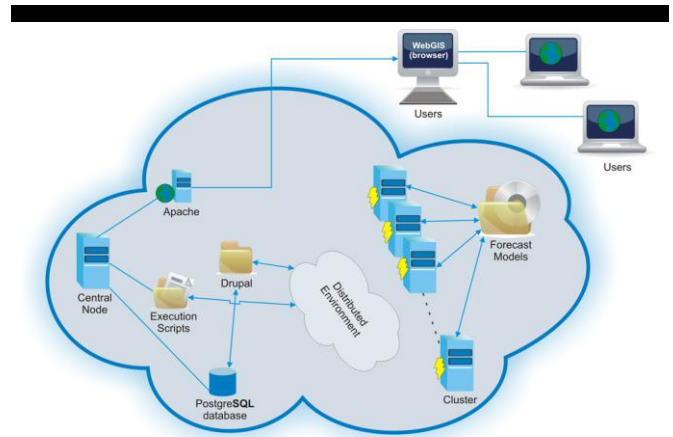


Figure 1. Physical architecture of the RDFS. Adapted from Jesus *et al.*, 2012.

The nowcast-forecast information system proposed herein, RDFS-PT, is based on the deployment of a generic forecasting platform, adaptable to any geographical location, and customizable for coastal applications, which was originally developed at CMOP (Center for Coastal Margin Observation & Prediction, U.S.A. – Baptista, 2006) and was adapted and extended by LNEC (Jesus *et al.*, 2012; 2013). The system integrates a set of numerical models that run in parallel automatically in a high-performance environment. The RDFS-PT platform is capable of coupling waves, tides, storm surges, river flows, precipitation and winds, providing forecasts of water levels, currents, water temperatures, salinity and waves for a target area. It was recently extended for water quality (fecal contamination in sewer systems and estuarine water bodies, and oil spills in coastal regions, Rodrigues *et al.*, 2013).

The usefulness of NFS and other decision-support systems for coastal management problems is also often hampered by the difficulties in the communication of the results. A broad spectrum of users, with different needs (e.g., water body managers, water utilities, general public) using different platforms (desktops, mobiles, tablets) should be reached.

A new intelligent platform for coastal management was developed, based on the integration of waves, hydrodynamics and water quality RDFS-PT forecasting and on real-time on-line monitoring networks, and the automatic comparison between data and predictions. The platform is devoted to the surveillance and real-time decision support, in particular to support the issues of early-warning during contamination events and the reliability analysis of data, through a combination of information from predictive models and sensors.

The platform is conceived in a user's service-oriented architecture, providing on-line access to both real-time model predictions and data-derived products, at different levels of detail and complexity. Real-time model predictions are generally stored in two distinct servers (a main server and a redundant one). In both cases data are stored in the file system via NETCDF standard format, allowing future use in other models. Regarding the mentioned user-oriented services, a set of webservices is provided at the RDFS-PT website, either through a geographic user-interface (geo-referenced imaging data by WMS services) or through an alpha-numeric webservice to scope timeseries from the data outputs in user-specific points of the model grid.

The platform is built in a modular and generic way, including both quick access products and a Web Geographic Information

System (WebGIS). This WebGIS allows the visualization of the existing network monitoring information, and can easily be extended in the future for new data sources, either publicly available or provided by the coastal authorities and other end-users. Services are automatically provided in the platform for comparison between model predictions and these data, granting robustness and long-term evaluation to the whole system to the end-users.

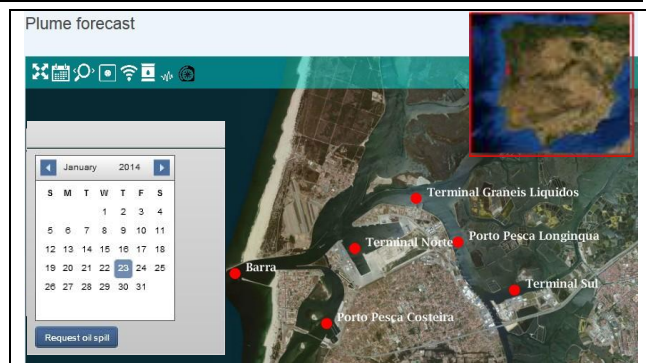


Figure 2. Location of oil spill hotspots in the Port jurisdiction area. The location of the Aveiro lagoon within the Iberian peninsula is shown in the inset

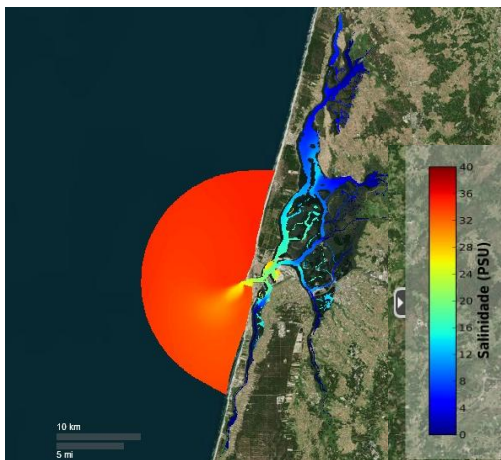


Figure 3. Example of forecast product for salinity.

### Architecture and technological approach

RDFS's physical architecture includes several computer servers and a shared file server. This central file server provides archival storage for model outputs, access to model results, and tools for managing the forecasts. Every day, each computer server runs one or more forecasts (depending on its capacity). The components of RDFS-PT and their interactions are illustrated in Figure 1.

The RDFS-PT forecasting process runs on Linux operating systems and, at its core, is composed of a set of Perl scripts scheduled on crontab. Running on a daily basis, these scripts prepare and launch the simulations for each model producing

forecasting results, among others. The scripts start by gathering all the necessary input data, mostly from a PostgreSQL database, to force the models and then launch the simulation. At the end of the simulation, all relevant output results are made available to the central node. Simulation requirements include the results of the previous run (and/or other forecast models simulation results), forecasts from regional circulation models and atmospheric models, and data from field sensors.

A cascade modeling approach is used, forced by external regional models. Each model is fed by the outputs of the previous model, customized for each model format.

Model output results are then processed in the forecast engine, using visualization tools such as VisTrails or the matplotlib library, to generate automatically model forecast products and data/model comparisons, to be included in the WebGIS platform.

The RDFS-PT platform is a customized deploy of Drupal, a PHP-based Content Management System (CMS), which is used to access model metadata, status and products. Web Map Services (WMS) and Geoserver map server provide GIS support for the generated products and a more interactive and intuitive user interface, allowing geospatial placement of products, as well as model output query capabilities. The WebGIS was developed in Flex, using the OpenScales library to handle geospatial information. This WebGIS was built in a modular and generic way, allowing the visualization of RDFS-PT data and the flexible integration of spatial data from other sources.

### Forecasting modeling system and model components

RDFS-PT includes models for circulation, wave generation and propagation, oil spill fate, ecosystem dynamics and fecal contamination, among others. Herein, the models used in the application of the platform to the oil spills in the Aveiro lagoon are briefly described.

Circulation is simulated with the community model SELFE (Zhang and Baptista, 2008). SELFE solves the 3D baroclinic shallow water equations for elevations, velocities, salinity and water temperature. The domain is discrete with finite elements in the horizontal and mixed S-Z coordinates in the vertical. A semi-implicit time stepping algorithm combined with an Eulerian-Lagrangian treatment of the advective terms in the momentum equations provides a robust and spurious-free solution, free of Courant number restrictions. SELFE is fully parallelized. In the Aveiro lagoon, SELFE is forced by water elevations, temperatures and salinities from a regional model ([www.myocean.org](http://www.myocean.org)) at the ocean boundary, quasi-real time river flows ([www.snirh.pt](http://www.snirh.pt)) and atmospheric forcings ([www.ncdc.noaa.gov/data-access/model-data/model-datasets/global-forecast-system-gfs](http://www.ncdc.noaa.gov/data-access/model-data/model-datasets/global-forecast-system-gfs); [climetua.fis.ua.pt/](http://climetua.fis.ua.pt/)).

Oil transport and weathering is computed with the 2D version of VOILS (Azevedo *et al.*, 2009; 2014). VOILS contains the most relevant processes for the transport and rheological changes of the oil, such as advection, evaporation, scattering at the surface, emulsification, dispersion and dissolution in the water column, and shoreline retention and reposition. It is particularly suited for the representation of complex coastlines and coastal studies, as it is based on unstructured meshes to simulate physical processes on a multi-scale approach. VOILS solves a transport-type equation for the thickness of the oil at the surface. The equations are solved with a combination of finite volumes and Eulerian-Lagrangian methods, which provide efficiency and mass conservation.

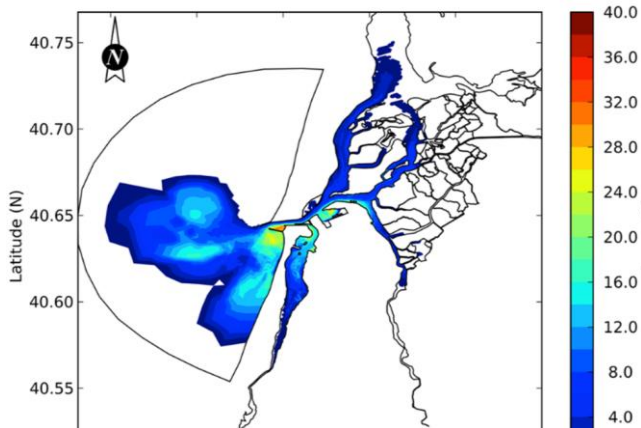


Figure 4. Oil exposure indicator (hours), which shows the time that a particular node of the simulation grid has been affected by the presence of oil during an oil spill model simulation.

### Real-time monitoring networks

Constraints for reliable, large-scale, operational use of hydraulic models in real-time forecasting have been minimized with the recent appearance of low cost and reliable automatic data acquisition and transmission systems, as well as with the usage of highly efficient and reliable numerical models.

An advanced, new monitoring framework, within the broad-range RDFS-PT system, was developed to provide dependable real-time monitored data. These data are essential to validate model predictions, issue alerts or to support decisions on mitigation measures to be performed in the areas at risk.

A wireless sensor network was built, where each node gathers and transfers data into a web-database system, setting up a real-time web-based management system. Two possible data transmission procedures are possible. In the first one, the data transmission process is triggered through a central server located at the National Civil Engineering Laboratory (LNEC). This server connects to the sensor via the GSM modem and requests the measurements stored in the data logger. Alternatively the sensor itself uploads the measurements data to an FTP server, hosted at

LNEC, triggering the communication process. This flexible approach allows for different types of sensor deployments and data acquisition rates and simplifies future sensor node integration.

Sensor measurements often contain faulty values and outliers whose detection may be of major importance in a dependable monitoring network supporting risk management. Alerts may be configured for all parameters, triggering the dispatch of emails or mobile messages whenever the defined limits are reached.

### Dependable requirements for risk management information systems

A cascade of uncertainties present in each part of a risk management system affects the reliability of the forecasts. The timeliness and quality of monitoring data gathered and used subsequently in forecasting models, is affected by external disturbances (e.g., biofouling, corrosion). Moreover, in a distributed computing system, where multiple scripts are running simultaneously and large quantities of data are being processed from different sources, an innocuous fault in one process may affect the outcome of a forecast and cause a system breakdown. Also, in RDFS-PT input, data from both forecast models and other sources are largely heterogeneous, due to their different origins and sensors. This heterogeneity makes it difficult to ensure the full reliability in the system, as complex scenarios arise from the specific effects of each technology.

New solutions to automatically adjust the sensors measurements are under development, taking into consideration all critical aspects of the sensor networks in the aquatic monitoring process. There is a strong need for reliable data collection in harsh coastal and marine environments, making dependable techniques important to improve the robustness of the sensors measurements.

Regarding software failures, the solution implemented was based on failure models mainly regarding the input and output of the forecast models. Redundancy and bypass methods were the preferred tactics to tackle problems originating from sources outside the forecasting system. If a data source is unavailable, similar sources are adopted or most likely information is used. In case of incomplete or unsuccessful forecasts, the use of redundant forecasts (ran on a different workstation) is the first option, or else a rerun is always tried. When all automated solutions fail, a maintenance team is alerted (automatically) on unsolvable

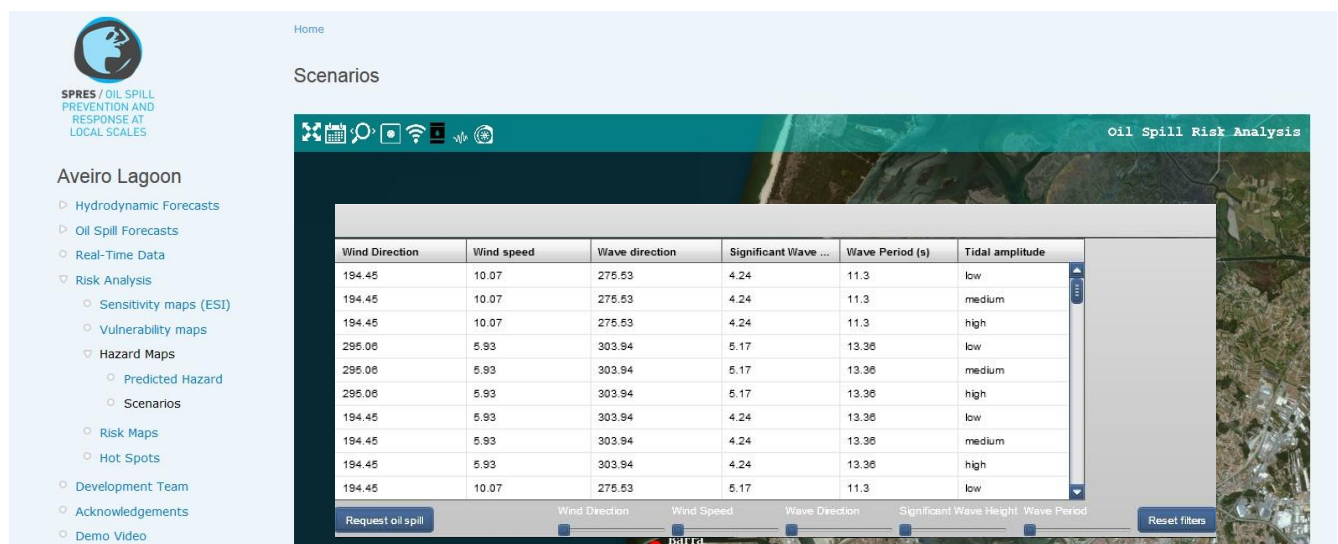


Figure 5. Filtering interface for quick search of oil hazard maps for specific scenarios.

situations, with resort to checklist mechanisms in the master scripts, so that human intervention may correct faulty processes. A fully reliable RDFS-PT is a future goal, but many failure causes remain to be identified and solved.

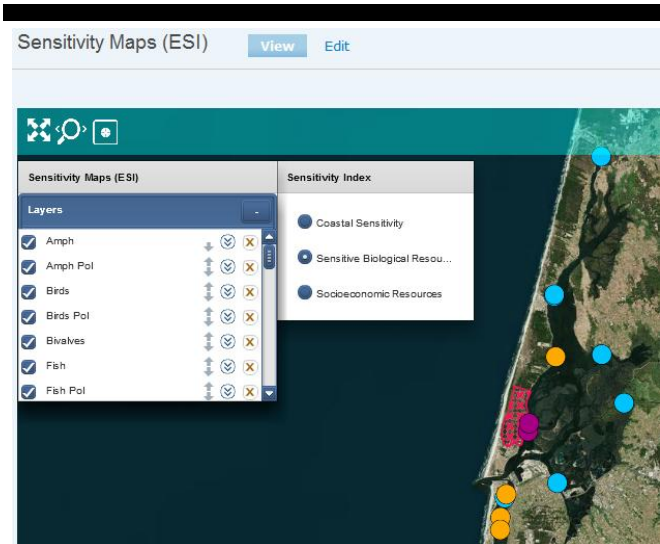


Figure 6. Partial view: choice of layers in Sensitivity Maps view.

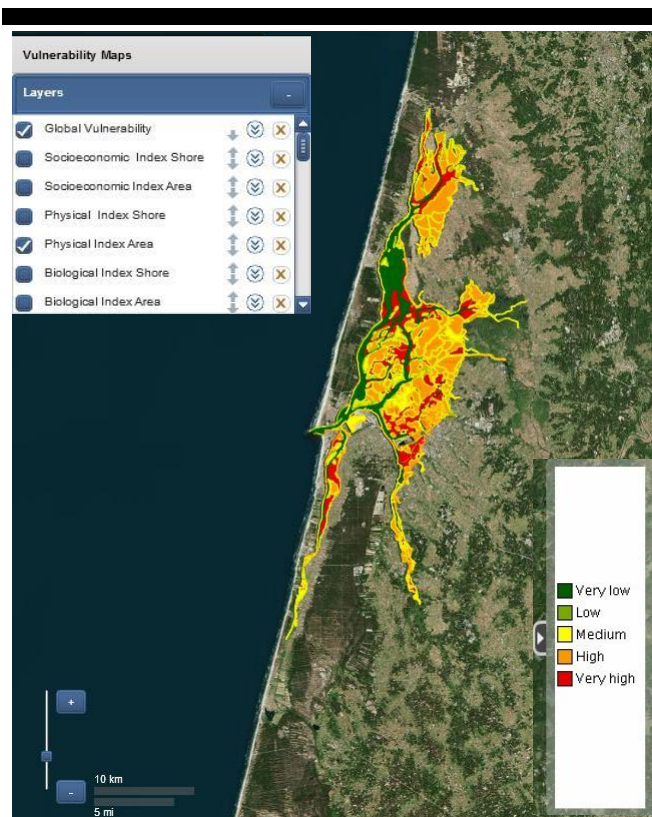


Figure 7. Global Vulnerability and Physical Index Area map.

## RDFS-SPRES: A WEBGIS OBSERVATORY PLATFORM FOR OIL SPILL RISK MANAGEMENT IN THE AVEIRO LAGOON

### Concept and general methodology

Natural and anthropogenic disasters worldwide, like oil spills, can lead to severe environmental and economic losses (Dietrich et al. 2012). Even for the accidents whose timing and location are unpredictable, many prevention and mitigation actions can be done to reduce the severity of the disaster. This issue motivated the development of a high-accuracy coastal oil spill nowcast-forecast system to assist emergency agents, taking into account the various forcing mechanisms and relevant processes of oil spill evolution and pathways in coastal environments. These advanced tools constitute an effective asset for coastal managers and emergency agents, as they can significantly improve local contingency plans and contribute to effective emergency management.

The advanced risk management tool presented herein addresses oil spill risks in two ways: 1) an enhanced risk assessment portal combining hazard maps, provided by high-resolution simulations based on a multi-scenario approach, and georeferenced vulnerability information, organized along physical, ecological and socioeconomic views (Oliveira *et al.*, 2014); and 2) georeferenced oil spill predictions produced by the real-time oil spill forecasting system. Both functionalities are available within the same WebGIS platform, as a “one-stop-shop” for all relevant information for coastal managers and emergency agents.

The adaptation of RDFS-PT for oils spill was done through the integration of the model VOILS (Azevedo *et al.*, 2009, 2014). Forced by daily hydrodynamic predictions, the oil model runs automatically also on a daily basis, for pre-specified locations. Given the time requirements for the availability of predictions and the need to provide a quick answer in the event of a spill, the 2D mode of VOILS is used, simulating the oil slick thickness at the surface, accounting for oil retention and reposition at the land margins, as well as all processes at the water surface.

Herein, the RDFS-PT platform is applied to the Aveiro lagoon, a coastal ecosystem located in the Northwest coast of Portugal, valuable both at ecological and economical levels. The lagoon holds several habitats and relevant anthropic activities (e.g. recreational activities, port activities, fisheries/bivalve harvesting). The application to the Aveiro lagoon is supported by a previous pilot deployment of the RDFS-PT (<http://ariel.lnec.pt/>, Rodrigues *et al.*, 2013) for the hydrodynamic prediction in the Aveiro lagoon. This deployment was improved through an update of bathymetry, integration of ocean boundary water elevations from MyOcean and by the integration of a real-time monitoring network at two key locations (Gomes *et al.*, 2012). This network provides automatic validation of the modeling system predictions besides the possibility of environmental analyses based on historical records of the water characteristics in the lagoon.

### Innovative emergency and risk management system

The Aveiro lagoon oil risk RDFS-PT platform was conceptualized for emergency management through pre-defined hot spots for oil spills (Figure 2), where a plume of 10 tons of RFO/HFO N.6 oil is released, all defined with the collaboration of the Port Authority. Oil spill predictions for all spots and all scenarios (Figure 3) are run in parallel processors, to provide the fastest availability of results. These results are then processed into indicators for oil impact analysis, such as the time of exposure to



oil at every node of the domain (Figure 4), for each oil spill model simulation. From the analysis of Figure 4 one can evaluate the areas affected by the oil for a particular simulation. Information on the surface slick and on the beached oil can be processed and visualized as different GIS layers, allowing for the quick specification of the most adequate response or mitigation action.

A detailed risk assessment, based on georeferenced hazard and vulnerability maps, can also be visualized in the interface. A multi-scenario approach, based on the most likely environmental scenarios for accident-prone conditions (wind, waves and tides) was used to generate hazard maps. To facilitate the oil pathways analysis, the platform provides a filtering service for each forcing factor and for the probability of the combination of factors, allowing a quick access to specific simulations (Figure 5).

The oil spill emergency component is closely linked to the formal risk management tool. While oil forecast runs are ongoing, a preliminary estimate of the potential oil pathways can be inferred, as the platform automatically selects and highlights the pre-run scenario closest to the forecasted environmental conditions. Likewise, the oil spill forecasts also contribute to progressively enrich the database of scenarios. Every day, each new set of oil runs is integrated in the risk analysis database and made available at the filtering menu. This closed loop will continuously increase the completeness of the platform and consequently its usefulness for real accidents.

The flexible and generic nature of the platform will enable at a later stage the possibility to combine, in a single screen, different layers of sensitivity, vulnerability and hazard maps, as well as relevant oil indicators at selected locations – receptor points. Receptor point information will be readily available as data time series for visualization, analysis and download. For the same points, the platform will provide the mitigation and response action fact sheets under development in the SPRES project.

## CONCLUDING REMARKS AND OUTLOOK

Herein, an interactive and flexible computational GIS-based platform is presented, which takes advantage of novel technologies to provide on-line, intuitive and geographically-referenced access to real-time data and model predictions, and to produce on-demand services in support of coastal resources and harbor operations management as well as emergency procedures. The forecasting engine behind the platform is supported by multi-scale, high-accuracy numerical models for both hydrodynamics and oil transport and weathering, which handle all relevant processes both in the water column and intertidal areas.

The platform, generally denoted as RDFS-PT, was customized for oil spill risk management and successfully applied to the risk of an oil spill within the Port of Aveiro jurisdiction area.

Future development efforts will include:

- the inclusion of additional oil indicators in support of local risk evaluation and emergency resources allocation;
- an on-demand oil spill simulator, in addition to the real-time forecast of the evolution of pre-defined plumes;
- the customization of the interface for the general public, with specific products for recreational purposes;
- the adaptation of the spatial data infrastructure developed for the River Basin Management Plans, compliant with the Inspire Directive, to the oil spill management system

## ACKNOWLEDGEMENTS

This work was funded by projects Pac:Man (PTDC/AAC-AMB/113469/2009), SPRES (Interreg Atlantic Area Transnational Cooperation Programme 2007-2013 project SPRES

- 2011-1/168) and FLAD (project C-WOS), as well as FCT's Grants (SFRH/BPD/73089/2010, SFRH/BPD/82489/2011, SFRH/BPD/87512/2012). The authors thank António Baptista and Paul Turner (CMOP) for the RDFS platform, and Joseph Zhang (VIMS), for the model SELFE. The team also thanks the Port of Aveiro authority for all the data and support provided in the development of the platform.

## LITERATURE CITED

- Azevedo, A., Oliveira, A., Fortunato, A. and Bertin, X., 2009. Application of an Eulerian-Lagrangian oil spill modeling system to the Prestige accident: trajectory analysis. *Journal of Coastal Research*, SI 56 (Proceedings of the 10th International Coastal Symposium), 777 – 781. Lisbon, Portugal, ISSN 0749-0258.
- Azevedo, A., Oliveira, A., Fortunato, A.B., Zhang, J., Baptista, A.M., 2014. A cross-scale numerical modeling system for management support of oil spill accidents. *Marine Pollution Bulletin*, (2014), in press, <http://dx.doi.org/10.1016/j.marpolbul.2014.01.028>
- Baptista, A.M., 2006. CORIE: the first decade of a coastal-margin collaborative observatory. *Computing in Science and Engineering*, 10/3, 53-58, doi:10.1109/MCSE.2008.83
- Costa, M., Oliveira, A., Rodrigues, M. and Azevedo, A., 2009. Application of Parallel, High-Performance Computing in Coastal Environmental Modeling: Circulation and Ecological Dynamics in the Portuguese Coast. *Proceedings da 3rd Iberian Grid Infrastructure*, pp. 375-386.
- Daniel, P., Josse, P., Dandin, P., Lefevre, J.M., Lery, G., Cabioc H, F., Gouriou, V., 2004. Forecasting the Prestige oil spills, Interspill 2004.
- David, L.M. Oliveira, A., Rodrigues, M., Jesus, G., Póvoa, P., David, C., Costa, R., Fortunato, A.B., Menaia, J., Frazão, M. and Matos, R., 2013. Development of an integrated system for early warning of recreational waters contamination, *Novatech 2013*, 10 pp.
- Dietrich, J.C., Trahan, C.J., Howard, M.T., Fleming, J.G., Weaver, R.J., Tanaka, S., Yu, L., Luettich Jr., R.A., Dawson, C.N., Westerink, J.J., Wells, G., Lu, A., Vega, K., Kubach, A., Dresback, K.M., Kolar, R.L., Kaiser, C. and Twilley, R.R., 2012. Surface trajectories of oil transport along the Northern Coastline of the Gulf of Mexico”, *Continental Shelf Research*, 41, 17-47.
- Gomes, J.L., Jesus, G., Rodrigues, M., Rogeiro, J., Azevedo, A. and Oliveira, A., 2013. Managing a Coastal Sensors Network in a Nowcast-forecast Information System, *Proc. of the Sixth Int. Workshop on Next Generation of Wireless and Mobile Networks (NGWMN-2013)*, 6 pp.
- González, M., Ferrer, L., Uriarte, A., Urtizberea, A. and Caballero, A., 2008. Operational Oceanography System applied to the Prestige oil-spillage event, *Journal of Marine Systems*, 72/1-4, 178-188.
- Jesus, G., Gomes, J., Ribeiro, N. and Oliveira, A., 2012. Custom deployment of a Nowcast-forecast information system in coastal regions, *Geomundus 2012*, Lisbon, Portugal, 6 pages.
- Jesus, G., Gomes, J., Oliveira, A., den Boer, S. and Azevedo, A., 2013. From a nowcast-forecast information system to an oil spill risk assessment and response tool, *Geomundus 2013*, Spain, 6 pages
- Oliveira, E.R., Silveira, B. and Alves F.L., 2014. Mechanisms for oil spill accident response in coastal lagoons (Aveiro, Portugal), *Journal of Sea Research*, SI: Atlantic Iberian Margin, in press-corrected proof., available online 14 November 2013, doi:10.1016/j.seares.2013.11.002.
- Rodrigues, M., Oliveira, A., Queiroga, H., Fortunato, A.B. and Zhang, Y., 2009. Three-dimensional modelling of the lower trophic levels in the Ria de Aveiro (Portugal). *Ecological Modelling*, 220, 1274–1290.
- Rodrigues M., Costa J., Jesus G., Fortunato A.B., Rogeiro J., Gomes J., Oliveira A. and David L.M., 2013. Application of an estuarine and coastal nowcast-forecast information system to the Tagus estuary. *Proceedings of the 6th SCACR – International Short Course/Conference on Applied Coastal Research* (Lisboa, Portugal), 10 pp.

# Coastal management and mis-management: comparing successes and failures at two lagoon outlets in KwaZulu-Natal, South Africa

Lisa Guastella<sup>†</sup>, Alan Smith<sup>‡</sup>, Tandi Breetzke<sup>#</sup>

<sup>†</sup>Oceanography Department  
University of Cape Town  
Private Bag X3, Rondebosch, 7700,  
South Africa  
lisagus@telkomsa.net

<sup>‡</sup>School of Geological Sciences  
University of KwaZulu-Natal  
Durban 4001, South Africa,  
asconsulting@telkomsa.net

<sup>#</sup>Royal HaskoningDHV  
6 Payne St, Pinetown, 3610  
South Africa  
Tandi.Breetzke@rhdhv.com



[www.cerf-jcr.org](http://www.cerf-jcr.org)



[www.JCRonline.org](http://www.JCRonline.org)

## ABSTRACT

Guastella, L.A., Smith, A. M., Breetzke T., 2014. Coastal management and mis-management: comparing successes and failures at two lagoon outlets in KwaZulu-Natal, South Africa. In: Green, A.N. and Cooper, J.A.G. (eds.), *Proceedings 13<sup>th</sup> International Coastal Symposium* (Durban, South Africa), *Journal of Coastal Research*, Special Issue No. 70, pp. 513-520, ISSN 0749-0208.

KwaZulu-Natal (KZN) has a high energy, dynamic coastline. The coast is a significant asset, utilised for residential, industrial, transport, nature conservation and recreational purposes. It is also the discharge point for many steep gradient, short-headed rivers. These rivers have highly variable discharges and, together with variable coastal erosion and deposition cycles, place stress on coastal resources and infrastructure. Many of the rivers, particularly those with smaller catchments, discharge into back-beach lagoons before discharging into the ocean. Lagoon outlet dynamics are variable and, when combined with ocean swells and/or river flooding, can cause erosion. Coastal managers need to be aware of the risks to coastal assets and to this end, informed decision-making is vital to ensure sustainability of coastal resources and protection of coastal infrastructure, albeit often inappropriately located. While a strategy of non-intervention of lagoon outlets is always preferable, there comes a point when intervention may be necessary to protect coastal infrastructure, particularly if the intervention can replicate natural processes. Fixed coastal webcams, backed up by on-site photography, are used to illustrate two contrasting examples of coastal management on the KZN south coast at: (a) Margate where intervention resulted in the saving of coastal infrastructure, and (b) Amanzimtoti where a lack of intervention resulted in a train derailment, loss of infrastructure, injuries and significant repair costs. This paper critically reviews these contrasting examples and concludes that a greater understanding of lagoon outlet dynamics can significantly contribute to improved coastal management practices, and in this instance, could have prevented this derailment.

**ADDITIONAL INDEX WORDS:** Coastal management, lagoon outlet, erosion, mouth dynamics, breaching.

## INTRODUCTION

The KwaZulu-Natal (KZN) coastline, on the east coast of South Africa (Fig. 1), is a high energy, dynamic coastline. It is a significant asset, utilised for residential, industrial, transport, nature conservation and recreational purposes. The coastline is also the discharge point for rivers that drain the hinterland. The climate is subtropical, characterised by summer rainfall and dry winters. Annual average rainfall along the KZN south coast varies from 1 009 mm at Durban to 1223 mm at Margate (source: SAWS), with approximately 70% of this occurring during the summer months. The variability in river discharge, together with variable coastal erosion and deposition cycles, results in various stresses on coastal resources and infrastructure. Many of the rivers, particularly those with smaller catchments, discharge into back-beach lagoons before discharging into the ocean, but the mouth dynamics are often variable and on occasions, combined with ocean swells and/or river flooding, can cause erosion (Cooper, 1990). A strategy of non-intervention of lagoon mouths is preferred by environmental regulators in order to maintain a natural outlet and natural ecosystem (Harrison and Cooper, 1991; National Estuarine Management Protocol, 2013), however occasionally intervention may be necessary to protect coastal infrastructure, albeit often inappropriately located, or prevent pollution. Fixed coastal webcams, backed up by on-site

photography are used to illustrate and compare different management decisions and consequences at two different beaches containing lagoon outlets on the KZN south coast at (a) Margate, and (b) Amanzimtoti.

## METHODS

Fixed coastal webcams have afforded an ideal opportunity to observe coastal and lagoon outlet variability on a seasonal, day-to-day and even hourly time scale (Guastella & Smith, 2014). These are used here to illustrate the change in character of the lagoon outlets that discharge at Margate beach and Chain Rocks beach, Amanzimtoti (Fig. 1). Daily low-tide images have been captured from beach webcams at Margate and Chain Rocks provided by a cell phone company (Vodacom) (refer Fig. 1) since 3 March 2010 and, in the case of Margate, also from a tourism website (South Coast Web) since 10 June 2011. The images are updated every minute in the case of the Vodacom webcams and one to three minutes in the case of the South Coast Web webcams. Images are captured manually from websites by saving the image coinciding with low tide for that day. Low tide is selected owing to the fact that changes in beach character are more evident, while the high tide mark is nonetheless usually easily discernible. High tide images are also collected on occasion, mainly to demonstrate lagoon mouth breaches and/or the impacts of high tide or swell

DOI: 10.2112/SI70-087.1 received 22 December 2013; accepted 21 February 2014. © Coastal Education & Research Foundation 2014

events. This information, together with site visits, has been used to analyse beach change and to evaluate the efficacy of interventions. In the case of Margate, only the imagery from the “Seagull” holiday flats on the South Coast Web site is used in this manuscript as it gives the best view of the lagoon and outlet.

## RESULTS AND DISCUSSION

### Margate

Margate Beach (30°51'45.85"S, 30°22'17.50"E) is located on the KwaZulu-Natal lower south coast within the Hibiscus Coast Municipal Area (Fig. 1). The beach is located within a 1.2 km long bay, which is topographically bounded by two low, but prominent rocky headlands (Fig. 2). The bay is subject to seasonal beach rotation in response to differing seasonal swell regimes, with the southern end of the beach generally depleted of sand during the winter months while the northern end experiences accretion; the reverse is true during summer (Guastella & Smith, 2014). The 6 km long Nkongweni River, which has a catchment of 18 km<sup>2</sup> (Begg, 1978), discharges at the southern end of the bay via a back-beach lagoon. During the dry winter months (late April to August) the lagoon outlet is generally closed. During the wet summer season the lagoon may breach seaward of the river or migrate south along the back beach until it opens at the southern end of the bay. The mouth opens for, on average, 3 to 6 days per month during summer (Breetzke, 2012). The baymouth bar that separates the lagoon outlet from the sea can be overtopped during high tide events, especially during spring tides coinciding with large swells, and the lagoon subject to inundation. This is more frequent if the beach is depleted of sand as usually occurs at the

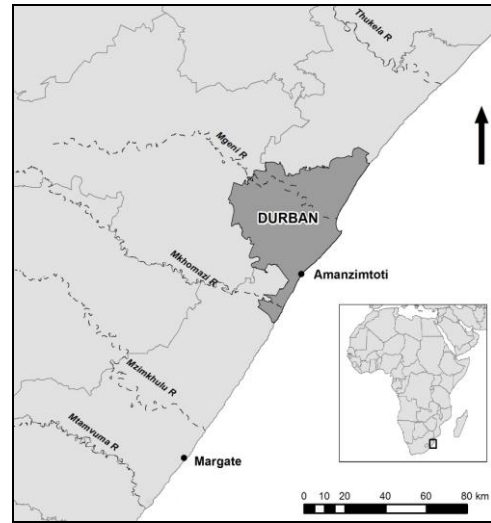


Figure 1. Location of Amanzimtoti and Margate on the east coast of South Africa.

end of winter.

Margate is an extremely popular holiday destination and is the second tourism node after the city of Durban; as such the beach and areas surrounding the river have become highly urbanised. A poorly designed and maintained sewage plant and illegal stormwater connections have further degraded the system (Breetzke, 2012). Backflooding is possible during the winter as



Figure 2. Google Earth imagery of Margate beach showing Nkongweni lagoon mouth position on 31 May 2011 and location of webcams in the south. The Vodacom webcam locality and view direction is indicated by the long, red arrow, while the short yellow arrows indicate the localities and view directions of the South Coast Web webcams. The inset for 2 June 2012 shows southward migration of the lagoon mouth, while that for 9 October 2012 shows a migration inland of the previous position.

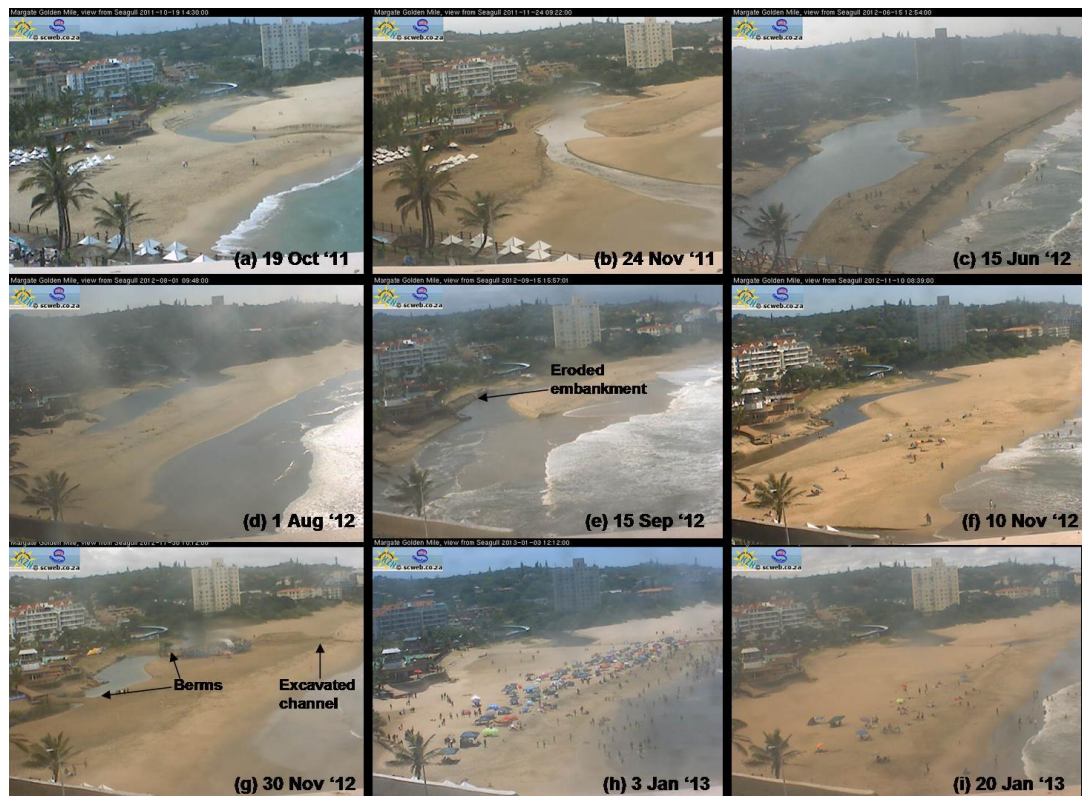


Figure 3. Sequence of webcam imagery from the Seagull webcam (South Coast Web) (refer locality in Fig 2) from (a) 19 October 2011 to (i) 20 January 2013 showing migration of the Nkongweni lagoon outlet southward and erosion of the embankment and infrastructure followed by (g) intervention during the last week of November 2012 and recovery of the beach in January 2013 (h & i). All images are at low tide except (c) showing backflooding of the lagoon on 15 June 2012 and limited beach area at high tide owing to winter erosion in the south of the bay, and (e) showing erosion of the south bank at high tide following copious rain (84 mm from 14-15 September 2012).

water (sometimes polluted from the poorly maintained sewage system), can accumulate without having the hydraulic power to breach. In spite of its poor water quality, the river and lagoon supports a “good” fish community (Cooper et al., 1994; Harrison et al., 2000).

The Margate main beach area (Fig. 2) is backed by a public Olympic size swimming pool, lifesaving facilities, superslide (waterpark) and a restaurant. These beach facilities were inappropriately located too close to the high-water mark. The baymouth bar (Fig. 2) constitutes the most important part of the Margate bathing beach area (Begg, 1978) and is the focal point of many recreational activities. While the Nkongweni lagoon is predominantly closed, the mouth can migrate southwards under natural conditions (Breetzke, 2012). From our database, this process commenced in October 2011 and continued in November (Fig. 3b) and December 2011, following above-average rainfall during those months (Fig. 5a). The lagoon outlet closed at times, but when the outlet was opened it still preferentially discharged to the south of the beach through most of 2012, apart from January and February 2012 when it was more centrally placed. This trend to preferentially discharge to the south was common along the KZN south coast during 2012, particularly during early summer (September – November) and was related to above-average rainfall (Fig. 5a). This transported sediment downstream and onto the coast where waves then reworked it back onto the beach and

inflated the beaches, preventing them from direct breaching at river mouths (Smith et al., this issue).

#### **Margate: the problem**

A topographically forced, localised reversal in the predominant south to north longshore drift flow and seasonal variations in wave climate from SSE in winter to easterly in summer (Guastella & Smith, 2014), forces the Nkongweni lagoon outlet southward. Backflooding during June 2012 left a narrow baymouth bar (Fig. 3c), which subsequently breached at the southern extremity of the bay, whereafter the lagoon receded (e.g. Fig. 3d). Persistent southward flow of the Nkongweni mouth following high rainfall episodes of September (Fig. 3e) to November 2012 (Fig. 3f), combined with tidal action, started to undermine infrastructure and compromised beach access. In addition, seasonal cyclical erosion by a megarip in the south of the bay (Guastella & Smith, 2014) left the beach area less protected and infrastructure more vulnerable to wave action during high tides (Fig. 3e). Crossing the fast flowing and potentially polluted lagoon outlet water in order to get onto the beach was considered extremely dangerous (Breetzke, 2012). By the end of October to November 2012 infrastructure was under threat (Fig. 4a-c) and the available recreational beach area, visible to potential visitors on the live webcam imagery (Fig. 3), was compromised leading to holiday booking cancellations and resultant negative financial impact on the tourism industry.

A solution was sought and with further summer rainfall due and the threat of infrastructural and tourism loss, the Hibiscus Coast Municipality (HCM) appointed consultants to find a short-term solution, which would ultimately lead to a longer-term management plan. While a non-intervention policy in terms of beach manipulation and artificial mouth breaching is preferred by coastal regulators, the impending risk to infrastructure and threat to the local economy posed by increased erosion of the river mouth necessitated intervention. The mouth previously had reportedly been artificially maintained in a more northerly position



Figure 4. Margate beach (a) erosion of the ramp in front of the lifeguard tower and reduced back-beach area, (b) erosion of the embankment in front of the Olympic-size swimming pool, (c) undermining of infrastructure supporting a smaller swimming pool at the extreme southern end of Margate beach, and (d) a similar view to (b) showing infilling of the back-beach area and draining of the previously southward extending outlet; the newly excavated channel and berm to prevent southward movement of the outlet can be seen in the distance.

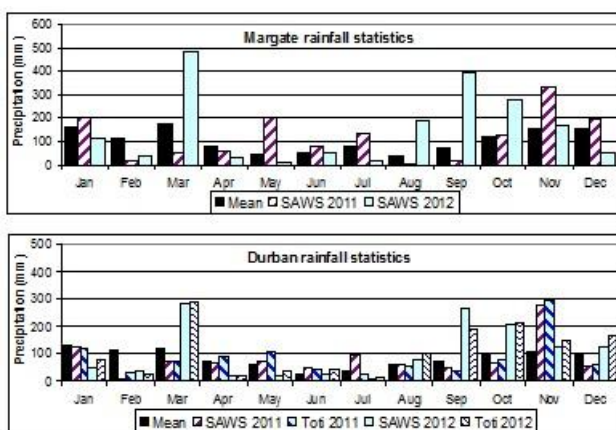


Figure 5: Monthly rainfall at (a) Margate and (b) Durban South and Amanzimtoti during 2011 and 2012 compared to the 30-year long-term mean. Margate and Durban South data are from the South African Weather Service (SAWS) and Amanzimtoti data are from eThekweni Municipality City Engineers. The SAWS Durban South station is located at the old airport site, some 12 km north of Amanzimtoti, and represents one of the longest and most reliable weather stations in the area.

by municipal officials in order to prevent negative effects on the recreational facilities and Margate Main Beach area (Begg, 1978; Breetzke, 2012). As an emergency measure it was therefore proposed to artificially breach the Nkongweni Estuary by digging a channel directly in front of the lagoon, where it had previously naturally breached under flood conditions, and dam the back-beach lagoon outlet and transfer sand from that accumulated in the adjacent sand berm to the Margate Main Beach back-beach area.

As such the consultants requested permission from the provincial Department of Agriculture and Environmental Affairs (DAEA) for emergency measures in terms of Section 24F(3) of the National Environmental Management Act (NEMA) and from Ezemvelo KZN Wildlife, which manages the artificial breaching of estuaries via an approved policy in terms of the 1994 Natal amendment to the Sea Shore Act No 21 of 1984. The application was approved and emergency work started in the last week of November. The excavated channel placed the outlet in a more northerly position and damming of the back-beach lagoon outlet prevented undermining of infrastructure (Fig. 3g). A berm was constructed alongside the excavated channel and sand was moved to create access ramps to the beach and replenish the back-beach area. Recovery of the beach was immediate (Fig. 3g) and by mid-December the area previously under threat from the southward migrating lagoon outlet was dry and filled with sand (Fig. 4d) and following a drier January the lagoon had receded (Fig. 3h & i). Seasonal replenishment of beach sand, as part of a seasonal beach rotation (Guastella & Smith, 2014) occurred (Fig. 3i) and the infrastructure and tourism industry was saved. While this short-term solution was a success, solutions are also required in the medium to long-term as the outlet naturally forces its way southward again. To this end an application for environmental authorisation for longer term measures is underway and a Mouth Management Plan has been drafted to manage the outlet. This proposes reinstatement and maintenance of the perpendicular berm to prevent southward migration of the mouth across the main beach, thereby allowing a natural build up and breach at the more northern location in front of the lagoon. A manual artificial breach will only be considered as a last resort should the berm not be effective (Breetzke, 2013) and will require prior approval from the relevant authorities (Ezemvelo KZN Wildlife and DAEA).

## Amanzimtoti

Amanzimtoti (30° 3'48.32"S, 30°52'54.61"E) is located on the KwaZulu-Natal upper south coast within the eThekweni Metropolitan Municipal Area (Fig. 1). The Amanzimtoti coastal area consists of shallowly indented sandy embayments separated by low rock outcrops (Cooper, 1995). The Chain Rocks embayment (Fig. 6) is a 1.6 km long, topographically bound bay, bounded by the Chain Rocks outcrop in the south and Inyoni Rocks outcrop to the north. A coastal railway line, a legacy of past bad planning practices, traverses both the seaward edge of the modified coastal dune and the Amanzimtoti River. The river catchment is urbanised and residential units are set on the vegetated dune above the railway line and a restaurant, paddleboats and a canoe club along the lagoon's northern edge. The river draining into the lagoon is polluted by urban run-off and a poorly maintained sewage system and is often clogged with an invasive alien water hyacinth *Eichhornia crassipes*. In spite of its degraded state, the lagoon is frequented by a thriving bird population and is on occasion well stocked with fish.

As in the case of Margate beach, the Chain Rocks embayment is subject to seasonal beach rotation - during the austral winter erosion is greatest in the south with deposition in the north of the bay, whilst during summer the reverse is true (Guastella & Smith,

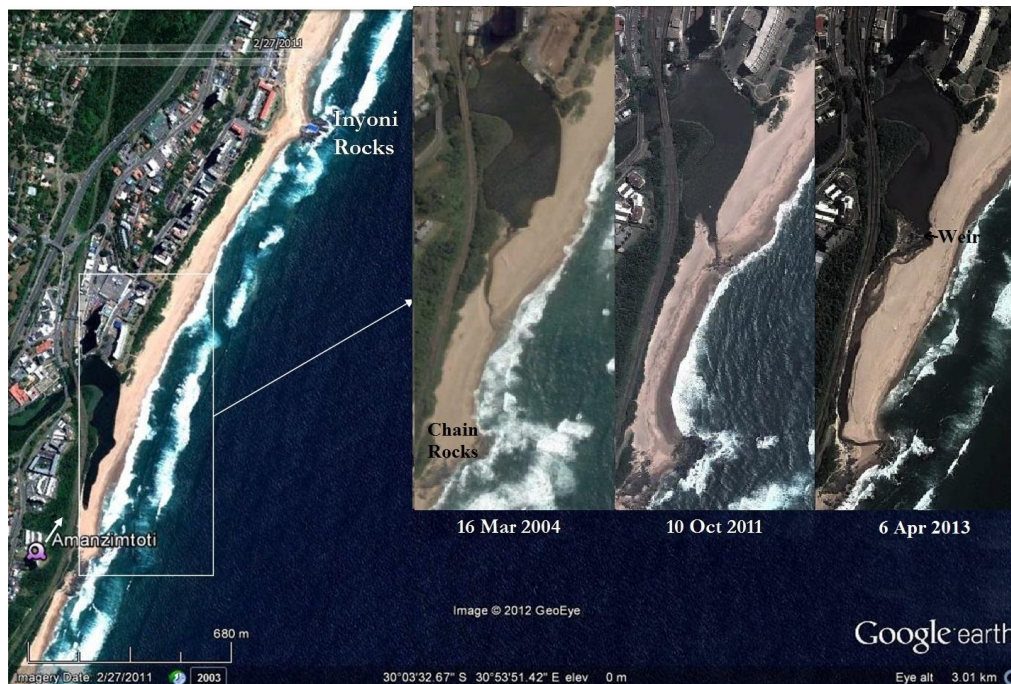


Figure 6. Location of Chain Rocks Beach and Amanzimtoti lagoon and the position of the Vodacom NNE-orientated webcam (bottom left of picture) (Google Earth). The inset illustrates the study area and a snapshot of changes in beach width and estuary mouth position. The inset image for 10 October 2011 shows the lagoon outlet being more centrally placed near the weir whereas on 6 April 2013 the lagoon outlet is in the extreme south and is hugging the embankment next to the railway line. Note also the decreased beach width during October 2011 and inflated state of the beach during April 2013.

2014). The Amanzimtoti River, which has a river length of 11.6 km and drains a catchment of 39 km<sup>2</sup> (Cooper 1991), discharges into the Indian Ocean via a lagoon. A detailed discussion of the beach and lagoon morphodynamics is contained in Smith et al., (this issue). The lagoon mouth is often closed by the baymouth bar (refer Fig. 1, Smith et al., this issue), but it can be breached during high rainfall and/or high swell activity, especially on a spring high tide. There is a systematic seasonal change of lagoon mouth morphodynamics driven by river run-off (Smith et al., this issue). The mouth tends to migrate along the beach, varying from being centrally placed to discharging some 400 m to the south alongside the Chain Rocks outcrop that marks the south edge of the bay, depending on the amount of rainfall, beach width and ocean swell regime. During 1979 a concrete weir was constructed on a diabase sill (Figs 6 & 7g) outcrop intermittently exposed along the dominant lagoon outlet channel, reportedly to control the extent to which the lagoon level dropped whenever the mouth was opened (Begg, 1984), however, it may have been constructed to prevent southward migration of the outlet or to control water levels for the paddle-boats on the lagoon. The outlet sometimes breaks through at this point. A 1909 photograph in Begg (1984) shows the mouth to be naturally open there.

#### **Amanzimtoti: the problem**

Analysis of webcam imagery, backed up by site visits, showed that the lagoon outlet breached on 8 August 2012 following widespread rain (99 mm over three days) and started to migrate southwards to a position about 100 m south of the weir (Fig. 7b). Low flow was maintained until the end of the month after which the mouth temporarily closed, only to breach again on 6 September 2012 following further heavy rains (140 mm over 3

days), but this time in a more southerly position some 180 m south of the weir. Progressive southward migration of the mouth to about 250 m south of the weir occurred on 16 September 2012 (Fig. 7c) following 80 mm of rain during 14-15 September. High rainfall (363% of normal for September 2012; refer Fig. 5b), resulted in increased and accelerated river flow and initiated erosion of the coastal dune upon which the railway line is constructed. The mouth remained open in this new southerly position and also breached opposite the weir position during 11-15 October 2012 (refer Fig. 7d) under the influence of tidal action, but then resumed a southerly position again with a meander (see 19 Nov 2012 image, Fig. 7e). Fieldwork showed slippage of the embankment (Fig. 8a) and that the railway line was being undermined.

A telephone discussion and email was sent on 6 November 2012 to the railway authority by the main author of this paper, warning that the slope was unstable and could fail in the event of more continued rain or future high seas coincident with spring tides, and that further slope failure could lead to infrastructure damage to the railway line. A short-term solution of breaching the river mouth to reduce water levels and erosion was advised and an emergency authorisation could be applied for with the relevant environmental authorities. This warning went unheeded and instead the railway authority embarked on a lengthy tender process for engineering services to propose a medium to long-term solution without addressing the immediate problem.

In the interim a meeting was held between the railway authority and representatives from the DAEA, EKZN Wildlife and the eThekweni Municipality. The environmental authorities reportedly advised that no hard defence structures were to be deployed. Permissions were put in place for the railway authority to breach



Figure 7: Sequence of webcam imagery from the Vodacom webcam (refer locality in Fig 6) from (a) 25 July 2012 to (i) 20 January 2013 showing southward and landward migration of the Amanzimtoti lagoon outlet at Chain Rocks. All images are at low tide except (d), (g) and (h) which were captured at mid-tide, and (f) which was taken on 30 November 2012 two hours before high tide following heavy rain; note the train crossing the railway line. Figure (h) shows the breached baymouth bar on 14 December 2012, following emergency intervention by the Municipality on 11 December 2012 after the railway line had failed. Note the standing train and yellow cranes on the railway line to remove the two derailed locomotives. Figure (i) shows the outlet extending even more southward towards Chain Rocks, a position which was maintained for most of 2013.

the baymouth bar at the central position (refer Fig. 6) to relieve the hydraulic pressure, however no formal application was made. The only action taken by the railway authority was to place a speed restriction of 30 km/hr on trains to reduce vibration from train traffic and so reduce destabilisation of the already unstable slope. A follow-up e-mail to the railway authority by the senior author on 30 November 2012, advising that heavy rains (intense rain of 22 mm within 15 minutes followed by a further 33 mm) had inflated the river flow, further undermining the unstable dune slope below the railway line, was ignored. This was further aggravated by wave action at high tide (refer Fig. 7f).

Yet more rain over 5-7 December 2012 pushed the lagoon mouth further southwards towards Chain Rocks (Fig. 7g), resulting in additional slope failure. A deluge on 10 to 11 December 2012 (97 mm from 14:00 on 10 December to 10:00 on 11 December) was the final straw and the embankment failed at approximately 03:30 am on 11 December 2012 during the passing of a goods train, resulting in the collapse of the railway line and train derailment (Fig. 8b & d), with injuries to four personnel. The intense rain coincident with high tide after midnight had further undermined the toe of the embankment, resulting in an initial collapse of a mast pole and subsequent collapse of the embankment under the weight of the train. After the incident the river mouth was breached by the Municipality at the concrete weir (Fig. 7h) as an emergency to relieve the hydraulic pressure and a

significant drop in river levels adjacent to the embankment occurred. However, the outlet returned to its southerly trajectory during January (Fig. 7i) and the mouth remained in the southerly position during most of 2013, ultimately also eroding away a ski-boat access ramp, which had previously been stabilised by waterloffels (Fig. 8c). Railway traffic was limited to one line as the broken south-bound line was out of commission and the remaining line was moved landward as a precaution. A diversion and repair plan started during November 2013 using geofabric sandbags, however this has not yet been authorised and has been permitted as an emergency procedure in the interim.

The Amanzimtoti River could easily have been artificially breached prior to the incident at minimal cost. Breaching would have reduced water levels and hydraulic pressure and caused a diversion of flow away from the embankment, reducing the risk of further erosion. Instead the railway authority are faced with a cost of approximately R20 million (source withheld) for repairs (installation of geofabric bags, sheet piles and embankment reconstruction). Loss of equipment (i.e. two locomotives, one wagon, signals and railway infrastructure) amounted to approximately R11 million (source withheld). Factoring in the cost of buses to transport commuters when the line was out of commission, emergency personnel, clean-up, temporary shifting of the railway line landward, planning and consultant fees, etc., the total amount is estimated to be about R50 million.



Figure 8: (a) Southward view of Amanzimtoti lagoon outlet showing slippage of the embankment on 4 November 2012. Note how close the slippage is occurring to the railway line and mast poles; (b) northward view of derailed locomotives and railway carriage on 11 December 2012; (d) inland (WSW) view of collapsed embankment and cranes to remove locomotives – note the lack of vegetation on the embankment compared to (a). Figure (c) is a southward view of the Amanzimtoti lagoon outlet on 25 October 2013, similar to that in (a), showing the outlet extended further south undermining the dune and ramp on which the white vehicle in the distance is parked. Note the absence of vegetation compared to Figure (a) as a result of continued slope failure.

### LESSONS LEARNT

While it is acknowledged that artificial breaching of river mouths may have an adverse effect on the natural functioning of these sensitive systems, in some critical cases it is politically/socially unavoidable. Each case needs to be assessed individually, based on sound scientific input. Artificial breaching should only be done if absolutely necessary and from a hydrodynamical point of view it is preferable to allow water levels to rise and breach the bar naturally (CSIR, 1990) – this is often achieved in combination with high swells. Breaching is a complex and controversial matter and the level at which it is done and the position and depth of the breached channel are very important. This must be carefully managed because if channels are dug too low the system could be drained entirely.

In this case timeous intervention at Margate Beach prevented infrastructure loss, which would have been costly if left unchecked. The limited beach width and inherited poorly placed infrastructure has intensified coastal squeeze, leaving little room for coastal retreat, hence requiring management. Knowledge of how lagoon outlets work can help to make an informed decision. Management with minimal intervention to achieve this is recommended, but this may require ongoing maintenance, depending on natural factors such as rainfall, sedimentation, erosion, tides and ocean swells. The case of Amanzimtoti illustrates how a “do nothing” approach resulted in costly infrastructural loss, injury and the potential for loss of life. It is fortunate that the train was a goods train and not a passenger train, as the repercussions could have been immense had it been a passenger train. A low impact intervention strategy to breach (and maintain) the lagoon at a point near the historic weir, where the

lagoon has previously naturally breached (e.g. Fig. 7d), would have relieved pressure on the system and avoided erosional damage. Analysis of our records of webcam imagery shows that in previous instances (e.g. 2010) where the lagoon naturally breached at this point after months of flowing southward, beach recovery in the southern corner was rapid. Mimicking this scenario would have avoided the erosion damage experienced. A carefully managed and maintained breaching programme would have avoided this disaster.

### CONCLUSION

Whereas interference with natural processes is incorrect from an ecological and geomorphological perspective, there comes a critical point where intervention may be required to protect infrastructural loss and thereby avoid future knock-on expenses. Each situation is different and needs to be treated on a case-by-case basis, with due consideration of ecological and geomorphological impacts and location and circumstances of previous breaches. In both cases the ecological functioning of the river-lagoon system has been compromised. However intervention was timely in the case of Margate, but not in the case of Amanzimtoti. Perhaps in both cases short-term remedies (an artificial breaching process) could have been instituted before the situations worsened. Emergency breaching should be the policy and not permanent diversions. Live webcams provide the opportunity to examine the baseline, and before and after intervention scenarios, and to use and apply the knowledge gained to other systems that may require similar management. Live webcams also provide an early warning system to alert when erosion is starting to occur and thereby plan for any corrective action that may be required. Dedicated webcams should be used by local authorities to monitor and manage known erosion hotspots.

### ACKNOWLEDGEMENTS

The South African Weather Service (SAWS) is acknowledged for the Durban South and Margate rainfall data, while eThekweni City Engineers are acknowledged for the Amanzimtoti rainfall data. Fig 1 was compiled by Riaan Botes of Geodynamic Systems. Webcam imagery was sourced from South Coast Web and Vodacom and satellite imagery was sourced from Google earth. This project is self-funded.

### LITERATURE CITED

- Begg, G., 1978. The Estuaries of Natal (Part 1), *Town and Regional Planning Report* 41, The Natal Town and Regional Planning Commission, Pietermaritzburg, South Africa, 657p.
- Breetzke, T., 2012. EMP for Margate Main Beach and Nkongweni Estuary: Short-Term Emergency Response, Specialist Report for Hibiscus Coast Municipality, *Royal HaskoningDHV Reference Number: E02.DUR.000643*, 23p, unpublished.
- Breetzke, T., 2013. Nkongweni Estuary Interim Mouth Management Plan: A project for the Hibiscus Coast Municipality, *Royal HaskoningDHV Reference Number: M01.DUR.0000017*, 12p, unpublished.
- Cooper, J.A.G., 1990. Ephemeral stream-mouth bars at flood-breach river mouths: comparison with ebb-tidal deltas at barrier inlets. *Marine Geology*, 95, 57-70.
- Cooper, J.A.G., 1991. *Sedimentary Models and Geomorphological Classification of River Mouths on a Subtropical, Wave-Dominated Coast, Natal, South Africa*. PhD Thesis, University of Natal, Durban, South Africa, unpublished.
- Cooper, J.A.G., 1995. Shoreline Changes on the Natal coast: Mtamvuna River mouth to the Mkomazi River mouth. *Natal Town and Regional Planning Commission Report*, 79, The Natal Town and Regional Planning Commission, Pietermaritzburg, South Africa, 53p.



- CSIR., 1990. Hydro factors affecting siltation in the lower reaches of Natal/KwaZulu rivers, submitted to Natal Town & Regional Planning Commission, *CSIR Report EMA-D 9006*, 22p.
- Guastella, L.A., Smith, A.M., 2014. Coastal dynamics on a soft coastline from serendipitous webcams: KwaZulu-Natal, South Africa, *Estuarine Coastal & Shelf Science*, <http://dx.doi.org/10.1016/j.ecss.2013.12.009>.
- Harrison, T.D. & Cooper, J.A.G., 1991. Active migration of juvenile grey mullet (Teleostei: mugilidae) into a small coastal lagoon against high current velocities. *South African Journal of Science*, 87, 395-396.
- Harrison, T.D., Cooper, J.A.G., Ramm, A.E.L., 2000. State of South African estuaries. Geomorphology, Ichthyofauna, Water quality and Aesthetics. *State of the Environment Series Report 2*. Department of Environmental Affairs and Tourism, Pretoria, pp. 1-127.
- National Estuarine Management Protocol., 2013. National Environmental Management Integrated Coastal Management Act (ICM) (2008), *Government Gazette* 36432, 10 May 2013.
- Smith, A.M., Guastella, L.A., Goble, B.J., (this issue). Forecasting lagoon outlet erosion: KwaZulu-Natal, southeast Africa, *Journal of Coastal Research*, Special Issue 66..
- South Coast Web website: <http://www.margate.co.za/index-goldenmile.htm>
- Vodacom website: <http://www.vodacom.co.za/personal/services/webcams/webcams/?pageUrl=/personal/services/webcams/webcams&firstLoad=true>.

## Beach users' profile, perceptions and willingness to pay for beach management in Cadiz (SW Spain)

†Bruna Alves, †Javier Benavente, ‡Óscar Ferreira

†Dept. Earth Sciences, CASEM  
Universidad de Cádiz  
11510 Puerto Real, Spain  
bruna.alvesrodrigues@alum.uca.es

‡FCMA/CIMA/CIACOMAR  
Universidade do Algarve  
8005-139 Faro, Portugal  
oferreir@ualg.pt



[www.cerf-jcr.org](http://www.cerf-jcr.org)



### ABSTRACT

Alves, B., Benavente, J., Ferreira, Ó., 2014. Beach users' profile, perceptions and willingness to pay in Cadiz (SW Spain). In: Green, A.N. and Cooper, J.A.G. (eds.), *Proceedings 13<sup>th</sup> International Coastal Symposium* (Durban, South Africa), *Journal of Coastal Research*, Special Issue No. 70, pp. 521-526, ISSN 0749-0208.

[www.JCRonline.org](http://www.JCRonline.org)

Beaches are complex systems on which different activities and interests are pursued. The most widespread activities relate to tourism and recreation. An individual's choice for a particular coast depends on the site characteristics and user's perception. In order to identify beach users' profiles and perceptions, a beach survey was carried out in the beaches of Cadiz, SW Spain, and subsequent sociodemographic factors affecting people's willingness to pay for beach management were identified. Despite part of the economic interests in Cadiz being related to tourism-related activities, most of the beach users are Cadiz residents. Respondents say that the elevated number of people in the beach during high season is problematic and causes unpleasant consequences, like accumulation of litter. Moreover, people mentioned the inadequate number of beach facilities (e.g. recreational services, showers, W.C.'s) and the perceived need for beach nourishment in some specific areas of the coast. The hypothetical implementation of a fee for beach management improvement was not supported by interviewees. A high number of local visitors of low economic status seemed to be the variables driving this finding. Regardless of beach users' assertions that the quality of the urban coast of Cadiz could be improved, they were not prepared to pay increased tax to achieve this.

**ADDITIONAL INDEX WORDS:** *coastal tourism, coastal recreation, beach management, contingent valuation method.*

### INTRODUCTION

Coastal zones are complex systems where different processes occur. They are also attractive and important for socioeconomic activities. The coastal zone generates economic activity and a local tax base (Houston, 2013).

Seaside tourism and recreation have rapidly increased in recent decades, becoming a "big business" and a primary contributor to the Gross Domestic Product (GDP) of several countries (Houston, 2013). Coastlines worldwide receive millions of visitors every year for activities such as beach going, swimming, fishing, etc.

According to Breton *et al.* (1996) the key factors that influence users' preferences when choosing a specific beach include beach development status, i.e. a functional, comfortable, user-friendly and safe beach. Considering coastal tourism as an important industry and that the provision of recreation services affects wellbeing and profits (Paudel *et al.*, 2011), when increasing the benefits of a coast, i.e. the recreational value, there must be an appropriate environmental status and leisure facilities.

The general public's attitudes and perceptions are important for identification and effective management of areas under concern (MacLeod *et al.*, 2002). However, in tourist coasts, local residents also are directly affected by holiday-related activities and hence have a strong moral case to be heard and heeded (Weaver and Lawton, 2013).

This paper analysed a questionnaire applied to beach end-users'

in Cadiz, SW Spain. Beach goers' profiles were described and sociodemographic factors affecting people's willingness to pay to improve beach management were identified.

### STUDY AREA

Cadiz is a coastal town in SW Spain (Figure 1). It has a population of approximately 130,000 inhabitants and one of the highest population densities in Europe (~11,000 per km<sup>2</sup>). The city is the second most important municipality in economic activity in the Cadiz province, but its economic dynamic, in terms of GDP, is low if tourism is excluded. Maritime trade and shipyard activities have been reduced as well as fishing activities. The strongest economic sector is commerce. Tourism has grown lately because of the beaches, historical and artistic heritage sightseeing, carnivals and year-round cruise ship tourism.

The coast comprises different beaches and tourist targets. The present study focused on three sandy beaches located within the town: Santa María del Mar, Victoria and Cortadura (Figure 1). Santa María del Mar is the smallest beach surveyed (900 m long), created in the early 1980's by beach nourishment. It is the closest beach to the centre, which causes intensive occupation during summer. The average number of users on summer day is 4,000 (D. García pers. comm. 2012). The high occupation is evident especially during high tide, when most of the beach disappears. Regular nourishment maintains the beach with the Andalucía-Atlántico Coastal Authority previously ordering replenishment of the area in 1991, 1997, 2000, 2004 and 2009 (Muñoz-Perez *et al.*, 2001, 2013).

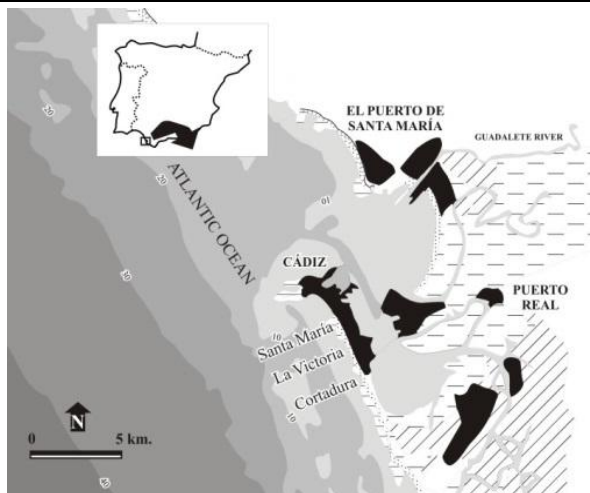


Figure 1. City of Cadiz, beaches (Santa María del Mar, Victoria and Cortadura) and surroundings, SW Spain.

Victoria is a long urban beach (2,800 m) with good accessibility, hotels and many amenities (game-courts, children's recreational space, tourism office, bars, etc). It is also the busiest beach in town. The wide surface and beach quality are maintained by a sand nourishment programme (placed in 1991, 2004 and 2010; Muñoz-Perez *et al.*, 2001, 2013). The average number of visitors on a peak season day is 20,000 people, reaching 60,000 on the busiest days (D. García pers. comm. 2012).

Cortadura is an isolated, semi-natural beach 1,600 m long. Dunes and coastal vegetation are protected by a project for dune restoration. Cortadura receives in average 10,000 people on a summer day (D. García pers. comm. 2012).

## METHODS

### Data collection

Data from 765 beach users were obtained by means of a questionnaire survey over May to August 2013. Reference for questions were obtained from previous publications (Ariza *et al.*, 2012; Blakemore and Williams, 2008; Breton *et al.*, 1996; Landry *et al.*, 2003; Lozoya, 2012; Roca *et al.*, 2008; Roca *et al.*, 2009). The questionnaire approached different topics, resulting in an evaluation of the end-user profile (sociodemographic profile, habits on beach use, motivation and suggestions), beach landscape and comfort, available facilities, and environmental, geomorphological and physical aspects.

Surveys were conducted *in situ* using a pseudorandom selection of respondents. The interviewer followed a zigzag path through the beach loungers, stopping at any group of people. The chosen candidate (minimum age of 15) was briefly introduced to the survey and instructed to answer the questions.

Data were later treated using descriptive statistical analysis and statistical models.

## RESULTS

### Beach users' profile

Descriptive statistical analysis is used in order to describe the respondents (Table 1).

The total sample was composed mostly of female respondents and the majority of users were between 25-55 years old. Santa María del Mar is characterised mostly by beach goers ranging from 25 to 55 years old. The group of 45-55 year old represents nearly one third of the users (28.2%), with the number of individuals over 65 years obtaining a significantly high number. In Victoria the average age of beach users was significantly younger than Santa María del Mar, with users mostly between 15-45 years old, with the majority of the users being between 25 to 35 years old (25.4%). Cortadura, as Santa María del Mar, also has people mainly between 25-55 years, although about one third of the sample is between 25-35 years (28%).

Education level is similar in the whole area with compulsory Secondary Education (*Educación Secundaria Obligatoria*) or less held by 17.4% of the total population and 27.8% have Post-Compulsory Schooling (*Bachillerato*). The majority of the candidates attained an undergraduate or a higher degree (44.8% are undergraduates and 10% obtained a master or a higher degree).

Beach goers in Santa María del Mar and Victoria have the same pattern of family monthly income. The population fits into two groups: one earning between €1,000-€2,000 and the other > €3,000. In Cortadura €1,000-€2,000 range is the most frequent mentioned household income interval, and there is a decrease in the number of families earning higher salaries.

Santa María has 70.8% of beach goers from Cadiz, whereas this number decreases in both Victoria and Cortadura (51% and 55.1%, respectively). At the same time, in Santa María del Mar the percentage of people from the province and the rest of Spain decreases followed by an increase in the beaches of Victoria and Cortadura, with Victoria representing the main beach chosen by foreigners with 7.7% more than at the other studied beaches.

The beaches are visited with a very specific purpose: sunbathing and resting (75.7%). A few observations demonstrate other visit reasons, such as the use of the beach as a space for children to play (12%) and to practise sports (8.5%). In general, respondents stayed primarily in their own houses, but slight differences are detected in housing arrangements detected. At Santa María del Mar 80.4% of the people came from their residence, decreasing to 51% and 44.2% in Victoria and Cortadura, respectively. In Santa María 9.5% of the candidates stay in a second residence and 6% do one-day-trips. In Victoria 19.2% of the visitors come for one day on the beach with only 13.4% of the candidates interviewed using their second residence. In Cortadura, the number of one-day tourist's increases to 35.2% with 8.5% of the beach goers using their second residence.

From all the surveys it was evident that most visitors walked to the beach (54.9%), followed by those who used car/motorcycles (34.9%) and urban buses (6.1%). Although, in Cortadura the percentage of people that use automotive transport was higher with a lower percentage of people who walk to the beach.

### Willingness to pay - "Would you be willing to pay to use the beach if this meant that the beach would be better maintained or improved?"

WTP (willingness to pay) was expressed by only 88 respondents (12.9%). The mean value was of €1.66 per adult visit to the beach, the median was €1. Respondents tended to use round numbers when giving a value; in this study, €1, €2 and €3 represented over half of the responses (71.6%). The variable WTP does not show a normal frequency distribution (Shapiro-Wilk,  $p < 0.001$ ).

Differences in the amount respondents stated to be willing to pay (amount WTP) and whether respondents were conceptually willing to pay or not (%WTP), were analysed with respect to

Table 1. General and individual sociodemographic characteristics, transport and accommodation type.

Variables	All sample (n = 765) %	Santa María del Mar (n = 171) %	Victoria (n = 393) %	Cortadura (n = 201) %
<b>Age (years)</b>				
15-25	16.4	9.4	20	15.5
25-35	25.1	21.2	25.4	28
35-45	23.4	24.7	23.5	22
45-55	18.7	28.2	12.5	22.5
55-65	10.2	7.1	12.5	8.5
>65	6.2	9.4	6.1	3.5
<b>Gender</b>				
Male	42.6	41.5	41.2	46.3
Female	57.4	58.5	58.8	53.7
<b>Education Level</b>				
Compulsory Sec. Educ. or less	17.4	15.4	18.3	17.3
Post-Compulsory Schooling	27.8	27.2	25.7	32.8
Undergraduate	44.8	46.3	45.5	42.1
MSc or higher	10	11.1	10.5	8.1
<b>Monthly Income (€)</b>				
0-1,000	8.6	9.1	9.6	6.3
1,000-2,000	35	31.8	32.4	42.8
2,000-3,000	28.3	26.5	28.1	30.2
3,000-4,000	16.9	16.7	20	10.7
>4,000	11.2	15.9	9.9	10
<b>Hometown</b>				
Cadiz City	56.5	70.8	51	55.1
Cadiz Province	17.3	12.3	18.5	19.2
Rest of Spain	20.7	14	22.8	22.2
Abroad	5.5	2.9	7.7	3.5
<b>Visit Purpose</b>				
Sunbathe & resting	75.7	72.8	75.2	79
Sports	8.5	6.2	9.1	9.2
For children's play	12	19.1	11.2	7.7
Other	3.8	1.9	4.4	3.1
<b>Accommodation</b>				
Second residence	11.2	9.5	13.4	8.5
Regular home	55.8	80.4	51	44.2
Campsite	0.1	0	0	0.5
Hotel	5.9	1.8	7.2	7.1
Renting	6.5	2.3	9.2	4.5
One day trip	20.5	6	19.2	35.2
<b>Transport</b>				
On foot	54.9	72.3	63.9	22.4
Bicycle	1.6	0.6	1.5	2.4
Car/motorcycle	34.9	20.6	24.8	66.7
Urban bus	6.1	4.1	6.7	7
Other	2.5	2.4	3.1	1.5

independent explanatory variables: age, gender, hometown, education level and beach (Table 2). The monthly family income was not taken into account because income and education level were found to be collinear, i.e. convey the same information. Respondents' likelihood of giving a positive conceptual valuation (%WTP) was analysed using Logistic Regression. Tobit Model (censored regression model) was used to verify, among the respondents willing to pay, the amount that they would assign to a hypothetical beach tax.

Significant variables for %WTP are (Table 2): age (range 45-55), hometown (Cadiz Province and rest of Spain), education level (undergraduate or higher) and beach. Significant variables used for variation in amount WTP were found to be the same as for %WTP (Table 2), this time also including the age category >65 years of age.

### Beach users' perception and suggestions

Interviewees were asked to name what they most disliked on the beach they were spending the day. There were 613 valid answers,

Table 2. Used variables for variation in conceptual and amount WTP and respective explanatory variables significance.

Variables	%WTP (n = 681)		Amount WTP (n = 81)	
	Odds Ratio	p	Coefficient	p
<b>Age (years)</b>				
<i>15-25</i>				
25-35	0.667	0.278	-0.877	0.141
35-45	0.728	0.389	-0.497	0.396
45-55	0.401	0.037*	-1.501	0.031**
55-65	0.859	0.741	-0.306	0.674
>65	0.329	0.108	-2.462	0.035**
<b>Gender</b>				
<i>Male</i>				
Female	1.257	0.361	0.151	0.706
<b>Hometown</b>				
<i>Cadiz City</i>				
Cadiz Province	2.308	0.009***	1.512	0.003***
Rest of Spain	2.652	0.001***	1.473	0.004***
Abroad	1.479	0.459	0.727	0.382
<b>Education Level</b>				
<i>Compulsory Sec. Educ. or less</i>				
Post-Compulsory Schooling	1.824	0.260	0.606	0.416
Undergraduation or higher	3.471	0.011**	1.792	0.009***
<b>Beach</b>				
<i>Santa María del Mar</i>				
Victoria	0.598	0.081*	-0.695	0.160
Cortadura	0.372	0.008***	-1.360	0.024***

Reference categories in *italic*. Logistic Regression Pseudo-R<sup>2</sup> 0.0772. Tobit Model Pseudo-R<sup>2</sup> 0.0554. \*Significant value at 0.1, \*\*significant value at 0.05 and \*\*\*significant value at 0.01.



Figure 2. Word cloud of the most frequent dislike aspects along the beaches studied.

out of which 4.2% were satisfied with beach conditions. The main complaint was crowding (Figure 2) mentioned by 23.2%, followed by presence of rocks and algae on the sand (16.8%) and litter (11.7%). Besides the three parameters mentioned above, 8.5% of respondents agreed that the parking condition is a problem as there is deficiency of available area and fees are high.

Other aspects listed were the presence of pigeons, nearby urbanisation development, excessive noise, uncivil attitudes and lack of beach nourishment (perceived as a reduction in beach area and scarped slope of the subaerial beach). Beach goers, especially in Santa María del Mar, declared that there is a notable lack of beach services and amenities.

People were also asked to add suggestions for the improvement of beach quality. From 122 comments, 13.9% mentioned the need of civic and environmental education and awareness, increased vigilance (12.3%) and the improvement in amenities and services (11.5%) i.e. more WC's, AP system in English and recycling bins. Other suggestions included requirement for beach nourishment (9.8%), more recreation options (9%) such as game courts, special areas for children, etc., and improvement in cleaning services (7.4%). Interestingly the traditional "night of barbecues", a local summer night festivity locally known as *Trofeo Carranza*, was suggested to be forbidden in 5.7% of the collected data, as it brings litter to the beaches and causes occurrence of uncivil attitudes.

## DISCUSSION

### Beach visitors: the identified end-users' profiles

The average beach user of Cadiz is an adult of 40 years old, living in town that walks to the beach walking directly from home for sunbathing and resting. This person finished an undergraduate or a higher degree and the total household income is approximately €2,200 per month. This description fits well to the town type as the urbanisation established along the oceanfront, makes it easier to reach the beach by merely walking from home. Forty years old expresses the mean age of a beach population which comprises young and elderly people, as the beaches are easily reachable and there is a great variety of beach services and amenities to be offered. Moreover, Cadiz is densely occupied, which makes the coastal space an extension of people's home where the sand is referred to as their backyard, i.e. citizens have a passionate bond with the beach.

Nevertheless, some minor differences appear in each of the beaches studied. In Cortadura beach users frequently come for a

day trip driving a car from Cadiz Province or from the rest of Spain. This behaviour is quite exclusive to Cortadura because it is located far from the town centre, out of the urbanised area and the public transport to the beach is not efficient, an aspect that is disadvantageous to elder users. Cortadura serves the population from neighbouring towns that can rely on private transport. Victoria beach receives the most diverse type of visitors as its beachfront has a high density and a great variety of development; the area is favoured by summer residents and tourists. Santa María del Mar is the preferred beach among the locals. It is close to the city centre and to other traditional neighbourhoods of Cadiz. People use the beach for long day stays, enjoying the space for social interaction. Picnics, family, reunions' and children's playground, are some of the common activities on the beach on a typical summer day.

### Visitors' perceptions and suggestions for beach management improvement

The expressed animosity towards the summer occupancy of the beaches refers to the concept of carrying capacity (MacLeod and Cooper, 2005; Valdemoro and Jimenez, 2006), i.e. the amount and type of visitors that can be accommodated within a given area without suffering any social consequences or detrimental impact on resources. The beach resting zone (MOP, 1970) corresponds to the area where most of the beach users lounge around placing their parasols and sunbeds. This is the typical pattern in wide beaches, like Victoria, that concentrates people in the rest zone whereas a large part of the beach is barely used. The sand in the beach back zone gets hot and uncomfortable, thus the space is basically for beach access and installation of services and amenities.

Conversely, in Santa María del Mar users settle all over the area as the beach is very short and narrow. This semi-artificial beach, morphologically comparable to a pocket beach, experiences severe erosion (Benavente *et al.*, 2006), which is clearly visible and is the origin of complaints by the traditional and loyal beach users who suggest beach nourishment. The reduction in beach surface is the determinant for the perception of crowding. Due to the continuous changes in the beach subaerial portion, coastal dynamics play an important role in use and exploitation of Santa María del Mar.

Deposition of rocks and algae on the shoreline can be compared to the presence of litter on sand and water. Although rocks and algae are natural elements of the coastal ecosystem, they seem to be disliked at urban coasts. Along the studied beaches, rocks cause uncomfortable irregularities on sand and the stranded algal wrack deposits produce an unpleasant smell. Moreover, the algal deposits interact with litter, creating a rough contour of debris at the high water line. As found by Ariza *et al.*, (2008) and Blakemore and Williams (2008) the presence of litter was a negative aspect and, in Cadiz, mentioned as an example of uncivil behaviour taking place anytime, but particularly during the "night of barbecues". End-users expect vigilance on the beach and application of fines to those not respecting social space and total prohibition of barbecues. Other users stated that the beaches need improvement in cleaning services: more frequent garbage collection and installation of more waste bins. A proactive measure suggestion was the implementation of campaigns for environmental education and awareness, so that people would be conscious of their importance in beach maintenance and potential coastal tourism.

End-users requested improvements in beach services and amenities. Similarly to what is described by Roca *et al.* (2008) the toilet facilities were said to be insufficient in relation to the high number of visitors (Santa María del Mar), sparse (Victoria) and nearly absent (Cortadura). Beach users in Santa María del Mar also pointed out the lack of other facilities, like regular and feet

showers. Foreign tourists complained about the P.A. system information being only in Spanish. This is an important observation, because Cadiz is recognised as a tourist destination.

The urbanisation that for decades has developed along the coast, was cited as a cause of disturbance, because it degrades the scenery and can actually be responsible for other identified problems, for example the presence of pigeons on the beach and the overcrowded parking areas. Roca *et al.* (2008) also found that parking is a problem in other urban coastal areas, as there is no available space and the private service implements high charges. In Cadiz, respondents, especially locals, do not agree with private parking and requested the construction of new lots to meet the excessive summer demand.

### Willingness to pay

Blakemore and Williams (2008) found 87% of the interviewed British tourists were willing to pay for beach use. They would pay in average £0.90 to visit Olu Deniz, a Turkish beach resort, i.e. €1.10 at November 2013 exchange rates. Voke *et al.* (2013) found that 63.25% of users would be willing to pay to visit a marine renewable deployment area in St. David's beach, Wales. Mean value for visitors was £6.70 per person (approximately €8, November 2013 exchange rates). Median values were slightly lower, £5 (circa €6).

These results are substantially different to those of the present study. Cadiz urban beaches are of great importance for daily and holiday life of local residents. Statistics show that local residents are much less willing to pay compared to visitors from the province and the rest of Spain. It does not apply to foreigners, although this might be explained by the few surveyed people coming from abroad. As the question was how much respondents would be willing to pay "per visit" it is logical that local residents would be willing to pay lower values, or not pay at all, as they visit the area more frequently than people with holiday purposes. Besides, local residents believe that they already pay enough taxes to the council and assume that beach facilities and maintenance must be covered by these taxes. Local residents consider the beach a public space, as any other, so they do not agree that it is something they must pay for. Moreover, there is a crucial difference between the monthly income of a British family that goes for holiday in a foreign country and the household income of a family from Cadiz that essentially uses the local beaches.

The hypothetical market bias is one aspect of the objection to the method. As the payment in question is theoretical, respondents can give answers which may relate to a token value, misrepresenting their WTP. Willingness to pay may represent the amount that people are prepared to pay at that moment, according to their current income and preferences, but does not necessarily correspond to their perceived value of the area, or in this case, the real cost of managing the beach. On the other hand, candidates can also overestimate their WTP as they are aware the payment is theoretical and in reality they will not be required to pay. As found in Blakemore and Williams (2008), the present survey found that most of the results for amount WTP were round values. Hence, these values may not necessarily correspond to a true market value, but they are possibly a good indication of revenue that could be collected.

Education had a positive influence on conceptual and amount WTP, i.e. people with higher levels of education are expected to better understand the need for managing environmental resources, and therefore they are more amenable to a beach visit tax. In the same sense a higher level of education contributes to people having a higher income.

Similar to Halkos and Matsiori (2012), age categories negatively affect WTP. People between 45-55 years old and older (>65 years), would pay less than other age groups. Interestingly, if %WTP and amount WTP are compared, results indicate that younger age categories are less inclined to pay, however when young people affirm to be willing to pay, they pay higher amounts than elder respondents. Older people may not be able to contribute much due to several reasons, such as more expenditure on health, preference for alternative recreation activities or economic dependence after their retirements.

Visitors to Cortadura are less prone to accept paying a visit tax. This beach has a semi-natural aspect and end-users might consider that intensive coastal management is not required, as services and amenities are sparse and are concentrated at one access to the beach. Cortadura visitor's economic profile indicates that nearly half of the sample (49.1%) is composed of households earning a maximum €2,000/month, which indicates that on this beach the economic status might be a setback for WTP. Moreover, people arrive at Cortadura mainly by car, a transport that includes extra expenses during a day on the beach.

## CONCLUSION

The survey provided good quality data to describe end-users in the urban beaches of Cadiz. Results which confirm that beach goers are mostly from town. Foreigners arrive in town all year round for cultural events and sightseeing, but summer tourists of sand-and-sun are few. The urban coast is essential to local residents for recreational and holiday options, factors explained by the densely populated urban area, low economic status and lack of public spaces.

Because beaches are such an important local resource, the high concentration of users during the peak days of summer is problematic as well as the associated uncivil actions. Additionally, some beach services did not satisfy public opinion. This suggests that to achieving a high quality environmental status, beach users' needs and implemented leisure services must be harmonious. Coastal authorities should review the management plan for urban beaches according to people's perceptions and needs.

The proposal of a beach tax does not seem to be the best approach for enhancement of beach functions (e.g. recreation and natural buffer zone), services and management. The economic status and high frequency of local visitors argue against the idea of implementing a toll.

## ACKNOWLEDGMENTS

The work is a contribution to the project GERICO (CGL 2011-25438), research group RNM-328 of the Andalusian Research Plan (PAI), supported by the Ministry of Economy and Competitiveness. The authors would like to thank Campus de Excelencia Internacional • Campus del mar (CEIMAR). Authors kindly thank Profs. Ramon Ballester and Ricard Rigall-I-Torrent from Department of Economics, University of Girona, for statistics guidance and review. Also, Daniel García, Environmental Services, Cadiz City Hall for information provided.

## LITERATURE CITED

- Ariza, E., Jiménez, J.A. and Sardá, R., 2008. Seasonal evolution of beach waste and litter during the bathing season on the Catalan coast. *Waste Management*, 28 (12), 2604-13.
- Ariza, E., Ballester, R., Rigall-i-Torrent, R., Saló, A., Roca, E., Villares, M., Jiménez, J.A. and Sardá, R., 2012. On the relationship between quality, users' perception and economic valuation in NW Mediterranean beaches. *Ocean & Coastal Management*, 63, 55-66.
- Benavente, J., Anfuso, G., Del Río, L., Ciavola, P., Rodríguez, S. and Nuño, T., 2006. Patrones de transporte sedimentario y cambios morfológicos en una playa urbana en bolsillo. In A. Pérez Alberti y J. López Bedoya (eds.): *Geomorfología y Territorio*. Serv. Publ. Universidad de Santiago de Compostela, 337-348.
- Blakemore, F. and Williams, A., 2008. British tourists' valuation of a Turkish Beach using Contingent Valuation and Travel Cost Methods. *Journal of Coastal Research*, 24, 1469-80.
- Breton, F., Clapés, J., Marquès, A. and Priestley, G.K., 1996. The recreational use of beaches and consequences for the development of new trends in management: the case of the beaches of the Metropolitan Region of Barcelona (Catalonia, Spain). *Ocean & Coastal Management*, 32(3), 153-80.
- Halkos, G. and Matsiori, S., 2012. Determinants of willingness to pay for coastal zone quality improvement. *The Journal of Socio-Economics*, 41(4), 391-99.
- Houston, J.R., 2013. The Economic Value of Beaches - a 2013 Update. *Shore & Beach*. 81(1), 3-11.
- Landry, C.E., Keeler, A. G. and Kriesel, W., 2003. An economic evaluation of beach erosion management alternatives. *Marine Resource Economics*. 18(2), 105-27.
- Lozoya, J.P., 2012. *Multi-risk assessment and users' perception: a further step towards ecosystem-based beach management*. Blanes, Spain: Centre d'Estudis Avançats de Blanes. Ph.D. thesis, 188p.
- MacLeod, M. and Cooper, J.A.G., 2005. Carrying Capacity of Coastal Areas. In: Schwartz, M. (ed), *Encyclopedia of Coastal Systems*. Kluwer, pp. 228.
- MacLeod, M., Pereira da Silva, C. and Cooper, J.A.G., 2002. A comparative study of the perception and value of beaches in Rural Ireland and Portugal: implications for coastal zone management. *Journal of Coastal Research*. 18, 14-24.
- Ministerio de Obras Públicas (MOP), 1970. Playas, modelos tipo y sugerencias para su ordenación. Madrid: Spain. Dirección General de Puertos y Señales Marítimas. 64p.
- Muñoz-Pérez, J.J., Medina, R. and Tejedor, B., 2001. Evolution of longshore beach contour lines determined by EOF method. *Scientia Marina* 65(4), 393-402.
- Muñoz-Pérez, J.J., Roman-Sierra, J., Navarro-Pons, M., Graça Neves, M. and Campo, J., 2013. Comments on "Confirmation of beach accretion by grain-size trend analysis: Camosoto beach, Cádiz, SW Spain" by E. Poizot et al., (2013) *Geo-Marine Letters* 33(4), *Geo-Marine Letters*, 1-4.
- Paudel, K.P., Caffey, R.H. and Devkota, N., 2011. An evaluation of factors affecting the choice of coastal recreational activities. *Journal of Agricultural and Applied Economics*. 43(2), 167-79.
- Roca, E., Villares, M. and Ortego, M.I., 2009. Assessing public perceptions on beach quality according to beach users' profile: A case study in the Costa Brava (Spain). *Tourism Management*. 30(4), 598-607.
- Roca, E., Riera, C., Villares, M., Fragell, R. and Junyent, R., 2008. A combined assessment of beach occupancy and public perceptions of beach quality: A case study in the Costa Brava, Spain. *Ocean & Coastal Management*, 51(12), 839-46.
- Valdemoro, H.I. and Jimenez, J.A., 2006. The influence of shoreline dynamics on the use and exploitation of Mediterranean tourist beaches. *Coastal Management*, 34(4), 405-23.
- Voke, M., Fairley, I., Willis, M. and Masters, I., 2013. Economic evaluation of the recreational value of the coastal environment in a marine renewables deployment area. *Ocean & Coastal Management*, 78, 77-87.
- Weaver, D.B. and Lawton, L.J., 2013. Resident perceptions of a contentious tourism event. *Tourism Management*, 37, 165-75.

# Evaluation of recreational quality, carrying capacity and ecosystem services supplied by sandy beaches of the municipality of Camaçari, northern coast of Bahia, Brazil



[www.cerf-jcr.org](http://www.cerf-jcr.org)

José R. de Souza Filho<sup>∞</sup>, Rodrigo C. Santos<sup>‡</sup>, Iracema R. Silva<sup>†</sup>, Carla I. Elliff<sup>‡</sup>

<sup>∞</sup> Federal Institute of Education, Science and Technology Baiano  
Salvador, Bahia, Brazil  
jrsouzageografia@gmail.com

<sup>†</sup> Department of Oceanography  
Federal University of Bahia  
Salvador, Bahia, Brazil  
iracema@pq.cnpq.br

<sup>‡</sup> Postgraduate Course in Geology  
Federal University of Bahia  
Salvador, Bahia, Brazil  
rodrigocerqueiras@yahoo.com.br  
carlaelliff@gmail.com



[www.JCRonline.org](http://www.JCRonline.org)

## ABSTRACT

Souza Filho, J. R., Santos, R. C., Silva, I R., Elliff, C.I., 2014. Evaluation of recreational quality, carrying capacity and ecosystem services supplied by sandy beaches of the municipality of Camaçari, northern coast of Bahia, Brazil. In: Green, A.N. and Cooper, J.A.G. (eds.), *Proceedings 13<sup>th</sup> International Coastal Symposium* (Durban, South Africa), *Journal of Coastal Research*, Special Issue No. 70, pp. 527-532, ISSN 0749-0208.

The coastal municipality of Camaçari is currently under great real estate pressure. It is located within one of the main urban growth vectors of the State of Bahia, Brazil. In this context, the main goal of this research was to assess the recreational quality and the carrying capacity, and qualitatively evaluate the ecosystem services supplied by the beaches of the municipality of Camaçari and its adjacent coastal area. In order to evaluate the recreational quality, the beaches of Busca Vida, Jauá, Interlagos, Arembepe, Barra de Jacuibe, Guarejuba and Itacimirim were classified according to twenty-three geoenvironmental quality indicators and eleven infrastructure indicators. Aiming to evaluate the similarity of geoenvironmental and recreational infrastructure characteristics among the studied beaches, a multivariate cluster analysis was used. The ecosystem services were assessed and gathered according to Regulation/Support Services, Provision Services and Information and Culture Services classes. Some beaches experienced a usage level above their carrying capacity, contributing to low geoenvironmental quality and compromising the supplied ecosystem services, mainly the ones concerning regulation and support. In beaches with low urbanization levels and predominance of natural or poorly human impacted environments, a greater diversification and quality of ecosystem services was identified, both of regulation and support services as well as of provision, information, culture and leisure services.

**ADDITIONAL INDEX WORDS:** *Ecosystem service, recreational quality, carrying capacity, coastal management.*

## INTRODUCTION

Ecosystems may be defined in a simplified way as systems that comprise the complex and dynamic interactions between living beings and their physical and biological environments (MA, 2003). This concept places the human being as an integrant and participative party and concerns not only the interactions between organisms, but also all physical factors that form the environment (Andrade and Romero, 2009). One of the main properties of ecosystems is their resilience, which represents their ability to return to their natural state, in other words, the measurement of the disturbances that may be absorbed by an ecosystem without changing its stable equilibrium (Andrade and Romero, 2009). The resilience of ecosystems is an essential property concerning the definition of their carrying capacity in order to assure the supply of ecosystem services.

There is, currently, a worldwide concern about the economic benefits of biodiversity, comparing the costs caused by its loss with the costs of conservation measures. Thus, Ecological Economy studies the relationships between ecosystems and economic systems (Constanza, 1989), broadening the Neoclassic Economy concepts and associating economic studies with

ecologic, social and environmental concepts, among others. Thus, Ecologic Economy evaluates and quantifies the services offered by ecosystems and sets their limits of resilience and their carrying capacity, aiming at the sustainability of these services.

With the increase on the demand for recreation and leisure, and the consequent increase on the pressure on resources and natural ecosystems, carrying capacity has been an increasingly present concern in several areas and in different evaluation scales. The concept of carrying capacity assumes that there is a certain number of people that the resources may withstand without deteriorating environmental and recreational quality (Archer and Cooper, 2001; Williams and Gill, 2001; Pereira da Silva, 2002; Polette and Raucci, 2003; Silva *et al.*, 2006; Silva *et al.*, 2009). However, in general, a greater emphasis is given on social issues than on the sustainability of the natural systems.

The municipality of Camaçari, located on the northern shore of the State of Bahia, Brazil, presents a narrow coastline of approximately 40 km in extension, and is limited, in its most inner area, by semi-consolidated deposits of the Barreiras Formation (Martin *et al.*, 1980; Dominguez *et al.*, 2009), of Miocene age (Suguio and Nogueira, 1999). Quaternary deposits, mainly represented by sandy Holocene and Pleistocene marine terraces are found across nearly the entire coastal area (Martin *et al.*, 1980), with the majority of them occupied and altered by human activities. Locally, there are fluvial-lacustrine deposits of



wetlands, dunes, lagoons, mangroves, coral reefs and beach sandstone banks (Martin *et al.*, 1980, Dominguez *et al.*, 1996, Leão and Kikuchi, 1999). This ecologic diversity, along with the easy access, creates a strong attraction towards tourism, recreation and leisure activities, and appeals to visitors and businessmen, which today represents an important vector of touristic growth of the State of Bahia (Silva *et al.*, 2008).

The occupation of this coastline did not happen homogeneously. The municipality of Camaçari presents two different situations regarding coastline occupation: beaches located within closed condos, such as Busca Vida and Interlagos, and beaches present along the greatest area of its length, open access to the public, such as Arembepe and Jauá. Despite the intense urbanization in both cases, spatial occupation occurs in different ways. In the first case, the occupation pattern presents a greater arrangement of space usage, which is not seen in the second case, where there is free occupation of the coastal area. There are also beaches – such as Barra do Jacuípe, Guarajuba and Itacimirim – that merge sectors occupied by closed condos, sectors with free occupation and sectors still without any type of human construction. In this context, besides the already available knowledge concerning coastal sediment dynamics of the area (Bittencourt *et al.*, 2010; Dominguez *et al.*, 1996), it is of crucial importance to perform studies concerning the recreational quality and carrying capacity of these beaches, as well as the ecological boundaries and ecosystem services supplied by the studied beaches that may subsidize usage and occupation plans for this shoreline.

Considering that recreational quality of beaches depends on their geoenvironmental and infrastructure characteristics, which set the limits – either ecological or accommodation – for their use, and that the ecosystem services supplied by these beaches may be compromised once these limits are not respected. This study had the objective to value qualitatively the ecosystem services supplied by the beaches of the municipality of Camaçari and estimate their recreational quality and carrying capacity.

## METHODS

All indicators were analyzed and classified based on walks along the studied beaches during field trips in different seasons, between January 2010 and December 2011. Since Jauá, Arembepe, Guarajuba and Itacimirim presented great variation in their natural and occupation characteristics and infrastructure, these beaches were divided in sectors with similar characteristics. Thus, the beach units were considered as: Busca Vida; Jauá, sectors 1 and 2; Interlagos; Arembepe, sectors 1, 2 and 3; Barra do Jacuípe; Guarajuba, sectors 1 and 2, and Itacimirim, sectors 1 and 2 (Figure 1).

### Evaluation of the Recreational Quality

The recreational quality of the beaches of the municipality of Camaçari was evaluated based on joint analysis of geoenvironmental and infrastructure quality analysis, described by Leatherman (1997), Silva *et al.* (2003), Araújo and Costa (2008) and Silva *et al.* (2012). To do so, 23 geoenvironmental quality indicators (exposure degree to wave energy, bathing area, big waves breaking directly on the beach face, rip currents, slope of the beach face, constituent material of the beach face, beach sand color, water transparency, width during low tide, coastal erosion vulnerability, human structures that hinder the movement of users in the beach, natural structures that hinder beach usage, shoreline typology according to the degree of urban occupation, fixed structures, habitat diversity, vegetation coverage at the backshore,

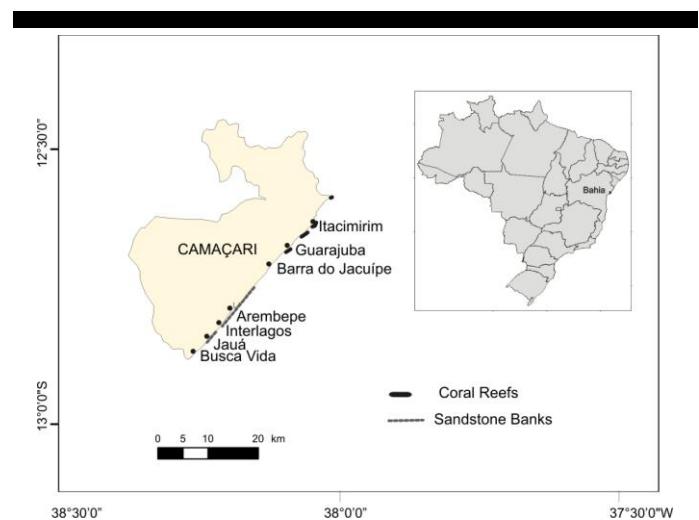


Figure 1. Location of the municipality of Camaçari and the studied beaches.

odors, oil or bitumen on the beach or in the water, marine litter accumulation, floating litter, algae on the sand or in the water column, sewage discharge, jellyfish) and 11 infrastructure indicators for recreational use (toilet facilities, snack bars, bars and restaurants, accommodation facilities, parking lots, trash cans, recreation facilities, public transportation, beach access, level difference down to the beach, usage intensity, life-guards) were selected. These indicators were classified in three categories, each one valued from 1 to 3 (1 – low quality; 2 – intermediate quality; 3 – high quality). The recreational quality of each beach was expressed as the total sum of the found values. Finally, aiming to assess the similarity between the studied beaches, a multivariate Cluster analysis was applied (McCune and Grace, 2002), using the PAST software, based on the values attributed to each indicator.

This way, according to Silva and collaborators (2012), evaluating bathing areas, which are conditioned to the degree of wave exposure, exposed beaches were considered as those with plain wave action; the ones where sandstone banks or coral reefs create a locally protected area were considered as partly sheltered; and, sheltered beaches were those in which these structures protect the coast from wave action in at least 50% of their length. Regarding water transparency, water with no turbidity was considered translucent; brown-colored waters, as high turbidity, and, water with intermediate coloration between the previous situations, as average turbidity. In this case, only the observations made over the summer period were considered.

Concerning the vulnerability of erosive processes, beaches were considered of low vulnerability to erosion when they did not present any erosion evidence; of average vulnerability, when there was local erosion evidences (low erosive scarp on the holocene marine terrace or on dune cordon); and, high vulnerability beaches were those with significant erosion evidences (erosive scarp on the holocene marine terraces or on the dune cordon, fallen coconut trees, coconut trees with exposed roots and the presence of protecting structures) over most of their length. Structures of human (usually erosion protection structures) or natural (usually sandstone banks) origin that hinder the user's movement or the use of the beach itself were considered as few when they covered an area smaller than 50% of the beach length and, with many covering and area greater than this.

Regarding the evaluation of the coastline typology, beaches with more than 70% fixed constructions along 50 m of the coast were considered highly urbanized; those with 30 to 70% constructions were considered of low urbanization; and below 30%, were considered as very low urbanization. Clear evidence of effluent discharge was considered via visual perception of the presence of sewage across the beaches (reaching the sea or not), information gained from local inhabitants or traders on the occurrence of discharge or the presence of structures (such as septic tanks) which may indicate eventual sewage discharges. Concerning the presence of oil or bitumen, algae or jellyfish, the occurrence of more than ten items per beach was considered as frequent.

Still according to Silva and collaborators (2012), in the evaluation of recreational infrastructure, the indicators regarding the presence of toilet facilities, snack bars, bars and restaurants, accommodation, trash cans and recreation facilities, were considered as few when less than three occurrences per kilometer were noticed along the analyzed beach and adjacent coastal area.

If there were parking lots, the availability of vacancies for vehicles, taking into account the demand of each beach, was considered by using a visual estimation of parking conditions during the summer. Public transportation was considered restricted when available at only one specific location along the evaluated beach. The intensity of usage was measured by the ratio between the available usage area of each beach and the number of users during high frequency periods (summer weekends, between 12 A.M. and 3 P.M.).

### Evaluation of the Carrying Capacity

The beaches of the municipality of Camaçari were divided into cells of 50 m in extension (comprising the backshore and beach face) and, these cells were used to measure the initial and final widths of the beach. The area of each cell was calculated based on these values. The number of people within each cell was counted. To do so, the walks were taken during the period of highest frequency, estimated from pictures taken every hour, to allow the identification of user flow during the day. The counting, as well as the measurements of each beach cell, was carried out during the days when this period corresponded to or was near low tide heights. Then, the relationship between each cell area and the number of users was calculated, thus, finding the available beach area for each user. The current load was determined through the ratio between the available area and the current usage level. To estimate the carrying capacity – understood as a situation of ideal accommodation – the number of people per day for each beach was determined, considering an ideal usage level of 10 m<sup>2</sup> per user, according to users' preference established by Silva and collaborators (2012), by interviewing beach users in the Northern Coast of the State of Bahia.

### Qualitative valuation of the ecosystem services

Considering that the ecosystems associated to the beach must also be valued, allowing a more integrated and broader analysis, the present proposal also considered the adjacent coastal area up to 200 m from the backshore towards the continent. For the studied beaches – and their associated ecosystems – the ecosystem services were grouped in Regulation and/or Support Services, Provision Services, and Information and Culture Services (De Groot *et al.*, 2002). Table 3 presents the characteristics and criteria adopted in this valuation, in which each service (or its absence) is attributed a low, medium or high value.

## RESULTS

The evaluation of geoenvironmental quality, according to the criteria adopted in this study, showed a higher quality for Guarajuba (sectors 1 and 2) and Itacimirim (sectors 1 and 2) beaches – further from the urban center of Salvador city – and a lower geoenvironmental quality for the Busca Vida, Interlagos, Jauá (sector 1) and Arembepe (sectors 1 and 2) beaches – closest to the urban center in the Salvador city. Some indicators had the same valuation on the studied beaches and did not serve as a comparison parameter. These indicators include the declivity of the beach, sediment color and presence of algae, jellyfish and litter. It is important to emphasize that litter accumulation was a negative indicator in all studied beaches.

The Cluster diagram divided the studied beaches into two major groups: the first represented by those with a high human occupation level and the second by those with lower occupation levels. In the first group there was a subdivision relating (with ca. 90% similarity) the Jauá (sector 1) and Arembepe (sector 2) beaches. These beaches are characterized by a disordered occupation of their backshore, with the loss of their natural characteristics, acceleration of coastal erosion processes and, consequently low geoenvironmental quality. This group also congregates the Guarajuba (sector 2) and Itacimirim (sector 1) beaches (with ca. 75% similarity). These latter beaches, despite the intense usage of their shoreline, have still kept some of their natural characteristics and a high geoenvironmental quality.

The second group gathers the Interlagos and Busca Vida beaches (with ca. 80% similarity) located within private condos, with ordered occupation and restricted access. These two beaches, on the other hand, are similar (ca. 70% similarity) to the Arembepe beach (sector 1), where the greatest area of its shoreline is also occupied by private condos. According to the Cluster diagram, Barra de Jacuípe and Itacimirim (sector 2) within this group presented similarity (ca. 80%). In these beaches, the occupation of the coastline is not continuous, with several sectors that still preserve their natural characteristics. The last grouping congregates the Jauá beach (sector 2) and the beaches of Guarajuba (sector 1) and Arembepe (sector 3) (with ca. 70% similarity) all with no urbanization, preserving their natural aspects.

The evaluation of the infrastructure quality indicated a greater availability of recreational infrastructure for Arembepe (sector 2), Guarajuba (sector 2) and Itacimirim (sector 1). On these beaches there is free access to the public and provision of toilet facilities, snack bars, restaurants, bars and accommodation facilities. These beaches presented high usage intensity, possibly due to the services offered, which motivates the accelerated occupation of their shoreline. The lowest values of infrastructure were presented by the Arembepe (sector 3), Jauá (sector 2), Guarajuba (sector 1), Interlagos and Busca Vida beaches. The first three beaches have a very low usage intensity with the total absence of recreational infrastructures. The last two beaches mentioned are located within private condos, with a greater usage intensity when compared to the previous ones, with recreational infrastructure offered in clubs within the condos and not along the beaches.

The Cluster diagram, applied to the infrastructure characteristics, also divided the beaches into two major groups: the first group consists of beaches with low infrastructure quality – Arembepe (sectors 1 and 3), Jauá (sector 2), Guarajuba (sector 1), Itacimirim (sector 2), Interlagos and Busca Vida and, the second group, consists of beaches with high infrastructure quality – Arembepe (sector 2), Guarajuba (sector 2), Itacimirim (sector 1), Barra do Jacuípe and Jauá (sector 1).

The joint evaluation of the geoenvironmental and infrastructure indicators resulted in the valuation of recreational quality of the studied beaches (Table 6). This evaluation indicated a medium recreational quality for every studied beach, except the Guarajuba (sector 2) and Itacimirim (sector 1) beaches, which presented high recreational quality. These two sectors of the Guarajuba and Itacimirim beaches were characterized by the presence of natural pools formed by coral reefs, appreciated for bathing and diving, and by the availability of restaurants and beach tents, with the provision of toilet facilities, showers, beach chairs and parasols, attracting tourism, recreational and leisure activities.

Despite the low variation results for the recreational quality evaluation, the grouping analysis indicated different levels of similarity between the studied beaches (Figure 2). Once more, two major groups were identified: the first with the beaches of higher occupation and demand for recreation and leisure activities, and the second with lower user frequency (as a reflex of various characteristics, both geoenvironmental and infrastructure). The first group maintains both groupings observed in the geoenvironmental quality diagram, with the degree of similarity ca. 80% for Guarajuba (sector 2) (Figure 3A) and Itacimirim (sector 1) – both with a high recreational quality – and, with the degree of similarity ca. 95%, for the Jauá (sector 1) and Arembepe (sector 2) (Figure 3B) beaches. The second group, also in agreement with the groupings observed in the geoenvironmental quality diagram, consists of Interlagos and Busca Vida beaches (ca. 80% similarity), the Barra do Jacuípe and Itacimirim (sector 2) beaches (also with ca. 80% similarity) and the Arembepe (sector 3) and Guarajuba (sector 1) beaches (with ca. 70% similarity) with the Jauá (sector 2) beach (with ca. 60% similarity).

The evaluation of the ecosystem services offered by the beaches of the municipality of Camaçari and its adjacent coastal zone clearly indicated a strong dependence on their natural conditions. Thus, the coastal sectors where wetlands, mangroves or estuaries occur associated to the beach – such as Busca Vida, Jauá, Interlagos, Arembepe (sectors 1 and 3), Barra do Jacuípe, Guarajuba (sector 1) and Itacimirim (sector 2) – offer, in a higher or lower degree, important water control and storage, assimilation and nutrient recycling services, as well as serving as a nursery and refuge area for several species and as sources of food production and ornamental and genetic resources.

Along the sectors where marine sand terraces were not waterproofed by human constructions – such as Jauá (sector 2), Arembepe (sector 3), Barra do Jacuípe, Guarajuba (sector 1) and Itacimirim (sector 2) – regulation services occur associated to the recharge of aquifers and with the preservation of the Restinga vegetation on the terraces, providing a terrestrial refuge and nursery. The preservation of this ecosystem also allows, in some cases, the provision of ornamental resources, food production and services associated to ecotourism activities.

The occurrence or preservation of the dune cordon and its vegetation – as in Arembepe (sector 3) – enables adjacent coastal area protection against coastal erosion, working as a natural barrier and contributing to sediment trapping. Support services associated to sediment trapping in the adjacent coastal area and the backshore are also provided where natural vegetation is preserved, as in Jauá (sector 2), Arembepe (sector 3), Barra do Jacuípe, Guarajuba (sector 1) and Itacimirim (sector 2).

Important regulation/support, provision and information services are provided by the shoreline sectors where reef ecosystems occur – as in Guarajuba (sectors 1 and 2) and Itacimirim (sectors 1 and 2). These ecosystems represent marine refuges and nursery areas, promote coastline protection (reducing

wave action power) and, many times, contribute to food production, provide genetic resources and offer services associated to ecotourism and recreation. By analyzing the values related to regulation and support services it is possible to observe that the beaches behave in different ways. Some, such as Arembepe (sector 3), Barra do Jacuípe and Itacimirim (sector 2), obtained a high grade. On the other hand, making up the lowest grades, there are Arembepe (sector 2), Guarajuba (sector 2), Itacimirim (sector 1) and Jauá (sector 1). Such a result confirms that this class of service is inversely proportional to the urbanization level, in other words, the more urbanized the coastline is, the less regulation and support services it offers. It is also important to highlight that regulation and/or support services allow, through their maintenance, the provision of information, culture and leisure

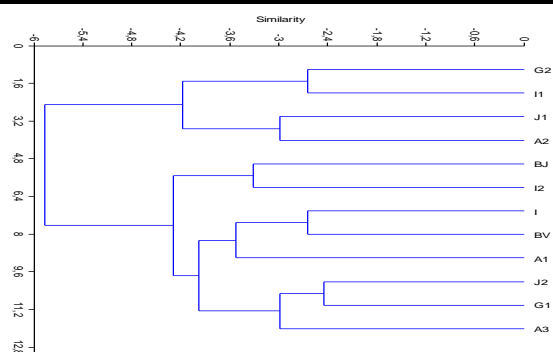


Figure 2. Cluster diagram for the studied beaches according to their Recreational Quality Indicators (Geoenvironmental + Infrastructure). BV: BuscaVida; J1: Jauá (sector 1); J2: Jauá (sector 2); I: Interlagos; A1: Arembepe (sector 1); A2: Arembepe (sector 2); A3: Arembepe (sector 3); BJ: Barra do Jacuípe; G1: Guarajuba (sector 1); G2: Guarajuba (sector 2); I1: Itacimirim (sector 1); I2: Itacimirim (sector 2).

services. The analysis of the provision services indicated that natural food production and the offer of ornamental resources contributed with equal importance in every area, presenting similar characteristics. These services also presented an inversely proportional relationship to the urbanization level.

Information, culture and leisure services, among others, obtained the highest values in areas with low urbanization and high geoenvironmental quality, critical for recreation and ecotourism activities and for the maintenance of scenic attraction. The services associated to historical and cultural tourism were not observed in any of the studied beaches.

According to the evaluation of the accommodation limits of the studied beaches (Table 1), the greatest areas available for user accommodation were found in the Barra do Jacuípe (160,000 m<sup>2</sup>), Busca Vida (120,000 m<sup>2</sup>) and Guarajuba (sector 1) (90,000 m<sup>2</sup>) beaches, and the smallest in the Jauá (sector 2) (28,750 m<sup>2</sup>), Itacimirim (sector 1) (25,000 m<sup>2</sup>) and Itacimirim (sector 2) (37,500 m<sup>2</sup>) beaches. However, the beaches with the greatest user accommodation areas do not currently offer adequate recreational infrastructure (i. e. provision of toilet facilities, restaurants, trash cans and life-guards), which decreases their recreational attraction. The beaches of Jauá (sector 1) and Arembepe (sector 2) presented usage levels of 6 and 2 m<sup>2</sup>/user, respectively. This corresponds to a current load of around 11,875 and 33,750 users per day (Table 1). These values exceed the carrying capacity – assuming for the ideal usage condition (10 m<sup>2</sup>/user) for beaches in the municipality of Camaçari. According to the study carried out by Silva *et al.*,

2012 – estimated in 7,185 users/day for Jauá (sector 1) and in 6,750 users/day for Arembepé (sector 2).

## DISCUSSION

The beaches of Jauá (sector 1) and Arembepé (sector 2) showed high similarity in their Cluster diagrams for recreational quality and, amongst the studied beaches, they were the ones which presented the lowest geoenvironmental quality values. The intense occupation of their coastline and the usage above their carrying capacity – with irregular constructions on the backshore area and the loss of coastal vegetation – might have created or intensified the severity of the coastal erosion impeding the usage of the these beaches, with the construction of containment structures and the loss of recreational beach during high tide periods. Besides the loss of geoenvironmental quality, this intense occupation compromises the offer of ecosystem services, especially those of regulation and support related to the recharge of aquifers (by waterproofing the sand terraces), sediment trapping (removal of vegetation in the backshore and dune cordon), water control and storage and pollutant assimilation and recycling (compromised by the irregular occupation of wetlands), marine and terrestrial refuge and/or nursery (compromised by the removal of Restinga vegetation and by the impact on turtle nesting areas), among others.

On the other hand, beaches such as Busca Vida, Interlagos, Guarajuba (sector 1), Arembepé (sectors 1 and 3) and Itacimirim (sector 2) presented a carrying capacity at least ten times greater than the current carrying capacity. However, it must be highlighted that those values refer to the social capacity, according to the comfort sensation indicated by users. Considering ecological limits, imposed by the need of ecosystem service maintenance, the Guarajuba (sector 1), Arembepé (sector 3) and Itacimirim (sector 2) beaches require more restricted use, especially on the prevention of human occupation in the backshore area and adjacent coastal areas. As these beaches have increased services offered (both of regulation and support), provisions, information and culture.

## CONCLUSION

The Cluster diagram analysis indicated different similarity levels among the studied beaches, identifying two major groups, for both the geoenvironmental quality analysis and for infrastructure: the first group consists of beaches with higher occupation, and demands for recreation and leisure activities,

Table 1. Carrying capacity, accommodation area, usage level and current carrying capacity of the beaches of the municipality of Camaçari.

CARRYING CAPACITY				
Beaches	Beach area available for users' accommodation (m <sup>2</sup> )	Current usage level per beach (average area per user in m <sup>2</sup> )	Current carrying capacity	Carrying capacity *
Busca Vida	120000	100	1200	12000
Jauá - 1	71250	6	11875	7125
Jauá - 2	28750	100	288	2875
Interlagos	60000	100	600	6000
Barra do Jacuípe	160000	35	4571	16000
Guarajuba - 1	90000	100	900	9000
Guarajuba - 2	60000	32	1875	6000
Arembepe - 1	60000	100	600	6000
Arembepe - 2	67500	2	33750	6750
Arembepe - 3	67500	100	675	6750
Itacimirim - 1	25000	13	1923	2500
Itacimirim - 2	37500	100	375	3750

\* considering an ideal usage of 10 m<sup>2</sup>/person

while the second group consists of beaches with lower user frequencies.

The geoenvironmental characteristics were preponderant in the recreational evaluation of the beaches and showed their dependence, in a higher or lower degree, on the usage and urbanization conditions and their impacts. According to the criteria adopted in this study, the Guarajuba (sectors 1 and 2) and Itacimirim (sectors 1 and 2) beaches presented a higher geoenvironmental quality, while the Busca Vida, Interlagos, Jauá (sector 1) and Arembepé (sectors 1 and 2) beaches, presented a



Figure 3. A: Guarajuba beach (sector 2), considered of high recreational quality; B: Intense use and high level of urbanization of the Arembepé Beach (sector 2).

lower quality. The evaluation of the recreational infrastructure showed that the Arembepe (sector 2), Guarajuba (sector 2) and Itacimirim (sector 1) beaches presented a higher quality, while the Arembepe (sector 3), Jauá (sector 2), Guarajuba (sector 1), Interlagos and Busca Vida beaches presented a lower recreational infrastructure quality. The fact that infrastructure conditions (such as the offer of toilet facilities, restaurants, trash cans, public transportation, and recreation facilities, etc.) are easily altered should be taken into account. However, once geoenvironmental conditions are altered, it is unlikely for them to return to their original conditions.

The identification of ecosystem services offered by the studied beaches and their adjacent coastal area (limit of 200 m of the backshore area) showed a greater variety of services, both of regulation and/or support, as well as provision and information, culture and leisure, for the beaches with low urbanization levels and the predominance of natural environments or with little human impact, such as the Arembepe (sector 3), Barra do Jacuípe, Guarajuba (sector 1) and Itacimirim (sector 2) beaches.

The Jauá (sector 1) and Arembepe (sector 2) beaches presented a usage level above their carrying capacity, which seems to have contributed to the long term decrease in their geoenvironmental quality and compromising of the ecosystem services offered, especially those of regulation and support.

Finally, the evaluation methods proposed in this study showed the need of usage management and planning measures for the beaches of the municipality of Camaçari, especially for those closest to Salvador's urban center, where it is possible to observe a compromise of the geoenvironmental quality and the offer of ecosystem services. For the beaches that still preserve their natural patrimony, it is urgent to implement preventive measures, since this entire municipality undergoes intensive real-estate pressure.

## ACKNOWLEDGEMENT

I. R. Silva thanks CNPq (National Council for Scientific and Technological Development) for the Research Fellowship-Grant and R. C. Santos thanks CAPES (Coordination of Improvement of Higher Education Personnel) for the Research Fellowship.

## LITERATURE CITED

- Andrade, D.C., Romeiro, A.R., 2009. Serviços ecossistêmicos e sua importância para o sistema econômico e o bem-estar humano, Campinas: IE/UNICAMP, 155p.
- Archer, B., Cooper, C., 2001. Os Impactos positivos e negativos do turismo. In: Theobald, W. F. (org.), Turismo Global, Editora Senac, São Paulo, Brasil, pp. 10-20.
- Bittencourt, A.C.S.P., Livramento, F.C., Dominguez, J.M.L., Silva, I.R., 2010. Tendências de longo prazo à erosão costeira num cenário perspectivo de ocupação humana: litoral norte do estado da Bahia. *Revista Brasileira de Geociências*, 40, 2-13.
- Constanza, R., 1989. What is Ecological Economics? *Ecological Economics*, 1, 1-7.
- De Groot, R.S., Wilson, M.A., Boumans, R.M.J., 2002. A typology for the classification, description, and valuation of ecosystem functions, goods and services. *Ecological Economics*, 41, 393-408.
- Dominguez, J.M.L., Leão, Z.M.A.N., Lyrio, R.S., 1996. Litoral Norte do Estado da Bahia. In: SBG, XXXIX Congresso Brasileiro de Geologia. Roteiro de Excursão. 67p.
- Dominguez, J.M.L., Andrade, A.C.S., Almeida, A.B., Bittencourt A.C.S.P., 2009. The Holocene Barrier Strandplains of the State of Bahia. In: Dillenburg, S.R., Hesp, P.A., Geology and Geomorphology of Holocene Coastal Barriers of Brazil. Lecture Notes in Earth Sciences, Springer-Verlag Berlin Heidelberg, Germany, 107, 253-288.
- Leão, Z.M.A.N., Kikuchi, R.K.P., 1999. The Bahian Coral Reefs – from 7000 years BP to 2000 years AD. *Ciência and Cultura*, 51, 262-273.
- Martin, L., Bittencourt, A.C.S.P., Vilas Boas G.S., Flexor J.M., 1980. Texto Explicativo para o Mapa Geológico do Quaternário Costeiro do Estado da Bahia, CPM/SME, Bahia, Brazil. 20p.
- McCune, B., Grace, J.B., 2002. Nonmetric Multidimensional Scaling. In: Analysis of Ecological Communities. MJM, Software, Oregon. 125p.
- Millennium Ecosystem Assessment. 2003. Ecosystem and Human Well-Being: a framework for assessment. Island Press, Washington, DC.
- Pereira, S.C., 2002. Beach Carrying Capacity Assessment: How important is it? *Journal of Coastal Research*, SI. 36, 190-197.
- Polette, M., Raucci, G.D., 2003. Methodological Proposal for Carrying Capacity Analysis in Sandy Beaches: A Case Study at the Central Beach of Balneário Comboriú (Santa Catarina, Brazil). *Journal of Coastal Research*, SI. 35, 94-106.
- Silva, J.S., Barbosa, S.C.T., Leal, M.M.V., Lins, A.R., Costa, M.F., 2006. Ocupação da praia da Boa Viagem (Recife/PE) ao longo de dois dias de verão: um estudo preliminar. *Pan-American Journal of Aquatic Sciences*, 1(2), 91-98.
- Silva, S.B.M., Silva, B.C.N., Carvalho, S.S., 2008. Metropolitização e turismo no litoral norte de Salvador: de um deserto a um território de enclaves? In: Carvalho, I., Pereira, G.C. (eds) Como anda Salvador, Edufba, Salvador, Bahia. pp. 189-211.
- Silva, I.R., Souza Filho, J.R., Barbosa, M., Rebouças, F., Machado, R.S., 2009. Diagnóstico Ambiental e Avaliação da Capacidade de Suporte das Praias do Bairro de Itapoã, Salvador, Bahia. *Revista Sociedade e Natureza*, 21(1), 71-84.
- Silva, I.R., Bittencourt, A.C.S.P., Alveirinho, D.J., Souza Filho, J.R., 2012. Qualidade recreacional e capacidade de carga das praias do Litoral Norte do Estado da Bahia, Brasil. *Gestão Costeira Integrada*, 12(2), 131-146.
- Suguio, K., Nogueira, A.C.R., 1999. Revisão Crítica dos Conhecimentos Geológicos sobre a Formação (Ou Grupo?) Barreiras do Neógeno e o seu Possível Significado como Testemunho de Alguns Eventos Geológicos Mundiais. *Geociências*, 18, 461-479.
- Williams, P.W., Gill, A., 2001. Questões de Gerenciamento da Capacidade de Carga Turística. In: Theobald, W. F. (org.). Turismo Global, Editora Senac, São Paulo, Brazil. pp. 45-55.

# Cross-shore variation of water surface elevation and velocity during bore propagation

Kwang-Ho Lee<sup>†</sup>, Sungwon Shin<sup>‡</sup>, Do-Sam Kim<sup>∞</sup>

<sup>†</sup> Dept. of Energy Resources and Plant Engineering, Kwandong University, Gangneung, Gangwon-do, Korea  
klee@kd.ac.kr

<sup>‡</sup> Experimental Center for Coastal & Harbor Engineering  
Chonnam National University  
Yeosu, Jeonnam, Korea  
sungwshin@gmail.com  
sungwshin@jnu.ac.kr  
(corresponding author)

<sup>∞</sup> Dept. of Civil Engineering, Korea Maritime University, Busan 606-791, Korea  
kimds@hhu.ac.kr



[www.cerf-jcr.org](http://www.cerf-jcr.org)



[www.JCRonline.org](http://www.JCRonline.org)

## ABSTRACT

Lee, K.-H., Shin, S., Kim, D.-S., 2014. Cross-shore variation of water surface elevation and velocity during the bore propagation. In: Green, A.N. and Cooper, J.A.G. (eds.), *Proceedings 13<sup>th</sup> International Coastal Symposium* (Durban, South Africa), *Journal of Coastal Research*, Special Issue No. 70, pp. 533-538, ISSN 0749-0208.

In this study, we have investigated the hydrodynamics of a turbulent bore generated by removing a gate suddenly with water impounded on one side. This bore generation method was referred to a general dam-break problem. In order to perform the numerical simulation of the bore formation and propagation, we considered the incompressible flows of two immiscible fluids, liquid and gas, governed by the Navier-Stokes equations. The interface between the two fluids (air and water) was tracked by the volume-of-fluid (VOF) technique, and the M-type Cubic Interpolated Propagation (MCIP) scheme was used to solve the Navier-Stokes equations. It is known that the MCIP method is a low diffusive and stable scheme and is generally extended the original one-dimensional CIP to higher dimensions, using a fractional step technique. A Large Eddy Simulation (LES) closure scheme, which is a cost-effective approach to turbulence simulation, was employed to predict the evolution of quantities associated with turbulence. In order to verify the applicability of this numerical model to the bore simulation, the simulation results were compared to the laboratory experimental data. The numerical model for the bore formation and propagation based on the two-phase fully nonlinear Navier-Stokes equations was well verified by comparing with the analytic model based on the fully nonlinear shallow water wave equations and the laboratory experimental results.

**ADDITIONAL INDEX WORDS:** bore, two-phase flow, MCIP method, Navier-Stokes equation, mean flow velocity variation, non-hydrostatic pressure

## INTRODUCTION

Bores, such as tsunami bores or tidal bores, are defined as discontinuous flows varying in time and spatial scale. The bore front generates large differences in the water surface level, propagates with high speed, and causes severe damages, such as impact loads (Ramsden, 1993, 1996; Abdolmaleki, *et al.*, 2004) and scouring (Tonkin *et al.*, 2003) on coastal and inland structures; in addition to the loss of human lives and properties. Many researchers have studied the generation and propagation of bores for a long period of time. Ritter (1892) was first to derive the analytic solution of the hydrodynamics of the bore movement generated by an instantaneous dam breaking with a rectangular shape. Dressler (1952) and Whitham (1955) suggested an analytic solution of the speed and height of a bore considering bottom resistance. Stoker (1957) extended Ritter's solution to derive the surface shape of the bore at the initial depth using a wet-bed condition in the down-stream side.

In the horizontal channel, the bore is usually generated by removing a wall between two fluids with different water surface levels. As the analytic solution of this kind of bore generation and its propagation with a hydrostatic pressure distribution is generally assumed, the shallow water wave equation (Saint Venant equation

in one-dimensional case) is used as the a governing equation of numerical models to predict these phenomena.

The finite difference method is typically used for the numerical analysis of the bore hydrodynamics. Many different schemes have been suggested to predict the bore generation, propagation, and impact accurately considering the numerical diffusion and the sensitivity of the solution (Madsen, *et al.*, 2005) such as approximate Riemann solutions (Glaister, 1988), modified Lax-Friedrich schemes (Rao and Latha, 1992), Godunov methods (Savic and Holly, 1993), space-time conservation methods (Molls and Molls, 1998), MacCormack schemes (Garcia-Navarro *et al.*, 1992), TVD (Total Variation Diminishing) schemes (Harten, 1983), flux vector splitting methods (Jha, *et al.*, 1995) or upwind conservative schemes (Ying *et al.*, 2004). Additionally, the finite element method (Katopodes and Strekoff, 1978) and the finite volume method (Hue, *et al.*, 1998) are used to predict the bore propagation velocity. Most of schemes which were mentioned above apply shallow water wave equations based on a non-viscous and homogeneous flow with a hydrostatic pressure distribution. Gharangik and Chaudhry (1991) and Mohapatra and Chaudhry (2004) used Boussinesq equations as a governing equation for the characteristic analysis of the bore. Mohapatra and Chaudhry (2004) have examined the bore simulation capability, the contribution of each term to the Boussinesq equations, and the effects of a roughness, bottom slope, and non-hydrostatic pressure.

Laboratory experiments have been conducted by several researchers. Pohle (1952) and Strelkoff (1986) showed that the bore pressure distribution is non-hydrostatic on the initial stage of the bore formation. Dressler (1954) showed that the water depth is not constant in its initial stage. According to these results, researchers used fully nonlinear Navier-Stokes equations with the MAC (Marker And Cell) method (Harlow and Welch, 1965; Nichols and Hirt, 1971) and the VOF (Volume Of Fluid) method (Hirt and Nichols, 1981; Abdolmaleki, et al., 2004). Moreover, an analytical method that combines VOF method and SMAC (Simplified Marker And Cell) method (Amsden and Harlow, 1970) based on Euler equations was attempted (Mohapatra, et al., 1999). Gotoh et al. (2002) and Dalrymple et al. (2006) applied a SPH (Smoothed Particle Hydrodynamics) method to simulate the bore formation and propagation generated by dam-breaking and tsunami generation (solitary wave).

It is also known that bores are highly turbulent flows (Yeh and Ghazali, 1986, 1988; Svenden and Madsen, 1984) and their propagation is affected by turbulence, air entrainment, and gas-liquid interaction. However, previous studies have not considered all those effects.

In this study, a numerical simulation was conducted by using two-phase fully nonlinear Navier-Stokes equations which can consider nonlinearity, non-hydrostatic pressure and viscosity in order to investigate water surface variations and velocity variations as the bore is formed and propagates. The LES (Large Eddy Simulation) model (Smagorinsky, 1963) was applied to evaluate the effect of turbulence and the VOF method was used to track the water surface variation. The MCIP (Multi-dimensional Cubic Interpolated Pseudo Particle) method (Nakamura and Yabe, 1999) was employed to enhance the capturing of impact waves and to minimize numerical diffusion.

The results of numerical simulations were compared with laboratory experimental data collected and analyzed by Arnason (2005) for model verification in terms of the water surface and velocity variations.

### Numerical Model

#### Governing equations

Assuming a viscous and incompressible fluid, the two-fluid motion is governed by the continuity equation and Navier-Stokes equations, given by

$$\frac{\partial \bar{u}_i}{\partial x_i} = 0 \tag{1}$$

$$\bar{u}_i \frac{\partial \bar{u}_i}{\partial x_j} = -\frac{1}{\bar{\rho}} \frac{\partial \bar{p}}{\partial x_i} + \frac{\partial}{\partial x_j} (-\tau_{ij} + 2\tilde{\nu} \bar{D}_{ij}) + g_i \tag{2}$$

where,  $\bar{u}_i$  the filtered velocity field,  $\bar{\rho}$  is the density,  $p$  is the pressure,  $g_j$  is the acceleration vector due to gravity,  $\tilde{\nu}$  is the dynamic viscosity,  $\tau_{ij}$  is subgrid scale (SGS) stress tensor,  $\bar{D}_{ij}$  is the strain stress tensor. In the above equations, the density  $\bar{\rho}$  and the viscosity  $\tilde{\nu}$  are functions of space and time determined by either the first (gas) or the second (water) fluid. The subgrid scale (SGS) stress tensor  $\tau_{ij}$  is defined as:

$$\tau_{ij} = -2\nu_e \bar{D}_{ij} \tag{3}$$

where,  $\nu_e$  is the eddy viscosity. In the present model, the most widely used Smagorinsky's model (Smagorinsky, 1963) is adapted to evaluate eddy-viscosity. In Smagorinsky's model, the LES eddy viscosity is proportional to the SGS characteristic

length (filter width)  $\Delta$  and to strength of strain stress tensor (Lesieur et al., 2005).

$$\nu_e = (C_s \Delta)^2 \sqrt{2\bar{D}_{ij}\bar{D}_{ij}} \tag{4}$$

where  $C_s$  is the Smagorinsky's constant and can be approximated by

$$C_s = \frac{1}{\pi} \left( \frac{3\alpha}{2} \right)^{-3/4} = 0.235 \alpha^{-3/4} \tag{5}$$

Applying a Kolmogorov constant  $\alpha = 1.5$  to Eq (5), Smagorinsky's constant yields  $C_s \approx 0.173$ .

Also, the SGS characteristic length  $\Delta$  and the strength of strain stress tensor  $\sqrt{2\bar{D}_{ij}\bar{D}_{ij}}$  are determined as follows, respectively

$$\begin{cases} \Delta = \sqrt[3]{\Delta x \Delta y \Delta z} \\ 2\bar{D}_{ij}\bar{D}_{ij} = 2(\bar{D}_{11}^2 + \bar{D}_{22}^2 + \bar{D}_{33}^2) + 4(\bar{D}_{12}^2 + \bar{D}_{23}^2 + \bar{D}_{31}^2) \end{cases} \tag{6}$$

#### Volume of Fluid (VOF) method

The Volume of fluid (VOF) method by Hirt and Nichols (1981), an interface tracking algorithm for the simulation of the two-phase flow, is coupled with the LES based two-phase flow model. Since the original Hirt and Nichols' VOF method, many modified and extended interface tracking methods including GENSMAC (Tome et al., 1994), TUMMAC (Miyata and Nishimura, 1985), FCT-

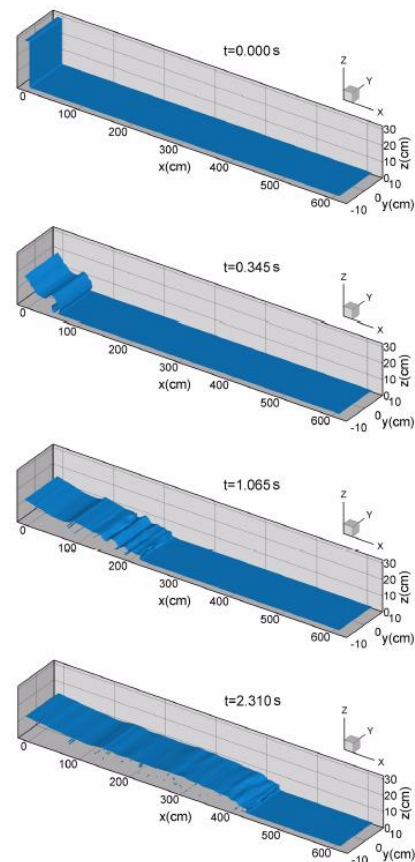


Figure 1. Time history of the computed water surface in case of  $h1=300$  mm

VOF (Rudman, 1997) and MARS(Kunugi, 2000) have been proposed as alternative schemes to lessen errors due to the interface reconstruction. However, these methods require additional computational time because of their algorithms, a serious issue in 3-dimensional numerical analysis. Although Hirt and Nichols' VOF method uses the simplified line interface calculation (SLIC) in interface reconstruction, its applicability has been demonstrated by many researchers.

The VOF method is based on the VOF function  $f$ , which is a color function ranged from 0 (air-phase) to 1 (water-phase). Using the VOF function, the interface is determined in each computational cell which has  $0 < f < 1$ . Further, considering both fluids, the density  $\tilde{\rho}$  and viscosity  $\tilde{\nu}$  in the interface cell are evaluated by the VOF function as follows:

$$\begin{cases} \tilde{\rho}_{i,j,k} = f_{i,j,k} \langle \rho_w \rangle_{i,j,k} + (1 - f_{i,j,k}) \langle \rho_a \rangle_{i,j,k} \\ \tilde{\nu}_{i,j,k} = f_{i,j,k} \langle \nu_w \rangle_{i,j,k} + (1 - f_{i,j,k}) \langle \nu_a \rangle_{i,j,k} \end{cases} \quad (7)$$

where, the subscript  $w$  and  $a$  represent water-phase and air-phase, respectively.

The advection of the VOF function is obtained by considering the conservation of fluid mass in each cell as follows:

$$\frac{\partial f}{\partial t} + \frac{\partial(\bar{u}_i f)}{\partial x_i} = 0 \quad (8)$$

The interface orientation is defined by the gradient of the VOF function  $\nabla f$  in each interface cell.

### Discretization of governing equations and boundary conditions

The governing equations (1) and (2) and the VOF advection equation (8) are discretized using the finite difference method within the orthogonal staggered grid. The discretized equations are calculated based on a simplified Marker and Cell (SMAC) method

developed by Amsden and Harlow (1970) and a Multi-dimensional Cubic Interpolated Pseudo-particle (MCIP) method proposed by Nakamura and Yabe (1999). Cubic Interpolated Pseudo Particle (CIP) method is a less-diffusive and stable algorithm for solving the hyperbolic equations (Nakamura and Yabe, 1999). In the CIP method, a quantity within a mesh is interpolated by a cubic polynomial and the first spatial derivatives are introduced as free parameters on each grid point. Nakamura and Yabe (1999) extended the one-dimensional CIP method to higher dimensions using the fractional step, which is called the MCIP method. An impermeable condition (for normal velocities) and a non-slip condition (for tangential velocities) are used to treat the bottom and lateral boundary conditions.

### LABORATORY EXPERIMENTAL DATA

Laboratory experiments for bore formation and propagation were conducted by Arnason (2005) in the wave tank (16.6 m (L) x 0.6m (W) x 0.45m (H)). This wave tank equips the bore generation system by using a vertically removable gate. Two different water depths can be set by this gate and the bore is generated by quickly removing gate by 0.2 s. This facility has been used to conduct the experiments for the bore generation (Yeh, et al., 1989; Ramsden, 1993, 1996).

Water depth behind the gate ( $h_1$ ) was set to 125, 200, 250, 300 mm and the water depth in the front side of the gate ( $h_0$ ) was fixed to 20 mm. The bore was generated by opening the gate. The water surface levels and the bore propagation velocities were measured by LDV (Laser Doppler velocimeter) and DPIV (Digital Particle Image Velocimetry).

Arnason (2005) also provided an analytic solution of the water surface and velocity variations based on fully nonlinear shallow water theory using characteristic lines (CL hereafter). Table 1 shows the results of his analytical approach.

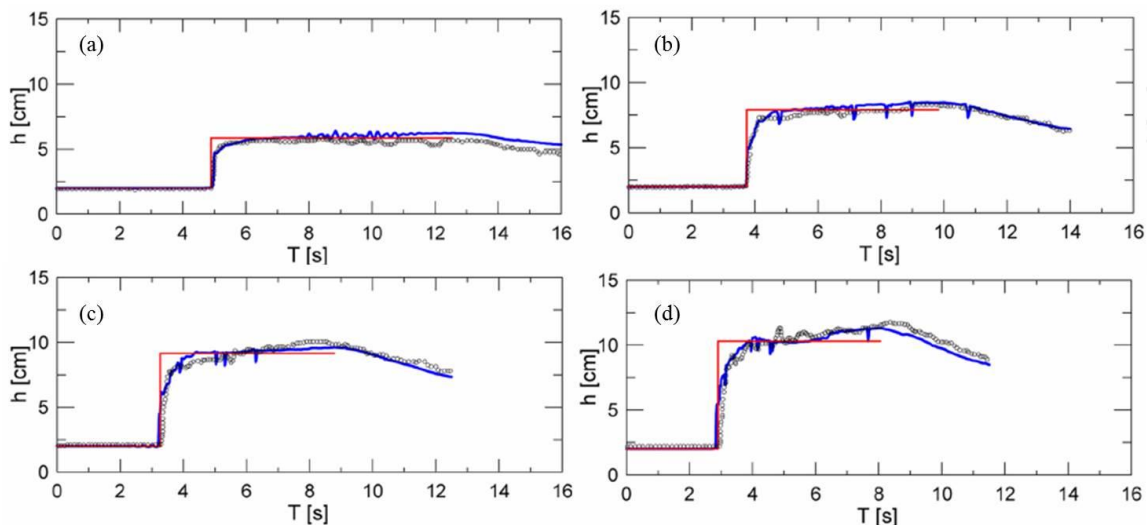


Figure 2. Comparison of the computed water surface levels and the experimental data. Blue lines are the results by MSLV and red lines are results by CL, and open circles are measured data.  $h_1$  = (a) 125mm, (b) 200 mm, (c) 250 mm, (d) 300 mm.



## RESULTS

In order to investigate the bore formation and propagation processes, MCIP-SMAC-LES-VOF (MSLV hereafter) a method based on two-phase fully nonlinear Navier-Stokes equations was employed. The VOF function ( $f$ ) in this computation was set to 0.5. The computational domain was 16.6m long ( $x$ -direction), 0.2m wide ( $y$ -direction), and 0.5m deep ( $z$ -direction) and the grid sizes were fixed to  $dx \times dy \times dz = 2 \times 2 \times 1$  cm. The snapshots of the model result are shown in Figure 1.

Figure 2 shows the water surface elevation as a function of time when the initial water depth behind the gate ( $h_1$ ) was set to 125, 200, 250, and 300 mm. In this figure the numerical simulations of this study based on the MSLV method, and the results of characteristic lines (CL) method proposed by Arnason (2005) were compared with each other.

From the point of view of the bore propagation speed ( $c$ ), two simulation results agreed well with the experimental results for all four cases. Even if there is a small difference between data and predictions in the bore front propagation due to the gate opening time in the experiments, the effect was negligible. Also in this figure, MSLV and CL results of the water surface variations as a function of time agreed well with the experimental results when  $h_1 \leq 200$ mm. However, when  $h_1 > 200$ mm, the water level in the experiment increases as time goes on. This phenomenon was shown more clearly as the bore is getting stronger, i.e.  $h_1/h_0$  is larger. These results show a bigger difference from the CL results as the bore strength is larger because the CL keeps the bore height constant. On the other hand, the MSLV results matched well with the experimental results in terms of the water level decrease due to the negative wave by wave reflection as well as the increase of the water surface level. Since the CL approach considers hydrostatic pressure, this method cannot predict water surface level increase.

Pohle (1952) and Strelkoff (1986) indicated that the pressure distribution in the initial stage of bore formation is non-hydrostatic as proved experimentally by Dressler (1954). Moreover, Mohapatra and Chaudhry (2004) used nonlinear Boussinesq equations to show that when  $h_1/h_0 \geq 0.4$ , the non-hydrostatic pressure distribution effect appears like the results above, but the

Table 1. Analytical model results of bore height ( $h_2$ ), propagation speed ( $c$ ), flow velocities ( $u_2$ ), and Froude number ( $F = u_2 / (gh_2)^{1/2}$ ).

$h_1$ (mm)	$h_0$ (mm)	$h_2$ (mm)	$c$ (m/s)	$u_2$ (m/s)	$F$
125	20	58.5	1.06	0.70	0.92
200	20	79.2	1.39	1.04	1.18
250	20	91.5	1.58	1.24	1.31
300	20	103.0	1.76	1.42	1.41

propagation speed is not affected by that pressure distribution. Therefore, the MSLV method is more suitable to predict water surface variation by non-hydrostatic pressure distribution in the initial stage of the bore formation. In contrast, Mohapatra, et al. (1999) and Mohapatra and Chaudhry (2004) concluded that the non-hydrostatic pressure distribution does not effect on the long term variation of water surface. Therefore, turbulence and viscosity might effect on the increase of the water surface level as the time step increases in the experiments.

Figure 3 shows the comparisons between two computed results by the CL and MSLV methods and the experimental results measured by the LDV and DPIV in terms of flow velocities. The flow velocities were measured 5.2m from the gate by using both the LDV and DPIV. In this figure, the asterisk indicates the arrival time of the negative wave reflected by the end wall. The results show that, when  $h_1 \geq 200$ mm, the flow velocity decreases as the bore passes through the measurement location and that the CL method over-estimates the flow velocity while it reproduced the water surface level accurately (when  $h_1$  is shallower-125mm). Because the experimental results of the flow velocities do not exceed the simulation results of the CL method in all cases, the velocity computed by the CL method can be regarded as an upper-critical flow velocity. On the contrary, the measured water surface level was lower than the CL prediction at the bore front and exceeded the predicted value as a time step increases. Therefore, the flux, which is calculated by the product of the water depth and the depth-averaged flow velocity, increases by 9% while the bore passes through the measurement location when  $h_1=250$ mm.

On the other hand, the results of the MSLV method regarding the flow velocity showed a good agreement with the experimental results regardless of the increase of the bore strength. The MSLV method predicted the flow velocity decrease as a function of time

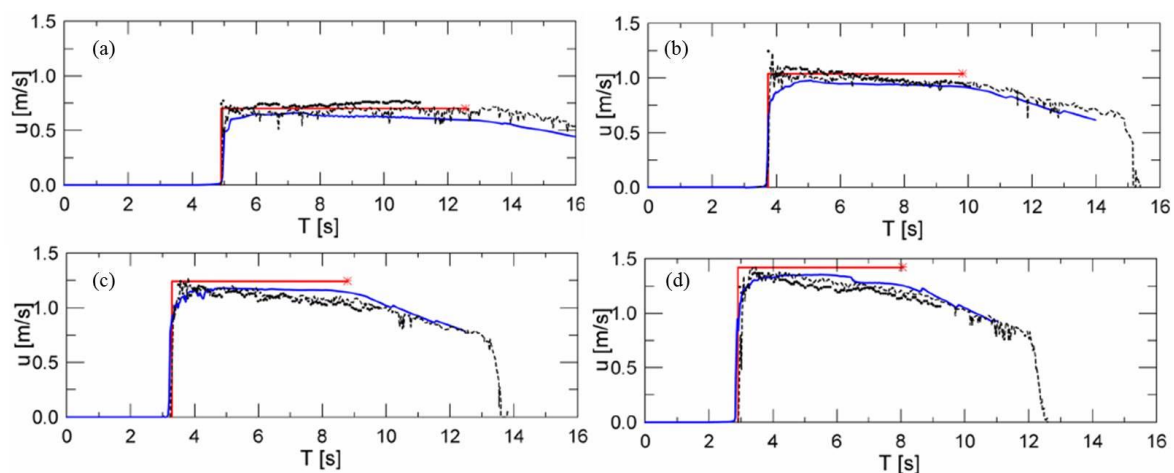


Figure 3. Comparison of the computed velocity with the experimental data. Blue lines are the results by MSLV and red lines are the results by CL. Black bold lines are measured data by LDV and black dashed lines are measured data by DPIV.  $h_1 =$  (a) 125mm, (b) 200 mm, (c) 250 mm, (d) 300 mm.

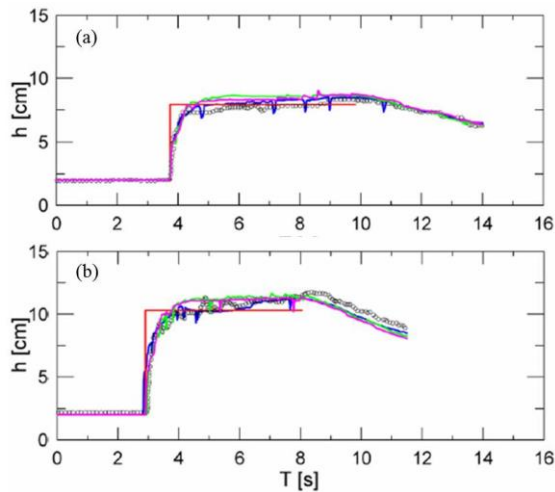


Figure 4. The effects of viscosity and LES model on water level. Red lines are results by CL and open circles are experimental results. Blue lines are results by MSLV, green lines are results by MNVI (no viscosity), and pink lines are results by MV1 (no LES).  $h_1 =$  (a) 200 mm and (b) 300 mm.

including the negative wave effect. However, the MSLV method slightly under-estimated the flow velocity at the bore front in comparison with the experimental results. One of the reasons can be because the air entrainment involves the bore formation at the initial stage and this air entrainment makes prediction harder in the MSLV method. In a comparison between the CL simulation and the MSLV simulation, the results by the CL method are always larger than those by the MSLV method in terms of the flow velocity. The difference increases with time step increases. However, as shown in Figure 1, the water surface elevation results of the MSLV method become larger than those of the CL method. These results can be affected by the turbulence and viscosity as mentioned before.

Figure 4 shows the comparisons between the simulation and the experimental results of water surface elevations considering the effect of turbulence and viscosity. In Figure 4a, the results of the MSLV method ignoring viscosity (MNVI) and the results of the CL method were similar to each other. The major difference between these two methods is the pressure distribution during the computations (MNVI: non-hydrostatic pressure distribution, CL: hydrostatic pressure distribution). The result thus shows that the pressure distribution mainly effects the area near the front of the bore. When the MSLV result takes viscosity into account (MV1) and is compared with the MNVI result, the viscosity effect does not appear at the bore front. In figure 4a, in the case of the smaller bore strength, the viscous effect appears when  $t > 4.3$ s, especially where the water surface level decreases when  $4.3 < t < 8.4$  s while it increase when  $t > 8.4$  s. However, when the bore is stronger, as shown in Figure 4b, the viscosity effect is negligible.

A comparison between the MSLV results (considering both turbulence and viscosity) and the MV1 results shows that the water surface level slightly increases at the bore front due to the effect of turbulence and the water surface level decreases with time step increase. The difference in the water surface level between the two methods is larger at the top corner of the bore front and the turbulence effect increases when the bore is stronger.

From these comparisons, the results show that the non-hydrostatic pressure and turbulence give a larger effect on the

water surface elevation while the viscosity effect is small. This tendency becomes larger as the bore is stronger.

Figure 5 shows the mean flow velocities as a function of time by both predictions and measurements with respect to the presence of viscosity and turbulence when  $h_1$  is 300 mm. Firstly, the result of the MNVI prediction for mean velocity is smaller than that of the CL prediction. Therefore, the computed mean velocity based on the hydrostatic pressure distribution shows a larger value, especially in the top corner of the bore front. Secondly, in the comparison between the results of the MV1 and that of the MNVI, the mean velocity prediction considering the viscosity effect is slower at the bore front while it is faster at the top corner of the bore front. Overall, the difference is small. Thirdly, the MSLV prediction for mean flow velocity considering both viscosity and turbulence is faster than the results from the MV1 method at the bore front and the top corner of the bore front. In contrast it is smaller when  $t > 6.5$ s. However, the difference between two simulations is small as shown in figure 5. Therefore, in terms of the effect on the mean flow velocity variation, the assumption of pressure distribution gives a large effect on the prediction while the considerations of viscosity and turbulence are quite small.

## CONCLUSION

In this study, high-precision numerical simulations were performed by applying the VOF method, LES model, SMAC and MCIP methods to the two-phase fully non-linear Navier-Stokes equations. The numerical model was able to consider nonlinearity, non-hydrostatic pressure, viscosity, turbulence, and gas layer above the water level. The model results were compared with the experimental results in terms of the water surface and the mean flow velocity variations. The conclusions drawn in this study are:

1) The numerical model for the bore formation and propagation based on the two-phase fully nonlinear Navier-Stokes equations was well verified by comparing with the analytic model based on the fully nonlinear shallow water wave equations and the laboratory experimental results.

2) If the non-hydrostatic pressure distribution is considered, the computed water surface level is lower than the result based on the hydrostatic pressure distribution at the bore front but the water surface level is constantly higher after that.

3) Considering viscosity and turbulence, the model results of water surface elevation is lower when both quantities are excluded, but there is no difference at the bore front and a large difference at the top corner of the bore front.

4) Among the non-hydrostatic pressure distributions, the viscosity, and turbulence factors, the non-hydrostatic pressure distribution and turbulence give a greater effect on the water surface elevation while the viscosity effect is small. This tendency increases with bore size.

5) Among the pressure distribution, the viscosity, and turbulence factors; the assumption of hydrostatic pressure distribution gives rise to a large impact on the mean flow velocity whilst over-estimating the mean flow velocity. The presence of viscosity and turbulence in the model give a smaller effect on the simulation of mean flow velocity than the actual result by considering the hydrostatic pressure distribution.

6) The smaller difference between the numerical simulations in this study and the experimental results could be a result of a basic numerical error, the gate opening time, and the bottom roughness, factors that were not considered in this study.

## ACKNOWLEDGEMENT

This work was partially funded by the RIC program (Kwandong University) of the Ministry of Trade, Industry and Energy and the Korea Institute of Marine Science & Technology Promotion funded by Ministry of Oceans and Fisheries (No. 20110131). The authors gratefully acknowledge Dr. H. Arnason for providing his experimental data set.

## LITERATURE CITED

- Abdolmaleki, A., Thiagarajan, K.P., and Morris-Thomas, M.T., 2004. Simulation of the dam break problem and impact flows using a Navier-Stokes solver. *15th Australasian Fluid Mech. Conference*, 13-17.
- Akanbi, A.A. and Katopodes, N.D., 1988. Model for flood propagation on initially dry land. *Journal of Hydraulic Engineering, ASCE*, 114, 7, 689-706.
- Akiyama, M. and Aritomi, M., 2002. *Advanced numerical analysis of two-phase flow dynamics -multi-dimensional flow analysis-*. Corona Publishing Co., LTD. Tokyo, JAPAN.
- Amsden, A.A. and Harlow, F.H., 1970. *The SMAC method : a numerical technique for calculating incompressible fluid flow*. Los Alamos Scientific Laboratory Report LA-4370, Los Alamos, N.M.
- Arnason, H., 2005. *Interactions between an incident bore and a free-standing coastal structure*. Ph.D Dissertation, University of Washington, USA.
- Dalrymple, R.A., Grilli, S.T., and Kirby, J.T., 2006. Tsunamis and challenges for accurate modeling. *Advances in Comput. Oceanography*, 19, 1, 142-151.
- Dressler, R.F., 1952. Hydraulic resistance effect upon the dambreak functions. *Journal of hydraulic Research*, 49, 3, 217-225.
- Dressler, R.F., 1954. Comparison of theories and experiments for hydraulic dam-break wave. *Int. Assoc. Sci. Pubs.*, Vol. 38, No. 3, pp. 319-328.
- Garcia-Navarro, P., Alcrudo, F., and Saviron, J.M., 1992. 1-D open channel flow simulation using TVD-MacCormack scheme. *Journal of Hydraulic Engineering, ASCE*, 118, 10, 1359-1372.
- Gharangik, A. and Chaudhry, M.H., 1991. Numerical simulation of hydraulic jump. *Journal of Hydraulic Engineering, ASCE*, 117, 9, 1195-1211.
- Glaister, P., 1988. Approximate Riemann solutions of shallow water equations. *Journal Hydraulic Research, Delft, The Netherlands*, 26, 3, 293-306.
- Gotoh, H. Sakai, T., and Hayashi, M., 2002. Lagrangian model of drift-timbers induced flood by using moving particle semiimplicit method. *Journal of Hydrosience and Hydraulic Engineering, JSCE*, 20, 1, 95-102.
- Harlow, F.H. and Welch, J.E., 1965. Numerical calculation of time dependent viscous incompressible flow of fluid with a free surface. *Physics in Fluids*, 8, 2182-2189.
- Harten, A., 1983. High resolution schemes for hyperbolic conservation laws. *Journal of Computational Physics.*, 49, 357-393.
- Hirt, C.W and Nichols, B.D., 1981. Volume of fluid (VOF) method for the dynamics of free boundaries. *Journal of Computational Physics*, 39, 201-225.
- Hu, K., Mingham, C.G., and Causon, D.M., 1998. A bore-capture finite volume method for open-channel flows. *International Journal of Numerical Methods in Fluids*, 28, 1241-1261.
- Jha, A.K., Akiyama, J., and Ura, M., 1995. First- and second-order flux difference splitting schemes for dam-break problem. *Journal of Hydraulic Engineering, ASCE*, 121, 12, 877-884.
- Katopodes, N.D. and Strelkoff, R., 1978. Computing two-dimensional dam-break flood waves. *Journal of Hydraulic Division, ASCE*, Vol. 104, No. 9, pp. 1269-1288.
- Kunugi, T., 2000. MARS for multiphase calculation. *CFD Journal*, 9, No. 1, IX-563.
- Madsen, P.A., Simonsen, H.J., and Pan, C.H., 2005. Numerical simulation of tidal bores and hydraulic jumps. *Coastal Engineering*, 52, 409-433.
- Miyata, H. and Nishimura, S., 1985. Finite-difference simulation of nonlinear waves generated by ships of arbitrary three-dimensional configuration. *Journal Computational Physics*, Vol. 60, pp. 391-436.
- Mohapatra, P.K. and Chaudhry, M.H., 2004. Numerical solution of Boussinesq equations to simulate dam-break flows. *Journal of Hydraulic Engineering, ASCE*, 130, 2, 156-159.
- Mohapatra, P.K., Eswaran, V., and Bhallamudi, S.M., 1999. Two dimensional analysis of dam-break flow in vertical plane. *Journal of Hydraulic Engineering, ASCE*, 125, 2, 183-192.
- Mollis, T. and Mollis, F., 1998. Space-time conservation method applied to Saint Venant equations. *Journal of Hydraulic Engineering, ASCE*, 124, 5, 501-508.
- Nakamura, T. and Yabe, T., 1999. Cubic interpolated propagation scheme for solving the hyper-dimensional Vlasov-Poisson equation in phase space. *Computational Physics Communications*, 120, 122-154.
- Nichols, B.D. and Hirt, C.W., 1971. Improved free surface conditions for numerical incompressible flow computations. *Journal of Computational Physics*, 1, 8, 434-448.
- Pohle, F.V., 1952. Motion of water due to breaking of a dam and related problems. *USNBS*, 521, 8, 47-53.
- Ramsden, J.D., 1993. *Tsunami : Forces on a vertical wall caused by long waves, bores, and surges on a dry bed*. Ph.D. Dissertation, California Institute of Technology.
- Ramsden, J.D., 1996. Forces on a vertical wall due to long waves, bores, and dry-bed surges. *Journal of Waterway, Port, Coastal, and Ocean Engineering, ASCE*, 122, 3, 134-141.
- Rao, V.S. and Latha, G., 1992. A slope modification method for shallow water equations. *International Journal of Numerical Methods in Fluids*, 14, 189-196.
- Ritter, A., 1892. Die fortpflanzung der wasserwellen, *Zeitschrift des Vereines deutscher Ingenieuer*. 36, 33, 947-954.
- Rudman, M., 1997. Volume-tracking methods for interfacial flow calculations. *International Journal of Numerical Methods in Fluids*, Vol. 24, pp. 671-691.
- Savic, L.J. and Holly, F.M., 1993. Dambreak flood waves computed by modified Gouunov method. *Journal of Hydraulic Research, Delft, The Netherlands*, 31, 2, 187-204.
- Smagorinsky, J., 1963. General circulation experiments with the primitive equations. *Mon. Weath. Rev.*, 91, 3, 99-164.
- Stoker, J.J., 1957. *Water waves*. Interscience, Wiley, New York, N.Y., pp. 331-341.
- Strelkoff, T., 1986. Dam-break flood waves. *Megatrends in Hydraulic Engineering, Albertson, M. L. and Papadakis, C. N. Editors*, California State University, 257-266.
- Svendsen, I.A. and Madsen, P.A., 1984. A turbulent bore on a beach. *Journal of Fluid Mechanics*, Vol. 148, pp. 73-96.
- Tome, M.F. and McKee, S., 1994. GENSMAC : A computational marker and cell method for free-surface flows in general domains. *Journal of Computational Physics*, 110, 1, 171-186.
- Tonkin, S., Yeh, H. Kato, F., and Sato, S., 2003. Tsunami scour around a cylinder. *Journal of Fluid Mechanics*, 496, 165-192.
- Wang, Z. and Shen, H.T., 1999. Lagrangian simulation of one-dimensional dam-break flow. *Journal of Hydraulic Engineering, ASCE*, 125, 11, 1217-1220.
- Whitham, G.B., 1955. The effect of hydraulic resistance in the dam-break problem. *Proceedings Series A, Royal Society of London*, 226-227.
- Yeh, H.H., 1991. Vorticity-generation mechanism in bores. *Proceedings of Royal Society, London A*, 432, 215-231.
- Yeh, H.H. and Ghazali, A., 1986. Nearshore behavior of bore on a uniformly sloping beach. *20th International Conference on Coastal Engineering, ASCE*, 877-888.
- Yeh, H.H. and Ghazali, A., 1988. On bore collapse. *Journal Geophysical Research*, 93, 6930-6936.
- Yeh, H.H., Ghazali, A., and Marton, I., 1989. Experimental study of bore run-up. *Journal of Fluid Mechanics*, 206, 563-578.
- Ying, X., Khan, A.A., and Wang, S.S.Y., 2004. Upwind conservative scheme for the Saint Venant equations. *Journal of Hydraulic Engineering, ASCE*, 130, 10, 977-987.

## Development of an oil spill hazard scenarios database for risk assessment



Sérgio den Boer<sup>†</sup>, Alberto Azevedo<sup>†</sup>, Leandro Vaz<sup>‡</sup>, Ricardo Costa<sup>∞</sup>, André B. Fortunato<sup>†</sup>, Anabela Oliveira<sup>†</sup>, Luís M. Tomás<sup>‡</sup>, João M. Dias<sup>‡</sup>, Marta Rodrigues<sup>†</sup>

<sup>†</sup>National Civil Engineering Laboratory  
Av. Do Brasil 101  
1700-066 Lisboa  
Portugal  
aazevedo@lnec.pt

<sup>‡</sup>CESAM, Physics Department  
University of Aveiro  
Campus Universitário de Santiago  
3810-193 Aveiro  
Portugal

<sup>∞</sup>CIIMAR, Interdisciplinary Centre of  
Marine and Environmental Research  
University of Porto  
Rua dos Bragas 289  
4050-123 Porto  
Portugal



[www.JCRonline.org](http://www.JCRonline.org)

### ABSTRACT

den Boer, S., Azevedo, A., Vaz, L., Costa, R., Fortunato, A.B., Oliveira, A., Tomás, L.M., Dias, J.M., Rodrigues, M., 2014. Development of an oil spill hazard scenarios database for risk assessment. In: Green, A.N. and Cooper, J.A.G. (eds.), *Proceedings 13<sup>th</sup> International Coastal Symposium* (Durban, South Africa), *Journal of Coastal Research*, Special Issue No. 70, pp. 539-544, ISSN 0749-0208.

The occurrence of oil spills in coastal regions may have catastrophic consequences on the environment and severe socio-economic impacts. This work presents a new methodology to evaluate the risk associated with oil spills in coastal zones and estuaries, and illustrates its application in a coastal lagoon (Ria de Aveiro, Portugal). A ranked list of the hydrodynamic scenarios under which oil spills are most likely generated through the analysis of 33 years of wave and wind data, retrieved from the ERA-INTERIM project database, and from the analysis of oil spills that occurred in the Atlantic Iberian shelf. Considering six spill locations and a single oil type spill inside the Aveiro harbor, the database resulted in approximately 3500 simulations. Hydrodynamic simulations were made with the MORSYS2D modeling system, a soft coupling of the hydrodynamic model ELCIRC and the wave model SWAN. The high-accuracy, unstructured grid, oil fate model VOILS was used in 2D mode to simulate the transport and the oil weathering processes at the surface and in the intertidal areas. The hazard assessment analysis included the determination of the trajectory of the plumes, the shoreline retention areas affected by the oil and their oil exposure time. Time evolution of the oil properties, such as the oil evaporation rate and emulsification processes of the mixture, are provided to support clean-up operations, as well as robustness controls such as oil mass balance.

**ADDITIONAL INDEX WORDS:** *climatology, oil spill modeling, risk assessment.*

### INTRODUCTION

Near shore and offshore oil spill events have huge social, economic and environmental impacts, which can ultimately cripple an entire coastal area for long periods of time, as recent examples demonstrate – Deep Sea Horizon in the Gulf of Mexico (Mackowsky *et al.* 2010), Prestige in the bay of Biscay (Albaigés *et al.* 2006) and Cercal in Northern Portugal (Costa *et al.* 2012). Simultaneously, adequate preparedness of harbor and maritime authorities to potential oil spills requires significant material and human resources. Hence, risk assessment studies can bring enormous benefits, by optimizing emergency resource allocation.

The development of hazard maps for oil spills constitutes a first step towards the generation of risk maps. These hazard maps should provide detailed indications on the areas which will most likely be affected by an oil spill in a given region, together with the associated probability. Such maps can be used for both long-term planning (i.e., before the occurrence of an accident)

and immediate response action (i.e., once the accident occurs).

Hence, the generation of these maps from existing information should be rapid so they can be updated as new information becomes available. For instance, a map developed for planning purposes has to rely on educated guesses on where the spill is more likely to occur. In contrast, once the accident does occur, the map can be updated to take into account the location of the spill or other information. Maps for specific conditions can also be useful. For instance, hazard maps for specific seasons can be used in the risk analyses, since the vulnerability can also vary seasonally.

The present paper describes a new methodology to develop hazard maps of oil spills in coastal regions, and illustrates its application in a coastal lagoon. The approach uses historical information on previous spills to restrict the range of environmental conditions associated with the accidents, as well as the combined probabilities of different environmental conditions (tides, waves and wind). A database of simulations of both hydrodynamics conditions and oil slick transport and weathering is then built, providing the building blocks for the hazard maps.

The paper starts by presenting the case study (the Aveiro lagoon in Northern Portugal). The new method is then described in detail, from the analysis of past accident records to the generation of the simulation database and the numerical models used in the study. Finally, the hazard maps are presented.

## STUDY AREA

The present study was focused on the Ria de Aveiro (**Error! Reference source not found.**), a complex lagoon system located on the western Portuguese coast (40.38°N, 8.45°W), spanning 45 km long and 10 km wide. This shallow system is mainly formed by four channels (Mira, Ílhavo, Espinheiro and S. Jacinto). The lagoon has freshwater inputs from five distinct rivers, but the circulation is mainly controlled by tides (Dias *et al.*, 2000; Lopes *et al.* 2005). Outside the inlet, wave-driven currents can be significant, since the wave climate is very energetic (Plecha *et al.*, 2012).

The Aveiro lagoon has many, and sometimes conflicting, uses such as harbor activities, industry, agriculture, fishery, aquaculture, tourism and nautical. Also, due to its rich biodiversity and fragile ecosystems, this region is highly vulnerable to oil spills events (Mendes *et al.*, 2009). The significant oil spill hazards associated to the presence of a large commercial harbor in the inner lagoon motivate the development of mitigation measures and risk assessment studies.

## METHODOLOGY

### General Approach

The present work aims at developing a methodology to build hazard scenarios databases. The methodology is illustrated for the region of the Aveiro lagoon. The oil spill hazard database consists of results from oil spill model simulations and their associated probabilities. The specification of the simulation conditions and the determination of the probabilities are based on the climatological conditions of the study region, historical records of past oil spill events and expert judgment on the most

likely locations for the occurrence of an oil spill in a particular port or coastal region. The methodology can be divided in four tasks:

1. Past oil spill occurrences are analyzed to determine the most favorable weather and ocean conditions for this type of event in the study area.
2. The climatological conditions for the region of interest are determined for wind, waves and tides. This analysis is performed from databases of past environmental conditions in the region (from hindcasts or measured data), constrained with the information determined in the first task. This task defines the climatological conditions propitious to the occurrence of spill accidents and their associated probabilities.
3. A numerical modeling system is used to generate a hydrodynamic database for the scenarios defined in the previous task. If computational costs are a limiting factor, the probabilities associated with each scenario can be used to restrict the simulations to the most likely conditions.
4. Finally, the hazard scenarios database is built using an oil spill model. For each of the hydrodynamic simulations included in the previous database, several oil spill simulations are performed considering the most likely locations, as well as different release times in the tidal cycle. The probability associated with each location is estimated from expert judgment, based on port activities.

Ultimately, the analysis of the final hazard scenarios database provides the information needed for the production of the hazard probability maps. The following sections explain in more detail each of these tasks.

### Accident Threshold Conditions

In order to define the weather conditions most prone for the occurrence of accidental oil spills along the Portuguese coast, all historical spill records were analyzed. Information was retrieved from CEDRE (Centre of Documentation, Research and Experimentation on Accidental Water Pollution – <http://www.cedre.fr/en/spill/alphabetical-classification.php>) and DGAM (Direção Geral da Autoridade Marítima) databases, which included 35 ship accidents that occurred along the Iberian Atlantic shelf between 32°- 46° N and 0°- 40°W (Figure 2).

The historical data was useful for identifying the frequency of these types of accidents and with weather and ocean conditions most favorable for their occurrence.

The monthly probability of occurrence of oil spill accidents in this region (Table 1) shows that ship accidents are most frequent

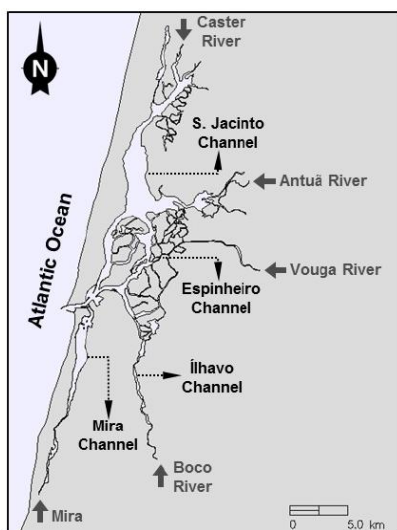


Figure 1: Aveiro's lagoon geography.



Figure 2: Location of the 35 ship accidents involving oil leakages in the Iberian Atlantic region. Each marker corresponds to an accident.

in the wintertime. Therefore, for oceanographic standardization purposes, the DJF period was selected as the study period. Together, these three months represent about two thirds of the oil spill occurrences in the region.

Table 1: Probability of occurrence of the 35 registered accidents in the region. No accidents are reported between April and September.

	Jan	Feb	Mar	Oct	Nov	Dec
Prob. (%)	21.2	6.1	9.1	12.1	15.1	36.4

The NCEP-GDAL and ERA-I global reanalysis project databases were selected to determine the weather and ocean conditions for the period defined due to their long-term series and availability. Wind speed, wind direction and significant wave height (Hs) were analyzed, as they are the variables with the greatest influence on sea navigation conditions.

A comparison between time series of wind and waves for all locations of the 35 historical spills show significant correlations between them. Wind and waves are highly correlated, in both magnitude and direction (Figure 3, Table 2).

Table 2: Correlation coefficients between wind speed and significant wave height (Magnitude Correlation), and between wind and wave direction (Direction Correlation).

Datasets	ERA-I	NCEP
Direction Correlation	0.53	0.54
Magnitude Correlation	0.86	0.71

Only the magnitudes of wind speed and significant wave height were used in the definition of the accident threshold values. The analysis of the wind and wave conditions at the time of the accidents (Figure 4) provided the thresholds for the occurrence of ship accidents. These thresholds were defined from the analysis of the ERA-I reanalysis dataset due to the existence of several outliers in the NCEP wave set. The thresholds were calculated following different criteria for wind and wave data. The minimum wind speed in the dataset was 3.9 m/s. Hence, a value of 3.0 m/s was specified as the threshold below which no accidents are expected to occur. The wave threshold was specified as the lowest value in which ocean conditions are

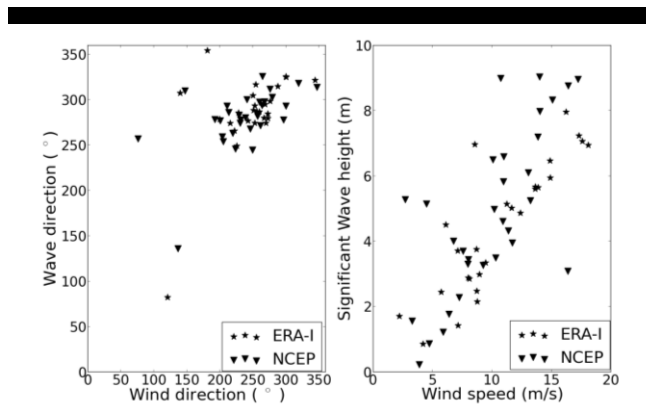


Figure 3: Comparison between the direction (left) and magnitude (right) of wind and waves, for NCEP and ERA-I reanalyses.

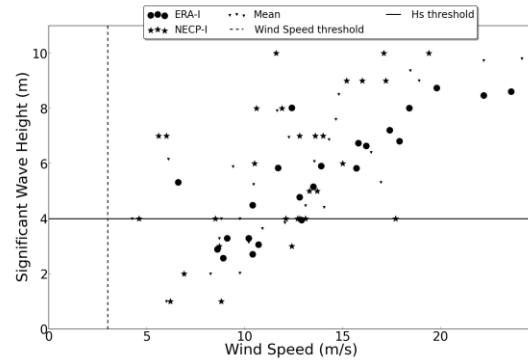


Figure 4: Accident retrieved values for wind speed and wave significant height from multiple data sources.

believed to be responsible for the accidents. This criterion was adopted because several accidents in the dataset, with wave heights lower than 4 m, were not due to the wave or wind conditions, but to other causes (e.g., engine failure, fires). Based on these data, threshold values of 3.0 m/s for wind speed and 4.0 m for Hs were specified.

### Climatological Analysis

The climatology of winds and waves was characterized based on the time series of the grid point, of the Era-Interim database, nearest the Aveiro lagoon and located at 40°31'N / 8°58'60.00"W. The global dataset is characterized by a time span of 33 years (1979-2012), with a temporal resolution of 6 hours and a spatial resolution of 1.5°. The variables considered in the climatological analysis were zonal and meridional wind components, combined significant wave height and swell, mean wave period and mean wave direction. From here on the combined dataset will be named simply significant wave height. Figure 5 and Figure 6 show the monthly means and their standard deviations as well as the minimum and maximum values and their comparison with the accident threshold values determined previously.

Both figures show a seasonal pattern, with lower (higher) standard deviations during summer (winter). The mean and median values of Hs are below the threshold value, although maximum values are above this level (Figure 5). In contrast, both mean and median magnitudes are above the wind speed threshold (Figure 6). This analysis shows that the Aveiro lagoon is climatologically prone to possible oil spill events caused by adverse atmospheric and ocean conditions.

### Hazard scenarios database setup

The generation of a scenarios database involved the definition of the environmental conditions and their associated probabilities. Environmental conditions are defined herein as a set of values for 5 variables: wind speed and direction, significant wave height, mean wave direction and mean wave period. A subset of time series of these values for the winter months alone (December-February) was retrieved from the ERA-Interim database. This subset was further reduced by eliminating the elements of the set in which the wind speed or the significant wave height were smaller than the corresponding thresholds defined above. The continuum range of each of these

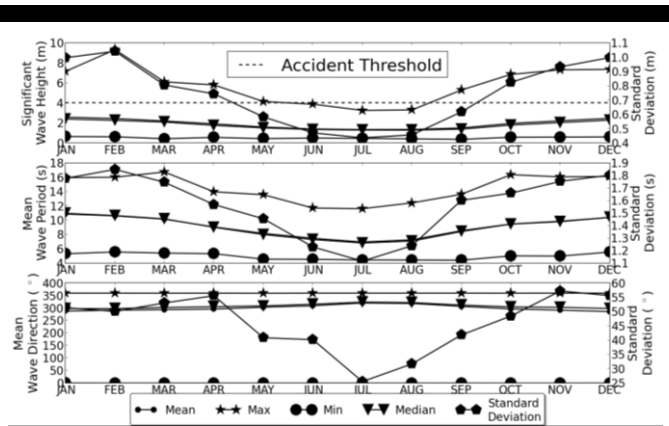


Figure 5: Monthly statistics for wave-related variables.

5 variables was then discretized into three intervals, limited by the 0<sup>th</sup>, 75<sup>th</sup>, 95<sup>th</sup> and 100<sup>th</sup> percentiles.

The choice of these limits was guided by the need to provide a higher refinement for the most extreme situations. The probability associated with each 5-dimensional bin was then calculated for the winter months, and the bins were ranked according to this probability.

Finally, a representative value for each of the five variables was determined for each bin, together with a standard deviation representative of the bin. The representative value is taken as the average of all the elements of the subset in the bin (Figure 7). The limits of the various bins and the standard deviations are represented in Table 4.

The total number of environmental conditions to consider in the simulations was further reduced to 64 by eliminating all bins that did not include any occurrence. Since this methodology was only applied to the wind and wave variables, the information regarding the tides was added *a posteriori*. Three tidal amplitudes were considered: spring tide, neap tide and mean tide. The final number of hydrodynamic simulations was set to 192. The parameterization from Table 4 was used to establish the hydrodynamic scenarios which feed the oil spill simulations.

Regarding the oil spill simulations and based on port activities and concerns, six locations were chosen as the most probable areas for the occurrence of an oil spill in the lagoon (Figure 8).

The oil spill simulations were started on three distinct tidal

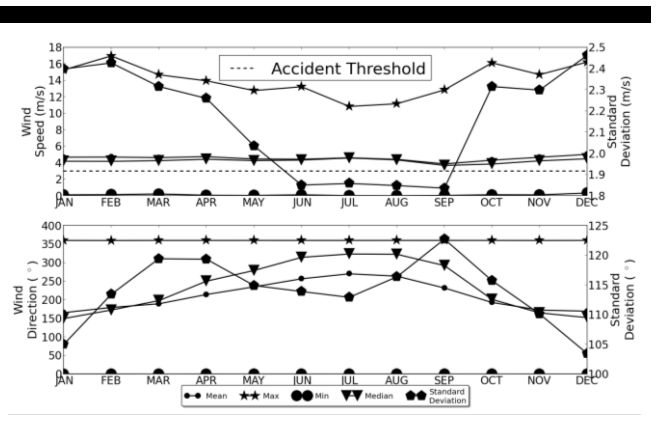


Figure 6: Monthly statistics for wind-related variables

phases: high tide, low tide and maximum flood. Maximum ebb was not considered since tidal ebb currents are very strong and consequently most of the oil would leave the lagoon soon after the spill, thereby minimizing the hazard. The final hazard scenarios database, which accounts for the hydrodynamic and oil spills setups, is constituted by 3456 simulations (192 hydrodynamic simulations × 6 spill locations × 3 tidal phases).

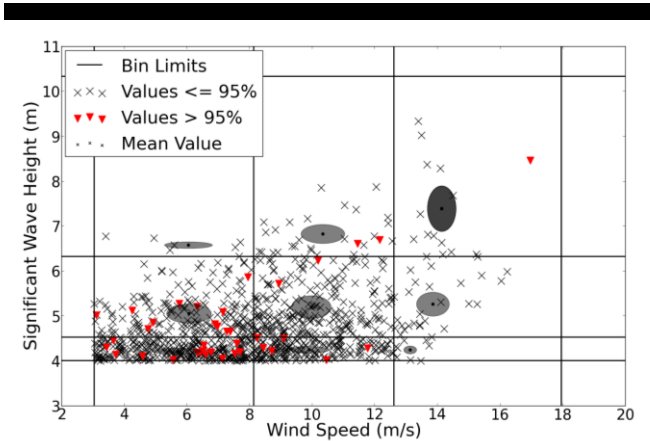


Figure 7: Wind speed vs. Hs bin constraints, representative values and error ellipses, for data above the thresholds.

Table 3: Representative values for each parameterized class (Mean, Standard deviation).

	frequent cases Percentiles (0 <sup>th</sup> -75 <sup>th</sup> ) ( $\mu \pm \sigma$ )	mildly observed cases Percentiles (75 <sup>th</sup> -95 <sup>th</sup> ) ( $\mu \pm \sigma$ )	less frequent cases Percentiles (95 <sup>th</sup> -100 <sup>th</sup> ) ( $\mu \pm \sigma$ )
Mean wave direction (°)	275.5±1.5	303.9±1.4	333.6±1.3
Wind direction (°)	194.4±11.1	295.1±4.4	351.1±0.2
Significant wave height (m)	4.2±0.02	5.2±0.1	6.9±0.3
Wind speed (m/s)	5.9±0.2	10.1±0.2	13.7±0.4
Mean wave period (s)	11.3±0.4	13.4±0.1	15.2±0.1

### Numerical models

Two modeling systems were used in this study: MORSYS2D and VOILS. MORSYS2D (Bertin *et al.*, 2009) consists of (1) a wave propagation model (SWAN, Booij *et al.*, 1999), (2) a circulation model (ELCIRC, Zhang *et al.*, 2004) and (3) a sand transport and bathymetry update model (SAND2D, Fortunato and Oliveira, 2004, 2007), sharing information and interacting through Perl scripts. This platform simulates morphological evolution under the combined action of tides, waves, freshwater discharge and wind. However, the bathymetry was fixed in the present study, and the sand transport model was not used. Therefore, all hydrodynamic simulations were made with the coupled system using ELCIRC and SWAN. VOILS (Azevedo *et al.* 2009, 2014; Azevedo, 2010) is an oil spill model, based on a Eulerian-Lagrangian approach to solve the transport equation and uses unstructured horizontal grids for domain representation. VOILS can be used in two distinct modes: a 2D



Figure 8: Location of the six predefined oil spills..

surface model, which was used herein, and a 3D mode, that results from the hard-coupling of the transport and transformation model with the hydrodynamic model SELFE (Zhang and Baptista, 2008), where the transport of the oil in the water column is calculated.

In both modes the model simulates the major transformation processes: evaporation, emulsification, spreading, dispersion, dissolution, and shoreline retention and reposition. Each process can be switched on and off, and solved with different formulations.

The information retrieved from the climatological analysis was used to setup the hydrodynamic simulations. The hydrodynamic simulations were forced with 12 tidal constituents (Z0, MSF, O1, K1, N2, M2, S2, MN4, M4, MS4, M6 and 2MS6), taken from the regional model of Fortunato *et al.* (2002). The simulation grid for the hydrodynamic and the oil spill models had about 70000 elements and 42000 nodes. The validation and calibration of MORSYS2D in the Aveiro lagoon is described in Vaz *et al.* (2013). The time steps were set to 90 s and 900 s in the hydrodynamic and oil spill runs, respectively.

### Hazard probability maps

The analysis of the hazard scenarios database provided useful information regarding the study region. One of the products developed is the hazard probability map ( $H_p$ ) that was determined using the expression (1):

$$H_p(x, y) = \frac{\sum_{i=1}^n P_i \sum_{j=1}^m \sum_{k=1}^l S_j T_k Q(x, y)_{ijk}}{\sum_{i=1}^n P_i} \quad (1)$$

where,  $H_p$  is the hazard probability map (Figure 9),  $n$  is the number of hydrodynamic simulations used in the analysis,  $m=6$  is the number of spill locations,  $P_i$  is the occurrence probability associated to the hydrodynamic simulation,  $S_j$  is the occurrence probability associated to spill location  $j$ .  $Q(x, y)_{ijk}$  is an indicator of the presence of oil at each node of the grid:  $Q$  is 1 if oil reached the point  $(x, y)$  during the simulation, and 0 otherwise.  $T_k$  is the probability associated to the tidal range of the simulation (neap, mean or spring tide), and  $l=3$  is the number of tidal ranges considered (Figure 9). The scaling by the sum of the probabilities in Eq. (1) allows estimating the hazard from a limited number of simulations.

Figure 10 shows the hazard probability maps for the first 20 simulations, which correspond, approximately, to the 40% most probable hydrodynamic conditions for the occurrence of an oil spill. Figure 10 shows the probability of a particular point in the Aveiro lagoon domain to be contaminated with oil, from a spill located in Barra (Figure 10a) and Terminal Sul (Figure 10b). The probability of a spill occurring in Barra or in Terminal Sul was estimated with the collaboration of the harbor authorities as approximately 35% and 5%, respectively. Because these maps were built considering only the 20 most probable hydrodynamic conditions and the maximum values found were 26.25%, in Barra and nearly 3.75% in Terminal Sul.

The hazard probability maps can be used by port administration to predict which areas of the lagoon are most likely to be affected, and make an effective management of the logistic capabilities and response strategies to mitigate oil spill events inside the Aveiro lagoon.

In the future, these hazard probability maps will be confronted with the vulnerability maps for the Aveiro lagoon region, to establish the high-resolution risk maps for this coastal domain.

### CONCLUSIONS

The approach presented herein allows the generation of hazard maps for oil spill accidents in coastal regions. The information required is now widely available worldwide: oil spill accidents (CEDRE-<http://www.cedre.fr/en/spill/alphabetical-classification.php>), hindcasts of weather and ocean conditions (ERA-I), and tidal constituents from tide gauges or numerical models. The association of probabilities to each environmental scenario has several advantages: 1) it opens the route to quantitative and rigorous risk analyses, which are critical for decisions on resource allocation; 2) it provides simple criteria to decide which simulations to perform, since the most likely scenarios are also those that affect the results the most; and 3) it provides a simple and rigorous way to generate new maps by including additional information. The maps generated herein are made available to the decision-makers through a WebGIS platform for both oil forecast and risk analysis, which allows their combination with vulnerability information (Oliveira *et al.*, this issue).

### ACKNOWLEDGEMENT

The European Union, under the European Regional Development Fund and INTERREG IV B: Atlantic Area Transnational Programme, supported this study through the research project SPRES-2011-1/168. The Portuguese Foundation for Science and Technology FCT also supported this study in the frame of the research project PTDC/AAC-AMB/113469/2009 - PAC:MAN, co-funded by COMPETE,

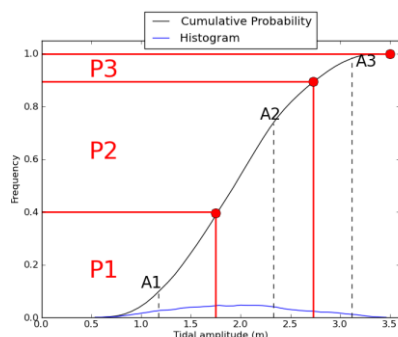


Figure 9: Histogram of tidal ranges at the Aveiro inlet, from a 19 years tidal synthesis. (A1, A2, A3) = (1.16, 2.33, 3.12) m correspond to the mean tidal amplitudes used in the scenarios simulations for each tidal range. Their associated probabilities of occurrence are (P1, P2, P3) = (40.7%, 48.7%, 10.6%), corresponding to neap, mean and spring tide, respectively.



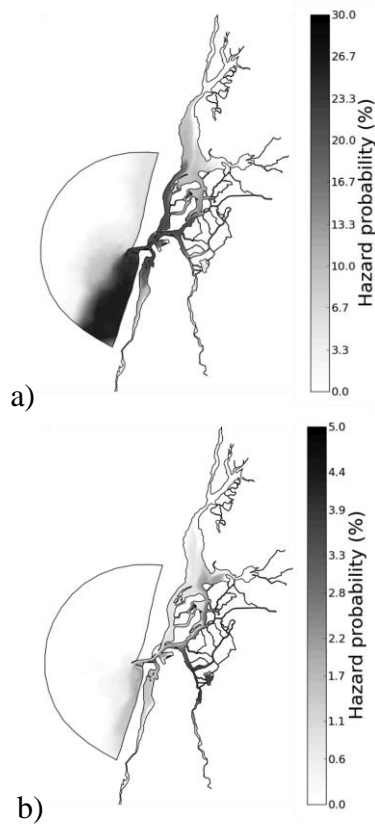


Figure 10: Hazard probability maps for the 20 most probable scenarios (approximately 40% of the total hazard scenarios dataset). a) oil spill in Barra and b) oil spill in Terminal Sul.

QREN, FEDER. The authors also thank to Luso-American Development Foundation, for funding project C-WOS, and also the grants of the second (SFRH/BPD/73089/2010) and ninth (SFRH/BPD/87512/2012) authors. The authors thank Prof. António M. Baptista (CMOP, USA) for the model ELCIRC. This work also makes use of results produced with the support of the Portuguese National Grid Initiative; more information in <https://wiki.ncg.ingrid.pt>.

### LITERATURE CITED

- Albaigés, J., Morales-Nin, B., Vilas, F., 2006. The Prestige oil spill: A scientific response. *Marine Pollution Bulletin* 53 (5-7), 205–207.
- Azevedo, A., Oliveira, A., Fortunato, A. and Bertin, X., 2009. Application of an Eulerian-Lagrangian oil spill modeling system to the Prestige, 777 – 781.
- Azevedo, A., 2010. *Sistema Integrado de Modelação para Apoio à Prevenção e Mitigação de Acidentes de Hidrocarbonetos em Estuários e Orla Costeira*. Lisboa, Portugal: Faculdade de Ciências da Universidade de Lisboa, Ph.D. Thesis, 224 pp. <http://hdl.handle.net/10451/2332>
- Azevedo, A., Oliveira, A., Fortunato, A.B., Zhang, J., Baptista, A.M., 2014. A cross-scale numerical modeling system for management support of oil spill accidents. *Marine Pollution Bulletin*, (2014), *in press*, <http://dx.doi.org/10.1016/j.marpolb.2014.01.028>
- Bertin, X., Oliveira, A. and Fortunato, A.B., 2009. Simulating morphodynamics with unstructured grids: description and validation of an operational model for coastal applications. *Ocean Modelling*, 28/1-3, 75-87.

- Booij, N., Ris, R.C. and Holthuijsen, L.H., 1999. A third-generation wave model for coastal regions, Part I, Model description and validation. *Journal of Geophysical Research*, C4, 104, 7649-7666.
- Costa, R.T., Azevedo, A., Da Silva, J.C.B. and Oliveira, A., 2012. Oil spill detection and modeling: Preliminary results for the Cercal accident. *European Spatial Agency (ESA) Special Publication*, SP-709, pp. 5.
- Dias, J.M., Lopes, J.F. and Dekeyser, I., 2000. Tidal Propagation in Ria de Aveiro Lagoon, Portugal. *Physics and Chemistry of the Earth*, 4, 25, 369-374.
- Fortunato, A., Pinto, L., Oliveira, A. and Ferreira, J., 2002. Tidally-generated shelf waves off the western Iberian coast. *Continental Shelf Research* 22/14, 1935–1950.
- Fortunato, A.B. and Oliveira, A., 2004. A modeling system for tidally driven long-term morphodynamics. *Journal of Hydraulic Research*, 42/4, 426-434.
- Fortunato, A.B. and Oliveira, A., 2007. Improving the stability of a morphodynamic modeling system. *Journal of Coastal Research*, SI 50, 486-490.
- Lopes, J.F., Dias, J., Cardoso, A.C. and Silva, C.I.V., 2005. The water quality of the Ria de Aveiro lagoon, Portugal: From the observations to the implementation of a numerical model. *Marine Environmental Research*, 60, 594–628.
- Mackowsky, R.M., Kende, C.B., Bennet, R.C. and Ziemanski, J.A., 2010. *The Deepwater Horizon Catastrophe: A Factual Overview and Preliminary First-Party Analysis*, Cozen O'Connor editions, 61 pp.
- Mendes, R., Dias, J.M. and Pinheiro, L.M., 2009. Numerical modeling estimation of the spread of maritime oil spills in Ria de Aveiro lagoon. *Journal of Coastal Research*, SI 56, 1375-1379.
- Plecha, S., Silva, P.A., Oliveira, A. and Dias, J.M., 2012. Establishing the wave climate influence on the morphodynamics of a coastal lagoon inlet. *Ocean Dynamics* 62, 5, 799-814.
- Vaz, L., Plecha, S. and Dias, J.M., 2013. Coastal wave regime influence on Ria de Aveiro inlet dynamics. *Journal of Coastal Research*, SI 65, 1605-1610.
- Zhang, Y., Baptista, A.M. and Myers, E.P., 2004. A cross-scale model for 3D baroclinic circulation in estuary-plume-shelf systems: I. Formulation and skill assessment. *Continental Shelf Research*, 24/18, 2187-2214.
- Zhang, Y.-L. and Baptista, A.M., 2008. SELFE: A semi-implicit Eulerian-Lagrangian finite-element model for cross-scale ocean circulation. *Ocean Modelling*, 21/3-4, 71-96.

# Tourism carrying capacity on estuarine beaches in the Brazilian Amazon region

Rosigleyse C. de Sousa†, Luci C.C. Pereira†, Rauquírio M. da Costa†, José A. Jiménez††

†Instituto de Estudos Costeiros,  
Universidade Federal do Pará,  
Bragança, 68600-000, Brazil.  
rosigleyse@yahoo.com.br  
cajueiro@ufpa.br  
raucosta@ufpa.br

††Universitat Politècnica de Catalunya.  
Carrer Jordi Girona, 1-3. Edificio D1,  
08034. Barcelona, Spain.  
jose.jimenez@upc.edu



[www.cerf-jcr.org](http://www.cerf-jcr.org)



[www.JCRonline.org](http://www.JCRonline.org)

## ABSTRACT

Sousa, R.C., Pereira, L.C.C., Costa, R.M. and Jiménez, J.A., 2014. Tourism carrying capacity on estuarine beaches in the Brazilian Amazon region. In: Green, A.N. and Cooper, J.A.G. (eds.), *Proceedings 13<sup>th</sup> International Coastal Symposium* (Durban, South Africa), *Journal of Coastal Research*, Special Issue No. 70, pp. 545-550, ISSN 0749-0208.

Tourism Carrying Capacity (TCC) can be defined as the level of human activity that an area can support without provoking deterioration of its physical and environmental characteristics. The present study aimed to estimate the maximum number of visitors that Colares, Marudá and Murubira beaches can receive during periods of peak visitation. The TCC was calculated considering the Physical Carrying Capacity (PCC), the Real Carrying Capacity (RCC), and the Effective Carrying Capacity (ECC) of each beach. In each survey, the number of visitors along a pre-established transect (central portion of each beach) was counted every hour (8 am until 6 pm). The maximum recommended ECC values indicated a maximum of 674 visitors per day at Colares, 812 visitors per day at Marudá and 97 visitors per day at Murubira. In comparison with these recommendations, the observed numbers of visitors were relatively high at Marudá (885 visitors) and Murubira beaches (297 visitors), while Colares was within the suggested limit (193 visitors). Peak visitation rates were recorded between 1 pm and 4 pm, and observed carrying values varied from 1.5 to over 5.000 m<sup>2</sup> per visitor at Colares beach, 0.7-426 m<sup>2</sup> per visitor at Marudá beach, and 1.7-42.9 m<sup>2</sup> at Murubira. The results of the present study indicated that the density of visitors on the study beaches exceeded tolerable limits, and that coastal management measures are necessary to improve local tourist activities.

**ADDITIONAL INDEX WORDS:** *Carrying capacity, vacation periods, Amazon littoral.*

## INTRODUCTION

Coastal tourism planning is often based on the concepts and parameters provided by carrying capacity assessments, which can be defined as the level of human activity that an area can support without provoking deterioration of its physical and environmental characteristics, or the quality of the visitors' experience (Tejada *et al.*, 2009). Carrying capacity evaluation is used to assess the impacts of tourism on both physical space and the quality of the environment, and to establish guidelines for sustainable tourism practices (De Ruyck *et al.*, 1997; Deacon and Kolstad, 2000). This approach depends on the availability of data on local resources and infrastructure, and is typically influenced by factors such as seasonality, the period of the day, the quality of the available infrastructure and the resources being exploited, as well as user satisfaction (Tejada *et al.*, 2009). Studies of this type have been important for the planning of the rational exploitation and sustainable development of beach environments (Williams and Lemckert, 2007).

The Federation of National Parks of Europe (FNNPE, 1993) has defined carrying capacity as the ability of the ecosystem to sustain itself and guarantee the unconditional establishment of human activities with no negative feedback effects. In Brazil, coastal tourism is very popular with both local and foreign visitors, especially in the tropical and subtropical regions of the country

(Silva *et al.*, 2008; Sousa *et al.*, 2013). The equatorial (Amazon) region has considerable potential for the development of a coastal tourism industry, although the lack of basic services and infrastructure in many areas tends to limit the numbers of visitors from abroad and from other regions of Brazil (Pinto *et al.*, 2011; Silva *et al.*, 2011a; Sousa *et al.*, 2011).

On the estuarine and oceanic beaches of the Amazon coast, the potential for tourism is limited by a number of factors, including the intense rainy season, the long distances from major urban centers, and the complexity of the local coastal ecosystems, characterized by vast tracts of mangrove forests and meandering tidal creeks, which limit access options considerably (Pessoa *et al.*, 2013). These factors combine to limit the recreational use of most of the coast to the school vacation period (July) and long bank holidays, principally during the second (dry season) half of the year (Oliveira *et al.*, 2011; Silva *et al.*, 2011a).

Given this, the present study investigated the tourism carrying capacity of three touristic Amazon beaches to estimate the maximum recommended number of visitors for a given time period. The results of this study should provide a valuable contribution to the elaboration of future management plans based on the sustainable development of recreational activities and the conservation of local natural resources.

## STUDY AREA

The macrotidal Amazon coast is dominated by dozens of estuaries, including that of the Amazon River itself, which discharge enormous quantities of freshwater, sediments, nutrients,

and organic matter into the western Atlantic Ocean (Geyer *et al.*, 1996). The climate of this region is characterized by a long and intense rainy season, between January and June, and a dry season during the second half of the year.

Located in the Brazilian state of Pará, the study area encompasses a number of estuarine beaches (Figure 1). Geomorphologically, this coast can be divided into three main sectors: I Coastal Atlantic (including 18 towns), II Continental Estuarine (10 towns and cities), and III Insular Estuarine (13 towns) (GERCO/PA, 1995). Marudá beach is located in sector I and Colares and Murubira beaches in sector II. Other relevant characteristics of each beach are:

(i) Colares beach is located on Colares Island, which is 96 km from the Pará state capital, Belém. The island is separated from the continent by the Guajará-Mirim River and Laura tidal creek.

(ii) Marudá beach is located at the mouth of the Marapanim estuary, 160 km from Belém.

(iii) Murubira beach is located on Mosqueiro Island, 60 km from Belém, a site of considerable historic and touristic importance.

## METHODS

### Field studies

Each one of the study beaches was surveyed on a Sunday in July 2012, the principal school vacation period. During each survey, the number of people present within a pre-established transect was counted every hour between 8 am and 6 pm.

The transects (100 m wide) were located near a beach access and divided into three zones: zone 1: promenade and backshore; zone 2: intertidal zone: (from the higher spring tide to the lower neap tide level); and zone 3: subtidal zone (15 m into water from the lower neap tide level). Measurements of the width of zone 2 were taken every hour due to the mesotidal and macrotidal conditions.

The analysis of the different types of use and the indices used for the evaluation of the management capacity of the three beaches were derived from direct observation and the application of a

checklist. The recreational carrying was estimated following the approach of Ruschman (1999) and Eugênio-Martin (2004), based on the density of visitors in each zone:

$$C = V / K \quad (\text{Eq. 1})$$

where **C** is Recreational Carrying, **V** is the area available for use, and **K** is the number of beachgoers.

### Carrying Capacity Assessment

The assessment of tourist carrying capacity was based on the model developed by Cifuentes (1992), which attempts to establish the maximum number of visits an area can tolerate based on its physical, biological, and management conditions, considering three main parameters: Physical Carrying Capacity, Real Carrying Capacity, and Effective Carrying Capacity (Cifuentes, 1992).

The Physical Carrying Capacity (PCC) was defined as the maximum number of users that can be accommodated within a certain area at a specific time. As beaches are open areas, the time parameter was not applicable, so the original formula was adapted following the approach of Ruschmann *et al.* (2008) and Zacarias *et al.* (2011), with the Physical Carrying Capacity (PCC) being given by:

$$PCC = A / A_u \quad (\text{Eq. 2})$$

where **A** is the size of the study area, and **A<sub>u</sub>** is the area available per user (= 10 m<sup>2</sup>; Ruschmann *et al.*, 2008).

The Real Carrying Capacity (RCC) is the maximum tolerable number of people within a given area, once correction factors (intrinsic physical, environmental, ecological, social, and management characteristics of the site) have been taken into account. This approach is based on the observation that certain factors, such as the quality of the water, incidence of sunlight, site accessibility, wind speeds, and in particular rainfall may affect visitation rates. The Real Carrying Capacity (RCC) was determined by:

$$RCC = PCC \times (cf_1 \times cf_2 \times \dots \times cf_n) \quad (\text{Eq. 3})$$

where **PCC** is the Physical Carrying Capacity and **Cf<sub>1</sub>...cf<sub>n</sub>** are the correction factors.

As tourism is highly dependent on climatic variables, one correction factor – rainfall – was considered in this study. This factor was selected because of its potential to limit touristic activities, the availability of reliable data, and its relevance for the evaluation of the potential sustainability of a destination (Cifuentes, 1992; Cifuentes *et al.*, 1999). Rainfall data were obtained from the Brazilian Institute of Meteorology (INMET, 2012) and the correction factor (Cf<sub>x</sub>) was calculated by:

$$Cf_x = 1 - Lm_x / Tm_x \quad (\text{Eq. 4})$$

where **Lm<sub>x</sub>** is the limiting magnitude of variable **x** and **Tm<sub>x</sub>** is the total magnitude of variable **x**.

The Effective Carrying Capacity (ECC) is the maximum number of visitors that a site can support considering the RCC and management capacity. This final parameter was based on the available infrastructure, services, and equipment, as observed during the survey period (Table 1). The ECC was determined by:

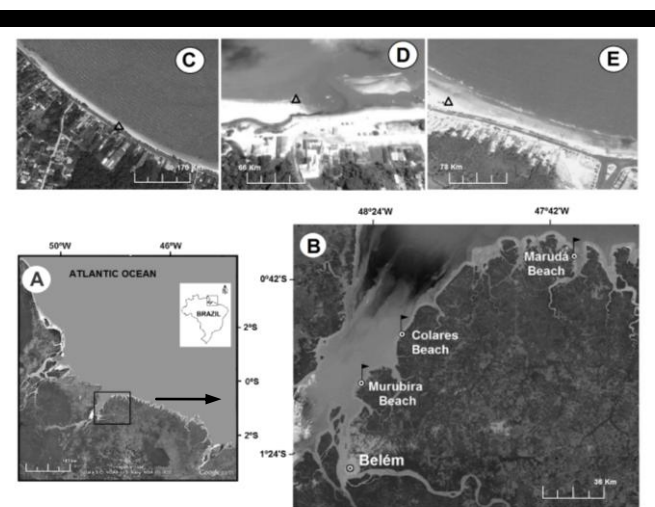


Figure 1. Study Area. Amazon Coast (A); Study area indicating Belém (Pará State Capital) and the three collection sites (B); Murubira 01°07'16.5"S, 48°26'39.4"W (C), Colares 00°55'54.1"S, 48°17'28.9"W (D) and Marudá 00°37'21.4"S, 47°38'00.0"W (E) beaches. Image from Google Earth.

$$\text{ECC} = \text{RCC} \times \text{Mc} \quad (\text{Eq. 5})$$

where **RCC** is the Real Carrying Capacity and **Mc** is Management Capacity.

### Statistical Analysis

The number of beachgoers and the variation in the recreational carrying values were analyzed according to tidal, spatial (zones), and temporal (hour of the day) conditions. When the data were normally distributed and presented homogeneous variance, ANOVA and the Fisher post-hoc test were applied. For non-normal data, Mann-Whitney's *U* or the Kruskal-Wallis nonparametric analysis of variance were used. All analyses were run in the STATISTICA 6.0 package, considering  $p < 0.05$ .

## RESULTS

### Beach Zonation

Based on recreational use patterns and topographic characteristics, each beach was divided into three zones:

- i) Zone 1: the promenade at Marudá and Murubira, and the backshore area at Colares. This area is characterized by the presence of musical attractions, as well as bars and restaurants (Figure 2A);
- ii) Zone 2: the use of this intermediate area depends on tidal conditions (high/low, spring/neap). During the ebb and low tides, this zone is used primarily for recreational activities, such as sports (football and volleyball), sunbathing, and the consumption of food and drinks at tables provided by the owners of local bars and guesthouses (Figure 2B). At Colares, however, this zone is used infrequently, due to the presence of muddy sediments;
- iii) Zone 3: the surf zone, located at the water's edge, is used by bathers and for other recreational activities, such as jet-skiing, kite-surfing, and motor-boating (Figure 2C). This zone is not used during low or ebb tides at Colares due to the presence of muddy sediments and the frequent occurrence of incidents involving stingrays.

### Infrastructure and services

The best services and infrastructure were found in Marudá and Murubira (Table 2). By contrast, Colares beach was characterized by rudimentary infrastructure and limited services, in addition to logistic difficulties, which include a ferry crossing (Table 2).

### Carrying Capacity Assessment

As transect width at all sites was 100 m, the area surveyed at each site was determined by the perpendicular extension of the

Table 1. Indicators of Management Capacity applied to assess the Effective Carrying Capacity at Amazon beaches.

Indicators	Classification		
	Low (1)	Medium (2)	High (3)
Public bathrooms	Absent	Little	Adequate
Payphones	Absent	Little	Adequate
Waste bins	Absent	Little	Adequate
Street lighting	Absent	Little	Adequate
Parking	Absent	Little	Adequate
Safety	Absent	Little	Adequate
Accommodation	Absent	Little	Adequate
Bars and restaurants	Absent	Little	Adequate
Accessibility	Absent	Little	Adequate
Presence of domestic animals	Frequent	Moderate	Absent

transect, which was 267.1 m at Colares (area of 26,710 m<sup>2</sup>), 254.4 m at Marudá (25,440 m<sup>2</sup>), and 32 m at Murubira (3,200 m<sup>2</sup>). Considering  $A_u = 10$  m<sup>2</sup>, the PCC was estimated to be 2670 visitors/day at Colares, 2560 visitors/day at Marudá and 320 visitors/day at Murubira.

For the calculation of the Real Carrying Capacity (RCC) in 2012, the months in which total rainfall exceeding 200 mm represented a total of 180 days, that is, 51% of the year (365 days). This corresponds to a correction factor of 0.51 for rainfall. Based on this, the RCC was estimated at 1282 visitors per day for Colares, 1229 for Marudá, and 154 for Murubira.

Given these findings, the management capacity recorded for each beach (Table 2) indicated that Colares has only 50% of the conditions necessary for the achievement of its recreational goals, while Marudá has 63% of this management capacity and Murubira, 60%. Given this, the Effective Carrying Capacity was estimated to be 674 visitors per day at Colares, 812 at Marudá, and 97 at Murubira. While the number of visitors observed at Colares (193) was well within this theoretical limit, it was far exceeded at both Marudá (885 visitors) and Murubira beaches (297 visitors).

### Carrying Capacity Assessment per zone

The carrying capacity was also estimated per zone and time period, although only zones 1 and 2 were considered here (Table 3) due to the problems of overcrowding.

In zone 1 (Table 3), at Colares, the effective carrying capacity was estimated to be 45 visitors, but during the peak visitation time



Figure 2. Zone 1 in Murubira beach (A), Zone 2 in Marudá beach (B) and Zone 3 in Colares beach.

Table 2. Management Capacity applied to assess the Effective Carrying Capacity at Amazon beaches.

Indicators	Classification		
	Colares	Marudá	Murubira
Public bathrooms	1	1	1
Payphones	1	1	1
Waste bins	1	2	2
Street lighting	1	3	3
Parking	1	2	1
Safety	3	3	3
Accommodation	2	2	2
Bars and restaurants	2	2	2
Accessibility	1	1	1
Presence of domestic animals	2	2	2
$\Sigma$	15	19	18

(2 pm) more than 80 beachgoers were found (Figure 3). At Marudá, a peak with 610 beachgoers was recorded at 6 pm, when the effective carrying capacity should be 44 visitors (Figure 3). At Murubira, the effective carrying capacity was estimated to be 10 visitors. However, during the peak visitation that occurred between 9 am and 3 pm, this beach reached almost 240 visitors (Figure 3).

At Marudá and Murubira, in zone 1, the density of visitors increased steadily over the course of the afternoon, due to the presence of musical attractions in this zone at the end of the day.

Table 3. Carrying capacity assessment - PCC, RCC and ECC (allowed visitors), and the Use level - UL (m<sup>2</sup>/person) and peak visitation time (h) for zones 1 and 2 on the three study beaches.

Beaches	Carrying capacity estimates					
	Zone 1	PCC	RCC	ECC	UL	Peak Time
Colares		333	163	45	42-333	2 pm
Marudá		136	67	44	0.7-12	6 pm
Murubira		40	20	10	1.7-20	6 pm
Zone 2	PCC	RCC	ECC	UL	Peak Time	
Colares	10-2000	5-1140	2-569	10-5000	4 pm	
Marudá	310-510	142-1230	89-778	8.9-426	12 pm	
Murubira	10-280	5-137	3-82	5-42.9	2 pm	

In zone 2 (Table 3), the effective carrying capacity at Colares was estimated between 2 and 569 visitors, and the peak number of beachgoers (44) was observed at 4 pm (Figure 3). At Marudá, the effective carrying capacity estimated ranged 89 to 778 visitors, and the peak (375 visitors) was recorded at 12 pm (Figure 3). At Murubira, the visitation peak was 102 beachgoers (around 2 pm), while the effective carrying capacity was calculated to be between 3 and 82 visitors (Figure 3).

At Marudá and Murubira beaches, in zone 2, the limits were exceeded during the flood and high tide, leading to overcrowding due to the considerable reduction in the size of the area available

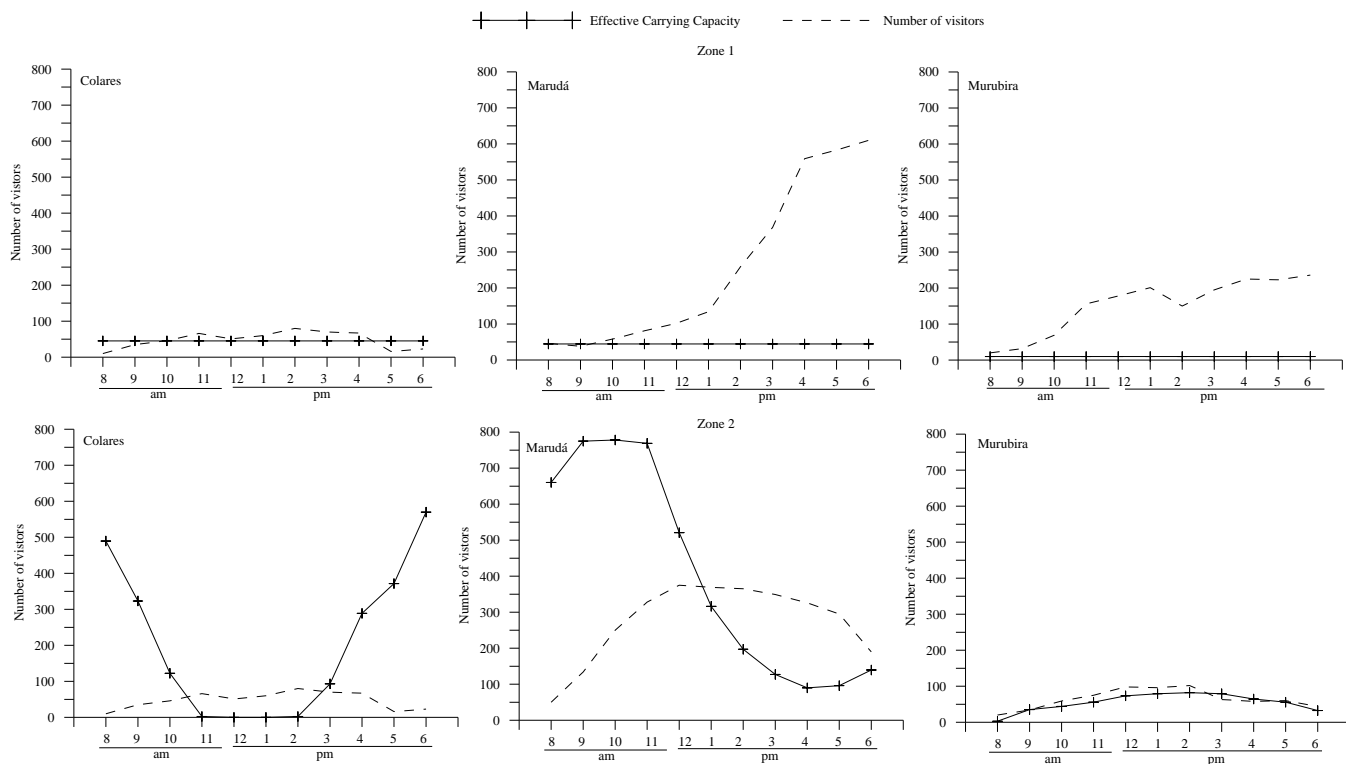


Figure 3. Number of visitors in zone 1 and zone 2 in all studied beaches per hour.

to beachgoers, accentuated by the region's macrotides.

It was possible to estimate the use level for each zone based on the area surveyed and the numbers of beachgoers. On Colares beach, these values varied from 42 to 333 m<sup>2</sup> per person in zone 1, 10 to 5000 m<sup>2</sup> per person in zone 2, and 1.5 to 75 m<sup>2</sup> per person in zone 3. At Marudá, these values ranged from 0.7 to 12 m<sup>2</sup> per person in zone 1, 8.9 to 426 m<sup>2</sup> per person in zone 2, and 1.9 to 18.8 m<sup>2</sup> in zone 3, while at Murubira, they ranged from 1.7 to 20 m<sup>2</sup> per person in zone 1, 5–42.9 m<sup>2</sup> per person in zone 2, and 3.8–37.5 m<sup>2</sup> per person in zone 3.

### Statistical Analysis

Significant differences were found among zones on Marudá ( $p = 0.00$ ;  $F = 16.45$ ) and Murubira ( $p = 0.00$ ;  $F = 18.56$ ) beaches, with zone 1 invariably presenting the highest values. On both beaches, this zone was characterized by high numbers of visitors attracted primarily by the presence of musical attractions and bars selling alcoholic beverages.

### DISCUSSION

Large numbers of tourists visit the beaches of the Amazon coast primarily during the school vacation period (July), which coincides with the start of the dry season in this region, and some of the long bank holidays occurring during the second half of the year (Sousa *et al.*, 2011; Sousa *et al.*, 2013; Pessoa *et al.*, 2013). During the first half of the year, by contrast, the high precipitation levels tend to limit the numbers of beachgoers.

In general terms, Amazonian beaches have a considerable potential for tourism due to the natural beauty of their landscapes and high levels of environmental preservation. However, this potential is limited considerably by the lack of services and infrastructure, in particular a public sanitation system. The unregulated discharge of sewage and other effluents directly onto many of the beaches is a major problem that affects not only the quality of the beach, but also public health (Krause and Glaser, 2003; Menezes *et al.*, 2009; Pereira *et al.*, 2007, Souza-Filho *et al.*, 2006; Pereira *et al.*, 2009; Silva *et al.*, 2011b; Oliveira *et al.*, 2011; Pinto *et al.*, 2011). These problems intensify during the July vacation period in particular, when the beaches are visited by large numbers of tourists.

Spatial and temporal visitation patterns on the study beaches were influenced strongly by factors such as the intensity of the sunlight, accessibility, the availability of attractions (musical shows), and oscillations in tidal levels (De Ruyck *et al.*, 1997; Deacon and Kolstad, 2000; Silva, 2002; Polette and Raucci, 2003; Silva *et al.*, 2008; Silva *et al.*, 2011b). Similar results were obtained at other Amazonian beaches (Silva *et al.*, 2011b; Sousa *et al.*, 2011).

At Colares, the spatial distribution of beachgoers was determined primarily by natural conditions, including the presence of muddy sediments in the intertidal zone (zone 2) and the occurrence of incidents involving stingrays in zone 3 during the ebb and low tide. These features limit visitation basically to zone 1.

In the present study, carrying capacity was estimated empirically based on field observations, given the lack of official data on the numbers of tourists that visit the study beaches. The observed capacity was consistent with that suggested by Zacarias *et al.* (2011). The results of the study indicate that the numbers of visitors on Marudá and Murubira beaches are higher than the recommended limits. As the number of tourists increases, so does the feeling of congestion, while the quality of the environment decreases gradually (Aranguren *et al.*, 2008), and the capacity of the beach to recover from these impacts declines. This process is

accompanied by the continuous accumulation of litter derived from the sale of refreshments demanded by the growing numbers of beachgoers.

Colares beach presents a number of distinct characteristics, including its even simpler infrastructure and more isolated location, as well as the fact that its principal attribute is its natural scenery, rather than man-made attractions. The combination of these factors contributes to the smaller numbers of visitors observed at this site.

While the present study focused on a high season period, the values recorded appear to be representative of the carrying capacity at the study sites during weekends in the holiday season. Overall, the results may be fundamentally important to the development of future coastal management plans, which should contribute to improvements in the region's tourism industry.

### FINAL CONSIDERATIONS

The study beaches all presented similar patterns of use and visitation, although Colares beach was distinct in a number of aspects, due to the restrictions imposed by some of its natural features and the lack of services and infrastructure. While there is room for growth in the touristic potential of Amazonian beaches, the lack of adequate coastal management policies impacts both the quality of local environments and public health standards. The implementation of management initiatives is urgently needed in order to improve the facilities available to local beachgoers and to guarantee the quality of the recreational experience for tourists in this sector of the Amazon coast. These initiatives should include (i) beach zoning, in order to guarantee the conservation of natural resources, (ii) the improvement of infrastructure (e.g., toilets and showers at 300 m intervals), (iii) the formal structuring of basic services and tourist facilities, (iv) prohibition of domestic animals from the beach area, (v) placement of stingray warning signs on Colares beach, and the prohibition of bathing during the ebb and low tides, and (vi) daily removal of litter from the beach.

### ACKNOWLEDGEMENTS

The authors would also like to thank CNPq for yours research grants. We are also indebted to Dr. Stephen Ferrari for his careful correction of the English.

### LITERATURE CITED

- Aranguren, J., Moncada, J. A., Naveda, J., Rivas, D., and Lugo, C., 2008. Evaluación de la capacidad de carga turística en la playa Conomita, Municipio Guanta, Estado Anzoátegui. *Revista de Investigación*, 64, 31-36.
- Cifuentes, M. A., 1992. Determinación de capacidad de carga turística en áreas protegidas. Costa Rica: Biblioteca Orton IICA/CATIE, 28p. Available in: <http://www.ulpgc.es/hege/almacen/download/23/23388/articulocifuentes.pdf>.
- Cifuentes, M. A., Mesquita, C. A. B., Méndez, J., Morales, M. E., Aguilar, N. and Cancino, D., 1999. Capacidad de carga turística de las áreas de Uso Público del Monumento Nacional Guayabo, Costa Rica. Costa Rica: WWF Centro America.
- De Ruyck, M.C., Alexandre, G.S. and McLachlan, A., 1997. Social carrying capacity as a management tool for sandy beaches. *Journal Coastal of Research*, 13 (3), 822–830.
- Deacon, R.T. and Kolstad, C.D., 2000. Valuing beach recreation lost in environmental accidents. *Journal of Water Resources. Planning and Management*, 126 (6), 374–381.
- Eugenio-Martin, J.L., 2004. Monitoring the congestion level of competitive destinations with mixed logic models. Available in: <http://www.nottingham.ac.uk>. Viewed, 2, June 2009.
- Federation of Nature and National Parks of Europe., 1993. *Loving Them to Death? Sustainable Tourism in Europe's Nature and National Parks*, FNNPE, Grafenau.

- Geyer, W.R., Beardsley, R.C., Lentz, S.J., Candela, J., Limeburner R., Johns, W.E., Castro, B.M. and Soares, I.D., 1996. Physical oceanography of the Amazon shelf. *Continental Shelf Research*, 16 (5), 575-616.
- Governo do Estado do Pará., 1995.-Lei Estadual do Programa Estadual de Gerenciamento da Zona Costeira (GERCO/PA)- Lei nº 5587/95.
- INMET (Instituto Nacional de Meteorologia)., 2012. Monitoramento de Estações Automáticas. <http://www.inmet.gov.br/sonabra/maps/automaticas.php>. Viewed 2 August 2012.
- Krause, G. and Glaser, M., 2003. Co-evolving geomorphological and socio-economic dynamics in a coastal fishing village of the Bragança region (Pará, North Brazil). *Ocean and Coastal Management*, 46 (9/10), 859-874.
- Menezes, M.O.B., Macedo, S.R.P., Corrêa, S.C. and Farage, E.R., 2009. Effects of the urban expansion on the islands of the low Amazon estuary: the case of Soure, Marajó Archipelago. *Revista da Gestão Costeira Integrada*, 9 (2), 113-126.
- Oliveira, S.M.O. de, Pereira, L.C.C., Vila-Concejo, A., Gorayeb, A., Sousa, R.C. de and Costa, R.M. da., 2011. Natural and anthropogenic impacts on a macrotidal sandy beach of the Brazilian Amazon (Ajuruteua): guidelines for coastal management. In: Furmanczyk, K., Giza, A. and Terefenko, P. (eds.), *Proceedings 11<sup>th</sup> International Coastal Symposium* (Szczecin, Poland), *Journal of Coastal Research*, Special Issue No. 64, pp.1385-1389.
- Pereira, L.C.C., Guimarães, D.de O, Costa, R.M. da, Souza-Filho, P.W.M., 2007. Use and Occupation in Bragança Littoral, Brazilian Amazon. *Journal of Coastal Research*, Special Issue No. 50, pp.1116-1120.
- Pereira, L.C.C., Mendes, C.M., Monteiro, M.C. and Asp, N.E., 2009. Morphological and Sedimentological Changes in a Macrotidal Sand Beach in the Amazon Littoral (Vila dos Pescadores, Pará, Brazil). In: Silva, C.P. da, Vaz, B., Abrantes, P. and Estanqueiro, R. (eds.), *Proceedings 10<sup>th</sup> International Coastal Symposium* (Lisbon, Portugal), *Journal of Coastal Research*, Special Issue No. 56, pp. 113-117.
- Pessoa, R.M.C., Pereira, L.C.C., Sousa, R.C., Magalhães, A., and da Costa, R.M., 2013. Recreational Carrying Capacity of an Amazon Macrotidal Beach During Vacation Periods. In: Conley, D.C., Masselink, G., Russell, P.E. and O'Hare, T.J. (eds.), *Proceedings 12<sup>th</sup> International Coastal Symposium* (Plymouth, England), *Journal of Coastal Research*, Special Issue No. 65, pp. 1027-1032.
- Pinto, K.S.T., Pereira, L.C.C., Vila-Concejo, A., Gorayeb, A., Sousa, R.C. de and Costa, R.M. da., 2011. Effects of the lack of coastal planning on water quality and land use on a macrotidal beach (Atalaia, Pará) in the amazon region. In: Furmanczyk, K., Giza, A., and Terefenko, P. (eds.), *Proceedings 11<sup>th</sup> International Coastal Symposium* (Szczecin, Poland), *Journal of Coastal Research*, Special Issue No. 64, pp. 1401-1405.
- Polette, M. and Raucci, G., 2003. Methodological Proposal for Carrying Capacity Analysis in Sandy Beaches: A Case Study at the Central Beach of Balneário Camboriú- SC- Brazil. *Journal of Coastal Research*, 35, 94-103.
- Ruschmann, D., 1999. Turismo e Planejamento Sustentável: a proteção do meio ambiente. Campinas: Papirus, 199p.
- Ruschmann, D., Paolucci, L. and Maciel, N., 2008. Capacidade de carga no planejamento turístico: estudo de caso da Praia Brava-Itajaí frente à implantação do Complexo Turístico Habitacional Canto da Brava. *Revista Brasileira de Pesquisa em Turismo*, 2 (2), 41-63.
- Silva, C.P. da., 2002. Beach Carrying Capacity Assessment: How Important is it? In: Silva, C.P. da, Vaz, B., Abrantes, P. and Estanqueiro, R. (eds.), *Proceedings 10<sup>th</sup> International Coastal Symposium* (Lisbon, Portugal), *Journal of Coastal Research*, Special Issue No. 56, pp. 190-197.
- Silva, I.R. da, Pereira, L.C.C., Sousa, R.C., Oliveira, S.M.O de, Guimarães, D. de O., Costa, R.M. da., 2011b. Amazon Beaches (São Luís, Brazil): Recreational Use, Environmental Indicators, and Perception of Beachgoers. In: Furmanczyk, K., Giza, A., and Terefenko, P. (eds.), *Proceedings 11<sup>th</sup> International Coastal Symposium* (Szczecin, Poland), *Journal of Coastal Research*, Special Issue No. 64, pp. 1287-1291.
- Silva, J.S., Leal, M.M.V., Araújo, M.C.B., Barbosa, S.C.T. and Costa, M.F., 2008. Spatial and Temporal Patterns of Use of Boa Viagem Beach, Northeast Brazil. *Journal of Coastal Research*, 24 (1A), 79-86.
- Silva, N.I.S. da, Pereira, L.C.C., Vila-Concejo, A., Gorayeb, A., Sousa, R.C. de, Asp, N.E. and Costa, R.M. da., 2011a. Natural and social conditions of Princesa, a macrotidal sandy beach on the Amazon Coast of Brazil. In: Furmanczyk, K., Giza, A., and Terefenko, P. (eds.), *Proceedings 11<sup>th</sup> International Coastal Symposium* (Szczecin, Poland), *Journal of Coastal Research*, Special Issue No. 64, pp. 1979-1983.
- Sousa, R.C., Pereira, L.C.C. and Costa, R.M., 2013. Water quality at touristic beaches on the Amazon coast. In: Conley, D.C., Masselink, G., Russell, P.E. and O'Hare, T.J. (eds.), *Proceedings 12<sup>th</sup> International Coastal Symposium* (Plymouth, England), *Journal of Coastal Research*, Special Issue No. 65, pp. 1057-1062.
- Sousa, R.C., Pereira, L.C.C., Silva, N.I.S., Oliveira, S.M.O. de, Pinto, K.S.T. and Costa, R.M. da., 2011. Recreational carrying capacity of three Amazon macrotidal beaches during the peak vacation season. In: Furmanczyk, K., Giza, A., and Terefenko, P. (eds.), *Proceedings 11<sup>th</sup> International Coastal Symposium* (Szczecin, Poland), *Journal of Coastal Research*, Special Issue No. 64, pp. 1292-1296.
- Souza-Filho, P.W.M., Martins, E.S.F. and Costa, F.R., 2006. Using mangroves as a geological indicator of coastal changes in the Bragança macrotidal flat, Brazilian Amazon: A remote sensing data approach. *Ocean and Coastal Management*, 49, 462-475.
- Tejada, M., Malvárez, G. C. and Navas, F., 2009. Indicators for the Assessment of Physical Carrying Capacity in Coastal Tourist Destinations. In: Silva, C.P. da, Vaz, B., Abrantes, P. and Estanqueiro, R. (eds.), *Proceedings 10<sup>th</sup> International Coastal Symposium* (Lisbon, Portugal), *Journal of Coastal Research*, Special Issue No. 56, pp. 1159-1163.
- Williams, P. and Lemckert, C., 2007. Beach Carrying Capacity: Has it been exceeded on the Gold Coast? *Journal of Coastal Research*, Special Issue No. 50, pp. 21-24.
- Zacarias, D.A., Williams, A.T. and Newton, A., 2011. Recreation carrying capacity estimations to support beach management at Praia de Faro, Portugal. *Applied Geography*, 31, 1075-1081.

## The impact of processes associated with risk assessment and categorization of bathing waters on the water safety system development on the Polish Baltic coast

Tomasz Zalewski<sup>†</sup>, Tomasz Czapiewski<sup>‡</sup>,

<sup>†</sup>Department of Tourism  
University of Szczecin, Szczecin  
70-383, Poland  
zalewski@univ.szczecin.pl

<sup>‡</sup>Institute of Political and European Studies  
University of Szczecin, Szczecin  
71-021, Poland  
tomasz.czapiewski@whus.pl



[www.cerf-jcr.org](http://www.cerf-jcr.org)



[www.JCRonline.org](http://www.JCRonline.org)

### ABSTRACT

Zalewski, T., Czapiewski, T., 2014. The impact of processes associated with risk assessment and categorization of bathing waters on the water safety system development on Polish Baltic coast. In: Green, A.N. and Cooper, J.A.G. (eds.), *Proceedings 13<sup>th</sup> International Coastal Symposium* (Durban, South Africa), *Journal of Coastal Research*, Special Issue No. 70, pp. 551-555, ISSN 0749-0208.

The present paper attempted to systematize contemporary Polish water safety systems and create a preliminary evaluation of water safety system changes on the Polish Baltic coast using new legislation. The main focus is a risk assessment in the form of audits of bathing waters along with a categorization thereof. Detailed analyses included assessments of: the Act of 18 August 2011 –concerning the safety of persons in water–, administrators of the water area, entities authorized to perform water rescue, operational standards and reporting, monitoring with respect to dangerous bathing spots and drownings. An analysis is presented on the basis of 90 bathing sites and guarded areas used for swimming in the West Pomeranian Province in 2013, which is then compared with statistics from 2010-2012. With the number of drownings in the West Pomeranian Province compared to that of the accepted international standard discussed within the final part of the publication.

**ADDITIONAL INDEX WORDS:** *Risk assessment, lifesaving, water safety policy, drowning*

### INTRODUCTION

Drowning is a global health hazard and social problem with limited related theories, models and frameworks dedicated to prevention or rescue (Connelly 2012). In 2000, 409,272 drownings were reported worldwide, making drowning the second leading global cause of unintentional injury or death after road traffic accidents (Avramidis 2012b; Cortes *et al.*, 2006). Drowning's are only one of the many forms of aquatic incidents but one of the easiest to measure and most extreme in consequence.

The risk of drowning (fatal and non-fatal) on the coast has many contributing factors. Accidental deaths due to drowning in coastal waters can usually be accounted for through a sequence of several factors known as the 'drowning chain', such as: a lack of knowledge, unrestricted access to the hazard, lack of supervision or surveillance and an inability to cope once in difficulty (ILFRC, 2008). An appropriate 'drowning prevention chain' consists of: activities that lead to adequate education and information, denial of access, acquisition of survival skills, improvement of infrastructure and/or provision of warning and supervision.

Aquatic areas can never be made to be completely safe but the consequences and the severity of the risk may vary. A risk assessment is vital as the vast majority of all drownings are preventable (Moon and Long, 2002). Risk assessment is central to the effective management of safety in aquatic areas and although risk is unique, some features are common. It is accepted that risk

mitigation should be practicable. This means that the level of risk needs to be balanced against the time taken, trouble involved and cost of precautions required to avoid it.

Many different strategies (e.g., prevention campaigns, lifeguard certification tests, changes in technology and rescue techniques, educational meetings or workshops, publication of water safety newsletters and literature, safety audio-visual materials, computer simulations for teaching lifesavers) are implemented to lower the number of drownings. Nevertheless drowning episodes continue to occur worldwide at epidemic rates (Avramidis and Butterly, 2012).

It is widely accepted that, in most countries, new legislation needs to be established in order to gauge the safety of bathing waters (Avramidis, 2011). It is recommended in literature that local authorities should take larger responsibility for safety by funding additional professional lifeguards to provide more professional lifeguard surveillance (Avramidis, 2010) and, more importantly, frequently assess procedural maintenance. Avramidis *et al.* (2009a, 2009b) even recommend stricter penalties for non-compliance with legislation and evidence of declining national standards, which should at least meet the standards of the International Lifesaving Federation (Avramidis 2011). Adequate screening procedures on the physical and psychological health of lifeguards is in place, as they have core similarities to that of individuals within public health-, safety- and security-based jobs.

### Policy Framework

The water safety system in Poland is currently based on the Act of 18 August 2011 concerning the safety of persons in water



(Journal of Laws, 2011). The Act was first enforced on the 1<sup>st</sup> January 2012, with 2013 being the second bathing season subjected to the regime of this Act. Previously, the legal system lacked a document dedicated to water safety and legal frameworks for building safety systems were scattered in various statutory acts.

The Act distinguishes bathing waters (with the highest safety standards required), swimming areas, open-air or indoor swimming pools and those having additional infrastructure. It should be noted that the law does not provide for the existence of "unguarded bathing waters", although many entities describe them as "a traditional swimming area" for economic reasons. This is because the maintenance of bathing waters or swimming areas involves specific financial burdens. Regulations (executive orders to the Act issued thereunder and for the implementation thereof) determine the rules for water rescue training, signs, protection of water areas, life-saving, signaling, sanitary equipment and the minimum number of lifeguards required.

The Act introduces two specific categories of entities which are crucial for the safety of persons in the water. The first are the "administrators of the water area", responsible for ensuring the safety in the water area. These are usually local government units who are engaged in sports or recreational activities. The administrator is required to ensure permanent control of the designated water area by providing lifeguards, by creating an observation position over the designated area –which should be equipped with lifesaving and auxiliary equipment–, and through the use of signs and warning devices.

The other category includes "entities authorized to perform water rescue" such as the Voluntary Water Rescue Service" (Wodne Ochotnicze Pogotowie Ratunkowe (WOPR)), which in Poland is traditionally the primary source of trained rescue personnel having such status under the law. Other entities (the Act does not introduce restrictions on the legal form) must apply for the registration in the Ministry of the Interior in order to be authorized as an entity to perform water rescue, after having met the adequate requirements. These requirements are set out in the Act in a seemingly broad manner, but are so general that the intervention of ministry officials has become crucial. Experience shows that the Act is liberal and beneficial for the applicants. More detailed criteria for the approval process (e.g., precisely described operational principles, clearly defined distribution of power and resources, coordination and documentation of activities, etc.) could contribute to the professionalization of the entire process. By the end of September 2013, the registry included 32 entities, most of which are local or regional bodies. Registered entities have a number of rights and responsibilities including the organization and conduct of water rescue operations, preventive and educational activities concerning safety in water areas, training of lifeguards and instructors in the field of water rescue and, most importantly from the perspective of the purposes of this article, indication of threats to safety of persons in water areas. The large number of entities that have obtained approval, their different provenances, incomparable standards of competence and the short durations of activity (often undertaken only during the holiday season) do not allow for government administrations to implement efficient control over such entities. The delegation of power to a more senior or provincial level could contribute to improving the quality of control on newly-created entities that are authorized to perform water rescue but which are not prepared for the fulfillment of the above responsibilities. In the area of the West Pomeranian Province, the most important entity authorized to perform water rescue is the local Voluntary Water Rescue Service (WOPR WZ).

The systemic relationships between the two categories of entities described above is based on the adoption of the model that 'the administrator of the designated water area can subcontract the organization, management and coordination of rescue actions to entities authorized to perform water rescue'. This turns out to be fairly common practice.

One of the most important activities carried out by WOPR WZ is the process of conducting audits of bathing waters along with risk assessment reports in accordance with the standards of the International Lifesaving Federation in Europe. The objective of this action is to increase the involvement of the relevant local government units, institutions, administrators and organizers in the preparation of bathing waters and aquatic sports, and the operation of recreational equipment during the holidays. At the request of the bathing administrators, or at least after having obtained their consent, WOPR auditors recently conducted audits and prepared risk assessment reports for various local designated swimming areas. Analysis of the results achieved during the audits highlight certain trends (Zalewski, 2011).

It is worth noting that the conduction of annual audits and the categorization of bathing waters is not clearly identified in the Act and that these are not conducted by central government authorities. They are, in fact, an independent initiative of the non-governmental organization WOPR, together with support (mainly financial) from local authorities of the region. Moreover, the ministry indicates that the entity responsible for ensuring the safety of a designated water area is not legally obliged to agree to an audit (i.e., presenting the documents proving rescue qualifications or rescue equipment). This is largely a consequence of inconsistencies in the Act, which, on the one hand, emphasizes the need to assess risks in water areas, but, on the other hand, does not specify any procedures, instruments and sanctions connected with it. This, in turn, renders the call for risk assessment null and void (Czapiewski, 2013).

Another factor that should be noted when discussing audit activities in relation to bathing waters is the nature of the relationship between the auditee and the auditor. There is no typical situation of internal audit, i.e., audits are not carried out by a specialized department within the organization. A security audit in bathing water is an external audit, as the auditor is a member of the organization (WOPR), which is usually independent of the bathing water administrator. It should be added, however, that the Voluntary Water Rescue Service (WOPR) –who conduct audits of bathing waters in the West Pomeranian Province– are also the main source providing lifeguards. It can be assumed with high certainty that any lifeguards working in bathing waters along the West Pomeranian Province are WOPR members.

Water area audits involving the assessment of water safety cover the following seven issues:

1. The analysis of the area
2. Access to emergency services
3. Public safety and auxiliary equipment
4. Signs
5. Information boards
6. The hazard analysis
7. Lifeguard's equipment

–all of which affect the potential for hazards occurring in the water area.

Categorization, an essential step in the auditing of designated water areas, allows the auditor to verify the various departments responsible for ensuring safe bathing conditions. The data obtained in this part of an audit allows for statistics to be measured but, most of all, helps in determining the level of safety a

designated water area. The categorization of bathing water includes the assessment of:

1. Bathing water organization
2. Bathing water facilities and equipment
3. Qualification of lifeguards
4. Alarm signaling
5. Social area for lifeguards
6. Documents concerning the bathing water and conducted rescue actions, including water quality control documentation

The degree of safety of each of these six factors is rated using a five-star rating system.

## RESULTS

### Audit and categorization of bathing waters and analysis of drowning statistics within the West Pomeranian Province

The distribution of designated bathing areas in West Pomeranian Province is as follows: 45 bathing areas are situated within 30 coastal locations, whilst 45 bathing areas are situated within 35 locations inland. Over 20% of designated water areas are still not guarded by lifeguards.

The audit covered 47 bathing waters (30 coastal and 17 inland) and 43 swimming areas (15 coastal and 28 inland). In 2012, audits were carried out for 50 bathing waters and 35 swimming areas. Unfortunately, in several locations municipalities did not take the appropriate measures to register bathing waters in time, resulting in 5 bathing waters losing their status. Changing the status of bathing waters to swimming areas resulted in a 2% decrease in the number of bathing waters in the province.

The audit of designated water areas was divided into two areas: coastal and inland. An important part of the audit process conducted in designated water areas was a comparison of the data collected for the years 2010-2013. The audit of bathing waters noted 50 locations (27 coastal and 23 inland) in 2010, whereas 82 sites were noted in the summer of 2011 (47 bathing waters, 35 swimming areas). In 2012, the audit included 85 bathing areas including 50 bathing waters and 35 swimming areas. In 2013, 90 designated water areas were audited and 83 hazard analyses were prepared. Comparing the results from inland areas for 2012 with the results of the current summer season, it can be noted that the same bathing waters have achieved a similar level of water safety. The average rating of inland bathing waters amounted to 59 points out of 115 points, which represents 51.3% of the maximum number of points. In 2013 there was a decrease of 0.67% compared to 2012. The trend recorded in the period 2010-2012 has ended. Average categorization ratings of coastal bathing waters amounted to 62 points out of 125 points, which represents 49.8% of the maximum number of points. The observed average decrease of 3.31%, when compared to 2012, indicates a disturbing trend of decline in the development of designated water areas.

When comparing the safety analyses of bathing waters and designated swimming areas, it can be observed that there is a significant difference in the degree of organization at these locations. The administrators of swimming areas, despite clear legal standards, are reluctant to equip their areas with professional rescue equipment. When it comes to inland locations, the main reason for the low safety level is a lack of involvement from those responsible for the construction of bathing areas and for the improvement of safety in designated water areas. They tend towards minimum expenditure on the organization and on rescue equipment. Very often those responsible for the purchase of professional rescue equipment do not have adequate knowledge in this field. In addition to a lack of equipment, another serious

problem for the administrators of designated water areas is the absence of social facilities for lifeguards. Administrators avoid creating professionally equipped medical stations and social rooms for employed lifeguards, who often use storage rooms as medical stations and as shelter during adverse weather.

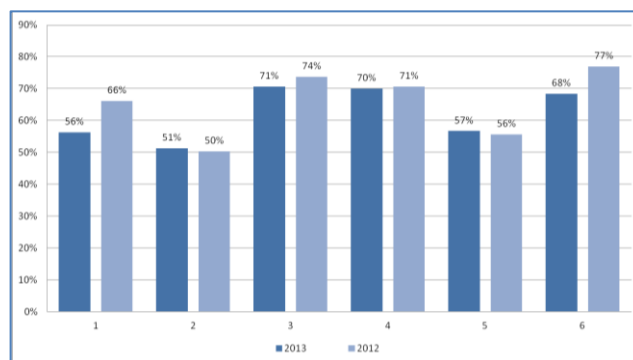


Figure 1. Comparison of the categorization results of coastal bathing waters for years 2012-2013.

1. Bathing water organization
2. Bathing water facilities and equipment
3. Qualification of lifeguards
4. Alarm signaling
5. Social facilities for lifeguards
6. Documents of the bathing water

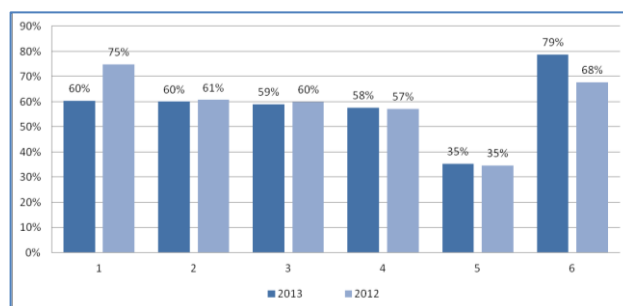


Figure 2. Comparison of the categorization results of inland bathing waters for years 2012-2013.

1. Bathing water organization.
2. Bathing water facilities and equipment.
3. Qualification of lifeguards.
4. Alarm signaling.
5. Social facilities for lifeguards.
6. Documents of the bathing water.

Analysis of individual categories for this year shows that the best rated category—‘documents of the bathing water’—obtained a score of 73.58% (an average between 68.33% for the coast and 78.82% inland). This category included the assessment of work logs, ready to use rescue protocols, medical aid sheets, emergency procedures and standard operating procedures. Administrators of designated bathing water areas were provided with these documents in past years during pre-season training and during on-site visits.

The lowest scoring category—‘social facilities for lifeguards’—possessed an average score of 45.98% (56.67% for the coast and 35.29% inland). This category analysed both the working conditions of lifeguards, as well as housing conditions. At most of bathing waters, lifeguards could use public toilets or toilets located

near their workplace and on the premises. However, in most inland bathing waters, sanitary rooms were limited to scruffy mobile toilets. Few coastal bathing waters had specially built lifeguard stations designed for this purpose, in contrast to Germany, where each bathing area has a well-equipped rescue campus located in the dune area. Warehouses and storage rooms for the equipment were often located right next to the workplace of lifeguards. On larger beaches, medical points were located directly in the workplace of lifeguards. Only a few bathing waters had well-equipped medical points with out-patient facilities. Unfortunately, few administrators of bathing waters seemed to recognize that social facilities should serve both as a shelter for lifeguards on duty (in case of bad weather conditions) and as a place of storing the relevant bathing waters' documents.

The rating of 'equipment belonging to bathing waters' was not favorable either; the average score amounted to only 55.65% (60% for the coast and 51.29% inland). Criteria that were taken into account included the number and type of first aid kits, the possession of an appropriate number of spinal boards (or stretchers), the type and location of stations (towers, medical points, equipment of medical points, coordination centers), lifeguard rescue equipment, public rescue equipment, boats and any additional equipment. At most of the bathing waters, lifeguards worked in observation towers; only a few stations were located directly on the beach or pier. Most of the administrators provided rescue buoys or rescue tubes for each member of the rescue team, but few individual ABCs or wetsuits. Thanks to the preventative action named "I don't do drugs and swim", lifeguards at several bathing waters were equipped with individual first aid kits for resuscitation and wound care. Lifeguards usually did use the rowboats on premises. More and more coastal bathing waters now possess hybrid motor boats or jet skis. Technological advances in this field are inevitable. The noticeable trend of replacing rowboats with motorized watercraft should convince legislators to amend the provision on compulsory rowboats.

'Bathing water organization' also achieved a poor result of 58.32% (56.29% for the coast and 60.32% for the inland areas). The appropriate use of land, local attractions and water activities effectively improve usability of recreational waters. One of the most important fields in the category of 'bathing water organization' is the issue of water hazard prevention. Leaflets, stickers, wristbands or other gadgets handed out to sunbathers encouraged them to participate with the use of dummies for CPR. Most prevention carried out at the coast included work by the West Pomeranian unit of WOPR within the previously mentioned category.

'Signage of bathing waters' and 'proper display of designated fairway for watercrafts' received the poor rankings. There were no updated information boards regarding water quality, which—in most cases—did not contain the necessary messages or were unreadable. Often incorrect placement of these signs caused them not to be visible to people vacationing by the water. Occasionally fairways were located outside of the guarded zones and were separated by the same buoys as the ones used to demarkate bathing waters; this led to these areas being treated as guarded swimming areas.

'Alarm signaling' has been rated with an average of 63.82% (70% for the coast, 57.65% for inland). There has been a lack of professional communication between stations and of direct communication with the Emergency Communication Center (CPR). Only a few beaches had information boards, flagpoles, sound sirens or a PA system.

'Qualifications of lifeguards' achieved an average score of 64.86% (70.67% for the coast and 59.06% for inland areas). Most

of the lifeguards had undergone Qualified First Aid training and were veritably qualified lifeguards. Some coastal bathing waters employed rescue teams consisting of two lifeguards and one rescuer with incomplete qualifications but who was trained in Qualified First Aid. Most coastal bathing waters had rescue teams consisting of four and even five members for each position, an attribute which was rewarded when categorizing. Unfortunately, when it comes to the inland bathing waters, there were rescue teams that did not meet the statutory requirements.

A summary of the results of all evaluated categories in the West Pomeranian Province during 2013 allowed the water safety of designated water areas to be valued at a level of 60.37%; while the result obtained in the previous year (2012) classed the level of safety as 62.36%. This demonstrates a decrease in the level of organization and the amount of equipment owned by bathing waters in the examined region of 1.99%.

Regarding the study of the number of drowning that occurred in 2013, available statistics allow for a separation of the number of drownings in the period before the summer season from those during the peak season. Six people had drowned in the province by 14<sup>th</sup> June, while 22 people drowned between 15<sup>th</sup> June and 15<sup>th</sup> September. Additionally, on the basis of information obtained from the media, reports of bathing waters and the Water Rescue Coordination Centre (CKRW) in Szczecin, there were six water-related events in which the immediate cause of death was not drowning (e.g., suicidal jump from the bridge). An analysis of the number of drownings during the bathing season carried out since 2008 indicates that the values fluctuate between 22 and 30 throughout the season.

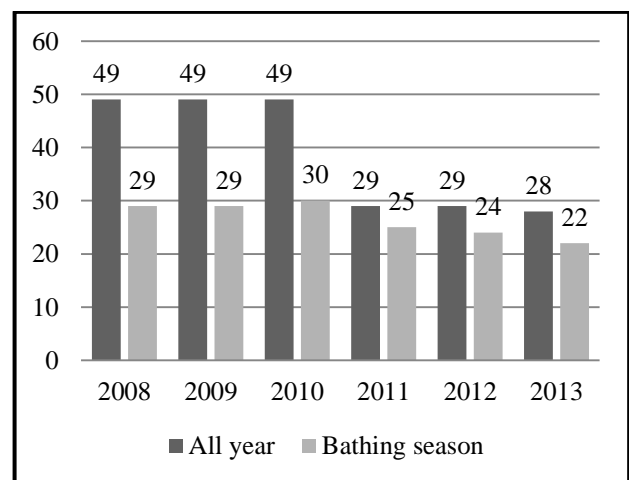


Figure 3. Number of drownings in the West Pomeranian Province between 2008 and 2013. \*Numbers by September 15, 2013

According to the Police, by the end of September 2013 there had been 439 drownings in Poland, whereas in the previous year 436 people drowned over the same period. The number of drownings in the West Pomeranian Province between January 1<sup>st</sup> and September 15<sup>th</sup> was 28; which represents a proportion of only 6.6% of the total number of drownings in the country as a whole over the same period. This result can be considered as satisfactory, taking into account the attractiveness of this region: 185km of Baltic Sea coastline, 172 lakes with an area of more than 50ha, several large rivers and hundreds of small water pools. West Pomeranian Province is an attractive region to tourists, especially during the summer months. During this time, this region is visited by over 1.5 million Polish tourists and more than 400 000 foreign

tourists. The vast majority of these people choose to spend their time by the water. 16 drownings between July and August in the province (including 11 by the sea), when compared with 250 drownings in the country, represents 6.4%. Water pool drownings within the province included 8 at lakes, 16 in the sea and 4 in rivers.

The most common causes of drowning were found to be foolhardiness, alcohol consumption, poor recognition of a water pool and a lack of swimming skills or of adequate preparation before swimming. There were also accidents linked to adverse weather circumstances. Territorial analysis of drownings indicates that the largest number of tragedies during the bathing season of June 15<sup>th</sup> and September 15<sup>th</sup> happened in Kołobrzeg county—8 people (including one minor)—which represents 28.5% of all drownings in the province over that interval.

The number of drownings in particular counties of the West Pomeranian Province was analyzed according to the accepted international standard for the assessment of drowning per number of residents. Drowning rates varied greatly based on the number of residents and tourists present. What is positive is the fact that this rate did not exceed 1.3 drownings as to 100,000 residents. An interesting situation is that of Kołobrzeg county, where a number of drownings (8) gives a rate of 10.35 drownings per 100,000 residents. However, when both local residents and tourists are taken into account, this rate is only 1.64 drownings per 100,000. This is due to the fact that Kołobrzeg county is particularly attractive to tourists, as shown by the influx of about 400,000 tourists per year. Counties such as the City of Szczecin, Koszalin, Gryfino, Łobez, Myślibórz, Pyrzyce, Stargard, Świdwin and Wałcz equals experienced no drownings during 2013. The rate of drownings per number of swimmers (both residents and tourists) in the province as a whole decreased from 0.87:100,000 in 2012 to 0.66:100,000 in 2013.

## CONCLUSIONS

An audit of bathing waters in the West Pomeranian Province has been developed for many years, even before the new Law on Safety in Water Areas entered into force. Audits of bathing waters indisputably contribute to the objectives set by the new law. The ambiguous nature of the Act and serious misinterpretations thereof, however, may weaken the effectiveness of the audit process in the future.

There are noticeable declines in some categories that make up the overall diagnosis of the safety level of bathing waters. In total, the decrease in safety level determined by the results of the categorization was 2%. If it were not for the 'documentation category'—which saw a significant improvement as a result of several years of popularizing work by the WOPR—a total decrease in water safety would have been significantly greater. In conjunction with an apparent decline in the number of bathing waters, this creates a negative picture of changes over the last year. The scale of audits and the separation of these audits by one-year intervals does not allow for a trend emphasized and create clear predictions to be made. It should, however, serve as a warning signal, particularly to the two types of entities controlling water safety: the central government administration, which is responsible for the control over the water safety system and which draws up amendments to the laws, and municipalities, which are mainly responsible for ensuring safety in water areas. These conclusions are in accordance with literature (Avramidis, 2010, 2011).

The above described, adverse trends are fortunately not correlated with changes in the number of drownings in the region over 2013. For several years this has been a stable value with only

minor fluctuations. Compared to other regions of the country, the number of drownings in West Pomerania can be assessed as moderately low. When one takes into account the number of people residing in water areas during the bathing season and, in particular, the extent of water areas.

The risk assessment for inland bathing waters and swimming areas indicates a lack of accountability from municipalities for water safety in their areas. Few municipalities utilize external resources for upgrades or new bathing infrastructure. Municipalities avoid costs associated with the creation of designated water areas and the equipping of these areas with the appropriate rescue tools, both of which would certainly improve water safety in the relevant municipalities. There is a need for increased involvement by local partners, so as to build safety and provide systematic solutions ranging from prevention in schools, through to proper signage located in water areas, to the equipping of lifeguards and WOPR Intervention Groups. Building such awareness is necessary considering the lack of governmental (central) pressure to increase the efficiency of the water safety system. Creating this system is a long process, which ultimately will reduce the number of drownings and accidents in the water.

## LITERATURE CITED

- Avramidis, S., 2011. Suggestions for Governing Actions Aiming to Enhance Water Safety in Swimming and Aquatic Activities. In: Vagenas, G., Athanasopoulos, S. And Chatoupis, K. (eds.), *Research and Application in Sport Science*, University of Athens, pp. 125.
- Avramidis, S., Butterly, R. and Llewellyn, D., 2009a. Under What Circumstances Do People Drown? Encoding the Fourth Component of the 4W Model. *International Journal of Aquatic Research and Education*, 3(4), 406-421.
- Avramidis, S., Butterly, R. and Llewellyn, D., 2009b. Where do People Drown? Encoding the third component of the 4W Model. *International Journal of Aquatic Research and Education*, 3(3), 236-254.
- Connolly, J., 2012. The C-Zones Framework. *International Journal of Aquatic Research and Education*, 6, 80-93.
- Cortés, L. M., Hargarten, S. W. and Hennes, H. M., 2006. Recommendations for Water Safety and Drowning Prevention for Travelers. *Journal of Travel Medicine*, 13, 21-34.
- Czapiewski T., 2013. Auditprozess der Badeorteaus der rechtlichen Perspektive und öffentlicher Politik. *Moderne Verwaltung der Sicherheitim Bereich des Grenzwassers von Polen und Deutschland* (Szczecin, Poland), 5-14p.
- International Lifesaving Federation (ILS) Rescue Committee, 2008. *Total Life Saving Service Plan*.
- Moon, R. E. and Long, R. J., 2002. Drowning and near-drowning. *Emergency Medicine*, 14, 377-386.
- Zalewski, T., 2011. Assumptions for the strategy of development of the water safety system on Polish Baltic coast. *Journal of Coastal Research*, Special Issue No. 64, Part II, 1306-1310.

## Recreational parameters as an assessment tool for beach quality

Camilo-Mateo Botero†, Cristina Pereira‡, Giorgio Anfuso∞, Omar Cervantes@, Allan T. Williams§, Enzo Pranzini+, Carlos P. Silva#

† Grupo Joaquín Aaron Manjarres, Universidad Sergio Arboleda, Calle 18 No. 14-18, Santa Marta, Colombia. playascol@yahoo.com, camilo.botero@usa.edu.co

@ Facultad de Ciencias Marinas (FACIMAR), Universidad de Colima. Carretera Manzanillo-Barra de Navidad Km 19.5. Colonia El Naranjo, 28860 Manzanillo, México omar\_cervantes@ucol.mx

# e-GEO, Faculdade de Ciências Sociais e Humanas, Universidade Nova de Lisboa, 1069-061 Lisboa, Portugal cpsilva@fch.unl.pt

‡ Grupo de Investigación en Sistemas Costeros, Playascol Corporation, Calle 19 NO. 8-44, Santa Marta, Colombia grupo.sistemas.costeros@gmail.com cpereira@playascol.com

+ Built Environment, Swansea Metropolitan University, Swansea, Wales SA1 6ED, UK allan.williams@virgin.net

∞ Departamento de Ciencias de la Tierra, Facultad Ciencias del Mar y Ambientales, Universidad de Cádiz, Polígono Río San Pedro s/n, 11510 Puerto Real, Spain giorgio.anfuso@uca.es

+ Dipartimento di Scienze della Terra, Università degli Studi di Firenze, Borgo Albizi 28, 50122 Florence, Italy enzo.pranzini@unifi.it



[www.cerf-jcr.org](http://www.cerf-jcr.org)



[www.JCRonline.org](http://www.JCRonline.org)

### ABSTRACT

Botero, C., Pereira, C., Anfuso, A., Cervantes, O., Williams, A.T., Pranzini, E., Silva, C.P. 2014. Recreational parameters as an assessment tool for beach. In: Green, A.N. and Cooper, J.A.G. (eds.), *Proceedings 13<sup>th</sup> International Coastal Symposium* (Durban, South Africa), *Journal of Coastal Research*, Special Issue No. 70, pp. 556-562 ISSN 0749-0208.

Beach quality can be understood according to uses established for this coastal system, the most common being tourism, fishing and conservation. This is especially true with regards to tourism, where quality is frequently measured with respect to two major areas: environmental and recreational. In 2002, an environmental quality index for tourist beaches was developed in Colombia, called ICAPTU (Índice de Calidad Ambiental en Playas Turísticas). ICAPTU had four indicators and eleven parameters, mainly focused in environmental aspects. In 2010, a research project started with the objective of updating ICAPTU with a more comprehensive scope, dividing environmental quality into three indicators: sanitary, eco-systemic and recreational. This research paper presents the progress on the design of five parameters considered in the newer version of ICAPTU, all related to recreational issues: a. Coastal Scenery, focused on an assessment tool tested in Europe, USA and Australia; b. Safety and security, measured from risk perception and real risk; c. Urbanization, related to ecosystem resilience to infrastructure on the shore; d. Zoning, understood as a spatial organization of beach activities; e. Environmental behaviour, assessed from a test focused on common attitudes of tourists when they visit the beach. These five parameters were used on-field techniques as a method for acquiring information. Several instruments were designed based on surveys, checklists and interpretation sheets. Every tool was applied and tested on Colombian beaches located in four Departments: La Guajira, Magdalena, Atlántico and Bolívar. Geospatial technologies are also explored as resources for improving the evaluation of beach environmental quality. Finally, this work concluded that beach quality can be assessed by recreational parameters, scientifically designed, supporting decision making of coastal zone management.

**ADDITIONAL INDEX WORDS:** *Integrated coastal zone management, sustainable tourism, coastal systems, Caribbean, Colombia.*

### INTRODUCTION

Tourism is the world's biggest industry with an average growth of 9% per annum since 1985 (Klein *et al.*, 2004). In 2011, global tourism employed 6-7% of the global workforce and was *circa* 5% of the worldwide gross domestic product (GDP; UNWTO, 2011). In 2011 South America recorded a great increase (+9 percent), continuing to lead growth in the region for the second consecutive year. In Colombia, tourism currently represents one of the most important activities with 1.692.822 international tourism arrivals

in 2012 and more than US\$12,000 million generated (PROEXPORT - Ministerio de Comercio, Industria y Turismo, 2012). In this sense, beaches are considered as a major player in this market and worth billions of tourist dollars (Houston, 2008).

Such interest in exploiting the characteristics of national beaches, is consistent with the great dependency that Caribbean coastal zones have on tourist activities, as they generate a considerable proportion of national incomes (Beharry-Borg and Scarpa, 2010; Gavio *et al.*, 2010). However sustainability of the beaches as natural systems is considered a limiting factor on the economic activities (Nelson and Botteril, 2002). As a coastal feature, beach quality is determined by both, the quality of the environment and the quality of the tourist experience (Duvat,

2011). Concerning the Caribbean coast of Colombia, Botero *et al.* (2013 a and b) have carried out studies concerning the interest of beach users and conclusions highlighted the pertinence of assessing beach quality from an integrated approach. Such is the case of the ICAPU project (in English “Index of Environmental Quality in Tourist Beaches”), whose context has hosted the present investigation aiming at characterizing different aspects related to environmental and recreational perceptions from tourist beaches.

### ICAPU - Index of Environmental Quality in Tourist Beaches

Within a research program held in Colombia since 2010, the ICAPU has been designed to work as a technical instrument that summarizes the criteria for assessing beach quality. The original model designed in 2002 had four indicators and eleven parameters, which mainly focused on environmental aspects (Botero, 2002). In 2010, a research project started with the main objective of updating the ICAPU index by enlarging its scope, dividing environmental quality aspects into three indicators: sanitary, eco-systemic and recreational.

In a recent development of the ICAPU project, all its thirty parameters underwent a calibration process within the newer ICAPU index, many of which related to recreational issues. This paper focuses on five of the most novel parameters, supported in several scientific documents: i) Coastal Scenery, focused on beach user perception of landscapes (Ergin *et al.*, 2004 and 2006); ii) Safety and security, aimed at understanding relationships between beach user risk perception and real risk due to environmental beach conditions (Scott, *et al.* 2007, 2009), anthropogenic hazards or human-made hazards (Espejel *et al.* 2007); iii) Urbanization, related to type and proportion of buildings and public works in the coastal zone and ecosystem resilience to human intervention (Leatherman, 1989, De Santiago, *et al.* 2013; Roig-Munar, F.X. 2013; iv) Zoning, concerning the spatial organization of beach activities (Zielinski and Botero, 2012, Yepes, 2002, 2004) ; v) Environmental behaviour, related to tourists attitudes when users visit the beach (Dovidio, J.F *et al.* 2003, Wolch and Zhang, 2004, Cervantes *et al.* 2008).

### Geospatial Techniques for Beach Quality

Geospatial Techniques, refers to all available means for generating, organizing, storing, and analysing spatial information, which may include advances in geodesy, photogrammetry, geophysics, computer science, statistics, remote sensing and geographic information systems (GIS) (Klemas, 2011; Bishop, *et al.*, 2012). Remote sensing in particular has been largely applied to the study of coastal systems, ranging from observation of chemical (suspended sediments, chlorophyll) and hydrological parameters, through to ocean processes affecting the seashore, as well as detecting changes of land use/cover, landscape, or ecosystems (Klemas, 2011). Within the coastal zone, the most popular application of remote sensing and GIS at the beach scale, is perhaps the evolution of erosion problems, usually addressed through the use of satellite and video imagery (Pranzini and Wetzel, 2007; Brignone, *et al.*, 2012).

There are several sensors available for retrieving data, which differ from platform (aircraft, satellite), mode (active and passive), application (imagers, profilers) and wavelength range detection (Klemas, 2009). Remotely sensed data are now going beyond bare-earth representation and consider the effects of human interventions projected on anthropogenic structures, vegetation canopies and short-term changes in terrain (Mitasova, *et al.*,

2012). Further elements on tourist beaches can also be studied with this instrument, such as the presence of human facilities and civil structures concerning zoning and urbanization, landscape and landform features that characterize coastal scenery and rip currents or near shore morphology associated to safety/security issues (Mitasova, *et al.*, 2012; Barrett and Houser, 2012). In this context, geospatial techniques figure as an asset that may contribute to the calibration process of the recreational parameters within ICAPU.

## METHODS

Recreational parameters referred to in this document may be considered as immeasurable concepts usually conceived for characterizing a beach as a tourist destination. However, these concepts need to be translated into beach quality units susceptible of being aggregated into the mathematical expression of the indicators that compose an index. Therefore, the methods considered in this research are framed on the methodology designed for calibrating the recreational parameters of ICAPU. Given the lack of measuring instruments and reference measurements, calibration of the recreational parameters considers five common stages (see figure 1).

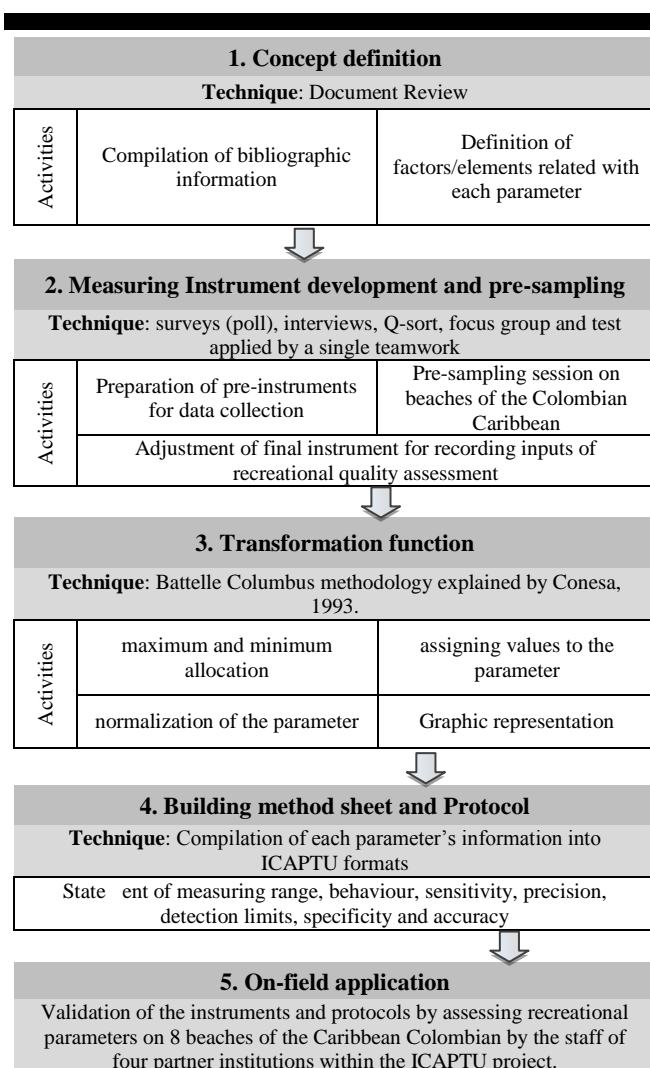


Figure 1. General methodology considered for the calibration process of recreational parameters within the ICAPU project.



Figure 2. Study area, adapted from IGAC (2013). Visited beaches of Caribbean Colombian departments: Riohacha (La Guajira), El Rodadero and Bahia Concha (Magdalena), Puerto Velero, Caño Dulce and Salgar (Atlántico) and Boca Grande (Bolívar).

The results described here, focuses on the exercise developed for building up the instrument for measuring each recreational parameter. During the process, different tools were applied and tested in the Caribbean Coast of Colombia, specifically at beaches located in four departments: La Guajira, Magdalena, Atlántico and Bolívar (see figure 2).

Regarding the specific methods used for each parameter, construction of the measuring instrument for *coastal scenery* focuses on adapting the assessment process of Rangel *et al.* (2013), which applied the methodology of Ergin *et al.* (2004 and 2006), based on the scoring of 26 elements, both natural (physical features of the beach) and human (those introduced to the landscape through anthropogenic activities). Such parameters were determined by interviewing more than 1,000 beach users in various European countries and the USA about their preferences and priorities concerning coastal scenery. Considering this background, the present research applied the idea of assessing coastal scenery according to the preferences of beach users in the study area.

After identifying all characteristic elements of the coastal landscape in the zone, these were then organized on a checklist that was used on a survey applied to four beaches of different municipalities of the Colombian Caribbean. Each element is composed of five categories characterizing the landscape element and beach users were asked to rank them on a 1 to 5 scale, from “no importance” to “great relevance”. The non-clustered ordinal data obtained from this pre-sampling sessions were brought under a frequency analysis to identify users' preferences. Categories with value of 1 represent the lowest recreational quality and a value of 5 is the highest.

Measurement instrument designs for the, *safety and security* parameter, were based on the definition of real and perceived risk of beach users. Concerning real risk it was designed as a tool for collecting information about the threats affecting the investigated coastal areas. This pre-instrument was a structured interview addressed to the staff responsible for security issues on beaches, such as, policemen, members of civil protection, Red Cross, lifeguards, doctors and nurses on duty at medical centres close to the investigated beaches.

Hence, the pre-instrument allowed drafting a measurement instrument to assess real risk on tourist beaches. This instruments figures as a quantitative matrix motivated by the methodology for risk assessment at the workplace proposed by the Colombia

Technical Guide No. 45, which was adapted to the beach context. The methodology incorporated variables such as the level of impairment (e.g. the relationship between hazards, its consequences and preventive action), the exposure level (user contact with the hazard), the level of probability (likelihood of occurrence of a hazardous event) and consequence (results in terms of injury or illness) and the risk level (combination of probability and consequence). Levels above the variables are combined to yield a score that indicated which risk level (low, moderate, high or extreme), describes an evaluated beach and the resulting equivalent level of safety/security.

For designing the measuring instrument of the *urbanization* parameter, the “focus group” technique was used, as described by Hurtado (2010). After an active literature review of scientific articles and technical documents related to the term “waterfront” and “beach urbanization” (Leatherman, 1989, De Santiago, et. al. 2013 and Roig-Munar, F.X. 2013), a set of impacts associated with the presence of civil structures on the beach according to two dimensions: landscape and environment, were identified. These impacts were organized on a matrix to determine the degree of ‘affectation’ according to the methodology of Conesa (2003) and Gomez–Orea (2007), for environmental impact assessments.

A diverse group of experts (environmental engineers, architects and civil engineers) were gathered at each of the four beaches evaluated (Riohacha, Bahia Concha, Puerto Velero and Boca Grande), each beach representing a different urbanization typology. Discussion sessions were held concerning the presence/absence, relevance and improvements of every impact registered on the matrix. When visiting every beach, experts were asked to score the impacts according to the 11 evaluation criteria established by: nature, intensity, extent, moment, persistence, reversibility, synergy, accumulation, effect, periodicity and recoverability (Conesa, 2003, Gomez–Orea, 2007).

The methodology used for the development of the *zoning* parameter was based on the document “Basic Guide for Certification of Tourist Beaches”, proposed by Zielinski and Botero (2012). This document presented the use of checklists for assessing the status of tourist beaches in an easy, quick and accurate manner.

Initially elements or factors were identified which characterize an organized beach, according to a comprehensive literature review along with field visits. This preliminary list was then evaluated by experts of the Ibero-American Network of Beach Management and Certification (PROPLAYAS, from its Spanish acronym). Using the Q-Sort technique, zoning factors were organized from the “most” to the “least important”. As a result, it produced a checklist of the zoning factors including different aspects and the relative importance of each one was established by the expert group.

The design of a tool for assessing the, *environmental attitude* of beach users took into account reliable instruments developed by other researchers and these were then adapted to the characteristics of tourist beaches (Mamat and Mokhtar, 2012). Initially five existing instruments for measuring environmental attitudes were chosen for creating a new one focused on the beach environment:

- New Ecological Paradigm (Dunlap *et al.*, 2000)
- New Environmental Paradigm (Dunlap and Van Liere, 1978 - Adapted by Kim and Weiler, 2012)
- Scale of attitudes toward environmental issues (Moreno *et al.*, 2005)
- Test of environmental attitudes (Mamat and Mokhtar 2012)
- Measurement of environmental attitudes based on behaviour (Kaiser, 2007)

Table 1. Coastal landscape elements considered for evaluating coastal scenery on the Caribbean Littoral of Colombia.

Physical Elements	Human Elements
Cliff height	Litter
Beach face width	Sewage
Sand colour	Soil use
Rocky shore width	Built environment
Valley	Beach Users' Density
Skyline landform	Recreational Equipment
Coastal landscape features (arches, caves, waterfalls, island, reefs, etc.)	Folklore
Vistas	Floating Surfaces (boat, vessels...)
Water colour	Facilities
Vegetation cover	
Waves	

Category of coastal landscape elements Example:

Beach face with				
Category A < 15 m	Category B 15-30 m	Category C 31-45 m	Category D 46-60 m	Category E > 60 m
Weighting factor: <b>0.08</b>	Weighting factor: <b>0.2</b>	Weighting factor: <b>0.2</b>	Weighting factor: <b>0.12</b>	Weighting factor: <b>0.4</b>

The items of each instrument were grouped, based on the classification made by Kim and Weiler (2012), which gathered their items into five variables according to their synergy. The variables used included the importance of resource protection, user support to management measures, negative and positive impacts perception (Cervantes, et. al. 2008) and feelings of concern over certain habits and behaviour.

## RESULTS AND DISCUSSION

### Coastal Scenery

Over 450 beach users were asked for their perception on the beaches of Riohacha, Puerto Velero, Bocagrande and El Rodadero. Table 1 registers the final list of physical and human elements considered on the surveys applied during the pre-sampling sessions. Out of the data collected and analyzed, a weighting factor may be defined for each category within each element as represented in the example in Table 1. The final instrument measures recreational quality (according to coastal scenery) by identifying from a checklist the category of the landscape elements present on the beach and calculating the average value of their weighting factor.

As research is ongoing, some of these elements are currently under review because of underlying inconsistencies between field data with previous work related with coastal scenery, such as, the case of natural elements, e.g. cliff height, rocky shore width, valley and waves. As previously observed by Botero *et al.* (2013 a and b), beach users at the Colombian Caribbean were not particularly interested in landscape but in having fun and enjoying sunshine and bathing, as recorded in many Mediterranean destinations. In this sense, natural elements of great scenic relevance, as highlighted in previous studies (Ergin *et al.*, 2004 and 2006), were not selected by beach users during the survey exercise and/or had a small score during data analysis.

Concerning beach width, it represented an important parameter and users preferred wide beaches, favoured sand colour being white, later grey, and the less attractive one being black sediments, which differ from previous studies where black sediments on Pacific islands are considered exotic because of its volcanic origin and "grey mouse" is less appreciated (Pranzini *et al.* 2010). Further contrast, with respect to results obtained by Ergin *et al.* (2004 and 2006), was evidenced by the importance given to

human parameters such as recreational infrastructures and activities, etc. Such results, are also probably linked to the fact that questionnaire surveys were carried out on urban beaches essentially frequented by local users, that were not used to visiting different beach types (natural ones) and, for this reason, their "ideal" beach, is the one they were used to and essentially chosen because of its proximity (Botero *et al.*, 2003 b).

### Safety and Security

Security is one of the fundamental attributes to measure the quality of a tourist destination, because it represents one of the aspects that tourists consider when making their choice. With the information gathered at four beaches in the study area (Riohacha, Puerto Velero, Bocagrande and El Rodadero), a classification of the identified hazards was made according to the damage they cause. These hazards were included in 6 groups: natural, environmental, physical, biological, social and institutional (see table 2).

Short and Holgan (1994), Scott, *et al.* (2007, 2009) and Espejel *et al.* (2007) argued that environmental characteristics are important in preventing accidents on beaches because these aquatic environments are variable and continuously evolving (Abraldes and Rubio, 2005). These environments present four major factors that can determine the degree of peril on a beach: the beach morphology, equipment and infrastructure, rescue and first aid service and circumstantial aspects. Therefore, this paper has defined a safe beach as the one that provides conditions for the protection of life and physical integrity of users through the following services: a) rescue and first aid, b) emergency care at sea and land, and c) surveillance and monitoring personal protection to safeguard users from common crime and criminal acts, this being an important issue along many areas of Colombia. All these services are achieved through joint work among lifeguards, health and police officers, and relief agencies.

Table 2. Hazard classification of beaches from interviews on the Caribbean coast of Colombia.

Natural	Environmental	Social
<ul style="list-style-type: none"> <li>· Natural disasters</li> <li>· Precipitations</li> <li>· Floods</li> <li>· Rip currents</li> <li>· Waves</li> <li>· Landslides</li> <li>· Coastal erosion</li> <li>· Beach topography</li> <li>· Reefs, bedrock, cliffs</li> </ul>	<ul style="list-style-type: none"> <li>· Microbiological pollution of water</li> <li>· Microbiological pollution of sand</li> <li>· Modification of sediment dynamics</li> <li>· Litter and hazard waste</li> <li>· Atmospheric emissions from vehicles</li> <li>· Sewer presence</li> </ul>	<ul style="list-style-type: none"> <li>· Criminal activities</li> <li>· Reckless behaviour</li> <li>· Harassment of street vendors</li> <li>· Ignorance of regulations</li> <li>· Lack of hygiene in food handling</li> <li>· Increased carrying capacity</li> </ul>
Biological	Physical	
<ul style="list-style-type: none"> <li>· Invasive species</li> <li>· Marine animals</li> <li>· Presence of birds and domestic animals.</li> </ul>	<ul style="list-style-type: none"> <li>· Solar radiation</li> <li>· Very high temperature</li> <li>· Water turbidity</li> </ul>	<ul style="list-style-type: none"> <li>· Noise (intermittent or continuous)</li> <li>· Insufficient lighting on the beach</li> </ul>
Institutional		
<ul style="list-style-type: none"> <li>· Police absence or insufficient beach patrol of authority.</li> <li>· Absence of first aid services</li> </ul>	<ul style="list-style-type: none"> <li>· Lack of safety measures and risk management</li> <li>· Informal provision of tourist services</li> <li>· Absence of emergency and rescue services</li> </ul>	<ul style="list-style-type: none"> <li>· Invasion of public space</li> <li>· Absence of lifeguards</li> <li>· Lack of nearby medical centres</li> </ul>



### Urbanization

Urbanization is defined as, the effect of construction of coastal civil structures, which produces a negative or positive contrast with the landscape and ecosystem functionality when satisfying human need for leisure. The following typologies of urbanization were also categorised from undisturbed natural beaches, natural or minimally altered beaches, moderately artificial beaches, artificial beaches, to very artificial beaches. Another progress on the calibration process of this parameter refers to identification of the impacts or effects associated to the urbanization on the beach (see table 3).

Urban development in coastal zones seeks for the development of tourism by incrementing foreign investments, job creation and the presence of transnational companies (Talesnik and Gutierrez, 2002). A high density of buildings can currently be recorded along several coastal areas of France, Italy and Spain, where the built up area exceeds 45% (EEA, 2006). In the same way, Breen and Rigby (1996) argued that such pressure produces important changes in land use by means of construction of shops, cafes and restaurants (Talesnik and Gutierrez, 2002). They observed others kinds of recreational buildings, such as, aquariums, amusement parks and yacht marinas as well as buildings for cultural purposes (e.g. theatres, concert halls and cinemas; Benseny, 2008).

### Zoning

As a pre-instrument for the zoning parameter, a checklist was designed for gathering all relevant factors defining this parameter, distributed in their respective typologies (see table 4). The maximum quality is then observed when the beach presents all of these factors and the minimum occurs when there is none. The Zoning parameter is necessary for evaluating the environmental quality of a tourist beach, in terms of its ability to satisfy the human needs for leisure and recreation. Therefore in order to facilitate the management of beach space, a strategic plan is required concerning beach zoning and the organization of local stakeholders, such as, beach users, peddlers, life-guards, fishermen, etc. Such kinds of studies were carried out in Spain over a decade ago, whilst in Colombia the topic has been developed only in the past few years (Yepes *et al.*, 2002, 2004; Botero, 2008, Herrera, 2010).

The most known antecedent is a study titled "Beaches: models, types and suggestion for its management", in which two types of spatial arrangement for Spanish beaches were proposed, e.g. lateral and cross-section zoning (MOP, 1970). This study clearly explained the proper way for the establishment of different areas in a beach, according to the main types of usage, which include a variety of activities ranging from recreational and sports to economic or contemplative (Botero, 2013a). Therefore, the

Table 3. Effects associated with the presence of buildings and structures on the beach within two dimensions.

<b>Environment</b>	· Solid waste generation	· Habitats (changes and fragmentation)
	· Atmospheric emissions	· Changing sediment dynamics
	· Discharges	· Microclimatic variations
	· Migration of species (disturbance)	· Modified waves
		· Noise pollution
<b>Landscape</b>	· Visual intrusion	· Human concentration
	· Changes in natural morphology	· Employment generation
		· Loss of vegetation cover

Table 4. Zoning Factors defined for measuring recreational quality at the Caribbean coast of Colombian.

<b>Spatial organization</b>	<b>Regulations</b>	<b>Commercial organization</b>
· Green zones	· Respect for beach public use	· Peddler identification
· Parking lot	· Absence of discharges	· Forbidden animals at food courts
· Tourism services area	· Solid waste management	· Clean sales sites
· Public space binding site	· Lifeguard service	· No disturbing advertising activities
· Transition area	· Presence of trash cans	· Legality of goods
· Users resting area	· Cleaning periodically	· Hygiene and sanitation with products
· Users active area	· Non-cemented structures	· Access to potable water
· Bathing area	· Ornamentation with native plants	
· Nautical sports area	· Beach management	
· Area for vessels transit		
· Vessel parking area		
· Promenade		
· Beach access		
· Signing and lighting Sports and recreational facilities		
	<b>Beach users organization</b>	
	· Carrying capacity	· Tourist information points
	· Beach information board	· Safety recommendations
	· Code of conduct for all	

zoning parameter encompasses the spatial arrangement of physical elements and services to reduce the negative interactions amongst them.

### Environmental Behaviour

In general, environmental attitudes are defined as, the provision or encouragement to perform an action that can help or affect the natural environment. These attitudes, condition people's habits and/or customs and are in turn associated with a number of cognitive, psychosocial and socio-demographic variables (Mamat and Mokhtar 2012b). Therefore, attitudes are the starting point for establishing environmentally responsible behaviour (Cervantes *et al.*, 2008; Dovidio, *et al.* 2003). The evaluation of environmental attitudes has an extensive literature, especially on assessment of attitudes in schools, universities, and industries, which leave aside the relationship between communities and natural resources as scenarios for socio-economic development (Wolch and Zhang, 2004, Cervantes *et al.* 2008).

Along with creation of a new test for environmental attitudes on tourist beaches, a list of 24 items was compiled that composed the new instrument. Within the instrument, items were organized by sections on: waste management, commitment to conservation concern for the community and responsible actions for the conservation of water, fauna and flora. Because several items were left out of the synergy of the proposed variables, they were gathered into an additional variable called "intention of intervention". On-field applications are being carried out on four beaches along the Northern Caribbean littoral of Colombia in Riohacha, El Rodadero, Salgar and Bocagrande. These pre-sampling sessions have contributed to improve the instrument by reorganizing items in order to fit into the proper variables. Further results on the validation of the text are also expected from field work currently in progress.

### CONCLUDING REMARKS

According to the improvements achieved in the present study, beach quality can be assessed by the use of scientifically designed recreational parameters that produces a measurable appreciation of the coastal system. The applied methodology and results obtained

constitute important tools for decision makers, especially along the Northern Caribbean coast of Colombia, which is increasing in occupation and development. Detailed monitoring of this parameter would be a warning system for authorities and managers, orienting in this way the definition and implementation of appropriate management measures (Botero, 2013). Thus, improvements of beach quality evaluation by innovative technologies fulfils a rising need with the interest of an automatic monitoring process and optimizing the available funding; in that way, the ICAPTU initiative is getting closer to becoming an efficient tool for coastal zone management.

## ACKNOWLEDGEMENT

Authors want to acknowledge institutions and researchers which are part of the project ICAPTU, especially students who support daily research activities in Santa Marta. Moreover acknowledge to the Iberoamerican Network of Beach Management and Certification – PROPLAYAS, which all authors are members. Finally, authors acknowledge the programme Expo-Master in Marine-Coastal Integrated Management, in which three authors participated as student, professors or supervisor.

## LITERATURE CITED

- Abraldes, J., Rubio, J. 2005. Factores de peligrosidad para la valoración del riesgo de accidentes en las playas. Departamento de Ciencias de la Actividad Física y del Deporte. Universidad Católica San Antonio de Murcia. UCAM. Revista Digital - Buenos Aires 91 - Diciembre de 2005.
- Barrett, G. and Houser, C., 2012. Identifying Hotspots of Rip Current Activity Using Wavelet Analysis at Pensacola Beach, Florida. *Physical Geography*, 33, 32-49.
- Beharry-Borg, N., & Scarpa, R., 2010. Valuing quality changes in Caribbean coastal waters for heterogeneous beach visitors. *Ecological Economics*, 69 (5), 1124-1139.
- Benseny, G., 2008. La problemática ambiental en urbanizaciones turísticas litorales. *Aportes y Transferencias*, 12 (1), 105-125.
- Benoit, G., and Comeau, A., 2005. In G. Benoit, and A. Comeau (Eds.), A sustainable future for the Mediterranean: The Blue Plan's environment and development outlook. London, UK: Earthscan.
- Bishop, M. P., James, L. A., Shroder Jr, J. F. and Walsh, S. J., 2012. Geospatial technologies and digital geomorphological mapping: Concepts, issues and research. *Proceedings of the 41st Annual Binghamton Geomorphology Symposium* (South Carolina, Columbia), *Geomorphology* 137 (1), pp. 5-26.
- Botero, C., 2002. Propuesta de un índice de calidad ambiental de playas turísticas. University of La Salle. Bogota, Colombia. Eng. Thesis, 108 p.
- Botero, C., 2008. Proposal of management framework for tourist beaches based on integrated coastal management. Faro, Portugal: Erasmus mundus European joint master, Msc. thesis, 100 pp.
- Botero, C., 2013. Evaluación de los esquemas de certificación de playas en América Latina y propuesta de un mecanismo para su homologación. Puerto Real, Spain: University of Cádiz, PhD thesis, 408 pp.
- Botero, C., Anfuso, G., Williams T. and Palacios, A., 2013 a. Perception of coastal scenery along the Caribbean littoral of Colombia. *Journal of Coastal Research*, Special Issue No. 65, pp. 1733-1738.
- Botero, C., Anfuso, A., Williams, A.T., Zielinski, S., Silva, C.P., Cervantes, O., Silva, L. and Cabrera, J.A., 2013. Reasons for beach choice: European and Caribbean perspectives. *Journal of Coastal Research*, Special Issue No. 65, pp. 880-885.
- Breen A. and Rigby, D., 1996. The new waterfront: a worldwide urban success story. McGraw-Hill. London: Thames and Hudson; New York. 224 pp.
- Brignone, M., Schiaffino, C. F., Isla, F. I. and Ferrari, M., 2012. A system for beach video-monitoring: Beachkeeper plus. *Computers & Geosciences*, 49, 53-51.
- Cervantes, O. and Espejel, I., Arellano, E., and Delhumeau, S., 2008. Users perception as a tool to improve urban beach planning and management. *Environmental Management*. 42,2, pp. 249-264.
- Conesa, V., 2003. Guía Metodológica para la Evaluación del Impacto Ambiental. *Ediciones Mundi-Prensa*, Madrid. 3ª edición. 412 p.
- De Santiago, I., Morichon, D., Abadie, S., Castelle, B., Liria, P. and Epelde, I., 2013. Video observation of the morphodynamics of nearshore sandbars on a partially engineered embayed beach. *Journal of Coastal Research*, Special Issue 65, 458-453.
- Dovidio, J.F., Kawakami, K and Beach, K.R., 2003. Implicit and explicit attitudes: Examination of the relationship between measures of intergroup bias. In: Brown, R. and Gaertner, S. (eds.), *Blackwell Handbook of Social Psychology: Intergroup processes*. United Kingdom. Blackwell Publishing, pp. 175-197.
- Dunlap, R. E., Van Liere, K. D., Mertig, A. G. And Jones, R. E., 2000. New trends in measuring environmental attitudes: Measuring endorsement of the new ecological paradigm: A revised NEP scale. *Journal of Social Issues*, 55 (3), 425-442.
- Duvat, V., 2011. Interest of quality-based policies for Integrated Coastal Zone Management implementation: Lessons learnt from a French case study. *Ocean & Coastal Management* 54 (2011), 831-843.
- EEA. 2006. The changing face of Europe's coastal areas. In Breton F. and Meiner A. (Eds.), EEA report no. 6. Luxembourg Office for Official Publications of the European Communities.
- Ergin, A., Karaesmen, E., Micallef, A., and Williams, A.T., 2004. A new methodology for evaluating coastal scenery: Fuzzy logic systems. *Area*. 36(4), 367-386
- Ergin, A., Williams, A.T., and Micallef A., 2006. Coastal Scenery: Appreciation and Evaluation.. *Journal of Coastal Research*. 22(2), 958-964.
- Espejel, I., Espinoza-Tenorio, A., Cervantes, O., Popoca, A., Mejía, A., and Delhumeau, S., 2007. Proposal for an integrated index for the planning of recreational beaches: use at seven mexican arid sites. *Journal of Coastal Research*. Special Issue 50, 47-51.
- Gavio, B., Palmer-Cantillo, S., & Mancera, J. E., 2010. Historical analysis (2000-2005) of the coastal water quality in San Andrés Island, SeaFlower Biosphere Reserve, Caribbean Colombia. *Marine Pollution Bulletin*, 60 (7), 1018-1030.
- Gómez-Orea, D., 2007. Evaluación ambiental estratégica. Un instrumento para integrar el medio ambiente en la elaboración de planes y programas. Madrid Spain: Mundi-prensa, 360p.
- Grünewald L., 1998. La Seguridad en la Actividad Turística". Secretaria de Turismo de la Nación, Universidad del Salvador y Cámara de Empresarios Hoteleros de Villa Gesell. 10pp.
- Herrera, J., 2010. Modelo de gestión costera para playas turísticas del Caribe Colombiano. Aplicación en Playa Blanca, Magdalena, Colombia. Santa Marta, Colombia: University of Magdalena, Msc thesis, 174 p.
- Houston, J. R., 2008. The economic value of beaches e a 2008 update. *Shore and Beach*, 76(3), 22-26.
- Hurtado, J., 2010. Metodología de la investigación. 4ª edición. *Ciea-Sypal*. Caracas, Venezuela. 168 p.
- IGAC-Instituto Geográfico Agustín Codazzi. 2013. Mapas Nacionales. Presidencia de la República. Available in: <http://geoportal.igac.gov.co/ssigl2.0/visor/galeria.req?mapaId=22> on 20-11-2013.
- Kaiser, F. G., Oerke, B. and Bogner, F. X., 2007. Behavior-based environmental attitude: development of an instrument for adolescents. *Journal of Environmental Psychology*, 27 (3), 242-251.
- Kim, A. and Weiler, B., 2013. Visitors' attitude towards responsible fossil collecting behaviour: An environmental attitude-based segmentation approach. *Tourism Management*, 36 (2013), 602-612).
- Klein, Y., J. Osleeb and Viola M., 2004. Tourism-generated earnings in the coastal zone: a regional analysis. *Journal of Coastal Research*, 20 (4), 1080-1088.
- Klemas, V., 2009. Sensors and Techniques for Observing Coastal Ecosystems. In: Yanf., X. (ed.), *Remote Sensing and Geospatial Technologies for Coastal Ecosystem Assessment and Management*. Berlin: Springer Heidelberg, pp. 17-44.
- Klemas, V., 2011. Remote sensing techniques for studying coastal ecosystems: An overview. *Journal of Coastal Research*, 27 (1), 2-17.
- Leatherman, S., 1989. National assessment of beach nourishment requirements associated with accelerated sea level rise. In Smith, J.B. and Tirpak D. A. (eds.), *The Potential Effects of Global Climate Change on the United States Appendix B: Sea Level Rise*. Washington, D.C.: U.S. EPA Office of Policy, Planning, and Evaluation Publication, EPA 230-05-89-057, 28p.

- Mamat, M. and Kokhtar, F., 2012a. Developing hadhair environmental attitude test as instrument for Malaysian Environmental Attitude. *Proceedings of the 1<sup>st</sup> National Conference on Environmental-Behaviour Studies* (Shah Alam, Malaysia), *Procedia- Social and Behavioral Sciences*, 49, pp. 75-84.
- Mamat, M. and Kokhtar, F., 2012b. Environmental attitude profile among Muslim students of environmental course in Malaysia. *ASEAN Conference on Environmental-Behaviour Studies (AcE-Bs)* (Kuching, Sarawak, Malaysia), *Procedia- Social and Behavioral Sciences*, 42, pp. 92-99.
- Mitasova, H., Harmon, R., Weaver, K., Lyons, N. and Overton, M., 2012. Scientific visualization of landscapes and landforms. *Proceedings of the 41st Annual Binghamton Geomorphology Symposium* (South Carolina, Columbia), *Geomorphology* 137 (1), pp. 122-137.
- Moreno, M., Corraliza, J. A. and Ruiz, J.P., 2005. Escala de actitudes ambientales hacia problemas específicos. *Psicothema*, 17, 412-418.
- Nelson, C. and Botteril, N., 2002. Evaluating the contribution of beach quality awards to the local tourism industry in Wales - the Green Coast Award. *Journal of Ocean & Coastal Management*, 45, 157-170.
- Pranzini, E., 2007. Remote sensing in beach erosion monitoring: from the origin, to OpTIMAL and further. In: Pranzini, E. and Wetzel, L. (ed.), *Beach erosion monitoring. Results from BEACHMED-e/OptIMAL Project*. Florence, Nuova Grafica Florentina, pp. 49-50.
- Pranzini, E., Simonetti, D., Vitale, G., 2010. Sand colour rating and chromatic compatibility of borrow sediments. *Journal of Coastal Research*, 26, 798-808.
- PROEXPORT. 2012. Informe Turismo Extranjero en Colombia. Ministry of Trade, Industry and Tourism. Bogota, Colombia. 37 p.
- Rangel, N., Correa, I., Anfuso, G., Ergin, A., and Williams, A.T., 2013. Assessing and managing scenery in the Caribbean coast of Columbia, *Journal of Tourism Management*. 35, 41-58.
- Roig-Munar, F.X., Mir-Gual, M., Rodríguez-Perea, A., Pons, G.X., Martín-Prieto, J.A., Gelabert, B. and Blázquez, M., 2013. Beaches of Ibiza and Formentera (Balearic Islands): a classification based on their environmental features, tourism use and management. *Journal of Coastal Research*, SI 65, 1844- 1849.
- Scott, T., Russell, P., Masselink, G., Wooler, A., and Short, A., 2007. Beach rescue statistics and their relation to nearshore morphology and hazards: a case study for southwest England. *Journal of Coastal Research*, SI 50. 1-6.
- Scott, T., Russell, P., Masselink, G., Wooler, A., 2009. Rip current variability and hazard along a macro- tidal coast. *Journal of Coastal Research*, SI 56. 895 - 899.
- Short, A., 1996. The role of wave height, period, slope, tide range and embaymentisation in beach classifications: a review. *Revista Chilena de Historia Natural*, 69, 586-604.
- Talesnik, D. and Gutierrez, A., 2002. Transformaciones de frentes de agua: la forma urbana como producto estándar. EURE (Santiago), Santiago, v.28, n. 84, sept. 2002. Available in <[http://www.scielo.cl/scielo.php?script=sci\\_arttext&pid=S025071612002008400002&lng=es&nrn=iso 20/11/2013](http://www.scielo.cl/scielo.php?script=sci_arttext&pid=S025071612002008400002&lng=es&nrn=iso 20/11/2013)>.
- UNWTO - United Nations World Tourism Organization. 2011. Tourism highlights, 2011 edition.
- Wolch, J. and Zhang, J., 2004. Beach recreation, cultural diversity and attitudes towards nature. *Journal of Leisure Research*. 36, 3, 414-443.
- Yepes, V., 2002. Ordenación y gestión del territorio turístico. Las playas, In: Blanquer, D. (ed.), *Ordenación y gestión del territorio turístico*. Valencia, Spain: Tirant lo Blanch press, pp. 549-579.
- Yepes, V., Sánchez, I. and Cardona, A., 2004. Criterios de diseño de aparcamientos y accesos a las playas. *Equipamientos y servicios municipales*, 112, 40-44.
- Zielinski, S and Botero, C., 2012. Guía básica para certificación de playas turísticas. Editorial Gente Nueva. Santa Marta, Colombia. 86 p. ISBN 978-958-8704-25-8 [www.sistemascosteros.org](http://www.sistemascosteros.org).

# Sedimentation and erosion patterns in a low shoot-density *Zostera noltii* meadow in the fetch-limited Berre lagoon, Mediterranean France

Anne-Éléonore Paquier†, Samuel Meulé†, Edward J. Anthony†, Guillaume Bernard‡

†Aix-Marseille Université, CNRS, IRD, CEREGE UM34  
13545 Aix en Provence, France.  
paquier@cerege.fr

‡Gipreb, cours mirabeau - 13130 Berre  
l'étang, France



[www.cerf-jcr.org](http://www.cerf-jcr.org)



[www.JCRonline.org](http://www.JCRonline.org)

## ABSTRACT

A.-E. Paquier, S. Meulé, E.J. Anthony, G. Bernard, 2014. Sedimentation and erosion patterns in a low shoot-density *Zostera noltii* meadow in the fetch-limited Berre Lagoon, Mediterranean France. In: Green, A.N. and Cooper, J.A.G. (eds.), *Proceedings 13<sup>th</sup> International Coastal Symposium* (Durban, South Africa), *Journal of Coastal Research*, Special Issue No. 70, pp. 563-567, ISSN 0749-0208

Seagrass meadows fulfill several coastal ecosystem services that include coastal protection, provision of shelter for fishes and fish nesting sites, and water oxygenation. These aspects are hinged in part on the capacity of these meadows to attenuate waves and to slow down currents. Berre lagoon (area: 155 km<sup>2</sup>) is a fetch-limited, micro-tidal brackish water body on the French Mediterranean coast. At the turn of the 20th century, the lagoon was occupied by extensive meadows of *Zostera marina* and *Zostera noltii*. Urban and industrial pollution and freshwater diversion into the lagoon contributed to the complete disappearance of *Zostera marina* while *Zostera noltii* declined dramatically. Since the 1970s, these sources of perturbation have been drastically reduced but with no appreciable effect on *Zostera noltii*. A study was carried out on a receding *Zostera noltii* meadow occupying a small shallow bay (< 2 m deep) fronting a beach over a 14-month period in order to monitor both patterns of shoot density and erosion and accretion in the bay. Berre lagoon experiences short-fetch waves generated by northwesterly "Mistral" winds that exhibit a seasonal pattern. Shoot density shows a markedly seasonal trend that does not appear to be related to bed changes, which evened out over the study period. The data show that bed changes are less marked over the *Zostera noltii* meadow, and are more important in non-colonized areas, as well as along the beach, which exhibits sediment rotation. These patterns are probably reflecting the influence of the meadow on wave dissipation patterns.

**ADDITIONAL INDEX WORDS:** *Sea grass, strong wind events, beach protection, beach rotation.*

## INTRODUCTION

Seagrass meadows are known to fulfil a number of coastal ecosystem services that include shoreline stabilization (Short *et al.*, 2007), provision of shelter and food for fishes and fish nesting sites (Gillanders, 2006) and water oxygenation (Borum *et al.*, 2006). These aspects are hinged in part on the capacity of these meadows to attenuate waves (Fonseca and Cahalan, 1992; Chen *et al.*, 2007; Lowe *et al.*, 2007; Paul and Amos, 2011; Paul *et al.*, 2012; Manca *et al.*, 2012; Koftis *et al.*, 2013) and to slow down currents (Neumeier, 2007). These meadows are decreasing under direct impacts from coastal development and dredging activities and indirect impacts from declining water quality (Waycott *et al.*, 2009). There is, therefore, a need to protect them; especially when they are in disturbed coastal ecosystems, such as coastal lagoons or estuaries, subject to changes in sedimentation and erosion patterns. In these fetch-limited environments, wind waves can have important impacts on seagrass meadows by inducing meadow burial from sediment fallout or erosion of the meadow bed. The aim of this paper is to link spatial sedimentation and erosion patterns in a fetch-limited lagoon setting in the western Mediterranean with shoot density patterns in a small *Zostera noltii* meadow that has suffered considerably over the last century.

## Study site

Berre lagoon, one of the largest Mediterranean coastal lagoons (155 km<sup>2</sup>), is a brackish water body located in southeastern France (Figure 1a). It is bordered on the seaward side by the Nerthe hill range (Figure 1b). This semi-enclosed ecosystem is connected to the Mediterranean Sea by the narrow Caronte channel (Figure 1b). The lagoon is composed of two main basins: "Grand étang" and "Etang de Vaïne". Berre lagoon receives water and sediments from three small river catchments: the Touloubre (730 km<sup>2</sup>), the Arc (400 km<sup>2</sup>) and the Cadière (73 km<sup>2</sup>) covering a total surface area of 1200 km<sup>2</sup> (Gouze *et al.*, 2008). Wind data from the nearby Marignane weather station, between 1949 and 2008 (Figure 1d.), show that the lagoon is dominantly affected by northwestern winds (the Mistral), which account for 41.4% of the record. Plants have been drastically reduced, with legally imposed limitation of freshwater and silt inputs since 1995. Between the 1970s and the 1990s urban and domestic pollution have also been drastically reduced. Notwithstanding, the area colonized by *Zostera noltii* has not increased significantly (Bernard *et al.*, 2007).

Our study was carried out on a receding *Zostera noltii* meadow (Figure 2) occupying a shallow bay (less than 2 m deep) at the southeast of "Grand étang" on Berre Point (Figures 1b and 1c). The elevation of the beach bordering the meadow attains 0.65 m and also exhibits the highest wind speeds (up to 30 m.s<sup>-1</sup>).

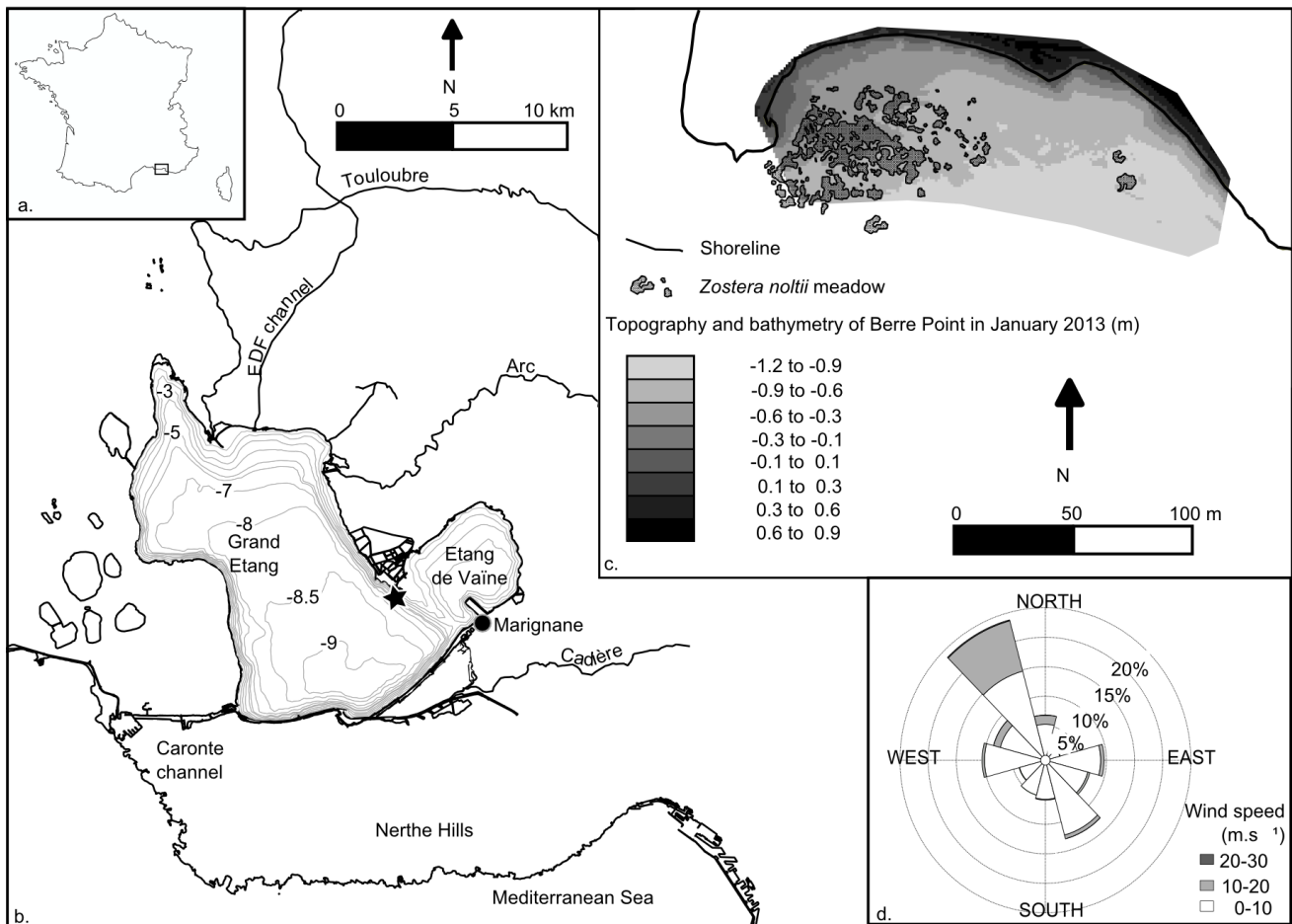


Figure 1. Study area. a. Location in France. b. Berre lagoon with star indicating the study site of Berre Point. c. Elevation and bathymetry of Berre point. d. Mean wind rose for Berre lagoon from the Météo France weather station in Marignane between 1949 and 2009.

Southeasterly winds are the next most abundant (29.1%, with a maximum of 23 m.s<sup>-1</sup>). Strong winds (speeds higher than 10 m.s<sup>-1</sup>) are nearly equally distributed throughout the year but are slightly more common in winter and spring (27.6% from January to March, 26.6% from April to June, 22.7% from July to September and 23.1% from October to December). Berre lagoon is a virtually tideless, fetch-limited setting in which the wave regime consists of only short-fetch waves with periods of 2 to 4s.

At the turn of the 20th century, the lagoon was occupied by extensive meadows of *Zostera marina* and *Zostera noltii*, probably exceeding 60 km<sup>2</sup> (Bernard *et al.*, 2007). Urban and industrial pollution and the diversion of Durance River for hydroelectric power in 1966 resulted in an increase in freshwater and silt inputs, perturbing the lagoon (Stora and Arnoux, 1988). *Zostera* meadows declined dramatically over the century. *Zostera marina* disappeared completely, whereas *Zostera noltii* has been reduced to four patches covering only 0.015 km<sup>2</sup>. Since the 1980s and 1990s, freshwater and silts inputs from the Durance hydroelectric plant have been drastically reduced, with legally imposed limitation of freshwater and silt inputs since 1995. The slope is 1.53% in the eastern part of the beach, 1.43% in the central part, and 1.46% in the western part (Figure 1 c). Berre Point is exposed

to the two dominant winds, but the Mistral fetch of 12 km is three times more important than that of the southeasterly winds.

## METHODS

Seven high-resolution topographic surveys covering both the beach and the submerged meadow bed were conducted with a DGPS Trimble RTK between February 2012 and March 2013. From the data, 1 m-cell digital elevation models (DEM) were computed using a Delaunay triangulation method. The surveys were referenced to 0 NGF (French sea-level datum). Each summer from 2009 to 2012, the meadow limits were mapped from aerial photographs and validated by the GPS measurements in the field. From March 2012 to March 2013, measurements of meadow biometry were also conducted monthly at Berre Point. Shoot densities were measured at 20 randomly chosen stations using a 0.2 x 0.2 quadrat. Due to low water temperatures, the number of measured stations was reduced during the three winter visits (2 in March 2012 and 1 in January 2013). Hourly wind speeds and directions (measurements at an elevation of 10 m) from Marignane weather station for our study period (Figure 1b) were used to constrain the forcing conditions in the lagoon.

## RESULTS

Figure 3 shows changes in bathymetry of the meadow and the topography of the adjacent beach between February 22, 2012 and March 21, 2013 (Figure 3a). The maps show that changes can attain up to +0.7 m, even when only time periods of a few months are considered. The period February 22, 2012 to June 8, 2012 was dominated by erosion of the meadow substrate, whereas the beach showed alongshore alternations of erosion and accretion (Figure 3a). The trend changed almost completely from June 9, 2012 to October 3, 2012 (Figure 3b), which is characterized by net overall accretion. The October 4, 2012 to January 22, 2013 (Figure 3c) pattern once again differs from that of the preceding months. The meadow zone showed hardly any change, but the beach showed alongshore alternations of erosion and accretion that are nearly the reverse of those observed between February 22, 2012 and June 8, 2012 (Figure 3a). From January 23, 2013 to March 21, 2013

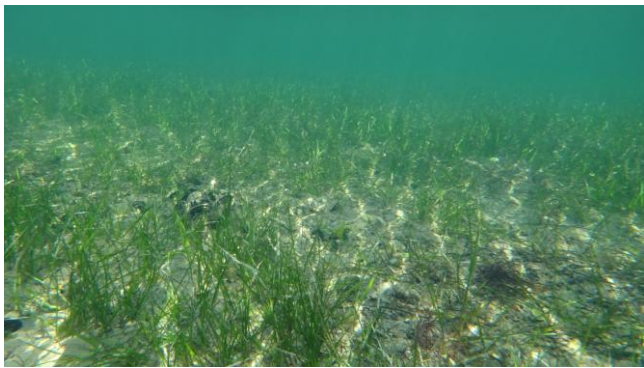


Figure 2. Photograph showing part of the low shoot-density meadow at Berre Point (March 28, 2012).

(Figure 3d), the trend along the beach showed anew the reverse of the pattern in the preceding three months with accretion dominating in the west and mild erosion in the east. Much of the meadow once again showed little change whereas the subtidal zone, between the beach and the meadow, underwent mild accretion. A specific feature of this last survey was a 20 m-long and 100 m-wide swath of erosion east of the meadow.

*Zostera noltii* shoot density over the period March 2012 to March 2013 showed a cyclic pattern of increase from spring to summer, followed by a decrease in autumn and winter and then, an increase in the following spring (Figure 4). The mean density increased from  $559.72 \pm 187$  shoot.m<sup>-2</sup> on March 1, 2012 to  $1037.5 \pm 480$  shoot.m<sup>-2</sup> on June 6, 2012. It then decreased down to  $531.25 \pm 221$  shoot.m<sup>-2</sup> on November 15, 2012, and further decreased to  $536.36 \pm 182$  shoot.m<sup>-2</sup> on January 8, 2013, before increasing once more to  $1098 \pm 412$  shoot.m<sup>-2</sup> on March 12, 2013.

The wind speed conditions corresponding to the four periods of time are shown in Figure 5. Spring 2012 wind speeds exceeding 10 m.s<sup>-1</sup> occurred 9.97% of the time (8.09% from the northwest and 1.87% from the southeast). Summer winds speeds higher than 10 m.s<sup>-1</sup> occurred 7.01% of the time (6.55% from the northwest and 0.46% from the southeast). The autumn months showed a higher frequency of strong winds, which composed 9.49% of all recorded winds (8.51% from the northwest and 0.52% from the southeast). The winter 2013 wind speeds are the highest with 19.31% of winds stronger than 10 m.s<sup>-1</sup> (15.43% from northwest and 1.29% from southeast). It is interesting to note that two exceptional events characterized by wind speeds from the northwest in excess of 22.3 and 22.9 m.s<sup>-1</sup> over periods of 24 hours occurred on March 4, 2013 and on March 17, 2013.

## DISCUSSION

The discussion will focus on three points: patterns of bathymetric and beach topographic change, tentative conclusions that can be drawn from these patterns regarding the role and the

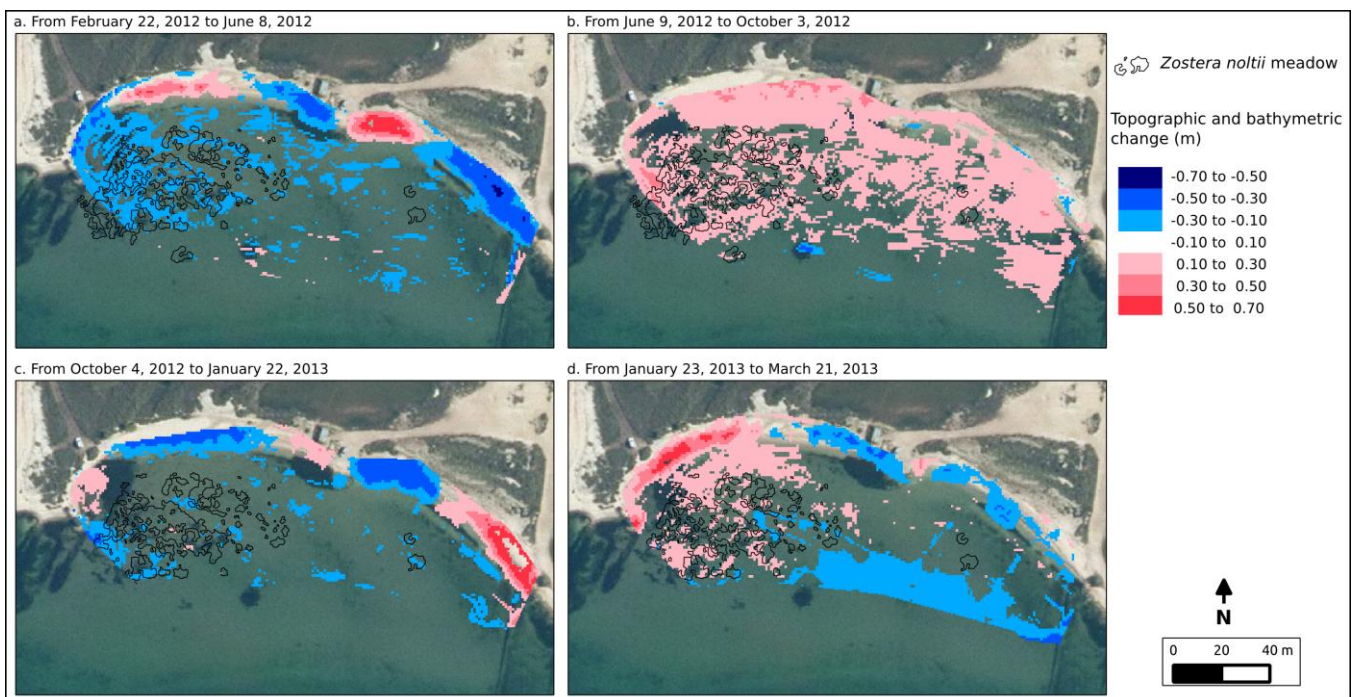


Figure 3. Seasonal topographic and bathymetric changes observed at Berre Point between February 2012 and March 2013. The margin error is evaluated to  $\pm 10$  cm.

fate of the subsisting *Zostera noltii* meadows in Berre lagoon, and the possible relationship between these patterns and shoot density.

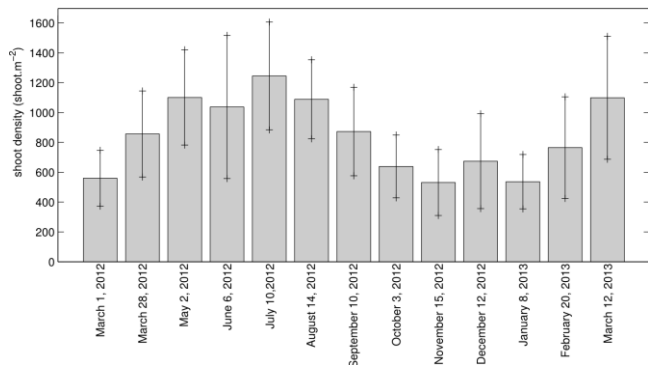


Figure 4. Mean shoot density measured at Berre Point between March 2012 and March 2013. Standard errors are represented by black crosses.

Figure 6 is a map synthesizing the net change over the study period. It shows that the western sector of Berre Point landward of the meadow underwent net accretion, especially the beach. Accretion diminished in the subtidal zone but was still notable in the *Zostera noltii* meadow. On the other hand, the central and eastern beach sectors show alternations of accretion and erosion. Overall, the areas that accreted from June 8, 2012 to October 3, 2012 (Figure 3b.) were eroded from October 4, 2012 to January 22, 2013 (Figure 3c.), with the inverse condition observed for areas that were stable or eroded from June 8, 2012 to October 3, 2012. The waves and currents generated by the winds affecting the lagoon resulted in a sediment circulation pattern that seem to correspond to a form of beach ‘rotation’ from one part of the headland-bound bay to the other. This rotation is clearly linked to the bay orientation relative to the two dominant winds because the beach shows in the same sector accretion during a northwest wind

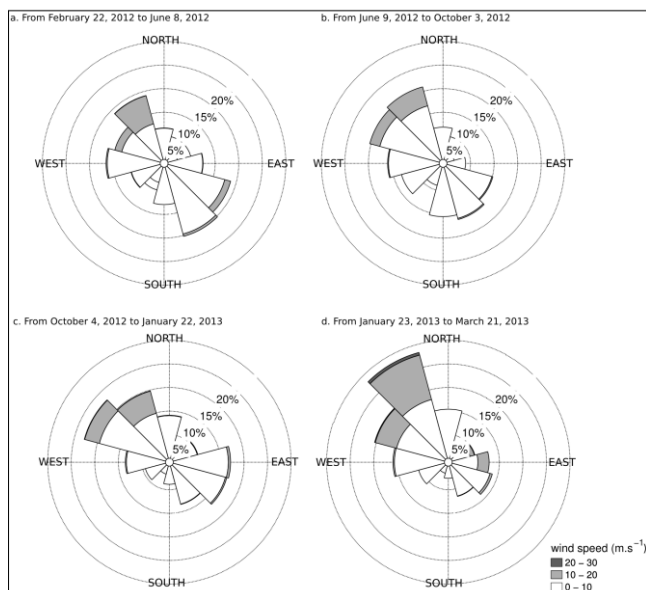


Figure 5. Winds observed in Marigane between February 2012 and March 2013.

event and erosion during a southeast event. Although the datasets are relatively short, they are interesting in that they highlight, to our knowledge, for the first time, rotation in a fetch-limited lagoon beach system. Rotation is a commonly described process on ocean-facing beaches exposed to larger waves (Thomas *et al.*, 2011). These observations suggest that the sediment exchanges are the response of a mobile sediment stock to forcing induced by the commonality of strong winds in the lagoon, in spite of the low fetch conditions. However, scrutiny of the spatial patterns of erosion and accretion shows that the meadow is not just a passive element in the overall sediment dynamic of the study site. Bernard *et al.* (2007) clearly demonstrated that the recession of Berre Point meadow is hinged on a low shoot density. It would be expected that this low-shoot density meadow does not play a role in seabed protection against erosion. Figure 6 shows that this is not the case. The largest accretion occurred in the bay sector occupied by *Zostera noltii*.

This spatial pattern may reflect the effect of refraction and diffraction of the dominant waves from the northwest around the western headland of the bay. These processes create a low-energy shadow zone in this sector that favours circulation of sediments derived from the east and from the subtidal zone. However, there is a strong likelihood that this accretion has also been favoured by wave and current dissipation over the meadow. The milder bathymetry of the western part of the bay (Figure 1), including the meadow, and the gentler beach slope suggests that this sector may be acting as a net sediment sink. At the same time, the presence of the meadow also generates a shelter effect for this sector from strong southeasterly wind-wave events. The eastern sector of the bay, where the *Zostera noltii* meadow is lacking, is more exposed to these events, just as it is to refracted waves from the northwest and the currents generated by winds from these two directions. The swathe of erosion between January 22, 2013 and March 21, 2013, mentioned earlier (Figure 3d), has been unique to this period as the earlier surveys did not highlight significant changes in this swathe. The net change corresponds to exceptional northwest wind events that occurred on March 4, 2013 and on March 17, 2013. On a seasonal basis, the summer period between June and October appears to be most favourable in terms of overall accretion of the bay (Figure 3b), although these results will need to be further confirmed by future studies. Finally, the cyclic shoot density pattern exhibited by the Berre lagoon meadow (Figure 4) follows a seasonal evolution that is similar to that of other meadows reported from other Mediterranean lagoons by Auby and Labourg (1996), with growth from spring to summer probably stimulated by the warmer temperatures and longer days.

### CONCLUSION

A study conducted over the period between March 2012 and March 2013 has shown patterns of erosion and accretion in a Mediterranean seagrass meadow and its adjacent beach, as well as trends in shoot density growth. The results show that although the meadow is of limited extent, it does play a role in pattern of sedimentation and erosion both in the subtidal zone and along the beach in the shelter of this meadow. In particular, though relatively short, the datasets highlight, to our knowledge, for the first time, beach rotation in a fetch-limited lagoon.

Although the beach sedimentation and erosion patterns may reflect the effect of bay orientation relative to the dominant northwesterly wind-waves and currents generated by these winds, it appears likely that the *Zostera noltii* meadow also contributes to beach protection by acting as a buffer between these events and the beach.

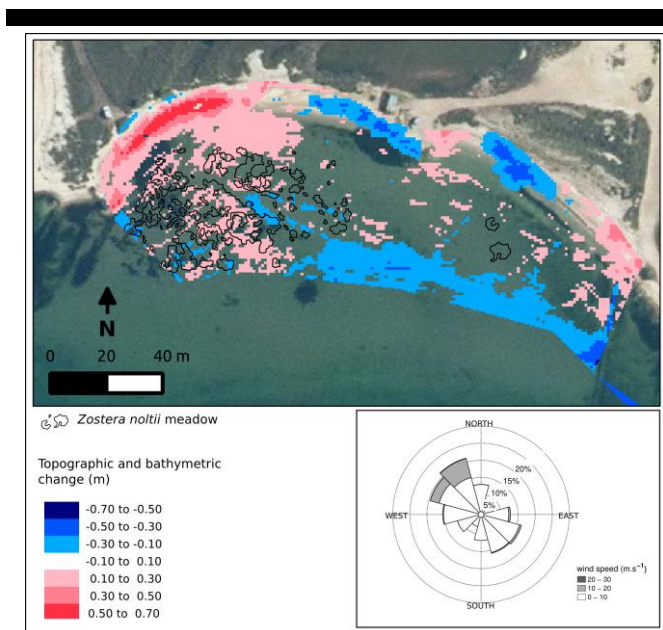


Figure 6. Net topographic and bathymetric change and wind conditions at Berre Point between February 22, 2012 and March 21, 2013. The margin error of Net topographic and bathymetric change is evaluated to  $\pm 10$  cm.

No apparent relationship between seasonal shoot density growth, characterised by an increase in summer, and the seasonal patterns of morphological change, seems to come out from the datasets. Further studies will be needed to confirm more clearly the results of this one year study.

### ACKNOWLEDGEMENT

This study was realized during a PhD study financed by the "Provence Alpes Côte d'Azur" region and the Gipreb (Gestion intégrée, prospective, restauration Étang de Berre). Gipreb and Météo France are respectively acknowledged for meadow mapping and weather data.

### LITERATURE CITED

- Auby, I. and Labourg, P.-J., 1996. Seasonal dynamics of *Zostera noltii* hornem. in the bay of Arcachon (France). *Journal of Sea Research*, 35(4), 269-277.
- Bernard, G., Boudouresque, C. F., and Picon, P., 2007. Long term changes in *Zostera* meadows in the Berre lagoon (Provence, Mediterranean sea). *Estuarine, Coastal and Shelf Science* 73(3-4), 617-629.
- Borum, J., Sand-Jensen, K., Binzer, T., Pedersen, O., and Greve, T., 2006. Oxygen movement in seagrasses. In: Larkum, A. W. D., Orth, R. J., Duarte, C. M. In *Seagrasses: Biology, Ecology and Conservation*, 255-270. Springer Netherlands.
- Chen, S.-N., Sanford, L., Koch, E., Shi, F., and North, E., 2007. A nearshore model to investigate the effects of seagrass bed geometry on wave attenuation and suspended sediment transport. *Estuaries and Coasts* 30, 296-310.
- Fonseca, M. S. and Cahalan, J. A., 1992. A preliminary evaluation of wave attenuation by four species of seagrass. *Estuarine, Coastal and Shelf Science* 35(6), 565-576.
- Gillanders, B. 2006. Seagrasses, fish, and fisheries. In: Larkum, A. W. D., Orth, R. J., Duarte, C. M. In *Seagrasses: Biology, Ecology and Conservation*, 255-270. Springer Netherlands.
- Gouze, E., Raimbault, P., Garcia, N., Bernard, G. and Picon, P., 2008. Nutrient and suspended matter discharge by tributaries into the Berre lagoon (France): The contribution of flood events to the matter budget. *Comptes Rendus Geoscience* 340(4), 233-244.

- Koftis, T., Prinos, P., and Stratigaki, V., 2013. Wave damping over artificial *Posidonia oceanica* meadow: A large-scale experimental study. *Coastal Engineering* 73, 71-83.
- Lowe, R. J., Falter, J. L., Koseff, J. R., Monismith, S. G. and Atkinson, M. J., 2007. Spectral wave flow attenuation within submerged canopies: Implications for wave energy dissipation. *Journal of Geophysical Research: Oceans* 112(C5).
- Manca, E., Cáceres, I., Alsina, J., Stratigaki, V., Townend, I., and Amos, C., 2012. Wave energy and wave-induced flow reduction by full-scale model *posidonia oceanica* seagrass. *Continental Shelf Research* 50-51(0), 100-116.
- Neumeier, U., 2007. Velocity and turbulence variations at the edge of saltmarshes. *Continental Shelf Research* 27(8), 1046-1059. Natural Coastal Mechanisms - Flume and Field Experiments on Links between Biology, Sediments and Flow.
- Paul, M. and Amos, C. L., 2011. Spatial and seasonal variation in wave attenuation over *Zostera noltii*. *Journal of Geophysical Research: Oceans* 116(C8).
- Paul, M., Bouma, T., and Amos, C., 2012. Wave attenuation by submerged vegetation: combining the effect of organism traits and tidal current. *Mar Ecol Prog Ser* 444, 31-41.
- Short, F., Carruthers, T., Dennison, W., and Waycott, M., 2007. Global seagrass distribution and diversity: A bioregional model. *Journal of Experimental Marine Biology and Ecology* 350(1-2), 3-20.
- Stora, G. and Arnoux, A., 1988. Effects on mediterranean lagoon macrobenthos of a river diversion: Assessment and analytical review. In: El-Sabh M. and Murty T. (Eds.), *Natural and Man-Made Hazards*, pp. 525-546. Springer Netherlands.
- Thomas, T., Phillips, M.R., Williams, A.T., and Jenkins, R.E. (2011). Short-term beach rotation, wave climate and the North Atlantic Oscillation (NAO). *Progress in Physical Geography* 35, 333-352.
- Waycott, M., Duarte, C. M., Carruthers, T. J. B., Orth, R. J., Dennison, W. C., Olyarnik, S., Calladine, A., Fourqurean, J. W., Heck, K. L., Hughes, A. R., Kendrick, G. A., Kenworthy, W. J., Short, F. T. and Williams, S. L., 2009. Accelerating loss of seagrasses across the globe threatens coastal ecosystems. *Proceedings of the National Academy of Sciences* 106(30), 12377-12381.



## Effects of mud flows from the LUSI mud volcano on the Porong River estuary, Indonesia

Shuichi Kure†, Bambang Winarta‡, Yuriko Takeda†, Keiko Udo†, Makoto Umeda∞, Akira Mano†, Hitoshi Tanaka∞

†International Research Institute of Disaster Science  
Tohoku University  
Sendai, Japan  
kure@irides.tohoku.ac.jp

‡Faculty of Civil Engineering & Planning  
Institut Teknologi Sepuluh Nopember  
Surabaya, Indonesia

∞ Department of Civil and Environmental Engineering  
Tohoku University  
Sendai, Japan



[www.cerf-jcr.org](http://www.cerf-jcr.org)



[www.JCRonline.org](http://www.JCRonline.org)

### ABSTRACT

Kure, S., Winarta, B., Takeda, Y., Udo, K., Umeda, M., Mano, A., Tanaka, H. 2014. Effects of Mud Flows from the LUSI Mud Volcano on the Porong River estuary, Indonesia. In: Green, A.N. and Cooper, J.A.G. (eds.), *Proceedings 13<sup>th</sup> International Coastal Symposium* (Durban, South Africa), *Journal of Coastal Research*, Special Issue No. 70, pp. 568-573, ISSN 0749-0208.

On May 29, 2006, mud and gases began erupting unexpectedly from a hydrocarbon exploration well near Sidoarjo, East Java, Indonesia. The eruption, called the LUSI (Lumpur Sidoarjo [Lumpur means mud in Indonesian]) mud volcano, has continued since then at rates as high as 180,000 m<sup>3</sup> per day. The mud inundated an area in excess of 6.5 km<sup>2</sup>, in spite of attempts to contain it via the construction of a series of levees. The mud is erupting and accumulating behind the levee system. It is also being pumped into the Porong River, which then carries the mud to the ocean approximately 20 km to the east. The main objective of this study is to assess the effect of mudflow from the LUSI volcano on the river and estuary environment such as sediment deposition and water quality using the observed river cross sections and bathymetry data after the eruption of the LUSI volcano. From the analysis it was found that a significant sediment deposition occurred at the river bed of Porong River due to increased sediment discharge from the volcano during the dry periods after which the sediment deposits on the river bed were gradually eroded and flushed away to the ocean by floods and high water flows during the wet periods. Environmental impacts due to increased sediment from the Porong River on the estuary and coastal region are discussed.

**ADDITIONAL INDEX WORDS:** *East Java, Sidoarjo, water quality, Sediment transport.*

### INTRODUCTION

On May 29, 2006, mud and gases began erupting unexpectedly from a hydrocarbon exploration well near Sidoarjo, East Java, Indonesia. The eruption, called the LUSI (Lumpur Sidoarjo [Lumpur means mud in Indonesian]) mud volcano, has continued since then at rates as high as 180,000 m<sup>3</sup> per day. The mud inundated an area in excess of 6.5 km<sup>2</sup>, in spite of attempts to contain it via the construction of a series of levees. The mud inundation has caused over 30,000 persons to be displaced from more than a dozen villages in the area. The inundation of numerous factories, farmland, and a major toll road has caused significant economic impacts on the region. The mud is erupting and accumulating behind the levee system. It is also being pumped into the Porong River, which then carries the mud to the ocean approximately 20 km to the east. However, the accumulation of mud in the river may result in sedimentation through the riverbank and spreading across the fisheries' aquaculture area along the coast. The local Marine and Fisheries Board stated that if the mudflow cannot be appropriately released to the sea, the sedimentation will affect the quality of the water's oxygen absorption in the river and estuary. Thus, it is an urgent issue to investigate the effects of the mud inflow into the Porong River on the river estuary environments.

Hydro and morpho dynamics of the river estuary have been

studied by many researchers based on observations and numerical simulations (e.g. Tanaka, 2007). Many dynamic models on the river mouth change and monitoring systems have been proposed in order to evaluate the river mouth environments (e.g. Totok and Mano, 2001; Tanaka and Lee, 2003). Tanaka and Lee (2003) evaluated the influence of a jetty construction on the morphology and wave set-up at a river mouth based on the field observations. Modeling and monitoring of the river estuary morphology change is important in order to evaluate the effects of human activities and hydrological changes in the river basin and coastal region on the river estuary environments.

In the Porong region, Nagrahadi and Yanagi (2003) investigated the sea surface water quality in the Madura Strait, Indonesia based on observations in 2000 and 2001 in order to evaluate the impact of the river discharge on the estuary area. The Madura Strait is located at the downstream area of the Porong River and Surabaya River. They concluded that the water quality distribution in the Madura Strait, especially near the Surabaya River and Porong River estuaries, is highly affected by the load from the river. Sukresno *et al.* (2008) investigated the total suspended matter in the Porong region after the mud eruption and inflow to the river using Aqua-Modis satellite data and a numerical model. They found that the total suspended matter of Porong region varies in the range of 22 – 130 mg/l, and is affected by rainfall due to the monsoon. Also, they concluded that the total suspended matter in the Porong region did not increase significantly regardless of the mud inflow from the LUSI. Yuanita *et al.* (2011) applied a cohesive sediment transport model to the Madura Strait, Indonesia.

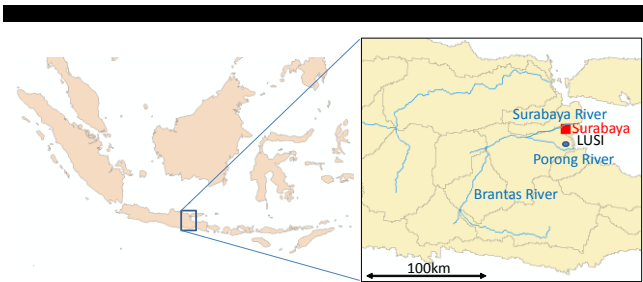


Figure 1. Location of the Brantas River basin, Surabaya city and the LUSI mud volcano.

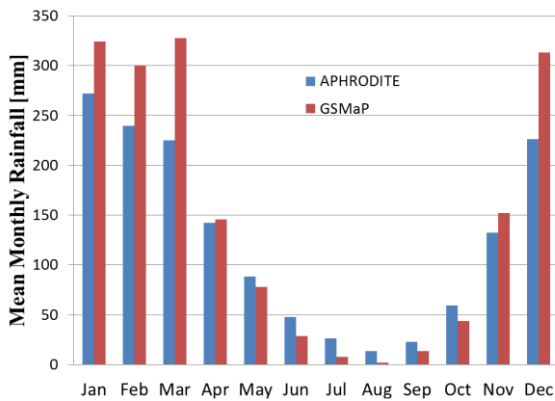


Figure 2. Mean monthly rainfall in the Brantas River basin (GSMaP and APHRODITE).

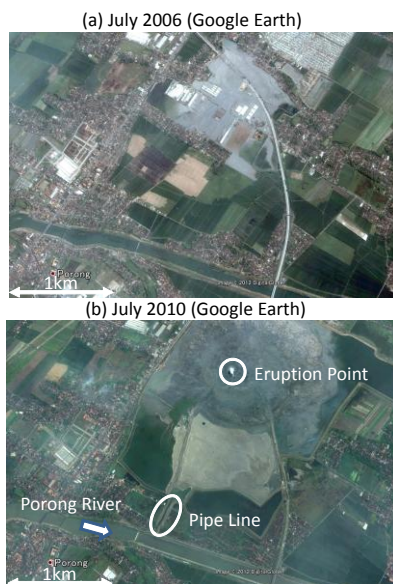


Figure 3. Mud inundation occurrences around the mud eruption point and the Porong River in (a) July 2006 and (b) July 2010 (Google Earth).

Based on the numerical simulation, they showed that the sediment discharge from the Porong River to the Madura Strait affected the area about 4 km from the river mouth.

As such, some studies focused on the effects of the mud inflow on the Porong region and Madura Strait. However, these studies focused mainly on the Madura Strait, not the Porong River itself,

and were based on the numerical simulation. Also, model validations used in those studies were insufficient due to the lack of available observation data. Thus, the effects of the mud inflow to the Porong River on the river morphology and environments should be quantitatively evaluated based on the observation data because there are serious concerns about flooding and water quality pollution problems in the Porong River due to the mud inflow from the LUSI.

The main objective of this study is to assess the effect of mudflow from the erupted LUSI volcano on the river and estuary environments such as sediment deposition and water quality using the observed river cross sections and bathymetry data.

### STUDY AREA

The Porong River, about 30 km south of Surabaya city (the second largest city in Indonesia), is nearly 60 km in total length and belongs to the downstream portion of the Brantas River (Figure 1). The Brantas River basin, the second largest river basin in Indonesia, originates in the Kelud Mountains (1,731 m), is about 320 km long and has a 12,000 km<sup>2</sup> catchment area. The Brantas River splits into the Surabaya River and Porong River downstream. Flood water is directed to flow into the Porong River through gate operations at the diversion point of the two rivers in order to protect Surabaya city from floods and high water flows.

Annual mean rainfall within the Brantas River basin is about 1500 – 2000 mm, and rainfall distribution over the Brantas River basin varies distinctly between the rainy (October–April) and dry (May–September) seasons. Figure 2 shows the mean monthly rainfall in the Brantas River basin obtained from APHRODITE (e.g. Yatagi *et al.*, 2012) and GSMaP (e.g. Aonashi *et al.*, 2009) datasets. GSMaP developed by JAXA is based on the satellite-derived rainfall data. It provides hourly and daily rainfall data at a 0.1-degree resolution over the world from March 2000 through today in near real time. The APHRODITE dataset, developed by Japan Meteorological Research Institute, is based on the spatial interpolation of ground observation data. It provides daily rainfall data at a 0.25-degree resolution over the Asia and Pacific region from 1956 through 2007. From Figure 2, the difference of rainfall depth between the rainy and dry periods can be seen. GSMaP is the satellite driven data and it has some biases and uncertainties. However, it can be seen from Figure 2 that the seasonal change of the mean monthly rainfall and climatology are very similar to those of the APHRODITE data.

Big cities such as Surabaya and Malang are located inside the Brantas River basin, and the basin is densely populated and many agricultural and industrial activities are being conducted. In order to protect these cities from flood related disasters, several river basin management and flood control projects have been implemented based on technical and budget supports from several countries. As a result, flood damage caused by the Brantas and Porong River has decreased. However, mud flow from the LUSI mud volcano may reduce the flood capacity of the Porong River due to sedimentation of the mud in the river bed. Thus, it is important to quantitatively evaluate the effects of the mud flows from the LUSI mud volcano on the river and estuary morphology.

### MUD INUNDATION

An unexpected eruption of mud and fluids took place on May 29, 2006 approximately 200 m away from a deep hydrocarbon exploration well in the Porong area, Sidoarjo, East Java. There are two opinions on the mechanism of the LUSI mud volcano in Porong.



Figure 4. Mud inundation situation. There are many houses buried in the mud after the LUSI eruption. The picture was taken from the levee system near the eruption point in October, 2010 by the authors.



Figure 5. The mud inflow situation at the 26 K.P. on November 13, 2013. The picture was taken from the right side levee of the Porong River by the authors.



Figure 6. Target river cross sections in the Porong River (Google Earth)

One states that the disaster was triggered by the Yogyakarta earthquake on May 27, 2006, whereas the other maintains it was caused by the misconduct of oil drilling activities by a private company. Both opinions concur at the point that the mechanism is a result of an underground explosion that was caused by higher pressure of fluid that pushed the weakest layer of sediment (Mazzini *et al.*, 2007; Fitrianto, 2012).

Mud volcanos are widely known phenomena in Java Island, but the LUSI is apparently different from the others in magnitude and volume. The maximum mud flow rate from the LUSI is about 180,000 m<sup>3</sup>/day, and the accumulation of the mud reached 30 million m<sup>3</sup> as of the fall of 2007 (USGS, 2008). Figure 3 shows satellite images (Google Earth) around the LUSI eruption point and the Porong River after the mud eruption (a: July 2007 and b: July 2010). The mud inundated and accumulated the area and a pipe line was constructed to deliver the mud to the Porong River (Figure 3). It can be seen from Figure 4 that many houses were buried due to the mud inundation and accumulation. It should be emphasized that the eruption of the LUSI and mud discharge to

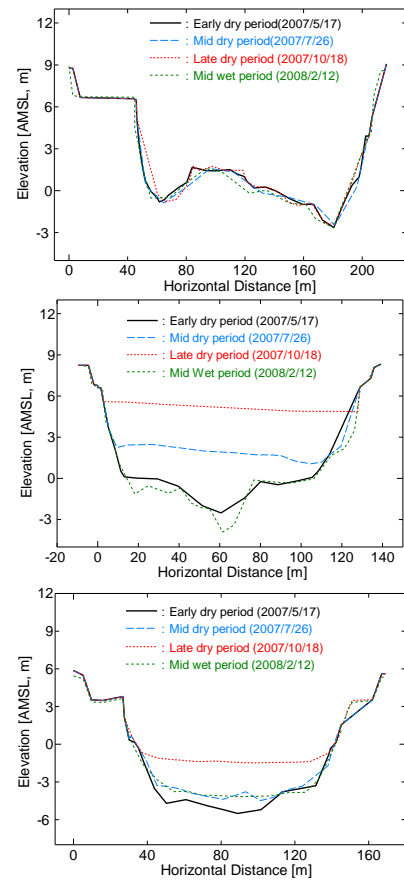


Figure 7. Time evolution of the river cross sections at the 18 (upper figure), 26 (middle figure) and 27.6 (lower figure) K.Ps. during the early and late dry periods and the wet period.

the Porong River are still continuing as of November 13, 2013 as confirmed by a field survey conducted by the authors. According to the probabilistic analysis of Davies *et al.* (2011), the mud eruption was projected to continue for several more decades. Figure 5 shows the situation of mud discharge from the LUSI through the constructed pipe line into the Porong River, 26 km from the river mouth (Hereinafter, referred to as the 26 K.P.). Particle sizes of the mud are within 0.1  $\mu\text{m}$  – 0.1 mm with dominant particle sizes are less than 10  $\mu\text{m}$  approximately. It can be said that the LUSI mud is substantially finer-grained than normal sediments (USGS, 2008).

### MUD DEPOSITION IN THE PORONG RIVER

The mud from the LUSI is being pumped into the Porong River, which then carries the mud to the ocean approximately 20 km to the east. The mud inflow to the Porong River may result in sedimentation throughout the river and estuary, and may reduce the flood capacity of the river. Thus, it is important to analyze the time and space evolution of river cross sections and bathymetry after the mud inflow to the Porong River.

BPLS (Badan Penanggulangan Lumpur Sidoarjo – Sidoarjo Disaster Recovery Agency), responsible for assessing the LUSI disaster, observed the river cross section data once per month from November 2006 through April 2010 in order to evaluate the effects of the mud inflow to the Porong River. In this paper the

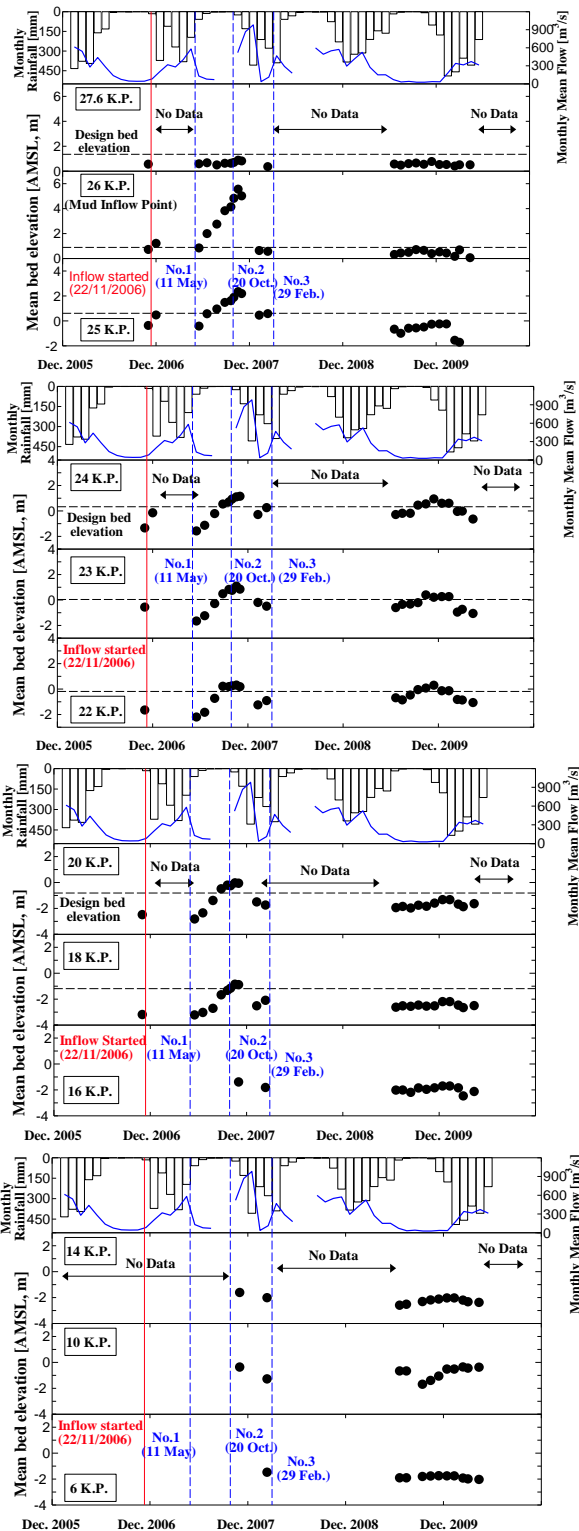


Figure 8. Time series of the monthly rainfall (GSMaP), monthly mean river flow discharge and mean river bed elevations at the 6 – 27.6 K.P.s. from December 2005 through December 2010.

Figure 6 shows the cross section points in the Porong River selected as the targets in this study. These target cross sections, located within 6 – 27.6 K.P.s. from the river mouth, provide more data for analysis compared to the other points. The point where the mud flows into the Porong River, via the pipe line, is the 26 K.P. Figure 7 shows the time evolution of the river cross sections at the 18, 26 and 27.6 K.P.s. during the early and late dry periods and wet period. Elevation values in the figures are based on the average mean sea level (AMS L, m). As shown in this figure, the bed elevation changes at the 18 and 26 K.P.s., especially the 26 K.P., were significant due to the mud discharge from the LUSI during the middle and late dry periods. However, the elevation was returned to almost the initial heights during the wet period due to the mud erosion and transport by the increased river flow discharge. These time evolutions of the bed elevation were not found at the 27.6 K.P. located in the upstream of the mud inflow point.

Figure 8 shows the time series of the monthly rainfall (GSMaP), monthly mean river flow discharge and averaged river bed elevations at the 6 - 27.6 K.P.s. The river flow discharge data was observed at the 27.6 K.P. by BPLS from January 1, 2004. A good correlation between monthly rainfall (GSMaP) and monthly mean river flow discharge can be seen from Figure 8 although GSMaP is satellite driven data with some biases and uncertainties. Figure 9 shows IKONOS satellite images around 26 K.P. of the river taken during the events, provided by Centre for Remote Imaging, Sensing and Processing (CRISP), National University of Singapore. The dates and timings when the satellite images were taken are represented in Figure 8 using the vertical dash lines of no.1 (May 11, 2007), no.2 (October 20, 2007) and no.3 (February 29, 2008). It was found from the figures that the mean river bed elevations increased during the dry periods due to the mud discharge from the LUSI and decreased during the wet period due to the increase of the river flow discharge. These behaviors are likely insignificant at the 6 – 16 K.P.s. although detailed discussion cannot be made due to lack of data at these points. Accordingly, it can be said that the mud influenced not only the points near the mud inflow point but also the lower river mouth and estuary points. The satellite images shown in Figure 9 represent the mud inflow situations and the differences between dry period and wet period. It is notable that a density flow was caused by suspended mud sediments as clearly shown by the satellite images of the dry period (no.2).

Figure 10 shows the time series of hourly river flow discharge data at the 27.6 K.P. and the mean river bed elevations at the 20, 23 and 26 K.P.s. during the 2007 and 2009 events when such data are available sufficiently compared to the events of other years. It was found that the sediment erosion and transport started at the flow rate about 500 – 600 m<sup>3</sup>/s, and took about 3 months to return to almost the same initial bed elevation levels by the erosion and flushing due to the increase of the hourly discharge volume.

Figure 11 shows the relationship between the mud deposition volume and the distance from the mud inflow point (26 K.P.) at the 2007 and 2009 events. In this paper the mud deposition volume (m<sup>2</sup>) was defined as the river width (m) multiplied by the increase of the average bed elevation (m). From Figure 11, high values of mud deposition are observed near the mud inflow point. Also, the mud deposition volume of the 2007 event is much higher than that of the 2009 event because the mud inflow volume decreases with the decrease of the mud eruption volume of the LUSI as shown in Table 1 (values obtained from Davies *et al.* (2011)). It can be said that the mud eruption from the LUSI and mud deposition in the Porong River is gradually decreasing year by year.

data provided by BPLS was used to analyze the river bed elevation changes in time and space.

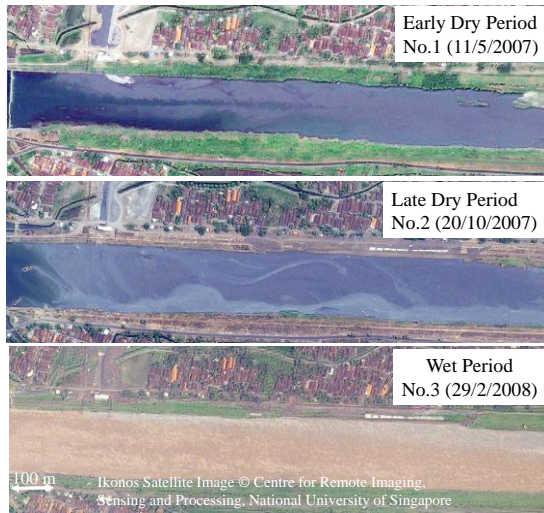


Figure 9. Ikonos Satellite Images around the mud inflow point (26 K.P.) during the dry period (May 2007 (No.1) and November 2007 (No.2)) and wet period (February 2008 (No.3)).

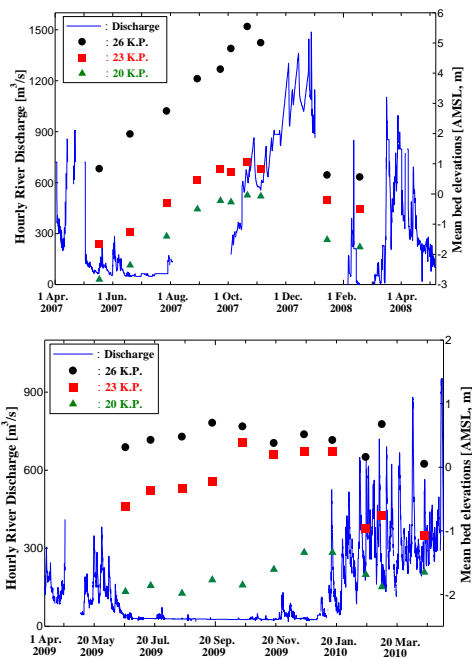


Figure 10. Time series of the hourly river discharge and mean bed elevations at the 20, 23, 26 K.P.s. during the 2007 and 2009 events.

As discussed above, the deposition of mud in the Porong River occurs during the dry periods due to the mud inflow from the LUSI, and the mud is flushed away by the floods and high water flows during the wet periods. This is because the particle sizes of the mud from the LUSI are substantially small (below 0.1 mm) and the deposition occurred due to the mud inflow from the LUSI, leading to the formation of another layer over the original river bed. Thus, it can be inferred that the critical shear stress of the mud causing erosion in the Porong River is relatively small, and it is easy for the mud sediments to be transported.

These results suggest that the effects of the mud inflow to the Porong River on the flood capacity of the river due to

sedimentation of the river cross sections are insignificant, and the mud inflow and deposition in the Porong River do not result in the increase of flood frequency.

### EFFECTS ON WATER QUALITY

As discussed in the previous chapter, flood related concerns of the mud inflow to the Porong River may be an insignificant problem because the accumulated mud in the river bed is gradually eroded and flushed away by the floods and high water flows during the wet periods. However, a main concern of the mud inflow to the Porong River is the effects on the water quality, environment and ecosystems of the river and estuary. The local Marine and Fisheries Board stated that if the mud cannot be released to the sea appropriately, the sedimentation will affect the quality of the water's oxygen absorption in the river and estuary.

Thus, it is important to quantitatively evaluate the effects of the mud inflow on the water quality, and to quantify these effects so that we might better improve the water quality in the river and estuary. Fitrianto (2012) provided a comprehensive review of the water quality survey of the Porong River, and several actions and innovations conducted by shrimp farmers living near the Porong River in order to overcome the LUSI disasters. According to McMichael (2009), evidence indicates that the mud polluted the Porong River with hazardous materials such as arsenic (As) and phenol. The mud has been assessed and found to contain phenol in concentrations exceeding the maximum residue limit. Phenol is toxic to fish, aquatic vegetation and humans. USGS (2008) found that several elements, notably As, are present in concentrations that exceed US government environmental guidelines for residential soil (McMichael, 2009). It can be assumed that the mud may seriously affect the livelihoods and health of shrimp and fishing communities located adjacent to the Porong River. In fact, based on the data of the Sidoarjo Fisheries and Marine Department, the fisheries production in the Porong, Tanggulangin and Jabon districts was 7,338,500 kg in 2007, but it reduced to 5,467,200 kg in 2008 (Fitrianto, 2012).

According to Fitrianto (2012), there were four actions and responses taken by farmers living near the Porong River in order to overcome the pollution of the river. These include:

- 1) The farmers reacted spontaneously by protesting the BPLS and sought a compensation for their losses.
- 2) The farmers sold their ponds and changed their business to another sector.
- 3) The farmers changed their commodities cultivated from shrimp to other pollution-tolerant fish.
- 4) The farmers still cultivate the shrimp but by modifying their technique and practices with new methods such as creating a water filtering technique, finding a new feeding method, etc.

From these literature reviews, it can be inferred that the Porong River and its estuary have faced several water quality problems, and this resulted in reducing the production of the fish and shrimps from the Porong River. However, some analyses

Table 1. The mud eruption rate from the LUSI mud volcano from 2006 through 2010 (made from the data of Davies et al. (2011)).

Year	Eruption rate [m <sup>3</sup> /day]
2006	90,000 - 180,000
2007	60,000 - 95,000
2008	20,000 - 80,000
2009	5,000 - 78,000
2010	1,000 - 76,000

classified the mud as non-hazardous and non-toxic (Pohl, 2007). Therefore, it is important to investigate the water quality situation of the Porong River and estuary after the mud inflow from the LUSI volcano. In the near future we will conduct water quality surveys on the Porong River from the several aspects concerning the water quality and mud deposition in the river bed.

## CONCLUSIONS

In this study, the effects of mud flows from the LUSI mud volcano on the Porong River were investigated from two aspects: One is the flood problem due to the sedimentation in the river, and the other is the water quality problem in the river and estuary.

The observed cross section data after the mud eruption and inflow to the Porong River were provided by BPLS and used to analyze the time evolutions of the cross sections. Our analysis found that a significant sediment deposition occurred at the river bed of Porong River due to increased sediment discharge from the volcano during the dry periods, and then the sediment deposits in the river bed were gradually eroded and flushed away to the ocean by floods and high water flows during the wet periods. Accordingly, it can be said that the mud flow from the LUSI mud volcano has no influence to reduce the flood capacity of the Porong River due to sedimentation of the mud in the river bed.

The environmental impacts due to increased sediment from the LUSI on the river and estuary was also discussed in the paper through the literature reviews. Pohl (2009) mentioned that some analyses classified the mud as non-hazardous and non-toxic. On the other hands, others mentioned that the evidence showed that the Porong River is polluted by hazardous materials such as arsenic and phenol (Fitrianto, 2012; McMichael, 2009). In fact, the fisheries production in the Porong and the other districts decreased 25 % in 2008, and the farmers living near the Porong River took several actions and innovations in order to survive from the disaster of the Porong River. Thus, further surveys on the water quality and environment and monitoring should be conducted in order to quantitatively evaluate the effects of the mud inflow on the water quality and ecosystem of the Porong River, estuary and coastal region. In the near future, several water quality surveys of the Porong River and estuary will be conducted by the authors.

## ACKNOWLEDGEMENT

This study was supported by the JSPS KAKENHI Grant Number 24404014. GSMaP satellite driven rainfall dataset developed and provided by JAXA (Japan Aerospace Exploration Agency) was employed in this study. Also, IKONOS satellite images were provided by Centre for Remote Imaging, Sensing and Processing (CRISP), National University of Singapore. The authors would like to thank Ms. Akiko Kanazawa and Ms. Atsuko Hashimoto of Tohoku University for their insightful comments and review of the paper.

## LITERATURE CITED

- Aonashi, K., Awaka, J., Hirose, M., Kozu, T., Kubota, T., Liu, G., Shige, S., Kida, S., Seto, S., Takahashi, N. and Takayabu, Y.N. 2009. GSMaP passive, microwave precipitation retrieval algorithm: Algorithm description and validation. *J. Meteor. Soc. Japan*, 87A, 119-136.
- Davies, R.J., Mathias, S.A., Swarbrick, R.E. and Tingay, M.J. 2011. Probabilistic longevity estimate for the LUSI mud volcano, East Java. *Journal of the Geological Society*, Vol.168, pp.517-523, doi: 10.1144/0016-76492010-129.
- Fitrianto, A. R. 2012. Shrimp Farmers' Innovation in Coping with the Disaster (A Case Study in Sidoarjo Mud Volcano Disaster Toward Shrimp Farmer's Responses). *Procedia Economics and Finance*, Vol. 4, pp.168-176, doi: 10.1016/S2212-5671(12)00332-2.

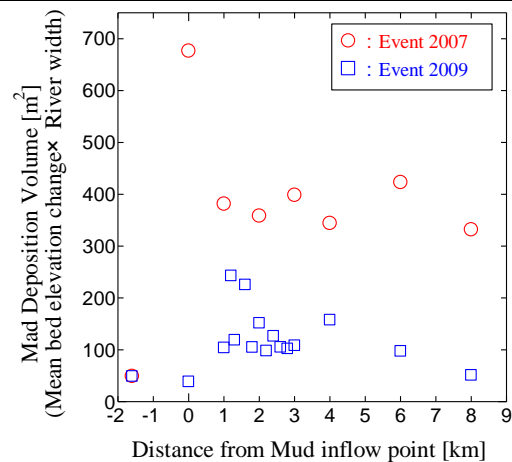


Figure 11. Relationship between the mud deposition volume and the distance from the mud inflow point.

- Tanaka, H., and Lee, H. 2003. Influence of Jetty Construction on Morphology and Wave Set-up at a River Mouth. *Coastal Engineering Journal*, 45(4), 659-683.
- Tanaka, H. 2007. Hydro- and Morpho-dynamics at River Entrance. *Annual Journal of Hydraulic Engineering*. JSCE, 51, K\_9-K\_11.
- Totok, S., and Mano, A. 2001. A dynamic model on the river mouth change, Proceedings of 2<sup>nd</sup> Conference on IAHR Symposium on River, *Coastal and Estuarine Morphodynamics*, 433-442.
- Martinelli G. and Pahahi B. 2005. Mud Volcanoes, geodynamics and seismicity, NATO Science Series, Series 4, 51, Springer, 288.
- Mazzini, A., Svensen, H., Akhmanov, G.G., Aloisi, G., Planke, S., Malthe-Sorensen, A., and Istadi, B. 2007. Triggering and dynamic evolution of the LUSI mud volcano, Indonesia. *Earth and Planetary Science Letters*, 261, 375-388, doi: 10.1016/j.epsl.2007.07.001.
- McMichael, H. 2009. The Lapindo mudflow disaster: environmental, infrastructure and economic impact. *Bulletin of Indonesian Economic Studies*, 45(1) 73-83, /doi/abs/10.1080/00074910902836189
- Pohl, C. 2007. Lapindo Brantas and the mud volcano sidoarjo, Indonesia. available from: [http://www.foeurope.org/publications/2007/LB\\_mud\\_volcano\\_Indones In.pdf](http://www.foeurope.org/publications/2007/LB_mud_volcano_Indones In.pdf)
- Nugrahadi, M.S., and Yanagi, T., 2003. Water Quality in Madura Strait, Indonesia. *Engineering Sciences Reports*, Kyushu University, 25(1), 7-15.
- Sukresno, B., Priyono, B., Zahrudin, D.A., and Subki, B.A. 2008. Investigation of Total Suspended Matter in Porong Region Using AQUA-MODIS Satellite Data and Numerical Model. *Pusat Pengkajian dan Perekayasa Teknologi Kelautan dan Perikanan (P3TKP)*, 3(3), <http://www.p3tkp.litbang.kkp.go.id/?q=Jurnal/Jurnal%202008/vol-3-no-3-desember>
- US Geological Survey. 2008. Preliminary Analytical Results for a Mud Sample Collected from the LUSI Mud Volcano, Sidoarjo, East Java, Indonesia. available from: [http://pubs.usgs.gov/of/2008/1019/pdf/OF08-1019\\_508.pdf](http://pubs.usgs.gov/of/2008/1019/pdf/OF08-1019_508.pdf) (accessed Apr. 4, 2013)
- Yatagai, A., Kamiguchi, K., Arakawa, O., Hamada, A., Yasutomi, N. and Kitoh, A. 2012. APHRODITE: Constructing a Long-term Daily Gridded Precipitation Dataset for Asia based on a Dense Network of Rain Gauges. *Bulletin of American Meteorological Society*, 1401-1415, doi:10.1175/BAMS-D-11-00122.1.
- Yuanita, N., Rini, M.A., and Heriawan, U. 2011. Cohesive Sediment Transport Modeling: Application to the Madura Strait, Indonesia. *ASCE. Coastal Engineering Practice*, 522-536, doi: 10.1061/41190(422).

# Influence of mean sea level rise on tidal dynamics of the Ria de Aveiro lagoon, Portugal

Carina L. Lopes<sup>†</sup>, João M. Dias<sup>†</sup>

<sup>†</sup> NMEC, CESAM  
Physics Department,  
University of Aveiro, Aveiro  
3810-193 Portugal  
carinalopes@ua.pt  
joao.dias@ua.pt



[www.cerf-jcr.org](http://www.cerf-jcr.org)



[www.JCRonline.org](http://www.JCRonline.org)

## ABSTRACT

Lopes, C.L., Dias, J.M., 2014. Influence of mean sea level rise on tidal dynamics of the Ria de Aveiro lagoon, Portugal. In: Green, A.N. and Cooper, J.A.G. (eds.), *Proceedings 13th International Coastal Symposium* (Durban, South Africa), *Journal of Coastal Research*, Special Issue No. 70, pp. 574-579, ISSN 0749-0208.

Global mean sea level rise is an important consequence of climate change because of its impact on coastal regions. Recent studies highlight that tidal propagation in shallow waters tends to be modified with mean sea level rise, intensifying coastal threats. This study aims to quantify changes in tidal patterns in Ria de Aveiro coastal lagoon, Portugal in response to the local mean sea level rise. To achieve this goal the hydrodynamic model ELCIRC, previously calibrated and validated for Ria de Aveiro, was applied, considering the present mean sea level and a local mean sea level rise projection of 0.42 m for the end of the 21<sup>st</sup> century, assuming no change in bed elevation. The model results for present mean sea level show that the amplitude of the main semidiurnal ( $M_2$ ) and diurnal ( $K_1$ ) constituents decrease whereas the respective phase increases towards the head of the estuary, while the  $M_4$  constituent shows an opposite pattern, due to the upstream lagoon shallowness. As consequence, the tidal distortion is higher in the lagoon upper reaches than at the lagoon mouth. Under mean sea level rise conditions, the tidal wave tends to be less distorted in the upper lagoon, given that the  $M_2$  amplitude tends to increase while the  $M_4$  amplitude tends to decrease. The results highlight that tidal current magnitude decreases toward the channel's head for both scenarios, but their magnitude tends to increase with mean sea level rise. The residual currents showed a net export of materials to the ocean, which will increase with mean sea level rise.

**ADDITIONAL INDEX WORDS:** *tidal asymmetry, tidal ellipses, residual circulation, ELCIRC.*

## INTRODUCTION

Global mean sea level has risen over the 20<sup>th</sup> century and several studies predict that the mean sea level will continue to rise during the 21<sup>st</sup> century as consequence of climate change. In general, the physical impacts of mean sea level rise on coastal areas are inundation of low-lying coastal areas, landward intrusion of salt water in estuaries and aquifers, landward migration of sandy beaches and barrier island coasts and habitat loss. Recent studies also show that tidal propagation in shallow waters will be modified, intensifying coastal threats (Pickering *et al.*, 2012; Ward *et al.*, 2012; Pelling *et al.*, 2013). These works show that the tidal modifications are strongly dependent on coastal geometry, presenting opposite tendencies in resonant and non-resonant areas. Therefore understanding the local tidal modification is crucial.

Coastal lagoons are shallow coastal landforms particularly sensitive to the mean sea level rise because they are found in low-lying coasts worldwide. Considering that they are extremely rich in fauna and flora, and that lagoonal species are dependent on the lagoon tidal conditions, it is crucial to quantify tidal changes in these environments induced by the mean sea level rise. Attending to these issues, the present study aims to quantify tidal changes in Ria de Aveiro coastal lagoon in response to the local mean sea

level rise. To achieve this goal the hydrodynamic model ELCIRC, previously calibrated and validated for Ria de Aveiro (Lopes *et al.*, 2013a; Lopes and Dias, submitted), was applied to this system, considering two scenarios: the present mean sea level and a local mean sea level rise projection of 0.42 m for the end of the 21<sup>st</sup> century. The 0.42 m sea level rise scenario corresponds to Lopes *et al.* (2011) estimation, considering the SRES A2 storyline and the results from the Atmosphere Ocean General Circulation Model GISS-ER for the Portuguese coast.

## STUDY AREA

The Ria de Aveiro is a shallow lagoon with a complex geometry, located on the northwest Portuguese coast (Figure 1). It is 45 km long and 10 km wide and covers an area of 89.2 km<sup>2</sup> at spring tide which is reduced to 64.9 km<sup>2</sup> at neap tide (Lopes *et al.*, 2013a). The lagoon contains four main channels Mira, S. Jacinto, Ílhavo and Espinheiro, and a large number of shallow narrow channels and is characterized by large areas of mud flats and salt marshes. The average depth in the navigation channel (15 m relative to chart datum) is higher than the average depth of the remaining lagoon (1 m relative to chart datum).

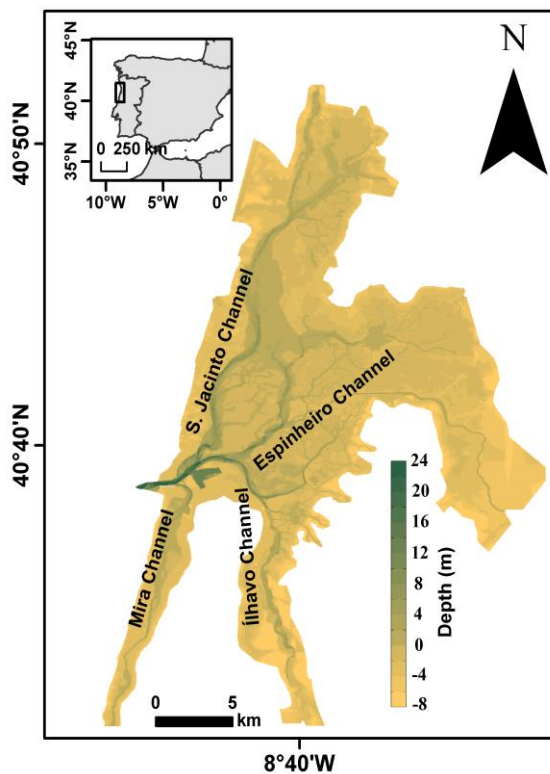


Figure 1. Location of Ria de Aveiro, indicating its main channels and the digital terrain model relative to chart datum, used in numerical simulations.

The lagoon connects with the Atlantic Ocean through a single artificial inlet built in 1808 and its hydrodynamics are dominated by the tide, which is semidiurnal with a small diurnal pattern. Furthermore, the fortnightly spring/neap tide cycle is evident at the lagoon inlet, generating tidal ranges between 0.46 m at neap tide and 3.52 m at spring tide (Lopes and Dias, submitted). The main source of freshwater is the Vouga River. The mean flow is about  $1.8 \times 10^6 \text{ m}^3$ , which is considerably lower than the tidal prism at the lagoon mouth that ranges between  $65.8 \times 10^6 \text{ m}^3$  and  $139.7 \times 10^6 \text{ m}^3$  (Lopes *et al.*, 2013a). The wind stress and wave influence is restricted to dispersed areas of the lagoon in rare situations of extreme weather conditions (Dias, 2001). The lagoon can be considered as vertically homogeneous, except occasionally when fresh water inflows are high and the upper parts of the lagoon can present vertical stratification (Dias *et al.*, 2000; Vaz *et al.*, 2009).

The residual circulation is determined essentially by flood/ebb asymmetry. As the lower lagoon is ebb-dominant there is a trend to export properties to the ocean (Oliveira *et al.*, 2006). The prolongation of the northern breakwater that fixed the lagoon entrance in 1987 and the generalized deepening observed at the lagoon main channels and at the navigation channel driven significant modifications on tidal propagation. Analysis of sea levels at several lagoon stations obtained in two distinct surveys in 1987/88 and 2002/03 revealed that the average amplitude of  $M_2$  constituent increased approximately 24.5 cm over this period, while the average phase decreased approximately  $17.41^\circ$  (Araújo *et al.*, 2008). Also, the collapse of salt pan walls and consequent increase in the total flooded area caused an increase of the tidal

currents, mainly on ebb, modifying the tidal asymmetry pattern, leading to an increase of the ebb dominance (Picado *et al.*, 2010).

## METHODOLOGY

The 2D hydrodynamic model ELCIRC (Zhang *et al.*, 2004) was applied to Ria de Aveiro lagoon in order to study the tidal propagation under different mean sea level conditions. The model configuration used was previously calibrated for tidal propagation by Lopes *et al.* (2013a) and Lopes and Dias (submitted) and validated for storm surge propagation by Lopes and Dias (submitted). Besides the description of water dynamics in the lagoon channels, the numerical grid allows the inundation of its marginal lands. This model ability is extremely important in sea level rise studies, considering that the channels marginal regions of Ria de Aveiro present low altitude and are potentially flooded during high sea levels.

Two scenarios were simulated, one considering the present mean sea level and other one considering the local mean sea level rise projection of 0.42 m obtained by Lopes *et al.* (2011) for the end of the 21<sup>st</sup> century. No change in bed elevation was considered. The model was forced by thirteen harmonic constituents ( $M_{SF}$ ,  $O_1$ ,  $K_1$ ,  $P_1$ ,  $Q_1$ ,  $N_2$ ,  $M_2$ ,  $S_2$ ,  $K_2$ ,  $M_4$ ,  $MN_4$ ,  $MS_4$  and  $M_6$ ) taken from the regional model developed by Fortunato *et al.* (2002). The freshwater input and wind effects were neglected considering their minor importance relative to the tide. The time step was 90 s and the model was run for 34 days. The numerical results were then analyzed discarding the first four days of outputs (spin up period). For both simulations, harmonic analysis of water levels and velocity was made at the numerical nodes which are permanently under water for the each scenario. The amplitude and phase of the most important water level harmonic constituents were determined using the matlab package T\_tide (Pawlowicz *et al.*, 2002) and the results were analyzed independently and used to assess tidal asymmetry for both simulations, through:

$$A_r = \frac{A_{M_4}}{A_{M_2}}$$

$$\varphi = 2\theta_{M_2} - \theta_{M_4}$$

Where  $A_r$  is the amplitude ratio,  $A_{M_4}$  and  $A_{M_2}$  are the amplitudes of  $M_4$  and  $M_2$  constituents, respectively,  $\varphi$  is the phase of  $M_4$  ( $\theta_{M_4}$ ) relative to the phase of  $M_2$  ( $\theta_{M_2}$ ). The  $A_r$  indicates the magnitude of tidal asymmetry; as the larger the amplitude ratio the more distorted is the tide. The  $\varphi$  indicates flood or ebb dominance ( $0^\circ < \varphi < 180^\circ$  indicates flood dominance and  $180^\circ < \varphi < 360^\circ$  indicates ebb dominance). The tidal asymmetry differences were assessed computing the ratio between  $A_r$  for both scenarios under analysis. Also, the regions that changed their dominance were identified.

The harmonic analysis of velocity was performed to compute tidal ellipses of  $M_2$  constituent for both scenarios, using the matlab package developed by Xu (2002). The semi-major axis and the eccentricity of tidal ellipses were analyzed. The differences in the tidal ellipses motivated by the increase in the mean sea level were assessed computing the ratio between the semi-major axis for the present and for the future mean sea level. Also, changes in the eccentricity were assessed identifying the regions with modifications in its rotation.

Finally, the residual currents were assessed averaging the currents over 29.56 days (two times the  $M_{SF}$  constituent period). The changes in the magnitude of residual currents were found



computing the ratio between residual currents intensity for both scenarios under analysis.

## RESULTS AND DISCUSSION

The model results were used to characterize the tide along the lagoon for both scenarios. Figure 2 presents the distribution of amplitude and phase of  $M_2$ ,  $K_1$  and  $M_4$  constituents for the present mean sea level. The results show that the  $M_2$  constituent is the most important in the establishment of the overall lagoon water levels. Indeed, its amplitude ranges from 0.5 m at the upper reaches of the lagoon channels to 1.1 m at the lagoon mouth. The diurnal contribution is one order of magnitude smaller, and ranges from 0.04 m at the upper reaches of the main channels to 0.05 m at the lagoon mouth. The  $M_4$  amplitude presents an opposite pattern, with amplitude values increasing towards the channel's head, following the decrease in lagoon depth. The  $M_4$  constituent amplitude at the lagoon mouth is close to zero while it can reach 0.2 m at the shallow channel's extremities. Concerning the phase results,  $M_2$  and  $K_1$  constituents show identical patterns, with values increasing towards the channel's head. Concerning the  $M_4$  constituent, the phase is almost constant between the lagoon mouth and the middle of the main channels, decreasing from there to the end of the narrow channels. The amplitude and phase

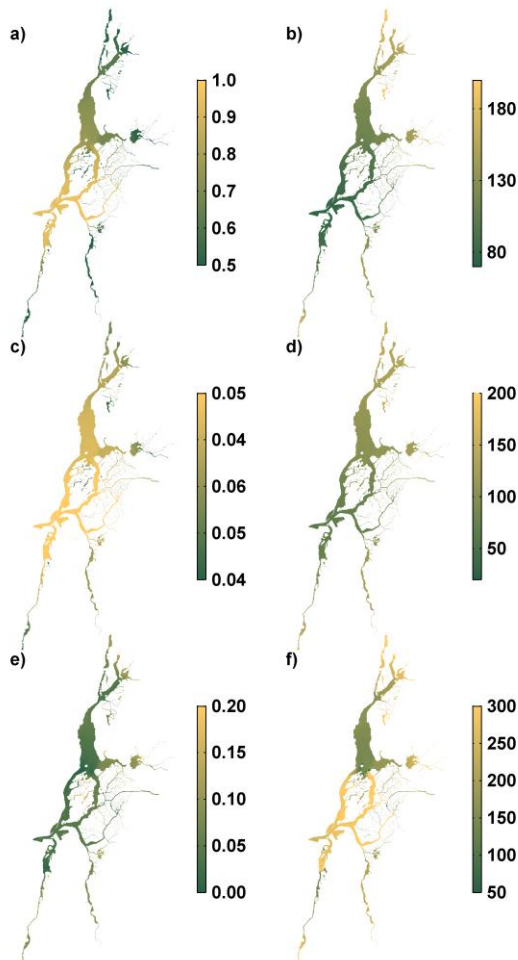


Figure 2. Amplitude (m) (a), (c) and (e)) and phase (b), (d) and (f)) of  $M_2$ ,  $K_1$  and  $M_4$  constituents, respectively, for the present mean sea level.

patterns for the 0.42 m mean sea level rise scenario are identical to those described for the present and therefore are not shown here. Despite the similarities in the patterns, important changes are identified in the phase and amplitude magnitudes in response to the decrease of friction motivated by the mean sea level rise. Indeed, the amplitude of  $M_2$  constituent decrease between 2% and 5% at the lagoon central area and increase between 5% and 20% at the channel's head. Its phase increases at the lagoon central area and decreases at the channel's head. Moreover, the differences found in the amplitude and phase of  $M_4$  constituent close to the lagoon mouth are negligible. Nevertheless, in the lagoon central area and channel's head its amplitude decreases between 10% and 20%.

Concerning the tidal asymmetry (Figure 3), the amplitude ratio results evidence that the tidal distortion patterns are similar for both scenarios, increasing its value from the lagoon mouth (close to zero) towards the channel's head (between 0.3 and 0.4). Despite the similarities in pattern, the tidal distortion tends to increase with the mean sea level rise (see Figure 3 c) from the lagoon mouth surroundings until the main channel's head and in one small area located at the S. Jacinto channel. For the remaining lagoon the tidal distortion tends to decrease with mean sea level rise. The tidal dominance results show that the lagoon is ebb-dominated at the lagoon mouth and central area, and flood-dominated at the channel's head. This pattern was observed for both mean sea levels, however, it should be noted that the ebb-dominance tends to be extended further upstream at the S. Jacinto channel (see Figure 3c) with the mean sea level rise.

The tidal features and propagation within Ria de Aveiro lagoon for the present mean sea level were previously studied by several authors (Dias *et al.*, 2000; Dias, 2001; Araújo, 2005; Lopes *et al.*, 2006; Oliveira *et al.*, 2006; Araújo *et al.*, 2008; Picado *et al.*, 2010; Lopes *et al.*, 2011; Valentim *et al.*, 2013). The patterns of amplitude and phase obtained in this study are similar to those obtained by these authors. Nevertheless, important differences in the magnitudes of amplitude and phase of tidal constituents were found. Generally, the amplitude of  $M_2$  constituent is higher and the amplitude of  $M_4$  constituent is lower than amplitudes obtained in those studies. Also, the phase of  $M_2$  constituent obtained here is lower than those obtained in the previous studies. These differences can be explained in great part by the geomorphologic changes in the last 25 years at the inlet regions and at the lagoon main channels, showing that the lagoon tidal features are highly dependent on bathymetric changes (Araújo *et al.*, 2008). In fact, previous works are based on bathymetric records obtained in a global survey performed in 1987/88 and in a survey restricted to the inlet region obtained in 2001, whereas the bathymetry used here was updated for the lagoon main channels and the inlet region with data measured in 2011 and 2012, respectively. Indeed, a deepening of the lagoon main channels was found between 1987 and 2011, being the S. Jacinto and Espinheiro channels the most affected, with changes of about 8 meters in some areas (Lopes *et al.*, 2013b).

The relation between tidal asymmetry and sediment dynamics was studied in other estuaries worldwide (Dronkers, 1986; Friedrichs and Aubrey, 1988; Bolle *et al.*, 2010; Brown and Davies, 2010; Jewell *et al.*, 2012). They found that in ebb-dominated estuaries there is a trend to export sediments, while in flood-dominated estuaries there is a trend to sediment import. Brown and Davies (2010) found that Dyfi Estuary presents a tidal dominance pattern similar to Ria de Aveiro lagoon, with ebb-dominance in the lower estuary and flood-dominance in the upper estuary. This pattern causes sediment export through the estuary

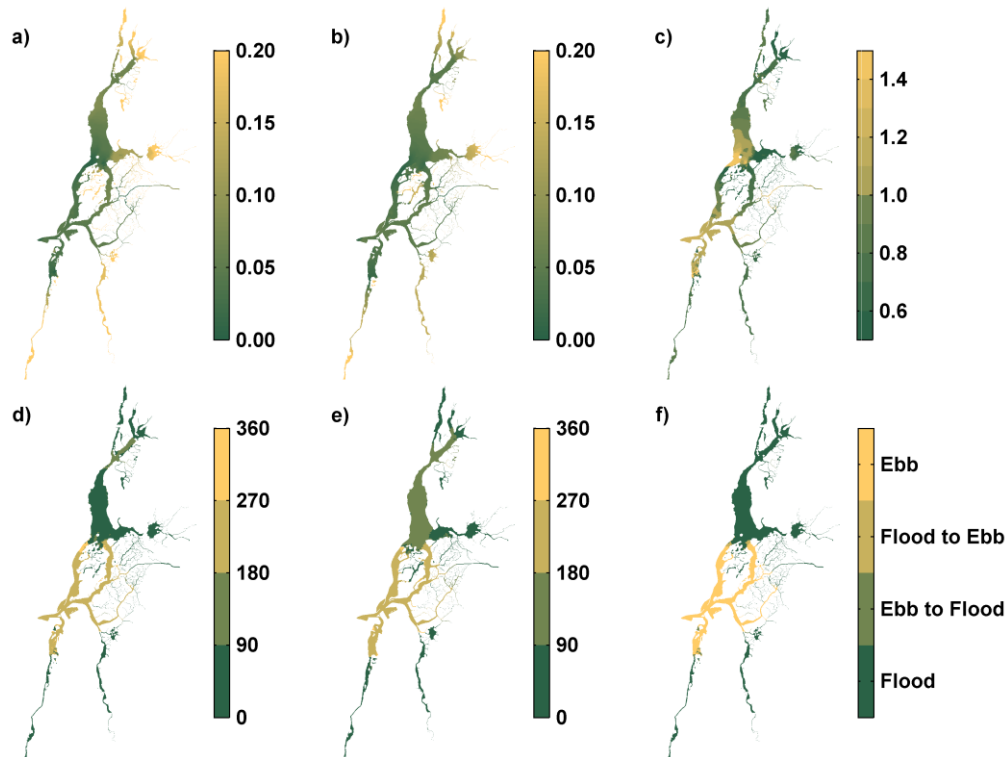


Figure 3. a) and b)  $A_t$  for present and sea level rise scenarios, respectively. c) Ratio between  $A_t$  for both scenarios. d) and e)  $\varphi$  ( $^\circ$ ) for present and sea level rise scenarios, respectively. f) Tidal dominance changes motivated by the mean sea level rise.

mouth and a redistribution of internal sediments in the upper estuary where the tidal energy is weaker.

Given the non-linear dependence between the water elevation and the velocity, the tidal currents were also analyzed within the lagoon for both scenarios through the computation of  $M_2$  constituent tidal ellipses (the most relevant). The ellipses semi-major axis and eccentricity are presented in Figure 4. The results show that the semi-major axis patterns are similar for both scenarios. The highest currents were found at the lagoon mouth (1.2 m/s), and its magnitude decreases towards the channel's head, where the currents are close to zero. Although the similarity of patterns (Figure 4) shows that, with the exception of some small isolated regions scattered along the lagoon, the tidal currents increase with the mean sea level rise. Concerning the eccentricity of tidal ellipses (Figures 4d, 4e and 4f); the results show the existence of regions with clockwise and anticlockwise current rotation. It is interesting to note that in the Mira channel the anticlockwise rotation is dominant, while in the S. Jacinto channel the clockwise rotation dominates. The rotation of tidal currents remains unchangeable with the mean sea level rise, except in one small region located at the half of S. Jacinto channel where tidal currents exchange from anticlockwise to clockwise rotation (see Figure 4f).

The residual currents are also computed in order to characterize the exchange of water properties within the lagoon. The analysis of results is emphasized at the lagoon mouth, where the exchange between the lagoon and the ocean occur. The residual current patterns are similar for both scenarios. The highest residual

currents were found at the lagoon mouth, decreasing in magnitude towards the channel's head (Figure 5). The ratio between the magnitude of residual currents for both scenarios evidences that they tend to increase at the lagoon mouth and deeper channels, highlighting higher transport rates in these regions for the future. In shallow areas and narrow channels a decrease on the magnitude of residual currents was found and consequently a decrease in the transport rates. The patterns of residual current directions are similar for both scenarios (only shown at the inlet region). The inlet channel presents high inland residual currents at the northern part ( $\sim 0.2$  m/s) and currents of similar magnitude directed to the ocean in the southern regions. Along the channel axis the residual currents are weaker and the residual flow presents two vortices rotating in a clockwise direction. Moreover, between the jetties the residual currents are directed seaward, highlighting the export of water, sediments, nutrients, etc. to the ocean. The residual circulation on Ria de Aveiro lagoon was studied previously by Dias (2001), Lopes and Dias (2007) and Valentim *et al.* (2013). The first two studies assessed residual currents averaging tidal currents over a  $M_2$  tidal cycle, and obtained similar residual patterns. The Valentim *et al.* (2013) study, investigated the influence of the mean sea level rise on residual currents in a small salt marsh located at the entrance of Mira channel. They found that residual currents direction remains unchangeable, while its intensity tends to decrease with the mean sea level rise in this salt marsh. The results described in this study are in accordance with those obtained in those studies.

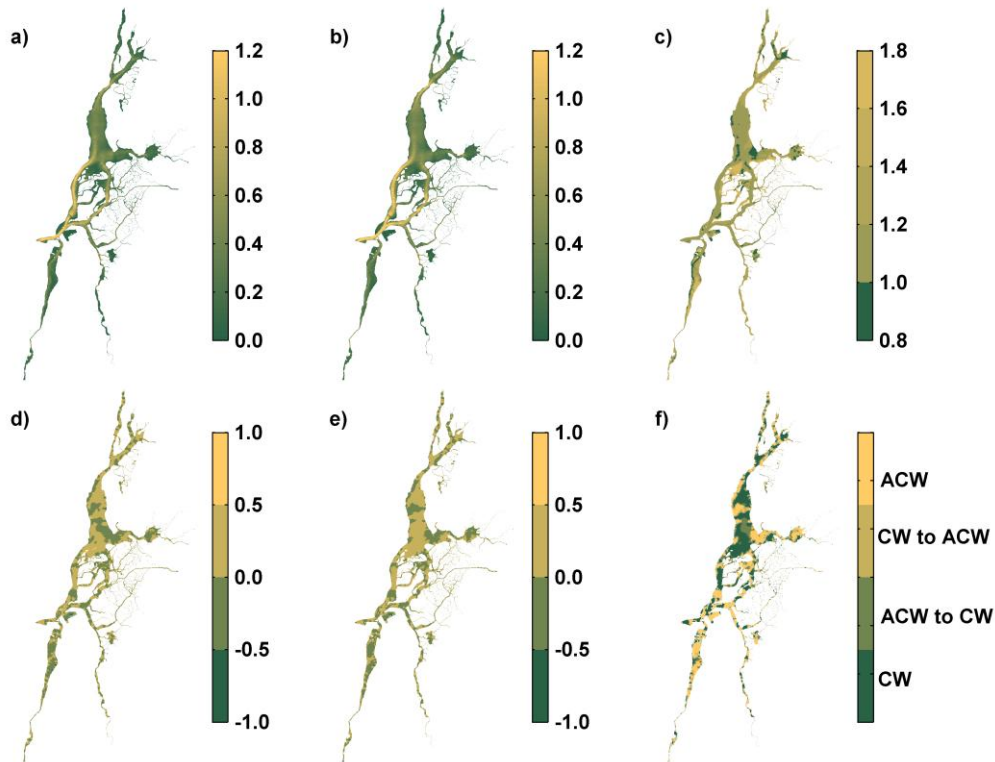


Figure 4. a) and b) Semi-major axis of  $M_2$  constituent velocity for present and sea level rise scenarios, respectively. c) Ratio between semi-major axis for both scenarios. d) and e) Tidal ellipses eccentricity for present and sea level rise scenarios, respectively. f) Eccentricity changes motivated by the mean sea level rise (ACW- anticlockwise; CW – clockwise).

## CONCLUSIONS

This work reports the main features of Ria de Aveiro tidal dynamics and expected modifications motivated by mean sea level rise. The results proved that the tidal influence is greatest at the

lagoon entrance and decreases towards the channel's head. Indeed, as the lagoon depth decreases the amplitude of  $M_2$  and  $K_1$  constituents reduces, whereas their phase increases. The first harmonic of  $M_2$ , the  $M_4$  constituent, presents an opposite pattern, increasing its amplitude as the lagoon depth decreases. As a consequence, the tidal wave is more distorted in the lagoon upper

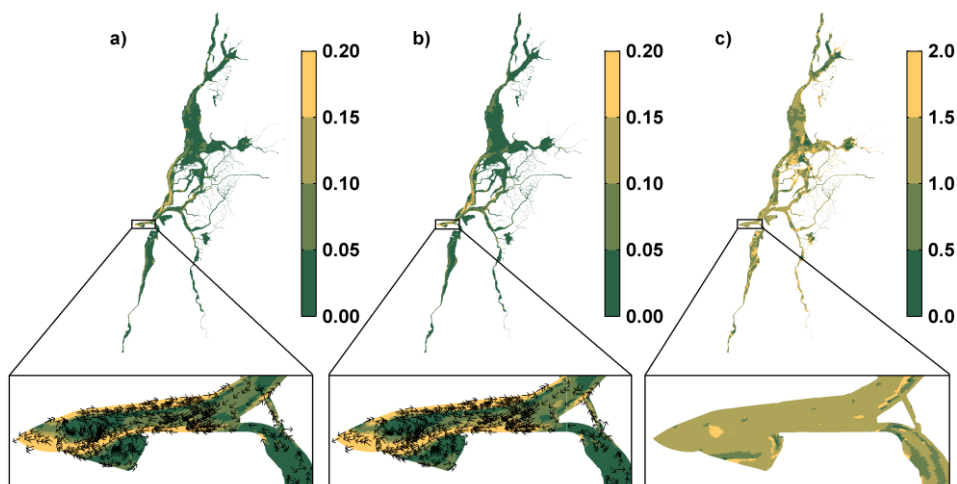


Figure 5. a) and b) Residual currents magnitude (m/s) and respective zoom at the inlet region showing also de currents direction, for present and sea level rise scenarios, respectively. c) Ratio between residual currents for both scenarios.

reaches, where the amplitude ratio can reach 0.4, than at the lagoon entrance where the amplitude ratio is close to zero. Moreover the tidal asymmetry results show that the upper lagoon is flood-dominated, while the lower lagoon is ebb-dominated. Important changes on the tidal wave propagation were found with the mean sea level rise, in response to the friction reduction within the lagoon, mainly at the lagoon upper reaches. Indeed, considering that  $M_2$  amplitude will increase and  $M_4$  amplitude will decrease, a reduction of the amplitude ratio at the upper lagoon is expected.

Concerning the tidal currents, the highest currents were found at the upper lagoon for both scenarios. Moreover, the tidal currents will be intensified and its direction remains unchangeable with mean sea level rise. The residual current patterns at the inlet show that the lagoon mouth tends to export material to the ocean and that this trend will remain with mean sea level rise. Globally, an intensification of residual currents with the mean sea level rise was found, highlighting the intensification of exchanges within the lagoon.

### ACKNOWLEDGEMENT

The first author benefits from a Ph.D. grant (SFRH/BD/78345/2011) given by the Portuguese Science Foundation FCT (Fundação para a Ciência e Tecnologia).

This work has been partly supported by FCT and by European Union (COMPETE, QREN, FEDER) in the frame of the research projects PTDC/AAC-CLI/100953/2008 - ADAPTARia; PTDC/AAC-AMB/121191/2010 - BioChangeR; PTDC/AAC-AMB/113469/2009 - PAC:MAN; LTER/BIA-BEC/0063/2009 - LTER-RAVE. The European Commission, under the 7th Framework Programme, also supported this study through the collaborative research project LAGOONS (contract n°283157).

### LITERATURE CITED

- Araújo, I.G.B., 2005. *Sea Level Variability: Examples from the Atlantic Coast of Europe*. Southampton, UK: University of Southampton, Ph.D. thesis, 411p.
- Araújo, I.B., Dias, J.M. and Pugh, D.T., 2008. Model simulations of tidal changes in a coastal lagoon, the Ria de Aveiro (Portugal). *Continental Shelf Research*, 28, 1010-1025.
- Bolle, A., Wang, Z.B., Amos, C. and De Ronde, J., 2010. The influence of changes in tidal asymmetry on residual sediment transport in the Western Scheldt. *Continental Shelf Research*, 30, 871-882.
- Brown, J.M. and Davies, A.G., 2010. Flood/ebb tidal asymmetry in a shallow sandy estuary and the impact on net sand transport. *Geomorphology*, 114, 431-439.
- Dias, J.M., 2001. *Contribution to the study of the Ria de Aveiro hydrodynamics*. Aveiro, Portugal: University of Aveiro, PhD, Physics Department, 288p (<http://hdl.handle.net/10773/4939>).
- Dias, J.M., Lopes, J.F. and Dekeyser, I., 2000. Tidal propagation in Ria de Aveiro lagoon, Portugal. *Physics and Chemistry of the Earth Part B-Hydrology Oceans and Atmosphere*, 25, 369-374.
- Dronkers, J., 1986. Tidal Asymmetry and Estuarine Morphology. *Netherlands Journal of Sea Research*, 20, 117-131.
- Fortunato, A.B., Pinto, L., Oliveira, A. and Ferreira, J.S., 2002. Tidally generated shelf waves off the western Iberian coast. *Continental Shelf Research*, 22, 1935-1950.
- Friedrichs, C.T. and Aubrey, D.G., 1988. Non-Linear Tidal Distortion in Shallow Well-Mixed Estuaries - a Synthesis. *Estuarine Coastal and Shelf Science*, 27, 521-545.
- Jewell, S.A., Walker, D.J. and Fortunato, A.B., 2012. Tidal asymmetry in a coastal lagoon subject to a mixed tidal regime. *Geomorphology*, 138, 171-180.
- Lopes, C.L. and Dias, J.M., submitted. Assessment of extreme sea levels and flood extension analysis on Ria de Aveiro (Portugal). *Journal of Hydrology*.
- Lopes, J.F. and Dias, J.M., 2007. Residual circulation and sediment distribution in the Ria de Aveiro lagoon, Portugal. *Journal of Marine Systems*, 68, 507-528.
- Lopes, C.L., Azevedo, A. and Dias, J.M., 2013a. Flooding assessment under sea level rise scenarios: Ria de Aveiro case study. *Journal of Coastal Research*, SI 65, 766-771.
- Lopes, C.L., Plecha, S., Silva, P.A. and Dias, J.M., 2013b. Influence of morphological changes in a lagoon flooding extension: case study of Ria de Aveiro (Portugal). *Journal of Coastal Research*, SI 65, 1158-1163.
- Lopes, C.L., Silva, P.A., Dias, J.M., Rocha, A., Picado, A., Plecha, S. and Fortunato, A.B., 2011. Local sea level change scenarios for the end of the 21st century and potential physical impacts in the lower Ria de Aveiro (Portugal). *Continental Shelf Research*, 31, 1515-1526.
- Lopes, J.F., Dias, J.M. and Dekeyser, I., 2006. Numerical modelling of cohesive sediments transport in the Ria de Aveiro lagoon, Portugal. *Journal of Hydrology*, 319, 176-198.
- Oliveira, A., Fortunato, A.B. and Dias, J.M., 2006. Numerical modeling of Ria de Aveiro inlet dynamics, in: Smith, J.M. (Ed.), *30th International Conference on Coastal Engineering*. World Scientific Publishing Co., San Diego, California, USA, pp. 3282-3294.
- Pawlowicz, R., Beardsley, B. and Lentz, S., 2002. Classical tidal harmonic analysis including error estimates in MATLAB using T-TIDE. *Computers & Geosciences*, 28, 929-937.
- Pelling, H.E., Green, J.A.M. and Ward, S.L., 2013. Modelling tides and sea-level rise: To flood or not to flood. *Ocean Modelling*, 63, 21-29.
- Picado, A., Dias, J.M. and Fortunato, A.B., 2010. Tidal changes in estuarine systems induced by local geomorphologic modifications. *Continental Shelf Research*, 30, 1854-1864.
- Pickering, M.D., Wells, N.C., Horsburgh, K.J. and Green, J.A.M., 2012. The impact of future sea-level rise on the European Shelf tides. *Continental Shelf Research*, 35, 1-15.
- Valentim, J.M., Vaz, N., Silva, H., Duarte, B., Cacador, I. and Dias, J.M., 2013. Tagus estuary and Ria de Aveiro salt marsh dynamics and the impact of sea level rise. *Estuarine Coastal and Shelf Science*, 130, 138-151.
- Vaz, N., Dias, J.M. and Leitão, P.C., 2009. Three-dimensional modelling of a tidal channel: The Espinheiro Channel (Portugal). *Continental Shelf Research*, 29, 29-41.
- Ward, S.L., Green, J.A.M. and Pelling, H.E., 2012. Tides, sea-level rise and tidal power extraction on the European shelf. *Ocean Dynamics*, 62, 1153-1167.
- Xu, Z., 2002. Ellipse parameters conversion and velocity profiles for tidal currents in Matlab (<http://woodshole.er.usgs.gov/operations/sea-mat/>).
- Zhang, Y.L., Baptista, A.M. and Myers, E.P., 2004. A cross-scale model for 3D baroclinic circulation in estuary-plume-shelf systems: I. Formulation and skill assessment. *Continental Shelf Research*, 24, 2187-2214.

## The influence of the Maputo and Incomati rivers on the mixing and outflow of freshwater from Maputo Bay (Mozambique)



[www.cerf-jcr.org](http://www.cerf-jcr.org)

Katrin Markull†, João D. Lencart e Silva† John H. Simpson‡, João Miguel Dias†

†Physics Department  
University of Aveiro,  
3810-193 Aveiro, Portugal  
katrinma@gmx.net  
j.lencart@ua.pt  
joao.dias@ua.pt

‡ School of Ocean Sciences  
Bangor University  
Anglesey, UK  
j.h.simpson@bangor.ac.uk



[www.JCRonline.org](http://www.JCRonline.org)

### ABSTRACT

Markull, K., Lencart e Silva, J.D., Simpson, J.H., Dias, J.M., 2014. The influence of the Maputo and Incomati rivers on the mixing and outflow of freshwater from Maputo Bay (Mozambique). In: Green, A.N. and Cooper, J.A.G. (eds.), *Proceedings 13<sup>th</sup> International Coastal Symposium* (Durban, South Africa), *Journal of Coastal Research*, Special Issue No. 70, pp. 580-585, ISSN 0749-0208.

Maputo Bay is a tidally-energetic embayment, influenced by strong rainfall and associated river runoff during the wet season. Literature shows that salinity can regulate the nutrient cycle in mangrove estuarine ecosystems affecting the early life stages in these habitats which sustain the economically important shrimp stocks. The freshwater flow into Maputo Bay is for a part controlled by dam systems on its main rivers. In this work we investigate how varying flows from the Incomati and Maputo rivers interact with the tide to influence the evolution of the bay's salinity field. A 3-dimensional hydrodynamic model was applied to Maputo Bay, improving a previously published model through vertical and temporal refinement and recalibration, leading to a more accurate representation of the semidiurnal and fortnightly stratification-mixing cycles occurring during the wet season. However, the model still predicts salinities lower than those found in observations. An analysis showed that uncertainties in the salinity field increased towards the mouth of the Maputo River indicating the uncertainty of the modeled flow at the catchment as a possible cause of the underestimation of salinity in the bay. A set of experiments of varying Maputo and Incomati river flows show that for a flow as frequent as 5 times per year, the buoyancy input and the associated density driven flow contributed less than the tide in forcing the bay-shelf exchange. The inverse is observed for results where a flow with a 5-year return period leads to a more efficient bay-shelf exchange during neap tides than during spring tides. For this scenario, the results suggest that the estuarine plume was arrested inside the bay by tidal stirring during spring tide and released during neap tide when tidal stirring was subdued. The analysis of the separate and joint effects of the two rivers in setting the salinity field in Maputo Bay show a difference in extent of influence area between the rivers. These results suggest that the management of the freshwater inflow from the Maputo River can be crucial for maintaining lower salinities over parts of the bay to sustain the economically important marine resources.

**ADDITIONAL INDEX WORDS:** *Tidal mixing, density gradient, river discharge, freshwater plume, salinity, buoyancy, hydrodynamic modeling.*

### INTRODUCTION

Estuaries are diverse and complex dynamic regions in the transitional zone between land and sea. Due to their rich ecosystems and natural navigational facilities, they often support human concentration and the associated economic activities such as fisheries, transport and tourism. These activities can pose threats on the ecosystems that need to be studied to be fully understood and prevented.

The importance of the several forcing mechanisms involved in estuarine dynamics varies from estuary to estuary. Density-driven circulation in estuaries is usually influenced by river inflow (Simpson *et al.*, 1990). Other possible factors of importance include tidal dynamics and wind-induced circulation on the continental shelf as well as locally. The competition between the various forcing mechanisms as well as other factors such as topography and Coriolis force determine the so-called buoyancy-

stirring interaction described by Simpson (1997). Different salinity distributions and circulation patterns are found in estuaries, depending on the relative importance of buoyancy/stratification and stirring.

Linden and Simpson (1988) undertook laboratory experiments on the influence of turbulence on mixing and frontogenesis. Through air bubbles, turbulence was induced to a fluid containing a horizontal density gradient. Those authors suggested that, during periods of large turbulence, e.g. through tidal mixing, the water column was vertically mixed and baroclinic circulation was weak. When turbulence was decreased, the baroclinic circulation increased while the water column stratified. A vertical density gradient developed due to the advection of the denser fluid under the lighter fluid. Depending on the duration of the absence of turbulence, a front developed, in which the horizontal density gradient was increased, leading to the development of a counter current. Once turbulence was increased again, the water column mixed vertically, reducing baroclinic circulation. The transport of density through baroclinic circulation in the absence of mixing was more efficient than the transport through turbulence when

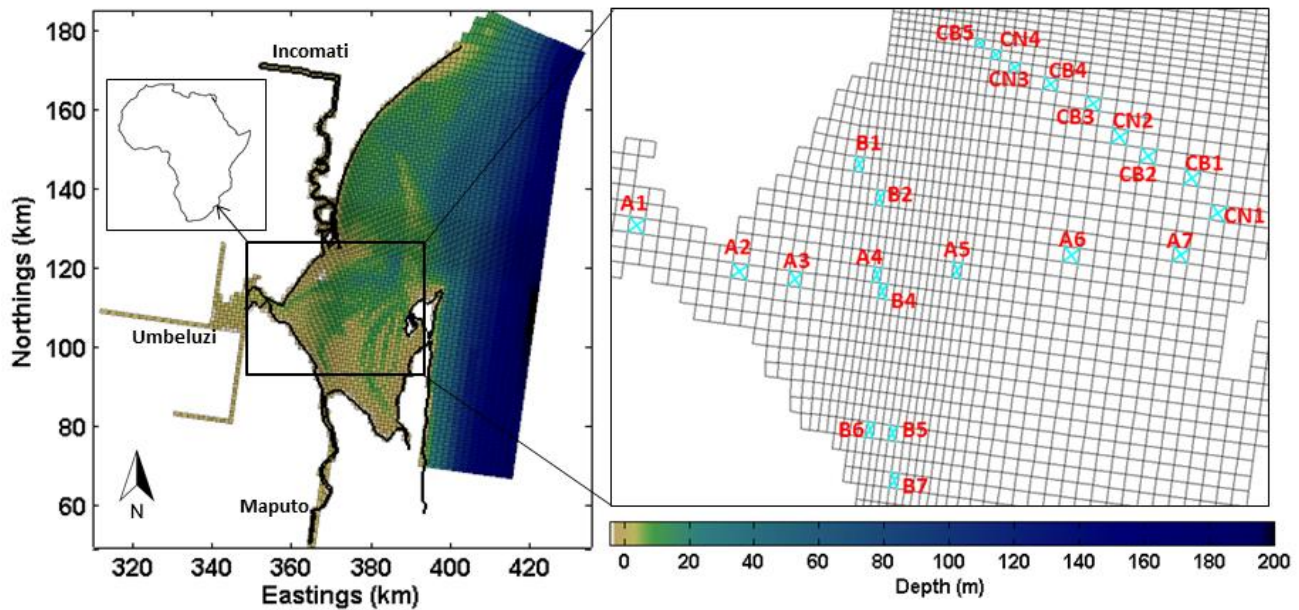


Figure 1. The bathymetry of Maputo Bay and the grid applied. The land boundary is indicated by the black line in the left plot. Light-blue crosses represent observation stations used for calibration (right plot).

mixing was increased. This process can be important for estuarine dynamics, especially in areas with a large spring-neap tidal ratio, due to the large differences in tidal mixing.

Maputo Bay is a shallow, subtropical estuary in the South of Mozambique with a surface area of 1875 km<sup>2</sup> (see Figure 1). It is tidally-energetic with a large spring-neap tide ratio, with a spring tidal range of approximately 3 m and a neap tidal range of around 1 m (Canhanga and Dias, 2005). There are two pronounced seasons: wet season between October and March and dry season between April and September (Canhanga, 2004), with a mean annual rainfall of 884 mm (de Boer *et al.*, 2000). River discharge is characterised by a strong seasonal cycle, maximum values exceeding 1000 m<sup>3</sup>s<sup>-1</sup> usually occur in the wet season between November and April (Lencart e Silva *et al.*, 2010). The Incomati River makes up around 57 % of the freshwater discharge into the bay, being characterised by a mean discharge of 133 m<sup>3</sup>s<sup>-1</sup>. The Maputo River accounts for a further 38 % of runoff, with a long-term mean discharge of 89 m<sup>3</sup>s<sup>-1</sup> (Milliman and Meade, 1983).

The Bay is also considered an important fishing ground due to the mangrove swamps and high productivity. The local population benefits from the collection and capture of fish, crabs and shellfish (De Boer & Longamane 1996 in de Boer *et al.*, 2000). Especially shrimp is an economically important resource for the area (Hoguane, 2007).

Ravikumar *et al.* (2004) have shown that salinity can regulate the nutrient cycle in mangrove estuarine ecosystems. Salinities outside the 20–30 range will hamper production in the mangroves and affect the early life stages in mangrove habitats that sustain the economically important shrimp stocks (Monteiro and Manchard, 2009). The salinity of Maputo Bay is, for a part, controlled by dam systems of its main rivers (Vas and v.d. Zaag, 2003).

Lencart e Silva (2007) suggested the occurrence of an arrestment of the estuarine plume of Maputo Bay, induced by the large freshwater discharge in the wet season, in combination with

decreased density forcing during high mixing periods of spring tide. This can decrease salinities during times of arrestment.

The objective of this article is to answer two questions: - what is the dominant source of freshwater in Maputo Bay leading to the reduction of salinity? - is it important for the salinity field when in the spring-neap cycle a freshwater plume is released?

## METHODS

### Numerical Model

The model Delft3D-Flow, a software for computations of coastal, estuarine and river areas developed by Deltares in the Netherlands, was applied to Maputo Bay.

Delft3D-Flow is a three-dimensional, finite differences hydrodynamic and transport model which simulates transport and flow forced by tidal and meteorological processes. The Navier-Stokes shallow water equations are solved with hydrostatic, Boussinesq and f-plane approximations (Deltares, 2011; Lesser *et al.*, 2004). Delft3D-Flow uses a horizontal Arakawa-C grid with control volumes and for most applications an Alternating Direction Implicit (ADI) integration method (Lencart e Silva *et al.*, 2013).

Delft3D has previously been applied to study several estuarine systems worldwide, e.g. the Rhine ROFI (de Boer *et al.*, 2008), Tomales Bay, California (Harcourt-Baldwin and Diedericks, 2006) and the Ria de Muros in North-West Spain (Carballo *et al.* 2009).

The model used here is based on a model published by Lencart e Silva *et al.* (2010). Those authors applied a curvilinear Cartesian grid with 96×135 cells to Maputo Bay. This irregular grid has a mean resolution of approximately 500 m, with higher resolution within parts of the embayment and lower resolution outside the bay (see Figure 1). The bathymetry of Maputo Bay used results from the interpolation to the numerical grid of a set of topo-

hydrographic surveys from the nineteen sixties to the nineteen eighties. The propagation of the tide is modelled by prescribing tidal harmonics, interpolated across the open boundary, and vertical mixing is determined by a k-epsilon closure scheme. A heat model is applied, taking into account air temperature, wind speed at a meteorological station at Mavalene Airport, atmospheric radiation, relative humidity as well as net solar and atmospheric radiation to calculate heat losses from convection, evaporation and back radiation. Wind data obtained from a station at Mavalene Airport is applied at the water surface. Salinities and temperatures, obtained from data from Sete *et al.* (2002), who developed a compilation of the available cruise data between 1977 and 1980, are defined for each of the vertical layers at the open oceanic boundary, divided into 14 horizontal sections. Salt transport is calculated based on inputs from freshwater of the rivers and salinities prescribed at the oceanic open boundary.

Lencart e Silva *et al.* (2010) concluded that the model represented tidal motion and dissipation and is calibrated to the first degree. Furthermore, the model was able to satisfactorily reproduce the tidal and subtidal features during the dry season. However, the model overestimated freshwater storage in the bay, probably related to exaggerated vertical mixing during the wet season spring tides. This problem is possibly related to an insufficient vertical resolution and an increased bottom roughness parameter applied to improve the relationship between water level and velocity.

To overcome the problem of vertical over-mixing without impairing the water level-velocity relationship, a number of changes were made to the model, especially refining temporal and vertical resolution. In comparison with the original model, the modeling time step was refined from 5 minutes to 1 minute to be in accordance with the Courant–Friedrichs–Lewy number. The vertical resolution was increased from five equally-spaced sigma layers to 15 sigma layers with refined surface layers. Background horizontal eddy viscosity and diffusivity were changed from 10 to 1 m<sup>2</sup>/s. Background vertical eddy viscosity and diffusivity were not specified in the original model and are 10<sup>-4</sup> m<sup>2</sup>/s in the new model.

**Calibration and Validation**

A calibration run was set up from a cold start, including wind forcing, river flow from the rivers Incomati, Maputo, Umbeluzi, Tembe and Matola, a heat flux model as well as open-boundary forcing with tidal harmonic water levels, salinities and temperatures. Model results were compared against observations, consisting of CTD profiles from Lencart e Silva (2007). The CTD profiles were taken in 21 stations within Maputo Bay, with 14 surveys taken for each station, spread over wet and dry season in 2003/04 (Figure 1).

The new model reproduces more accurately the semidiurnal and fortnightly stratification-mixing cycles occurring during the wet season as well as water temperatures. However, the model still predicts salinities lower than those found in observations (wet season bay-average salinities of 30 in the model and 33 in observations). An analysis was conducted to investigate the spatial distribution of the uncertainty.

Root Mean Square Errors (RMSE) of salinity were calculated for all observation stations. Figure 2 shows the RMSE values interpolated over a part of the bay, for 6 different survey dates. High values of RMSE are generally found due to the model predicting lower salinities than those found in observations. The RMSE increases in the wet season and with decreasing distance from the inflow of the Maputo River. This is especially evident in the areas of very high RMSE on the 26<sup>th</sup> of March and the 20<sup>th</sup> of

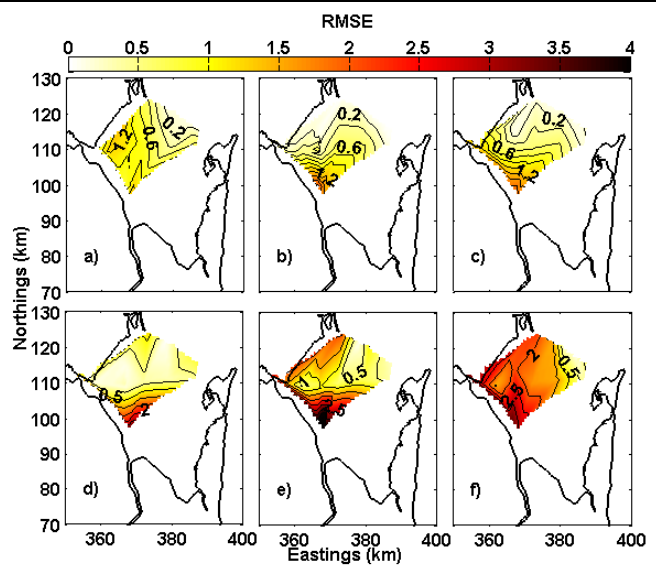


Figure 2. RMSE values of salinities interpolated over part of the bay for a) 29<sup>th</sup> of July, b) 25<sup>th</sup> of October, c) 18<sup>th</sup> of November, d) 26<sup>th</sup> of January, e) 26<sup>th</sup> of March and f) 20<sup>th</sup> of May of 2003/04.

May, where large RMSE values are found in the southern part of the bay and along a stretch towards the opening along the west. This high RMSE area can be explained by the spreading of the freshwater from the Maputo towards the west along the coast, which has been observed in the model runs.

**Initial Conditions and Scenarios**

Different scenarios were developed to investigate the hydrodynamic response of Maputo Bay to river and tidal forcing. All production runs had duration of 20 days and began after a 3 month warm start under dry season conditions, produced under the same conditions as the calibration run. An overview of all scenarios used in the simulations can be found in table 1.

Two total amounts of discharge, introduced over 3 days, were used: an average wet season discharge, with a return period of five times per wet season and an extreme wet season discharge, with a return period of five years. All values were calculated from a data set of daily values for the Maputo and Incomati river discharge for a period of 10 years. A generalized extreme value inverse cumulative distribution function was fitted to the data (RMSE 0.0746) and the discharges for the various return periods were calculated. Only the rivers Incomati and Maputo were taken into

Table 1. Overview of the scenarios used for simulations

Nr	Incomati (m <sup>3</sup> s <sup>-1</sup> )	Maputo (m <sup>3</sup> s <sup>-1</sup> )	Ratio Incomati: Maputo	Timing of Discharge
1	612	408	3:2	Spring
2	612	408	3:2	Neap
3	2160	1440	3:2	Spring
4	2160	1440	3:2	Neap
5	816	204	4:1	Spring
6	816	204	4:1	Neap
7	2880	720	4:1	Spring
8	2880	720	4:1	Neap
9	204	816	1:4	Spring
10	204	816	1:4	Neap
11	720	2880	1:4	Spring
12	720	2880	1:4	Neap

account for the production runs, as the remaining rivers play a much less significant role in forcing the hydrodynamics of Maputo Bay. To find out whether the influences of the Incomati and Maputo on the bay's hydrodynamics differ, the relative discharge ratios were varied. As a base case, a ratio of 3:2 (discharge Incomati : discharge Maputo) was chosen, which is approximately the ratio found in reality. The other ratios applied were 4:1 (more Incomati discharge) and 1:4 (more Maputo discharge). To find out whether the timing of the arrival of the freshwater pulse in the bay, in relation to the moment in the spring-neap tidal cycle, has an influence on the dynamics, the pulses were introduced either during spring or during neap tide.

Wind and waves were not taken into account in the production runs, as Lencart e Silva (2007) concluded that the wind from the observation station at Mavalene Airport could not be directly related to the bay's hydrodynamics and no other wind data was available.

A passive tracer was introduced in all model runs with a concentration of 1 kg/m<sup>3</sup> to investigate the exchange between bay and continental shelf.

### RESULTS

Bay-average salinities were calculated and the tidal signal was filtered out. Results are shown in Figure 3. Initial salinities were approximately 35.1. By the end of the discharge of the freshwater pulse, after 72 hours, bay-average salinities had dropped considerably. In the runs where an average discharge was induced (Figures 3 a and b), bay-average salinities for the 3:2 ratio (discharge Incomati : discharge Maputo) dropped to 34.8. Runs with the extreme discharge (Figures 3 c and d) dropped to around 33.5.

Average wet season discharge runs showed slightly decreasing bay-average salinities over most of the research period, with values plateauing around neap tide. If discharge was introduced

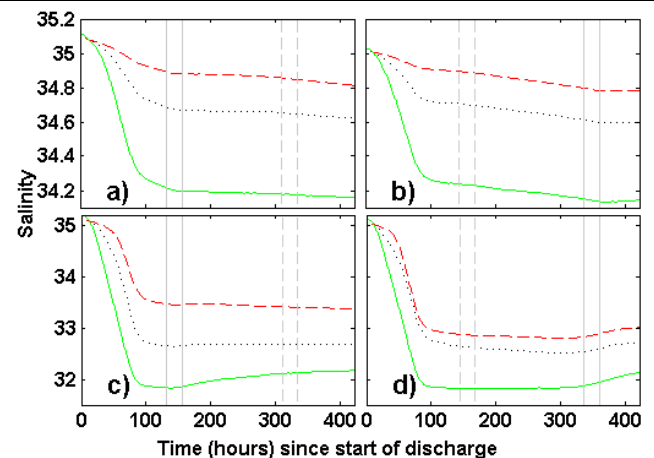


Figure 3. Development of tidally-filtered bay-average salinities over time for a) average discharge during spring tide, b) average discharge during neap tide, c) extreme discharge during spring tide and d) extreme discharge during neap tide. Dotted black line: 3:2 ratio; dashed red line: 4:1 ratio; solid green line: 1:4 ratio. Solid vertical lines indicate timing of neap tide and dashed vertical lines indicate timing of spring tide. .

during neap tide, slightly increasing bay-average salinities can be observed after the following neap tide towards the end of the research period. Extreme wet season discharge runs showed increasing bay-average salinities during and after neap tide (except for a ratio of 4:1 introduced during spring tide) and stable bay-average salinities during spring tide.

Generally, bay-average salinities were lower when the discharge of the Maputo was larger than that of the Incomati (1:4 ratio),

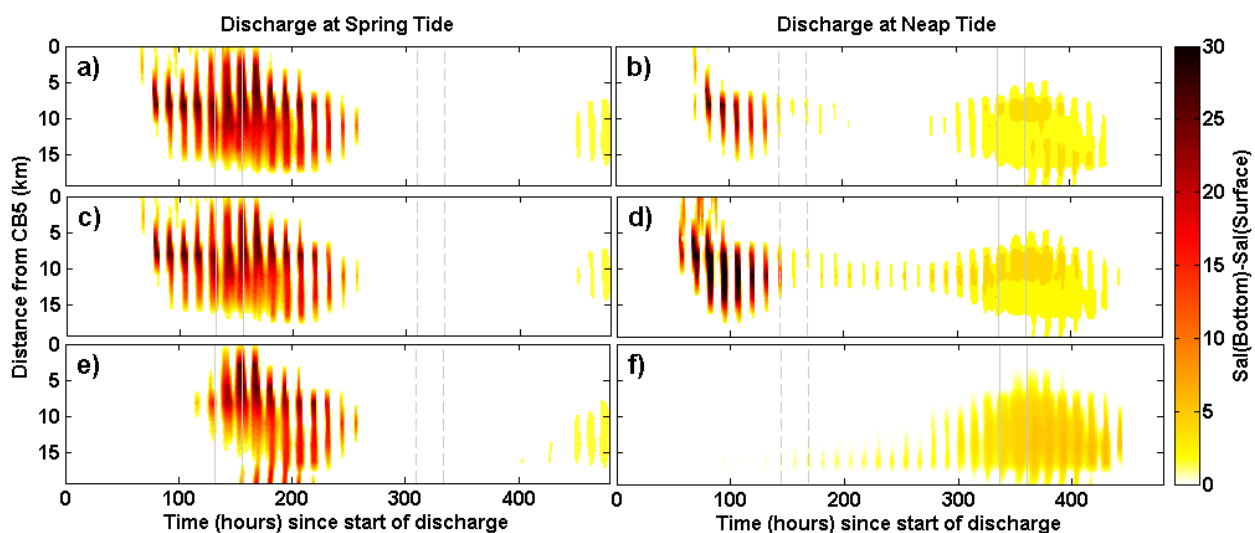


Figure 4. Development of vertical salinity differences across the bay's opening over time. Positive values indicate salinities in the bottom layer larger than in the surface layer. The left column represents an extreme discharge during neap tide with Incomati:Maputo discharge ratios of a) 3:2, c) 4:1 and e) 1:4. The right column represents an extreme discharge during spring tide with Incomati:Maputo discharge ratios of b) 3:2, d) 4:1 and f) 1:4. Solid vertical lines indicate timing of neap tide and dashed vertical lines indicate timing of spring tide.



independent of timing or amount of discharge.

Vertical salinity differences between the bottom and the top layer over a cross section across the bay's mouth were calculated and are shown in Figure 4. Only runs with extreme discharge are represented here. All runs showed an alternating strengthening and weakening/absence of vertical salinity differences with semidiurnal frequencies.

Earliest signs of significant vertical salinity differences were found after approximately 50 hours for discharge introduced during neap tide (Figure 4, right column) and 72 hours for discharge during spring tide (Figure 4, left column). When discharge occurred during neap tide, the vertical salinity differences in the beginning of the simulation were larger than when discharge occurred during spring tide, however, they did not remain present over a long period of time. Vertical salinity differences were generally first found approximately 5 – 9 km southwest of station CB5, located at the northeastern part of the bay's opening, later spreading further across the opening.

Generally, vertical salinity gradients were largest during and just after neap tide and usually near zero during spring tide.

Comparing different ratios of river discharge, it can be seen that the vertical salinity gradients were present earlier when the discharge of the Incomati was larger (4:1 ratio, Figures 4 c and d). For a larger Maputo discharge, on the other hand, vertical salinity differences were present over a longer period of time and extended over a larger section of the bay's opening. If this discharge ratio was introduced during neap tide (Figure 4 f), the vertical salinity gradients only appeared just before the following neap tide, approximately 300 hours after the beginning of discharge. However, these later vertical differences were stronger than for other discharge ratios.

Figure 5 shows the development of bay-wide concentration of a tracer introduced evenly throughout the bay at the beginning of the discharge, with a concentration of  $1 \text{ kg/m}^3$ .

After the discharge of freshwater (72 hours), tracer concentrations had dropped to approximately  $0.92 \text{ kg/m}^3$  for average-discharge runs and  $0.86 \text{ kg/m}^3$  for extreme-discharge runs.

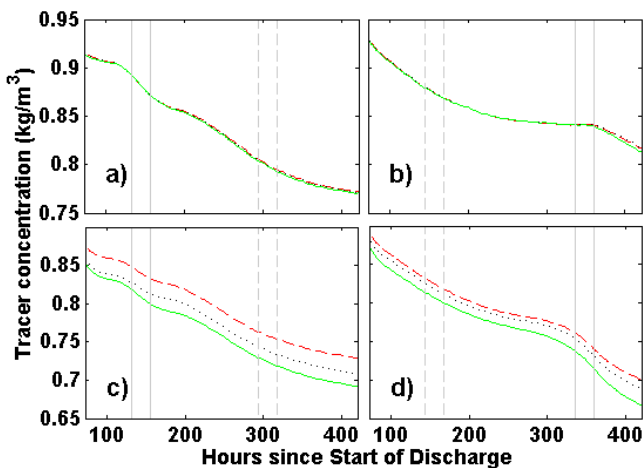


Figure 5. Development of tidally-filtered bay-average tracer concentration over time for a) average discharge during spring tide, b) average discharge during neap tide, c) extreme discharge during spring tide and d) extreme discharge during neap tide. Dotted black line: 3:2 ratio; dashed red line: 4:1 ratio; solid green line: 1:4 ratio. Solid vertical lines indicate timing of neap tide and dashed vertical lines indicate timing of spring tide.

Afterwards, the average discharge runs showed a large rate of change during neap tide (for runs with discharge during spring tide) or just after neap tide (for runs with discharge during neap tide) and in the transition from neap to spring tide. During spring tide and in the transition from spring to neap tide the rate of change was smaller, decreasing even further just before neap tide.

The extreme-discharge runs showed very large rates of change during neap tide and significant rates of change in the transition from neap to spring tide. During spring tide and in the transition from spring to neap tide, the rate of change of tracer concentration was smaller.

The average discharge runs did not show significant differences for varying discharge ratios, while for the extreme-discharge runs, tracer concentrations dropped more when the discharge of the Maputo was larger (1:4 ratio), indicating larger residence times.

## DISCUSSION

In the first 72 hours of the simulations, corresponding to the duration of the input of river discharge, bay-average salinities decreased for all runs. Rates of change for bay-average salinities and tracer concentrations were larger for the runs with a larger discharge. When an extreme discharge occurred during neap tide, bay-average salinities after 3 days were larger and tracer concentrations were smaller than for a discharge during spring tide. The differences between discharge during spring and neap tide can be explained by tidal mixing. A discharge that is introduced during spring tide is, in the first days in the bay, influenced by decreasing tidal mixing. This produces the large vertical salinity differences. When a discharge is introduced during neap tide, however, tidal mixing increases over the first days, leading to smaller vertical salinity differences.

This pattern was also observed further on in the simulations, when neap tides generally coincided with large decreases in tracer concentrations and increases in bay-average salinities, especially in the runs with an extreme wet season discharge. Here again, neap tide lead to a stratification of the water column, whereas larger mixing during spring tide eroded the stratification.

Taking into account the dynamics described above it is assumed that low tidal mixing during neap tide allows the intensification of baroclinic circulation, in accordance with the conclusions by Linden and Simpson (1988), which is more efficient in the bay-shelf exchange than the barotropic circulation from the larger tidal forcing during spring tide. The larger bay-shelf exchange during neap tide leads to larger rates of change in salinities and tracer concentrations. During spring tide, the stratification and the baroclinic circulation are eroded.

Over a large part of the simulation, bay-average salinities for the average discharge runs were dropping even after all discharge occurred. This was due to the freshwater still present in the river arms which were not taken into account for calculating bay-average salinities.

The relative differences between runs with different discharge ratios can be explained by the locations of the river mouths in the bay. The Incomati River mouth is located close to the northwestern part of the opening of Maputo Bay, whereas the Maputo River mouth is located in the southern part of the bay. Discharge introduced to the Incomati therefore tends to leave the bay quicker, without influencing a large area of the bay, which is confirmed by the earlier arrival of vertical salinity differences for a larger Incomati discharge. Discharge induced to the Maputo, on the other hand, influences a larger area of the bay and takes longer to reach the bay's opening. Therefore, a larger discharge of the Maputo decreases bay-average salinities more significantly.

Furthermore this increase in salinity during weaker mixing associated with neap tide can also be found in the runs with a 1:4 discharge ratio introduced at spring tide. After an initially strong decrease of salinities in the first 100 hours, the bay-average salinities reach a minimum at around neap tide and then increase visibly, at a decreasing rate towards the larger mixing associated with spring tide. The effect is largest for an extreme discharge with a ratio of 1:4 (more Maputo discharge), as the Maputo plume influences a larger area of the bay.

The stronger vertical salinity differences during the last neap tide in the run with an extreme discharge during neap tide with a 1:4 ratio, indicates the presence of larger buoyancy forcing inside the bay. Also taking into account the small rates of change in tracer concentration during the spring tide and large rates of change during neap tide it is assumed that the estuarine plume is in fact arrested during spring tide and released during neap tide, especially when controlled by a larger Maputo discharge.

### CONCLUSION

The three-dimensional hydrodynamic model Delft3D was applied to Maputo Bay to investigate the effect of different river discharges on the salinity field. The improvements in a previous implementation of the model conducted to generally successful calibration of the model, representing the stratification-mixing cycles of the bay. However, salinities remained lower than those observed in the field. The availability of only forecasted data for the Maputo River catchment is a possible source for the underestimation of salinity, which increased towards the mouth of the Maputo River.

The results for an extreme discharge suggest a confirmation of the findings by Linden and Simpson (1988), with lower turbulent mixing during neap tide assumedly leading to efficient density currents and larger mixing during spring tide associated with an erosion of baroclinic circulation. If an average discharge was introduced, on the other hand, buoyancy input and the associated density forcing were smaller and tidal advection played a larger role in forcing the bay-shelf exchange.

Even though varying the moment of the release of the freshwater into the bay between spring and neap tide has created significantly different results for the duration of the simulation, it remains difficult to come to any conclusions on the effect of the timing of discharge after several spring-neap cycles.

Varying the ratios between Incomati discharge and Maputo discharge has shown that the different locations of the river mouths influence the salinity field and exchange with the shelf significantly. When the discharge of the Incomati is larger, discharging close to the bay's opening, much of the freshwater leaves the bay early in the simulation, without influencing a large area of the bay. The Maputo river plume, discharged in the southern part of the bay, needs longer to reach the bay's opening and influences a larger area of the bay.

The results suggest that the Maputo River has a larger influence on the salinity field in Maputo Bay. Through its dam system, the input of freshwater can be managed, helping to sustain the salinities needed for an optimal growth of the economically important resources.

Furthermore, the results suggest that the estuarine plume was in fact arrested during high mixing periods of spring tide and released during stratified periods of neap tide.

Future research should be taken to investigate how the effect of varying the river discharge over different time intervals influences the exchange with the shelf and the salinity field. The dynamics of the plume arrestment in dry and wet season conditions would be another interesting topic for further investigations.

### ACKNOWLEDGEMENT

The observations used in the recalibration and original modelling work were funded by the European project Catchment2Coast, FP5 INCO-DEV (ICA4-CT-2002-10059).

### LITERATURE CITED

- de Boer, W.F., Rydberg, L. and Saide, V., 2000. Tides, tidal currents and their effects on intertidal ecosystems of the southern bay, Inhaca Island, Mozambique. *Hydrobiologia*, 428, 187-196.
- de Boer, G.B., Pietrzak, J.D. and Winterwerp, J.C., 2008. Using the potential energy anomaly equation to investigate tidal straining and advection of stratification in a region of freshwater influence. *Ocean Modelling*, 22, 1-11.
- Canhanga, S.J.V., 2004. *Modelação Hidrodinâmica da Baía de Maputo*. Aveiro, Portugal. Universidade de Aveiro, MSc Thesis, 134 pp.
- Canhanga, S. and Dias, J.M., 2005. Tidal characteristics of Maputo Bay, Mozambique. *Journal of Marine Systems*, 58, 83-97.
- Carballo, R., Iglesias, G. and Castro, A., 2009. Residual circulation in the Ria de Muros (NW Spain): a 3D numerical model study. *Journal of Marine Systems*, 75, 116-130.
- Deltares, 2011. *Delft3D-Flow User Manual Version 3.15*. Delft, The Netherlands, 672 pp.
- Harcourt-Baldwin, J.L. and Diedericks, G.P.J., 2006. Numerical modelling and analysis of temperature controlled density currents in Tomales Bay, California. *Estuarine, Coastal and Shelf Science*, 66, 417-428.
- Hogwane, A.M., 2007. Perfil Diagnóstico da Zona Costeira de Moçambique. Diagnosis of Mozambique Coastal Zone. *Revista de Gestão Costeira Integrada*, 7(1), 69-82.
- Lencart e Silva, J.D. (2007). *Controls on Exchange in a Subtropical Tidal Embayment, Maputo Bay*. Anglesey, UK.. University of Wales, PhD Thesis, 111 pp.
- Lencart e Silva, J.D., Azevedo, A., Lillebø, A.I. and Dias, J.M., 2013. Turbidity and seagrass meadows under changing physical forcing. *Journal of Coastal Research*, SI 65, 2023-2028.
- Lencart e Silva J.D., Simpson, J.H., Hogwane, A.M. and Harcourt-Baldwin, J.-L., 2010. Buoyancy-stirring interactions in a subtropical embayment: a synthesis of measurements and model simulations in Maputo Bay, Mozambique. *African Journal of Marine Science*, 32:1, 95-107.
- Lesser, G.R., Roelvink, J.A., van Kester, J. and Stelling, G.S., 2004. Development and validation of a three-dimensional morphological model. *Coastal Engineering*, 51, 883-915.
- Linden, P.F. and Simpson, J.E., 1988. Modulated mixing and frontogenesis in shallow seas and estuaries. *Continental Shelf Research*, 8(10), 1107-1127.
- Milliman, J.D. and Meade, R.H., 1983. World-wide delivery of river sediment to the oceans. *Journal of Geology*, 91, 1-21.
- Monteiro, P.M.S. and Marchand, M., 2009. Catchment2Coast: A Systems Approach to Coupled River-coastal Ecosystem Science and Management. *Deltares Select Series Volume 2*. IOS Press, 92 pp.
- Ravikumar, S., Kathiresan, K., Thadedus Maria Ignatimall, S., Babu Selvam, M. and Shanthi, S., 2004. Nitrogen-fixing azobacters from mangrove habitat and their utility as marine biofertilizers. *Journal of Experimental Marine Biology and Ecology*, 312, 5-17.
- Sete, C., Ruby, J. and Dove, V.F., 2002. Seasonal variation of tides, currents, salinity and temperature along the coast of Mozambique, Maputo. Technical report. Maputo: Centro Nacional de Dados Oceanográficos (CENADO), 72 pp.
- Simpson, J.H., 1997. Physical Processes in the ROFI regime. *Journal of Marine Systems*, 12, 3-15.
- Simpson, J.H., Brown, J., Matthews, J. and Allen, G., 1990. Tidal Straining, Density Currents, and Stirring in the Control of Estuarine Stratification. *Estuaries*, 13(2), 125-132.
- Vas, Á.C. and v.d. Zaag, P., 2003. Sharing the Incomati Waters: Cooperation and Competition in the Balance. *Water Policy*, 5(4), 349-368.

## Salinity modelling accuracy of a coastal lagoon: a comparative river flow analysis of basin model vs. traditional approaches



[www.cerf-jcr.org](http://www.cerf-jcr.org)

L.M. Tomas<sup>†</sup>, M. Rodrigues<sup>‡</sup>, A.B. Fortunato<sup>‡</sup>, A. Azevedo<sup>‡</sup>, P.C. Leitão<sup>∞</sup>, A. Oliveira<sup>‡</sup>, A. Rocha<sup>†</sup>, J.F. Lopes<sup>†</sup>, J.M. Dias<sup>†</sup>

<sup>†</sup>CESAM, Department of Physics  
University of Aveiro  
Campus Universitário de Santiago  
3810-193 Aveiro, Portugal  
lmatomas@ua.pt

<sup>‡</sup> National Civil Engineering Laboratory  
Av. do Brasil, 101  
1700-066 Lisbon, Portugal

<sup>∞</sup> MARETEC, Instituto Superior Técnico  
Av. Rovisco Pais, n°1  
1049-011 Lisbon, Portugal



[www.JCRonline.org](http://www.JCRonline.org)

### ABSTRACT

Tomas, L.M., Rodrigues, M., Fortunato, A.B., Azevedo, A., Leitão, P.C., Oliveira, A., Rocha, A., Lopes, J.F., Dias, J.M., 2014. Salinity modelling accuracy of a coastal lagoon: a comparative river flow analysis of basin model vs. traditional approaches. In: Green, A.N. and Cooper, J.A.G. (eds.), *Proceedings 13th International Coastal Symposium (Durban, South Africa)*, *Journal of Coastal Research*, Special Issue No. 70, pp. 586-591, ISSN 0749-0208..

The main purpose of this study is to investigate the uncertainties in the modelling of salinity fields in the Ria de Aveiro lagoon associated with the estimation of river flow discharges. The prediction of fresh water inputs is necessary to properly implement forcing conditions and consequently to provide accurate forecasts of baroclinic circulation in coastal lagoons. Located in the north-western Portuguese coast, the Ria de Aveiro is a shallow vertically homogeneous mesotidal coastal lagoon with a complex geometry. Although it is tidally dominated, it receives freshwater from five rivers, the Vouga, Antuã, Cáster, Boco and Ribeira dos Moínhos, whose contributions are responsible for the salinity variation within the system. This research concerns the accurate prediction of river flow to be used in the operational forecast system of the lagoon. Given the lack of observed data for river discharges, as there are only two real time measuring stations located in the Vouga and Antuã river basins, but far from the lagoon, alternative estimation approaches are needed. In order to estimate the river discharges for all five rivers, two different approaches were considered: the first estimates the Vouga river flow, the major fresh water source, based on the nearest real time measuring station and estimates the other river flows based on river basin areas proportionality; the second establishes river flows based on the precipitation/river flow relationships for the Vouga and Antuã rivers and on the areas of the other river basins using the SWAT model. The methodology comprises the exploitation of the 3D unstructured-grid hydrodynamic model SELFE, required to adequately simulate the flow and transport of salt in very complex domains such as the Ria de Aveiro. The model is forced by water elevations at the ocean boundary and river flows at the river boundaries, and atmospheric drivers at the surface (wind stress, atmospheric pressure and heat fluxes). The salinity model predictions were compared with data from seven stations, and its accuracy was assessed through Root Mean Square Error (RMSE). The river flows estimated by the first method led to the best fit between observed and predicted salinity.

**ADDITIONAL INDEX WORDS:** *salinity field; river flow estimation; Ria de Aveiro; SELFE 3D; circulation forecasts.*

### INTRODUCTION

The successful implementation of hydrodynamical models in coastal areas depends greatly on the forcing conditions in place (Dias *et al.*, 2006a,b, Rodrigues *et al.*, 2009a). For coastal and estuarine areas, the salinity variation depends on the fresh water/salt water ratio; the fresh water from the rivers discharging and the salt water from the ocean (Vaz *et al.*, 2009). As observations for river flows are not always available for all fresh water sources, different strategies are used to estimate the river flows to be implemented in a numerical model. Correct fresh water flow estimation is necessary in order to properly simulate the salinity fields across the domain.

An increasing number of accidental oil spills have been occurring in the Iberian Peninsula area, mainly due to weather events (Azevedo *et al.*, 2014). It can be expected that extreme weather events, causing most of the accidents, will increase with changing climate (Easterling *et al.*, 2000; Morss *et al.*, 2011) and causing an increase in economic losses (Barredo, 2009). Rising human and economic impacts of natural and accidental hazards

have triggered the European Commission to develop legal frameworks to increase prevention, preparedness, protection and response to such events and to promote research and acceptance of risk prevention measures within society (Alfieri *et al.*, 2012). An important part of a holistic approach to risk management of hazards is the establishment of early warning systems (Alfieri *et al.*, 2012). Recent studies have illustrated that early warning systems can have significant benefits exceeding their development and maintenance cost (Rogers and Tsirkunov, 2011; Teisberg and Weiher, 2009). At the present, these systems are mainly in use for weather related events, but its implementation for other events is now being done. In this frame, oil spill accidents can be considered important hazards induced by several risk factors related to environmental conditions and associated with maritime transport and port activities, which cannot always be predicted or controlled. The number of accidental oil spills affecting the Atlantic coast of Europe in recent decades has led to a growing concern regarding oil spill preparedness and response, and has motivated the development and implementation of different tools to be used in these emergency situations. Therefore, it is essential to support the development of accurate hydrodynamic models that

can be coupled to oil spill forecast models to build up operational platforms that can be used to simulate oil spill events.

Nowcast-forecast systems (NFS) are 4D (space-time) simulation environments that integrate state-of-the-art numerical models and near-real time data. In the scope of the INTERREG project SPRES, NFS applied to oil spills were developed for four coastal sites in the Atlantic Area (<http://spres.ihcantabria.com/>). State-of-the-art numerical hydrodynamic models driven by real-time data and meteorological, oceanographic, and/or river flow rate forecasts form the core of these end-to-end systems. The Rapid Deployment Forecasting System (RDFS-PT) is an operational system in use in the Ria de Aveiro lagoon (<http://ariel.lnec.pt/>) (Oliveira *et al.*, 2011), to provide real-time data about the weather and ocean conditions and, in addition, near real-time forecast information. At the present, its application is already in use to predict hydrodynamic conditions, which are being coupled with a model to forecast oil spills drift (Azevedo *et al.*, 2014). The operational system will be used as a tool to prepare and deploy the necessary measures to minimise the effects of an oil spill within the vicinity of the lagoon.

The oil slick drift simulations rely on the outputs from the hydrodynamic model. Consequently the simulation accuracy of the different variables is very important to adequately forecast the slick drift. The oil behaviour depends on several variables such as water salinity and temperature, influencing the oil weathering (Azevedo *et al.*, 2014). Although the Ria de Aveiro is tidally dominated (Dias *et al.*, 2000), its water circulation and especially its longitudinal salinity gradients are also influenced by the fresh water/sea water ratio (Dias *et al.*, 1999; Vaz and Dias, 2008; Vaz *et al.*, 2009). Despite its importance river discharges at the lagoon are not monitored permanently; there are only two real time measuring stations located in the Vouga and Antuã river basins, but far from the lagoon. Consequently, alternative estimation approaches are needed to estimate the river discharges for all five rivers, in order to give appropriate boundary conditions to the hydrodynamic model. To fulfil this gap, two different approaches were considered in this study: the first estimates the Vouga River flow based on the nearest real time measuring station and estimates the other river flows based on river basin areas proportionality; the second determines the river flows using a local application of the SWAT watershed model based on the precipitation/river flow relationships for the Vouga and Antuã rivers and on the areas of the other river basins.

## STUDY AREA

The Ria de Aveiro (Figure 1) is a shallow vertically homogeneous lagoon with a very complex geometry, located on the northwest coast of Portugal (40° 38' N, 8° 45' W). It is 45 km long and 10 km wide and covers an area of 89.2 km<sup>2</sup> at spring tide which is reduced to 64.9 km<sup>2</sup> at neap tide (Lopes *et al.*, 2013). The lagoon is separated from the ocean by a sand spit. An artificial inlet connects the lagoon to the open ocean. The lagoon is characterized by narrow channels and by large areas of mud flats and salt marshes (Dias *et al.*, 1999; Dias, 2001). An important national harbour, including several terminals, for commercial and fisheries activities is located within the lagoon. Due to the increase in maritime traffic, this area is more prone to accidents and possible oil spills within the vicinity. One of the terminals receives hydrocarbon products, such as unleaded gasoline, for storage and distribution for retailers. This infrastructure is quite important for the local and national economy, and justifies the actual concern with oil spill accidents.

Ria de Aveiro is a mesotidal lagoon (Dias *et al.*, 2000), within which the semidiurnal tides are the main forcing mechanism of its

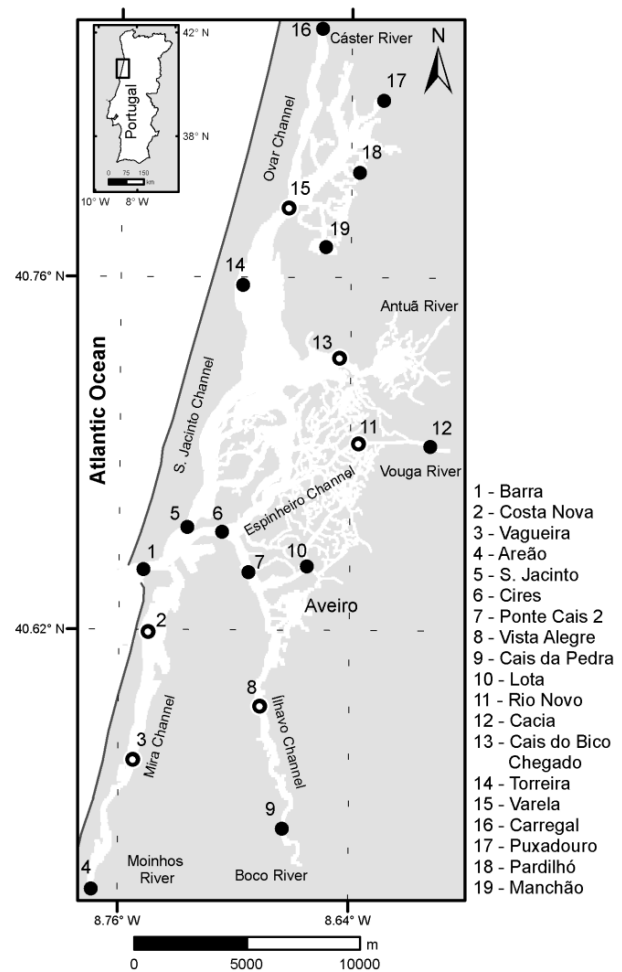


Figure 1. Map of the Ria de Aveiro with its main fresh water contributors. All stations represented by black circles, except Varela, are used for hydrodynamic calibration; for salt and heat transport, the stations used in the calibration have a white dot in its symbol.

dynamics. The lagoon has several fresh water sources composed by rivers and small streams and ponds, which contribute to the fresh water input in the lagoon (Figure 1). The main source of freshwater is the Vouga River which discharges into the Espinheiro channel, and represents approximately 2/3 of the overall lagoon fluvial input. Its mean flow is about  $1.8 \times 10^6$  m<sup>3</sup>, which is considerably lower than the tidal prism at the lagoon mouth that ranges between  $65.8 \times 10^6$  m<sup>3</sup> and  $139.7 \times 10^6$  m<sup>3</sup> (Lopes *et al.*, 2013). In the Laranjo bay inflows the Antuã, while at the heads of S. Jacinto, Ílhavo and Mira channels inflow the Cáster, Boco and Ribeira dos Moínhos, respectively. The wind stress and waves influence are restricted to disperse areas of the lagoon in rare situations of extreme weather conditions (Dias, 2001). The lagoon can be considered vertically homogeneous, except occasionally when fresh water inflows are high and the upper parts of the lagoon can present vertical stratification (Dias *et al.*, 2000; Vaz *et al.*, 2009).

## METHODOLOGY

The complexity of the geometry of the Ria de Aveiro requires a multi-scale model based on unstructured grids, in order to resolve properly the narrow and meandering channels of the lagoon. The choice fell on the community model SELFE 3D ([www.stccmop.org/CORIE/modeling/selfe/](http://www.stccmop.org/CORIE/modeling/selfe/)), from the Centre for Coastal Margin Observation and Prediction (CMOP), located in Beaverton, Oregon, USA ([www.stccmop.org](http://www.stccmop.org)). This numerical model adopts a semi-implicit Eulerian-Lagrangian scheme applied to unstructured grid of finite elements (Zhang and Baptista, 2008). SELFE solves the 3D shallow-water equations, with hydrostatic and Boussinesq approximations, and transport equations for salt and heat. The primary variables that SELFE solves are the free-surface elevation and 3D velocity, 3D salinity and 3D water temperature; further details are presented in Zhang and Baptista (2008).

SELFE can be run in parallel mode, which reduces computational time significantly (Zhang and Baptista, 2008). This is a particularly relevant factor as this model is to be applied as part of an operational forecasting system, for real time forecast of hydrodynamics.

SELFE was used in previous applications to the Ria Aveiro lagoon (Rodrigues *et al.*, 2009a, b, 2012; Azevedo, 2010), proving to be an adequate tool to forecast the local dynamics. The implementation described in this study integrates the expansion of the numerical domain used in those applications, which is enlarged to the Atlantic Ocean. The domain used is based on a grid available from previous work (Oliveira *et al.*, 2007; Picado *et al.*, 2010; Rodrigues *et al.*, 2012; Lopes *et al.*, 2013). The domain was extended from the shore till the edge of the continental platform, approximately 65 km from shore, to the west of the Iberian Peninsula. This extension was necessary to test the model robustness using atmospheric variables forcing.

Additionally, inside the lagoon, the resolution was increased in some areas, depending on their relevance. Changes were performed mainly in areas where the configuration and depth of the lagoon were altered due to the dredging or other interventions. The enlarged domain has an area of approximately 6400 km<sup>2</sup>, comprising 62252 elements and 36486 nodes; the finite elements have a side length ranging from 2 to 8000 m. The domain has six open boundaries, one at the sea that covers all nodes in the ocean, and five fluvial boundaries at the main fresh water contributors.

As SELFE is a 3D model, a vertical structure has to be defined, and this vertical grid can use S coordinates or hybrid SZ coordinates, which can resolve both bottom and surface layer. For this application, the grid has a hybrid SZ coordinates system, with seven pure sigma coordinates levels, equally spaced, for the top surface layer, based on the previous work from Rodrigues *et al.* (2009a, b, 2012). Below the pure Sigma coordinates, eight layers are defined from 100 to 3000 m, as the domain extension reaches the edge of the platform. Both bottom and surface layers are resolved, thus simulating the bottom friction effect and resolving the surface horizontal velocities

The domain bathymetry was also updated with the most contemporary bathymetric data collected from recent surveys, mainly for the main channels. The data used is from 2011, for the main channels, and 2012 for the area of the commercial port, providing a good coverage and resolution for these parts of the lagoon. For the secondary channels and smaller water courses, datasets from the 1987/88 surveys were used. For the offshore part of the grid, dataset from the 2011 GEBCO surveys provided bathymetric data for the Iberian Peninsula west coast and open sea.

### Sea Surface Elevation Model Calibration

The numerical model uses as open boundary conditions the input from the five fresh water contributors and tide from the Atlantic Ocean (salinity equals to 36). The model also takes into account the atmospheric forcing, such as air temperature, wind, atmospheric pressure, humidity and flux radiation. The aim is to have the best quality boundary conditions to implement in the numerical model, thus expecting better results in the simulations.

The initial salinity and water temperature fields are built based on the spatial distribution of the grid nodes in the domain. The highest salinity values, 36, are located in the open sea and in the area located right in front of the tidal inlet, station 1 (Figure 1). Then salinity gradually decreases towards the channels heads, reaching zero closer to the fresh water contributors. For the initial temperature conditions, the values vary from 14.7 to 16.5 °C; the highest values are in the oceanic part of the grid and its variation is similar to salinity.

The hydrodynamic model was calibrated using sea surface elevation data from 18 measuring stations (Figure 1) located across the domain. The calibration used observations from several surveys performed in 2002/2003.

The direct comparison between observations and simulations led to the calculation of the Root Mean Square Error (RMSE) (eq. 1), Skill (eq. 2) and the relative error ( $\Delta$ ) (eq. 3). The equations used to obtain these values were the following (Dias, 2001; Dias and Lopes, 2006a,b):

$$RMSE = \frac{1}{N} \sum_{i=1}^N \zeta_o(t_i) - \zeta_m(t_i)^2 \quad (1)$$

$$Skill = 1 - \frac{\sum_{i=1}^N \zeta_m(t_i) - \zeta_o(t_i)^2}{\sum_{i=1}^N \zeta_m(t_i) - \zeta_o + \zeta_o(t_i) - \zeta_o^2} \quad (2)$$

$$\Delta \% = \frac{RMSE}{Tidal\ Range} \times 100 \quad (3)$$

where  $\zeta_o$  and  $\zeta_m$  are observed and predicted sea surface elevation, respectively,  $\zeta_o$  is the average observed elevation and  $N$  is the number of measurements in the time series.

### River flow estimation

The Ria de Aveiro simulation comprises the contribution of five fresh water sources namely, the Vouga, Boco, Cáster, Antuã and Ribeira dos Moínhos. The main contributor is the Vouga river, followed by the Cáster and the Antuã. The Boco is a small contributor and Ribeira dos Moínhos is composed by a network of pounds and underwater sources, which are not entirely known (Figure 1). There are only two real-time fresh water stations from Sistema Nacional de Informação de Recursos Hídricos (SNIRH) located in Vouga and Antuã basins, recording periodically river flow data (Figure 2). The data available is measured far from the lagoon, and is scarce and incomplete; thus fresh water inputs to the lagoon have to be estimated from climatological analysis supported with previous *in-situ* observations.

In order to include the fresh water flows into the hydrodynamic model, two different strategies for river flow estimation were used: the first adopts, as a reference, data from a measuring station in the river Vouga (Ponte Redonda), this will be designated as method A; the second uses the SWAT watershed model (Neitsch *et al.*, 2011) to estimate the flow, this will be designated as method B.

Method A uses observations from an *in-situ* flow measuring station located at the Ponte Redonda, Vouga river, located a few kilometres upstream from the lagoon.

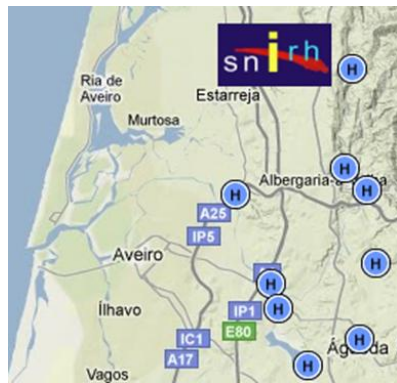


Figure 2. Location of fresh water measuring stations for the Vouga and Antuã river basins (<http://snirh.pt>).

The flow for the Vouga at the lagoon entrance is estimated with the following equation, which takes into account the Vouga basin area:

$$flow\ Vouga = flow\ Ponte\ Redonda \cdot 0.35$$

The estimated flows for the other fresh water contributors are based in river basin areas proportionality.

Method B applies the SWAT watershed numerical model to estimate the flow according to the terrain conditions, such as basin area, basin run-off, precipitation, soil infiltration (Arnold *et al.*, 1998; Neitsch *et al.*, 2011).

The hydrologic cycle is simulated based on the water balance (Setegn *et al.*, 2008, Akiner *et al.*, 2012):

$$SW_t = SW_0 + \sum_{i=1}^t (R_{day} - Q_{surf} - E_a - W_{seep} - Q_{gw})$$

where  $SW_t$  (mm) is the final soil water content;  $SW_0$  (mm) is the initial soil water content on day  $i$ ,  $t$  (days) is the time;  $R_{day}$  (mm) is the amount of precipitation on day  $i$ ,  $Q_{surf}$  (mm) is the amount of surface runoff on day  $i$ ,  $Q_{gw}$  (mm) is the amount of return flow on day  $i$ ,  $E_a$  (mm) is the amount of evapotranspiration on day  $i$ , and  $W_{seep}$  (mm) is the amount of water entering the unsaturated zone from the soil profile on day  $i$ .

The SWAT model was implemented to the Vouga basin using, as a base, the topography obtained from SRTM (<http://srtm.usgs.gov/>). The soil usage, which is also important in terms of terrain run-off, was built based on a map from 2006, whilst the soil physical properties were gathered from a 1:1000000 map; both maps were supplied by the European Environment Agency. In order to complete the initial conditions, meteorological data, such as monthly air temperature, relative humidity, wind velocity and direction and solar radiation was gathered for the area concerned; these datasets were for a 30 years period, for 8 stations from the Portuguese Institute for the Sea and Atmosphere (IPMA). Precipitation gauges were chosen according to data availability, thus 6 stations were selected because they had over 30 years of daily precipitation values available (SNIRH). Flow data was collected for several stations along the Vouga basin to be used for model calibration and validation. Based on the model calibration and validation, the flow, for the lagoon fresh water contributors, was estimated for the period necessary for this study.

### Salt and heat transport simulations

To compare both methods for flow estimation, the period from December 1<sup>st</sup>, 2012 till January 18<sup>th</sup>, 2013 was simulated; this period was chosen because adequate quality data, for several

stations, was available for the whole period. For this particular exercise, seven stations were used for water free surface elevation and six stations for salinity and water temperature (Figure 1). The 7th station is located at the entrance of the inlet, which is important in assessing the quality of the tidal signal arriving from the ocean. The data was obtained from a tide gauge in use since the 1970s.

The boundary conditions implemented for the simulations were water elevation, water temperature and salinity for the ocean open boundary (data obtained from reanalysis available from <http://www.myocean.eu/>). Atmospheric conditions obtained from the WRF model from the University of Aveiro (<http://climetua.fis.ua.pt/weather>) for the whole grid. These boundary conditions were implemented in both sets of simulations, the first with flows estimated from method A and the second with the flows obtained from method B.

## RESULTS AND DISCUSSION

### SSE Model Calibration

According to Dias *et al.* (2009), the RMSE values should be compared with the local tidal amplitude. Typically, if the error is lower than 5%, the agreement between observed and simulated data is considered excellent; if the error is between 5 to 10%, the agreement is considered good.

An excellent fit is found at the measuring stations located nearest the lagoon inlet (Table 1), where the tidal signal is strongest and less energy is dissipated. As the morphology of the channel increases in complexity, the model has more difficulties to replicate the hydrodynamic conditions. At the lagoon central area the fit is still good, while for the stations located the furthest away from the inlet the model encountered some difficulties in replicating the hydrodynamics, mainly when the model simulates the flow in the narrow channels. As the most relevant area for the oil spill forecast is concentrated in the Port jurisdiction area, close to the tidal inlet, considering it is more prone to an accident due to maritime traffic from the Aveiro harbour, the lower values that were found in this area reveal that the quality of the simulation is considered good for these purposes. Consequently, the calibration and validation was successful, considering the RMSE, Skill values and also by direct comparison between observations and simulations.

Table 1. Values for RMSE, Skill and relative error ( $\Delta$ ) error obtained for the hydrodynamic model calibration for the whole 18 measuring stations.

Station	RMSE	Skill	Tidal range (m)	$\Delta$ (%)
Barra	0.0867	0.9967	3.39	2.56
Costa Nova	0.0982	0.9954	3.01	3.27
Vagueira	0.2407	0.9590	2.79	8.62
Areão	0.4163	0.7627	1.59	26.10
Cais de Pedra	0.3460	0.8844	1.81	19.14
Vista Alegre	0.2759	0.9322	1.97	13.97
Ponte Cais 2	0.1088	0.9945	2.92	3.76
Lota	0.1807	0.9843	3.19	5.67
Cires	0.1599	0.9888	3.06	5.22
São Jacinto	0.1712	0.9839	2.82	6.06
Rio Novo	0.9432	0.4203	2.58	36.61
Cacia	0.2844	0.9432	2.26	12.57
Laranjo	0.3587	0.8984	2.54	14.12
Torreira	0.3335	0.9014	1.97	16.96
Manchão	0.5255	0.6667	1.92	27.42
Pardilhó	0.5180	0.6063	1.76	29.37
Puxadouro	0.5200	0.5943	1.44	36.23
Carregal	0.3640	0.8261	1.78	20.43

**Salt and heat transport simulations**

The two methods for estimating river flows were evaluated against salinity and water temperature (not show in this study) data at the six stations (Figure 1). Figure 3 shows the comparison between salinity observations and model predictions using both flow estimation methods. This variable was selected considering variable it is particularly sensible to freshwater flows. To quantify the accuracy of the model predictions, the RMSE and Skill between observed and predicted salinity were determined (Table 2). The results show that the simulation with method A provides a better fit between observations and predictions for all stations, although the predicted salinity values are most of the times lower than the observations, especially at low tide (Figure 3). Both methods overestimate the freshwater flows being imposed at the model open boundaries. The only exception is for Chegado (Figure 3), where the best fit was obtained with method B, and method A underestimates the fresh water from Cáster River.

When analysing the RMSE for both strategies, method A provides the best results; the same occurs for the Skill. The RMSE present major differences mainly for the stations located in the main channels (Costa Nova, Vagueira and Varela); when the stations are located further away from the tidal entrance and therefore closer to the river’s mouth, in the narrowest parts of the lagoon, the difference in RMSE values decreases significantly. For the Rio Novo station, located in the Vouga River, similar RMSE values are found for both methods. Method B was primarily implemented to replicate the Vouga River, as this area has the best coverage in terms of hydrological and meteorological stations;

Table 2. RMSE and Skill values obtained for both flow estimation methods, for the 6 measuring stations.

Station	RMSE	Skill	RMSE	Skill
	A	A	B	B
Costa Nova	3.9425	0.8674	16.0973	0.4346
Varela	5.7349	0.7111	11.7804	0.4162
Rio Novo	9.4886	0.4620	10.1195	0.3672
Vagueira	5.7479	0.8871	13.4164	0.4526
Chegado	8.4000	0.7191	10.1021	0.5308
Vista Alegre	7.7904	0.6613	17.8931	0.3971

thus both methods have similar estimations for the Vouga. When analysing the Skill, significant differences are observed between simulations, with the best fit found again for method A, except for Rio Novo station where the values do not differ significantly. For this station the agreement between predictions and observations is poor, revealing that the Vouga River flow is probably overestimated. The best fit is found for the Costa Nova and Vagueira stations, which are located in the same channel; this may be due to a good estimation of the freshwater discharge in this channel and to the high resolution of the numerical grid in this area of the domain.

**CONCLUSIONS**

The SELFE implementation developed for Ria de Aveiro reproduces accurately the tidal propagation and salinity patterns in the central area of the lagoon. This is the most relevant area for

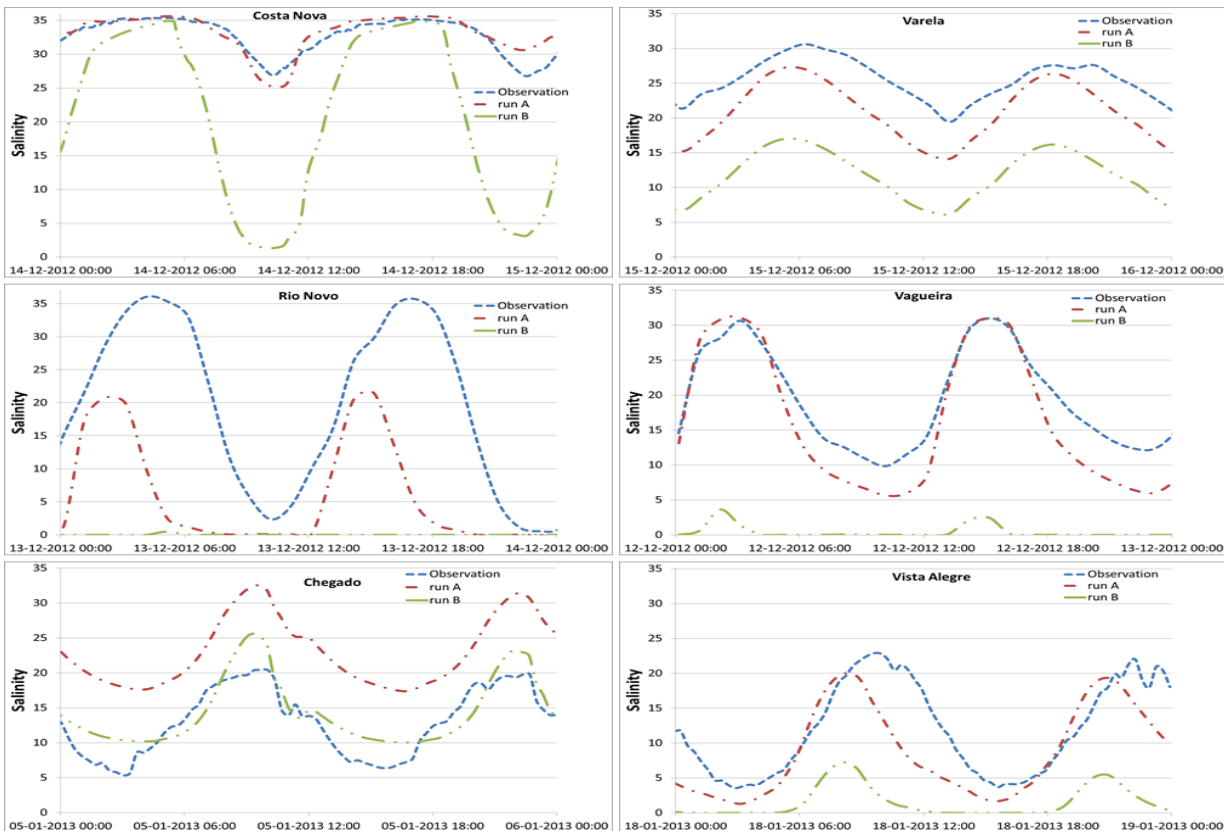


Figure 3. Salinity variation during a full tidal cycle, for the 6 measuring stations. ....: Observed data; -.-: runs with flow estimation using method A; -.-: runs with flow estimation using method B

this study, considering it is more prone to accident due to maritime traffic from the Aveiro harbour. The best results for salinity simulations are found when the fresh water flows are estimated using the method A, based on the use of freshwater flows measured at Ponte Redonda, which is the nearest real time measuring hydrologic station, rather than the use of the SWAT basin model. This application is therefore ready to use to predict hydrodynamic conditions in the frame of the operational system developed for the Ria de Aveiro.

### ACKNOWLEDGEMENTS

The European Union, under the European Regional Development Fund and INTERREG IV B: Atlantic Area Transnational Programme, supported this study through the research project SPRES-2011-1/168. The Portuguese Foundation for Science and Technology FCT also supported this study in the frame of the research project PTDC/AAC-AMB/113469/2009 - PAC:MAN, co-funded by COMPETE, QREN, FEDER. The second and fourth authors are co-funded by the Portuguese Foundation for Science and Technology FCT grants SFRH/BPD/87512/2012 and SFRH/BPD/73089/2010, respectively. The authors thank António Baptista, from CMOP, and Joseph Zhang, from VIMS, for the model SELFE. The team also thanks the Port of Aveiro authority for all the data and support provided in the development of this study and Polis Ria de Aveiro for the data provided.

### LITERATURE CITED

- Akiner, M. and Akkoyunlu, A., 2012. Modeling and forecasting river flow rate from the Melen Watershed, Turkey. *Journal of Hydrology*, 456 – 457, 121-129.
- Alfieri, L., Salamon, P., Pappenberger, F., Wetterhall, F. and Thielen, J., 2012. Operational early warning systems for water-related hazards in Europe. *Environmental Science & Policy*, 21, 35-49.
- Arnold, J.G., Srinivasan, R., Mutiah, R.S. and Williams, J.R., 1998. Large area hydrologic modelling and assessment: Part I – model development. *Journal of American Water Resources Association*, 34(1), 73-90.
- Azevedo, A., Oliveira, A., Fortunato, A.B., Zhang, J., Baptista, A.M., 2014. A cross-scale numerical modeling system for management support of oil spill accidents. *Marine Pollution Bulletin*, (2014), in press, <http://dx.doi.org/10.1016/j.marpolbul.2014.01.028>
- Barredo, J.L., (2009). Normalised flood losses in Europe: 1970–2006. *Natural Hazards and Earth System Sciences*, 9, 97-104.
- Dias, J.M., 2001. *Contribution to the Study of the Ria de Aveiro Hydrodynamics*. Aveiro, Portugal: University of Aveiro, Ph.D. Thesis, 288 pp. <http://hdl.handle.net/10773/4939>.
- Dias, J.M. and Lopes, J.F., 2006a. Calibration and validation of hydrodynamic, salt and heat transport models for the Ria de Aveiro lagoon (Portugal). *Journal of Coastal Research*, S.I. 39, 1680-1684.
- Dias, J.M. and Lopes, J.F., 2006b. Implementation and assessment of hydrodynamic, salt and heat transport models: the case of the Ria de Aveiro lagoon (Portugal). *Environmental Modelling & Software*, 21, 1-5.
- Dias, J.M., Lopes, J.L. and Dekeyser, I., 1999. Hydrological characterisation of Ria de Aveiro, Portugal, in early Summer. *Oceanologia Acta*, 22(5), 473-485.
- Dias, J.M., Lopes, J.F. and Dekeyser, I., 2000. Tidal Propagation in Ria de Aveiro Lagoon, Portugal. *Physics and Chemistry of the Earth*, 4(25), 369-374.
- Dias, J.M., Sousa, M., Bertin, X., Fortunato, A. and Oliveira, A., 2009. Numerical modelling of the impact of the Ancão Inlet relocation (Ria Formosa, Portugal). *Environmental Modelling & Software*, 24, 711-725.
- Easterling, D.R., Meehl, G.A., Parmesan, C., Changnon, S.A., Karl, T.R. and Meams, L.O., 2000. Climate extremes: observations, modelling, and impacts. *Science*, 289, 2068-2074.
- Lopes, C.L., Azevedo, A. and Dias, J.M., 2013. Flooding assessment under sea level rise scenarios: Ria de Aveiro case study. *Journal of Coastal Research*, SI 65, 766-771.
- Morss, R., Wilhelmi, O., Meehl, G. and Dilling, L., 2011. Improving societal outcomes of extreme weather in a changing climate: an integrated perspective. *Annual Review of Environment and Resources*, 36, 1-25.
- Neitsch, S.L., Arnold, J.G., Kiniry, J.R. and Williams, J.R., 2011. Soil and Water Assessment Tool, Theoretical Documentation Version 2009, Texas Water Resources Institute, Technical report N° 406, Texas A&M University System.
- Oliveira, A., Fortunato, A.B. and Dias, J.M., 2007. Numerical Modeling of the Aveiro Inlet Dynamics. In: *Coastal Engineering 2006*, Editor: Jane McKee Smith, World Scientific Publishing Co., ISBN 978-981-270-636-2, Vol. 4, 3282 – 3294.
- Oliveira, A., Rodrigues, M., Fortunato, A. B., Jesus, G., Ribeiro, N.A., Dodet, G., Dias, J.M., 2011. Previsão em tempo real da circulação na Ria de Aveiro, In: Almeida, A., Alves, F.L., Bernardes, C., Dias, J.M., Gomes, N.C.M., Pereira, E., Queiroga, H., Seródio, J. e Vaz, N. (Eds.), 2011. Actas das Jornadas da Ria de Aveiro 2011. Universidade de Aveiro, CESAM – Centro de Estudos do Ambiente e do Mar. Aveiro. 373 pp., 310-315. [http://la.cesam.ua.pt/documentos/LivroActasJornadasRiaAveiro2011\\_Cores.pdf](http://la.cesam.ua.pt/documentos/LivroActasJornadasRiaAveiro2011_Cores.pdf)
- Picado, A., Dias, J.M. and Fortunato, A.B., 2010. Tidal changes in estuarine systems induced by local geomorphologic modifications. *Continental Shelf Research*, 30 1854-1864.
- Rodrigues, M., Oliveira, A., Costa, M., Fortunato, A.B. and Zhang, Y., 2009a. Sensitivity analysis of an ecological model applied to the Ria de Aveiro. *Journal of Coastal Research*, SI56, 448-452.
- Rodrigues, M., Oliveira, A., Queiroga, H., Fortunato, A.B. and Zhang, Y., 2009b. Three-dimensional modelling of the lower trophic levels in the Ria de Aveiro (Portugal). *Ecological Modelling*, 220, 1274-1290.
- Rodrigues, M., Oliveira, A., Queiroga, H. and Brotas, V., 2012. Seasonal and diurnal water quality modelling along a salinity gradient (Mira channel, Aveiro lagoon, Portugal). *Procedia Environmental Sciences*, 899-918.
- Rogers, D. and Tsirkunov, V., 2011. *Costs and Benefits of Early Warning Systems, Global Assessment Report on Risk Reduction*. World Bank, Washington DC, 16 pp.
- Setegn, S.G., Srinivasan, R. and Dargahi, B., 2008. Hydrological modelling in the Lake Tana basin, Ethiopia using SWAT model. *The Open Hydrology Journal*, 2, 49-62.
- Teisberg, T.J. and Weiher, R.F., 2009. *Benefits and Costs of Early Warning Systems for Major Natural Hazards*. Background Paper, World Bank, Washington, DC, 68 pp.
- Vaz, N. and Dias, J.M., 2008. Hydrographic Characterization of an Estuarine Tidal Channel. *Journal of Marine Systems*, 70, 168-181.
- Vaz, N., Dias, J.M. and Leitão, P.C., 2009. Three-dimensional modelling of a tidal channel: The Espinheiro Channel (Portugal). *Continental Shelf Research* 29, 29-41.
- Zhang Y. and Baptista, A.M., 2008. SELFE: A semi-implicit Eulerian–Lagrangian finite-element model for cross-scale ocean circulation. *Ocean Modelling*, 21, 71-96.



# Hydrodynamics of a river-associated tidal inlet and maintenance of dynamic equilibrium: preliminary findings



Mauricio Villagran<sup>†‡</sup>, Diego Caamaño<sup>‡</sup>, Rodrigo Cienfuegos<sup>†§</sup>

<sup>†</sup> Pontificia Universidad Católica de Chile, mvillagranv@uc.cl, racienfu@ing.uc.cl

<sup>‡</sup> Universidad Católica de la Santísima Concepción, UCSC mvillagran@ucsc.cl, dcaamano@ucsc.cl

<sup>§</sup> Centro Nacional de Investigación para la Gestión Integrada de Desastres Naturales (CIGIDEN), Pontificia Universidad Católica de Chile

[www.cerf-jcr.org](http://www.cerf-jcr.org)



[www.JCRonline.org](http://www.JCRonline.org)

## ABSTRACT

Villagran M., Caamaño D., Cienfuegos R., 2014. Hydrodynamics of a river-associated tidal inlet and maintenance of dynamic equilibrium: preliminary findings. In: Green, A.N. and Cooper, J.A.G. (eds.), *Proceedings 13<sup>th</sup> International Coastal Symposium* (Durban, South Africa), *Journal of Coastal Research*, Special Issue No. 70, pp. 592-597, ISSN 0749-0208.

Detailed video images and ADCP measurements were used to describe the processes of suspended sediment transport by the Mataquito River into the Pacific Ocean. It is found that, in the absence of fluvial flood discharges, suspended sediment transport to the sea only takes place during low tide periods and it is characterized by pulses of different frequencies that in turn are related to the spatial velocity distribution at the river inlet. It was observed that at low tide the highest velocities are near the mouth of the river, presenting an heterogeneous spatial distribution. In this high speed zone, we hypothesized the shear stresses are big enough to re-suspend fine sediment that is transported into the ocean by the main river current. A simple conceptual explanation based on these findings is presented, seeking to explain the observed dynamic equilibrium of the Mataquito River inlet after the significant alterations produced by the 2010 M8.8 earthquake and tsunami.

**ADDITIONAL INDEX WORDS:** *River inlet, Hydrodynamics, ADCP measurements, Video monitoring.*

## INTRODUCTION

River inlets and associated barriers are highly sensitive and dynamic areas in coastal environments (Cooper, 2001; Lichter *et al.*, 2011). In this regard, river inlet morphodynamics and river mouth evolution has been related to changes on discharge, sediment transport rates, channel migration and/or closure (Tung *et al.*, 2009). Studying this natural ecosystem provides background information for predicting and estimating possible alterations induced by human intrusion, or natural responses to significant changes at local or reach scale.

Estuary classification has been widely used to understand/classify hydrodynamic processes and its resultant patterns at large spatial scales (Fitzgerald, 1996; Lichter *et al.*, 2011). The morphological diversity can be explained by several factors (Fitzgerald, 1996; Cooper, 2001), such as: tidal range, sediment transport rates, relative influence of waves, tidal and fluvial processes, and other abiotic factors as tectonics, latitude, topography, etc. (Hume *et al.*, 2007). However, the mechanism that explains how they change or maintain equilibrium is characteristic of each particular inlet.

There are many ways to assess the evolution of coastal inlets, however, one of the most novel is based on video coastal monitoring systems. This technique can provide high temporal and spatial resolution of a study site; and during the last decade has become a very useful tool (Paterson *et al.*, 2000; Morris *et al.*,

2001, 2007; Freire *et al.*, 2011). We have used these monitoring systems complemented by ADCP hydrodynamic measurements at the river inlet to identify the forcing processes involved in the dynamic equilibrium observed at the Mataquito River mouth.

The Mataquito River and adjacent coastal area (34°52'S, 72°09'W) is associated with a narrow and shallow estuary, located in central Chile, with a pre-earthquake landform and morphologic configuration condition characterized by a 9 km-long sand spit. This scenario changes dramatically after the Chilean Tsunami of February 27<sup>th</sup>, 2010. We followed its recovery process through *in situ* detailed field measurements and video coastal monitoring. The recovery of the system was surprisingly fast, indicating a high degree of resilience for this natural landform (Villagran *et al.*, 2011). After the tsunami event a new configuration of the river inlet emerged, changing from a "normally open, river-dominated barred estuary", into a configuration close to a coastal lagoon with a unique and well-defined outlet. This new arrangement shows an apparent equilibrium in time, under the observed scenarios i.e. highly energetic wave conditions, micro-tidal range and little variation in river discharge.

## Site Description

The central Chile coast has a Mediterranean climate, with storms and floods concentrated during winter (May–August) and a marked dry season during summer (December–March). The coastline has a predominant south to north orientation, widely open to the action of the Pacific Ocean's waves (Figure 1). The local topography is steep and narrow, mainly because of the presence of a mountain range near the coast.

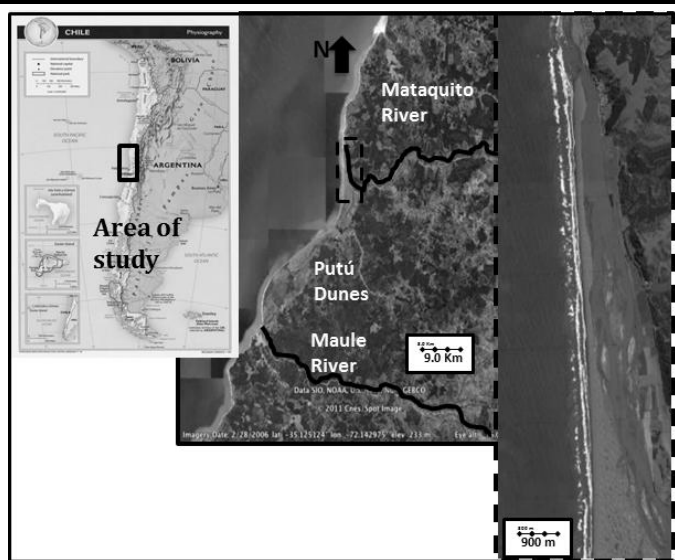


Figure 1. Mataquito River study area overall location, showing coastline northing direction and a portion of the 9 km-long sand spit. (images source: Adapted from Googlearth)

The Mataquito River originates in the Andes and it drains a basin of approximately 6,200 km<sup>2</sup>. The mean annual river discharge is 150 m<sup>3</sup>/s, but it may vary between 30 m<sup>3</sup>/s during the dry season up to several thousands of m<sup>3</sup>/s during flood periods.

The Mataquito River mouth is located 50 km north of the Maule River mouth (Figure 1). At the river mouth, the flow is diverted northward by a dune system (Putú dunes). The shoreline at the river mouth is completely exposed to the action of South Pacific swells, forming a long barrier system and a sheltered estuary behind it.

Historically, this estuary has been protected by a long sand spit, which is shaped by the south-north longshore current induced by the wave climate. The location of the mouth was fixed ten years ago by the construction of a small rocky groin. This sand spit suffered heavy erosion after the 2010 Chilean tsunami, where most of the barrier was washed away (Figure 2, upper left panel). During the following year, the barrier reformed very rapidly (Villagran *et al.*, 2011). After the 2010 event, the Mataquito River discharge has consistently been below its average yearly value. These low river discharges have given rise to a slightly different configuration of the sand spit than existed before the 2010 earthquake and tsunami. The main difference being the location of the river mouth, which is now 3.5 km south of its former position. In Figure 2 we show a set of consecutive images that were taken from a drone, where the impact of the 2010 earthquake and tsunami can be assessed, and the recovery of the coastal system during the following months can be appreciated.

## METHODS

### Field Campaign

The characterization of pre-tsunami condition was done using satellite images and topographic surveys when available. The post-tsunami evolution was assessed through several field surveys carried out between April 2010 and July 2013. Topographic data was related to known points located within the study area and surveyed using a Spectra Precision Epoch 50 RTK DGPS. Rectified aerial pictures obtained from drones complemented this information. Hydrodynamic measurements at the river mouth were performed during two campaigns in December 2012 and July 2013. A Rio Grande (1200 kHz) Acoustic Doppler Current Profiler (ADCP) was used to profile velocity cross sections at the intertidal area. A single transect was defined and continuous sampling performed from both banks. It was noticed that operating the zodiac became complicated during the low tide levels. At this point focused currents were observed and the presence of eddies was recognized.

In addition, more than 20 years of daily river discharge data is available from the Licanten gauge station (34°59'S, 72°00'W), and wave climate was characterized using NOAA database at node (35°S).

As part of a research project funded by the Chilean National Commission for Science and Technology (CONICYT), two video cameras were installed pointing towards the Mataquito River mouth. The cameras were mounted on a pole at more than 155 m above MSL, facing southwest, and averaged images are captured to characterize the river and sand spit evolution. (Cienfuegos *et al.*, 2014 *this issue*). Camera 1 (Cam1) takes images from a straight reach of nearly 1 km, while Camera 2 (Cam2) provides an overview of the whole system over a long stretch of 3 km, including the estuary and the river mouth.

The oblique images captured by both video cameras are transferred via Wifi to a computer where the video is pre-processed to save only images (i.e. timex, snapshot and timestacks) and then uploaded to an internet server (see also Cienfuegos *et al.*, 2014 *this issue*).



Figure 2. Recovery process of Mataquito River mouth after Chilean Tsunami of 2010. Red arrows are used to compare in time similar spatial locations on each image. (Villagran *et al.*, 2011)

### Measurements

The video monitoring system stores daylight averaged images over 15 minutes of video, plus a snapshot of the sea state at the beginning of each period of video recording. This information

provides some information regarding the wave forcing, and the morphodynamic evolution at the study site

Cameras were installed in December of 2012, however, only from August 15<sup>th</sup> of 2013 has a continuous record of images has been obtained. Before that, several gaps exist due to intermittent energy supply. Both cameras were used to track and characterize the sediment plume that exits the river.

Using Cam2 (panoramic view) it was possible to observe the extension of the plume in the sea, how and where it travels from the river mouth along the coast. This camera was also used to monitor the sand spit extension and to observe the slow migration of the river mouth towards the north (Figure 2, lower panel). *In situ* measurements using RTK DGPS measurements and aerial photographs were also used to record the barrier recovery after the 2010 earthquake and tsunami (Villagran *et al.*, 2011). Using Cam1 (close view) it was possible to observe the suspended sediment plume alongshore, providing rough estimates of its migration velocity towards the north.

Combining both images, many different patterns have been observed, that can be classified into 4 qualitative conditions:

- No Plume: When no plume was observed during the video recording or on the snapshot
- Small Plume: When water presents mild turbidity and was not possible to visually identify the plume.
- Medium Plume: When a well-defined and narrow (i.e. hundred meters from the shoreline) sediment plume extending along the coast was observed.
- Large Plume: When a well-defined and wider than the previous condition (i.e. 2 to 4 kilometers from the shoreline) sediment plume extending along the coast was observed.

Suspended sediment plumes could be identified during low tides, while at high tides they were non-existent or negligible. The plume usually appeared a couple of hours before the lowest tide level and was visible for about 6 hours. A different situation occurred during river floods, where the sediment plume was visible for a much longer time being less sensitive to tide variations. However, during the time the video cameras have been recording, we have witnessed only one flood where these features could be observed. More flood events are necessary in order to characterize the river flood influence on the sediment plume.

Occasionally, images show a different type of plume with many front lines or “pulses” of sediment, suggesting that some differentiated flushing of sediment is occurring at the river mouth during a single tidal cycle. That was the case of July 31<sup>st</sup>, where pulses did not occur regularly and the frequency of appearance of fronts was not uniform during the day.

ADCP measurements during the field campaign of July 30th-31st of 2013, show localized high-speed currents at the river mouth. Figure 4 exhibits the flow speed at different tide stages during July 31<sup>st</sup>. It is possible to observe a cluster of high velocities that moves as the tide levels diminish. This translation stops when the ocean levels start rising again. Higher velocities have a magnitude close to 1 m/s, whereas the mixed cross section scenario indicates velocities around 0.2 m/s. This coincides with the surface velocity field observations.

## PRELIMINARY RESULTS

Combining three types of data (ADCP, Video and historical), we were able to construct a database to study the inlet, separating the results into two fields: suspended sediment plume description and river mouth hydrodynamics.

## Sediment Plume Description

Table 1 shows the occurrence of the different patterns of the sediment plume at the sand spit. Those patterns are correlated with tidal range, qualitative wave conditions and mean hourly river discharge. Changes in water turbidity were used to classify the type of plume, which varied in extent and sediment concentration. The averaged images of Cam2 allow us to qualitatively estimate the wave climate, specially identifying the number of submerged sandbars in the image (many sand bars indicate more energetic conditions). These conditions affect the plume extension and spreading in the sea more than in the flushing itself, but it may be related to the availability of sediment in the river mouth that is transported by ebb currents.

Tidal range in the study area is micro-tidal and fluctuates between 0.5 m and 1.8 m. Tidal variability seems to influence the appearance of the plume in the sea, rather than its magnitude or extent. The influence of river discharge is obvious during river floods (Image 1, Table 1), but strong river discharge is not the only influence on the occurrence of the suspended sediment plume.

Additionally Figure 5 shows the pulse of sediment occurring at the plume (yellow lines in the pictures). The pulse captured was very weak, mainly because of a lack of sediment at the river mouth (low discharge and calm wave conditions). However, it seems to have a frequency close to 5 minutes at some point (see right image on Figure 5b) and is reduced to shorter frequencies at different stages of the tide

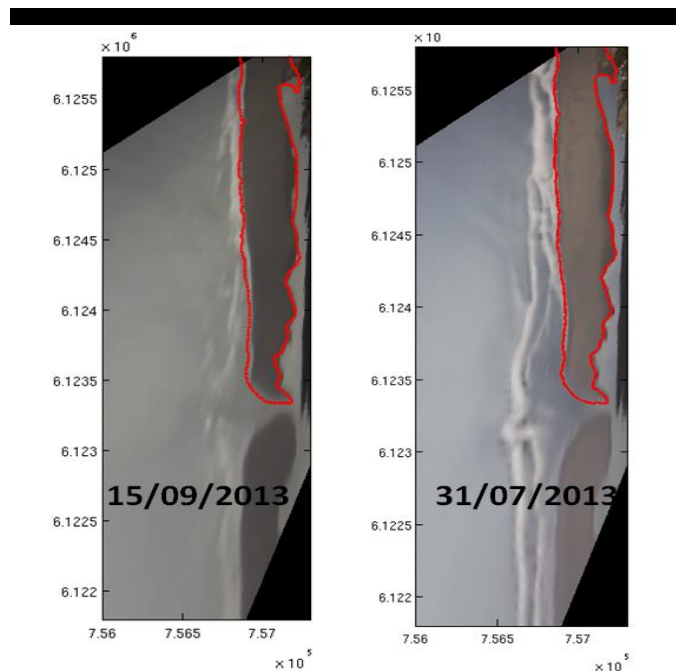








Figure 3. Cam2 rectified images of Mataquito sand spit and river mouth. Red dots show validation tracks taken on July 31<sup>st</sup> of 2113.

Table 1. Qualitative description of different turbid river plume at Mataquito river Mouth.

<b>Date/ Time</b>	<b>Tidal Range (m)</b>	<b>Daily Discharge Range(m<sup>3</sup>/s)</b>	<b>Wave Condition/ Plume size</b>	<b>Image of river mouth at low tide</b>
<b>21/12/2012 15:00UTC</b>	0.8	289.2-179.7	Mild/ Large	
<b>20/06/2013 16:30UTC</b>	1.1	42.4- 41.7	Low Energetic/ Small	
<b>21/08/2013 18:30UTC</b>	1.8	75.1- 71.6	Very Energetic/ Small	
<b>12/09/2013 16:30UTC</b>	1.0	126.9-113.0	Energetic/ Medium	
<b>03/10/2013 17:45UTC</b>	1.2	25.5- 26.2	Very Energetic/ Medium	
<b>26/11/2013 15:30UTC</b>	0.8	75.2 – 63.1	Energetic/ Medium	

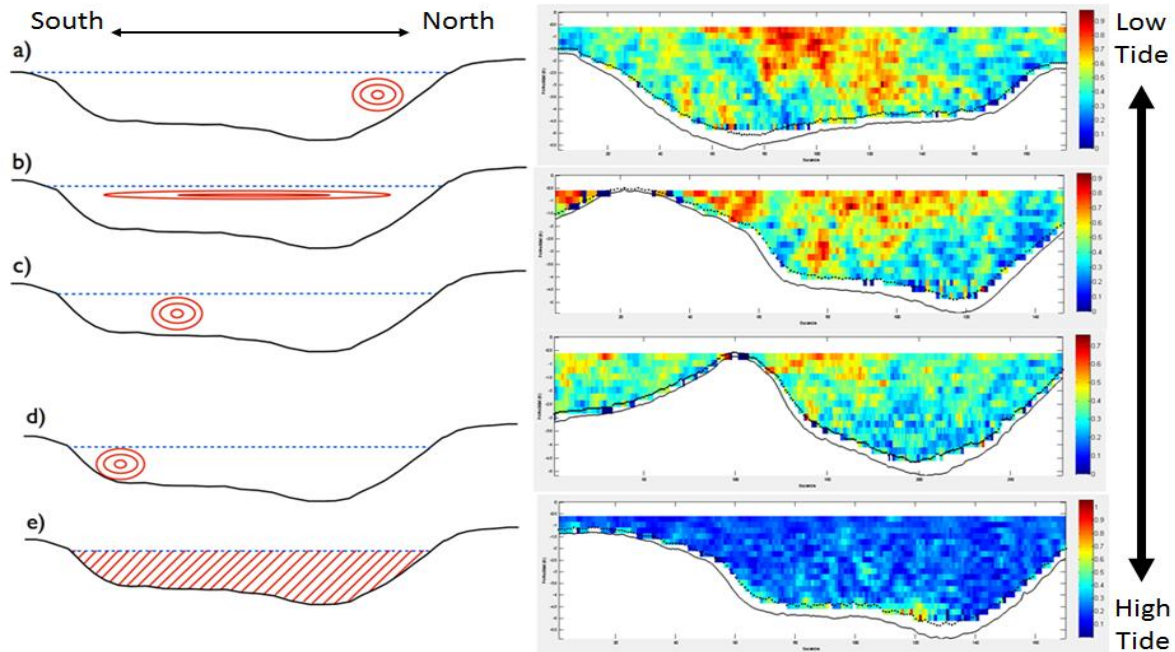


Figure 4. Left: Schematics showing location of observed zones of high velocities concentration at decreasing stages towards the low tide level (a through d), and the beginning of increasing tide levels (e). Red line indicates high velocity zone or velocity equalization (e). Right: ADCP measurements at different stage of the tidal cycle. Red colours indicate places with velocities around 1 m/s.

### River Mouth Hydrodynamics

River mouth hydrodynamics were assessed mainly using the ADCP device which shows the behavior of the currents at the river inlet (Figure 4). Currents are completely different from low tide to high tide. During low tide the outgoing speed reaches 1 m/s and, in contrast, at high tide, the speed decreases to values lower than 0.2 m/s. There are many fluctuations in the speed patterns observed at the inlet varying mostly in magnitude and the location of peak velocities. As the tide level falls a core of high velocities forms in the central portion of the cross section. As the tide level decreases this group of high velocities moves towards the south bank where it maintains its position until the increment on the tidal level. Once the tidal level starts rising again, the magnitude of the higher velocities decreases and the cross section reaches a mixed condition on which is not possible to identify high velocity clusters, because the outgoing current is being equalized by the incoming tide fluxes (Figure 4).

These fluctuations, occurring mostly during the lower part of the tide cycle, generate shear zones that favor the development of vertical eddies. It is hypothesized that these entrain fine-grained bottom sediment, which is then distributed in the water column. At this point the particles are carried into the ocean producing the observed sediment plume even for low river discharges. The turbulence appears at the north bank of the river mouth and moves towards the south bank as the tide falls. It maintains its position for a few hours until the water levels start rising again. This behavior favors erosion and deposition processes which shift location with the tide. These are the cause of sediment pulses. It is suggested then that this mechanism is involved in keeping the river mouth morphology (i.e. depth and width) constant in time. The mouth moves towards north due to longshore currents, but not

significant change in width has been observed during post Tsunami recovery.

Another important feature observed at the river mouth was the differentiated wave-breaking pattern at each side of the river mouth (Figure 6 a & b). Waves mostly approach to shore from a south-west direction. When those waves interact with the river current going out the inlet, a current refraction phenomenon occurs with the waves. This refraction in combination with a gentle slope due to the sedimentation on the south bank of the inlet generated by the longshore currents (Fitzgerald 1996), and spilling wave breaking. In contrast, on the north bank, waves break by plunging, with a much steeper beach slope and frequently under an erosion profile. This breaking process transports sand from the spit into the river channel, explaining the main mechanism of migration for the sand barrier towards the north.

## CONCLUSION

### Conceptual Model of the River Inlet

Our preliminary observations show that flushing occurs during ebb tides and river floods. Furthermore, the ebb currents fluctuate through the tidal cycle, generating a vertical mixing of water that seems to travel along the cross section of the channel. According to pressure sensor observations, this phenomenon could be related to difference in water table between the river and the estuary behind the sand spit.

Differentiated wave breaking and beach slope at the river mouth induced by wave refraction due to ebb tidal currents and sedimentation process due to longshore currents, explain the migration mechanism of the sand spit to the north (Figure 6c). Pulses of fine sediment flushing, continuous sediment delivery and no delivery alternate daily in the inlet. These pulses are flushed away by the river at erratic intervals, but it seems to be

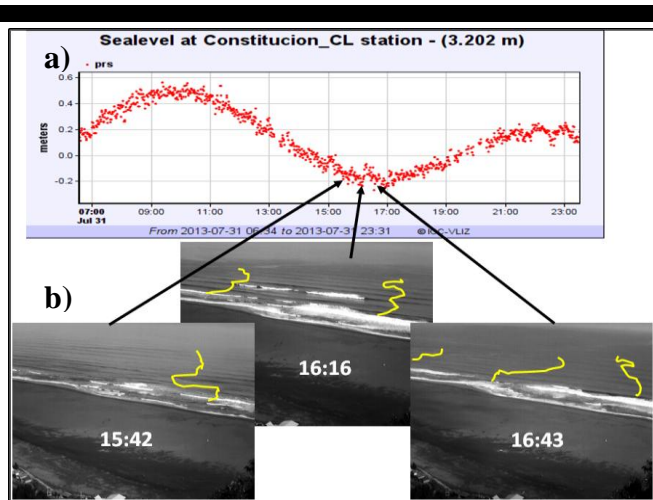


Figure 5. a) Part of the tidal curve at Constitución tidal gauge (nearest point to Mataquito river mouth), (source IOC-UNESCO). b) Averaged images of Cam1 showing in yellow the sediment pulses at July 31<sup>st</sup> 2013.

connected to periods of water storage at the estuary and periods of water discharge and hydrodynamics from the estuary. Although South-West predominantly wave climate control the longshore current and dominate the shape of the river mouth, it does not heavily influence the occurrence of sediment flushing from the inlet

The combination of video monitoring system with field measurements (ADCP and others), proves to be an effective way to investigate the hydrodynamic-morphodynamic evolution of the river inlet. The accuracy in temporal and spatial resolution obtained using these techniques allows us to quantify qualitatively and sometimes quantitatively the forces involved on this process.

In the Mataquito river mouth, a minimum tidal range of 0.8 m seem to be necessary to produce an effective flushing of sediment

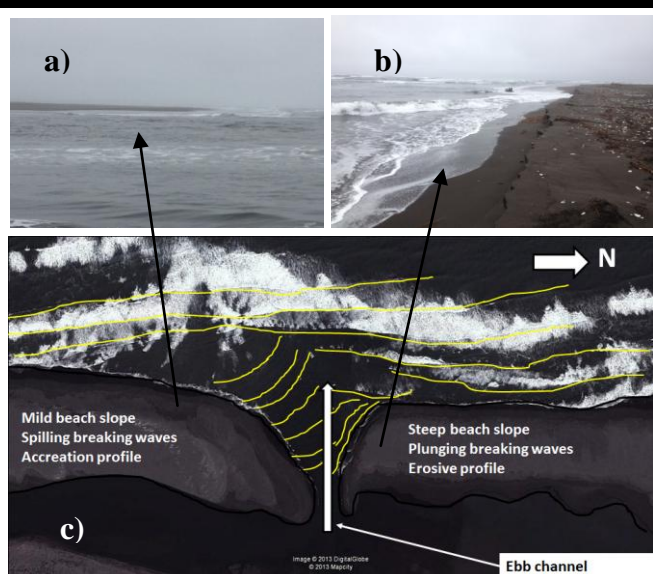


Figure 6. a) & b) South and North images of beach face respectively. c) Concept model of river inlet migration (Image source: Google Earth).

and develop a turbid sediment plume in the sea. Moreover, under river flooding conditions, this limit seems not to be necessary, since the flushing is then controlled by river discharge.

The apparent equilibrium achieved by the inlet is controlled by a sum of factors including: longshore current, tidal range, river discharge, river inlet hydrodynamics and waves conditions. The inlet migration is generated by a differentiated wave breaking and sedimentation/erosion process, induced at each side of the inlet. Hence, the random behavior of the inlet flushing during low tide, alternate with the appearance of vertical eddies, regulating periods of water storage at the estuary and water discharge at the river mouth.

## ACKNOWLEDGEMENT

This work has been funded by the Chilean National Science and technology Committee CONICYT through the Fondecyt project N°1120878. Mauricio Villagran has been supported by CONICYT through a PhD scholarship. The CONICYT/FONDAP/15110017 program is also acknowledged

## LITERATURE CITED

- Cienfuegos R., Villagran M., Aguilera J.C., Catalán P., Castelle B., and Almar R., 2014. Video Monitoring and Field Measurements of a Rapidly Evolving Coastal System: the River Mouth and Sand Spit of the Mataquito River in Chile. *J. Coastal Research*, S.I. 65, (this volume).
- Cooper, J.A.G. 2001. Geomorphological variability among microtidal estuaries from the wave-dominated South African coast. *Geomorphology*, 40, 99-122.
- Fitzgerald, D. M., 1996. Geomorphic Variability and Morphologic and Sedimentologic Controls on Tidal Inlets. *J. Coastal Research*, S.I. 23, 47-71.
- Freire, P., Taborda, R., Bertin, X., Guerreiro, M., Fortunato, A. B., Silva, A. M., Andrade, C., Oliveira, A., Antunes, C., Freitas, M. C., Nahon, A., Rodrigues, M. and Bruneau, N., 2011. Medium-term morphodynamic evolution of a small coastal inlet. *J. Coastal Research*, S.I. 64, 666-670. Szczecin, Poland
- Holland, K.T., Holman, R., Lippmann, T., Stanley, J. and Plant, N., 1997. Practical use of video imagery in nearshore oceanographic field studies. *J. Oceanic Engineering*, 22, 81-92.
- Hume T., Snelder, T., Weatherhead M. and Liefing M., 2007 A controlling factor approach to estuary classification. *Ocean & Coastal Management* 50, 905-929
- Lichter, M., Klein M., and Zviely D. 2011. Dynamic morphology of small south-eastern Mediterranean river mouths: a conceptual model. *Earth Surf. Process. Landforms* 36, 547-562.
- Morris D., Coco G., Bryan, K. and Turner I., 2007. Video-derived mapping of estuarine evolution. *J. Coastal Research*, S.I. 50, 410-414.
- Morris B., Davidson M. and Huntley D. 2001. Measurements of the response of a coastal inlet using video monitoring techniques. *Marine Geology* 175, 251-272.
- Paterson A., Hume T., and Healy T. 2001. River Mouth Morphodynamics on a Mixed Sand-Gravel Coast. *J. Coastal Research* S.I. 34, 288 – 294.
- Tung, T. T., Walstra, D. J. R., Graaff, J. van de and Stive, M. J. F. 2009. Morphological modeling of tidal inlet migration and closure, Lisbon, Portugal. *J. Coastal Research*, S.I. 56, 1080-1084.
- Villagran M., Cienfuegos R., Almar R., Gironás J., Catalán P., Camaño C. and Dominguez J.C. 2011. Natural post tsunami recovery of Mataquito river mouth after 2010 Chilean tsunami. *Proc. AGU Fall Meeting Conference* (San Francisco, USA).

# Tidal dispersion and flushing times in a multiple inlet lagoon



[www.cerf-jcr.org](http://www.cerf-jcr.org)

João D. Lencart e Silva†, Carina L. Lopes†, Ana Picado†, Magda C. Sousa† and João M. Dias†

†NMEC, CESAM  
Departamento de Física  
Universidade de Aveiro  
3810-193 Aveiro, Portugal  
j.lencart@ua.pt  
carinalopes@ua.pt  
ana.picado@ua.pt  
mcsousa@ua.pt  
joao.dias@ua.pt



[www.JCRonline.org](http://www.JCRonline.org)

## ABSTRACT

Lencart e Silva, J. D., Lopes, C. L., Picado, A., Sousa, M. C., Dias, J. M., 2014. Tidal dispersion and flushing time in a multiple inlet lagoon. In: Green, A.N. and Cooper, J.A.G. (eds.), *Proceedings 13<sup>th</sup> International Coastal Symposium* (Durban, South Africa), *Journal of Coastal Research*, Special Issue No. 70, pp. 598-603, ISSN 0749-0208.

The Ria Formosa is a tidal multi-inlet shallow-water coastal lagoon located in the south of Portugal, subjected to the dry Mediterranean climate. The tide controls the Ria's exchange with the adjacent shelf for most of the hydrological year except for isolated torrential run-off events. Episodes of low hypoxia reported in the literature may be related to the lagoon's flushing time, affecting its shellfish production valued at 20 – 50 million €y<sup>-1</sup>. Over the past decades several observational and modelling studies presented values for the capacity of the tide to renovate the water inside the Ria. However, these studies lack either the spatial resolution to yield results unaffected by numerical diffusion or analyze a very limited part of the lagoon's territory. In this work, we use a very-high resolution hydrodynamic model to assess the flushing time exclusively due to tidal forcing inside the Ria Formosa. A bi-dimensional implementation of the finite-volume/finite-difference Eulerian–Lagrangian hydrodynamic and transport model (ELCIRC) was used, allowing for the local refinement of the computational domain, which best suits the lagoon's complex morphology. The present model configuration was validated for tidal propagation with sea surface elevation collected in 1979/80 at 11 lagoon stations. The validation results show a good agreement between predicted and observed elevations, with root mean square errors lower than 20 cm and skill values higher than 0.98. A set of experiments were carried out by releasing a conservative tracer at different stages of the tide at discrete points of the Ria, where possible environmental hazard hot-spots are located and the flushing e-folding time calculated from the tracer's dilution. The results are discussed taking into account the propagation of the tide in this multi-inlet, meandering topography. Evidence is presented of topographic trapping due to the complex spatial distribution of the phase lags of the semi-diurnal tidal constituents. This evidence explains the significant increase of the flushing time from the inlets to the head of the channels, thus justifying the use of detailed spatial resolution when modelling such a complex system.

**ADDITIONAL INDEX WORDS:** *topographic trapping, Ria Formosa, contamination risk, exchange dynamics.*

## INTRODUCTION

Lagoons are transitional zones between terrestrial and marine aquatic environments, usually providing shelter and nursery areas for a variety of species and often hosting anthropogenic activities which may pose a significant threat to these ecosystems. Their main characteristic of buffer zone between open ocean and land can be the source of their vulnerability to hazards related to the time the lagoon takes to exchange water through its inlets.

The Ria Formosa is a mesotidal multi-inlet shallow-water coastal lagoon located in the south of Portugal, subjected to the dry Mediterranean climate (36°06'N, 8°02'W to 37°03'N, 7°32'W, Figure 1), spanning ~55 km along the coast and ~6 km across its widest zone (Dias *et al.*, 2009). The tide controls the Ria's exchange with the adjacent shelf through 6 inlets, Ancão, Faro-Olhão, Armona, Fuseta, Tavira and Cacela on most of the hydrological year, except for isolated torrential run-off events (Newton and Mudge, 2003). The lagoon is composed of salt

marshes, sand flats and a network of natural and partly dredged channels. Its complex geometry, with innumerable channels and straits and multiple inlets, makes it a considerably challenging study area. However, the study of the controls of the circulation of its water is essential to assist the management of its conflicting uses, such as tourism, fisheries, aquaculture and salt extraction industries, as well as a natural habitat for various species of birds which gives the Ria its status of Natural Reserve.

The tide in the Ria Formosa is mainly semidiurnal with the range varying from 1.3 m in neaps tides to more than 3 m in spring tides, resulting in a submerged surface area between 14 - 43 km<sup>2</sup> (Instituto Hidrográfico, 1986). This results in a large tidal prism in relation to its volume, with 50% to 75% of the lagoon's volume flowing through its inlets (Salles *et al.*, 2005). Nevertheless, episodes of low hypoxia reported in the literature at the inner zones of the lagoon may be related to the lagoon's flushing efficiency there, affecting its shellfish production valued at 20 - 50 million €y<sup>-1</sup> (Ferreira *et al.*, 2012).

DOI: 10.2112/SI70-101.1 received 1 December 2013; accepted 21 February 2014. © Coastal Education & Research Foundation 2014

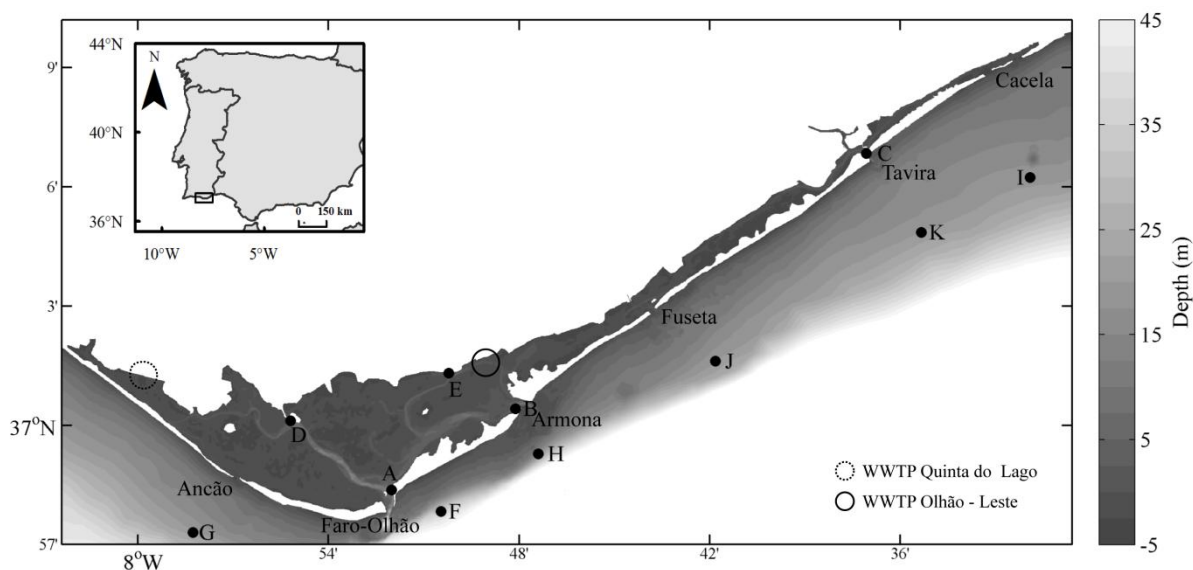


Figure 1. Location map of the Ria Formosa lagoon showing: bathymetry; location of the SSE calibration stations (A to K); names of the 6 inlets; location of the wastewater treatment plants.

The Ria can be broadly divided into 3 cells: i) the westernmost cell served by the Ancão, Faro-Olhão and Armona inlets; ii) the central cell served by the Fuseta inlet; and iii) the easternmost cell served by the Tavira and Cacela inlets (Fig. 1). Of these three cells the westernmost is the largest, most complex and subjected to more anthropogenic influence.

Over the past decades several observational and modelling studies presented values for the capacity of the tide to renew the water inside the Ria. Newton and Mudge (2003) and Mudge *et al.* (2008) used water temperature and salinity as tracers to describe the circulation around the western part of the Ria and give a measurement of the water residence time inside that area. Neves (1988) applied a numerical model to study the Ria's tidal exchange with ocean, however, the low resolution of the model used in this study was unable to resolve the more intricate morphology of the lagoon, thus giving good results for the areas near the inlets, but failing to do so in the higher reaches where higher risk to long water residence is expected. Dias *et al.* (2009) studied the Ria with a high-resolution model, but their work was mainly focused on the effects of the relocation of the Ancão inlet.

In this article we aim to give an overall, high spatial resolution account of the flushing time in the Ria Formosa solely forced by the tide, highlighting the main features of its distribution and providing an analysis of the risk of exposure to a hypothetical release of a harmful pollutant from two risk sites reported in APA and ARH (2012).

Tidal flushing of the lagoon's water can occur by advection of the water by a coastal current away from the inlets tidal excursion, by tidal shear dispersion (Fisher, 1979), tidal rectification (Li and O'Donnell, 1997) and chaotic dispersion (Ridderinkhof and Zimmerman, 1992). On the other hand, several methods have been suggested to assess the exchange and transport processes between restricted zones and the ocean. We choose to adopt the definition of flushing time ( $\tau$ ) of a time varying tracer concentration  $C(t)$  as proposed by Takeoka (1984), where:

$$\tau = \int_{t_0}^{\infty} C t \, dt \quad (1)$$

For our case we assumed the continuously stirred tank reactor (CSTR) simplification, as in Monsen *et al.* (2002) where  $C(t)$  can be found from:

$$C t = C_0 e^{-\frac{t}{\tau}} \quad (2)$$

where  $\tau$  can be found by linear regression, and  $C_0$  is the initial tracer concentration:

$$\ln C t = -\frac{t}{\tau} + \ln(C_0) \quad (3)$$

## METHODS

### Model

In order to best accommodate the complex morphology of interconnect channels and tidal flats of the Ria Formosa, we used for this study a hydrodynamic model relying on an unstructured grid. The ELCIRC (Zhang *et al.*, 2004) hydrodynamic model uses a finite-volume/finite difference Eulerian-Lagrangian algorithm to solve the shallow water equations on a horizontal unstructured grid. In this application the model solves the Navier-Stokes shallow water equations for surface elevation and the bi-dimension water velocity with hydrostatic, Boussinesq and f-plane approximations. The integration in time is done with a semi-implicit scheme, where the barotropic pressure gradient in the momentum equation and the flux term in the continuity equation are treated semi-implicitly; the bottom boundary condition for the momentum equations is treated fully implicitly; and all other terms are treated explicitly.

For this study the tide was the only forcing applied, and was determined from the harmonic constituents calculated by Fortunato *et al.* (2002). A set of 11 harmonic Sea Surface



Elevation (SSE) constituents and mean sea level ( $Z_0$ ,  $M_{sf}$ ,  $O_1$ ,  $K_1$ ,  $N_2$ ,  $M_2$ ,  $S_2$ ,  $MN_4$ ,  $M_4$ ,  $MS_4$ ,  $M_6$ , and  $2MS_6$ ) were prescribed at the boundary. The bed roughness was prescribed using the Manning formulation. For all of the scenarios described below, the model was started with unperturbed SSE and elevation, and a 2 day warm-up period was carried out by ramping-up the tidal forcing to production values. A 60 s time step was adopted to comply with the Courant-Friedrichs-Lewy stability parameter.

The model used in this study is based on the one used by Dias *et al.* (2009) and Dias and Sousa (2009), with further refinement in the horizontal where new bathymetric data was available. Based on the new bathymetric data, the Manning roughness coefficient was changed using the same depth-dependence strategy applied in Dias *et al.* (2009).

Given that no lagoon-wide survey of SSE or velocities were available under the most up-to-date bathymetric conditions, we chose to run the refined horizontal grid with the bathymetric data and respective bed roughness used in Dias *et al.* (2009) to check our model against the available SSE observations and the previously published model. The validation was done by comparing the measured and predicted time series of SSE for 11 stations (Fig. 1) from a 1979/1980 dataset using contemporary bathymetry. The validation results show a good agreement between predicted and observed elevations and in line with the previously published version of the model, with root mean square errors lower than 20 cm and skill values higher than 0.98.

The production scenarios were then run with an up-to-date bathymetry and inlet configuration.

## Scenarios

In order to assess the flushing times in the Ria Formosa the lagoon was filled with a uniformly distributed passive tracer with a concentration of  $1 \text{ kgm}^{-3}$ . The model was then run for 75 days and the concentration outputted every hour of model calculation time.

After filtering the semidiurnal tidal signal out with a pl33 low-pass filter (Flagg *et al.* 1976; Beardsley *et al.*, 1985) transient flushing times were calculated for spring and neap tide conditions using Equation 3 by least-squares fitting a 5-day window and extracting  $\tau$ . These fits add  $r^2$  in a range 0.64-0.99 and p-values < 0.001. The calculation of an aggregated fortnightly value for the flushing time was made by extending the regression window to one full neap to spring cycle with the same satisfactory fit.

To assess the risk of exposure to a hypothetically harmful pollutant concentration (LD), was emitted from the locations of 2 wastewater treatment plants (WWTP – Fig. 1) a discharge of passive tracer in spring and neap tide conditions. The discharges were carried out in separate runs for each WWTP, for each of the tidal conditions with the same flow and concentration of  $1 \text{ kgm}^{-3}$  for 2 days. Hourly in each calculation point, the exceedance of LD was counted for 7 days of the simulation run ( $N_{LD}$ ). An empirical probability of exceeding LD was calculated by dividing  $N_{LD}$  by the total simulation hours. For the purpose of this study we defined LD as 10% of the concentration at the discharge outlet.

## RESULTS AND DISCUSSION

### Spatial distribution of flushing time

Figures 2a and 2b show the residence times calculated for 5-day window around neap and spring tides, respectively. Common to both scenarios the zones near all of the inlets, with exception to the westernmost Ancão inlet, present very low flushing times of less than 50 hours. On the opposite extreme, the westernmost

region served by the Ancão inlet shows flushing times reaching about 40 days under neap tide conditions.

As expected, the neap tide snapshot shows considerably longer flushing times, with channel margins near the Armona inlet and between this inlet and the Fuseta inlet assuming a relatively longer flushing than in the spring tide.

Comparing the  $M_{sf}$  constituent in the margins and in the deeper channel shows larger amplitude ( $\sim 14 \text{ cm}$ ) in the former in phase with the spring tide. During neaps the semidiurnal mean sea level is lower and quadratic friction is distributed by a smaller water column, thus reducing the efficiency of tidal dispersion.

Over the full fortnightly cycle (Figure 2c), apart from the western cell serviced by the Ancão, Faro-Olhão and Armona inlets, the lagoon is efficiently flushed by the tide.

For the lagoon's western cell the results show that the main contributor for the flushing is the Faro-Olhão inlet, with very low flushing times in its vicinity and in the channel connecting this and the Armona inlet. This is due to the combined effect of a larger tidal prism exiting through the Faro-Olhão inlet and the higher tidal velocities inducing efficient tidal dispersion. In the main channel leaving the Faro-Olhão inlet to the northwest, outside the reach of the tidal excursion of this inlet, flushing time rises considerably, reaching 15 days for the western end of the lagoon.

### Remarkably confined areas in the lagoon

Hill (1994) shows that in a single inlet lagoon, the  $M_{sf}$  phase lag on the spring tide indicates the level of choking of a lagoon. In the Ria Formosa, the  $M_{sf}$  constituent is roughly in phase with the spring tide, so in this aspect the Ria can be considered a leaky lagoon according to Kjerfve (1986) terminology. However, there are significant differences in amplitude of the  $M_{sf}$ , which can be negligible near the inlets and be as high as 0.5 m near the head of the channels in the more confined areas such as the westernmost area of Ancão peninsula. This indicates that within these areas exists a fortnightly cycle of water storage, which contributes to the decrease in the lagoon's flushing.

Another aspect leading to the confinement of the water in the lagoon is its meandering morphology, which leads to topographic trapping due to the complex spatial distribution of the semidiurnal tidal phases. Figure 3 shows the phase of the  $M_2$  tide for the Ramalhete region. Between point A and point B, the tide lags  $\sim 40^\circ$  where the mean  $M_2$  velocity is  $\sim 0.3 \text{ ms}^{-1}$  for an extension of  $\sim 3000 \text{ m}$ . By the time the water, which started the flood at point A of the channel reaches point B, the tide there is already ebbing, channeling the water to the longer channel leading to the Faro-Olhão inlet. This water will return to the A-B segment in the next tide, thus resuming the trapping mechanism. This confirms the findings of Newton and Mudge (2003) and Mudge *et al.* (2008) who observed this behaviour using salinity and water temperature as tracers. Of the four flushing mechanisms mentioned in the introduction, the water in this channel is mainly affected by tidal shear dispersion and rectification. Given that the flow is essentially confined to the channel, the water is not affected significantly by chaotic dispersion nor advection by offshore, since the reversing trapping mechanism keeps the water from reaching the inlets, with a flushing time between 5 and 7 days.

### Risk analysis

Figure 4 shows that a discharge at the Quinta do Lago WWTP (QdL) has higher values of LD spread by a wider area when released at spring tide. Inversely, the discharge at the Olhão-Leste WWTP (OL) has its main effect when discharged at neap tides.

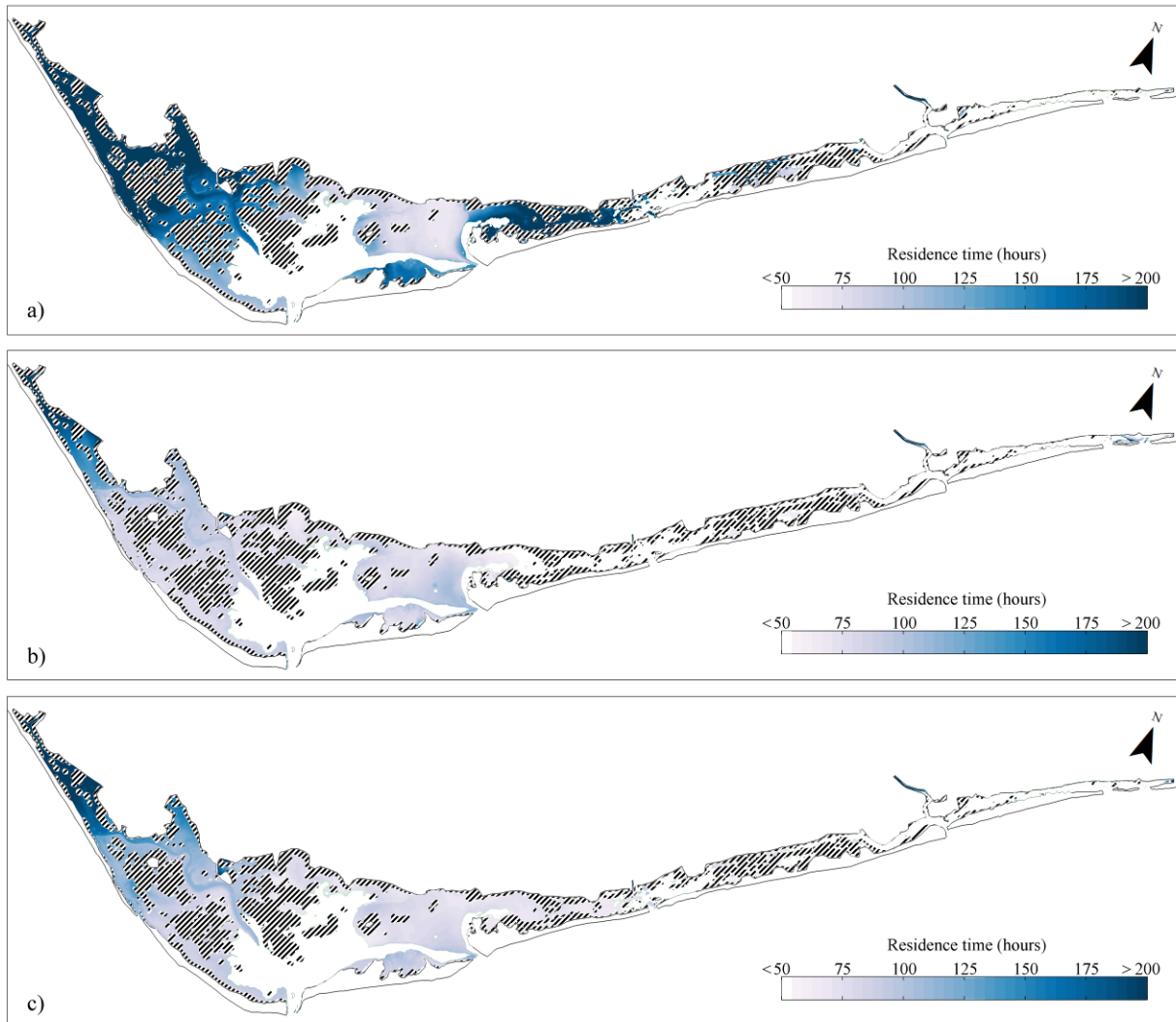


Figure 2. Flushing time in the Ria Formosa Lagoon (invalid regions in stripes): a) calculation for neap tide conditions; b) calculation spring tide conditions; c) calculation for full fortnightly cycle.

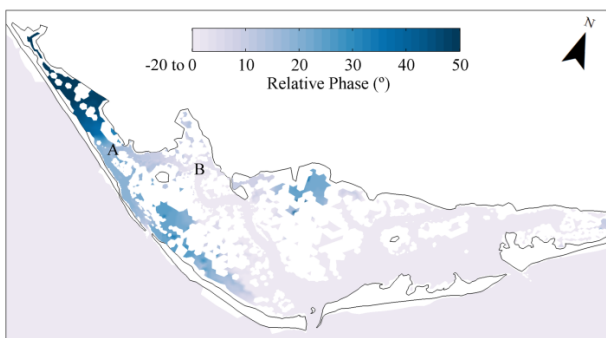


Figure 3.  $M_2$  tidal constituent phase relative in the western cell of the lagoon relative to point. Segment AB representing the Ramalhete channel.

This contrast can be attributed to proximity of each of the discharge sites to a main inlet.

The OL site connects to the Armona inlet, which on a spring tide quickly flushes the affected area reducing the LD exceedance probability. Following the same rationale, the larger currents in neap tides in this area in comparison to the QdL site manage to spread the pollutant to a wider area before the Armona inlet is able to flush the water.

For the QdL case, low flushing in neap tides is responsible for the minute dissipation of the pollutant during the beginning of the neap to spring cycle, thus reducing the area exposed to LD. In the spring tide discharge scenario at QdL, low flushing of this western area combined with the enhanced tidal dispersion at spring tides works to spread the pollutant through a wider area before its concentration is diluted.

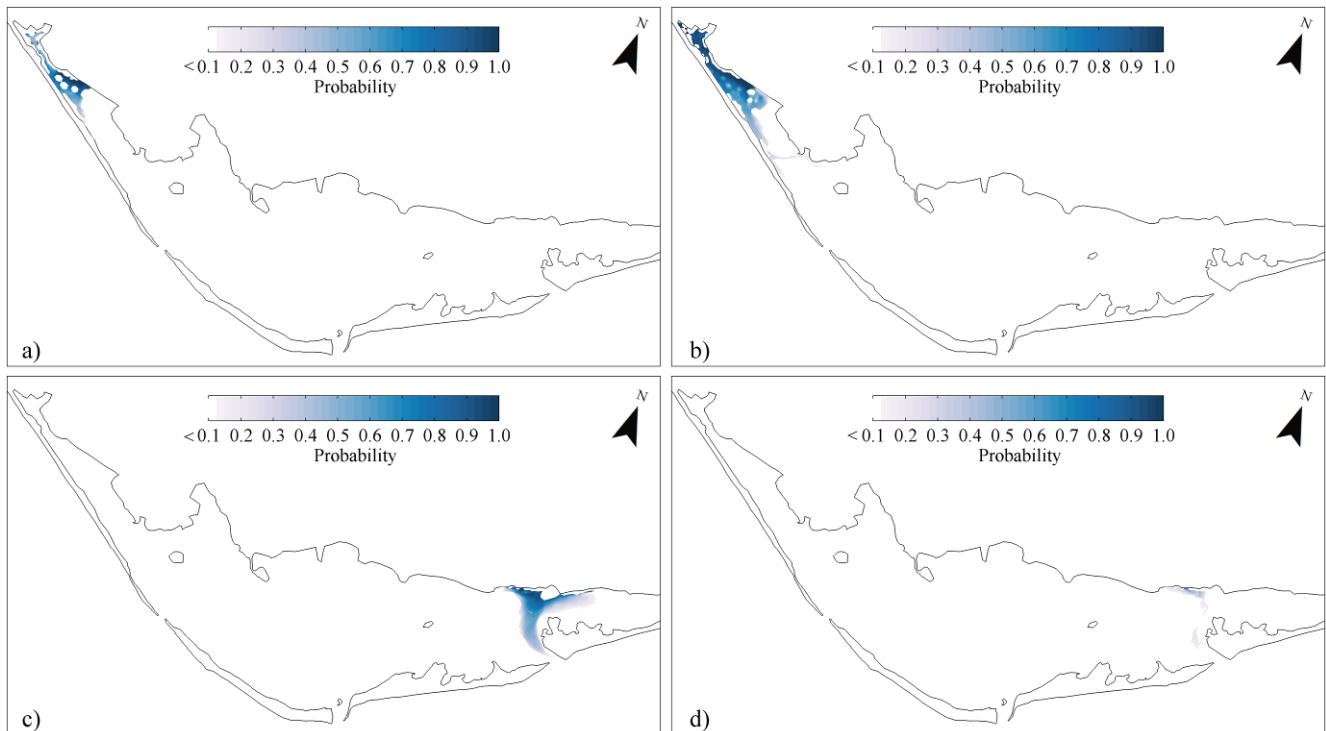


Figure 4. Probability of exceedance of LD: a) discharge in neap tide conditions at Quinta do Lago WWTP (QdL); b) discharge in spring tide conditions at QdL; c) discharge in neap tide conditions at Olhão-Leste WWTP (OL); d) discharge in spring tide conditions at OL.

## CONCLUSIONS

A high resolution unstructured grid hydrodynamic model was used to assess the spatial distribution of the flushing time in the Ria Formosa lagoon solely due to tidal forcing.

It was found that although near the inlets the lagoon has very low flushing of less than 50 hours, further away from the inlets the residence time rises considerably, reaching about 15 days in problematic areas such as Ancão peninsula.

The main tidal controls found to these remarkably confined zones are the  $M_{st}$  amplitudes there, reaching as high as 0.5 m in areas where depths are under 2 m, and topographic trapping due to the complex spatial distribution of the phase of semidiurnal tidal constituents.

Furthermore, a marked neap to spring cycle of flushing was found where the tide can efficiently flush the lagoon at springs but is unable to do so at neaps.

The release of a hypothetically harmful pollutant concentration (LD) in two locations of the bay showed tidal dispersion and the distance from an efficient exchange inlet combine to disperse LD for a wider area of increased exposure.

This work only takes into account the role of the tide in the control of the exchange between the Ria Formosa and the Atlantic Ocean. Although the tide is the main driver inside the Ria, due to the absence of significant density driven flow or relevant wind fetch, the shelf outside of the Ria is controlled by nearshore wind, remote wind, thermohaline circulation and mesoscale features of the Gulf of Cadiz. The circulation at the shelf may contribute to the lagoon's flushing through enhanced mixing with the ocean waters or by advecting the lagoon water away from the tidal excursion of its inlets. Conversely, trapping mechanisms such as downwelling and the formation of an inner shelf (Lenz, 1995) may

lead to the permanence of the lagoon water within reach of its inlets and promote offshore connectivity between its 3 cells. Future modelling studies of the Ria's flushing time and the connectivity between its 3 cells should take into account the currents and mixing conditions at the Ria's neighbouring shelf.

## ACKNOWLEDGEMENTS

The work described in this publication was supported by the European Community's 7th Framework Programme through the grant to the budget of the Integrating Activity HYDRALAB IV, contract no. 261520. The second, third and fourth authors have been supported by the Portuguese Science Foundation through a doctoral grants (SFRH/BD/78345/2011), (SFRH/BD/79920/2011) and (SFRH/BD/60209/2009), respectively.

## LITERATURE CITED

- APA and ARH, 2012. PGBH que integram a Região Hidrográfica das Ribeiras do Algarve (RH8): Parte 2, Tomo 4. Agência Portuguesa do Ambiente, 358 pp.
- Beardsley, R. C., Limeburner, R. and Rosenfeld, L. K., 1985 *Introduction to the CODE-2 moored array and large-scale data report*, edited by: Limeburner, R., Woods Hole Oceanographic Institution.
- Dias J.M. and Sousa M., 2009. Numerical modeling of Ria Formosa tidal dynamics. *Journal of Coastal Research*, S.I. 56, 1345-1349.
- Dias, J.M., Sousa, M.C., Bertin, X., Fortunato, A. and Oliveira A., 2009. Numerical modeling of the impact of the Ancão Inlet relocation (Ria Formosa, Portugal). *Environmental Modelling & Software*, 24, 711-725.
- Ferreira, J.G., Saurel, C., Nunes, L., Lencart e Silva, J.D., Vazquez F., Bergh, Ø., Dewey, W., Pacheco, A., Pinchot, M., Ventura Soares, C., Taylor, N., Verner-Jeffreys, D., Baas, J., Petersen, J.K., Wright, J., Calixto, V. and Rocha M., in press. *FORWARD - Framework for Ria Formosa Water Quality, Aquaculture, and Resource Development*. Lisbon. IMAR- Institute of Marine Research, pp. 224.

- Fisher, H. B., List, E.J., Koh, R.C.Y., Imberger, J. and Brooks, N.H., 1979. *Mixing in Inland and Coastal Waters*. Academic Press, New York, NY.
- Flagg, C.N., Vennerssch, J.A. and Beardsley, R.C., 1976. 1974 M.I.T. New England Shelf dynamics experiment (March, 1974) Data Report Part II: The moored array: M.I.T. Report 76-1. Cambridge, MA, Massachusetts Institute of Technology.
- Fortunato, A.B., Pinto, L., Oliveira, A. and Ferreira, J.S., 2002. Tidally generated shelf waves off the western Iberian coast. *Continental Shelf Research*, 22(14), 1935-1950.
- Hill, A.E., 1994. Fortnightly tide in a lagoon with variable choking. *Estuarine, Coastal and Shelf Science*, 38, 423-434.
- Instituto Hidrografico, 1986. Marés 81/82 Ria de Faro. Estudo das marés de oito estações da Ria de Faro. Instituto Hidrografico, Lisbon, 13 pp.
- Kjerfve, B., 1986. *Comparative oceanography of coastal lagoons*. In: Wolfe, D.A. (Ed.), *Estuarine Variability*. Academic Press, New York, 63-81.
- Lentz, S. J., 1995. Sensitivity of the Inner-Shelf Circulation to the Form of the Eddy Viscosity Profile. *Journal of Physical Oceanography*, 25, 19-28.
- Li, C. and O'Donnell, J., 1997. Tidally driven residual circulation in shallow estuaries with lateral variation. *Journal of Geophysical Research*, 102: 27,915-27,929.
- Monsen, N.E., Cloern, J.E. and Lucas, L.V., 2002. A comment on the use of flushing time, residence time, and age as transport time scales. *Limnology and Oceanography*, 47(5), 1545-1553.
- Mudge, S.M., Icely, J.D. and Newton, A. 2008. Residence times in a hypersaline lagoon: using salinity as a tracer. *Estuarine, Coastal and Shelf Science*, 77(2), 278-284.
- Neves, R.J., 1988. Flow process modelling in a salt marsh. In: Schrefler, A., Zienkiewicz, A. (Eds.), *Computer Modelling in Ocean Engineering*. Balkema, Rotterdam, 303-310.
- Newton, A. and Mudge, S.M., 2003. Temperature and salinity regimes in a shallow, mesotidal lagoon, the Ria Formosa, Portugal. *Estuarine, Coastal and Shelf Science*, 57, 73-85.
- Ridderinkhof, H. and J.T.F. Zimmerman, 1992. Chaotic stirring in a tidal system. *Science*, 258, 1107-1111.
- Salles, P., Voulgaris, G. and Aubrey, D.G., 2005. Contribution of nonlinear mechanisms in the persistence of multiple tidal inlet systems. *Estuarine, Coastal and Shelf Science*, 65, 475-491.
- Takeoka, H., 1984. Fundamental concepts of exchange and transport time scales in a coastal sea. *Continental Shelf Research*, 3(3), 311-326.
- Zhang, Y., Baptista, A. and Meyers, E., 2004. A cross-scale model for 3D baroclinic circulation in estuary-plume-shelf systems: I. Formulation and skill assessment. *Continental Shelf Research*, 24, 2187-2214.

# Study of suspended sediment dynamics in a temperate coastal lagoon: Ria de Aveiro (Portugal)

Sandra Plecha<sup>†</sup>, Ana Picado<sup>†</sup>, Pedro Chambel-Leitão<sup>‡</sup>, João M. Dias<sup>†</sup>, Nuno Vaz<sup>†</sup>

<sup>†</sup>NMEC, CESAM  
University of Aveiro  
Aveiro, Portugal  
{sandraplecha, ana.picado, joao.dias,  
nuno.vaz}@ua.pt

<sup>‡</sup> MARETEC  
Technical University of Lisbon  
Lisbon, Portugal  
chambelpc@ist.utl.pt



[www.cerf-jcr.org](http://www.cerf-jcr.org)



[www.JCRonline.org](http://www.JCRonline.org)

## ABSTRACT

Plecha, S., Picado, A., Chambel-Leitão, P., Dias, J.M., Vaz, N., 2014. Study of suspended sediment dynamics in a temperate coastal lagoon: Ria de Aveiro (Portugal). In: Green, A.N. and Cooper, J.A.G. (eds.), *Proceedings 13<sup>th</sup> International Coastal Symposium* (Durban, South Africa), *Journal of Coastal Research*, Special Issue No. 70, pp. 604-609, ISSN 0749-0208.

Suspended sediment concentrations are simulated at Ria de Aveiro, a lagoon located in a temperate climate area in the northwest of Portugal. The fine-grained suspended sediment concentration is analyzed using the numerical model MOHID ([www.mohid.com](http://www.mohid.com)) and spatial maps of instantaneous and maximum concentration and also temporal variability at specified locations are analyzed in order to characterize the influence of the tide and sea level conditions in the suspended sediment concentrations within the lagoon. The highest suspended sediment concentrations were found in upstream areas during ebb conditions due to the river's proximity, while the minimum concentrations were observed near the inlet due to the presence of marine water poor in suspended sediments. When a 0.42 m sea-level rise (an estimate of conditions in 2100) is modelled, a decrease in suspended sediment concentration is observed for the overall study area, as result of an increase in the tidal prism.

**ADDITIONAL INDEX WORDS:** *Suspended sediment, sea level rise, sediments modeling, MOHID.*

## INTRODUCTION

Tidal dominated coastal systems, such as estuaries and lagoons, have experienced over the time, changes in geomorphology (especially erosion), which may be attributed to sea level rise (SLR), variations in the amount of sediment deposited on the coast and to anthropogenic degradation (Santos and Miranda, 2006). These changes could increase marginal inundation risk, salinity intrusion on adjacent land, marginal and bottom erosion, as well as restricting the navigation in shallow channels. Moreover, SLR may also contribute to changes in estuarine patterns of dissolved and non-dissolved matter, such as fine-grained cohesive sediments.

The importance of cohesive sediments in coastal regions has been widely recognized, playing an important role in the functioning of healthy ecosystems, since their transport, propagation and concentration influence the development of flora and fauna in estuaries and lagoons. Additionally, changes in sea level could induce changes in the spatial distribution of cohesive sediments and influence ecosystem biogeochemistry.

The variation in composition and spatial variability in suspended sediment dynamics render them difficult to study in the field. This is further hindered by complex interactions between tide and freshwater discharge. One way to overcome difficulties and study spatial and temporal variability of suspended sediments is to use high resolution numerical models.

In this study a numerical model is used to evaluate cohesive sediment dynamics in Ria de Aveiro (Figure 1), under both present mean sea level and a future sea level rise (SLR) scenario (+0.42 m).

Several studies have been undertaken on the effect of SLR in Ria de Aveiro. For example, Lopes *et al.* (2001) analyzed numerically the influence of tides and river inputs on suspended sediment concentration (SSC) in Ria de Aveiro lagoon, emphasizing Laranjo Bay from a bio-geophysical point of view. Also, Dias *et al.* (2003), Lopes *et al.* (2006) and Abrantes *et al.* (2006) used numerical models to investigate the spatial and temporal variability of SSC in this lagoon. Those authors concluded that tidal, wind- and river-induced residual currents contribute to the net export of water and sediments seaward, which is consistent with the ebb dominant nature of the system.

In this study, a high resolution numerical model is used to investigate the impact of SLR in the spatial and temporal patterns of suspended sediment in the Ria de Aveiro.

## STUDY AREA

The Ria de Aveiro lagoon (Figure 1), is located in a temperate climate area on the northwest coast of Portugal. Between the Vouga river basin and the Atlantic Ocean, this lagoon is highly influenced by marine and fluvial interaction. The lagoon is characterized by a complex geometry comprising several channels and intertidal areas, and is connected to the Atlantic Ocean through a narrow channel of 1.3 km length, 350 m wide and more than 30 m deep.

The Ria de Aveiro is a mesotidal system (with an average range at the inlet of 2.0 m) with a tidal semidiurnal pattern (Dias *et al.*, 2000). The tidal prism of the lagoon is approximately  $139.7 \times 10^6$  m<sup>3</sup> for maximum spring tide and  $65.8 \times 10^6$  m<sup>3</sup> for minimum neap tide (Picado *et al.*, 2010), with the water flux through the inlet ranging between  $6.26 \times 10^3$  m<sup>3</sup>s<sup>-1</sup> for spring tide and  $2.95 \times 10^3$  m<sup>3</sup>s<sup>-1</sup> for neap tide (Lopes *et al.*, 2013).

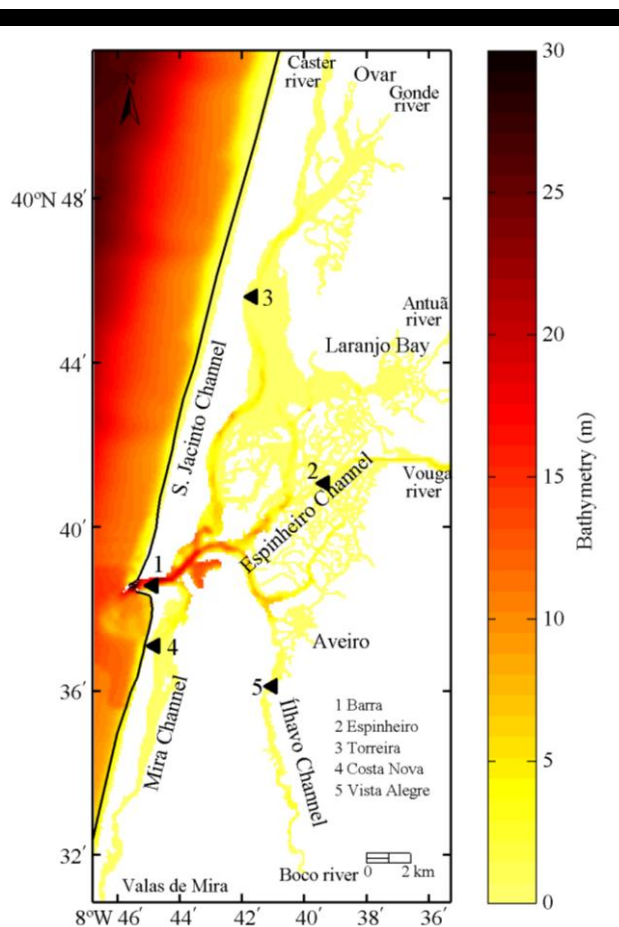


Figure 1. Location of Ria de Aveiro, identifying its main channels and the stations used in the study.

The lagoon receives freshwater from several rivers: the Antuã, Cáster, Gonde, Boco and Vouga rivers and Valas de Mira (see Figure 1). However the major fluvial input comes from the Vouga River which contributes 2/3 of the freshwater entering the lagoon, with an annual average flow of approximately  $70 \text{ m}^3 \text{ s}^{-1}$ .

The residual circulation is determined essentially by flood/ebb asymmetry, with higher velocities on ebb than on flood. As the lower lagoon is ebb-dominant, it shows a trend to export sediments to the ocean (Oliveira *et al.*, 2006, Plecha *et al.*, 2012).

The bottom granulometry of Ria de Aveiro channels is highly variable, being characterized by a combination of medium to fine sands with a variable content of finer particles (silt and clay), which increases with distance from the lagoon mouth. The inner zone of intertidal flats is mainly composed of medium to fine sand, silty clay and sandy clay (Freitas *et al.*, 2005).

## METHODS

The cohesive sediment concentration was analyzed using the numerical model MOHID ([www.mohid.com](http://www.mohid.com)) which encompasses a 2D advection-diffusion equation coupled to the hydrodynamic model.

### Numerical model

The numerical model used in this work is the two-dimensional baroclinic model MOHID ([www.mohid.com](http://www.mohid.com)), developed by the Instituto Superior Técnico (Universidade Técnica de Lisboa)

(Martins *et al.*, 2001). A finite volume discretization approach has been implemented (Martins *et al.*, 2001), allowing the use of a generic vertical coordinate. MOHID has been applied to several different coastal and estuarine areas and has shown its ability to simulate complex features of the flows (Ruiz-Villarreal *et al.*, 2002, Vaz *et al.*, 2005, 2009, Saraiva *et al.*, 2007, Mateus *et al.*, 2012). The hydrodynamic application described in this study is based on previous implementations for Ria de Aveiro (Vaz *et al.*, 2009, 2011).

The cohesive sediment transport model considers an Eulerian approach to compute fine sediment concentration in the water column. A 3D advection-diffusion equation integrated in MOHID is used in which the particle settling velocity is represented by the vertical advection (Cancino and Neves, 1994 a, b; 1995a, b). A differential control volume is used in computations considering the sediment accumulation rate and the sediment fluxes in and through the volume, respectively.

The governing equation can be written in the conservative form as:

$$\begin{aligned} \frac{\partial C}{\partial t} + \frac{\partial uC}{\partial x} + \frac{\partial vC}{\partial y} + \frac{\partial (w+W_s)C}{\partial z} \\ = \frac{\partial}{\partial x} \left( \varepsilon_x \frac{\partial C}{\partial x} \right) + \frac{\partial}{\partial y} \left( \varepsilon_y \frac{\partial C}{\partial y} \right) + \frac{\partial}{\partial z} \left( \varepsilon_z \frac{\partial C}{\partial z} \right) \end{aligned} \quad (1)$$

Where  $C$  is the suspended sediment concentration,  $t$  is time,  $x, y$  are the horizontal co-ordinates,  $z$  is the vertical co-ordinate,  $\varepsilon_x, \varepsilon_y$  and  $\varepsilon_z$  are the sediment mass diffusion coefficients,  $W_s$  the sediment fall velocity and  $u, v, w$  the flow velocity components in  $x, y, z$  directions.

### Numerical Setup

Numerical simulations are performed considering a numerical grid with spatial resolution of 100 m in order to minimize computational costs and a time step of 5 s.

The freshwater inputs from 6 main rivers are considered as landward boundary conditions. Each river inflow was predicted through the SWAT numerical model (Arnold *et al.*, 1998), which is a river basin scale model developed to quantify the impact of land management practices in large, complex watersheds.

The cohesive sediment transport model is initialized with a constant sediment concentration of  $0.01 \text{ mgL}^{-1}$  for the whole domain. The suspended sediment concentration fluctuation is simulated by imposing a specific suspended sediment concentration for each river discharge. Due to the lack of *in-situ* data for cohesive sediment concentration associated to each river inflow, reference values between 8 and  $10 \text{ mgL}^{-1}$  were used as boundary conditions. For sediment deposition a settling velocity of  $0.00001 \text{ ms}^{-1}$  is used.

The initial simulation period was between 1st December 2009 and 15th January 2010, integrating a spin-up period of 30 days, in order to encompass two times the maximum Ria de Aveiro residence time. The numerical results analyzed and presented here relate to the final 15 days of simulation.

Several numerical simulations were performed in order to characterize the cohesive sediment concentration under two sea level scenarios: current mean sea level (MSL) and a predicted rise of 0.42 m (SLR) to 2100 (Lopes *et al.*, 2011). Then, the sediment concentration patterns were analyzed along the tidal cycle and also in the spring-neap cycle, in order to evaluate differences due to tidal propagation.

Spatial maps of instantaneous and maximum concentrations as well as the temporal variability of sediments concentrations at specified locations (along the main channels of the lagoon) were analyzed in order to characterize the influence of the tide and sea

level conditions in the cohesive sediment concentrations distribution within the lagoon. The future RSL condition assumes no change in bed levels.

## RESULTS AND DISCUSSION

### Cohesive sediment dynamics

Simulations show that cohesive sediment dynamics in the Ria de Aveiro are characterized by a fortnightly pattern, related to the spring and neap tide, as illustrated in Figure 2 for five stations located within the lagoon. These five stations (Figure 1) were chosen in order to encompass distinct areas of the lagoon. The Barra station is located near the inlet and is the most downstream station, being under oceanic influence. The remaining four stations are located in the main channels of the Ria de Aveiro. The Espinheiro station is located in the central area of the lagoon under the influence of the major freshwater source: the Vouga River. The Torreira station is located in the S. Jacinto channel and is influenced by two rivers: the Cáster and Gonde. The Mira and Ílhavo channels are represented by the Costa Nova and Vista Alegre stations under the influence of Valas de Mira and Boco rivers, respectively. An additional river (Antuã) located in Laranjo Bay region (see Figure 1) was also considered in simulations.

The results depicted in Figure 2 show that the rivers are the main cohesive sediment source, which is evidenced by the high

concentrations found at the Espinheiro station located close to the Vouga river mouth. Additionally, higher concentrations are observed during ebb than flood conditions, since the main cohesive sediment source is the river discharge. The wide range in cohesive sediment concentration observed, between  $0.01 \text{ mgL}^{-1}$  at Barra and  $10 \text{ mgL}^{-1}$  at Espinheiro, shows the influence of marine and fluvial water in the lagoon.

The range of cohesive sediment concentration in upstream stations (Figure 2) is higher during spring tide than on neap tides, reflecting the higher intrusion of marine water (low concentration) that dilutes the fluvial waters (high concentration). The riverine influence on sediment concentration is also evident for neap tide periods when minimum cohesive sediment concentrations are higher than  $2.5 \text{ mgL}^{-1}$ .

For the SLR scenario, a decrease in cohesive sediment concentration is observed, induced by an increase of the lagoon tidal prism (Lopes *et al.*, 2013) and consequent higher intrusion of marine water with low cohesive sediment concentration.

A concentration decrease is predicted at the Torreira station, located in the S. Jacinto channel, with an average decrease of  $0.60 \text{ mgL}^{-1}$ . This reduction is caused by the importance of this channel in the water distribution through the lagoon, since 33% of the total volumetric flux of the lagoon crosses this channel.

The concentration in Espinheiro and Vista Alegre stations presents a decrease of about  $0.50 \text{ mgL}^{-1}$  (on average), since the tidal prism, due to the SLR at these channels increase at a higher rate (25%) than for the remaining channels (14%) (Lopes *et al.*, 2013).

### Maximum suspended sediment concentration

The spatial distribution of maximum suspended sediment concentration was computed for 15 days and is illustrated in Figure 3, for a spring/neap tide period and for the MSL and SLR scenarios.

The highest sediment concentrations are observed at the upstream regions of S. Jacinto channel, Laranjo Bay and Mira and Ílhavo channels, justified by the weak influence of the tide when compared with the river influence. In addition the cohesive sediment concentration maximums occur at spring tide (Figures 3a-c), since the stronger ebb currents at this tidal stage produce a downstream advection of water with high suspended sediment concentration.

For the Ria de Aveiro northern area, high concentrations are observed in spring tide (Figures 3a-c), with values ranging between  $4$  and  $8 \text{ mgL}^{-1}$ , while in neap tide period (Figures 3d-f) it ranges between  $3.5$  and  $8 \text{ mgL}^{-1}$ . For the central region of Ria de Aveiro, which encloses the Espinheiro channel, the Vouga river influence is noticeable, with maximum cohesive sediment concentrations of  $10 \text{ mgL}^{-1}$ . At Ílhavo and Mira channels, the maximum cohesive sediment concentrations are observed at spring tide, with values of  $8.2 \text{ mgL}^{-1}$ , while in neap tide they are 10% smaller.

For the SLR scenario, the maximum cohesive sediment concentrations are illustrated in Figure 3b,e. To better analyze the changes induced by the SLR, the differences between MSL and SLR concentrations were computed and are illustrated in Figures 3c and f. It is found that the SLR induces a generalized decrease in the maximum concentrations, in particular for spring tide (Figure 3a-c) due to an increase in seawater volume entering the lagoon. On the other hand, a slightly increase in maximum concentration is observed in Mira channel.

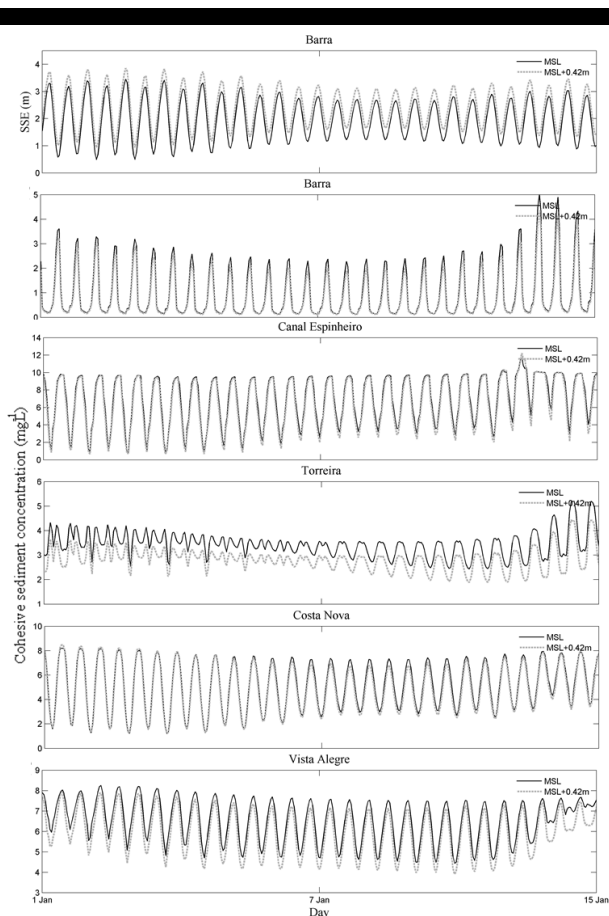


Figure 2. Water level (m) at Barra and suspended sediment concentration ( $\text{mgL}^{-1}$ ) for five stations within Ria de Aveiro, for a 15 day period.

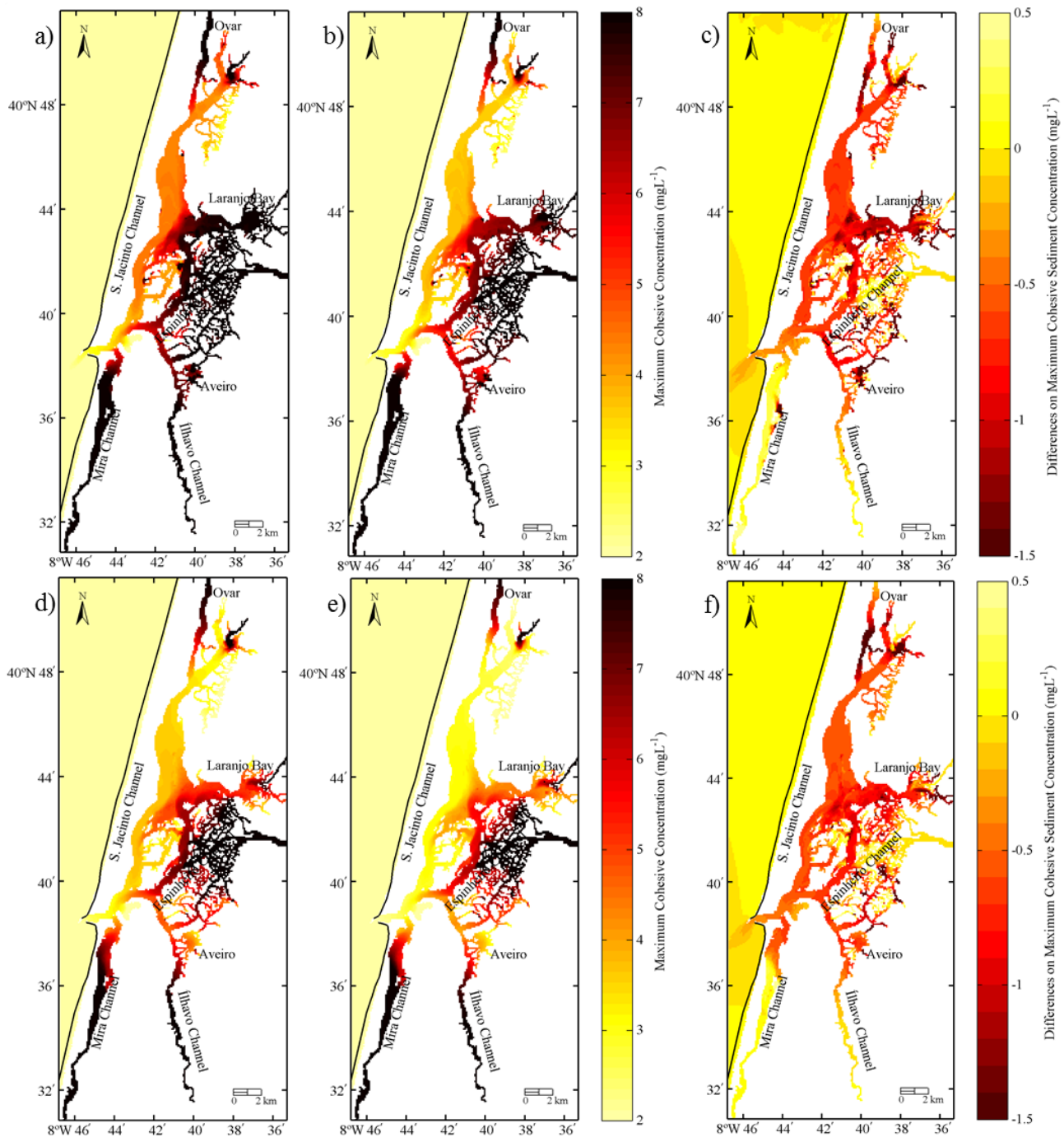


Figure 3. Maximum cohesive sediment concentration ( $\text{mgL}^{-1}$ ) in Ria de Aveiro for spring (a, b, c) and neap (d, e, f) tide periods, under contemporary mean sea level (a, d) and a sea level rise of 0.42 m (b, e). Differences between the two sea levels are shown in (c) and (f).

### Suspended sediment concentration – tidal cycle dependence

The suspended sediment concentration dependence on the tidal stage is illustrated in Figure 4 for four conditions: flood (a,e), high

tide (b,f), ebb (c,g) and low tide (d,h), for spring (a-d) and neap (e-h) tide periods, respectively.

The spatial distribution of suspended sediment concentrations reveals a spatial gradient. In the upstream regions high suspended sediment concentrations are found, close to those in the inflowing rivers which are cohesive sediment sources. Elsewhere, in downstream regions, the influence of sea water is evidenced by



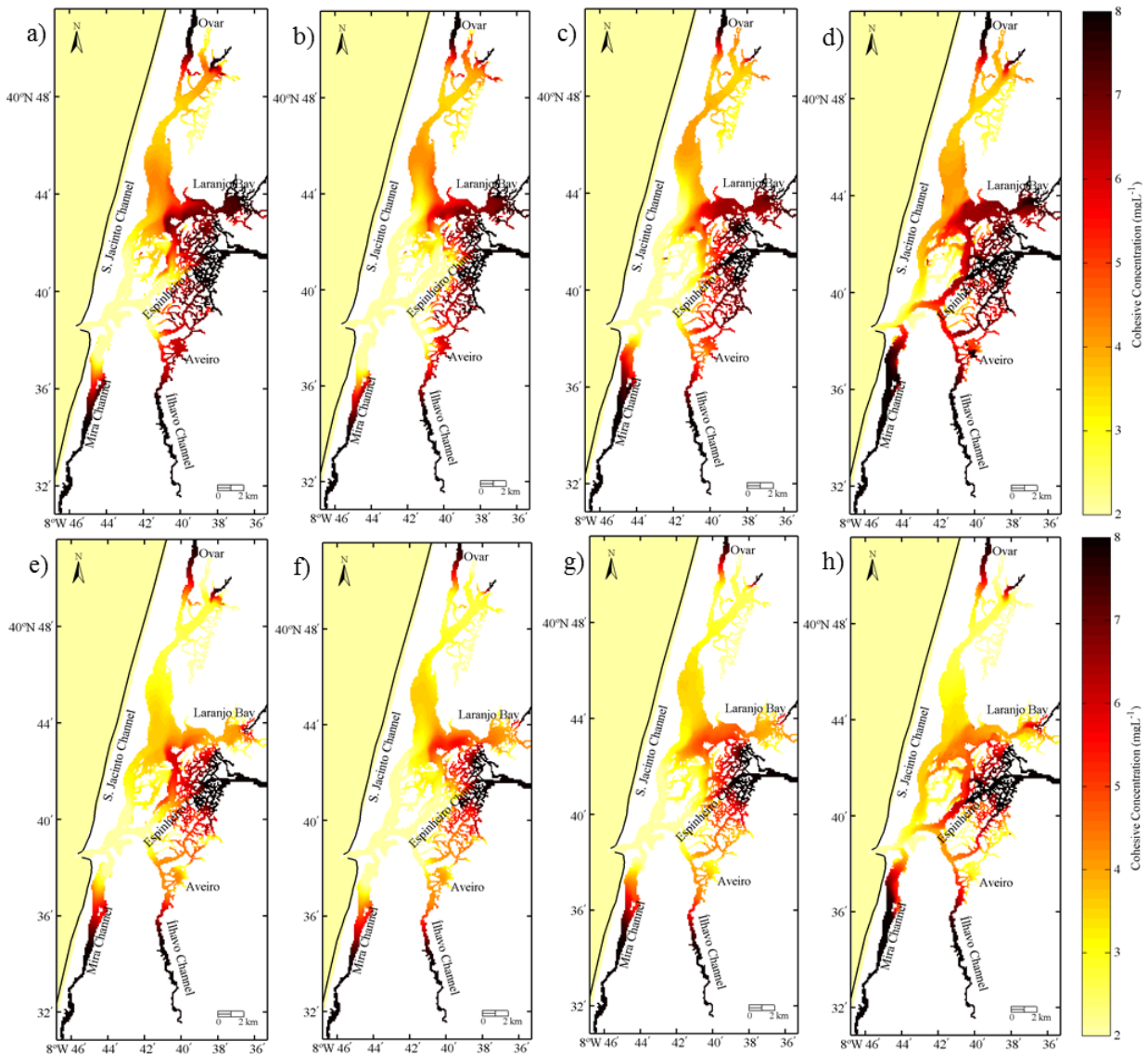


Figure 4. Cohesive sediment concentration ( $\text{mgL}^{-1}$ ) in a tidal cycle for a spring (a-e) and neap (e-h) tide periods at flood (a,e), high tide (b,f), ebb (c,g) and low tide (d,h).

the observed patterns of low concentrations ( $2 \text{ mgL}^{-1}$ ). Similarly to what was observed in Figure 3, the suspended sediment concentration is higher on spring than neap tides.

The highest concentrations are observed in the central area of the lagoon at low tide, with values ranging from  $3 \text{ mgL}^{-1}$  at the inlet to  $8 \text{ mgL}^{-1}$  at the middle of the channels. During flood and at high tide the influence of sea water is higher during spring tide than neap tide, reaching 12 km and 10 km in the S. Jacinto and Espinheiro channels, respectively. At high tide, the suspended sediment concentration in the central area of the lagoon is approximately  $0.5 \text{ mgL}^{-1}$  lower on spring tide than during neap tide.

The suspended sediment concentration along the tidal cycle (Figure 4d,h) is higher at low tide in the central area of the lagoon, with values of  $6\text{-}10 \text{ mgL}^{-1}$  and  $7\text{-}10 \text{ mgL}^{-1}$  for spring and neap tide periods, respectively. At the upstream regions of S. Jacinto, Mira

and Ílhavo channels, the suspended sediment concentrations are smaller, ranging between  $3$  and  $8 \text{ mgL}^{-1}$ .

Furthermore, at spring tide the sea water intrusion is higher than during neap tide, due to high tidal prism, and consequently the sediment concentration is lower.

In the inlet region, the suspended sediment concentration is on average 30% higher in spring tide than in neap tide. This is evident during flood and high tide, due to the high propagation of low suspended sediment concentration marine water. This lower concentration during neap tide is due to the weak tidal currents that transport less sea water volume into the lagoon (small sediment concentration), turning the river flow the main suspended sediment source in the lagoon. The regions close to the river mouths also have higher concentrations during spring tide due to the intense ebb currents that re-suspend the sediments, enhanced by the river inflow velocity.

In the Mira and Ílhavo channels, and due to their smaller extension and inlet proximity, the sediment concentration is similar for both spring and neap tide, being slightly higher (10%) in spring than in neap tide, as a result of the strongest tidal and fluvial influence on the water flow, with higher sediment concentration in the upstream-downstream direction.

On the other hand, in S. Jacinto and Espinheiro channels, the sediment concentrations depend strongly on the tidal period.

## CONCLUSION

The suspended sediment dynamics in the Ria de Aveiro have a fortnightly pattern related to spring and neap tide and sediment concentration is highly dependent on the concentrations imposed at each river boundary.

The maximum sediment concentrations were found at the upstream areas during ebb conditions, due to the combined effect of tide and river discharge. The minimum suspended sediment concentrations were observed near the inlet under flood conditions, revealing the effect of seawater propagation into the lagoon. The highest suspended sediment concentrations were found at the central area of the lagoon (Espinheiro channel), which connects the main freshwater source (Vouga River) to the ocean.

When considering a sea level rise as consequence of climate change, a decrease in the cohesive sediment concentration is predicted for the overall study area, due to the higher intrusion of marine water scarce of sediments.

The cohesive sediment model developed in this study constitutes a promising tool to study the local sediment dynamics under different forcing conditions. Building on this work it is planned to implement a biogeochemical model that uses the results of the transport model to compute the dynamics of Chlorophyll in Ria de Aveiro, evaluating the limiting factor for phytoplankton growth. The model described here constitutes the first step toward the development of a predictive biogeochemical model for the Ria de Aveiro lagoon.

## ACKNOWLEDGEMENT

This work has been partly supported by FCT and by European Union (COMPETE, QREN, FEDER) in the frame of the research project PTDC/AAC-AMB/121191/2010 - BioChangeR: Biogeochemical Processes induced by Climate and Anthropogenic Circulation Changes - The Case Study of Ria de Aveiro. The European Commission, under the 7th Framework Programme, also supported this study through the collaborative research project LAGOONS (contract n°283157). The second author has been supported by the Fundação para a Ciência e Tecnologia through the doctoral grants SFRH/BD/79920/2011. The last author is supported by the Ciência 2008 program.

## LITERATURE CITED

- Abrantes, I., Dias, J.M. and Rocha, F., 2006. Spatial and Temporal Variability of Suspended Sediments Concentration in Ria de Aveiro Lagoon and Fluxes between the Lagoon and the Ocean. *Journal of Coastal Research*, S.I. 39, 718-723.
- Arnold, J.G., Srinivasan, P., Muttiah, R.S. and Williams, J.R., 1998. Large area hydrologic modeling and assessment. Part I. Model development. *Journal of the American Water Resources Association*, 34, 73-89.
- Cancino, L. and Neves, R., 1994a. Numerical Modelling of Three-Dimensional Cohesive Sediment Transport in an Estuarine Environment. In: Belorgey, M., Rajaona, R.D., Sleath, J.F.A. (eds.), *Sediment Transport Mechanisms in Coastal Environments and Rivers*. World Scientific, pp. 107-121.
- Cancino, L. and Neves, R., 1994b. 3D-Numerical Modelling of Cohesive Suspended Sediment in the Western Scheldt Estuary (The Netherlands). *Netherlands Journal of Aquatic Ecology*, 28(3-4), 337-345.
- Cancino, L. and Neves, R., 1995a. *Biogeochemistry of the Maximum Turbidity Zone in Estuaries*. Final Report on Hydrodynamic and Transport Modelling Contribution for CEC-Environment Programme, Inst. Superior Técnico. Lisbon, 80 p.
- Cancino, L. and Neves, R., 1995b. Three-Dimensional Model System for Baroclinic Estuarine Dynamics and Suspended Sediment Transport in a Mesotidal Estuary. In: *Computer Modelling of Seas and Coastal Regions*. Computational Mechanics Publications, pp. 353-360.
- Dias, J.M., Lopes, J.F. and Dekeyser, I., 2000. Tidal propagation in Ria de Aveiro lagoon, Portugal. *Physics and Chemistry of the Earth Part B-Hydrology Oceans and Atmosphere*, 25, 369-374.
- Dias, J.M., Lopes, J.F. and Dekeyser, I., 2003. A Numerical Model System Application to the Study of the Transport Properties in Ria de Aveiro Lagoon. *Ocean Dynamics*, 53, 220-231.
- Freitas, R., Sampaio, L., Rodrigues, A. and Quintino, V., 2005. Seabottom classification across a shallow water bar channel and near-shore shelf, using single-beam acoustics. *Estuarine Coastal and Shelf Science*, 65, 625-632.
- Lopes, C.L., Silva, P.A., Dias, J.M., Rocha, A., Picado, A., Plecha, S. and Fortunato, A.B., 2011. Local sea level change scenarios for the end of the 21st century and potential physical impacts in the lower Ria de Aveiro (Portugal). *Continental Shelf Research*, 31, 1515-1526.
- Lopes, C.L., Azevedo, A. and Dias, J.M., 2013. Flooding assessment under sea level rise scenarios: Ria de Aveiro case study. *Journal of Coastal Research*, SI65, 766-771.
- Lopes, J.F., Dias, J.M. and Dekeyser, I., 2001. Influence of Tides and Rivers Input in the Suspended Sediment Transport in Ria de Aveiro Lagoon, Portugal. *Physics and Chemistry of the Earth*, 26(9), 729-734.
- Lopes, J.F., Dias, J.M. and Dekeyser, I., 2006. Numerical Modelling of Cohesive Sediments Transport in the Ria de Aveiro Lagoon, Portugal. *Journal of Hydrology*, 319, 176-198.
- Martins, F., Leitão, P., Silva, A. and Neves, R., 2001. 3D modelling in the Sado estuary using a new generic vertical discretization approach. *Oceanologica Acta*, 24(1), 1-12.
- Mateus, M., Vaz, N. and Neves R., 2012. A process-oriented model of pelagic biogeochemistry for marine systems. Part II: Application to a mesotidal estuary. *Journal of Marine Systems*, 94, S90-S101.
- Oliveira, A., Fortunato, A.B. and Dias, J.M., 2006. Numerical modeling of the Aveiro inlet dynamics. In: Smith, J.M. (eds.), *Proceedings of 30th International Conference on Coastal Engineering*, World Scientific Publishing Co, pp. 3282-3294.
- Picado, A., Dias, J.M. and Fortunato, A.B., 2010. Tidal changes in estuarine systems induced by local geomorphologic modifications. *Continental Shelf Research*, 30, 1854-1864.
- Plecha, S., Silva, P.A., Oliveira, A. and Dias, J.M., 2012. Establishing the wave climate influence on the morphodynamics of a coastal lagoon inlet. *Ocean Dynamics*, 62, 799-814.
- Ruiz-Villarreal, M., Montero, P., Taboada, J.J., Prego, R., Leitão, P.C. and Pérez-Villar, V., 2002. Hydrodynamic Model Study of the Ria de Pontevedra Under Estuarine Conditions. *Estuarine, Coastal and Shelf Science*, 54, 101-113.
- Santos, F.D. and Miranda, P., 2006. *Alterações Climáticas em Portugal. Cenários, Impactes e Medidas de Adaptação. — Projecto SIAM II*. Lisboa, Portugal. Gradiva, 506 p.
- Saraiva, S., Pina, P., Martins, F., Santos, M., Braunschweig, F., and Neves, R., 2007. Modelling the influence of nutrient loads on portuguese estuaries. *Hydrobiologia*, 587, 5-18.
- Vaz, N., Dias, J.M., Leitão, P. and Martins, I., 2005. Horizontal patterns of water temperature and salinity in an estuarine tidal channel: Ria de Aveiro. *Ocean Dynamics*, 55, 416-429.
- Vaz, N., Dias, J.M. and Leitão, P.C., 2009. Three-dimensional modelling of a tidal channel: the Espinheiro Channel (Portugal). *Continental Shelf Research*, 29, 29-41.
- Vaz, N. and Dias, J.M., 2011. Cross-sectional and stratification patterns induced by tidal and river discharge changes in a tidal channel: a modelling study. *Journal of Coastal Research*, S.I. 64, 1614-1618.

# Residual currents and transport pathways in the Tagus estuary, Portugal: the role of freshwater discharge and wind

Nuno Vaz †, João M. Dias†

†CESAM, Physics Department  
University of Aveiro  
Aveiro, Portugal  
nuno.vaz@ua.pt  
joao.dias@ua.pt



[www.cerf-jcr.org](http://www.cerf-jcr.org)



[www.JCRonline.org](http://www.JCRonline.org)

## ABSTRACT

Vaz, N., Dias, J.M., 2014. Residual currents and transport pathways in the Tagus estuary, Portugal: the role of freshwater discharge and wind. In: Green, A.N. and Cooper, J.A.G. (eds.), *Proceedings 13<sup>th</sup> International Coastal Symposium* (Durban, South Africa), *Journal of Coastal Research*, Special Issue No. 70, pp. 610-615, ISSN 0749-0208.

Estuaries are interface areas between rivers and the coastal sea. They also receive point discharges of contaminants which can affect estuarine biogeochemistry. The study of residual circulation in estuaries is a key issue since it is related to the transport and dispersal of dissolved and non-dissolved substances. This study investigates the residual flows in a coastal plain estuary (the Tagus estuary, Portugal) taking into account the major forcing factors: tide, river discharge and wind stress. The methodology used is the implementation of a high resolution estuarine model in a 2D mode to simulate the tidal dynamics of the estuary. Tidal flows were calculated by tidally-averaging the flow currents along the whole estuary. The complex bathymetry of the estuary, tides, river discharge and wind stress modulate the residual flow in the Tagus estuary. The combine effect of the tide and river discharge creates preferential corridor flows in the deeper areas of the estuary. On the other hand, wind intensity and direction generate changes in residual currents in the shallow areas near the south shore of the estuary. River runoff changes the residual current intensity from values higher than  $0.3 \text{ ms}^{-1}$  (high discharge) to values of about  $0.05 \text{ ms}^{-1}$  (low discharge). The wind direction also induces changes in the residual flow patterns, inducing a rotation of the residual flow, according to the wind direction. Thus, the estuarine model of the Tagus estuary is a tool that sheds new insight about its fundamental hydrodynamics processes and consequently about the long term circulation patterns.

**ADDITIONAL INDEX WORDS:** *Estuarine model, residual circulation, tides, river discharge, wind stress, Tagus Estuary.*

## INTRODUCTION

Estuaries are interface areas between rivers and the coastal sea. They are important feeding and nursery areas for many marine species. In recent years, due to an increasing urban and suburban development, they are being used as point source discharge of contaminants, which can affect estuarine biogeochemistry. The transport of dissolved matter in estuaries is closely related to residual circulation estuarine processes. Therefore, it is critical to study residual currents, which can modulate transport pathways in estuarine environments. In temperate estuaries, tidal motion is a key factor in the forcing of local circulation. However, the residual circulation which modulates the transport of contaminants and other passive tracers is mainly forced by the freshwater discharge from the major tributaries and also local wind stress.

Understanding residual flows is important for issues like aquaculture, fisheries and understanding the estuarine environment. The influence of the tide in the residual circulation has been studied by several authors (Fischer *et al.*, 1979; Wei *et al.* 2004; Lopes and Dias, 2007). Other authors have explored the

influence of river discharge and wind stress in the establishment of residual flows (Garvine *et al.*, 1992; Jay and Flinchem, 1997; Lopes and Dias, 2007).

Residual circulation is often related to along- and cross-channel salinity structures, which could be used as proxy to establish transport pathways of dissolved water properties, since salinity is considered a natural tracer. As noted by MacCready and Banas (2012) residual circulation in many estuaries has the form of an exchange flow, which brings ocean water into the deeper part of a channel or estuary and exports low salinity surface water out of the estuary.

Estuarine regions present, in many cases, high temporal and spatial variability in terms of current velocity due to complex topography. This, associated with scarce current velocity measurements, renders numerical models a common tool to study the generation of residual flows in estuaries (Lopes and Dias, 2007; Valentim *et al.*, 2013).

The Tagus Estuary (Figure 1) is a coastal plain estuary located near Lisbon, and it is characterized by semidiurnal mesotidal tides and exposure to mean-to-high hydrological and meteorological conditions. In estuarine systems with fast tidal currents, long-term

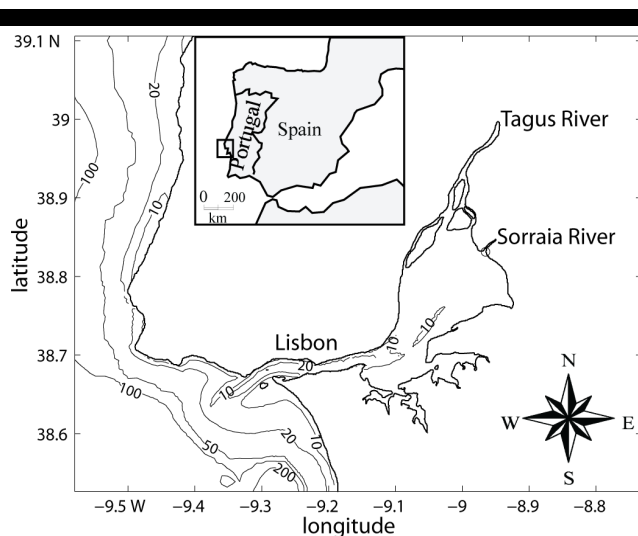


Figure 1. The Tagus Estuary bathymetry and location (isolines in meters related to the local datum).

residual circulation plays a key role in the transport of materials and their export to the coastal waters. Valentim *et al.* (2013) explored the effect of sea level rise in the establishment of residual flows (actual and future climate change scenarios), studying their generation through the interaction between tidal motion and topographic features of the Tagus Estuary.

In this article a step forward is taken, and the depth-integrated high resolution model of the Tagus Estuary is applied to study the generation of residual flows inside the estuary. The forcing factors taken into account are tidal propagation, river discharge and wind intensity and direction for the actual climate scenario. This paper is structured as follows: first the study and model is described; then the residual circulation driven by different forcing is characterized and discussed and the general conclusions are presented.

### THE TAGUS ESTUARY

The Tagus Estuary is coastal plain system located near Lisbon (Portugal). Tides are semidiurnal with amplitude ranging from 1 to 4 m (over the local datum). With a surface area of about 320 km<sup>2</sup> and an average volume of 1900×10<sup>6</sup> m<sup>3</sup>, it is the largest Portuguese estuarine system (Figure 1). Intertidal areas, composed mainly of mudflats, occupy between 20 and 40% of the total estuarine area.

The hydrography of the estuary is modulated by the tidal propagation and fluvial discharge from the major tributaries (Tagus, Sorraia). These interconnected elements induce the generation of sharp gradients of salinity (and other variables) inside the estuary with the formation of three distinct regions: a marine region (lower estuary), a mixing region (middle estuary) and a region where the freshwater inflow dominates (upper estuary). This is consistent with the observations by Vaz and Dias (2008) for other Portuguese estuarine systems, where they spatially characterized the salinity gradients of a tidal channel under different tidal forcing and river inflow conditions.

The Tagus is considered as ebb-dominated, with floods typically 1 h longer than ebbs (stronger velocities during ebbs), and thus inducing a net export of sediments (Fortunato *et al.*, 1997). The area affected by tides reaches 80 km landward of Lisbon and maximum tidal currents are about 2.0 m/s (Gameiro *et al.*, 2007).

The major source of freshwater is the Tagus River, with an annual average inflow between 300 – 400 m<sup>3</sup>s<sup>-1</sup>. The estuary also receives effluent discharges, mainly from several urban, industrial and agricultural sources. Another important freshwater tributary is the Sorraia River, which contributes approximately 1/10 of the freshwater outflow of the Tagus River. In general, the Tagus estuary is well-mixed and has an average tidal prism of 600×10<sup>6</sup> m<sup>3</sup>.

The wind regime in the region exhibits a marked seasonal pattern, presenting south/southwest predominant winds during the wet seasons, rotating to north/northwest during the dry season. The seasonal variability of meteorological conditions and river inflow induces a strong seasonal variability in the estuary hydrography and biogeochemical conditions (Vaz *et al.*, 2011; Mateus *et al.*, 2012).

### THE TAGUS ESTUARY MODEL

The Tagus Estuary predictive model is an implementation of Mohid ([www.mohid.com](http://www.mohid.com)) for the study area. It is a baroclinic finite volume model, designed for coastal and estuarine shallow water applications, like the Tagus estuary, where flow over complex topography, flooding and drying of intertidal areas, changing stratification or mixing conditions are all important. Mohid allows an integrated modeling approach of physical and biogeochemical processes. A complete description of the model's physics can be found in Leitão *et al.* (2005).

The model has been used to different coastal and estuarine areas, showing its capability to simulate complex flows features (e.g. Vaz *et al.*, 2009a, 2011; Santos *et al.*, 2006; Bernardes, 2007; Malhadas *et al.*, 2009). In this study, a previously validated setup of the MOHID-2D model for the Tagus estuary (Vaz *et al.*, 2011, Valentim *et al.*, 2013) is applied. Details of its accuracy in reproducing the tidal dynamics after model validation are described in Vaz *et al.* (2011).

Given the intense vertical mixing of the estuary, the model was set in a 2D mode (Vaz *et al.*, 2011). The numerical grid encompasses the whole extension of the Tagus estuary, having 335×212 cells of 200 m each. This resolution was considered adequate to simulate hydrodynamic processes inside the estuary. Tides, meteorological variables and variable river inflow are the main forcing mechanisms for the circulation. On the open ocean boundary, the model input is the tidal forcing from a 2D tidal model (Vaz *et al.*, 2009b). Meteorological forcing (wind intensity and direction, air temperature, relative humidity) and river discharge from the major tributaries (constant values representing mean and extreme discharges) are imposed at the surface and landward boundaries, respectively. Atmosphere-water interactions (e.g. heat fluxes, solar radiation and wind stress) and the interaction between the estuary bottom and the water column (e.g. cohesive sediments re-suspension and deposition) are handled by the model.

The model was spun-up for 5 days, which is considered appropriate to achieve a stable estuarine hydrodynamic and the results from the spin-up period were not considered in the analysis. The time step is 15 s and the horizontal viscosity 5m<sup>2</sup>s<sup>-1</sup>. Initial conditions for the hydrodynamic model are null free surface gradient and null velocity in all points.

The simulation period is generic, since the main objective of this work is to study the generation of residual flows due to wind stress and freshwater discharge. Several simulations were performed, imposing constant wind direction from the main quadrants in the model (N, NW, NE, S, SW directions) and considering a constant intensity for all the simulations (8 ms<sup>-1</sup>). Mean and extreme freshwater inflows from the Tagus River were

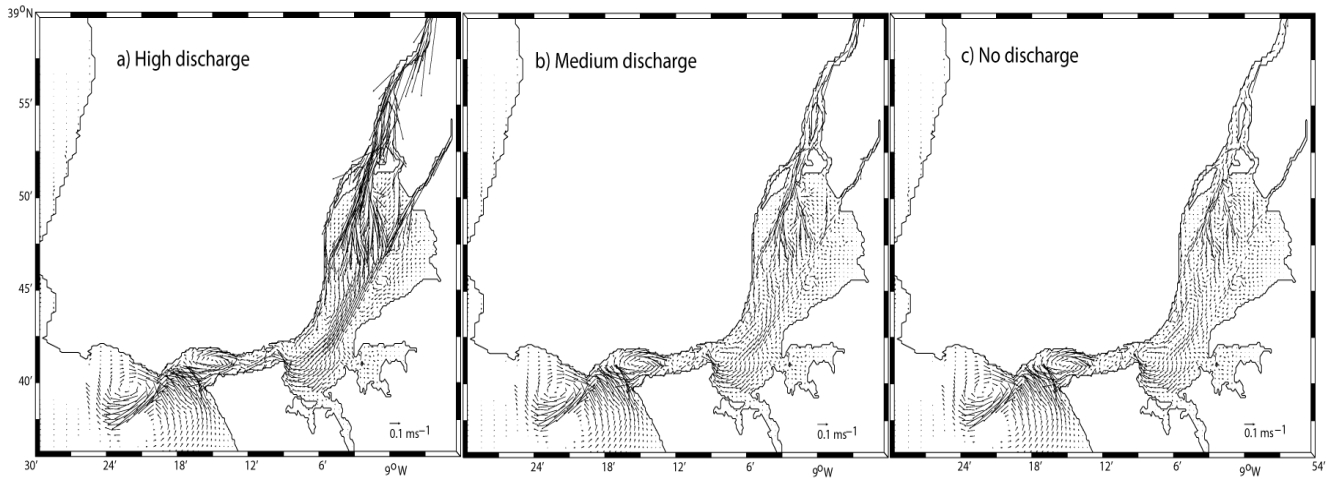


Figure 2. Residual flow in the Tagus Estuary for a) High freshwater discharge of  $2000 \text{ m}^3 \text{ s}^{-1}$ ; b) Medium freshwater discharge of  $350 \text{ m}^3 \text{ s}^{-1}$  of the Tagus River and c) No freshwater discharge. The small arrow at the lower right corner represents a velocity of  $0.1 \text{ ms}^{-1}$ .

imposed as constant values of  $350 \text{ m}^3 \text{ s}^{-1}$  and  $2000 \text{ m}^3 \text{ s}^{-1}$ , respectively. Freshwater inflows for the Sorraia River for the proposed scenarios are 1/10 of the Tagus river discharge.

A simulation without freshwater discharge and null wind stress was also performed in order to simulate the tidally induced residual circulation.

## RESULTS

Taking into account that the numerical model was previously validated (Vaz *et al.*, 2011), generic simulations were conducted to determine the residual circulation in the Tagus Estuary. In this study the procedure adopted by Valentim *et al.* (2013) was followed, meaning that residual circulation was computed for all grid cells averaging the transient eulerian components of the velocity ( $u$ ,  $v$ ) during a fortnight cycle (multiple of the  $M_2$  and  $S_2$  tidal periods).

The tidal effect was removed from the results by subtracting the tidally induced residual velocity to the results of the simulations with wind stress and freshwater discharge, in order to study their isolated effects.

The local wind in the Tagus Estuary is highly variable. During the winter, the wind circulation has predominant directions from northwest (NW), north (N) and southeast (SE) (SMN, 1974), and the predominant wind intensity ranges from  $1.5 \text{ ms}^{-1}$  (8.5% occurrence) to  $14 \text{ ms}^{-1}$  (7.5% occurrence). During the spring, predominant winds are mainly from the north, northwest and northeast (NE) and their intensity range from  $1 \text{ ms}^{-1}$  (~5% occurrence) to  $15 \text{ ms}^{-1}$  (~20% occurrence) (SMN, 1974). For the analysis of the wind driven residual circulation, the model was run with the wind stress and tidal forcing and then the tidal effect was removed following the procedure previously described. For this paper, will be shown results only for three predominant directions (N, NE and SW) considering the wind intensity equal to  $8 \text{ ms}^{-1}$ .

### Residual circulation induced by freshwater discharge

The residual flows induced by the freshwater inflow are depicted in Figure 2. In general, higher velocities are generated due to the high freshwater discharge (Figure 2a). Also, higher residual velocities are found in the deeper areas of the estuary for

all three cases. The freshwater discharge generates residual flows higher than  $0.3 \text{ ms}^{-1}$  in the deeper channels of the estuary (Figure 2a), reducing to values of about  $0.1$  ( $0.05$ )  $\text{ms}^{-1}$  in the medium (No) discharge scenario.

From the results two corridor flows are evident in the upstream and central region of the estuary. In fact, the flow associated with the Tagus and Sorraia River favors the generation of two visible corridor flows near the north margin and central region, respectively.

In the central region of the estuary, outside the corridor flow (shallow region near the south margin), no influence of the river discharge is visible. In this area, the residual currents are of the order of  $0.01 \text{ ms}^{-1}$  and driven by the back and forth movement of the tide.

Near the estuary mouth a less organized pattern exists. Here, the residual currents range between  $0.1$  (medium and no discharge) to  $0.3 \text{ ms}^{-1}$  in the high discharge scenario. Moreover, a noticeable feature of this region is the generation of eddies due to interaction of the estuarine circulation with the complex local bathymetry, which increases the nonlinearity of transport processes in this region. In a previous study of the Tagus Estuary mouth, Fortunato *et al.* (1997) observed the generation of these eddies, relating them with the spring and neap tidal cycle, and highlighting their importance to mixing processes in this region.

### Residual circulation induced by winds

The model was forced with wind from three dominant directions with an intensity of  $8 \text{ ms}^{-1}$ , a value which represents the mean value for the Tagus Estuary region. The resulting circulation (Figure 3) is similar for the three scenarios. However, looking closely there are some differences in the horizontal spatial variability, especially in the shallow areas near the south margin of the estuary. The residual flows are generally one order of magnitude lower than the flows induced by the freshwater discharge. Typically, the wind induced residual flows can reach  $0.07 \text{ ms}^{-1}$  for a wind intensity of  $8 \text{ ms}^{-1}$ . For the scenario of northerly wind (Figure 3a), the residual currents present the lowest values, with a maximum residual flow of  $0.02 \text{ ms}^{-1}$ . This may be due to the orientation of the estuary, where the main channels are orientated from NE to SW. For the NE scenario (Figure 3b), the

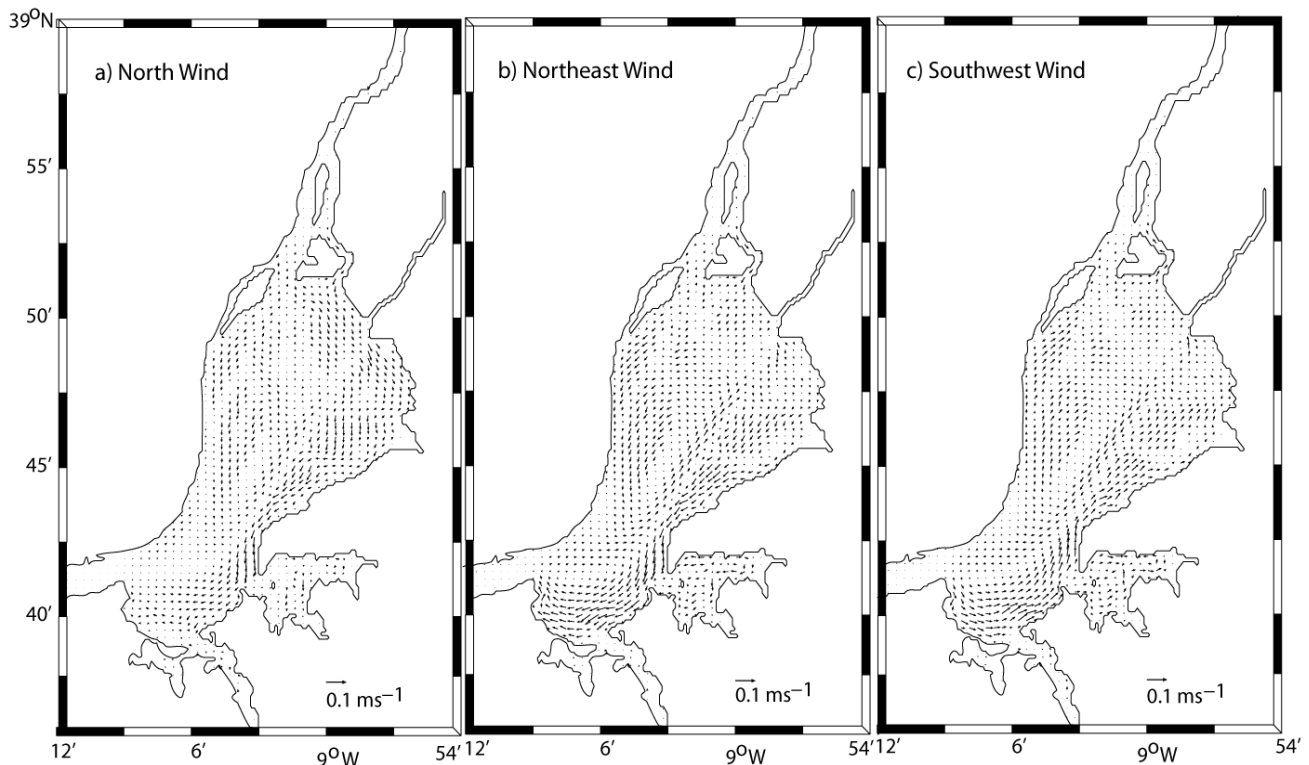


Figure 3. Residual flow in the Tagus Estuary for a) North wind scenario; b) Northeast wind c) Southwest wind. The small arrow at the lower right corner represents a velocity of  $0.1 \text{ ms}^{-1}$ .

maximum residual flow is higher, presenting values of  $\sim 0.07 \text{ ms}^{-1}$ . In this scenario, the residual flow vectors are orientated to SW due to the northeastern wind. For the SW scenario (Figure 3c), the maximum values of residual are again of  $0.08 \text{ ms}^{-1}$ , and the flow vectors are orientated toward the NE due to the southwestern wind forcing.

In the deeper channels of the estuary, the wind induced residual flows are of the order of  $0.01 \text{ ms}^{-1}$ , a low value that shows that in deeper areas the residual flows are mainly driven by the freshwater discharge or tidal propagation.

Near the south margin of the estuary (close to the estuary corridor) is located the region where the influence of the wind is more visible. In fact, the shallowness of this region, with depths of about 1 m over the local datum, turns the surface circulation in this region quite susceptible to the wind stress effect.

### Theoretical transport pathways inside the estuary

Residual currents generated by freshwater discharge and wind stress forcing may induce different theoretical transport pathways of dissolved material. In Figure 4 the proposed transport pathways are depicted for the Tagus Estuary.

In an estuarine region a parcel of water will move up and down the estuary during the flood and ebb due to the tidal propagation. In the absence of residual currents and other perturbing influences, the parcel of water will return to its original position after one tidal period. But, if the effects of the residual circulation are incorporated, then the parcel position at the end of the ebb will be somehow different from its position in absence of residual currents. The difference between these two positions defines the residual displacement.

The results presented in this paper allow the definition of different paths for dissolved properties within the estuary. In fact, the river discharge may induce the dispersion and transport of properties through two well defined corridors passing through the deeper areas of the estuary (the navigation channels). The outflow of the Tagus and Sorraia produces a downward transport of properties (black arrows in Figure 4), which is visible in the central area of the estuary, corresponding to its mixing area. Then, the transport turns more chaotic due to the particular features of the bathymetry of the estuary in the area close to its mouth. Moreover, the corridor flow is highly dependent on the river discharge. A Tagus river discharge of  $2000 \text{ m}^3 \text{ s}^{-1}$  (and a  $200 \text{ m}^3 \text{ s}^{-1}$  for the Sorraia) produces two well-defined corridor flows. Under the average and no river outflow scenarios, these corridor flows decrease their extent and are confined to the upstream region of the estuary.

The wind stress plays a key role in the establishment of residual flow in the shallow areas of the estuary (close to its south margin). In this region, the wind direction may induce clockwise or counterclockwise residual flows according to the direction of the wind. A southwest wind generates a counterclockwise circulation and a north/northeast wind may induce a clockwise circulation as depicted in gray color in Figure 4.

### DISCUSSION

In a coastal plain estuary with complex bathymetry and high tidal currents, the residual circulation can be modulated by the spring-neap tidal variability of the turbulent mixing due to tidal

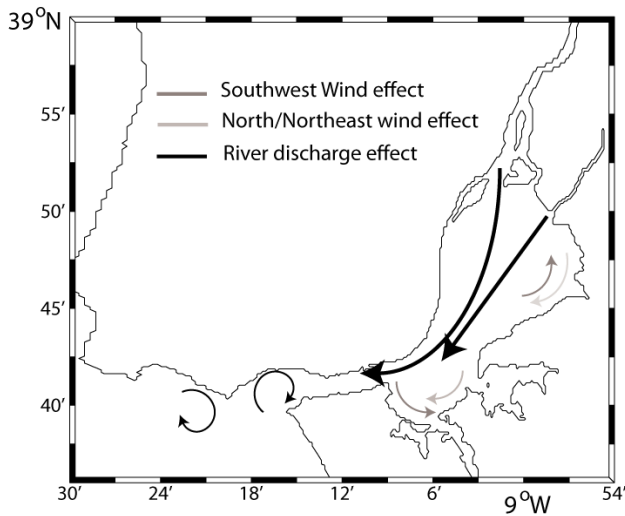


Figure 4. Sketch of the transport pathways inside the estuary. In black is depicted the theoretical river discharge effect and in gray is depicted the wind effect on the transport pathways.

currents (Ribeiro *et al.*, 2004). At longer time scales, variations in river flow may change vertical and horizontal gradients of density, promoting a decrease in vertical mixing and intensifying the gravitational circulation. Moreover, river flow can vary by an order of magnitude or more just over a few days due to storms or dam releases, changing the circulation patterns inside an estuary (MacCready, 1999). Therefore, estuarine circulation results from a complex interaction, between several forcing factors, over a wide range of time scales.

In the Tagus Estuary, Neves (2010) revealed that the residual circulation is modulated by the spring-neap cycle by setting the vertical thermohaline structure. But no clues were revealed about the role of river discharge or wind stress in the residual circulation patterns.

In this paper the tidal role is not directly explored and the study is focused in the river discharge effect and wind stress role. In a shallow system like the Tagus Estuary, which is considered a well-mixed system (Vaz *et al.*, 2011; Valentim *et al.*, 2013), a 2D approach was considered the best to study subtidal dynamics inside the estuary.

The freshwater inflow from the main tributaries (Tagus and Sorraia rivers) produces significantly residual flows in the deeper areas of the estuary, generating two corridor flows in the central area of the estuary. In shallow areas, the freshwater discharge induces a more chaotic circulation pattern strongly dependent on the bathymetry of the area. In fact, this freshwater inflow forcing appears to generate a kind of nonlinear interaction with the bathymetry, producing this chaotic pattern, similar to the one produced by the tide as studied by Guyondet and Koutitonsky (2008). The residual flows due to the freshwater discharge are of the same magnitude as the ones due to tidal motion, presenting values of about  $0.05 \text{ ms}^{-1}$ . As observed by Carballo *et al.* (2009) for their study of the Muros (NW Spain), the river driven case causes an outflow throughout the water column in the upstream region of the Tagus Estuary, close to the river's mouth.

Near the mouth of the estuary, the river inflow driven case shows the formation of two eddies, one inside the estuary and another just outside. The generation of these eddies were studied by Fortunato *et al.* (1997) in a 3D modeling study of the dynamics of this region. They related the eddy formation with asymmetry

between ebb and flood currents and the particular bathymetry of the region.

The analysis of wind driven scenarios revealed that the higher wind induced residual flows are generated in the shallow areas of the estuary near the south margin. In this region, the wind, depending on the direction induces the generation of clockwise and counterclockwise patterns. Moreover, the higher velocities are visible in the NE and SW wind scenarios, mainly due to the natural orientation of the estuary (NE-SW direction). In this case, the wind creates a torque which causes the estuarine water to rotate. Moreover, the wind may induce the generation of surface waves that may induce changes in the circulation of shallow areas of the estuary. However, this issue will be studied in the future.

The estuarine dynamics inside the Tagus Estuary allow the identification of channels of preferential flows. This is a common feature of many estuarine systems where the bathymetry and orientation of the channels induces preferential flow corridors (Vaz *et al.*, 2009a). In the Tagus Estuary, these corridor flows are visible in the deeper channels in the central area of the estuary. These corridor flows are dependent on the freshwater discharge from the main tributaries, being highlighted by a strong river outflow.

## CONCLUSIONS

In this work, the results of a two-dimensional depth integrated hydrodynamic model (MOHID, [www.mohid.com](http://www.mohid.com)) were used to study the residual circulation in a coastal plain estuary: the Tagus Estuary, Portugal. The main objectives of this study were to study the generation of residual flows, highlighting the role of the freshwater discharge and wind stress in their generation and also the spatial patterns of variability.

The simulations considered three scenarios of freshwater discharge, comprising extreme, mean and no river inflow. The results depicted show the effect of different freshwater discharges. Among the effects, the generation of specific corridor flows in the central region of the estuary is visible. As stated, these corridor flows are highly dependent on the magnitude of the river outflow. In fact, under extreme river inflow, these corridor flows are visible in all the central area of the estuary, occupying the navigation channels. The river inflow driven circulation also highlighted the generation of two eddies located near the estuary mouth. This eddies are generated due to asymmetries between ebb and flood currents and the particular topography of the estuary mouth.

The wind driven residual circulation results highlighted the generation of residual currents in the shallow areas of the estuary, near the south shore. In fact, depending on the direction of the wind forcing, it is visible a cyclonic or anti-cyclonic rotation of the water in this particular region of the estuary.

The spatial patterns of residual circulation allow the establishment of preferential transport pathways of dissolved properties. In fact, along the deepest areas of the estuary, a downstream long term transport may be induced by downstream residual flows. On the contrary, the wind may turn and modulate the transport of dissolved matter in periods of low river outflow.

It was also noted that the high spatial residual flow variability is closely connected not only with the major forcing, but also with the interaction between estuarine circulation and the bottom topography of the estuary, which is highly non-linear.

This study reveals that a simple approach as the one followed here may produce sound results, which reveal much of the common features of a classical coastal plain estuary like the Tagus. Improved simulations may be made with the implementation of a three-dimensional model to study the generation of residual flows inside the estuary and its influence in

the horizontal and vertical mixing processes. To that end, a salt and heat transport model is being implemented, and the results will be explored in future studies of estuarine circulation.

### ACKNOWLEDGMENTS

This work has been partly supported by FCT and by European Union (COMPETE, QREN, FEDER) in the frame of the research project PTDC/AAC-AMB/121191/2010 - BioChangeR: Biogeochemical Processes induced by Climate and Anthropogenic Circulation Changes - The Case Study of Ria de Aveiro. The first author of this work is supported by the FCT program Ciência 2008.

### LITERATURE CITED

- Bernardes, B., 2007. *Hydrodynamical and Ecological Modelling of the North Sea*. Technical University of Lisbon, Lisbon, Portugal, MSc thesis, 81p.
- Carballo, R., Iglesias, G., Castro, A., 2009. Residual circulation in the Ria de Muros (NW Spain): a 3D numerical model study. *Journal of Marine Systems*, 75, 116 – 130.
- Fischer, H.B., List, E.J., Koh, R.C.Y., Imberger, J., Brooks, N.H., 1979. *Mixing in Inland and Coastal Waters*. Academic Press, New York.
- Fortunato, A.B.; Baptista, A.M. and Luettich jr., R.A., 1997. A three-dimensional model of tidal currents in the mouth of the Tagus estuary. *Continental Shelf Research*, 17, 14, 1689–1714.
- Gameiro, C., Cartaxana, P., Brotas, V., 2007. Environmental drivers of phytoplankton distribution and composition in Tagus estuary, Portugal. *Estuarine, Coastal and Shelf Science*, 75, 21–34.
- Garvine, R.W., McCarthy, R.K., Wong, K., 1992. The axial salinity distribution in the Delaware Estuary and its weak response to river discharge. *Estuarine, Coastal and Shelf Science*, 35(2), 157–165.
- Guyondet, T., Koutitonsky, V.G., 2008. Tidal and residual circulations in coupled restricted and leaky lagoons. *Estuarine, Coastal and Shelf Science*, 77(3), 396–408.
- Jay, D.A., Flinchem, E.P., 1997. Interaction of fluctuating river flow with a barotropic tide: a demonstration of wavelet tidal analysis methods. *Journal of Geophysical Research – Oceans*, 102(C3), 5705–5720.
- Leitão, P.; Coelho, H.; Santos, A. and Neves, R., 2005. Modelling the main features of the Algarve coastal circulation during July 2004: A downscaling approach. *Journal of Atmospheric & Ocean Science*, 10, 421-462.
- Lopes, J.F., Dias, J.M., 2007. Residual circulation and sediment distribution in the Ria de Aveiro lagoon, Portugal. *Journal of Marine Systems*, 68(3-4), 507-528.
- MacCready P., Banas N.S (2012) Residual circulation, mixing, and dispersion. In: Wolanski, E. and McLusky, D.S. (eds.), *Treatise on Estuarine and Coastal Science*, Elsevier, chapter 2.05.
- MacCready, P., 1999. Estuarine Adjustment to Changes in River Flow and Tidal Mixing. *Journal of Physical Oceanography*, 29, 708-726.
- Malhadas, M.S., Silva, A., Leitão, P.C., Neves, R., 2009. Effect of the Bathymetric changes on the hydrodynamic and residence time in Óbidos lagoon (Portugal). *Journal of Coastal Research*, 56, 549–553.
- Mateus, M., Vaz, N., Neves R., 2012. A process-oriented model of pelagic biogeochemistry for marine systems. Part II: Application to a mesotidal estuary. *Journal of Marine Systems*, 94, S90-S101.
- Neves, F.J., 2010. Dynamics and Hydrology of the Tagus Estuary: Results from in Situ Observations. University of Lisbon, Portugal, PhD thesis, 210p.
- Ribeiro, C., Wanick, J., Sharples, J., 2004. Observations of the spring-neap modulation of the gravitational circulation in a partially mixed estuary. *Ocean Dynamics*, 54, 299-306.
- Santos, M., Neves, R., Leitão, P., Pereira, P., Pablo, H., Fernandes, L.D., Carvalho, S.M., Alves, C.P., 2006. Qualidade da água da Lagoa de Óbidos: Que futuro? In: XII Encontro Nacional de Saneamento Básico, Cascais 2006.
- SMN, 1974. *Atlas Climatológico de Portugal Continental*. Serviço Meteorológico Nacional, Lisboa.
- Valentim J.M., Vaz N., Silva H., Duarte B., Caçador I., Dias J.M., 2013. Tagus Estuary and Ria de Aveiro Salt Marsh Dynamics and the Impact of Sea Level Rise. *Estuarine, Coastal and Shelf Science*, 130, 138-151.
- Vaz N., Mateus M., Dias J.M., 2011. Semidiurnal and spring-neap variations in the Tagus Estuary: Application of a process-oriented hydro-biogeochemical model. *Journal of Coastal Research*. S.I.64, 1619-1623.
- Vaz, N.; Dias, J.M. and Leitão, P.C., 2009a. Three-dimensional modeling of a tidal channel: The Espinheiro Channel (Portugal). *Continental Shelf Research*, 29, 29-41.
- Vaz, N.; Fernandes, L.; Leitão, P.C.; Dias, J.M. and Neves, R. 2009b. The Tagus estuarine plume as a response to wind and river runoff: Winter 2007 case study. *Journal of Coastal Research*, S.I. 56, 1090-1094.
- Vaz, N. and Dias, J.M., 2008. Hydrographic characterization of an estuarine tidal channel. *Journal of Marine Systems* 70 (1-2), 168-181.
- Wei, H., Hainbucher, D., Pohlmann, T., Feng, S., Suendermann, J., 2004. Tidal induced Lagrangian and Eulerian mean circulation in the Bohai Sea. *Journal of Marine Systems*, 44(3-4), 141-15.



# Analysis of the recent evolution of the sand spit at the Solís Chico river mouth

Sebastián Solari, Christian Chreties, Guillermo López, Luis Teixeira

IMFIA – Facultad de Ingeniería  
Universidad de la República  
Montevideo, Uruguay  
ssolari@fing.edu.uy



[www.cerf-jcr.org](http://www.cerf-jcr.org)



[www.JCRonline.org](http://www.JCRonline.org)

## ABSTRACT

Solari, S., Chreties, Ch., López, G., Teixeira, L., 2014. Analysis of the recent evolution of the sand spit at the Solís Chico river mouth. In: Green, A.N. and Cooper, J.A.G. (eds.), *Proceedings 13<sup>th</sup> International Coastal Symposium* (Durban, South Africa), *Journal of Coastal Research*, Special Issue No. 70, pp. 616-620, ISSN 0749-0208.

The Solís Chico river, located on the southern Uruguayan coast, flows into the Río de la Plata estuary. The seaside resorts La Floresta and Parque del Plata are located on the estuary. In recent years the river mouth has migrated westward, away from the river axis, forming a sand spit that hinders the recreational use of Parque del Plata beach. In turn, at La Floresta there is a beach nourishment project whose main objective is to mitigate the erosion of the beach and the adjoining cliffs. This work aims to identify the causes of the recent migration of the river mouth and to analyze the possibility of using the sand spit as a borrow area for the beach nourishment. The river sediment supply to the coast for the period 1900-2010 was estimated, along with the long-shore and cross-shore sediment transport produced by sea waves. Furthermore, the plan-view stability of the river was studied in order to determine if the long-term evolution of the river is affecting the migration of the mouth. It was found that the migration of the mouth is mainly due to an extraordinarily high river sediment supply in 2002, combined with an increase in the net westward potential long-shore transport rate since the late 90s, and that the meander dynamics of the river are not affecting the evolution of the mouth. Additionally, the most likely area of natural breaching of the sand spit was identified, recommending its use as a borrow area for nearby beach nourishment.

**ADDITIONAL INDEX WORDS:** River mouth, sand spit, morphology, sediment transport.

## INTRODUCTION

Solís Chico river, located on the south coast of Uruguay (34 ° 46'S, 55 ° 42'W), flows into the estuary of the Río de la Plata forming a sand spit. On the margins of the estuary mouth are the beach resorts Parque del Plata to the west and La Floresta to the east (see Figure 1).

In recent times the mouth of the river has moved westward, as the sand spit elongated. This evolution of the mouth affects the accessibility to the Parque del Plata beach, reducing its potential for recreational use, and exposes the dunes to river bank erosion. In turn, at La Floresta a beach nourishment project is planned whose objectives are to recover dry beach for recreational activities and to protect the coastal cliffs from wave action.

Thus, the objective of this work is twofold: (a) identify the causes of the migration of the Solís Chico river mouth and (b) assess the possibility of artificially migrating the mouth of the river to the east, using the extracted sand to nourish La Floresta beach.

## METHODOLOGY

Firstly the migration of the river mouth and the elongation of the sand spit were quantified from historical records. Then, riverine aspects that could affect the behavior of the mouth were quantified: river flows, levels and sediment supplies to the coast at different temporal scales were estimated, and long-term plan view stability of the river was analyzed (i.e. meander evolution). Finally the action of maritime agents on the coast was considered by estimating and analyzing long-shore and cross-shore sediment transport at the river mouth zone. The methodology used for each

stage of the work is described next. For a detailed description of river studies the reader is referred to Chreties (2014).

The temporal evolution of the river mouth position and the length of the sand spit were quantified using aerial and satellite images for the period 1966-2012 (11 images in total).

In order to characterize the behavior of the river a hydrologic model (NRCS, 2010) and a one-dimensional hydraulic model (HEC-RAS 4.1; USACE, 2010) were implemented for the basin and the last stretch of the river (close to the mouth) respectively. From the latter, time series of daily mean water level and daily sediment transport rate were obtained at several river sections, and

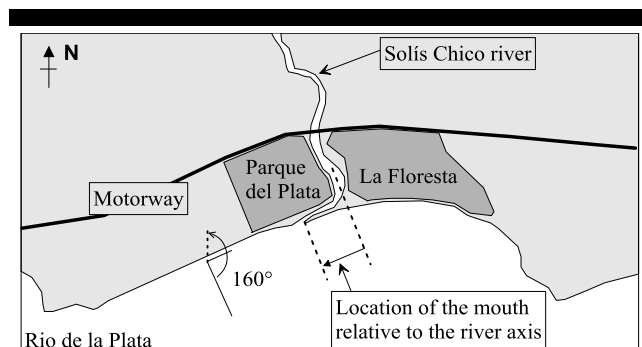


Figure 1. Study area, indicating the mean direction of the perpendicular to the beach and the reference axis used for measuring the relative position of the river mouth.

particularly at the last stretch of the river. Sediment transport was estimated by means of the Engelund-Hansen formulation (USACE 2010, Molinas and Boasheng 2001). For the implementation of these two models daily precipitation in a nearby basin was available for the period 1985-2002, along with information about topography and sediment characteristics of the river.

Then the formula proposed by Komura (1969) was used, along with the relation between flow rate and sediment transport obtained with the hydraulic model, to extend the sediment transport data series to a longer period. To this end, monthly precipitation data for the period 1900-2010, available at a nearby basin, was incorporated to the analysis. This way, a series of annual total sediment transport in the river for the period 1900-2010 was estimated (i.e. annual sediment supplied to the coast).

Three different criteria were used to analyze the plan-view stability of the river, namely: Leopold and Woman (1957), Lane (1957) and Millar (2000). All three results show that the final stretch of the river has a meandering pattern. The analysis of the meandering dynamics of the river was conducted using historical records (aerial images from 1966 compared with satellite images from 2006 to 2010), empirical formulations (Nanson and Hickin 1983) and the process-based numerical model RVR Meander (Abad and García 2006).

Regarding the influence of the maritime agents on the mouth, firstly the wave climate was estimated from the six-hourly time series of wind and wave reanalysis data from the ERA-Interim program (Dee et al., 2011), provided by the European Centre Medium-Range Weather Forecasts for the period 1979-2010. The local nearshore shallow waters wave climate was estimated using the hybrid downscaling methodology proposed by Camus et al. (2011). This methodology allows reconstructing of the time series of wave conditions at a nearshore location without propagating every sea state of the series. The methodology uses the maximum dissimilarity selection algorithm to select a given number of representative sea states from the deep water series (in this work 1024 sea states were used). Then, using the SWAN model (see e.g. Holthuijsen, 2010) each of these representative sea states is propagated under stationary conditions. Lastly, the entire offshore series is propagated to nearshore using a non-linear interpolation technique based on radial basis functions. Thus a 6-hourly time series of sea state parameters is constructed off the Solís Chico river mouth for the period 1979-2010. Before using the wind reanalysis data in the propagation, they were calibrated with wind data measured in the Rio de la Plata, using the directional quantile-matching methodology proposed by Minguéz et al. (2011).

From the sea state time series off the river mouth the time series of directional wave power and potential littoral sediment transport were estimated. The directional wave power was estimated using linear theory (see e.g. Dean and Dalrymple 1991). Notwithstanding the difficulties in estimating longshore sediment transport (Cooper and Pilkey, 2004) the littoral sediment transport was estimated using the CERC formula (see e.g. USACE 2002, Dean and Dalrymple 2002). For both variables the time evolution, mean annual cycle and interannual variability was analyzed.

Lastly the numerical model PETRA was used to analyze the stability of the sand spit under the action of severe wave conditions, so as to identify where and under what conditions waves are able to create a secondary open. PETRA is a cross-shore process-based beach model, which does not establish any "a priori" final profile (open-loop). The model evaluates the sediment transport along the beach profile due to local hydrodynamic and computes the conservation of sand within the beach profile. PETRA allows the users to determine the profile

shape response to a storm event and, in particular, to estimate coastline recession (González et al. 2007).

## RESULTS

The results obtained with the proposed methodology are presented next. Discussion and synthesis of these results is presented in the following sections.

### Quantifying the evolution of the sand spit

Six aerial photos (1966-2001) and four satellite photos (2006-2010) were used to quantify the evolution of the mouth. For each images the distance between the end of the sand spit and the river axis was measured, as shown in Figure 1. It was found that the length of the sand spit increased significantly between 2001 and 2006, with the river mouth migrating westward. The length of the spit increased from 500-800m before 2001 to 1000-1350m from 2006 to present. The volume of the sand spit increased by 13,200 m<sup>3</sup> between 2001 and 2006. Figure 2 shows the time series of spit length. Also included in the figure is the location of secondary breaches in the spit when they were present.

### River dynamics

Figure 3 shows the time series of river flow in a section near the mouth (upper panel) and the relation between the flow rate and the sediment rate (lower panel), obtained with the daily precipitation series of the period 1985-2002. It shows that the maximum flow occurred during an extreme event in 2002. This event is responsible for 34% of total sediment transport estimated for the period 1985-2002. Also, the analysis of the time series of water levels (not presented) shows that the water level in the river only exceeds the level of the sand spit for flows with return period greater than 20 years.

Figure 4 shows the annual sediment transport estimated for a section of river located 1.8 km upstream of the mouth, calculated with the hydrodynamic numerical model for the period 1985-2002 and with the simplified method Komura (1969) for the period 1900 - 2010. It shows that the sediment transport of 2002 was significantly higher than the other years of 1960-2010, exceeded only in 1959 and 1922.

Regarding the plan-view stability of the river meanders, the analysis based on historical records shows that the lateral migration rate of the meanders is between 0.6 and 0.85 m/year; i.e. in the last 40 years no significant changes were registered in the

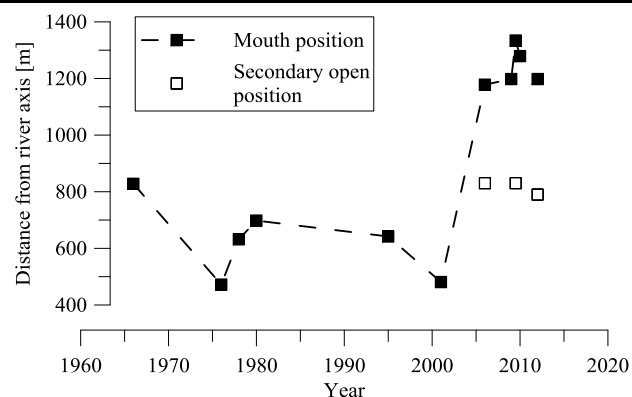


Figure 2. Distance from the river axis to the river mouth, measured as shown in Figure 1 (filled dots). Position of the secondary opens (empty dots).

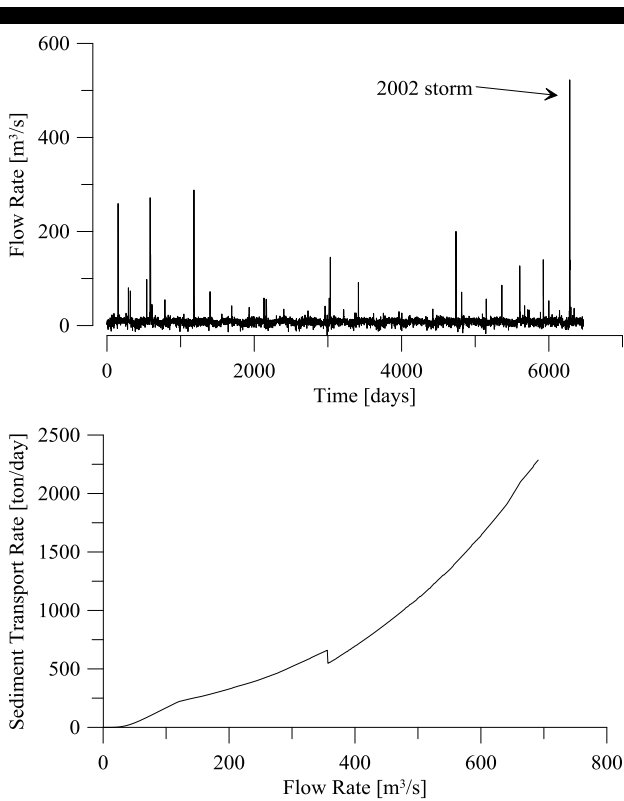


Figure 3. Upper panel: Flow rates at the last stretch of the river, near the mouth, obtained from the hydraulic model. Lower panel: relation between flow rate and sediment transport rate at the same section.

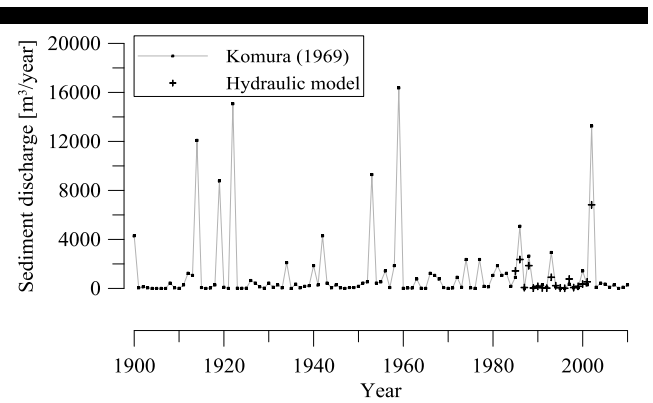


Figure 4. Time series of the annual sediment transport at the mouth of the river obtained from the hydraulic model (crosses) and using the Komura (1969) formula (black squares).

evolution of the river meanders, despite the existence of several anthropogenic interventions in the system, like the construction of a bridge and a roadway at the river bank. In agreement with this result, using the empirical formulation of Nanson and Hickin (1983) an average migration rate of 0.4 m/year was obtained, with a maximum rate of approximately 2.5 m/year. Also, with the numerical model RVR Meander it was found that the meander migration rate is not significant, with only some localized high values reaching migration rates between 2 and 3 m/year.

**Coastal dynamics**

Figure 5 shows the one year moving average of the direction of the wave power for the period 1979-2010. The mean direction of the wave power for the whole period is 158°, approximately equal to the direction perpendicular to the beach (160°) obtained from satellite images (see Figure 1). Figure 5 shows that the direction of the wave power has a decreasing trend (i.e. is rotating eastward).

Figure 6 shows the annual potential net littoral transport estimated with the CERC formula for the period 1979 to 2010, assuming that the coast direction remains constant during the whole period, perpendicular to 160°. It indicates a high variability of the annual net littoral transport, which ranges from 60,000 m<sup>3</sup>/year to -40,000 m<sup>3</sup>/year, with positive values corresponding to westward transport and negative values corresponding to eastward transport. The average net annual transport rate of the period is about 28,000 m<sup>3</sup>/year. The accumulated transport, starting on January 1979, is shown in Figure 7, evidencing a change in the slope of the cumulative transport around 1998. This change is in agreement with Figure 6, which shows that from 1998 on, there

are no years with negative net littoral transport. Therefore, the average annual net transport of 28,000 m<sup>3</sup>/year is not representative of the analyzed period. Taking as a turning point the year 1998, a mean annual littoral transport rate of 16,400 m<sup>3</sup>/year is obtained for the period 1979-1997, while for the period 1998-2010 it is approximately 45,500 m<sup>3</sup>/year.

Lastly, Figure 8 shows the location on the sand spit of beach profiles modeled with PETRA. The evolution of each profile was modeled under the action of severe waves, considering several sea level conditions. The return period of the significant wave height used in the analysis is about one year. The results show that the opening of the sand spit by wave action is only feasible in profile 2 with sea levels whose return period is greater than 10 years. From the analysis of profiles 3 and 4 (not shown) it seems that the height of the sand spit is not reduced significantly by wave action, even considering extreme sea levels.

**DISCUSSION**

**River mouth migration**

The analysis of aerial and satellite imagery shows that the sand spit has grown between 400 and 500 m westward from 2001 to 2006. This growth implies an increase in the volume of the sand

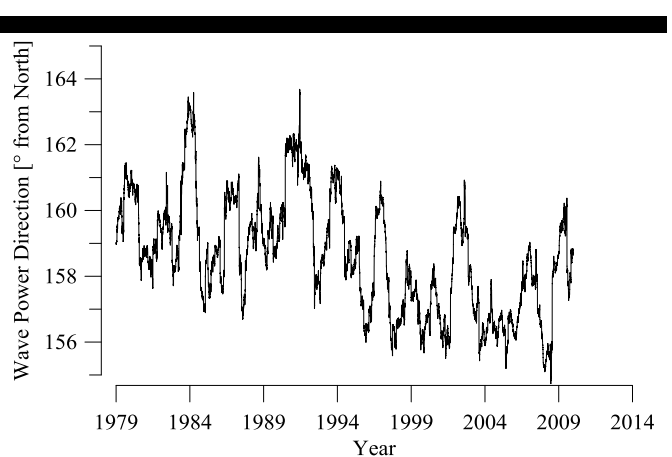


Figure 5. Time series of the annual moving average of direction of the wave power.

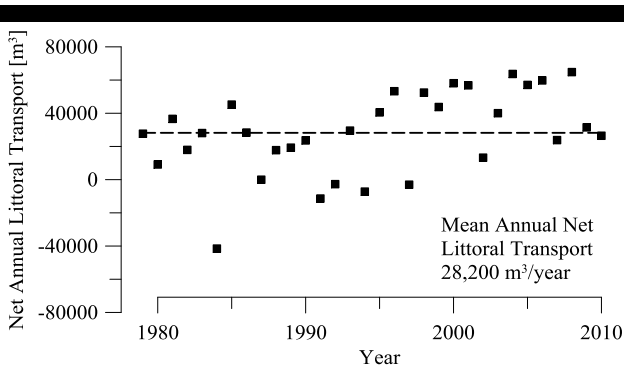


Figure 6. Annual net littoral transport for the period 1979-2010. It is assumed that the beach perpendicular remains constant (160°).

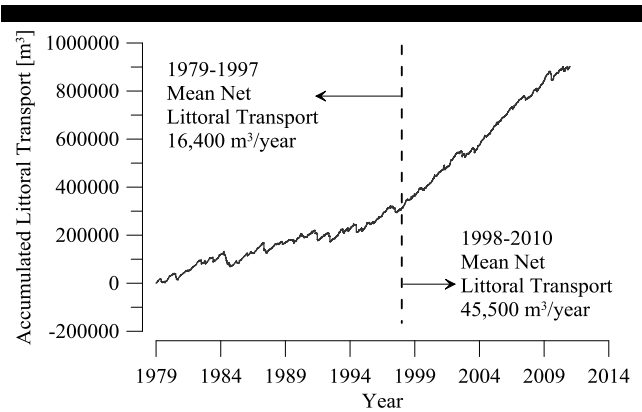


Figure 7. Accumulated littoral transport, starting from 1979.

spit of about 13,200 m<sup>3</sup>.

The estimated annual sediment transport of the river in the period 1900-2010 confirmed that the river sediment supply to the coast in 2002 (4500 m<sup>3</sup> according to the hydraulic model) is an order of magnitude higher than the average of previous years (350 m<sup>3</sup> according to the hydraulic model). To get a river sediment discharge greater than 4500 m<sup>3</sup> it is necessary to go back to 1959. It is observed that the sediment supplied to the coast by the river in 2002 is of the same order of magnitude as the increase in volume of the sand spit observed in 2001-2006.

Comparing the time series of the river sediment discharge to the coast with the migration of the mouth (see Figure 9), it follows that the elongation of the sand spit coincides with the increase in the river sediment supply. So in the pre-2002 images the sand spit is shorter than it is now, and then an increase in its length is observed between the 2001 and 2006 images, coinciding with the extraordinary river sediment discharge occurred during 2002. Moreover, according to the result obtained with Komura (1969), from 2003 to 2010 the average river sediment transport was 208 m<sup>3</sup>/year, lower than the 1960-2010 average value (882 m<sup>3</sup>/year), in agreement with the small variation of the length of the sand spit shown by the latest available images (2006, 2009, 2009 and 2010).

Analysis of coastal dynamics shows that the potential littoral transport increases from the year 1998, from an average net westward transport of approximately 16,400 m<sup>3</sup>/year in the period 1979-1998 to an average of 45,500 m<sup>3</sup>/year for the period 1999-2010. 2002 is within the period of increasing westerly transport.

Regarding the long-term stability of the mouth, neither the

analysis of river dynamics nor the analysis of coastal dynamics provide evidence suggesting long-term effects. From the long-term stability analysis of the river it appears that the meanders have no effect on river mouth evolution. Both the Nanson and Hickin (1983) formulation and the RVR Meander numerical model show that the dynamics of the plan-view configuration of the river are very limited. Particularly, no trend of migration of meanders in the flow direction, with potential to affect the mouth, is identified. Regarding coastal processes, it was found that the mean direction of wave energy is almost perpendicular to the beach, suggesting that this stretch of coast is close to equilibrium.

### Secondary breaches in the sand spit

From the satellite images several events were identified with secondary openings in the sand spit. The analysis of the conditions that may produce secondary openings shows that its occurrence is most likely in the stretch located between section 2 and the mouth (see Figure 8). This stretch is most vulnerable to wave action. Also, it was found that the breakage of the sand spit by the sole action of the river is limited to flow conditions whose return period is greater than 20 years, suggesting that a sudden eastward migration of the mouth is a possible but not very likely event.

### CONCLUSIONS

It is concluded that the migration of the mouth is mainly due to an extraordinary river sediment supply in 2002, combined with an increase in the net (westward) potential littoral transport rate since the late 90s. Cooper (1990) described similar influxes of sediment

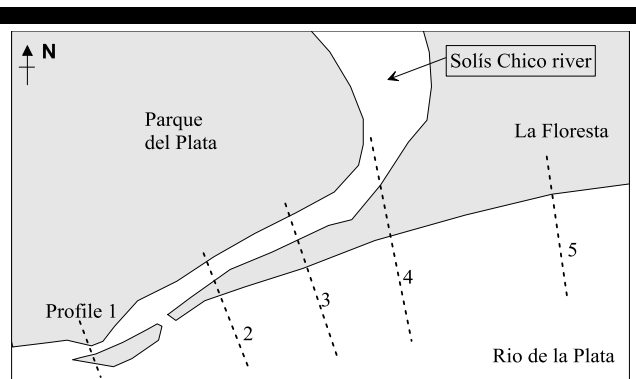


Figure 8. Outline of the beach profiles analyzed with the numerical model PETRA.

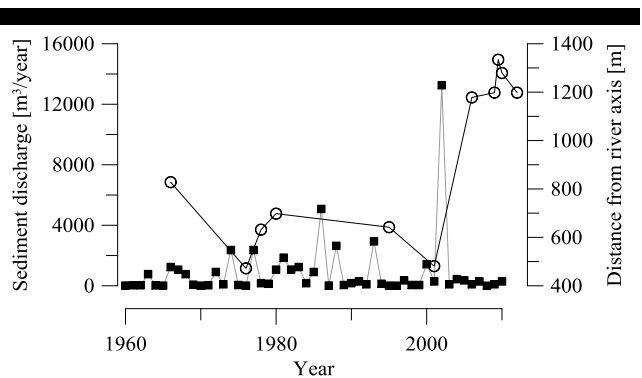


Figure 9. River sediment discharge to the coast (black squares) and evolution of the position of the river mouth (empty circles).



Figure 10. Outline of the borrow area proposed for La Floresta beach nourishment project.

to the South African coast during river floods, forming ephemeral deltas that were reworked landwards

In turn, given the natural variations in the position of the river mouth, as well as the rates of river sediment supply, it is concluded that the sand spit could be partially used for the nourishment of La Floresta beach, 1,700 m eastward of the present mouth location, without affecting the natural dynamics of the river mouth or the upstream stability of the river. In order to keep the river mouth within the limits of previously recorded positions, the borrow area shown in Figure 10 is proposed. This area is the most vulnerable to natural openings by wave action.

It is expected that the migration of the mouth eastward from its current location (i.e. towards the axis of the river), determines the natural filling and closing of the last stretch of the river, that now runs parallel to the coast, favouring the recovering of the direct connection between Parque del Plata resort and its beach. However, due to the complexity of the hydro-sedimentological fluvial and coastal processes involved, and taking into account that there is no measured data of the sediment transport rates in the area, it is advised to implement a monitoring system in the river mouth area, including systematic measurements of the position of the sand spit and the evolution of the profile of the adjacent beaches.

### ACKNOWLEDGEMENT

This study was partially funded by the National Hydrographic Administration of the Ministry of Public Works of Uruguay (Dirección Nacional de Hidrografía del Ministerio de Transporte y Obras Públicas).

### LITERATURE CITED

- Abad, J.D., García, M.H., 2006. RVR Meander: A toolbox for re-meandering of channelized streams. *Computers & Geosciences*, 32(1), 92-101.
- Camus, P., Méndez, F.J., Medina, R., 2011. A hybrid efficient method to downscale wave climate to coastal areas. *Coastal Eng.*, 58, 851-862.
- Chetries, Ch., Solari, S., López, G., Teixeira, L., 2014. Analysis of the Solís Chico river mouth migration. *Proceedings of River Flow 2014* (Lausanne, Switzerland), IAHR. Abstract accepted.
- Cooper, J.A.G., 1990. Ephemeral stream mouth bars at flood breach river mouths on a wave-dominated coast: comparison with ebb-tidal deltas at tidal inlets. *Mar. Geol.*, 95, 57-70
- Cooper, J.A.G. and Pilkey, O.H., 2004. Longshore drift: trapped in an expected universe. *Journal of Sedimentary Research*, 74, 599-606.
- Dean, R.G., Dalrymple, R.A., 1991. *Water Wave Mechanics for Engineers & Scientists* (Advanced Series on Ocean Engineering-Vol2). World Scientific, Singapore. 353 p.
- Dean, R.G., Dalrymple, R.A., 2002. *Coastal Processes with Engineering Applications*. Cambridge University Press. Cambridge, U.K. 488p.
- Dee D. P., Uppala, S. M., Simmons, A. J., Berrisford P. et al. 2011. The ERA-Interim reanalysis: configuration and performance of data assimilation system. *Quart. Journ. Roy. Met. Soc.*, 137, 553-597.
- González, M., Medina, R., González-Ondina, J., Osorio, A., Méndez, F.J., García E., 2007. An integrated coastal modeling system for analyzing beach processes and beach restoration projects, SMC. *Computers & Geosciences*, 33, 916-931.
- Holthuijzen, L.H., 2010. *Waves in Oceanic and Coastal Waters*. Cambridge University Press. Cambridge, U.K. 404 p.
- Komura, S., 1969. Computation of Dominant Discharge. *Proceedings of the 13th Congress of IAHR* (Kyoto, Japan), Vol. 5.1, pp. 265-268.
- Lane, E.W., 1957. *A study of the shape of channels formed by natural streams flowing in erodible material*. Omaha: US Army Engineer Division, Missouri River.
- Leopold, L. and Woman, M., 1957. *River Channel Patterns: Braided, Meandering and Straight*. U.S. Geol. Surv. Prof. Paper, 282-B.
- Millar, R.G., 2000. Influence of bank vegetation on alluvial channel patterns. *Water Resources Research*, 36(4), 1109-1118.
- Mínguez, R., Espejo, A., Tomás, A., Méndez, F.J., Losada, I.J., 2011. Directional calibration of wave reanalysis databases using instrumental data. *Journal of Atmospheric and Oceanic Technology*, 28, 1466-1485.
- Molinas, A., Boasheng, W., 2001. Transport of sediment in large sand-bed rivers. *Journal of Hydraulic Research*, 39, 135-146
- Nanson, G.C., Hickin, E.J., 1983. Channel migration and incision on the Beatton River. *Journal of Hydraulic Engineering*, 109, 327-337.
- NRCS, 2010. *National Engineering Handbook 210-630-Hidrology*. National Resources Conservation Service, United States Department of Agriculture. Washington, USA.
- USACE, 2002. *Coastal Engineering Manual*. Engineer Manual 1110-2-1100, U.S. Army Corps of Engineers, Washington, D.C. (in 6 volumes).
- USACE, 2010. *HEC-RAS, River Analysis System. Hydraulic Reference Manual*. U.S. Army Corp of Engineers. Hydrologic Engineering Center. Report Number CPD-69.

## Differential short- and medium-term behavior of two sections of an urban beach

Javier Benavente †, Theocharis A. Plomaritis †, Laura del Río †, María Puig †, Cristina Valenzuela †, Bruno Minuzzi †

† Dept. of Earth Sciences, Faculty of Marine and Environmental Sciences, University of Cádiz, 11510, Puerto Real, Cádiz, Spain  
javier.benavente@uca.es



[www.cerf-jcr.org](http://www.cerf-jcr.org)



[www.JCRonline.org](http://www.JCRonline.org)

### ABSTRACT

Benavente, J., Plomaritis, T.A., del Río, L., Puig, M., Valenzuela, C., Minuzzi, B. 2014. Differential short- and medium-term behavior of two sections of an urban beach. In: Green, A.N. and Cooper, J.A.G. (eds.), *Proceedings 13<sup>th</sup> International Coastal Symposium* (Durban, South Africa), *Journal of Coastal Research*, Special Issue No. 70, pp. 621-626, ISSN 0749-0208.

The present study aims to identify factors that control the different morphological evolution of two sections of an urban beach. The study area is the Victoria Beach in Cadiz city (SW Spain). The beach comprises two sectors: Cortadura zone (CZ) and Victoria zone (VZ), both subject to the same offshore wave conditions. The area is a typical low energy coast with dissipative beach morphology, where storm conditions are generally recorded in the winter season. Variability of beach profiles was analyzed through the use of empirical orthogonal functions (EOF). For short-scale processes, nearshore wave and current measurements were collected simultaneously at both zones during a tidal cycle. Additionally, medium term beach evolution from the last 50 years was evaluated using aerial photos. Results of medium term beach changes show a clear retreat that in fact led to several artificial nourishments of the beach over the last years. Erosion observed in CZ was greater than in VZ. In the short term, VZ presented greater morphological variability than CZ, which only experienced some changes in beach volume. Wave and current measurements showed a higher wave height and longshore current velocity in CZ under the same offshore wave conditions, which might account for the higher erosive trend in this area and development of a more dissipative profile. The reason for this differential behavior is related to the different characteristics of wave propagation in the outer surf and shoaling zone of both sections.

**ADDITIONAL INDEX WORDS:** *Beach morphodynamics, swash bars, geological framework, coastal erosion, Gulf of Cadiz.*

### INTRODUCTION

Seasonal changes in beach profiles constitute an important aspect of the variability of the coastal environment and reach utmost importance in the case of urban beaches. Since the late 1940's and the early work of Shepard (1950) on southern California beaches, it is known that seasonal beaches generally experience sand transport towards the beach during spring and summer, resulting in a steeper beach face and a well-developed berm at the end of the summer, with a wider dry beach. During fall and winter, storm-generated waves that cut away the berm cause an offshore sediment motion which results in the accumulation of sediment on a winter bar located offshore beyond the surf zone.

The ability of a given beach type to shift between different morphodynamic states shows the health of that beach. This capacity allows the beach to adapt to changes in energy conditions, so its absence could be an indicator of erosion trends (Benavente *et al.*, 2000, Benavente *et al.*, 2002).

These morphological and morphodynamic changes are usually altered on urban beaches strongly modified by human interventions, especially on nourished beaches. As a consequence,

these type of beaches commonly lack the ability to adapt to changes in incident wave energy. In fact, nourishment works have often had limited durability, due to factors like the type of artificial beach profile, sediment grain size, contouring conditions (i.e. nearshore bathymetry), etc. (Anfuso *et al.*, 2001).

Apart from that, it is frequent that diverse sectors of a single beach show contrasting behavior, with a different response during storm conditions and, mainly, during the recovery period. This constitutes a problem from the management perspective for two reasons. On one hand, sometimes interventions are undertaken in the entire beach but with a correct knowledge of differential beach behavior, they could be done only where they are really necessary, with fewer expenses. On the other hand, this different behavior is usually related to the presence of artificial coastal engineering structures, like groins or breakwaters. According to this general belief, coastal managers often act over these structures several times instead of analyzing the beach as a natural environment probably controlled by natural factors. Among these natural factors, geological framework is commonly one of the most important (Jackson *et al.*, 2005; Lentz & Hapke, 2011) because it controls the energy that arrives to the beach, by determining nearshore bathymetry and other boundary conditions.

The objective of this paper is to analyze the medium and short term evolution of two different sectors of the same urban beach, and to identify the reasons for their differential behavior.

### STUDY SITE

The study area, La Victoria beach, is located in the Gulf of Cadiz (SW Spain) facing the Atlantic Ocean (Figure 1). It is a mesotidal coast with 3.2 m and 1.1 m of spring and neap tidal ranges, respectively. Dominant winds blow from ESE (19.6% of annual occurrence) and WNW (12.8%), although the first is not significant in wave generation due to its short fetch. These conditions together with coastline orientation make sea and swell waves approach generally from the third and fourth quadrants (Benavente *et al.*, 2000). According to this, prevailing longshore drift is directed southeastwards. Significant wave height is usually lower than 1 m, with waves over 4 m high being uncommon and occurring only during the most significant storms, which usually take place between November and March and approach from the third quadrant (Del Río *et al.*, 2012). In fact, waves greater than 1.5 m are considered storm waves by the National Ports Authority, so the area can be classified as a low-energy one.

Concerning the geological setting, this area is located in the southern part of Cádiz Bay. It belongs to the end of the Guadalquivir Neogene depression, characterized by soft, sub-horizontal sedimentary deposits which give rise to a linear NNW-SSE oriented, low-lying coastline. The most important river courses in this area are the Guadalquivir and Guadalete rivers, which flow North of the study site. From a geomorphological point of view, La Victoria beach is located on a sandy tombolo attached to the rocky outcrop of Cádiz city (Figure 1). Bathymetric contours in the study site are broadly parallel to the coastline and the nearshore zone shows a generally gentle slope, interrupted by several shore-parallel rocky outcrops.

In detail, La Victoria is an urban beach around 3000 m long, located in Cádiz city and backed by a seafront. Outside the limits of the city, on its southernmost sector, it is backed by foredunes and a low, mostly non-vegetated dune ridge artificially stabilized by fences. It is a flat beach, with slope values ranging from 0.025 to 0.02, composed by medium to fine quartz-rich sands ( $D_{50}=201\mu\text{m}$ ). It is between 5-90 m wide, with a narrower north and south ends and a wider central sector (Plomaritis *et al.*, 2009).

From the morphodynamic point of view, it is an intermediate-dissipative beach where flat bars are often observed on the foreshore. According to this classification the beach shows a wide surf zone with prevailing spilling breakers.

### METHODS

Medium-term shoreline changes were determined on six sets of aerial photographs and orthophotographs dating from 1956 to 2005, at scales between 1:18,000 and 1:33,000. The images were processed in GIS environment in order to digitize the shorelines and calculate rates of shoreline change, by means of DSAS extension for ArcGIS™ (Thieler *et al.*, 2009). Due to the absence of dunes or beach vegetation in the study area, the HWL was used as a valid shoreline proxy (Del Río & Gracia, 2013).

Short-term variability was assessed through beach topographic monitoring carried out from February 2012 to May 2013. Surveys were conducted almost every spring tide (every 15 days) using a DGPS-RTK (Leica GPS 900) and a Total Station (Leyca Geosystem TC 407). Profiles were surveyed in two sections of La Victoria beach with a different behavior (Muñoz-Pérez *et al.*, 2001): Cortadura zone (CZ) and Victoria zone (VZ).

The processing of the topographic data led to the calculation of the erosion/accretion volumes of sand per unit of beach length up

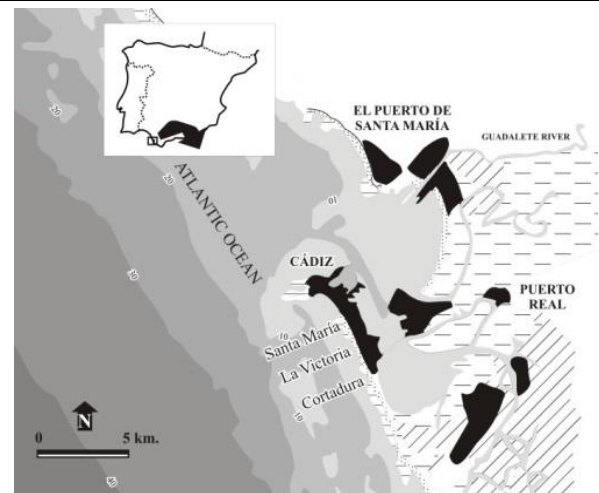


Figure 1. Study area in SW Spain showing two different sectors of the same beach: La Victoria (VZ) and Cortadura (CZ).

to mean low-water level, as well as beach gradient, width of the dry beach and intertidal beach gradient between mean high and low water levels. During the surveys surface sediment samples were collected with a seasonal periodicity and the granulometric parameters were calculated.

In order to separate the spatial and temporal variability of the beach profile the method of the Empirical Orthogonal Functions (EOFs), also known as Principal Component Analysis (Lorenz, 1956) was used. EOF is one of the most widely and extensively used methods for decomposing a space-time field into spatial patterns and associated time indices. Winant *et al.* (1975) were among the first to apply it for studying the seasonal changes in cross-shore beach profiles. Since then it has been used in beach morphodynamics (review in Larson *et al.*, 2003). The method is purely statistical and tries to represent the complex field of spatiotemporal variability through a number of basic spatial patterns coupled with time-dependent function (Kroon *et al.*, 2008). Although the resulting patterns lack any direct physical meaning they are often linked with coastal processes and behavior (Harley *et al.*, 2011). This method was already applied on La Victoria beach in order to identify profile variations (Muñoz-Pérez *et al.*, 2000) and different longshore evolution patterns (Muñoz-Pérez *et al.*, 2001).

Hourly wave height and period data were obtained from the offshore Wave Rider buoy "Cádiz", which belongs to the Spanish Sea Wave Recording Network (REMRO). Energy values were calculated, as well as the *erosivity* parameter proposed by Benavente *et al.* (2000):

$$E_r = E\Omega = \rho g H^3 / 8 W_s T \quad (1)$$

where  $\Omega$  is the Dean Parameter with  $W_s$  being the sediment fall velocity parameter,  $\rho$  is the density of water,  $H$  is the mean significant offshore wave height of the period prior to the beach profiling and  $T$  is its associated period.

Finally, an intensive field experiment was undertaken on 10th and 11th October 2012. Measurements of nearshore waves and currents were collected at the two zones of La Victoria beach simultaneously during this tidal cycle. An ADV (acoustic Doppler velocimeter) and a pressure sensor with an electromagnetic current meter were deployed in the VZ and in the CZ respectively. They

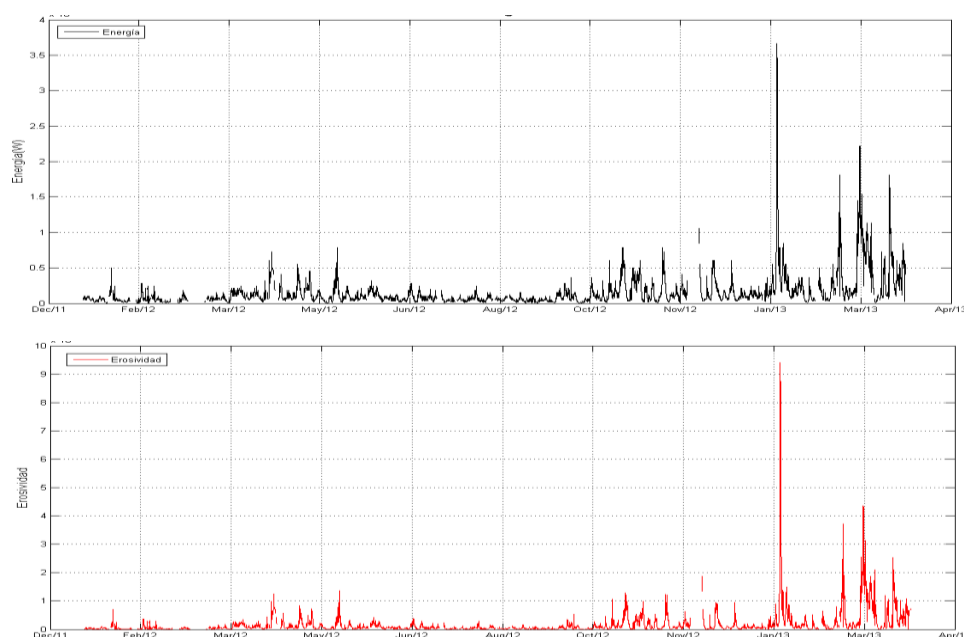


Figure 2. Energy and *erosivity* conditions between February 2012 and May 2013.

were programmed in a burst of ten minutes, with a frequency of 2 Hz in the case of the electromagnetic current meter, 4 Hz in the pressure sensor and 32 Hz in the ADV.

## RESULTS

### Medium-term evolution

The aerial photographs reveal a moderate advance of the HWL along the whole beach over the last decades. However, shoreline trends vary in space and time. Accretion rates are higher in the central sector of the beach (VZ), reaching up to 1,2 m/yr for the whole analysed period, but it is remarkable that shoreline advance occurred only after the massive nourishment works performed in 1991, when 2,000,000 m<sup>3</sup> of sand were poured on the beach (Muñoz-Pérez *et al.*, 2001). As a consequence of the nourishment, beach width was increased about 80 m on average, especially in the central sector of the beach. Shoreline accretion decreases towards the southern end of La Victoria, and in fact no net changes are recorded in CZ across the studied period. Considering that three nourishment works have been carried out in La Victoria since 1991 (Muñoz-Pérez *et al.*, 2013), the contrast between the aforementioned HWL advance in VZ and the apparent stability recorded in CZ reveals a clear trend of sand loss in CZ.

### Energy conditions

During 2012 significant wave heights were around 1 m and the maximum wave heights rarely were higher than 2 m. Therefore, along 2012 wave conditions never crossed the threshold values proposed for the storm conditions in this area (Ribera *et al.*, 2011; Del Río *et al.*, 2012). This situation changed at the beginning of 2013, so during this year four storms were recorded, in January,

February, March and April. Approach direction was WSW in all cases, typical for storms in this area (Del Río *et al.*, 2012).

According to this, the most energetic periods were the winter and the beginning of spring 2013, and the less energetic were the first winter and summer 2012 (Figure 2). Regarding the *erosivity* parameter, the most erosive periods were January and March 2013. These results indicate that 2012 was a year when beach accretion would be expected, and erosive conditions occurred only during short periods of 2013. It is also interesting to remark that the intensity of the January 2013 storm was very high but the duration was extremely short (Figure 2).

### Profile evolution

Profiles on CZ (Figure 3) show a clearly dissipative state without any important features along the entire profile; however, a small berm is developed during the summer till the beginning of November. Along the spring season, a very low bar system can be observed in the lower part of the beach.

In the central sector of the beach (VZ), profile morphology is steeper and more variable according to Muñoz-Pérez *et al.* (2001). A well developed berm can be seen during the whole year 2012, with a width around 90 m. Only between January and April 2013 this morphology disappeared, with part of the sediment being deposited in the lower portion of the intertidal zone building a well developed bar system.

Regarding the volumetric evolution, both areas showed a similar behavior, with remarkable variations only from the beginning of 2013. Values showed significant erosion in winter 2013, most important in CZ, and small recovery in May, most important in VZ. Intertidal slopes showed the same behavior as the sediment volume.



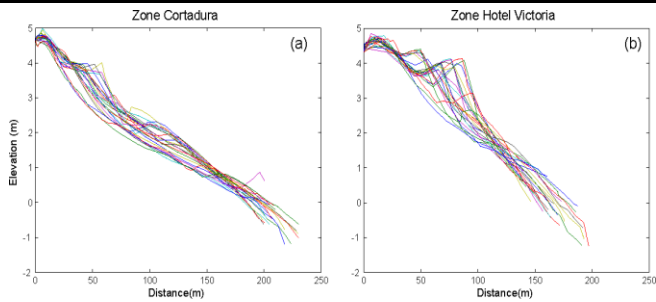


Figure 3. Profile evolution in Victoria beach in CZ (a) and VZ (b).

**EOFs**

Results of the variance of each profile for the five first eigenfunctions are ranked in Table 1. For each profile an eigenvalue is assigned, which represents percentage of the variability which they explain, defined as the Mean Squared Value (MSV) of the data. Values from EOF4 onwards are related to very small morphological changes with a temporal scale shorter than the frequency of the surveys, hence outside the scope of this work.

Table 1. Variance explains by each eigenfunction in two profiles representative from both areas.

	CZ1	CZ2	VZ1	VZ2
EOF1	58,9	67,4	38,5	37,1
EOF2	15,8	15,4	22,2	22
EOF3	8,9	9	20,4	20,2
EOF4	4,5	2,3	8	9,6
EOF5	3,5	1,5	4,3	4,4

The first eigenfunction (EOF1) explains most of the MSV of the data and represents the average profile of the beach. Values are lower in VZ than in CZ due to the higher variability of the first zone; therefore, the low variability of CZ allows building a mean profile significantly accurate for this area (Figure 4).

The second eigenfunction (EOF2) explains the major part of the remaining MSV. Both EOF1 and EOF2 are needed in order to explain the mean profile and its variability in the case of VZ.

The third eigenfunction was no so important for CZ but it explained around 20% of the variance in VZ. This eigenfunction use to be related with sediment transport processes.

In CZ, the second eigenfunction explains the presence of the berm and its variability, located at around 65 m from the profile base (Figure 4). Also, the variability that appears around 100 m would explain the presence or absence of the bar system during the period when the upper part of the beach was eroded.

The third eigenfunction (EOF3) just explain these movement of sand between the berm and the bar system, large variability around 25 m from the start of the profile during accretion periods and around 60m during erosive situations. Variations of the EOFs during the study period were really low, only they increased during the beginning of 2013. It must be noted that temporal variation of EOF1 coincided with the evolution of beach volume.

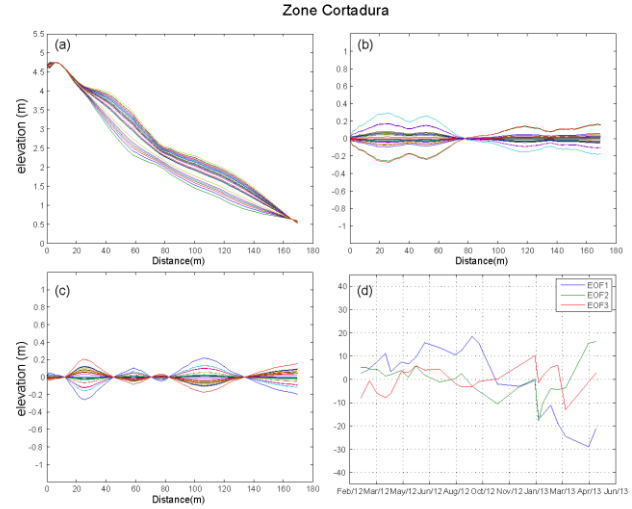


Figure 4. Variation of the first three eigenfunctions across the profile in CZ. a) EOF1, b) EOF2, c) EOF3 and d) temporal variations of these.

In VZ (Figure 5) the movement of the berm makes it impossible to design a mean profile from EOF1. The second eigenfunction explains this variability of the berm between 40 and 80 m, as well as the presence of a bar beyond 90 m during erosive periods. Finally, the third eigenfunction explains the high variability of the berm around 80 m. Also here temporal variation of the eigenfunctions was low until the beginning of 2013. In that case the evolution of EOF1 is mostly related to the intertidal slope of this area, and as mentioned above, EOF2 is also needed to explain volumetric evolution.

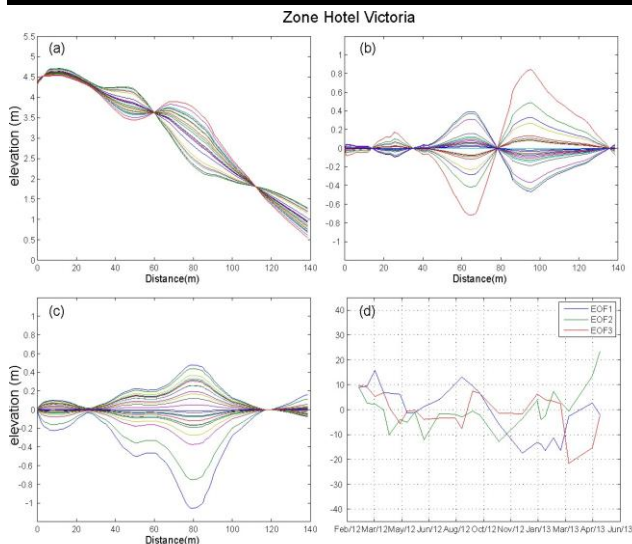


Figure 5. Variation of the first three eigenfunctions across the profile in VZ. a) EOF1, b) EOF2, c) EOF3 and d) temporal variations of these three.

**Intensive survey**

Results of the intensive survey show that the wave energy in CZ was barely higher than in VZ and only during high tide. This way, in CZ a maximum height of 0.77 m was recorded, with an average height of 0.35 m, while in VZ the maximum wave height was 0.69 m and the average was 0.21 m.

Data from current measurements were more interesting (Figure 4). It can be observed that the velocity in the cross-shore direction was higher in CZ, with a mean value around 0.7 m/s while in VZ it was around 0.4 m/s. It is also evident that the direction of the most intensive fluxes was towards SW, i.e. offshore with a small longshore component. Nevertheless, in VZ the most intense currents were directed towards the coast.

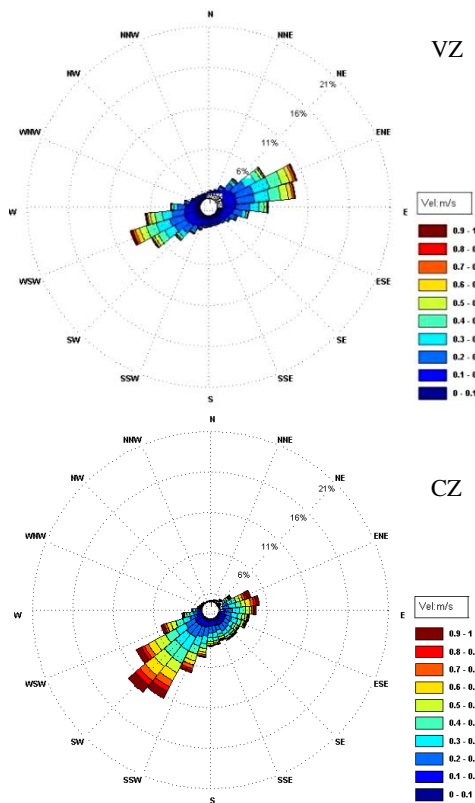


Figure 6. Current roses obtained during the intensive survey for the both areas: VZ (upper) and CZ (lower). Coastal orientation is NNW-SSE.

**DISCUSSION**

In the medium term, the apparent advance of the HWL in VZ can be directly attributed to the diverse artificial nourishments performed on the beach, aimed at keeping an adequately wide dry beach. In CZ the apparent stability of the shoreline is also a result of these replenishments, and therefore the natural trend of the beach is clearly erosive in the medium term.

Regarding short-term beach changes and their relation with wave conditions, it must be pointed out that according to Del Río *et al.* (2012), the most intensive storm episodes generally occur in December and the greatest erosion in January, due to the high seasonality of the storminess. However, during 2012 no storms were recorded and during 2013 they occurred during the second

part of the winter and the beginning of the spring. Despite these low energy conditions, erosion was observed in CZ but not in VZ. Nevertheless, important morphological changes were recorded in VZ but not in CZ.

Several studies used volumetric variations as indicator of the state of the beach (e.g. Allen, 1981; Carr *et al.*, 1982; Oyegun, 1991; Thom and Hall, 1991) instead of morphological changes. In this study, it has been obtained that morphological and volumetric changes in VZ occur in the same sense, but this is not the case in CZ. In this area morphological changes were really low compared to the volumetric ones. In spite of the similar behavior of both parameters in VZ, the correlation between them was also poor. This result, according to Benavente *et al.* (2000), would mean that the beach could adapt its morphology to the energetic conditions, but there is not enough sediment to increase beach volume during fair weather conditions.

When comparing changes in beach profiles and wave conditions, a good agreement was observed between profile slope and erosivity parameter in VZ (Figure 7) but not in CZ. Conversely, in CZ, due to the little morphological changes recorded, a good agreement was found between volumetric changes and erosivity parameter (Figure 7).

Therefore, an increase in energetic conditions generates volumetric changes in CZ, while in VZ it generates morphological changes not linked to beach erosion. This differential behavior reveals a higher adaptability of VZ to changes in wave energy, and a lower adaptability of CZ, hence the latter being more vulnerable to erosion (Benavente *et al.*, 2002).

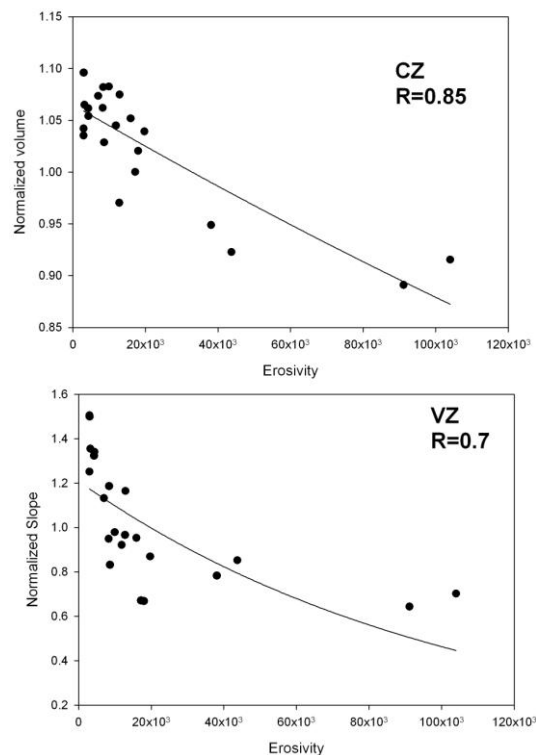


Figure 7. Relationship between erosivity parameter and normalized volume in CZ and relationship between the same parameter and normalized slope in VZ. Correlation made by an exponential decay equation with a significance level higher than 0.9 in both cases.

It is important to note that although energetic conditions along the studied period were quite low, erosion was recorded in CZ and beach recovery was limited. This could be observed during the intensive survey when under a mild wave situation, for the same energetic conditions, in VZ there would be accretion, while in CZ there would be erosion due to the stronger rip currents and a higher longshore transport transferring sediment out of this area.

The contrasting energy levels measured in the intensive survey supports the data from López-Dóriga *et al.* (2010). These authors observed, through wave propagation, the wave refraction and diffraction processes on the rocky shoal located in front of CZ, which generates energy concentration on this area of the beach.

Regarding the EOFs, they reveal that the first eigenfunction is related to energetic changes in both study areas, although in CZ is linked to volumetric variations while in VZ is linked to slope changes. This method has also been useful for quantifying the higher variability of VZ, where sediment exchange between the berm and the bars, together with berm changes, reveal the sedimentary stability of this area.

In a similar study performed also in la Victoria beach, Muñoz-Pérez *et al.* (2001) related the first eigenfunction (EOF1) to shoreline recession and dry beach reduction, highlighting the seasonal behavior as responsible for changes in beach slope. However, in the present work the first eigenfunction is not strictly related to beach retreat. These differences might be due to two main reasons. The first one is related to differences in the energetic regime considered in each study. The above authors assume a dominant seasonal behavior, with a nearly complete recovery of the beach profile at the beginning of the spring, but this situation did not occur during the present study due to the special conditions recorded in 2012. The second reason would be related to changes in beach characteristics, as the field work by Muñoz-Pérez *et al.* (2001) was performed shortly after the massive beach nourishment in 1991 and they assumed that the whole beach showed the same behavior.

In the present work most of the principal components are defined in a similar way to that proposed by Winant *et al.* (1975), where EOF1 represents the average level of beach profile, while EOF2 represents the seasonal changes in slope according to the position of the bar and the berm.

## CONCLUSIONS

In this study the differential behavior of two sectors of the same urban beach has been demonstrated and analysed using diverse methods in the short and medium term. It has been found that the southern area of the beach (CZ) shows a clearly erosive trend at both time scales. The use of Principal Component Analysis on topographic beach profiles has revealed that the limited morphodynamic response of CZ indicates a higher vulnerability to storm conditions, compared to the central part of the beach (VZ).

This differential behavior can be attributed to geological controls. As pointed out by previous works, the presence of a rocky shoal in the nearshore area determines differential conditions of incident energy in both areas. This study supports this conclusion through in-situ surveys of waves and currents in the breaker zone.

From the methodological perspective, this work shows that PCA on beach profiles can be considered a useful tool to identify the kind of beach response to storms.

## ACKNOWLEDGEMENT

This work is a contribution to the project GERICO (CGL2011-25438) (Spanish National R & D Programme), project RNM-6547 (Andalusian Excellence Research Program) and to the research

group RNM-328 of the Andalusian Research Plan (PAI). The authors would like to acknowledge Puertos del Estado for providing wave data.

## LITERATURE CITED

- Benavente, J., Gracia, F.J. and López-Aguayo, F., 2000. Empirical model of morphodynamic beachface behaviour for low energy mesotidal environments. *Marine Geology*, 167, 375-390.
- Benavente, J., Del Río, L., Anfuso, G., Gracia, F.J. and Reyes, J.L., 2002. Utility of morphodynamic characterization in the prediction of beach damage by storms. *Journal of Coastal Research*, SI 36, 56-64.
- Del Río, L., Plomaritis, T.A., Benavente, J., Valladares, M. and Ribera, P., 2012. Establishing storm thresholds for the Spanish Gulf of Cádiz coast. *Geomorphology*, 143-144, 13-23.
- Del Río, L. and Gracia, F.J., 2013. Error determination in the photogrammetric assessment of shoreline changes. *Natural Hazards*, 65(3), 2385-2397.
- Jackson, D.W.T., Cooper, J.A.G. and Del Río, L., 2005. Geological control of beach morphodynamic state. *Marine Geology*, 216, 297-314.
- Larson, M., Capobianco, M., Jansen, H., Rózyński, G., Southgate, H.N., Stive, M., Wijnberg, K.M. and Hulscher, S., 2003. Analysis and modeling of field data on coastal morphological evolution over yearly and decadal time scales. Part 1: background and linear techniques. *Journal of Coastal Research*, 19-4, 760-775.
- Lentz, E.E. and Hapke, C.J., 2011. Geologic framework influences on the geomorphology of an anthropogenically modified barrier island: assessment of dune/beach changes at Fire Island, New York. *Geomorphology*, 126, 82-96.
- López-Dóriga, U., Benavente, J. and Plomaritis, T.A., 2010. Natural recovery processes in an urban beach, La Victoria (Cádiz, SW Spain). In: Mimsa, H., Sedrati, M., El Moumi, B. and Menier, D. (eds.), *Proceedings 1er Colloque International Littoraux Méditerranéens: états passés, actuels et futurs* (Asilah, Morocco), p. 9.
- Lorenz, E.N., 1956. Empirical orthogonal functions and Statistical Weather Prediction. *Technical report, Statistical Forecast Project Report 1*, Dep. of Meteor., MIT, 49p.
- Muñoz-Pérez, J.J. and Medina, R., 2000. Profile changes due to a fortnightly tidal cycle. *International Conference on Coastal Engineering (ASCE)*, Sydney, pp. 3063-3075.
- Muñoz-Pérez, J.J. and Tejedor, L., 2001. Las funciones empíricas ortogonales y los cambios en el perfil de playa a corto, medio, y largo plazo. *Física de la Tierra*, 13, 139-166.
- Muñoz-Pérez, J.J., Román-Sierra, J., Navarro-Pons, M., Neves, M.G. and Del Campo, J.M. (in press). Comments on "Confirmation of beach accretion by grain-size trend analysis: Camosoto beach, Cádiz, SW Spain" by E. Poizot *et al.* (2013) *Geo-Marine Letters*, 33(4). DOI 10.1007/s00367-013-0344-0
- Plomaritis, T., Anfuso, G., Benavente, J. and Del Río, L., 2009. Storm impact and recovery patterns in natural and urbanised beaches in Cadiz (SW Spain): *Geophysical Research Abstracts*, 11. EGU2009-1409.
- Thieler, E., Himmelstoss, E.A., Zichichi, J.L. and Ergul, A., 2009. The Digital Shoreline Analysis System (DSAS) Version 4.0- An ArcGIS Extension for Calculating Shoreline Change. *U.S. Geological Survey open-file report*, 2008-1278.
- Winant, C.D., Inman, D.L. and Nordstrom, C.E., 1975. Description of seasonal beach changes using empirical eigefunctions. *Journal of Geophysical Research*, 80(15), 1979-1986.

# Estimating the impact threshold for wind-blown sand

Bailiang Li<sup>†</sup>, Jean T. Ellis<sup>‡</sup>, Douglas J. Sherman<sup>∞</sup>

<sup>†</sup> Department of Environmental Science  
Xi'an Jiaotong – Liverpool University  
Suzhou, Jiangsu 215123, China  
bailiang.li@xjtlu.edu.cn

<sup>‡</sup> Geography and Marine Science  
University of South Carolina  
Columbia, SC 29208, USA  
jtellis@sc.edu

<sup>∞</sup> Department of Geography  
University of Alabama  
Tuscaloosa, AL 35487, USA  
sherman@ua.edu



[www.cerf-jcr.org](http://www.cerf-jcr.org)



[www.JCRonline.org](http://www.JCRonline.org)

## ABSTRACT

Li, B., Ellis, J. T., Sherman, D. J., 2014. Estimating the Impact Threshold for Wind-Blown Sand. In: Green, A.N. and Cooper, J.A.G. (eds.), *Proceedings 13<sup>th</sup> International Coastal Symposium* (Durban, South Africa), *Journal of Coastal Research*, Special Issue No. 70, pp. 627-632, ISSN 0749-0208.

In many aeolian studies, it is commonplace to use Bagnold's (1936) equation to calculate threshold shear velocity ( $u_{*t}$ ), which includes an empirical constant,  $A$ , typically set at about 0.082 for maintaining saltation (the dynamic, or impact, threshold). Here, we present data from a pilot study to assess the variability of  $A$  to improve estimations of  $u_{*t}$ , which in turn, should improve transport rate predictions. Using field data from three coastal environments, we measured or calculated all parameters within the Lettau and Lettau (1978) model and  $u_{*t}$  equation. In Jericoacoara, Brazil (BRA), Inch, Ireland (IRE), and Esposende, Portugal (POR) wind velocities were measured with cup anemometer towers and transport rates were measured using traps for 31 data runs lasting 120 to 1020 seconds each. Mean grain sizes were 0.17 mm (IRE), 0.31 mm (POR), and 0.30 mm (BRA), and mean shear velocities were 0.38 m s<sup>-1</sup> (IRE), 0.40 m s<sup>-1</sup> (POR), and 0.49 m s<sup>-1</sup> (BRA). Empirically determined, adjusted  $A$  values ranged from 0.02 to 0.21 with a mean and standard deviation of 0.11 and 0.04. No relationship exists between estimates of  $A$  and grain Reynolds number. A statistically significant ( $p < 0.001$ ), negative relationship was found between  $A$  and mass transport rate, leading to substantial over-prediction of transport rates near the threshold and under-prediction during fast winds if a constant of 0.082 is used.

**ADDITIONAL INDEX WORDS:** *Aeolian processes, Bagnold's A, Sediment transport.*

## INTRODUCTION

Aeolian processes are important for sculpting landscapes on Earth and extraterrestrial bodies such as Mars, Venus, and Titan (Iversen and White, 1982; Greeley and Arvidson, 1990; Greeley *et al.*, 1992). Because of the challenges of field experiments and the limited access to extraterrestrial surfaces, most of our understanding of the dynamics of aeolian sand transport is based on wind tunnel research (Greeley *et al.*, 1980; Merrison *et al.*, 2007) or theoretical numerical simulations (White, 1979; Kok, 2010a). Therefore, the prediction of sediment transport rates for conditions common to natural environments is lacking a strong empirical foundation for the representation of the complexities of prototype systems. As a consequence, the prediction of sediment transport rates has been shown to be generally problematic. For example, Sherman *et al.*, (1998) and more recently Sherman and Li (2012) evaluated the performance of seven commonly used transport models (i.e. Bagnold, 1937; Kawamura, 1951; Zingg, 1953; Owen, 1964; Kadib, 1965; Hsu, 1973; Lettau and Lettau, 1978) with regard to their ability to approximate measurements of sand transport on beaches in Ireland. They found that almost all the models over-predicted the measured transport rates, especially at slower wind speeds, which may limit their applicability in coastal and arid environments. The over-prediction issues have also been observed by many others (e.g. Chapman, 1990; Dong *et al.*, 2004; Bauer *et al.*, 2009; Delgado-Fernandez and Davidson-Arnott, 2009). Several factors that confound the applicability of these models have been identified, such as the slope of the sand surface (White and Tsoar, 1998; Iversen and Rasmussen, 1999),

the presence of vegetation (Hesp, 1989; Lancaster and Baas, 1998; Allgaier, 2008), surface moisture content (Namikas and Sherman, 1995; Jackson and Nordstrom, 1997; Cornelis and Gabriels, 2003; Niels and Wiggs, 2011), saltation intermittency (Stout and Zobeck, 1997; Davidson-Arnott and Bauer, 2009), the spatial and temporal variability of saltation (Jackson and McCloskey, 1997; Baas and Sherman, 2006; Baas, 2008; Udo *et al.*, 2008; Ellis *et al.*, 2012), and fetch length (Nordstrom and Jackson, 1992; Jackson and Cooper, 1999; Dong *et al.*, 2004; Lynch *et al.*, 2009; Delgado-Fernandez, 2010).

However, the over-prediction issue still exists even when predicting time-averaged sand transport rates across long, dry, un-vegetated, flat, sandy surfaces. Sherman and Li (2012) argued that this can be attributed to the poor understanding and representations of the physics in aeolian processes. For example, they suggested that shear velocity is often over-estimated when using the Law of the Wall because of the assumption of a value of 0.4 for the von Kármán constant. Instead, they argued for the use of an apparent von Kármán parameter that varies substantially (decreases) as a function of the transport rate (saltation intensity). Accordingly, the shear velocity estimates used in the transport models were corrected using the empirical relationship between total sand transport rate  $Q$  (in kg m<sup>-1</sup> s<sup>-1</sup>) and the apparent von Kármán parameter  $\kappa_a$  (Li *et al.*, 2010):

$$\kappa_a = -3.03Q + 0.40 \quad (1)$$

After correcting the shear velocity estimates used in the models (using Eqn. 1), the over-prediction issues were greatly reduced, but still present. Sherman *et al.* (2013) posited that this might be a result of the inaccuracy of the values of empirical constants used in the models. They recalibrated six sand transport prediction models (those of Bagnold, 1937; Kawamura, 1951; Zingg, 1953;

Owen, 1964; Hsu, 1973; Lettau and Lettau, 1978) using the field data collected in three coastal environments and proposed a set of new coefficients. The recalibration of the constants improved the overall accuracy of the predictions. However, when the total, measured transport rates were less than  $5 \text{ g m}^{-1} \text{ s}^{-1}$ , the models still over-predicted transport. They argued that this problem is probably from errors in estimating the threshold shear velocity necessary to maintain saltation.

Bagnold (1936) argued that the threshold shear velocity required to initiate saltation (fluid threshold) is greater than that needed to maintain active saltation (impact threshold). He proposed a parameter  $A$  similar to the Shields parameter (Shields, 1936), to represent the mechanical efficiency of momentum transfer from the wind or a wind and sand system, to the surface sediments:

$$A = \frac{u_{*f}}{\sqrt{gd \left( \frac{\rho_s}{\rho} - 1 \right)}} \quad (2)$$

where  $u_{*f}$  is threshold shear velocity (in  $\text{m s}^{-1}$ ),  $g$  is gravitational acceleration ( $9.81 \text{ m s}^{-2}$ ),  $d$  is grain diameter (in m), and  $\rho_s$  and  $\rho$  are sand and air densities ( $2650$  and  $1.2 \text{ kg m}^{-3}$ ), respectively. Note that the Shields parameter is equal to  $A^2$  and both are a function of grain Reynolds number,  $Re_*$ , defined as:

$$Re_* = u_* d / \nu \quad (3)$$

Here,  $u_*$  is shear velocity (in  $\text{m s}^{-1}$ ) and  $\nu$  is kinematic viscosity of air ( $1.8 \cdot 10^{-5} \text{ m}^2 \text{ s}^{-1}$ ). However, studies of the Shields parameter in water indicate that  $A$  has a narrow range (0.14 to 0.26) when  $Re_*$  is greater than 10 (c.f. Figure 3 in Paphitis, 2001). Greeley (1974) also found  $A$  in the air flow becomes insensitive to  $Re_*$  when  $Re_* > 0.65$ . For a typical air flow on a sandy surface,  $u_*$  ranges from 0.2 to 0.5  $\text{m s}^{-1}$ ,  $d$  values are 0.1 to 1 mm, and thus  $Re_*$  should range from 1.1 to 28. This indicates values of  $A$  between 0.12 and 0.14 for the fluid threshold. These values correspond to  $A$  values found from some wind tunnel experiments, e.g., 0.12 (Zingg, 1953) and 0.11-0.12 (Nickling, 1988), but inconsistent with other experiments, e.g., 0.10 (Bagnold, 1936), 0.09-0.11 (Chepil, 1945) and 0.17-0.20 (Lyles and Krauss, 1971). There is very little research on the value of  $A$  for conditions when momentum transfer is mainly by the grain impact threshold. For example, the most commonly used  $A$  value of 0.082 was proposed by Bagnold (1937) based on a minimal set of wind tunnel experiments with sieved 0.18 to 0.30 mm sand. More recently, Sørensen (2004) derived values of 0.08-0.09 for homogenous sands with 0.125 to 0.320 mm diameter and 0.11 for natural heterogeneous sand with modal size of 0.23 mm. The data of Shao and Mikami (2005) translate to a value of  $A = 0.17$  (after correction for altitude: Ellis and Sherman, 2013). Because of the ambiguity in these results and because the variability of  $A$  values may lead to substantial errors in predicting sand transport rates, it is desirable to revisit the potential variability of  $A$  for impact threshold of the wind-blown sand in natural environments.

## METHODS

### Study Sites and Instrumentation

Data were collected in three coastal environments: Inch, Ireland (IRE), Esposende, Portugal (POR), and Jericoacoara, Brazil (BRA). The characteristics of these environments have been detailed in Sherman *et al.* (1998), Li *et al.* (2009), and Li *et al.* (2010), respectively. All experiments were conducted on flat sandy surfaces with very little slope ( $< 0.05$ ) and an upwind fetch

Table 1. Summary of the data collected at three sites. Note: Run duration  $T$ , median grain size  $d$ , and total sand transport rate  $Q$  for each run are reported in Sherman *et al.* (2013, 173).

Site+ Run#	$T$ (s)	$u_*$ ( $\text{ms}^{-1}$ )	$d$ (mm)	$Q$ ( $\text{gm}^{-1}\text{s}^{-1}$ )	$Re_*$	$A$
<b>IRE1</b>	1020	0.37	0.17	6.83	3.54	0.10
<b>IRE2</b>	1020	0.44	0.17	1.88	4.17	0.21
<b>IRE3</b>	1020	0.35	0.17	1.93	3.33	0.15
<b>IRE4</b>	1020	0.30	0.17	1.37	2.85	0.13
<b>IRE5</b>	1020	0.43	0.17	4.83	4.06	0.17
<b>Mean</b>	1020	0.38	0.17	3.37	3.59	0.15
<b>Std</b>	0	0.06	0.00	2.37	0.54	0.04
<b>POR1</b>	600	0.46	0.31	8.72	8.07	0.13
<b>POR2</b>	600	0.46	0.31	7.32	8.02	0.14
<b>POR3</b>	900	0.40	0.31	1.61	7.21	0.15
<b>POR4</b>	900	0.40	0.30	1.69	6.92	0.15
<b>POR5</b>	360	0.47	0.32	8.64	8.57	0.14
<b>POR6</b>	360	0.47	0.32	9.34	8.43	0.14
<b>POR7</b>	900	0.36	0.35	14.40	7.28	0.02
<b>POR8</b>	600	0.33	0.34	6.21	6.26	0.07
<b>POR9</b>	600	0.37	0.33	3.32	6.91	0.11
<b>POR10</b>	600	0.38	0.33	2.56	7.13	0.13
<b>POR11</b>	900	0.32	0.28	0.32	4.96	0.13
<b>POR12</b>	600	0.37	0.27	2.38	5.80	0.13
<b>Mean</b>	660	0.40	0.31	5.54	7.13	0.12
<b>Std</b>	198	0.05	0.02	4.24	1.08	0.04
<b>BRA1</b>	120	0.54	0.30	31.49	8.98	0.09
<b>BRA2</b>	180	0.49	0.22	24.04	5.91	0.07
<b>BRA3</b>	213	0.53	0.23	21.83	6.95	0.12
<b>BRA4</b>	170	0.49	0.30	26.11	8.26	0.07
<b>BRA5</b>	240	0.50	0.29	20.43	8.13	0.10
<b>BRA6</b>	240	0.50	0.28	18.03	7.74	0.11
<b>BRA7</b>	240	0.47	0.28	15.55	7.42	0.10
<b>BRA8</b>	240	0.45	0.30	15.01	7.44	0.09
<b>BRA9</b>	240	0.51	0.30	18.05	8.41	0.12
<b>BRA10</b>	240	0.48	0.25	26.31	6.62	0.05
<b>BRA11</b>	300	0.41	0.27	20.31	6.19	0.02
<b>BRA12</b>	240	0.50	0.33	22.68	9.24	0.09
<b>BRA13</b>	299	0.50	0.43	16.35	11.98	0.11
<b>BRA14</b>	240	0.49	0.44	27.31	4.64	0.07
<b>Mean</b>	225	0.49	0.30	21.68	7.71	0.09
<b>Std</b>	47	0.03	0.06	4.93	1.76	0.03

length at least 80 m. Vertical profiles of streamwise velocities were measured using arrays of four Gill-type, 3-cup anemometers at 0.25, 0.50, 0.75, and 1.00 m above the surface. At the BRA site, one RM Young 81000 ultrasonic anemometer at 1 m was deployed. Sand samples were collected using either Leatherman/Rosen type cylindrical traps (IRE site) or vertical arrays of hose-type traps (POR and BRA sites). Traps were deployed for sample periods of 120-1020 s (Table 1). The captured sand was dry-sieved and weighed to calculate the time-averaged total sand transport rate and median grain size. We recognize that the use of data from different environments, obtained using different types of anemometers and sand traps, might produce bias in our results. On the other hand, if the results are to be considered robust, then they should be relatively immune to such bias. Indeed, in our analysis of these same data (Sherman *et al.*, 2013, especially Figs. 2 and 3), no systematic bias was found. These data were also used to calibrate the empirical constants used in the sand transport prediction models evaluated in the assessment by (Sherman *et al.*, 2013).

### Evaluation Procedure

Following the quality control protocol detailed in Sherman *et al.* (2013), only runs with well-measured, fully developed air flows (defined as  $r^2$  values exceeding 0.98 for the semi-log, curve-fitting of the wind profile), dry sand (defined as sand moisture content < 2%) and equilibrium saltation conditions (defined as total sand transport rate > 0.28 g m<sup>-1</sup> s<sup>-1</sup> or 1.0 kg m<sup>-1</sup> h<sup>-1</sup>) were selected to ensure the validity of these transport models. After the screening, there were 31 data sets comprising five runs from IRE, twelve runs from POR and fourteen runs from BRA. Mean grain sizes were 0.17 mm (IRE), 0.31 mm (POR), and 0.30 mm (BRA), and the mean shear velocities ( $u_*$ ) were 0.38 m s<sup>-1</sup> (IRE), 0.40 m s<sup>-1</sup> (POR), and 0.49 m s<sup>-1</sup> (BRA) after the  $\kappa_a$  corrections (as described above). The summary of the data is presented in Sherman *et al.*'s (2013) Table 1.

Sherman *et al.* (2013) concluded that the most robust model to estimate mass transport rates is the Lettau and Lettau (1978) model with the  $\kappa_a$  correction:

$$Q = C\sqrt{d/D}(\rho/g)u_*^2(u_* - u_{*t}) \quad (4)$$

where  $C = 2.47$ , and  $D$  is a reference grain size of 0.25 mm. The  $A$  value for each run can be calculated by combining Eqns. 2 and 4:

$$A = \frac{u_* - \frac{gQ}{C\rho(d/D)^{1/2}u_*^2}}{\sqrt{gd(\rho_s/\rho - 1)}} \quad (5)$$

### RESULTS AND DATA ANALYSIS

The values of  $A$  calculated with Eqn. 5 are reported in Table 1. The estimates, based on the data from the disparate environments, range from 0.02 to 0.21, with a mean and standard deviation of 0.11 and 0.05. Detailed examination shows that  $A$  varies between 0.10 and 0.21 for IRE, between 0.02 and 0.15 for POR, and between 0.02 and 0.12 for BRA, indicating substantial overlapping ranges between these three sites. The means and standard deviations are 0.15 and 0.04, 0.12 and 0.04, and 0.09 and 0.03, respectively. These results demonstrate that average values of  $A$ , based on field data, are generally larger than that found by Bagnold in his laboratory experiments.

For each run,  $u_*$ ,  $d$ ,  $Q$ , and  $Re_*$  are presented in Table 1. The  $u_*$  values are derived from direct measurement from the ultrasonic anemometer for BRA and from wind profile measurements and Eqn. 1 for IRE and POR (for detailed procedure, c.f., Sherman and Li, 2012). In order to examine the dependency of  $A$  upon  $u_*$ ,  $d$ ,  $Q$ , and  $Re_*$ , each variable is plotted against  $A$  (Figures 1a-d) and regression analyses were conducted between these variables and  $A$  (Table 2). Both visual examination and correlation analysis lead to the conclusion that there is no significant relationship between  $A$  and  $u_*$ ,  $d$  or  $Re_*$  and that there is a statistically significant linear relationship between  $A$  and  $Q$  ( $p < 0.001$ ). This empirical relationship is:

$$A = -0.0028Q + 0.1452 \quad (6)$$

Regression analysis was also conducted for the data from each site (Table 2). None of the sites had a statistical relationship between  $Re_*$  and  $A$ . The relationship between  $A$  and  $Q$  found for

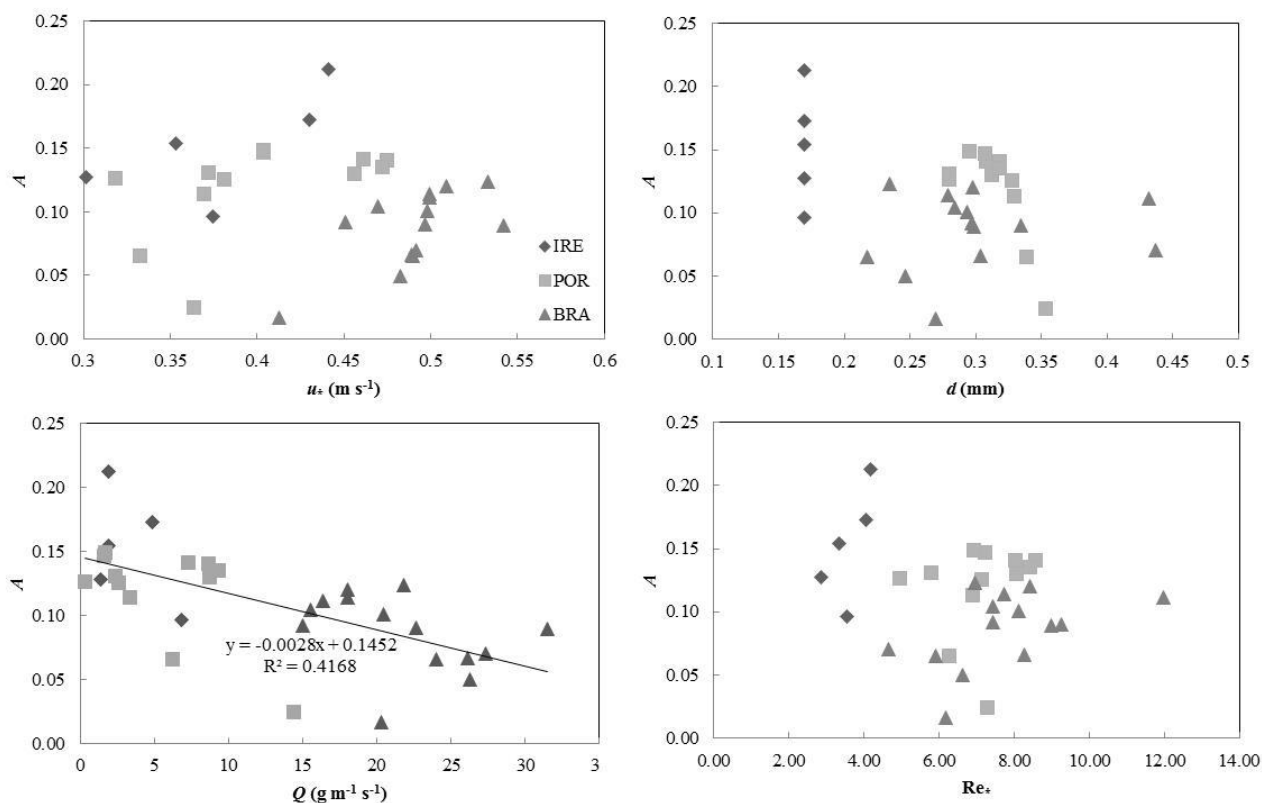


Figure 1. Scatterplots between  $u_*$  and  $A$  (a), between  $d$  and  $A$  (b), between  $Q$  and  $A$  (c) and between  $Re_*$  and  $A$  (d). Note: The only statistically significant relationship is between  $Q$  and  $A$ , as depicted in panel c.

Table 2. Results of linear regression between  $u_*$ ,  $d$ ,  $Q$ ,  $Re_*$ , and  $A$ . N/A means the p value is not available when  $R^2 = 0$ .

Site		$u_*$ vs. $A$	$d$ vs. $A$	$Q$ vs. $A$	$Re_*$ vs. $A$
All	$R^2$	0.01	0.12	0.42	0.09
	p	0.628	0.053	< 0.001	0.109
IRE	$R^2$	0.47	0.00	0.24	0.47
	p	0.204	N/A	0.397	0.204
POR	$R^2$	0.25	0.51	0.32	0.02
	p	0.097	0.009	0.054	0.634
BRA	$R^2$	0.42	0.02	0.17	0.09
	p	0.012	0.638	0.145	0.306

the combined data becomes weaker for the individual sites and is not statistically significant for IRE. However, statistically significant relationships were found between  $u_*$  and  $A$  for BRA ( $p = 0.012$ ) and between  $d$  and  $A$  for POR ( $p = 0.009$ ).

## DISCUSSION

Results from this study suggest that for  $2.85 < Re_* < 11.98$ ,  $A$  is independent of  $Re_*$ , which is consistent with the findings of Greeley *et al.* (1974). The negative relationship between  $Q$  and  $A$  found for the combined data indicates that under conditions with more intense saltation, the degree of mechanical efficiency associated with maintaining saltation becomes easier to achieve. This can be explained by the relative importance of momentum transfer to the surface associated with the impact threshold and fluid threshold processes. At slow mass transport rates, the motion of most sand particles is initiated by fluid shear stress directly. Only a few sand particles are actively in saltation, which means the fluid threshold dominates the process. According to Bagnold (1937), the value of  $A$  for initiation of motion by fluid-induced stresses alone is larger than that for the threshold associated with momentum transfer caused by saltating grains impacting the surface. Presumably, there is a gradient in the value for  $A$  caused by the transition from fluid-dominated to impact-dominated conditions. Therefore it is not surprising to find larger  $A$  values for slower saltation (transport) rates.

According to Eqn. 6, when  $Q$  is small,  $A$  is approximately 0.15. Even though the impact threshold should be less than the fluid threshold, the value of  $A = 0.15$  is substantially greater than most estimates associated with the fluid threshold, where wind tunnel experiments have set  $A$  from 0.09 to 0.12 (Bagnold, 1936; Chepil, 1945; Zingg, 1953; Nickling, 1988), but less than the estimates of 0.17 to 0.20 derived by Lyles and Krauss (1971). However, with increasing transport rates the proportion of total stress borne by saltating grains increases relative to the fluid-borne stress, which should lead to a reduced threshold shear velocity or a smaller value of  $A$ . A statistically significant, linear relationship exists between  $Q$  and  $A$  (Eqn. 6 and Figure 1c). However, the relationship should be assumed valid only for the range of data used to derive the equation ( $0.32 \text{ g m}^{-1} \text{ s}^{-1} < Q < 31.49 \text{ g m}^{-1} \text{ s}^{-1}$ ). Extrapolation of the linear relationship leads to nonsensical results. For example, if we extrapolate the regression line to  $Q = 51.86 \text{ g m}^{-1} \text{ s}^{-1}$ , we obtain the result  $A = 0$ , which contradicts the assumption of a positive threshold velocity.

We cannot determine if the finding of a variable  $A$  is genuine, or arises as an artifact of our experimental design and analytic approaches. There are several issues that could contribute to this ambiguity: 1) we used Leatherman/Rosen type traps at Inch, and these are notorious for losing efficiency at faster transport rates; 2) the use of  $r^2 \geq 0.98$  might not be a stringent enough criterion for using velocity profiles; 3) we estimated shear velocity using two different methods, and may have introduced a bias thereby; 4) the

estimation of the apparent von Kármán parameter requires iteration between transport rates and the parameter. Because both variables appear on the right hand side of Eqn. 5, their interdependence, modulated through estimated shear velocity, may also contribute to a non-stationary  $A$ ; 5) we have not tried to account for the distribution of grain sizes present at the different sites. The distributions were different, and this may contribute to the segregation of results by site that we see in Figure 1-c, for example; 6) spatial variability in transport rates (e.g., Ellis *et al.*, 2012) might cause a reduced correspondence between wind and transport measurements; and 7) we have ignored potential electrostatic charging of the wind and the sediments. Such triboelectrification, if present, should be expected to change with wind speed (and, consequently, sand transport rate) according to Rasmussen *et al.* (2009), Merrison (2012), or Bo *et al.* (2013).

Bagnold (1937) proposed  $A = 0.082$  for the impact threshold, which has since been widely used in aeolian studies. However, our study shows that average  $A$  value for the impact threshold is 0.11, but may have substantial variability. These differences have important implications for the accuracy of threshold shear velocity estimates and, consequently, the performance of sand transport models. For example, consider a median sand grain size of  $d = 0.25 \text{ mm}$  and wind shear velocity that varies from the impact threshold to  $0.6 \text{ m s}^{-1}$ . The threshold shear velocity for  $A = 0.082$  is a constant of about  $0.018 \text{ m s}^{-1}$  while for  $A = -0.0032Q + 0.1481$ , the threshold shear velocity (Eqn. 6), becomes a variable. Accordingly, the predicted sand transport rates ( $Q$ ) for  $A = 0.082$  (denoted as  $Q_{A=0.082}$ ) and for  $A = -0.0032Q + 0.1481$  (denoted as  $Q_{\text{Eqn6}}$ ) can be obtained (c.f., Figure 2). Then the potential error in sand transport prediction, defined as  $((Q_{A=0.082}/Q_{\text{Eqn6}}) - 1) \cdot 100\%$ , can be calculated (c.f., Figure 3). Note that  $u_*$  should be directly measured from Reynolds stresses or derived from velocity profiles using the  $\kappa_a$  correction method described in Li *et al.* (2010). From Figure 2, it is possible to determine that  $u_{*(A=0.082)}$  is less than  $u_{*(\text{Eqn 6})}$  when  $u_* < 0.49 \text{ m s}^{-1}$  and greater when  $u_* > 0.49 \text{ m s}^{-1}$ . Figures. 2 and 3 also show that the potential error in transport predictions is infinite if  $u_* < 0.33 \text{ m s}^{-1}$ . Beyond  $u_* = 0.33 \text{ m s}^{-1}$ , with the increase of  $u_*$  the error decreases until  $u_* = 0.49 \text{ m s}^{-1}$ , at which the two impact threshold estimates are identical. At faster shear velocities, the prediction error becomes negative and reaches -34% when  $u_* = 0.55 \text{ m s}^{-1}$ . This indicates that using a constant  $A$  value may substantially over predict the sand transport near threshold and under predict the sand transport in very strong wind field.

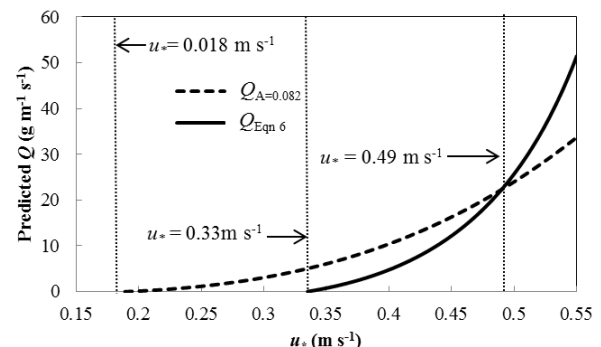


Figure 2. Predicted mass transport rates from  $A = 0.082$  and Eqn. 6.

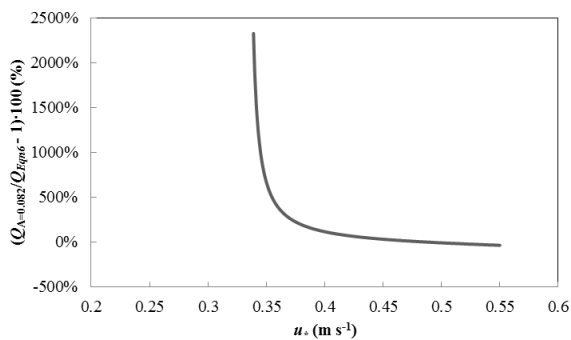


Figure 3. Potential error in sand transport prediction as a function of shear velocity.

### IMPLICATION AND CONCLUSION

It is clear that the concept of an impact threshold and the specification of its appropriate estimation deserve further attention, especially because small errors in the estimate may translate to large absolute errors in predictions using transport models, (as demonstrated by Figure 3). Some considerations arise from this study.

First, our data suggest that Bagnold's estimate of  $A = 0.082$  should not be uncritically applied. For typical transport rates found on beaches, values of  $A$  in the range of 0.10 to 0.15 are more reasonable, based on this analysis. Given the expected ratio of impact to fluid threshold shear velocity, this suggests that values of  $A$  for the latter should range from about 0.12 to 0.18. Such a relative valuation of the respective versions of  $A$  is necessary to maintain saltation hysteresis, whereby transport can be maintained at shear velocities inadequate to initiate movement (Kok, 2010b). These results imply that for natural sand systems it is much more difficult for the wind alone to initiate movement than reported by Bagnold (1937).

Second, the variability of  $A$  for the impact threshold is intuitive for conditions when transport rates are small and it can be expected that the contribution of wind-borne stresses are still large, but decreasing progressively as the saltation intensity increases, relative to the grain-borne stresses. However, we also expect that with increasing sand transport rates,  $A$  should attain a minimum value and become independent of further increases in  $Q$ . Our data do not allow us to identify this condition.

Greater attention to, and specification of, the values of empirical constants such as the  $A$  in the threshold shear velocity equation is critical as aeolian saltation models become more sophisticated, and their practical applications to environmental problems on Earth and on extraterrestrial surfaces become more valuable. Surprisingly little attention has been paid to details such as this, but clearly more work is needed.

### ACKNOWLEDGEMENTS

Support from field work came from several sources. Ireland: from EC IMPACTS Project No. EV5V-CT93-0258, supervised by Julian Orford and Robert Devoy, and from the US Fulbright Scholar Program. Portugal: US and Portuguese Fulbright Scholars Programs (with Helena Granja). Brazil: National Science Foundation, Geography and Regional Science Program (#0727775 and #0822482). The authors received valuable support from LABOMAR, at the University of Ceara especially Luis Parente Maia, and from Eugene Farrell. The Brazilian portion of this work

is registered with the Brazilian Ministry of the Environment, Sistema de Autorizaço e Informaçoem Biodiversidade, Registration Number 18038-1.

### LITERATURE CITED

- Allgaier, A., 2008. Aeolian sand transport and vegetation cover. In: S. W. Breckle, Yair, A. and Veste, M. (ed.), *Arid Dune Ecosystems*. Berlin: Springer Berlin Heidelberg, pp. 211-224.
- Baas, A.C. and Sherman, D.J., 2006. Spatiotemporal variability of aeolian sand transport in a coastal dune environment. *Journal of Coastal Research*, 22, 1198-1205.
- Baas, A.C.W. 2008 Challenges in aeolian geomorphology: investigating aeolian streamers, *Geomorphology*, 93(1), 3-16.
- Bagnold, R.A., 1936. The movement of desert sand. *Proceedings of the Royal Society of London. Series A, Mathematical and Physical Sciences*, 157, 594-620.
- Bagnold, R.A. 1937. The transport of sand by wind. *Geographical journal*, 89, 409-438.
- Bauer, B.O., Davidson-Arnott, R.G.D., Hesp, P.A., Namikas, S.L., Ollerhead, J., and Walker, I.J., 2009. Aeolian sediment transport on a beach: Surface moisture, wind fetch, and mean transport. *Geomorphology*, 105, 106-116.
- Bo, T.L., Zhang, H., Hu, W.W., and Zheng, X.J., 2013. The analysis of electrification in windblown sand. *Aeolian Research*, 11, 15-21.
- Chapman, D.M., 1990. Aeolian sand transport-an optimized model. *Earth Surface Processes and Landforms*, 15, 751-760.
- Chepil, W. 1945. Dynamics of wind erosion: II. Initiation of soil movement. *Soil Science*, 60, 397.
- Cornelis, W.M. and Gabriels, D., 2003. The effect of surface moisture on the entrainment of dune sand by wind: an evaluation of selected models. *Sedimentology*, 50, 771-790.
- Davidson-Arnott, R.G.D. and Bauer, B.O., 2009. Aeolian sediment transport on a beach: Thresholds, intermittency, and high frequency variability. *Geomorphology*, 105, 117-126.
- Delgado-Fernandez, I. and Davidson-Arnott, R., 2009. Sediment input to foredunes: description and frequency of transport events at Greenwich Dunes, PEI, Canada. *Journal of Coastal Research*, SI 56, pp. 302-306.
- Delgado-Fernandez, I., 2010. A review of the application of the fetch effect to modelling sand supply to coastal foredunes. *Aeolian Research*, 2, 61-70.
- Dong, Z., Wang, H., Liu, X., and Wang, X., 2004. The blown sand flux over a sandy surface: a wind tunnel investigation on the fetch effect. *Geomorphology*, 57, 117-127.
- Ellis, J.T., Sherman, D.J., Farrell, E.J., and Li, B., 2012. Temporal and spatial variability of aeolian sand transport: Implications for field measurements. *Aeolian Research*, 3, 379-387.
- Ellis, J.T. and Sherman, D.J., 2013. Fundamentals of Aeolian Sediment Transport: Wind-Blown Sand. In: Shroder, J. F. (ed.), *Treatise on Geomorphology*. San Diego: Academic Press, pp. 85-108.
- Greeley, R. and Arvidson, R.E., 1990. Aeolian processes on Venus. *Earth, Moon, and Planets*, 50, 127-157.
- Greeley, R., Iversen, J., Pollack, J., Udovich, N., and White, B., 1974. Wind tunnel studies of Martian aeolian processes. *Proceedings of the Royal Society of London. Series A, Mathematical and Physical Sciences*, 341, 331-360.
- Greeley, R., Lancaster, N., Lee, S., and Thomas, P., 1992. Martian aeolian processes, sediments, and features. *Mars*, 1, 730-766.
- Greeley, R., Leach, R., White, B., Iversen, J., and Pollack, J., 1980. Threshold windspeeds for sand on Mars: Wind tunnel simulations. *Geophysical Research Letters*, 7, 121-124.
- Hesp, P.A., 1989. A review of biological and geomorphological processes involved in the initiation and development of incipient foredunes. *Proceedings of the Royal Society of Edinburgh. Section B. Biological Sciences*, 96, 181-201.
- Hsu, S.A., 1973. Computing eolian sand transport from shear velocity measurements. *The Journal of Geology*, 81, 739-743.
- Iversen, J. and White, B., 1982. Saltation threshold on earth, mars and venus. *Sedimentology*, 29, 111-119.
- Iversen, J.D. and Rasmussen, K.R., 1999. The effect of wind speed and bed slope on sand transport. *Sedimentology*, 46, 723-731.



- Jackson, D.W.T. and McCloskey, J., 1997. Preliminary results from a field investigation of aeolian sand transport using high resolution wind and transport measurements. *Geophysical Research Letters*, 24, 163-166.
- Jackson, D.W.T., and Cooper, J.A.G., 1999. Beach fetch distance and aeolian sediment transport. *Sedimentology*, 46, 517-522.
- Jackson, N.L., and Nordstrom, K.F., 1997. Effects of time-dependent moisture content of surface sediments on aeolian transport across a beach, Wildwood, New Jersey, USA. *Earth Surface Processes and Landforms*, 22, 611-621.
- Kadib, A.A., 1965. A function for sand movement by wind. In *University of California Hydraulics Engineering Laboratory Report HEL 2-8* Berkeley, CA: UCLA-Berkeley. 91p.
- Kawamura, R., 1951. Study of sand movement by wind. In: *The reports of the Institute of Science and Technology*. Tokyo, Japan: University of Tokyo. Volume 5, pp. 95-112.
- Kok, J.F., 2010a. Difference in the wind speeds required for initiation versus continuation of sand transport on Mars: Implications for dunes and dust storms. *Physical Review Letters*, 104, 074502.
- Kok, J.F., 2010b. An improved parameterization of wind-blown sand flux on Mars that includes the effect of hysteresis. *Geophysical Research Letters*, 37, L12202.
- Lancaster, N. and Baas, A., 1998. Influence of vegetation cover on sand transport by wind: field studies at Owens Lake, California. *Earth Surface Processes and Landforms*, 23, 69-82.
- Lettau, K. and Lettau, H., 1978. Experimental and micrometeorological field studies of dune migration. In: K. Lettau and Lettau, H. (ed.), *Exploring the World's Driest Climate*. Center for Climatic Research, University of Wisconsin-Madison, IES Report 101, pp. 110-147.
- Li, B., Granja, H., Farrell, E.J., Ellis, J.T., and Sherman, D.J., 2009. Aeolian Saltation at Esposende Beach, Portugal. In: *Proceedings 10<sup>th</sup> International Coastal Symposium* (Lisbon, Portugal), *Journal of Coastal Research*, Special Issue No. 56, pp. 327-331.
- Li, B., Sherman, D.J., Farrell, E.J., and Ellis, J.T., 2010. Variability of the apparent von Kármán parameter during aeolian saltation. *Geophysical Research Letters*, 37, L15404.
- Lyles, L. and Krauss, R., 1971. Threshold velocities and initial particle motion as influenced by air turbulence. *Transactions of the ASAE*, 14, 563-566.
- Lynch, K., Jackson, D.W.T and Cooper, J.A.G., 2009. Foredune accretion under offshore winds. *Geomorphology*, 105, 139-146.
- Merrison, J. P., 2012. Sand transport, erosion and granular electrification. *Aeolian Research*, 4, 1-16.
- Merrison, J.P., Gunnlaugsson, H.P., Nørnberg, P., Jensen, A.E., and Rasmussen, K.R., 2007. Determination of the wind induced detachment threshold for granular material on Mars using wind tunnel simulations. *Icarus*, 191, 568-580.
- Namikas, S.L. and Sherman, D.J., 1995. A review of the effects of surface moisture content on aeolian sand transport. In: T Tchakerian, V. P. (eds.), *Desert Aeolian Processes*. London: Chapman & Hall, pp. 269-293.
- Nields, J.M., and Wiggs, G.F.S., 2011. The application of terrestrial laser scanning to aeolian saltation cloud measurement and its response to changing surface moisture. *Earth Surface Processes and Landforms*, 36, 273-278.
- Nickling, W.G., 1988. The initiation of particle movement by wind. *Sedimentology*, 35, 499-511.
- Nordstrom, K.F., and Jackson, N.L., 1992. Effect of source width and tidal elevation changes on aeolian transport on an estuarine beach. *Sedimentology*, 39, 769-778.
- Owen, P.R., 1964. Saltation of uniform grains in air. *Journal of Fluid Mechanics*, 20, 225-242.
- Paphitis, D., 2001. Sediment movement under unidirectional flows: an assessment of empirical threshold curves. *Coastal Engineering*, 43, 227-245.
- Rasmussen, K.R., Kok, J.F., and Merrison, J.P., 2009. Enhancement in wind-driven sand transport by electric fields. *Planetary and Space Science*, 57, 804-808.
- Shao, Y. and Mikami, M., 2005. Heterogeneous saltation: Theory, observation and comparison. *Boundary-layer meteorology*, 115, 359-379.
- Sherman, D.J., Jackson, D.W.T., Namikas, S.L., and Wang, J., 1998. Wind-blown sand on beaches: an evaluation of models. *Geomorphology*, 22, 113-133.
- Sherman, D.J. and Li, B., 2012. Predicting aeolian sand transport rates: a reevaluation of models. *Aeolian Research*, 3, 371-378.
- Sherman, D.J., Li, B., Ellis, J.T., Farrell, E.J., Maia, L.P., and Granja, H., 2013. Recalibrating aeolian sand transport models. *Earth Surface Processes and Landforms*, 38, 169-178.
- Shields, A., 1936. *Application of Similarity Principles and Turbulence Research to Bedload Movement (English Translation of the original German Manuscript)*. Hydrodynamics Laboratory, California Institute of Technology, Publication No. 167.
- Sørensen, M., 2004. On the rate of aeolian sand transport. *Geomorphology*, 59, 53-62.
- Stout, J.E. and Zobeck, T.M., 1997. Intermittent saltation. *Sedimentology*, 44, 959-970.
- Udo, K., Kuriyama, Y. and Jackson, D. W. T., 2008. Observations of wind-blown sand under various meteorological conditions at a beach. *Journal of Geophysical Research - Earth Surface*, 113, F04008.
- White, B.R., 1979. Soil transport by winds on Mars. *Journal of Geophysical Research: Solid Earth*, 84, 4643-4651.
- White, B.R. and Tsoar, H., 1998. Slope effect on saltation over a climbing sand dune. *Geomorphology*, 22, 159-180.
- Zingg, A.W., 1953. Wind-tunnel studies of the movement of sedimentary materials. In *Proceedings of Fifth Hydraulic Conference*, State Univ. of Iowa Studies in Engineering, pp. 111-135.

## Rip currents and circulation on a high-energy low-tide-terraced beach (Grand Popo, Benin, West Africa)

Bruno Castelle†, Rafael Almar‡, Matthieu Dorel‡, Jean-Pierre Lefebvre‡, Nadia Sénéchal†, Edward J. Anthony∞, Raoul Laibi+, Rémy Chuchla‡+, Yves du Penhoat‡+

† CNRS, Université Bordeaux 1, UMR 5805-EPOC Avenue des Facultés, F-33405, Talence, France  
b.castelle@epoc.u-bordeaux1.fr  
n.senechal@epoc.u-bordeaux1.fr

‡ IRD-LEGOS  
rafael.almar@ird.fr  
matthieu.dorel@ird.fr  
jean-pierre.lefebvre@ird.fr  
remy.chuchla@ird.fr  
Yves.Du-Penhoat@ird.fr

∞ Aix-Marseille Univ, IUF, CEREGE UMR 34, Europôle de l'Arbois, B.P. 80, 13545 Aix en Provence cedex 04, France  
anthony@cerege.fr

+ Université Abomey Calavi  
Département des Sciences de la Terre,  
Faculté des Sciences et Techniques  
Cotonou, Republic of Benin  
raoulaibi@yahoo.fr



[www.cerf-jcr.org](http://www.cerf-jcr.org)



[www.JCRonline.org](http://www.JCRonline.org)

### ABSTRACT

Castelle, B., Almar, R., Dorel, M., Lefebvre, J.P., Sénéchal, N., Anthony, E.J., Laibi, R., Chuchla, R., du Penhoat, Y., 2014. Rip currents and circulation on a high-energy low-tide-terraced beach (Grand Popo, Benin, West Africa). In: Green, A.N. and Cooper, J.A.G. (eds.), *Proceedings 13<sup>th</sup> International Coastal Symposium* (Durban, South Africa), *Journal of Coastal Research*, Special Issue No. 70, pp. 633-638, ISSN 0749-0208.

Rip currents are wave-driven intense seaward-flowing jets of water that are important to both beach morphodynamics and the overall ecosystem. Rip currents are also the leading deadly hazard to recreational beach users worldwide. More specifically, the African region is reported to have the highest rates of drowning in the world, yet both the occurrence and the type of rips developing along the African beaches are unknown. In February 2013, a 12-day field experiment was performed at the high-energy low-tide-terraced sandy beach of Grand Popo beach (Benin, West Africa). Human drifter data and video imagery are combined to address wave-driven circulation and rip current activity. Results show two prevailing rip current types. (1) Low-energy (~ 0.2-0.4 m/s) swash rips, with short life-spans of about 1 minute, extend about 5-10 m offshore and occur preferably at mid to high tide at fixed locations in the center of beach cusps. (2) Higher-energy (0.2 – 0.8 m/s) surfzone flash rips become active with the onset of intense wave breaking across the low-tide terrace. They tend to migrate downdrift with a longer time-span of about 2-5 minutes. The relatively weak longshore current (0.2 – 0.55 m/s) measured during the experiment suggests that flash rips were driven by vortices generated by wave breaking rather than shear instabilities of the longshore current. Swash rips and flash rips are common at Grand Popo and often co-exist. We propose a conceptual model of both flash and swash rip activity on this stretch of the West African coast.

**ADDITIONAL INDEX WORDS:** *Flash rips, swash rips, longshore current, drifters, video monitoring, beach safety.*

### INTRODUCTION

Rip currents are unsteady concentrated flows of water jetting offshore at  $O(1)$  m/s which are ubiquitous along wave-dominated sandy beaches (Dalrymple *et al.*, 2011). Rip currents are important in the transport and dispersal of pollutants, nutrients and biological species in mixed nearshore waters (Shanks *et al.*, 2010) as well as in offshore sediment transport (Aagaard *et al.*, 1997), short-term (from days to weeks) sandy beach morphodynamics (Michallet *et al.*, 2013) and localized beach and dune erosion during storms (Thornton *et al.*, 2007; Birrien *et al.*, 2013).

Rip currents are also one of the most dangerous natural hazards in the world, and arguably the leading deadly hazard to recreational beach users (*e.g.* Scott *et al.*, 2011; Brander *et al.*, 2013). In high-income countries (HICs) such as the United States and Australia, rip current hazard assessment, lifesaving services

and community education programs have been performed for a long time. Yet, fatal drownings at beaches still occur with about 100 reported in the United States (United States Lifesaving Association, 2011) and 29 in Australia (Surf Life Saving Australia, 2011) in 2011. Worldwide, 96% of all unintentional drowning deaths occur in low- and middle-income countries (LMICs; WHO, 2010), which are mostly situated in tropical and subtropical regions with long stretches of coastline exposed to high-energy ocean wave conditions (Hammerton *et al.*, 2013). For instance, the African region is reported to have the highest rates of drowning in the world (Peden and McGee, 2003; WHO, 2010), although there is a wide range of uncertainty around the estimate of global drowning deaths (Hammerton *et al.*, 2013). A necessary step to overcome these tragic statistics is to assess both the occurrence and the type of rips developing along the African beaches. There are many causes of rip current and a wide range of rip types (Dalrymple *et al.*, 2011). One can distinguish (1) rips

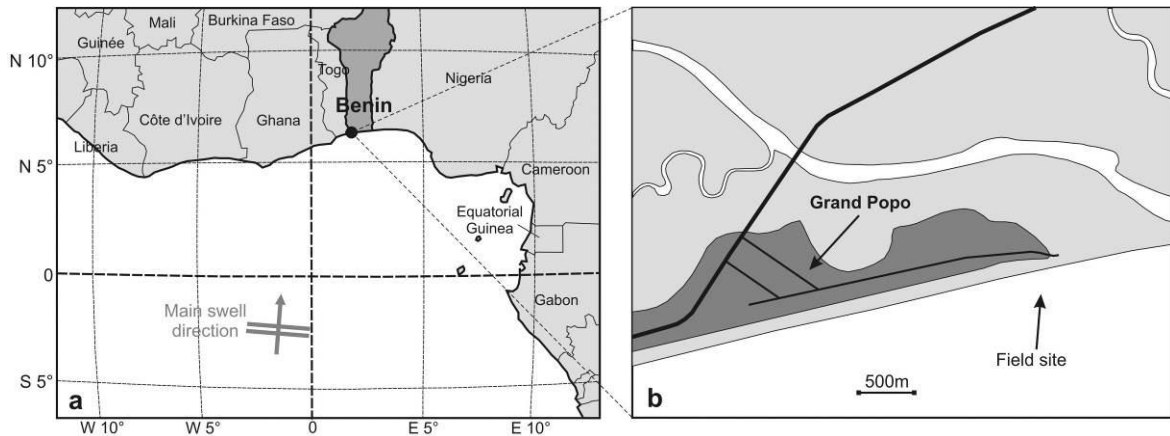


Figure 1. Location of the study site (Grand Popo beach) in Benin, West Africa

that are fixed at a given location and (2) those that are episodic and tend to migrate alongshore. In the former type, rips driven by alongshore variations in bathymetrically-controlled wave breaking along rip-channeled beaches (Bruneau *et al.*, 2011; Austin *et al.*, 2013) have been documented for decades (*e.g.* MacMahan *et al.*, 2006). Rip currents against headlands, groins or piers (Pattiaratchi *et al.*, 2009) are driven by wave shadowing (Castelle and Coco, 2012) or the deflection of the longshore current (Castelle and Coco, 2013) when located at the downwave or upwave side of this fixed rigid boundary, respectively. Nearshore rip currents can also be controlled by offshore bathymetric anomalies such as canyons (Long and Ozkan-Haller, 2005; Castelle *et al.*, 2012). Swash rips, often found in the center of beach cusps (Masselink and Pattiaratchi, 1998; Dalrymple *et al.*, 2011), are also fixed in location but are not surfzone rip currents in contrast to all the other rips described herein. The second type of rip currents, episodic and migrating alongshore, known as flash rips (also called transient rips; Johnson and Pattiaratchi, 2004; Murray *et al.*, 2013) have received far less attention. Whether shear instabilities of the longshore current (Ozkan-Haller and Kirby, 1999) or vorticity generated by wave breaking (Clark *et al.*, 2012) is the major driving mechanism for surfzone eddies and flash rips remains an open question. The lack of understanding is partly due to the difficulty of measuring flash rips in the field because of their unpredictable nature. Flash rips are preferably found along alongshore-uniform beaches exposed to groundswells or wind-wave conditions.

Along the high-energy low-tide-terraced beaches of the Benin Coast, which are representative of a lot of beaches in West Africa, rip currents are readily ubiquitous, although nothing is known about the dominant rip current types. In addition, nothing is known about the nature and cause of beach drownings and reliable data on the number of drowning incidents are non-existent. In February 2013, a 12-day field experiment was performed at Grand Popo beach (Almar *et al.*, this issue). In this paper we address wave-driven circulation and rip current activity during the experiment using Lagrangian and video data.

## METHODS

### Study site

Grand Popo beach (6.2°N, 1.7°E; Figure 1) is located in Benin, West Africa. Grand Popo is representative of the natural

undisturbed reflective sandy beaches of the Gulf of Guinea (for an extensive description, see Laibi *et al.*, this issue). This is an open wave-dominated and microtidal beach (mean spring tide range: ~1.8 m) exposed to long period swells with a mean significant wave height  $H_s = 1.36$  m and a mean peak wave period  $T_p = 9.4$  s. The combination of the medium to coarse quartz sand (0.4–1 mm,  $D_{50}$ : 0.6 mm) and dominant groundswell regime generated in the South Atlantic results in a modal intermediate, rather reflective,

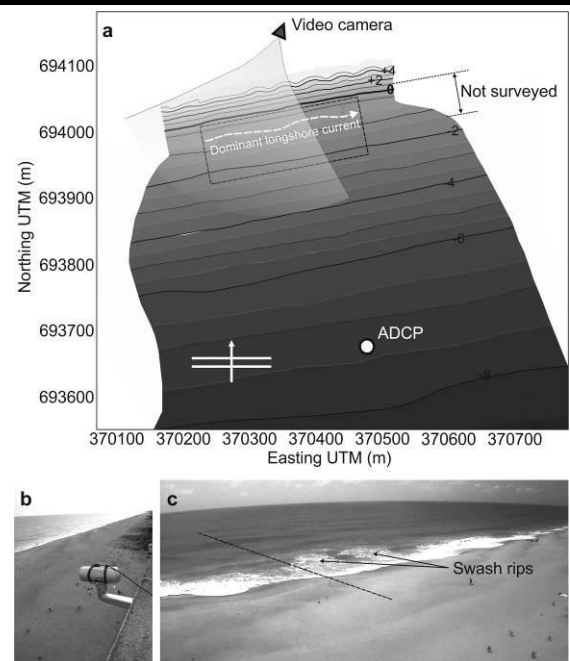


Figure 2. (a) Grand Popo beach bathymetry surveyed in February 2013 (note that the terrace was not surveyed due to breaking waves; the terrace shape is therefore indicated loosely based on observations by the human drifters) with locations of the ADCP and the video camera. (b) Video camera mounted on a 15-m high semaphore located about 80 m from the mean sea water shoreline and (c) example of snapshot showing 2 swash rips with the black line indicating the time stack location.

beach state corresponding to the low-tide terrace classification in Wright and Short (1984). The combined effect of persistent S swells throughout the year and the beach steepness results in an intense easterly longshore drift of about  $0.8 \times 10^6 \text{ m}^3/\text{year}$  (Laïbi *et al.*, this issue).

### Field experiment

The field experiment was conducted from February 17 to 28, 2013 (for an extensive field experiment description, see Almar *et al.*, this issue). The experiment was designed both to measure beach changes on short timescales and to test the applicability of a low-cost video monitoring system in such remote environments. Figure 2 shows the measured nearshore bathymetry with the location of the video system and that of the ADCP moored in 8-m depth to obtain the wave and tide conditions throughout the experiment. The beach exhibited an alongshore-uniform low tide terrace, a steep and rather alongshore-uniform lower shoreface and a well-developed cusped morphology in the high tide zone that were spaced at about 30 m.

During the experiment, shifting from a neap tide (0.4-m range) to a spring tide (1.5-m range) cycle, Grand Popo beach was exposed to 2 successive groundswell regimes from the South with a significant wave height  $H_s$  peaking at 1.1 m and 1.6 m and a peak wave period peaking at 12 s and 16 s, respectively (see Figure 3). During this experiment, morphological changes were restricted to the beach cusp system (Sénéchal *et al.*, this issue). The dominant swell regime combined with the coastline orientation resulted in a persistent, yet varying in intensity, easterly longshore current throughout the experiment. Wave breaking type was mostly plunging across the terrace and surging across the beach cusp system during low and high tide, respectively.

### Data collection

Mostly because of logistic difficulties, it was not possible to deploy traditional PVC GPS-equipped drifters (see for instance MacMahan *et al.*, 2009). Instead we resorted to the use of human operators that drifted with the currents, each equipped with a GPS with a 3-m horizontal accuracy. This enabled a fair representation of the current structure. In total, 7 human drifter experiments were performed at low tide for about 1-1.5 hours with 2 or 3 operators. Human drifters were released updrift in the video camera view field and willingly went ashore about 250 m downdrift (Figure 2a).

Rip current activity was also identified from the video camera which was mounted on a 15-m high semaphore located about 80 m from the mean sea water shoreline (Figures 2b, c). The camera recorded continuous video footage at 2 Hz. Timestacks and timex were generated every 15 minutes.

## RESULTS

Figure 4 shows the human drifter results for the 7 experiments together with the corresponding directional wave spectra and representative video snapshots. These results are further analyzed in Table 1 with an overall description of both the sea state and wave-driven circulation using Lagrangian data and visual inspection of the video runs.

Results show a large variability in wave-driven circulation during the experiment although the 2 successive groundswells regimes were not that much contrasted. For both wave regimes, the wave period peaked about 2-3 days before the peak in significant wave height (Figure 2) as waves originate from storm far out to sea in the South Atlantic. In addition, the first pulses of

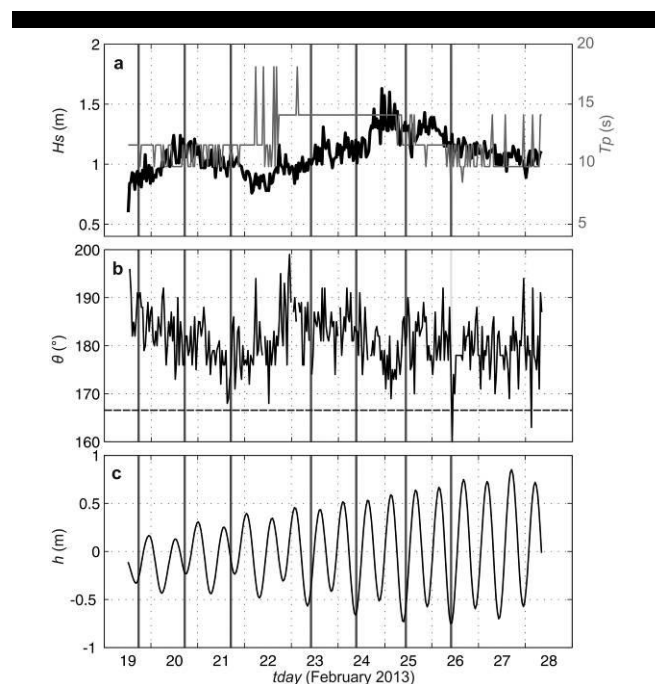


Figure 3. Time series of offshore wave conditions and tides measured by the ADCP (Figure 2) during the field experiment with the indication of the performed human drifter experiments (gray vertical lines). (a) Significant wave height  $H_s$  (black) and peak wave period  $T_p$  (gray); (b) angle of wave incidence  $\theta$  with the horizontal dotted black line indicating shore-normal incidence and (c) tide elevation  $h$ .

swell typically have a S-SW incidence that progressively shifts to the S as the remote storms tracked W-E. Given that Grand Popo is primarily exposed to long-period swells ( $T_p \sim 10-16$  s), wave are strongly refracted which resulted in an overall S incidence that progressively, and slightly, shifted from W to E as  $H_s$  increased (see for instance February 22 – 25 in Figure 3). Accordingly, for each wave regime the nearshore circulation was initially dominated by a longshore current with the subsequent (within 1 or 2 days) increase in rip current activity as both  $H_s$  peaked and wave incidence became more shore-normal.

We first describe the nearshore circulation during the first swell regime (February 19, 20 and 21). On February 19, the low-energy S groundswell combined with a SW sea resulted in a weak (0.2 m/s) longshore current (Figures 4a, b and c). Low-energy swash rips extending about 5-10 m offshore were observed as the low-tide water level was relatively high because of the neap tidal range. On February 20 (Figures 4d, e and f), the increase in  $H_s$  combined with a more shore-normal incidence resulted in the formation of both swash and flash rips, with a weak longshore current. Among the 14 human drifter pathlines measured that day, 7 were caught in a flash rip (Figure 4d) with a rip speed of about 0.5 m/s. When these drifters exited the surf zone, they subsequently slowly migrated alongshore. Some of them re-entered the surf zone, before being transported by the alongshore current. A detailed visual inspection of the video runs indicates that flash rips were episodic, characterized by short life-spans of 2-5 minutes, in agreement with the observations of Murray *et al.* (2013) on the Gold Coast (Australia), and tended to migrate slowly downdrift. The next day (February 21, Figures 4g, h and i) the fading S swell combined with the increase in SW sea resulted in a dominant weak longshore current (0.2 m/s) with occasional swash rips.

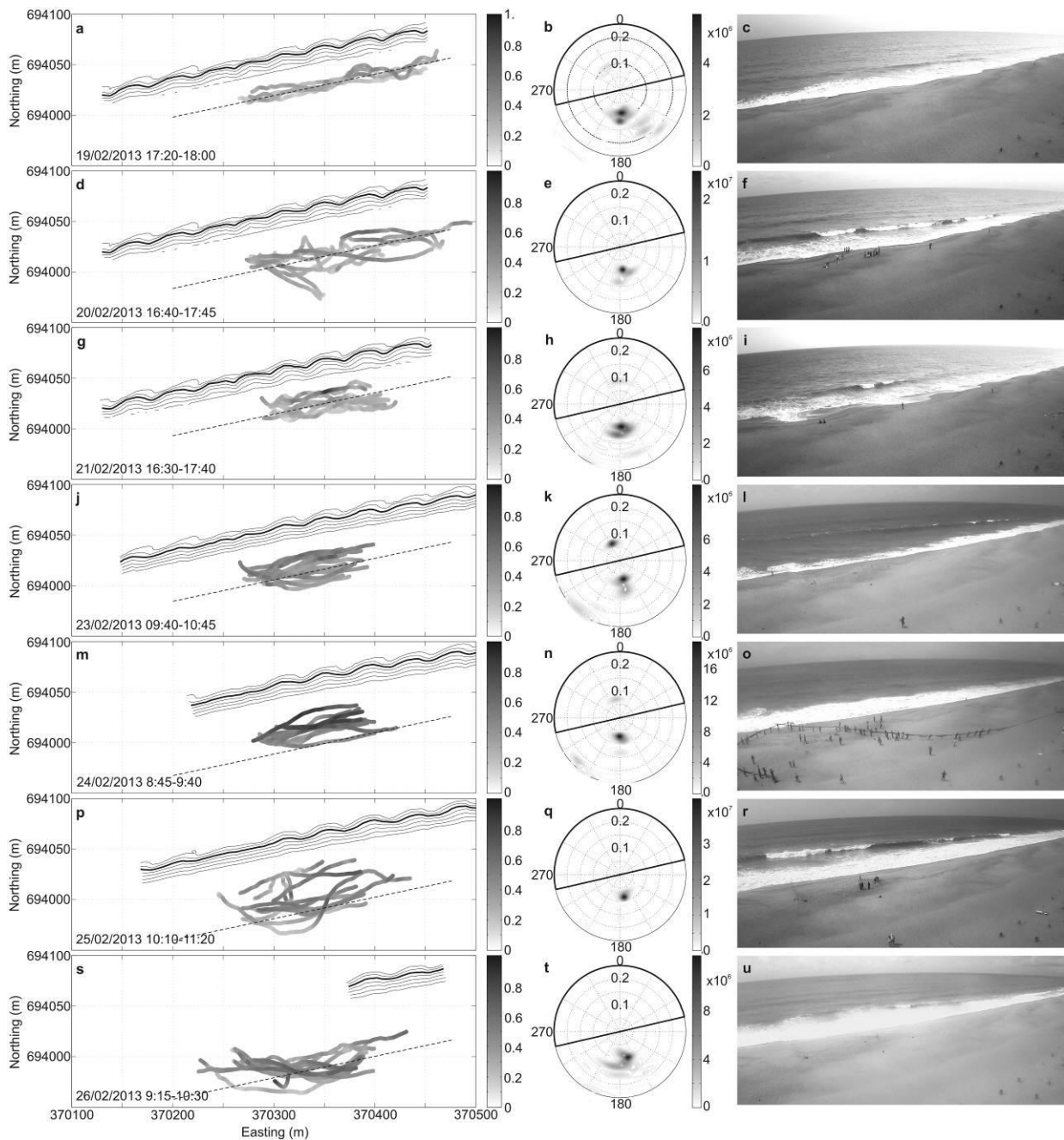


Figure 4. Wave-driven circulation and wave conditions for the 7 human drifter experiments. Left-hand panels: pathlines of the human drifters with color bar and the dashed black line indicating drifter velocity in m/s and the outer edge of the surf zone loosely based on visual observations, respectively. The beach cusp topography is contoured at a 0.5-m interval (the thick contour corresponds to  $z = 4$  m). Middle panels: directional wave spectra measured by the ADCP with color bar indicating energy density in  $\text{m}\cdot\text{Hz}^{-0.5}\cdot\text{deg}^{-0.5}$ . Right-hand panels: snapshot during the corresponding experiment.

The second swell regime (February 23, 24, 25 and 26) coincided with a progressive shift towards spring tides. Although swash rips were ubiquitous during mid- and high-tide phases, they progressively disappeared during the human drifter experiments which were performed at low tide ( $-0.7 \text{ m} < h < -0.4 \text{ m}$ ). During the first 2 days, the S wave incidence combined with a SW sea resulted in a dominant longshore current increasing in speed (0.35 to 0.55 m/s, see also drifter pathlines in Figure 4). This relatively strong longshore current pulled fishnets nearby and forced the local fisherman to pass over our instrumented site (Figure 4o). On

February 25 (Figures 4p, q and r), the fading SW sea and the building S swell ( $H_s = 1.4 \text{ m}$ ) with an increasingly shore-normal incidence resulted in ubiquitous flash rips ( $\sim 0.4 - 0.8 \text{ m/s}$ ). Yet, a rather small number of human drifters actually exited the surfzone compartment (Figure 4p) as they were mostly transported by the longshore current ( $\sim 0.3 \text{ m/s}$ , Table 1). Flash rips remained active the subsequent day (Figures 4s, t and u) with similar characteristics. As for the first swell regime, flash rips were episodic and tended to migrate slowly downdrift.

Table 1. Overview of wave conditions and wave-driven circulation for the 7 human drifter experiments ( $U_l$  is the mean surface longshore current computed from the Lagrangian data).

Date	$h$ (m)	$H_s$ (s)	$T_p$ (m)	$\theta$ (°)	Sea state	Circulation description	$U_l$ (m/s)
19/02/2013 17:20-18:00	-0.3	0.9	12	190	Low-energy S swell + SW sea	Dominant weak longshore current, occasional swash rips	0.2
20/02/2013 16:40-17:45	-0.2	1.1	10-12	180	Building S swell + low-energy SW sea	Weak longshore current with flash and swash rips	0.25
21/02/2013 16:30-17:40	-0.1	1.0	12	175	Fading S swell + SW sea	Dominant weak longshore current, occasional flash rips	0.2
23/02/2013 9:40-10:45	-0.4	1.0	14-16	185	Slowly building S swell + low-energy SW sea	Dominant longshore current increasing in speed, rare swash rips	0.35
24/02/2013 8:45-9:40	-0.6	1.1	14	185	Slowly building S swell + SW sea	Dominant longshore current further increasing in speed, rare rips	0.55
25/02/2013 10:10-11:20	-0.6	1.4	12-14	180	S swell peaking + low-energy SW sea	Weak longshore current, active flash rips, no swash rip	0.3
26/02/2013 9:15-10:30	-0.6	1.2	10-12	180	Slowly fading S swell + low-energy SW sea	Weak longshore current, active flash rips, no swash rip	0.3

## DISCUSSION AND CONCLUSION

This paper presents the first assessment of rip current activity on a West African beach. Our results indicate that, at Grand Popo beach, there are 2 common types of rips. (1) Low-energy (~0.2 - 0.4 m/s) swash rips extending about 5-10 m offshore (see Figure 2c) occur preferably at mid to high tide in the center of beach cusps with no significant influence of the incoming wave characteristics. Although swash rips are fixed at a given location, they have a very short life-span (typically less than 2 minutes, see for instance the video time stack in Figure 5). (2) Surfzone flash rips, episodic and tending to migrate downdrift, become active with the onset of intense wave breaking across the low-tide terrace. Given that the latter type of rips was observed under relatively low longshore current speeds (< 0.5 m/s), flash rips were not driven by shear instabilities of the longshore current. Instead, vorticity generated by wave breaking was likely the major driving mechanism for surfzone eddies and flash rips at Grand Popo beach. Flash rips were occasionally intense (0.8 m/s) and were preferably observed at low tide during the experiment.

Given the high rate of beach-user drownings in West Africa, assessing the occurrence and the types of rip developing along this stretch of coast was a necessary first step. Figure 6 presents a conceptual model of rip current activity at Grand Popo as a function of wave and tide conditions. All the configurations in the left-hand and middle panels were observed during the experiment. Although the circulations shown in the right-hand panels ( $H_s > 2$

m) in Figure 6 were not observed during the experiment, they were based on a detailed visual inspection of the video data from March to November 2013 for which a number of high-energy events were monitored (see Figure 6b, c). Interestingly enough, Grand Popo beach remained low-tide terraced even during storms with  $H_s > 2.5$  m, suggesting that the up-state transition towards a bar and rip morphology, for which rips driven by alongshore variations in bathymetrically-controlled wave breaking are ubiquitous (Bruneau *et al.*, 2011), may never be reached.

To conclude, this study is the first one on rips in West Africa. Another experiment is planned at Grand Popo in March 2014 for which expected higher-energy waves and the deployment of a large number of PVC GPS-equipped drifters will arguably further increase our understanding of rip current dynamics in West Africa.

## ACKNOWLEDGEMENT

The work described in this publication was supported by the French INSU LEFE and EC2CO programs, the IRD (Action Initiative program), and the UNESCO co-chair CIPMA. We are greatly indebted to the naval services of Benin at Grand Popo for their logistic support during the field experiment and for allowing the installation of the permanent video system on the semaphore. BC funded by project BARBEC (ANR N2010 JCJC 602 01).

## LITERATURE CITED

- Aagaard, T., Greenwood, B. and Nielsen, J., 1997. Mean currents and sediment transport in a rip channel. *Marine Geology*, 140, 25-45.
- Almar, R., *et al.* 2014. The Grand Popo beach 2013 experiment, Benin, West Africa: from short timescale processes to their integrated impact over long-term coastal evolution. In: Green, A.N. and Cooper, J.A.G. (eds.), *Proceedings 13<sup>th</sup> International Coastal Symposium* (Durban, South Africa), *Journal of Coastal Research*, Special Issue No. 66.
- Austin, M., Scott, T.M., Russell, P.E. and Masselink, G., 2013. Rip Current Prediction: Development, Validation and Evaluation of an Operational Tool. *Journal of Coastal Research*, 29, 283-300.
- Birrien, F., Castelle, B., Dailloux, D., Marieu, V., Rihouey, D. and Price, T.D., 2013. Video observation of megacusp evolution along a high-energy engineered sandy beach: Anglet, SW France. In: Conley, D.C., Masselink, G., Russell, P.E. and O'Hare, T.J. (eds.), *Proceedings 12<sup>th</sup> International Coastal Symposium* (Plymouth, England), *Journal of Coastal Research*, Special Issue No. 65, pp. 1727-1732.
- Brander, R.W., Dominey-Howes, D., Champion, C., Del Vecchio, O. and Brighton, B., 2013. Brief Communication: A new perspective on the Australian rip current hazard. *Natural Hazards and Earth Science System Sciences*, 13, 1687-1690.
- Bruneau, N., Bonneton, P., Castelle, B. and Pedreros, R., 2011. Modeling rip current circulations and vorticity in a high-energy mesotidal-

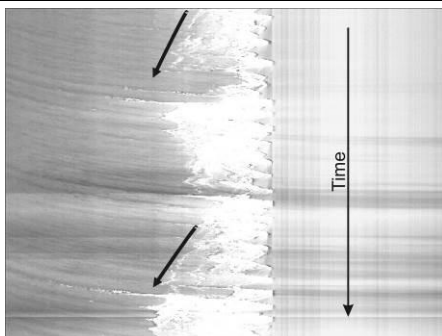


Figure 5. 5-minute timestack showing the occurrence of 2 swash rips identified by the foam streaks migrating seaward. Both swash rips have a life-span of about 1 minute.

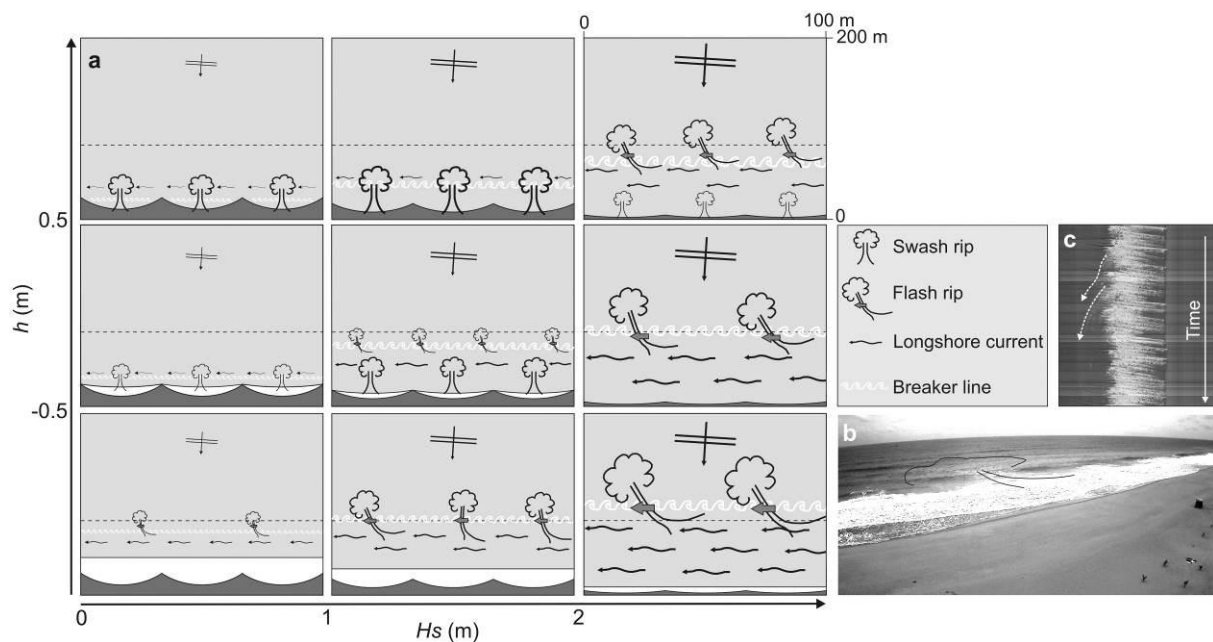


Figure 6. Conceptual model of rip current activity at Grand Popo beach (W Africa) as a function of the significant wave height  $H_s$  and tide level  $h$ . (b,c) Snapshot and corresponding 10-min time stack of a flash rip for  $H_s > 2$  m on May 6, 2013.

- macrotidal environment. *Journal of Geophysical Research*, 116(C07026), doi: 10.1029/2010JC006693.
- Castelle, B. and Coco, G., 2012. The morphodynamics of rip channels on embayed beaches. *Continental Shelf Research*, 43, 10–23.
- Castelle, B., Marieu, V., Coco, G., Bonneton, P., Bruneau, N. and Ruessink, B.G., 2012. On the impact of an offshore bathymetric anomaly on surf zone rip channels. *Journal of Geophysical Research*, 117(F01038), doi: 10.1029/2011JF002141.
- Castelle, B. and Coco, G., 2013. Surf zone flushing on embayed beaches. *Geophysical Research Letters*, 40(L1-5), doi:10.1002/grl.50485.
- Clark, D.B., Elgar, S. and Raubenheimer, B., 2012. Vorticity generation by short-crested breaking waves. *Geophysical Research Letters*, 39(L24604), doi:10.1029/2012GL054034.
- Dalrymple, R.A., MacMahan, J.H., Reniers, A.J.H.M. and Nelko, V., 2011. Rip Currents. *Annual Review of Fluid Mechanics*, 43, 551–581.
- Hammerton, C.E., Brander, R.W., Dawe, N., Riddington, C. and Engel, R., 2013. Approaches for beach safety and education in Ghana: a case study for developing countries with a surf coast. *International Journal of Aquatic Research and Education*, 7, 254–265.
- Johnson, D. and Pattiaratchi, C.B., 2004. Transient rip currents and nearshore circulation on a swell-dominated beach. *Journal of Geophysical Research*, 109(C02026), doi:10.1029/2003JC001798.
- Laibi, R., Anthony, E.J., Almar, R., Castelle, B., Sénéchal, N., Kestenare, E., 2014. Longshore drift cell development on the human-impacted Bight of Benin sand barrier coast, West Africa. In: Green, A.N. and Cooper, J.A.G. (eds.), *Proceedings 13<sup>th</sup> International Coastal Symposium* (Durban, South Africa), *Journal of Coastal Research*, Special Issue No. 66.
- Long, J. W. and Özkan-Haller, H.T., 2005. Offshore controls on nearshore rip currents. *Journal of Geophysical Research*, 110(C12007), doi:10.1029/2005JC003018.
- MacMahan, J.H., Thornton, E.B. and Reniers, A.J.H.M., 2006. Rip current review. *Coastal Engineering*, 53, 191–208.
- Masselink, G. and Pattiaratchi, C.B., 1998. Morphological evolution of beach cusps and associated swash circulation patterns. *Marine Geology*, 146, 93–113.
- Michallet, H., Castelle, B., Barthélemy, E., Berni, C. and Bonneton, P., 2013. Physical modeling of three-dimensional intermediate beach morphodynamics. *Journal of Geophysical Research*, 118(2), 1045–1059, doi:10.1002/jgrf.20078.
- Murray, T., Cartwright, N. and Tomlinson, R., 2013. Video-imaging of transient rip currents on the Gold Coast open beaches. In: Conley, D.C., Masselink, G., Russell, P.E. and O'Hare, T.J. (eds.), *Proceedings 12<sup>th</sup> International Coastal Symposium* (Plymouth, England), *Journal of Coastal Research*, Special Issue No. 65, pp. 1809–1814.
- Özkan-Haller, H. and Kirby, J., 1999. Nonlinear evolution of shear instabilities of the longshore current: A comparison of observations and computations. *Journal of Geophysical Research*, 104(C11), 25953–25984, doi:10.1029/1999JC900104.
- Pattiaratchi, C.B., Olson, D., Hetzel, Y. and Lowe, R., 2009. Wave-driven circulation patterns in the lee of groynes. *Continental Shelf Research*, 29, 1961–1974.
- Peden, M.M. and McGee, K., 2003. The epidemiology of drowning worldwide. *Injury Control and Safety Promotion*, 10, 195–199.
- Scott, T.M., Russell, P.E., Masselink, G., Austin, M.J., Wills, S. and Wooler, A., 2011. Rip current hazards on large-tidal beaches in the United Kingdom. In: Leatherman, S. and Fletemeyer, J. (eds.), *Rip Currents: Beach Safety, Physical Oceanography, and Wave Modelling*, CRC Press, pp. 225–242.
- Sénéchal, N., Laibi, R.A., Almar, R., Castelle, B., Biaisque, M., Lefebvre, E. Anthony, J.-P., Dorel, M., Chuchla, R., Hounkonnou, M.H., Du Penhoat, Y., 2014. Observation of the destruction of a beach cusp system in presence of a double coupled cusp system: the example of Grand Popo – Benin. In: Green, A.N. and Cooper, J.A.G. (eds.), *Proceedings 13<sup>th</sup> International Coastal Symposium* (Durban, South Africa), *Journal of Coastal Research*, Special Issue No. 66.
- Shanks, A.L., Morgan, S.G., MacMahan, J.H. and Reniers, A.J.H.M., 2010. Surf zone physical and morphological regime as determinants of temporal and spatial variation in larval recruitent. *Journal of Experimental Marine Biology and Ecology*, 392, 140–150.
- Surf Lifesaving Australia, 2011. National Coastal Safety Report 2011. Sydney, Australia.
- Thornton, E.B., MacMahan, J.H. and Sallenger Jr., A.H., 2007. Rip currents, mega-cusps, and eroding dunes. *Marine Geology*, 240, 151–167.
- United States Lifesaving Association, 2011. 2011 National Lifesaving statistics. Available at <http://arc.usla.org/Statistics/public.asp>
- World Health Organization, 2010. Drowning Fact Sheet 347. Available at <http://www.who.int/mediacentre/factsheets/fs347/en/>
- Wright, L.D. and Short, A.D., 1984. Morphodynamics variability of surf zones and beaches: a synthesis. *Marine Geology*, 70, 251–285.

# Video monitoring and field measurements of a rapidly evolving coastal system: the river mouth and sand spit of the Mataquito River in Chile



[www.cerf-jcr.org](http://www.cerf-jcr.org)

Rodrigo Cienfuegos<sup>†,§</sup>, Mauricio Villagran<sup>†‡</sup>, Juan C. Aguilera<sup>†</sup>, Patricio Catalán<sup>∞,§</sup>, Bruno Castelle<sup>#</sup>, Rafael Almar<sup>+</sup>

<sup>†</sup>Pontificia Universidad Católica de Chile, [racienfu@ing.puc.cl](mailto:racienfu@ing.puc.cl), [mwillagranv@uc.cl](mailto:mwillagranv@uc.cl)

<sup>‡</sup> Departamento de Ingeniería Civil, Universidad Católica de la Santísima Concepción, UCSC [mwillagran@ucsc.cl](mailto:mwillagran@ucsc.cl)

<sup>∞</sup> Departamento de obras civiles, Universidad Técnica Santa María, Valparaíso, Chile, [patricio.catalan@usm.cl](mailto:patricio.catalan@usm.cl)

<sup>+</sup> Institut de Recherche pour le développement (IRD)/ LEGOS, Toulouse, France. [rafael.almar@ird.fr](mailto:rafael.almar@ird.fr)

<sup>#</sup> EPOC- OASU, University of Bordeaux, Bordeaux, France. [b.castelle@epoc.u-bordeaux1.fr](mailto:b.castelle@epoc.u-bordeaux1.fr)

<sup>§</sup> Centro Nacional de Investigación para la Gestión Integrada de Desastres Naturales (CIGIDEN), Pontificia Universidad Católica de Chile



[www.JCRonline.org](http://www.JCRonline.org)

## ABSTRACT

Cienfuegos R., Villagran M., Aguilera J.C., Catalán P., Castelle B., Almar R., 2014. Video monitoring and field measurements of a rapidly evolving coastal system: the river mouth and sand spit of the Mataquito River in Chile. In: Green, A.N. and Cooper, J.A.G. (eds.), *Proceedings 13<sup>th</sup> International Coastal Symposium* (Durban, South Africa), *Journal of Coastal Research*, Special Issue No. 70, pp. 639-644, ISSN 0749-0208.

The understanding of morphological processes controlling the evolution of sand spit reformation after a tsunami impact is a challenging and interesting topic, especially in highly energetic and micro tidal environments. A field campaign performed during December 2012 at the Mataquito River mouth in Chile, allowed us to simultaneously monitor topobathymetry evolution, wave climate, tidal range, swash zone dynamics and upper beach face evolution over a portion of its sand spit. A video system was set up for a continuous and long-term monitoring of the evolution of the river mouth and sand spit. Primarily, in this work we focus on the application of a video-derived shoreline detection method to assess shoreline evolution and beach cusps migration at hourly scales. We test the method performance on short-term episodic migration of beach cusps recorded during the campaign. Beach face variations at a daily scale were observed, which can be attributed to the migration of beach cusps in the alongshore direction, and linked to wave forcing and alongshore sediment transport.

**ADDITIONAL INDEX WORDS:** Coastal monitoring, video system, river mouth, sand spit, beach cusps migration

## INTRODUCTION

The coast of central Chile is characterized by highly energetic wave conditions and micro-tidal range generally affected by strong swells coming from the South West Pacific Ocean. Moreover very often, rivers that come from the Andes provide continuous discharge into the sea supplying abundant amount of sediment into coastal systems. This highly dynamic environment offers the opportunity to witness short-term beach evolution because changes occur very fast. An empirical proof of this was the fast reformation of the Mataquito River sand spit (34°52', 72°09'W) after the Chilean earthquake and tsunami of February 27<sup>th</sup>, 2010 that hit this area. Before the tsunami, its morphologic configuration was characterized by the presence of a large sand spit (~3 millions m<sup>3</sup> of emerged sand) oriented South to North, that forced the river to run parallel to the rocky shoreline over ca. 9 km. During the tsunami, the sand spit was almost completely washed away under the combined action of strong currents and land subsidence (~1 m) thus evidencing the drastic impact that

these extreme events can have on coastal morphology (Villagran *et al.*, 2011). Somewhat surprisingly, the sand spit almost completely reformed during the following year, reaching a very similar configuration as the one that existed before, but with the river outlet slightly updrift. This rapid evolution is suggestive of a strong littoral transport driven by the energetic wave climate of central Chile.

Previous works had investigated the morphologic variation of coastal features using video images. Migration behavior of discharge channels (e.g. Paterson *et al.*, 2003; Morris *et al.*, 2001), the estimation of sand volume changes (e.g. Smith & Bryant, 2007) or the migration of submerged sand bars (e.g. Armaroli and Ciavola, 2011; van Enckevort & Ruessink, 2003; Ruessink *et al.*, 2013; Holland *et al.*, 1997) and shoreline detection (Plant *et al.*, 2007; Almar *et al.*, 2012). These examples had proved the interest of using video monitoring systems to evaluate morphological changes occurring at different time scale along the coast, complementing the data obtained using traditional in situ measurements.



## Site Description

The Mataquito River is an Andean river draining a 6,200 Km<sup>2</sup> basin located 300 km South-West of Santiago de Chile. Main hydrologic and catchment characteristics are summarized in Table 1. The Mataquito river mouth is located 50 km north of the Maule River. The Mataquito river exits north of the Putu dune system (aligned South-East) over a strait shoreline aligned in the South-North direction. The change of direction relative to the more frequent wave climate coming from Southwest direction favors the accumulation of sand and the formation of a long sand spit system and a calm estuary behind it (see Figure 1). This sand spit suffered heavy erosion after the 2010 Chilean tsunami, but was rapidly reformed over the following year (Villagran *et al.*, 2011). We focus on a 3 km long strait beach located at the sea front of the sand spit where a highly dynamic sub-aqueous triple bar system exists. The intertidal bars closely follow the shoreline configuration. The wave height along the sand spit is fairly constant over the year, with strong swells coming from the South Pacific Ocean that produce a highly energetic longshore current. In situ wave measurements are not available, but NOAA nearest node provide a yearly mean significant wave height of 2.7 m with peak period of 11.7 s. The tide in Mataquito is semi-diurnal and micro-tidal with tidal ranges between 0.3 m (neap tide) to 1.5 m (spring tide). During storms, sea level may increase by 1 to 2 m due to storm surges and wind set up.

The plentiful supply of sediment is another important aspect regarding morphological changes. The Mataquito River ensures sand availability, together with the Putu dunes system and the Maule River located to the South. Long-shore currents generated by the dominant Southwest wave climates can transport this loose material to the north.

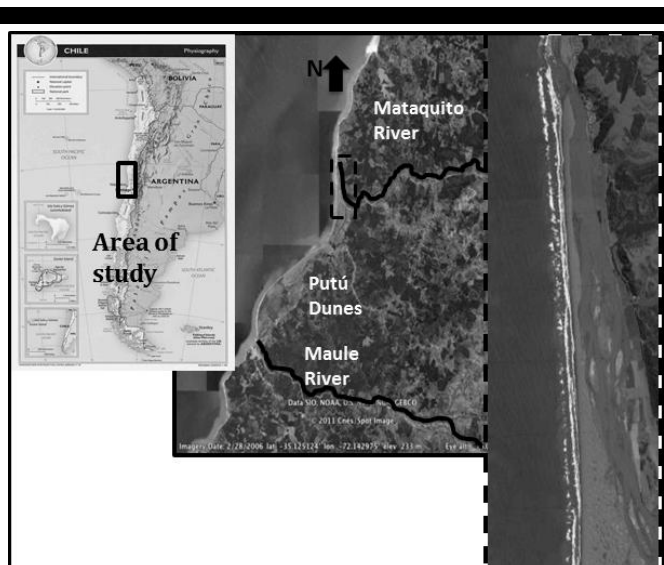


Figure 1. Location of the Mataquito River mouth, shoreline geometry, and zoom over the sand spit barrier.

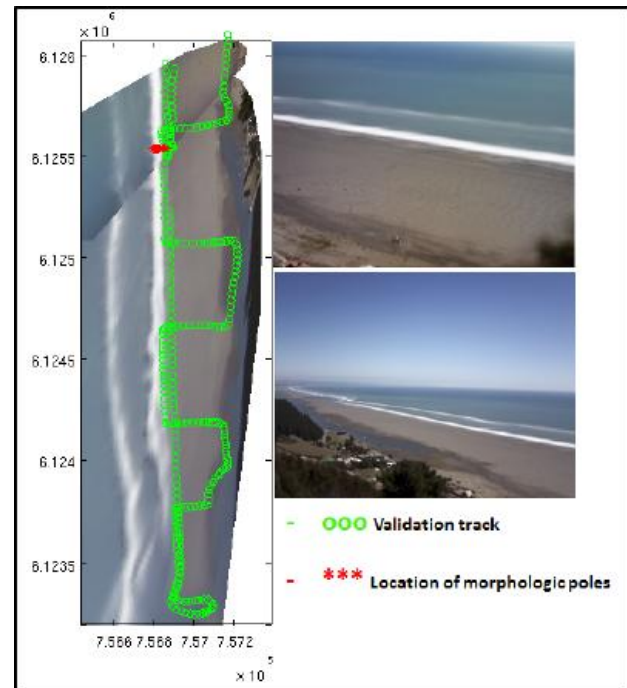


Figure 2. Averaged images provided by the coastal video monitoring system (right panels) and rectified images compared to DGPS tracks (green dots) and surveys at the location where vertical rods were deployed on the beach face (red dots).

## METHODS

### Instruments and Measurements

Waves, tides and river discharge are the main hydrodynamic factors influencing the morphological changes in the area. Therefore, the first two were measured during our short field campaign to complement the video data, and river discharge are continuously acquired from the Licanten station, which is the closest gauge station to the river mouth whose data is freely available from the internet ([www.dga.cl](http://www.dga.cl)).

In order to better understand the forcing and processes that control the evolution of the sand spit, we conducted, for the first time in Chile, a field campaign in the area of the Mataquito River mouth over 3 weeks. The field campaign took place between November 28<sup>th</sup> and December 14<sup>th</sup> of 2012. Different instruments were deployed in the area, and many researchers and students participated in the data collection (more than 30 people in total). It was the first surf zone survey campaign of this extent taking place in Chile ever. During this campaign we performed simultaneous measurements of topo-bathymetry, wave climate, tidal range, swash zone and upper beach face evolution, while a video system was continuously acquiring images of the coastal system.

For topo-bathymetry surveys we used a RTK DGPS instrument and a sonar altimeter with GPS antenna. Wave climate and tidal range was measured with the help of a Teledyne ADCP (1,200Hz) moored at 11.6 m depth and 900 m from the shoreline. The swash and beach face evolution at daily scales were studied using GPS and topographic levels. Eleven morphological rods were installed in the swash zone to measure beach face evolution in a way similar to Kulkarni *et al.* (2004). The rods were painted

in yellow to clearly discriminate them from the grey color of the sand, and a high-resolution video camera was installed on the beach to monitor the waves passing through the rods. Four wired pressure sensors (Kepler, acquisition sampling of 100 Hz) were placed in the intertidal zone to measure water surface elevation around high tide. Additionally, a LiDAR sensor was mounted during low tide at an elevation of 9 m above the beach to provide measurements of the swash free-surface profile for comparison with those detected by the video camera and pressure sensors. Nonetheless, in this work we do not exploit swash dynamics detected through video images, pressure sensors nor LiDAR data, which will be presented elsewhere. The coastal monitoring video system consists of two IP cameras with 2 MegaPixel resolution each (Vivotek IP7161), mounted on a 6 m timber pole located on the top of the hill surrounding the Mataquito River mouth

Table 1. Main hydrologic and sediment characteristics of the Mataquito River watershed. Sediment size is representative of the river mouth.

Hydrologic parameter	Units
Basin dimension	6,200 Km <sup>2</sup>
Mean monthly river discharge	150 m <sup>3</sup> /s
Maximum peak river discharge observed	Nearly 8,000 m <sup>3</sup> /s
Sediment D <sub>50</sub>	0.12 – 0.22 mm
Hydraulic regime	Mixed (rain/snowmelt)
Annual Mean precipitation in the watershed	740 mm/year

(34°58'28"S 72°10'46,8"O, altitude 155m above msl) pointing towards the Southwest.

Moreover, a switch with Power over Ethernet (PoE) energy supply plus a Wifi antenna was installed on the pole to transmit the video signal continuously to a computer station located near the beach. The system is completely autonomous, with power requirements supplied by batteries charged by a dedicated solar panel array. Video images are transmitted during daylight from the tower to the PC housing base. The video signal is post-processed in order to record 15 min averaged images and timestacks from both cameras at an acquisition sampling rate of 2 fps. In order to save batteries, an on/off switch was included on the system to turn it off during night.

Camera 1 (Cam1) was adjusted with a zoom lens, obtaining more detailed images of the beach face, pointing to the north part of the aerial view. Camera 2 (Cam2) has a panoramic view of the whole sand spit system, pointing to the Southward part of it (see Figure 2).

Implementation of photogrammetric post-processing routines was necessary to transform video images into rectified almost undistorted linear coordinate images. This process was necessary to be able to quantify qualitatively and quantitatively the morphologic changes in the study area. Several control points (CCP) were measured using DGPS within cameras field of view, applying a similar methodology as the one described by Holland *et al.* (1997).

A validation of the rectification process was made comparing the rectified images with a survey track of the whole sand spit made with an RTK mounted on AWD truck (see Figure 2). Both images were merged creating a single view of the sand spit (see Figure 2). We obtained a good level of agreement between the RTK survey and the GPS control points in the rectified images. The average error for Cam1 is about 5 m, while the average error for Cam2 is around 20 m.

## DATA ANALYSIS

### ADCP's Data Analysis

The data collected with the ADCP allow us to characterize the wave climate during the field campaign. The hydrodynamic conditions observed during the campaign were representative of average wave climates though a superposition of Southwest and Northwest wave climates could be observed, as suggested by the bimodal wave spectrum sample presented in Figure 3. The wave record obtained during the field campaign (see Figure 4) shows the occurrence of an energetic swell between December 3<sup>rd</sup> and 4<sup>th</sup>, with a significant wave height reaching 3 to 4 m, a peak period of 14 to 16 s and a wave direction of 270°. The wave direction remained relatively constant during the field campaign (270° on average), while the peak period showed some variations between 10 s and 17 s. Beside the most energetic wave conditions observed between December 3<sup>rd</sup> and 4<sup>th</sup>, the rest of the time the significant wave height remained below 2 m.

### Beach Slope Variation

Using eleven morphological rods for monitoring beach slope variations at daily scale we were able to assess its profile evolution during the surveyed period (see Figure 5). Most of the time, little variations were observed on the beach face. However, during the last 2 days of measurements (December 9<sup>th</sup> and 10<sup>th</sup>), 50 cm of accretion was observed at the upper part of the beach slope. This process might be associated to a change on the peak wave period (longer waves) and a bi-modal wave climate (see Figure 3) that should be further analyzed. Moreover the

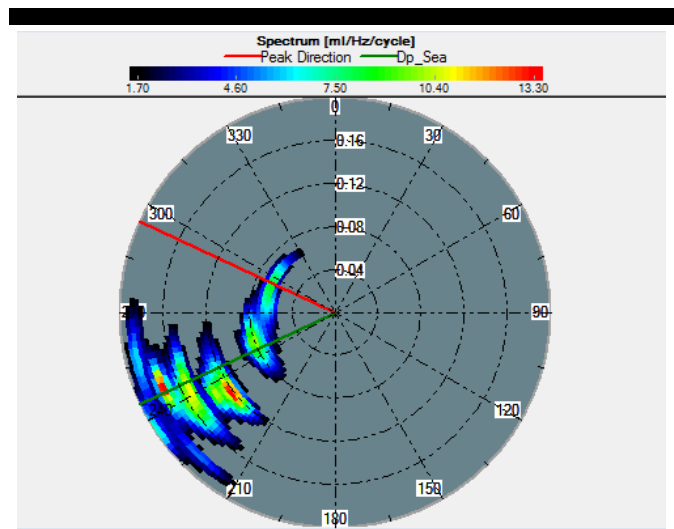


Figure 3. Sample of a 20 minutes wave spectrum at the Mataquito site obtained during the field campaign on December 10<sup>th</sup>, 2012. bathymetric change (accretion) in the beach face can be attributed to the beach cusp migration observed by video images during December 9<sup>th</sup> and 10<sup>th</sup> as will be shown in the next section

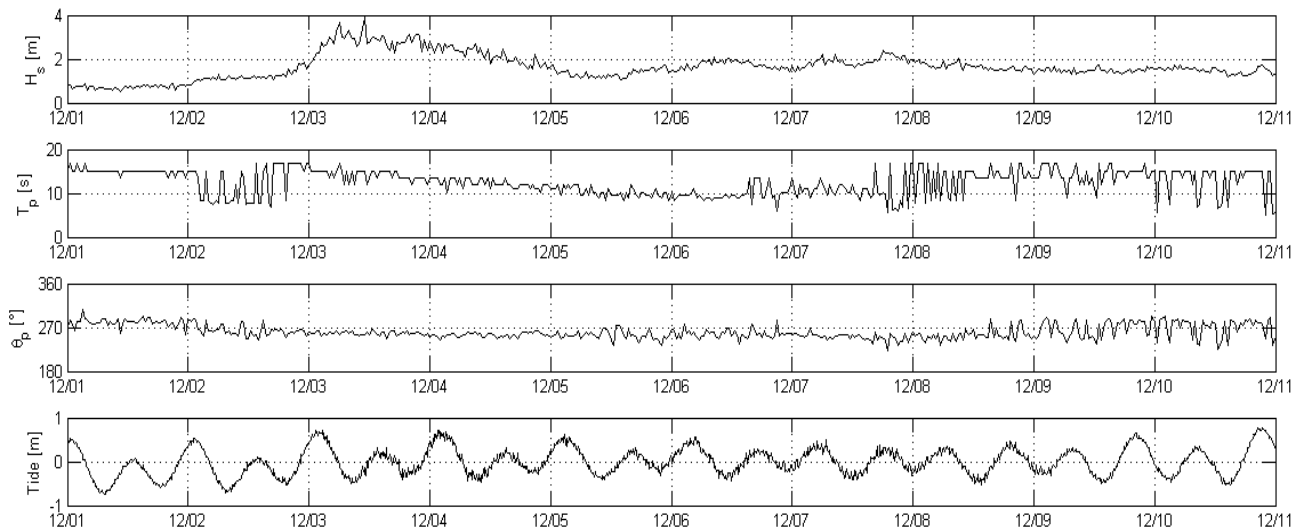


Figure 4. Time series of ADCP record during the field deployment. First panel: Significant wave height,  $H_s$ . Second panel: Peak wave period,  $T_p$ . Third panel: Peak wave direction,  $\theta_p$ . Fourth panel: Tidal level.

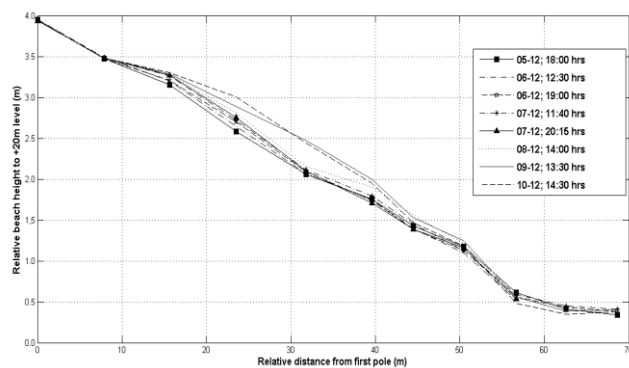


Figure 5. Beach face evolution during the field campaign

### Shoreline Detection Using Video

Each averaged video image (one every 15 minutes), corresponding to December 9<sup>th</sup> and 10<sup>th</sup>, 2012, was analyzed to detect the shoreline. The chosen shoreline detection algorithm is based on the edge detection gradient operator method from Gonzalez and Woods (2002). Other methods were also explored for comparison (e.g.: Almar *et al.*, 2012) but are not shown here. Pixels corresponding to the shoreline were rectified to compute their corresponding UTM coordinates using the transformation matrix obtained from the rectification process described before.

Using a shoreline detection algorithm, a set of shoreline curves was extracted from averaged images of December 9<sup>th</sup> and 10<sup>th</sup> for Cam1. In Figure 6 we present an example of the application of the shoreline detection algorithm. We have tested the method over different video images and light conditions obtaining in general a good agreement between the automated detection process and visual inspections. For the following analysis, we use averaged

images obtained from Cam1, which has a better resolution to perform the shoreline detection and analysis.

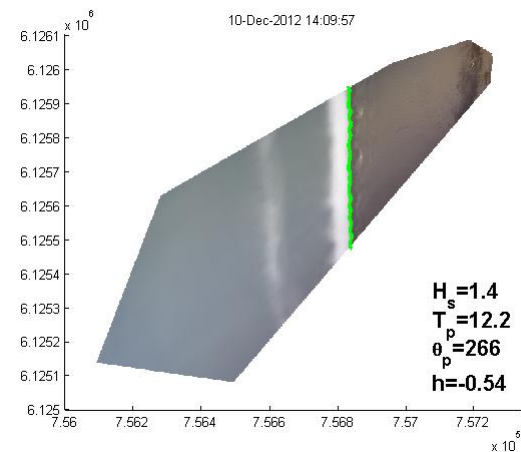


Figure 6. Example of a rectified 15 minute averaged image and the application of the shoreline detection algorithm.

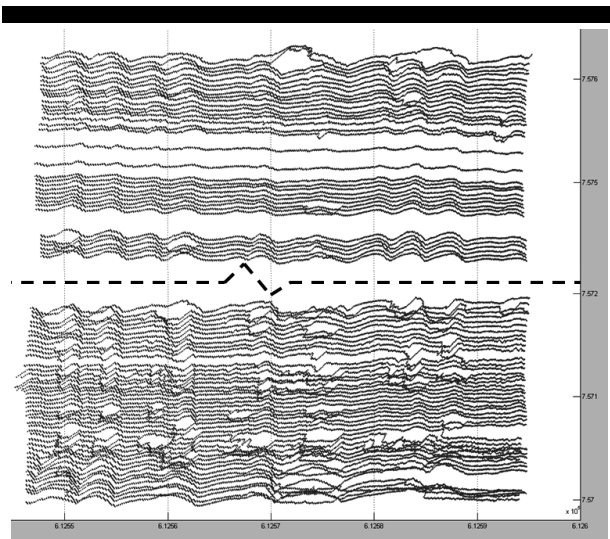


Figure 7. Set of detected shorelines for averaged images during December 9<sup>th</sup> and 10<sup>th</sup>. Shoreline curves were shifted to avoid overlapping between them. The dashed line represents the night time that separates both days. Blank spaces between shoreline curves correspond to downtimes of the Cam1.

### Shoreline Analysis

Although the algorithm occasionally fails, we succeeded in acquiring a large number of shoreline-detected curves at a high acquisition rate. In Figure 7, time series of shoreline evolution over the two days of observation are presented. It can be seen that cusp evolution and migration is visible at an hourly scale.

In Figure 8 we show results for the shoreline detection for images obtained under high and low tide conditions over the two days of observation. With the help of this figure we can get an overview of beach evolution at a daily scale. Some variability in the shoreline, both in the onshore-off-shore direction and in the beach cusps' geometry is observed. It appears that the beach is accreted from South to North resulting in an off-shore shoreline migration that could reach 10 m. The latter is consistent with the beach face evolution depicted in Figure 5 for December 9<sup>th</sup> and 10<sup>th</sup>. Cusp migration and evolution can also be observed at this short time scales. Note that wave conditions were mild but with long peak periods, that were fairly constant during these days.

### Cusp Migration

To assess beach cusp geometry and migration, we use shoreline-detected curves from 15 minutes averaged images taken every hour during December 10<sup>th</sup>. A zoomed region of the shoreline-detected curves can be seen in Figure 9.

From Figure 9, typical alongshore wavelengths of beach cusps are comprised between 30 to 50 m (validated also with in situ topographical measurements). More interestingly, with the help of the video system, cusp evolution can effectively be observed at hourly scales. The cusp horn migrate towards the North at an estimated rate of 1 – 1.5 m/h., while the alongshore shape of the cusp appears to increase in time in the longshore direction.

In order to better understand beach cusps dynamics and its link with inner and outer bar systems present in the area, longer time series of shoreline and bar evolution are necessary. Indeed, during the field campaign we observed that the cusps' growth could be associated to the formation of a second, more seaward, cusp system as tide cycles progressively shifted from spring to neap. This feature, which certainly deserves more studies, illustrates the complexity and extremely fast evolution of beach morphodynamics in the site.

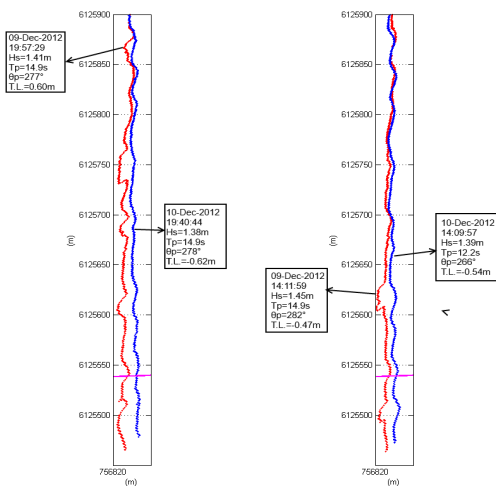


Figure 8. Shoreline evolution between high and low tides in December 9<sup>th</sup> and 10<sup>th</sup>. The horizontal line in the low part of the image shows the location of the topographic rods. Left panel: High tides. Right panel: Low tides.

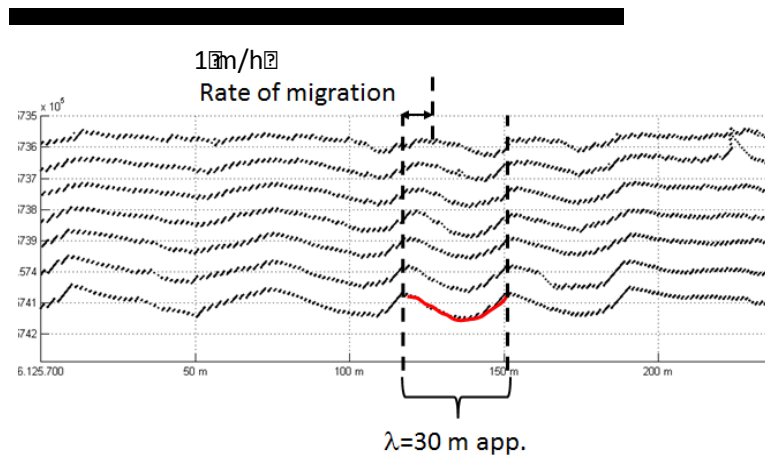


Figure 9. Shoreline-detected curves separated every 1 hour observed in December 10<sup>th</sup>. Typical wavelength of beach cusps is estimated at 30 m, and its rate of migration in the North direction is comprised between 1 to 1.5 m/h.

## CONCLUDING REMARKS

In this work we have described the field campaign that we have conducted in the coastal area of the Mataquito River mouth in the Maule Region in Chile. This coastal system was heavily affected by the 2010 Maule earthquake and tsunami, which produced land subsidence and strong erosion of a large sand spit.

Because a very rapid coastal reformation of this system was observed during the following years, this site attracted our attention and we started making sporadic surveys of its topographic evolution in order to better understand the morphodynamic processes at play. In December 2012, we conducted for the first time a 3-week field campaign where wave conditions were continuously measured with the help of an ADCP, while in situ topo-bathymetric surveys were performed on the beach face of the reformed sand spit. In parallel, we set up a coastal monitoring video system capable of acquiring images in the area of interest.

Using video information, we focused on the detection of shoreline evolution at hourly scales over a 1 km straight beach. The employed shoreline detection algorithm showed a good performance when compared to visual inspections thus enabling us to further analyze the coastal evolution during the campaign. Analysis of a two day time framework under mild wave heights but long peak wave periods, showed an accretive behavior of the beach with an off-shore migration of the shoreline that could reach 10 m within 24 hours, consistent with in situ measurements. Similarly, beach cusp wavelengths could be estimated from video images to be comprised between 30 to 50 m, and a consistent migration pattern was observed. Beach cusp migration to the North at an average rate of the order of 100-150 cm/hr was estimated. Even though longer time series and observations are necessary to understand the conditions that enhance this accretive behavior, the coastal monitoring video system that is currently installed in the area has proven to be a cost-effective method to quantify the morphodynamic evolution of the highly dynamic coast of the Maule Region. Future studies will focus on the understanding of the beach cusps dynamics and its coupling with inner and outer bars.

## ACKNOWLEDGEMENT

This work has been funded by the Chilean National Science and technology Committee CONICYT through the Fondecyt project N°1120878. Mauricio Villagran has been supported by CONICYT through a PhD scholarship. The CONICYT/FONDAP/15110017 program is also acknowledged.

## LITERATURE CITED

- Almar, R., Ranasinghe, R., Sénéchal, N., Bonneton, P., Roelvink, D., Bryan, K. R., ... & Parisot, J. P., 2012. Video-Based Detection of Shorelines at Complex Meso-Macro Tidal Beaches. *Journal of Coastal Research*, 28(5), 1040-1048.
- Armaroli, C., Ciavola, P., 2011. Dynamics of a nearshore bar system in the northern Adriatic: a video-based morphological classification. *Geomorphology*, 126, 201–216.
- Gonzalez, R. C., and Woods, R. E., 2002. *Digital Image Processing*, 2° Edición. Prentice Hall, New York
- Holland, K.T., Holman, R., Lippmann, T., Stanley, J., Plant, N., 1997. Practical use of video imagery in nearshore oceanographic field studies. *Journal of Oceanic Engineering* 22, 81–92.
- Kulkarni C., Levoy F., Monfort O. and Miles J. 2004. Morphological variations of a mixed sediment beachface (Teignmouth, UK). *Continental Shelf Research*. 24, 1203-1218
- Morris B., Davidson M. and Huntley D., 2001. Measurements of the response of a coastal inlet using video monitoring techniques. *Marine Geology* 175, 251-272.
- Paterson A., Hume T., and Healy T., 2001. River Mouth Morphodynamics on a Mixed Sand-Gravel Coast. *Journal of Coastal Research* SI 34, (ICS 2000 New Zealand)
- Plant, N.G., Aarninhhof, S.G.J., Turner, I.L. and Kingston, K.S., 2007. The performance of shoreline detection models applied to video imagery. *Journal of Coastal Research*, 23(3), 658-670.
- Ruessink G., Price T. and Castelle B., 2013. Finite-Amplitude Behaviour of alongshore variability in nearshore sandbars: observations and modelling. *Procc. of Coastal Dynamics 2013* (Arcachon, France) SHOM pp 1-15.
- Smith, R.K. and Bryan, K.R., 2007. Monitoring beach face volume with a combination of intermittent profiling and video imagery. *Journal of Coastal Research*, 23(4), 892–898.
- Van Enckenvort I. and Ruessink G., 2003. Video observation of nearshore bar behavior. Part I alongshore uniform variability. *Continental Shelf Research*. 23. 501-512.
- Villagran M., Cienfuegos R., Almar R., Gironás J., Catalán P., Camaño C. and Dominguez J.C., 2011. Natural post tsunami recovery of Mataquito river mouth after 2010 Chilean tsunami. *Procc. AGU Fall Meeting Conference* (San Francisco, USA).

## Storm-driven cusp behaviour on a high energy gravel beach

Poate, T.G.†, Masselink, G.†, McCall, R.M.‡, Russell, P.E.†, Davidson, M.A.†

†School of Marine Science and  
Engineering  
Plymouth University  
Plymouth  
Timothy.poate@plymouth.ac.uk

‡Deltares,  
The Netherlands



[www.cerf-jcr.org](http://www.cerf-jcr.org)



[www.JCRonline.org](http://www.JCRonline.org)

### ABSTRACT

Poate, T.G., Masselink, G., McCall, R.T., Russell, P.E., Davidson, M.A., 2014. Storm-driven cusp behaviour on a high energy gravel beach. In: Green, A.N. and Cooper, J.A.G. (eds.), *Proceedings 13<sup>th</sup> International Coastal Symposium* (Durban, South Africa), *Journal of Coastal Research*, Special Issue No. 70, pp. 645-650, ISSN 0749-0208.

Gravel and mixed sand-gravel beaches are characterised by steep reflective profiles which provide effective forms of wave absorption and therefore coastal defence to many mid-latitude regions, including northwestern Europe and North America. In the UK the combination of energetic wave conditions and large tides creates very dynamic and responsive morphology often dominated by cusped features. Recent storm-responsive field campaigns at Loe Bar, Cornwall, UK, have captured highly energetic wave conditions ( $H_s = 2.5\text{--}5.8$  m) using temporary video camera installations, low tide 3D topographic surveys with real time kinematic GPS, local tide level measurements and inshore directional wave data. Characterised by fine gravel ( $D_{50} = 3$  mm) and a steep reflective profile ( $\tan\beta = 0.118$ ), the barrier at Loe Bar is exposed to an annual 10% exceedence significant wave height  $H_{s10\%}$  of 2.4 m arriving predominantly from the southwest (Atlantic Ocean) and shore-normal to the beach. Under medium-wave conditions ( $H_s = 2\text{--}3$  m), contrasting cusp behaviour was recorded with accretion and erosion, principally, through horn growth and decay (bed-level change  $\Delta z = c. 1$  m). During more energetic conditions ( $H_s = 5.8$  m), the morphological response is more consistent and the waves drive erosion of the lower profile causing bed-level changes over a tide in excess of 1.5 m. Very rapid recovery to pre-storm bed levels is observed with defined cusp evolution occurring within 12 hours during the falling limb of the storm as incident wave energy decreases. The unique gravel cusp dataset suggests free behavior due to cusp morphodynamic feedback, rather than hydrodynamic forcing, plays an dominant role in cusp evolution.

**ADDITIONAL INDEX WORDS:** *Gravel, storms, cusps, wave steepness, morphology.*

### INTRODUCTION

Rhythmic topographic features known as beach cusps are ubiquitous on a wide range of beaches globally. Beach cusps are characterised by rhythmic wavelengths made up of regularly spaced ridges (horns) interspaced by shoreline depressions (embayments). Despite their prominence on both sandy and gravel coasts, and subsequent extensive study numerically and in-situ, there is little agreement within the literature as to the prediction and formation of cusps. Numerous theories have been presented to explain the evolution and uniform nature of these features, including the role of swash dynamics, standing edge waves and self-organisation theories (for detailed reviews see Werner and Fink 1993; Holland and Holman 1996; Coco *et al.*, 1999).

Found on beaches with grain sizes from fine sand to coarse pebbles, the favourable conditions for cusp formation are reflective conditions with incident waves normal to the shoreline under steady water levels/low tidal ranges (Guza and Inman, 1975; Holland and Holman, 1996; Holland, 1998). As well as the hydrodynamic forcing required for cusp evolution, other controlling factors include: dependence on underlying larger scale morphology (van Gaalen *et al.*, 2011) and sediment grain size distributions, with cusp formation a result of gravel “structures”

atop underlying finer material (Buscombe and Masselink 2006). There is disparity in agreement whether cusps represent erosional or accretionary features with Almar *et al.* (2008) observing favourable formation under mildly accretionary conditions while also stating their formation can occur through erosion of upper berm features, supported by Antia (1987).

Removal of cusps under storm conditions is well supported by numerous authors (Miller *et al.*, 1989; Almar *et al.*, 2008; van Gaalen *et al.*, 2011), although conversely Almar *et al.* (2008) also shows removal of cusps through infilling under accretionary conditions. The complexities of cusp dynamics are further compounded by diversity in cusp formation rates with time spans of minutes (Komar 1973) to days (Holland and Holman 1996) cited as lag times for cusp development.

The work presented in this paper focuses on three short term events of cusp formation and removal from a reflective gravel barrier at Loe Bar, Cornwall (Figure 1). It is not the intention of this paper to compare observed beach cusp characteristics with cusp formation theories (cf., Masselink, 1998); rather, the work is motivated by the morphodynamic response of beach cusp morphology under storm waves.

## METHOD

### Site

Loe Bar is situated 2 km south-east of Porthleven, Cornwall, UK (Figure 1) and forms a bay-bar which encloses a freshwater lagoon (Loe Pool) (Poate *et al.* 2013). The bar itself, perhaps better termed the barrier, represents a 4.3 km long fine-gravel beach ( $D_{50} = 2-4$  mm) that extends from Porthleven, to the north, and Gunwallow, to the south, with a steep reflective profile ( $\tan\beta = 0.118$ ) (Figure 1). At its widest point the barrier is 250 m wide between Loe Pool and the sea and extends 430 m between the adjacent headlands. The barrier consistently displays extensive three-dimensional beach morphology with an upper, more stable, cusp system (alongshore wavelength  $\lambda = 40$  m) and lower more responsive cusp features ( $\lambda = 25$  m). Wave statistics from a nearshore directional wave buoy which has been deployed for 1 year in  $\sim 10$  m Chart Datum shows an annual significant wave height  $H_s = 1.2$  m,  $H_{s10\%} = 2.4$  m, peak  $H_s = 6.1$  m and peak wave period  $T_p$  of 9.8 seconds. Orientated at  $320^\circ$  (NW) the site is exposed to a dominant energetic wave approach of  $235^\circ$  (SW) with limited directional variation (Figure 1).

### Field Measurements

Field data presented in this paper cover two separate field campaigns at Loe Bar (Figure 1) which will be further split into three events for clarity. The first dataset was collected during a 6-week deployment between 23 February and 28 March 2012 (cf. Poate *et al.*, 2013). The two periods of interest from this dataset occurred at the end of February (LB1) and at the end of March (LB2). The third event (LB3) occurred in November 2012 and was a separate deployment timed to capture the arrival of a significant storm at the site.

For each of the datasets topographical data was collected using real-time kinematic GPS (RTK GPS) mounted on an all-terrain vehicle (ATV). This method allows rapid data collection over a

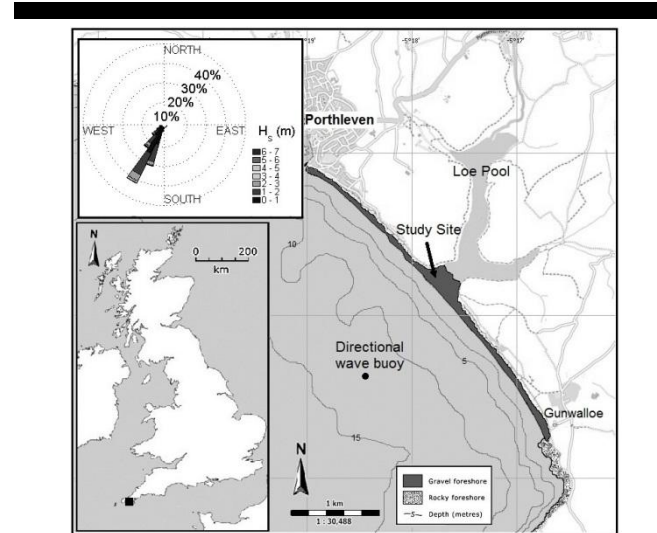


Figure 1. Location of study site close to Porthleven, including position of the nearshore directional wave buoy. The directional wave plot is based on data collected from October 2011, from Poate *et al.* (2012).

wide area ensuring the highly 3D nature of the site is recorded. ATV sampling was done by logging continuously, generating an approximately gridded dataset with a resolution of 5–10 m line spacing. 3D survey data were translated and rotated onto a local coordinate system before being interpolated onto a regular  $1\text{ m} \times 1\text{ m}$  grid (Figure 2), using the quadratic loess scale-controlled interpolation method (Plant *et al.*, 2002). Surface change maps were derived from consecutive surveys and sediment volumes were calculated for fixed regions (within all surveys) down to mean sea level (MSL).

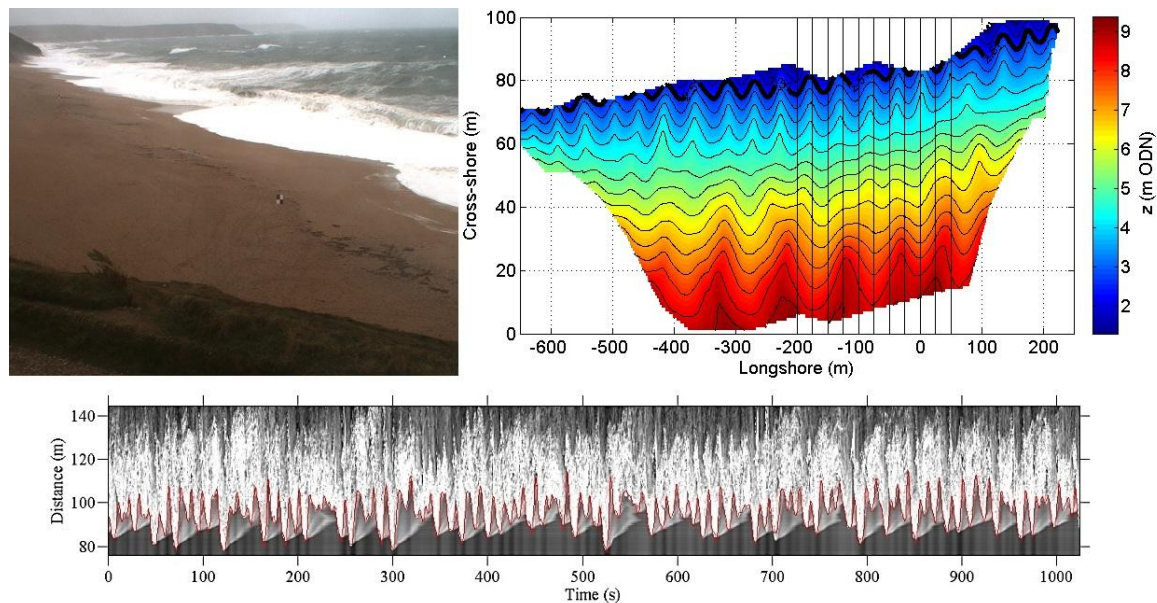


Figure 2. Camera view at Loe Bar (top left) and 3D supratidal surface morphology (during LB3). The morphology is overlaid with the location of cross-shore pixel stack transects which are presented in Figure 7, thick black contour marks Mean High Water Springs (MHWS), elevation ( $z$ ) above Ordnance Datum (ODN). Example pixel stack (bottom panel) with semi-automatic edge detection (red line).

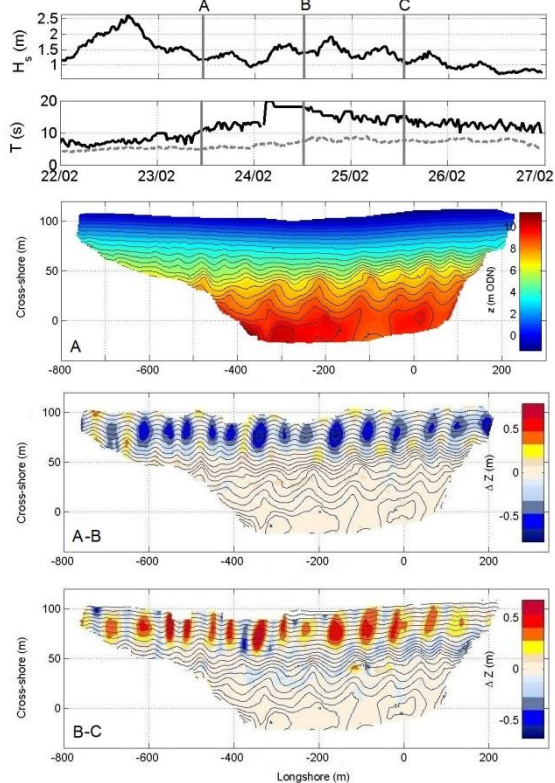


Figure 3. Morphological response during February LB1. From the top: significant wave height ( $H_s$ ); peak wave period ( $T_p$ , black), mean wave period ( $T_z$ , dashed grey), vertical grey lines indicate survey dates; 3D surface plot of initial morphology; and 3D surface plots showing morphological change ( $\Delta z$ ). In the lower two panels accretion is in red and erosion is in blue, and the contours represent the resulting morphology.

Swash dynamics were measured using digital video cameras (Pointgrey Grasshopper 2MP) mounted on the headland (Figure 2). The cameras were installed to provide an overview of the beachface and logged at a rate of 3 Hz during daylight hours. This approach provides the greatest flexibility for post-processing allowing various image “products” such as time-averaged images and pixel stacks to be generated for any temporal or spatial region of interest. In line with the topographic data, the video images were translated and rotated onto the local coordinate system for extraction of the runup. Pixel timestacks were generated for 17-min periods at regular alongshore intervals (Figure 2) to capture the variability in runup in response to the horn and embayment profiles of the cusp morphology. The two percent exceedance value ( $R_2$ ) was derived in line with previous work by Stockdon *et al.* (2006). A semi-automatic process was used to map the cross-shore position of the swash with the vertical runup extent related to the still water level for that time period (Figure 2).

Local water levels were logged using a single RBR® TWR 2050 wave-tide recorder logging at 4 Hz deployed at mean low water spring (MLWS).

## RESULTS

The first dataset, LB1 (Figure 3), was characterised by steady wave heights, somewhat tidally modulated, with  $H_s$  between 1.5 m and 2 m, while the peak wave period ( $T_p$ ) increased rapidly from 12 to 20 seconds on 24 February. Initially, and shown in Figure 3 (A), the beach was characterised by larger (secondary) cusps

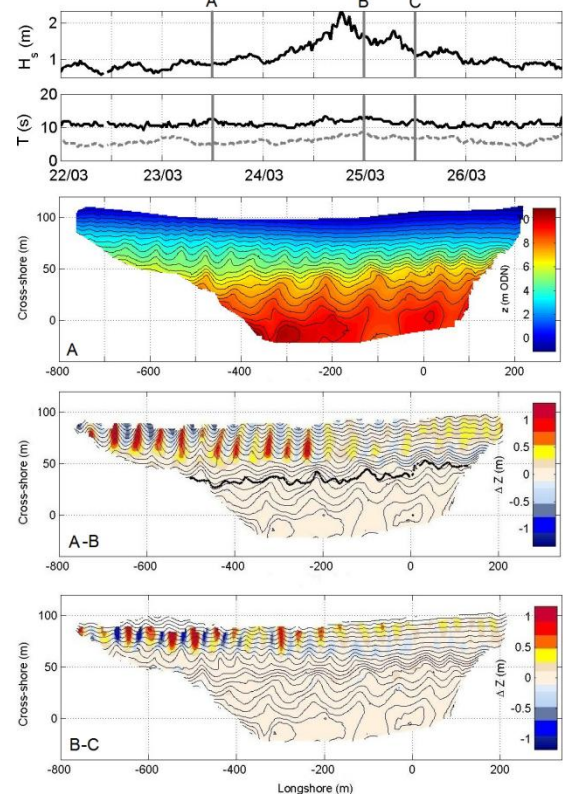


Figure 4. Morphological response during March LB2. From the top: significant wave height ( $H_s$ ); peak wave period ( $T_p$ , black), mean wave period ( $T_z$ , dashed grey), vertical grey lines indicate survey dates; 3D surface plot of initial morphology; and 3D surface plots showing morphological change ( $\Delta z$ ). In the lower two panels accretion is in red and erosion is in blue, and the contours represent the resulting morphology.

across the upper beach ( $> 6$  m ODN) while the lower beach ( $< 4$  m ODN) was highly planar. Figure 3 (A-B) shows the surface change in response to the arrival of the long period waves on 24 February, dominated by pockets of erosion across the lower beachface ( $\Delta z = c. 0.5$  m). The removal of material extends the secondary cusps, evident in the upper beach, down the profile, through deepening of the embayments. There are small patches of accretion on the cusp horns; however, the primary response is one of offshore movement of material from the embayments and subsequent increased cusp definition. During the following tide, the wave period drops while the wave height remains steady. This results in a recovery phase which mirrors the extent ( $\Delta z = c. 0.5$  m) and distribution of the erosive regions previously described. The accretion is focused on the cusp embayments, resulting in a return to the initial planar profile of the lower profile (Figure 3; B-C).

During the second event (LB2) the significant wave height increased from 1 m to 2.3 m while the peak wave period remained steady at 11 seconds. The initial morphological state was very similar to that observed during LB1 with a secondary cusp system at the upper section of the barrier and a highly planar lower profile (Figure 4; A). The surface change in response to the increased waves was characterised by rhythmic areas of accretion which acted to extend the cusps from the upper profile across the lower beach (Figure 4; A-B). The development of these accretionary features corresponds with the location of the cusp horns and yet there was little evidence of any deepening of the embayments as



observed during LB1. The following low tide revealed widespread smoothing of the lower profile, after wave heights reduced, with redistribution of material through erosion of the cusp horns and deposition within the embayments (Figure 4; B-C). The cusp dynamics during LB2 were most pronounced at the eastern part of the beach; this was also where the secondary cusp morphology on the upper beach was most pronounced.

The storm event recorded during LB3 (Figure 5), the second largest wave event at this site during 2012, peaked at a significant wave height of 5.83 m (9 m  $H_{max}$ ) with a peak wave period of 11 seconds. Initial morphology (Figure 5; A) consisted of rhythmic shallow cusps extending across the upper and lower profile. The response to the rapid increase in wave height was the widespread loss of material from the beachface with  $\Delta z = c. 1.75$  m vertical change observed; no accretion or onshore movement of material was evident (Figures 5; A-B). The secondary cusps across the upper section of the barrier were unaffected by this erosion, while the lower profile had become highly planar through removal of the cusp horns. During the following tide, the significant wave heights reduced to 2.5 m while the peak period remained constant. The subsequent survey shows the response was dominated by

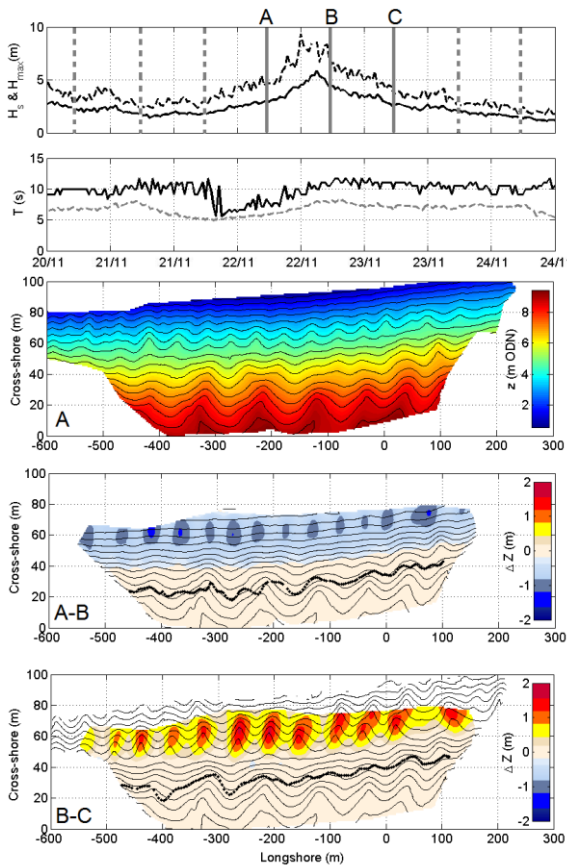


Figure 5. Morphological response during LB3. From the top; significant wave height ( $H_s$ , solid,  $H_{max}$ , dashed); peak wave period ( $T_p$ , black), mean wave period ( $T_z$ , dashed grey), vertical grey lines indicate survey dates presented in the panels below, vertical dashed lines indicate survey data presented in Figure 6; 3D surface plots show initial morphology and subsequent surface change ( $\Delta z$ ), with accretion shown in red and erosion shown in blue. Solid black line in A-B and B-C shows in-situ runup line. Contours in the lower two panels show the resulting morphology.

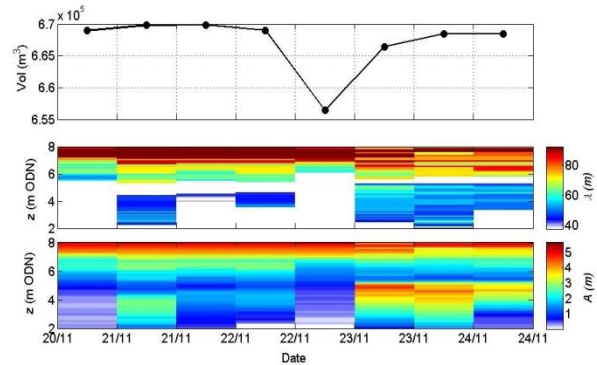


Figure 6. Beach volume and cusp dynamics during LB3. From the top: total beach volume ( $m^3$ ); cross-shore cusp wavelength ( $\lambda$ ); and cross-shore cusp amplitude ( $A$ ). White colour in the lower two panels indicates that cusp wavelength and amplitude could not be determined.

accretion across the lower barrier with  $\Delta z = 1.75$  m deposition and no evidence of removal from the upper profile (Figure 5; B-C). The accretion occurred in a rhythmic pattern, creating well defined horns as part of an established cusp system across the beachface.

### ANALYSIS

The change in volume and development/removal of the cusps system during LB3 is explored in more detail in Figure 6. The sharp drop in volume ( $12,600 m^3$ ) highlights the response to the increased wave conditions (Figure 6); however, the rapid recovery phase almost matches the total loss ( $10,050 m^3$ ). The cusp wavelength ( $\lambda$ ) and amplitude ( $A$ ; wavelength depth) also quantify the swift recovery phase through the cross-shore variation in cusp size (Figure 6). The beach remains stable from 20 November with some cusp definition increasing on 21 November; however, the removal of features across the lower beach between 22 and 23 November dominates the plot. The accretion which occurred on 23 November created a well-defined cusped system with a high amplitude (5 m) and a short wavelength (60 m). Some smoothing

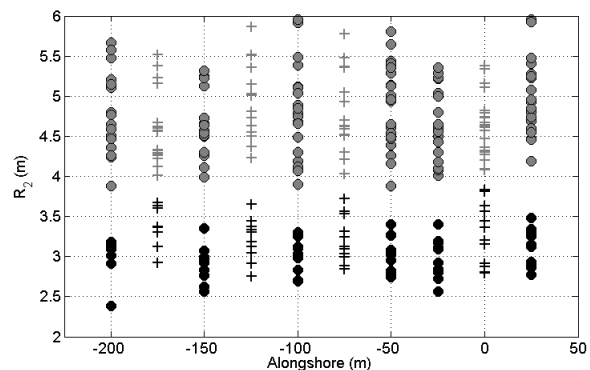


Figure 7. Alongshore variability in two percent exceedence runup values ( $R_2$ ) derived from video images during LB3. Circles identify cusp embayment locations and crosses represent cusp horns. Black symbols were recorded during calm conditions (21 November) and grey symbols represent energetic conditions (23 November). Pixel stack locations are shown in Figure 2.

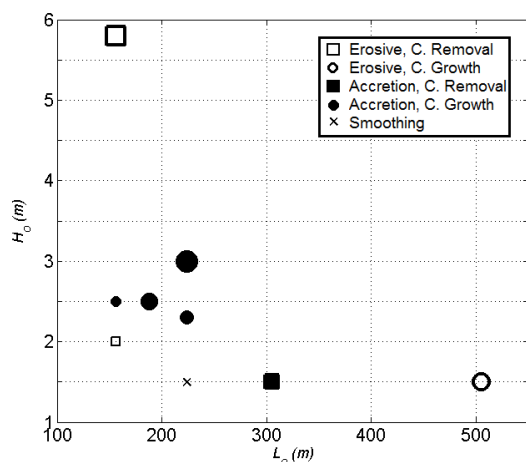


Figure 8. Distribution of cusp (C) response during LB1, 2 and 3 to different wave heights ( $H_o$ ) and wave length ( $L_o$ ). The size of the symbol infers the magnitude of the response.

of the cusps occurred in the following days; yet, these accretionary features still dominated the beachface (Figure 6).

The change in morphology during LB3 provides an excellent opportunity to study of the alongshore variability in runup during the different hydrodynamic conditions and cusp features. Under moderate waves at the start of LB3, runup is higher on the horns (0.5 m) driven by the difference in the profile steepness between the horns ( $\tan\beta = 0.181$ ) and the embayments ( $\tan\beta = 0.117$ ) (Figure 7). For energetic conditions during LB3 (23 November) the difference in  $R_2$  is less clear with embayments slightly higher than the horns. This pattern is likely to lead to smoothing of the cusps, which is evident in Figure 6, as the cusp wavelength and amplitude decreases on the 24 November.

## DISCUSSION

The generation and evolution of the cusp system at Loe Bar is strongly driven by the dominant wave conditions, acting on morphology which retains rhythmic features, with rapid growth and decay observed. The three events presented were characterised by different hydrodynamics and contrasting responses to the cusp morphology. In previous work (Masselink *et al.*, 2010) wave steepness has been used to explain gravel transport and beach response with low steepness waves ( $H_o/L_o = < 0.01$ ) associated with accretionary phases while high steepness short period waves generating erosive conditions ( $H_o/L_o = > 0.02$ ), where  $H_o$  is deepwater wave height and  $L_o$  is the deepwater wavelength. LB1 was dominated by very low steepness waves with  $H_o/L_o = 0.003$  at the arrival of the long period waves; however, the morphological response was erosive with material removed from the survey beach face. Recovery of the beach face followed waves steepening slightly with  $H_o/L_o = 0.005$ . Wave steepness during LB2 rose to  $H_o/L_o = 0.01$ , as the waves increased and the period remained short, which resulted in accretionary cusps developing. Subsequent smoothing of the cusps system followed the steepness decreasing ( $H_o/L_o = 0.007$ ) as the waves reduced. Erosive conditions dominated LB3 under large steep waves ( $H_o/L_o = 0.037$ ), while the rapid recovery occurred as the wave steepness reduced significantly to 0.013 during the following tide (Figures 5; B-C).

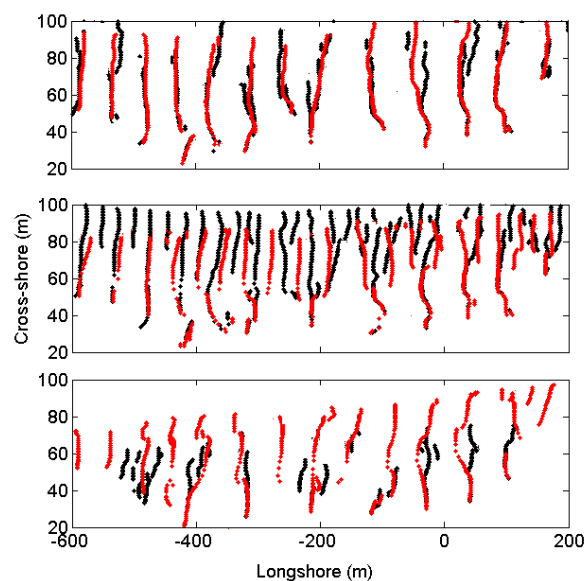


Figure 9. Cusp horn positions, extracted from surface contours at 0.25 m intervals, during “planar” states (black dots) and cusped states (red dots); From the top; LB1, LB2 and LB3.

The types of beach cusp responses, observed during the three events (LB1, LB2 and LB3) are shown with reference to the offshore wave height ( $H_o$ ) and wave length ( $L_o$ ) in Figure 8. The plot does not offer a clear pattern of behaviour which is due, in part, to the limited data points, but also due to the importance of the antecedent (cusp) morphology in driving the morphological response (i.e., free or self-organised behaviour).

The morphological response during LB1 is an embayment deepening erosive event dominated by horn divergent swash flows (Bagnold 1940, Russell and McIntire 1962, Dean and Maurmeier 1980) leading to cusp formation. Conversely LB2 is a horn accretionary event again resulting in cusp development (Dyer 1986). While the initial morphology during LB1 and LB2 was highly planar rhythmic features were still present. Identification of “horns” within this rhythmicity, and from the upper secondary cusped system, line up strongly with the resulting cusps which evolve (Figure 9). The large storm during LB3 also lead to a highly planar beach face, however, like LB1 and LB2 the resulting cusp features appear to develop in line with the secondary cusp system and previous horn locations, suggesting self-organised behaviour (Figure 9). This supports previous cusp observations under storm conditions which have led to removal of cusps or growth (horn divergence) (Miller *et al.*, 1989; Almar *et al.*, 2008; van Gaalen *et al.*, 2011).

What is unique, and not previously reported within the literature, is the rapid (12 hr) and extensive cusp growth which takes place following the storm. As conditions decrease, following the storm peak, onshore transport returns 80% of the sediment that was removed back onshore into the new cusp system. Holland *et al.* (1998) found a three-day lag in cusp development following a storm event at Duck, USA, a coarse sandy beach, while there are no comparable gravel cusp datasets available.

The behaviour of swash excursions, under moderate conditions, within a rhythmic cusp field are in line with previous runup studies which shows greater vertical swash under steeper (horn) slopes (Stockdon *et al.*, 2006) and suggest morphological feedback a dominant force over swash oscillations (Masselink and

Pattiaratchi, 1998), particularly under moderate waves. During energetic conditions the presence of cusps may help drive horn divergent flows to increase the embayment  $R_2$  (Figure 7), (Masselink *et al.*, 1998).

Each of the events presented focuses on the primary “active” cusp system located on the lower profile, while the secondary, larger, cusp system is located between 3 and 6 m above MHWS. Based on the observations presented here their generation could only come from a significant (likely decadal) event required to generate suitable swash excursions to reach this region and result in cusp formation. Whether they are created through removal of an upper berm (Antia, 1987), embayment deepening or horn deposits is unclear.

### CONCLUDING REMARKS

The formation and evolution of cusps remains a complex and divided issue with a combination of hydrodynamic and morphologic factors driving their development. There remains a lack of specific long term studies of cusp behaviour on gravel beaches; however, this paper has presented unique cusp response under moderate to storm waves;

- In contrast to earlier studies, this dataset does not show a simple relation between wave steepness and beach erosion and accretion. Wave steepness and cusp behaviour at Loe Bar include;
  - $H_0/L_0 < 0.003$  = Erosive swash (embayment deepening = cusp growth)
  - $0.003 > H_0/L_0 < 0.01$  = Accretionary swash (horn deposit = cusp growth)
  - $0.01 > H_0/L_0 < 0.03$  = Smoothing (cusp removal)
  - $0.03 > H_0/L_0$  = Erosive swash (cusp re-set)
- Existing cuspat morphology and “relic” rhythmicity accelerates cusp development
- Rapid gravel cusp growth (<12hrs)

Longer monitoring studies, at different gravel sites, incorporating a range of grain sizes and beach slopes, utilising the methodology outlined above, would be a great addition to any future cusp work. These observations not only highlight the resilience and stability of gravel barriers to extreme waves but also highlight their relevance as responsive and dynamic sites.

### ACKNOWLEDGEMENT

This work was funded by the Engineering and Physical Sciences Research Council (EPSRC) grant EP/H040056/1 in partnership with the Channel Coastal Observatory (CCO), HR Wallingford and The Environment Agency. The authors would like to thank all those who helped with the field work: Pedro Almeida, Peter Ganderton, Jack Puleo. RM would like to acknowledge support given by Deltas under the Strategic Research Projects 1204516 and 1202362.

### LITERATURE CITED

Almar, R.; Coco, G.; Bryan, K.R.; Huntley, D.A.; Short, A.D. and Senechal, N., 2008. Video observations of beach cusp morphodynamics, *Journal of Marine Geology*, 254, 216–223.

Antia, E.E., 1987. Preliminary field observations on beach cusp formation and characteristics on tidally and morphodynamically distinct beaches on the Nigerian coast. *Mar. Geol.*, 78, 23–33.

Bagnold, R.A., 1940. Beach formation by waves: some model experiments in a wave tank. *J. Inst. Civ. Eng. Pap.*, 5237, 27–52.

Buscombe, D., and Masselink, G., 2006. Concepts in Gravel Beach Dynamics. *Earth Science Reviews*, 79, 33–52.

Coco, G., O'Hare, T., Huntley, D., 1999. Beach cusps: a comparison of data and theories for their formation. *Journal of Coastal Research*, 15, 741–749.

Dean, R.G., Maurmeyer, E.M., 1980. Beach cusps at Point Reyes and Drakes Bay beaches, California. Proc. 17th Int. Gould, J., Eliot, I.G., 1997. *Conf. Coastal Engineering*, ASCE, pp. 863–884.

Dyer, K.R., 1986. *Coastal and Estuarine Sediment Dynamics*, Wiley and Sons, Chichester.

van Gaalen, J.F., Kruse, S.E., Coco, G., Collins, L. and Doering, T., 2011. Observations of beach cusp evolution at Melbourne Beach, Florida, USA. *Geomorphology*, 129, 131–140.

Holland, K.T., Holman, R.A., 1996. Field observations of beach cusps and swash motions. *Mar. Geol.*, 134, 77–93.

Guza, R.T., Inman, D.L., 1975. Edge waves and beach cusps. *Journal of Geophysical Research*, 80(21), 2997D3012.

Komar, P.D., 1973. Observations of beach cusps at Mono Lake, California. *Geological Society of America Bulletin*, 84(11), 3593D3600.

Masselink, G., Pattiaratchi, C.B., 1998. Morphological evolution of beach cusp morphology and associated swash circulation patterns. *Mar. Geol.*, 146, 93–113.

Masselink, G., Hegge, B.J. and Pattiaratchi, C.B., 1997. Beach cusp morphodynamics. *Earth surface processes and landforms*, 22(12): 1139–1155.

Masselink, G., Russell, P., Blenkinsopp, C.E., Turner, I.L., 2010. Swash zone sediment transport, step dynamics and morphological response on a gravel beach. *Marine Geology*, 274(1–4), 50–68.

Miller, J.R., Miller, S.M.O., Torzynski, C.A., Kochel, R.C., 1989. Beach cusp destruction, formation, and evolution during and subsequent to an extratropical storm, Duck, North Carolina. *J. Geol.*, 97(6), 749–760.

Nolan, T.J., Kirk, R.M., Shulmeister, J., 1999. Beach cusp morphology on sand and mixed sand and gravel beaches, South Island, New Zealand. *Mar. Geol.*, 157, 185–198.

Plant, N.G., Holland, K.T., Puleo, J.A., 2002. Analysis of the scale of errors in nearshore bathymetric data. *Marine Geology*, 191(1–2), 71–86.

Poate, T., Masselink, G., Davidson, M., McCall R., Russell, P., Turner, I., 2013. High frequency in-situ field measurements of morphological response on a fine gravel beach during energetic wave conditions. *Marine Geology*, 342(0), 1–13.

Russell, R.J., McIntire, W.G., 1965. Beach cusps. *Geol. Soc. Am. Bull.*, 76, 307–320.

Stockdon, H.F., Holman, R.A., Howd, P.A., Asbury, H.S., 2006. Empirical parameterization of setup, swash, and runup. *Coastal Engineering*, 53(7), 573–588.

Werner, B.T., Fink, T.M., 1993. Beach cusps as self-organised patterns. *Science*, 260, 968–971.

# The Grand Popo beach 2013 experiment, Benin, West Africa: from short timescale processes to their integrated impact over long-term coastal evolution



[www.cerf-jcr.org](http://www.cerf-jcr.org)

Rafael Almar<sup>†</sup>, Norbert Hounkonnou<sup>‡</sup>, Edward J. Anthony<sup>∞</sup>, Bruno Castelle<sup>§</sup>, Nadia Senechal<sup>§</sup>, Raouf Laibi<sup>+</sup>, Trinity Mensah-Senoo<sup>#</sup>, Georges Degbe<sup>@</sup>, Mayol Quenum<sup>‡</sup>, Matthieu Dorel<sup>†</sup>, Remy Chuchla<sup>†</sup>, Jean-Pierre Lefebvre<sup>†</sup>, Yves du Penhoat<sup>†</sup>, Wahab Sowah Laryea<sup>#</sup>, Gilles Zodehougan, Zacharie Sohou<sup>@</sup>, Kwasi Appeaning Addo<sup>#</sup>, Raimundo Ibaceta<sup>†\*</sup>, Elodie Kestenare<sup>†</sup>

<sup>†</sup>IRD-LEGOS  
Université Paul  
Sabatier/CNRS/CNES/IRD  
Toulouse, France  
rafael.almar@ird.fr  
matthieu.dorel@ird.fr  
remy.chuchla@ird.fr  
jean-pierre.lefebvre@ird.fr  
Yves.Du-Penhoat@ird.fr  
elodie.kestenare@ird.fr

<sup>§</sup>EPOC  
Université de Bordeaux/CNRS  
Talence, France  
b.castelle@epoc.u-bordeaux1.fr  
n.senechal@epoc.u-bordeaux1.fr

<sup>@</sup> IRHOB  
Cotonou, Republic of Benin  
gdegbe@yahoo.fr  
zsohou@yahoo.fr

<sup>‡</sup> University of Abomey-Calavi  
ICMPA-UNESCO Chair  
International Chair in Mathematical  
Physics and Applications  
Cotonou, Republic of Benin  
norbert.hounkonnou@cipma.uac.bj  
malgdaq2000@yahoo.fr

<sup>+</sup> Université Abomey Calavi  
Département des Sciences de la Terre,  
Faculté des Sciences et Techniques  
Cotonou, Republic of Benin  
raoulaibi@yahoo.fr

<sup>\*</sup>Universidad Técnica Federico Santa  
Maria, Valparaíso, Chile  
raimundo.ibaceta@alumnos.usm.cl

<sup>∞</sup> Aix-Marseille Université, IUF,  
CEREGE, UMR 34 Europôle de l'Arbois,  
B.P. 80, 13545 Aix en Provence cedex 04,  
France  
anthony@cerge.fr

<sup>#</sup> University of Ghana  
Department of Marine and Fisheries  
Sciences,  
Accra, Ghana  
tri\_box3@hotmail.com  
kappeaning-addo@ug.edu.gh  
sowah\_laryea@yahoo.com



[www.JCRonline.org](http://www.JCRonline.org)

## ABSTRACT

Almar, R., Hounkonnou, N., Anthony, E., Castelle, B., Senechal, N., Laibi, R., Mensah-Senoo, T., Degbe, G., Quenum, M., Dorel, M., Chuchla, R., Lefebvre, J-P, du Penhoat, Y., Laryea, W.S., Zodehougan, G., Sohou, Z., and Appeaning Addo, K., Kestenare, E., 2014. The Grand Popo beach 2013 experiment, Benin, West Africa: from short timescale processes to their integrated impact over long-term coastal evolution. *In: Green, A.N. and Cooper, J.A.G. (eds.), Proceedings 13<sup>th</sup> International Coastal Symposium* (Durban, South Africa), *Journal of Coastal Research*, Special Issue No. 70, pp. 651-656, ISSN 0749-0208.

The first large nearshore field experiment in the Gulf of Guinea was conducted at Grand Popo Beach, Benin, in February 2013, on an open wave-dominated micro- to meso-tidal coast, located mid-way between Cotonou and Lome harbours. The overall project aims at understanding at multi-scale (from event to interannual) the causes of the dramatic erosion observed throughout the Bight of Benin, and caused by the interaction of a large littoral drift with human engineering works. Grand Popo 2013 experiment was designed to measure the processes over the short term and to test the ability of an installed video system to monitor the evolution of this stretch of coast over the longer term. The beach, characterized by a low-tide terrace and a high tide reflective part, experiences a long swell ( $H_s=1.6$  m,  $T_p=16$  s, oblique incidence  $\sim 15-20^\circ$ ). Topographic surveys showed a double beach cusp system interaction and repeated surf-zone drifter runs revealed high flash and swash rip activity driven by wave dissipation over the terrace and energetic swash dynamics at the upper reflective beach. Swash was measured over a cusp system at two locations using video poles. Wave reanalyses (ERAInterim) were used to determine the wave climate and its variability, and to quantify sediment transport. This robust methodology is thought to be replicated elsewhere in different coastal environments in West Africa, in particular with the objective to monitor various sites within the framework of the new West African Coastal Observatory.

**ADDITIONAL INDEX WORDS:** low-tide terrace, long swell, micro-meso tidal environment, beach cusps, energetic swash, wave reflection, littoral drift, Gulf of Guinea, erosion

## INTRODUCTION

Multi-scale coastal evolution is poorly known, mainly due to lack of observational datasets, and this is even more pertinent on

tropical coasts. Understanding the processes responsible for coastal evolution at different timescales is crucial for socio-economic development, especially in the present context of vulnerability to climate change. 80 % of the economic activity of the Gulf of Guinea countries is concentrated along the coast,

DOI: 10.2112/SI70-110.1 received 29 November 2013; accepted 21 February 2014. © Coastal Education & Research Foundation 2014

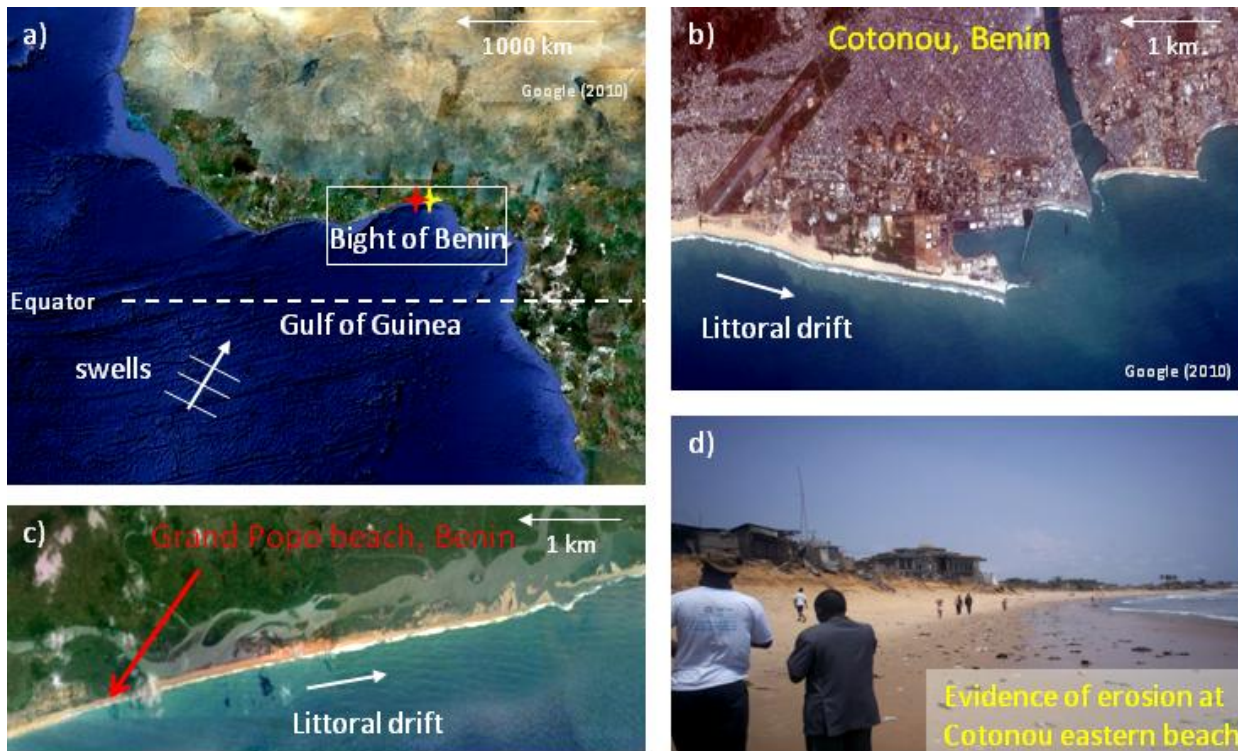


Figure 1. The Bight of Benin coast. a) regional map, with red and yellow crosses indicating respectively the study site at Grand Popo, and the city of Cotonou b) part of the city of Cotonou showing the main harbour breakwater with updrift accretion and downdrift erosion, c) Grand Popo beach and d) a picture of Cotonou showing beach erosion.

together with large population densities (main cities: Abidjan, Accra, Lomé, Cotonou, Lagos). Erosion in Cotonou currently reaches 10 m/year (Dossou and Glehouenou-Dossou, 2007) due to recent coastal constructions (i.e. harbour jetty, see Addo *et al.*, 2011, Angnuureng *et al.*, 2013; Laïbii *et al.*, this issue). It is important to move towards more integrated coastal zone management, and a first step is to adequately characterise the natural coastal system, the prevailing processes and their integrated effects. In this framework, an international project has been designed to better understand the processes responsible for the observed erosion and monitor the long term evolution of this stretch of coast.

We believe that our observations are crucial, not only to understand the causes of erosion in the Gulf of Guinea (Anthony and Blivi, 1999; Blivi *et al.*, 2002; Blivi and Adjoussi, 2004), but to improve our fundamental knowledge on the morphodynamics of low-tide terrace beaches (Wright and Short, 1984). These beaches are mostly described in the literature for micro-tidal and fairly low energetic waves and remain poorly documented in energetic swell-wave dominated environments. As such, our project has the following specific objectives:

1) **Describe nearshore wave-driven circulation (scale  $L \sim 10$  m,  $T \sim$ hour).** This is conducted through the characterization of both alongshore currents and more variable cross-shore currents (e.g. flash and cusp rips), the influence of relative tide, wave conditions, and interactions between swash and surf zone processes.

2) **Explore the small-scale swash zone hydro-morphodynamics ( $L \sim$ metre,  $T \sim$ second).** How is wave energy transferred to lower frequencies, and energy dissipated and reflected in the swash zone (see the current research challenges proposed by Brocchini and

Baldock, 2008)? This includes the study of individual swash and swash-to-swash interactions and the influence of tide in generating beach slope changes in the course of the tidal excursion. The objective is also to be able to monitor bed evolution at the swash event scale, and wave groups, and link these events to longer-term beach profile evolution.

3) **Characterize beach cups dynamics and beach profile evolution ( $L \sim 10$  m,  $T \sim$ hour to day).** Routine field observations show that the Gulf of Guinea beaches remain most of the time in the Low Tide Terrace state, following the beach morphodynamic classification of Wright and Short (1984) and the dominant variability is due to the upper beach alternating from rather alongshore-uniform to a periodically steep morphology. The conditions for these transitions and the mechanisms involved are still poorly known, as well as the influence of antecedent morphology; this includes, for instance mechanisms involved in the construction and interaction of stacked beach cusp systems (Vousdoukas, 2013).

4) **Establish at a longer timescale the link between wave forcing, littoral drift and morphological evolution ( $L \sim 10$  km,  $T \sim$ month to decades).** The understanding of the integrated effect of short-scale processes is crucial although linking these scales remains a challenging task. To address this aspect, we provide a general description of the Gulf of Guinean morphological system and its wave forcing. This includes an analysis of the strong wave's variability at seasonal and interannual scales, as well as littoral drift.

In this paper we provide an overview of the project, including objectives, field experiment set-up, long term video monitoring system, and main achievements up to now. Closely related to the project are three other papers. The first gives a general overview

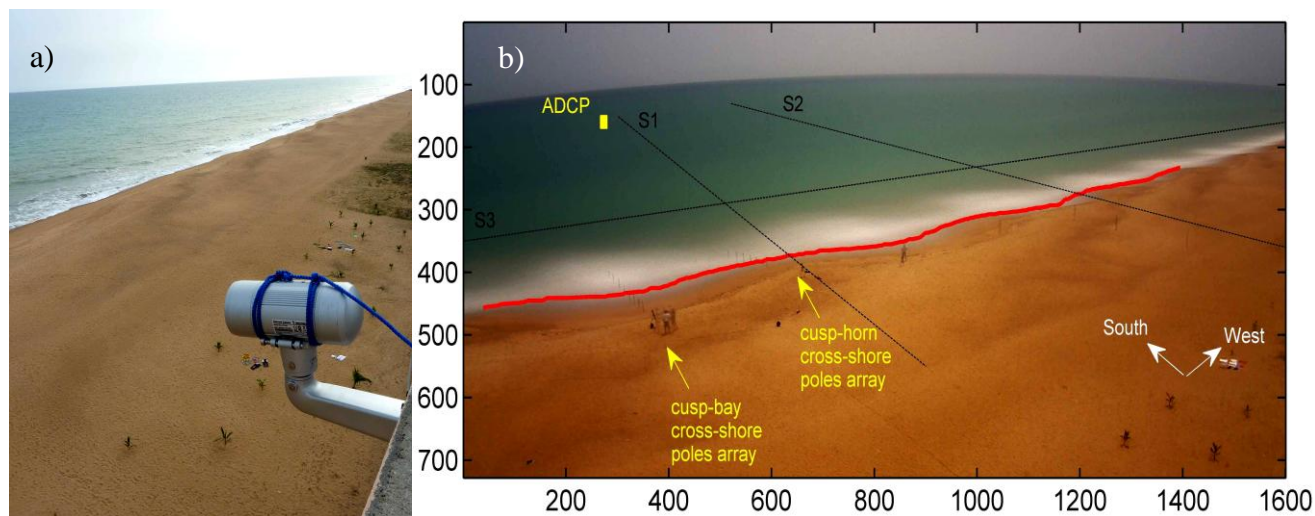


Figure 2. a) Grand Popo video system and b) a 15-min time-averaged image. Black lines stand for the time stack image locations (2 cross-shore and 1 alongshore), red line is the shoreline automatically detected using method described in Almar et al., 2012a. Pole arrays in the instrumented cusp (horn and bay) are visible in the left part of the image.

of the Bight of Benin beach system (Laïbi et al., this issue), whereas the other two address, respectively, the dynamics of double beach cusps (Senechal et al., this issue) and the occurrence of flash and swash rips (Castelle et al., this issue) at the Grand Popo beach experimental site, described below.

### STUDY SITE

The field study was conducted in 2013 at Grand Popo beach (6.2°N, 1.7°E, Figure 1) in Benin, Gulf of Guinea, midway (80 km) between Cotonou (Benin) and Lomé (Togo). Like much of the Bight of Benin coast, Grand Popo beach bounds a sand barrier system extending from Ghana to Nigeria (Anthony and Blivi, 1999; Anthony et al., 2002). Grand Popo is representative of the beaches of the Bight of Benin. This bight coast is an open wave-dominated and microtidal environment (from 0.3 m to 1.8 m for neap and spring tidal ranges, respectively) exposed to long period swells (ECMWF 1957-2013 annual wave averages:  $H_s=1.36$  m,  $T_p=9.4$  s,  $Dir=S-SW$ ) generated at high latitudes in the South Atlantic. The beach (Figures 2 and 3) presents an alongshore-uniform low tide terrace (LTT) and a steep and rather alongshore-uniform lower beachface and persistent upper beachface cusped morphology cut into a well-developed berm. The grain size is medium to coarse ( $D_{50} = 0.6$  mm). An eastward littoral drift of 0.8 to 1.5 m<sup>3</sup>/yr has been reported in the literature (Tastet et al., 1985; Anthony and Blivi, 1999; Blivi et al., 2002), driven by persistent oblique long swells year-round.

### DATA

#### Grand Popo beach 2013 experiment

As a first step in setting up a robust methodology to be replicated, a field experiment was conducted at Grand Popo beach from 17 to 28 February 2013. The experiment was designed both to measure beach changes at the short timescale and to test the applicability of a low-cost video monitoring system. Incident waves were measured with an acoustic Doppler current profiler (ADCP RDI WORKHORSE) moored on the shoreface at a depth of 8 m (Figure 3). Surf zone currents were measured by means of repeated human operators acting as drifters (~10 runs per series)

daily, at selected moments, over the entire experiment duration (see Castelle et al., this issue, for a description of the method). Swash was measured over a beach cusp system (~30-m wavelength, Figure 2) along two cross-shore transects, in a cusp bay and horn. This was done using conventional pressure sensors (10 NKE SP2T10-SI) and a new technique of dense arrays of poles deployed on the beach. Measurements were conducted daily over daylight hours. Water surface and bed vertical levels were monitored using 2 high frequency video cameras HD (SONY HDR-CX 250, 30 Hz, 1920x1080 pixels, Figure 4). These levels are detected through colour band divergence at the transition between the pole painted in black, the reddish beach sand, and the white-blue water (Figures 4.b, 4.c). A large-scale bathymetric survey was also conducted on the last day of the experiment using an echosounder (GARMIN GPS MAP526S) mounted on a fishing

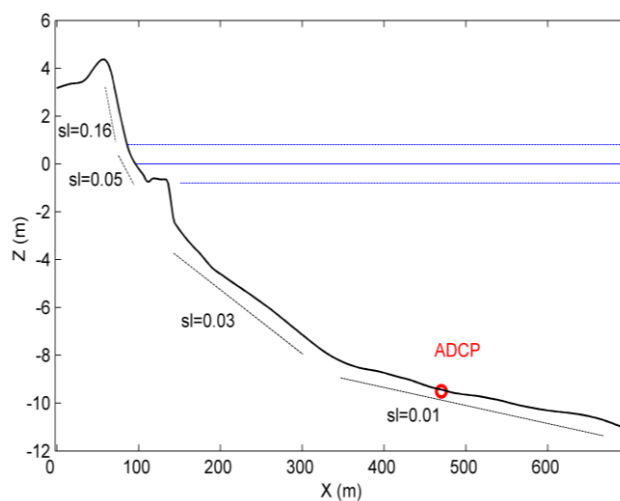


Figure 3. Alongshore-averaged bathymetric cross-shore profile at Grand Popo.  $Z = 0$  m, the mean water level (solid blue line), dashed blue lines are spring high and low tide levels ( $\pm 0.8$  m). Dashed black lines stand for local slopes.

boat (Figure 3). Elevations were corrected from the tidal elevations of the ADCP measurements and the Cotonou harbour gauge. Beach surveys were performed daily using a GPS (TOPCON, post-processed using PPP - Precise Point Positioning, see Ebner and Featherstone, 2008). Atmospheric data (wind and pressure) are provided by the Cotonou Airport weather services (<http://rp5.ru/>).

### Offshore wave data

Wave data (Total Swell, wind waves,  $H_s$ ,  $T_p$  and  $Dir$ ) in deep water were extracted from the ECMWF ERAinterim reanalyses (Dee *et al.*, 2011) from the ECMWF data server ([www.ecmwf.int/research/era](http://www.ecmwf.int/research/era)) which are on a  $1 \times 1^\circ$  grid and based on the WAM model. Data are available from 1979 to the present, with a 6-hr temporal resolution.

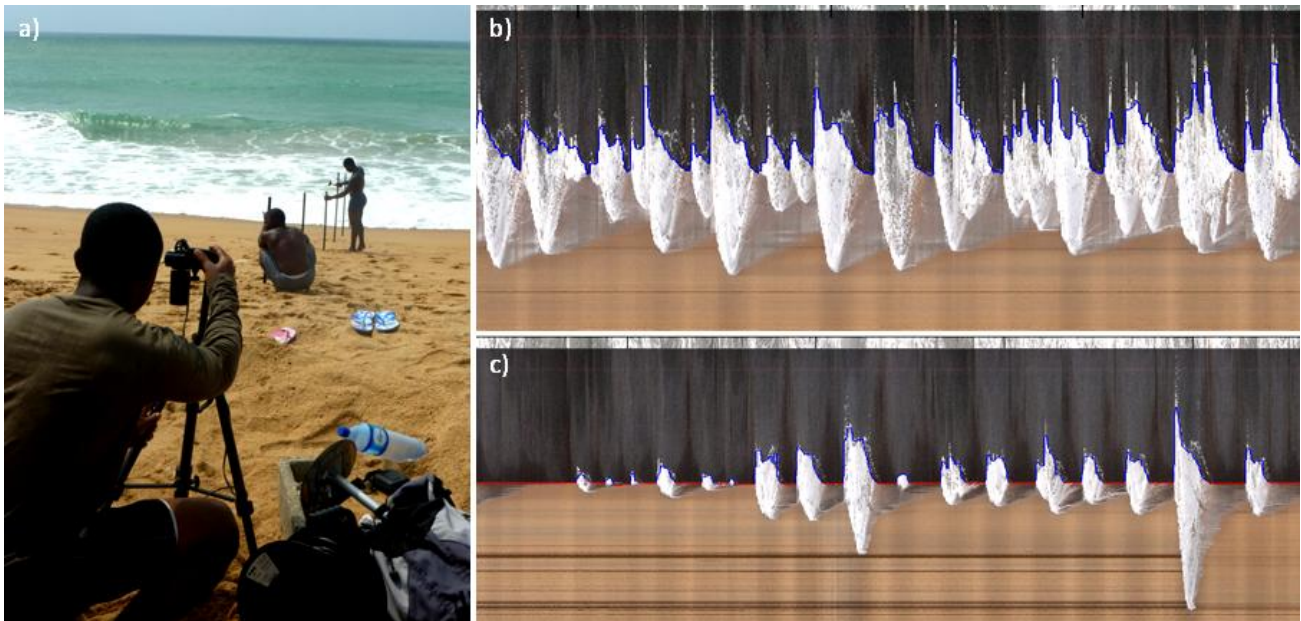


Figure 4. Illustration of the high frequency video/poles measurements. a) Camera mounted on a tripod on the berm aligned with a cross-shore transect of poles and results of a 30 Hz vertical time stack ( $\sim 1$  min) on poles located in the lower (b) and upper (c) swash zone.

### Permanent video system

In parallel, a long-term video station was deployed (camera VIVOTEK IP7361,  $1600 \times 1200$  pixels, Figure 2.a) on a 15 m-high semaphore belonging to the navy of the Republic of Benin, 80 m distant from the shore (i.e. which is the approximate beach width). This autonomous system is powered by a solar panel. A computer on site processes the raw images and store data. Three types of secondary images are stored: instant, 15-min averages (Figure 2.b, and time stacks (Figure 6). 3 time stacks are generated, 2 across-shore, to cope with alongshore non-uniformity, and 1 alongshore, offshore of the low-tide terrace, at the breaker point (Figure 2). This station gives continuous and long-term information on beach morphological change as well as on waves, tides and currents. During the experiment, 2 Hz raw videos were stored.

Rectification of images from pixels into real world coordinates was accomplished by direct linear transformation using GPS ground survey points (Holland *et al.*, 1997) after a correction of the lens radial distortion (Heikkila and Silven, 1997). Although varying somewhat throughout the field of view, the pixel footprint was less than 0.1 and 0.05 m in the region of interest (surf-swash zones of the instrumented cusp) for cross-shore and alongshore direction, respectively.

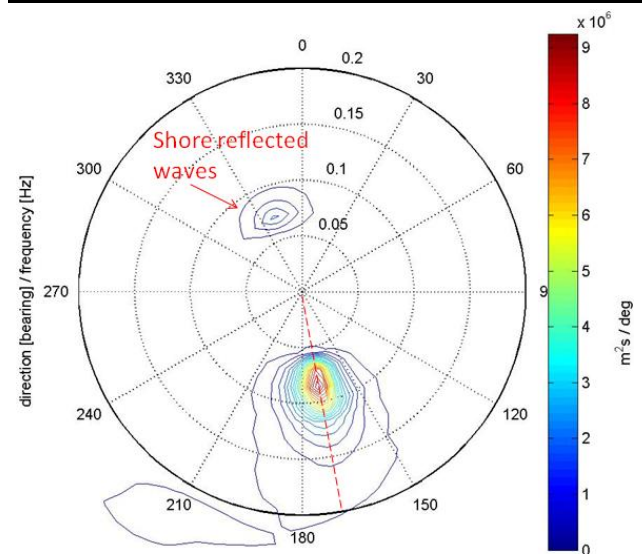


Figure 5. Average energy spectrum from the ADCP over the experiment duration. Red dashed line is the shore normal direction.

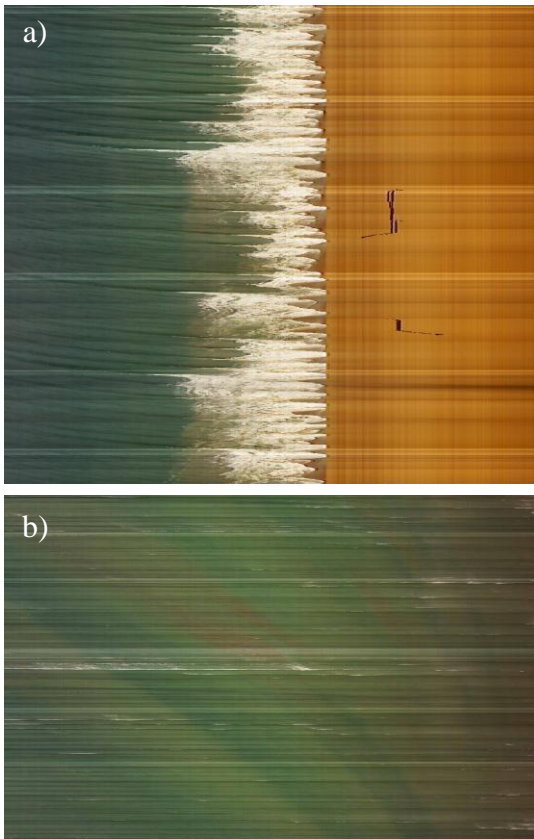


Figure 6. Secondary images from the video system. a) Cross-shore and b) along-shore time stacks.

## PRELIMINARY RESULTS

Various aspects of the experiment are discussed by Senechal et al., (this issue) and Castelle et al. (this issue). Here, some of the results recorded by the ADCP and obtained from the swash poles are presented.

Figure 7 shows the long swell conditions at Grand Popo beach from 22 to 26 March. A noteworthy element is that the long distance between the swell generation zone in the South Atlantic and Grand Popo beach results in the the maximum in peak wave period  $T_p$  preceding that of the significant wave height  $H_s$  for about 3 days, which is long compared to the lag generally encountered elsewhere in smaller oceanic basins. Another key specificity of this site is that the energy spectrum (Figure 5) reveals a large shore reflection of incoming swell waves energy ( $8 \text{ s} < T_p < 20 \text{ s}$ ), the swash playing the role of a low-pass filter (see Almar et al., 2012b). A time series (not shown) of this reflection value denotes a large influence of both incoming period and tidal level; the reflection peaking when the swash occurs on the steep upper beachface and when breaking in the surf zone is reduced.

The recently developed method of video pole arrays (Figures 4 and 8, see also Lefebvre et al., this issue, for a description) shows good skills at describing both bed and swash elevation. This set up enables a description of the wave-by-wave impact of breakers on the beach morphology, and swash energy frequency-transfer and reflection. Large variations (of the order of 1 to 10 cm) of the bed level are observed at periods longer than group periods (typically 5 – 10 min), suggesting a substantial morphological control on swash-surf zone dynamics. This will be further investigated.

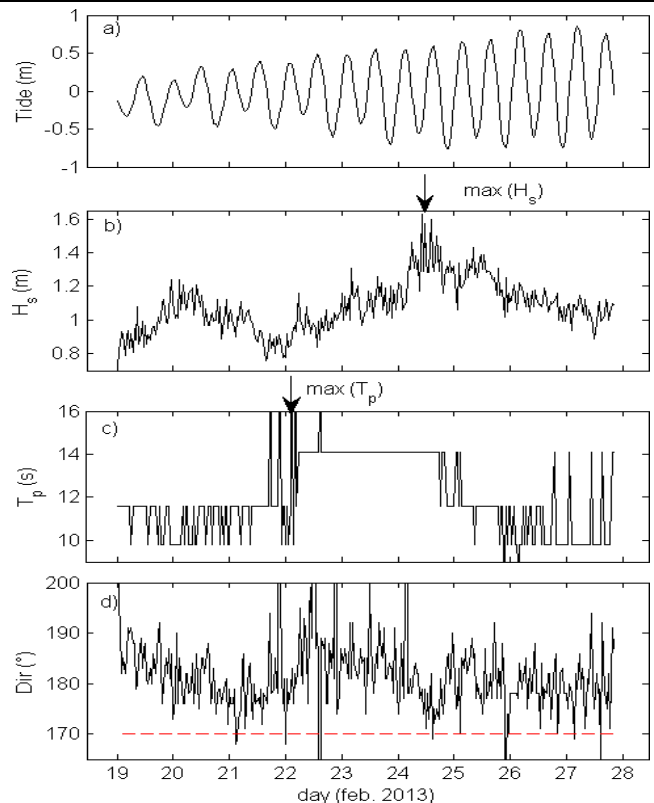


Figure 7. Hydrodynamic conditions recorded by the ADCP from 19 to 28 Feb. 2013. a) tidal elevation, b) significant wave height  $H_s$ , c) peak period  $T_p$  and d) peak direction  $Dir$ . Red dashed line stands for shore-normal incidence.

The first results on the wave climatology characterization using reanalyses indicate a strong seasonal and interannual variability. Monthly swell and wind waves are significantly correlated at -0.2 with the South Antarctic Modulation (SAM) and at 0.4 with the Intertropical Convergence zone (ITCZ), respectively.

## CONCLUDING REMARKS

The Grand Popo 2013 experiment, the first of such importance to be conducted in the Gulf of Guinea, took place from 17 to 28 February 2013 and involved 17 scientists from 7 institutions in Benin, Ghana and France. The experiment was aimed at describing processes at event scale responsible for observed dramatic erosion in the Gulf of Guinea and placed emphasis on a description of the nearshore circulation (pulsations or rips), morphological interactions between stacked cusps systems, and swash hydro- and morphodynamics including energy dissipation, reflection and bed level change. The experiment also involved the testing of an original video monitoring system. At a larger scale, empirical and quantitative (from ECMWF reanalyses) results were obtained, allowing a global description of the Bight of Benin wave forcing and coastal behaviour.

It is still too early to draw conclusions on seasonal and interannual patterns of the evolution of this stretch of coast, but the quantitative information obtained from such permanently operating low-cost coastal video systems is key to building long-term robust systems of observation and analysis of beach dynamics and long-term coastal stability in the region. Following the success of this first system, similar video monitoring systems are currently being deployed along the West Africa coast within



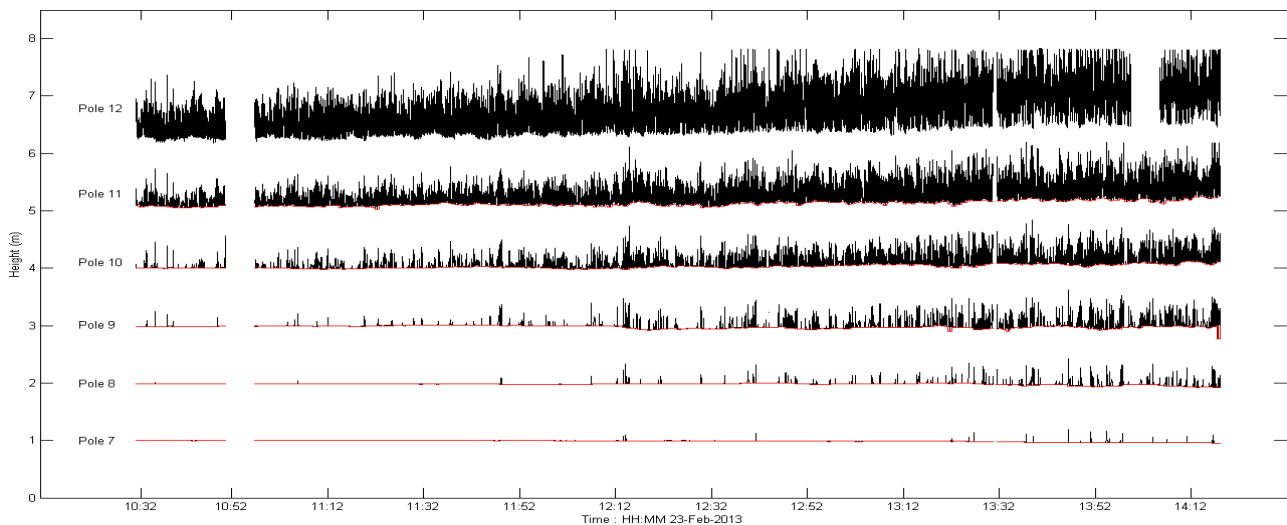


Figure 8. Illustration of the bed/swash detection at the 6 poles of a cross-shore line (23 feb. 2013). Black and red lines are water and bed levels, respectively.

the framework of the recently set up West African Coastal Observatory (MOLOA) and ALOC-GG projects. The current overall project methodology thus provides a basis for replicated elsewhere in West Africa in the next years.

#### ACKNOWLEDGEMENT

This study was funded by the French INSU LEFE and EC2CO programs, the IRD (Action Incitative program), and the UNESCO co-chair CIPMA. We benefited the ECMWF ERA Interim dataset ([www.ECMWF.Int/research/Era](http://www.ECMWF.Int/research/Era)), made freely available. We are greatly indebted to the naval services of Benin at Grand Popo for their logistic support during the field experiment and for allowing the installation of the permanent video system on the semaphore.

#### LITERATURE CITED

- Addo, K.A., Jayson-Quashigah, P.N., Kufogbe, K.S., 2011. Quantitative analysis of shoreline change using medium resolution satellite imagery in Keta, Ghana. *Marine Science*, 1, 1-9.
- Almar R., Ranasinghe R., Senechal N., Bonneton P., Roelvink D., Bryan K., Marieu V., Parisot J.P., 2012. Video based detection of shorelines at complex meso- macrotidal beaches, *Journal of Coastal Research*. COAS\_49646, vol. 28(5), 1040-1048.
- Almar, R., Cienfuegos, R., Gonzalez, E., Catalán, P., Michallet, H., Bonneton, P., Castelle, B., & Suarez, L., 2012. Barred-beach morphological control on infragravity motion. *Coastal Engineering Proceedings*, 1(33), currents.24. doi:10.9753/icce.v33.currents.24
- Angnuureng B.D., Appeaning, A.K. and Wiafe, G., 2013. Impact of sea defense structures on downdrift coasts: The case of Keta in Ghana. *Acad. J. Environ. Sci.*, 1(6), 104-121.
- Anthony, E.J., Blivi, A.B., 1999. Morphosedimentary evolution of a delta-sourced, drift-aligned sand barrier-lagoon complex, western Bight of Benin. *Marine Geology*, 158, 161-176.
- Anthony, E.J., Oyede, L.M., Lang, J., 2002. Sedimentation in a fluvially infilling, barrier-bound, estuary on a wave-dominated, microtidal coast: The Ouémé River estuary, Benin, West Africa. *Sedimentology*, 49, 1095-1112.
- Blivi, A., Anthony, E.J., Oyédé, L.M., 2002. Sand barrier development in the Bight of Benin, West Africa, *Ocean & Coastal Management*, 45, 185-200.
- Blivi, A.B., and Adjoussi, P., 2004. Moving of the Togo shoreline detected by remote sensing. *Geo-Eco-Trop*, 28(1-2), 27-38
- Brocchini, M., and Baldock, T.E., 2008. Recent advances in modeling swash zone dynamics: Influence of surf-swash interaction on nearshore hydrodynamics and morphodynamics, *Rev. Geophys.*, 46, RG3003, doi: 10.1029/2006RG000215
- Castelle, B., Almar, R., Dorel, M., Lefebvre, J-P, Sénéchal, N., Anthony, E., Laibi, R., Chuchla, R., du Penhoat, Y., 2014. Flash rip dynamics on a high-energy low-tide-terraced beach (Grand Popo, Benin, West Africa) *In Proceedings 13th International Coastal Symposium (Durban, South Africa)*, *Journal of Coastal Research, Special Issue No. 66*.
- Dee D. P. et al., 2011. The ERA-Interim reanalysis: configuration and performance of the data assimilation system, *Q. J. R. Meteorol. Soc.* 137, 553–597, doi:10.1002/qj.828
- Dossou, K. and Glehouenou-Dossou, B., 2007. The vulnerability to climate change of Cotonou (Benin): the rise in sea level. *Environment and Urbanization*, 19(1), 65-79.
- Ebner, R., Featherstone, W.E., 2008. How well can online GPS PPP post-processing services be used to establish geodetic survey control networks? *Journal of Applied Geodesy*, 2, 149-1576.
- Heikkila, J., Silven, O., 1997. A four-step camera calibration procedure with implicit image correction, *Computer Vision and Pattern Recognition. In Proceedings of the IEEE Computer Society Conference from 17-19 Jun 1997*, 1106-1112.
- Holland, K.T., Holman, R.A., Lippmann, T.C., Stanley, J., Plant, N., 1997. Practical use of video imagery in nearshore oceanographic field studies. *Oceanic Engineering* 22(1), 81–92.
- Laibi, R., Anthony, E., Almar, R., Castelle, B., Senechal, N., 2014. Longshore drift cell development on the human-impacted Bight of Benin sand barrier coast, West Africa. *In Proceedings 13th International Coastal Symposium (Durban, South Africa)*, *Journal of Coastal Research, Special Issue No. 66*, ISSN 0749-0208
- Lefebvre J-P., Viêt N.T., Almar R., Uu D.V., Thuan D.H., Binh L.T., My, T.V., 2014. Contribution of the swash generated by low energy wind waves in the recovery process of a beach impacted by extreme events: Nha Trang, Vietnam. *Journal of Coastal Research, Special Issue No. 66*.
- Masselink, G., Short, A.D., 1993. The effect of tide range on beach morphodynamics and morphology: a conceptual model. *Journal of Coastal Research* 9, 785 – 800.
- Miles, J.R., Russell, P.E., 2004. Dynamics of a reflective beach with a low tide terrace, *Continental Shelf Research*, 24 (11), 1219-1247.
- Senechal et al., 2014. Observation of the destruction of a beach cusp system in presence of a double coupled cusp system : the example of Grand Popo – Benin. *In Proceedings 13th International Coastal Symposium (Durban, South Africa)*, *Journal of Coastal Research, Special Issue No. 66*, ISSN 0749-0208
- Vousdoukas, M., 2013. Characteristics and Interactions of Multiple Beach Cusp Systems on a Meso-Tidal, Steeply-Sloping Beach. *Proceedings of the Twenty-second (2012) International Offshore and Polar Engineering Conference, Rhodes, Greece, June 17–22, 2012*, ISSN 1098-6189
- Wright, L.D., Short, A.D., 1984. Morphodynamics variability of surf zones and beaches: a synthesis, *Marine Geology*, 56, 93-118.

# Intertidal beach classification in infrared images

Bas Hoonhout †‡, Fedor Baart †∞, Jaap van Thiel de Vries †

†Delft University of Technology  
Department of Coastal Engineering  
Delft, The Netherlands

‡ Deltares  
Unit of Hydraulic Engineering  
Delft, The Netherlands  
bas.hoonhout@deltares.nl

∞ Deltares  
Software Centre  
Delft, The Netherlands



[www.cerf-jcr.org](http://www.cerf-jcr.org)



[www.JCRonline.org](http://www.JCRonline.org)

## ABSTRACT

Hoonhout, B.M., Baart, F., Van Thiel de Vries, J.S.M. 2014. Intertidal Beach Classification in Infrared Images. In: Green, A.N. and Cooper, J.A.G. (eds.), *Proceedings 13<sup>th</sup> International Coastal Symposium* (Durban, South Africa), *Journal of Coastal Research*, Special Issue No. 70, pp. 657-662, ISSN 0749-0208.

Digital imagery is a powerful data source for coastal monitoring, maintenance and research. It provides high-resolution measurements in both time and space. The size and resolution of long-term imagery datasets provide great opportunities, but also pose problems of tractability in the data analysis. In order to fully use the possibilities of these datasets, reliable and automated classification of images is essential. This paper discusses an automated classification approach based on Conditional Random Fields (CRF). The algorithm is applied in pixel space only. Therefore it does not rely on in-situ measurements, nor is there a need for image rectification. The algorithm consists of three steps: segmentation, feature extraction and model training and prediction. We applied the method to a coastal thermal infrared image stream that monitors the wetting and drying of the upper intertidal beach in relation to tide and meteorological parameters. Classification of the upper intertidal beach provides information on the potential sources of Aeolian sediment. The use of 62 extracted features and structured learning proves to provide significantly better classification results compared to algorithms solely based on intrinsic intensity features.

**ADDITIONAL INDEX WORDS:** Coastal imagery, classification, segmentation, superpixels, infrared, Aeolian transport, intertidal beach, features, conditional random fields, CRF.

## INTRODUCTION

Digital imagery is a powerful data source for coastal monitoring, maintenance and research. It provides high-resolution measurements in both time and space. Remote sensing applications make long-term monitoring feasible, providing unprecedented datasets. In the last couple of decades many coastal applications of in-situ imagery have been developed. Holland *et al.* (1997) used a generic coastal video system for nearshore monitoring. This system inspired many applications, like an intertidal beach mapper (Aarninkhof *et al.*, 2003), subtidal bathymetry extraction (Holman *et al.*, 2013), rip-current detection (van Dongeren *et al.*, 2013) and vegetation mapping (Schretlen and Wijnberg, 2012). Vousdoukas *et al.* (2012) uses a similar system for run-up monitoring. More advanced algorithms use multiple cameras for stereo rectification, for example of waves (de

Vries *et al.*, 2009) or extract entire surface moisture maps from intensity images using a reference plate (Darke *et al.*, 2009).

The size and resolution of long-term imagery datasets provide great opportunities, but also pose problems of tractability in the data analysis. In order to fully use the possibilities of these datasets, reliable and automated classification of images is essential (Baart, 2013). Traditionally classification of coastal images relies on algorithms tailored to a specific purpose (e.g. Aarninkhof *et al.*, 2003). By definition such algorithms have limited applicability. More generic approaches exist, but are often not fully automated, limiting the feasibility of handling large datasets (e.g. Quartel *et al.*, 2006). This paper discusses a fully automated classification approach based on probabilistic graphical networks. In contrast with most coastal classification algorithms, we not only use intrinsic intensity features, but also include a large



Figure 1. a) Raw infrared image. b) Arbitrary time-variance image. c) Spatial gradient in time-variance.

set of extracted features in our discriminative pixel descriptors. Although the approach is generic for any kind of imagery, we focus on the use of coastal infrared imagery. Coastal infrared images are a valuable data source for monitoring beach moisture content as supply limiter for Aeolian sediment transport.

### COASTAL INFRARED IMAGERY

Coastal infrared imagery provides high resolution and long-term information on surface temperatures. We use coastal infrared imagery to monitor beach temperatures, which are related to beach moisture content (Edwards *et al.*, 2013). Moisture content is important for Aeolian sediment transport in supply-limited environments (de Vries *et al.*, 2014). Large moisture content hampers the development of a saltation cascade and hence decreases the sediment transport rates compared to transport-limited environments where fetch is limited (Pye and Tsoar, 1990).

The intertidal area is of particular interest since its moisture content changes continuously under influence of tide, solar radiation, rain and wind. The intertidal area is also expected to be an important source of sediment for Aeolian transport (de Vries *et al.*, 2010). The delicate balance between meteorology and tide is expected to explain when and what sediment is transported from the intertidal area to the dry beach and dunes.

A long-term monitoring campaign is initiated in the southern part of Holland, The Netherlands. The research area includes the 20Mm<sup>3</sup> mega-nourishment known as the Sand Motor (or Sand Engine; Stive *et al.*, 2013) that will feed large amounts of sediment to the Holland coast in the coming years. In context of this campaign we monitor accretional aeolian processes, amongst others, using a COX CX320 thermal infrared camera looking down at the dune, beach and sea (Figure 1a). In view of the camera we have about 120m dry sandy beach, an intertidal area with a tidal range of about 1.5m, a relatively low vegetated dune and a small road. In summertime a construction of the coastguard is present as well. Tide and weather conditions are measured at nearby meteorological stations. First results show indeed clear correlations between tide, meteorology and the wetting and drying of the beach. Tide and rain increase the moisture content in the intertidal area, and thereby decrease the temperature. In contrast, either high solar radiation or strong winds decrease the moisture content and thus increase the potential Aeolian transport rate (Figure 2). These correlations are not obvious in regular CCD images that are available at the same site.

These first results are obtained by tracking individual pixels in time. For a full analysis of intertidal moisture content it is necessary to know the location of the intertidal area. This location varies in time due to variability in tide and morphology. We use a generic and automated classification algorithm for coastal imagery to recognize the area that is a potential source for Aeolian sediment in an infrared variance image. Infrared images are single channel, non-normalized and relatively low resolution images that provide special challenges for classification that are not widely covered in other disciplines. The algorithm is applied in pixel space only. Therefore it does not rely on in-situ measurements, nor is there a need for image rectification.

### CLASSIFICATION ALGORITHM

Like in normal coastal CCD images, the intertidal area is not always very distinct in coastal infrared images either. Unlike CCD images, however, thermal infrared images are non-normalized. Their output is always in degrees of temperature and the frame of reference is fixed as long as the view is fixed. Therefore subsequent thermal infrared images can easily be compared over a

fairly long time span and sequences of images can be used for classification. Such sequences hold much more information than

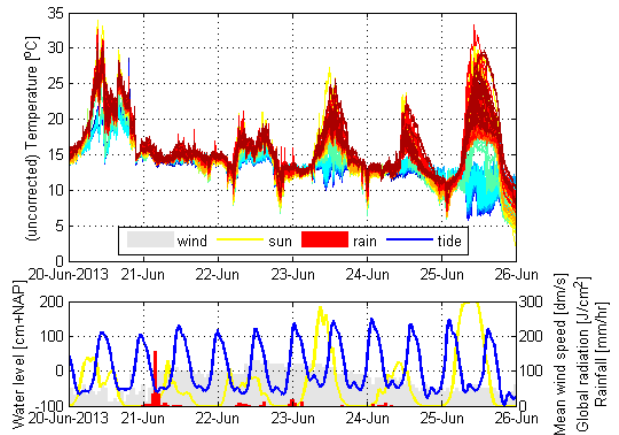


Figure 2. Uncorrected infrared surface temperatures with influence of 24 hours cycle, tide, solar radiation, wind and rain. Each line corresponds to a specific pixel indicated by the raster in Figure 1a.

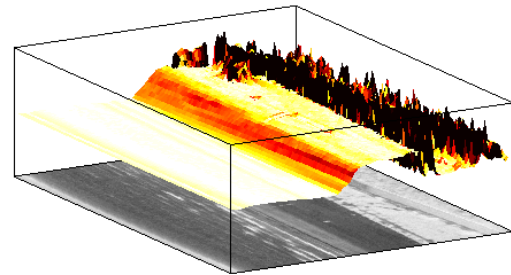


Figure 3. Raw infrared image (bottom), time-variance (surface height) and spatial gradient (surface color). The red, sloped area corresponds to the upper part of the intertidal area.

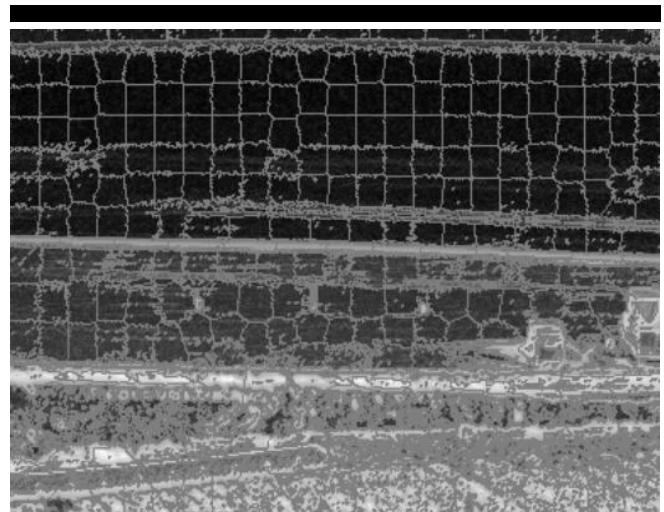


Figure 4. Segmented artificially constructed two-channel infrared variance image.

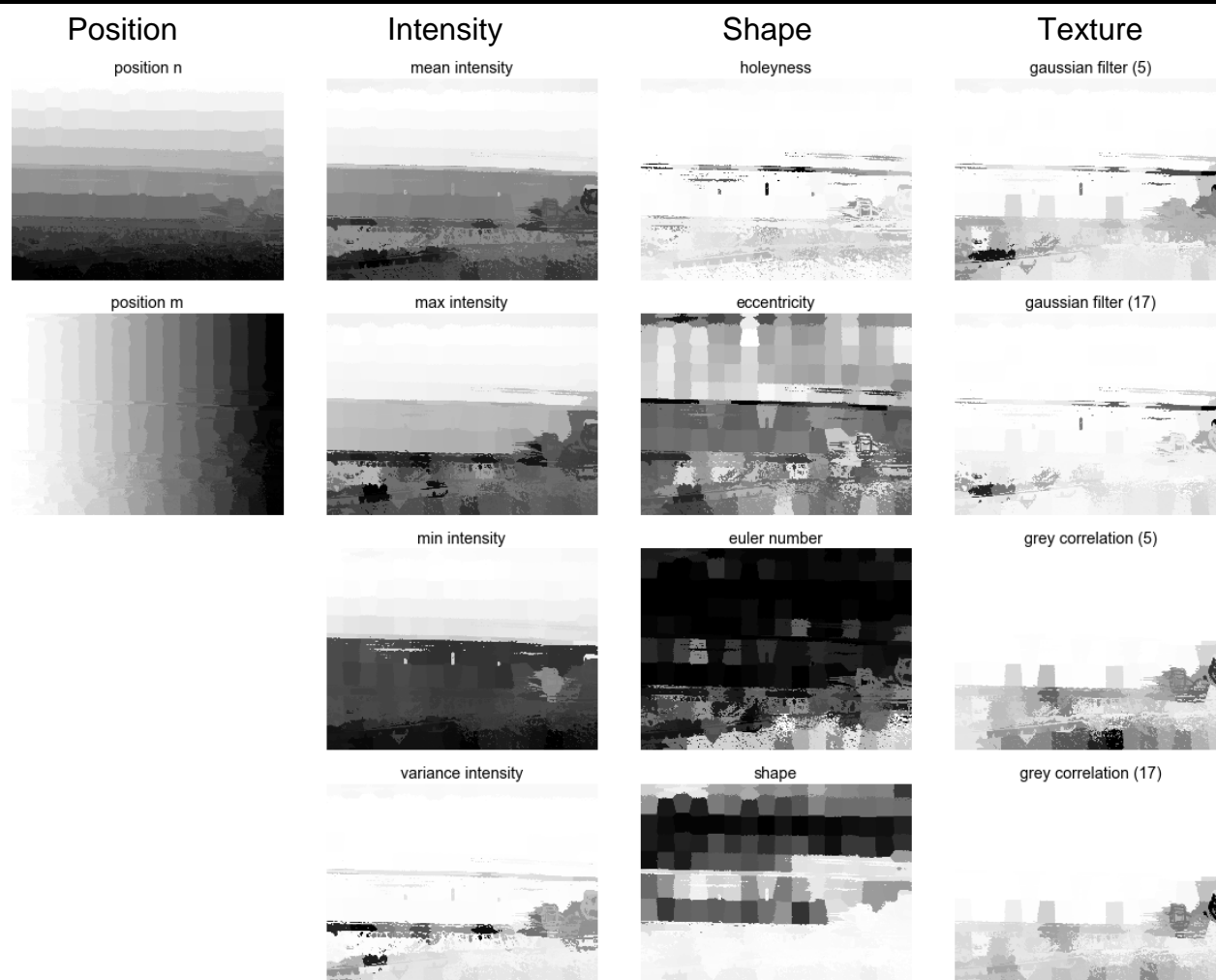


Figure 5. Several features extracted from the infrared variance image in Figure 1b. Low values are white, high values are black. The position and intensity features are referred to as intrinsic features, whereas the shape and texture features are referred to as extracted features.

single images, which makes classification of the intertidal area feasible.

The classification algorithm is based on Conditional Random Fields (CRF), which is a probabilistic graphical model with pairwise potentials (Koller and Friedman, 2009). The algorithm is based on 3 steps that are explained in the following:

1. Segmentation
2. Feature extraction
3. Model construction and training

### Segmentation

Building an algorithm that classifies individual pixels will most likely result in an intractable algorithm that is very sensitive to local scatter. Instead, the image is first segmented into superpixels. A superpixel is a cluster of pixels with similar intrinsic features<sup>1</sup>. The classification algorithm subsequently classifies all

superpixels. All pixels in a superpixel by definition share the same class. The algorithm discussed uses four intrinsic features in particular for segmentation:

1. Pixel coordinate M
2. Pixel coordinate N
3. Time-variance of infrared pixel
4. Spatial gradient in the time-variance

Figures 1b and 1c show an example of the latter two features for an arbitrary 24 hours sequence of infrared images. Figure 3 shows both features in a single 3D plot. A part that coincides with the upper part of the intertidal area is clearly visible, especially in the spatial gradient. Besides, the sea and beach part of the image are distinct through their difference in time variance. Vegetation is characterized in highly scattered values in both time-variance and spatial gradient. The differences in variance related to tide and meteorology are also visible from the plain time series depicted in Figure 2.

<sup>1</sup> We define intrinsic features as those features directly related to the input image and hence to either pixel location or pixel intensity (first 2 columns in Figure 5). In the following sections we will introduce extracted features that are related to second-order properties of the image, like cluster size and shape (last two columns in Figure 5).

From the time-variance and spatial gradient features we artificially construct a two-channel infrared variance image. We use the SLIC segmentation algorithm (Achanta *et al.*, 2010) for segmentation of these images (Figure 4). Segmentation consists of clustering pixels in a space stretched by the four features listed above using a K-means algorithm. The number of superpixels (clusters) is given as input. We use approximately 400 superpixels per image. A second parameter to the clustering algorithm is the compactness, which determines the weight of the pixel coordinate features  $M$  and  $N$  compared to the time-variance features. A high compactness results in relatively square and heterogeneous superpixels whereas a low compactness results in scattered, but homogeneous superpixels. We use a relatively high compactness of 40.

### Feature extraction

In order to classify a superpixel we need features to distinct a superpixel of one class from a superpixel of another. For segmentation we already used four features regarding location and time-variance of the pixels. These features were determined based on individual pixels. When dealing with superpixels more features can be extracted that help us discriminate between classes of pixels. An important property of CRFs is that features are normalized and therefore are independent of each other. As a consequence interdependent features may be used without risking the result to be biased (Koller and Friedman, 2009). We use 62 features from the main categories shown in the columns of Figure 5. This figure shows a subset of the features in use.

The successful classification depends on the distinctive quality of the different features. The example features of position and intensity are computed using trivial functions. The shape and texture definitions are computed as follows. Holeyness is defined as the superpixel convex hull area divided by the total pixel area. The eccentricity is the ratio of the minor and major axis of an ellipsis fitted to the shape of the superpixel. The Euler number is computed as one divided by the number of holes. Shape is defined as the area divided by the squared perimeter.

The Gaussian filter (5) and (7) correspond to the variance left in a superpixel after a Gaussian filter with sigma 5 and 17 has been applied. The grey correlation correspond to the correlation with a Grey Level Co-occurrence Matrix (GLCM; Haralick *et al.*, 1973) with interval of 5 and 17 pixels. In the full feature set the angles of the grey patterns vary by angle. Figure 5 shows that the Gaussian filter textures feature correspond to both intertidal and vegetation, whereas the GCLM texture corresponds with vegetation only. Several features show a strong correspondence with the upper intertidal zone.

### Model construction and training

The final step of the algorithm is the construction of a model that classifies all superpixels (and thereby all pixels) in a new unseen segmented infrared variance image. The output of the model is thus an assignment for each pixel to a single class taken from a set of predetermined classes. The set of predetermined classes we use is: sky, sea, intertidal, beach, dune, vegetation, construction.

The model we construct is a Conditional Random Field (CRF). A CRF is a probabilistic graphical model, which is a graphical representation of the conditional probability distribution over all classes given a set of features, and constructed as a graph: with nodes and edges (Figure 6). We use a node for each superpixel. Each node can be interpreted as a logistic regressor for the class assignment of that superpixel over all 62 extracted features of that superpixel. The class with the largest probability is defined as the

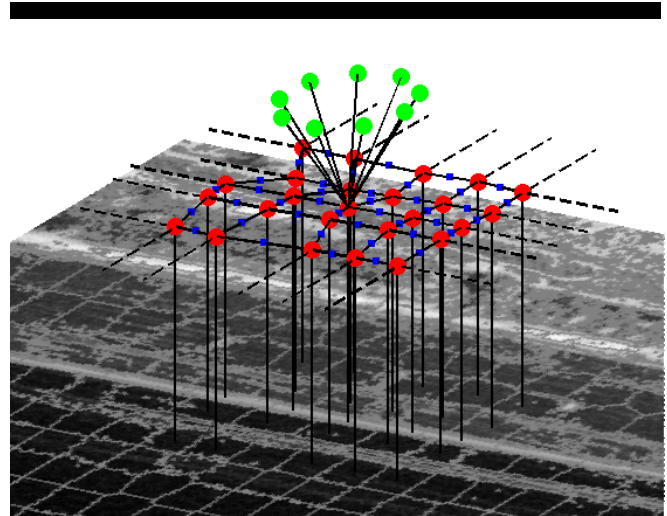


Figure 6. Impression of partial Conditional Random Field for segmented infrared variance image. Each node (red dot) is connected to a specific superpixel. All nodes are connected to adjacent nodes by edges. Each of those edges hosts a potential function (blue squares) that penalizes differences between the nodes connected by the edge. For the middle node a small number of feature nodes are shown (green dots).



Figure 7. Infrared variance image classified using trained Conditional Random Field.

assignment of that superpixel. Without edges the class assignment of each superpixel would be independent of the class assignments of other superpixels and solely based on the unary potentials given by the logistic regressor.

However, the nodes are connected by edges that represent dependencies of the nodes. We use a two-dimensional grid as graph. Each node is connected to its neighboring superpixels: two at the corners of the image, three at the edges and four elsewhere. The dependencies of adjacent superpixels are governed by pairwise potentials. Potentials are factors in the conditional probability distribution of the graph describing the relation<sup>2</sup> of the class assignment of a superpixel given the assignment of adjacent superpixels. The reasoning behind this is that the probability of a

<sup>2</sup> This relation is not to be confused with the marginal distribution over the edge, which is a compromise given all pairwise potentials in the graph.

superpixel next to a superpixel classified as “sea” is more likely to be sea itself. Also the probability of a superpixel to be classified as “dune” is less likely when their neighbors are all classified as “sea”. The class “beach” or “sky” is more likely to be appropriate. In order to stimulate adjacent superpixels to be “common” neighbors, potentials penalize the adjacent superpixels that have classes assigned that are not likely to be found next to each other.

So far we constructed the structure of the conditional probability distribution over all classes in the form of a graph. In order to classify unseen images we need to provide the parameter weights involved in this graphical representation. First, the unary potentials need a weight for each combination of class and feature indicating the likelihood that feature to have a high value given that assignment of the class. Similarly, we need weights for the pairwise potential factors that describe the relation between a class assignment given the assignment of neighboring superpixels. Both sets of weights are trained using a manually annotated dataset.

By manually annotating a series of infrared variance images we construct a dataset that can be used to fit the CRF (unary + pairwise potentials) to this data. A set of images is segmented into superpixels and intrinsic and extrinsic features are extracted like described in the previous section. Subsequently each of these superpixels is manually annotated with a class. From the combined information of extracted features and manual annotations, the CRF can be fitted (or trained or learned) including both the unary and pairwise potentials. The result is two sets of parameter weights for the unary and pairwise potentials separately. The first set of parameter weights generally contains a bias term, which is related to the a-priori probability of a class assignment. This bias term is not used in our model prediction.

When fitting a logistic regressor, including a CRF, we always have the risk of under- or overfitting. Especially when dealing with many features and little data we risk overfitting, which causes the fit to match the data well, but without being generic. To prevent overfitting we use a simple  $L^2$ -norm regularization. The regularization parameter, however, is uncalibrated due to an insufficient amount of data. The data we used for training are 24 hours infrared variance images from Kijkduin, The Netherlands. We used about 19 images for training and another 8 for testing. These images are segmented and manually annotated. More annotated images are necessary to obtain a sufficiently large set for regularization calibration (or validation) as well. It is assumed that the fixed view and relative low variance in the data already limits the risk of overfitting considerably. When extending the approach to multiple views, however, a validation dataset and the calibration of the regularization parameter cannot be omitted.

CRFs like described above include many features, weights and relations. Finding the optimal solution, the class assignment for all superpixels with the absolute largest likelihood, is often intractable. Therefore iterative methods are used to approximate the most likely class assignment for the image. There are several methods available for such structured learning, like message passing or structured Support Vector Machines. We use the latter because of its efficiency and availability (Andersen *et al.*, v1.1.5). The learning algorithm iteratively approximates the maximum a-posteriori (MAP) class assignment for each node in the grid. This is the class assignment for all nodes with the maximum likelihood.

## RESULTS

Figure 7 shows an example of a classification result of the trained Conditional Random Field (CRF). The major parts of the image are well recognized. This is mainly due to the use of pairwise potentials and a large set of extracted superpixel features like shape and holeyness. Figure 8 shows a classification result

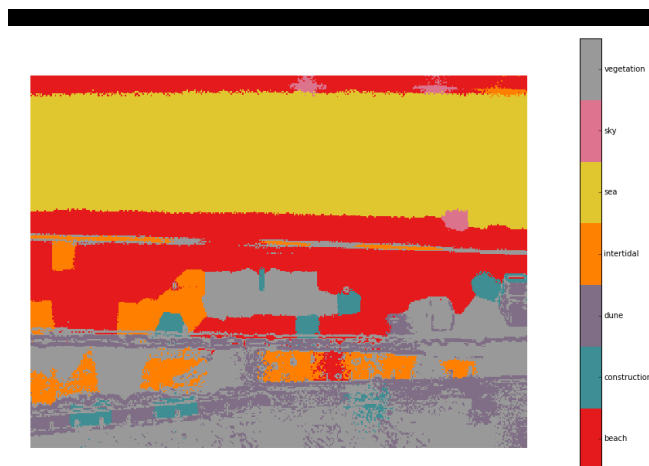


Figure 8. Infrared variance image classified using trained Conditional Random Field with intrinsic features only and no pairwise potentials.

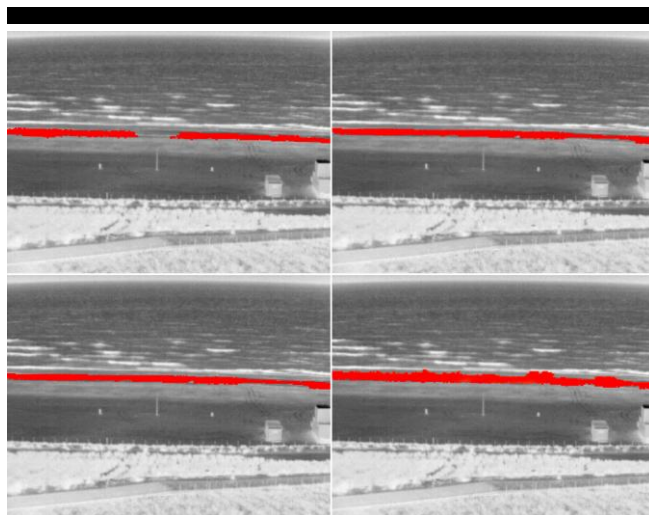


Figure 9. Four examples of classifying the upper part of the intertidal area as a potential source for Aeolian sediment. All classification is based on 24 hours infrared variance images, except the lower right image. The latter is based on a 14 days variance image and consequently shows a larger area as potential sediment source.

where only intrinsic intensity features and no pairwise potentials are used. Vegetation and intertidal area, beach, surfzone and sky and even constructions and vegetation are easily interchanged if we only rely on intensity related features. This shows the great potential of structured learning of segmented images with extracted features.

Unfortunately we didn't obtain distinctive results as shown in Figure 7 for every image. Solving a 7-class classification problem with only 3 or 4 intrinsic features (and many extracted from the segmentation result) and a very limited number of training images appeared to be an extremely complex task. Even manual classification was sometimes difficult. The scarce dataset of infrared variance images apparently still provides too much variance compared to the size of the training dataset. Compared to regular CCD image classification, infrared images are very scarce datasets for several reasons:

- Only two channels (time and spatial variance) compared to many channels in CCD images (RGB, HSV, LAB, etc.).
- Single view at single station for a couple of months compared to many views over many stations for years in a row.
- Low resolution (380x290) compared to high resolution (2000x1500 or more).

Since the purpose of developing an automated classification algorithm was to spot potential sources for Aeolian sediment, we trained another, simpler model that better fits the amount of data available and limits the risks of overfitting. This model distinguishes between two classes only: the upper intertidal area and all other areas. This model appears to be very robust (Figure 9). Still, on rainy days no clear distinction can be made between wet sand due to rain and wet sand due to tide, but then no potential source of Aeolian sediment is found, which is adequate behavior.

## CONCLUSIONS

Image classification using Conditional Random Fields (CRF) appears to be a very generic and versatile approach also for coastal imagery. The segmentation and feature extraction routines used are generic and can be used in any classification algorithm based on CRFs. Both the segmentation and feature extraction are likely to perform even better with full color images and larger heterogeneous datasets, which in turn will increase the applicability and robustness of the approach.

A very specialized application on coastal infrared variance images for monitoring of intertidal beach moisture content and morphology appears to benefit from this general approach. However, the limitations of the data available for this specialized application are reflected in the complexity of tasks the model can perform.

For more extensive validation and comparison of classification algorithms for coastal images, a large and heterogeneous benchmark dataset of coastal images is needed. This benchmark dataset should contain a variety of coastal images from different locations, seasons and view angles. Currently we are working on such benchmark dataset by manually classifying a large number of coastal images.

## OPEN SOURCE

The three main steps of the classification algorithm (segmentation, feature extraction and model construction and training) are part of an open-source toolbox for coastal image analysis hosted by the OpenEarth repository (van Koningsveld *et al.*, 2010). The toolbox relies on the Scikit Image toolbox (Scikit-image, v0.7.2) for segmentation and feature extraction and on the PyStruct toolbox<sup>3</sup> (Mueller, v0.1) for model construction and training. The toolbox also provides a tool for efficient manual classification.

## ACKNOWLEDGEMENTS

For their work discussed in this paper the authors are supported by the ERC-Advanced Grant 291206 – Nearshore Monitoring and Modeling (NEMO).

<sup>3</sup> By using the PyStruct toolbox we actually train a structured Support Vector Machine (SSVM) rather than a Conditional Random Field (CRF). The two are methods are virtually the same, except that the SSVM is based on a Hinge loss function rather than a logistic regressor. As a consequence the tight relation between the graph and its logarithmic representation of the corresponding conditional probability distribution is abandoned.

## LITERATURE CITED

- Aarninkhof, S.G.J., Turner, I.L., T, D.T.D., Caljouw, M. and Nipius, L., 2003. A video-based technique for mapping intertidal beach bathymetry. *Coastal Engineering*, 49(4), 275-289.
- Achanta, R., Shaji, A., Smith, K., Lucchi, A., Fua, P. and Süsstrunk, S., 2010. Slic superpixels. *Ecole Polytechnique Federal de Lausanne (EPFL), Tech. Rep.*, 149300.
- Andersen, M., Dahl, J. and Vandenberghe, L., Python Software for Convex Optimization (CVXOPT), v1.1.5. <http://cvxopt.org/>.
- Baart, F., 2013. Confidence in coastal forecasts. *Delft University of Technology*. PhD thesis. doi:10.4233/uuid:64161304-4714-4214-9790-e0da4a71399d
- Darke, I., Davidson-Arnott, R. and Ollerhead, J., 2009. Measurement of Beach Surface Moisture Using Surface Brightness. *Journal of Coastal Research*. 25(1), 248-256.
- van Dongeren, A.P., van Ormondt, M., Sembiring, L., Sasso, R., Austin, M., Briere, C., Swinkels, C., Roelvink, J.A. and van Thiel de Vries, J.S.M., 2013. Rip current prediction through model-data assimilation on two distinct beaches. *Coastal Dynamics 2013*, Arcachon, France, 1775 - 1786.
- Edwards, B.L., Namikas, S.L. and D'Sa, E.J., 2013. Simple infrared techniques for measuring beach surface moisture. *Earth Surface Processes and Landforms*, 38(2), 192-197.
- Haralick, R.M., Shanmugam, K. and Dinstein, I.H., 1973. Textural features for image classification. *Systems, Man and Cybernetics, IEEE Transactions on*, SMC-3(6), 610-621.
- Holland, K.T., Holman, R.A., Lipmann, T., Stanley, J. and Plant, N.G., 1997. Practical use of video imagery in nearshore oceanographic field studies. *Journal of Oceanographic Engineering*, 22, 81-92.
- Holman, R., Plant, N. and Holland, T., 2013. Cbathy: A robust algorithm for estimating nearshore bathymetry. *Journal of Geophysical Research: Oceans*, 118(5), 2595-2609.
- Koller, D. and Friedman, N., 2009. Probabilistic graphical models: Principles and techniques. The MIT Press.
- van Koningsveld, M. *et al.*, 2010. Openearth - inter-company management of: Data, models, tools & knowledge. *Proceedings WODCON XIX Conference*, Beijing, China. <http://www.openeearth.eu/>.
- Mueller, A., Pystruct - structured learning in python, v0.1. <http://pystruct.github.io/>.
- Pye, K. and Tsoar, H., 1990. Aeolian sand and sand dunes. Unwin Hyman, London.
- Quartel, S., Addink, E.A. and Ruessink, B.G., 2006. Object-oriented extraction of beach morphology from video images. *International Journal of Applied Earth Observation and Geoinformation*, 8(4), 256 - 269.
- Schretlen, J.L.M. and Wijnberg, K.M., 2012. Argus video imagery in support of aeolian transport studies: An exploratory study at vlugtenburg beach, Twente University.
- Scikit-image - image processing in python, v0.7.2. The scikit-image development team. <http://scikit-image.org/>.
- Stive, M.J.F., de Schipper, M. A., Luijendijk, A. P., Aarninkhof, S. G. J., van Gelder-Maas, C., van Thiel de Vries, J. S. M., de Vries, S., Henriquez, M., Marx, S. and Ranasinghe, R., 2013. A new alternative to saving our beaches from sea-level rise: The sand engine. *Journal of Coastal Research*, 29(5), 1001 - 1008.
- Vousdoukas, M., Wziatek, D. and Almeida, L., 2012. Coastal vulnerability assessment based on video wave run-up observations at a mesotidal, steep-sloped beach. *Ocean Dynamics*, 62(1), 123-137.
- de Vries, S., de Schipper, M.A., Stive, M.J.F. and Ranasinghe, R., 2010. Sediment exchange between sub-aqueous and sub-aerial coastal zones. *Coastal Engineering Proceedings*.
- de Vries, S., Hill, D.J., de Schipper, M.A. and Stive, M.J.F., 2009. Using stereo photogrammetry to measure coastal waves. *Journal of Coastal Research*, SI 56: 1484-1488.
- de Vries, S., van Thiel de Vries, J.S.M. and van Rijn, L.C., 2014. Aeolian sediment transport in supply limited situations. *Aeolian Research*.

# Contribution of swash processes generated by low energy wind waves in the recovery of a beach impacted by extreme events: Nha Trang, Vietnam

Jean-Pierre Lefebvre<sup>†</sup>, Rafael Almar<sup>†</sup>, Nguyen T. Viet<sup>‡</sup>, Dinh V. Uu<sup>∞</sup>, Duong H. Thuan<sup>‡</sup>, Le T. Binh<sup>+</sup>, Raimundo Ibaceta<sup>\*</sup>, Nguyen V. Duc<sup>@</sup>



[www.cerf-jcr.org](http://www.cerf-jcr.org)

<sup>†</sup>IRD-LEGOS  
Université Paul  
Sabatier/CNRS/CNES/IRD  
Toulouse, France  
jean-pierre.lefebvre@ird.fr  
rafael.almar@ird.fr

<sup>‡</sup> Water Resources University  
Faculty of Marine and Coastal Eng.  
Hanoi, Vietnam  
nguyentrungviet@wru.edu.vn  
duonghaithuan@gmail.com

<sup>∞</sup> Hanoi University of Sciences  
Department of Oceanology  
Vietnam National University  
Hanoi, Vietnam  
uudv50@gmail.com

<sup>+</sup> Hydraulic Engineering Consultants  
Hydrology and Environment Division  
Hanoi, Vietnam  
Lebinh.hec@gmail.com

<sup>\*</sup>Universidad Técnica Federico Santa  
Maria, Valparaíso, Chile  
raimundo.ibaceta@alumnos.usm.cl

<sup>@</sup> Central Vietnam Construction and  
Consultancy, JSC  
Vietnam  
nguyenvietduch1978@gmail.com



[www.JCRonline.org](http://www.JCRonline.org)

## ABSTRACT

Lefebvre, J.-P., Almar, R., Viet, N.T., Uu, D.V., Thuan, D.H., Binh, L.T., Ibaceta, R., Duc, N.V., 2014. Contribution of swash processes generated by low energy wind waves in the recovery of a beach impacted by extreme events: Nha Trang, Vietnam. In: Green, A.N. and Cooper, J.A.G. (eds.), *Proceedings 13<sup>th</sup> International Coastal Symposium* (Durban, South Africa), *Journal of Coastal Research*, Special Issue No. 70, pp. 663-668, ISSN 0749-0208.

Nha Trang beach experiences southerly sediment drift during winter monsoons and northerly sediment drift during summer monsoons. In addition, the area is likely to be impacted by tropical storms or typhoons. Due to the presence of islands at the south east border of the bay, the strongest impact on the shoreline apart from extreme events is due to NE swell from October to April. The mechanism responsible for the sediment drift generated by low energetic locally generated wind waves is insufficiently understood. It involves the functioning of the swash zone for weak conditions. Two field experiments were scheduled before and after the period of cyclonic activity. The aim of the first experiment was to describe the site's bathymetry and the geomorphology of the upper beach and hydrologic functioning of the bay. A new method of measurements in the swash and surf zone based on processing of data extracted from HD video processing was tested successfully for wind wave conditions in a reflective beach. Here, we present some data obtained during the field experiment at different time scales. The data provides a first quantification of the impact on sediment transport from typical low energy conditions which are encountered during spring and summer in Nha Trang.

**ADDITIONAL INDEX WORDS:** *swash zone, surf zone, low energetic waves regime, video processing, typhoon.*

## INTRODUCTION

Vietnam experiences a tropical monsoon climate, dominated from April to September by southwest monsoons and from October to late March or early April, by northeast monsoons. From May to November, central Vietnam is likely to be impacted by tropical storms or typhoons, with possible events occurring outside this period (Takahashi, 2011; Nguyen-Thi *et al.*, 2012). In 2013, the site was impacted in October by typhoon Nari and in November by super typhoon Haiyan. Although regularly impacted by these extreme events, the economy of Khanh Hoa province is largely related to seaside tourism activities. At present, the hotel and catering industry is intensifying in the vicinity of the beach of Nha Trang. Although typically containing low energy, these short (largely wind-) waves tend to counterbalance the result of

southward drift by a transport of sediment. The swash zone likely plays a significant role in this recovery, due particularly to its infra-gravity oscillation (Masselink and Hugues, 1998; Butt and Russel, 2000).

Because of its shallow, turbulent and unsteady nature, measurements of the physical parameters in the swash zone using conventional data collection systems can be highly problematic (Longo *et al.*, 2002; Jackson *et al.*, 2007; Gómez-Pujol *et al.*, 2011). Recently, various field studies involving increasingly complex experimental set-ups have been conducted (Blenkinsopp *et al.*, 2011; Almeida *et al.*, 2013). More than a decade ago, different techniques taking advantage of video have been proposed (Holman *et al.*, 1993; Foote and Horn, 1999; Holland *et al.*, 2001; Vousdoukas *et al.*, 2014).

The present paper provides a description of the first of two field experiments scheduled before and after the cyclonic season, one



during the summer monsoon, the other during the winter monsoon. In order to investigate the role of the swash zone in the recovery phases generated by low energy waves, different techniques were used to collect data at different time scales (swash event scale, tide scale and month scale). A new method based on video monitoring of swash and surf zone was also tested for low energetic, high-frequency conditions.

## METHODS

### Site presentation

A field experiment was conducted from 26<sup>th</sup> to 30<sup>th</sup> May, 2013 in Nha Trang, Vietnam facing the China Sea. Located in a semi-enclosed bay, the beach of Nha Trang (12°15'N–109°11'E) is sheltered from SE winds and waves by Tre, Mieu and Tam islands. Apart from extreme events, the beach is impacted by waves generated locally by moderate south-eastern winds and by north-eastern swells responsible for a strong southward longshore sediment drift. The beach is about 7 km long, oriented South-North and composed by medium sand ( $\phi = 2$ ). The average slope in the swash zone is of approximately 6°, and approximately 3° in the surf zone. The tide is of micro-tidal varying from mixed to diurnal.

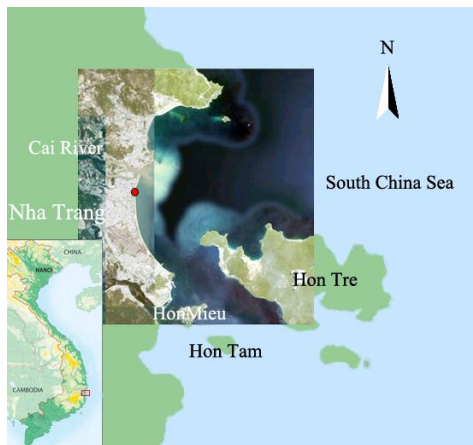


Figure 1. Nha Trang bay. Site of experiment is circled in red.

## DATA

### Instruments and Measurements

A suite of instruments were deployed along a cross-shore transect from beyond the depth of closure to the swash zone (Figure 2). The incident wave parameters were measured by two AWACs (Nortek) moored together with two grain size analyzers (LISST-25X, Sequoia Scientific, Inc) at depth 7.0 and 9.2m, respectively. A pressure type wave gauge DNW-5M and a multi-parameter sensor: water height, wave height and period, turbidity) (OBS-3A, OSIL), both coupled with an electromagnetic current meter (COMPACT) were moored at depth 4.8m and 2.6m, respectively. Measurement of the bathymetry of the bay was achieved with a dual frequency echo-sounder during the first day of the field experiment. Daily topographic measurements of the beach were conducted with a theodolite (Topcon, GTP101) and differential GPS. The experimental setting was completed by an alignment of 20 black painted metallic poles each with a 30mm wide red tape adhered near their tops. They were deployed cross-shore from the backshore toward the surf zone; the 13 landward-most poles were spaced one meter apart and the last 7, two meters apart. The actual position and elevation of the top of each pole was measured with a theodolite. A high definition video camera (HDR-CX 250, Sony) was used to monitor the waves along the poles over daylight hours with an acquisition rate of 25Hz. A micro-profiler ADV (Vectrino II, Nortek) was deployed in the vicinity of the poles, at either end of the surf zone or at the highest point of the run up, following the tide-induced displacement of the swash zone. Topographic surveys were carried out three times a day with a theodolite from the backshore up to approximately 1.5 meter depth. During two days, hourly surveys of the elevation of the bed at each pole, was conducted by manually measuring the elevation between the top and the base of each pole. This pole-related measurement was referenced with the three-dimensional position of the top of the pole.

A permanent video station made up of two video cameras (IP7361 Vivotek) deployed on the same lamp-post, one pointing to the North, the other installed before the field experiment. This system allows a real time evaluation of changes in the intertidal bed elevation. The description of the system and image processing are detailed in Almar *et al.* (2014). The bed elevation of the intertidal domain is obtained by plotting the averaged water line.

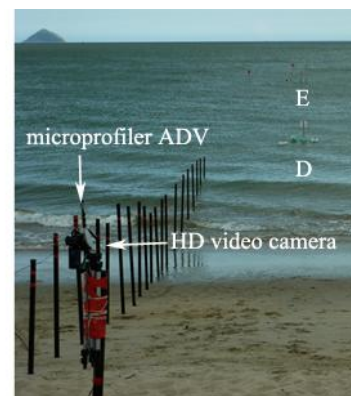
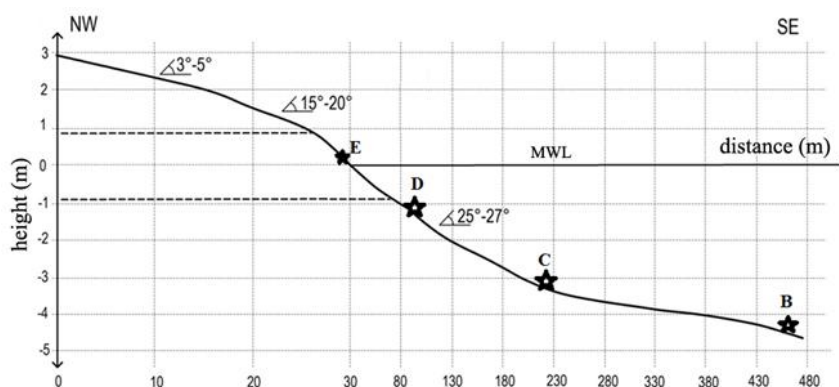


Figure 2. Experimental setup. Left: AWAC and LISST 25X (B), pressure sensor and electromagnetic current meter (C), multi-parameters sensor OBS-3A (D), poles and micro-profiler ADV (E). Right: photo of alignment of poles and the ADV micro-profiler.

### Video processing

The wave height in the swash and surf zone simultaneously at each pole was obtained at a sample rate of 25Hz using an unsupervised method. In each frame of a video recording of 250s duration, the red, green and blue component of the pixels located on lines passing along each pole are extracted and stacked into a

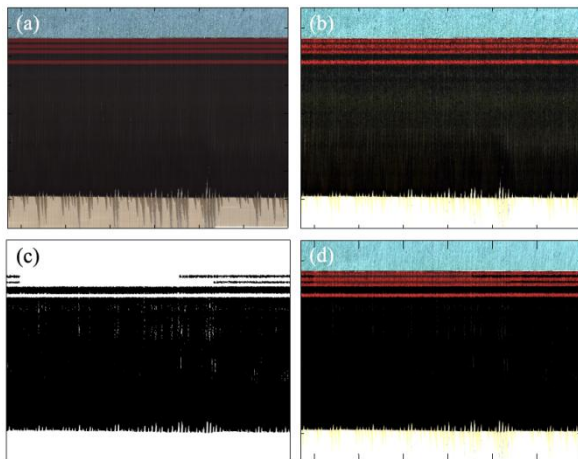


Figure 3. Normalization-enhancement of timestack. Initial timestack (a) RGB intensity normalized stack (b) Mask obtained by selection of ochre-red color band (c) enhanced stack obtained by masking of the RGB intensity normalized stack (d).

matrix. The red component is used to detect the width of the tape and to calculate the pixel to mm conversion factor for a given pole.

In order to minimize the influence of variation of ambient light, uncertainty between water with suspended sediment and bed, variation of bed color with saturation, shadow and reflection of the pole on wet sand amongst other sources of perturbation, the stacks are normalized and enhanced in hue and intensity. First, the intensity of each red, green and blue raster is maximized separately. The stack is then converted in Hue-Saturation-Value coding and the ochre to red band corresponding to the sediment color is enhanced. A binary mask is obtained and the smallest gaps are filled. This mask is finally applied to the enhanced stack which reduces the noise in the final stack and enhances the transitions between water and pole (Figure 3). The water level is obtained by detection of dark /light transition in the blue raster of the enhanced stack. The wave spectral density is calculated from the temporal water level. The bed is estimated by statistical analysis of the time variations of detected water level. In order to limit the influence of uncertainty of the method, only emerged episodes of more than one second are considered, and locations with at least 1/20 of time emerged are considered as in the swash zone

### PRELIMINARY RESULTS

The field experiment was carried out from neap to neap tide, with a tide range varying from 1.2 to 1.8m. The waves originated mostly from the SE with a mean height of approximately 0.2m (Figure 4).

The wave spectral density obtained from the processing of sequences of 250s of swash-surf video indicated a rapid dissipation of 75% of the wave power at the transition between the surf zone to the swash zone (Figure 5) and a peak period of 2.7s which is consistent with the measurements by the AWACs

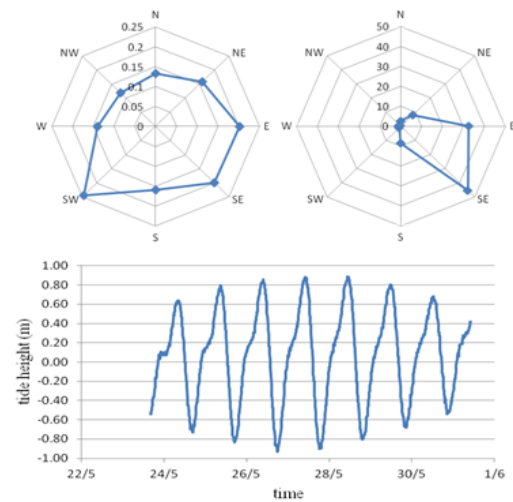


Figure 4. Mean height in meters of waves measured at B during the field experience (left) and percentage of occurrence of the wave from a given direction (right).

(2.15s). A group period of 20s was observed in the upper swash zone. At the upper part of the swash zone, the bed evolution showed an accretion at the rate of 0.04mm s<sup>-1</sup> (Figure 6).

The hourly monitoring of bed elevation measured manually at the eleven first poles of the alignment (swash and surf zone) during an ebb tide (29/05 - tide range 1.47m) and a rising tide (30/09 - tide range 1.36m) is presented in figure 4, the distance between poles measured from the most landward one. During the two days, the waves originated from the ESE with a mean height and period of 0.30m and 3s, respectively, the 29/05 and 0.19m and 6s, the 30/05.

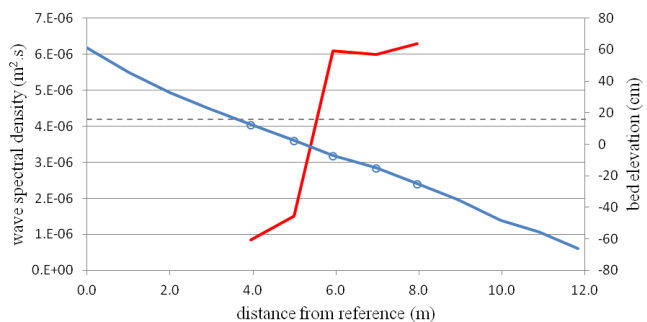


Figure 5. Decay of wave spectral density at the boundary between surf zone and swash zone (red). The bed elevation is represented in blue with the circle indicating the position of the poles 5 to 9 (from left to right). The dashed line marks the tidal height at the moment of the measurement.

At the beginning of ebb tide, the upper swash zone was accreting (from reference to 3.9m seaward) and the surf zone was eroding. After mid-tide, (tide elevation of 0.3m) a significant accretion was noted in the surf zone (poles between 7m to 8.9m seaward from reference). At the end of ebb tide, an accretion was measured at every emerged pole. During 8 hours of the ebb tide, the 10m portion comprising the swash zone and a part of the surf zone accreted at the rate of 0.8cm m<sup>-2</sup> h<sup>-1</sup> (Figure 7).

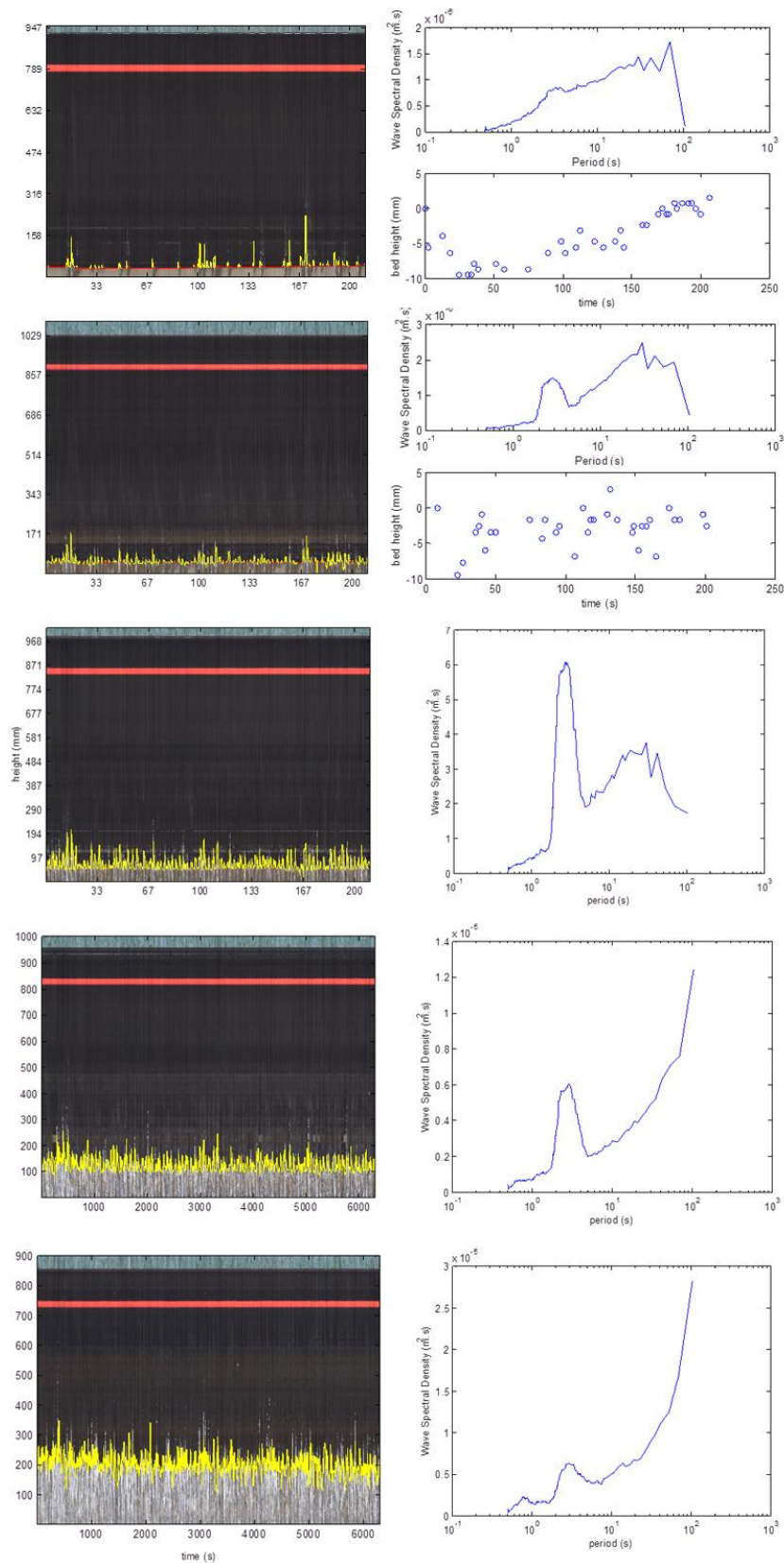


Figure 6. Monitoring of variation of bed elevation in the swash- surf zone from pole #5 to #9 (top to bottom). The water height detection is plotted on the timstack in yellow and the detected bed in red (centre). The corresponding water spectral density is shown with bed elevation (for pole located in the swash zone) (left).

From the video survey system, we extracted at a different date, the bed elevation in the intertidal zone along a cross-shore line close to the field experiment (Figure 8). The area was accreting from May to October. After 12<sup>th</sup> October, significant erosion occurred, probably due to the North-East wave regime associated with winter monsoons. In the night of 13<sup>th</sup> and 14<sup>th</sup> October, Nha Trang experienced strong waves associated with the passage of

typhoon Nari. The effect of this event caused an accretion that counter-balanced the erosion generated by the NE swell of the winter monsoon. During the night of 10<sup>th</sup> and 11<sup>th</sup> November, Nha Trang beach was impacted by waves generated by the passage of super typhoon Haiyan (Figure 9).

**DISCUSSION AND CONCLUSIONS**

During the first field experiment of our two-year project, the hydrodynamics of the site was described both by conventional techniques (mooring of wave gauges and current meters, bathymetry and topography surveys) and by less usual and low cost methods (video survey of the beach, high frequency monitoring of swash and surf zone). The processing of information extracted from surveys allows a quantification of variation of bed elevation of the intertidal domain, in a radius of approximately 1 km around the video survey station. The setting successfully resisted to two major tropical storms induced by the passage of typhoons Nari and Haiyan.

The measurements of bore propagation in the swash and surf zones by video acquisition of poles proved to be efficient. It provided consistent wave spectral density for location spaced every meter. The water height was detected precisely enough to allow a wave to wave analysis of the run up and run down. The simultaneity of measurements at different locations is inherent to the method. The bed can be detected even between short laps between a run up and run down events. The field experiment confirmed the sediment transport landward due to the swash generated by weak wave. Finally, the asymmetry of sediment transport in the surf and swash zone for the rising and ebb tide during similar wave conditions was shown.

**ACKNOWLEDGEMENT**

The work described in this publication was supported by the Vietnamese Ministry for Science and Technology (BKHCN/NDT-HD/2013/110). We thank the National Institute of Oceanography of Nha Trang for its help in the preparation and carrying out of this field experiment.

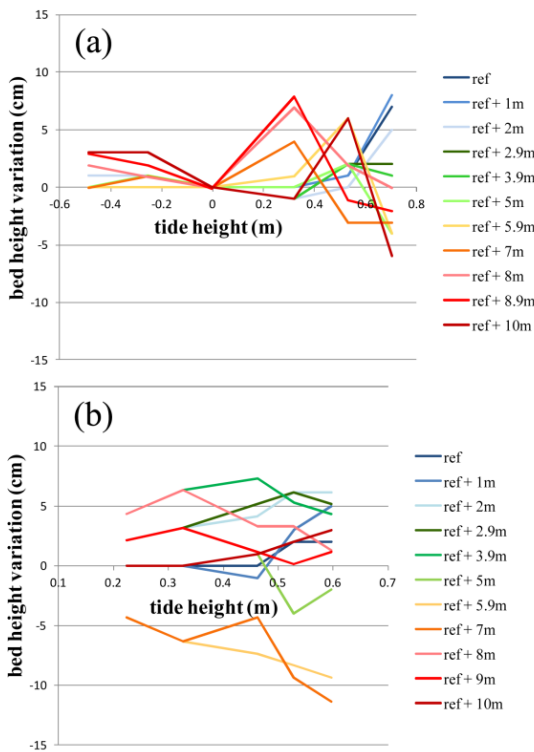


Figure 7. Monitoring of variation of bed elevation in the swash-surf zone.

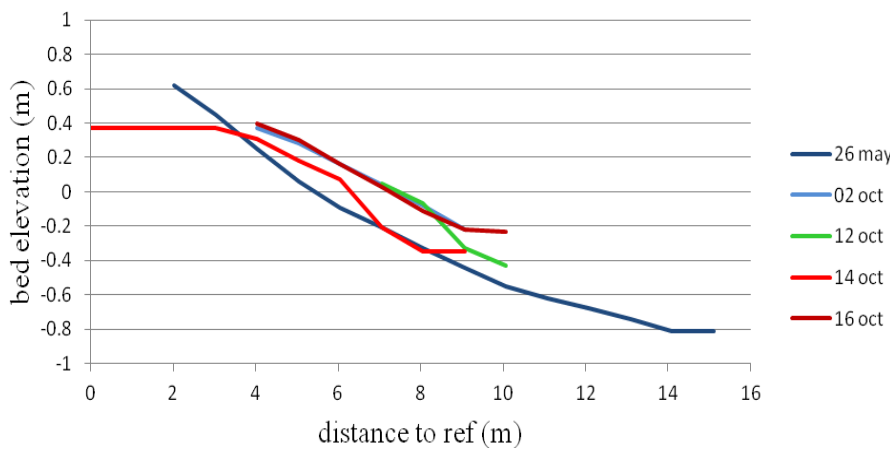


Figure 8. Bed elevation of the inter-tidal domain estimated by processing of images from the video survey (left) trajectory of typhoon Nari (right).

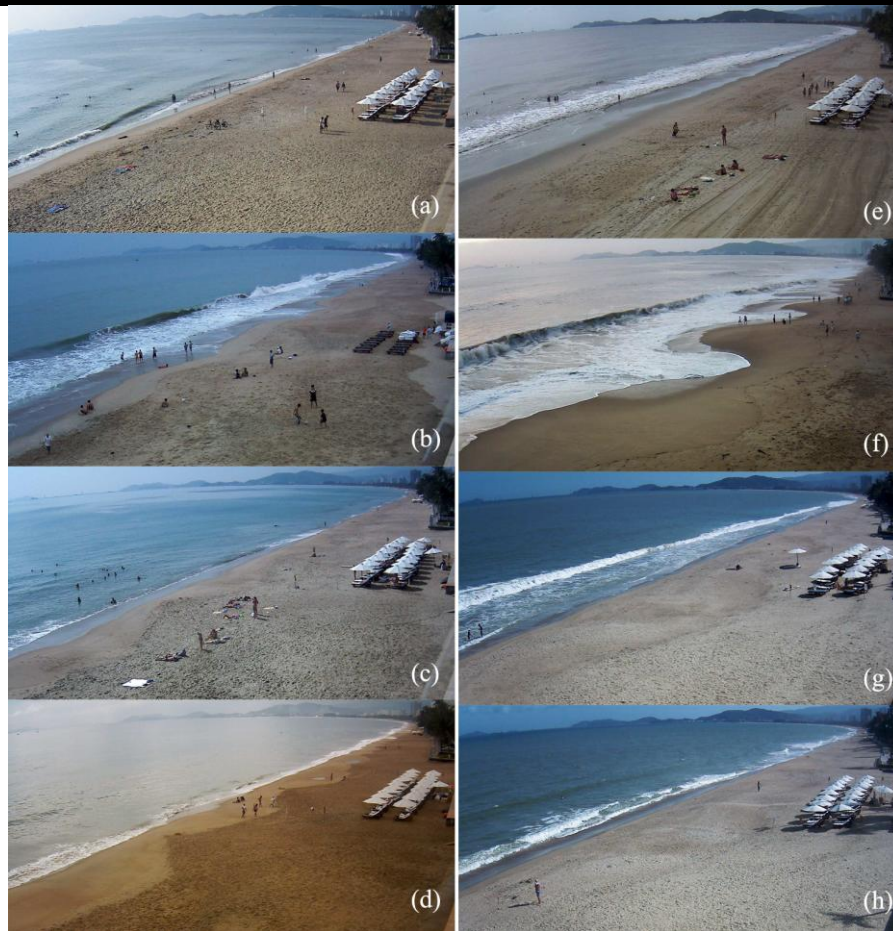


Figure 9. Monitoring of the location of field experiment: left: before and after typhon Nari (13 October): 12/10(a), 14/10 (b), 16/10(c) and 18/10 (d) and right: before and after typhoon Haiyan (10 November): 9/11 (e), 10/11 (f), 11/11(g) and 12/11 (h).

### LITERATURE CITED

- Almeida, L.P., Masselink G., Russell, P., Davidson, M., Poate, T., McCall, R., Blenkinsopp, C., Turner, I., 2013. Observations of the swash zone on a gravel beach during a storm using a laser-scanner (Lidar). *Journal of Coastal Research*, Special Issue No. 65, 636–641.
- Almar, R., Hounkonnou, N., Anthony, E., Castelle, B., Senechal, N., Laibi, R., Mensah-Senoo, T., Degbe, G., Quenum, M., Dorel, M., Chuchla, R., Lefebvre, J-P, du Penhoat, Y., Laryea, W.S., Zodehougan, G., Sohoun, Z., and Appeaning Addo, K., and Kestenare, E., 2014. The Grand Popo beach 2013 experiment, Benin, West Africa: from short timescale processes to their integrated impact over long-term coastal evolution. In: Green, A.N. and Cooper, J.A.G. (eds.), Proceedings 13th International Coastal Symposium (Durban, South Africa), *Journal of Coastal Research*, Special Issue No. 66
- Baldock, T.E., Hughes M.G., 2006. Field observations of instantaneous water slopes and horizontal pressure gradients in the swash-zone. *Continental Shelf Research*, 26, 574–588.
- Blenkinsopp, C.E., Turner, I.L., Masselink, G., Russell, P.E., 2011. Swash zone sediment fluxes: Field observations. *Coastal Engineering*, 58, 28–44
- Butt, T., Russel, P., 2000. Hydrodynamics and Cross-Shore Sediment Transport in the Swash-Zone of Natural Beaches: A Review. *Journal of Coastal Research*, 16, 2, 255–268
- Foote, M., Horn, D., 1999. Video measurement of swash zone hydrodynamics. *Geomorphology*, 29, 59–76.
- Holland, K.T., Puleo, J.A., Kooney, T.N., 2001. Quantification of swash flows using video-based particle image velocimetry. *Coastal Engineering*, 44, 65–77.
- Gómez-Pujol, Luis, Jackson, Derek, Cooper, Andrew, Malvarez, Gonzalo, Navas, Fatima, Loureiro, Carlos and Smyth, Thomas, 2011. Spatial and temporal patterns of sediment activation depth on a high-energy microtidal beach. *Journal of Coastal Research*, SI 64. pp. 85–89.
- Holman, R.A., Sallenger, Jr., A.H., Lippmann, T.C., Haines, J.W., 1993. The application of video image processing to the study of nearshore processes. *Oceanography*, 6(3), 18–85.
- Jackson, D.W.T., Anfuso, G. and Lynch, K., 2007. Swash bar dynamics on a high-energy mesotidal beach. *Journal of Coastal Research*, SI 50. pp. 738–745.
- Longo, S., Petti, M., Losada, I.J., 2002. Turbulence in the swash and surf zones: a review. *Coastal Engineering*, 45, 129–147.
- Masselink, G., Hugues, M., 1998. Field investigation of sediment transport in the swash zone. *Continental Shelf Research*, 18, 1179–1199.
- Nguyen-Thi, H.A., Matsumoto, J., Ngo-Duc, T., Endo, N., 2012. Long-term trends in tropical cyclone rainfall in Vietnam. *Journal of Agroforestry and Environment*, 6(2), 89–92.
- Takahashi, H.G., 2011. Long-term changes in rainfall and tropical cyclone activity over South and Southeast Asia. *Advances in Geosciences*, 30, 17–22.
- Vousdoukas, M.I., Kirupakaramoorthy, T., Oumeraci, H., de la Torre, M., Wübbold, F., Wagner, B., Schimmels, S., 2014. The role of combined laser scanning and video techniques in monitoring wave-by-wave swash zone processes. *Coastal Engineering*, 83, 150–165.

## Observed destruction of a beach cusp system in presence of a double-coupled cusp system: the example of Grand Popo, Benin

Nadia Senechal †, R.A. Laibi‡, R. Almar∞, B. Castelle†, M. Biauxque†, J.-P. Lefebvre∞, E. J. Anthony#, M. Dorel∞, R. Chuchla∞+, M.H. Hounkonnou+, Y. Du Penhoat∞+

†University of Bordeaux  
UMR CNRS EPOC  
Talence, France  
[n.senechal@epoc.u-bordeaux1.fr](mailto:n.senechal@epoc.u-bordeaux1.fr)  
[b.castelle@epoc.u-bordeaux1.fr](mailto:b.castelle@epoc.u-bordeaux1.fr)  
[Melanie.biauxque@etu.u-bordeaux1.fr](mailto:Melanie.biauxque@etu.u-bordeaux1.fr)

‡ Université Abomey Calavi  
Département des Sciences de la Terre,  
Faculté des Sciences et Techniques  
Cotonou, Republic of Benin  
[raoulaibi@yahoo.fr](mailto:raoulaibi@yahoo.fr)

∞ IRD-LEGOS  
Université Paul  
Sabatier/CNRS/CNES/IRD  
Toulouse, France  
[rafael.almar@ird.fr](mailto:rafael.almar@ird.fr)  
[matthieu.dorel@ird.fr](mailto:matthieu.dorel@ird.fr)  
[remy.chuchla@ird.fr](mailto:remy.chuchla@ird.fr)  
[jean-pierre.lefebvre@ird.fr](mailto:jean-pierre.lefebvre@ird.fr)  
[Yves.Du-Penhoat@ird.fr](mailto:Yves.Du-Penhoat@ird.fr)

+ University of Abomey Calavi  
ICMPA-UNESCO Chair  
International Chair in Mathematical  
Physics and Applications  
Cotonou, Republic of Benin  
[norbert.hounkonnou@cipma.uac.bj](mailto:norbert.hounkonnou@cipma.uac.bj)  
[malgdaq2000@yahoo.fr](mailto:malgdaq2000@yahoo.fr)

# Aix-Marseille Univ, IUF,  
CEREGE UMR 34,  
Europôle de l'Arbois, B.P. 80,  
13545 Aix en Provence cedex 04,  
France  
[anthony@cerege.fr](mailto:anthony@cerege.fr)



[www.cerf-jcr.org](http://www.cerf-jcr.org)



[www.JCRonline.org](http://www.JCRonline.org)

### ABSTRACT

Senechal, N., Laibi, R.A., Almar, R., Castelle, B., Biauxque, M., Lefebvre, E. J. Anthony, J.-P., Dorel, M., Chuchla, R., Hounkonnou, M.H., Du Penhoat, Y., 2014. Observed destruction of a beach cusp system in presence of a double-coupled cusp system: the example of Grand Popo, Benin. *In: Green, A.N. and Cooper, J.A.G. (eds.), Proceedings 13<sup>th</sup> International Coastal Symposium* (Durban, South Africa), *Journal of Coastal Research*, Special Issue No. 70, pp. 669-674, ISSN 0749-0208.

Beach cusps are common features of steep reflective and intermediate beaches. However, very few observations have reported double coupled cusp systems. Here, we present a dataset of observations of a beach exhibiting two sets of beach cusps. Data were collected at Grand Popo Beach (Benin, West Africa) in February 2013. Daily topographic surveys along a 380 m long stretch of shore allowed observation of the dynamics of the two sets of beach cusps. At the beginning of the field survey, we clearly observe two sets of cusps; the upper beach cusps system is relatively asymmetric with a typical wavelength of about 45 m, while the lower beach cusps system is relatively symmetric with a typical wave length slightly shorter (about 35 m). After two days, we measured the total destruction of the lower set of beach cusps while the upper set of beach cusps was only partially destroyed. The data suggest that destruction of the lower beach cusp system may be related to persistent accretionary conditions and/or calm conditions but probably also to the transition from wave-driven circulation (dominated by weak alongshore currents with flash and swash rips), to a second period characterized by dominant longshore currents further increasing in speed (with rare swash rips). Conversely, the disappearance of the western upper beach cusp may be related to an accretionary pattern and to the coalescence of two individual features. Our observations, consistent with previous works, suggest that beach cusps certainly arise as a result of some combination of erosion and accretion.

**ADDITIONAL INDEX WORDS:** *reflective beach, topographic survey, cusp migration.*

### INTRODUCTION

Forecasting the shoreline position is a key issue for coastal planning and management. Shoreline position along sandy coasts varies over a broad spectrum of time and space scales in response to a variety of processes. The beachface sometimes displays 3D

geometry associated with undulating patterns usually known as 'beach cusps'. Beach cusps are crescentic morphological features found on the foreshores of beaches and characterized by distinctive alongshore periodicity, usually defined as a sequence of horns and bays with the horns extending seaward, coupled with steeper slopes, and bays landward coupled with milder slopes.

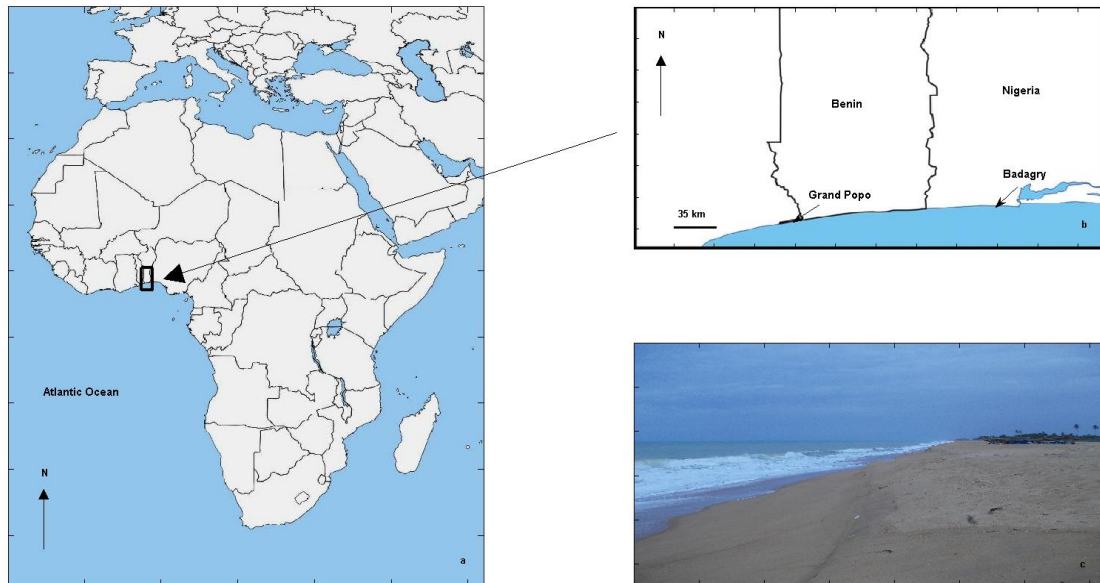


Figure 1. Field area location. (a) General location of Benin. (b) Focus on the Benin coast. (c) Oblique view of the Grand Popo beach.

Beach cusp's wavelengths, defined as the distance between consecutive horns, can range from decimeters (Komar, 1973) to tens of meters (see Coco *et al.*, 1999 for a review of existing observations).

Beach cusps have been observed over a variety of beach types featuring a large range of sediment sizes, from fine sand to boulders (Mii, 1958; Russell and McIntire, 1965) but more commonly develop on beaches exposed to relatively low wave energy in the presence of medium to coarse sediment. Size sorting of materials between the horns and the bays is generally observed, bays being made up of finer sediment than the horns (Komar, 1983; Antia 1987).

Beach cusps have received a great deal of interest over past decades, focusing either on the formation mechanisms underlying their initiation (e.g. Guza and Inman, 1975; Inman and Guza, 1982; Werner and Fink, 1993; Masselink, 1999; Coco *et al.*, 1999, 2000) or on the processes influencing the subsequent development and shape of beach cusps (e.g. Masselink and Pattiaratchi, 1998; Masselink *et al.*, 1997; Werner and Fink, 1993; Coco *et al.*, 1999, 2003). Beach cusps are thought to shape the beach by either breaching of a previously deposited berm, or deposition of cusps horns under net accretionary conditions (Masselink and Pattiaratchi, 1998). The role of erosion/accretion in cusp growth has been generally contradictory and recent extensive observations of cusps (van Gaalan *et al.*, 2011) have confirmed that beach cusps certainly arise as a result of some combination of erosion and accretion with tides complicating the temporal and spatial patterns of net morphological changes (Coco *et al.*, 2004). On the other hand, beach cusp destruction has received less interest. It has been generally related to erosive conditions with the action of storm and/or the presence of strong longshore currents. However, recent studies have also reported that persistent beach accretion conditions may result in bay infilling resulting in pattern disappearance (e.g. Almar *et al.* 2008).

Here we present a data set of a double-coupled, beach cusp field. Double beach cusp fields have been rarely examined in the literature (Antia, 1987) and the data presented in this work are

collected at Grand Popo beach on the sandy coast of Benin, in the course of a 10-day field experiment in February 2013. In particular, observations allowed investigation of the natural destruction of the lower beach cusp field under moderate wave energy and rising tidal range conditions with concurrent slow alongshore migration of the upper beach cusp field.

## METHODS

### Site presentation

Data were collected at Grand Popo (GPP) beach during the Grand Popo field experiment conducted in February 2013 (Almar *et al.*, 2014). GPP beach is situated on the Benin coast (West Africa, Figure 1a) and consists of a low sandy coast, almost W-E orientated (Figure 1b). The sediment is primarily of a relatively homogeneous suite of iron-coated medium to coarse sand (0.4–1 mm,  $D_{50}$ : 0.6 mm). GPP is typical of the natural undisturbed reflective beaches of the Gulf of Guinea, in an open wave-dominated and microtidal environment (mean spring tide range: ~1.8 m) exposed to long period swells (ECMWF 1957-2013 average,  $H_s=1.36$  m,  $T_p$ , 9.4 s) generated in the South Atlantic. The incident waves, dominantly in the plunging regime, and grain-size conditions result in a relatively steep-faced (slope ~12-17°) reflective beach year-round with milder gradients in summer when southwesterly swell waves are higher, as a result of northward migration of zone of wave-generation in the South Atlantic (Laibi *et al.*, 2014).

### Data

Data were collected at Grand Popo beach during a 10-days field experiment conducted in February 2013. The main goal of this experiment was to provide the first high intensive hydro-morphodynamic data set of the area; including remote sensing high frequency surveys (see Almar *et al.*, 2014 for a full description of the field experiment). The resulting morphological evolution was evaluated by both in-situ measurements and remote sensing. Daily topographic surveys of the intertidal area on ~300 m longshore

coastal stretch were performed at each low tide using a pedestrian-operated GPS. Twenty five cross-shore lines were surveyed from the water line at low tide up to the berm and extending onshore to the high tide mark. Due to satellite limitations during the field experiment, the accuracy was about  $\pm 0.05$  m in the horizontal and  $\pm 0.15$  m in the vertical.

A cusp system was defined here as the presence of a well formed bay associated with the presence of two horns. Beach cusp wavelength was defined as the distance between two consecutive horns. To examine the evolution of the cusp systems a 'global analysis' of beach evolution (Garnier *et al.*, 2006, 2010; Castelle *et al.*, 2012) was also used. This involved analysing variables that are integrated over the whole acquisition domain. The notation  $\bar{Z}$  is defined as the alongshore-averaged elevation over the measured domain and was estimated for each topographic survey.

The first value to be estimated was the perturbation defined as:

$$p_i(x, y) = Z_i(x, y) - \bar{Z}_i(y) \quad \text{Equation 1}$$

where:  $i$  indicates each individual survey and  $x$  and  $y$  are the alongshore and cross-shore coordinates, respectively. An additional variable that is considered in this study is the energy of the perturbation per unit surface defined as:

$$V_i = \frac{\sum (Z_i(x, y) - \bar{Z}_i(y))^2}{\text{Surface}} \quad \text{Equation 2}$$

where: Surface is the surface of the topographic survey. Finally, using the same definition as in Garnier *et al.* (2010), the global growth rate,  $\Sigma_i$  is given by:

$$\Sigma_i = \frac{1}{2V_{i-1}} \frac{(V_i - V_{i-1})}{dt} \quad \text{Equation 3}$$

Incident waves were measured with an ADCP (RDI WORKHORSE) moored in 8-m water depth (see Almar *et al.*, 2014). Surf zone currents were measured by means of repeated human operators acting as drifters (~10 runs per series) daily, at selected moments, over the entire experiment duration (see Castelle *et al.*, 2014).

## PRELIMINARY RESULTS

### Overall evolution

Figure 2 represents the topographic surveys of the Grand Popo field area at the beginning of the survey period (upper panel) and after 5 days (middle panel). Clearly, on the first day of the observations (February 20) we note that the beachface displays 3D patterns associated with a double beach cusp system. Along the 300 m long beach section, we clearly observe two sets of cusps: 7 beach cusps on the mid- foreshore and 6 beach cusps on the upper foreshore. The upper beach cusps system is relatively asymmetric with a typical wavelength of about 40 m. In contrast, the lower beach cusp system is relatively symmetric with a typically slightly shorter wave length (about 35 m). The larger spacing of the higher cusps is consistent with those observations of Russell and McIntire (1965) and Williams (1973). The mean wavelengths are also consistent with previous observations in the area. Based on a long-term data set (2-years) that consisted in bi-monthly to monthly field visits, Antia (1987) also reported several cases of multiple sets of cusps at Badagry and Victoria beaches, also

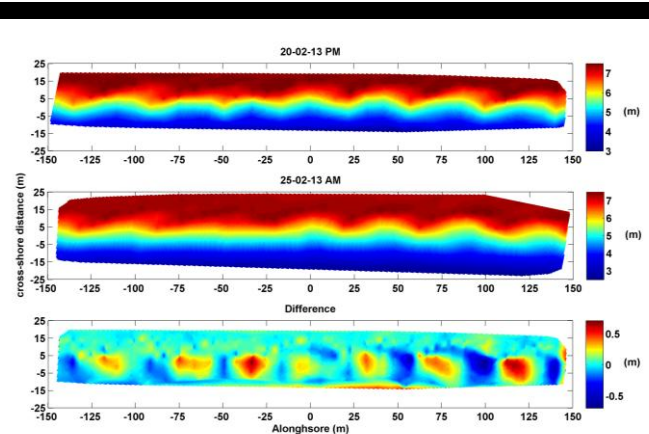


Figure 2. Topographic survey at (upper) the beginning of Grand Popo topographic survey and (middle) five days later. (Lower) Difference in elevation between the two surveys.

situated on the Bight of Benin coast in Nigeria (Figure 1b). After 5 days of observations (middle panel, February 25), our results clearly show that only one set of cusps are present and that it has been strongly modified. Indeed, we only observe the higher cusps and clearly identify 4 beach cusps on the eastern beach (positive alongshore position) while on the western beach (negative alongshore position) we observe the disappearance of the pattern and the formation of a uniform berm between alongshore positions -25m and -90m. The difference map between the two topographic surveys (lower panel) indicates a relatively stable sediment budget (even with a slight positive shift) for this part of the beach. In particular, accretion spots are observed at locations of the initial lower bay cusps (e.g. alongshore positions -35 m, 120 m) although erosive spots are also observed on the eastern cusp horns (positive alongshore positions). Figure 3 provides further insight on the sequence of lower cusps destruction and higher cusp evolution.

### Detailed evolution of beach cusp patterns

Figure 3 represents the perturbation maps (see equation 1) derived from each topographic survey. Starting on February 20 (Figure 2, upper panel), we observe that the two sets of cusps persist until the afternoon of February, 21. The first major evolution appears in the night from February 21 to February 22. We clearly observe that the lower beach cusp begins to disappear. The disappearance process continues on February 22 so that in the evening, the patterns have completely disappeared and we observe an alongshore uniform contour level. At the same time, we observe a slight smoothing of the western upper beach cusps. This smoothing process is ongoing until the evening of February 23<sup>rd</sup> when we observe only four remaining upper beach cusps on the eastern part of the beach. On February 24<sup>th</sup> the morphology is similar to that observed on February 25<sup>th</sup>. As previously observed (Antia, 1987), the higher level cusps demonstrated a greater degree of stability compared with the lower set of cusps on the mid-foreshore. Beach cusp destruction has been generally related to erosive conditions with the action of storm and/or the presence of strong longshore currents. However, recent studies have also reported that persistent beach accretion conditions may generate bay infilling, resulting in pattern disappearance (e.g. Almar *et al.* 2008).



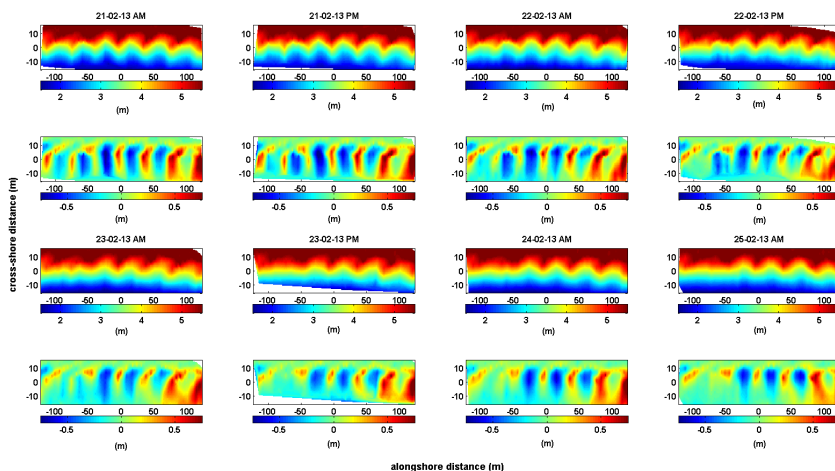


Figure 3. (Upper) Topographic surveys showing elevation in meters and (lower) associated perturbation maps showing the deviation elevations from the alongshore averaged profile in meters (see equation 1) for each survey.

**Detailed evolution of beach cusp patterns**

Figure 3 represents the consecutive topographic surveys and their associated perturbation maps (see equation 1). Starting on February 20<sup>th</sup> (Figure 2, upper panel), we observe that the two sets of cusps persist until February, 21 (pm). The first major evolution occurs during the night from February 21<sup>st</sup> to February 22<sup>nd</sup> as the lower beach cusp system is already substantially smoothed. This smoothing process continues on February 22<sup>nd</sup> and 23<sup>rd</sup> so that, in the evening of February 23<sup>rd</sup>, the patterns had nearly disappeared resulting in an alongshore-uniform contour. At the same time, we observe a slight smoothing of the western upper beach cusps. This smoothing process is ongoing until pm of February 23<sup>rd</sup> when we only observe 4 remaining upper beach cusps on the eastern part of the beach. On February 24<sup>th</sup> we observe that the lower beach cusp set reforms, coupled to the upper beach cusp set, before being rapidly smoothed the next day. As previously observed (Antia,

1987), the higher level cusps showed a larger degree of stability compared with the lower set of cusps.

These observations are further quantified through the time series of both the energy of the perturbation and the global growth (Figure 5). We observe that the energy of the perturbation is decreasing, which is the signature of the smoothing of the lower beach cusp set and that of the western upper beach cusp set. Similarly, the global growth rate is relatively high on February 22 and 23 and negative. Then on February 24 when the lower beach cusp reformed, the energy of perturbation increases, resulting in a positive global growth of rate before decreasing again on February 25<sup>th</sup>. Beach cusp destruction has been generally related to erosive conditions with the action of storm and/or the presence of strong longshore currents. However, recent studies also reported that persisting beach accretion conditions may result in a pattern of cusp disappearance through bay infilling (e.g. Almar *et al.* 2008).

Figure 4 provides further insight into the conditions of cusp

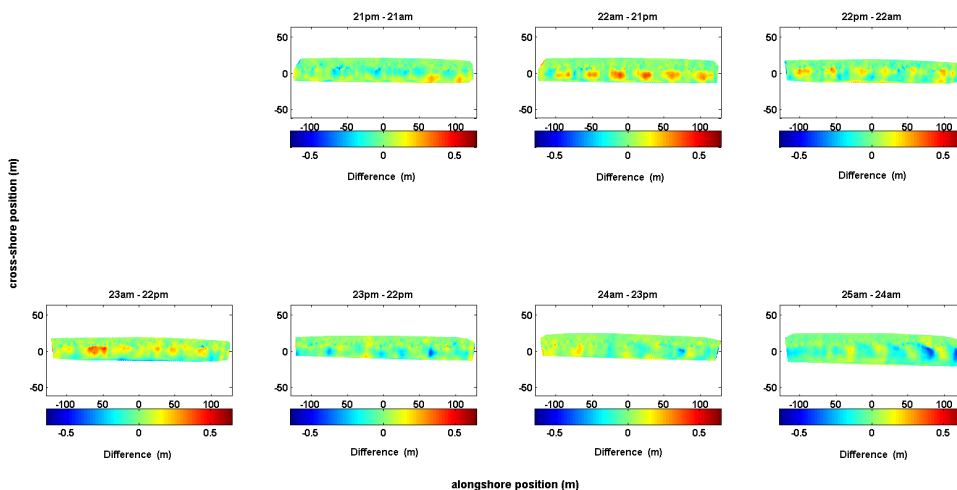


Figure 4. Difference maps between consecutive topographic surveys starting on February 21am and ending February 25am.

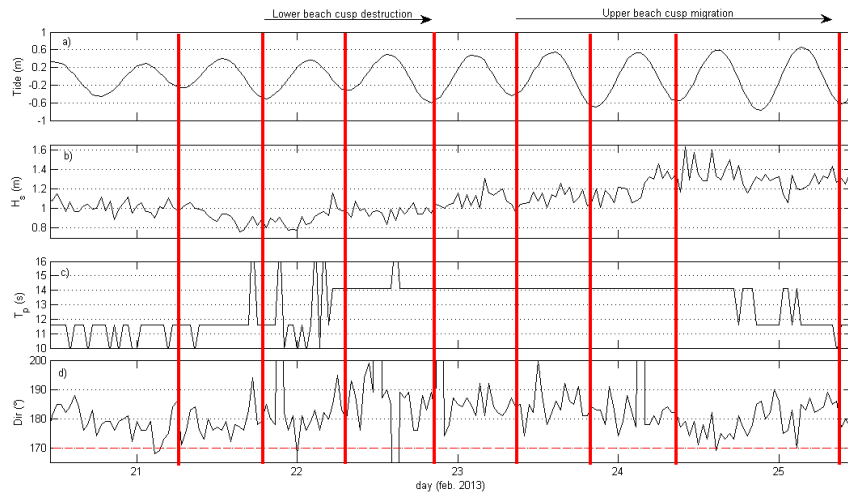


Figure 6. Hydrodynamic forcing observed from ADCP data from 21<sup>st</sup> to 25<sup>th</sup> Feb. 2013 showing a) tidal elevation, b) significant wave height  $H_s$ , c) peak period  $T_p$  and d) peak direction  $Dir$ . Red dashed line stands for shore normal incidence and red solid lines indicate times of the topographic surveys.

destruction through the difference between consecutive topographic surveys. We observe that, at the beginning of the survey period and consistent with morphological observations, topographic variations are not significant (or at least below the accuracy of the method). The only notable evolution is observed on the eastern part of the beach with two accretion patterns located in the bays of the lower cusp system. During the night from February 21<sup>st</sup> to February 22<sup>nd</sup> we observe an overall accretionary phase of the beach with significant accretion located in the bays of the lower cusp system. These results suggest that lower beach cusp decay might not be ascribed to the erosive conditions but rather to the persistence of accretionary conditions leading to the infilling of beach cusp bays (Almar *et al.*, 2008) or to the persistence of calm conditions (Masselink *et al.*, 1997).

Similarly, the disappearance of the western upper beach cusp may be related to an accretion pattern and to the merging of two individual cusps. The work of Almar *et al.* (2008), based on 3-year data set of video images collected at Tairua Beach (New Zealand), reported several cases of cusp merging. Interestingly, the two cusps that merged during the experiment are the two with the shortest spacings. This is in agreement with existing nonlinear

modeling of nearshore bedforms dynamics showing that coalescence and splittings are an attempt of the bedforms to self-organize into a more alongshore-uniform pattern as splitting is confined to the longest bedforms, whereas merging usually combines the smaller spacings into a longer one (Castelle and Ruessink, 2011). Starting from February 23<sup>rd</sup>, we observe significant erosion patterns associated in some cases with accretion patterns, suggests a slow alongshore eastward migration of the remaining beach cusp systems.

## DISCUSSION AND CONCLUSIONS

This paper presents the first observations on beach cusp dynamics at Grand Popo Beach. Our results indicate that GPP beach sometimes exhibits a double beach cusp system, consistent with other observations in the same area (Antea, 1987). Along the 300-m long stretch of beach surveyed, we clearly observed two systems of cusps at the early stage of the experiment: seven beach cusp wavelengths in the lower system and six wavelengths in the upper system. The upper beach cusp system was relatively asymmetric with a wavelength of about 40 m. In contrast, the lower beach cusp system was relatively symmetric with a slightly shorter wavelength ( $\sim 35$  m). This data set is unique because it catches in detail the destruction of the lower beach cusp system and the partial destruction of the upper beach cusp one but also the a very short sequence of formation/destruction of the lower beach cusp system. Consistent with previous observations (Masselink, 1997; Almar *et al.*, 2008), the destruction of the lower beach cusps at the beginning of the survey may be associated to calm conditions and/or persistent accretion conditions. Figure 6 illustrates the hydrodynamic conditions during the field experiment. We clearly observe that at the onset of the lower beach cusp destruction, swell is of low energy and long, favoring accretionary conditions. Castelle *et al.* (2014) also noticed a change in the wave-driven circulation. While during the first period of the survey, wave-driven circulation was characterized by weak longshore currents with flash and swash rips, the second period of the field survey was characterized by dominant longshore currents further increasing in speed, and rare swash rips.

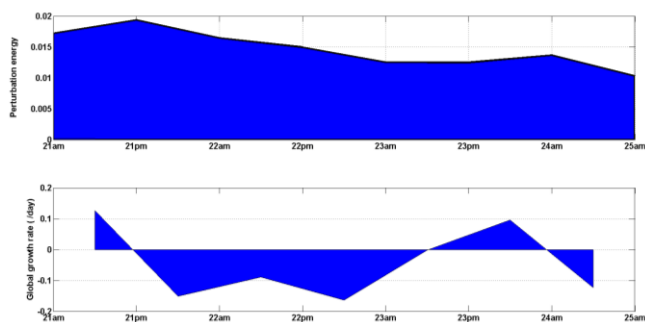


Figure 5. (upper) Energy of the perturbation per unit surface (equation 2) and (lower) global growth rate of the energy of perturbation per unit surface in  $\text{day}^{-1}$  (equation 3).

The swash rips occur preferably at mid- to high-tide in the center of beach cusps with no significant influence of the incoming wave characteristics. Their presence at the beginning of the field survey may explain the persistence of the lower beach cusp set, despite moderate and essentially accretion conditions possibly induce bay infilling. Indeed, Almar *et al.* (2008) indicated that with respect to the accretionary events, the processes that allow beach cusps to be maintained or grow cannot cope with a large increase in beach volume. The change in wave-driven circulation coinciding with a shift from neap to spring tide cycle can explain the progressive decay of the upper beach cusp system and its slow alongshore migration. Visual observations clearly indicate bench of erosion at the cusp horns (Figure 7). Our observations, consistent with previous studies, suggest that beach cusps certainly arise as a result of some combination of the erosion and accretion with tides complicating the temporal and spatial patterns of net morphological changes (Coco *et al.*, 2004, van Gaalan *et al.*, 2013). Nevertheless, the growth of the lower beach cusp system, coupled with the upper one on February 24 is not clear at the moment and further investigations should be undertaken. Detailed analysis of the swash hydrodynamics using either the video data (timestacks) or the video pole arrays (details concerning the method are provided in Lefevre *et al.*, 2014) should allow better insight.

### ACKNOWLEDGEMENT

This study was funded by the French INSU LEFE and EC2CO programs, the IRD (Action Incitative program), and the ICMIPA-UNESCO Chair. NS was also financially supported by ANR Barbec. We are greatly indebted to the Beninese Navy at Grand Popo, for their logistic support during the field experiment and allowing the installation of the permanent video system on the semaphore.

### LITERATURE CITED

- Almar, R., Coco, G., Bryan, K.R., Huntley, D.A., Short, A.D., Senechal, N., 2008. Video observations of beach cusp morphodynamics. *Marine geology*, 254, 216-233.
- Almar, R., Hounkonnou, N., Anthony, E., Castelle, B., Senechal, N., Laibi, R., Mensah-Senoo, T., Degbe, G., Quenum, M., Dorel, M., Chuchla, R., Lefebvre, J-P, du Penhoat, Y., Laryea, W.S., Zodehougan, G., Sohoul, Z., and Appeaning Addo, K., Kestenare, E., 2014. The grand Popo beach experiment, Benin, West Africa: from short timescale processes to their integrated impact over long-term coastal evolution. In Proceedings 13th International Coastal Symposium (Durban, South Africa), *Journal of Coastal Research*, Special Issue No. 66, ISSN 0749-0208.
- Antia, E.E., 1987. Preliminary field observations on beach cusp formation and characteristics on tidally and morphodynamically distinct beaches on the Nigerian coast. *Marine Geology*, 78, 23-33.
- Castelle, B., Mariou, V., Coco, G., Bonneton, P., Bruneau, N., Ruessink, B.G., 2012. On the impact of an offshore bathymetric anomaly on surf zone rip channels. *Journal of Geophysical Research*, 117, F01038. doi:10.1029/2011JF002141.
- Castelle, B., Ruessink, B.G., 2011. Modeling formation and subsequent nonlinear evolution of rip channels: time-varying versus time-invariant wave forcing. *Journal of Geophysical Research*, 116(F04008), doi: 10.1029/2011JF001997,
- Castelle, B., Almar, R., Dorel, M., Lefebvre, J-P, Sénéchal, N., Anthony, E., Laibi, R., Chuchla, R., du Penhoat, Y., 2014. Flash rip dynamics on a high-energy low-tide-terraced beach (Grand Popo, Benin, West Africa). In Proceedings 13th International Coastal Symposium (Durban, South Africa), *Journal of Coastal Research*, Special Issue No. 66, ISSN 0749-0208.
- Coco, G., O'Hara, T.J., Huntley, D.A., 1999. Beach cusps: a comparison of data and theories for their formation. *Journal of Coastal Research*, 15(3), 741-749.



Figure 7. Erosion patterns at the horn cusps.

- Coco, G., Huntley, D.A., O'Hara, T.J., 2000. Investigation of a self-organization model for beach cusp formation and development. *Journal of Geophysical Research*, 105(C9), 21991-22002.
- Coco, G., Burnet, T.K., Werner, B.T., Elgard, S., 2003. Test of self-organization in beach cusp formation. *Journal of Geophysical Research*, 108(C3), 46.&-46.11.
- Coco, G., Burnet, T.K., Werner, B.T., Elgard, S., 2004. The role of tides in beach cusp development. *Journal of Geophysical Research*, 109(C4), C04011.
- Garnier, R., Calvete, D., Falques, A., Caballeria, M., 2006. Generation and nonlinear evolution of shore-oblique/transverse sand bars. *Journal of Fluid Mechanics*, 567, 327-360.
- Garnier, R., Dodd, N., Falques, A., Calvete, D., 2010. Mechanisms controlling crescentic bar amplitude. *Journal of Geophysical Research*, 115, F02007, doi:10.1029/2009JF001407.
- Guza, R.T., Inman, D.L., 1975. Edge waves and beach cusps. *Journal of Geophysical Research*, 80(21), 2997-3012.
- Inman, D.L., Guza, R.T., 1982. The origin of swash cusps on beaches. *Marine Geology*, 49, 133-148.
- Komar, P.D., 1973. Observations of beach cusps at Mono lake, California. *Geol. Soc. Amer. Bull.* 84, 3593-3600.
- Komar, P.D., 1983. Rhythmic shoreline features and their origin. In: Gardner, R., Scoging, H. (eds.), *Mega-geomorphology*. Oxford Univ. Press, Oxford, 92-112.
- Laibi, R., Anthony, E., Almar, R., Castelle, B., Senechal, N., 2014. Morphodynamic characterisation of the human-impacted Bight of Benin sand barrier coast, West Africa. In Proceedings 13th International Coastal Symposium (Durban, South Africa), *Journal of Coastal Research*, Special Issue No. 66, ISSN 0749-0208.
- Lefebvre J-P., Viêt N.T., Almar R., Uu D.V., Thuan D.H., Binh L.T., My, T.V., 2014. Contribution of the swash generated by low energy wind waves in the recovery process of a beach impacted by extreme waves. In Proceedings 13th International Coastal Symposium (Durban, South Africa), *Journal of Coastal Research*, Special Issue No. 66, ISSN 0749-0208.
- Masselink, G., 1999. Alongshore variation in beach cusp morphology in a coastal embayment. *Earth Surface Process. Landf.*, 24(4), 335-348.
- Masselink, G., Pattiaratchi, C.B., 1997. Morphological evolution of beach cusp morphology and associated swash circulation patterns. *Marine Geology*, 146, 93-113.
- Masselink, G., Hegge, B.J., Pattiaratchi, C.B., 1997. Beach cusp morphodynamic. *Earth Surface Process. Landf.*, 22, 1139-1155.
- Mii, H., 1968. Beach cusps on the Pacific coast of Japan. *Tohoku Univ. Sci. Rep. 2<sup>nd</sup> Ser.*, 29, 77\_107.
- Russell, R.J., McIntire, W.G., 1965. Beach cusps. *Geol. Soc. Amer. Bull.* 76, 307-320.
- Van Gaalan, J.F., Kruse, S.E., Coco, G., Collins, L., Doering, T., 2011. Observations of beach cup evolution at Melbourne beach, Florida, USA. *Geomorphology*, 129, 131-140.
- Werner, B.T., Fink, T.M., 1993. Beach cusps as self-organised patterns. *Science*, 260, 968-971.
- Williams, A.T., 1973. The problem of the beach cusp development. *J. Sediment. Petrol.*, 43, 857-866.

# Nearshore and foreshore influence on overwash of a barrier island

Ana Matias†, Ana R. Carrasco†, Carlos Loureiro‡∞, Sílvia Almeida†, Óscar Ferreira†

† CIMA, Universidade do Algarve, Campus de Gambelas, 8005-139 Faro, Portugal  
ammatias@ualg.pt

azarcos@ualg.pt  
cloureiro@ualg.pt  
smalmeida@ualg.pt  
oferreir@ualg.pt

‡ Centre for Coastal and Marine Research School of Environmental Sciences University of Ulster Coleraine, Northern Ireland, UK

∞ Geological Sciences School of Agriculture, Earth and Environmental Sciences University of KwaZulu-Natal Westville, Durban, South Africa



[www.cerf-jcr.org](http://www.cerf-jcr.org)



[www.JCRonline.org](http://www.JCRonline.org)

## ABSTRACT

Matias, A., Carrasco, A.R., Loureiro, C., Almeida, S., Ferreira, Ó., 2014. Nearshore and foreshore influence on overwash of a barrier island. In: Green, A.N. and Cooper, J.A.G. (eds.), *Proceedings 13<sup>th</sup> International Coastal Symposium* (Durban, South Africa), *Journal of Coastal Research*, Special Issue No. 70, pp. 675-680, ISSN 0749-0208.

Accurate prediction of the occurrence and morphological consequences of overwash are important for coastal flood risk assessment and management. A number of morphological and oceanographic factors controlling overwash have been identified by several authors, including nearshore bathymetry. This work intends to identify alongshore variations in storm impact and evaluate the role of sub-aerial and submerged morphological variations in overwash occurrence. For this study, 24 cross-shore topo-bathymetric profiles were set on Barreta Island (Ria Formosa barrier island system, Portugal), extending from the nearshore to the lagoon level on the island backbarrier. Pre- and post-overwash surveys were made between August 2012 and April 2013. Offshore wave characteristics were obtained during overwash events including offshore significant wave height (Hs), peak period and wave direction. Wave propagation and wave parameters at breaking were obtained from SWAN model simulations. During the study period, overwash occurred both under storm conditions (e.g., Hs = 3.8 m) and non-storm conditions (e.g., Hs = 0.8 m), the latter coincident with spring high-tide. Overwash water intrusion distance across the barrier varied alongshore between 0 m (no overwash) and 40 m (reaching lagoon waters). Beach morphology was spatially variable, and changeable from one overwash episode to the next. Important morphological variations of the barrier include modification of barrier crest elevation, beach slope, and presence of swash bars in the vicinity of Ancão Inlet. Predictions of overwash occurrence were made by means of the computation of the Overwash Potential (OP), defined as the difference between the wave runup and the barrier elevation. Several runup equations were tested, and the results of obtained OP were compared to the observations of actual overwash occurrence to determine the most reliable approach. The selected predictor provided an accuracy of 88% for the identification of the locations where overwash processes occurred along the barrier. The predictions were variable alongshore due to variations in breaking waves and beach slope, which in turn are related to the existence of nearshore bars, associated with the presence of the updrift Ancão Inlet. This study proves that nearshore and foreshore morphologies have a major impact on the longshore variation of overwash distribution.

**ADDITIONAL INDEX WORDS:** *Swan, runup predictor, beach, storm, coastal hazards.*

## INTRODUCTION

Overwash associated with major storms may seem catastrophic, however, in the longer term point (hundreds of years), overwash can be considered as a nearly continuous process, shaping and reshaping coastal barriers (Leatherman, 1988). Where overwash processes are allowed to occur, the net volume of sand is often maintained, with the morphology translating shoreward (Dolan and Godfrey, 1973). Accurate prediction of the occurrence and morphological consequences of overwash is of obvious importance for coastal flood risk assessment and management (Matias *et al.*, 2008).

Factors controlling the frequency and intensity of overwash, and the resulting morphologies, include marine conditions (e.g. Fisher *et al.*, 1974), the orientation of the coast relative to the storm (e.g. Fletcher *et al.*, 1995), nearshore bathymetry (e.g. Ritchie and Penland, 1988), beach topography (e.g. Leatherman, 1976), backbeach elevations (e.g. Morton and Sallenger, 2003), dune morphology (e.g. Donnelly and Sallenger, 2007), and engineering structures (e.g. Hayden and Dolan, 1977). Sallenger (2000) developed a conceptual model for predicting storm responses and

scaling magnitudes of coastal changes, including an overwash regime. In this model, overwash occurrence depends on the relation between the maximum elevation of runup on the beach (dependent on astronomical tide, storm surge, wave height and wavelength, and beach slope) and dune crest level. This approach has been tested using field data with reasonable results (e.g. Wetzell *et al.*, 2007) and run-up formulae have been empirical parameterized (e.g. Stockdon *et al.*, 2006). However a detailed analysis of the influence of other foreshore factors in overwash occurrence and alongshore variability is still needed. The objectives of the current work are (1) to identify and describe longshore variations in storm impacts along a barrier island; and (2) to evaluate the role of sub-aerial and submerged morphological variations in overwash occurrence.

## STUDY AREA

The study area is located on the western section of Barreta Island, which is part of the Ria Formosa barrier island system, in southern Portugal (Figure 1). The barrier island chain extends for 55 km alongshore and is presently composed of five islands and two peninsulas, separated by six tidal inlets.

The western part of Barreta Island starts downdrift of Ancão Inlet (Figure 1). This inlet was artificially relocated in June 1997,

reached dynamic equilibrium as a “mature migrating inlet” in May-July 1999 (Vila-Concejo *et al.*, 2003), and has been migrating eastward towards the study area. The mechanism of washover formation in the study area is inlet dynamics (Matias *et al.*, 2008), which promotes downdrift erosion, shoreline retreat and overwash. The typical barrier sedimentary environments found in the study area are: a reflective beach face on the seaward side of the barrier; a beach berm present only during high-volume stages, a washover crest, an extensive washover terrace surface, and the washover terminus on the landward side of the barrier.

Tides are semi-diurnal and mesotidal, with a mean tidal range of about 2 m that can reach up to 3.5 m during spring tides. Average high tide elevation is 1.4 m and 0.6 m above mean sea level (MSL) for spring and neap tide, respectively. An analysis of 2 years of records from a tidal gauge on the Algarve Coast (Lagos, Figure 1) showed a maximum observed storm surge level of +0.75 m (Gama *et al.*, 1994). The offshore wave climate is dominated by west-southwest waves (71% of occurrences, Figure 1; Costa *et al.*, 2001). SE waves that are short-period and generated by regional winds (locally called “Levante”) are also frequent (about 23%, Costa *et al.*, 2001). Average annual significant offshore wave height ( $H_s$ ) is 1.0 m and average peak period ( $T_p$ ) is of 8.2 seconds (Costa *et al.*, 2001). Storm events in the region (defined as  $H_s \geq 3.0$  m, Pessanha and Pires, 1981) corresponded to 1% of the offshore wave climate, between 1986 and 1993 (Costa, 1994). Western Barreta has a northwest-southeast orientation (Figure 1) such that it is directly exposed to dominant W-SW waves, and is relatively protected from SE waves.

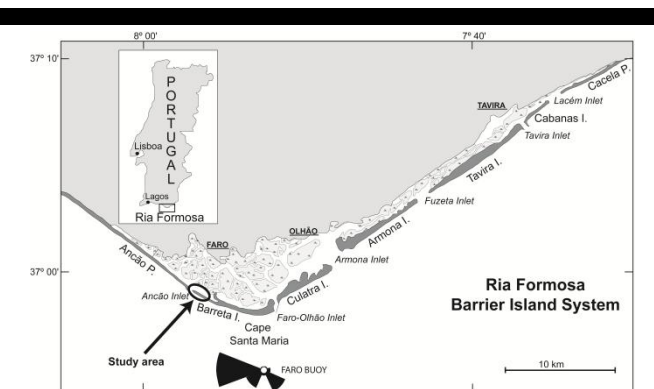


Figure 1. Locations of the study area within the Ria Formosa barriers (P.= Peninsula; I.= Island), tidal inlets and mainland cities. Wave rose positioned on the Faro buoy location using data from Costa *et al.* (2001).

## METHODS

### Hydrodynamics

Tidal and offshore wave data for each of the field surveys undertaken between 30 August 2012 and 26 April 2013 were used for this study. Predicted levels from the Instituto Hidrográfico de Portugal were used, and storm surge evaluated by the comparison between predicted levels and the observations from a tidal gauge located in Huelva, Spain (60 Km to the East). Offshore wave data were recorded by the Instituto Hidrográfico de Portugal using a directional wave-rider buoy offshore Cape Santa Maria (Figure 1) in a depth of 93 m (COSTA, 1994). Records were obtained for 20 minutes every 3 hours, except during storm periods when data were recorded every half hour. Overwash occurrence was determined by field comparison and observation and therefore the

exact timing of the start and end of the overwash events was not recorded. To obtain the most likely hydrodynamic conditions that promoted overwash, maximum significant wave heights ( $H_s$ ) coincident with high-tides were extracted for the days before the surveys, together with corresponding peak period ( $T_p$ ), and wave direction ( $\Theta$ ).

Numerical wave modelling with SWAN (Simulating Waves Nearshore; Booij *et al.*, 1999) was used to explore nearshore wave conditions during overwash. SWAN was run in stationary mode, using a nested scheme composed of three regular grids. Selected grid resolutions were 50 m x 50m for the regional grid, 18 mx 18m for the background grid (larger map of Figure 2) and 5 m x 5m for each of the detailed grids (smaller map of Figure 2, as an example), respectively. Model predictions were initialized on the open boundaries of the regional grid with the parametric input from the wave buoy time-series, using a JONSWAP spectral shape to represent the wave field. Input boundary conditions for the background and detailed grids were determined from the computations over the regional and background grids, respectively. Breaking wave heights were obtained for several positions alongshore.

### Morphology

To study longshore variations in overwash, 24 cross-shore topographic profiles were set on Barreta Island (Ria Formosa barrier island system, Portugal). Reference surveys were performed from August 30, 2012 until April 24, 2013, in order to measure pre-overwash conditions and afterwards repeated following overwash occurrence (Table 1).

Table 1. Fieldwork number, date and beach conditions during topographic surveys and bathymetric survey dates.

Survey	Topography date	Beach conditions	Bathymetry date
#1	30-08-2012	Reference pre-overwash	4/5-06-2012
#2	02-10-2012	Post-overwash	03-10-2012
#3	31-10-2012	Post-overwash	
#4	14-11-2012	Reference pre-overwash	13/14-11-2012
#5	19-11-2012	Post-overwash	
#6	28-12-2012	Reference pre-overwash	
#7	21-01-2013	Reference pre-overwash	
#8	30-01-2013	Post-overwash	04-02-2013
#9	13-02-2013	Post-overwash	
#10	13-03-2013	Post-overwash	
#11	26-04-2013	Fair-weather	26-04-2013

Profile measurements during surveys were made using a Real-Time Kinematic Differential Global Positioning System (RTK-GPS), sampling at 1 Hz. Topographic profiles covered the barrier from the low-tide level at the beach (depth  $\approx -1$  m, referred to mean sea level, MSL) until the lagoon level on the island backbarrier, with distances between consecutive profiles ranging from 60 m to 90 m, over a total extent of 1600 m. Also, an alongshore alignment was measured during the surveys, consisting of maximum runup (in the absence of overwash) or furthest overwash intrusion line (in the presence of overwash). These alignments were recognisable in the field by differences in the sand grain-size, sand tone (due to differences in moisture content),

alignments of debris or shells, and only seldomly by superficial sedimentary structures.

The bathymetric profile surveys were undertaken less frequently because changes in the nearshore morphology are smaller during non-storm conditions and also because occasionally the oceanographic conditions would not guarantee the safety of equipment and people aboard. Bathymetric surveys had the same spacing and followed the orientation of topographic profiles until a depth of about -12 m MSL. They were made using an RTK-GPS, coupled with an eco-sounder, with data-synchronization and navigation assured by the software Hypack. This method has an estimated average error of 0.030 m (Horta, J. and Pacheco, A., oral communication).

Post-processing of bathymetric data included data-quality check, de-spiking and smoothing of profiles.

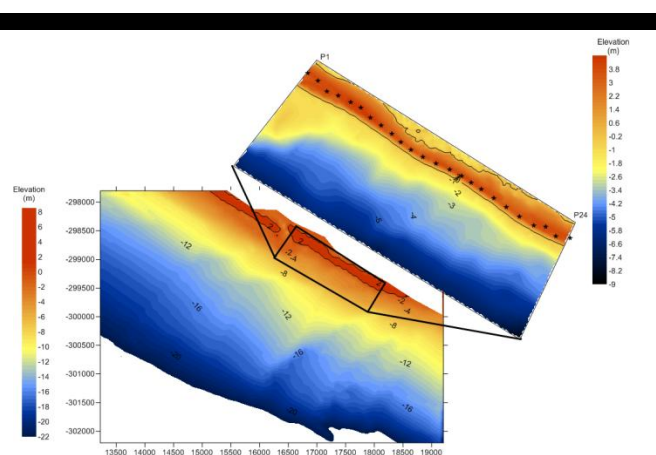


Figure 2. Topo-bathymetric maps of the study area, including the extensive background survey (until -22 m) and a detailed survey from 2<sup>nd</sup> and 3<sup>rd</sup> of October 2012. Ancão Inlet is visible in the background survey, at NW of the study area. The stars on the top map represent the location of the barrier crest in each of the 24 profiles.

### Overwash potential

According to the hydrodynamic and morphological characteristics recorded for each of the studied events, the likelihood of overwash occurrence was estimated. This was made by the computation of the overwash potential, OP (described in Matias *et al.*, 2012):

$$OP = R_{\text{high}} - h_c = R_2 + \eta - h_c \quad (1)$$

where:  $R_{\text{high}}$  is the highest elevation of the landward margin of swash relative to a fixed vertical datum (Sallenger, 2000),  $h_c$  is the barrier crest elevation,  $R_2$  is the 2% exceedance level for vertical runup, including setup and swash, and  $\eta$  is sea level. When OP is negative, wave runup is lower than the barrier crest and insignificant morphological changes are noticed at the barrier crest. When OP is positive, overwash occurs because the predicted runup elevation is higher than the barrier crest. Positive OP values are indicative of overwash water depth over the crest; therefore greater OP values imply larger overwash events and larger morphological changes. The results from one of the events were used to investigate the applicability of a number of wave runup

predictors ( $R_2$ ), similarly to what was done with data from overwash laboratory experiments BARDEX (Matias *et al.*, 2012) and BARDEX II (Matias *et al.*, 2013). The wave runup equations that were tested in this study can be found in Hunt (1959), Guza and Thornton (1982), Holman (1986), Mase (1989), Powell (1990), Nielsen and Hanslow (1991), van der Meer and Stam (1992), Komar (1998), Ruggiero *et al.* (2001), Lorang (2002), Hughes (2004) and Stockdon *et al.* (2006). The description of each equation can be found in Matias *et al.* (2012).

## RESULTS AND DISCUSSION

Throughout all surveys of the monitoring period the barrier profile was variable alongshore. The barrier was generally narrower in the middle section (around profile P10, Figure 3) where the barrier width reached only about 70 m at MSL. The wider barrier was permanently located on the northwestern end of the study area (profiles P1 to P5, Figure 3), where the barrier is about 150 m wide at MSL. The barrier crest, herein defined as the portion of the barrier with highest elevation, and most of the backbarrier, were generally composed of bare sand. Along the northwestern section recent dune development was noticed together with the colonization by pioneer dune vegetation. On the southeastern area dunes were also present as isolated patches, which are relict remnants of a former dune crest that has been destroyed by overwash and breaching. Generally, a single barrier crest was present, but on profiles P1 to P3, two or three barrier crests existed (Figure 3).

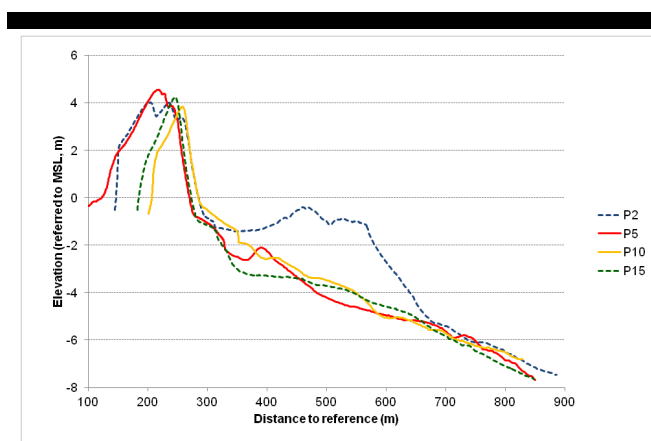


Figure 3. Topo-bathymetric profiles extracted from the survey undertaken on the 3<sup>rd</sup> October 2012. Represented profiles are from locations P2, P5, P10 and P15, as examples of different barrier sub-aerial and submerged morphologies.

The overall shoreline alignment was not rectilinear; rather it exhibited prominent and reentrant areas, visible in Figure 2 by the orientation of the barrier crest (represented by stars). The irregularities were not rhythmic and display variable locations from one survey to the next. The backbarrier slope facing the lagoon was steep and always sandy until the MSL contour. At lower elevations the backbarrier margin was often occupied by overwash fans or tidal flats.

The beach face was generally intermediate to reflective (Figure 3), with average beach slope ranging from 0.09 to 0.14. The beach

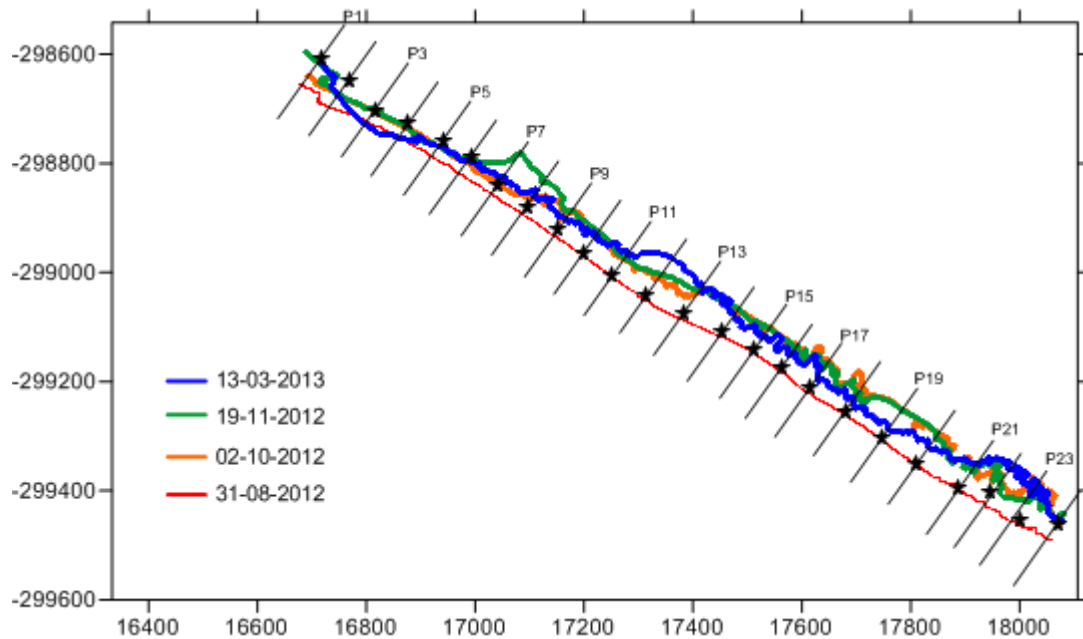


Figure 4. Maximum overwash intrusion lines along the study area, for dates 02-10-2012, 19-11-2012 and 13-03-2013; and maximum runup on the top of the beach face on 31-08-2012. The position of the crest of each profile in 02-10-2012 is represented by a star.

face occasionally exhibited beach cusps with variable wave-length and changing location but that rarely extended throughout the entire study area. On the lower foreshore, some profiles intersected a flat low-tide terrace (slope of 0.01 to 0.02) at elevations around -1 to -1.5 m (MSL; profile P10 of Figure 3 is an example). These low-lying morphologies had restricted longshore extension, generally less than 200 m. In the nearshore, between -3.5 m to -4 m MSL, sand bars with larger alongshore and cross-shore extensions were observed (around profiles P9, P10 and P11 of Figure 2). These morphologies, often related to rip-bar systems, are not rhythmic topography *sensu stricto* as a wavelength could not be attributed. There was no systematic alongshore repetition of features with similar characteristics; rather there were sand bars with somewhat different dimensions along the nearshore of the barrier (Figure 2). The comparison between surveys suggests that the bars changed in shape and position. Nevertheless, the most striking morphological feature of the nearshore is the ebb tidal delta of Ancão Inlet (Figure 2), that limits the study area to the northwest. The delta and associated swash bars are large features that changed dramatically the nearshore (profile P2 of Figure 3), affecting directly the barrier, most notably until the location of profile P4 (Figure 2). The additional volume of sediments in the nearshore (from 0 to -8.0 m, MSL) of profile P2 in relation to other profiles located further downdrift from Ancão Inlet (e.g. P10 or P15, Figure 3) is approximately 900 m<sup>3</sup>/m, which corresponds to about 30% more for the beach profile volume at those depths.

The effects of six overwash events were measured (Table 1) during the study period. For these six events, overwash occurred twice under storm conditions (25 October 2012 and 15 to 17 November 2012) while the other four occurred under non-storm conditions, but coinciding with spring high-tides. Overwash occurrence of November 2012 was related to a storm event, over which  $H_s$  reached maximum values of 3.8 m (the highest value recorded during the monitoring period), with a tidal level of 1.4 m MSL). Non-storm overwash was, on the other hand, promoted by significantly lower waves ( $H_s = 0.8$  m) recorded on March 12, 2013, but coincident with equinoctial spring tides, which reached

a level of about 1.5 m above MSL. However, for this last event overwash did not occur in many of the profiles (Figure 4).

Pre-overwash crest elevation was 3.5 m to 4.7 m, and although morphologic variations occurred during overwash throughout the study area, the same range of crest elevations was observed after overwash. Overwash water intrusion distance across the barrier varied alongshore between 0 m (no overwash) and 40 m (Figure 4). Particularly relevant, however, was the fact that more energetic waves present during storm overwash did not generate longer intrusions than non-storm overwash. In some profiles, overwash water intrusion reached the furthest position during the non-storm event measured on the 13<sup>th</sup> March 2013 (such as profile P12), while for the more energetic storm in November 2012, overwash intrusion reached further inland on profiles P7, P8 and P19, for example (Figure 4).

To further investigate the differences in overwash characteristics along the study area, the overwash episode that generated the most variable barrier response was selected as case study. This corresponded to non-storm overwash episode measured on the 2<sup>nd</sup> of October 2012, promoted by waves with offshore  $H_s = 0.89$  m,  $T_p = 9.1$  s and a tide level of 1.35 m above MSL. The storm surge level for that day, obtained from the tidal gauge, was negligible. The results of SWAN model for the breaking conditions in the nearshore showed that  $H_{sb}$  varied from 0.80 m to 1.25 m (Figure 5). The highest waves were breaking on top of the ebb delta of Ancão Inlet, on profile P2, at Northwest of the study area. At profiles P20 and P21,  $H_{sb}$  also reached 1.0 m (Figure 5). During this event, overwash was observed from profiles P9 until P23, however, water intrusion was variable, reaching the lagoon waters in profiles P11 to P16, P19 and P20. In places, such as P23, the existence of remnants of vegetated dunes on the backbarrier limited the overwash water progression into landward positions. The beach slope varied between 0.10 and 0.14, and the barrier crest elevation varied between 3.48 m and 4.54 m above MSL.

Because overwash was not uniform alongshore, the evaluation of Overwash Potential (OP) to accurately predict overwash was

more demanding. OP was computed using the 12 equations mentioned above for the computation of the runup. Alongshore variable breaking wave conditions were used for the computation of runup instead of a unique value that represents offshore conditions. All equations, except one failed to accurately predict more than 75% of swash/overwash cases for this survey. The most

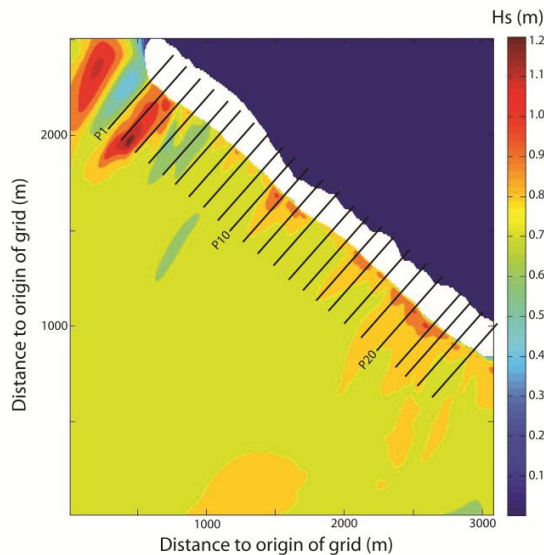


Figure 5. Distribution of significant wave height ( $H_s$ ) on the study area during the overwash event of October 2012. The profile location is also represented.

accurate predictor of runup was Mase's (1989) equation, which correctly predicted the storm impact for 21 profiles (P3 to P7 and P9 to P24, Figure 6). Such predictions imply that OP had an 88% accuracy using Mase's equation. Therefore, OP is given by the following equation:

$$OP = 1.86H_b\zeta^{0.71} + \eta + h_c \quad (2)$$

where  $\zeta$  is the Iribarren Number (Battjes, 1974) given by:

$$\zeta = \tan\beta(H_s/L_o)^{-0.5} \quad (3)$$

where  $\tan\beta$  is beach slope and  $L_o$  is the deep-water wave length. OP computed with equation 2 has been previously considered to over-estimate runup (Matias *et al.*, 2012; 2013). Moreover, the application of the most widely used runup equation, developed by Stockdon *et al.* (2006), failed to produce overwash in any of the profiles, clearly underestimating actual overwash occurrence. This is in agreement with previous studies undertaken in the Ria Formosa barrier system (specifically in Ancão Peninsula) where it was concluded that Stockdon *et al.* (2006) equation underestimated runup (Vousdoulas *et al.*, 2012) and therefore incorrectly predicted the storm impact regime in 55% of cases (Almeida *et al.*, 2012).

The cases where OP was inaccurately predicted using equation 2 were the ones located closer to Ancão Inlet (P1 and P2) and at P8 (Figure 4). For profiles P1 and P2, overwash occurrence was predicted but it did not occur. The swash bars that form part of the ebb delta of Ancão Inlet induced higher breaking waves (Figure 5), but also breaking positions seaward than in other parts of the barrier. The dissipation of energy at such seaward locations frequently caused wave reformation and a second wave breaker. These conditions induced a runup excursion that did not reach the barrier crest, and consequently did not promote overwash. It must

be stressed that the sand retention in the Ancão Inlet associated morphologies promotes downdrift sediment starvation (Vila-Concejo *et al.*, 2003), which is the main cause of overwash in the study area (Matias *et al.*, 2009). Furthermore, inlet dynamics was identified as the most important process contributing to the occurrence of overwash in the barrier islands of the Ria Formosa, accounting for 57% of all washover morphologies formed between 1947 and 2001 (Matias *et al.*, 2008). For profile P8 was the reverse; no overwash was predicted (OP = -0.22 cm, Figure 6) because of a combination of the lowest  $H_{sb}$  (0.8 m, Figure 5) with a flatter beach face slope (0.11). It is possible that small variations in morphology occurred between the overwash episode (28 September 2012) and the survey (2-3 October 2012) that influenced important factors such as the position of nearshore bars and variability in beach slope.

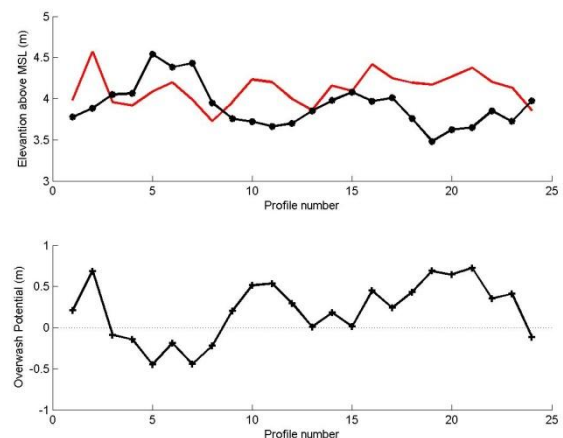


Figure 6. Upper panel: Barrier crest elevation (in black and connected dots) along the study area, from Northwest (to the left) to Southeast (to the right) and computed runup elevation (in red) for the same locations, for October 2012 event. Overwash is expected when the red line is above the black line. Lower panel: Overwash potential computed for all profiles. Positive values of Overwash Potential in the lower panel are indicative of overwash.

## CONCLUSIONS

This paper highlights the importance of foreshore and nearshore morphological features in storm impacts along a barrier island. The barrier exhibits significant alongshore variations, including variable barrier width and beach slope, presence of beach cusps and swash bars. Irregularities in the nearshore of the study area are mostly related to sand bars that are either moving downdrift from Ancão Inlet or are remnants of ebb delta sediments from previous Ancão Inlet positions.

Overwash occurrence was predicted using the Overwash Potential, which was tested using several runup predictors. Mase (1989) equation proved to be the most accurate, being able to correctly predict swash/overwash on 88% of the analyzed profiles. Shortcomings in the application of OP as presented here may arise from the lack of a parameter that relates the distance between the breaker position and the barrier crest. It is relevant to consider that nearshore bars influence wave shoaling and breaking, which in turn is important to promote alongshore gradients, and hence variations in overwash occurrence. This can only be partially accounted for in the computation of runup by the use of variable  $H_{sb}$ , obtained from the application of wave propagation models.



However, other important spatial variables may also need to be taken into account to improve predictions. These include the distance between the barrier crest and the breaker positions, or between the barriers crest and beach berm positions. The incorporation of these morphological variables is a crucial step towards more accurate predictions.

### ACKNOWLEDGEMENT

The data reported were collected within RUSH project (From Runup to Overwash), PTDC/CTE-GIX/116814/2010 financed by Fundação para a Ciência e a Tecnologia (FCT). Ana Matias was supported by Programme Investigator FCT. Ana Rita Carrasco and Carlos Loureiro were supported by the FCT, grant references SFRH/BPD/88385/2012 and SFRH/BPD/85335/2012, respectively. We would like to thank RUSH collaborators for their contributions during fieldwork: André Pacheco, Isabel Mendes, Mara Nunes, Margarida Ramires.

### LITERATURE CITED

- Almeida, L.P., Voudoukas, M.I., Ferreira, Ó., Rodrigues, B. and Matias, A., 2012. Thresholds for storm impacts on a sandy exposed coastal area. *Geomorphology*, 143, 3-12.
- Battjes, J.A., 1974. Runup distributions of waves breaking on slopes. *Journal of Waterways, Harbors, and Coastal Engineering*, 97(WW1), 91-114.
- Booij, N., Ris, R.C. and Holthuijsen, L.H., 1999. A third-generation wave model for coastal regions – 1. Model description and validation. *Journal of Geophysical Research* 104(C4), 7649-7666.
- Costa, C., 1994. *Final Report of Sub-Project A. Wind Wave Climatology of the Portuguese Coast*. IH/LNEC, Portugal, Report PO-WAVES 6/94-A, 80 p.
- Costa, C., Silva, R. and Vitorino, J., 2001. Contribuição para o estudo do clima de agitação marítima na costa portuguesa. *Proceedings of 2as Jornadas Portuguesas de Engenharia Portuária*, Sines, Portugal, PIANC, CD-ROM.
- Dolan, R. and Godfrey, P., 1973. Effects of Hurricane Ginger on the barrier islands of North Carolina. *Geological Society of America Bulletin*, 84, 1329-1334.
- Donnelly, C. and Sallenger, A.H., 2007. Characterisation and modeling of washover fans. *Proceedings of Coastal Sediments '07*, ASCE, New Orleans, USA, pp. 2061-2073.
- Fisher, J.S., Leatherman, S.P., and Perry, F.C., 1974. Overwash processes on Assateague Island. *Proceedings of 14th Conference on Coastal Engineering*, ASCE, Copenhagen, Denmark, pp. 1194-1211.
- Fletcher, C.H., Richmond, B.M., Barnes, G.M., and Schroeder, T.A., 1995. Marine flooding on the coast of Kauai during Hurricane Iniki: Hindcasting inundation components and delineating washover. *Journal of Coastal Research*, 11(1), 188-204.
- Gama, C., Dias, J.A., Ferreira, Ó. and Taborda, R., 1994. Analysis of storm surge in Portugal, between June 1986 and May 1988. *Proceedings of the 2nd International Symposium on Coastal Zone Research – Management and Planning*, Lisbon, Portugal, EUROCOAST, pp. 381-387.
- Guza, R.T. and Thornton, E.B., 1982. Swash oscillations on a natural beach. *Journal of Geophysical Research*, 87 (C1), 483-491.
- Holman, R.A., 1986. Extreme value statistics for wave run-up on a natural beach. *Coastal Engineering*, 9, 527-544.
- Hughes, S.A., 2004. Estimation of wave run-up on smooth, impermeable slopes using the wave momentum flux parameter. *Coastal Engineering*, 51, 1085-1104.
- Hunt, I.A., 1959. Design of seawalls and breakwaters. *Journal of Waterways and Harbors*, Division 85 (WW3), 123-152.
- Komar, P.D., 1998. *Beach processes and sedimentation*. Prentice Hall, New Jersey, 544 pp.
- Leatherman, S.P., 1976. *Quantification of overwash processes*. Ph.D. Thesis, University of Virginia, USA, 245 pp.
- Leatherman, S.P., 1988. *Barrier island handbook*. Coastal Publications Series, Laboratory for Coastal Research, University of Maryland, 92 p.
- Mase, H., 1989. Random wave runup height on gentle slope. *Journal of Waterway, Port, Coastal, and Ocean Engineering*, 115, 649-661.
- Matias, A., Ferreira, Ó., Vila-Concejo, A., Garcia, T., Dias and J.A., 2008. Classification of washover dynamics in barrier islands. *Geomorphology*, 97, 655-674.
- Matias, A., Vila-Concejo, A., Ferreira, Ó., Morris, B., and Dias, J.A. 2009. Sediment dynamics of barriers with frequent overwash. *Journal of Coastal Research*, 25(3), 768-780.
- Matias, A., Williams, J., Masselink, G. and Ferreira, Ó., 2012. Overwash threshold for gravel barriers. *Coastal Engineering*, 63, 48-61.
- Matias, A., Masselink, G., Kroon, A., Blenkinsopp, C. and Turner, I.L., 2013. Overwash experiment on a sandy barrier. *Journal of Coastal Research*, SI 65, 778-783.
- Morton, R.A. and Sallenger, A.H., 2003. Morphological impacts of extreme storms on sandy beaches and barriers. *Journal of Coastal Research*, 19(3), 560-573.
- Nielsen, P. and Hanslow, D.J., 1991. Wave runup distributions on natural beaches. *Journal of Coastal Research*, 7 (4), 1139-1152.
- Pessanha, L.E. and Pires, H.O. 1981. *Elementos sobre o clima de agitação marítima na costa sul do Algarve*. Report of Instituto Nacional de Meteorologia e Geofísica, Portugal, 66 p.
- Ritchie, W. and Penland, S., 1988. Rapid dune changes associated with overwash processes on the deltaic coast of South Louisiana. *Marine Geology*, 81, 97-122.
- Ruggiero, P., Komar, P.D., McDougal, W.G., Marra, J.J. and Beach, R.A., 2001. Wave runup, extreme water levels and the erosion of properties backing beaches. *Journal of Coastal Research*, 17(2), 407-419.
- Sallenger, A.H., 2000. Storm impact scale for barrier islands. *Journal of Coastal Research*, 16(3), 890-895.
- Stockdon, H.F., Holman, R.A., Howd, P.A. and Sallenger, A.H., 2006. Empirical parameterization of setup, swash, and runup. *Coastal Engineering*, 53, 573-588.
- van der Meer, J.W. and Stam, C.M., 1992. Wave runup on smooth and rock slopes of coastal structures. *Journal of Waterway, Port, Coastal, and Ocean Engineering*, 118, 534-550.
- Vila-Concejo, A., Ferreira, Ó., Matias, A., and Dias, J.A., 2003. The first two years of an inlet: sedimentary dynamics. *Continental Shelf Research*, 23, 1425-1445.
- Voudoukas, M.I., Ferreira, Ó., Almeida, L.P., Pacheco, A., 2012. Towards reliable storm-hazard forecasts: XBeach calibration and its potential application in an operational early-warning system. *Ocean Dynamics*, 61, 1001-1015.
- Wetzell, L.M., Howd, P.A. and Sallenger, A.H., 2003. Simple models for predicting dune erosion hazards along the Outer Banks of North Carolina. *Proceedings of Coastal Sediments '03*, ASCE, CD-ROM.

# Morphodynamic variations of a macrotidal beach (Atalaia) on the Brazilian Amazon Coast

Luci C.C. Pereira†, Ketellyn S.T. Pinto†, Ana Vila-Concejo‡

† Instituto de Estudos Costeiros, Alameda  
Leandro Ribeiro, s/n, Aldeia, Bragança,  
68600-000, Brazil  
cajueiro@ufpa.br  
ket\_ufpa@yahoo.com.br

‡ School of Geosciences F09,  
The University of Sydney, Sydney, NSW  
2006, Australia  
ana.vilaconcejo@sydney.edu.au



[www.cerf-jcr.org](http://www.cerf-jcr.org)



[www.JCRonline.org](http://www.JCRonline.org)

## ABSTRACT

Pereira, L.C.C., Pinto, K.S.T., Vila-Concejo, A., 2014. Morphodynamic variations of a macrotidal beach (Atalaia) on the Brazilian Amazon Coast. In: Green, A.N. and Cooper, J.A.G. (eds.), *Proceedings 13<sup>th</sup> International Coastal Symposium* (Durban, South Africa), *Journal of Coastal Research*, Special Issue No. 70, pp. 681-686, ISSN 0749-0208.

Beach morphology, waves, tides, and current speeds were measured in a moderate-energy macrotidal environment of the Amazon coast (Atalaia beach, Brazil). The study was based on two complementary sets of data: (i) hydrodynamic and topographic data collected in four 25-hour campaigns during equinoctial and non-equinoctial periods, and (ii) climatological data (wind speed and direction, and rainfall) obtained from the Brazilian Institute of Meteorology. The results indicate that tidal currents run predominantly to the northwest during the flood tide and southeast during the ebb. The highest current speeds were recorded during the equinoctial period, reaching a maximum of 0.5 m/s in the flood tide. In March and June (rainiest months), ebb tide currents reached a maximum speed of 0.4 m/s. The tidal cycle was weakly asymmetric with the ebb tide lasting up to 6 hours and 40 minutes. High tides ranged from 4 m (non-equinoctial) to 5.7 m (equinoctial). Wave energy was modulated slightly during the low tide due to wave attenuation on the sandbanks, but substantial changes were not observed during ebb and flood tides. Modal wave height ( $H_b$ ) varied from 1.1 to 1.43 m, associated with wave periods of 5.0–7.5s, with the highest values being recorded in November (intense winds). This beach can be classified as tide-modified, presenting primarily dissipative ( $\Omega > 5$ ) characteristic. Wave-dominated characteristics were observed in November, when  $H_s$  values were around 1.5 m and tidal elevation was approximately 4 m (non-equinoctial period).

**ADDITIONAL INDEX WORDS:** *Modal wave heights, macrotidal beach, Amazon littoral.*

## INTRODUCTION

Variations in the morphodynamics of beaches are determined primarily by oscillations in hydrodynamic conditions, the morphological configuration of the coastal region and adjacent continental shelf, and the available stock of sediments (Wright *et al.*, 1985; Scott *et al.*, 2007; Camacho-Valdéz *et al.*, 2008). Early studies of beach morphodynamics focused on the wave patterns and sedimentary characteristics of microtidal environments (Wright and Short, 1984). However, Masselink and Short (1993) examined the effects of waves and tidal currents on macrotidal beaches using the relative tidal range (RTR). Subsequently, dimensionless fall velocity, or  $\Omega$  (Short, 1987), and the tidal reach were considered to be essential parameters for the study of the morphodynamics of macrotidal beaches worldwide (Masselink and Hegge, 1995; Jackson *et al.*, 2005; Scott *et al.*, 2007; Short and Jackson, 2013).

Few studies have described the seasonal variation in the morphodynamics of equatorial environments characterized by the presence of sandbanks and bars which attenuate the wave energy in the nearshore zone (see Alves and El-Robrini, 2006; Monteiro *et al.*, 2009; Pereira *et al.*, 2013a). The coastal processes observed on the Amazon littoral result from a combination of forces, including the occurrence of asymmetrical semidiurnal macrotides, strong tidal currents, moderate energy waves, and the input of dozens of estuaries, which discharge vast amounts of freshwater

and sediments into the ocean (Cavalvante *et al.*, 2010; Anthony *et al.*, 2013; Pereira *et al.*, 2012a; Pereira *et al.*, 2013b). An additional factor of increasing importance is the impact of anthropogenic activities (Oliveira *et al.*, 2011; Pinto *et al.*, 2011; Silva *et al.*, 2011, 2013).

The present study focused on the seasonal variation in the morphodynamic state of Atalaia beach on the Amazon Coast affected by spring macrotides (4–6 m) and wave heights ( $H_s$ ) typically of over 1.0 m. This beach is located in the northeastern extreme of the Brazilian state of Pará, and is one of its principal tourist attractions (Sousa *et al.*, 2011; Sousa *et al.*, 2013; Pessoa *et al.*, 2013).

In comparison with the region's other beaches, this coastline is relatively exposed to wave action (Pereira *et al.*, 2012a; Pereira *et al.*, 2012b; Pereira *et al.*, 2013a; Pereira *et al.*, 2013b), although a subtle attenuation of the wave energy can be observed at low tide. Atalaia beach is currently subject to an intense process of erosion resulting from the high local hydrodynamic energy, associated with the ongoing occupation of its dune fields, cliffs, and intertidal zone (Pinto *et al.*, 2011; Pereira *et al.*, 2012b).

Given these considerations, the present study aimed to evaluate the influence of climatological and hydrodynamic factors on the morphodynamics and sediment balance of Atalaia beach under nearshore and offshore conditions. In the case of the nearshore conditions, seasonal (dry and rainy) and tidal (flood/ebb, equinoctial/non-equinoctial) variables were also taken into account.

## STUDY AREA

Atalaia beach is located in the northeastern extreme of the Brazilian state of Pará (Figure 1), in the municipality of Salinópolis. The beach has a NW–SE orientation, with a total length of 12 km and a width of 200–400 m (Pinto *et al.*, 2011). The western sector is occupied by holiday homes that sit on cliffs (Barreiras Formation), while the eastern sector is characterized by a large number of bars and restaurants housed in wooden stilt buildings built on sand-dunes or in the intertidal zone (Sousa *et al.*, 2011; Pinto *et al.*, 2011).

The region's equatorial climate is hot and humid, and highly seasonal, with two principal seasons (dry and rainy). The dry season normally occurs between July and December, when around 10–15% of the total annual precipitation is recorded, and mean temperatures are typically between 27°C and 30°C. The rainy season lasts from January to June, and is characterized by high rainfall (1500–2500 mm), reduced sunlight and evaporation, and mean temperatures of around 26°C. The region is dominated by northeasterly trade winds (Geyer *et al.*, 1996), which are more intense during the dry season (INMET, 2010).

## METHODS

The present study was conducted between November, 2008, and September, 2009, considering two distinct time scales: (i) short term, with campaigns of 25 hours' duration for the collection of nearshore hydrodynamic and morphological data, and (ii) medium term, based on climatological and hydrodynamic data obtained from national agencies for the evaluation of offshore conditions.

### Physical variables

Meteorological data (wind velocity and rainfall) were obtained from the Brazilian Institute of Meteorology's Salinópolis-A215 station for the period between November, 2008, and September, 2009. The data included monthly average wind speeds (m/s), derived from hourly readings, and total monthly precipitation (mm).

Four intensive campaigns were conducted in order to sample distinct wave/weather conditions:

- (i) Dry season/non-equinoctial tide (DSNE): November, 2008, period characterized by intense winds;
- (II) Rainy season/equinoctial tide (RSE): March, 2009;
- (iii) Rainy season/non-equinoctial tide (RSNE): June, 2009, period characterized by the least intense winds;

- (iv) Dry season/equinoctial tide (DSE): September, 2009.

Waves and currents were measured using a bottom-mounted mooring at a depth of 4.7 m (MLW), to which a mini-current meter (Sensordata SD 6000), and wave and tide data loggers (TWR 2050) were attached for 25 h under spring tide conditions. Mean current velocity and direction were recorded at 10-min intervals. Wave data was taken in 512 samples at a 4 Hz burst rate of over a period of 10 min. Tidal range data were acquired every 2 s and mean values were obtained every 10 min.

Data on offshore waves, including significant wave height ( $H_{os}$ ), period ( $T_p$ ), and direction ( $\theta$ ), were provided by the INPE Weather Forecasting and Climatic Studies Center (CPTEC-INPE). Offshore hydrodynamic data were analyzed on a daily basis during the four months in which the nearshore campaigns were undertaken.

### Morphodynamic data

Two topographic surveys (P1 and P2) were carried out during the study period. At each low tide, beach profiles were surveyed in the eastern sector from a depth of 0.5 m to the aeolian foredunes, a distance of around 200–400 m. The profiles were used to assess morphological changes and to calculate beach slopes at high and low tides. Surface sediment samples were collected along the whole of the beach profile, and were later separated in the laboratory using a Ro-Tap sieve shaker with meshes ranging from -1.0 to 4.0  $\phi$ . Grain sizes were classified according to Wentworth (1922) and statistical analyses followed Folk and Ward (1957).

This study adopted the empirical expression of the relationship between the state of the beach and the dimensionless fall velocity  $\Omega = H_b/w_s T$ , where  $H_b$  is breaking wave height,  $w_s$  is sediment fall velocity (m/s), and  $T$  is the wave period (s). The dimensionless fall velocity (Dean's number,  $\Omega$ ) is a dimensionless parameter first proposed by Gourlay (1968) and Dean (1973), that incorporates both wave and sediment characteristics. Masselink and Short (1993) proposed an additional parameter, the relative tidal range (RTR), which takes the tide-induced migration of hydrodynamic processes into consideration. The RTR ( $RTR = TR/H_b$ , where  $TR$  is the mean spring tidal range and  $H_b$  is the breaking wave height) quantifies the effects of tidal processes on the beach. The morphodynamic beach model used in this study was first applied by Masselink and Short (1993) and is based on both these parameters ( $\Omega$  and RTR), which were calculated using modal wave heights and periods.

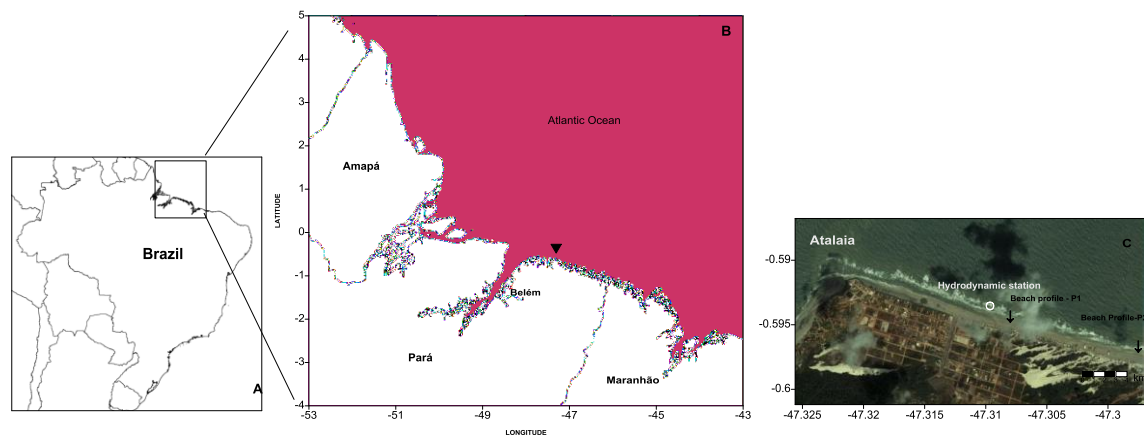


Figure 1. Location of the study area: **A** – Location of Brazil in South America; **B** – Northern coast of Brazil; **C** – Atalaia beach showing the data collection points.

## RESULTS

### Offshore conditions

The highest hydrodynamic energy was recorded during the equinoctial months (March and September) and in November, period characterized by strong winds. In March, the winds blew predominantly from between 40°N and 70°N, and the highest waves ( $H_{os}$ ), varying from 1.1 m to 1.5 m, came from 35°–55°N. These waves also had relatively long periods (5–9 s). In September, by contrast, the winds blew mainly from the east and northeast (75°–90°N), generating waves from 70°–80°N, with heights of 1.0–1.3 m, with shorter periods (4–5s). In November, the winds were slightly less intense than those recorded in September, generating waves of 0.7–1.2 m in height coming from 40°–70°N, with periods of 4–9s. In June, wave energy was at its lowest ( $H_{os} = 0.7$ –1.1 m), due to the reduced intensity of the winds. The highest daily  $H_{os}$  values (1.21 m) were recorded in March, and the lowest values in November (1.0 m) and June (1.08 m).

### Nearshore conditions

The tides (Figure 2A) are asymmetrical, with a slightly longer ebb phase (~6 h and 40 min) in comparison with the flood tide. The tidal currents flow predominantly SE-NW during the flood phase, and NW-SE during the ebb (Figure 3). The highest tides and strongest currents were recorded during the equinoctial months, with tides reaching 5.0 m in March and 5.7 m in September (Figure 2A). Related to this, the most intense currents (Figure 3) were also recorded during this period, principally during the flood tide (around 0.5 m/s). In November, the highest waves ( $H_s = 1.1$  m) and shortest periods ( $T = 5$ s) were recorded as a result of the strong local winds. During this period, the tidal currents were less evident in comparison with other months, due

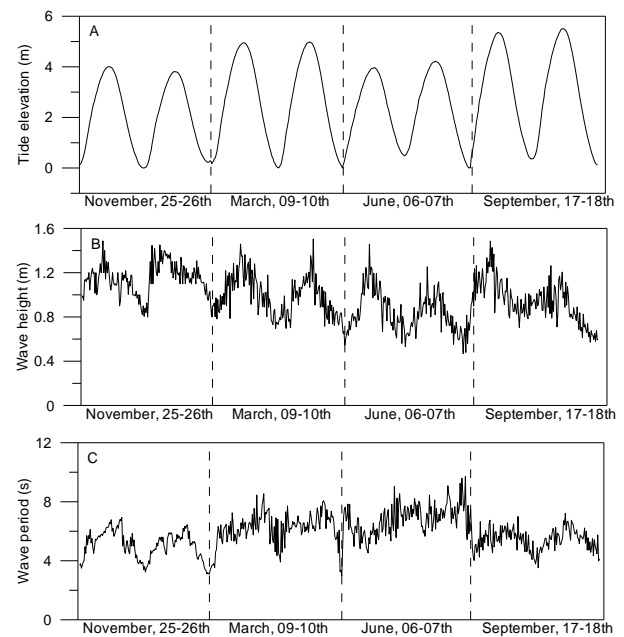


Figure 2. Nearshore variables: A – tidal elevation (m); B – wave height (m); C – wave period (s).

to the reduced levels of fluvial discharge, strong winds, and the predominance of drift currents flowing to the north.

The smallest waves were recorded in June ( $H_s = 0.8$  m,  $T = 6.8$ s; Figure 2B-C), coinciding with the weak winds blowing during this period. During the rainy season, the ebb currents reached a maximum velocity of 0.4 m/s. A slight tendency for wave attenuation was observed during the low tide in all study months, as a result of the presence of offshore sandbanks.

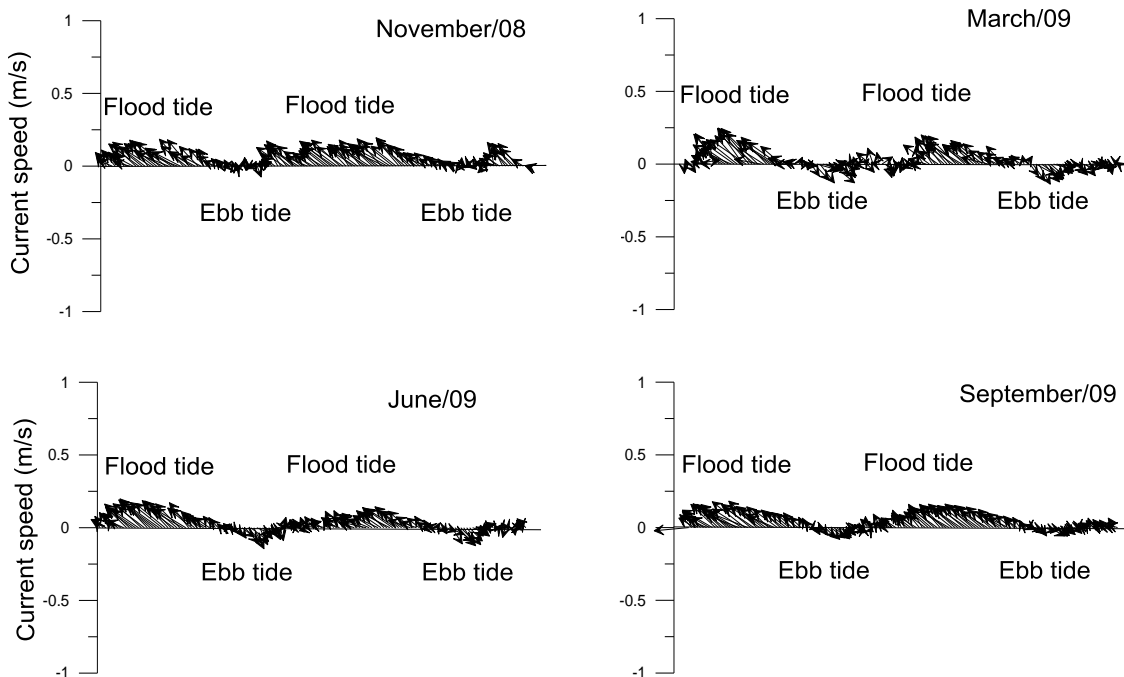


Figure 3. Current direction and intensity.

## Beach morphology

Both beach profiles are characterized by their shallow inclination ( $1^\circ$ ) during low tide. By contrast, during high tide period these beaches have moderate to high beach slope ( $>3^\circ$ ). The P1 is approximately 300 m long, from the reference point (backshore) to the water's edge at the low spring tide. This sector is highly erosive, with a loss of  $-1.61 \text{ m}^3/\text{m}$  of sediment between November, 2008, and September, 2009 (Figure 4). In March and June, 2009, however,  $0.49 \text{ m}^3/\text{m}$  of sediment was deposited, with winds blowing from the southeast, which contributed to the protection of the sector from the direct action of the waves incoming from the same quadrant (SE), resulting in an increase in the profile during this period in comparison with the other months.

The P2 sector is more extensive, stretching approximately 400 m from the frontal dunes (interrupted by wooden buildings and an access road) to the low spring tide line. This area is more stable in comparison with the P1 sector. The sediment balance recorded between November, 2008, and September, 2009, was  $-0.028 \text{ m}^3/\text{m}$ . A small accumulation of sediment ( $0.062 \text{ m}^3/\text{m}$ ) was recorded between November, 2008 and March, 2009, and from June to September, 2009 ( $0.048 \text{ m}^3/\text{m}$ ), when the winds blew from the northeast, and provided better protection from the direct action of the waves coming in from the northeast.

A predominance of fine (83%) and very fine (17%) sand was recorded. The distribution of these sediments was moderately to well selected, with positive asymmetry, mesokurtic to platykurtic. The sediments were slightly finer overall in June, coinciding with a period of reduced hydrodynamic energy and high fluvial discharge. A strong correlation ( $R^2 = 0.9759$ ) was found between the mean and median values for the sediment characteristics, with only slightly weaker tendencies being found between the mean values and asymmetry ( $R^2 = 0.8178$ ) and selection, and a less marked relationship between the means and kurtosis ( $R^2 = 0.6449$ ). These findings indicate that the marked predominance of fine sand (as observed in November, when wave energy was greatest) results in a better selection of the grains, with a strong tendency for the distribution to be positive and mesokurtic. When the proportion of very fine sand increases, as observed in June, the distribution tends to be more moderately selected, asymmetric, and platykurtic.

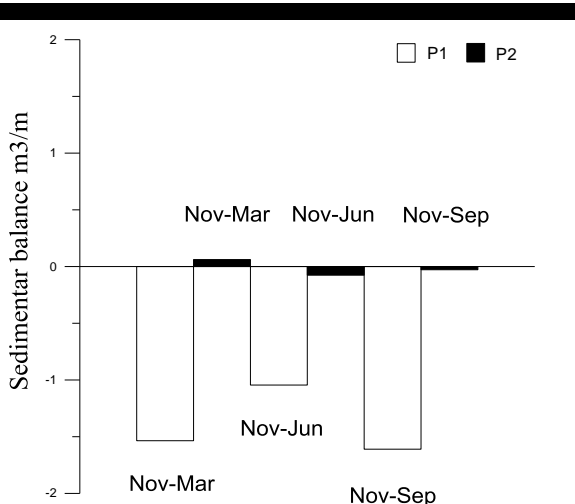


Figure 4. Sedimental balance (P1 and P2), based on November, 2008, as the reference month.

## Morphodynamic features

Considering the offshore data for the four months of the study period, Atalaia can be classified as a dissipative beach of the non-barred type (Figure 5), except for June, 2009, when it was classified as barred-dissipative. When the nearshore data are also considered however, it is possible to confirm that the effects of the attenuation of the wave energy on the sandbanks, that occurs during some phases of the tide, has contributed to a dissipative type of morphodynamic state, but with “non-barred” characteristics in March, June, and September (Figure 5). In November this was classified as a “barred” type of dissipative environment.

A similar pattern was observed in relation to the tidal phases, with non-barred characteristics being recorded during both flood and ebb tides, except in November, which was once again classified as a barred-type dissipative period during both tidal phases.

## DISCUSSION

High-energy events cause accentuated and erosive morphological changes. In the study area, events of this type resulted from the equinoctial spring tides occurring in March and September, 2009, and also during the period of most intense winds (November, 2008).

While the Amazon coast is dominated by macrotides, waves may reach heights ( $H_w$ ) of over 1.5 m, making a major contribution to temporal changes in the beach profile. In this region, wave energy is often modified at low tide by the presence of sandbanks or bars (Pereira *et al.*, 2012a, 2013b; Anthony *et al.*, 2013).

In comparison with most other Amazonian beaches, however, Atalaia is characterized by reduced attenuation of wave energy, due to the lack of extensive sandbanks offshore. Another characteristic of the region is tidal asymmetry (Pereira *et al.*, 2012a, 2013a), and Atalaia beach is characterized by a slightly shorter flood tide period with stronger tidal currents than those observed during the longer ebb tide.

The P1 sector presented erosive characteristics throughout most of the study period. The dunes were well scarped during the equinoctial spring tides, when the hydrodynamic energy was at its greatest. However, more sediment was deposited during the rainy season (low hydrodynamic energy) in comparison with the first month of the study period (November, 2008). This sector is also affected by the occupation of both the intertidal zone (wooden buildings) and the dune fields, in which guesthouses, hotels and holiday homes have been constructed.

In P2, the sandbanks located off the mouth of the Sampaio River may also contribute to the attenuation of wave energy (Figure 1), contributing to the stability of this sector, even during the equinoctial months. Erosion was observed in this sector during June (low energy), when the winds blew from the southeast.

The tidal asymmetry and the attenuation of the waves during low tide contributed to the differentiated classification of the nearshore and offshore conditions of Atalaia beach. In general, the beach was classified as being of the dissipative non-barred type. In the nearshore environment in November, the high energy of the waves contributed to its classification as barred. The largest waves and shortest periods (wind-waves) were recorded in this month. The offshore area of the beach was also classified as barred in June. In this case, the model proposed by Masselink and Short (1993) does not appear to be appropriate for beaches like Atalaia, where the wave energy is modified slightly by sandbanks during certain phases of the tide.

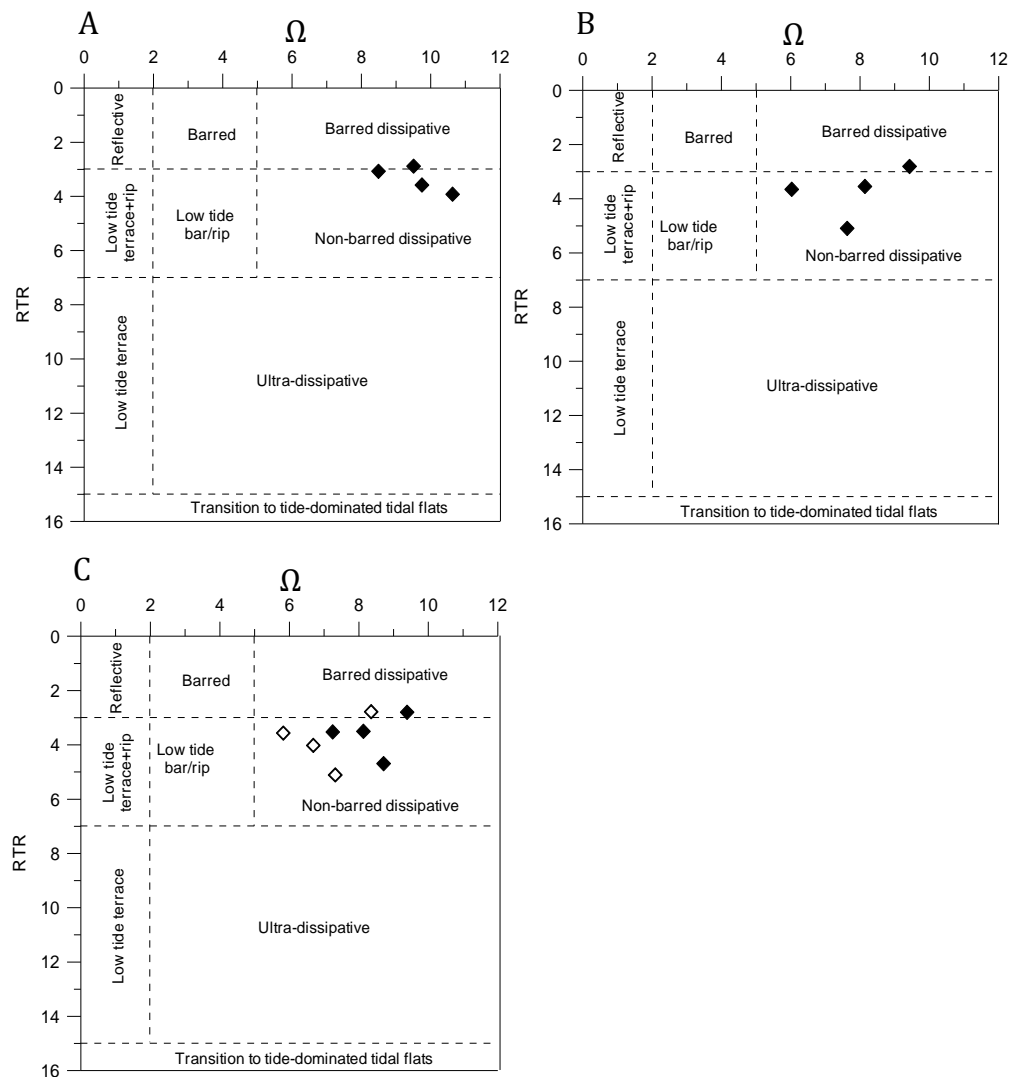


Figure 5. Relationship between RTR and  $\Omega$  in Atalaia. Offshore (A), Nearshore (B) and Ebb tide  $\diamond$  and flood tide  $\blacklozenge$  (C).

## CONCLUSIONS

Atalaia beach presents dissipative characteristics for the majority of the variables analyzed, with a gently-sloping intertidal zone, fine to very fine sediments, and waves of moderate energy.

Marked seasonal variation was recorded in all hydrodynamic and morphological parameters. High-energy events were related to the equinoctial spring tides in March and September, 2009, as well as the strong northwesterly winds in the dry season, which caused erosion in the P1 sector of the beach, and deposition in the P2 sector. The opposite pattern (erosion in the east and deposition in the west) was recorded during periods of low energy. These natural processes, together with the inadequate occupation of the dunes and intertidal zone, have contributed significantly to the intensification of local erosion.

In general, then, Atalaia presents characteristics typical of a dissipative beach (gently sloping substrate made up of fine or very fine sand) influenced by macrotides and waves of moderate hydrodynamic energy. The study site was classified as a non-

barred dissipative beach during most of the months of the study period, and the analytical model used here did not appear to be appropriate for beaches influenced by the presence of bars that attenuate the wave energy.

Emergency measures are clearly required in order to correct the problems of erosion identified on this beach. For this, studies over a longer time scale will be necessary for a better understanding of the coastal dynamics of Atalaia beach.

## ACKNOWLEDGEMENTS

This study was financed by Fapespa through Universal Project No. 115/2008. Pereira is grateful CNPQ for her research grant. Vila-Concejo acknowledges Future Fellowship award from the Australian research council (FT100100215).

## LITERATURE CITED

Alves, M.A.M.S. and El-Robrini, M., 2006. Morphodynamics of the macrotidal beach: Ajuruteua, Bragança North Brazil. Proceedings of

- the 8th International Coastal Symposium (Itajaí, Brazil), *Journal of Coastal Research*, Special Issue 39, pp. 949-951.
- Anthony, J.E., Gardel, A., Proisy, C., Fromard, F., Gensac, E., Peron, C., Walcker, R. and Lesourd, S., 2013. The role of fluvial sediment supply and river-mouth hydrology in the dynamics of the muddy, Amazon-dominated Amapá-Guianas coast, South America: a three-point research agenda. *Journal of South American Earth Sciences*, 44 (No Spécial), 18-24.
- Camacho-Valdéz, V., Murillo-Jiménez, J.M., Nava-Sánchez, E.H. and Turrent-Thompson, C., 2008. Dune and beach morphodynamics at Cabo Falso, Baja California Sur, Mexico: response to natural, Hurricane Juliette (2001) and anthropogenic influence. *Journal of Coastal Research*, 24(3), 553-560.
- Cavalcante, G.H., Kjerfve, B., Knoppers, B. and Feary, D.A., 2010. Coastal currents adjacent to the Caeté estuary, Pará region, North Brazil. *Estuarine, Coastal and Shelf Science*, 88 (1), 84-90.
- Dean, R. G., 1973. Heuristic models of sand transport in the surf zone. *Proceeding of the Conference on Engineering Dynamics in the surf Zone* (Sydney, Australia), Institute of Engineers, pp. 208-214.
- Folk, R.L. and Ward, W.C., 1957. Brazos river bar: A study in the significance of grain size parameters. *Journal of Sedimentology Petrology*, 27, 3-27.
- Geyer, W.R., Beardsley, R.C., Lentz, S.J., Candela, J., Limeburner, R., Johns, W.E., Castro, B.M. and Soares, I.D., 1996. Physical oceanography of the Amazon shelf. *Continental Shelf Research*, 16, 575-616.
- Gourlay, M.R., 1968. *Beach and Dune Erosion Tests*. Delft Hydraulics Laboratory, Report no. M935/M936.
- Instituto Nacional de Meteorologia (INMET), 2010. Monitoramento das Estações automáticas. URL: [www.inmet.gov.br/sonabra/maps/automaticas.php](http://www.inmet.gov.br/sonabra/maps/automaticas.php). Accessed between 10th October 2009 and 14th November 2010.
- Jackson, D.W.T., Cooper, J.A.G. and del Rio, L., 2005. Geological control of beach morphodynamic state. *Marine Geology*, 216, 297-314.
- Masselink, G. and Hegge, B., 1995. Morphodynamics of meso- and macrotidal beaches: examples from central Queensland, Australia. *Marine Geology*, 129, 1-23.
- Masselink, G. and Short, A.D., 1993. The effect of tide range on beach morphodynamics and morphology: A conceptual beach model. *Journal of Coastal Research*, 9 (3), 785-800.
- Monteiro, M.C., Pereira, C.C.L. and Oliveira, S.M.O., 2009. Morphodynamic changes of a macrotidal sand beach in the Brazilian Amazon coast (Ajuruteua-Pará). Proceedings of the 10th International Coastal Symposium (Lisboa, Portugal), *Journal of Coastal Research*, Special Issue, No.56, pp. 103-107.
- Oliveira, S.M.O. de, Pereira, L.C.C., Vila-Concejo, A., Gorayeb, A., Sousa, R.C. de, Souza-Filho, P.W.M. and Costa, R.M. da, 2011. Natural and anthropogenic impacts on a macrotidal sandy beach of the Brazilian Amazon (Ajuruteua): guidelines for coastal management. Proceedings of the 11th International Coastal Symposium (Szczecin, Poland), *Journal of Coastal Research*, Special Issue No. 64, pp. 1385-1389.
- Pereira, L.C.C., Oliveira, S.M. de O., Costa, R.M., Costa, K.G. da and Vila-Concejo, A., 2013b. What happens on an equatorial beach on the Amazon coast when La Niña occurs during the rainy season? *Estuarine, Coastal and Shelf Science*, 135, 116-127.
- Pereira, L.C.C., Pinto, K.S.T., Costa, K.G., Vila-Concejo, A. and Costa, R. M. da, 2012b. Oceanographic conditions and human factors on the water quality at an Amazon macrotidal beach. *Journal of Coastal Research*, 285, 1627-1637.
- Pereira, L.C.C., Silva, N.I.S. da, Costa, R.M., Asp, N.E., Costa, K.G. da and Vila-Concejo, A., 2012a. Seasonal changes in oceanographic processes at an equatorial macrotidal beach in northern Brazil. *Continental Shelf Research*, 43, 95-106.
- Pereira, L.C.C., Vila-Concejo, A. and Short, A.D., 2013a. Influence of subtidal sand banks on tidal modulation of waves and beach morphology in Amazon macrotidal beaches. In: Conley, D.C., Masselink, G., Russell, P.E. and O'Hare, T.J. (eds.), Proceedings 12th International Coastal Symposium (Plymouth, England), *Journal of Coastal Research*, Special Issue No. 65, pp. 1821-1826.
- Pessoa, R.M.C., Pereira, L.C.C., Sousa, R.C., Magalhães, A. and da Costa, R.M., 2013b. Recreational Carrying Capacity of an Amazon Macrotidal beach during vacation periods. In: Conley, D.C., Masselink, G., Russell, P.E. and O'Hare, T.J. (eds.), Proceedings 12th International Coastal Symposium (Plymouth, England), *Journal of Coastal Research*, Special Issue No. 65, pp. 1027-1032.
- Pinto, K.S.T., Pereira, L.C.C., Vila-Concejo, A., Gorayeb, A., Sousa, R.C. de and Costa, R.M. da, 2011. Effects of the lack of coastal planning on water quality and land use on a macrotidal beach (Atalaia, Pará) in the Amazon Region. Proceedings of the 11th International Coastal Symposium (Szczecin, Poland), *Journal of Coastal Research*, Special Issue No. 64, pp. 1385-1389.
- Scott, T., Russell, P., Masselink, G., Wooler, A. and Short, A., 2007. Beach rescue statistics and their relation to nearshore morphology and hazards: a case study for southwest England. Proceedings of the 9th International Coastal Symposium (Gold Coast, Australia), *Journal of Coastal Research*, Special Issue No. 50, pp. 1-6.
- Short, A.D., 1987. A note on the controls of beach type and change, with S.E. Australian examples. *Journal of Coastal Research*, 3, 387-395.
- Short, A.D. and Jackson, D.W.T. (2013) *Beach Morphodynamics*. In: Treatise on Geomorphology. (Eds: Shroder, John F.), Elsevier, Academic Press, Amsterdam, San Diego, pp. 106-129. ISBN 9780123747396.
- Silva, I.R. da, Pereira, L.C.C., Trindade, W.N., Magalhães, A. and Costa, R.M., 2013. Natural and anthropogenic processes on the recreational activities in urban Amazon beaches. *Ocean & Coastal Management*, 76, 75-84.
- Silva, N.I.S., Pereira, L.C.C., Gorayeb, A., Vila-Concejo, A., Sousa, R.C., Asp, N.E. and Costa, R.M. da, 2011. Natural and social conditions of Princesa, a macrotidal sandy beach on the Amazon Coast of Brazil. Proceedings of the 11th International Coastal Symposium (Szczecin, Poland), *Journal of Coastal Research*, Special Issue No. 64, pp 1979-1983.
- Sousa, R. C., Pereira, L. C. C., Silva, N. I. S., Oliveira, S. M. O., Pinto, K. S. T. and Costa, R. M., 2011. Recreational carrying capacity of Amazon macrotidal beaches during the peak vacation season. Proceedings of the 11th International Coastal Symposium (Szczecin, Poland), *Journal of Coastal Research*, Special Issue No. 64, pp. 1292-1296.
- Sousa, R.C., Pereira, L.C.C. and Costa, R.M., 2013. Water quality at touristic beaches on the Amazon coast. In: Conley, D.C., Masselink, G., Russell, P.E. and O'Hare, T.J. (eds.), Proceedings 12th International Coastal Symposium (Plymouth, England), *Journal of Coastal Research*, Special Issue No. 65, pp. 1057-1062.
- Wentworth, C.K., 1922. A scale of grade and class terms for clastic sediments. *Journal of Geology*, 30, 377-392.
- Wright, L.D. and Short, A.D., 1984. Morphodynamic variability of surf zones and beaches: A synthesis. *Marine Geology*, 56, 93-118.
- Wright, L.D., Short, A.D. and Green, M.O., 1985. Short-term changes in the morphodynamic states of beaches and surf zones: An empirical predictive model. *Marine Geology*, 62, 339-364.

## Stratigraphic analysis applied on the recognition of the interface between marine and fluvial depositional systems

Eduardo G. Barboza<sup>†‡</sup>, Maria L.C.C. Rosa<sup>†</sup>, Sérgio R. Dillenburg<sup>†‡</sup>, Anderson B. da Silva<sup>‡</sup>, Luiz J. Tomazelli<sup>†‡</sup>

Centro de Estudos de Geologia Costeira e Oceânica, Instituto de Geociências, Universidade Federal do Rio Grande do Sul

Caixa Postal 15.001 - Porto Alegre - RS - Brasil

eduardo.barboza@ufrgs.br

luiza.camara@ufrgs.br

sergio.dillenburg@ufrgs.br

luiz.tomazelli@ufrgs.br

<sup>‡</sup> Programa de Pós Graduação em Geociências, Universidade Federal do Rio Grande do Sul, Porto Alegre - RS - Brasil  
anderson.biancini@ufrgs.br



[www.cerf-jcr.org](http://www.cerf-jcr.org)



[www.JCRonline.org](http://www.JCRonline.org)

### ABSTRACT

Barboza, E.G., Rosa, M.L.C.C., Dillenburg, S.R., Biancini da Silva, A., Tomazelli, L.J., 2014. Stratigraphic analysis applied on the recognition of the interface between marine and fluvial depositional systems. In: Green, A.N. and Cooper, J.A.G. (eds.), *Proceedings 13<sup>th</sup> International Coastal Symposium* (Durban, South Africa), *Journal of Coastal Research*, Special Issue No. 70, pp. 687-692, ISSN 0749-0208.

Coastal areas contain interfaces between complex depositional systems as a consequence of the convergence of marine and continental environments. The knowledge of such complex depositional systems is important in understanding of coastal evolution and for coastal management. The present study deals with the subsurface identification of interfaces between fluvial and beach/shallow marine systems, using Ground Penetrating Radar (GPR). GPR profiles were measured along dip direction, at two sites on the coastal plain of Santa Catarina state (Pinheira and Passo de Torres), where deposits of fluvial and beach/foredune ridge systems occur. GPR data showed that fluvial and beach deposits are interdigitated in subsurface, with reflectors showing different downlap directions. The results of this study allow a more complete knowledge of the complex interfaces between marine and continental systems. Also, the identification of hidden older fluvial deposits in the subsurface of coastal plains gives important geotechnical information to be considered in the use and occupation of coastal areas and during prospection for placer deposits.

**ADDITIONAL INDEX WORDS:** *GPR, remote sensing, depositional architecture, Geomorphology.*

### INTRODUCTION

The stratigraphic relationships in coastal deposits are quite complex as a consequence of the superposition of depositional processes of marine and continental environments. Among the depositional systems that converge are river and beach/shallow marine systems. The geometry related to the interface between these systems has been observed in outcrops of ancient rocks. In modern systems observation of the geometry is more difficult. The use of GPR has allowed the observation of a great variety of geometries and stratigraphies of coastal depositional systems at high resolution (Bridge *et al.*, 1995; Bristow and Jol, 2003; Bristow *et al.*, 2007; FitzGerald *et al.*, 2007; Johnston, *et al.*, 2007; Barboza *et al.*, 2009, 2010, 2011a, 2013; Caron *et al.*, 2010; Silva *et al.*, 2010; Buynevich *et al.*, 2011; Dillenburg *et al.*, 2013, 2014; Rocha *et al.*, 2013; Moulton *et al.*, 2013).

The Holocene coastal system of the northern sector of the Pelotas Basin in Southern Brazil has excellent examples of interaction between different depositional systems (Figure 1). This coastal system was initiated as a complex barrier system at around 7 ka (Dillenburg *et al.*, 2006, 2009). Presently this complex barrier exhibits contemporaneous sectors showing opposing stacking

patterns, with progradational segments separated by retrogradational segments cut by inlets or river mouths (Dillenburg and Barboza, 2014). Similar setting was identified by Green *et al.* (2013) for the South African Coast. In progradational segments barrier morphology is marked by the presence of foredune ridges, transgressive dunefields/parabolic dunes and fluvial paleochannels (Barboza *et al.*, 2011b; Hesp *et al.*, 2005, 2007; Dillenburg *et al.*, 2000, 2005, 2009). This Holocene barrier system corresponds to a high-frequency depositional sequence stratigraphy, and was first recognized in southern Brazil as barrier-lagoon depositional system IV (Rosa *et al.*, 2011; Villwock *et al.*, 1986).

Ground Penetrating Radar (GPR) data acquired in two different sectors of the coastal plain of Santa Catarina state (Pinheira and Passo de Torres) (Figure 1), show geometric relationships between river and beach deposits, with seaward dipping reflectors being truncated by sigmoidal landward dipping reflectors. Due to the relatively thick aeolian cover these geometrical relationships are not observed on the barrier surface. This paper presents GPR data of these complex interfaces between marine and continental depositional systems, and highlights the geotechnical importance of identification of buried older fluvial deposits in the subsurface of coastal plains.



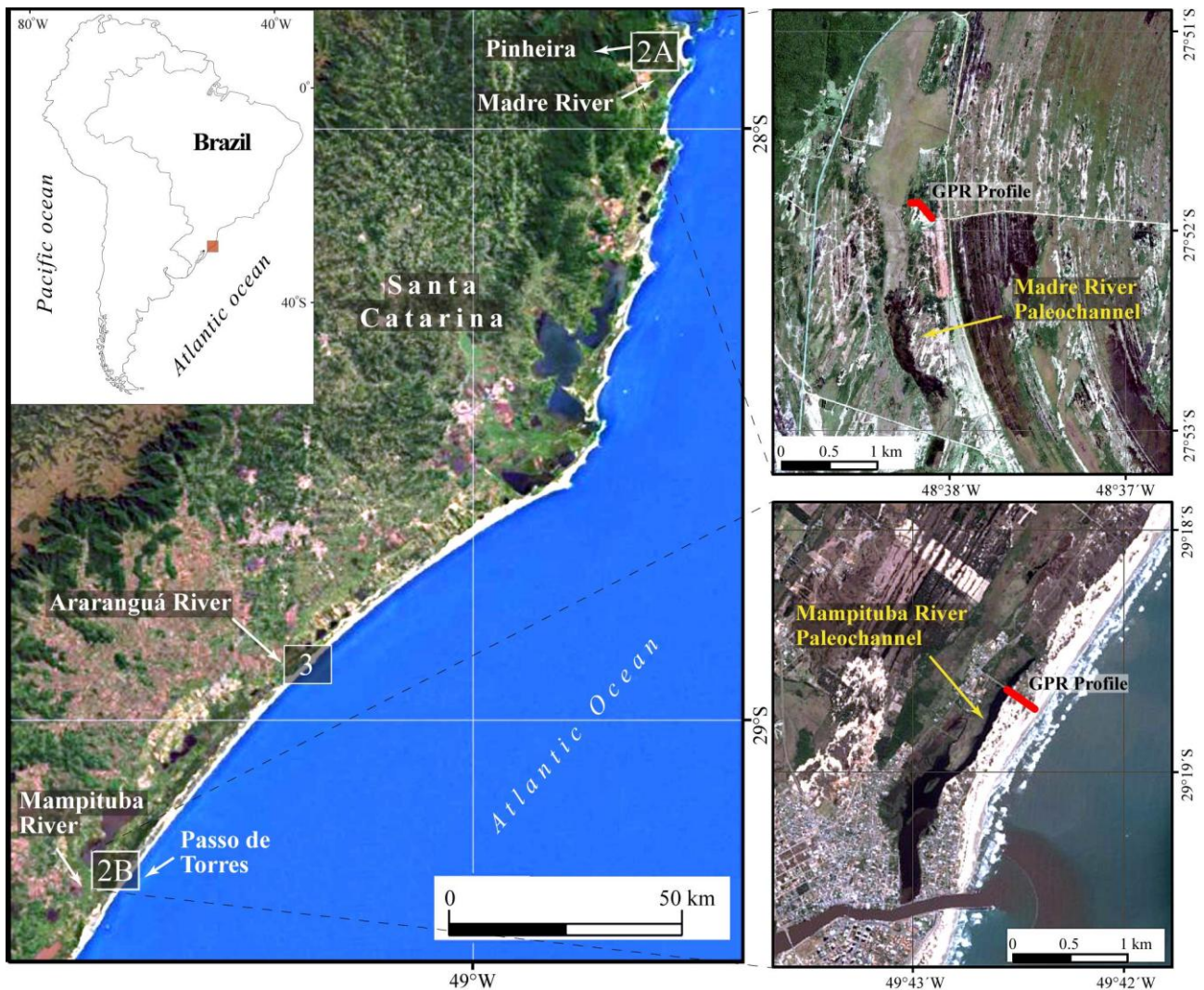


Figure 1. Location of the three analyzed areas along the northern sector of the Pelotas Basin. The numbers and letters indicate the figures for subsequent details. In the right detail of the location of GPR profiles. Satellite image from LANDSAT 7 R5G4B3 (ETM+).

## REGIONAL SETTING

The long-term northward littoral drift and processes of sand transfer from the adjacent shelf were responsible by the delivery of a huge volume of sand used to build the Holocene barrier (Dillenburg and Barboza, 2014). The climate is temperate or humid subtropical with generally warm to hot temperatures in summer and cool temperatures in winter. The NE wind is dominant, especially from September to March. From April to August winds from S and SW are dominant. Rainfall ranges from 1,000 to 1,500 mm and is evenly distributed throughout the year (Nimer, 1990).

The swell is from southern and eastern quadrants, although less frequent, have high energy and a long period, the control the alongshore transport of sediments (littoral drift) is to the northeast (Siegle and Asp, 2007). Significant wave height is 1.5 m, but during storms sea level can surge up to 1.3 m (Barletta and Calliari, 2001; Calliari *et al.*, 1998). This relatively high wave energy limits the seaward extent of the shoreface to between -16 and -25 m depths (Gruber *et al.*, 2003 and 2006). The coast has

semidiurnal tides and is microtidal with a mean range of 0.5 m (Dillenburg *et al.*, 2009). The maximum sea level of the Postglacial Marine Transgression (PMT) reached +2 to +3 m at around 6 – 5 cal ka, subsequently followed by a slow sea level fall (Angulo *et al.*, 2006; Barboza and Tomazelli, 2003).

## METHODS

The GPR profiles were collected in the Common Offset method. For a real time topographic survey the GPR system was connected to a Global Navigation Satellite System (GNSS). The GPR system utilized comprises a GSSI™ (Geophysical Survey Systems, Inc.) SIR-3000 data collector for bistatic antennas (150 MHz – Radarteam Sweden AB) and for monostatic antenna (200 MHz – GSSI™), with a two-way-traveltime (TWTT) range of 360 – 300 ns, this configuration penetrated 17 – 13 m deep, respectively (Figure 2). Noise and gain filters were applied during time of data acquisition. Data were post-processed with Radan™, Reflex-Win® and Prism2® software packages, proceeding with background removal, band-pass frequency filters, gain equalization,

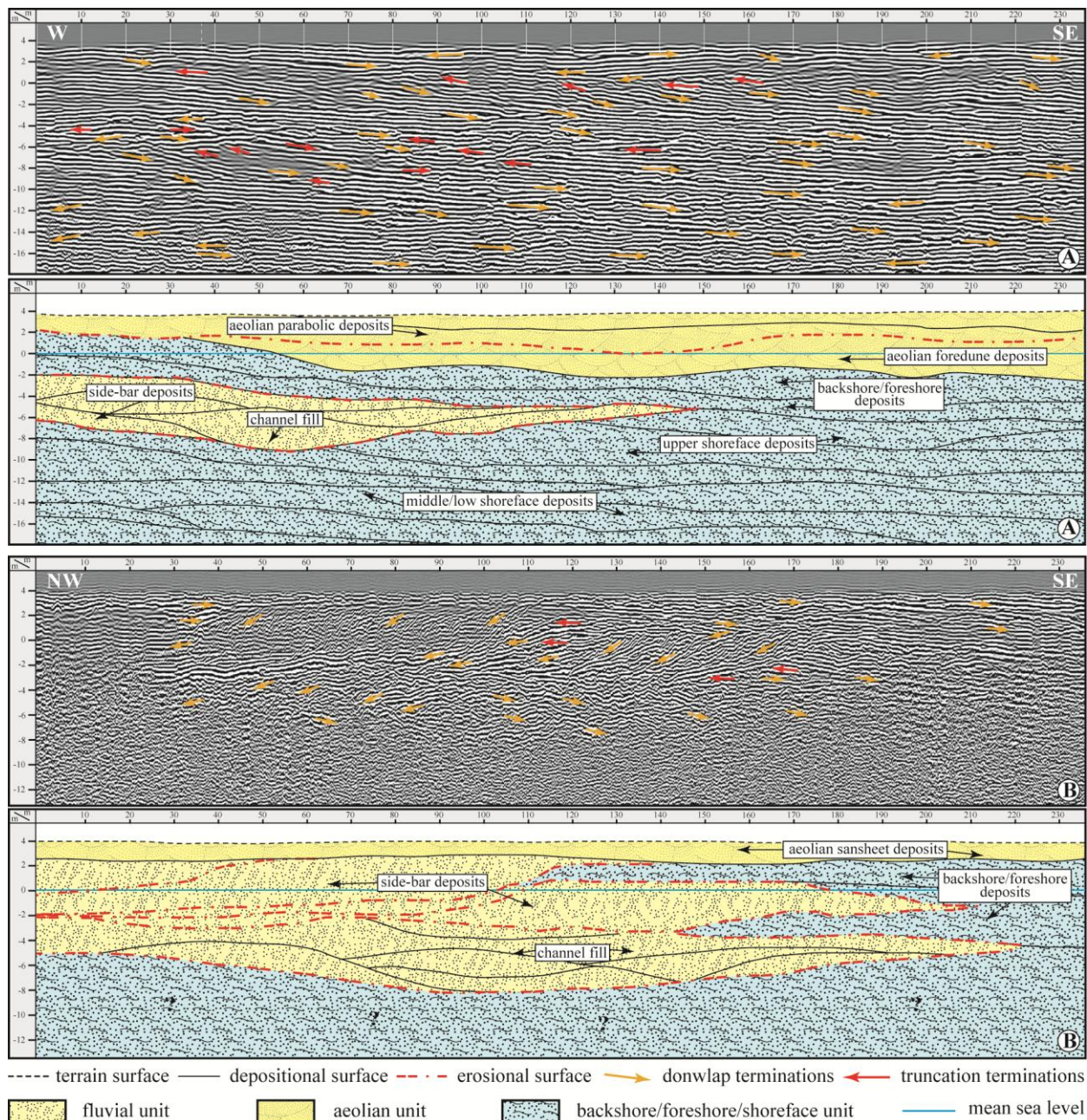


Figure 2. A) Pinheira profile acquired with a frequency of 150 MHz. B) Passo de Torres GPR profile acquired with a frequency of 200 MHz. Both profiles show similarities regarding their depositional environment, but they are distinct by the presence of a unit of aeolian sand at Pinheira. The question marks in the interpretation of (B) represent undefined shoreface units.

topographic corrections and time to deep conversion. A dielectric constant of 10 was used to convert travel-time to depth, representing a velocity of 0.09 m/ns (Davis and Annan, 1989). This constant was validated by lithological data obtained by drilling. GPR profiles were topographically corrected using GNSS post-processed elevation data points collected along the profile lines at 1 second interval time. These data were acquired using a Trimble PROXRT GNSS unit with GLONASS option (datum: WGS84) and analyzed in a Geographic Information Systems (GIS).

The interpretation was based in the method of seismostratigraphy (Payton, 1977) adapted to GPR (Neal, 2004). The method was based on termination (onlap, downlap, toplap and truncations), geometry and pattern of reflectors (Mitchum Jr. *et al.*, 1977; Vail, 1987; Catuneanu *et al.*, 2009; Abreu *et al.*, 2010).

It was performed a simulation of future progradation of the Araranguá River region using the cloning tool in Adobe® Photoshop® software (Figure 3B). As reference of the rate of progradation the value of ~1 km/1,000 yrs was used (Hesp *et al.*, 2009).

## RESULTS AND DISCUSSIONS

Figure 2 shows two GPR profiles 230 m long, where the following units were interpreted: a basal upper/middle shoreface unit, characterized by an alternation between continuous, sub-parallel and low angle reflectors, with undulating and non-continuous reflectors; a middle unit characterized by the interfingering of fluvial and backshore/foreshore deposits, with the first presenting continuous, parallel and low to medium angle

reflectors dominantly dipping landwards (in general to the west), sometimes concave reflectors, characterizing typical bar and channel fill deposits; and the second characterized by continuous, parallel reflectors, with very low angle seaward-dipping reflectors; and finally a top aeolian unit formed by very continuous, horizontal and parallel reflectors representing a strike profile of deposits of parabolic dunes and transgressive sand sheets.



Figure 3. The modern Araranguá River mouth, an example of how an interfingering between fluvial and backshore/foreshore deposits could have been formed. The red ellipse (A) shows different phases of the river mouth location. A new mouth position results in the partial rework of backshore/foreshore/shoreface deposits, but later (after the mouth closure), the formed fluvial deposits were partially reworked by waves action, resulting in a record in the form of a lens of fluvial deposits inside a shore depositional unit (Fig. 2A and 2B). (B) Simulation of subsequent barrier progradation for 1 ka and potential of preservation the record of interfingering between the river and beach deposits systems. Satellite Image base from Google Earth 2012.

In Figure 2A the top aeolian unit is marked by parabolic dune deposits that cover foredune deposits. These foredunes show noncontinuous and high angle undulating GPR reflectors. In the section of the Figure 2B, the aeolian unit is thinner and formed by sand sheets which cover directly the backshore/foreshore and fluvial deposits. The fluvial record of Figure 2A and 2B corresponds to a paleochannel, and it was developed in the form of a shore-parallel fluvial channel, probably similar to the modern Araranguá River (Figure 3), but which remained active, in a south-north orientation even after the substantial development of barrier progradation.

Simultaneously, or slightly after the onset of progradation, fluvial action resulted in the erosion of the upper units of the prograded deposits (foredune and backshore/foreshore deposits), down to a depth of approximately 8 m below present sea-level, forming the general GPR record of Figure 2A. With lens geometry and extending until approximately 150 m in the GPR record in Figure 2A, the record of a fluvial transverse erosion or lateral channel migration of the shore deposits occurs. This channel erosion may have resulted from a combination of high precipitation and high energy waves.

Consequently a temporary mouth of the Madre River was positioned right at the location of the GPR profile. This positioning of the river mouth resulted in the partial reworking of deposits of the backshore/foreshore/shoreface, to a seawards distance of 200 – 250 m, but later (after the mouth closure), the fluvial deposits were partially reworked by wave action, resulting in a record in the form of a lens of fluvial deposits inside a shore depositional unit.

At Passo de Torres similar characteristics are observed. One difference between Pinheira and Passo de Torres is related to the aeolian unit, which is formed by parabolic and foredune deposits at Pinheira and by sand sheets at Passo de Torres. In this area the fluvial erosion occurs until approximately 4 m below present sea level. Channel fill and side bar deposits are identified among the top aeolian and an undefined, but probably, middle/low shoreface unit with mud presence. Differently of Pinheira, the interfingering between this and the fluvial deposits is thinner with a fluvial dominance in the top of the section, which is cover by the aeolian unit. This difference is related to the dynamic of Madre and Mampituba fluvial systems.

The setting of both areas was probably similar to the modern Araranguá River mouth situation (Figure 3), where the active river mouth is located slightly to the south-southwest of an older mouth, which is now under wave attack, a condition that forms a laterally composite record of fluvial and shore deposits. This provides a comparative modern environment in which the interfingering between fluvial and shore units, as presented in the GPR records of Figure 2A and 2B could have formed.

This interfingering between fluvial and beach deposits is part of the evolutionary model of the two studied prograded barriers. This complex characteristic of the subsurface relationship between fluvial and beach deposits has important implications for geotechnical studies related to future development of urban areas on the coastal. Also, fluvial sands reworked under high energy conditions (beach), provide the potential for development of heavy mineral deposits.

## CONCLUSION

GPR data revealed important complex interfaces between fluvial and beach deposits in the subsurface of two prograded barriers. This kind of information is not only important in a descriptive or in an evolutionary scope of the coastal plain of the two studied areas, but it is also of great importance as geotechnical information. Usually such information is obtained by

measurement of the mechanical resistance of subsurface deposits on development projects of urban areas, but without considering their lateral variation. The identification of this subsurface complex interfaces has also importance on the prospection of placer deposits.

## ACKNOWLEDGEMENT

This study was funded by Conselho Nacional de Desenvolvimento Científico e Tecnológico (CNPq – Brazil) via project n° 473227/2010-0. Eduardo G. Barboza, Sérgio R. Dillenburg and Luiz J. Tomazelli thank CNPq for providing their research fellowships.

## LITERATURE CITED

- Abreu, V.S., Neal, J. and Vail, P.R., 2010. Integration of Sequence Stratigraphy concepts. In: Abreu, V.S., Neal, J., Bohacs, K.M. and Kalbas, J.L. (eds.), *Sequence Stratigraphy of siliciclastic systems – The ExxonMobil Methodology: atlas of exercises*, 209-224.
- Angulo, R.J., Lessa, G.C. and Souza, M.C., 2006. A critical review of Mid- to Late-Holocene sea-level fluctuations on the eastern Brazilian coastline. *Quaternary Science Reviews*, 25, 486-506.
- Barboza, E.G. and Tomazelli, L.J., 2003. Erosional features of the eastern margin of the Patos Lagoon, southern Brazil: significance for Holocene history. *Journal of Coastal Research*, SI 35, 260-264.
- Barboza, E.G., Dillenburg, S.R., Rosa, M.L.C.C., Tomazelli, L.J. and Hesp, P.A., 2009. Ground-penetrating radar profiles of two Holocene regressive barriers in southern Brazil. *Journal of Coastal Research*, SI 56, 579-583.
- Barboza, E.G., Rosa, M.L.C.C., Dillenburg, S.R. and Tomazelli, L.J., 2010. The Holocene Coastal Barrier of Rio Grande do Sul (Southern Brazil): an Evaluation Based on GPR Data. In: 2010 Meeting of the Americas. Eos Trans. AGU, *Meet. Am. Suppl.*, v. 91. p. NS11A-03.
- Barboza, E.G., Rosa, M.L.C.C., Hesp, P.A., Dillenburg, S.R., Tomazelli, L.J. and Ayup-Zouain, R.N., 2011a. Evolution of the Holocene Coastal Barrier of Pelotas Basin (Southern Brazil) - a new approach with GPR data. *Journal of Coastal Research*, SI 64, 646-650.
- Barboza, E.G., Rosa, M.L.C.C., Dillenburg, S.R., Tomazelli, L.J. and Ayup-Zouain, R.N., 2011b. Comportamento Regressivo/Transgressivo da linha de costa na Bacia de Pelotas durante o Holoceno Médio e Tardio. In: López R.Á. and Marcomini S.C. (eds.), *Problemática de Los Ambientes Costeros*. 1ed. Buenos Aires - Argentina: Editorial Croquis, v. 1, 15-30.
- Barboza, E.G., Rosa, M.L.C.C., Dillenburg, S.R. and Tomazelli, L.J., 2013. Preservation potential of foredunes in the stratigraphic record. *Journal of Coastal Research*, SI 65, 1265-1270.
- Barletta, R.C. and Calliari, L.J., 2001. Determinação da intensidade das tempestades que atuam no litoral do Rio Grande do Sul, Brasil. *Pesquisas em Geociências*, 28(2), 117-124.
- Bridge, J.S., Alexander, J., Collier, R.E.L.L., Gawthorpes, R.L. and Jarvis, J., 1995. Ground-penetrating radar and coring used to study the large-scale structure of point-bar deposits in three dimensions. *Sedimentology*, 42, 839-852.
- Bristow, C.S. and Jol, H.M., 2003. An introduction to ground penetrating radar (GPR) in sediments. *Geological Society, Special Publications*, 211, 1-7.
- Bristow, C.S., Jones, B.G., Nanson, G.C., Hollands, C., Coleman, M. and Price, D.M., 2007. GPR surveys of vegetated linear dune stratigraphy in central Australia: Evidence for linear dune extension with vertical and lateral accretion. In: Baker, G.S. and Jol, H.M. (eds.), *Stratigraphic Analyses Using GPR. The Geological Society of America, Special Publication*, 432, 19-34.
- Buynevich, I.V., Klein, A.H.F., FitzGerald, D.M., Cleary, W.J., Hein, C.J., Veiga, F., Angulo, R.J., Asp, N.E. and Petermann, R.M., 2011. Geological legacy of storm erosion along a high-energy indented coastline: northern Santa Catarina, Brazil. *Journal of Coastal Research*, SI 64, 1840-1844.
- Calliari, L.J., Tozzi, H.A.M. and Klein, A.H.F., 1998. Beach morphology and coastline erosion associated with storm surges in southern Brazil – Rio Grande to Chuí, RS. *Anais da Academia Brasileira de Ciências*, 70(2), 231-247.

- Caron, F., Lima, L.G., Dillenburg, S.R., Tomazelli, L.J., Barboza, E.G., Antikeira, J.A.F., Rosa, M.L.C.C.; Manzolli, R.P. and Silva, A.B., 2010. Morphology, stratigraphy and factors controlling evolution of a transgressive barrier in southern Brazil. In: 2010 Meeting of the Americas. Eos Trans. AGU, *Meet. Am. Suppl.*, v. 91, p. OS21A-01.
- Catuneanu O., Abreu, V.S., Bhattacharya, J.P., Blum, M.D., Dalrymple, R.W., Eriksson, P.G., Fielding, C.R., Fisher, W.L., Galloway, W.E., Gibling, M.R., Giles, K.A., Holbrook, J.M., Jordan, R., Kendall, C.G.S.T.C., Macurda, B., Martinsen, O.J., Miall, A.D., Neal, J.E., Nummedal, D., Pomar, L., Posamentier, H.W., Pratt, B.R., Sarg, J.F., Shanley, K.W., Steel, R.J., Strasser, A., Tucker, M.E. and Winker, C., 2009. Towards the standardization of sequence stratigraphy. *Earth-Science Reviews*, 92, 1-33.
- Davis, J.L. and Annan, A.P., 1989. Ground-penetrating radar for high-resolution mapping of soil and rock stratigraphy. *Geophysical Prospecting*, 37, 531-551.
- Dillenburg, S.R. and Barboza, E.G., 2014. The Dip and Strike-Fed Sandy Coast of Southern Brazil. In: Martini, I.P. and Wanless H.R. (eds.), *Sedimentary Coastal Zones from High to Low Latitudes: Similarities and Differences*, Geological Society, London, Special Publications 388, 1-15.
- Dillenburg, S.R., Roy, P.S., Cowell, P.J. and Tomazelli, L.J., 2000. Influence of antecedent topography on coastal evolution as tested by the shoreface translation-barrier model (STM). *Journal Coastal Research*, 16, 71-81.
- Dillenburg, S.R., Tomazelli, L.J., Martins, L.R. and Barboza, E.G., 2005. Modificações de Longo Período da Linha de Costa das Barreiras Costeiras do Rio Grande do Sul. *Gravel*, 3 (1), 4-9.
- Dillenburg, S.R., Tomazelli, L.J., Hesp, P.A., Barboza, E.G., Clerot, L.C.P. and Silva, D.B., 2006. Stratigraphy and evolution of a prograded, transgressive dunefield barrier in southern Brazil. *Journal of Coastal Research*, SI 39, 132-135.
- Dillenburg, S.R., Barboza, E.G., Tomazelli, L.J., Hesp, P.A., Clerot, L.C.P. and Ayup-Zouain, R.N., 2009. The Holocene Coastal Barriers of Rio Grande do Sul. In: Dillenburg, S.R. and Hesp, P.A. (eds.), *Geology and Geomorphology of Holocene Coastal Barriers of Brazil. Lecture Notes in Earth Sciences*, 107, 53-91.
- Dillenburg, S.R., Barboza, E.G., Tomazelli, L.J., Rosa, M.L.C.C. and Maciel, G.S., 2013. Aeolian Deposition and Barrier Stratigraphy of the Transition Region between a Regressive and a Transgressive Barrier: an example from Southern Brazil. *Journal of Coastal Research*, SI 65, 464-469.
- Dillenburg, S.R., Barboza, E.G., Hesp, P.A., Rosa, M.L.C.C., Angulo, R.J., Souza, M.C., Giannini, P.C.F. and Sawakuchi, A.O., 2014. A Transgressive barrier at Pinheira, Southern Brazil around 3 ka? Discussion of Hein et al. (2013). Evidence for a transgressive barrier within a regressive strandplain system: Implications for complex response to environmental change. *Sedimentology*, 61 (2), 1300-1320.
- Fitzgerald, D.M., Cleary, W.J., Buynevich, I.V., Hein, C.J., Klein, A.H.F., Asp, N. and Angulo, R., 2007. Strandplain Evolution along the Southern Coast of Santa Catarina, Brazil. *Journal of Coastal Research*, SI 50, 152-156.
- Green, A.N., Cooper, J.A.G. and LeVieux, A., 2013. Unusual barrier/inlet behaviour associated with active coastal progradation and river-dominated estuaries. *Journal of Coastal Research*, SI 69, 35-45.
- Gruber, N.L.S., Toldo Jr., E.E., Barboza, E.G. and Nicolodi, J.L., 2003. Equilibrium beach and shoreface profile of the Rio Grande do Sul coast - south of Brazil. *Journal of Coastal Research*, SI 35, 253-259.
- Gruber N.L.S., Corrêa, I.C.S., Nicolodi, J.L. and Barboza, E.G., 2006. Morphodynamic limits of shoreface and inner shelf at the northern coast of Rio Grande do Sul, Brazil. *Journal of Coastal Research*, SI 39, 664-668.
- Hesp, P.A., Dillenburg, S.R., Barboza, E.G., Tomazelli, L.J., Ayup-Zouain, R.N., Esteves, L.S., Gruber, N.L.S., Toldo Jr., E.E., Tabajara, L.L.C.A. and Clerot, L.C.P., 2005. Beach Ridges, Foredunes or Transgressive Dunefields? Definitions and an Examination of the Torres to Tramandaí Transgressive Dunefield Barrier System, Southern Brazil. *Anais da Academia Brasileira de Ciências*, 77 (3), 493-508.
- Hesp, P.A., Dillenburg, S.R., Barboza, E.G., Clerot, L.C.P., Tomazelli, L.J. and Ayup-Zouain, R.N., 2007. Morphology of the Itapeva to Tramandaí transgressive dunefield barrier system and mid- to late Holocene sea level change. *Earth Surface Processes and Landforms*, 32, 407-414.
- Hesp, P.A., Giannini, P.C.F., Martinho, C.T., Miot da Silva, G. and Asp, N.E., 2009. The Holocene Barrier Systems of the Santa Catarina Coast, Southern Brazil. In: Dillenburg, S.R. and Hesp, P.A. (eds.), *Geology and Geomorphology of Holocene Coastal Barriers of Brazil. Lecture Notes in Earth Sciences*, 107, 93-133.
- Johnston, J.W., Thompson, T.A. and Baedke, S.J., 2007. Systematic pattern of beach-ridge development and preservation: Conceptual model and evidence from ground penetrating radar. In: Baker, G.S. and Jol, H.M. (eds.), *Geological Society of America Special Papers* 432, 47-58.
- Mitchum Jr., R.M., Vail, P.R. and Sangree, J.B., 1977. Seismic Stratigraphy and Global Changes of Sea Level, Part 6: Stratigraphy interpretation of seismic reflection patterns in depositional sequences. In: Payton, C.E. (ed.), *Seismic Stratigraphy — Applications to Hydrocarbon Exploration*. Tulsa, AAPG, 26, 117-133.
- Moulton, M.A.B., Oliveira Filho, S.R., Rocha, T.B., Fernandez, G.B., 2013. Foredunes of Rio de Janeiro coast: genesis, structure and morphology. *Journal of Coastal Research*, SI 65, 1319-1324.
- Neal, A., 2004. Ground-penetrating radar and its use in sedimentology: principles, problems and progress. *Earth Science Reviews*, 66, 261-330.
- Nimer, E., 1990. *Clima*. In: IBGE. Fundação Instituto Brasileiro de Geografia e Estatística. Geografia do Brasil: Região Sul, 151-187.
- Payton, C.E., 1977. *Seismic Stratigraphy — Applications to Hydrocarbon Exploration*. Tulsa, AAPG, (Memoir # 26), 516 p.
- Rocha, T.B., Fernandez, G.B. and Peixoto, M.N.O., 2013. Applications of ground-penetrating radar to investigate the Quaternary evolution of the south part of the Paraíba do Sul river delta (Rio de Janeiro, Brazil). *Journal of Coastal Research*, SI 65, 570-575.
- Rosa, M.L.C.C., Barboza, E.G., Dillenburg, S.R., Tomazelli, L.J. and Ayup-Zouain, R.N., 2011. The Rio Grande do Sul (southern Brazil) shoreline behavior during the Quaternary: a cyclostratigraphic analysis. *Journal of Coastal Research*, SI 64, 686-690.
- Siegle, E. and Asp, N.E., 2007. Wave Refraction and Longshore Transport Patterns along the Southern Santa Catarina Coast. *Brazilian Journal of Oceanography*, 55, 109-120.
- Silva, A.B., Barboza, E.G., Rosa, M.L.C.C. and Fracalossi, F.G., 2010. Caracterização dos Depósitos Sedimentares em Subsuperfície no Setor Meridional da Planície Costeira Sul de Santa Catarina. *Gravel*, 8 (1), 1-7.
- Villwock, J.A., Tomazelli, L.J., Loss, E.L., Dehnhardt, E.A., Horn Filho, N.O., Bachi, F.A. and Denhardt, B.A., 1986. Geology of the Rio Grande do Sul Coastal Province. In: Rabassa, J. (ed.), *Quaternary of South America and Antarctic Peninsula*, 4, 79-97.

# Alongshore variations in beach-dune system response to major storm events on the Danube Delta coast

Florin Tătui†, Alfred Vespremeanu-Stroe†, Luminița Preoteasa†

†Faculty of Geography  
University of Bucharest  
Bucharest, Romania  
ionflorin.tatui@g.unibuc.ro  
vsalfred@yahoo.com  
luminita@geo.unibuc.ro



[www.cerf-jcr.org](http://www.cerf-jcr.org)



[www.JCRonline.org](http://www.JCRonline.org)

## ABSTRACT

Tătui, F., Vespremeanu-Stroe, A., Preoteasa, L., 2014. Alongshore variations in beach-dune system response to major storm events on the Danube Delta coast. In: Green, A.N. and Cooper, J.A.G. (eds.), *Proceedings 13<sup>th</sup> International Coastal Symposium* (Durban, South Africa), *Journal of Coastal Research*, Special Issue No. 70, pp. 693-699, ISSN 0749-0208.

Deltaic beach-dune systems are extremely dynamic, responding to processes operating on scales from short-term variations related to storm and floods to long-term evolution driven by large-scale sediment dynamics (including lobe switching). On Danube Delta beaches, coastal storms and associated processes lead to a wide range of morphological impacts from moderate deposition to significant erosion. Coastal processes develop with marked temporal differences as a result of variations in storminess related to changes in climatic systems (North Atlantic Oscillation). In order to assess the variations in vulnerability to extreme storms, different sectors along the study site were examined using two storm impact indexes: *Storm Impact Categories* of Sallenger, 2000 and *Dune Stability Factor* of Armaroli *et al.*, 2012, based on specific storm thresholds. There is a very good correspondence between the effects of the December 1997 – January 1998 extreme storm cluster and the vulnerability of the beach-dune system predicted with both indicators, with significant alongshore variations of storm impact. The driving factors imposing this variability at different time scales are also discussed, ranging from nearshore slope (which imposes different wave heights and storm induced water level increase) and sediment availability (in direct connection with the evolution of different deltaic lobes, position into the littoral cell and the distance to the Sf. Gheorghe arm mouth, river discharge variability and human interventions) to beach-dune morphology (accommodation space and pre-existing coastal morphology).

**ADDITIONAL INDEX WORDS:** *Coastal erosion, flooding, vulnerability, storm impact, storm surge, dune recovery.*

## INTRODUCTION

Coastal storms and associated processes are widely recognized as some of the most important driving agents for morphological changes observed in the beach-dune systems. Foredunes are crucial features in these systems as they play important roles in their functioning through protection from flooding, ecological as well as aesthetical value. Short term water level changes due to wind and wave set-up play a major role in the dynamics of the coastal zones. Sudden increases in water levels combined with wave action during storms can have important effects leading to significant erosion, shoreline retreat, over-wash, dune disappearance and flooding.

Many studies analyze hurricane impact on the North American coast (Morton, 2002; Stone *et al.*, 2004; Zhang *et al.*, 2005) and the response of European Atlantic coasts to storms (Cooper *et al.*, 2004; Regnaud *et al.*, 2004; Ciavola *et al.*, 2007; Anthony, 2013), but an accurate prediction of these impacts is still lacking (Smyth *et al.* 2013).

The extreme storm impact on coastal systems has been documented as being related to a wide spectrum of control parameters ranging from storm characteristics (Morton, 2002) to beach morphology (Hequette *et al.*, 2001; Backstrom *et al.*, 2007,

2008, 2009; Houser, 2012; Jackson *et al.*, 2005; Jackson and Cooper, 2009; Gervais *et al.*, 2013; Armaroli *et al.*, 2013). Several site-specific storm definitions and thresholds applicable to a number of coastal sites in Europe have recently been presented in the EU-funded ‘MICORE’ project (Trifonova *et al.*, 2012; Armaroli *et al.*, 2012; Almeida *et al.*, 2012; Del Rio *et al.*, 2012).

To predict general storm impacts on coastal morphology and assess the associated dune system vulnerability, a number of storm indexes have been developed in recent years (e.g. Sallenger, 2000; Judge *et al.*, 2003; Armaroli *et al.*, 2012). These works have shown generally good agreement between the effects of extreme storms and the predicted levels of dune vulnerability.

This paper focuses on the analysis of the longshore differences in beach-dune system response to major storm events on a deltaic, low-lying, sandy coast, using two such storm vulnerability indexes: the storm impact scale of Sallenger (2000) and Dune Stability Factor from Armaroli *et al.* (2012) which is based on specific critical thresholds for the forcing agents and coastal morphology. Analysis of this natural beach along the Sulina – Sfântu Gheorghe coastline is important as it is highly sensitive to any changes from storm activity and can offer valuable information on the driving agents of storm impact variability.

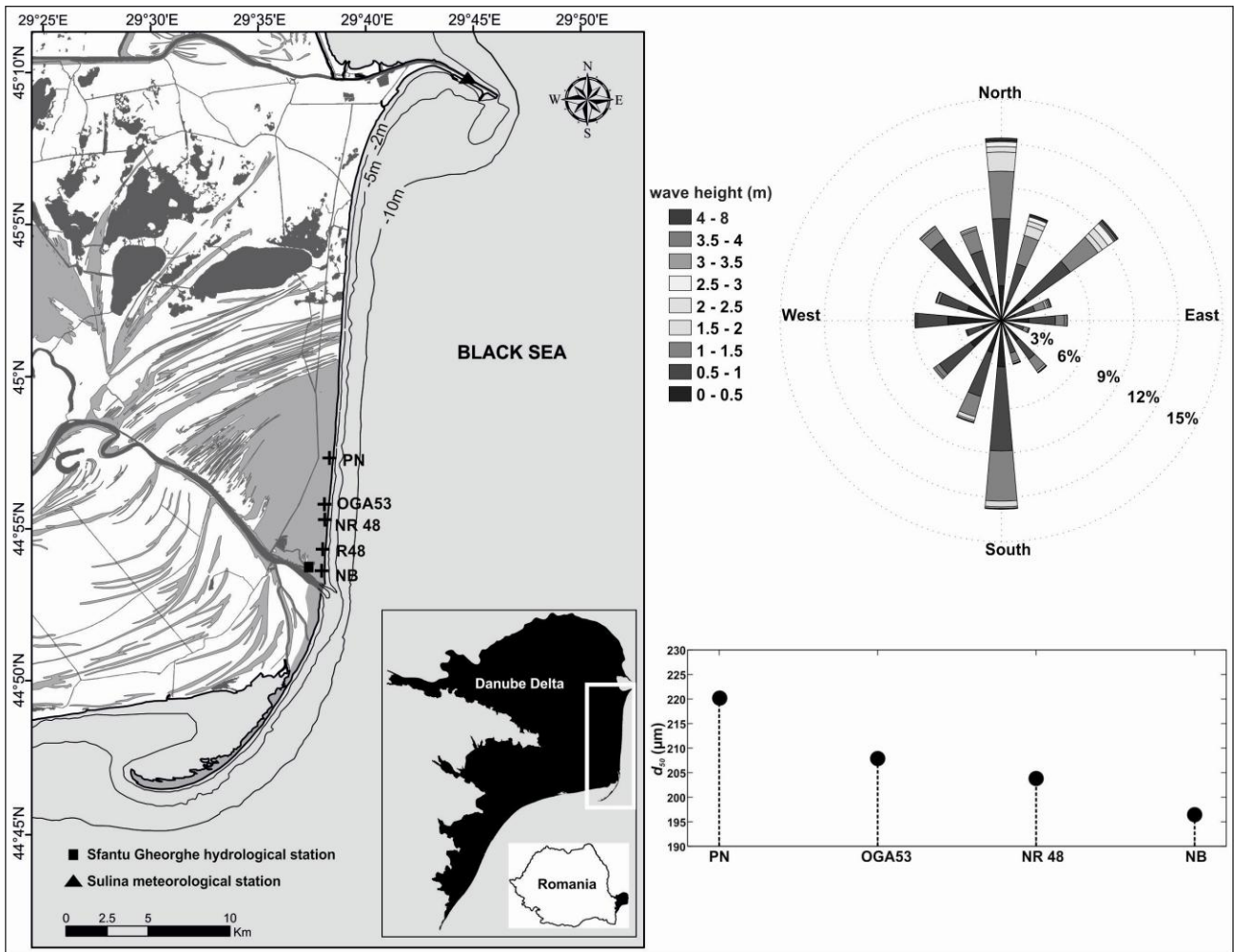


Figure 1. Study site and profiles location. Rose plot of offshore wave heights and directions modelled for 1991 – 2000 period (Vespremeanu-Stroe, 2007) and correspondent beach sediment grain-size  $d_{50}$  for each profile (Preoteasa and Vespremeanu-Stroe, 2010).

## STUDY AREA

The study area is a 16 km stretch of sandy beaches along Sulina – Sfântu Gheorghe coastline (Danube Delta, Romanian Black Sea coast), located northward of Sfântu Gheorghe arm mouth (Figure 1). According to longshore and cross-shore consistency in beach characteristics (morphology, slope, grain size) and shoreline dynamics, the study site is divided into three morphologically distinct sectors: i) a slightly prograding southern sector (0 – 1 km; NB profile), with a current shoreline advance of 1 – 2 m yr<sup>-1</sup> on average, large sub-aerial beaches (40 – 60 m), wide foredunes with contemporary volumes of 100 – 150 m<sup>3</sup> m<sup>-1</sup>; ii) the stable central sector (1 – 6 km in length; R48, NR48 and OGA53 profiles), with wide berms (25 – 40 m across) and high (2.5 – 4 m) and wide foredunes (current volumes of 120 – 180 m<sup>3</sup> m<sup>-1</sup>), and iii) the erosional northern sector (6 – 16 km long; PN profile), characterized by retreating rates between 1 – 2 m yr<sup>-1</sup> at 6 km and 6 – 7 m yr<sup>-1</sup> at 16 km, narrow beaches (20 – 30 m) and small foredunes (5 – 30 m<sup>3</sup> m<sup>-1</sup> from 6 km to 9 km, after that they become discontinuous and, finally, after 11 km, disappear).

The nearshore zone is characterized by the presence of one to four longshore quasi-linear sandbars, which are progressing offshore in a cyclic manner (Tăţui *et al.*, 2011). The average slope

of the nearshore is ranging from 0.4 degrees in south, 0.45 degrees along the central sector and 0.5 degrees in north.

Both the beach and the dunes consist of fine quartz sand with a median grain diameter of about  $d_{50} \sim 200 \mu\text{m}$ . The coast is tideless (Bondar *et al.*, 1973); the mean annual offshore significant wave height is 1.43 m and the corresponding wave period is 5.5 s (Tăţui *et al.*, 2011). Waves from the northeastern direction are dominant in terms of both magnitude and frequency (Figure 1). They induce a net southward longshore sediment transport of 0.65 – 1 × 10<sup>6</sup> m<sup>3</sup> yr<sup>-1</sup>, increasing downdrift (Vespremeanu-Stroe, 2004; Dan *et al.*, 2009).

## METHODS

We used a three step methodology: i) detection and characterization of coastal storms on the Romanian Black Sea coast; ii) determination of climatological, hydrodynamic and morphological storm thresholds and iii) assessment of beach-dune system vulnerability to extreme storms.

Data are represented by mean wind speed and direction measured at Sulina meteo station for more than 50 years (1960 – 2012); wave height, direction and period modelled along the study site for 1990 – 2000 interval (Vespremeanu-Stroe, 2007; Dan,

Table 1. Description of storm categories and thresholds (based on wind data measured at Sulina meteo station: 1960 – 2013).

CATEGORY	I	II	III	IV	V
Minimal conditions (V, D)	≥10 m/s, ≥24 h	≥15 m/s, ≥12 h	≥20 m/s, ≥6 h	≥24 m/s, ≥6 h	≥28 m/s, ≥2 h
Total number (storms)	862	446	99	24	7
Frequency (%)	59.9	31	6.9	1.7	0.5
H <sub>s</sub> (m)	1.5 – 2.5	2.5 – 4	4 – 5	5 – 6	> 6
Return period (yr)	0.06	0.11	0.5	2.08	7.4
Storm surge / Water level (m)	< 0.3 / 0.5	0.3 – 0.5 / 0.5 – 0.8	0.5 – 0.7 / 0.8 – 1.2	0.7 – 0.9 / 1.2 – 1.5	> 0.9 / 1.5

2013); beach and dune surveys between 1997 – 2013 on 5 cross-shore profiles and water levels measured at Sf. Gheorghe hydrological station and modelled during different storm scenarios (Dan, 2013).

The climatological analysis uses several parameters such as mean wind speed ( $V$ ), maximum wind speed ( $V_{max}$ ), resultant wind direction ( $RWD$ ) and total duration ( $D$ ) of each storm and two indicators – an energetic one: Storm Severity Index –  $SSI = \Sigma(V^3 \times T)/1000$ , where  $T$  is the time step of the wind data, and a morphological one: Storm Impact Potential –  $SIP = \Sigma(V^3 \times T \times \sin \alpha)/1000$ , where  $\alpha$  is the angle between instantaneous wind direction and shoreline

In order to assess the beach-dune vulnerability along the study area, we computed two storm impact indicators: the impact scale proposed by Sallenger (2000), which compares the water levels reached on the beach ( $R_{HIGH}$  – elevation due to storm surge and the vertical height of the wave run-up and  $R_{LOW}$  – elevation below which the beach is continuously subaqueous) with the dune foot height ( $D_{LOW}$ ) and dune crest height ( $D_{HIGH}$ ), and a simple morphological index (Dune Stability Factor,  $DSF = (A_{hmax} / A_{dunefoot}) \times 100$ ; Armaroli *et al.*, 2012), based on maximum water level and beach cross-sectional area. If the DSF is below or equal to 20%, the dunes are susceptible to complete removal (vulnerable to overwash, overtopping, dune obliteration); if the percentage is between 20% and 75%, the dunes are vulnerable to frontal erosion and for  $DSF \geq 75\%$ , the dunes are not considered vulnerable (profile intersection: safe conditions). These two storm impact indicators were calculated and compared to the pre- and post-storm topographical profiles (between October/December 1997 and February 1998), similar with the methodology described by Armaroli *et al.* (2013). The run-up ( $R_{2\%}$ ) was estimated based on the formulae of Holman (1986) modified by Komar (1998) and Stockdon *et al.* (2006).

## RESULTS

Storm distribution on the Danube Delta coast (Table 1) shows significant temporal variations in the last five decades. This temporal variability of storms indicates three active intervals: 1961-1973, 1975-1978, 1995-1998 and two calmer ones: 1989–1994 and 2005-2012; the last interval is characterized by an exceptional negative anomaly, with the storm frequency and SIP parameter lowered to half, respectively, one third of the multi-decadal average. The overall storm frequency is inversely correlated with North Atlantic Oscillation ( $r^2 = 0.76$ ), which further affects the multi-decadal coastline evolution of the Danube delta (Vespremeanu-Stroe and Tătu, 2011).

Taking into account the low-intensity storms (categories I and II), the maximum frequency occurs in February with 7.3 stormy days; for severe storms (categories III to V), the stormiest months are December and January. A marked dominance of the northern storms (71% of the total number of storms and 87% of the severe storms are from northern sector) occurs (Figure 1).

Based on our data and previous studies conducted along the study area (Vespremeanu-Stroe, 2007; Dan, 2013), several relevant thresholds have been established for each identified storm category; only the onshore storms have been taken into consideration due to their potential of inducing significant morphological changes of the beach-dune system) – Table 1.

The low-energy storms (category I:  $V_{max} < 15$  m/s,  $H_s \leq 2.5$  m) induce constructive processes in the foredunes helping aeolian transport (Udo *et al.*, 2008; Jackson, 1996) of important sediment volumes from the foreshore and berms, while the sub-aerial beach is affected by moderately erosive wave-driven processes. Their impact is not significant per single event, but the high frequency (17 storms per year or 60% of the total) imposes cumulative morphological changes which contribute the most in creating an equilibrium profile of the subaerial beach.

Medium-energy storms (category II – III:  $V_{max} < 25$  ms<sup>-1</sup>,  $H_s$ : 2.5 – 5 m) are predominantly conservative for the foredunes as wind usually erodes their stoss slope moving the sediment to the dune crest or beyond, to the landward slope. The beaches register significant erosion along the study area (dissipative and intermediate beaches), with maximum water elevation reaching up to 1 m.

Extreme storms (categories IV and V) are erosive for all beach-dune system subunits, inducing storm surges of more than 0.7 m (maximum water level > 1.5 m) and high waves ( $H_s > 5$  m) driven by wind speeds higher than 25 ms<sup>-1</sup>. The return period for these storms is 0.4 years, but two thirds of them are offshore storm events. During the last 50 years we registered only 12 category IV onshore storms and 5 category V onshore storms (a 10 year return period).

The strongest storm ( $SSI = 1031$ ) registered during the last half century occurred in January 1998 (Figure 2) and had the highest total morphological impact ( $SIP = 633$ ). It was a category V storm with a total duration of 157 hours. The wind blew onshore ( $RWD = 35^\circ$ ) with maximum speeds of 28 ms<sup>-1</sup>, inducing a theoretical maximum  $H_s$  of 7.4 m (corresponding peak period of 9.2 s) and a storm surge of almost 1 m. It was the second event of a storm cluster because it was preceded by another extreme storm (15-18 December 1997): category V ( $SSI = 768$ ,  $SIP = 329$ ),  $D = 82$  hours,  $RWD = 19^\circ$ , maximum wind speed of 28 ms<sup>-1</sup> and  $H_{smax} = 6.8$  m, with a similar storm surge of 1 m.



This storm cluster yielded a pronounced morphological impact on the deltaic coast. Most of the low-lying coastal sectors were overwashed-up by the waves, which overtopped the highest units of the sub-aerial coast and formed extensive wash-over fans. The pre-storm (October/December 1997) and post-storm (February 1998) measurements allowed evaluation of this impact along the study area (Figure 3). Here, the storm induced shoreline erosion accounting for 10 m along the central sector to 15 – 20 m on the southern sector and 25 – 50 m on the northern erosive sector (up to ten times higher than the mean annual shoreline retreat rate of 5.8 m). Despite the very high rates of shoreline retreat, along the Sf. Gheorghe beach (6 km northward of arm mouth), the most consolidated sector on the Danube Delta coast, the dunes resisted well, except for several breaches only in the southern part (NB profile). Nevertheless, the sedimentary losses were quite high ( $> 15 \text{ m}^3 \text{ m}^{-1}$  for all sectors), varying between 15 – 20  $\text{m}^3 \text{ m}^{-1}$  in center (R48 profile – the storm displaced important quantities of sediment to offshore and reconfigured the beach-foredune boundary) and 40 – 50  $\text{m}^3 \text{ m}^{-1}$  in south (across the NB profile, where storm waves washed-up the foredune crests creating a large individualized wash-over fan); on the southern sector there appeared only three wash-over fans. On the northern sector, the dunes were completely removed, leading to massive sediment loss.

Considering this storm cluster as a 30-year return period storm or even higher and noting the above mentioned variability in storm impact, we assessed the alongshore vulnerability variations along the study area for such an extreme event. Dan (2013) modelled the water level elevation along the study area for a wind scenario similar to that of January 1998 storm (wind from northeast at  $28 \text{ ms}^{-1}$ ). The simulated values show significant variations along the study site, water levels during the storm decreasing from north to south (85 cm on the erosive sector, 65 cm on the central area and 55 cm on the southern sector). Moreover, the run-up values computed for the same storm conditions showed similar inter-site variability, with values decreasing from 1.45 m on the northern sector to 1.3 m on the central sector and to 1.2 m on the southern sector. Hence, the maximum simulated water levels

Table 2. Statistics of profile configurations and measured storm response for January 1998 storm.

Profile statistic	South	Center			North
	NB	R48	NR48	OGA53	PN
Dune crest height (m)	2.2	3.4	2.8	2.6	2
Shoreline retreat (m)	16	12	13	13	50
Volume lost above MSL ( $\text{m}^3/\text{m}$ )	46	17	16	26	>50
Recovery time (yr)	4	1.5	1.5	1.7	6
DSF% (Armaroli, 2012)	19	37	32	32	1
Storm Impact Level (Sallenger, 2000)	2-3	2	2	2	3

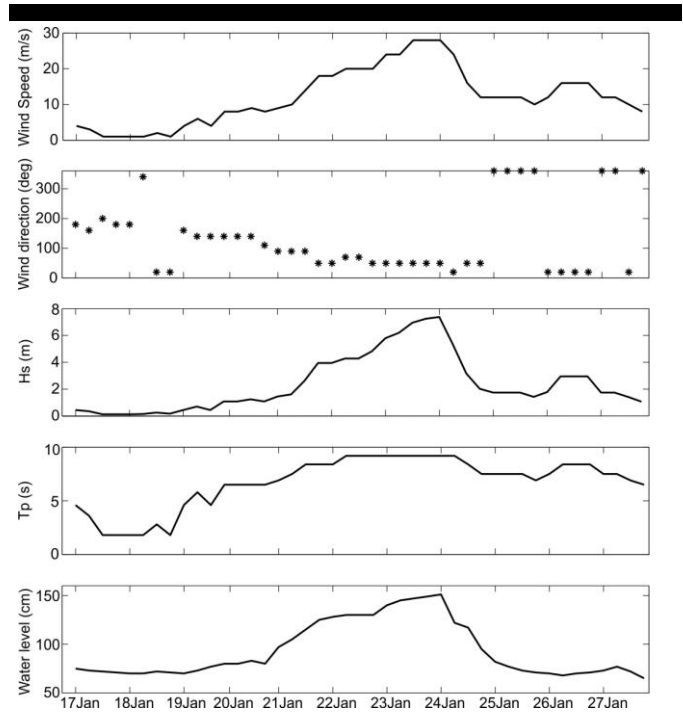


Figure 2. Characteristics of the January 1998 storm used for evaluating the vulnerability of the beach-dune system: wind speed, wind direction, significant wave height ( $H_s$ ), peak period ( $T_p$ ) and water level.

during the January 1998 storm decreased from 2.3 m (north) to 1.95 m (center) and 1.75 m (south). The maximum topographic elevations were registered on the central sector (wide sub-aerial beaches, unitary and robust dune area with widths of 60 – 80 m and heights of 2.5 – 4 m), while the lowest widths and elevations of the dune system were encountered on the southern ( $< 50 \text{ m} / 2.5 \text{ m}$ ) and northern sector ( $< 30 \text{ m} / 2 \text{ m}$ ) – Table 2. North of the PN profile, dunes were constantly decreasing in height becoming gradually discontinuous and, finally, disappearing. According to the variability of the cross-shore profile morphology and of the storm induced water levels along the study site, there are considerable variations in the beach-dune system vulnerability to such extreme events, expressed by different values of the two indicators (Table 2). The southern sector is characterized by impact level 2 to 3 according to storm impact scale of Sallenger (2000) and the DSF is less than 20%, which means that this sector records collision to over-wash regimes. The central sector is susceptible to collision regime (impact level 2) expressed by frontal erosion (DSF between 30 and 40%). The northern area has an impact level 3 confirmed by the smallest values of the DSF, corresponding to an overwash regime.

## DISCUSSION

Beach-dune system vulnerability to storm impact has been evaluated along a short deltaic coastal sector where highly variable responses have been identified in relation to alongshore unidirectional differences in morphological, hydrodynamic and environmental characteristics.

A synthesis of the relevant data of December 1997 – January 1998 storm cluster vulnerability degree and storm impact is shown in Table 3. The lowest vulnerability to extreme events along the study area is specific to the central sector. Here, the storm impact on morphology is characterized by frontal dune erosion and

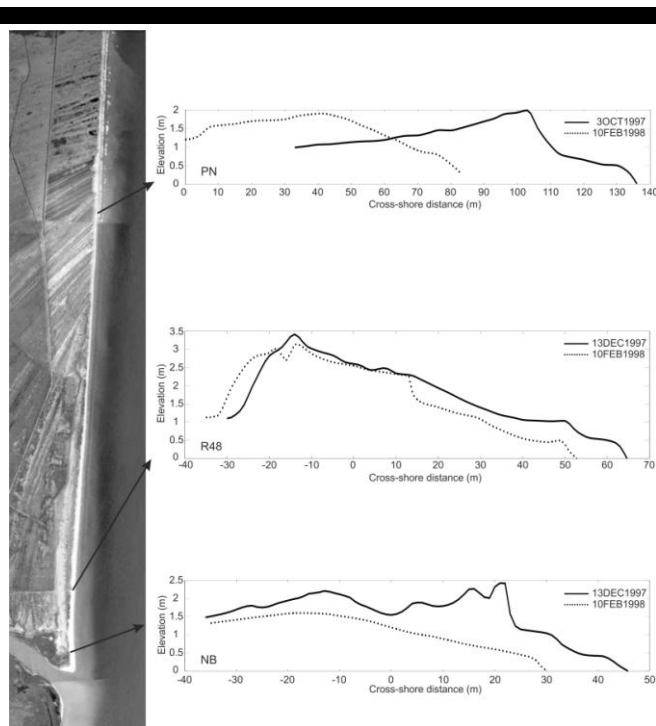


Figure 3. Examples of representative profiles for the extreme storm impact on the beach-dune system morphology.

profile lowering (collision regime). Run-up collides with the dune foot and the sediment is eroded from the seaward slope of the foredunes and transported offshore – contributing to a net sediment loss as the eroded sand is not returned to the dunes. The degree of vulnerability of the southern sector is medium (collision to over-wash regime), extreme storms inducing dune over-wash, local dune obliteration and profile flattening. Most of reworked sediments are transported offshore and hardly returns to the beach-dune system. The northern sector is the most vulnerable area to moderate to extreme storms along the study site. The morphological impact of the extreme events includes dramatic shoreline retreat, dune over-wash, overtopping and obliteration (over-wash regime). Most of the sediment is exported offshore; however, small quantities are transported landward by over wash (net deposition landward).

All these variations in vulnerability and morphological impact of extreme events are controlled mainly by differences in nearshore slope and sediment availability (alongshore sand reservoir distribution). The nearshore slope imposes, during the same event, alongshore differences in wave heights seen in the variations of water levels along different coastal sectors and, further, in the impact of storm waves on the beaches and dunes.

The variability of beach and foredune sand volumes is also very important, where shoreline dynamics (erosion/accretion processes) impose different equilibrium morphologies of the beach-dune system which play a major role in the storm impact magnitude.

Even though the analyzed storm cluster had a long return period (30 years) and resulted in a major impact on the beach-dune morphology (inducing important shoreline retreat and massive sediment loss), the system recovered relatively quickly. The sedimentary volumes recovered rapidly on the stable sectors (1.5 years), and later on the southern and northern sectors (4 – 6 years; Table 2).

The current morphological situation of the study area is quite different in comparison with January 1998. On the southern sector, the storm cluster created a large accommodation space for secondary landforms which allowed long aeolian fetches which, together with the slow but constant advance of the shoreline (continued until 2010) and with the low storm regime afterwards conducted to a fast growing foredune. This reflects into an increase of the dune stability and a more efficient protection from future storms. This was the case during an energetic phase between 2002 – 2004, when the continuous increase in width and height of beaches and dunes attenuated the impact of storm waves. Moreover, the aeolian fetch extended as a consequence of the increase in the berms width. This situation lead to rapid development of dunes and the initialization in 2011 when an incipient foredune ridge at approximately 40 m was formed in front of the foredunes between 1998 and 2010.

On the central sector, due to the stable shoreline and wide beaches, the beach-dune volumes are highest and the foredunes are unitary and continuous alongshore, dictating a low impact from the severe storms. The mobility of this sector is seasonally modulated by storms and calmer intervals, without expressing any tendency of multi-annual evolution. Hence, the negative variations of beach-dune system volumes are the result of sediment dynamics during energetic events. The 2002 – 2004 stormy interval determined narrower beaches and shorter aeolian fetches negatively impacted the foredune seaward slope, especially its lower half, but the overall impact (sediment loss) was minor ( $2 - 5 \text{ m}^3 \text{ m}^{-1}$ ). It is possible for this sector to be affected by significant erosion in the case of an 100 year return period event (the worst scenario described in Dan, 2013), characterized by wind from north-east reaching 40 m/s, a combination between the highest ever-recorded wind speed and the onshore prevalent direction.

On the northern sector, based on the continuous shoreline retreat (higher rates in northward direction), the beaches are narrow and the dunes (where they are present) are small ( $\leq 2 \text{ m}$  high) and eroded even during medium-energy storms. The dunes are frequently overtopped and, sometimes, washed-up by the waves, with the northern sector becoming a succession of wide wash-over fans following the onshore extreme storms.

The succession of the erosional/stable/prograding sectors along the study area is determined by i) position into the littoral cell and the distance to the Sf. Gheorghe (Danube) mouth, which acts as a sediment trap during fair-weather conditions; ii) river discharge variability, and iii) human interventions (e.g. Sulina jetties), which breakdown the longshore sediment transport and changes the longshore distribution of sediment budgets. Taking into account long-term scales (multi-annual, decadal), the primary factor modulating the evolution of this deltaic coast is climatic

Table 3. Vulnerability degree and storm impact along the study area.

<i>Coastal Sector</i>	<i>Vulnerability degree</i>	<i>Storm Impact</i>
<i>South</i>	Medium	Overwash, profile flattening
<i>Center</i>	Low	Dune erosion, profile lowering
<i>North</i>	High	Overtopping, shoreline retreat, dune obliteration

variability (e.g. NAO) expressed by variations in storm frequency and intensity, wave climate and, ultimately, in shoreline behavior and beach-dune system morphology. On shorter time scales (events, seasons), the longshore variations in beach-dune system response to major storm events are a matter of differences in antecedent morphology (shoreface slope, nearshore morphology, sub-aerial beach morphometry, foredune morphology and volume) and secondary to minor differences in storm waves, which would be slightly smaller on the northern sector than in the rest, due to smaller fetches.

## CONCLUSION

The use of the two storm impact indicators provided good agreement in estimating beach-dune system vulnerability to an extreme event along a deltaic coast. The beaches studied showed significant variability of the morphodynamic response to this event. Generally, the natural areas characterized by sufficient sediment availability show low vulnerability to extreme storms and a higher frequency (than recorded) of such events have to occur to damage them. The impact on erosional areas is much higher in terms of shoreline retreat and sediment loss, but it is in fact only a short term spike superposed on the multi-decadal erosional trend (driven by the local negative sediment budget).

At short time scales (daily-to-seasonally), the coastal erosion is controlled by storm wave climate, storm surge and wave run-up, associated with the cross-shore profile morphology. At the medium and long-term scale (multi-annual to centennial), erosion of the deltaic coasts is controlled to a large extent by large-scale sediment dynamics (seen as a shifting of the active sedimentation between different distributaries of a delta), rather than by hydrodynamics.

The prediction of dune erosion and vulnerability to storms is important for assessing the resilience of deltaic coastal areas, but the use of storm impact indicators, morphodynamic classifications and models should be treated with caution. It is not enough to extrapolate the impact of extreme events to predict future conditions. It is necessary to also take into account the past long-term evolution of the coastal sector and other critical local dynamic factors which drive this evolution (sediment availability, river discharge variability, geological constraints etc.).

## ACKNOWLEDGEMENTS

This study was funded by the Romanian National Authority for Scientific Research, CNCS – UEFISCDI under the grant no. PN-II-RU-TE-2011-3-0293 awarded to AVS. Florin Zăinescu is thanked for his help in the analysis of storms data sets. The topographic and bathymetric measurements were conducted in the frame of Sfântu Gheorghe Marine and Fluvial Research Station (Faculty of Geography, University of Bucharest).

## LITERATURE CITED

- Anthony E.J., 2013. Storms, shoreface morphodynamics, sand supply, and the accretion and erosion of coastal dune barriers in the southern North Sea. *Geomorphology*, 199, 8-21.
- Almeida, L.P., Voudoukas, M.V., Ferreira, O., Rodrigues, B.A. and Matias, A., 2012. Thresholds for storm impacts on an exposed sandy coastal area in southern Portugal. *Geomorphology*, 143-144, 3-12.
- Armaroli, C., Ciavola, P., Perini, L., Lorito, S., Valentini, A. and Masina, M., 2012. Critical storm thresholds for significant morphological changes and damage along the Emilia-Romagna coastline, Italy. *Geomorphology*, 143-144, 34-51.
- Armaroli, C., Grottoli, E., Harley, M.D. and Ciavola, P., 2013. Beach morphodynamics and types of foredune erosion generated by storms along the Emilia-Romagna coastline, Italy. *Geomorphology*, 199, 22-35.
- Backstrom, J.T., Jackson, D.W.T. and Cooper, J.A.G., 2007. Shoreface dynamics of two high-energy beaches in Northern Ireland. *Journal of Coastal Research*, 50, 594-598.
- Backstrom, J.T., Jackson, D.W.T., Cooper, J.A.G. and Malvarez, G.C., 2008. Storm-driven shoreface morphodynamics on a low-wave energy delta: the role of nearshore topography and shoreline orientation. *Journal of Coastal Research*, 24, 1379-1387.
- Backstrom, J. T., Jackson, D.W.T. and Cooper, J.A.G., 2009. Shoreface morphodynamics of a high-energy, steep and geologically constrained shoreline segment in Northern Ireland. *Marine Geology*, 257(1-4), 94-106.
- Bondar, C., State, I. and Roventă, V., 1973. *Black Sea in the area of the Romanian coast. Hydrological monograph* (in Romanian). Bucharest: Institutul de Meteorologie și Hidrologie, 516p.
- Ciavola, P., Armaroli, C., Chiggiato, J., Valentini, A., Deserti, M., Perini, L. and Luciani, P., 2007. Impact of storms along the coastline of Emilia-Romagna: the morphological signature on the Ravenna coastline (Italy). In: Lemckert, C.J. (ed.), *Proceedings 9<sup>th</sup> International Coastal Symposium* (Gold Coast, Australia), *Journal of Coastal Research*, Special Issue No. 50, 540-544.
- Cooper, J.A.G., Jackson, D.W.T., Navas, F., McKenna, J. and Malvarez, G., 2004. Identifying storm impacts on an embayed, high-energy coastline: examples from western Ireland. *Marine Geology*, 210, 261-280.
- Dan, S., Stive, M.J.F., Walstra, D.J.R. and Panin, N., 2009. Wave climate, coastal sediment budget and shoreline changes for the Danube Delta. *Marine Geology*, 262, 39-49.
- Dan, S., 2013. Coastal dynamics of the Danube Delta. Enschede, the Netherlands: Delft University of Technology Ph.D thesis, 159p.
- Del Rio L., Plomaritis T.A., Benavente J., Valladares M. and Ribera P., 2012. Establishing storm thresholds for the Spanish Gulf of Cadiz coast. *Geomorphology*, 143-144, 13-23.
- Gervais, M., Balouin, Y. and Certain, R., 2013. The major control parameters of storm morphological evolution on a microtidal barred beach. *Proceedings of Coastal Dynamics 2013*, Arcachon, France.
- Hequette, A., Desrosiers, M., Hill, P.R. and Forbes, D.L., 2001. The influence of coastal morphology on shoreface sediment transport under storm-combined flows, Canadian Beaufort Sea. *Journal of Coastal Research*, 17, 507-516.
- Holman, R.A., 1986. Extreme value statistics for wave run-up on a natural beach. *Coastal Engineering*, 9, 477-491.
- Houser, C., 2013. Alongshore variation in the morphology of coastal dunes: Implications for storm response. *Geomorphology*, 199, 48-61.
- Jackson, D.W.T., 1996. Potential inertial effects in aeolian sand transport: Preliminary results. *Sedimentary Geology*, 106(3-4), 193-201.
- Jackson, D.W.T., Cooper, J.A.G. and del Rio, L., 2005. Geological control of beach morphodynamic state. *Marine Geology*, 216(4), 297-314.
- Jackson, D.W.T. and Cooper, J.A.G., 2009. Geological Control on Beach Form: Accommodation Space and Contemporary Dynamics. *Journal of Coastal Research*, Sp. Iss. 56, 69-72.
- Judge, E.K., Overton, M.F. and Fisher, J.S., 2003. Vulnerability indicators for coastal dunes. *Journal of Waterway, Port, Coastal and Ocean Engineering*, 129, 270-278.
- Komar, 1998. *Beach Processes and Sedimentation*. New York: Prentice Hall. 544 p.
- Morton, R.A., 2002. Factors controlling storm impacts on coastal barriers and beaches— a preliminary basis for near real-time forecasting. *Journal of Coastal Research*, 18, 486-501.
- Preoteasa, L. and Vespreamanu-Stroe, A., 2010. Grain-Size Analysis of the Beach-Dune Sediments and the Geomorphological Significance. *Revista de Geomorfologie*, 12, 73-79.
- Regnaud, H., Pirazzoli, P.A., Morvan, G. and Ruz, M.H., 2004. Impacts of storms and evolution of the coastline in western France. *Marine Geology*, 210, 325-337.
- Sallenger, A.H., 2000. Storm impact scale for barrier islands. *Journal of Coastal Research*, 16, 890-895.
- Smyth, T.A.G., Jackson, D.W.T. and Cooper, J.A.G., 2013. Three dimensional airflow patterns within a coastal trough-bowl blowout during fresh breeze to hurricane force winds. *Aeolian Research*, 9, 111-123.
- Stockdon, H.F., Holman, R.A., Howd, P.A. and Sallenger Jr., A.H., 2006. Empirical parameterization of setup, swash, and runup. *Coastal Engineering*, 53, 573-588.

- Stone, G.W., Liu, B., Pepper, D.A. and Wang, P., 2004. The importance of extratropical and tropical cyclones on the short-term evolution of barrier islands along the northern Gulf of Mexico, USA. *Marine Geology*, 210, 63-78.
- Tătui, F., Vespremeanu-Stroe, A. and Ruessink, B.G., 2011. Intra-site differences in nearshore bar behavior on a nontidal beach (Sulina-Sf. Gheorghe, Danube Delta coast). In: Furmanczyk, K., Giza and Terefenko (eds.), *Proceedings 10<sup>th</sup> International Coastal Symposium* (Szczecin, Poland), *Journal of Coastal Research*, Special Issue No. 64, 873-878.
- Trifonova, E.V., Valchev, N.N., Andreeva, N.K. and Eftimova, P.T., 2012. Critical storm thresholds for morphological changes in the western Black Sea coastal zone. *Geomorphology*, 143-144, 81-94.
- Udo, K., Kuriyama, Y. and Jackson, D. W. T., 2008. Observations of wind-blown sand under various meteorological conditions at a beach. *Journal of Geophysical Research –Earth Surface*, 113 (F4). pp. F04008.
- Vespremeanu-Stroe, A., 2004. Longshore sediment transport and wave climate along the Danube Delta coast (in Romanian). *Studii și Cercetări de Oceanografie Costieră*, 1, 67-82.
- Vespremeanu-Stroe, A., 2007. Danube Delta coast: geomorphological study (in Romanian). Editura Universitară, Bucharest, Romania: University of Bucharest Ph.D thesis, 226p.
- Vespremeanu-Stroe, A. and Tătui, F., 2011. North-Atlantic Oscillation signature on coastal dynamics and climate variability of the Romanian Black Sea coast. *Carpathian Journal of Earth and Environmental Sciences*, 6(1), 308-316.
- Zhang, K., Whitman, D., Leatherman, S.P. and Robertson, W., 2005. Quantification of beach changes caused by Hurricane Floyd along Florida's Atlantic coast using airborne laser surveys. *Journal of Coastal Research*, 21, 123-134.

# Bedform Dynamics in a Rip Current

Antony Thorpe, Jon Miles, Gerd Masselink, Paul Russell

School of Marine Science and Engineering,  
University of Plymouth, Plymouth,  
PL4 8AA, UK  
athorpe1@plymouth.ac.uk  
j.r.miles@plymouth.ac.uk  
gerd.masselink@plymouth.ac.uk  
p.russell@plymouth.ac.uk



[www.cerf-jcr.org](http://www.cerf-jcr.org)



[www.JCRonline.org](http://www.JCRonline.org)

## ABSTRACT

Thorpe, A., Miles, J., Masselink, G., Russell, P., 2014. Bedform Dynamics in a Rip Current, *Proceedings 13<sup>th</sup> International Coastal Symposium* (Durban, South Africa), *Journal of Coastal Research*, Special Issue No. 70, pp. 700-705, ISSN 0749-0208.

A Sand Ripple Profiler (SRP) was deployed in a rip channel on a dissipative sandy beach to measure bedform height ( $\Delta$ ), length ( $\lambda$ ) and migration rate ( $M_r$ ) throughout a macro-tidal cycle.

Data were collected in significant wave heights ranging from 0.5 m to 2.1 m and water depths of between 0.9 m and 7.4 m. Periods when the rip current was active were identified by comparing measured cross-shore velocity ( $U$ ) with predicted cross-shore velocity from a bed return flow model. Rip flow was found to commence when offshore velocities reached approximately 0.1 m/s, maximum rip velocity as a 5 minute mean was 0.74 m/s.

At lower tidal elevations ( $h < 2.5$  m), in the strong offshore flow of the rip current megaripples were found to migrate offshore ( $M_r = 0 - 4$  cm/min). When migration occurred in a rip current migration rates were correlated with  $U$  with the highest migration rates found in the strongest flows.

In non-rip current conditions megaripples exhibited two types of migration behaviour; (1) migrating onshore at a maximum rate of 2.1 cm/min when  $h$  was in the range of 2.5 m to 5 m and wave skewness was high and (2) megaripples were stable when mean flows and skewness were low, this occurred at higher tidal elevations when  $h > 5$  m.

**ADDITIONAL INDEX WORDS:** *Rip Currents, Megaripples, Field Measurements, Bedform Migration*

## INTRODUCTION

Rip currents are a unique feature of the nearshore zone exhibiting a channel of strong, quasi-steady, offshore-directed flow (in the order of 0.5 m/s) that dissects the wave dominated surfzone and dissipates beyond the breaker zone (MacMahan *et al.*, 2005; Austin *et al.*, 2010). Wave breaking is focused on sandbars and minimized in the rip channel; as a consequence of this water travels alongshore in feeder channels before flowing seaward within the rip neck (MacMahan *et al.*, 2006). Rip currents are typically found at lower tidal elevations where they are associated with bar/rip morphology (Brander, 1999a).

Bedform dynamics are principally governed by the flow characteristics, and to a lesser extent grain size and the water depth in which they are situated (Allen, 1985). In the combined flows of the surfzone (waves > currents), Gallagher *et al.* (1998) found megaripples (height ( $\Delta$ ) = 0.2 – 0.3 m, length ( $\lambda$ ) = 2 – 5 m) present 60 % of the time (in a trough where  $h = 1.5 - 2$  m) during a 6 week field work campaign. The megaripples generally took the form of oval shaped holes and occurred under a wide range of wave conditions ( $H_s = 0.5 - 4$  m). Onshore migration was attributed to wave skewness with typical migration rates of 0.5 cm/min (maximum = 2.5 cm/min). Gallagher *et al.* (2003) proposed that megaripples found in the surfzone were dynamically similar to asymmetric, steady flow features present in rivers and estuaries.

In a tidal shoal of an estuary mouth (currents > waves) Hoekstra *et al.* (2004) found megaripples ( $\Delta = 0.03 - 0.05$  m,  $\lambda = 0.6 - 1$  m) were consistently present and were shown to increase in wavelength with increasing mean flows and migrated in the direction of tidal flow (maximum = 0.5 m/s) at maximum rates of 1.1 to 1.4 cm/min.

Megaripples have also been observed to be present in rip currents (Greenwood and Davidson-Arnott, 1979; Nielsen, 1992; Aagaard *et al.*, 1997; Brander, 1999b). Field observations suggest that in rip currents megaripples migrate offshore and are current dominated (Nielsen, 1992). Sherman *et al.* (1993) observed megaripples in a rip feeder channel ( $V = 0.4$  to 0.6 m/s) by visually measuring a pre-selected megaripple with a 'meter long aluminium comb'. They observed lunate bedforms of megaripple dimension ( $\Delta = 0.16$  m,  $\lambda = 1.6$  m) migrating at an average of 1.65 cm/min in the direction of flow.

The aim of this paper is to quantify bedform dynamics, with particular focus on bedform migration, in a rip current and to investigate the processes responsible. This is achieved by comparing bedforms and their behaviour in an active rip current to that in non-rip conditions.

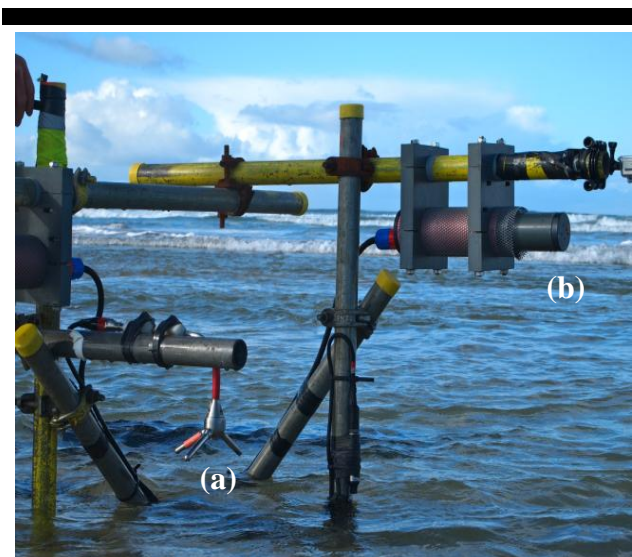


Figure 1. Mobile instrument frame and position of instruments; (a) ADV head and (b) Sand Ripple Profiler (SRP). The picture was taken at low tide in the first field experiment; at mid tide and high tide the rig is completely submerged.

## METHODS

### Study Site

The data in this study were collected from Perranporth on the North Cornwall Coast, UK during two separate experiments. Perranporth is a highly energetic beach with an annual significant wave height ( $H_s$ ) of 1.6 m and a peak period ( $T_p$ ) of 10.5 s (Austin *et al.*, 2010). It faces west-northwest, is exposed to Atlantic swell and also receives locally generated wind waves. It is a macro-tidal beach with a mean spring range of 6.3 m and consists of medium sized sand ( $D_{50} = 0.28 - 0.34$  mm). The beach is dissipative with pronounced low tide bar/rip morphology on a seasonal time scale (Austin *et al.*, 2010).

During both fieldwork campaigns the beach exhibited a low tide rhythmic bar/rip system throughout its length. The rip used for the study was chosen because it offered a clearly defined channel with offshore flow dissecting the intertidal bar.

### Field Measurements

Offshore wave data were collected from a wave buoy located approximately 1 km offshore of the study site. *In-situ* data were collected using a range of instruments secured to a mobile frame (Figure 1). The frame was assembled prior to deployment and carried into the rip channel at spring low tide.

The flow velocities, waves and tidal elevation in the rip channel were recorded with a Nortek Vector 3D-Acoustic Doppler Velocimeter (ADV) fitted with an internal Pressure Transducer (PT). The head of the ADV was carefully aligned to measure cross-shore and longshore flows with the sensing volume set at 0.55 m above the bed. The PT, used to measure wave statistics and tidal elevation was housed in the ADV casing unit with the sensor positioned at a height of 0.2 m above the bed. Data from the ADV, PT and OBS were logged autonomously at 8 Hz during the first experiment and 4 Hz in the second deployment.

A Sand Ripple Profiler (SRP) was used to measure bedform dynamics. The SRP is a pencil beam sonar scanner that collects data as a range ( $R$ ) and angle ( $\theta$ ) from the scanner. Data

processing involved transforming the ( $R$ ,  $\theta$ ) data to polar coordinates ( $x$  = cross-shore distance;  $z$  = distance below the scanner). The data were post-processed to produce a profile of the bed from which  $\Delta$ ,  $\lambda$  and  $M_r$  were deduced. The SRP was aligned to scan in the cross-shore direction positioned 0.9 m above the bed, giving a footprint of approximately 2 m with a horizontal resolution of 14 mm directly below the scanner. In the second experiment a second SRP was deployed, also with a cross-shore orientation, giving a 4.4 m footprint. The data logger was programmed to log autonomously scanning the bed once every minute. Analysis is limited to sections of data where the acoustic scans by the SRP are unaffected by aeration in the water column from breaking waves.

Bedform statistics were calculated following Masselink *et al.* (2007). Bedform length was found using the auto-correlation of the scan where the wavelength is twice the spatial lag corresponding to the strongest negative auto-correlation peak. For this method to work, at least half a megaripple wavelength should be captured in the scan. Bedform height was estimated as the root mean square of the bed elevation using,  $\sqrt{8\sigma}$ , where  $\sigma$  is the standard deviation of the bed level profile (Crawford and Hay, 2001). Migration rate was determined by cross-correlating scans 5 minutes apart, with the strongest positive correlation assumed to represent migration distance. This value was divided by the elapsed time to give migration rate in centimetres per minute.

## RESULTS

### Environmental Conditions

Data presented here were collected from six full tidal cycles (during the first field experiment) and the flood of a seventh (during a second field experiment), thus giving 13 periods when the rip current was active (accounting for flood and ebb parts of the tidal cycle). Offshore  $H_s$  ranged from 0.5 to 1.9 m and peak period was between 10 to 15 seconds.

*In-situ* hydrodynamic parameters were calculated as 5-minute means and synchronised to periods when good SRP data were collected (Figure 2). Water depths ranged from 0.9 m (the depth at which the SRP was deployed) to a maximum of 7.4 m. Wave heights ( $H_s$ ) were corrected for depth attenuation and ranged from 0.5 m in Tide 1 to 2.1 m in Tide 5. In relatively shallow water, the rip current is active and offshore-directed flows are typically in excess of 0.3 m/s, with a maximum of 0.74 m/s in run number 294. Mean cross-shore flows ( $U$ ) are close to zero in relatively deep water. Wave skewness is a measure of wave shape, with positively shaped waves having a faster onshore than offshore stroke and therefore having the potential to induce onshore sediment transport or onshore bedform migration (Gallagher *et al.*, 1998). Normalised short-wave skewness was calculated as  $S = \langle U^3 \rangle / \langle U^2 \rangle^{2/3}$  following Elgar *et al.* (1988) using velocity data high-pass filtered at 0.05 Hz. The mobility number ( $\psi$ ), calculated following Gallagher *et al.* (2003), includes both the mean and the oscillatory component of the velocity time series where;  $\psi = (u^2 + v^2)/(s-1)gD$ , and  $s$  is the specific gravity (a ratio of sediment to water density, 2.65 for quartz sand),  $g$  is acceleration due to gravity and  $D$  is grain diameter. Wave skewness and mobility number exhibit a similar trend with the highest values found at lower tidal elevations and in larger waves.

To define when the rip current was active, a simple model by Masselink and Black (1995) was used to predict cross-shore velocities (as a result of bed return flow) and compared to measured cross-shore velocities (Figure 3). To consistently isolate the rip from non-rip conditions it was deemed that four consecutive observations of measured  $U$  exceeding predicted  $U$

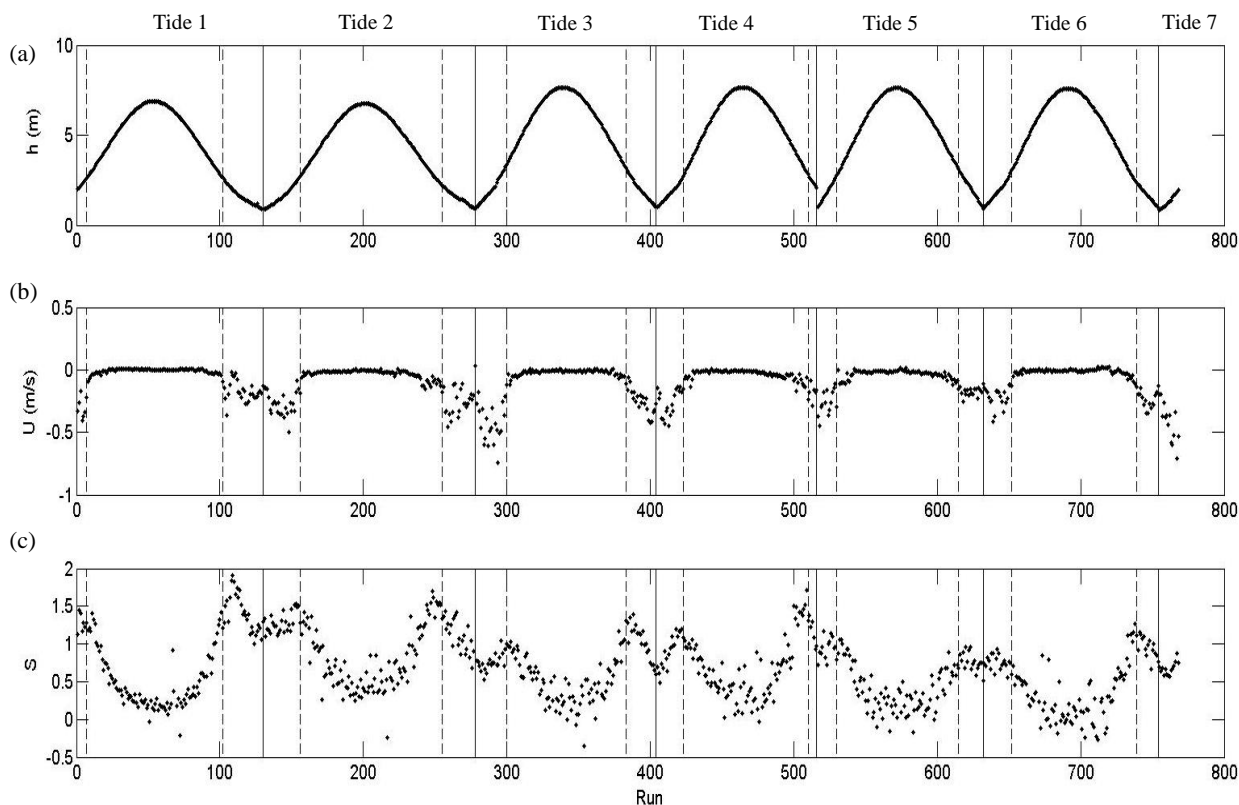


Figure 2. Hydrodynamic parameters calculated from 5 minute bursts. (a) Water depth ( $h$ ), (b) mean cross-shore velocity ( $U$ ) and (c) wave skewness ( $S$ ). The solid lines represent the boundaries between individual tides; the dashed lines mark the rip boundaries.

were rip current conditions, and similarly four consecutive observations where predicted  $U$  exceeded measured  $U$  (after a period of rip conditions) was a return to non-rip conditions.

Periods of rip current conditions are marked with a vertical dashed line in the time series plots of hydrodynamic conditions in Figure 2.

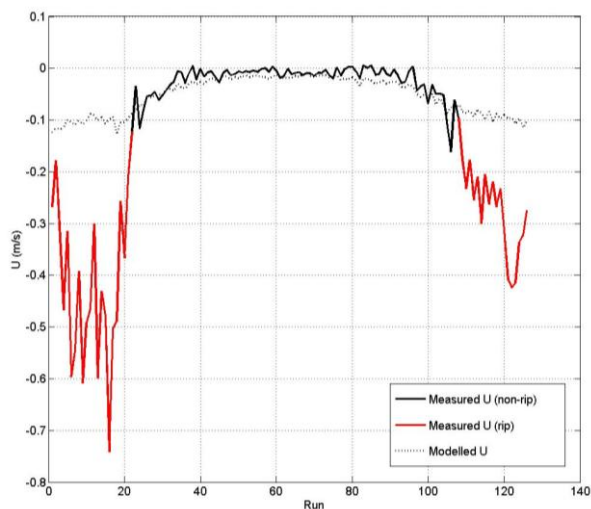


Figure 3. Rip identification. Measured  $U$  against modelled  $U$  with rip and non-rip conditions marked (-ve is offshore).

### Bedform Dimensions

During the study bedforms of megaripple scale were found to be present in the rip channel throughout the tidal cycle (Figure 4). Bedform length and height in non-rip conditions were found to be stable with minimal change during each tide and consistent values between each tide, with  $\lambda$  ranging from 0.92 to 1.35 m and  $\Delta$  from 0.04 to 0.09 m (though in Tide 5, megaripple height is as high as 0.15 m).

During rip current conditions measurements of  $\lambda$  was found to be quite variable, though the observed trend is an increase in  $\lambda$  compared to non-rip conditions, with  $\lambda$  often of the order of 2 m, and in some cases in excess of 3 m. Bedform  $\Delta$  in the rip current was of similar scale as in non-rip conditions, with heights ranging from 0.04 to 0.20 m.

### Bedform Migration

Megaripple migration direction and speed varied over the tidal cycle, but the variation was consistent between tides. This is shown in Figure 5a, which was produced by collapsing 5 tides of data (from Tides 3 to 7, all of which were of similar tidal range, allowing each data run to be averaged) onto one plot.

Typically in rip current conditions, megaripple migration was offshore at rates ranging from 0 to 4 cm/min, with the majority of offshore migration occurring at  $h < 2.5$  m. Figure 6 shows an example of 60 minutes of bed data collected from within the rip current, with  $h$  increasing from 0.8 to 1.7 m and  $U$  peaking at 0.6 m/s. The average  $\lambda$  and  $\Delta$  were 2.9 m and 0.1 m, respectively (far exceeding the typical measurements made in the non-rip conditions, where  $\lambda = 0.92$  to 1.35 m and  $\Delta = 0.04$  to 0.09 m) and

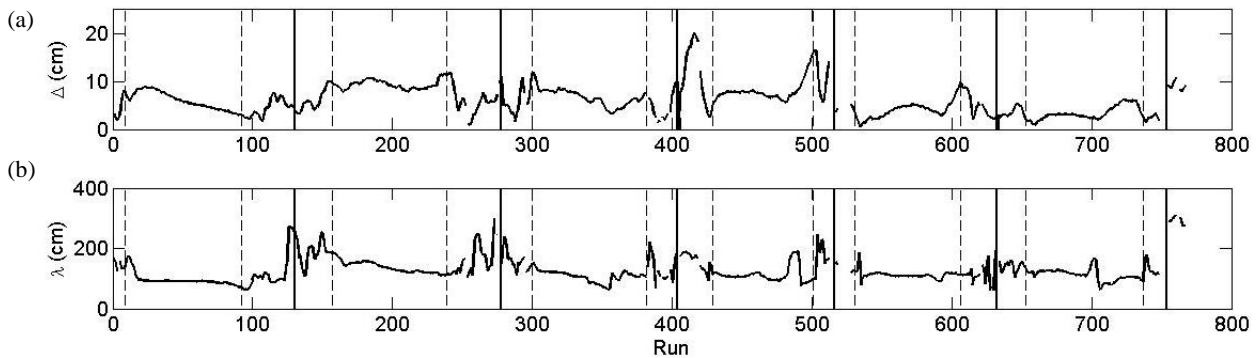


Figure 4. Time series of (a) bedform height ( $\Delta$ ) and (b) length ( $\lambda$ ). The solid lines represent the boundaries between individual tides; the dashed lines mark the rip boundaries.

average migration rate for the period was 0.75 cm/min with a 5 minute maximum of 2.1 cm/min.

In non-rip conditions megaripples showed two different forms of migration behaviour. As tidal elevation increased ( $h = 2.5$  to 5 m) and mean flows became weaker as the rip became inactive the direction of migration switched to onshore at similar speeds as

the offshore migration ( $M_r = 0$  to 2.1 cm/min). As the tidal elevation increased further ( $h > 5$  m), the megaripples remained

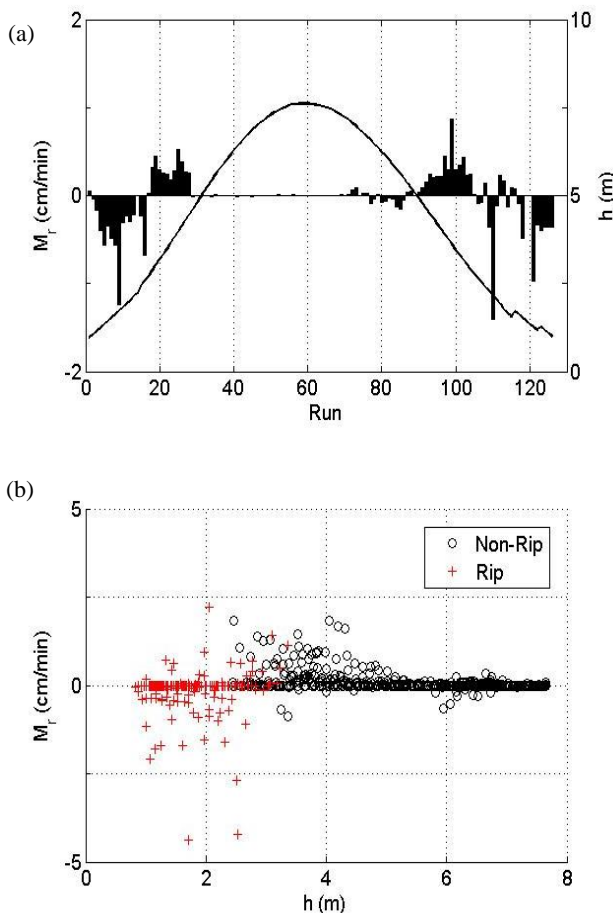


Figure 5. (a) Migration rate and direction (-ve is offshore) alongside water depth. Data from Tides 3 to 7 collapsed onto one plot. (b) Migration rate and direction as a function of water depth.

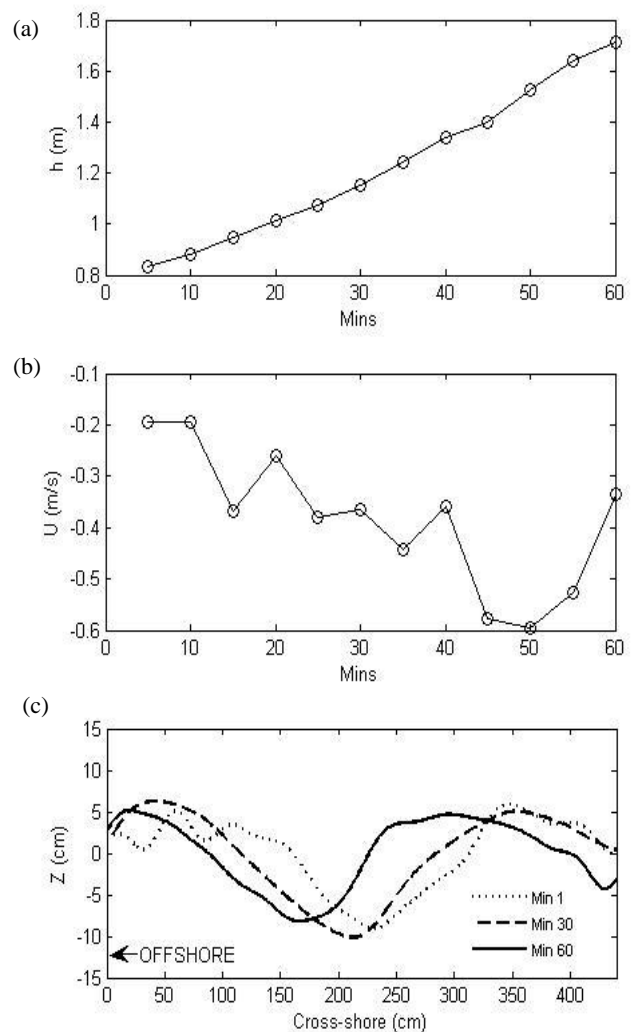


Figure 6. (a) Water depth ( $h$ ), (b) cross-shore velocity ( $U$ ) and (c) individual SRP bed scans (every 30 minutes) showing offshore megaripple migration.



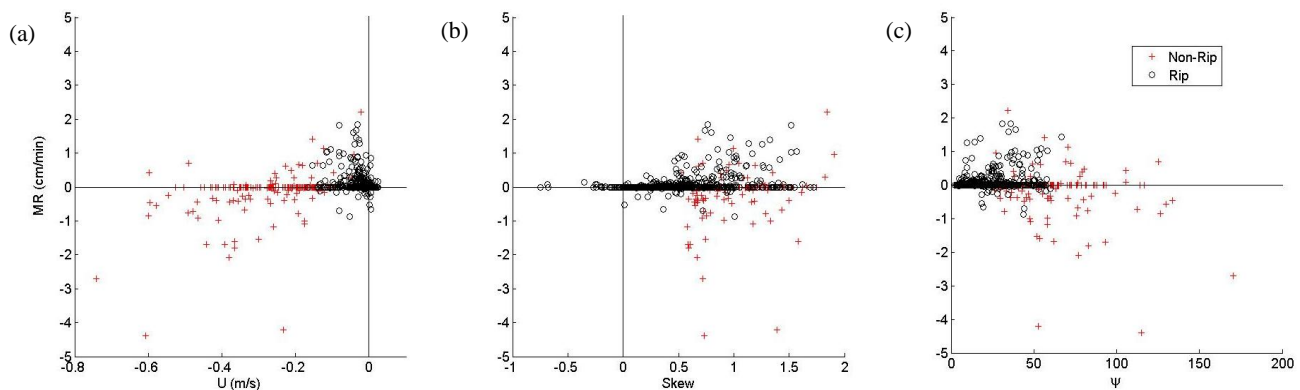


Figure 7. Hydrodynamic forcing on megaripple migration; (a) Wave skewness, (b) cross-shore velocity and (c) mobility number.

stable until the process was reversed on the flooding tide. The importance of water depth with regard to migration behaviour is shown in Figures 5a and 5b. The partitioning of data into rip and non-rip conditions (Figure 5b) describes offshore migration in rip conditions well.

The hydrodynamic variables responsible for the different megaripple migration behaviours are investigated in Figure 6. The rip flow shows a reasonable relationship with megaripple migration. The fastest offshore migration is found in the strongest offshore flows, with little offshore migration occurring when  $U < 0.2$  m/s and all onshore migration taking place in weaker flows of  $< 0.3$  m/s. At wave skewness values of below 0.5 there is no migration in any direction, whilst beyond this onshore migration rate shows an increase with increasing skewness for non-rip conditions. In rip conditions migration shows no relationship with wave skewness and there are periods of reasonably high skewness values (1.2 to 1.6) and moderate flow (0.2 – 0.4 m/s) when offshore migration occurs (Figure 6b). The fastest offshore migration rates are found at mobility numbers of above 50. The majority of onshore migration was found to occur at lower

mobility numbers.

The combined forcing of megaripple migration by mean offshore flows and wave skewness is investigated in Figure 8. Following figure 5a, the same method has been applied for  $U$  and  $S$ . There are three well defined parameter spaces within the figure with low  $S$  and weak  $U$  resulting in a stable bed. Weak  $U$  and high  $S$  result in onshore migration and strong offshore directed  $U$  and low  $S$  resulting in offshore migration.

## DISCUSSION

Bedforms of megaripple scale were found to be consistently present in rip currents in the data collected, confirming field observations by Greenwood and Davidson-Arnott, (1979), Aagaard *et al.* (1997) and Brander (1999b). The megaripples in the rip were, at times, over twice the length of the bedforms in non-rip conditions, suggesting an increase in wavelength was the result of conditions becoming increasingly current dominated, agreeing with observations made by Hoekstra *et al.* (2004) in a tidal inlet.

The partitioning of the data into rip and non-rip conditions based on a comparison with predicted offshore flows works well as a means of identifying rip flow, with the boundary between rip and non-rip conditions closely matching the change in migration direction. Rip flow ceased at velocities weaker than 0.1 m/s but this value would possibly depend on the hydrodynamic forcing of the rip and the scale of the controlling morphology.

Bedform migration in a rip current was found to undergo three phases over an entire tidal cycle; offshore migration in the strong offshore flows of the rip, onshore migration when skewness was high and mean flows were low and stable around high tide ( $h > 5$  m) when both mean flows and skewness was low.

Though offshore migration did not always occur in a rip the migration rate was positively correlated to the rip velocity, supporting the assertion by Nielsen (1992) that bedforms in a rip current are current dominated. The rates of migration in a rip current recorded in this study (0 to 4 cm/min) compare favourably to measurements made by Sherman *et al.* (1993) in a feeder channel of an average of 1.35 cm/min with similar mean flows.

If the waves are positively skewed the onshore stroke of the wave is stronger than the offshore stroke resulting in net onshore sediment transport. Gallagher *et al.* (2003) proposed this may result in onshore migration of bedforms. In the data presented here, skewness values are low in deep water, and peak when  $h = 2$  to 3 m, coinciding with periods of onshore migration. Migration rates of megaripples in non-rip conditions increase with increasing

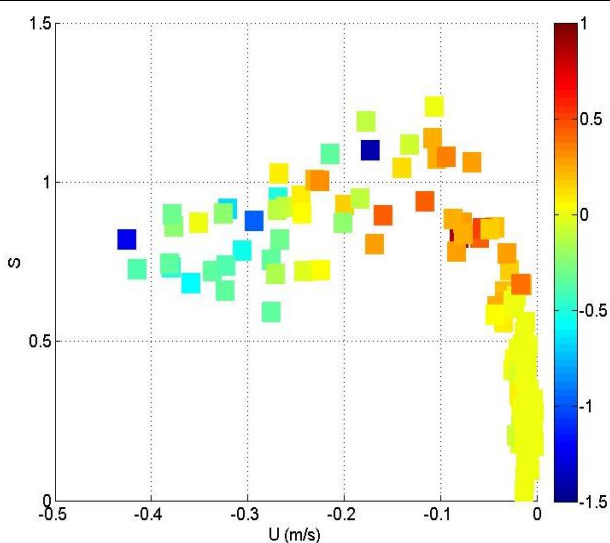


Figure 8. Migration rate (cm/min) and direction (represented by the colour bar; 'cool' colours indicating offshore migration) as a function of cross-shore velocity and wave skewness. Data from Tides 3 to 7.

skewness. Wave skewness and strong offshore-directed mean flows peak at similar times and the clear change in migration direction at  $h = \sim 2.5$  m suggests that they compete for control over megaripple migration and there is a fine balance between which is the dominant forcing. However, the fact that offshore migration is shown to take place in relatively high skewness values suggests that mean flows can dominate even if skewness is high.

The apparent change in hydrodynamic forcing over the tidal cycle is not possible to describe with a single parameter. The form of mobility number used by Gallagher *et al.* (2003) was chosen as it includes both an oscillatory and mean flow component. It shows a reasonable relationship with offshore migration, though no correlation with onshore migration. This may be because skewness is a measure of wave shape and not oscillatory flow.

### CONCLUSION

New measurements within a rip channel have found bedform migration rate and direction to be dependent on the occurrence of offshore directed flows of the rip current, wave skewness and water depth. In an active rip current ( $U = 0.1$  to  $0.74$  m/s) bedforms were found to migrate offshore at rates of 0 to 4 cm/min, with migration rates showing an approximately linear relationship with rip velocity. In non-rip conditions bedforms were observed to migrate onshore in water of intermediate depths ( $h = 2.5$  to  $5$  m) and when skewness was high ( $> 0.5$ ). When  $h > 5$  m and both skewness and mean flows were low the bed was stable.

### ACKNOWLEDGEMENTS

This work is part of the first author's PhD. We would like to acknowledge the Natural Environment Research Council (NERC) for their funding of the PhD studentship (ref no: NE/I528550/1).

We would also like to thank the DRIBS (Dynamics of Rip Currents and Implications for Beach Safety) project (grant ref no: NE/H004262/1) for providing technical assistance and use of the infra-structure in place for their fieldwork.

### LITERATURE CITED

- Aagaard, T., Greenwood, B., Nielsen, J., 1997. Mean currents and sediment transport in a rip channel. *Marine Geology*, 140, 25-45.
- Allen, J. R. L., 1985. *Principles of Physical Sedimentology*. London: George Allen, Unwin Ltd.
- Austin, M., Scott, T., Brown, J., MacMahan, J., Masselink, G., Russell, P. 2010. Temporal observations of rip current circulation on a macro-tidal beach. *Continental Shelf Research*, 30, 1149-1165.
- Brander, R. W., 1999a. Field observations on the morphodynamic evolution of a low-energy rip current system. *Marine Geology*, 157, 199-217.
- Brander, R. W., 1999b. Sediment Transport in Low Energy Rip Current Systems. *Journal of Coastal Research*, 15, 839-849.
- Crawford, A., Hay, A. 2001. Linear transition ripple migration and wave orbital velocity skewness: Observations. *Journal of Geophysical Research*, 106, 14133-14128.
- Elgar, S., Guza, R. T., Freilich, M. H., 1988. Eulerian measurements of horizontal accelerations in shoaling gravity waves. *Journal of Geophysical Research: Oceans*, 93, 9261-9269.
- Gallagher, E. L., Elgar, S., Thornton, E. B., 1998. Megaripple migration in a natural surf zone. *Nature*, 394, 165-168.
- Gallagher, E. L., Thornton, E. B., Stanton, T. P. 2003. Sand bed roughness in the nearshore. *Journal of Geophysical Research: Oceans*, 108, 3039.
- Greenwood, B., Davidson-Arnott, R. G. D., 1979. Sedimentation and equilibrium in wave-formed bars: a review and case study. *Canadian Journal of Earth Sciences*, 16, 312-332.
- Hoekstra, P., Bell, P., van Santen, P., Roode, N., Levoy, F., Whitehouse, R., 2004. Bedform migration and bedload transport on an intertidal shoal. *Continental Shelf Research*, 24, 1249-1269.
- MacMahan, J. H., Thornton, E. B., Reniers, A. J. H. M., 2006. Rip current review. *Coastal Engineering*, 53, 191-208.
- MacMahan, J. H., Thornton, E. B., Stanton, T. P., Reniers, A. J. H. M. 2005. RIPEX: Observations of a rip current system. *Marine Geology*, 218, 113-134.
- Masselink, G., Austin, M., O'Hare, T., Russell, P., 2007. Geometry and dynamics of wave ripples on the nearshore of a coarse sandy beach. *Geophysical Research Letters*, 112
- Masselink, G., Black, K.P., 1995. Magnitude and cross-shore distribution of bed return flow measured on natural beaches. *Coastal Engineering*, 25, 165-190.
- Nielsen, P., 1992. *Coastal bottom boundary layers and sediment transport*. Advanced series on ocean engineering. London: World Scientific.
- Sherman, D. J., Short, A.D., Takeda, I., 1993. Sediment Mixing-Depth and Bedform Migration in Rip channels. *Journal of Coastal Research*, 15, 39-48.

# Determining the role of exposure, wave force, and rock chemical resistance in marine notch development.

Paweł Terefenko†, Olga Terefenko‡

†Faculty of Geosciences  
University of Szczecin  
70-383 Szczecin, Poland  
pawel.terefenko@univ.szczecin.pl

‡ Faculty of Geosciences  
University of Szczecin  
70-383 Szczecin, Poland  
olga.terefenko@univ.szczecin.pl



[www.cerf-jcr.org](http://www.cerf-jcr.org)



[www.JCRonline.org](http://www.JCRonline.org)

## ABSTRACT

Terefenko, P., Terefenko, O., 2014. Determining the role of exposure, wave force, and rock chemical resistance in marine notch development. In: Green, A.N. and Cooper, J.A.G. (eds.), *Proceedings 13<sup>th</sup> International Coastal Symposium* (Durban, South Africa), *Journal of Coastal Research*, Special Issue No. 70, pp. 706-711, ISSN 0749-0208.

In order to assess the role of coastal exposure, wave force, and rock chemical resistance in marine notch development a study was undertaken along 28km of the Algarve region in southern Portugal between Gale and Portimão. Notches were identified in the field, and exposure to wave force was calculated on the basis of wave refraction estimates. Almost 100 samples were collected and analyzed to assess calcium carbonate content of the coastal lithology. Finally with the use of GIS geostatistical methods, values of chemical resistance were calculated. Statistical correlation analysis enabled the definition of the importance of each investigated factor in the process of the formation of marine notches and the resulting shape. Since shape is a quantitative factor, several additional statistical calculations such as the Kruskal-Wallis test and analysis with tree classification methods were performed. The final results show that the importance of each factor controlling coastal morphology is changeable and depends generally on coastal exposure. Bigger wave force is assisted with lower diversity of coastal forms. The shape of the coastal notches depends on the notch exposure and wave force. The bigger the wave force the higher the probability that V-shape notches occur. The effect of the chemical resistance factor was less prominent though it does influence notch shape at specific levels of wave force.

**ADDITIONAL INDEX WORDS:** *Marine notch, Rocky shoreline, Algarve coast*

## INTRODUCTION

In order to understand the functioning of the coastal system it is important to connect causative factors with their effects. Such an approach is vital from the cognitive point of view, and it allows for the undertaking of practical activities aimed at providing safety in the coastal zone, as well as to emphasize the significance of coastal protection.

Although there have been significant advances in the understanding of rocky coastal systems (Sunamura, 1977, 1983; Sunamura, 1992; Griggs and Trenhaile, 1994; Trenhaile, 2000, 2002; Dickson and Woodroffe, 2002, Haslett 2009; Wziątek et al., 2011) their evolution, which depends on marine and sub-aerial processes as well as on rock properties, has still not been exactly defined. Several landforms of varied scale such as coastal cliffs, shore platforms, bays, pocket beaches, marine caves, and marine notches exist in such environments. A commonly observed morphological feature on rock coasts are marine notches which are often used as indicators for present and past mean sea level (Kershaw et al., 2001; Benac et al., 2004, 2008) but very rarely for determining principles that regulate processes in the rocky coast environment (Wziątek et al. 2011).

A general definition describes marine notches as undercuts or groove forms, developing in vertical profiles of cliff faces as a result of sea corrosion (Pirazzoli, 1986). Two key erosion processes that are of particular relevance in this definition are the

mechanical action of wave spray, wind, or sand and pebbles and chemical action which includes rock dissolution.

Basic classification of marine notches, groups those most measured features of rocky coast into four genetic types. (Pirazzoli, 1986, Wziątek et al., 2011). Tidal notches appear at the intertidal zone as a result of sea corrosion and are the most commonly recognizable notches. Abrasion notches are generated by waves, and the mechanical action of sand and pebbles. They usually occur at the boundary between hard cliffs and loose sediment (eg. rocky cliffs bordering pocket beaches). Surf notches are formed above high tide level and are directly correlated with the action of water spray. Structural notches are related to the presence of weaker lithological layers favouring local marine erosion or weathering processes (Kershaw and Guo, 2001).

Notches are also classified on the basis of the shape as *U-*, *V-*, and *ripple notches*, and their occurrence in the cliff profile – notch combination (Figure 1). When more than two distinct tidal or surf notches occur at the cliff profile, they create one of four possible combinations (Wziątek et al. 2011): 1) *W*: combination of two tidal notches (Pirazzoli, 1986), 2) *3-W*: combination of three tidal notches, 3) *2-step*: combination of tidal notch and surf notch in an upper part (Moura et al., 2006), 4) *3-step*: combination of two tidal notches and surf notch (Figure 1). *Ripple notches* – two or more small notches in the cliff profile close to each other can be considered as a ripple shape or as a notch combination depending on the spacing between them and applied classification rules.

This paper provides a description and the results of an analysis that set the spatial distribution of notches, their shape, and combination against the selected factors which are considered to be crucial in the processes of controlling coastal morphology such as: coast exposition, wave force, and rock chemical resistance.

**STUDY AREA**

The study area is located in the Algarve region in South Portugal (Figure 2a). It covers 28 kilometers of coastline (Figure 2c) between the cities of Galé and Portimão (Figure 2b). This meso-tidal area generally consists of Mesozoic limestone, marls, and calcarenites (Lagos-Portimão Formation (LP)) which have been karstified (Antunes *et al.*, 1981). Karstification occurred in two periods. The first before the Pliocene and the younger 40,000 years later (Roberts and Plater, 1999, Moura *et al.* 2006). The LP Formation are the most common Miocene units in the western Algarve.

**METHODS**

**Notch identification and classification**

The presence of wave-cut notches was investigated during organized field campaigns (September 2009 – December 2012). In the first stage the location of the notches was mapped. Each notch was noted and geo-located using Differential GPS. In the case of an inaccessible cliff the notch was located on a 1:25000 scale topographic map (Portuguese Military Maps) and aerial photos at 1:10000 scale. Only active notches were classified. These occur between the spring low tide and the upper limit of the spray zone.

In the second step the identification and classification process was performed on only two selected cliffs but with the use of remote sensing methods. A laser-based survey technique allowing for rapid and accurate collection of large amounts of topographical data (Xharde *et al.*, 2006, Buckley *et al.*, 2008) was used. The characteristics of the notch shapes and their genetic types were described using high precision laser scanning data. The terrestrial LiDAR survey methodology was found to be accurate and useful. It enabled identification of some small notches that were not visible in the field.

The data characterizing the spatial distribution and shape of wave-cut notches in the studied area was augmented with information on the nature of the coexistence of those objects with other notches. All data were saved in the geomorphological dataset in a graphic layer with line geometry. The notch parameters, such as shape and combinations were recognized (Figure 3) and placed in a non-spatial table linked with the graphic part using a relationships layer. The form of recording allowed for the direct import of data to statistical programs in which the basic statistical analysis was conducted.

**Estimations of notch exposure and wave forcing**

Off-shore wave datasets were analyzed for the period May 1995 to December 2012. Data was obtained from a wave buoy deployed in 120m water depth by the Portuguese Hydrographic Institute ([www.hidrografico.pt](http://www.hidrografico.pt)), south of the city of Faro (7°53'54''W ; 36°54'7''N).

Wave refraction estimations were necessary in order to obtain values of wave height and direction close to the coast. Calculations were carried out according to Snell's law (US Army Corps of Engineers, 2002):

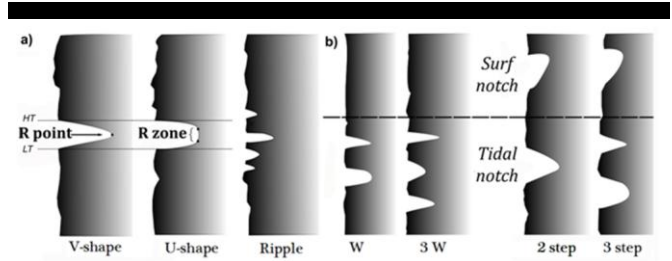


Figure 1. Notch shapes (a) and notch combinations (b) (Wziątek *et al.*, 2011).

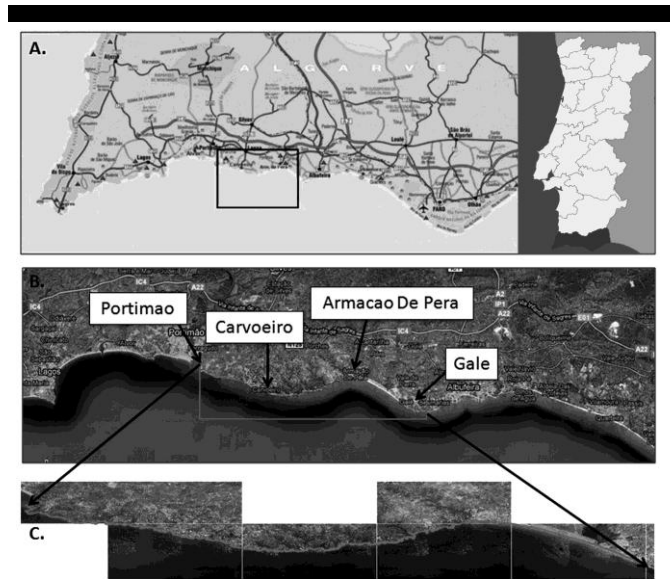


Figure 2. A) Map of Algarve region showing the location of the study area; B) Satellite image of the study area; C) coastline of the investigated area.

$$\frac{\sin \theta}{C} = \frac{\sin \theta_0}{C_0} \tag{1}$$

where  $\theta$  corresponds to the wave angle and  $C=L/T$  to the wave celerity. The subscript  $0$  denotes off-shore conditions. For wave celerity  $T$  represents the wave period and  $L$  is the wave length expressed by the wave dispersion equation (US Army Corps of Engineers, 2002, Wziątek *et al.*, 2011).

While the used methodology provided the wave direction at a desired depth of 10 m., the wave height was obtained by the equation  $H=H_0 K_s \cdot K_r$ , where

$$K_s = \sqrt{\frac{C_{g0}}{C}} \quad K_r = \left[ \frac{1 - \sin^2 \theta_0}{1 - \sin^2 \theta} \right]^{1/4} \tag{2}$$

In this equation  $C_g$  is the group velocity, equal to  $C_g=n \cdot C$  with  $n$  equivalent to:

$$n = 0.5 \left[ 1 + \frac{4\pi d/L}{\sinh(4\pi d/L)} \right] \tag{3}$$

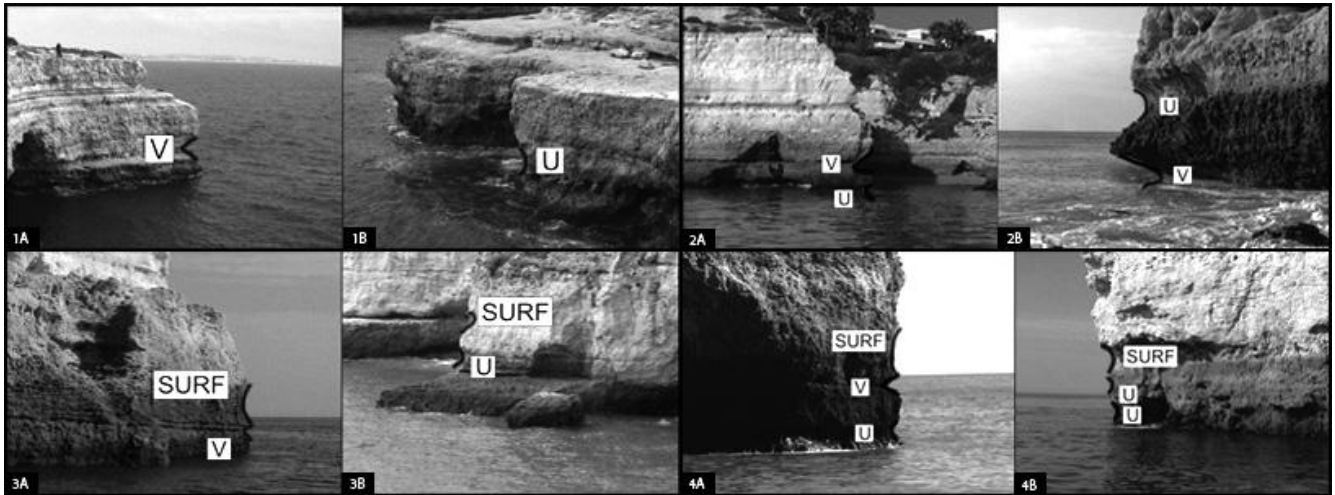


Figure 3. Photos showing examples of the spatial distribution of notches on the cliff profile together with their shape and combination: (1A) Single V-shape notch (without combination); (1B) single U-shape notch. (2A) U-shape and V-shape notches in “W” combination; (2B) V-shape and U-shape notches in “W” combination; (3A) V-shape notch and surf notch in “2 step” combination; (3B) U-shape and surf notch in “2 step” combination; (4A) U-shape, V-shape and surf notch in “3 step” combination; (4B) V-shape, U-shape and surf notch in “3 step” combination.

All performed wave refraction estimations have been calculated for average wave conditions from all analyzed periods and for the average coastline orientation of the study area ( $113^\circ$ ).

Having calculated the wave incidence angle at the coast area, the exposure angle for all sectors along each notch was calculated. Wave power was estimated for each fragment of the constant local orientation angle for all notches. At selected positions wave power was determined as  $P = E \cdot C_g \cdot \cos \theta_{exp}$ , where  $E$  was the wave energy  $E = 0.125 \cdot \rho \cdot g \cdot H^2$  and  $\theta_{exp}$  the wave incidence angle on the notch.

The sum of  $P$  for all segments alongshore of single notch length provided the total power. The acquired results were considered as the final feature of notch exposure and wave force.

### Estimations of rock chemical resistance

In order to gather information about the chemical resistance of the study area's coastal rock 117 rock samples were collected from 71 cliff profiles. Samples were obtained from accessible parts of the coast, generally if possible from layers of notches, platforms, and on vertical cliffs walls. The samples were analyzed with a use of a Carlo Erba CN Elemental Analyzer. Their  $CaCO_3$  content was used as a proxy of chemical resistance (Leontjew *et al.*, 1982). In order to obtain resistance values for all identified notches a geostatistical method (Kriging interpolation) was used. Based on the statistical model including the data autocorrelation, the biggest advantage of this interpolation was the possibility to get not only the most probable value in any cell of the generated raster, but above all the evaluation of the expected error in resulting datasets (Urbański, 2010).

Having collected samples on vertical cliff walls, transformation to a horizontal plane was necessary in order to perform interpolation. During the transformation it was assumed that two coordinates would be used: the height of the sample collection and its distance from the initial point measured along the coastline. While performing this process the horizontal depth of the sample resulting from the diversified cliff profile was not considered.

### Statistical analysis

In order to investigate the variability of influencing factors, descriptive statistics, histograms, and standard box plots were used.

Due to the non-measurability of the analyzed feature of shapes and combinations which are qualitative data, and due to the lack of the normal distribution of variables the non-parametric Kruskal-Wallis test was used. This is the equivalent of a one-way analysis of variance. The value of the Kruskal-Wallis test is calculated in the following way:

$$H_{obl} = \frac{12}{n(n+1)} \left( \sum_{j=1}^k \frac{R_j^2}{n_j} \right) - 3(n+1) \quad 4$$

For samples including more than 5 observations, the distribution of the statistics of the H test is well-approximated through the chi-square distribution with  $k-1$  degrees of freedom. Comparing the calculated value of the H test with the critical value of the distribution for the adopted significance level and for the  $k-1$  degrees of freedom opens one of two possible decisions (Aczel, 2000):

if  $H_{obl} \geq \chi^2_{\alpha; k-1}$ , then reject  $H_0$  in favour of  $H_1$ ,

if  $H_{obl} < \chi^2_{\alpha; k-1}$ , then there are no important reasons for rejecting  $H_0$ .

In case of rejecting the zero hypothesis, i.e. stating that not all averages are identical, it is necessary to indicate between which averages (populations) there are statistically significant differences. Further analysis of differences between the averages identified by the Kruskal-Wallis test is based on the average ranges from samples calculated for each pair of the populations that are to be compared (for example,  $i$  and  $j$  population):

$$\bar{R}_i = \frac{R_i}{n_i} \quad \text{and} \quad \bar{R}_j = \frac{R_j}{n_j} \quad 5$$

The verification of the zero hypothesis stating that the averages of  $i$  and  $j$  populations are identical is D statistics:

$$D = \left| \bar{R}_i - \bar{R}_j \right| \quad 6$$

The test was conducted by comparing the value of D statistics and the value of the critical point calculated according to the following formula:

$$D^* = \sqrt{\chi^2_{\alpha k-1} \left[ \frac{n(n+1)}{12} \right] \left\{ \frac{1}{n_i} + \frac{1}{n_j} \right\}} \quad 7$$

When  $D > D^*$ , the zero hypothesis is rejected and states that between the averages of  $i$  and  $j$  population there are statistically significant differences.

## RESULTS

### Basic notch shapes and combination statistics

Based on introductory analysis performed on Table 1 242 notches were documented and classified based on shape and combination.

According to this classification the notches with regard to their shape constitute a group of 131 U-shaped objects (54,13%), 107 V-shaped (44,21%) and 4 notches of the ripple profile (1,65%).

Notches occurring individually without any combination included 31,4% of examined cases and the remaining 68,6% are the objects occurring altogether with other notches in the W, 3step, 2step, and W3 combinations. On the examined area, almost the half of analyzed elements (48,76%) occur in the W combinations. The remaining combinations appear more rarely and come to 19,83%, including 11,16% occurring in the 3 step combination, 7,44% in 2step, and only 1,24% in the W3 combination.

The number of U-shaped and V-shaped cavities is about equal. There is a majority of W combinations, whose distribution into two basic groups of shapes (U and V) is quite even. The second most common occurrence is the single combination. Objects with this characteristic have a U-shaped profile more often.

Analysis of exposure, wave force, and chemical resistance for marine notch development was therefore performed based on the U-shaped and V-shaped notches. The 4 cases of ripple-shaped objects were excluded from further analysis as well as the secluded case of the W3 combination.

### Influence of exposure on notch shape and combination

Descriptive statistics and analysis of the box plots show that the smallest diversity occurs among notches with the highest exposure. Half of the examined objects occur in cliffs with exposures higher than 67,33%, and their diversification reduces with more exposure, (proved by the range of the third quartile ( $Q3 \in <67,33 ; 94,74>$ ) and the fourth quartile ( $Q4 \in <94,74 ; 100>$ )). The similar range of the first and second quartiles indicates that this tendency does not occur for notches with exposure lower than the middle value.

Through distribution of exposures with regard to the classification of notches into U- and V-shaped and the categorized histograms for the same groups of data, it may be seen that the majority of V-shaped notches occur on sheltered cliffs. Both types of notches occur throughout the examined range of exposures from 0% to 100%. However, the occurrence of V-shaped notches in areas with very high exposure is explicitly emphasized. U-shaped notches have a much more even distribution.

The relationship between the exposure of cliffs and the shape of notches was confirmed with a non-parametric Kruskal-Wallis test. The value of the Kruskal-Wallis test was  $H=122,1940$ , and the critical value of the chi-square distribution was  $\chi^2=42,28$  at the level of test probability  $p=0,0000$ . Since the Kruskal-Wallis test

Table 1. Overview of the number of notch shapes (SH) and combinations (COM) identified on the investigated area.

COM \ SH	W	single	3step	W3	2step	total
U	60	45	13	3	10	<b>131</b>
V	58	28	14	0	7	<b>107</b>
ripple	0	3	0	0	1	<b>4</b>
<b>total</b>	<b>118</b>	<b>76</b>	<b>27</b>	<b>3</b>	<b>18</b>	<b>242</b>

was higher than  $\chi^2$ , the zero hypothesis (there is no relationship between exposure and the shape of the notches) was rejected. The analysis clearly shows that exposure has a statistically significant influence on notch shape.

The exposure of cliffs has a smaller influence on the diversification of the notches occurring in particular combinations or individually. The box plots and histograms for combinations 2step, 3step, W, and single show that three out of four groups (3step, single, and W) occur in the whole examined range of exposures. The biggest distribution may be observed within notches occurring in the W combination, half of which are located in the cliffs moderately exposed or sheltered, and the remaining combinations, in which over half occur in very exposed cliffs (exposure higher than 80%).

The result of the performed Kruskal-Wallis analysis testing relationships between the exposure of cliffs and the notch combination reached  $H=9,99$  in comparison to  $\chi^2=14,49$  showed the lack of the relationship of the exposure and the combinations in which notches occur. The table of multiple comparison, shows differences between W and other combinations, but all p values for these comparisons reached at least the limit value  $p=0,0187$ , which means that these differences are not statistically significant.

### Influence of the chemical resistance on the notch shape and combination

Descriptive statistics and analysis of the box plots, show that the majority of notches (75%) were created in rocks with at least 89,16% calcium carbonate, with a maximum of 92,12% observed. The average content of calcium carbonate in examined rocks was 88,17%.

Both box plots and categorized histograms indicate significant differences between the amount of calcium carbonate in cliffs where U-shaped notches occur and cliffs with V-shaped notches. Despite the fact that the ranges of the graphs are similar, the boundaries of the areas of the most typical units (interval  $< Q1, Q3 >$ ) are significantly different. The most typical units among U-shaped notches occur in rocks consisting of 88,6 – 90,49% calcium carbonate content, whereas the most typical V-shaped notches occur in rocks with the content of calcium carbonate at levels from 90,03 to 91%.

These differences are weakly visible in the analysis divided into combinations. Each group of combinations, occurs in rocks with a similar content of calcium carbonate, which is proved by the location of medians and typical areas on the same level.

The relationship between the content of calcium carbonate in the cliff rocks and the shape of the notches that occur in them was confirmed using the non-parametric Kruskal-Wallis test. It confirms the considerable statistical diversification of the notches of the particular profile with regard to the content of calcium carbonate based on comparing the values  $H=18,68$  and  $\chi^2=12,37$ , where  $H$  is bigger than  $\chi^2$ . This result is emphasized by the difference between the value of the average ranges, which comes to 38,77 ( $R''U'' = 102,07$  and  $R''V'' = 140,84$ ). The result of the conducted test is statistically significant since both values of  $p$  for

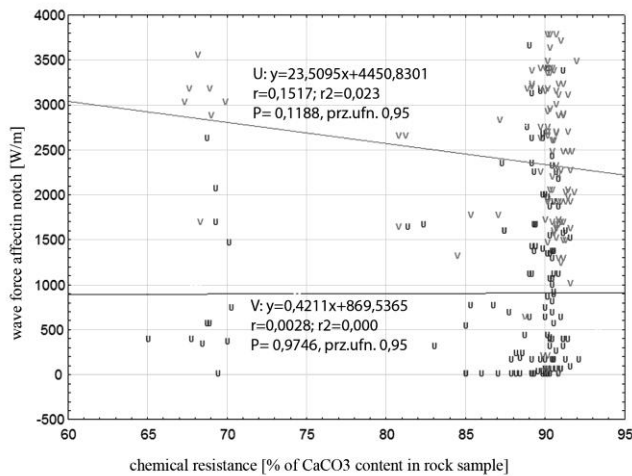


Figure 4. Scatter graph of wave force and chemical resistance.

U-shaped and V-shaped cavities are lower than the limit value  $p=0,000023$ .

Smaller differences of the average ranges (23,06) definitely occur between the particular combinations of cavities ( $R''2step'' = 107,72$ ,  $R''3step'' = 130,78$ ,  $R''single'' = 112,18$  and  $R''W'' = 124,44$ ). In this situation, despite the result of the Kruskal-Wallis test, in which  $H > \chi^2$  ( $H=2,68$  and chi-square  $\chi^2=1,429$ ), which enables elimination of the hypothesis about the identical distributions of the compared groups, the results are statistically insignificant ( $p < 0,4432$ ).

### Influence of wave force on notch shape and combination

Values of the wave force range from 0 [W/m] to 3783,31 [W/m]. The smallest may be observed in 25% of documented places, where the notches that are influenced by the smallest value may be found. This is confirmed by the range of the first quartile ( $Q1 < 0 ; 373,93 >$ ). The remaining 75% of analyzed objects are characterized by a similar dispersion which is proved by the range of three subsequent quartiles.

Regarding the distribution of the wave force influencing U-shaped and V-shaped notches it could be noticed that both types occur in almost the whole examined range. There is a clear dominance of V-shaped notches in more exposed places. The majority of U-shaped notches occur in areas less open to wave action. This characteristic confirms the results of the distribution of the shape groups with regard to exposure. This result indicates the mutual correlation of wave force and exposure variables.

The introductory analysis of the diversification of the wave power and its influence on the shape and combinations was confirmed by the detailed analysis. The value of the Kruskal-Wallis test ( $H=91,31$ ), although close to the value of chi-square ( $\chi^2=90,48$ ), enables elimination of the hypothesis of similar distributions of the wave force variable in the analysis of notches divided into U- and V- shaped. This result is statistically significant and means that there is a relationship between the wave force and the shape of notches.

Wave force influence on the type of the combination is, however, statistically insignificant.

### Correlation between features controlling marine notch development

There is a slight linear correlation ( $r=-0,1517$ ) between the wave force and chemical resistance.

The affinity value  $r^2 = -0,023$  for U-shaped notches indicates that based on the set regression model  $y = -23,5095x + 4450,8301$  only a 2,3% change of one variable may be explained by the change of another variable (Figure 4). Besides, the level of significance  $p=0,1188$  at the critical level 0,05 does not allow this relationship to be considered statistically significant. In the case of V-shaped notches, the correlation between these variables is totally insignificant.

Correlation of exposure and wave force was analysed. In the case of these two variables, the correlation both in cases of V-shaped notches ( $r=0,8754$ ) as well as U-shaped ones ( $r=0,8857$ ) is very strong. Based on the analyzed scatter graph (Figure 5), a relationship between exposure and wave force is confirmed.

### DISCUSSION

Exposure of the coast with regard to the dominant wave direction is one of the most important factors that determines how the power of waves directly affects the cliff face. In this work, it was shown that shapes of notches change with coastal exposure, and even more so with increasing wave force. The results show a dominance of the V-shaped profile of cavities in cliffs with a high exposure and U-shaped cavities with small exposure confirming the findings of Pirazzoli (1986). The results also confirm the generally accepted theory that states that factors such as wave force and exposure directly influence the rate of erosion of rocky coasts (Carter and Woodroffe, 1994; Masselink and Hughes, 2003; Bird, 2008; Haslett, 2009; Davis and Fitzgerald, 2010; Evelpidou *et al.*, 2011).

Single notches are created under conditions of strong wave force and high cliff exposure. However, there is no confirmed relationship of these factors with other types of notch combinations. Such results indicate an interesting relationship. The stronger the wave force the lower the diversity of coastal features. Conversely, with a decrease in wave force, the number of morphological features increases.

Lack of confirmation for the direct influence of exposure and wave force on the combination type indicates that these must be related to other factors or conditions. Since nearly 50% of all

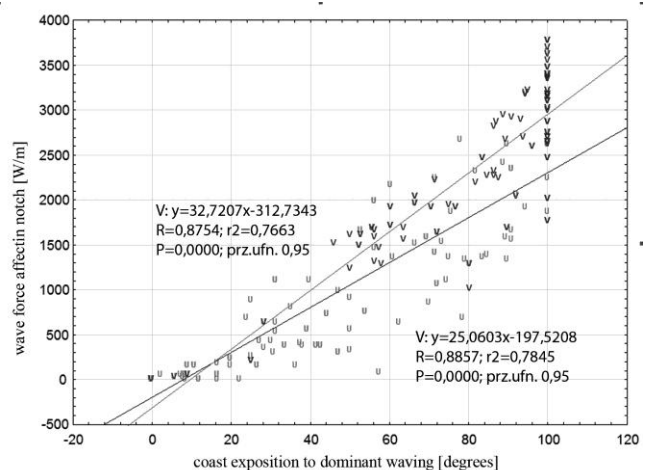


Figure 5. Scatter graph of wave force and coast exposition.

documented combinations belong to the “W” type, their occurrence is probably related to the semi-diurnal tidal regime. It would mean that this combination is mainly the reflection of two characteristic states: average high tide and average low tide. Such a statement confirms the theory that the occurrence of more than one notch in the profile of the cliff is related to tidal conditions and changes of sea level (Pirazzoli, 1986; Bird, 2008; Kogure *et al.*, 2006; Benac *et al.*, 2008).

Although a correlation of notch shapes and chemical resistance lacks statistical significance, this feature does play a role in some specific situations. In cliffs influenced by a wave force lower than a specific value (in the analyzed area this is 1197,73 [W/m]) U-shaped notches are usually formed. In the remaining cliffs, where the wave force is higher than 1197,73, the shape depends mainly on the chemical resistance of the rocks in which they are created.

## CONCLUSION

In the system of the rocky coastal zone the variability of the dominating factors depends directly on the exposure of the cliff. Observed dependency indicates that that on strongly exposed cliffs the wave force is the factor initiating the creation of notches, whereas the chemical resistance decides the shape of the created object. In the case of sheltered fragments of coast where waves attack with much less force, the second factor – rock chemical resistance, does not cause a significant diversification of shapes.

Single notches occur in conditions of high wave force and high exposure of the cliff. However no relationship of both those factors with the occurrence of a different notch combination was confirmed. The shape of the notches changes together with the exposure of the cliff and wave force. V-shaped profiles dominate in areas of high exposure and U-shaped in areas of low exposure. The creation of more than one notch in the profile of the cliff is connected with the condition of the tides and the changes of sea level and neotectonic movements.

The dominant combination is the W-shaped profile occurring in cliffs with variable exposure and diversified chemical resistance. There is no relationship between the type of the combination formed by the notches and the exposure of the cliff, wave force, or the rock chemical resistance.

## ACKNOWLEDGEMENT

The work described in this publication was supported by The National Science Center, Poland within the project “GIS analysis of features controlling coastal morphology of Algarve (Portugal)”. Project number: UMO-2011/01/N/ST10/06987.

## LITERATURE CITED

- Antunes M.T., Bizon G., Naseimento A., Pais J., 1981, Nouvelles donnes sur l'adulation des depots miocenes de l'Algarve (Portugal) et l'evolution geologique regionale. *Ciencias da Terra (UNL)* 6, Lisboa, 153- 168.
- Benac C., Juracic M., Blasković I., 2008, Tidal notches in Vinodol Channel and Bakar Bay, NE Adriatic Sea: Indicators of recent tectonics. 2008, *Marine Geology* 248, 151-160.
- Benac C., Juracic M., Blasković I., 2008. Tidal notches in Vinodol Channel and Bakar Bay, NE Adriatic Sea: Indicators of recent tectonics. 2008, *Marine Geology* 248, 151-160.
- Benac, C., Juracic, M., and Bakran-Petricioli, T. 2004. Submerged tidal notches in the Rijeka Bay NE Adriatic Sea: indicators of relative sea-level change and of recent tectonic movements. *Marine Geology* 212 (1-4):21-33.
- Bird, E., 2008. Coastal Geomorphology - An Introduction. Sussex : John Wiley & Sons, LTD.
- Buckley S. J., Howell J.A., Enge H.D., Kurz T.H., 2008, Terrestrial laser scanning in geology: data acquisition, processing and accuracy. *Journal of the Geological Society* 165, 625–638.
- Carter R., Woodroffe C., 1994. Coastal evolution. Late Quaternary shoreline morphodynamics. Cambridge University Press.
- Davis R., Fitzgerald D., 2010. Beaches and coasts. Blackwell Publishing.
- Dickson, M.E., Woodroffe, C.D., 2002. Rocky coastline around Lord Howe Island and potential changes in the dynamics of coastal erosion with global climate change. Proceedings Australia's National Coastal Conference, Coast to Coast 2002— Source to Sea, Geoscience Australia, Australia, pp. 515–518.
- Evelpidou N., Pirazzoli P.A., Sali J.-F., Vassilopoulos A., 2011. Submerged notches and doline sediments as evidence for Holocene subsidence., *Continental Shelf Research* 31., 1273–1281.
- Griggs, G.B., Trenhaile, A.S., 1994. Coastal cliff and platform. In: Carter, R.W.G., Woodroffe, C.D. (Eds.), *Coastal Evolution*. Cambridge Univ. Press, Cambridge, UK, pp. 425–450.
- Haslett S., 2009. Coastal Systems. Rutledge Introduction to Environmental Series. Rutledge Taylor & Francis Group.
- Haslett S.H., 2009. Coastal Systems, Rutledge Introduction to Environment Series, Rutledge Taylor & Francis Group, London and NewYork, p.216.
- Kershaw, S., and Guo, L. 2001. Marine notches in coastal cliffs: indicators of relative sea-level change, Perachora Peninsula, Central Greece. *Marine Geology* 179:213-228.
- Kogure T., Aoki H., Hirose T., Matsukura Y., 2006. Effect of the development of notches and tension cracks on instability of limestone coastal cliffs in the Ryukyus, Japan. *Geomorphology* 80, 236-244.
- Leontjew O.K., Nikiforow L.G., Safjanow G.A., 1982. Geomorfologia brzegów morskich, Wydawnictwo Geologiczne, Warszawa.
- Masselink G., Hughes M.G., 2003. Introduction to Coastal Processes & Geomorphology. London : Hodder Education.
- Moura D., Albardeiro L., Veiga-Pires C., Boski T., Tigano E., 2006, Morphological features and processes in the central Algarve rocky coast (South Portugal). *Geomorphology*. 81, 345-360.
- Pais, J., Legoinha, P., Elderfield, H., Sousa, L., and Estevens, M. 2000. The Neogene of Algarve (Portugal). *Ciencias da Terra (UNL)* 14:277-288.
- Pirazzoli P.A., 1986, Marine notches, Orson Van de Plassche. *Sea-Level Research: A Manual for the Collection and Evaluation of Data*. Zurich. 361-400.
- Roberts, H.M., Plater, A.J., 1999. U- and Th disequilibria in coastal infill sediments from Praia da Rocha (Algarve Region, Portugal): a contribution to the study of Late Quaternary weathering and erosion. *Geomorphology* 26, 223–238.
- Sunamura, T., 1977. A relationship between wave-induced cliff erosion and erosive force of waves. *J. Geol.* 85, 613–618.
- Sunamura, T., 1983. Processes of sea cliff and platform erosion. In: Komar, P.D. (Ed.), *CRC Handbook of Coastal Processes and Erosion*. CRC Press, Boca Raton, FL, pp. 233–265.
- Sunamura, T., 1992. *Geomorphology of Rocky Coast*. Wiley, New York, p. 302.
- Trenhaile, A.S., 2000. Modeling the development of wave-cut shore platform. *Mar. Geol.* 166, 163–178.
- Trenhaile, A.S., 2002. Rock coasts, with particular emphasis on shore platform. *Geomorphology* 48, 7–22.
- US Army Corps of Engineers. 2002. *Coastal Engineering Manual, Engineer Manual 1110-2-1100* (in 6 volumes). Washington, DC: U.S. Army Corps of Engineers.
- Wziątek D., Voudoukas M.V., Terefenko P., 2011, Wave-cut notches along the Algarve coast, S. Portugal: Characteristics and formation mechanisms, *Journal of Coastal Research*, SI 64, str. 855 – 859.
- Xharde R., Long B.F., Forbes D.L., 2006, Accuracy and Limitations of Airbone LiDAR Surveys in Coastal Environments. McGill University , 2412-2415.





[www.cerf-jcr.org](http://www.cerf-jcr.org)

## Beach oscillation and rotation: local and regional response at three beaches in southeast Australia

Andrew D. Short<sup>†</sup>, Melissa A. Bracs<sup>‡</sup>, Ian L. Turner<sup>‡</sup>

<sup>†</sup>School of Geosciences  
University of Sydney  
Sydney, NSW 2006, Australia  
andrew.short@sydney.edu.au

<sup>‡</sup> Water Research Laboratory  
School of Civil and Environmental Engineering,  
University of New South Wales,  
NSW 2052, Australia  
m.bracs@unsw.edu.au  
ian.turner@unsw.edu.au



[www.JCRonline.org](http://www.JCRonline.org)

### ABSTRACT

Short, A.D., Bracs, M.A., Turner, I.L., 2014, Beach oscillation and rotation: local and regional response on three beaches in southeast Australia. In: Green, A.N. and Cooper, J.A.G. (eds.), *Proceedings 13<sup>th</sup> International Coastal Symposium* (Durban, South Africa), *Journal of Coastal Research*, Special Issue 70, pp. 712-717, ISSN 0749-0208.

Six years of monthly subaerial surveys across three embayed beaches in southeast Australia located 270 km apart are utilized to compare the response of the beaches at the local and regional scale. The three beaches (Narrabeen, Moruya and Pedro) are exposed to a similar deep water wave climate ( $H_s \sim 1.5$  m,  $T \sim 10$  s), identical tides (spring range 1.6 m) and have similar lengths ( $\sim 3$  km), easterly orientation and medium to fine sand. Over the six years all three beaches had synchronous oscillation and rotation, though at different magnitudes. The lower energy Moruya beach undergoes greater beach oscillation (up to 100 m) and rotation than the higher energy Narrabeen and Pedro. The results highlight the regional scale of synchronous beach response, as well as have implication for our understanding of sediment transport and shoreline stability in relation to beach state, with the lower energy beach having a more dynamic shoreline. Furthermore the six years of data is insufficient to detect longer term trends observed at Narrabeen since 1976.

**ADDITIONAL INDEX WORDS:** *Beach oscillation, rotation, Australia*

### INTRODUCTION

Beaches on Australia's southeast coast are exposed to a highly variable wave climate, with waves generated from five sources and arriving from north through east to south quadrants (Short and Trenaman, 1992). Tropical, east coast and mid-latitude cyclones provide the highest levels of wave energy, and their seasonality, frequency and intensity dominate beach behaviour. On exposed beaches the shoreline oscillates (erodes-accretes) as much as 100 m in response to variable wave height, and on embayed beaches beach rotation, as a result of changes in wave direction, has been found to account for up to 30% of beach change (Short and Trembanis, 2004; Ranasinghe, *et al.*, 2004; Harley, *et al.*, 2011). To date detailed information on this phenomenon has been derived from two beaches located near Sydney. Utilizing six years of monthly beach surveys this paper takes one of these beaches, Narrabeen, and compares its behaviour to two adjoining beaches located 270 km to the south.

The aims of this paper are to examine the nature of change between two adjoining beaches possessing different levels of wave energy and beach state, and then compare their response with Narrabeen to determine the extent of regional response. In this preliminary analysis, the cause of the rotation, the wave climate, will not be discussed.

### FIELD SITES AND METHODS

The 3000 km long open southeast Australian coast extends from Fraser Island to Tasmania (Figure 1) and includes 1253 beaches with an average length of 1.5 km ( $\sigma=3.8$  km). These occupy 62% of the coast and the remainder being predominately rocky shore. The relatively short beach length is a result of geological inheritance, which forms numerous headlands and reefs along the coast and predominately embayed beaches (Short, 2010). Figure 1 shows the coast and location of the three field sites, Narrabeen on Sydney's northern beaches and Moruya and Pedro to the south.

Narrabeen beach has been surveyed monthly along five profile lines (NB1, 2, 4, 6, 8) since 1976, initially using the Emery method, then since 2006 using a quadbike-mounted DGPS (Harley, *et al.*, 2011) and since 2011 partly using surfcams (Mole, *et al.*, 2013). It is an east-facing 3.6 km long embayed beach with average breaker wave height decreasing from 1.5 m in the north to 1 m in the south. The sand is 70% quartz and 30% carbonate with a  $D_{50}=0.3$  mm. Modal beach state likewise changes from TBR/LTT in the north to LTT/R in the south (Table 1). Moruya and Pedro have been surveyed monthly since 2007 using the Emery method, each having three profile lines (M1-M3, P4-P6). Moruya is 2.4 km long and partly sheltered by a submerged rock reef, with breaker wave height averaging 1.2 m in the north,

decreasing to less than 1 m in the south and maintaining a TBR/LTT to R beach state. Adjoining Pedro beach is 2.5 km long with wave heights averaging 1.4 m, which maintain a RBB-TBR beach state. Both beaches have predominately quartz sand with a  $D_{50}=0.35$  mm. Surveys were undertaken during spring low tides. On all profile lines, elevation was recorded every 10 m seaward of a fixed benchmark down to at least mean sea level. In this work, surveys between November 2007 and October 2013 are analysed, with a total of 72 surveys for each of the three beaches.

Deepwater directional wave data are recorded at both sites. The Sydney buoy, operating since 1992, is located 7 km east of Long Reef Point has recorded an average  $H_s$  of 1.62 m,  $T_p=9.8$  s and direction  $134^\circ$ , while the Batemans Bay buoy operating since 1986 is located 35 km northeast of Moruya-Pedro has an average  $H_s$  of 1.44 m,  $T_p=9.4$  s and direction  $128^\circ$ . With the coastline oriented approximately north-south, both wave buoys receive waves arriving from between  $33-191^\circ$ .

**ANALYSIS**

At each profile line the position of 0.7 m AHD (Australian Height datum, or approximately Mean High Water Springs, MHWS) was obtained, and used to define horizontal beach width relative to a fixed shoreward benchmark. The mean beach width was then calculated for each survey line over the six year study. The time series of the deviation of each survey from the mean width was then used to graphically and statistically compare variations in profile behaviour within and between the three beaches, using correlation and principle components analysis (PCA).

**Profile configuration**

The profile envelopes of the nine survey lines are shown in Figure 2, while Table 1 lists their mean width and variation. All three beaches have very dynamic shorelines, oscillating from between 34 to 97 m. Interestingly on Moruya and Pedro the greatest variation occurs on the lower energy southern profiles, particularly M3, which regularly undergoes substantial shifts in shoreline position. In contrast, Narrabeen exhibits the greatest oscillation at the more exposed northern profile and least at the sheltered southern profile. Obviously local processes are at work here, though other possible causes of the extreme M3 oscillation are discussed later. The plots also indicate that Narrabeen and Pedro have similar height berms (~3 m) compared to a lower berm at Moruya (~2.5 m). These elevations are expected to reflect the higher wave energy at Narrabeen and Pedro compared to Moruya.

The deviations of beach width at each survey line from the mean are plotted in Figure 3. These plots clearly show the negative



Figure 1. Map of southeast Australia showing the location and details of Narrabeen, Moruya and Pedro beaches and location of survey lines.

Table 1. Variability and trends in MHWS beach width and beach state at the three beach sites over 2007-2013. Width  $\sigma$  is calculated after subtracting the linear trend.

Profile	Linear trend (m yr <sup>-1</sup> )	Mean width (m)	$\sigma$ (m)	Range (m)	Beach state <sup>1</sup> mean	Beach state <sup>1</sup> $\sigma$
NB1	-1.7	76	8.5	41	2.4	0.9
NB4	-1.4	57	9.6	45	2.3	0.9
NB8	+2.0	55	6.7	34	1.5	0.7
M1	-2.8	53	8.7	47	2.5	0.5
M2	-0.7	61	12.2	49	1.8	0.5
M3	+0.7	75	21.1	97	1.7	0.4
P1	-2.0	43	8.0	38	3.4	0.9
P2	-0.5	47	8.1	46	3.5	0.8
P3	-0.7	62	9.7	40	3.2	0.7

<sup>1</sup> Beach state: 1=reflective, 2=low tide terrace, 3=transverse bar & rip, 4=rhythmic bar & beach.

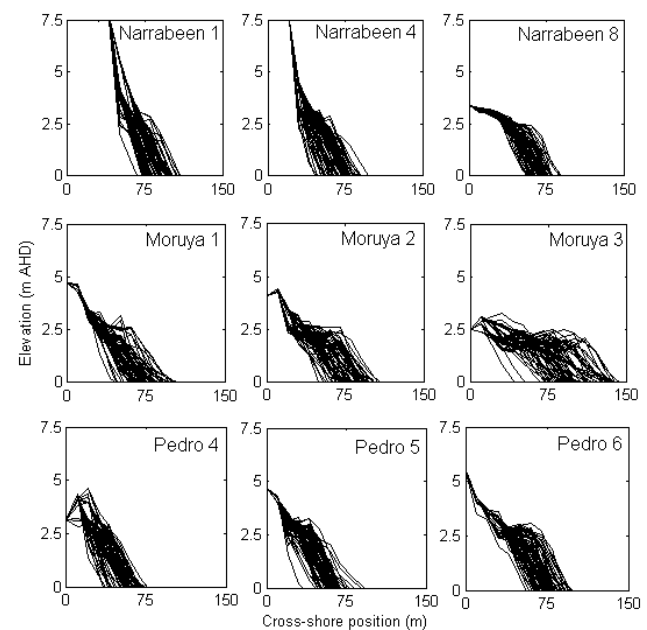


Figure 2. Profile envelopes of the Narrabeen, Moruya and Pedro survey lines.

phase relation between the northern and southern profiles within each beach, that is, the rotation. They also indicate the similarity in this relationship between the three sites, which are quantified in the correlation analysis (Table 2).

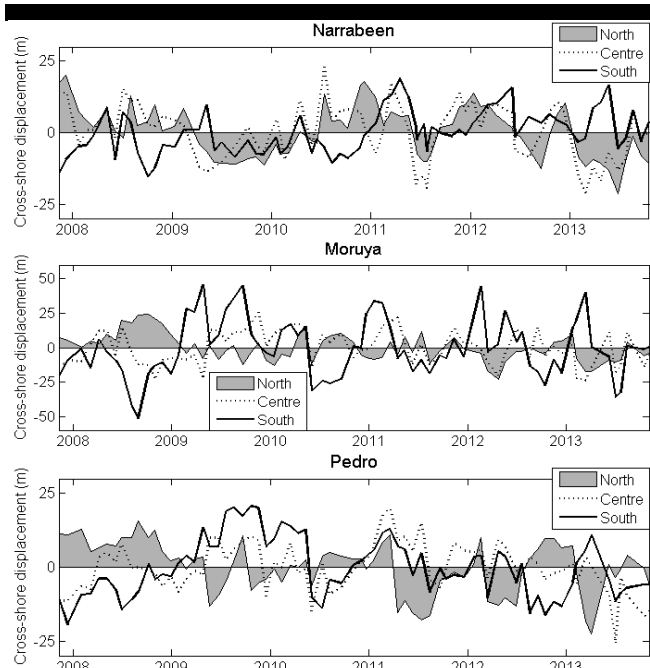


Figure 3. Plot of beach width deviation at each profile line from the mean position. Note the strong negative phase relations between the north and south profiles within each beach.

Table 2. Correlation matrix amongst the nine profile lines<sup>1</sup>

Correlation within sites			
Moruya	1 (North)	2 (Centre)	3 (South)
1	-	0.15	<b>-0.38</b>
2	-	-	0.18
3	-	-	-
Pedro	4	5	6
4	-	-0.14	<b>-0.31</b>
5	-	-	0.52
6	-	-	-
Narrabeen	1	4	8
1	-	0.71	0.003
4	-	-	0.08
8	-	-	-
Correlation between sites			
	Pedro 4	Pedro 5	Pedro 6
Moruya 1	0.55	0.02	<b>-0.24</b>
Moruya 2	0.04	0.49	0.37
Moruya 3	-0.12	0.40	0.68
	Narrabeen 1	Narrabeen 4	Narrabeen 8
Moruya 1	0.31	0.37	<b>-0.33</b>
Moruya 2	-0.05	0.18	0.14
Moruya 3	-0.06	<b>-0.29</b>	0.21
	Narrabeen 1	Narrabeen 4	Narrabeen 8
Pedro 4	0.40	0.46	<b>-0.33</b>
Pedro 5	0.10	0.02	0.38
Pedro 6	<b>-0.28</b>	<b>-0.33</b>	0.06

<sup>1</sup> Significant negative correlation in **bold**, significant positive correlation in *italics*.

## Correlation

The correlation analysis (Table 2) highlights several significant features of the three beaches. At Moruya and Pedro the northern end of each beach is significantly negatively correlated with the southern, indicating that rotation is the dominant mode at both sites. Further, the northern, central and southern profiles are significantly correlated between the two sites, which together with the significant negative correlation between M1 and P6 indicates that their behaviour is synchronous, as may be expected from two adjoining beaches.

When compared with Narrabeen, located 270 km to the north, there is significant positive correlation between the three northern and central profiles. There is also significant negative correlation between the southern profiles at Moruya and Pedro and northern profile at Narrabeen; and vice versa. However while there is positive correlation between the three southern profiles, it is not significant.

## Principal Components Analysis

PCA was performed on the Moruya and Pedro profiles, the Narrabeen profiles and on all three beaches combined. Figure 4 shows the results for Moruya and Pedro. The dominant mode (58%) is synchronised rotation, with the greatest magnitude at M3. Mode 2 (19%) indicates oscillation, with the centre of both beaches having the largest signal suggesting the shoreline straightens as it widens. The negative signal at M3 may be related to the large magnitude of rotation at this point. Mode 3 (12%) is another rotation signal with M3 again having the opposite signal.

Figure 5 shows that Narrabeen is dominated by oscillation (60%), though it shows some rotational influence as indicated by the larger magnitude of the northern profiles, which accrete or erode more than the southern profiles. Mode 2 (30%) is all rotation around a central neutral nodal point, while Mode 3 (10%) may be another indication of the beach straightening during accretion phases, with the maximum signal in the centre.

Figure 6 displays the PCA for all three beaches and here the dominant Mode 1 (41%) is synchronised rotation, with the greatest magnitude at the southern ends of Moruya (M3) and Pedro (P6); while the second mode (20%) is synchronised oscillation, with the greatest magnitude again in the centre of all three beaches.

## DISCUSSION

Moruya and Pedro beaches display synchronised shoreline behaviour, as would be expected for adjacent sites, with both strong oscillation and rotation. The oscillation is illustrated graphically in Figure 2 with the magnitude noted in Table 1. The rotation is illustrated in Figure 3 and quantified by the negative correlation between the northern and southern profiles at each beach, while their synchronous behaviour is shown by the significant positive correlation between the matching profiles on both beaches (Table 2). Both beaches therefore respond in unison to changing wave height which drives oscillation, and changing wave direction which drives rotation. What is interesting at this site is that the lower energy Moruya beach undergoes both greater oscillation and rotation, than Pedro, with the greatest shoreline change occurring at the lowest energy M3 profile location (Figure 2).

An explanation may lie in the respective beach states as the lower energy Moruya beach switches between an LTT and R state, usually with full recovery between erosion events, resulting in substantial sediment transport across the shoreline. This supports Harley, *et al.*, 2011, who found that rotation on Narrabeen beach was due more to on-offshore movement of sand, rather than

alongshore transport. In contrast, the higher energy Pedro beach exhibits a characteristically fully detached bar which moves seaward and landward within the surf zone between events. The adjoining beach face undergoes less cross-shore movement, as it is partially sheltered by the bar and will not widen substantially until the bar attaches and migrates onshore, which it rarely does. As these data only record the subaerial beach, the dynamic bar system is not documented.

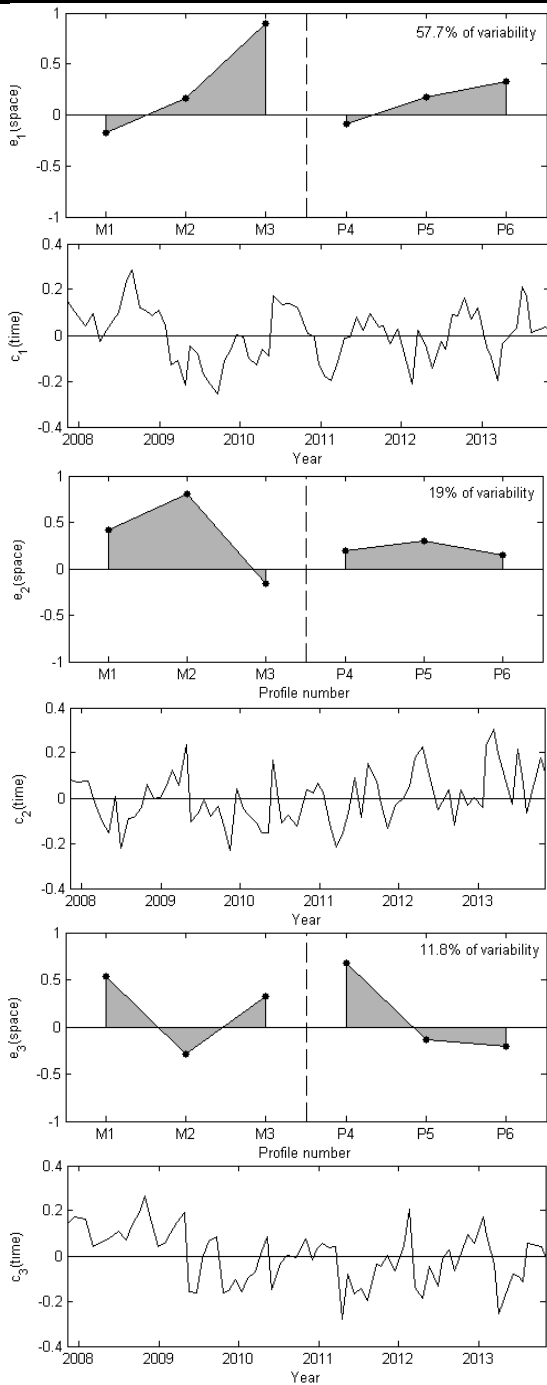


Figure 4. PCA of MHWS beach width time series for Moruya profiles 1-3 and Pedro 4-6 after record mean has been removed.

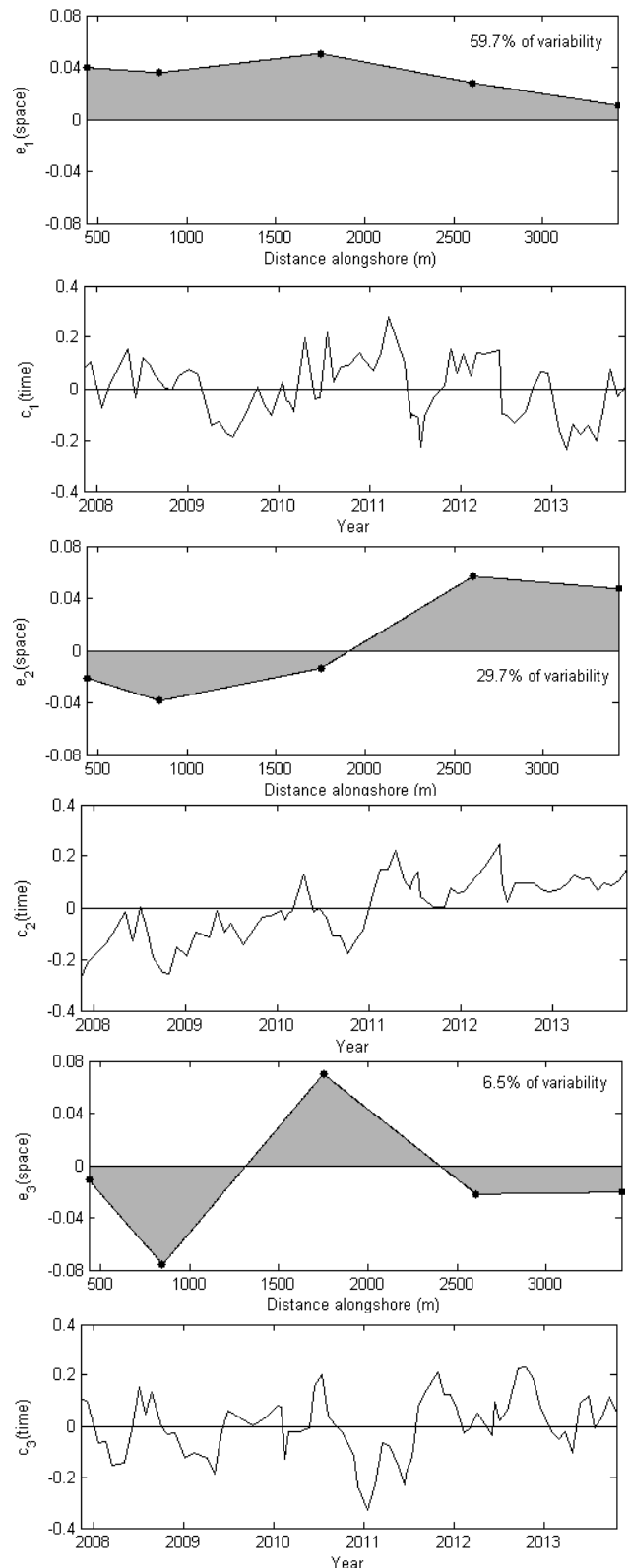


Figure 5. PCA of MHWS beach width for the five Narrabeen profile (NB1, 2, 4, 6, 8) after the record mean has been removed.

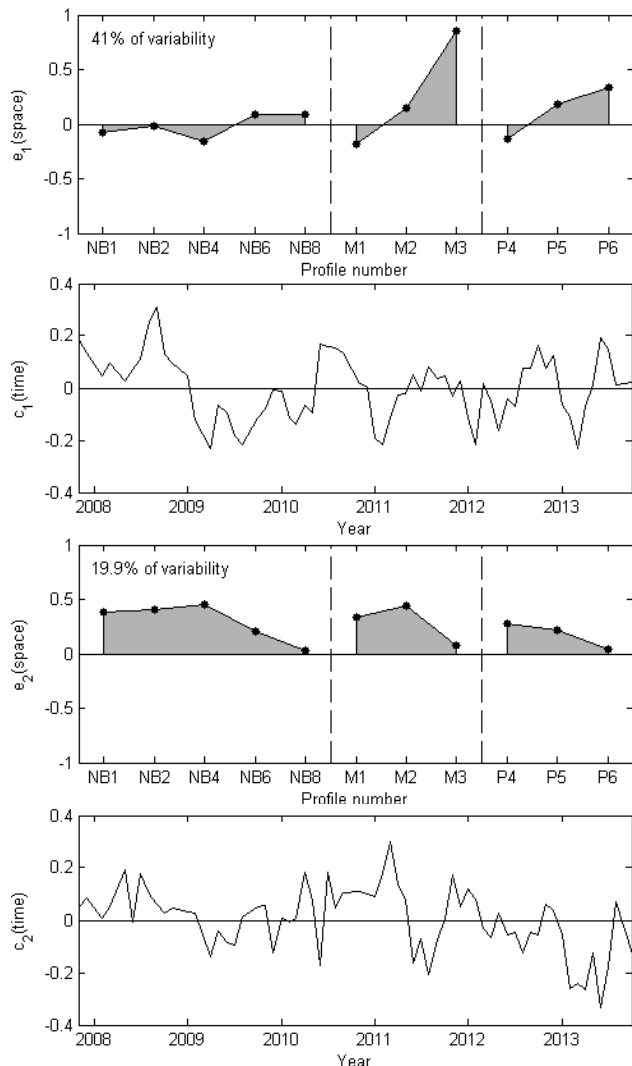


Figure 6. PCA of MHWs beach width at Narrabeen (NB1-8), Moruya (M1-3) and Pedro (P4-6) profile lines after the record mean has been removed.

Narrabeen beach also displays a highly variable shoreline (Table 2) with evidence of strong oscillation and rotation (Figure 5). Between 2007 and 2013, the shoreline position varied by as much as 34 to 45 m, though significantly less than the maximum range observed since 1976; 49 to 82 m across the five profile locations. When the longer term shoreline record is examined (Figure 7) it shows that profiles NB1 and 8 in particular have periods where they deviate from the mean position. NB1 has a negative trend since 2000, while NB8 has experienced a positive trend, quantified from 2007-2013 at  $-1.5$  m/yr and  $+2.2$  m/yr respectively. These trends greatly exceed the 1976-2013 linear trends which are  $-0.05 \pm 0.11$  m/yr at NB1 and  $-0.001 \pm 0.10$  m/yr at NB8, both not significantly different from zero. Likewise the 2007-2013 Narrabeen dataset does not have the significant north-south negative correlation ( $-0.25$ ), which is apparent in the 1976-2013 time series. The six-year record therefore reflects the present phase of inter-annual variability, which diverge from the decadal scale trends.

When all three beaches are compared it is interesting that Narrabeen and Pedro have a similar scale of shoreline variability, while the lower energy Moruya is more mobile, though as previously noted Narrabeen has experienced greater variability in the past. Also interesting is that all Moruya-Pedro profiles, apart from M3, have undergone negative trends in shoreline position during the six-year survey period. However because of their relatively short length and the nature of the longer term behaviour of Narrabeen beach these are unlikely to represent long-term erosion trends. It should also be noted that at Moruya-Pedro the zero benchmark for all six survey lines lies at least several meters seaward of the 1974 erosion scarp, indicating that longer term events and trends are not revealed by the 2007-2013 time series.

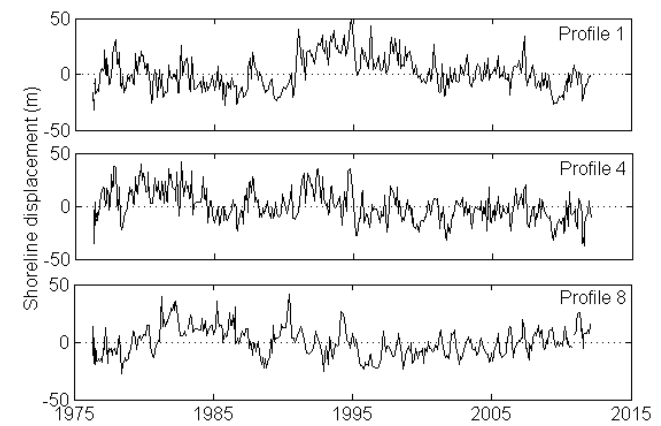


Figure 7. Time series of shoreline variability at Narrabeen profiles 1, 4 and 8, 1976-2013.

The correlation analysis (Table 2) supports the strong rotation on Moruya and Pedro during this study, and to a lesser extent Narrabeen, as discussed above. It also supports the synchronized behaviour amongst the three beaches located 270 km apart. Finally the PCA (Figure 7) indicated that synchronized rotation was the dominant mode, followed by synchronized oscillation across the three sites.

While this paper has examined the shoreline behaviour within and between the three beaches, it has not examined the causes of this behaviour. Previous studies of Narrabeen beach have firmly established a link between the shoreline behaviour and wave climate. Short, *et al.*, 1995; Ranasinghe, *et al.*, 2004; Short and Trembanis, 2004; and Harley, *et al.*, 2011 have all noted the link between wave climate and shoreline behaviour, as well as the link between changes in wave climate and the Southern Oscillation Index (SOI). This study does not pursue this link aside from noting that during the study period there has been a dominant positive SOI (La-Nina) pattern. The earlier studies found this pattern was associated with slightly higher energy, more easterly waves and a lagged anti-clockwise beach rotation, as observed in the shoreline trends (Table 1), together with a strong southerly rotation signal (Figure 7).

## CONCLUSION

Three embayed beaches with similar orientation, dimensions, and deepwater wave climate, but located 270 km apart were surveyed monthly between 2007-2013. An analysis of their shoreline behavior using graphical, correlation and PCA analysis has shown that they have strong synchronized behavior both in

terms of the direction and magnitude of beach oscillation and beach rotation, as well as the linear trend in shoreline position.

The synchronized behavior of the beach systems indicates that waves can drive synchronized regional scale behavior. This is of significance in itself suggesting that embayed beaches along long (100's km) of coast will behave in a similar manner, as well as indicating that data on behavior from single beaches may be representative of general trends over large section of similar coast. However while a single beach may record regional trends the result show there is still significant variation in the scale of these trends, with the oscillation ranging from 34 to 97 m, and the location of maximum oscillation being in the north at Narrabeen and the south at Moruya and Pedro. Clearly local factors are also contributing to shoreline dynamics on each of the beaches.

While the surveys cover a six year period the longer (37 year) Narrabeen study and the presence of the 1974 erosion scarp at Moruya and Pedro indicate that decadal duration studies are required to observe the full range of beach behaviour.

Finally, the Moruya-Pedro surveys indicate that lower energy intermediate beaches may experience greater shoreline oscillation compared to adjoining higher energy intermediate beaches, owing to the rapid transfer of sand between the R-LTT state compared to those with a detached bar.

## ACKNOWLEDGEMENT

The Narrabeen research was funded by the Australian Research Council (LP100200348). M. Bracs is funded by a UNSW Faculty of Engineering, Women in Engineering Research Scholarship.

## LITERATURE CITED

- Harley, M.D., Turner, I.L., Short, A.D. and Ranasinghe, R., 2011. A re-evaluation of coastal embayment rotation in SE Australia: the dominance of cross-shore versus alongshore sediment transport processes. *Journal of Geophysical Research*, 116, F04033.
- Mole, M.A., Mortlock, T.R.C., Turner, I.L., Goodwin, I.D., Splinter, K.D. and Short, A.D., 2013. Capitalizing on the surfcam phenomenon: a pilot study in regional-scale shoreline and inshore wave monitoring utilizing existing camera infrastructure. *Journal of Coastal Research*, Special Issue 65.
- Ranasinghe, R., McLoughlin, R., Short, A.D. and Symonds, G., 2004. The Southern Oscillation Index, wave climate and beach rotation. *Marine Geology*, 204, 273-287.
- Short, A.D., 2010. Role of geological inheritance in Australian beach morphodynamics. *Coastal Engineering*, 57, 92-97.
- Short, A.D., Cowell, P.J., Cadee, M., Hall, W. and van Dijk, B., 1995. Beach rotation and possible relation to the Southern Oscillation. *Ocean and Atmosphere Pacific*, Adelaide
- Short, A.D. and Trembanis, A., 2004. Decadal scale patterns in beach oscillation and rotation Narrabeen Beach, Australia- time series, PCA and wavelet analysis. *Journal of Coastal Research*, 20, 523-532
- Short, A.D. and Trenaman, N.L., 1992. Wave climate of the Sydney region: an energetic and highly variable ocean wave regime. *Australian Journal Marine and Freshwater Research*, 43, 765-791.

# A preliminary classification of coastal sand dunes of KwaZulu-Natal

D.W.T. Jackson,<sup>†</sup> J.A.G. Cooper<sup>‡</sup> and A.N. Green<sup>‡</sup>

<sup>†</sup>School of Environmental Sciences  
University of Ulster, Cromore Road,  
Coleraine, Co. Londonderry,  
Northern Ireland, UK  
d.jackson@ulster.ac.uk;  
jag.cooper@ulster.ac.uk

<sup>‡</sup> University of KwaZulu-Natal Marine  
Geoscience Unit, School of Geological  
Sciences, University of KwaZulu-Natal,  
Westville, Private Bag X54001, South  
Africa. greenal@ukzn.ac.za



[www.cerf-jcr.org](http://www.cerf-jcr.org)

## ABSTRACT

Jackson, D.W.T., Cooper, J.A.G., Green, A.N., 2014. A preliminary classification of sand dunes of the KwaZulu-Natal coast. In: Green, A.N. and Cooper, J.A.G. (eds.), *Proceedings 13<sup>th</sup> International Coastal Symposium* (Durban, South Africa), *Journal of Coastal Research*, Special Issue No. 70, pp. 718-722, ISSN 0749-0208.

The 550 km-long KwaZulu-Natal coast broadly divides into a bedrock-framed southern section and northern coastal plain section, each of approximately equal length. Seven types of coastal dune are identified on this coast: estuary barrier dunes; mainland beach foredunes; prograded beachridge dunes; headland bypass dunes; transverse dune fields; parabolic/migrating dunefield; and climbing dunes. The development and distribution of the various dune forms is more strongly controlled by the geological setting, than the aerodynamic regime.

**ADDITIONAL INDEX WORDS:** *coastal dunes, foredunes, transverse dune fields, climbing dunes, South Africa,*



[www.JCRonline.org](http://www.JCRonline.org)

## INTRODUCTION

Coastal dunes are important features on many of the world's coastlines. Not only are they a vital part of the contemporary coastal sedimentary system, but they are sedimentary archives that reflect climatic shifts, sea level changes and sediment availability. Coastal dunes assume a wide variety of geomorphological forms (Tsoar, 1971, Goldsmith, 1978, Pye, 1983) and those of the southern African coast have been reviewed by Tinley (1981). The supply of sediment available to the aeolian system and suitable wind regimes to transport material are well-known influences on the form of coastal dunes. The role of antecedent topography has received less attention, although it is known to exert a strong influence on the wind regime at the local scale (e.g. Lynch *et al.*, 2010, Jackson *et al.*, 2011, 2013, Delgado-Fernandez *et al.*, 2013, Smyth *et al.* 2012, 2013). In this paper, we examine the coastal dunes of KwaZulu-Natal, developing a classification of dune forms and investigating the role of aeolian dynamics, sediment supply and antecedent topography on dune morphology.

Little work has been conducted on the contemporary form and dynamics of dunes along the dune-fringed KwaZulu-Natal (KZN) coast, South Africa, where vast quantities of sand are currently occupying modern dune fields along a relatively narrow coastal shelf environment. Most of these modern dunes front much older Pleistocene forms ramped up against these, to form distinctively different dune fields in terms of their orientation, shape and extent. Green *et al.* (2004) conducted a detailed short-term analysis of windflow patterns over a blowout system near Sodwana Bay. Olivier and Garland (2003) described the

development of foredunes on the prograding coast north of the Tugela River. Van Aarde *et al.* (1996) give an account of vegetation restoration on dunes that have been mined for heavy minerals in northern KZN.

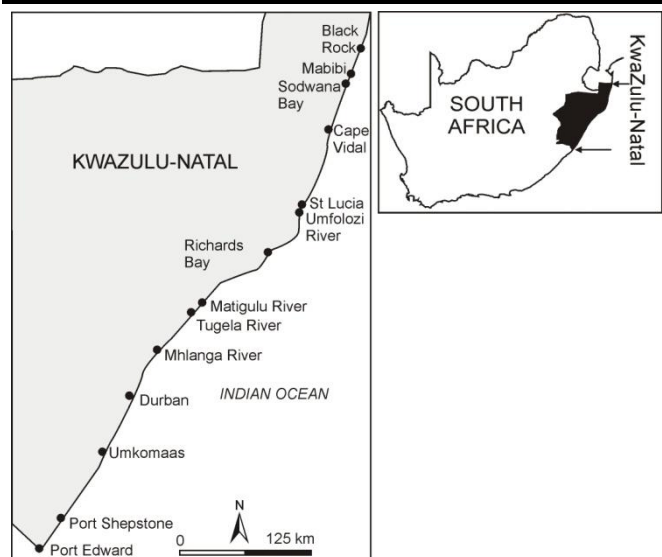


Figure 1. Locality map of the study area.



Figure 2. Estuary barrier dunes (TOP) frequent the barrier fronting estuaries emerging into the coast. Headland bypass dunes (BOTTOM) maintain their dune forms whilst travelling over and/or around headland features.

## ENVIRONMENT

The KZN coastline (Fig. 1) extends over approximately 560 km. Of this, roughly half is coastal plain and half is bedrock-framed coast in which sand deposits are best developed in shallow re-entrants at estuary mouths. A large semi-continuous Pleistocene dune ridge is developed along both the bedrock and coastal plain coasts (Porat and Botha, 2008).

Tides on the Natal coast are semi-diurnal. At Durban, mean spring tidal range is 1.72 m and mean neap tidal range is 0.5 m. The Natal coast is therefore microtidal in the classification of Davies (1980) or low mesotidal in the sense of Hayes (1979). The coastal sedimentary regime is wave dominated. Recorded wave heights over a 2 year period ranged from 0.3 to 7.6m (Hydraulics Research Unit, HRU, 1968) with a median wave height of 1.49 m. The dominant direction of wave approach at Durban is ESE to SE. The greatest significant wave heights were recorded from SSE to SW directions and the lowest from E to ESE directions. Maximum wave periods (> 17 s) occurred from SE to SSE, while the shortest wave periods (5-7 s) came from E to NE. The median wave period is 10.7 s. The KZN coast is also impacted by easterly to SE swells associated with tropical cyclones and cut-off low (COL) storms.

Longshore transport is enhanced during the winter swell regime (Smith *et al.*, 2010) and the annual longshore transport volume was calculated at 500,000 m<sup>3</sup> at Richards Bay, (Schoonees, 2000). Although they are infrequent, tropical cyclones also occur; for example, Tropical Storm Imboa (February, 1984) produced 9 m (H<sub>s</sub>) swells in the Richards Bay area

The climate of the KZN hinterland is dominated by the subtropical high pressure belt (Tyson, 1987). The mean annual rainfall of 900-1000mm is largely restricted to the summer months when 80% of the rain falls (Tyson, 1987); rapid altitudinal rise inland produces orographic forcing of rainfall. Winter rainfall is typically associated with coastal low pressure systems moving northwards and produces only a minor proportion of the annual total.

Due to the latitudinal position of the region, it is influenced by both tropical and temperate weather systems. The major winds at the coast are bi-directional (Tinley, 1985) oriented oblique and almost parallel to the coastline these are therefore south-westerly with north-easterly (Preston-Whyte and Tyson, 1988). Winds from these broad sectors occur with frequencies in excess of 255 days a year. Onshore north-easterly sea breezes are common along the KZN coast, particularly during the summer months and help strengthen the prevailing north-easterly gradient winds from anti-cyclonic circulations. Lighter land breezes (1-2ms<sup>-1</sup>) also occur at night and blow offshore as a north-westerly wind.

## METHODS

Using Google Earth, a simple visual examination of the nature and distribution of the dominant dune forms along the coast was carried out. This was supplemented with the authors' own field knowledge of the dune systems in order to develop a preliminary classification of dune forms and to assess the controls on their form and development.

## RESULTS

The following seven main dune types were identified:

1. Estuary barrier dunes
2. Headland bypass dunes
3. Mainland beach foredunes
4. Prograded beach ridge dunes
5. Transverse dunefields
6. Parabolic/migrating dunefield
7. Climbing dunes

Estuary barrier dunes develop on the numerous sand barriers that front the estuaries of southern KZN (Green *et al.*, 2013) (Fig. 2). They are usually of limited extent (<100m long and <10m high) and are susceptible to erosion during periodic river floods that erode the barriers (Cooper *et al.*, 1990). Occasionally, the migration or opening of stream outlets causes the erosion of dunes developed on barriers. Such was the case on the Mhlanga lagoon, where a well-developed foredune over 10m high was eroded by several phases of mouth opening at various positions on the barrier.

Mainland foredunes are generally shore-parallel dunes developed behind beaches with little or no influence from estuaries. They are common on the KZN south coast and are usually thickly vegetated with woody vegetation that indicates their long-term stability (Fig. 3). During extreme storm events, however, scarps form on these dunes, re-introducing dune sand into the nearshore system (Smith *et al.*, 2010). Headland bypass dunes (McLachlan *et al.* 1994) are relatively uncommon features due to the low degree of indentation on the KZN coast. Small features are locally developed on the KZN south coast and across





Figure 3. Mainland beach foredunes (TOP) are found on the back beach and parallel the beach orientation. They are maintained by cross-shore processes and waves and aeolian action. Prograded beachridge dunes (BOTTOM) are sequences of parallel aeolian dune ridges.

some of the prominent aeolianite/beachrock headlands of northern KZN (Fig. 2).

A particularly striking example is present at Black Rock. These features transfer sand alongshore in the direction of dominant winds, taking a route across the terrestrial landscape.

Prograded beach ridge dunes are extensive sequences of aeolian dune ridges that in most cases parallel the adjacent beach (Fig. 3). They are developed north of the Tugela River, where an abundant, though episodic supply of sediment enables coastal progradation (Olivier and Garland, 2003).

Transverse dunefields are large, strongly asymmetrical, elongated dunes perpendicular to the prevailing wind direction (Fig. 4). Containing gently sloping windward sides and steeply sloping leeward sides they form in areas of sparse vegetation and abundant sand supply. Extensive sets of unvegetated transverse dunes are present in northern KZN where they occur in dunefields over 10 km long and 250 m wide (Fig. 4). They have straight to undulating crests (up to 10m high) that appear to oscillate in position rather than migrating. The inter-dune troughs contain distinctive coarse lag deposits (Cooper *et al.* 2013). The best examples occur in the iSimangaliso Wetland Park north of Cape Vidal.

Parabolic/migrating dunefields (Green *et al.*, 2004) are sediment-rich dune forms migrating inland from beach source areas. They move rapidly through and/or over antecedent topography relying on strong dominant winds to maintain their form and extent. They are best developed in northern KZN at the north and south extremities of transverse dunefields (Fig. 4). The largest example is at Whitesands, north of Sodwana Bay, where a 500 m-wide migrating dunefield extends 2.5 km inland. The feature has two components, each related to one of the two dominant wind fields. Climbing dunes (Tsoar, 2001) are dune forms initially retarded by high topography but then abundant sand supply and strong winds surmount this to orientate the parabolic-like dune forms further inland. Such features are developed in northern KZN, where they climb on the high vegetated Pleistocene dunes (Fig. 5).

## DISCUSSION

The southern sections of the KZN coast where estuaries are prevalent and the intervening bedrock topography is generally low are dominated by dune types 1-4. The semi-continuous sandy beach that runs across estuary mouths and continues as a veneer on the intervening bedrock is the source of dune sand. Wind blows obliquely onshore and sand is trapped in the vegetated dunes to landward. Occasional embryo dunes do form seaward of the forested foredune but these are usually ephemeral features related to temporary sediment abundances. Dunes that form on estuary barriers are subject to periodic erosion related to rivermouth processes. Consequently they have less-developed vegetation cover that seldom includes woody vegetation. Whether on barriers or mainland stretches, foredunes experience occasional scarping during storms, however, the preponderance of woody vegetation points to long-term stability of many dunes. Contemporary sediment supply on the southern KZN coast involves both longshore transport (Schoonees, 2000) and periodic fluvial influxes (McCormick *et al.*, 1992), neither of which has been quantified with a high degree of certainty.

On the coastal plain north of the Tugela River dune types 5-7 are more common. In these northern sectors the Pleistocene dune topography (up to 100m high) is more dominant. Its presence restricts accommodation space for contemporary dune development. Consequently, modern dunes either form in a narrow zone seaward of the Pleistocene dunes (transverse dunefields), climb over them (climbing dunes), or migrate landwards across topographic depressions (migrating dunes). Periodic sediment influxes in the northern KZN coast are restricted to the Tugela, Matigulu and Umfolozi river mouths, north of which sediment supply is restricted to longshore transport. Most of the dunes have therefore developed under conditions of low contemporary sediment supply. The climbing dunes and transverse dunefields have shown little long-term progressive morphological change since the earliest air photography (1937), suggesting that they are in equilibrium with the windfield. This may well be linked to the paucity of contemporary sediment supply. In these cases, coastal orientation relative to the bi-directional wind field may play an important role in dictating the local dune dynamics.

## CONCLUSIONS

The contemporary sand dunes of the KZN coast can be divided into seven basic types: 1. Estuary barrier dunes; 2. Headland bypass dunes; 3. Mainland beach foredunes; 4. Prograded beach ridge dunes; 5. Transverse dunefields; 6. Parabolic-migrating dunefields and 7. Climbing dunes.

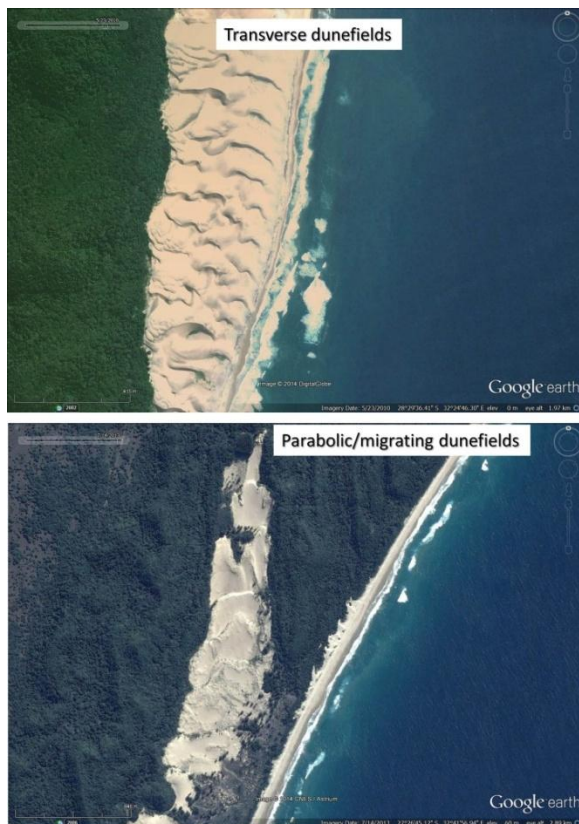


Figure 4. Transverse dune fields (TOP) are supplied with abundant sediment and maintained by strong wind flows. Generally free of vegetation they have crestal ridges perpendicular to the predominant wind direction. Parabolic/Migration dunes (BOTTOM) are also mainly free of vegetation and driven by strong winds and sediment supply that pushes them through and over pre-existing topography.



Figure 5. Climbing dunes are dunes that have overcome topographic relief to allow them to progress over into higher terrain. Very strong winds are usually funnelled through pre-existing topography to accelerate airflow (and sediment) to maintain these dune types. Vegetation across the surface is usually absent due to the accelerated flow and aeolian abrasion.

The distribution of contemporary sand dune systems of the KZN coast is affected strongly by the antecedent geomorphology. Of the seven dune types identified, types 1-4 are most prevalent in the southern bedrock-framed coast.

The larger number of estuaries and relatively low-lying bedrock coast has meant that well-vegetated dunes have developed since sea level stabilisation in the mid-Holocene. These have been sustained by fluvial and longshore sediment supply. In northern KZN, accommodation space for modern dunes is limited by the presence of large Pleistocene dunes. Types 5-7 dominate this stretch of the coast and the bi-directional wind regime helps maintain a 'steady state' dune position in which large quantities of sand pulse back and forth along /oblique to the shoreline.

## LITERATURE CITED

- Cooper, J.A.G., Mason, T.R., Reddering, J.S.V. and Illenberger, W.K. 1990. Geomorphological effects of catastrophic flooding on a small subtropical estuary. *Earth Surface Processes and Landforms*, 15, 25-41.
- Cooper, J.A.G., Smith, A.M. and Green, A.N., 2013. Backbeach deflation aprons: morphology and sedimentology. *Journal of Sedimentary Research*, 83, 395-405.
- Davies, J.L., 1980. *Geographical Variation in Coastal Development*, Second Edition. New York, Longman, 204 pp.
- Delgado-Fernandez, I., Jackson, D.W.T., Cooper, J.A.G., Baas, A.C.W., Beyers, J.H. and Lynch, K. 2013. Field characterization of three-dimensional lee-side airflow patterns under offshore winds at a beach-dune system. *Journal of Geophysical Research - Earth Surface*, 118, pp. 706-721.
- Goldsmith, V. 1978. Coastal Dunes. In: Davis, R.A. (ed) *Coastal Sedimentary Environments*, Springer-Verlag, New York, 171-230.
- Green, A.N., Cooper, J.A.G. and Le Vieux, A.M., 2013. Unusual barrier/inlet behavior associated with active coastal progradation and river-dominated estuaries. *Journal of Coastal Research*, S.I. 69, 35-45.
- Green, A.N., Garland, G.G. and Diab, R. 2004. Wind characteristics and blowout formation near Mabibi, northern KwaZulu-Natal. *South African Journal of Geography*, 86, 104-112.
- Hayes, M.O., 1979. Barrier island morphology as a function of tidal and wave regime. In: Leatherman, S.P. (ed.) *Barrier Islands*. Academic Press, New York, pp. 1-27.
- Jackson, D.W.T., Beyers, J.H.M., Lynch, K., Cooper, J.A.G., Baas, A.C.W. and Delgado-Fernandez, I. 2011. Investigation of three-dimensional wind flow behaviour over coastal dune morphology under offshore winds using computational fluid dynamics (CFD) and ultrasonic anemometry. *Earth Surface Processes and Landforms*, 36, 1113-1134.
- Jackson, D.W.T., Beyers, M., Delgado-Fernandez, I., Baas, A.C.W., Cooper, J.A.G. and Lynch, K. 2013. Airflow reversal and alternating corkscrew vortices in foredune wake zones during perpendicular and oblique offshore winds. *Geomorphology*, 187, 86-93.
- Lynch, K., Jackson, D.W.T. and Cooper, J.A.G., 2010. Coastal foredune topography as a control on secondary airflow regimes under offshore winds. *Earth Surface Processes and Landforms*, 35, 344-353.
- McCormick, S., Cooper, J.A.G., and Mason, T.R. 1992. Fluvial sediment yield to the Natal coast: a review. *South African Journal of Aquatic Sciences*, 18, 74-88.
- McLachlan, A., Illenberger, W.K., Burkinshaw, J.R. and Burns, M.E.R., 1994. Management Implications of Tampering with Littoral Sand Sources. , S.I. 12, 51-59
- Olivier, M. J. and Garland, G. G. 2003. Short-term monitoring of foredune formation on the east coast of South Africa. *Earth Surface Processes and Landforms*, 28, 1143-1155.
- Preston-Whyte, R.A. and Tyson, P.D. 1988. *The atmosphere and weather of South Africa*. Oxford University Press, Cape Town, 374pp.
- Porat, N., and Botha, G. 2008. The luminescence chronology of dune development on the Maputaland coastal plain, southeast Africa. *Quaternary Science Reviews*, 27, 1024-1046.
- Pye, K., 1983. Coastal dunes. *Progress in Physical Geography* ,7, 531-557

- Schoonees, J.S., 2000. Annual variation in the net long-shore sediment transport rate. *Coastal Engineering*, 40, 141-160.
- Smith, A., Mather, A., Guastella, L., Cooper, J.A.G., Ramsay, P.J., and Theron, A., 2010. Contrasting styles of swell-driven coastal erosion: examples from KwaZulu-Natal, South Africa. *Geological Magazine*, 147, 940-953.
- Smyth, T.A.G., Jackson, D.W.T. and Cooper, J.A.G. 2012. High resolution measured and modelled three-dimensional airflow over a coastal bowl blowout. *Geomorphology*, 177-178. pp. 62-73.
- Smyth, T.A.G., Jackson, D.W.T and Cooper, J.A.G. 2013. Three-dimensional airflow patterns within a coastal trough-bowl blowout during fresh breeze to hurricane force winds. *Aeolian Research*, 9, 111-123.
- Tinley, K.L. 1985. *Coastal Dunes of South Africa*. CSIR, South African National Scientific Programmes Report No. 109, Pretoria, South Africa, 300 pp.
- Tsoar, H. 1971. Types of Aeolian Sand Dunes and their Formation. In: N.J. Balmforth and A. Provenzale (Eds.): *The language of Pattern and Form*. Springer Verlag, Berlin, pp. 403-429.
- Tyson, P.D., 1987. *Climatic Change and Variability in Southern Africa*. Oxford University Press, Cape Town, 220 pp.
- van Aarde, R. J., Ferreira, S. M. Kritzing, J. J. van Dyk, P. J. Vogt, M. and Wassenaar, T. D. 1996. An evaluation of habitat rehabilitation on coastal dune forest in northern KwaZulu-Natal, South Africa. *Restoration Ecology*, 4, 334-345.

# Integrating different records to assess coastal hazards at multi-century timescales

Adam D. Switzer<sup>†‡</sup>, Fengling Yu<sup>†</sup>, Chris Gouramanis<sup>†</sup>, Janneli Lea A. Soria<sup>†‡</sup>, Dat T. Pham<sup>†‡</sup>

<sup>†</sup> Earth Observatory of Singapore  
Nanyang Technological University,  
50 Nanyang Avenue,  
Singapore 639798, Singapore  
aswitzer@ntu.edu.sg

<sup>‡</sup> Division of Earth Sciences  
Nanyang Technological University,  
50 Nanyang Avenue,  
Singapore 639798, Singapore



[www.cerf-jcr.org](http://www.cerf-jcr.org)



[www.JCRonline.org](http://www.JCRonline.org)

## ABSTRACT

Switzer, A.D., Yu, F., Gouramanis, C., Soria, J., Pham, T.D. 2014. An integrated approach to assessing coastal hazards at multi-century timescales. *In: Green, A.N. and Cooper, J.A.G. (eds.), Proceedings 13<sup>th</sup> International Coastal Symposium* (Durban, South Africa), *Journal of Coastal Research*, Special Issue No. 70, pp. 723-728, ISSN 0749-0208.

In many places on earth, the written record of coastal flooding events from tropical cyclones (typhoons, hurricanes) and tsunamis is too short or inconsistent to accurately assess the hazard posed by both kinds of event on scales beyond those of the average human lifespan. In this paper we summarize an integrated research paradigm that incorporates instrumental, historical, archaeological and geological records to extend the record of coastal flooding events to generate a multi-century analysis of recurrence interval for coastal flooding, thus, improving long-term risk assessment. The two primary factors in assessing risk from coastal hazards are frequency and magnitude. These can be addressed through field and modeling studies of washover deposits where they are found. We also summarize recent advances in the identification of overwash events from the geological record and report on the progress to distinguish storm and tsunami deposits. The recent advances have increased the utility of tsunami and storm deposits to improve coastal risk assessment.

**ADDITIONAL INDEX WORDS:** *Storms, Tropical cyclones, Tsunamis, Coastal flooding, Coastal infrastructure, Nuclear Power Plants, Harbors, Airports, Extreme waves*

## INTRODUCTION

The coastal zone hosts a high concentration of the world's populace (Small and Nicholls, 2003) and a significant portion of global Gross Domestic Product (GDP) is produced in the coastal zone (Turner *et al.*, 1996). Assessing the recurrence interval of coastal hazards on any coast is a key requirement for developing a baseline understanding of the potential impacts of future climate and sea level change, and natural-hazard events, such as, coastal flooding from storms and tsunamis. Such assessments, incorporating an evaluation of coastal hazard and vulnerability, are essential for developing adequate risk management strategies for large (e.g. ports) or potentially hazardous (e.g. nuclear power plants) coastal infrastructure projects (Figure 1).

To assess the vulnerability of any coastal development it is important to consider not only the hazard but the sum of the social, economic and physiographic properties of the region, and to note that vulnerability is also inherently linked to a communities' ability to respond to and recover from adverse impacts, i.e. a society's resilience. Assessing coastal vulnerability is a very important prerequisite to determine "where", "why" and "how" questions related to coastal flooding risk, e.g., where to place Nuclear Power plants, hospitals, airports, and industrial parks (Figure 1). Only when armed with such knowledge, can those tasked with disaster preparedness take steps to prepare for

and reduce the risk of coastal flooding leading to coastal disasters. While cyclone and tsunami warning systems facilitate the monitoring and prediction of the impact of modern events, it would be dangerous to ignore the history of a coastal site, or the prehistoric record potentially preserved in the archaeological and geological record. For some hazards, like tropical cyclones, their occurrence is essentially seasonal, and reasonably predictable, although the question must always be asked 'What is the worst cyclone to have ever affected this coast?'. It is also apparent that on many coasts a similar question can and should then be asked for tsunamis. At almost all coastal locations the only way to adequately answer this question is to turn to the historical, archeological and geological records. For example, the Bay of Bengal has a long history of earthquakes and tsunamis, but the documented record is unfortunately fraught with inconsistencies that make recurrence interval analysis difficult. (e.g. Dominey-Howes *et al.*, 2007a; Kumar and Achyuthan, 2006; Alam *et al.*, 2013).

In this paper, we outline and synthesize the emerging research paradigm that incorporates instrumental, historical, archaeological and geological records to integrate the record of coastal flooding events to generate a multi-century analysis of recurrence interval for coastal flooding.



Figure 1. Upper Left) Guangdong (foreground) and Ling Ao (background) nuclear power plants in southern China (photo courtesy of L-3 Communications MAPPS (mapps.1-3com.com)). This region has experienced historical storm surges of more than 4 m. Upper Right) A destroyed cooking oil facility at Tanuan, Leyte Province, the Philippines (photo courtesy heraldsun.com.au). The area was devastated by a 3m storm surge caused by Typhoon Haiyan in November 2013. Lower Left) Tacloban airport following a 6 m storm surge caused from Typhoon Haiyan (photo EPA). Lower Right) Two steamships, Leonor and Albay, and other sunken vessels at the Hong Kong Central waterfront following an unnamed typhoon of 1874 (Courtesy Hong Kong Museum of History).

## METHODOLOGY

The approach described here is designed to evaluate the recurrence intervals of coastal flooding events only. In doing so we recognize that during events like cyclones, the coastal flooding should be considered in the context of the whole event including storm surge, wind damage and flooding from rainfall. The approach described here has three integral steps, which commonly overlap in time (Figure 2). The key steps in this integrated approach are:

- 1) examine and validate the instrumental record
- 2) compare and contrast the historical and archaeological record
- 3) incorporate archaeological, geomorphological and geological records to extend the record back to statistically significant lengths of time.

### The instrumental record of coastal hazard events: tide gauges and satellite altimetry

#### Tide gauges

For the study of sea level change, storm surge and tsunamis, the primary instrumental record of interest is the global network of tide gauges (Church and White, 2006). A summary of the techniques used to characterize extreme sea level events (primarily storm surge) based on tide gauge data was recently published by Mendez and Woodworth (2010) and they noted that there are several primary techniques that have been applied to analyzing extreme sea level events including the assessment of high annual percentiles (e.g., Woodworth and Blackman, 2004) and the investigation of sea level maxima over a block of time (e.g. Araújo and Pugh, 2008). In contrast, others have chosen to look at the number of events per year (e.g., Marcos *et al.*, 2009) or examine only events over a certain threshold (Zhang *et al.*, 2000).

In tsunami studies, the use of tide gauges is limited due to the low recurrence interval of tsunami events globally and limitations from the spatial distribution and length of tide gauge records. Despite this, there are a few notable examples where tide gauges have been of some use in evaluating the return interval of tsunami events, e.g. in Western Australia (Dominey-Howes *et al.*, 2007b) and the Black Sea (Yalciner *et al.*, 2004). In terms of instrumental records, the modern Deep-ocean Assessment and Reporting of Tsunamis (DART) buoy system, combined with a near global network of tide gauges now provides a high spatial resolution for assessing tsunami events as and after they happen.

#### Satellite altimetry

Altimeters mounted on orbiting satellites (e.g. Jason 1 and 2) were primarily designed to observe sea level variability (Henry, *et al.*, 2013). However, as both storms and tsunami waves disturb the sea level locally, they leave physical signals that can only be recorded with local altimetry. The detection of storm and tsunami waves by satellite altimetry is limited to opportunities where satellites move over a storm or tsunami during their passage across the ocean. Notable examples include tsunami observations from the Indian Ocean tsunami in 2004 (Ablain *et al.*, 2006) along with storm observations of Hurricanes Katrina in 2005 (Scharoo *et al.*, 2005) and Sandy in 2012 (Lillibridge *et al.*, 2013). Given the short record (since 1992) and the limitation that a satellite needs to be passing at the time along with the processing time and the need for background corrections, satellite altimetry is unlikely to ever be a tool for detection and warning of storm surges and tsunamis. However, satellite altimetry does provide useful datasets for validating models of storm surge developments and tsunami propagation and dissipation.

### Using historical documents and archeological information

The second invaluable source of data in assessing coastal hazards is at the availability of archaeological and historical records (e.g. Liu *et al.*, 2001; Louie and Liu, 2003; Lau *et al.*, 2010; Scheitlin *et al.* 2010; Chague-Goff *et al.*, 2011; Paris *et al.*, 2014). To adequately assess the historical records of catastrophic events, a database is commonly created and the material is assessed and validated to remove errors and misinterpretations, and the robustness of the dataset tested (e.g., Liu *et al.*, 2001, Lau *et al.*, 2010; Lee *et al.*, 2012). Unfortunately, those studying the historical record of hazards are often frustrated by inconsistencies in descriptions, and inaccuracies in translation between different languages, calendars and location names (e.g. Paris *et al.*, 2014).

Archaeology and geoarchaeology also lend themselves to the analysis of coastal hazard recurrence as many ancient settlements are located on coastlines. Thus, it is not surprising that many coastal archaeological sites include evidence for cyclones (e.g. Bird, 1992) and catastrophic flooding from storms or tsunamis (e.g. Mahabalipuram, India (Rajani and Kasturirangan, 2013)). For example, McFadgen and Goff (2007) synthesised the geoarchaeological record of tsunamis in New Zealand, and Vott *et al.*, (2011), based on a combination of geoarchaeological and sedimentological techniques, presented evidence of multiple tsunami on the Bay of Palairos-Pogonia, NW Greece, during the Holocene.

Recently, combining the instrumental, historical and geoarchaeological datasets has become popular in coastal hazards research. Examples for tsunamis (e.g. Dominey-Howes *et al.*, 2007b) and storm surges (e.g. see review of Nott, 2004; Elsner *et al.*, 2008) demonstrate the clear potential of this type of integrated research in sustaining future coastal communities.

### Using the geological record

The geological and geomorphological record provides opportunities to assess coastal hazards over centennial timespans or to assess the history of extreme coastal events on coastlines without archaeological or historical records (Donnelly *et al.*, 2001; Nott, 2004). Analysis of geological records indicated precursors to the 26 December 2004 Indian Ocean (e.g., Jankaew *et al.*, 2008; Monecke *et al.*, 2008) and 11 March 2011 Tohoku (Minoura *et al.*, 2001) tsunamis, poignantly showing that catastrophic tsunami washover events are too infrequent to be adequately characterized by historical records alone.

Research on the geological or geomorphological record has led to the discovery of long records of coastal flooding spanning many thousands of years in numerous locations around the world (e.g., Liu and Fearn, 2003, Woodruff *et al.*, 2009). Such records can be depositional (e.g. see reviews of Nott, 2004; Goff *et al.*, 2012) or in rarer instances erosional (Switzer *et al.*, 2006; Buynevich *et al.*, 2004). One notable example is the study of Nanayama *et al.* (2003) from Hokkaido, Japan, where tsunami deposited sand sheets (some extending several kilometers inland) indicated that large tsunamis inundated the coast on average every 500 years, between 2000 and 7000 years BP. It is important to note that a large tsunami does not equate to a large earthquake (Hill *et al.*, 2012).

Most coastal washover records come from low-energy coastal environments, such as coastal marshes or lakes (e.g. Bondevik *et al.*, 1997; Liu and Fearn, 2001; Switzer and Jones, 2008). Storm and tsunami overwash events can leave behind sandy deposits that can yield information that allows the investigation of the physical characteristics of the flooding event including the reconstruction of water depths and velocities of past inundations; estimation of source locations (of tsunamigenic events); and the mapping of the

likely inundation distance of future events (e.g. Paris *et al.*, 2007; Gonzalez *et al.*, 2009).

The majority of work on the depositional record of coastal flooding events has been conducted in sub-tropical and temperate latitudes that are home to salt marshes and coastal lagoons which favor preservation of deposits (e.g. Minoura *et al.*, 1994; Clague and Bobrowsky, 1994; Benson *et al.*, 1997; Liu and Fearn, 2001; Tuttle *et al.*, 2004; Switzer and Jones, 2008). The Indian Ocean Tsunami of 2004 (Jankaew *et al.* 2008, Monecke *et al.* 2008), Cyclones Nargis of 2008 (e.g. Fritz *et al.*, 2009) and Typhoon Haiyan of 2013 indicate a real need for such research in tropical environments. Unfortunately, such environments come with a myriad of challenges including poor preservation of the deposit, intensive bioturbation, seasonal flooding and limited or difficult access. Additionally, many tropical countries have few resources for such studies (e.g. Bangladesh, Philippines, Myanmar, and Indonesia) and considerable socio-economic issues preventing the adequate evaluation of past events.

## RESULTS AND DISCUSSION

Despite the challenges of working in different latitudes with differing preservation issues, long-term coastal flooding records provide the only method for assessing the recurrence of large coastal flooding events capable of leaving lasting sedimentary signatures (e.g. Woodruff *et al.*, 2008). Determining such recurrence intervals is critical for planning large coastal infrastructure projects (Figure 1).

### Determining long term recurrence intervals

Assessing the archaeological, geological and geomorphological record invariably requires dating techniques, such as radiocarbon <sup>14</sup>C and optically stimulated luminescence (OSL) to provide chronologies of events that allows the determination of recurrence intervals. If using sandsheets two approaches can be applied. The first approach dates the deposit directly, for example the OSL dating of tsunami or storm laid sands (e.g. Huntley and Clague, 1996; Murari *et al.*, 2007; Brill *et al.*, 2012) and the second focuses on dating material from the confining deposits, thereby bracketing the age of the event (e.g. Jankaew *et al.*, 2008; Switzer and Jones, 2008). Recently, new approaches to the treatment of age data have helped to narrow uncertainties of event timing, for example the summing of probability density functions for <sup>14</sup>C dates (Kelsey *et al.*, 2005). As accurate dating is fundamental to the determination of recurrence intervals, coastal stratigraphers

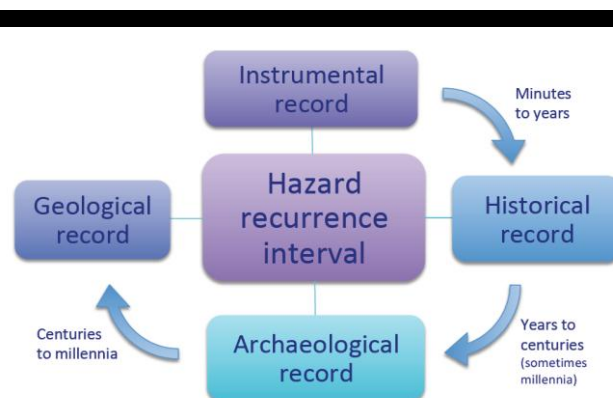


Figure 2. Schematic diagram of the integrated approach to different records of coastal hazards that cover differing timeframes. A similar approach can be applied to other hazards, such as, earthquakes and volcanic eruptions (e.g. Paris *et al.*, 2014).

face the limitations of the geological and analytical uncertainties in estimating event ages, and the uncertainties in some cases may be as large as the recurrence intervals.

### Storm or tsunami?

Commonly, the assessment of any record beyond the historical timeframe will result in the question “are the deposit(s) the result of a storm(s) or tsunami(s)?” Although the presence of washover sandsheets or coastal boulders may provide a primary source of information on the past occurrence of an overwash event, it is often necessary to attempt to distinguish between tsunami and storm deposits in the prehistoric record.

There will never be a single analytical technique that can unambiguously distinguish between storms and tsunamis as the depositional mechanism of paleo-washover deposits (Morton *et al.*, 2007; Switzer and Jones, 2008; Chague-Goff *et al.*, 2011). In all paleo-washover studies, a series of criteria based on the local geography and stratigraphy must be evaluated against known storm and tsunami events in the region. What commonly occurs in paleo-washover studies is the evaluation of known or recent overwash deposits to develop modern analogues for comparison with the paleo-deposits. Both the modern and paleo-approaches use similar techniques that combine field observations with the analysis of geomorphic, sedimentological, geochemical and paleontological signatures to understand and compare each deposit. From this comparison, a depositional agent may be inferred.

Using modern analogues to infer a depositional agent in boulder studies is difficult and the comparison of paleo and recent deposits are commonly inconclusive (e.g. Switzer and Burston, 2010). In contrast, comparative stratigraphic studies of both storm and tsunami deposits reveal some differences in sedimentology, stratigraphy, faunal composition, wave height and inland extent (e.g. Goff *et al.*, 2012; Phantuwongraj and Choowong, 2011). Generally, coastal flooding events deposit sandsheets that contrast with the sediments of the coastal plain, lake, marsh or lagoon (Minoura *et al.*, 1994; Clague and Bobrowsky, 1994; Benson *et al.*, 1997; Bondevik *et al.* 1997; Liu and Fearn, 2001; Tuttle *et al.*, 2004; Switzer and Jones, 2008, Jankaew *et al.* 2008, Moneke *et al.* 2008). The internal sedimentology of such sandsheets (e.g. bedding structures), the local physiography (e.g. height above sea level) and the three dimensional distribution (e.g. landward extent and taper and regional continuity), can also assist in determining the origin of a washover sandsheet (See discussions of Nott, 2004 and Chague-Goff *et al.*, 2011). The presence of marine fossils or exotic (deep water) heavy mineral assemblages within a terrestrial environment may indicate transport via a tsunami as opposed to a storm (e.g. Switzer *et al.*, 2005; Hawkes *et al.*, 2007; Mamo *et al.*, 2009). Additionally, salinity changes caused by short-lived marine inundation events can cause notable changes in the assemblages of ostracods, diatoms, foraminifera and aquatic plants. Although several researchers have proposed criteria to distinguish these two types of deposits it is apparent that each deposit must be carefully considered in the context of its regional setting (Switzer and Jones, 2008; Goff *et al.*, 2001; Morton *et al.*, 2007).

Despite these limitations, storm or tsunami characteristics in some locations have been successfully reconstructed from geological evidence. For example, Woodruff *et al.* (2009) successfully reconstructed the mid-Holocene periodicity of typhoons in southern Japan providing a commentary on mid-Holocene storminess in the Western Pacific. Using beach ridges, Nott (2011) reconstructed the landfall of large tropical cyclones at Shark Bay in northern Australia for the last 6000 years.

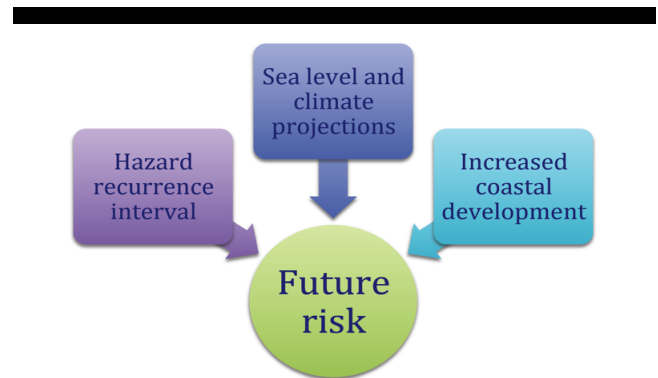


Figure 3. Schematic diagram of the conceptual paradigm for assessing the future risk of any coastal community (based on the work of Lin *et al.*, 2012).

In tsunami studies, similar work by Atwater *et al.* (2005), demonstrated that tsunami deposits from Japan and North America, in conjunction with modeling of the tsunami heights that were inferred from written historical records in Japan, suggesting that a ~M9 megathrust earthquake centred offshore northwest North America occurred on the 26 January 1700.

Approaches integrating the historical and geological record of coastal flooding events with climate and sea level predictions (Figure 3) are also becoming increasingly popular (e.g. Lin *et al.*, 2012). In their study, Lin *et al.*, (2012) assumed sea level would rise by ~1 m by 2100 and added this to surge predictions from synthetic storms based on future potential storminess. They concluded that when both sea level and the future of severe storms were taken into account, the models projected a considerable risk of more frequent coastal flooding on the northeast US coast including New York City.

### Communication – Science to policy transfer

While the integrated approach outlined here provides a paradigm for extending the historical record of coastal flooding events for which there are no written or oral records, transferring this information to coastal planning policy and practices remains problematic. The integration of different records is not necessarily straightforward and as there remains no ‘recipe’ for distinguishing between storms and tsunamis in the geological record, the true ‘hazard’ message may be lost in the scientific arguments of whether a deposit is a tsunami deposit or a storm.

Although limitations clearly exist, the careful examination of the integrated record outlined here can yield valuable information to coastal planners and disaster management agencies. Although the need to adequately communicate and integrate the available science into policy is paramount to effective hazard mitigation and adaptation, many examples exist where the threat of catastrophic events was known from either the geological or historical records but not incorporated into policy. Two recent examples of this failure to appreciate the geological and historical data of washover events that have had catastrophic results occurred in Tohoku, Japan and Tacloban, Philippines (Figure 1D). In Tohoku it is tragically apparent that although geological evidence for previous large tsunamis on the Sendai coastal plain had been identified (Minoura *et al.*, 2001), the science did not convey the likelihood of a similar future event to the management of the coastal communities of central Japan. In the Tacloban example, historical records from a Jesuit priest (Algue, 1898) along with an inscription in front of the Church of Tanauan describe a typhoon

in October 1897 that shows striking similarities to Typhoon Haiyan of November 2013. The historical records from 1897 provide clear evidence of the threat and impact of catastrophic typhoons in Tacloban and nearby low-lying coastal towns. It will be of great interest to observe how future generations perceive and adapt to the threat of the recent catastrophic events.

#### When scientific argument limits application

In many instances, while the long term integrated records of coastal flooding events are deemed to be of interest to the scientific community and to a less extent to reinsurers and disaster management professionals, unfortunately this information fails to be transferred into meaningful action and policy in local and regional governments. Today such records are only just starting to be used as a basis for signage, evacuation maps and emergency planning (e.g. Gonzalez *et al.*, 2009; Lin *et al.*, 2012).

At times it is apparent that it may be best to step away from the scientific arguments of storm versus tsunami and call a deposit a coastal flooding event. This will avoid loss of the true 'hazard' message in the scientific arguments of whether a deposit is a tsunami deposit or a storm. This will also remove the ambiguity that non-specialists face when confronted with the dilemma of associating a cause of the coastal flooding. By focusing on the impacts of coastal flooding events and not the cause, the basic premise of coastal hazard implications and ramifications for coastal planning and emergency management can be sustainably implemented. By adopting this approach, the sedimentary deposit's genesis becomes less relevant and the fact that the deposit is present is indicative of coastal flooding. This simple concept will still yield invaluable information on the recurrence of 'large marine overwash events' that can be managed accordingly. That information is of key importance for future coastal and hazard mapping and planning to coastlines that have short historical records.

#### CONCLUSION

The Earth's coastal environments are locations of immense population growth and infrastructure development. Globally we must address not only the potential for sea level rise but the potential for coastal flooding events from storms and tsunamis. A primary aspect of any debate concerning what management and planning practices to employ is how often will the flooding events happen? The development of policy, planning and management strategies should be framed in a context of risk perception around regional government planning and the demand for development. Coastal engineers, geomorphologists, modelers and risk managers can contribute to the task, but often this contribution can confound the problem through differences in contextual paradigms and or approaches to the problem. The management and preparation for coastal flooding currently sits in an uncomfortable paradigm of building on experiences learnt from past 'mistakes'. This paradigm is no longer valid and truly integrated coastal flooding assessments can no longer be bound by historical experiences. Only through the integration of geological, archaeological and historical records with computer modeling and foresight analysis will coastal communities be better equipped to actively manage coastal hazard events. A plethora of recent coastal disasters and the increasing technological savvy of the global population means that the populace of coastal communities will no doubt be increasingly lobbying for coastal hazard mitigation and participating in coastal planning discussions in the future. Only through integrating different records and effectively transferring the science to the policy will coastal hazards be adequately managed.

#### ACKNOWLEDGEMENTS

This is Earth Observatory of Singapore contribution 64. This research is supported by National Research Foundation Singapore under its Singapore NRF Fellowship scheme (National Research Fellow Award No. NRF-RF2010-04) and administered by Earth Observatory of Singapore. This paper is a contribution to the IGCP project "IGCP-588 Preparing for Coastal Change".

#### LITERATURE CITED

- Ablain, M., J. Dorandeu, P.-Y. Le Traon, A. Sladen, The Indian Ocean Tsunami of December 26, 2004 (2006) High Resolution Altimetry Reveals New Characteristics of the December 2004 Indian Ocean Tsunami, *Geophysical Research Letters*, 33 (21)
- Alam, E., Dominey-Howes, D., Chagué-Goff, C., and Goff, J. (2012). Tsunamis of the northeast Indian Ocean with a particular focus on the Bay of Bengal region—a synthesis and review. *Ear. Sci. Rev.*, 114(1), 175-193.
- Algue, J. and Manila Observatory. (1898). *El baguio de Samar y Leyte, 12-13 de octubre de 1897.* Manila : J. Marty. 74 pp.
- Araújo, I. B., and Pugh, D. T. (2008). Sea levels at Newlyn 1915-2005: analysis of trends for future flooding risks. *Journal of Coastal Research*, 24(sp3), 203-212.
- Atwater, B. F., Musumi-Rokkaku, S., Satake, K., Tsuji, Y., Ueda, K., Yamaguchi, D (2005), The Orphan Tsunami of 1700: 2005 Japanese clues to a parent earthquake in North America, *Prof. Pap. U.S. Geol. Surv.*, 1707, 3-123.
- Benson, B. E., Grimm, K. A., and Clague, J. J. (1997). Tsunami deposits beneath tidal marshes on northwestern Vancouver Island, British Columbia. *Quaternary Research*, 48(2), 192-204.
- Bird, M. K. (1992). The impact of tropical cyclones on the archaeological record: an Australian example. *Arch. in Oceania*, 75-86.
- Bondevik, S., Svendsen, J. I., and Mangerud, J. A. N. (1997). Tsunami sedimentary facies deposited by the Storegga tsunami in shallow marine basins and coastal lakes, western Norway. *Sedimentology*, 44(6), 1115-1131.
- Brill, D., Klasen, N., Brückner, H., Jankaew, K., Scheffers, A., Kelletat, D., and Scheffers, S. (2012). OSL dating of tsunami deposits from Phra Thong Island, Thailand. *Quaternary Geochronology*, 10, 224-229.
- Buynovich, I. V., FitzGerald, D. M., and van Heteren, S. (2004). Sedimentary records of intense storms in Holocene barrier sequences, Maine, USA. *Marine Geology*, 210(1), 135-148.
- Chagué-Goff, C., Schneider, J. L., Goff, J. R., Dominey-Howes, D., and Strotz, L. (2011). Expanding the proxy toolkit to help identify past events—lessons from the 2004 Indian Ocean Tsunami and the 2009 South Pacific Tsunami. *Earth-Science Reviews*, 107(1), 107-122.
- Chowong, M., Murakoshi, N., Hisada, K. I., Charoentitirat, T., Charusiri, P., Phantuwongraj, S., and others (2008). Flow conditions of the 2004 Indian Ocean tsunami in Thailand, inferred from capping bedforms and sedimentary structures. *Terra Nova*, 20(2), 141-149
- Church, J. A., and White, N. J. (2006). A 20th century acceleration in global sea-level rise. *Geophysical Research Letters*, 33(1).
- Clague, J. J., and Bobrowsky, P. T. (1994). Tsunami deposits beneath tidal marshes on Vancouver Island, British Columbia. *Geological Society of America Bulletin*, 106(10), 1293-1303.
- Donnelly, J. P., S. Roll, M. Wengren, J. Butler, R. Lederer, and T. Webb (2001), Sedimentary evidence of intense hurricane strikes from New Jersey. *Geology*, 29(7), 615-618
- Dominey-Howes, D., Cummins, P., and Burbidge, D. (2007a). Historic records of teletsunami in the Indian Ocean and insights from numerical modelling. *Natural Hazards*, 42(1), 1-17.
- Dominey-Howes, D. (2007b). Geological and historical records of tsunami in Australia. *Mar. Geol.*, 239(1), 99-123.
- Elsner, J. B., Jagger, T. H., and Liu, K. B. (2008). Comparison of Hurricane Return Levels Using Historical and Geological Records. *J. Applied Meteorology and Climatology*, 47(2).
- Fritz, H. M., C. D. Blount, S. Thwin, M. K. Thu, and N. Chan (2009), Cyclone Nargis storm surge in Myanmar, *Nature Geos.*, 2(7), 448-449
- Goff, J., C. Chagué-Goff, and S. Nichol (2001), Paleotsunami deposits: a New Zealand perspective, *Sediment. Geol.*, 143(1-2), 1-6
- Goff, J., Chagué-Goff, C., Nichol, S., Jaffe, B., and Dominey-Howes, D. (2012). Progress in paleotsunami research. *Sediment. Geol.*, 243, 70-88.



- González, F. I., Geist, E. L., Jaffe, B., Kânoğlu, U., Mofjeld, H., and others (2009). Probabilistic tsunami hazard assessment at Seaside, Oregon, for near and far field seismic sources. *JGR:Oceans*, 1978–2012, 114(C11).
- Hawkes, A. D., Bird, M., Cowie, S., Grundy-Warr, C., Horton, B. P., and others (2007). Sediments deposited by the 2004 Indian Ocean tsunami along the Malaysia–Thailand Peninsula. *Mar. Geol.*, 242(1), 169–190.
- Henry, O., Ablain, M., Meyssignac, B., Cazenave, A., and others (2013). Effect of the processing methodology on satellite altimetry-based global mean sea level rise over the Jason-1 operating period. *J. of Geodesy*, 1–11.
- Hill, E. M., Borrero, J. C., Huang, Z., Qiu, Q., Banerjee, P., and others (2012). The 2010 Mw 7.8 Mentawai earthquake: Very shallow source of a rare tsunami earthquake determined from tsunami field survey and near-field GPS data. *JGR Solid Earth* (1978–2012), 117(B6).
- Huntley, D. J., and Clague, J. J. (1996). Optical dating of tsunami-laid sands. *Quat. Research*, 46(2), 127–140.
- Ishii, M., Kiser, E., and Geist, E. L. (2013). Mw 8.6 Sumatran earthquake of 11 April 2012: Rare seaward expression of oblique subduction. *Geology*, 41(3), 319–322.
- Jankaew, K., B. F. Atwater, Y. Sawai, M. Choowong, T. Charoentitirat, M. E. Martin, and A. Prendergast (2008). Medieval forewarning of the 2004 Indian Ocean tsunami in Thailand. *Nature*, 455(7217), 1228–1231.
- Kelsey, H. M., A. R. Nelson, E. Hemphill-Haley, and R. C. Witter (2005). Tsunami history of an Oregon coastal lake reveals a 4600 yr record of great earthquakes on the Cascadia subduction zone. *Geol. Soc. Am. Bull.*, 117(7–8), 1009–1032.
- Kumar, K. A., and Achyuthan, H. (2006). A record of paleo-tsunami in the Indian Ocean. *Marine Geodesy*, 29(4), 253–263.
- Lau, A. Y. A., A. D. Switzer, D. Dominey-Howes, J. C. Aitchison, and Y. Zong (2010). Written records of historical tsunamis in the northeastern South China Sea – challenges associated with developing a new integrated database. *Nat. Hazards Earth Syst. Sci.*, 10(9), 1793–1806.
- Lee, Y., Yu, F., Switzer, A. D., Lau, A. Y., Terry, J., and Gouramanis, C. (2012). *Developing a historical typhoon database for the southeastern Chinese coastal provinces, 1951–2010*. In *Proceedings of the Annual International Conference on Geological and Earth Sciences* (pp. 8–12).
- Lillibridge, J., Lin, M., and Shum, C. K. (2013). Hurricane sandy storm surge Measured by satellite altimetry. *Oceanography*, 26(2), 8–9.
- Lin, N., K.A. Emanuel, M. Oppenheimer and E. Vanmarcke (2012). Physically based assessment of hurricane surge threat under climate change. *Nature Climate Change*, 2(6), 462–467.
- Liu, K. B., and Fearn, M. L. (2000). Reconstruction of prehistoric landfall frequencies of catastrophic hurricanes in northwestern Florida from lake sediment records. *Quat. Res.*, 54(2), 238–245.
- Liu, K.-b., C. Shen, and K.-s. Louie (2001). A 1,000-Year History of Typhoon Landfalls in Guangdong, Southern China, Reconstructed from Chinese Historical Documentary Records. *Ann. Ass. Am. Geogr.*, 91(3), 453–464.
- Louie, K.-s., and K.-b. Liu (2003). Earliest historical records of typhoons in China. *J. Hist. Geogr.*, 29(3), 299–316.
- Mamo, B., Strotz, L., and Dominey-Howes, D. (2009). Tsunami sediments and their foraminiferal assemblages. *Earth-Science Reviews*, 96(4), 263–278.
- Marcos, M., Tsimplis, M. N., and Shaw, A. G. (2009). Sea level extremes in southern Europe. *JGR:Oceans* (1978–2012), 114(C1).
- McFadgen, B. G., and Goff, J. R. (2007). Tsunamis in the New Zealand archaeological record. *Sediment. Geol.*, 200(3), 263–274.
- Menéndez, M., and Woodworth, P. L. (2010). Changes in extreme high water levels based on a quasi- global tide- gauge data set. *Journal of Geophysical Research: Oceans* (1978–2012), 115(C10).
- Minoura, K., Nakaya, S., and Uchida, M. (1994). Tsunami deposits in a lacustrine sequence of the Sanriku coast, northeast Japan. *Sediment. Geol.*, 89(1), 25–31.
- Minoura, K., F. Imamura, D. Sugawara, Y. Kono, and T. Iwashita (2001). The 869 Jogan tsunami deposit and recurrence interval of large-scale tsunamis on the Pacific coast of northeast Japan. *J. Nat. Disaster Sci.*, 23, 83–88.
- Monecke, K., Finger, W., Klarer, D., Kongko, W., McAdoo, B. G., Moore, A. L., and Sudrajat, S. U. (2008). A 1,000-year sediment record of tsunami recurrence in northern Sumatra. *Nature*, 455(7217), 1232–1234.
- Morton, R. A., Gelfenbaum, G., and Jaffe, B. E. (2007). Physical criteria for distinguishing sandy tsunami and storm deposits using modern examples. *Sediment. Geol.*, 200(3), 184–207.
- Murari, M. K., Achyuthan, H., and Singhvi, A. K. (2007). Luminescence studies on the sediments laid down by the December 2004 tsunami event: prospects for the dating of paleo tsunams events and for the estimation of sediment fluxes. *Current Science*, 92(3), 367–371.
- Nanayama, F., K. Satake, R. Furukawa, K. Shimokawa, B. F. Atwater, K. Shigeno, and S. Yamaki (2003). Unusually large earthquakes inferred from tsunami deposits along the Kuril trench. *Nature*, 424(6949), 660–663.
- Nott, J. (2004). Paleotempestology: the study of prehistoric tropical cyclones--a review and implications for hazard assessment. *Environ. Int.*, 30(3).
- Nott, J. (2011). A 6000 year tropical cyclone record from Western Australia. *Quat. Sci. Rev.*, 30(5–6), 713–722.
- Okal, E. A., et al. (2010). Field Survey of the Samoa Tsunami of 29 September 2009. *Seismol. Res. Lett.*, 81(4), 577–591.
- Paris, R., F. Lavigne, P. Wassmer, and J. Sartohadi (2007). Coastal sedimentation associated with the December 26, 2004 tsunami in Lhok Nga, west Banda Aceh (Sumatra, Indonesia). *Mar. Geol.*, 238(1–4), 93–106, doi: 10.1016/j.margeo.2006.12.009.
- Paris, R., Switzer, A. D., Belousova, M., and others (2014). Volcanic tsunamis: a review of source mechanisms, past events and hazards in Southeast Asia (Indonesia, Philippines, Papua New Guinea). *Natural Hazards*, 70(1), 447–470.
- Phantuwoongraj, S., and M. Choowong (2011). Tsunamis versus storm deposits from Thailand. *Nat. Hazards*, 1–20.
- Rajani, M. B., and Kasturirangan, K. (2013). Sea-level changes and its impact on coastal archaeological monuments: seven pagodas of Mahabalipuram, a case study. *J.Indian Soc. of Rem. Sens.*, 41(2), 461–468.
- Scharroo, R., Smith, W. H., and Lillibridge, J. L. (2005). Satellite altimetry and the intensification of Hurricane Katrina. *Eos, Transactions American Geophysical Union*, 86(40), 366–366.
- Scheitlin, K. N., Elsner, J. B., Malmstadt, J. C., Hodges, R. E., and Jagger, T. H. (2010). Toward increased utilization of historical hurricane chronologies. *JGR:Atmospheres* (1984–2012), 115(D3).
- Small, C. and Nicholls, R.J. 2003, A Global Analysis of Human Settlement in Coastal Zones, *Journal of Coastal Research*, 19(3), 584–599.
- Switzer, A. D., and B. G. Jones (2008). Large-scale washover sedimentation in a freshwater lagoon from the southeast Australian coast: sea-level change, tsunami or exceptionally large storm?, *The Holocene*, 18(5), 787–803.
- Switzer, A. D., K. Pucillo, R. A. Haredy, B. G. Jones, and E. A. Bryant (2005). Sea Level, Storm, or Tsunami: Enigmatic Sand Sheet Deposits in a Sheltered Coastal Embayment from Southeastern New South Wales, Australia. *J. Coast. Res.*, 655–663.
- Switzer, A. D., Bristow, C. S., and Jones, B. G. (2006). Investigation of large-scale washover of a small barrier system on the southeast Australian coast using ground penetrating radar. *Sediment. Geol.*, 183(1), 145–156.
- Turner, R. K., Subak, S. and Adger, W. N. 1996, Pressures, trends, and impacts in coastal zones: interactions between socioeconomic and natural systems, *Environmental Management*, 20(2), 159–173.
- Tuttle, M. P., Ruffman, A., Anderson, T., and Jeter, H. (2004). Distinguishing tsunami from storm deposits in eastern North America: the 1929 Grand Banks tsunami versus the 1991 Halloween storm. *Seismological Research Letters*, 75(1), 117–131.
- Vött, A., Lang, F., Brückner, H., Gaki-Papanastassiou, K., Maroukian, H., Papanastassiou, D., and Zander, A. (2011). Sedimentological and geoarchaeological evidence of multiple tsunamigenic imprint on the Bay of Palairos-Pogonia (Akarnania, NW Greece). *Quat. Int.*, 242(1), 213–239.
- Woodruff, J. D., J. P. Donnelly, D. Mohrge, and W. R. Geyer (2008). Reconstructing relative flooding intensities responsible for hurricane-induced deposits from Laguna Playa Grande, Vieques, Puerto Rico. *Geology*, 36(5), 391–394, doi: 10.1130/g24731a.1.
- Woodruff, J. D., J. P. Donnelly, and A. Okusu (2009). Exploring typhoon variability over the mid-to-late Holocene: evidence of extreme coastal flooding from Kamikoshiki, Japan. *Quat. Sci. Rev.*, 28(17–18), 1774–1785.
- Woodworth, P. L., and Blackman, D. L. (2004). Evidence for systematic changes in extreme high waters since the mid-1970s. *J. of Climate*, 17(6).

- Yalçiner, A., Pelinovsky, E., Talipova, T., and others (2004). Tsunamis in the Black Sea: comparison of the historical, instrumental, and numerical data. *JGR:Oceans* (1978–2012), 109(C12).
- Zhang, K., Douglas, B. C., and Leatherman, S. P. (2000). Twentieth-century storm activity along the US east coast. *Journal of Climate*, 13(10).

# Wind-driven waves in a shallow estuarine lake with muddy substrates: St Lucia, South Africa

Vulindlela Zikhali<sup>†</sup>, Katrin Tirok<sup>‡</sup>, Derek Stretch<sup>†</sup>

<sup>†</sup>School of Engineering  
University of KwaZulu-Natal  
Durban, South Africa  
208501353@stu.ukzn.ac.za

<sup>‡</sup> School of Life Sciences  
University of KwaZulu-Natal  
Durban, South Africa  
Tirok@ukzn.ac.za

School of Engineering  
University of KwaZulu-Natal  
Durban, South Africa  
stretchd@ukzn.ac.za



[www.cerf-jcr.org](http://www.cerf-jcr.org)



[www.JCRonline.org](http://www.JCRonline.org)

## ABSTRACT

Zikhali, V., Tirok, K., Stretch, D., 2014. Wind-driven waves in a shallow estuarine lake with muddy substrates: St Lucia, South Africa. In: Green, A.N. and Cooper, J.A.G. (eds.), *Proceedings 13<sup>th</sup> International Coastal Symposium* (Durban, South Africa), *Journal of Coastal Research*, Special Issue No. 70, pp. 729-735, ISSN 0749-0208.

Wind-waves in shallow lakes or estuaries with muddy substrates can drive sediment re-suspension and cause high turbidity levels that can negatively impact the productivity of photosynthetic organisms. This investigation evaluates the efficacy of a simple semi-empirical model (Young and Verhagen, 1996 : *Coastal Engineering*, 29, 47–78) for predicting the wave characteristics in these systems in order to include their effects in ecosystem models. The southern basin of the St Lucia estuarine lake in South Africa was used for a case study. Average depths are about 1 m with fetches up to approximately 10 km. Substrate materials vary from sandy to muddy with deeper locations predominantly the latter. An array of pressure sensing wave poles was deployed to measure significant wave heights and periods to compare with model predictions. The influence of the wind speed, fetch, fetch-averaged depth, and substrate composition were evaluated. Most of the observed waves were fetch limited during the conditions that prevailed during the two field trips. The results indicate that the model adequately captures the high energy wave events for persistent wind speeds and directions, but that there is considerable variability in its performance generally. Some of this variability can be attributed to difficulties in estimating appropriate fetch and depth parameters for variable winds and in the context of a lake with compound shape and variable bathymetry. There was no clear evidence of significant wave attenuation due to the muddy substrates.

**ADDITIONAL INDEX WORDS:** *wind-driven waves, fetch and depth limitations, muddy substrates, Lake St Lucia.*

## INTRODUCTION

The biological functioning of shallow lakes or estuaries with muddy substrates can be significantly influenced by wind waves that drive sediment resuspension and associated high turbidities. For example high turbidity affects primary production processes (Cloern , 1987) while zooplankton may also be adversely affected with reduced feeding rates and increased mortality rates (Carrasco et al., 2013).

To apply simple quantitative biological models to explore these issues requires a means to estimate wave energy directly from easily accessible parameters such as wind speeds, fetches and depths. For shallow lakes and estuaries the growth of wind-waves are often affected by fetch and/or depth limited conditions. The prediction of wave characteristics under these conditions was addressed by Young and Verhagen (1996) who proposed a semi-empirical model based on an extensive field study at Lake George in Australia. However, Young and Verhagen (1996) did not consider the effects of muddy substrates on the growth of wind-waves, since their case study site had sandy substrates. It is well known that waves can be attenuated by the dissipative effects of induced shear stresses within the fluid-mud layers of shallow systems (e.g. Mehta and Jiang, 1990; Kranenburg et al., 2011; Elgar and Raubenheimer, 2008; Sheremet et al., 2003; Winterwerp et al., 2007; Torres-Freyermouth et al., 2010). Apparently these

effects have not yet been incorporated into simplified semi-empirical models.

Lake St Lucia is a large estuarine lake system located in KwaZulu-Natal, South Africa (Fig. 1). It is part of the iSimangaliso Wetland Park, which was declared a UNESCO World Heritage site in 1999. The area is also a Ramsar wetland of international importance due to its significant role as a biodiversity hotspot (Perissinotto et al., 2013). The shallow lake conditions and muddy substrates make the estuarine habitat particularly susceptible to the effects of high turbidity due to the stirring effects of wind-driven waves. The system is increasingly threatened by increased catchment sediment yields due to land-use changes and land degradation. Similar challenges are faced by many estuarine and lake systems worldwide due to intensive developments of their catchments (e.g. Wolanski, 2007). There is a need to develop models that can be used to understand and evaluate the impacts of these changes, and to manage and mitigate them in the future.

This study aims to contribute towards developing and testing simplified models to investigate the above-mentioned issues. In particular a key question addressed was whether substrate characteristics need to be explicitly included in the model?

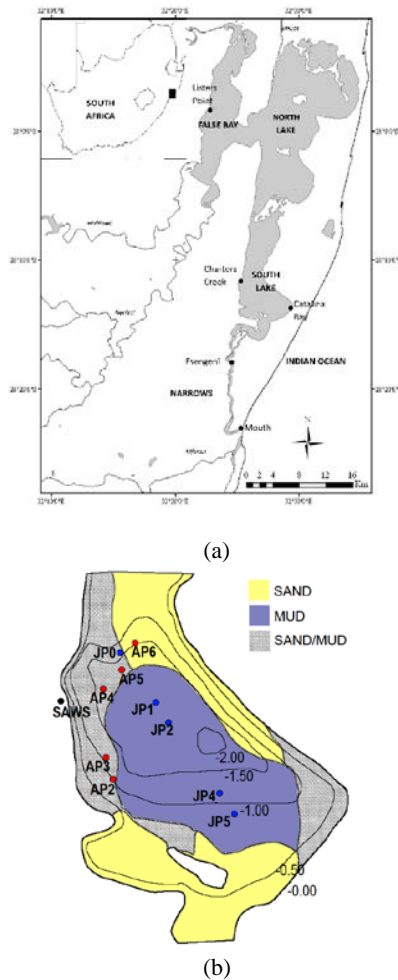


Figure 1. a) Map of St Lucia estuarine lake system on the east coast of South Africa. (b) Detailed map of the southern basin showing bathymetry, substrate distribution, location of wave measuring stations (APx – stations used in April 2013, JPx – stations used in July 2013, for details see Field Measurements), and location of the weather station (SAWS).

## METHODS

### Study Site

The St Lucia lake system comprises three interconnected basins – False Bay, North Lake and South Lake – that are linked to the sea via a 22 km long sinuous channel called the Narrows (Figure 1(a)). The inlet to the system from the sea can close for prolonged time periods due to near-shore littoral transport processes (Lawrie and Stretch, 2011a, b). Tidal effects are present for about 14 km up the Narrows when the inlet is open - the lake itself is not tidal.

The lake has a surface area of approximately 350 km<sup>2</sup> and an average depth of 1.0 m when the inlet is open and when water levels are near the estuary mean water level (EMWL), which is a datum that is 0.25m above sea level. When the inlet is closed the water level can differ strongly from EMWL depending on rainfall, river inflow and evaporation. We measured waves in the lower part of Lake St Lucia South Lake in April and July 2013 (Figure 1(b)). For the period of this investigation, the water level was  $\pm 0.3$  m above EMWL. The lower South Lake has a surface area of

approximately 30 km<sup>2</sup>, extending approximately 6 km from north to south and 5 km east to west. The sediment of lower South Lake shows spatial variability with sandy areas around the edges and muddy area around the deeper center of the lake (Figure 1(b)).

The wind climate is characterised by prevailing north-easterly and south-westerly winds, with north-east winds being dominant in the summer (Perissinotto et al., 2013). These wind directions were characteristic of the strongest winds observed during the course of this investigation. There is a strong diurnal cycle in the wind. Typical wind speeds during the day are 4ms<sup>-1</sup> or higher, whereas during the night wind speeds tend to be below 4ms<sup>-1</sup>. The lighter night-time winds tend to come from the west and are thermally driven land breezes.

### Field Measurements

We measured waves at ten different locations over a total period of 15 days in April and July 2013 using pressure transducers (Figure 1(b)). Each pressure transducer and its digital controller and logger was mounted inside a perforated tube to form a “wave pole” (Figure 2). In April the wave poles were arranged approximately parallel to the main wind directions (north-easterly and south westerly) to provide data for wave growth along a varying fetch. The poles were placed at depths between 1 and 1.7m at positions with a mix of mud/sand sediments. The poles deployed in July were arranged in a way that kept the fetch fairly constant for the north-easterly wind direction and the depth at the poles ranged from 0.9 to 2.1m with mainly muddy sediment. The water depth at each wave pole was measured using a survey staff. This allowed us to gauge the accuracy of average water depth changes derived from the pressure transducers’ measurements.

Each pressure transducer was contained inside an air-tight, flexible plastic bag and attached to the end of an impermeable plastic manometer tube. The flexible plastic bag automatically adjusts for variations in atmospheric pressure so that the transducer measures differential pressures due to water level changes alone. The transducers were statically calibrated to establish the relationship between their voltage output and depth below the water surface. Measured pressures were logged to an SD memory card at a burst sampling frequency of 4Hz for durations of 5 minutes (1200 readings) every 15 minutes. The plastic manometer tube was weighted and the depth at which it was initially set was typically 0.5 m. The pressure transducer (MPX5010) had a range of 10 kPa (1 m of water) and an accuracy of about 0.5%. The output voltage of the sensor (0–5 V) was digitised with 10 bit resolution using an Arduino microcontroller. The electronics and battery power supply were packaged together with the pressure sensor in the waterproof bag installed at the top of the pole.

### Data Analysis

The recorded pressure data were transformed into significant wave heights ( $H_s$ ) for each five minute sampling period. In this procedure, the pressure time series were decomposed into Fourier modes, each with a specific frequency. These modes were individually corrected for attenuation of the pressure with depth according to linear wave theory. An inverse Fourier transform was then used to recreate the actual observed wave heights. The amplitude  $a$  of a surface wave of wavelength  $L$  and period  $T$  can be related to the pressure  $p$  measured at depth  $z$  in water of total depth  $h$  by (e.g. Holthuijsen, 2007)

$$\frac{p}{\rho g} = a \sin(kx - \omega t) \frac{\cosh[k(h+z)]}{\cosh(kh)} \quad (1)$$

with  $k = 2\pi/L$ ,  $\omega = 2\pi/T$ ,  $L = (gT^2/2\pi)\tanh(kh)$ , and where  $\rho$  is the water density and  $g$  is acceleration due to gravity. The significant wave height  $H_s$  can be computed as the average of the highest one third of the wave heights recorded during each five minute sampling period. Other parameters derived from the recorded pressure fluctuations were the peak period and the average water depth.

Significant wave heights smaller than 50mm were excluded from further analysis because the attenuation of the pressure signal from these small waves were not accurately resolved by the pressure transducer.

**Wave Model**

We used a simple semi-empirical model (Young and Verhagen, 1996, YandV henceforth) to predict significant wave heights at the individual wave pole positions based on fetch, average depth over the fetch and wind speed. We then compared the predicted wave heights with the measured wave heights to test the efficacy of the YandV model for Lake St Lucia. Our study site differs from the system used for calibration by YandV by having a smaller surface area and having muddy sediment instead of sandy sediment. The fetch was estimated for each of the pole positions under the different wind directions using Google Earth™ imagery. The average depth over the fetch was estimated using a bathymetry contour map (refer to Hutchison (1974), Figure 1(b)).

Wind speeds and directions were provided by the South African Weather Service, which collects wind data from a weather station located near the western bank of the lake (SAWS in Figure 1(b)) with the anemometer installed at a height of approximately 10 m.

The YandV model is formulated in terms of non-dimensional quantities. The relevant dimensionless depth and fetch from the field measurements were calculated for each five minute data set at each wave pole position. These dimensionless values together with the corrected wind speeds were used as inputs to the model. The dimensionless forms of the wave energy ( $\epsilon$ ), depth ( $d$ ) and fetch ( $x$ ) used for the model are defined by

$$\epsilon = \frac{g^2 \cdot E}{U^4}, \quad \delta = \frac{d \cdot g}{U^2}, \quad X = \frac{x \cdot g}{U^2} \tag{2}$$

YandV suggested a semi-empirical relationship between  $\epsilon$ ,  $\delta$  and  $X$  given by the following equation

$$\epsilon = C_0 \left[ \tanh(C_1 \delta^{0.75}) \tanh\left(\frac{C_2 X^{0.57}}{\tanh(C_1 \delta^{0.75})}\right) \right]^{1.74} \tag{3}$$

Table 1. Asymptotic limits of Equation 10 following YoungandVerhagen (1996).

Conditions	Equation 10
Depth limited: $\chi \rightarrow \infty$	$\epsilon = 1.06 \times 10^{-3} \delta^{2.3}$
Fetch limited: $\delta \rightarrow \infty$	$\epsilon = 1.6 \times 10^{-7} \chi$
$\chi \rightarrow \infty, \delta \rightarrow \infty$	$\epsilon = 3.64 \times 10^{-2}$

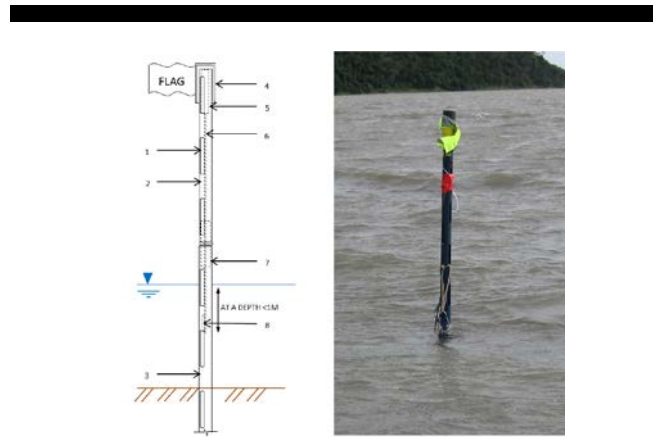


Figure 2. Schematic diagram of the wave pole components. The labelled items are: (1) plastic pole slots; (2) plastic pole; (3) metal base pole; (4) plastic cap; (5) differential pressure transducer device and data logger; (6) plastic manometer tube; (7) connection; (8) weight. A multiparameter sonde containing various sensors (temperature, salinity, pH, DO, turbidity) was attached to selected wave poles during their deployment.

with constants  $C_0 = 3.64 \times 10^{-2}$ ,  $C_1 = 0.493$ , and  $C_2 = 3.13 \times 10^{-2}$ . Equation 10 predicts the wave energy in the limits of both depth and fetch limited conditions and is consistent with results deduced from previous experimental data ().

Due to different characteristics of the boundary layer over land compared to water (Walmsley et al., 1989) wind speeds were corrected according to their direction and fetch over the water to the location of the individual wave poles. Winds measured at the weather station were corrected by a factor  $\Delta R$  as described by YandV, whence

$$U_x = U_i + \Delta R U_i \tag{4}$$

where  $U_i$  is the (measured) reference wind speed prior to crossing the shoreline,  $U_x$  is the wind speed at a fetch  $x$  downwind from the shoreline crossing point, and  $\Delta R$  is a correction given by

$$\Delta R = 0 \quad \text{for } z \geq \delta_i \tag{5}$$

$$\Delta R = \frac{\ln(z/z_0) \cdot \ln(\delta_i/z_{0w})}{\ln(z/z_{0w}) \cdot \ln(\delta_i/z_0)} - 1 \quad \text{for } z < \delta_i \tag{6}$$

where  $z$  is the reference height of the velocity,  $z_0$  is the roughness length over water,  $z'_0$  is the upwind terrestrial roughness length, and  $\delta_i$  is the internal boundary layer height over water given by

$$\delta_i = 0.75 z_0 \left(\frac{x}{z_0}\right)^{4/5} \tag{7}$$

The roughness length over the water  $z_0$  is assumed to vary with wind speed as given by

$$z_0 = A \frac{u_*^2}{g} \quad (8)$$

$$u_*^2 = C_{10} U_{10}^2 \quad (9)$$

$$C_{10} = (0.8 + 0.065 U_{10}) \times 10^{-3} \quad (10)$$

where  $A=0.0185$ ,  $u_*$  is the friction velocity,  $U_{10}$  is the wind speed at a reference height of 10 m, and  $C_{10}$  is a drag coefficient.

After experimenting with various terrestrial roughness lengths appropriate for the case study site ( $\approx 0.5$  m) it was found that the wind correction factor was generally close to unity i.e.  $\Delta R \approx 1$ . For simplicity this value was subsequently adopted as a uniform wind correction for all locations and wind directions.

Once the measured wind-speeds have been corrected for roughness changes, and given the measured fetch and depth parameters at each wave pole and for each wind direction, the significant wave height may be predicted from Equation 10 using the definition  $H_s = 4\sqrt{E}$ . These predicted wave heights can then be compared with the measured wave heights from the wave poles.

## Results

### Measured wave and time series

The range of depths, fetches, and wave heights sampled during the field experiments at each of the wave pole locations (Figure 1(b)) are summarised in Table 2. Maximum fetches were about 10 km and mostly associated with winds from northerly directions. Fetch-averaged depths during the July field trip were generally larger than for the April field trip due to the re-positioning of the wave poles.

Figure 5 shows time histories of water levels, wave heights and wind vectors measured during the two field trips in April and July 2013. There are strong diurnal variations in the wind speed at this location, which are evident in the time series. During the night-time hours wind speeds typically reduce to  $4 \text{ ms}^{-1}$  or less, and comprise of mainly land breezes from the west. Winds greater than  $4 \text{ ms}^{-1}$  generally occur during the day (peaking in the afternoons) and are typically from the south-west or north-east (Figure 5). It is these stronger winds that drive the generation of waves in the lake with significant wave heights typically in the range 200 – 400 mm.

It is evident from figure 5 that waves increase rapidly as the wind increases and also dissipate rapidly once wind speeds reduce again. The increases in wave energy are accompanied by re-suspension of fine muddy sediments that make the water column highly turbid.

In addition to the generation of waves the surface wind stress also drives significant water exchanges between the lake basins that are evident as changes in average water levels in figure 5. When the wind blows from southerly directions water is pushed north in the system and water levels fall in the South Lake, and vice versa for winds from northerly directions. These wind setup processes and their time scales have been described in detail by Schoen et al. (2014); Hutchison and Midgely (1978). Water level changes of up to 400 mm were observed during the field study (Figure 5). During calm periods after high winds the system relaxes towards a state where the water levels across all the basins are equal.

During the April field trip most of the energetic wave events were driven by winds from the south-south westerly direction (Figure 5). The pole arrangement used (Figure 1(b)) means that almost half of the data set experienced similar fetch conditions.

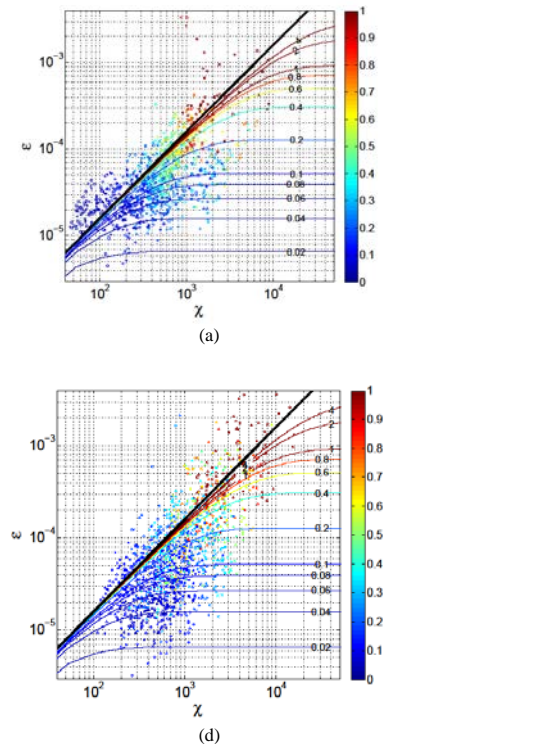


Figure 3. Non-dimensional plots of observed wave energy ( $\varepsilon$ ) versus fetch ( $\chi$ ) for various depths ( $\delta$ , shown colour-coded). Wave energies predicted by the Young and Verhagen (1996) model are shown as lines for comparison with the measurements. (a) April - all data, (b) April -  $\delta < 0.2$ , (c) April -  $\delta > 0.2$ , (d) July - all data, (e) July -  $\delta < 0.2$ , (f) July -  $\delta > 0.2$ .

During the July field trip the strongest winds were more evenly split between the northerly and the southerly directions. Fetches for the southerly winds were generally slightly larger than those for northerly winds for this pole arrangement.

### Comparison with Young and Verhagen model

Scatter plots show general consistency between the measured and modelled wave heights (Figure 4). The model shows some bias towards under prediction of wave heights for small fetches and/or small depths, but its performance improves at intermediate fetch and depth values. However, considerable scatter is evident in the data.

A more detailed comparison between the model and measurements is given in Figure 4 (a) – (b), that show a series of non-dimensional plots of measured wave energy  $\varepsilon$  as a function of fetch number  $\chi$ . Values for the non-dimensional depths  $\delta$  are colour-coded to the data points. Wave energies predicted by the Y and V model for various depth numbers are plotted for comparison with the measurements, and indicate which conditions were fetch or depth limited in terms of wave growth. It is evident that most of the measurements were in fetch-limited or transitional conditions according to the model, although there are also significant occasions that experienced depth-limited wave growth. The trends in the measurements are broadly consistent with the

Table 2: Range of depths at sampling positions, average depths, significant wave heights and fetches observed during field trips. The average depth is the depth at each sampling position averaged over the fetch (which varies with the wind direction).

SAMPLING LOCATIONS (REFER FIG. 1(b))	POLE DEPTH (mm)		FETCH AVG DEPTH (mm)		FETCH (m)		Hs (mm)	
	min	max	min	max	min	max	min	max
<i>April Field Trip</i>								
AP2	1540	1850	760	1680	660	11600	10	310
AP3	1420	1730	810	1650	50	11000	10	350
AP4	1090	1380	930	1630	600	9600	10	330
AP5	890	1170	930	1630	1000	9000	10	310
AP6	710	990	890	890	1200	9300	10	270
<i>July Field Trip</i>								
JP0	820	1070	540	540	700	10200	10	240
JP1	1640	2160	890	890	650	10300	10	370
JP2	1420	2330	950	950	1400	9700	10	380
JP4	1970	2310	570	570	1700	7500	10	410
JP5	1920	2180	350	350	1800	10300	10	350

model but again show considerable variability as is evident in the scatter of the data. There are a significant number of measurements that lie outside the predicted bounds i.e. the measured wave energies are lower than predicted by the model.

Given the scatter in the data it is not possible to unambiguously attribute these effects to wave attenuation associated with muddy substrates, but that is one possible explanation. Figure 4 (a) and (b) reveal that the model tends to consistently overestimate the wave energy for small fetch numbers  $X < 100$  and depth numbers  $D < 0.1$ . These data are from the April field trip and come from the wave poles near the western side of the basin (AP2, AP3 – see Figure 1(b)), and for wind from the south/south-west. Samples of measured and modelled significant wave height time series indicate that the major wind-wave events are generally well captured by the model when the wind comes from specific directions (Figure 5). When the wind speed and/or direction changes the model can produce large prediction errors. This seems to be associated with estimation of the appropriate fetch and depth parameters that are applicable during those periods.

## Discussion and Conclusion

In this study we have tested the application of the YandV semi-empirical model for predicting wave heights in a shallow estuarine lake with compound shape and variable bathymetry. A notable difference from previous applications of the model is the substrate's composition at our case study site. St Lucia comprises large areas with soft, unconsolidated muddy substrates, particular in the deeper locations, while previous case studies have focussed mainly on systems with sandy substrates. This difference was a key motivation for the present study, namely to evaluate how muddy substrates affect wind-wave predictions from simple models.

The comparison between modelled and measured significant wave heights showed broad consistency with considerable variability in the results. There were examples of both significant underestimation as well as overestimation of wave energy, but the reason(s) for these errors are difficult to isolate. Some of the model underestimation seems to be associated with short fetch

and/or shallow water, which is consistent with findings of previous investigators (e.g. Young, 1997).

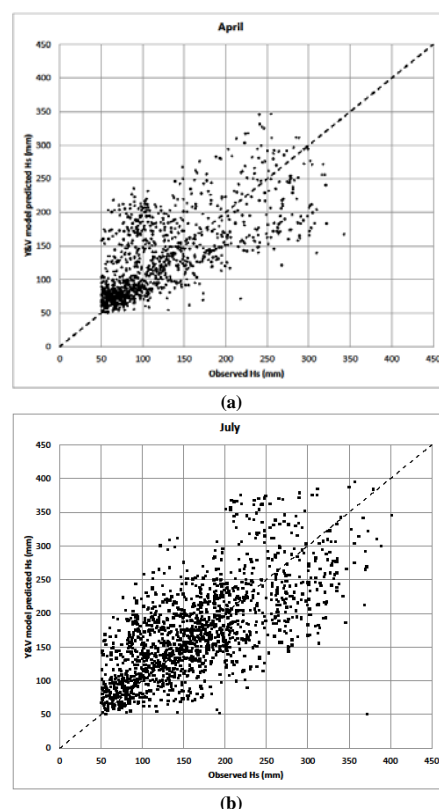


Figure 4. Wind vector and water level time series from the (a) April field trip, pole AP3; (b) July field trip, poles JP4 and JP5 (concatenated). The pole positions are shown in (Fig 1(b)). Wind measurements (uncorrected) are from the weather station shown as location SAWS in Fig 1(b).

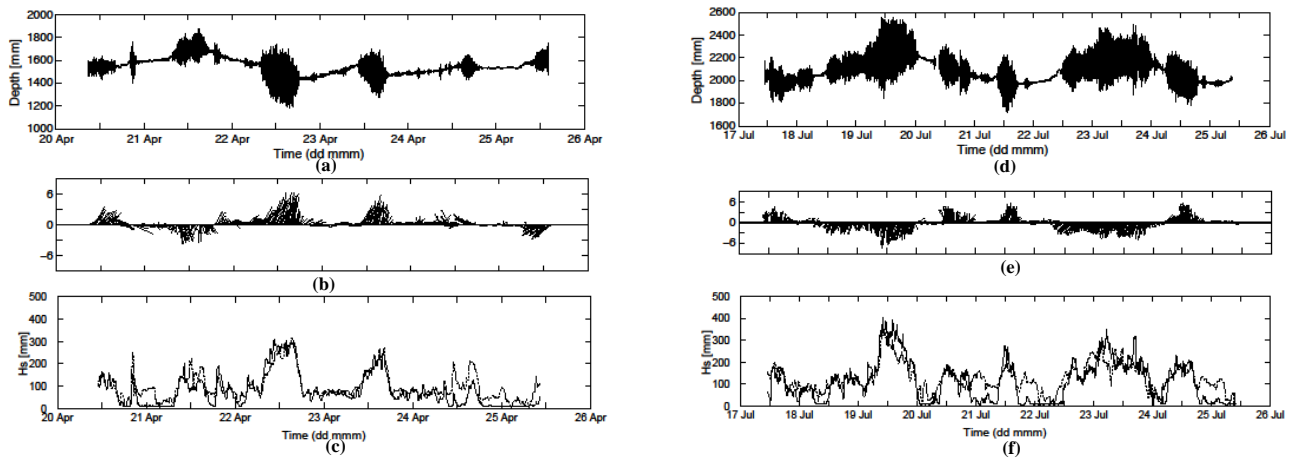


Figure 5: Water level (a), wind vector (b) and time series (c) from the April field trip, pole AP3; (d), (e) and (f) are corresponding data sets from the July field trip, poles JP4 and JP5 (concatenated). The pole positions are shown in (Fig 1(b)). Wind measurements (uncorrected) are from the weather station shown as location SAWS in Fig 1(b). Sample time series show measured (solid lines) and predicted (dashed lines) wave heights for wave poles (c) AP5; (d) JP4 and JP5 (concatenated).

No clear evidence of wave attenuation due to the muddy substrates was evident from the data. These effects, if present, may have been masked by scatter in the results. The compound shape of the lake system means that the estimation of the applicable fetch and depth parameters was difficult to do and is prone to errors that may explain much of the variability in the data and model predictions. For example small changes in wind direction can make large differences in the estimated fetch and associated fetch-averaged depths. Furthermore the method of correcting the wind from a single local terrestrial weather station to account for roughness changes over the water is also difficult to do accurately and can also significantly impact the model predictions.

If simple semi-empirical models such as the Young and Verhagen model are to be used to model wind-wave generation in shallow, muddy systems with complex geometry, our results suggest that considerable care is required to accurately specify insitu wave-generation parameters such as wind speed, direction, fetch, and fetch-averaged water depth. The simultaneous measurement of insitu wind speeds and directions for calibration of the wave-generation model may reduce some of these uncertainties. However, alternative modelling approaches, such as the 2D spectral wave model SWAN (Booij et al., 1999; Winterwerp et al., 2007; Kranenburg et al., 2011), can account for complex lake geometry and bathymetry in a natural way and may therefore be preferable in these cases.

## ACKNOWLEDGEMENTS

We thank the following: iSimangaliso Wetland Park Authority for supporting this research; SA National Research Foundation and SANPAD for funding; Caroline Fox for field work support, Zane Thackeray for the data loggers; Henk-Jan Verhagen for his MATLAB script; Julia Schoen for help with field work and data analysis; Sydney Mpungose and Logan Govender for fabricating field equipment.

## LITERATURE CITED

Booij, N., Ris, R. C., and Holthuijsen, L. H. (1999). A third-generation wave model for coastal regions. Part I: Model

description and validation. *Journal of Geophysical Research*, 104(C4), 7649 – 7666.

- Carrasco, N., Perissinotto, R., and Jones, S. (2013). Turbidity effects on feeding and mortality of the copepod *Acartiella natalensis* (Connell and Grindley, 1974) in the St. Lucia Estuary, South Africa. *Journal of Experimental Marine Biology and Ecology*, 45–51.
- Cloern, J. (1987). Turbidity as a control on phytoplankton biomass and productivity in estuaries. *Continental Shelf Research*, 7, 1367–1381.
- Elgar, S., Raubenheimer, B. (2008). Wave dissipation by muddy seafloors. *Geophysical Research Letters*. 35, 1–5.
- Holthuijsen, L. (2007). *Waves in Oceanic and Coastal Waters*. New York: Cambridge University Press.
- Hutchison, IPG., (1974). *St Lucia Lake and estuary - hydrographic data*. Report No. 3/74, Hydrological Research Unit, University of the Witwatersrand, Johannesburg, South Africa.
- Hutchison, IPG and Midgely, DC., (1978). Modelling the water and salt balance in a shallow lake. *Ecological Modelling*, 4, 211–235.
- Kranenburg, W. M., Winterwerp, J. C., de Boer, G. J., Cornelisse, J. M. and Zijlema, M. (2011). SWAN-Mud: Engineering Model for Mud-Induced Wave Damping. *Journal of Hydraulic Engineering*, 137, 959 – 975.
- Lawrie, R.A. and Stretch, D.D., (2011a). Anthropogenic impacts on the water and salinity budgets of St Lucia estuarine lake in South Africa. *Estuarine, Coastal and Shelf Science*, 93, 58 – 67.
- Lawrie, R.A. and Stretch, D.D. (2011b). Occurrence and persistence of water level/salinity states and the ecological impacts for St Lucia estuarine lake, South Africa. *Estuarine, Coastal and Shelf Science*, 95, 67–76.
- Mehta, A., and Jiang, F. (1990). *Some field observations on bottom mud motion due to waves*. Florida: South Florida Water Management District.
- Perissinotto R, Stretch, DD, Taylor, RH (eds), 2013. *Ecology and Conservation of Estuarine Ecosystems: Lake St. Lucia as a Global Model*. Cambridge University Press.
- Schoen, J, Stretch, DD and Tirok, K., (2014). Wind-driven circulation in a shallow estuarine lake: St Lucia, South Africa. *Estuarine, Coastal and Shelf Science*, submitted.



- Sheremet, A., Stone, G.W. (2003). Observations of near shore wave dissipation over muddy sea beds, *Journal of Geophysical Research*, 108, 1–11
- Stretch, DD, Chrystal, CP, Chrystal, RA, Main, CM and Pringle, JJ., (2013). Estuary and Lake Hydrodynamics. In: Perissinotto R, Stretch, DD, Taylor, RH (eds) *Ecology and Conservation of Estuarine Ecosystems: Lake St. Lucia as a Global Model*. Cambridge University Press.
- Torres-Freyermuth, A., and Hsu, T.-J. (2010). On the dynamics of wave-mud interaction: A numerical study. *Journal of Geophysical research*, 115, 1–18.
- Walmsley, J.L., Taylor, P.A., and Salmon, J.R. (1989). *Simple guidelines for estimating wind speed variations due to small-scale topographic features*. Climatological Bulletin, 23, 3-14
- Winterwerp, J. C., de Graaff, R., Groeneweg, J., and Luijendijk, A. (2007). Modelling of wave damping at Guyana mud coast. *Coastal Engineering*, 54 (3), 249 – 261.
- Wolanski, E., 2007. *Estuarine Ecohydrology*. Netherlands: Elsevier.
- Young, I., and Verhagen, L. (1996). The growth of fetch limited waves in water of finite depth. Part 1. Total energy and peak frequency. *Coastal Engineering*, 29, 47–78.
- Young, I. (1997). The growth rate of finite depth wind-generated waves. *Coastal Engineering*, 32, 181-195

# Beachrock facies variability and sea level implications: a preliminary study

Christopher S. Kelly<sup>†</sup>, Andrew N. Green<sup>†</sup>, J. Andrew G. Cooper<sup>†‡</sup>, Errol Wiles<sup>†</sup>

<sup>†</sup>Geological Sciences  
School of Agriculture, Earth and  
Environmental Sciences  
University of KwaZulu-Natal, Westville,  
South Africa  
[christopher.kelly@fulbrightmail.org](mailto:christopher.kelly@fulbrightmail.org)  
[greenal@ukzn.ac.za](mailto:greenal@ukzn.ac.za)  
[eawiles@yahoo.com](mailto:eawiles@yahoo.com)

<sup>‡</sup>School of Environmental Sciences  
Centre for Coastal and Marine Research  
University of Ulster  
Coleraine, UK  
[jag.cooper@ulster.ac.uk](mailto:jag.cooper@ulster.ac.uk)



[www.cerf-jcr.org](http://www.cerf-jcr.org)



[www.JCRonline.org](http://www.JCRonline.org)

## ABSTRACT

Kelly, C.S., Green, A.N., Cooper, J.A.G. and Wiles, E. 2014. Beachrock facies variability and sea level implications: a preliminary study. In: Green, A.N. and Cooper, J.A.G. (eds.), *Proceedings 13<sup>th</sup> International Coastal Symposium* (Durban, South Africa), *Journal of Coastal Research*, Special Issue No. 70, pp. 736-742, ISSN 0749-0208.

In spite of the worldwide abundance of beachrocks and their acknowledged utility as an indicator of former sea level position, some studies have expressed doubt as to their position of cementation on paleo shorelines. These criticisms are not, however, coupled with nuanced sedimentological studies of beachrocks. Instead, few beachrock studies acknowledge any facies and therefore disregard important signatures of the depositional environment and, consequently, utility as paleo sea level indicators. This study presents detailed sedimentological descriptions and interpretations from two beachrock localities along the subtropical, microtidal, wave-dominated eastern coastline near Durban, South Africa. The outcrops record the migration of a paleo inlet and deposition in sub, inter, and supra tidal environments. Understanding the inferred depositional environment, and observed stratigraphic relationships between various beachrock facies is critical to teasing out the local evolution of shoreline and relative sea level. The outcrops studied here record multiple episodes of Holocene sea level rise and fall.

**ADDITIONAL INDEX WORDS:** beachrock, facies, sea level, South Africa

## INTRODUCTION

Beachrocks are common features of tropical and subtropical coastlines. They exhibit diverse sedimentological and morphological characteristics (Vasdoukas *et al.*, 2007). Beachrocks form at or near mean sea level, due to cementation of clasts by calcium carbonate (High-Magnesian Calcite or Aragonite) in the vadose/phreatic zone of the intertidal zone (e.g. Vasdoukas *et al.*, 2007). They have important implications for coastal evolution by preferentially preserving shorelines (Cawthra, 2012; Green *et al.*, 2014) and modifying shoreline dynamics (Cooper, 1991). In microtidal settings beachrocks have been particularly useful in constraining former sea level positions (Ramsay, 1995; Ramsay and Cooper, 2002; Desruelles *et al.* 2009; Cooper, 2011, Vacchi *et al.* 2012). Some concerns, however, have been expressed regarding the reliability of these features as sea-level indicators due to the often diachronous nature of their cementation, the range in thicknesses in relation to the known tidal range and the argument that they may also be supratidal in origin (Kelleat, 2006). Most authors implicitly dismiss or under-describe the facies variations that may occur within beachrocks and superimpose this term broadly on all rocks formed at or near

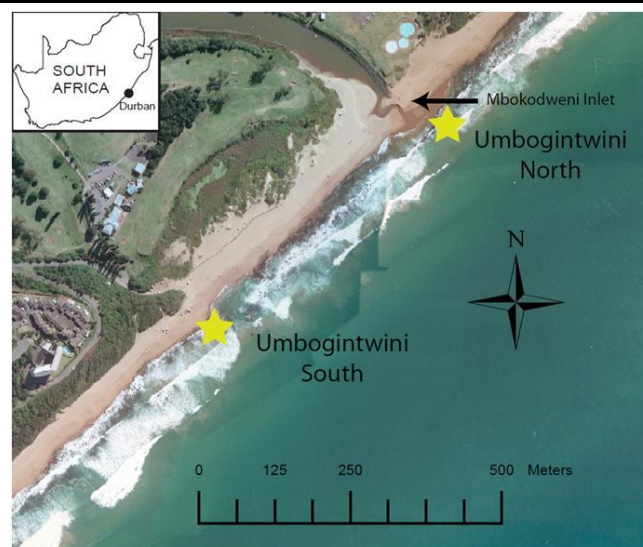


Figure 1. The two study sites from the east coast of South Africa. Umbogintwini North (30.0089° S, 30.9368° E) and South (30.0118° S, 30.9329° E) are denoted by the yellow stars. The study area is approximately 19.5 km south of Durban.

DOI: 10.2112/SI70-124.1 received 08 November 2013; accepted 21 February 2014.

© Coastal Education & Research Foundation 2014

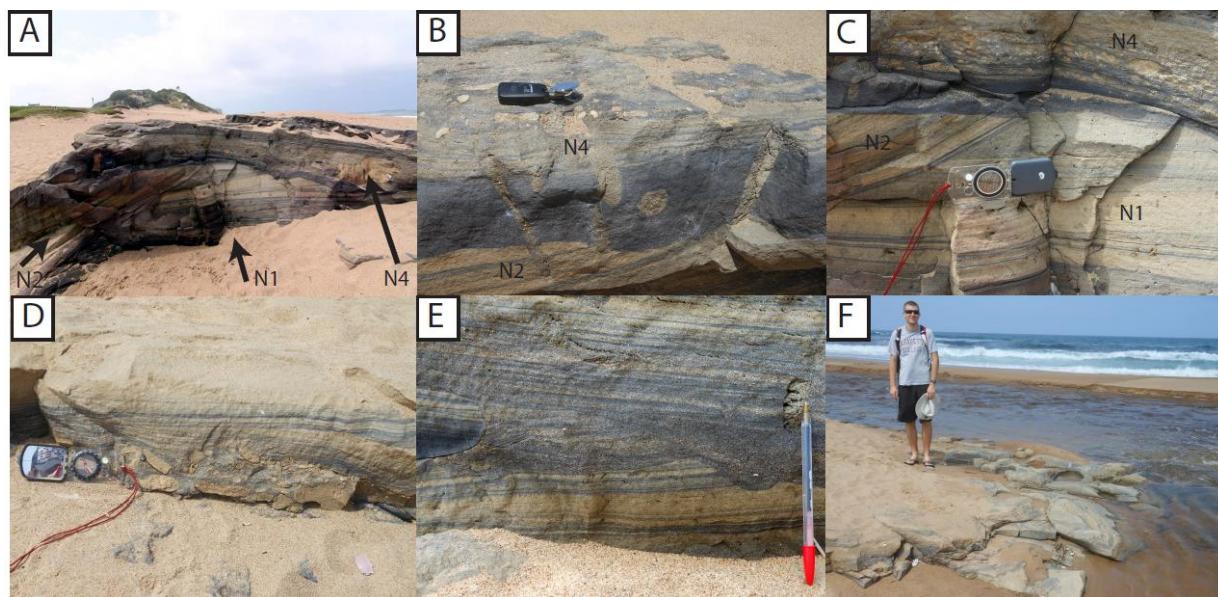


Figure 2. Beachrock units at Umbogintwini North (A-F). **A.** Dip section of Umbogintwini North. Note the erosional surface marking the contact between planar cross bedded sandstone of Facies N1 and overlying steeply dipping Facies N2. **B.** The erosional contact between Facies N2 and N4 with overlying heavy mineral layer and sandy infills of crab burrows (Facies N4). Note the intraformational beachrock and pebbles included as larger clasts. **C.** The contacts between Facies N1, N2, and Facies N4. Note the steeply dipping trough cross bedding of Facies N2 as an inlet migration indicator. **D.** Seaward imbricated pebbles at the base of Facies N4 and overlying antidunes. **E.** Landward oriented antidunes truncating seaward- dipping heavy mineral laminae of Facies N4. **F.** Upper surface of Facies N4 potholed to seaward

mean sea level by carbonate diagenesis. This may be the result of the variability within beachrocks worldwide (Voudoukas *et al.*, 2007) and the seemingly less diverse sedimentary structures preserved in more temperate occurrences of beachrock (Vacchi *et al.*, 2012; Kelletat, 2006; Knight, 2007) Despite the potential for detailed sedimentological description and interpretation from beachrocks in subtropical settings (Caron, 2011), relatively little attention has been given to the nature of the sedimentary facies preserved and their original environment of deposition. This paper investigates a series of beachrocks on the east coast of South Africa that exhibit major facies variability.

## REGIONAL SETTING

The east coast of KwaZulu-Natal South Africa is predominantly a microtidal, wave dominated coastline (Davis and Hayes, 1984; Davis, 1964; Schumann and Orren, 1980). The Quaternary coastal geology surrounding Durban is mainly comprised of Pleistocene-Holocene aged calcareous arenites (Krige, 1932; McCarthy, 1967). These abut a series of rubified palaeo-dune sands that comprise an ancient dune complex of suspected Mio-Pliocene age, termed the Berea Ridge (Krige, 1932; McCarthy, 1967). The Berea Ridge forms a ~ 100 km long coast-parallel ridge that in many instances extends all the way to the shoreline where it is exposed amidst younger Holocene dune sands. The calcareous arenites around Durban have been described by several authors (Cooper and Flores, 1991; Cooper and Liu, 2004; Cawthra, 2012) and are considered to represent the intertidal and supratidal cementation of beachrock and aeolianite respectively.

This paper examines two such outcrops from the East coast of South Africa at Umbogintwini, approximately 19.5 km south of Durban (Figure 1) (Jukes, 1976). The sites are spaced approximately 500 m from each other, situated on either side of

the modern Mbokodweni Estuary, a small, temporarily-open closed estuary (Figure 1).

## OBSERVATIONS

The sedimentary facies for both Umbogintwini North (Figure 2) and South (Figure 3) are described in terms of their sedimentary features and stratigraphic relationships. Facies of each site are described below.

### Umbogintwini North

The exposed portion of outcrop at Umbogintwini North is approximately 30m long and 10 m wide, preserved under the sand of a contemporary barrier beach. Presently, the Mbokodweni inlet abuts the outcrop. Historical literature (Jukes, 1976) from Umbogintwini South and recent aerial photography (Google Earth), however, show that beach cover and inlet position are in perpetual flux. The position of the modern inlet, and even the degree of exposed beachrock, is ephemeral.

#### Facies N1

This facies is a flat lying to very shallowly dipping planar cross-bedded medium sandstone (Figure 2a). Cross beds dip to the northeast and southwest, the laminae of which are marked by heavy mineral lags. These are truncated by isolated J-shaped sandy burrows (*Psilonichnus* ichnofacies) (Figure 2b). The upper surface of the unit is marked by a strongly erosional boundary that truncates the foresets of Facies 1N (Figure 2a). This surface dips landwards at 30° forming a broad coast-perpendicular scour depression.

**Facies N2**

Sandstone with high-angle (25°) trough cross beds infills the lower scoured surface. The trough cross-beds are marked by abundant heavy mineral laminae that dip to the south-southwest (Figure 2c). The unit is 50 cm thick and has a notable absence of gravel or shell debris. Facies N2 is truncated laterally to the north by Facies 3.

**Facies N3**

This facies comprises high angle, planar cross bedded medium sandstone. Bedding planes are marked by heavy mineral laminae that dip to the east at 20° (Figure 2c). Isolated burrows are present. The unit is <40 cm thick and pinches to the north forming a lens like structure. Facies N3 is in turn truncated by a well-defined erosional surface, undulating along strike to form a series of runnels, each approximately 15-20 cm wide and 10 cm deep. This surface itself dips seaward at approximately 15-20 degrees.

**Facies N4**

This Facies rests on an erosional surface, and its base comprises a 10-20 cm-thick heavy mineral horizon of almost pure heavy minerals interspersed with cobbles to small boulders of intraformational beachrock (Figure 2b, c, and d). This unit is heavily bioturbated, burrows occurring as sandy, quartz-rich infills of material derived from the upper unit (*Skolithos* ichnofacies). The basal surface is marked by smaller cobbles and pebbles in a heavy mineral matrix. On the basal erosion surface, pebbles are seaward imbricated with long axis in the direction of current flow and grade into a crudely planar bedded pebble horizon (Figure 2d). Gravel clasts decrease in frequency with stratigraphic height, with occasional isolated shell debris evident in this horizon. The upper portions of Facies 4 are marked by seaward dipping heavy mineral laminae, some of which are truncated by a series of antidunes that overlie the pebble clasts (Figure 2e). Antidunes grade into smaller scale, rippled trough cross-sets. The upper surface of the outcrop is potholed to seaward (Figure 2f).

**Umbogintwini South**

Beachrock at Umbogintwini South is exposed in a 30 m outcrop, thinning to the south to just 5-10 meters, and stretching 100 m south. There is undoubtedly more beachrock buried underneath several meters of sand to both the north and south of the outcrop. Jukes (1976) described a bone-bearing beachrock just seaward of this study site temporarily exposed in the wake of an intense storm in 1966. He also discovered intact fossilized crabs in some of the burrows preserved in now-buried beachrock at the same locality.

**Facies S1**

This basal facies is a >2m thick, planar laminated fine to medium sandstone with occasional large sigmoidal trough cross-beds (Figure 3a). The planar laminations dip seawards at 4° and are marked by laminae scale heavy mineral partings. Several heavy mineral-rich foresets converge tangentially to seaward forming a thick seaward-pinching horizon (Figure 3b). Some small antidunes are preserved in dip section. This layer is truncated by several sand-filled sub-horizontal burrow structures (*Thalassinoides* ichnofacies). The upper surface of this unit is truncated by a landward dipping 9° erosional surface with a well-developed heavy mineral lag (Figure 3c). This erosional surface is most prominent moving seaward in downdip section.

**Facies S2**

This comprises a series of steeply both landward and seaward dipping trough cross beds with 20 cm thick cosets, dipping at approximately 20° (Figure 3c). Each set is marked by gritty to very coarse sand horizons in an overall medium sand dominated succession. In strike section, Facies S2 forms a lens-like unit within Facies S1.

**Facies S3**

Overlying Facies S2, with an erosional contact is Facies S3, a <20 cm thick flat-lying, finely planar laminated medium to fine sandstone (Figure 3d). Occasional heavy mineral layers are evident.

**Facies S4**

This is a thin, <50 cm thick, veneer of trough cross-bedded, pebbly medium sandstone (Figure 3d). The pebbles comprise bioclasts including bivalves and oysters (*Crassostrea* sp.), occasional intraformational calcareous arenite clasts, and well-rounded dolerite (Figure 3e). The trough cross-bed sets vary in thickness (between 5-20 cm) and dip both seaward and landward.

**Facies S5**

This consists of re-cemented blocks of Facies S1 and 3S. Blocks are slabby (0.3 m x 1 m x 1 m) and appear to have collapsed and have been subsequently re-cemented onto the outcrop (Figure 3e). The contact itself forms a stylolite core where the blocks have sutured to the underlying platform, in addition to a thin coating of mixed bioclastic and pebble rich gully-fill (Figure 3d). This takes the form of a loosely consolidated and crudely bedded conglomeritic veneer, onlapping the sutured contact (Figure 3e).

**Facies S6**

Facies S6 includes an alongshore-oriented gully fill that extends for over 100 m (Figure 3f). The fill is a polymict conglomerate of pre-existing cobbles and small boulders of serpulid bioherms, mixed whole shells of non-life position oysters (*Saccostrea* sp.), cobbles of beachrock, arkosic sandstone, dolerite and sparse shale pebbles. These components rest in a very poorly sorted fine sand to grit matrix.

**Facies S7**

This occurs as a thin drape of rhizolithic, poorly consolidated, fine sandstone (Figure 3g). Facies S7 is mixed with red sands of the Berea Ridge, against which the succession onlaps, that have cascaded via the processes of slope creep and wash. The surface of the outcrop of Facies S6 and Facies S7 is marked by a series of small (20 cm diameter, 10 cm depth) potholes that have not been infilled (Figure 3h).

**DISCUSSION****Northern study site interpretations**

Given the planar cross-bedded sand together with the heavy mineral laminae and *Psilonichnus* ichnofacies, we interpret Facies 1 as being deposited in the swash zone. The bidirectional upper flow regime planar sets are in keeping with swash runup and backwash, marked by thin lags of heavy minerals in the intertidal zone (Reineck and Singh, 1986). Facies N2 and Facies N3 are interpreted as inlet facies that record both northward and southward migration of the inlet.

The large scale scour geometry and steeply dipping cross-sets of the scour fill are akin to records described by Reddering (1983) for the migration of microtidal inlets.

In describing the mesoscale migration of inlets, Seminack and Buynevich (2013) show steeply dipping sigmoidal-oblique foresets overlying channel lag facies in a broad "cut-and-fill" structure. The abrupt basal contacts observed also resemble those previously described in the inlet facies models of Fitzgerald *et al.* (2012).

The prominent erosional surface that truncates the inlet migration sequence represents an increasing energy regime associated with the deposition of Facies N4; this interpretation is supported by the overlying thick heavy mineral accumulations, seaward imbricated pebbles, upper flow regime planar bedding and antidunes. The most commonly observed occurrences of modern antidunes on the foreshore are in the swash zone (Hayes *et al.*, 1972; Hayes, 1976). Broome and Komar (1979) found that the formation of "backwash ripples" in the swash zone, instead of mirroring stream antidunes, is initiated by supercritical backwash flow colliding with the subcritical wave bore and undergoing an hydraulic jump. In gravelly microtidal settings, gravel imbrication in the swash zone is attributed to the forces of entrainment of blade-shaped gravel clasts via swash and winnowing of spherical gravel via backwash (Postma and Nemeč, 1990). When extrapolated to pebble-sized clasts on a sandy beach, energy requirements increase, although the process itself is similar, and

consequently the only likely zone of deposition is the swash zone. Thus, the facies assemblages of this unit are characteristic of storm-deposited antidune sequences in the swash zone as neither the process of massive scale winnowing nor pebble imbrication are typical of a normal fair-weather swash regime. As such, these provide a reliable indicator of the palaeo-swash zone in a microtidal setting.

### Southern study site interpretations

The predominant planar cross-bedding structures, *Thalassinoides* ichnofacies and isolated antidunes suggest deposition of Facies S1 in a swash-dominated intertidal environment. The antidunes similarly represent occasions of storminess when flows reached supercritical levels (See Facies N4 Discussion); the heavy mineral layers are associated with current winnowing during the build-up, development, and decay of, these bedforms.

The trough cross-bedded and coarser components of the overlying Facies S2 are representative of a longshore trough associated with a low tide terrace at a shallow subtidal shoreline position. This unit is well-established in sedimentary literature and steeply dipping, coarse sand deposits, and trough cross-bedding, are classic markers of the longshore trough facies (Hunter *et al.*, 1979 and Greenwood and Mittler, 1985).

Facies S3 is interpreted as a backbeach unit.

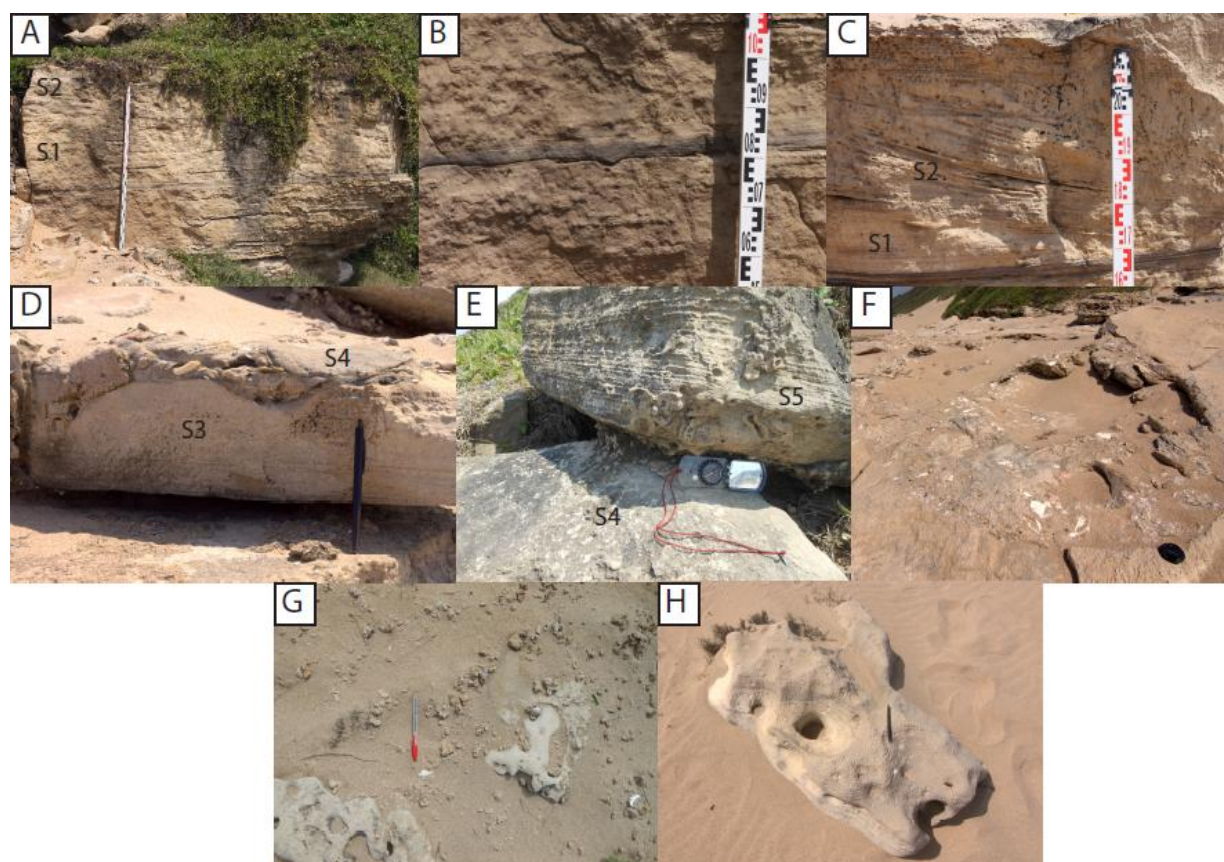


Figure 3. Outcrop photographs from Umbogintwini South (A-H). **A.** Facies 1 truncated by an erosional surface on which Facies S2 occurs. **B.** Seaward-pinching heavy mineral-rich laminae in Facies S1. **C.** Erosional contact between Facies S1 and trough cross bedded Facies S2. **D.** Facies S3 flat-lying planar laminated sandstone and overlying bioclastic gully-fill of Facies S5. **E.** Re-cemented Facies S5 collapsed blocks with stylolite-core cement of bioclastic and pebble composition attached to Facies S4, a bioclast-rich, trough cross bedded medium sandstone. **F.** Polymict conglomeratic gully fill (Facies S6) comprised of serpulid bioherms, *Saccostrea* sp. oysters, beachrock cobbles and pebbles. **G.** Loosely consolidated rizolithic fine sandstone of Facies S7. **H.** Between Facies S6 and S7 potholes occur that have not been infilled.

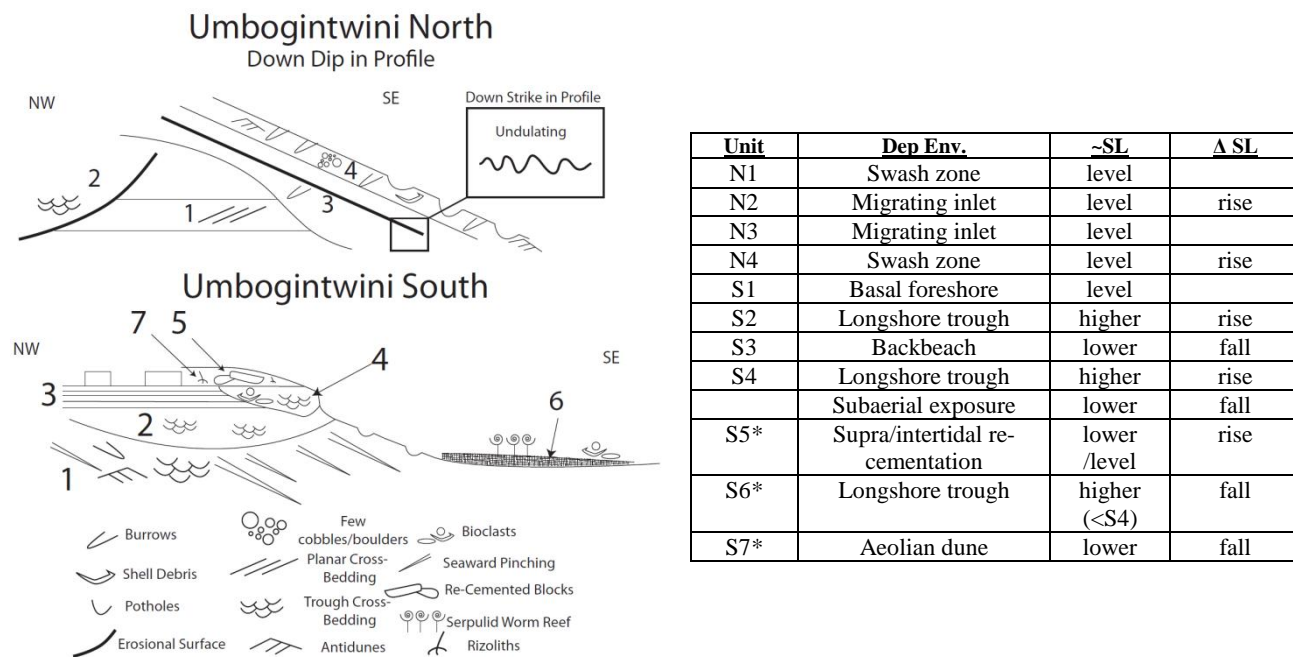


Figure 4. Schematic figure depicting the stratigraphic relationships, sedimentary structures, and basic geometry of the beachrock facies, and table summarizing depositional interpretations for each facies along with inferred relative sea level position. Chronology for the starred facies is not constrained. Abbreviations: Depositional Environment (Dep Env.), SL (sea level), and change in (Δ)

The flat-lying, planar bedded sand and the reduced presence of heavy minerals suggests a higher position up the shore profile with fewer high energy events. This unit is similar to the backbeach facies reported by Ramsay and Mason (1990) at Sodwana Bay 1, ~300 km north of Durban.

We interpret the trough cross-bedding of Facies S4 to represent conditions produced by 3-D barform migration in a subtidal longshore trough depositional environment. Bioclastic debris were likely derived from the reworking of bioherm features to seaward, together with the incorporation of dolerite pebble ejecta from the palaeo-inlet and reworking of intraformational beachrock.

Facies S5 (re-cemented blocks of older facies), seems to represent a previously unrecognised beachrock facies. Additionally, the cementation style is unique to sea level position (an *intertidal* gully fill), and, as such, has remarkable potential in identifying palaeo-shoreline position.

Facies S6 is comparable with the longshore runnel complex of Cooper and Flores (1991). The inclusion of coarse material as rip up clasts of whole serpulid reef, pebbles of reworked Facies S1-S4S and the inclusion of non-life-position oyster clasts suggest storm deposition and subsequent winnowing by longshore currents in the shallow intertidal zone to leave a lag. The scoured runnel morphology lends further credence to this interpretation. The rizo-lithic nature of Facies S7 points to deposition by an aeolian dune. Similar facies were documented by Cooper and Flores (1991) in the area and signify a regional phase of dune building.

### Local sea level history

Our interpretations of depositional environments in light of the microtidal setting of the coastline permits an interpretation of relative sea level fluctuations during the Holocene period. These

are described in figure 4, a schematic of the two outcrops in section and the relative fluctuations in sea level for each facies.

### Umbogintwini North

During the deposition of Facies N1 in the swash zone, sea level was approximately level with the modern position of the unit. The two migrating inlet facies, Facies N2 and N3, potentially record a shifting base level and consequent change in sea level. The contact between the intertidal Facies N1 and inlet Facies N2 marks the base of the inlet channel which incised to base level. Sea level thus rose from the time of deposition of Facies N1 to Facies N2. The transition from Facies N2 to Facies N3 marked the southward and seaward migration of the inlet, evidenced by its overall orientation. This configuration can be explained by changing longshore sediment supply that caused the reconfiguration of the inlet (e.g. Cooper, 1989; Green *et al.*, 2013). The later transition to the swash zone of Facies N4 implies a rise in sea level and translation of the shoreline over the inlet sequence.

### Umbogintwini South

Sea level would have been at approximately the elevation of the basal foreshore Facies S1 at the time of its deposition. From the time of cementation of Facies S1 to S2, sea level had risen, as evidenced by the imposition of a subtidal longshore trough with an erosion surface truncating the lower unit. The along-strike depression formed in this erosional surface is interpreted as a rip channel, and the coarser material as the infill deposit. This is also consistent with rising sea levels. This phase of deposition was followed by a fall in sea level marked by the deposition of Facies S3 in the backbeach. Sea levels then rose again, causing an additional longshore trough to be superimposed over Facies S3

and infilled by the bioclastic-rich Facies S4. The inclusion of reworked beachrock, inlet pebbles, and bioclasts implies a lengthy period of shoreline stability during the deposition of Facies S4.

A sea level low was likely to have followed this period, exposing the previously cemented facies and causing the collapse of the blocks of Facies S2. The stylolitic contacts between these clasts would have initially developed in the supratidal environment where the blocks had collapsed and been shifted into position by possible wave activity (e.g Reddering, 1988) with a later cementation phase as intertidal gully fill once sea level had risen to that elevation. At the point of deposition of Facies S6, sea level would have been at a relatively higher position, but lower than that experienced during the time of deposition of Facies S4, due to Facies 4's similar depositional environment but higher vertical elevation. A key indicator constraining the age disparity between Facies S6 and the stratigraphically higher complex of Facies S4 and S5, is an unfilled pothole surface between the two. The unfilled nature of the potholes also suggests that sea level never subsequently reached this point. Finally, the aeolian Facies S7 was deposited at a time of lower relative sea level than Facies S4, and probably also Facies S6. This inference is consistent with the distance from mean sea level to modern dune cordons.

## CONCLUSION

Our detailed sedimentological analysis of beachrock from two sites along the microtidal east coast of South Africa reveals the migration of a paleo inlet, and formation of beachrock in sub, inter, and supratidal settings. Particularly from the latter, we infer at least three cycles of Holocene sea level rise/fall. Although we cannot yet assess this history chronologically, three full cycles of transgression and regression are broadly consistent with previous regional sea level studies conducted by Ramsay and Cooper (2002), Compton (2006), and Norström *et al.* (2012). By more completely understanding the sedimentological characteristics of beachrock at a given locality, geoscientists can more accurately assess the coastal environment in which it formed. This study demonstrates the utility of such an analysis to the position of formation of beachrock, and thus relative sea level history.

Future efforts to age-date the cement of key sea level datums from these sites will help to further resolve the poorly-constrained Holocene sea level history of southeast Africa.

## ACKNOWLEDGEMENTS

We are grateful to Mr Riaan Botes for his assistance with GIS-based figures. Additionally, we thank the U.S. Fulbright Student Program and the University of KwaZulu-Natal in their support of this research collaboration.

## LITERATURE CITED

- Broome, R. and Komar, P.D., 1979. Undular hydraulic jumps and the formation of backlash ripples on beaches. *Sedimentology*, 26, pp.543–559.
- Caron, V., 2011. Contrasted textural and taphonomic properties of high-energy wave deposits cemented in beachrocks (St. Bartholomew Island, French West Indies). *Sedimentary Geology*, 237(3–4), pp.189–208.
- Cawthra, H.C., 2012. New Insights into the Geological Evolution of the Durban Bluff and Adjacent Blood Reef, South Africa. *South African Journal of Geology*, 115, pp.291–308.
- Cooper, J.A.G., 1989. Fairweather versus flood sedimentation in Mhlanga Lagoon, Natal: implications for environmental management. *South African Journal of Geology*, 92, pp. 279–294.
- Cooper, J.A.G. 1991. Beachrock formation in low latitudes: implications for coastal evolutionary models. *Marine Geology*, 98, 145–154.
- Cooper, J.A.G. 2011. Sea Level Studies: Sedimentary indicators of relative sea-level changes - high energy coasts. In: Elias, S.A. (ed) Encyclopedia of Quaternary Science. Second Edition. Elsevier, 4, 385–395.
- Cooper, J.A.G. and Flores, R.M., 1991. Shoreline deposits and diagenesis resulting from two Late Pleistocene highstands near +5 and +6 metres, Durban, South Africa. *Marine Geology*, 97, pp.325–343.
- Cooper, M.R. and Liu, K., 2004. The Cainozoic palaeontology and stratigraphy of KwaZulu-Natal. Part 4. The post-Karoo geology of the Durban area, with special reference to the Isipingo Formation. *Durban Museum Novitates*, 29, pp.1–23.
- Compton, J.S., 2006. The mid-Holocene sea-level highstand at Bogenfels Pan on the southwest coast of Namibia. *Quaternary Research*, 66(2), pp.303–310.
- Davies, J. L., 1964. A morphogenic approach to world shorelines. *Zeitschrift für Geomorphologie*, 8, 127–142.
- Davis, R. A., & Hayes, M. O., 1984. What is a wave-dominated coast?. *Marine Geology*, 60(1), 313–329.
- Desruelles, S., Fouache, É., Ciner, A., Dalongeville, R., Pavlopoulos, K., Kosun, E., Coquinot, Y., and Potdevin, J.-L., 2009. Beachrocks and sea level changes since Middle Holocene: Comparison between the insular group of Mykonos–Delos–Rhenia (Cyclades, Greece) and the southern coast of Turkey: Global and Planetary Change, v. 66, no. 1–2, p. 19–33.
- Fitzgerald, D.M., Buynevich, I. V and Hein, C., 2012. Morphodynamics and Facies Architecture of Tidal Inlets and Tidal Deltas. In R. a. Davis, R. a. J. Davis, and R. W. Dalrymple, eds. *Principles of Tidal Sedimentology*. Springer Netherlands, pp. 301–333.
- Google Earth, 2013. <http://www.earth.google.com> [Nov. 15, 2013].
- Green, A.N., Cooper, J.A.G., Le Vieux, A.M., 2013. Unusual barrier/inlet behaviour associated with active coastal progradation and river-dominated estuaries, *J. Coast. Res.* 69, 35–45.
- Green, A.N, Cooper, J.A.G. and Satzmann, L. 2014. Holocene shelf stratigraphy in the context of a stepped sea level rise: stratigraphic signature of meltwater pulses. *Geology*. (in press)
- Greenwood, B. and Mittler, P.R., 1985. Vertical Sequence and Lateral Transitions in the Facies of a Barred Nearshore Environment. *Journal of Sedimentary Petrology*, 55(3), pp.0366–0375.
- Hayes, M.O., 1976. Transitional-coastal depositional environments. In M. O. Hayes and T. K. Kana, eds. *Terrigenous Clastic Depositional Environments: Am. Assoc. Petroleum Geologists Field Course Notes*. University of South Carolina, pp. 32–111.
- Hayes, M.O., Anan, F.S. and Bozeman, R.N., 1972. Sediment dispersal trends in the littoral zone; a problem in paleogeographic reconstruction. In *Coastal Environments of Northeastern Massachusetts and New Hampshire*. University of Massachusetts, pp. 290–315.
- Jukes, L.M., 1976. A bone-bearing beachrock at Umbogintwini, Natal. *Transactions of the Geological Society of South Africa*, 79, pp.301–303.
- Hunter, R.E., Clifton, E.H. and Phillips, L.R., 1979. Depositional Processes, Sedimentary Structures, and Predicted Vertical Sequences in Barred Nearshore Systems, Southern Oregon Coast. *Journal of Sedimentary Petrology*, 49(3), pp.0711–0726.
- Kelletat, D., 2006. Beachrock as Sea-Level Indicator? Remarks from a Geomorphological Point of View. *Journal of Coastal Research*, 226, pp.1558–1564.
- Knight, J., 2007. Beachrock Reconsidered. Discussion of: Kelletat, D., 2006. Beachrock as Sea-Level Indicator? Remarks from a Geomorphological Point of View. *Journal of Coastal Research*, 22(6), 1558–1564. *Journal of Coastal Research*, 234(July), pp.1074–1078.
- Krige, L.J., 1932. The Geology of Durban. *Transactions of the Geological Society of South Africa*, 35, pp.37–67.
- McCarthy, M.J., 1967. Stratigraphical and Sedimentological Evidence from the Durban Region of Major Sea-level Movements since the Late Tertiary. *Transactions of the Geological Society of South Africa*, 70, pp.135–165.
- Norström, E., Risberg, J., Gröndahl, H., Holmgren, K., Snowball, I., Mugabe, J.A., and Siteo, S.R., 2012. Coastal paleo-environment and sea-level change at Macassa Bay, southern Mozambique, since c 6600 cal BP: *Quaternary International*, v. 260, p. 153–163.
- Postma, G. and Nemeč, W., 1990. Regressive and transgressive sequences in a raised Holocene gravelly beach, southwestern Crete. *Sedimentology*, 37, pp.907–920.
- Ramsay, P.J., 1995. 9000 Years of Sea-Level Change Along the Southern African Coastline. *Quaternary International*, 31(1989), pp.71–75.
- Ramsay, P.J. and Cooper, J.A.G., 2002. Late Quaternary Sea-Level Change in South Africa. *Quaternary Research*, 57(1), pp.82–90.

- Ramsay, P.J. and Mason, T.R., 1990. Development of a Type Zoning Model for Zululand Coral Reefs, Sodwana Bay, South Africa. *Journal of Coastal Research*, 6(4), pp.829–852.
- Reddering, J.S. V., 1983. An inlet sequence produced by migration of a small microtidal inlet against longshore drift : the Keurbooms Inlet , South Africa. *Sedimentology*, 30, pp.201–218.
- Reddering, J.S. V. 1988. Pseudo-stylolites produced by abrasion, Robberg, southern Cape. *South African Journal of Geology* , 91, pp. 415-416.
- Reineck, H.E. and Singh, I.B., 1986. *Depositional Environments* 2nd ed., New York: Springer.
- Schumann, E. H., & Orren, M. J. , 1980. The physico-chemical characteristics of the south-west Indian Ocean in relation to Maputaland. in M.N. Bruton and K.H. Cooper, eds. *Studies on the ecology of Maputaland*. Rhodes University and The Wildlife Society of Southern Africa, Grahamstown-Durban, 8-11.
- Seminack, C.T. and Buynevich, I. V., 2013. Sedimentological and Geophysical Signatures of A Relict Tidal Inlet Complex Along A Wave-Dominated Barrier: Assateague Island, Maryland, U.S.A. *Journal of Sedimentary Research*, 83(2), pp.132–144.
- Vacchi, M., Rovere, A., Zouros, N., Desruelles, S., Caron, V., and Firpo, M., 2012, Spatial distribution of sea-level markers on Lesbos Island (NE Aegean Sea): Evidence of differential relative sea-level changes and the neotectonic implications: *Geomorphology*, v. 159-160, p. 50–62.
- Vousdoukas, M.I., Velegrakis, a. F. and Plomaritis, T. a., 2007. Beachrock occurrence, characteristics, formation mechanisms and impacts. *Earth-Science Reviews*, 85, pp.23–46.